Virchows Arch (2006) 449: 1–13
DOI 10.1007/s00428-006-0190-9

REVIEW ARTICLE

Rodolfo Montironi · Remigio Vela Navarrete · Antonio Lopez-Beltran · Roberta Mazzucchelli · Gregor Mikuz · Aldo V. Bono

Histopathology reporting of prostate needle biopsies. 2005 update

Received: 3 October 2005 / Accepted: 15 November 2005 / Published online: 22 April 2006
© Springer-Verlag 2006

Abstract This report reviews the diagnostic and prognostic importance of the pathologic findings in prostate needle biopsies. The morphological findings of the needle biopsy may be placed into one of the following five categories: prostate cancer, atypical small acinar proliferation, high-grade prostatic intraepithelial neoplasia, inflammation, and benign prostatic tissue. While the prime goal of the biopsy is to diagnose prostatic adenocarcinoma, once carcinoma is detected, further descriptive information regarding the type, amount of cancer, and grade forms the cornerstone for contemporary management of the patient and for assessment of the potential for local cure and the risk for distant metastasis. The information provided in the needle biopsy report regarding the attributes of carcinoma is used depending on the individual patient's medical condition and preference and on the treating physician's evaluation to determine whether any form of treatment is indicated and, if so, the type of therapy.

Keywords Prostate cancer · Needle biopsy · Prognostic factor · Gleason score · Perineural invasion · Tumor volume

Issues on the pathology reporting of prostate needle biopsies have been dealt with in recent consensus conferences organized under the auspices of the Uropathology Working Group (European Society of Pathology), European Society of Uropathology (a full section office member of the European Association of Urology) (Florence, Italy, June 2003, and Palermo, Sicily, June 2005), World Health Organization (Lyon, France, December 2002, and Stockholm, Sweden, September 2004), and International Society of Urologic Pathology (San Antonio, TX, USA, March 2005). The authors of this review have been involved in these conferences.

R. Montironi (✉) · R. Mazzucchelli
Institute of Pathological Anatomy and Histopathology,
Polytechnic University of the Marche Region (Ancona),
School of Medicine, United Hospitals,
Via Conca 71, 60020 Torrette, Ancona, Italy
e-mail: r.montironi@univpm.it
Fax: +39-071-889985

R. Vela Navarrete
Urology Service and Renal Transplantation Unit,
Autonomous University of Madrid,
Madrid, Spain

A. Lopez-Beltran
Department of Pathology, Reina Sofia University Hospital and
Cordoba University Medical School,
Cordoba, Spain

G. Mikuz
Department of Pathology,
University of Innsbruck School of Medicine,
Innsbruck, Austria

A. V. Bono
Department of Urology,
Ospedale di Circolo,
Varese, Italy

Introduction

The detection of prostate cancer (PCa) has tripled during the past decade, chiefly because of the widespread use of serum prostate-specific antigen testing, digital rectal examination, and transrectal ultrasound. Needle biopsy of the prostate plays a central role in the morphologic evaluation of prostate cancer [2, 54, 72]. The morphological diagnosis may be placed into one of the following five categories: PCa, atypical small acinar proliferation (ASAP), high-grade prostatic intraepithelial neoplasia (HGPIN), inflammation, and benign prostatic tissue [56]. The pathology report of a biopsy with cancer should include a number of morphological features that may help urologists to assess the risk of extraprostatic disease and progression: the cancer's location, extent and volume of the cancer in each specimen, and the Gleason score; optional features that may add predictive value include the presence of perineural invasion, vascular/lymphatic invasion, microvessel density (MVD), and DNA ploidy expression. Furthermore, the cancer's expression of select biomarkers may be of value [58]. This report reviews the diagnostic and prognostic importance of the pathologic findings in prostate needle biopsies.

Prostate cancer

Diagnostic criteria

The diagnosis of carcinoma relies on a combination of architectural and cytologic findings. The light microscopic features are usually sufficient, but cases with small suspicious foci may benefit from immunohistochemical studies (Table 1).

Architectural features

Architectural features are usually assessed at low- to medium-power magnification, with emphasis on spacing, size, and shape of acini. The arrangement of the acini is diagnostically useful and is the basis of the Gleason grade. Malignant acini usually have an irregular, haphazard arrangement, randomly scattered in the stroma in clusters or singly (Fig. 1a). The spacing between malignant acini often varies widely. Variation in acinar size is a useful criterion for cancer, particularly when small, irregular, abortive acini with primitive lumens are seen at the periphery of a focus of well-differentiated carcinoma.

The acini in suspicious foci are usually small or medium sized, with irregular contours that contrast with the typical smooth, round to elongated contours of benign and hyperplastic acini. Comparison with the adjacent benign prostatic acini is always of value in the diagnosis of cancer. Well-differentiated carcinoma and the large acinar variant of Gleason grade 3 carcinoma are particularly difficult to separate from benign acini in needle biopsies because of the uniform size and spacing of acini; in such cases, greater emphasis is placed on cytologic features, immunohistochemical findings, and the presence of smaller diagnostic acini at the edge of the focus.

The basal cell layer is absent in prostate cancer, whereas an intact basal cell layer is present with benign acini. This is an important diagnostic feature that is not always easy to evaluate in routine tissue sections, owing to false negative findings with atrophy and other mimics of cancer. Compressed stromal fibroblasts may mimic basal cells but are usually seen only focally at the periphery of acini. Small foci of adenocarcinoma sometimes cluster around or infiltrate near larger benign acini that have intact basal cell layers, compounding the difficulty.

Table 1 Diagnostic criteria for carcinoma

Architectural features
Infiltrative pattern of malignant acini
Arrangement: irregular and haphazard
Spacing between acini varies widely
Variation in size
Irregular contour
Basal cell layer
Absent
Cytological features (secretory cells in single layer)
Nuclear hyperchromasia
Nuclear enlargement
Nucleolar enlargement or prominence
Mitotic figures
Amphophilic cytoplasm
Luminal findings
Crystalloids
Intraluminal blue mucin and/or pink amorphous secretions
Stromal findings
Collagenous micronodules
Immunohistochemical findings
Prostate-specific antigen
Prostatic acid phosphatase
34βE12
p63
Racemase
Additional feature
Adjacent prostatic intraepithelial neoplasia

Cytologic features

The cytologic features of adenocarcinoma include nuclear and nucleolar enlargement, which occurs in most malignant cells (Fig. 1b). Every cell has a nucleolus, so "prominent" nucleoli (at least 1.50 μm in diameter or larger) are sought. Pathologists do not routinely measure nucleoli for diagnosis; this determination is based on comparison with benign epithelial cells elsewhere in the specimen.

Artifacts often obscure the nuclei and nucleoli, and overstaining of nuclei by hematoxylin creates one of the most common and difficult problems in the interpretation of suspicious cells. Differences in the fixation and handling of biopsy specimens influence nuclear size and chromasia, so comparison with cells from the same specimen is useful as an internal control. Many pathologists prefer pale staining with eosin, but this approach fails to accentuate nucleoli, which are often enlarged. In specimens with nuclear hyperchromasia and pale eosinophilic staining, we often increase the light source and magnification of suggestive foci to identify hidden enlarged nucleoli.

Luminal findings

Crystalloids are sharp, needle-like eosinophilic structures that are often present in the lumens of well-differentiated and moderately differentiated carcinomas (Fig. 1c) [18]. They are not specific for carcinoma and can be found in other conditions. The presence of crystalloids in metastatic adenocarcinoma of unknown site of origin is strong presumptive evidence of prostatic origin, although it is an uncommon finding and not conclusive [53]. Special stains highlight the presence of crystalloids that otherwise cannot be seen by light microscopy [53]. Crystalloids stain red with trichrome stain, blue with toluidine blue, and violet with Mallory's staining. Crystalloids are argyrophilic with silver stain methods. No staining is observed with PAS,

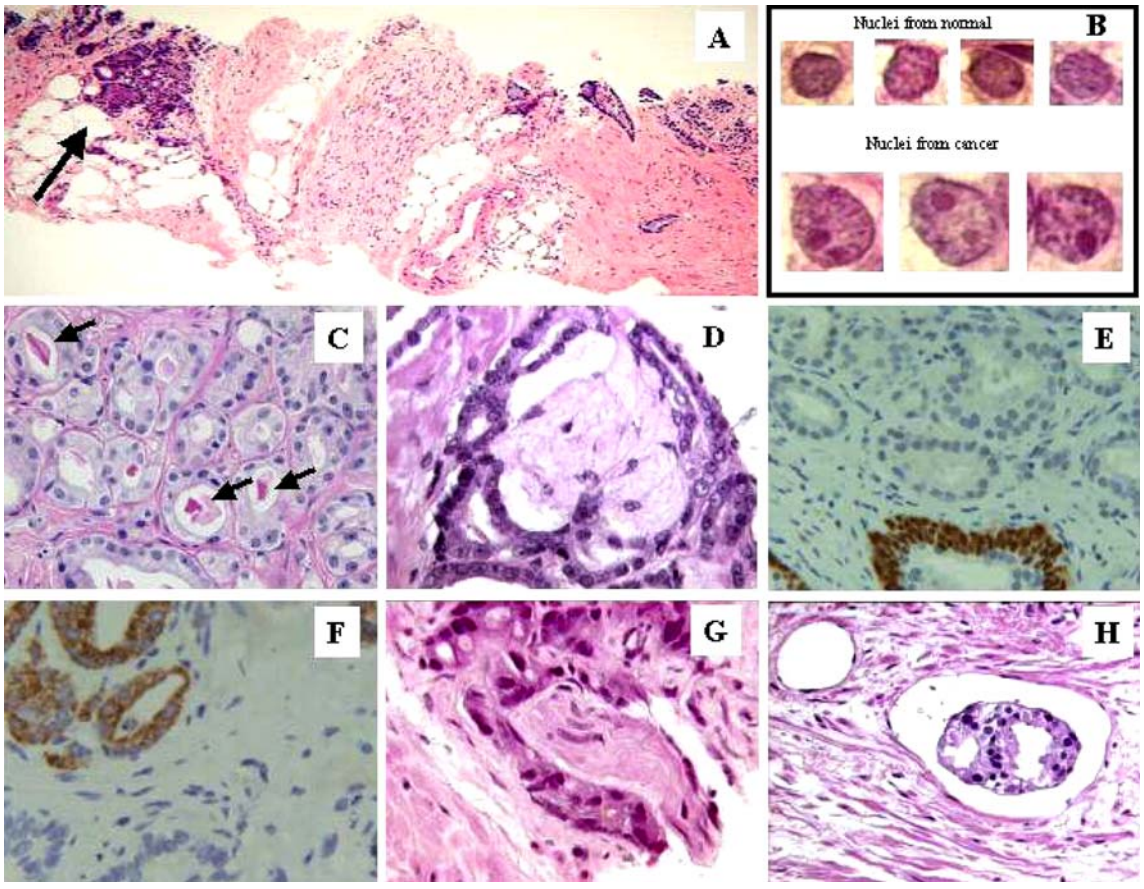

Fig. 1 **a** Prostate biopsy with cancer: acini with an irregular, haphazard arrangement, randomly scattered in the stroma in clusters. Extraprostatic extension is present (*arrow*). **b** The cytologic features of adenocarcinoma include nuclear and nucleolar enlargement, which occurs in most malignant cells (nuclei from normal cells are shown for comparison). **c** Prostate cancer with crystalloids (*arrows*). **d** Collagenous micronodules. **e** Prostate cancer lacks basal cells (a nonneoplastic duct/acinus with basal cells is shown for comparison) (cocktail including 34betaE12 and p63). **f** Prostate cancer with racemase expression (a nonneoplastic duct/acinus without racemase is shown for comparison). **g** Perineural invasion. **h** Lymphovascular invasion

Alcian blue, Prussian blue, and Congo red. Immunohistochemical stains for prostate-specific antigen (PSA) and prostatic acid phosphatase (PAP) are negative. The pathogenesis of crystalloids is not known, but they probably result from abnormal protein and mineral metabolism within benign and malignant acini. Ultrastructurally, they are composed of electron-dense material that lacks the periodicity of crystals. Radiographic microanalysis reveals abundant sulfur, calcium, and phosphorus and a small amount of sodium [18]. Hard, proteinaceous secretions are almost always present in adjacent acini and are probably the source of the crystalloids.

Luminal acidic sulfated and nonsulfated mucin is often seen in acini of adenocarcinoma, appearing as amorphous or delicate, threadlike, faintly basophilic secretions in routine sections. This mucin stains with Alcian blue and is best displayed at pH 2.5, whereas normal prostatic epithelium contains periodic acid Schiff-reactive mucin that is neutral. Acidic mucin is not specific for carcinoma; it may be found in prostatic intraepithelial neoplasia (PIN), atypical adenomatous hyperplasia, sclerosing adenosis, and, rarely, nodular hyperplasia [31].

Occasionally, PCa may show the presence of intraluminal corpora amylacea. These are usually seen in normal ducts and acini, adenosis, and verumontanum mucosal gland hyperplasia.

Stromal findings

The stroma in cancer frequently contains young collagen, which appears lightly eosinophilic, although desmoplasia may be prominent. Muscle fibers in the stroma are sometimes split or distorted. However, this is a difficult feature to appreciate and cannot be relied upon because of the resemblance of the stroma associated with benign acini.

Collagenous micronodules (or *mucinous fibroplasia*) are a specific but infrequent and incidental finding in prostatic adenocarcinoma. They consist of microscopic nodular masses of paucicellular eosinophilic fibrillar stroma that impinge on acinar lumens (Fig. 1d) [12]. They are usually present in mucin-producing adenocarcinoma and result from extravasation of acidic mucin into the stroma. Collagenous micronodules are present in about 13% of

cases of adenocarcinoma; they are not observed in benign epithelium, nodular hyperplasia, or PIN. They are an infrequent finding, present in 0.6% of needle biopsies and 12.7% of prostatectomies. Collagenous micronodules may be particularly valuable in challenging needle biopsy specimens [12].

Immunohistochemical findings

The most important immunohistochemical markers in prostate pathology are PSA, PAP, and high-molecular-weight keratin 34βE12. Promising new markers include prostate-specific membrane antigen and human glandular kallikrein 2 [17]. Useful confirmatory immunohistochemical stain to demonstrate urothelial origin is the combination of cytokeratin 7, cytokeratin 20, and thrombomodulin.

The immunohistochemical expression of PSA is useful for distinguishing high-grade prostate cancer from urothelial carcinoma, colonic carcinoma, granulomatous prostatitis, and lymphoma [8]. PSA also facilitates the identification of the site of tumor origin in metastatic adenocarcinoma. PSA can be detected in frozen sections, paraffin-embedded sections, cell smears, and cytologic preparations of normal and neoplastic prostatic epithelium. Staining is invariably heterogeneous. Microwave antigen retrieval is usually not necessary, even in tissues that have been immersed in formalin for years. Formalin fixation is optimal for the localization of PSA, and variation in staining intensity is only partially the result of fixation and embedding effects. Immunoreactivity is preserved in decalcified specimens and may be enhanced. PAP is a valuable immunohistochemical marker for identifying prostate cancer when used in combination with PSA [48]. The intensity of PAP immunoreactivity correlates with patient survival, probably because immunoreactive cancer has greater androgen responsiveness.

In problem cases, using monoclonal antibodies directed against *high-molecular-weight cytokeratin* (for example, clone *34βE12*) may be useful for evaluation of the basal cell layer. We use this infrequently (in fewer than 5% of cases), however, and only as an adjunct to the light microscopic findings. The findings with this immunohistochemical stain should not be the basis for a diagnosis of malignancy, particularly in small suggestive foci. It is most useful in confirming the benignancy of a suggestive focus by showing an immunoreactive basal cell layer. Anti-keratin 34βE12 stains nearly all of the normal basal cells of the prostate; no staining occurs in the secretory and stromal cells.

Because the uniform absence of a basal cell layer in prostatic acinar proliferations is one important diagnostic feature of invasive carcinoma, and because basal cells may be inapparent by hematoxilin–eosin (H&E) stain, basal cell specific immunostains may help to distinguish invasive prostatic adenocarcinoma from benign small acinar cancer—mimics which retain their basal cell layer, e.g., glandular atrophy, postatrophic hyperplasia, atypical adenomatous hyperplasia, sclerosing adenosis (atypical adenomatous hyperplasia), and radiation-induced atypia [24, 32, 79]. Because the basal cell layer may be interrupted or not demonstrable in small numbers of benign glands, the complete absence of a basal cell layer in a small focus of acini cannot be used alone as a definitive criterion for malignancy; rather, the absence of a basal cell layer is supportive of invasive carcinoma only in acinar proliferations which exhibit suspicious cytologic and/or architectural features on H&E stain [32]. Conversely, some early invasive prostatic carcinomas, e.g., microinvasive carcinomas arising in association with or independent of HGPIN, may have residual basal cells [60]. The intraductal spread of invasive carcinoma and entrapped benign glands are other proposed explanations for residual basal cells [24, 79]. Rare prostatic adenocarcinomas contain sparse neoplastic glandular cells that are immunoreactive for 34βE12, yet these are not in a basal cell distribution [24, 69]. The use of antibodies for 34βE12 is especially helpful for the diagnosis of deceptively appearing variants of prostate cancer. Immunohistochemistry for cytokeratins 7 and 20 have a limited diagnostic use in prostate pathology with the exception that negative staining for both markers, which can occur in prostate adenocarcinoma, would be unusual for transitional cell carcinoma [29].

p63, a nuclear protein encoded by a gene on chromosome 3q27–29 with homology to p53 (a tumor suppressor gene), has been shown to regulate growth and development in epithelium of the skin, cervix, breast, and urogenital tract. Specific isotypes are expressed in basal cells of stratified and pseudostratified epithelia (prostate, bronchial), reserve cells of simple columnar epithelia (endocervical, pancreatic ductal), myoepithelial cells (breast, salivary glands, cutaneous apocrine/eccrine glands), urothelium, and squamous epithelium [42]. A monoclonal antibody is active in paraffin-embedded tissue following antigen retrieval. p63 has similar applications to those of high-molecular-weight cytokeratins in the diagnosis of prostatic adenocarcinoma (Fig. 1e), but with the advantages that p63 (1) stains a subset of 34βE12-negative basal cells, (2) is less susceptible to the staining variability of 34βE12 (particularly in transurethral prostatectomy specimens with cautery artifacts), and (3) is easier to interpret because of its strong nuclear staining intensity and low background. Interpretative limitations related to the presence or absence of basal cells in small numbers of glands for 34βE12 apply to p63, requiring correlation with morphology [69]. Prostatic adenocarcinomas have occasional p63 immunoreactive cells, most representing entrapped benign glands or intraductal spread of carcinoma with residual basal cells [42].

α-Methyl-coenzyme A racemase (*AMACR*) mRNA was recently identified as being overexpressed in prostatic adenocarcinoma by cDNA library subtraction utilizing high-throughput RNA microarray analysis [77]. This mRNA was found to encode a racemase protein, for which polyclonal and monoclonal antibodies have been produced which are active in formalin-fixed, paraffin-embedded tissue [4, 38, 77, 81]. Immunohistochemical studies on biopsy material with an antibody directed against AMACR (P504S) demonstrate that more than 80% of prostatic adenocarcinomas are labeled [39]. Certain

subtypes of prostate cancer, such as foamy gland carcinoma, atrophic carcinoma, pseudohyperplastic, and treated carcinoma show lower AMACR expression. However, AMACR is not specific for prostate cancer and is present in nodular hyperplasia (12%), atrophic glands (36%), HGPIN (>90%) [81], and atypical adenomatous hyperplasia (17.5%) [78]. AMACR may be used as a confirmatory stain for prostatic adenocarcinoma, in conjunction with H&E morphology and a basal cell specific marker (Fig. 1f) [81]. AMACR is expressed in other nonprostatic neoplasms, including urothelial and colon cancer. An immunoperoxidase cocktail containing monoclonal antibodies to cytokeratin 34betaE12 and p63 is an effective basal cell stain (Fig. 1e). A cocktail containing 34betaE12, p63, and racemase is also used.

Prognostic morphologic factors

The information provided in the surgical pathology report of a prostate needle biopsy with carcinoma has become critical in the subsequent management and prognostication of the cancer. The surgical pathology report should thus be comprehensive and yet succinct in providing relevant information consistently to urologists, radiation oncologists, and oncologists, and, thereby, to the patient (Table 2) [2, 7, 15, 58].

Site of sampling (specific location of the biopsy)

While obtaining multiple systematic biopsies is relatively standard in urologic practice, the submission of needle cores in two containers (left and right side) or individual containers for each site [site-specific labeling (e.g., right apex, right mid, right base, etc.)] remains a matter of urologist/institutional preference. The potential importance of knowing the specific location of the biopsy and, by extension, the location of the cancer may be summarized into seven headings (Table 3) [26, 59, 80]:

1. *Correlation with digital rectal examination and imaging studies*
2. *Prognostic importance*. Tumor involvement of base biopsies may influence bladder neck-sparing radical prostatectomy; extensive cancer in base biopsies correlates with extraprostatic extension; and the dominant side of prostate biopsy correlates with ipsilateral positivity of surgical margins and extraprostatic extension [2]
3. *Importance in planning therapy*. Mapping distribution of the cancer in needle biopsies may help plan the field of radiation therapy or may influence nerve sparing or bladder neck sparing during radical prostatectomy
4. *Importance in subsequent patient sampling*. In a patient with atypical glands without cancer, knowledge of the site allows for more focused repeat biopsies
5. *Importance in subsequent prostate gland sampling*. Biopsy samples with site-specific labeling usually contain only one or two cores, which is advantageous for block and slide preparation and allows for complete visualization of cores and detection of small foci of cancer; and knowledge of the location of the cancer may help target additional tissue or block sampling in cases with no apparent cancer in radical prostatectomy sections
6. *Technical superiority in needle biopsy material examination*. Limited number of cores in site-specific labeled specimens reduces fragmentation, thereby allowing for more confident assessment of the number of cores involved
7. *Knowledge of the biopsy site helps recognize potential diagnostic pitfalls*. This includes seminal vesicle epithelium or central zone epithelium, seen most frequently in base biopsies and the rare Cowper's glands in apex biopsies

Table 2 Prognostic factors in prostate biopsies with cancer

Location and distribution of tumor
Histopathologic type
Gleason score including primary and secondary patterns
Extent of involvement
Local invasion: extraprostatic extension and seminal vesicle involvement
Perineural invasion: extent (focal vs multifocal) and diameter of nerve bundles
Lymphovascular invasion

Table 3 The potential importance of knowing the specific location of the biopsy and the location of the cancer

Correlation with digital rectal examination and imaging studies
Prognostic importance
Importance in planning therapy
Importance in subsequent patient sampling
Importance in subsequent prostate gland sampling
Technical superiority in needle biopsy material examination
Knowledge of biopsy site helps to recognize potential diagnostic pitfalls

Histologic type (variants and variations of acinar adenocarcinoma)

Greater than 99% of all carcinomas of the prostate seen in needle biopsy specimens are referred to as acinar, microacinar, or conventional type. Because this is the overwhelming histologic type of cancer in needle biopsy specimens, it is not necessary to specify such cancers as acinar or conventional type in pathology reports (Table 4).

Carcinomas of the prostate with architectural or cytologic variations, such as atrophic, pseudohyperplastic, hypernephroid, etc., are descriptive terms used to describe variations in prostate cancer to help pathologists recognize diagnostic pitfalls, but have no known prognostic sig-

Table 4 Histological type in prostate needle biopsy specimens

Adenocarcinoma of prostate (conventional, acinar, microacinar or usual type, and variations)
Adenocarcinoma of prostate with ductal features
Adenocarcinoma of prostate with mucinous differentiation
Adenocarcinoma of prostate with signet ring cell features
Sarcomatoid carcinoma of prostate
Adenosquamous carcinoma
Small cell carcinoma of prostate
Urothelial carcinoma (involving prostatic ducts and acini without stromal invasion and involving prostatic ducts and acini with stromal invasion)
Basal cell (adenoid cystic) carcinoma

Table 5 Issues on the application of the Gleason grading system

General applications of the Gleason grading system
Grading variations of acinar adenocarcinoma
Grading variants of adenocarcinoma
Reporting secondary patterns of lower grade when present to a limited extent
Reporting secondary patterns of higher grade when present to a limited extent
Tertiary Gleason patterns
Percentage of Gleason 4 pattern in Gleason score 7 tumors
Percent pattern 4–5
Needle biopsy with different cores showing different grades

nificance. They may be commented upon in a microscopic description and do not deserve specific mention in the final diagnosis.

Several variants of prostate cancer have been described, including ductal, mucinous, signet ring cell, adenosquamous, small cell carcinoma, and sarcomatoid carcinoma [19]. The former three are diagnoses tenable only on examination of radical prostatectomy or transurethral resection specimens. If seen in needle biopsy specimens, the diagnostic terminology used must be adenocarcinoma of prostate with ductal features; adenocarcinoma of prostate with signet ring cell features; and adenocarcinoma of prostate with mucinous differentiation. Small cell carcinoma, sarcomatoid carcinoma, and adenosquamous carcinoma may be diagnosed on needle biopsies. There are no formal studies that have demonstrated that the presence of these histologic variants in needle biopsies is of prognostic or predictive importance, although the often-aggressive outcome associated with such tumors suggests the value of this exercise [2].

Cancer grade

The Gleason grading system is recommended as the international standard for grading prostate cancer. The Gleason score is a scalar measurement that combines discrete primary and secondary groups (patterns or grades) into nine groups (scores 2 to 10). The Gleason score should be reported as the composite score and its component patterns, e.g., Gleason $7 = 4 + 3$. The method of reporting in needle biopsies needs the clarification of some issues, including some not addressed in the original Gleason system [57] (Table 5). A recent consensus conference organized by the members of the International Society of Urological Pathology has dealt with the current application of the Gleason system [23]. The recommendations are summarized as follows:

1. *General applications of the Gleason grading system*. A Gleason score of $1 + 1 = 2$ is a grade that should not be diagnosed regardless of the type of specimen, with extremely rare exceptions. The diagnosis of Gleason 2–4 should not be made on needle biopsies [20]. The reasons for not making this diagnosis are compelling: (1) Gleason score 2–4 cancer is extraordinarily rare in needle biopsies, as compared to transurethral resection specimens; (2) there is poor reproducibility among experts for lower-grade tumors [1]; (3) the correlation with the prostatectomy score for Gleason 2–4 tumors is poor, and approximately half of the prostatectomies in one study had extraprostatic extension; and (4) a "low" score of Gleason 2–4 may misguide clinicians and patients into believing that there is an indolent tumor. "Individual cells" would not be allowed within Gleason pattern 3. The vast majority of cribriform patterns are diagnosed as Gleason pattern 4 with only rare cribriform lesions satisfying diagnostic criteria for cribriform pattern 3C
2. *Grading variations of acinar adenocarcinoma*. One should grade the tumor solely based on the underlying architecture
3. *Grading variants of adenocarcinoma*. Ductal adenocarcinomas should be graded as Gleason score $4 + 4 = 8$, while retaining the diagnostic term of ductal adenocarcinoma to denote their unique clinical and pathological findings. There is no consensus on the way colloid (mucinous) carcinoma should be scored. Some authors think that all colloid carcinomas should be assigned a Gleason score of 8, while others say that one should ignore the extracellular mucin and grade the tumor based on the underlying architectural pattern. Small cell carcinoma should not be assigned a Gleason grade
4. *Reporting secondary patterns of lower grade when present to a limited extent*. In the setting of high-grade cancer, one should ignore lower-grade patterns if they occupy less than 5% of the tumor area
5. *Reporting secondary patterns of higher grade when present to a limited extent*. High-grade tumors of any quantity on needle biopsy, as long as it was identified at low to medium magnification, should be included within the Gleason score
6. *Tertiary Gleason patterns*. The typical situation with tertiary patterns on biopsy includes tumors with patterns 3, 4, and 5, in various proportions. Such tumors should be classified overall as high grade (Gleason score 8–10) given the presence of a high-grade tumor (patterns 4 and 5) on needle biopsy. On needle biopsies with patterns 3, 4, and 5, both the

primary pattern and the highest grade should be recorded. For a radical prostatectomy specimen, one assigns the Gleason score based on the primary and secondary patterns with a comment as to the tertiary pattern

7. *Percentage of Gleason 4 pattern in Gleason score 7 tumors*. In recently generated nomograms, patients with Gleason score 4+3 vs 3+4 are stratified differently, underscoring the importance of the relative amount of pattern 4 [49]
8. *Percent pattern 4–5*. Whether the actual percentage of pattern 4 tumors should be included in the report is not clear based on published data to date, and, if this emerges as an important parameter, meaningful discriminatory cut-off points for the percentage of pattern 4 will need to be defined. It remains an option if one wants to include this information in addition to the routine Gleason score
9. *Needle biopsy with different cores showing different grades*. The pathologist should assign individual Gleason scores to separate cores, as long as the cores are submitted in separate containers or the cores are in the same container, yet specified by the urologist as to their location (i.e., by different color inks). In addition to giving separate cores individual Gleason scores, one has the option to also give an overall score at the end of the case. If more than one core contained cancer in the setting of multiple cores per container, some authors think that one should still grade each core separately, with the other authors saying that one should give an overall grade for the involved cores per specimen container. In cases where a container contains multiple pieces of tissue and one cannot be sure if one is looking at an intact core, one should only give an overall score for that container

The WHO nuclear grading system should be used in addition to the Gleason scheme, but, in practice, is rarely or never reported. Nuclear anaplasia is scored as 1, 2, and 3, corresponding to slight, moderate, and marked nuclear changes, respectively. Nuclear grade is based on the predominant nuclear grade, but there may also be value to report the highest nuclear grade [57].

Extent of involvement of needle core (tumor volume)

The amount of tumor in prostate needle cores is an important pathologic parameter that must be reported in needle biopsies. The extent of involvement of needle cores by prostatic adenocarcinoma has been shown to correlate with the Gleason score, tumor volume, surgical margins, and pathologic stage in radical prostatectomy specimens [26, 41]. The extent of needle core involvement, including bilateral involvement, has also been shown to predict biochemical recurrence, postprostatectomy progression, and radiation therapy failure in univariate, and often in multivariate, analysis [25, 26, 28, 41, 44]. The extent of this involvement is a parameter included in some recent nomograms created to predict pathologic stage and seminal vesicle invasion after radical prostatectomy and radiation therapy failure [25, 27, 43, 44].

The amount of cancer in a biopsy specimen depends on many factors, including prostate volume, cancer volume, cancer distribution, technical procedure, number of biopsy cores obtained, and cohort of patients being evaluated.

There is lack of consensus in the literature as to the best method of reporting the extent of tumor involvement. The report should provide the number of involved cores (if possible, it should include the percentage of cores involved) (Table 6). In addition, one or both of the following more detailed methods of tumor extent should be performed: One method is to report the linear length of cancer in millimeters (total tumor length in all biopsies; longest single length of tumor; linear length in increments of 0.5 mm) [46]. The other method is to provide a percentage estimate of involvement of each of the cores derived by visual estimation (overall percentage of cancer in all biopsies, percentage of each core involved; reporting the percentage of cancer involvement in increments of 5 or 10% is appropriate) [21, 72]. The correlation is with greater involvement of the cores. While the correlation for high tumor burden in needle biopsies is directly proportional to the likelihood of an adverse outcome, low tumor burden in needle biopsies is not necessarily an indicator of low volume and low-stage cancer in the prostatectomy specimen [74].

One problem encountered with this otherwise straightforward method is when there is extreme fragmentation of the needle biopsy specimen, making the assessment of the number of cores and the percentage of cancer within each core difficult. In case of highly fragmented tissue, this may be overcome by providing a composite (global) percentage of involvement of cancer in all needle biopsy tissue, and this may be a slightly more accurate correlate of the amount of cancer in the prostate gland itself.

Bilateral cancer, which indicates multifocality, is indirectly suggestive of greater tumor volume. This parameter is easily deduced from the pathology report findings of each of the cores submitted. In patients not subsequently treated by radical prostatectomy, this is a critical factor in assigning "pathologic stage."

Table 6 Diagnostic reporting of amount of tumor in needle cores

Number of cores involved
Amount of cancer in biopsy (either method is optional)
Linear measurement in mm (total tumor length in all biopsies, longest single length of tumor)
Percent of sampled tissue (overall % of cancer in all biopsies, % of each core involved)
Bilaterality

Local invasion (location of carcinoma)

Routine biopsy sampling may occasionally contain extraprostatic fat or seminal vesicle tissue. If the cancer were noted to involve these structures, the finding would indicate pT3 disease. The presence of seminal vesicle invasion or extraprostatic fat involvement in the staging biopsy is highly correlative of similar findings at radical prostatectomies. Extraprostatic fat invasion (Fig. 1a) at needle biopsy is highly predictive of biochemical recurrence (79%, compared to 43% failure rate in cases with extraprostatic extension not detected by needle biopsy).

Only exceptionally rarely is fat present within the normal prostate. Hence, a tumor in adipose tissue in a needle biopsy specimen can safely be interpreted as an extraprostatic extension [16, 21]. Ganglion cells and skeletal muscle involvement by the tumor are not equivalent to extraprostatic extension, as they may both be found frequently within the prostate.

Distinction between the seminal vesicle epithelium and ejaculatory duct epithelium may be impossible in limited samples, although occasionally the seminal vesicle can be distinguished if its smooth muscle wall is present. In contrast, the ejaculatory duct epithelium has a rim of fibrous tissue that is rich in thin blood vessels. If the distinction between seminal vesicle tissue/ejaculatory duct is not feasible, diagnostic terminology such as "adenocarcinoma of the prostate with invasion of seminal vesicle/ejaculatory duct tissue" may be used.

In seminal vesicle or extraprostatic fat targeted biopsies, it is important to not only diagnose cancer, but to also determine whether the targeted tissue is represented. In a positive biopsy, if the intended tissue is not present and its absence is not specified in the report, there is a high likelihood of misinterpretation of a locally advanced disease that is not present. Also, seminal vesicle containing/targeted biopsies should demonstrate tumor within the muscular wall.

Perineural invasion

Perineural, circumferential, or intraneural invasion is defined as the presence of prostate cancer juxtaposed intimately along, around, or within a nerve (Fig. 1g). Other descriptors of perineural invasion that may strengthen the prognostic significance of this parameter include extensive (multifocal) perineural invasion and greater nerve diameter [50]. Involvement of nerves present within adipose tissue (extraprostatic nerves) by cancer indicates extraprostatic extension and deserves notation in the pathology report when present.

Although perineural invasion in needle biopsy specimens is not an independent predictor of prognosis when the Gleason score, serum PSA, and extent of cancer are factored in, most studies indicate that its presence correlates with extraprostatic extension (38–93%) [3, 61, 76]. Recent data suggest that this finding may independently predict lymph node metastasis and postsurgical progression [61, 68]. This parameter may also be used to plan nerve-sparing surgery [33]. Some of the data from the radiation oncology literature suggest that this parameter is an independent risk factor for predicting adverse outcome after external beam radiation therapy, and in patients with high Gleason scores and perineural invasion, adjuvant hormonal therapy or dose escalation has been advocated [5, 61].

Vascular/lymphatic invasion

Microvascular invasion consists of tumor cells within endothelial-lined spaces. The presence of a cellular reaction in the adjacent stroma is not required for diagnosis. Also, we do not differentiate between vascular and lymphatic channels because of the difficulty and lack of reproducibility among different observers by routine light microscopic examination [64]. Microvascular invasion may be confused with a fixation-associated retraction artifact of acini. Immunohistochemical stains directed against endothelial cells, such as factor VIII-related antigen, *Ulex europaeus*, CD31, or CD34, may increase the detection rate [64].

Because lymphovascular invasion (Fig. 1h), as studied in radical prostatectomy specimens, correlates with lymph node metastasis, biochemical recurrence, and distinct metastasis, its presence in the needle biopsy is likely to have similar correlations. This feature is very rarely seen in needle biopsy specimens. This finding should be reported in needle biopsy specimens only if identified [37, 71].

Prognostic molecular markers (and methods)

Other preoperative factors may improve the predictive accuracy for pathologic stage, including neuroendocrine (NE) differentiation, nuclear DNA content, and MVD [36, 66] (Table 7).

Table 7 Prognostic molecular markers (methods)

Neuroendocrine differentiation
Karyometric factors including DNA
Microvessel density
Proliferation markers (MIB-1, Ki-67)
Tumor suppressor gene (p53)
GSTP1 gene methylation
PTEN mutation
Hepsin
Pim-1 kinase
EZH2
p21
p27
ECPA and nuclear matrix proteins
Apoptosis-related: Bcl-2, Bax (radiotherapy patients)
Chromosomal alterations, especially 8p allelic imbalance
Others

Neuroendocrine (NE) differentiation

Prostate cancer may show divergent differentiation towards a NE phenotype in the form of NE small cell carcinoma or carcinoid-like tumors. Much more common is focal NE differentiation in prostate cancer, which may be pronounced in approximately 10% of carcinomas. The prognostic significance of focal NE differentiation is controversial, but current evidence suggests an influence on prognosis related to hormone-resistant tumors and/or a role in the conversion to a hormone-resistant phenotype. Chromogranin A appears to be the best overall tissue and serum marker of NE differentiation.

Nuclear DNA content

DNA ploidy analysis of prostate cancer by flow cytometry and digital image analysis provides important prognostic information that supplements histopathologic examination. Controversy exists, however, about whether this analysis is a significant predictor above Gleason score in multivariate analysis. DNA ploidy pattern correlates with cancer grade, tumor volume, and stage [40]. Most low-stage tumors are diploid, and high-stage tumors are nondiploid, but many exceptions occur [75].

Microvessel density (MVD)

A significant increase in MVD occurs in PIN [73] and carcinoma, compared with normal prostatic tissue [47, 73]. The mean blood vessel count is higher in tumors with metastases than in those without metastases [70], and most studies [47, 73], but not all [55], show a correlation with pathologic stage. MVD appears to be an independent predictor of cancer progression in some studies [14, 55]. The cumulative data suggest that increased MVD contributes to the extraprostatic spread of adenocarcinoma, perhaps by facilitating microvascular invasion.

Other molecular markers

The discovery of new molecular markers that, in a needle biopsy setting, are of prognostic significance is very much the need of the hour (Table 7) [58, 66].

Atypical small acinar proliferation (ASAP) suspicious for but not diagnostic of malignancy

About 2.5% of contemporary needle biopsies contain minute collections of small acini that raise the suspicion of carcinoma but fall below the diagnostic threshold [34, 65]. This problem is invariably the result of the small size of the focus. Quantitative criteria for malignancy are not employed for diagnosis in the prostate, but very small foci with only a few malignant acini are evaluated cautiously and invariably with intradepartmental consultation. We have rarely diagnosed adenocarcinoma with as few as three malignant acini, and only when frank cytologic anaplasia was present that stood in stark contrast with the adjacent benign epithelium; further, confounding factors are excluded, such as inflammation near the focus of concern; serial sections are obtained; and the possibility of seminal vesicle or ejaculatory duct epithelium was excluded. Of the foci suspicious for cancer, 30% can be correctly diagnosed when AMACR immunohistochemistry is applied [81].

Other causes of difficulty with small suspicious foci include the presence of distorted acini that lack convincing cytologic features, prominent inflammation in which the adjacent benign acini show distortion, and inflammatory reactive atypia with nuclear and nucleolar enlargement. Calling such a case "ASAP suggestive but not diagnostic of malignancy" is appropriate. This is a valid diagnostic category based on our "absolute uncertainty" regarding the diagnosis. In such cases, the diagnosis of carcinoma cannot be made, but the possibility cannot be definitively excluded.

The diagnosis of malignancy should only be made when one has absolute confidence in the histologic findings. Other supportive evidence, including patient age; serum PSA concentration; and immunohistochemistry findings related to the expression of 34βE12, p63, and AMACR, is useful but is not a substitute for the light microscopic findings. These other findings should be evaluated only after microscopic examination to avoid bias.

There are a variety of benign and malignant lesions that may be included in the ASAP group. Suspicious small acinar proliferations are stratified by some authors into three groups based on the level of suspicion: "suspicious, favor benign," "suspicious," and "highly suspicious." The expected clinical response to each of these diagnoses is identical, and it is recommended that patients have follow-up repeat biopsies. As a subsequent diagnosis of invasive carcinoma has been made in up to 57% of patients with ASAP, rebiopsy is recommended. The biopsy protocol recommended includes biopsies from the initial atypical site, adjacent sites, and the standard sextant sites [22].

Prostatic intraepithelial neoplasia (PIN)

PIN refers to the putative precancerous end of the morphologic continuum of cellular proliferations within preexisting prostatic ducts, ductules, and acini. PIN is divided into two grades (low and high) to replace the previous three-grade system (PIN 1 is considered low grade; PIN 2 and 3 are considered high grade) [9, 10, 13]. The continuum from low-grade PIN to HGPIN and early invasive cancer is characterized by basal cell layer disruption; progressive loss of markers of secretory differentiation; and increasing nuclear and nucleolar abnormalities, proliferative activity, MVD, genetic instability, and DNA content. Autopsy studies indicate that

PIN precedes carcinoma by 10 years or more; low-grade PIN first emerges in men in the third decade of life [63].

The incidence of PIN in needle biopsies varies according to the patient population under consideration (screening population vs urology office population) and the number of biopsies obtained. The American Cancer Society National Prostate Cancer Detection Project identified PIN and cancer in 17 (5.2%) and 58 (15.8%) men, respectively, from a series of 330 biopsies from men participating in an early detection project [52]. Other studies have found HGPIN in up to 16.5% of contemporary needle biopsy specimens in urology office practice [11].

The diagnosis of HGPIN has no prognostic significance, although its presence is predictive of subsequent cancer detection in 27–31% (recent data) of patients [6, 30, 45, 51, 62]. Due to the lower predictive value for cancer in recent years, studies have focused on HGPIN parameters in needle core biopsies that may be more useful in subsequent detection of cancer. Whether the extent of involvement of HGPIN is a better predictor of subsequent prostate cancer detection is controversial [6, 51, 62]. The pattern of HGPIN (micropapillary, cribriform, etc.) is not correlated with increased prostate cancer recognition [6, 51].

Attempts have been made to identify those HGPIN lesions with close relationships with cancer. For instance, intensely AMACR-stained HGPIN ducts and acini are preferentially located in close proximity to adenocarcinoma, whereas weakly stained HGPINs are at a distance from cancer (B. Helpap, Singen, Germany, personal communication).

Biopsy is the only definitive method for detecting PIN and early invasive cancer. If all procedures fail to identify coexistent carcinoma, close surveillance and follow-up are indicated. Follow-up is suggested at 3- or 6-month intervals for 2 years, and then at 12-month intervals for life. Identification of PIN in the prostate should not influence or dictate therapeutic decisions.

The cancer detection rate in patients with low-grade PIN is identical to that in patients who underwent repeat biopsies for persistent elevated serum PSA or for abnormal digital rectal examinations. Because the clinical significance or biologic relevance of low-grade PIN is not known and appears insignificant, this diagnosis should not be made in needle biopsies.

Inflammation

Pathologists often diagnose prostate needle biopsies with acute or chronic inflammation as acute or chronic prostatitis, respectively. Several studies have shown that there is no correlation of the finding of acute or chronic inflammation on needle biopsy with clinical symptoms of acute or chronic prostatitis. There are conflicting data on the relationship of acute or chronic inflammation on needle biopsy with serum PSA in men without clinical evidence of prostatitis [35, 67]. It is recommended to note acute inflammation and prominent chronic inflammation in the pathology report without using the term prostatitis, recognizing that the clinical relevance of these findings remains unclear. Table 8 shows the features a pathologist should evaluate on a biopsy with inflammation.

Table 8 Inflammation-related features

Type inflammatory cells (lymphocytes, neutrophils, etc.)
Extent
Relationship with stroma and epithelium

Benign prostate tissue

Table 9 shows a list of items a pathologist should include in the pathology report when no malignancy is seen in the biopsy. A number of pathologists interpret prostate needle biopsies without evidence of carcinoma as benign prostatic hyperplasia (BPH). However, the morphology of needle biopsy tissue cannot predict prostate size and does not correlate with the presence or degree of lower urinary tract symptoms. Furthermore, most needle biopsies of the prostate do not sample the transition zone, which is the area of origin of BPH. Thus, biopsies without carcinoma or other atypical features should simply be diagnosed as benign prostate tissue [22].

Conclusions

While the prime goal of the needle biopsy is to diagnose prostatic adenocarcinoma, once carcinoma is detected, further descriptive information regarding the type, amount of cancer, and grade forms the cornerstone for contemporary management of the patient and for assessing the potential for local cure and the risk for distant metastasis. The information provided in the needle biopsy report regarding the attributes of carcinoma is used to determine whether any form of treatment is indicated and, if so, the type of therapy that is required. Furthermore, the information in the biopsy report that may be valuable in further, potentially determining treatment strategies includes the field and/or type of radiation therapy, the need of adjuvant hormonal therapy, the eligibility for clinical trials, the type of surgery, and, sometimes, the intraoperative course [2, 58].

Table 9 No malignancy

Insufficient sample(s) (basis)
Total length of the biopsies
Mean length
Sample not representative
Nonprostatic tissue
Only stroma
Type of tissue not corresponding to the prostate zone the urologist intended to sample
Normal tissue
Atrophy, postatrophic hyperplasia, etc.

Acknowledgements The publication of this paper is in part supported by a grant from the Italian Ministry of University and Scientific Research (RM) (MIUR 2003).

References

1. Allsbrook WC Jr, Mangold KA, Johnson MH, Lane RB, Lane CG, Epstein JI (2001) Interobserver reproducibility of Gleason grading of prostatic carcinoma: urologic pathologists. Hum Pathol 32:74–80
2. Amin MB, Boccon-Gibod L, Egevad L, Epstein JI, Humphrey PA, Mikuz G, Newling D, Nilsson S, Sakr W, Srigley JR, Wheeler TM, Montironi R (2005) Prognostic and predictive factors and reporting of prostate carcinoma in prostate needle biopsy specimens. Scand J Urol Nephrol Suppl 216:20–33
3. Anderson PR, Hanlon AL, Patchefsky A, Al-Saleem T, Hanks GE (1998) Perineural invasion and Gleason 7–10 tumors predict increased failure in prostate cancer patients with pretreatment PSA<10 ng/ml treated with conformal external beam radiation therapy. Int J Radiat Oncol Biol Phys 41:1087–1092
4. Beach R, Gown AM, De Peralta-Venturina MN, Folpe AL, Yaziji H, Salles PG, Grignon DJ, Fanger GR, Amin MB (2002) P504S immunohistochemical detection in 405 prostatic specimens including 376 18-gauge needle biopsis. Am J Surg Pathol 26:1588–1596
5. Beard CJ, Chen MH, Cote K, Loffredo M, Renshaw AA, Hurwitz M, D'Amico AV (2004) Perineural invasion is associated with increased relapse after external beam radiotherapy for men with low-risk prostate cancer and may be a marker for occult, high-grade cancer. Int J Radiat Oncol Biol Phys 58:19–24
6. Bishara T, Ramnani DM, Epstein JI (2004) High-grade prostatic intraepithelial neoplasia on needle biopsy: risk of cancer on repeat biopsy related to number of involved cores and morphologic pattern. Am J Surg Pathol 28:629–633
7. Boccon-Gibod L, van der Kwast TH, Montironi R, Boccon-Gibod L, Bono A (2004) Handling and pathology reporting of prostate biopsies. Eur Urol 46:177–181
8. Bostwick DG (1994) Prostate-specific antigen: current role in diagnostic pathology of prostate cancer. Am J Clin Pathol 102:531–537
9. Bostwick DG (1995) High-grade prostatic intraepithelial neoplasia: the most likely precursor of prostate cancer. Cancer 75:1823–1836
10. Bostwick DG, Brawer MK (1987) Prostatic intra-epithelial neoplasia and early invasion in prostate cancer. Cancer 59:788–794
11. Bostwick DG, Qian J, Frankel K (1995) The incidence of high-grade prostatic intraepithelial neoplasia in needle biopsies. J Urol 154:1791–1794
12. Bostwick DG, Wollan P, Adlakha K (1995) Collagenous micronodules in prostate cancer: a specific but infrequent diagnostic finding. Arch Pathol Lab Med 119:444–447
13. Bostwick DG, Pacelli A, Lopez-Beltran A (1996) Molecular biology of prostatic intraepithelial neoplasia. Prostate 29:117–134
14. Bostwick DG, Wheeler TM, Blute M (1996) Optimized microvessel density analysis improves prediction of cancer stage from prostate needle biopsies. Urology 48:47–57
15. Bostwick DG, Adolfsson J, Burke HB, Damber J-E, Huland H, Pavone-Macaluso M, Waters DJ (2005) Epidemiology and statistical methods in prediction of patient outcome. Scand J Urol Nephrol Suppl 216:94–110
16. Cohen RJ, Stables S (1998) Intra-prostatic fat. Hum Pathol 29:424–425
17. Darson MF, Pacelli A, Roche P, Rittenhouse HG, Wolfert RL, Young CY, Klee GG, Tindall DJ, Bostwick DG (1997) Human glandular kallikrein 2 (hK2) expression in prostatic intraepithelial neoplasia and adenocarcinoma: a novel prostate cancer marker. Urology 49:857–862
18. Del Rosario AD, Bui HX, Abdulla M, Ross JS (1993) Sulfur-rich prostatic intraluminal crystalloids: a surgical pathologic and electron probe x-ray microanalytic study. Hum Pathol 24:1159–1167
19. Eble J, Sauter G, Epstein JI, Sesterhenn IA (eds) (2004) WHO classification of tumours. Tumours of the urinary system and male genital organs. (Tumours of the prostate). IARC, Lyon, pp 111–112
20. Epstein JI (2000) Gleason score 2–4 adenocarcinoma of the prostate on needle biopsy: a diagnosis that should not be made. Am J Surg Pathol 24:477–478
21. Epstein JI (2004) Diagnosis and reporting of limited adenocarcinoma of the prostate on needle biopsy. Mod Pathol 17:307–315
22. Epstein JI, Potter SR (2001) The pathological interpretation and significance of prostate needle biopsy findings: implications and current controversies. J Urol 166:402–410
23. Epstein JI, Allsbrook WC Jr, Amin MB, Egevad LL, The ISUP Grading Committee (2005) The 2005 International Society of Urological Pathology (ISUP) consensus conference on gleason grading of prostatic carcinoma. Am J Surg Pathol 29:1228–1242
24. Foster CS, Bostwick DG (eds) (1998) Pathology of the prostate. Saunders, Philadelphia, PA, pp 253–281
25. Freedland SJ, Csathy GS, Dorey F, Aronson WJ (2002) Percent prostate needle biopsy tissue with cancer is more predictive of biochemical failure or adverse pathology after radical prostatectomy than prostate specific antigen or Gleason score. J Urol 167:516–520
26. Freedland SJ, Aronson WJ, Terris MK, Kane CJ, Amling CL, Dorey F, Presti JC Jr (2003) The percentage of prostate needle biopsy cores with carcinoma from the more involved side of the biopsy as a predictor of prostate specific antigen recurrence after radical prostatectomy: results from the Shared Equal Access Regional Cancer Hospital (SEARCH) database. Cancer 98:2344–2350
27. Freedland SJ, Aronson W, Presti JC Jr, Kane CJ, Terris MK, Elashoff D, Amling CL, The SEARCH Database Study Group (2003) Percent of prostate needle biopsy cores with cancer is significant independent predictor of prostate specific antigen recurrence following radical prostatectomy: results from SEARCH database. J Urol 169:2136–2141
28. Gancarczyk KJ, Wu H, McLeod DG, Kane C, Kusuda L, Lance R, Herring J, Foley J, Baldwin D, Bishoff JT, Soderdahl D, Moul JW (2003) Using the percentage of biopsy cores positive for cancer, pretreatment PSA, and highest biopsy Gleason sum to predict pathologic stage after radical prostatectomy: the Center for Prostate Disease Research nomograms. Urology 61:589–595
29. Genega EM, Hutchinson B, Reuter VE, Gaudin PB (2000) Immunophenotype of high-grade prostatic adenocarcinoma and urothelial carcinoma. Mod Pathol 13:1186–1191
30. Gokden N, Roehl KA, Catalona WJ, Humphrey PA (2005) High-grade prostatic intraepithelial neoplasia in needle biopsy as a risk factor for detection of adenocarcinoma. Current level of risk in a screening population. Urology 65:538–542
31. Goldstein NS, Qian J, Bostwick DG (1995) Mucin expression in atypical adenomatous hyperplasia of the prostate. Hum Pathol 26:887–891
32. Hendrick L, Epstein JI (1989) Use of keratin 903 as an adjunct in the diagnosis of prostate carcinoma. Am J Surg Pathol 13:389–396
33. Holmes GF, Walsh PC, Pound CR, Epstein JI (1999) Excision of the neurovascular bundle at radical prostatectomy in cases with perineural invasion on needle biopsy. Urology 53:752–756
34. Iczkowski K, MacLennan GT, Bostwick DG (1997) Atypical small acinar proliferation of the prostate suspicious for malignancy in needle biopsies: histologic features and clinical significance in 33 cases. Am J Surg Pathol 21:1489–1495
35. Irani J, Levillain P, Goujon JM, Bon D, Dore B, Aubert J (1997) Inflammation in benign prostatic hyperplasia: correlation with prostate specific antigen value. J Urol 157:1301–1303

36. Isaacs JT (1997) Molecular markers for prostate cancer metastases: developing diagnostic methods for predicting aggressiveness of prostate cancer. Am J Pathol 150:1511–1521
37. Ito K, Nakashima J, Mukai M, Asakura H, Ohigashi T, Saito S, Tachibana M, Hata J, Murai M (2003) Prognostic implication of microvascular invasion in biochemical failure in patients treated with radical prostatectomy. Urol Int 70:297–302
38. Jiang Z, Woda BA, Rock KL, Xu Y, Savas L, Khan A, Pihan G, Cai F, Babcook JS, Rathanaswami P, Reed SG, Xu J, Fanger GR (2001) P504S: a new molecular marker for the detection of prostate carcinoma. Am J Surg Pathol 25:1397–1404
39. Jiang Z, Wu CL, Woda BA, Dresser K, Xu J, Fanger GR, Yang XJ (2002) P504S/ Alpha-Methylacyl-CoA racemase: a useful marker for diagnosis of small foci of prostatic carcinoma on needle biopsy. Am J Surg Pathol 26:1169–1174
40. Jones EC, McNeal J, Bruchovsky N, Bruchovsky N, de Jong G (1990) DNA content in prostatic adenocarcinoma: a flow cytometry study of the predictive value of aneuploidy for tumor volume, percentage Gleason grade 4 and 5, and lymph node metastases. Cancer 66:752–757
41. Kattan MW, Eastham JA, Wheeler TM, Maru N, Scardino PT, Erbersdobler A, Graefen M, Huland H, Koh H, Shariat SF, Slawin KM, Ohori M (2003) Counseling men with prostate cancer: a nomogram for predicting the presence of small, moderately differentiated, confined tumors. J Urol 170:1792–1797
42. Kaufmann O, Fietze E, Mengs J, Dietel M (2001) Value of p63 and cytokeratin 5/6 as immunohistochemical markers for the differential diagnosis of poorly differentiated and undifferentiated carcinomas. Am J Clin Pathol 116:823–830
43. Kestin LL, Goldstein NS, Vicini FA, Martinez AA (2002) Percentage of positive biopsy cores as predictor of clinical outcome in prostate cancer treated with radiotherapy. J Urol 168:1994–1999
44. Koh H, Kattan MW, Scardino PT, Suyama K, Maru N, Slawin K, Wheeler TM, Ohori M (2003) A nomogram to predict seminal vesicle invasion by the extent and location of cancer in systematic biopsy results. J Urol 170:1203–1208
45. Kronz JD, Allan CH, Shaikh AA, Epstein JI (2001) Predicting cancer following a diagnosis of high-grade prostatic intraepithelial neoplasia on needle biopsy: data on men with more than one follow-up biopsy. Am J Surg Pathol 25:1079–1085
46. Lewis JS Jr, Vollmer RT, Humphrey PA (2002) Carcinoma extent in prostate needle biopsy tissue in the prediction of whole gland tumor volume in a screening population. Am J Clin Pathol 118:442–450
47. Lo J, Kerns BJ, Amling CL, Robertson CN, Layfield LJ (1996) Correlation of DNA ploidy and histologic diagnosis from prostate core-needle biopsies: is DNA ploidy more sensitive than histology for the diagnosis of carcinoma in small specimens? J Surg Oncol 63:41–45
48. Lowe FC, Trauzzi SJ (1993) Prostatic acid phosphatase in 1993: its limited clinical utility. Urol Clin North Am 20:589–595
49. Makarov DV, Sanderson H, Partin AW, Epstein JI (2002) Gleason score 7 prostate cancer on needle biopsy: is the prognostic difference in Gleason scores 4 + 3 and 3 + 4 independent of the number of involved cores? J Urol 167:2440–2442
50. Maru N, Ohori M, Kattan MW, Scardino PT, Wheeler TM (2001) Prognostic significance of the diameter of perineural invasion in radical prostatectomy specimens. Hum Pathol 32:828–833
51. Mendrinos SE, Amin MB, Lim SD, Herrera CM, Srigley JR (2004) Predictive value of pathologic parameters of high-grade prostatic intraepithelial neoplasia (HGPIN) in the initial biopsy for the subsequent detection of prostatic carcinoma (Pca). Mod Pathol 171:168A
52. Mettlin C, Lee F, Drago J, Murphy GP (1991) The American Cancer Society National Prostate Cancer Detection Project: findings on the detection of early prostate cancer in 2425 men. Cancer 67:2949–2958
53. Molberg KH, Mikhail A, Vuitch F (1994) Crystalloids in metastatic prostatic adenocarcinoma. Am J Clin Pathol 101:266–268
54. Montironi R (2001) Prognostic factors in prostate cancer. BMJ 322:378–379
55. Montironi R, Magi-Galluzzi C, Diamanti L, Taborro R, Scarpelli M, Pisani E (1993) Prostatic intraepithelial neoplasia: qualitative and quantitative analysis of the blood capillary architecture on this tissue sections. Pathol Res Pract 189:542–548
56. Montironi R, Mazzucchelli R, Scattoni V, Bostwick DG (2002) Pathological findings in TRUS prostatic biopsy — diagnostic, prognostic and therapeutic importance. Eur Urol Suppl 1:60–75
57. Montironi R, Mazzucchelli R, Scarpelli M, Lopez-Beltran A, Fellegara G, Algaba F (2005) Gleason grading of prostate cancer in needle biopsies or radical prostatectomy specimens: contemporary approach, current clinical significance and sources of pathology discrepancies. BJU Int 95:1146–1152
58. Montironi R, Mazzucchelli R, Lopez-Beltran A, Algaba F, Scarpelli M, Mikuz G, Boccon-Gibod L (2006) Prostate carcinoma II. Prognostic factors in prostate needle biopsies. BJU Int 97:492
59. Naya Y, Slaton JW, Troncoso P, Okihara K, Babaian RJ (2004) Tumor length and location of cancer on biopsy predict for side specific extraprostatic cancer extension. J Urol 171:1093–1097
60. Oliai BR, Kahane H, Epstein JI (2002) Can basal cells be seen in adenocarcinoma of the prostate? An immunohistochemical study using high molecular weight cytokeratin (clone 34betaE12) antibody. Am J Surg Pathol 26:1151–1160
61. Quinn DI, Henshall SM, Brenner PC, Kooner R, Golovsky D, O'Neill GF, Turner JJ, Delprado W, Grygiel JJ, Sutherland RL, Stricker PD (2003) Prognostic significance of preoperative factors in localized prostate carcinoma treated with radical prostatectomy: importance of percentage of biopsies that contain tumor and the presence of biopsy perineural invasion. Cancer 97:1884–1893
62. Roscigno M, Scattoni V, Freschi M, Raber M, Colombo R, Bertini R, Montorsi F, Rigatti P (2004) Monofocal and plurifocal high-grade prostatic intraepithelial neoplasia on extended prostatic biopsies: factors predicting cancer detection on extended repeat biopsy. Urology 63:1105–1110
63. Sakr WA, Grignon DJ, Haas GP, Schomer KL, Heilbrun LK, Cassin BJ, Powell J, Montie JA, Pontes JE, Crissman JD (1995) Epidemiology of high-grade prostatic intraepithelial neoplasia. Pathol Res Pract 191:838–841
64. Salomao DR, Graham SD, Bostwick DG (1995) Microvascular invasion in prostate cancer correlates with pathologic stage. Arch Pathol Lab Med 119:1050–1054
65. Scattoni V, Roscigno M, Freschi M, Deho F, Raber M, Briganti A, Fantini G, Nava L, Montorsi F, Rigatti P (2005) Atypical small acinar proliferation (ASAP) on extended prostatic biopsies: predictive factors of cancer detection on repeat biopsies. Arch Ital Urol Androl 77:31–36
66. Schalken JA, Bergh A, Bono A, Foster C, Gospadarowicz M, Isaacs WB, Rubin M, Schroder F, Tribukait B, Tsukamotot T, Wiklund P (2005) Molecular prostate cancer pathology: current issues and achievements. Scand J Urol Nephrol Suppl 216:82–93
67. Schatteman PH, Hoekx L, Wyndaele JJ, Jeuris W, Van Marck E (2000) Inflammation in prostate biopsies of men without prostatic malignancy or clinical prostatitis: correlation with total serum PSA and PSA density. Eur Urol 37:404–412
68. Sebo TJ, Cheville JC, Riehle DL, Lohse CM, Pankratz VS, Myers RP, Blute ML, Zincke H (2001) Predicting prostate carcinoma volume and stage at radical prostatectomy by assessing needle biopsy specimens for percent surface area and cores positive for carcinoma, perineural invasion, Gleason score, DNA ploidy and proliferation, and preoperative serum prostate specific antigen: a report of 454 cases. Cancer 91:2196–2204
69. Shah RB, Zhou M, LeBlanc M, Snyder M, Rubin MA (2002) Comparison of the basal cell-specific markers, 34betaE12 and p63, in the diagnosis of prostate cancer. Am J Surg Pathol 26:1161–1168

70. Shankey TV, Kallioniemi OP, Koslowski JM, Lieber ML, Mayall BH, Miller G, Smith GJ (1993) Consensus review of the clinical utility of DNA content cytometry in prostate cancer. Cytometry 14:497–500
71. Shariat SF, Khoddami SM, Saboorian H, Koeneman KS, Sagalowsky AI, Cadeddu JA, McConnell JD, Holmes MN, Roehrborn CG (2004) Lymphovascular invasion is a pathological feature of biologically aggressive disease in patients treated with radical prostatectomy. J Urol 171:1122–1127
72. Srigley JR, Amin MB, Boccon-Gibod L, Egevad L, Epstein JI, Humphrey PA, Mikuz G, Newling D, Nilsson S, Sakr W, Wheeler TM, Montironi R (2005) Prognostic and predictive factors in prostate cancer: historical perspectives and recent international consensus initiatives. Scand J Urol Nephrol Suppl 216:8–19
73. Takai K, Goellner JR, Katzmann JA et al. (1994) Static image and flow DNA cytometry of prostatic adenocarcinoma: studies of needle biopsy and radical prostatectomy specimens. J Urol Pathol 2:39–48
74. Thorson P, Vollmer RT, Arcangeli C, Keetch DW, Humphrey PA (1998) Minimal carcinoma in prostate needle biopsy specimens: diagnostic features and radical prostatectomy follow-up. Mod Pathol 11:543–551
75. Tribukait B (1993) Nuclear deoxyribonucleic acid determination in patients with prostate carcinoma: clinical research and application. Eur Urol 23:64–76
76. Vargas SO, Jiroutek M, Welch WR, Nucci MR, D'Amico AV, Renshaw AA (1999) Perineural invasion in prostate needle biopsy specimens. Correlation with extraprostatic extension at resection. Am J Clin Pathol 111:223–228
77. Xu J, Stolk JA, Zhang X, Silva SJ, Houghton RL, Matsumura M, Vedvick TS, Leslie KB, Badaro R, Reed SG (2000) Identification of differentially expressed genes in human prostate cancer using subtraction and microarray. Cancer Res 60:1677–1682
78. Yang XJ, Wu CL, Woda BA, Dresser K, Tretiakova M, Fanger GR, Jiang Z (2002) Expression of Alpha-Methylacyl-CoA racemase (P504S) in atypical adenomatous hyperplasia of the prostate. Am J Surg Pathol 26:921–925
79. Young RH, Srigley JR, Amin MB, Ulbright TM, Cubilla AL (2000) Tumors of the prostate gland, seminal vesicles, male urethra and penis (Fascicle 28), 3rd edn. AFIP, Washington, DC
80. Zhou M, Epstein JI (2003) The reporting of prostate cancer on needle biopsy: prognostic and therapeutic implications and the utility of diagnostic markers. Pathology 35:472–479
81. Zhou M, Chinnaiyan AM, Kleer CG, Lucas PC, Rubin MA (2002) Alpha-Methylacyl-CoA racemase: a novel tumor marker over-expressed in several human cancers and their precursor lesions. Am J Surg Pathol 26:926–931

Virchows Arch (2006) 449: 14–23
DOI 10.1007/s00428-006-0192-7

ORIGINAL ARTICLE

Luca Morandi · Gianluca Marucci · Maria P. Foschini · Maria G. Cattani · Annalisa Pession Cristina Riva · Vincenzo Eusebi

Genetic similarities and differences between lobular in situ neoplasia (LN) and invasive lobular carcinoma of the breast

Received: 13 January 2006 / Accepted: 11 February 2006 / Published online: 13 April 2006
© Springer-Verlag 2006

Abstract One of the most controversial issues in breast pathology is whether lobular neoplasia (LN) is a risk factor or a precursor lesion of invasive lobular carcinoma (ILC). This is consequent to the fact that no conclusive data on the biology of LN exist. Molecular studies of LN and ILC are scanty, variable, and not consistent. Clonality of 12 cases of LN and ILC present simultaneously in the same block has been studied. Cells from both lesions were obtained by microdissection and were studied for mitochondrial DNA (mtDNA), D-loop sequencing, and neighbor-joining trees. Eight of the same cases were studied with comparative genomic hybridization (CGH) array to have additional data consistent with mtDNA. In all cases, loss of heterozygosity was studied for D16S496,locus 16q22.1 related to e-cadherin. It appears that no fewer than eight cases were genetically very similar (clonal) with mtDNA. Seven of these cases appeared also clonal with CGH array. It is concluded that in the present series, LN and ILC are genetically related lesions in the majority of cases and that LN might be the precursor of ILC.

Keywords CGH array · mtDNA · Lobular neoplasia · Invasive lobular carcinoma

L. Morandi · G. Marucci · M. P. Foschini · A. Pession · V. Eusebi
Section of Pathology, Department of Oncology, University of Bologna, Ospedale Bellaria, Bologna, Italy

M. G. Cattani
Section of Pathology, Department of Oncology, University of Bologna, Ospedale Maggiore, Bologna, Italy

C. Riva
Section of Pathology, Department of Human Morphology, University of Insubria, Varese, Italy

V. Eusebi (✉)
Anatomia Patologica, Ospedale Bellaria, Via Altura 3, 40139 Bologna, Italy
e-mail: vincenzo.eusebi@ausl.bo.it
Tel.: +39-051-6225523
Fax: +39-051-6225759

Introduction

Lobular carcinoma in situ (LCIS) of the breast has been recognized for many years [12] and along this period, it has run a parallel story with ductal carcinoma in situ (DCIS). It has been originally described as having well-differentiated cells with monotonous nuclei (LCIS) [12]. However recently, cases formed by poorly differentiated cells with pleomorphic nuclei have been reported (pleomorphic LCIS, PLCIS) [14] similarly to what is seen in poorly differentiated DCIS. In addition as in DCIS, variants of LCIS showing neuroendocrine [8], apocrine [9], mucinous [15], and myoepithelial cell differentiation [35] have been described. The same does not apply to the outcome of the lobular and ductal in situ lesions. There is a general consensus that duct flat epithelial atypia and atypical duct hyperplasia, as defined by WHO, are indicators of increased risk of invasive carcinoma [10, 39], and that DCIS are precursor lesions [31]. On the contrary, it is not clear yet if atypical lobular neoplasia/lobular carcinoma in situ (LN) is a risk factor or a precursor lesion of invasive carcinoma [39].

Multifocality and bilaterality in LN [1] are in favor of a risk indicator. This is also shown by a meta-analysis study from nine centers in which it was found that ipsilateral invasive carcinoma developed in 15.1% of patients with previous LN treated only with excision. In the same study, 9.3% of patients developed contralateral invasive carcinoma [2]. In another study of over 1,100 patients, about 15% of women with LN treated by biopsy alone eventually developed invasive breast carcinoma; 8.7% of the subsequent carcinomas were in the ipsilateral breast, while 6.7% were in the contralateral breast [36].

As an opposite view, contralateral occurrence of invasive carcinoma after a diagnosis of LN was denied by Ottensen et al. [29] who believed that LN was a precancerous lesion rather than a marker of increased risk. Invasive carcinoma was diagnosed in the same breast with atypical lobular hyperplasia in 68% of patients, and in the contralateral breast in 24% of patients as studied by Page et al. [30] who stated that atypical lobular hyperplasia was intermediate between a local precursor and a generalized risk factor for both breasts. In a metanalysis study, of 439 cases of ALH and LN (from 22 centers) diagnosed on excisional tissue, there was residual underestimated carcinoma (in situ or invasive) in 89 cases (20.2%) and accordingly LN was regarded as a high-risk lesion [6].

Controversial data also exist whether LN and classical invasive lobular carcinoma [38] are related lesions especially in view of the fact that nearly half of the invasive carcinomas associated to LN are ductal and not lobular in type [5].

In a recent three-dimensional study using large (macro) sections, Foschini et al. [13] have shown that a total of 234 foci of LN were observed in the 12 cases where LN and ILC were present at the same time in the same breast, and it appeared that 184 LN (78.6%) were located inside the areas of ILC, indicating a profound relationship between LN and ILC.

The genetic relation between synchronous LN and ILC, evaluated with array comparative genomic hybridization (CGH), suggested clonal features in a majority of paired specimens studied [16]. In addition, there are also direct mutational data where concurrent LN and ILC harbor same truncating mutations and same loss of heterozygosity (LOH) pattern supporting clonal evolution [38]. LOH studies by Nayar et al. [26] identified LOH at 11q13 in LN and ILC in one-third of informative cases. Similarities between LN and ILC with LOH were also seen by Lakhani et al. [22, 26].

To further evidence genetic differences or similarities between LN and ILC, a study of clonality based on mitochondrial (mt) and nuclear DNA evaluation in 12 cases harboring at the same time LN and ILC is presented in this study.

Materials and methods

Patients

Twelve patients randomly selected were included in the present study. The patients were all females who had undergone quadrantectomy with axillary dissection in five cases and mastectomy with axillary dissection in six cases (Table 1). In case 12, simple mastectomy had been performed. The surgically resected material had the following preoperative procedures: FNA in three cases, frozen sections in three cases, and core biopsy in six cases. The age of patients ranged from 44 to 81 years (mean 61.9 years).

Table 1 Anatomoclinical findings of cases

Case	Age	ILC	LN	Grade	T	N	Surgery
1	73	Class.	Class.	2	T1b	N0	M+LD
2	81	Class.	Class.	2	T1b	N+	M+LD
3	66	Class.	Class.	2	T3	N+	M+LD
4	60	Class.	Class.	2	T1c	N0	Q+LD
5	44	Class.	Class.	2	T2	N+	Q+LD
6	69	Class.	Class.	2	T1b	N0	Q+LD
7	56	Pleo.	Class.	3	T2	N+	M+LD
8	53	Class.	Class.	2	T1c	N0	Q+LD
9	69	Class.	Class.	2	T1c	N0	M+LD
10	71	Class.	Class.	2	T1c	N0	M+LD
11	56	Class.	Class.	2	T1c	N0	Q+LD
12	45	Pleo.	Pleo.	3	T4	Nx	M

M Mastectomy, *Q* quadrantectomy, *LD* lymph node dissection, *Class.* classical, *Pleo.* pleomorphic

Tissue processing and histological analysis

Tissues were fixed in 10% buffered formalin, paraffin-embedded as routine, and stained with Hematoxylin–Eosin (H&E). All cases were stained with anti e-cadherin antibody (DAKO, monoclonal NCH-38, dilution 1:50). For immunohistochemistry, the ABC method was employed and antigen retrieval was performed, submitting sections at high pressure for 6 min at 100°C in citrate buffer, pH 8.

Cases were selected when in the same tissue block there were foci of LN admixed to ILC areas. The in situ lesions were LN/lobular intraepithelial neoplasia 2 (LIN 2) [5] in all cases with the exception of case 12 which showed LN with pleomorphic cells (LIN 3). In accordance, LN/LIN 2 cases showed monotonous noncohesive cells that filled the ductules; on the contrary, LN with pleomorphic cells (LIN 3) from case 12 was composed of large cells with eosinophilic cytoplasm and pleomorphic nuclei. The number of LN foci ranged from three to 12 in various cases (mean 6). In the same paraffin block, from all cases, areas of classical ILC (single files of monotonous noncohesive cells) [24, 37] were present with the exception of cases 7 and 12 that showed the features of the lobular invasive pleomorphic variant, composed of cells with eosinophilic cytoplasm and often multiple irregular nuclei [11]. In case 7, the in situ lesion was LN/LIN 2, while in case 12, the features were consistent with those of LN with pleomorphic nuclei (LIN 3).

Immunohistochemistry for e-cadherin, performed in all cases, was consistently negative, both in in situ and invasive lesions.

Microdissection and DNA extraction

Pertinent lesions were microdissected using the laser-assisted SL μcut Microtest (MMI GmbH distributed by Nikon, Firenze, Italy, http://www.mmi-micro.com). Five-micrometer-thick sections were obtained, and unstained

sections were deparaffinized with Bio-Clear (Bio-optica, Milano, Italy), rinsed in ethanol 100 to 80%, and stained with H&E. Care was taken in microdissecting cells from LN foci (Fig. 1), and from ILC areas (Fig. 2) that were kept separate. Breast glandular tissue uninvolved by the neoplastic process and lymphocytes from reactive lymph nodes were also microdissected, as control reference DNA for mtDNA analysis.

DNA was extracted as previously described [25].

Mitochondrial displacement-loop (D-loop) region analysis by automatic direct sequencing

The mtDNA D-loop sequence analysis was evaluated, amplifying two segments of about 600 bp covering the region since position 16045 through position 650 according to Anderson et al. [3] as described in the human mitochondrial databank (*MITOMAP: a human mitochondrial genome database*. Center for Molecular Medicine, Emory University, Atlanta, GA, USA http://www.gen.emory.edu/mitomap.html).

Primers used in this study were designed using primer3 (http://www.genome.wi.mit.edu/cgi-bin/primer3_www.cgi): region 16045–60: for 5′-CCACCCAAGTATTGACT CACCCATCAA-3′, Rev: 5′-CATGGAGAGCTCCCGT GAGTGGTTAAT-3′; region 50-650 For 5′–CTCCATG CATTTGGTATTTTCGTCTGG-3′, Rev 5′-GTTTATGGG TGATGTGAGCCCGTCTA-3′, and were selected to avoid amplification of human mitochondrial pseudogenes in the nuclear genome [40]. In addition, a portion of two coding regions, *ND4* and *Cytochrome B* (*CytB*) of mtDNA, was sequenced using the following primers: *ND4* forward: 5′-TTTGAATCAACACAACCACCCACAGC-3′; *ND4* reverse: 5′-CGGCAAGTACTATTGACCCAGCGATG-3′; *CytB* forward: ACAGTCCCACCCTCACACGATTCTTT-3′, and *CytB* reverse: 5′-GCTTACTGGTTGTCCTCCGATT CAGG.

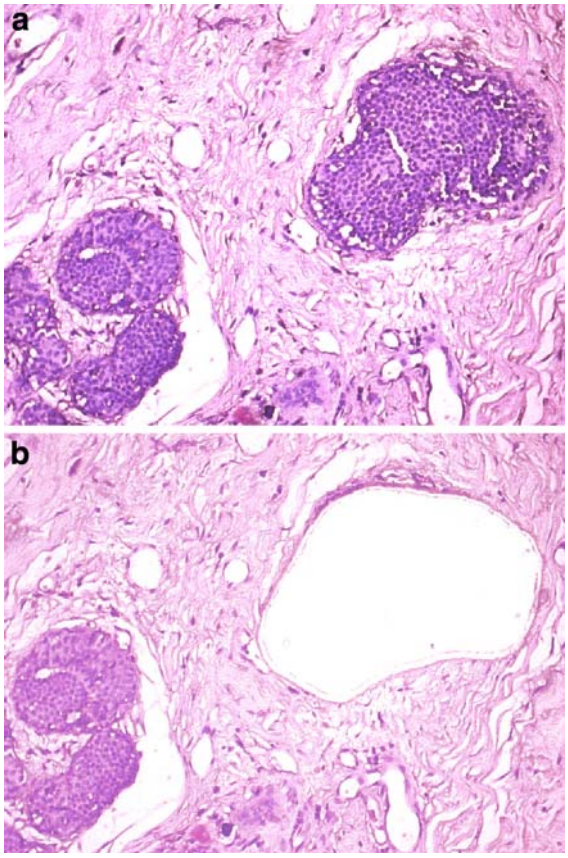

Fig. 1 **a** Case number 8. LIN 2. Ductules are filled by monotonous cell population. **b** Same case. The cells contained in one ductule have been removed by microdissection

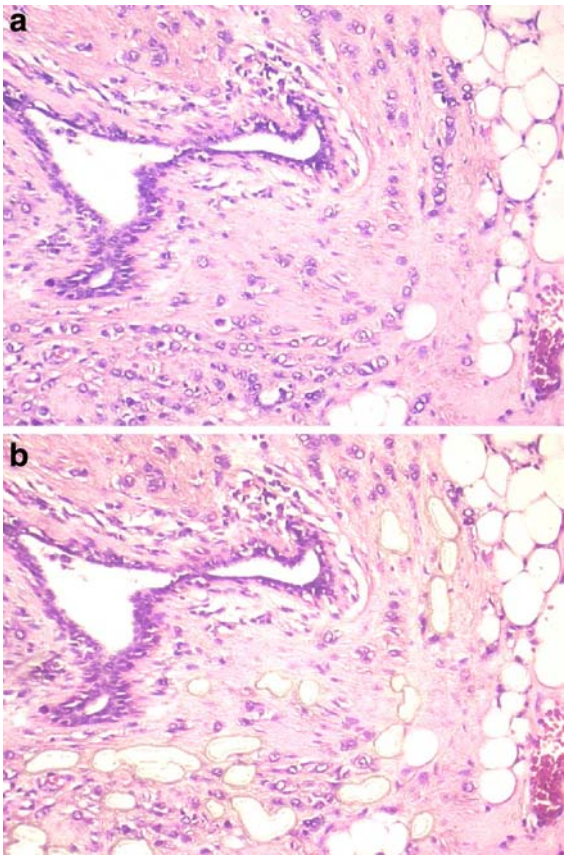

Fig. 2 **a** Case number 5. ILC classical subtype. The neoplastic cells show single file arrangement. **b** Same case. Neoplastic cells removed by microdissection

PCR products were separated by electrophoresis on 2% agarose gel and purified using the MiniElute Gel Extraction kit (Qiagen GmbH, Hilden, Germany). Sequencing analysis was then performed on purified product using the DTCS-Quick Start kit (Beckman Coulter, Fullerton, CA, USA) and a CEQ2000 XL automatic DNA sequencer. The strands were screened using the forward and reverse primers. Sequences were compared against a comprehensive human mitochondrial databank and each other by multiple sequence alignment ClustalW software (http://www.ebi.ac.uk/clustalw).

Phylogenetic and cluster analyses were conducted using ClustalW and MEGA version 3.1 [20, 21, 32] (http://www.megasoftware.net) using the neighbor-joining (NJ) method

[27] and Kimura-2 parameter with Gamma model that corrects for multiple hits taking into account transitional and transversional substitution rates and differences in substitution rates among sites [19]. Every NJ tree was tested for standard error by Bootstrap method [19]. The same software calculated the pairwise distance value which has been annotated in Table 2.

The following notations for ambiguous nucleotides are used in case of heteroplasmy: R: A/G; Y: C/T; M: A/C; W: A/T; S: C/G; K: G/T; B: C/G/T; D: A/G/T; H: A/C/T; V: A/C/G; and N: A/G/C/T.

As a control of the method, an additional case of bilateral LN was studied for mtDNA. LN 1 cells from both sides (genetically independent lesions) were microdissected together with the respective ipsilateral, morphologically normal glands and lymphocytes.

Oligonucleotide CGH microarrays

Eight pair cases only were studied (case numbers 2, 5, 6, 7, 8, 10, 11, and 12) as LN did not offer enough material to be microdissected for this purpose.

For each CGH, genomic DNA from the experimental sample was random primer-amplified using components from the BioPrime Array CGH labeling kit (Invitrogen, Milan). The reaction consisted of 300 ng/μl random oligodeoxyribonucleotide primers, 20 U of Klenow enzyme, 200 μM dNTPs, and the total DNA extracted from the microdissected specimen. Total DNA and the random primers were denatured at 95°C for 5 min and then immediately cooled on ice. The remaining reactants were then added, and the reaction was incubated at 37°C for 2 h. Amplified DNA was further purified by MiniElute spin columns (Qiagen GmbH, Hilden, Germany).

One microliter of amplified DNAs were further analyzed for quantity and length by the Agilent 2100 Bioanalyzer. A second round of the same linear amplification system was used to label amplified DNA using Cy3-dCTP for reference DNA and Cy5-dCTP (Perkin Elmer) for test-DNA following the protocol of Barrett et al. [4]. Labeling reactions were performed in a volume of 50 μl with a modified dNTP pool containing 120 μM each of dATP, dGTP, and dTTP, 60 μM of dCTP and Cy5-dCTP or Cy3-dCTP, and 60 μM of dCTP. Labeled targets were subsequently purified by MiniElute spin columns (Qiagen) and eluted in ultra pure water (Invitrogen). Experimental and reference targets for each hybridization were pooled and mixed with 100 μg of human Cot-1 DNA (Invitrogen)/50 μl of 1× hybridization control targets (SP310, Operon Technologies, Alameda, CA, USA)/50 μg of yeast tRNA (Invitrogen) in a final volume of 250 μl and mixed together with 250 μl of 2× hybridization solution (Agilent). Before hybridization to the array, the 500-μl hybridization mixtures were denatured at 100°C for 1.5 min and incubated at 37°C for 30 min. To remove any precipitate, the mixture was centrifuged at 14,000×*g* for 5 min and transferred to a new tube, leaving a small residual volume (<5 μl). The sample was applied to the array by using an Agilent hybridization chamber, and hybridization was carried out for 17 h at 65°C in a rotating oven (Robbins Scientific, Mountain View, CA, USA) at 4 rpm. The arrays were then disassembled in 6× SSPE/0.00025% of *N*-Laurylsarcosine, and washed once for 1 min with 6× SSPE/0.005% of *N*-Laurylsarcosine and once more for 1 min with 0.06× SSPE/0.005% *N*-Laurylsarcosine, both at room temperature. Slides were immerged in the stabilization solution (Agilent Cod. 5185–5979), dried, and scanned by using an Agilent 2565A scanner with 5 μm resolution [4].

Reference DNAs for CGH hybridization were derived from a pool of wild-type female DNA extracted from 10 different healthy women's lymphocytes. The starting materials of these samples were paraffin-embedded lymph nodes to recover fragmented DNA as it occurred to the test samples. This minimized internal variability length among reference DNA and DNA from carcinomas. Samples were similar in magnitude and ranged from 500 to 1,000 cells in different cases, as indicated by Sieben et al. [34].

Table 2 Results from the pairwise distance calculations using Kimura-2 parameter and the total number of loci found to be mutated in LN and/or ILC

Case	Kimura-2 parameter	Number of point mutations
12	0	12
5	0.001	7
4	0.0014	19
1	0.002	18
10	0.0027	28
2	0.0031	47
8	0.0045	34
11	0.005	12
3	0.0065	13
7	0.0068	45
9	0.0068	45
6	0.0121	27

Image and data analysis

Microarray images were analyzed by using the Feature Extraction Software (Agilent version 7.5) following the protocol described from Barrett et al. [4]. In brief, default settings were employed, using signals from negative control features for background subtraction. Several filtering procedures were applied, eliminating: (1) features that did not cross the threshold of calculated background for both channels; (2) outlier features for each experiment; (3) features not included between −0.1 and 0.1 values obtained in the female/male CGH experiment (see SupplInf1CGHdata.zip, rough CGH data). The discovery of gains and losses was made using the CGH-Explorer (http://www.ifi.uio.no/bioinf/Papers/CGH/) software for analysis of copy errors (ACE) [23]. Single genes were partitioned into subsequences, or "runs", of positive or negative copy numbers (after calculating the running mean

of the data, with five neighbors). Each run was characterized by its length and height (average value), and the collection of (length, height) pairs were compared to the distribution of (length and height) pairs in a theoretical null population of normal copy number ratios, available from the male/female experiment. This method computes an estimate of the positive false discovery rate (pFDR) and provides a table of different pDFR values and corresponding numbers of significant genes. The pDFR value was chosen to select the maximum number of mutated genes compared to the minimum number of false positive mutations found by male/female hybridization control. A data table was obtained by this algorithm with converted values (wild type = 0, gain = +1, loss = −1; see SupplInf2.zip).

To verify the genetic distance among different lobular lesions, a hierarchical cluster analysis was obtained using the expression profiler software [18] (http://www.ebi.ac.uk/expressionprofiler). For this, purpose we used as parameter the correlation-based distance and the complete linkage analysis (Fig. 4).

The concordance between the paired in situ and invasive components was calculated using the following formula [16, 17, 31]: (number of changes in common to LN and ILC)/(number of changes in common to LN and ILC)+1/2 (number of changes in ILC only + number of changes in LN only) (see supplementary information 4 synthetic view of the whole-arm alterations).

LOH by microsatellite analysis for 16q

The microsatellite D16S496, mapped on 16q22 (accession number Z23639) close to *CDH1* gene, was tested for loss of heterozygosity in the same cases studied with array CGH.

PCR products were loaded on a CEQ 2000 XL automatic DNA sequencer (Beckman Coulter, Fullerton, CA, USA).

Fragment analysis was evaluated comparing raw data with 600 bp standard by CEQ 2000 fragment analysis software.

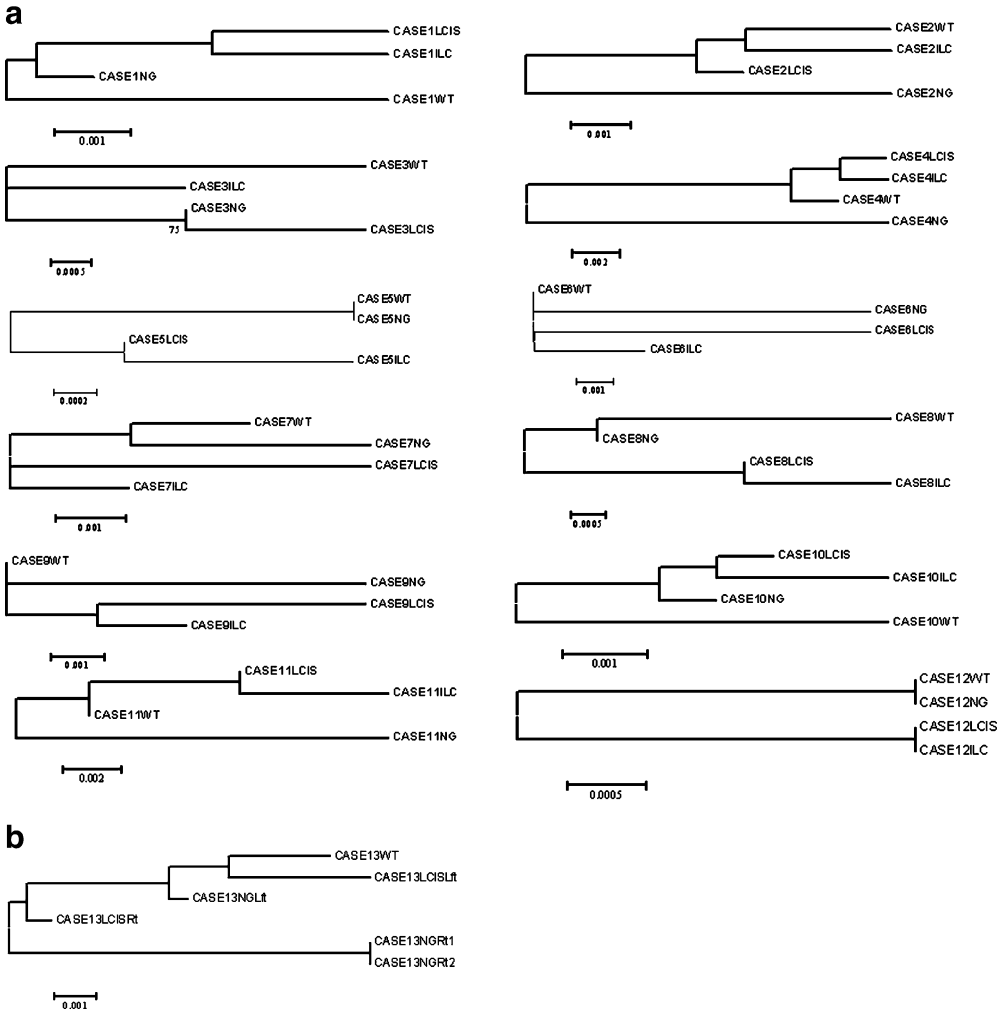

Fig. 3 **a** Neighbor-joining trees based on D-loop mutations found in 12 cases tested. *NG* Normal gland, *WT* lymphocytes, *ILC* invasive lobular carcinoma, *LCIS* lobular neoplasia. **b** Neighbor-joining tree for the case of bilateral LN used as control of the test. *NGRt1* Normal gland, right breast; *NGRt2* normal gland, same block other area, right breast; *NGLft* normal gland, left breast; *LCISRt* lobular neoplasia, right breast; *LCISLft* lobular neoplasia, left breast; *WT* lymphocytes

Results

mtDNA results

Twelve pairs of concurrent LN and ILC lesions were analyzed by mtDNA sequencing.

D-loop regions

The sequences of D-loop regions showing somatic point mutations are reported in supplementary information (Suppl. inf. 3.zip). The NJ trees as seen in eight cases (1, 2, 4, 5, 8, 10, 11, and 12) showed little genetic distance (clonality) between LN foci and ILC areas (Fig. 3a), as they clustered on the same secondary branch. These data were further confirmed by the bootstrap test, especially in case 12 which showed six mutations in common between LN and ILC among nine informative loci found in the D-loop region, which were not shared by lymphocytes and normal gland, indicating total genetic similarity between the paired lesions.

On the contrary, cells from classic ILC and elements from foci of LN/LIN 3 of case 7 were genetically distant as also were those from paired lesions of cases 3 and 6 (Fig. 3a).

Case 9 had an intermediate pattern as ILC and LN were located on the same secondary branch, but the Kimura-2 distance parameter showed high score (0.00679) (Table 2, Fig. 3a).

Case control for the mtDNA test: the case of bilateral LN showed 33 nucleotide positions in which a mutation in at least one tissue specimen (lesional or normal) was found. The NJ tree of this case, as visualized in Fig. 3b, showed wide genetic distance between right and left LN confirmed by the Kimura-2 distance parameter value of 0.00955. The right and left normal glands also appeared genetically very distant with value of 0.0134. On the contrary, LN foci were genetically related to the respective ipsilateral normal gland. In addition, microdissected normal glands from different sites of the same tissue block of the right breast were genetically identical (Kimura-2 distance parameter value = 0) as also demonstrated by the bootstrap test of this NJ tree indicating a common cell of origin.

mtDNA coding regions

The mtDNA coding regions (*ND4* and *CytB*) revealed only a limited number of mutations : in case 6, the *CytB* gene of mtDNA contained a heteroplasmic mutation in codon 29 that produces an amino acid substitution from Leu to Ile only for ILC. Case 11 showed in *ND4*, position 11.125, a heteroplasmic mutation that produces an amino acid change from Ser to Phe in both LCIS and ILC.

In the remaining cases, the *ND4* and *CytB* regions scanned gave only five synonymous mutations.

CGH array data

The original filtered file (SupplInf1CGHdata.zip) and the computed one by ACE algorithm (SupplInf2.zip) are available as supplementary information.

Gains and losses were very similar in no fewer than seven out of 12 cases studied when LN cells were compared to those composing ILC. Case 7 (pleomorphic ILC associated with LIN 2) was the one showing the lowest concordance index (0.235) (supplementary information 4 synthetic view of the whole-arm alterations).

These data were in agreement with those offered by the mtDNA test as all cases that were clonal with it appeared also similar from a genomic point of view. In accordance, in case 7, the paired lesions that were genetically distant as shown by the NJ tree had also the lowest concordance index with CGH array.

Cluster analysis (Fig. 4) showed similar data to those illustrated in supplementary synthetic view of the whole-arm alterations, where only case 7 showed no association between paired lesions.

Case 12 (LIN 3 and pleomorphic ILC) clustered as an individual group.

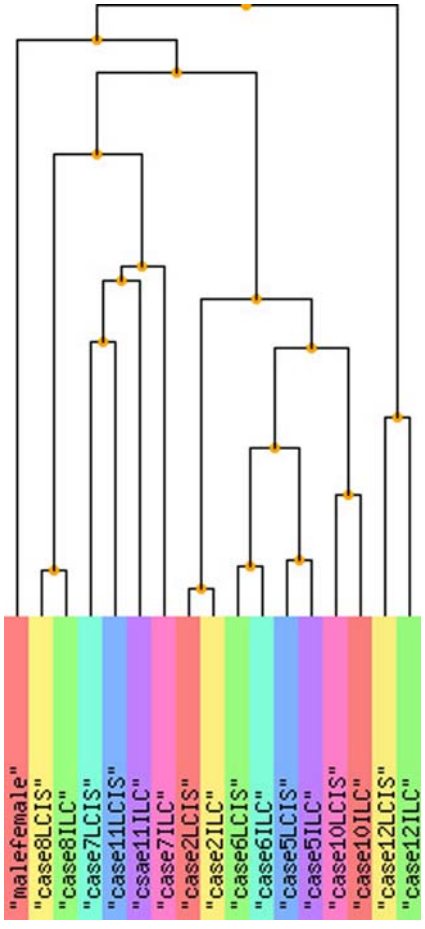

Fig. 4 Cluster analysis from array CGH data: seven out of eight cases showed association between the paired lesions, while only case 7 did not. Case 12 (LIN 3 and pleomorphic ILC) clustered as an individual group as well as male/female test control but on the other side

Table 3 Summary of the most frequent genetic alterations found (the total number of gains and losses are provided as supplementary information, SupplInf2.zip)

bp	name	chro	2ILC	5ILC	6ILC	7ILC	8ILC	10ILC	11ILC	12ILC	Frequency (%)	2LN	5LN	6LN	7LN	8LN	10LN	11LN	12LN	Frequency (%)
778831	AZU1	19p	0	1	1	0	1	0	0	0		0	1	1	1	1	0	1	0	
791961	PRTN3	19p	0	1	1	0	1	0	0	0		0	1	1	1	1	0	1	0	
810452	DF	19p	0	1	1	0	1	0	0	0		0	1	1	1	1	0	1	0	
880041	DRIL1	19p	0	1	1	0	1	0	0	0		0	1	1	1	1	0	1	0	
976984	CNN2	19p	0	1	1	0	1	0	0	0		0	1	1	1	1	0	1	0	
991100	ABCA7	19p	0	1	1	0	1	0	0	0		0	1	1	1	1	0	1	0	
1156750	STK11	19p	0	1	1	0	1	0	0	0		0	1	1	1	1	0	1	0	
1237168	EFNA2	19p	0	1	1	0	1	0	0	0		0	1	1	1	1	0	1	0	
1334872	NDUFS7	19p	0	1	1	0	1	0	0	0		0	1	1	1	1	0	1	0	
1432427	PCSK4	19p	0	1	1	0	1	0	0	0		0	1	1	1	1	0	1	0	
1766241	EloA-BP1	19p	0	1	1	0	1	0	0	0		0	1	1	1	1	0	1	0	
1856364	SCAMP-4	19p	0	1	1	0	1	0	0	0		0	1	1	1	1	0	1	0	
1936438	BTBD2	19p	0	1	1	0	1	0	0	0		0	1	1	1	1	0	1	0	
1988468	MKNK2	19p	-1	1	1	0	1	0	0	0		-1	1	1	1	1	0	1	0	
2115148	DOT1L	19p	0	1	1	0	1	0	0	0		0	1	1	1	1	0	1	0	
2184146	GNRPX	19p	0	1	1	0	1	0	0	0		0	1	1	1	1	0	1	0	
2199673	AMH	19p	0	1	1	0	1	0	0	0		0	1	1	1	1	0	1	0	
5574059	SAFB	19p	0	1	0	1	1	0	0	0		0	1	0	1	1	0	0	0	
5641327	RPL36	19p	0	1	0	1	1	0	0	0		0	1	0	1	1	0	0	0	
5642525	PRSS15	19p	0	1	0	1	1	0	0	0		0	1	0	1	1	0	0	0	
5865418	CAPS	19p	0	1	0	1	1	0	0	0		0	1	0	1	1	0	0	0	
7874755	MAP2K7	19p	0	1	1	0	1	0	0	0		0	1	0	1	1	0	1	1	
7897590	TIMM44	19p	0	1	1	0	1	0	0	0		0	1	0	1	1	0	1	1	
8036287	FBN3	19p	0	1	1	0	1	0	0	0		0	1	0	1	1	0	1	1	
8273002	8D6A	19p	0	1	1	0	1	0	0	0		0	1	0	1	1	0	1	1	
8292289	RPS28	19p	0	1	1	0	1	0	0	0		0	1	0	1	1	0	1	1	
9825391	OLFM2	19p	0	1	1	0	1	0	0	0		0	1	0	1	1	0	1	1	
10064013	ANGPTL6	19p	0	1	1	0	1	0	0	0		0	1	0	1	1	0	1	1	
10077955	PPAN	19p	0	1	1	0	1	0	0	0		0	1	0	1	1	0	1	1	
10223584	MRPL4	19p	0	1	1	0	1	0	0	0		0	1	0	1	1	0	1	1	
10261655	ICAM5	19p	0	1	1	0	1	0	0	0		0	1	0	1	1	0	1	1	
10305416	ICAM3	19p	0	1	1	0	1	0	0	0	62,5	0	1	0	1	1	0	1	1	87,5
3063538	BPHL	6p	1	1	0	0	1	1	0	0		1	1	0	0	1	1	0	0	
16346681	GMPR	6p	1	1	0	0	1	1	0	0		1	1	0	0	1	1	0	0	
25830977	HIST1H2AA	6p	1	1	1	0	1	1	0	-1		1	1	1	0	1	0	0	0	
25953312	SLC17A3	6p	1	1	1	0	1	1	0	-1		1	1	1	0	1	0	0	0	
26129845	HIST1H4A	6p	1	1	1	0	1	1	0	-1		1	1	1	0	1	0	0	0	
26139796	HIST1H3B	6p	1	1	1	0	1	1	0	-1		1	1	1	0	1	0	0	0	
26139796	HIST2H3C	6p	1	1	1	0	1	1	0	-1		1	1	1	0	1	0	0	0	
26296901	HIST1H4D	6p	1	1	1	0	1	1	0	-1		1	1	1	0	1	0	0	0	
26304298	HIST1H3D	6p	1	1	1	0	1	1	0	-1		1	1	1	0	1	0	0	0	
26306991	HIST1H2AD	6p	1	1	1	0	1	1	0	-1		1	1	1	0	1	0	0	0	
26307706	HIST1H2BF	6p	1	1	1	0	1	1	0	-1		1	1	1	0	1	0	0	0	
26312406	HIST1H4E	6p	1	1	1	0	1	1	0	-1		1	1	1	0	1	0	0	0	
26325127	HIST1H2AE	6p	1	1	1	0	1	1	0	-1		1	1	1	0	1	0	0	0	
26358349	HIST1H3F	6p	1	1	1	0	1	1	0	-1	62,5	1	1	1	0	1	0	0	0	62,5
9766801	CRBPIV	1p	0	1	0	1	1	0	0	0		0	1	0	0	1	0	0	0	
15181445	CASP9	1p	1	0	0	0	0	0	0	0		1	1	0	0	0	0	0	0	
30686594	MATN1	1p	1	0	0	0	1	0	0	-1		1	1	0	0	1	0	0	0	
39919683	CAP1	1p	0	0	0	0	1	0	0	0		0	0	0	0	1	0	0	1	
58616379	JUN	1p	0	0	1	0	1	0	0	0	62,5	1	0	1	0	1	0	0	0	62,5
47853642	MAP4	3p	0	1	0	0	1	0	-1	0		0	0	0	0	1	0	-1	1	
49413223	AMT	3p	1	1	0	0	1	0	0	0		1	1	0	0	1	0	0	0	
49419392	NICN1	3p	1	1	0	0	1	0	0	0		1	1	0	0	1	0	0	0	
50289273	HYAL3	3p	1	1	0	0	1	0	0	0		1	1	0	0	1	0	0	0	
50296763	HYAL1	3p	1	1	0	0	1	0	0	0		1	1	0	0	1	0	0	0	
124106757	PDIR	3p	1	0	1	0	1	0	0	0		1	0	0	0	1	0	0	0	
124653417	MYLK	3p	1	0	1	0	1	0	0	0	62,5	1	0	0	0	1	0	0	0	62,5
2153802	CASKIN1	16p	1	1	1	0	1	0	0	-1		1	1	0	0	1	0	0	0	
2229393	DCI	16p	1	1	1	0	1	0	0	0		1	1	0	0	1	0	0	0	
2419346	CCNF	16p	1	1	1	0	1	0	0	0		1	1	0	0	1	0	0	0	
2461057	NTN2L	16p	1	1	1	0	1	0	0	0		1	1	0	0	1	0	0	1	
2503267	ATP6V0C	16p	1	1	1	0	1	0	0	0		1	1	0	0	1	0	0		
2762338	MPN	16p	1	1	1	0	1	0	0	0	50	1	1	0	0	1	0	0	1	50
57834565	MMP15	16q	0	0	-1	0	1	0	-1	0		-1	-1	-1	0	1	0	0	-1	
67248161	ATP6V0D1	16q	-1	-1	0	0	1	0	-1	0	50	-1	-1	0	0	1	0	0	0	50
46189008	CYP2B6	19q	0	-1	-1	0	1	0	0	0		-1	-1	-1	0	1	0	0	0	
46390967	CYP2S1	19q	0	-1	-1	0	1	0	0	0		-1	-1	-1	0	1	0	0	0	
46817184	CEACAM4	19q	0	-1	-1	0	1	0	0	0		-1	-1	-1	0	1	0	0	0	
46869072	CEACAM7	19q	0	-1	-1	0	1	0	0	0		-1	-1	-1	0	1	0	0	0	
47394592	DEDD2	19q	0	-1	-1	0	1	0	0	0		-1	-1	-1	0	1	0	0	0	
51942909	FKRP	19q	-1	0	0	0	1	0	0	0		-1	0	0	0	1	0	0	-1	
53520394	EMP3	19q	0	0	0	0	1	0	0	-1	50	0	0	0	0	1	0	0	-1	50
45731605	COL18A1	21q	1	1	1	0	1	0	0	0		1	1	1	0	1	0	0	0	
46257853	COL6A1	21q	1	1	1	0	1	0	0	0		1	1	1	0	1	0	0	0	
46374244	COL6A2	21q	1	1	1	0	1	0	0	0		1	1	1	0	1	0	0	0	
46412376	FTCD	21q	1	1	1	0	1	0	0	0	50	1	1	1	0	1	0	0	0	50
143845844	KYNU	2q	1	1	0	0	1	1	0	0		1	1	0	0	0	0	0	0	
162196010	TANK	2q	1	1	0	0	1	1	0	0		1	1	0	0	0	1	0	0	
162558208	ELYS	2q	1	1	0	0	1	1	0	0		1	1	0	0	0	1	0	0	
169861650	NOSTRIN	2q	1	1	0	0	1	1	0	0		1	1	0	0	0	1	0	0	
172581402	CYBRD1	2q	1	1	0	0	1	1	0	0		1	1	0	0	0	1	0	0	
173067391	BC029123	2q	1	1	0	0	1	1	0	0		1	1	0	0	0	1	0	0	
173152012	DLX1	2q	1	1	0	0	1	1	0	0	50	1	1	0	0	0	1	0	0	37,5
184508238	DCTD	4q	1	1	1	0	1	0	0	0		0	0	0	0	0	0	0	0	
184654703	I_1944379	4q	1	1	1	0	1	0	0	0		0	0	0	0	0	0	0	0	
184714078	FLJ30277	4q	1	1	1	0	1	0	0	0		0	0	0	0	0	0	0	0	
185705743	AK057370	4q	1	1	1	0	1	0	0	0		0	0	0	0	0	0	0	0	
186958918	MGC24125	4q	1	1	1	0	1	0	0	0		0	0	0	0	0	0	0	0	
186984173	DKFZp761O04	4q	1	1	1	0	1	0	0	0	50	0	0	0	0	0	0	0	0	0
117809906	ATP5L	11q	0	0	0	-1	0	0	0	-1		0	0	0	0	0	0	0	0	
117843064	MGC13053	11q	0	0	0	-1	0	0	0	-1		0	0	0	0	0	0	0	0	
117844957	AF272392	11q	0	0	0	-1	-1	0	0	-1	37,5	0	0	0	0	0	0	0	0	0

Red Gains, *green* losses, *blank* no alterations found

Genomic clonality was found in the lesions of case 6 by array CGH. Clonality was not confirmed by mtDNA that showed remarkable genetic distance in this same case.

The most common genomic alterations found both in LN and ILC are illustrated in Table 3. These included gains in 19p which were found in 87.5% of ILC and 62.5% of LN from AZU1 located at 778.831 bp to ICAM3 located at 10.305.416 bp.

Gains of 6p were found in cases 2, 5, 6, 8, and 10 (63% of cases). This region is associated to the Histone gene family.

1p+, where *JUN* and *CASP9* are located, was found in cases 2, 5, 6, 7, and 8 (63% of cases) and in LN only in case 12.

Gains in 3p, where *MAP4* (microtubule-associated protein 4) was located, were found in cases 2, 5, 6, 8, and 11 (63% of cases) for both LN and ILC, and 12 for LN only.

16p+ was found in cases 2, 5, 6, and 8 (50% of cases) and in 12 for LN only, where *CASKIN1*, *CCNF*, *NTN2L*, *ATP6VOC*, and *MPN* are located.

16q22.1 loss, which includes the locus of e-cadherin (*CDH1*), was observed in four cases of ILC (cases 2, 5, 6, and 11). The same locus was lost in LN in cases 2, 5, 6, and 12 (Table 3, Fig. 5).

19q deletions were found in cases 2, 5, 6, 8, and 12.

21q+ (in which are present *COL18A1*, *COL6A1*, *COL6A2*, and *FTCD*) was found in cases 2, 5, 6, and 8.

Gains in 2q were found in cases 2, 5, 8, and 10 (50% of cases) where *KYNU*, *TANK*, *DLX1*, and *NOSTRIN* are located.

Case 2 had a deletion in 7p22, corresponding to *NUDT1* (human 8-oxo-dGTPase). This gene has a role in eliminating oxidized-free dGTP and prevents incorporation of an oxidized guanine base into DNA during replication [17].

Case 5 showed a gain at 10q21 (nucleotide 59815182, see SupplInf2.zip). This locus corresponds to *TFAM* gene (transcription factor A, mitochondrial), which has been described to bind mtDNA in a sequence-independent manner in a nucleosome like structure called nucleoid.

A subset of genetic alterations present only in ILC and not in LN consisted of gain of 4q where the *DCTD* gene is

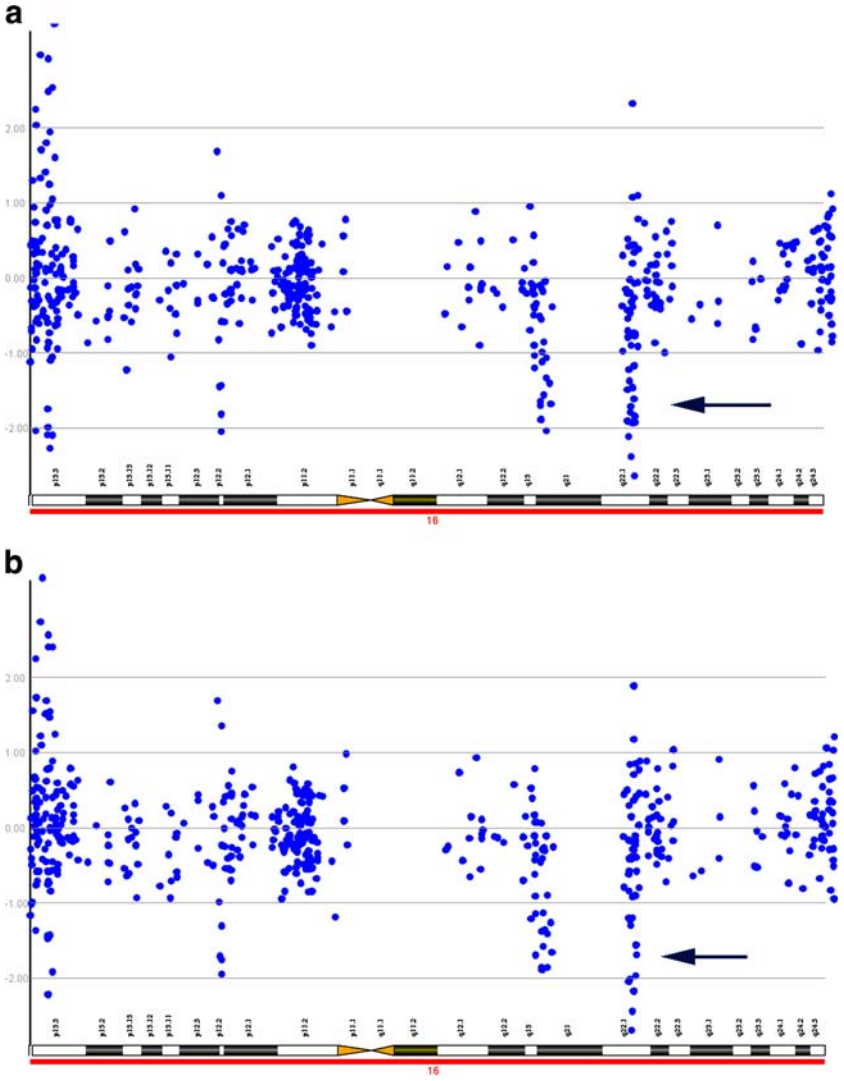

Fig. 5 Scatter plot of case 2 visualized by CGH-Explorer for chromosome 16: **a** LN, **b** ILC; deletions in 16q22.1 shown (*arrows*). Same pattern of genetic alterations is seen

located (cases 2, 5, 6, and 8), and of loss of 11q where *ATP5L* gene is located (cases 7, 8, and 12).

LOH by microsatellite analysis of 16q22.1

LOH data obtained by microsatellite analysis confirmed CGH data when the D16S496 (chromosome 16, nucleotide 67506219) mapped close to *CDH1* (chromosome 16, nucleotide 67328696) was found to be informative (cases 2, 5, 8, 10, and 12). The same allele was lost in ILC and LN of cases 2 and 5, an additional evidence for clonality.

Discussion

There are several methods to assess clonality in pathology. One of these is constituted by the mtDNA test, which is a method that is repeatedly validated [25]. In accordance, eight out of the 12 cases of simultaneous LN and ILC studied here appeared to have a genetic clonal profile as demonstrated by the vicinity in the NJ tree of the respective paired lesions and by the Kimura-2 distance parameter score, that the more are close to 0, the more the lesions are clonal.

Clonality was not seen in the cells from the case of bilateral LN used as test control, but genetic identity was seen in normal glands obtained from the same paraffin block.

Similar results were confirmed in the eight cases of this series studied with CGH array, a further method that indicates clonality. Chromosomal numerical aberrations, particularly regional amplifications and deletions, are a hallmark of solid tumor genomes, and these genetic changes were used to demonstrate common cells of origin among different tumor cell populations [16, 28, 31]. In accordance, seven cases displayed similar genomic profile in the paired lesions (LN and ILC). In case 7 (LIN 2 and pleomorphic ILC), the genomic profile was different in the paired lesions, a finding confirmed by mtDNA NJ tree.

Case 11 was consistent with a clonal lesion as it showed at the same time in LN and ILC heteroplasmic mutation of *ND4* with amino acid change from Ser to Phe. Case 6, on the contrary, contained a heteroplasmic mutation of *CytB* gene in codon 29 only in ILC and not in LN.

Admittedly, a potential pitfall in this study might be related to the cross-contamination between cells from LN and ILC especially consequent to the fact that both lesions were taken from the same paraffin block. Nevertheless, to minimize this possible confounder, special care was taken during the microdissection of each lesion that was processed separately.

The data offered by the two methods (mtDNA and CGH array) were consonant in the various cases, with the exception of case 6 that appeared clonal at CGH level, while on the contrary, LN and ILC were genetically distant when mtDNA was evaluated. We cannot offer a clear-cut explanation to this phenomenon, which might simply be the consequence of stochastic events related to the same genetic changes at the nuclear level in different cells of origin.

Nuclear gains and losses were more numerous in ILC than LN as it appears from supplementary synthetic view of the whole-arm alterations. This was also observed by Hwang et al. [16] who suggested a greater genomic stability for LN compared to ILC. Gains of 4q (cases 2, 5, 6, and 8) and losses of 11q (cases 7, 8, and 12) constituted a subset of genetic alterations present only in ILC, which probably indicates progression of the tumor.

CGH alterations found in the present series were similar to those seen in previous works [16, 31], such as: 6q−, 1q+, 16p+, 17p−, 8q+, but here, additional changes were identified: 19p+, 6p+, 19q−, 1p+, 2q+, 6q+, 11p−.

Locus 16q22.1 was deleted both in ILC and LN in their respective four cases (Table 3, Fig. 5). This locus includes the e-cadherin gene (*CDH1*). All lesions studied were e-cadherin negative at immunohistochemical level. This phenomenon is not necessarily consequent to deletion only of the gene but also to its inactivation via hypermethylation or point mutation [33]. In fact, there are contrasting data in the literature that vary from 100 to 50% for loss of *CDH1* [7, 16], from 22 to 29% for point mutation [7, 33], and from 41 to 77% for promoter hypermethylation of the same gene [7, 33]. It is possible that the three cases of the present series that did not show loss of the e-cadherin locus (as demonstrated by CGH array and LOH) had probably *CDH1* inactivation by the two other mechanisms.

In the two cases of pleomorphic ILC, of which one also showed LIN 3, a genetic portrait different from classic lobular neoplasia was evidenced (17p loss, 19q gain, no alteration in 1p and 2q, 4q, 6p, 16p). These data are dissonant from those offered by the one case reported by Reis-Fihlo et al. [31] who found gains on 1q, 7p, 8p, 9p and 20p and losses on 1p and 16q. This is probably consequent to the fact that the number of cases evaluated is still too limited and the techniques employed are not totally superimposable yet.

Admittedly, the present cases were selected as LN and ILC were present in the same block. Consequently, these might represent a subset of lesions with high malignant potential. Nevertheless, the clinical implication for these lesions appears to be related not only to the fact that frequently, LN and ILC are intermingled [12], but also that they appear genetically similar. If the data offered in this study are confirmed by other similar studies, then it would be difficult to escape from the admission that LN is a precursor lesion of ILC, at least from genetic point of view.

Acknowledgements This work was supported by grants number 2002064975 and 2005063089 (COFIN) from the Ministry of University and Research (MIUR).

The authors thank Dr. Alberto Goldoni (from Medical Genetics Unit, S. Orsola-Malpighi Hospital, University of Bologna) for the bioinformatics support.

References

1. Andersen JA (1974) Multicentric and bilateral appearance of lobular carcinoma in situ of the breast. Acta Pathol Microbiol Scand 82:730–734
2. Andersen JA (1977) Lobular carcinoma in situ of the breast. Cancer 39:2597–2602
3. Anderson S, Bankier AT, Barrel BG, de Bruijn MH, Coulson AR, Drouin J, Eperon IC, Nierlich DP, Roe BA, Sanger F, Schreier PH, Smith AJ, Staden R, Young IG (1981) Sequence and organization of the human mitochondrial genome. Nature 290:457–465
4. Barrett MT, Scheffer A, Ben-Dor A, Sampas N, Lipson D, Kincaid R, Tsang P, Curry B, Baird K, Meltzer PS, Yakhini Z, Bruhn L, Landerman S (2004) Comparative genomic hybridization using oligonucleotide microarrays and total genomic DNA. Proc Natl Acad Sci U S A 101:1765–1777
5. Bratthauer GL, Tavassoli FA (2002) Lobular intraepithelial neoplasia: previously unexplored aspects assessed in 775 cases and their clinical implications. Virchows Arch 440:134–138
6. Elsheikh TM, Silverman JF (2005) Follow-up surgical excision is indicated when breast core needle biopsies show atypical lobular hyperplasia or lobular carcinoma in situ. A correlative study of 33 patients with review of the literature. Am J Surg Pathol 29:534–543
7. Etzell JE, DeVries S, Chew K, Florendo C, Molinaro A, Ljung BM (2001) Loss of chromosome 16q in lobular carcinoma in situ. Hum Pathol 32:292–296
8. Eusebi V, Azzopardi JG (1980) Lobular endocrine neoplasia in fibroadenoma of the breast. Histopathology 4:413–428
9. Eusebi V, Betts CM, Haagensen DE, Gugliotta P, Bussolati G, Azzopardi JG (1984) Apocrine differentiation in lobular carcinoma of the breast. Hum Pathol 15:134–140
10. Eusebi V, Feudale E, Foschini MP, Micheli A, Conti A, Riva C, Di Palma S, Rilke F (1994) Long term follow up of in situ carcinoma of the breast. Semin Diagn Phathol 11(n 3):223–235
11. Eusebi V, Magalhaes F, Azzopardi JG (1992) Pleomorphic lobular carcinoma of the breast: an aggressive tumor showing apocrine differentiation. Hum Pathol 23:655–662
12. Foote FW, Stewart FW (1941) Lobular carcinoma in situ. Am J Pathol 17:491–500
13. Foschini MP, Righi A, Cucchi MC, Ragazzini T, Merelli S, Santeramo B, Eusebi V (2006) The impact of large sections and 3D technique on the study of lobular in situ and invasive carcinoma of the breast. Virchows Arch 448:256–261
14. Frost AR, Tsangaris TN, Silverberg SG (1996) Pleomorphic lobular carcinoma in situ. Pathol Case Rev 1:27–31
15. Gad A, Azzopardi JG (1975) Lobular carcinoma of the breast: a special variant of mucin-secreting carcinoma. J Clin Pathol 28:711–716
16. Hwang ES, Nyante SJ, Chen Y-Y, Moore D, DeVries S, Korkola JE, Esserman LJ, Waldman FM (2004) Clonality of lobular carcinoma in situ and synchronous invasive lobular carcinoma. Cancer 100:2562–2572
17. Kang D, Hamasaki N (2005) Mitochondrial DNA in somatic cells: a promising target of routine clinical tests. Clin Biochem 38:687–695
18. Kapushesky M, Kemmeren P, Culhane AC, Durinck S, Ihmels J, Korner C, Kull M, Torrente A, Sarkans U, Vilo J, Brazma A (2004) Expression profiler: next generation—an online platform for analysis of microarray data. Nucleic Acids Res 1:465–470
19. Kimura M (1980) A simple method for estimating evolutionary rate of base substitution through comparative studies of nucleotide sequences. J Mol Evol 16:111–116
20. Kumar S, Gadagkar SR (2000) Efficiency of the neighbor-joining method in reconstructing deep and shallow evolutionary relationships in large phylogenies. J Mol Evol 51:544–553
21. Kumar S, Tamura K, Jakobsen IB, Nei M (2001) MEGA2: molecular evolutionary genetics analysis software. Bioinformatics 17:1244–1245
22. Lakhani SR, Collins N, Sloane JP (1995) Loss of heterozygosity in lobular carcinoma in situ of the breast. J Clin Pathol 48:74–78
23. Lingjaerde OC, Baumbusch LO, Liestol K, Glad IK, Borresen-Dale AL (2005) CGH-Explorer: a program for analysis of array-CGH. Bioinformatics 21:821–822
24. Martinez V, Azzopardi JG (1979) Invasive lobular carcinoma of the breast: incidence and variants. Histopathology 3:467–488
25. Morandi L, Pession A, Marucci G, Foschini MP, Pruneri G, Viale G, Eusebi V (2003) Intraepidermal cells of Paget's carcinoma of the breast can be genetically different from those of the underlying carcinoma. Hum Pathol 34(12):1321–1330
26. Nayar R, Zhuang Z, Merino MJ, Silverberg SG (1997) Loss of heterozygosity on chromosome 11q13 in lobular lesions of the breast using tissue microdissection and polymerase chain reaction. Hum Pathol 28:277–282
27. Nei M, Kumar S (1994) MEGA: Molecular Evolutionary Genetics Analysis software for microcomputers. Comput Appl Biosci 10:189–191
28. O'Hagan RC, Brennan CW, Strahs A, Zhang X, Kannan K, Donovan M, Cauwels C, Sharpless NE, Wong WH, Chin L (2003) Array comparative genome hybridization for tumor classification and gene discovery in mouse models of malignant melanoma. Cancer Res 63:5352–5356
29. Ottesen GL, Graversen HP, Blichert-Toft M, Zedeler K, Andersen JA (1993) Lobular carcinoma in situ of the female breast short-term results of a perspective nationwide study. Am J Surg Pathol 17(1):14–21
30. Page DL, Schuyler PA, Dupont WD, Jensen RA, Plummer WD, Simpson JF (2003) Atypical lobular hyperplasia as a unilateral predictor of breast cancer risk: a retrospective cohort study. Lancet 361:125–129
31. Reis-Filho JS, Simpson PT, Jones C, Steele D, Mackay A, Iravani M, Fenwick K, Valgeirsson H, Lambros M, Ashworth A, Palacious J, Schmitt F, Lakhani SR (2005) Pleomorphic lobular carcinoma of the breast: role of comprehensive molecular pathology in characterization of an entity. J Pathol 207:1–13
32. Saitou N, Nei M (1987) The neighbor joining method: a new method to reconstructing phylogenetic trees. Mol Biol Evol 4:406–425
33. Sanchez-Estevez C, Guo M, Herman JG, Gamallo C, Esteller M, Palacios J (2003) Epigenetic and genetic alterations of APC and CDH1 genes in lobular breast cancer: relationships with abnormal E-cadherin and catenin expression and microsatellite instability. Int J Cancer 106:208–215
34. Sieben NLG, Haar NT, Cornelisse CJ, Fleuren GJ, Cleton-Jansen AM (2000) PCR artifacts in LOH and MSI analysis of microdissected tumor cells. Hum Pathol 31:1415–1419
35. Soares J, Tomasic G, Bucciarelli E, Eusebi V (1994) Intralobular growth of myoepithelial cell carcinoma of the breast. Virchows Arch 425:205–210
36. Tavassoli FA (1999) Pathology of the breast. Appleton—Lange, Stamford, CT
37. Tot T (2003) The diffuse type of invasive lobular carcinoma of the breast: morphology and prognosis. Virchows Arch 443:718–724
38. Vos CB, Cleton-Jansen AM, Berx G (1997) E-cadherin inactivation in lobular carcinoma in situ of the breast: an early event in tumori-genesis. Br J Cancer 76:1131–1133
39. WHO (2003) Tumours of the breast and female genital organs. IARC Press, Lyon
40. Woischnik M, Moraes CT (2002) Pattern of organization of human mitochondrial pseudogenes in the nuclear genome. Genome Res 12:885–893

Virchows Arch (2006) 449: 24–30
DOI 10.1007/s00428-006-0213-6

ORIGINAL ARTICLE

Walter Schippinger · Peter Regitnig · Nadia Dandachi · Klaus-Dieter Wernecke · Thomas Bauernhofer · Hellmut Samonigg · Farid Moinfar

Evaluation of the prognostic significance of androgen receptor expression in metastatic breast cancer

Received: 8 February 2006 / Accepted: 1 April 2006 / Published online: 21 April 2006
© Springer-Verlag 2006

Abstract The purpose of this study was to investigate the influence of androgen receptor (AR) expression in tumour tissue on survival of patients with metastatic breast cancer. Tumour specimens from 232 patients with metastatic breast cancer were examined for presence of AR by immunohistochemistry. According to the extent of immunostaining, AR expression was classified as score 0, 1+, 2+, or 3+. AR positivity was observed in 164 (70.7%) tumours. The median survival after disease recurrence (SAR) of patients with AR-expressing tumours was significantly longer compared to that of patients with AR-negative tumours (21.89 months, 95% CI 17.23–26.55 vs 11.99 months, 95% CI 9.36–14.62; log-rank test 0.0282). In addition, patients with AR score 3+ had a significantly longer disease-free survival (DFS) compared to patients with AR score 0, 1+, and 2+, (24.67 months, 95% CI 13.72–35.62 vs 16.36 months, 95% CI 13.18–19.54, log-rank test 0.0043). Multivariate Cox analyses showed no statistically significant influence of AR expression on DFS or SAR. In conclusion, SAR is significantly longer in patients with AR-expressing breast carcinoma. However, AR expression is not an independent prognostic factor for SAR in metastatic breast cancer.

Keywords Metastatic breast cancer · Androgen receptor · Prognostic factors

W. Schippinger (✉) · N. Dandachi · T. Bauernhofer · H. Samonigg
Division of Oncology, Department of Internal Medicine, Medical University of Graz, Auenbruggerplatz 15, 8036 Graz, Austria
e-mail: walter.schippinger@klinikum-graz.at
Tel.: +43-316-3853115
Fax: +43-316-3854167

P. Regitnig · F. Moinfar
Institute of Pathology, Medical University Graz, 8036 Graz, Austria

K.-D. Wernecke
Institute of Medical Biometry, Humboldt University of Berlin, 13344 Berlin, Germany

Introduction

Determination of oestrogen and progesterone receptor (ER and PgR) status is a standard procedure in histopathological assessment of breast cancer. In early stage breast cancer, the ER and PgR status is a commonly accepted prognostic factor for survival. Absence of ER and PgR expression has been shown to be associated with early disease recurrence and poor survival [2, 12, 16]. Primary invasive breast carcinomas express ER and PgR in approximately 55–65 and 45–55% of cases, respectively [4, 20, 21]. Androgen receptor (AR) expression has been reported in 60% of invasive breast carcinomas and, moreover within ER-negative tumours, almost 50% have been shown to be AR positive [1, 15]. Whereas the prognostic value of ER and PgR is well established, little information exists on the prognostic value of AR expression in breast cancer [1, 5, 13, 19]. Several authors reported a prognostic advantage for patients with AR expression in early breast cancer compared to patients with AR-negative tumours [1, 5, 13]. In patients with metastasised breast cancer, prognostic factors influencing survival are less well defined than in patients with early-stage disease. Survival and clinical course varies widely in patients with metastatic cancer. Studies have demonstrated that characteristics of the primary breast carcinoma, such as oestrogen receptor expression, are determinants for the prognosis of patients after disease relapse [6, 7, 10].

The purpose of the present study was to analyse the prognostic significance of AR expression on disease-free and post-recurrence survival for patients with metastatic breast cancer within a multiple model including clinical and histopathological prognostic covariates.

Materials and methods

To examine the frequency of AR expression and the impact of AR expression on survival of patients with metastatic breast cancer, 250 patients with metastatic breast carcinoma were randomly selected from the database of the

Division of Oncology at the Medical University of Graz (Graz, Austria). From 232 of the selected patients, paraffin-embedded tumour samples were available at the Institute of Pathology at the Medical University of Graz. The primary breast carcinomas of the selected patients were resected between February 1989 and September 1997.

The following patient data were retrieved from the database: age, menopausal status, date of surgery of the primary tumour, histological tumour type, histopathological tumour size (T), grade (G), nodal status (N) and date of first tumour recurrence, and date of death, when appropriate. All cases were graded histopathologically using the modified Bloom and Richardson's system [8].

Immunohistochemical analyses of ER, PgR, AR, and HER-2/neu were carried out on tissue microarrays using a custom-made precision instrument (Beecher Instruments, Silver Spring, MD, USA). For tissue microarrays, representative regions were selected on routinely haematoxylin–eosin-stained sections. On the average, five tissue cylinders (0.6 mm in diameter) were taken from each tumour.

From the tissue microarrays, 4-μm serial sections were deparaffinised, rehydrated, and rinsed in distilled water. Immunohistochemical assays for AR, ER, PgR, and HER-2/neu were performed using standardised automated procedures (Ventana Medical Systems, Tucson, AZ, USA and Dako Cytomation, Glostrup, Denmark). As primary antibodies, the monoclonal antihuman mouse antibody clone 6F11 was used for ER and antibody clone 1A6 for PgR (both Ventana medical Systems). To determine AR expression, the monoclonal mouse antihuman androgen receptor antibody clone AR441 (Dako) was used. Antigen retrieval was achieved by microwave treatment (ER and PgR) or heating in a water bath (AR). A Ventana ES (Ventana Medical Systems) or Chem-Mate (Dako) autostainer was used in conjunction with an indirect streptavidin–biotin method. After incubation with the primary antibody, incubation with the secondary (link), biotinylated antibody was performed for 30 min. The sections were washed and then incubated with streptavidin–peroxidase for another 30 min. Finally, the enzyme was visualised after a 15-min incubation with diaminobenzidine. Counterstaining was performed using haematoxylin. For ER, PgR, and AR, samples were scored as positive when at least 10% of the nuclei were immunoreactive. A simple semiquantitative scoring system was used: score 0 was defined as lack of staining or staining below cut-off level. Score 1+ was defined as weakly positive, corresponding to weak nuclear staining intensity in more than 10% of cells. Score 2+ was defined as moderately positive, equal to moderate nuclear staining intensity in 10 to 80% of cells and score 3+ as strongly positive, equal to strong staining intensity in 51 to 100% of cells or moderate staining intensity in more than 80% of cells.

HER-2/neu expression was determined using the HercepTest (Dako) according to the manufacturer's protocol and scoring guidelines (scoring range 0 to 3+). Score 3+ was regarded as a positive result for HER-2/neu overexpression. All immunoslides were evaluated independently by at least two investigators (FM and PR). Cases in which disagreement occurred were reevaluated using a multiheaded microscope; a final agreement was reached in all cases examined.

Survival after disease recurrence (SAR) was defined as the time period from first manifestation of metastatic disease until death. Disease-free survival (DFS) was defined as the time from surgery of primary breast cancer to occurrence of metastases.

This retrospective study has been approved by the ethic committee of the Medical University of Graz. Informed consent was not requested for immunohistochemical analyses of ER, PgR, AR, and HER-2/neu in the stored tumour samples. Our procedure was in accordance to

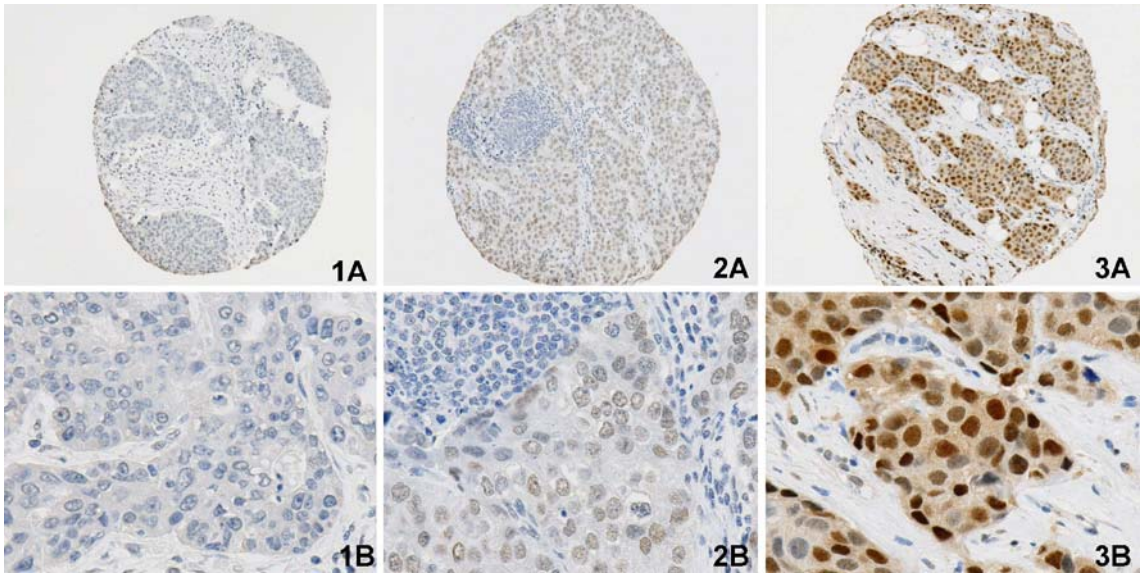

Fig. 1 Examples of immunoreactions in invasive breast carcinomas on tissue microarrays. **a** and **b***1* Lack of immunoreaction for androgen receptor (score 0); *2* weak positive reaction for androgen receptor (score 1+); *3* strong positivity for androgen receptor (score 3+)

national law. In addition, most of the patients were deceased when the study was initiated.

Statistics

Patient's characteristics were expressed in absolute numbers (%). The SAR and DSF according to the AR status categories AR negative (AR score 0) vs AR positive (AR score 1+, 2+, and 3+) and AR score 3+ vs AR scores (0, 1+, and 2+), respectively, were estimated according to Kaplan–Meier and compared univariately with log-rank statistics as well as multivariately with Cox' proportional hazard regression. Cox' proportional hazard regression analysis was performed to evaluate the prognostic value of AR status multivariately. Hazard ratios with 95% confidence intervals for all included variables are given. Statistical analyses were performed using Statistical Package for the Social Science (SPSS) for Windows. Significance was assessed at the $p<0.05$ level (two-sided).

Results

Expression of AR, ER, PgR, and HER-2/neu

Of the 232 cases of breast carcinoma examined, 164 (70.7%) cases expressed AR: 59 (25.4%) score 1+, 72 (31.0%) score 2+, and 33 (14.2%) score 3+. One hundred and fifty-two (65.5%) tumours were ER and/or PgR positive and 61 (26.8%) of the tumours showed a positive HER-2/neu status as defined by an immunohistochemical score 3+. Examples for immunoreactions on tissue microarrays for AR are shown in Fig. 1.

From 164 tumours expressing AR, 120 (73.2%) were ER positive and 77 (47.0%) were PgR positive. Fifty tumours (30.9%) showed co-expression of AR and HER-2/neu score 3+, whereas only 11 (16.7%) cases with HER-2/neu score 3+ were seen within the 68 AR-negative tumours.

Patient characteristics are shown in Table 1.

Within the subset of cases with co-expression of AR and HER-2/neu score 3+, the following clinicopathological characteristics were found: the median age of patients was 59.1 years (range 28–80) and 11 (22.0%) patients were premenopausal and 39 (78.0%) postmenopausal. The distribution of tumour size and nodal status was found as followed: pT1 in 13 (26%), pT2 in 19 (38%), pT3 in 10 (20%), and pT4 in 8 (16%) cases; N0 in 8 (16%), N1 in 37 (74%), and N2 in 4 (8%) patients. Forty-three (86.0%) cases of this subset were invasive ductal carcinomas and seven (14.0%) were mixed ductal/lobular carcinomas or other tumour types; 16 (32.0%) tumours were classified as G1/2 and 32 (64.0%) as G3/4; 27 (54.0%) cases were ER and PgR negative, 14 (28%) cases ER or PgR positive, and 9 (18.0%) cases ER and PgR positive; AR score 1+ was found in 20 (40.0%), AR score 2+ in 25 (50.0%), and AR score 3+ in 5 (10.0%) tumours. The site of first metastasis was visceral in 31 (62%) and non-visceral in 19 (38%) patients; disease-free survival was 0 months in 10 (20%), ≤ 24 months in 29 (58%), and >24 months in 11 (22%) patients of this subset. Thirteen (26%) of these 50 patients

Table 1 Patient characteristics

Characteristics	No. of patients (%)
All patients	232 (100)
Age (years)	
Median	59.4
Range	28–80
Histology	
Invasive ductal	188 (81.0)
Invasive lobular	14 (6.0)
Mixed ductal/lobular and others	30 (12.9)
Adjuvant treatment	
Endocrine therapy only	65 (28.0)
Chemotherapy only	50 (21.6)
Endocrine and Chemotherapy	3 (1.3)
Menopausal status	
Premenopausal	66 (28.4)
Postmenopausal	166 (71.6)
Tumour size	
pT1	79 (34.1)
pT2	82 (35.3)
pT3	16 (6.9)
pT4	55 (23.7)
Nodal status	
N0	51 (22.9)
N1	150 (67.3)
N2	22 (9.8)
Grading	
G1/2	84 (38.4)
G3/4	135 (61.6)
ER/PgR status	
ER− and PgR−	80 (34.5)
ER+ or PgR+	72 (31.0)
ER+ and PgR+	80 (34.5)
AR expression	
Score 0	68 (29.3)
Score 1+	59 (25.4)
Score 2+	72 (31.1)
Score 3+	33 (14.2)
HER-2 expression	
Score 0	117 (51.3)
Score 1+	21 (9.2)
Score 2+	29 (12.7)
Score 3+	61 (26.8)
Site of first metastasis	
Visceral	120 (51.7)
Non-visceral	112 (48.3)
Disease-free survival	
0 months	57 (24.6)
≤24 months	89 (38.4)
>24 months	86 (37.1)

ER Oestrogen receptor, *PgR* progesterone receptor, *AR* androgen receptor, *HER-2* human epidermal growth factor 2

received adjuvant endocrine therapy and seven (14%) were treated with adjuvant chemotherapy.

AR status and survival after disease recurrence in univariate analysis

The median follow-up after disease recurrence was 76.6 months. Two hundred (86.2%) patients died during the observation period.

The median SAR of patients with AR-expressing tumours (AR score 1+, 2+, and 3+) was significantly longer compared to that of patients with AR-negative tumours (AR score 0) (21.89 months, 95% CI 17.23–26.55 and 11.99 months, 95% CI 9.36–14.62, respectively; log-rank test 0.0282). An additional comparison of patients with strong AR expression (AR score 3+) and patients with weak, moderate, or no AR expression (AR score 1+, 2+, and 0) in tumour tissue revealed a statistically significant longer median SAR for patients with tumours showing strong AR expression (31.31 months, 95% CI 9.77–52.85 vs 17.61 months, 95% CI 14.75–20.47; log-rank test 0.0405). The median SAR of patients with co-expression of AR and HER-2/neu score 3+ was similar to that of patients with AR-negative tumours (10.89 months, 95% CI 5.40–16.38).

The Kaplan–Meier curves for SAR of patients with AR-positive (AR score 1+, 2+, and 3+) and patients with AR-negative (AR score 0) tumours are shown in Fig. 2.

AR status and disease-free survival in univariate analysis

The median DFS of patients with AR-expressing tumours (AR score 1+, 2+, and 3+) and of those patients with AR-negative tumours (AR score 0) was 17.51 and 15.64 months, respectively, which was not statistically different (log-rank test p=0.6862). To examine whether strong AR expression influences DFS, a univariate analysis was performed comparing patients with strong AR expression (AR score 3+) with patients showing weak, moderate, or no AR expression (AR score 1+, 2+, and 0) in tumour tissue: this analysis showed a statistically significant longer DFS for patients with strong AR expression (median DFS 24.67 months, 95% CI 13.72–35.62) compared to patients with AR score 0, 1+, or 2+ in the primary tumour (median DFS 16.36 months, 95% CI 13.18–19.54; log-rank test 0.0043). The Kaplan–Meier curves for DFS of patients with AR score 3+ and patients with AR score 0, 1+, and 2+ are shown in Fig. 3. The median DFS in the subset of patients with co-expression of AR and HER-2/neu score 3+ was 9.07 months (95% CI 2.63–15.52).

AR expression and survival after disease recurrence in the multivariate model

Multivariate analyses included variables determinable at the time of primary tumour assessment.

The included variables and the results of Cox' multivariate regression analysis are shown in Table 2. The significant prognostic factors for SAR are menopausal status, number of axillary lymph node metastases, and ER and PgR status. Age, tumour size, histopathological tumour grading, and HER-2/neu status had no significant impact on SAR as well as AR status in the categories AR negative (AR score 0) vs AR positive (AR score 1+, 2+, and 3+) and AR score 3+ vs AR scores (0, 1+, and 2+), respectively.

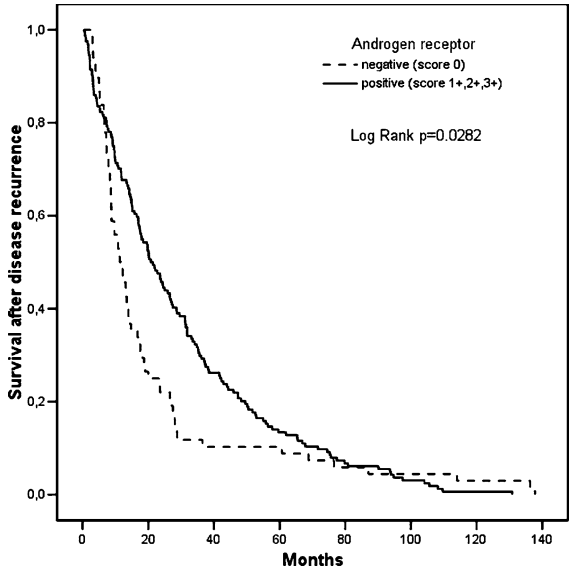

Fig. 2 Survival after disease recurrence of patients with androgen receptor score (1+, 2+, and 3+) and patients with AR score 0

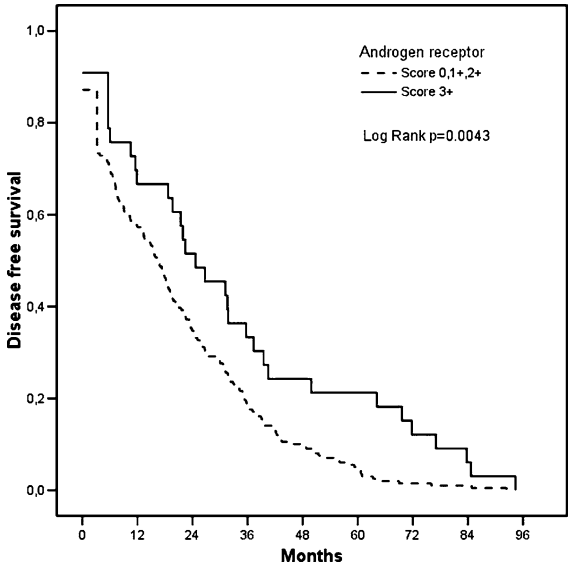

Fig. 3 Disease-free survival of patients with androgen receptor score 3+ and patients with AR score (0, 1+, and 2+)

Table 2 Multivariate Cox' regression analysis: evaluation of prognostic factors for survival after disease recurrence

	Hazard ratio	95% CI	*p*-value
Age	0.799	0.325–1.967	0.626
Menopausal status	0.646	0.450–0.927	**0.018**
Tumour size (pT)			0.674
pT1	1.264	0.831–1.922	0.273
pT2	1.183	0.795–1.762	0.407
pT3	1.346	0.722–2.507	0.349
Metastatic axillary lymph nodes			**0.004**
1–3	0.500	0332–0.751	**0.001**
≥3	0.865	0.604–1.238	0.428
Grading	0.908	0.670–1.229	0.532
Oestrogen receptor status	1.601	1.081–2.371	**0.019**
Progesterone receptor status	1.437	1.016–2.032	**0.040**
Androgen receptor status	1.208	0.839–1.737	0.309
HER-2/neu status			0.286
Score 2+	0.748	0.521–1.072	0.114
Score 3+	0.790	0.455–1.371	0.402

For the HR, the reference category for categorical covariates was <35 years for age, premenopausal for menopausal status, pT4 for tumour size, 0 metastatic lymph nodes for metastatic axillary lymph nodes, G1/2 for grading, negative oestrogen receptor status for oestrogen receptor status, negative progesterone receptor status for progesterone receptor status, negative androgen receptor status for androgen receptor status, and HER-2/neu scores (0 and 1+) for HER-2/neu status. Significant *p*-values are printed in bold

Table 3 Multivariate Cox' regression analysis: evaluation of prognostic factors for disease-free survival

	Hazard ratio	95% CI	*p*-value
Age	1.063	0.468–2.412	0.884
Menopausal status	0.700	0.496–0.989	**0.043**
Tumour size (pT)			**0.043**
pT1	0.554	0.362–0.850	**0.007**
pT2	0.648	0.431–0.976	**0.038**
pT3	0.541	0.293–1.001	**0.050**
Metastatic axillary lymph nodes			**0.037**
1–3	0.872	0.604–1.260	0.467
≥3	0.629	0.442–0.896	**0.010**
Grading	0.972	0.723–1.307	0.853
Oestrogen receptor status	1.343	0.936–1.926	0.109
Progesterone receptor status	1.338	0.959–1.866	0.086
Androgen receptor status	0.803	0.567–1.138	0.218
HER-2/neu status			0.424
Score 2+	0.880	0.628–1.234	0.460
Score 3+	0.704	0.415–1.194	0.193

For the HR, the reference category for categorical covariates was <3 years for age, premenopausal for menopausal status, pT4 for tumour size, 0 metastatic lymph nodes for metastatic axillary lymph nodes, G 1/2 for grading, negative oestrogen receptor status for oestrogen receptor status, negative progesterone receptor status for progesterone receptor status, negative androgen receptor status for androgen receptor status, and HER-2/neu scores (0 and 1+) for HER-2/neu status. Significant *p*-values are printed in bold

AR expression and disease-free survival in the multivariate model

The included variables and the results of Cox' multivariate regression analysis are shown in Table 3. The significant prognostic factors for DFS are menopausal status, tumour size, and number of axillary lymph node metastases. Age, histopathological tumour grading, and ER, PgR, and HER-2/neu status had no significant impact on DFS as well as AR status in the categories AR negative (AR score 0) vs AR positive (AR score 1+, 2+, and 3+) and AR score 3+ vs AR scores (0, 1+, and 2+), respectively.

Discussion

This is the first study analysing the prognostic value of AR expression in breast carcinoma for post-recurrence survival in a large number of patients with metastatic breast cancer.

Whereas in early-stage breast cancer the prognostic significance of characteristics of the primary tumour, such as ER and PgR expression, is well documented and generally accepted for use in determining prognosis, parameters influencing the survival after disease relapse are less well defined [2, 9, 16]. Several studies revealed a significant influence of ER and PgR status of the primary breast carcinoma on patient outcome after development of metastatic disease [6, 7, 10]. The objective of this study was to examine whether post-recurrence outcome is influenced by the presence of AR in primary breast carcinoma tissue.

The results of our study show in univariate analysis a statistically significant advantage in SAR for patients with AR-expressing tumours compared to patients with AR-negative breast carcinomas. In addition, patients with strong AR expression in tumour tissue had a significantly longer median SAR than the group of patients with weak, moderate, or no AR expression in the tumours. In multivariate analyses, neither AR positivity nor strong AR expression maintained statistical significance as prognostic parameters for SAR. Univariate analyses examining the impact of AR expression on DFS revealed strong AR expression to influence DFS significantly; however, in the multivariate model, AR expression had again no significant effect on DFS. These findings show that assessment of AR expression does not confer information independently from other prognostic parameters in terms of SAR or DFS in patients with breast cancer who develop metastatic disease. Co-expression of AR and HER-2/neu score 3+ was seen in 30.9% of the tumours examined in this study. SAR as well as DFS of this subset was short, suggesting that AR positivity cannot compensate the unfavourable effect of HER-2/neu overexpression on the patient's prognosis. The present study revealed menopausal status, number of axillary lymph node metastases, and ER and PgR status to be significant prognostic factors for post-recurrence survival in multivariate analysis. Tumour size, histopathological grading, and HER-2/neu status of the primary

tumour have been shown to have no statistically significant impact on SAR in the multivariate analysis.

Up to now, only a few studies examined the impact of AR expression on the prognosis of patients with breast carcinoma. These studies investigated the role of AR expression in early breast cancer. One of the largest studies, reported by Bryan et al., assessed survival data of 1,181 patients with breast cancer and the AR status of primary and recurrent breast carcinomas. Patients with AR-negative tumours were shown in this study to have a statistically significant trend toward shorter overall survival in univariate analysis than those patients with AR-positive tumours [5]. Unfortunately, in this study, the prognostic significance of AR expression was not investigated in a multivariate model including other histopathological prognostic parameters.

In another study evaluating the role of AR expression in early breast cancer, AR content was assessed in breast carcinomas of 224 patients. Approximately 91% of the tumours examined were classified as AR positive. A multivariate analysis revealed levels of AR content to be an independent predictor of the likelihood of axillary lymph node metastases but did not show any prognostic significance concerning relapse-free survival [19].

In the study reported by Kuenen-Boumeester et al. which included 153 patients with breast cancer, AR proved to be prognostic for DFS in univariate analysis. However, the multivariate model showed lymph node status, tumour size, and ER status to be the only independent prognostic factors for DFS. In that study also, AR expression was not shown to be a significant prognostic parameter for DFS in multivariate analysis [13]. A recently published study on 88 patients with predominantly ER-negative breast carcinomas found AR expression in 49% of ER-negative and in 89% of ER-positive tumours. Follow-up data for disease recurrence were available for 66 patients. Although univariate analysis showed that patients with ER-negative, AR-positive tumours had only 33% the risk of disease recurrence compared with that of patients with ER- and AR-negative breast cancer, AR expression was not a significant factor in the multivariate analysis [1].

The findings of studies suggesting positive AR expression status in univariate analyses to be associated with better prognosis could be affected by co-expressions of AR with other tumour characteristics affecting patient prognosis. AR expression was shown in several previous studies to be associated with ER and PgR positivity of breast carcinoma tissue [3, 11, 14, 15, 18]. The frequent co-expression of AR, ER, and PgR could also be an explanation for the advantage in SAR for patients with AR-expressing tumours, as observed in the present study.

Of the 232 breast carcinomas examined in this study, 70.7% expressed androgen receptors. This fact demonstrates that AR expression is a common characteristic in breast cancer and AR could be a possible target for endocrine antitumour therapy strategies. Results of a small, phase II trial testing the efficacy of the antiandrogen drug flutamide in patients with metastatic breast cancer were disappointing [17]. However, in that study, AR status of tumour tissue was not assessed. Future studies on antiandrogen treatment in breast cancer should include measurement of AR expression using a scoring system for AR positivity as performed in the present study to test whether response to antiandrogen therapy is associated with the extent of AR expression in tumour tissue.

References

1. Agoff SN, Swanson PE, Linden H, Hawes SE, Lawton TJ (2003) Androgen receptor expression in estrogen receptor-negative breast cancer. Immunohistochemical, clinical, and prognostic associations. Am J Clin Pathol 120:725–731
2. Allemani C, Sant M, Berrino F, Aareleid T, Chaplain G, Coebergh JW, Colonna M, Contiero P, Danzon A, Federico M (2004) Prognostic value of morphology and hormone receptor status in breast cancer—a population-based study. Br J Cancer 91:1263–1268
3. Brentani MM, Franco EL, Oshima CT, Pacheco MM (1986) Androgen, estrogen, and progesterone receptor levels in malignant and benign breast tumors: a multivariate analysis approach. Int J Cancer 38:637–642
4. Britton JA, Gammon MD, Schoenberg JB, Stanford JL, Coates RJ, Swanson CA, Potischman N, Malone KE, Brogan DJ, Daling JR (2002) Risk of breast cancer classified by joint estrogen receptor and progesterone receptor status among women 20–44 years of age. Am J Epidemiol 156:507–516
5. Bryan RM, Mercer RJ, Bennett RC, Rennie GC, Lie TH, Morgan FJ (1984) Androgen receptors in breast cancer. Cancer 54:2436–2440
6. Chang J, Clark GM, Allred DC, Mohsin S, Chamness G, Elledge RM (2003) Survival of patients with metastatic breast carcinoma: importance of prognostic markers of the primary tumor. Cancer 97:545–553
7. Clark GM, Sledge GW Jr, Osborne CK, McGuire WL (1987) Survival from first recurrence: relative importance of prognostic factors in 1,015 breast cancer patients. J Clin Oncol 5:55–61
8. Elston CW, Ellis IO (1991) Pathological prognostic factors in breast cancer. I. The value of histological grade in breast cancer: experience from a large study with long-term follow-up. Histopathology 19:403–410
9. Hahnel R, Woodings T, Vivian AB (1979) Prognostic value of estrogen receptors in primary breast cancer. Cancer 44:671–675
10. Howell A, Barnes DM, Harland RN, Redford J, Bramwell VH, Wilkinson MJ, Swindell R, Crowther D, Sellwood RA (1984) Steroid-hormone receptors and survival after first relapse in breast cancer. Lancet 1:588–591
11. Isola JJ (1993) Immunohistochemical demonstration of androgen receptor in breast cancer and its relationship to other prognostic factors. J Pathol 170:31–35
12. Knight WA, Livingston RB, Gregory EJ, McGuire WL (1977) Estrogen receptor as an independent prognostic factor for early recurrence in breast cancer. Cancer Res 37:4669–4671
13. Kuenen-Boumeester V, Van der Kwast TH, Claassen CC, Look MP, Liem GS, Klijn JG, Henzen-Logmans SC (1996) The clinical significance of androgen receptors in breast cancer and their relation to histological and cell biological parameters. Eur J Cancer 32A:1560–1565
14. Miller WR, Telford J, Dixon JM, Hawkins RA (1985) Androgen receptor activity in human breast cancer and its relationship with oestrogen and progestogen receptor activity. Eur J Cancer Clin Oncol 21:539–542
15. Moinfar F, Okcu M, Tsybrovskyy O, Regitnig P, Lax SF, Weybora W, Ratschek M, Tavassoli FA, Denk H (2003) Androgen receptors frequently are expressed in breast carcinomas: potential relevance to new therapeutic strategies. Cancer 98:703–711

16. Molino A, Micciolo R, Turazza M, Bonetti F, Piubello Q, Corgnati A, Sperotto L, Recaldin E, Spagnolli P, Manfrin E (1997) Prognostic significance of estrogen receptors in 405 primary breast cancers: a comparison of immunohistochemical and biochemical methods. Breast Cancer Res Treat 45:241–249
17. Perrault DJ, Logan DM, Stewart DJ, Bramwell VH, Paterson AH, Eisenhauer EA (1988) Phase II study of flutamide in patients with metastatic breast cancer. A National Cancer Institute of Canada Clinical Trials Group study. Invest New Drugs 6:207–210
18. Riva C, Dainese E, Caprara G, Rocca PC, Massarelli G, Tot T, Capella C, Eusebi V (2005) Immunohistochemical study of androgen receptors in breast carcinoma. Evidence of their frequent expression in lobular carcinoma. Virchows Arch 447:695–700
19. Soreide JA, Lea OA, Varhaug JE, Kvinnsland S (1992) Androgen receptors in operable breast cancer: relation to other steroid hormone receptors, correlations to prognostic factors and predictive value for effect of adjuvant tamoxifen treatment. Eur J Surg Oncol 18:112–118
20. Stanford JL, Szklo M, Brinton LA (1986) Estrogen receptors and breast cancer. Epidemiol Rev 8:42–59
21. Wittliff JL (1974) Specific receptors of the steroid hormones in breast cancer. Semin Oncol 1:109–118

Virchows Arch (2006) 449: 31–39
DOI 10.1007/s00428-005-0144-7

ORIGINAL ARTICLE

Lilach Kleinberg · Vivi Ann Flørenes · Martina Skrede · Hiep Phuc Dong · Søren Nielsen · Michael T. McMaster · Jahn M. Nesland · Ie-Ming Shih · Ben Davidson

Expression of HLA-G in malignant mesothelioma and clinically aggressive breast carcinoma

Received: 11 September 2005 / Accepted: 7 December 2005 / Published online: 16 March 2006
© Springer-Verlag 2006

Abstract The aim of the present study was to evaluate HLA-G expression in breast carcinoma and malignant mesothelioma (MM). Malignant breast carcinoma effusions (46) and corresponding solid tumors (39) and 104 MM (26 effusions, 78 solid tumors) were analyzed using immunohistochemistry (IHC). HLA-G protein and mRNA expression were further studied using immunoblotting (IB) and RT-PCR. HLA-ABC expression was analyzed using flow cytometry (FCM). IHC showed predominantly focal HLA-G expression in 12 of 46 (26%) breast carcinoma effusions and 16 of 39 (41%) solid lesions. In MM, 20 of 78 (26%) solid lesions and 14 of 26 (54%) effusions were focally HLA-G positive. Expression in MM was higher in effusions (p=0.008). IB showed more frequent HLA-G expression in MM compared with breast carcinoma effusions, while RT-PCR showed HLA-G mRNA expression in both tumors. FCM showed conserved HLA-ABC expression in 15 of 15 effusions. Breast cancer patients with HLA-G-positive tumor cells had shorter disease-free survival (mean 37 vs 85, median 25 vs 31 months), though not significantly (p=0.14). In conclusion, HLA-G is focally expressed in MM and breast carcinoma, while HLA-ABC expression is conserved. However, the up-regulated expression of HLA-G in MM effusions and its possible association with shorter disease-free survival in advanced stage of breast carcinoma suggest a possible role in immune response evasion in some tumors.

Keywords Breast carcinoma · Malignant mesothelioma · Effusions · Immune response

L. Kleinberg · V. A. Flørenes · M. Skrede · H. P. Dong · J. M. Nesland · B. Davidson (✉)
Department of Pathology, Norwegian Radium Hospital, University of Oslo,
Montebello, 0310 Oslo, Norway
e-mail: ben.davidson@radiumhospitalet.no
Tel.: +47-22934871
Fax: +47-22508554

S. Nielsen
Department of Pathology, Aalborg Hospital,
Ålborg, Denmark

M. T. McMaster
Department of Stomatology, University of California,
San Francisco, CA, USA

I.-M. Shih
Department of Pathology, Gynecology and Oncology, Johns Hopkins University Medical Institutions,
Baltimore, MD, USA

Introduction

The evolution and progression of malignant tumors involve the acquisition of genetic and phenotypic advantages that mediate cancer cell survival. One of the mechanisms in this process is evasion of host immune response effectors. Cytotoxic T lymphocytes (CTL) and natural killer (NK) cells are able to identify cells that have lost or express insufficient amounts of MHC class I molecules and attack them [30]. However, in vitro and in vivo models show that tumor cells are able to escape the immune response by down-regulating the expression of classic HLA antigens or by expressing nonclassic antigens such as HLA-G and HLA-E [1, 40]. NK- and T-cell-mediated lysis of target cells is inhibited by HLA-G through interaction with the inhibitory receptors ILT2 and ILT4 [20], and the differential expression of inhibitory and activating NK receptors, such as NKG2 family members, may decide the effectiveness of the immune response in certain conditions [4].

HLA-G is present as a membrane-bound or a soluble form, and its expression in normal tissues is limited to trophoblastic cells, where it is postulated to mediate immune tolerance during pregnancy [28, 29, 40]. A variety of tumors shows HLA-G expression. In melanomas [22, 32, 33] and renal cell carcinomas [5, 6, 21], HLA-G is up-regulated in both cell lines and clinical specimens compared to normal tissue and benign lesions. In the largest study of melanomas, Ibrahim et al. [22] found up-regulated HLA-G expression in melanomas compared to nevi (22/79 vs 1/71 cases), but HLA-G expression was not elevated in metastases compared to primary tumors and showed no

correlation with survival. HLA-G is up-regulated in renal carcinoma cell lines in response to interferon-γ stimulation and inhibits lysis of renal cell carcinoma cells by effector cells [5, 21]. Similarly, treatment of short-term cultures of ovarian carcinoma cells with interferon-γ results in increased expression of HLA-E mRNA and HLA-G protein and a tumor-protective effect via CD94/NKG2A receptors [27]. HLA-G is expressed by 100% (66/66) trophoblastic tumors of different degree of malignancy but is uniformly absent in epithelial and stromal tumors of the uterine cervix and corpus [36]. HLA-G1 and HLA-G5 were shown to be up-regulated in 19 lung carcinoma specimens compared to normal controls using real-time PCR [38]. Protein expression was detected at the membrane in 9 of 34 (26%) tumors, with expression of the soluble form in 6 of 34 (18%) specimens, and membrane expression was associated with higher histological grade [38]. Similar to lung carcinomas, real-time PCR detected HLA-G mRNA in 45 of 45 B- and T-cell lymphomas, with protein expression limited to 23 of 45 (51%) specimens [39]. In gastric cancer, HLA-G mRNA expression was limited to 2 of 35 tumors, with no expression in 35 normal specimens [18]. Data for breast cancer are controversial, with reported expression in 14 of 36 (39%), 0 of 25 (0%), and 22 of 88 (25%) tumors in three studies [24, 31, 37]. Korkola et al. [23] performed microarray analysis of breast carcinomas and found that the HLA-G gene is one of the differentiators of lobular from ductal carcinomas, being higher in the latter tumor type.

The abovementioned data provide evidence that HLA-G is expressed by tumor types of different lineage. However, the clinical significance of HLA-G expression is still unknown for the majority of cancer types, thereby leaving unanswered the question as to whether HLA-G-mediated immune evasion has a central clinical role in cancer progression. We recently showed that despite the elevated levels of secreted HLA-G in malignant compared to reactive (benign) effusions [37], higher HLA-G expression on tumor cells at this anatomic site predicts better survival in ovarian carcinoma [16]. To further investigate this issue, the present study analyzed the expression of HLA-G in two cohorts of patients with clinically aggressive tumors: breast carcinoma patients who developed metastatic disease in the serosal cavities and patients with malignant mesotheliomas (MM). HLA-G expression data in these two cancer types were compared to our previous findings in ovarian carcinoma [16] to evaluate potential differences between these three tumor types that have propensity to involve the serosal cavities. We report that HLA-G is expressed in both breast carcinoma and MM, though focally, with up-regulation in MM effusions compared to solid tumors. MM effusions have higher HLA-G expression than metastatic adenocarcinomas, with opposite results in solid lesions. In addition, HLA-G protein expression shows a trend for worse survival in breast carcinoma effusions. These data may suggest a role for HLA-G in a subset of cases in these cancer types.

Materials and methods

Breast carcinomas

Patients and material The study cohort consisted of 43 female patients (aged 33–83, mean 59 years) with histologically verified breast cancer. Thirty-seven tumors were diagnosed as infiltrating duct carcinoma, three as lobular carcinoma, and two as carcinoma containing both histological types. Forty-six effusions (41 pleural, 4 peritoneal, 1 pericardial) from these 43 patients were submitted for routine diagnostic purposes to the Department of Pathology at the Norwegian Radium Hospital during the period of 1998–2004. Submitted specimens arrived within minutes after tapping and were processed immediately. Paraffin-embedded cell blocks were prepared from all 46 effusions. Additional material was suspended and frozen in equal volumes of RPMI supplemented with 20% fetal calf serum and 20% DMSO. All specimens underwent morphological evaluation and were further characterized using immunocytochemistry, as previously detailed [8, 9]. Patient consent was obtained according to institutional and national guidelines.

Seventeen corresponding primary tumors, 13 lymph node metastases, and 9 locoregional recurrence specimens from 17 of the 43 breast carcinoma patients were available for comparative analyses. Diagnoses, histologic typing, and tumor grade were reviewed for all cases.

Malignant mesotheliomas

Patients and material The studied material consisted of 104 specimens (26 effusions, 78 biopsies) submitted to the Department of Pathology both at the Norwegian Radium Hospital and Aalborg Hospital during the period of 1998–2003. The MM material consisted of 32 peritoneal (8 effusions, 24 biopsies) and 72 pleural (18 effusions, 54 biopsies) specimens. MM specimens were obtained from 86 patients (62 males, 24 females) aged 39–91 (mean 64 years). Seventy-four patients had one specimen available for analysis, six had two specimens, and six had three specimens. The diagnostic procedure and the informed consent protocol were as described for breast carcinomas.

Immunohistochemistry

Immunohistochemistry (IHC) was performed using an HLA-G-specific mouse monoclonal antibody, 4H84 [29], which reacts with the denatured HLA-G heavy chain. Pretreatment consisted of microwave oven antigen retrieval (four times, 5 min) in low pH citrate buffer. A 1:600 dilution of the antipeptide antibody was used. Visualization was achieved using the EnVision+ peroxidase system (DakoCytomation, Glostrup, Denmark). Positive controls for these antibodies consisted of an ovarian carcinoma case shown to be positive and specific in our previous study [16]. Negative controls were stained with an antibody for

mouse myeloma protein (IgG1 kappa, catalog no. M-9035; Sigma-Aldrich, St. Louis, MO).

Staining was scored in tumor cells in effusions and solid tumors. Membrane or combined membrane and cytoplasmic expression were interpreted as positive. Staining extent was scored on a scale of 0–4, corresponding to percentage of immunoreactive tumor cells of 0, 1–5, 6–25, 26–75, and 76–100%, respectively. At least 500 tumor cells were scored, when present (>90% of cases). No specimen contained less than 100 tumor cells.

Immunoblotting

Nineteen effusions (10 MM, 9 breast carcinomas) and four breast cancer cell lines (T47-D, SKBr3, MCF-7, MDA-MB-231) were analyzed for HLA-G expression using immunoblotting (IB). Eight breast carcinomas and seven MM specimens were of pleural origin. The remaining breast carcinoma and three MM effusions were peritoneal. The JEG-3 choriocarcinoma cell line (kindly provided by Professor Shih) was used as positive control. Frozen samples were thawed, washed twice in cold PBS, and lysed in NP-40 ice-cold lysis buffer [1% NP-40, 10% glycerol, 20 mM Tris–HCl (pH 7.5), 137 mM NaCl, 100 mM NaF, 1 mM sodium vanadate, 1 mM phenylmethyl sulfonyl fluoride, and 0.02 mg/ml each of leupeptin, pepstatin, and aprotinin, and 10 μl/ml phosphatase inhibitor cocktail I). All inhibitors were from Sigma-Aldrich. Lysates were then sonicated and centrifuged, and protein was quantified by Bradford analysis. Twenty-five micrograms of total cellular protein was loaded into each lane, separated by electrophoresis through SDS–12% polyacrylamide gels (SDS-PAGE), blotted onto immobilon-P-membranes (Millipore Corporation, Bedford, MA) and blocked in 5% nonfat dry milk in TBS-T. The filters were subsequently hybridized with the 4H84 antibody using a concentration of 1 μg/ml. A mouse monoclonal antibody against α-tubulin (clone 57) (Oncogene, San Diego, CA) was used as loading control at a concentration of 1:5,000. After washing in TBS-T, bound antibody was visualized using peroxidase-conjugated anti-mouse IgG and the ECL detection system (Amersham Pharmacia, Buckinghamshire, UK). Negative controls consisted of antibody in the absence of lysate.

RNA isolation and RT-PCR analysis

HLA-G mRNA expression was analyzed in four breast carcinoma and four MM effusions. The JEG-3 cell line was

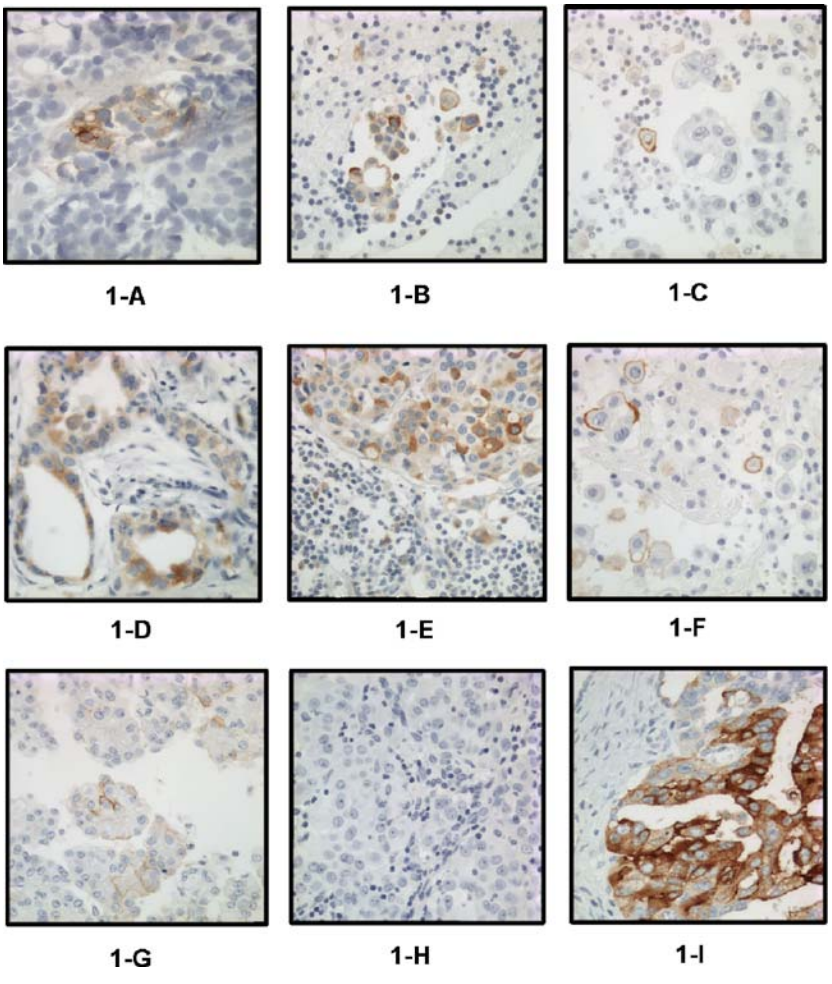

Fig. 1 Breast carcinoma and malignant mesothelioma (MM) cells show focal expression of HLA-G. **a–c** Breast carcinoma effusions. **a** Specimen with less than 5% expression in carcinoma cells. **b** Effusion with HLA-G expression in 25–75% of tumor cells, a rare finding in our cohort. Lymphocytes in the vicinity of tumor cells are negative. **c** HLA-G-negative specimen. Few macrophages in the vicinity of tumor cell clusters are positive. **d, e** Solid breast carcinoma. **d** Primary infiltrating duct carcinoma with HLA-G expression in 25–75% of tumor cells. As in the case of effusions, this was a rare finding in our cohort. **e** HLA-G expression in a lymph node metastasis. **f–g** MM. **f** MM effusion with membrane staining for HLA-G in more than 75% of tumor cells. **g** Solid epithelioid MM in which only cells that are dissociating express HLA-G, a total of less than 5% of all tumor cells. **h** HLA-G-negative epithelioid MM. **i** Ovarian carcinoma control. Twenty-five to seventy-five percent of cells in this primary serous ovarian carcinoma expressed HLA-G in a combined membrane and cytoplasmic pattern (×400 magnification for all figures)

Table 1 HLA-G expression in malignant mesothelioma (MM) and breast carcinoma

Tumor	Site	Staining extent					Total
		0%	1–5%	6–25%	26–75%	76–100%	
Breast carcinoma	Effusion	34	10	0	2	0	46
	Primary	9	5	2	1	0	17
	Lymph node	7	5	1	0	0	13
	Locoregional recurrences	7	1	1	0	0	9
MM	Effusion	12	9	0	4	1	26
	Solid	58	15	3	2	0	78

used as positive control. Total RNA was isolated using the Trizol reagent (Life Technologies, Gaithersburg, MD) according to the manufacturer's recommendations. cDNA was prepared from 5 μg total RNA using the SuperScript First Strand Synthesis System (Invitrogen, Paisley, UK). Polymerase chain amplification of HLA-G transcripts was performed in a total volume of 30 μl containing 6 μl of the RT product, 0.75 U Taq polymerase, 200 μmol of each dNTP, and 7 pmol of each primer. The following set of primers was used: G.257F (exon 2, 5′-GGA AGA GGA GAC ACG GAA-CA-3′) and G.963R (exon 5, 5′-GCA-GCT-CCA-GTG ACT GG-3′) [34]. PCR conditions were as follows: 35 cycles at 94°C/1 min, 62°C/30 s, and 72°C/2 min, final extension at 72°C/7 min. As an internal control, β-actin was reverse-transcribed using the following primers: MOD-59 (5′-ATC ATG TTT-GAG ACC-TTC-3′) and MOD-60 (5′-CAT-CTC TTG-CTC-GAA-GTC-CA-3′). PCR conditions were as follows: 25 cycles at 94°C/30 s, 58°C/30 s, and 72°C/30 s [26]. PCR products were analyzed by polyacrylamide gel electrophoresis and SYBR green staining.

Flow cytometric immunophenotyping

Four-color flow cytometry (FCM) was performed on ten breast carcinoma and five MM effusions using a FACSCalibur flow cytometer (Becton-Dickinson, San Jose, CA) equipped with a 15-mW argon-ion laser (488 nm) and 12-mW red diode laser (635 nm).

Direct staining procedure This has been previously described [10]. An anti-HLA-ABC antibody was purchased from DakoCytomation (clone W6/32, 1:10 dilution). The remaining antibodies were previously shown to be reliable markers of the different cell populations in effusions [10]. These consisted of Ber-EP4 (DakoCytomation, clone Ber-EP4, 1:10 dilution) and anti-epithelial membrane antigen (EMA; clone E-29, 1:10 dilution) as markers of epithelial (Ber-EP4, EMA) and mesothelial (EMA) cells and anti-CD45 (Becton-Dickinson, clone 2D1, 1:10 dilution) and anti-CD14 (Diatec, Oslo, Norway, clone 18D11, 1:5 dilution) as markers of leukocytes and macrophages, respectively. Antibodies were directly conjugated to fluorescein isothiocynate (FITC), phycoerythrin (PE), peridinin chlorophyll protein (PerCP), or allophycocyanin (APC). The combinations used were as follows:

- FITC-Ber-EP4/PE-HLA-ABC/PerCP-CD45/APC-CD14
- FITC-EMA/PE-HLA-ABC/PerCP-CD45/APC-CD14
- FITC− isotype/PE− isotype /PerCP− isotype /APC− isotype

Prediluted monoclonal antibodies were added to each tube. Cells were incubated with antibodies and filtered as previously described [10].

Table 2 The association between HLA-G expression and c-erbB-2 status in 28 breast carcinoma effusions

HLA-G status	c-erbB-2 expression			*p* value
	1–10%	11–50%	51–100%	
Negative	0	6	12	0.029
Positive	3	4	3	

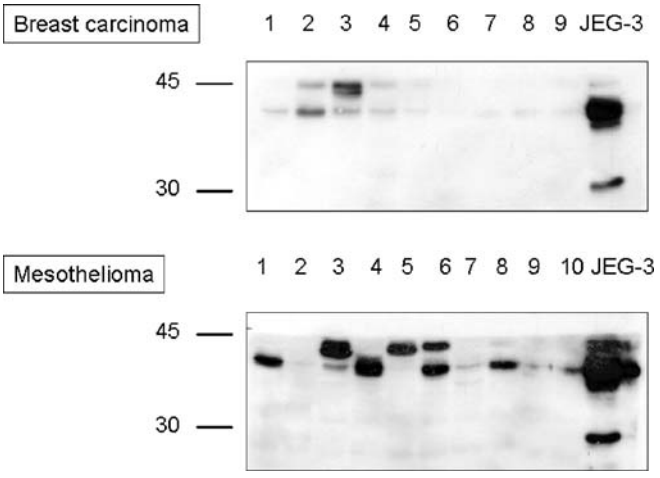

Fig. 2 HLA-G immunoblotting using the 4H84 antibody. *First panel:* breast carcinoma effusions (*lanes 1–9*). The specimen in *lane 2* shows two bands, the more pronounced one at 37 kDa. The effusion in *lane 3* shows 3 bands, corresponding to expression of the 37-kDa form and two larger forms, presumably the result of differently glycosylated isoforms. The remaining specimens show weak or negative expression. The JEG-3 choriocarcinoma cell line shows pronounced expression at 37 kDa and two additional bands at 30 kDa and (weakly) at 45 kDa. *Second panel:* MM effusions (*lanes 1–10*, seven pleural, three peritoneal). MM specimens in *lanes 1, 3, 4, 5, 6, 8, and 10* express one or both of the abovementioned HLA-G forms. As with breast carcinomas, JEG-3 cells show higher expression than that observed in clinical specimens, with three bands at 30, 37, and 45 kDa

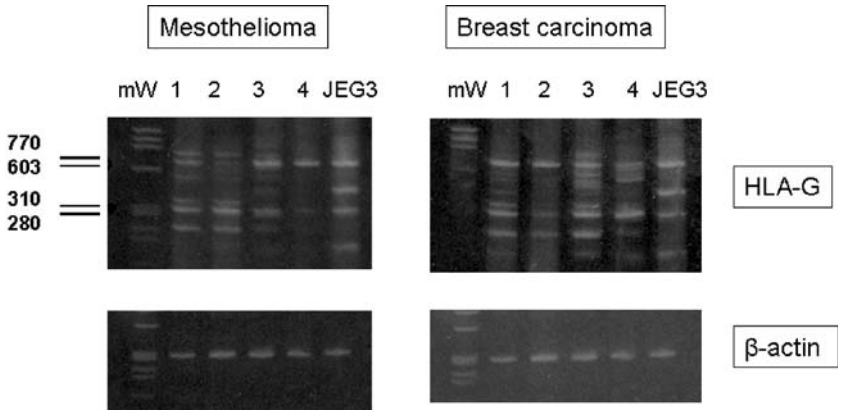

Fig. 3 HLA-G RT-PCR. RT-PCR analysis of four breast carcinoma and four MM effusions shows HLA-G mRNA expression in all specimens, as well as in the JEG-3 choriocarcinoma cell line used as positive control. β-Actin (*lower panel*) was used as internal control

Controls, instrument calibration, and evaluation of results The Ber-EP4-positive breast carcinoma cell line T47-D was chosen as positive control based on pilot studies. A mixture of a T47-D cells and peripheral blood leukocytes (PBL) was analyzed in each run. Data analysis was undertaken using the CellQuest software (version 3.4, Becton Dickinson). The gating procedure excluded cell debris and leukocytes by including only cells that were CD45 negative and with higher forward scatter (FSC) and side scatter (SSC) than the values for lymphocytes. Quadrant cursors were set by using isotype-matched negative controls. Quadrant setting was undertaken, so that in negative controls, 99% of the cells were localized to the left lower quadrant. Cell populations were interpreted as immunoreactive for Ber-EP4, EMA, and HLA-ABC only when unequivocal separation from the negative controls (carcinoma cell lines in the case of CD45) could be demonstrated. Expression in less than 1% of cells was scored as negative. For each measurement, data from 50,000 to 200,000 events were acquired.

Statistical analysis

Statistical analysis was performed applying the SPSS-PC package (version 12.0, Chicago, IL). Probability of less than 0.05 was considered statistically significant. Studies of the association between HLA-G expression and specimen type (effusion vs solid) or site (pleural vs peritoneal) were undertaken using the two-sided chi-square test. Comparative analysis of HLA-G expression in MM and breast carcinoma compared to the previously analyzed ovarian carcinomas was done using the same method. Comparative analyses of staining results in tumor cells in effusions vs corresponding primary tumors and lymph node metastases in breast carcinoma were performed using the Wilcoxon signed-rank test. Univariate survival analysis for 28 breast carcinoma patients with clinicopathologic data was performed using the Kaplan–Meier method and log-rank test. Expression categories in the latter test were clustered as negative vs positive to allow for a sufficient number of cases to be included in each category. Clinical data were not available for MM patients.

Results

Breast carcinomas

HLA-G is focally expressed in breast carcinoma cells at all anatomic sites The dissemination of breast carcinoma cells to effusions is a clinical marker of aggressive and rapidly fatal disease. Tumors that are metastatic to this site may therefore possess unique biological features, among which is the resistance to elimination by the host immune system. IHC analysis of HLA-G expression at various anatomic sites showed cancer cell expression in 12 of 46 (26%) effusions and 16 of 39 (41%) corresponding solid lesions (Fig. 1a–e; Table 1). Staining was focal in the majority of

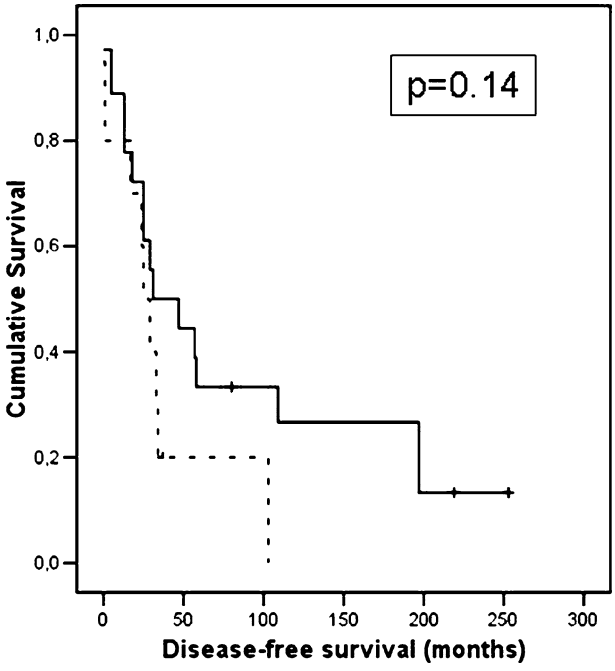

Fig. 4 HLA-G expression in tumor cells in breast carcinoma effusions is associated with a trend for poor disease-free survival (DFS) in Kaplan–Meier survival analysis. Patients with carcinoma cells showing any level of expression (n=10, *dashed line*) had significantly worse DFS than those with effusions showing negative expression (n=18, *solid line*; 37 vs 85 months for mean DFS, 25 vs 31 for median DFS; p=0.14)

cases, as reflected by expression in more than 25% of cells in only 3 of 85 (4%) specimens. The three lobular carcinomas showed no HLA-G expression in the effusion specimens, although one of these cases that had a corresponding primary tumor for evaluation showed focal expression in the latter specimen. In view of the small case number, however, this does not allow us to draw conclusions regarding potential differences between ductal and lobular carcinomas.

HLA-G expression has been previously reported to be independent of hormone receptor or c-erbB-2 expression [24]. We analyzed this association and the relation between HLA-G and clinicopathologic parameters in our material. HLA-G expression in effusions showed no correlation with clinicopathologic parameters (data not shown) but was inversely correlated with c-erbB-2 expression (Table 2). Comparative analysis of HLA-G in effusions, primary tumors, and lymph node metastases showed no site-related differences (Wilcoxon signed-rank test, $p>0.05$). IB showed variable expression of different HLA-G isoforms in effusions, with more pronounced expression in the JEG-3 cell line (Fig. 2). The T47-D, MDA-MB-231, and MCF-7 cell lines all expressed HLA-G (data not shown). RT-PCR showed mRNA expression in four of four breast carcinoma effusions, of which two expressed the protein (Fig. 3).

HLA-G expression may predict worse disease-free survival in breast carcinoma effusions We recently showed that HLA-G expression in carcinoma cells in post-chemotherapy effusions predicts improved survival in ovarian carcinoma [19]. Despite the focal nature of HLA-G expression in breast carcinoma, we wished to analyze the predictive role of this marker in 28 specimens with clinicopathologic data. Follow-up period (overall survival) ranged from 2 to 330 months (mean 88 months). The period from primary diagnosis to disease recurrence ranged from 0 (simultaneous) to 253 months (mean 60 months). Breast cancer patients with any number of HLA-G-positive tumor cells in effusions had shorter disease-free survival (mean 37 vs 85, median 25 vs 31 months), but this finding failed to reach statistical significance ($p=0.14$; Fig. 4).

Malignant mesotheliomas

HLA-G expression is significantly elevated in malignant mesothelioma effusions Malignant mesothelioma (MM) classically presents with pleural plaques or diffuse peritoneal disease with a concomitant malignant effusion. As in breast carcinoma, the majority of MM cases in our study

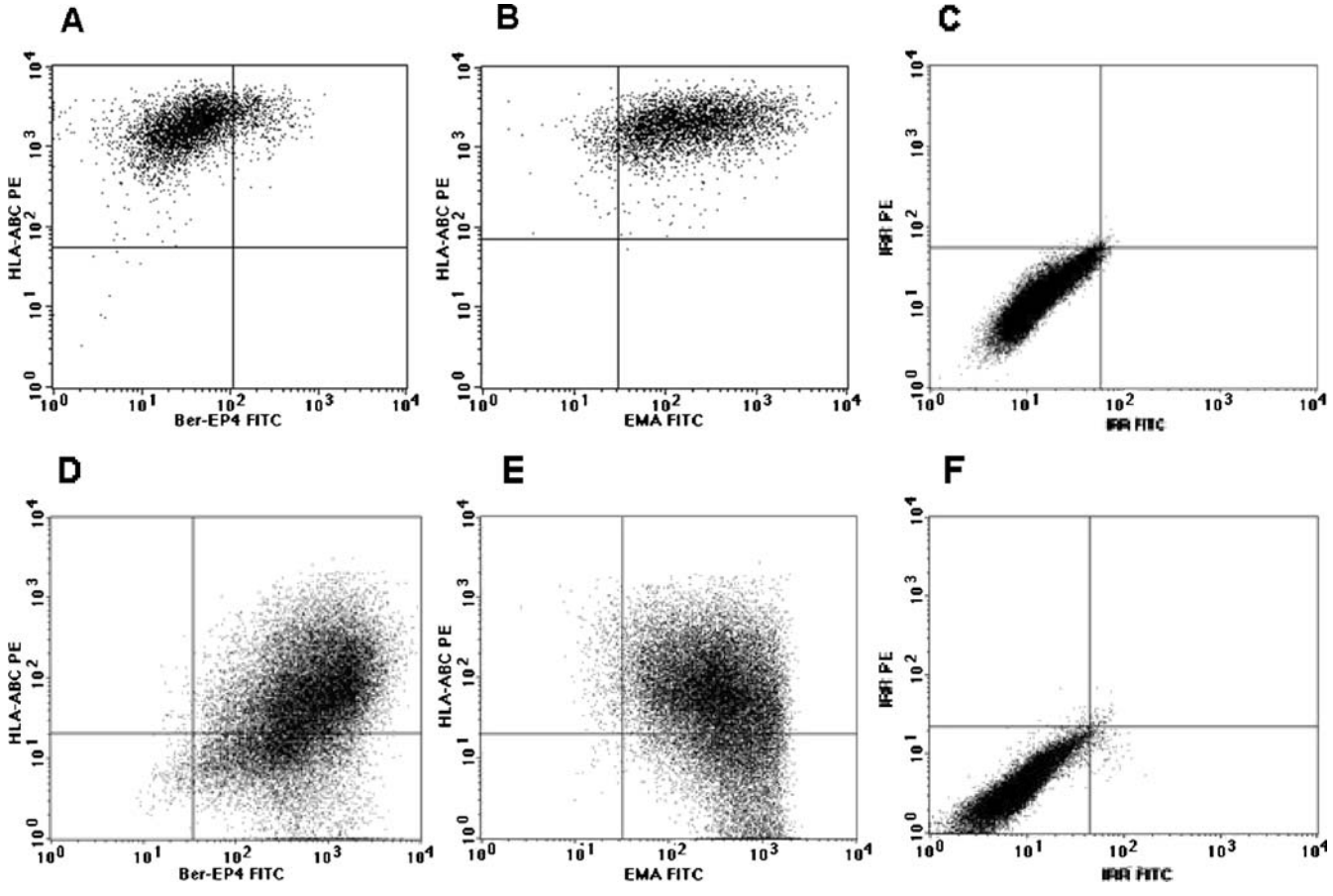

Fig. 5 Flow cytometric (FCM) analysis of HLA-ABC expression in effusions. **a, b** FCM dot plot of an MM effusion. Tumor cells show strong expression of HLA-ABC and EMA but, with the exception of few cells, are negative for Ber-EP4. **c** Negative staining using isotype control antibodies. **d, e** FCM data for a pleural effusion with breast carcinoma metastasis. Tumor cells show strong expression of the epithelial markers Ber-EP4 and EMA. The majority is positive for HLA-ABC. **f** Negative staining using isotype control antibodies

were HLA-G negative, the remaining specimens showing predominantly focal expression (Fig. 1f–h; Table 2). Staining with isotypic controls was negative. Peritoneal and pleural MM showed comparable HLA-G expression (chi-square test, $p>0.05$). However, MM cells in effusions showed significantly higher HLA-G expression compared to solid tumors (chi-square test, $p=0.008$), a finding that was supported by frequent HLA-G expression in MM effusions by IB analysis (Fig. 2). The ovarian carcinoma specimen used as positive control using IHC showed consistent staining in all reactions (Fig. 1i). RT-PCR showed mRNA expression in four of four MM carcinoma effusions, of which two of three cases analyzed using IHC and/or IB expressed the protein (Fig. 3).

To evaluate the possibility that HLA-G is a marker of malignancy in mesothelial cells, we looked at benign reactive mesothelial cells in our 46 breast carcinoma effusions and in 54 of our previously analyzed ovarian carcinoma effusions. Mesothelial cell populations were seen in 50 of 100 specimens and showed HLA-G expression in only 2 of 50 specimens (data not shown).

Comparison between malignant mesotheliomas and metastatic adenocarcinomas

HLA-ABC protein is expressed in breast carcinoma and malignant mesothelioma effusions In view of the focal nature of HLA-G expression in both malignancies, we wished to investigate the possibility that reduced HLA-ABC expression is a central mechanism involved in immune response evasion in MM and breast carcinoma. Both MM and breast cancer tumors expressed HLA class I in more than 75% (most often 100%) of tumor cells (Fig. 5).

HLA-G expression is more frequently expressed in malignant mesothelioma in effusions and in adenocarcinomas at solid sites MM shares many of the histogenetic features of adenocarcinomas in general and ovarian carcinoma in particular. We wished to analyze the potential differences in HLA-G expression between MM and breast carcinoma and our previously analyzed ovarian carcinoma cohort, in which HLA-G was detected in cancer cells in 49 of 148 (33%) effusions, 33 of 66 (50%) primary tumors, and 59 of 122 (48%) solid metastases [16]. MM cells in effusions showed higher HLA-G expression compared to both ovarian and breast carcinomas (chi-square analysis, $p=0.045$), with opposite results for tumor cells at solid sites (chi-square analysis, $p=0.001$; Table 3).

Table 3 HLA-G expression in MM, breast carcinoma, and ovarian carcinoma

Tumor type	Site	HLA-G expression		*p* value
		Negative	Positive	
MM	Effusion	12	14	0.045
Breast	Effusion	34	12	
Ovarian	Effusion	99	49	
MM	Solid	58	20	0.001
Breast	Solid	23	16	
Ovarian	Solid	96	92	

Discussion

Cancer cell dissemination is a demanding process, in which only selected cells are able to form viable metastases. Unlike cells in the primary tumor, metastatic cells are far less susceptible to elimination by the host defense mechanisms or externally applied therapy. This selection process is especially apparent in the serosal cavities, where cells face reduced levels of oxygen and nutrients by undergoing extensive alterations compared to their counterparts in solid tumors (reviewed in [7, 11]). In the present study, we analyzed the expression of HLA-G in two tumors that involve the serosal cavities, breast carcinoma and MM.

MM is an aggressive and rapidly fatal cancer [3, 41]. Leukocyte infiltration is present in both solid tumors and effusions in MM, but its role in modulating or halting the progression of this disease is unproven. Thus, immunotherapy is not a part of current treatment protocols for MM. We observed frequent, though predominantly focal, expression of HLA-G in MM, with little or no loss of HLA-ABC expression. HLA-G was similarly expressed in tumors of pleural and peritoneal origins but was significantly up-regulated in effusions compared to solid tumors, in agreement with our recent reports of altered expression of angiogenic molecules and growth factor receptors at this site [12, 14]. Whether this difference confers any survival advantages for MM cells in effusions remains to be established. However, it may suggest a role for HLA-G in mediating immune response evasion in at least some of the tumors that metastasize to effusions. Furthermore, the up-regulation of sHLA-G in malignant effusions [37] and its rare expression in reactive mesothelial cell populations may suggest a tumor-specific role for this membrane protein in MM.

Another cancer type that involves the serosal cavities is breast cancer [19, 25, 42]. Breast cancer metastasis to this anatomic site, predominantly to the pleural cavity, may occur at any point of time along the clinical course [17] and portends a uniformly poor prognosis [2, 17]. We recently published data that support extensive alterations in breast carcinoma cells in effusions compared to corresponding primary tumors and lymph node metastases [13, 15].

A recent study of a different patient cohort that was not selected for disease progression or outcome by our group showed that HLA-G is expressed in 22 of 88 (25%) primary ductal breast carcinomas [37]. An additional report of predominantly ductal carcinomas found expression in 14 of 36 (39%) primary tumors [24]. Our current findings are in agreement with these figures, as evident from the expression rates of 41 and 26% in solid lesions and effusions, respectively. They differ from the report of Palmisano et al. [31], where no expression was found in 25 tumors. The latter cases were, however, selected for down-regulated HLA class I, possibly implying that the modulation of one

HLA-related cellular mechanism renders additional ones superfluous. In fact, none of our effusion specimens showed loss of HLA-ABC expression. Another reason for this discrepancy may be related to technical factors since Palmisano et al. also reported lack of HLA-G expression in three breast carcinoma cell lines that were unequivocally positive in our IB experiments.

In agreement with our data for ovarian carcinoma [16], we found no differences in HLA-G expression between primary carcinomas, lymph node metastases, locoregional recurrences, and effusions, with focal expression of this molecule at all anatomic sites in our cohort. As in MM, the focal pattern of expression may suggest a role for HLA-G in immune response evasion in small tumor subpopulations rather than the entire tumor, suggesting that other mechanisms (e.g., HLA-E expression) may promote tumor survival in this setting.

The clinical significance of HLA-G expression in cancer cells is uncertain at present. Urosevic et al. [38] reported higher HLA-G expression in lung carcinomas of higher histological grade. In contrast, Ibrahim et al. [22] reported that HLA-G expression in melanomas does not correlate with survival. In breast carcinoma, no association was found between expression of this marker and tumor grade or hormone receptor and c-erbB-2 status [24]. In the present study, HLA-G expression showed no association with clinicopathologic parameters, including receptor status in the primary tumor. Nor did it show any relation to the previously analyzed hormone receptor status in effusions [17]. However, we did observe two apparently contradictory findings: HLA-G protein expression had an inverse correlation with protein expression of c-erbB-2, an established marker of clinical aggressiveness in breast carcinoma, but patients with HLA-G-positive tumor cells relapsed earlier than those with no expression of this membrane protein, though not significantly so. Seen collectively, these data suggest that the clinical relevance of HLA-G in cancer, and in breast carcinoma in particular, is unsettled at present.

As shown by other investigators, HLA-G is by no means a universal marker for all cancer types [35]. However, even in tumors that express the molecule, such as lung carcinomas and lymphomas, marked differences are seen between mRNA and protein expression [38, 39]. Although our analysis of HLA-G mRNA expression was limited to eight specimens, it was in agreement with these results. This suggests that posttranscriptional mechanisms affect HLA-G mRNA and protein expression. Several cytokines, including IL-10 and interferon-γ, may have a role in this setting [39], an issue that we are currently analyzing.

In our effort to compare the biological characteristics of tumors involving the serosal cavities, we analyzed the present findings together with our previous data for ovarian carcinomas. When we compared the site-related expression of HLA-G in the three tumors, we found higher HLA-G expression in MM effusions compared to breast and ovarian carcinoma, whereas the opposite was true for expression in solid lesions. These data further support a different sequence of phenotypic and genotypic alterations in MM compared to adenocarcinomas of different types. As discussed above, the clinical significance of these changes is dependent upon the specific tumor type in question.

In conclusion, HLA-G is focally but frequently expressed in MM and in clinically aggressive breast carcinoma, suggesting a role for this molecule in mediating immune response evasion in subpopulations of these tumor cells. The up-regulated expression of HLA-G in MM effusions compared to solid tumors, and in MM cells compared to reactive mesothelial cells, provides evidence supporting anatomic site-specific biological differences in this tumor and may be a marker of malignant transformation, disease progression, and metastasis in MM. Assessment of the predictive role of HLA-G in breast carcinoma requires further research.

Acknowledgements We gratefully acknowledge the competent technical help of Ms. Inger-Liv Nordli, Ms. Mai Nguyen, Ms. Ann Larsen, and Ms. Esther Hasper (IHC) and Mr. Arild Holth (FCM) at the Department of Pathology, Norwegian Radium Hospital.

References

1. Algarra I, Garcia-Lora A, Cabrera T, Ruiz-Cabello F, Garrido F (2004) The selection of tumor variants with altered expression of classical and nonclassical MHC class I molecules: implications for tumor immune escape. Cancer Immunol Immunother 53:904–910
2. Banerjee AK, Willetts I, Robertson JF, Blamey RW (1994) Pleural effusion in breast cancer: a review of the Nottingham experience. Eur J Surg Oncol 20:33–36
3. Britton M (2002) The epidemiology of mesothelioma. Semin Oncol 29:18–25
4. Brostjan C, Bellon T, Sobanov Y, Lopez-Botet M, Hofer E (2002) Differential expression of inhibitory and activating CD94/NKG2 receptors on NK cell clones. J Immunol Methods 264:109–119
5. Bukur J, Rebmann V, Grosse-Wilde H, Luboldt H, Ruebben H, Drexler I, Sutter G, Huber C, Seliger B (2003) Functional role of human leukocyte antigen-G up-regulation in renal cell carcinoma. Cancer Res 63:4107–4111
6. Bukur J, Malenica B, Huber C, Seliger B (2003) Altered expression of nonclassical HLA class Ib antigens in human renal cell carcinoma and its association with impaired immune response. Hum Immunol 64:1081–1092
7. Davidson B (2004) Malignant effusions: from diagnosis to biology. Diagn Cytopathol 31:246–254
8. Davidson B, Risberg B, Kristensen G, Kvalheim G, Emilsen E, Bjåmer A, Berner A (1999) Detection of cancer cells in effusions from patients diagnosed with gynecological malignancies. Evaluation of five epithelial markers. Virchows Arch 435:43–49
9. Davidson B, Nielsen S, Christensen J, Asschenfeldt P, Berner A, Risberg B, Johansen P (2001) The role of desmin and N-cadherin in effusion cytology: a comparative study using established markers of mesothelial and epithelial cells. Am J Surg Pathol 25:1405–1412
10. Davidson B, Dong HP, Berner A, Christensen J, Nielsen S, Johansen P, Bryne M, Asschenfeldt P, Risberg B (2002) Detection of malignant epithelial cells in effusions using flow cytometric immunophenotyping: an analysis of 92 cases. Am J Clin Pathol 118:85–92
11. Davidson B, Risberg R, Reich R, Berner A (2003) Effusion cytology in ovarian cancer—new molecular methods as aids to diagnosis and prognosis. Clin Lab Med 23:729–754

12. Davidson B, Reich R, Lazarovici P, Flørenes VA, Risberg B, Nielsen S, Sert B, Bedrossian C (2004) Expression of the nerve growth factor receptors TrkA and p75 in malignant mesothelioma. Lung Cancer 44:159–165
13. Davidson B, Reich R, Lazarovici P, Flørenes VA, Nielsen S, Nesland JM (2004) Altered expression and activation of the nerve growth factor receptors TrkA and p75 provide the first evidence of tumor progression to effusion in breast carcinoma. Breast Cancer Res Treat 83:119–128
14. Davidson B, Vintman L, Zcharia E, Bedrossian C, Berner A, Nielsen S, Ilan N, Vlodavsky I, Reich R (2004) Heparanase and basic fibroblast growth factor are co-expressed in malignant mesothelioma. Clin Exp Metastasis 21:469–476
15. Davidson B, Konstantinovsky S, Nielsen S, Dong HP, Berner A, Vyberg M, Reich R (2004) Altered expression of metastasis-associated and regulatory molecules in effusions from breast cancer patients—a novel model for tumor progression. Clin Cancer Res 10:7335–7346
16. Davidson B, Bukholt Elstrand M, McMaster MT, Berner A, Kurman RJ, Risberg B, Trope CG, Shih IM (2005) HLA-G expression in effusions is a possible marker of tumor susceptibility to chemotherapy in ovarian carcinoma. Gynecol Oncol 96:42–47
17. Dieterich M, Goodman SN, Rojas-Corona RR, Emralino AB, Jimenez-Joseph D, Sherman ME (1994) Multivariate analysis of prognostic features in malignant pleural effusions from breast cancer patients. Acta Cytol 38:945–952
18. Dutta N, Majumder D, Gupta A, Mazumder DNG, Banerjee S (2005) Analysis of human lymphocyte antigen class I expression in gastric cancer by reverse transcriptase-polymerase chain reaction. Hum Immunol 66:164–169
19. Hausheer FH, Yarbro JW (1985) Diagnosis and treatment of malignant pleural effusion. Semin Oncol 12:54–75
20. Hofmeister V, Weiss EH (2003) HLA-G modulates immune responses by diverse receptor interactions. Semin Cancer Biol 13:317–323
21. Ibrahim EC, Guerra N, Lacombe MJ, Angevin E, Chouaib S, Carosella ED, Caignard A, Paul P (2001) Tumor-specific up-regulation of the nonclassical class I HLA-G antigen expression in renal carcinoma. Cancer Res 61:6838–6845
22. Ibrahim EC, Aractingi S, Allory Y, Borrini F, Dupuy A, Duvillard P, Carosella ED, Avril MF, Paul P (2004) Analysis of HLA antigen expression in benign and malignant melanocytic lesions reveals that upregulation of HLA-G expression correlates with malignant transformation, high inflammatory infiltration and HLA-A1 genotype. Int J Cancer 108:243–250
23. Korkola JE, DeVries S, Fridlyand J, Hwang ES, Estep AL, Chen YY, Chew KL, Dairkee SH, Jensen RM, Waldman FM (2003) Differentiation of lobular versus ductal breast carcinomas by expression microarray analysis. Cancer Res 63:7167–7175
24. Lefebvre S, Antoine M, Uzan S, McMaster M, Dausset J, Carosella ED, Paul P (2002) Specific activation of the non-classical class I histocompatibility HLA-G antigen and expression of the ILT2 inhibitory receptor in human breast cancer. J Pathol 196:266–274
25. Martinez-Moragon E, Aparicio J, Sanchis J, Menendez R, Cruz Rogado M, Sanchis F (1998) Malignant pleural effusion: prognostic factors for survival and response to chemical pleurodesis in a series of 120 cases. Respiration 65:108–113
26. Maelandsmo GM, Hovig E, Skrede M, Engebraaten O, Florenes VA, Myklebost O, Grigorian M, Lukanidin E, Scanlon KJ, Fodstad O (1996) Reversal of the in vivo metastatic phenotype of human tumor cells by an anti-CAPL (mts1) ribozyme. Cancer Res 56:5490–5498
27. Malmberg KJ, Levitsky V, Norell H, de Matos CT, Carlsten M, Schedvins K, Rabbani H, Moretta A, Soderstrom K, Levitskaya J, Kiessling R (2002) IFN-gamma protects short-term ovarian carcinoma cell lines from CTL lysis via a CD94/NKG2A-dependent mechanism. J Clin Invest 110:1515–1523
28. McMaster MT, Librach CL, Zhou Y, Lim KH, Janatpour MJ, DeMars R, Kovats S, Damsky C, Fisher SJ (1995) Human placental HLA-G expression is restricted to differentiated cytotrophoblasts. J Immunol 154:3771–3778
29. McMaster M, Zhou Y, Shorter S, Kapasi K, Geraghty D, Lim KH, Fisher SJ (1998) HLA-G isoforms produced by placental cytotrophoblasts and found in amniotic fluid are due to unusual glycosylation. J Immunol 160:5922–5928
30. Moretta L, Biassoni R, Bottino C, Cantoni C, Pende D, Mingari MC, Moretta A (2002) Human NK cells and their receptors. Microbes Infect 4:1539–1544
31. Palmisano GL, Pistillo MP, Fardin P, Capanni P, Nicolo G, Salvi S, Spina B, Pasciucco G, Ferrara GB (2002) Analysis of HLA-G expression in breast cancer tissue. Hum Immunol 63:969–976
32. Paul P, Rouas-Freiss N, Khalil-Daher I, Moreau P, Riteau B, Le Gal FA, Avril MF, Dausset J, Guillet JG, Carosella ED (1998) HLA-G expression in melanoma: a way for tumor cells to escape from immunosurveillance. Proc Natl Acad Sci U S A 95:4510–4515
33. Paul P, Cabestre FA, Le Gal FA, Khalil-Daher I, Le Danff C, Schmid M, Mercier S, Avril MF, Dausset J, Guillet JG, Carosella ED (1999) Heterogeneity of HLA-G gene transcription and protein expression in malignant melanoma biopsies. Cancer Res 59:1954–1960
34. Paul P, Rouas-Freiss N, Moreau P, Cabestre FA, Menier C, Khalil-Daher I, Pangault C, Onno M, Fauchet R, Martinez-Laso J, Morales P, Villena AA, Giacomini P, Natali PG, Frumento G, Ferrara GB, McMaster M, Fisher S, Schust D, Ferrone S, Dausset J, Geraghty D, Carosella ED (2000) HLA-G, -E, -F preworkshop: tools and protocols for analysis of non-classical class I genes transcription and protein expression. Hum Immunol 61:1177–1195
35. Real LM, Cabrera T, Collado A, Jimenez P, Garcia A, Ruiz-Cabello F, Garrido F (1999) Expression of HLA-G in human tumors is not a frequent event. Int J Cancer 81:512–518
36. Singer G, Kurman RJ, McMaster M, Shih I-M (2002) HLA-G immunoreactivity is specific for intermediate trophoblast in gestational trophoblastic disease and can serve as a useful marker in differential diagnosis. Am J Surg Pathol 26:914–920
37. Singer G, Rebmann V, Chen YC, Liu HT, Ali SZ, Reinsberg J, McMaster MT, Pfeiffer K, Chan DW, Wardelmann E, Grosse-Wilde H, Cheng CC, Kurman RJ, Shih IM (2003) HLA-G is a potential tumor marker in malignant ascites. Clin Cancer Res 9:4460–4464
38. Urosevic M, Kurrer MO, Kamarashev J, Mueller B, Weder W, Burg G, Stahel RA, Dummer R, Trojan A (2001) Human leukocyte antigen G up-regulation in lung cancer associates with high-grade histology, human leukocyte antigen class I loss and interleukin-10 production. Am J Pathol 159:817–824
39. Urosevic M, Willers J, Mueller B, Kempf W, Burg G, Dummer R (2002) HLA-G protein up-regulation in primary cutaneous lymphomas is associated with interleukin-10 expression in large cell T-cell lymphomas and indolent B-cell lymphomas. Blood 99:609–617
40. van der Ven K, Pfeiffer K, Skrablin S (2000) HLA-G polymorphisms and molecule function—questions and more questions—a review. Placenta 21(Suppl A):S86–S92
41. van Ruth S, Baas P, Zoetmulder FAN (2003) Surgical treatment of malignant pleural mesothelioma. Chest 123:551–561
42. Wilkes JD, Fidias P, Vaickus L, Perez RP (1995) Malignancy-related pericardial effusion. 127 cases from the Roswell Park Center Institute. Cancer 76:1377–1387

Virchows Arch (2006) 449: 40–47
DOI 10.1007/s00428-006-0212-7

ORIGINAL ARTICLE

So Yeon Park · Hye Seung Lee · Gheeyoung Choe · Jin Haeng Chung · Woo Ho Kim

Clinicopathological characteristics, microsatellite instability, and expression of mucin core proteins and p53 in colorectal mucinous adenocarcinomas in relation to location

Received: 2 January 2006 / Accepted: 30 March 2006 / Published online: 28 April 2006
© Springer-Verlag 2006

Abstract It has been suggested that right-sided and left-sided colorectal cancer may arise by different mechanisms. However, there have been few studies of mucinous adenocarcinoma (MA) in relation to location. Therefore, we analyzed clinicopathological characteristics, microsatellite instability (MSI), and expression of MUC1, MUC2, MUC5AC mucin core proteins, and p53 by immunohistochemistry in relation to tumor location. Ninety-six consecutive colorectal MAs and ninety-eight nonmucinous adenocarcinomas (nMAs) were investigated. Right-sided MAs, by comparison with those on the left side, were characterized by older age, larger tumor size, lower stage at presentation, peritumoral lymphocytic response, background of serrated adenoma, MSI-H phenotype, higher MUC2 and MUC5AC expression, and lower p53 protein overexpression. Right-sided nMAs, relative to those on the left side, were associated with MSI-H phenotype, higher MUC2 and MUC5AC expression, and lower p53 protein overexpression. Thus, MSI-H phenotype, expression of MUC2 and MUC5AC, and infrequent p53 protein overexpression are associated with right-sided location as well as mucinous histology. In univariate analysis, right-sided location had a favorable effect on disease specific survival of the patients with MA, although it is not an independent predictor of survival. Our results indicate that MA is a distinctive form of colorectal cancer and has different phenotypes depending on tumor location.

S. Y. Park · H. S. Lee · G. Choe · J. H. Chung
Department of Pathology,
Seoul National University Bundang Hospital,
Seongnam, Gyeonggi, South Korea

S. Y. Park · G. Choe · J. H. Chung · W. H. Kim (✉)
Department of Pathology,
Seoul National University College of Medicine,
28 Yongon-Dong,
Seoul 110-799, South Korea
e-mail: woohokim@snu.ac.kr
Tel.: +82-2-7408269
Fax: +82-2-7655600

Keywords Mucinous adenocarcinoma · Tumor location · Microsatellite instability · MUC2 · MUC5AC

Abbreviations MA: Mucinous adenocarcinoma · nMA: Nonmucinous adenocarcinoma · MSI: Microsatellite instability

Introduction

The molecular genetic pathways implicated in colorectal carcinogenesis can be divided into at least two groups on the basis of their presumed functions. One is the chromosomal instability pathway and involves the activation of oncogenes such as K-ras and the inactivation of tumor-suppressor genes such as APC, p53, and DCC [7, 32]. The other is the microsatellite instability (MSI) pathway, characterized by genomic instability associated with defective DNA mismatch repair. Alteration of mismatch repair genes is responsible for hereditary nonpolyposis colorectal cancers and sporadic colorectal cancers with high frequency MSI (MSI-H) that make up 10–15% of sporadic colorectal cancers [1, 31]. Histologically, MSI-H colorectal cancers are poorly differentiated or mucinous and have increased numbers of tumor infiltrating lymphocytes, Crohn's-like peritumoral lymphoid reaction and expansile growth pattern [10, 14, 18]. They are predominantly found in the right colon, whereas p53 and K-ras mutations occur frequently in the left colon. Thus, it has been suggested that right-sided and left-sided colorectal cancers may arise through different mechanisms [6].

Mucinous adenocarcinoma (MA) is a histologic subtype of colorectal carcinoma characterized by abundant pools of extracellular mucin. It accounts for 10 to 15% of colorectal carcinomas and is located more often in the right colon and rectum than other parts of the colon [30, 33]. It is generally thought that patients with MA present at a more advanced stage of disease and have a poorer prognosis than those with other types of carcinoma [30, 33, 34]. However, MSI-H MAs were recently reported to have a better prognosis than microsatellite-stable (MSS) ones, although MSI status

is not an independent predictor of survival [16, 24]. Wu et al. [33] proposed that differences in survival of colorectal MAs could be related to differences in tumor location or stage at presentation rather than to histological type. However, few studies of MAs of the colorectum have focused on its location.

The expression of mucin genes is relatively organ- and cell type-specific, and alteration of mucin expression is a common feature of colonic neoplasia [19]. Expression of MUC1 is elevated in colorectal cancer and is correlated with tumor progression and metastasis [2, 23, 25]. MUC2 expression is decreased in nonmucinous adenocarcinomas (nMAs) and increased in MAs of colon and rectum [4, 12, 23]. MUC5AC is not expressed in the normal colon but is expressed in adenomas and carcinomas [3, 4, 12, 20, 21, 29]. It is interesting to note that increased expression of secretory mucins MUC2 and MUC5AC has been reported in sporadic MSI-H cancers, suggesting serrated pathway of morphogenesis [4]. There are a few reports concerning the association between expression of MUC2 or MUC5AC and tumor location or histology [4, 20, 21], but the expression of mucin core proteins in colorectal MA has not been intensively studied in relation to tumor location.

Hence, the aim of this study is to analyze the clinicopathological characteristics, MSI status, and expression of mucin core proteins and p53, in mucinous and nonmucinous colorectal adenocarcinomas as a function of tumor location.

Materials and methods

Patients

Ninety-six consecutive MAs of the large bowel were collected from Seoul National University Hospital from January 1993 to December 1999 and from Seoul National University Bundang Hospital from May 2003 to December 2004. Ninety-eight consecutive nMAs from Seoul National University Bundang Hospital from May 2003 to December 2004 served as controls. MA was defined as carcinoma with >50% area showing extracellular mucin. Ten of the 194 patients had a synchronous carcinoma on the other side of the colon and one had a synchronous gastric carcinoma. None of the patients received preoperative irradiation or chemotherapy.

Tumors were classified and staged according to the sixth edition of the TNM Classification of the American Joint Committee on Cancer [9]. Eleven cases were classified as stage I, 67 as stage II, 65 as stage III, and 51 as stage IV. One hundred fifteen of the patients were male (59%), and 79 female (41%), with a mean age of 57.1±12.8 years (mean±SD; range, 21–94 years). Seventy-six cases were located in the right colon (from cecum to transverse colon) and one hundred eighteen were in the left colon (from descending colon to rectum).

Histopathologic evaluation

The histologic sections of tumors were examined and the following features were recorded: tumor configuration, location, size, depth of invasion, venous, angiolymphatic, and perineural invasion, peritumoral lymphocytic response, pattern of growth at tumor periphery, and background of serrated adenoma. Peritumoral lymphocytic response was regarded as conspicuous when there was a distinct cuff of lymphocytes at the invasive margin of the tumor [13]. The growth pattern of the tumor was recorded as pushing when the advancing edge of the tumor was sharply defined at low power examination, and infiltrating when there was irregular infiltration of tumor cells at advancing front [13].

Analysis of microsatellite instability

In all 194 cases, tumor and corresponding normal tissue were obtained from formalin-fixed and paraffin-embedded tissue samples by microdissection. DNA was extracted from the microdissected tissues with phenol/chloroform after digestion by proteinase K. Polymerase chain reaction (PCR) amplification of BAT26 microsatellite marker was performed with reaction mixtures with the following ingredients: 0.3 μM each of forward and reverse primers, 1.5 mM $MgCl_2$, 100 μM deoxynucleotide triphosphate, 0.75 U of Taq polymerase, and 50 ng of DNA in a total volume of 25 μl. PCR conditions were 95°C for 5 min, followed by 30 cycles of 94°C for 30 s, 51°C for 45 s, and 72°C for 30 s with a final elongation at 72°C for 10 min. Aliquots of PCR products (1 μl) were mixed with 0.4 μl of 1 M methylmercury hydroxide (Johnson Mattey Electronics, Ward Hill, MA), 2 μl of 15% wt/vol Ficoll (molecular weight 400,000) loading buffer containing 0.25% bromophenol blue and 0.25% xylene cyanol, and 1.6 μl of 0.5 × TBE buffer (90 mM Tris, 92 mM boric acid, 2.5 mM EDTA). The mixture was heated to 100°C for 5 min and rapidly transferred to ice before being loaded into the gel. Four microliters of this mixture was electrophoresed on 6% polyacrylamid gel containing 6 M urea for 2 h at 1,800 V. Products were then visualized by silver staining by the protocol of Schlegel et al. [28]. Cases with MSI in BAT26 microsatellite locus were regarded as MSI-H.

Immunohistochemistry

Four micron sections were deparaffinized, rehydrated in graded alcohol, and processed using avidin–biotin immunoperoxidase method. Briefly, antigen was retrieved by exposure in a microwave oven for 15 min in 10 mM citrate buffer pH 6.0. Endogenous peroxidase activity was blocked with a 3% H_2O_2-methanol solution, and the slides were incubated in 10% normal goat serum for 30 min to prevent nonspecific staining. They were then incubated for 1 h at room temperature or overnight at 4°C (for hMLH1 and hMSH2) in appropriately diluted primary antibody. The

following mouse antihuman monoclonal antibodies were used: MUC1 (clone Ma552; 1:100; Novocastra, Newcastle, UK), MUC2 (clone Ccp58; 1:100; Novocastra), MUC5AC (clone CLH2; 1:100; Novocastra), p53 (clone DO-7; 1:600; DakoCytomation, Glostrup, Denmark), hMLH1 (clone G168-15; 1:100; BD Pharmingen, San Diego, CA), hMSH2 (clone FE11; 1:50; Oncogene Research Products, Boston, MA), hMSH6 (clone 44; 1:100; BD Biosciences, Frankline Lakes, NJ), and hPMS2 (clone A16-4; 1:100; BD Pharmigen). Thereafter, the sections were incubated with biotinylated secondary antibodies, followed by avidin–biotin peroxidase complexes for 30 min. Diaminobenzidine was used as chromogen, and Mayer's hematoxylin as counterstain. As a negative control, nonimmune serum was substituted for the primary antibody.

The staining intensity of MUC1, MUC2, MUC5AC, and p53 was fairly homogeneous in all positive cases and therefore was not scored. Hence, tumor sections were classified as follows: 0, no staining or staining in less than 10% of the tumor cells; 1+, staining in 10 to 25% of the cells; 2+, staining in 26 to 50% of the cells; 3+, staining in 51 to 75% of the cells; 4+, staining in more than 75% of the cells. For statistical analysis of MUC1, MUC5AC, and p53, all cases with any degree of positive staining were grouped as positive. For MUC2, cases were classified as either high (≥2+) or low staining (0 or 1+) after consideration of the distribution of staining, to allow statistical comparison.

The results of hMLH1, hMSH2, hMSH6, and hPMS2 were scored without knowledge of the MSI status. The nuclei of normal colonic epithelium and lymphocytes are strongly stained for hMLH1, hMSH2, hMSH6, and hPMS2 and this served as a positive internal control for staining of these proteins. Loss of expression was recorded when nuclear staining was absent in all malignant cells. Diffuse nuclear staining of these proteins in tumor cells was interpreted as intact.

Statistical analysis

Statistical analysis was performed with SPSS software (version 11.0, SPSS, Chicago, IL). Chi-square or Fisher's exact tests were used when comparing frequencies between groups. All numerical data are expressed as means±SD and differences between means of groups were compared by independent samples *T* test. The period from the date of resection to the date of death or last contact (if alive) was used for survival analysis. Outcome analysis was based on patients who were alive or had died of colorectal cancer.

Table 1 Clinicopathological features of colorectal adenocarcinomas stratified by histological type

	Nonmucinous adenocarcinoma (*n*=98)	Mucinous adenocarcinoma (*n*=96)	*P* value
Age (year)	63.1±12.8	56.7±13.1	0.001[a]
Gender			
Male	57 (58.2%)	58 (60.4%)	0.749
Female	41 (41.8%)	38 (39.6%)	
Tumor size (cm)	5.11±2.06	7.03±2.56	<0.001[a]
Tumor location			
Righ-sided	25 (25.5%)	51 (53.1%)	<0.001[a]
Left-sided	73 (74.5%)	45 (46.9%)	
TNM stage			
I–II	42 (42.9%)	36 (37.5%)	0.447
III–IV	56 (57.1%)	60 (62.5%)	
Angiolymphatic invasion			
Absent	27 (27.6%)	37 (38.5%)	0.104
Present	71 (72.4%)	59 (61.5%)	
Venous invasion			
Absent	76 (77.6%)	81 (84.4%)	0.226
Present	22 (22.4%)	15 (15.6%)	
Perineural invasion			
Absent	52 (53.1%)	60 (62.5%)	0.183
Present	46 (46.9%)	36 (37.5%)	
Tumor border			
Pushing	43 (43.9%)	46 (47.9%)	0.572
Infiltrating	55 (56.1%)	50 (52.1%)	
Peritumoral lymphocytic response			
Inconspicuous	79 (80.6%)	78 (81.3%)	0.910
Conspicuous	19 (19.4%)	18 (18.7%)	
Background of serrated adenoma			
Absent	98 (100%)	79 (82.3%)	<0.001[a]
Present	0 (0%)	17 (17.7%)	

[a]Statistically significant

The log-rank test was used to compare Kaplan–Meier survival curves. The covariates, which were statistically significant in the univariate analysis, were then included in the multivariate analysis using Cox proportional hazards regression model; the hazard ratio (HR) and its 95% confidence interval (CI) were assessed for each factor. All tests were two-sided, and $P<0.05$ was considered statistically significant.

Results

Microsatellite instability and expression of mucin core proteins and p53

Twenty-seven (13.9%) of the 194 colorectal carcinomas were MSI-H. Twenty-six cases failed to express one or two mismatch repair proteins; loss of hMLH1 and hPMS2 in18 cases, loss of hMSH2 and hMSH6 in six cases, and loss of hPMS2 alone in two cases. All cases with loss of expression were MSI-H. One of the 27 MSI-H cases showed intact staining on all four mismatch repair proteins.

MUC1 was expressed in 79 (40.7%) of the 194 cases. It was present in the apical membrane or intracytoplasmic lumen of the tumor cells. The mucinous material around the immunoreactive tumor cells was also stained for MUC1. Although MUC1 was mainly localized on the cell membrane, some of the cases displayed a cytoplasmic pattern of expression. MUC2 was expressed in 127 (65.5%) of the 194 cases, although the proportion of positive cells was variable. It was detected in the cytoplasm of the tumor cells with goblet cell features. Twenty-eight cases were 1+, 17 cases were 2+, 24 cases were 3+, and 58 cases were 4+. High MUC2 expression, defined as immunoreactivity of 2+ or more, was observed in 51.0% of cases. MUC5AC was expressed in 60 (30.9%) of the 194 cases. It was present in the cytoplasm of the tumor cells with goblet or columnar cell features.

p53 protein overexpression, defined as positivity in ≥10% of the tumor cells, was found in 82 (42.3%) of the cases.

Using the chi-square test, MSI-H phenotype showed significant positive correlations with MUC2 ($P<0.001$) and MUC5AC ($P=0.003$). In addition, expression of p53 was inversely correlated with MUC2 ($P<0.001$), MUC5AC ($P<0.001$), and MSI-H phenotype ($P<0.001$).

Mucinous vs nonmucinous adenocarcinomas

Tables 1 and 2 list the characteristics of the 194 colorectal carcinomas, stratified by mucinous and nonmucinous histological type. When compared with nMA, MA developed in younger age (56.7±13.1 vs 63.1±12.8 year; $P=0.001$). MAs were larger (7.03±2.56 vs 5.11±2.06 cm; $P<0.001$) and more often located in the right colon (53.1 vs 25.5%; $P<0.001$) than nMAs. In addition, the background of serrated adenomas was noted only in MAs (17.7 vs 0%; $P<0.001$). There was no significant difference in gender, stage, angiolymphatic, venous, and perineural invasion, or tumor border type between mucinous and nonmucinous cancers.

MSI-H phenotype was more common in MAs than in nMAs (25.0 vs 3.1%; $P<0.001$), whereas p53 protein overexpression was less common in MAs (31.3 vs 53.1%; $P=0.002$).

High MUC2 expression was predominantly found in MAs than in nMAs (89.6 vs 13.3%; $P<0.001$). MUC5AC expression was also significantly associated with MAs (49.0 vs 13.3%; $P<0.001$). MUC1 expression showed no significant difference between mucinous and nonmucinous cases.

Characteristics of mucinous and nonmucinous adenocarcinoma in relation to location

To explore the factors associated with tumor location, we examined clinicopathological features, MSI, and expression of mucin core proteins and p53 in the 96 MAs in relation to tumor location. When compared with left-sided tumors, right-sided MAs were characterized by older age (59.7±12.5 vs 53.2± 13.0 year; $P=0.014$), larger tumor size (7.6±2.6 vs 6.4±2.4 cm; $P=0.026$), lower TNM stage at presentation (47.1 vs 26.7%, stage I and II; $P=0.040$), peritumoral lymphocytic response (27.5 vs 8.9%; $P=0.020$), background of serrated adenoma (25.5 vs 8.9%; $P=0.033$), MSI-H phenotype (39.2 vs 8.9%; $P<0.001$), high MUC2 expression

Table 2 Microsatellite instability and expression of p53, MUC1, MUC2, and MUC5AC, in relation to mucinous vs nonmucinous histology and tumor location

	Colorectal adenocarcinomas (total)			Nonmucinous adenocarcinomas			Mucinous adenocarcinomas		
	Nonmucinous adenocarcinomas (*n*=98)	Mucinous adenocarcinomas (*n*=96)	*P* value	Right-sided (*n*=25)	Left-sided (*n*=73)	*P* value	Right-sided (*n*=51)	Left-sided (*n*=45)	*P* value
MSI-H	3 (3.1%)	24 (25.0%)	<0.001[a]	3 (12.0%)	0 (0%)	0.003[a]	20 (39.2%)	4 (8.9%)	<0.001[a]
P53 (+)	52 (53.1%)	30 (31.3%)	0.002[a]	9 (36.0%)	43 (58.9%)	0.048[a]	11 (21.6%)	19 (42.2%)	0.029[a]
MUC1 (+)	40 (40.8%)	39 (40.6%)	0.978	9 (36.0%)	31 (42.5%)	0.570	19 (37.3%)	20 (44.4%)	0.474
MUC2 (+)	13 (13.3%)	86 (89.6%)	<0.001[a]	7 (28.0%)	6 (8.2%)	0.012[a]	49 (96.1%)	37 (82.2%)	0.027[a]
MUC5AC (+)	13 (13.3%)	47 (49.0%)	<0.001[a]	10 (40.0%)	3 (4.1%)	<0.001[a]	30 (58.8%)	17 (37.8%)	0.040[a]

[a]Statistically significant

(96.1 vs 82.2%; P=0.027), MUC5AC expression (58.8 vs 37.8%; P=0.040), and low p53 protein overexpression (21.6 vs 42.2%; P=0.029) (Table 2; Fig. 1).

To see whether the characteristics associated with tumor location in MAs were also observed in nMAs, we performed a similar analysis of the 98 cases of the nonmucinous type. When compared with the left-sided tumors, right-sided nMAs were characterized by MSI-H phenotype (12.0 vs 0%; P=0.003), high MUC2 expression (28.0 vs 8.2%; P=0.012), and MUC5AC expression (40.0 vs 4.1%; P<0.001), as well as low p53 protein overexpression (36.0 vs 58.9%; P=0.048) (Table 2). There was no significant difference in other clinicopathologic characteristics and MUC1 expression.

Association of mucinous adenocarcinoma with serrated adenoma

Seventeen MAs were found in association with adjacent serrated adenomas (Fig. 2). Of these, 13 cases were right-sided (five in the cecum, six in the ascending colon, and two in the transverse colon) and four were left-sided (three in the sigmoid colon and one in the rectum). All 17 showed papillary infolding and eosinophilic cytoplasm in addition to the typical saw-tooth appearance of serrated adenoma (Fig. 2). Serrated tufts or papillary fronds were also found in inspissated mucin of the carcinoma tissue in those cases. When compared with MAs without background of serrated adenoma, those with serrated adenoma were significantly associated with MUC5AC expression (88.2 vs 40.5%; P<0.001). MSI, MUC1, MUC2, and p53 expression did not differ between the two types of MA.

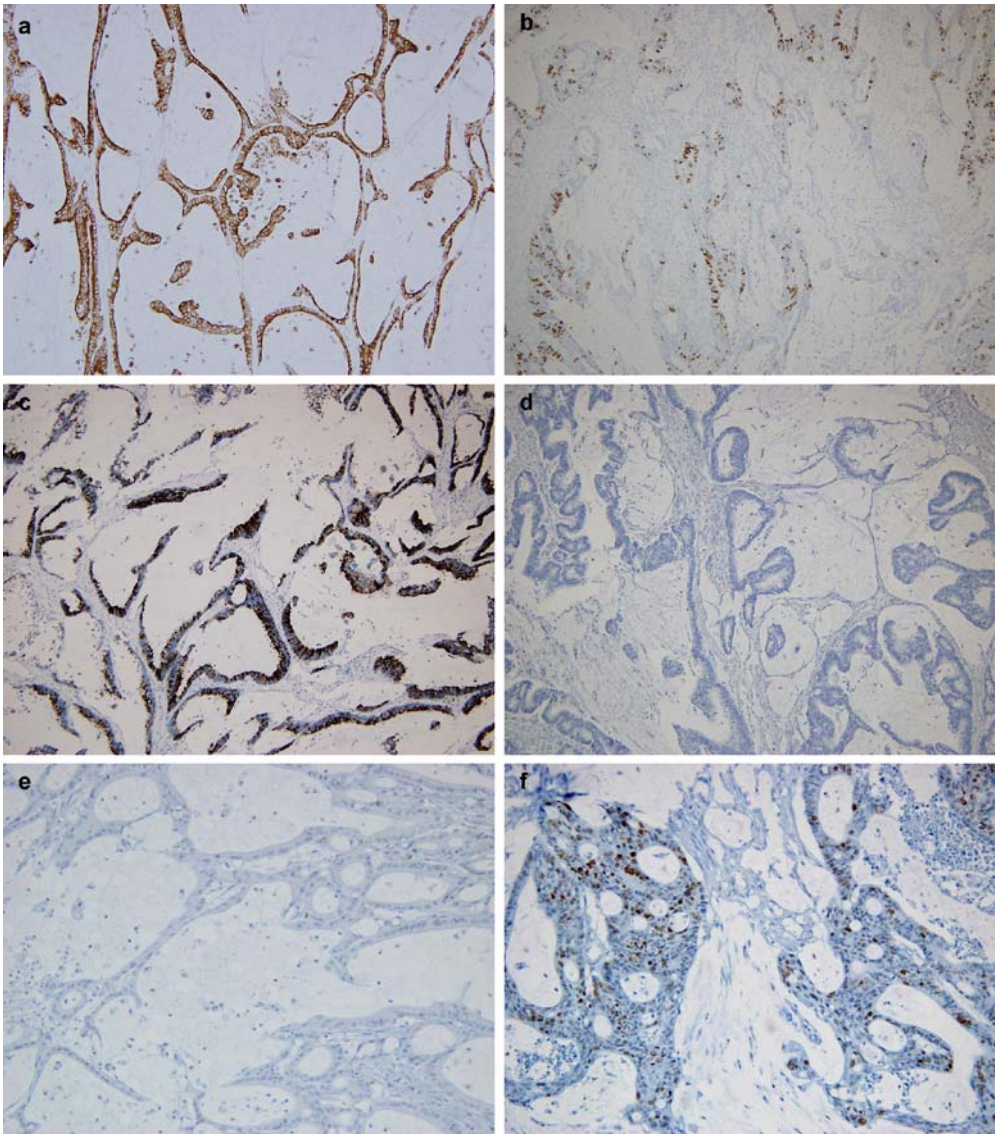

Fig. 1 MUC2 (**a**, **b**), MUC5AC (**c**, **d**), and p53 (**e**, **f**) expression in right-sided (**a**, **c**, **e**) and left-sided (**b**, **d**, **f**) mucinous adenocarcinomas

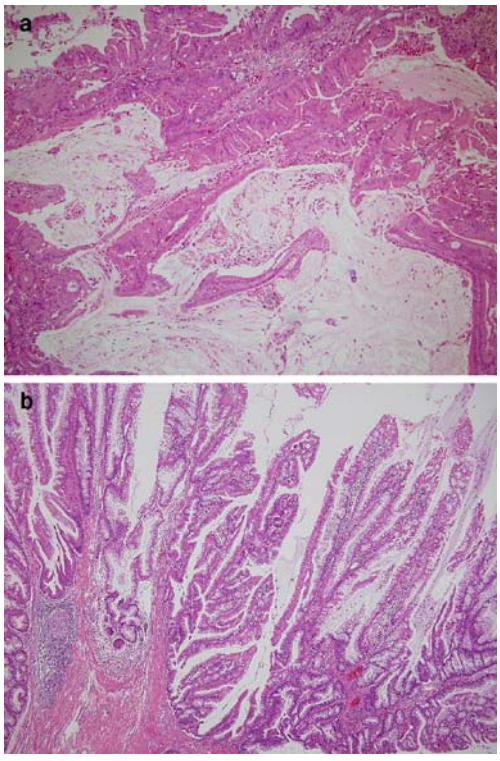

Fig. 2 Serrated feature of right-sided mucinous carcinoma (**a**) associated with serrated adenoma (**b**)

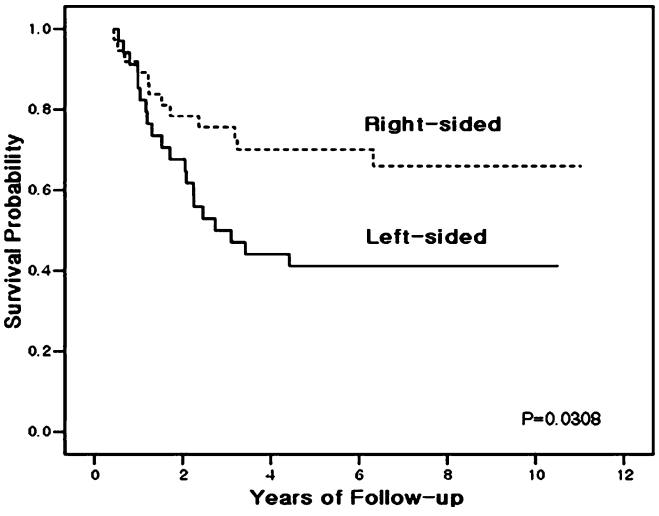

Fig. 3 Kaplan–Meier survival curves showing the disease-specific survival of patients with mucinous adenocarcinoma according to tumor location

Survival analysis

Of the 96 MAs, 72 cases operated in Seoul National University Hospital from January 1993 to December 1999 were followed to December 2003 and were suitable for survival analysis. In univariate analysis, low stage (log rank, $P<0.0001$), absence of venous invasion ($P<0.0001$), pushing border ($P=0.0189$), right-sided location ($P=0.0308$), MSI-H phenotype ($P=0.0203$), and peritumoral lymphocytic response ($P=0.0233$) showed a favorable influence on survival (Fig. 3). In multivariate analysis, advanced stage (HR, 5.463; 95% CI, 1.752–17.033; $P=0.003$) and venous invasion (HR, 3.021; 95% CI, 1.199–7.609; $P=0.019$) were identified as independent predictors of survival. Neither tumor location nor MSI status was significant prognostic factors in multivariate analysis.

Discussion

In this study, we evaluated the clinicopathologic characteristics, MSI, and expression of mucin core proteins and p53 of MA of the colorectum in relation to tumor location. We found that expression of MUC2 and MUC5AC was associated with mucinous histology and right-sided tumor location. Expression of MUC2 in colorectal MAs has been documented in many studies [4, 12, 23] and has been shown to be associated with proximal (right-sided) location [4]. MUC5AC expression was also reported to be associated with MAs and right-sided tumors [4, 20, 21]. We observed that MUC2 and MUC5AC expression was positively correlated with MSI-H phenotype. Hence, the association of MUC2 and MUC5AC expression with mucinous histology and right-sided tumor location may be partly related to MSI, because MAs, especially right-sided MAs, were significantly correlated with MSI-H phenotype. There has been a similar report that MSI-H colorectal cancers are more often positive for both MUC2 and MUC5AC than MSS tumors [4]. In addition, Losi et al. [21] recently reported a relationship between the presence of MUC5AC and altered expression of MLH1 in colorectal carcinomas. It has been shown that serrated polyps including hyperplastic polyps, mixed polyps, and serrated adenoma, are characterized by increased expression of intestinal mucin MUC2, inappropriate expression of gastric mucin MUC5AC, and high frequency of MSI [3, 4]. Thus, it was suggested that serrated epithelial polyps may represent precursors of MSI-H cancers [4].

In our study, 17 (17.7%) of the 96 colorectal MAs were associated with serrated adenoma and most of those cases showed serrated feature, whereas none of the nMAs showed this association. In addition, the MAs associated with serrated adenoma were predominantly right-sided. Makinen et al. [22] reported that 27 (5.8%) of 466 colorectal carcinomas were found in association with adjacent serrated adenomas, and nine of the 27 carcinomas was mucinous, with a mucinous component present in 11 additional cases. Moreover, of the nine MAs associated with serrated adenoma, seven originated in the cecum. Although further study is needed, it seems that mucin production is a common feature of serrated colorectal adenocarcinoma and that MAs associated with serrated adenoma are a distinct subtype of colorectal MAs, predominantly found in the right colon. Our study also revealed that serrated MAs expressed high levels of MUC5AC. This could be related to gastric differentiation of the serrated adenoma, leading to expression of gastric mucin, MUC5AC [15].

Our analysis revealed that MSI-H phenotype and a peritumoral lymphocytic response, which is a feature of MSI-H colorectal cancers [10, 14, 18], are characteristics of right-sided MAs and not of left-sided MAs. Kakar et al. [16] reported that MSI-H mucinous carcinomas were more often right-sided than MSS mucinous carcinomas. In their study, 41.4% of right-sided mucinous carcinomas were MSI-H compared to 11.8% of left-sided mucinous carcinomas. Recently, Kazama et al. [17] also showed that in mucinous carcinoma, MSI tumors were significantly more frequent in the proximal colon (55.6%) than in the distal colon (9.5%). Thus, although mucinous histology is a characteristic feature of MSI-H colorectal cancers, this does not apply to left-sided MAs. Moreover, we observed that although p53 overexpression is infrequent in MAs than in nMAs [11], it is even less in right-sided MAs. It, therefore, seems that right-sided and left-sided MAs arise through different carcinogenetic pathway. It was proposed that right- and left-sided colorectal cancers are different tumors because of their embryonic origin, genetic change, and biologic identity [6]. Glebov et al. [8] showed that more than 1,000 genes were differentially expressed in adult ascending vs descending colon and 87 genes in ascending vs descending fetal colon, indicating that anatomically relevant differences are already established in embryonic colon and additional changes in gene expression occur in postnatal development. Thus, distinct biological and genetic characteristics of right- and left-sided colonic mucosa may be associated with different responses to carcinogenic stimuli, leading to different carcinogenic pathways of right- and left sided colorectal cancer.

Our patients with right-sided MA had significantly better survival than did those with left-sided MA (P=0.0308). However, tumor location showed no statistical difference in survival in the same stage and was not an independent prognostic factor in multivariate analysis. Patients with right-sided MA presented at lower stage than those with left-sided MA (P=0.040), accounting for its favorable prognosis.

Our immunohistochemical analysis of four mismatch repair proteins provided 96.3% sensitivity and 100% specificity for the MSI-H phenotype, which confirmed the previous reports that immunohistochemistry of mismatch repair proteins is a rapid, cost-effective, sensitive, and extremely specific method for detection of MSI-H cancers [5, 26, 27, 35]. We found that entire group of tumors lacking hMLH1 protein showed loss of hPMS2. Similarly, all of the tumors lacking hMSH2 showed loss of hMSH6. This association of hMLH1 and hPMS2, and hMSH2 and hMSH6 has already been reported previously [5, 26, 27, 35]. The complete association of these proteins verifies the heterodimerization-dependent stability of hMSH6 and hPMS2 [26]. We observed isolated loss of hPMS2 protein in two out of 27 MSI-H cases. de Jong et al. [5] also reported that eight (23%) of 35 colorectal tumors with a known hMLH1 mutation showed loss of PMS2 without loss of hMLH1 protein by immunohistochemistry. The loss of PMS2 protein suggests the presence of hMLH1 or hPMS2 mutation or somatic abrogation of hMLH1. Although our study didn't find cases with isolated loss of hMSH6, previous studies revealed some cases with isolated loss of hMSH6 among MSI-H tumors [5, 26, 27, 35]. Therefore, it is necessary to include hMSH6 and hPMS2 in the panel of antibodies to be used when evaluating MSI status by immunohistochemistry.

In summary, we found that clinicopathological characteristics, MSI status, and expression of mucin core proteins and p53 differed according to tumor location and mucinous histology. MSI-H phenotype, expression of MUC2 and MUC5AC mucin core proteins, and low p53 overexpression were associated with right-sided tumor location as well as mucinous histology. In addition, older age, larger tumor size, lower stage at presentation, peritumoral lymphocytic response, and association with serrated adenoma were characteristics of right-sided MA. Our findings, therefore, indicate that MA is a distinctive type of colorectal cancer, with different features depending on its location.

Acknowledgements This work is supported by a grant from the Seoul National University Bundang Hospital Research Fund, Seongnam, Korea. So Yeon Park and Hye Seung Lee contributed equally to this work.

References

1. Aaltonen LA, Peltomaki P, Leach FS, Sistonen P, Pylkkanen L, Mecklin JP, Jarvinen H, Powell SM, Jen J, Hamilton SR, Petersen GM, Kinzler KW, Vogelstein B, de la Chapelle A (1993) Clues to the pathogenesis of familial colorectal cancer. Science 260:812–816
2. Baldus SE, Monig SP, Huxel S, Landsberg S, Hanisch FG, Engelmann K, Schneider PM, Thiele J, Holscher AH, Dienes HP (2004) MUC1 and nuclear beta-catenin are coexpressed at the invasion front of colorectal carcinomas and are both correlated with tumor prognosis. Clin Cancer Res 10:2790–2796
3. Biemer-Huttmann AE, Walsh MD, McGuckin MA, Ajioka Y, Watanabe H, Leggett BA, Jass JR (1999) Immunohistochemical staining patterns of MUC1, MUC2, MUC4, and MUC5AC mucins in hyperplastic polyps, serrated adenomas, and traditional adenomas of the colorectum. J Histochem Cytochem 47:1039–1048
4. Biemer-Huttmann AE, Walsh MD, McGuckin MA, Simms LA, Young J, Leggett BA, Jass JR (2000) Mucin core protein expression in colorectal cancers with high levels of microsatellite instability indicates a novel pathway of morphogenesis. Clin Cancer Res 6:1909–1916
5. de Jong AE, van Puijenbroek M, Hendriks Y, Tops C, Wijnen J, Ausems MG, Meijers-Heijboer H, Wagner A, van Os TA, Brocker-Vriends AH, Vasen HF, Morreau H (2004) Microsatellite instability, immunohistochemistry, and additional PMS2 staining in suspected hereditary nonpolyposis colorectal cancer. Clin Cancer Res 10:972–980
6. Distler P, Holt PR (1997) Are right- and left-sided colon neoplasms distinct tumors? Dig Dis 15:302–311
7. Fearon ER, Vogelstein B (1990) A genetic model for colorectal tumorigenesis. Cell 61:759–767
8. Glebov OK, Rodriguez LM, Nakahara K, Jenkins J, Cliatt J, Humbyrd CJ, DeNobile J, Soballe P, Simon R, Wright G, Lynch P, Patterson S, Lynch H, Gallinger S, Buchbinder A, Gordon G, Hawk E, Kirsch IR (2003) Distinguishing right from left colon by pattern of gene expression. Cancer Epidemiol Biomarkers Prev 12:755–762

9. Green FL, Balch CM, Fleming ID, Fritz AG, Balch CM, Haller DG, Morrow M (eds) (2002) AJCC cancer staging manual, 6th edn. Springer, Berlin Heidelberg New York
10. Greenson JK, Bonner JD, Ben-Yzhak O, Cohen HI, Miselevich I, Resnick MB, Trougouboff P, Tomsho LD, Kim E, Low M, Almog R, Rennert G, Gruber SB (2003) Phenotype of microsatellite unstable colorectal carcinomas: Well-differentiated and focally mucinous tumors and the absence of dirty necrosis correlate with microsatellite instability. Am J Surg Pathol 27:563–570
11. Hanski C, Tiecke F, Hummel M, Hanski ML, Ogorek D, Rolfs A, Schmitt-Graff A, Stein H, Riecken EO (1996) Low frequency of p53 gene mutation and protein expression in mucinous colorectal carcinomas. Cancer Lett 103:163–170
12. Ishizu H, Kumagai J, Eishi Y, Takizawa T, Koike M (2004) Mucin core protein expression by colorectal mucinous carcinomas with or without mucus hyperplasia. J Gastroenterol 39:125–132
13. Jass JR, Love SB, Northover JM (1987) A new prognostic classification of rectal cancer. Lancet 1:1303–1306
14. Jass JR, Do KA, Simms LA, Iino H, Wynter C, Pillay SP, Searle J, Radford-Smith G, Young J, Leggett B (1998) Morphology of sporadic colorectal cancer with DNA replication errors. Gut 42:673–679
15. Jass JR (1999) Serrated adenoma and colorectal cancer. J Pathol 187:499–502
16. Kakar S, Aksoy S, Burgart LJ, Smyrk TC (2004) Mucinous carcinoma of the colon: correlation of loss of mismatch repair enzymes with clinicopathologic features and survival. Mod Pathol 17:696–700
17. Kazama Y, Watanabe T, Kanazawa T, Tada T, Tanaka J, Nagawa H (2005) Mucinous carcinomas of the colon and rectum show higher rates of microsatellite instability and lower rates of chromosomal instability: a study matched for T classification and tumor location. Cancer 103:2023–2029
18. Kim H, Jen J, Vogelstein B, Hamilton SR (1994) Clinical and pathological characteristics of sporadic colorectal carcinomas with DNA replication errors in microsatellite sequences. Am J Pathol 145:148–156
19. Kim YS, Gum J Jr, Brockhausen I (1996) Mucin glycoproteins in neoplasia. Glycoconj J 13:693–707
20. Kocer B, Soran A, Erdogan S, Karabeyoglu M, Yildirim O, Eroglu A, Bozkurt B, Cengiz O (2002) Expression of MUC5AC in colorectal carcinoma and relationship with prognosis. Pathol Int 52:470–477
21. Losi L, Scarselli A, Benatti P, Ponz de Leon M, Roncucci L, Pedroni M, Borghi F, Lamberti I, Rossi G, Marino M, Ponti G, Zangardi G, Menigatti M, Di Gregorio C (2004) Relationship between MUC5AC and altered expression of MLH1 protein in mucinous and nonmucinous colorectal carcinomas. Pathol Res Pract 200:371–377
22. Makinen MJ, George SM, Jernvall P, Makela J, Vihko P, Karttunen TJ (2001) Colorectal carcinoma associated with serrated adenoma-prevalence, histological features, and prognosis. J Pathol 193:286–294
23. Manne U, Weiss HL, Grizzle WE (2000) Racial differences in the prognostic usefulness of MUC1 and MUC2 in colorectal adenocarcinomas. Clin Cancer Res 6:4017–4025
24. Messerini L, Ciantelli M, Baglioni S, Palomba A, Zampi G, Papi L (1999) Prognostic significance of microsatellite instability in sporadic mucinous colorectal cancers. Hum Pathol 30:629–634
25. Nakamori S, Ota DM, Cleary KR, Shirotani K, Irimura T (1994) MUC1 mucin expression as a marker of progression and metastasis of human colorectal carcinoma. Gastroenterology 106:353–361
26. Plaschke J, Kruger S, Pistorius S, Theissig F, Saeger HD, Schackert HK (2002) Involvement of hMSH6 in the development of hereditary and sporadic colorectal cancer revealed by immunostaining is based on germline mutations, but rarely on somatic inactivation. Int J Cancer 97:643–648
27. Rigau V, Sebbagh N, Olschwang S, Paraf F, Mourra N, Parc Y, Flejou JF (2003) Microsatellite instability in colorectal carcinoma. The comparison of immunohistochemistry and molecular biology suggests a role for hMSH6 [correction of hMLH6] immunostaining. Arch Pathol Lab Med 127:694–700
28. Schlegel J, Bocker T, Zirngibl H, Hofstadter F, Ruschoff J (1995) Detection of microsatellite instability in human colorectal carcinomas using a non-radioactive PCR-based screening technique. Virchows Arch 426:223–227
29. Sylvester PA, Myerscough N, Warren BF, Carlstedt I, Corfield AP, Durdey P, Thomas MG (2001) Differential expression of the chromosome 11 mucin genes in colorectal cancer. J Pathol 195:327–335
30. Symonds DA, Vickery AL (1976) Mucinous carcinoma of the colon and rectum. Cancer 37:1891–1900
31. Thibodeau SN, Bren G, Schaid D (1993) Microsatellite instability in cancer of the proximal colon. Science 260:816–819
32. Vogelstein B, Fearon ER, Hamilton SR, Kern SE, Preisinger AC, Leppert M, Nakamura Y, White R, Smits AM, Bos JL (1988) Genetic alterations during colorectal-tumor development. N Engl J Med 319:525–532
33. Wu CS, Tung SY, Chen PC, Kuo YC (1996) Clinicopathological study of colorectal mucinous carcinoma in Taiwan: a multivariate analysis. J Gastroenterol Hepatol 11:77–81
34. Yamamoto S, Mochizuki H, Hase K, Yamamoto T, Ohkusa Y, Yokoyama S, Ushitani Y, Tamakuma S (1993) Assessment of clinicopathologic features of colorectal mucinous adenocarcinoma. Am J Surg 166:257–261
35. Young J, Simms LA, Biden KG, Wynter C, Whitehall V, Karamatic R, George J, Goldblatt J, Walpole I, Robin SA, Borten MM, Stitz R, Searle J, McKeone D, Fraser L, Purdie DR, Podger K, Price R, Buttenshaw R, Walsh MD, Barker M, Leggett BA, Jass JR (2001) Features of colorectal cancers with high-level microsatellite instability occurring in familial and sporadic settings: parallel pathways of tumorigenesis. Am J Pathol 159:2107–2116

Virchows Arch (2006) 449: 48–61
DOI 10.1007/s00428-006-0179-4

ORIGINAL ARTICLE

Riccardo Alessandro · Maria Antonietta Di Bella · Anna Maria Flugy · Simona Fontana · Francesca Damiani · Chiara Corrado · Paolo Colomba · Matilde Todaro · Domenica Russo · Alessandra Santoro Elise C. Kohn · Giacomo De Leo

Comparative study of T84 and T84SF human colon carcinoma cells: in vitro and in vivo ultrastructural and functional characterization of cell culture and metastasis

Received: 3 October 2005 / Accepted: 14 February 2006 / Published online: 13 April 2006
© Springer-Verlag 2006

Abstract To better understand the relationship between tumor heterogeneity, differentiation, and metastasis, suitable experimental models permitting in vitro and in vivo studies are necessary. A new variant cell line (T84SF) exhibiting an altered phenotype was recently selected from a colon cancer cell line (T84) by repetitive plating on TNF-α treated human endothelial cells and subsequent selection for adherent cells. The matched pair of cell lines provides a useful system to investigate the extravasation step of the metastatic cascade. Since analysis of morphological differences can be instructive to the understanding of metastatic potential of tumor cells, we compared the ultrastructural and functional phenotype of T84 and T84SF cells in vitro and in vivo. The reported ultrastructural features evidence differences between the two cell lines; selected cells showed a marked pleomorphism of cell size and nuclei, shape, and greater surface complexity. These morphological differences were also coupled with biochemical data showing a distinct tyrosine phosphorylation-based signaling, an altered localization of β-catenin, MAPK, and AKT activation, as well as an increased expression in T84SF cells of Bcl-X_L, a major regulator of apoptosis. Therefore, these cell lines represent a step forward in the development of appropriate models in vitro and in vivo to investigate colon cancer progression.

Keywords Colon carcinoma · Tumor cells · Ultrastructure · Metastasis · Apoptosis · Bcl-X_L

R. Alessandro (✉) · M. A. Di Bella · A. M. Flugy · S. Fontana · F. Damiani · C. Corrado · P. Colomba · G. De Leo
Dipartimento di Biopatologia e Metodologie Biomediche, Sezione di Biologia e Genetica, Università di Palermo,
Via Divisi 83,
90133 Palermo, Italy
e-mail: ricale@unipa.it
Tel.: +39-091-6554600
Fax: +39-091-6554624

M. Todaro
Dipartimento di Discipline Chirurgiche ed Oncologiche, Università di Palermo,
Palermo, Italy

D. Russo
Istituto di Biomedicina ed Immunologia Molecolare "Alberto Monroy", Centro Nazionale delle Ricerche,
Palermo, Italy

A. Santoro
Laboratorio di Ematologia,
Dipartimento di Ricerca Clinica e Biotecnologia,
A.O. "V.Cervello",
Palermo, Italy

E. C. Kohn
Molecular Signalling Section, Laboratory of Pathology, Center for Cancer Research, National Cancer Institute,
Bethesda, MD, USA

Introduction

Tumor cell heterogeneity with regard to morphological, biochemical, functional, and genetic features has been widely documented [4, 18, 25, 43]. Metastasis, a major complication of cancer disease, is a highly selective process that favors the emergence of cell clones able to establish specific cell–cell and cell–matrix interactions, to resist to hypoxia and to immune response [18, 41, 46]. However, to better understand the relationship between tumor heterogeneity and metastasis, suitable experimental models permitting in vitro and in vivo studies are necessary. For this purpose, the selection and establishment inside a cell population of clones showing high metastatic potential can highlight specific molecular properties correlated with metastatic phenotype [44]. Our group has recently derived a novel metastatic variant cell line, termed T84SF, by a selection procedure based on repetitive plating of colon cancer cells on TNF-α activated human endothelial cells. The matched pair of cell lines provides a useful system to investigate the extravasation step of the metastatic cascade. T84SF cells displayed in vitro a higher proliferation rate and a more invasive behavior compared

to the parental cells, while a greater number of metastatic colonies in nude mice formed in vivo [4].

Electron microscopy (EM), together with biochemical and immunological analysis, may greatly contribute to the problem of intraneoplastic heterogeneity [19]. The morphological aspects of cells, strictly related to their functional properties, are highly relevant to the full phenotypic characterization of neoplastic cells. EM studies have been helpful, for example, in evaluating the surface changes that occur in malignant progression, such as alterations of cell–cell interactions, modifications of microvilli structure and distribution, as well as increase in the release of membrane vesicles. Vesicles shedding, which affects the ability of proliferating and invasive cancer cells to infiltrate and metastasize, is an active process [6, 55]. Several studies have demonstrated that cancer cells release membrane vesicles containing proteinases and, as such, may aid in the metastatic process [21, 23]. Vesicle membranes also contain surface antigens expressed on the plasma membrane [12]; they originate from domains of the plasma membrane selectively enriched in membrane components, including HLA class I molecules, β1 integrins, membrane-bound matrix metalloproteinase (MMP)-9 [13], and apoptosis-inducing molecules [32].

Considerable insight into carcinoma progression has been obtained from studies of relevant cell adhesion molecules such as E-cadherin and catenins [57]. It is known that loss of E-cadherin expression is associated with more aggressive tumors and with the acquisition of a mesenchymal and dedifferentiated phenotype. β-catenin is normally localized to the cell membrane and is bound to E-cadherin thus composing cell adhesion structures important for epithelial integrity. Genetic alterations occurring during colon progression lead to a cytoplasmic and nuclear accumulation of β-catenin, where it acts as a transcriptional activator of genes involved in invasive growth and metastasis [27]. To find support of suitability of our in vitro model, we analyzed the expression patterns of β-catenin and E-cadherin in T84 cells and selected cells.

Aberration in regulation of apoptosis has been recognized as an important mechanism in oncogenesis and tumor progression [24]; we have previously demonstrated that T84SF cells showed a lower apoptotic index compared to parental cell line. In this paper, we identify Bcl-X_L as a promising molecular player in the augmented apoptosis resistance of selected cells.

In the present study, with the purpose to investigate the early phases of the extravasation process, electron microscopic and biochemical investigations have been performed using T84 and T84SF cell lines. We have particularly evaluated (a) the in vitro and in vivo ultrastructural features of T84 parental and T84SF selected cells; (b) the expression of cell adhesion molecules; (c) the MAPK (ERK 1/2) and AKT signaling, which occurs in the two cell lines; (d) the content of vesicles shed by T84 and T84SF; and (e) the expression of Bcl-X_L and caspase-3.

The ultrastructural and biochemical data reported here show interesting differences between parental and selected cell line, which support the value of this model for a better understanding of the extravasation step of the metastatic cascade.

Materials and methods

Cell culture

T84 (ICLC, Genova, Italy) and T84SF human colon cancer cells were maintained in DMEM-F12 (BioWhittaker, Verviers, Belgium) supplemented with 10% fetal calf serum (FCS) (BioWhittaker), 100 U/ml penicillin and 100 μg/ml streptomycin (Euroclone, UK).

In vitro ultrastructural characterization of T84 and T84SF cell lines

For conventional transmission electron microscopy (TEM), confluent T84 and T84SF tumor cells were rinsed briefly in prewarmed phosphate-buffered saline (PBS) pH 7.5 and then fixed as a pellet and in situ as an intact sheet by addition of a volume of 2.5% glutaraldehyde buffered in 0.1 M sodium cacodylate buffer. After several washes with buffer, the cells were postfixed with 1% OsO_4 for 1 h at 4°C, rinsed and dehydrated in a graded ethanol series, gently scraped and then embedded in epoxy resin. Ultrathin sections were stained with uranyl acetate and lead citrate and finally examined under a Philips CM10 electron microscope at 80 kV. The ultrastructure features were evaluated by analysis of at least 50 cells of the two cell lines.

Ultrastructural characterization and gelatinase content of vesicles

For the preparation of the vesicles, subconfluent T84 and T84SF cells were washed with PBS then successively incubated in serum-free DMEM-F12 for 24 h and in 10% FCS growth medium for 3 h to stimulate vesicles shedding [53]. Culture media were then collected and centrifuged at 4,500 rpm for 10 min to remove cell debris. The cell-free supernatants were further centrifuged for 3 h at 4°C at 27,000 rpm. Pelleted vesicles were resuspended in PBS, and the amount of isolated vesicles was determined by measuring protein concentration using bovine serum albumin (BSA; Sigma Chemical, St. Louis, MO, USA) as a standard.

For analysis of the ultrastructural morphology of the shed vesicles, the vesicles pellet was resuspended in PBS and then applied to collodion-coated grids. After washing, the vesicles were negatively stained with uranyl acetate or 1% phosphotungstic acid and examined by transmission electron microscopy.

For zymographic analysis of vesicle-associated gelatinases, vesicles were obtained by stimulating T84 and T84SF cells with gelatin Sepharose-treated MMP-free serum, to avoid MMP contamination from serum [13].

Zymography was performed using 8% polyacrylamide gel containing 0.1% gelatin. Vesicle samples were diluted in sodium dodecyl sulfate-polyacrylamide gel electrophoresis (SDS-PAGE) sample buffer in nonreducing conditions without heating. After electrophoresis, gel was washed twice for 30 min in 2.5% Triton X-100 at room temperature and incubated overnight in 50 mM Tris–HCl, pH 7.5, 10 mM $CaCl_2$, 150 mM NaCl, at 37°C. Gel was stained in Coomassie Blue R 250 for 1 h. Gelatinase activities were visualized as clear bands, on a stained background. As standards for gelatinases, a cell culture media from human fibroblasts treated with TPA (Sigma, St. Louis, MO), was used.

Ultrastructural characterization of metastasis

T84 and T84SF metastasis were obtained by injecting viable single cells suspensions (2×10^6) into tail veins of athymic male nude mice [4].

Anesthetized animals were perfused with an isotonic buffered saline solution containing 2% dextran for 10 min followed by a 15 min treatment with 2.5% glutaraldehyde buffered in 0.1 M sodium cacodylate. Lungs were removed, cut into small pieces and immersed in the same solution for 2 h. After rinsing in cacodylate buffer, biopsies were postfixed in 1% OsO_4 for 1 h, and finally embedded in Epoxy resin. Ultrathin sections were cut, stained, and analyzed at the transmission electron microscope.

Reverse transcription-polymerase chain reaction analysis

Total RNA from subconfluent cells was isolated with the Rneasy Mini kit (QIAGEN, Hilden, Germany) according to the manufacturer's instructions. Five micrograms of total RNA from each cell line were used for first strand cDNA synthesis using the 1st Strand cDNA Synthesis kit (Amersham, Little Chalfont, UK). One-tenth of the reverse transcribed cDNA was amplified with the following polymerase chain reaction (PCR) primer sets: 5′-AAA TGTCTCAGAGCAACCG-3′ (sense), 5′-TACGCTTTC CACGCACAGT-3′ (antisense) for Bcl-X_L; 5′-GAGGA GAGCGGTGGTCAAAG-3′ (sense), 5′-GTTCAGGGA GCTCAGACTAG-3′ (antisense) for E-Cadherin; and 5′-CAAGAGATGGCCACGGCTGCT-3′ (sense), 5′-TCCTT CTGCATCCTGTCGGCA-3′ (antisense) for β-actin (used as an internal standard). Standard amplifications were performed with a total of 40 cycles at an annealing temperature of 56°C. All the oligonucleotides were designed to recognize a unique sequence for each mRNA. The PCR products were separated in 1% agarose gels. The expected product sizes were 467, 361, and 275 bp for Bcl-X_L, E-Cadherin, and β-actin, respectively.

Western blot analysis

T84 parental cell line and T84SF cells grown at subconfluence were washed with PBS and resuspended in lysis buffer (300 mM NaCl, 50 mM Tris–HCl pH 7.6, 0.1% Triton, 1 mM PMSF, 10 μg/ml Leupeptin, 10 μg/ml Aprotinin, 4 mM EDTA, 2 mM sodium orthovanadate, 10 mM PP_I, 100 mM NaF) on ice for 1 h. The cell lysates were clarified at high-speed centrifugation for 15 min, and an aliquot of the supernatant was assayed to determine protein concentration by Bradford method. Proteins were separated by a 6% SDS-PAGE and transferred to nitrocellulose membrane (Protran Schleicher and Schuell, Dassel, Germany). The membrane was incubated in block solution (1 M glycine, 1.25% dry milk, 0.1% ovalbumin) and probed overnight at 4°C with specific antibodies against Bcl-X_L (H5 mouse IgG1, Santa Cruz Biotechnology, Santa Cruz, CA, USA), caspase-3 (rabbit polyclonal, Santa Cruz Biotechnology), p44/42 MAP (Cell Signalling Technology, Beverly, MA, USA), phospho-p44/42 MAP kinase (Cell Signalling Technology), total AKT (rabbit polyclonal, Cell Signalling, Danvers, MA, USA), pAKT (mouse monoclonal, Becton and Dickinson, Franklin Lakes, NJ, USA), E-Cadherin (G10 mouse IgG1, Santa Cruz Biotechnology), and β-catenin (mouse monoclonal, Santa Cruz Biotechnology). After three washes with WS, the membrane was incubated with proper horseradish peroxidase-conjugated secondary antibody, and proteins were detected by the enhanced chemiluminescence detection system (Super Signal, Pierce, Rockford, IL, USA).

Confocal microscopy

Cells were allowed to attach for 3 h to glass coverslips precoated with 25 nM collagen IV (Sigma Chemical). They were then fixed in 3.7% formaldehyde in PBS, permeabilized with 0.5% Triton X-100, and blocked with 1% BSA (Fraction V) (Sigma Chemical) in PBS for 1 h. Coverslips were incubated with β-catenin antibody (mouse monoclonal, Becton and Dickinson) at a 1:200 dilution in PBS overnight at 4°C. Antibody-treated cells were washed in PBS and incubated with Alexa-Fluor 594 conjugated with goat IgG anti-mouse antibody (Molecular Probes, Eugene, OR, USA) at a 1:500 dilution in PBS for 1 h. Coverslips were washed and mounted using Vectashield with DAPI (Vector Labs, Burlingame, CA). The cells were examined with the use of a Nikon Diaphot-TDM (Eclipse 200) confocal microscope equipped with a 65× objective.

Immunohistochemistry and immunofluorescence

Immunohistochemical stainings were performed on 5-μm thick paraffin sections of mouse lung metastasis obtained after tail vein injections of T84 and T84SF human colon cancer cell lines. Deparaffinized sections were permeabilized in PBS with 0.1% Triton X-100 for 10 min and then incubated with 3% BSA to block the unspecific staining.

After several washes in PBS, sections were incubated overnight at 4°C with specific antibody against Bcl-X_L (1:50 dilution; H5 mouse IgG1, Santa Cruz Biotechnology). After two rinses in PBS, sections were incubated for 30 min at room temperature with biotinilated anti-mouse immunoglobulins (Dako LSAB2 Kit, Dako, Carpinteria, CA, USA) and then incubated with streptavidin peroxidase for 30 min (Dako LSAB2 Kit, Dako). Staining was detected by AEC (3-Amino-9-ethylcarbazole) as a colorimetric substrate. Nuclei were counterstained using aqueous hematoxylin (Dako).

For immunofluorescence studies, T84 and T84SF cells were plated at 3×10^5 cells/well on coverslips previously coated with gelatin (2 μg/well). After 1 hr of adhesion, cells were washed with PBS, fixed in 3.7% paraformaldehyde for 10′, permeabilized for 5′ in 0.5% Triton X-100, and blocked in 1% BSA for 60′. Cells were incubated with an anti-phosphotyrosine antibody (PY20, Santa Cruz Biotechnology) for 60′ at 37°C, washed three times with PBS, and then incubated with the fluorescein-conjugated secondary antibody for 60′. After several washes, coverslips were mounted in moviol and viewed by fluorescence microscopy (Olympus BX50).

Results

Ultrastructural analysis of T84 and T84SF cell lines

Electron microscopy analysis of T84 and T84SF colon carcinoma cells confirmed and extended the previously described data on morphological differences between the two cell lines [4]. The prominent difference observed was the pronounced cellular and nuclear polymorphism.

T84 cells showed a spindle or polygonal shape. The nuclei displayed homogeneous chromatin and one or two round or elongated nucleoli. The cytoplasm contained elements of rough endoplasmic reticulum, some mitochondria, and free scattered ribosomes. Lipid droplets and glycogen granules were observed in small quantities (Fig. 1a–c). The cells were connected by desmosomes and some junctions appeared as long regions of adhesion even though no specific structure was evident. The cell surfaces exhibited prominent processes and sometimes long cytoplasmic projections; microvilli were pleomorphic in both size and distribution (Fig. 1c,d).

T84SF cells, harvested in suspensions or in a monolayer, revealed a significant heterogeneity in cell shape and size and were characterized by a high nucleus-to-cytoplasm ratio (Fig. 2a,c,i). Nuclei were enlarged and well-distinguished, often irregular in shape and highly segmented with crude chromatin structure; the nuclear profile was

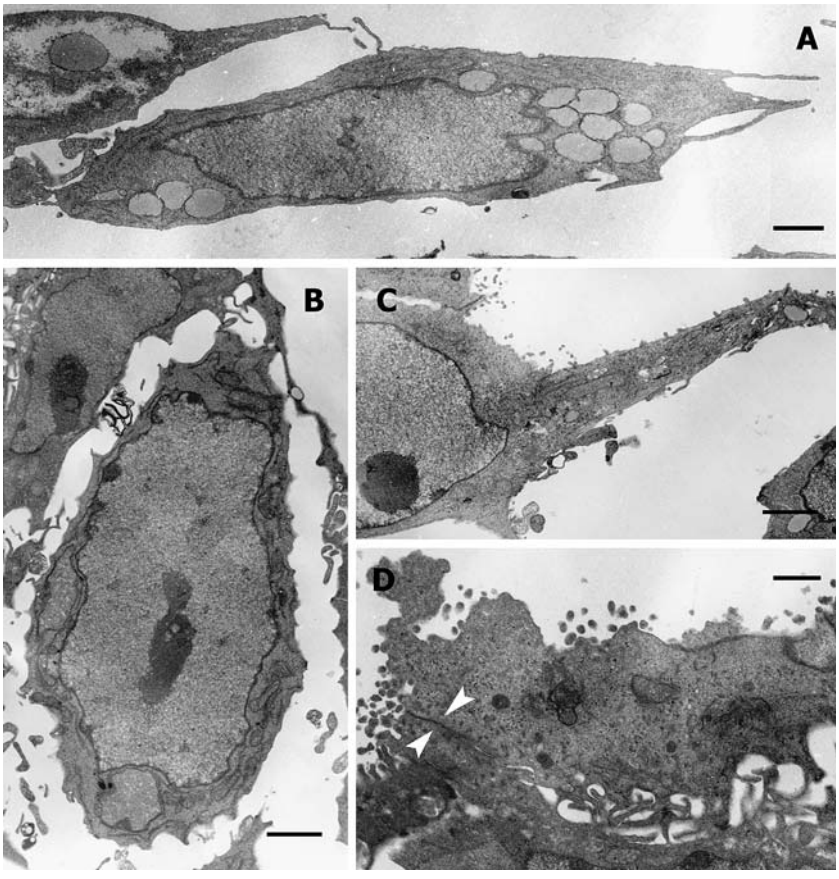

Fig. 1 Ultrastructural features of T84 cells. Cells range from oval to spindle shape (**a**,**b**) and are connected to each other by cell junctions (*arrowheads*) (**d**). The cytoplasm contains some lipid droplets and organelles. Note the long cytoplasmic projections (**a**,**c**). *Scale bars* 1 μm (**a**,**d**), 2 μm (**b**,**c**)

sometimes indented by a nuclear pocket (Fig. 2b). One or two prominent nucleoli with evident fibrillar centers could be identified (Fig. 2a,c). The cytoplasm was reduced and showed few cell organelles. T84SF had well-developed lysosomal granules in their cytoplasm and numerous lipid droplets; mitochondria were more irregular and swollen. The cytoplasm often showed electron lucent cleft-like space, multivesicular bodies, or vacuoles and microfilament bundles (Fig. 2d,i). Myelin figures were also encountered (Fig. 2a,i). Several cells showed some crystal-like intracellular structures (Fig. 2e).

T84SF cells displayed a very convoluted cell surface forming many interdigitations with neighboring cells (Fig. 2a,i); these were connected by regular junctional complexes as desmosomes or regions of adhesion occurring along the lateral borders. Networks of intermediate filaments were anchored to the desmosomes (Fig. 2g,h).

Cell surfaces exhibited abundant, branched, and randomly orientated protrusions, as well as an increased number of pleomorphic microvilli making contact with each other. In many cases, intracellular lumina with well-developed microvilli were formed (Fig. 2f,i).

These differences in cellular and nuclear polymorphism and distribution of cytoplasmic organelles in the two cell lines are summarized in Table 1.

Ultrastructural features and proteolytic activity of T84- and T84SF-released vesicles

The most striking characteristic of T84SF was the amount of vesicles shed from the plasma membrane and also found in the peripheral cytoplasm (Figs. 2d and 3a). As shown in Fig. 3b, purified vesicles analyzed by TEM with negative staining appeared homogeneous in form, with a roughly spherical shape and a size ranging between 90 and 140 nm. No morphological differences between the vesicles collected by the two cancer cell lines were observed by ultrastructural analysis, although T84SF cell consistently released a greater amount of vesicles compared to T84 parental cells.

The presence of matrix metalloproteinases in T84 and T84SF vesicles was analyzed by gelatin zymography (Fig. 4) to assess whether the invasive nature of the T84SF cells was correlated with an increased release of vesicle-

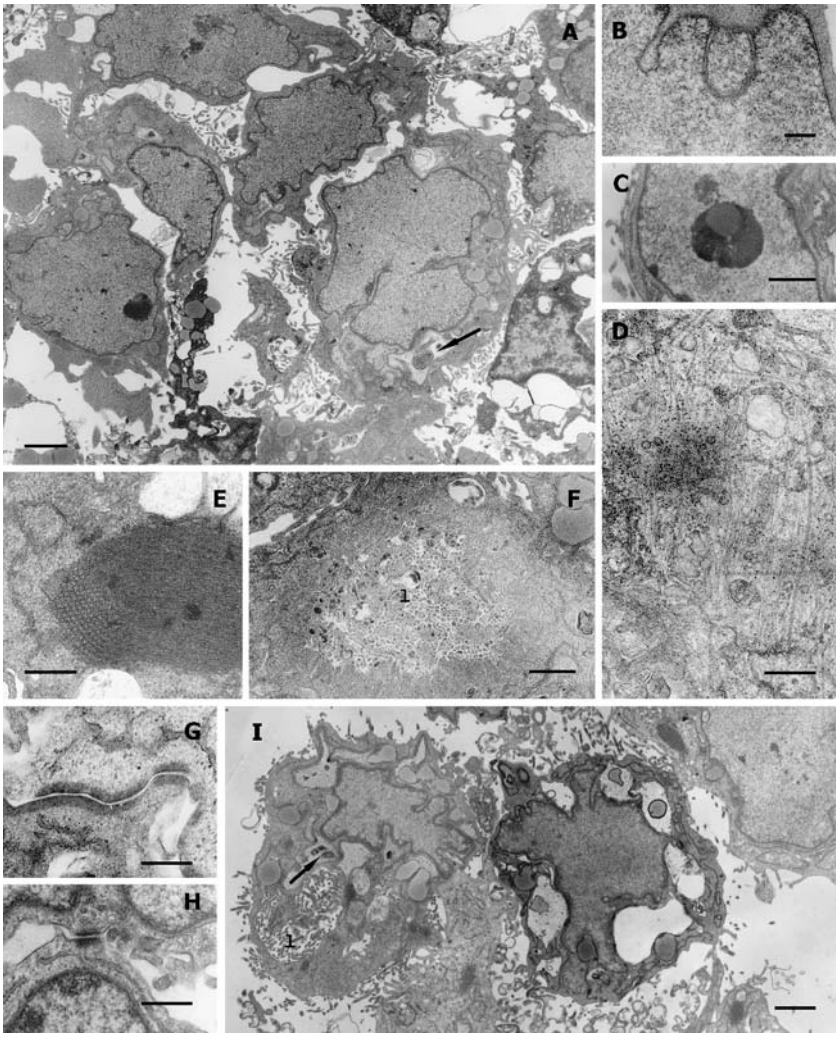

Fig. 2 TEM view of T84SF cells. Neoplastic cells present irregularity in size and shape, different cell projections and abundant microvilli, well-demarcated enlarged nuclei often irregular in shape, and prominent nucleoli (**a**,**c**). Nuclear pockets can be observed (**b**). In the cytoplasm, lipid droplets, electron-lucent cleft-like spaces (**a**,**i**), microfilament bundles, microtubuli (**d**) and some myelin figures can be observed (*arrows*) (**a**,**i**). Details of junctional complexes and desmosomes between lateral membranes are shown in **g** and **h**; intracellular lumina, where numerous microvilli are projecting into the lumen, can be clearly seen (**f**,**i**). Figure **e** shows a detail of a cytoplasmic paracrystalline inclusion. *Scale bars* 2 μm (**a**), 1 μm (**c**,**f**,**i**), 0.5 μm (**b**,**d**), 0.4 μm (**e**,**g**,**h**). *l* Lumen

Table 1 Evaluation of noteworthy ultrastructural features

	Cellular polymorphism				Nuclear polymorphism			Cell membranes structures		
	Size	Shape	Nucleus-to-cytoplasm ratio	Cytoplasmic organelles	Nucleolus	Nuclear membrane	Chromatin	Cell junctions	Interdigitations	Microvilli
T84	Homogeneous	Spindle or polygonal	High	Mitochondria +++ RER++ Free ribosomes ++ Glycogen granules ++ Lipid droplets ++ Vesicles + Intracellular lumina —	One or two round	Regular profile	Homogeneous, well-preserved euchromatin	++	+	++
T84SF	Heterogeneous	Irregular	High	Mitochondria + RER ++ Free ribosomes ++ Glycogen granules ++ Lipid droplets +++ Vesicles +++ Intracellular lumina +++	One or two, irregular	Indented profile and invaginations	Peripheral heterochromatin often in blocks	+++	+++	+++

+++ Well-represented, ++ moderately represented, + poorly represented, — Not observed

Fig. 3 Micrograph **a** illustrates the numerous vesicles released from the surface of T84SF tumour cells. Microvesicles were isolated from cell-free supernatants of tumour cells and observed also by electron microscope with negative staining (**b**). *Scale bars* 1 μm (**a**), 0.1 μm (**b**)

associated gelatinases with respect to T84 parental cells. Since the enzymatic forms observed by zymographic analysis show a lower molecular weight than the proMMP-9 and proMMP-2 standards, we may hypothesize that the activated forms of gelatinases are selectively restricted in vesicles. In addition, unidentified bands with a molecular weight of more than 200 kDa were also detected.

Analysis of signaling pathways in T84 and T84SF cells

To verify if T84 and T84SF cells were characterized by different signaling pathways, we looked at both basal signal transduction pathways and more specific cellular signaling involved in cell proliferation and survival. Immunofluorescence analysis, with a monoclonal antibody that specifically recognizes phosphorylated tyrosine residues, allowed to detect changes in global cellular tyrosine phosphorylation. As shown in Fig. 5a, the two cell lines

Fig. 4 Zymographic analysis of T84 and T84SF vesicles-associated gelatinases. Cell culture media from human fibroblasts treated with TPA was used as a standard for proMMP-2 and proMMP-9 (STD). Only activated forms of MMP-2 could be detected in vesicles-derived samples, although no quantitative differences were observed between the two cell lines

displayed a different basal intensity and localization of tyrosine-phosphorylated proteins.

Since several reports have indicated activation of extracellular signal-regulated kinase (ERK) in several human cancer cell lines, including colon cancer cell lines [34, 50], we next examined whether the basal ERK signaling pathway was differentially activated in T84SF selected cells compared to T84 parental cells. To determine whether ERK was activated, T84 and T84SF cells were cultured up to 60% of confluence; whole cell extracts were prepared and immunoblotted with antibodies specifically recognizing the phosphorylated and active forms of ERK1/2. Figure 5b shows the almost exclusive phosphorylation of ERK1/2 in T84SF cells compared to parental cells (upper panel). Total ERK proteins showed a slight increase of 15% in T84SF cells with respect to T84 cells (Fig. 5b, lower panel).

Another critical intracellular signaling, often deregulated in various human malignancies, is the AKT/PKB signal transduction pathway that is involved in the regulation of cell survival [20]. Our Western blot analysis, using antibodies against the phosphorylated and active forms of AKT, shows a 20% increase of the phosphorylated form of AKT in T84SF cells compared to the parental cells (Fig. 5c, upper panel). The amount of total AKT did not change between the two cell lines (Fig. 5c, lower panel).

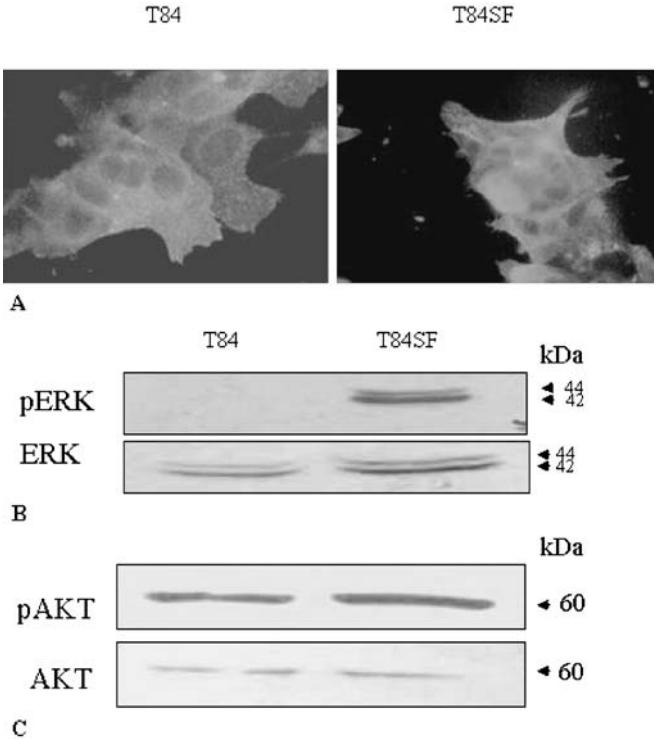

Fig. 5 Analysis of proteins involved in signalling pathways of T84 and T84SF cells. **a** Immunofluorescence analysis of tyrosine phosphorylated proteins in T84 parental and selected cells shows a clear difference in the intensity and localization of **b** Western blot analysis of phospho ERK1/2 (*upper panel*) and total ERK1/2 (*lower panel*) in T84 and T84SF cells. One hundred micrograms of cell lysates was loaded for both T84 and T84SF cells. The Western blot results presented are representative of at least three different experiments

Ultrastructural analysis of lung metastasis

Electron microscopy analysis of the tumor T84 and T84SF cells in athymic mice confirmed the histological aspects of colon carcinoma metastatic foci and added several ultrastructural details on differentiative features of colon histological organization (Fig. 6).

T84SF carcinoma cells formed cellular nests consisting of closely apposed oval cells with large, centrally located nuclei; these showed oval or irregular shape and they were frequently indented. The cells exhibited high nuclear-to-cytoplasmic ratios, with one or two nucleoli sometimes marginally attached to the nuclear profiles, and the chromatin was visible as distinct amount of peripheral heterochromatin (Fig. 6a,b). Some cells showed a columnar shape forming a tubular atypical gland (Fig. 6b); small nodular aggregates with a well-developed basal lamina at the base could be seen inside a larger one (Fig. 6c). In metastatic foci formed by T84SF cells, the cell borders were in contact with each other (Fig. 6a,c), while in T84 cells there was ultrastructural discontinuity with pericellular space or gaps between adjacent cells (Fig. 6d,e). However, in both cell types, the apico-lateral junctional complexes between adjacent cells were well-developed; tight junctions, intermediate junctions, and desmosomes were frequently formed (Fig. 7a–c).

Several peculiar aspects indicative of glandular epithelial differentiation were observed in metastasis formed by T84 parental and T84SF selected cells. The presence of numerous intercellular lumina, lined by junctions, could be frequently detected (Fig. 7b,c). On the luminal surface, the apical portion of the cells showed well-developed microvilli with a central core of filaments (Fig. 7b–d). Sometimes microvilli presented a covering of glycocalyceal bodies or filaments and granules (Fig. 7b,c); sometimes interdigitating microvilli were observed deeply indenting the adjacent cell membrane, and apical protrusions like bleb or blunt pseudopod-like projections could be seen on the cell surface (Fig. 7e,h,i). Intercellular lumina were of different sizes, sometimes too small to be easily recognized, sometimes so large to contain cellular debris and cellular remnants or whole cells (Fig. 7c). The luminal space was filled with a large variety of structures like flocculent and secretory materials and particles (Fig. 7b,c). Microvilli were also observed at the surface of intracytoplasmic lumen found entirely within a single cell (Fig. 8b).

The cells contained abundant mature organelles, such as Golgi complex, rough endoplasmic reticulum, and numerous free ribosomes throughout the cytoplasm; numerous round mitochondria with transverse parallel cristae occupied over 60% of the cytoplasm; however, they appeared poorly preserved (note washed-out matrix) (Fig. 7f).

Dense core granules, vesicles, multivesicular bodies, lysosome-like structures, and lamellar bodies were also present (Fig. 7f,g).

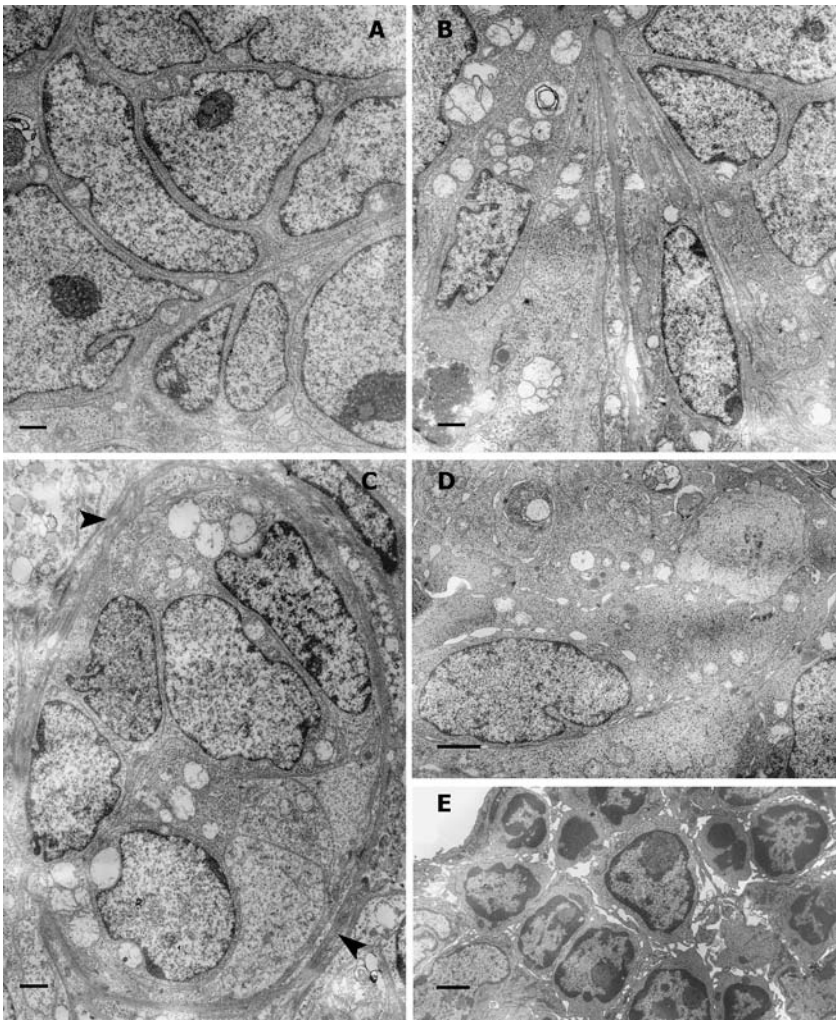

Fig. 6 Lower power view of metastasis foci observed in the lung of athymic nude mice injected with T84SF (**a**,**b**,**c**) or T84 cells (**d**,**e**). T84SF tumor cells are closely attached to each other and can have a columnar shape; widening of the intercellular spaces can be observed between T84 cells. A small confined nodular aggregate, delimited by an evident basal lamina (*arrowheads*), is shown inside a metastatic nest (**c**). *Scale bars* 1 μm (**a**,**b**,**c**), 2 μm (**d**,**e**)

Both in the T84 and T84SF foci, cells in division could be observed at different phases, but the number of mitotic figures observed was increased in the T84SF cell line; desmosomal junctions were maintained in rounded tumor cells during mitosis (Fig. 8a).

The most notable difference found between the two carcinoma cells was the occurrence of centrosomal amplification; T84SF cells displayed abnormality including supernumerary centrioles that were, in fact, observed loosely dispersed in the cytoplasm during interphase (Fig. 8b).

E-cadherin and β-catenin expression in T84 and T84SF cell lines

Next, we analyzed whether the observed histopathological patterns of tumor growth were accompanied by in vitro alterations in the expression patterns and localizations of two important molecules involved in cell–cell adhesion: E-cadherin and β-catenin. Figure 9a,b shows a reduction of E-cadherin expression in T84SF cells compared to parental cells both at RNA and protein levels, as evidenced by reverse transcription-polymerase chain reaction (RT-PCR) semiquantitative and Western blot analyses, respectively. When we determined the levels of β-catenin in the two cell lines, we found a less significant reduction of protein expression in T84SF cells with respect to the parental cells (Fig. 9c), whereas there was a clear difference in the cellular localization. Confocal images show a distinct membranous β-catenin staining of T84 cells, while a cytoplasmic and nuclear localization was observed in selected T84SF cells (Fig. 9d).

Bcl-X_L expression in T84-and T84SF-derived metastasis and in vitro cell cultures

To assess the expression of Bcl-X_L in parental and selected T84 cells, we next carried out a comparative analyses at both mRNA and protein levels. As shown in Fig. 10a, the RT-PCR semiquantitative analysis showed a higher Bcl-X_L mRNA level in T84SF than in T84 cells. Moreover, Western blot analysis revealed that expression of Bcl-X_L protein was also markedly increased in metastatic T84SF cells compared with parental cells (Fig. 10b). To confirm

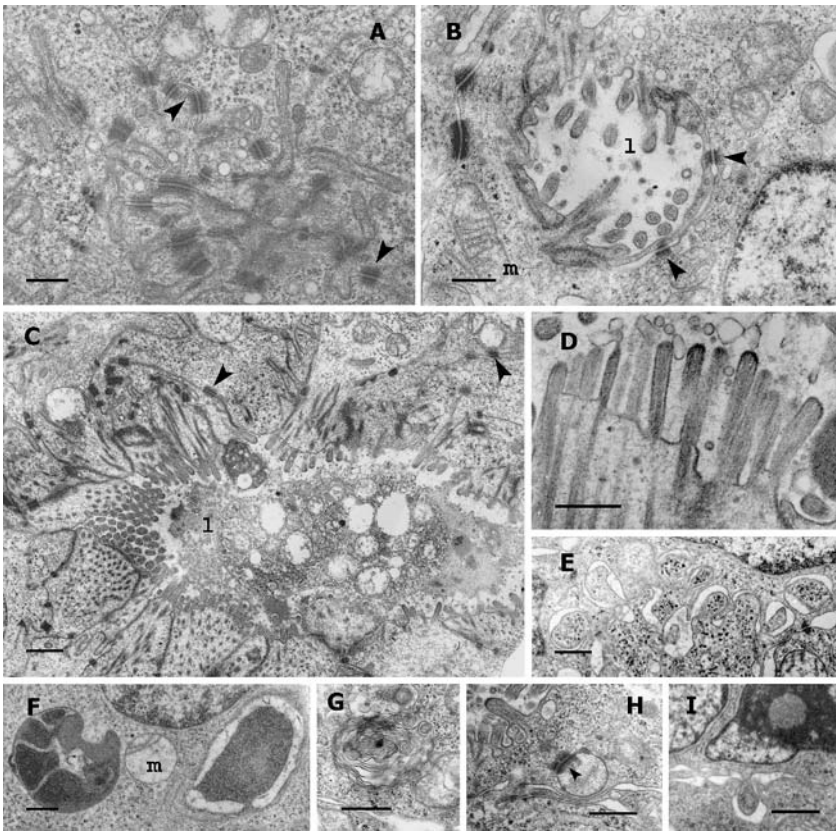

Fig. 7 Representative transmission electron micrographs of the cancer cells in the nests. Cells frequently form intercellular lumina that are sealed by specialized junctions and, frequently, desmosomes (*arrowheads*) tether the plasma membranes (**a**,**b**,**c**,**e**,**h**). The cell membranes can be seen forming numerous folds and invaginations or tiny processes that deeply indent the cytoplasm (**e**,**h**,**i**). Long microvilli project into the luminal surface of tumor cells (**b**,**c**); a high-power view of microvilli with a core of microfilaments is shown in **d**. Figure **c** shows a lumen with a large remnant of cells. Membrane-bound dense granules, mitochondria (**f**), and myelin figures (**g**) can be also observed. *m* Mitochondria, *l* lumen. *Scale bars* 1 μm (**c**,**e**), 0.5 μm (**a**,**b**,**d**,**f**–**i**)

these results, we performed an immunohistochemical staining of Bcl-X_L protein on the two cell lines and on corresponding lung metastatic foci. Figure 11a,b illustrates the Bcl-X_L staining patterns on cultured cells and tissue sections, respectively. The images show a higher Bcl-X_L expression in T84SF cells and related metastasis compared to the parental T84 cell line and tissues, in which a weak immunoreactivity was observed. To further validate the reduced susceptibility of T84SF colon cancer cells to apoptosis, we analyzed the levels of one of the main apoptosis effectors, caspase-3. Western blot analysis showed a 35% decrease of caspase-3 in selected cells compared to parental T84 cells (Fig. 10c).

Discussion

The establishment and thorough characterization of cancer cell lines derived from experimental in vitro or in vivo selections allow the development of new approaches to understand specific steps of tumor progression and metastasis formation. We recently established a new metastasis model by selecting a colon cancer cell line (T84SF) through repeated cycles of adhesion to E-selectin expressing endothelial cells (EC). This cell line represents a good working model to investigate tumor–EC interactions during metastasis because it shows increased growth rate, chemoinvasivity, MMP production, diminished apoptosis,

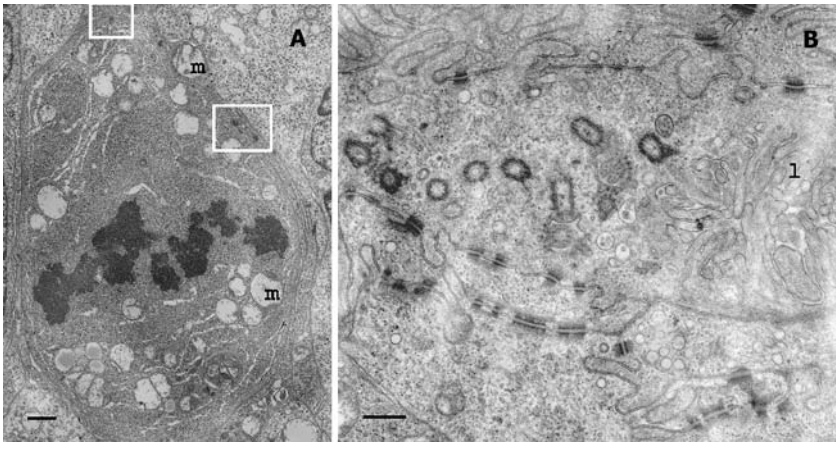

Fig. 8 Mitotic figure in thin section of tumor cells in metastatic foci (**a**). The cell has a typical metaphase plate and a bipolar spindle; it maintains desmosomal junctions (*framed area*) with the other cells. Supernumerary centrioles in metastatic T84SF cell (**b**); at least ten centrioles can be observed. Note an intracellular lumen with well-developed microvilli. *Scale bars* 1 μm (**a**), 0.5 μm (**b**). *l* Lumen, *m* mitochondria

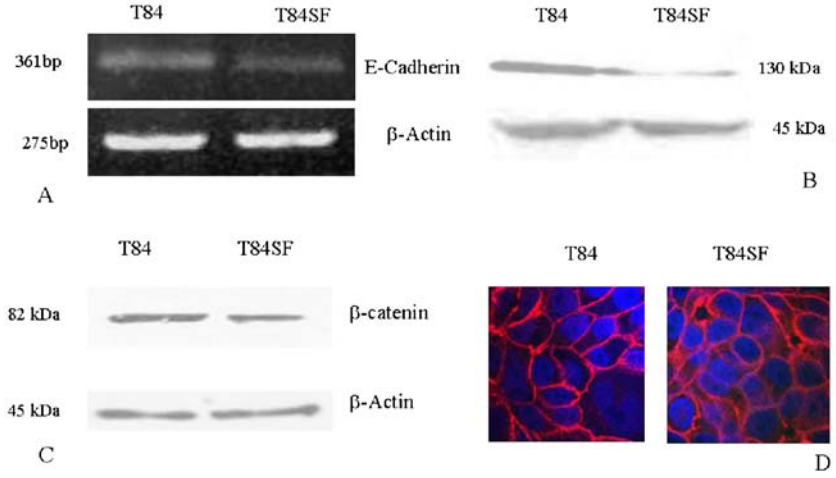

Fig. 9 E-cadherin expression and β-catenin localization. **a** Semi-quantitative RT-PCR of E-cadherin and actin used as standard (*lowerpanel*). **b** Western blot analysis for evaluation of E-cadherin protein expression. **c** Western blot analysis for evaluation of β-catenin and actin protein evaluation, *upper* and *lowerpanels*, respectively. Fifty micrograms of cell lysates was loaded for both T84 and T84SF cells. These results are representative of at least three different experiments. **d** Confocal laser scanning microscopy showing staining for β-catenin. Note that in T84SF cells, β-catenin is cytoplasmic and weakly nuclear, while in T84 cells, β-catenin is markedly localized at the cell membrane

as well as a higher number of metastasis in nude mice compared to parental cells [4]. It has been reported that specific changes indicative of cancer process can be correlated with morphology, such as anchorage independent growth, invasiveness ability, and tumorigenicity [9, 29, 43]. The purpose of this work was to further detail our characterization of T84 and T84SF cells by adding an ultrastructural approach together with a biochemical investigation of molecular players involved in the higher invasive and metastatic phenotype of selected cells.

Comparison between the parental T84 colon cancer cells and the T84SF cells using transmission electron microscopy evidenced a greater complexity in selected cells as denoted by a marked pleomorphism of cell size and nuclei, shape, adhesion structures, and greater surface complexity. These morphological features were previously correlated with a greater metastatic potential in characterized cell lines such as 8701 BC, MCF-7, and others [3, 9, 43].

T84SF cells exhibited, with respect to parental cells, numerous branched and randomly oriented protrusions, as well as a greater amount of microvilli of different size and shapes. Changes in the plasma membrane are probably of unique importance in the manifestation of several properties of metastatic phenotype. The functional significance of microvillous projections and blebs is poorly understood, but the variety of molecules found on such projections suggests a role in cell–cell interactions [5, 11, 16]. Several authors have shown that immortalized or transformed tumorigenic cell lines exhibited an increased number of microvillous projections compared with normal cells, and they also suggested that such projections may represent a morphological marker of neoplastic transformation [10, 30, 36, 47, 48].

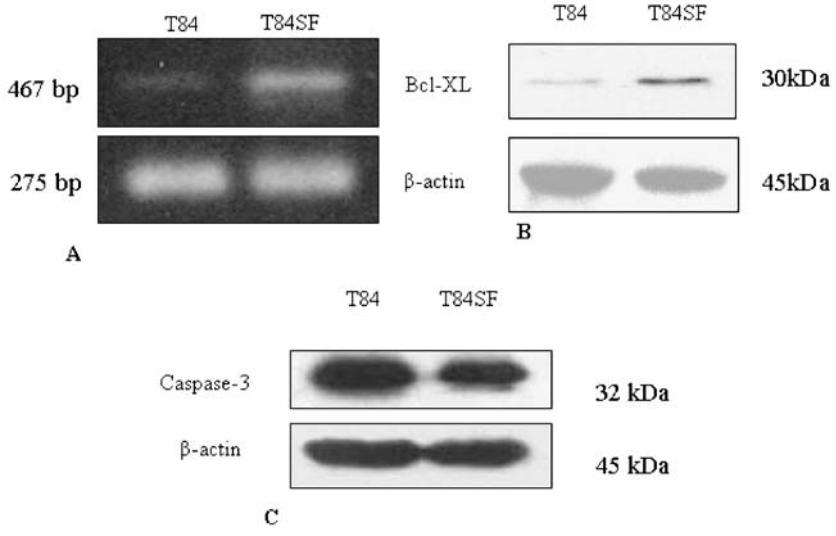

Fig. 10 Analyses of Bcl-X_L and caspase 3 expression in T84 and T84SF cells. **a** Semi-quantitative RT-PCR of Bcl-X_L and actin used as standard (*lowerpanel*). **b** Western blot analysis for evaluation of Bcl-X_L protein expression. Fifty microgram of cell lysate was loaded for both T84 and T84SF cells. This result is representative of at least three different experiments. **c** Lysates from T84 and T84SF cells were evaluated for caspase 3 expression by Western blot analysis. A 30% decrease in the amount of this apoptotic effector was observed in T84SF cells compared to parental ones

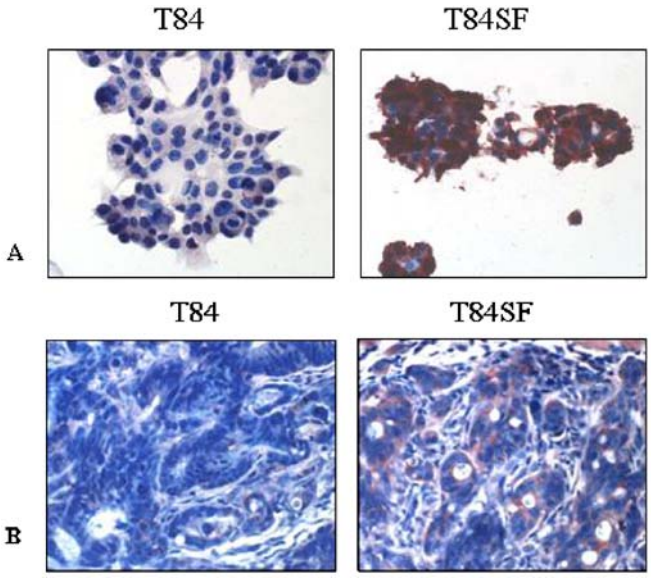

Fig. 11 **a** Immunohistochemical staining of Bcl-X_L on the two cell lines and **b** on corresponding lung metastatic foci

T84 cells have been shown to keep in culture several differentiated traits such as the ability to form functional tight junctions and desmosomes [35]. Our results confirm and extend these observations on samples derived from metastases formed by i.v. injection of cells in nude mice vein tail. Both cell lines produced multicellular aggregates displaying an acinar organization with well-developed apico-lateral junctional complexes. The metastases of colorectal adenocarcinomas often show histopathological features of the primary tumor and exhibit well-organized epithelial structures despite the acquisition of invasive properties and mesenchyme-like phenotypes during tumor progression. Such observations suggest that neoplastic cells may recover, probably influenced by local microenvironment, the same differentiated epithelial growth patterns characteristics of primary site [8].

In this scenario, the presence of regular junctional complexes in T84SF selected cells, although it may look incongruous with the more malignant phenotype of these cells, finds (1) a rationale in the procedure we adopted to select the cells and (2) confirmation from data obtained by other groups.

It is well-known that modifications in cancer cell adhesion play an important role in tumor progression, invasiveness, and metastasis [31]. Initially, a decrease in homotypic and heterotypic cancer cell adhesion, caused by the reduced expression of adhesion molecules and elevated activity of proteases including numerous metalloproteinases, promotes their escape from the primary tumor and intravasation [37]. During post-intravasation steps, however, the increased ability of blood-borne metastatic cells to form new heterotypic and homotypic adhesive interactions could be critically important for establishing secondary lesions in distant tissues and organs [42]. In several different types of cancer, the in vivo selection of tumor cells for high metastatic potential resulted in a selection of malignant cells exhibiting increased homotypic aggregation properties [2, 22]. In addition, cancer cell lines selected in vitro for enhanced homotypic aggregation kinetics demonstrated significantly higher in vivo experimental metastatic potential than parental cells [54]. An intriguing finding is the different cellular localization of β-catenin concomitant to a loss of plasma membrane-associated E-cadherin in T84SF cells compared to the parental T84 cells. A number of evidences show that delocalization of β-catenin is involved in tumor progression, and nuclear β-catenin may regulate target genes, such as matrilysin, CD44, uPAR, and fibronectin [27]. Qi et al. [45] recently showed that during transendothelial migration of melanoma cells, Src activation leads to the phosphorylation of N-cadherin and subsequent dissociation of β-catenin. It is interesting to note that we previously demonstrated that T84SF cells have an increased Src activity and our present data on cytoplasmic and nuclear localization of β-catenin fit well with the possibility of this protein having a role in transendothelial migration of colon cancer cells. Therefore, our data strengthen the evidence that metastatic cells are able to modulate adhesive abilities during tumor progression, thus representing a facilitator mechanism in metastasis formation.

We have previously demonstrated a marked difference in the tumorigenicity and metastasis formation of T84 and T84SF cells [4]. T84SF cells have been shown having a higher growth rate in vitro than T84 parental cells. This is consistent with our ultrastructural observations of an increased number of mitotic figures, as well as of supernumerary centrioles in metastatic foci formed by T84SF cells. It is intriguing that amplification of the centrosome has been found in numerous forms of cancers [56]. This higher proliferation rate is associated with a decrease in apoptosis and related with an in vitro and in vivo augment of anti-apoptotic molecules such as Bcl-X_L. Aberration in regulation of apoptosis has been recognized as an important mechanism in oncogenesis and tumor progression [24]. Different authors have evidenced that Bcl-X_L overexpression may enhance metastatic potential by counteracting the proapoptotic signals in the microenvironment, thus favoring the successful development of metastasis in specific organs [17, 38]. We demonstrated that T84SF cells express, at mRNA and protein levels, both in vitro and in lung metastatic foci a greater amount of Bcl-X_L compared to T84 parental cells. It is known that the expression of Bcl-X_L prevents the redistribution of cytochrome c from mitochondria to cytosol, a prominent requisite for caspase activation and apoptosis [33]. In accordance, we found a decreased amount of caspase-3 in T84SF cells with respect to the parental cells. Our results stress the involvement of Bcl-X_L in metastasis formation pointing to a role of the interaction of cancer cell to endothelial cells in the modulation of anti-apoptotic molecules.

Another ultrastructural feature we observed by analysis of T84 and T84SF cancer cells was the striking surface activity in T84 selected cells as testified by the release of membrane vesicles. The release of vesicles from living cells is considered to be a normal physiological process,

but it is particularly active in proliferating cells, such as cancer cells where it can occur continuously, and is often related to enhanced proteolytic activity [55]. It is well-established that tumor cells use proteolytic activity to modify their environment; these enzymes may include tumor cell surface molecules or soluble molecules [15]. Proteases such as MMP-2, MMP-9, and u-PA were shown to play an active role in colon cancer invasion and metastasis [40]; positivity for MMP-2 expression was found more frequently in colon carcinoma with a more aggressive phenotype [39]. Previous investigations have demonstrated the presence of these molecules in membrane vesicles shed from different tumor cell lines, including melanoma, breast, ovarian, and fibrosarcoma cancer cell lines, while few information are available in colon cancer cell lines [13, 14, 21, 53]. Although the process of shedding remains unclear, it has been associated with the release of growth factors, tumor antigens, increased cellular invasiveness, and suppression of immune surveillance. It is interesting to note that the present data show the presence of lytic bands likely corresponding to the activated forms of MMP-2 and MMP-9 in vesicles of both T84 and T84SF cells. These results fit well with the specific role described for vesicles in proliferating and invasive cancer cells [6]. We have previously reported that the increased invasiveness of T84SF cells was associated to a higher MMP-2 lytic activity than in parental cells. We believe that the major amount of vesicles shed by T84SF cells may explain the invasive phenotype of these cells. Moreover, to better understand the molecular events regulating the invasiveness of T84SF cells, we should investigate the role of other enzymes involved in extracellular matrix degradation such as other MMPs (stromalisin, matrilysin) or serine proteases.

To examine the cellular signaling underlying the phenotypic modifications evidenced in T84SF cells, we studied different interconnected cellular signaling known to be involved at various levels in cell proliferation and survival: protein tyrosine phosphorylation, MAPK, and AKT activation. The level of phosphorylation within a cell is a reflection of the balance between kinase and phosphatase activities. It is now well-established that tyrosine kinases play a central role in signal transduction, acting as relay points for a complex network of interdependent signaling molecules that ultimately lead to dramatic changes in tumor growth and survival, development, and metastasis [7]. Many growth factors have been reported to modulate metastasis-related phenotypes through the activation of receptor tyrosine kinase involving Ras/MAPK signal pathway [28]. A vast body of literature has documented the involvement of the AKT kinase as a final effector in the modulation of cell survival [20]. The complex nature of these interactions continues to be a challenge for the cancer biologist. Proper dissection and analysis of all these signaling systems hold the key for elucidating which target molecules are the most credible for the design of future successful therapeutics. The present data demonstrate the following: (1) T84SF cells undergo an increase in cytoplasmic and nuclear tyrosine-phosphorylated proteins, as shown by immunofluorescence analysis; (2) a striking difference in ERK 1/2 phosphorylation between parental and selected cells; and (3) a 20% increase in AKT phosphorylation in T84SF cells compared to T84 cells.

Abdel-Ghany et al. [1] have proven that, in a model of lung colonization by B16-F10 cells, the interaction of cancer cells to the endothelium is mediated by β4 integrin ligation to the lung endothelial Ca^{2+}-activated chloride channel protein CLCA1, and that this interaction leads to the activation of downstream signaling to extracellular signal-regulated kinase. It has been reported that the activation of the ERK1/2 pathway in hematopoietic cells leads to transcriptional activation of AP-1 and AP-1-dependent Bcl-X_L gene expression [52], while inhibition of ERK1/2 causes downregulation of Bcl-family proteins in human intestinal epithelial cells [26]. In a similar model of cells derived by colon mucosa, Sanders and Basson [49] showed that the collagen-mediated spreading and migration functions were dependent on ERK activation and that phosphorylation of ERK 1/2 required Src activity, thus suggesting that ERK is downstream of Src-mediated signaling pathway. Our present data show an increased ERK phosphorylation in T84SF cells compared to T84 parental cells. We previously demonstrated that the expression of the metastatic phenotype is correlated in T84SF cells with an augmentation of Src activity. Further work is necessary to investigate the correct correlation of these two pathways during transendothelial colon cancer migration.

AKT regulates a number of critical cellular pathways, including those leading to cellular proliferation and inhibition of apoptosis [20]. The survival signals of AKT upon its phosphorylation and activation are mediated in part via identified downstream targets of this kinase. Phosphorylation of BAD, Caspase 9, and Forkhead transcription factor by AKT suppresses the proapoptotic function of these proteins. Sekharam et al. [51] demonstrated that overexpression in colon cancer cells of insulin-like growth factor 1 and insulin-like growth factor 1 receptor causes the activation of AKT and upregulation at the transcriptional level of Bcl-X_L, with a consequent increase in expression of Bcl-X_L protein. We have found a 20% increase in AKT phosphorylation in T84SF cells compared to the parental cells. These data, together with our results on Bcl-X_L expression, increased ERK activation and β-catenin localization bring us to speculate that our selection procedure has determined the isolation of a clone with specific overexpressed signaling pathways leading to the expression of a metastatic phenotype. Further work is in progress to identify the molecules whose levels in tyrosine phosphorylation are modulated in T84SF cells and the specific processes affected by these important signaling pathways.

In conclusion, our findings indicate that appropriate phenotypic features and critical cellular signaling have been retained by T84 parental and T84SF selected cells despite long-term culture in vitro and the selection procedure.

These cell lines therefore represent a step forward in the development of appropriate models in vitro and in vivo

to investigate the process of extravasation during colon cancer progression.

Acknowledgements This work was supported by grants from the Italian Ministero della Istruzione, della Università e della Ricerca Scientifica 60% (MIUR) to R.A, M.A.D, A.M.F and G.D.L and by the Associazione Italiana per la Ricerca sul Cancro (AIRC) to R.A and G.D.L.

We thank Prof. F. Aragona for helpful discussions on the ultrastructural pathology of metastatic colonies.

Riccardo Alessandro and Maria Antonietta Di Bella contributed equally to this work.

Francesca Damiani and Chiara Corrado are PhD students in Immunopharmacology at the University of Palermo.

References

1. Abdel-Ghany M, Cheng H, Elble R, Pauli B (2002) Focal adhesion kinase activated by B4 integrin ligation to mCLCA1 mediates early metastatic growth. J Biol Chem 277: 34391–34400 (Sep 13)
2. Al-Mehdi A, Tozawa K, Fisher A, Shientag L, Lee A, Muschel RJ (2000) Intravascular origin of metastasis from the proliferation of endothelium-attached tumor cells: a new model for metastasis. Nat Med 6:100–102
3. Alessandro R, Minafra S, Pucci-Minafra I, Onisto M, Garbisa S, Melchiori A, Tetlow L, Woolley D (1993) Metalloproteinase and TIMP expression by the human breast carcinoma cell line 8701-BC. Int J Cancer 55:250–255
4. Alessandro R, Flugy A, Russo D, Stassi G, De Leo A, Corrado C, Alaimo G, De Leo G (2005) Identification and phenotypic characterization of a subpopulation of T84 human colon cancer cells, after selection on activated endothelial cells. J Cell Physiol 203:261–272
5. Berlin C, Bargatze R, Campbell JJ, von Andrian U, Szabo M, Hasslen S, Nelson R, Berg E, Erlandsen S, Butcher E (1995) Alpha 4 integrins mediate lymphocyte attachment and rolling under physiologic flow. Cell 80:413–422
6. Black P (1980) Shedding from the cell surface of normal and cancer cells. Adv Cancer Res 1:75–197
7. Blume-Jensen P, Hunter T (2001) Oncogenic kinase signalling. Nature 411:355–365
8. Brabletz T, Jung A, Reu S, Porzner M, Hlubek F, Kunz-Schughart L, Knuechel R, Kirchner T (2001) Variable beta-catenin expression in colorectal cancers indicates tumor progression driven by the tumor environment. Proc Natl Acad Sci USA 98:10356–10361
9. Calaf G, Russo J, Tait L, Estrad S, Alvarado ME (2000) Morphological phenotypes in neoplastic progression of human breast epithelial cells. J Submicrosc Cytol Pathol 32:83–96
10. Calaf G, Alvarado M, Hei T (2005) Beta catenin is associated with breast cancer progression in vitro. Int J Oncol 26:913–921
11. Carpen O, Pallai P, Staunton D, Springer T (1992) Association of intercellular adhesion molecule-1 (ICAM-1) with actin-containing cytoskeleton and alpha-actinin. J Cell Biol 118: 1223–1234
12. Dolo V, Pizzurro P, Ginestra A, Vittorelli M (1995) Inhibitory effects of vesicles shed by human breast carcinoma cells on lymphocyte 3H-thymidine incorporation, are neutralised by anti TGF-beta antibodies. J Submicrosc Cytol Pathol 27:535–541
13. Dolo V, Ginestra A, Cassara D, Violini S, Lucania G, Torrisi MR, Nagase H, Canevari S, Pavan A, Vittorelli ML (1998) Selective localization of matrix metalloproteinase 9, beta1 integrins, and human lymphocyte antigen class I molecules on membrane vesicles shed by 8701-BC breast carcinoma cells. Cancer Res 58:4468–4474
14. Dolo V, D'Ascenzo S, Violini S, Pompucci L, Festuccia C, Ginestra A, Vittorelli, M, Canevari S, Pavan A (1999) Matrix-degrading proteinases are shed in membrane vesicles by ovarian cancer cells in vivo and in vitro. Clin Exp Metastasis 17:131–140
15. Egeblad M, Werb Z (2002) New functions for the matrix metalloproteinases in cancer progression. Nat Rev Cancer 2: 161–174
16. Erlandsen S, Hasslen S, Nelson R (1993) Detection and spatial distribution of the beta 2 integrin (Mac-1) and L-selectin (LECAM-1) adherence receptors on human neutrophils by high-resolution field emission SEM. J Histochem Cytochem 41:327–333
17. Espana L, Fernandez Y, Rubio N, Torregrosa A, Blanco J, Sierra A (2004) Overexpression of Bcl-xL in human breast cancer cells enhances organ-selective lymph node metastasis. Breast Cancer Res Treat 87:33–44
18. Fidler I (1990) Critical factors in the biology of human cancer metastasis: twenty-eighth G.H.A. Clowes memorial award lecture. Cancer Res 50:6130–6138
19. Fidler I (2003) The pathogenesis of cancer metastasis: the 'seed and soil' hypothesis revisited. Nat Rev Cancer 3:453–458
20. Franke T, Kaplan D, Cantley L (1997) PI3K: downstream AKTion blocks apoptosis. Cell 88:435–437
21. Ginestra A, La Placa M, Saladino F, Cassara D, Nagase H, Vittorelli M (1998) The amount and proteolytic content of vesicles shed by human cancer cell lines correlates with their in vitro invasiveness. Anticancer Res 18:3433–3437
22. Glinsky V, Glinsky G, Rittenhouse-Olsen K, Huflejt M, Glinskii O, Deutscher S, Quinn T (2001) The role of Thomsen–Friedenreich antigen in adhesion of human breast and prostate cancer cells to the endothelium. Cancer Res 61: 4851–4857
23. Graves L, Ariztia E, Navari J, Matzel H, Stack M, Fishman D (2004) Proinvasive properties of ovarian cancer ascites-derived membrane vesicles. Cancer Res 64:7045–7049
24. Hanahan D, Weinberg R (2000) The hallmarks of cancer. Cell 100:57–70
25. Harada K, Nishizaki T, Ozaki S, Kubota H, Ito H, Sasaki K (1998) Intratumoral cytogenetic heterogeneity detected by comparative genomic hybridization and laser scanning cytometry in human gliomas. Cancer Res 58:4694–4700
26. Harnois C, Demers M, Bouchard V, Vallee K, Gagne D, Fujita N, Tsuruo T, Vezina A, Beaulieu J, Cote A, Vachon P (2004) Human intestinal epithelial crypt cell survival and death: Complex modulations of Bcl-2 homologs by Fak, PI3-K/Akt-1, MEK/Erk, and p38 signalling pathways. J Cell Physiol 198: 209–222
27. Harris T, Peifer M (2005) Decisions, decisions: beta-catenin chooses between adhesion and transcription. Trends Cell Biol 15:234–247
28. Hartmann G, Weidner K, Schwarz H, Birchmeier W (1994) The motility signal of scatter factor/hepatocyte growth factor mediated through the receptor tyrosine kinase met requires intracellular action of Ras. J Biol Chem 269(35):21936–21939
29. Hewitt RE, McMarlin A, Kleiner D, Wersto R, Martin P, Tsokos M, Stamp GW, Stetler-Stevenson WG (2000) Validation of a model of colon cancer progression. J Pathol 192:446–454
30. Jackson S, Strausbauch P, Finley J, Laich D, Hewan-Lowe K (2003) Desmosomes and microvilli mean a lot: diagnosis of neoplasms of unknown origin using electron microscopy. Ultrastruct Pathol 27:155–161
31. Jothy S, Munro S, LeDuy L, McClure D, Blaschuk O (1995) Adhesion or anti-adhesion in cancer: what matters more? Cancer Metastasis Rev 14:363–376
32. Kim J, Wieckowski E, Taylor D, Reichert T, Watkins S, Whiteside T (2005) Fas ligand-positive membranous vesicles isolated from sera of patients with oral cancer induce apoptosis of activated T lymphocytes. Clin Cancer Res 11:1010–1020
33. Kluck R, Bossy-Wetzel E, Green D, Newmeyer D (1997) The release of cytochrome c from mitochondria: a primary site for Bcl-2 regulation of apoptosis. Science 275:1132–1136

34. Laferriere J, Houle F, Huot J (2004) Adhesion of HT-29 colon carcinoma cells to endothelial cells requires sequential events involving E-selectin and integrin beta4. Clin Exp Metastasis 21:257–264
35. Liu Y, Nusrat A, Schnell FJ, Reaves TA, Walsh S, Pochet M, Parkos CA (2000) Human junction adhesion molecule regulates tight junction resealing in epithelia. J Cell Sci 113(Pt 13): 2363–2374 (July)
36. Malick L, Langenbach R (1976) Scanning electron microscopy of in vitro chemically transformed mouse embryo cells. J Cell Biol 68:654–664
37. Martin G (2003) Cell signalling and cancer. Cancer Cell 4: 167–174
38. Martin S, Ridgeway A, Pinkas J, Lu Y, Reginato M, Koh E, Michelman M, Daley G, Brugge J, Leder P (2004) A cytoskeleton-based functional genetic screen identifies Bcl-xL as an enhancer of metastasis, but not primary tumor growth. Oncogene 23:4641–4645 (Jun 3)
39. Matsuyama Y, Takao S, Aikou T (2002) Comparison of matrix metalloproteinase expression between primary tumors with or without liver metastasis in pancreatic and colorectal carcinomas. J Surg Oncol 80:105–110
40. Mook O, Frederiks W, Van Noorden C (2004) The role of gelatinases in colorectal cancer progression and metastasis. Biochim Biophys Acta 1705:69–89
41. Nicolson G, Menter D, Herrmann J, Yun Z, Cavanaugh P, Marchetti D (1996) Brain metastasis: role of trophic, autocrine, and paracrine factors in tumor invasion and colonization of the central nervous system. Curr Top Microbiol Immunol 213: 89–115
42. Orr F, Wang H (2001) Tumor cell interactions with the microvasculature: a rate-limiting step in metastasis. Surg Oncol Clin N Am 10:357–381
43. Pucci-Minafra I, Minafra S, Alessandro R, Faccini AM (1989) An ultrastructural evaluation of cell heterogeneity in invasive ductal carcinomas of the human breast. II. An in vitro study. J Submicrosc Cytol Pathol 21:489–499
44. Putz E, Witter K, Offner S, Stosiek P, Zippelius A, Johnson J, Zahn R, Riethmuller G, Pantel K (1999) Phenotypic characteristics of cell lines derived from disseminated cancer cells in bone marrow of patients with solid epithelial tumors: establishment of working models for human micrometastases. Cancer Res 59:241–248
45. Qi J, Wang J, Romanyuk O, Siu C (2005) Involvement of Src family kinases in N-cadherin phosphorylation and {beta}-catenin dissociation during transendothelial migration of melanoma cells. Mol Biol Cell 17(3):1261–1272
46. Radinsky R (1995) Modulation of tumor cell gene expression and phenotype by the organ-specific metastatic environment. Cancer Metastasis Rev 14:323–338
47. Rovensky Y, Komissarova E, Topol L, Kisseljov F (1992) Changes in surface relief of suspended cells are morphological signs of the initial stage of neoplastic transformation in fibroblastic monolayer cultures. Cell Biol Int Rep 16:557–565 (Jun)
48. Russo J, Tait L, Russo I (1991) Morphological expression of cell transformation induced by c-Ha-ras oncogene in human breast epithelial cells. J Cell Sci 99(Pt 2):453–463 (Jun)
49. Sanders M, Basson M (2004) Collagen IV regulates Caco-2 migration and ERK activation via alpha1beta1- and alpha2beta1-integrin-dependent Src kinase activation. Am J Physiol Gastrointest Liver Physiol 286:G547–G557
50. Seddighzadeh M, Zhou J, Kronenwett U, Shoshan M, Auer G, Sten-Linder M, Wiman B, Linder S (1999) ERK signalling in metastatic human MDA-MB-231 breast carcinoma cells is adapted to obtain high urokinase expression and rapid cell proliferation. Clin Exp Metastasis 17:649–654
51. Sekharam M, Zhao H, Sun M, Fang Q, Zhang Q, Yuan Z, Dan H, Boulware D, Cheng J, Coppola D (2003) Insulin-like growth factor 1 receptor enhances invasion and induces resistance to apoptosis of colon cancer cells through the Akt/Bcl-x(L) pathway. Cancer Res 63:7708–7716
52. Sevilla L, Zaldumbide A, Pognonec P, Boulukos K (2001) Transcriptional regulation of the bcl-x gene encoding the anti-apoptotic Bcl-xL protein by Ets, Rel/NF-kB, STAT and AP-1 transcription factor families. Histol Histopathol 16:595–601
53. Taraboletti G, D'Ascenzo S, Borsotti P, Giavazzi R, Pavan A, Dolo V (2002) Shedding of the matrix metalloproteinases MMP-2, MMP-9, and MT1-MMP as membrane vesicle-associated components by endothelial cells. Am J Pathol 160: 673–680
54. Updyke T, Nicolson G (1986) Malignant melanoma cell lines selected in vitro for increased homotypic adhesion properties have increased experimental metastatic potential. Clin Exp Metastasis 4:273–284
55. Vittorelli M (2003) Shed membrane vesicles and clustering of membrane-bound proteolytic enzymes. Curr Top Dev Biol 54:411–432
56. Wang Q, Hirohashi Y, Furuuchi K, Zhao H, Liu Q, Zhang H, Murali R, Berezov A, Du X, Li B, Greene M (2004) The centrosome in normal and transformed cells. DNA Cell Biol 23:475–489
57. Wijnhoven B, Dinjens W, Pignatelli M (2000) E-cadherin-catenin cell–cell adhesion complex and human cancer. Br J Surg 87:992–1005

Virchows Arch (2006) 449: 62–68
DOI 10.1007/s00428-006-0222-5

ORIGINAL PAPER

An-Hang Yang · Chih-Wei Hsu · Jui-Yu Chen · Ling-Ming Tseng · Ging-Shing Won · Chen-Hsen Lee

Normocalcemic primary hyperparathyroidism in patients with recurrent kidney stones: pathological analysis of parathyroid glands

Received: 16 January 2006 / Accepted: 6 April 2006 / Published online: 3 May 2006
© Springer-Verlag 2006

Abstract The lack of overt elevation of serum calcium concentration in some patients suffering from primary hyperparathyroidism is an intriguing clinical phenomenon. Previous studies have substantiated abnormal parathyroid tissue in these patients, but the extent and mode of derangements remained largely undefined. The parathyroid tissues from patients of normocalcemic primary hyperparathyroidism (NCPHPT) and those having normal parathyroid glands, hypercalcemic primary hyperplasia, secondary hyperplasia, and adenoma were compared by undertaking quantitative immunohistochemistry analysis on tissue microarray. The statistic results suggested that the parathyroid tissue of NCPHPT approximates more to normal gland than to its counterpart in other groups of parathyroid proliferative diseases in terms of the lack of significant alterations of calcium-sensing receptor (CaSR), chromogranin A (CGA), parathyroid hormone (PTH), and proliferation index (Ki67). On the other hand, the depressed vitamin D receptor (VitDR) and elevated cyclin D1 (CyD1) of NCPHPT indicated the inherent functional abnormalities in parathyroid cells. Our results imply that inherent functional disengagement may exist between CaSR and CyD1 or between CaSR and VitDR or both in parathyroid cells of symptomatic NCPHPT. Lack of enhanced release of CGA and PTH and discordance between proliferative activity and CyD1 expression in parathyroid cells may further hinder the development of hypercalcemia.

Keywords Normocalcemia · Hyperparathyroidism · Immunohistochemistry · Nephrolithiasis

Abbreviations PHPT: Primary hyperparathyroidism · NCPHPT: Normocalcemic primary hyperparathyroidism · CaSR: Calcium-sensing receptor · CGA: Chromogranin A · PTH: Parathyroid hormone · VitDR: Vitamin D receptor · CyD1: Cyclin D1 · IDV: Integrated density value · ADV: Average density value

A.-H. Yang
Division of Ultrastructural and Molecular Pathology,
Department of Pathology, Taipei Veterans General Hospital,
Taipei, Taiwan

C.-W. Hsu · J.-Y. Chen · L.-M. Tseng · C.-H. Lee
Division of General Surgery, Department of Surgery,
Taipei Veterans General Hospital,
Taipei, Taiwan
e-mail: cwhsu3@vghtpe.gov.tw
e-mail: chenjy@vghtpe.gov.tw
e-mail: lmtseng@vghtpe.gov.tw

G.-S. Won
Division of Metabolism and Endocrinology,
Department of Medicine, Taipei Veterans General Hospital,
Taipei, Taiwan
e-mail: gswon@vghtpe.gov.tw

G.-S. Won
Department of Medicine, School of Medicine,
National Yang-Ming University,
Taipei, Taiwan

A.-H. Yang
Department of Pathology, School of Medicine,
National Yang-Ming University,
Taipei, Taiwan
e-mail: ahyang@vghtpe.gov.tw

C.-H. Lee (✉)
Department of Surgery, School of Medicine,
National Yang-Ming University,
Taipei, Taiwan
e-mail: chlee@vghtpe.gov.tw
Tel.: +886-2-28757555
Fax: +886-2-28757655

Introduction

The parathyroid gland plays a key role in the calcium homeostatic system by sensing fluctuations in extracellular calcium concentration and responding with rapid changes of parathyroid hormone. Regardless of the underlying causes, hyperparathyroid diseases are manifested by inappropriate secretion of parathyroid hormone (PTH). Except for the secondary hyperplasia and other rare situations, overproduction of PTH usually results in hypercalcemia, being asymptomatic or symptomatic. However, a significant fraction of the patients with primary

hyperparathyroidism (PHPT) can maintain a normal serum calcium concentration despite the primary increase in PTH secretion [17, 19]. They were categorized to the normocalcemic PHPT (NCPHPT) in the earlier studies mainly based on the normal total serum calcium concentration [11, 12, 14, 21, 24, 26, 27, 30], but various proportions of thus defined NCPHPT patients were later found to have persistent or intermittent elevation of ionized serum calcium [8, 17–20, 31]. However, still other patients exhibiting symptomatic PHPT maintained normocalcemia in terms of both ionizing and total serum calcium concentrations [19, 20]. The rationale behind symptomatic NCPHPT with both normal total and ionizing serum calcium is not completely elucidated [19, 20]. Previous studies inferred that the maintenance of normal serum calcium might be related to mild hypersecretion in PTH or the bone and kidney resistance to the PTH [8, 19]. The pathological examination of resected specimens from the patients with NCPHPT revealed adenomatous or hyperplastic process in parathyroid tissues despite that some glands were morphologically normal [14, 24, 26]. The assessments of calcium-sensing receptor (CaSR) expression, dose response-intracellular calcium concentration, and PTH release in the parathyroid tissue showed that the patients of NCPHPT shared the similar patterns, albeit less extensive, of functional derangement to those of hypercalcemic patients [17]. The ultrastructural study of normal-appearing parathyroid in NCPHPT also revealed the so-called "hyperfunctional changes" with increased cellular organelles, enhanced cell membrane complexity, and diminished intracellular fat [24]. Although these findings substantiate that parathyroid tissue of NCPHPT is indeed abnormal, the extent and mode of functional derangements remain largely undefined.

Materials and methods

Study cohort and clinicopathological definitions of parathyroid lesions

The parathyroid surgical specimens of formalin-fixed and paraffin-embedded tissue and histological slides of a total of 82 patients were retrieved from the pathology archive of Taipei Veterans General Hospital; the corresponding clinical data were also collected. These specimens included normal parathyroid tissue from 17 patients (group N), parathyroid adenoma from 15 patients (group A), primary diffuse hyperplasia from 16 patients (group PH), secondary hyperplasia from 14 patients (group SH), and parathyroid tissue of normocalcemic hyperparathyroidism from 20 patients (group NC). Group A, group SH, and group PH were collectively referred as proliferative group. Group N was defined as control group. The patients in group N were selected based on the normal histology of incidentally resected parathyroid gland from elective thyroid surgery; they showed neither preoperative episode of abnormal total serum calcium nor clinical evidence of urinary tract stone. Group NC consisted of the symptomatic patients who suffered from recurrent kidney stones but exhibited total and ionizing serum calcium concentration in the normal range. All patients in this group had intact serum PTH concentration above normal range on at least three occasions; they also lacked any known causes for secondary hyperparathyroidism such as impaired renal function. The patients who failed to achieve symptomatic relief after surgery were not included in this group. Group PH included the patients who not only had high serum calcium and PTH but also exhibited diffuse symmetric or asymmetric parathyroid gland hyperplasia involving at least two glands. The parathyroid lesions in this group lacked complete circumscription and showed lobular arrangement. Group SH was exclusively composed of the uremic patients who exhibited diffuse nodular hyperplasia involving all parathyroid glands. Group A included the patients with solitary parathyroid gland enlargement. The pathological features of parathyroid adenoma included distinct circumscribed lesion and lack of lobular pattern; a rim of normal-appearing or atrophic parathyroid tissue located immediately outside the adenomatous lesion was also counted as a pathological criterion of adenoma.

Preparation of tissue microarray and quantitative immunohistochemistry

The parathyroid tissue in each original paraffin block was mapped with reference of its corresponding histological slide. Two randomly sampled tissue cores 1. 2 mm in diameter from the defined area(s) of paraffin block(s) were obtained in each patient using a self-made hand punch. We then inserted the tissue cores to a predrilled multiwell (12×15 wells) recipient block to construct the tissue array. The loaded array block was mildly heated in a 40°C oven for 10 min and then subjected to routine process of paraffin section. The serial 6-μm sections were carefully transferred to the silane-coated microslides (Muto Glass, Muto Pure Chemicals, Japan). The first and the last of the consecutive slides for every group of immunohistochemical analysis were stained for hematoxylin and eosin to survey the slide quality. The paraffin sections for immunohistochemical analysis were deparaffinized in xylene substitute (Paraclean, Earthsafe Tech, USA), and rehydrated and immersed in 3% H_2O_2 for 10 min. Table 1 shows the primary antibodies and working dilutions used in tissue array analysis. Before incubation with primary antibodies, sections were microwaved either in 0. 01 M sodium citrate buffer (pH 6. 0) for 10 min or with pressure cooker in 1.0 mM EDTA buffer for 5 min and blocked with blocking serum in phosphate-buffered saline (PBS) for 20 min at room temperature. The sections were incubated with primary antibody for 40 min and subsequently with labeled polymer-HRP (EnVision DAB kit, Dako). The sections were thoroughly washed between incubations. After the final wash in 1% Triton X-100/PBS, sections were stained using DAB-H_2O_2 as substrate. Negative controls included replacing primary antibodies with normal serum or omission of EnVision-DAB reagents or both. Selected tissue sections (normal thyroid for CaSR, CGA, VitDR,

Table 1 Primary antibodies used for immunohistochemical analysis

Antibodies/hosts or clones	Dilution	[a]Source (cat. #)
Vitamin D receptor/clone 9A7	1/100	ABR (MA1-710)
Calcium-sensing receptor/rabbit polyclonal	1/100	ABR (PA1-934)
Cyclin D1/clone AM293	1/200	Zymed (18-0220)
Ki67/clone MIB-1	1/75	Immunotech (0505)
Chromogranin A/clone LK2H10	1/150	BioGenex (MU126-UC)
Parathyroid hormone/clone 3B3	1/30	Dako (M7070)

[a]Affinity Bioreagents (ABR), Golden, CO, USA; Zymed Laboratories, South San Francisco, CA, USA; Immunotech, Cedex, France; BioGenex, San Ramon, CA, USA; Dako, Glostrup, Denmark

and PTH; intestinal mantle cell lymphoma for CyD1; and Burkitt's lymphoma for Ki67) were prepared from surgical specimens to serve as positive controls. The optimal sections, which showed homogeneous staining and the least tissue dot loss, were selected for quantitative immunohistochemical analysis. The stained slides were photographed using a light microscope (Olympus BX50) equipped with digital camera (Coolpix 4500, Nikon, Japan); the image acquisitions were performed under the condition of fixed settings of objective lens, condenser, illumination light, shutter speed, and aperture size. In all assessments, each tissue dot was represented by four randomly selected image fields. The staining intensity and labeling index were digitalized using an image-processing software (AlphaEaseFC 4.0, Alpha Innotech, USA). The cytoplasmic or nuclear staining intensity of individual cell is defined as integrated density value (IDV) of selected cytoplasmic or nuclear area; the average staining intensity of an image field is defined as average density value (ADV=total IDV/total nuclear or cytoplasmic area). The nuclear labeling index is defined as percentage of positive stained nuclei of parathyroid cells in an image field.

Statistics

The unqualified tissue pairs that resulted from tissue exhaustion, partial or complete detachment during processing, or defective staining were excluded from the statistical analysis. One-way ANOVA with Tukey–Kramer post test was performed using GraphPad Prism version 3.00 for Windows (GraphPad Software, San Diego, CA, USA).

Results

Clinicopathological analysis

The clinical profiles of all patient groups are listed in Table 2. The initial pathological descriptions of parathyroid lesions in NC group were hyperplasia (13/20), adenoma (3/20), and normal-appearing gland (4/20). The linear regression analysis of preoperative PTH vs serum calcium in the NC group shows a positive slope (0.01) (Fig. 1).

Immunohistochemical analysis

The randomly sampled tissue cores were assessed independently to reduce the bias resulting from the heterogeneity of tissue distribution. Figure 2 shows the representative immunohistochemical staining patterns of parathyroid tissues of all patient groups. Figure 3 depicts the scattergrams of the expression of CaSR, PTH, VitDR, CGA, Ki67, and CyD1 on tissue arrays. Compared with normal control, the group NC fails to show significant alterations of CaSR, CGA, PTH, and Ki67 (Fig. 3a,b,d, and f). On the other hand, group NC shares the expression patterns of other hyperparathyroidism groups to show significant upregulation of CyD1 and downregulation of VitDR (Fig. 3c,e). Hyperparathyroidism groups show no significant difference of PTH expression from normal control despite that they have lower numerical statistic means (Fig. 3d). CaSR and CGA have similar profile to constantly exhibit the greatest degree of downregulation in group SH and lack of significant deviation

Table 2 Clinical profiles

	N	SH	A	PH	NC
Age (year)	49±16	48±8	52±14	51±15	52±14
Sex ratio (F/M)	0.5	1.4	0.6	1.3	0.5
$[Ca^{2+}]_t$ (mg/dl)	9.2±0.6	11.2±1.6	11.8±0.7	11.6±0.8	9.3±0.6
$[Ca^{2+}]_i$ (mmol/l)	NA	NA	NA	NA	1.23±0.28
iPTH (pg/dl)	NA	965.4±450.8	226.1±302.3	223.0±309.2	50.0±9.3

Data presented as mean±SD
Normal range: total serum calcium $[Ca^{2+}]_t$: 8.4–10.6 mg/dl; ionizing serum calcium $[Ca^{2+}]_i$: 1.13–1.31 mmol/l; intact PTH (iPTH): <35.3 pg/ml
NA not available

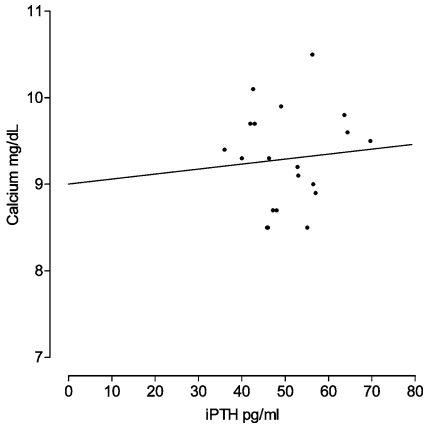

Fig. 1 Regression of preoperative total serum calcium vs intact PTH levels in NC group patients

from normal in group NC; the group A and group PH have intermediate attenuation of CaSR and CGA between group SH and group NC (Fig. 3a,b). The expression trend for Ki67 in the non-NC hyperparathyroidism groups is reciprocal to that of CaSR and CGA (Fig. 3f). CyD1 and VitDR also show mutually reciprocal trends in all hyperparathyroidism groups (Fig. 3c,e). Both Ki67 and CyD1 elevate in the hyperparathyroidism groups except Ki67 of NC group that shows no significant difference from normal control (Fig. 3e,f).

Discussion

In several earlier studies, relatively high frequency (31–81%) of normal-appearing parathyroid gland was found in those patients who manifested PHPT and recurrent kidney stone but maintained normal serum calcium concentration [14, 21, 26]. A proportion of them (22–52%) was reported to have cessation of stone formation after surgery [14, 21]. These reports imply that parathyroid glands may be morphologically normal but functionally deranged. Recently, Silverberg and Bilezikian [25] proposed the concept of "incipient" PHPT based on the pathophysiological profiles of a cohort of patients who manifested normocalcemic PHPT without evidence of preferential cortical bone loss but exhibited abnormal relationship between serum

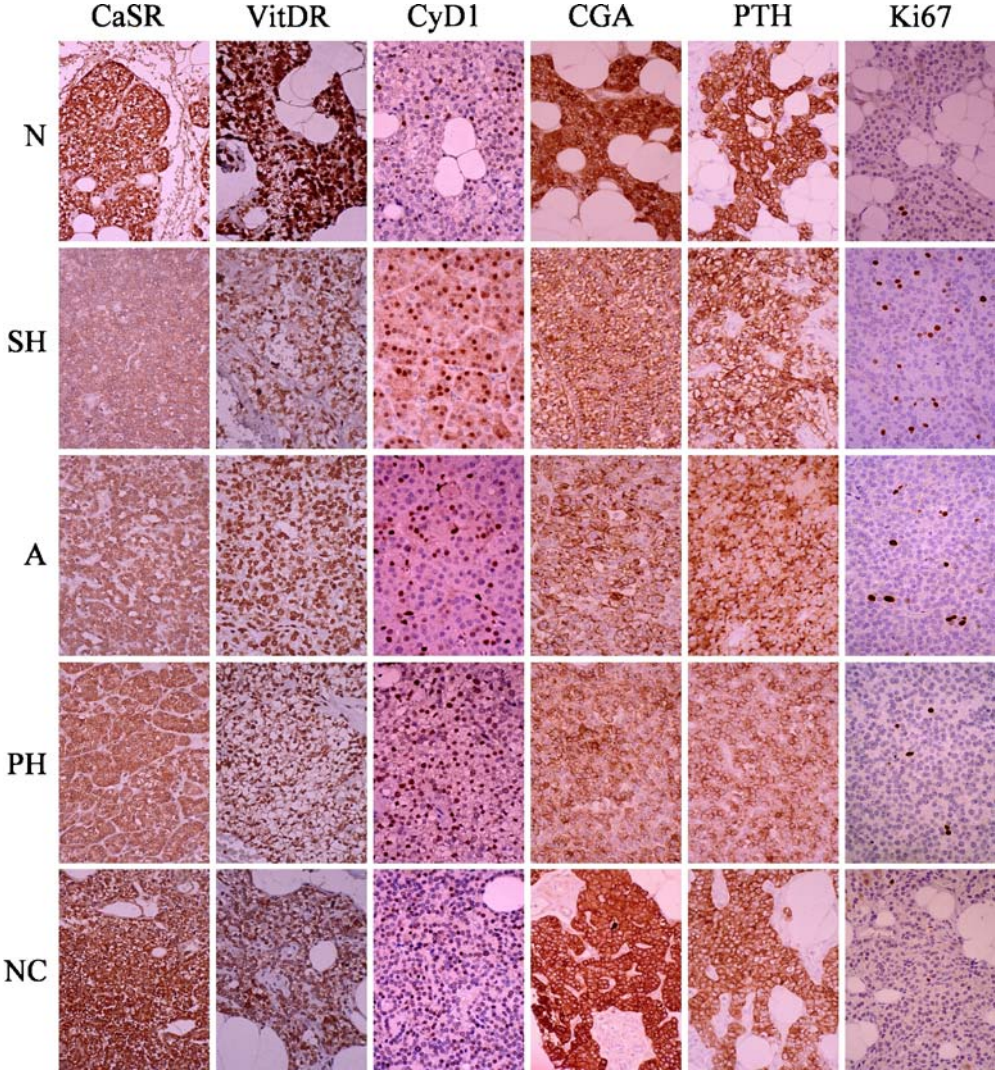

Fig. 2 Representative immunohistochemical staining patterns of parathyroid tissues on tissue array

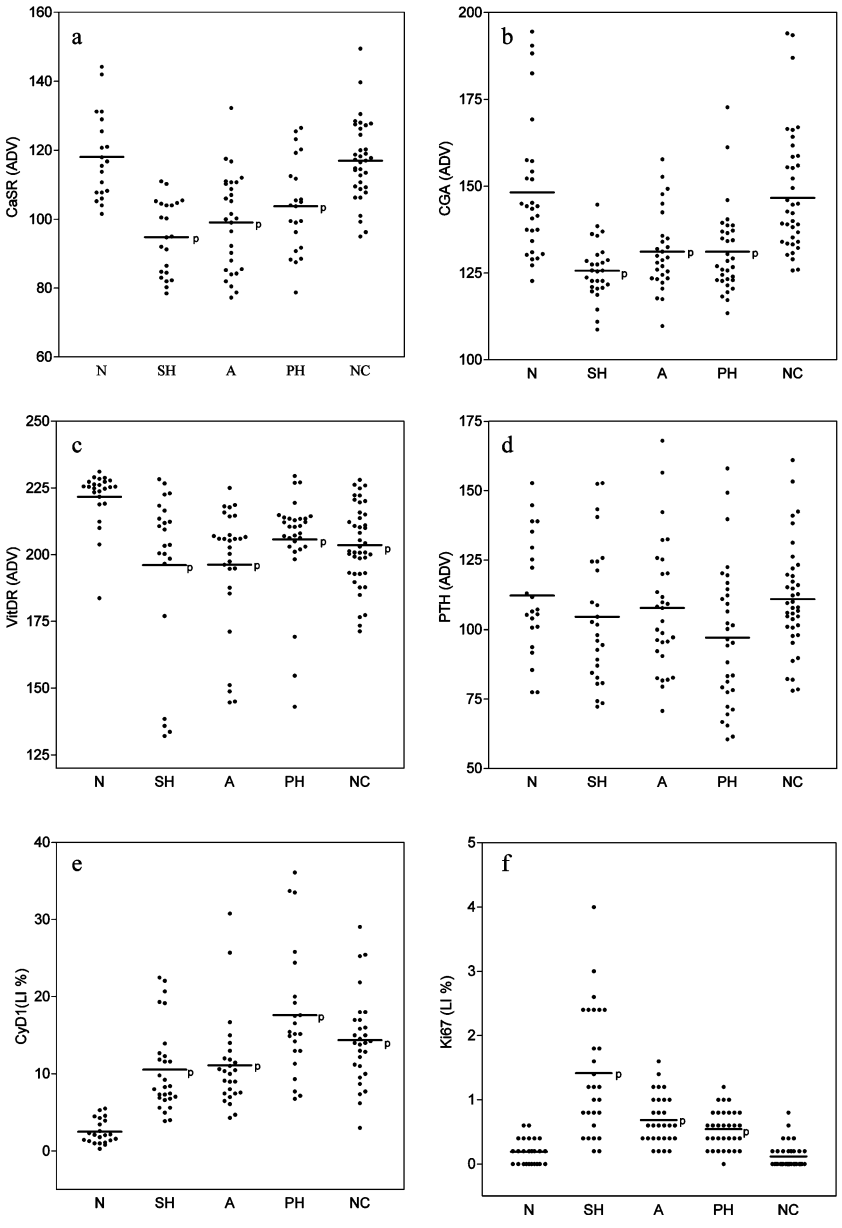

Fig. 3 Quantitative immunohistochemical analyses. "*p*" indicates $P<0.05$ vs normal control (N)

calcium and PTH levels, suggesting that these patients showed no difference in their biochemical profiles from those with hypercalcemia. The evolving of normocalcemic to hypercalcemic status in some patients in the study of Silverberg and Bilezikian [25] made them speculate that NCPHPT might be a transient form of PHPT that could not be explained by abnormal ratio of PTH (1–84)/PTH (7–84), PTH resistance, or primary abnormality of CaSR alone. In our study, we also found that 20% of the patients in NC group have normal-appearing glands. The lack of a negative slope relationship between serum calcium and PTH in NCPHPT patients before surgery implies the deviation from the normal physiological setting.

The emerging alteration of CyD1 and VitDR while maintaining normal profiles of CaSR, CGA, Ki67, and PTH in the NC group is the key feature of NCPHPT and further suggests that the CyD1 and VitDR might be the inciting molecular basis of hyperparathyroidism. Depression of CaSR was reported in parathyroid cells of primary or secondary hyperparathyroidism [2, 5, 10, 15, 32]. Using a *PTH-cyclin D1* transgenic mouse as a model of human hyperparathyroidism, Imanishi et al. [13] showed that CyD1 overexpression could suppress parathyroid CaSR, which was thought to contribute to the elevation in calcium-PTH set point and the proliferation of parathyroid cells. Based on these results, we speculate that there might be functional derangement between CyD1 and CaSR in our NCPHPT patients, and the lack of secondary down-regulation of CaSR might contribute to the maintenance of normocalcemic status.

The molecular mechanism by which VitDR is down-regulated in the primary or secondary hyperparathyroidism is still unclear. Reduced VitDR transcripts in hyperparathyroidism might reflect a defective promoter in the

regulation of tissue-specific VitDR expression [4]. In a rat model, Garfia et al. [9] found that downregulation of VitDR prevented the inhibitory effects of active vitamin D on the PTH synthesis and might represent an important pathogenic mechanism of hyperparathyroidism. The reduction of VitDR in NC group in our study implies that similar inherent functional abnormalities of VitDR might also exist in these patients and substantiates, in addition to CyD1, another pathogenic basis of hyperparathyroidism in normocalcemic patients.

The lack of concurrent alteration of CaSR with the reduction of VitDR is also a special feature of our NCPHPT patients. It was proposed that decreased CaSR expression in primary or secondary hyperparathyroidism might be secondary to the reduced VitDR expression because CaSR gene was found to have a functional vitamin D-responsive element in the 5′-flanking region [1]. Based on this finding, we speculate that failure of functional engagement between VitDR and CaSR might contribute to the maintenance of normocalcemic status in hyperparathyroidism.

CGA is a glycoprotein present in secretory granules of endocrine cells. In the parathyroid cells, it is usually costored and cosecreted with PTH in response to hypocalcemia [3, 28]. CGA is also the precursor of several bioactive peptides that inhibit stimulated release of PTH and costored CGA [3, 6, 7, 22, 34]. Reduced expression of both CGA and PTH has been described in the parathyroid tissue with primary or secondary hyperparathyroidism [23, 28, 33]. The lack of concordant downregulation of mRNA levels of PTH and CGA in parathyroid cells of hyperparathyroidism indicates that the alteration of secretory rather than the synthetic capacity is responsible for the decreased cellular content of CGA and PTH [16, 29]. Based on these studies, we speculate that the lack of enhanced release of CGA and PTH in our NCPHPT patients might contribute to the maintenance of normocalcemic status in NCPHPT patients.

In conclusion, our results imply that an inherent functional disengagement may exist between CaSR and CyD1 or between CaSR and VitDR or both to play a crucial role in maintaining normal calcium level in PHPT. The lack of enhanced release of CGA and PTH and discordance between proliferative activity and CyD1 expression in parathyroid cells may also hinder the development of hypercalcemia.

Acknowledgements This work was supported by Taipei Veterans General Hospital Research Grant 94-02-48A (to Y.A.H.), National Science Council Grant NSC 91-2314-B-075-066 (to Y.A.H.), and Yen Tjing Ling Medical Foundation Grant CI-92-1-1 (to Y.A.H. and C.H.L.).

All experiments comply with the laws of Taiwan.

References

1. Canaff L, Hendy GN (2002) Human calcium-sensing receptor gene. Vitamin D response elements in promoter P1 and P2 confer transcriptional responsiveness to 1,25-dihydroxyvitamin D. J Biol Chem 277:30337–30350
2. Chattopadhyay N (2000) Biochemistry, physiology and pathophysiology of the extracellular calcium-sensing receptor. Int J Biochem Cell Biol 32:789–804
3. Cohn DV, Fasciotto BH, Reese BK, Zhang JX (1995) Chromogranin A: a novel regulator of parathyroid gland secretion. J Nutr 125:2015S–2019S
4. Correa P, Akerstrom G, Westin G (2002) Exclusive underexpression of vitamin D receptor exon 1f transcripts in tumors of primary hyperparathyroidism. Eur J Endocrinol 147:671–675
5. Farnebo F, Hoog A, Sandelin K, Larsson C, Farnebo LO (1998) Decreased expression of calcium-sensing receptor messenger ribonucleic acids in parathyroid adenomas. Surgery 124:1094–1098
6. Fasciotto BH, Trauss CA, Greeley GH, Cohn DV (1993) Parastatin (porcine chromogranin A347–419), a novel chromogranin A-derived peptide, inhibits parathyroid cell secretion. Endocrinology 133:461–466
7. Fasciotto BH, Denny JC, Greeley GH Jr, Cohn DV (2000) Processing of chromogranin A in the parathyroid: generation of parastatin-related peptides. Peptides 21:1389–1401
8. Gardin JP, Paillard M (1984) Normocalcemic primary hyperparathyroidism: resistance to PTH effect on tubular reabsorption of calcium. Miner Electrolyte Metab 10:301–308
9. Garfia B, Canadillas S, Canalejo A, Luque F, Siendones E, Quesada M, Almaden Y, Aguilera-Tejero E, Rodriguez M (2002) Regulation of parathyroid vitamin D receptor expression by extracellular calcium. J Am Soc Nephrol 13:2945–2952
10. Gogusev J, Duchambon P, Hory B, Giovannini M, Goureau Y, Sarfati E, Drueke TB (1997) Depressed expression of calcium receptor in parathyroid gland tissue of patients with hyperparathyroidism. Kidney Int 51:328–336
11. Grimelius L, Johansson H, Lindquist B, Thoren L, Werner I (1973) Normocalcemic primary hyperparathyroidism. Acta Chir Scand 139:42–44
12. Hagag P, Revet-Zak I, Hod N, Horne T, Rapoport MJ, Weiss M (2003) Diagnosis of normocalcemic hyperparathyroidism by oral calcium loading test. J Endocrinol Invest 26:327–332
13. Imanishi Y, Hosokawa Y, Yoshimoto K, Schipani E, Mallya S, Papanikolaou A, Kifor O, Tokura T, Sablosky M, Ledgard F, Gronowicz G, Wang TC, Schmidt EV, HallC, Brown EM, Bronson R, Arnold A (2001) Primary hyperparathyroidism caused by parathyroid-targeted overexpression of cyclin D1 in transgenic mice. J Clin Invest 107:1093–1102
14. Johansson H, Thoren L, Werner I, Grimelius L (1975) Normocalcemic hyperparathyroidism, kidney stones, and idiopathic hypercalciuria. Surgery 77:691–696
15. Kifor O, Moore FD Jr, Wang P, Goldstein M, Vassilev P, Kifor I, Hebert SC, Brown EM (1996) Reduced immunostaining for the extracellular Ca2+-sensing receptor in primary and uremic secondary hyperparathyroidism. J Clin Endocrinol Metab 81:1598–1606
16. Levine MA, Dempsey MA, Helman LJ, Ahn TG (1990) Expression of chromogranin-A messenger ribonucleic acid in parathyroid tissue from patients with primary hyperparathyroidism. J Clin Endocrinol Metab 70:1668–1673
17. Lundgren E, Ridefelt P, Akerstrom G, Ljunghall S, Rastad J (1996) Parathyroid tissue in normocalcemic and hypercalcemic primary hyperparathyroidism recruited by health screening. World J Surg 20:727–734

18. Luong KV, Nguyen LT (2000) Normocalcemic hyperparathyroidism in Vietnamese immigrants living in southern California. Am J Med Sci 319:380–384
19. Maruani G, Hertig A, Paillard M, Houillier P (2003) Normocalcemic primary hyperparathyroidism: evidence for a generalized target-tissue resistance to parathyroid hormone. J Clin Endocrinol Metab 88:4641–4648
20. Monchik JM (1995) Normocalcemic hyperparathyroidism. Surgery 118:917–923
21. Poole GV Jr, Albertson DA, Myers RT (1983) Normocalcemic hyperparathyroidism revisited. Am Surg 49:668–671
22. Russell J, Gee P, Liu SM, Angeletti RH (1994) Inhibition of parathyroid hormone secretion by amino-terminal chromogranin peptides. Endocrinology 135:337–342
23. Schmid KW, Hittmair A, Ladurner D, Sandbichler P, Gasser R, Totsch M (1991) Chromogranin A and B in parathyroid tissue of cases of primary hyperparathyroidism: an immunohistochemical study. Virchows Arch A Pathol Anat Histopathol 418:295–299
24. Shieber W, Birge SJ, Avioli LV, Teitelbaum SL (1971) Normocalcemic hyperparathyroidism with “normal” parathyroid glands. Arch Surg 103:299–302
25. Silverberg SJ, Bilezikian JP (2003) “Incipient” primary hyperparathyroidism: a “forme fruste” of an old disease. J Clin Endocrinol Metab 88:5348–5352
26. Siminovitch JM, James RE, Esselstyn CB Jr, Straffon RA, Banowsky LH (1980) The effect of parathyroidectomy in patients with normocalcemic calcium stones. J Urol 123:335–337
27. Siperstein AE, Shen W, Chan AK, Duh QY, Clark OH (1992) Normocalcemic hyperparathyroidism. Biochemical and symptom profiles before and after surgery. Arch Surg 127:1157–1160
28. Tanaka R, Umemura S, Kakuta T, Fujisaki T, Sakai H, Saitoh A, Osamura RY (2003) Co-expression of parathyroid hormone and chromogranin A in secondary hyperparathyroidism: a functional marker for secretory activity of hyperplastic nodules. Pathol Res Pract 199:93–99
29. Weber CJ, Russell J, Chryssochoos JT, Hagler M, McGarity WC (1996) Parathyroid hormone content distinguishes true normal parathyroids from parathyroids of patients with primary hyperparathyroidism. World J Surg 20:1010–1014
30. Wills MR, Pak CY, Hammond WG, Bartter FC (1969) Normocalcemic primary hyperparathyroidism. Am J Med 47:384–391
31. Wu PH, Wang CJ (2002) Normocalcemic primary hyperparathyroidism with fractures. J Arthroplasty 17:805–809
32. Yano S, Sugimoto T, Tsukamoto T, Chihara K, Kobayashi A, Kitazawa S, Maeda S, Kitazawa R (2000) Association of decreased calcium-sensing receptor expression with proliferation of parathyroid cells in secondary hyperparathyroidism. Kidney Int 58:1980–1986
33. Yong JL, Vrga L, Warren BA (1994) A study of parathyroid hyperplasia in chronic renal failure. Pathology 26:99–109
34. Zhang JX, Fasciotto BH, Darling DS, Cohn DV (1994) Pancreastatin, a chromogranin A-derived peptide, inhibits transcription of the parathyroid hormone and chromogranin A genes and decreases the stability of the respective messenger ribonucleic acids in parathyroid cells in culture. Endocrinology 134:1310–1316

Virchows Arch (2006) 449: 69–77
DOI 10.1007/s00428-006-0200-y

ORIGINAL ARTICLE

Iannis E. Adamopoulos · Lynett Danks · Ichiro Itonaga · Rachel M. Locklin · Afsie Sabokbar · David J. P. Ferguson · Nicholas A. Athanasou

Stimulation of osteoclast formation by inflammatory synovial fluid

Received: 15 September 2005 / Accepted: 8 March 2006 / Published online: 21 April 2006
© Springer-Verlag 2006

Abstract Peri-articular bone resorption is a feature of arthritis due to crystal deposition and rheumatoid disease. Under these conditions, the synovial fluid contains numerous inflammatory cells that produce cytokines and growth factors which promote osteoclast formation. The aim of this study was to determine whether inflammatory synovial fluid stimulates the formation of osteoclasts. Synovial fluid from rheumatoid arthritis (RA), pyrophosphate arthropathy (PPA) and osteoarthritis (OA) patients was added to cultures (n=8) of human peripheral blood mononuclear cells (PBMCs) in the presence and absence of macrophage colony-stimulating factor (M-CSF) and the receptor activator of NF-κB ligand (RANKL). Osteoclast formation was assessed by the formation of cells positive for tartrate-resistant acid phosphatase (TRAP) and vitronectin receptor (VNR) and the extent of lacunar resorption. The addition of 10% OA, RA and PPA synovial fluid to PBMC cultures resulted in the formation of numerous multinucleated or mononuclear $TRAP^+$ and VNR^+ cells which were capable of lacunar resorption. In contrast to PBMC cultures incubated with OA synovial fluid, there was marked stimulation of osteoclast formation and resorption in cultures containing inflammatory RA and PPA synovial fluid which contained high levels of tumour necrosis factor alpha, a factor which is known to stimulate RANKL-induced osteoclast formation.

Keywords Synovial fluid · Rheumatoid arthritis · Crystal · Pyrophosphate · Osteoclast

I. E. Adamopoulos · L. Danks · R. M. Locklin · A. Sabokbar
Institute of Musculoskeletal Sciences, Botnar Research Centre, University of Oxford,
Oxford, UK

I. Itonaga
Department of Orthopaedic Surgery, Oita Medical University,
1-1 Idaigaoka, Hasama-machi,
Oita-gun, Oita 879-5593, Japan

D. J. P. Ferguson
Nuffield Department of Clinical Laboratory Science,
John Radcliffe Hospital,
Oxford, UK

I. E. Adamopoulos · N. A. Athanasou (✉)
Department of Pathology, Nuffield Orthopaedic Centre,
Windmill Road,
Headington, Oxford, OX3 7LD, UK
e-mail: nick.athanasou@ndos.ox.ac.uk
Tel.: +44-1865-227619
Fax: +44-1865-227354

Introduction

Bone resorption is a common feature of a number of inflammatory joint conditions including rheumatoid arthritis (RA) and crystal (e.g. urate, pyrophosphate) arthropathy. In both RA and acute crystal arthritis, the synovial fluid is characterised as inflammatory; it contains abundant neutrophil polymorphs and other leucocytes, including macrophages and lymphocytes [12, 29]. These activated inflammatory cells produce abundant cytokines and growth factors as well as proteolytic enzymes and immune components that are known to promote osteoclastic bone resorption [11].

Osteoclasts are multinucleated cells which are specialised to carry out lacunar bone resorption [4]. Osteoclasts are formed by the fusion of mononuclear osteoclast precursors that are found in the bone marrow and the monocyte fraction of peripheral blood; osteoclasts can also be formed from tissue macrophages, including synovial macrophages [13, 14]. Osteoclast formation occurs in the presence of macrophage colony-stimulating factor (M-CSF) and receptor activator of nuclear factor κ beta ligand (RANKL), a tumour necrosis factor (TNF)-related protein [26, 33]. RANKL is expressed on the membrane of osteoblasts, some fibroblasts (e.g. synovial fibroblasts) and inflammatory cell (e.g. T lymphocyte) populations, and is released locally as a soluble factor [16]. Osteoclastogenesis involves binding of RANKL to the receptor activator of NF-κB (RANK), which is present on osteoclast precursors. This process is inhibited by osteoprotegerin (OPG), a

soluble decoy receptor for RANK, which is produced by many cells, including osteoblasts, synovial fibroblasts and T lymphocytes [16, 37, 40].

The concentration of inflammatory cytokines, such as TNFα and interleukin (IL)-1, is elevated in the synovial fluid of various forms of inflammatory arthritis [28, 32]. This is of interest because it has recently been shown that inflammatory cytokines can influence the expression of RANKL and OPG by bone stromal cells [15, 16]; this cytokine effect could account for the recent observation that the soluble RANKL to OPG ratio is increased in the synovial fluid of patients with RA compared with those with OA [22]. The increase in inflammatory cytokines found in various forms of inflammatory and non-inflammatory arthritis may also directly contribute to osteoclast formation and bone resorption under these conditions because it has recently been shown that cytokine factors, such as TNFα, IL-6 and IL-11, are capable of inducing osteoclast differentiation (in the presence of M-CSF) by a RANKL-independent mechanism [8, 21, 24, 25].

In this study, we have sought to determine the effect of inflammatory and non-inflammatory synovial fluid on osteoclast formation and lacunar resorption. We have analysed the effect of synovial fluid taken from uninflamed OA joints and compared it with that of inflammatory synovial fluid taken from joints affected by RA and crystal (pyrophosphate) arthritis on monocyte–osteoclast differentiation. Our findings indicate that inflammatory synovial fluid is capable of stimulating osteoclast formation and that, in this way, it may contribute to the joint destruction that occurs under these conditions.

Materials and methods

Reagents

All cell incubations were performed in alpha minimal essential medium (αMEM) (Gibco, UK) supplemented with glutamine (2 mM), benzyl penicillin (100 IU/ml) and streptomycin (10 μg/ml). Positive control cultures were supplemented with 10% foetal bovine serum (FBS). Test cultures were supplemented with 10% RA, pyrophosphate arthritis (PPA) or OA synovial fluid. Cell cultures were incubated at 37°C in a humidified atmosphere with 5% CO_2. Hyaluronidase was purchased from Sigma-Aldrich (UK). Amgen Inc. (Thousand Oaks, CA, USA) kindly provided the soluble RANKL. Human M-CSF was purchased from R&D Systems (UK).

Preparation of synovial fluid

Synovial fluid was aspirated from the hip and knee joints of five seropositive RA patients (five women; average age, 49.3 years), six OA patients (four women and two men; average age, 67.7 years) and three PPA patients (one woman and two men; average age, 66.6 years). The patient diagnoses of OA, RA and PPA were made on the basis of clinical, radiological and relevant serological examination as well as histology of the synovial tissues (Fig. 1) [2]. Using the grading system of Krenn et al. [23] for the degree of synovitis, the inflammatory changes in the joints examined ranged from 0 to 1 in OA, 2 to 3 in RA and 1 to 3 in PPA. Each synovial fluid was defined as inflammatory or non-inflammatory on the basis of the white blood cell count per cubic millimetre (WBC/mm^3) as previously described [12, 29]; non-inflammatory synovial fluids contained less than 1,500 WBC/mm^3, and inflammatory synovial fluids contained more than 1,500 WBC/mm^3. The presence of typical, positively birefringent crystals in PPA synovial fluid samples was confirmed by polarization microscopy. A sample of each fluid was also sent for microbiological culture to confirm the absence of infection. Each synovial fluid sample was incubated with hyaluronidase (1,000 U/ml) at 37°C for 45 min and then centrifuged at 700×*g* for 10 min to remove all cells.

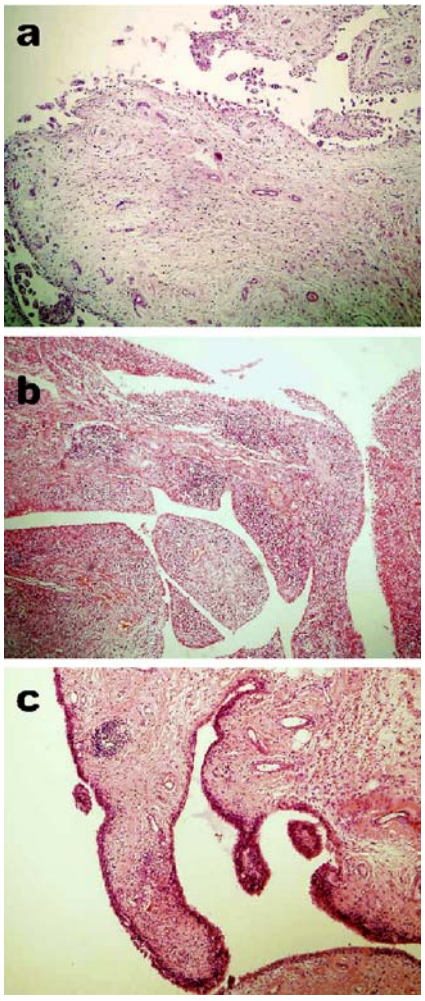

Fig. 1 Representative histology of **a** OA, **b** RA and **c** PPA synovium of joints from which synovial fluid was obtained. In RA and PPA synovium, there is, respectively, a diffuse and focal chronic inflammatory cell infiltrate. Haematoxylin and eosin, original magnification ×40

Aliquots of the synovial fluid were then placed in vials and stored at −80°C.

Isolation and culture of human monocytes

The peripheral blood of eight healthy male donors (age 25–40) was collected into tubes containing EDTA, diluted 1:1 in αMEM, layered over Ficoll-Hypaque (Pharmacia, UK) and centrifuged at 693×*g* for 18 min at 4°C. The peripheral blood mononuclear cell (PBMC) layer was removed and washed in αMEM, and the cell pellet was then resuspended in αMEM/FBS. The number of PBMCs in the cell suspension was counted in a haemocytometer after lysis of red cells with a 5% v/v acetic acid solution. PBMCs (2×10^5) were added to 4-mm-diameter dentine slices and 6-mm-diameter glass cover-slips and incubated for 2 h at 37°C in 5% CO_2. After 2 h of incubation, non-adherent cells were then removed by vigorous washing. Dentine slices and glass cover-slips were then transferred to 16-mm-diameter wells of a 24-well tissue culture plate and incubated for up to 21 days in αMEM supplemented with 10% RA, PPA or OA synovial fluid in the presence and absence of human M-CSF (25 ng/ml) and RANKL (30 ng/ml). Positive controls consisted of PBMCs cultured in the presence of 10% FBS with M-CSF (25 ng/ml) and RANKL (30 ng/ml). The culture medium and respective supplements were entirely replaced every 3 days.

Analysis of CD44 receptor expression on human PBMCs by flow cytometry

Cells were washed once in 1 ml wash buffer (PBS containing 0.5% BSA), resuspended in 100 μl wash buffer and labelled with mouse anti-human CD44 (R&D Systems) or an isotype control mouse IgG2 for 30 min. After washing, cells were labelled with a rabbit anti-mouse fluorescein isothiocyanate (FITC)-conjugated secondary antibody (Dako) for 30 min. Cells were then washed twice in PBS and resuspended in 300 μl PBS for flow cytometric analysis. The level of FITC fluorescence was measured using a FACSCalibur flow cytometer (Becton Dickinson).

Cytochemical assessment of osteoclast formation

Cell preparations on cover-slips at 24 h and 14 days were assessed histochemically for the expression of the osteoclast-associated enzyme, tartrate-resistant acid phosphatase (TRAP). Histochemical staining for TRAP was carried out using a commercially available kit (Sigma, UK). Cell preparations were fixed in citrate/acetone solution and stained for acid phosphatase, using naphthol AS-BI phosphate as a substrate, in the presence of 1.0 M tartrate; the product was reacted with fast garnet GBC salt [30]. Cell preparations on cover-slips were also stained immunohistochemically by an indirect immunoperoxidase technique with the monoclonal antibody 23C6 (Serotec, UK), which is directed against CD51; the vitronectin receptor (VNR), a highly osteoclast-associated antigen [10]; 3G5, a mouse anti-human CD44 (anti-CD44 v3, subclass IgG_{2a}) (R&D Systems Europe) expressed by PBMC and osteoclasts; Tuk 4 (Dako, Japan), which is directed against CD14, a monocyte antigen which is not expressed by osteoclasts [5, 20]; and M7254 (Dako, UK), which is directed against CD3, a T-cell marker. The cell preparations on cover-slips were counterstained with haematoxylin. Positive controls for $CD14^+$ and $CD44^+$ staining consisted of cell preparations on cover-slips of peripheral blood monocytes and, for VNR staining, osteoclasts from giant cell tumour of the bone. Negative controls consisted of cover-slips with no added primary antibody and isotype control for each antibody (IgG_2 or IgG_1).

Functional evidence of osteoclast differentiation

Functional evidence of osteoclast differentiation was determined by a lacunar resorption assay system using cell culture on dentine slices [13, 17]. Dentine provides a smooth-surface mineralised substrate for the assessment of lacunar resorption. After cells had been cultured on dentine slices for 24 h and for 3, 7, 10, 14, 18 and 21 days, the slices were removed from the wells, rinsed in PBS and placed in 0.25% trypsin for 15 min. The slices were then washed vigorously in distilled water and left overnight in 1 M ammonium hydroxide. The dentine slices were then sonicated to remove cell debris and stained with 0.5% toluidine blue. Dentine slices were examined by light microscopy and the percentage surface area of lacunar resorption in each dentine slice then measured using Adobe PhotoShop 5.5 image analysis software.

Ultrastructural evidence of osteoclast differentiation

Ultrastructural evidence of osteoclast differentiation was determined by transmission electron microscopy (TEM) and scanning electron microscopy (SEM). SEM was performed after cells had been cultured on dentine slices for 24 h and for 3, 7, 10, 14, 18 and 21 days. The cell cultures on dentine slices were fixed in a 4% glutaraldehyde solution and then dehydrated by passing through graded alcohols and then through graded hexamethyldisilazane solution (Sigma, UK) before being air dried. The dentine slices were then mounted onto aluminium stubs using double-sided Sellotape, sputtered with gold and examined using a Philips SEM 505 scanning electron microscope. TEM was performed after cells had been cultured on dentine slices for 15 days. The cell cultures were fixed with 2.5% glutaraldehyde/0.1 M cacodylate buffer, pH 7.2, postfixed in osmium tetroxide, dehydrated by passing through graded alcohols and then embedded in epoxy resin. Serial thin sections were cut and then stained with uranyl acetate and lead citrate before examination in a Joel 1200EX transmission electron microscope.

The effect of OA, RA and PPA synovial fluid on osteoclast resorption activity

The effect of OA, RA and PPA synovial fluid on osteoclast resorption activity was determined using cultures of mature osteoclasts obtained from two giant cell tumours of bone. Giant cell tumour tissue was curetted with a scalpel blade and the resultant cell suspension added to dentine slices in 96-well tissue culture plates. Cells were settled on the dentine slices for 2 h, washed in MEM, and then placed in 24-well tissue culture plates containing 1 ml MEM/FCS and 10% RA, PPA or OA synovial fluid. Cell cultures were incubated for 24 h, after which time the extent of lacunar resorption was assessed as described above.

Enzyme-linked immunosorbent assay for OPG/TNFα

Aliquots of synovial fluid were assayed to determine the concentration of OPG and TNFα by an enzyme-linked immunosorbent assay (ELISA) system (Duoset; R&D Systems). The 96-well plates were coated with 2 μg/ml mouse monoclonal anti-human OPG or with mouse monoclonal anti-human TNFα (R&D Systems). The OPG standard curve was generated using recombinant human OPG (R&D Systems) at concentrations from 2,000 to 31.25 pg/ml, and the TNFα standard curve was generated using recombinant human TNFα from 1,000 to 15.65 pg/ml (R&D Systems). The secondary antibodies were biotinylated anti-human OPG and anti-human TNFα (R&D Systems) at 200 ng/ml, and detection was done using streptavidin–horseradish peroxidase (R&D Systems). The reaction was stopped after 30 min of incubation in the dark by addition of 50 μl 2 M H_2SO_4. The plate was read at 450 nm on a Dynatech plate reader using Revelation software.

Statistical analysis

Each experiment was carried out in triplicate. Data are presented as the mean percentage lacunar resorption +/− standard error of the mean. Statistical analysis on measurements of mean percentage area resorbed was performed using Student's *t* test. Values less than $p=0.05$ were considered significant.

Results

Phenotypic characteristics of isolated PBMCs

Isolated PBMCs incubated for 24 h on glass cover-slips, in the presence or absence of synovial fluid, expressed the monocyte/macrophage marker CD14 and were negative for CD3 and the osteoclast markers TRAP and VNR. Twenty-four-hour PBMC cultures on dentine slices showed no evidence of lacunar resorption. Isolated cells thus expressed the cytochemical and functional phenotype of monocytes and not osteoclasts. Flow cytometry and immunohistochemistry showed that isolated PBMCs incubated for 24 and 72 h on glass cover-slips in the presence of M-CSF and RANKL also expressed CD44, an antigen which is associated with substrate adhesion and cell–cell fusion (Fig. 2).

The effect of inflammatory (RA, PPA) and non-inflammatory (OA) synovial fluid on osteoclast formation

In control cultures, PBMCs were incubated for up to 21 days with 10% FBS in the presence of M-CSF and RANKL. Under these conditions, numerous $TRAP^+$ and VNR^+ multinucleated cells were seen in 14-day cultures on cover-slips, and numerous resorption pits were formed in 21-day cultures on dentine slices. Substitution of RA, PPA or OA synovial fluid for either M-CSF or RANKL in these monocyte cultures did not result in the formation of $TRAP^+/VNR^+$ cells.

PBMCs incubated for up to 21 days with 10% RA, PPA or OA synovial fluid, in the presence of M-CSF and RANKL, also showed formation of $TRAP^+$ and VNR^+ cells and evidence of lacunar resorption (Figs. 3, 4 and 5a). In contrast to PBMC cultures incubated in the absence of synovial fluid, where $TRAP^+$ and VNR^+ cells first appeared after 5 and 7 days of incubation, respectively, $TRAP^+$ and VNR^+ mononuclear and multinucleated cells

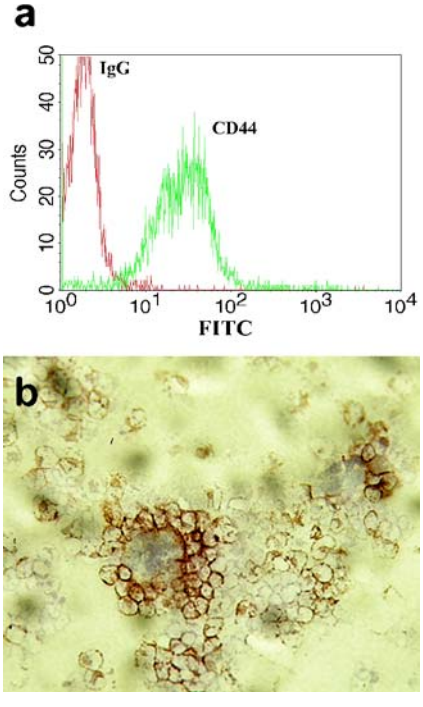

Fig. 2 Seventy-two-hour PBMC cultures incubated with M-CSF and RANKL, analysed for CD44 expression by **a** flow cytometry utilizing antibodies directed against CD44 and its isotype IgG2 and by **b** immunohistochemistry showing expression of the CD44 receptor on mononuclear cells. Original magnification ×400 immunoperoxidase

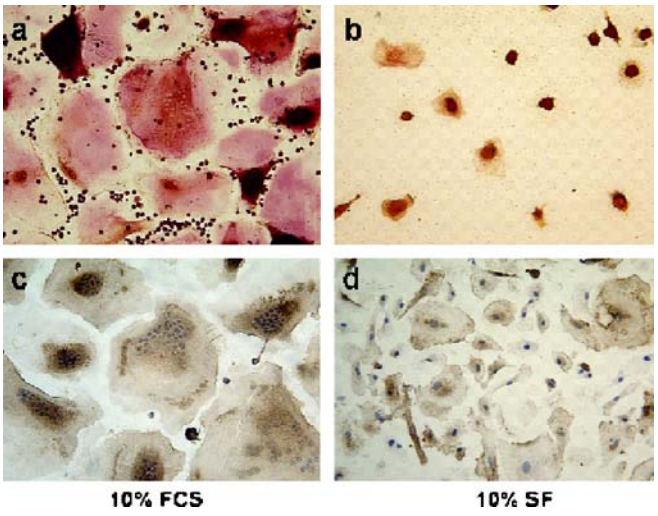

Fig. 3 Fourteen-day PBMC cultures incubated with M-CSF and RANKL, showing **a** large multinucleated $TRAP^+$ cells in control cultures and **b** numerous small largely mononuclear $TRAP^+$ cells, in the presence of 10% RA synovial fluid, and **c** large multinucleated VNR^+ cells in control cultures and **d** small multinucleated mononuclear VNR^+ cells, in the presence of 10% RA synovial fluid. Original magnification ×200

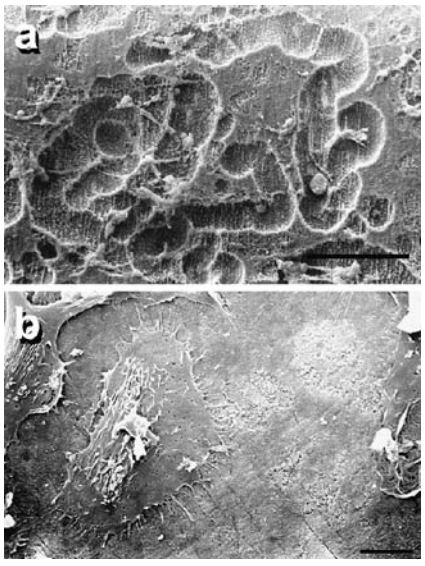

Fig. 5 SEM photomicrograph of an 18-day PBMC culture on a dentine slice incubated with M-CSF, RANKL and 10% RA synovial fluid showing **a** low- and **b** high-power views of lacunar resorption and **c** low-grade surface resorption. Size bar=10 μm

were seen as early as 3 days after PBMC cultures containing 10% OA, RA or PPA synovial fluid were commenced.

More $TRAP^+$ and VNR^+ cells were formed in PBMC cultures to which RA and PPA synovial fluids were added. The majority of $TRAP^+$ and VNR^+ cells present in synovial-fluid-treated cultures appeared mononuclear. Few large $TRAP^+$ and VNR^+ multinucleated cells were formed in PBMC cultures containing synovial fluid, most multinucleated cells being relatively small and containing less than four nuclei. A significant increase in the number of VNR^+ cells was noted in PBMC cultures treated with 10% RA and PPA compared to OA synovial fluid (Fig. 4). The latter was not significantly different from control cultures to which FBS was added. TEM examination of the mononuclear cells formed in PBMC cultures on dentine slices in 10% RA synovial fluid showed that actively resorbing mononuclear cells had a well-developed ruffled border, a characteristic ultrastructural feature of osteoclasts (Fig. 6).

The effect of inflammatory (RA, PPA) and non-inflammatory (OA) synovial fluid on lacunar resorption.

In PBMC control cultures, lacunar resorption on dentine slices was first detected on day 14 of culture (Fig. 5a). However, in PBMC cultures to which OA, RA or PPA synovial fluid was added, resorption began between the seventh and tenth day of incubation. Extensive resorption pit formation was noted in PBMC cultures to which RA and PPA synovial fluids were added; this increased resorption was significant both relative to control PBMC

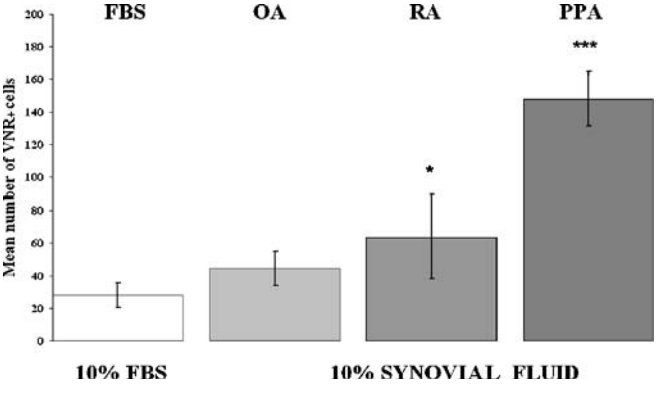

Fig. 4 Mean number of VNR^+ cells formed in 14-day PBMC cultures incubated with M-CSF and RANKL in the presence of 10% FBS (control) and 10% OA, RA and PPA synovial fluid. *p<0.005 and ***p<0.0001 relative to control

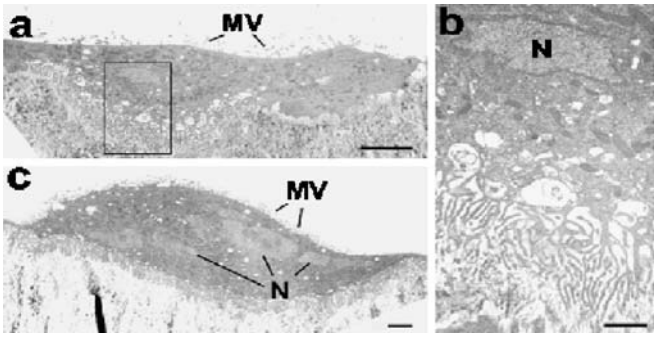

Fig. 6 TEM photomicrograph of an 18-day PBMC culture on a dentine slice incubated with M-CSF, RANKL and 10% RA synovial fluid showing **a** mononuclear cell with a ruffled border [shown in (**b**) at high power] actively resorbing bone and **c** multinucleated cell resorbing bone. *N* nucleus, *MV* microvilli. In (**a**) and (**c**), size bar=10 μm, and in (**b**), the size bar=2 μm

cultures and to cultures containing OA synovial fluid (p=0.03 and p=0.02, respectively) (Fig. 7). Although most resorption seen in the cultures was lacunar in type, a form of non-lacunar resorption characterised by superficial roughening of the dentine surface was also noted both around resorption pits and in direct relation to cells on the bone surface (Fig. 5b). PBMC cultures to which 10% OA synovial fluid had been added showed a similar level of resorption to that seen in control cultures. The addition of synovial fluid from OA, RA and PPA joints had no significant difference on the extent of lacunar resorption by mature osteoclasts isolated from giant cell tumour of bone (Fig. 8); this finding suggests that the increased resorption seen in cultures treated with RA and PPA synovial fluid was due to increased osteoclast formation rather than increased osteoclast resorption activity.

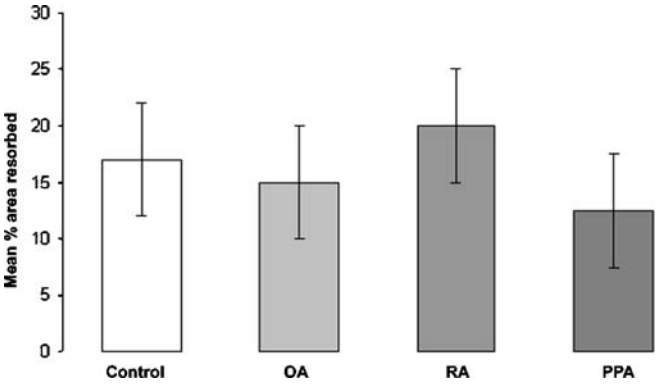

Fig. 8 Mean percentage area resorption produced by mature osteoclasts isolated from giant cell cultures incubated in the presence of 10% non-inflammatory (OA) and inflammatory (RA/PPA) synovial fluid

TNFα and OPG concentration in OA, RA and PPA synovial fluids

Although there was some variation in the concentration of TNFα in the synovial fluid samples taken from individual RA (5.7–20 pg/ml) and PPA (4.7–8.2 pg/ml) joints, the concentration of TNFα in RA and PPA joint synovial fluid was higher than that seen in OA joint fluid, where the TNFα concentration was much less variable (4.3–5.5 pg/ml). Osteoclast formation and lacunar resorption were most pronounced in PBMC cultures to which RA and PPA synovial fluids containing the highest levels of TNFα were added. Only small variations in the concentration of OPG were observed in OA, RA and PPA joints, all fluids tested exhibiting OPG concentrations below 3.5 pg/ml.

Discussion

Mononuclear osteoclast precursors are present in the synovial macrophage population of RA and OA joints, and osteoclast formation by these cells occurs in the presence of M-CSF and RANKL [13, 17]. Variations in the cellular and humoral composition of synovial fluid reflect changes in the synovial tissues with which the fluid is in continuity. Normal synovial fluid is a dialysate of plasma, containing hyaluronan, glycoproteins, albumin and small quantities of larger proteins decreasing in amount with an increase in molecular size. In inflammatory synovial fluid, increasing amounts of all proteins, including high molecular weight proteins found in the plasma, enter the joint. These factors may significantly influence cell differentiation and function, as may cytokines and growth factors produced by activated fibroblasts and leucocytes found in inflamed synovial tissue. RA synovium contains a significant macrophage infiltrate; this is reflected in the high number of macrophages found in the synovial fluid of inflamed RA joints. The extent of synovial macrophage infiltration correlates strongly with the degree of joint erosion in arthritis [42], and increased osteoclast formation has been noted in cultures of synovial macrophages from RA compared with OA joints [17].

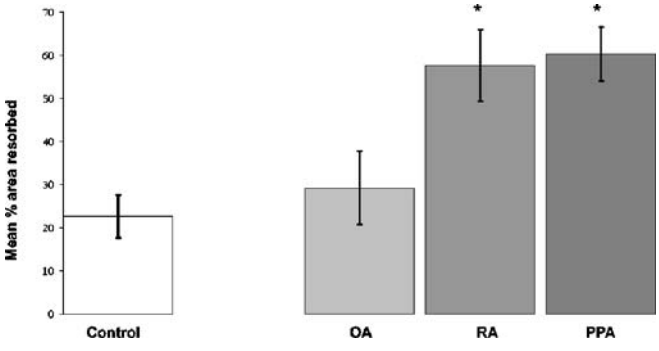

Fig. 7 Mean percentage area resorption produced by osteoclasts formed in PBMC cultures incubated with M-CSF and RANKL in the presence of 10% non-inflammatory (OA) and inflammatory (RA/PPA) synovial fluid. *p<0.05 relative to 10% OA synovial fluid

In the present study, we have shown that the synovial fluid derived from inflamed (RA/crystal arthropathy) joints stimulates RANKL-induced macrophage–osteoclast differentiation. We found that the addition of synovial fluid to monocyte cultures incubated with RANKL and M-CSF resulted in the formation of mononuclear cells and small multinucleated cells that expressed TRAP and VNR, markers of the osteoclast phenotype; these cells possessed a ruffled border and fulfilled the essential functional criterion of osteoclasts, being capable of lacunar resorption. We also found that inflammatory synovial fluid from RA and PPA joints markedly stimulated osteoclast formation and lacunar resorption. In the presence of non-inflammatory OA synovial fluid, osteoclast formation and lacunar resorption were similar to that seen in control cultures, but in the presence of RA and PPA synovial fluid, there was a twofold increase in lacunar resorption relative to OA and control cultures.

In the presence of 10% synovial fluid, many of the $TRAP^{+}/VNR^{+}$ cells in monocyte cultures were either mononuclear or contained fewer than four nuclei. These

cells exhibited cytochemical, functional and ultrastructural characteristics of osteoclasts, being $TRAP^+/VNR^+$ and capable of lacunar resorption pit formation; these cells also had a ruffled border, an area of membrane specialisation which is essential for bone resorption. Mononuclear cells that express the cytochemical and functional characteristics of osteoclasts have previously been noted in cultures of marrow cells and tissue macrophages [6, 7, 34]. Our findings are similar to those of a recent study which found that a significant proportion of bone-resorbing osteoclasts that form in cultures of synovial fluid macrophages are small and contain fewer than four nuclei [1]. The reason for the limited capacity mononuclear phagocytes incubated in synovial fluid to form polykaryons is not known, but it may be related to the fact that synovial fluid contains abundant hyaluronic acid. The CD44 receptor, which we have shown in this study to be expressed by monocytes, is indispensable for cell fusion, and fusion of mononuclear phagocytes is associated with osteoclast differentiation [41]. Since CD44 is the principal receptor for hyaluronic acid [3], it is possible that occupancy of the CD44 receptor by hyaluronic acid and its breakdown products results in a limited capacity of this macrophage population to carry out cell fusion. Occupancy of the CD44 receptor by hyaluronic acid and CD44 antibodies has been reported to inhibit cell fusion without altering osteoclast resorption activity [19, 39].

There was an increase in the number of bone-resorbing cells formed in monocyte cultures to which inflammatory (RA and PPA) synovial fluids were added compared with OA synovial fluid. Although most of the resorption carried out by these cells was lacunar in type, many of the cells exhibited a form of low-grade (non-lacunar) resorption of the dentine surface. This type of resorption has previously been described in arthroplasty-derived and tumour-derived macrophage cultures [18, 35]; however, the extent of the low-grade resorption seen in the monocyte cultures treated with inflammatory synovial fluid was much more extensive than in previous studies, and it is possible that the mononuclear and small multinucleated osteoclastic cells that form in cultures treated with RA and PPA synovial fluid exhibit an increased capacity for this type of resorption.

The resorption activity of mature osteoclasts was not stimulated when inflammatory synovial fluid was added to cultures of osteoclasts derived from giant cell tumours of bone. This suggests that the increased resorption that followed the addition of inflammatory synovial fluid occurred through stimulation of osteoclast formation rather than mature osteoclast activity. Pigmented villonodular synovitis (PVNS) is a condition in which there is periatricular bone resorption associated with heavy macrophage and giant cell infiltrate in synovial tissues. The giant cells in PVNS exhibit the phenotypic characteristics of mature osteoclasts [9, 31]. These osteoclast-like giant cells are most likely formed from synovial macrophages, and stimulation of osteoclast formation under this condition may be similarly promoted by a factor present in PVNS synovial fluid, which is known to contain giant cells.

Levels of RANKL are known to be increased in RA compared with OA synovial fluid [22], but it is unlikely that RANKL alone represents the pro-osteoclastogenic factor in inflammatory synovial fluid because osteoclast formation did not occur when inflammatory synovial fluid was added to monocyte cultures (in the presence of M-CSF). Likewise, although M-CSF has been reported to be increased in RA synovial fluid [38], M-CSF is unlikely to be the factor promoting osteoclast formation in inflammatory synovial fluid because the addition of inflammatory synovial fluid to monocyte cultures (in the presence of RANKL) did not stimulate osteoclast formation and resorption. It has been noted that the level of OPG in synovial fluid is decreased in RA compared with OA joints [22]. We measured the concentration of OPG by ELISA and found in our samples that it was not significantly different in OA, RA and PPA joint fluids. RANKL, however, is known to exist in a soluble form, and it remains possible that the RANKL to OPG ratio could be increased by stimulation of RANKL production by fibroblasts and activated T and B lymphocytes, all of which have been shown to support osteoclast formation in RA [36, 40].

The synovial membrane and synovial fluid in RA and crystal arthritis are known to contain large amounts of TNFα [28, 32], and TNFα has been reported to stimulate RANKL-induced osteoclastogenesis by modulating stromal cell expression of RANKL and OPG [15, 16]. Osteoclast differentiation, however, could not have been stimulated by stromal cells in inflammatory synovial fluid because our cultures contained only monocytes. Recent studies have shown that TNFα can stimulate osteoclast formation from marrow precursors in the presence of permissive levels of RANKL [27], and it is possible that the high levels of TNFα in inflammatory synovial fluid could have stimulated osteoclast formation in this way. Another means whereby TNFα in inflammatory synovial fluid could have stimulated osteoclast formation is through a RANKL-independent mechanism. We and others have shown that TNFα (in the presence of M-CSF) can induce osteoclast formation from mouse marrow precursors and human monocytes and macrophages [8, 21, 24]. We have also recently shown that TNFα can induce osteoclast formation from synovial fluid macrophages isolated from RA and PPA joints [1]. Whether TNFα alone or in concert with other growth factors and cytokines stimulates osteoclast formation by RANKL-dependent and/or RANKL-independent mechanism in inflammatory arthritis is not certain, but a role for TNFα is suggested by our finding that the most extensive resorption was seen in the monocyte cultures to which RA and PPA inflammatory synovial fluids containing the highest levels of TNFα were added.

Acknowledgements This study was approved by the Oxford Research Ethics Committee. The authors wish to thank all the volunteers who kindly donated blood samples for this study. We also extend our thanks to Dr. David Lacey, Amgen Inc., for providing the soluble RANKL. This work was funded by Action Research and the Frances and Augustus Newman Foundation. I.A. is the recipient of a Research into Ageing DPhil studentship.

References

1. Adamopoulos IE, Sabokbar A, Wordsworth BP, Carr A, Ferguson DJ, Athanasou NA (2006) Synovial fluid macrophages are capable of osteoclast formation and resorption. J Pathol 208:35–43
2. Arnett FC, Edworthy SM, Bloch DA, McShane DJ, Fries JF, Cooper NS, Healey LA, Kaplan SR, Liang MH, Luthra HS et al (1998) The American Rheumatism Association 1987 revised criteria for the classification of rheumatoid arthritis. Arthritis Rheum 31:315–24
3. Aruffo A, Stamenkovic I, Melnick M, Underhill CB, Seed B (1990) CD44 is the principal cell surface receptor for hyaluronate. Cell 61:1303–13
4. Athanasou NA (1996) Cellular biology of bone-resorbing cells. J Bone Joint Surg Am 78:1096–112
5. Athanasou NA, Quinn J (1990) Immunophenotypic differences between osteoclasts and macrophage polykaryons: immunohistological distinction and implications for osteoclast ontogeny and function. J Clin Pathol 43:997–1003
6. Athanasou NA, Quinn J, Ferguson DJ, McGee JO (1991) Bone resorption by macrophage polykaryons of giant cell tumour of tendon sheath. Br J Cancer 63:527–533
7. Athanasou NA, Quinn J, Bulstrode CJ (1992) Resorption of bone by inflammatory cells derived from the joint capsule of hip arthroplasties. J Bone Joint Surg Br 74:57–62
8. Azuma Y, Kaji K, Katogi R, Takeshita S, Kudo A (2000) Tumor necrosis factor-alpha induces differentiation of and bone resorption by osteoclasts. J Biol Chem 275:4858–4864
9. Darling JM, Goldring SR, Harada Y, Handel ML, Glowacki J, Gravallese EM (1997) Multinucleated cells in pigmented villonodular synovitis and giant cell tumor of tendon sheath express features of osteoclasts. Am J Pathol 150:1383–1393
10. Davies J, Warwick J, Totty N, Philp R, Helfrich M, Horton M (1989) The osteoclast functional antigen, implicated in the regulation of bone resorption, is biochemically related to the vitronectin receptor. J Cell Biol 109:1817–1826
11. Feldmann M, Brennan FM, Maini RN (1996) Role of cytokines in rheumatoid arthritis. Annu Rev Immunol 14:397–440
12. Freemont A, Denton J (1991) Atlas of synovial fluid cytopathology. Kluwer Academic Publishers, Boston
13. Fujikawa Y, Quinn JM, Sabokbar A, McGee JO, Athanasou NA (1996) The human osteoclast precursor circulates in the monocyte fraction. Endocrinology 137:4058–4060
14. Fujikawa Y, Sabokbar A, Neale S, Athanasou NA (1996) Human osteoclast formation and bone resorption by monocytes and synovial macrophages in rheumatoid arthritis. Ann Rheum Dis 55:816–822
15. Hofbauer LC, Lacey DL, Dunstan CR, Spelsberg TC, Riggs BL, Khosla S (1999) Interleukin-1beta and tumor necrosis factor-alpha, but not interleukin-6, stimulate osteoprotegerin ligand gene expression in human osteoblastic cells. Bone 25:255–259
16. Hofbauer LC, Khosla S, Dunstan CR, Lacey DL, Boyle WJ, Riggs BL (2000) The roles of osteoprotegerin and osteoprotegerin ligand in the paracrine regulation of bone resorption. J Bone Miner Res 15:2–12
17. Itonaga I, Fujikawa Y, Sabokbar A, Murray DW, Athanasou NA (2000) Rheumatoid arthritis synovial macrophage–osteoclast differentiation is osteoprotegerin ligand-dependent. J Pathol 192:97–104
18. Itonaga I, Schulze E, Burge PD, Gibbons CL, Ferguson D, Athanasou NA (2002) Phenotypic characterization of mononuclear and multinucleated cells of giant cell reparative granuloma of small bones. J Pathol 198:30–36
19. Kania JR, Kehat-Stadler T, Kupfer SR (1997) CD44 antibodies inhibit osteoclast formation. J Bone Miner Res 12:1155–1164
20. Knapp W, Dorken B, Gilks WR, Rieber EP, Schmidt RE, Stein H, von dem Borne AEGK (1989) Leukocyte typing IV: white cell differentiation antigen. Oxford University Press, New York
21. Kobayashi K, Takahashi N, Jimi E, Udagawa N, Takami M, Kotake S, Nakagawa N, Kinosaki M, Yamaguchi K, Shima N, Yasuda H, Morinaga T, Higashio K, Martin TJ, Suda T (2000) Tumor necrosis factor {alpha} stimulates osteoclast differentiation by a mechanism independent of the ODF/RANKL-RANK interaction. J Exp Med 191:275–286
22. Kotake S, Udagawa N, Hakoda M, Mogi M, Yano K, Tsuda E, Takahashi K, Furuya T, Ishiyama S, Kim KJ, Saito S, Nishikawa T, Takahashi N, Togari A, Tomatsu T, Suda T, Kamatani N (2001) Activated human T cells directly induce osteoclastogenesis from human monocytes: possible role of T cells in bone destruction in rheumatoid arthritis patients. Arthritis Rheum 44:1003–1012
23. Krenn V, Morawietz L, Haupl T, Neidel J, Petersen I, Konig A (2002) Grading of chronic synovitis—a histopathological grading system for molecular and diagnostic pathology. Pathol Res Pract 198(5):317–325
24. Kudo O, Fujikawa Y, Itonaga I, Sabokbar A, Torisu T, Athanasou NA (2002) Proinflammatory cytokine (TNFalpha/IL-1alpha) induction of human osteoclast formation. J Pathol 198:220–227
25. Kudo O, Sabokbar A, Pocock A, Itonaga I, Fujikawa Y, Athanasou NA (2003) Interleukin-6 and interleukin-11 support human osteoclast formation by a RANKL-independent mechanism. Bone 32:1–7
26. Lacey DL, Timms E, Tan HL, Kelley MJ, Dunstan CR, Burgess T, Elliott R, Colombero A, Elliott G, Scully S, Hsu H, Sullivan J, Hawkins N, Davy E, Capparelli C, Eli A, Qian YX, Kaufman S, Sarosi I, Shalhoub V, Senaldi G, Guo J, Delaney J, Boyle WJ (1998) Osteoprotegerin ligand is a cytokine that regulates osteoclast differentiation and activation. Cell 93:165–176
27. Lam J, Takeshita S, Barker JE, Kanagawa O, Ross FP, Teitelbaum SL (2000) TNF-[alpha] induces osteoclastogenesis by direct stimulation of macrophages exposed to permissive levels of RANK ligand. J Clin Invest 106:1481–1488
28. Lettesjo H, Nordstrom E, Strom H, Nilsson B, Glinghammar B, Dahlstedt L, Moller E (1998) Synovial fluid cytokines in patients with rheumatoid arthritis or other arthritic lesions. Scand J Immunol 48:286–292
29. McCarty D (1993) Synovial fluid. In: McCarty D, Koopman WJ (eds) Arthritis and allied conditions. Lea & Febiger, Philadelphia
30. Minkin C (1982) Bone acid phosphatase: tartrate-resistant acid phosphatase as a marker of osteoclast function. Calcif Tissue Int 34:285–290
31. Neale SD, Kristelly R, Gundle R, Quinn JM, Athanasou NA (1997) Giant cells in pigmented villo nodular synovitis express an osteoclast phenotype. J Clin Pathol 50:605–608
32. Partsch G, Steiner G, Leeb BF, Dunky A, Broll H, Smolen JS (1997) Highly increased levels of tumor necrosis factor-alpha and other proinflammatory cytokines in psoriatic arthritis synovial fluid. J Rheumatol 24:518–523
33. Quinn JM, Elliott J, Gillespie MT, Martin TJ (1998) A combination of osteoclast differentiation factor and macrophage-colony stimulating factor is sufficient for both human and mouse osteoclast formation in vitro. Endocrinology 139:4424–4427
34. Quinn JM, Whitty GA, Byrne RJ, Gillespie MT, Hamilton JA (2002) The generation of highly enriched osteoclast-lineage cell populations. Bone 30:164–170
35. Sabokbar A, Fujikawa Y, Neale S, Murray DW, Athanasou NA (1997) Human arthroplasty derived macrophages differentiate into osteoclastic bone resorbing cells. Ann Rheum Dis 56: 414–420
36. Shigeyama Y, Pap T, Kunzler P, Simmen BR, Gay RE, Gay S (2000) Expression of osteoclast differentiation factor in rheumatoid arthritis. Arthritis Rheum 43:2523–2530

37. Simonet WS, Lacey DL, Dunstan CR, Kelley M, Chang MS, Luthy R, Nguyen HQ, Wooden S, Bennett L, Boone T, Shimamoto G, DeRose M, Elliott R, Colombero A, Tan HL, Trail G, Sullivan J, Davy E, Bucay N, Renshaw-Gegg L, Hughes TM, Hill D, Pattison W, Campbell P, Boyle WJ et al (1997) Osteoprotegerin: a novel secreted protein involved in the regulation of bone density. Cell 89:309–319
38. Smith JB, Bocchieri MH, Smith JB Jr, Sherbin-Allen L, Abruzzo JL (1990) Colony stimulating factor occurs in both inflammatory and noninflammatory synovial fluids. Rheumatol Int 10:131–134
39. Sterling H, Saginario C, Vignery A (1998) CD44 occupancy prevents macrophage multinucleation. J Cell Biol 143:837–847
40. Takayanagi H, Iizuka H, Juji T, Nakagawa T, Yamamoto A, Miyazaki T, Koshihara Y, Oda H, Nakamura K, Tanaka S (2000) Involvement of receptor activator of nuclear factor kappaB ligand/osteoclast differentiation factor in osteoclastogenesis from synoviocytes in rheumatoid arthritis. Arthritis Rheum 43:259–269
41. Vignery A (2000) Osteoclasts and giant cells: macrophage–macrophage fusion mechanism. Int J Exp Pathol 81:291–304
42. Yanni G, Whelan A, Feighery C, Bresnihan B (1994) Synovial tissue macrophages and joint erosion in rheumatoid arthritis. Ann Rheum Dis 53:39–44

Virchows Arch (2006) 449: 78–87
DOI 10.1007/s00428-005-0123-z

ORIGINAL ARTICLE

Ida Münster Ikonomou · Anne Tierens · Gunhild Troen · Hege Vangstein Aamot · Sverre Heim · Grete F. Lauritzsen · Helen Vålerhaugen · Jan Delabie

Peripheral T-cell lymphoma with involvement of the expanded mantle zone

Received: 29 June 2005 / Accepted: 21 September 2005 / Published online: 22 April 2006
© Springer-Verlag 2006

Abstract Peripheral T-cell lymphoma (PTCL) with a nodular architecture is rare. Recently, two variants have been described with infiltration of the B-cell follicle, one variant that localizes to the marginal zone with a so-called perifollicular growth pattern, and a variant that localizes to the germinal center. These lymphomas have a CD4+ phenotype and may express Bcl-6. We have studied five similar cases of PTCL with involvement of the B-cell follicle. However, our cases differ from the cases previously described by their predominant and frequently patchy involvement of the expanded mantle zone of the B-cell follicle at onset. Later biopsies in three of the cases show diffuse infiltration of the lymph node, without features of angioimmunoblastic TCL (AILT). All cases expressed Bcl-6 in addition to CD4. Cytogenetics was available in four of the cases but revealed no recurrent chromosomal aberrations or changes associated with other types of PTCL. No mutations of the *BCL-6* gene were observed. Together, the cases seem to have an intermediately aggressive clinical behavior. Whether our cases are part of a spectrum of PTCLs that encompasses previously described variants with predominant marginal zone or germinal center infiltration or they represent a separate T-cell lymphoma type remains to be demonstrated by a study of more of such cases.

Keywords Lymphoma · T-cell · Peripheral · Bcl-6

I. M. Ikonomou (✉) · A. Tierens · G. Troen · H. Vålerhaugen · J. Delabie
Department of Pathology,
The Norwegian Radium Hospital,
University of Oslo,
Oslo, Norway
e-mail: ida.m.munster.ikonomou@radiumhospitalet.no
Tel.: +47-22934151
Fax: +47-22935426

H. V. Aamot · S. Heim
Department of Cancer Genetics,
The Norwegian Radium Hospital,
University of Oslo,
Oslo, Norway

G. F. Lauritzsen
Department of Oncology,
The Norwegian Radium Hospital,
University of Oslo,
Oslo, Norway

Introduction

Recently, nine cases of CD4+ peripheral T-cell lymphoma (PTCL) with distinct perifollicular growth pattern have been described [24]. On the basis of the typical growth pattern and uniform immunophenotype, the authors proposed that those cases belonged to a potentially novel type of nodal PTCL (nPTCL). Also recently, three cases and one additional case report of CD4+/Bcl6+ PTCL with follicular involvement have been described [6, 13]. The authors speculate that these cases may also represent a novel type of nPTCL, based on the intrafollicular growth pattern and Bcl-6 expression [6]. Bcl-6 expression in those lymphomas as well as the localization in the germinal center may indicate that those lymphomas arise from a previously described but poorly characterized subset of Bcl-6 expressing intrafollicular T-cells [4, 29].

The present article reports five similar well-documented cases, but with predominant involvement of the expanded mantle zone at onset.

Clinical history

The clinical findings of the cases are summarized in Table 1.

Briefly, four of the five patients were men. All patients presented with lymphadenopathy with or without B symptoms. One patient also presented with erythroderma, but no skin disease was noted in the other patients at onset of the disease. The patients received different treatment regimens including chemotherapy, radiotherapy or high-dose chemotherapy with autologous stem cell support. One patient died with a disease at 24 months, whereas four patients are alive with a follow-up ranging from 12 to 124 months.

Table 1 Clinical features of the cases

Case no.	Age (years)/ sex	Signs and symptoms	Sites of involvement	Treatment	Clinical course/follow-up
1	48/F	Lymphadenopathy, fatigue, weight loss, generalized itching	Cervical region, mediastinum, stage IIA, bulky	CHOP-21 ×8, RT, MIME ×4, BEAM with ASCT	First relapse: inguinal region, distal ileum, bone marrow; second relapse: cervical region and abdomen with hemophagocytic syndrome; DOD 24 months from diagnosis
2	32/M	Lymphadenopathy	Bilateral cervical regions, axillae, left groin, stage IIIA	CHOP-21 ×8, MIME ×3, BEAM with ASCT, IKE ×6, alemtuzumab 735 mg	First relapse: right cervical region; second and third relapse: lymph nodes on both sides of diaphragm; CR at 113 months from diagnosis
3	51/M	Lymphadenopathy	Cervical region, axillae, inguinal region, stage IIIA	CHOEP-14 ×6, BEAM with ASCT, RT skin, local	First relapse: skin; second relapse: skin; alive with skin affection 27 months after diagnosis
4	64/M	Lymphadenopathy, fatigue, weight loss, fever, erythroderma	Generalized lymphadenopathy, spleen, bone marrow, stage IVB	CHOP-14 ×5, prophylactic intrathecal treatment, CHOEP ×1, BEAM with ASCT	Clinical CR at 12 months from diagnosis, but with minimal residual disease in the bone marrow
5	52/M	Lymphadenopathy	Submental, axillae, stage IIA	CHOP-21 ×8, MIME ×3, BEAM with ASCT	First relapse: lymph nodes on both sides of diaphragm, bone marrow infiltration; CR at 124 months after diagnosis

F Female; *M* male; *CHOP* cyclophosfamide 750 mg/m^2, doxorubicin 50 mg/m^2, vincristin 1.4 mg/m^2, prednisolon, new course every 14 or 21 days; *RT* radiation therapy; *MIME* mitoguazone 500 mg/m^2 day 1 and 15, ifosfamide 1,000 mg/m^2 day 1–5, etoposide 100 mg/m^2 day 1–3 and metothrexate 30 mg/m^2 day 3; *BEAM* carmustine 300 mg/m^2 day 1, etoposide 150 mg/m^2×2 day 1–4, cytarabin 200 mg/m^2×2 day 1–4, and melphalan 140 mg/m^2 day 5; *ASCT* autologous stem cell transplantation; *IKE* ifosfamide 5,000 mg/m^2 day 2, carboplatin AUC5 day 2, etoposide 100 mg/m^2 day 1–3; *CHOEP-14* chop + etoposide 100 mg/m^2 day 1–3, new course every 14 days; *DOD* dead of disease; *CR* complete remission

Three of the latter patients are alive without disease and one patient currently has lymphoma affection.

Materials and methods

Tissues, blood, and bone marrow samples

The five cases we report were identified by reviewing a set of 80 archival T-cell lymphomas (with the exclusion of mycosis fungoides and T-lymphoblastic lymphoma) in adult patients diagnosed between 1990 and 2002 and of which full clinical documentation was available. Three of the five cases were sent to us in consultation.

All samples were taken for diagnosis or staging. Part of the lymph node biopsies were submitted for cytogenetic analysis, part was submitted for flow cytometric analysis (one patient), part was formalin-fixed, another part was B5-fixed, and a part was snap-frozen in liquid nitrogen and stored at −70°C until further use. Bone marrow biopsies were taken in all cases for staging purposes. Those biopsies were fixed in B5. Blood and bone marrow samples were available for cases 1 and 2 at diagnosis and follow-up and were analyzed by flow cytometry as well as molecular analysis.

Histologic, immunophenotypic and in situ hybridization studies

For histologic examination, sections were stained with hematoxylin and eosin.

Primary antibodies used for immunohistochemistry were anti-CD20 (Dako, Glostrup, Denmark), anti-CD21 (Novo Castra Laboratories, Newcastle upon Tyne, UK), anti-CD3 (Dako), anti-CD2 (Novo Castra), anti-CD4 (Novo Castra), anti-CD5 (Novo Castra), anti-CD7 (Novo Castra), anti-CD8 (Novo Castra), anti-CD30 (Dako), anti-CD57 (Novo Castra), anti-CD45RO (Dako), anti-TIA1 (Coulter Immunology Immunotech, Marseille, France), anti-granzyme B (Monosan, Uden, Netherlands), anti-CD10 (Novo Castra), anti-Bcl-6 (Dako), and anti-IgD (Dako). For most of the immunohistochemical stainings, rabbit anti-mouse antibody labeled with a peroxidase-conjugated polymer (DAKO EnVision System, Dako) was used according to the instructions of the manufacturer. For some antibodies (anti-CD20 and anti-CD57), the peroxidase-labeled avidin–biotin technique according to Hsu et al. was used [11]. Epstein Barr virus (EBV) small nuclear RNA was detected using a fluorescein-labeled PNA probe and a secondary peroxidase-labeled anti-FITC antibody (Dako). The color reaction for immunohistochemistry and in situ hybridization was developed using diaminobenzidine and H_2O_2 as substrates.

Molecular studies

Genomic DNA was extracted from three to five 5-μm frozen tissue sections or from whole blood or bone marrow samples using the Geno-M48 automatic nucleic acid extractor following the instructions of the manufacturer (Qiagen, Oslo, Norway). DNA was eluted in water. DNA at 100 ng was used for each single polymerase chain reaction (PCR) test.

For the detection of T-cell receptor (TCR) gamma gene rearrangements, a multiplex PCR with subsequent denaturing gradient gel analysis or fragment analysis was used. The primers have been described before [10]. Briefly, a set of three primers to detect the junction genes was combined

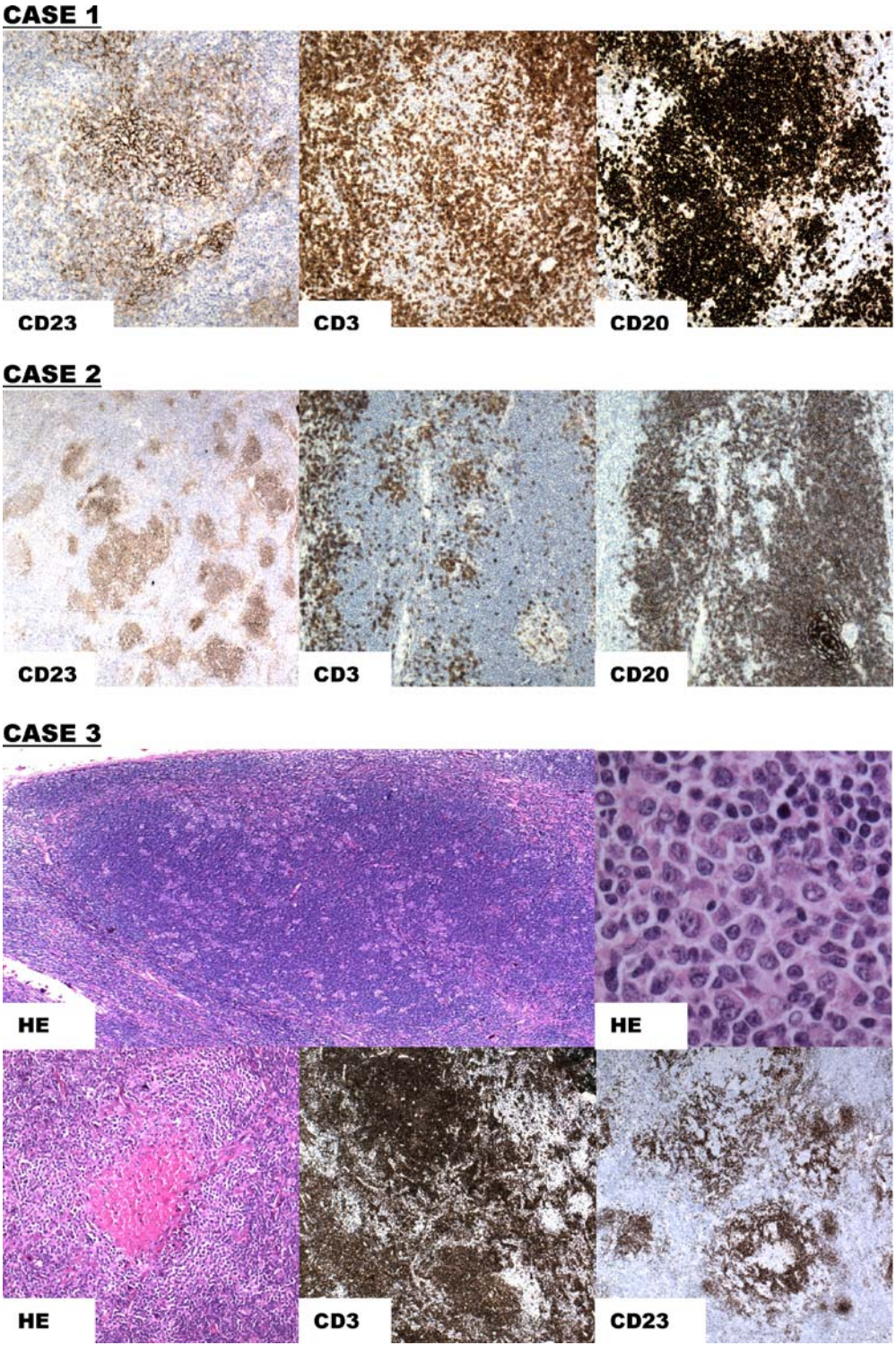

Fig. 1 Case 1. Semi-serial sections of the first lymph node biopsy (×10). CD23 immunostaining shows an expanded network of follicular dendritic cells, with clusters of clear tumor cells within the network. CD3 staining highlights infiltration of the network with T-cell lymphoma. CD20 staining highlights residual germinal center B-cells. Case 2. CD23 staining (×2) reveals multiple expanded networks of follicular dendritic cells. The subsequent panels represent semi-serial sections (×10) showing CD3 and CD20 staining, respectively. Numerous clusters of T-cells are detected within the expanded mantle zone of this follicle. Case 3. All illustrations are from a first lymph node biopsy in this case. The lymph node shows a nodular architecture (HE section, ×2). A detail of the medium- to large-sized tumor cells is shown in the *upper right-hand* panel (HE section, ×60) whereas a tumor nodule with central coagulation necrosis is shown in the *lower left-hand* panel (HE section, ×1X). CD3 staining (×2) on a semi-serial section reveals massive infiltration of T-cell lymphoma within the expanded follicles. CD23 staining (×2) reveals expanded nodular networks of follicular dendritic cells with clusters of clear tumor cells within the network

with one of the four GC-clamped primers or fluoresceinated primers to detect variable gene families 1–8, 9, 10, and 11, respectively. PCR products were subsequently run on a denaturing gradient gel and analyzed after ethidium bromide staining or run on an ABI Prism 3100 DNA analyzer (Applera Corporation, Foster City, CA).

To analyze mutations in the 5′-untranslated part of the *BCL-6* gene in the lymphoma cells, lymphoma cells were microdissected from CD3-stained frozen tissue sections of patients 1, 2, and 4, respectively. Microdissection of lymphoma cells was done to avoid contaminating B-cells, potentially harboring mutated *BCL-6* genes, from the analysis. Sections of the tissue were cut onto uncoated glass slides and immunohistochemical staining was performed as described above, with the single modification that all incubation steps were reduced to 5 min. Tumor cells were located as enlarged CD3+ cells within the CD3− nodular areas. Laser-capture microdissection was performed according to the instructions of the manufacturer (Arcturus, Mountain View, CA). Microdissected cells were lysed using proteinase K digestion (200 μg/ml proteinase K in PCR buffer at 37°C for 1 h). Lysed cells were directly used as template in the PCR reaction. For the amplification of part of the 5′-untranslated region of the *BCL-6* gene, the E1.21B (5′-CTCTTGCCAAATGCTTTG-3′) and E1.26 (5′-CACGATACTTCATCTCATC-3′) primer set encompassing nucleotides +404 to +1,142 were used. PCR conditions were as previously described [17]. The products were directly sequenced using BigDye dideoxynucleotide terminators and the ABI Prism 3100 DNA analyzer (Applera Corporation). Sequencing was performed from both ends of the PCR products, using the PCR primers.

Flow cytometry

Four-parameter flow cytometric analysis was performed on a single-cell suspension from part of a fresh lymph node obtained from patient 1 to confirm the immunophenotype of the malignant cells. Primary FITC- or PE-labeled antibodies used were anti-CD3 (clone SK7, Becton Dickinson, Franklin Lakes, NJ), anti-CD5 (clone DK23, Dako), anti-

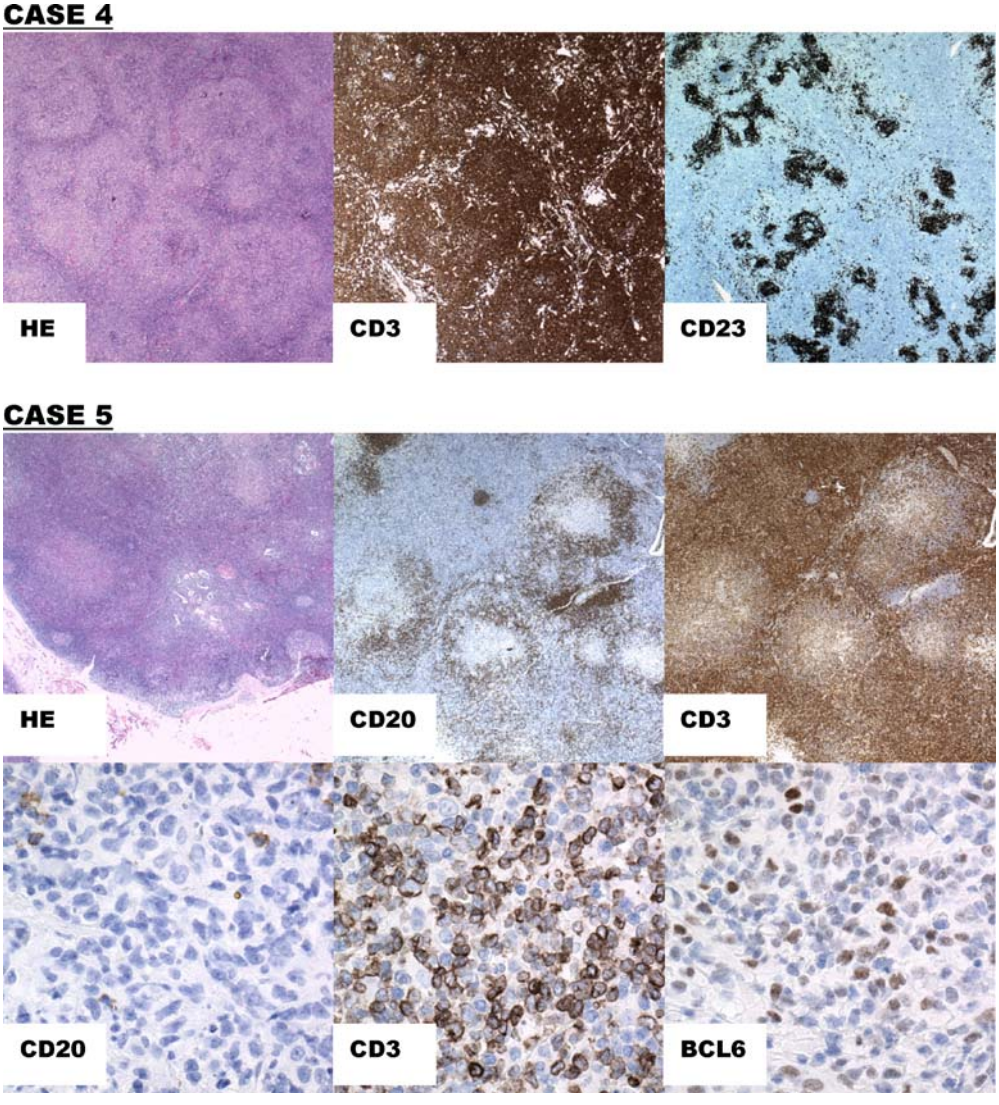

Fig. 2 Case 4. The T-cell lymphoma has a vaguely nodular pattern (HE, ×2). CD3 staining reveals a nodular T-cell lymphoma. A semi-serial section stained with CD23 staining reveals expanded but disrupted networks of follicular dendritic cells in the background of the lymphoma. Case 5. The lymph node shows partial infiltration with a pale-staining nodular T-cell lymphoma (HE, ×2). Staining for CD20 reveals a rim of small B-cells surrounding the nodular tumor infiltrate. Staining for CD3 on a semi-serial section reveals numerous medium-sized lymphoma cells within the nodules and abundant small T-cells outside the nodules. Further panels show a detail of the tumor nodules stained for CD20, CD3 and Bcl-6, respectively

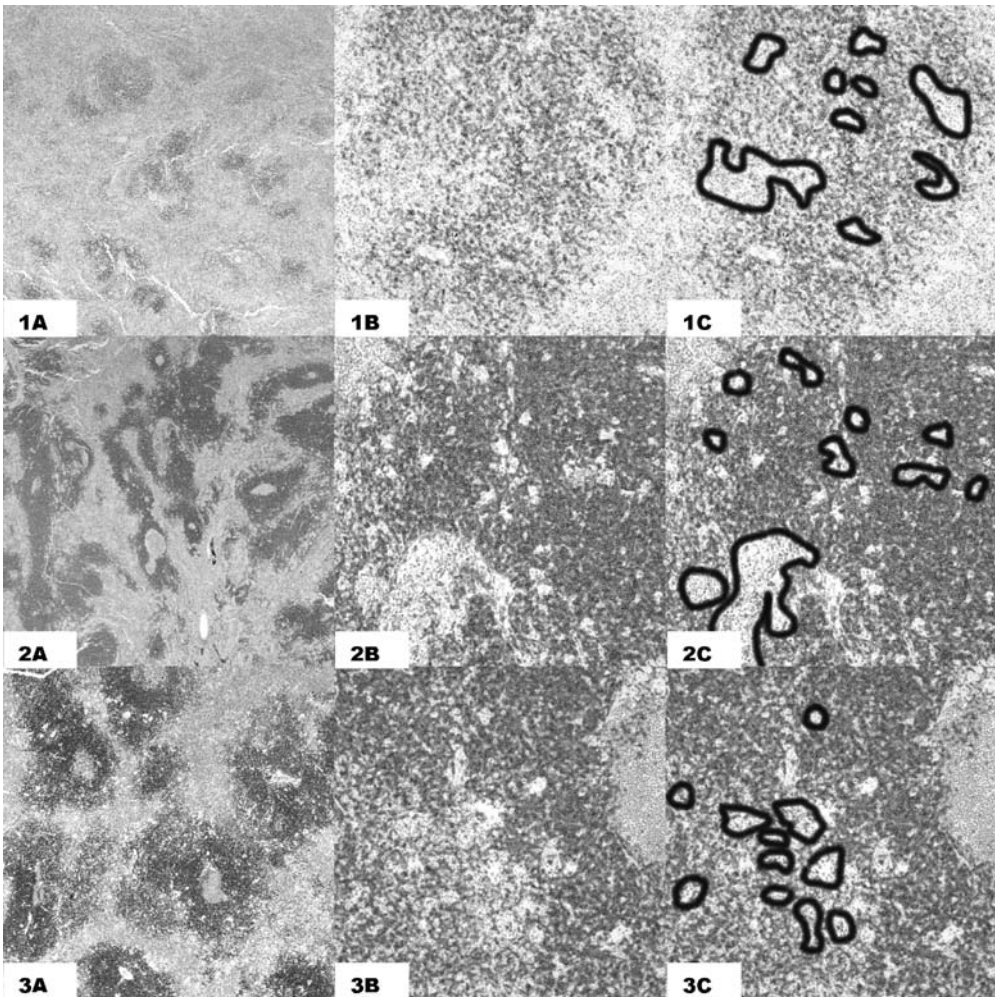

Fig. 3 The panels 1, 2 and 3 show IgD staining in cases 1, 2 and 3, respectively, with object lens magnifications ×2 (panels A) and ×10 (panels B). Those panels reveal the expansion of the mantle zones in those cases. Panels C are copies of panels B but with *circles* drawn around the T-cell lymphoma clusters within the mantle zones

CD4 (clone MT310, Dako), anti-CD8 (clone DK25, Dako), anti-CD10 (clone HI10a, Becton Dickinson), and anti-CD19 (clone SJ25C1, Becton Dickinson). Flow cytometry was performed on a FacsCalibur (Becton Dickinson) and analyzed using the Paint-a-GatePRO software (Becton Dickinson).

Cytogenetic methods

G-banding and karyotyping

Cells from lymph node biopsies were cultured for a short-term (24 h) at 37°C in McCoy's 5A medium supplemented with 20% fetal calf serum, L-glutamine, heparin, and antibiotics. The harvested dividing cells were stained according to standard G-banding protocols, using trypsin (DIFCO

Table 2 Immunophenotype of the neoplastic cells

Case	CD20	CD3	Bcl-6	CD2	CD5	CD7	CD4	CD8	Gr B	CD45RO	TIA-1	CD30	CD57	CD10	EBER
1a[a]	−	+	−	+	+	+	+	−	−	+	−	−	−	+	−
1b[a]	−	+	+	+	+	−	+	−	−	−	−	−	−	−	−
2	−	+	+	+	+	−	+	−	−	+	−	+/−	−	−	−
3	−	+	+	+	+	+	+	−	−	+	−	+/−	−	−	−
4	−	+	+	+	+	−	+	−	−	+	−	−	+	−	−
5	−	+	+	+	+	+	+	+	−	+	−	−	−	−	−

+ positive, − negative, +/− partly positive, *Gr B* Granzyme B, *TIA-1*
[a]1a represents the interfollicular small-cell component whereas 1b represents the intrafollicular large-cell component

Table 3 Genotype of the neoplastic cells

Case	Test	Lymph node	Bone marrow	Blood
1[a]	TCRgamma	3R	3R	2R
	IgH	neg.	neg.	neg.
2[a]	TCRgamma	3R	3R	NA
	IgH	neg.	neg.	NA
3	TCRgamma	1R	NA	NA
	IgH	neg.	NA	NA
4	TCRgamma	2R	NA	NA
	IgH	neg.	NA	NA
5	TCRgamma	neg.	NA	NA
	IgH	neg.	NA	NA

[a]The same TCRgamma gene rearrangement as judged by denaturing gradient gel electrophoresis was detected in the respective samples of the patients

TCR T-cell receptor, *R* clonal rearrangement, *NA* not analyzed, *neg.* no monoclonal rearrangements detected

Laboratories, Detroit, MI, USA) and Leishman solution (BHD, Poole, England). Metaphase cells were captured and analyzed on a CytoVision system (Applied Imaging, Santa Clara, CA, USA) and karyotyped in accordance with ISCN guidelines [18].

M-FISH

M-FISH analysis of the chromosomes was attempted in cases 1–3, but was unsuccessful in case 3 because only few metaphases of sub-standard technical quality were present. Freshly dropped chromosome preparations were used for M-FISH analysis. Following a pre-hybridization treatment, the chromosome preparations were denatured in 70% formamide solution at 72°C for 2.5 min, dehydrated in 70, 85, and 100% ethanol series, and air-dried. During the dehydration, 10 μl of SpectraVysion probe (Vysis, Downers Grove, IL, USA) was denatured at 72°C for 5 min and then placed on the preparation. After hybridization in a moist chamber at 37°C for 72 h, a series of post-hybridization washes were performed. The SpectrumGreen signal was amplified once. The chromosome preparation was counterstained with DAPI III (Vysis, Downers Grove, IL, USA). The fluorescence signals were captured on a CytoVision system using a single bandpass filter for Spec-

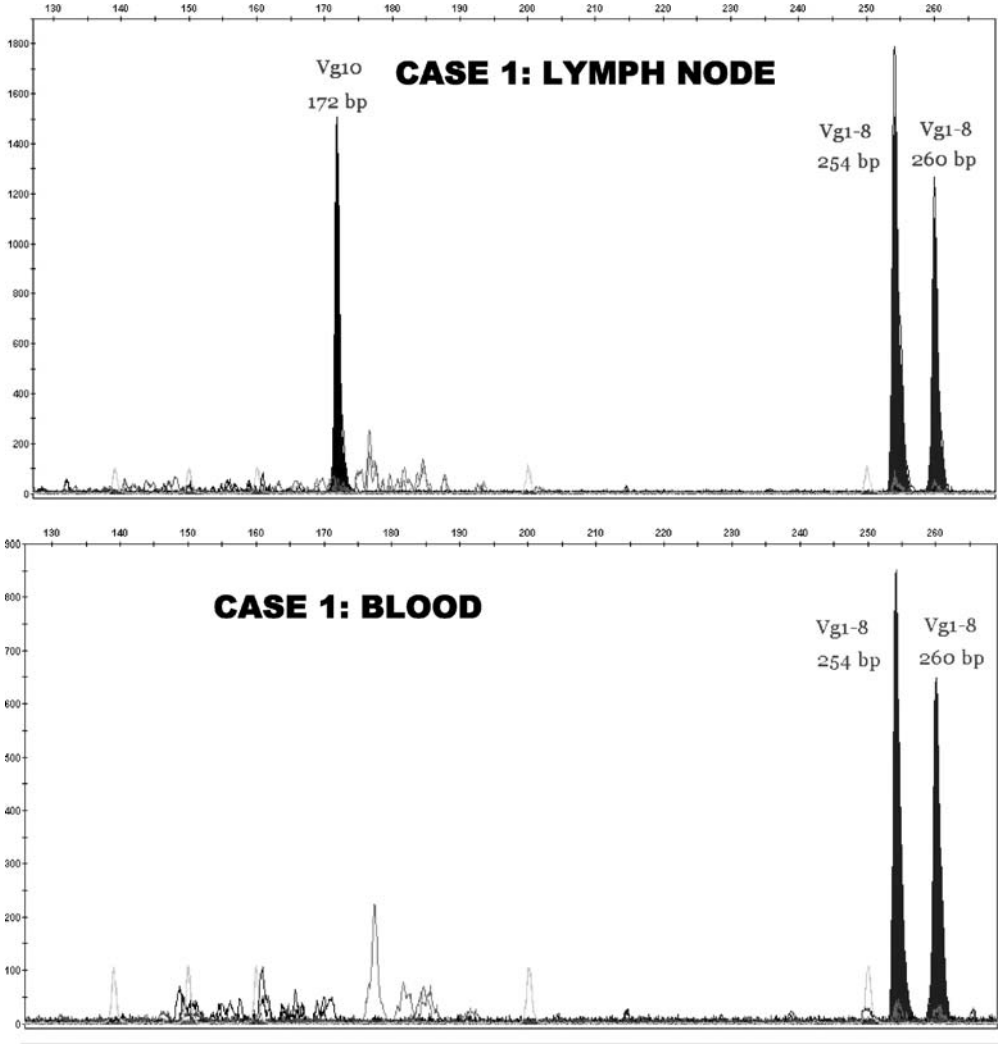

Fig. 4 Electrophoregrams showing fragment analysis of TCRgamma gene PCR products obtained from the lymph node and blood in case 1. Three prominent rearranged TCRgamma genes are seen in the lymph node, whereas only two, but identical rearranged TCRgamma genes, are observed in the blood

trumGold and SpectrumAqua, a 83.500 filter set for SpectrumGreen, SpectrumRed, and DAPI, and a 84.000 Quad filter set for SpectrumRed. The analysis was performed using the composite image of the five fluorophores and computerized pseudocoloring of the chromosomes.

Results

Histology

Representative histological and immunohistochemical features are illustrated in Fig. 1 for cases 1–3 and in Fig. 2 for cases 4 and 5.

Sequential lymph node biopsies were taken in cases 1–3, revealing progressive changes.

The most typical early change observed was the vaguely nodular architecture of the lymph node. The nodules were mainly composed of small IgD+ mantle cells (Fig. 3). Some nodules contained regressive germinal centers. Within these nodules, sprinkled clusters (cases 1–3) or larger sheets (case 4) of intermediate- to large-sized atypical T-cells were present (Fig. 2). The latter usually had clear cytoplasm and one or more visible nucleoli. The clusters of lymphoma cells were variably present within remnant germinal centers. The latter was especially prominent in case 5 (Fig. 2). In two cases, coagulation necrosis was focally seen within larger clusters of tumor cells (Fig. 1, case 3). In addition, lymphoma cells could also be observed to varying degrees in the internodular area. In sequential biopsies, the latter component predominated. No proliferation of high endothelial vessels was noted in any of the cases. No fibrosis was noted in the background. In addition, no eosinophilic granulocyte infiltration was noted.

In addition to these changes, case 1 revealed a monotonous small-cell lymphoma component in the internodular areas. These small lymphoid cells displayed slightly irregular hyperchromatic nuclei without discernable nucleoli (not illustrated).

Case 3 showed relapse of his lymphoma in the skin, but no skin biopsies were available for review.

Bone marrow biopsies showed lymphoma infiltration at diagnosis only in case 4 and at follow-up also in cases 1, 3, and 5. When involved with lymphoma, the bone marrow showed spread clusters of T-cell lymphoma, without the cellular background typically found in the lymph node (not illustrated).

Immunohistochemical and in situ hybridization studies

The immunophenotype of the malignant cells in the five cases is summarized in Table 2.

For control purposes, six cases of angioimmunoblastic T-cell lymphoma (AILT) were immunostained. The neoplastic T-cells in these six control cases were convincingly positive for CD10 in five of the six cases and for bcl-6 in two cases.

Molecular studies

Results of the genotypic studies are summarized in Table 3. Four of the five patients revealed one or more monoclonal TCR gamma gene rearrangements. Two of the patients showed at least three TCR gamma gene rearrangements, compatible with the presence of at least two neoplastic T-cell clones. We could not demonstrate clonal TCR gamma gene rearrangements in case 5. This might be due to the limited tumor infiltration in the frozen tissue sample used for the analysis. PCR products from the diagnostic lymph node and follow-up bone marrow and/or blood samples of patients 1 and 2 revealed the same monoclonal gene rearrangements (Fig. 4). This is consistent with the presence of the same clone or clones in the respective samples of each of the two patients.

Results of sequence analysis of the 5′-untranslated part of the *BCL-6* gene in the lymphoma cells showed no mutations (not illustrated).

Flow cytometry

A flow cytometric analysis on a lymph node suspension of case 1 confirmed the existence of two distinct T-cell populations, a small cell CD3+/CD4+/CD10+ and a larger cell CD3+/CD4+/CD10− population.

Table 4 Karyotype of the lymphoma cases

Case	Cytogenetics
1	46,XX,del(6)(q15q25) [8]/46,XX,der(11)t(3;11)(q13;q25),der(13)t(X;13)(q22;p11) [6]/46,XX,der(9)t(1;9)(q21;p24),der(15;17)(q10;q10),+17[4]
2	33~41,der(X)t(X;10)(q28;q24),Y,ins(1;22)(q31;q11q13),der(2)t(1;2)(q32;q37),der(3)t(3;17)(p21;q11),−4,der(5)t(4;5)(q11;p15),der(7)(qter-p22::13q?::6p21-6pter),der(7)t(4;7)(q11:p22),−9,−10,t(13;15)(q22;q22),der(14)t(9;14)(q32;p11),der(14)(qter-p11::10q22–10q26::2q23-2qter)[cp7]
3	45,XY,der(7)t(1;7)(q21;q32),add(12)(q24),+2mar,inc [9]
5	47,XY,+add(X)(p22),+Y,add(1)(p34),−2,add(3)(q29),del(3)(q12q21),add(5)(q35),−6,del(6)(q15),+7,del(8)(q22),del(12)(q22),+add(12)(q24),−13,der(1;16)(q10;p10),+mar [10]/46,XY [5]

Cytogenetics

In four of the cases (cases 1–3 and 5), abnormal karyotypes were detected. The addition of M-FISH analysis to the G-banding analysis in cases 1 and 2 enhanced the karyotypic information obtained. Whereas three cytogenetically unrelated clones were detected in case 1, only one abnormal clone was found in cases 2, 3, and 5. No results are available for case 4. The composite abnormal karyotypes, as they emerged from the combined analyses, are given in Table 4.

Discussion

We describe five cases of a variant of nPTCL with infiltration of a markedly expanded follicle mantle zone. These cases have some similarities with three cases reported by de Leval et al. and a more recently described case [6, 13]. As in those cases, our cases also have a CD3+, CD4+, CD57−, and Bcl-6+ phenotype and involve the B-cell follicle. However, whereas our cases predominantly involve the follicle mantle, lymphoma cells are typically seen in the germinal centers in the previously reported cases. Focal coagulation necrosis as described by de Leval et al. in their cases was also seen in two of our cases [6]. As in one of the cases previously reported, a correct diagnosis of lymphoma in the first lymph node biopsy was postponed due to only minimal infiltration with lymphoma cells [6]. The latter is similar to AILT, in which initial lymphoma involvement of lymph nodes can be minimal and a reactive component predominates [21]. Our cases also bear similarities to the nine cases of CD4+ PTCL with distinct perifollicular growth pattern described by Rüdiger et al. [24]. However, in their cases, the lymphoma diffusely occupied the marginal zones at diagnosis but was not typically present within an expanded mantle zone nor within the germinal centers. It was not reported whether the cases of Rüdiger et al. expressed Bcl-6 or not. It is not excluded that the T-cell lymphoma cases we describe here and the cases de Leval et al. have reported, as well as the cases of Rüdiger et al., represent one entity with a spectrum of infiltration of the B-cell follicle, ranging from a predominantly intrafollicular or mantle zone infiltration to a predominantly perifollicular growth pattern. Alternatively, our cases may be distinct. Indeed, the typical infiltration of the markedly expanded mantle zone at initiation (Fig. 5) may set our cases apart from the previously described T-cell lymphoma cases with involvement of the follicle. More cases and further genetic as well as clinical data will need to be reported to support the hypothesis that our cases represent a novel T-cell lymphoma entity. Other nodular variants of PTCL have been described previously, but the variants reported by de Leval et al., Rüdiger et al., and the cases described here are clearly distinctive by their propensity to localize to the B-cell follicle. Indeed, in previously reported nodular variants of PTCL lymphomas, the lymphoma was typically located in the T-cell area of the lymph node [16, 27]. However, interestingly, the cases described by Macon et al. were all characterized by what the authors describe as tumor nodules abutting lymphoid follicles [16]. It is therefore not excluded that those cases also might be related to the cases we describe here.

Attygalle et al. [2] point to the similarities of AILT and T-cell lymphoma with follicular involvement and suggest that the latter may be an early stage of AILT. Their argument is based on the expression of CD10 by both lymphoma types. However, the histologic features of the cases described by de Leval et al. and the cases we describe here are different from those described as type I AILT by Attygalle et al. [2, 6]. Notably, the presence of the clusters of tumor cells in the B-cell follicle (germinal center or mantle), the variable expression of CD10 (two out of three cases of de Leval et al., no expression in our cases, except on one of the clones in case 1, i.e., the interfollicular component), and the absence of B-immunoblasts and EBV positive cells in T-cell lymphoma with follicular involvement are major differences. In addition, sequential biopsies in our patients did show evolution to a diffuse lymphoma but not to a pattern typical of type II or type III AILT as described by Attygalle et al. Also, as discussed below, the cytogenetic findings are not typical of those that are described in AILT.

In contrast to the previously described cases, two of our cases contained at least two malignant clones as evidenced by TCR gamma gene rearrangement studies. In case 1, but not in case 2, the additional clone had a different morphology, phenotype, and karyotype and likely represents a composite T-cell lymphoma. The second clone consisted of CD3+, CD4+, CD10+, and Bcl-6− small cells that infiltrated exclusively the extrafollicular area but not the germinal centers. In case 2, only one morphologically and immunophenotypically homogeneous tumor population

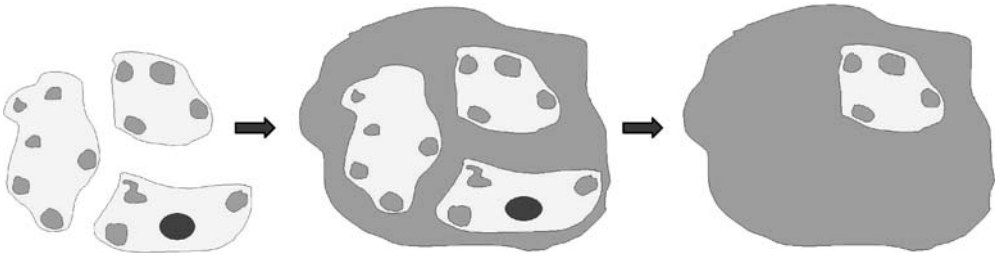

Fig. 5 The drawing depicts the progressive changes of the architectural pattern seen in our cases. Initially, clusters of T-cell lymphoma (*dark gray areas*) are seen within expanded mantle zones (*light gray areas*). Some regressive germinal centers (*black area*) may be seen. Later biopsies reveal internodular extension of the T-cell lymphoma and, ultimately, destruction of the B-cell area

was seen. Multiple clones are not unusual for T-cell lymphoma and have been reported especially for mycosis fungoides and AILT and occasionally in adult T-cell lymphoma–leukemia [26, 28]. The presence of multiple tumor clones in case 2 suggests an external triggering factor for tumorigenesis for those lymphomas such as, for example, super-antigens or the presence of a virus.

Cytogenetics in four of the cases did reveal different karyotypes, of which two were complex karyotypes. Although very few cytogenetic findings are typical for defined T-cell lymphoma types, none of the findings in our cases are similar to those described in these T-cell lymphoma entities. Notably, trisomy 5, trisomy 7, or an extra X chomosome as observed frequently in AILT were not seen in our cases [15, 25].

It is of interest that the cases reported by de Leval et al. and our cases typically infiltrate B-cell follicles and have a CD4+/Bcl-6+ phenotype [6]. The localization in the B-cell follicle as well as the immunophenotype might indicate an origin from an as yet poorly characterized subset of intrafollicular T-cells with similar phenotype [4, 22, 29]. Bcl-6 expression in T-cells is important to inhibit their differentiation into T-helper 2 cells, but the significance of this for germinal center cell development is not clear [7]. Interestingly, intrafollicular T-cells in the mice show somatic hypermutation of their antigen receptor genes as typically observed in both murine and human germinal center B-cells as well as lymphomas derived from those cells [20, 30]. Somatic hypermutation affects also the 5′-untranslated region of the *BCL-6* gene, although the latter has only been shown for B-cells [19]. Whether or not somatic hypermutation occurs in human germinal center T-cells is controversial [5, 9, 23]. Bcl-6 expression is a recurrent finding in anaplastic large-cell lymphoma, in T-lymphoblastic lymphoma, and in a subset of PTCL as well as AILT. However, only a minority of T-cell lymphomas displays *BCL-6* mutation [3, 12, 14]. We could not document *BCL-6* gene mutation in our cases described here.

Clinically, nPTCL with involvement of the mantle zone seems to behave as an intermediately aggressive lymphoma with widespread lymph node involvement at diagnosis and multiple relapses with progression of the disease following treatment with chemotherapy. These findings are similar to those of the cases reported by de Leval et al. [6]. Only limited clinical follow-up information is available for the cases described by Rüdiger et al. Of interest is the fact that some of our patients had prolonged lymphadenopathy prior to the final diagnosis of lymphoma. They also had various additional symptoms. More cases and a longer follow-up are necessary to make any firm conclusions as to the prognosis of the disease. Three of our cases received high-dose chemotherapy (HDC) with autologous stem cell support at relapse after conventional chemotherapy and two received this treatment as part of first-line therapy. Four have experienced relapses after the HDC. Case number 2 received anti-CD52 antibody treatment (alemtuzumab) at the third relapse (second relapse after high-dose treatment) and is in a complete remission 16 months after termination of treatment. One of our cases died with hemophagocytosis after high-dose therapy with stem cell support. No viral infection was documented. Hemophagocytosis complicating autologous stem cell transplantation is rare but has been reported before [1, 8]. Alternatively, hemophagocytosis might have been secondary to the relapsed T-cell lymphoma. Hemophagocytosis is a known complication of T-cell lymphoma.

In conclusion, PTCL with involvement of the B-cell follicle has special morphologic features that distinguish these cases from other PTCL. Larger series will have to be reported to establish whether or not PTCL with involvement of the various structures (germinal center, mantle, or marginal zone) of the B-cell follicle represents one or more clinico-pathologic entities.

References

1. Abe Y, Choi I, Hara K, Matsushima T, Nishimura J, Inaba S, Nawata H, Muta K (2002) Hemophagocytic syndrome: a rare complication of allogeneic nonmyeloablative hematopoietic stem cell transplantation. Bone Marrow Transplant 29:799–801
2. Attygalle A, Al-Jehani R, Diss TC, Munson P, Liu H, Du M-Q, Isaacson PG, Dogan A (2002) Neoplastic T cells in angioimmunoblastic T-cell lymphoma express CD10. Blood 99:627–633
3. Carbone A, Gloghini A, Gaidano G, Dalla-Favera R, Falini B (1997) *BCL-6* protein expression in human peripheral T-cell neoplasms is restricted to CD30+ anaplastic large-cell lymphomas. Blood 90:2445–2450
4. Cattoretti G, Chang C-C, Cechova K, Zhang J, Ye BH, Falini B, Louie DC, Offit K, Chaganti RSK, Dalla-Favera R (1995) Bcl-6 protein is expressed in germinal-center B cells. Blood 86:45–53
5. Cheynier R, Henrichwark S, Wain-Hobson S (1998) Somatic hypermutation of the T cell receptor Vβ gene in microdissected splenic white pulps from HIV-1-positive patients. Eur J Immunol 28:1604–1610
6. de Leval L, Savilo E, Longtine J, Ferry JA, Harris NL (2001) Peripheral T-cell lymphoma with follicular involvement and a CD4+/bcl-6+ phenotype. Am J Surg Pathol 25:395–400
7. Dent AL, Hu-Li J, Paul WE, Staudt LM (1998) T helper type 2 inflammatory disease in the absence of interleukin 4 and transcription factor STAT6. Proc Natl Acad Sci USA 95:13823–13828
8. Fukuno K, Tsurumi H, Yamada T, Oyama M, Moriwaki H (2001) Graft failure due to hemophagocytic syndrome after autologous peripheral blood stem cell transplantation. Int J Hematol 73:262–265
9. Golby SJC, Dunn-Walters DK, Spencer J (1999) Human tonsillar germinal center T cells are a diverse and widely disseminated population. Eur J Immunol 29:3729–3736
10. Greiner TC, Raffeld M, Lutz C, Dick F, Jaffe ES (1995) Analysis of T cell receptor-gamma gene rearrangements by denaturing gradient gel electrophoresis of GC-clamped polymerase chain reaction products. Correlation with tumor-specific sequences. Am J Pathol 146:46–55
11. Hsu SM, Raine L, Fanger H (1981) Use of avidin–biotin–peroxidase complex (ABC) in immunoperoxidase techniques: a comparison between ABC and unlabeled antibody (PAP) procedures. J Histochem Cytochem 29:577–580
12. Hyjek E, Chadburn A, Liu YF, Cesarman E, Knowles DM (2001) *BCL-6* protein is expressed in precursor T-cell lymphoblastic lymphoma and in prenatal and postnatal thymus. Blood 97:270–276
13. Jiang L, Jones D, Medeiros LJ, Orduz YR, Bueso-Ramos CE (2005) Peripheral T-cell lymphoma with a "follicular" pattern and the perifollicular sinus phenotype. Am J Clin Pathol 123:448–455

14. Kerl K, Vonlanthen R, Nagy M, Bolzonello NJ, Gindre P, Hurwitz N, Gudat F, Nador RG, Borisch B (2001) Alterations on the 5′ noncoding region of the *BCL-6* gene are not correlated with *BCL-6* protein expression in T cell non-Hodgkin lymphomas. Lab Invest 81:1693–1702
15. Lepretre S, Buchonnet G, Stamatoullas A, Lenain P, Duval C, d'Anjou J, Callat M-P, Tilly H, Bastard C (2000) Chromosome abnormalities in peripheral T-cell lymphoma. Cancer Genet Cytogenet 117:71–79
16. Macon WR, Williams ME, Greer JP, Cousar JB (1995) Paracortical nodular T-cell lymphoma. Identification of an unusual variant of peripheral T-cell lymphoma. Am J Surg Pathol 19:297–303
17. Migliazza A, Martinotti S, Chen W, Fusco C, Ye BH, Knowles DM, Offit K, Chaganti RSK, Dalla-Favera R (1995) Frequent somatic hypermutation of the 5′ noncoding region of the *BCL-6* gene in B-cell lymphoma. Proc Natl Acad Sci USA 92:12520–12524
18. Mitelman F (ed) (1995) An international system for human cytogenetic nomenclature. Karger, Basel
19. Pasqualucci L, Migliazza A, Fracchiolla N, William C, Neri A, Baldini L, Chaganti RSK, Klein U, Küppers R, Rajewsky K, Dalla-Favera R (1998) *BCL-6* mutations in normal germinal center B cells: evidence of somatic hypermutation acting outside Ig loci. Proc Natl Acad Sci USA 95:11816–11821
20. Rajewsky K (1996) Clonal selection and learning in the antibody system. Nature 27 381(6585):751–758
21. Ree HJ, Kadin ME, Kikuchi M, Ko YH, Go JH, Suzumiya J, Kim DS (1998) Angioimmunoblastic lymphoma (AILD-type T-cell lymphoma) with hyperplastic germinal centers. Am J Surg Pathol 22:643–655
22. Ree HJ, Kadin ME, Kikuchi M, Ko YH, Suzumiya J, Go JH (1999) Bcl-6 expression in reactive follicular hyperplasia, follicular lymphoma, and angioimmunoblastic T-cell lymphoma with hyperplastic germinal centers: heterogeneity of intrafollicular T-cells and their altered distribution in the pathogenesis of angioimmunoblastic T-cell lymphoma. Hum Pathol 30:403–411
23. Roers A, Hansmann ML, Rajewsky K, Küppers R (2000) Single-cell PCR analysis of T helper cells in human lymph node germinal centers. Am J Pathol 156:1067–1071
24. Rüdiger T, Ichinohasama R, Ott MM, Müller-Deubert S, Miura I, Ott G, Müller-Hermelink HK (2000) Peripheral T-cell lymphoma with distinct perifollicular growth pattern. A distinct subtype of T-cell lymphoma? Am J Surg Pathol 24:117–122
25. Schlegelberger B, Zhang Y, Weber-Matthiesen K, Grote W (1994) Detection of aberrant clones in nearly all cases of angioimmunoblastic lymphadenopathy with dysproteinemia-type T-cell lymphoma by combined interphase and metaphase cytogenetics. Blood 84:2640–2648
26. Smith JL, Hodges E, Quin CT, McCarthy KP, Wright DH (2000) Frequent T and B cell oligoclones in histologically and immunophenotypically characterized angioimmunoblastic lymphadenopathy. Am J Pathol 156:661–669
27. van den Oord JJ, de Wolf-Peeters C, O'Connor NTJ, de Vos R, Tricot G, Desmet VJ (1988) Nodular T-cell lymphoma. Report of a case studied with morphologic, immunohistochemical, and DNA hybridization techniques. Arch Pathol Lab Med 112:133–138
28. Vega F, Luthra R, Medeiros LJ, Dunmire V, Lee S-J, Duvic M, Jones D (2002) Clonal heterogeneity in mycosis fungoides and its relationship to clinical course. Blood 100:3369–3373
29. Ye BH, Cattoretti G, Shen Q, Zhang J, Hawe N, de Waard R, Leung C, Nouri-Shirazi M, Orazi A, Chaganti RSK, Rothman P, Stall AM, Pandolfi P-P, Dalla-Favera R (1997) The *BCL-6* proto-oncogene controls germinal-centre formation and Th2-type inflammation. Nat Genet 16:161–170
30. Zheng B, Xue W, Kelsoe G (1994) Locus-specific somatic hypermutation in germinal centre T cells. Nature 372:556–559

Virchows Arch (2006) 449: 88–95
DOI 10.1007/s00428-006-0197-2

ORIGINAL ARTICLE

Ivo Steiner · Petra Hájková · Jiří Kvasnička · Ivana Kholová

Myocardial sleeves of pulmonary veins and atrial fibrillation: a postmortem histopathological study of 100 subjects

Received: 25 November 2005 / Accepted: 7 February 2006 / Published online: 13 April 2006
© Springer-Verlag 2006

Abstract Atrial fibrillation (AF) is triggered by ectopic beats originating from extensions of the left atrial myocardium over the pulmonary veins (PVs), so-called myocardial sleeves. A total of 100 hearts (393 PVs) obtained at autopsy were studied. Of these, 50 were from patients with chronic AF and 50 from controls in sinus rhythm. Out of a total of 393 PVs studied, a sleeve was present in 349 PVs (88.8%). The myocardial sleeves frequently harboured senile atrial amyloid and scarring. These two changes were evaluated semi-quantitatively (grade 0–3). Amyloidosis was found in 68% of all hearts and in 55% of all sleeves. It was more frequent in patients with AF (58.5%) than in those without (51.7%), however, without statistical significance (p values 0.948, 0.306, 0.166 and 1). Scarring was present in all 349 sleeves studied. It was significantly more severe in patients with AF (average grade 2.44) than in those without (average grade 2.00) (p values <0.001, <0.1, <0.05 and <0.01). In conclusion, amyloidosis and particularly scarring of the myocardial sleeves of the pulmonary veins, appear to be common in the elderly population as an arrhythmogenic substrate for AF.

Keywords Atrial fibrillation · Pathogenesis · Pulmonary veins · Myocardial sleeves of pulmonary veins · Senile heart amyloid

I. Steiner (✉) · P. Hájková · I. Kholová
The Fingerland Department of Pathology,
Charles University Faculty of Medicine and Faculty Hospital,
Hradec Králové, Czech Republic
e-mail: steiner@lfhk.cuni.cz
Tel.: +420-495-514673
Fax: +420-495-832004

J. Kvasnička
First Department of Internal Medicine,
Charles University Faculty of Medicine and Faculty Hospital,
Hradec Králové, Czech Republic

Introduction

Atrial fibrillation (AF) is the most common sustained cardiac arrhythmia and is characterised by rapid and irregular activation of the atrium (400–600/min.). Its prevalence increases with age, rising from 0.5% of subjects in their 50s to nearly 10% of octogenarians. Its prevalence is almost certain to increase in the coming decades [27]. Key risk factors for development of AF include, in addition to age, systemic hypertension, congestive heart failure, myocardial infarction, valvular disease (particularly mitral stenosis) and thyrotoxicosis. In 30–50% of cases, AF occurs in individuals without any evidence of cardiac or other disease, so-called lone AF. AF is a source of considerable morbidity and mortality, increasing the risk of heart failure, thromboembolic phenomena, particularly ischemic stroke, and death [1, 10, 26, 31, 32, 35, 47].

The pathogenesis of AF has not been fully elucidated. The cardiac rhythm in AF is controlled not by the sinoatrial node but by multiple ectopic pacemakers in the atrial chambers. The groundbreaking electrophysiological work of French authors in 1997 and 1998 demonstrated that, in most patients with AF, the ectopic beats originate in the region of pulmonary veins (PVs), mostly the superior ones [13, 20]. Because of these findings, the pulmonary veins, formerly rather neglected structures, became a subject of interest to cardiologists and pathologists [11, 19, 37, 45]. It was subsequently shown that the ectopic impulses originate in extensions of left atrial myocardium over the PVs, structures described as ‘myocardial sleeves of pulmonary veins’.

The precise morphology of these sleeves is relevant for ablation treatment of chronic AF, involving selective catheter destruction of arrhythmia-generating tissue in the PVs or complete electrical isolation of the PVs from the left atrium [17]. To date, however, a paucity of data exists about this subject. We present herein the results of our investigation of PVs from the most extensive cohort so far studied of 100 hearts at autopsy, focusing on two pathological conditions of the sleeves in particular, senile isolated atrial amyloidosis and scarring, and their possible relationship to AF.

Fig. 1 Left atrium and pulmonary veins after fixation and cross sections of the veins for histology

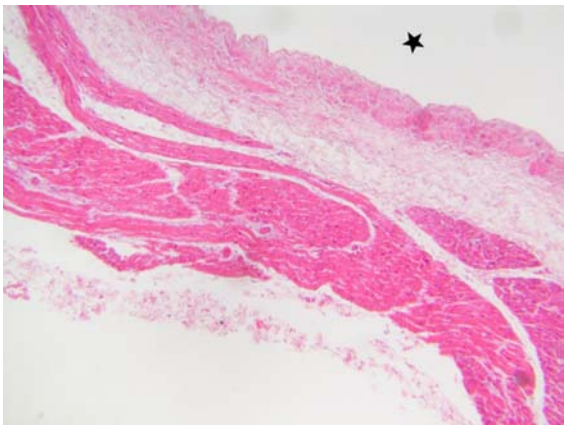

Fig. 2 Segment of a well-developed myocardial sleeve of a pulmonary vein. *Asterisk* indicates vein lumen. HE, ×50

Materials and methods

During the period October 2003 to May 2005, 100 hearts with PVs obtained at autopsy were studied: 50 from consecutive patients with chronic AF and 50 control hearts from patients without this arrhythmia. The latter were selected so that the two groups did not significantly differ with regard to demographic or clinical characteristics.

In all subjects, the heart was excised together with PVs, with excision being extended into the pulmonary hila. The entire specimen was fixed in buffered formalin with glass tubes of appropriate diameter inserted into the PVs to maintain their shape. Complete cross sections of the PVs, namely, right superior, right inferior, left superior and left inferior, were cut at 4–5 mm intervals from the periphery towards the venoatrial junction (Fig. 1). Specimens were taken also from the free walls of all the four heart chambers. The sections were routinely processed and stained by hematoxylin–eosin (HE), resorcin-fuchsin Van Gieson (El VG) and, for the detection of amyloid by a modified Sweat and Puchtler method, using the direct cotton dye Sirius (Saturn) red. The isolated atrial amyloid (IAA) character of the amyloid deposits was confirmed by their immunoreactivity with the human atrial natriuretic peptide antibody (CBL 66, Cymbus Biotechnology; 1:6,000).

The extent and severity of both amyloid deposits and scarring in the myocardial sleeves of PVs was graded subjectively on a scale of 0 to 3 by the following criteria:

- Isolated atrial amyloid: 0=not present; 1=occasional fine fibers around cardiomyocytes and/or in the walls of small intramyocardial vessels, mostly in the inner layers of the sleeve; 2=more frequent fibers in the entire thickness of the sleeve; 3=dense network of fibers and/or solid foci
- Scarring: 0=absent; 1=isolated foci of fibrosis affecting only a part of the sleeve and/or mild diffuse interstitial fibrosis; 2=isolated foci of fibrosis affecting the entire thickness of the sleeve and/or moderately severe diffuse interstitial fibrosis; 3=multiple confluent foci affecting the entire thickness of sleeve and/or severe scarring completely replacing the myocardium

Histological examination with grading of amyloidosis and of scarring was done blind to clinical data. Only after assessing all hearts were clinical records reviewed by a cardiologist (JK) unaware of the morphological findings. The subjects were classified into two groups:

- AF group: Comprising patients with permanent AF recorded repeatedly during at least the last 2 years, patients with paroxysmal AF and patients with AF recorded during their hospitalisation immediately preceding death but with no previous documentation regarding heart rhythm

Table 1 Baseline demographic and clinical data in patients with atrial fibrillation and wihout the arrhythmia (controls)

	Number		Age (mean, years)		HD	DM	Cause of death				
	Male	Female	Male	Female			IHD	Valvular disease	Malignancy	Cor pulmonale	Other
AF	50		76.9±7.3		34	22	16	5	8	6	15
	21	29	75.9	77.6							
Controls	50		71.7±9.5		34	17	11	3	17	2	17
	20	30	74.0	70.2							

AF Atrial fibrillation, *DM* diabetes mellitus, *HD* hypertensive disease, *IHD* ischemic heart disease

– Control group: Comprising patients in sinus rhythm and patients with terminal AF in whom sinus rhythm had been documented during the last year

The baseline demographic and clinical data for all subjects are presented in Table 1.

According to the clinical case notes, there were 68 patients with systemic hypertension, 39 with diabetes (30 patients had both), 50 with chronic atrial fibrillation, 27 with ischemic heart disease, 8 with valvular disease, and 8 with chronic cor pulmonale. At autopsy, 76 hearts were hypertrophic (>400 g in men or >350 g in women); in the remaining 24, the weight was within the normal range. Coronary atherosclerosis was assessed as mild (<50% luminal stenosis) in 44 hearts and as significant (>50% stenosis) in 56. In 17 hearts, there was marked atrial dilatation (both atria in 11, the right atrium only in 5 and the left atrium only in 1). None of the hearts showed an either primary or secondary tumor [8]. The SA and AV node were not sampled.

In all subjects, a complete autopsy was performed with appropriate sampling; there was no case of systemic amyloidosis.

The data obtained were evaluated by Fisher's exact test in contingency tables and analysis of variance with multiple comparisons. A value of $p<0.05$ was considered to be statistically significant.

Results

The 100 subjects studied comprised 41 men aged 56–92 years (mean age 75.0±8.1 years) and 59 women aged 51–95 years (mean age 73.8±9.3 years). There was a total of 393 PVs (seven hearts had a common right PV).

Myocardial sleeves are formed by left atrial myocardium extending over the PVs, covering them for a variable distance towards the pulmonary hilus and even beyond it. The sleeve is, therefore, always positioned on the adventitial side of the PV, separated from the media by a fibrofatty layer (Fig. 2).

Of the total of 393 PVs, a sleeve was revealed in 349 (88.8%), most frequently in the right superior PV (right superior PV 95.7%; left superior 89%; right and left inferior PVs 85%; all seven common right PVs had a sleeve). In the 93 hearts with four PVs, there were 64 in which all PVs had sleeves, 19 in which 3 had sleeves, 8 in which 2 had sleeves and 2 in which only 1 had a sleeve. Sleeves were generally longer in the upper than in the lower PVs and in the left than in the right ones. Features of the sleeves, e.g. frequency and distribution among individual PVs, did not differ significantly between the AF and the control group.

Isolated atrial amyloid was present in the atrial walls in 80 hearts (80%), in both atria in 65, in the left atrium only (right atrium negative) in 13 and in the right atrium only (left atrium negative) in two. It was more frequent in women (88.1%) than in men (68.3%). The deposits were immunoreactive for atrial natriuretic peptide.

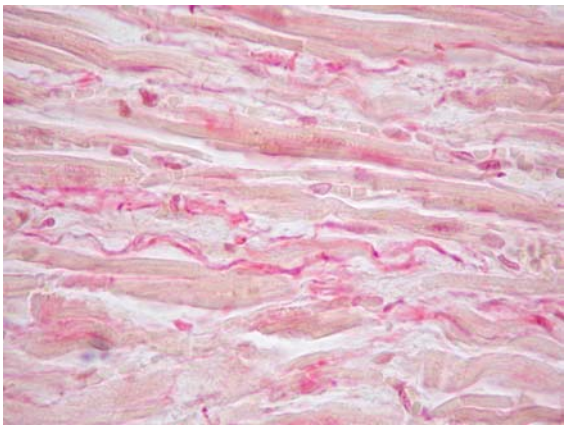

Fig. 3 Grade 1 amyloid in sleeve myocardium. Sirius red, ×250

In the myocardial sleeves of PVs, IAA was present in 68 hearts (68%) in a total of 192 sleeves (55%) (Figs. 3 and 4). The deposits were slightly more marked in the central parts of the sleeves than at their periphery. The severity (average grade) of amyloidosis in all 349 sleeves was: right superior PV=1.03, right inferior PV=0.82, common right PV=1.86, left superior PV=0.76 and left inferior PV=0.60. The distribution of the grades in individual PVs in the AF and the control group is shown in Table 2. Although amyloid in the sleeves was more common in the AF group than in the controls (76 vs 60% of hearts and 58.5 vs 51.7% of sleeves) and more severe (average grade 0.89 vs 0.76), we failed to find a statistically significant relation (right superior PV $p=0.948$; right inferior PV $p=0.306$; left superior PV $p=0.166$ and left inferior PV $p=1$).

In eight hearts, there were, in addition to IAA, deposits of senile systemic amyloid (transthyretin immunoreactive) in the ventricular myocardium.

Scarring of the myocardial sleeves was universal, present at least mildly in all 349 sleeves. It was much more pronounced at their periphery (towards the lungs) than centrally (close to the left atrium). In the mild cases, intercellular fibrosis affected only a part of the sleeve thickness, sometimes only an isolated muscle bundle

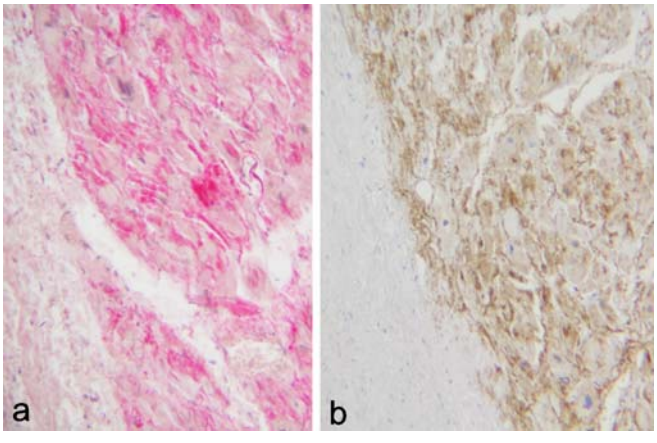

Fig. 4 Grade 3 amyloid in sleeve myocardium. **a** Sirius red, ×125. **b** Immunostaining for atrial natriuretic peptide. ×125

Table 2 The degree of isolated atrial amyloid in myocardial sleeves of pulmonary veins

	Gr. 0		Gr. 1		Gr. 2		Gr. 3		Σ		Average grade		*p*
	AF	Controls	AF	Controls	AF	Controls	AF	Controls	AF	Controls	AF	Controls	
RS	14	19	16	14	9	7	3	7	42	47	1.02	1.04	n.s.
RI	17	18	12	14	7	8	2	1	38	41	0.84	0.80	n.s.
Comm. R	1	0	1	1	1	0	3	0	6	1	2.00	1.00	
LS	15	24	17	17	10	4	1	1	43	46	0.93	0.61	n.s.
LI	24	25	12	12	4	5	2	1	42	43	0.62	0.58	n.s.
Σ	71	86	58	58	31	24	11	10	171	178	0.89	0.76	

AF Atrial fibrillation, *Comm. R* common right pulmonary vein (PV), *Gr.* grade, *LI* left inferior PV, *LS* left superior PV, *n.s.* not significant, *p* statistical significance, *RI* right inferior PV, *RS* right superior PV

(Fig. 5). In the advanced cases, the entire thickness was collagenised (Fig. 6) and the sleeve became thinner, most markedly at the periphery; the fibrosed fingerlike projections of its myocardium acquired a serpentine shape (Fig. 7). In a totally scarred sleeve, the structure of the myocardium was smudged, appearing homogeneous, glassy and hyaline, sometimes even with finely granular calcification (Fig. 8). The El VG stain revealed numerous elastic fibers within the collagen matrix—'fibroelastosis' (Figs. 9 and 10). The microvasculature showed no obvious changes.

Because of the irregular distribution of scarring along the sleeves, its grading was assessed from a mid-length section. The severity (average) of scarring in all 349 sleeves was: right superior PV=2.14, right inferior PV=2.08, common right PV=2.0, left superior PV=2.27 and left inferior PV=2.41. The distribution of the grades in individual PVs in the AF and the control group is shown in Table 3. The grade of scarring was statistically significantly higher in the AF group compared with the controls in the right superior PV ($p<0.001$), the left superior PV ($p<0.05$) and the left inferior PV ($p<0.01$); in the right inferior PV, the difference was marginal ($p=0.08$). An association ($p<0.05$) between sleeve scarring and the patient's age was found for both superior PVs.

In a search for the genesis of the scarring, we have shown that the myocardial sleeves are supplied by coronary arteries; an injection of a solution of gelatine stained by black Indian ink into both coronary orifices in six isolated hearts with PVs revealed the black material to be histologically demonstrable in small intramyocardial sleeve vessels. This raised the obvious question of whether there is relationship between the degree of coronary atherosclerosis and the grade of myocardial sleeve scarring but, in fact, neither the entire cohort (Table 4) nor the separate AF or control group showed such a relation. As regard to other possible causes of scarring, there has been no case with either inflammation (myocarditis) or obvious apoptosis in the myocardial sleeves.

In addition to amyloidosis and scarring, other pathological findings were occasionally encountered in the myocardial sleeves, e.g. lipomatous atrophy, vacuolar degeneration, chronic inflammatory infiltrates, deposits of systemic senile amyloid, septic emboli, leukaemic infiltrates and metastatic carcinoma.

Discussion

The extensions of left atrial myocardium onto pulmonary veins, now known as myocardial sleeves of pulmonary veins, were first described in 1836 by a medical student Raeuschel, under the tutorship of Purkyně in then Prussian Breslau [33, 41]. In 1966, Nathan and Eliakim published a detailed gross anatomical description of them [30], but it

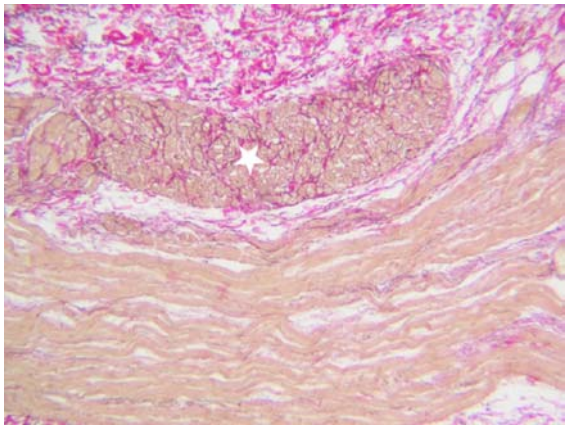

Fig. 5 Grade 1 scarring of a myocardial sleeve. An isolated muscle bundle (*asterisk*) shows interstitial fibrosis. The remaining myocardium appears normal. El VG, ×125

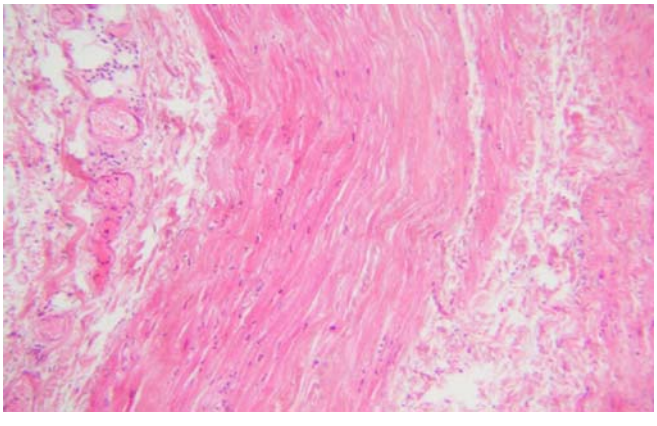

Fig. 6 Grade 3 scarring of a myocardial sleeve. Smudged structure and hyalinisation of the muscle. HE, ×125

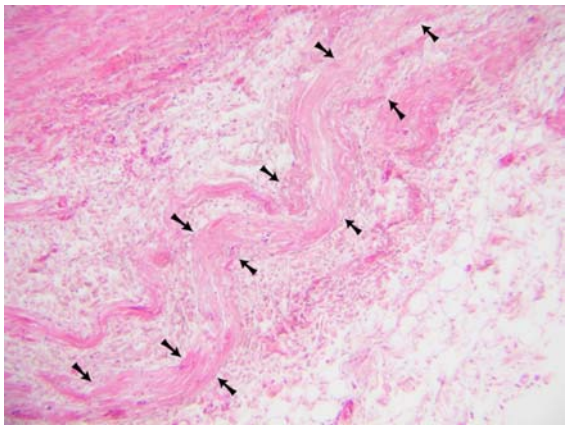

Fig. 7 Totally scarred, hyalinised peripheral projection of a sleeve (*between arrows*) acquiring a serpentine shape. HE, ×125

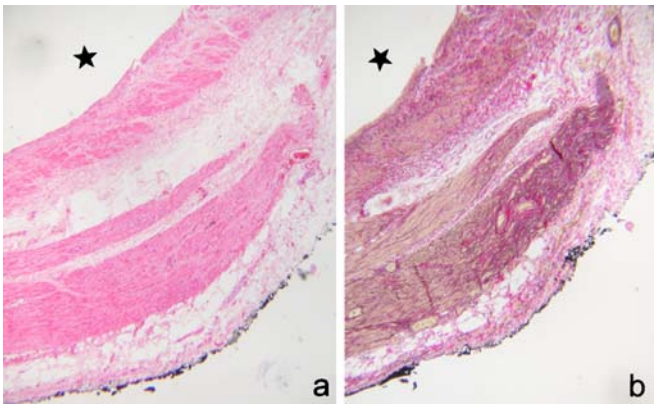

Fig. 9 Fibroelastosis of the peripheral part of a myocardial sleeve. *Asterisk* indicates vein lumen. **a** HE, ×50. **b** El VG, ×50

was only in the late 1990s, after the pioneering electrophysiological studies of Jaïs et al. [20] and Haïssaguerre et al. [13] established the crucial role of PVs in the initiation of AF, that the sleeves became of interest to morphologists. There is, nevertheless, a paucity of data about PV morphology as an arrhythmogenic substrate, and we are aware of only eight previous anatomopathological studies [15, 16, 23, 29, 35, 36, 42, 46]. These were limited investigations of between 10 [35] and 43 [23] hearts and their results can be summarised as follows.

Myocardial sleeves are developed in 68–100% of PVs and their length is 4–48 mm, mostly 10–13 mm. Their mean thickness is 1.1 mm but may be up to 5 mm; they are thickest at the venoatrial junction, thinning out peripherally. The sleeves are more extensive around the superior PVs. Their peripheral margin is irregular, usually not circumferential, with multiple, small fingerlike projections. The myocardial bundles of the sleeves are arranged circularly, longitudinally and obliquely. There is marked interindividual and intraindividual variability in character of the sleeves. Specialised cells, particularly node-like cells, were not seen [14].

The current study more or less confirms all these findings. In our group of 100 hearts from patients both with and without AF, the frequency of myocardial sleeves was 100% of hearts and 89% of PVs. The right superior PV was the single most often coated vein (96%). There was no obvious difference in the pattern of the sleeves between the AF and control groups.

To the best of our knowledge, this is the first study dealing with the presence of amyloid in the myocardial sleeves. The entity known nowadays as senile heart amyloid was first described by Soyka in 1876 [39]. In 1979, Westermark et al. [5] showed that there are two types of senile heart amyloid, the more common type, limited to the atria and designated ‘isolated atrial amyloid’, and the rarer and clinically more relevant ‘systemic senile amyloid’, affecting the entire myocardium and sometimes extracardiac tissues [24]. In 1986, Kaye et al. [22] demonstrated that IAA’s protein precursor is atrial natriuretic peptide (ANP). In our previous study [40], it was shown that IAA deposits in the atrial walls first appear in the fourth decade of life, their prevalence increasing roughly linearly by 15–20% with each subsequent decade to reach 95% in nonagenarians; the prevalence is higher in females than in males. For the identification of IAA, the Sirius red method is superior to the Congo red method, the difference mainly with regard to very small deposits which

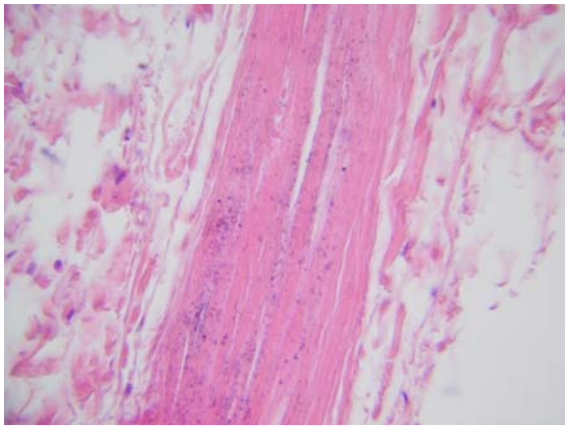

Fig. 8 Totally scarred, hyalinised sleeve with fine microcalcifications. HE, ×250

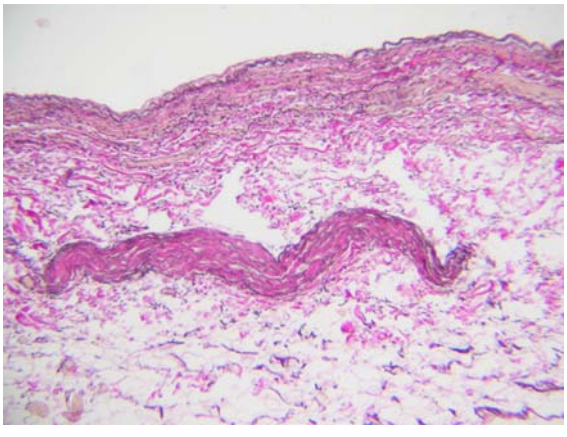

Fig. 10 Thin fingerlike sleeve peripheral projection with marked fibroelastosis. El VG, ×125

Table 3 The degree of scarring in myocardial sleeves of pulmonary veins

	Gr. 0		Gr. 1		Gr. 2		Gr. 3		Σ		Average grade		*p*
	AF	Controls	AF	Controls	AF	Controls	AF	Controls	AF	Controls	AF	Controls	
RS	0	0	6	13	12	28	24	6	42	47	2.43	1.85	<0.001
RI	0	0	6	12	16	21	16	8	38	41	2.26	1.90	0.08
Comm. R	0	0	0	1	5	0	1	0	6	1	2.17	1.00	
LS	0	0	5	11	13	21	25	14	43	46	2.47	2.07	<0.05
LI	0	0	3	6	10	22	29	15	42	43	2.62	2.21	<0.01
Σ	0	0	20	43	56	92	95	43	171	178	2.44	2.00	

AF Atrial fibrillation, *Comm. R* common right pulmonary vein (PV), *Gr.* grade, *LI* left inferior PV, *LS* left superior PV, *n.s.* not significant, *p* statistical significance, *RI* right inferior PV, *RS* right superior PV

may not be evident with Congo red staining. Unlike Congo red, the Sirius red method gives uniform results as it does not require differentiation.

A relationship between senile amyloidosis of the heart (not of the sleeves) and AF has already been described [5, 18]; in a recent study of surgically removed right atrial appendages, Röcken et al. [34] showed more frequent and more severe deposits of IAA in patients with AF than in those in sinus rhythm.

We have demonstrated in the current study that IAA is deposited not only in the atrial walls but also in the myocardial sleeves of the PVs; it was present in 68% of hearts and in 55% of sleeves. The deposits were more marked in the central parts of the sleeves than at their periphery. The superior PVs contained more amyloid than the inferior ones, and the right PVs were more affected than the left. The amyloid was present in 76% of patients with AF and its average grade was 0.89, while in patients in sinus rhythm, the values were 60 and 0.76, respectively. The differences, however, do not reach statistical significance.

The characteristic scarring (fibrosis) of the myocardial sleeves has been noted in several previous autopsy studies, but reports of its significance vary. In some, it was correlated with AF [16, 23, 29, 36, 46]; in others, it was not [15, 42]. It was more marked in the left-sided PVs than in the right-sided ones and did not correlate with age [16]. Only Hassink et al. [15] graded systematically the degree of fibrosis.

Similarly inconsistent are the results of biopsy studies in which the wall and/or appendage of the left or right atria (not the sleeves) were examined. Patients with chronic AF, compared with those in sinus rhythm, showed more fibrosis of the atrial myocardium [3, 6, 21, 25, 48], often associated with atrial dilatation, so-called atrial structural remodelling [10, 32]. Other authors, however, failed to find this correlation [34, 43]. In one study [12], the degree of fibrosis was related to age. There is also a report by Frustaci et al. [9] describing myocarditis in endomyocardial biopsies of the right atrial walls in 8 out of 12 patients with lone AF. An autopsy study from the "pre-PV" era [7] on the pathology of AF demonstrated changes in the sinoatrial node and internodal tracts.

Table 4 Relation of the degree of scarring in myocardial sleeves of pulmonary veins to the degree of coronary artery atherosclerosis (n=100)

Coronary atherosclerosis	*n*	Average grade of sleeve scarring
Mild (<50% stenoses)	44	2.23
Significant (>50% stenoses)	56	2.21

In the current series, scarring of the myocardium was seen in all 349 sleeves. It was more pronounced in the left PVs than in the right, with the left inferior PV most affected. Patients with AF had significantly more marked scarring (average grade 2.44) than those in sinus rhythm (average grade 2.0). The lesion was most severe in the peripheral parts of the sleeves, with the fingerlike projections often totally sclerotic.

Scarring of the myocardial sleeves of the PVs, therefore, seems to play an important role in the pathogenesis of AF. This premise concurs with the findings of the original work by Haïssaguerre et al. [13] and also of others [19] that the ectopic foci of AF are located not near the venoatrial ostium but 2–4 cm inside the veins, which corresponds with the site of peripheral projections of the sleeves with the most severe scarring.

The histological appearance of the scars was unusual. With a HE stain, they were homogeneous and glassy (rarely with microcalcifications), with the El VG stain revealing a high content of elastic fibers, probably the basis for the glassy appearance. The character of these fibroelastotic scars differs from postnecrotic myocardial scars in ischemic heart disease. As a matter of fact, we never encountered necrosis/infarction in the sleeve myocardium.

There is a crucial question concerning the genesis of the scarring. Although we have demonstrated by an injection method the coronary origin of the sleeves' nutrient vessels, we failed to find a relation between the degree of coronary artery atherosclerotic narrowing and the grade of sleeve scarring. The microcapillary density [4] apparently was not reduced. We presume that the peripheral parts of the sleeves, which are located at the very periphery of the coronary circulation, are in a state of chronic hypoxia with consequent progressive degeneration of the myocardium resulting in fibroelastotic scarring. The genesis of the scarring is, therefore, probably not postnecrotic but degenerative. Further research on this topic is required [2].

Our results confirm the finding of Röcken et al. [34], in right atrial appendages, of an inverse correlation between amyloidosis and scarring. In the myocardial sleeves, the amyloid deposits were more extensive centrally, near the atrium, while scarring affected mostly their periphery. The distribution of both lesions correlated inversely also in individual PVs; the difference was most obvious between the right superior PV (most amyloid, least scarring) and the left inferior PV (least amyloid, most scarring). This inverse relation might be explained, on the one hand, by the proven toxicity of amyloid proteins (including ANP) for cardiomyocytes [28, 38], leading to their injury and scarring or, alternatively, by the presumption that the fibrosed myocardium fails to produce ANP, which is the precursor of IAA [44].

To summarise, in our currently most extensive pathological analysis of 100 hearts of subjects with and without atrial fibrillation, we have shown that scarring and amyloidosis of the myocardial sleeves of the pulmonary veins are a universal feature in the elderly population and a likely substrate for triggering and sustaining atrial fibrillation.

Acknowledgements The authors are grateful to RNDr. E. Čermáková for statistical evaluation and to Dr. J. Gosney for English edition. This study was supported by the Czech Republic Ministry of Health (Grant IGA 7592-3).

References

1. Allessie MA, Boyden PA, Camm AJ, Kléber AG, Lab MJ, Legato MJ, Rosen MR, Schwartz PJ, Spooner PM, Van Wagoner DR, Waldo AL (2001) Pathophysiology and prevention of atrial fibrillation. Circulation 103:769–777
2. Bauer A, McDonald AD, Donahue JK (2004) Pathophysiological findings in a model of persistent atrial fibrillation and severe congestive heart failure. Cardiovasc Res 61:764–770
3. Boldt A, Wetzel U, Lauschke J, Weigl J, Gummert J, Hindricks G, Kottkamp H, Dhein S (2004) Fibrosis in left atrial tissue of patients with atrial fibrillation with and without underlying mitral valve disease. Heart 90:400–405
4. Boldt A, Scholl A, Garbade J, Resetar ME, Mohr FW, Gummert JF, Dhein S (2005) ACE-inhibitor treatment attenuates atrial structural remodeling in patients with lone chronic atrial fibrillation. Basic Res Cardiol 100:1–7
5. Cornwell GG, Murdoch WL, Kyle RA, Westermark P, Pitkänen P (1983) Frequency and distribution of senile cardiovascular amyloid. A clinicopathologic correlation. Am J Med 75:618–623
6. Corradi D, Callegari S, Benussi S, Nascimbene S, Pastori P, Calvi S, Maestri R, Astorri E, Pappone C, Alfieri O (2004) Regional left atrial remodeling in patients with chronic atrial fibrillation undergoing mitral-valve surgery. Virchows Arch 445:498–505
7. Davies MJ, Pomerance A (1972) Pathology of atrial fibrillation in man. Br Heart J 34:520–525
8. DeGiorgio F, Arena V, DeMercurio D, Pascali VL, Capelli A (2004) Right atrial lipoma with "satellite" atrial fibrillation? Virchows Arch 444:392–394
9. Frustaci A, Chimenti C, Bellocci F, Morgante E, Russo MA, Maseri A (1997) Histological substrate of atrial biopsies in patients with lone atrial fibrillation. Circulation 96:1180–1184
10. Fuster V, Rydén LE, Asinger RW et al (2001) ACC/AHA/ESC guidelines for the management of patients with atrial fibrillation: executive summary. Circulation 104:2118–2150
11. Fynn SP, Kalman JM (2004) Pulmonary veins: anatomy, electrophysiology, tachycardia, and fibrillation (review). Pacing Clin Electrophysiol 27:1547–1559
12. Goette A, Juenemann G, Peters B, Klein HU, Roessner A, Huth Ch, Röcken Ch (2002) Determinants and consequences of atrial fibrosis in patients undergoing open heart surgery. Cardiovasc Res 54:390–396
13. Haïssaguerre M, Jaïs P, Shah DC, Takahashi A, Hocini M, Quiniou G, Garrigue S, Le Mouroux A, Le Métayer P, Clémenty J (1998) Spontaneous initiation of atrial fibrillation by ectopic beats originating in the pulmonary veins. N Engl J Med 339:659–666
14. Haïssaguerre M, Sanders P, Hocini M, Jaïs P, Clémenty J (2004) Pulmonary veins in the substrate for atrial fibrillation. The "venous wave" hypothesis. J Am Coll Cardiol 43:2290–2292
15. Hassink RJ, Aretz HT, Ruskin J, Keane D (2003) Morphology of atrial myocardium in human pulmonary veins. A postmortem analysis in patients with and without atrial fibrillation. J Am Coll Cardiol 42:1108–1114
16. Ho SY, Cabrera JA, Tran VH, Farré J, Anderson RH, Sánchez-Quintana D (2001) Architecture of the pulmonary veins: relevance to radiofrequency ablation. Heart 86:265–270
17. Hocini M, Sanders P, Jaïs P, Hsu L-F, Takahashi Y, Rotter M, Clémenty J, Haïssaguerre M (2004) Techniques for curative treatment of atrial fibrillation. J Cardiovasc Electrophysiol 15:1467–1471
18. Hodkinson HM, Pomerance A (1977) The clinical significance of senile cardiac amyloidosis: a prospective clinico-pathological study. Q J Med 46:381–387
19. Hsieh M-H, Tai C-T, Tsai C-F, Yu W-C, Lee S-H, Lin Y-K, Ding Y-A, Chang M-S, Chen S-A (2000) Pulmonary vein electrogram characteristics in patients with focal sources of paroxysmal atrial fibrillation. J Cardiovasc Electrophysiol 11:953–959
20. Jaïs P, Haïssaguerre M, Shah DC, Chouairi S, Gencel L, Hocini M, Clémenty J (1997) A focal source of atrial fibrillation treated by discrete radiofrequency ablation. Circulation 95:572–576
21. Janse MJ (1997) Why does atrial fibrillation occur? Eur Heart J 18(Suppl. C):C12–C18
22. Kaye GC, Butler MG, D'Ardenne AJ, Edmondson SJ, Camm AJ, Slavin G (1986) Identification of immunoreactive atrial natriuretic peptide in atrial amyloid (letter to the editor). J Clin Pathol 39:581–582
23. Kholová I, Kautzner J (2003) Anatomic characteristics of extensions of atrial myocardium into the pulmonary veins in subjects with and without atrial fibrillation. Pacing Clin Electrophysiol 26:1348–1355
24. Kholová I, Niessen HWM (2005) Amyloid in the cardiovascular system: a review. J Clin Pathol 58:125–133
25. Kostin S, Klein G, Szalay Z, Hein S, Bauer EP, Schaper J (2002) Structural correlate of atrial fibrillation in human patients. Cardiovasc Res 54:361–379
26. Lin W-S, Prakash VS, Tai C-T, Hsieh M-H, Tsai C-F, Yu W-C, Lin Y-K, Ding Y-A, Chang M-S, Chen S-A (2000) Pulmonary vein morphology in patients with paroxysmal atrial fibrillation initiated by ectopic beats originating from the pulmonary veins. Implications for catheter ablation. Circulation 101:1274–1281
27. Lloyd-Jones DM, Wang TJ, Leip EP Larson MG, Levy D, Vasan RS, D'Agostino RB, Massaro JM, Beiser A, Wolf PA, Benjamin EJ (2004) Lifetime risk for development of atrial fibrillation. The Framingham Heart Study. Circulation 110:1042–1046
28. Merlini G, Bellotti V (2003) Molecular mechanisms of amyloidosis. N Engl J Med 349:583–596
29. Moubarak JB, Rozwadowski JV, Strzalka CT, Buck WR, Tan WS, Kish GF, Kisiel T, Fronc HC, Maloney JD (2000) Pulmonary veins–left atrial junction: anatomic and histological study. Pacing Clin Electrophysiol 23:1836–1838

30. Nathan H, Eliakim M (1966) The junction between the left atrium and the pulmonary veins. An anatomic study of human hearts. Circulation 34:412–422
31. Nattel S (2002) New ideas about atrial fibrillation 50 years on. Nature 415:219–226
32. Pedersen OD, Køber L, Torp-Pedersen C (2004) Atrial fibrillation and atrial cardiomyopathy—two sides of the same coin? Am Heart J 147:953–955
33. Raeuschel F (1954) De arteriarum et venarum structura. Dissertatio inauguralis anatomico-physiologica. Vratislaviae, 1836. In: Purkyně JE, Opera omnia, Tomus 6—dissertation theses of Purkyně's students. SZN, Praha, pp 165–183
34. Röcken C, Peters B, Juenemann G, Saeger W, Klein HU, Huth Ch, Roessner A, Goette A (2002) Atrial amyloidosis. An arrhythmogenic substrate for persistent atrial fibrillation. Circulation 106:2091–2097
35. Roux N, Havet E, Mertl P (2004) The myocardial sleeves of the pulmonary veins: potential implications for atrial fibrillation. Surg Radiol Anat 26:285–289
36. Saito T, Waki K, Becker AE (2000) Left atrial myocardial extension onto pulmonary veins in humans: anatomic observations relevant for atrial arrhythmias. J Cardiovasc Electrophysiol 11:888–894
37. Scharf C, Sneider M, Case I, Chugh A, Lai SWK, Pelosi F, Knight BP, Kazerooni E, Morady F, Oral H (2003) Anatomy of the pulmonary veins in patients with atrial fibrillation and effects of segmental ostial ablation analyzed by computed tomography. J Cardiovasc Electrophysiol 14:150–155
38. Schubert D, Behl C, Lesley R, Brack A, Dargusch R, Sagara Y, Kimura H (1995) Amyloid peptides are toxic via a common oxidative mechanism. Proc Natl Acad Sci U S A 92:1989–1993
39. Steiner I (1984) The first description of senile cardiac amyloidosis-I Soyka, 1876, Praha. Cs Patol 20:11–13 (In Czech)
40. Steiner I (1987) The prevalence of isolated atrial amyloid. J Pathol 153:395–398
41. Steiner I (2005) A hitherto unknown priority of Jan Ev Purkyně—myocardial sleeves of the pulmonary veins. Contribution to the pathogenesis of atrial fibrillation. Cas Lek ces 144:709-710 (In Czech)
42. Tagawa M, Higuchi K, Chinushi M, Washizuka T, Ushiki T, Ishihara N, Aizawa Y (2001) Myocardium extending from the left atrium onto the pulmonary veins: a comparison between subjects with and without atrial fibrillation. Pacing Clin Electrophysiol 24:1459–1463
43. Todd DM, Skanes AC, Guiraudon G, Guiraudon C, Krahn AD, Yee R, Klein GJ (2003) Role of the posterior left atrium and pulmonary veins in human lone atrial fibrillation. Electrophysiological and pathological data from patients undergoing atrial fibrillation surgery. Circulation 108:3108–3114
44. Van den Bergh MP, Tjeerdsma G, de Kam PJ, Boomsma F, Crijns HJGM, van Veldhuisen DJ (2002) Longstanding atrial fibrillation causes depletion of atrial natriuretic peptide in patients with advanced congestive heart failure. Eur J Heart Fail 4:255–262
45. Verheule S, Wilson EE, Arora R, Engle SK, Scott LR, Olgin JE (2002) Tissue structure and connexin expression of canine pulmonary veins. Cardiovasc Res 55:727–738
46. Weiss C, Gocht A, Willems S, Hoffmann M, Risius T, Meinertz T (2002) Impact of the distribution and structure of myocardium in the pulmonary veins for radiofrequency ablation of atrial fibrillation. Pacing Clin Electrophysiol 25:1352–1356
47. Wellens HJJ (2004) Cardiac arrhythmias: the quest for a cure. A historical perspective. J Am Coll Cardiol 44:1155–1163
48. Yoshihara F, Nishikimi T, Sasako Y et al (2002) Plasma atrial natriuretic peptide concentration inversely correlates with left atrial collagen volume fraction in patients with atrial fibrillation. Plasma ANP as a possible biochemical marker to predict the outcome of the maze procedure. J Am Coll Cardiol 39:288–294

Virchows Arch (2006) 449: 96–103
DOI 10.1007/s00428-006-0176-7

ORIGINAL ARTICLE

Christina Mayerl · Melanie Lukasser · Roland Sedivy · Harald Niederegger · Ruediger Seiler · Georg Wick

Atherosclerosis research from past to present—on the track of two pathologists with opposing views, Carl von Rokitansky and Rudolf Virchow

Received: 21 November 2005 / Accepted: 9 February 2006 / Published online: 13 April 2006
© Springer-Verlag 2006

Abstract It is now clear that inflammation plays a key role in atherogenesis. As a matter of fact, signs of inflammation of atherosclerotic plaques have been observed for centuries and also constituted the basis for a fierce controversy in the 19th century between the prominent Austrian pathologist Carl von Rokitansky and his German counterpart, Rudolf Virchow. While the former attributed a secondary role to these inflammatory arterial changes, Virchow considered them to be of primary importance. We had the unique opportunity to address this controversy by investigating atherosclerotic specimens from autopsies performed by Carl von Rokitansky up to 178 years ago. Twelve atherosclerotic arteries originally collected between the years 1827 to 1885 were selected from the Collectio Rokitansky of the Federal Museum of Pathological Anatomy, Vienna Medical University. Using modern sophisticated immunohistochemical and immunofluorescence techniques, it was shown that various cellular intralesional components, as well as extracellular matrix proteins, were preserved in the historic atherosclerotic specimens. Most importantly, CD3 positive cells were abundant in early lesions, thus, rather supporting Virchows's view, that inflammation is an initiating factor in atherogenesis. Furthermore, we hope to have opened a new and intriguing possibility to study various pathological conditions using valuable historical specimens.

C. Mayerl · M. Lukasser · H. Niederegger · G. Wick (✉)
Division of Experimental Pathophysiology and Immunology,
Department Biocenter, Innsbruck Medical University,
Fritz-Pregl Str. 3,
6020 Innsbruck, Austria
e-mail: georg.wick@i-med.ac.at
Tel.: +43-512-5073100
Fax: +43-512-5072867

R. Sedivy
Department of Clinical Pathology, University Hospital Vienna,
Vienna, Austria

R. Seiler
Department of Vascular Surgery,
University Hospital Innsbruck,
Innsbruck, Austria

Keywords Atherosclerosis · Inflammation · Historical material

Introduction

Atherosclerosis is a disease that has plagued mankind for millennia, as exemplified by findings of degenerative changes in the aorta, coronary, and peripheral arteries of Egyptian mummies [13, 14, 27]. These lesions from ancient Egyptians are no different from those currently observed in vascular surgery and morbid histology.

Medical researchers began to take a closer look at vascular alterations in the beginning of the 19th century. In 1829, the German-born French surgeon and pathologist Jean Lobstein introduced the term "arteriosclerosis" in his unfinished Traité d'Anatomie Pathologique, a four-volume treatise on pathological anatomy, based upon his lifelong personal experience [6].

In the middle of the 19th century, two opposing schools of pathology, that of Rudolf *Virchow* in Berlin, Germany, and that of Carl *von Rokitansky* in Vienna, Austria, described cellular inflammatory changes in atherosclerotic vessel walls [11, 17]. Although *von Rokitansky* considered these changes secondary in nature, *Virchow* supported their primary role in atherogenesis. Contrary to the "humoral pathology" and the "crases" theory of the Viennese school, Virchow saw the causes of diseases in changes of cells and coined the term "cellular pathology".

Virchow strongly criticized Carl *von Rokitansky* and the Viennese Medical School for their dogmatism and support of outdated humoralism. In fact, the humoral disease theory included in the first edition of *Rokitansky's* famous pathology textbook "A Manual of Pathological Anatomy" was eliminated entirely from the second edition.

In 1910, the German chemist Windaus showed that atherosclerotic plaques consist of calcified connective tissue and cholesterol [23]. Three years later, Anitschkow and Chaltow succeeded in inducing atherosclerosis in rabbits by feeding a cholesterol-rich diet [1] unequivocally identifying a classical risk factor for progression of

atherosclerotic alterations. Several other risk factors, such as smoking, high blood pressure, high emotional stress, improper diet, diabetes, etc., were later found to contribute to disease progression.

However, the crucial first pathogenetic events of the disease remained unclear. Classical concepts of atherogenesis did not attribute a major relevance to inflammatory-immunologic processes as possible pathogenetic factors. A comprehensive review on historical papers dealing with inflammatory aspects of atherosclerosis has been compiled by Nieto [9].

The "response to injury hypothesis", summarized by Ross in 1993, originally postulated an alteration of the endothelium and intima due to, e.g., mechanical injury, toxins, and oxygen radicals, as the initiating event leading to endothelial dysfunction [12].

Alternatively, the "altered lipoprotein hypothesis", favored by Steinberg and others, postulated an initiating role of chemically altered lipoproteins, notably oxidized low-density lipoprotein (oxLDL), leading to the primary formation of foam cells in the intima [16]. The group of Fogelman [8] pointed out that native LDL, rather than oxLDL, is transported into the intima through the endothelium, where it is then modified and retained, acting as a chemoattractant for monocytes and smooth muscle cells (SMC), and being later taken up by these cells, resulting in foam cell formation. This concept was termed the "retention of modified LDL hypothesis". However, atherogenesis seems to be a far more complex process than simple lipid deposition.

Intriguingly, accumulations of activated T cells, macrophages, and dendritic cells were identified in severely afflicted arteries [2] and were also found to be common in arteries of young adults and even children, at predilection sites for the later occurrence of atherosclerotic lesions [18, 25]. We have called these foci of intimal mononuclear cells the "vascular-associated lymphoid tissue"—VALT [7, 22]. With respect to these findings, the question arose, as to which antigens are recognized by the immune system, leading to a local immune reaction in the arterial wall. An extended series of experiments revealed a stress protein, heat shock protein 60 (HSP 60), as the potential (auto) antigen inciting an immune response at the beginning of atherosclerotic changes in the vessel wall [4, 24]. Classical atherosclerosis risk factors, such as high blood pressure, smoking, diabetes, biochemically modified LDL, etc., result in the expression of HSP60 by endothelial cells (EC), especially at sites that are subjected to major (turbulent) haemodynamic stress and known to be predilection sites for the later development of atherosclerotic lesions. Thus, pre-existing cellular and humoral immunity to microbial HSP60 may encompass pathogenetically relevant cross-reactivity with HSP60 expressed on the surface of arterial EC and leads to the initial inflammatory stage of atherosclerosis [10]. In addition, bona fide autoimmunity triggered by biochemically altered autologous HSP60 may also occur [26]. Based on this concept, the "immunological hypothesis" of atherogenesis was formulated [21]. Accordingly, the latter results strongly support Virchow's theory of atherosclerosis as a primarily inflammation-induced disease.

We recently had the unique opportunity to investigate paraffin sections of early atherosclerotic lesions from specimens secured by *von Rokitansky* in the middle of the 19th century, which were stored in the archives of the Institute for Pathological Anatomy, Vienna. We used these historical materials to confirm the presence and role of an early inflammatory process in atherogenesis, and also present methodological data on the successful use of various modern immunohistochemical techniques on such historical resources.

Materials and methods

Twelve atherosclerotic arteries, originally collected between 1827 and 1885, were selected from the Collection of Pathological Specimens procured by *Rokitansky* and thereafter stored at the Federal Museum of Pathological Anatomy, Vienna, Austria (see Table 1). In the early 19th

Table 1 Origin of historical vessels from the Rokitansky collection

Museum archive number	Sex/age	Year	Tissue origin
MN1819[a]	Male	1837	A. brachialis
MN3590	Male/51	1878	Aorta ascendens
MN1943[a]	Female/64	1840	A. lienalis
MN3854	n.k.	1881	Aorta abdominalis
MN2460[a]	n.k.	1853	Aorta thoracis
MN1184[a]	n.k.	1828	A. lienalis
MN1637[a]	Female/21	1834	A. lienalis
MN1347[a]	Male/47	1831	A. lienalis
MN1150	n.k.	<1827	A. iliaca communis dexter
MN2918[a]	Male/43	1863	A. cerebri media sinister
MN4207	n.k.	1885	A. cerebri media sinister
MN2343[a]	Male/49	1850	A. cerebri media sinister

n.k. not known
[a]Specimens collected by *Rokitansky*

century, specimens were stored in pure alcohol ("Weingeist"), and subsequently in "Kaiserling's fluid" (750 ml formaldehyde, 1,000 ml distilled water, 10 g potassium nitrate, 30 g potassium acetate) [15]. In the beginning of the 20th century, Kaiserling's fluid was replaced with lower graded formaldehyde to preserve tissue to the present [3]. Historical human lymph node (1893) and human skin (1849) proved to be unusable as positive control tissue as either black deposits (lymph node) or section detachment from the slides made successful processing impossible. Formaldehyde (4% formaldehyde in phosphate buffered saline, PBS, pH 7.2)-fixed recent samples of human skin, tonsil, lymphnode, and arterial fragments were, therefore, used for control purposes. For the final analysis, 3 of 12 vessels were excluded because of signs of autolytic degeneration.

Historical and contemporary tissues were dehydrated and paraffin embedded. Sections 5-μm thick were cut and placed onto silane-coated slides. Sections were rehydrated and the crucial step of antigen retrieval was performed either with proteinase XXIV (P8038, Sigma, 1 mg/ml in PBS, 5-min incubation) or microwave irradiation (750 W,

Table 2 Antibodies, optimized conditions, and results from recent control tissues

Antibody against	Clone	Source	Code	Dilution[a]	Antigen retrieval	Conjugate	Positive control tissue	Control staining
CD 3 (T cells)	Polyclonal	Dako	A 0452	1:50	Citrate	EnVision, AP	Human tonsil	+++
CD 3 (T cells)	Polyclonal	Neo Markers	RB-360-A	1:10	Citrate	EnVision, AP	Human tonsil	++
CD 68 (macrophages)	KP-1	Dako	M0814	1:50	Citrate	G. a-m. AP	Human tonsil	+++
CD 68 (macrophages)	PG-M1	Dako	M0876	1:50	Citrate	G. a-m. AP	Human tonsil	+++
CD 68 (macrophages)	Kp-1	Neo Markers	MS-397-S	1:30	Citrate	G. a-m. AP	Human tonsil	++
Smooth Muscle Actin	1A4	Dako	M0851	1:50	Citrate	EnVision, AP	Human tonsil	+++
von Willebrand Faktor	Polyclonal	Dako	A 0082	1:200	Citrate	EnVision, AP	Human tonsil	+++
S 100 Protein	4C4.9	Neomarkers	MS-296-P	1:50	Proteinase XXIV or EDTA	G. a-m. AP	Human tonsil	+++
HLA-DP, DQ, DR (MHC II)	CR3/43	Dako	M 0775	1:50	Citrate	G. a-m. AP	Human tonsil	+++
CD 25 (IL-2 rezeptoe)	4C9	Novo Castra	NCL-CD25-305	1:50	Citrate	EnVision, AP	Human tonsil	+++
Fibroblasts	TE-7	Cymbus	CBL 271	1:50	Proteinase XXIV or EDTA	G. a-m. AP	Human breast skin	+++
CD106 (VCAM)	1.4C3	Neo Markers	MS-1101-S	1:5	EDTA	EnVision AP	Human tonsil	+++
CD 54 (ICAM)	54C04	Neo Markers	MS-1094-S	1:10	Citrate	EnVision AP	Human tonsil	+++
CD 62-E (E-Selectin)	G4	Novo Castra	NCL-CD62E-382	1:50	EDTA	G. a-m. AP	Human tonsil	++
CD 62-P (P-Selectin)	1E3	Dako	M 7199	1:50	Proteinase XXIV	G. a-m. AP	Human lymphnode	+++
Collagen type I	Polyclonal	Cedarlane	CL50111AP	1:60	Citrate	G. a-rb. 488	Human breast skin	+++
Collagen type III	Polyclonal	Cedarlane	CL50311AP	1:30	Citrate	G. a-rb. 488	Human breast skin	+++
Collagen type IV	CIV 22	Dako	M 0785	1:25	Citrate or n.p.	G. a-m. AP	Human kidney	++
Fibronectin	Polyclonal	Dako	A 0245	1:100	Citrate or n.p.	EnVision, AP	Human breast skin	+++

– to +++: semiquantitative assessment of staining intensity
G. a-m. AP Goat anti mouse AP, *n.p.* no pretreatment, *G. a-rb. 488* goat anti rabbit IgG, Alexa 488
[a]Determined in pilot studies

10 min) with citrate buffer (10 mM, pH 6.0) or EDTA buffer (0.1 mM, pH 8.0). After a final washing step in PBS, samples were treated with antibodies listed in Table 2. The two-step indirect method yielded the best results of several tested detection systems. Therefore, for immunohistochemistry staining, a goat anti-mouse immunoglobulin (D0487, Dako, Glostrup, Denmark) or Envision polymer (K4017, Dako), both conjugated with alkaline phosphatase, were used. Nuclei were stained with hematoxylin (S3309, Dako).

Immunofluorescence detection was performed with an Alexa488-labeled goat anti-rabbit immunoglobulin (A-11008, Molecular Probes, Eugene, OR, USA). For nuclear staining in immunofluorescence tests, diaminophenylindol (D1306, Molecular Probes) was used. Controls were performed with normal mouse serum (X0910, Dako), normal rabbit serum (prepared in our laboratory) and rabbit total immunoglobulin fraction (X0903, Dako) or appropriate mouse immunoglobulin isotype preparations, i.e., mouse IgG1 (X0931, Dako), mouse IgG2a (X0943, Dako) and mouse IgG2b (X0944, Dako). Finally, slides were mounted in Kayser's glycerol gelatine (109242, Merck, Darmstadt, Germany).

Microscopic analyses were carried out either with a Nikon Eclipse E800 microscope or a Zeiss Axiovert 100M confocal laser scanning microscope.

Results

Immunohistochemical and immunofluorescence analyses using monoclonal and polyclonal antibodies recognizing

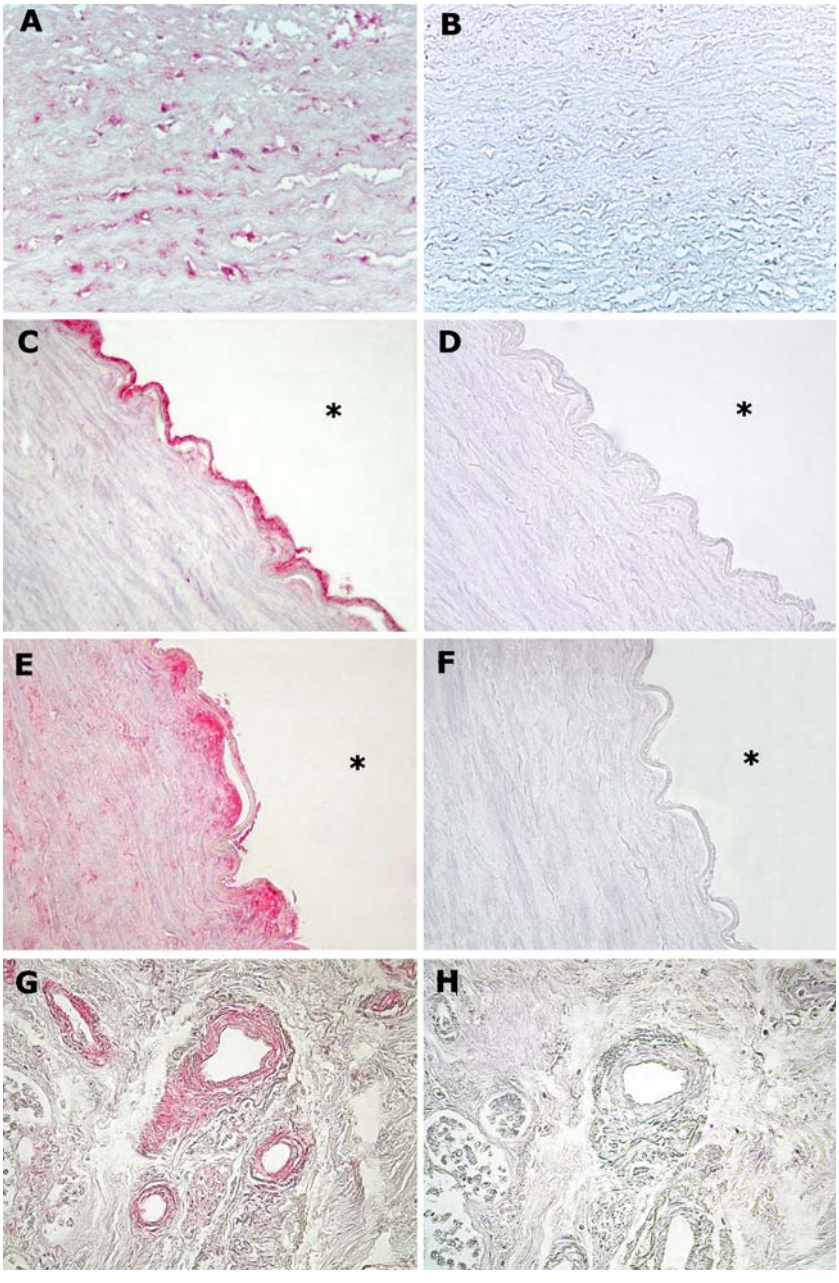

Fig. 1 Immunohistochemical staining on 5-μm thick paraffin sections of arterial vessels collected in the 19th century by Carl von Rokitansky. Positive cells are visualized with an alkaline phosphatase labelled conjugate. * Arterial lumen: **a** staining for CD3+ T-cells (*red*); aorta ascendens, 51-year-old male died in 1878 (Protocol Nr. MN3590 see Table 1). Original magnification ×400; **b** negative control—rabbit Ig fraction; aorta ascendens, 51-year-old male died in 1878 (MN3590). Original magnification ×400; **c** Von Willebrand factor (*red*); arterial intima, male (age unknown) died in 1837 (MN1819). Original magnification ×200; **d** Negative control—rabbit Ig fraction; arterial intima, male (age unknown) died in 1837 (MN1819). Original magnification ×200; **e** Fibronectin (*red*); arterial intima; male (age unknown) died in 1837 (MN1819). Original magnification ×200; **f** Negative control—normal rabbit serum; male (age unknown) died in 1837 (MN1819). Original magnification × 200; **g** Collagen type IV (*red*); arteria lienalis, 47-year-old male died in 1831 (MN1347). Original magnification ×200; **h** Negative control—mouse IgG1, arteria 47-year-old male died in 1831 (MN1347)

various cell surface markers, adhesion molecules, and extracellular matrix (ECM) components were adapted and successfully used for these studies. The T-cell surface marker CD3, the endothelial marker von Willebrand factor (vWF), and the epitopes of the extracellular matrix proteins collagen type I, III, and IV and fibronectin were preserved and, thus, could be visualized.

In two of nine vessels, CD3-positive cells could be detected in atherosclerotic lesions (Fig. 1a). To exclude unspecific staining, negative controls were also performed showing no staining (Fig. 1b). None of the historical vessels were positive for the macrophage surface marker CD68, the smooth muscle cell antigen alpha-actin, the dendritic cell marker S100, HLA-DR (MHC II), a fibroblast marker as well as the adhesion molecules CD62-P (P-selectin) or CD106 (vascular cell adhesion molecule-1–VCAM-1) (see Table 3). In contrast, vWF was found in the vasa vasorum of almost all vessels examined. However, only a few specimens also showed a vWF positive endothelium lining the main arterial lumen (Fig. 1c,d). Fibronectin-expressing structures were present ubiquitously in almost all analyzed lesions, particularly in adventitia and thickened areas of the intima (Fig. 1e,f). In half of the arteries, collagen type IV-positive structures were found in the vasa vasorum (Fig. 1g,h). A specimen of the arteria lienalis additionally showed collagen type IV-positive filaments in intima and media. Collagen type I was also detected in the adventitia and media of two vessels (Fig. 2a). All atherosclerotic lesions examined showed abundant collagen type III in the adventitia and media. In contrast, collagen type III-positive fibres were rarely found in the intima (Fig. 2b–d).

Discussion

Methodological aspects

Human pathological specimens have been collected and stored in anatomical museums for centuries [15]. This large pool of historical material could, in principle, serve as a rich resource for various types of research. However, thus far, only a limited number of methods were available for the examination of such sensitive samples, and immunohistochemistry could not be successfully implemented [15]. Our laboratory has extensive experience in this area [19] and, in fact, introduced immunohistological techniques into paleontological research, thus creating a new subdiscipline, paleoimmunology [20].

The arterial vessels examined derived from pathological human samples collected by *von Rokitansky* and his antecessor Wagner and successor Heschl between 1827 and 1885. Intriguingly, autopsy reports compiled approximately 170 years ago are often still available [15], a remarkable sign of a well-organized storage system throughout the centuries.

Implementing the application of modern immunological techniques to atherosclerosis research has been a challenge, as available supply of historical arteries was limited, and some vessels had to be excluded due to autolytic degeneration. The historical control tissues, intended to be used for establishing the assays, turned out to be unsuitable due to black deposits of unknown origin. Additionally, some of the chemicals used for tissue fixation and storage conditions (exposure to light or air) might have altered the specimens. The sensitivity of different epitopes to the extraordinary extended fixation time (up to 17 decades) is clearly distinguished by comparing the results found with polyclonal and monoclonal antibodies, respectively. CD3, vWF, collagen type I, collagen type III, fibronectin positive

Table 3 Expression pattern of different atherosclerosis markers on historical vessels from the 19th century Rokitansky collection

	MN 1819	MN 1150	MN 3590	MN 1943	MN 3854	G 2460	MN 1184	MN 1637	MN 1347
CD3 (T-cells)	–	–	+	+	–	–	–	–	–
CD68 (macrophage) Clone KP1	–	–	–	–	–	–	–	–	–
CD68 (macrophage) Clone PG-M1	–	–	–	n.t.	–	–	n.t.	n.t.	n.t.
SMA (alpha-Actin)	–	–	–	n.t.	–	–	n.t.	n.t.	n.t.
vWF	+++	+++	+	++	+++	+++	+++	–	+
S 100-protein	–	–	–	n.t.	–	–	–	–	–
HLA-DR (MHC II)	–	–	–	n.t.	–	–	–	–	–
Fibroblasts	–	–	–	n.t.	–	–	–	–	–
CD62-P (P-selectin)	–	–	–	n.t.	–	–	–	–	–
CD106 (VCAM-1)	–	–	–	n.t.	–	n.t.	n.t.	n.t.	n.t.
Collagen type I	+	–	–	n.t.	–	+	n.t.	n.t.	n.t.
Collagen type III	+++	+++	+++	n.t.	+++	+++	n.t.	n.t.	n.t.
Collagen type IV	–	–	–	n.t.	+++	–	++	+	++
Fibronectin	+++	+++	+++	n.t.	+++	++	+++	+++	+++

– to +++: semiquantitative assessment of staining intensity
n.t. not tested

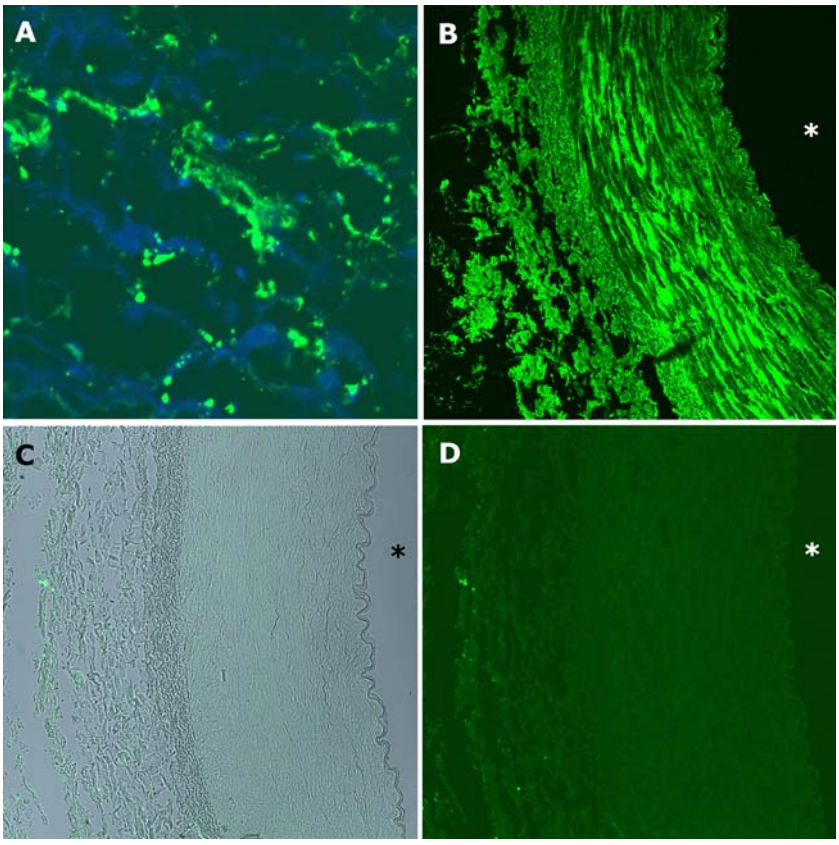

Fig. 2 Indirect immunofluorescence staining on 5-μm thick paraffin sections of historical human arterial vessels. *Arterial lumen: **a** Collagen type I (FITC, *green*) and nuclear staining (DAPI, *blue*); adventitia of an arteria iliaca (MN1150). Original magnification ×400; **b** Collagen type III (FITC, *green*); arteria brachialis, male (age unknown) died in 1837 (MN1819). Original magnification ×200; **c** Transmission image from negative control for **d**; arteria brachialis, male (age unknown) died in 1837 (MN1819). Original magnification ×200; **d** Negative control—rabbit Ig fraction; arteria brachialis, male (age unknown) died in 1837 (MN1819). Original magnification ×200

fibers and cells were all detected with polyclonal antibodies, whereas, monoclonal antibodies generally failed to detect these structures, with the exception of collagen type IV, in historical tissue. In view of the unique nonfibrillar procollagen-like structure of collagen type IV, which includes several non-helical domains that are susceptible to conventional proteases, the latter observation was rather surprising.

It is, thus, probable that epitopes in tissue specimens, especially after extended fixation time and harsh storage conditions, deteriorate or are masked by chemical processes such as methylen bridges formed between reactive sites of tissue proteins. Thus, destruction or masking of the epitope recognized by a monoclonal antibody results in the lack of any signal. On the other hand, the use of a polyclonal antibody greatly enhances the possibility that at least one of the several epitopes these immunoglobulins bind to has resisted deterioration. Accordingly, the antigen retrieval procedure, has turned out to be a crucial step. Finally, the optimal technique for visualization of histological structures in historical tissue samples, i.e., immunohistochemistry or immunofluorescence, must be determined for each antigen–antibody system in pilot studies.

General aspects

It has long been known that both humoral and cellular immune reactions take place in atherosclerotic lesions, but it has not been clear whether these processes were primary or secondary in nature. Already in the middle of the 19th century, Carl *von Rokitansky* and Rudolf *Virchow* pointed out an association of histologic signs of inflammation with atherosclerotic lesions. Both described cellular inflammatory changes in atherosclerotic vessel walls, but while *von Rokitansky* considered these changes secondary in nature, *Virchow* supported their primary role in atherogenesis.

Atherosclerosis is a multifactorial disease, and advanced lesions are by definition complex encompassing various inflammatory and non-inflammatory hallmarks [28]. In principle, one can distinguish three major types of this disease, viz.

(a) Those that develop exclusively on a genetic basis and for which valuable murine knockout models have been developed [29], e.g., familial hypercholesterolemia (FH) due to a heterozygous or homozygous deficiency of the LDL receptor on one end of the spectrum.
(b) Mainly immunologically caused variants, i.e., allotransplant-associated atherosclerosis, are positioned at the other end of the spectrum.
(c) Between these two extremes, the large majority of atherosclerotic patients can be placed who develop what we call *poor man's atherosclerosis*, i.e., the form that can afflict nearly everybody and that represents killer number one in the developed world. Advanced lesions of the latter type are characterized by the presence of macrophages, smooth muscle cells, T cells, dendritic cells, mast cells, fibroblasts, and abundant

collagenous and non-collagenous extracellular matrix proteins. Endothelial cells in the atherosclerotic region differ in their expression of adhesion molecules from other, non-affected vascular territories [7]. Macrophages and smooth muscle cells possess non-saturable scavenger receptors and are transformed into foamcells that have the tendency to disintegrate and release their lipid-rich content into the extracellular space where cholesterol crystals may even be formed. Lymphocytes are preferentially of the Th1 phenotype and include both, effector and regulatory cells, as reflected by their respective cytokine profiles [28]. B cells are scarce, both in early as well as in late lesions [4, 7], but antibodies against plaque antigens, inhibitory Fc-receptors, and cytokines are deemed to play a major role in the advanced atherogenic process [30].

It now seems clear that inflammatory immunologic processes on an appropriate genetic background are operative in incipient atherogenesis, but the very first pathogenetic event remains to be elucidated. In our "autoimmune concept of atherogenesis" [21], we postulate that classical atherosclerosis risk factors, such as hypertension, smoking, diabetes, the life-long infectious load or an altered lipid metabolism first act as stressors of endothelial and intimal cells leading to the expression of HSP60 that then triggers adaptive and innate immune processes that start the disease. With respect to the activity of oxidized LDL as an endothelial stressor, it is of interest that lipid-lowering statins have anti-inflammatory [31] and immunosuppressive [32] effects. The initiating role of adaptive immune mechanisms is, e.g., supported by the fact that atherosclerosis can be induced in normocholesterolemic rabbits by immunization with recombinant HSP60 [24] and that the transfer of the disease in mice is possible by both anti-HSP60 antibodies [33] or T cells [34]. Alternatively, components of the innate immune system operative via the activation of Toll-like receptors (TLRs) [35] or in the form of natural killer T (NKT) [36] cells may initiate the disease.

Immunohistological studies in rabbits and humans have identified activated T cells as the first intima-infiltrating elements, clearly preceding macrophages and smooth muscle cells [25]. The present results further support our previous findings that $CD3^+$ T cells are present in the earliest phases of atherosclerosis and, thus, seem to agree with *Virchow's* view that inflammation plays a primary role in initiating the atherogenic process rather than *Rokitansky's* concept assigning them a secondary role only.

This investigation of historical biological sources and the application of modern technologies thereto has opened new perspectives for the use of this valuable material for all types of pathohistological studies.

Acknowledgements We want to thank Ruth Pfeilschifter-Resch and the medical technologists at the Department of Clinical Pathology in Vienna for preparing paraffin sections as well as Ilona Lengenfelder for assistance in the preparation of figures and Dr. Beatrix Patzak for consulting in sample selection. The Clinical Department of Plastic and Reconstructive Surgery, University Hospital Innsbruck, Austria and Dr. Felix Offner from the Department of Pathology, County Hospital Feldkirch, kindly provided recent control tissue. The authors want to acknowledge the Austrian Science Fund (FWF-project no.14741 to G.W.) and the European Union (Molecular basis of vascular events leading to thrombotic stroke, MOLSTROKE; LSHM-CT-2004-005206) for supporting the project.

References

1. Anitschkow N, Chalatow S (1913) Ueber experimentelle Cholesterinsteatose und ihre Bedeutung für die Entstehung einiger pathologischer Prozesse. Zentralbl Allg Pathol 24:1–9
2. Hanson GK, Holm J, Jonasson L (1989) Detection of activated T lymphocytes in the human atherosclerotic plaque. Am J Pathol 135(1):169–175
3. Kaisering C (1896) Über die Conservierung von Sammlungspräparaten mit Erhaltung der natürlichen Farben. Berlin Klin Wschr 33:775–777
4. Kleindienst R, Xu Q, Willeit J, Waldenberger FR, Weimann S, Wick G (1993) Immunology of atherosclerosis: demonstration of heat shock protein 60 expression and T-lymphocytes bearing alpha/beta or gamma/delta receptor in human atherosclerotic lesions. Am J Pathol 142(6):1927–1937
5. Libby P, Ridker P, Maeri A (2002) Inflammation and atherosclerosis. Circulation 105(9)1135–1143
6. Lobstein J (1833) Traité d'Anatomie Pathologique, vol 2. Levrault, Paris
7. Millonig G, Schwentner C, Müller P, Mayerl C, Wick G (2001) The vascular-associated lymphoid tissue: a new site of local immunity. Curr Opin Lipidol 12(5):547–553
8. Navab M, Berliner JA, Watson AD, Hama SY, Territo MC, Lusis AJ, Shih DM, Van Lenten BJ, Frank JS, Demer LL, Edwards PA, Fogelman AM (1996) The Yin and Yang of oxidation in the development of the fatty streak. A review based on the 1994 George Lyman Duff Memorial Lecture. Arterioscler Thromb Vasc Biol 16(7):831–842
9. Nieto FJ (1998) Infections and atherosclerosis: new clues from an old hypothesis? Am J Epidemiol 148(10):937–948
10. Perschinka H, Mayr M, Millonig G, Mayerl C, van der Zee R, Morrison SG, Morrison RP, Xu Q, Wick G (2003) Cross-Reactive B-Cell Epitopes of Microbial and Human Heat Shock Protein 60/65 in Atherosclerosis. Arterioscler Thromb Vasc Biol 23(6):1060–1065
11. Rokitansky C (1855) A manual of pathological anatomy. Blanchard and Lea, Philadelphia
12. Ross R (1993) The pathogenesis of atherosclerosis: a perspective for the 1990s. Nature 362(6423):801–809
13. Ruffer MA (1911) On arterial lesions found in Egyptian mummies. J Pathol Bacteriol 15:453–462
14. Sandison AT (1962) Degenerative vascular disease in the Egyptian mummy. Med Hist 6:77–81
15. Sedivy R, Patzak B (2002) Pancreatic diseaes past and present: a historical examination of exhibition specimens from the Collectio Rokitansky in Vienna. Virchows Arch 441(1):12–18
16. Steinberg D, Witztum JL (1990) Lipoproteins and atherogenesis: current concepts. JAMA 264(23):3047–3052
17. Virchow R (1971) Cellular pathology as based upon physiological and pathological histology (English translation of second German edition). JB, Lippincott, Philadelphia
18. Waltner-Romen M, Falkensammer G, Rabl W, Wick G (1998) A previously unrecognized site of local accumulation of mononuclear cells: the vascular-associated lymphoid tissue. J Histochem Cytochem 46(12):1347–1350

19. Wick G, Haller M, Timpl R, Cleve H, Ziegelmayer G (1980) Mummies from Peru: demonstration of antigenic determinants of collagen in the skin. Int Arch Allergy Appl Immunol 62 (1):76–80
20. Wick G, Kalischnig G, Maurer H, Mayerl C, Mueller PU (2001) Really old—Paleoimmunology: immunohistochemical analysis of extracellular matrix proteins in historic and prehistoric material. Exp Gerontol 36:1565–1579
21. Wick G, Knoflach M, Xu Q (2004) Autoimmune and inflammatory mechanisms in atherosclerosis. Annu Rev Immunol 22:361–403
22. Wick G, Romen M, Amberger A, Metzler B, Mayr M, Falkensammer G, Xu Q (1997) Atherosclerosis, autoimmunity, and vascular-associated lymphoid tissue. FASEB J 11 (13):1199–1207
23. Windaus A (1910) Ueber den Gehalt normaler und atheromatoeser Aorten an Cholesterol and Cholesterinester. Zeitschrift Physiol Chem 67:174–176
24. Xu Q, Dietrich H, Steiner HJ, Gown AM, Schoel B, Mikuz G, Kaufmann SH (1992) Induction of arteriosclerosis in normocholesterolemic rabbits by immunization with heat shock protein 65. Arterioscler Thromb Vasc Biol 12(7):789–799
25. Xu Q, Oberhuber G, Gruschwitz M, Wick G (1990) Immunology of atherosclerosis: cellular composition and major histocompatibility complex class II antigen expression in aortic intima, fatty streaks and atherosclerotic plaques in young and aged human specimens. Clin Immunol Immunopathol 56 (3):344–359
26. Xu Q, Schett G, Perschinka H, Mayr M, Egger G, Oberhollenzer F, Willeit J, Kiechl S, Wick G (2000) Serum soluble Heat Shock Protein 60 is elevated in subjects with atherosclerosis in a general population. Circulation 102(1):14–20
27. Zimmerman MR (1993) The paleopathology of the cardiovascular system. Texas Heart Inst J 20:252–257
28. Hansson GK (2005) Inflammation, atherosclerosis, and coronary artery disease. N Engl J Med 352(16):1685–1695
29. Breslow JL (1996) Mouse models of atherosclerosis. Science 272:685–88
30. Caligiuri G, Nicoletti A, Poirier B, Hansson GK (2002) Protective immunity against atherosclerosis carried by B cells of hypercholesterolemic mice. J Clin Invest 109(6):745–753
31. Sposito AC, Chapman MJ (2002) Statin therapy in acute coronary syndromes: mechanistic insight into clinical benefit. Arterioscler Thromb Vasc Biol 22(10):1524–1534
32. Jurgens G, Xu Q, Huber L, Bock G, Howanietz H, Wick G, Traill KN (1989) Promotion of lymphocyte growth by high density lipoproteins (HDL). Physiological significance of the HDL binding site. J Biol Chem 264(15):8549–8556
33. Foteinos G, Afzal AR, Mandal K, Jahangiri M, Xu Q (2005) Anti-heat shock protein 60 autoantibodies induce atherosclerosis in apolipoprotein E-deficient mice via endothelial damage. Circulation 112(8):1206–1213
34. George J, Afek A, Gilburd B, Shoenfeld Y, Harats D (2001) Cellular and humoral immune responses to heat shock protein 65 are both involved in promoting fatty-streak formation in LDL-receptor deficient mice. J Am Coll Cardiol 38(3):900–905
35. Edfeldt K, Swedenborg J, Hansson GK, Yan ZQ (2002) Expression of toll-like receptors in human atherosclerotic lesions: a possible pathway for plaque activation. Circulation 105(10):1158–1161
36. Tupin E, Nicoletti A, Elhage R, Rudling M, Ljunggren HG, Hansson GK, Berne GP (2004) CD1d-dependent activation of NKT cells aggravates atherosclerosis. J Exp Med 199(3): 417–422

Virchows Arch (2006) 449: 104–111
DOI 10.1007/s00428-006-0207-4

CASE REPORT

Gabriella Nesi · Antonella Lombardi · Giacomo Batignani · Ferdinando Ficari · Carlos A. Rubio · Francesco Tonelli

Well-differentiated endocrine tumor of the distal common bile duct: a case study and literature review

Received: 16 November 2005 / Accepted: 27 March 2006 / Published online: 3 May 2006
© Springer-Verlag 2006

Abstract Primary carcinoid tumors of the extrahepatic biliary tree are exceedingly rare, accounting for 0.2–2% of all digestive carcinoids. The authors in this study describe a case of biliary duct primary well-differentiated endocrine tumor in a 30-year-old man with symptoms of biliary obstruction and watery diarrhoea. Abdominal ultrasound showed a 2-cm solid lesion in the head of the pancreas, compressing the distal common bile duct. A computed tomography scan confirmed these findings, revealing the hypervascular pattern of the tumor. Gastrointestinal hormonal screening demonstrated an increase in plasma serotonin. The patient underwent standard pylorus-preserving pancreatoduodenectomy. Pathological examination showed a neuroendocrine tumor of the distal common bile duct measuring 1.8 cm in greatest dimension. The tumor cells were immunopositive for neuron-specific enolase (NSE), chromogranin A, synaptophysin, serotonin, and cytokeratin. Stains for gastrin and somatostatin were negative. Seven years later, the patient is well, with no evidence of disease. Given the site of these tumors and the difficulty in differentiating them from periampullary lesions, decisions as to the appropriate surgical approach may be problematic. After an exhaustive review of the literature, the authors conclude that pancreatoduodenectomy is the treatment of choice.

A. Lombardi · G. Batignani · F. Ficari · F. Tonelli
Department of Clinical Physiopathology, Surgical Unit,
University of Florence,
Florence, Italy

C. A. Rubio
Department of Pathology, Karolinska Institute,
Stockholm, Sweden

G. Nesi (✉)
Department of Human Pathology and Oncology,
University of Florence,
Viale GB Morgagni 85,
Florence, 50134, Italy
e-mail: gabriella.nesi@unifi.it
Tel.: +39-055-4478114
Fax: +39-055-4379868

Keywords Biliary tree · Carcinoid · Endocrine tumors · Prognosis · Surgery

Introduction

Extrahepatic bile duct tumors are uncommon, with the majority being adenocarcinomas (80%), mostly of the well-differentiated type. Carcinoid tumors located in the biliary tree are exceedingly rare [3, 33, 36], accounting for 0.2–2% of all digestive carcinoids.

In the recent World Health Organization classification by Capella et al. [12], the term carcinoid tumor has been replaced with the term endocrine tumor to designate all gastrointestinal lesions with evidence of endocrine differentiation. It includes the total number of endocrine tumors, ranging from well-differentiated (traditionally known as carcinoid tumors) to poorly-differentiated malignancies with endocrine features, typified by small cell carcinoma. The review of the literature indicates that only 50 cases have been described since 1959 [16], the report in this study being the 7th case of endocrine tumor (well-differentiated type) arising in the distal common bile duct [7, 30, 34, 38, 44, 50].

Case report

A 30-year-old man was admitted to hospital with a 1-month history of sudden diarrhoea with pale stools, painless jaundice, pruritus, dark urine, and weight loss. Stool cultures gave negative results. The patient's medical history was otherwise unremarkable. Physical examination revealed a mild tenderness in the right hypochondrium on deep palpation. Laboratory tests showed abnormal liver function with signs of biliary obstruction. Tumor markers (CEA, CA19-9, and CA125) were not elevated. Multihormonal screening demonstrated an increase in plasma serotonin (350 ng/ml: normal 90–180) and platelet serotonin (1470 ng/109 plt: normal: 200–600). Somatostatin, gastrin, insulin, glucagon, pancreatic polypeptide (PP), and

vasoactive intestinal peptide (VIP) were within the normal range.

Abdominal ultrasonography (US) disclosed a mild dilation of the intra- and extrahepatic biliary tree, and a 2-cm solid, hypoechoic mass in the head of the pancreas, obstructing the distal bile duct. A spiral computed tomography (CT) scan confirmed these findings and, during the arterial phase, revealed the hypervascular pattern of the lesion. No distal bile duct infiltration was detected by endoscoscopic US. ^{111}In-pentetreotide scintigraphy at 4 and 24 h identified a region of abnormal uptake in the head of the pancreas.

At laparotomy, a nodular lesion was found in the common bile duct, seemingly invading the head of the pancreas. After a complete abdominal and liver examination, no other neoplastic lesion was noted. The patient underwent standard pylorus-preserving pancreatoduodenectomy.

Pathological findings

Macroscopic examination of the surgical specimen showed a yellowish mass (1.8×1.0×0.7 cm in size) encircling the distal common bile duct and partly adherent to the pancreatic head, with no infiltration of the adjacent connective tissue or the pancreas (Fig. 1).

The operative specimen was fixed in 10% neutral buffered formalin. Immunohistochemical studies were performed with the streptavidin–biotin complex method (DAKO LSAB kit, Carpinteria, CA), using a panel of antibodies against the following antigens: cytokeratin (MoAb clone AE1/AE3, BioGenex, San Ramon, CA), neuron-specific enolase (NSE) (MoAb clone MIG-N3, BioGenex), chromogranin A (MoAb clone LK2H10, BioGenex), synaptophysin (MoAb clone Snp88, BioGenex), serotonin (MoAb clone 5HT-H209, Lab Vision, Fremont, CA), gastrin (polyclonal, Novocastra, Newcastle upon Tyne, UK), somatostatin (polyclonal, DAKO), and Ki-67 (MoAb clone MIB-1, DAKO).

Histologically, the tumor consisted of nests and sheets of fairly uniform cells, separated by hyalinized fibrous bands (Fig. 2). The tumor cells displayed lightly eosinophilic cytoplasm and their nuclei were spherical to ovoid, with inconspicuous nucleoli. Mitotic figures were not visible. There was no evidence of necrosis or vascular invasion. Immunohistochemical analysis showed neoplastic cells diffusely positive for NSE, chromogranin A, synaptophysin, and cytokeratin and focally reactive for serotonin (Fig. 3). Stains for gastrin and somatostatin were negative. The percentage of Ki-67 positive cells was assessed by scoring a minimum of 2,000 tumor cells in areas of highest immunostaining, giving a labeling index of 6%. The final pathological diagnosis was well-differentiated endocrine tumor of the common bile duct. No regional lymph nodes were positive and pancreas, gallbladder, and resection lines were free from tumor.

The postoperative course was unremarkable, with serum bilirubin and plasma serotonin rapidly decreasing to normal values. The patient is well with no evidence of disease 7 years after surgery.

Discussion

Most tumors arising in the extrahepatic bile ducts are adenocarcinomas (roughly 80%), mostly of the well-differentiated type. Primary endocrine tumors of the extrahepatic biliary tree are uncommon, accounting for 0.2–2% of all digestive well-differentiated carcinoid tumors [12, 33, 36].

In 1959, Davies [16] described the first case of carcinoid tumor of the biliary ducts and since then, 50 cases, including the present one, have been reported in the literature. On account of the site of these neoplasms and the difficulty in differentiating them from periampullary lesions, it may be problematic to decide on the diagnostic and surgical approach. To this respect, we reviewed the literature (see Table 1).

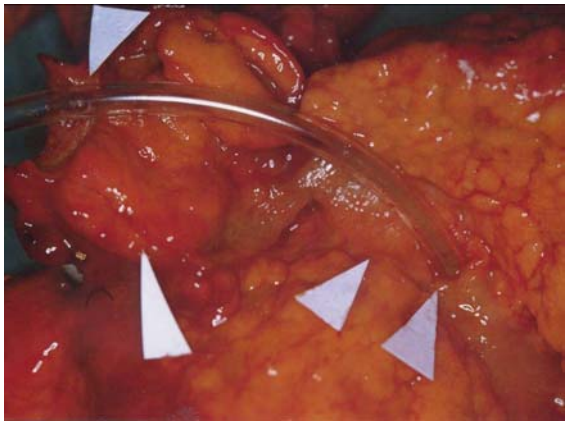

Fig. 1 Gross specimen showing a well-circumscribed, yellowish mass encircling the common bile duct and growing within the lumen

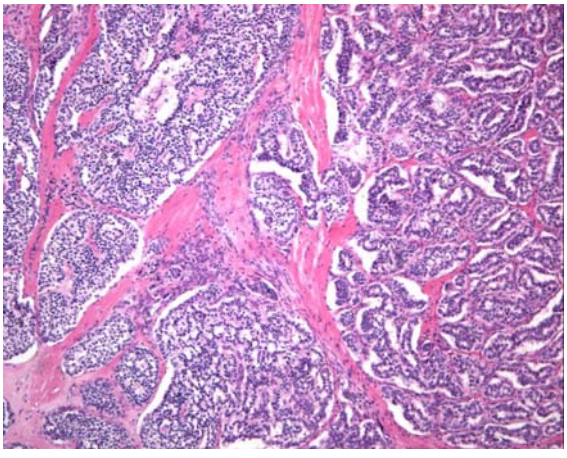

Fig. 2 The tumour exhibited small round cells arranged in nests, separated by dense connective tissue (H&E; original magnification ×200)

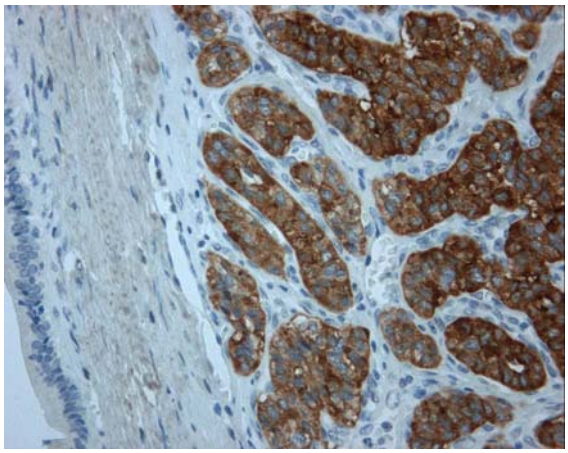

Fig. 3 Diffuse cytoplasmic positivity to chromogranin A in the neoplastic cells (LSAB; original magnification ×350)

Endocrine tumors of the extrahepatic biliary tree occur more frequently in women than in men (1.9:1) and the mean patient age is 2–3 decades below that of patients with nonendocrine neoplasms in the same anatomic site (39 vs 64 years).

Apart from the gallbladder and the ampulla, the most frequent site for extrahepatic endocrine tumors is the proximal/middle tract of the common bile duct, with only six cases [7, 30, 34, 38, 44, 50] reported in the distal bile duct. The intrahepatic location is exceedingly rare [4, 18, 34].

These tumors do not appear to be associated with cholelithiasis. Indeed, only three of 50 patients (6%) had gallstones. Presenting symptoms (i.e., jaundice, biliary colic, abdominal or back pain, and weight loss) seem to be directly related to tumor invasion of adjacent structures or to metastases [13, 18, 21, 34]. In only three previous cases, urinary 5-hydroxyindoleacetic acid (5-HIAA) was measured and found slightly elevated [29, 32, 50]. One patient had a history of recurrent duodenal and gastric ulcers, with immunohistochemistry and electron microscopy detecting abundant gastrin production and limited synthesis of serotonin and pancreatic polypeptide [35]. None of the reported cases showed evidence of the carcinoid syndrome. Obstructive jaundice may occur in about 60% of patients, enabling timely medical evaluation [14, 18, 34].

To establish a preoperative diagnosis, brush cytology is of use, but the incidence of false negative results may be high due to the submucosal location of the neoplasm. Most neuroendocrine tumors of the common bile duct were found accidentally (i.e., incidentalomas) during biliary tract operations performed for other indications. An endocrine choledochal tumor was suspected preoperatively in three patients with elevated urinary 5-HIAA [29, 32, 50].

Although many diagnostic tools are available, including abdominal ultrasound, CT scan, endoscopic retrograde cholangiopancreatography (ERCP), echoendoscopy, and percutaneous transhepatic cholangiography (PTC), the correct diagnosis of endocrine tumor is usually made postoperatively after histological and immunohistochemical examination of the surgical specimen [14, 23, 25].

Microscopically, these neoplasms exhibit combined patterns with trabecular anastomosing structures, solid nests and occasional tubule formation. Tumor cells show positive staining for chromogranin, NSE, and several hormones such as gastrin and somatostatin. Serotonin is immunohistochemically identified in fewer than 50% of cases [34, 40]. In the present case, focal serotonin reactivity of tumor cells was evident, along with raised levels of both plasma and platelet serotonin. However, given that circulating serotonin is mostly carried in platelets by specific granules, it follows that, in neuroendocrine tumors with relatively low serotonin production, the serotonin measured in the serum or plasma is not so sensitive a marker as the serotonin content in the platelets.

Differently to other sites, endocrine tumors of the extrahepatic biliary ducts tend to have indolent biological behavior, even when metastatic. Metastases were more frequently reported in the liver, pancreas, gallbladder, and regional lymph nodes and were found at the time of diagnosis in fewer than 34% of cases. Death was attributed to tumor invasion in only three patients with liver involvement and advanced disease at the time of diagnosis [4, 21, 27]. A 20-year survival was described in a fourth case, despite the presence of widespread metastases [16].

Treatment depends on the location of the tumor and the extent of the disease. Hepatic, cystic, and proximal common bile duct neoplasms may be treated with en bloc resection of the tumor and adjacent bile ducts, regional lymphadenectomy and Roux-en-Y reconstruction hepaticojejunostomy [34, 40]. Only three patients with a tumor in the cystic duct were treated with simple cholecystectomy [22, 26, 37]. Hepatolobectomy may be performed when the liver is involved [8, 47].

Due to the difficulty in differentiating distal common bile duct tumors from periampullary or pancreatic tumors, pancreatoduodenectomy is recommended. Five of the seven patients with distal common duct neoplasm, including the present case, had undergone pancreatoduodenectomy [30, 34, 38, 50]. All these five patients, who underwent curative surgical resection, were alive and disease-free, with a follow-up ranging from 4 months to 20 years.

No absolute histological criteria exist by which to judge the malignant potential of biliary endocrine tumors. Size seems to correlate best with the probability of metastasis. However, a minute carcinoid tumor of the cystic duct that metastasized has been reported [26]. Lymphovascular invasion is a common finding in these tumors [34] and, although quantitative assessment of Ki-67 reactive cells may help to determine prognosis and survival, a Ki-67 index higher than 5% does not necessarily predict aggressive development [31]. Accordingly, it is generally

Table 1 Case review of carcinoid tumors of the extrahepatic biliary tract

Author	Year	Site/size	MTS	Sex/age	Symptoms	Diagnosis	Immunohistochemistry	Treatment/follow-up
Davies [16]	1959	CBD, N/A	Yes, liver	N/A	N/A	At operation (histology)	Not determined	N/A, well at 20 years
Pilz [43]	1961	CBD, N/A	No	F/55	Weakness	At operation (histology)	Argyroph. ?, Argentaff. +	Biopsy, N/A
Little [32]	1968	Proximal CBD, N/A	Portal vein	F/41	RUQ pain, jaundice, ↑ urinary 5-HIAA	Preoperative suspect	Argyroph. ?, Argentaff. +	Laparotomy and biopsy, cholecystectomy, died of pulmonary thromboembolism 3 weeks after surgery
Godwin [21]	1975	BD, N/A	Yes, liver	N/A	N/A	At operation (histology)	Argyroph. ?, Argentaff. +	Laparotomy and biopsy, died at 1 day
Bergdahl [7]	1976	Distal CBD, N/A	No	F/79	Incidental finding	Autopsy	N/A	Incidental autopsy finding
Judge [27]	1976	Left HD, 5 cm	Liver, LN	M/19	Hepatic disease, RUQ pain, jaundice, cholelitiasis	Autopsy	Argyroph. +, Argentaff. −	Inoperable, died 6 days after admission
Gerlok [20]	1979	Proximal CBD, N/A	No	M/32	Painless jaundice	At operation (histology)	Argyroph. ?, Argentaff. ?	N/A
Vitaux [50]	1981	Distal CBD, N/A	LN, pancreas	M/30	Jaundice, ↑ urinary 5-HIAA	Preoperative suspect	Argyroph. ?, Argentaff. +	Pancreatoduodenectomy, well 48 months later
Abe [1]	1983	CBD, N/A	Liver	M/64	RUQ pain	N/A	N/A	Local resection, died 10 months later
Goodman [22]	1984	CD, N/A	LN	F/28	RUQ pain	At operation (histology)	Argyroph. −, Argentaff. − Somatostatin +	Cholecystectomy, LND, well 9 months later
Alexander [2]	1986	BD, N/A	No	F/64	Cholelitiasis, hematemesis	N/A	N/A	N/A, well 8 months later
Jutte [28]	1986	CHD, N/A	No	M/62	Back pain	At operation (histology)	Argyroph. +, Argentaff. ? α1-antitrypsin −, gastrin −, glucagon −, insulin −, somatostatin −	Tumor resection, Roux-en-Y hepaticojejunostomy, well 24 months later
Nicolescu [39]	1986	CBD, N/A	No	F/50	Biliary colic, cholelitiasis	N/A	N/A	N/A
Bickerstaff [9]	1987	BD, N/A	No	F/57	Jaundice	N/A	N/A	N/A, well 4 months later
Fujita [19]	1989	CHD, N/A	No	M/55	Jaundice	At operation (histology)	Gastrointestinal hormonal screening −	N/A, well 6 months later
Chittal [15]	1989	CD, N/A	No	F/46	Biliary colic	At operation (histology)	Argyroph. −, Argentaff. +, CEA +, Ck +, EMA +, Leu7 +	Well 3 years later
van der Wal [49]	1989	CHD-CBD N/A	No	M/55	RUQ pain	At operation (histology)	N/A	Tumor resection, Roux-en-Y hepaticojejunostomy, well 12 months later
Bumin [11]	1990	Proximal CBD, N/A	No	F/38	Jaundice	At operation (histology)	N/A	Tumor resection, Roux-en-Y hepaticojejunostomy, N/A

Table1 (continued)

Author	Year	Site/size	MTS	Sex/age	Symptoms	Diagnosis	Immunohistochemistry	Treatment/follow-up
Brown [10]	1990	HD, N/A	No	F/35	Painless jaundice	At operation (histology)	Argyroph. +, Argentaff. −, Chromogranin +, Ck +, EMA +, NSE +, Serotonin +	Resection of tumor, Roux-en-Y hepaticojejunostomy, N/A
Besznyak [8]	1991	HD, N/A	No	F/13	Jaundice	At operation (histology)	N/A	Hepatic lobectomy, well at 2 years
Barron-Rodriguez [4]	1991	CHD, N/A	Liver	M/36	RUQ pain jaundice, pruritus	At operation (histology)	Argyroph. +, Argentaff. ?, chromogranin +, Ck +, Leu7 +, NSE +, Synaptophysin +	Inoperable, died 4 days after admission
Newman [38]	1992	Distal CBD, N/A	N/A	F/15	N/A	N/A	Serotonin +, Glucagon +, PP +	Pylorus-preserving pancreatoduodenectomy, N/A
Dixon [17]	1992	CBD, N/A	N/A	F/60	N/A	N/A	N/A	N/A
Rugge [46]	1992	CD-CBD, 2 cm	No	F/64	Biliary colic, jaundice	At operation (histology)	Chromogranin +, Ck +, EMA +, Serotonin −, Glucagon −, Somatostatin −, Insulin −, Gastrin −	Resection of tumor, Roux-en-Y hepaticojejunostomy, well 12 months later
Sankary [47]	1995	CHD, N/A	No	F/47	Jaundice	At operation (histology)	N/A	Tumor resection, Roux-en-Y hepaticojejunostomy, trisegmentectomy, well 4 years later
Belli [5]	1996	Proximal CBD, N/A	No	M/78	Jaundice	At operation (histology)	N/A	Resection of tumor, Roux-en-Y hepaticojejunostomy, well at 15 months
Kopelman [30]	1996	Distal CBD, N/A	Yes, liver	F/44	Jaundice	At operation (histology)	N/A	Pylorus-preserving pancreatoduodenectomy, well at 18 months
Hao [24]	1996	Proximal CBD, N/A	No	M/42	Liver disease	At operation (histology)	Chromogranin +, serotonin +, gastrin +, glucagon −, NSE −, somatostatin −, insulin −	Orthotopic liver transplant, tumor resection, well at 5 months
Nahas [37]	1998	CHD, N/A	No	N/A	N/A	N/A	N/A	Tumor resection, Roux-en-Y hepaticojejunostomy, well 6 months later
Shah [48]	1998	CD, N/A	No	F/52	Jaundice, cholelitiasis, RUQ pain	At operation (histology)	N/A	Cholecystectomy, N/A
Bembenek [6]	1998	CHD-CBD, 1.5 cm	Yes, LN	F/12	Jaundice, RUQ pain, nausea, vomiting, weight loss	At operation (histology)	Chromogranin +, gastrin +, NSE +, Ck +	Tumor resection, Roux-en-Y hepaticojejunostomy, N/A
Ross [45]	1999	CBD, N/A	No	F/65	Jaundice	At operation (histology)	N/A	Pancreatoduodenectomy, well 17 months later
Perakath [42]	1999	CBD, N/A	LN	F/36	Acute cholangitis	At operation (histology)	N/A	Resection of tumor, LND, Roux-en-Y hepaticojejunostomy

Table1 (continued)

Author	Year	Site/size	MTS	Sex/age	Symptoms	Diagnosis	Immunohistochemistry	Treatment/follow-up
Hermina [26]	1999	CD, 5.4 cm	No	M/69	RUQ pain	At operation (histology)	N/A	Cholecystectomy
Chamberlain [13]	1999	Bifurcation CBD, 2.7 cm	No	F/37	Jaundice	At operation (histology)	Chromogranin +, PP +, synaptophysin +, serotonin −, glucagon −, insulin −, gastrin −, CEA −	Resection of tumor, LND, Roux-en-Y hepaticojejunostomy, well 18 months later
Chamberlain [13]	1999	Bifurcation CHD right, 2.5 cm	No	F/67	Incidental finding	At operation (histology)	N/A	Tumor resection, LND, Roux-en-Y hepaticojejunostomy, well 15 months later
Chan [14]	2000	Bifurcation CBD, N/A	LN	M/14	Jaundice	At operation (histology)	Ck +, chromogranin +, synaptophysin +, serotonin +, VIP +	Resection of tumor, Roux-en-Y bilateral hepaticojejunostomy N/A
Juturi [29]	2000	CBD, 4 cm	LN	M/30	Abdominal pain, jaundice, nausea, vomiting, weight loss, ↑ urinary 5-HIAA	Preoperative suspect	N/A	Pancreatoduodenectomy, N/A
Maitra [34]	2000	(7 points) CBD: mid: 2 points, distal: 1 point, CBD: 1 point, CHD: 3 points, 1.1–2.7 cm∅	Hilar LN, (2 points)	F/49.8 37–67	Painless jaundice, diarrhoea, acholia, peptic ulcer (1 point), pruritus	At operation (histology)	Chromogranin + (7 points), synaptophysin + (2 points), gastrin + (2 points), serotonin + (3 points), glucagon − (7 points), insulin − (7 points), PP + (2 points), somatostatin + (2 points)	Resection of tumor, Roux-en-Y hepaticojejunostomy, LND, well at 2–11 years
Pawlik [41]	2003	CHD bifurcation, 2.1 cm	LN	M/59	Jaundice	At operation (histology)	Chromogranin +	Resection of tumor, Roux-en-Y hepaticojejunostomy, N/A
Podnos [44]	2003	CBD 2 cm	LN/1.5×2.5cm	F/65	Cholecystitis	At operation (histology) postoperative	NSE +, chromogranin +, serotonin −, gastrin −, glucagon −, insulin −	Cholecystectomy, resection of tumor, Roux-en-Y hepaticojejunostomy, well at 37 months
Podnos [44]	2003	Distal CBD, 2 cm	N/A	M/27	Sclerosing cholangitis, pruritus, jaundice	At operation (histology)	N/A	Orthotopic liver transplant with Roux-en-Y hepaticojejunostomy, well at 7.5 years

Table1 (continued)

Author	Year	Site/size	MTS	Sex/age	Symptoms	Diagnosis	Immunohistochemistry	Treatment/follow-up
Ligato [31]	2005	Right-CHD, 3 cm	No	F/33	N/A	At operation	Gastrin + −	N/A
Present case	2005	Distal CBD, 1.8 cm	No	M/30	Jaundice, pruritus, diarrhoea with pale stools, ↑ plasmatic serotonin	At operation (histology)	NSE +, chromogranin +, synaptophysin +, Ck +	Pancreatoduodenectomy, well at 7 years

CBD common bile duct, *BD* bile duct (NOS), *HD* hepatic duct, *CHD* common hepatic bile duct, *CD* cystic duct, *LN* lymph-nodes, *LND* LN dissection, *N/A* not available, *RU* right upper quadrant

agreed that curative surgical resection is the most relevant prognostic factor in endocrine tumors of the extrahepatic biliary ducts.

References

1. Abe V, Itoh H, Yoshida M (1983) Carcinoid tumor of the common bile duct: report of a case. Stomach Intestine 18:543–548
2. Alexander IA, Thomson KR, Kune GA (1986) Primary common bile duct carcinoid: demonstration by computerised tomography, ultrasonography and angiography. Australas Radiol 30:34–37
3. Angeles-Angeles A, Quintanilla-Martìnez L, Larriva-Sahd J (1991) Primary carcinoid the common bile duct. Immunohistochemical characterization of a case and review of the literature. Am J Clin Pathol 96:341–344
4. Barron-Rodriguez LP, Manivel JC, Mendez-Sanchez N, Jessurun J (1991) Carcinoid tumor of the common bile duct: evidence for its origin in metaplastic endocrine cells. Am J Gastroenterol 86:1073–1076
5. Belli G, Rotondano G, D'Agostino A, Marano I (1996) Primary extrahepatic bile duct carcinoids. HPB Surg 9:101–105
6. Bembenek A, Lotterer E, Machens A, Cario H, Krause U, Holzhausen HJ, Fleig WE, Dralle H (1998) Neuroendocrine tumor of the common hepatic duct: a rare case of extrahepatic jaundice in adolescence. Surgery 123:712–715
7. Bergdahl L (1976) Carcinoid tumours of the biliary tract. Aust N Z J Surg 46:136–138
8. Besznyak I, Tasnadi G, Hirsch T, Koves I, Schaff Z, Lapis K (1991) Hepato-lobectomy for carcinoid tumor of the hepatic duct. Orv Hetil 132:591–594
9. Bickerstaff DR, Ross WB (1987) Carcinoid of the biliary tree: a case report and review of the literature. J R Coll Surg Edinb 32:48–51
10. Brown WM, Henderson JM, Kennedy JC (1990). Carcinoid tumour of the bile duct. A case report and literature review. Am Surg 56:343–346
11. Bumin C, Ormeci N, Dolapci M, Gungor S (1990) Carcinoid tumor of the biliary duct. Int Surg 75:262–264
12. Capella C, Solcia E, Sobin LH, Arnold R (2000) Endocrine tumours of the gallbladder and extrahepatic bile ducts. In: Hamilton R, Aaltonen LA (eds) Pathology and Genetics of Tumours of the Digestive System. WHO Classification of Tumours. IARC Press, Lyon, pp 214–266
13. Chamberlain RS, Blumgart LH (1999) Carcinoid tumors of the extrahepatic bile duct. A rare cause malignant biliary obstruction. Cancer 86:1956–1965
14. Chan C, Medina-Franco H, Bell W, Lazenby A, Vickers S (2000) Carcinoid tumor of the hepatic duct presenting as a Klatskin tumor in an adolescent and review of world literature. Hepatogastroenterology 47:519–521
15. Chittal SM, Ra PM (1989) Carcinoid of the cystic duct. Histopathology 15:643–646
16. Davies AJ (1959) Carcinoid tumors (argentaffinomata). Ann R Coll Surg Engl 25:277–280
17. Dixon J, Lisehora G, Lee MY (1992) Carcinoid tumour of the common bile duct. Contemp Surg 41:37–40
18. El Rassi ZS, Mohsine RM, Berger F, Thierry P, Partensky CC (2004) Endocrine tumors of the extrahepatic bile ducts. Pathological and clinical aspects, surgical management and outcome. Hepatogastroenterology 51:1295–1300
19. Fujita N, Mochizuki F, Lee S, Satoh K, Kobayashi G, Yano A, Shimoda T (1989) Carcinoid tumour of the bile duct: case report. Gastrointest Radiol 14:151–154
20. Gerlock AJ Jr, Muhletaler CA (1979) Primary common bile duct carcinoid. Gastrointest Radiol 4:263–264
21. Godwin JD (1975) Carcinoid tumours. An analysis of 2,837 cases. Cancer 36:560–569
22. Goodman ZD, Albores-Saavedra J, Lundblad DM (1984) Somatostatinoma of the cystic duct. Cancer 53:498–502
23. Hammond PJ, Jackson JA, Bloom SR (1994) Localization of the pancreatic endocrine tumours. Clin Endocrinol 40:3–14
24. Hao L, Friedman AL, Navarro VJ, West B, Robert ME (1996) Carcinoid tumor of the common bile duct producing gastrin and serotonin. J Clin Gastroenterol 23:63–65
25. Henson DE, Albores-Saavedra J, Compton CC (2000) Protocol for the examination of the specimens from patients with carcinomas of the extrahepatic bile ducts, exclusive of the sarcomas and carcinoid tumours: a basis for checklists. Cancer Committee of the College of American Pathologists. Arch Pathol Lab Med 124:26–29
26. Hermina M, Starling J, Warner TF (1999) Carcinoid tumor of the cystic duct. Pathol Res Pract 195:707–710
27. Judge DM, Dickman PS, Trapukdi BS (1976) Nonfunctioning argyrophilic tumour (APUDoma) of the hepatic duct: simplified methods of detecting biogenic amines in tissue. Am J Clin Pathol 66:40–45
28. Jutte DL, Bell RH Jr, Penn I, Powers J, Kolinjivadi J (1986) Carcinoid tumor of the biliary system. Case report and literature review. Dig Dis Sci 32:763–769
29. Juturi JV, Maghfoor I, Doll DC, Evans ML (2000) A case of biliary carcinoid presenting with pancreatitis and obstructive jaundice. Am J Gastroenterol 95:2973–2974
30. Kopelman D, Schein M, Kerner H, Bahuss H, Hashmonai M (1996) Carcinoid tumor of the common bile duct. HPB Surg 10:41–43

31. Ligato S, Furmaga W, Cartun RW, Hull D, Tsongalis GJ (2005) Primary carcinoid tumor of the common hepatic duct: a rare case with immunohistochemical and molecular findings. Oncol Rep 13:543–546
32. Little JM, Gibson AA, Kay AW (1968) Primary common bile-duct carcinoid. Br J Surg 55:147–149
33. Loftus JP, van Heerden JA (1995) Surgical management of the gastrointestinal carcinoid tumors. Adv Surg 28:317–336
34. Maitra A, Krueger JE, Tascilar M, Offerhaus GJ, Angeles-Angeles A, Klimstra DS, Hruban RH, Albores-Saavedra J (2000) Carcinoid tumors of the extrahepatic bile ducts: a study of seven cases. Am J Surg Pathol 24:1501–1510
35. Mandujano-Vera G, Angeles-Angeles A, de la Cruz-Hernandez J, Sansores-Perez M, Larriva-Sahd J (1995) Gastrinoma of the common bile duct: immunohistochemical and ultrastructural study of a case. J Clin Gastroenterol 20:321–324
36. Michelassi F, Erroi F, Dawson PJ, Pietrabissa A, Noda S, Handcock M, Block GE (1989) Experience with 647 consecutive tumors of the duodenum, ampulla, head of the pancreas, and distal common bile duct. Ann Surg 210:544–556
37. Nahas SC, Lourencao JL, Gazoni E, Mott Cde B, Borba MR, Pinto Filho JO, Lopes LH, Varella D, Nahas CS, Pinotti HW (1998) Tumour carcinoide de ducto biliar comum: relato de um caso. Rev Hosp Clin Fac Med Sao Paulo 53:26–28
38. Newman K, Vates T, Duffy L, Anderson K (1992) Pancreatoduodenectomy with preservation of the stomach and pylorus: a safe and effective alternative in children. J Pediatr Surg 27:1334–1335
39. Nicolescu PG, Popescu A (1986) Carcinoid tumor of the cystic duct. Morphol Embryol (Bucur) 32:275–277
40. Parks RW, Johnston GW, Rowlands BJ (1997) Surgical biliary bypass for benign and malignant extrahepatic biliary tract disease. Br J Surg 84:488–492
41. Pawlik TM, Shah S, Eckhauser FE (2003) Carcinoid tumor of the biliary tract: treating a rare cause of duct obstruction. Am Surg 69:98–101
42. Perakath B, Chandran BS, Srivastava VM, Nair A, Sitaram V (1999) Carcinoid tumor of common hepatic duct. Indian J Gastroenterol 18:127
43. Pilz E (1961) Uber ein karzinoid des ductus choledochus. Zentralbl Chir 86:1588–1590
44. Podnos YD, Jimenez JC, Zainabadi K, Ji P, Cooke J, Busuttil RW, Imagawa DK (2003) Carcinoid tumors of the common bile duct: report of two cases. Surg Today 33:553–555
45. Ross AC, Hurley JB, Hay WB, Rusnak CH, Petrunia DM (1999) Carcinoids of the common bile duct: a case report and literature review. Can J Surg 42:59–63
46. Rugge M, Sonego F, Militello C, Guido M, Ninfo V (1992) Primary carcinoid tumor of the cystic and common bile ducts. Am J Surg Pathol 16:802–807
47. Sankary HN, Foster P, Frye E, Williams JW(1995) Carcinoid tumours of the extrahepatic bile duct: an unusual cause of bile duct obstruction. Liver Transpl Surg 1:122–123
48. Shah IA, Schlageter MO, Wong SX, Gani OS (1998) Carcinoid tumor of the cystic duct. Dig Surg 15:372–373
49. van der Wal AC, Van Leeuwen DJ, Walford N (1989) Small cell neuroendocrine (oat cell) tumour of the common bile duct. Histopathology 16:398–400
50. Vitaux J, Salmon RJ, Languille O, Buffet C, Martin E, Chaput JC (1981) Carcinoid tumor of the common bile duct. Am J Gastroenterol 76:360–362

Virchows Arch (2006) 449: 112–116
DOI 10.1007/s00428-006-0214-5

CASE REPORT

Shinichi Ban · Yoshihisa Naitoh · Fumihiro Ogawa · Yoshihiko Shimizu · Michio Shimizu · Akihiro Yasumoto · Isamu Koyama

Intraductal papillary mucinous neoplasm (IPMN) of the gastric-type with focal nodular growth of the arborizing papillae: a case of high-grade transformation of the gastric-type IPMN

Received: 10 February 2006 / Accepted: 28 March 2006 / Published online: 26 April 2006
© Springer-Verlag 2006

Abstract We present a case of intraductal papillary mucinous neoplasm (IPMN) of the pancreas, demonstrating a process of high-grade transformation of the gastric-type IPMN. An 83-year-old Japanese woman underwent pylorus-preserving pancreatoduodenectomy for removal of a multicystic mass of the pancreas head, which had been followed up for 7 years. The removed tumor was a low-grade gastric-type IPMN spreading in the branch ducts, focally forming an intraluminal nodular lesion. The nodular lesion was comprised of arborizing papillotubular proliferation of cuboidal to columnar epithelia with high-grade atypia, and was characterized by diffuse MUC1 expression and a gastric mucin phenotype (focal MUC5AC and MUC6 expressions). Therefore, the nodular lesion was consistent with the pancreatobiliary-type IPMN, and the present case suggests that the low-grade gastric-type IPMN may progress to a focal intraductal carcinoma over the years, and the pancreatobiliary-type IPMN may be one of the forms of such high-grade transformation of the gastric-type IPMN. One of the cystic lesions was an oligocystic-type serous cystic neoplasm (serous cystadenoma), which might be an incidental concomitance or have a common basis.

Keywords Intraductal papillary mucinous neoplasm · Mucin · Serous cystic neoplasm

S. Ban (✉) · Y. Naitoh · F. Ogawa · Y. Shimizu · M. Shimizu
Department of Pathology, Saitama Medical School,
38 Morohongo, Moroyama, Iruma,
Saitama 350-0495, Japan
e-mail: shinba@saitama-med.ac.jp
Tel.: +81-49-2761164
Fax: +81-49-2761583

A. Yasumoto · I. Koyama
Department of Surgery, Saitama Medical School,
Saitama, Japan

Introduction

Intraductal papillary mucinous neoplasm (IPMN) of the pancreas is non-invasive epithelial neoplasms that grow through the main pancreatic duct and/or branch ducts, although development of invasive carcinomas from IPMNs is also demonstrated [9, 13]. Recent studies have shed light on morphological and mucin-phenotypical heterogeneity of neoplastic epithelia of IPMNs [1, 2, 10, 11, 14, 15], which seems to be converging on the following four subclassifications: gastric, intestinal, pancreatobiliary, and oncocytic types [3, 4]. However, the relationship among those types (subclassifications), namely, the progression from one type to another, has not been fully clarified yet [4]. Herein, we present a case of IPMN, which, through careful histopathological examinations, seems to demonstrate a process of high-grade transformation of the gastric-type IPMN, and to give us a hint with regard to the relationship among the subclassification of IPMNs.

Clinical history

The patient was an 83-year-old Japanese woman who had been on medication for diabetes mellitus, hypertension, and arrhythmia. She had been followed for a cystic mass of the pancreas head for 7 years. The mass had gradually increased in size, and at the time of operation, abdominal computed tomography revealed a lesion measuring 8.5 cm in diameter and comprised of multilocular cysts. The patient underwent pylorus-preserving pancreatoduodenectomy. No evidence of lymph node metastases or other organ metastases was noted.

Materials and methods

The excised specimen was routinely fixed in formalin and the pancreas head was studied by whole-step sectioning. Each block was embedded in paraffin and cut for hematoxylin and eosin staining, PAS and diastase digestive PAS

reactions, and immunohistochemistry. The lesions identified by light microscopy were mapped on the macroscopic photographs of each step section of the pancreas (Fig. 1). Immunohistochemistry using an ENVISION/HRP kit (DakoCytomation, Glostrup, Denmark) after antigen retrieval by autoclaving was performed with monoclonal antibodies directed against mucin core proteins, all purchased from Novocastra Laboratories, Newcastle upon Tyne, UK (clones, dilution): MUC1 (Ma695, 1:100); MUC2 (Ccp58, 1:100); MUC5AC (CLH2, 1:50); and MUC6 (CLH5, 1:50). The staining was visualized with diaminobenzidine as a chromogen, followed by light counterstain with hematoxylin.

Results

On gross examination, the pancreas head was occupied by three cystic lesions with sizes depicted in Fig. 1 (tentatively named as a, b, and c). Cyst (a) had a sessile nodular lesion that protruded into the cystic lumen.

The histological findings and the results of immunohistochemistry are summarized in Table 1. The nodular lesion of cyst (a) was comprised of arborizing papillotubular proliferation of cuboidal to columnar atypical cells with round nuclei and weakly eosinophilic cytoplasm (Fig. 2a). The atypia was sufficiently high-grade to be designated as a carcinoma, but obvious invasion into the surrounding tissue was not observed. In another part of cyst (a), the epithelium was almost denuded. Cyst (b) was lined by flat to low-papillary mucinous (PAS-positive) columnar epithelium of low-grade atypia, which was reminiscent of gastric foveolar epithelium (Fig. 2b). Microscopic branch-duct lesions comprised of low-papillary proliferation of mucinous columnar epithelium were observed between and around cystic lesions (a) and (b) (Fig. 1). These lesions showed a low-grade atypia similar to that of the (b) lesion (Fig. 2c). A similar epithelium was involved in a part of the non-dilated main pancreatic duct. Careful examination revealed a transition between the high-grade epithelium of the nodular lesion of (a) and the low-grade epithelium of the adjacent branch-duct lesion (Fig. 2d, e). The above lesions were often accompanied by chronic inflammation, but lacked ovarian-type stroma. The nodular lesion of (a) was partly positive for MUC5AC and MUC6, but negative for MUC2, and MUC1 was diffusely positive in a linear fashion along the luminal sides (Fig. 3a–d). Low-grade epithelium of (b) and microscopic branch-type lesions were only positive for MUC5AC (Fig. 3e–h).

The cystic lesion (c) was lined by flat monolayer epithelium comprised of small cuboidal cells with clear cytoplasm and low-grade atypia (Fig. 2f). The epithelium was PAS-positive and sensitive to diastase digestion, which suggested that it contained glycogen. Then, cyst (c) was diagnosed as an oligocystic-type serous cystic neoplasm (serous cystadenoma). Immunohistochemically, the mucins were all negative.

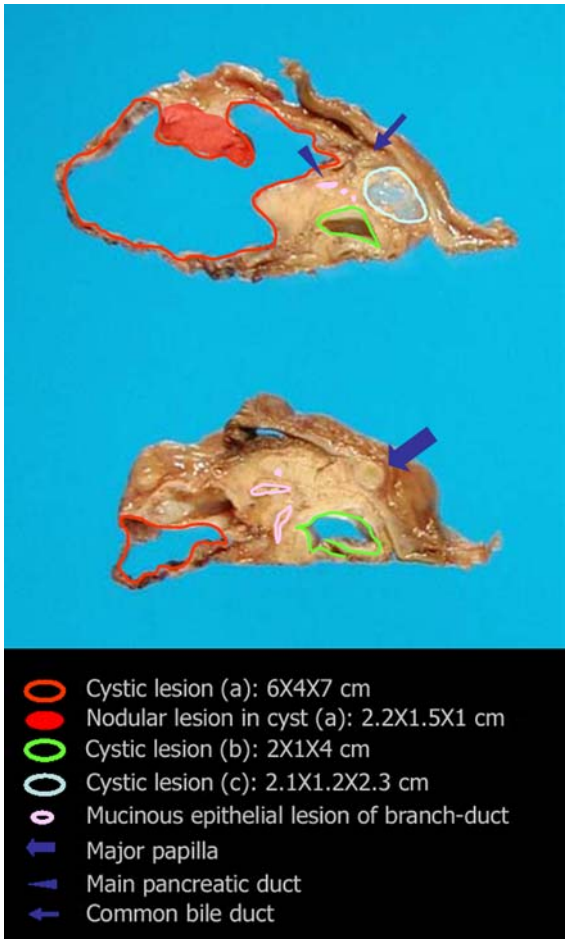

Fig. 1 Gross appearance of the representative cut sections of the pancreas head tumor, whole-step sectioning of which was performed. Each lesion is mapped in *color* indicated below

Discussion

The microscopic branch-duct lesions of the present case showed a low papillary proliferation of mucinous columnar epithelium of low-grade atypia positive only for MUC5AC. Thus, we regarded them as the gastric-type IPMN. The differential diagnosis to be considered is pancreatic intraepithelial neoplasia (PanIN) [6], and the accompanying macroscopic cystic lesions such as (b) suggest the present case to be IPMN rather than PanIN based on the recent conceptual consensus of PanIN and IPMN [6]. However, from another point of view, the gastric-type IPMNs seem to frequently represent PanIN-like histological architecture [3], and a histological continuum between PanIN and IPMN, especially in the gastric-type IPMN, should be reconsidered.

In the present case, a transition to the intracystic nodular lesion from the microscopic branch-duct lesion was observed, and we interpreted that the nodular lesion progressed from the branch-duct low-grade lesion through its high-grade transformation. One problem is to which type of IPMN the nodular lesion should be categorized. Arborizing papillotubular proliferation of cuboidal to columnar epi-

Table 1 Histology and immunohistochemistry of each lesion

Lesion	Histology	MUC1	MUC2	MUC5AC	MUC6
Cystic lesion (a) (nodular lesion)	Pancreatobiliary-type IPMN	+, D[a]	−	+, P	+, P
Cystic lesion (b)	Gastric-type IPMN	−	−	+, P	−
Microscopic branch-duct lesions	Gastric-type IPMN	−	−	+, P/D	−
Cystic lesion (c)	Oligocystic-type serous cystadenoma	−	−	−	−

D Diffusely positive, *P* partly positive, + positive staining, − negative staining
[a]Positive in a linear fashion along the luminal side

thelia with high-grade atypia, and the MUC1-positive and MUC2-negative mucin phenotype compel us to place it into the pancreatobiliary-type [1, 2, 4]. Besides, MUC5AC expression is also consistent with the pancreatobiliary-type [4], and a most recent presentation has demonstrated MUC6 expression in pancreatobiliary-type IPMNs [7]. Therefore, the pancreatobiliary-type IPMNs seem to be gastric in the mucin phenotype, and the present case suggests that the low-grade gastric-type IPMN may progress to a focal intraductal carcinoma over the years, and

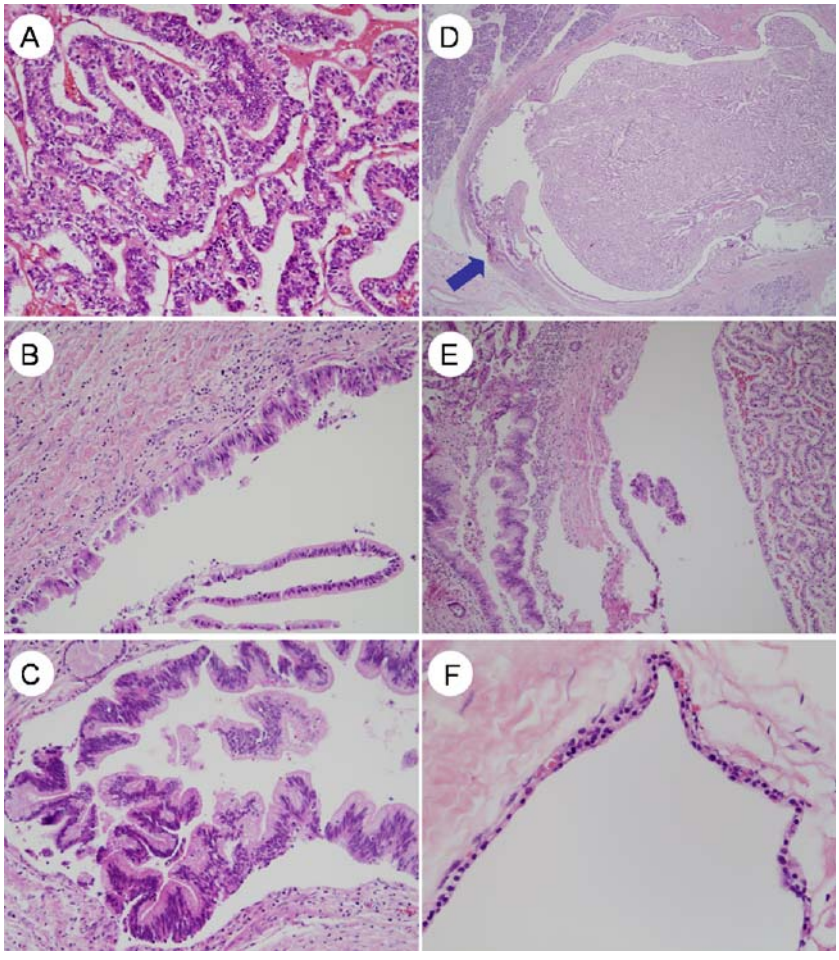

Fig. 2 Microscopic findings. **a** The nodular lesion of cyst (*a*) is comprised of an arborizing papillotubular proliferation of cuboidal to columnar cells with round nuclei and weakly eosinophilic cytoplasm, showing high-grade atypia (hematoxylin-eosin, original magnification ×200). **b** Cyst (*b*) is lined by flat to low-papillary mucinous columnar epithelium of low-grade atypia, which is reminiscent of gastric foveolar epithelium (hematoxylin-eosin, original magnification ×200). **c** Microscopic branch-duct lesions observed between and around cystic lesions (*a*) and (*b*) are comprised of low-papillary proliferation of mucinous columnar epithelium similar to that of (*b*) (hematoxylin-eosin, original magnification ×200). **d** A careful examination of the opposite side of the lower cut surface of Fig. 1 reveals a transition between the high-grade epithelium of the nodular lesion (*a*) and the low-grade epithelium of the adjacent branch-duct lesion at the portion indicated by the *arrow* (hematoxylin-eosin, original magnification ×20). **e** High-power view of the portion indicated by the *arrow* in **d** (hematoxylin-eosin, original magnification ×100). **f** Cyst (*c*) is lined by flat monolayer epithelium comprised of small cuboidal cells with clear cytoplasm and low-grade atypia, which is diagnosed as oligocystic-type serous cystic neoplasm (serous cystadenoma) (hematoxylin-eosin, original magnification ×400)

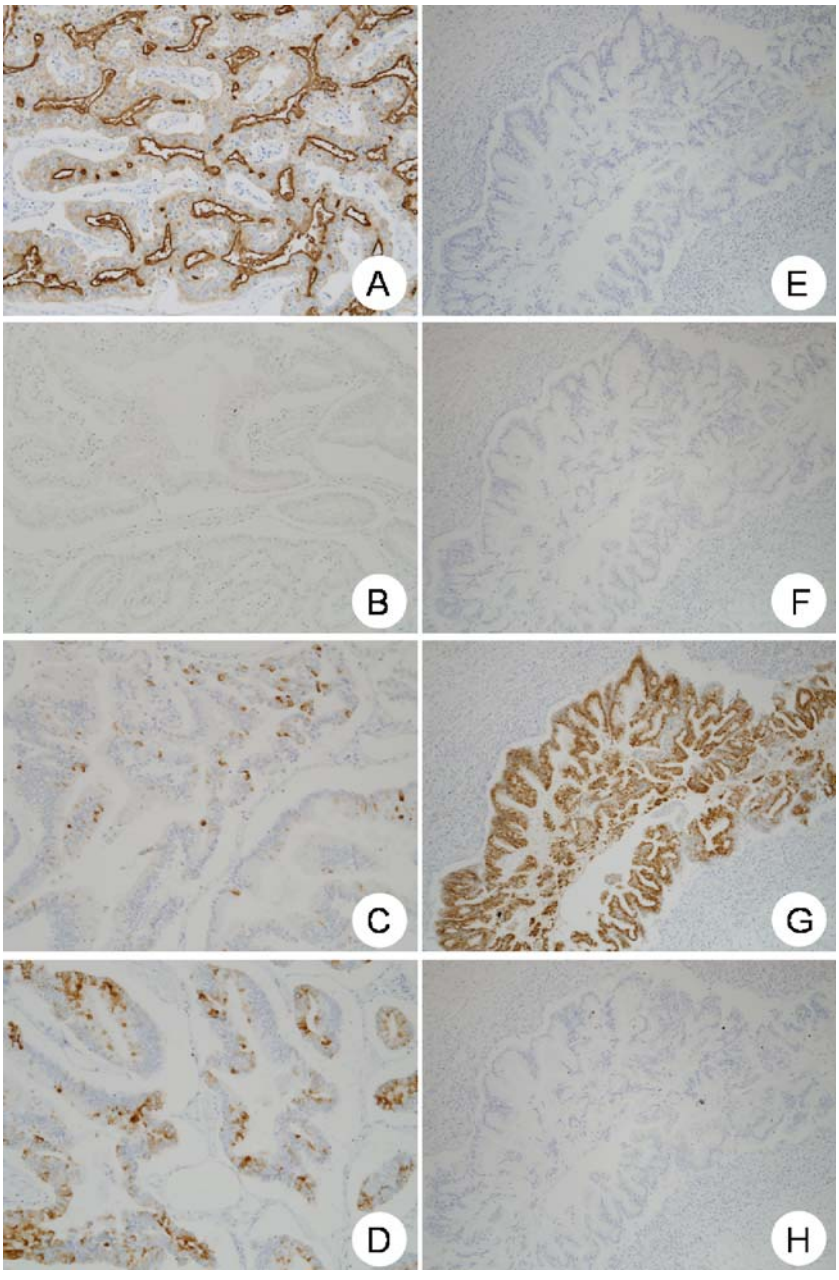

Fig. 3 Immunohistochemical findings. **a–d** The nodular lesion of cyst (*a*) is diffusely positive for MUC1 in a linear fashion along the luminal side (**a**), negative for MUC2 (**b**), and focally positive for MUC5AC (**c**) and MUC6 (**d**) (original magnification ×200). **e–h** Microscopic branch-duct lesions comprised of low-papillary proliferation of mucinous columnar epithelium of low-grade atypia are positive for MUC5AC (**g**), but negative for MUC1 (**e**), MUC2 (**f**), and MUC6 (**h**) (original magnification ×100)

the pancreatobiliary-type IPMN may be one of the forms of such high-grade transformation of the gastric-type IPMN.

Some histological similarities of the pancreatobiliary-type IPMNs to the oncocytic-type IPMNs or intraductal oncocytic papillary neoplasms (IOPNs) have been noted even in the original description of the pancreatobiliary-type by Adsay et al. [1, 2]. These two types also share mucin profiles, that is, expression of MUC1, MUC5AC, and MUC6 [4, 7]. As for the MUC6 expression, a report on mucin-producing bile duct tumors (MPBTs), counterparts of pancreatic IPMNs, is interesting because a subset of MPBTs, called cuboidal-type by the authors, showed pancreatobiliary or oncocytic patterns and MUC6 expression [12]. We should further study the pancreatobiliary-type and oncocytic-type IPMNs with regard to this point.

In the present case, an oligocystic-type serous cystic neoplasm (serous cystadenoma) was observed in the vicinity of the IPMN. The concomitant occurrence of both neoplasms seems to be very rare and little evidence has been presented to determine that the concomitant occurrence is an incidental event or has a common basis such as similar genetic abnormalities [5]. Not constant but frequent MUC6 expression of serous cystic neoplasms has been reported, suggesting the differentiation of serous cystic neoplasms toward centroacinar cells [8]. However, the oligocystic-type serous cystic neoplasm of the present case did not show MUC6 positivity.

Acknowledgements The authors thank Mr.Yoshiya Goto and Mr. Yusuke Hosonuma for their technical assistance.

References

1. Adsay NV, Conlon KC, Zee SY, Brennan MF, Klimstra DS (2002) Intraductal papillary-mucinous neoplasms of the pancreas: an analysis of in situ and invasive carcinomas in 28 patients. Cancer 94:62–77
2. Adsay NV, Merati K, Basturk O, Iacobuzio-Donahue C, Levi E, Cheng JD, Sarkar FH, Hruban RH, Klimstra DS (2004) Pathologically and biologically distinct types of epithelium in intraductal papillary mucinous neoplasms: delineation of an "intestinal" pathway of carcinogenesis in the pancreas. Am J Surg Pathol 28:839–848
3. Ban S, Naitoh Y, Sakurai T, Kuroda M, Shimizu M (2005) Two major types of intraductal papillary mucinous neoplasm (IPMN) of the pancreas: their distinct histological and mucin phenotypic features. Mod Pathol 18(Suppl 1)1:275A (Abstract)
4. Furukawa T, Klöppel G, Adsay NV, Albores-Saavedra J, Fukushima N, Horii A, Hruban RH, Kato Y, Klimstra DS, Longnecker DS, Lüttges J, Offerhaus GJ, Shimizu M, Sunamura M, Suriawinata A, Takaori K, Yonezawa S (2005) Classification of types of intraductal papillary-mucinous neoplasm of the pancreas: a consensus study. Virchows Arch 447:794–799
5. Goh BK, Loh HL, Soo KC (2005) Synchronous pancreatic serous cystic tumor, intraductal papillary mucinous tumor and gastric carcinoma: report of a case. Pancreas 31:195–197
6. Hruban RH, Takaori K, Klimstra DS, Adsay NV, Albores-Saavedra J, Biankin AV, Biankin SA, Compton C, Fukushima N, Furukawa T, Goggins M, Kato Y, Klöppel G, Longnecker DS, Lüttges J, Maitra A, Offerhaus GJ, Shimizu M, Yonezawa S (2004) An illustrated consensus on the classification of pancreatic intraepithelial neoplasia and intraductal papillary mucinous neoplasms. Am J Surg Pathol 28:977–987
7. Khayyata S, Basturk O, Klimstra D, Hruban R, Zamboni G, Levi E, Adsay NV (2006) Muc6 expression distinguishes oncocytic and pancreatobiliary type from intestinal type papillae in pancreatic neoplasia: delineation of a pyloro-pancreatic pathway. Lab Invest 86 (Suppl 1):275A (Abstract)
8. Kosmahl M, Wagner J, Peters K, Sipos B, Klöppel G (2004) Serous cystic neoplasms of the pancreas: an immunohistochemical analysis revealing alpha-inhibin, neuron-specific enolase, and MUC6 as new markers. Am J Surg Pathol 28:339–346
9. Longnecker DS, Hruban RH, Adler G, Klöppel G (2000) Intraductal papillary-mucinous neoplasms of the pancreas. In: Hamilton R, Aaltonen LA (eds) Tumors of the digestive system. IARC, Lyon, pp 237–240
10. Lüttges J, Zamboni G, Longnecker D, Klöppel G (2001) The immunohistochemical mucin expression pattern distinguishes different types of intraductal papillary mucinous neoplasms of the pancreas and determines their relationship to mucinous noncystic carcinoma and ductal adenocarcinoma. Am J Surg Pathol 25:942–948
11. Nakamura A, Horinouchi M, Goto M, Nagata K, Sakoda K, Takao S, Imai K, Kim YS, Sato E, Yonezawa S (2002) New classification of pancreatic intraductal papillary-mucinous tumour by mucin expression: its relationship with potential for malignancy. J Pathol 197:201–210
12. Shibahara H, Tamada S, Goto M, Oda K, Nagino M, Nagasaka T, Batra SK, Hollingsworth MA, Imai K, Nimura Y, Yonezawa S (2004) Pathologic features of mucin-producing bile duct tumors: two histopathologic categories as counterparts of pancreatic intraductal papillary-mucinous neoplasms. Am J Surg Pathol 28:327–338
13. Solcia E, Capella C, Klöppel G (1997) Tumors of the pancreas (Atlas of tumor pathology, 3rd series, Fascicle 20). AFIP, Washington, District of Columbia, pp 53–64
14. Terris B, Dubois S, Buisine MP, Sauvanet A, Ruszniewski P, Aubert JP, Porchet N, Couvelard A, Degott C, Flejou JF (2002) Mucin gene expression in intraductal papillary-mucinous pancreatic tumours and related lesions. J Pathol 197:632–637
15. Yonezawa S, Horinouchi M, Osako M, Kubo M, Takao S, Arimura Y, Nagata K, Tanaka S, Sakoda K, Aikou T, Sato E (1999) Gene expression of gastric type mucin (MUC5AC) in pancreatic tumors: its relationship with the biological behavior of the tumor. Pathol Int 49:45–54

Virchows Arch (2006) 449: 117–120
DOI 10.1007/s00428-006-0205-6

CASE REPORT

Eva Markert · Ulrike Gruber-Moesenbacher · Christian Porubsky · Helmut H. Popper

Lung osteoma—a new benign lung lesion

Received: 22 December 2005 / Accepted: 23 March 2006 / Published online: 26 April 2006
© Springer-Verlag 2006

Abstract Extraskeletal osteomas have not been described in the lung. Tumors with osseous elements can be found, such as hamartoma and amyloid tumor, and reactive lesions such as osseous metaplasia. A 39-year-old male patient was treated for multiple myeloma and got a bone marrow transplantation 2 years and a few months before he presented with a solitary well-circumscribed tumor in the right middle lobe. The patient underwent surgical resection. The tumor presented with a fibrous capsule and consisted of mature bone trabecules. Within the tumor, fatty tissue was seen. There were small bone spicules interpreted as areas of new bone formation and appositional growth. No amyloid deposition, no immature epithelial tubules as in hamartomas, and no normal lung structure as in osseous metaplasia were seen. Within the osseous elements, a positive reaction was seen with antibodies for osteonectin, whereas the reaction for calcitonin was negative. To the best of our knowledge, this is the first case of an osteoma being reported in the lung looking like any other extraskeletal osteoma. This tumor might have been induced by circulating stem cells; however, due to autologous bona marrow transplantation, this cannot be proven.

E. Markert · H. H. Popper (✉)
Institute of Pathology, Laboratories for Molecular Cytogenetics, Environmental and Pulmonary Pathology,
Medical University of Graz,
Auenbruggerplatz 25,
Graz 8036, Austria
e-mail: helmut.popper@meduni-graz.at
Tel.: +43-316-3804405
Fax: +43-316-384329

U. Gruber-Moesenbacher
Institute of Pathology,
Teaching Hospital Feldkirch,
Carinagasse 47, Feldkirch 6800, Austria

C. Porubsky
Medical University of Graz,
Department of Thoracic and Hyperbaric Surgery,
Auenbruggerplatz 29, Graz 8036, Austria

Keywords Pulmonary osteoma · Hamartoma · Ossification · Osteonectin

Introduction

The most common benign mesenchymal neoplasm of the lung is hamartoma. A primary extraskeletal osteoma of the lung has never been reported. Within its differentials, hamartoma with osseous foci, osseous metaplasia, tracheobronchiopathia chondro-osteoplastica, and nodular amyloidosis or amyloid tumors with ossification have to be excluded.

Clinical history

In February 2002, the diagnosis of a multiple myeloma (subtype IgA-kappa, stage IIIb, Salmon, and Durie) was established in a 37-year-old male patient, current smoker (34 pack years). He was treated with interferon α and got autologous bone marrow transplantation the same year but relapsed in 2004. While prepared for a second bone marrow transplantation, in the absence of respiratory symptoms, a tumor, 1.7 cm in diameter was detected in the right upper lobe of the lung and subsequently removed. The tumor was of hard consistency and ossification could be identified macroscopically.

Material and methods

The VATS lung tissue specimen including the tumor was cut and a frozen tissue section was done for an intraoperative diagnosis. To be able to cut the tumor for frozen sections, the cut surface was decalcified for 1 min with hydrochloric acid (10%). Then the lung tissue was inflated with 10% neutral-buffered formaldehyde solution, fixed, decalcified with EDTA, and processed routinely. Immunohistochemistry was applied to decalcified paraffin sections using antibodies for osteonectin and calcitonin. Dilution

and processing was done as recommended by the manufacturer (Biodesign and Dako).

Results

Macroscopically, an osseous tumor with a diameter of 1.7 cm was identified, incompletely encapsulated by fidbrous tissue. Histological examination showed a network of mature lamellar bone trabecules with central lacunes in the tumor. At its periphery, a rim of typical osteoblasts was seen and areas with immature bone formation, characterized by calcified spicules and closely attached osteoblasts (Figs. 1 and 2). Within the delicate bone trabecules, there was fatty tissue with dilated thin walled vessels, similar, as it would be seen in mature lamellar bone. No chondroid cells, no epithelial tubules could be identified, however, in two areas entrapped bronchioles were seen. Both bronchioles had well-developed mucosa and a smooth muscle layer, which is not seen in hamartoma (Fig. 3). By immunohistochemistry, most osteoblasts, some osteocytes within the mature bone, and some histiocyte- and fibroblast-like cells expressed osteonectin (Fig. 4). The reaction for calcitonin was negative within the osteoma, whereas a few scattered positive cells could be seen within the lung tissue.

Discussion

Osteomas are benign osseous tumors. They are rare lesions and most frequently involve the skull, facial bones, or the spine protruding from the underlying bone. On histological examination the osteomas are characterized by mostly broad trabecules of mature bone. The intratrabecular tissue can be variably composed of vascular, fibrous, adipose, and hematopoetic elements [2].

Extraskeletal osteoma has rarely been reported. In 1997, Lekas et al. [7] published a case report about an 11-year-old

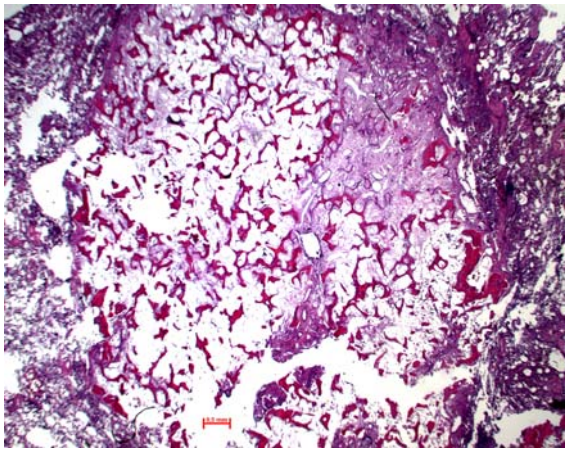

Fig. 1 Low power micrograph of the osteoma. Note areas of fat as well as fibrous tissue. The osteoma is well encapsulated by fibrous tissue. The surrounding lung is unremarkable. H&E, *bar* 0.5 mm

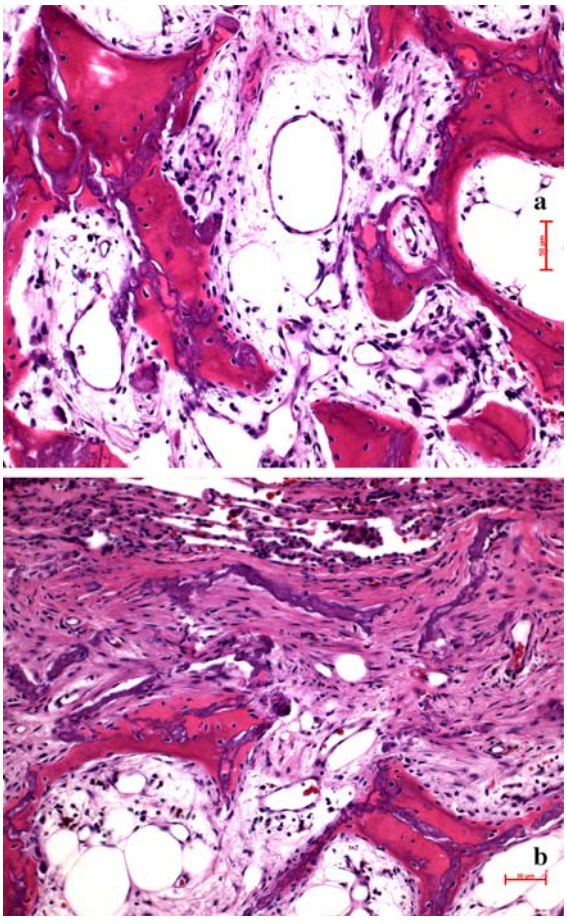

Fig. 2 Osteoma of the lung. **a** The central part is shown with mature lamellar bone. Within the bone, trabecules spicules are still present, which represent the initial stage of the bone formation. In addition, there are activated osteoblasts and osteoclasts, indicating restructuring of the bone. In **b**, the peripheral part of the osteoma is shown. This is characterized by calcified spicules embedded in dense fibrous tissue and surrounded by osteoblasts. H&E, *bars* 50 μm

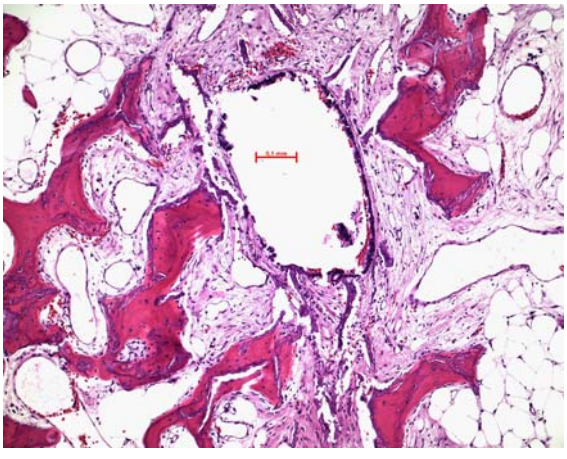

Fig. 3 Central portion of the osteoma with entrapped bronchioles. Regular epithelium and a thin muscular coat, usually 2–3 cell layers without cartilage, characterize these. Notably, bone spicules are seen approaching the bronchiolar wall and coming close to the surface epithelium. H&E, *bar* 100 μm

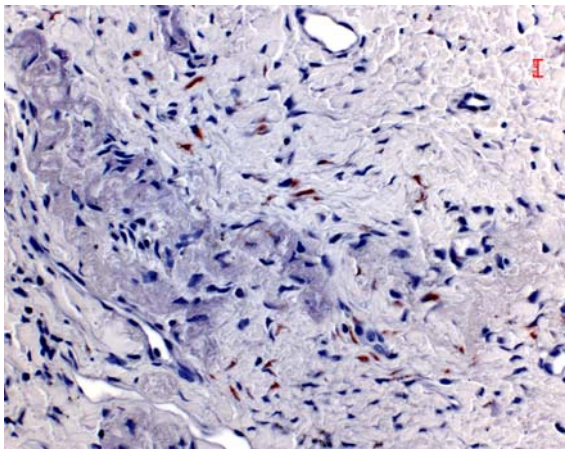

Fig. 4 Immunohistochemistry for osteonection; a focal positive staining is seen in fibroblast-like cells. *Bar*, 100 μm

girl, who developed an osteoma on the base of her tongue. One case of bilateral choroidal osteoma in association to histiocytosis X was documented by Kline et al. [6] in 1982. Extraskeletal osteomas were also described in animals, such as a benign osseous lesion in the leg of a cat [5].

More likely than osteomas in the lung are pulmonary hamartomas most frequently discovered in middle aged or elderly adults [11]. A Male predominance of 2:1 is reported [4]. Hamartomas usually manifest as solitary lung nodules evenly distributed throughout both lungs. Endobronchial localization is rare [3]. Histologically, they can be composed of hyaline cartilage, fibromyxoid stroma, smooth muscle cells, and adipose tissue. Any of the main tissue types can predominate. This is cartilage in 51.3%, fibromyxoid stroma in 10.5%, and less frequently adipose tissue (2.1%). In approximately 40%, smooth muscle cell proliferation can be found; sometimes calcification or bone-formation can be observed, a predominance of mature bone is exceptionally rare [3]. One frequent and pathognomonic finding in hamartoma is the coexistence of mesenchymal elements and epithelial tubules reminiscent of bronchiolar epithelium [10]. These tubules are composed of a simple layer of primitive cuboidal epithelium on a basal lamina and embedded in a primitive mesenchymal stroma. A smooth muscle cell layer is absent. Because of the absence of epithelial elements in our nodule, we were able to exclude hamartoma. The entrapped bronchioles were characterized by a well-developed bronchiolar epithelium and a muscular layer.

Peripheral pulmonary ossification is frequently found in lungs of elderly people. In this case, bone trabecules develop within the walls of alveoli. They can contain bone marrow. The lung structure is preserved and no fibrous capsule is present. In pulmonary ossification, calcification often precedes the bone formation. In contrast, our case shows a de novo formation of bone, which is also substantiated by the expression of osteonectin in the fibroblast-like cells at the periphery of the tumor.

A further disorder has to be excluded: tracheobronchopathia osteochondroplastica. The ossification is usually confined to preexisting bronchial or tracheal cartilage, but ossous metaplasia can occur [1]. In contrast, the tumor reported herein is a well-circumscribed single nodule without cartilage, localized in peripheral lung parenchyma; thus, unlikely to be mistaken for tracheobronchopathia osteochondroplastica.

Nodular amyloidosis might be another source of osseous metaplasia. Nodular amyloidosis or amyloid tumor could have been a consequence of the patient's plasmocytoma. Usually, there is deposition of congophilic amyloid, chronic inflammation with foreign body granulomas, and there can be calcification and even bone formation [8]. In our case, there was no evidence of amyloid deposits in the tumor and surrounding normal lung tissue.

Our patient suffers from multiple myeloma, which induces osteolytic lesions with consecutive hypercalcemia/hyperphosphatemia. There are reported cases of secondary neoplasm as a consequence of chemotherapy; nevertheless, a benign extraskeletal bone tumor has ever been associated to multiple myeloma [12].

One case of pulmonary ectopic ossification developed in a dog almost 3 years after allogenic bone marrow transplantation. The extensive bone formation was oriented along the bronchial walls, had normal trabecular architecture and marrow with normal cellularity. The authors postulated a bone formation of donor origin, although DNA analysis could not be performed.

It may well be that in our patient the osteoma could be formed by circulating stem cells derived from the bone marrow [9]; however, due to an autologous transplantation, this cannot be proven. We suppose that this bone tumor in the patient's lung is independent from his major diagnosis myeloma. In our opinion, this tumor is clearly identified as osteoma, although its localization in peripheral lung tissue is extraordinary.

References

1. Castella J, Puzo C, Cornudella R, Curell R, Tarres J (1981) Tracheobronchopathia osteochondroplastica. Respiration 42:129–134
2. Frassica FJ, Waltrip RL, Sponseller PD, Ma LD, McCarthy EF, Jr. (1996) Clinicopathologic features and treatment of osteoid osteoma and osteoblastoma in children and adolescents. Orthop Clin North Am 27:559–574
3. Gjevre JA, Myers JL, Prakash UB (1996) Pulmonary hamartomas. Mayo Clin Proc 71:14–20
4. Hansen CP, Holtveg H, Francis D, Rasch L, Bertelsen S (1992) Pulmonary hamartoma. J Thorac Cardiovasc Surg 104:674–678
5. Jabara AG, Paton JS (1984) Extraskeletal osteoma in a cat. Aust Vet J 61:405–407
6. Kline LB, Skalka HW, Davidson JD, Wilmes FJ (1982) Bilateral choroidal osteomas associated with fatal systemic illness. Am J Ophthalmol 93:192–197
7. Lekas MD, Sayegh R, Finkelstein SD (1997) Osteoma of the base of the tongue. Ear Nose Throat J 76:827–828
8. Lynch LA, Moriarty AT (1993) Localized primary amyloid tumor associated with osseous metaplasia presenting as bilateral breast masses: cytologic and radiologic features. Diagn Cytopathol 9:570–575

9. Sale GE, Storb R (1983) Bilateral diffuse pulmonary ectopic ossification after marrow allograft in a dog. Evidence for allotransplantation of hemopoietic and mesenchymal stem cells. Exp Hematol 11:961–966
10. Salminen US (1990) Pulmonary hamartoma. A clinical study of 77 cases in a 21-year period and review of literature. Eur J Cardiothorac Surg 4:15–18
11. van den Bosch JM, Wagenaar SS, Corrin B, Elbers JR, Knaepen PJ, Westermann CJ (1987) Mesenchymoma of the lung (so called hamartoma): a review of 154 parenchymal and endobronchial cases. Thorax 42:790–793
12. Zarrabi MH, Rosner F (1989) Second neoplasms in Hodgkin's disease: current controversies. Hematol Oncol Clin North Am 3:303–318

Virchows Arch (2006) 449: 121–123
DOI 10.1007/s00428-006-0202-9

CASE REPORT

J. Fernando Val-Bernal · Marta Cuadrado ·
M. Francisca Garijo · José M. Revuelta

Incidental in vivo detection of an isolated hemangioma of the aortic valve in a man with a history of renal transplantation

Received: 10 March 2006 / Accepted: 18 March 2006 / Published online: 25 April 2006
© Springer-Verlag 2006

Abstract Hemangiomas of the cardiac valves are exceptional. To our knowledge, only ten cases of valve hemangiomas, six in the mitral and four in the tricuspid valve, have been reported in the English literature. We describe an incidentally detected aortic valve hemangioma of a 62-year-old man with chronic, degenerative aortic valve stenosis, who underwent renal transplantation 7 years before. We believe that this is the first report of a hemangioma in this localization and the first one in association with solid organ transplantation. The review of the literature of the adult cases of valve hemangioma, including this report, revealed that the average age was 47.2 years (range, 24 to 68 years). No clear sex predominance has been noted. Patients can be asymptomatic or experience sudden death. Symptomatic patients have complaints of palpitations, dyspnea, or syncopal episodes. Histologically, these valve tumors are classified as capillary, cavernous, and mixed. Mean tumor size is 1.1 cm (range, 0.6 to 2 cm). In 50% of cases the hemangioma is an incidental finding at autopsy or in a removed valve. Valve aortic hemangioma, despite its rarity, should be considered in the differential diagnosis of vascular lesions of this cardiac valve.

Keywords Heart · Cardiac valves · Aortic valve · Hemangioma · Organ transplantation

J. F. Val-Bernal (✉) · M. Cuadrado · M. F. Garijo
Departamento de Anatomía Patológica,
Hospital Universitario Marqués de Valdecilla,
Avda. Valdecilla 1,
Santander 39008, Spain
e-mail: apavbj@humv.es
Tel.: +34-942-202599
Fax: +34-942-201903

J. M. Revuelta
Department of Cardiovascular Surgery Service,
Marqués de Valdecilla University Hospital, Medical Faculty,
University of Cantabria,
Santander, Spain

Introduction

Primary benign vascular tumors of the heart are quite uncommon representing about 4% of cardiac tumors [2, 3]. Thus, in a series of cardiac tumors covering a period of two decades, no case of hemangioma was observed [11].

Most cardiac hemangiomas are asymptomatic and incidentally detected at autopsy or cardiac surgery [2]. On the other hand, cardiac valve tumors are rare and the great majority of which are papillary fibroelastomas [4].

Valve hemangiomas are very rare neoplasms. In fact this location is not mentioned in a recent and authoritative monograph on cardiac tumors [13]. To the best of our knowledge, only ten cases of valve hemangiomas have been reported in the English literature [1, 4, 5, 7, 9, 10, 12, 14, 16]. In this report, we present a new case incidentally detected in the aortic valve and review the literature on the subject. To the best of our knowledge, this the first report of hemangioma of the aortic valve and the first one in association with solid organ transplantation.

Case report

A 62-year-old man presented in the casualty ward with syncope and dyspnea. Past medical history was significant for diabetes mellitus type II, hypertension, and chronic renal failure treated with renal transplantation 7 years before. Echocardiography revealed calcific aortic valve stenosis and mitral incompetence with left ventricular enlargement. Aortic valve replacement with a bileaflet, mechanical device, type CarboMedics (CarboMedics, Austin, Texas, USA) of 21 mm, and a mitral annuloplasty with Sovering annulus (Sorin Biomedica Cardio S.p.A, Saluggia, Italy) of 30 mm were performed. After the operation, the left valves were sound on function. The echocardiogram did not reveal abnormalities. The patient's recovery was uneventful. He was discharged in good condition on postoperative day 15.

Results

The operative excised three-cuspid aortic valve measured 3×2.2×0.9 cm. The cusps showed extensive fibrous thickening and nodular calcific deposits. As commissural fusion was absent, the etiology of stenosis was considered degenerative.

Microscopic examination of the noncoronary cusp of the aortic valve showed an incidental, small, circumscribed nodule situated just beneath the endocardium (Fig. 1a). The nodule measured 6 mm and it consisted of medium-sized and large, thin-walled, interconnecting vascular channels occupied by red blood cells. They were lined by single-layered thin endothelial cells. A pseudopapillary pattern reminiscent of sinusoidal hemangioma was noted. The intervening stroma was scanty and myxoid (Fig. 1b). Pleomorphism, hyperchromasia, mitotic figures, or thrombosis were not seen. Cells lining vascular channels stained for CD31 and CD34. Alpha-smooth muscle actin stained some pericytic cells around vascular spaces. There was no reactivity for human herpes virus-8 (HHV-8) antibody. The rest of the valve revealed diffuse fibrosis and extensive calcification.

Discussion

Hemangiomas of the heart may occur in all locations. Most of the tumors are sporadic, without evidence of extracardiac vascular lesions. The most common sites are the atria (33.3%), the left ventricle or ventricular septum (26.7%), the right ventricle (24.4%), and the pericardium or epicardium (13.3%) [2].

Hemangiomas of the cardiac valves are exceptional. Cardiac valves are avascular structures except for one third of the proximal portion near the valve ring. This fact explains the rarity of the valve hemangioma.

As far as we are aware, only ten cases of valve hemangioma have been reported [1, 4, 5, 7, 9, 10, 12, 14, 16] in the English literature, six in the mitral valve and four in the tricuspid valve. To the best of our knowledge, the present is the first case reported located in the aortic valve. Including this case, the average age of the adults is 47.2 years (range, 24 to 68 years). There is no preference for gender. Patients can be asymptomatic or experience sudden death. Symptomatic patients have complaints of palpitations, dyspnea, or syncopal episodes.

Histologically these valve tumors are classified as capillary, cavernous, and mixed types. Average tumor size in adults is 1.1 cm (range, 0.6 to 2 cm). In 50% of the cases, the hemangioma was an incidental finding at autopsy or in a removed valve.

Organ transplantation with immunosuppression is associated with an increased incidence of some neoplasms occurring in the recipient. However, hemangioma does not show an increased incidence. Therefore, it is difficult to know the influence of immunosupression or the status of the organ transplant in the development of the hemangioma in our patient. As a related phenomenon Kuvin et al. [6] reported a blood cyst of the mitral valve apparatus in a woman with a history of orthotopic liver transplantation.

Differential diagnosis includes blood cyst, varix, neovascularization of the valve, organized thrombus, and hemangioendothelioma.

A blood cyst [2, 6, 9, 17] is usually congenital, lined by endothelial cells, located along the lines of closure of heart valves. The lesion results of invagination of endothelium and its lumen are connected to the cardiac lumen. It is a rare finding in adults [6]. Varices [2, 9] are endocardial, unilocular cysts, filled with blood. They are dilated thrombosed veins most commonly located in the inferior rim of the fossa ovalis. Neovascularization of the leaflets is a proliferation diffuse, irregular in size of blood vessels separated from abundant fibrous stroma. Intravascular papillary endothelial hyperplasia is a benign intravascular process thought to arise from an organizing thrombus. The lesion may present clinically as an abnormal mass and may be confused with a benign or malignant vascular neoplasms

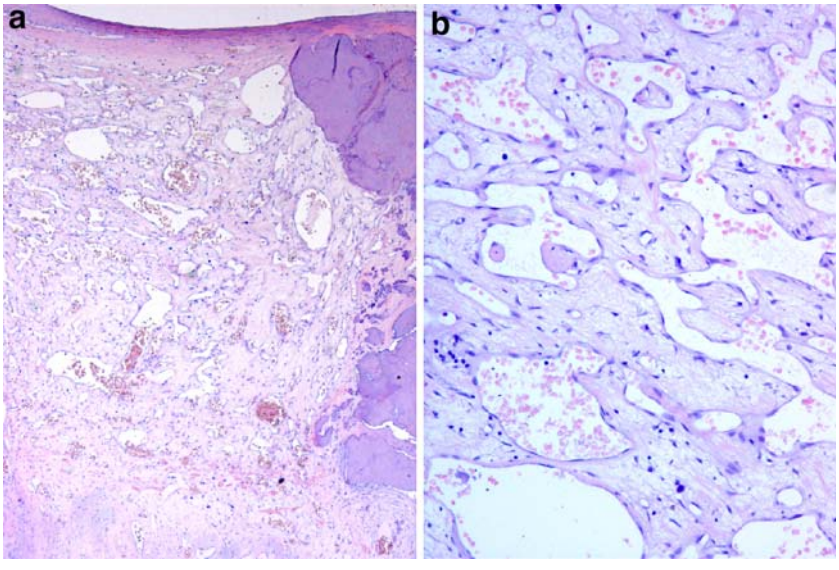

Fig. 1 **a** Panoramic view of the hemangioma arising from the aortic valve in subendothelial location. The lesion retains circumscription without encapsulation. Vessels of cavernous and capillary type are intermingled. In the vicinity, valve calcification can be seen. **b** The interconnecting vascular channels are lined by single-layered thin endothelial cells. These cells show uniform, bland nuclei. The intervening stroma is myxoid

[8]. Cardiac hemangioendothelioma [15] is a vascular tumor of intermediate malignancy that can be difficult to differentiate from hemangioma. Malignant features include mitotic activity, solid growth, some degree of cellular atypia, and necrosis. The epithelioid variant shows epithelial-like endothelial cells with cytoplasmic vacuoles.

In conclusion, valve aortic hemangioma, despite its rarity, should be considered in the differential diagnosis of vascular lesions of this cardiac valve.

References

1. Ahmed U, Khurshid SG (2004) Mitral valve hemangioma with superimposed infective endocarditis. J Gen Intern Med 19 (Suppl 1):60–61
2. Burke A, Virmani R (1996) Tumors of the heart and great vessels. In: Rosai J, Sobin LH (eds) Atlas of tumor pathology, third series, fascicle 16. Armed Forces Institute of Pathology, Washington, DC, pp 1–11
3. Burke A, Johns JP, Virmani R (1990) Hemangiomas of the heart. A clinicopathologic study of ten cases. Am J Cardiovasc Pathol 3:283–290
4. Edwards FH, Hale D, Cohen A, Thompson L, Pezzella AT, Virmani R (1991) Primary cardiac valve tumors. Ann Thorac Surg 52:1127–1131
5. Kutay V, Yakut C, Ekim H (2006) Mitral annular tumors: report of two cases in childhood. J Card Surg 21:191–194
6. Kuvin J, Saha P, Rastegar H, Salomon RN, Pandian N, Denofrio D (2004) Blood cyst of the mitral valve apparatus in a woman with a history of orthotopic liver transplantation. J Am Soc Echocardiogr 17:480–482
7. Lapenna E, De Bonis M, Torracca L, La Canna G, Dell'Antonio G, Alfieri O (2003) Cavernous hemangioma of the tricuspid valve: minimally invasive surgical resection. Ann Thorac Surg 76:2097–2099
8. Massetti M, Babatasi G, Saloux E, Bhoyroo S, Grollier G, Khayat A (1999) Spontaneous native aortic valve thrombosis. J Heart Valve Dis 8:157–159
9. McAllister HA, Fenoglio JJ (1978) Tumors of the cardiovascular system. In: Hartman WH, Cowan WR (eds) Atlas of tumor pathology, second series, fascicle 15. Armed Forces Institute of Pathology, Washington, DC, pp 46–51
10. Nye SW, Orsinelli DA, Baker PB, Brown DA (2001) Surgical treatment of a hemangioma of the mitral valve. Ann Thorac Surg 71:345–347
11. Odim J, Reehal V, Laks H, Mehta U, Fishbein MC (2003) Surgical pathology of cardiac tumors. Two decades at an urban institution. Cardiovasc Pathol 12:267–270
12. Ray R, Rishi A, Venugopal P, Chopra P (2004) Hemangioma of the tricuspid valve: a report of two cases with review of the literature. Cardiovasc Pathol 13:120–122
13. Tazelaar H, Burke AP, Watanabe G, Basson CT (2004) Haemangioma. In: Travis WD, Brambilla E, Müller-Hermelink, Harris CC (eds) Pathology and Genetics of tumours of the lung, pleura, thymus and heart. World Health Organization Classification of Tumours. IARC Press, Lyon, pp 266–267
14. Ugras S, Bayram I (2005) Cavernous hemangioma of the mitral valve in a child: report of a case and review of the literature. Pathology 35:396–398
15. Val-Bernal JF, Garcia-Alberdi E, Gutierrez JA, Garijo MF (2005) Incidental in vivo detection of an epithelioid hemangioendothelioma of the mitral valve. Pathol Int 55:644–648
16. Wong KK, Sandor GGS, Sett SS (2004) Isolated hemangioma of the tricuspid valve. Cardiol Young 14:324
17. Yamamoto H, Nakatani S, Niwaya K, Ohnishi T, Uematsu M, Kitakaze M (2005) Images in cardiovascular medicine. Giant blood cyst of the mitral valve: echocardiographic and intraoperative images. Circulation 112:e341

Virchows Arch (2006) 449: 124–128
DOI 10.1007/s00428-006-0211-8

CASE REPORT

Vassiliki Zolota · Vassiliki Tzelepi · Nicolaos Charoulis · Efstratios Apostolakis · Demetrios Dougenis

Mediastinal rhabdomyoma: case report and review of the literature

Received: 12 December 2005 / Accepted: 28 March 2006 / Published online: 25 April 2006
© Springer-Verlag 2006

Abstract Rhabdomyomas are benign tumors in which at least some cells are differentiated as skeletal muscle cells with cytoplasmic cross-striations. Extracardiac adult rhabdomyoma is an extremely uncommon benign neoplasm that usually involves the head and neck region. Rare cases have been reported to involve other sites of the body including mediastinum. We report the fourth case of mediastinal adult rhabdomyoma.

Keywords Adult · Rhabdomyoma · Mediastinum

Introduction

Rhabdomyomas are benign tumors in which at least some cells are differentiated as skeletal muscle cells with cytoplasmic cross-striations [11]. They are rare lesions that consist of two types, cardiac and extracardiac. The cardiac rhabdomyomas are often associated with tuberous sclerosis and are considered hamartomatous [3]. Extracardiac rhabdomyomas consist of three clinical and histological subtypes: adult, fetal, and genital accounting for 50, 40, and 10% of these tumors, respectively [11]. The extracardiac adult rhabdomyoma (EAR) is an extremely uncommon benign neoplasm that usually involves the head and neck region [11]. In the literature, only three cases of EAR have been reported to arise in mediastinum [5, 8, 10]. Possible origin from the myoid cells of the thymus has been postulated [10]. We report the fourth case of adult rhabdomyoma presenting as a mediastinal mass.

Clinical history

A 75-year-old, white woman presented to her family doctor with 1 month history of fever and chills. No weight loss or fatigue was reported. She also denied tobacco and alcohol use. Physical examination was unremarkable apart from a palpable thyroid gland and varicosities. She was treated with antibiotics and had resolution of her symptoms. However, 2 months later, she was referred to our hospital because of fever recurrence. Routine laboratory tests showed moderate anemia and elevated HER. Chest radiography revealed a mediastinal mass (Fig. 1a) which was subsequently confirmed on chest computed tomography (Fig. 1b). The mass was located behind the trachea, esophagus, and the right branchiocephalic vessels extending to the prevertebral space of the neck.

A cervical approach was undertaken with incision "collar" type at suprasternal notch including a partial upper sternotomy. The tumor was found to wrap around the esophagus and the trachea. It was encapsulated without invasion of mediastinal structures and was easily dissected free and removed completely. A right lobectomy of the thyroid gland was also performed because of a palpable lesion. Frozen section was reported negative for malignancy.

The postoperative course of the patient was uneventful and she was discharged home on the 6th postoperative day. A repeat chest X-ray a month later was normal. She is alive with no evidence of disease 10 months later.

V. Zolota · V. Tzelepi
Department of Pathology, University of Patras, Medical School, 26504 Rio, Greece

N. Charoulis · E. Apostolakis · D. Dougenis
Department of Surgery, University of Patras, Medical School, 26504 Rio, Greece

Present address:
V. Zolota (✉)
10 Spirou Mpleri str.,
Nafpaktos 30300, Greece
e-mail: vtzelepi@yahoo.com
Tel.: +30-2634025814
Fax: +30-2634025814

Present address:
V. Tzelepi
12 Agias Anastasias str.,
Patras 26225, Greece

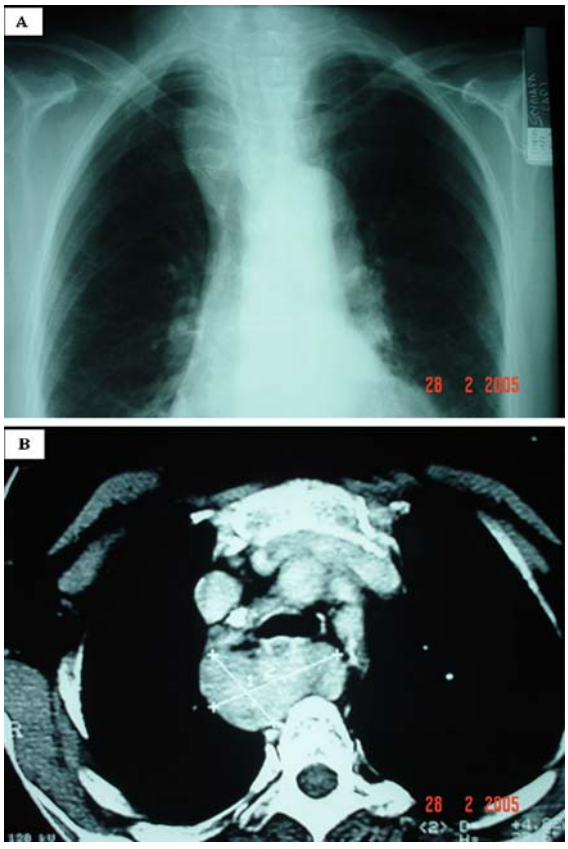

Fig. 1 **a** Plain chest radiography depicting a mediastinal mass extending towards the upper lobe of the lung. **b** Computed tomography of the chest revealing a mass at the upper posterior mediastinal in contact with esophagus and tracheal carina, anteriorly to the prevertebral fascia

Materials and methods

The surgical specimen was fixed in 10% formalin and representative sections were embedded in paraffin and stained with hematoxylin–eosin (H&E) and periodic acid-Schiff (PAS) with and without prior diastase digestion.

For immunohistochemical analysis, the avidin–biotin complex technique and antibodies against a-smooth muscle actin (a-SMA), muscle specific actin (MSA), desmin, S-100 protein, CD56, carcinoembryonic antigen (CEA), myoglobin, myogenin, MyoD1, and cytokeratin "cocktails" AE1 and AE3 were employed. Clones and sources of the antibodies used are showed in Table 1. Diaminobenzidine was used as the chromogen. Nuclei were counterstained with hematoxylin.

Results

Pathology

The mediastinal neoplasm was a multilobulated, redish-tan, and firm mass with smooth external surface that measured 16×8.7×2.5 cm and weighed 100 g. There was a thin capsule that was not penetrated by the tumor. On cross-section, it was homogenous and fleshy and had fibroelastic consistency. Part of the tumor that measured 3.1×2.5×1.2 cm was submitted for intraoperative evaluation (frozen section). The intraoperative diagnosis was "neoplasm composed of cells with abundant eosinophilic granular cytoplasm. There is no sign of malignancy".

The right lobe of the thyroid was also submitted at the Pathology Department. It measured 4.1×3.2×2.1 and weighed 8 g. On cross-section, a nodule with colloidal consistency measuring 0.4 cm on greatest dimension was seen.

Microscopy showed that the neoplasm was composed of closed packed round to polygonal cells of variable size, separated by connective tissue septa and blood vessels (Fig. 2a). The neoplastic cells had small eccentric nuclei with prominent nucleoli and a deeply eosinophilic granular cytoplasm with occasional vacuoles (Fig. 2b). A few cells had peripheral intracytoplasmatic vacuolation and centrally located nuclei that imparted a spider web appearance (Fig. 2b). There was no atypia, mitotic figures, or necrosis (Fig. 3a). Cross-striations were not evident on H&E staining. The tumor cell cytoplasm was PAS positive (Fig. 3b). Most of the PAS positive material was removed by prior diastase treatment. No thymic tissue was identified in any of the tissue sections.

Table 1 Clone and sources of the antibodies used

Antibody	Clone–source
a-SMA	1A4, BioGenex, USA
MSA	HHF-5, BioGenex, USA
Desmin	33, BioGenex, USA
S100	15E2E2, BioGenex, USA
CD56	123C3.D5, Neomarker, CA
CEA	CEA 88, BioGenex, USA
AE1	BioGenex, USA
AE3	BioGenex, USA
Myoglobin	Dako, Denmark
Myogenin	F5D, Dako, Denmark
MyoD1	5,8A, Dako, Denmark

Immunohistochemistry

Tumor cells were positive for MSA, desmin, myoglobin, and CD56 (Figs. 4a,b and 5). S-100 protein was expressed in approximately 20% of the tumor cells. No immunostaining was observed for CD56, a-SMA, CEA, myogenin, MyoD1, AE1, and AE3.

Discussion

Rhabdomyoma is a rare entity, accounting for only 2% of all tumors with skeletal muscle differentiation [8, 11]. Most patients are between 40 and 70 years old, although the age range extends from 2 to 82 years [11]. The mean age at

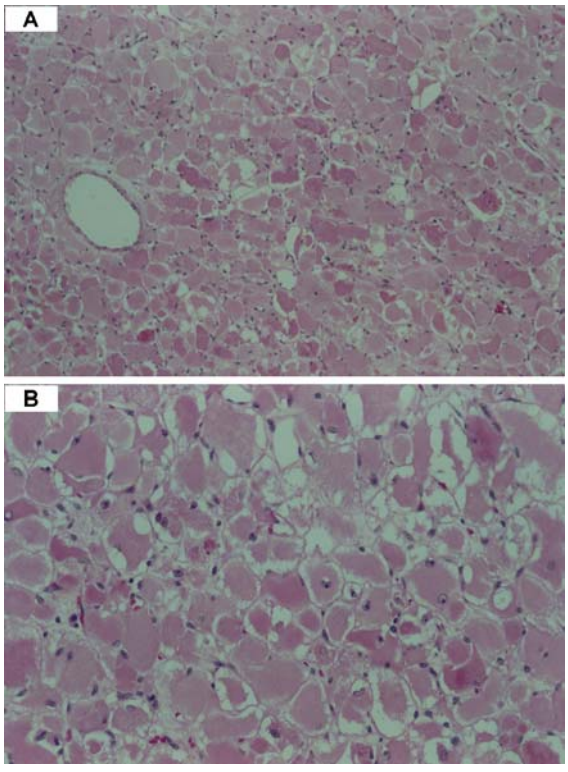

Fig. 2 **a** The tumor consists of closely packed, large polygonal cells and scant stroma containing thin-walled vascular channels (H&E, ×100). **b** The tumor cells have small round nuclei and abundant eosinophilic, granular or peripherally vacuolated cytoplasm. Numerous cells have a spider web appearance. (H&E, ×200)

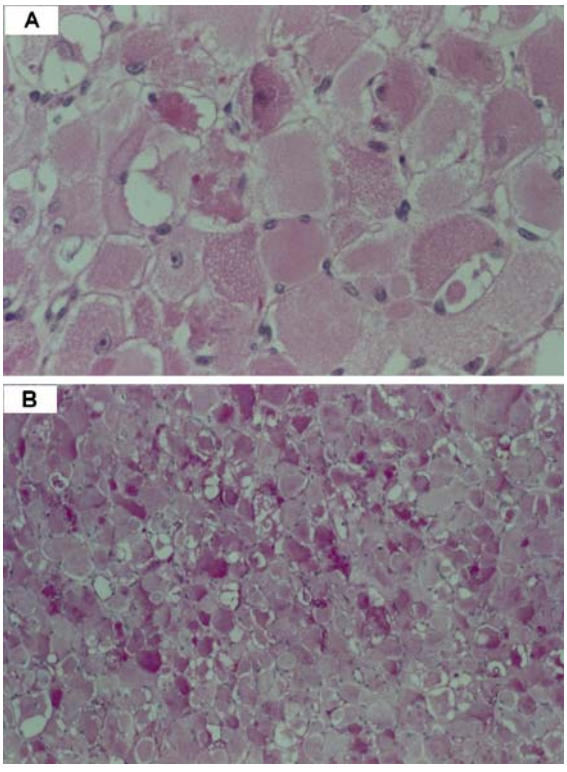

Fig. 3 **a** Nuclei are centrally or peripherally located and have prominent nucleoli but show no prominent variation in size and shape (H&E, ×400). **b** The tumor cell cytoplasm is PAS positive (×100)

presentation is 54–60 years [10]. The male to female ratio is 3–4 to 1 [10, 11].

Seventy to 75% of extracardiac adult rhabdomyomas (EAR) occur in the head and neck region. The most common site is the mucosa of the pharynx, followed by the mucosa of the oral cavity, and the larynx and the branchial musculature of the neck in the distribution of the third and fourth branchial arches. Rare cases have been reported to occur in the extremities [5], esophagus [15], stomach [18], and mediastinum [2, 12, 17]. To our knowledge, this is the fourth case of adult rhabdomyoma occurring in the mediastinum.

The neoplasm is usually unifocal, but 15% of the cases are multifocal [1, 6, 7, 11] and 26% of the tumors can be multinodular at onset [10]. The lesions are often symptomatic. The most common presenting symptoms are slowly growing soft tissue masses, airway obstruction, dysphagia, hoarseness, and nasal obstruction. The symptoms depend upon the site and size of the tumor [1, 8, 10, 11, 15]. Occasionally, the tumor is asymptomatic [6, 10, 12, 17]. Two of the three previously reported mediastinal cases were incidental findings at autopsy, whereas the third patient presented with bronchitis and cough.

On gross examination the tumor is usually reddish-tan, well-circumscribed, encapsulated, and lobulated with a median size of 3.0 cm and a maximum of 7 to 8 cm [11]. There have been reported cases with a larger size [5, 9] as

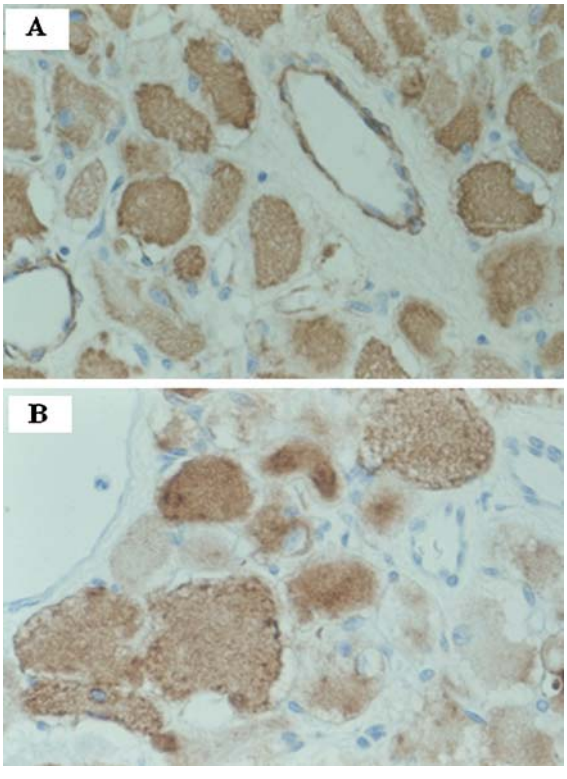

Fig. 4 **a** Diffuse, strong positive staining of the tumor cells for MSA (×200). **b** The tumor cells stain for Desmin (×400)

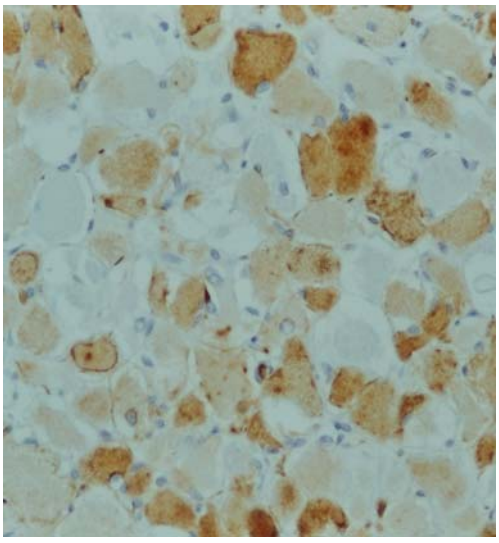

Fig. 5 The tumor cells stain for myoglobin (×200)

was in our case, in which the tumors' greatest diameter was 14 cm (not the mediastinal ones).

Histologically, the tumor is composed of well-demarcated lobules that consist of closely packed, large polygonal cells and scant stroma containing thin-walled vascular channels [1, 6, 8, 10, 16, 17]. The tumor cells have small round centrally or peripherally located nuclei with prominent nucleoli and abundant eosinophilic, granular or peripherally vacuolated cytoplasm [1, 7, 11, 16, 17]. The peripherally located vacuoles are a result of the removal of intracellular glycogen by the fixative. When they are surrounded by residual radially oriented cytoplasm, they impart a spider web appearance to the cell [7, 10, 16]. Cytoplasmic cross-striations and crystal-like structures can be found focally in hematoxylin–eosin stained sections in most but not all of the cases. The former is more prominent with the Masson trichrome and the phosphotungstic acid stains [7, 10, 15]. The cytoplasm is rich in glycogen which gives the Periodic-Acid Schiff reaction positive but sensitive to prior diastase treatment [5, 9, 7, 15]. Mitoses are absent [1, 10, 16]. Foci of inflammation and necrosis with reactive nuclear features can rarely be seen [10].

Ultrastructurally, the tumor cells show abundant mitochondria and glycogen, hypertrophic Z bands, and hazardly arranged clusters of myofilaments [12, 15, 17].

Immunohistochemical staining for desmin and muscle-specific actin (MSA) is strongly positive in the tumor cells as was in our case [1, 6, 9, 10, 15, 17]. Strong positivity for myoglobin is another feature of adult rhabdomyoma. The tumor cells may also demonstrate focal or rare immunoreactivity for vimentin, Leu7, a-smooth muscle actin (a-SMA), CD56, CD57, and S-100 protein [10, 11]. No reactivity is observed for glial fibrillary acid protein (GFAP), cytokeratins, CD68, and neurofilaments [1, 9, 10].

The differential diagnose includes a variety of neoplasms with abundant eosinophilic, vacuolated, or granular cytoplasm such as granular cell tumor, hibernoma, oncocytoma, and paraganglioma [10]. Granular cell tumor has poorly defined cell borders, is often associated with pseudoepitheliomatous hyperplasia, is strongly positive for S-100 protein, and lacks the light microscopic (cross-striations) and immunohistologic evidence (expression of MSA, myoglobin) of striated muscle differentiation. Paragangliomas express neuronal specific enolase (NSE), synaptophysin and/or chromogranin, which are not a feature of adult rhabdomyoma. Hibernomas and oncocytomas also lack skeletal muscle markers. Alveolar soft part sarcoma may have an immunologic profile similar to rhabdomyoma. However, the tumor cells of alveolar soft part sarcoma have an alveolar pattern of growth and contain intracytoplasmic crystalline rods and granules that are demonstrated with the Pas/diastase stains [11]. Rhabdomyosarcoma can easily be excluded because the cells exhibit high degree of pleomorphism and atypia, findings that are not features of adult rhabdomyoma. Thymoma [13], thymic carcinoma [14] and thymic cysts [4] with rhabdomyomatous features have been described in the literature and should be excluded before making the diagnosis of mediastinal rhabdomyoma. Rhabdomyomatous thymoma [13] and thymic carcinoma [14] exhibit two distinct cell populations, an epithelial and a myoid one. Yet even the rhabdomyomatous cells of these neoplasms are different from rhabdomyoma cells, having eccentrically placed nuclei and less amount of eosinophilic cytoplasm. Normal thymic tissue is found at the periphery of the tumor and this is also the case for rhabdomyomatous thymic cyst [4].

Unlike cardiac rhabdomyoma which is hamartoma rather than true neoplasm, extracardiac adult rhabdomyoma is considered to be a true neoplasm. Clonal chromosomal abnormalities such as a balanced translocation between chromosome 15 and 17 and abnormalities involving the band 10q126 have been observed in adult rhabdomyoma which supports the notion that it is a true neoplasm [9]. However, some authors believe that adult rhabdomyoma is a result of degeneration and regeneration of striated muscle rather than a neoplasm [1].

It has been suggested that mediastinal rhabdomyoma arises from the thymic myoid cells [12]. The normal fetal and infant thymus gland contains myoid cells that are associated with Hassal's corpuscles. There have been reported thymomas with groups of myoid cells [12, 13]. However, multiple sections of the mediastinal tumor in our case and the previous ones have failed to demonstrate any residual thymic elements [12, 17].

Adult rhabdomyoma is cured after complete resection. However, recurrences have been reported to happen after 1 month to 35 years [9–11, 16] and are probably due to incomplete resection of the primary tumor. Uncontrolled focal growth, metastases, or death due to the neoplasm has not been reported [11].

In summary, we report a rare case of rhabdomyoma which should be included in the differential diagnosis of tumors presenting as a large, asymptomatic, mediastinal mass.

References

1. Blaauwgeers LLG, Troost D, Dingemans KP, Traat CW, Van den Tweel JG (1989) Multifocal rhabdomyoma of the neck. Am J Surg Pathol 13:91–799
2. Box CJ, Newman CL, Anastasiades KD, Lucas WG, Latouf OM (1995) Adult rhabdomyoma: Presentation as a cervicomediastinal mass (case report and review of the literature). Am Surg 61:271–276
3. Burke AP, Virmany R (1991) Cardiac rhabdomyoma: a clinicopathologic study. Mod Pathol 4:70–74
4. Chetty R, Reddi A (2003) Rhabdomyomatous multilocular thymic cyst. Am J Clin Pathol 119:816–821
5. Cronin CT, Keel SB, Graabe J, Schuler JG (2000) Adult rhabdomyoma of the extremity: case report and review of the literature. Human Pathol 31:1074–1080
6. Delides A, Petrides N, Banis K (2005) Multifocal adult rhabdomyoma of the head and neck: a case report and literature review. Eur Arch Otorhinolaryngol 262:504–506
7. Enzinger FM, Weiss SW (1994) Rhabdomyoma. In: Gay MS (ed) Soft tissue tumors, 3rd edn. Mosby, St Luis, pp 523–537
8. Favia G, Muzio LL, Serpico R, Maiorano E (2003) Rhabdomyoma of the head and neck: clinicopathologic features of two cases. Head Neck 25:700–704
9. Gibas Z, Miettinen M (1992) Recurrent parapharyngeal rhabdomyoma. Evidence of the neoplastic nature of the tumor from cytogenetic study. Am J Surg Pathol 16:721–728
10. Kapadia SB, Meis JM, Frisman DM, Ellis GL, Heffner DK, Hyams VJ (1992) Adult rhabdomyoma of the head and neck: a clinicopathologic and immunophenotypic study. Hum Pathol 24:608–617
11. Kempson RL, Fletser CD, Evans HL, Hendrickson MR, Sibley RK (2001) Skeletal muscle tumors. In: Rosai J (ed) Atlas of tumor pathology. Tumors of the soft tissues. Armed Forces Institute of Pathology, Washington, pp 257–267
12. Miller R, Kurtz SM, Powers JM (1978) Mediastinal rhabdomyoma. Cancer 42:1983–1988
13. Moran CA, Koss MN (1993) Rhabdomyomatous thymoma. Am J Surg Pathol 17:633–636
14. de Queiroga EM, Chicota H, Bacchi CE, Moran CA, Suster S (2004) Rhabdomyomatous carcinoma of the thymus. Am J Surg Pathol 28:1245–1250
15. Roberts F, Kirk AJ, More IA, Butler J, Reid RP (2000) Oesophageal rhabdomyoma. J Clin Pathol 53:554–557
16. Scrivner D, Meyer JS (1980) Multifocal recurrent adult rhabdomyoma. Cancer 46:790–795
17. Sidhu JS, Nicolas MM, Taylor W (2002) Mediastinal rabdomyoma. A case report and review of the literature. Int J Surg Pathol 10:313–318
18. Tuazon R (1969) Rhabdomyoma of the stomach. Report of a case. Am J Clin Pathol 52:37–41

Virchows Arch (2006) 449: 129–133
DOI 10.1007/s00428-006-0215-4

CASE REPORT

S. Lanzafame · R. Caltabiano · L. Puzzo · A. Cappellani

Thyroid transcription factor 1 (TTF-1) and p63 expression in two primary thyroid papillary carcinomas of branchial cleft cysts

Received: 16 February 2006 / Accepted: 30 March 2006 / Published online: 21 April 2006
© Springer-Verlag 2006

Abstract Malignant lateral cervical cysts can be related to metastatic tumors or rarely to primary thyroid carcinoma arising in branchial cleft cysts. This study evaluates the expression of thyroid-associated transcription factor-1 (TTF-1) and p63 in three branchial cleft cysts and in two primary thyroid papillary carcinoma of branchial cleft cysts. TTF-1 was negative in the nuclei of the lining epithelia of branchial cleft cysts, but positive in the adjacent normal thyroid tissue, while TTF-1 was positive in the nuclei of the lining epithelia and in the nuclei of the papillae and follicles in branchial cleft cysts with ectopic thyroid carcinoma. P63 was positive in the nuclei of the lining epithelia of branchial cleft cysts, but negative in the adjacent normal thyroid tissue. Papillary thyroid carcinoma of branchial cleft cysts displayed p63-positive foci. In conclusion, our results demonstrate that TTF-1 cannot distinguish between primary and metastatic tumors of branchial cleft cysts. The detection of p63 in papillary thyroid carcinomas of branchial cleft cysts could suggest that p63 contributes to the onset of this tumor. It is really important to evaluate if the case has a metastatic derivation or represents papillary thyroid carcinoma arising in ectopic thyroid tissue in a branchial cleft cyst.

Keywords Branchial cleft cyst · Ectopic thyroid papillary carcinoma · TTF-1 · p63

S. Lanzafame (✉) · R. Caltabiano · L. Puzzo
Department G.F. Ingrassia, Section of Anatomic Pathology,
University of Catania,
Santa Sofia 87 street,
95123 Catania, Italy
e-mail: lanzafas@unict.it
Fax: +39-095-3782023

A. Cappellani
Department of Surgery,
University of Catania,
Catania, Italy

Introduction

The thyroid-associated transcription factor-1 (TTF-1) is a 38-kDa DNA-binding protein, with 378 amino acids, belonging to the homeobox-containing gene family. TTF-1 is required for maximal expression of the TSHR gene in thyroid cells and is essential for morphogenesis of the thyroid, lung, and ventral forebrain. Considering that the expression of TTF-1 is restricted to thyroid, brain, and lung, the detection of this antigen may suggest the origin of unknown metastases [9].

P63 is a member of the p53 gene family, located at 3q27–29 region [11]. P63 gives rise to an array of multiple protein isoforms due to differential mRNA splicing and to alternative promoter usage. In conclusion, p63 encodes six different isoforms: three with the transactivating domain (TA) and three lacking the N-terminal domain (ΔN). The TAp63 forms are capable of transactivating p53 target genes also inducing apoptosis, while ΔNp63 forms behave in a dominantly negative fashion toward their own TA proteins and toward p53 in vivo in the mouse and in transfected human cells [21]. Strikingly, squamous cell carcinomas of the skin and other organs produce high levels of ΔNp63 [12].

Lateral cervical cysts are usually benign lesions occurring predominantly in young people. Malignant lateral cervical cysts are less frequent and can be related to metastatic tumors arising mainly from carcinomas in the oronasopharyngeal area and the thyroid gland or, rarely, to primary thyroid carcinoma arising in branchial cleft cysts.

Branchial cleft cysts were considered a result of impaired obliteration of branchial clefts or pouches. However, at the moment, there is much controversy about the genesis of branchial cleft cysts with more recent theories suggesting epithelial inclusions within cervical lymph nodes as triggering event. The detection of thyroid tissue within a branchial cleft cyst is a matter of debate in the literature.

The aim of this study is to evaluate, through immunohistochemistry, the expression of TTF-1 and p63 in branchial cleft cysts with ectopic normal thyroid tissue

and, for the first time, in two primary thyroid papillary carcinomas of branchial cleft cysts, and to evaluate the embryology and the oncogenetic pathway of these lesions.

Materials and methods

From a retrospective review of patients undergoing surgery for solitary cervical cysts, we found three branchial cleft cysts with ectopic normal thyroid tissue; one branchial cleft cyst with ectopic thyroid papillary carcinoma, classic type; and one branchial cleft cyst with ectopic thyroid papillary carcinoma, follicular type. In the last two cases, there was no evidence of papillary carcinoma found within the thyroid gland when it was subsequently removed and subjected to meticulous histological examination. The totally embedded thyroid was subjected to sectioning of all the blocks so the authors could be sure there was no thyroid primary carcinoma. Clinical data of the patients are summarized in Table 1.

All specimens were fixed in 10% neutral-buffered formalin at room temperature. They were embedded in paraffin wax, and 4-μm serial sections were collected on silane-coated glass slides. Immunohistochemistry was performed with the mouse antibody against TTF-1, clone 8G7G3/1 (DAKO, USA), at a dilution of 1:50 in phosphate-buffered saline (PBS) with microwave pretreatment; the mouse antibody against thyroglobulin (TG), clone DAK-Tg6 (DAKO), at a dilution of 1:100 in PBS with microwave pretreatment; and the mouse antibody against p63, clone BC4A4 (Biocare Medical, USA), at a dilution of 1:50 in PBS with microwave pretreatment. All antibodies were applied directly to each section and the slides were incubated overnight (4°C). Immunocomplexes were subsequently treated with the secondary antibody for 30 min at room temperature and then detected by means of streptavidin peroxidase for 30 min at room temperature (Vectastain ABC kit; Vector Laboratories, Burlingame, CA, USA). Immunoreactivity was visualized by development for 2 min with 0.1% 3,3′-diaminobenzidine and 0.02% hydrogen peroxide (DAB substrate kit; Vector Laboratories). Sections were counterstained with Mayer hematoxylin, mounted with permount, and examined by light microscopy. Immunoreactivity was evaluated blindly by two observers, who independently assessed the immunostainings by means of light microscopy. Amongst serial sections, two of every six were stained with hematoxylin and eosin (Bio-optica, Milan, Italy) for morphological studies. Negative controls consisted of sections in which primary antibodies were omitted and replaced with either nonimmune murine serum (X 0910; DAKO) or with 1% PBS–bovine serum albumin. Positive controls consisted of thyroid tissue sections.

Results

In cases of branchial cleft cysts with ectopic thyroid papillary carcinomas, classic and follicular types, histological examination demonstrated a cyst lined by a single layer of columnar epithelium with subepithelial lymphoid aggregates. Within the cyst wall, we found thyroid papillary carcinomas, classic and follicular types (Figs. 1 and 2) and foci of normal thyroid follicles (Fig. 3). In fact, in the first case papillae with delicate fibrovascular cores, sclerotic stroma, ground glass, grooved nuclei with small distinct nucleoli and pseudoinclusions were evident. In the second, irregularly shaped follicles with typical nuclear features of papillary carcinoma were evident.

As already reported in the literature [8], TTF-1 was negative in the nuclei of the lining epithelia of branchial cleft cysts, but stained positive in the adjacent normal thyroid tissue (Fig. 4). On the other hand, TTF-1 was positive both in the nuclei of the lining epithelia and in the nuclei of the papillae and follicles in the branchial cleft

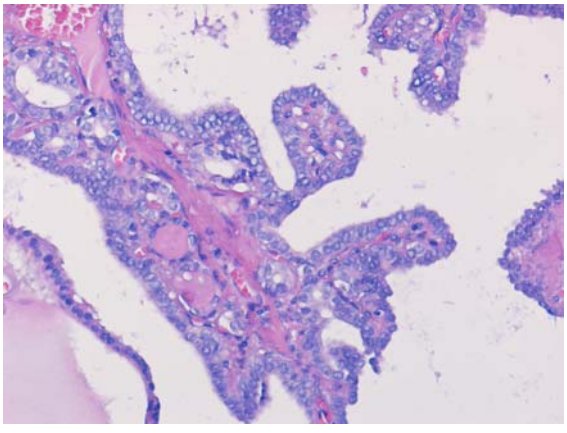

Fig. 1 Thyroid papillary carcinoma, classic type in branchial cleft cyst (E.E. 20×)

Table 1 Clinical data of the patients

Case no.	Gender	Age	Gross examination	Diagnosis	Other investigations
1	Female	11	Cyst, 3×2×0.5 cm	Branchial cleft cyst	
2	Male	20	Cyst, 2.6×1×0.5 cm	Branchial cleft cyst	
3	Male	54	Cyst, 3×2.5×1 cm	Branchial cleft cyst	
4	Female	29	Cyst, 4×2.5×1 cm with white nodule (1 cm)	Thyroid papillary carcinoma in branchial cleft cyst	No evidence of carcinoma within the thyroid gland after thyroidectomy
5	Female	21	Cyst 2.5×1×0.5 cm with white nodule (0.5 cm)	Thyroid papillary carcinoma follicular type in branchial cleft cyst	No evidence of carcinoma within the thyroid gland after thyroidectomy

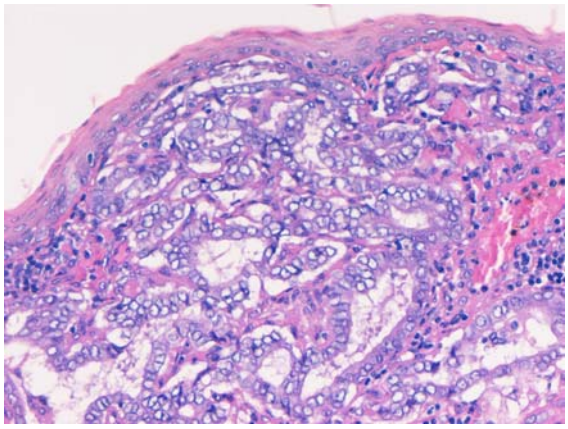

Fig. 2 Thyroid papillary carcinoma, follicular type in branchial cleft cyst (E.E. 10×)

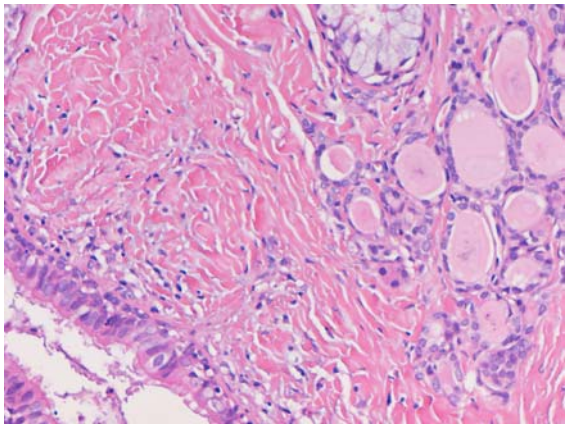

Fig. 3 Normal thyroid tissue next to thyroid papillary carcinoma in branchial cleft cyst (E.E. 10×)

cysts with ectopic thyroid carcinoma (Fig. 5). The results also showed that p63 expression was positive in the nuclei of the lining epithelia of branchial cleft cysts, but negative in the adjacent normal thyroid tissue (Fig. 6). Papillary thyroid carcinoma of branchial cleft cyst displayed p63-positive foci in the papillae and the lining epithelia (case no. 4). Staining was focal rather than extensive or confluent; the extent of staining varied from multiple positive foci to scattered or rare foci (Fig. 7). On the other hand, the follicular variant of papillary carcinoma in branchial cleft cyst was negative for p63 (case no. 5). Only thyroid tissue of branchial cleft cysts and ectopic thyroid carcinoma in branchial cleft cysts demonstrated cytoplasmic staining for TG.

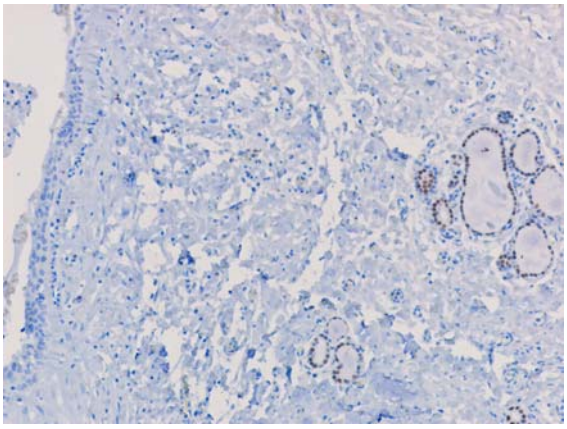

Fig. 4 TTF-1 immunostaining in branchial cleft cysts (10×)

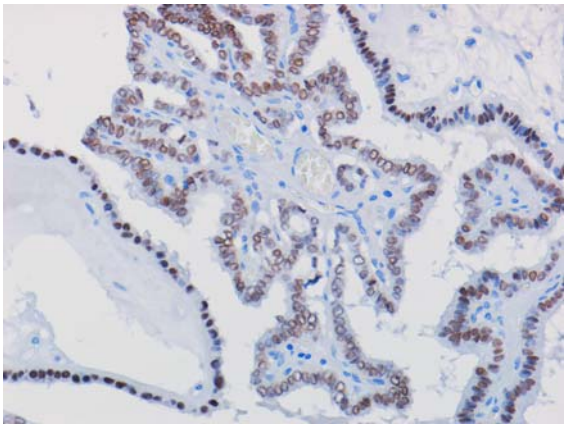

Fig. 5 TTF-1 immunostaining in branchial cleft cysts with ectopic thyroid carcinoma, classic type (20×)

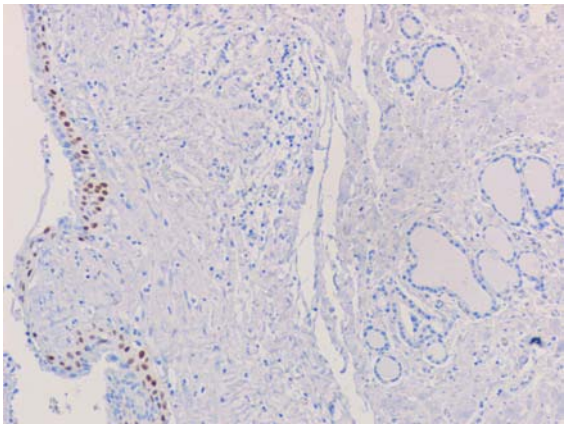

Fig. 6 P63 immunostaining in branchial cleft cysts and ectopic normal thyroid tissue (10×)

Discussion

Heterotopic thyroid tissue can be found anywhere along the thyroglossal duct. The most frequent location is at the base of the tongue, where it may cause respiratory obstruction and difficulty in swallowing [16]. Other sites are the anterior tongue, submandibular area, larynx, trachea, mediastinum, and the heart [13]. In a few cases, thyroid tissue may also be found in branchial cleft cysts. In any of these locations, the tissue is subject to the same disease that can affect the main gland, including inflammation, hyperplasia, and tumors. Although the majority of the cystic lesions in the lateral neck containing a focus of papillary thyroid carcinoma represent lymph node metastases from a thyroid primary tumor that have undergone secondary cystic change [17], in the literature there are four case

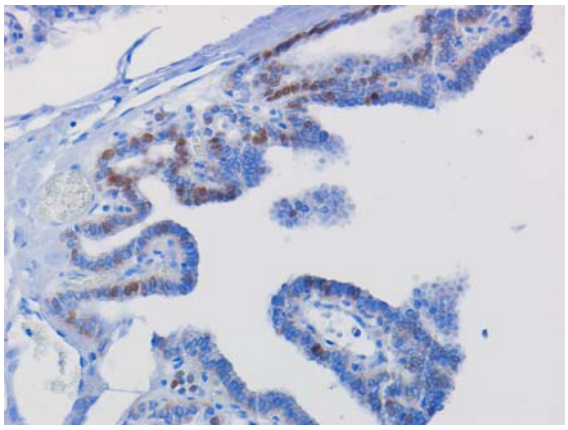

Fig. 7 P63 immunostaining in branchial cleft cysts with ectopic thyroid carcinoma, classic type (20×)

reports about primary thyroid papillary carcinoma arising from branchial cleft cysts [1, 7, 10, 18]. We believe that our cases are really primary thyroid papillary carcinoma arising from ectopic thyroid tissue of the branchial cleft cyst because they fit Sidhu's criteria [18] consistent with this diagnosis. In fact, we found an epithelial lining layer and a subepithelial collection of lymphoid tissue typical of branchial cleft cyst, normal thyroid tissue within the cyst wall adjacent to the focus of papillary carcinoma, positive staining for thyroglobulin in tumor tissue and no evidence of papillary carcinoma in the thyroid gland when it was removed and subjected to meticulous histological examination. Considering Kreft et al.'s [8] article about expression of TTF-1 in metastatic papillary thyroid cancer of cystic lesions of the neck and Carrizo and Luna's [4] article about expression of TTF-1 in thyroid-like nasopharyngeal papillary adenocarcinoma, we performed TTF-1 immunostaining in primary thyroid papillary carcinoma of branchial cleft cysts to identify different staining between the two lesions. Unfortunately, a strong nuclear staining was evident in the nuclei of the lining epithelia and in the nuclei of the papillae and follicle, both in primary and metastatic thyroid papillary carcinoma. Therefore, our results demonstrate that this antibody cannot distinguish between primary and metastatic tumors of branchial cleft cyst.

Considering that solid cell nests of the thyroid gland, recently proposed as adult stem cells [14] and usually considered as remnants of the ultimobranchial body, are p63 positive structures with a possible histogenetic link with papillary thyroid carcinoma [2], we performed p63 immunostaining on our patients. The detection of p63 in the papillary thyroid carcinomas of the branchial cleft cysts but not in the follicles of the follicular variant of papillary carcinoma nor in normal thyroid tissue could suggest that follicular cells in the branchial cleft cysts, already damaged by oncogenic mutations, induce p63, a potentially oncogenic protein, that would contribute to the onset of papillary carcinoma. The focal staining pattern, characteristically seen in papillary carcinoma, was similar to patchy p63 staining found in adenocarcinomas and contrasted with the extensive to confluent staining seen in squamous carcinomas [19]. However, according to the literature, the involvement of p63 immunoreactive cells in the tumorigenic process remains to be proven because they may simply reflect squamous differentiation of papillary thyroid carcinoma [3]. Our finding of ectopic thyroid tissue and carcinoma within a branchial cleft cyst raises the question of the mechanism whereby this situation arises. At the moment, there are two explanations for the formation of the lateral branchial cleft cysts. According to the congenital hypothesis, they represent a remnant of the structures lying in the lateral aspect of the embryo (branchial clefts/pouch, cervical sinus, thymopharyngeal duct) [15]. According to the acquired hypothesis, they develop as a result of cystic transformation of cervical lymph nodes [6, 20]. The presence of thyroid tissue within a branchial cleft cyst may be explained by either theory. In fact, the thyroid develops from one median anlage and two lateral anlage. The median anlage develops from the base of the tongue in the foramen cecum and descends to its final position along the thyroglossal duct. The thyroglossal duct then atrophies, although it may persist, become cystic, and even develop papillary thyroid carcinoma in the thyroid tissue present in its wall. The lateral anlage develops from the fourth–fifth branchial pouch, so some thyroid cells may be entrapped in a lateral branchial cleft cyst. We can also explain the presence of ectopic thyroid tissue in an acquired branchial cleft cyst, considering the possible occurrence of benign thyroid inclusions in cervical lymph node [18]. According to the acquired hypothesis, epithelial cell inclusions from upper airway and gastrointestinal tract enter lymphatic vessels and reach the lateral neck lymph nodes. This colonization would promote a cystic degeneration of the lymph nodes. As previously described, thyroid cells can also reach the cervical lymph node and explain the possible occurrence of thyroid carcinoma arising in branchial cleft cysts [18].

In conclusion, ectopic thyroid tissue in a branchial cleft cyst is a rare abnormality, and papillary carcinoma arising in this tissue is extremely rare [5]. It is really important, for adequate therapy, to evaluate if the case has a metastatic derivation with a missed primary tumor or represents papillary thyroid carcinoma arising in ectopic thyroid tissue in a branchial cleft cyst. Hence, thyroidectomy would be performed even if the gland were clinically and radiologically free of nodules.

References

1. Balasubramaniam GS, Stillwell RG, Kennedy JT (1992) Papillary carcinoma arising in ectopic thyroid tissue within a branchial cyst. Pathology 24:214–216
2. Cameselle-Teijeiro J, Febles-Perez C, Sobrinho-Simoes M (1995) Papillary and mucoepidermoid carcinoma of the thyroid with anaplastic transformation: a case report with histologic and immunohistochemical findings that support a provocative histogenetic hypothesis. Pathol Res Pract 191:1214–1221
3. Cameselle-Teijeiro J, Preto A, Soares P, Sobrinho-Simoes M (2005) A stem cell role for thyroid solid cell nests. Hum Pathol 36:590–591

4. Carrizo F, Luna MA (2005) Thyroid transcription factor-1 expression in thyroid-like nasopharyngeal papillary adenocarcinoma: report of 2 cases. Ann Diagn Pathol 9:189–192
5. Choi SS, Zalzal GH (1995) Branchial anomalies: a review of 52 cases. Laryngoscope 105:909–913
6. Golledge J, Ellis H (1994) The aetiology of lateral cervical (branchial) cysts: past and present theories. J Laryngol Otol 108:653–659
7. Jadusingh W, Shah DJ, Shaw H, Lyn C (1996) Thyroid papillary carcinoma arising in a branchial cleft cyst. West Indian Med J 45:122–124
8. Kreft A, Hansen T, Kirkpatrick CJ (2005) Thyroid transcription factor 1 expression in cystic lesions of the neck: an immunohistochemical investigation of thyroglossal duct cysts, branchial cleft cysts and metastatic papillary thyroid cancer. Virchows Arch 447:9–11
9. Lau SK, Luthringer DJ, Eisen RN (2002) Thyroid transcription factor-1: a review. Appl Immunohistochem Mol Morphol 10:97–102
10. Matsumoto K, Watanabe Y, Asano G (1999) Thyroid papillary carcinoma arising in ectopic thyroid tissue within a branchial cleft cyst. Pathol Int 49:444–446
11. Moll UM, Erster S, Zaika A (2001) p53, p63 and p73-solos, alliances and feuds among family members. Biochim Biophys Acta 1552:47–59
12. Nylander K, Vojtesek B, Nenutil R, Lindgren B, Roos G, Zhanxiang W, Sjostrom B, Dahlqvist A, Coates PJ (2002) Differential expression of p63 isoforms in normal tissues and neoplastic cells. J Pathol 198:417–427
13. Osammor JY, Bulman CH, Blewitt RW (1990) Intralaryngotracheal thyroid. J Laryngol Otol 104:733–736
14. Preto A, Cameselle-Teijeiro J, Moldes-Boullosa J, Soares P, Cameselle-Teijeiro JF, Silva P, Reis-Filho JS, Reyes-Santias RM, Alfonsin-Barreiro N, Forteza J, Sobrinho-Simoes M (2004) Telomerase expression and proliferative activity suggest a stem cell role for thyroid solid cell nests. Mod Pathol 17:819–826
15. Regauer S, Gogg-Kamerer M, Braun H, Beham A (1997) Lateral neck cysts—the branchial theory revisited. A critical review and clinicopathological study of 97 cases with special emphasis on cytokeratin expression. APMIS 105:623–630
16. Seoane JM, Cameselle-Teijeiro J, Romero MA (2002) Poorly differentiated oxyphilic (Hurthle cell) carcinoma arising in lingual thyroid: a case report and review of the literature. Endocr Pathol 13:353–360
17. Seven H, Gurkan A, Cinar U, Vural C, Turgut S (2004) Incidence of occult thyroid carcinoma metastases in lateral cervical cysts. Am J Otolaryngol 25:11–17
18. Sidhu S, Lioe TF, Clements B (2000) Thyroid papillary carcinoma in lateral neck cyst: missed primary tumour or ectopic thyroid carcinoma within a branchial cyst? J Laryngol Otol 114:716–718
19. Unger P, Ewart M, Wang BY, Gan L, Kohtz DS, Burstein DE (2003) Expression of p63 in papillary thyroid carcinoma and in Hashimoto's thyroiditis: a pathobiologic link? Hum Pathol 34:764–769
20. Wild G, Mischke D, Lobeck H, Kastenbauer E (1987) The lateral cyst of the neck: congenital or acquired? Acta Otolaryngol 103:546–550
21. Yang A, Kaghad M, Wang Y, Gillett E, Fleming MD, Dotsch V, Andrews NC, Caput D, McKeon F (1998) p63, a p53 homolog at 3q27–29, encodes multiple products with transactivating, death-inducing, and dominant-negative activities. Mol Cell 2:305–316

Virchows Arch (2006) 449: 134
DOI 10.1007/s00428-006-0201-x

LETTER TO THE EDITOR

Raphael Schiffmann

The significance of lysosomal inclusions in Fabry disease

Received: 21 February 2006 / Accepted: 8 March 2006 / Published online: 12 April 2006
© Springer-Verlag 2006

Dear Editor,

We read the comments of Dr. Politei with great interest. The point of our paper was not to state that enzyme replacement therapy (ERT) does not work (although we do think that it has a modest effect only), but to indicate that, at least in this patient, long-term ERT depletes lysosomal storage only from vascular endothelial cells. This suggests a limited cellular availability of the infused enzyme. This impediment may be a major cause of the limited effect of ERT. ERT did stabilize the renal function of this patient. It is true that early treatment may do better than late, but this remains to be demonstrated in prospective controlled studies.

Sincerely,

Dr. Raphael Schiffmann

R. Schiffmann (✉)
National Institutes of Health—Developmental and Metabolic Neurology Branch, NINDS,
Bldg. 10, Rm. 3D03, 9000 Rockville Pike,
Bethesda, MD 20892-1260, USA
e-mail: SchiffmR@ninds.nih.gov

Virchows Arch (2006) 449: 135–136
DOI 10.1007/s00428-006-0171-z

LETTER TO THE EDITOR

Aurelia Noske · Stefan Pahl

Combined adenosquamous and large-cell neuroendocrine carcinoma of the gallbladder

Received: 6 July 2005 / Accepted: 28 November 2005 / Published online: 29 March 2006
© Springer-Verlag 2006

Dear Editor,
Although featuring a relatively simple microscopic anatomy, the gallbladder may give rise to a wide variety of malignant tumors. Beside pure forms of carcinomas, there are different admixed types. We report on a combined adenosquamous and large-cell neuroendocrine carcinoma of the gallbladder, a histological subtype which, to the best of our knowledge, has not been described before.

Case report

A 81-year-old female patient was admitted to our hospital with a history of abdominal pain, weight loss, and jaundice for 3 months. At the time of admission, clinical signs of a fracture of the right femoral neck were also present. Cholelithiasis was diagnosed by abdominal ultrasound, whereas conventional radiography of the hip indicated a pathological fracture. The operative findings showed an advanced and unresectable large tumor of the gallbladder with infiltration of the extrahepatic bile ducts and liver. A palliative resection of the tumor with establishment of a biliodigestive anastomosis was performed. The femoral head was removed and an endoprothesis implanted.

Pathological gross examination revealed a protruding polypoid-exophytic tumor in the neck region of the gallbladder with continuous diffuse infiltration of the gall bladder wall and adjacent liver tissue (50 mm max. diameter). Additionally, there were three gallstones of (respectively) 20 mm diameter in the gallbladder. Separately, we received an extrahepatic bile duct segment (50×35×30 mm) with inconspicuous mucosa but extensive periductal, necrotic tumor infiltration of 45×30×30 mm. We also obtained the femoral head (45 mm diameter).

Microscopically, the tumor consisted of two components, a moderately differentiated adenosquamous carcinoma and a poorly differentiated large-cell neuroendocrine carcinoma. The adenocarcinoma was composed of small- and medium-sized glands lined by a columnar epithelium with moderate atypical nuclei (Fig. 1a). Abrupt transitions to the squamous component showing keratin pearls were found (Fig. 1b). Adjacent mucosa of the gallbladder showed severe dysplasia, whereas preexisting squamous metaplasia could not be detected. In addition, the tumor was composed of a substantial component exhibiting round cells growing in solid sheets, nests, and cords (Fig. 1c). The formation of rosettes could be focally demonstrated. The cells tended to be larger than those of a small-cell carcinoma and had pleomorphic nuclei and a high mitotic rate. The neuroendocrine differentiation of this component could be confirmed by immunohistochemistry. Diffuse and strong cytoplasmic expression of synaptophysin (Fig. 1d) and CD56, but only focal and low immunoreactivity for chromogranin A, was found. Adenoid and squamous carcinoma complexes were distributed between the neuroendocrine component (Fig. 1e,f). Histological examination of the femoral head revealed only a metastasis of the neuroendocrine component.

Discussion

Carcinomas of the gallbladder are rare neoplasms of the gastrointestinal tract and associated with a poor outcome. This is mainly because most tumors are diagnosed at an advanced stage. Prognosis depends not only on the stage of the disease process but also on the exact histological type [4]. Adenocarcinomas and other differentiated carcinomas are generally associated with a comparatively favorable prognosis, while small-cell (neuroendocrine) and undifferentiated carcinomas exhibit a highly aggressive clinical behavior [2, 3]. Most common malignant tumors of the gallbladder are adenocarcinomas, whereas primary ade-

A. Noske · S. Pahl (✉)
Institute of Pathology, Charité Hospital,
Campus Mitte, Schumannstr. 20/21,
10117 Berlin, Germany
e-mail: stefan.pahl@charite.de
Tel.: +49-30-450536043
Fax: +49-30-450536900

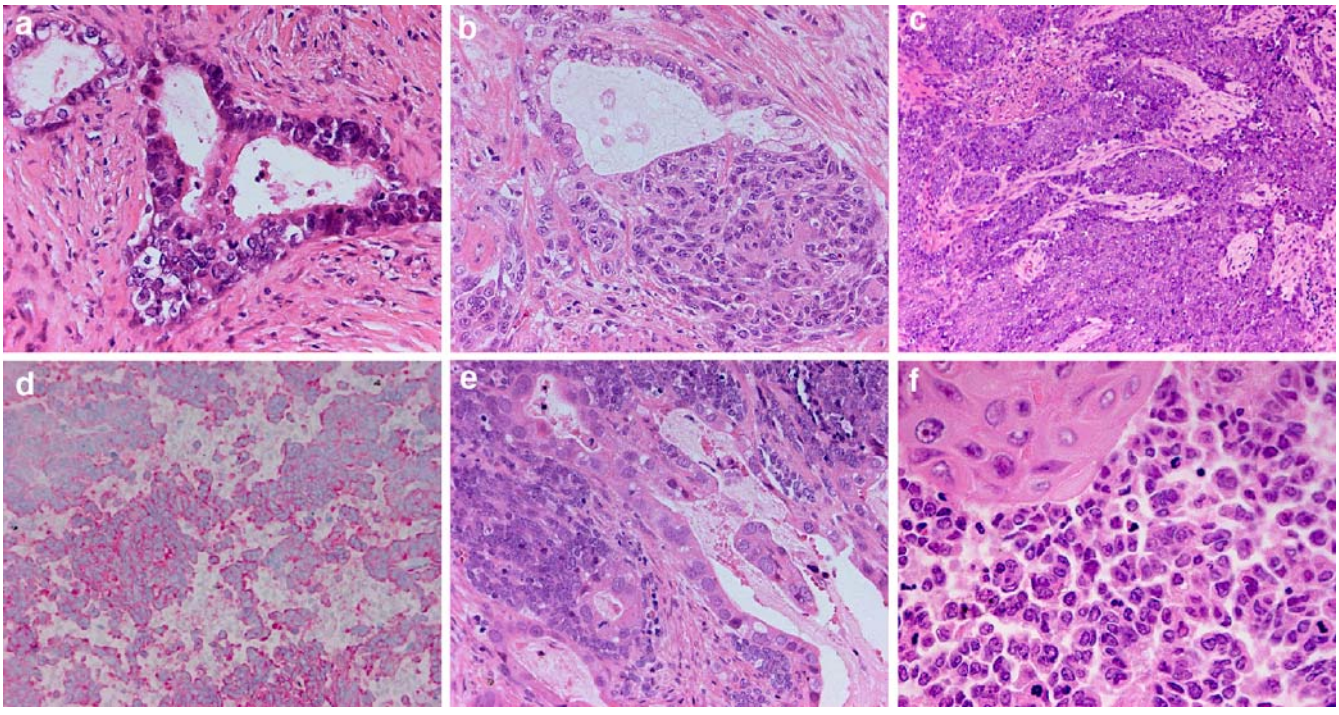

Fig. 1 Histological appearance of the combined gallbladder carcinoma. **a** Well-differentiated adenocarcinomatous glands infiltrating the muscular wall of the gallbladder. H & E, ×200. **b** Transitional area between glandular and squamous differentiated carcinoma formations. H & E, ×200. **c** Area of the large-cell (neuroendocrine) carcinoma component growing in solid nests and cords. H & E, ×100. **d** Immunohistochemical staining for synaptophysin. Tumor cells of the neuroendocrine component are diffusely positive (×200). **e** Admixed area of the adenocarcinomatous and neuroendocrine component. H & E, ×200. **f** Transitional region between squamous and neuroendocrine carcinoma complexes. The latter component is composed of large cells with irregular nuclei. H & E, ×400

nosquamous, pure squamous, and neuroendocrine carcinomas are rare. Among the spectrum of neuroendocrine carcinomas are well-differentiated carcinoid tumors, small-cell (oat cell) carcinomas, and large-cell neuroendocrine carcinomas.

We present an unusual case of an adenosquamous carcinoma in combination with a substantial large-cell neuroendocrine component, which resembled the corresponding tumor type of the lung. It is known that adenosquamous carcinomas may contain scattered endocrine cells admixed with the neoplastic columnar and squamous cells in approximately 20% [1]. In the opposite way, small-cell (neuroendocrine) carcinomas may show foci of squamous differentiation and areas of well-differentiated neoplastic glands. Neuroendocrine tumors of the large cell type, similar to the large-cell neuroendocrine carcinoma of the lung, are extremely rare [5]. Normally, neuroendocrine cells cannot be found in the gallbladder, but may occur in non-neoplastic epithelium that exhibits hyperplastic or metaplastic changes [5]. Until now, the histogenesis of the neuroendocrine differentiated tumors is not clear. Whether those cells stem from a common pluripotent precursor or from metaplastic neuroendocrine cells is still debatable. Nevertheless, recognition of divergent differentiation in gallbladder carcinoma is important, as a neuroendocrine component may be associated with paraneoplastic syndromes and a different chemotherapeutical regimen can be indicated. More importantly, however, the neuroendocrine component usually follows a more aggressive clinical course, as shown in our case, where the bone metastasis was composed of the neuroendocrine component.

References

1. Albores-Saavedra J, Nadji M, Henson DE, Angeles-Angeles A (1989) Entero-endocrine cell differentiation in carcinomas of the gallbladder and mucinous cystadenocarcinomas of the pancreas. Pathol Res Pract 183:169–175
2. Carriaga MT, Henson DE (1995) Liver, gallbladder, extrahepatic bile ducts, and pancreas. Cancer 75:171–190
3. Fujii H, Aotake T, Horiuchi T, Chiba Y, Imamura Y, Tanaka K (2001) Small cell carcinoma of the gallbladder: a case report and review of 53 cases in the literature. Hepatogastroenterology 48:1588–1593
4. Henson DE, Albores SJ, Corle D (1992) Carcinoma of the gallbladder. Histologic types, stage of disease, grade, and survival rates. Cancer 70:1493–1497
5. Papotti M, Cassoni P, Sapino A, Passarino G, Krueger JE, Albores-Saavedra J (2000) Large cell neuroendocrine carcinoma of the gallbladder. Am J Surg Pathol 24:1424–1428

Virchows Arch (2006) 449: 137–139
DOI 10.1007/s00428-006-0210-9

LETTER TO THE EDITOR

Taisuke Mori · Hideki Orikasa · Takeharu Shigematsu · Kazuto Yamazaki

An ultrastructural and immunohistochemical study of a combined submucosal granular cell tumor and lipoma of the colon showing a unique nodule-in-nodule structure: putative implication of CD34 or prominin-2-positive stromal cells in its histopathogenesis

Received: 14 October 2005 / Accepted: 3 April 2006 / Published online: 4 May 2006
© Springer-Verlag 2006

Dear Editor

We recently had a patient with a unique combination of a granular cell tumor and a lipoma of the colon showing a nodule-in-nodule appearance by histopathological examination.

Our patient, a 55-year-old Japanese man, underwent colonoscopic examination as part of a routine health check. A whitish, polypoid lesion was found in the cecum (Fig. 1a, inset). Benign, submucosal tumor, such as a carcinoid tumor or a lipoma, was suspected and the lesion was resected endoscopically. The excised specimen measured 9×6 mm in size (Fig. 1a, inset).

Low-power light microscopic examination of the tumor revealed nodular proliferation of mature fat cells in the submucosal layer of the colon (Fig. 1a) without a definitive fibrous capsule. In the proliferative submucosal lipomatous nodule, a cluster of small fibrous granular cell tumors was sitting upon the lipoma nodule beneath the slightly thickened layer of the muscularis mucosa (Fig. 1a), forming a nodule-in-nodule (a granular cell tumor nodule in a lipoma nodule) structure (Fig. 1a). In the smaller granular cell tumor nodule, tumor cells with rich, finely granulated, clear cytoplasm formed cell nests in an alveolar or fasciculated pattern, sometimes in proximity to bundles of peripheral nerve fibers (Fig. 1b). Dense fibrous collagen, spindle-shaped or stellate stromal cells, and some small vasculature blood vessels were seen in the extracellular stromal tissue of the granular cell tumor (Fig. 1b). The boundary between the granular cell tumor and the lipoma tissue was not well defined, which consisted of mixed intervening fibrous stroma containing abundant spindle-shaped or stellate stromal cells (Fig. 1b). Most of the immunohistochemical characteristics were consistent with many previous literal descriptions of the immunohistochemical characteristics of granular cell tumors and lipomas. Briefly, negative controls were prepared by substituting the primary antibodies with nonimmunune immunoglobulin G. External organs served as positive controls. CD34 was expressed in endothelial cells, and prominin-2 was expressed in normal epithelial cells of the adult kidney and digestive tract. The granular cell tumor cells expressed various neurogenic markers of Schwann cells, including S-100, neuron-specific enolase, and CD56. Other neurogenic markers characteristic of neurons or neuroendocrine cells were also faintly positive, e.g., synaptophysin and chromogranins. Strong expression of markers of phagosomes or phagocytes (CD68) was also detected in the cells of the granular cell tumor component. Positive expression of CD34 was observed not only in the endothelial cells of the small vasculature, but also in the spindle-shaped or stellate stromal cells. Spindle-shaped or stellate stromal cells showing positive immunohistochemical staining for CD34 and/or prominin-2 were more conspicuous in the tumor nodules than other nontumorous areas of the colonic wall. (Fig. 1a). However, no expression of c-kit, myogenic cell markers (e.g. alpha smooth muscle actin, muscle actin of HHF35, desmin, and MEF-2), and CD10 was observed in the spindle-shaped or stellate stromal cells. A few spindle-shaped or stellate stromal cells among the cell nests of granular cell tumor were labeled by the antiprominin-2 antibody (Fig. 1c).

Ultrastructual examination of the granular cell tumor tissue specimens by transmission electron microscope revealed alveolar aggregations of granular cell tumor cells with rather clear cytoplasm demarcated by thin

T. Mori · H. Orikasa · K. Yamazaki (✉)
Department of Pathology, Saiseikai Central Hospital,
l-4-17, Minatoku,
Tokyo, 108-0073, Japan
e-mail: KazutoYamazaki@aol.com
Tel.: +81-3-34518211
Fax: +81-3-34577949

T. Shigematsu
Department of Internal Medicine, Saiseikai Central Hospital,
Tokyo, Japan

T. Mori
Department of Pathology, School of Medicine, Keio University,
Tokyo, Japan
e-mail: taisuke@sc.itc.keio.ac.jp

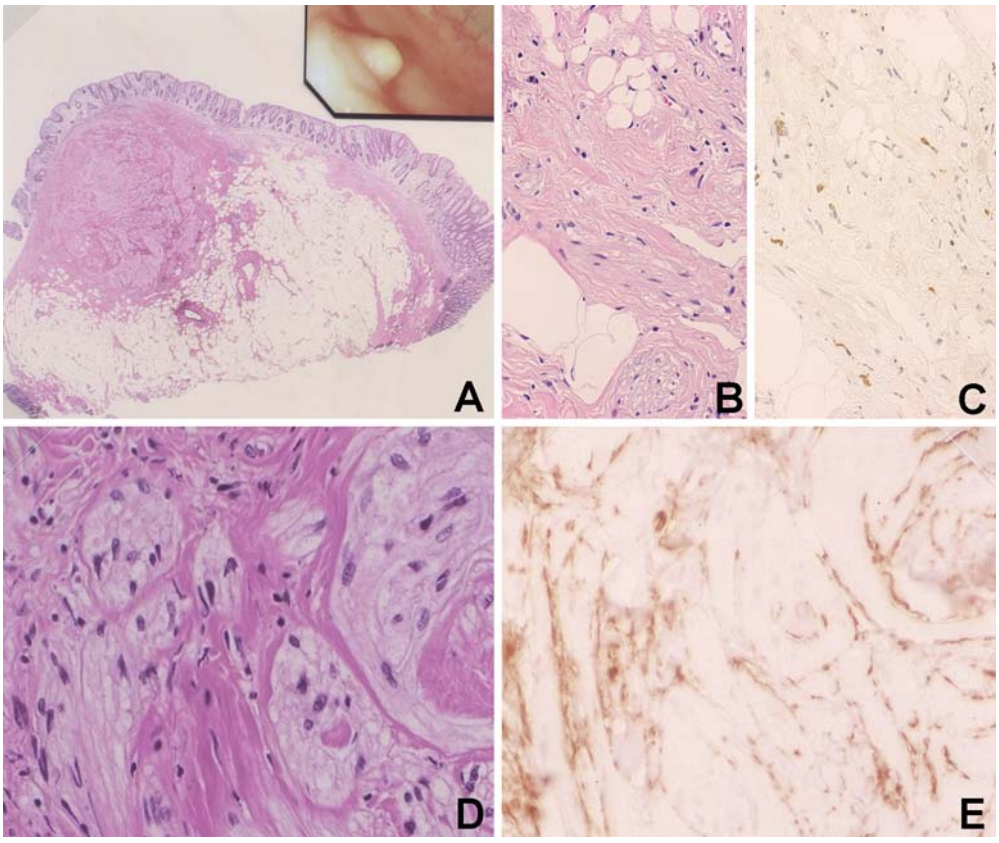

Fig. 1 Light microscopic and light microscopic immunohistochemical findings in the endoscopically resected polypoid lesion. **a** Low-power view of a section prepared from the resected polypoid lesion. Combined submucosal granular cell tumor (*upper left*) and lipoma (*lower right*) of the colon showing a nodule-in-nodule structure. Hematoxylin and eosin (H&E) stain, ×9. *Inset*: endoscopic view of the elevated *whitish* polypoid lesion. **b** Medium-power view of the granular cell tumor. H&E stain, ×190. **c** Immunostaining for prominin-2 in the granular cell tumor tissue. A few spindle-shaped stromal cells appeared in the stroma surrounding the granular cell tumor nests showing positive staining, ×190. **d** H&E stain in the granular cell tumor tissue. **e** Immunostaining for CD34 in the granular cell tumor tissue. Not only vascular endothelial cells, but also spindle-shaped stromal cells showing positive staining, ×190. A consequent section to subpanel **d** in the H&E section

lamina-like structures from the extracellular collagenous matrix. Either spindle-shaped, stellate stromal, or fibroblastic cells were embedded in the extracellular collagenous matrix, extending their thin cytoplasmic processes around the alveolar cell nests of the granular cell tumor (Fig. 2a,b).

Small electron-dense granular contents, possibly lipid-rich secondary lysosomes, and copious amount of vacuolated structure, which the contents were extracted during tissue processing for electron microscopy, were found in the vacuolated clear cytoplasm. The tumor cells had rather large nuclei with irregular nuclear membranes that were rich in euchromatin without conspicuous heterochromatin aggregation or large nucleoli. Their thin cytoplasm often extended far between their perikaryon and became embedded in the well-developed fibrous collagen-rich extracellular matrix in the tumor tissue. Occasional isolated cilia arising from the perikaryonic basal bodies were seen in both the spindle-shaped and stellate stromal or fibroblastic cells and granular cell tumor cells (Fig. 2b).

In the presented distinctive polypoid lesion of the colon, the positive immunohistochemical staining for cell proliferation markers and the detection of occasional isolated cilia on electron-microscopic examination [1] were consistent with the benign or slowly growing nature of this unique tumor. The tumor showed a unique nodule-in-nodule structure. The development of this peculiar tumor could be interpreted as a two-stage sequence, initiated by the formation of a lipoma component followed by the generation of a granular cell component.

Multipotent stromal stem cells in the tissue stroma may have a significant role in the histopathogenesis of this uncommon submucosal tumor characterized by the combination of a submucosal granular cell tumor and a lipoma of the colon demonstrating a nodule-in-nodule appearance. Previous reports describe clonal, plastic adherent stem cells from the bone marrow stroma to be capable of differentiating into osteoblasts, adipocytes, and chondrocytes. Recently, many investigators have demonstrated that multipotent stem cells can be recovered from a variety of other adult tissues and can differentiate into numerous tissue lineages, including myoblasts, cardiomyocytes, hepatocytes, and possibly even neural tissue. It is noteworthy that the primitive mesenchymal stem cells can be labeled by anti-CD133 (prominin, AC133), prominin-2 [2], or anti-low-affinity nerve growth factor receptor (p75, LNGFR) [4]. Prominin-2 is a pentaspan membrane glycoprotein predominantly expressed in neuroepithelial cells, hematopoietic stem cells, and epithelial cells of the adult kidney and the digestive tract. Tumor cells of PC3 prostate adenocarcinoma are also known to express prominin-2. CD34 showed diffusely positive staining in the cytoplasm of spindle-shaped stromal cells in the granular tumor cells. Gastrointestinal stromal tumors with neural differentiation are less likely to express CD34 compared to the neoplasms of the colon. CD34 molecule was once considered as one of the stem cell markers [1, 5]. CD34-positive stromal cells were shown to be distributed in the connective tissue surrounding mammary acini, salivary grand acini, thyroid follicles, hair follicles, sweat glands, and endocervical

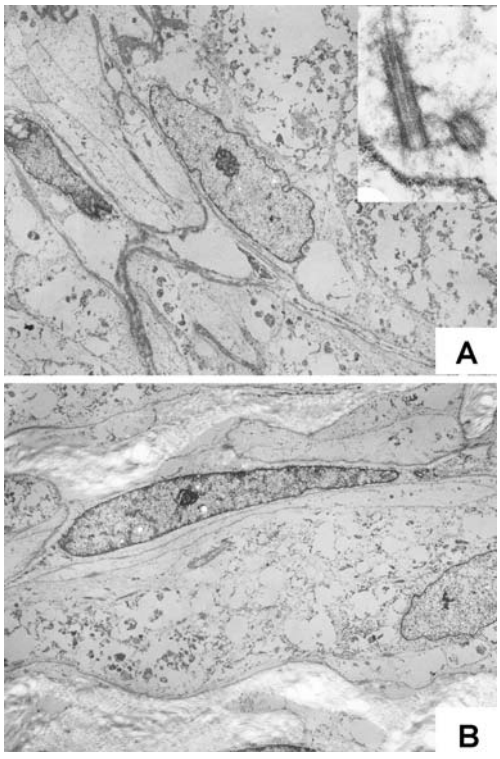

Fig. 2 Electron micrographs of the granular cell tumor in the resected polypoid lesion. **a** Higher-power view of the granular cell tumor cells with clear or vacuolated cytoplasm. Rather electron-dense and large aggregations of granular structures of possibly secondary lysosomes in the cytoplasm, ×7,000. *Inset*: isolated cilium arising from the perikaryonic basal bodies of the granular cell tumor cells, ×35,000. **b** High-power view of the granular cell tumor cells and spindle-shaped stromal or fibroblastic cells with elongated thin cytoplasmic processes, ×7,000

glands of the uterus, whereas no CD34-positive stromal cells were reported in the lamina propria of the colorectum or stomach [3]. In the colorectum and stomach, CD34-positive stromal cells were reported only in the submucosa, subserosa, muscularis propria, and muscularis mucosa [1]. It is also well known that tissue stromal cells might have the microenvironmental function of regulating the growth or differentiation of adjacent cell populations [1, 5].

Based on the immunoreactivity for CD34 and prominin-2 in spindle/stellate stromal cells, the authors speculate that these cells may have the potential to differentiate into neoplastic fat and granular cells.

In the present case, the strong predilection for spindle-shaped or stellate stromal cells to show positive staining for CD34 molecule in the tumor tissue is striking [5]. In addition to expression of CD34 in this exclusive population of spindle-shaped or stellate stromal cells, expression of prominin-2, a promising stem cell marker, was also observed in some of the cells [2]. We examined a few cases of spindle cell lipoma and granular cell tumors for expression of both markers (CD34/prominin-2). As a result, the spindle cell lipomas were positive for both markers and the granular cell tumors were positive in the spindle stromal cells for CD34. However, faintly positive staining for prominin-2 was detected around stromal cells.

As for markers of proliferating cells, topoisomerase II, proliferating cell nuclear antigen (PCNA), and Ki-67 showed various staining patterns among the three major cellular components of this rare tumor, namely, (1) tumor cells of granular cell tumor, (2) spindle-shaped or stellate stromal cells, and (3) lipoma cells. P53 expression was not conspicuous in any of these three cell components. MEF2 is a transcription factor considered as a specific marker for myogenic or cardiomyocytic lineages. Although its precise mechanism is yet to be defined, some mesenchymal stem cell and intrathoracic sarcoma exhibit positive staining for MEF2. PCNA and Ki-67 are well known as proliferation markers. PCNA and Ki-67 were expressed in the granular cell tumor cells more frequently compared with spindle-shaped/stellate stromal cells and lipoma cells. However, MEF2 were not expressed in granular/spindle/adipocyte cells of the presented tumor.

It is interesting that these cells showed no expression of c-kit and some myogenic markers (alpha smooth muscle actin, muscle actin of HHF35, desmin, and MEF-2) and CD10 in the present study [1, 5]. Our ultrastructural analysis also revealed that well-developed thin cytoplasmic processes of the spindle-shaped or stellate stromal cells could generate intimate cell-to-cell or cell-to-matrix interaction through the wide surface area of the cell membrane [5]. This cell-to-cell or cell-to-matrix interaction may be a fundamental process in tissue microenvironmental functions [5]. Our results suggest that CD34-positive stromal cells are essential for the integrity of gastrointestinal mesenchymal elements, including smooth muscles, neural elements, and fat tissue [5]. CD34-positive stromal cells or a few similar cells labeled by prominin-2 [2] may have the potential to differentiate into neoplastic fat cells in the lipoma and tumor cells in the granular cell tumor. These cells may play some role in regulating the growth or the differentiation of both types of tumor cells in this unique submucosal tumor displaying a nodule-in-nodule appearance as a combination of a granular cell tumor and a lipoma.

References

1. Dabbs D (2002) Diagnostic immunohistochemistry. Churchill Livingstone, New York
2. Fargeas CA, Corbeil D, Huttner WB (2003) AC133 antigen, CD133, prominin-1, prominin-2, etc.: prominin family gene products in need of a rational nomenclature. Stem Cells 21:506–508
3. Fenoglio-Preiser CM, Noffsinger AE, Stemmermann GN, Lantz PE, Listrom MB, Rilke FO (1998) Gastrointestinal mesenchymal neoplasms. In: gastrointestinal pathology: an atlas and text. Lippincot Williams & Wilkins, Philadelphia, PA, pp 1169–1215
4. Gregory CA, Prockop DJ, Spees JL (2005) Non-hematopoietic bone marrow stem cells: molecular control of expansion and differentiation. Exp Cell Res 306:330–335
5. Yamazaki K, Eyden BP (1996) Ultrastructural and immunohistochemical studies of intralobular fibroblasts in human submandibular gland: the recognition of a 'CD34 positive reticular network' connected by gap junctions. J Submicrosc Cytol Pathol 28:471–483

Virchows Arch (2006) 449: 140
DOI 10.1007/s00428-006-0235-0
© Springer-Verlag 2006

ANNOUNCEMENTS

4–8 September 2006
Postgraduate Course
Diagnostic Breast Pathology
Department of Pathology
Medical University Graz, Austria

Course Director
Farid Moinfar, MD (Graz)

Guest faculty
Fattaneh A. Tavassoli, MD (New Haven, USA)

Course Objectives
This intensive course is designed for pathologists in training as well as practicing pathologists. During the course, the participants will review 100 cases dealing with a variety of benign and malignant breast neoplasms and tumor-like lesions. Several common diagnostic problems including papillary neoplasms, intraductal proliferative lesions, variants of ductal and lobular intraepithelial neoplasias, and infiltrating carcinomas are included.

On each day, 20 cases will be extensively discussed by an interactive approach. Particular attention will be paid to the diagnostic criteria with systematic analysis of differential diagnoses. Value and limitations of immunohistochemistry as a diagnostic adjunct will be demonstrated.

Course fee:
Euro 600,- Practicing pathologists
Euro 400,- Pathologists in training

For more information and registration please contact:
Edith Kleinferchner
Department of Pathology, Medical University Graz
Auenbruggerplatz 25
8036 Graz, Austria
Fax: 0043 (0) 316 385 3432
e-mail: edith.kleinferchner@meduni-graz.at
http://pathologie.meduni-graz.at/Pathologie/veranstaltungen.htm

11–13 October 2006
Postgraduate Course
Diagnostic Hepatopathology
Department of Pathology
Medical University Graz, Austria

Course Director
Carolin Lackner, MD (Graz)

Faculty
Helmut Denk, MD, FRCPath (Graz)

Guest faculty
Stefan G. Hübscher, MD (Birmingham)

Course Objectives
The differential diagnosis of chronic hepatitis is a problem frequently encountered in liver pathology. This three day course provides a comprehensive review of the histological features and differential diagnosis of chronic hepatitis in adults; i.e., viral hepatitis, autoimmune hepatitis, overlap syndromes, as well as recurrent chronic hepatitis in the transplanted liver. Liver injury due to drugs, toxins and metabolic disorders and steatohepatitis (ASH/NASH) will also be discussed.

Every day two key lectures, each dealing with a main diagnostic topic will be given. The course covers approx. 50 cases and per day approx. 15-20 cases will be discussed in an interactive approach. Additionally the participants will have ample opportunity for microscopic evaluation of each case.

Course fee:
Euro 400,- (Practicing pathologists)
Euro 280,- (Pathologists in training)

For more information and registration please contact:
Edith Kleinferchner
Department of Pathology, Medical University Graz
Auenbruggerplatz 25
8036 Graz, Austria
Fax: 0043 (0) 316 385 3432
e-mail: edith.kleinferchner@meduni-graz.at
http://pathologie.meduni-graz.at/Pathologie/veranstaltungen.htm

24–26 January 2007
Theorico-practical Course on Bone and Soft Tissue Tumors
Department of Pathology, Hospital del Mar, Barcelona, Spain

Faculty
Christopher Fletcher, M.D. (Brigham and Women's Hospital, Boston, USA)
Andrew Rosenberg, M.D. (Massachusetts General Hospital, Boston, USA)
Angelo Paolo Dei Tos, M.D. (Hospital of Treviso, Italy)
John Goldblum, M.D. (Cleveland Clinic, Cleveland, USA)
Paola Dal Cin, Ph.D. (Brigham and Women's Hospital, Boston, USA)

For further information please contact:
Francisco Alameda, M.D.
Department of Pathology
Hospital del Mar, Spain
E-mail: 86780@imas.imim.es
or
Esther Oliva, M.D.
Department of Pathology
Massachusetts General Hospital
55 Fruit Street, WRN-2
Boston, MA 02114, USA
E-mail: eoliva@partners.org

Virchows Arch (2006) 449:141–147
DOI 10.1007/s00428-006-0232-3

ORIGINAL ARTICLE

HPV subtypes in cervical cancer biopsies between 1930 and 2004: detection using general primer pair PCR and sequencing

Bjørn Inge Bertelsen · Kalaiarasy Kugarajh · Robert Skar · Ole Didrik Laerum

Received: 24 February 2006 / Accepted: 5 May 2006 / Published online: 10 June 2006
© Springer-Verlag 2006

Abstract Our objective was to investigate the practicability of sequencing DNA from formalin fixed, paraffin embedded tissue stored for up to 75 years and to study human papillomavirus subtype distribution in cervical neoplasias between 1931 and 2004. Three protocols for DNA retrieval were tested, and magnetic bead DNA extraction proved advantageous, as it gave superior specimen purity and effortless sequencing. Successful sequencing was achieved in more than 70% of the specimens from 1931 to 1960. This technique was utilized in the study of papillomavirus subtypes using general primer pair PCR with sequencing of the products in a series of 97 cases of neoplastic and non-neoplastic cervical specimens from 1931 to 1960 and 73 similar cases from 1992 to 2004. HPV was detected in 61% of neoplastic specimens from 1931 to 1960, and in 89% of those from 1992 to 2004. In specimens from 1931 to 1934, only HPV type 16 was detected, whereas in the specimens from 1940 and up, other HPV subtypes were identified in one-third of the cases. The difference was significant and suggests an increase in papillomavirus subtype heterogeneity in Western Norway during 1930–2000. The results strongly support the feasibility of using DNA from paraffin-embedded specimens for studying cancer etiology and genotypes over extended time periods.

Keywords Uterine cervical neoplasms · Human papillomavirus · Base sequence · History

B. I. Bertelsen (✉) · R. Skar · O. D. Laerum
Department of Pathology, Haukeland University Hospital,
5021 Bergen, Norway
e-mail: mgpbb@webmail.uib.no

K. Kugarajh · O. D. Laerum
The Gade Institute, University of Bergen,
5021 Bergen, Norway

Abbreviations

CIN 3	Cervical intraepithelial neoplasia grade 3
HPV	Human papilloma virus
PBGD	Porphobilinogen deaminase gene
SD	Standard deviation

Introduction

Cervical carcinoma is the second most common cancer in women worldwide [33]. Recent studies show that human papillomavirus (HPV) DNA is present in practically all cervical carcinomas, with some geographical variation in viral subtypes [1, 4, 22]. The incidence of cervical cancer in Norway rose from the 1950s to the mid-1970s, after which a decline began [3]. At the same time, a tendency towards a poorer prognosis in younger women was noted [3]. Thus, temporal variation in exposure to the viral factor cannot be excluded. In addition, alternative tumorigenic mechanisms may have been important in other time periods and different geographic areas. In a recent study of HPV types associated with more than 1,900 cases from nine different countries, Munoz and co-workers found that about 66% of the patients had infection with HPV types 16 or 18 out of altogether 30 high-risk types [22]. Their data indicated that, in contrast to the others, HPV type 16 decreased significantly with patient age. Therefore, they could not exclude a cohort effect due to altered incidence of infection over the last 40–50 years. The facts that life style and cultural determinants of human viral exposition may change over time, and that the HPV prevalence two or three generations back is largely unknown, prompted us to look for the presence of HPV DNA in archival cervical cancer tissue [32]. Improved DNA retrieval methods make gene analyses

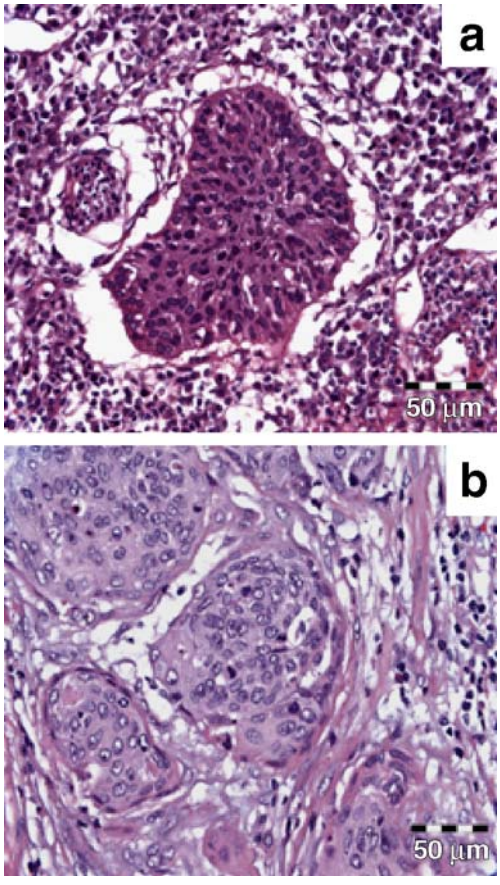

Fig. 1 Cervical squamous cell carcinomas from 1932 (**a**) and 2004 (**b**). Tissue blocks from the 1930s and up could usually be cut with a standard microtome, rendering valid hematoxylin-eosin stained sections

and viral genome identification in archival paraffinized tissue a realistic task [2, 12, 13, 16, 17, 21, 27]. This laboratory has been providing histopathological service in western Norway since 1912. Diagnostic tissue specimens, including more than 2 million formalin-fixed, paraffin-embedded tissue blocks, have been filed from 1930 until present for the purpose of quality control, and clinical information exists in most cases.

On this background, our aim was to assess the utility of sequencing DNA from paraffin-embedded uterine cervical specimens stored for more than 70 years using sequencing of *p53* exons 7 and 8 as test system and to examine the distribution of HPV subtypes in a larger series of neoplastic and non-neoplastic cervical tissues from 1931 to 1960 with controls from 1992 to 2004 using general primer pair PCR with sequencing of the products.

Materials and methods

All paraffin-embedded tissue had been stored at 10–20°C in ambient air and humidity of the local mild, wet climate. Pre-tests showed that most tissue blocks from the 1930s and up could be cut with a standard microtome, rendering acceptable histological sections. In some cases where the paraffin surrounding the tissue had become brittle and unsuited for cutting, the tissue was cut out with a scalpel and re-embedded in paraffin to make new blocks. They could then easily be sectioned using a standard microtome. A total of 173 cases were chosen on the basis of availability of tissue in the pathology archives. Fifty five cases of neoplastic cervical tissue, i.e., squamous cell carcinoma (n=50), adenocarcinoma (n=3), and cervical intraepithelial neoplasia grade 3 (CIN 3) (n=2) from 1931 to 1960 (Fig. 1) with a mean age of 48.5 years (SD 10.1 years) and 42 cases of non-neoplastic cervical tissue, i.e., polyps (n=10), mucosa with inflammation or erosion (n=13), condyloma (n=1), and normal mucosa in uterine prolapse or leiomyoma (n=18) from 1931 to 1960 were retrieved.

The control material from 1992 to 2004 included 43 cases of cervical neoplastic lesions (i.e., biopsies or surgical specimens from 39 squamous cell carcinomas, one CIN 3 and three adenocarcinomas) with a mean age of 48.0 years (SD 15.3 years) and 33 cases of cervical non-neoplastic epithelium (i.e., cervical curettages or surgical specimens in cases of infertility, endometrial hyperplasia, leiomyoma, or descensus genitalis) with a mean age of 55.9 years (SD 13.2 years) (Fig. 1). One representative tissue block was selected from each lesion. The diagnoses were assessed by reviewing the histological sections and the patient records. Only cases with unequivocal histological verification were included. All specimens had been fixed in 4% formaldehyde. Neutral phosphate-buffered 4% formaldehyde was used after 1970. The fixation times are not known.

Isolation of DNA

Two 10 µm thick sections were cut from each specimen after cleaning both tissue block and microtome with absolute alcohol. Three DNA retrieval protocols were tested. Protocol 1 consisted of xylene deparaffinization, consecutive washings with absolute ethanol and acetone, followed by proteinase K treatment at 37°C overnight as described [5]. In protocol 2, the specimens were deparaffinized and washed in ethanol as above, then incubated with proteinase K at 37°C for 6 days, treated with Chelex-100 and Tween 20 [14]. Protocol 3 consisted of automated DNA extraction using the GenoPrep DNA from Tissue Kit on a GenoM-48 robotic workstation (both from QIAGEN GmbH, Hilden, Germany) employed in accordance with the manufacturer's recommendations. DNA was detected on agarose gel electrophoresis (1% NuSieve GTG agarose, Biowhittaker Molecular Applications, Walkersville, ME, USA) with 0.5 µg/ml ethidium bromide) and visualized under ultraviolet light. The purity of the retrieved DNA was estimated as the ratio between the spectrophotometric absorption at 260 and 280 nm (OD_{260}/OD_{280}) [25].

P53 analysis

Eight specimens from each decade, i.e., the 1930s, the 1940s, the 1950s, the 1960s, and five cases from the 1990s, a total of 37 specimens, were used in the analyses. Amplifications of the *p53* exons 7 and 8 were carried out using primers as reported, with product sizes of 171 bp for exon 7 and 230 bp for exon 8 [34]. PCR was carried out in 50 μl reaction volumes containing 2 μl of the tissue extract, 0.025 U/μl of Amplitaq Gold (Applera Corporation, Norwalk, CT, USA), 0.25 μM of each primer, 0.25 mM of each dNTP, 1×Amplitaq PCR buffer (Applera) and 1.5 mM Mg^{2+}. In some cases, PCR was successful only after 1:10 dilution of DNA [19]. Thermal cycling consisted of an initial denaturing step at 95°C for 10 min, followed by 45 cycles of denaturation at 95°C for 50 s, 50 s of annealing at 63°C and 58°C for exon 7 and exon 8, respectively, elongation at 72°C for 1 min, and final completion by a 7-min post-elongation step at 72°C.

Standard precautions to avoid cross-contamination between specimens and PCR product carryover were employed [20].

Human blood DNA (50 ng/μl) was used as positive control and distilled water as negative control. The reaction products (10 μl) were electrophoresed on agarose gel with ethidium bromide. The *p53* PCR products were purified using the QIAquick PCR Purification Kit-250 (QIAGEN) according to the manufacturer's specifications. The PCR products were forward and reverse cycle-sequenced using ABI Prism BigDye terminator kit version 2.0 (Applera) and the oligonucleotide primers used in the PCR reactions. The sequencing reaction mix consisted of 2.5 to 7 μl of purified PCR product, 0.25 to 0.5 μM of primer, 2 μl of Big Dye and water up to a total of 10 μl. The cycle sequencing reaction consisted of an initial denaturing step (96°C, 20 s), followed by 25 cycles of denaturation (96°C, 10 s), annealing (55°C, 5 s) and elongation (60°C, 4 min). The sequencing reaction products were purified on Sephadex spin columns, and electrophoresed on an ABI 377 or 3100 Sequence Analyzer (both from Applied Biosystems). The data were analyzed using the ABI Sequence Analysis software version 3.7 (Applied Biosystems) and manually compared to the exon 7 and exon 8 sequences from the nucleotide database at NCBI http://www.ncbi.nlm.nih.gov, accession AF135120). Mutations were verified by independent PCR amplification and sequencing from tumor DNA.

HPV subtype detection

HPV analysis was performed in 159 cases where a control gene could be amplified, rendering a distinct band on agarose gel electrophoresis. The control genes used were either *p53* exon 7 or 8 with amplification as stated above, or the porphobilinogen deaminase gene (*PBGD*) (forward primer 5′-CATACAAGAGACCATGCAGG-3′, reverse primer 5′-CATCCTCAGGGCCATCTTCA-3′, PCR product size 153 bp). In nine cases from 1931 to 1941, the control gene could not be amplified, while the others gave acceptable results, a success rate of 88%. Five cases in the control group could not be tested because tissues were used up. HPV DNA was detected using a PCR-based assay with the general primer pair GP5+/GP6+ rendering a 150-bp product [9]. The PCR reaction mix for HPV and PBGD contained 1×GeneAmp PCR buffer II, 1.5 mM $MgCl_2$, 0.2 mM dNTP, 0.2 μM of each primer, 0.2 U Amplitaq Gold (Applera), 50 ng DNA. The GP5+ primer was biotinylated at the 5′-end. The thermal cycling consisted of an initial denaturing step (95°C, 15 min), followed by 45 cycles of denaturation (94°C, 30 s), annealing (43°C for HPV and 61°C for PBGD, 30 s) and elongation (72°C, 30 s), and terminated by a post-elongation step (72°C, 10 min). The HPV PCR products were forward sequenced as described above, except that PCR product and sequencing product were both purified using streptavidin-coated magnetic beads employing the DYNAPURE Dye Terminator Removal version 2 kit and protocol (Dynal Biotech, Oslo, Norway). Following arrangement of the sequence data using the Staden computer package (Medical Research Council, London, UK), the HPV subtypes were identified through alignment with the HPV DNA sequences published in the NCBI BLAST database (see www.ncbi.nlm.nih.gov/BLAST).

Statistics

The Wilcoxon signed rank-sum test in the MATLAB v.6 statistics software (The MathWorks, Natick, MA, USA) was used for statistical evaluation of differences in DNA purity. Frequency data in independent groups were compared using two-tailed Fisher's exact test at http://www.unc.edu/~preacher/fisher/fisher.htm. *P* values less than 0.05 indicated significant differences.

Results

DNA isolation and *p53* sequencing

DNA could for the most part be retrieved from old and recent specimens using all three protocols. Agarose gel electrophoresis showed that DNA from formalin-fixed, paraffin-embedded tissue consisted of markedly smaller fragments than that from the control human blood, and that DNA from the old samples (1931–1960) showed more decomposition than that from recent specimens (1990–2004) (data not shown). The purity of the DNA was mainly dependent on the extraction protocol used, while specimen age was of little significance. The magnetic bead technique

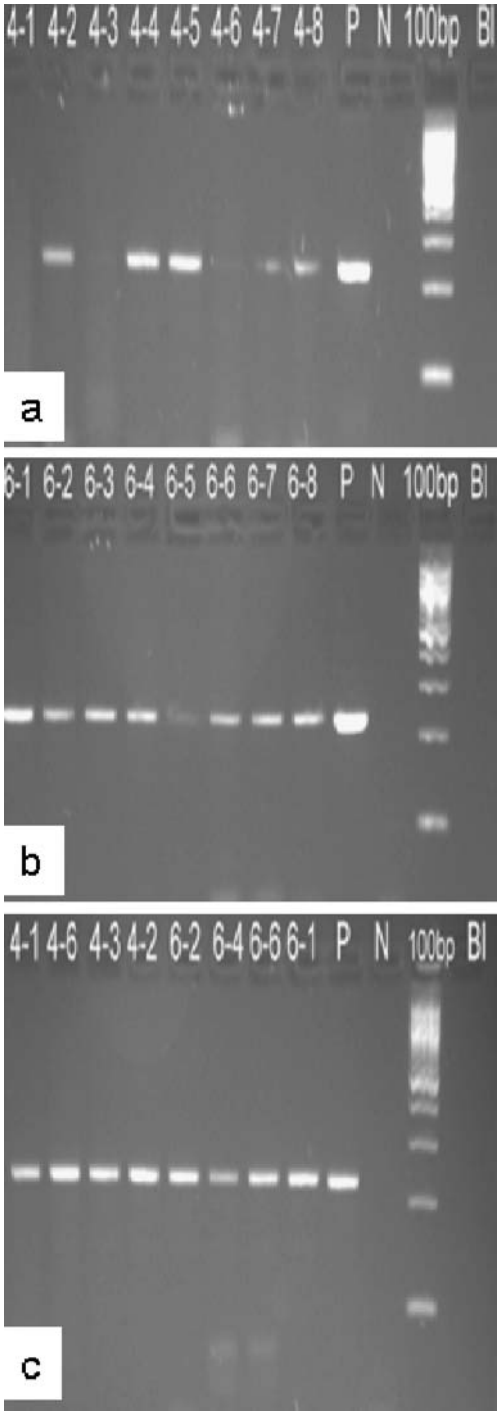

Fig. 2 PCR products of *p53* exon 8 on agarose gel. Examples of DNA retrieved using proteinase K (protocol 2) on specimens from the 1940s (**a**), specimens from the 1960s (**b**), and DNA extraction using magnetic beads (protocol 3) on specimens from the 1940s (**c**, *left*) and specimens from the 1960s (**c**, *right*). Specimens that rendered no PCR product when proteinase K DNA retrieval was used, often gave successful PCR when DNA had been extracted using magnetic beads

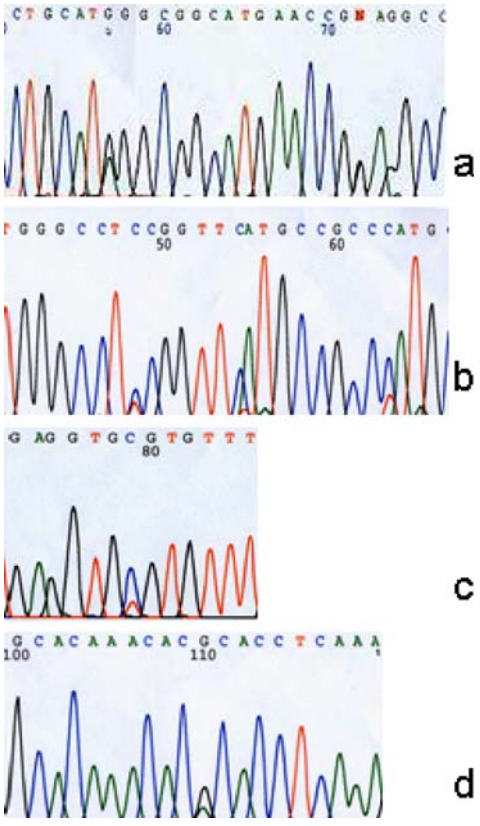

Fig. 3 The *p53* mutations detected. A section of the forward (**a**) and reverse (**b**) sequence of the *p53* exon 7 in a sample from the 1960 showing the codon 243 guanine to adenine transition and the codon 248 guanine to adenine transition, and a section of the forward (**c**) and reverse (**d**) sequence of the *p53* exon 8 in a sample from 1992 showing the cytosine to thymidine transition in codon 273

(protocol 3) rendered DNA of high purity (mean 1.801, SD 0.056) and significantly purer than that brought about using the proteinase-K methods, protocol 1 (mean 1.23, SD 0.101) and protocol 2 (mean 1.333, SD 0.105) (p=0.006 and p=4.5×10^{-10}, respectively).

P53 exon 7 and 8 forward and reverse sequencing of specimens from 1930 to 1960 was successful in 21 of 32 specimens purified using protocol 2 and in 8 of 8 specimens purified using protocol 3 (Fig. 2). Three single base substitutions were found (Fig. 3). Two mutations were detected in one sample from 1960. One was an exon 7 codon 243 guanine to adenine transition, resulting in a nonconservative missense mutation (M243I). The second mutation was a change from guanine to adenine at the third position of exon 7 codon 248, which is a synonymous substitution (R248R). The third mutation was in a sample from 1992 with a transition from cytosine to thymidine at the first position of exon 8 codon 273, a nonconservative missense mutation (R273C).

HPV sequencing and typing

The results are summarized in Table 1. HPV was found in 73% of all, old and recent, cervical neoplastic specimens. No significant difference was found between the HPV

Table 1 HPV subtype distribution related to diagnoses and year

Diagnoses	Years	No. of cases	Age mean (SD)	HPV positive	HPV subtypes					
					16	18	31	33	45	Other
Neoplastic	1931–1934	22	50(8.2)	15(68%)	15	–	–	–	–	–
	1940–1941	16	47(6.7)	8(50%)	3	–	–	1	2	2[c]
	1950–1960	13	48(15.2)	8(62%)	6	2	–	–	–	–
	1992–2004[a]	38	48(15.7)	34(89%)	23	5	1	1	2	2[b]
Non-neoplastic	1931–1934	20	46(11.1)	4(20%)	4	–	–	–	–	–
	1940–1941	14	43(9.9)	2(14%)	2	–	–	–	–	–
	1950–1960	3	44(10.0)	0	–	–	–	–	–	–
	1992–2004	33	56(13.2)	2(6%)	2	–	–	–	–	–

Four specimens of squamous cell carcinoma and five specimens of normal mucosa from 1931–60 were excluded because of negative control gene amplification

SD Standard deviation

[a] Five cases could not be examined because of used up tissue

[b] That is, HPV 56 in one case and HPV 82 in one case

[c] That is, HPV 52 in one case and HPV 73 in another case

prevalence in the neoplastic specimens from 1931 to 1960 (61%) and that in those from 1992 to 2004 (89%) (p=0.397, two-tailed Fisher's exact test). There was a marked domination of type 16, as it made up 72% of HPV subtypes detected. In the non-neoplastic specimens, HPV was detected in 11% of the specimens, all of them type 16. It is of special note that only HPV type 16 was detected in the neoplastic and non-neoplastic specimens from 1931 to 1934, whereas HPV subtypes other than 16 made up one-third of the infections in the specimens from 1940 and up. The difference was statistically significant (p=0.004, two-tailed Fisher's exact test). However, there was no significant difference between the proportions of non-16 HPV types in the 1931–1960 group compared to the 1992–2004 group (19% compared to 31%, respectively) (p=0.3, two-tailed Fisher's exact test).

Discussion

We have demonstrated the practicability of sequencing DNA from formalin-fixed, paraffin-embedded cervical cancer specimens stored for more than 70 years. The fixative and fixation time used reportedly affect the quality and fragment sizes of the DNA that can be retrieved [10, 12, 15, 17]. Fixation times are basically unknown in this material, and extensive variation must be presumed. The use of unbuffered formalin (up to 1970) paired with lengthy storage times in paraffin wax would be expected to cause suboptimal DNA preservation [11, 35]. Nevertheless, despite abundant DNA fragmentation in the cervical cancer specimens from 1931–1960, magnetic bead DNA extraction produced high-purity DNA well-suited for sequencing of *p53* exons 7 and 8, as well as HPV GP5+/GP6+ general primer pair products with product lengths of 171, 230, and 142 bp, respectively. The omission of organic solvents combined with active DNA separation, may account for the marked increase in DNA purity over the conventional proteinase K-based techniques that were also tested.

The presence of HPV DNA in most cervical cancers from the 1930s and up underpins the notion that the viral etiology of cervical carcinogenesis has been stable over several generations. Earlier studies using in situ hybridization, Southern blotting, and PCR give credence to the same conclusion [8, 27, 30]. Thompson and co-workers examined similar material of paraffin-embedded cervical carcinomas from Australia. During the period from the 1920s to the 1980s, they found no significant change in the prevalence of HPV DNA, with HPV 16 accounting for more than 90% of the cases. As the study did not include non-neoplastic control tissue from the same period and HPV DNA sequencing was not performed, their data must be taken with some reservation. However, it indicates that over the investigated period, the HPV pattern and incidence in Norway show important dissimilarities. This is mainly relating to changing patterns of HPV subtypes in Norway, which is supported in this paper by findings in both tumors and non-neoplastic tissue.

Indeed, the lack of viral subtypes other than HPV 16 in specimens from 1931 to 1934, in contrast to findings in the later specimens where other subtypes made up one-third, may suggest increasing papillomavirus subtype heterogeneity in western Norway during 1930–2000. The fact that no significant difference in viral heterogeneity could be found when the 1931–1960 group was compared to the 1992–2004 group brings up the possibility that an increase in HPV subtype heterogeneity could have occurred early in the period covered by this study. We are not aware of other

data on this specific subject. However, our results on HPV subtype distribution in cervical neoplasia generally correspond with the current status that subtypes 16, 18, 45, 31, 33, 52, 58, 35, 59, 56, 39, 51, 73, 68, and 66 prevail [23]. Our results on HPV subtypes after the 1930s are also compatible with both recent Norwegian data and the findings from this geographical region that HPV 16 was present in 63% of high-grade squamous intraepithelial lesions [7, 18].

Mutations in *p53* exons 7 and 8 were scarce, compatible with earlier reports on cervical cancer [6]. As HPV DNA was generally present, non-mutational inactivation of *p53*, as well as pRb, by HPV oncoproteins must be expected in these cases [26, 28].

Rekand and coworkers have recently demonstrated isolation and analysis of poliovirus RNA from paraffin-embedded specimens stored for 50 years at this department [24]. The value of historic material in viral studies is further substantiated by the recent characterization of the 1918 influenza virus isolated from frozen lung tissue found in an Alaskan graveyard [29, 31].

In conclusion, optimized DNA extraction and gene amplification procedures make huge tissue archives from diagnostic pathology laboratories available for research. DNA sequencing can be used to trace causative disease factors and genetic hallmarks of cancer after more than 70 years of storage.

Acknowledgements We thank Professor Anders Molven for expert advice and fruitful discussion. The Haukeland University Hospital Research Fund and The Norwegian Cancer Society provided the funds for this study.

References

1. Andersson S, Rylander E, Larsson B, Strand A, Silfversvard C, Wilander E (2001) The role of human papillomavirus in cervical adenocarcinoma carcinogenesis. Eur J Cancer 37:246–250
2. Bertelsen B, Steine S, Sandvei R, Molven A, Laerum O (2006) Molecular analysis of the PI3K-AKT pathway in uterine cervical neoplasia: frequent PIK3CA amplification and AKT phosphorylation. Int J Cancer 118:1877–1883
3. Bjørge T, Thoresen SØ, Skare GB (1993) Incidence, survival and mortality in cervical cancer in Norway, 1956–1990. Eur J Cancer 29A:2291–2297
4. Bosch FX, Lorincz A, Munoz N, Meijer CJ, Shah KV (2002) The causal relation between human papillomavirus and cervical cancer. J Clin Pathol 55:244–265
5. Brüstle O, Ohgaki H, Schmitt HP, Walter GF, Ostertag H, Kleihues P (1992) Primitive neuroectodermal tumors after prophylactic central nervous system irradiation in children. Association with an activated K-ras gene. Cancer 69:2385–2392
6. Busby-Earle RMC, Steel CM, Williams ARW, Cohen B, Bird CC (1994) p53 mutations in cervical carcinogenesis—low frequency and lack of correlation with human papillomavirus status. Br J Cancer 69:732–737
7. Baak JP, Kruse AJ, Garland SM, Skaland I, Janssen EA, Tabrizi S, Fagerheim S, Robboy S, Nilsen ST (2005) Combined p53 and retinoblastoma protein detection identifies persistent and regressive cervical high-grade squamous intraepithelial lesions. Am J Surg Pathol 29:1062–1066
8. Collins JE, Jenkins D, McCance DJ (1988) Detection of human papillomavirus DNA sequences by in situ DNA-DNA hybridisation in cervical intraepithelial neoplasia and invasive carcinoma: a retrospective study. J Clin Pathol 41:289–295
9. de Roda Husman A-M, Walboomers JMM, van den Brule AJC, Meijer CJLM, Snijders PJF (1995) The use of general primers GP5 and GP6 elongated at their 3′ ends with adjacent highly conserved sequences improves human papillomavirus detection by PCR. J Gen Virol 76:1057–1062
10. Dubeau L, Chandler LA, Gralow JR, Nichols PW, Jones PA (1986) Southern blot analysis of DNA extracted from formalin-fixed pathology specimens. Cancer Res 46:2964–2969
11. Goelz SE, Hamilton SR, Vogelstein B (1985) Purification of DNA from formaldehyde fixed and paraffin embedded human tissue. Biochem Biophys Res Commun 130:118–126
12. Greer CE, Wheeler CM, Manos MM (1994) Sample preparation and PCR amplification from paraffin-embedded tissues. PCR Methods Appl 3:S113–S122
13. Hummel S (2003) Ancient DNA typing. Methods, strategies and applications, 1st edn. Springer, Berlin Heidelberg New York
14. Ibrahim SO, Vasstrand EN, Johannessen AC, Idris AM, Magnusson B, Nilsen R, Lillehaug JR (1999) Mutations of the p53 gene in oral squamous-cell carcinomas from Sudanese dippers of nitrosamine-rich toombak and non-snuff-dippers from the Sudan and Scandinavia. Int J Cancer 81:527–534
15. Isola J, DeVries S, Chu L, Ghazvini S, Waldman F (1994) Analysis of changes in DNA sequence copy number by comparative genomic hybridization in archival paraffin-embedded tumor samples. Am J Pathol 145:1301–1308
16. Iwamoto KS, Mizuno T, Ito T, Akiyama M, Takeichi N, Mabuchi K, Seyama T (1996) Feasibility of using decades-old archival tissues in molecular oncology/epidemiology. Am J Pathol 149:399–406
17. Karlsen F, Kalantari M, Chitemerere M, Johansson B, Hagmar B (1994) Modifications of human and viral deoxyribonucleic acid by formaldehyde fixation. Lab Invest 71:604–611
18. Kraus I, Molden T, Erno LE, Skomedal H, Karlsen F, Hagmar B (2004) Human papillomavirus oncogenic expression in the dysplastic portio; an investigation of biopsies from 190 cervical cones. Br J Cancer 90:1407–1413
19. Kösel S, Graeber MB (1994) Use of neuropathological tissue for molecular genetic studies: parameters affecting DNA extraction and polymerase chain reaction. Acta Neuropathol (Berl) 88:19–25
20. Lehmann U, Kreipe H (2001) Real-time PCR analysis of DNA and RNA extracted from formalin-fixed and paraffin-embedded biopsies. Methods 25:409–418
21. Lewis F, Maughan NJ, Smith V, Hillan K, Quirke P (2001) Unlocking the archive-gene expression in paraffin-embedded tissue. J Pathol 195:66–71
22. Munoz N, Bosch FX, de Sanjose S, Herrero R, Castellsague X, Shah KV, Snijders PJ, Meijer CJ (2003) Epidemiologic classification of human papillomavirus types associated with cervical cancer. N Engl J Med 348:518–527
23. Munoz N, Bosch FX, Castellsague X, Diaz M, de Sanjose S, Hammouda D, Shah KV, Meijer CJ (2004) Against which human papillomavirus types shall we vaccinate and screen? The international perspective. Int J Cancer 111:278–285
24. Rekand T, Male R, Myking AO, Nygaard SJ, Aarli JA, Haarr L, Langeland N (2003) Detection of viral sequences in archival spinal cords from fatal cases of poliomyelitis in 1951–1952. J Virol Methods 114:91–96
25. Sambrook J, Fritsch EF, Maniatis T (1989) Molecular cloning. A laboratory manual, 2nd edn. Cold Spring Harbor Laboratory, New York

26. Scheffner M, Werness BA, Huibregtse JM, Levine AJ, Howley PM (1990) The E6 oncoprotein encoded by human papillomavirus types 16 and 18 promotes the degradation of p53. Cell 63:1129–1136
27. Shibata D, Martin W, Arnheim N (1988) Analysis of DNA sequences in forty-year-old paraffin-embedded thin-tissue sections: A bridge between molecular biology and classical histology. Cancer Res 48:4564–4566
28. Spandidos DA, Dokianakis DN, Kallergi G, Aggelakis E (2000) Molecular basis of gynecological cancer. Ann N Y Acad Sci 900:56–64
29. Taubenberger JK, Reid AH, Lourens RM, Wang R, Jin G, Fanning TG (2005) Characterization of the 1918 influenza virus polymerase genes. Nature 437:889–893
30. Thompson CH, Rose BR, Cossart YE (1992) Detection of HPV DNA in archival specimens of cervical cancer using in situ hybridisation and the polymerase chain reaction. J Med Virol 36:54–59
31. Tumpey TM, Basler CF, Aguilar PV, Zeng H, Solorzano A, Swayne DE, Cox NJ, Katz JM, Taubenberger JK, Palese P, Garcia-Sastre A (2005) Characterization of the reconstructed 1918 Spanish influenza pandemic virus. Science 310:77–80
32. WHO (1995) Human papillomaviruses, 1st edn. World Health Organization, Lyon
33. WHO (1997) The world health report 1997: conquering suffering, enriching humanity. World Health Organization, Geneva
34. Zariwala M, Schmid S, Pfaltz M, Ohgaki H, Kleihues P, Schafer R (1994) p53 gene mutations in oropharyngeal carcinomas: a comparison of solitary and multiple primary tumours and lymph-node metastases. Int J Cancer 56:807–811
35. Zsikla V, Baumann M, Cathomas G (2004) Effect of buffered formalin on amplification of DNA from paraffin wax embedded small biopsies using real-time PCR. J Clin Pathol 57:654–656

Virchows Arch (2006) 449:148–158
DOI 10.1007/s00428-006-0231-4

ORIGINAL ARTICLE

Extranodal follicular dendritic cell sarcoma: clinical, pathologic, and histogenetic characteristics of an underrecognized disease entity

Jinru Shia · Wen Chen · Laura H. Tang · Diane L. Carlson · Jin Qin · Jose G. Guillem · Jennifer Nobrega · W. Douglas Wong · David S. Klimstra

Received: 24 February 2006 / Accepted: 5 May 2006 / Published online: 7 June 2006
© Springer-Verlag 2006

Abstract It has been more than 10 years since follicular dendritic cell (FDC) sarcoma was first reported to occur in extranodal sites, yet extranodal FDC sarcoma still appears underrecognized, and its clinical and pathological characteristics remain to be defined. This study analyzed the clinical and pathological findings of three such cases that the authors encountered recently and 43 previously reported cases identified in the literature. Assessment of all 46 cases showed a slight female predominance (1.2:1) with a median age of 41.5 years. One-third of the cases were misdiagnosed at initial evaluation mainly because the possibility of FDC sarcoma was not considered. When considered, this disease had distinct pathological characteristics that allowed an accurate diagnosis. Staining for FDC markers, CD21, CD35, and clusterin was particularly helpful. The pathogenesis of the disease appeared heterogeneous, and associated factors included Epstein–Barr virus infection (in hepatic cases) and inflammatory pseudotumor-like conditions. Treatment modality varied widely although surgical resection was often included. With a median follow-up of 18 months, 43% of the cases recurred and 7% died of disease. The 5-year recurrence-free survival was 27.4%. From data available at the current time, we were not able to identify prognostically significant pathologic factors.

Keywords Sarcomas · Literature review · Reticulum cell · Extranodal · Dendritic cell

J. Shia · W. Chen · L. H. Tang · D. L. Carlson · J. Nobrega · D. S. Klimstra (✉)
Department of Pathology,
Memorial Sloan-Kettering Cancer Center,
1275 York Avenue,
New York, NY 10021, USA
e-mail: Klimstrd@mskcc.org

J. Qin
Biostatistics Research Branch,
National Institute of Allergy and Infectious Disease, NIH,
Bethesda, MD, USA

J. G. Guillem · W. D. Wong
Department of Surgery, Memorial Sloan-Kettering Cancer Center,
New York, NY, USA

Introduction

Follicular dendritic cells (FDCs) belong to the accessory immune system. They normally reside in the primary and secondary lymphoid follicles, serving as antigen-presenting cells and playing a major role in the induction and maintenance of humoral immune response [19, 46].

Tumors showing features of FDCs were first recognized in 1986 by Monda et al. [30] who described four cases. Since then, many reports have documented FDC sarcomas, predominantly arising in lymph node [9, 22, 34]. In general, nodal FDC sarcomas tend to affect axillary or cervical lymph nodes of young to middle-aged adults without sex predilection. The behavior is believed to be more akin to that of a low-grade sarcoma than a malignant lymphoma [9, 34]. As the morphological features of FDC sarcomas (storiform arrangement of plump spindle cells with admixed lymphocytes) have become better known, the possibility of this diagnosis is now commonly being considered for node-based spindle cell lesions, and the availability of antibodies that recognize FDCs (CD21, CD35, and clusterin) has allowed the diagnosis to be established more readily.

FDC sarcoma of extranodal sites, on the other hand, appears much less well recognized, although its occurrence has been known since the early 1990s [8]. In these loca-

Table 1 Clinical characteristics of patients with extranodal FDC sarcoma

Case number	Reference	Age	Sex	Site	Initial treatment	Recurrence (time to recurrence in months)	Last follow-up (month)	Outcome status
	New cases							
1	Case 1	30	M	Rectum	Surgery	Intra-abdominal (10)	15	AWD
2	Case 2	29	F	Lesser omentum	Surgery		17	NED
3	Case 3	69	F	Tonsil	Neoadjuvant RT + surgery	Hilar lymph nodes (96)	108	AWD
	Cases from literature							
4	Shek et al. 1996 [41]	35	F	Liver	Surgery	Local, two times (30 and 48)	60	AWD
5	Shek et al. 1998 [42]	37	M	Liver	Surgery		24	NED
6	Chen et al. 2001 [11]	57	F	Liver	Observation		36	AWD
7	Chen et al. 2001[11]	51	F	Liver	Surgery		12	NED
8	Selves et al. 1996 [39]	68	F	Liver	Neoadjuvant chemo + surgery		30	NED
9	Torres et al. 2005 [43]	82	M	Liver	Surgery		18	NED
10	Han et al. 2000 [24]	45	M	Stomach	Surgery		10	NED
11	Geerts et al. 2004 [21]	40	F	Stomach	Surgery		5	AWD
12	Shek et al. 1998 [42]	61	F	Ampulla	Surgery (whipple)		9	NED
13	Hollowood et al. 1995 [25] and Chan et al. 1997 [9]	23	F	Small bowel	Surgery	Local, two times (6 and 24)	24	AWD
14	Chang et al. 2001 [10]	37	F	Right colon	Surgery		7	NED
15	O'Malley 2004 [33]	38	M	Cecum	surgery		NA	NA
16	Hollowood et al. 1995 [25] and Chan et al. 1997 [9]	63	M	Head of pancreas	Surgery	Local (8)	11	DOD
17	Chan et al. 1997 [9]	42	M	Mesocolon (also involves mesenteric lymph nodes, and with small peritoneal deposits)	Surgery + chemo (lymphoma regimen)	Local (18)	"Shortly after recurrence"[a]	DOD
18	Chiaramonte et al. 2001 [13]	39	M	Retroperitoneum	Surgery	Pericardial LN and lung (6)	"Shortly after recurrence"[a]	DOD
19	Schwarz et al. 1999 [38]	62	M	Lower abdominal wall	Surgery + RT		8	NED
20	Perez-Ordonez et al. 1996 [34]	40	F	Abdomen	Surgery + chemo	Local, and then liver (12 and 24)	24	AWD
21	Grogg et al. 2004 [22]	62	M	Left-thigh soft tissue	Surgery		18	NED
22	Shah et al. 2001 [40]	33	M	Lung	Chemo + surgery (no response to chemo)		NA	NA
23	Fisher et al. 1999 [18]	41	F	Breast	Surgery	Local ("within a few months")	36	NED
24	Nayler et al. 1996 [31] and Chan et al. 1997 [9]	18	F	Tonsil	Surgery + chemo		NA	NA
25	Perez-Ordonez et al. 1996 [34]	62	F	Tonsil	Surgery		12	NED
26	Chan et al. 1994 [8] and Chan et al. 1997 [9]	44	M	Tonsil	Surgery		36	NED

27	Chan et al. 1997 [9]	32	M	Tonsil	Surgery + RT	Local and cervical LN (54)	54	AWD
28	Biddle et al. 2002 [3]	48	F	Tonsil	Surgery with neck dissection		6	NED
29	Biddle et al. 2002 [3]	48	M	Tonsil	Surgery		8	NED
30	Satoh et al. 2003 [37]	16	M	Tonsil	Surgery + chemo + RT (PEP, UFT, MTX, CDDP; 30Gy RT)		24	NED
31	Vargas et al. 2002 [45]	54	F	Tonsil	Surgery w neck dissection		8	NED
32	Grogg et al. 2004 [22]	57	F	Tonsil	None		8	AWD
33	Araujo et al. 1999 [1]	14	M	Hard palate	Surgery		5	NED
34	Chan et al. 1994 [8] and Chan et al. 1997 [9]	63	F	Palate	Neoadjuvant RT + surgery with neck dissection		54	NED
35	Beham-Schmid et al. 1998 [2]	44	M	Nasopharynx	Surgery + RT		20	NED
36	Biddle et al. 2002 [3]	33	M	Nasopharynx, oropharynx	Surgery + RT	Lung (10)	10	AWD
37	Chan et al. 2001 [7]	34	M	Nasopharynx	Neoadjuvant chemo (CHOP) + surgery		36	NED
38	Desai et al. 1999 [16]	45	F	Parapharyngeal	Surgery	Local (31)	57	NED
39	Chan et al. 1997 [9]	40	F	Parapharyngeal mass	Surgery	Local (12)	12	AWD
40	Vargas et al. 2002 [45]	54	F	Left parotid	Surgery + RT	Local (6)	8	AWD
41	Galati et al. 1999 [20]	65	F	Thyroid	Surgery + neck dissection + RT		36	NED
42	Chan et al. 1997 [9]	17	M	Neck soft tissue	Neoadjuvant chemo + surgery (CHOP followed by ifosfamide, carboplatin, epiadriamycin)		NA	NA
43	Chan et al. 1997 [9]	25	F	Neck soft tissue	Surgery + RT	Lung (20)	20	AWD
44	Choi et al. 2000 [14]	28	F	Neck soft tissue	Surgery	Lung (324)	324	AWD
45	Choi et al. 2000 [14]	66	F	Neck soft tissue	Surgery + RT	Lung (24)	24	AWD
46	Bradshaw et al. 2005 [5]	9	M	Neck soft tissue	Surgery	Local (60)	96	NED

[a] For statistical purposes, the time to recurrence was used as last follow up time

LN Lymph node, *chemo* chemotherapy, *RT* radiotherapy, *AWD* alive with disease, *NED* no evidence of disease, *DOD* died of disease

tions, FDC sarcoma does not usually enter the differential diagnosis clinically or pathologically, particularly when it occurs in visceral organs, and the morphological features suggest a wide variety of other diagnoses such as carcinoma, meningioma, malignant fibrous histiocytoma, and schwannoma. We have recently encountered three cases of extranodal FDC sarcoma, two involving intraabdominal sites and one involving the tonsil. All three were misdiagnosed at the time of initial evaluation, as the possibility of FDC sarcoma was not entertained in any of them. This prompted us to perform a detailed analysis of extranodal examples of this disease based on these cases as well as other well-characterized, previously reported cases. We identified 43 previously reported cases with adequate information. In this study, we detail the features of extranodal FDC sarcoma, providing an overview of the current knowledge about the clinical, pathological and histogenetic characteristics of this disease entity.

Materials and methods

Assessment of new cases

For the three new cases, a detailed clinical history was obtained from the medical records and from discussions with the responsible clinicians. Pathological materials were processed in a routine manner with formalin fixation and paraffin embedding for H&E and immunohistochemical staining. Antibodies used for immunohistochemistry included vimentin (Dako, CA, Carpinteria, CA, USA; 1:4000), CD21 (Dako, 1:10), CD35 (Dako, 1:100), clusterin (Upstate Biotech, CA, USA 1:200), AE1:AE3 (Boehringer-Mannheim, Indianapolis, IN, USA, monoclonal, 1:1,000), CAM5.2 (Becton Dickinson, Franklin Lakes, NJ, USA, monoclonal, 1:1,000), 34BE12 (Enzo, Farmingdale, NY, USA, 1:50), S100 protein (Dako, 1:500), HMB45 (Dako, 1:10), A103 (Ventana Medical Systems, prediluted), tyrosinase (Novocastra, Newcastle upon Tyne, UK, 1:200), LCA (Dako, 1:1,000), SMA (Dako, 1:1,000), Desmin (Dako, 1:200), and c-kit (Dako, 1:100). Appropriate positive and negative controls were evaluated simultaneously. Electron microscopy was performed in one case, for which ultrathin sections were cut from epoxy resin-embedded, 2% glutaraldehyde-fixed, and 1% osmium tetroxide postfixed tissues. These sections were stained with uranyl acetate and lead citrate and examined with a Zeiss 906 transmission electron microscope. In situ hybridization for Epstein–Barr virus (EBV)-encoded RNA (EBER) was performed in one case on formalin-fixed, paraffin-embedded tissue using a fluoresceinated EBV-specific RNA probe (Dako). Positive signal was detected with a biotin-free, antifluorescein horseradish peroxidase-conjugated antibody.

Literature review

Review of the literature was performed with a MEDLINE search using the terms “follicular dendritic cell tumor” or “follicular dendritic cell sarcoma” combined with “extranodal” or with specific sites (e.g., liver or hepatic, stomach or gastric, etc). References from articles retrieved by this method were also reviewed to identify other relevant publications. An effort was made to identify cases that were reported more than once in different settings, and only one entry with the most updated information was included for such cases. Nodal and splenic FDC tumors were not included.

Statistical analysis

Data obtained from the literature and the three new cases were analyzed. Recurrence-free survival rates were calculated by Kaplan–Meier estimation. Associations between pathological factors and adverse outcome were analyzed using the Cox regression method.

Results

Clinical and pathological findings of the three new cases

Pertinent clinical data on all three cases are listed in Table 1. In case 1, the disease occurred in the rectum of a 30-year-old male patient. The patient presented with a 6-month history of blood per rectum, and an endoscopy showed a mass protruding into the rectal lumen. The initial biopsy of the mass was thought to be a “mesenchymal tumor with neural differentiation”. The patient underwent a low anterior resection and opted not to receive any adjuvant therapy postoperatively. Sixteen months after the diagnosis, a follow-up CT scan demonstrated perihepatic intraperitoneal masses consistent with recurrent disease. No further workup or treatment was carried out at the time of last follow-up, which was 19 months after the initial diagnosis.

Case 2 was a 29-year-old female patient who presented with a mass in the left upper quadrant of the abdomen. A workup including ultrasound, CT scan, and MRI revealed a mass in close proximity to the stomach and liver. The mass was resected without a preoperative biopsy. At operation, the 12.0×9.0×4.0-cm mass appeared to have arisen from the lesser omentum, adjacent but not adherent to the neighboring organs. The pathological diagnosis rendered for this tumor at the referring institution was “a high-grade neoplasm, possibly a malignant fibrous histiocytoma, giant cell type”. Because of the presence of giant cells and close proximity to the pancreas, a concern of “a sarcomatoid giant cell carcinoma of the pancreas” was also raised. At

Table 2 Pathological findings of the three new cases of extranodal FDC sarcoma

Cases	Histology	Mitosis	Necrosis	IHC				
				CD21	CD35	Clusterin	S100	Cytokeratin
1	Growth: fascicular; cells: spindle and oval	3/10HPF	Present	Pos	Pos	Pos	Neg	Neg
2	Growth: fascicular; cells: spindle and ovoid; multinucleated tumor cells present	0	Present	Neg	Pos	Not done	Neg	Neg
3	Growth: diffuse; cells: epithelioid; multinucleated tumor giant cells present	0	Absent	Pos	Pos	Not done	Pos	Neg

IHC Immunohistochemistry, *HPF* high-power field, *Pos* positive, *Neg* negative

last follow-up, 17 months after initial diagnosis, the patient remained alive with no evidence of disease; no additional therapy was given.

Case 3 involved the tonsil of a 69-year-old female patient. Pathological diagnosis for the initial excisional biopsy was "squamous cell carcinoma of the tonsil", and the patient underwent adjuvant radiation therapy followed by a radical neck dissection. The patient had then remained disease-free for 8 years, at which point she developed a persistent cough and was found to have hilar and lung lesions. A mediastinoscopic biopsy of the hilar lesion showed a metastatic FDC sarcoma involving a lymph node. Retrospective review of the patient's prior tonsillar lesion revealed an FDC sarcoma as well. No further therapy was given. At last follow-up, 9 years after the initial tonsillar lesion, the patient was alive with radiographic evidence of stable disease.

Pathological features of all three cases are summarized in Table 2. Grossly, the tumors were well circumscribed with a fleshy cut surface, similar to sarcoma or lymphoma (Fig. 1). Microscopically, cases 1 and 2 showed a more spindled cell morphology with a whorled, fascicular, or storiform growth pattern (Fig. 2), while in case 3, the cells were more epithelioid and the growth pattern was more diffuse (Fig. 3). In all three cases, the cells had eosinophilic fibrillary cytoplasm with indistinct cell borders (Fig. 4), and there were small lymphocytes scattered throughout the tumor and clustered around vessels (Fig. 5). In case 3, the epithelioid tumor cells had irregular nuclei and prominent round nucleoli. Some nuclei contained round intranuclear inclusions (Fig. 3). In all three cases, mitoses were not prominent, being absent in two cases and 3/10 high power fields (HPF) in one (case 1). Necrosis was noted in two cases. Regional lymph node involvement was present in case 1. Immunohistochemically, all three cases showed diffuse positivity for CD21, two of three showed positivity for CD35, and one of one for clusterin (Fig. 6). All cases were negative for cytokeratins, and two of three were negative for S100 protein. Cases 1 and 2 were tested for c-kit, and muscle markers (desmin and SMA) with negative results. Melanoma markers, HMB45 and tyrosinase, were negative in all three. Ultrastructural studies were performed in case 1, as was in situ hybridization for EBER. Ultrastructurally, the tumor cells showed prominent cell processes that were focally joined by well-formed cell junctions and desmosomes (Fig. 7). EBER showed no evidence of EBV.

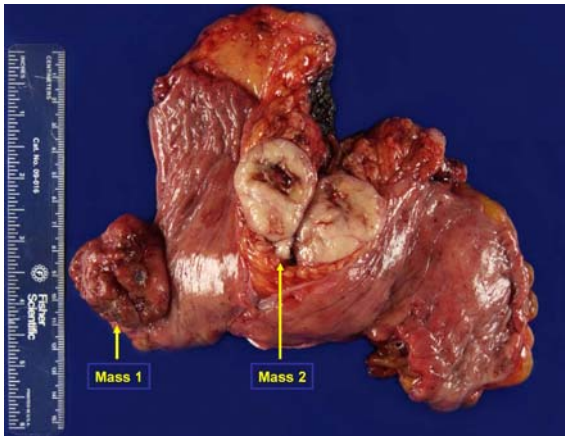

Fig. 1 Gross picture of an FDC sarcoma of the rectum (case 1). There are two main mass lesions, both affecting the bowel wall. Note the fleshy homogeneous cut surface with focal hemorrhage and necrosis

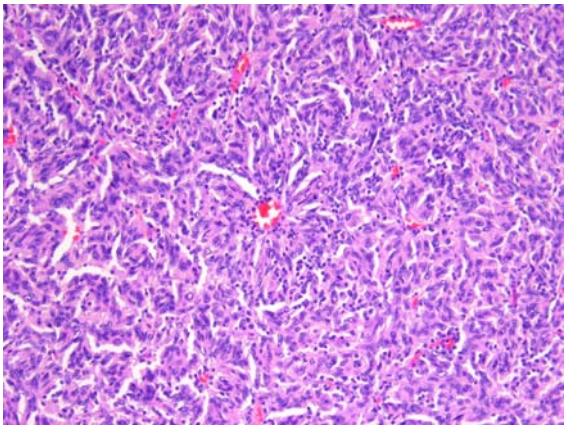

Fig. 2 Microscopic appearance of an FDC sarcoma of the rectum (case 2). The tumor has a whorled and storiform growth pattern. The tumor cells are spindled

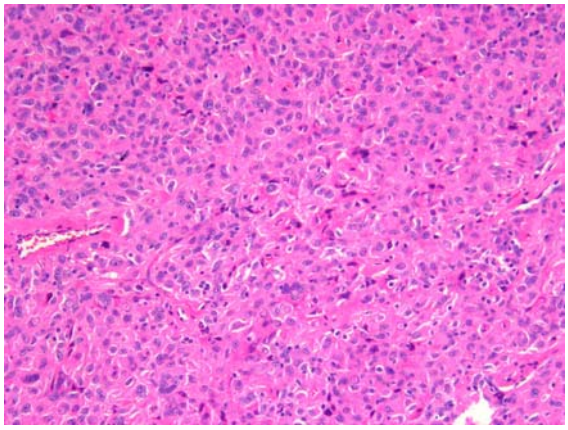

Fig. 3 An FDC sarcoma of the tonsil (case 3) showing a diffuse growth pattern. The tumor cells are plump and epithelioid with pink, vaguely fibrillary cytoplasm. The nuclei are irregular and cleaved in some cells. Prominent nucleoli are present. Some nuclei contain round intranuclear inclusions. Multinucleated tumor giant cells are also apparent

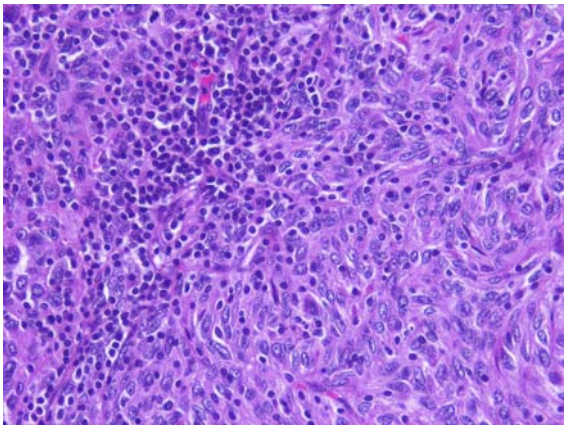

Fig. 5 FDC sarcoma showing small lymphocytes scattered about and clustered around blood vessels (case 1)

Literature review

A total of 43 cases of extranodal FDC sarcoma were retrieved from the literature. Clinical information on these 43 cases, along with the three new cases, is detailed in Table 1.

Patient demographic characteristics

There were 25 women and 21 men (female to male ratio, 1.2:1). The age range was 9–82 years, with a median of 41.5 years and a mean of 43.5 years. The geographic distribution of the cases covered both Eastern and Western countries, although more reports appeared to have originated from Asian countries.

Tumor anatomic distribution

The tumors affected various anatomic sites. Six involved the liver. Another six involved the tubular gastrointestinal tract (three in large bowel, one in small bowel, and two in stomach). Other organ sites included the ampulla of Vater, pancreas, lung, breast, and thyroid (one case each). Three cases were intraabdominal but extravisceral (one in lesser omentum, one in mesocolon, and one in retroperitoneum). Eight cases involved soft tissues of the neck (five cases), the abdominal wall (two cases), and the thigh (one case). Seventeen cases involved the oral cavity and upper aerodigestive regions (ten in tonsil, seven in palate and pharynx) and one the parotid gland. Of note, the three cases that were intraabdominal and extravisceral, and the eight cases of soft tissues of various sites were included as extranodal FDC tumors based on lack of convincing evidence of nodal origin.

Clinical management and patients' outcome

Eight of the 46 cases (17%) had lymph node involvement at the time of presentation, and one of the eight also had a liver metastasis. Except in two cases (cases 6 and 32), all patients underwent surgical resection of the tumor. Eighteen of the 44 patients (41%) who had surgery also had some

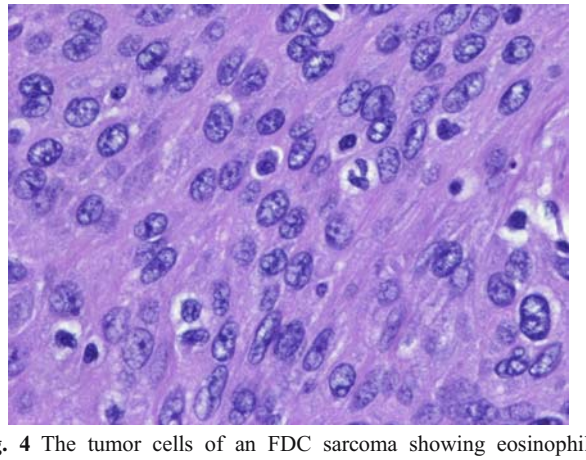

Fig. 4 The tumor cells of an FDC sarcoma showing eosinophilic fibrillary cytoplasm with indistinct cell borders (case 1)

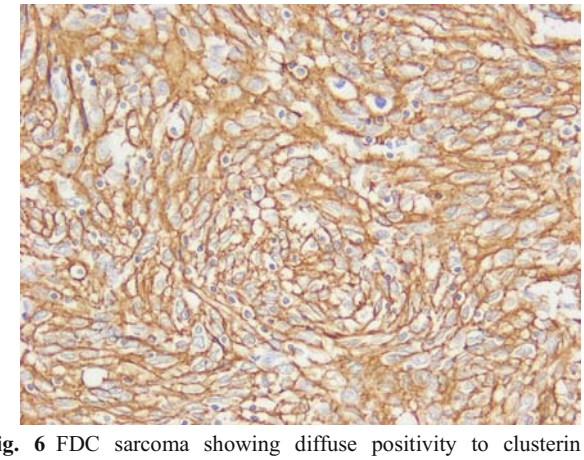

Fig. 6 FDC sarcoma showing diffuse positivity to clusterin by immunohistochemistry (case 1)

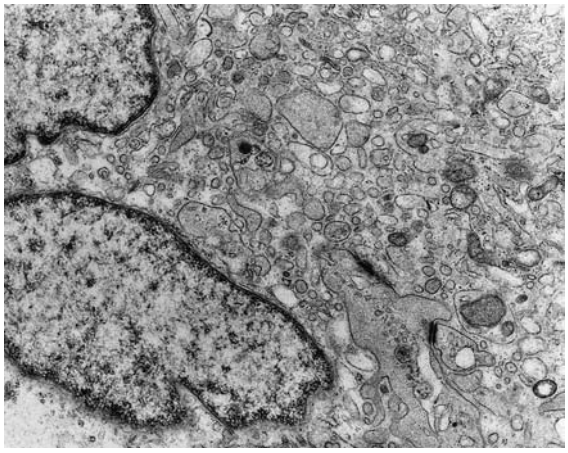

Fig. 7 Ultrastructurally, the tumor cells show prominent cell processes that are focally joined by well-formed cell junctions and desmosomes (case 1)

form of adjuvant treatment: 4 had neoadjuvant chemotherapy, 3 had adjuvant chemotherapy, 2 had neoadjuvant radiotherapy (RT), 8 had adjuvant RT, and 1 had adjuvant chemo and RT. The chemotherapeutic agents varied among reports but usually included the cytoxan, hydroxydaunomycin (adriamycin), vincristine (oncovin), and prednisone (CHOP) regimen.

Follow-up information was available in 42 cases. The follow-up time ranged from 5 to 324 months (mean, 32 months; median, 18 months). Overall, 18 of the 42 patients (43%) had local and/or distant recurrence after initial treatment. Local recurrence occurred in 11 patients (26%) at a median of 15 months after resection (range, 6–60 months). Distant metastases occurred in nine patients (21%) at a median of 24 months after resection (range, 6–324 months). Metastatic sites included lung (five cases), liver (one case), intraabdominal soft tissues (one case), and lymph nodes (two cases). Two cases (cases 20 and 27) had both local and distant recurrence. At last follow-up, three patients (7%) died of disease, 15 (36%) were alive with disease, and 24 (57%) were alive with no evidence of disease. Two-year and 5-year recurrence-free survival for the entire group were 62.3% (95% CI, 0.469, 0.827) and 27.4% (95% CI, 0.102, 0.739), respectively (Fig. 8).

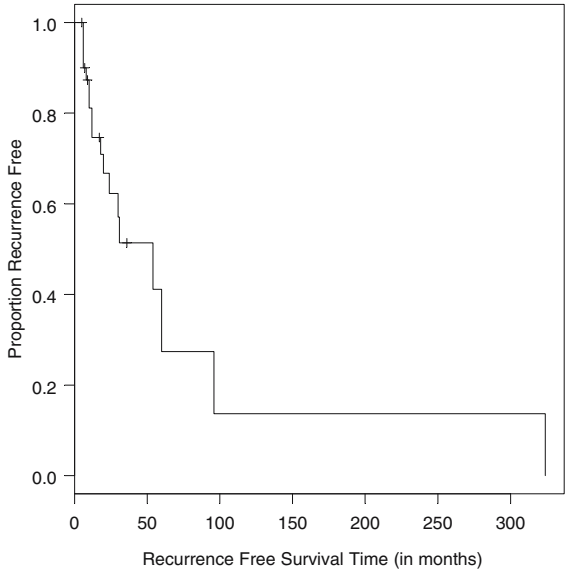

Fig. 8 Recurrence-free survival curve for patients with extranodal FDC sarcoma

Discordant diagnoses entertained at initial evaluation

Overall, 15 cases (33%) were misdiagnosed at the time of initial evaluation. In all three new cases, and in some reported cases, the diagnosis of FDC sarcoma was not entertained at initial evaluation. In some cases, such erroneous interpretations were the reasons that neoadjuvant or adjuvant therapy was rendered. Disease entities considered included: reactive response (one case), carcinoma (five cases), inflammatory pseudotumor (IPT) (two cases), malignant fibrous histiocytoma (two cases), meningioma (one case), mesenchymal tumor with neural differentiation (or neural origin) (two cases), schwannoma (one case), and stromal tumor (one case).

Pathological findings

The average size of tumors of all sites was 7.4 cm, ranging from 1 to 20 cm (median, 6 cm). Intraabdominal tumors (n=18) had an average tumor size of 10.3 cm (range, 4–20 cm; median, 11 cm), whereas the average tumor size of the tumors outside the abdominal cavity (n=19) was only 4.7 cm (range, 1–14 cm; median, 3 cm) (p<0.001).

The gross and microscopic findings of the reported cases were similar to those observed in our three cases as described above. The most helpful diagnostic features were the syncytial arrangement of tumor cells with fibrillary cytoplasm and indistinct cytoplasmic borders and the presence of small lymphocytes scattered throughout the tumor. The cells varied from plump and spindled to epithelioid. It is of interest to note that FDC sarcomas arising in the liver tended to have a prominent plasma cell component in the inflammatory infiltrate, whereas plasma cells were nonexistent or inconspicuous in extrahepatic cases. Binucleated and multinucleated neoplastic cells and intranuclear inclusions were features that were seen in some cases. Although the tumors were often hypercellular, most reports suggested that the tumors had a low-grade histology with only mild to moderate atypia. However, high-grade examples with marked cytological atypia were reported. A mitotic count was available in 31 cases, ranging from 0 to 50/10 HPF with a median of 3/10 HPF.

Table 3 Immunohistochemical staining results of extranodal FDC sarcoma

Markers	Number of cases positive/ number of cases tested	Cases positive (%)
CD21	45/46	98
CD35	38/41	93
Clusterin	3/3	100
Fascin	6/6	100
Desmoplakin	8/11	73
CD68	7/21	33
S100 protein	11/34	32
EMA	16/22	27
Cytokeratin	1/18	6

Nineteen of 31 (61%) had a mitotic count of <5/10 HPF. Information on necrosis was available in 33 cases, of which ten (30%) exhibited coagulative necrosis.

Immunohistochemical staining results are summarized in Table 3. CD21 and CD35 were commonly used, and both had a high positive rate (98% for CD21 and 93% for CD35). Clusterin and fascin were relatively recently employed markers [22, 23] and were tested in only a few cases, having uniform positivity. CD68, S100 protein, and EMA showed variable staining results among different reports. Desmoplakin, a desmosome-associated protein [17], was detected in 73% of the cases, while cytokeratin was positive in only 1 of 18 cases. In the one cytokeratin-positive case, the positivity was only seen in <10% of the tumor cells.

Ultrastructural findings were reported in ten cases, and all showed typical findings as described in our case 1.

Correlation between clinical and pathological findings and patients' outcome

Associations between the various clinical and pathological factors and recurrence-free survival were analyzed, and the results are summarized in Table 4. Factors assessed included age, gender, intraabdominal involvement, size, lymph node involvement or distant metastasis at time of presentation, mitotic rate, necrosis, and the use of neoadjuvant or adjuvant therapy. No statistical significance was identified for any of these factors.

Possible etiology and associated conditions

Of the six tumors that occurred in the liver, five were positive for the EBER as tested by in situ hybridization. Furthermore, Southern blot analysis in two cases showed clonal and episomal EBV in the tumor cells [41]. On the other hand, all 24 extra-hepatic cases that were tested by EBER failed to demonstrate any evidence of EBV.

In addition, two cases (cases 16 and 37) [7, 9] had an association with Castleman's disease of hyaline-vascular type [9]. In case 16, the main tumor mass showed small foci of residual hyaline-vascular Castleman's disease [9]. In case 37, hyaline-vascular Castleman's disease occurred at the same site 11 years before development of a frank FDC sarcoma [7]. Another two cases (cases 1 and 5), both occurring in the liver, exhibited a morphological resemblance to the so-called IPT and were diagnosed as such initially [39, 41].

Discussions

Given the fact that FDCs are present in all lymphoid follicles, including extranodal lymphoid follicles, it is not

Table 4 Correlation between clinicopathological findings and clinical outcome in patients with extranodal FDC sarcoma

		Local or distant recurrence (number with positive events/ total number of patients)	Two-year recurrence-free survival	*p*-value
Age[a]		–	–	0.32
Sex	Male	7/18	0.672	0.86
	Female	11/24	0.603	
Intraabdominal involvement	Present	7/18	0.676	0.19
	Absent	11/24	0.552	
Size[a]		–	–	0.18
Lymph-node involvement at presentation[b]	Present	1/7	0.618	0.71
	Absent	17/35	0.667	
Mitotic rate[a]		–	–	0.98
Necrosis	Present	4/10	0.587	0.32
	Absent	10/19	0.686	
Use of adjuvant therapy	Yes	8/15	0.72	0.96
	No	10/27	0.565	

[a] Calculated as continuous variables

[b] One case had both lymph-node involvement and liver metastasis

surprising that tumors of these cells occur in extranodal sites. Yet, extranodal FDC sarcoma appears to be significantly underrecognized, particularly when it affects visceral organs. This entity did not enter the differential diagnosis at the time of initial evaluation in any of the three cases we encountered.

When suspected based on histology, the diagnosis of FDC sarcoma can be relatively straightforward. As illustrated by this review study, extranodal FDC sarcomas, like their nodal counterparts, typically have distinct histological, immunophenotypical, and ultrastructural findings to allow a definitive diagnosis. In terms of immunohistochemical markers, in addition to CD21 and CD35, clusterin has been shown to be a highly sensitive and specific FDC marker [23]. Fascin, another relatively recently discovered marker, however, has been shown to be very nonspecific among spindle cell tumors and thus does not imply a dendritic lineage [23]. Desmoplakin is a desmosome-associated protein found on epithelial cells and nonepithelial cells with desmosomes [17]. Positive staining was detected in 73% of the cases. However, because the antibody does not yield consistent results on paraffin-embedded sections, often producing only patchy or focal staining, it is of limited value for the diagnosis of FDC sarcoma. Additionally, FDCs may show variable staining for EMA, S100 protein, and CD68. Keratin stains, however, appear consistently negative in FDC sarcoma; in only 1 of the 18 cases tested was there focal keratin staining in <10% of the tumor. These immunohistochemical results for extranodal FDCs are essentially identical to the more extensive results reported for nodal FDCs.

It is difficult to determine the frequency of extranodal FDC sarcoma given that almost all reports are case-based and the denominator necessary for the determination of the frequency is essentially unknown. Overall, the disease is uncommon. Lack of a high index of suspicion is the main reason for this uncommon disease to be misdiagnosed in most instances, as illustrated in all three new cases we encountered and those reported in the literature. When evidence of FDC differentiation is not sought, the fact that FDC sarcomas can show variable staining for EMA, CD68, and S100 protein, coupled with an epithelioid cell-predominant or a spindle cell-predominant morphology, may lead to such diagnoses as carcinoma, meningioma, sarcoma of neural origin, malignant fibrous histiocytoma, or simply a stromal tumor not further specified. As documented in case 3 of our series and several cases reported in the literature, such erroneous diagnoses have then led to divergent treatment modalities for this disease entity.

Correct identification of this disease entity is clinically important. As our analyses have shown, this disease carries an overall recurrence rate of 43% (local recurrence in 26% and distant recurrence in 21%). The 5-year recurrence-free survival rate was only 27.4%. A small but definite proportion of patients (7%) died of the disease. These figures may still underestimate the biology of this tumor given the relatively short follow-up time available for these cases.

How to predict which patients will experience a worse outcome is a question still, however, to be answered. Previous reports suggested that intraabdominal involvement, a high mitotic count (≥5/10 HPF), coagulative necrosis, and significant cellular atypia are potentially helpful morphological predictors of unfavorable outcome [9]. In this study, we were not able to perform a statistical analysis on cellular atypia because data were not uniformly recorded in the literature reports. However, none of the other factors mentioned above showed significant statistical power in predicting tumor recurrence. With increasing recognition of FDC sarcomas, cases with more marked nuclear pleomorphism are being diagnosed more frequently, and it remains to be established whether a more poorly differentiated FDC sarcoma may also be more clinically aggressive. Similarly, more experience is needed to determine any other prognostic factors.

With regard to the etiology and predisposing factors for FDC sarcoma, there have been a number of interesting observations that deserve attention and further investigation. First, as outlined in this review study, five of six hepatic FDCs exhibited positive EBER by in situ hybridization, whereas none of the 24 extrahepatic cases tested was positive for the virus. EBV has also been demonstrated in some but not all splenic and nodal FDC sarcomas [6, 26]. In the hepatic cases, Southern blotting analysis showed that the EBV infection occurred before the clonal proliferation of neoplastic FDCs, suggesting its causative role in the development of FDC sarcoma [39, 41]. These findings therefore suggest a pathogenetic difference between hepatic (and some splenic and nodal) FDC sarcomas and other types of FDC sarcomas.

Second, as illustrated by cases 17 and 37, some extranodal FDC sarcomas appear to be associated with the hyaline-vascular type Castleman's disease, similar to some of their nodal counterparts [7, 27, 28]. This finding is not surprising because Castleman's disease affects extranodal sites as well. Several reports have suggested that the FDC proliferation and dysplastic changes occurring in Castleman's disease can form the background from which an FDC sarcoma develops. As such, the relationship of Castleman's disease and FDC sarcomas has been suggested to parallel the hyperplasia–dysplasia–neoplasia sequence that is seen in other tumor types [9, 29, 35, 36].

Third, there have been emerging data suggesting an association between FDC sarcoma and the so-called IPT [6, 12, 32, 39, 41]. In this study, IPT refers to the morphologically reactive fibroinflammatory mass lesions of

uncertain nature and etiology. Such an association appears to be particularly apparent in hepatic cases. Two of the reported hepatic cases (cases 4 and 8) were initially diagnosed as IPT. More importantly, Cheuk et al. [12] in 2001 reported a series of seven hepatic, three splenic, and one peripancreatic FDC proliferations that bore a "striking histological resemblance to IPT because of the admixture of lymphocytes, plasma cells, and spindle cells". Although only one splenic case showed a component that was indistinguishable morphologically from a conventional FDC tumor, the authors believed that such FDC proliferations were neoplastic. Cossu et al. [15] in 2005 reported a classic FDC tumor developing in a 31-year-old woman, at a site where a nodal IPT-like proliferation was removed 6 years earlier. It is of great interest that in the initial IPT-like lesion, groups of irregularly and loosely arranged CD21-positive cells were noted. All these observations suggest that either FDC sarcoma can present at a very early stage as an IPT-like condition or a subset of IPT has the potential to evolve into an FDC sarcoma. Of interest also is the fact that all hepatic cases [39, 41, 42] (including that reported by Cheuk et al. [12]) exhibited EBV genome in the tumor cells whereas the nodal FDC sarcoma that developed at the site of a previously excised IPT did not [15].

Viewing the above observations together, it appears that FDC sarcomas, nodal or extranodal, are pathogenetically heterogeneous. Most hepatic FDC sarcomas and some splenic and nodal tumors might be related to EBV infection and might present as a fibroinflammatory mass like the so-called IPT. The cases reported by Cheuk et al. [12] might represent an earlier stage of FDC sarcoma when compared to those reported by others [11, 39, 41]. All these cases seem to share a heavy inflammatory infiltrate that may contain plasma cells. Most nonhepatic FDC sarcomas, on the other hand, may have an inciting factor not related to EBV [15]. Some such cases might also undergo an IPT-like proliferation at an early stage or might have evolved from an IPT-like condition.

It is apparent that much more investigation is required, including perhaps clonality studies, before we can firmly accept the pathogenetic relationship between some IPT-like conditions and FDC sarcoma. The association between IPT and FDC sarcoma, however, is not unreasonable from a conceptual point of view and has already been suggested by other investigators [32]. After all, FDCs are believed to be of mesenchymal origin. Phenotypic marker studies and in vitro experiments with fibroblast-like cell lines have demonstrated development of FDCs from fibroblast-like cells [4, 44]. It is possible that under certain oncogenic stimuli, such as EBV infection, the mesenchymal cells in IPT-like conditions undergo transformation into FDCs, and as has been observed in Castleman's disease, such cells then undergo "dysplasia" and eventually become neoplastic.

In summary, this study illustrates the need for wider recognition of extranodal FDC sarcoma. In analyzing all reported cases, we have outlined the clinical and pathological characteristics of this disease entity and brought forth evidence for associations between FDC sarcoma and IPT-like conditions which should prompt further exploration of the histogenesis and classification of both IPT and FDC sarcoma.

References

1. Araujo VC, Martins MT, Salmen FS, Araujo NS (1999) Extranodal follicular dendritic cell sarcoma of the palate. Oral Surg Oral Med Oral Pathol Oral Radiol Endod 87:209–214
2. Beham-Schmid C, Beham A, Jakse R, Aubock L, Hofler G (1998) Extranodal follicular dendritic cell tumour of the nasopharynx. Virchows Arch 432:293–298
3. Biddle DA, Ro JY, Yoon GS, Yong YW, Ayala AG, Ordonez NG, Ro J (2002) Extranodal follicular dendritic cell sarcoma of the head and neck region: three new cases, with a review of the literature. Mod Pathol 15:50–58
4. Bofill M, Akbar AN, Amlot PL (2000) Follicular dendritic cells share a membrane-bound protein with fibroblasts. J Pathol 191:217–226
5. Bradshaw EJ, Wood KM, Hodgkinson P, Lucraft H, Windebank KP (2005) Follicular dendritic cell tumour in a 9-year-old child. Pediatr Blood Cancer 45:725–727
6. Brittig F, Ajtay E, Jakso P, Kelenyi G (2004) Follicular dendritic reticulum cell tumor mimicking inflammatory pseudotumor of the spleen. Pathol Oncol Res 10:57–60
7. Chan AC, Chan KW, Chan JK, Au WY, Ho WK, Ng WM (2001) Development of follicular dendritic cell sarcoma in hyaline-vascular Castleman's disease of the nasopharynx: tracing its evolution by sequential biopsies. Histopathology 38:510–518
8. Chan JK, Tsang WY, Ng CS, Tang SK, Yu HC, Lee AW (1994) Follicular dendritic cell tumors of the oral cavity. Am J Surg Pathol 18:148–157
9. Chan JK, Fletcher CD, Nayler SJ, Cooper K (1997) Follicular dendritic cell sarcoma. Clinicopathologic analysis of 17 cases suggesting a malignant potential higher than currently recognized. Cancer 79:294–313
10. Chang KC, Jin YT, Chen FF, Su IJ (2001) Follicular dendritic cell sarcoma of the colon mimicking stromal tumour. Histopathology 38:25–29
11. Chen TC, Kuo TT, Ng KF (2001) Follicular dendritic cell tumor of the liver: a clinicopathologic and Epstein–Barr virus study of two cases. Mod Pathol 14:354–360
12. Cheuk W, Chan JK, Shek TW, Chang JH, Tsou MH, Yuen NW, Ng WF, Chan AC, Prat J (2001) Inflammatory pseudotumor-like follicular dendritic cell tumor: a distinctive low-grade malignant intra-abdominal neoplasm with consistent Epstein–Barr virus association. Am J Surg Pathol 25:721–731
13. Chiaramonte MF, Lee D, Abruzzo LV, Heyman M, Bass BL (2001) Retroperitoneal follicular dendritic cell sarcoma presenting as secondary amyloidosis. Surgery 130:109–111
14. Choi PC, To KF, Lai FM, Lee TW, Yim AP, Chan JK (2000) Follicular dendritic cell sarcoma of the neck: report of two cases complicated by pulmonary metastases. Cancer 89:664–672
15. Cossu A, Lissia A, Dedola MF, Deiana A, Faedda R, Palmieri G, Tanda F (2005) Classic follicular dendritic reticulum cell tumor of the lymph node developing in a patient with a previous inflammatory pseudotumor-like proliferation. Hum Pathol 36:207–211

16. Desai S, Deshpande RB, Jambhekar N (1999) Follicular dendritic cell tumor of the parapharyngeal region. Head Neck 21:164–167
17. Ennas MG, Chilosi M, Scarpa A, Lantini MS, Cadeddu G, Fiore-Donati L (1989) Isolation of multicellular complexes of follicular dendritic cells and lymphocytes: immunophenotypical characterization, electron microscopy and culture studies. Cell Tissue Res 257:9–15
18. Fisher C, Magnusson B, Hardarson S, Smith ME (1999) Myxoid variant of follicular dendritic cell sarcoma arising in the breast. Ann Diagn Pathol 3:92–98
19. Fonseca R, Yamakawa M, Nakamura S, van Heerde P, Miettinen M, Shek TW, Myhre Jensen O, Rousselet MC, Tefferi A (1998) Follicular dendritic cell sarcoma and interdigitating reticulum cell sarcoma: a review. Am J Hematol 59:161–167
20. Galati LT, Barnes EL, Myers EN (1999) Dendritic cell sarcoma of the thyroid. Head Neck 21:273–275
21. Geerts A, Lagae E, Dhaene K, Peeters M, Waeytens A, Demetter P, Cuvelier C, Defreyne L, De Vos M, Pattyn P (2004) Metastatic follicular dendritic cell sarcoma of the stomach: a case report and review of the literature. Acta Gastroenterol Belg 67:223–227
22. Grogg KL, Lae ME, Kurtin PJ, Macon WR (2004) Clusterin expression distinguishes follicular dendritic cell tumors from other dendritic cell neoplasms: report of a novel follicular dendritic cell marker and clinicopathologic data on 12 additional follicular dendritic cell tumors and 6 additional interdigitating dendritic cell tumors. Am J Surg Pathol 28:988–998
23. Grogg KL, Macon WR, Kurtin PJ, Nascimento AG (2005) A survey of clusterin and fascin expression in sarcomas and spindle cell neoplasms: strong clusterin immunostaining is highly specific for follicular dendritic cell tumor. Mod Pathol 18:260–266
24. Han JH, Kim SH, Noh SH, Lee YC, Kim HG, Yang WI (2000) Follicular dendritic cell sarcoma presenting as a submucosal tumor of the stomach. Arch Pathol Lab Med 124:1693–1696
25. Hollowood K, Stamp G, Zouvani I, Fletcher CD (1995) Extranodal follicular dendritic cell sarcoma of the gastrointestinal tract. Morphologic, immunohistochemical and ultrastructural analysis of two cases. Am J Clin Pathol 103:90–97
26. Horiguchi H, Matsui-Horiguchi M, Sakata H, Ichinose M, Yamamoto T, Fujiwara M, Ohse H (2004) Inflammatory pseudotumor-like follicular dendritic cell tumor of the spleen. Pathol Int 54:124–131
27. Katano H, Kaneko K, Shimizu S, Saito T, Irie T, Mori S (1997) Follicular dendritic cell sarcoma complicated by hyaline-vascular type Castleman's disease in a schizophrenic patient. Pathol Int 47:703–706
28. Lee IJ, Kim SC, Kim HS, Bang D, Yang WI, Jung WH, Chi HS (1999) Paraneoplastic pemphigus associated with follicular dendritic cell sarcoma arising from Castleman's tumor. J Am Acad Dermatol 40:294–297
29. Lin O, Frizzera G (1997) Angiomyoid and follicular dendritic cell proliferative lesions in Castleman's disease of hyaline-vascular type: a study of 10 cases. Am J Surg Pathol 21:1295–1306
30. Monda L, Warnke R, Rosai J (1986) A primary lymph node malignancy with features suggestive of dendritic reticulum cell differentiation. A report of 4 cases. Am J Pathol 122:562–572
31. Nayler SJ, Verhaart MJ, Cooper K (1996) Follicular dendritic cell tumour of the tonsil. Histopathology 28:89–92
32. Nonaka D, Birbe R, Rosai J (2005) So-called inflammatory myofibroblastic tumour: a proliferative lesion of fibroblastic reticulum cells? Histopathology 46:604–613
33. O'Malley D (2004) Diagnosis: follicular dendritic cell tumor mimicking GI stromal tumor. http://socforheme.org/case-nov-04.htm
34. Perez-Ordonez B, Erlandson RA, Rosai J (1996) Follicular dendritic cell tumor: report of 13 additional cases of a distinctive entity. Am J Surg Pathol 20:944–955
35. Perez-Ordonez B, Rosai J (1998) Follicular dendritic cell tumor: review of the entity. Semin Diagn Pathol 15:144–154
36. Ruco LP, Gearing AJ, Pigott R, Pomponi D, Burgio VL, Cafolla A, Baiocchini A, Baroni CD (1991) Expression of ICAM-1, VCAM-1 and ELAM-1 in angiofollicular lymph node hyperplasia (Castleman's disease): evidence for dysplasia of follicular dendritic reticulum cells. Histopathology 19:523–528
37. Satoh K, Hibi G, Yamamoto Y, Urano M, Kuroda M, Nakamura S (2003) Follicular dendritic cell tumor in the oro-pharyngeal region: report of a case and a review of the literature. Oral Oncol 39:415–419
38. Schwarz RE, Chu P, Arber DA (1999) Extranodal follicular dendritic cell tumor of the abdominal wall. J Clin Oncol 17:2290–2292
39. Selves J, Meggetto F, Brousset P, Voigt JJ, Pradere B, Grasset D, Icart J, Mariame B, Knecht H, Delsol G (1996) Inflammatory pseudotumor of the liver. Evidence for follicular dendritic reticulum cell proliferation associated with clonal Epstein–Barr virus. Am J Surg Pathol 20:747–753
40. Shah RN, Ozden O, Yeldandi A, Peterson L, Rao S, Laskin WB (2001) Follicular dendritic cell tumor presenting in the lung: a case report. Hum Pathol 32:745–749
41. Shek TW, Ho FC, Ng IO, Chan AC, Ma L, Srivastava G (1996) Follicular dendritic cell tumor of the liver. Evidence for an Epstein–Barr virus-related clonal proliferation of follicular dendritic cells. Am J Surg Pathol 20:313–324
42. Shek TW, Liu CL, Peh WC, Fan ST, Ng IO (1998) Intra-abdominal follicular dendritic cell tumour: a rare tumour in need of recognition. Histopathology 33:465–470
43. Torres U, Hawkins WG, Antonescu CR, DeMatteo RP (2005) Hepatic follicular dendritic cell sarcoma without Epstein–Barr virus expression. Arch Pathol Lab Med 129:1480–1483
44. Van Nierop K, de Groot C (2002) Human follicular dendritic cells: function, origin and development. Semin Immunol 14:251–257
45. Vargas H, Mouzakes J, Purdy SS, Cohn AS, Parnes SM (2002) Follicular dendritic cell tumor: an aggressive head and neck tumor. Am J Otolaryngol 23:93–98
46. Wu J, Qin D, Burton GF, Szakal AK, Tew JG (1996) Follicular dendritic cell-derived antigen and accessory activity in initiation of memory IgG responses in vitro. J Immunol 157:3404–3411

Virchows Arch (2006) 449: 159–163
DOI 10.1007/s00428-006-0208-3

ORIGINAL ARTICLE

Stephan Ihrler · Andrea Sendelhofert · Christoph Weiler · Hjalmar Hagedorn · John D. Harrison

Preinvasive intraductal neoplasia in salivary adenocarcinoma, not otherwise specified

Received: 22 December 2005 / Accepted: 27 March 2006 / Published online: 4 May 2006
© Springer-Verlag 2006

Abstract Preinvasive intraductal neoplasia of the salivary glands has only been identified in the rare salivary-duct carcinoma, whereas, it is an established feature of carcinomas of other glands. A fortuitous observation of what appeared to be intraductal tumor in a salivary adenocarcinoma, not otherwise specified, led to the present investigation to determine whether intraductal neoplasia is a significant feature of this carcinoma. Intraductal tumor confined by normal CK14-positive, actin-negative ductal basal cells was identified in 15 of 22 cases (68%). The degree of cellular atypia and the pattern of growth of intraductal tumor was similar to that of the invasive tumor. Cases with intraductal tumor devoid of invasive tumor were not found. Intraductal tumor is identified as the preinvasive precursor of adenocarcinoma, not otherwise specified, and apparently develops in excretory ducts. The findings support the possibility that different salivary tumors arise from different types of parenchymal cell. Possibly intraductal neoplasia is a universal feature of many types of salivary tumor, but has been overlooked because of the need to use immunohistology to demonstrate it and because it may no longer be present as such when the tumor presents as a clinical lesion.

S. Ihrler (✉) · A. Sendelhofert · C. Weiler
Institute of Pathology, Ludwig Maximilian University,
Thalkirchnerstraße 36,
80337 Munich, Germany
e-mail: Stephan.Ihrler@med.uni-muenchen.de
Tel.: +49-89-51604011
Fax: +49-89-51604043

H. Hagedorn
Department of ENT, Head and Neck Surgery,
Ludwig Maximilian University,
Munich, Germany

J. D. Harrison
Department of Oral Pathology, King's College London Dental Institute at Guy's, King's College and St. Thomas' Hospitals,
London, England, UK

Keywords Salivary gland · Carcinogenesis · Immunohistochemistry

Introduction

Intraductal neoplasia has been identified as a precursor, preinvasive state of different types of invasive adenocarcinoma in many glands, such as the mammary gland, prostate, and pancreas [4, 5, 15, 18]. However, an intraductal component of adenocarcinomas of salivary glands has only been described in salivary duct carcinoma, which is rare [6–9, 20]. A fortuitous observation of what appeared to be intraductal tumor in a salivary adenocarcinoma, not otherwise specified, which is the second most common malignant tumor of the salivary glands [1, 17], led to the present investigation to determine whether preinvasive intraductal neoplasia is a significant feature of this tumor. Immunohistochemistry has been found to be of great value in identifying the cellular components of salivary glands in health and disease [8, 13, 14], and was, therefore, applied in the present investigation.

Materials and methods

Patients and tumor specimens

Surgical specimens from 22 cases of adenocarcinoma, not otherwise specified, were retrieved from the files from 1990 to 2004 of the Institute of Pathology, Ludwig Maximilian University, Munich. There were 15 males and seven females; the ages ranged from 39 to 80 years with an average of 63.5 years; and 18 tumors were located in the parotid and four in submandibular glands (Table 1). Sixteen of the 22 cases were part of an investigation into the value of different histochemical markers on the differential diagnosis of adenocarcinoma, not otherwise specified, and acinic cell carcinoma of salivary glands [12].

The diagnosis of adenocarcinoma, not otherwise specified, was established according to the accepted structural

Table 1 Clinical and morphological features of salivary adenocarcinoma, not otherwise specified, with special reference to invasive and intraductal components

Case	Sex, age	Gland	pTN	Invasive tumor			Intraductal tumor					
				Histol. grade [a]	Pattern of growth	Proliferation (%)	Area (in %)	Histol. grade[b]	Pattern of growth	Proliferation (%)	Necrosis	Extension[c] (mm)
1	F64	P	pT2Nx	3	Sol	32.1	15	3	Sol	19.2	+	–
2	M50	P	pT2N2b	3	Sol	18.1	20	3	Sol	21.5	+	–
3	M60	S	pT2N0	3	Sol	25.4	10	3	Sol	27.0	+	–
4	M59	P	pT2N2b	3	Sol	29.3	5	3	Sol	15.6	+	1
5	M60	P	pT1N2b	2	Tub	8.0	–[d]					
6	M80	P	pT2N2b	3	Sol	11.7	5	2	Crib	9.8	–	–
7	F59	P	pT2N2b	2	Crib	11.9	25	2	Crib	23.3	+	–
8	F70	P	pT3N2b	3	Crib	4.4	–[d]					
9	M67	S	pT3N1	3	Sol	41.0	–[d]					
10	M64	P	pT1Nx	3	Sol	12.7	30	3	Sol	14.7	+	–
11	M52	P	pT1N2b	3	Sol	NE	–[d]					
12	F66	P	pT1N2b	3	Sol	13.3	–[d]					
13	F39	P	pT1N0	3	Sol	7.5	–[d]					
14	F66	P	pT4N1	3	Sol	38.9	10	3	Sol	28.6	+	4
15	M70	P	pT1Nx	3	Sol	18.7	40	3	Crib	29.9	+	3
16	M62	S	pT3N2b	3	Sol	15.3	2	3	Sol	-[e]	–	–
17	F78	P	pT1N0	2	Crib	18.2	5	2	Crib	12.2	–	5
18	M72	P	pT3N3	3	Sol	45.4	2	3	Crib	15.2	+	–
19	M63	S	pT3N2b	3	Sol	28.8	25	3	Sol	13.7	+	5
20	M64	P	pT4N0	3	Sol	32.0	2	2	Crib	-[e]	–	–
21	M69	P	pT4N2b	3	Sol	37.4	–[d]					
22	M62	P	pT2Nx	2	Crib	6.7	2	2	Crib	-[e]	–	–

M male, *F* female, *P* parotid, *S* submandibular gland, *Sol* solid, *Tub* tubular, *Crib* cribriform, *NE* not evaluable
[a]Histological grading of invasive tumor according to Auclair et al. [1];
[b]Histological grading of intraductal tumor according to Tavassoli et al. [18]
[c]Extension of intraductal tumor beyond area of invasive tumor (in mm)
[d]No intraductal tumor found;
[e]Intraductal tumor component too small for accurate calculation of proliferation

and cytological criteria, which exclude more specifically characterized types of salivary adenocarcinoma [1–3, 10, 17, 20]. Clinical and histologic data were analyzed to exclude cases representing metastatic disease to the salivary glands or to intraparotid lymph nodes. On the basis of the TNM system [16] of 2002, seven cases were pT1, seven were pT2, five were pT3, and three were pT4; 14 cases had metastases to the lymph nodes (pN1,2,3) and four cases had no such metastases (pN0); and in four cases a neck dissection had not been performed (Table 1).

Histology and immunohistochemistry

The specimens had been fixed in 4% buffered formaldehyde and embedded in paraffin wax, and serial sections were cut at 4 μm. Modifications of the avidin–biotin complex method (ABC), the labeled streptavidin–biotin staining method (LSAB), and the alkaline-phosphatase anti-alkaline-phosphatase method (APAAP) were used. In accordance with previous studies of our group on the cellular composition of normal glands and glands with different reactive and neoplastic lesions [13, 14], antibodies for p63, α-actin and cytokeratin (CK) subtypes 7, 18, 14, and K_s8.12, and the proliferation-associated antibody Ki67 (MIB-1) were applied. Quantification of proliferation of the different cellular components was enabled by immunohistochemical double-staining for CK14 and Ki67 [13, 14]. Owing to the high level of endogenous biotin, especially in striated and excretory ductal cells, an avidin–biotin blocking system (DAKO Biotin Blocking System X0590) was added to the ABC and LSAB methods. Non-neoplastic salivary parenchyma served as a positive internal control.

Analysis

A combination of topographical, cytological, and immunohistological criteria was used to identify the different types of normal cell and the neoplastic cells in the salivary glands [12–14]. Acinar cells were identified by positivity for CK18, intercalated ductal cells and columnar cells of striated and excretory ducts by positivity for CK7 and CK18, myoepithelial cells by positivity for α-actin, CK14,

and p63, and basal cells by positivity for CK14, CK K_s8.12 and p63 (Fig. 2).

Analogous to tumor models of other glands [4, 5, 15, 18], intraductal tumor was defined as an intraductal expansion of cells with a variable degree of structural and cellular atypia and increased cellular proliferation that is confined by a continuous layer of regular basal or myoepithelial cells that are devoid of atypia. Owing to an absence of established criteria in salivary tumors, the WHO guidelines for histological grading of intraductal neoplasia in mammary glands were applied [18].

The cases were analyzed with respect to the following criteria: 1) area of intraductal tumor in comparison to the total invasive and intraductal area of tumor; 2) separate histological gradings of 1, low; 2, intermediate; and 3, high for intraductal tumor [18] and invasive tumor [1]; 3) identification of the predominant pattern of growth in intraductal tumor [18] and in invasive tumor [1] (solid, cribriform, or tubular); 4) separate quantifications of cellular proliferation for intraductal and invasive tumors; 5) presence of comedo-type necrosis and associated calcification in intraductal tumor; 6) extension of intraductal tumor beyond the area of invasive tumor; 7) localization of intraductal tumor in relation to the different parts of the salivary parenchyma.

Results

The presence of intraductal tumor could not be established in sections stained with hematoxylin and eosin in most cases; immunohistological staining, particularly with CK14, was necessary to identify and quantify the intraductal tumor within the quantitatively dominating invasive tumor (Fig. 1a1, 2). The intraductal tumors were mainly found in excretory ducts with normal basal cells that were positive for CK14, CK K_s8.12, and p63 and negative for α-actin (Figs. 1a1,b2,c1, 2). Both intraductal and invasive tumors were positive for CK7 and 18.

Details of the intraductal and invasive tumors are shown in Table 1. Intraductal tumors were found in 15 of the 22 cases (68%). The amount of intraductal tumor in relation to

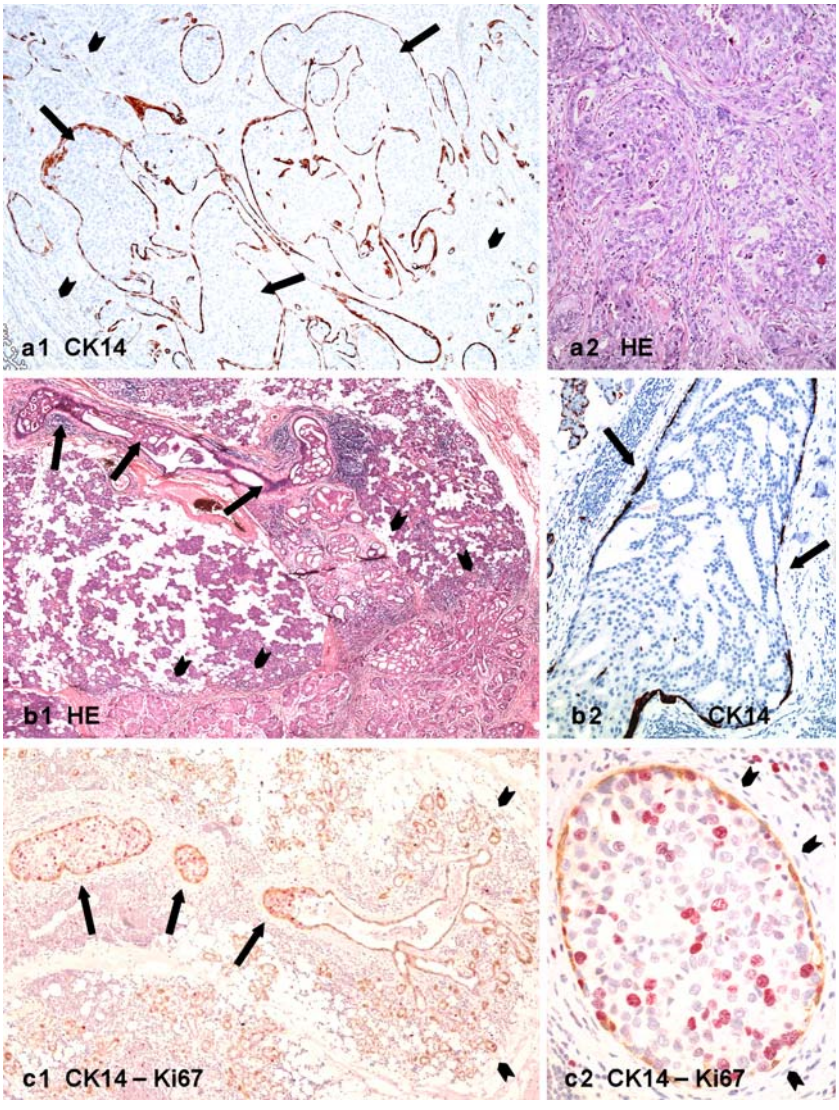

Fig. 1 Representative examples of intraductal neoplasia in adenocarcinoma, not otherwise specified. **a**1 Case 2 with a large component of intraductal tumour confined by CK14 positive basal cells (*arrows*) within invasive tumour (*arrowheads*). **a**2 Higher magnification of an adjacent section stained by haematoxylin and eosin shows the solid pattern and high degree of atypia, but the intraductal localization of tumour shown in **a**1 is not obvious. **b**1 Case 17 with a predominantly cribriform pattern both in invasive tumour (*bottom*: *arrowheads*) and in intraductal tumour in an excretory duct (*top*: *arrows*) that extends 5 mm beyond the invasive tumour, the junction of which was established in an adjacent section stained for CK14. **b**2 Higher magnification shows the cribriform pattern and intermediate grade atypia of the intraductal tumour that is confined by normal CK14 positive basal cells (*arrows*). **c**1 Case 14 with intraductal tumour in an excretory duct (*arrows*) with secondary ductal dilatation and surrounding acinar atrophy and chronic inflammation (*arrowheads*). **c**2 Higher magnification of CK14 Ki67 double staining shows solid intraductal tumour with high grade atypia and enhanced proliferation that is confined by normal CK14 stained basal cells without cellular atypia or enhanced proliferation (*arrowheads*)

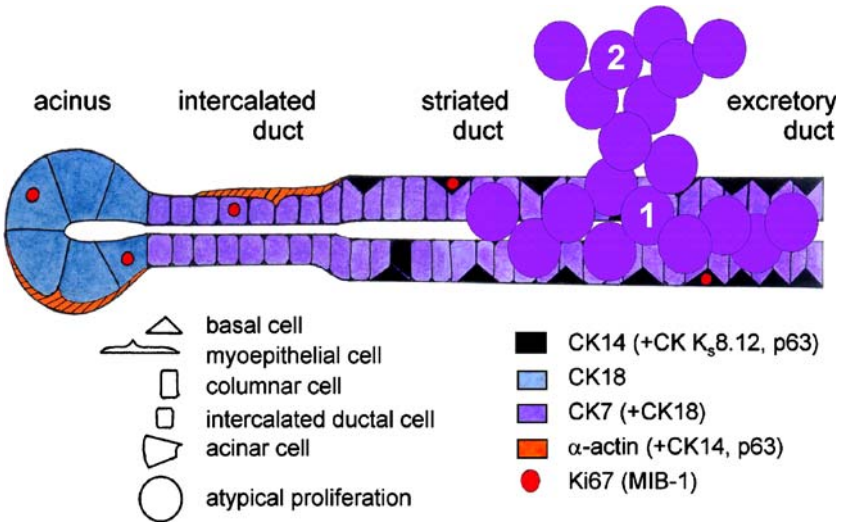

Fig. 2 Schematic illustration of the proposed development of adenocarcinoma, not otherwise specified, (2) from preinvasive intraductal neoplasia (1)

the total area of tumor ranged from 2 to 40%, with an average of 13%. An extension of the intraductal tumor beyond the borders of the invasive tumor was found in five cases, with a maximum of 5 mm (Fig. 1b1,c1). There was no case of intraductal tumor without an invasive tumor. There were eight cases of solid intraductal tumor, which were all grade 3 with comedo-type necrosis in seven, and seven cases of cribriform intraductal tumor, two of which were grade 3 with comedo-type necrosis and five were grade 2 with comedo-type necrosis in one (Fig. 1b2,c2). Microcalcification was found in comedo-type necrosis in one case. Solid intraductal tumor was always associated with solid invasive tumor (Figs. 1a1, 2) and cribriform intraductal tumor was associated with solid invasive tumor in four cases and with cribriform invasive tumor in three cases (Figs. 1b1, 2). Grade 3 intraductal tumor was associated with grade 3 invasive tumor in all ten cases (Fig. 1a1, 2); and grade 2 intraductal tumor was associated with grade 3 invasive tumor in two cases and with grade 2 invasive tumor in three cases (Fig. 1b1, 2). The mean proliferation rate of intraductal tumors (Fig. 1c2) was 19.2%, with a minimum of 9.8% and a maximum of 29.9%, and was slightly lower than the 22.8% of invasive tumors.

Discussion

That immunohistological staining, especially for CK14, was usually necessary to demonstrate intraductal tumor and that it was demonstrated in 68% of all cases and occupied from 2 to 40% of the total tumor area indicates that it is probably present much more often than is realized in routinely prepared sections of adenocarcinoma, not otherwise specified. That cases with exclusively intraductal tumor were not found indicates that intraductal tumor of the salivary gland is symptomless. Unlike the situation in the breast, where intraductal tumor is detected radiologically in many cases owing to associated calcification in comedo-type necrosis [4, 18], there is a lack of calcification in the salivary adenocarcinoma, which possibly relates to a low level of calcium, as has been found in ductal cells of salivary glands and in pleomorphic adenoma [11].

The term intraductal neoplasia covers a group of atypical intraductal proliferations associated with an increased risk of development of invasive carcinoma. The intraductal neoplasia described in the present investigation is analogous to what is well-established in other glands, such as the mammary glands, pancreas, and prostate [4, 5, 15, 18, 19]. It appears to be a precursor, preinvasive state that develops in the ductal system, apparently in excretory ducts in adenocarcinoma, not otherwise specified (Fig. 2). The different cribriform and solid patterns of growth of this intraductal neoplasia correspond to the patterns of growth of the invasive carcinoma and also correspond to the patterns of growth of intraductal neoplasia of the mammary gland [18]. However, although the predominance of high-grade atypia in this salivary intraductal neoplasia corresponds to the usually high histological grade of invasive salivary adenocarcinoma, not otherwise specified, it contrasts to the coexistence of low-grade and high-grade variants of intraductal neoplasia of the mammary gland [18].

The only other salivary carcinoma in which intraductal neoplasia has been described is the salivary duct carcinoma, and this is mainly in the recently described rare variant with low-grade histology, which is termed ‘low-grade cribriform cystadenocarcinoma’ in the new WHO classification [2, 6–9, 20]. However, the intraductal neoplasm of salivary duct carcinoma has been reported to be confined by myoepithelial cells, which indicates a development from intercalated ducts, which normally contain myoepithelial cells [6, 7, 9, 20]. Whereas, the intraductal neoplasm of adenocarcinoma, not otherwise specified, described in the present investigation, is confined by normal basal cells in excretory ducts, which indicates a development from excretory ducts and, possibly, the basal cells that have been found capable of proliferation [13, 14, Fig. 2]. This difference is compatible with the possibility that different salivary tumors arise from different types of parenchymal cell rather than from a putative population of stem cells, as

all the different types of parenchymal cell are capable of proliferation [13, 14].

The demonstration of an intraductal component may help to distinguish between primary and metastatic adenocarcinoma, which is a diagnostic problem more often encountered in the parotid, owing to relatively frequent metastases to intraparotid lymph nodes, as it is unlikely that a metastatic tumor would invade the parenchyma and extend into the ducts with the maintenance of the surrounding basal cells. The demonstration of extension of intraductal tumor up to 5 mm beyond the invasive tumor indicates how resection of a salivary adenocarcinoma could be incomplete and be followed by recurrence originating from persistent intraductal tumor, as can occur with mammary carcinoma [18].

Preinvasive intraductal neoplasia possibly occurs in many other types of salivary tumor, but has been overlooked because of the difficulty in establishing its presence in routinely stained sections and because continuing expansion of the invasive tumor destroys ducts so that intraductal tumor is no longer present as such. Thus, the application of the techniques used in the present investigation to other salivary tumors is necessary to investigate the possibility that intraductal neoplasia occurs in other types of salivary tumor.

Acknowledgement This study was supported by a grant from the Friedrich-Baur-Stiftung, Munich, Germany (Grant no. 0016/2003).

References

1. Auclair PL, Ellis GL (1991) Adenocarcinoma, not otherwise specified. In: Ellis GL, Auclair PL, Gnepp DR (eds) Surgical pathology of the salivary glands. WB Saunders, Philadelphia, pp 318–332
2. Auclair PL, van der Wal JE (2005) Adenocarcinoma, not otherwise specified. In: Barnes L, Eveson JW, Reichart P, Sidransky D (eds) World Health Organization classification of tumours. Pathology and genetics of head and neck tumours. IARC, Lyon, pp 238–239
3. Batsakis JG, El-Naggar AK, Luna MA (1992) "Adenocarcinoma, not otherwise specified": a diminishing group of salivary carcinomas. Ann Otol Rhinol Laryngol 101:108–110
4. Böcker W, Bier B, Freytag G (1992) An immunohistochemical study of the breast using antibodies to basal and luminal keratins, alpha-smooth muscle actin, vimentin, collagen IV and laminin. Part II. Epitheliosis and ductal carcinoma in situ. Virchows Arch A Pathol Anat Histopathol 421:323–330
5. Bonkhoff H, Remberger K (1998) Morphogenetic concepts of normal and abnormal growth in the human prostate. Virchows Arch 433:195–202
6. Brandwein-Gensler M, Hille J, Wang BY, Urken M, Gordon R, Wang LJ, Simpson JRM, Simpson RHW, Gnepp DR (2004) Low-grade salivary duct carcinoma. Description of 16 cases. Am J Surg Pathol 28:1040–1044
7. Cheuk W, Miliauskas JR, Chan KC (2004) Intraductal carcinoma of the oral cavity. A case report and a reappraisal of the concept of pure ductal carcinoma in situ in salivary duct carcinoma. Am J Surg Pathol 28:266–270
8. De Araujo VC, Loducca SVL, Sobral APV, Kowalski LP, Soares F, de Araujo NS (2002) Salivary duct carcinoma: cytokeratin 14 as a marker of in-situ intraductal growth. Histopathology 41:244–249
9. Delgado R, Klimstra D, Albores-Saavedra J (1996) Low-grade salivary duct carcinoma—a distinctive variant with a low grade histology and a predominant intraductal growth pattern. Cancer 78:958–967
10. Ellis GL, Auclair PL (1996) Adenocarcinoma, not otherwise specified. In: Ellis GL, Auclair PL (eds) Atlas of tumor pathology. Tumors of the salivary glands. Armed Forces Institute of Pathology, Washington, District of Columbia, pp 175–183
11. Harrison JD, Triantafyllou A, Baldwin D, Schäfer H (1993) Histochemical and biochemical determination of calcium in pleomorphic adenoma. Virchows Arch B Cell Pathol 64:123–125
12. Ihrler S, Blasenbreu-Vogt S, Sendelhofert A, Lang S, Zietz C, Löhrs U (2002) Differential diagnosis of salivary acinic cell carcinoma and adenocarcinoma (NOS). A comparison of (immuno-) histochemical markers. Pathol Res Pract 198:777–783
13. Ihrler S, Zietz C, Sendelhofert A, Sendelhofert A, Lang S, Blasenbreu-Vogt S, Löhrs U (2002) A morphogenetic concept of salivary duct regeneration and metaplasia. Virchows Arch 440:519–526
14. Ihrler S, Blasenbreu-Vogt S, Sendelhofert A, Rössle M, Harrison JD, Löhrs U (2004) Regeneration in chronic sialadenitis: an analysis of proliferation and apoptosis based on double immunohistochemical labelling. Virchows Arch 444:356–361
15. Klöppel G, Hruban RH, Longnecker DS, Adler G, Kern SE, Partanen TJ (2000) Ductal adenocarcinoma of the pancreas. In: Hamilton SR, Aaltonen LA (eds) World Health Organization classification of tumours. Pathology and genetics of tumours of the digestive system. IARC, Lyon, pp 221–228
16. Sobin LH, Wittekind C (2002) Salivary glands. In: Sobin LH, Wittekind C (eds) TNM Classification of malignant tumours—International Union Against Cancer. 6th edn. Wiley, New York, pp 52–56
17. Spiro RH, Huvos AG, Strong EW (1982) Adenocarcinoma of salivary origin. Clinicopathologic study of 204 patients. Am J Surg 144:423–431
18. Tavassoli FA, Hoefler H, Rosai J (2003) Intraductal proliferative lesions. In: Tavassoli FA, Devilee P (eds) World Health Organization classification of tumours. Pathology and genetics of tumours of the breast and female genital organs. IARC, Lyon, pp 63–72
19. Wick MR, Ockner DM, Mills SE, Ritter JH, Swanson PE (1998) Homologous carcinomas of the breast, skin, and salivary glands. A histologic and immunohistochemical comparison of ductal mammary carcinoma, ductal sweat gland carcinoma, and salivary duct carcinoma. Am J Clin Pathol 109:75–84
20. Zarbo RJ (2002) Salivary gland neoplasia: a review for the practicing pathologist. Mod Path 15:298–323

Virchows Arch (2006) 449:164–170
DOI 10.1007/s00428-006-0239-9

ORIGINAL ARTICLE

Survivin expression in pre-invasive lesions and non-small cell lung carcinoma

Nalan Akyürek · Leyla Memiş · Özgür Ekinci · Nurdan Köktürk · Can Öztürk

Received: 1 April 2006 / Accepted: 17 May 2006 / Published online: 30 June 2006
© Springer-Verlag 2006

Abstract Survivin is an inhibitor of apoptosis protein, which is overexpressed in many carcinomas, including lung carcinoma. The aim of this immunohistochemical study was to investigate the role of survivin in the early steps of lung carcinogenesis and non-small cell lung carcinomas (NSCLC), and its relationship with expression of p53 protein, a tumor suppressor gene involved in cell cycle control. In the normal bronchial epithelium, low-grade atypical adenomatous hyperplasia (AAH) and non-neoplastic lung parenchyma adjacent to tumor, survivin was found completely negative. Expression of survivin was detected in the areas of squamous metaplasia and dysplasia as well as high-grade AAH lesions adjacent to tumor. Survivin was expressed in 50 (64%) and p53 in 41 (53%) NSCLC. Survivin expression was significantly correlated with lymph node metastasis (p=0.02). There was no correlation between survivin and p53 expression. The patients with expression of survivin had significantly worse prognosis (Log-rank test, p=0.003). Multivariate Cox regression analysis showed TNM stage (p<0.001) and survivin expression (p=0.003) as independent prognostic indicators. In conclusion, survivin expression might be an early step in lung carcinogenesis. Survivin expression might also be used as a prognostic indicator predicting the worse outcome in NSCLC, and might be a novel target for the treatment of patients with preinvasive lesions of lung and NSCLC.

N. Akyürek (✉) · L. Memiş · Ö. Ekinci
Department of Pathology, Gazi University Medical School,
Besevler, 06500 Ankara, Turkey
e-mail: akyurek@gazi.edu.tr

N. Köktürk · C. Öztürk
Department of Pulmonary Medicine,
Gazi University Medical School,
Ankara, Turkey

Keywords Survivin · Preinvasive lesions · Non-small cell lung carcinoma · Prognosis · Immunohistochemistry

Introduction

Lung cancer is the most common cause of cancer death in majority of the countries. Prediction of prognosis is quite difficult, predominantly due to marked clinical heterogeneity among the patients, even into the same stage [4]. Lung carcinogenesis is a multistep process, in most cases driven by genetic, epigenetic, and molecular abnormalities involving oncogenes, tumor suppressor genes, proliferation factors and apoptosis [26]. Preneoplastic cells also contain several molecular genetic and epigenetic abnormalities identical to some of those found in overt lung cancer cells [3, 11].

Abnormal inhibition of apoptosis during homeostasis is thought to be a critical step for lung carcinogenesis. Survivin is the well-known member of the inhibitor of the apoptosis protein (IAP) family and is a bifunctional protein that suppresses apoptosis and regulates cell division [2]. Survivin directly inhibits caspase-3 and caspase-7 activity, thus preventing apoptosis. Survivin is cell-cycle-regulated and is expressed in the G2/M phase of the cell cycle. Its interaction with the mitotic spindle tubules leads to an increase in caspase-3 activity and accelerated apoptotic cell death. Overexpression of survivin has oncogenic potential because it may overcome the G2/M phase checkpoint to enforce progression of cells through mitosis, favoring the development of neoplastic clones [1].

In contrast to other IAPs, survivin is abundantly expressed in fetal tissues, but undetectable in most of normal adult tissues [2]. Most importantly, survivin is upregulated in most human cancers, including lung, breast, colon, stomach, esophagus, pancreas, bladder, uterus, ovary, liver carcinomas,

neuroblastoma, glioma, melanoma, soft tissue sarcoma, leukemias, and high-grade non-Hodgkin lymphoma [1, 2, 27].

Several studies indicated that survivin expression is present in precancerous lesions and in very early stages of cancer in the uterine cervix [6], colon [13], skin [7], and oral mucosa [17]. New biological markers are needed to define the stepwise process of lung cancer development, to function as a diagnostic marker, and to provide new specific treatment options for preinvasive lesions of the lung. Although expression of survivin has been reported for atypical adenomatous hyperplasia (AAH) in the lung [23], the biologic role of survivin in preinvasive lesions, including squamous dysplasia and AAH, and non-small cell lung carcinomas (NSCLC), is still controversial.

Currently, expression of survivin protein is being used as a novel prognostic factor in several human neoplasms. High survivin expression in tumors correlates with more aggressive behavior and poorer prognosis [27]. Defects in apoptotic mechanisms also play an important role in resistance to chemotherapy and radiation. Therefore, there is great interest in survivin as a diagnostic marker and potential drug target because of its predominantly tumor-specific expression in adult tissues [1, 22, 27].

Several studies have demonstrated that transcription of survivin expression is suppressed by p53, another cell cycle checkpoint regulating protein that induces apoptosis. Thus, loss of p53 might result in derepression of survivin expression [8, 19, 24].

In this study, to detect the time of appearance of survivin in early neoplastic processes of lung cancer, we investigated the expression of survivin normal lung tissue, preinvasive lesions, and NSCLC and sought to determine its association with clinicopathological parameters and its impact on prognosis. The relevance of p53 regulation on survivin expression was also evaluated in NSCLC.

Materials and methods

Patients

Seventy-eight patients with NSCLC, who consecutively underwent surgical resection or biopsy between 1994 and 2001, were investigated retrospectively in this study. There were 72 men and six women, ranging in age from 39 to 78 years (mean±SD, 60.8±9.9 years, median 63 years). All patients underwent surgery (27 patients) or biopsy (51 patients) without preoperative treatment. Histological classifications of the tumors were determined according to the World Health Organization (WHO) criteria [30] and included 58 squamous cell carcinomas, 16 adenocarcinomas, and four large cell carcinomas. Tumor staging was performed according to International System for Staging Lung Cancer [21]. The patient population composed of two patients with clinical or pathological stage I, four patients with stage II, 43 patients with stage III, and 29 patients with stage IV. Median follow-up time was 18 months (range 1–80 months). During follow-up, 45 patients died of lung cancer.

In addition, we included 46 bronchial biopsy samples, which contained areas of normal bronchial epithelia in ten samples, squamous metaplasia in eight samples, low-grade dysplasia in ten, and high-grade dysplasia in 18 samples that were taken from healthy smokers. Specimens of 11 low-grade atypical adenomatous lesions (AAH) of the lung were obtained from ten patients. Additionally, specimens of high-grade AAH lesions adjacent to bronchioloalveolar carcinoma in eight patients were included. Preinvasive lesions were classified according to the WHO classification criteria [30] by the two experienced pathologists (L.M. and N.A.). Moderate dysplasia and severe dysplasia were considered as high-grade squamous dysplasia [11]. The grade of AAH was defined according to increased cellularity and cytological atypia [30].

Immunohistochemistry

Formalin-fixed, paraffin-embedded-tumor-tissue sample sections were cut into 4-μm thick sections. Then the slides were deparaffinized in xylene, rehydrated in alcohol, and blocked for endogenous peroxidase using 3% H_2O_2. Antigen retrieval was performed using 0.01 M sodium citrate buffer (pH 6.0) through microwave processing, and then tissue sections processed with standard streptavidin–biotin–immunoperoxidase method. The sections were incubated with rabbit polyclonal antibody survivin (diluted 1:100; NeoMarkers, Freemont, CA, USA) and mouse monoclonal prediluted antibody p53 (DO-7, NeoMarkers) 2 h at room temperature. We used 3-amino-9-ethylcarbazole substrate (AEC, LabVision, NeoMarkers) as the chromogen and Mayer's hematoxylin as the counterstain. Staining without antibody was performed as a negative control procedure. Sections of normal gastric mucosa for survivin and colon carcinoma for p53 were used as positive control.

Immunohistochemical staining was evaluated semiquantitatively by two pathologists (N.A. and O.E.) according to the percentage of cells demonstrating cytoplasmic or nuclear staining. Survivin staining was generally cytoplasmic, and nuclear staining was found in only one case. For statistical purposes, as 10% cutoff was used for survivin expression. Nuclear staining in more than 10% of tumor cells was considered positive for p53 expression.

Statistical analysis

Fisher's exact test and Mann–Whitney *U* test were used to evaluate the correlation of survivin expression with clini-

copathological parameters. The Spearman rank correlation coefficient was applied to evaluate the strength of association between survivin and p53. A univariate survival analysis was performed according to Kaplan–Meier method. The statistical significance of differences of survival among the groups was evaluated by the log-rank test. The variables included in the multivariate Cox regression analysis were gender, age, histological types, stage, and survivin immunoreactivity. A value of $p<0.05$ was considered as statistically significant. SPSS software program 10.0 (SPSS, Chicago, IL, USA) was used for statistical analysis.

Results

Survivin expression in normal and pre-invasive lesions

In the samples from normal bronchial epithelium and low-grade AAH lesions from healthy smokers, and from the normal pulmonary tissue adjacent to tumour, survivin expression was found to be completely negative (Figs. 1a and 2a). Expression of survivin was observed in 25% (2/8) of squamous metaplasia samples. On the other hand, survivin expression was tended to increase from low-grade dysplasia (40%; 4/10) to high-grade dysplasia (61%; 11/18) samples ($p=0.08$). Furthermore, survivin was observed to be present in squamous metaplasia, dysplasia, and carcinoma in situ lesions adjacent to squamous cell carcinoma, and high-grade AAH lesions adjacent to bronchioloalveolar carcinoma (Fig. 1b–d and Fig. 2b).

Survivin expression in NSCLC

Survivin expression was detected in 64% (50/78) tumor specimens obtained from NSCLC (Fig. 3a and b). The relationship between survivin expression and clinicopathological parameters is shown in Table 1.

The frequency of lymph node metastasis was significantly higher in survivin positive group (68.6 vs 31.4%, $p=0.02$). However, there was no significant correlation between the survivin expression and age, gender, smoking status, histological type, tumor size, TNM stage, and distant metastasis.

p53 expression was observed in 53% (41/78) tumor specimens of the NSCLC. However, no significant correlation was noted between the expression of survivin and p53 (Spearman correlation test, $rho=0.156$, $p=0.218$).

Survivin expression and prognosis

By univariate analysis, survivin expression was observed to be significantly associated with poorer survival (log-rank test, $p=0.003$; Fig. 4). In 50 patients with survivin expression, the mean survival time was 25.1 months, whereas in 28 patients with negative expression of survivin, it was 40.7 months. There was no significant relationship between p53 expression and survival ($p=0.11$).

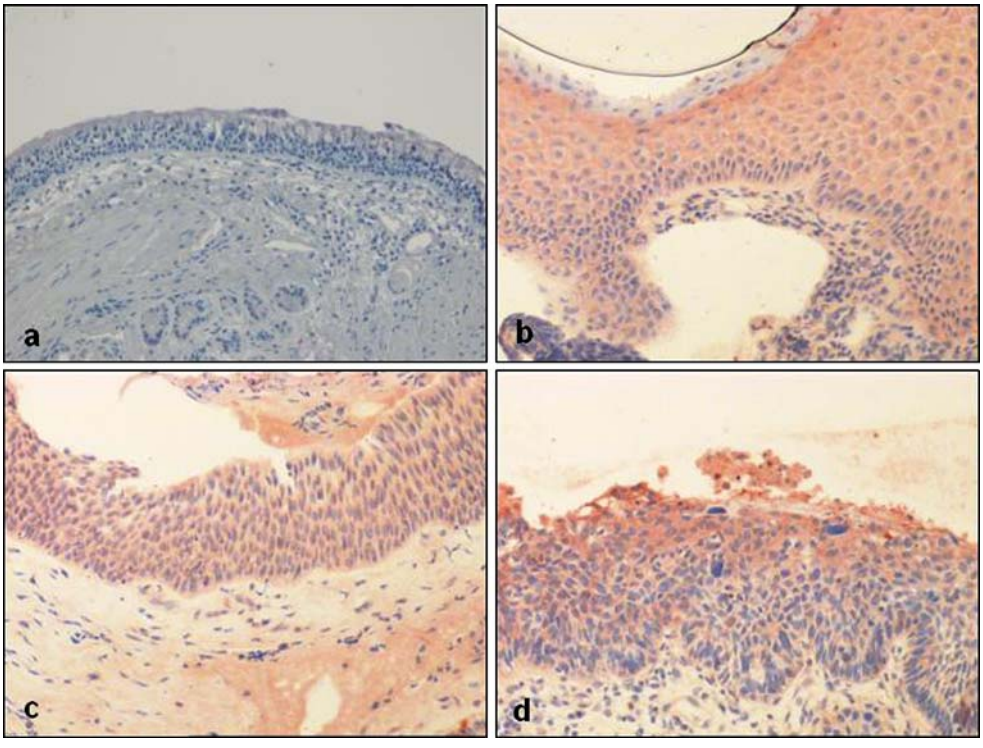

Fig. 1 **a** Negative survivin staining in normal bronchial epithelium, ×200. **b** Survivin expression in squamous metaplasia, ×400. **c** Survivin expression in low-grade dysplasia, ×400. **d** Survivin expression in high-grade dysplasia, ×400

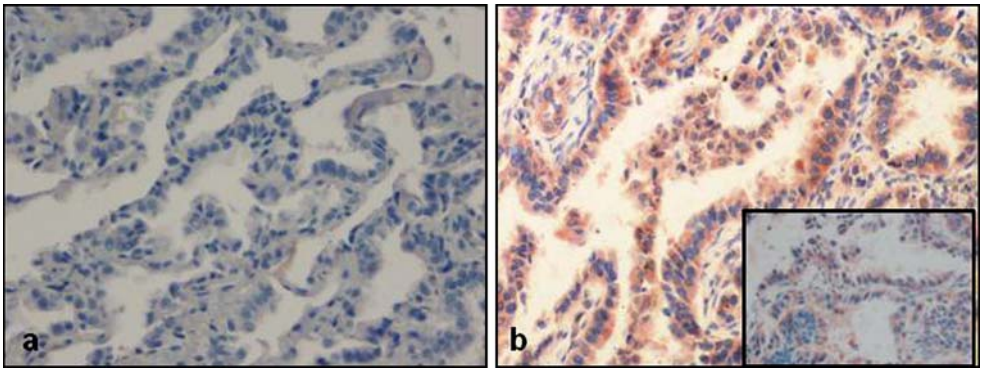

Fig. 2 **a** Negative survivin staining in low-grade AAH, ×400. **b** Survivin expression in non-mucinous bronchioloalveolar carcinoma, ×400; *inset*: survivin expression in high-grade AAH lesion adjacent to bronchioloalveolar carcinoma, ×400

On multivariate analysis, in which age, gender, histologic subtype, TNM stage, expression of survivin, and p53 were investigated, survivin was found to be an independent prognostic predictor (p=0.003), along with TNM stage (p<0.001).

Discussion

Survivin is expressed in fetal tissues, whereas it is completely downregulated in normal adult tissues [2]. Survivin is also overexpressed in the most common human carcinomas, suggesting that reactivation of the survivin gene frequently occurs in many cancers [1, 2, 27]. However, the exact timing of reexpression of survivin during carcinogenesis is still unknown. In the present study, both normal bronchial epithelium and non-neoplastic lung tissue did not express survivin. Additionally, survivin immunoreactivity was negative in all patients that had only low-grade AAH lesions without lung carcinoma, these lesions showing discontinuous lining of cells with small nuclei and minimal nuclear atypia. Therefore, low-grade AAH may not be related to bronchioloalveolar carcinoma. High-grade AAH lesions are characterized by a more continuous single-cell layer with moderate atypia, and less frequently pseudopapillae and tufts. We did expect that high levels of survivin expression in high-grade AAH lesions, which were in continuity with the margin of bronchioloalveolar adenocarcinoma, would be similar to that of adenocarcinoma. Nakanishi et al. [23] showed that the positivity of survivin significantly increased in the low-grade AAH lesions (9%) to high-grade AAH lesions (89%) to non-mucinous bronchioloalveolar carcinomas (100%). These results indicate an important role of survivin in lung carcinogenesis and provide some important clues that high-grade AAH is a precancerous lesion or early-stage lesion of non-mucinous bronchioloalveolar carcinoma.

In bronchial carcinogenesis, survivin expression has been first studied; we observed that survivin overexpression was associated with metaplastic or early neoplastic lesions. Recently, survivin expression has been found in several preneoplastic lesions, including Bowen disease, hypertrophic actinic keratosis [7], polyps of colon [13], cervical squamous intraepithelial lesions [6], and oral precancerous lesions [17]. In the colon, survivin protein expression is detected in all non-neoplastic colonic mucosa adjacent to tumor as well as hyperplastic and adenomatous polyps. During colorectal tumorigenesis, survivin protein expression is significantly and progressively increased during the transition from dysplasia to carcinoma, supporting the theory that survivin plays a crucial role in the earliest phases of the malignant transformation [13].

High levels of survivin overexpression were found at both mRNA and protein levels in NSCLC [5, 9, 10, 12, 14, 16, 18, 20, 23–25, 28, 29, 31, 32]. In the current study, we found that definite cytoplasmic expression of survivin had a

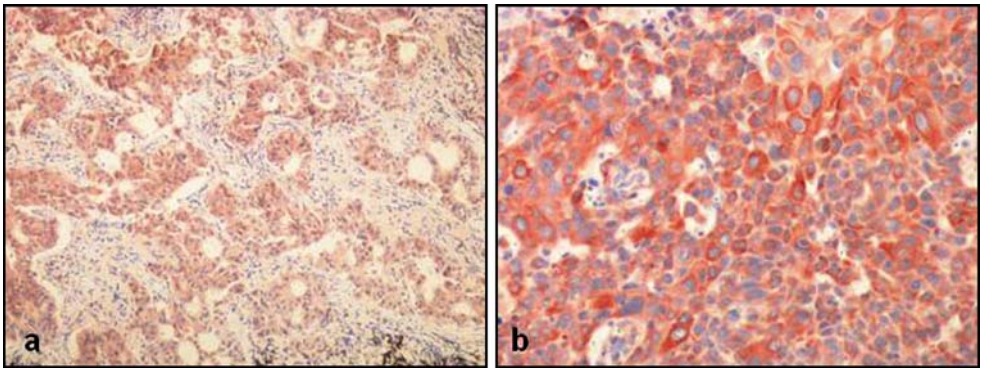

Fig. 3 **a** Survivin expression in adenocarcinoma, ×200. **b** Survivin expression in squamous cell carcinoma, ×400

Table 1 Relationship between clinicopathologic parameters and expression of survivin in NSCLC

Clinicopathologic parameters	No. of cases (%)	Expression of survivin		
		Positive (%)	Negative (%)	*p* value
Age	78	60.68±10.55	61.21±8.89	0.821
Gender				
Men	72	47 (65.3)	25 (34.7)	0.661
Women	6	3 (50)	3 (50)	
Histology				
Epidermoid carcinoma	58	38 (65.5)	20 (34.5)	0.239
Adenocarcinoma	16	11 (68.8)	5 (31.3)	
Large cell carcinoma	4	1 (25)	3 (75)	
Tumor status				
T1	3	1 (33.3)	2 (66.6)	0.628
T2	9	5 (55.6)	4 (44.4)	
T3	28	19 (67.9)	9 (32.1)	
T4	38	25 (65.8)	13 (34.2)	
Nodal status				
N0	8	2 (25)	6 (75)	0.022
N1–N3	70	48 (68.6)	22 (31.4)	
Distant metastasis				
M0	49	31 (63.3)	18 (367)	1
M1	29	19 (65.5)	10 (34.5)	
Stage				
IA–IIB	6	2 (33.3)	4 (66.7)	0.394
IIIA	21	15 (71.4)	6 (28.6)	
IIIB	22	14 (63.6)	8 (36.4)	
IV	29	19 (65.5)	10 (34.5)	
Smoking status				
Smoker	72	47 (65.3)	25 (34.7)	0.661
Non-smoker	6	3 (50)	3 (50)	
p53				
Positive	41	32 (78.8)	9 (21.2)	0.269
Negative	37	24 (65.5)	13 (34.5)	

significant association with a shorter overall survival. Previous studies have similarly shown that expression of survivin might estimate worse survival in patients with resected NSCLC [10, 12, 14, 16, 18, 20, 25, 28]. As we aimed at examining the association between survivin expression and survival, we also used endobronchial biopsies, which were taken from tumor during bronchoscopy procedure in this study. In patients with advanced stage, this information should be preferably known at the time of diagnosis to help clinicians in the treatment design.

Regarding the localization of survivin, there are reports in the literature both nuclear and cytoplasmic [5, 18, 28, 31], or only cytoplasmic immunoreactivities [10, 14, 23] in NSCLC. Two of these studies reported that nuclear survivin expression was significantly associated with poor prognosis [18, 28], whereas one study showed that nuclear survivin expression was significantly associated with favorable prognosis [31]. In addition, two of these publications indicated that cytoplasmic expression of survivin in NSCLC correlated with unfavorable prognosis [10, 14]. There is also conflicting data regarding the predictive value of nuclear staining vs cytoplasmic staining in several cancers. The distinct roles of survivin have been described depending on its subcellular, cytoplasmic, or nuclear localizations. The differential localization might reflect different functions of survivin, with respect to inhibition of apoptosis or regulation of the cell proliferation. The nuclear pool of survivin has been suggested to be mostly involved in promoting cell proliferation, while the cytoplasmic pool of survivin is thought to be involved in controlling cell survival [15, 16]. Additionally, it has been regarded that different antibodies may have different affinities for different splice variants of survivin.

Another important observation of the present study was positive correlation between survivin expression and lymph node metastasis. Wang et al. [32] also reported that survivin expression has been linked to lymph node metastasis. In the current study, no significant correlation between survivin expression and tumor size, distant metastasis, and stage was found. This finding can be explained by the fact that most of the cases in this study were in the advanced stage. The majority of publications with expression of survivin in

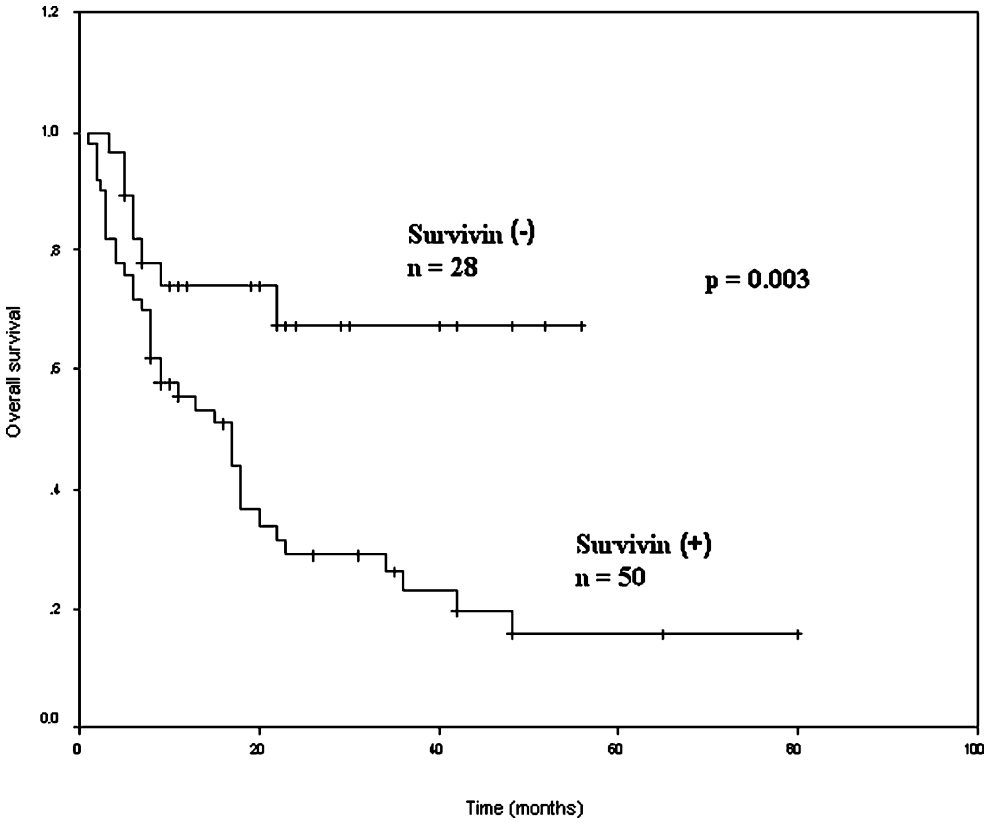

Fig. 4 Kaplan–Meier survival curves for positive (n=50) and negative (n=28) patiens of NSCLC regarding survivin expression

NSCLC were restricted to patients who were at the early stage [5, 25, 28] or advanced stages [20, 31]. Falleni et al. [5] found that survivin levels were elevated consistently in Stage I lung carcinoma samples and that cytoplasmic survivin was correlated with T status (T1 vs T2). Recently, it was shown that survivin mRNA was significantly higher in stages III–IV than stage I and II [32].

Although we did not find any correlation with histological type of tumor, several studies showed that squamous cell carcinomas had higher survivin expression than adenocarcinomas, and there was positive correlation between survivin expression and tumor differentiation [5, 14, 24, 32].

Previous studies have also shown that survivin is a gene repressed by wild-type p53 and have suggested that loss of this protein produces derepression of survivin in NSCLC [8, 19, 24]. In contrast to previous studies in NSCLC, survivin expression did not correlate with p53 immunoreactivity in this study. It could be explained by the fact that survivin derepression is not only due to mutations in the p53 gene, but also to other still unknown factors or different antibody reactions against a specific survivin epitope that was used in our study.

Our current study suggested that the cytoplasmic expression of survivin might provide additional prognostic information for NSCLC. Various studies using antisense oligonucleotides or peptide inhibitors of survivin have suggested that these proteins are important for maintaining tumor cell survival or for developing resistance to apoptosis induction by anticancer drugs [1, 22, 27]. As a result of this widespread expression in tumors and generally low-level expression in normal tissue, survivin may potentially be a valuable new target for apoptosis-based chemotherapy and a useful prognostic marker in NSCLC. Additionally, these future drugs might become important members of chemopreventive agents for therapy in high-risk patients such as heavy smokers presenting preinvasive lesions with survivin expression.

References

1. Altieri DC (2003) Validating survivin as a cancer therapeutic target. Nat Rev Cancer 3:46–54
2. Ambrosini G, Adida C, Altieri DC (1997) A novel anti-apoptosis gene survivin expressed in cancer and lymphoma. Nat Med 3:917–921
3. Brambilla C, Fievet F, Jeanmart M, de Fraipont F, Lantuejoul S, Frappat V, Ferretti G, Brichon PY, Moro-Sibilot D (2003) Early detection of lung cancer: role of biomarkers. Eur Respir J 39:36s–44s
4. Brundage MD, Davies D, Mackillop WJ (2002) Prognostic factors in non-small cell lung cancer: a decade of progress. Chest 122:1037–1057
5. Falleni M, Pellegrini C, Marchetti A, Oprandi B, Buttitta F, Barassi F, Santambrogio L, Coggi G, Bosari S (2003) Survivin gene expression in early-stage non-small cell lung cancer. J Pathol 200:620–626
6. Frost M, Jarboe EA, Orlicky D, Gianani R, Thompson LC, Enomoto T, Shroyer KR (2002) Immunohistochemical localiza-

tion of survivin in benign cervical mucosa, cervical dysplasia, and invasive squamous cell carcinoma. Am J Clin Pathol 117:738–744
7. Grossman D, McNiff JM, Li F, Altieri DC (1999) Expression of the apoptosis inhibitor survivin in nonmelanoma skin cancer and gene targeting in a keratinocyte cell line. Lab Invest 79:1121–1126
8. Hofmann HS, Simm A, Hammer A, Silber RE, Bartling B (2002) Expression of inhibitors of apoptosis (IAP) proteins in non-small cell human lung cancer. J Cancer Res Clin Oncol 128:554–560
9. Ichiki Y, Hanagiri T, Takenoyama M, Baba T, Fukuyama T, Nagata Y, Mizukami M, So T, Sugaya M, Yasuda M, So T, Sugio K, Yasumoto K (2005) Tumor specific expression of survivin-2B in lung cancer as a novel target of immunotherapy. Lung Cancer 48:281–289
10. Ikehara M, Oshita F, Kameda Y, Ito H, Ohgane N, Suzuki R, Saito H, Yamada K, Noda K, Mitsuda A (2002) Expression of survivin correlated with vessel invasion is a marker of poor prognosis in small adenocarcinoma of the lung. Oncol Rep 9:835–838
11. Jeanmart M, Lantuejoul S, Fievet F, Moro D, Sturm N, Brambilla C, Brambilla E (2003) Value of immunohistochemical markers in preinvasive bronchial lesions in risk assessment of lung cancer. Clin Cancer Res 9:2195–2203
12. Karczmarek-Borowska B, Filip A, Wojcierowski J, Smolen A, Pilecka I, Jablonka A (2005) Survivin antiapoptotic gene expression as a prognostic factor in non-small cell lung cancer: in situ hybridization study. Folia Histochem Cytobiol 43:237–242
13. Kawasaki H, Toyoda M, Shinohara H, Okuda J, Watanabe I, Yamamoto T, Tanaka K, Tenjo T, Tanigawa N (2001) Expression of survivin correlates with apoptosis, proliferation, and angiogenesis during human colorectal tumorigenesis. Cancer 91:2026–2032
14. Kren L, Brazdil J, Hermanova M, Goncharuk VN, Kallakury BV, Kaur P, Ross JS (2004) Prognostic significance of anti-apoptosis proteins survivin and bcl-2 in non-small cell lung carcinomas: a clinicopathologic study of 102 cases. Appl Immunohistochem Mol Morphol 12(1):44–49
15. Li F, Yang J, Ramnath N, Javle MM, Tan D (2005) Nuclear or cytoplasmic expression of survivin: what is the significance? Int J Cancer 114(4):509–512
16. Ling X, Yang J, Tan D, Ramnath N, Younis T, Bundy BN, Slocum HK, Yang L, Zhou M, Li F (2005) Differential expression of survivin-2B and survivin-DeltaEx3 is inversely associated with disease relapse and patient survival in non-small-cell lung cancer (NSCLC). Lung Cancer 49:353–361
17. Lo Muzio L, Pannone G, Leonardi R, Staibano S, Mignogna MD, De Rosa G, Kudo Y, Takata T, Altieri DC (2003) Survivin a potential early predictor of tumor progression in the oral mucosa. J Dent Res 82:923–928
18. Lu B, Gonzalez A, Massion PP, Shyr Y, Shaktour B, Carbone DP, Hallahan DE (2004) Nuclear survivin as a biomarker for non-small-cell lung cancer. Br J Cancer 91:537–540
19. Mirza A, McGuirk M, Hockenberry TN, Wu Q, Ashar H, Black S, Wen SF, Wang L, Kirschmeier P, Bishop WR, Nielsen LL, Pickett CB, Liu S (2002) Human survivin is negatively regulated by wild-type p53 and participates in p53-dependent apoptotic pathway. Oncogene 21:2613–2622
20. Monzo M, Rosell R, Felip E, Astudillo J, Sanchez JJ, Maestre J, Martin C, Font A, Barnadas A, Abad A (1999) A novel anti-apoptosis gene: re-expression of survivin messenger RNA as a prognosis marker in non-small-cell lung cancers. Clin Oncol 17:2100–2104
21. Mountain CF (1997) Revisions in the international system for staging lung cancer. Chest 111:1710–1717
22. Nachmias B, Ashhab Y, Ben-Yehuda D (2004) The inhibitor of apoptosis protein family (IAPs): an emerging therapeutic target in cancer. Semin Cancer Biol 14:231–243
23. Nakanishi K, Kawai T, Kumaki F, Hiroi S, Mukai M, Ikeda E (2003) Survivin expression in atypical adenomatous hyperplasia of the lung. Am J Clin Pathol 120:712–719
24. Nakano J, Huang CL, Liu D, Ueno M, Sumitomo S, Yokomise H (2005) Survivin gene expression is negatively regulated by the p53 tumor suppressor gene in non-small cell lung cancer. Int J Oncol 27:1215–1221
25. Oshita F, Ito H, Ikehara M, Ohgane N, Hamanaka N, Nakayama H, Saito H, Yamada K, Noda K, Mitsuda A, Kameda Y (2004) Prognostic impact of survivin, cyclin D1, integrin beta1, and VEGF in patients with small adenocarcinoma of stage I lung cancer. Am J Clin Oncol 27:425–428
26. Rom WN, Hay JG, Lee TC, Jiang Y, Tchou-Wong KM (2000) Molecular and genetic aspects of lung cancer. Am J Respir Crit Care Med 161:1355–1367
27. Schimmer AD (2004) Inhibitor of apoptosis proteins: translating basic knowledge into clinical practice. Cancer Res 64:7183–7190
28. Shinohara ET, Gonzalez A, Massion PP, Chen H, Li M, Freyer AS, Olson SJ, Andersen JJ, Shyr Y, Carbone DP, Johnson DH, Hallahan DE, Lu B (2005) Nuclear survivin predicts recurrence and poor survival in patients with resected nonsmall cell lung carcinoma. Cancer 103:1685–1692
29. Tanabe H, Yagihashi A, Tsuji N, Shijubo Y, Abe S, Watanabe N (2004) Expression of survivin mRNA and livin mRNA in non-small-cell lung cancer. Lung Cancer 46:299–304
30. Travis WD, Brambilla E, Muller-Hermelink HK, Harris CC (eds) (2004) World Health Organization classification of tumours. Pathology and genetics of tumours of the lung, Pleura and Heart. IARC, Lyon
31. Vischioni B, van der Valk P, Span SW, Kruyt FA, Rodriguez JA, Giaccone G (2004) Nuclear localization of survivin is a positive prognostic factor for survival in advanced non-small-cell lung cancer. Ann Oncol 15:1654–1660
32. Wang XY, Yao Z, Li Y, Liu T, Zheng HY, Zhu CZ, Sun CY, Wang AX, Zhao M, Wu XY (2005) Expression and significance of survivin mRNA in lung cancer tissue microarray detected by FISH. Chin Med Sci J 20:214–216

Virchows Arch (2006) 449:171–174
DOI 10.1007/s00428-006-0225-2

ORIGINAL ARTICLE

Genetic clonality is a feature unifying nephroblastomas regardless of the variety of morphological subtypes

Barbara Guertl · Ivo Leuschner · Dieter Harms · Gerald Hoefler

Received: 2 March 2006 / Accepted: 13 April 2006 / Published online: 20 May 2006
© Springer-Verlag 2006

Abstract Nephroblastomas are embryonal tumors exhibiting a wide variety of different morphological features and genetic changes. Some of the genetic aberrations were associated with a certain histological subtype. It is generally assumed that nephroblastomas develop as subclonal proliferations from nephrogenic rests. However, so far, a very limited amount of tumors from only part of the morphological spectrum of nephroblastomas was investigated. We therefore investigated the clonality of 45 tumors of all different histological subtypes. The number of each subtype was in accordance with the percentage of occurrence of the respective subtype. We analyzed a highly polymorphic locus of the human androgen receptor gene for nonrandom X-inactivation of genomic DNA using a methylation-sensitive restriction enzyme. Data were obtained for 39 tumors. Eighteen of the tumors included were noninformative in the genetic locus examined, the remaining 21 tumors were monoclonal regardless of the histological subtype. Our findings therefore support the hypothesis that Wilms' tumors are monoclonal proliferations despite their large variety of morphological features.

B. Guertl (✉)
Institute of Pathology,
Paracelsus Private Medical University Salzburg,
Salzburg Landeskrankenanstalten, Müllner Straße 48,
Salzburg 5020, Austria
e-mail: b.guertl-lackner@salk.at

I. Leuschner · D. Harms
Kiel Pediatric Tumor Registry, Institute of Pathology,
Christian Albrechts University Kiel,
Michaelisstr. 11,
24105 Kiel, Germany

G. Hoefler
Institute of Pathology, Medical University of Graz,
Auenbruggerplatz 25,
Graz 8036, Austria

Keywords Nephroblastoma · HUMARA analysis · Clonality

Introduction

Nephroblastomas (Wilms' tumors, WT) are triphasic embryonal neoplasms of the kidney, affecting 1 in 8,000 to 10,000 children [7]. WT can arise either in conjunction with a congenital malformation syndrome or, more frequently, as sporadic and familial tumors [8].

Histological and ultrastructural nephroblastoma often recapitulates normal embryonal kidney development [21] with a variety of cell types differentiating toward blastema, epithelium, and stroma. Each component can be present within the tumor to a varying degree. The diverse cell types may also express a varying degree of differentiation. The blastema can be arranged in different patterns, the epithelial structures can also show a wide morphological spectrum, such as tubules, glomeruloid structures, or a tubulopapillary pattern. Almost any type of differentiation can be observed within the stromal component of nephroblastomas, such as myoblastic elements, mature skeletal muscle, adipose tissue, cartilage, bone and osteoid, mature ganglionic cells, and neuroglial tissue [23].

The molecular pathogenesis of nephroblastomas appears to be heterogeneous. One of the first genes described to be involved not only in the pathogenesis of WT, but also controlling the early stages of kidney organogenesis, was the WT1 gene located at 11p13 [9, 18]. Over the past few years, numerous other genes and genetic loci, contributing to the pathogenesis of nephroblastomas, were described, such as the WT2 gene at 11p15 [16] and genes located at chromosome 1, 17p13 and p53 [14]. Methylation abnormalities in glypican 3 and involvement of tumor suppressor genes such as SLIT2 and RASSF1A were also demonstrat-

Table 1 PCR primer pairs for nested PCR of the analytical region of the HUMARA gene

Primer pairs PCR 1 (outer)	15–98	5′TGTGGGGCCTCTACGATG3′
	16–98	5′CCGTCCAAGACCTACCGA3′
Primer pairs PCR 2 (inner)	47–97	5′TACGATGGGCTTGGGGAGAA3′
	48–97 (fluorescent)	5′CCGAGGAGCTTTCCAGAATC3′

ed [1, 6]. An involvement of the Wingless-type MMTV integration site family member (Wnt) signaling pathway by gain of function mutations in exon 3 of beta-catenin and stabilization of beta-catenin pending on the WT1 function [19], and loss of heterozygosity and microsatellite instability of the APC gene were also discovered [24].

Additional studies were performed to correlate genetic alterations and histological subtypes of nephroblastomas. Tumors with heterologous differentiation showed lower levels of WT1 gene transcripts [13]. In contrast, tumors with WT1 wild type showing blastemal-predominant or epithelial-predominant histology revealed high levels of WT1 protein [22]. A correlation of WT1 gene mutations with a stromal-predominant histology was discovered [25]. In WT1 negative tumors, the nuclear accumulation of beta-catenin and Bcl-2 expression were demonstrated to be associated with rhabdomyogenesis [12].

In our study, we wanted to investigate whether nephroblastomas with such a variety of morphological and genetic features could indeed be derived from a single neoplastic cell. So far, to our knowledge, only one study was attempted, including 11 nephroblastomas, for two of which the histological typing was not available [26].

Materials and methods

Samples

All samples were obtained from the children's tumor registry at the Institute of Pediatric Pathology, University of Kiel and were reviewed and subclassified by the International Society of Pediatric Oncology (SIOP) panel. Tissue samples had been fixed in 10% buffered formaldehyde solution and embedded in paraffin wax. Four-micrometer-thick sections were obtained.

DNA isolation

If the sample uniformly consisted of tumor or normal tissue, between 1 and 3 sections were directly transferred for DNA isolation. From the remaining cases, areas were selected for microdissection after deparaffination and stained with Papanicolaou's stain. They were microdissected manually under microscopic control from approximately three sections, depending on the size of the selected area [15]. Genomic DNA was extracted with the Nucleospin C+T system (Macherey and Nagel, Düsseldorf, Germany) according to the manufacturer's recommendations.

Human androgen receptor gene assay

Between 100 and 500 ng of genomic DNA samples was digested for 4 h at 37°C in a 20-µl restriction enzyme reaction using 10 U of Hpa II (Roche, Penzburg, Germany), followed by inactivation of the enzyme at 95°C for 3 min. Amplification of the human androgen receptor (HUMARA) gene was carried out by nested polymerase chain reaction (PCR). Digested genomic DNA (10 µl of the restriction enzyme reaction) was included in a 50-µl PCR reaction with the Qiagen Hot Start Taq DNA polymerase reaction. A fluorescent downstream primer was used for the inner PCR product; primer sequences are given in Table 1. After a hot start (95°C for 15 min), DNA was amplified in a first PCR for 30 cycles (94°C for 30 s, 53°C for 45 s, and 72°C for 30 s) followed by a final extension at 72°C for 10 s. Ten microliters of the reaction product was used as a template for a second (nested) PCR with 45 cycles (94°C for 30 s, 57°C for 45 s, and 72°C for 45 s) and the same denaturing and final extension steps as described for the first PCR.

PCR products were analyzed on a 0.35-mm-thick 5% urea gel at 1,200 V using an automated sequencing system (ALF, Amersham-Pharmacia Biotech). The principle of this analysis is based on the Lyon hypothesis that in every female somatic cell, one X chromosome is randomly inactivated by methylation during early embryogenesis [20]. The HUMARA gene is located on the X chromosome and contains a differential methylation site only about 100 bp upstream of a CAG trinucleotide repeat locus. Both the activated and nonactivated alleles can thus be detected by methylation-sensitive restriction endonucleases. This CAG locus is informative in a high percentage of females and because of the short length of the PCR product, this method can also be used with formalin-fixed, paraffin-embedded material. The allele intensity and corrected ratio for determining clonality of the samples were calculated. According to Kopp et al. [17], monoclonality was assumed when one of the alleles was represented in ≥50% in comparison with the other allele (corrected ratio ≤0.33 or ≥3).

Results

Tumor histology

All samples were retrieved from the Children's Tumor Registry at the Department of Pediatric Pathology, Christian-Albrechts

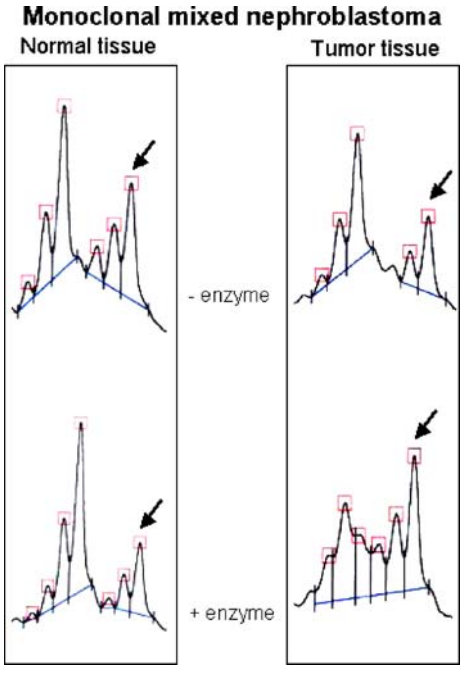

Fig. 1 Clonality analysis of a mixed nephroblastoma using the HUMARA assay. A clear change in the proportion of the peaks is seen after enzyme digestion in the monoclonal tumor (*arrow*)

University of Kiel, Germany. The tumors had routinely been reviewed by the SIOP panel and the classification was according to the decision of the SIOP panel. The distribution of anaplasia was classified according to the characterization published by Faria et al. [11]. Seventeen nephroblastomas of mixed type were included, six of stromal type, four of epithelial type, eight of blastemal type, three showing focal anaplasia, and seven showing diffuse anaplasia. On a second review by the SIOP panel, one of the nephroblastomas of mixed type was defined to be a large intralobar nephrogenic rest. The sample selected for analysis from the subgroup of nephroblastomas with focal anaplasia always contained the respective anaplastic area. Two of the tumors of epithelial type were obtained from one patient with bilateral nephroblastoma.

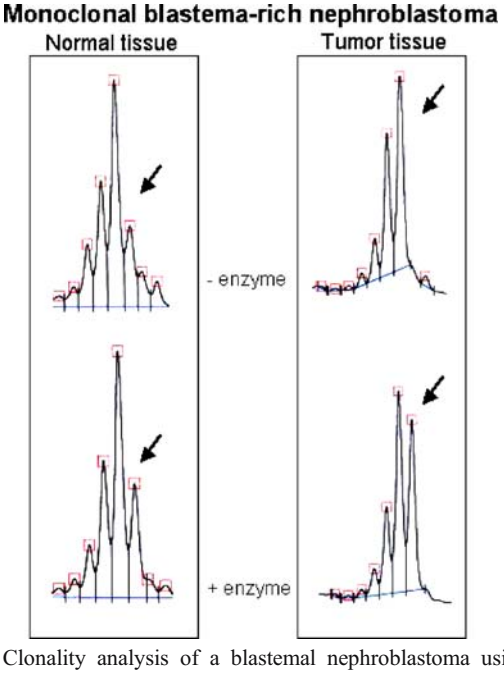

Fig. 2 Clonality analysis of a blastemal nephroblastoma using the HUMARA assay. The same change in the proportion of the peaks is seen as indicated in Fig. 1 (*arrow*)

Human androgen receptor assay

Out of the 16 nephroblastomas of mixed type included in the study (see also classification of tumor histology), data were obtained for 14 samples: 7 were noninformative and 7 were monoclonal (for example, see Fig. 1). Out of the six nephroblastomas of stromal type, four proved to be monoclonal and two were noninformative. For all nephroblastomas of the blastemal type, results were obtained. Three of the tumors appeared to be noninformative and five were monoclonal (for example, see Fig. 2). Three of the nephroblastomas of the epithelial type included were demonstrated to be monoclonal. For the sample of the right kidney of the bilateral epithelial nephroblastoma, no result was obtained for technical reasons. Two of the nephroblastomas with focal anaplasia were also monoclonal, one of them was noninformative. From the seven nephroblastomas with diffuse anaplasia included in the study, five were shown to be noninformative; for the remaining two, an analysis was not possible for technical reasons.

Discussion

Nephroblastomas can contain different cellular components to a varying degree. Each cell type in turn can show a varying degree of maturation. Nephroblastomas therefore display a wide variety of morphological features and are classified accordingly with nine different subclasses in the current classification of renal tumors for childhood [5]. The genetic background of the development of these tumors has already been the focus of extensive research [1, 6, 9, 14, 16, 18, 19, 24]. Additional studies showed some genetic patterns correlating with certain histological phenotypes. Different levels of WT1 gene transcripts, for example, were found with different subtypes of nephroblastoma [13, 22]. Rhabdomyogenesis within the stromal component of nephroblastoma is associated with changes in the molecules of the Wnt signaling pathway [12]. A high correlation of p53 mutation with the anaplastic subtype of nephroblastoma, a subgroup with an extremely poor prognosis, was described [2] and these appear to be confined to anaplastic loci [3].

The origin of nephroblastomas remains to be verified. From morphological and genetic data obtained so far, it is generally believed that nephroblastomas develop from nephrogenic rests by accumulating genetic alterations [5] and thus, are considered to be subclonal proliferations of nephrogenic rests [4, 10]. This hypothesis also postulates that in the development of some tumors, there may be no rest stage of nephrogenic rests [4].

So far, the clonality of WT, although postulated in several papers [4, 5, 10], was only investigated in one study including 11 patients. One of these patients histologically turned out to have clear cell sarcoma, two of the patient's nephroblastomas were anaplastic, six of them showed favorable histology, and no histological diagnosis was available for the remaining two [26]. Considering the genetic and the morphological diversity of nephroblastoma, we wondered whether all the different subtypes with this large variety of genetic changes would reveal a monoclonal growth pattern.

Forty-five tumors were included into the study, the number of different subtypes is in accordance with the incidence of occurrence. All tumors analyzed showed monoclonality in a representative part of the tumor.

Our results therefore strongly support the current hypothesis of monoclonal development of WT regardless of their exact morphological subtype.

Acknowledgement The experiments carried out comply with the current laws in this country.

References

1. Astuti D, DaSilva NF, Dallol A, Gentle D, Martinsson T, Kogner P, Grundy R, Kishida T, Yao M, Latif F, Maher ER (2004) SLIT2 promoter methylation analysis in neuroblastoma, Wilms' tumour and renal cell carcinoma. Br J Cancer 90:515–521
2. Bardeesy N, Falkoff D, Petruzzi MJ, Nowak N, Zabel B, Adam M, Aguiar MC, Grundy P, Shows T, Pelletier J (1994) Anaplastic Wilms' tumour, a subtype displaying poor prognosis, harbours p53 gene mutations. Nat Genet 7:91–97
3. Bardeesy N, Beckwith JB, Pelletier J (1995) Clonal expansion and attenuated apoptosis in Wilms' tumor are associated with p53 gene mutations. Cancer Res 55:215–219
4. Beckwith JB (1993) Precursor lesions of Wilms tumor: clinical and biological implications. Med Pediatr Oncol 21:178–181
5. Beckwith JB, Kiviat NB, Bonadio JF (1990) Nephrogenic rests, nephroblastomatosis, and the pathogenesis of Wilms' tumor. Pediatr Pathol 10:1–36
6. Boily G, Saikali Z, Sinnett D (2004) Methylation analysis of the glypican 3 gene in embryonal tumours. Br J Cancer 90:1606–1611
7. Breslow NE, Olshan A, Beckwith JB, Green DM (1993) Epidemiology of Wilms tumor. Med Pediatr Oncol 21:178–181
8. Breslow NE, Olson J, Moksness J, Beckwith JB, Grundy P (1996) Familial Wilms' tumor: a descriptive study. Med Pediatr Oncol 27:398–403
9. Call KM, Glaser T, Ito CY, Buckler AJ, Pelletier J, Haber DA, Rose EA, Kral A, Yeger H, Lewis WH, Jones C, Housman DE (1990) Isolation and characterization of a zinc finger polypeptide gene at the human chromosome 11 Wilms' tumor locus. Cell 60:509–520
10. Charles AK, Brown KW, Berry PJ (1998) Microdissecting the genetic events in nephrogenic rests and Wilms tumor development. Am J Pathol 153:991–1000
11. Faria P, Beckwith JB, Mishra K, Zuppan C, Weeks DA, Breslow N, Green DM (1996) Focal versus diffuse anaplasia in Wilms tumor—new definitions with prognostic significance: a report from the National Wilms Tumor Study Group. Am J Surg Pathol 20:909–920
12. Fukuzawa R, Heathcott RW, Sano M, Morison IM, Yun K, Reeve AE (2004) Myogenesis in Wilms' tumors is associated with mutations of the WT1 gene and activation of Bcl-2 and the Wnt signaling pathway. Pediatr Dev Pathol 7:125–137
13. Gerald WL, Gramling TS, Sens DA, Garvin AJ (1992) Expression of the 11p13 Wilms' tumor gene, WT1, correlates with histologic category of Wilms' tumor. Am J Pathol 140:1031–1037
14. Grundy P, Coopes M (1996) An overview of the clinical and molecular genetics of Wilms' tumor. Med Pediatr Oncol 27:394–397
15. Guertl B, Ratschek M, Harms D, Jaenig U, Leuschner I, Poremba C, Hoefler G (2003) Clonality and loss of heterozygosity of WT genes are early events in the pathogenesis of nephroblastomas. Hum Pathol 34:278–281
16. Karnik P, Chen P, Paris M, Yeger H, Williams BR (1998) Loss of heterozygosity at chromosome 11p15 in Wilms tumors: identification of two independent regions. Oncogene 7:237–240
17. Kopp P, Jaggi R, Tobler A, Borisch B, Oestreicher M, Sabacan L, Jameson JL, Fey MF (1997) Clonal X-inactivation analysis of human tumours using the human androgen receptor gene (HUMARA) polymorphism: a non-radioactive and semiquantitative strategy applicable to fresh and archival tissue. Mol Cell Probes 11:217–228
18. Kreidberg JA, Sariola H, Loring JM, Maeda M, Pelletier J, Houseman D, Jaenisch R (1993) WT-1 is required for early kidney development. Cell 74:679–691
19. Li Cm, Kim CE, Margolin AA, Guo M, Zhu J, Mason JM, Hensle TW, Murty VV, Grundy PE, Fearon ER, D´Agati V, Licht JD, Tycko B (2004) CTNNB1 mutations and overexpression of Wnt/beta-catenin target genes in WT1-mutant Wilms tumors. Am J Pathol 165:1943–1953
20. Lyon MF (1961) Gene action in the X-chromosome of the mouse. Nature 190:372–373
21. Mierau GW, Beckwith JB, Weeks DA (1987) Ultrastructure and histogenesis of the renal tumors of childhood: an overview. Ultrastruct Pathol 11:313–333
22. Miwa H, Tomlinson GF, Timmons CF, Huff V, Cohn SL, Strong LC, Saunders GF (1992) RNA expression of the WT1 gene in Wilms' tumors in relation to histology. J Natl Cancer Inst 84:181–187
23. Murphy WM, Beckwith JB, Farrow GM (1994) Tumors of the kidney, bladder, and related urinary structures. In: Atlas of tumor pathology, 3rd series, fascicle 11. Armed Forces Institute of Pathology, Washington, pp 12–54
24. Ramburan A, Oladiran F, Smith C, Hadley GP, Govender D (2005) Microsatellite analysis of the adenomatous polyposis coli (APC) gene and immunoexpression of beta catenin in nephroblastoma: a study including 83 cases treated with preoperative chemotherapy. J Clin Pathol 58:44–50
25. Schumacher V, Schneider S, Figge A, Wildhardt G, Harms D, Schmidt D, Weirich A, Ludwig R, Roya-Pokora B (1997) Correlation of germ-line mutations and two-hit inactivation of the WT1 gene with Wilms tumors of stromal-predominant histology. Proc Natl Acad Sci USA 94:3972–3977
26. Wilimas JA, Dow LW, Douglass EC, Jenkins JJIII, Jacobson RJ, Moohr J, Fialkow PJ (1991) Evidence for clonal development of Wilms' tumor. Am J Pediatr Hematol Oncol 13:26–28

Virchows Arch (2006) 449: 175–191
DOI 10.1007/s00428-006-0220-7

ORIGINAL ARTICLE

Roland Moll · Hans-Jürgen Holzhausen · Hans-Dieter Mennel · Caecilia Kuhn · Renate Baumann · Christiane Taege · Werner W. Franke

The cardiac isoform of α-actin in regenerating and atrophic skeletal muscle, myopathies and rhabdomyomatous tumors: an immunohistochemical study using monoclonal antibodies

Received: 6 September 2005 / Accepted: 8 April 2006 / Published online: 20 May 2006
© Springer-Verlag 2006

Abstract The two sarcomeric isoforms of actins, cardiac and skeletal muscle α-actin, are highly homologous so that their immunohistochemical distinction is extremely difficult. Taking advantage of monoclonal antibodies distinguishing the two conservative amino acid exchanges near the aminoterminus, we have performed an extended immunohistochemical analysis of the cardiac α-actin (CAA) isoform in normal, regenerating, diseased and neoplastic human muscle tissues. Intense and uniform CAA staining is seen in fetal and adult myocardium and in fetal skeletal muscle while adult skeletal muscle is essentially negative, except for muscle spindle myocytes and a few scattered muscle fibres with overall reduced diameter. By contrast, CAA synthesis is markedly induced in regenerating skeletal muscle cells, in Duchenne muscular dystrophy and upon degenerative atrophy. CAA has also been detected in certain vascular and visceral smooth muscle cells. Among tumors, CAA has consistently been seen in rhabdomyosarcomas and rhabdomyomatous cells of nephroblastomas, whereas, smooth muscle tumors have shown only occasional staining. While the synthesis of this actin isoform is less restricted than previously thought, monoclonal antibodies against CAA provide a well-defined, reliable and sensitive diagnostic tool for the definition and detection of aberrant differentiation in diseased skeletal muscle and of striated muscle differentiation in rhabdomyosarcomas.

Keywords Heart · Immunohistochemistry · Myopathies · Sarcomas

R. Moll (✉) · R. Baumann
Institute of Pathology,
Philipp University of Marburg,
Baldingerstrasse,
D-35033 Marburg, Germany
e-mail: mollr@med.uni-marburg.de
Tel.: +49-6421-2862270
Fax: +49-6421-2865640

H.-D. Mennel
Department of Neuropathology,
Philipp University of Marburg,
D-35033 Marburg, Germany

H.-J. Holzhausen · C. Taege
Institute of Pathology, Medical Faculty,
University of Halle-Wittenberg,
D-06097 Halle (Saale), Germany

C. Kuhn · W. W. Franke
Division of Cell Biology,
German Cancer Research Center,
D-69120 Heidelberg, Germany

Introduction

Multigene families of structural proteins that are synthesized in cell type-specific patterns often provide valuable markers for cell typing in cell and developmental biology and in pathology. In particular, the detection of such molecules or isoforms has made possible subtle analyses of the cell type of origin and the state of differentiation of normal, diseased and malignantly transformed cells. A paramount example for the tumor diagnostic value of such cell type markers is provided by the families of intermediate filament proteins and their anchorage structures, the desmosomes [29, 56, 59, 60, 62].

A ubiquitously represented, albeit less complex, multigene family of cytoskeletal proteins are the actins, usually forming extended cytoplasmic microfilament arrays (for a recent review, see [35]). In the human body, six different genes encode closely related actin isoforms synthesized in specific combinations in the diverse muscle and non-muscle cells [55, 88, 89]. Among the various muscle types, smooth muscle cells contain smooth muscle-type α-actin and/or smooth muscle-type γ-actin, while sarcomeric α-actins, i.e. cardiac and skeletal muscle α-actin, form the microfilaments of striated muscles. In addition, co-expression of some of these genes in specific muscle cell types has been reported and appears to be common in certain embryonic tissues (e.g. [2, 39–41, 44, 72, 97]; for further reference, see [82]).

In pathology, specific antibodies against smooth muscle α-actin and sarcomeric α-actins have been accepted as valuable immunohistochemical markers, particularly for the differential diagnosis of soft tissue tumors (e.g. [75, 81, 91]). The two sarcomeric α-actins, however, are much more difficult to distinguish by selective antibodies in immunohistochemistry, due to their extremely close relationship, differing in only four of the total 374 amino acid residues [88]. Studies on their differential distribution have, thus, been restricted for a long time to analyses of their mRNAs both in tissue homogenates (e.g. [39, 44, 55, 57, 68, 85]) and in situ [45, 73, 84], without providing information at the protein level. Detailed immunohistopathologic studies have, therefore, been rare, although it is obvious that antibodies discriminating between the two sarcomeric α-actin isoforms might be valuable in diagnoses of myocardial diseases in which the detection of early cell damage is an important diagnostic problem and for the recognition of sarcomeric muscle differentiation in tumors. Moreover, specific determinations of the cardiac α-actin (CAA) isoform might also be of potential value in the serodiagnostic detection of early or masked cardiac infarction events.

Cardiomyocyte markers, therefore, appear to be especially desired in medicine and developmental biology (for anthologies, see, e.g. [42, 98]). However, only two groups have reported specific CAA antibodies [18, 30]. Taking advantage of the two amino acid substitutions near the aminoterminus, we have generated several monoclonal antibodies that recognize the cardiac isoform of sarcomeric α-actin and do not cross-react with the highly related skeletal muscle α-isoform [30–32]. Using one of these antibodies, mAb cAc1-20.4.2, on sections from formalin-fixed, paraffin-embedded tissues, we have established the specific CAA distribution pattern in human fetal and adult tissues. We report on its detection in various types of diseases of muscle cells, including myopathies, regenerative and atrophic processes and tumors. As this antibody also shows wide cross-species reactivity from chicken to man (e.g. [1, 6, 15, 21, 71]), it also invites potential studies in developmental biology and animal pathology.

Materials and methods

Tissues

Paraffin blocks containing various embedded human tissues were taken from the files of the Institutes of Pathology of Marburg and Halle (Saale). They were mostly derived from surgical specimens that had been routinely formalin-fixed immediately after removal. Some tissue samples were from autopsies, and mostly also had been formalin-fixed and paraffin-embedded; some samples of heart and tongue tissue were snap-frozen in isopentane precooled in liquid nitrogen. The specimens included, among other tissue types, fetal and adult heart and various skeletal muscle tissues, the latter either being normal or pathologically altered. In addition, various types of muscle and non-muscle tumors were examined. All cases were routinely stained with hematoxylin and eosin; for some tissues, Heidenhain's Azan trichrome staining was applied. For morphometric analyses (see below), frozen archival specimens of normal skeletal muscle biopsies from various regions (mostly quadriceps femoris and deltoideus) derived from 13 patients were processed to cryostat sections. In the case of Duchenne muscular dystrophy, frozen archival tissue blocks were—without previous thawing—fixed in formalin, routinely embedded in paraffin and further processed as described above for the other human tissues. In all cases, clinical data and pathological reports were available. Bovine heart and tongue tissue samples were obtained from a local slaughterhouse and immediately frozen as described above.

Antibodies and immunohistochemistry

The CAA-specific murine monoclonal antibody (mAb) cAc1-20.4.2 (IgG1 [30]) was used throughout the study, available from Progen Biotechnik (Heidelberg, Germany) and the following non-European distributors (USA: American Research Products, Belmont, MA; Research Diagnostics, Flanders, NJ; Maine Biotechnology Services, Portland, ME; Japan: Funakoshi and Cosmo Bio, both in Tokyo). In selected cases, additional staining was performed, with identical results, using mAb cAc2-12.3.1 (IgG1 [30]; for further details see also [31, 32]). In addition, mAb 1A4 against smooth muscle α-actin, mAb D33 against desmin (both from DakoCytomation, Hamburg, Germany), mAb VIM 3B4 against vimentin (Progen), mAb MNF116 against cytokeratins (DakoCytomation), mAb DP-2.17 (Progen) or rabbit antibodies (NatuTec, Frankfurt/Main, Germany) against desmoplakin and mAb PP2-150.2.3 against plakophilin 2 (Progen) were used.

For immunohistochemistry, 3- to 4-μm thick paraffin sections were mounted on poly-L-lysine-coated slides, incubated at 58°C, deparaffinized and treated by microwave oven heating in a plastic jar in 10-mM sodium citrate buffer (pH 6.0) four times for 5 min each at 600 W [79]. After cooling to room temperature, a conventional avidin–biotin-peroxidase complex (ABC) method (Vectastain Elite ABC-Kit; Vector, Burlingame, CA) was applied, all with physiological ionic strength buffer. Primary mAbs cAc1-20.4.2 and cAc2-12.3.1 were applied at a concentration of 1 μg/ml, diluted in phosphate-buffered saline (PBS) containing 2% dried skim milk. Similar microwave oven pre-treatment was applied for mAbs 1A4 and D33. For mAbs VIM 3B4, MNF116 and DP-2.17, the microwave procedure was followed by a very mild trypsinization step using 0.001% trypsin. Secondary antibodies were biotin-coupled horse antibodies against mouse immunoglobulins (Vector). The staining reaction was developed using 3,3′-diaminobenzidine (DAB) and H_2O_2; for mild counterstaining, Mayer's hematoxylin solution was used. For negative controls, the primary antibody was replaced by buffer or an irrelevant mAb.

For immunofluorescence microscopy (for details, see [9, 30, 37, 50, 51]), approximately 5-μm thick cryostat sections of frozen specimens of bovine and human heart and tongue tissue were fixed with cold (−20°C) acetone and air-dried. Primary mAbs cAc1-20.4.2 and cAc2-12.3.1 were usually applied at a concentration of ca 5 μg/ml (in PBS) for 30–45 min at room temperature. Sections were rinsed twice for 5 min each in PBS of increased ionic strength (PBS brought with 0.6-M NaCl to a final concentration to 0.74-M NaCl), followed by two rinses in PBS for 5 min each. Secondary antibodies (Cy3-coupled antibodies against mouse immunoglobulins; Dianova, Hamburg, Germany) were then added for 30- to 40-min exposure in a moist chamber at room temperature. After two rinses with PBS (for 5 min each) and a brief rinse with distilled water, the sections were exposed to absolute ethanol for 5 min, air-dried and mounted in Fluoromount G (Biozol Diagnostica, Eching, Germany).

For comparison, cultured neonatal rat cardiomyocytes [9] and rat vascular smooth muscle-derived cells (RV [26]) grown on coverslips were treated and incubated with mAb cAc1-20.4.2 and rabbit antibodies against desmoplakin essentially as described elsewhere [50, 51]. Secondary antibodies used were Alexa 564-labelled antibodies against mouse immunoglobulins and Alexa 488-labelled antibodies against rabbit immunoglobulins (MobiTec, Göttingen, Germany). For double label immunofluorescence microscopy, both primary antibodies were applied simultaneously, as were both secondary antibodies.

Slides were viewed and photographed using the Axiophot fluorescence microscope or the confocal laser scanning 510 microscope (both from Carl Zeiss MicroImaging, Oberkochen, Germany).

Morphometry

For morphometry, cryostat sections containing transversely cut skeletal muscle fibres were obtained from frozen normal muscle biopsies. After performing enzyme histochemistry for nicotinamide adenine dinucleotide (NADH)-tetrazolium reductase (not shown in this paper), ABC peroxidase staining for CAA was performed using mAb cAc1-20.4.2 (ABC reagents from DakoCytomation). The staining reaction was again developed using DAB and H_2O_2.

To quantify the frequency of CAA-positive skeletal muscle fibres, a simple counting device was chosen in the cases of CAA-immunostained frozen sections. These sections were strictly cut in a manner that only transverse sections were obtained. In 13 specimens of normal skeletal muscle biopsies, fibres were counted in five random areas each, using a quadrangular eyepiece counting device. Specifically, the whole number of fibre profiles and the number of CAA-positive fibres were counted.

A similar approach, using an eyepiece micrometer, has been used to measure the muscle fibre diameters in the same 13 cases of normal skeletal muscle biopsies. As muscle fibre diameters are more commonly used in muscle morphometry as compared to fibre areas, we decided to base our morphometric analysis on the shortest muscle fibre diameter [95]. Thus, for each CAA-positive muscle fibre, the shortest diameter was measured. The same was done with an immediately adjacent muscle fibre negative for CAA. For a total of 49 CAA-positive muscle fibres and 49 CAA-negative control muscle fibres, the mean values were calculated. The Whitney–Mann *U* test was applied for statistical evaluation.

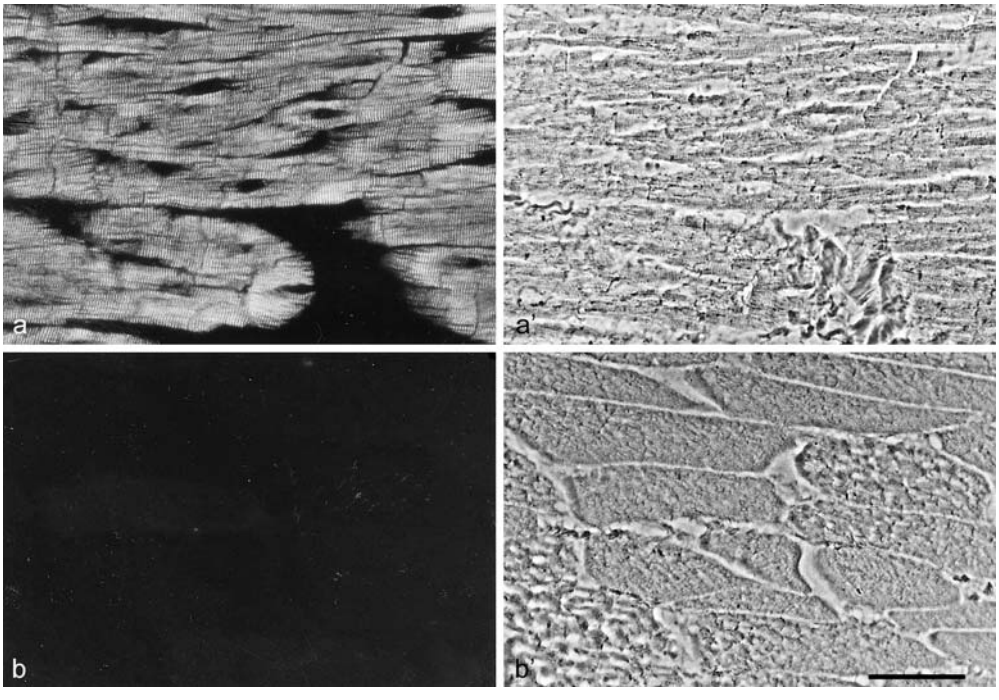

Fig. 1 Immunofluorescence microscopy of cryostat sections of bovine myocardium (**a**) and skeletal muscle of bovine tongue (**b**), using mAb cAc1-20.4.2 against cardiac α-actin (**a′**, **b′**, corresponding phase contrast images). Note the specificity of the finely striated immunostaining for cardiac muscle (**a**). *Bar*: 50 μm

Results

CAA specificity of immunostaining with monoclonal antibodies cAc1-20.4.2 and cAc2-12.3.1

The high specificity and binding stability of the CAA antibodies used is illustrated in Figs. 1 and 2. When cryostat sections of bovine myocardium or from tongue and other skeletal muscles were stained with mAbs cAc1-20.4.2 or cAc2-12.3.1, strong and uniform immunofluorescence staining of the cardiomyocytes was obtained, often revealing the cross-striated pattern corresponding to I-bands (Fig. 1a,a′). By contrast, skeletal muscle tissue of tongue and other organs was essentially negative (Fig. 1b,b′), except for a few scattered, mostly isolated muscle cells showing weak immunostaining (not shown). Similar results were obtained with cryostat sections of human heart and tongue tissue (not shown). Thus, using the protocol detailed in the Materials and methods section (for the short wash treatment with high salt buffer see also [31, 32]), any cross-reactivity of the two sarcomeric actin isoforms could be excluded.

The CAA antibodies also showed specific myofibrillar immunostaining in cardiomyocyte-derived cell cultures. For example, in primary rat cardiomyocyte cultures, parallel arrays of myofibers anchored at the junctions of the intercalated disks (Fig. 2a) were intensely immunostained, with cross-striations being visible in occasional cells (Fig. 2b). These junctions were intensely stained by desmoplakin antibodies (Fig. 2a,b), and these two markers were used throughout the study to identify cardiomyocytes (for cardiomyocyte specificity of desmoplakin see [27, 28, 37]. Smooth muscle-derived RV-cells were negative for both CAA and desmoplakin (not shown).

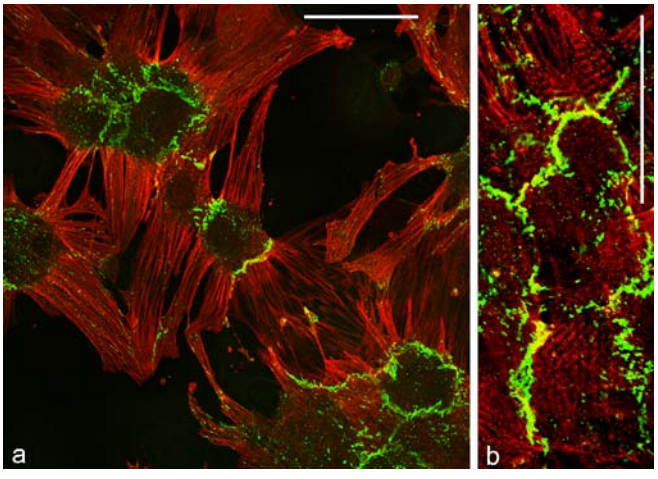

Fig. 2 Double-label confocal laser scanning immunofluorescence microscopy of cultured neonatal rat cardiomyocytes, immunostained for cardiac α-actin (Alexa 564, *red*) and desmoplakin (Alexa 488, *green*). Only the merged image is presented. The desmoplakin reaction identifies the junctions of the myocardiac intercalated disks (and of endocytosed vesicles derived therefrom) at which the α-actin-containing myofibrillar bundles anchor (**a** survey micrograph; **b** higher magnification, in some regions revealing the cross-striated pattern). *Bars*: 50 μm

Immunolocalization of CAA in normal fetal and adult human muscle tissues

The immunohistochemical results on normal human tissues are summarized in Table 1. As expected from previous data (e.g. [30, 55, 88]), cardiomyocytes from both fetal (Fig. 3a) and adult (Fig. 3b) heart showed nearly uniform reaction with both CAA mAbs, strongly decorating the myofibers and in many places revealing the typical sarcomeric pattern. The intercalated disks were specifically stained by the mAb against desmoplakin (see above) and by the mAb against plakophilin 2 (not shown).

Skeletal muscles from various human fetuses (Table 1) also exhibited an intense and almost uniform immunostaining (Fig. 4a,b), and even stronger staining was noted in the myocytes of the muscle spindles (not shown). Smooth muscle α-actin, on the other hand, was detected only in the youngest fetus studied (week 11), and only in about one-third of skeletal muscle cells (Fig. 4a, inset) but not in those of older fetuses.

In normal adult skeletal muscle (Fig. 4c–e), the vast majority of myocytes remained unstained. However, a small and variable proportion of muscle fibres, scattered in an apparently random distribution, exhibited significant CAA staining, which in longitudinal sections appeared in a

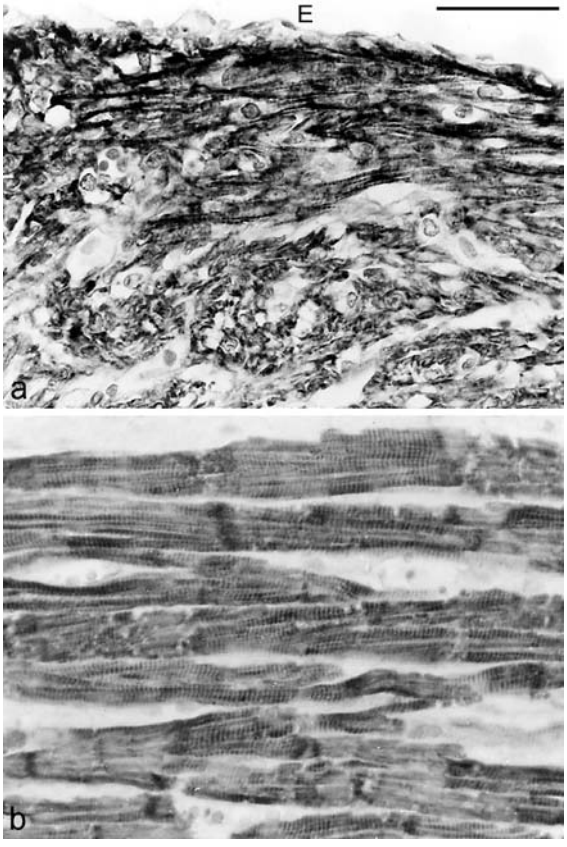

Fig. 3 Immunolocalization on sections through heart tissue, showing intense reaction of cardiac α-actin in human fetal and adult heart. **a** Subendocardial myocardium of 22-week-old fetus. *E*, endocardium. **b** Adult left-ventricular myocardium (68-year-old man), revealing the cross-striation pattern. *Bar*: 50 μm

striated pattern (Fig. 4c). The CAA-positive fibres were on average thinner than the negative ones, as confirmed by morphometric analyses (see below, next chapter). The immunostaining for CAA was particularly strong in thin fibres (Fig. 4c,d), and was relatively weak in fibres of regular diameter. Muscle spindle myocytes were consistently positive (Fig. 4e). No significant staining for smooth muscle α-actin was seen in adult skeletal muscle tissues (not shown).

Several types of smooth muscle cells also were found to be positive for CAA. While some CAA synthesis in the walls of certain muscular blood vessels has previously been noted [6, 18], we were surprised by the broad spectrum of smooth muscle cells potentially expressing CAA in

Table 1 Immunohistochemical detection of α-cardiac actin in non-neoplastic human tissues[a]

Tissue	No. of cases	α-Cardiac actin[b]
Myocardium		
Fetal (wk[c] 11, 12, 22)	3	+++
Infantile	1	+++
Adult	5	+++
Normal skeletal muscle		
Fetal		
Extremities (wk 11, 12, 20, 21, 22, 26)	6	+++
Tongue (wk 22, 23)	2	+++
Newborn	1	(+)
Adult		
Trunk, extremities[d]	12	(+)
Muscle spindle myocytes	3	+++
Tongue	3	+ to ++
Esophagus	1	++
Pathologically altered skeletal muscle		
Regenerating muscle (adult)[e]	16	
Activated satellite cells		+++
Regenerating myotubes		+++
Regenerating (thin) muscle fibers		+++
Myogenic giant cells		+++
Degenerative-atrophic muscle cells (adult)[f]	14	++, +++
Duchenne muscular dystrophy	1	++
Neurogenic muscular atrophy[g]	3	
Atrophic fibers		+ to ++
Non-atrophic fibers		(+) to ++
Muscle spindles		+++
Visceral smooth muscle		
Stomach, colon (normal)	3	− to +
Appendix vermiformis (without acute inflammation)	5	
Muscularis mucosae		_[h]
Muscularis propria, circular layer		+
Muscularis propria, longitudinal layer		−
Gall bladder (normal)	12	++ to +++
Gall bladder (muscle layer hypertrophy in chronic cholecystitis)	11	+ to ++
Uterine myometrium (normal)	12	−, (+)[i]
Vagina (postoperative fibrosis)	1	+
Vascular smooth muscle		
Umbilical cord vessels (arteries, vein)	12	+++
Various adult arteries and veins	26	− to ++
Aorta	13	+, ++[j]
Musculus arrector pili of skin	4	++
Non-muscle tissues		
Thymus, medulla (fetal, wk 18, 22; adult, 9, 28 and 35 years)	5	(+)[k]
Epithelia (fetal, adult)[l]	54	−
Ovary (adult)	2	−

Table 1 (continued)

Tissue	No. of cases	α-Cardiac actin[b]
Lymph node (adult)	4	–

[a]As determined by immunohistochemistry (paraffin sections, mAb cAc1-20.4.2)
[b]– Negative, *(+)* 1–10% of muscle cells positive, + 11–50% positive, ++ 51–90% positive, +++ 91–100% positive
[c]*wk* Week of gestation
[d]The muscle tissues comprised morphologically normal specimens from ventral neck, pectoralis muscle, axillary and scapular region and leg (musculus gastrocnemius, musculus soleus)
[e]Two weeks after heavy trauma, *n*=1; granulating inflammation around infected hip joint prosthesis, *n*=1; organizing hematoma, *n*=1; postoperative and inflammatory fibrosis, *n*=6; infiltrating malignant tumor, *n*=7
[f]Postoperative and inflammatory fibrosis, *n*=7; infiltrating malignant tumor, *n*=7
[g]Four- to six-month-old infants suffering from spinal muscular atrophy (Werdnig-Hoffmann; *n*=2) or severe cerebral damage (*n*=1)
[h]In one case (+)
[i]In four cases, very focal positivity
[j]In three cases >50% of smooth muscle cells of aortic media were positive. In addition, in some small atherosclerotic intimal plaques scattered spindle cells (probably representing myofibroblasts) were positive
[k]Scattered cells in the medulla, possibly representing myoid cells
[l]Various fetal and adult stratified squamous and simple epithelia (see the organs listed above, other than thymus)

addition to their characteristic smooth muscle-type α-actin. Among vascular smooth muscles, a relatively intense and widespread reaction was observed in the *tunica media* of umbilical cord vessels (not shown), and more variable positive reactions were seen in some media myocytes of variously-sized arteries and veins from adult specimens (Fig. 5a). The proportion of CAA-positive vessels in a given specimen varied considerably. Correlations between vascular CAA synthesis and specific organs or body sites or regional pathological processes (inflammatory, fibrotic) were not observed. We, here, report for the first time, the consistent, albeit variably extensive presence of CAA in all 13 specimens of the human aorta tissues studied (Table 1).

In normal visceral smooth muscle of the gastrointestinal tract, very limited and focal CAA staining was noted (Fig. 5b) while fetal intestinal *muscularis propria* showed

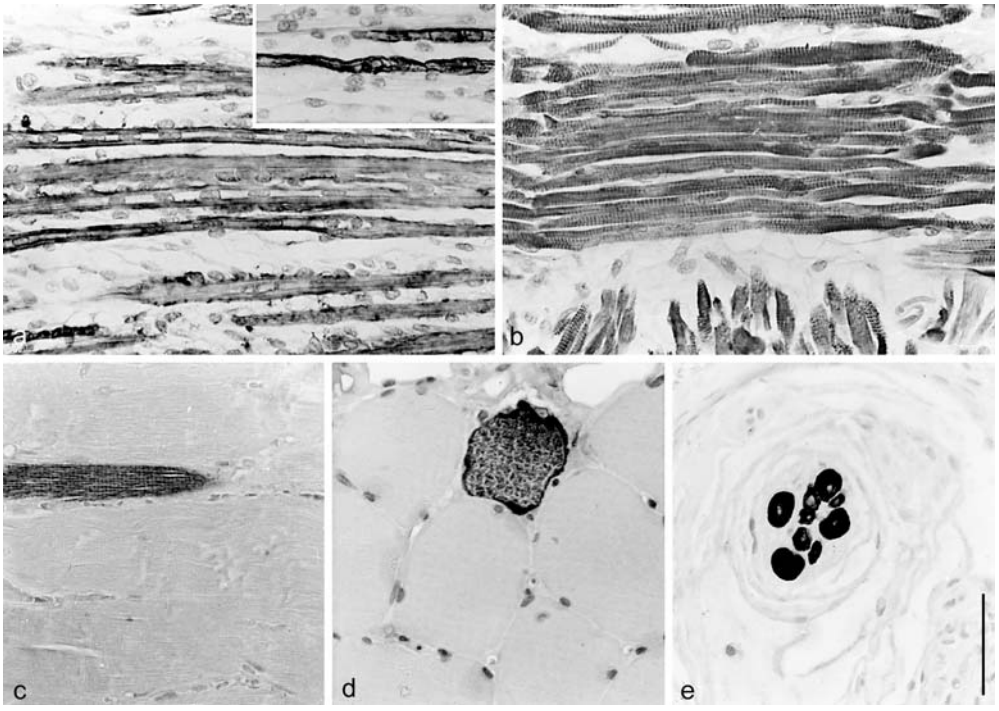

Fig. 4 Immunolocalization of cardiac α-actin in human fetal skeletal muscle and its down-regulation in adult skeletal muscle. **a** Skeletal muscle from 11-week-old fetus, showing uniformly strong cardiac α-actin staining while smooth muscle α-actin (*inset*) is still focally present. **b** Intense cross-striated pattern of cardiac α-actin in tongue muscle of 22-week-old fetus. **c**–**e** Absence of cardiac α-actin immunostaining in the vast majority of mature skeletal muscle fibres of adults (**c** and **d** *pectoralis* muscle, 67-year-old woman; **e** scapular muscle, 59-year-old man). Significant immunostaining is only seen in scattered fibres, usually of smaller diameters (near-longitudinally sectioned in **c** and cross-sectioned in **d**), probably reflecting minimal regeneration activity and in the neuromuscular spindle myocytes (thicker nuclear bag fibres and thinner nuclear chain fibres) which are prominently reactive (**e**). *Bar*: 50 μm

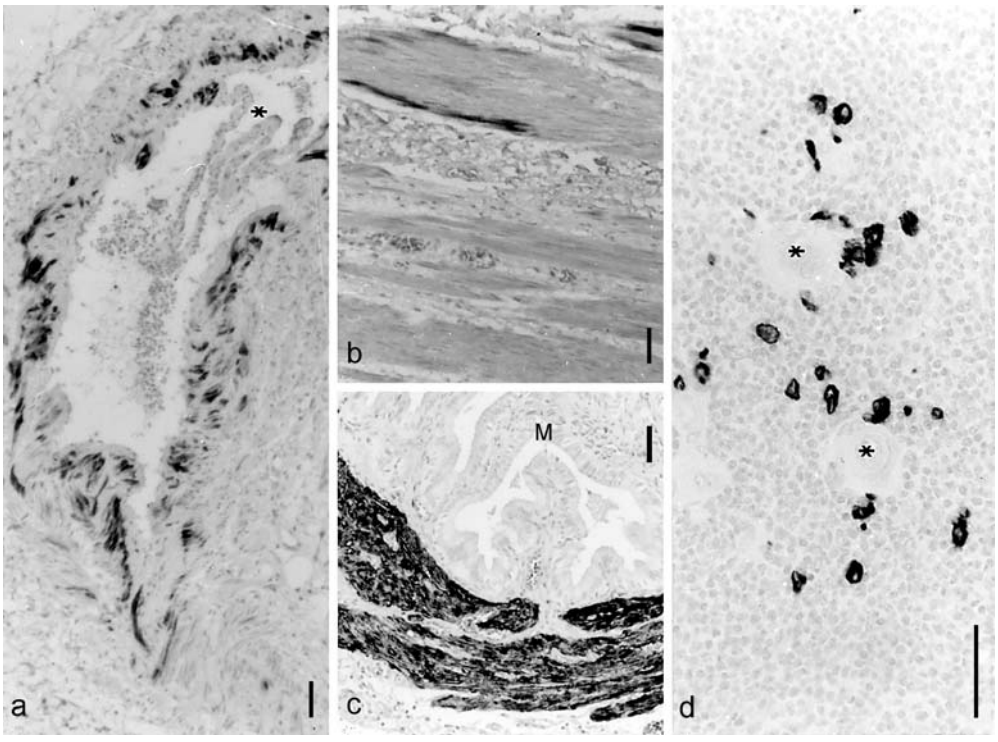

Fig. 5 Cardiac α-actin in certain cells of smooth muscle tissue and thymus. **a** Heterogeneous cardiac α-actin immunostaining among media cells of a small vein from chest wall. Note the negative valve (*asterisk*). **b** Focal cardiac α-actin reaction in visceral smooth muscle cells of gastric *tunica muscularis propria* (*top*; *facing the submucosa*). **c** In contrast, intense and extended reaction is seen in gall-bladder *muscularis*. *M*, mucosa. **d** Cardiac α-actin in scattered (probably myoid) medullary cells of human fetal (22 weeks) thymus. Note also some enrichment around Hassall bodies (*asterisks*) which remain unstained. *Bars*: 50 μm

more prominent staining (not shown). Interestingly, a remarkably intense and extended CAA immunostaining was regularly seen in normal gall bladder muscle (Fig. 5c), and this staining appeared somewhat reduced in chronic cholecystitis (Table 1). By contrast, normal uterine myometrium was completely negative in the cases studied.

Among the various non-muscle tissues studied (Table 1), only thymus showed a positive reaction for CAA, localized in scattered, round or elongated cells of the medulla which represented myoid cells (Fig. 5d), as also indicated by desmin staining in these cells as seen in sequential sections (not shown; see also [20, 22, 48, 74, 94]; for thymomas see also [63]). When sections of thymus were stained for cytokeratins, decorating the epithelial reticulum cells, and sequentially stained for CAA, no co-expression of CAA and cytokeratins was observed. The double staining experiments also showed that at some places, CAA-positive myoid cells and cytokeratin-positive epithelial reticulum cells were closely adjacent to each other (not shown), in line with previous observations on the localization of myoid cells in the thymus [48].

Morphometry of CAA-containing muscle fibres in normal adult skeletal muscle

The frequency of CAA-positive muscle fibres was determined morphometrically, based on frozen muscle biopsies of 13 patients. In the measurements based on rectangular counting areas, a mean frequency value of 1.4% of CAA-positive fibres (range: 0–8%) was found in normal skeletal muscle.

The reduction of fibre diameter in CAA-positive fibres was already apparent by directly comparing single positive fibres to the adjacent negative ones. This finding was corroborated by morphometric analysis. In measurements using an eyepiece micrometer, the mean value of the shortest diameter of CAA-positive fibres in normal skeletal muscle was 47 vs 63 μm for CAA-negative fibres. These values, calculated from 49 single CAA-positive fibres and 49 CAA-negative adjacent control fibres, were significantly different when the Whitney—Mann *U* test was applied. This test resulted in a critical value of −3.8333 and a *p* value of 0.0001, thus allowing the conclusion that in normal skeletal muscle, the mean diameter of CAA-positive fibres is significantly smaller than that of CAA-negative fibres.

Immunolocalization of CAA in pathologically altered skeletal muscle

Results with pathologically altered skeletal muscle from adults are also listed in Table 1. In certain muscle specimens taken from regions in the vicinity of tumors or fibroses, no or only minimal pathological changes were seen, but CAA staining disclosed individual scattered, very small positive cells closely adjacent to normal, CAA-negative muscle fibres (Fig. 6a). On the basis of their position and morphology, these cells most likely represented satellite cells in early stages of activation (cf. [11]; for reviews see also [43, 77]). Similar but larger cells present in such specimens (Fig. 6b) seemed to correspond to a slightly more advanced stage of regeneration.

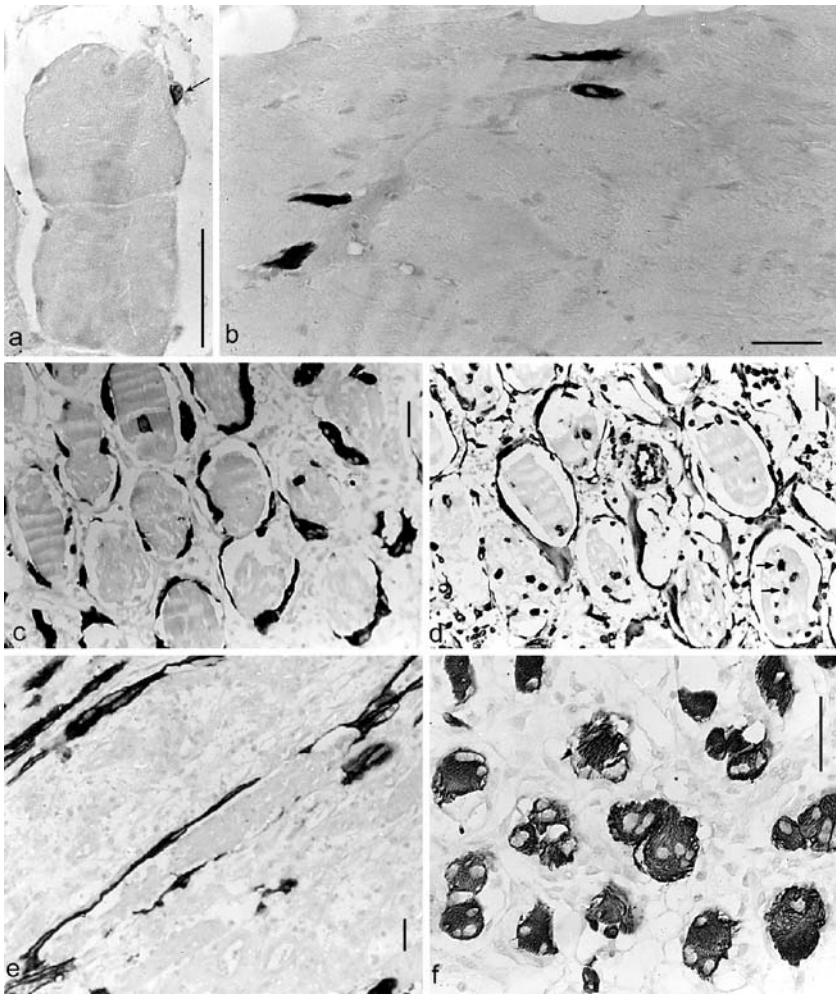

Fig. 6 Immunolocalization showing the induction of cardiac α-actin in adult human skeletal muscle during regeneration. **a** Early activation of a still small satellite cell with selective cardiac α-actin staining (*arrow*) of skeletal muscle tissue in the further surrounding of a leiomyosarcoma. **b** Larger, more advanced regenerating satellite cells showing strong cardiac α-actin staining (at higher magnification some of these cells reveal cross-striations; not shown) in *pectoralis* muscle close to a ductal breast carcinoma. **c**–**f** Thigh muscle from a 31-year-old man's leg that had been run over by a truck 14 days before surgical removal. Note cardiac α-actin in satellite cell-derived regenerating cells surrounding unstained necrotic skeletal muscle fibres (**c** seen in cross-sections, and **e** seen in near-longitudinal sections). Some of the regenerating cells are multinucleated, similar to myotubes. The regenerating cells are also positive for vimentin (**d**). Note further the vimentin-positive macrophages (some are denoted by *arrows*) probably involved in the uptake of the old, necrotic muscle fibres (**d**). In regions of complete resorption of old muscle, multinucleated myotubes have developed (**f**) which again are rich in cardiac α-actin. *Bars*: 50 μm

In grossly damaged muscle tissue with muscle fibre necrosis, e.g. after traumatic injury or upon severe inflammation, regenerating skeletal muscle fibres derived from activated satellite cells, as characterized by cytoplasmic basophilia and a centrally located nucleus and giant-like cells corresponding to multinucleated myotubes (Fig. 6f) always were conspicuous by strong CAA immunoreactivity (Fig. 6c,e). This was especially impressive in the case of a patient whose thigh had been extensively damaged 2 weeks before surgery during which necrotic thigh muscle was removed. The strongly CAA-positive regenerating cells (myoblasts and multinucleated myotubes), derived from activated satellite cells, surrounded the "old", necrotic muscle fibres in a corona-like fashion (Fig. 6c). These regenerating cells and the associated macrophages were also rich in vimentin (Fig. 6d; cf. also [8]).

Moreover, skeletal muscle fibres adjacent to—or included in—fibrotic lesions such as postoperative and post-inflammatory scars, fibromatoses or fibres localized close to the invasion front of malignant tumors also often contained CAA (Fig. 7a–e). In the transition zone between normal muscle and fibrosis, the—predominantly negative—normal staining pattern changed to extended positivity of the mostly still thick, morphologically normal-looking fibres, suggestive of de novo synthesis of CAA in preexisting muscle fibres (Fig. 7a,b). In addition, early regenerating, activated small satellite cells were present in these areas and were characterized by particularly strong immunostaining (Fig. 7b). In the fibrotic zone proper, thin

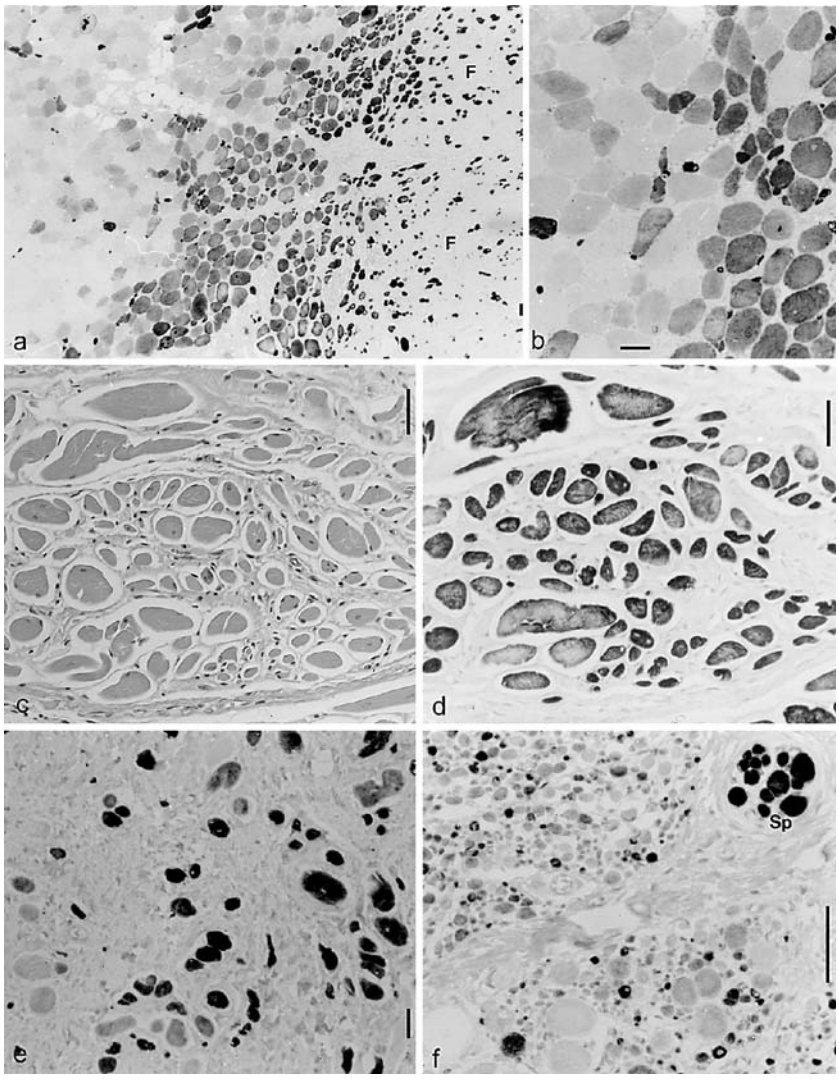

Fig. 7 Immunolocalization on sections, showing induction of cardiac α-actin gene expression in human cases of degenerative (**a**–**e**) and neurogenic (**f**) atrophy. **a** and **b** Abdominal wall muscle of a 40-year-old woman, bordering on a hypertrophic postoperative scar (*to the right*). Note the gradient of cardiac α-actin immunostaining over three zones: (*1*) predominantly negative staining of healthy muscle tissue (*left*); (*2*) zone characterized by moderate increase of cardiac α-actin in the majority of original muscle fibres, probably as the result of a beginning degeneration, in addition to the strong staining of the adjacent activated satellite cells (**a** *middle part*; *right part* in **b**); (*3*) fibrotic zone containing scattered cardiac α-actin-positive regenerating myocytes (**a** *right part*). **c** and **d** Degenerative atrophy of neck muscle (59-year-old man) due to interstitial fibrosis, 6 months after thyroid gland surgery (**c** hematoxylin & eosin staining), showing extensive cardiac α-actin staining (**d**). **e** Degenerative atrophy and regeneration of skeletal muscle fibres with mostly strong cardiac α-actin synthesis in grossly fibrotic pelvic floor muscle of a 73-year-old woman with recurrent rectal carcinoma. **f** In neurogenic atrophy of type Werdnig—Hoffmann (6-month-old boy, lower leg muscle), the small atrophic fibres show a heterogeneous pattern of cardiac α-actin-positive cells while the thicker non-atrophic fibres (*bottom*) display much weaker, if any significant staining. Note also the strongly positive myocytes of the conspicuous muscle spindle (*Sp*, *top right*). *Bars*: 50 μm

regenerating fibres and muscle giant-like cells again displayed strong CAA-staining (Fig. 7a, right-hand portion). In other less severe fibrotic lesions muscle fibres with variable, often reduced diameter also showed marked CAA synthesis (Fig. 7c,d). Because of their generally small nuclei, these might be regarded as mainly degenerative-atrophic cells. Atrophic fibres in regions occupied by dense, old fibrosis also showed strong CAA immunostaining (Fig. 7e). The relationship between muscle fibrosis and CAA synthesis was supported by parallel Azan trichrome staining that highlighted the collagenous matrix in which strongly CAA-positive muscle cells were embedded (Fig. 8a,b).

In cases of neurogenic muscle atrophy of the Werdnig–Hoffmann type, regionally variable patterns were seen, showing heterogeneous CAA immunostaining of the atrophic fibres (Fig. 7f). Here, the strongly stained muscle spindles were particularly conspicuous.

In specimens of Duchenne muscular dystrophy, CAA synthesis was clearly induced and many cells displayed strong and extended immunoreactivity (Fig. 9a,b), with more than half of the muscle fibres being positive with

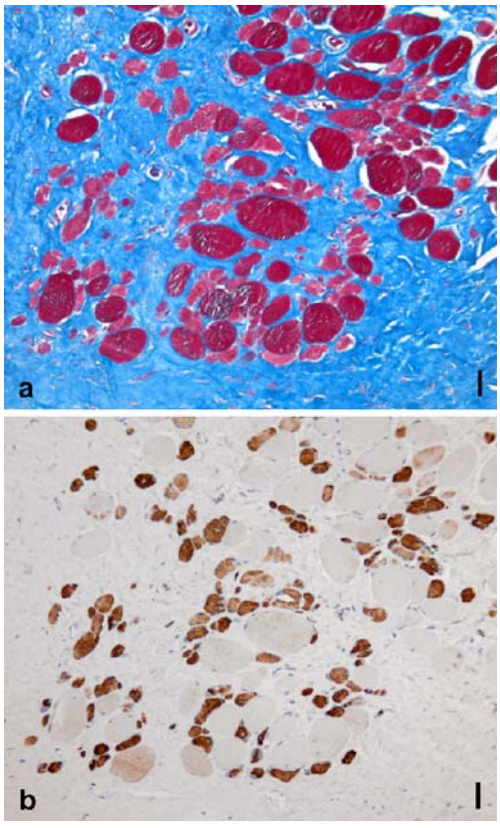

Fig. 8 Relationship between skeletal muscle fibrosis and cardiac α-actin expression as illustrated by the comparison of Heidenhain's Azan staining (**a**) and cardiac α-actin immunostaining (**b**) on consecutive serial sections. Skeletal muscle tissue from the left thoracic wall with interstitial fibrosis and scarring due to previous mammary gland surgery is shown. Note abundant deep blue-staining collagen (**a**) encircling skeletal muscle fibres, of which mainly the thin atrophic ones produce cardiac α-actin (**b**). *Bar*: 50 μm

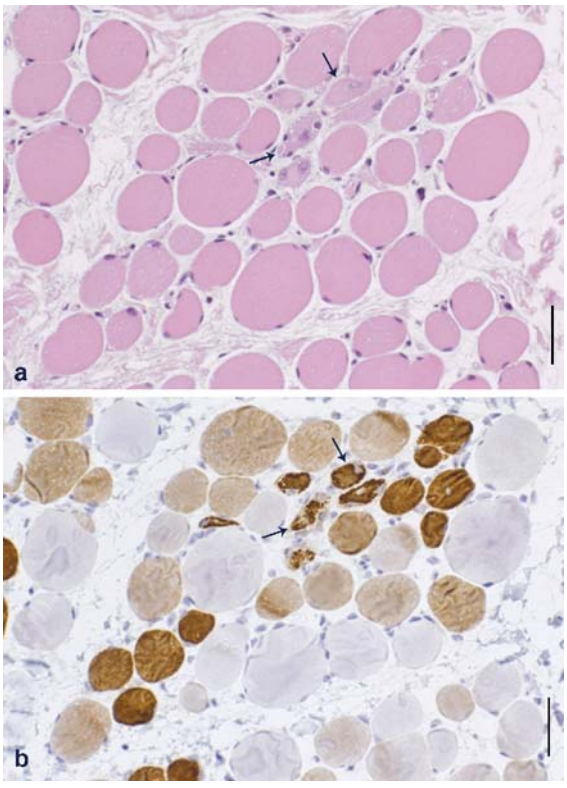

Fig. 9 Immunolocalization of cardiac α-actin in Duchenne muscular dystrophy (paraffin sections derived from an initially frozen muscle biopsy subsequently fixed in formalin). **a** Hematoxylin & eosin stained biopsy from *quadriceps* muscle (3-year-old boy), showing pronounced variability of muscle fibre diameters and a focus of small regenerating fibres with enlarged nuclei (*arrows*). **b** Immunohistochemically, cardiac α-actin is detected in more than half of the muscle fibres, with particularly strong staining of some thin fibres and—consistently—of regenerating fibres (*arrows*). *Bar*: 50 μm

mAb cAc1-20.4.2. Here, the typical thin and regenerating fibres which were focally present were characterized by particularly intense immunostaining.

Immunolocalization of cardiac and smooth muscle α-actin in tumors

Table 2 summarizes the data on cardiac and smooth muscle α-actin in human tumors. Rhabdomyosarcomas of embryonal (Fig. 10a), alveolar (Fig. 10b) and pleomorphic (not shown) types consistently exhibited strong but heterogeneous immunostaining for CAA, often involving the majority of the tumor cells. In the embryonal type tumors, differentiated, frequently strap-shaped, myotube-like tumor cells were rather regularly immunostained, sometimes exhibiting local cross-striation but occasional smaller, undifferentiated tumor cells were also positive (Fig. 10a). In alveolar rhabdomyosarcomas, CAA immunostaining of the tumor cells often appeared in a peripheral rim-like fashion or as a dense plaque (Fig. 10b, inset). Smooth muscle α-actin was focally detected in embryonal tumors but not in our cases of alveolar and pleomorphic rhabdomyosarcomas (not shown). Rhabdomyosarcomatous portions of mixed mesodermal tumors of the female genital tract (not shown) and differentiated rhabdomyomatous cells of nephroblastomas (Fig. 10c) were also strongly stained for CAA.

Among the leiomyomatous tumors, all of which were strongly positive for smooth muscle-α-actin, the majority of uterine leiomyomas examined were CAA negative, but some cases exhibited relatively large proportions of positive cells (Table 2). Leiomyosarcomas were either negative or showed minor, very focal staining (Fig. 10d).

No CAA staining was found in a large diversity of non-myogenic tumors, including malignant fibrous histiocytomas, Ewing's sarcomas and various types of carcinomas (Table 2). As expected, cardiac myxomas were also negative (Table 2) which, however, is not overly surprising in view of the non-myoid character of these tumors [69].

Discussion

Specific immunolocalization of the cardiac isoform of α-actin

Because of their high amino acid sequence homology, the two sarcomeric actins, cardiac and skeletal α-actin, are extremely difficult to distinguish by immunohistochemistry (for refs. see Introduction). However, by immunization of mice with synthetic peptides containing the two amino acid substitutions near the aminoterminus, mAbs have been obtained which specifically recognize the cardiac (cardiac/fetal) α-actin (CAA) isoform in immunohistochemistry and in immunoblot reactions [30] and in enzyme-linked immunosorbent assay (ELISA) assays of body liquids (cf. [31, 32]), in a wide range of species and with excellent optical resolution of the reactive fibril structures (e.g. [1, 6, 15, 21, 71]).

Subsequent to the introduction of our CAA-specific monoclonal antibodies [30], polyclonal antibodies specific for either skeletal [17] or cardiac [18] α-actin, respectively, have also been described. The specificity of our monoclonal CAA antibodies is strongly supported by the completely negative reaction in cryostat and paraffin sections of the vast majority of normal adult skeletal muscle fibres all of which contain abundant skeletal muscle α-actin. Any cross-reactivity with the skeletal muscle α-actin isoform is, therefore, excluded, in agreement with the aforementioned reports using other species and techniques [1, 6, 15, 21, 71]. In agreement with these reports, we reemphasize the cardiac α-isoform specificity of our monoclonal antibodies, and this also holds for cultured mammalian cells as shown in the present study (Fig. 2; cf. also [1]) and for avian cardiomyocytes growing in culture (e.g. [21, 71]). Thus, in contrast to a recent statement by Clément et al. ([18]; see also [14]) that mAb cAc1-20.4.2 would suffer from "obvious difficulties in interpretation, particularly in routine diagnostic procedures", it is our experience and that of several other groups that these monoclonal CAA-specific antibodies are highly reliable reagents that can be recommended for use in a wide range of species and diagnostic problems, in particular when—for cryostat sections—care is taken to challenge the intensity and specificity of antibody binding by an additional wash in high salt buffer (see Materials and methods).

Uniform synthesis of CAA in fetal and adult myocardium

CAA has been reported from several studies to be the predominant actin isoform in cardiomyocytes of fetal and adult heart, both at the mRNA and the protein level, although there are also considerable amounts of skeletal

Table 2 Immunohistochemical detection of α-cardiac and α-smooth muscle actin in various human tumors[a]

Tumor type	No. of cases	Age of patients (years)	α-Cardiac actin[b]	α-Smooth muscle actin[b]
Rhabdomyosarcoma				
Embryonal	3	5/12 to 9	++	(+)
Alveolar	8	6 to 60	+[c], ++	−
Pleomorphic	3	38 to 68	(+), +	−
Malignant mixed mesodermal tumor (uterus, ovary), rhabdomyosarcomatous portion	3	59 to 80	+, ++	(+)
Nephroblastoma[d], rhabdomyomatous differentiation	5	2 to 8	+++	n. d.
Cardiac myxoma	4	61 to 73	−	−, +[e]
Leiomyoma (uterus)	8[f]	32 to 62	−	+++
	3	43, 63, 86	(+)	+++
	1	46	+	+++
	2	48, 62	++	+++
Leiomyosarcoma (uterus, neck, arm, thigh)	6	49 to 81	−, (+)	+++
Gastrointestinal stromal tumor	6	44 to 81	−	−, +[e], ++[e]
Malignant fibrous histocytoma	9	39 to 76	−	−, +
Fibrosarcoma	8	46 to 82	−[g]	− to ++
Extraskeletal Ewing's sarcoma	1	58	−	n. d.
Alveolar soft part sarcoma	1	33	−	(+)
Various carcinomas[h]	9	43 to 78	−	−

[a] As determined by immunohistochemistry (paraffin sections; mAbs cAc1-20.4.2, anti-αsm-1)
[b] − Negative, *(+)* 1–10% of tumor cells positive, + 11–50% positive, ++ 51–90% positive, +++ 91–100% positive, *n.d.* not determined
[c] In two cases, +
[d] In all but one cases, the patients had been treated preoperatively by chemotherapy
[e] One case
[f] Late pregnancy in one case
[g] In one case (+), showing ~1% positive tumor cells
[h] These cases comprised breast carcinomas, oral squamous cell carcinomas and colorectal adenocarcinomas

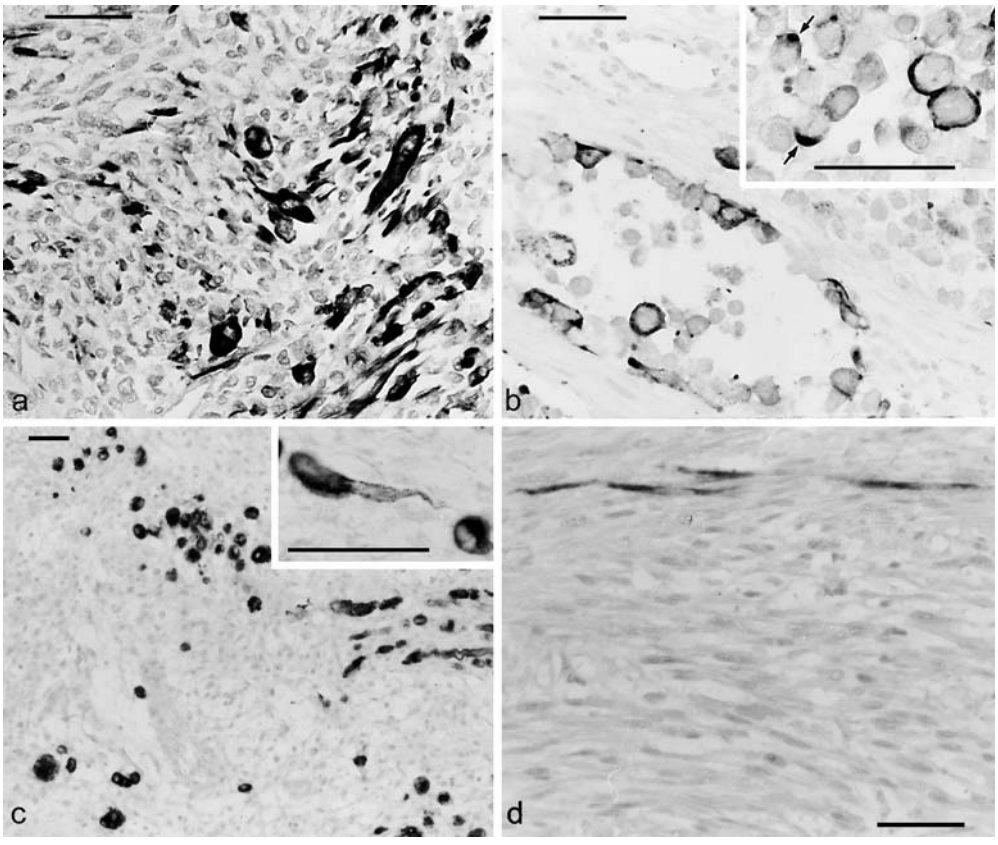

Fig. 10 Immunohistochemistry showing the synthesis of cardiac α-actin in soft tissue sarcomas and nephroblastoma. **a**, **b** Heterogeneous cardiac α-actin immunostaining in embryonal (**a** 27-year-old man) and alveolar (**b** 63-year-old man) rhabdomyosarcoma. Note intense staining of differentiated, strap-shaped, myotube-like rhabdomyoblasts but also of some undifferentiated small cells. The *arrows* in the *inset* in **b** denote plaque-like immunostaining in some primitive tumor cells of alveolar rhabdomyosarcoma. **c** In nephroblastoma after chemotherapy (8-year-old girl), differentiated rhabdomyomatous cells are strongly reactive for cardiac α-actin (the *inset* shows a cell with a process with delicate cross-striation). **d** Only very low and focal synthesis of cardiac α-actin in leiomyosarcoma of left upper arm (78-year-old man). *Bars*: 50 μm

muscle α-actin present in the fetal heart (cf. [39, 54, 55, 73, 89]). In diverse vertebrate species, human included, heart development and neonatal growth have been shown to be characterized by the reduction of skeletal muscle α-actin (for references, see above) and by the induced synthesis of myocardium-specific isoforms of a range of other proteins, notably various contractile fibre molecules (for review, see Wu [98]). Our immunohistochemical results based on mAbs have confirmed the uniform occurrence of CAA in all fetal and adult human cardiomyocytes (see also [30]), without noticeable exception. As to fetal myocardium, our results confirm previous data obtained with polyclonal antibodies [83].

The significance and importance of the CAA isoform for the development and the functions of the heart is not yet clear. However, essential specific functions are evident from gene "knock-out" experiments [49], its specific organization in early chicken sarcomeres [21] and the discovery that mutations in the human CAA gene cause both idiopathic dilated cardiomyopathy and familial hypertrophic cardiomyopathy [58, 64]. The present study also confirms the constitutive role of two specific desmosomal plaque proteins, desmoplakin and plakophilin 2, in the intercalated disks of both fetal and adult human heart where they occur in specific complex adhering junctions recently characterized as "areae compositae" [10]. Recently, it has also been reported that both desmoplakin and plakophilin 2 are of central importance for the integrity of the myocardial tissue and cardiac functioning ([37]; see also [10, 34]).

Down-regulation of CAA in developing skeletal muscle but persistence in neuromuscular spindle myocytes

Previous biochemical studies have shown that fetal skeletal muscle of various species contains considerable amounts of CAA [44, 55, 57, 68, 73, 85, 89]. In fact, in early embryogenesis, CAA is generally the predominant sarcomeric actin isoform (e.g. [44, 55, 68, 73]), and expression of the CAA gene appears to precede that of the gene encoding skeletal muscle α-actin ([21, 85] and refs. cited therein). This has also been demonstrated in cultures of chicken embryonic myoblasts in which CAA is detected in postmitotic cells, whereas, skeletal muscle α-actin appears only later, i.e. in differentiated multinucleated myotubes (e.g. [45, 84]). Our present results extend these findings to the cellular level and allow the conclusion that at least until the second third of pregnancy, most human fetal skeletal muscle cells contain CAA in addition to skeletal muscle α-actin (see also [44, 55, 57, 68, 73, 85, 89]). Moreover, developing skeletal muscle cells can transiently synthesize still another α-actin, i.e. smooth muscle-type α-actin (see Fig. 4a; cf. [7, 44, 55, 65, 96, 97]; for refs. see also [82]).

In adult skeletal muscle, the synthesis of CAA as the "fetal" isoform is known to be grossly down-regulated [57]. However, as a low amount of this isoform, representing less than 5% of the total α-actin present, has been reported in biochemical studies after tissue homogenization at the mRNA [39, 57] and at the protein [89] level, it has, so far, not been possible to decide whether

every skeletal muscle cell contains such a low amount or whether a few muscle cells are characterized by relatively high amounts of CAA while the majority of the cells contains very little, if any. Our present study has demonstrated that the second possibility, i.e. cell type heterogeneity, is correct: only a minor proportion of adult skeletal muscle cells has been identified to contain the CAA isoform, with particular enrichment in relatively thin fibres, as also verified by morphometric analysis. Some of these might represent regenerating fibres that—at least in part—might result from activation upon occult microtraumatization or nonspecific fibre necrosis. Clearly, the scattered, apparently random localization pattern of the CAA-positive skeletal muscle cells argues against a nerve-dependent distribution of this population of fibres. An apparent absence of CAA in neonatal and in normal adult skeletal muscle fibres has been noted by Chen et al. [15], whereas, most of our normal skeletal muscle specimens exhibited some CAA-positive myofibres. Future experiments will have to show how the CAA-positive subpopulation of myofibres is structurally and functionally distinguished from the major population of CAA-negative myofibres.

In addition, however, a consistent source of CAA in adult skeletal muscle are the modified muscle fibres of neuromuscular spindles. These relatively thin fibres, believed to act as sensors of muscle tension (e.g. [25]), obviously maintain a more fetal stage of differentiation as reflected by their actin pattern. Which special functions the CAA may serve in these spindle myocytes is presently an open question.

In summary, the previous and the present results collectively show that co-expression of cardiac and skeletal muscle α-actin isoforms is a feature of both fetal myocardium and fetal skeletal muscle, with inverse dynamics of down-regulation during development. In the regulation of this co-expression, the expression of the CAA gene seems to play a primary role, suggestive of a negative *trans* effect on the synthesis of skeletal muscle α-actin (for discussion, see [23, 49]).

Induction of CAA synthesis in pathologically altered skeletal muscle

Of particular interest in biology and medicine is our finding of strongly increased CAA synthesis in regenerating skeletal muscle. Resting satellite cells, considered to represent a tissue-bound reservoir of stem cells for skeletal muscle repair ([4, 5, 77]; for special aspects see also [70, 78]), seem to lack this actin isoform, as in healthy adult skeletal muscle, no small round cells immunostained for CAA are found in the fibre periphery (see also Fig. 4c,d of this study). However, when satellite cells are activated at the onset of regeneration, CAA synthesis appears to be induced and up-regulated. In our studies, we have been impressed that—within 2 weeks after necrotizing muscle trauma—activated satellite cells, myoblasts and multinucleated myotubes become strongly positive for CAA (see, e.g., Fig. 6c). The exact onset and mechanism of CAA synthesis during early skeletal muscle regeneration remains to be elucidated (for a relevant in vitro culture study, see [4]; for a study at the mRNA level in rats, see [86]).

In diagnostic muscle pathology, regenerating skeletal muscle fibres, being similar to myotubes, are routinely recognized by certain morphological criteria such as cytoplasmic basophilia, acridine orange positivity and central nuclei, but unequivocal identification is often difficult. Therefore, immunohistochemical markers of fibre regeneration are of potential diagnostic value. Several such markers have been proposed in the literature, notably intermediate filament proteins such as vimentin [8, 33], desmin [33, 46] and nestin [80]. Among them, vimentin seems to be a marker of early regeneration while nestin and increased desmin contents seem to be characteristic of later stages [80]. Perhaps surprisingly, molecules of the muscular contractile apparatus have, so far, not been included in the diagnostic armamentarium for muscular regeneration (see also [86]). Clearly, CAA can now be added as a reliable marker indicative of skeletal muscle regeneration.

The immunohistochemical diagnostic potential of CAA is particularly obvious in Duchenne's muscular dystrophy (DMD). For this disease, our study generally confirms and extends previous results of upregulation of the transcription of the CAA gene [3, 15]. Chen et al. [15] have found a majority of DMD muscle fibres (60–80%) to be CAA positive, using the same mAb as in the present study on cryostat sections. These authors suggested that the marked abnormal persistence of CAA after birth in all types of DMD muscle protein deficiency, including its presence in morphologically fully developed myofibres, may not be due to regenerative processes but rather may reflect a chronic dysregulation resulting in some kind of undifferentiated state (see also [3]). We, however, have noted in DMD, a particularly strong staining of small fibres displaying typical regenerative morphology (e.g., Fig. 9), which suggests some association with muscle fibre regeneration. Whether the DMD muscle fibres expressing the CAA gene are identical to the fast type IIb fibres that have been shown to be preferentially affected in DMD [92] will be examined in a separate study. From these findings, it now seems also mandatory to apply CAA immunostaining to further myopathies potentially associated with regenerative processes such as neurogenic conditions and other atrophic muscular processes of various etiologies, including true myopathies, inflammatory and congenital myopathies [16].

Another significant and interesting finding is the highly increased level of CAA synthesis upon non-necrotizing skeletal muscle damage such as in areas of fibrosis and scarring or at the invasion front of malignant tumors. Although in these situations, regenerative processes through activation of satellite cells can also occur, it appears that at least some CAA-positive skeletal muscle fibres that lack criteria of regeneration such as cytoplasmic basophilia have survived the damage but have undergone some sort of "dedifferentiation" in the sense of a degenerative atrophy due to inactivity and/or loss of innervation. Indeed, CAA may well be induced very early during

degeneration when fibrosis and morphological changes of muscle fibres are not yet obvious (see, e.g., Fig. 7a,b). Thus, CAA may emerge as a general marker for a reactive state of skeletal muscle, including true regeneration and reaction to non-specific damage and degeneration, and this reaction pattern may be interpreted as another example of atavism to a fetal state of gene expression (for other examples in pathology see, e.g., [36, 61]).

CAA in certain smooth muscle cells

For the first time, we have demonstrated the unexpected finding of variable and focal synthesis of CAA in certain subtypes of visceral smooth muscle cells. Quite surprisingly, in gall bladder muscle—both normal and hypertrophic (in the setting of chronic cholecystitis)—this actin isoform has been generally observed, the functional significance of which, however, remains to be elucidated. By contrast, gastrointestinal and uterine smooth muscle have been totally negative or positive only in relatively sparse cells (for an observation of isolated small groups of positive myometrial cells see [6]). McHugh et al. [55] have suggested an ectopic CAA gene expression in certain visceral smooth muscle tissues such as the ileum, but their Northern blot results have not provided information on the actual cell type involved.

As to vascular smooth muscle cells, focal CAA positivity has already been reported in umbilical cord arteries and in atherosclerotic lesions [6] and—apparently rarely—in some small arteries and intratumoral vessels [18]. The present study confirms these findings and extends the spectrum of CAA-positive vascular smooth muscle cells to media cells of the human aorta.

CAA as a marker for striated muscle differentiation in malignant tumors

In the pathological diagnosis of soft tissue tumors, the detection or confirmation of striated muscle differentiation to prove a rhabdomyosarcoma may be difficult, in particular, when cells with pathognomic cross-striations are absent [93]. In such cases, immunohistochemical markers gain special importance for accurate diagnosis, including desmin as a broad myogenic marker which, however, does not discriminate between rhabdo- and leiomyosarcomatous tumors. Moreover, desmin can also occur in certain non-muscle tumors such as malignant mesotheliomas [47], malignant peripheral nerve sheath tumors, primitive neuroectodermal tumors and epithelioid sarcomas [12]. Available markers specific for striated muscle differentiation include myoglobin, which, however, is of limited value [19], the heavy chain of fetal skeletal myosin [24], titin [67], and the myogenic regulatory proteins myogenin and MyoD1 ([90]; for further refs., see also [14]). Although the last two proteins, as nuclear transcription factors, have been reported to be of diagnostic value in a number of studies, they also face limitations [13].

In addition, antibodies against sarcomeric α-actin such as the IgM mAb α-sr1, reactive with both CAA and skeletal muscle α-actin, have been used on cryostat or paraffin sections [14, 75, 76, 81, 91], and here, positive reactions of rhabdomyosarcomas might as well reflect the synthesis of CAA. However, in one study, 27% of rhabdomyosarcomas studied as paraffin-embedded tissue have failed to stain with the α-sr1 antibody [91]. Using polyclonal antibodies, Clément et al. ([18]; for review, see also [14]) have published the immunohistochemical detection of CAA in all 17 rhabdomyosarcomas of different subtypes. This is well in line with the present results showing cytoplasmic CAA staining in all 14 rhabdomyosarcoma cases studied, albeit to a variable extent (see also [30]). With mAb cAc1-20.4.2, showing superior performance on routine paraffin sections, we here introduce a reliable, simple to use, "permanent" reagent for the specific detection of CAA, specifically for the recognition of rhabdomyogenic differentiation in malignant tumors.

That rhabdomyosarcomas, believed to be derived from relatively undifferentiated mesenchymal cells, synthesize CAA as the major sarcomeric actin isoform has previously been suggested on the basis of mRNA analyses [76, 85]. We, here, present evidence that in these tumors, CAA is present not only in morphologically differentiated cells (rhabdomyoblasts) but also in some undifferentiated tumor cells (see also [18]). The occurrence of CAA in malignant rhabdomyogenic cells is not surprising in the light of its general sarcomeric occurrence in embryonic and fetal striated muscles. Understandable in this context are also our novel findings that CAA can be found in the rhabdomyosarcomatous elements of mixed Müllerian tumors of the female genital tract and in the "mature", differentiated rhabdomyomatous (skeletal muscle-type) cells present in nephroblastomas, in particular, after chemotherapy. Our finding of an occasional, focal presence of CAA in leiomyosarcomas is in agreement with previous reports of two cases of such tumors showing immunostaining for sarcomeric α-actin [75] and of 2 out of 8 leiomyosarcomas being focally positive with the polyclonal antibody preparations against CAA [18]. Thus, similar to the situation of normal smooth muscle cells, this might again indicate a low level of CAA synthesis in malignantly transformed smooth muscle cells. Clearly, the maintained predominance of the autochthonous smooth muscle α-actin prevents diagnostic misinterpretations of such smooth muscle tumors as rhabdomyosarcomas.

Important in this context and as a basis for the general histodiagnostic application of CAA as a marker for rhabdomyosarcomas is the practical exclusion of any unspecific occurrence of this isoform in non-myogenic soft tissue sarcomas. In the course of the present study, we found complete absence of CAA immunostaining in 25 malignant, non-myogenic soft tissue tumors, including fibrosarcomas and malignant fibrous histiocytomas, underscoring the high specificity of the CAA marker.

Conclusions and perspectives

Besides the various immunohistological applications discussed above, specific antibodies against CAA might also be useful in the serological detection of this actin isoform in patients with myocardial damage. Indeed, this protein appears to be a particularly interesting myocardial infarction marker candidate as it is present in cardiomyocytes in large amounts and is relatively stable against proteolytic degradation (for references, see [30–32]). Because of the low CAA content in normal skeletal muscle, traumatization of such muscles should not give rise to false-positive serological results as may be the case for several other myocardial infarction markers. In preliminary experiments, we have also encountered some interesting positive serological findings in certain patients suffering from chronic skeletal muscle diseases, including DMD cases.

In conclusion, we have shown that antibodies specific for the cardiac isoform of α-actin can be used in routine pathology to detect or exclude specific diseases or regenerative and degenerative processes of skeletal muscle. These antibodies may also contribute to a better understanding of physiological and pathological processes in muscle biology and myogenic tumor formations. Therefore, it can be expected that monoclonal CAA antibodies will find their place within the immunohistochemical marker panel for the diagnosis of soft tissue tumors, as they are already successfully used in developmental biology (e.g. [1, 21, 71]). They also might be applied for monitoring of the differentiation state of stem cells on their way to myocardiac repair (e.g. [38, 52, 53, 66, 87, 90]). The ultimate specific marker combination to recognize cardiomyogenesis, however, should include myocardium-specific contractile proteins such as CAA and intercalated disk components absent from skeletal muscle such as desmoplakin and plakophilin 2 (cf. [10, 28, 34, 37]), as there is no other cell differentiation pathway known that combines the myocardial contractile apparatus with the desmosomal ensemble of junction proteins.

Acknowledgements We would like to thank Gabriele Bauer, Christine Grund, Angela Hartmann, Heike Geissel, Anke Roeper and Heidemarie Schumacher for excellent technical assistance, Petra Krupitza and Jutta Osterholt for preparing the figures and Eva Gundel and Tanja Wolf for typing the manuscript.

The authors declare that the experiments comply with the current laws of Germany.

Supported by the Deutsche Krebshilfe (Förderungsschwerpunkt "Zelladhäsion, Migration und Invasion", grants 10-2049-Fr I and 10-2026-Schm I)

References

1. Ahuja P, Perriard E, Perriard J-C, Ehler E (2004) Sequential myofibrillar breakdown accompanies mitotic division of mammalian cardiomyocytes. J Cell Sci 117:3295–3306
2. Babai F, Musevi-Aghdam J, Schürch W, Royal A, Gabbiani G (1990) Coexpression of alpha-sarcomeric actin, alpha-smooth muscle actin and desmin during myogenesis in rat and mouse embryos. I. Skeletal muscle. Differentiation 44:132–142
3. Bakay M, Zhao P, Chen J, Hoffman EP (2002) A web-accessible complete transcriptome of normal human and DMD muscle. Neuromuscul Disord 12(Suppl 1):S125–S141
4. Baroffio A, Bochaton-Piallat M-L, Gabbiani G, Bader CR (1995) Heterogeneity in the progeny of single human muscle satellite cells. Differentiation 59:259–268
5. Baroffio A, Hamann M, Bernheim L, Bochaton-Piallat M-L, Gabbiani G, Bader CR (1996) Identification of self-renewing myoblasts in the progeny of single human muscle satellite cells. Differentiation 60:47–57
6. Bea F, Bär H, Watson L, Blessing E, Kübler W, Kreuzer J, Jahn L (2000) Cardiac α-actin in smooth muscle cells: detection in umbilical cord vessels and in atherosclerotic lesions. Basic Res Cardiol 95:106–113
7. Bochaton-Piallat M-L, Ropraz P, Gabbiani G, Santeusanio G, Palmieri G, Schiaroli S, Spagnoli LG (1992) Actin isoform and intermediate filament protein expression in human developing skeletal muscle. Basic Appl Myol 2:83–87
8. Bornemann A, Schmalbruch H (1992) Desmin and vimentin in regenerating muscles. Muscle Nerve 15:14–20
9. Borrmann C (2000) Molekulare Charakterisierung der Adhärens-Zellverbindungen des Herzens: Identifizierung einer neuen Art, der Area composita. Ph.D. Thesis. University of Heidelberg, Heidelberg, Germany, 119 pp
10. Borrmann CM, Grund C, Kuhn C, Hofmann I, Pieperhoff S, Franke WW (2006) The *area composita* of adhering junctions connecting heart muscle cells of vertebrates. II. Colocalizations of desmosomal and *fascia adhaerens* molecules in the intercalated disk. Eur J Cell Biol Apr 3 [Epub ahead of print]
11. Campion DR (1984) The muscle satellite cell: a review. Int Rev Cytol 87:225–251
12. Cerilli LA, Wick MR (2002) Immunohistology of soft tissue and osseous neoplasms. In: Dabbs DJ (ed) Diagnostic immunohistochemistry. Churchill Livingstone, New York. pp 59–112, Chapter 3
13. Cessna MH, Zhou H, Perkins SL, Tripp SR, Layfield L, Daines C, Coffin CM (2001) Are myogenin and myoD1 expression specific for rhabdomyosarcoma? A study of 150 cases, with emphasis on spindle cell mimics. Am J Surg Pathol 25:1150–1157
14. Chaponnier C, Gabbiani G (2004) Pathological situations characterized by altered actin isoform expression. J Pathol 204:386–395
15. Chen Y-W, Zhao P, Borup R, Hoffman EP (2000) Expression profiling in the muscular dystrophies: identification of novel aspects of molecular pathophysiology. J Cell Biol 151:1321–1336
16. Clarkson E, Costa EF, Machesky LM (2004) Congenital myopathies: diseases of the actin cytoskeleton. J Pathol 204: 407–417
17. Clément S, Chaponnier C, Gabbiani G (1999) A subpopulation of cardiomyocytes expressing alpha-skeletal actin is identified by a specific polyclonal antibody. Circ Res 85:e51–e58
18. Clément S, Orlandi A, Bocchi L, Pizzolato G, Foschini MP, Eusebi V, Gabbiani G (2003) Actin isoform pattern expression: a tool for the diagnosis and biological characterization of human rhabdomyosarcoma. Virchows Arch 442:31–38
19. Dodd S, Malone M, McCulloch W (1989) Rhabdomyosarcoma in children: a histological and immunohistochemical study of 59 cases. J Pathol 158:13–18
20. Drenckhahn D, von Gaudecker B, Müller-Hermelink HK, Unsicker K, Gröschel-Stewart U (1979) Myosin and actin containing cells in the human postnatal thymus. Virchows Arch B Cell Pathol 32:33–45
21. Ehler E, Fowler VM, Perriard J-C (2004) Myofibrillogenesis in the developing chicken heart: role of actin isoforms and of the pointed end actin capping protein tropomodulin during thin filament assembly. Dev Dyn 229:745–755
22. Eimoto T, Kusano T, Ando K, Kikuchi M, Shirakusa T, Kawanami S (1990) Nonneoplastic and nonhyperplastic thymus in myasthenia gravis. Am J Clin Pathol 94:36–43

23. Einat P, Shani M, Yaffe D (1990) The amount of the endogenous and exogenous skeletal muscle actin mRNA in the heart of transgenic mice is affected by the genotype of the cardiac actin gene. Differentiation 44:36–41
24. Eusebi V, Ceccarelli C, Gorza L, Schiaffino S, Bussolati G (1986) Immunocytochemistry of rhabdomyosarcoma. The use of four different markers. Am J Surg Pathol 10:293–299
25. Fawcett DW (1994) Bloom and Fawcett—a textbook of histology, 12th edn. Chapman & Hall, New York. pp 287–292
26. Franke WW, Schmid E, Vandekerckhove J, Weber K (1980) A permanently proliferating rat vascular smooth muscle cell with maintained expression of smooth muscle characteristics, including actin of the vascular smooth muscle type. J Cell Biol 87:594–600
27. Franke WW, Schmid E, Grund C, Müller H, Engelbrecht I, Moll R, Stadler J, Jarasch E-D (1981) Antibodies to high molecular weight polypeptides of desmosomes: specific localization of a class of junctional proteins in cells and tissues. Differentiation 20:217–241
28. Franke WW, Moll R, Schiller DL, Schmid E, Kartenbeck J, Müller H (1982) Desmoplakins of epithelial and myocardial desmosomes are immunologically and biochemically related. Differentiation 23:115–127
29. Franke WW, Moll R, Müller H, Schmid E, Kuhn C, Krepler R, Artlieb U, Denk H (1983) Immunocytochemical identification of epithelium-derived human tumors with antibodies to desmosomal plaque proteins. Proc Natl Acad Sci USA 80:543–547
30. Franke WW, Stehr S, Stumpp S, Kuhn C, Heid H, Rackwitz H-R, Schnölzer M, Baumann R, Holzhausen H-J, Moll R (1996) Specific immunohistochemical detection of cardiac/fetal α-actin in human cardiomyocytes and regenerating skeletal muscle cells. Differentiation 60:245–250
31. Franke WW, Stumpp S, Stehr S (1999) Antibodies against heart muscle actin. United States Patent No. 5,972,633
32. Franke WW, Stumpp S, Stehr S (2001) Antikörper gegen Herzmuskel-Actin. Europäische Patentschrift EP 0 820 471 B1
33. Gallanti A, Prelle A, Moggio M, Ciscato P, Checcarelli N, Sciacco M, Comini A, Scarlato G (1992) Desmin and vimentin as markers of regeneration in muscle diseases. Acta Neuropathol (Berl) 85:88–92
34. Gerull B, Heuser A, Wichter T, Paul M, Basson CT, McDermott DA, Lerman BB, Markowitz SM, Ellinor PT, MacRae CA, Peters S, Grossmann KS, Drenckhahn J, Michely B, Sasse-Klaassen S, Birchmeier W, Dietz R, Breithardt G, Schulze-Bahr E, Thierfelder L (2004) Mutations in the desmosomal protein plakophilin-2 are common in arrhythmogenic right ventricular cardiomyopathy. Nat Genet 36:1162–1164
35. Goodson HV, Hawse WF (2002) Molecular evolution of the actin family. J Cell Sci 115:2619–2622
36. Gröne HJ, Weber K, Gröne E, Helmchen U, Osborn M (1987) Coexpression of keratin and vimentin in damaged and regenerating tubular epithelia of the kidney. Am J Pathol 129:1–8
37. Grossmann KS, Grund C, Huelsken J, Behrend M, Erdmann B, Franke WW, Birchmeier W (2004) Requirement of plakophilin 2 for heart morphogenesis and cardiac junction formation. J Cell Biol 167:149–160
38. Guan K, Fürst DO, Wobus AM (1999) Modulation of sarcomere organization during embryonic stem cell-derived cardiomyocyte differentiation. Eur J Cell Biol 78:813–823
39. Gunning P, Ponte P, Blau H, Kedes L (1983) α-Skeletal and α-cardiac actin genes are coexpressed in adult human skeletal muscle and heart. Mol Cell Biol 3:1985–1995
40. Gunning P, Ferguson V, Brennan K, Hardeman E (1997) Impact of α-skeletal actin but not α-cardiac actin on myoblast morphology. Cell Struct Funct 22:173–179
41. Gunning PW, Ferguson V, Brennan KJ, Hardeman EC (2001) α-Skeletal actin induces a subset of muscle genes independently of muscle differentiation and withdrawal from the cell cycle. J Cell Sci 114:513–524
42. Harvey RP, Rosenthal N (eds) (1999) Heart Development. Academic Press, San Diego, CA, USA, 530 pp
43. Hawke TJ, Garry DJ (2001) Myogenic satellite cells: physiology to molecular biology. J Appl Physiol 91:534–551
44. Hayward LJ, Schwartz RJ (1986) Sequential expression of chicken actin genes during myogenesis. J Cell Biol 102: 1485–1493
45. Hayward LJ, Zhu YY, Schwartz RJ (1988) Cellular localization of muscle and nonmuscle actin mRNAs in chicken primary myogenic cultures: the induction of α-skeletal actin mRNA is regulated independently of α-cardiac actin gene expression. J Cell Biol 106:2077–2086
46. Helliwell TR, Gunhan O, Edwards RHT (1989) Lectin binding and desmin expression during necrosis, regeneration, and neurogenic atrophy of human skeletal muscle. J Pathol 159:43–51
47. Hurlimann J (1994) Desmin and neural marker expression in mesothelial cells and mesotheliomas. Hum Pathol 25:753–757
48. Kirchner T, Hoppe F, Schalke B, Müller-Hermelink HK (1988) Microenvironment of thymic myoid cells in myasthenia gravis. Virchows Arch B Cell Pathol 54:295–302
49. Kumar A, Crawford K, Close L, Madison M, Lorenz J, Doetschman T, Pawlowski S, Duffy J, Neumann J, Robbins J, Boivin GP, O'Toole BA, Lessard J (1997) Rescue of cardiac alpha-actin-deficient mice by enteric smooth muscle gamma-actin. Proc Natl Acad Sci USA 94:4406–4411
50. Langbein L, Grund C, Kuhn C, Praetzel S, Kartenbeck J, Brandner JM, Moll I, Franke WW (2002) Tight junctions and compositionally related junctional structures in mammalian stratified epithelia and cell cultures derived therefrom. Eur J Cell Biol 81:419–435
51. Langbein L, Pape U-F, Grund C, Kuhn C, Praetzel S, Moll I, Moll R, Franke WW (2003) Tight junction-related structures in the absence of a lumen: occludin, claudins and tight junction plaque proteins in densely packed cell formations of stratified epithelia and squamous cell carcinomas. Eur J Cell Biol 82:385–400
52. Makino S, Fukuda K, Miyoshi S, Konishi F, Kodama H, Pan J, Sano M, Takahashi T, Hori S, Abe H, Hata J-I, Umezawa A, Ogawa S (1999) Cardiomyocytes can be generated from marrow stromal cells in vitro. J Clin Invest 103:697–705
53. Malouf NN, Coleman WB, Grisham JW, Lininger RA, Madden VJ, Sproul M, Anderson PA (2001) Adult-derived stem cells from the liver become myocytes in the heart in vivo. Am J Pathol 158:1929–1935
54. Mayer Y, Czosnek H, Zeelon PE, Yaffe D, Nudel U (1984) Expressing of the genes coding for the skeletal muscle and cardiac actins in the heart. Nucleic Acids Res 12:1087–1100
55. McHugh KM, Crawford K, Lessard J (1991) A comprehensive analysis of the developmental and tissue-specific expression of the isoactin multigene family in the rat. Dev Biol 148:442–458
56. Mertens C, Kuhn C, Moll R, Schwetlick I, Franke WW (1999) Desmosomal plakophilin 2 as a differentiation marker in normal and malignant tissues. Differentiation 64:277–290
57. Minty AJ, Alonso S, Caravatti M, Buckingham ME (1982) A fetal skeletal muscle actin mRNA in the mouse and its identity with cardiac actin mRNA. Cell 30:185–192
58. Mogensen J, Klausen IC, Pedersen AK, Egeblad H, Bross P, Kruse TA, Gregersen N, Hansen PS, Baandrup U, Borglum AD (1999) α-Cardiac actin is a novel disease gene in familial hypertrophic cardiomyopathy. J Clin Invest 103:R39–R43
59. Moll R, Franke WW, Schiller D, Geiger B, Krepler R (1982) The catalog of human cytokeratins: patterns of expression in normal epithelia, tumors and cultured cells. Cell 31:11–24
60. Moll R, Cowin P, Kapprell H-P, Franke WW (1986) Desmosomal proteins: new markers for identification and classification of tumors. Lab Invest 54:4–25
61. Moll R, Hage C, Thoenes W (1991) Expression of intermediate filament proteins in fetal and adult human kidney: modulations of intermediate filament patterns during development and in damaged tissue. Lab Invest 65:74–86

62. Moll R (1993) Cytokeratins as markers of differentiation: expression profiles in epithelia and epithelial tumors. Progress in Pathology, vol. 142, Gustav Fischer, Stuttgart, pp 1–197
63. Moran CA, Koss MN (1993) Rhabdomyomatous thymoma. Am J Surg Pathol 17:633–636
64. Olson TM, Michels VV, Thibodeau SN, Tai Y-S, Keating MT (1998) Actin mutations in dilated cardiomyopathy, a heritable form of heart failure. Science 280:750–752
65. Ordahl CP (1986) The skeletal and cardiac alpha-actin genes are coexpressed in early embryonic striated muscle. Dev Biol 117:488–492
66. Orlic D, Kajstura J, Chimenti S, Jakoniuk I, Anderson SM, Li BS, Picel J, McKay R, Nadal-Ginard B, Bodine DM, Leri A, Anversa P (2001) Bone marrow cells regenerate infarcted myocardium. Nature 410:701–705
67. Osborn M, Hill C, Altmannsberger M, Weber K (1986) Monoclonal antibodies to titin in conjunction with antibodies to desmin separate rhabdomyosarcomas from other tumor types. Lab Invest 55:101–108
68. Paterson BM, Eldridge JD (1984) α-Cardiac actin is the major sarcomeric isoform expressed in embryonic avian skeletal muscle. Science 224:1436–1438
69. Pucci A, Gagliardotto P, Zanini C, Pansini S, di Summa M, Mollo F (2000) Histopathologic and clinical characterization of cardiac myxoma: review of 53 cases from a single institution. Am Heart J 140:134–138
70. Rouger K, Brault M, Daval N, Leroux I, Guigand L, Lesoeur J, Fernandez B, Cherel Y (2004) Muscle satellite cell heterogeneity: in vitro and in vivo evidences for populations that fuse differently. Cell Tissue Res 317:319–326
71. Rudy DE, Yatskievych TA, Antin PB, Gregorio CC (2001) Assembly of thick, thin, and titin filaments in chick precardiac explants. Dev Dyn 221:61–71
72. Ruzicka DK, Schwartz RJ (1988) Sequential activation of α-actin genes during avian cardiogenesis: vascular smooth muscle α-actin gene transcripts mark the onset of cardiomyocyte differentiation. J Cell Biol 107:2575–2586
73. Sassoon DA, Garner I, Buckingham M (1988) Transcripts of α-cardiac and α-skeletal actins are early markers for myogenesis in the mouse embryo. Development 104:155–164
74. Schmid E, Tapscott S, Bennett GS, Croop J, Fellini SA, Holtzer H, Franke WW (1979) Differential location of different types of intermediate-sized filaments in various tissues of the chicken embryo. Differentiation 15:27–40
75. Schürch W, Skalli O, Seemayer TA, Gabbiani G (1987) Intermediate filament proteins and actin isoforms as markers for soft tissue tumor differentiation and origin. I. Smooth muscle tumors. Am J Pathol 128:91–103
76. Schürch W, Bochaton-Piallat ML, Geinoz A, d'Amore E, Laurini RN, Cintorino M, Begin LR, Boivin Y, Gabbiani G (1994) All histological types of primary human rhabdomyosarcoma express alpha-cardiac and not alpha-skeletal actin messenger RNA. Am J Pathol 144:836–846
77. Seale P, Asakura A, Rudnicki MA (2001) The potential of muscle stem cells. Dev Cell 1:333–342
78. Sherwood RI, Christensen JL, Conboy IM, Conboy MJ, Rando TA, Weissman IL, Wagers AJ (2004) Isolation of adult mouse myogenic progenitors: functional heterogeneity of cells within and engrafting skeletal muscle. Cell 119:543–554
79. Shi SR, Key ME, Kalra KL (1991) Antigen retrieval in formalin-fixed, paraffin-embedded tissues: an enhancement method for immunohistochemical staining based on microwave oven heating of tissue sections. J Histochem Cytochem 39: 741–748
80. Sjoberg G, Edstrom L, Lendahl U, Sejersen T (1994) Myofibers from Duchenne/Becker muscular dystrophy and myositis express the intermediate filament nestin. J Neuropathol Exp Neurol 53:416–423
81. Skalli O, Gabbiani G, Babai F, Seemayer TA, Pizzolato G, Schürch W (1988) Intermediate filament proteins and actin isoforms as markers for soft tissue tumor differentiation and origin. II. Rhabdomyosarcomas. Am J Pathol 130:515–531
82. Springer ML, Ozawa CR, Blau HM (2002) Transient production of α-smooth muscle actin by skeletal myoblasts during differentiation in culture and following intramuscular implantation. Cell Motil Cytoskelet 51:177–186
83. Suurmeijer AJ, Clément S, Francesconi A, Bocchi L, Angelini A, van Veldhuisen DJ, Spagnoli LG, Gabbiani G, Orlandi A (2003) α-Actin isoform distribution in normal and failing human heart: a morphological, morphometric, and biochemical study. J Pathol 199:387–397
84. Taneja KL, Singer RH (1990) Detection and localization of actin mRNA isoforms in chicken muscle cells by in situ hybridization using biotinated oligonucleotide probes. J Cell Biochem 44:241–252
85. Tonin PN, Scrable H, Shimada H, Cavenee WK (1991) Muscle-specific gene expression in rhabdomyosarcomas and stages of human fetal skeletal muscle development. Cancer Res 51:5100–5106
86. Toyofuku T, Hoffman JR, Zak R, Carlson BM (1992) Expression of α-cardiac and α-skeletal actin mRNAs in relation to innervation in regenerating and non-regenerating rat skeletal muscles. Dev Dyn 193:332–339
87. Urbanek K, Quaini F, Tasca G, Torella D, Castaldo C, Nadal-Ginard B, Leri A, Kajstura J, Quaini E, Anversa P (2003) Intense myocyte formation from cardiac stem cells in human cardiac hypertrophy. Proc Natl Acad Sci USA 100: 10440–10445
88. Vandekerckhove J, Weber K (1979) The complete amino acid sequence of actins from bovine aorta, bovine heart, bovine fast skeletal muscle, and rabbit slow skeletal muscle. A protein-chemical analysis of muscle actin differentiation. Differentiation 14:123–133
89. Vandekerckhove J, Bugaisky G, Buckingham M (1986) Simultaneous expression of skeletal muscle and heart actin proteins in various striated muscle tissues and cells. J Biol Chem 261:1838–1843
90. Verfaillie CM (2002) Adult stem cells: assessing the case for pluripotency. Trends Cell Biol 12:502–508
91. Wang NP, Marx J, McNutt MA, Rutledge JC, Gown AM (1995) Expression of myogenic regulatory proteins (myogenin and MyoD1) in small blue round cell tumors of childhood. Am J Pathol 147:1799–1810
92. Webster C, Silberstein L, Hays AP, Blau HM (1988) Fast muscle fibers are preferentially affected in Duchenne muscular dystrophy. Cell 52:503–513
93. Weiss SW, Goldblum JR (2001) Enzinger and Weiss's soft tissue tumors. Chapter 22: Rhabdomyosarcoma, 4th edn, Mosby, St. Louis, pp 785–835
94. Wekerle H, Paterson B, Ketelsen U-P, Feldman M (1975) Striated muscle fibres differentiate in monolayer cultures of adult thymus reticulum. Nature 256:493–494
95. Weller RO, Cumming WJK, Mahon M (1997) Diseases of muscle. In: Graham DI, Lantos PL (eds) Greenfield's neuropathology, 6th edn. Arnold, London, pp 489–581 (Chapter 8)
96. Wiens D, Spooner BS (1983) Actin isotype biosynthetic transitions in early cardiac organogenesis. Eur J Cell Biol 30:60–66
97. Woodcock-Mitchell J, Mitchell JJ, Low RB, Kieny M, Sengel P, Rubbia L, Skalli O, Jackson B, Gabbiani G (1988) α-Smooth muscle actin is transiently expressed in embryonic rat cardiac and skeletal muscles. Differentiation 39:161–166
98. Wu AHB (ed) (1998) Cardiac markers. Humana Press, Totowa, NJ, USA, 300 pp

Virchows Arch (2006) 449: 192–199
DOI 10.1007/s00428-006-0216-3

ORIGINAL ARTICLE

Christian August · Jens Brockmann · Thorsten Vowinkel · Heiner Wolters · Karl-Heinz Dietl · Bodo Levkau · Stefan Heidenreich · Detlef Lang · Hideo A. Baba

Stress associated proteins metallothionein, HO-1 and HSP 70 in human zero-hour biopsies of transplanted kidneys

Received: 16 January 2006 / Accepted: 4 April 2006 / Published online: 1 June 2006
© Springer-Verlag 2006

Abstract Light microscopic alterations reflecting both previous and preservation-induced changes in the donor organ are usually not very distinctive. The ischemia/reperfusion-associated injury depends primarily on the conditions of donor organ preservation. The present study examined human kidney biopsies with special attention paid to the molecular mechanisms of preservation-induced injury preceding reperfusion. Stress-associated proteins hemeoxygenase-1 (HO-1), heat shock protein 70 (HSP 70), and metallothionein (MT) were studied in human zero-hour biopsies of transplanted kidneys prior to reperfusion in 29 patients. Protein expression was evaluated by semiquantitative immunohistochemistry and Western blotting for HO-1 and HSP 70. These findings were correlated with terminal deoxynucleotidyltransferase-mediated 2′-deoxyuridine 5′-triphosphate-digoxigenin nick end labeling (TUNEL) staining and follow up. Compared to controls, MT and HSP 70 expression was significantly higher at zero hour. In contrast, HO-1 and the number of TUNEL-positive cells were not elevated. MT and HO-1 immunoexpression were inversely associated with graft function, and hence, were of prognostic relevance. MT and HSP 70 were sensitive to the duration of cold ischemia. MT and HO-1 are suitable indicators for tissue injury during ischemia and may serve as new predictive markers that need to be validated in further independent studies.

Keywords Heme-oxygenase-1 · HSP-70 · Metallothionein · Prognosis · Renal transplantation · Zero-hour biopsies

This work was supported by the Interdisciplinary Clinical Research Center (IZKF), Muenster University Hospital, Germany.

C. August (✉)
Institute of Pathology, Muenster University Hospital,
University of Muenster,
Domagkstr. 17,
48149 Muenster, Germany
e-mail: augustc@uni-muenster.de
Tel.: +49-251-8355439

J. Brockmann · T. Vowinkel · H. Wolters
Department of Surgery, Muenster University Hospital,
Muenster, Germany

K.-H. Dietl
Department of Surgery, Raphaelsklinik Muenster,
Muenster, Germany

B. Levkau
Institute of Pathophysiology, University of Duisburg-Essen,
Essen, Germany

S. Heidenreich · D. Lang
Department of Internal Medicine
Muenster University Hospital,
Muenster, Germany

H. A. Baba
Institute of Pathology, University of Duisburg-Essen,
Essen, Germany

Introduction

Zero-hour biopsies are suitable for obtaining information on both preexisting base-line alterations in donor organs [4] and changes during cold storage or warm ischemia. Baseline changes seem to have an impact on cadaveric kidneys, but are of limited importance in living donor organs [22].

Structural changes caused by injury of grafts during the organ preservation and/or the surgical procedure have so far not been extensively investigated in human kidneys. In renal transplantation, prolonged cold ischemia was found to be associated with delayed graft function [19]. Multivariate analysis established the duration of cold ischemia as an independent risk factor for graft failure [17]. In a rat model of kidney transplantation, grafts with preservation times of more than 6 h developed more severe endothelial vascular injury followed by enhanced intragraft procoagulant capacity and inflammatory response [3].

The immunohistochemical changes associated with reperfusion in transplanted human kidneys are well documented [14], but data reflecting the alterations at the zero-hour time point prior to reperfusion are scarce. Because structural differences are difficult to assess using

conventional light microscopy, we investigated the proteins hemeoxygenase-1 (HO-1), metallothionein (MT), and heat shock protein 70 (HSP 70) associated with ischemic stress on renal tissue [13, 20, 23] to detect possible protective functions of these endogenous proteins.

The cytoprotective effect of the HO-1 system may result from the oxidative elimination of heme, from the system's anti-inflammatory potential, and from the maintenance of microcirculation [12]. The functional mechanisms of HSP 70, which can be induced by heat stress and cold injury are not clearly understood to date, but results suggest that heat shock proteins protect stressed cells, serving as molecular "chaperones" that reactivate denatured proteins and maintain intracellular homeostasis [5]. MT is a ubiquitous, low-molecular-weight protein, which is inducible in various cell systems under both ischemic and toxic conditions. MT's protective function seems to be based on its capacity of binding heavy metal ions and its scavenger function for free radicals [24].

The aim of this study was to prove the hypothesis that these stress-associated proteins are predictive for graft outcome after the early postoperative interval of renal transplantation.

Materials and methods

Wedge biopsies from 29 renal allografts (26 of cadaveric and 3 of living donors) obtained immediately before performing vascular anastomoses (zero-hour point) were examined by light microscopy and immunohistochemistry and by terminal deoxynucleotidyltransferase-mediated 2′-deoxyuridine 5′-triphosphate-digoxigenin nick end labeling (TUNEL) staining. Additionally, snap-frozen samples of 20 cases were used for protein isolation and Western blotting. Patients with clinical or histologic signs of rejection were not included in the study. Seven renal needle biopsies from nontransplanted human kidneys without structural abnormalities served as control.

Histological analysis

The specimens were fixed in buffered formalin (4%) and embedded in paraffin. Tissue sections 4 μm thick were cut and stained with periodic acid Schiff's reagent and Masson–Goldner. The fibrosis index was calculated by the ratio of obsolescent and intact glomeruli expressed as percentage. All included renal allografts had a fibrosis index of 30% or less.

Immunohistochemistry

Following deparaffinization and rehydration, the slides were exposed to an autoclave pretreatment for antigen retrieval. Immunohistochemical staining was performed using antibodies against HO-1 (SPA-895, StressGen, rabbit, polyclonal, 1:1,500); MT (E9, mouse, monoclonal, 1:20,000), which was donated from Jasani [8]; and HSP 72, which is the inducible form of HSP 70 (SPA-810, StressGen, mouse, monoclonal, 1:200), incubated in a moist chamber overnight at 4°C. After the application of a bridging antibody (DAKO, mouse anti-rabbit, 1:125) and a second bridging antibody against mouse (DAKO 1.30), the immunoreactivity was detected by the alkaline phosphatase anti-alkaline phosphatase-complex (1:100) using the Neufuchsin chromogene. The specificity of staining was examined using negative controls in which was substituted the primary antibody through rabbit IgG for polyclonal and mouse IgG for monoclonal antibodies. Two experienced pathologists (C. August, H.A. Baba) independently evaluated the staining results semiquantitatively. Only the cytoplasmatic immunoreactivity was included in the score. Complete lack of immunostained cells was scored as 0, scattered positive cells (up to 10%) as 1, focal moderate to strong staining (up to 50%) as 2, and more than 50% of cells positive for MT/HO-1/HSP 70 as 3.

Western blotting

For immunoblotting of HO-1 and HSP 70, snap frozen kidney tissue was homogenized and all the protein was extracted. Each lane contained 40 μg of protein. Frozen kidney samples were ground to fine powder under liquid nitrogen, dissolved in lysis buffer, and sonicated five times for 4 s (VibraCell 72434, Bioblock Scientific). Cell debris was separated by centrifugation (2 min, 14,000×*g* at 4°C), and the total protein content was measured in the supernatants using the bicinchoninic acid protein assay (Pierce). The 40 μg of protein was separated on 10–12% sodium dodecyl sulfate polyacrylamide gel electrophoresis, transferred to membranes, immunoblotted with specific antibodies, and visualized by enhanced chemiluminescence (Amersham). For each sample, signals were normalized to a positive control that was loaded on each membrane. The intensity of the scanned immunoblot signals was quantified using the commercially available "scion image" program.

TUNEL technique

Apoptosis of tubular cells was analyzed by the TUNEL method. Briefly, paraffin sections were dewaxed, rehydrated by a graded alcohol series, and washed. Sections were digested with proteinase K (25 μg/ml) and incubated (1 h, 37°C) with terminal deoxynucleotidyl transferase (TdT) (0.3 U/μl, Boehringer, Mannheim, Germany) and digoxigenin-labeled nucleotides (digoxigenin-11-dUTP, 5 μl; Oncor, Amersham, UK), which were inserted into DNA strand breaks. After stopping the reaction by stop-wash buffer (300 mM NaCl, 30 mM sodium citrate, 30 min at room temperature), sections were incubated with alkaline phosphatase-conjugated antidigoxigenin sheep Fab fragments (Boehringer; 1:200 in 0.05 M Tris–HCl) for 45 min. Sections were washed three times in Tris-buffered

saline and color development was achieved with a substrate solution containing Fast Red (Sigma Chemical, Munich, Germany). For negative controls, distilled water was used instead of TdT in the reaction mixture. Counterstaining of nuclei was performed with hematoxylin. The number of apoptotic signals was counted in 10 HPF within the renal cortex.

Statistical analysis

The graft prognosis was assessed by the 3-month creatinine level. To dichotomize the cohort, the median was used as threshold to establish two groups, i.e., recipients with favorable or unfavorable prognoses. Correspondingly, longer and shorter ischemic times and the urine volume during the first 24 h were both dichotomized using their medians. The Mann–Whitney U test was used because it is capable of detecting a location shift without assuming a special form of distribution. Results of $p<0.05$ were considered significant. The ranking correlation in order with that of Spearman, applicable on data without normal distribution, was used to analyze the dependency of semiquantitiative data of immunohistochemistry and of data of immunoblotting from the duration of ischemia. All statistical analyses were performed using the Statistical Package of the Social Sciences.

Table 1 Data of cold ischemic time, age or donor, fibrosis index, the urine volume during the first 24 h after transplantation, and the concentration of creatinine in the blood of the recipient after 3 months are reviewed

Case no.	Cold ischemic time (h)	Age of donor	Fibrosis index (%)	Primary function (ml/24 h)	Graft function after 3 months (crea)
5	2	41	0	5,300	1.7
6	2	39	0	2,900	1.2
19	13	60	16	3,500	1.2
20	34	59	0	1,840	1.8
1	2	46	0	3,130	1.4
2	22	86	12	920	1.7
3	26	64	11	8,000	1.5
8	18	72	0	20	3.3
9	13	69	15	3,500	1.2
25	17	52	3	2,420	1.3
26	17	52	18	1,500	1.8
27	18	73	0	6,500	2
28	15	40	0	3,100	1.3
29	10	34	0	3,580	1.2
30	18	41	12	500	2.1
32	19	43	5	3,940	1.5
33	17	49	7	1,560	2.4
35	21	53	10	250	1.2
36	19	65	0	200	3.5
37	16	36	0	2,340	0.7
38	21	40	0	460	1.2
22	14	22	0	980	1.5
39	24	69	16	40	2.1
18	21	42	0	20	4.2
34	11	66	25	170	5.5
17	17	43	10	650	10
31	13	59	30	1,900	2
7	23	66	25	1,350	3
23	23	52	0	1,450	1.4

The fibrosis index was calculated by the ratio of obsolescent and intact glomeruli expressed as percentage

Results

Clinical findings

The donor age ranged from 22 to 86 years (mean 52.8 years), whereas the age of controls ranged from 15 to 62 years (mean 46). Kidneys were stored in histidine–tryptophane–ketoglutarate solution at a temperature of 4°C. The duration of cold ischemic time ranged from 2 h (living donors) to 34 h (cadaveric donors), with a combined median of 17 h. The primary function of the transplanted kidney was measured by urine production during the first 24 h after transplantation. The urine volume ranged from 0 to 8,000 ml (median 1,560 ml). Duration of cold ischemia was not significantly correlated with both the primary function during the first 24 h and the graft function after 3 months. In contrast, a reduced primary function (urine output <1,560 ml) was associated with a trend toward reduced function after 3 months ($r=-0.36$, $p=0.056$) (Table 1).

Light microscopy

Approximately 50% of cases (14 of 29 patients) showed regular cortical renal tissue without any obsolescent glomeruli. The remaining cases exhibited a different proportion of glomeruli with global sclerosis ranging from 3 to 30% (Fig. 1a,b). No significant association was detected between the proportion of obsolescent glomeruli (fibrosis index) functional parameters and stress protein immunoexpression. None of the controls showed obsolescent glomeruli. Vacuolizations of tubular epithelial cells were only occasionally observed, and tubular necrosis was completely absent.

Evaluation of apoptosis

Apoptotic signals in controls ($n=7$) were nearly absent (mean 0.33/10 HPF, range 0–1) and specimens of zero-hour biopsies similarly showed only few apoptotic signals in tubular cells (mean 1.46/10 HPF, range 0–12). No significant difference was detected between controls and zero-hour biopsies. Functional parameters and stress protein immunoexpression were not significantly associated with the number of TUNEL-positive cells.

Immunohistochemistry

All the controls (n=7) from human kidneys not stored in cold ischemia showed weak cytoplasmatic staining for MT as well as for HO-1 and HSP 70 in distal tubular cells, and, to a considerably lesser degree, in proximal tubules (Fig. 2, middle panel). Compared to controls, cytoplasmatic immunoexpression of inducible HSP 70, HO-1, and MT in the proximal tubules was increased in zero biopsies (Fig. 2, right panel). MT and HSP 70 were stained in remained and detached tubular cells as well. Stained and unstained cells occurred together in single tubules, in contrast, HO-1 showed a more diffuse staining pattern. Additionally, MT and HSP 70 showed weak nuclear staining both in controls and following cold ischemia. Endothelial cells of peritubular capillaries or arteries did not show any immunoreactivity in our study. Only glomerular capillaries showed an immunostaining with antibodies against HO-1 after cold ischemia, as well as in controls (not demonstrated in this work).

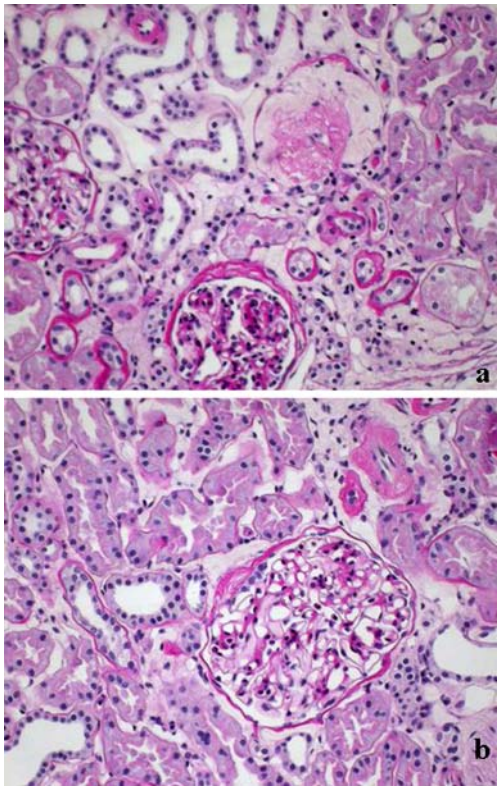

Fig. 1 Light microscopy of zero-hour biopsies stained with periodic acid Schiff's reagent: **a** Sclerotic glomerulus and capsular fibrosis representing preexisting tissue damage. The mild tubular atrophy is suggestive of preexisting mild ischemic injury (200×). **b** Glomerulus with regularly shaped tuft. The arteriolar hyalinization is indicative of preexisting changes, but does not show any signs of acute tubular injury (200×)

Western blotting

Immunoblots of HO-1 and HSP 70 are shown in Fig. 3. There was a significant correlation between Western blotting data and immunohistochemistry for HO-1 (r=0.58, p=0.02), but not for HSP 70 (r=0.29, p=0.26).

Cold ischemic time

Using the median of 17 h as a threshold, grafts with shorter ischemic intervals were separated from those which had been exposed to extended ischemia. Prolonged ischemia (>17 h) was associated with the elevated immunohistochemical expression of MT (p=0.001) and HSP 70 (p=0.007) according to the semiquantitative score. This result also appears to be in order with Spearman's correlation between the duration of ischemia and the amount of immunohistochemical MT (r=0.689, p=0.004) and HSP 70 expression (r=0.685, p=0.006), respectively (Fig. 4). In contrast, the content of HSP 70 obtained by immunoblotting of frozen tissue did not reach significance (p=0.211) in relation to the duration of cold ischemia. Additionally, the amount of HO-1 expression measured immunohistochemically and by Western blotting did not show any significant correlation with the duration of cold ischemia (r=0.239, p=0.23), although the HO-1 expression after cold ischemia measured in Western blotting (mean 1.34) was increased when compared to that of controls (mean 0.16).

Primary function

With reference to the median of primary graft function, grafts with sufficient (>1,560 ml) primary and reduced function (<1,560 ml) were separated into two groups. Western blotting of HO-1 and HSP 70 and immunohistochemical results for MT, HO-1, and HSP 70 did not reach any significance when compared with primary graft function. Initially, higher urine production was correlated with better graft function after 3 months, but this finding did not reach significance (r=−0.36, p=0.56).

Graft function after 3 months (prognosis)

Three months after transplantation, the creatinine levels ranged from 0.7 to 10 mg/dl. The median of 1.7 mg/dl was used as a threshold to set apart recipients with favorable outcomes from those with unfavorable outcomes after the postoperative 3-month interval. The immunohistochemical results and immunoblotting findings of graft outcome after 3 months are shown in Fig. 4. Grafts with favorable outcomes were associated with lower immunohistochemical MT (p=0.041) and HO-1 (p=0.001) scores. This also holds true for the content of HO-1 detectable by immunoblotting (p=0.019). In contrast, the degree of HSP 70 determined by immunohistochemistry (p=0.37) and by

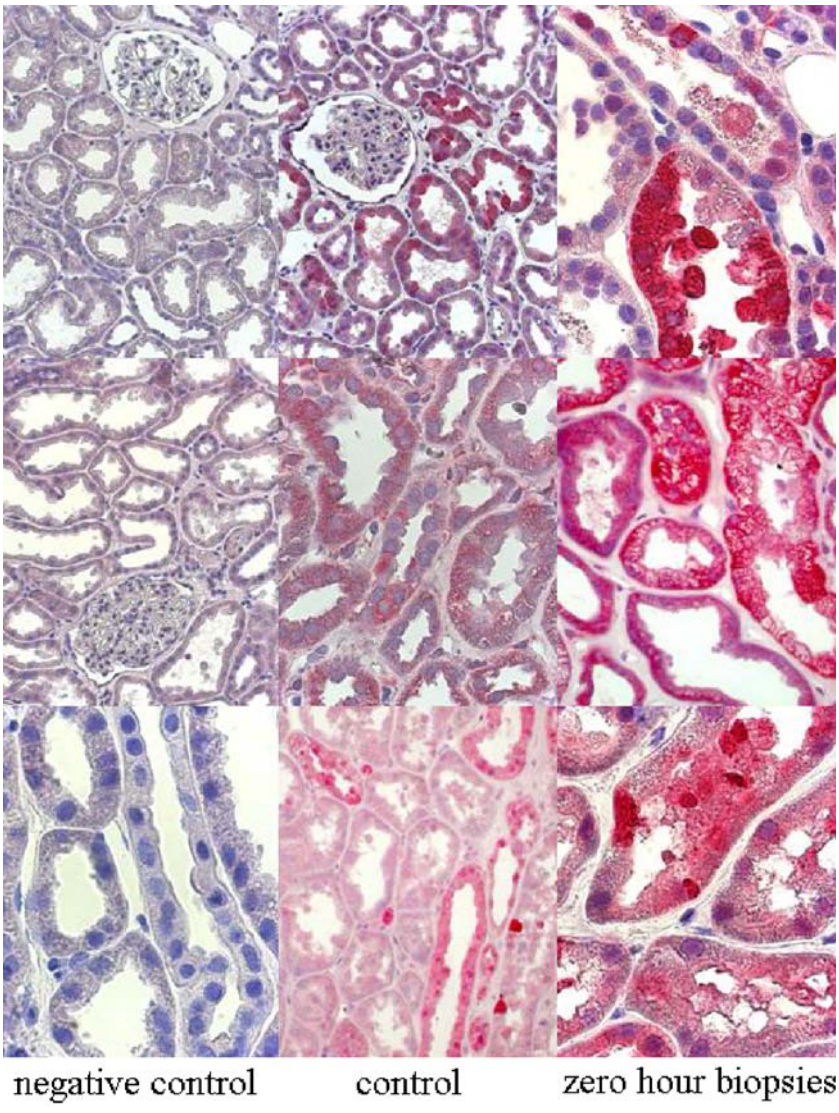

Fig. 2 Immunohistochemical staining of human zero-hour kidney biopsies after 17 h of cold ischemia (*right panel*) compared with controls (*middle panel*); in the *left panel* are documented negative controls to show the specificity of immunostaining: MT (200×, 200×, 630×; top); HO-1 (200×, 400×, 400×; middle); inducible form of HSP 70 (400×, 200×, 630×; below): Compared with controls, all proteins in zero-hour biopsies (*right panel*) show stronger immunoreactive signals cytoplasmatically in tubular epithelial cells. MT (*top line*) and HSP 70 (*bottom line*) were also stained in the nuclei of detached tubular cells. The HO-1 expression (*middle line*) was only cytoplasmatic and more diffuse in almost all cells of the involved tubules. Sometimes, the HO-1 staining was associated with tubular vacuolization

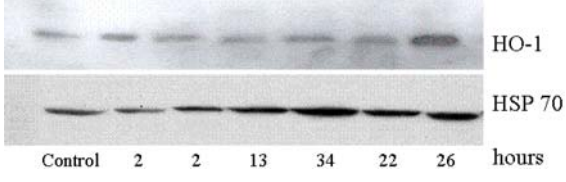

Fig. 3 Immunoblots of HO-1 and inducible HSP 70 of analyzed human frozen bioptic tissue obtained after varying periods of cold ischemia: The protein content of HO-1 and HSP 70 depends on the duration of cold ischemia. While HSP 70 was correlated with the ischemic time, HO-1 did not show significance in Spearman's correlation (see Fig. 4). The *control lane* originates from renal tissue not stored in cold ischemia

immunoblotting (p=0.57) did not reveal a prognostic significance.

Discussion

This study focused on the prognostic implications of stress proteins over a period of 3 months postoperatively and associated these results with clinical data. The main findings were:

1. MT, HO-1, and HSP 70 immunoexpression were significantly higher compared to controls.
2. MT and HSP 70 were sensitive to the duration of cold ischemia.
3. HO-1 and MT immunoexpression were inversely associated with graft function after 3 months.

The HO-1 system is an important cellular protective mechanism against various forms of toxic or hypoxic injury [1], and overexpression was shown to have beneficial effects in ischemia/reperfusion (I/R) injury and allograft rejection [12]. Interestingly, in our study, HO-1 expression detectable in zero-hour biopsies was shown to be inversely correlated with the kidney function after 3 months. Whether HO-1 is protective or an indicator for adverse organ function depends probably on the time of protein induction. If HO-1 is induced prior to the surgical procedure in transplantation, it diminishes the I/R injury on grafts in rat models of transplanted kidneys [25, 26], as

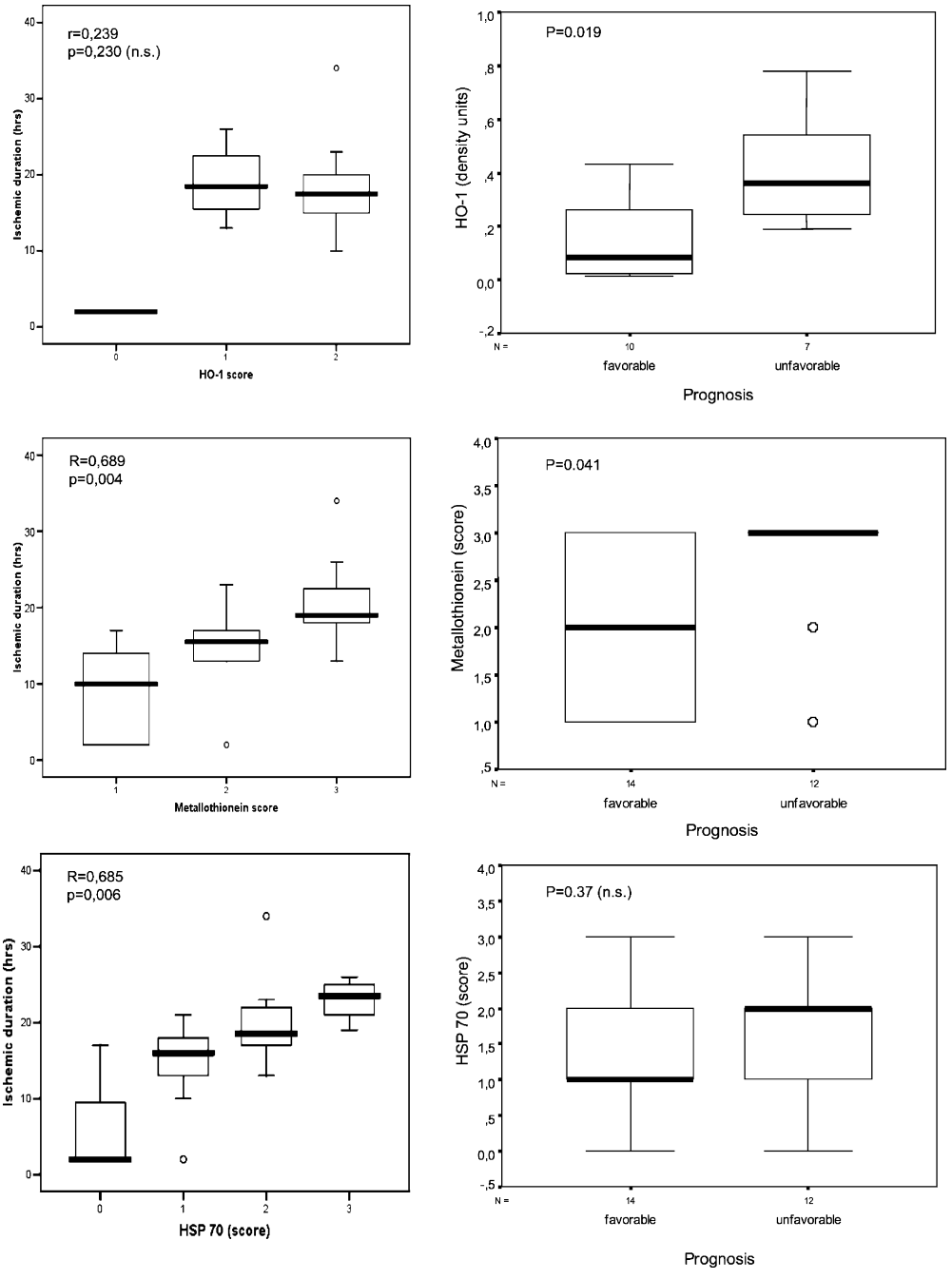

Fig. 4 Semiquantitative results of immunohistochemistry of MT, HO-1, and HSP 70 related with cold ischemic time (*left panel*) using Spearman's correlation (see also Fig. 3) and related with graft function after 3 months (*right panel*) assessed by the creatinine level. Grafts with a favorable outcome (creatinine more than 1.7 mg/100 ml) were associated with a lower immunohistochemical MT (p=0.041) and HO-1 (p=0.001) score (*n.s.* not significant)

well as those of livers [10] and hearts [11]. Similar effects of induced HO-1 in the early phase of transplantation might be responsible for the attenuation of the long-term prognosis in transplanted rat hearts [21] and kidneys [25]. When HO-1 is induced prior to the injury, the function seems to be rather protective [18, 25]. In contrast, our results suggest that the elevated expression of HO-1 during cold ischemia indicates the degree of tissue injury and is thus of inverse prognostic relevance. Such an indicative function of HO-1 reflecting the degree of cell stress was recently demonstrated on human myocardium after left ventricular mechanical support [6], suggesting a general biological function rather than a function restricted to the kidney. The functional impact of HO-1 following tissue injury might also be associated with its topochemical distribution in renal tissue. In our study, ischemically induced HO-1 was found in proximal tubular epithelial cells, which was in contrast to the distal tubular and only weak proximal tubular expression in the controls. We did not detect any immunohistochemical HO-1 staining of small arteries or arterioles of renal tissue as described in mouse cardiac allografts [7] and, more recently, in human renal biopsies [15]. In our study, tubular expression of HO-1 did not significantly depend on the duration of cold ischemia compared to controls. This might be attributed to other factors not explored here, such as donor or retrieval issues and/or previous catecholamine application.

In our study, the degrees of tubular expression of MT and HSP 70 were associated with longer durations of cold ischemia, but only MT showed inversely prognostic significance in semiquantitatively evaluated immunohistochemistry. MT and HSP 70 seem to reflect the degree of injury acquired during cold ischemia and might possibly serve as indicators for injury assessment. The function of MT for the preservation of cellular homoeostasis seems to be linked with its potential of binding and exchanging zinc ions between various apoforms and between zinc clusters in the cellular signal transduction [16]. It is widely accepted that complications with grafts during the early postoperative course are reduced to the same extent that duration of cold ischemia is minimized [17]. Our results do not justify the assumption that elevated MT expression has a genuine protective function with a prognostic impact in ischemically damaged donor kidneys. Such a functional benefit was only demonstrated by diminished I/R injury to transplanted rat kidneys [23]. Heart transplantation with MT transgenic mice showed decreased I/R-induced myocardial apoptosis [9]; however, our TUNEL staining results suggest that tubular apoptosis might not have any impact during the period of cold ischemic injury.

The inducible HSP 70 expression assessed by immunohistochemistry increased with the duration of cold ischemia. Whereas the semiquantitative evaluated cytoplasmatic expression of HSP 70 significantly increased compared with the control group, the corresponding Western blotting findings did not reach significance in regression analysis. This might be attributed to the fact that the measured content of HSP 70 using the more sensitive Western blotting technique included both the basic nuclear content of control and the overexpressed cytoplasmatic HSP 70, while by immunohistochemistry, only the cytoplasmatic reactivity was scored. One of the most important functions of HSP 70 seems to be the inhibition of intracellular mechanisms resulting in apoptosis [2]. Thus, possible protective effects of HSP 70 against renal tubular injury might be limited under the conditions prevailing in this study. No significant correlation between HSP 70 expression in zero-hour biopsies and the graft outcome after 3 months could be demonstrated. Our findings support the assumption that the putative protective capacity of HSP 70 might crucially depend on its having been induced at some earlier stage. Induction of HSP 70 prior to the ischemic insult was protective to the organ in a rat model of renal I/R [13]. In our study, this heat shock protein seems to indicate the degree of ischemic injury in zero-hour biopsies.

In this study, we found that elevated MT and HO-1 immunoexpressions were associated with declined graft function and may function as prognostic biomarkers. In this biological setting, the function of MT and HO-1 is indicative rather than protective, probably depending on the time point of induction. A possible protective acting of these proteins might, however, be diminished or masked by other mechanisms. Further independent investigations on larger cohorts will be necessary to validate these markers as prognostic tools.

Acknowledgements The authors thank Maria Wolters and Beate Naber for their excellent technical assistance.

References

1. Agarwal A, Kim Y, Matas AJ, Alam J, Nath KA (1996) Gas-generating systems in acute renal allograft rejection in the rat. Co-induction of heme oxygenase and nitric oxide synthase. Transplantation 61:93–98
2. Beere HM, Wolf BB, Cain K, Mosser DD, Mahboubi A, Kuwana T et al (2000) Heat-shock protein 70 inhibits apoptosis by preventing recruitment of procaspase-9 to the Apaf-1 apoptosome. Nat Cell Biol 2:469–475
3. Dragun D, Hoff U, Park JK, Qun Y, Schneider W, Luft FC et al (2001) Prolonged cold preservation augments vascular injury independent of renal transplant immunogenicity and function. Kidney Int 60:1173–1181
4. Escofet X, Osman H, Griffiths DF, Woydag S, Adam JW (2003) The presence of glomerular sclerosis at time zero has a significant impact on function after cadaveric renal transplantation. Transplantation 75:344–346
5. Georgopoulos C, Welch WJ (1993) Role of the major heat shock proteins as molecular chaperones. Annu Rev Cell Biol 9:601–634
6. Grabellus F, Schmid C, Levkau B, Breukelmann D, Halloran PF, August C et al (2002) Reduction of hypoxia-inducible heme oxygenase-1 in the myocardium after left ventricular mechanical support. J Pathol 197:230–237
7. Hancock WW, Buelow R, Sayegh MH, Turka LA (1998) Antibody-induced transplant arteriosclerosis is prevented by graft expression of anti-oxidant and anti-apoptotic genes. Nat Med 4:1392–1396
8. Jasani B, Elmes ME (1991) Immunohistochemical detection of metallothionein. Methods Enzymol 205:95–107
9. Kang YJ, Li Y, Sun X, Sun X (2003) Antiapoptotic effect and inhibition of ischemia/reperfusion-induced myocardial injury in metallothionein-overexpressing transgenic mice. Am J Pathol 163:1579–1586
10. Kato H, Amersi F, Buelow R, Melinek J, Coito AJ, Ke B et al (2001) Heme oxygenase-1 overexpression protects rat livers from ischemia/reperfusion injury with extended cold preservation. Am J Transplant 1:121–128
11. Katori M, Buelow R, Ke B, Ma J, Coito AJ, Iyer S et al (2002) Heme oxygenase-1 overexpression protects rat hearts from cold ischemia/reperfusion injury via an antiapoptotic pathway. Transplantation 73:287–292
12. Katori M, Busuttil RW, Kupiec-Weglinski JW (2002) Heme oxygenase-1 system in organ transplantation. Transplantation 74:905–912
13. Kelly KJ, Baird NR, Greene AL (2001) Induction of stress response proteins and experimental renal ischemia/reperfusion. Kidney Int 59:1798–1802
14. Koo DD, Welsh KI, Roake JA, Morris PJ, Fuggle SV (1998) Ischemia/reperfusion injury in human kidney transplantation: an immunohistochemical analysis of changes after reperfusion. Am J Pathol 153:557–566
15. Lemos FB, IJzermans JN, Zondervan PE, Peeters AM, van den Engel S, Mol WM et al (2003) Differential expression of heme oxygenase-1 and vascular endothelial growth factor in cadaveric and living donor kidneys after ischemia-reperfusion. J Am Soc Nephrol 14:3278–3287
16. Li CY, Lee JS, Ko YG, Kim JI, Seo JS (2000) Heat shock protein 70 inhibits apoptosis downstream of cytochrome c release and upstream of caspase-3 activation. J Biol Chem 275:25665–25671
17. Roodnat JI, Mulder PG, Van Riemsdijk IC, IJzermans JN, van Gelder T, Weimar W (2003) Ischemia times and donor serum creatinine in relation to renal graft failure. Transplantation 75:799–804

18. Salahudeen AA, Jenkins JK, Huang H, Ndebele K, Salahudeen AK (2001) Overexpression of heme oxygenase protects renal tubular cells against cold storage injury: studies using hemin induction and HO-1 gene transfer. Transplantation 72:1498–1504
19. Salahudeen AK, Haider N, May W (2004) Cold ischemia and the reduced long-term survival of cadaveric renal allografts. Kidney Int 65:713–718
20. Shimizu H, Takahashi T, Suzuki T, Yamasaki A, Fujiwara T, Odaka Y et al (2000) Protective effect of heme oxygenase induction in ischemic acute renal failure. Crit Care Med 28:809–817
21. Soares MP, Lin Y, Anrather J, Csizmadia E, Takigami K, Sato K et al (1998) Expression of heme oxygenase-1 can determine cardiac xenograft survival. Nat Med 4:1073–1077
22. Sund S, Reisaeter AV, Fauchald P, Bentdal O, Hall KS, Hovig T (1999) Living donor kidney transplants: a biopsy study 1 year after transplantation, compared with baseline changes and correlation to kidney function at 1 and 3 years. Nephrol Dial Transplant 14:2445–2454
23. Takahashi T, Itano Y, Noji S, Matsumoto K, Taga N, Mizukawa S et al (2001) Induction of renal metallothionein in rats with ischemic renal failure. Res Commun Mol Pathol Pharmacol 110:147–160
24. Thornalley PJ, Vasak M (1985) Possible role for metallothionein in protection against radiation-induced oxidative stress. Kinetics and mechanism of its reaction with superoxide and hydroxyl radicals. Biochim Biophys Acta 827:36–44
25. Tullius SG, Nieminen-Kelha M, Buelow R, Reutzel-Selke A, Martins PN, Pratschke J et al (2002) Inhibition of ischemia/reperfusion injury and chronic graft deterioration by a single-donor treatment with cobalt-protoporphyrin for the induction of heme oxygenase-1. Transplantation 74:591–598
26. Wagner M, Cadetg P, Ruf R, Mazzucchelli L, Ferrari P, Redaelli CA (2003) Heme oxygenase-1 attenuates ischemia/reperfusion-induced apoptosis and improves survival in rat renal allografts. Kidney Int 63:1564–1573

Virchows Arch (2006) 449:200–206
DOI 10.1007/s00428-006-0223-4

ORIGINAL ARTICLE

Identity of M2A (D2-40) antigen and gp36 (Aggrus, T1A-2, podoplanin) in human developing testis, testicular carcinoma in situ and germ-cell tumours

Si Brask Sonne · Amy S. Herlihy · Christina E. Hoei-Hansen · John E. Nielsen · Kristian Almstrup · Niels E. Skakkebaek · Alexander Marks · Henrik Leffers · Ewa Rajpert-De Meyts

Received: 19 January 2006 / Accepted: 18 April 2006 / Published online: 31 May 2006
© Springer-Verlag 2006

Abstract Testicular germ-cell tumours of young adults are derived from a pre-invasive intratubular lesion, carcinoma in situ (CIS). In a recent genome-wide gene expression screening using cDNA microarrays, we found *PDPN* over-expressed in CIS compared to normal adult testis. *PDPN* encodes podoplanin (Aggrus, human gp36, T1A-2), a transmembrane glycoprotein expressed in lymphatic endothelium and various solid tumours. To examine a potential role for *PDPN* in testicular neoplasms and during testicular development, we investigated its expression pattern during the development of human testis and in a series of testicular CIS, gonadoblastoma and overt germ-cell tumours. We established by RT-PCR and by immunohistochemistry with a gp36 antibody that *PDPN* mRNA and the protein product were expressed in testes with germ-cell neoplasms but not in the normal adult testis. We also found gp36 expression in early foetal gonocytes and immature Sertoli cells, similar to the expression pattern of M2A antigen, a previously identified marker for CIS and seminoma. This reinforced our previous proposal that M2A (D2-40) antigen was identical to gp36 (podoplanin, Aggrus, T1A-2). Our findings also suggest that podoplanin has a function in developing testis, most likely at the level of cell–cell interactions among pre-meiotic germ cells and immature Sertoli cells.

Keywords M2A · *PDPN* · Intratubular germ-cell neoplasia (IGCN) · Testicular germ-cell neoplasm · Testicular development · Sertoli cells

S. B. Sonne (✉) · A. S. Herlihy · C. E. Hoei-Hansen · J. E. Nielsen · N. E. Skakkebaek · H. Leffers · E. Rajpert-De Meyts
University Department of Growth and Reproduction, Section GR-5064, Rigshospitalet, Blegdamsvej 9, 2100 Copenhagen, Denmark
e-mail: si@bsonne.dk

A. Marks
Banting and Best Department of Medical Research, University of Toronto, Toronto, Ontario, Canada

K. Almstrup
Novo Nordisk, Molecular Genetics, Building 6A1.060, DK-2880 Bagsvaerd, Denmark

Introduction

Testicular germ-cell tumours (TGCTs) of adolescents and young adults, which have two main histological forms, seminomas and non-seminomas, are derived from a common pre-invasive precursor, carcinoma in situ testis (CIS, also known as intratubular germ-cell neoplasia, IGCN) [33]. Over the years, we have investigated the biology of CIS cells and pursued a search for novel markers of CIS and TGCTs, which could be valuable in clinical practice [12, 27].

Among the earliest identified sensitive markers of CIS was an onco-foetal antigen M2A [4, 10, 11, 24]. We established that M2A antigen was a marker of foetal gonocytes and Sertoli cell differentiation [5, 15, 17]. Using a panel of monoclonal antibodies, the molecular structure of M2A antigen was defined as a 40-kDa *O*-glycosylated glycoprotein [22]. One of these antibodies, D2-40, which did not require sialic acid residues to recognise the M2A antigen, was subsequently shown to be a marker of lymphatic endothelium [18, 19] and adopted for studies of lymphatic invasion in a variety of tumours [2, 9, 25].

In a recent genome-wide gene expression study of the CIS transcriptome using cDNA microarrays, we compared testicular tissue containing increasing amounts of CIS cells to normal testicular tissue, and found that *PDPN* was

Table 1 Summary of the immunohistochemical staining for podoplanin with anti-gp36 and M2A antibodies

Tissue	Age	*N*	gp36	M2A
Normal testis				
Foetal	GW 10	1	Gon +	Gon +
Foetal	GW 14	1	Gon ++, Sertoli +/−	Gon +, Sertoli +/−
Foetal	GW 24	1	Gon ++, Sertoli +	Gon ++, Sertoli +
Infantile	1 1/2 Y	1	Spg neg, Sertoli +/−	Spg neg, Sertoli +
Prepubertal	4 1/2 Y	1	Spg neg, Sertoli +/−	neg
Prepubertal	6 Y	1	Spg neg, Sertoli ++	Spg neg, Sertoli +
Prepubertal	8 Y	1	Spg neg, Sertoli ++	Spg neg, Sertoli ++
Prepubertal	10 Y	1	Spg neg, Sertoli +/−	Spg neg, Sertoli +
Adult	25–32 Y	8	neg	neg
Neoplastic testicular tissue				
Infantile teratoma	3 M	1	+/− (focal)	+/− (focal)
Gonadoblastoma	14–18 Y	2	+++	+++
CIS	25–36 Y	14	+++	+++
Seminoma	26–39 Y	10	Heterogeneous +/++	Heterogeneous +/++
Non-seminoma	25–39 Y	9	+/− (focal)	+/− (focal)
Spermatocytic seminoma	61 Y	1	neg	neg
Non-testicular tissue				
Lymphatic vessels		1	+/−	++
Pituitary gland		1	++	+/−
Stomach		1	++ (Crypt cells)	–
Lung, skeletal muscle, heart muscle, skin, small intestine, colon, liver, spleen, pancreas, oesophagus, salivary gland, adrenal gland, thyroid gland, parathyroid gland, thymus gland, tonsil, bone marrow, breast, uterus, cervix, adult ovary, kidney, prostate gland, omentum, peripheral nerve, cerebral cortex, cerebellum		1 of each	neg	neg

N Number, *GW* gestational week, *Y* year, *M* month, *CIS* carcinoma in situ, *Gon* gonocytes, *Spg* spermatogonia, *neg* no positive cells detected
Staining intensity: +++, strong staining in nearly all cells; ++, moderate staining or only a minority of cells positive; +, weak staining or a low percentage of cells stained; +/−, very weak staining in single cells

among the genes selectively expressed at high levels in CIS [1]. The *PDPN* gene encodes podoplanin and has been independently cloned by several groups and designated as Aggrus, human gp36 or T1A-2 [6, 20, 35]. Podoplanin is a transmembrane glycoprotein first identified in the podocytes of rat kidney [6, 23] and later reported as a marker of lymphatic endothelial cells [7]. A recent update on histological diagnosis of mesothelioma [26] described D2-40 as a promising marker for epitheloid mesothelioma and also mentioned podoplanin as a putative candidate. The similar molecular structure of M2A antigen and podoplanin and the selective distribution of these antigens on lymphatic endothelium—as demonstrated in studies with D2-40 antibody—suggested that these antigens might be the same proteins. In fact, we have previously reported in a preliminary communication using gp36-transfected cells that the M2A (D2-40) antibody was indeed binding to gp36 [3]. This conclusion was supported by the recent results of others who have also shown in transfection studies that the D2-40 antibody recognises podoplanin [31].

In the present study, we have investigated the expression of podoplanin at the mRNA and protein levels, using RT-PCR with primers specific for the *PDPN* sequence and immunohistochemistry (IHC) with M2A and anti-gp36 antibodies in a panel of specimens from normal human testes during development as well as CIS, gonadoblastoma (a CIS-resembling pre-invasive lesion of severely dysgenetic gonads) and different types of invasive TGCTs. We present results that reinforce the proposed identity between M2A antigen and gp36 (podoplanin, Aggrus, T1A-2) and suggest a role for the protein in cell–cell adhesion in developing seminiferous tubules.

Materials and methods

Tissue samples

The Regional Committee for Medical Research Ethics in Denmark approved the use of human tissue samples for this project. Tissue samples from adults with testicular neoplasms were obtained directly after orchidectomy and macroscopic pathological evaluation. Each testicular sample was divided into several tissue fragments, which were either snap-frozen at −80°C for nucleic acid extraction or fixed overnight at 4°C in Stieve's fluid, modified Stieve's (GR fixative), paraformalde-

hyde (PFA), or formalin, and subsequently embedded in paraffin. Tissue sections were stained with haematoxylin and eosin or with antibodies against placental alkaline phosphatase (PLAP or ALPP) for histological evaluation [10]. A series of 21 overt testicular tumours were analysed by IHC, including classical seminomas, various non-seminomatous tumour types (including embryonal carcinoma, EC), two gonadoblastomas, an infantile immature teratoma, and a spermatocytic seminoma. Fourteen samples of testicular CIS were analysed, of which 13 were from tissue adjacent to a TGCT, and one which had not progressed to an overt tumour (Table 1).

Furthermore, we included three samples of normal foetal testicular tissue of gestational weeks (GW) 10–24 (obtained from abortions or autopsies of stillbirths), five samples of infantile and prepubertal tissues (biopsies previously used to monitor testicular relapses in boys with leukaemia) and eight specimens of normal adult testes. The foetal and prepubertal testicular tissue samples were obtained for our previous studies as described earlier [15, 17, 29]. Finally, we included a commercially available tissue microarray containing samples of a broad variety of normal human tissues (MaxArray Human Normal Tissue, Zymed, S. San Francisco, CA, USA). All tissue types present on the array are listed in Table 1.

PDPN expression by reverse-transcriptase (RT)-PCR

Total RNA was purified using the Nucleospin RNAII kit (Macherey-Nagel, Düren, D) as described by the manufacturer. RNA samples were DNase-digested, and cDNA was synthesised using dT_{20} primers. RT-PCR was performed using specific primers spanning intron–exon boundaries, including an analysis of β2-microglobulin (*B2M*) as an internal control (*PDPN*: CCAAGCGCCACAGCCTCAA and GGCACAGA GTCAGAAACGGT, *B2M*: CGAGACATGTAAGCAGCAT CA and AGATTAACCACAACCATGCCTT). PCR conditions were: 5 min, 95°C; 35 cycles of: 30 s, 95°C; 1 min, 62°C; 1 min, 72°C; and finally 5 min, 72°C. The resulting PCR product was loaded on a 1% agarose gel, and bands were visualised by ethidium bromide staining.

Immunohistochemistry

A commercially available mouse monoclonal anti-gp36 antibody (ab10288, Abcam, Cambridge, UK) and previously described mouse monoclonal M2A antibody [4] were used. In addition, mouse monoclonal anti-PLAP antibody (BioGenex, San Ramon, CA, USA) and mouse monoclonal TRA-1-60 antibody (kindly provided by P. Andrews, University of Sheffield, UK) were used as controls to detect CIS and aid in distinguishing between seminoma and EC. The IHC stainings were performed using a standard indirect peroxidase method, as previously described for M2A, with slight modifications [10, 11]. Briefly, the dewaxed and rehydrated sections were heated in a microwave oven in citrate buffer, 10 mM, pH=6, to unmask the antigen. Subsequently, the sections were incubated with 0.5% H_2O_2 to inhibit the endogenous peroxidase, followed by diluted non-immune goat serum to block unspecific binding sites (Zymed, San Francisco, CA, USA). The sections were incubated overnight at 4°C with the primary antibodies diluted 1:250, 1:2000, 1:100 and 1:300 for anti-gp36, M2A, PLAP and TRA-1-60, respectively. Antibodies were diluted in Trizma Base Sodium Chloride buffer, pH=7.4. As a negative control, a serial section from each block was incubated with the dilution buffer. Subsequently, a secondary biotinylated goat–anti-mouse link antibody was applied (Zymed, San Francisco, CA, USA), followed by the horseradish peroxidase–streptavidin complex (Zymed, San Francisco, CA, USA). The sections were thoroughly washed between steps. The bound antibody was visualised using aminoethyl carbazole substrate (Zymed, San Francisco, CA, USA). Sections were lightly counterstained with Mayer's haematoxylin to mark cell nuclei.

The sections were examined under a light microscope (Zeiss Oberkochen, D) and scored systematically by two investigators (SBS and ERM). The staining was assessed using an arbitrary semi-quantitative score of the staining intensity and the proportion of cells stained: +++: strong staining in nearly all cells, ++: moderate staining or only a minority of cells positive, +: weak staining or a low percentage of cells stained, +/−: very weak staining in single cells, and neg: no positive cells detected.

Results

We first investigated the expression of *PDPN* mRNA by RT-PCR. As shown in Fig. 1, there was no visible *PDPN* expression in three different samples of preserved normal adult testicular tissue. In contrast, *PDPN* was moderately expressed in all seminoma and non-seminoma samples investigated, with subtle variations in expression level. The expression in samples with CIS (which contained variable numbers of tubules with CIS cells) ranged from very weak to strong.

Having confirmed that *PDPN* was not expressed in the adult testis, and indeed was specific for neoplastic germ cells, we then investigated a panel of CIS and TGCT specimens for expression at the protein level by IHC. To confirm the identity of M2A antigen with gp36, we performed staining using M2A and anti-gp36 antibodies on serial sections of all specimens. The staining was present exclusively in the cell membrane and cytoplasm. In general, the intensity of staining varied somewhat depending on the fixative used,

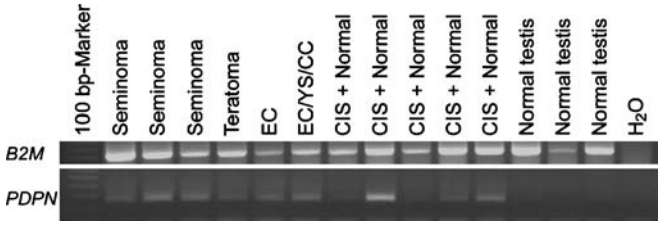

Fig. 1 *PDPN* mRNA expression in testicular tissue. *B2M* β2-microglobulin, *EC* embryonal carcinoma, *YS* yolk sac tumour, *CC* choriocarcinoma, *CIS* carcinoma in situ, *bp* base pairs

with stronger staining and less background in tissues fixed with Stieve's fluid or modified Stieve's compared to those fixed in PFA or formalin. The complete results of the IHC staining are listed in Table 1, and representative examples are shown in Fig. 2.

We demonstrated a high abundance of gp36/M2A antigen in approximately 70–90% of CIS cells in all specimens containing CIS (Fig. 2a), regardless of whether the CIS cells were adjacent to a seminoma or non-seminoma, or if the CIS cells were not from the surroundings of an overt tumour. A strong staining with both antibodies was also seen in neoplastic germ cells in both samples of gonadoblastoma. Classical seminoma showed a moderate to strong heterogeneous staining, whilst only focal staining of single elements was

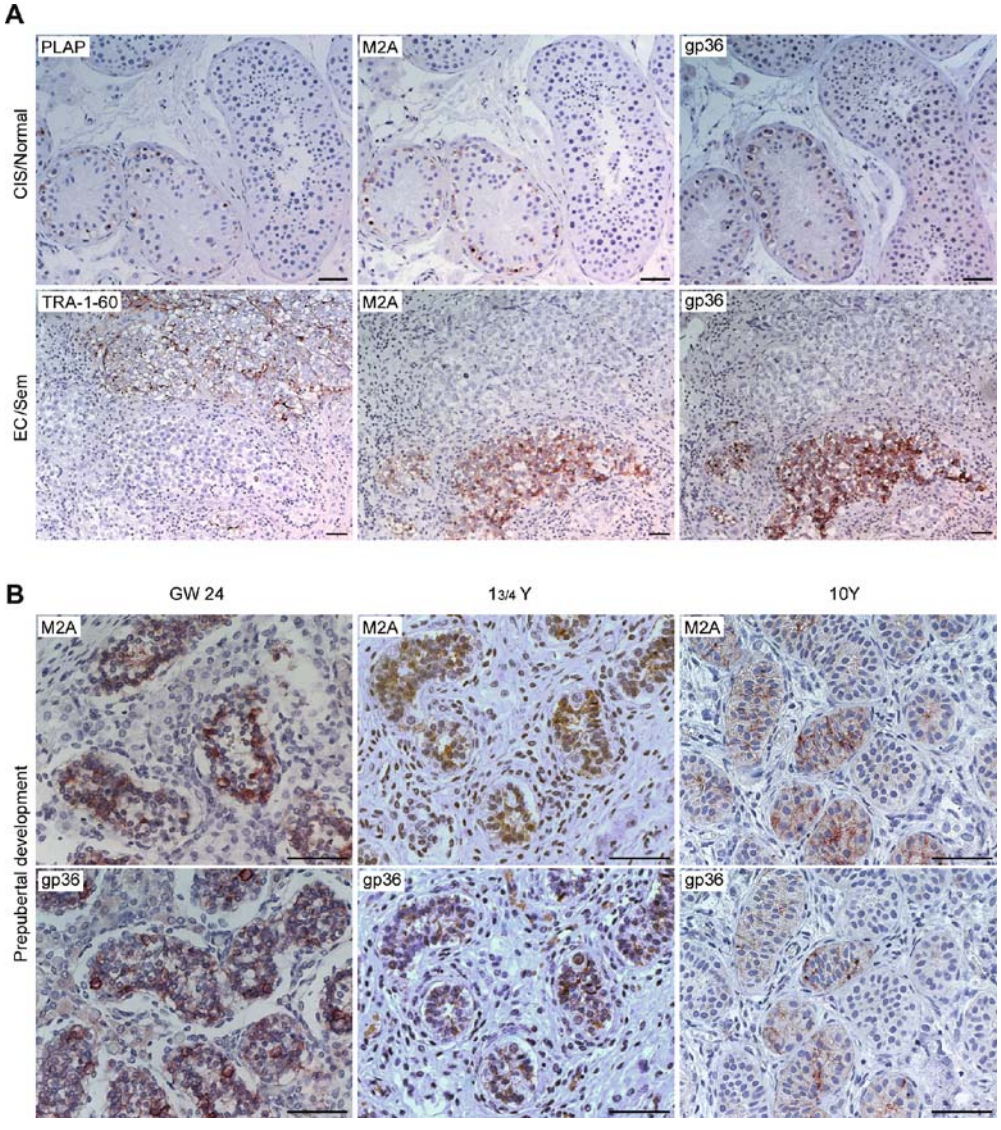

Fig. 2 Podoplanin expression in testicular neoplasms and normal foetal and prepubertal testes at the protein level. Immunohistochemical staining of serial sections with anti-gp36 and anti-M2A antigen antibodies. PLAP was used as control for carcinoma in situ (CIS) and seminoma (Sem), and TRA-1-60 for embryonal carcinoma (EC). *Scale bar* 25 μm. **a** (*Top*) Adult testis, normal tubules with preserved spermatogenesis are *on the right* (negative), CIS tubules are *on the left*. (*Bottom*) Seminoma and EC components in a mixed GCT. **b** Foetal testis of 24 gestational weeks (GW) and prepubertal testes ($1^3/_4$ and 10 years of age); staining for M2A antigen in the *top panel* and for gp36/podoplanin *at the bottom*

observed in non-seminomas. Some structures resembling remnants of seminiferous tubules were weakly positive in areas of immature teratomas, but in general, gp36/M2A antigen expression decreased with tissue differentiation. No staining was present in EC. An infantile teratoma from a 3-month-old patient showed weak focal staining of single structures, whilst spermatocytic seminoma was both gp36- and M2A-negative.

To establish whether the expression of gp36/podoplanin was the same as M2A antigen during testicular development, we performed staining with M2A and anti-gp36 antibodies on serial sections (Fig. 2b). Foetal testes showed strong expression of gp36 in gonocytes whilst there was no expression in germ cells in any of the postnatal specimens (Table 1). In specimens older than GW 14, gp36 was also present in immature Sertoli cells, where it continued until 10 years of age at which point the expression pattern became patchy with stronger expression in the tubules containing more immature Sertoli cells. Gp36 staining was somewhat stronger in gonocytes, whereas M2A antigen had a tendency to be more strongly reactive in foetal Sertoli cells.

Finally, we analysed the pattern of immunohistochemical expression of the M2A antigen and gp36 in a panel of extra-gonadal tissues and detected strong staining in cells of the lymphatic endothelium, pituitary gland and crypt cells in stomach. With a few exceptions (stomach), the pattern of expression of both antigens was nearly identical.

Discussion

This study is based in part on our previous global gene expression profiling study, which revealed a number of genes highly expressed in CIS [1]. Among those genes was *PDPN*, which encodes podoplanin (Aggrus, T1A-2, human gp36). In the present study, we comprehensively investigated the pattern of expression of *PDPN* in normal testis and germ-cell neoplasms. We demonstrated a similar expression pattern using anti-gp36 and M2A antibodies. This confirmed our previous preliminary observation that antibodies to M2A antigen recognise gp36 [3], thus reinforcing the identity between M2A antigen and gp36 (podoplanin, Aggrus, T1A-2).

The M2A antibody was originally raised against the human ovarian epithelial carcinoma cell line, HEY, but the identity of the M2A antigen has until recently been uncertain. We have previously reported that antibody D2-40 to the M2A antigen reacts with gp36 in gp36-transfected cells [3]. Independently from our studies, Schacht et al. [31] studied podoplanin in human carcinomas, including ovarian GCTs. They confirmed that the D2-40 antibody recognises podoplanin by transfecting podoplanin into podoplanin-negative rat myoblasts and knocking it out in human lymphatic endothelial cells using siRNA. Immunostaining of the rat cells with the D2-40 antibody showed a strong cytoplasmic staining after transfection with the podoplanin vector but no reaction in cells transfected with control vector, and the human lymphatic endothelial cells showed a marked reduction in M2A reactivity after *PDPN* siRNA transfection. In their study, ovarian GCTs showed a comparable expression pattern to their testicular counterparts as 4/4 dysgerminomas and 1/3 granulosa cell tumours were podoplanin-positive [31].

As far as testicular GCTs are concerned, podoplanin (Aggrus) expression was studied in only one earlier study which found Aggrus mRNA and protein in 10/11 seminomas, but no expression in four ECs or normal testicular tissue [21]. They did not investigate CIS, which is the focus of our current study. We found a high expression of podoplanin at the RNA and protein levels (M2A antigen, gp36) in all CIS specimens and a high protein expression in two gonadoblastomas as reported earlier for M2A [16]. We also demonstrated that in contrast to the classical seminoma, spermatocytic seminoma, a rare tumour of elderly men which does not arise from CIS [27, 34], was negative for both gp36 and M2A antigen.

We confirmed that gp36 has an identical expression pattern to that of M2A during testicular development. In agreement with our previous studies of M2A expression [5, 17], we show in this study that gp36/podoplanin is expressed in foetal but not in adult testes, and that it is a marker not only for gonocytes and neoplastic germ cells but also for immature Sertoli cells. Sertoli cells were increasingly gp36/M2A-positive towards the end of foetal development, whilst staining of germ cells decreased to become negative when gonocytes differentiated into infantile pre-spermatogonia. The same observation was made in a recent study, where infantile spermatogonia were named stage T_2-spermatogonia [8].

Furthermore, we have confirmed the expression of gp36 and M2A antigen in lymphatic vessels, pituitary gland and stomach, whereas no expression was seen in a large number of other tissues (see Table 1), of which staining in a subset had been previously reported by Schacht et al. [31] (including lung, thyroid gland, thymus, tonsil, ovary and prostate gland). Some differences in reported expression could be due to small tissue samples on the analysed tissue array.

Our study supports the identity between the M2A antigen and gp36 (podoplanin Aggrus, T1A-2). Based on the perinatal lethality of podoplanin knock-out mice, a role for this protein during development is likely [30, 32]. Podoplanin knock-out mice show defects in lung ad lymphatic vessel formation, but there is no information concerning their gonadal development [30, 32]. The molecular structure of M2A antigen as a membrane *O*-linked sialoglycoprotein (mucin) [22] suggests a possible function in intercellular adhesion. Indeed,

changes in M2A antigen/gp36 expression coincide with transitions in the functional differentiation of both germ cells and Sertoli cells in seminiferous epithelium. Downregulation of M2A antigen/gp36 in germ cells coincides with the movement of gonocytes towards the basement membrane as they loose embryonic stem-cell-like phenotype and differentiate into spermatogonia [13, 14, 28]. Similarly, downregulation of the M2A antigen/gp36 in Sertoli cells at puberty coincides with their functional maturation and lining up on the basement membrane of the seminiferous tubules [5]. Thus, we postulate a role for the podoplanin (M2A antigen/gp36) in cell migration and cell interaction during prenatal and postnatal testicular development.

Acknowledgements The authors wish to thank L. Andersen and H. Kistrup for the skilful technical assistance, Drs. N. Jørgensen and N. Græm for providing some foetal and prepubertal testis samples, and Dr. P. Andrews for kindly providing TRA-1-60 antibody. This work was supported by grants from the Danish Cancer Society, Svend Andersen's Foundation, the Danish Medical Research Council, the Kirsten and Freddy Johansen's Foundation, Willumsen's Foundation and the Vissing Foundation. The experiments presented in the present manuscript comply with the Danish law.

References

1. Almstrup K, Hoei-Hansen CE, Wirkner U, Blake J, Schwager C, Ansorge W, Nielsen JE, Skakkebaek NE, Rajpert-De Meyts E, Leffers H (2004) Embryonic stem cell-like features of testicular carcinoma in situ revealed by genome-wide gene expression profiling. Cancer Res 64:4736–4743
2. Arigami T, Natsugoe S, Uenosono Y, Arima H, Mataki Y, Ehi K, Yanagida S, Ishigami S, Hokita S, Aikou T (2005) Lymphatic invasion using D2-40 monoclonal antibody and its relationship to lymph node micrometastasis in pN0 gastric cancer. Br J Cancer 93:688–693
3. Avivi-Green C, Kahn HJ, Zimmer G, Sutherland R, Letarte M, Law J, Chen L, Herrler G, Marks A (2004) D2-40 antigen and endoglin are complementary markers of lymphatic and blood capillaries, respectively, in breast cancer. Proceedings of the 95th annual meeting of the American Association for Cancer Research, vol 45, abstract 3243
4. Bailey D, Baumal R, Law J, Sheldon K, Kannampuzha P, Stratis M, Kahn H, Marks A (1986) Production of a monoclonal antibody specific for seminomas and dysgerminomas. Proc Natl Acad Sci U S A 83:5291–5295
5. Baumal R, Bailey D, Giwercman A, Skakkebaek N, Stratis M, Marks A (1989) A novel maturation marker for human Sertoli cells. Int J Androl 12:354–359
6. Breiteneder-Geleff S, Matsui K, Soleiman A, Meraner P, Poczewski H, Kalt R, Schaffner G, Kerjaschki D (1997) Podoplanin, novel 43-kd membrane protein of glomerular epithelial cells, is down-regulated in puromycin nephrosis. Am J Pathol 151:1141–1152
7. Breiteneder-Geleff S, Soleiman A, Kowalski H, Horvat R, Amann G, Kriehuber E, Diem K, Weninger W, Tschachler E, Alitalo K, Kerjaschki D (1999) Angiosarcomas express mixed endothelial phenotypes of blood and lymphatic capillaries: podoplanin as a specific marker for lymphatic endothelium. Am J Pathol 154:385–394
8. Franke FE, Pauls K, Rey R, Marks A, Bergmann M, Steger K (2004) Differentiation markers of Sertoli cells and germ cells in fetal and early postnatal human testis. Anat Embryol (Berl) 209:169–177
9. Fukunaga M (2005) Expression of D2-40 in lymphatic endothelium of normal tissues and in vascular tumours. Histopathology 46:396–402
10. Giwercman A, Cantell L, Marks A (1991) Placental-like alkaline phosphatase as a marker of carcinoma-in-situ of the testis. Comparison with monoclonal antibodies M2A and 43-9F. APMIS 99:586–594
11. Giwercman A, Marks A, Bailey D, Baumal R, Skakkebaek NE (1988) A monoclonal antibody as a marker for carcinoma in situ germ cells of the human adult testis. APMIS 96:667–670
12. Giwercman A, von der MH, Skakkebaek NE (1993) Epidemiological and clinical aspects of carcinoma in situ of the testis. Eur Urol 23:104–110
13. Hoei-Hansen CE, Almstrup K, Nielsen JE, Brask SS, Graem N, Skakkebaek NE, Leffers H, Rajpert-De Meyts E (2005) Stem cell pluripotency factor NANOG is expressed in human fetal gonocytes, testicular carcinoma in situ and germ cell tumours. Histopathology 47:48–56
14. Honecker F, Kersemaekers AM, Molier M, Van Weeren PC, Stoop H, De Krijger RR, Wolffenbuttel KP, Oosterhuis W, Bokemeyer C, Looijenga LH (2004) Involvement of E-cadherin and beta-catenin in germ cell tumours and in normal male fetal germ cell development. J Pathol 204:167–174
15. Jorgensen N, Giwercman A, Muller J, Skakkebaek NE (1993) Immunohistochemical markers of carcinoma in situ of the testis also expressed in normal infantile germ cells. Histopathology 22:373–378
16. Jorgensen N, Muller J, Jaubert F, Clausen OP, Skakkebaek NE (1997) Heterogeneity of gonadoblastoma germ cells: similarities with immature germ cells, spermatogonia and testicular carcinoma in situ cells. Histopathology 30:177–186
17. Jorgensen N, Rajpert-De Meyts E, Graem N, Muller J, Giwercman A, Skakkebaek NE (1995) Expression of immunohistochemical markers for testicular carcinoma in situ by normal human fetal germ cells. Lab Invest 72:223–231
18. Kahn HJ, Bailey D, Marks A (2002) Monoclonal antibody D2-40, a new marker of lymphatic endothelium, reacts with Kaposi's sarcoma and a subset of angiosarcomas. Mod Pathol 15:434–440
19. Kahn HJ, Marks A (2002) A new monoclonal antibody, D2-40, for detection of lymphatic invasion in primary tumors. Lab Invest 82:1255–1257
20. Kato Y, Fujita N, Kunita A, Sato S, Kaneko M, Osawa M, Tsuruo T (2003) Molecular identification of Aggrus/T1alpha as a platelet aggregation-inducing factor expressed in colorectal tumors. J Biol Chem 278:51599–51605
21. Kato Y, Sasagawa I, Kaneko M, Osawa M, Fujita N, Tsuruo T (2004) Aggrus: a diagnostic marker that distinguishes seminoma from embryonal carcinoma in testicular germ cell tumors. Oncogene 23:8552–8556
22. Marks A, Sutherland DR, Bailey D, Iglesias J, Law J, Lei M, Yeger H, Banerjee D, Baumal R (1999) Characterization and distribution of an oncofetal antigen (M2A antigen) expressed on testicular germ cell tumours. Br J Cancer 80:569–578
23. Matsui K, Breiteneder-Geleff S, Kerjaschki D (1998) Epitope-specific antibodies to the 43-kD glomerular membrane protein podoplanin cause proteinuria and rapid flattening of podocytes. J Am Soc Nephrol 9:2013–2026
24. Meng FJ, Zhou Y, Skakkebaek NE, Marks A, Giwercman A (1996) Detection and enrichment of carcinoma-in-situ cells in semen by an immunomagnetic method using monoclonal antibody M2A. Int J Androl 19:365–370

25. Niakosari F, Kahn HJ, Marks A, From L (2005) Detection of lymphatic invasion in primary melanoma with monoclonal antibody D2-40: a new selective immunohistochemical marker of lymphatic endothelium. Arch Dermatol 141:440–444
26. Ordonez NG (2005) Immunohistochemical diagnosis of epithelioid mesothelioma: an update. Arch Pathol Lab Med 129:1407–1414
27. Rajpert-De Meyts E, Bartkova J, Samson M, Hoei-Hansen CE, Frydelund-Larsen L, Bartek J, Skakkebaek NE (2003) The emerging phenotype of the testicular carcinoma in situ germ cell. APMIS 111:267–278
28. Rajpert-De Meyts E, Hanstein R, Jorgensen N, Graem N, Vogt PH, Skakkebaek NE (2004) Developmental expression of POU5F1 (OCT-3/4) in normal and dysgenetic human gonads. Hum Reprod 19:1338–1344
29. Rajpert-De Meyts E, Jorgensen N, Graem N, Muller J, Cate RL, Skakkebaek NE (1999) Expression of anti-Mullerian hormone during normal and pathological gonadal development: association with differentiation of Sertoli and granulosa cells. J Clin Endocrinol Metab 84:3836–3844
30. Ramirez MI, Millien G, Hinds A, Cao Y, Seldin DC, Williams MC (2003) T1alpha, a lung type I cell differentiation gene, is required for normal lung cell proliferation and alveolus formation at birth. Dev Biol 256:61–72
31. Schacht V, Dadras SS, Johnson LA, Jackson DG, Hong YK, Detmar M (2005) Up-regulation of the lymphatic marker podoplanin, a mucin-type transmembrane glycoprotein, in human squamous cell carcinomas and germ cell tumors. Am J Pathol 166:913–921
32. Schacht V, Ramirez MI, Hong YK, Hirakawa S, Feng D, Harvey N, Williams M, Dvorak AM, Dvorak HF, Oliver G, Detmar M (2003) T1alpha/podoplanin deficiency disrupts normal lymphatic vasculature formation and causes lymphedema. EMBO J 22:3546–3556
33. Skakkebaek NE (1972) Possible carcinoma-in-situ of the testis. Lancet 2:516–517
34. Skakkebaek NE, Berthelsen JG, Giwercman A, Muller J (1987) Carcinoma-in-situ of the testis: possible origin from gonocytes and precursor of all types of germ cell tumours except spermatocytoma. Int J Androl 10:19–28
35. Zimmer G, Oeffner F, Von M, V, Tschernig T, Groness HJ, Klenk HD, Herrler G (1999) Cloning and characterization of gp36, a human mucin-type glycoprotein preferentially expressed in vascular endothelium. Biochem J 341(Pt 2):277–284

Virchows Arch (2006) 449: 207–214
DOI 10.1007/s00428-006-0219-0

ORIGINAL ARTICLE

Kerstin Amann · Jürgen Hofstetter · Valentina Câmpean · Andreas Koch · Marie-Luise Gross · Roland Veelken · Eberhard Ritz

Nonhypotensive dose of β-adrenergic blocker ameliorates capillary deficits in the hearts of rats with moderate renal failure

Received: 4 January 2006 / Accepted: 8 April 2006 / Published online: 12 May 2006
© Springer-Verlag 2006

Abstract Renal failure causes sympathetic overactivity and inadequate capillary growth in response to cardiomyocyte hypertrophy in experimental renal failure, as well as in uremic patients. In nonuremic animals, sympathetic overactivity was shown to suppress capillary growth. The purpose of this study was to examine whether blockade with α- and β-adrenoblockers ameliorates the capillary deficit that was documented in the hearts of rats with moderate renal failure. Male Sprague–Dawley rats, 3 days after surgical ablation [subtotal nephrectomy (SNX)] or sham operation (sham), were treated with phenoxybenzamine, metoprolol, or a combination of both: After 12 weeks, the hearts were investigated using morphometric and stereologic techniques. The length density of myocardial capillaries was lower ($p<0.05$) in untreated SNX than in sham (2,786±372 vs 3,397±602 mm/mm^3); the decrease was abrogated by metoprolol (3,305±624 mm/mm^3), but not by phenoxybenzamin (2,628±480 mm/mm^3). The intercapillary distance increased ($p<0.05$) in SNX (20.5±1.5 μm) and tended to be lower after metoprolol treatment (19.0±1.9 μm). The media area of intramyocardial arterioles was significantly higher in untreated SNX (1,158±1,343 vs 686±771 μm^2 in sham). Metoprolol in nonhypotensive doses prevents the capillary deficit in the hearts of rats with moderate renal failure and presents an argument for an important role of sympathetic overactivity in the genesis of the capillary deficit in moderate chronic renal insufficiency.

Keywords Sympathetic overactivity · β-blockade · Heart · Capillaries · Renal failure · Myocardial perfusion

Abbreviations SNX: Subtotal nephrectomy · PBZ: Phenoxybenzamine · MET: Metoprolol · EPO: Erythropoietin · LVH: Left ventricular hypertrophy · BP: Blood pressure · MAP: Mean arterial blood pressure · SAP: Systolic arterial blood pressure · DAP: Diastolic arterial blood pressure · HR: Heart rate · S-creatinine: serum creatinine · VEGF: Vascular endothelial growth factor

K. Amann (✉) · V. Câmpean
Department of Pathology, University of Erlangen-Nürnberg,
Krankenhausstr. 8-10,
91054 Erlangen, Germany
e-mail: kerstin.amann@patho.imed.uni-erlangen.de
Tel.: +49-9131-8522291
Fax: +49-9131-8522601

J. Hofstetter · A. Koch · M.-L. Gross
Department of Pathology, University of Heidelberg,
Heidelberg, Germany

R. Veelken
Department of Medicine IV, University of Erlangen-Nürnberg,
Erlangen, Germany

E. Ritz
Department of Internal Medicine, University of Heidelberg,
Heidelberg, Germany

Introduction

Sympathetic overactivity is a known feature of renal failure and has been documented in both experimental [16] and clinical studies [19, 27, 31]. It has been shown that even in patients with normal glomerular filtration rates [27], or in experimental studies even after minimal renal injury [46], activating signals emanate from the damaged kidney via the dorsal roots, ascending into the hypothalamus. The sympathetic tone is raised by central mechanisms, causing increased efferent nerve traffic [16, 17]. Increased sympathetic activity is an important factor contributing to hypertension in renal failure [29] and to the progression of renal failure independent of blood pressure (BP) [9, 10, 12].

In experimental renal failure, as well as in patients with chronic kidney disease (CKD), the heart undergoes marked structural changes, which are important to explain the high cardiovascular mortality in CKD patients [22]. These changes occur very early on in the course of renal disease and comprise left ventricular hypertrophy (LVH), secondary to hypertrophy of cardiomyocytes, in part, independent of BP [38]; cardiac interstitial fibrosis [4, 32]; arteriolar wall thickening as a result of both hypertrophy and

hyperplasia [5]; and, finally, a capillary deficit [6, 7] resulting from a mismatch between cardiomyocyte hypertrophy and capillary growth. The causes of the capillary deficit, however, have not been elucidated. Previous studies in subtotally nephrectomized (SNX) rats showed that deficiency of erythropoietin (EPO) does not play a role [7], a finding which is relevant because EPO interacts with endothelial cells and recruits endothelial cell precursors [7].

Furthermore, in animal studies, angiotensin converting enzyme inhibitor treatment failed to normalize the capillary density in the heart [43], although other parameters, such as LVH and cardiac fibrosis, were prevented or at least ameliorated. The only intervention which, so far, has been shown to normalize capillary density in moderate experimental renal failure was endothelin (ET-1) receptor blockade [11, 35]. Although this finding points to a causal role of ET-1, the issue remains whether sympathetic overactivity is a contributory cause. This hypothesis was based on the observation that excess sympathetic activity causes a capillary deficit in the heart of normotensive and hypertensive rats [40, 44].

To address this issue, we compared untreated SNX rats with moderate chronic renal failure with SNX rats treated with nonhypotensive doses of the β-adrenoblocker metoprolol (MET). As further controls, we examined the effects of the α-adrenoblocker phenoxybenzamine (PBZ) and those of the combination of MET and PBZ.

Materials and methods

Animals

Male, 200-g Sprague–Dawley rats were housed individually in separate cages at constant room temperature (20°C) and humidity (75%) under a controlled light–dark cycle. The rats were fed a diet containing 40 g protein and 0.6 g NaCl per 100 g (Altromin, Lage/Lippe, Germany). After a 3-day adaptation period, the animals were randomly allotted to the following seven groups (n=5–11 animals per group):

Sham-operated control groups (sham)	
1. Untreated	(sham, n=8)
2. MET (150 mg/kg body weight/day)	(sham+MET, n=5)
3. PBZ (5 mg/kg body weight/day)	(sham+PBZ, n=5)
SNX groups	
4. Untreated	(SNX, n=9)
5. MET (150 mg/kg body weight/day)	(SNX+MET, n=11)
6. PBZ (5 mg/kg body weight/day)	(SNX+PBZ, n=8)
7. MET+PBZ (PBZ 2.5 mg/kg body weight/day and MET 50 mg/kg body weight/day)	(SNX+MET+PBZ, n=11)

Groups 1–3 were sham-operated, whereas groups 4–7 underwent standardized, two-step subtotal surgical nephrectomy: In the first operation, the right kidney was removed under general anesthesia (Ketamin, Xylazin) and weighed. Sham operation consisted in the decapsulation of the kidney, taking special care not to damage the adrenals. After 1 week, SNX was completed by resection of the lower and upper poles of the left kidney. To standardize the procedure, an amount of cortex corresponding to 75% of the weight of the removed right kidney was resected [4, 43]. Sham operation was performed as described above. This standardized procedure of a two-step, weight-controlled surgical resection of renal cortex resulted in a very moderate and stable degree of renal failure with no or only minor increase in systolic BP. Using the above-described procedure of moderate two-step SNX, the nephron number per kidney was reduced from approximately 30,000 to 15,000.

Forty-eight hours after the second operation, treatment was begun with nonhypotensive doses of MET, PBZ, and a combination of both which, in pilot experiments, proved to affect the release of effector peptides of the sympathetic nervous system, i.e., catecholamines, despite MET and PBZ having no effect on systemic BP or heart rate (HR), respectively. The animals were offered food pellets containing the respective drugs at a concentration designed to deliver the above-specified doses. Water and food consumption were monitored daily and the amount of food offered was adjusted accordingly to keep the drug dosage constant. With this protocol, food consumption was comparable between the groups, as was documented by the fact that no significant differences in body weight between the groups were observed at the end of the experiment. Before terminating the experiment, the animals were placed in metabolic cages and 24-h urine was collected for the determination of urine volume and albumin excretion.

BP measurements

Mean arterial, systolic arterial, and diastolic arterial BPs and HRs (derived from the peak systolic BP signal, per minute) were measured in three animals per group during the whole 12-week study period using a telemetry system (Data Sciences, St Paul, MM 55113, USA) [8]. Transmitters (TL 10-M2-C50-PE, TL11-M2-C50-PXT) were implanted in the abdominal aorta. For electrocardiography, two electrodes were implanted subcutaneously. Receivers (RLA 1000, RA 1000) were placed underneath the animal's cage. The maximum transmitter range was 40 cm. Implantation of the telemetry transmitter was performed as described elsewhere [9]. For logistical reasons, it was not possible to perform telemetry measurements in every animal. Thus, to monitor BP development over time in all animals, systolic BP was measured at weeks 1, 2, and 11 using tail plethysmography in conscious rats as described before in detail [8].

Tissue preparation

After 12 weeks, blood samples were taken and the experiment was terminated by retrograde perfusion fixation

via the abdominal aorta [43]. After the perfusion, the heart of each animal was taken out and the total heart weight, as well as the left ventricular weight, was determined. Tissue samples and sections were obtained and stained according to the orientator method [34]. Briefly, uniformly random sampling of the myocardium was achieved by preparing a set of equidistant slices of the left ventricle and the interventricular septum with a random start. Two slices were selected by area-weighted sampling and processed accordingly. Eight pieces of the left ventricular muscle including the septum were prepared and, afterwards, embedded in epon–araldite. Semithin sections (0.8 μm) were stained with methylen-blue and basic fuchsin and examined by light microscopy with oil immersion and phase contrast at a magnification of 1,000:1.

All investigations were performed in a blinded manner, i.e., the observer was unaware of the study group the animal belonged to. Stereological analyses were performed on eight random samples of differently orientated sections of the left ventricular myocardium per animal according to the orientator method [34]. Volume densities (V_V) of the capillaries, interstitial tissue, and myocytes were obtained using the point counting method according to the equation $P_P=V_V$ (with P_P as point density). Using the point counting method and a magnification of ×1,000, these structures can be easily identified and counted on semithin sections using standard criteria [43]. Reference volume was the total myocardial tissue (exclusive of noncapillary vessels, i.e., arterioles and veins, and tissue clefts). The vascular geometry of intramyocardial arterioles, i.e., vessels with lumen diameters between 30 and 150 μm and at least one muscular layer, was analyzed using planimetry and a semiautomatic image analysis system (Analysis, SIS, Münster, Germany) as described previously in detail [43]. Thereby, mean wall thickness, lumen diameter, and media and lumen area were determined in every arteriole that was present in the eight semithin sections per animal.

Statistics

Data are given as mean±standard deviation. After testing for normal distribution, Kruskal–Wallis test and one-way ANOVA were chosen for ANOVA, followed by Duncan's multiple range test to determine whether the differences between the groups were significant. The zero-hypothesis was rejected at $p<0.05$.

Results

Animal data

Daily food intake was comparable in all groups (sham operated, 16.9±1.29 g; untreated SNX, 18.5±2.01 g; SNX+MET, 18.4±1.63 g; SNX+PBZ, 18.8±1.6 g; SNX+MET+PBZ, 19.0±2.04 g). Daily water intake was also similar in the sham group (33.9± 6.2 ml/day), the SNX+MET group (38.8±8.4 ml/day), and the SNX+MET+PBZ (39.6± 8.3 ml/day) group; daily water intake was significantly higher in untreated (50.4±4.2 ml/day) and PBZ-treated SNX animals (49±10.1 ml/day). Because the values of the different measurements in sham-operated animals treated with MET and PBZ did not differ from the values in untreated sham-operated rats, only the values for the untreated sham-operated group will be reported and discussed in the following paragraphs.

At the end of the experiment, body weight, serum (S)-triglyceride, hemoglobin, and hematocrit were comparable in all groups. S-cholesterol was significantly higher in all SNX groups compared to that of the sham operation group. Absolute and relative (factored for body weight) weight of residual renal tissue (left kidney), S-urea (data not shown), and S-creatinine concentrations were significantly higher after SNX (0.8±0.09 mg/dl vs 0.6± 0.03 mg/dl in sham, $p<0.05$) with no differences between the SNX groups (0.78±0.13 mg/dl in SNX+PBZ, 0.76± 0.09 mg/dl in SNX+MET, and 0.77±0.08 mg/dl in SNX+PBZ+MET). Urinary albumin excretion at the end of the study was also significantly higher in untreated SNX (133± 74 mg/24 h) than in sham (0.3±0.21 mg/24 h) and all treated SNX groups (64±50 mg/24 h in SNX+PBZ, 54± 40 mg/24 h in SNX+MET, and 44±36 mg/24 h in SNX+PBZ+MET). Heart weight and relative left ventricular weight, i.e., left ventricular weight per body weight ratio, were significantly higher in the untreated SNX group than

Table 1 Animal data

Groups	Body weight (g)	Heart weight (g)	Relative left ventricular weight (mg/g body weight)	S-cholesterol (mg/dl)	Hematocrit (%)
Untreated sham (n=8)	416±26.0	1.63±0.22	2.24±0.19	61.7±11.4	46.6±3.3
Untreated SNX (n=9)	423±15.7	1.97± 0.39*	2.77±0.16*	108±26.6*	43.9±3.1
SNX+MET (n=11)	405±19.7	1.76±0.28	2.47±0.43	113±29.7*	43.0±4.3
SNX+PBZ (n=8)	409±25.3	1.55±0.14	2.51±0.26	118±38.9*	45.5±4.5
SNX+MET+PBZ (n=11)	415±28.7	1.83±0.26	2.49±0.41	98.7±26.8*	42.2±2.9
ANOVA	n.s.	$p<0.05$	$p<0.05$	$p<0.05$	n.s.

n.s. not significant
*$p<0.05$ vs sham

Table 2 Telemetric blood pressure measurements

Groups	Systolic blood pressure (mmHg)	Mean arterial blood pressure (mmHg)	Diastolic blood pressure (mmHg)
Untreated sham (n=3)	107±17.4	92±16.7	79±16.5
Untreated SNX (n=3)	121±11.3*	105±13.3*	91±18.6*
SNX+ MET (n=3)	133±11.1*	111±10.5*	103±21.3*
SNX+PBZ (n=3)	121±14.8*	111±16.9*	103±21.3*
ANOVA	p<0.05	p<0.05	p<0.05

*p<0.05 vs sham

in sham-operated rats. There was a tendency toward lower values in all treated SNX groups; the difference, however, was not statistically significant.

Mean, systolic, and diastolic BP values (as means of the 12-week telemetric measurements) were significantly higher in all SNX groups compared to sham-operated rats. HRs were comparable in sham-operated rats (317± 44 bpm) and all SNX groups (in untreated SNX, 316± 31 bpm; in SNX+MET, 316±49 bpm; and in SNX+PBZ, 308±38 bpm).

Using tail plethysmography, systolic BP was comparable in all experimental groups at the beginning of the experiment (sham, 89±9 mmHg; SNX, 96±16.6 mmHg; SNX+MET, 91±7.4 mmHg; SNX+PBZ, 90±33.7 mmHg; SNX+MET+PBZ, 90±12.9 mm H). After 11 weeks, systolic BP was significantly higher in SNX groups (113± 14.4 mmHg) than in the sham group (91±14.0 mmHg), with no significant differences between untreated SNX and the three intervention groups (SNX+MET, 109± 10.7 mmHg; SNX+PBZ, 113±23.5 mmHg; SNX+MET+ PBZ, 110±17.4 mm Hg) (Tables 1 and 2).

Cardiac capillary length density, intercapillary distance, and interstitial myocardial tissue

In sham-operated animals, the length density of myocardial capillaries, i.e., the total capillary length per volume myocardium, was significantly higher than in untreated SNX (3,397±602 vs 2,786±372 mm/mm^3, p<0.05). This decrease in myocardial capillary supply was prevented by the administration of MET (3,305±624 mm/mm^3, p<0.05), but not by that of PBZ (2,628±480 mm/mm^3) or combined MET+PBZ treatment (2,888±400 mm/mm^3). Conversely, the intercapillary distance, 18.6±1.5 μm in sham, was significantly increased in SNX (20.5±1.5), and this increase was prevented partly only by MET (19.0± 1.9, not significant). In PBZ-treated SNX, the intercapillary distance was 21.2±2.3 μm, and in MET+PBZ-treated SNX, 20.1± 1.4 μm (Fig. 1).

The volume density of the myocardial interstitial tissue was significantly higher (p<0.05) in the untreated SNX group (3.64±0.50%) compared to the sham (1.93±0.32%) and all treatment groups (SNX+ MET, 2.83±0.45; SNX+PBZ, 2.57±0.29%; SNX+MET+ PBZ, 2.47±0.42).

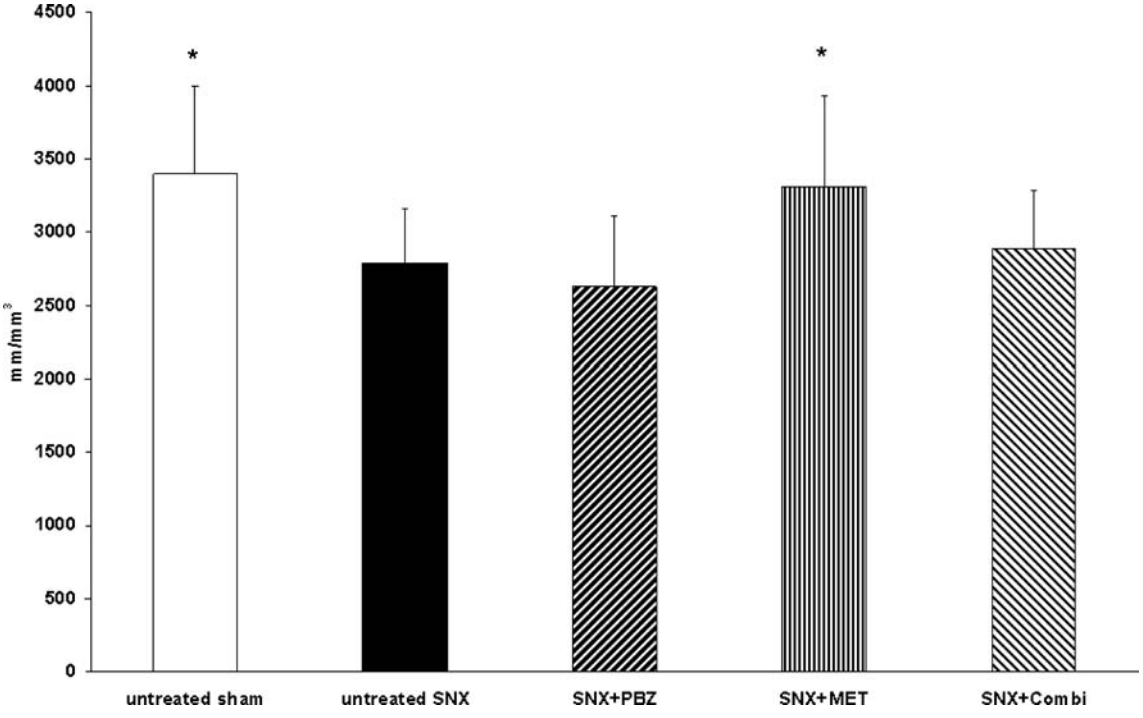

Fig. 1 The decrease in capillary length density in untreated SNX compared to sham-operated control animals is prevented by MET treatment of SNX. * represents p<0.05 vs untreated SNX

Table 3 Changes of intramyocardial arterioles

Groups	Intramyocardial arterioles		
	Wall thickness (μm)	Wall: lumen ratio ($\mu m/\mu m \times 10^{-2}$)	Media area (μm^2)
Untreated sham (n=8)	2.71±1.27	6.63±2.63	686±771
Untreated SNX (n=9)	4.18±1.94*	10.1±3.71*	1,158±1,343*
SNX+MET (n=11)	3.88±2.09*,**	9.13±3.50*,**	1,075±1,221*
SNX+PBZ (n=8)	4.15±1.84*	10.0±3.75*	1,094±1,236*
SNX+MET+PBZ (n=11)	3.73±1.96*,**	8.95±3.06*,**	1,007±1,309*
ANOVA	$p<0.05$	$p<0.05$	$p<0.05$

*$p<0.05$ vs sham
**$p<0.05$ vs untreated SNX

Intramyocardial arterioles

A total of 208 to 334 intramyocardial arterioles with lumen diameters between 30 and 150 μm were analyzed per group. The cumulative frequency distribution of lumen diameters was not different between the groups, thus excluding a systematic sampling error. The lumen diameter and the lumen area were not significantly different between the groups, either (data not shown). The wall thickness of intramyocardial arterioles, however, was significantly higher in all SNX rats (4.18±1.94 μm) than in sham-operated rats (2.71±1.27 μm), and this increase in arteriolar wall thickness had a tendency to be prevented ($p<0.059$) by MET treatment of SNX (3.88±2.09 μm), as well as by combined MET+PBZ treatment (3.73±1.96); however, the differences were not statistically significant (Table 3).

Discussion

The salient feature of the present study is the documentation that nonhypotensive doses of MET completely prevented the capillary deficit in the hearts of SNX rats with moderate renal failure. BP independence of this beneficial effect was clearly demonstrated by telemetric BP measurement. This effect was not seen in the PBZ-treated group or in the group that received MET+PBZ. The complete normalization of the length density of capillaries was accompanied by some improvement of the parameters of cardiac morphology, particularly, less thickening of the walls of intramyocardial arterioles, as well as by less-pronounced cardiac interstitial fibrosis. Whether the latter is related to the normalization of heart capillaries is unknown (Fig. 2).

In interpreting the results, it is important to consider several methodological problems. One potential confounder could be less-severe LVH in SNX with MET treatment. The relative left ventricular weight was significantly higher in untreated SNX compared to sham animals and was not significantly lowered by any treatment, however. Nevertheless, we caution that cardiac weight was measured after perfusion fixation, which could have confounded the measurements of LVH.

Potential artifacts may arise because the myocardium, and, in particular, the cardiac vascular tree, is an anisotropic tissue, i.e., the distribution of structures follows preferential orientations. To avoid this confounder, the orientator technique [34] was used to obtain random samples of the

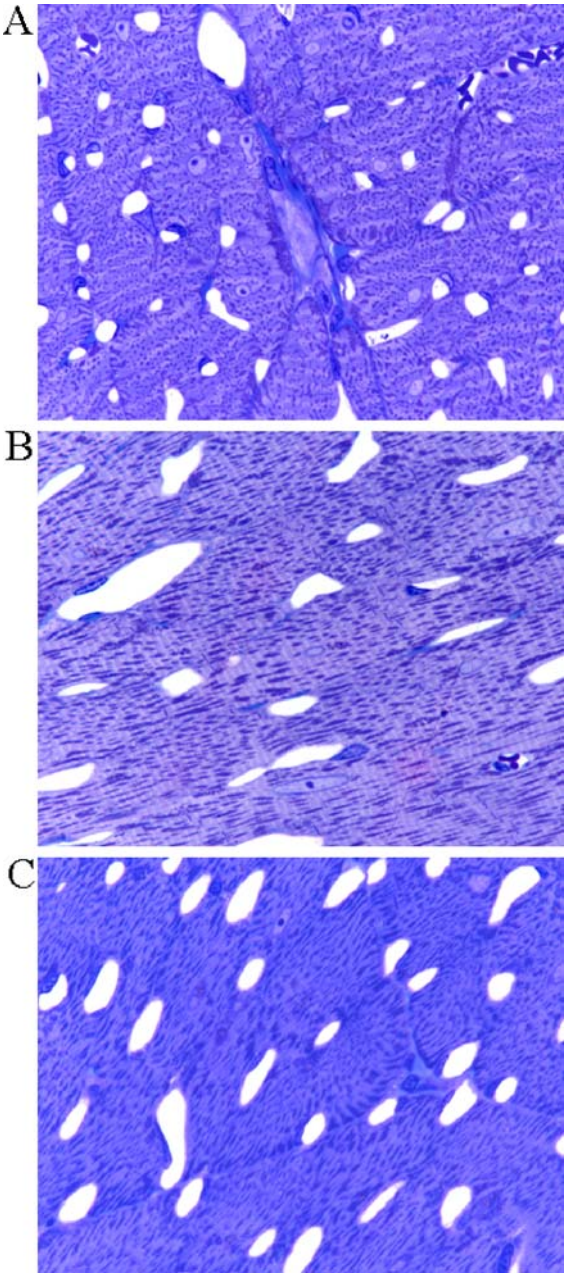

Fig. 2 Representative figures of changes in cardiac capillarization in untreated sham (**a**) and SNX (**b**), as well as in the MET-treated SNX (**c**). Note the lower number of capillary profiles in the untreated SNX rat with moderate renal failure (**b**) compared to the normal cardiac capillary density in a sham-operated control rat (**a**) and a MET-treated SNX rat (**c**)

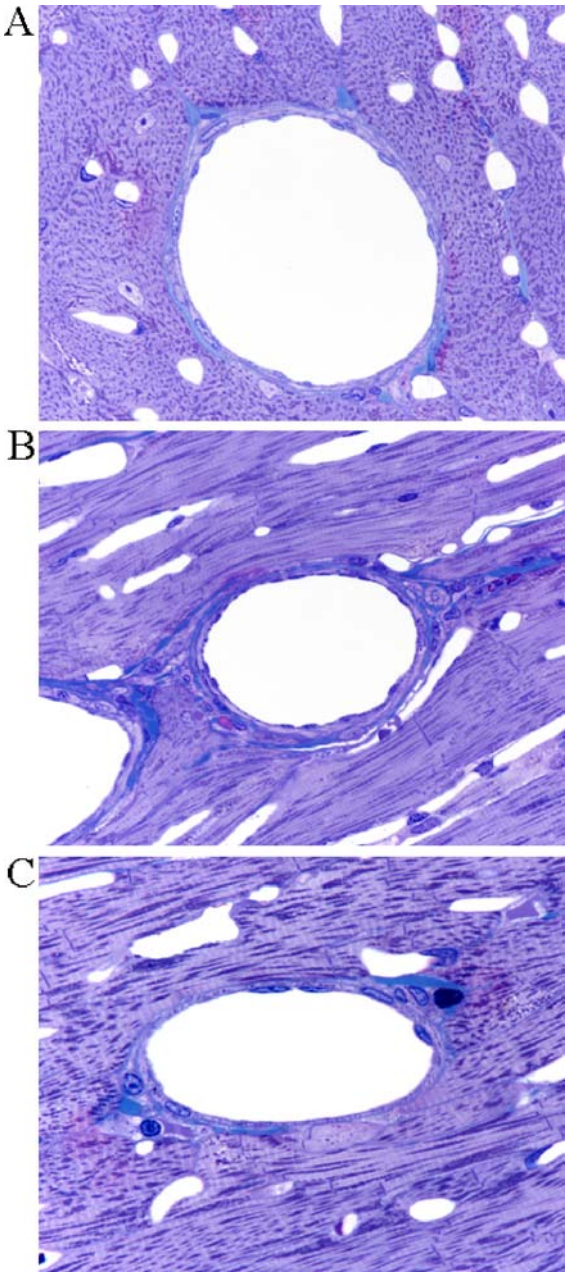

Fig. 3 Representative figures of changes in intramyocardial arterioles in untreated sham (**a**) and SNX (**b**) rats, as well as in the MET-treated SNX rats (**c**). Wall thickness of intramyocardial arterioles is increased in untreated SNX rats (**b**) compared to that of untreated sham-operated controls (**a**), and is also slightly higher than in MET-treated SNX rats (**c**)

myocardium, thus preventing any systematic error of spatial preference.

Although a pair-feeding protocol could not be used because of the considerable number of parallel groups, water and food consumption was monitored and intake was adjusted so as to keep the body weights in the different groups comparable. This protocol also guaranteed controlled intake of the medications.

We intentionally selected low doses of the adrenoreceptor blockers to avoid confounding effects of BP lowering. Lowering of BP would have been of concern because BP is one of the most potent determinants of LVH and accompanying structural alterations of the heart. Telemetry, i.e., the state-of-the-art technique, was used to exclude changes in BP, in addition to tail plethysmographic measurements.

In a previous study, Rambausek and coworkers [38] had investigated the effect of α- and β-adrenoreceptor blockade on LVH in SNX rats with renal failure. Using comparable doses of MET and prazosin i.p., they also found no significant effect on LVH, despite normalization of BP.

In the present study, we did not directly measure sympathetic activity. It is known from previous studies [9, 10] that, in the SNX model with only very moderate degrees of renal failure, the norepinephrine content of the kidney (and presumably also the heart) is decreased in parallel with increased norepinephrine turnover. This constellation indicates an increase in the firing rate of a reduced number of neurons [9, 10].

On the one hand, there is compelling experimental and clinical evidence [16, 17, 24, 29] that sympathetic activity is increased in renal disease, and particularly in chronic renal failure. On the other hand, there is evidence of diminished β-adrenergic responsiveness [20, 30, 33], as evidenced by measurements of receptor binding, of postreceptor signaling steps and of the HR response in SNX after stimulation with isoproterenol. α-Adrenoreceptor responsiveness of peripheral vessels is decreased as well [39].

A specific role of the sympathetic nerves in the regulation of mitochondrial and myofibril growth during the development of cardiac hypertrophy was shown in hypertensive rats [41]. In the perfusion of fixed hearts of normotensive (Wistar–Kyoto) and spontaneously hypertensive rats using similar stereological techniques, Tomanek showed that chronic sympathectomy by lifelong treatment with 6-hydroxydopamine significantly improved myocardial capillary supply independent of BP lowering or the prevention of LVH. He concluded that sympathetic nerves inhibit capillary proliferation either directly or indirectly during pressure-overload-induced cardiac enlargement [40].

In brown fat tissue of lean and obese rats, a specific role of the sympathetic nerve system for the control of vascular endothelial growth factor (VEGF) expression via noradrenalin was found [42]. VEGF gene and protein expression is significantly lower in the heart of untreated SNX with moderate renal failure [15]. Whether VEGF expression was increased in the MET-treated group could not be investigated in the present experiment because glutaraldehyd fixation precluded immunohistochemical or molecular analyses.

The present study extends previous experiments on the effect of the central sympathoplegic agent moxonidine on cardiac capillaries in SNX rats [43], which had documented a selective beneficial effect of moxonidine, but not of ramipril or nifedipine, on the capillary deficit of the heart in moderate renal failure. We emphasize, however, that

activation of the sympathetic system does not only cause the release of catecholamines, but also that of sympathetic cotransmitters such as adenosine triphosphate and neuropeptide Y (NPY) [37]. The beneficial effect of moxonidin in the study of Törnig et al. [43] did not allow the conclusion that it was the catecholamines per se which had modified the myocardial capillary density. In the present study, however, specific β-adrenoreceptor blockade completely prevented the capillary deficit in the hearts of SNX rats. Consequently, this observation indicates that this is a specific effect of catecholamines independent of the cotransmitters.

Blockade of the ET-1 system by either selective or nonselective antagonists has so far been the only intervention which prevents the capillary deficit in the heart in SNX [35]. It is therefore of interest that the ET-1 and the sympathetic systems interact. In anesthetized normotensive rats, intracerebroventricular injection of ET-1 increased sympathetic nerve activity [36], and ET-1 also modulated the release of the sympathetic transmitters NPY and norepinephrine in the mesenteric bed [25] and cardiac sympathetic innervation [26]. Whether blockade of the sympathetic nerve system conversely reduced ET-1 and whether this may have impacted on the cardiac parameters examined in this study could not be analyzed. Nevertheless, the similarity of the findings of improved capillary supply in SNX treated with ET-1 antagonists in a previous study [35] and with MET in the present study would be consistent with the hypothesis that ET-1 overactivity is a distal consequence of catecholaminergic stimulation.

The salient finding in the present study concerns the myocardial capillaries. It is intriguing that nonhypotensive doses of β-adrenoblockers tended to affect the structure of intramyocardial arterioles as well (Fig. 3). These structures are less frequent; consequently, the numbers sampled for analysis are less than those of capillaries and thus, the sensitivity was probably less. This may account for the fact that the finding was not significant. Nevertheless, we find the result remarkable, because in a recent experimental study [11], we had documented abnormal ET-1-dependent adaptive remodeling in response to changes in arterial flow in the mesenteric beds of SNX rats with moderate renal failure.

Sympathetic overactivity is of clinical relevance. In one prospective trial, hemodialyzed diabetic patients dying from cardiovascular causes had used β-adrenoblockers less frequently than survivors [28], and this prompted the postulation of more frequent use of β-blockers in this high-risk population [47]. The uncontrolled observations of Agarwal documented remarkable efficacy and tolerability of β-adrenoblockers in treatment-resistant hypertensive dialysis patients [2], and in observational studies, better survival was noted [3, 14, 23]. A recent analysis from the US Renal Data system found that, in dialysis patients without previously documented histories of heart failure, β-adrenoblocker use was associated with lower risks of new heart failure, cardiovascular death, and death from any cause [1]. Finally, in a prospective controlled study, the β-adrenoblocker carvedilol reduced mortality in hemodialysis patients with heart failure [18]. This observation is remarkable, because in the high-risk population of dialysis patients, other interventions, such as the rising of hemoglobin concentrations with EPO [13]; raising Kt/V, and thus, small solute removal [21]; and the administration of statins [45], have so far failed to improve outcome. It is tempting to speculate that the beneficial effect of sympathetic blockade on the cardiac microvasculature contributed to the clinical efficacy of β-adrenoblockade on outcome.

In conclusion, although β-adrenoblockers exert effects unrelated to heart structure, improved myocardial capillary perfusion after β-adrenoblockade may contribute to the survival benefit derived from β-adrenoblockers in CKD patients.

Acknowledgements The study was supported by the Deutsche Forschungsgemeinschaft (KFO 106, TP 6). The authors thank Z. Antoni, M. Klewer, P. Rieger, S. Söllner, M. Weckbach, and H. Ziebart for excellent technical support.

References

1. Abbott KC, Trespalacios FC, Agodoa LY, Taylor AJ, Bakris GL (2004) Beta-blocker use in long-term dialysis patients: association with hospitalized heart failure and mortality. Arch Intern Med 164:2465–2471
2. Agarwal R (1999) Supervised atenolol therapy in the management of hemodialysis hypertension. Kidney Int 55:1528–1535
3. Agarwal R (2003) Systolic hypertension in hemodialysis patients. Semin Dial 16:208–213
4. Amann K, Ritz E, Wiest G, Klaus G, Mall G (1994) A role of parathyroid hormone for the activation of cardiac fibroblasts in uremia. J Am Soc Nephrol 4:1814–1819
5. Amann K, Gharehbaghi H, Stephen S, Mall G (1995) Hypertrophy and hyperplasia of smooth muscle cells of small intramyocardial arteries in spontaneously hypertensive rats. Hypertension 25:124–131
6. Amann K, Breitbach M, Ritz E, Mall G (1998) Myocyte/capillary mismatch in the heart of uremic patients. J Am Soc Nephrol 9:1018–1022
7. Amann K, Buzello M, Simonaviciene A, Miltenberger-Miltenyi G, Koch A, Nabokov A, Gross ML, Gless B, Mall G, Ritz E (2000) Capillary/myocyte mismatch in the heart in renal failure—a role for erythropoietin? Nephrol Dial Transplant 15:964–969
8. Amann K, Münter K, Wessels S, Wagner J, Balajew V, Hergenröder S, Mall G, Ritz E (2000) Endothelin A receptor blockade prevents capillary/myocyte mismatch in the heart of uremic animals. J Am Soc Nephrol 11:1702–1711
9. Amann K, Rump LC, Simonaviciene A, Oberhauser V, Wessels S, Orth SR, Gross ML, Koch A, Bielenberg GW, Van Kats JP, Ehmke H, Mall G, Ritz E (2000) Effects of low dose sympathetic inhibition on glomerulosclerosis and albuminuria in subtotally nephrectomized rats. J Am Soc Nephrol 11:1469–1478
10. Amann K, Koch A, Hofstetter J, Gross ML, Haas C, Orth SR, Ehmke H, Rump LC, Ritz E (2001) Glomerulosclerosis and progression: effect of subantihypertensive doses of alpha and beta blockers. Kidney Int 60:1309–1323
11. Amann K, Miltenberger-Miltenyi G, Simonoviciene A, Koch A, Orth S, Ritz E (2001) Remodeling of resistance arteries in renal failure: effect of endothelin receptor blockade. J Am Soc Nephrol 12:2040–2050
12. Amann K, Veelken R (2003) Mechanisms and consequences of sympathetic hyperactivity in renal disease. Clin Nephrol 60 (Suppl 1):S81–S92

13. Besarab A, Bolton WK, Browne JK, Egrie JC, Nissenson AR, Okamoto DM, Schwab SJ, Goodkin DA (1998) The effects of normal as compared with low hematocrit values in patients with cardiac disease who are receiving hemodialysis and epoetin. N Engl J Med 339:584–590
14. Bragg JL, Mason NA, Maroni BJ, Held PJ, Young EW (2001) Beta-adrenergic antagonist utilization among hemodialysis patients. J Am Soc Nephrol 12:321A
15. Campean V, Haas CS, Acker T, Ritz E, Plate KH, Amann K (2003) The role of angiogenic factors in the genesis of maladaptation of capillary growth in uremia. J Am Soc Nephrol 14:208A
16. Campese VM (2000) Neurogenic factors and hypertension in renal disease. Kidney Int Suppl 75:S2–S6
17. Campese VM, Kogosov E (1995) Renal afferent denervation prevents hypertension in rats with chronic renal failure. Hypertension 25:878–882
18. Cice G, Ferrara L, D'Andrea A, D'Isa S, Di Benedetto A, Cittadini A, Russo PE, Golino P, Calabro R (2003) Carvedilol increases two-year survival in dialysis patients with dilated cardiomyopathy: a prospective, placebo-controlled trial. J Am Coll Cardiol 41:1438–1444
19. Converse RL Jr, Jacobsen TN, Toto RD, Jost CM, Cosentino F, Fouad-Tarazi F, Victor RG (1992) Sympathetic overactivity in patients with chronic renal failure. N Engl J Med 327:1912–1918
20. Dhein S, Rohnert P, Markau S, Kotchi-Kotchi E, Becker K, Poller U, Osten B, Brodde OE (2000) Cardiac beta-adrenoceptors in chronic uremia: studies in humans and rats. J Am Coll Cardiol 36:608–617
21. Eknoyan G, Beck GJ, Cheung AK, Daugirdas JT, Greene T, Kusek JW, Allon M, Bailey J, Delmez JA, Depner TA, Dwyer JT, Levey AS, Levin NW, Milford E, Ornt DB, Rocco MV, Schulman G, Schwab SJ, Teehan BP, Toto R (2002) Effect of dialysis dose and membrane flux in maintenance hemodialysis. N Engl J Med 347:2010–2019
22. Foley RN, Parfrey PS, Sarnak MJ (1998) Epidemiology of cardiovascular disease in chronic renal disease. J Am Soc Nephrol 9:S16–S23
23. Foley RN, Herzog CA, Collins AJ (2002) Blood pressure and long-term mortality in United States hemodialysis patients: USRDS Waves 3 and 4 Study. Kidney Int 62:1784–1790
24. Hausberg M, Kosch M, Harmelink P, Barenbrock M, Hohage H, Kisters K, Dietl KH, Rahn KH (2002) Sympathetic nerve activity in end-stage renal disease. Circulation 106:1974–1979
25. Hoang D, Macarthur H, Gardner A, Westfall TC (2002) Endothelin-induced modulation of neuropeptide Y and norepinephrine release from the rat mesenteric bed. Am J Physiol Heart Circ Physiol 283:H1523–H1530
26. Ieda M, Fukuda K, Hisaka Y, Kimura K, Kawaguchi H, Fujita J, Shimoda K, Takeshita E, Okano H, Kurihara Y, Kurihara H, Ishida J, Fukamizu A, Federoff HJ, Ogawa S (2004) Endothelin-1 regulates cardiac sympathetic innervation in the rodent heart by controlling nerve growth factor expression. J Clin Invest 113:876–884
27. Klein IH, Ligtenberg G, Oey PL, Koomans HA, Blankestijn PJ (2001) Sympathetic activity is increased in polycystic kidney disease and is associated with hypertension. J Am Soc Nephrol 12:2427–2433
28. Koch M, Thomas B, Tschope W, Ritz E (1993) Survival and predictors of death in dialysed diabetic patients. Diabetologia 36:1113–1117
29. Koomans HA, Blankestijn PJ, Joles JA (2004) Sympathetic hyperactivity in chronic renal failure: a wake-up call. J Am Soc Nephrol 15:524–537
30. Leineweber K, Heinroth-Hoffmann I, Ponicke K, Abraham G, Osten B, Brodde OE (2002) Cardiac beta-adrenoceptor desensitization due to increased beta-adrenoceptor kinase activity in chronic uremia. J Am Soc Nephrol 13:117–124
31. Ligtenberg G, Blankestijn PJ, Oey PL, Klein IH, Dijkhorst-Oei LT, Boomsma F, Wieneke GH, van Huffelen AC, Koomans HA (1999) Reduction of sympathetic hyperactivity by enalapril in patients with chronic renal failure. N Engl J Med 340:1321–1328
32. Mall G, Rambausek M, Neumeister A, Kollmar S, Vetterlein F, Ritz E (1988) Myocardial interstitial fibrosis in experimental uremia—implications for cardiac compliance. Kidney Int 33:804–811
33. Mann JF, Jakobs KH, Riedel J, Ritz E (1986) Reduced chronotropic responsiveness of the heart in experimental uremia. Am J Physiol 250:H846–H852
34. Mattfeld T, Mall G, Gharebhaghi H, Möller P (1990) Estimation of surface area and length with the orientator. J Microsc 159:301–317
35. Nabokov AV, Amann K, Wessels S, Münter K, Wagner J, Ritz E (1999) Endothelin receptor antagonists influence cardiovascular morphology in uremic rats. Kidney Int 55:512–519
36. Nakamura K, Sasaki S, Moriguchi J, Morimoto S, Miki S, Kawa T, Itoh H, Nakata T, Takeda K, Nakagawa M (1999) Central effects of endothelin and its antagonists on sympathetic and cardiovascular regulation in SHR-SP. J Cardiovasc Pharmacol 33:876–882
37. Oberhauser V, Vonend O, Rump LC (1999) Neuropeptide Y and ATP interact to control renovascular resistance in the rat. J Am Soc Nephrol 10:1179–1185
38. Rambausek M, Ritz E, Mall G, Mehls O, Katus H (1985) Myocardial hypertrophy in rats with renal insufficiency. Kidney Int 28:775–782
39. Rascher W, Schömig A, Kreye VA, Ritz E (1982) Diminished vascular response to noradrenaline in experimental chronic uremia. Kidney Int 21:20–27
40. Tomanek RJ (1989) Sympathetic nerves modify mitochondrial and capillary growth in normotensive and hypertensive rats. J Mol Cell Cardiol 21:755–764
41. Tomanek RJ, Carlson DW, Palmer PJ, Bhatnagar RK (1987) Role of sympathetic nerves during developing cardiac hypertrophy in Grollman hypertensive rats. Am J Physiol 253: H818–H825
42. Tonello C, Giordano A, Cozzi V, Cinti S, Stock MJ, Carruba MO, Nisoli E (1999) Role of sympathetic activity in controlling the expression of vascular endothelial growth factor in brown fat cells of lean and genetically obese rats. FEBS Lett 442:167–172
43. Törnig J, Amann K, Ritz E, Nichols C, Zeier M, Mall G (1996) Arteriolar wall thickening, capillary rarefaction and interstitial fibrosis in the heart of rats with renal failure: the effects of ramipril, nifedipine and moxonidine. J Am Soc Nephrol 7:667–675
44. Torry RJ, Connell PM, O'Brien DM, Chilian WM, Tomanek RJ (1991) Sympathectomy stimulates capillary but not precapillary growth in hypertrophic hearts. Am J Physiol 260:H1515–H1521
45. Wanner C, Krane V, Marz W, Olschewski M, Mann JF, Ruf G, Ritz E (2005) Atorvastatin in patients with type 2 diabetes mellitus undergoing hemodialysis. N Engl J Med 353:238–248
46. Ye S, Zhong H, Yanamadala V, Campese VM (2002) Renal injury caused by intrarenal injection of phenol increases afferent and efferent renal sympathetic nerve activity. Am J Hypertens 15:717–724
47. Zuanetti G, Maggioni AP, Keane W, Ritz E (1997) Nephrologists neglect administration of beta blockers to dialysed diabetic patients. Nephrol Dial Transplant 12:2497–2500

Virchows Arch (2006) 449: 215–219
DOI 10.1007/s00428-006-0193-6

ORIGINAL ARTICLE

Tetsuya Ueo · Kenji Kashima · Tsutomu Daa · Yoshiyuki Kondo · Shigeo Yokoyama

Coexistence of Epstein–Barr virus-associated gastric carcinoma with malignant lymphoma: report of two cases

Received: 3 November 2005 / Accepted: 9 December 2005 / Published online: 12 April 2006
© Springer-Verlag 2006

Abstract Epstein–Barr virus (EBV)-associated gastric carcinoma (EBV-GC) is not rare, accounting for 5 to 18% of all gastric carcinomas. Recently, we encountered two cases of EBV-GC of ordinary histopathological type coexistent with malignant lymphoma. One patient was a 71-year-old Japanese man who had two lesions, one in the cardia and the other in the antrum of the stomach. The former was EBV-GC without lymphoma, and antral one was EBV-GC with diffuse large B-cell lymphoma (DLBCL). The other patient was a 49-year-old Japanese man who had received chemotherapy for pelvic DLBCL 3 years earlier. He had EBV-GC with follicular lymphoma in the fundus of the stomach. In both cases, gastric carcinomas were positive for EBV-encoded small RNA by in situ hybridization, whereas the lymphoma cells, infiltrating nonneoplastic lymphocytes, and nonneoplastic epithelial cells were negative. The present cases suggest that focal immunosuppression by adjacent gastric lymphomas might be related to the alteration of the microenvironment and development of EBV-GC.

Keywords Epstein–Barr virus · Gastric carcinoma · Gastric lymphoma

Introduction

Five to 18% of all gastric carcinomas are reported to be associated with Epstein–Barr virus (EBV)-infection, while the incidence of gastric carcinoma with lymphoid stroma (lymphoepithelioma-like carcinoma) is more than 90% [6]. EBV-associated gastric carcinoma (EBV-GC) occurs at nearly the same relative frequency independent of its clinical stage [17]. In EBV-GC, most malignant cells are positive by in situ hybridization (ISH) for EBV-encoded small RNA (EBER), whereas adjacent cells including nonneoplastic epithelial and inflammatory cells are negative [12, 17]. These findings imply that EBV infects mucosal epithelial cells to immortalize them, or infects carcinoma cells at early stage of their life. According to a clinicopathological study of a large number of cases, EBV-GC occurs predominantly in proximal stomach, particularly in the gastric cardia, compared with other parts of the stomach [21]. Although EBV-infection pathway to epithelial or carcinoma cells is not clear at present, some environmental alterations in the stomach might be related to the infection.

In immunocompromised patients, such as those with HIV infection or transplantation, malignant lymphoma frequently develops, in which EBV is considered to be one of the causative agents [9, 18]. EBV-associated lymphomas preceded by chronic pyothorax or Hashimoto's thyroiditis have a chronic inflammatory background that may constitute localized immunosuppressive state. Hence, it is hypothesized that malignant lymphoma as well as the inflammatory background provides abnormal immunological milieu that might contribute to EBV infection.

Coexistence of primary carcinoma and lymphoma in the stomach is an extremely uncommon event, accounting for 0.098% of all gastric malignancies [15]. In such cases, EBV-infection is extremely rare, and to our knowledge, only two cases of gastric EBV-GC and lymphoma have been reported [8, 15]. Recently, we encountered two cases of EBV-GC with malignant lymphoma. We present in this study the morphologic, immunophenotypic, and clinical features of the two cases.

T. Ueo · K. Kashima (✉) · T. Daa · Y. Kondo · S. Yokoyama
Department of Pathology, Faculty of Medicine,
Oita University,
Hasama-machi,
Oita 879-5593, Japan
e-mail: kkashima@med.oita-u.ac.jp
Tel.: +81-97-5866098
Fax: +81-97-5865686

Clinical history

Case 1 A 71-year-old Japanese man was admitted to the hospital for investigation of melena. Colonic endoscopic examination revealed a 5×2.5 cm tumor in the rectum. In addition, endoscopic examination of the upper digestive

tract showed a broad depressed lesion with focal elevated component (type IIc + IIa) in the antrum of the stomach. The histopathological diagnosis of the biopsy specimens from the colonic and gastric lesions was moderately differentiated adenocarcinoma and poorly differentiated adenocarcinoma, respectively. Rectosigmoidectomy and gastrectomy were performed.

Case 2 The patient was a 49-year-old Japanese man who had undergone chemotherapy for pelvic diffuse large B-cell lymphoma (DLBCL) 3 years earlier. Gastric endoscopy conducted as part of a periodic medical check-up showed a slightly depressed lesion in the fundus of the stomach. Under a diagnosis of gastric carcinoma, total gastrectomy and regional lymph node resection were performed. During the operation, swollen mesenteric lymph nodes were also resected.

Materials and methods

The excised tumor tissues were formalin-fixed and paraffin-embedded in the routine manner. Four-micrometer-thick sections were stained with hematoxylin and eosin (H&E). Representative specimens were also stained with the Giemsa stain to detect *Helicobacter pylori*. ISH and immunohistochemical methods were also performed for EBV analysis.

In situ hybridization

In situ hybridization (ISH) for detection of EBV-specific RNAs was performed on paraffin sections with a commercially available EBV oligonucleotide probe complementary to EBV-encoded small RNAs (EBER) (Falma, Tokyo). A commercially available poly T oligonucleotide probe (Falma) was also used to verify the integrity and lack of degradation of mRNA in each sample.

ISH was performed according to minor modification of previously described cDNA-mRNA in situ hybridization method (20) using the Microprobe Manual Stain System (Fisher Scientific, Pittsburgh, PA, USA). Briefly, tissue sections (4 μm) of formalin-fixed, paraffin-embedded specimens were mounted on silane-treated ProbeOn slides (Fisher Scientific). The slides were placed in Microprobe slide holder, dewaxed, and rehydrated with Autodewaxer and Autoalcohol (Research Genetics), followed by enzymatic digestion with pepsin. Hybridization of the probe was performed for 30 min at 45°C, and the samples were then washed three times with 2× SCC for 2 min at 45°C. The samples were incubated with alkaline phosphatase-labeled avidin for 12 min at 45°C, rinsed in 50 mM Tris buffer (pH 7.6), and signal localization was obtained with alkaline phosphatase enhancer (BCIP-NBT). The slides were then washed with distilled water, counterstained with hematoxylin for 5 s, and cover slipped with Universal Mount (Research Genetics). A poly T probe (Falma) showed that the integrity of mRNA in each sample were intact.

Immunohistochemistry

Immunohistochemical staining was performed after bleaching technique with 0.25% potassium permanganate with monoclonal antibodies against latent membrane protein 1 (LMP-1; clone CS1-4, Dako, Carpinteria, CA,

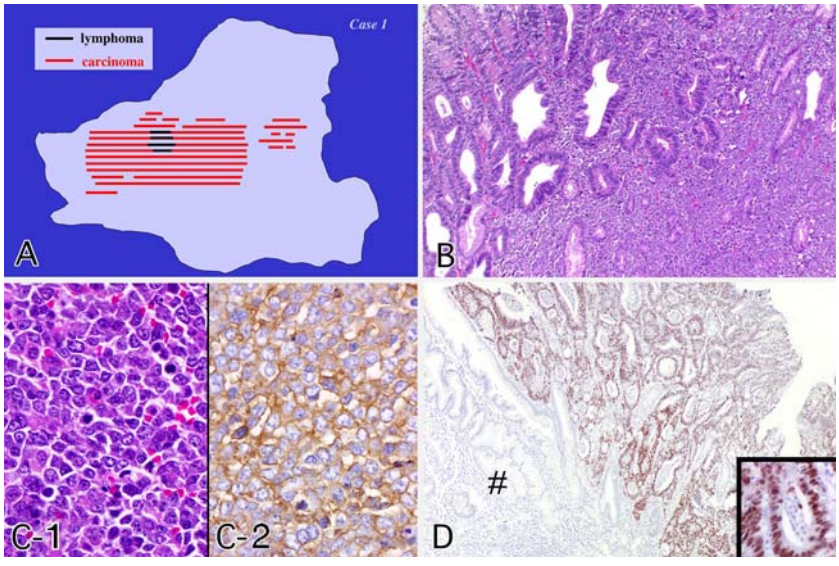

Fig. 1 **a** Schematic diagram of the resected stomach of case 1. Two isolated carcinomas (*red lines*) are located in the cardia (type IIc) and in the antrum (type IIa + IIc). The *black lines* (elevated part) within the antral lesion corresponds to malignant lymphoma. **b** Antral lesion of case 1 is composed of well-differentiated adenocarcinoma (*left*) and malignant lymphoma (*right*). **c** The elevated part within the antral lesion of the case 1 is composed of diffuse large B-cell lymphoma (*1*) which is positive for CD20 (*2*). **d** The carcinoma cells in the cardiac lesion of case 1 are positive for EBER, but normal epithelial cells and inflammatory cells (#) are negative. Inset shows nuclear positive signals for EBER

USA), EBV-encoded nuclear antigen 2 (EBNA 2; clone PE2, Dako), CD20 (clone L26, Dako), CD79a (Clone JCB117, Dako), CD10 (Clone 56C6, Novocastra Newcastle upon Tyne, UK), and bcl-2 (Clone 124, Dako).

Pathologic findings

Case 1 The colonic lesion was an adenocarcinoma. In the resected stomach, two isolated lesions were found in the cardia and antrum (Fig. 1a). The cardiac lesion was small and slightly depressed (type IIc), while the antral one was broadly depressed with focal elevated part (type IIc + IIa). The tumors were 2.2×1.5 cm and 8.0×4.2 cm in diameter, respectively. Microscopically, both lesions were well-differentiated adenocarcinoma with tubular and papillary structures. The cardiac lesion invaded the submucosa and the antral one was restricted to the mucosa. In addition, in the elevated part of the antral lesion, malignant lymphoma (DLBCL) was observed, which was positive for CD20 (Fig. 1a–c). The majority of tumor cells in the cardiac lesion were positive for EBV-encoded small RNA (EBER) by ISH. But tumor cells in the antral lesion was partially positive for EBER-ISH in spite of their preserved mRNA indicated by poly T ISH. On the contrary, adjacent normal epithelial cells, lymphoma cells and nonneoplastic lymphocytes were all negative for EBER-ISH (Fig. 1d). Further studies for the expression of the EBV-encoded nuclear antigen 2 (EBNA 2) and the latent membrane protein 1 (LMP 1) by immunohistochemistry were negative in both lesions. Nonneoplastic mucosa was slightly atrophic with mild intestinal metaplasia and mild to moderate lymphocytic infiltrates. No *Helicobacter pylori* was detected in Giemsa-stained sections.

Case 2 In the resected stomach, the depressed lesion (type IIc) 2.0×1.8 cm in diameter was located in the posterior wall of the fundus (Fig. 2a). The lesion was moderately differentiated adenocarcinoma, which was mostly restricted to the mucosa with minimal invasion of the submucosa (Fig. 2b). Intramucosal carcinoma showed tubular strictures with so-called "lace pattern" (Fig. 2c1). In addition, a small focus of follicular lymphoma composed of centrocytes (grade 1) was identified in the submucosa just beneath the mucosal carcinoma (Fig. 2b,c2), which was positive for CD20, CD 79a, CD 10, and bcl-2. Follicular lymphoma also involved the regional and mesenteric lymph nodes. The cancer cells were positive for EBER-ISH, but lymphoma cells, nonneoplastic lymphocytes, and nonneoplastic epithelial cells were all negative (Fig. 2d). EBNA 2 and LMP-1 were immunohistochemically negative for all cells mentioned above. The signal of EBER was also absent in regional and mesenteric lymph nodes and previously resected pelvic lymphoma. No *H. pylori* was detected in Giemsa-stained sections. The surrounding nonneoplastic mucosa showed mild atrophy with mild intestinal metaplasia, moderate lymphocytic, and slight neutrophilic infiltration.

Discussion

EBV is the causative agent of infectious mononucleosis, and has been also known as the etiological agent of human neoplasms such as Burkitt lymphoma [26], nasopharyngeal carcinoma (lymphoepithelioma) [4], malignant lymphoma arising in immunosuppressive patients [9, 18], and lymphoepithelial-like carcinoma in various organs [5, 7, 10]. In 1990, Burke et al. [3] were the first group to demonstrate EBV genomes in gastric carcinomas with similar histology to nasopharyngeal lymphoepitheliomas. The morphological features of the lymphoepithelioma-like gastric carcinoma include small nests of poorly differentiated/undifferentiated carcinoma with intense lymphoid stroma. The EBV genomes were detected at high frequency (92.3%) in these lymphoepithelioma-like gastric carcinomas [17], but the association with EBV was also observed in some conventional gastric adenocarcinomas. Tokunaga et al. [21]

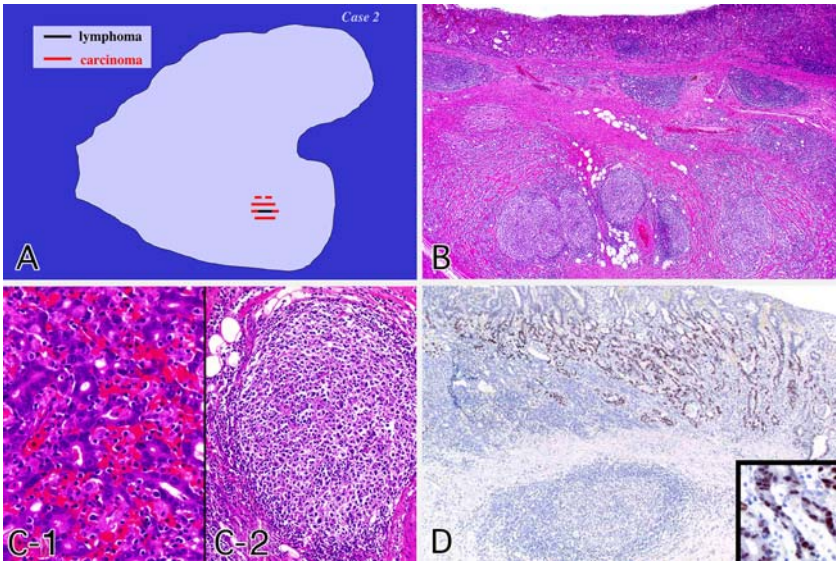

Fig. 2 **a** Schematic diagram of the resected stomach of case 2. The depressed lesion (type IIc, *red lines*) is located in the posterior wall of the fundus, beneath which follicular lymphoma (*black line*) exists. **b** Case 2. Low-power view showing mucosal adenocarcinoma and submucosal follicular lymphoma. **c** High-power views of intramucosal carcinoma with "lace pattern" (*1*) and follicular lymphoma (*2*) in case 2. **d** Most of the cancer cells in case 2 are positive for EBER, but lymphoma cells and nonneoplastic lymphocytes are all negative. Inset shows nuclear positive signals for EBER

reported that 104 of 1,828 (5.7%) gastric carcinomas, excluding lymphoepithelioma-like type, were positive for EBER. Hence, EBV-GC consists of two types: lymphoepithelioma-like carcinoma with high infection rate and ordinary carcinomas with low infection rate [3, 21].

The clinicopathological features of the EBV-GC have been well described. It shows male predominance, occurs predominantly in the proximal stomach, particularly in the cardia, and tends to be multiple lesions [14, 21]. Although EBV-GC is very frequently associated with lymphoid stroma (lymphoepithelioma-like appearance), EBV-GC without lymphoid stroma also exhibits some characteristic features. It tends to be composed predominantly of moderately differentiated tubular or poorly differentiated solid types, while papillary and scirrhous types are extremely rare [6]. In particular, a unique "lace pattern" of the intramucosal carcinoma in EBV-GC is an important finding [1]. In the present two cases, Case 1 had a well-differentiated tubular/papillary adenocarcinoma, which was considered an uncommon histological type of EBV-GC. In contrast, case 2 showed typical histological findings of moderately differentiated tubular adenocarcinoma with intramucosal "lace pattern". In addition, current studies reveals that EBV-GC are a distinct entity of carcinomas, characterized not only by unique genomic aberration [25], but also by distinct clinicopathologic features associated with significantly better prognosis [22].

Three types of EBV gene latency have been described for lymphoid cell lines based on the variable expression of the latent gene products, and they are used to classify EBV-associated neoplasms [6]. EBV-associated gastric carcinoma is categorized as latency type I that also includes Burkitt lymphomas. In latency type I pattern, antigen expression is restricted to EBNA1, while EBNA2 and LMP1 are not expressed. But some investigators reported exceptional LMP1 immunoreactivity in several patients of gastric carcinoma [2, 11, 20]. To ascertain the latency type of EBV, we have examined immunohistochemically EBNA2 and LMP1, but both were not expressed in the present two cases as most of previous reports.

The most interesting aspect of the present two cases is that the EBV-GC coexisted with gastric lymphoma. Coexistence of primary gastric lymphoma and carcinoma is extremely uncommon. Nakamura et al. [15] reported that its incidence accounts for only 0.098% of all examined gastric carcinomas (nine of 9,150 cases). Furthermore, EBV infection in such cases is extremely rare; to our knowledge only two cases of EBV-GC coexistent with gastric lymphoma have been reported. One was lymphoepithelioma-like carcinoma with mucosa-associated lymphoid tissue (MALT) lymphoma [8], and the other was a poorly differentiated adenocarcinoma with low-grade T-cell lymphoma of pleomorphic small cell type [15]. Besides the EBV-infected cancer cells, *H. pylori* infection was also observed in the previously reported two cases [8, 15]. *H. pylori* infection is generally considered to cause chronic active gastritis, intestinal metaplasia, ulcer, and gastric neoplasms including adenocarcinoma and malignant lymphoma, especially MALT type lymphoma [24]. The frequency of *H. pylori* infection has been reported to be 45–90% in patients with gastric adenocarcinoma, and 56–100% in those with gastric lymphoma [15, 16, 24]. However, in the two cases reported in this study, *H. pylori* was not detected. Therefore, it is speculated that *H. pylori* infection is not related to the development of gastric carcinoma and malignant lymphoma.

It is interesting to note that almost all carcinoma cells in the cardiac lesion of case 1 and case 2 were positive for EBV, whereas those in the antral lesion of case 1 were partially positive. EBV involvement in EBV-GC is thought to precede the clonal growth of carcinoma cells [6, 19]. Therefore, the finding that partial EBV-infection of gastric carcinoma cells in the antrum lesion of the case 1 is thought to be exceptional contradiction to the current literature. EBV infection in the antral lesions of case 1 might be superimposed on the developed carcinoma. Unfortunately, because we have only formalin-fixed paraffin-embedded tissue, we could not satisfactorily carry out EBV clonality analyses by using Southern blot hybridization method on fresh samples as previously described [12]. If we could clarify the clonality of EBV on our unusual case 1, it might help to understand the role of EBV in gastric carcinogenesis. Although we have no idea which of carcinoma or lymphoma developed first, it is conceivable that lymphoma might induce focal environment of immunosuppression in the stomach, which might facilitate EBV-infection or growing of EBV-positive tumor cells.

With regard to the predisposing factors for EBV-GC, severe atrophic gastritis in the background is reported to be important [13]. In addition, current literature by Wong et al. [23] suggests that immunosuppression and active inflammation contribute to development of colorectal EBV-positive lymphomas. They stress that EBV infection and neoplastic transformation of lymphocytes are promoted by the inflammatory milieu in inflammatory bowel disease and/or by immunosuppressive milieu [23]. However, as mentioned above, the present two cases lacked *H. pylori* infection, atrophic changes and inflammation in the background mucosa were not so conspicuous. In the present two cases, although we could not exclude the possibilities that epithelial damage due to mild atrophic gastritis or other unknown causative factors were the underlining mechanism of EBV-GC, we could not deny that immunosuppressive microenvironment due to adjacent gastric lymphoma may potentially be one of predisposing factor for EBV-infection and related to development of EBV-GC.

Acknowledgements The authors thank Mr. S. Yano and Ms. T. Nakamatsu for their skilled technical assistance.

References

1. Arikawa J, Tokunaga M, Satoh E, Tanaka S, Land CE (1997) Morphological characteristics of Epstein–Barr virus-related early gastric carcinoma: a case-control study. Pathol Int 47:360–367
2. Andal N, Shanthi P, Krishnan KB, Taralaxmi V (2003) The Epstein Barr virus and gastric carcinoma. Indian J Pathol Microbiol 46:34–36
3. Burke AP, Yen TS, Shekitka KM, Sobin LH (1990) Lymphoepithelial carcinoma of the stomach with Epstein–Barr virus demonstrated by polymerase chain reaction. Mod Pathol 3:377–380
4. Dickens P, Srivastava G, Loke SL, Chan CW, Liu YT (1992) Epstein–Barr virus DNA in nasopharyngeal carcinomas from Chinese patients in Hong Kong. J Clin Pathol 45:396–397
5. Dimery IW, Lee JS, Blick M, Pearson G, Spitzer G, Hong WK (1988) Association of the Epstein–Barr virus with lymphoepithelioma of the thymus. Cancer 61:2475–2480
6. Fukayama M, Chong JM, Kaizaki Y (1998) Epstein–Barr virus and gastric carcinoma. Gastric Cancer 1:104–114
7. Gal AA, Unger ER, Koss MN, Yen TS (1991) Detection of Epstein–Barr virus in lymphoepithelioma-like carcinoma of the lung. Mod Pathol 4:264–268
8. Greiner A, Kirchner T, Ott G, Marx A, Fischbach W, Muller-Hermelink HK (1996) Occurrence of multiple lymphoepithelioma-like carcinomas and MALT-type lymphoma in the stomach: detection of EBV in carcinomas but not in lymphoma. Histopathology 29:51–56
9. Hamilton-Dutoit SJ, Pallesen G, Franzmann MB, Karkov J, Black F, Skinhoj P, Pederson C (1991) AIDS-related lymphoma: histopathology, immunophenotype, and association with Epstein–Barr virus as demonstrated by in situ nucleic acid hybridization. Am J Pathol 138:149–163
10. Hamilton-Dutoit SJ, Therkidsen MH, Nielsen NH, Jensen H, Hansen JP, Pallesen G (1991) Undifferentiated carcinoma of the salivary gland in Greenlandic Eskimos: demonstration of Epstein–Barr virus DNA by in situ nucleic acid hybridization. Hum Pathol 22:811–815
11. Harn HJ, Chang JY, Wang MW, Ho LI, Lee HS, Chiang JH, Lee WH (1995) Epstein–Barr virus-associated gastric adenocarcinoma in Taiwan. Hum Pathol
12. Imai S, Koizumi S, Sugiura M, Tokunaga M, Uemura Y, Yamamoto N, Tanaka S, Sato E, Osato T (1994) Gastric carcinoma: monoclonal epithelial malignant cells expressing Epstein–Barr virus latent infection protein. Proc Natl Acad Sci USA 91:9131–9135
13. Kaizaki Y, Sakurai S, Chong JM, Fukuyama M (1999) Atrophic gastritis, Epstein–Barr virus infection, and Epstein–Barr virus-associated gastric carcinoma. Gastric Cancer 2:101–108
14. Matsunou H, Konishi F, Hori H, Ikeda T, Sasaki K, Hirose Y, Yamamichi N (1996) Characteristics of Epstein–Barr virus-associated gastric carcinoma with lymphoid storm in Japan. Cancer 77:1998–2004
15. Nakamura S, Aoyagi K, Iwanaga S, Yao T, Tsuneyoshi M, Fujishima M (1997) Synchronous and metachronous primary gastric lymphoma and adenocarcinoma: a clinicopathologic study of 12 patients. Cancer 79:1077–1085
16. Nakamura S, Yao T, Aoyagi K, Iida M, Fujishima M, Tsuneyoshi M (1997) *Helicobacter pylori* and primary gastric lymphoma. A histopathologic and immunohistochemical analysis of 237 patients. Cancer 79:3–11
17. Oda K, Tamaru J, Takenouchi T, Mikata A, Nunomura M, Saitoh N, Sarashina H, Nakajima N (1993) Association of Epstein–Barr virus with gastric carcinoma with lymphoid stroma. Am J Pathol 143:1063–1071
18. Saemundsen AK, Purtilo DT, Sakamoto K, Sullivan JL, Synnerholm AC, Hanto D, Simmons R, Anvret M, Collins R, Klein G (1981) Documentation of Epstein–Barr virus infection in immunodeficient patients with life-threatening lymphoproliferative disease by Epstein–Barr virus complementary RNA/DNA and viral DNA/DNA hybridization. Cancer Res 41: 4237–4242
19. Shibata D, Weiss LM (1992) Epstein–Barr virus-associated gastric adenocarcinoma. Am J Pathol 140:769–774
20. Shin WS, Kang MW, Kang JH, Choi MK, Ahn BM, Kim JK, Sun HS, Min KW (1996) Epstein–Barr virus-associated gastric adenocarcinomas among Koreans. Am J Clin Pathol 105: 174–181
21. Tokunaga M, Uemura Y, Tokudome T, Ishidate T, Masuda H, Okazaki E, Kaneko K, Naoe S, Ito M, Okamura A, Shimada A, Sato E, Land CE (1993) Epstein–Barr virus related gastric cancer in Japan: a molecular patho-epidemiological study. Acta Pathol Jpn 43:574–581
22. van Beek J, zur Hausen A, Klein Kranenbarg E, van de Velde CJ, Middeldrop JM, van den Brule AJ, Meijer CJ, Bloemena E (2004) EBV-positive gastric adenocarcinomas: a distinct clinicopathologic entity with a low frequency of lymph node involvement. J Clin Oncol 22:664–670
23. Wong NA, Herbst H, Herrmann K, Kirchner T, Krajewski AS, Moorghen M, Niedobitek F, Rooney N, Shepherd NA, Niedobitek G (2003) Epstein–Barr virus infection in colorectal neoplasms associated with inflammatory bowel disease: detection of the virus in lymphomas but not in adenocarcinomas. J Pathol 201:312–318
24. Wotherspoon AC, Doglioni C, Diss TC, Pan L, Moschini A, de Boni M, Isaacson PG (1993) Regression of primary low-grade B-cell gastric lymphoma of mucosa-associated lymphoid tissue type after eradication of Helicobacter pylori. Lancet 342: 575–577
25. zur Hausen A, van Grieken NC, Meijer GA, Hermsen MA, Bloemena E, Meuwissen SG, Baak JP, Meijer CJ, Kuipers EJ, van den Brule AJ (2001) Distinct chromosomal aberrations in Epstein–Barr virus-carrying gastric carcinomas tested by comparative genomic hybridization. Gastroenterology 121:612–618
26. zur Hausen H, Schulte-Holthausen H, Klein G, Henle W, Henle G, Clifford P, Santesson L (1970) EBV DNA in biopsies of Burkitt tumors and anaplastic carcinomas of the nasopharynx. Nature 228:1056–1058

Virchows Arch (2006) 449: 220–224
DOI 10.1007/s00428-006-0217-2

ORIGINAL ARTICLE

Hend Braham · Mounir Trimeche · Sonia Ziadi · Sarra Mestiri · Moncef Mokni · Khaled Amara · Mohamed Hachana · Badreddine Sriha · Sadok Korbi

CD10 expression by fusiform stromal cells in nasopharyngeal carcinoma correlates with tumor progression

Received: 15 December 2005 / Accepted: 4 April 2006 / Published online: 4 May 2006
© Springer-Verlag 2006

Abstract CD10 is a cell surface zinc metalloprotease expressed through a variety of normal cell types, including lymphoid precursor cells, germinal center B lymphocytes, and some epithelial cells. Many studies showed that CD10 expression is associated with the tumor progression of a large variety of cancers, such as breast and colorectal carcinomas. The aim of this study was to investigate the expression of CD10 in nasopharyngeal carcinoma (NPC). The expression of CD10 was immunohistochemically examined in 47 paraffin embedded NPC biopsies from Tunisian patients compared with 16 reactional nasopharyngeal mucosas. A significant expression of CD10 was observed in stromal fusiform cells in 46.8% of NPC cases but was not in malignant and normal epithelial cells. There was no significant expression of CD10 in control group. The stromal expression of CD10 was more frequently detected in advanced clinical stage than early stage (56 vs 23%; p=0.04) and in patients older than 25 years than in patients under 25 years (56.2 vs 26.5%; p=0.05). Our study is the first in investigating CD10 expression in nasopharyngeal carcinoma and showed that CD10 expression by stromal cells in this malignancy play an important role in tumor progression, particularly in older patients.

Keywords Nasopharyngeal carcinoma · CD10 · Immunohistochemistry · Tumor progression

This work was in part presented at the East–West Symposium on Nasopharyngeal Cancer, Toronto, Canada, June 16–18, 2005.

H. Braham · M. Trimeche · S. Ziadi · S. Mestiri · M. Mokni · K. Amara · M. Hachana · B. Sriha · S. Korbi
Laboratory of Pathology, CHU Farhat Hached, Sousse, 4000, Tunisia

M. Trimeche (✉)
Laboratoire d'Anatomie et de Cytologie Pathologiques, CHU Farhat Hached, Sousse, 4000, Tunisia
e-mail: m_trimech@yahoo.fr
Tel.: +216-73210355
Fax: +216-73210355

Introduction

Nasopharyngeal carcinoma (NPC) is rare in most population of the world, but frequent in a few well-defined ethnic groups. The highest incidence rates of NPC are found in Cantonese in China, Hong Kong, and Singapore. Other high-risk populations include Eskimos in Alaska, Canada, and Greenland, the Maghrebians in North Africa and in various parts of the world migrants from high-risk regions [14]. Although NPC is not as frequent in North Africa as it is in Southeast Asia, it remains the most frequent head and neck cancer in Tunisia, Algeria, and Morocco [3, 26]. The biology and natural history of nasopharyngeal carcinoma are still incompletely understood. Several clinical and routine histological factors of primary NPC with prognostic significance have been described; that is, tumor thickness according to localization, tumor and nodal stage, presence of tumor-infiltrating lymphocytes, biologic markers, patient's age, and gender. However, to these days, there is no conclusive molecular understanding of the pathogenesis of NPC.

CD10 is a 90- to 110/kDa cell surface zinc-dependent metalloprotease that has been called neutral endopeptidase 24.11. This enzyme is known to regulate biological activities of peptide substrates by reducing the local concentrations available for receptor binding and signal transduction [30]. This molecule can be normally expressed by numerous tissues and, accordingly, loss or decrease of CD10 expression has been shown to contribute to the development or the progression in many types of malignancies, including renal cancer [9], invasive bladder cancer [20], poorly differentiated stomach cancer [29], small cell and non-small cell lung cancer [6], endometrial cancer [27, 28], and prostate cancer [7, 33]. Indeed, reduced CD10 expression may promote peptide-mediated proliferation by allowing and accumulating higher peptide concentrations at the cell surface and may facilitate the development or progression of neoplasia [21]. On another hand, many reports have shown a significant correlation of stromal cell CD10 expression with tumor progression in a large variety of cancers such as melanoma [2], colorectal

[25], and breast cancer [12]. However, according to our knowledge, no reports concerning CD10 expression in NPC have been published yet. But CD10 belongs to the metalloprotease (MMP) family groups and it had been shown that MMP1 [22], MMP3, [32], and MMP9 [11] overexpression in NPC correlates with tumor progression and metastasis. Thus, it is interesting to explore CD10 expression in NPC.

In this study, we investigated the expression of CD10 by immunohistochemical analysis in NPC biopsies and we assessed correlations of these expressions with clinicopathologic parameters.

Materials and methods

Patients and specimens

Forty-seven paraffin embedded NPC biopsies were randomly selected, before any treatment, from the Laboratory of Pathology at Farhat Hached Hospital, Sousse, Tunisia. The ages ranged from 9–78 years. They included 33 male and 14 female patients. NPC histological type was determined on tissue sections according to the World Health Organization classification [1], resulting in the following distribution: 2/47 (4.2%) keratinizing squamous cell carcinoma, 8/47 (17.1%) nonkeratinizing differentiated carcinoma, and 37/47 (78.7%) nonkeratinizing undifferentiated carcinoma. The EBV status of the tumor cells was determined using in situ hybridization for the detection of the small EBV-nuclear RNAs (EBERs) as described previously [35] (data not shown). EBV infection was detected in the neoplastic cells of all undifferentiated NPC biopsies and nonkeratinizing carcinoma. In contrast, squamous cell NPCs were EBV-negative. The clinical staging NPC was performed according to International Union Against Cancer Tumor-Node-Metastasis (TNM) classification and stage grouping (5th edition 1997). T classification was divided into low T (T1, T2) and high T classification categories (T3, T4). N classification was divided into low lymph node (N0, N1) and high lymph node (N2, N3) categories. Stage grouping was divided into early stage (stage I or II) and advanced stage categories (stage III or IV). The control group consisted of 16 biopsy specimens of reactional nasopharyngeal mucosa obtained from noncancer patients.

Immunohistochemical staining of CD10

Five-micrometer sections of paraffin embedded tissues were deparaffinized in toluene. Subsequently, the sections

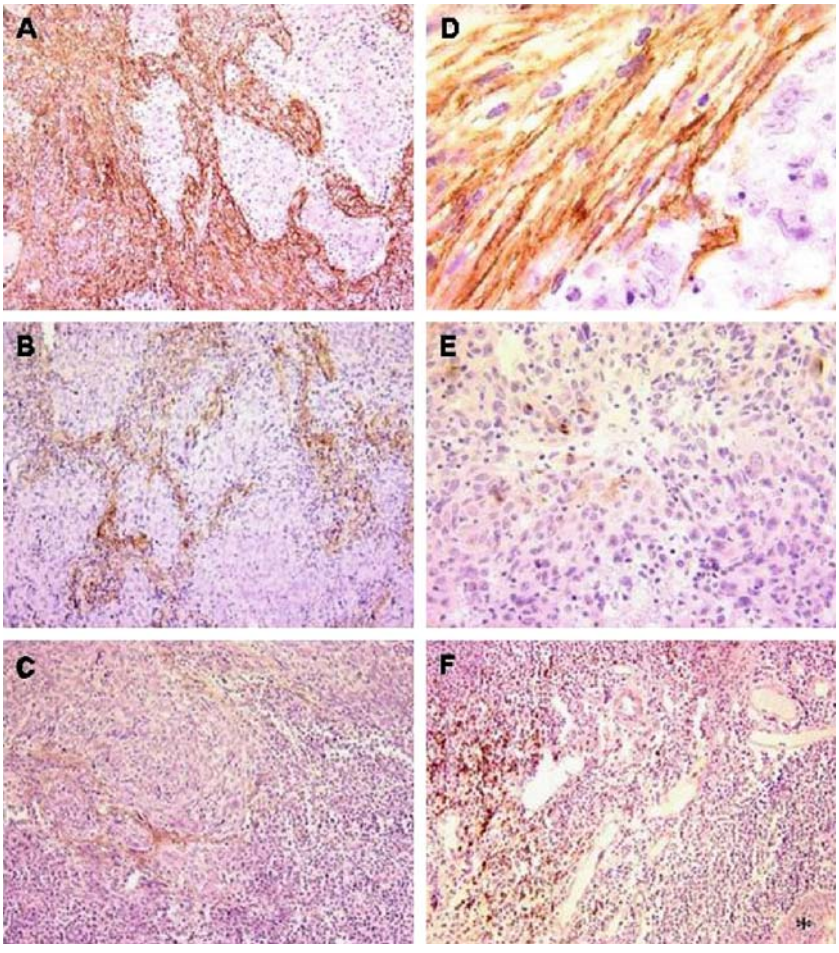

Fig. 1 Pattern of CD10 expression in nasopharyngeal carcinoma. **a**, **b**, and **c** Nasopharyngeal carcinoma samples showing CD10 expression in more than 10% of the stromal cells, whereas tumor cells are negative (original magnification ×100). **d** CD10 is detected in the fusiform stromal cells (*at the left*), whereas tumor cells are negative (*at the right*) (original magnification ×1,000). **e** Nasopharyngeal carcinoma showing CD10 expression in rare tumor cells (original magnification ×400). **f** CD10 staining on tissue section sample of reactional nasopharyngeal mucosa obtained from control group. No immunostaining for CD10 is detected in normal epithelial cells (*), whereas CD10 expression is observed in some lymphocytes (original magnification ×100)

were hydrated with a graded alcohol series, and rehydrated in water. Slides were microwaved in 0.01 M citrate buffer, first at pH 6.0, then at pH 9.0 for 20 min at 750 W. After boiling, the sections were allowed to cool at room temperature for 20 min, rinsed thoroughly with water, and placed in Tris–buffered saline (TBS) (0.05 M Tris–HCl, 1.15 M NaCl, pH 7.6). Endogenous peroxidase activity was blocked with hydrogen peroxide solution for 7 min, and sections were rinsed gently with TBS. Then, the sections were incubated at 4°C overnight with the primary antibody CD10 (clone 56C6; NeoMarker, Fremont, USA) diluted to 1:15. The sections were rinsed in TBS and incubated with a biotinylated secondary antibody (DakoCytomation, Glostrup, Denmark) for 30 min, followed by incubation with streptavidin–peroxidase reagent (DakoCytomation) for 30 min. After being washed in TBS, sections were incubated in 3, 3′-diaminobenzidine a substrate–chromogen solution for 30 min. Finally, the slides were counterstained with hematoxylin and mounted.

Evaluation of immunostaining

The degree of staining was determined by two independent observers. CD10 expression was delaminated in tumoral, stromal, lymphocytes, and normal epithelial cells. A case was considered positive if more than 10% of the cells exhibited immunostaining for this antigen, otherwise it was negative [12, 25].

Statistical analysis

The correlation between the patient's clinicopathologic features and CD10 expression was analyzed by the chi-square (χ^2) test. A p value ≤0.05 was considered to indicate statistical significance.

Results

Immunohistochemical features of CD10

A significant expression of CD10 was observed in stromal cells in 22 of 47 NPC cases (46.8%). This enzyme was immunolocalized in the fusiform stromal cells (Fig. 1a–d) but wasn't in lymphoid stroma cells. Furthermore, there was no CD10 positivity in normal and tumor epithelial cells except for one case which CD10 expression was expressed in rare tumor cells (Fig. 1e).

There was no expression of CD10 in epithelial cells in control group, but CD10 immunoreactivity was noted in germinal center cells and in some clusters lymphocytes (Fig. 1f).

Association of CD10 with clinicopathologic data

As shown in Table 1, stromal CD10 expression was more frequently detected in high T and lymph node categories (55.2 and 60%, respectively) than in low T and lymph node categories (33.3 and 37%, respectively), but the difference was not statistically significant (p=0.14 and p=0.11, respectively). Conversely, there was significant correlation of CD10 expression with stage grouping. Indeed, the frequency of stromal expression of CD10 was more frequently detected in advanced clinical stage than in early stage (56 vs 23%; p=0.04). Furthermore, only 26.5% of specimens were CD10 positive for patients under 25 years of age compared with 56.2% for older patients (p=0.05). In addition, immunohistochemical detection of CD10 did not correlate with gender and NPC histological type.

Discussion

The major clinicopathologic application of CD10 immunoreactivity has been in the diagnosis of precursor B-cell leukemia, follicular lymphoma, and Burkitt lymphoma [10, 13]. In addition, it has been proven that CD10 has a wide distribution on the surfaces of various normal cell types and that it may play specific roles in the control of cell growth

Table 1 Correlation between Stromal CD10 Expression and clinicopathologic features of nasopharyngeal carcinoma

Clinicopathologic features	Number of cases	CD10 expression in stromal cells[a]	
		n (%)	*P* Value
Gender			
Male	33	16 (48.5)	*P*>0.50
Female	14	6 (43)	
Age (years)			
≤25	15	4 (26.6)	0.05
>25	32	18 (56.2)	
Histology (WHO)			
Keratinizing squamous cell carcinoma	2	1 (50)	*p*>0.50
Nonkeratinizing differentiated carcinoma	8	4 (50)	
Nonkeratinizing undifferentiated carcinomas	37	18 (48.7)	
T classification			
T1, T2	18	6 (33.3)	0.14
T3, T4	29	16 (55.2)	
N classification			
N0, N1	27	10 (37)	0.11
N2, N3	20	12 (60)	
Stage grouping			
I, II	13	3 (23)	0.04
III, IV	34	19 (56)	

[a]Positive staining >10% of stromal cells

and differentiation in both hemopoietic and epithelial systems [16, 29].

Many reports have been published about CD10 expression by the tumor cells in different organs and its association with differentiation and growth of tumor cells such as lung, renal, endometrial, and mesenchymal [5, 31, 34]. Others reports showed that CD10 expression in stromal cells of a large variety of cancers such as melanoma, colorectal, and breast cancer may also contribute to tumor progression [2, 12, 25]. Our study is the first in investigating CD10 expression in NPC and demonstrated that CD10 was significantly expressed by the stromal cells of 46.8% of NPC but not in malignant epithelial cells.

We have shown that the CD10 stromal cell expression was more frequently detected in advanced clinical stage (III/IV than I/II stage) suggesting that this molecule may contribute to the invasion and, thus, probably facilitate metastasis in NPC. Although metastasis is a cascade of linked sequential steps involving multiple host–tumor interactions, disruption of the extra cellular matrix is a crucial step in which neoplastic cells leave the primary lesion and invade local and distant host tissues [11]. Matrix metalloproteases (MMPs), a gene family of zinc-containing endopeptidases, degrade extra cellular matrix and play an essential role in the metastatic process [8, 23, 24]. As other MMP family, CD10 stromal cell expression may contribute to the tumor progression. In support of this hypothesis, an interesting study [12] showed that CD10 is expressed by the stromal cells within the area of invasive ductal carcinoma, but not in the stromal cells of noninvasive carcinoma. A similar observation has also been made in colorectal carcinoma [25], in which stromal CD10 expression was significantly higher in severe dysplasia, intramucosal carcinoma, and invasive carcinoma than in adenomas with mild to moderate dysplasia. Furthermore, strong CD10 expression was detected only at the growth front of invasive carcinoma, and not in dysplastic lesions. In malignant melanoma [2], CD10 was expressed in stromal cells of more advanced primary melanomas and their association with higher proliferation rate suggests that stromal cells may have an important role in tumor progression. These data strongly suggest that the proliferation of CD10-positive stromal cells is a part of the mechanism of invasive growth.

Previous researches [11, 22] showed significant positive correlation of MMP1 and MMP9 protein expression with lymph nodes metastasis NPC, and close association between MMP1 and MMP9 and Epstein–Barr virus oncoprotein such as latent membrane protein (LMP1). The main question arises from such findings: it is possible that, because CD10 belongs to the metalloprotease family, its increased expression is induced by Epstein–Barr virus oncoproteins. Additional studies are required to clarify this hypothesis. However, several studies showed that CD10 levels, in vitro, are influenced by several factors. Indeed, certain cytokines such as interleukin-1α, tumor necrosis factor, interleukin-6, and granulocyte macrophage colony stimulating factor increase lung fibroblasts CD10 expression during the inflammatory process [21]. On the other hand, transforming growth factor-β1 could decrease CD10 activity by reducing gene transcription or mRNA stability [4]. Furthermore, CD10 activity may be regulated by prostaglandin synthesis and cAMP [21]. These factors secreted from the tumor cells may stimulate or inhibit stromal cell expression of CD10, singularly or in combination. In our study, whether the stronger stromal expression of CD10 in advanced clinical stage was induced by others factors, or was a primary event remains speculative and warrants further evaluation.

While in South China, most NPC patients are between 40 and 60 years old, in North Africa, the distribution of NPC according to age is bimodal. Beside the main peak of incidence around 50 (80% cases), there is a secondary peak between the age of 10 and 25 (20% cases). Previous reports [15, 17–19] have shown that the juvenile and adult forms of NPC have distinct oncogenic mechanisms. For example, P53 and Bcl2 are more abundantly expressed in the adult forms, whereas c-kit is more frequently detected in the juvenile form [17, 18]. In our study, stromal expression of CD10 was more frequently detected in adult NPC form than in young age form. Based on these data, we propose that the juvenile and adult forms of NPC have distinct biological characteristics regarding not only carcinogenesis pathways but also tumor progression. In conclusion, our study is the first in investigating CD10 expression in nasopharyngeal carcinoma and showed that CD10 expression by stromal cells in this malignancy play an important role in tumor progression, particularly in older patients. However, the prognostic value and mechanisms of the induction of CD10 remain to be elucidated.

Acknowledgements This work was funded by the "Ministère de la Recherche Scientifique et de la Technologie" of Tunisia. We thank Intissar Toumi and Samir Jaafar for their skilled technical assistance.

Competing interests The authors declare that they have no competing interests.

References

1. Barnes L, Eveson JW, Reichart P, Sidransky D (eds) (2005) World Health Organization classification of tumours. Pathology and genetics of head and neck tumours. IARC Press, Lyon
2. Bilalovic N, Sandstad B, Golouh R, Nesland JM, Selak I, Torlakovic EE (2004) CD10 protein expression in tumor and stromal cells of malignant melanoma is associated with tumor progression. Mod Pathol 17:1251–1258
3. Cammoun M, Hoerner V, Mourali N (1974) Tumors of the nasopharynx in Tunisia. An anatomic and clinical study based on 143 cases. Cancer 33:184–192
4. Casey ML, Smith JW, Nagai K, MacDonald PC (1993) Transforming growth factor-beta 1 inhibits enkephalinase (EC 3.4.24.11) gene expression in human endometrial stromal cells and sex skin fibroblasts in culture. J Clin Endocrinol Metab 77:144–150

5. Chu P, Arber DA (2000) Paraffin-section detection of CD10 in 505 nonhematopoietic neoplasms. Frequent expression in renal cell carcinoma and endometrial stromal sarcoma. Am J Clin Pathol 113:374–382
6. Cohen AJ, Bunn PA, Franklin W, Magill-Solc C, Hartmann C, Helfrich B, Gilman L, Folkvord J, Helm K, Miller YE (1996) Neutral endopeptidase: variable expression in human lung, inactivation in lung cancer, and modulation of peptide-induced calcium flux. Cancer Res 56:831–839
7. Cutrona G, Leanza N, Ulivi M, Melioli G, Burgio VL, Mazzarello G, Gabutti G, Roncella S, Ferrarini M (1999) Expression of CD10 by human T cells that undergo apoptosis both in vitro and in vivo. Blood 94:3067–3076
8. Egeblad M, Werb Z (2002) New functions for the matrix metalloproteinases in cancer progression. Nat Rev Cancer 2:161–174
9. Gohring B, Holzhausen HJ, Meye A, Heynemann H, Rebmann U, Langner J, Riemann D (1998) Endopeptidase 24.11/CD10 is down-regulated in renal cell cancer. Int J Mol Med 2:409–414
10. Greaves MF, Hariri G, Newman RA, Sutherland DR, Ritter MA, Ritz J (1983) Selective expression of the common acute lymphoblastic leukemia (gp 100) antigen on immature lymphoid cells and their malignant counterparts. Blood 61:628–639
11. Horikawa T, Yoshizaki T, Sheen TS, Lee SY, Furukawa M (2000) Association of latent membrane protein 1 and matrix metalloproteinase 9 with metastasis in nasopharyngeal carcinoma. Cancer 89:715–723
12. Iwaya K, Ogawa H, Izumi M, Kuroda M, Mukai K (2002) Stromal expression of CD10 in invasive breast carcinoma: a new predictor of clinical outcome. Virchows Arch 440:589–593
13. Jaffe ES, Harris NL, Stein H, Vardiman JW (eds) (2001) World Health Organization classification of tumors. Pathology and genetics of tumors of haematopoietic and lymphoid tissues. IARC Press, Lyon
14. Jeannel D, Bouvier G, Hubert A (1999) Nasopharyngeal carcinoma: an epidemiological approach to carcinogenesis. Cancer Surv 33:125–155
15. Karray H, Ayadi W, Fki L, Hammami A, Daoud J, Drira MM, Frikha M, Jlidi R, Middeldorp JM (2005) Comparison of three different serological techniques for primary diagnosis and monitoring of nasopharyngeal carcinoma in two age groups from Tunisia. J Med Virol 75:593–602
16. Kenny AJ, O'Hare MJ, Gusterson BA (1989) Cell-surface peptidases as modulators of growth and differentiation. Lancet 30:785–787
17. Khabir A, Sellami A, Sakka M, Ghorbel AM, Daoud J, Frikha M, Drira MM, Busson P, Jlidi R (2000) Contrasted frequencies of p53 accumulation in the two age groups of North African nasopharyngeal carcinomas. Clin Cancer Res 6:3932–3936
18. Khabir A, Ghorbel A, Daoud J, Frikha M, Drira MM, Laplanche A, Busson P, Jlidi R (2003) Similar BCL-X but different BCL-2 levels in the two age groups of North African nasopharyngeal carcinomas. Cancer Detect Prev 27:250–255
19. Khabir A, Karray H, Rodriguez S et al (2005) EBV latent membrane protein 1 abundance correlates with patient age but not with metastatic behavior in North African nasopharyngeal carcinomas. J Virol 2:39–46
20. Koiso K, Akaza H, Ohtani M, Miyanaga N, Aoyagi K (1994) A new tumor marker for bladder cancer. Int J Urol 1:33–36
21. Kondepudi A, Johnson A (1993) Cytokines increase neutral endopeptidase activity in lung fibroblasts. Am J Respir Cell Mol Biol 8:43–49
22. Kondo S, Wakisaka N, Schell MJ, Horikawa T, Sheen TS, Sato H, Furukawa M, Pagano JS, Yoshizaki T (2005) Epstein–Barr virus latent membrane protein 1 induces the matrix metalloproteinase-1 promoter via an Ets binding site formed by a single nucleotide polymorphism: enhanced susceptibility to nasopharyngeal carcinoma. Int J Cancer 115:368–376
23. Liotta LA, Stetler-Stevenson WG (1991) Tumor invasion and metastasis: an imbalance of positive and negative regulation. Cancer Res 51(supp l):5054–5059
24. McCawley LJ, Matrisian LM (2000) Matrix metalloproteinases: multifunctional contributors to tumor progression. Mol Med Today 6:149–156
25. Ogawa H, Iwaya K, Izumi M, Kuroda M, Serizawa H, Koyanagi Y, Mukai K (2002) Expression of CD10 by stromal cells during colorectal tumor development. Hum Pathol 33:806–811
26. Parkin DM, Whelan SL, Ferlay J, Raymond L, Youg J (eds) (1997) Cancer incidence in five continents, vol VII. IARC Scientific Publication No. 143. IARC Press, Lyon
27. Pekonen F, Nyman T, Ammala M, Rutanen EM (1995) Decreased expression of messenger RNAs encoding endothelin receptors and neutral endopeptidase 24.11 in endometrial cancer. Br J Cancer 71:59–63
28. Potlog-Nahari C, Feldman AL, Stratton P, Koziol DE, Segars J, Merino MJ, Nieman LK (2004) CD10 immunohistochemical staining enhances the histological detection of endometriosis. Fertil Steril 82:86–92
29. Sato Y, Itoh F, Hinoda Y, Ohe Y, Nakagawa N, Ueda R, Yachi A, Imai K (1996) Expression of CD10/neutral endopeptidase in normal and malignant tissues of the human stomach and colon. J Gastroenterol 31:12–17
30. Shipp MA, Look AT (1993) Hematopoietic differentiation antigens that are membrane-associated enzymes: cutting is the key! Blood 82:1052–1070
31. Shipp MA, Tarr GE, Chen CY, Switzer SN, Hersh LB, Stein H, Sunday ME, Reinherz EL (1991) CD10/neutral endopeptidase 24.11 hydrolyzes bombesin-like peptides and regulates the growth of small cell carcinomas of the lung. Proc Natl Acad Sci USA 188:10662–10666
32. Sternlicht MD, Lochter A, Sympson CJ, Huey B, Rougier JP, Gray JW, Pinkel D, Bissell MJ, Werb Z (1999) The stromal proteinase MMP3/stromelysin-1 promotes mammary carcinogenesis. Cell 98:137–146
33. Tawfic S, Niehans GA, Manivel JC (2003) The pattern of CD10 expression in selected pathologic entities of the prostate gland. Hum Pathol 34:450–456
34. Tran NL, Nagle RB, Cress AE, Heimark RL (1999) N-Cadherin expression in human prostate carcinoma cell lines. An epithelial–mesenchymal transformation mediating adhesion with Stromal cells. Am J Pathol 155:787–798
35. Trimeche M, Ziadi S, De Leval L, Hmissa S, Sriha B, Mokni M, Toumi I, Elomri H, Laatiri A, Kehlif A, Boniver J, Korbi S (2005) Prevalence of Epstein–Barr virus in non-Hodgkin's lymphomas in central region of Tunisia. Ann Pathol 25:95–102

Virchows Arch (2006) 449:225–229
DOI 10.1007/s00428-006-0236-z

ORIGINAL ARTICLE

Lung disease 35 years after aspiration of activated charcoal in combination with pulmonary lymphangioleiomyomatosis

A histological and clinicopathological study with scanning electron microscopic evaluation and element analysis

M. Huber · W. Pohl · G. Reinisch · J. Attems · S. Pescosta · F. Lintner

Received: 1 February 2006 / Accepted: 14 May 2006 / Published online: 15 June 2006
© Springer-Verlag 2006

Abstract Activated charcoal provides effective treatment for most toxic ingestions. Accidental aspiration of activated charcoal is rare. Previously, there have been a few single cases reported on charcoal-related pulmonary complications. We describe an unusual case of pulmonary lesions 35 years after accidental aspiration of activated charcoal. The 38-year-old female patient presented with recurrent pneumothorax. A routinely performed chest roentgenogram revealed pulmonary lesions, highly suggestive to lymphangioleiomyomatosis (LAM). Histopathological investigation of the lung tissue demonstrated some features of LAM but showed prominent pneumoconiotic lesions with cystic tissue destruction. The pneumoconiotic reaction was characterized by prominent black deposits accompanied by foreign-body granuloma formation and minimal fibrosis. Scanning electron microscopic investigation of these deposits showed particles measuring up to 300 μm in greatest diameter. Energy-dispersive X-ray spectra of these particles revealed carbon-rich material, presumably charcoal. The aspiration event was confirmed by the clinical history. To our knowledge, this is the first report not only on a long-term follow-up after aspiration of activated charcoal but also on charcoal-related pulmonary lesions in combination with LAM.

Keywords Activated charcoal · Aspiration · Pneumoconiosis · Lymphangioleiomyomatosis

M. Huber (✉) · J. Attems · F. Lintner
Otto Wagner Hospital, Institute of Pathology and Bacteriology,
Baumgartner Hoehe 1,
Vienna, Austria
e-mail: Monika.Huber@wienkav.at

W. Pohl · S. Pescosta
Grimmenstein Hospital, Landesklinik Hochegg,
Grimmenstein, Austria

G. Reinisch
Institute for Micro Technique and Precision Engineering,
Vienna University of Technology,
Vienna, Austria

G. Reinisch
Biomechanische Forschungs-Gesellschaft m.b.H,
Vienna, Austria

Introduction

Activated charcoal usually provides effective treatment for most toxic ingestions. It is known as an inert substance and is considered a benign therapy for enhancing elimination of drug overdose. The incidence of aspiration pneumonia after application of activated charcoal is considered low [15]. Previously, there have only been a few single cases reported on charcoal-related pulmonary complications [4, 6, 7, 10, 16].

In contrast, lymphangioleiomyomatosis (LAM) is known as a rare disorder characterized by proliferation of atypical smooth muscle cells within the lung and the lymphatic system, without associated inflammation and fibrosis [17]. It leads to progressive loss of lung parenchyma and to the development of cystic lesions. One of the most common presenting symptoms of the disease is pneumothorax. The etiology of LAM is still unknown.

To our knowledge, this is the first report not only on a long-term follow-up after aspiration of activated charcoal but also on charcoal-related pulmonary lesions in combination with LAM.

Clinical history

A 38-year-old female who presented with recurrent spontaneous pneumothorax was admitted to the hospital. A routinely performed chest roentgenogram revealed a diffuse bilateral reticular pattern, cystic spaces, and pneumothorax on the right side, highly suggestive to lymphangioleiomyomatosis (LAM). Computer tomography (CT) scan of the chest demonstrated fibrotic and cystic pulmonary lesions. Multiple thin-walled cysts were distributed diffusely throughout both lungs (Fig. 1). Arterial blood gas values while breathing ambient air were PaO_2, 83 mmHg and $PaCO_2$, 87.5 mmHg at pH 7.43. Pulmonary function testing revealed the presence of obstruction with a reduced FEV1 and FEV1/FVC ratio. Clinical examination showed no further abnormalities.

The patient's history revealed previous bilateral spontaneous pneumothoraces 8 and 7 months before the actual admittance, respectively. Seven years ago, bilateral renal angiomyolipomas were detected, followed by consecutive surgical partial nephrectomy. At the age of three, accidental aspiration of activated charcoal after treatment of drug intoxication was reported. At this time, consecutive charcoal removal by bronchoscopy was performed. The patient had never been smoking.

At surgery, wedge resections of each lobe of the right lung were performed by video-assisted thoracoscopy. Both surgery and the postoperative course of the excision site were uneventful.

Fig. 1 CT scan shows bilateral replacement of pulmonary parenchyma with cysts. Pneumothorax *on the right side*. CT scan at the level of lower lobes

Materials and methods

Light microscopy

The specimens were fixed in 10% buffered formaldehyde solution and embedded in paraffin according to standard procedures. Sections were routinely stained with hematoxylin–eosin, elastica van Gieson, and Berlin blue stain. In addition, sections were stained immunohistochemically by the streptavidin biotin technique. Tissue sections were incubated according to the instructions of the manufacturer with antibodies against HMB-45 (Dako, diluted 1:50), alpha-smooth muscle actin (Dako, diluted 1:30), desmin (Dako, diluted 1:200), progesterone receptor (PRICA) (Dako, diluted 1:150), and Estrogen receptor (ERICA) (Dako, diluted 1:500).

Scanning electron microscopy and element analysis

Unstained sections were performed for electron microscope analysis. The unstained slides were sputtered with gold before investigation and were inspected by the use of a scanning electron microscope (SEM, Philips XL40, Netherlands) at 17.5 keV. To identify elements, energy dispersive X-ray analysis (EDAX, Netherlands) was done on spots and in a two-dimensional area mapping mode.

Results

Gross and light microscopic findings

The wedge specimens were three small rims of lung tissue from the lobes of the right lung, measuring 4.5×1.5×0.8, 5×3×2, and 6×2.5×1 cm. On gross examination, the cut surfaces revealed multiple cysts measuring up to 10 mm in greatest diameter distributed in lung parenchyma and subpleural, being most pronounced in specimens of the middle and lower lobes.

Microscopic examination of the lung tissue showed emphysema, prominent cystic lesions without lining epithelium, and numerous black pigmented deposits with irregular borders (Fig. 2a). Particles—accompanied by foreign-body giant-cell reaction—were Fe (Berlin blue stain) negative. By polarized light, intracellular birefringence was absent. Particles of various sizes were distributed to all regions of the lung, including connective tissue surrounding bronchi and vessels, in subpleural connective tissue, and in walls of bronchioles and cystic lesions (Fig. 2a,b). Black particles were also found in the interstitium without any obvious relation to structures of the bronchovascular bundle. Elastica van Gieson stain revealed minimal fibrosis in areas of accumulated particles with giant-cell reaction and pigment-

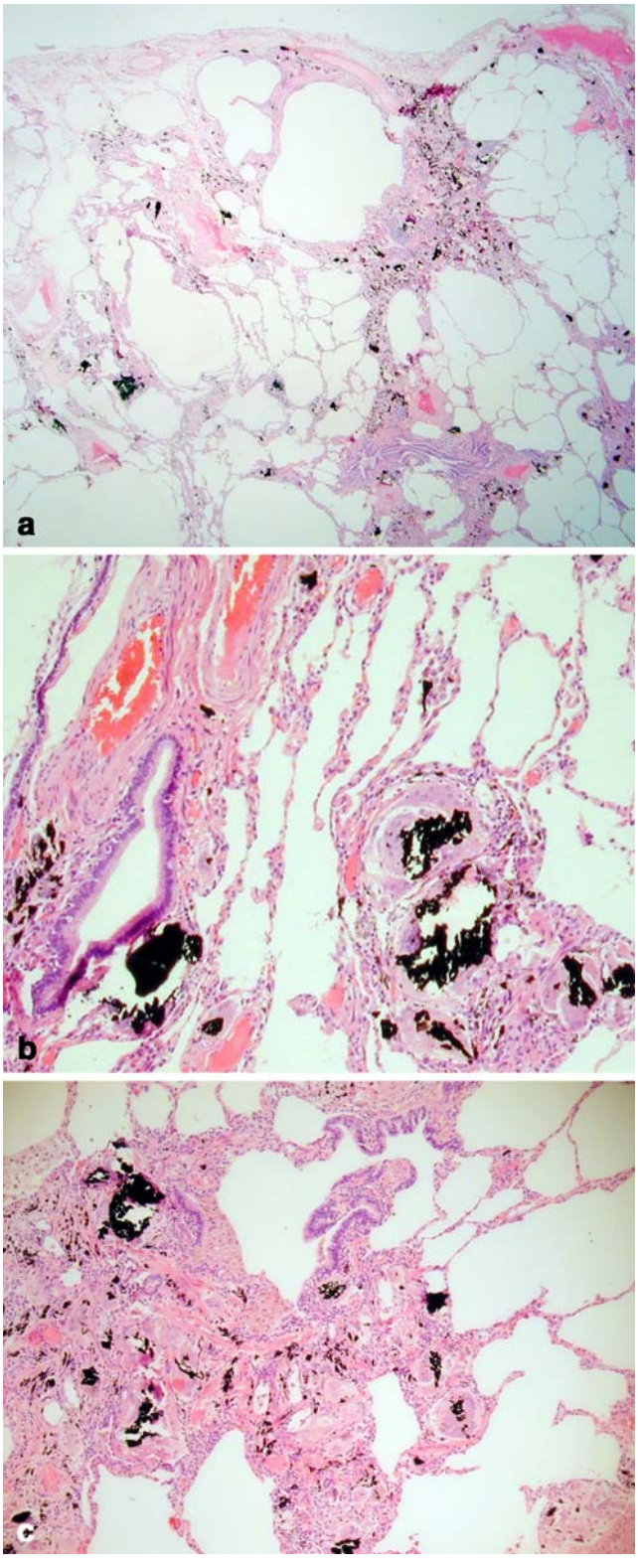

◀**Fig. 2** **a** Lung parenchyma with distributed pigment deposits, adjacent enlarged airspaces, and large cystic lesions (hematoxylin and eosin stain, ×10). **b** *Black particles* in the wall of bronchioles and distributed in the interstitium with giant-cell reaction (hematoxylin and eosin stain, ×40). **c** Accumulations of particles with giant-cell reaction and minimal fibrosis, fibrosis of adjacent small airways (hematoxylin and eosin stain, ×40)

laden macrophages and showed occasional arrangements of elastic fibers indicating remnants of obliterated bronchioles within fibrotic areas. These areas were of various sizes scattered in the parenchyma. Focally, epithelium-covered fibrous tissue extended into the parenchyma (Fig. 2c). Adjacent enlarged airspaces and large cysts were developed. Some inflammatory responses were focally minimal to moderate. Black particles accompanied by foreign-body giant-cell reaction were distributed in greatest number in tissue from the middle and lower lobes.

In addition, the walls of a few cysts showed small clusters of spindle cell proliferation of immature smooth muscle fibers (Fig. 3). Immunohistochemically, these cells showed reactivity with HMB-45 (Fig. 3, inset), smooth muscle actin, desmin, ERICA, and PRICA in various proportions, indicating lesion of LAM.

Scanning electron microscopic investigation showed particles measuring up to 300 μm in greatest diameter. Energy-dispersive X-ray spectra of these particles revealed carbon-rich material, presumably charcoal (Fig. 4); the small silica peak was associated with components of the glass slide.

Discussions

Occupational lung disease includes a wide spectrum of disorders caused by inhalation of particles or noxious chemicals. Most of these disorders—including pneumoconiosis, asbestos-related lung disease, and chemical pneumonitis—lead to diffuse lung disease.

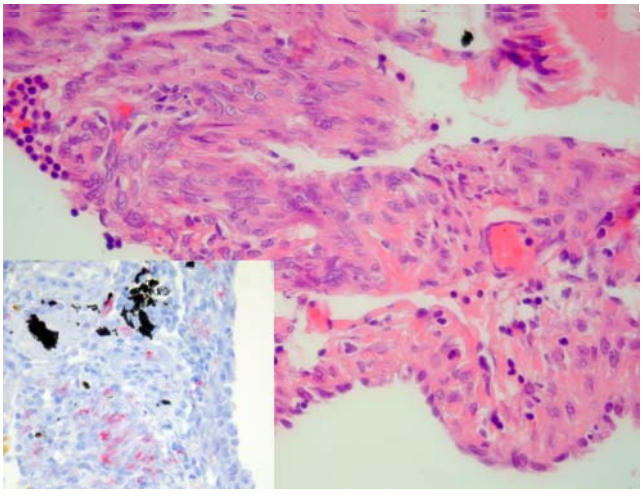

Fig. 3 Dilated airspace showing spindle cell proliferation of immature smooth muscle fibers as an indication for LAM (hematoxylin and eosin stain, ×60). *Inset*: HMB-45-positive LAM cells

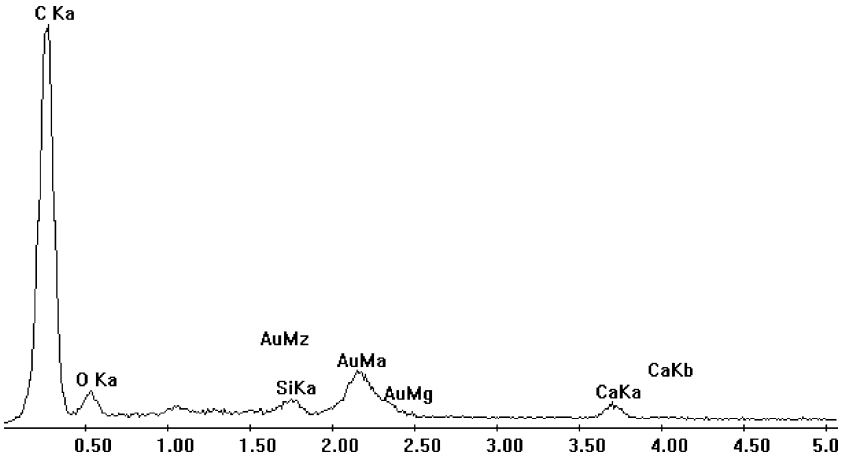

Fig. 4 Energy dispersive X-ray spectrum of the deposit. The photograph is showing a deposit rich in carbon. The peaks indicate the relative proportion of the individual elements (C Ka: carbon; O Ka: oxygen; Si Ka: silica; Ca Ka: calcium)

Commonly, in pneumoconiotic lesions, inhaled dust particles—in contrast to fibers (e.g., asbestos)—are generally within the respirable range of less than 5 μm in diameter. After deposition of particles in the lower respiratory tract, acute or chronic reactions occur, depending on the reactivity of the inhaled substance. Acute reactions comprise inflammation and edema. Chronic reactions result in fibrosis or granuloma formation [8].

Depending on the tissue reactions, particles are categorized as nonfibrogenic or fibrogenic dusts. Relatively inert dusts (e.g., carbon, barium, and tin) or dusts with moderate fibrogenic potential (such as coal mine dust) reveal particle-laden macrophages with minimal or no accompanying fibrosis. Fibrogenic dusts (e.g., silica and asbestos) result in nodular or diffuse fibrosis. Depending on the components and amount of a dust mixture, fibrotic reactions may occur in various proportions. After exposure, an ongoing lymphatic clearance of particles starts, which leads to a particle accumulation adjacent to bronchovascular bundles and subpleural connective tissue [8].

The acute complication after charcoal aspiration includes immediate airway obstruction with severe bronchospasm and reduced vital capacity [4, 6, 10]. Acute pulmonary damage after charcoal aspiration was thought to follow aspiration of gastric contents and the suspension of activated charcoal [16]. While charcoal is considered to be inert, the pulmonary injury was attributed to sorbitol in the charcoal preparation [10].

Previous experimental studies after intratracheal installation of activated charcoal demonstrated acute changes in pulmonary microvascular permeability and the development of lung edema [2]. The pulmonary changes after prolonged installation of charcoal included airway injury and inflammation and led to the development of bronchiolitis obliterans [13].

The development of chronic lung disease after aspiration of activated charcoal has been described in two previous case reports, including one postmortem study [4, 7]. The periods of evaluation were 16 weeks and two and a half years after the charcoal aspiration event, respectively. Biopsies in both cases revealed particle deposits within the airways as well as an obliteration of the bronchioles and a giant-cell reaction. In addition, the postmortem study revealed scarring and fibrous obliteration of the bronchioles associated with airway stenosis and bronchiolectasis [4].

It has been postulated that exposure to carbonaceus dusts other than coal, including activated carbon, graphite, lampblack, carbon black, and fumes, can cause pneumoconiosis similar in appearance to coal worker pneumoconiosis (CWP) [9].

CWP comprises coal dust macules composed of pigment-laden macrophages and associated focal emphysema. The secretion of proteolytic enzymes by dust-activated macrophages and mechanical forces is regarded as a potential mechanism of dust-induced emphysema [14].

However, our case showed features of chronic pneumoconiotic reactions characterized by particle deposits accompanied by foreign-body granuloma formation. These findings have been demonstrated after inhalation of many environmental agents, including talc. For instance, the latency for slowly progressing talc pneumoconiosis is greater than 15 years [8].

It is suggested that the mechanism of induction of foreign-body giant cells depends on surface chemistry of the underlying substrate where degradative enzymes, reactive oxygen intermediates, or other products are secreted and the protein adsorption occurs before cell adhesion [1]. In our case, the prominent giant-cell reaction may result not only due to the surface properties but also due to the particle dimension of up to 300 μm, which is caused by an accidental aspiration. An ongoing fracture of particles may contribute to the release of free radicals such as oxygen.

Like in the above-mentioned postmortem report [4], adjacent to fibrotic areas, airspace enlargement and tissue destruction were evident in our case as well.

Emphysema of lung parenchyma and cystic tissue destruction are also common in LAM. LAM is known as a disease of abnormal proliferation of smooth muscle cells, which results in the obstruction of airways, lymphatics, and vessels [11]. There are different theories on the mechanism of cyst development in LAM. It is assumed that tissue destruction in LAM occurs either due to obstruction of lymphatic channels causing rupture or bronchiolar obstruction followed by alveolar rupture. Other investigators conclude that the lesions result in the degradation of elastic fibers caused by an imbalance between elastase and alpha1-antitrypsin, which are released by proliferated muscle cells [5, 6]. The proteinase hypothesis is supported by other authors who suggest that the expression of matrix metalloproteinase 2 by the LAM cells may play an important role in the cystic destruction of the lung parenchyma [12].

Pulmonary LAM is associated with various diseases, including tuberous sclerosis complex (TSC), renal angiomyolipomas, and uterine leiomyomas. In our case, the patient's history revealed bilateral renal angiomyolipomas. This rare hamartomatous tumor may occur in isolation or as part of TSC [17].

The predilection of LAM for women during their reproductive age leads to the assumption that hormonal factors play an important role in the pathogenesis of this disease. Apart from the hormonal influence, an additional factor may be existent. The trigger that starts the smooth muscle cell proliferation in LAM in the lung and occasionally in lymph nodes is still unknown. There are speculations that LAM might be the result of local cytokine effects transferred by lymphatics [3].

In the present case, a chronic pneumoconiotic reaction with granuloma formation after charcoal aspiration is evident. The release of proteolytic enzymes may contribute to the airspace enlargement in both pneumoconiotic lesion and LAM. It is likely that the present LAM lesions—in combination with TSC-associated angiomyolipomas—may be considered an isolated process.

References

1. Anderson J (2000) Multinucleated giant cells. Curr Opin Hematol 7:40–47
2. Arnold TC, Willis BH, Xiao F, Conrad SA, Carden DL (1999) Aspiration of activated charcoal elicits an increase in lung microvascular permeability. J Toxicol Clin Toxicol 37 (1):9–16
3. Bittmann I, Dose TB, Müller C, Dienemann H, Vogelmeier C, Löhrs U (1997) Lymphangioleiomyomatosis: recurrence after single lung transplantation. Hum Pathol 28(12): 1420–1423
4. Elliott CG, Colby TV, Kelly TM, Hicks HG (1989) Charcoal lung. Bronchiolitis obliterans after aspiration of activated charcoal. Chest 96(3):672–674
5. Fukuda Y, Kawamoto M, Yamamoto A, Ishizaki M, Basset F, Musugi Y (1990) Role of elastic fiber degradation in emphysema-like lesions of pulmonary lymphangiomyomatosis. Hum Pathol 21 (12):1252–1261
6. Golej J, Boigner H, Burda G, Hermon M, Trittenwein G (2001) Severe respiratory failure following charcoal application in a toddler. Resuscitation 49(3):315–318
7. Graff GR, Stark J, Berkenbosch JW, Holcomb GW 3rd, Garola RE (2002) Chronic lung disease after activated charcoal aspiration. Pediatrics 109(5):959–961
8. Green FHY, Churg A (1998) Pathologic features of occupational lung disease. In: Churg A, Green FHY (eds) Pathology of occupational lung disease, 2nd edn. pp 21–45
9. Green FHY, Vallyathan V (1998) Coal workers' pneumoconiosis and pneumoconiosis due to other carbonaceous dusts. In: Churg A, Green FHY (eds) Pathology of occupational lung disease, 2nd edn. pp 129–207
10. Harris CR, Filandrinos D (1993) Accidental administration of activated charcoal into the lung: aspiration by proxy. Ann Emerg Med 22(9):1470–1473
11. Kalassian KG, Doyle R, Kao P, Ruoss S, Raffin T (1997) Lymphangioleiomyomatosis: new insights. Am J Respir Crit Care Med 155:1183–1186
12. Hayashi T, Fleming MV, Stetler-Stevenson WG, Liotta LA, Moss J, Ferrans VJ, Travis WD (1997) Immunohistochemical study of matrix metalloproteinases (MMPs) and their tissue inhibitors (TIMPs) in pulmonary lymphangioleiomyomatosis (LAM). Hum Pathol 28:1071–1078
13. Lee AG, Wagner FM, Chen MF, Serrick C, Giaid A, Shennib H (1998) A novel charcoal-induced model of obliterative bronchiolitis-like lesions: implications of chronic non-specific airway inflammation in the development of posttransplantation obliterative bronchiolitis. J Thorac Cardiovasc Surg 115(4): 822–827
14. Li K, Keeling B, Churg A (1996) Mineral dusts cause elastin and collagen breakdown in the rat lung: a potential mechanism of dust-induced emphysema. Am J Respir Crit Care Med 153:644–649
15. Moll J, Kerns W 2nd, Tomaszewski C, Rose R (1999) Incidence of aspiration pneumonia in intubated patients receiving activated charcoal. J Emerg Med 17(2):279–283
16. Pollak MM, Dunbar BS, Holbrook PR, Fields AI (1981) Aspiration of activated charcoal and gastric contents. Ann Emerg Med 10(10):528–529
17. Sullivan EJ (1998) Lymphangioleiomyomatosis. A review. Chest 114:1689–1703

Virchows Arch (2006) 449: 230–233
DOI 10.1007/s00428-006-0221-6

ORIGINAL ARTICLE

Anja Dankof · Veit Krenn

C4d deposits mark sites of meniscal tissue disintegration

Received: 9 November 2005 / Accepted: 8 April 2006 / Published online: 4 May 2006
© Springer-Verlag 2006

Abstract Although the frequent occurrence of meniscal degeneration is a well-known fact and its consequences include rupture and even loss of the meniscus, the pathogenetic factors are established insufficiently. Because complement factors and leukocytes are present in synovial fluid, we tried to detect complement deposits and macrophages in menisci, which displayed degenerative changes. We therefore performed a retrospective analysis by immunohistochemical staining of C4d and CD68 in meniscal tissue derived from patients (n=15) who underwent meniscectomy because of meniscal tears and from three autopsy cases (n=3). In this study, focal C4d deposits in the meniscal extracellular matrix in areas of mucoid degeneration or fibrillation were demonstrated for the first time, while no C4d deposits in the avascular zone of menisci without signs of degeneration or injury could be detected. In addition, colocalization of C4d and CD68+ cells was found at sites of meniscal tissue disintegration in five cases. These results represent the first evidence for an involvement of complement and macrophages in meniscal tissue disintegration, indicating a complement mediated reaction at the site of tissue alteration.

Keywords Cartilage · Immunohistochem · Extracell matrix

A. Dankof
Institute of Pathology, Humboldt-University,
University Hospital Charité,
Schumannstrasse 20/21,
10117 Berlin, Germany

V. Krenn (✉)
Institute of Pathology Trier,
Moltkestrasse 32,
54292 Trier, Germany
e-mail: krenn@patho-trier.de
Tel.: +49-651-24024
Fax: +49-651-149586

Introduction

Meniscal degeneration (MD) is a common disorder of the fibrous cartilage of the human knee joint. Although the first descriptions of characteristic histopathological changes in MD are nearly 30 years old, studies concerning the pathogenesis are scarce. All we know today about MD almost exclusively derives from diagnostic imaging techniques [14] and conventional HE or EvG staining, while no immunohistochemical marker for MD is available.

Histomorphologically, three different variances of MD have been described: calcification, acellular hyalin degeneration, and mucoid or myxoid degeneration [5, 6]. The latter is the most frequent degenerative lesion and can further be subdivided into intrameniscal stromal mucoid degeneration (mD) and cystic parameniscal degeneration.

In the past, mD has usually been considered to be the result of endogenous or exogenous trauma [15, 19, 20]. In addition, synthesis of mucopolysaccharides after malnutrition of the meniscal tissue was suspected to be of pathogenetic relevance [19]. Stromal mD was even considered to represent a physiological condition in the meniscus [5]. Furthermore, vascular disturbance/posttraumatic hematoma due to trauma and accumulation of proteoglycans after altered mechanical strains were accused to give rise to degenerative lesions [7, 11, 12]. Some studies demonstrated MD to be age- and stress-related [8, 10, 18].

Although trauma has been repeatedly accused over the last decades to be the source of MD, Weber [21] questioned the existence of isolated traumatic injury and stated that the conventional criteria to distinguish between traumatic and degenerative meniscal lesions were not longer necessary.

These conflicting concepts can be brought together by considering the basic distinction between primary [8] and secondary MD. According to Aufdermaur [2], secondary degenerative lesions are massive and show only few changes due to repair. Especially in cases with preceding primary degeneration, trauma may aggravate degenerative lesions [4].

So apart from mechanical factors, are there any additional factors, which are involved in the development,

maintenance, or even aggravation of degenerative lesions? Are there any signs of an immunoresponse at sites of MD?

Because complement factors and leukocytes are present in synovial fluid [3], we tried to detect complement deposits and macrophages by immunohistochemical staining of C4d and CD68 in menisci, which displayed degenerative changes.

Materials and methods

Medial menisci, obtained from 15 patients (n=15, 6 women and 9 men, ages 13–68, average age 41 years) who underwent meniscectomy because of meniscal tears were selected for this study. In addition, three medial menisci (n=3) of the right knee, which did not display macroscopic signs of degeneration or injury, were obtained from autopsy cases (comparison group, average age 62 years). These menisci were removed totally and triangular slices were cut to evaluate both the vascular and the avascular zones of the tissue.

Histology

After fixation in formalin (4%), the meniscal tissue was embedded in paraffin. The microtomed sections of 1–3 μm width were stained with hematoxylin and eosin. In addition, an EvG staining was performed and an immunohistochemical staining was carried out using antibodies to C4d and CD68.

After the tissue sections were deparaffinized, epitopes were demasked (pressure cooker, citrate buffer, pH 6). Staining was performed using commercially available rabbit polyclonal antibody against C4d (Biomedica, Austria) and CD68, which was appropriately diluted (1:10).

Antibody binding was detected by using the labeled streptavidin–biotin method (LSAB-Kit+, DAKO, Denmark). Peroxidase-linked streptavidin binds to biotin, which again is linked to the secondary antibody. DAB (3,3-diaminobenzidine; DAKO, Denmark) served as a chromogen for the reaction with peroxidase. Endogenous peroxidase was blocked by H_2O_2. In a final step, nuclear counterstaining with hematoxylin according to Mayer was performed. Successful IH was controlled using tonsil tissue treated as described above; negative controls were obtained by omitting the primary antibody. Immunostainings were evaluated by two pathologists (V.K. and A.D.).

Five selected cases additionally underwent IH double staining to validate colocalization of macrophages and C4d deposits. The EnVision Doublestain System (DAKO, Denmark) was used according to the manufacturer's instructions: after epitope demasking (pressure cooker, citrate buffer, pH 6) anti-C4d antibody (polyclonal, Biomedica, Austria) and anti-CD68 antibody (DAKO, Denmark) were successively added. DAB (C4d) and Fast Red (CD68) were used as chromogens. Tonsil tissue served as a positive control; negative controls were obtained by omitting the primary antibody.

Results

Hematoxylin–eosin

Comparison group

Although only menisci without macroscopic signs of tears and degeneration were selected from the comparison group, two of three menisci (n=3) histologically showed discrete signs of mD and two displayed slight fibrillation of the extracellular matrix. Proliferating chondrocytes were seen in all cases. The vascular zone presented with several small vessels, fibrous tissue, and fat.

Meniscal degeneration

Thirteen of 15 menisci (n=15) displayed discrete to severe mD. Menisci without signs of mD belonged to a 22-year-old man and an 18-year-old woman. Fibrillation of the extracellular matrix was seen in 14 of 15 patients, the meniscus without fibrillation deriving from a 19-year-old man. Tears of the meniscal tissue could be demonstrated in 14 patients, four with sharp edges, three with smooth tear contours, and six displaying both features. Smooth tear edges were in all cases accompanied by deposits of fibrin. Fourteen menisci showed proliferating chondrocytes. Small areas of fibrous cartilage necrosis were only seen in three cases.

C4d

Comparison group No C4d deposits were detected within the extracellular matrix of the avascular zone of the meniscal tissue; only one case showed weak focal staining in a small area with signs of mD. Linear C4d deposits were seen along the meniscal surface (Fig. 1a,b), while the vascular zone presented with positive perivascular and endothelial C4d staining.

Meniscal degeneration Twelve menisci (n=15) displayed diffuse C4d deposits in the extracellular matrix with strong relation to areas of mD or fibrillation, partially in the vicinity of meniscal tears (Fig. 2a,b). No correlation between deposition of C4d and the age of traumatic changes could be demonstrated. In addition, as it was seen in the comparison group, linear C4d deposits were detected along the meniscal surface, surrounding vessels, and along endothelial cells in the vascular zone.

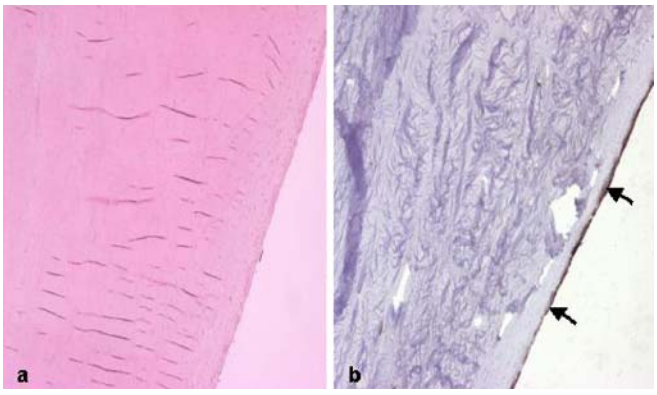

Fig. 1 Unaltered meniscal tissue from a 63-year-old man (HE, 25×) (**a**). Linear C4d deposits (*arrows*) are only detected along the meniscal surface (IH C4d, 25×) (**b**)

CD68

Comparison group CD68+ cells were predominantly located in the vicinity of vessels in the vascular zone. No macrophages were detected in the extracellular matrix of the avascular zone.

Meniscal degeneration Twelve menisci (n=15) showed CD68+ macrophages, while the distribution pattern differed. If the examined tissue specimen included the vascular zone of the meniscus, CD68+ cells could be demonstrated in the vicinity of blood vessels. Regarding the avascular zone, macrophages were in some cases located directly beyond the meniscal surface. Three menisci presented with solitary CD68+ macrophages distributed diffusely in the extracellular matrix, while five menisci displayed colocalization of mD/tissue fibrillation, C4d deposits, and macrophages.

C4d/CD68

Five menisci, which presented with macrophages in areas, which also showed C4d deposits in IH single staining, were selected for IH double staining of CD68/C4d. As expected, colocalization of macrophages and C4d deposits was clearly detectable (Fig. 3).

Discussion

Although histopathology of bradytrophic tissue has not received much attention in the past, some studies just recently were able to highlight its importance and amend the diagnostic repertoire [9, 13]. In this study, focal C4d deposits in the meniscal extracellular matrix of areas of mD or fibrillation were demonstrated for the first time. Because no intrameniscal deposits in menisci without signs of degeneration or injury could be detected, these complement deposits specifically trace disintegration of fibrocartilage. In addition, colocalization of C4d and CD68+ cells could be demonstrated in these lesions, indicating that C4d deposits are not an unspecific sign of inflammation but reflect a complement mediated reaction at the site of tissue alteration.

As up to now, only histomorphological descriptions of degenerative meniscal changes, based on conventional staining methods like HE and EvG staining, exist; these results represent the first immunohistochemical evidence for an involvement of complement and macrophages in MD.

Degeneration of the meniscal tissue is subdivided into primary and secondary changes [1, 2, 8], depending on preexisting conditions like trauma or biomechanically defective positions of the joint. Beyond this, three morphologically different types can be distinguished: calcification, acellular hyalin degeneration, and mucoid or myxoid degeneration [5, 6]. mD is the most frequent form and, depending on the location of the degenerative lesions, is again divided into intrameniscal stromal mD and cystic parameniscal degeneration [5, 6].

Although the frequent occurrence of MD is a well-known fact and its consequences include rupture and even loss of the meniscus, the pathogenetic factors are established insufficiently.

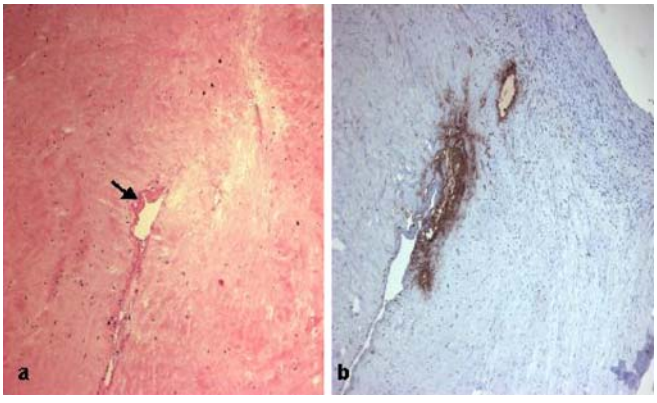

Fig. 2 Meniscal tear with depositions of fibrin along its edges (*arrow*) and an adjacent area with fibrillation and beginning mucoid degeneration (HE, 100×) (**a**). C4d deposits in the same area, corresponding to **a** (IH C4d, 100 ×) (**b**)

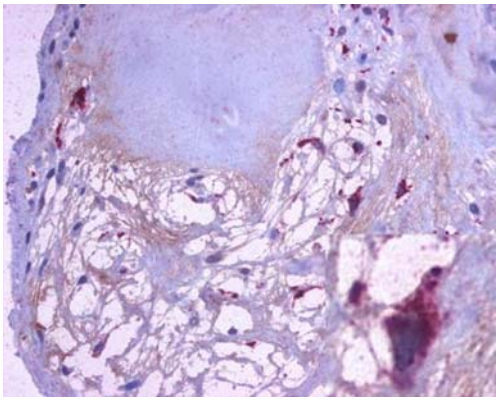

Fig. 3 Area of mucoid degeneration with colocalization of C4d deposits and CD68+ macrophages (IH C4d/CD68, 400×). *Insertion* CD68+ macrophage

Besides endogenous and exogenous trauma [14, 19, 20], posttraumatic changes like hematoma or vascular disorders [7], synthesis of mucopolysaccharides arising from nutritional deficiencies, and accumulation of proteoglycans after altered mechanical strains [11, 12] are suspected to be the source of MD. While an aggravating effect of traumatic changes on preexisting MD is well accepted [4], the existence of isolated traumatic ruptures of unaltered meniscal tissue is doubted [21].

In this study, C4d deposits in areas of mD or fibrillation were demonstrated for the first time, indicating complement activation within this lesions, possibly resulting in perpetuation of preexisting tissue disintegration.

Activation of the complement cascade by immunocomplexes via the classical pathway results in enzymatic cleavage of the complement component C4, whose final split product is C4d [16]. As C4d exposes a thioester group, which leads to the formation of a covalent bond to the closest protein or carbohydrate near the site of C4 activation, it is not as transient as other complement fragments and can therefore be detected much easier by immunohistochemistry.

The fact that degenerative lesions with C4d deposits were seen in unvascularized areas raises the question of from what kind of source complement factors derive. On the one hand, complement may originate from the serum, invading the extracellular matrix in the course of trauma. On the other hand, complement factors could derive from inside the joint because they have been demonstrated in synovial fluid [3].

Although colocalization of C4d and CD68+ macrophages suggests that complement activation is involved in the development or aggravation of MD because macrophages are known to be activated by the formation of immunocomplexes by IgG and complement components (C5a) [17] and are capable of synthesizing complement factors (C4 and C3), the functional relevance of C4d deposits at sites of MD remains to be elucidated. Measurement of intraarticular complement turnover could supply further evidence for an involvement of complement activation in MD.

Nevertheless, complement deposits and macrophages were demonstrated for the first time in MD, indicating that apart from mechanical mechanisms, complement mediated processes may be involved.

Taken together, detection of C4d deposits could serve as an immunohistochemical marker for disintegration of fibrocartilage, providing an auxiliary tool for the histopathological diagnosis of MD.

References

1. Andreesen M (1956) Praktische Erfahrung bei der Begutachtung von Meniskusschäden. Hefte Unfallheilkd 52:214
2. Aufdermaur M (1971) Die Bedeutung der histologischen Untersuchung des Kniegelenksmeniskus. Schweiz Med Wochenschr 101:1405–1441
3. Brodeur JP, Ruddy S, Schwartz LB, Moxley G (1991) Synovial fluid levels of complement SC5b-9 and fragment Bb are elevated in patients with rheumatoid arthritis. Arthritis Rheum 34(12):1531–1537
4. Burri C (1976) Meniscusverletzungen. Hefte Unfallheilkd 128:73
5. Ferrer-Roca O, Vialalta C (1980) Lesions of the meniscus. I. Macroscopic and histologic findings. Clin Orthop 146:289–300
6. Ferrer-Roca O, Vialalta C (1980) Lesions of the meniscus. II. Horizontal cleavages and lateral cysts. Clin Orthop 146:301–307
7. Kleinberg S (1938) Cysts of external semilunar cartilage: report of three cases. Arch Surg 37:827–834
8. Könn G (1985) Möglichkeiten und Grenzen der histologischen Altersbestimmung von Zusammenhangstrennungen des Kniegelenkmeniskus. Unfallchirurgie 88:1
9. Krenn V, Morawietz L, Burmester GR, Haupl T (2005) Synovialitis score: histopathological grading system for chronic rheumatic and non-rheumatic synovialitis. Z Rheumatol 64 (5):334–342
10. Lindström A (1950) Trauma and ganglia of the semilunar cartilages of the knee. Acta Orthop Scand 23:237–246
11. McDevitt CA, Muir H (1976) Biochemical changes in the cartilage of the knee in experimental and natural osteoarthritis in the dog. J Bone Joint Surg Br 58:94–101
12. McDevitt CA, Webber RJ (1990) The ultrastructure and biochemistry of meniscal cartilage. Clin Orthop 252:8–18
13. Morawietz L, Gehrke T, Classen RA, Barden B, Otto M, Hansen T, Aigner T, Stiehl P, Neidel J, Schroder JH, Frommelt L, Schubert T, Meyer-Scholten C, Konig A, Strobel P, Rader ChP, Kirschner S, Lintner F, Ruther W, Skwara A, Bos I, Kriegsmann J, Krenn V (2004) Proposal for the classification of the periprosthetic membrane from loosened hip and knee endoprotheses. Pathologe 25(5):375–384
14. Richter J, Grifka J, Fisseler-Eckhoff A, Müller KM, Kramer J (1996) Ultrasound morphologic criteria in evaluating meniscus changes—an experimental study. Z Orthop Ihre Grenzgeb 134 (2):137–143
15. Romanini L, Calvisi V, Collodel M, Masciocchi C (1988) Cystic degeneration of the lateral meniscus. Pathogenesis and diagnostic approach. Ital J Orthop Traumatol 14:493–500
16. Sacks SH, Chowdhury P, Zhou W (2003) Role of complement system in rejection. Curr Opin Immunol 15(5):487–492
17. Shushakova N, Skokowa J, Schulman J, Baumann U, Zwirner J, Schmidt RE, Gessner JE (2002) C5a anaphylatoxin is a major regulator of activating versus inhibitory Fcgammas in immune complex-induced lung disease. J Clin Invest 110:1823–1830
18. Slany A (1941) Autoptische Reihenuntersuchungen an Kniegelenken mit besonderer Berücksichtigung der Meniskuspathologie. Arch Orthop Unfallchir 41:256
19. Smillie IS (1978) Surgical pathology of the menisci. In: Smillie IS (ed) Injuries of the knee joint. Churchill Livingstone, Edinburgh, pp 83–111
20. Walter JB, Talbot IC (1996) Connective tissue: its normal structure and the effects of disease. In: Walter JB, Talbot IC (eds) General pathology. Churchill Livingstone, Edinburgh, pp 103–116
21. Weber M (1994) Die Beurteilung des Unfallzusammenhangs von Meniskusschäden. Orthopäde 23:171–178

Virchows Arch (2006) 449: 234–237
DOI 10.1007/s00428-006-0218-1

CASE REPORT

Junichi Shiraishi · Hiroaki Nomori · Hideki Orikasa · Taisuke Mori · Kazuto Yamazaki

Atypical thymoma (WHO B3) with neuroendocrine differentiation: report of a case

Received: 27 February 2006 / Accepted: 5 April 2006 / Published online: 4 May 2006
© Springer-Verlag 2006

Abstract We report a case of type-B3 thymoma manifesting neuroendocrine differentiation. The patient was a 42-year-old woman who complained of shoulder pain but had no symptoms of myasthenia gravis or anemia. The tumor was located in the anterior mediastinum and had directly invaded the pericardium and left lung. Histological examination revealed that the tumor was lobulated by bands of fibrous tissue, perivascular spaces were scattered throughout the tumor, and there were a few intraepithelial lymphocytes. The vast majority of lymphocytes in the perivascular spaces and in the lobulated tumor were immunohistochemically positive for TdT, MIC2, and CD1a. The majority of tumor cells were polygonal and medium or large in size. The tumor cells were weakly positive for synaptophysin, chromogranin A, CD56, and NSE. Small nests of small, relatively uniform polygonal cells were observed facing the fibrous bands. These cells resembled the cells of carcinoid tumors and were strongly positive for NSE, synaptophysin, chromogranin A, and CD56. Ultrastructurally, sparse dense-core granules were observed in the cytoplasm of a few tumor cells. This is a unique case of thymoma with neuroendocrine differentiation, and to the best of our knowledge this is the first such case ever reported.

Keywords Thymoma · Carcinoid tumor · Neuroendocrine differentiation

Introduction

Neuroendocrine differentiation in epithelial neoplasms of the thymus has been investigated immunohistochemically and ultrastructurally [4, 5, 7, 11, 12]. Thymic tumors with neuroendocrine differentiation consist of nonneuroendocrine tumors with neuroendocrine differentiation and pure neuroendocrine tumors, that is, carcinoid tumors, small-cell carcinomas, and large-cell neuroendocrine carcinomas. Thymic carcinomas often contain a variable number of tumor cells having a neuroendocrine phenotype, but thymomas with neuroendocrine differentiation are extremely rare. We describe a case of type-B3 thymoma that exhibited a unique pattern of neuroendocrine differentiation.

Clinical history

A 42-year-old woman complained of shoulder pain, and a computed tomography (CT) scan revealed a large tumor in the anterior mediastinum that had directly invaded the pericardium and left lung (stage III, according to the Masaoka classification). A diagnosis of thymoma was made based on the histological findings in a CT-guided needle biopsy specimen. The patient was treated with three courses of combination chemotherapy consisting of cisplatin (50 mg/m^2), adriamycin (40 mg/m^2), oncovin (0.6 mg/m^2), and etoposide (700 mg/m^2), but there was no marked reduction in tumor size (decrease in diameter from 7 to 6 cm, evaluated as stable disease). Total thymectomy and partial resection of the pericardium and left lung were performed. The serum NSE level was

J. Shiraishi (✉)
Department of Pathology, Japanese Red Cross Medical Center,
4-1-22 Hiroo, Shibuya-ku,
Tokyo 150-8935, Japan
e-mail: jshira@chive.ocn.ne.jp
Tel.: +81-3-34001311
Fax: +81-3-34091604

H. Nomori
Department of Thoracic Surgery, Saiseikai Central Hospital,
Tokyo, Japan

H. Orikasa · K. Yamazaki
Department of Pathology, Saiseikai Central Hospital,
Tokyo, Japan

T. Mori
Department of Pathology, Keio University School of Medicine,
Tokyo, Japan

elevated to 110 ng/dl before surgery, but the serum acetylcholine receptor antibody level was not elevated. There were no symptoms and signs of myasthenia gravis, multiple endocrine neoplasia I, or Cushing's syndrome.

Materials and methods

The surgical specimen was fixed with 10% formalin and embedded in paraffin. Sections were cut 4 μm thick and stained with hematoxylin and eosin (H&E). Immunohistochemical staining was performed using primary antibodies against MIC2 (monoclonal, mouse, DAKOCytomation, diluted 1:50), terminal deoxynucleotidyl transferase (TdT) (polyclonal, rabbit, DAKOCytomation, diluted 1:20), CD1a (monoclonal, mouse, Novocastra, Newcastle, UK, diluted 1:30), synaptophysin (monoclonal, mouse, DAKOCytomation, diluted 1:50), chromogranin A (polyclonal, rabbit, DAKOCytomation, diluted 1:150), CD56 (monoclonal, mouse, Novocastra, diluted 1:50), NSE (monoclonal, mouse, DAKOCytomation, diluted 1:400), hCG (polyclonal, rabbit, DAKOCytomation), ACTH (polyclonal, rabbit, DAKOCytomation, diluted 1:1), CD5 (monoclonal, mouse, Novocastra, diluted 1:100), bcl-2 (monoclonal, mouse, DAKOCytomation, diluted 1:25), and c-kit (polyclonal, rabbit, Oncogene, Darmstadt, Germany, diluted 1:50). Before staining for anti-MIC2, the sections were autoclaved in citrate buffer for 20 min, and before staining for anti-TdT, CD1a, synaptophysin, CD56, bcl-2, c-kit, and CD5, they were autoclaved in citrate buffer for 5 min. Before staining for anti-hCG and calcitonin, the sections were immersed in 0.015 mol/l protease K at room temperature for 6 min. The peroxidase reaction was developed with 0.06% 3,3-diaminobenzidine tetrahydrochloride in phosphate-buffered saline, pH 7.4, containing 0.003% hydrogen peroxide.

For ultrastructural examination, tissue fragments were fixed in 2.5% phosphate-buffered glutaraldehyde, and then processed and embedded in epoxy resin. Ultrathin sections mounted on copper grids and stained with uranyl acetate and lead citrate were examined with an electron microscope.

Results

Macroscopically, the tumor was an infiltrating mass measuring 5.7×5.0×3.7 cm, which had involved the pericardium and left lung (Fig. 1). The cut surface was firm and whitish and contained small hemorrhagic foci.

Microscopic examination of the tumor revealed lobulation by fibrous bands, scattered perivascular spaces, and a few intraepithelial lymphocytes (Fig. 2a). Most of the lymphocytes were immunohistochemically positive for immature T-cell markers (MIC2, TdT, and CD1a) (Fig. 2c). The majority of the tumor cells were polygonal, medium or large in size, arranged in a vague epidermoid pattern with palisading of the cells around perivascular spaces (Fig. 2b), and contained round to oval nuclei with distinct nucleoli.

Fig. 1 Cut surface of the tumor. The tumor measured 5.7×5.0×3.7 cm and had extended into the left lung. The tumor was firm and whitish, and it contained scattered small hemorrhagic areas

The Hassall corpuscle-like keratin pearls were focally aggregated in some lobules (Fig. 2d). There were scattered small nests of small, relatively uniform polygonal cells facing the fibrous bands (Fig. 3a), the nests being reminiscent of carcinoid tumor. Immunohistochemical staining revealed that the small cells were strongly positive for NSE, synaptophysin, chromogranin A, and CD56 (Fig. 3b,c). Most of the medium to large tumor cells, on the other hand, were weakly positive for these neuroendocrine markers. The tumor cells were completely negative for c-kit, bcl-2, and several hormones (hCG, ACTH, and calcitonin). Only a few tumor cells were positive for CD5. Grimelius staining was negative. The mitotic rate was low (1–2 mitoses per 10 HPFs). The diagnosis classification was so-called atypical thymoma (type-B3 thymoma according to the WHO) with foci of neuroendocrine differentiation. Chemotherapy was only slightly effective.

Ultrastructural examination revealed sparse dense-core granules with a halo about 100 nm in diameter in the cytoplasm of a few tumor cells (Fig. 4). The medium to large tumor cells were rich in tonofibrils, and occasional desmosomes were observed at the cell junctions.

Discussion

Thymic carcinomas often exhibit neuroendocrine differentiation [4, 5, 8]. However, reports of thymomas with neuroendocrine differentiation have been extremely rare.

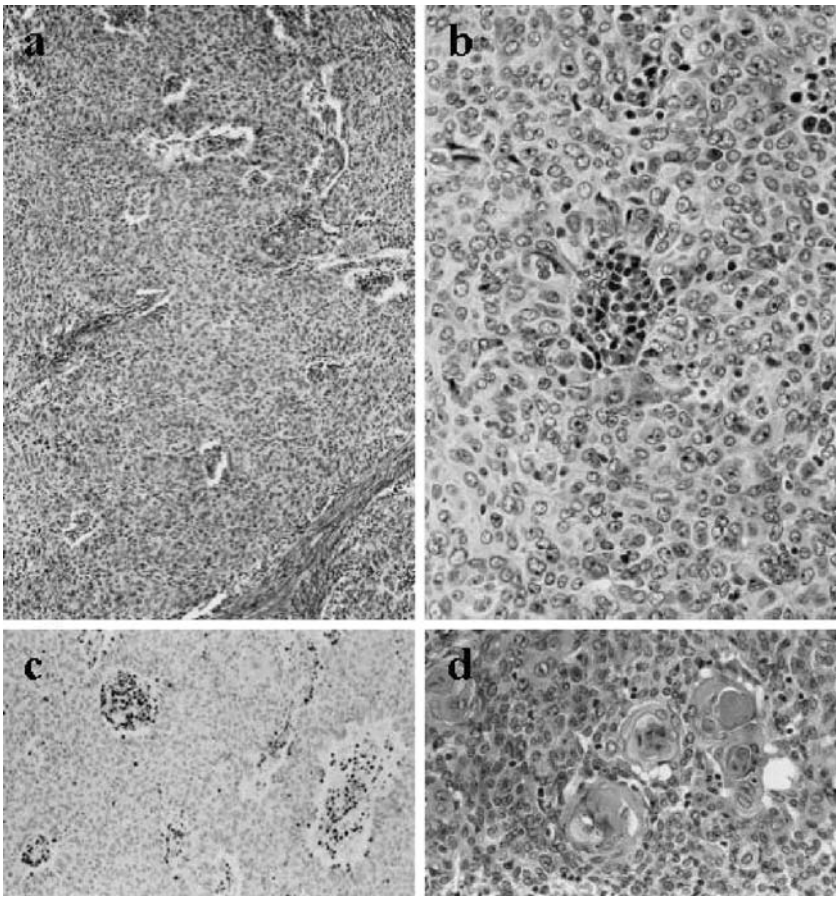

Fig. 2 Histological and immunohistochemical findings in the tumor. Low magnification of an H&E-stained section of the tumor showing a lobulated tumor with scattered perivascular spaces and a few intraepithelial lymphocytes (**a**). High magnification showing that the tumor cells are polygonal, medium to large in size, and somewhat epidermoid in arrangement. A perivascular space containing lymphocytes is bordered by palisading tumor cells (**b**). The lymphocytes present in the perivascular spaces and scattered among tumor cells are TdT-positive (**c**). Hassall corpuscle-like keratin pearls are aggregated in this lobule (**d**)

Lauriola et al. [7] showed that thymomas are negative for neuroendocrine markers except for focal NSE immunoreactivity in areas of medullary differentiation in half of lymphocyte-rich thymomas. Hishima et al. found that only a few thymomas are positive for several neuroendocrine markers (synaptophysin, alpha subunit of a guanine nucleotide binding protein, Go, and small-cell lung carcinoma cluster 1 antigen). However, the marker positive cells were dispersed, *and did not have apparentmorphological features of neuroendocrine differentiation* [4]. Only two cases of combined thymoma and carcinoid tumor have ever been reported. In one of the cases, a large carcinoid tumor was surrounded by thymoma [1], and in the other case, neuroendocrine differentiation was detected in limited areas of the tumor [3, 9].

The degree of neuroendocrine differentiation in our case varied from area to area. Marked neuroendocrine differentiation was observed at the margin of the lobules facing the fibrous bands, and the tumor cells in those areas resembled the cells of carcinoid tumors and were strongly positive for neuroendocrine markers. By contrast, the majority of tumor cells with the appearance of ordinary thymoma cells showed a slight tendency toward neuroendocrine differentiation. *Different from reported cases*, *our case showed that most of tumor cells had neuroendocrine differentiation with different degrees*, *and morphological features were clearly consistent with the degree of neuroendocrine differentiation*.

Because several thymic carcinomas and thymomas have been found to be immunoreactive for hormones (hCG, ACTH, calcitonin, serotonin, somatostatin, growth hormone, etc.) [2, 4, 6], we tested the tumor cells for hCG, ACTH, and calcitonin immunoreactivity; however, they were completely negative.

We have reported a case of an unusual thymoma that exhibited a unique pattern of neuroendocrine differentiation that to the best of our knowledge is the first such case ever reported. It is used to be thought that neuroendocrine tumors in many organs were of neural crest origin, but the source of many neuroendocrine tumors is now thought to be primitive cells or epithelial cells that have capacity for bidirectional differentiation toward both nonneuroendocrine and neuroendocrine cells [1, 9, 10]. The presence of multiple foci of neuroendocrine cell nests contiguous with ordinary thymoma cells in the thymoma in our case supports the latter concept, that is, the thymic epithelial cell origin of the neuroendocrine cells. *In one case of combined B3 thymoma and large-cell neuroendocrine carcinoma*, *shared genetic alterations were observed by CGH*, *suggesting a common clonal origin of both tumor components* [10].

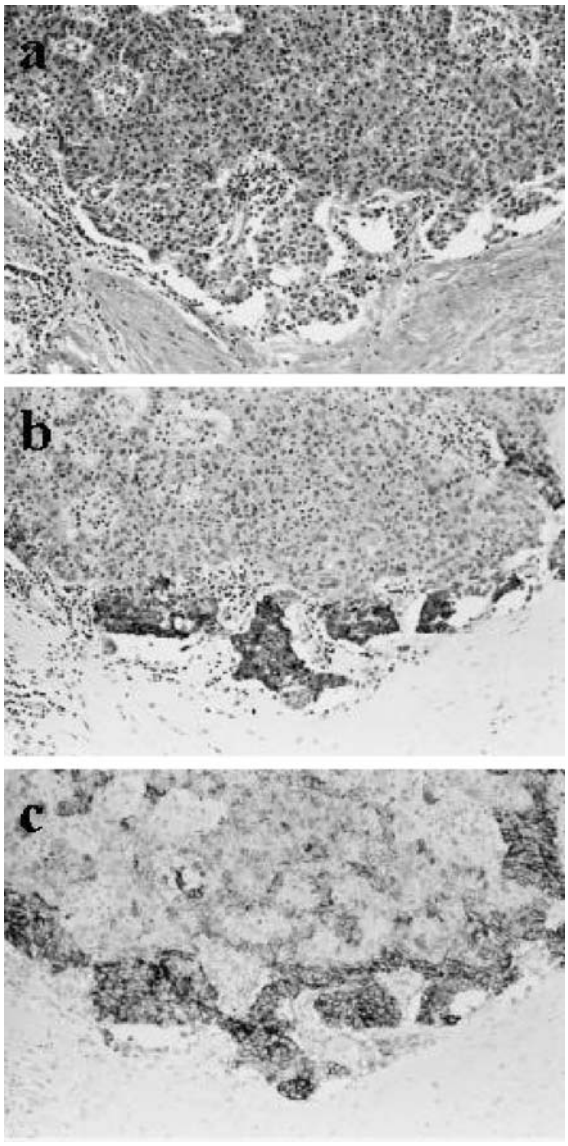

Fig. 3 Histological and immunohistochemical findings in a tumor lobule. Nests of small tumor cells are seen facing the fibrous band (**a**). These tumor cells are strongly positive for chromogranin A (**b**) and CD56 (**c**). The medium to large tumor cells in the upper half of the photographs are weakly positive for CD56 (**c**) and faintly positive for chromogranin A (**b**)

Acknowledgements The authors thank Yukio Shimosato, MD, Keio University, Yoshihiro Matsuno, MD, National Cancer Center Research Institute and Hospital, and Tsunekazu Hishima, MD, Tokyo Metropolitan Komagome Hospital for reviewing the surgical specimen and for critical discussion of the case. The authors also thank Toshihiro Nagai of Keio University for preparing the electron micrographs.

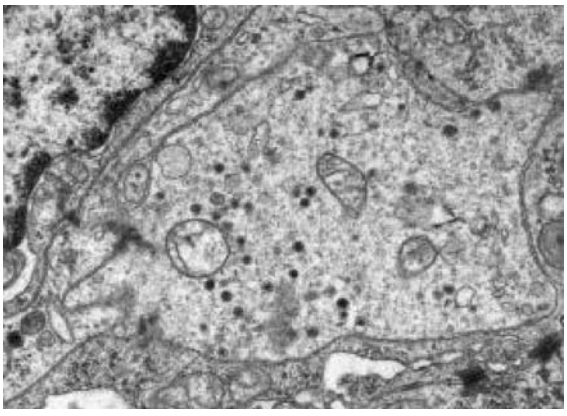

Fig. 4 Ultrastructure of the tumor cells. Dense-core granules of about 100 nm in diameter are seen in the cytoplasm of a tumor cell. Some dense-core granules possess a peripheral halo

References

1. Cho KJ, Ha CW, Koh JS, Zo J, Jang J (1993) Thymic carcinoid tumor combined with thymoma-neuroendocrine differentiation in thymoma? J Korean Med Sci 8:458–463
2. Fukayama M, Hayashi Y, Shiozawa Y, Maeda Y, Koike M (1990) Human chorionic gonadotropin in the thymus. An immunocytochemical study on discordant expression of subunits. Am J Pathol 136:123–129
3. Goto K, Kodama T, Matsuno Y, Yokose T, Asamura H, Kamiya N, Shimosato Y (2001) Clinicopathologic and DNA cytometric analysis of carcinoid tumors of the thymus. Mod Pathol 14:985–994
4. Hishima T, Fukayama M, Hayashi Y, Fujii T, Arai K, Shiozawa Y, Funata N, Koike M (1998) Neuroendocrine differentiation in thymic epithelial tumors with special reference to thymic carcinoma and atypical thymoma. Hum Pathol 29:330–338
5. Kuo TT (2000) Frequent presence of neuroendocrine small cells in thymic carcinoma: a light microscopic and immunohistochemical study. Histopathology 37:19–26
6. Lauriola L, Maggiano N, Serra FG, Nori S, Tardio ML, Capelli A, Piantelli M, Ranelletti FO (1997) Immunohistochemical and in situ hybridization detection of growth-hormone-producing cells in human thymoma. Am J Pathol 151:55–61
7. Lauriola L, Erlandson RA, Rosai J (1998) Neuroendocrine differentiation is a common feature of thymic carcinoma. Am J Surg Pathol 22:1059–1066
8. Moran CA, Suster S (2000) Thymic neuroendocrine carcinomas with combined features ranging from well-differentiated (carcinoid) to small cell carcinoma. A clinicopathologic and immunohistochemical study of 11 cases. Am J Clin Pathol 113:345–350
9. Shimosato Y, Mukai K (1997) Tumors of the mediastinum. Atlas of tumor pathology, third series, fascicle 21. Armed Forces Institute of Pathology, Washington, DC, pp 181–183
10. Travis WD, Brambilla E, Müller-Hermelink HK, Harris CC (2004) Tumours of the lung, pleura, thymus and heart. IARC Press, Lyon, pp 145–197
11. Wich MR, Scheithauer BW, Weiland LH, Bernatz PE (1982) Primary thymic carcinomas. Am J Surg Pathol 6:613–630
12. Zoltowska A, Pawelczyk T, Stopa M, Skokowski J, Stepinski J, Roszkiewicz A, Nyka W (1998) Myoid cells and neuroendocrine markers in myasthenic thymuses. Arch Immunol Ther Exp (Warsz) 46:253–257

Virchows Arch (2006) 449: 238–243
DOI 10.1007/s00428-006-0182-9

CASE REPORT

Pierre Mongiat-Artus · Catherine Miquel · Jean-François Fléjou · Florence Coulet · Jérôme Verine · Olivier Buhard · Hany Soliman · Pierre Teillac · Françoise Praz

Spectrum of molecular alterations in colorectal, upper urinary tract, endocervical, and renal carcinomas arising in a patient with hereditary non-polyposis colorectal cancer

Received: 19 September 2005 / Accepted: 22 February 2006 / Published online: 26 April 2006
© Springer-Verlag 2006

Abstract Hereditary nonpolyposis colon cancer (HNPCC) syndrome is the most frequent hereditary cancer syndrome predisposing to cancers of various locations, especially colon, endometrium, stomach, and upper urinary tract. Carcinomas of the kidney parenchyma are not considered as an HNPCC-related tumor. HNPCC tumors are characterized by microsatellite instability (MSI) due to a defect in mismatch repair (MMR) and carry somatic frameshift mutations in mononucleotide repeats within the coding regions of key genes. We report the first case of a papillary carcinoma of the kidney in an HNPCC patient who developed carcinomas of the upper urinary tract, endocervix, and colon. Whereas the HNPCC-related tumors demonstrated MSI phenotype, loss of MSH2 protein expression, and frameshift mutations in several of the 13 target genes analyzed, the kidney cancer displayed MSS phenotype, normal MMR protein expression, and no frameshift mutation in target genes. Our observations do not support the possibility that papillary carcinomas are part of HNPCC syndrome.

Keywords Hereditary nonpolyposis colorectal cancer · Papillary renal carcinoma · Microsatellite instability · Upper urinary tract carcinomas

Abbreviations HNPCC: Hereditary nonpolyposis colorectal cancer · MMR: Mismatch repair · MSI: Microsatellite instability · UCC: Urothelial cell carcinoma · UUT: Upper urinary tract

P. Mongiat-Artus (✉) · P. Teillac
Department of Urology, Saint-Louis Hospital,
Paris 7 University, 1 avenue Claude Vellefaux,
75010 Paris, France
e-mail: pierre.mongiat-artus@sls.aphp.fr
Tel.: +33-1-42499615
Fax: +33-1-42499616

C. Miquel
Department of Pathology,
Saint-Anne Hospital, INSERM U752, Paris 5 University,
Paris, France

J.-F. Fléjou
Department of Pathology, Saint-Antoine Hospital,
Paris 6 University, Paris, France

F. Coulet
Department of Genetics,
Pitié-Salpétrière Hospital, Paris 6 University,
Paris, France

J. Verine
Department of Pathology,
Saint-Louis Hospital, Paris 7 University,
Paris, France

O. Buhard · F. Praz
INSERM U762, Paris 6 University,
Paris, France

H. Soliman
Department of Biochemistry,
Saint-Louis Hospital, Paris 7 University,
Paris, France

Introduction

HNPCC is the most frequent hereditary cancer syndrome, characterized by an increased risk for colorectal cancer affecting more than 70% of cases and representing about 5% of all colorectal cancers. A variety of extracolonic tumors are also associated with HNPCC, particularly cancers of endometrium, stomach, small bowel, biliary system, ovary, and upper urinary tract (renal pelvis and proximal ureter). Most HNPCC-related tumors are due to germline mutations of mismatch repair (MMR) genes with the majority of cases caused by mutations in either of *MLH1* or *MSH2* [10]. Tumors with MMR defects are characterized by the presence of microsatellite instability (MSI) in simple repeated sequences and loss of immunostaining for MMR proteins. MSI is a feature of more than 90% of HNPCC-related tumors representing small deletion/insertion in mono- and dinucleotide repeats distributed throughout the genome. The underlying genetic mecha-

nism of carcinogenesis in MSI tumors is thought to be mainly related to somatic frameshift mutations of repeats contained within genes having putative roles in growth control, apoptosis, and DNA repair [3]. To date, only two studies investigated the occurrence of mutations in target genes in MSI upper urinary tract (UUT) carcinomas [6, 9].

We report the case of a female HNPCC patient whose first tumor was an UUT carcinoma. She later developed a second carcinoma in the endocervix and a third in the colon. Subsequent tumors consisted of UUT urothelial cell carcinoma (UCC) recurrences, and a tubulopapillary renal adenocarcinoma, a tumor that had not been reported in HNPCC patients so far. We describe MSI analysis, MMR gene expression, and the mutation profile of MSI target genes in the different tumors.

Clinical history

A nonsmoking 61-year-old woman unexposed to occupational carcinogens had a father affected by a duodenal cancer at age 45 and a father's mother affected by a colon cancer. She was diagnosed on a segmental ureterectomy specimen with a pTaG1 UCC of the left ureter (#1) at 32 years old. She received a right nephrectomy at the same time for a nonfunctional multicystic kidney. She developed a pT1b endocervical adenocarcinoma (#2) at 48 years old. She then received a left ureterectomy with an ileo-ureteroplasty for a first UCC recurrence pTaG2 in the proximal left ureter (#3) at 54 years old. At 56, she presented with a well-differentiated pT3 adenocarcinoma of the left transverse colon (#4) without any lymph node invasion or metastasis and underwent left colectomy. She was diagnosed with HNPCC syndrome as she was fulfilling the Amsterdam criteria II. At 61, she received left nephro-ureterectomy and cystectomy for a second UCC recurrence in the left middle calyx (#5) that was too large for a conservative endoscopic removal.

Materials and methods

DNA extraction

For molecular analysis, matched normal and tumoral DNA were extracted from microdissected paraffin-embedded blocks using the DNeasy Tissue Kit (Qiagen GmbH, Germany). Renal parenchyma or lamina muscularis propria of the ureter without tumor infiltration were used as normal tissue. Sections from each paraffin block were stained to select the tumor site containing the largest amount of tumor tissue (>80% of tumor tissue) that was further microdissected.

MSI analysis and genetic analysis

The MSI status of the tumors was established using the new pentaplex PCR recommended by the National Cancer Institute including five quasimonomorphic mononucleotide repeats: BAT-25, BAT-26, NR-21, NR-24, and NR-27 [1, 14, 15]. PCR products were run in a capillary array on the ABI PRISM 3100 genetic analyzer and the fragment sizes analyzed using the GeneScan 3.1 software (Applied Biosystems). The tumors were classified as MSI if three or more markers showed instability, and MSS (microsatellite stable) if none did. The coding exons of the *MSH2* gene were amplified by PCR and analyzed by single strand conformation polymorphism; exons displaying abnormal profiles were sequenced by PCR amplification with intronic flanking primers.

Mutation analysis of target genes

Tumor DNA and their normal counterpart were analyzed for frameshift mutations in 13 selected mononucleotide repeats located within coding sequences, except for MRE11, whose T11 tract is located at a splicing site. Shortening of the MRE11(T)11 tract impairs the correct splicing process leading to significant decrease in the MRE11 protein level [5]. The regions encompassing the repeated sequences were amplified and analyzed as already reported [8]. The presence of frameshift mutations is based on peak pattern alterations compared with the reference peak size and pattern established for the normal counterpart.

Immunohistochemical analysis of mismatch repair protein expression

Immunohistochemical stainings were performed on formalin-fixed paraffin-embedded sections after antigen retrieval using microwave or pressure cooking at pH 6. The mouse monoclonal antibodies were raised against MLH1 (G168-728, 1:70, BD PharMingen, San Diego, CA, USA), MSH2 (FE11, 1:100, Calbiochem, Darmstadt, Germany), and MSH6 (clone 44, 1:100, Becton Dickinson, Lexington, MA, USA). The immunoreactivity was revealed using biotinylated anti-mouse secondary antibody followed by incubation with a final layer of peroxidase labeled streptavidin (Super Sensitive Detection kit, Biogenex, San Ramon, CA, USA).

Results and discussion

Histological findings

Macroscopic examination of the left nephro-ureterectomy specimen revealed a mass measuring 3×2×4.5 cm in the middle calyx (#5). This tumor appeared to invade the peripelvic fat. Furthermore, in the subcapsular and middle part of the renal parenchyma, a renal cyst measuring 1 cm was identified (#6). Microscopically, the mass of the calix (#5) was an invasive UCC with a histological grade of 3 according to the World Health Organization classification, invading the peripelvic fat (pT3). The tumor showed

Table 1 Description of several tumors arising in the HNPCC patient

Tumors	Age (years)	Location	Histological type	Stage	MSI status	Immunohistochemistry
#1	32	Left ureter	UCC	pTa	ND	MSH2−, MSH6−
#2	48	Endocervix	Adenocarcinoma	pT1b	MSI	MSH2−, MSH6−
#3	54	Left ureter (first recurrence)	UCC recurrence	pTa	MSI	ND
#4	56	Colon	Adenocarcinoma	pT3	MSI	MSH2−, MSH6−
#5	61	Left middle calix (second recurrence)	UCC recurrence	pT3	MSI	MSH2−, MSH6−
#6	61	Renal	Papillary renal carcinomas	PT1a	MSS	MSH2+, MSH6+

ND Not determined, *MSI* microsatellite instability, *MSS* microsatellite stable, *UCC* urothelial cell carcinoma

malignant urothelial cells with hyperchromasia and a high mitotic activity (23 mitosis per 10 high-power fields), and evidence of lymphatic invasion. The renal cyst (#6) was a type-2 tubulopapillary renal carcinoma (Furhman grade II nuclear features). The tumor size was 1 cm and was limited to the renal parenchyma without extracapsular extension. The regional lymph node (n=1) and the surgical margins were tumor-free.

Molecular and immunohistochemical findings

Among the six tumors collected from this HNPCC patient, five were analyzed for MSI; one tumor (#1) was fixed in Bouin solution rendering it unsuitable for molecular analysis (Table 1). The endocervical adenocarcinoma (#2), the UUT UCC (#3 and #5), and the colon adenocarcinoma (#4) displayed a widespread MSI in all five markers tested (Fig. 1). The allelic size shifts for the BAT markers were smaller for the first UUT recurrence (#3) than for the second UUT recurrence (#5). By contrast, the renal papillary carcinoma (#6) was MSS without any instability (Fig. 1).

All six tumors from this HNPCC patient were studied for MMR protein expression. Immunohistochemical staining revealed that the first five MSI tumors displayed loss of MSH2 and MSH6 expression and retained MLH1 expression (Fig. 2). In the tumor fixed in Bouin whose MSI analysis could not be performed (#1), the pattern of expression was similar to the other tumors indicating that this tumor was also MMR-deficient. On the contrary, the tubulopapillary renal carcinoma (#6) showed normal expression of MLH1, MSH2, and MSH6 in accordance with its MSS status.

Sequencing revealed that the patient carried a germline nonsense mutation of the *MSH2* gene within exon 7. This 1165C>T substitution leads to Arg389X, due to the change of CGA Arg codon to a TGA nonsense codon.

We have studied 13 target genes and found somatic frameshift mutations in the two UCC recurrences and in the colon and endocervical carcinoma (Fig. 3). UCC recurrences and colon carcinoma displayed *BAX* and *MRE11* mutations. In the colon carcinoma (#4), mutations in *TCF-4*, *MBD4*, and *RAD50* were also found. In the first UCC recurrence (#3), no other mutation was found while in the second one (#5), additional mutations were found in *TCF-4*, *RAD50*, *MSH6*, *MSH3*, and *DNA-PKcs*. The endocervical carcinoma displayed *BLM* and *ATR* mutations. As expected, no mutation could be found in any of the target genes in the kidney cancer.

Discussion

We report a 61-year-old woman with HNPCC syndrome who presented three different tumors of the HNPCC spectrum, being chronologically UCC, endocervical carcinoma, and colon carcinoma. In addition, she later developed a papillary renal carcinoma. In HNPCC patients, it is very uncommon that UCC occurs as the first tumor in

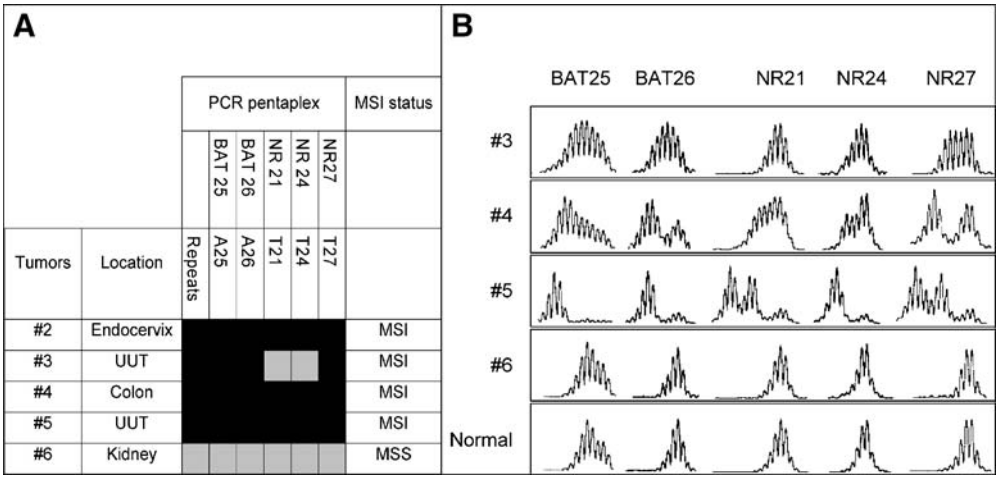

Fig. 1 MSI status in several tumors from an HNPCC patient using the PCR pentaplex of five quasimonomorphic markers. The regions encompassing the repeated sequences were amplified by PCR using fluorescent primers and migrated on an ABI3100 genetic analyzer (Applied Biosystems). **a** Frameshift mutations are scored as present (*black*), absent (*gray*), or not determined (*white*). **b** The profiles were analyzed using the GeneScan 3.2 software

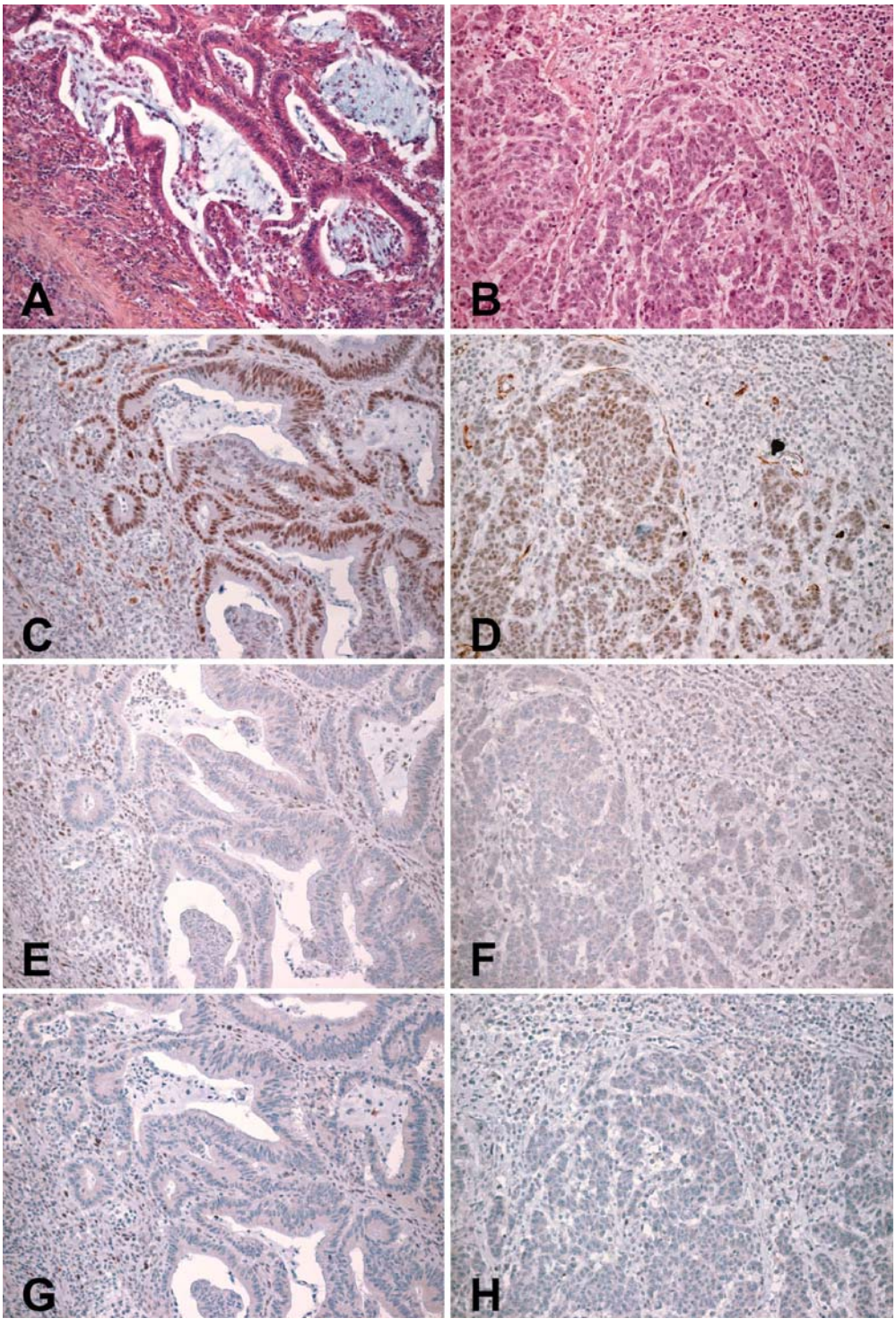

Fig. 2 Histological features and immunohistochemical analysis of both UUT (**b**, **d**, **f**, and **h**) and colon carcinomas (**a**, **c**, **e**, and **g**) (original magnification ×200). **a**, **b** Hematoxylin and eosin; **c**, **d** anti-MLH1. Note the nuclear staining of the malignant cells in both tumors; **e**, **f** anti-MSH2. Absence of MSH2 expression in tumor cells; **g**, **h** anti-MSH6. Absence of MSH6 expression in tumor cells

medical history, but this fact may be explained by the relatively low incidence of UCC in HNPCC patients which has been estimated as 10% [13]. We demonstrate that the four HNPCC-related cancers displayed an MSI phenotype and loss of MSH2/MSH6 expression, in keeping with the presence of a *MSH2* germline mutation in this patient. Yet, concomitant extinction of MSH2 and MSH6 expression is common because the absence of MSH2 leads to degradation of the partnerless MSH6 while the reverse is not true. Previous studies demonstrated loss of immunostaining for at least one of the MMR proteins, mostly MLH1 or MSH2, in about 80% of MSI UUT carcinomas [2, 4, 6, 11]. Loss of MSH2 expression has been reported in 33 to 60% of MSI UUT tumors, while isolated loss of MSH6 has rarely been described [4, 6].

MSI tumor progression is thought to result from the accumulation of somatic frameshift mutations within various genes involved in key cellular pathways [3]. It is

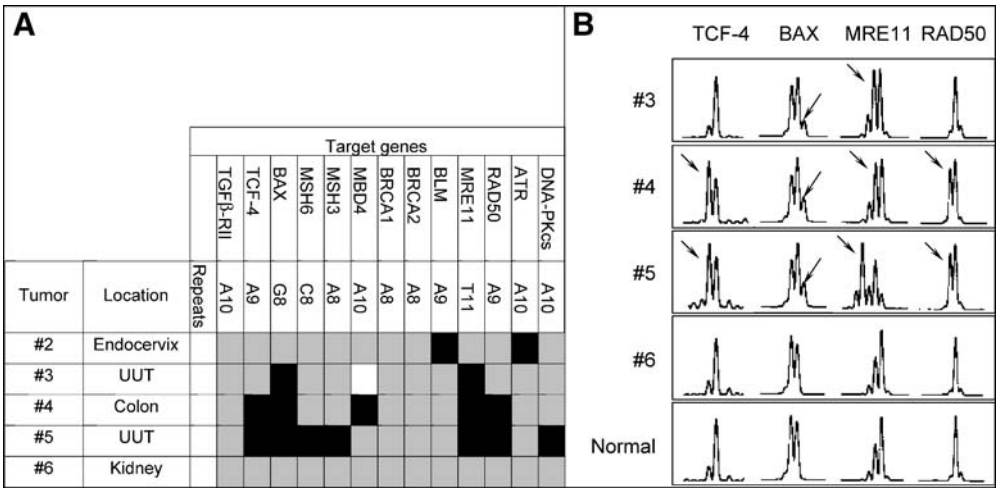

Fig. 3 MSI-driven target gene mutations in several tumors from an HNPCC patient. The regions encompassing the repeated sequences were amplified by PCR using fluorescent primers and migrated on an ABI3100 genetic analyzer (Applied Biosystems). **a** Frameshift mutations are scored as present (*black*), absent (gray), or not determined (*white*). **b** The profiles were analyzed using the GeneScan 3.1 software. The mutated allele is indicated by an *arrow*

interesting to note that the pattern of target gene mutations differs between gastrointestinal and endometrial tumors, indicating that the selection of mutations is a tissue-specific process [3]. Little is known regarding the possible target genes in MSI UUT [6, 9]. In our patient, mutations in *BAX* and *MRE11* are shared by the UUT and the colon carcinomas. Frameshift mutations in the proapoptotic *BAX* gene arise in half MSI colorectal cancers and one-fourth MSI UUT carcinomas [3, 6]. MRE11, a key element in the control of genomic stability, is frequently inactivated in MSI gastrointestinal carcinomas [5]. In our study, it is interesting to note that *BAX* and *MRE11* mutations were already present in the first recurrence of the UUT carcinoma suggesting that it is probably an early event in UUT tumor progression. As already reported in MSI UUT, we have confirmed the presence of mutations in other MMR genes, *MSH6* and *MSH3* [6]. In addition, we describe mutations in genes playing major role in tumor growth and damage signaling in MSI UUT: *MRE11*, *TCF-4*, *RAD50*, *DNA-PKcs*.

To our knowledge, we describe the first occurrence of a papillary renal carcinoma in an HNPCC patient. Papillary renal carcinoma represents 7 to 14% of primary renal cell carcinoma, with most of renal carcinomas being clear cell carcinomas. The age at diagnosis varies from the third to the eighth decade of life with a peak incidence in the sixth and seventh decades. Although renal carcinomas are not considered to belong to the HNPCC spectrum, some clear cell kidney cancers have been described in HNPCC families, occurring at a frequency identical to that of the general population. The renal papillary tumor arising in this HNPCC patient was MSS, did not display any target gene mutation, and showed normal MMR protein expression. Papillary renal carcinoma occurs rarely in a hereditary context at a not-yet-estimated frequency. Mutations in c-Met protooncogene (7q31.1-q34) have been implicated in 80% of type-1 hereditary papillary renal carcinoma and in 13% of the sporadic cases, but other genomic alterations including trisomy 7, 16, and 17, as well as loss of chromosome Y or t (X;1)(p11.2;q21), have been described in early phase of sporadic papillary renal carcinomas [7, 12].

We describe target gene mutations profiles in different tumors arising in an HNPCC patient and provide some evidence that *BAX* and *MRE11* mutations may take place early in MSI UUT tumorigenesis. Our observations further document that the tubulopapillary carcinoma arose independently through a molecular pathway that does not involve MSI.

Acknowledgements Pierre Mongiat-Artus received support from the "Association Française d'Urologie". Catherine Miquel was supported by the "Fondation pour la Recherche Médicale". This research was supported by grants from the "Association pour la Recherche sur le Cancer" (#4683 to F.P.).

References

1. Buhard O, Suraweera N, Lectard A, Duval A, Hamelin R (2004) Quasimonomorphic mononucleotide repeats for high-level microsatellite instability analysis. Dis Markers 20:251–257
2. Catto JW, Azzouzi AR, Amira N, Rehman I, Feeley KM, Cross SS, Fromont G, Sibony M, Hamdy FC, Cussenot O, Meuth M (2003) Distinct patterns of microsatellite instability are seen in tumours of the urinary tract. Oncogene 22:8699–8706
3. Duval A, Hamelin R (2002) Mutations at coding repeat sequences in mismatch repair-deficient human cancers: toward a new concept of target genes for instability. Cancer Res 62:2447–2454
4. Ericson KM, Isinger AP, Isfoss BL, Nilbert MC (2005) Low frequency of defective mismatch repair in a population-based series of upper urothelial carcinoma. BMC Cancer 5:23
5. Giannini G, Ristori E, Cerignoli F, Rinaldi C, Zani M, Viel A, Ottini L, Crescenzi M, Martinotti S, Bignami M, Frati L, Screpanti I, Gulino A (2002) Human MRE11 is inactivated in mismatch repair-deficient cancers. EMBO Rep 3:248–254
6. Hartmann A, Zanardo L, Bocker-Edmonston T, Blaszyk H, Dietmaier W, Stoehr R, Cheville JC, Junker K, Wieland W, Knuechel R, Rueschoff J, Hofstaedter F, Fishel R (2002) Frequent microsatellite instability in sporadic tumors of the upper urinary tract. Cancer Res 62:6796–6802
7. Iliopoulos O, Eng C (2000) Genetic and clinical aspects of familial renal neoplasms. Semin Oncol 27:138–149
8. Jacob S, Miquel C, Sarasin A, Praz F (2005) Effects of camptothecin on double-strand break repair by non-homologous end-joining in DNA mismatch repair-deficient human colorectal cancer cell lines. Nucleic Acids Res 33:106–113

9. Mongiat-Artus P, Miquel C, Van der Aa M, Buhard O, Hamelin R, Soliman H, Bangma C, Janin A, Teillac P, van der Kwast T, Praz F (2006) Microsatellite instability and mutation analysis of candidate genes in urothelial cell carcinomas of upper urinary tract. Oncogene 25:2113–2118
10. Peltomaki P (2001) Deficient DNA mismatch repair: a common etiologic factor for colon cancer. Hum Mol Genet 10:735–740
11. Roupret M, Catto J, Coulet F, Azzouzi AR, Amira N, Karmouni T, Fromont G, Sibony M, Vallancien G, Gattegno B, Meuth M, Hamdy FC, Cussenot O (2004) Microsatellite instability as indicator of MSH2 gene mutation in patients with upper urinary tract transitional cell carcinoma. J Med Genet 41:e91
12. Schmidt L, Junker K, Nakaigawa N, Kinjerski T, Weirich G, Miller M, Lubensky I, Neumann HP, Brauch H, Decker J, Vocke C, Brown JA, Jenkins R, Richard S, Bergerheim U, Gerrard B, Dean M, Linehan WM, Zbar B (1999) Novel mutations of the MET proto-oncogene in papillary renal carcinomas. Oncogene 18:2343–2350
13. Sijmons RH, Kiemeney LA, Witjes JA, Vasen HF (1998) Urinary tract cancer and hereditary nonpolyposis colorectal cancer: risks and screening options. J Urol 160:466–470
14. Suraweera N, Duval A, Reperant M, Vaury C, Furlan D, Leroy K, Seruca R, Iacopetta B, Hamelin R (2002) Evaluation of tumor microsatellite instability using five quasimonomorphic mononucleotide repeats and pentaplex PCR. Gastroenterology 123:1804–1811
15. Umar A, Boland CR, Terdiman JP, Syngal S, de la Chapelle A, Ruschoff J, Fishel R, Lindor NM, Burgart LJ, Hamelin R, Hamilton SR, Hiatt RA, Jass J, Lindblom A, Lynch HT, Peltomaki P, Ramsey SD, Rodriguez-Bigas MA, Vasen HF, Hawk ET, Barrett JC, Freedman AN, Srivastava S (2004) Revised Bethesda Guidelines for hereditary nonpolyposis colorectal cancer (Lynch syndrome) and microsatellite instability. J Natl Cancer Inst 96:261–268

Virchows Arch (2006) 449:244–247
DOI 10.1007/s00428-006-0228-z

CASE REPORT

Extramammary myofibroblastoma is genetically related to spindle cell lipoma

Francesca Maggiani · Maria Debiec-Rychter · Guy Verbeeck · Raf Sciot

Received: 15 March 2006 / Accepted: 25 April 2006 / Published online: 20 May 2006
© Springer-Verlag 2006

Abstract Extramammary-type myofibroblastoma is a rare, benign spindle cell lesion, strictly resembling the breast counterpart, but occurring in extramammary sites, mainly in the inguinal/groin area. In this paper, we describe an extramammary-type myofibroblastoma in the groin of a 37-year-old male patient. The tumor showed a typical morphological and immunophenotypical profile, including staining for both CD34 and desmin. Dual-color interphase florescent in situ hybridization analysis revealed losses of *RB*/13q14 and *FKHR*/13q14 loci within tumor cells. The chromosome 13 rearrangements associated with the loss of the 13q14 chromosomal region are typically seen in spindle cell lipoma, and have been previously recognized in mammary myofibroblastoma, providing strong evidence for a pathogenetic link between these lesions.

Keywords Mammary-type myofibroblastoma · Spindle cell lipoma · Immunohistochemistry · Cytogenetics · Chromosome 13

F. Maggiani · R. Sciot
Department of Morphology and Molecular Pathology,
University Hospital, Catholic University Leuven,
Leuven, Belgium

M. Debiec-Rychter
Human Genetics, University Hospital,
Catholic University Leuven,
Leuven, Belgium

G. Verbeeck
Department of Pathology,
St. Elisabeth Hospital,
Turnhout, Belgium

R. Sciot (✉)
Department of Pathology,
University Hospital St. Rafaël,
Minderbroedersstraat 12,
B-3000 Leuven, Belgium
e-mail: raf.sciot@uz.kuleuven.be

Introduction

Mammary myofibroblastoma is a rare mesenchymal tumor arising in breast soft tissue [12, 13]. Extramammary locations have been described in recent years, and the most common site is the inguinal/groin area, with an apparent predilection for the embryonic milk-line that extends from the axilla to the medial groin [9]. This benign mesenchymal tumor usually arises in elderly male patients or in postmenopausal women, with an age range of 35 to 67 years (median 53 years) similar to its mammary counterpart.

Extramammary myofibroblastoma usually occurs subcutaneously, presenting as a slowly growing, well circumscribed, painless mass measuring between 1 and 4 cm. Lesions larger than 10 cm in diameter have also rarely been reported [1]. The tumor is mainly composed of spindle-shaped cells with myofibroblastic differentiation, embedded in a hyalinized stroma with ropy collagen and containing a variable amount of mature adipose tissue and mast cells. The spindle cell component stains diffusely for CD34 and desmin, in accordance with its myofibroblastic differentiation [6, 8, 10].

Cytogenetic analysis of the mammary counterpart has revealed rearrangements or losses of 13q and 16q, as typically seen in spindle cell lipoma, thus suggesting a link between these two lesions [11]. It is not known whether the extramammary counterpart of myofibroblastoma shows the same chromosomal changes. This prompted us to investigate this rare variant of mammary myofibroblastoma.

Patient

A 37-year-old man presented with a solitary lesion in his groin. The mass was nodular and had a subcutaneous location. The lesion appeared painless, firm, and well circumscribed on physical examination. A complete surgical

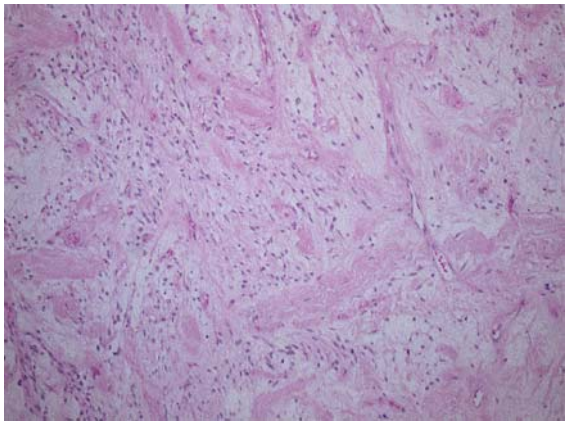

Fig. 1 Fasicles of spindle cells with thick, irregular bands of hyalinized collagen in between

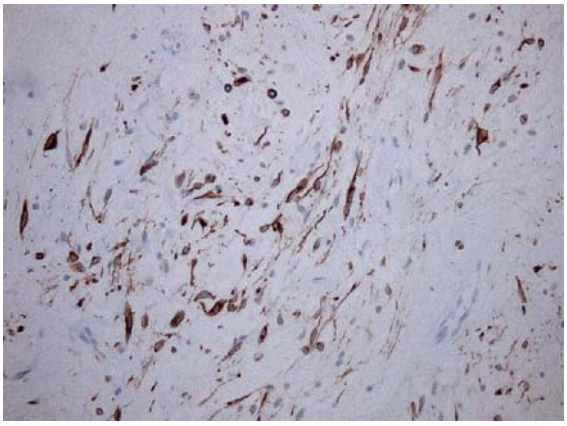

Fig. 3 Desmin staining, with strong spindle cell positivity

excision was performed. No recurrence or other complaints have been reported 10 months following surgery.

Materials and methods

Part of the excised tumor was fixed in 4% formalin, followed by conventional processing and embedding in paraffin wax. Sections were cut and stained with hematoxylin & eosin. Immunohistochemical stainings were also performed for a panel of antibodies using the avidin–biotin peroxidase complex technique. The antibodies used include S-100 protein (polyclonal, DAKO, Glostrup, Denmark; dilution 1:300), alpha smooth muscle actin [monoclonal (mc), DAKO; dilution 1:100], desmin (mc, Biomedicals, Aurora, OH, USA; dilution 1:20), and CD34 (mc, Becton Dickinson, Franklin Lakes, NJ, USA; dilution 1:10).

Dual-color interphase florescent in situ hybridization (FISH) was performed on 5-μm sections of ethanol-fixed paraffin-embedded tumor tissue, as previously described [5]. For the assessment of chromosome 13 loss, directly labeled SpectrumGreen and SpectrumOrange DNA LSI 13q14 (*FKHR*-locus) and LSI 13q14 (*Rb*-locus) (Vysis, Downers Grove, IL, USA) probes, respectively, were cohybridized on one slide. For the control, directly labeled SpectrumGreen chromosome 9 enumeration DNA probe (CEP9; Vysis) was cohybridized with locus specific SpectrumOrange-labeled LSI 9p21 (*p16*-locus) DNA probe (Vysis). The FISH data were collected on a Leica DMRB (Leica, Wetzlar, Germany) fluorescence microscope run by Quips SmartCapture FISH imaging software. For each set of probes, 100 interphase nuclei were evaluated and the percentage of tumor nuclei containing 0–1, 2, or more signals was recorded. A specimen was interpreted as monosomic if only one signal for each respective probe was detected in >40% of the nuclei evaluated (more than three standard deviations above the average false-positive rate observed in control FISH experiments on normal paraffin-embedded tissue).

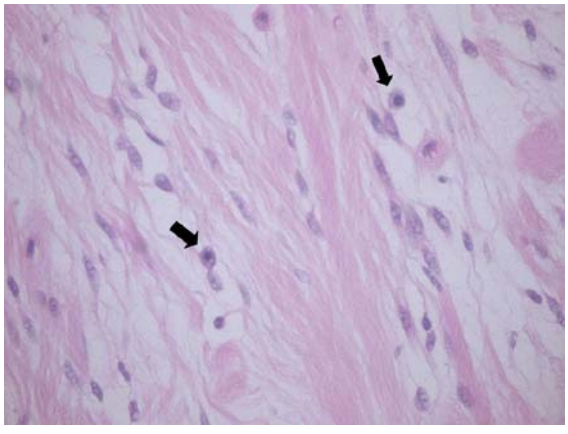

Fig. 2 Bland spindle cells with scattered mast cells (*arrow*)

Results

Histological features

On histology, the lesion consisted of uniform, haphazardly arranged spindle cells with, focally, a vague fascicular pattern. The matrix was loose to prominently collagenized, with thick hyalinized and ropy collagen bands (Fig. 1). Adipocytes were very rare, while mast cells were dispersed throughout the lesion (Fig. 2). The spindle cells showed an eosinophilic cytoplasm with an ill-defined margin and an oval nucleus with one or two distinct nucleoli. There was no significant pleomorphism and no mitoses were observed. Immunohistochemistry showed a diffuse positive for CD34 and desmin in the spindle cells (Fig. 3). No staining was obtained with the other antibodies.

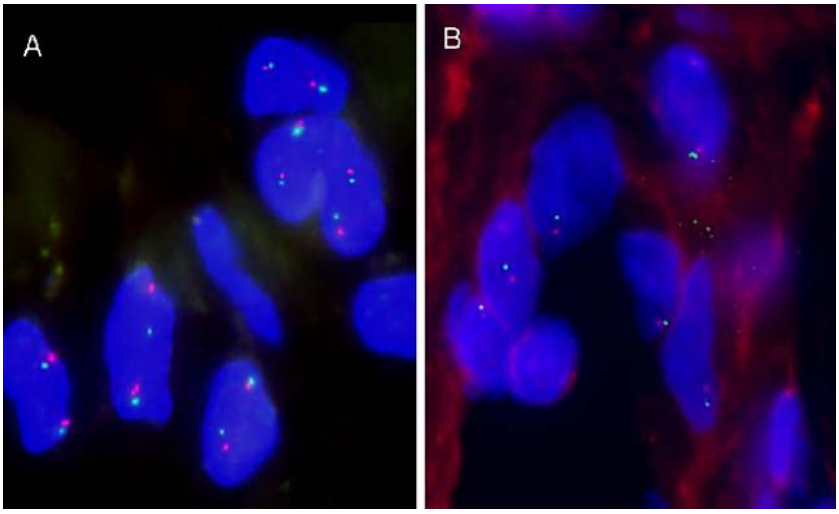

Fig. 4 Representative images of double-color FISH analysis of extramammary myofibroblastoma. Normal (diploid) copy number of chromosome 9 is indicated by the presence of the double red and green signals from centromeric SpectrumGreen-labeled CEP9 and locus specific SpectrumOrange-labeled LSI *p16*/9p21 probes in the majority of tumor nuclei (**a**). Loss of *RB*/13q14 and *FKHR*/13q14 loci as indicated by the presence of single red and green signals from both differentially labeled locus specific probes in the majority of tumor cells (**b**)

FISH studies

By interphase FISH using control chromosome 9 specific probes, the tumor cells revealed normal, biallelic chromosome 9 centromeric and *p16*-locus specific copy number components in 73% of analyzed nuclei (Fig. 4a). In contrast, 87% of nuclei showed only single cohybridized green and red signals using *RB*- and *FKHR*-locus specific probes, indicating the 13q14 loss (Fig. 4b).

Discussion

Spindle cell lipoma and (extra) mammary myofibroblastoma are benign mesenchymal tumors typically occurring in elderly men, with clear predilections of the subcutaneous tissue. In spite of the different typical locations, the lesions share several clinical, morphological, and immunophenotypical features. The tumors have the same clinical indolent behavior: a painless, well-circumscribed, slowly enlarging mass with no evidence of recurrence after surgical removal. Histologically, a close resemblance between (extra) mammary myofibroblastoma and spindle cell lipoma can be easily appreciated [2]. They are both unencapsulated nodular proliferations of bland-looking spindle cells, embedded in a collagenized stroma, with a variable amount of adipocytic mature tissue. Concerning the immunophenotypical profile, the spindle cell component of both lesions typically presents CD34 immunoreactivity. No desmin or smooth muscle actin expression is observed in spindle cell lipoma, while the latter markers are present in myofibroblastoma. This discrepancy could be explained by considering spindle cell lipoma as a proliferation of a stromal precursor cell undergoing a fibroblastic/lipocytic differentiation and (extra) mammary-type myofibroblastoma as the result of a myofibroblastic differentiation of the same uncommitted cell. A similar histogenetic hypothesis, indicating a presumptive mesenchymal CD34+ stem cell capable of fibro-myofibroblastic or lipocytic differentiation, has just been suggested for a group of mesenchymal tumors, including myofibroblastoma, spindle cell lipoma and tumors with hybrid morphological and immunophenotypical features, arising from the mammary stroma [8, 7].

It is well known that spindle cell lipoma, as well as pleomorphic lipoma, show characteristic (total or partial) losses of 13q and/or 16q [4, 3]. We reported similar chromosomal changes in mammary-type myofibroblastoma, which supports a strong relation between these entities [11]. In the present case, FISH analysis revealed an analogous loss of the genetic material from the 13q14 region, as indicated by the monoallelic presence of *RB* and *FKHR* loci in tumor cells. The hitherto unreported presence of 13q14 chromosomal loss in the extramammary type of myofibroblastoma, in combination with immunophenotypical and morphological features, further supports a pathogenetic link between these entities. Although it is clear that additional cases should be examined, this finding underscores that mammary and extramammary myofibroblastomas most likely represent the same entity. In addition, the question of whether these tumors are phenotypic variants of spindle cell lipoma should be seriously taken under consideration.

Acknowledgements This text presents research results of the Belgian program on Interuniversity Poles of Attraction initiated by the Belgian Sate, Prime Minister's Office, Science Policy Programming. The authors of the text assume the scientific responsibility. The authors would like to acknowledge the Cooperation in Scientific and Technical Research (COST) support through the COST ACTION B19 "Molecular cytogenetics of solid tumors" in carrying out this work. The authors would like to thank Belinda Carleer and Venessa Vanspauwen for their excellent technical assistance.

References

1. Ali S, Teichberg S, DeRisi DC (1994) Giant myofibroblastoma of the male breast. Am J Surg Pathol 18:1170–1176
2. Chan K-W, Ghadially FN, Alagaratnam TT (1984) Benign Spindle cell tumor of the breast: a variant of spindle cell lipoma or fibroma of breast. Pathology 16:331–336
3. Dahlen A, Debiec-Rychter M, Pedeutour F, Domanski HA, Hoglund M, Bauer HC, Rydholm A, Sciot R, Mandahl N, Mertens F (2003) Clustering of deletions on chromosome 13 in benign and low-malignant lipomatous tumors. Int J Cancer 103:616–623
4. Dal Cin P, Sciot R, Polito P, Stas M (1997) Lesions of 13q may occur independently of deletion of 16q in spindle cell/pleomorphic lipomas. Histopathology 31:222–225
5. Debiec-Rychter M, Lasota J, Sarlomo-Rikala M, Kordek R, Miettinen M (2001) Chromosomal aberrations in malignant gastrointestinal stromal tumors: correlation with c-KIT gene mutation. Cancer Genet Cytogenet 128:24–30
6. Lee AH, Sworn MJ, Theaker JM (1993) Myofibroblastoma of breast: an immunohistochemical study. Histopathology 22:75–78
7. Magro G, Michal M, Bisceglia M (2001) Benign spindle cell tumors of the mammary stroma: diagnostic criteria, classification, and histogenesis. Pathol Res Pract 197:453–466
8. Magro G, Bisceglia M, Michal M, Eusebi V (2002) Spindle cell lipoma-like tumor, solitary fibrous tumor and myofibroblastoma of the breast: a clinico-pathological analysis of 13 cases in favor of a unifying histogenetic concept. Virchows Arch 440:249–260
9. McMenamin, Fletcher CD (2001) Mammary-type myofibroblastoma of soft tissue: a tumor closely related to spindle cell lipoma. Am J Surg Pathol 25:1022–1029
10. Nucci MR, Fletcher CD (1999) Myofibroblastoma of the breast: a distinctive benign stromal tumor. Pathol Case Rev 4:214–219
11. Pauwels P, Sciot R, Croiset F, Rutten H, Van den Berghe H, Dal Cin P (2001) Myofibroblastoma of the breast: genetic link with spindle cell lipoma. J Pathol 191:282–285
12. Toker C, Tang C-K, Whitely JF (1981) Benign spindle cell breast tumor. Cancer 48:1615–1622
13. Wargotz ES, Weiss SW, Norris HJ (1987) Myofibroblastoma of the breast: sixteen cases of a distinctive benign mesencymal tumor. Am J Surg Pathol 11:493–502

Virchows Arch (2006) 449:248–252
DOI 10.1007/s00428-006-0224-3

CASE REPORT

An unusual case of malignant pilocytic astrocytoma occurring in the eye

Alessandra Canesso · Marina Gardiman · Roberto Salmaso · Rita Alaggio · Vito Ninfo

Received: 18 September 2005 / Accepted: 10 April 2006 / Published online: 20 May 2006
© Springer-Verlag 2006

Abstract Pilocytic astrocytoma is a central nervous system neoplasia that arises during pediatric age. Only few cases have been documented in patients older than 50 years old. It is a low-grade lesion that can rarely undergo malignant changes presenting the histologic features of a high-grade glioma. We report a case of a pilocytic astrocytoma arising in the eyeball of a 53-year-old man affected by glaucoma that underwent malignant evolution.

Keywords Pilocytic astrocytoma · Glioma · Malignant evolution

Introduction

Pilocytic astrocytoma is a low-grade neoplasia of the central nervous system that occurs in pediatric age without any sexual distinction. Some cases have also been detected in young adults and only rarely after fifth decade [14].

It is located more frequently in the cerebellum, where it grows as a quite well-restricted mass, often cystic with mural nodule. Other possible locations are the chiasmatic–hypothalamic region, the optic nerve and, rarely, the cerebral emispheres and the spinal cord.

Its typical imaging shows hypointensive images in T1 sequences and hyperintensive images in T2 sequences with enhancement of the tumoral nodule after administration of contrast material [4].

A. Canesso (✉) · M. Gardiman · R. Salmaso · R. Alaggio · V. Ninfo
Section of Pathology, Department of Oncological and Surgical Sciences, University of Padova,
Via Gabelli 61,
Padova 35100, Italy
e-mail: canalex@hotmail.it

Its clinical course is generally favorable. Even after a subtotal resection, its growth is slow and leptomeningeal spread is rare. Some cases have been reported, however, in which pilocytic astrocytoma underwent malignant evolution presenting the histologic features of high-grade malignant glioma, including palisading necrosis, vascular proliferation, and mitotic index increase [14].

We report a case of a pilocytic astrocytoma with histologic features of malignancy occurring in the eyeball of a 53-year-old man with a clinical history of glaucoma.

Case report

Clinical history

A 53-year-old man underwent an enucleation and an endoprosthesis implant for a glaucoma of the right eye.

He had undergone a surgical operation for a congenital cataract when he was 6 years old and another one for glaucoma at the age of 45.

There are no previous tumor diagnosis

Surgical specimen showed deformed eyeball with diffuse increased consistency and scleral darkening; crystalline lens was entirely embebbed in a relatively friable yellowish mass. On cut surface, the tumor occupied the whole posterior chamber of the eye replacing the vitreous body and infiltrating the optic nerve and the iris that appeared pale.

No preoperative RMN of the facial bones was carried out, while postoperative RMN, with and without administration of contrast material, revealed that the extrinsic muscle structures and part of the optic nerve were normal and there

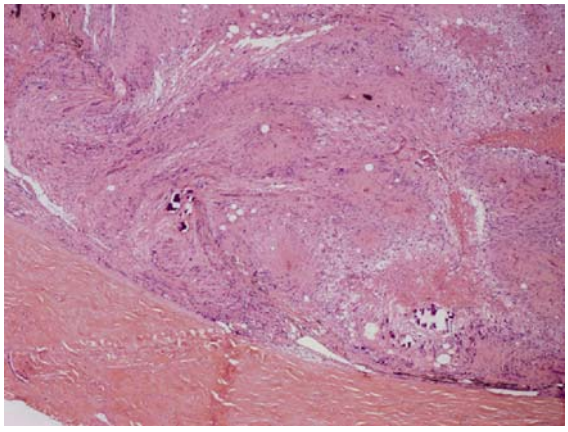

Fig. 1 Tumor shows a typical area of pilocytic astrocytoma (*on the left*) composed of spindle cells arranged in fascicles with calcifications associated with foci of necrosis with pseudopalisading (*on the upper right*). H&E, 3×

were no signs of chiasma alteration. Sixteen months after the operation, the patient is alive and free of disease.

Methods

The material obtained from the eyeball was fixed in formalin, embedded in paraffin and stained with hematoxylin and eosin using standard methods. The following immunohistochemical stainings were performed: MIB-1 (Neomarkers, dilution 1:20), glial fibrillary acidic protein (GFAP) (Novocastra, dilution 1:100), S100 protein (Neomarkers, dilution 1:1,200), HMB-45 (Novocastra, dilution 1:60), AE1/AE3 (Neomarkers, dilution 1:500), and p53 (Novocastra, dilution 1:100).

Results

Microscopically, the lesion showed different areas: typical features of pilocytic astrocytoma associated with foci of necrosis with pseudopalisading (Fig. 1). Areas of pilocityc astrocytoma were focally evident and characterized by the classic byfasic pattern formed by compact piloid tissue intermingled with calcification and microcysts (Fig. 2a). Rosenthal fibers were prominent in solid areas, whereas granular bodies were easily detected in the cystic component (Fig. 2b).

Most of the tumor was composed by highly cellular areas of spindle cells with oval hyperchromatic and pleomorphic nuclei; in this areas, more than one mitosis/10 HPF were detected (average two mitosis/10 HPF) as well as vascular proliferation and necrosis with pseudopalisading (Fig. 3). Vascular proliferation was characterized by medium-sized vascular channels with multilayered endothelial cells around foci of necrosis. Typical glomeruloid vasculature of pylocitic astrocytoma was not present.

The immunohistochemical stainings showed a strong and diffuse positivity for S-100 protein, GFAP, and p53 especially in the compact fibrillar areas (Figs. 4 and 5). Mib-1 highlighted the different proliferative rate in the area of classic pilocytic astrocytoma (6.97%) and in area of malignant transformation (19.52%) (evaluation with Roche Image Analysis System) (Fig. 4).

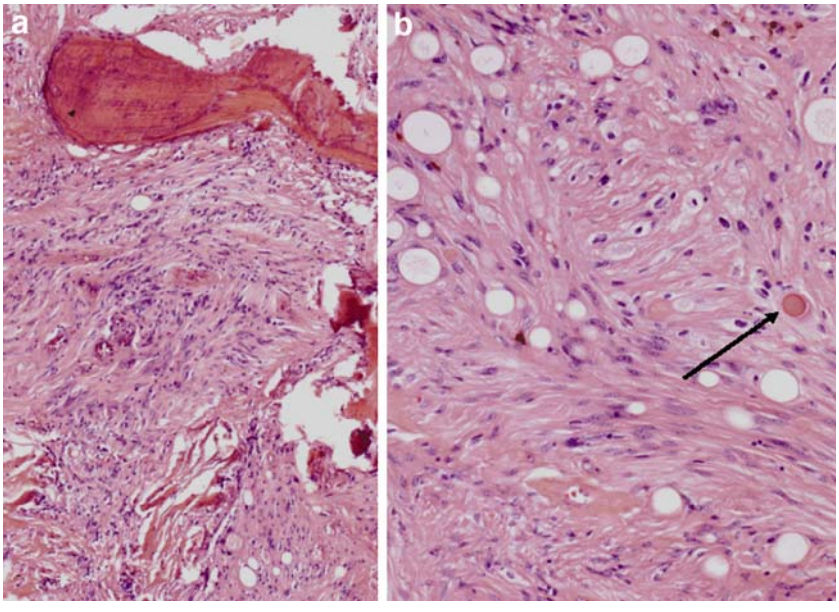

Fig. 2 Typical features of pilocytic astrocytoma: calcification (**a**) and microcystic areas with granular bodies (*arrow*, **b**). H&E, 12×; 15×

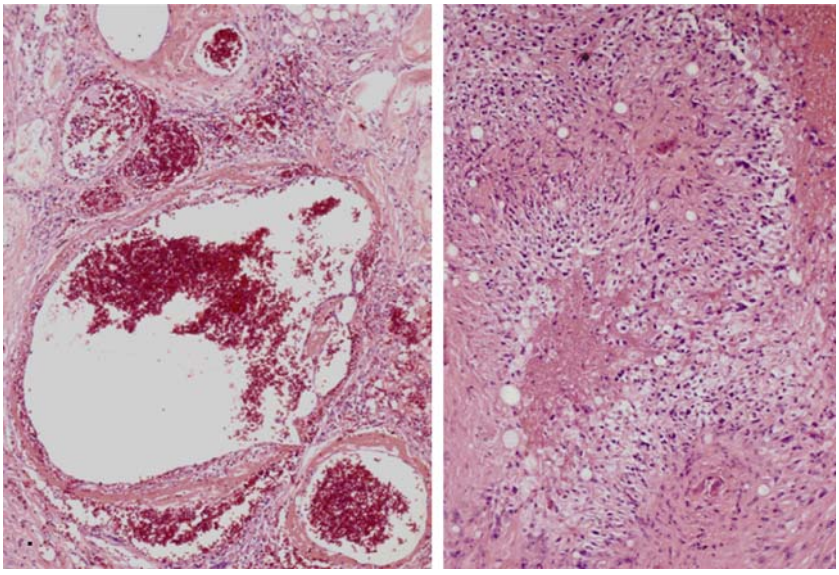

Fig. 3 Areas of necrosis with peripheral palisading mimicking glioblastoma multiforme (*right*) and rich vascular proliferation (*left*). H&E, 12×

Cytokeratins and HMB-45 were negative. Our final diagnosis was pilocytic astrocytoma with malignant transformation.

Discussion

A wide range of neoplasia occur in the orbit such as soft tissue tumor, lymphoid tumor, metastatic tumor, glioma, and meningioma.

Soft tissue tumor are infrequent; the list includes fibrous histiocytoma (the most commonly diagnosed mesenchymal lesion at this anatomic site) hemangioma, hemangiopericytoma and solitary fibrous tumor, giant cell angiofibroma, rhabdomyosarcoma, particularly in childhood, and a variety of soft tissue lesions [5, 10].

Lymphoid tumors generally develop in the course of a previously recognized non-Hodgkin's malignant lymphoma or leukemia [10]. Direct spread from adjacent structures can occur with primary intraocular tumors such as retinoblastoma or

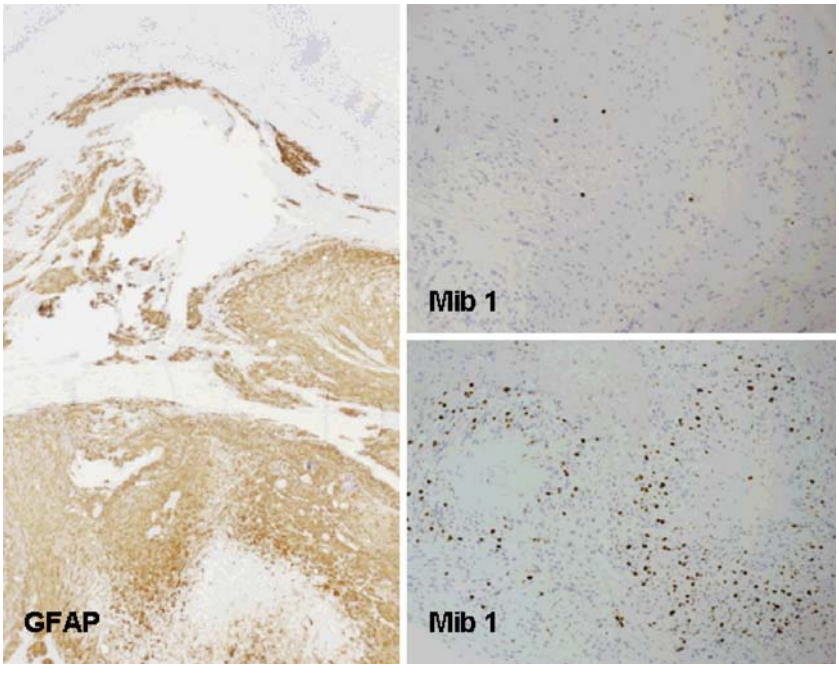

Fig. 4 Strong and diffuse positivity for GFAP (*left*). Mib 1 staining highlights the different proliferative rate in the area of classical pilocytic astrocytoma (*upper right*) and in area of malignant transformation (*down*) (6×; 25×)

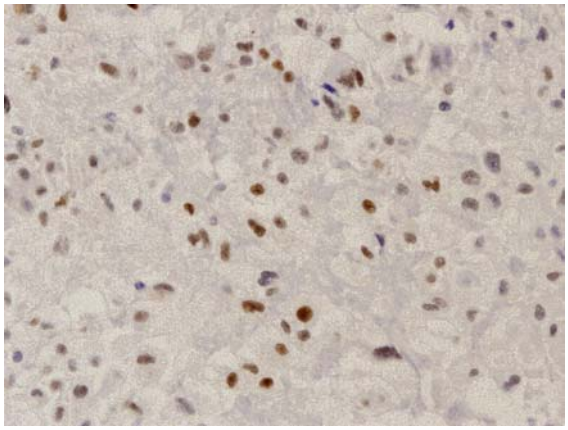

Fig. 5 Positivity for p53 in compact fibrillar areas (40×)

uveal malignant melanoma. Hematogenous metastases to the orbit may be seen: carcinoma of the breast, bronchus, kidney or prostate in adults, and neuroblastoma in children [10].

Most optic gliomas are low grade pilocytic astrocytoma [8]. Typically make their presence with minimal exophtalmos, optic nerve atrophy or papilledema. Generally, these tumors can be adequately managed by surgical [10].

Pilocytic astrocytoma is a slowly growing neoplasia defined a low-grade malignancy in WHO classification [14] characterized by rare leptomeningeal spread and recurrences after an incomplete resection. Transformation into high-grade astrocytoma is even a rarer occurrence. Only few cases of cerebellar [1–3, 7, 12] and chiasmatic–hypothalamic [6, 9, 15] pilocytic astrocytomas had recurrences within 4 to 48 years after the original diagnosis manifesting the histologic features and the clinical behavior of glioblastoma multiforme or anaplastic astrocytoma.

All initial lesions occurred during pediatric age and were treated by surgical excision and/or radiation therapy. The histologic examination showed neoplasias with the typical features of pilocytic astrocytoma, e.g., solid areas alternating with microcystic areas, spindle-shaped monomorphous cells, eosinophilic granular bodies, and Rosenthal fibers.

Recurrent lesions occurred in the same locations as the initial ones, except one reported by Yukitaka et al. [13], but their morphological features only partly reminded those of a low-grade astrocytoma [15]; this was due to their high-cellular polymorphism, endothelial proliferation, brisk mitotic index, and palisading necrosis. Only one case showed areas formed by small cells mixed with others typical features of pilocytic astrocytoma, which were considered as anaplastic astrocytoma [9].

In most cases, the authors linked the malignant evolution of the low-grade initial lesions to radiation therapy that can be also involved in the development of some other types of tumors such as meningiomas, astrocytomas, and fibrosarcomas [12]; on the other hand, malignant evolution seems almost unlikely in patients who did not receive any radiation therapy.

The case described herein can be included in those reported by literature because it shows the features of pilocytic astrocytoma, such as the typical cellularity located in some areas of the neoplasia, eosinophile granular bodies, Rosenthal fibers, and calcification as well as palisading necrosis, vascular endothelial proliferation, and nuclear abnormalities.

These last morphological findings are in favor of the diagnosis of malignancy. Vascular proliferation is common in pilocytic astrocytoma and numerous eosinophilic hyaline droplets were described in glioblastoma multiforme [11].

In our case, vascular proliferation was characterized by medium-sized vascular channels with multilayered endothelial cells around foci of necrosis. Typical glomeruloid vasculature of pylocitic astrocytoma was not present.

Eosinophilic granular bodies are an important diagnostic feature of several neoplasms including ganglion cell tumors, pleomorphic xanthoastrocytoma, and pilocytic astrocytoma [14]. Sasaki et al. [11] reported a case of glioblastoma multiforme with unusual histological features in a 79-year-old woman. In the tumor, there were marked nuclear atypism, frequent mitotic figures, small areas of necrosis with pseudopalisading, microvascular proliferation, and numerous eosinophilic round bodies within the cytoplasm of large neoplastic cells. Nevertheless, there are no areas of low-grade astrocytoma.

For these reasons, we concluded for a diagnosis of malignant pilocytic astrocytoma and not for glioblastoma multiforme despite the presence of vascular proliferation and presence of eosinophile granular bodies.

The difference from the cases reported by literature lies in the fact that neoplasia underwent malignant evolution even though this was not induced by typical factors such as radiation therapy.

We can hypothesize that the only symptom was treated by surgery but not the growing neoplastic mass that was overlooked and remained in the eyeball. Longstanding tumor mass with an inadequate treatment can have induced malignant transformation in an otherwise typical pilocytic astrocytoma.

In conclusion, if this kind of low-grade lesions are not diagnosed because their locations allow them to grow without manifesting clear symptoms, in time, they can undergo malignant transformation even in absence of an history of radiation therapy.

Acknowledgement Special thanks to Ms. Elena Leonardi for the linguistic revision of this text.

References

1. Alpers CE, Davis RL, Wilson CB (1982) Persistence and late malignant transformation of childhood cerebellar astrocytoma. Case report. J Neurosurg 57:548–551
2. Bernell WR, Kepes JJ, Seitz EP (1972) Late malignant recurrence of childhood cerebellar astrocytoma. Report of two cases. J Neurosurg 37:470–474

3. Budka H (1975) Partially resected and irradiated cerebellar astrocytoma of childhood: malignant evolution after 28 years. Acta Neurochir (Wien) 32(1–2):139–146, Abstract
4. Burger PC, Scheithauer BW (ed) (1994) Atlas of tumors pathology: tumors of the central nervous system. Armed Forces Institute of Pathology, Washington, DC, pp 77–96
5. Dei Tos AP, Seregard S, Calonje E et al (1995) Giant cell angiofibroma a distinctive orbital tumor in adults. Am J Surg Pathol 19(11):1286–1293
6. Dirks PB, Jay V, Becker LE et al (1994) Development of anaplastic changes in low grade astrocytomas of childhood. Neurosurgery 34(1):68–78
7. Kleinman GM, Schoene WC, Walshe TM et al (1978) Malignant transformation in benign cerebellar astrocytoma. Case report. J Neurosurg 49:111–118
8. Marquardt MD, Zimmerman LE (1982) Histopathology of meningiomas and gliomas of the optic nerve. Human Pathol 13 (1):226–235
9. Nishio S, Takeshita I, Fukui M et al (1988) Anaplastic evolution of childhood optico-hypothalamic pilocytic astrocytoma: report of an autopsy case. Clin Neuropathol 7(5):254–258
10. Rosai J (2004) Rosai and Ackerman's surgical pathology, vol 2, pp 2725–2730
11. Sasaki A, Yoshida S, Kurihara H et al (2001) Glioblastoma with large numbers of eosinophilic hyaline droplets in neoplastic astrocytes. Clin Neuropathol 20(4):156–162
12. Schwartz AM, Ghatak NR (1990) Malignant transformation of benign cerebellar astrocytoma. Cancer 65:333–336
13. Yukitaka U, Norio A, Toshiki Y et al (1987) Malignant recurrence of childhood cerebellar astrocytoma: case report. Neurosurgery 21 (2):251–255
14. WHO Classification of Tumors (ed) (2000) Pathology and genetic of tumors of the nervous system. IARC Press, Lyon, pp 47–49
15. Wilson WB, Feinsod M, Hoyt WF et al (1976) Malignant evolution of childhood chiasmal pilocytic astrocytoma. Neurology 26:322–325

Virchows Arch (2006) 449:253–257
DOI 10.1007/s00428-006-0226-1

CASE REPORT

Nodular glomeruloid pleuroblastoma: a biphasic pleural-based malignant tumor with immature elements

Pinias Mukonoweshuro · Richard L. Attanoos · Mark E. F. Smith

Received: 23 October 2005 / Accepted: 24 April 2006 / Published online: 1 June 2006
© Springer-Verlag 2006

Abstract An unusual diffuse pleural-based tumor arising in an elderly asbestos-exposed male is presented. The tumor presented in a 72-year-old male with a 30-year history of dockyard work and likely significant asbestos exposure. Macroscopically, at post mortem, the pleural tumor diffusely encased the right lung and was composed of an admixture of neoplastic macro-, and by light microscopy, micro-nodules. Histologically, the tumor had a biphasic growth pattern with glomeruloid epithelioid elements and immature blastematous mesenchymal stroma. Immunophenotypically, the tumor had a complex pattern with epithelioid elements expressing cytokeratins, desmin, carcinoembryonic antigen (CEA), Ber EP4 and E-cadherin. The diagnostic problems and medicolegal issues surrounding the diagnosis and differentiation from malignant pleural mesothelioma and other tumors are discussed.

Keywords Biphasic · Pleura · Glomeruloid · Blastoma

Introduction

Biphasic neoplasms encompass tumors containing an admixture of malignant epithelial and mesenchymal elements, both probably arising from the same progenitor cell. In the pleura, the most common primary biphasic tumor is malignant mesothelioma. Accurate diagnosis of malignant mesothelioma is important for clinical and medicolegal reasons as the tumor is often related to prior occupational asbestos exposure and is compensatable. Other rare primary pleural biphasic tumors such as synovial sarcoma also exist and should be considered in the differential diagnosis. Local pleural extension from peripheral bronchogenic carcinoma is common and when associated with a florid desmoplastic response, may impart a biphasic growth pattern in the pleura. In the thoracic setting, immature blastematous stroma is not a feature of these tumors but may be seen in both pleuro-pulmonary blastoma and pulmonary blastoma, both tumors usually seen in the young.

We describe a diffuse biphasic pleural-based malignant tumor with immature blastematous elements and glomeruloid epithelial structures. To our knowledge, this is the first published report of this tumor type.

P. Mukonoweshuro · M. E. F. Smith (✉)
Department of Histopathology, Level 04, Derriford Hospital,
Derriford Road,
Plymouth PL6 8DH, UK
e-mail: mark.smith@phnt.swest.nhs.uk

R. L. Attanoos
Department of Histopathology, Llandough Hospital,
Penlan Road, Llandough, Penarth, Vale of Glamorgan,
CF64 2XX Wales, UK

Clinical history

A 72-year-old male electrical fitter with a 30-year history of dockyard work that is likely to have been associated with significant occupational asbestos exposure, presented with a short history of breathlessness. Investigation demonstrated a right-sided pleural effusion associated with nodular pleural thickening. Pleural needle core biopsy and cytologic study of the effusion did not reveal evidence of malignancy. However, he later presented with a chest-wall mass, biopsy of which showed a malignant biphasic tumor not typical of malignant mesothelioma. Trial of chemotherapy was attempted but with limited clinical response, followed by some palliative radiotherapy, again with limited response. The patient died of the effects of the pleural tumor at the

Table 1 Antibodies

Antibody	Clone/source	Dilution	Pretreatment
Ber-EP4	Ber-EP4/Dako	1:40	Trypsin, 10 mins
Calretinin	5A5/Vector	1:300	Pressure cooker, 1.5 mins
CD15	MNA/Becton Dickinson	1:40	Microwave, 30 mins
CD31	JC/70A/Dako	1:100	Microwave, 30 mins
CEA	85A12/Skybio	1:2,500	Microwave, 30 mins
Cytokeratin5/6	D5/16B4/Dako	1:1,000	Microwave, 30 mins
Cytokeratin	MNF116/Dako	1:100	Trypsin, 10 mins
Desmin	DE-R-11/ Dako	1:1,200	Microwave, 20 mins
E-Cadherin	NCH-38/Dako	1:200	Microwave, 30 mins
EMA	E29/Dako	1:200	Microwave, 10 mins
Laminin	Polyclonal/Sigma	1:100	Trypsin, 30 mins
Myogenin	F5D/Dako	1:300	Pressure cooker, 1.5 mins
P53	DO-7/Dako	1:1,500	Microwave, 20 mins
S100	Polyclonal/Dako	1:6,000	Trypsin, 10 mins
WT-1	Polyclonal, Dako	1:100	Trypsin, 30 mins

age of 73, 15 months after initial clinical presentation. His past medical history included systemic hypertension and diabetes. A post mortem was performed.

Materials and methods

Postmortem tissues were fixed in 10% formalin and embedded in paraffin. Sections, 3-μm thick, were stained with hematoxylin and eosin. Some of the sections were stained for mucin [alcian blue/diastase periodic acid Schiff (DPAS) stain] and reticulin. Immunohistochemistry was performed using antibodies listed in Table 1. A streptavidin–biotin method (Vectastain Elite, commercial source—Vector laboratories, California) was used to visualize the immunolocalisation.

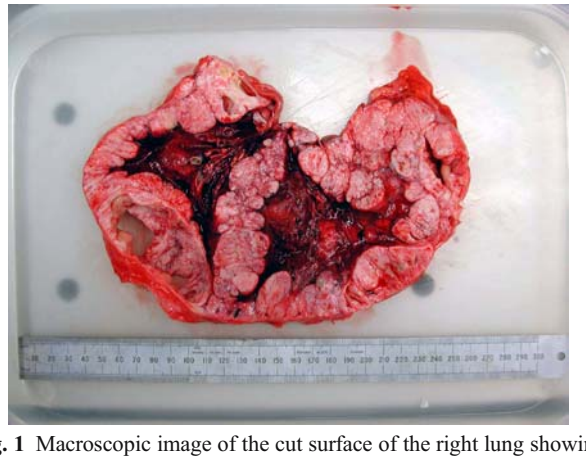

Fig. 1 Macroscopic image of the cut surface of the right lung showing a multi-nodular pleural-based tumor with areas of cystic degeneration

Results

Post mortem examination revealed a right-sided pleural multi-nodular tumor consisting of whitish mucoid tissue with focal areas of necrosis (Fig. 1). The largest macroscopic nodule measured approximately 60 mm in diameter. Several cystic spaces, probably degenerative in origin and up to 70 mm in maximum diameter, were present within the tumor. The right lung with tumor weighed 3,610 g. The left lung weighed 590 g and did not show tumor. A left pleural plaque was identified. No further significant abnormalities were detected. No systemic metastases or other primary tumors were detected.

Histological examination of the tumor showed a complex biphasic multi-nodular pleural tumor (Fig. 2a) with focal necrosis. The microscopic tumor nodules varied from 1 to 14 mm in diameter. Some of the nodules had a pronounced glomeruloid appearance characterised by cystic spaces with a thin lining of malignant epithelium and filled by papillary tufts of epithelium, often with blastematous cores (Fig. 2b). Some of the smaller papillary structures showed hyalinised cores only. The stroma of the nodules was blastematous, characterised by short spindle cells with plump hyperchromatic nuclei and scanty cytoplasm (Fig. 3). In some nodules, the blastematous spindle cell element was dominant, and in some, it appeared to imperceptibly merge with the epithelium. There was focal myxoid change within the stroma, but no specific mesenchymal differentiation was identified. Mitoses were present (0–3/10 high power fields), including abnormal forms, within the epithelial and blastematous elements. A further tumor stromal component consisted of fascicles of tumor spindle cells disposed in a collagenous background between

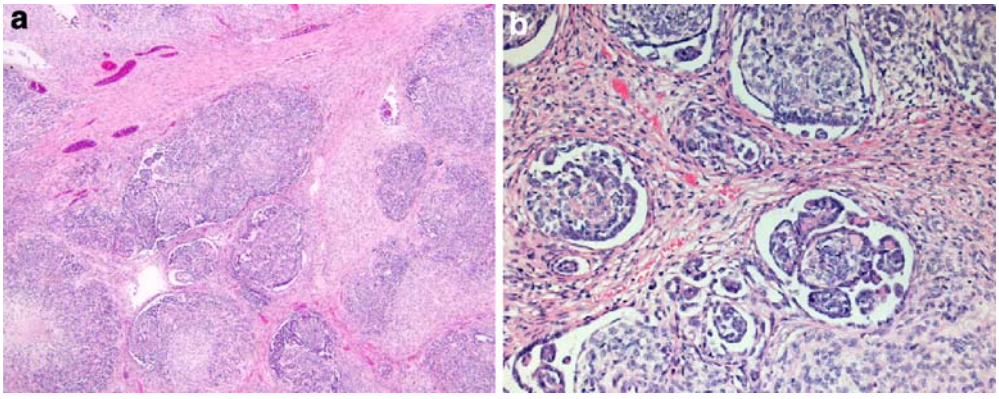

Fig. 2 **a** Low-power view showing a nodular biphasic tumor. (hematoxylin and eosin ×25). **b** Glomeruloid structures with blastematous stroma and hyalinised cores (hematoxylin and eosin ×200)

the tumor nodules. The cells in this component showed elongated, sometimes wavy, mildly pleomorphic nuclei. No rhabdomyoblasts were seen. Asbestos bodies and pulmonary fibrosis were not found in either lung.

Immunohistochemical staining demonstrated strong positive staining for cytokeratins (MNF116) (Fig. 4a) and desmin and focal positive staining for cytokeratin 5/6, in the epithelial component. The desmin-staining pattern showed accentuated basal staining with some dot-like positivity (Fig. 4b). The epithelial component also showed focal positive staining for E-cadherin, Ber-EP4 and carcinoembryonic antigen (CEA). In the spindle cell component, there was focal WT-1 expression. Where the blastematous spindle cell component apparently merged with the epithelial component, there was some positive spindle cell staining for cytokeratin (MNF116) and desmin (Figs. 4a and b), highlighting the transition between these two elements. Elsewhere, the tumor spindle cell component showed negative staining for cytokeratins and desmin. There was positive staining for laminin around epithelial cell groups and in the hyalinised papillary cores of glomeruloid structures. Though the stromal element was generally not associated with laminin, it was identified in those areas where it was suspected that blastematous stroma merged with epithelium.

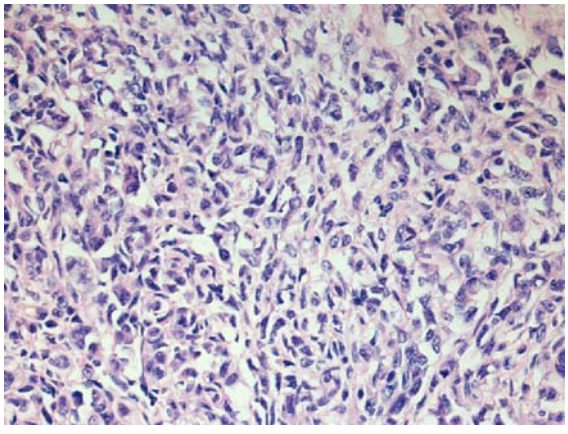

Fig. 3 Blastematous spindle cell stroma (hematoxylin and eosin ×400)

Calretinin, EMA, p53, CD15, CD31, myogenin and S100 were not detected in either the epithelial or spindle cell components. A mucin stain (PAS/diastase) was negative. Abundant reticulin was present between individual spindle cells in the stroma and also delineated epithelial cell groups.

Discussion

Malignant tumors of the pleura can be primary or metastatic. Correct diagnosis, therefore, requires appropriate clinical and radiological information in addition to a thorough histological work-up with immunohistochemistry, and to a lesser extent, ultrastructural studies. Biphasic tumors involving the pleura pose a diagnostic challenge and require careful consideration of a differential diagnosis that includes malignant mesothelioma [7], carcinosarcoma [6, 9], other rare entities such as synovial sarcoma [2], pulmonary blastoma, and in children, pleuro-pulmonary blastoma [1].

The presence of immature elements including a blastematous component and glomeruloid epithelial structures in a pleural-based tumor occurring in an elderly individual is not typical of any tumor known to us including malignant mesothelioma, carcinosarcoma, pleuro-pulmonary blastoma and pulmonary blastoma. The latter two tumors normally arise in children and young adults.

The macroscopic growth pattern of the tumor is an important consideration with respect to diagnosis. Diffuse pleural growth by malignant mesothelioma is typical but not a specific or constant feature. A number of "pseudomesotheliomatous" tumors have been reported with an identical macroscopic growth pattern and these tumors clinically are indistinguishable from malignant mesothelioma. Such tumors often represent peripheral bronchogenic adenocarcinoma (although all histologic types of lung carcinoma may occur). A number of other histogenetic tumor types may show such a similar macroscopic growth pattern including varied malignant sarcomas, thymic epithelial tumors, malignant melanoma, primitive neuroectodermal tumor and varied

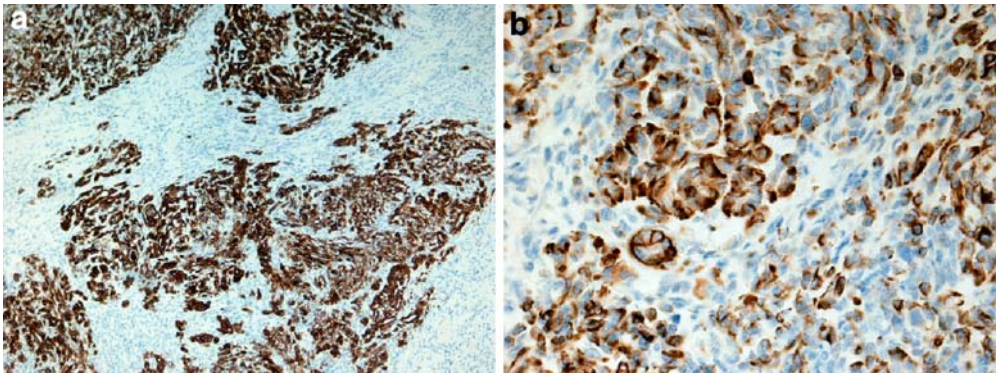

Fig. 4 **a** Immunohistochemistry showing positive staining for cytokeratin (MNF116) in the epithelial component. **b** Immunohistochemistry showing basal, dot-like staining for desmin in the epithelium and blastematous spindle cells

lymphomas. In this case, the tumor showed a diffuse encasement of the lung and was composed of conglomerates of small and large tumor nodules.

The nodular macroscopic appearance and the tumor morphology on light microscopy would be atypical for a diagnosis of malignant mesothelioma. Although it is recognised that the morphologic diversity of malignant mesothelioma is wide, a primitive spindle cell component with blastematous features associated with glomeruloid structures is not a recognised feature of malignant mesothelioma. Such stromal blastematous features are analogous to those seen in paediatric tumors such as Wilms tumor and hepatoblastoma [3].

In the lung and pleura, tumors with somewhat similar morphology are pleuro-pulmonary blastoma and pulmonary blastoma. The pleuro-pulmonary blastoma, however, is mainly a malignant tumor of infancy and childhood. A few case reports describe these tumors in adults [3–5] demonstrating that, although uncommon, adults can occasionally develop primitive neoplasms that are generally associated with the paediatric population. The histology of the pleuro-pulmonary blastoma is characterised by a cystic and/or solid pattern. The cystic component is lined by benign epithelium. The stromal component is primitive in appearance and contains a rhabdomyoblastic element. Malignant epithelial elements have not been identified in this tumor in contrast to the pulmonary blastoma [8]. The classic pulmonary blastoma is a biphasic tumor whose strict definition requires a primitive epithelial component that resembles well-differentiated or high-grade fetal adenocarcinoma set in a primitive blastematous stroma [8]. The epithelial component of the present case falls short of this strict definition, lacking the "fetal" endometrioid glands, and itself, showing curious glomeruloid structures. Biphasic synovial sarcoma of the pleura is recognised, but it does not have glomeruloid structures.

The morphology of the present tumor is not that of biphasic synovial sarcoma. A further possibility is that of primary pulmonary carcinosarcoma with diffuse growth. However, no primary intraparenchymal tumor was identified at necropsy. It is feasible that a carcinosarcoma may show a poorly differentiated stroma but a blastematous stroma is not a recognised feature, and careful search, usually reveals areas of specific mesenchymal differentiation. The epithelial component is most often squamous cell carcinoma followed by adenocarcinoma and large cell carcinoma [8]. None of these diagnostic features were present in the described tumor.

With respect to the tumor immunophenotype, it is of note that the most specific and sensitive mesothelial marker, calretinin, was negative and that epithelial markers CEA, E-cadherin and Ber -EP4, were focally positive. Importantly, this immunophenotype excludes a diagnosis of malignant mesothelioma. The expression of desmin in the epithelial element of a tumor is unusual. However, malignant mesothelioma and desmoplastic small round cell tumor, both tumors associated with serosal surfaces, provide precedents for co-expression of desmin and cytokeratin in their epithelioid elements.

Given the history of occupational asbestos exposure and the presence of a pleural plaque, it is possible that the development of the tumor described in this report may be asbestos-related. However, the occupational history of many further cases will be needed before this tumor's relationship to asbestos exposure can be clarified.

Conclusion

We present an unusual malignant biphasic pleural tumor with immature stromal elements and glomeruloid epithelial structures. We suggest that this is a distinct tumor that pathologists need to be aware of. Especially in asbestos-exposed subjects, distinction from malignant mesothelioma is important. The presence of an occupational history of asbestos exposure may be seen to suggest that the tumor is

asbestos-related but such conclusions are considered premature and further validation is necessary before the recognition of the tumor as of asbestos causation.

References

1. Dehner LP (1994) Pleuropulmonary blastoma is the pulmonary blastoma of childhood. Sem Diagn Pathol 11:144–151
2. Gaertner E, Zeren EH, Fleming MV, Colby TV, Travis WD (1996) Biphasic synovial sarcomas arising in the pleural cavity. A clinicopathologic study of five cases. Am J Surg Pathol 20:36–45
3. Hill DA, Sadeghi S, Schultz MZ, Burr JS, Dehner LP (1999) Pleuropulmonary blastoma in an adult: an initial case report. Cancer 85:2368–2374
4. Kern WH, Stiles QR (1976) Pulmonary blastoma. J Thorac Cardiovasc Surg 72:801–808
5. Koss MN, Hochholzer L, O'Leary T (1991) Pulmonary blastomas. Cancer 67:2368–2381
6. Mayall FG, Gibbs AR (1992) 'Pleural' and pulmonary carcinosarcomas. J Pathol 167:305–311
7. Moran CA, Suster S (2000) Tumors of the lung and pleura. In: Fletcher CDM (ed) Diagnostic histopathology of tumors, vol 1, 2nd edn. Churchill Livingstone, London, pp 183–184
8. Travis WD, Brambilla E, Müller-Hermelink HK, Harris CC (eds) (2004) Tumors of the lung, pleura, thymus and heart. World Health Organization classification of tumors, pathology and genetics. IARC, Lyon, pp 56–57, 99–100, 126–144
9. Zimmerman KG, Sobhonya RE, Payne CM (1981) Histochemical and ultrastructural features of an unusual pulmonary carcinosarcoma. Human Pathol 12:1046–1051

Virchows Arch (2006) 449:258–261
DOI 10.1007/s00428-006-0230-5

CASE REPORT

Extramedullary hematopoiesis mimicking acute appendicitis: a rare complication of idiopathic myelofibrosis

Gülsüm Özlem Elpek · Sevgi Bozova · Gülgün Erdoğan · Kamil Temizkan · Mehmet Öğüş

Received: 16 December 2005 / Revised: 3 March 2006 / Accepted: 2 May 2006 / Published online: 1 June 2006
© Springer-Verlag 2006

Abstract Extramedullary hematopoiesis (EMH) is rarely found in the gastrointestinal tract. To our knowledge, EMH involving the appendix was not described. We report a case with a previous history of idiopathic myelofibrosis, which presented with clinical findings of acute appendicitis that necessitate appendectomy after the relief of his anemia. Microscopic examination and immunohistochemistry revealed foci of EMH throughout the mucosa and the submucosa. In the latter, small clusters of hematopoietic cells were also detected in a few dilated vascular structures. The histopathological features of acute appendicitis were not observed. Our case supports that EMH might develop in organs that are not involved in hematopoiesis. Although in gastrointestinal system, obstruction and bleeding are the most common symptomatic manifestations, this case emphasizes that EMH might also present clinically as acute appendicitis. The absence of histopathological features of acute appendicitis raises the possibility that local production of some mediators from hematopoietic precursor cells might contribute to this clinical presentation.

Keywords Hematopathology · Intestine · Immunohistochemistry

G. Ö. Elpek (✉) · S. Bozova · G. Erdoğan
Department of Pathology, Akdeniz University Medical School, Dekanlık, Antalya 07070, Turkey
e-mail: elpek@akdeniz.edu.tr

K. Temizkan
Department of Haematology, Akdeniz University Medical School, Dekanlık, Antalya 07070, Turkey

M. Öğüş
Department of General Surgery, Akdeniz University Medical School, Dekanlık, Antalya 07070, Turkey

Introduction

Characterized by the development and growth of hematopoietic tissue outside of the bone marrow, extramedullary hematopoiesis (EMH) is an essential process in fetal life. However, its occurrence after birth is considered abnormal and takes place in a number hematological disorders in which the normal function of the bone marrow is disturbed [3, 6]. In these diseases, while organs with hematopoietic capacity like the spleen and liver are most commonly involved, EMH has also occasionally been found in a myriad of other tissues and organs including the bowels [1, 7, 9–12, 14, 16]. Although rare cases of EMH involving the intestines are in records, to our knowledge, EMH involving the appendix was not described.

Reported in this study is a patient with a previous history of idiopathic myelofibrosis, who presented with right iliac fossa pain, nausea, and constipation necessitating urgent laparatomy for clinical diagnosis of acute appendicitis. Histopathological and immunohistochemical evaluation revealed that the cause of this presentation was EMH located at multiple sites throughout the mucosa and the submucosa of the appendix.

Clinical history

A 57-year-old man was admitted to the Department of General Surgery with right-lower abdominal pain, nausea, and constipation. The patient had suffered from idiopathic myelofibrosis since 2003. During the course of his illness, he was treated intermittently with α-interferon. One year before the present admission, he underwent elective splenectomy for relief of anemia and left-sided, upper

quadrant abdominal pain caused by infarcted and enlarged spleen (4,650 g) and histology showed EMH.

Abdominal examination revealed tenderness on the right-iliac fossa with positive McBurney sign and hepatomegaly 2 cm below the costal margin.

Laboratory values included a hemoglobin level of 6.3 g/dl, hematocrit of 18.50%, platelet count 224×10^3, and white blood cell count of 38,000/μl with differential count of 49% segmented neutrophils, 21% band forms, 12% lymphocytes, 2% eosinophils, 9% monocytes, and 7% myelocytes and metamyelocytes. Abdominal ultrasonography revealed no pathology other than a slightly edematous appendix. After the correction of anemia with a blood transfusion, an urgent laparatomy was performed with a preliminary diagnosis of acute appendicitis. At operation, the sole pathology was a slightly edematous appendix that was removed for further evaluation. The gastrointestinal complaints of the patient disappeared soon after the operation. He was managed with α-interferon and until present his condition remains relatively stable.

Materials and methods

Four micrometer thick hematoxylin and eosin (H&E) stained tissue sections from the surgical specimen divided into three segments from tip to base, originally fixed in 10% buffered formalin and embedded in paraffin were prepared for histopathological evaluation.

Immunohistochemical staining was performed by using streptavidin-biotinylated-peroxydase method. Primary antibodies used in the study are as follows: Myeloperoxidase (Dako, polyclonal, dilution: 1/300), glycophorin C (Dako, monoclonal, dilution: 1/50), and CD31 (Dako, monoclonal, dilution: 1/50). For CD31 staining, antigen retrieval by microwave heating (750 W, 4×5 min in citrate buffer 0.01 mol/l, pH 6) was also performed.

Results

Surgical specimen consisted of slightly edematous appendix with 5×0.7×0.8 cm dimensions. On cut surface, the wall thickness was between 0.3–0.4 cm without any luminal obliteration.

Microscopic examination revealed clusters of megakaryocytes, with myeloid and eryhtroid precursors throughout the lamina propria and submucosa. In the latter, lymphatics and blood vessels were found to be dilated. In a few of these vascular structures, hematopoietic cells were also present either in their lumen or as small clusters attached to their wall (Fig. 1).

Immunohistochemical staining for CD31, glycophorin C, and myeloperoxidase confirmed the presence of megakaryocytes, eryhtroid cells, and myeloid cells, respectively (Fig. 1).

Discussion

Gastrointestinal system is an unusual site for EMH and is rarely reported in the medical literature. We could find only seven previously such reported cases with the site of predilection being small bowel (three cases) [8, 10, 11], followed by rectum (two cases) [2, 12] and cecum (one case) [14]. Involvement of the colon, together with small bowel, was also described [1]. In these cases, EMH presented mostly with gastrointestinal bleeding and obstruction. The case presented in this study is the first situation where the EMH presented with right-iliac fossa pain together with nausea and constipation, mimicking acute appendicitis. In contrast to this clinical presentation, the typical histopathological findings of acute appendicitis were not observed. At present, it is not possible to conclude the exact mechanisms that contribute to the clinical presentation of acute appendicitis due to EMH. In our case, no luminal obliteration was detected. Therefore, the characteristic sequence of events starting with luminal obliteration which leads to an impaired blood flow, destruction of local epithelial barrier, bacterial invasion, and subsequently leukocyte infiltration is not an explanation for the clinical presentation of the EMH of the appendix. Recently, it was pointed out that in histologically normal appendices removed at surgery for a diagnosis of acute appendicitis, local production of cytokines, and the release of hyperalgesic mediators (cyclooxygenase metabolites and sympathomimetic amines) might be the cause of the clinical symptoms before the appearance of the typical histopathological features of acute inflammation [15]. In our patient, another possibility, which cannot be excluded is an appendectomy performed too early before the appearance of an inflammatory reaction. For this reason, it is not possible to conclude if EMH was the lesion underlying the clinical picture or simply a “bystander lesion”. However, we suggest that local production of some cytokines and/or hyperalgesic mediators from hematopoietic precursor cells might also contribute to the clinical presentation of the disease.

From the clinical point of view, the present case support that, in patients prone to EMH, presenting with gastrointestinal complaints including acute appendicitis, infiltration of the intestines by EMH should be taken in consideration.

In our case, the precursor cells of myeloid and eryhtroid series are scattered throughout the mucosa, submucosa together with clusters of megakaryocytes in a background of fibrous tissue, without forming a tumoral mass. The fibrotic background especially with megakaryocytes could

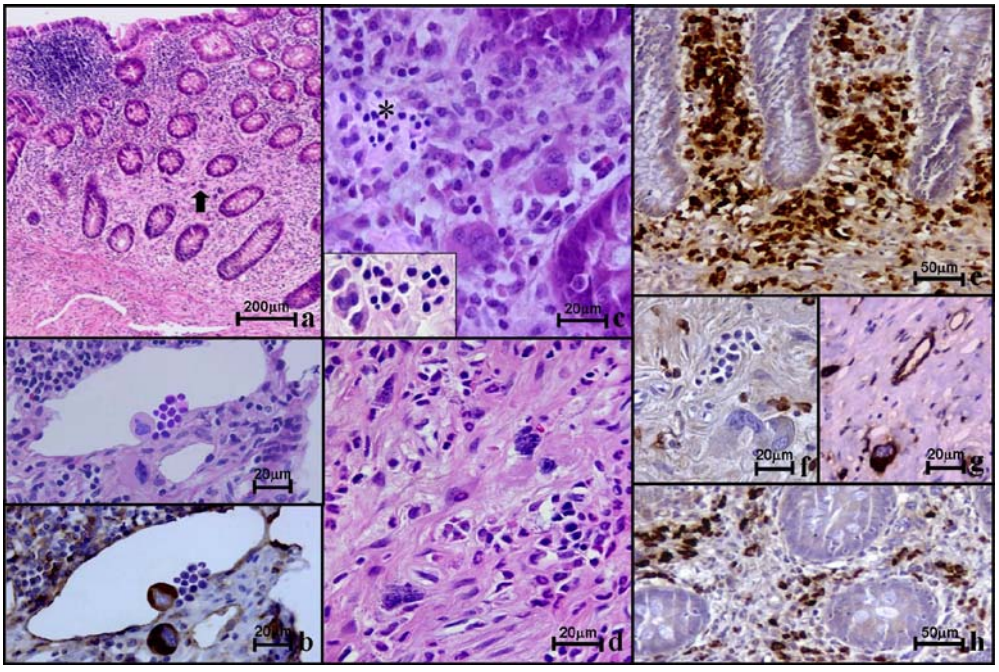

Fig. 1 Foci of EMH in the appendix. **a** Hematopoietic cells are located in the lamina propria and submucosa. Scattered large cells representing megakaryocytes (*large arrow*) may be appreciated even at lower magnifications **b** Intravascular EMH composed of a small cluster of hematopoietic cells which is attached to the vessel wall in the submucosa. CD31 staining highlights megakaryocytes and vascular structures in the same area. **c** and **d** All three lineages of hematopoiesis were present: multinuclear megakaryocytes, the eryhtroid precursors, and the myeloid precursors. *Inset* Higher magnification of area indicated by *asterisk* in **c** demonstrates eryhtroid precursors with small dense nuclei and myeloid precursors with ovoid nuclei. **e** Myeloperoxidase expression in foci of EMH in the lamina propria and submucosa. **f** While myeloid precursors stain positively with myeloperoxidase, eryhtroid precursors and megakaryocytes are negative. **g** CD31 expression by megakaryocytes. **h** Eryhtroid precursors in the lamina propria expressing glycophorin C

be mistaken microscopically for a sarcoma or a carcinoma. However, the presence of maturing hematopoietic precursors of all three myeloid cell lines and our immunohistochemical findings enabled us to distinguish between EMH and other lesions.

Our case had splenic EMH which required splenectomy before the development of EMH in the appendix. Although the exact pathogenesis of EMH is not completely clarified, one theory to explain splenic EMH is "splenic filtration" in which circulating hematopoietic stem cells filtered by this organ, accumulate and establish hematopoiesis [17]. It was suggested that the development of EMH in other organs could be related to the cessation of filtration by the removal of the spleen [2]. Nevertheless, in our case, EMH was located in the appendix, an organ that does not filter the blood. For this reason, the theory is not sufficient to explain the development of EMH in this case.

The myelostimulatory theory, postulating that EMH is the result of the aberrant secretion of an unknown myelostimulatory factor that results in up-regulation of hematopoiesis in the bone marrow and embryonic sites of hematopoiesis, is not an explanation for EMH occurring in appendix because this organ is not an embryonic site of hematopoiesis [5]. In addition, like our patient, EMH could be discovered in organs not to be involved in adult and fetal hematopoiesis.

Recently, "redirected differentiation theory" have been proposed to explain the occurrence of EMH in multiple different organs [2]. According to this hypothesis, unidentified circulating factor(s) induces adult stem cell populations to differentiate into cells of hematopoietic lineage. Indeed, numerous tissues in the body contain stem cell population retaining the capacity to proliferate and differentiate into many different cell types [13]. Although appendix was found to carry c-kit positive stem cells, it was shown that these cells do not give rise to myeloid cells but only basophilic granular cells and extratymic T cells [4].

In our case, hemoglobin value was consistent with an anemic state, supporting the view that EMH is a compensatory phenomenon in response to replacement of bone marrow by fibrosis [18]. Another interesting feature in our case is the presence of hematopoietic cells in the dilated vascular structures of the submucosa. We suggest that the presence of EMH in the appendix might be related to a compensatory phenomenon to the anemic state that allows homing of hematopoietic progenitor cells via vascular structures. However, as in other nonhematopoietic organs, the etiology of EMH of the appendix remains to be

elucidated and further studies are needed to clarify if only one mechanism is sufficient to its development or not.

Acknowledgements The authors thank Dr. Bahar Akkaya from Akdeniz University, Medical School, Department of Pathology for her collaboration in providing recent histopathological data about the presented case. The technical assistance of Mrs. Nuran Keleş and Dr. Gökbay Elpek is gratefully acknowledged.

References

1. Glew RH, Haese WH, McIntyre PA (1973) Myeloid metaplasia with myelofibrosis: the clinical spectrum of extramedullary haematopoiesis and tumor formation. Johns Hopkins Med J 132:253–270
2. Koch CA, Li CY, Mesa RA, Teferi A (2003) Nonhepatosplenic extramedullary hematopoiesis: associated diseases, pathology, clinical course, and treatment. Mayo Clin Proc 78:1223–1233
3. Korsten J, Grossman H, Winchester PH, Canale VC (1970) Extramedullary haematopoiesis in patients with thalassemia anaemia. Radiology 95:257–263
4. Koya T, Honda S, Narita J, Watanabe H, Arakawa M, Abo T (1999) Enrichment of c-kit^{+} Lin^{-} haemopoietic progenitor cells that commit themselves to extratymic T cells in vitro culture of appendix mononuclear cells. Immunology 96:447–456
5. Laszlo J (1975) Myeloproliferative disorders (MPD): myelofibrosis, myelosclerosis, extramedullary hematapoiesis, undifferentiated MPD, and hemorrhagic thrombocythemia. Semin Hematol 12:409–432
6. Lieberman PH, Rosvoli RV, Ley AB (1965) Extramedullary myeloid tumors in primary myelofibrosis. Cancer 139:325–327
7. Lopez-Guillermo A, Cervantes F, Bruguera M, Pereira A, Feliu E, Rozman C (1991) Liver dysfunction following splenectomy in idiopathic myelofibrosis: a study of 10 patients. Acta Haematol 85:184–188
8. MacKinnon S, McNicol AM, Lee FD, McDonald GA (1986) Myelofibrosis complicated intestinal extramedullary haematopoiesis and acute small bowel obstruction. J Clin Pathol 39:677–679
9. Pitcock JA, Renhard EH, Justin BW, Mendelsohn RS (1962) A clinical and pathological study of seventy cases of myelofibrosis. Ann Intern Med 57:73–84
10. Schreibman D, Brenner B, Jacobs R, Ben-Arieh Y, Tatarsky I, Alroy G (1988) Small intestinal myeloid metaplasia. JAMA 259:2580–2582
11. Sharma BK, Pounder RE, Cruse JP, Knowles SE, Lewis AA (1986) Extramedullary haematopoiesis in the small bowel. Gut 27:873–875
12. Solomon D, Goodman H, Jacobs P (1994) Case report: rectal stenosis due to extramedullary haemopoiesis-radiological features. Clin Radiol 49:726–728
13. Spradling A, Drummond-Barbosa D, Kai T (2001) Stem cells find their niche. Nature 414:98–104
14. Sunderland K, Barratt J, Pidcock M (1994) Extramedullary hemopoiesis arising in the gut mimicking carcinoma of the cecum. Pathology 26:62–64
15. Wang Y, Reen DJ, Puri P (1996) Is a histologically normal appendix following emergency appendicectomy always normal? Lancet 347:1076–1079
16. Wilkins BS, Green A, Wild AE, Jones DB (1994) Extramedullary haemopoiesis in fetal and adult human spleen: a quantitative immunohistological study. Histopathology 24:241–247
17. Wolf BC, Neiman RS (1987) Hypothesis: splenic filtration and the pathogenesis of extramedullary hematopoiesis in agnogenic myeloid metaplasia. Hematol Pathol 1:77–80
18. Wyatt JP, Sommers SJ (1950) Chronic marrow failure, myelosclerosis and extramedullary hematopoiesis. Blood 5:329–347

Virchows Arch (2006) 449:262–267
DOI 10.1007/s00428-006-0234-1

CASE REPORT

Diagnosis of primary esophageal synovial sarcoma by demonstration of t(X;18) translocation: a case report

Catherine Butori · Véronique Hofman · Rita Attias · Jerôme Mouroux · Florence Pedeutour · Paul Hofman

Received: 13 March 2006 / Accepted: 12 May 2006 / Published online: 21 June 2006
© Springer-Verlag 2006

Abstract Synovial sarcoma (SS) is an uncommon soft tissue tumor occurring mainly in the periarticular region of the extremities of young adults. In this report, we describe a very rare occurrence of primary SS of the esophagus in a 72-year-old woman. Histologically, the tumor demonstrated biphasic morphologic findings associated with poorly differentiated areas. Tumor cells expressed vimentin, epithelial (EMA, CK7, AE1/3), bcl-2 and neuroectodermal (CD56, CD57, CD99) antigens. Differential diagnose included esophageal sarcomatoid carcinoma. Cytogenetic analysis confirmed the diagnosis of SS by identifying t(X;18) translocation. The literature of this very uncommon entity of the esophagus is reviewed.

Keywords Oesophagus · Sarcoma · Cytogenetic · Fluorescence in situ hybridization · Sarcomatoid carcinoma

C. Butori · V. Hofman · P. Hofman (✉)
Laboratory of Clinical and Experimental Pathology
and Human Tissue Biobank Unit, 30 Avenue de la Voie Romaine,
Louis Pasteur Hospital,
06002 Nice, France
email: hofman.p@chu-nice.fr

R. Attias · F. Pedeutour
Laboratory of Solid Tumors Genetics,
Centre Hospitalier Universitaire de Nice and CNRS UMR 6543,
Faculté de Medecine,
Nice, France

J. Mouroux
Department of Thoracic Surgery, 30 Avenue de la Voie Romaine,
Louis Pasteur Hospital,
06002 Nice, France

Synovial sarcoma (SS) is a malignant mesenchymal tumor of uncertain histogenesis, involving the soft tissue of the extremities, and less frequently the head and neck, mediastinum, lungs, pleura, heart, mesentery and retroperitoneum [6, 21]. SS of the digestive tract is an exceptional tumor. To our knowledge, nine cases have been previously reported, eight occurring in the esophagus [1–5, 7, 17, 18] and one in the gastric antrum [3]. The histological, immunohistochemical, and ultrastructural features of these digestive tumors usually support the diagnosis of SS [1–5, 7, 17, 18, 21]. However, these different criteria for diagnosis are not specific of SS and can be demonstrated in other malignant tumors. Particularly in the esophageal location, these different features can be observed both in SS and in sarcomatoid carcinoma (carcinosarcoma) [3, 11, 13, 16]. The recognition of SS in this unexpected site is probably often mistaken. Cytogenetic approach with fluorescence in situ hybridization (FISH) showing t(X;18) translocation in SS is then crucial for allowing the diagnosis [21]. We report a case of primary SS of the esophagus, for which the diagnosis suspected histologically was made by cytogenetic studies.

Report of a case

The patient was a 72-year-old woman who presented with dysphagia for 6 months already, without weight loss and other symptoms. Physical examination showed no masses in the abdomen, the chest or extremities. An upper gastrointestinal endoscopy showed a partially obstructing 11-cm polypoid mass in the middle and distal esophagus, with a nonulcerating overlying mucosa. The gastroesophageal junction was normal. Computed tomographic scan of

the chest showed a well-circumscribed large mass measuring 112×55 mm (Fig. 1a,b) that was inseparable from the left wall of the esophagus. An incisional biopsy showed a mitotic spindle cell proliferation with some neoplastic epithelial cells resembling a sarcomatoid carcinoma. The patient underwent a transhiatal total esophagectomy with gastric pull-up through the posterior mediastinum and cervical esophagogastric anastomosis. First histologic examination showed a biphasic proliferation compatible with a sarcomatoid carcinoma or more probably with a SS. Immunohistochemical and cytogenetical studies confirmed the diagnosis of SS. The patient was discharged on the 28th postoperative day and was scheduled to receive high-dose ifosfamide. There was no recurrence of the disease 6 months after the surgery.

Materials and methods

Histological and immunohistological studies

For histologic analysis, representative sections were taken from the tumor, fixed in 10% formaldehyde and processed to paraffin blocks. Four-micrometer sections of the paraffin blocks were stained with hematoxylin-eosin-safran (HES). Immunohistochemical stains for epithelial membrane antigen (EMA; Dako Corporation, Carpinteria, CA, USA; 1:60), vimentin (Dako; 1:200), cytokeratins CK7 (Dako; 1:40), CK20 (Dako; 1:50), AE1/3 (Dako; 1:50), bcl-2 (Dako; 1:50), CD99 (Dako; 1:50), muscle actin (HHF-35, Dako; 1:50), desmin (Dako; 1:50), S-100 (Immunotech, Luminy, France; 1:50), HMB45 (Immunotech, Luminy,

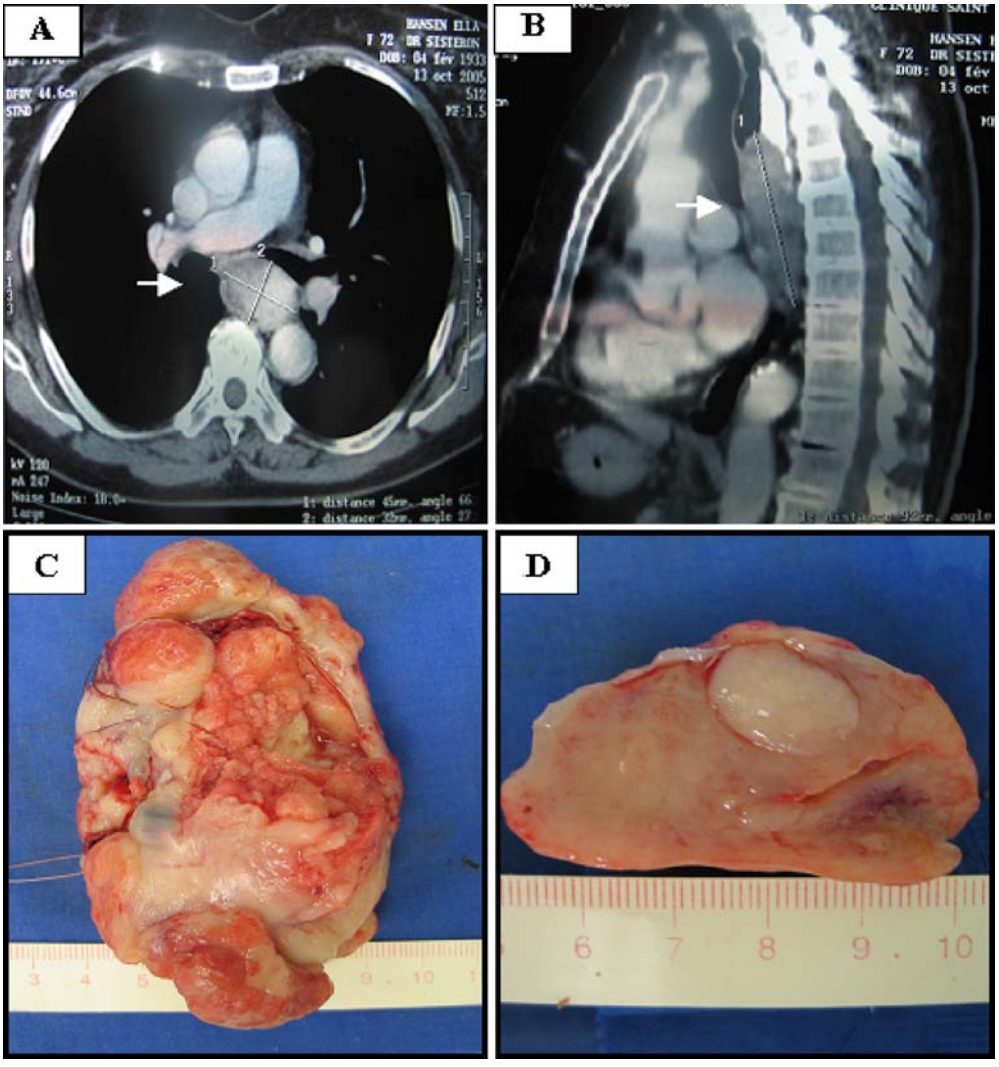

Fig. 1 **a** Transversal computed tomographic scan of the chest showing a well-circumscribed mass inseparable from the esophagus (*arrow*). **b** Saggital computed tomographic scan of the chest showing a mass developed into the esophageal lumen (*arrow*). **c** and **d** Macroscopic appearance of the esophageal synovial sarcoma. **c** The surface of the tumor is friable and not covered by the esophageal mucosa. **d** Transversal section of the tumor: white-tan and yellow nodular mass

France; 1:50), CD31 (Dako; 1:50), CD34 (Immunotech, Luminy, France; 1:100), CD56 (Dako; 1:50), CD57 (Becton-Dickinson, San José, CA, USA), CD117 (Dako; 1:100) and Ki67 (Dako; 1:100) were performed using the streptavidin–biotin complex method.

Cytogenetic and fluorescence in situ hybridization (FISH) analysis

A fresh fragment of the tumor was reserved for cytogenetic analysis. After mechanical and enzymatical dissociation of the fragment, and short-term culture of cells (5 days), metaphase cells preparations were done according to established procedures [12]. Fluorescence in situ hybridization (FISH) was performed on metaphase and interphase cells using the dual-color probe for the *SYT* gene (18q11.2) and the chromosome X centromere (DXZ1) probe according to the manufacturer's instructions (Vysis, Abbott Molecular Diagnostics, Rungis, France). Microscopic analysis was performed using an Axioplan II imaging microscope (Carl Zeiss, Jena, Germany) coupled with the ISIS software (MetaSystems, Altlussheim, Germany).

Pathologic findings

Gross findings

The resected specimen consisted of the esophagus, which measured 23.5 cm in length and 2.5 cm in diameter, with an attached 7.5-cm portion of the stomach. An 11×5.5 cm white-tan and yellow, ulcerated, firm mass (Fig. 1c,d) was observed in the middle third esophagus, 5 cm above the gastroesophageal junction.

Histologic findings

Histologically, the tumor was predominantly composed of a monotonous atypical spindle cell proliferation admixed with well-formed glandular structures (Fig. 2a,b). The intervening stromal spindle cell population comprised of cells containing elongated, vesicular nuclei with tapered ends that were surrounded by scant, lightly eosinophilic cytoplasm. The epithelial glandular component was focal, adopting a pseudopapillary configuration (Fig. 2b). These glandular and pseudopapillary structures were lined by

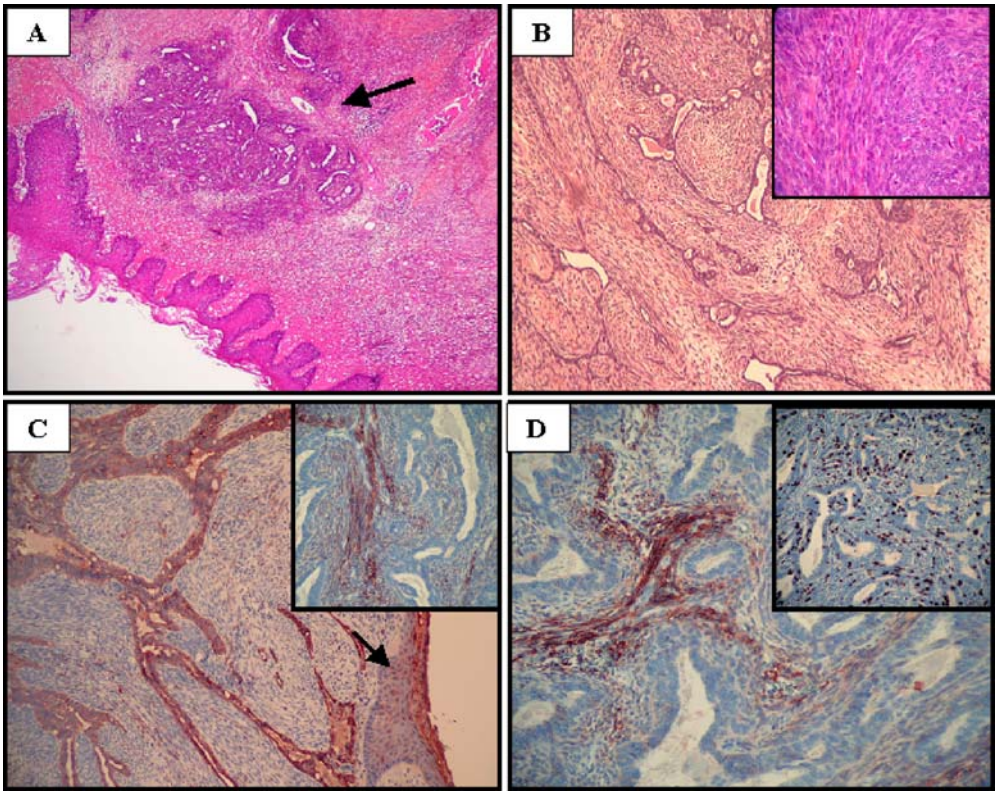

Fig. 2 **a** Synovial sarcoma involving the subepithelial area of the esophagus (*arrow*) (HES ×200). **b** Biphasic synovial sarcoma showing a glandular proliferation surrounded by a spindle cell stroma (HES ×200); *inset*: area of monotonous proliferation of atypical spindle cells with scant cytoplasm (HES ×320) **c** Immunohistochemical stain for cytokeratin AE1/3 showing diffuse positivity in glandular elements associated with focal cytoplasmic positivity in the tumor spindle cells. *Arrow*: esophageal epithelium (×200); *inset*: staining of the spindle cell component with anti-CD99 antibody (×200) **d** Immunohistochemical stain for CD56 showing strong positivity in the majority of the tumor spindle cells (×320); inset: Anti-Ki67 antibody staining showing high-index mitotic activity (×200)

round, cuboidal or columnar cells containing round or oval nuclei with abundant, eosinophilic cytoplasm. Some of the glandular lumens were filled with homogeneous eosinophilic material. In some areas, an abrupt transition from the biphasic to poorly differentiated areas in the tumor was observed. In these latter areas, the cells showed a spindle shape, and no glandular structures were observed (Fig. 2b, inset). None of the tissue sections examined displayed areas of hemorrhage or necrosis. Vascular invasion was noted in some tissue sections. Mitoses ranged from five to eight per ten high-power fields. No tumor cells were observed at surgical resection margins.

Immunohistochemical findings

Immunohistochemical analysis revealed positive stainings of the glandular elements with all epithelial markers (Fig. 2c). Focal membrane or cytoplasmic positivity for antibodies against EMA and AE1/3 was noted in the spindle cells. The spindle cell component stained strongly

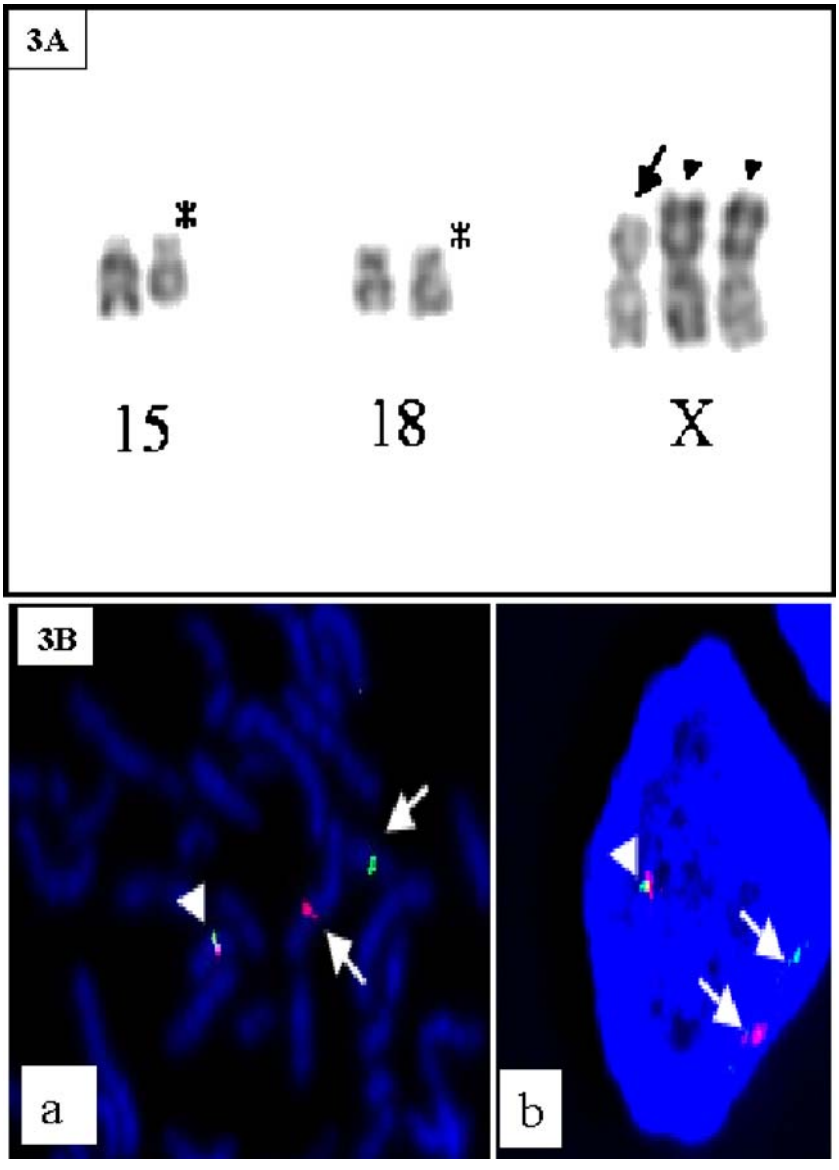

Fig. 3 **a** Partial R-banded karyotype showing the t(X;18) characteristic of synovial sarcomas and secondary anomalies. The abnormal chromosome X involved in the t(X;18) translocation is indicated by an *arrow*. The two abnormal chromosomes X derived from the t(X;15) translocation are indicated by *arrowheads*. The abnormal chromosomes 18 and 15 are marked with an *asterisk*. **b** Rearrangement of the *SYT* gene (18q11.2) detected by FISH analysis with the dual-color *SYT* gene (18q11.2) probe on a partial metaphase cell (**a**) and interphase cell nucleus (**b**). The 5′ (*red signal*) and 3′ (*green signal*) parts of *SYT* are split on the abnormal chromosomes X and 18 derived from the t(X;18) translocation (*arrows*), respectively, whereas they are juxtaposed on the normal chromosome 18 (*arrowhead*)

with vimentin. The majority of the spindle cells (>80%) was strongly positive for bcl-2. Focal positivity for CD99 (Fig. 2c, inset), CD56 (Fig. 2d) and CD57, was observed in these latter cells. Stains for muscle actin, desmin, S-100 protein, HMB45, CD31, CD34, CD117 were uniformly negative in the tumor cells. Anti-Ki67 immunostaining showed numerous stained nuclei (from 20 to 25 per ten high-power fields) (Fig. 2d, inset).

Cytogenetic findings

Sixteen R-banded metaphase cells were analyzed. The tumor cells were hyperdiploid (51 chromosomes) and showed structural abnormalities in addition to the numerical alterations. Both chromosomes X were abnormal (Fig. 3a). One of them was involved in a reciprocal translocation with chromosome 18. The location of the breakpoints of this translocation, suspected to be at Xp11 and 18q11.2 was confirmed by FISH analysis: a rearrangement of the *SYT* gene, located at 18q11.2 and specific of synovial sarcomas was observed on all metaphase and interphase cells (Fig. 3b,a,b). The other chromosome X was involved in a reciprocal translocation with chromosome 15. The abnormal chromosome X derived from a t(X;15) was duplicated (Fig. 3a). In addition, trisomies for chromosomes 2, 12, 19 and 20 were also observed. According to the International System for Human Cytogenetic Nomenclature [14], the karyotype was: 51,t(X;18)(p11;q11.2),t(X;15)(p21;q12), +der(X)t(X;15)(p21;q12),+2,+12,+19,+20.ish t(X;18) (5'SYT+,3'SYT-;5'SYT-,3'SYT+).

Comment

Esophageal mesenchymal tumors are rare conditions, mostly corresponding to gastrointestinal stromal tumors [8]. SS originating from the esophagus is very rare, and only eight cases have been reported so far [1–5, 7, 17, 18]. The patients' ages range from 14 to 75 years, and 4/8 were male [1–5, 7, 17, 18]. Dysphagia was the most frequent complaint [1–5, 7, 17, 18]. Radiologically, an intraluminal mass into esophagus was present in all cases, involving the cervical or proximal esophagus (seven cases) [1, 2, 4, 5, 8, 15, 16] or the gastroesophageal junction (one case) [3]. Macroscopically, the tumors ranged from 4.5 to 21 cm in size and were mostly solid, polypoid, without or with few areas of necrosis and hemorrhage [1–5, 7, 17, 18]. In this digestive site, SS may be mostly biphasic and rarely monophasic or poorly differentiated [1–5, 7, 17, 18]. By immunohistochemistry, the epithelial and mesenchymal elements of the digestive SS have essentially the same pattern of reactivity with antibodies directed against epithelial markers and vimentin, and can express neuroectodermal antigens such as CD99, CD56 and CD57 [1–5, 7, 17, 18]. Esophageal SS demonstrated ultrastructural findings as found in SS [3]. Finally, one previous reported case established the presence of the t(X;18) translocation in two SS of the upper digestive tract [3].

Though SS can have a distinctive histological and immunohistochemical appearance, establishing a precise diagnosis requires cytogenetic studies, especially in unusual locations such as the digestive tract, to differentiate these tumors from other esophageal tumors, specially sarcomatoid carcinoma. Cytogenetic analysis is a powerful method allowing for differentiation between esophageal SS and esophageal sarcomatoid carcinoma [3, 11, 13]. The distinction of these two different tumors has therapeutic implications, as SS may respond to adjuvant chemotherapy with regimens including high-dose ifosfamide [19]. Histologic grade of SS (which depends on necrosis and mitotic activity) is a predictor of outcome [9, 20]. However, other significant predictors of outcome include the UICC/AJCC stage, tumor size, vascular invasion, increased rate of apoptosis and pathologic resection margins [10, 20]. SS is regarded as a high-grade sarcoma, but it seems that not all SS share the same poor outcome [20]. Particularly, the follow-up from previous reports indicates that esophageal SS may have a better prognosis than SS arising elsewhere [1–5, 7, 17, 18].

Finally, esophageal SS is probably underdiagnosed in the absence of cytogenetic studies. The presence of the t (X;18) translocation can be detected either by conventional cytogenetic or directly by FISH or by reverse-transcription-polymerase chain reaction (RT-PCR) on frozen or paraffin-embedded tumor sections. While FISH analysis allows a rapid result without nucleic acids extraction procedures, the RT-PCR method provides the advantage to identify which one of the SSX1 or SSX2 genes is the fusion partner of SYT, an information that might be useful as a prognosis indicator [15]. These methods should be largely indicated in case of sarcomatoid carcinoma of the esophagus, as prognosis and therapeutic strategy are different from those of SS in the digestive tract.

Acknowledgements We are grateful to Elodie Basc and Mireille Mari for skilful technical assistance. This work was supported by the Programme Hospitalier de Recherche Clinique National 2003 du CHU de Nice, The Ligue Nationale Contre le Cancer, Comité des Alpes-Maritime and the Cancéropôle Provence Alpes-Côte d'Azur.

References

1. Amr SS, Shihabi NK, Al Hajj H (1984) Synovial sarcoma of the esophagus. Am J Otolaryngol 5:266–269
2. Anton-Pacheco J, Cano I, Cuadros J, Vilarino A, Berchi F (1996) Synovial sarcoma of the esophagus. J Pediatr Surg 31:1703–1705

3. Billings SD, Meisner LF, Cummings OW, Tjada E (2000) Synovial sarcoma of the upper digestive tract : a report of two cases with demonstration of the X;18 translocation by fluorescence in situ hybridization. Mod Pathol 13:68–76
4. Bloch MJ, Iozzo RV, Edmunds LH Jr, Brooks JJ (1987) Polypoid synovial sarcoma of the esophagus. Gastroenterology 92:229–233
5. Bonavina L, Fociani P, Asnaghi D, Ferrero S (1998) Synovial sarcoma of the esophagus simulating achalasia. Dis Esophagus 11:268–271
6. Fisher C (1998) Synovial sarcoma. Ann Diagn Pathol 2:401–421
7. Habu S, Okamoto E, Toyosaka A, Nakai Y, Takeuchi M (1998) Synovial sarcoma of the esophagus: report of a case. Surg Today 28:401–404
8. Hamilton SR, Aaltonen LA (eds) (2000) World Health Organization classification of tumours of the digestive system. IARC, Lyon
9. Hasegawa T, Yamamoto S, Nojima T, Hirose T, Nikaido T, Yamashiro K, Matsuno Y (2002) Validity and reproducibility of histologic diagnosis and grading for adult soft-tissue sarcomas. Hum Pathol 33:111–115
10. Kawauchi S, Kukuda T, Oda Y, Saito T, Olga A, Takeshita M, Yokohama K, Chuman H, Iwamoto Y, sasaki K, Tsuneyoshi M (2000) Prognostic significance of apoptosis in synovial sarcoma: correlation with clinicopathologic parameters, cell proliferative activity, and expression of apoptosis-related proteins. Mod Pathol 13:755–765
11. Kwon MS, Hong SJ, Cho HA, Ahn GH, Lee SS, Lee KY, Rhyu MG (2003) Extensive and divergent chromosomal losses in squamous and spindle-cell components of esophageal sarcomatoid carcinoma. Virchows Arch 443:635–642
12. Limon J, Dal Cin P, Sandberg AA (1986) Application of long-term collagenase disaggregation for the cytogenetic analysis of human solid tumors. Cancer Genet Cytogenet 23:305–313
13. Matsumoto T, Fujii H, Arakawa A, Yamasaki S, Sonoue H, Hattori K, Kajiyama Y, Hirose S, Tsurumaru M (2004) Loss of heterozygosity analysis shows monoclonal evolution with frequent genetic progression and divergence in esophageal carcinosarcoma. Hum Pathol 35:322–327
14. Mitelman F (ed) (1995) ISCN: an international system for human cytogenetic nomenclature. Karger, Basel
15. Nilsson G, Skytting B, Xie Y, Brodin B, Perfekt R, Mandahl N, Lundeberg J, Uhlen M, Larsson O (1999) The SYT-SSX1 variant of synovial sarcoma is associated with a high rate of tumor cell proliferation and poor clinical outcome. Cancer Res 59:3180–3184
16. Ohtaka M, Kumasaka T, Nobukawa B, Hirai S, Suda K, Ohno Y, Iwasaki R, Ikegami Y, Fukasawa M (2002) Carcinosarcoma of the esophagus characterized by myoepithelial and ductal differentiations. Pathol Int 52:657–663
17. Palmer Bv, Levene A, Shaw HJ (1983) Synovial sarcoma of the pharynx and esophagus. J Laryngol Otol 97:1173–1176
18. Perch SJ, Soffen EM, Whittington R, Brooks JJ (1991) Esophageal sarcomas. Surg Oncol 48:194–198
19. Rosen G, Forsher C, Lowenbraun S, Eilber F, Eckardt J, Holmes C, Fu YS (1993) Synovial sarcoma. A study of intensive chemotherapy in 14 patients with localized disease. Cancer 73:2506–2511
20. Trassard M, Le Doussal V, Hacene K, Terrier P, Ranchere D, Guillou L, Fiche M, Collin F, Vilain MO, Bertrand G, Jacquemier J, Sastre-Garau X, Bui NB, Bonichon F, Coindre JM (2001) Prognostic factors in localized primary synovial sarcoma: a multicenter study of 128 adult patients. J Clin Oncol 19:525–534
21. Weiss SW, Goldblum JR (2001) Malignant soft tissue tumors of uncertain type. In: Weiss SW, Goldblum JR (eds) Enzinger and Weiss's soft tissue tumors, 4th edn. Mosby, St Louis, MO, pp 1483–1571

Virchows Arch (2006) 449: 268–271
DOI 10.1007/s00428-006-0153-1

CASE REPORT

Jan Koren · Jana Mensikova · Petr Mukensnabl · Michal Zamecnik

Mullerianosis of the urinary bladder: report of a case with suggested metaplastic origin

Received: 29 November 2005 / Accepted: 23 December 2005 / Published online: 11 July 2006
© Springer-Verlag 2006

Abstract Mullerianosis of the urinary bladder is a very rare and morphologically complex tumor-like lesion. It is composed of several types of mullerian-type lesions, including endometriosis, endocervicosis, and endosalpingiosis. This disease occurs in women of the reproductive age group. In the pathogenesis, implantative and metaplastic origins have been suggested, and they are still under discussion. In the present report, a rare case of this lesion in a 41-year-old woman is described. The bladder contained, in addition to typical mullerianosis, glandular cystitis with focal intestinal metaplasia. An interesting and, to our knowledge, hitherto unreported feature was a rare continuity between the glands of mullerianosis and glands of glandular cystitis. The histologic and immunohistochemical findings in the present case support strongly the metaplastic origin of mullerianosis.

Keywords Mullerianosis · Urinary bladder · Chronic glandular cystitis · Intestinal type · Metaplasia

Introduction

The so-called mullerianosis of the urinary bladder is a rare tumor-like lesion composed of various types of mullerian-derived tissues such as glands lined with endometrial, endocervical and tubal epithelium, and endometrial stroma [3, 6]. The lesion occurs in female patients of reproductive age, and its pathogenesis appears to be similar to that of ordinary endometriosis [1–4, 6]. In this paper, we would like to describe an additional case, in which an unusual association with glandular cystitis of intestinal type was observed besides the typical clinicopathological features. In addition, the lesion contained rare and, to our knowledge, hitherto undescribed direct connections between urothelial and mullerian epithelium. This finding, along with absence of history of any pelvic surgery, favors metaplastic histogenesis of this lesion.

J. Koren (✉) · J. Mensikova
Department of Pathology, Roosevelt's Faculty Hospital,
General Svoboda's Square No 1,
975 17 Banska Bystrica, Slovak Republic
e-mail: koren.jan@stonline.sk
Tel.: +421-48-4412432

P. Mukensnabl · M. Zamecnik
Sikl's Department of Pathology, Medical Faculty Hospital,
Charles University,
Pilsen, Czech Republic

Clinical history

A 41-year-old woman with a 5-year history of dysuria, chronic pelvic pain, and hematuria intra mensem was admitted. The patient had no history of pelvic surgery or cesarean section. Cystoscopic examinations revealed many hemorrhagic tumor-like deformations of the posterior bladder wall beneath an intact surface urothelium. The endoscopist supposed endometriosis but it was necessary to rule out a neoplasm; therefore, a diagnostic transurethral resection was performed.

Materials and methods

The formol-fixed tissue was completely routinely processed, paraffin-embedded, and stained with hematoxylin and eosin, periodic acid–Schiff (PAS) with and without diastase, and alcian blue at pH 2.5. Immunohistochemical studies were performed on formalin-fixed, paraffin-embedded sections, using the following antibodies: pancytokeratins (AE1/AE3, 1:1,000, Neo Markers, Westinghouse), CK7 (OV-TL12/30, 1:200, Dako, Glostrup), CK20 (KS20.8, 1:100, Dako, Glostrup), carcinoembryonic antigen (II-7, 1:1,000, Dako, Glostrup), vimentin (V9, 1:1,000, Neo Markers, Westinghouse), progesterone receptor (PR) (1A6, 1:50, Immunotech, Marseille), estrogen receptor (ER) (ER1D5, 1:1,000, Immunotech, Marseille), chromogranin A (DAK-A3, 1:400, Dako, Glostrup), synaptophysin (polyclonal, without dilution, Neo Markers, Westinghouse), and CD10 (56C6, 1:40, Neo Markers,

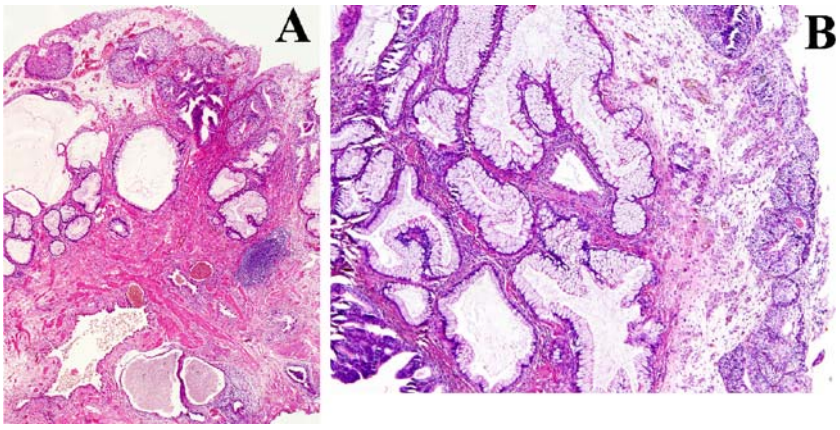

Fig. 1 **a** Low-power view shows both glandularis cystitis (*top*) and mullerianosis (*bottom*). **b** Glandular cystitis of intestinal type contains glands with numerous goblet cells

Westinghouse). A streptavidin–biotin–peroxidase complex (Dako, Glostrup) was employed in the immunohistochemical studies.

Results

The resected tissue fragments measured from several millimeters to 1.5 cm, varied in shape, possessed "fibrous" consistence, and varied in color from gray to rusty brown. Histologically, they showed features of the chronic glandular cystitis of the intestinal type with typical glands and with solid von Brunn's nests. The glands of cystitis were lined by epithelium of the intestinal type with many goblet cells. The stroma was myxoid, with interspersed stromal lymphoid aggregates and hemosiderin-ladden macrophages. Lamina propria and muscularis propria contained numerous glands and stroma typical of mullerianosis [3, 6] (Fig. 1). A majority of the glands was of endometrial type and was associated with endometrial stroma (Fig. 2). The epithelium of some glands showed focal tubal features, with typical ciliated, intercalated, and peg cells [6]. In addition, a minority of the glands contained columnar mucinous epithelium of the endocervical type [2]. The glands of mullerianosis were dilated focally and were seen often near intestinal-type glands of the glandular cystitis. This apparent juxtaposition prompted us to search for a transition between mullerian and urothelial epithelium, as such finding could help in histogenetic considerations on mullerianosis. After an extensive search, a synchronous presence of urothelium and ciliated tubal-type epithelium in some glands was found (Fig. 3). Histochemically, mucin in metaplastic epithelial cells of intestinal type and endocervical cells was strongly positive with alcian blue at pH 2.5 and PAS, whereas urothelial and mullerian cells were mucin-negative.

The immunohistochemical expressions of the epithelium are summarized in Table 1. Pancytokeratin was positive in urothelial and mullerian-type epithelium and negative in epithelial cells of intestinal type. CK7 stained urothelial and mullerian-type epithelium. CD10 showed focal membranous luminal positivity in intestinal metaplasia and diffuse reactivity in endometrial stromal cells. Vimentin positivity was limited to the stroma except for areas of typical endometrial stroma. ER and PR positivity were

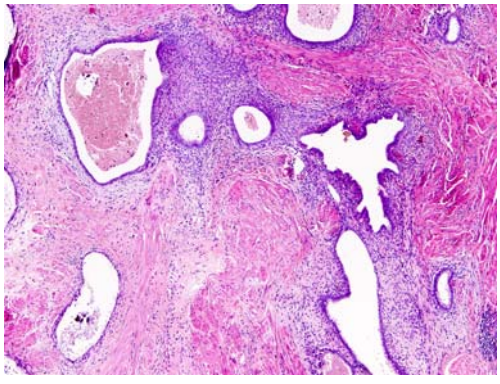

Fig. 2 An area of endometriosis (a part of mullerianosis) with typical endometrial glands and endometrial stroma in lamina mucosa and muscularis propria of the urinary bladder

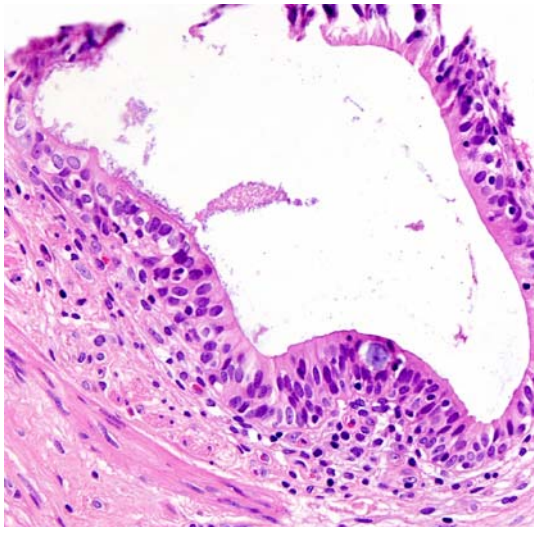

Fig. 3 A detail of the gland shows synchronous presence of urothelium and ciliated tubal-type epithelium. This finding suggests metaplastic origin of mullerianosis

Table 1 The immunohistochemical expressions in epithelial cells of various types in normal urothelium, glandular cystitis and mullerianosis of the bladder (except for CK20, CEA, synaptophysin, and chromogranin A, which were all negative in all cells)

	AE1-AE3	CK7	CD10	ER	PR	Vimentin
Urothelial cells	Positive	Positive	Negative	Negative	Negative	Negative
Cells of intestinal type in glandular cystitis	Negative	Negative	Focal membranous luminal positive	Negative	Negative	Negative
Endometrial cells	Positive	Positive	Positive	Focal positive	Positive	Negative
Tubal cells	Positive	Positive	Negative	Focal positive	Positive	Negative
Endocervical cells	Positive	Positive	Negative	Focal positive	Positive	Negative

scattered in epithelial cells of mullerian types and were diffusely positive in endometrial stroma. These hormone receptor immunostains highlighted well in rare glands a transition between receptor-positive mullerian epithelium and receptor-negative urothelial epithelium (Fig. 4).

Discussion

The present lesion showed features of mullerianosis of the urinary bladder, as it contained structures of endometriosis, endocervicosis, and endosalpingiosis in lamina propria and lamina muscularis [3, 6]. The term "mullerianosis of the urinary bladder" was firstly used by Young and Clement [6] in 1996 to designate a tumor-like lesion located usually in the posterior bladder wall in a woman of reproductive age and associated with cystitis glandularis chronica and solid von Brunn's nests. An additional case in a 27-year-old patient without history of pelvic surgery was described by Donne et al. in 1998 [3]. These authors discuss two different pathogenetic ways of mullerianosis of the urinary bladder: metaplastic and implantative. They prefer metaplastic origin, and they suggest that the presence of various types of mullerian tissue can be explained by a capacity of mullerian metaplasia to differentiate toward tubal, endometrial, or endocervical phenotype. An invariable localization of mullerianosis in the posterior wall and fundus of the bladder corresponds to its peritoneal covering that is particularly receptive to female hormones [3]. On the other hand, Young and Clement [6] prefer an implantative origin of the endocervicosis (a part of mullerianosis), supposing that the origin is related to the implantation of endocervical cells during cesarean section.

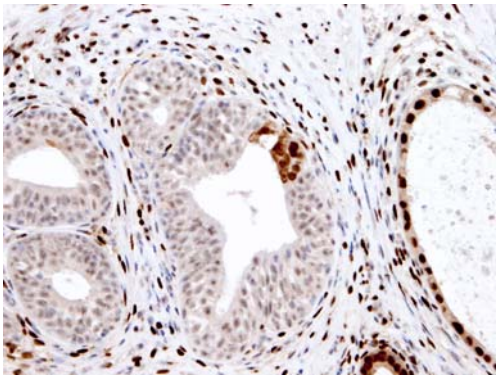

Fig. 4 Immunoreactivity for PR. The epithelium of glandular cystitis is PR-negative (*left*) whereas that of mullerianosis is PR-positive (*right*). A group of PR-positive mullerian cells with cilia in the gland of glandular cystitis is seen in the center of the photomicrograph. A majority of the cells in this gland are PR-negative urothelial cells

In the present case, we were able to find very rare foci of the metaplastic ciliated epithelium of the tubal type in continuity with the urothelium. It seems that, in such foci, urothelium underwent metaplasia to the tubal (i.e., mullerian) phenotype, acquiring besides the tubal morphology also immunohistochemical positivity for PR and ER. The metaplasia in urothelial cells in association with cystitis chronica is in keeping with a general view that the metaplastic changes are more frequent in mucosa affected by chronic inflammation. The implantative origin of mullerianosis in our case is not probable because the patient has no history of any pelvic surgery that would cause an implantation of the endometrium or endocervical epithelium into the bladder wall [2, 3].

A differential diagnosis of mullerianosis of the urinary bladder includes cystitis glandularis, nephrogenic adenoma, and adenocarcinoma arising in mullerianosis [2, 6]. Glandular cystitis and nephrogenic adenoma lack morphological and immunohistochemical (particularly positivity for sex-steroid hormone receptor) features of the mullerian lesion. As was seen in our case, some glands of mullerianosis in the bladder wall, especially those without endometrial stroma, can simulate adenocarcinoma arising in mullerianosis. Although a malignant tumor arising in mullerianosis of the urinary bladder was still not described, one can suppose that such possibility can occur in analogy with malignization of endometriosis. A single case of endometrioid carcinoma in endometriosis of the urinary bladder [1] and four cases of clear cell carcinoma associated with endometriosis or mullerian cysts [5] were described till now. The carcinomatous epithelium in these cases was distinguishable by its malignant nuclear features, irregular gland architecture, and, at least, focal stromal desmoplastic reaction.

In conclusion, we described the sixth case of mullerianosis of the urinary bladder. It was associated with cystitis glandularis chronica of the intestinal type. From a histogenetic point of view, the spatial association between glands of mullerianosis and glandular cystitis as well as rare continuity between mullerian and urothelial epithelium in a single gland indicates that mullerianosis had arisen in the present case through metaplasia of the urothelium in a setting of chronic inflammation.

References

1. Al-Izzi MS, Horton LWL, Kelleher J, Fawcett D (1994) Malignant transformation in endometriosis of the urinary bladder. Histopathology 14:191–198
2. Clement PB, Young RH (1992) Endocervicosis of the urinary bladder. Am J Surg Pathol 16:533–542
3. Donne C, Vidal M, Buttin X, Becerra P, Carvia R, Zuluaga A, Nogales FF (1998) Mullerianosis of the urinary bladder. Clinical and immunohistochemical findings. Histopathology 33:290–292
4. New NE, Roberts PF (1990) Mucinous metaplasia in endometriosis of the bladder. Histopathology 16:307–308
5. Oliva E, Amin MB, Jimenez R, Young RH (2002) Clear cell carcinoma of the urinary bladder: a report and comparision of four tumors of mullerian origin and nine of probable urothelial origin with discussion of histogenesis and diagnostic problems. Am J Surg Pathol 26:190–197
6. Young RH, Clement PB (1996) Mullerianosis of the urinary bladder. Mod Pathol 9:731–737

Virchows Arch (2006) 449: 272
DOI 10.1007/s00428-006-0209-2

LETTER TO THE EDITOR

Girish Venkataraman · Vijayalakshmi Ananthanarayanan · Gladell P. Paner

Accessible calculation of multirater kappa statistics for pathologists

Received: 20 March 2006 / Accepted: 27 March 2006 / Published online: 4 May 2006
© Springer-Verlag 2006

Dear Editor:
Multirater kappa statistics are relatively underused by pathologists to study interobserver agreement [1, 3]. While several methods are available for measuring agreement when there are only two raters, there is little awareness of the appropriate software programs geared to handle measures of agreement when there are more than two raters or when there are more than three categories to be rated for this kind of analysis. There are two major options for performing this analysis—free online open-source software or routine statistical packages like SPSS, SAS, or STATA to calculate kappa statistics.

We personally use SPSS 13 (SPSS Inc., Chicago, IL, USA) for agreement studies; unfortunately, the current version of SPSS does not calculate kappa statistics when there are more than two raters or more than two categories of rating. To circumvent this problem, there is an SPSS macrofile called "MKAPPASC" that is freely available on the Internet for users of SPSS version 6 and above to implement similar studies within the SPSS environment. Still, this method will give only the overall interrater agreement rather than category-specific agreements, which is generally the preferred statistic.

A weighted version of the kappa coefficient is sometimes suggested as a reliability measure for data from ordered scales [1]. The idea is that one should distinguish between different types of disagreement. Specifically, two ratings that differ by a small amount on an ordered scale should be considered a "lesser disagreement" than two scores that are far apart. Weighted kappas can be calculated in STATA software using the "kap" and "kapwgt" commands. A default weights matrix is supplied or one can define one's own.

The SAS procedure PROCFREQ can provide the kappa statistic for two raters and multiple categories, provided that the data are in a 2×2 format. A SAS macro MAGREE, on the other hand, can compute the estimates and tests of agreement between multiple raters/categories. An excellent article is available at http://www2.sas.com/proceedings/sugi30/155-30.pdf

In the interest of other investigators who might wish to perform a similar analysis (unweighted multirater kappa) without using these software, there is a free Excel spreadsheet-based program that calculates category-specific kappa statistics for more than three raters and three categories available at http://www.ccit.bcm.tmc.edu/jking/homepage/genkappa.doc with confidence interval based on the method of Fleiss [2]. Interested investigators may consider all these options whenever they plan to utilize multirater kappa statistics in the field of pathology.

G. Venkataraman (✉) · G. P. Paner
Department of Pathology, Loyola University Medical Center,
Building 110, Room 2233, 2160 South First Avenue,
Maywood, IL, 60153, USA
e-mail: gvenkat@lumc.edu
Tel.: +1-708-3272572
Fax: +1-708-3272620

V. Ananthanarayanan
Department of Pathology, UIC
University of Illinois at Chicago,
Chicago, IL, USA
e-mail: viju@uic.edu

References

1. Cohen J (1968) Weighted kappa: nominal scale agreement with provision for scaled disagreement or partial credit. Psychol Bull 70:213–220
2. Fleiss JL (1981) Statistical methods for rates and proportions, 2nd edn. Wiley, New York
3. O'Malley FP, Mohsin SK, Badve S, Bose S, Collins LC, Ennis M, Kleer CG, Pinder SE, Schnitt SJ (2006) Interobserver reproducibility in the diagnosis of flat epithelial atypia of the breast. Mod Path 19:172–179

Virchows Arch (2006) 449: 273–276
DOI 10.1007/s00428-006-0206-5

LETTER TO THE EDITOR

Gregor Mikuz · Rodolfo Montironi · Antonio Lopez-Beltran · Gianni Bussolati

The dilemma of multiorgan donors with high serum PSA—a pathologist's proposal

Received: 22 December 2005 / Accepted: 20 March 2006 / Published online: 5 May 2006
© Springer-Verlag 2006

Organ transplantation has become the standard treatment for patients with end stage organ failure. Because of this tremendously increased demand, transplantation is perforce limited by organ shortage. At present in the U.S., 90,669 patients are waiting for a transplantation, but only 23,522 were carried out in 2005 [31]. The organ exchange organization Eurotransplant[1] has a deficit of about 9000 organs/year [12]. About 10% of patients on the waiting list will die before organ transplantation [17].

With the so called "extended or aggressive criteria" [27, 29] the number of organs suitable for transplantation can be markedly increased (by up to 80%) without impairing medium term results [2, 27]. In the past, one of the most important eligibility criteria was the age of the donors, who usually were not older than 50. Extended criteria permit using organs of patients older then 55. The proposal has even been made to include donors who have cancers with low transmission risk (brain tumors) or with a remote (>5 years) cancer history [20]. With the exception of malignant melanoma, choriocarcinoma and gynaecological malignancies [9, 10] donors with other potentially more aggressive tumors are nowadays no longer rejected [18, 29]. The occurrence of donor transmitted tumors is surprisingly low, accounting for a mere 9 out of 34,933 (0.025%) cadaveric donors (1 transmitted tumor for every 3881 cadaveric donors) and 13 out of 108,062 (0.012%) transplanted organs (1 transmitted tumor for 8312 transplanted organs) [18]. In a series of 582 liver transplants 6 cases (1.03%) of genitourinary tumors (4 renal cell and 2 prostate carcinomas) did not show any evidence of tumor transmission after a follow up of 55± 20 months (range 14–68 months) [30]. Another cohort's study showed that the risk of a donor having an undetected malignancy is 8 in 626 (1.3%) and the risk of a transmitted tumor is 1 in 626 (0.2%) [6].

Prostate cancer has become the most commonly diagnosed cancer in the western world. Due to PSA screening, the number of prostate cancers detected in men younger than 50 is on the increase [19]. Not all prostate cancer patients have total PSA values exceeding the cut-off of 4 ng/ml and not all patients with high tPSA values have a prostate cancer. Many of them have "innocuous" diseases like infarction or prostatitis. In a volunteer screening area [26] 8% of the 21,078 screened volunteers had elevated PSA and of the 778 who underwent biopsies only 198 (25%) were positive for carcinoma.

This simplified epidemiological data implies that some men with end stage organ failure waiting for transplantation as well as some organ donors are harboring a prostate cancer, which nowadays can be detected by PSA screening. In fact, the incidence of prostate cancer in male donors amounts to about 3% [16] However, kidneys and other organs were transplanted long before PSA screening was introduced. That means many patients were transplanted in spite of having a clinical silent prostate cancer and probably many donors also had a silent cancer. One might therefore have expected an enormous increase of prostate cancer in men who underwent transplantation. In actual fact, the epidemiologic study shows an increase of lymphomas (28- to 49- fold), skin carcinomas (29-fold), vulvar and anal carcinomas (100-fold), hepatocellular

G. Mikuz (✉)
Institute of Pathology, Medical University Innsbruck,
Muellerstrasse 44 A,
6020 Innsbruck, Austria
e-mail: Gregor.Mikuz@i-med.ac.at
Fax: +43-512-5073650

R. Montironi
Institute of Pathological Anatomy and Histopathology,
Polytechnic University of the Marche Region,
Ancona, Italy

A. Lopez-Beltran
Department of Pathology, Reina Sofia University Hospital
and Cordoba University Medical School,
Cordoba, Spain

G. Bussolati
Department of Biochemical Sciences and Human Oncology,
University of Torino,
Torino, Italy

[1] Members: Austria, Belgium, Luxemburg, Germany, Slovenia, and The Netherlands

carcinoma (20- to 38- fold), Kaposi sarcoma (400- to 500-fold) and a small increase in other sarcomas and renal carcinomas. These tumors are not donor transmitted but tumors *de novo* arising in immunosupressed recipients. The incidence of prostate cancer in transplanted patients, however, shows no increase [24]. Moreover, up to now only one case of donor transmitted prostate cancer has been reported in a heart recipient [15]. Prostate cancer in organ recipients is also not a contraindication for organ transplantation, provided the prostatectomy was carried out about 2 years before transplantation [23].

In donors with high serum PSA, pathologists are faced with the request of a quick histological assessment of the prostate. Mostly clinicians want to have frozen sections of biopsies or of the prostate after autopsy. Frozen sections can even be performed on whole mounted prostate [22]. The prostate of adult men has a volume of 20–30 cc and small cancers can measure less than 0.5 cc. The cancer could of course be found with the first biopsy. If it isn't, however, using the standard method up to 50–100 frozen sections might be needed to find a small cancer. With multiple biopsies, the chance of finding the cancer is even better than with frozen section. If the cancer is missed in frozen section and/or biopsy, it means that the cancer is small and probably clinically unimportant. Frozen sections of core biopsies are categorically to be refused, for the diagnoses are not reliable and the material for paraffin histology is more or less destroyed. The assessment of Gleason grade in frozen sections is extremely unreliable [3].

The kidney is only rarely the site of a secondary (metastatic) neoplasm and in the series of Bates and Baithun [5] not a single case of prostate cancer metastatic to the kidney has been reported. There are no recent references to such metastases in other organs which are currently being transplanted. Even in an old autopsy series from the pre-PSA era, the only organ commonly involved was the lung (55%); however, only cases with widespread organ metastases have been analyzed regardless of the stage, Gleason score and duration of disease [13, 28]. Seventy-six percent of patients with an initially untreated localized pT2 prostate cancer are still alive and without metastases 15 years after diagnosis [25]. All these statistics underscore the fact that haematogenous metastases appear very late in patients with prostate cancer. Even vascular or lymphatic invasion in prostatectomy specimens seem not to be an independent prognostic factor, but a factor which depends on the grade of malignancy [4]. Bone metastases appear only in 2.3% and 5.3% of patients with a PSA levels ≤10 ng/ml and 11–20 ng/ml respectively, but the detection rate in patients with carcinoma Gleason ≤7 is even lower (1.2%). Lymph node metastases can be excluded in patients with a PSA <20 ng/ml [1].

Other sites of metastases include lungs, liver, soft tissue and brain. But these organs can be reached only through arterial dissemination after the tumor cells have reached and passed the pulmonary circulation. That means it takes a long time for cancer cells to migrate from the bone or lymphnodes to the lung. However, also in large series no kidney metastases have been observed [13, 28]. Obviously, these data are valid only for conventional prostate cancer (about 98% of cases). Donors with rare and unusual prostate carcinoma variants (prostate duct carcinoma, foamy cell carcinoma, signet ring carcinoma, small cell carcinoma, etc.) must be rejected because these cancer types are more aggressive.

For a baseline staging of the donor prostate, multiple paraffin embedded biopsies (at least 15) not only of the prostate but especially of the prostate capsule and the periprostatic tissue of the peripheral zone and neurovascular bundles should be performed. Multiple transrectal biopsies should be combined with the transperineal approaches which are more appropriate for the sampling from the anterior half of the prostate. Such biopsies could be quickly processed in as little as 4 h, a reasonable time to make a decision.

The assessment of extraprostatic extension in biopsy material is, however, not a simple matter. A rough semiquatitative assessment of the biopsies combined with the PSA values is very helpful for the prediction of extraprostatic extension. Small foci of carcinoma with a linear length of less then 3 mm in 6–10 biopsies are very characteristic of organ confined cancer (92% of cases) [7]. Ninety-eight percent of the patients with a PSA ≤10 ng/ml

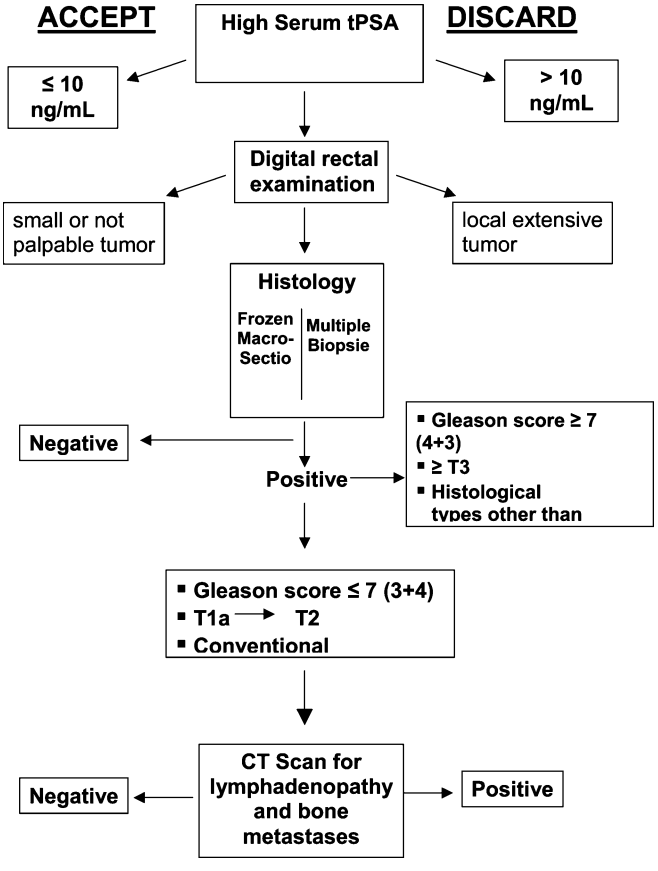

Fig. 1 Flow chart summarizing important cut-offs for organ use from donors with high serum PSA

have an organ confined tumor [7]. Unfortunately the staging with MRI has an accuracy of less then 70% and a very low predictive value [8, 14].

Men with a history of transurethral prostate resection (TURP) and the diagnosis of a stage pT1a /pTb carcinoma will probably be refused as donors. However pT1a-b cancers in TURP material mostly correspond to a pT2 cancer in prostatectomy specimen [21]. More than 70% of men with stage pT1b prostate cancer have a disease free survival of 15 years [25], which means that even organs of such donors could safely be transplanted.

In our opinion, the organs (heart, kidney, liver, and pancreas) from donors with prostate cancer can be safely used for transplantation, provided the following criteria are fulfilled: Serum tPSA ≤10 ng/ml, conventional prostate carcinoma, Gleason score ≤7 (3+4), clinical stage T1a–T2c, negative CT scan for lympadenopathy and bone metastases (Fig. 1). It should however be stressed that there is a difference between Gleason 3+4 and Gleason 4+3. Both correspond to Gleason score 7, but 4+3 predicts a more advanced stage and an increased rate of progression [11]. The above proposed cut-offs are extremely low because as already mentioned even patients with a PSA ≤20 ng/ml rarely have bone and lymphnode metastases.

This proposal reflects the personal experience of the authors and can obviously be used only as a general framework, subject to future revising or alteration. There is no doubt that a broad discussion among the involved specialists is necessary to achieve a general consensus. But we should not forget that the recipient's risk of dying from a donor-transmitted prostate cancer is more than 100-fold lower than the risk of dying while waiting for an organ.

References

1. Abuzallouf S, Dayes I, Lukka H (2004) Baseline staging of newly diagnosed prostate cancer: a summary of the literature. J Urol 171:2122–2127
2. Aigner C, Winkler G, Jaksch P, Seebacher G, Lang G, Taghavi S, Wisser W, Klepetko W (2005) Extended donor criteria for lung transplantation—a clinical reality. Eur J Cardio-thorac Surg 27:757–761
3. Algaba F, Arce Y, Lopez-Beltran A, Montironi R, Mikuz G, Bono AV, European Society of Uropathology; Uropathology Working Group (2005) Intraoperative frozen section diagnosis in urological oncology. Eur Urol 47:129–136
4. Amin M, Boccon-Gibod L, Egevad L, Epstein JI, Humphrey PA, Mikuz G, Newling D, Nilsson S, Sakr W, Srigley JR, Wheeler TM, Montironi R (2005) Prognostic and predictive factors and reporting of prostate carcinoma in prostate needle biopsy specimens. Scand J Urol Nephrol 216:20–33 (Suppl)
5. Bates AW, Baithun SI (2002) The significance of secondary neoplasms of the urinary and male genital tract. Virchows Arch 440:640–647
6. Birkeland SA, Storm HH (2002) Risk for tumor and other disease transmission by transplantation: a population-based study of unrecognized malignancies and other diseases in organ donors. Transplantation 74:1409–14013
7. Boccon-Gibod LM, Dumonceau O, Toublanc M, Ravery V, Boccon-Gibod LA (2005) Micro-focal prostate cancer: a comparison of biopsy and radical prostatectomy specimen features. Eur Urol 48:895–899
8. Borre M, Lundorf E, Marcussen N, Langkilde NC, Wolf H (2005) Phased array magnetic resonance imaging for staging clinically localised prostrate cancer. Acta Oncol 44:589–592
9. Buell JF, Trofe J, Hanaway MJ, Lo A, Rosengard B, Rilo H, Alloway R, Beebe T, First MR, Woodle ES (2001) Transmission of donor cancer into cardiothoracic transplant recipients. Surgery 130:660–666
10. Buell JF, Beebe TM, Trofe J, Gross TG, Alloway RR, Hanaway MJ, Woodle ES (2004) Donor transmitted malignancies. Ann Transplant 9:53–56
11. Chan TY, Partin AW, Walsh PC, Epstein JI (2000) Prognostic significance of Gleason score 3+4 versus Gleason score 4+3 tumor at radical prostatectomy. Urology 56:823–827
12. Cohen B, Wight C (1999) A European perspective on organ procurement: breaking down the barriers to organ donation. Transplantation 68:985–990
13. de la Monte SM, Moore GW, Hutchins GM (1986) Metastatic behavior of prostate cancer. Cluster analysis of patterns with respect to estrogen treatment. Cancer 58:985–993
14. Futterer JJ, Engelbrecht MR, Huisman HJ, Jager GJ, Hulsbergen-van De Kaa CA, Witjes JA, Barentsz JO (2005) Staging prostate cancer with dynamic contrast-enhanced endorectal MR imaging prior to radical prostatectomy: experienced versus less experienced readers. Radiology 237:541–549
15. Gazdar AF (1997) Tumors arising after organ transplantation. Sorting out their origins. JAMA 277:154–155
16. Gonzalez Segura C, Pascual M, Canizares R, Garcia- Huete L, Torras J, Riera L, Condom E (2003) Importance of tumoral markers in donors: study of prostate-specific antigen. Transplant Proc 35:1647–1649
17. Gridelli B, Remuzzi G (2000) Strategies for making more organs available for transplantation. N Engl J Med 343: 404–410
18. Kauffman MH, McBride MA, Cherikh WS, Spain PC, Marks WH, Roza AM (2002) Transplant tumor registry: donor related malignancies. Transplantation 74:358–362
19. Khan MA, Han M, Partin AW, Epstein JI, Walsh PC (2003) Long-term cancer control of radical prostatectomy in men younger than 50 years of age: update. Urology 61:86–91
20. Loren AW, Desai S, Gorman RC, Schuchter LM (2003) Retransplantation of a cardiac allograft inadvertently harvested from a donor with metastatic melanoma. Transplantation 76:741–743
21. Mai KT, Isotalo PA, Green J, Perkins DG, Morash C, Collins JP (2000) Incidental prostatic adenocarcinomas and putative premalignant lesions in TURP specimens collected before and after the introduction of prostrate-specific antigen screening. Arch Pathol Lab Med 124:1454–1456
22. Mazzucchelli R, Scarpelli M, Lopez-Beltran A, Montironi R (2006) Complete sampling and macrocryosectioning of the prostate in a potential multiorgan donor candidate. J Clin Pathol (in press)
23. Neugut AI, Grann VR (2004) Waiting time in prostate cancer. JAMA 291:2757–2758
24. Penn I (1993) The effect of immunosuppression on pre-existing cancers. Transplantation 55:742–747
25. Puthawala AA, Syed AM, Austin PA, Cherlow JM, Perley JM, Shanberg AM, Sawyer DE, Ingram JE, Baghdassarian R, Wachs BH, Perley JE, Londrc A, Espinoza-Ferrel T (2001) Long-term results of treatment for prostate carcinoma by staging pelvic lymph node dissection and definitive irradiation using low-dose rate temporary iridium-192 interstitial implant and external beam radiotherapy. Cancer 92:2084–2094
26. Reissigl A, Horninger W, Fink K, Klocker H, Bartsch G (1997) Prostate carcinoma screening in the county of Tyrol, Austria: experience and results. Cancer 80:1818–1829
27. Renz JF, Kin C, Kinkhabawala M, Jan D, Varadrajan R, Goldstein M, Varadarajan R, Brown R Jr, Emond JC (2005) Utilization of extended donor criteria liver allografts maximizes donor use and patient access to liver transplantation. Ann Surg 242:556–563

28. Saitoh H, Hida M, Shimbo T, Nakamura K, Yamagata J, Satoh T (1984) Metastatic patterns of prostatic cancer. Correlation between sites and number of organs involved. Cancer 54: 3078–3084
29. Salim A, Velmahos GC, Brown C, Belzberg H, Demetriades D (2005) Aggressive organ donor management significantly increases the number of organs available for transplantation. J Trauma 58:991–994
30. Serralta AS, Orbis FC, Sanjuan FR, Moya AH, Lopez-Andujar R, Pareja EI, Vila JC, Juan MB, Mir JP (2003) If the donor had an early stage genitourinary carcinoma and the liver has already been implanted, should we perform the transplantectomy? Liver Transplant 9:1281–1285
31. UNOS United Network for Organ Sharing http://www.unos.org 2006

Virchows Arch (2006) 449: 277–278
DOI 10.1007/s00428-006-0227-0

LETTER TO THE EDITOR

Rosa Noguera · Marta Piqueras · Manish Subramaniam · Julia Cruz · Adela Cañete · Antonio Llombart Bosch · Samuel Navarro

Immunohistochemical evaluation of a novel clone of monoclonal anti-MYCN antibody B8.4B in neuroblastic tumours: a correlation with MYCN gene status

Received: 27 March 2006 / Accepted: 24 April 2006 / Published online: 10 May 2006
© Springer-Verlag 2006

Abbreviations NTs: Neuroblastic tumours · MNA: MYCN-amplified neuroblastic tumours · MNNA: MYCN non-amplified neuroblastic tumours · TMA: Tissue microarray · INPC: International Neuroblastoma Pathology Classification · HE: Hematoxylin and eosin

To the Editor,

Amplification of the MYCN protooncogene is recognised as a reliable, established and an independent prognostic factor in neuroblastic tumours (NTs), identifying children with rapidly progressive disease often refractory to conventional therapy [5]. Detection of MYCN amplification is routinely carried out in the clinical staging of NTs; however, very few studies investigating the clinical significance of MYCN expression were reported. The biological value of over-expression of MYCN RNA or its protein remains controversial. Some reports have indicated a significant correlation between MYCN protein over-expression and poor prognosis [2, 4], whilst others deny its prognostic value [3]. The aim of this report was to test a novel clone of mouse monoclonal anti-human MYCN antibody B8.4B for detecting the MYCN protein on formalin-fixed paraffin embedded specimens and to compare the MYCN protein expression determined by this marker with the MYCN gene status in a series of 210 neuroblastic tumours.

The 210 neuroblastic tumours included in the study were classified according to the International Neuroblastoma Pathology Classification criteria. Forty-six of the 210 archival specimens were assembled in a tissue microarray comprising duplicate tissue cores, and the remaining 164 were analysed using conventional tissue sections. Hematoxylin and eosin sections were examined to estimate the percentage of tumour cells. Antigen retrieval was performed by boiling in pressure cooker for 3 min in 10 mM citrate buffer (pH 6.0). Immunohistochemical staining was carried out using primary mouse monoclonal anti-human N-Myc antibody (clone B8.4.B, BD PharMingen, Heidelberg, Germany) at 1:100 dilution using the DAKO ENVISION system (Dako Diagnostics, Denmark). The clone B8.4B recognises an epitope in the N terminus of human MYCN. Nuclear positivity in more than 5% of the tumour cells was considered as positive staining. Although this cutoff percentage of 5% was low, majority of the tumours showed more than 25% positivity, and only few cases displayed around 5 to 25% positivity. The topographical distribution and intensity of the staining were considered. Staining pattern was classified as focal when only one positive focus is present in the tumour sections examined, heterogeneous when multiple scattered positive foci are present with intervening negative areas and homogenous if the staining is uniform and diffuse. The range of the tumour cells positive for MYCN was grouped as 5–25%, 26–75% and more than 75%, and the number of cases under each group was calculated. The staining intensity was classified as mild, moderate and intense. Dual colour fluorescence in situ hybridization (FISH) analysis was performed according to standard protocol on touch preparations of all the 210 specimens using a cocktail DNA probe (Q-BIOgene) consisting of 2p24 MYCN red/D2Z green probes. The number of signals was analysed in at

R. Noguera (✉) · M. Piqueras · M. Subramaniam · J. Cruz · A. L. Bosch · S. Navarro
Department of Pathology, Medical School,
University of Valencia,
Avda. Blasco Ibañez, 17,
46010 Valencia, Spain
e-mail: rnoguera@uv.es
Tel.: +34-96-3864146
Fax: +34-96-3864173

A. Cañete
Pediatric Oncology Unit, Hospital La Fe,
Valencia, Spain

least 500 nuclei, and the MYCN gene status was defined according to the recommendations of the European Neuroblastoma Quality Assessment group [1].

MYCN protein was expressed in 37 of the 54 MYCN-amplified (MNA) cases (68.5%), whilst all the 15 MYCN gain cases were negative. Only 1 of the 141 MYCN non-amplified (MNNA) cases showed immunoreactivity for MYCN. Table 1 outlines the immunostaining results of MYCN protein and the clinical stages of the various histological types of MNA neuroblastomas.

The MYCN is a 60- to 63-kDa nuclear protein, which is essential in embryogenesis. MYC proteins interact with Max, a helix-loop-helix leucine zipper protein forming a sequence-specific complex, and compete with Mad and MxiI to regulate differentiation. Because the choice to undergo proliferation or differentiation may depend on the level of MYCN expression, a more aggressive phenotype in NTs might be conferred if the threshold of MYCN protein-mediated, transcription-regulatory activity is reached, whether this is due to gene amplification. Increased gene dosage necessary for up-regulating gene expression produces multiple gene copies leading to higher RNA levels, but the latter is not necessarily the result of an increased gene dosage. Thus, it is still not clear whether the MYCN protein expression without gene amplification is regulated at the transcriptional, translational or post-translational level [2].

Immunohistochemical assessment of the MYCN protein is important as high MYCN RNA levels do not necessarily suggest high-protein levels. In the present study, we report a novel clone of an anti-MYCN antibody that is highly effective in detecting the MNA NTs fixed in formalin and embedded in paraffin. This marker was positive in 68.5% of the MYCN-amplified cases. In spite of the low sensitivity, a positive immunostaining to anti-MYCN B8.4 antibody is a definite and reliable evidence of MYCN amplification in NTs. Moreover, all MYCN gain cases were negative, and only 1 of the 141 MNNA NTs showed positive immunostaining, thereby proving to be specific for MNA NTs. However, a negative test does not exclude MYCN amplification in the NTs. Our results differed from earlier reports in the sense that the MYCN markers used by them were positive in many MNNA cases [2, 4].

We conclude that this antibody promises to be a rapid, specific and cost-effective screening tool for the detection of NTs with MYCN amplification especially in peripheral health centres with no access to FISH or PCR techniques. In the near future, we plan to analyse the MYCN protein expression by Western blotting and quantify the MYCN mRNA by real-time quantitative PCR in a large series of neuroblastic tumours.

Acknowledgements This work is supported by grants PI-05/0383 and G03/089 (RITSI) from the thematic network of cooperative research of the Instituto Carlos-III, Madrid, Spain.

References

1. Ambros PF, Ambros IM (2001) Pathology and biology guidelines for resectable and unresectable neuroblastic tumos and bone marrow examination guidelines. Med Pediatr Oncol 37:492–504
2. Chan HSL, Gallie BL, DeBoer G, Haddad G, Ikegaki N, Dimitrouloakos J, Yeger H, Ling V (1997) MYCN protein expression as a predictor of neuroblastoma prognosis. Clin Cancer Res 3:1699–1706
3. Cohn SL, London WB, Huang D, Katzenstein HM, Salwen HR, Reinhart T, Madafiglia J, Marshall GM, Norris MD, Haber M (2000) MYCN expression is not prognostic of adverse outcome in advanced-stage neuroblastoma with non-amplified MYCN. J Clin Oncol 18:3604–3613
4. Hiyama E, Hiyama K, Yokoyama T, Ishii T (1991) Immunohistochemical analysis of N-myc protein expression in neuroblastoma: correlation with prognosis of patients. J Pediatr Surg 26:838–843
5. Seeger RC, Brodeur GM, Sather H, Dalton A, Siegel SE, Wong KY, Hammond D (1985) Association of multiple copies of the N-myc oncogene with rapid progression of neuroblastomas. N Engl J Med 313:1111–1116

Virchows Arch (2006) 449:279
DOI 10.1007/s00428-006-0270-x

ERRATUM

A murine model of NKT cell-mediated liver injury induced by alpha-galactosylceramide/D-galactosamine

Hideki Fujii · Shuichi Seki · Sawako Kobayashi · Takuya Kitada · Nobuyoshi Kawakita · Keishi Adachi · Hiroko Tsutsui · Kenji Nakanishi · Hiromi Fujiwara · Yoshinori Ikarashi · Masaru Taniguchi · Mitchell Kronenberg · Masaru Ikemoto · Yuji Nakajima · Tetsuo Arakawa · Kenji Kaneda

Published online: 4 August 2006
© Springer-Verlag 2006

The online version of the original article can be found at: http://dx.doi.org/10.1007/s00428-005-1265-8

H. Fujii (✉) · S. Seki · S. Kobayashi · T. Kitada · N. Kawakita
Departmet of Hepatology,
Osaka City University Graduate School of Medicine,
1-4-3 Asahimachi, Abeno-ku,
Osaka 545-8585, Japan
e-mail: rolahideki@med.osaka-cu.ac.jp

H. Fujii · M. Ikemoto · Y. Nakajima · K. Kaneda
Departmet of Anatomy,
Osaka City University Graduate School of Medicine,
Osaka, Japan

K. Adachi · H. Tsutsui · K. Nakanishi
Core Research for Evolutional Science and Technology,
Japan Science and Technology Agency,
Kawaguchi, Japan

H. Tsutsui · K. Nakanishi
Departmet of Immunology and Medical Zoology,
Hyogo College of Medicine,
Nishinomiya, Japan

H. Fujiwara
Biomedical Research Center,
Osaka University Graduate School of Medicine,
Suita, Japan

Y. Ikarashi
Pharmacology Division,
National Cancer Center Research Institute,
Tokyo, Japan

M. Taniguchi
Institute of Physical and Chemical Research,
Research Center for Allergy and Immunology,
Tokyo, Japan

M. Taniguchi
Chiba University Graduate School of Medicine,
Chiba, Japan

M. Kronenberg
La Jolla Institute for Allergy and Immunology,
San Diego, CA, USA

T. Arakawa
Department of Gastoroenterology,
Osaka City University Graduate School of Medicine,
Osaka, Japan

Virchows Arch (2005) 446:663–673

The name of the twelveth author is Mitchell Kronenberg not Kronenberg Mitchell.

Virchows Arch (2006) 449: 280
DOI 10.1007/s00428-006-0272-8
© Springer-Verlag 2006

ANNOUNCEMENTS

4–8 September 2006
Postgraduate Course
Diagnostic Breast Pathology
Department of Pathology
Medical University Graz, Austria

Course fee:
Euro 600,- Practicing pathologists
Euro 400,- Pathologists in training

For more information and registration please contact:
Edith Kleinferchner
Department of Pathology, Medical University Graz
Auenbruggerplatz 25
8036 Graz, Austria
Fax: 0043 (0) 316 385 3432
e-mail: edith.kleinferchner@meduni-graz.at
http://pathologie.meduni-graz.at/Pathologie/veranstaltungen.htm

11–13 October 2006
Postgraduate Course
Diagnostic Hepatopathology
Department of Pathology
Medical University Graz, Austria

Course fee:
Euro 400,-(Practicing pathologists)
Euro 280,-(Pathologists in training)

For more information and registration please contact:
Edith Kleinferchner
Department of Pathology, Medical University Graz
Auenbruggerplatz 25
8036 Graz, Austria
Fax: 0043 (0) 316 385 3432
e-mail: edith.kleinferchner@meduni-graz.at
http://pathologie.meduni-graz.at/Pathologie/veranstaltungen.htm

21–22 October 2006
Diseases and Tumors of the Salivary Glands
12th Salzburg Weekend Seminar
Auditorium of the Landeskliniken Salzburg, Austria

Course fee:
Euro 150.- Until 30 September 2006 (students: Euro 75.-)
Euro 180 after 1 October 2006
Euro 50.-Histopathological Slide Session (CD-Rom included)

For further information please contact:
Univ.-Doz. Dr. Johann Beck-Mannagetta
Dept. of Oral and Maxillofacial Surgergy/LKS
Müllner Hauptstrasse 48
5020 Salzburg, Austria
Fax: 0043-662-4482884
e-mail: j.beck-mannagetta@salk.at

29 November-1 December 2006
Combined Adult and Congenital Cardiovascular Pathology Course
London, UK

Course Organisers:
M. N. Sheppard, Y. Ho

Course fee:
£ 400.-
£300.- special fee for juniors in training

For further information please contact:
Short Course Office
National Heart and Lung Institute
Dovehouse Street
London SW3 6LY, UK
Fax: 0044 -020-7351-8346
e-mail: shortcourse.NHLI@IC.AC.UK

24–26 January 2007
Theorico-practical Course on Bone and Soft Tissue Tumors
Department of Pathology, Hospital del Mar, Barcelona, Spain

Faculty
Christopher Fletcher, M.D. (Brigham and Women's Hospital, Boston, USA)
Andrew Rosenberg, M.D. (Massachusetts General Hospital, Boston, USA)
Angelo Paolo Dei Tos, M.D. (Hospital of Treviso, Italy)
John Goldblum, M.D. (Cleveland Clinic, Cleveland, USA)
Paola Dal Cin, Ph.D. (Brigham and Women's Hospital, Boston, USA)

For further information please contact:
Francisco Alameda, M.D.
Department of Pathology
Hospital del Mar, Spain
E-mail: 86780@imas.imim.es
or
Esther Oliva, M.D.
Department of Pathology
Massachusetts General Hospital
55 Fruit Street, WRN-2
Boston, MA 02114, USA
E-mail: eoliva@partners.org

Virchows Arch (2006) 449:281–287
DOI 10.1007/s00428-006-0247-9

ORIGINAL ARTICLE

Assessment of epidermal growth factor receptor (EGFR) expression in primary colorectal carcinomas and their related metastases on tissue sections and tissue microarray

Frédéric Bibeau · Florence Boissière-Michot · Jean-Christophe Sabourin · Sophie Gourgou-Bourgade · Michèle Radal · Frédérique Penault-Llorca · Philippe Rochaix · Laurent Arnould · Marie-Pierre Bralet · David Azria · Marc Ychou

Received: 3 April 2006 / Accepted: 1 June 2006 / Published online: 25 July 2006
© Springer-Verlag 2006

Abstract Metastatic colorectal carcinomas (CRC) resistant to chemotherapy may benefit from targeting monoclonal therapy cetuximab when they express the epidermal growth factor receptor (EGFR). Because of its clinical implications, we studied EGFR expression by immunohistochemistry on tissue sections of primary CRC (n=32) and their related metastases (n=53). A tissue microarray (TMA) was generated from the same paraffin blocks to determine whether this technique could be used for EGFR screening in CRC. On tissue sections, 84% of the primary CRC and 94% of the metastases were EGFR-positive. When matched, they showed a concordant EGFR-positive status in 78% of the cases. Moreover, staining intensity and extent of EGFR-positive cells in the primary CRC correlated with those observed in the synchronous metastases. On TMA, 65% of the primary CRC, 66% of the metastases, and 43% of the matched primary CRC metastases were EGFR-positive. There was no concordant EGFR status between the primary and the metastatic sites. A strong discrepancy of EGFR status was noted between TMA and tissue sections. In conclusion, EGFR expression measured in tissue sections from primary CRC and their related metastases was found to be similar and frequent, but it was significantly underestimated by the TMA technique.

Keywords Epidermal growth factor receptor · Colorectal carcinoma · Metastases · Tissue microarray

F. Bibeau (✉) · F. Boissière-Michot · M. Radal
Department of Pathology, Centre Régional de Lutte Contre le Cancer Val d'Aurelle,
34298 Montpellier, Cedex 5, France
e-mail: fbibeau@valdorel.fnclcc.fr

S. Gourgou-Bourgade
Department of Biostatistics, Centre Régional de Lutte Contre le Cancer Val d'Aurelle,
Montpellier, France

J.-C. Sabourin
Department of Pathology, Hôpital Charles Nicolle,
Rouen, France

F. Penault-Llorca
Department of Pathology, Centre Jean Perrin,
Clermont Ferrand, France

P. Rochaix
Department of Pathology, Institut Claudius Regaud,
Toulouse, France

L. Arnould
Department of Pathology, Centre Georges-François Leclerc,
Dijon, France

M.-P. Bralet
Department of Pathology, Hôpital Paul Brousse,
Villejuif, France

D. Azria · M. Ychou
Department of Oncology, Centre Régional de Lutte Contre le Cancer Val d'Aurelle,
Montpellier, France

Introduction

Epidermal growth factor receptor (EGFR), also called HER1, is a member of the transmembrane tyrosine kinase receptor family. In normal and malignant cells, the activation of EGFR receptor cascades has multiple consequences, such as cell growth, differentiation, and proliferation [10]. The EGFR signaling pathway may also

promote malignant transformation, angiogenesis, and metastatic dissemination [10]. To block the activation of this receptor, targeted therapies have been developed, representing a new and promising strategy for cancer management [15]. Thus, antibodies directed against EGFR have recently been integrated into the treatment of metastatic colorectal carcinomas (CRC) resistant to chemotherapy [3, 23]. Such a strategy requires an EGFR immunohistochemical assessment by the pathologist to ensure that the targeted receptor is present in the tumor. Cancer patients included in these protocols are not always treated in the same institute for their primary disease and for their metastatic disease. Moreover, metastases are not always available for histology. It is thus possible that EGFR expression be evaluated in only one of the tumor locations (i.e., primary or metastatic). However, few and controversial data are available concerning the EGFR status in its primary site and the related metastatic sites [6, 11, 13, 24].

The first goal of our study was to analyze whether EFGR expression in colorectal primary tumors and their metastatic sites was similar or not. To answer this question, formalin-fixed and paraffin-embedded primary CRC from 32 patients and their related synchronous metastases (n=45) were examined using a standardized EGFR immunohistochemical procedure. Additionally, metachronous metastases (n=8) from four out of 32 patients were also processed for EGFR immunohistochemistry.

The second goal of this study was to evaluate EGFR expression on a tissue microarray (TMA) generated from the same paraffin blocks and to compare these results with those obtained by using the whole tissue sections. This comparison was carried out to determine whether the increasingly used TMA technology is a reliable tool for high-throughput EGFR screening in CRC [17, 26].

Materials and methods

Patient characteristics

Clinical and histopathological characteristics of the patients are reported in Table 1. Thirty-two patients, having undergone surgical resection of both the primary tumor and the corresponding metastatic sites in our institution between 2000 and 2004, were selected from a pathological database of colorectal cancer cases. There were 15 men (47%) and 17 women (53%). Median age at surgery was 60 years (ranging from 45 to 81 years). Twenty-one patients (66%) had colon cancer and 11 (34%) had rectal cancer. The most common histological type was adenocarcinoma (91%), the remaining three cases (9%) being mucinous carcinomas. According to the latest TNM classification [28], all the patients had stage-IV disease because of synchronous metastases at the time of diagnosis. Among them, four patients received neoadjuvant radiotherapy (n=2) or radiochemotherapy (n=2) for rectal carcinomas and six others received neoadjuvant chemotherapy before surgical resection of their metastases. Eighty-five paraffin-embedded tumor samples from CRC (n=32) and liver, pulmonary, and ovarian metastases (n=51, 1, and 1, respectively) were available. Synchronous metastases (n=45) were unique in 23 patients and multiple (n=22) in nine patients, consisting of two, three, or four locations in the liver (Table 1). Metachronous metastases (n=8) from four patients were also collected and assessed for EGFR immunohistochemistry. They consisted of five multiple liver metastases for one patient, one single liver metastasis for two patients, and one pulmonary metastasis for one patient. Synchronous and metachronous metastases were obtained by metastasectomy. All resected samples were received fresh, then immediately fixed in 10% pH neutral formalin for 48 h and embedded in paraffin before processing.

EGFR immunohistochemistry

EGFR immunohistochemistry was carried out on freshly sectioned tissue slides which has been shown to be critical for optimal EGFR immunoreactivity [1]. Immunohistochemistry of the tumors was performed by using the Dako autostainer and the EGFR pharmDx™ kit (K1494, Dako, Glostrup, Denmark), according to the manufacturer's instructions. Briefly, 4-μm-thick sections were mounted on silanized slides and allowed to dry overnight at 37°C. After deparaffinization and rehydratation, slides were incubated with 3% hydrogen peroxide for 5 min. After washing with the supplied buffer, tissue sections were covered for 5 min with a proteinase K solution. The slides were then incubated for 30 min with the primary mouse anti-EGFR monoclonal antibody (clone 2-18C9), which binds to a formalin-resistant epitope near the ligand-binding site on the extracellular domain of EGFR. After two rinses in buffer, the slides were incubated with a horseradish peroxidase-labeled polymer coupled to secondary antibodies for 30 min. Tissue staining was visualized with diaminobenzidine as substrate-chromogen solution. Slides were counterstained with hematoxylin, dehydrated, and mounted. Negative control sections were processed without the primary antibody but with an irrelevant murine IgG1 supplied with the kit. Negative and positive control cell slides (CAMA-1 and HT29 cell lines, respectively), provided with the EGFR pharmDx™ kit, were also used to ensure that each assay run was performed appropriately and according to protocol specifications. Furthermore, perineurium and normal mucosae on primary CRC and hepatocytes surrounding the metastases were considered as positive internal controls on tumor slides.

Table 1 Clinical data and EGFR status among primary CRC and their related metastases

Clinical data						EGFR status[a] on tissue sections									
Case no.	Sex	Age (years)	pTNM	Location	Neoadjuvant treatment	Primary site	Synchronous metastases (location number)				Metachronous metastases (location number)				
							1	2	3	4	1	2	3	4	5
1	M	60	T3N1M1	C		+	+	+	+	+					
2	M	60	T3N2M1	R	RCT	+	+	+	+						
3	M	66	T2N0M1	R		+	+	+	+						
4	M	49	T3N2M1	R	CT	+	+	+			+	+	+	+	+
5	M	70	T3N1M1	C		+	+	+							
6	F	74	T3N1M1	R	RCT	+	+	+							
7	F	59	T3N2M1	R	CT	+	+	+			−				
8	M	71	T3N2M1	C		+	+	+							
9	F	55	T3N2M1	R		−	+	−							
10	F	61	T4N1M1	C	CT	+	+				+				
11	F	68	T3N1M1	C	CT	+	+				+				
12	M	75	T3N1M1	R		+	+								
13	M	72	T3N1M1	C		+	+								
14	M	54	T3N0M1	C		+	+								
15	F	55	T4N1M1	C		+	+								
16	F	57	T4N2M1	C		+	+								
17	F	52	T3N1M1	R		+	+								
18	M	53	T3N0M1	C		+	+								
19	M	62	T4N2M1	C		+	+								
20	F	77	T3N2M1	C		+	+								
21	F	49	T3N1M1	C		+	+								
22	F	51	T3N2M1	C		+	+								
23	M	62	T3N2M1	R	RT	+	+								
24	F	65	T3N1M1	C	CT	+	+								
25	M	56	T4N1M1	C	CT	+	+								
26	F	47	T3N1M1	R	RT	+	+								
27	F	59	T3N1M1	C		+	−								
28	F	45	T3N2M1	C		+	−								
29	F	81	T3N1M1	R		−	+								
30	M	58	T2N0M1	C		−	+								
31	M	69	T3N1M1	C		−	+								
32	F	68	T3N2M1	C		−	+								

Liver metastases in all cases except for a metachronous pulmonary metastasis and a synchronous ovarian metastasis in patients 7 and 15, respectively

C colon, *R* rectum, *RCT* radio-chemotherapy, *CT* chemotherapy before surgical resection of metastasis, *RT* radiotherapy

[a]Positive if >1% of tumor cells expressed EGFR

Tissue microarray

Tissue blocks appearing to have enough material upon gross inspection were initially selected and hematoxylin–eosin-stained sections were evaluated by two observers (F. Bibeau and F. Boissière-Michot) for the presence of carcinoma. The areas to be used for the construction of the TMAs were marked on the slide and the donor block. Particular attention was made to select invasive cells near the tumor front. The tissues corresponding to selected areas were sampled using a manual arraying instrument (Manual Tissue Arrayer 1, Beecher Instruments, Sun Prairie, WI, USA). Two TMAs were constructed using 0.6-mm tissue cores. The sampling consisted of three malignant cores from different areas of the tumor from a single case of invasive colorectal cancer, placed at specified coordinates. When possible, normal mucosa was also sampled as internal control. After the arraying

was completed, TMA blocks were sectioned at a thickness of 4 μm. One section was stained with hematoxylin–eosin, and EGFR immunostaining using the immunohistochemical system kit EGFR pharmDx™ was performed on the adjacent section. Among the 32 cases sampled, 31 primary CRC, 29 metastatic sites, and 28 matched sites were assessable with this technology.

EGFR immunohistochemical staining scoring system

EGFR assessment was realized according to the EGFR pharmDx™ scoring guidelines. EGFR expression was evaluated on sections including the deepest region of tumor invasion as this region was shown to contain the greatest density of EGFR-positive cells [6]. Results were reported as positive when a complete or incomplete circumferential membrane staining was observed in at least 1% of the tumor cells. Staining was defined as immunostaining of tumor cell membranes above background level and scored as follows: 1+=weak, 2+=moderate, and 3+=strong. The absence of membrane staining or cytoplasmic staining was reported as negative. The percentage of stained cells was assessed as follows: 1–10, 10–50, and >50%. Slides were scored by two pathologists (F. Bibeau and J.C. Sabourin), who were blinded to the patients' characteristics. In the case of disagreement (three out of 91 specimens), the EGFR status was determined by consensus after simultaneous dual reexamination.

In addition to these standardized criteria, a semiquantitative analysis was performed taking into account both the staining intensity and the percentage of positive tumor cells.

Statistical analysis

The cut-off value for negative/positive expression of EGFR was 1% of tumor cells displaying a membranous staining, as specified by the EGFR pharmDx™ scoring guidelines. Data were summarized by frequency and percentage for categorical variables and by means, standard deviations, median, and range for continuous variables. For TMA analysis, the percentage of positive cells was calculated from the mean of triple cores.

The correlation between the percentage of positive cells observed on primary tumors and matched metastases was evaluated with the Spearman correlation coefficient. Associations between categorical variables were examined using McNemar's chi2 test. A P value of less than 0.05 was considered statistically significant. Due to the small number of patients with metachronous metastases, only the correlation between the matched primary CRC and the synchronous metastatic sites was made.

Results

EGFR expression of primary CRC and their related metastases on tissue sections

EGFR reactivity was not homogeneous throughout the tumors. EGFR immunostaining was mainly observed in the deepest region of the primary CRC or at the periphery of metastases, especially in the liver. Of note, EGFR immunoreactivity was often greater in isolated tumor cells and in small clusters of tumor cells.

Eighty-four percent of primary CRC (27 out of 32) and 94% of the synchronous metastases (30 out of 32) displayed EGFR reactivity in more than 1% of the tumor cells (Table 1). Overall, all patients displayed an EGFR-positive status considering EGFR-expression in the primary tumor and/or the metastatic sites. EGFR expression was positive at both sites in most of the cases (25 out of 32; 78%) and rarely in only one site, i.e., primitive (two out of 32; 6%) or metastastic (five out of 32; 16%). However, the discordant cases (i.e., positive primary sites with negative metastasis and conversely) were not statistically significant (P=0.453).

Nine (28%), 10 (31%), and eight (25%) of the primary CRC and seven (22%), 14 (44%), and nine (28%) of the synchronous metastases displayed a weak, moderate, and strong positivity, respectively. According to the extent of EGFR immunoreactivity, five (16%) primary CRC had no reactivity, 12 (37.5%) had <10% reactive cells, eight (25%) had >10–50% positive cells, and seven (22%) had >50% labeled cells. In the synchronous metastases, two cases (6%) were negative, 13 (41%) had <10% reactive cells, 11 (34%) had >10–50% positive cells, and six (19%) had >50% labeled cells.

Interestingly, the percentage of EGFR-positive tumor cells in the primary site was significantly correlated with that observed in the synchronous metastases (r^2=0.616, P=0.0002). This correlation was also demonstrated when combining EGFR scoring (labeling intensity) with the percentage of EGFR-positive tumor cells (r^2=0.559, P=0.0009). One example of the pattern of EGFR labeling in both sites is shown in Fig. 1. EGFR expression was positive among the multiple synchronous liver metastases in eight out of nine patients (i.e., 21 out of 22 samples, Table 1). The related primary site of the discordant case (two synchronous metastases: one was EGFR-positive, the other was EGFR-negative) displayed an EGFR-negative status (case number 9, Table 1).

Regarding the analysis of EGFR expression in metachronous metastases, we observed an analogous EGFR-positive status between all the available liver metastases (i.e., five metastases for one patient, one metastasis for two patients) and their related primary sites and synchronous

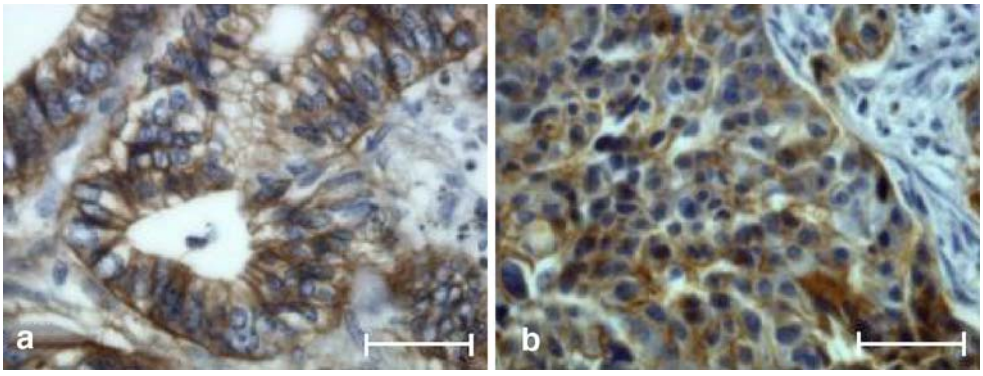

Fig. 1 Example of EGFR expression in tissue sections in a primary colorectal carcinoma (**a**) and the matched metastasis (**b**). Strong membranous staining of numerous cells in both sites (immunoperoxidase; *bar* 50 μm)

metastases (case numbers 4, 10, and 11, Table 1). The only metachronous pulmonary metastasis available for analysis did not show any EGFR immunoreactivity, whereas both the corresponding hepatic synchronous metastases and the primary site expressed EGFR (case number 7, Table 1).

EGFR expression of primary CRC and their related metastases on TMA

On the first TMA block, the EGFR status was found to be positive in 18 out of the 31 (58%) assessable primary tumors and 18 out of 29 metastases (62%) (Table 2). Only nine out of 28 (32%) assessable matched tumors were positive for both the primary and the metastatic sites, whereas four out of 28 (14%) were negative. Fifteen out of 28 (54%) cases were discordant (i.e., seven positive primary and negative metastases, and eight, conversely).

On the second TMA block, 14 out of 31 (45%) primary tumors and 16 out of 29 (55%) metastases were EGFR-positive (Table 2). Eight out of 28 (29%) assessable matched tumors were positive for both sites, whereas nine (32%) were negative. Eleven out of 28 cases (39%) were discordant (i.e., four positive primary sites and negative metastases, and seven, conversely).

When combining the two TMAs (six tissue cores), the number of positive cases increased, to reach 20 out of 31 of the primary tumors (65%) and 19 out of 29 of the metastases (66%) (Table 2). Twelve out of 28 (43%) assessable matched tumors were positive for both sites, whereas three (11%) were negative. Nevertheless, 13 cases (46%) remained discordant (i.e., six positive primary and negative metastases, and seven, conversely). Moreover, using the TMA technology and whatever the number of cores (three or six), we failed to demonstrate any correlation of EGFR expression between primitive sites and matched metastases.

Table 2 Comparison of EGFR expression in primary CRC and their synchronous metastatic sites on whole tissue sections and TMA

	Primary site	Metastases	Matched sites
Tissue sections	27/32 (84%)	30/32 (94%)	25/32 (78%)
First TMA	18/31 (58%)	18/29 (62%)	9/28 (32%)
Second TMA	14/31 (45%)	16/29 (55%)	8/28 (29%)
Both TMAs	20/31 (65%)	19/29 (66%)	12/28 (43%)

Data are expressed as the number of positive cases/total number of specimens

Comparison of EGFR expression between tissue sections and TMA

The EGFR status on the triple core-tissue array was significantly underestimated at both sites when compared with tissue sections (P=0.011 for both primitive and metastatic sites for the first TMA; P=0.0005 and P=0.0023 for primitive and metastatic sites, respectively, for the second TMA). When combining both TMAs (six tissue cores), although the number of positive cases increased, we still observed a significant discrepancy between both techniques for primitive sites (P=0.034) and metastases (P=0.0001).

Discussion

EGFR is a 170-kDa transmembrane cell surface receptor encoded by the human *HER1* gene, which promotes malignant cell proliferation and cancer progression [15]. Interfering with EGFR cell signaling by targeting strategies represents a novel approach to the treatment of solid tumors [15]. Among them, cetuximab (Erbitux®), a chimeric monoclonal human–mouse antibody, is used for the treatment of EGFR-expressing metastatic CRC that have progressed following chemotherapy [3, 23]. To identify patients eligible for this treatment, an immunohistochemical evaluation of EGFR expression is required. Although numerous studies have demonstrated EGFR expression in 70–97% of CRC [4, 6, 29], only few and controversial data are available on the EGFR status in distant metastases [6, 11, 13, 24]. Consequently, knowledge of EGFR metastastic status could be of potential value for therapeutic decisions, particularly if it differs from the primary tumors.

To answer the question as to whether EGFR expression is similar in different tumor sites, we compared the EGFR status of a set of primary CRC and their corresponding synchronous distant metastases, using a standardized immunohistochemistry test (EGFR pharmDx™, Dako). We also analyzed EGFR expression in metachronous metastases, when available, to study possible changes of EGFR expression during the metastatic process of CRC.

On whole tissue sections, our results demonstrated that EGFR expression was frequent and similar in both the primary and the metastatic sites. In our study, immunoreactivity was observed in 84 and 94% of the primary tumors and the metastases, respectively (Table 1). The 32 matched primary and synchronous metastatic CRC expressed a concordant EGFR status in 78% of the cases, all immunopositive, and the discordant cases were not statistically significant (P=0.453). Our data are in agreement with three recent studies that showed a high frequency and concordance of EGFR expression in matched primary tumors and distant metastatic lesions of CRC [8, 11, 13]. To our knowledge, only one study reported no correlation of EGFR expression on primary CRC and related metastases [24].

In addition to the concordant EGFR status between primary and metastatic locations, our study showed that both the staining intensity and the percentage of EGFR-positive cells in the primary site were significantly correlated with those observed in synchronous metastases (Fig. 1). Our work also emphasized the EGFR-positive status among multiple synchronous and metachronous metastatic sites in most of the patients (Table 1). Furthermore, we noticed an analogous EGFR-positive status between all metachronous metastases but one, their related synchronous metastases, and their primary CRC (Table 1). Such data, to our knowledge, have never been reported in clinical samples and seem to agree with the preclinical results, suggesting that EGFR expression is required for the tumor to acquire metastatic potential [19, 22, 27]. Moreover, in our cohort, all the patients displayed an EGFR-positive status. This would mean that most of the patients are potentially eligible for therapy with EGFR-targeted monoclonal antibodies, given the results of the immunohistochemistry.

The clinical relevance of EGFR immunohistochemical detection is today a matter of debate because EGFR-negative patients might respond to cetuximab and EGFR-positive patients might not [2, 3, 5, 23]. One reason proposed to explain this lack of correlation is a possible difference in the EGFR status between the primary tumor and the metastatic sites [24]. Our results do not support this hypothesis. The lack of response in EGFR-positive patients could more likely be explained by alterations in the critical downstream signals, activated via other receptors or other pathways. It is also plausible that the lack of correlation between EGFR expression and antitumor activity could be due to the potential for cetuximab to induce antibody-dependent cell-mediated cytotoxicity and to the absence of discrimination between the high- and low-affinity receptors with the commonly used antibodies [2, 14, 16]. Moreover, negative immunohistochemical results may be linked to the heterogeneity of EGFR expression and could, in part, represent false negative cases that might respond to EGFR-targeted therapy.

The second goal of our study was to perform the same analysis on TMA generated with the same paraffin blocks used for EGFR assessment on the whole tissue sections. TMA has been employed to study the molecular profile of different cancer types and to test hypotheses regarding colorectal carcinogenesis and prognosis [9, 12, 20]. However, EGFR expression in primary CRC and their related metastases has rarely been studied with this approach and the few published results are controversial [8, 25]. In our work, TMA was carried on multiple (three) cores, selected from the deepest region of tumor invasion. Nevertheless, the results obtained were systematically lower than those observed on the whole tissue sections. Even when combining the two TMAs, EGFR positivity only reached 65 and 66% in primary CRC and their related metastases, respectively (Table 2). In contrast to what we observed on tissue sections, we failed to demonstrate a correlation of EGFR expression between both sites using the TMA technology. The discordant results between the two technologies may be explained by cases containing rare stained cells (i.e., <10%) or small invasive clusters, which may be not selected when TMA is performed even using three or six cores. These small tumor clusters, also called tumor "budding," belong to a phenomenon which might be involved in metastatic spreading and seem to represent a poor prognostic factor [18, 21, 30]. Such data are of importance because TMA has been recognized as a useful and powerful tool for screening immunohistochemical markers for prognostic purposes and for carcinogenesis studies, as well.

In conclusion, we demonstrated that EGFR expression on whole tissue sections is frequent and similar in primary CRC and their related metastases. Our results also indicated that the EGFR status of the primary is concordant with those of metastases, whatever the number of sites and the time of occurrence, i.e., synchronous or metachronous. This may have clinical implications because patients are not always treated in the same institute for their primary disease and for their metastatic disease. In our experience, TMA does not represent an appropriate technique for EGFR screening in CRC because it significantly underestimates EGFR expression and does not provide data similar to those obtained with whole tissue sections. Undoubtedly, this technology is a reliable tool for the high-throughput

assessment of homogeneously distributed proteins [7], but it appears to generate unreliable information with very heterogeneous markers such as EGFR.

Acknowledgement We thank Dr. S.L. Salhi for presubmission editorial assistance.

References

1. Atkins D, Reiffen KA, Tegtmeier CL, Winther H, Bonato MS, Storkel S (2004) Immunohistochemical detection of EGFR in paraffin-embedded tumor tissues: variation in staining intensity due to choice of fixative and storage time of tissue sections. J Histochem Cytochem 52:893–901
2. Chung KY, Shia J, Kemeny NE, Shah M, Schwartz GK, Tse A, Hamilton A, Pan D, Schrag D, Schwartz L, Klimstra DS, Fridman D, Kelsen DP, Saltz LB (2005) Cetuximab shows activity in colorectal cancer patients with tumors that do not express the epidermal growth factor receptor by immunohistochemistry. J Clin Oncol 23:1803–1810
3. Cunningham D, Humblet Y, Siena S, Khayat D, Bleiberg H, Santoro A, Bets D, Mueser M, Harstrick A, Verslype C, Chau I, Van CE (2004) Cetuximab monotherapy and cetuximab plus irinotecan in irinotecan-refractory metastatic colorectal cancer. N Engl J Med 351:337–345
4. Cunningham MP, Essapen S, Thomas H, Green M, Lovell DP, Topham C, Marks C, Modjtahedi H (2005) Coexpression, prognostic significance and predictive value of EGFR, EGFRvIII and phosphorylated EGFR in colorectal cancer. Int J Oncol 27:317–325
5. Dei Tos AP, Ellis I (2005) Assessing epidermal growth factor receptor expression in tumours: what is the value of current test methods? Eur J Cancer 41:1383–1392
6. Goldstein NS, Armin M (2001) Epidermal growth factor receptor immunohistochemical reactivity in patients with American Joint Committee on Cancer Stage IV colon adenocarcinoma: implications for a standardized scoring system. Cancer 92:1331–1346
7. Gomaa W, Ke Y, Fujii H, Helliwell T (2005) Tissue microarray of head and neck squamous carcinoma: validation of the methodology for the study of cutaneous fatty acid-binding protein, vascular endothelial growth factor, involucrin and Ki-67. Virchows Arch 447:701–709
8. Gupta M, Varma V, Costonis G, Lawson D, Cohen C (2005) Epidermal Growth Factor Receptor (EGFR) in primary and metastatic colorectal carcinoma. Mod Pathol 18(Suppl 1):105A
9. Hernandez BY, Frierson HF, Moskaluk CA, Li YJ, Clegg L, Cote TR, McCusker ME, Hankey BF, Edwards BK, Goodman MT (2005) CK20 and CK7 protein expression in colorectal cancer: demonstration of the utility of a population-based tissue microarray. Hum Pathol 36:275–281
10. Holbro T, Civenni G, Hynes NE (2003) The ErbB receptors and their role in cancer progression. Exp Cell Res 284:99–110
11. Italiano A, Saint-Paul MC, Caroli-Bosc FX, Francois E, Bourgeon A, Benchimol D, Gugenheim J, Michiels JF (2005) Epidermal growth factor receptor (EGFR) status in primary colorectal tumors correlates with EGFR expression in related metastatic sites: biological and clinical implications. Ann Oncol 16:1503–1507
12. Jourdan F, Sebbagh N, Comperat E, Mourra N, Flahault A, Olschwang S, Duval A, Hamelin R, Flejou JF (2003) Tissue microarray technology: validation in colorectal carcinoma and analysis of p53, hMLH1, and hMSH2 immunohistochemical expression. Virchows Arch 443:115–121
13. Khalifa MA, Rowsell CH, Gladdy RA, Ko YJ, Hanna S, Smith A, Law C (2006) Expression of epidermal growth factor receptor in primary colorectal adenocarcinoma predicts expression in recurrent disease. Am J Clin Pathol 125:229–233
14. Lax I, Bellot F, Howk R, Ullrich A, Givol D, Schlessinger J (1989) Functional analysis of the ligand binding site of EGF-receptor utilizing chimeric chicken/human receptor molecules. EMBO J 8:421–427
15. Lockhart C, Berlin JD (2005) The epidermal growth factor receptor as a target for colorectal cancer therapy. Semin Oncol 32:52–60
16. Mattoon DR, Lamothe B, Lax I, Schlessinger J (2004) The docking protein Gab1 is the primary mediator of EGF-stimulated activation of the PI-3K/Akt cell survival pathway. BMC Biol 2:24
17. Mobasheri A, Airley R, Foster CS, Schulze-Tanzil G, Shakibaei M (2004) Post-genomic applications of tissue microarrays: basic research, prognostic oncology, clinical genomics and drug discovery. Histol Histopathol 19:325–335
18. Park KJ, Choi HJ, Roh MS, Kwon HC, Kim C (2005) Intensity of tumor budding and its prognostic implications in invasive colon carcinoma. Dis Colon Rectum 48:1597–1602
19. Parker C, Roseman BJ, Bucana CD, Tsan R, Radinsky R (1998) Preferential activation of the epidermal growth factor receptor in human colon carcinoma liver metastases in nude mice. J Histochem Cytochem 46:595–602
20. Prall F, Ostwald C, Nizze H, Barten M (2004) Expression profiling of colorectal carcinomas using tissue microarrays: cell cycle regulatory proteins p21, p27, and p53 as immunohistochemical prognostic markers in univariate and multivariate analysis. Appl Immunohistochem Mol Morphol 12:111–121
21. Prall F, Nizze H, Barten M (2005) Tumour budding as prognostic factor in stage I/II colorectal carcinoma. Histopathology 47:17–24
22. Radinsky R, Risin S, Fan D, Dong Z, Bielenberg D, Bucana CD, Fidler IJ (1995) Level and function of epidermal growth factor receptor predict the metastatic potential of human colon carcinoma cells. Clin Cancer Res 1:19–31
23. Saltz LB, Meropol NJ, Loehrer PJ Sr, Needle MN, Kopit J, Mayer RJ (2004) Phase II trial of cetuximab in patients with refractory colorectal cancer that expresses the epidermal growth factor receptor. J Clin Oncol 22:1201–1208
24. Scartozzi M, Bearzi I, Berardi R, Mandolesi A, Fabris G, Cascinu S (2004) Epidermal growth factor receptor (EGFR) status in primary colorectal tumors does not correlate with EGFR expression in related metastatic sites: implications for treatment with EGFR-targeted monoclonal antibodies. J Clin Oncol 22:4772–4778
25. Shia J, Klimstra DS, Li AR, Qin J, Saltz L, Teruya-Feldstein J, Akram M, Chung KY, Yao D, Paty PB, Gerald W, Chen B (2005) Epidermal growth factor receptor expression and gene amplification in colorectal carcinoma: an immunohistochemical and chromogenic in situ hybridization study. Mod Pathol 18:1350–1356
26. Simon R, Mirlacher M, Sauter G (2004) Tissue microarrays. Biotechniques 36:98–105
27. Singh RK, Tsan R, Radinsky R (1997) Influence of the host microenvironment on the clonal selection of human colon carcinoma cells during primary tumor growth and metastasis. Clin Exp Metastasis 15:140–150
28. Sobin LH, Wittekind CH (eds) (2002) TNM classification of malignant tumours, 6th edn. Wiley-Liss, New York
29. Spano JP, Fagard R, Soria JC, Rixe O, Khayat D, Milano G (2005) Epidermal growth factor receptor signaling in colorectal cancer: preclinical data and therapeutic perspectives. Ann Oncol 16:189–194
30. Ueno H, Murphy J, Jass JR, Mochizuki H, Talbot IC (2002) Tumour 'budding' as an index to estimate the potential of aggressiveness in rectal cancer. Histopathology 40:127–132

Virchows Arch (2006) 449:288–296
DOI 10.1007/s00428-006-0233-2

ORIGINAL ARTICLE

Routine assessment of prognostic factors in breast cancer using a multicore tissue microarray procedure

Anna Sapino · Caterina Marchiò · Rebecca Senetta · Isabella Castellano · Luigia Macrì · Paola Cassoni · Giampiero Ghisolfi · Milena Cerrato · Enrico D'Ambrosio · Gianni Bussolati

Received: 20 March 2006 / Accepted: 5 May 2006 / Published online: 13 June 2006
© Springer-Verlag 2006

Abstract We propose multicore tissue microarray (TMA) as an alternative to whole section for routine assessment of prognostic factors in breast cancer. Since 2004, we introduced the multicore TMA for testing estrogen (ER) and progesterone receptors (PR), proliferation activity by Ki67, and HER2 overexpression and amplification in routine work. At least four tumor foci were selected on the whole section, and a dedicated technician used a stereomicroscope for accurate sampling of the selected areas. To identify a specific case in the TMA, a separate file and a computerized reporting form with the TMA map were created. A preliminary pilot study comparing the TMA results with those obtained on whole sections showed the specificity of the procedure. Moreover, in everyday diagnosis, hormone receptors were repeated on full section when negative in TMA, without significant discrepancy. Retrospective analysis of the 237 breast carcinomas studied by TMA showed the expected correspondence of tumor-grade differentiation with the hormone receptor pattern, the proliferation activity, and HER2 immunohistochemical and FISH values. In conclusion, multicore TMA may be an efficient approach in the routine study of prognostic factors in breast cancer, significantly reducing costs, time, and burden of slides necessary to accomplish these mandatory tests.

A. Sapino (✉) · C. Marchiò · R. Senetta · I. Castellano · L. Macrì · P. Cassoni · G. Ghisolfi · M. Cerrato · G. Bussolati
Department of Biomedical Sciences and Human Oncology, University of Turin,
Via Santena 7,
10126 Turin, Italy
e-mail: anna.sapino@unito.it

E. D'Ambrosio
Division of Pathology, Vito Fazzi Hospital, Piazza F. Muratore, 73100 Lecce, Italy

Keywords Multicore TMA · Diagnosis · Prognostic factors

Introduction

The tissue microarray (TMA) is a technical procedure that allows combining tens to hundreds of paraffin-embedded tissue specimens into a single paraffin block, so that it is possible to have a great number of different tissues or of different pathological entities of the same organ onto a single slide for analysis at one time.

First described by Kononen et al. [10], the use of TMA has increased over the last few years as more researchers have recognized novel applications across a wide variety of scientific disciplines. In fact, TMA represents a solution for studying correlation of gene and protein expression in a large-scale tissues of either the same or of different origin [1, 5, 14, 16, 18]. It is commonly used in the development of diagnostic and prognostic indicators for clinical applications, with a wide range of techniques such as RNA in situ hybridization, fluorescence in situ hybridization, and immunohistochemistry [3, 10, 13, 20].

In breast cancer, the study of prognostic and predictive biomarkers has become a mandatory step of the pathological workup, so that for each case of breast carcinoma, pathologists are due to perform at least four immunohistochemical reactions to study estrogen (ER) and progesterone receptors (PR), HER2 protein, and at least a marker of proliferation activity such as Ki67. This involves at the same time a critical loss of precious material and a great burden of slides to be stocked in the pathology files [3]. In addition, in laboratories managing high number of breast cancer surgical specimens, the cost for this immunophenotyping in terms of technician's workload, costs of reagents, and time for evaluation of the reactions is very high.

Table 1 Clinical data of 237 patients

Age >50 years	197
Age <50 years	40
pT1c	140
pT2	69
pT3	8
pT4	7
Local recurrence	7
Distant metastases	6
pNx	13
pN0	104
pN0(i+) SN	4
pN1mi	7
pN1	56
pN2	31
pN3	9
Infiltrating ductal carcinoma	156
Infiltrating lobular carcinoma	30
Infiltrating mixed histotype	19
Infiltrating special type	32
G1	63
G2	92
G3	82

Zhang et al. [19] conducted a feasibility study by investigating the efficiency and effectiveness of immunohistochemical and FISH analyses in TMA of breast cancers constructed using a single 0.6-mm core biopsy per specimen. They found a high concordance comparing the results obtained from both TMA and full section (95%) and asserted the reliability of an immunophenotyping evaluation based on the analysis of a single tissue core. Recently, Bhargava et al. [2] using four cores demonstrated that the FISH scores were consistent among the two to four cores in the majority of the cases and that the TMA and full-section results were concordant in 99% of cases.

Taking all these data together, we decided to introduce TMA technology in routine diagnosis of prognostic and predictive factors of breast tumors. In a pilot study, we confirmed the results reported in literature [2] on the reliability of four cores to reproduce the immunophenotyping and the *HER2* gene status of the tumor. As a result, we extended this approach to the everyday diagnosis of breast tumors. We in this study report the protocol used and the analysis in terms of costs, time, archival slide load and workload of our laboratory using multicore TMA technology in breast cancer immunophenotyping and FISH testing, comparing them to the traditional examination on full sections.

Materials and methods

Case series

Thirty-six TMAs were prepared for immunohistochemical and FISH tests from a total of 237 consecutive cases of carcinomas of the breast, comprehensive of 126 cases operated in the Breast Unit of the San Giovanni Battista-Molinette Hospital of Torino from December 2004 to October 2005 and of 111 outsource cases sent for immunohistochemical testing of prognostic factors from the Vito Fazzi Hospital of Lecce. Tumors with a diameter less than 1 cm were excluded from TMA preparation. Patients' clinical data are summarized in Table 1.

Selection of areas for punching cores

For each case, we selected the tumor foci for the TMA construction during routine diagnosis by marking them on the more representative hematoxylin–eosin (H&E)-stained slide with a waterproof pencil (Fig. 1). The number of selected

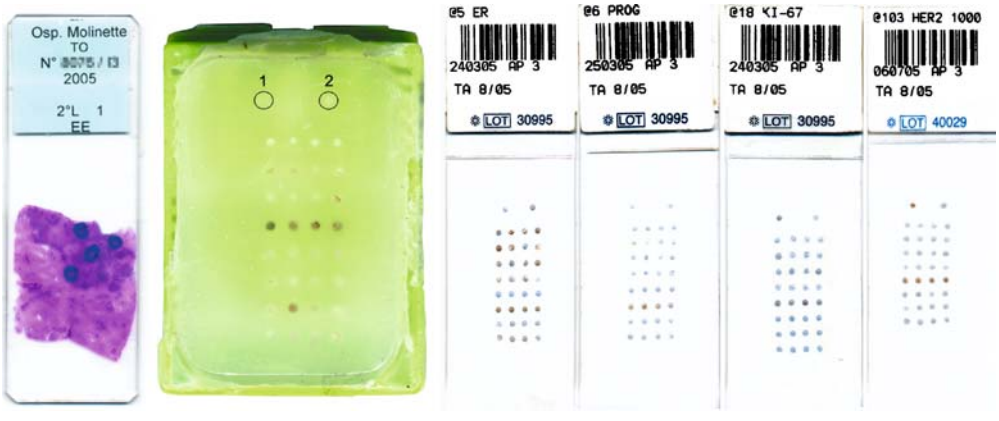

Fig. 1 Selection of areas for punching cores: the more representative foci are *marked both at the edge and at the center of the tumor* on the H&E-stained full section. Multicore TMA block: *within the circles* are ER+/PR+/HER2− (*1*) and ER−/PR−/HER2+ (*2*) controls. The correspondent sections placed in the center of the slides show a homogeneous immunostaining

fields varied from four to seven per slide, depending on the heterogeneity both of the histological pattern and of the grade of differentiation of the invasive breast cancer component. Moreover, care was taken to select areas from both the leading edge and the center of the tumor. In some cases, two different slides of the same tumor (corresponding to two different tissue blocks) were marked. One area of normal tissue was selected whenever possible to build up an internal control.

TMA construction

A serial number followed by the year, for example TMA 1/2005, was given to each TMA so that it was possible to record it on the computer database used for routine diagnosis (Win Sap v.6.2.1 Engineering Sanita' Enti Locali. Italia). The number of invasive breast carcinomas for each TMA varied from four to eight, depending on the weekly workload. When more than five fields of a tumor were selected, two lines of the same case were placed in the same TMA. TMA blocks were prepared and sliced by a dedicated technician and processed for immunohistochemical staining every Wednesday. Using the advanced tissue arrayer (mod. ATA-100, Chemicon International, Tamecula, CA, USA), tissue cylinders with a diameter of 1 mm were punched under the stereomicroscope from the specific areas of the "donor" block and brought into the "recipient" paraffin block. One core of an ER/PR-positive and HER2-negative (score 0) breast cancer and one core of an ER/PR-negative and HER2-positive (score 3+) amplified breast tumor were inserted as controls on the top of each recipient block (Fig. 1). The block was incubated in an oven at 45°C for 20′ to allow complete embedding of the grafted tissue cylinders in the paraffin of the recipient block, and then stored at 4°C until microtome sectioning. For immunohistochemical reaction and for FISH, sections were collected on Super Frost Plus slides (Menzel Glaser, Braunschweig, Germany).

Immunohistochemical and FISH procedures

TMA slides were stained using the Ventana automated immunostainer (BenchMark AutoStainer, Ventana Medical Systems, Tucson, AZ, USA). The technician took care to collect the sections on the center of the glass to avoid nonhomogeneous staining of the cores. Six sections were cut: section 1 was stained with H&E; sections 2–5 were processed for immunohistochemistry to test the following prognostic markers: ER (monoclonal antibody, clone 6F11, prediluted, Ventana-Diapath, Tucson, AZ, USA), PR (monoclonal antibody, clone 1A6, prediluted, Ventana-Diapath, Tucson, AZ, USA), Ki67 (monoclonal antibody, clone Mib1, diluted 1:200, DAKO, Glostrup, Denmark), and HER2 (polyclonal antibody, A0485 c-erbB-2 oncoprotein, diluted 1:800, DAKO, Glostrup, Denmark).

Section 6 was processed for *HER2* gene FISH analysis using PathVysion HER2/neu probe kit (Vysis, Downers Grove, IL, USA). Briefly, sections were baked overnight at 56°C, dewaxed in xylene, dehydrated in 100% ethanol, and air-dried. Slides were then treated with proteases for 45–60 min, denatured, and hybridized overnight at 37°C with the probes (HER2/neu/CEP17 SG probe 35-171060, Vysis, Downers Grove, IL, USA). Slides were washed with posthybridization buffer at 72°C, counterstained with 40,60-diamidino-2-phenylindole (DAPI), mounted, and stored in the dark before signal enumeration. For FISH analysis, the slides were examined by Olympus Bx41 fluorescence microscope equipped with a 100× oil immersion objective and a triple band pass filter for simultaneous detection of Spectrum Orange, Spectrum Green, and DAPI signals. Slides were first scanned at low power with a DAPI filter to recognize the TMA map. Areas of optimal tissue digestion and no overlapping nuclei were then selected in each core for counting. Forty to 60 cells for each case were counted. Cases were scored as amplified when the final ratio obtained in *HER2*/chromosome 17 signals was ≥2.0.

Microscopic examination

As a pilot study, the first 20 cases were immunostained on conventional full sections as well. The same protocol was then used in the routine work when a case in the TMA was found to be negative for the expression of ER/PR.

The correspondence between the fields selected on the original slide and the tissue areas pulled out of the donor block was verified on H&E-stained slides (section 1). For study purposes, the immunohistochemical results of each single core of a tumor were recorded. The results were assessed following the method published by Barghava et al. [2] that used a four-core/case TMA similar to our procedure. Briefly, for ER and PR, both the mean percentage value of stained nuclei in the four cores and the most intensively stained score (expressed by a score, from 0 to 3) were evaluated and reported together with the "quick score" [12]. This is obtained by a combination of the proportion of cell staining plus the measure of intensity, and the final value predicts the response of tumors to endocrine therapy. HER2 staining was assessed on a 0- to 3-point score [6] on each core. The highest score from different cores of the same tumor was reported. To control the results of HER2 status evaluated by TMA, we correlated the immunohistochemical and FISH results to the hormone receptor status and the Ki67 values and to the histological grades (G1, G2, and G3) of tumors, which was performed using the Elston and Ellis grading system of diagnosis [7]. After the results were obtained from the pilot study for Ki67, we reported the value of the core with the highest proliferative activity. The cut-off value to identify high or low proliferating

Table 2 Correlation of immunohistochemical and FISH results on TMA and full section (preliminary pilot study of 20 breast carcinomas)

	ER		PR		Ki67		HER2		FISH	
	q.s. ≥3	q.s. <3	q.s. ≥3	q.s. <3	>20%	<20%	Score 2+/3+	Score 0, 1+	A	NA
TMAvs full section	17/17	3/3	16/19[a]	4/1	12/13	8/7	1/2	19/18	1/1	19/19

q.s. Quick-score value 3 indicates a small (20%) chance of response to endocrine therapy (12); *ER agreement* 100%, *PR agreement* 85%
[a]In three cases, the final "quick score" was downgraded by 1 point due to either the lower percentage or the lower intensity of staining in the TMA compared to the full-section staining

activity was 20%, which corresponded to the mean proliferation of a series of 200 consecutive breast carcinomas.

Results

TMA's slides constructed with a limit of eight lines containing four to five tissue cores each (Fig. 1) were optimal in terms of staining consistency using the automated immunostainer, without discrepancy between central-placed cores and cores located at the periphery of the section. The presence of positive and negative controls and of normal tissues, when available, ensured the efficiency of the staining (Fig. 1).

Pilot study

The pilot study conducted on the first 20 cases showed high agreement between the results obtained on the full section and those obtained on TMA (Table 2). Perfect agreement was reached for ER, considering both the "quick score" and the percentage of stained nuclei, because in positive cases, the intensity of staining was almost homogeneous in all cores, the percentage of the receptor expression varied less than 5%, and no false negative results were obtained. Good agreement (85%) was achieved for PR. In fact, no false negative cases were observed in TMA. However, in two cases (10%), the percentages of receptor expression were 15 and 30% lower, respectively, in TMA than in the full section, and in three cases, the intensity varied by one point; thus, the final "quick score" value was downgraded in three cases of TMA. Good agreement (95%) was reached for Ki67 percentage results taking ≥20% of positive nuclei as the threshold value to define high proliferating tumors. In fact, only in one case of infiltrating lobular carcinoma the percentage of proliferating cells counted on TMA was 6%, while on the full section was 20%. In one case (5%), HER2 was negative (score 1+) in TMA and moderately positive in the full section (score 2+), but FISH testing on the full section confirmed that the case was not amplified. FISH results reached an agreement of 100%, considering cases as amplified or not amplified.

Routine multicore TMA

For routine tests, each TMA was constructed with four to eight cases, depending on the weekly workload (Table 3). The evaluation of TMA performance in terms of correspondence between the fields selected on the original slide and the tissue areas pulled out of the donor block showed that in about 90% of cases, the areas were correctly selected by the technician during TMA construction. As shown in Table 4, only one single core in 9.7% of cases and two cores in 0.8% of cases were not appropriate, having normal gland or fibrous tissue pulled out instead of the tumor tissue. In six cases, three or four cores floated off during the immunohistochemical processing (Table 4). The tumor in these six cases was highly sclerotic, and the cores were cracked on H&E-stained sections as well; thus, testing was performed on the full section. The results in three cases with only one core available on TMA slide corresponded to that on the full section. In cases where only one or two cores were lost, the reactions were not repeated on full section because the immunophenotype on TMA corresponded to that expected by the histology and the grade of tumors.

In the routine examination by TMA, we performed the ER and PR study on the full section of 22 cases completely negative on TMA. All these hormone receptor negative cases were G2 and G3, had a proliferation index evaluated by Ki67 ranging from 24 to 70%, and HER2 was overexpressed in nine cases. In seven of these cases, *HER2* gene was amplified. Only two out of 22 of ER/PR-negative cases resulted positive on the full section with 3% of ER and 2% of PR expression and an intensity score of 1 for both. In a case of infiltrating ductal carcinoma, only one core out of four was PR-positive. The reaction performed on the whole section confirmed that the tumor had two cell populations, one PR-positive at the leading edge, and one PR-negative in the center of tumor (Fig. 2a–d). Actually, a slightly

Table 3 Routine testing of prognostic factors in 237 cases of breast cancer: number of cases per single TMA, number of TMA and of full-section slides repeated for technical reason and/or for verifying ER/PR-negative immunostaining

Cases per TMA	4	5	6	7	8	Total number of TMA	Total number of slides
Number of TMA	2	6	7	11	10	36	
TMA slides	12	30	42	66	60		210
Repeated full-section slides	5	0	25	20	24		74

different cytohistological pattern was evident also at the retrospective examination on H&E-stained slide (Fig. 2e,f, insets). In other two cases, the tumor had a mixed ductal and lobular histotype, and the TMA was constructed with two lines of the same tumors. The immunohistochemical results were similar in the two histotypes (ER- and PR-positive, Ki67 <20%, HER2: negative).

All the 237 breast tumors were analyzed for HER2 overexpression and gene amplification by FISH (Table 5). Sixty-one cases were positive in immunohistochemistry (score 2+, 3+), and 33 of these (54%) exhibited *HER2* amplification. One case negative for HER2 overexpression (score 1+) was amplified with monosomy of chromosome 17 at FISH analysis. In addition, as reported in Table 5, HER2 was never overexpressed with score 3+ or amplified in G1 tumors, while 84% of HER2 with score 3+ were G3. HER2-negative cases showed high level of ER and PR in about 90% of cases against 56% of ER and PR nuclear expression in HER2 scored as 3+. Finally, 40% of HER2-negative cases showed high level of proliferation (≥20%) against 84% of HER2 (with score 3+)-positive cases.

Diagnostic reports

To speed up the turnaround time of the diagnostic report as smoothly as possible, a computerized report for each TMA was created. The report included a map of the TMA slide examined with the line position of the cases and the number of cores for each lines, and a table summarizing the results, as shown in Fig. 3. A final separate report was then prepared for each single case of invasive breast cancer examined on TMA. On the top of this report, the following standard phrase was added: "Prognostic factor performed on TMA number... Cores performed on block number... after selection of fields on H&E-stained sections of the tumor. The correspondence between the histology of selected fields and that of cores was assessed."

Table 4 Technical performance of TMA on 237 breast carcinomas

Number of cores	Not appropriate	Missing
1	23 (9.7%)	15 (6.3%)
2	2 (0.8%)	3 (1.2%)
3	0 (0%)	3 (1.2%)
4	0 (0%)	3 (1.2%)

Number of cores either not appropriate or missing on slides

Working time and cost analysis

The time and the cost for technical procedures and assessment of results using TMA or whole-section traditional procedure are reported in Table 6. The technical time required for preparing and sectioning one TMA constructed for example with eight cases is almost comparable to that needed for preparing eight traditional blocks and 40 slides. On the other hand, owing to the slide loads, two rounds of automated immunohistochemical staining are needed for testing eight cases using whole sections (32 slides) instead of one round using multicore TMA (four slides). The same is true for FISH because no more than six slides are processed every time by the technician to guarantee correct digestion and incubation. In addition, the time required for pathologists to read the immunohistochemical and FISH reactions is reduced by about 1 h. Finally, the costs are reduced by a factor of seven for immunohistochemical staining and FISH.

Discussions

The amount of work and responsibility for breast pathologists have notably increased in the last decade, since the assessment of prognostic and predictive factors in breast cancer has become mandatory for the therapeutic decision making. In the present study, we propose TMA of breast cancers constructed with multiple tissue cores of each tumor as an alternative to the whole section for studying ER, PR, proliferation activity by Ki67, and HER2 gene expression and amplification in routine work. In addition, we show that management of routine prognostic factors by multicore TMA carries on a significant reduction in reagent cost, technical time, and number of slides. For example, in our series of 237 breast carcinomas, we would have a burden of 1,185 slides to be stocked in the pathology file against 284 produced with 36 TMA.

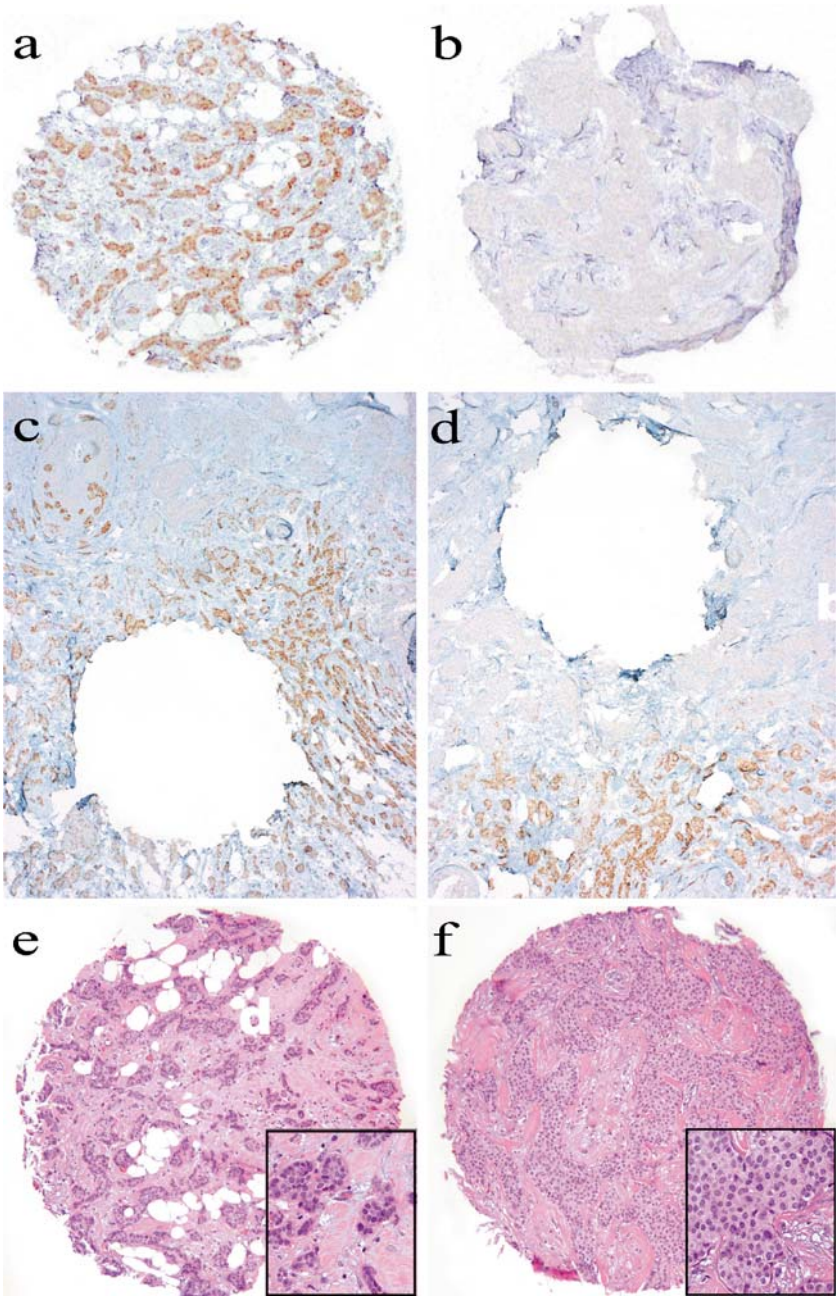

Fig. 2 Case of infiltrating ductal carcinoma with only one positive core out of four. The PR-positive core (**a**) comes from the edge of the tumor (**c**). PR-negative core (**b**) corresponds to a central area of the tumor (**d**). Slightly different histological pattern is evident in H&E staining (**e**, **f**, and insets)

However, to reach a good performance of the TMA technique in the routine assessment of prognostic factors of breast cancer, the following points are, in our opinion, mandatory: (a) specific selection of at least four tumor foci for each case and evaluation of the correspondence of the selected foci on TMA and on the full section, (b) dedicated technician, (c) use of stereomicroscope for accurate sampling and extraction of the selected area from the donor block, (d) repetition on full section of cases with negative hormonal receptor immunostaining, and (e) quality control of the results by comparing the immunophenotyping obtained by TMA with that expected by histology and grade of the tumor. In addition, to speed up the diagnostic report and to easily identify a specific case in the TMA, it was useful to create a separate file for TMA block and slide storing and a computerized reporting form with the TMA map. All these points, together with the sinking cost of the tissue microarrayer, obviously limit the

Table 5 Correlation of immunohistochemical expression of HER2 with HER2 gene amplification, tumor grade differentiation, hormone receptor status, and proliferation activity in the series of 237 breast carcinomas

HER2 score value (number of cases)	FISH amplified	G1	G2	G3	ER quick score ≥3	PR quick score ≥3	Ki67 >20%
Score 0 (79) (33%)	0 (0%)	24 (30%)	36 (46%)	19 (24%)	70 (90%)	68 (86%)	31 (39%)
Score 1+ (97) (41%)	1 (1%)	32 (33%)	42 (43%)	23 (24%)	90 (92.7%)	86 (88.6%)	41 (42%)
Score 2+ (36) (15%)	10 (27%)	7 (19%)	10 (28%)	19 (53%)	28 (77.7%)	30 (83.3%)	20 (55%)
Score 3+ (25) (11%)	23 (92%)	0 (0%)	4 (16%)	21 (84%)	14 (56%)	14 (56%)	21 (84%)
Total 237 (100%)	34 (14%)	63 (26%)	92 (39%)	82 (35%)	198 (84%)	154 (65%)	113 (48%)

use of TMA for routine to centers with high number of cases.

A limit to the use of TMA for routine immunohistochemical procedures may be the intratumoral heterogeneity and the different protein expression on cells from the leading edge vs those from the center of the tumor mass [4]. However, it has been shown that two to three cores of breast tumor are sufficiently representative of the entire lesion for assessing prognostic factors by TMA [4]. Moreover, even in highly heterogeneous tumors, such as ovarian cancer, the analysis of a single readable core matches the staining pattern of a whole section more than 90% of the time and analysis of two core increases that value to more than 95% [15]. In the present work, the selection of at least four areas on the original H&E-stained slides, which was carried out during assessment of the histological grade, guarantees that the most significant intratumoral variations in terms of tubular formation, nuclear atypia, and mitosis number are identified. In addition, in agreement with others [2], in the pilot study we confirmed that four tissue cores highly represent the original tumor, even considering the possibility of tissue

TISSUE ARRAY N. TMA 8/2005

MAP:

CONTROLS

ER/PR: +

HER2: +

	1	2	3	4	5	6	7	8
a	•	•	•	•	•	•	•	•
b	•	•	•	•	•	•	•	•
c	•	•	•	•	•	•	•	•
d	•	•	•	•	•	•	•	•
e								
f								

RESULTS

LINE	HISTOLOGICAL NUMBER	PROGNOSTIC FACTORS NUMBER	ER%	PR%	HER2	KI67%
1	4552/05 1L1	5630/05	95 3+	5 1+	0	5
2	4762/05 2N1	5634/05	95 3+	75 2+	1+	14
3	4896/05 1N1	5635/05	90 2+	8 2+	0	29
4	5013/05 3N2	5640/05	90 3+	50 2+	0	10
5	5185/05 2N	5641/05	*0	*0	3+	40
6	5220/05 1N1	5643/05	95 3+	80 3+	0	7
7	5300/05 1N2	5644/05	85 2+	35 1+	0	24
8	5312/05 2N1	5645/05	95 2+	50 2+	1+	5

*Revised on the whole section.

Turin,

Signature: ……

Fig. 3 Multicore TMA computerized form reporting the serial number of TMA and the year of construction. The map of the TMA slide includes: the controls, the line position, and the cores performed for each case. Results are reported in the table. To each line/case corresponds the histological and the prognostic factor number. The immunohistochemical results for each case are tabulated. For ER- and PR-negative cases (line 5), it is indicated that the reaction is repeated on the whole section (*)

Table 6 Comparative analysis of time and cost for studying eight cases using the traditional procedure on whole section and one TMA block (four immunohistochemical reactions, one FISH)

	Traditional procedure (eight blocks/40 slides)		TMA procedure (one block/five slides)	
	Time (h)	List price (€)	Time (h)	List price (€)
Block preparation	0.10	–	1.30	–
Sectioning	0.40	–	0.05	–
Automated immunoreactions and slides mounting	8	640	4	80
FISH reactions	96	5,600	48	700
Reading of immunohistochemical slides	1		0.30	
FISH slides	1.30		1	
Total	107.2	6,240	55.05	780

cores floating off on the slide during the immunostaining procedure. In fact, in only 2.4% of cases the reactions were repeated on the full sections because of missing cores on TMA, with a minimal impact on the final workload. Another possible bias to the use of TMA technology in routine is that a proportion of individual tissue cores may not be representative of the diagnostic section [8]. Our results show that when the TMA is prepared by a dedicated technician using a stereomicroscope for accurate sampling and extraction of the selected area from the donor block, the numbers of not appropriate cores are very low (1 core in 9.8% and 2 cores in 0.8% of cases).

Another important point is to ensure the reliability of the immunohistochemical results on multicore TMA. For this reason, first, we inserted control cores both for hormone receptors and HER2 analysis. Second, keeping in mind that the evaluation of hormone receptors is the parameter that highly influences prognosis and therapy of breast cancers [9], we decided to repeat the ER/PR test on whole section in case of negative results on TMA. A cut-off value for reporting hormone receptors as positive or negative has not been specifically defined in the literature; therefore, we use to report the percentage, the intensity, and the "quick score" [12] value that gives indication of the responsiveness of tumor to endocrine therapy separately. Using TMA, we showed some variations of PR "quick score" results compared to the full sections. The ER "quick score" was always confirmed. In addition, the retrospective analysis on the whole section of ER-negative tumors showed only in some cases a low percentage (≤3%) of ER expression that would not modify the treatment decisions. HER2 immunohistochemical reaction showed instead more variable results (95%). On the other hand, FISH test on multicore TMA had a correlation to whole-section test of 100% as was shown also in a previous work [2]. For this reason and to guarantee a quality control on the HER2 immunohistochemical results, we decided to study by FISH every TMA, with a final cost that was affordable also for routine testing. In a previous work, we showed that G1 ductal carcinomas and carcinomas of lobular and of special histological type did not show HER2 amplification even in the presence of protein overexpression [17]. The present results confirm these data with the exception of a case of lobular pleomorphic carcinoma that showed low level of gene amplification. Moreover, the retrospective analysis of the whole series of cases studied by TMA showed the expected correspondence of HER2 immunohistochemical values and FISH with the grade of tumor differentiation, the hormone receptor pattern, and the proliferation activity. In fact, the results of our series of breast cancers studied by multicore TMA match those recently published by Lal et al. [11] in a series of 3,655 breast carcinomas studied on whole histological sections.

In conclusion, multicore TMA technique may be an efficient and useful approach for routine management of prognostic factor in breast cancer, particularly for laboratories running high number of breast cancer surgical specimens, where the costs for this immunophenotyping in terms of reagents, technician's workload, and time for evaluation of the reactions are quite high.

Acknowledgements This work was supported by grants from the Ministry for Universities, Instruction and Research (MIUR), Rome, Italy; MURST (ex 60%), Rome, Italy; the Compagnia di San Paolo/FIRMS, Torino, Italy, and Regione Piemonte "Ricerca Scientifica Applicata" 2004 (Decreto Dirigenziale 59).

References

1. Abd El-Rehim DM, Ball G, Pinder SE, Rakha E, Paish C, Robertson JF, Macmillan D, Blamey RW, Ellis IO (2005) High-throughput protein expression analysis using tissue microarray technology of a large well-characterised series identifies biologically distinct classes of breast cancer confirming recent cDNA expression analyses. Int J Cancer 116:340–350
2. Bhargava R, Lal P, Chen B (2004) Feasibility of using tissue microarrays for the assessment of HER-2 gene amplification by fluorescence in situ hybridization in breast carcinoma. Diagn Mol Pathol 13:213–216

3. Bubendorf L, Nocito A, Moch H, Sauter G (2001) Tissue microarray (TMA) technology: miniaturized pathology archives for high-throughput in situ studies. J Pathol 195:72–79
4. Camp RL, Charette LA, Rimm DL (2000) Validation of tissue microarray technology in breast carcinoma. Lab Invest 80:1943–1949
5. Dhanasekaran SM, Barrette TR, Ghosh D, Shah R, Varambally S, Kurachi K, Pienta KJ, Rubin MA, Chinnaiyan AM (2001) Delineation of prognostic biomarkers in prostate cancer. Nature 412:822–826
6. Ellis IO, Bartlett J, Dowsett M, Humphreys S, Jasani B, Miller K, Pinder SE, Rhodes A, Walker R (2004) Updated recommendations for HER2 testing in the UK. J Clin Pathol 57:233–237
7. Elston CW, Ellis IO (1991) Pathological prognostic factors in breast cancer. I. The value of histological grade in breast cancer: experience from a large study with long-term follow-up. Histopathology 19:403–410
8. Gillett CE, Springall RJ, Barnes DM, Hanby AM (2000) Multiple tissue core arrays in histopathology research: a validation study. J Pathol 192:549–553
9. Goldhirsch A, Glick JH, Gelber RD, Coates AS, Thurlimann B, Senn HJ; Panel members (2005) Meeting highlights: international expert consensus on the primary therapy of early breast cancer 2005. Ann Oncol 16:1569–1583
10. Kononen J, Bubendorf L, Kallioniemi A, Barlund M, Schraml P, Leighton S, Torhorst J, Mihatsch MJ, Sauter G, Kallioniemi OP (1998) Tissue microarrays for high-throughput molecular profiling of hundreds of specimens. Nat Med 4:844–847
11. Lal P, Tan LK, Chen B (2005) Correlation of HER-2 status with estrogen and progesterone receptors and histologic features in 3,655 invasive breast carcinomas. Am J Clin Pathol 123:541–546
12. Leake R, Barnes D, Pinder S, Ellis I, Anderson L, Anderson T, Adamson R, Rhodes T, Miller K, Walker R (2000) Immunohistochemical detection of steroid receptors in breast cancer: a working protocol. UK Receptor Group, UK NEQAS, The scottish breast cancer pathology group, and the receptor and biomarker study group of the eortc. J Clin Pathol 53:634–635
13. Moch H, Kononen T, Kallioniemi OP, Sauter G (2001) Tissue microarrays: what will they bring to molecular and anatomic pathology? Adv Anat Pathol 8:14–20
14. Nocito A, Kononen J, Kallioniemi OP, Sauter G (2001) Tissue microarrays (TMAs) for high throughput molecular pathology research. Int J Cancer 94:1–5
15. Rosen DG, Huang X, Deavers MT, Malpica A, Silva EG, Liu J (2004) Validation of tissue microarray technology in ovarian carcinoma. Mod Pathol 17:790–797
16. Rubin MA, Dunn R, Strawderman M, Pienta KJ (2002) Tissue microarray sampling strategy for prostate cancer biomarker analysis. Am J Surg Pathol 26:312–319
17. Sapino A, Coccorullo Z, Cassoni P, Ghisolfi G, Gugliotta P, Bongiovanni M, Arisio R, Crafa P, Bussolati G (2003) Which breast carcinomas need HER-2/neu gene study after immunohistochemical analysis? Results of combined use of antibodies against different c-erbB2 protein domains. Histopathology 43:354–362
18. Torhorst J, Bucher C, Kononen J, Haas P, Zuber M, Kochli OR, Mross F, Dieterich H, Moch H, Mihatsch M, Kallioniemi OP, Sauter G (2001) Tissue microarrays for rapid linking of molecular changes to clinical endpoints. Am J Pathol 159:2249–2256
19. Zhang D, Salto-Tellez M, Putti TC, Do E, Koay ES (2003) Reliability of tissue microarrays in detecting protein expression and gene amplification in breast cancer. Mod Pathol 16:79–84
20. Zhang D, Salto-Tellez M, Do E, Putti TC, Koay ES (2003) Evaluation of HER2/neu oncogene status in breast tumors on tissue microarrays. Hum Pathol 34:362–368

Virchows Arch (2006) 449:297–301
DOI 10.1007/s00428-006-0259-5

ORIGINAL ARTICLE

Tissue shrinkage after fixation with formalin injection of prostatectomy specimens

Sara Jonmarker · Alexander Valdman · Anna Lindberg · Magnus Hellström · Lars Egevad

Received: 22 May 2006 / Accepted: 16 June 2006 / Published online: 15 August 2006
© Springer-Verlag 2006

Abstract Prostate cancer volume correlates with stage, grade, and progression after prostatectomy. When tumor volume is measured planimetrically, results are multiplied by a correction factor to compensate for tissue shrinkage caused by processing. Injection of formalin into prostatectomy specimens was suggested for improved fixation. Our aim was to investigate how this affects the prostate volume. We studied 142 radical prostatectomy specimens. All prostates were immersed in 10% formalin. In 84 prostates (59%) we also injected 20 ml of formalin before routine fixation. The prostates were weighed unfixed after injection and after final fixation. The specimens were sliced and totally embedded. The transverse diameters of the prostates were measured on unfixed specimens and microscopic sections. The average weight loss after final fixation was 5.8 and 8.6% for formalin-injected specimens and standard-fixed specimens, respectively (p<0.001). However, when total shrinkage was estimated from the transverse diameters, there was no difference related to fixation technique (p=0.59). The average linear shrinkage was 4.5%, corresponding to a volume correction factor of 1.15. We conclude that formalin injection for fixation of prostate tissue does not influence tumor volume calculation compared to conventional fixation.

S. Jonmarker · A. Valdman · A. Lindberg · L. Egevad (✉)
Department of Oncology and Pathology,
Karolinska University Hospital,
Stockholm 171 76, Sweden
e-mail: lars.egevad@ki.se

M. Hellström
Department of Urology,
Karolinska University Hospital,
Stockholm, Sweden

Keywords Prostate cancer volume · Tissue shrinkage · Formalin · Prostatectomy

Introduction

Numerous studies on prostate cancer were based on estimates of tumor volume [1, 2, 6, 11, 17–20, 23, 26]. Tumor volume in radical prostatectomy specimens was first reported by McNeal et al. [19] in 1986. The authors demonstrated that tumor volume correlates with histopathological parameters such as extraprostatic extension, positive surgical margins, and seminal vesicle invasion. Moreover, tumor volume was shown to correlate with histological grade [20] and to predict tumor stage and the risk of progression after radical prostatectomy [2, 6, 8, 17–19, 21, 23, 26].

For planimetric measurement of prostate cancer volume, the prostate is sliced at 3–5 mm, totally embedded, and the tumor is outlined on the glass slides [19]. Tumor volume is calculated by measuring the tumor areas on the slides and by multiplying by the slice thickness. The total tumor volume is the sum of volumes of each tissue slice.

Tissue shrinkage during specimen processing is one of the factors that may significantly affect the accuracy of prostate volume calculations [21]. To compensate for tissue shrinkage during specimen processing, a correction factor is used. The purposes of using a correction factor are to estimate the true volume of the unfixed tumor as it was in vivo and to obtain data sets that are comparable between laboratories. Published correction factors vary from 1.0 to 1.5 [1, 3, 9, 11, 13, 23–25] with 1.22 [23] and 1.5 [19] being the most cited ones. In all of these studies, the correction factor was calculated for specimens that were

fixed by standard procedures, i.e., by immersion of the entire specimen in buffered formalin. However, some laboratories routinely use formalin injection [12]. This method provides a quicker and more uniform fixation than conventional fixation by immersion in formalin [12]. Furthermore, formalin injection improves staining for several immunohistochemical markers [4]. However, to the best of our knowledge the effects of formalin injection on the prostate volume have not been studied yet. Thus, it is not clear whether the correction factor used for standard fixation can also be applied on formalin-injected specimens. The aim of the present study was to measure the effects of formalin injection on prostate tissue shrinkage.

Materials and methods

The study included 142 consecutive radical prostatectomy specimens collected from April 2003 to July 2004 at the Karolinska Hospital. Immediately after surgery, the prostatectomy specimen was immersed in ice and usually arrived at the Department of Pathology within 20 min. The seminal vesicles were removed and the unfixed prostate weighed. The transverse, sagittal, and vertical diameters of the prostate were measured with a slide caliper (Fig. 1a). The prostates were cut in halves by a horizontal section (Fig. 1b). Where tumor was seen macroscopically, a small tissue block was excised from the cut surfaces for other research purposes. The prostates were weighed before and after the tissue sampling. The weight before sampling was routinely registered in our laboratory procedure, but the weight after sampling was used for analysis of the effect of formalin fixation, which is reasonably independent of the weight of the excised tissue.

Of the 142 prostatectomy specimens, 84 (59%) were formalin-injected and 58 (41%) were immediately immersed in formalin according to the standard protocol. The prostates of the first group were injected at multiple sites with a total of 20 ml 10% buffered formalin solution (4% formaldehyde). The procedure was performed with a 20-ml syringe and a 23-G (0.6-mm) needle (Fig. 1c). To ensure more homogeneous fixation, the solution was injected deep into the prostate while slowly retracting the needle. The specimens were weighed after injection. The remaining 51 (41%) prostates were fixed without formalin injection.

The halves of the gland were mounted on a cork plate (Fig. 1d) and immersed in 10% buffered formalin for overnight fixation. After fixation, the weight was measured again. The surgical margins were inked with four different colors, one for each side, for optimal orientation on the glass slides. The prostate was sliced horizontally at 4 mm from apex to base. All specimens were dehydrated, embedded in paraffin, cut at 4 μm, and stained with hematoxylin and eosin. Of all slices, 77 (54%) were processed as whole-mount sections and 65 (46%) as standard sections, usually by cutting the horizontal slices in four quadrants.

The microscopic sections were measured on glass slides with a ruler at 1-mm precision. Only slices 3, 4, and 5 were

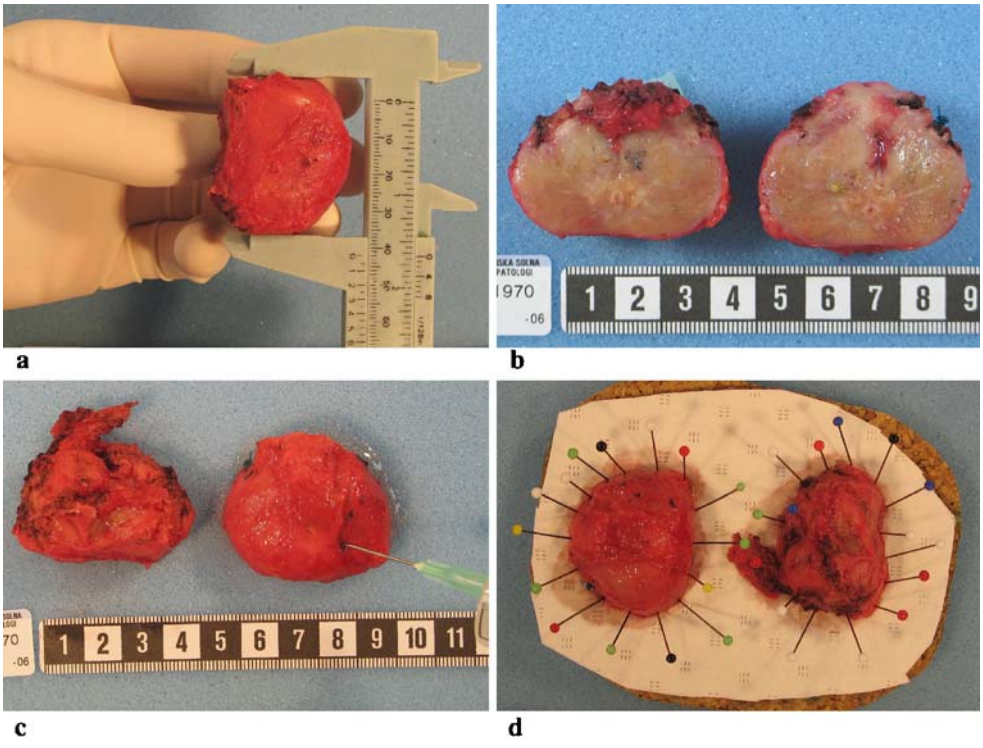

Fig. 1 The radical prostatectomy specimen processing. **a** The transverse, sagittal, and vertical diameters of the prostate were measured with a slide caliper. **b** The prostate was cut in halves by a horizontal section. **c** The prostate was injected at multiple sites with a total of 20 ml 10% buffered formalin solution. **d** Two halves of the prostate gland mounted on a cork plate

used for tissue shrinkage analysis because they corresponded to the level where the width of the unfixed specimens was measured. On whole-mount slides, the maximum width between the lateral boundaries of the prostate was measured. On quadrant sections, the widths of two adjacent quadrants were added.

Unpaired *t* test was used for calculations of weight differences and differences in percent of shrinkage between groups. A p value <0.05 was considered significant.

Results

The prostate weights before and after sampling for research, after formalin injection, and after final fixation are summarized in Table 1. The average weight of the unfixed specimens was 41.9 g (median 37.6, range 14–122). The average weights in the injection and standard fixation groups were 41.2 and 42.9 g, respectively (p=0.57). The average loss of weight after tissue sampling for research purposes was 0.7 g (range 0–3.3). The average gain of weight after formalin injection was only 1.7 g (range 0.2–4.1). The average weight loss after final fixation was 5.8 and 8.6% for formalin-injected specimens and standard-fixed specimens, respectively (p<0.001), (Fig. 2).

The tissue shrinkage is summarized in Table 2. For all specimens, the average linear shrinkage (as determined by measurements on glass slides compared to unfixed specimens) was 4.5%, which translates into a linear correction factor of 1.047 (100/95.5). Because the volumetric shrinkage correction must take into account linear shrinkage in three dimensions [25], the volume correction factor obtained in this study was $(1.047)^3$=1.15. There was no significant difference in shrinkage between formalin-injected specimens and standard-fixed specimens (4.1 and 4.9%, p=0.59), indicating that formalin injection does not have any effect on calculations of prostate cancer volume. The theoretical tumor volumes of the processed specimens (i.e., based on microscopic sections) were derived by dividing the weights of unfixed prostates with the correction factors calculated for the formalin injection and standard fixation groups (1.13 and 1.16, respectively). The mean volumes obtained were almost identical (mean 36.3 and 36.9 ml, respectively; p=0.83). The average linear shrinkage of whole-mount sections vs quadrant section was 4.7 and 4.3%, respectively (p=0.79).

Discussion

Prostate cancer volume has long been recognized as one of the tools capable of predicting postoperative progression rate [2, 6, 7, 14, 16, 27]. Epstein et al. [7] found that 26% of men with tumors smaller than 4 ml experienced recurrence 5 years after prostatectomy, as opposed to 49% of men with tumors larger than this. According to Stamey et al. [27], the recurrence rate after prostatectomy was 14, 39, 67, and 97% with tumor volumes of 0.5–2, 2–6, 6–12, and >12 ml, respectively. Some authors [7, 15] have claimed that tumor volume does not provide additional prognostic information beyond that obtained from Gleason score, extraprostatic extension, surgical margin status, and seminal vesicle invasion. This may be true when the majority of tumors are small. In other studies based on series of larger cancers, tumor volume was found to be an independent prognostic factor [14, 22]. Despite the dramatic decrease of tumor volume observed in prostatectomy specimens in recent years [5], there are still populations with relatively large prostate cancers [10], indicating that determination of tumor volume remains clinically significant.

Formalin fixation is known to shrink biological tissue [25]. The degree of shrinkage depends on type of specimen and laboratory-specific circumstances such as formalin concentration and duration of the fixation. After fixation, the specimen is dehydrated and paraffin-embedded, which may further affect volumes. The paraffin block is cut at approximately 4 μm and the sections are then usually allowed to expand on warm water. To some extent, this counterbalances the tissue shrinkage induced by formalin fixation and dehydration. However, the tissue expansion

Table 1 Weight measurements at four processing stages in formalin-injected (INJ) and immersion-fixed (IMM) specimens

	Average weight (g)			Weight difference (%)		
	Unfixed	After sampling	After formalin injection	After fixation	After injection vs after sampling	After fixation vs after sampling
All	41.9±17.6	41.2±17.4	42.1±18.6	38.3±16.4		−6.9±4.1
IMM	42.9±16.1	42.2±15.9		38.6±15.0		−8.6±4.3
INJ	41.2±18.5	40.4±18.4	42.1±18.6	38.0±17.3	+4.4±2.6	−5.8±3.6
p value (IMM vs INJ)	0.57	0.54		0.83		<0.001

Weight differences (%)±SD

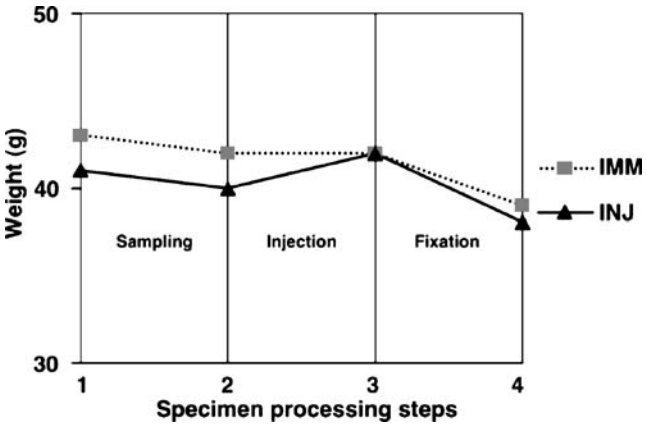

Fig. 2 The average weight changes at four specimen processing stages (*1* Unfixed, *2* after research sampling, *3* after formalin injection, and *4* after final fixation) in immersion-fixed (*IMM*) and formalin-injected (*INJ*) specimens

depends on the temperature and duration of the water bath. These factors may be variable between laboratories and are therefore sources of interlaboratory variability of tissue shrinkage. Finally, sections are rehydrated. At this point, the sections are attached to glass slides and tissue rehydration could not possibly counterbalance tissue shrinkage. A correction factor is used for accurate calculation of prostate cancer volume in radical prostatectomy specimens. Laboratories use different tissue fixation techniques and, hence, shrinkage correction factors must be calculated for each laboratory. Formalin injection ensures more uniform fixation compared to standard fixation by immersion in formalin [12] and significantly improves the staining for a number of immunohistochemical markers [4]. The present study was designed to investigate the effects of formalin injection on prostate tissue shrinkage. To our knowledge, this is the largest study of its kind.

By injecting 20 ml of formalin, the average specimen weight only increased by 1.7 g, a surprisingly low figure given that the weight of 20 ml formalin is approximately 20 g. The explanation for this is that most of the formalin will pass directly through the specimen and could be seen penetrating from the surfaces of the prostate. Artifacts like tissue edema or needle tracks were never seen microscopically in injected prostates.

Table 2 Tissue shrinkage (%) and differences in shrinkage between groups ±SD

	Quadrant sections	Whole-mounts	Formalin-injected	Standard-fixed	All
Shrinkage (%)	4.3±8.6	4.7±8.8	4.1±8.7	4.9±8.7	4.5±8.7
p values (paired differences)	0.79		0.59		

The specimens were both measured and weighed during tissue processing. The average weight loss after final fixation of formalin-injected specimens was significantly less than that of standard-fixed specimens. However, this did not result in any significant difference in shrinkage measured directly on the slides. This depends on the reversing effects of postfixation steps (rehydration and flotation on a water bath) on prostate tissue shrinkage.

The volumetric tissue shrinkage correction factor obtained in the present study was 1.15, which is almost identical to the one reported by Schned et al. [25]. Furthermore, similar to Schned et al., we showed that shrinkage is independent of the section type and the same correction factor can conveniently be used for all section types. A major reason for using injection fixation is to obtain better preservation of epitopes for immunohistochemistry. A limitation of the current study is that we have not compared the immunoreactivity between the study groups. However, such a comparison would be rather difficult to perform in the current series. There is a substantial interindividual variability in the immunoreactivity of these markers and it is also very likely that there is some variation of immunoreactivity because of differences in prostate size leading to different formalin diffusion velocity. Yet, we believe that a faster fixation will lead to improved immunohistochemistry in at least some cases.

In summary, we demonstrate here that the addition of formalin injection does not have any effect on tissue shrinkage as measured on the microscopic slides and, hence, does not affect prostate cancer volume calculations. Our findings support the routine usage of formalin injection fixation.

Acknowledgement We thank the laboratory technicians Ingeborg May and Ulf Hörnberg for excellent assistance with the handling of prostatectomy specimens.

References

1. Blackwell KL, Bostwick DG, Myers RP, Zincke H, Oesterling JE (1994) Combining prostate specific antigen with cancer and gland volume to predict more reliably pathological stage: the influence of prostate specific antigen cancer density. J Urol 151:1565–1570
2. Boswick DG, Graham SDJ, Napalkov P, Abrahamsson PA, di Sant'agnese PA, Algaba F, Hoisaeter PA, Lee F, Littrup P, Mostofi FK, Denis L, Schroeder F, Murphy GP (1993) Staging of early prostate cancer: a proposed tumor volume-based prognostic index. Urology 41:403
3. Cupp MR, Bostwick DG, Myers RP, Oesterling JE (1995) The volume of prostate cancer in the biopsy specimen cannot reliably predict the quantity of cancer in the radical prostatectomy specimen on an individual basis. J Urol 153:1543–1548
4. De Marzo AM, Fedor H, Gage WR, Rubin MA (2002) Inadequate formalin fixation decreases reliability of p27Kip1 immunohistochemical staining: probing optimal fixation time using high-density tissue microarrays. Human Pathol 33:756–760

5. DeMarzo AM, Nelson WG, Isaacs WB, Epstein JI (2003) Pathological and molecular aspects of prostate cancer. Lancet 361:955–964
6. Epstein JI, Oesterling JE, Walsh PC (1988) Tumor volume versus percentage of specimen involved by tumor correlated with progression in stage A prostatic cancer. J Urol 139:980–984
7. Epstein JI, Carmichael M, Partin AW, Walsh PC (1993) Is tumor volume an independent predictor of progression following radical prostatectomy? A multivariate analysis of 185 clinical stage B adenocarcinomas of the prostate with 5 years of follow up. J Urol 149:1478–1481
8. Epstein JI, Walsh PC, Carmichael M, Brendler CB (1994) Pathologic and clinical findings to predict tumor extent of nonpalpable (stage T1c) prostate cancer. JAMA 271:368–374
9. Greene DR, Egawa S, Neerhut G, Flanagan W, Wheeler TM, Scardino PT (1991) The distribution of residual cancer in radical prostatectomy specimens in stage A prostate cancer. J Urol 145:324–329
10. Häggarth L, Busch C, Norberg M, Häggman M, Norlen BJ, Egevad L (2005) Prediction of the volume of large prostate cancers by multiple core biopsies. Scand J Urol Nephrol 39:380–386
11. Häggman M, Nybacka O, Nordin B, Busch C (1994) Standardized in vitro mapping with multiple core biopsies of total prostatectomy specimens: localization and prediction of tumour volume and grade. Br J Urol 74:617–625
12. Hoedemaeker RF, Ruijter ET, Ruizeveld-de Winter JA, van der Kaa CA, the Biomed II MPC Study Group, van der Kwast TH (1998) Processing radical prostatectomy specimens. J Urol Pathol 9:211–222
13. Humphrey PA (1993) Complete histologic serial sectioning of a prostate gland with adenocarcinoma. Am J Surg Pathol 17:468–472
14. Humphrey PA, Walther PJ, Currin SM, Vollmer RT (1991) Histologic grade, DNA ploidy, and intraglandular tumor extent as indicators of tumor progression of clinical stage B prostatic carcinoma. A direct comparison. Am J Surg Pathol 15:1165–1170
15. Kikuchi E, Scardino PT, Wheeler TM, Slawin KM, Ohori M (2004) Is tumor volume an independent prognostic factor in clinically localized prostate cancer? J Urol 172:508–511
16. Lerner SE, Blute ML, Zincke H (1996) Risk factors for progression in patients with prostate cancer treated with radical prostatectomy. Semin Urol Oncol 14:12–20; discussion 21
17. McNeal JE (1992) Cancer volume and site of origin of adenocarcinoma in the prostate: relationship to local and distant spread. Hum Pathol 23:258–266
18. McNeal JE (1997) Prostate cancer volume. Am J Surg Pathol 21:1392
19. McNeal JE, Bostwick DG, Kindrachuk RA, Redwine EA, Freiha FS, Stamey TA (1986) Patterns of progression in prostate cancer. Lancet 1:60–63
20. Miller GJ (1989) Histopathology of prostate cancer: prediction of malignant behavior and correlation with ultrasonography. Urology 33:18–26
21. Noguchi M, Stamey TA, McNeal JE, Yemoto CE (2000) Assessment of morphometric measurements of prostate carcinoma volume. Cancer 89:1056–1064
22. Norberg M, Holmberg L, Wheeler T, Magnusson A (1994) Five year follow-up after radical prostatectomy for localized prostate cancer-a study of the impact of different tumor variables on progression. Scand J Urol Nephrol 28:391–399
23. Partin AW, Epstein JI, Cho KR, Gittlesohn AM, Walsh PC (1989) Morphometric measurement of tumor volume and percent of gland involvement as predictors of pathological stage in clinical stage B prostate cancer. J Urol 141:341–345
24. Schmid H-P, McNeal JE (1992) An abbreviated standard procedure for accurate tumor volume estimation in prostate cancer. Am J Surg Pathol 16:184–191
25. Schned AR, Wheeler KJ, Hodorowski K, Heaney JA, Ernstoff MS, Amdur RJ, Harris RD (1996) Tissue-shrinkage correction factor in the calculation of prostate cancer volume. Am J Surg Pathol 20:1501–1506
26. Stamey TA, McNeal JE, Freiha FS, Redwine E (1988) Morphometric and clinical studies on 68 consecutive radical prostatectomies. J Urol 139:1235–1241
27. Stamey TA, McNeal JE, Yemoto CM, Sigal BM, Johnstone IM (1999) Biological determinants of cancer progression in men with prostate cancer. JAMA 281:1395–1400

Virchows Arch (2006) 449:302–307
DOI 10.1007/s00428-006-0237-y

ORIGINAL ARTICLE

Morphometric sum optical density as a surrogate marker for ploidy status in prostate cancer: an analysis in 180 biopsies using logistic regression and binary recursive partitioning

Girish Venkataraman · Vijayalakshmi Ananthanarayanan · Gladell P. Paner · Rui He · Saeedeh Masoom · James Sinacore · Robert C. Flanigan · Eva M. Wojcik

Received: 21 March 2006 / Accepted: 14 May 2006 / Published online: 3 August 2006
© Springer-Verlag 2006

Abstract We sought to identify morphometric descriptors predictive of nondiploidy in prostatic adenocarcinoma on prostate needle biopsies using logistic regression (LR) and binary recursive partitioning (BRP) and compare the equivalence of both methods. A total of 180 prostate needle biopsies diagnosed as prostatic adenocarcinoma were selected. Deoxyribonucleic acid ploidy and morphometry were performed separately on Feulgen-stained sections from these biopsies using the CAS-200 system and Nuclear Morphometry Suite, respectively. Seven morphometric predictors were tested as predictor variables, including nuclear area, circularity, elongation, sum optical density (OD), configuration run length, coefficient of variation (CV), and angularity. Logistic regression (LR) identified a two-parameter model including sum OD and circularity that had a 93.9% overall correct prediction rate (area under curve = 0.950; 95% CI: 0.913, 0.987). A reduced model including only sum OD was equally good without any significant loss of predictive accuracy (93.3% correct overall classification rate). BRP also selected sum OD as the most predictive parameter; a sum OD cut-off of 7.73 in this model identified 93.3% of the nondiploid cases correctly. Morphometric OD can be used as a surrogate marker of nondiploidy. LR and BRP models are both equivalent in identifying and correctly classifying non-diploid cases of prostate cancer using sum OD as the predictor variable.

Keywords Prostate · Biopsy · Morphometry · Ploidy · Logistic regression · Binary recursive partitioning

G. Venkataraman (✉) · G. P. Paner · R. He · S. Masoom · E. M. Wojcik
Department of Pathology, Loyola University Medical Center, 2160, South First Avenue, Bldg. 110, Room 2233, Maywood, IL 60153, USA
e-mail: gvenkat@lumc.edu

R. C. Flanigan
Department of Urology, Loyola University Medical Center, Maywood, IL, USA

J. Sinacore
Department of Preventive Medicine/Biostatistics, Loyola University Medical Center, Maywood, IL, USA

V. Ananthanarayanan
Department of Pathology, University of Illinois, Chicago, IL, USA

Introduction

Several investigators have used morphometric measurements to determine differences in the nuclear size and shape of normal and neoplastic prostatic tissue. Changes in nuclear morphometric parameters have also been shown to correlate with prognosis in prostatic adenocarcinomas [6, 10, 11]. Many morphometric parameters that measure size, shape, texture, and Markovian texture descriptors have been used to predict patient outcomes in prostate cancer. Recently, a number of software programs have emerged that compute an increasing number of morphometric parameters derived from the same basic set of image data, which raises the question of whether the additional parameters are providing new information or simply additional measurement variables. If it is the latter, data reduction should be among the steps taken before modeling.

On the other hand, nuclear ploidy has also been shown to have prognostic significance in prostate cancer [2, 7]. The

observation of nondiploidy may be due to internal nuclear expansion secondary to increased cellular deoxyribonucleic acid (DNA) ploidy. Given this background, it is conceivable that the information gleaned from assessment of nuclear ploidy and nuclear morphometry may sometimes be overlapping and redundant. Hence, there is a need to determine which of the morphometric parameters can give the same information as ploidy—even better, if a single morphometric parameter contains all the information about ploidy status, separate assessment of ploidy may be obviated.

Materials and methods

Case selection and Feulgen staining

We selected 180 cases of prostatic adenocarcinoma, with pathologic Gleason scores (GS) ranging from 5 to 9, diagnosed by prostatic needle biopsy. Two cases with prior history of hormonal therapy and radiation therapy were excluded from the study. All cases had between 6 and 14 cores taken per patient. Clinical data including age, prebiopsy PSA, and transrectal ultrasound findings were also available for analysis. Cases with GS<7 were assigned as low-grade cancers, and cases with GS≥7 were assigned as high-grade cancers. Once the biopsy was diagnosed as adenocarcinoma, the biopsy site with the highest GS was selected for subsequent ploidy and morphometry analysis, and one 5 to 7-μm-thick section from the formalin-fixed, paraffin-embedded biopsy tissue was cut and stained with Feulgen, a stain that is specific for nuclear DNA. The process of staining involves hydrolysis with concentrated hydrochloric acid. The acid treatment extracts out the nonnuclear substances and then hydrolyzes the nuclear chromatin into its constituent nucleic acids. This is followed by binding of the dye to the nucleic acids, which, in turn, imparts a blue color to the nuclei.

Ploidy analysis

DNA image cytometry-based assessment of ploidy was evaluated by computer-assisted image analysis using a CAS-200 image analysis system (Becton-Dickinson, San Jose, CA, USA) equipped with CellSheet version 2.0 software (Bacus Laboratories, Lombard, IL, USA). A total of 80–120 nuclei were manually analyzed per case giving data from approximately 18,000 nuclei across the 180 cases. Areas on the Feulgen-stained sections that contained pathological lesions, as defined by adjacent H&E stained slides, were marked for DNA content analysis. For calibration, nuclei of rat hepatocytes with a known content of DNA were used. The calibration slide was initially used to adjust the focus of the microscope (40×) and set the proper light intensity (8.4–9.6 mV). Twenty hepatocytes were then located on the slide and measured to produce a relative DNA mass calibration histogram with a predefined CV of 0–3%.

The CAS-200 software generates a gallery of image file for each case termed as an image list mode (ILM) file, containing the nuclear data. Thereafter, the software automatically categorizes cases as nondiploid based on the upper limit of normal G0/G1 peak DI (using DI=1.1 as the upper limit of the normal euploid range). All the nondiploid cases in our study had a 4c peak percentage of cells ranging from 12% (DNA index 1.38) to 70% (DNA index 1.48). Cells not immediately classified were selected manually by drawing new boundaries around the desired nuclei. Incomplete cells, overlapping nuclei, and debris were deleted manually as well. After adjusting the field image, selected nuclei were measured and were added to a cell analysis histogram.

Sections from hydatidiform moles with a known set of triploid or tetraploid DNA were used as controls in the ploidy analysis.

Morphometry

Nuclear morphometry analysis was performed on the same CAS-200 ILM files generated for ploidy analysis using the Nuclear Morphometry Suite (Bacus Laboratories, Lombard, IL, USA). Cells were selected for acquisition via digital filter. Cell images were initially screened by a pathologist as well as technician after acquisition for quality-control purposes. Overlapping or irregularly shaped nuclei were excluded before morphometry analysis. A total of seven morphometric parameters were tested as predictor variables—including mean nuclear area and sum optical density (OD) (size features), circularity, elongation and angularity (shape features), configuration run length (general texture descriptor), and coefficient of variation (CV) (Markovian descriptor). Markovian texture features characterize variations between adjacent pixels in an image based on mathematical algorithms using a gray-level transition probability matrix, thus providing an overall quantitative assessment of fine changes in chromatin structure. All morphometry output files were exported as Excel CSV files and then imported into an MS Access 2000 database before analysis.

Statistical analysis

Baseline correlation between the various parameters was performed using the Pearson's product-moment correlation. All scale data were checked for significant deviations from a normal distribution using the Kolmogorov–Smirnov test. Chi-square analysis was performed to test the significance of difference of proportions. The phi (ϕ) coefficient was used to test the strength of associations after a significant chi-square.

Multivariate LR (MLR) modeling was performed using the forward Wald model. Using the predicted probabilities of the LR model for each case, a receiver operator characteristics (ROC) analysis was performed to identify the ability of the models to predict nondiploidy. An area under the ROC curve (AUROC) of 1 indicates perfect discrimination, while an area ≤0.5 indicates discrimination no better than random chance.

Thereafter, binary recursive partitioning was performed using the Classification and Regression Tree (CART) algorithm to identify the morphometric variables that best predicted nondiploidy. CART belongs to a family of nonparametric regression methods and is based on the recursive partitioning method [9]. The CART model builds a decision tree structure that begins by splitting the sample space into two partitions; each partition, or node, is split into two more partitions, and so on until further splitting cannot improve the performance of the classifier into diploid and nondiploid groups. Parameters with the most discriminative abilities figure at the higher nodes in the tree diagram. A minimum parent node size of 60 and a minimum child node size of 30 were used in the analysis, implementing the Gini algorithm and pruning to prevent overfitting. Analysis was performed using cross-validation. All CART analysis was implemented using the tree function in Statistical Package for the Social Sciences (SPSS) Answertree (SPSS 13; SPSS, Chicago, IL, USA).

The percentages of correct classification in both methods (MLR and CART) were compared to each other. The clustered bar graph (Fig. 1), scatter plot matrices (Fig. 2), and jittered dot density (Fig. 4) were generated using SYSTAT 11; the ROC plot (Fig. 3) was constructed using SPSS 13.

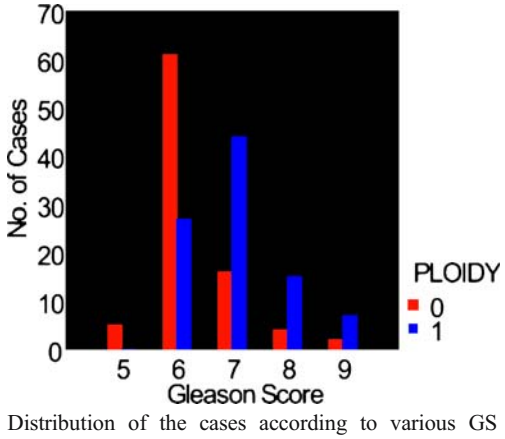

Fig. 1 Distribution of the cases according to various GS groups stratified by the ploidy status. There was a significant trend toward nondiploidy with higher GS [*red bars* (0), diploid; *blue bars* (1), nondiploid]

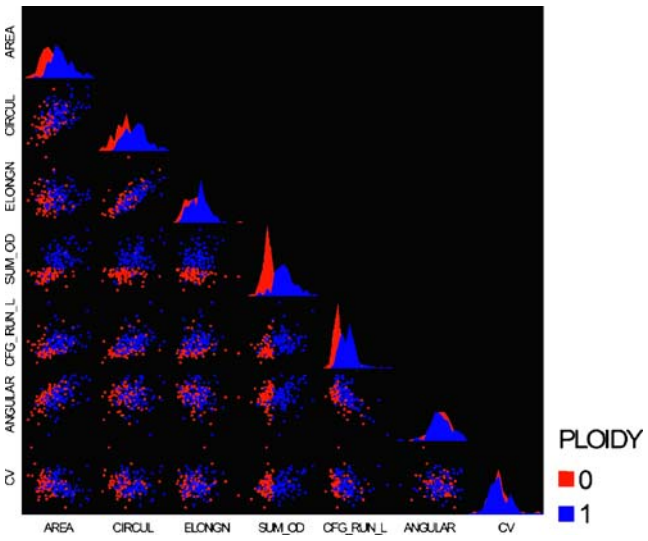

Fig. 2 Scatter Plot Matrix (SPLOM) depicting the density distributions of the seven morphometric classifiers by the ploidy status [*red dots*/*bars* (0), diploid; *blue dots*/*bars* (1), nondiploid). The best separation of diploid and nondiploid is seen with sum OD where there is minimal overlap of the histograms

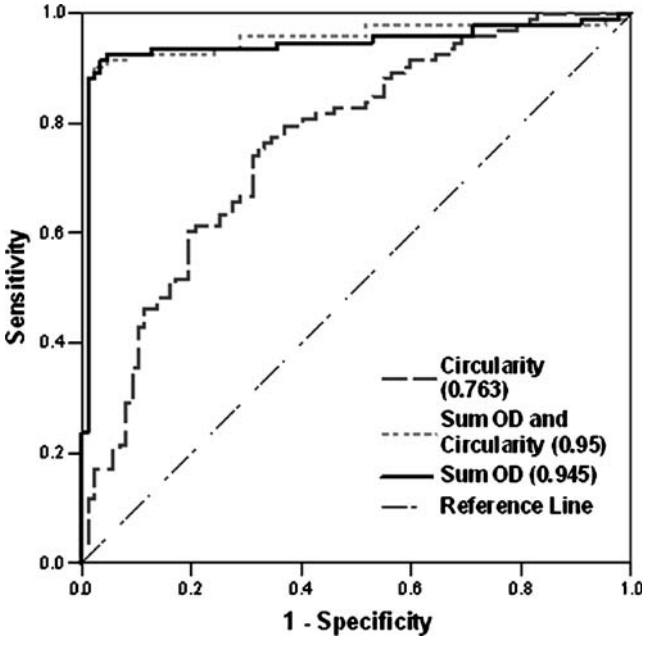

Fig. 3 ROC curves of the three LR models using morphometric sum OD only, circularity only, and a combination of sum OD and circularity. The ROC curve for each parameter is plotted using 1-specificity on the *x*-axis and sensitivity on the *y*-axis. The specific model corresponding to each curve is indicated in the *legend* along with the AUROC for that respective curve in *parentheses*. As apparent from the curves, a reduced model utilizing morphometric sum OD only (AUROC=0.945) is equally good at predicting nondiploidy as the combined model using circularity and sum OD (AUROC=0.95). The *reference line* indicates the AUROC cut-off of 0.50 (*n*=180)

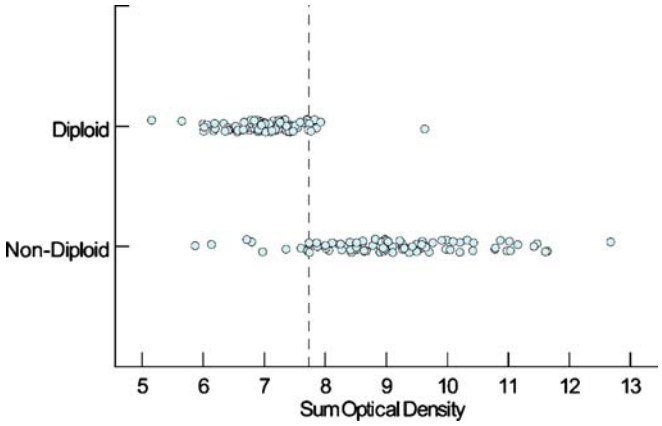

Fig. 4 Jittered dot plot of the sum OD measurements for diploid and nondiploid cases with *reference line* at 7.73 derived from CART analysis (n=180)

Results

There were a total of 87 diploid and 93 nondiploid cases with GS ranging from 5 to 9 (Fig. 1). There was a statistically significant association of nondiploidy with high GS (Pearson's χ^2=39.47; p=0.0001; ϕ coefficient=0.47). Among the morphometric parameters, sum OD was found to have the highest correlation with nondiploidy (Pearson's r=0.77, p=0.0001). The correlation for nuclear area, configuration run length, and circularity were also found to be good but lesser than sum OD (Table 1). Angularity and CV did not have any significant association with nondiploidy (Fig. 2).

In the MLR analysis, only two of the seven morphometric features were included in the final model, namely, sum OD (odd's ratio [OR]=14.13; 95% CI: 6.15, 32.43) and circularity (OR=5.196; 95% CI: 1.35, 19.97). This two-feature model including morphometric sum OD and circularity had an AUROC of 0.950 (95% CI: 0.913, 0.987) with 93.9% of the cases correctly classified as diploid or nondiploid. A reduced nested model using only sum OD correctly classified 93.3% of the cases correctly (AUROC=0.945; 95%CI: 0.905, 0.985) (Fig. 3).

CART is widely used in the behavioral sciences and has recently been applied to the high-dimensional data of proteomic assays. In the CART analysis using the C&RT algorithm as the tree growing method, again, sum OD was selected as the most discriminative feature with a 93.9% correct overall classification rate. CART chose a cut-off of 7.73 for sum OD above which to classify cases as nondiploid (with this, 96.6% of the nondiploid cases were correctly classified). None of the other parameters was selected in the final CART model, although the second most important feature selected by the CART model was configuration run length (Fig. 4).

Discussions

In prostate cancer, the introduction of new technologies, designed to assess biologically relevant alterations in tumor cells, has the potential to provide additional prognostic and predictive information from biopsies [1]. One such technique is the assessment of DNA ploidy in tumors. DNA ploidy studies, using various technologies, are abundant in the literature, but questions remain as to how such studies should be translated into evidence-based practice [8].

Table 1 Correlation matrix of the seven morphometric parameters with the ploidy status assessed

	Area	Circularity	Elongation	Sum OD	Config RL	Angularity	CV	Ploidy
Area	1.00							
Circularity	0.54	1.00						
Elongation	0.07	0.79	1.00					
Sum OD	0.62	0.44	0.18	1.00				
Config RL	0.46	0.56	0.34	0.47	1.00			
Angularity	0.45	0.02	−0.19	0.22	−0.49	1.00		
CV	−0.27	−0.10	0.03	0.17	−0.17	−0.06	1.00	
Ploidy	**0.56**	0.46	0.24	**0.77**	0.52	0.02	0.01	1.00

The most significant correlations are highlighted in bold
Config RL Configuration run length

Nuclear morphometry too, on the other hand, is based on evaluation of subtle changes in chromatin texture and nuclear contours in the cell of interest. Studies modeling outcomes based on morphometry as well as ploidy need to be interpreted with caution, as morphometry data are inherently redundant and multivariate in nature owing to the large number of correlated predictors. A single summary measure or computer models that select only the relevant information hold an obvious appeal.

One of the early studies correlating nuclear morphometry with ploidy in rectal cancer indicated that nuclear circularity correlated significantly with ploidy [4]. This is well in agreement with our data wherein circularity and sum OD were selected as the two significant parameters in the LR model to predict nondiploidy; it is interesting to note that almost all information about ploidy was contained within sum OD itself. Hence, we believe that the information offered by nuclear circularity is redundant. In a subsequent study in prostate cancer on fine needle aspirates, nondiploid tumors were found to have a higher mean nuclear area but none of the other factors was discriminative [12]. In another study, the mode of the OD was predictive of lymph node metastases after radical prostatectomy; this fact is corroborative of the fact that sum OD was the only factor predictive of nondiploidy in our study [3].

CART has two distinct advantages over LR. Firstly, the classifier is not assumed to be linear in x; and secondly, it is not necessary for the analyst to specify which interactions are to be tested, assuming the model is not simply additive. In a dataset with eight predictors, there are at least 20 possible two-way interactions and more than 40 three-way interactions.

In a more recent study on prostatic biopsies, a multivariate discriminant model identified configurable run length, difference variance, contrast, inverse difference moment, sum entropy, and diagonal variance as histomorphometry features capable of distinguishing diploid from nondiploid tumors [5]. These results are partly at variance with the features selected in our study. We believe that this is, in part, due to the larger size of our dataset. Even so, configuration run length did have a significant association with nondiploidy in our analysis too; but this was not included in our final model because it was highly correlated with circularity and sum OD.

We developed another LR model utilizing the parameters in the aforementioned study along with sum OD; this model included only sum OD and configurable run length as significant parameters with an AUC of 0.949. Once again, sum OD was the most important contributor in this model (data not shown). The CAS-200 ploidy determination of any individual cell partly takes into account the DNA index, the OD, and size and shape of the nucleus, among other parameters, for assessing ploidy class; this, we believe, is a probable explanation for why sum OD has such strong predictive ability.

There are, however, a few limitations to our study, which merit consideration. Firstly, we could not perform a systematic split-sample validation on our data because we were concerned that a reduced number of cases due to splitting the dataset as training and validation sets may lead to overfitted unstable models with unacceptable power. Addressing this issue partly, we have performed CART modeling to verify the information obtained from LR analysis insofar as both these modeling techniques (CART and LR), among other modeling techniques including kernel density and linear discriminant analysis, have recently shown to have the lowest misclassification rates in a study analyzing morphometric features in lung carcinoma cell lines [13].

Secondly, it could be argued that the same ILM gallery file could be used to derive ploidy information and morphometric information separately using the features available in the software; we believe that the more important information to keep in mind—when assessing morphometry as well as ploidy using the same software—is that morphometric features containing ploidy information should be excluded from the list of "morphometric predictors" so that redundant and duplicated information about ploidy will not be included in the final models predicting outcomes. Despite these limitations, our data represent the largest study to date studying the association of ploidy and nuclear morphometry on prostate biopsies. In conclusion, a single surrogate marker of nondiploidy like morphometric sum OD may give all the information offered by nuclear ploidy—possibly obviating the need to perform separate assessment of ploidy on prostate biopsies to predict survival outcomes.

References

1. Baak JP, Janssen E (2004) DNA ploidy analysis in histopathology. Morphometry and DNA cytometry reproducibility conditions and clinical applications. Histopathology 44:603–614
2. Cheng L, Sebo TJ, Slezak J, Pisansky TM, Bergstralh EJ, Neumann RM, Iczkowski KA, Zincke H, Bostwick DG (1998) Predictors of survival for prostate carcinoma patients treated with salvage radical prostatectomy after radiation therapy. Cancer 83:2164–2171
3. Epstein JI, Pizov G, Steinberg GD, Carter HB, Pitcock R, Armas OA, Partin A, Walsh PC (1992) Correlation of prostate cancer nuclear deoxyribonucleic acid, size, shape and Gleason grade with pathological stage at radical prostatectomy. J Urol 148:87–91
4. Heimann TM, Cohen RD, Szporn A, Gil J (1991) Correlation of nuclear morphometry and DNA ploidy in rectal cancer. Dis Colon Rectum 34:449–454
5. Kay PA, Riehle DL, Cheville JC, Lohse CM, Pankratz VS, Hill EM, Sebo TJ (2002) Comparison of quantitative histomorphom-

etry and DNA ploidy in tissue sections of prostate carcinoma. Anal Quant Cytol Histol 24:7–14
6. Khan MA, Walsh PC, Miller MC, Bales WD, Epstein JI, Mangold LA, Partin AW, Veltri RW (2003) Quantitative alterations in nuclear structure predict prostate carcinoma distant metastasis and death in men with biochemical recurrence after radical prostatectomy. Cancer 98:2583–2591
7. Lau WK, Blute ML, Bostwick DG, Weaver AL, Sebo TJ, Zincke H (2001) Prognostic factors for survival of patients with pathological Gleason score 7 prostate cancer: differences in outcome between primary Gleason grades 3 and 4. J Urol 166:1692–1697
8. Martinez Jabaloyas JM, Jimenez Sanchez A, Ruiz Cerda JL, Sanz Chinesta S, Sempere A, Jimenez Cruz JF (2004) Prognostic value of DNA ploidy and nuclear morphometry in metastatic prostate cancer. Actas Urol Esp 28:298–307
9. Stewart PW, Stamm JW (1991) Classification tree prediction models for dental caries from clinical, microbiological, and interview data. J Dent Res 70:1239–1251
10. Veltri RW, Miller MC, Partin AW, Coffey DS, Epstein JI (1996) Ability to predict biochemical progression using Gleason score and a computer-generated quantitative nuclear grade derived from cancer cell nuclei. Urology 48:685–691
11. Veltri RW, Partin AW, Epstein JE, Marley GM, Miller CM, Singer DS, Patton KP, Criley SR, Coffey DS (1994) Quantitative nuclear morphometry, Markovian texture descriptors, and DNA content captured on a CAS-200 Image analysis system, combined with PCNA and HER-2/neu immunohistochemistry for prediction of prostate cancer progression. J Cell Biochem Suppl 19:249–258
12. Wang N, Stenkvist BG, Tribukait B (1992) Morphometry of nuclei of the normal and malignant prostate in relation to DNA ploidy. Anal Quant Cytol Histol 14:210–216
13. Wolfe P, Murphy J, McGinley J, Zhu Z, Jiang W, Gottschall EB, Thompson HJ (2004) Using nuclear morphometry to discriminate the tumorigenic potential of cells: a comparison of statistical methods. Cancer Epidemiol Biomarkers Prev 13:976–988

Virchows Arch (2006) 449:308–314
DOI 10.1007/s00428-006-0238-x

ORIGINAL ARTICLE

Oncofetal protein glypican-3 in testicular germ-cell tumor

Satoshi Ota · Michiyo Hishinuma · Naoko Yamauchi · Akiteru Goto · Teppei Morikawa · Tetsuya Fujimura · Tadaichi Kitamura · Tatsuhiko Kodama · Hiroyuki Aburatani · Masashi Fukayama

Received: 5 April 2006 / Accepted: 15 May 2006 / Published online: 4 August 2006
© Springer-Verlag 2006

Abstract The expression of an oncofetal protein, the glypican-3 (GPC3), was immunohistochemically evaluated in a wide variety of primary testicular germ-cell tumors (GCTs) in comparison with other markers, alpha-fetoprotein (AFP), human chorionic gonadotropin (hCG)-beta, and OCT3/4. Eighty-nine cases of GCT including 22 cases of mixed GCT were evaluated with reference to each tumor component. GPC3 expression was observed in neoplastic cells of yolk-sac tumor (YST) (25/25), teratoma (2/10), components of syncytiotrophoblastic giant cells (STGCs) (10/14), and choriocarcinoma (1/3), but none in intratubular germ-cell neoplasias, unclassified type (0/33), seminomas (0/61), or embryonal carcinoma (0/19). All cases of YST showed diffuse labeling of neoplastic cells in cytoplasmic and membranous patterns, and the positive area of GPC3 was much larger than that of AFP. Glandular structures in teratomas showed GPC3 immunostaining as well as AFP. Although the number of GPC3-positive cells was smaller in STGC components and choriocarcinoma, there was no diffusion artifact in GPC3 immunostaining, as was frequently encountered in hCG-beta staining. Thus, GPC3 is a unique oncofetal protein, which is useful as an immunohistochemical marker for GCT differentiated to extraembryonic tissue, especially YST.

Keywords Testis · Glypican-3 · Germ-cell tumor · Neoplasia · Yolk-sac tumor · Biomarker

S. Ota (✉) · M. Hishinuma · N. Yamauchi · A. Goto · T. Morikawa · M. Fukayama
Department of Pathology, Graduate School of Medicine, University of Tokyo, Hongo 7-3-1, Bunkyo, Tokyo 113-0033, Japan
e-mail: soota-path@umin.ac.jp

T. Fujimura · T. Kitamura
Department of Urology, Graduate School of Medicine, University of Tokyo, Hongo 7-3-1, Bunkyo, Tokyo 113-0033, Japan

T. Kodama · H. Aburatani
Genome Science Division, Research Center for Advanced Science and Technology, University of Tokyo, Tokyo 153-8904, Japan

Gypican-3 (GPC3) is a cell-surface heparan sulfate proteoglycan linked to the extracytoplasmic cell-surface membrane by a glycosilphosphatidylinositol anchor [6]. Heparan sulfate proteoglycans are important regulators of heparin-binding growth factors, such as fibroblast growth factors (FGFs) and WNTs [2, 7], thought to regulate different growth factors in a tissue-specific manner. Recent studies have shown a marked elevation of GPC3 mRNA in hepatocellular carcinoma (HCC) over the level observed in corresponding normal tissues. Applying highly specific monoclonal antibodies against GPC3 to paraffin-embedded tissues of the liver, we recently demonstrated that GPC3 expression was specific to the fetal liver and to malignant neoplasms of hepatocyte lineage (HCC and hepatoblastoma) [24]. Subsequent study of GPC3 expression in AFP-producing gastric carcinoma demonstrated that GPC3 was concordantly expressed with alpha-fetoprotein (AFP), but discordantly with other hepatocyte markers, such as PIVKA-II and hepatocellular antigen [10]. These findings suggest that GPC3 is an oncofetal protein closely associated with AFP, and this raises the possibility that GPC3 can be used as an immunohistochemical marker for the classification of testicular germ-cell tumor (GCT).

GCT is the most common malignant neoplasm of the testis [5]. There are multiple types of testicular GCT that each shows a different degree of tissue differentiation.

Seminoma and intratubular germ-cell neoplasia, unclassified (IGCNU), and embryonal carcinoma are defined as pluripotent potential tumors [5, 23]. Other GCTs, including yolk-sac tumor (YST), teratoma, and choriocarcinoma, are more differentiated [5, 23]. Among the differentiated tumor components, YST remains the most commonly overlooked component of the mixed form of GCT [19, 20]. Most patients with tumors with YST component have elevated levels of serum AFP [14, 22]; however, small foci of YST are sometimes not detected even with the use of AFP immunostaining.

The aim of this study was to establish the sensitivity of immunohistochemical staining against GPC3 in the diagnosis of a large variety of primary testicular tumors, especially differentiated GCTs.

Materials and methods

Tissue samples

Testicular tissue specimens were retrieved from the file of the Department of Pathology, Tokyo University Hospital, which were surgically resected from 1984 to 2005. The 89 GCT samples included 22 MGCTs (Table 1). The histological components were classified by hematoxylin and eosin staining with the help of immunohistochemical stainings of AFP, placental alkaline phosphatase (PLAP), human chorionic gonadotropin (hCG)-beta, and OCT3/4. OCT3/4 was recently identified as the sensitive marker for seminoma and embryonal carcinoma [15]. Each component was counted, respectively, such as seminoma (n=61), spermatocytic seminoma (n=1), IGCNU (n=33), components of syncytiotrophoblastic giant cells (STGCs) (n=14), embryonal carcinoma (n=19), YST (n=25), teratoma (n=10), choriocarcinoma (n=3), and others. In addition, we examined sections from malignant lymphoma (n=4), adenomatoid tumor (n=1), undifferentiated sarcoma (n=1), solitary fibrous tumor (n=1), inflammatory disease (n=6), cryptorchism (n=3), and ovotestis (n=1). Diagnoses of testis GCTs were according to the accepted criteria [5].

Table 1 Demographical features of testicular neoplasms and lesions in this study

Histology	Total cases	Age	Median
Nonneoplastic	10	0.3–50	40
IGCNU	1	40	40
Seminoma	53	22–71	36
Spermatocytic seminoma	1	30	30
Embryonal carcinoma	2	26	26
Yolk-sac tumor	4	0.1–2.1	0.8
Choriocarcinoma	1	25	25
Teratoma	4	2.0–23	12
Carcinoid	1	65	65
Mixed germ-cell tumor	22	16–49	28.5
Nongerm-cell tumor	7	5–70	64
Total	106		

IGCNU Intratubular germinal cell neoplasm, unclassified

Antibodies and immunohistochemistry

Monoclonal antibodies for GPC3 were generated in our laboratory and previously reported [9, 10, 24]. For immunohistochemical staining, the primary antibodies against GPC3 (monoclonal, GPC-C02, dilution 1:2,500), AFP (rabbit polyclonal, 1:200, Dako, Copenhagen, Denmark), PLAP (monoclonal, 8A9, 1:50, Dako), hCG-beta (monoclonal, C6405, Nichirei, Tokyo, Japan), OCT3/4 (1:500, goat polyclonal, Santa Cruz Biotechnology, Santa cruz, CA, USA) were used. Tissue sections on silanated slides were deparaffinized with xylene, rehydrated with a series of graded ethanols, processed with an autoclave in 10 mmol/l citrate buffer for 5 min, pH 6.0, treated with horse serum albumin to block nonspecific staining, and immunostained. The detection of antibody binding was visualized by the avidin–biotin complex technique using diaminobenzidine as a chromogen. The sections were counterstained with hematoxylin.

The degree of immunohistochemical staining in the evaluation of GCT was defined as positive when the percentage of positive cells was more than 5% of the entire tumor cells for each histological type. For GPC3 and AFP immunostaining in YST, immunohistochemical expression was further graded as follows: +, 5–10% cells stained; ++, 10–50% cells stained; +++, >50% cells stained.

Results

Immunohistochemistry of GPC3 in nonneoplastic and neoplastic testis

The immunohistochemical results in nonneoplastic and neoplastic testes are presented in Table 2. Immunoreactivity for GPC3 was entirely negative in normal testicular components, such as Sertoli cells, spermatocytes, and Leydig cells. Inflammatory cells in both inflammatory lesions and tumors were also negative. On the other hand, GPC3-positive staining was observed in neoplastic cells of STGCs, YST, choriocarcinoma, and teratoma.

IGCNU, seminoma, and STGCs

Immunoreactivity for GPC3 was negative in both typical and spermatocytic seminomas. GPC3 expression was also negative in IGCNU, which was identified as accompanying

Table 2 GPC3, AFP, hCG-beta, and OCT3/4 expression in testis germ-cell tumors

	Total number	Positive cases (%)			
		GPC3	AFP	hCG-beta	OCT3/4
Nonneoplastic testis	10	0	0	0	0
IGCNU	33	0	0	0	32(97%)
STGCs	14	10(71%)	0	14(100%)	0
Seminoma	61	0	0	0	61(100%)
Spermatocytic seminoma	1	0	0	0	0
Embryonal carcinoma	19	0	0	0	18(95%)
Yolk-sac tumor	25	25(100%	23(92%)	0	0
Choriocarcinoma	3	1(33%)	0	3(100%)	0
Teratoma	10	2(20%)	2(20%)	0	0
Carcinoid	1	0	0	0	0

GPC3 Glypican-3; *AFP* alpha-fetoprotein; *hCG-beta* human chorionic gonadotropin-beta; *IGCNU* intratubular germinal cell neoplasm, unclassified; *STGCs* syncytiotrophoblastic giant cells

seminoma, embryonal carcinoma, and MGCT. On the other hand, most scattered neoplastic cells of STGCs in seminoma and MGCT were positive for GPC3 (10/14) (Fig. 1a,b).

Embryonal carcinoma

No immunohistochemical staining of GPC3 was found in either pure embryonal carcinomas or the embryonal carcinoma component in MGCT (Fig. 2).

Yolk-sac tumor (YST)

YST consisted of four infantile and 21 adult cases. All cases of infantile YST presented as the pure form, and adult cases as one of the components of MGCT. The most striking finding in GPC3 immunohistochemistry was the diffuse labeling of neoplastic cells in YST (25/25, 100%) (Fig. 2), whether in isolated form (Fig. 2a) or in combination with other components (Fig. 2c), in "the double layer pattern", glandular structures of embryonal carcinoma encircled by a row of flattened YST cells [1, 3], in MGCT. GPC3 positivity showed membranous and cytoplasmic staining patterns (Fig. 2a, inset). Among various histologic patterns of YST, most areas of reticular (Fig. 2a), macrocystic, and glandular patterns in YST showed diffuse positivity for GPC3. In the solid pattern, staining was not diffuse, but there were occasional neoplastic cells positive for GPC3 (Fig. 2e).

Choriocarcinoma

One of the three cases of choriocarcinoma exhibited focal immunoreactivity with antibodies to GPC3 (Fig. 3a). Some cytotrophoblasts and syncytiotrophoblasts in the choriocarcinoma were positive for GPC3 (Fig. 3b).

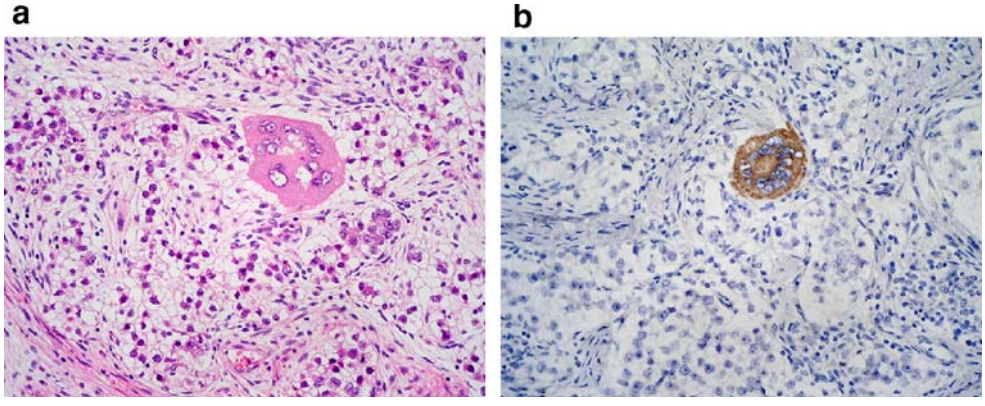

Fig. 1 GPC3 expression in syncytiotrophoblastic giant cells (STGCs) in seminoma. **a** Seminoma with STGCs. **b** GPC3 immunostaining in STGCs. Seminoma cells are totally negative

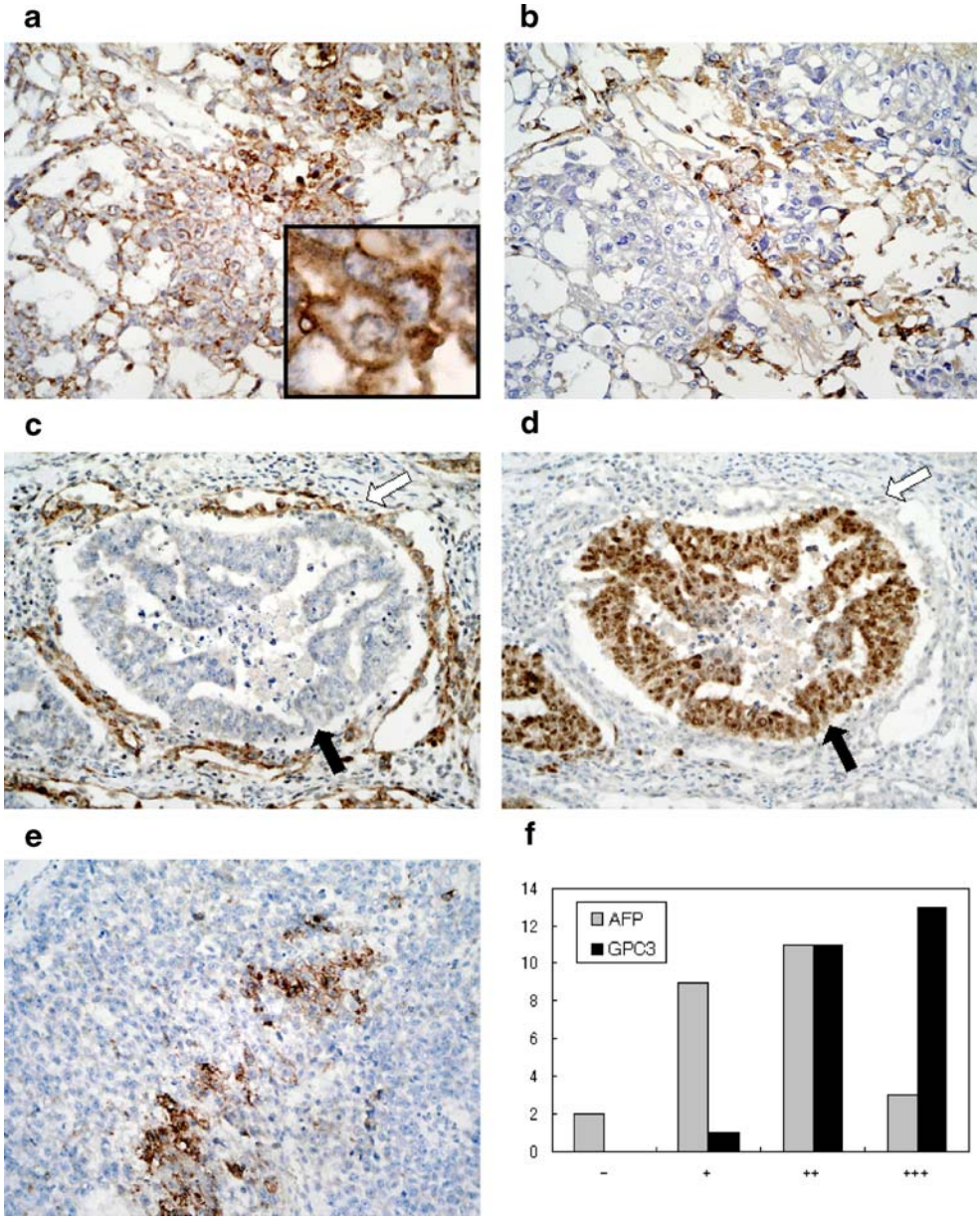

Fig. 2 GPC3 expressions in yolk-sac tumor(YST). **a** GPC3 immunostaining in YST with reticular pattern. *Inset* Membranous and cytoplasmic staining of GPC3. **b** AFP immunostaining in YST with reticular pattern. Parallel section to **a**. **c** GPC3 immunostaining in the "double layer pattern" of YST, *open arrow*, and embryonal carcinoma, *solid arrow*. **d** OCT3/4 immunostaining in the "double layer pattern" of YST, *open arrow*, and embryonal carcinoma, *solid arrow*. Note that GPC3 and OCT3/4 immunostaining is mutually exclusive. **e** GPC3 immunostaining in YST with a solid pattern. AFP staining was restricted to a smaller number of cells. **f** Staining intensity of GPC3 and AFP in YST cases. +, 5–10% cells stained; ++, 10–50% cells stained; +++, >50% cells stained

Teratoma and others

Some immature glandular structures showed weak GPC3 staining in two cases of immature teratoma (Fig. 4a). GPC3 was negative in most teratoma components, resembling the epidermis, smooth muscle, fat, neural tissue, cartilage, and bone. One carcinoid tumor was also negative for GPC3.

Comparison with representative marker molecules for germ-cell tumors

AFP

AFP staining was observed in the cytoplasm of neoplastic cells in YST (23/25) and teratoma (2/10). There were two cases of MGCT, in which AFP immunohistochemistry

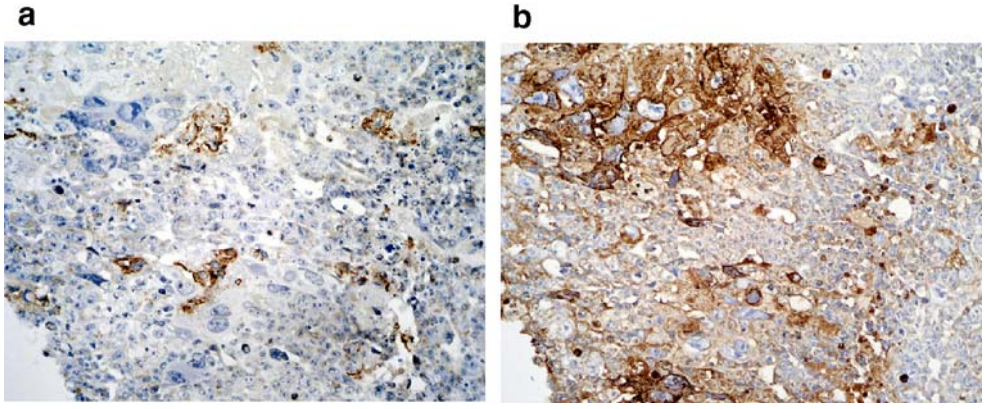

Fig. 3 GPC3 expressions in choriocarcinoma. **a** Focal immunostaining for GPC3 in choriocarcinoma. **b** hCG-beta immunostaining in choriocarcinoma. Note the diffusion artifacts, which were frequently observed in hCG-beta immunohistochemistry in necrotic and hemorrhagic lesions

failed to label the component of YST (Table 3). The proportion of AFP-positive cells in YST was much smaller than that of GPC3 positivity in 13 of 19 AFP-positive MGCT (Fig. 2a,b and f and Table 3).

AFP labeled some glandular structures in immature teratoma, but the luminal membranous staining pattern was more prominent for GPC3 compared to AFP (Fig. 4).

hCG-beta

Most STGCs were positive for hCG-beta. Stronger cytoplasmic staining of hCG-beta was shown with two cell types of choriocarcinoma (Fig. 3). Although the sensitivity and intensity of GPC3 for STGCs were almost identical to those of hCG-beta staining, no diffusion artifact was observed with GPC3 immunohistochemical staining in the area involving necrosis, where hCG-beta staining showed strong background labeling.

OCT3/4

OCT3/4 exhibited immunoreactivity in most neoplastic cells of IGCNU, seminoma, and embryonal carcinoma (Table 1) as reported [15]. No overlapped staining was detected for GPC3 and OCT3/4, which was illustrated in "the double layer pattern", glandular structures of embryonal carcinoma encircled by a row of flattened YST cells [1, 3], in MGCT (Fig. 2c,d).

Discussions

GPC3 is a cell-surface heparan sulfate proteoglycan, encoded by the gene on the X-chromosome. Kawakami et al. [16] investigated GPC3 expression in testicular GCT to prove the role of the extra X-chromosome. Using RT-PCR, they demonstrated GPC3 expression irrespective of the amount of X-chromosome. Otherwise, there has been no study to investigate the significance of GPC3 in testicular GCT. Applying highly specific monoclonal antibodies against GPC3 to paraffin-embedded tissues, we confirmed the expression of GPC3 in GCT, especially in differentiated tumors. The finding is concordant with our previous observation in hepatic and gastric neoplasms: GPC3 is an oncofetal protein closely associated with AFP [10, 24].

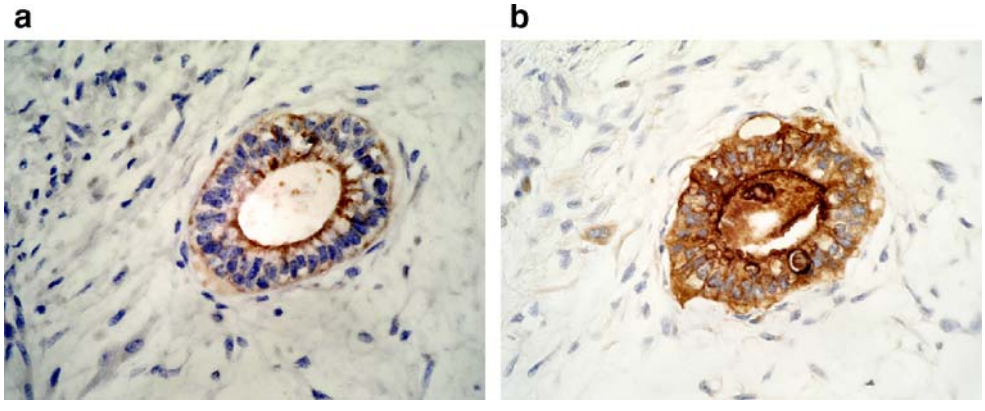

Fig. 4 GPC3 expressions in immature teratoma. **a** Focal immunostaining for GPC3 in immature glandular structures of teratoma. **b** AFP immunostaining in teratoma. Parallel section to **a**

Table 3 GPC3 and AFP immunostaining sensitivity for yolk-sac tumor component in mixed germ-cell tumor

MGCT case	YST area (%)	GPC3	AFP
1	90	+	+
2	5	++	++
3	10	++	++
4	20	++	++
5	20	++	++
6	20	++	+
7	20	++	+
8	20	++	+
9	20	+++	+++
10	5	++	+
11	20	++	++
12	20	++	−
13	20	+++	+++
14	20	+++	++
15	10	+++	++
16	10	+++	+
17	20	+++	+
18	0	−	−
19	10	+++	+
20	30	+++	++
21	10	+++	++
22	5	++	−

GPC3 Glypican-3, *AFP* alpha-fetoprotein, *MGCT* mixed GCT, *YST* yolk-sac tumor
−, 0–5% cells stained; +, 5–10% cells stained; ++, 10–50% cells stained; +++, >50% cells stained

In this study, immunohistochemical staining for GPC3 was observed more frequently in neoplastic cells of YST than of AFP. Because GPC3 immunostaining is more sensitive than that of AFP, there are two applications of the pathology of testicular GCT. YST has numerous patterns that produce an array of appearances. Among the relatively frequent patterns, solid pattern YST consists of a sheet-like arrangement of polygonal cells with clear to eosinophilic cytoplasm, which should be differentiated from seminoma and embryonal carcinoma. GPC3 could label occasional cells in this pattern, and thus may be useful for the differential diagnosis of the infrequent pattern of YST. Also, GPC3 is a useful immunohistochemical marker to identify the small amount of YST in MGCT. Commonly overlooked in MGCT is the small focus of YST components with a reticular, myxomatous, or solid pattern, contiguous with other histologic subtypes.

GPC3 showed immunoreactivity for STGCs and some choriocarcinoma in this study, appearing to indicate the unique characteristic of GPC3 as an oncofetal protein, which is different from AFP. However, AFP mRNA and protein are reported to be present in the human early villous placenta [4, 17]. Therefore, further studies are necessary to investigate the significance of the concordant and discordant expression of GPC3 and AFP. Nevertheless, GPC3 immunohistochemistry is an auxiliary tool for hCG-beta, since GPC3 immunohistochemistry was free from diffusion artifacts, which are a serious problem when interpreting hCG-beta staining in choriocarcinoma with hemorrhage and necrosis.

The list of immunohistochemical markers for GCT is now expanding. Pluripotent potential germ-cell neoplasms, like IGCNU, seminoma, and embryonal carcinoma, are labeled with antibodies against PLAP, c-KIT [12], OCT3/4 (POU5F1) [15], and CD30 [18]. On the other hand, for differentiated GCT, several growth factors, growth factor receptors, and transcription factors have been reported in neoplastic cells but with various frequencies and variable specificity [8, 11, 21]. This study confirmed the outstanding specificity of GPC3 to differentiated GCT, such as in “the double layer pattern”, glandular structures of embryonal carcinoma encircled by a row of flattened YST cells [1, 3], in MGCT in which OCT3/4 and GPC3 immunoreactivities were mutually exclusive.

The American Joint Committee on Cancer–TNM classification system has adopted the serum level of tumor markers as one of the determinants of the staging system, since it has been shown to have prognostic importance and plays an important role in the management of patients with testicular GCT. In addition to AFP as a marker for YST, elevated serum hCG-beta in patients with seminoma, correlating with the presence of STGCs in the tumor, is closely related with the metastatic potential of the tumor [13]. Therefore, further studies are necessary to test the feasibility of GPC3 as a serum marker for nonseminomatous GCT. Furthermore, when GPC3 becomes a target molecule in monoclonal antibody-based therapy, the importance of GPC3 might exceed that of AFP and hCG-beta.

Acknowledgements We are grateful to Ms. Y. Ohno for her technical assistance. This study was supported by the program for the Promotion of Fundamental Studies in Health Sciences of the National Sciences of the National Institute of Biomedical Innovation (NIBIO).

References

1. Cardoso de Almeida PC, Scully RE (1983) Diffuse embryoma of the testis. A distinctive form of mixed germ cell tumor. Am J Surg Pathol 7:633–642
2. De Cat B, Muyldermans SY, Coomans C, Degeest G, Vanderschueren B, Creemers J, Biemar F, Peers B, David G (2003) Processing by proprotein convertases is required for glypican-3 modulation of cell survival, Wnt signaling, and gastrulation movements. J Cell Biol 163:625–635
3. de Peralta-Venturina MN, Ro JY, Ordonez NG, Ayala AG (1994) Diffuse embryoma of the testis. An immunohistochemical study of two cases. Am J Clin Pathol 102:402–405

4. Duc-Goiran P, Mignot TM, Robert B, Machavoine F, Mondon F, Hagnere AM, Vacher-Lavenu MC, Danan JL, Vaiman D, Benassayag C, Ferre F (2005) Expression and Localization of Alpha-fetoprotein mRNA and Protein in Human Early Villous Trophoblasts. Placenta (in press)
5. Eble JN, Sauter G, Epstein JI, Sesterhenn IA (eds) (2004) World Health Organization classification of tumors. Pathology and genetics tumours of the urinary system and male genital organs. IARC Press, pp 218–249
6. Filmus J (2001) Glypicans in growth control and cancer. Glycobiology 11:19R–23R
7. Grisaru S, Cano-Gauci D, Tee J, Filmus J, Rosenblum ND (2001) Glypican-3 modulates BMP- and FGF-mediated effects during renal branching morphogenesis. Dev Biol 231:31–46
8. Hechelhammer L, Storkel S, Odermatt B, Heitz PU, Jochum W (2003) Epidermal growth factor receptor is a marker for syncytiotrophoblastic cells in testicular germ cell tumors. Virchows Arch 443:28–31
9. Hippo Y, Watanabe K, Watanabe A, Midorikawa Y, Yamamoto S, Ihara S, Tokita S, Iwanari H, Ito Y, Nakano K, Nezu J, Tsunoda H, Yoshino T, Ohizumi I, Tsuchiya M, Ohnishi S, Makuuchi M, Hamakubo T, Kodama T, Aburatani H (2004) Identification of soluble NH2-terminal fragment of glypican-3 as a serological marker for early-stage hepatocellular carcinoma. Cancer Res 64:2418–2423
10. Hishinuma M, Ohashi K, Yamauchi N, Kashima K, Uozaki H, Ota S, Kodama T, Aburatani H, Fukayama M (2006) Heptocellular oncofetal protein, Glypican 3 is a sensitive marker for alpha-fetoprotein producing gastric carcinoma. Histopathology (in press)
11. Hoei-Hansen CE, Nielsen JE, Almstrup K, Sonne SB, Graem N, Skakkebaek NE, Leffers H, Rajpert-De Meyts E (2004) Transcription factor AP-2gamma is a developmentally regulated marker of testicular carcinoma in situ and germ cell tumors. Clin Cancer Res 10:8521–8530
12. Honecker F, Stoop H, de Krijger RR, Chris Lau YF, Bokemeyer C, Looijenga LH (2004) Pathobiological implications of the expression of markers of testicular carcinoma in situ by fetal germ cells. J Pathol 203:849–857
13. Hori K, Uematsu K, Yasoshima H, Yamada A, Sakurai K, Ohya M (1997) Testicular seminoma with human chorionic gonadotropin production. Pathol Int 47:592–599
14. Jacobsen GK (1983) Alpha-fetoprotein (AFP) and human chorionic gonadotropin (HCG) in testicular germ cell tumours. A comparison of histologic and serologic occurrence of tumour markers. Acta Pathol Microbiol Immunol Scand [A] 91:183–190
15. Jones TD, Ulbright TM, Eble JN, Baldridge LA, Cheng L (2004) OCT4 staining in testicular tumors: a sensitive and specific marker for seminoma and embryonal carcinoma. Am J Surg Pathol 28:935–940
16. Kawakami T, Okamoto K, Sugihara H, Hattori T, Reeve AE, Ogawa O, Okada Y (2003) The roles of supernumerical X chromosomes and XIST expression in testicular germ cell tumors. J Urol 169:1546–1552
17. Lafuste P, Robert B, Mondon F, Danan JL, Rossi B, Duc-Goiran P, Mignot TM, Nunez EA, Benassayag C, Ferre F (2002) Alpha-fetoprotein gene expression in early and full-term human trophoblast. Placenta 23:600–612
18. Looijenga LH, Stoop H, de Leeuw HP, de Gouveia Brazao CA, Gillis AJ, van Roozendaal KE, van Zoelen EJ, Weber RF, Wolffenbuttel KP, van Dekken H, Honecker F, Bokemeyer C, Perlman EJ, Schneider DT, Kononen J, Sauter G, Oosterhuis JW (2003) POU5F1 (OCT3/4) identifies cells with pluripotent potential in human germ cell tumors. Cancer Res 63:2244–2250
19. Mostofi FK, Sesterhenn IA, Davis CJ Jr (1988) Developments in histopathology of testicular germ cell tumors. Semin Urol 6:171–188
20. Sesterhenn IA, Weiss RB, Mostofi FK, Stablein DM, Rowland RG, Falkson G, Rivkind SE, Vogelzang NJ (1992) Prognosis and other clinical correlates of pathologic review in stage I and II testicular carcinoma a report from the Testicular Cancer Intergroup Study. J Clin Oncol 10:69–78
21. Suzuki K, Tokue A, Kamiakito T, Kuriki K, Saito K, Tanaka A (2001) Predominant expression of fibroblast growth factor (FGF) 8, FGF4, and FGF receptor 1 in nonseminomatous and highly proliferative components of testicular germ cell tumors. Virchows Arch 439:616–621
22. Talerman A, Haije WG, Baggerman L (1980) Serum alphafetoprotein (AFP) in patients with germ cell tumors of the gonads and extragonadal sites: correlation between endodermal sinus (yolk sac) tumor and raised serum AFP. Cancer 46:380–385
23. Ulbright TM (2005) Germ cell tumors of the gonads: a selective review emphasizing problems in differential diagnosis, newly appreciated, and controversial issues. Mod Pathol 18(Suppl 2): S61–S79
24. Yamauchi N, Watanabe A, Hishinuma M, Ohashi K, Midorikawa Y, Morishita Y, Niki T, Shibahara J, Mori M, Makuuchi M, Hippo Y, Kodama T, Iwanari H, Aburatani H, Fukayama M (2005) The glypican 3 oncofetal protein is a promising diagnostic marker for hepatocellular carcinoma. Mod Pathol 18:1591–1598

Virchows Arch (2006) 449:315–319
DOI 10.1007/s00428-006-0244-z

ORIGINAL ARTICLE

The high frequency of EBV infection in pediatric Hodgkin lymphoma is related to the classical type in Bahia, Brazil

Iguaracyra Araujo · Achiléa Lisboa Bittencourt · Helenemarie S. Barbosa · Eduardo Martins Netto · Núbia Mendonça · Hans-Dieter Foss · Michael Hummel · Harald Stein

Received: 9 March 2006 / Accepted: 29 May 2006 / Published online: 1 August 2006
© Springer-Verlag 2006

Abstract Pediatric Hodgkin lymphoma (HL) occurring in developing regions is different from HL in industrialized countries due to the higher frequency of association with Epstein–Barr virus (EBV) infection. This infection is related to classical HL (cHL) but is virtually absent in nodular lymphocyte predominant HL (nLPHL). We studied the phenotype and the expression of EBV gene products in 90 pediatric cases by immunohistochemistry and in situ hybridization. EBV-positive tumor cells were found exclusively in cHL. The infection occurred with high frequency in all cHL subtypes, but it predominated in the mixed cellularity and lymphocyte depletion subtypes. These results reinforce the hypothesis that EBV plays a major role in the etiology of pediatric cHL in developing areas. Curiously, the frequency of EBV infection in HL was identical to the previously described for Burkitt's lymphoma in the same pediatric population. As both lymphomas have a postulated precursor cell in the germinal center (GC), the pattern of latently EBV-infected GC cells previously described in Bahia may be related to the development of these lymphomas.

Keywords Epstein–Barr virus infection · Classical Hodgkin lymphoma · Nodular lymphocyte predominant Hodgkin lymphoma · Pediatric Hodgkin lymphoma

I. Araujo · A. L. Bittencourt · H. S. Barbosa
Department of Pathology, Federal University of Bahia (UFBA), Bahia, Brazil

E. M. Netto
Hospital Universitário Prof. Edgard Santos, UFBA, Bahia, Brazil

N. Mendonça
Pediatric Oncology (ONCO), Bahia, Brazil

H.-D. Foss · M. Hummel · H. Stein
Institute of Pathology, Charite-Universitätmedizin Berlin, Campus Benjamin Franklin, Berlin, Germany

A. L. Bittencourt (✉)
Hospital Universitário Prof. Edgard Santos (HUPES), Rua Augusto Viana s/n, Canela 40110-160, Salvador, Bahia, Brazil
e-mail: achilea@uol.com.br

Introduction

Epstein–Barr virus (EBV) is a lymphotropic virus associated with some human malignancies such as endemic Burkitt's lymphoma (BL), Hodgkin's lymphoma (HL), AIDS-associated lymphomas and nasopharyngeal carcinoma [4, 12, 14, 20, 24]. In the case of HL, several findings support the notion that EBV may be involved in the pathogenesis of this disease: 1) an approximately threefold increase in the occurrence of HL after infectious mononucleosis [26], 2) the increase in antibody titers to EBV both before and after the onset of lymphoma [10], and 3) the finding of a monoclonal pattern of EBV infection in HL tissue [2]. However, the precise pathogenic role of this virus is unclear, as the mechanism of cell malignization has not been demonstrated [17].

HL in industrialized countries is associated with EBV infection in 40–60% of cases, whereas in developing countries this association reaches 100% [1, 7, 13, 15, 19]. The high frequency of EBV infection in HL is likely to be related to age and histological subtypes [10, 11, 16, 18, 19, 25]. The prevalence of the EBV-association is considered to be higher in children and in adults ≥50 years of age [16, 19, 25, 33].

Two types of HL have now been recognized by the World Health Organization (WHO) as two distinct entities, the classical HL (cHL) comprising four subypes, and the nodular lymphocyte predominant HL (nLPHL) [28, 29]. According to WHO, EBV infection is related exclusively to cHL, whereas nLPHL is consistently negative for this infection [28, 29]. However, Chang et al. [6] have recently demonstrated that in Vietnamese children nLPHL may be associated to EBV infection.

As studies dealing with EBV and its relation to cHL and nLHPL in pediatric patients in developing areas are very limited, we decided to investigate the EBV status of 90 consecutive cases of pediatric HL occurring in the same population and period of previously reported EBV-related BL. The diagnosis of cHL and nLPHL was done according to the WHO criteria [28, 29]. This study may also contribute to clarify whether this EBV association in developing regions is related exclusively to the cHL.

Materials and methods

Cases

Ninety consecutive cases of pediatric HL diagnosed at the pediatric Hospital Martagão Gesteira (Salvador, Bahia, Brazil) from 1976 through 1993 were revised. The cases were obtained from patients without clinically overt immune dysfunction. Relapse cases were excluded from this study.

Formalin-fixed and paraffin-embedded tissues were cut at 4 μm, and stained with hematoxylin–eosin (H&E). The diagnosis was verified in all cases by three pathologists (I.A., A.B., and H-D F.) who applied the criteria of WHO classification [28, 29].

Immunohistochemical studies

Formalin-fixed and paraffin-embedded tissue sections (4 μm) were stained by the immunoalkaline phosphatase (APAAP) or Envision method from DakoCytomation, Glostrup, Denmark [30]. The primary reagents were monoclonal antibodies specific for B-cell-associated antigens such as CD20 (L26) and CD79a (JCB117). In addition, CD3, a polyclonal antibody specific for T cells, Ber-H2, an antibody specific for the activation antigen CD30, C3D1 antibody specific for the CD15 molecule as well as antibodies against the B-cell characteristic transcription factors Oct-2 and Bob-1 were applied. With the exception of Oct-2 and BOB.1, which were purchased from Santa Cruz Biotechnology, CA, USA, all antibodies were from DakoCytomation, Glostrup, Denmark. All antibodies were used after high-pressure cooking (2 min in 0.1 M citrate buffer) to demask antigenic epitopes in paraffin sections.

EBV in situ hibridization

Probes specific for the EBER1 and EBER2 (nuclear EBV-encoded RNA molecules) were prepared using the plasmids pJJJ1 and pJJJ2. After linearization, anti-sense and sense (negative control) cRNA EBERs probes were obtained by run-off transcription with incorporation of Digoxigenin-labeled nucleotides.

Under RNAse-free conditions, in situ hybridization for the detection of EBER transcripts was performed as described previously [3]. Briefly, dewaxed and rehydrated paraffin sections were exposed to 0.2 N HCl, 0.6 mg/ml pronase (Boehringer, Mannheim, Germany), followed by post-fixation with 4% paraformaldehyde, and dehydration through graded ethanols. Slides were hybridized to 0.1 μg of labeled probes overnight at 50°C. EBER 1 and EBER 2 specific probes were combined to increase sensitivity. After washing, bound Digoxigenin-labeled EBER probes were detected using a monoclonal Digoxigenin-specific alkaline phosphatase conjugated antibody (Boehringer-Mannheim, Germany) and an alkaline phosphatase detection system (DakoCytomation). The positive signals were localized exclusively in the nuclei, with the exception of mitotic figures showing cytoplasm staining. In situ hybridization experiments with the sense (control) probe did not show any signal.

Statistical methods

The Program SPSS version 11.5 was used for statistical analyses. The correlation between EBV infection and age and histological subtypes of HL was analyzed by the Chi-square test. We considered statistic significance when $p<0.05$.

Results

All patients were less than 15 years old (3–14 years), the median age was 8.6 (±3.4) years. Seventy-two patients were boys and 18 were girls (ratio 3.8:1). All cases displayed a primary lymph node involvement: cervical (58 cases), axillar (five cases), abdominal (five cases), inguinal (six cases), supraclavicular (two cases), and mediastinal (one case). In 13 cases, the precise location of the affected lymph nodes was not available.

Histopathological and immunohistochemical findings

All cases fulfilled the morphological criteria for cHL or nLPHL as defined by the WHO classification [28, 29] The tumors were composed of RS cells and their variants in a heterogeneous background in accordance with each histo-

logical subtype. Of the 90 cases, 83 (92.2%) showed the morphological characteristics of a cHL with expression of CD30 in 100% of cells and CD15 in a variable proportion of cells. Of the 83 cHL cases, 11 (13%) showed some neoplastic cells positive for CD20. The T-cell antigen CD3 was observed only in small reactive lymphocytes in all cases. Fifty of the 83 cHL cases (60%) were of mixed cellularity (MC) subtype, 30 of nodular sclerosis (NS) subtype, and three of lymphocyte depletion (LD) subtype. The diagnosis of nLPHL was established in seven cases (7.7%), all displaying a strong expression of CD20 in all neoplastic cells and negativity for CD30. Oct-2 and BOB.1 were consistently co-expressed in these seven cases. These cases were previously diagnosed using the Rye classification [21] as LP (two cases) and LP subtype of NS (five cases). At that time, NS cases were further subdivided into LP, MC, and LD [8].

EBV in situ hybridization

A strong nuclear signal specific for EBER was observed in virtually all tumor cells in 78/90 of the cases (86.7%). (Fig. 1). All LPHL cases were negative for EBV (Table 1). The age distribution of EBER-positive and negative cases is shown in Fig. 2. There was a trend to have more positive cases within younger age groups (P=0.051) when excluding the LPHL cases (Fig. 2). All the EBV-associated cases were categorized as cHL being 50/50 (100%) of MC subtype, 25/30 (83.3%) of NS subtype and 3 (100%) of LD subtype (Table 1). Only five of the 83 cHL cases (6%) were EBV-negative, all of the NS subtype. In two of these cases, EBV-positive bystander lymphocytes were observed. In one nLHPL case EBV-positive bystander lymphocytes were also detected.

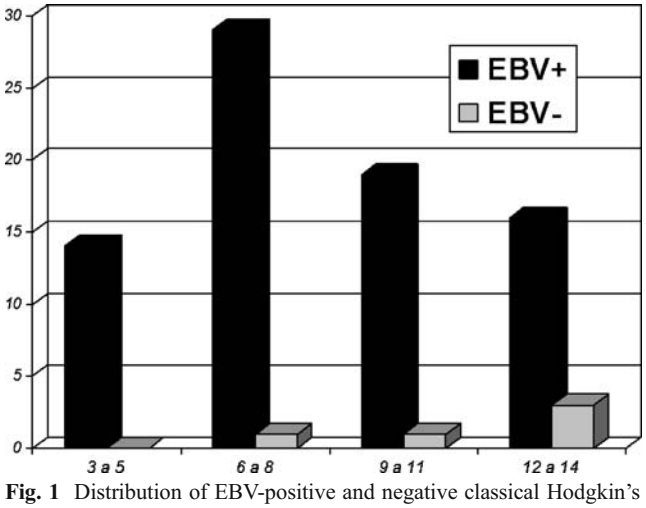

Fig. 1 Distribution of EBV-positive and negative classical Hodgkin's lymphomas by age

Table 1 The frequency of EBV infection in tumor cells among different subtypes of Hodgkin lymphoma

Classification	EBV-positive	EBV-negative
nLHPL	0	7
NS	25	5
MC	50	0
DL	3	0
Total	78 (86.7%)	12 (13.3%)

Discussion

Our study on EBV in cases of HL in the state of Bahia, a region in the Northeast of Brazil, represents the first extensive investigation into pediatric HL in Brazil and the basic findings were: 1) 86.7% of the cases expressed EBER molecules in tumor cells; 2) the EBV infection was present exclusively in cHL and was associated with all subtypes; 3) nLPHL was consistently negative for EBV in tumor cells; 4) the frequency of EBV infection (86.7%) was analogous to the previously described in BL in a similar pediatric population [3].

A high frequency of childhood EBV-associated HL is also described in other developing regions such as Malaysia, China, Kenya, Honduras, and Kuwait [1, 19, 22, 25, 33]. Bahia (Brazil) shows a higher frequency of EBV association with pediatric HL in comparison to Argentina [9]. This difference is possibly related to lower socio-economic condition of the population in the former. In agreement with this hypothesis, a high frequency of EBV related pediatric HL was also described in Ceará, another state of northeast Brazil [11].

The prevalence of EBV in tumor cells varies according to the histological subtypes of cHL [9, 16, 29]. As observed in previous studies in developing countries [1, 7, 11, 13, 19], we have found a significantly higher frequency of EBV in

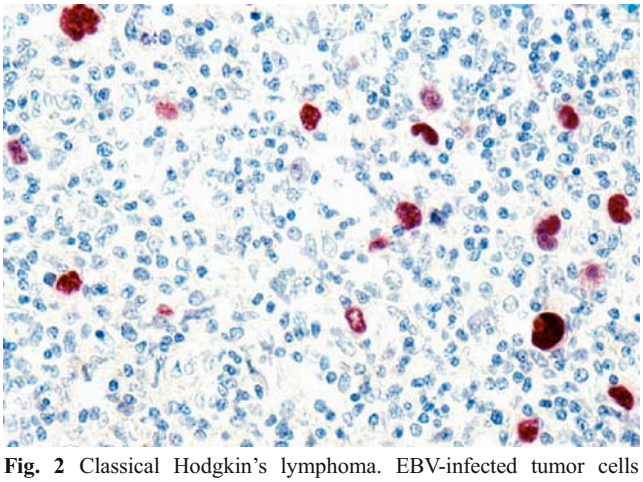

Fig. 2 Classical Hodgkin's lymphoma. EBV-infected tumor cells consistently show a strong expression of EBER in their nuclei (in situ hybridization, ×300)

MC as compared to NS subtype ($P<0.006$). However, other authors have not found association between EBV infection and histological subtypes in childhood in developing countries [6, 33]. The high frequency of EBV-associated HL in childhood reinforces the hypothesis that EBV plays a major role in the pathogenesis of pediatric HL, probably determining the first age incidence peak of cHL, which is lower than in developed countries [5].

Biological and clinical trials in recent years have demonstrated that HL consists of two disease types: nLPHL and cHL, which differ in their clinical behavior, morphology, immunophenotype, and EBV association. The EBV infection in neoplastic cells has been described exclusively in cHL [28, 29]. However, recently Chang et al. [2005] found EBV infection in 100% of nLPHL in Vietnamese children [6]. In the present study, we did not find EBV infection in tumor cells of nLHPL. However, we found EBV-positive small lymphocytes in one case of nLPHL. As demonstrated in cases of cHL, these EBV-positive lymphocytes are probably unrelated to nLPHL tumor cells but rather are persistently EBV-infected memory B cells [27].

Interestingly, the overall frequency of EBV infection in pediatric HL (86.7%) in Bahia is the same as that published previously for pediatric BL (87%) in the same hospital and period [3]. A possible consonance of geographical distribution of EBV-related HL and BL was suggested by Weinreb et al. [32]. It is known that both tumors originate from germinal center cells [23, 31]. We described previously that latent EBV-infected cells were found more frequently in germinal center in tonsils from children in our region compared to those from children in industrialized countries, and these germinal center cells abnormally express the oncogenic protein LMP-1 [4]. These findings could at least in part explain the high incidence of EBV-associated lymphomas derived from germinal center cells, such as cHL and BL, occurring in the pediatric population in developing areas.

In conclusion, this study has shown a high frequency of EBV-associated pediatric HL in agreement with other studies carried out in developing regions [19, 25, 33]. We observed that histological subtypes represent a strong risk factor for EBV-associated HL. In contrast, in other developing regions no correlation was found between EBV infection and subtypes of HD [6, 33]. The high association of EBV with all subtypes of pediatric cHL supports the hypothesis that EBV plays a major role in the development of pediatric HL. In the present cases, the infection was restricted to cHL, indicating that EBV infection is probably not related to the pathogenesis of nLHPL in our region. The present data corroborate the hypothesis that in developing areas the frequency of EBV-associated HL is similar to the EBV-associated BL in the same pediatric population. This is probably related to LMP-1 expression in EBV-infected germinal center cells [4], which are the postulated precursors of both HL and BL.

Acknowledgements We are indebted to Erica Berg for technical support.

Financial support was provided by the National Research Council (CNPq), Brazil and Deutsche Forschungsgemeinschaft (DFG), Germany.

References

1. Ambinder RF, Browning PJ, Lorenzana I, Leventhal BG, Cosenza H, Mann RB, MacMahon EM, Medina R, Cardona V, Grufferman S (1993) Epstein–Barr virus and childhood Hodgkin's disease in Honduras and United States. Blood 8:462–467
2. Anagnostopoulos I, Herbst H, Niedobitek G, Stein H (1989) Demonstration of monoclonal EBV genomes in Hodgkin's disease and Ki-1 positive anaplastic large cell lymphoma by combined southern blot and in situ hybridization. Blood 74:810–816
3. Araujo I, Foss HD, Bittencourt A, Hummel M, Demel G, Mendonça N, Herbst H, Stein H (1996) Burkitt's lymphoma in Northeast Brazil: expression of Epstein–Barr virus-gene products in Burkitt's lymphoma in Northeastern Brazil. Blood 87: 5279–5286
4. Araujo I, Foss HD, Hummel M, Anagnostopoulos I, Barbosa HS, Bittencourt A, Stein H (1999) Frequent expansion of Epstein–Barr virus (EBV) infected cells in germinal centres of tonsils from an area with a high incidence of EBV-associated lymphoma. J Pathol 187:326–330
5. Armstrong AA, Alexander FE, Paes RP, Morad NA, Gallagher A, Krajewski AS, Jones DB, Angus B, Adams J, Cartwright RA, Onions DE, Jarret RF (1993) Association of Epstein–Barr virus with pediatric Hodgkin's disease. Am J Pathol 142:1683–1688
6. Chang KL, Albujar PF, Chen Y-Y, Jonhson RM, Weiss LM (1993) High prevalence of Epstein–Barr virus in Reed–Sternberg cells of Hodgkin's disease occurring in Peru. Blood 81:496–501
7. Chang KC, Khen NT, Jones D, Su IJ (2005) Epstein–Barr virus is associated with all histological subtypes of Hodgkin lymphoma in Vietnamese children with special emphasis on the entity of lymphocyte predominance subtype. Hum Pathol 36:747–755
8. Cionini L, Argonini L, Mungai V, Biti GP, Bondi R (1978) Prognostic significance of histologic subdivision of Hodgkin's disease nodular sclerosis. Acta Radiol Oncol 17:65–73
9. De Matteo E, Baron AV, Chabay P, Porta J, Dragosky M, Preciado MV (2003) Comparison of Epstein–Barr virus presence in Hodgkin lymphoma in pediatric versus adult Argentine patients. Arch Pathol Lab Med 127:1325–1329
10. Engel M, Essop MF, Close P, Hartley P, Pallesen G, Sinclair-Smith C (2000) Improved prognosis of Epstein–Barr virus associated childhood Hodgkin's lymphoma: study of 47 South African cases. J Clin Pathol 53:182–186
11. Elgui de Oliveira D, Bacchi MM, Abreu ES, Niero-Melo L, Bacchi CE (2002) Hodgkin disease in adult and juvenile groups from two different geographic regions in Brazil: characterization of clinicopathologic aspects and relationship with Epstein–Barr virus infection. Am J Clin Pathol 118:25–30
12. Geser A, Lenoir GM, Anvret M, Bornkamm G, Klein G, Williams EH, Wright DH, De-The G (1983) EBV markers in a series of Burkitt's lymphoma from West Nile District of Uganda. Eur J Cancer Clin Oncol 19:1394–1404
13. Glaser SL, Lin RJ, Stewart SL, Ambinder RF, Jarrett RF, Brousset P, Pallesen G, Gulley ML, Khan G, O'Grady J, Hummel M, Preciado MV, Knecht H, Chan JK, Claviez A (1997) Epstein–Barr

virus-associated Hodgkin's disease: epidemiologic characteristics in international data. Int J Cancer 70:375–382
14. Herbst H, Steinbrecher E, Niedobitek G, Young LS, Brooks L, Muller-Lantzsch N, Stein H (1992) Distribution and phenotype of Epstein–Barr virus-harboring cells in Hodgkin's disease. Blood 80:484–491
15. Hummel M, Anagnostopolos I, Dallenbach F, Korbjuhn P, Dimmler C, Stein H (1992) EBV infection patterns in Hodgkin's disease and normal lymphoid tissue; expression and cellular localization of EBV products. Br J Haematol 82:689–694
16. Jarrett RF, Krajewski AS, Angus B, Freeland J, Taylor PR, Taylor GM, Alexander FE (2003) The Scotland and Newcastle epidemiological study of Hodgkin's disease: impact of histopathological review and EBV status on incidence estimates. J Clin Pathol 56:811–816
17. Khan G (2006) Epstein–Barr virus, cytokines, and inflammation: a cocktail for the pathogenesis of Hodgkin's lymphoma? Exp Hematol 34:399–406
18. Khan G, Norton AJ, Salvin G (1993) Epstein–Barr virus in Hodgkin's disease: relation to age and subtype. Cancer 71:3124–3129
19. Kusuda M, Toriyama K, Kamidigo NO, Itakura H (1998) A comparison of epidemiologic, histologic and virologic studies on Hodgkin's disease in Western Kenya and Nagasaki, Japan. Am J Trop Med Hyg 59:801–807
20. Levine AM, Shibata D, Sullivan-Halley J, Nathwani B, Brynes R, Slovak ML, Mahterian S, Riley CL, Weiss L, Levine PH (1992) Epidemiological and biological study of acquired immunodeficiency syndrome-related lymphoma in County of Los Angeles: preliminary results. Cancer Res (Suppl) 52:5482–5484
21. Lukes RJ, Butler JJ (1966) The pathology and nomenclature of Hodgkin's disease. Cancer Res 26:1063–1081
22. Makar RR, Saji T, Junaid TA (2003) Epstein–Barr virus expression in Hodgkin's lymphoma in Kuwait. Pathol Oncol Res 9:159–165
23. Marafioti T, Hummel M, Foss HD, Laumen H, Korbjuhn P, Anagnostopoulos I, Lammert H, Demel G, Theil J, Wirth T, Stein H (2000) Hodgkin and Reed–Sternberg cells represent an expansion of a single clone originating from a germinal center B cell with functional immunoglobulin gene rearrangements but defective immunoglobulin transcription. Blood 95:1443–1450
24. Niedobitek G, Herbst H, Young LS (1993) Epstein–Barr virus and carcinomas. Int J Clin Lab Res 23:17–24
25. Peh SC, Looi LM, Pallesen G (1997) Epstein–Barr virus (EBV) and Hodgkin's disease in a multi-ethnic population in Malaysia. Histopathology 30:227–233
26. Rosdahl N, Larsen SO, Clemmesen J (1974) Hodgkin's disease in patients with previous infectious mononucleosis. 30 years' experience. Br Med J 2:253–256
27. Spieker T, Kurth J, Kuppers R, Rajewsky K, Brauninger A, Hansmann ML (2000) Molecular single-cell analysis of the clonal relationship of small Epstein–Barr virus-infected cells and Epstein–Barr virus-harboring Hodgkin and Reed/Sternberg cells in Hodgkin disease. Blood 96:3133–3138
28. Stein H, Deisol G, Pileri S, Said J (2001). Nodular lymphocyte predominance Hodgkin lymphoma. In: Jaffe ES, Harris NL, Stein H, Vardiman JW (eds) World Health Organization classification of tumors. Pathology and genetics. Tumors of haematopoietic and lymphoid tissues. IARC, Lyon, pp 240–243
29. Stein H, Deisol G, Pileri S, Said J (2001) Classical Hodgkin lymphoma. In: Jaffe ES, Harris NL, Stein H, Vardiman JW (eds) World Health Organization classification of tumors. Pathology and genetics. Tumors of haematopoietic and lymphoid tissues. IARC, Lyon, pp 244–271
30. Stein H, Gatter K, Asbar H, Mason DY (1985) Use of freeze-dried paraffin-embedded sections for immunohistological staining with monoclonal antibodies. Lab Invest 652:676
31. Tamaru J, Hummel M, Marafioti T, Kalvelage B, Leoncini L, Minacci C, Tosi P, Wright D, Stein H (1995) Burkitt's lymphomas express VH genes with a moderate number of antigen-selected somatic mutations. Am J Pathol 147:1398–1407
32. Weinreb M, Day PJ, Niggli F, Powell JE, Raafat F, Hesseling PB, Schneider JW, Hartley PS, Tzortzatou-Stathopoulou F, Khalek ER, Mangoud A, El-Safy UR, Madanat F, Al Sheyyab M, Mpofu C, Revesz T, Rafii R, Tiedemann K, Waters KD, Barrantes JC, Nyongo A, Riyat MS, Mann JR (1996) The role of Epstein–Barr virus in Hodgkin's disease from different geographical areas. Arch Dis Child 74:27–33
33. Zhou X, Hamilton-Dutoit S, Yan Q, Pallesen G (1993) The association between Epstein–Barr virus and Chinese Hodgkin's disease. Int J Cancer 55:359–363

Virchows Arch (2006) 449:320–327
DOI 10.1007/s00428-006-0242-1

ORIGINAL ARTICLE

Overlapping morphologic and immunophenotypic profiles in small B-cell lymphoma. A report of two cases

Ioannis Kostopoulos · Mario Cocco · Chiara Ginanneschi · Alessandro D'Amuri · Stefano Lazzi · Alberto Fabbri · Francesco Forconi · Maria Margherita De Santi · Lorenzo Leoncini

Received: 9 February 2006 / Accepted: 31 May 2006 / Published online: 18 July 2006
© Springer-Verlag 2006

Abstract We present two cases of small B-cell lymphomas of particular diagnostic interest because the histological patterns were at variance with their immunophenotype. One of these lymphomas, involving the gallbladder and duodenum, showed a marginal zone lymphoma-like (MALT type) pattern of cellular infiltration with CD5 negativity but (unexpectedly) Cyclin D1 positivity. Fluorescence in situ hybridization analysis of this case was performed because of the aberrant expression of Cyclin D1, and was clearly positive for the Cyclin D1 gene translocation. The second case, occurring in a lymph node, showed the typical growth pattern of a follicular lymphoma but it had an atypical immunophenotype, namely, expression of Cyclin D1, CD10, and Bcl2 and focally Bcl6, accompanied by a lack of CD5 and CD23. The Cyclin D1 gene translocation was detected by fluorescence in situ hybridisation (FISH), whereas c-myc and Bcl2 genes translocation were absent. Numerical chromosomal changes, which were visualized for chromosomes 8, 11, and 18 could be correlated to the aberrant immunoprofile. In this context, we discuss the diagnostic value of Cyclin D1, CD5, CD23, CD10, Bcl6 markers revealed by immunohistochemistry, as well as the significance of detection by FISH of chromosomal translocations such as t(11;14) and t(14;18). The question still remains as to whether such cases should be designated as specific lymphoma entities or reported as unclassifiable and the chromosome aberration reported.

Keywords Cyclin D1 · Differential diagnosis · FISH · Immunohistochemistry · Overlapping immunophenotype · Small B-cell lymphomas

Abbreviations

CCND1	cyclin D1
FISH	fluorescence in situ hybridization
FL	follicular lymphoma
IHC	immunohistochemistry
MCL	mantle cell lymphoma
MZL	marginal zone lymphoma
SLL/CLL	small lymphocytic lymphoma/chronic lymphocytic leukemia

Introduction

Precise diagnosis is a prerequisite for the accurate classification of small B-cell lymphomas: this term is usually used for all B-cell lymphomas that are not in the category of diffuse large B-cell lymphoma and a panel of antibodies against CD5, CD10, CD20, CD23, CD43, and Cyclin D1 (CCND1) is widely used in the differential diagnosis of these disorders [5]. However, the diagnosis of small B-cell lymphomas is complicated when the neoplastic cells show morphologic and immunophenotypic heterogeneity. Small

M. Cocco · C. Ginanneschi · A. D'Amuri · S. Lazzi · M. M. De Santi · L. Leoncini (✉)
Department of Human Pathology and Oncology,
University of Siena,
Via delle Scotte 6,
53100 Siena, Italy
e-mail: leoncinil@unisi.it

I. Kostopoulos
Department of Pathology, Aristotle University of Thessaloniki,
Thessaloniki, Greece

A. Fabbri · F. Forconi
Department of Clinical Medicine and Immunological Sciences,
Section of Hematology, University of Siena,
Siena, Italy

B-cell lymphoma subtypes with morphology mimicking other types in this category have been reported in the literature [33, 34]. Potential misdiagnosis can arise from erroneous interpretation of the site of occurrence or morphologic features (such as marginal/mantle zone distribution, MALT-like infiltration, and follicular growth pattern). Aberrant immunohistochemical findings, such as loss or acquisition of antigens can also cause confusion [33, 34].

A number of methods [e.g., Southern blot analysis, polymerase chain reaction (PCR), real time PCR (RT-PCR), and fluorescence in situ hybridisation (FISH)] are available for the detection of chromosomal abnormalities specific for mantle cell lymphoma (MCL), follicular lymphoma (FL), extranodal marginal zone lymphoma (MZL) (MALT-type), and Burkitt lymphoma [t(11;14), t(14;18), t(11;18), and c-myc rearrangement, respectively] [11, 12, 25, 29, 32, 38]. In particular, the t(11;14)(q13;q32) translocation and overexpression of the product of the rearranged CCND1 gene [22, 35, 36, 40, 41] are considered hallmarks of mantle cell lymphoma [2, 3]. However, CCND1 protein can also sometimes be expressed in multiple myeloma [27], hairy cell leukemia [4], and, rarely, in splenic MZL/lymphoplasmacytic lymphoma [13]. This can occur in multiple myelomas as a result of a t(11;14) arising from illegitimate switch recombination of the IgH gene and scattered breakpoints on chromosome 11q13 (i.e., not within the major translocation cluster region involved in MCLs [30]). In contrast to MCLs and multiple myeloma, the expression of CCND1 in hairy cell leukemia is not associated with a t (11;14) translocation [4].

We have reviewed the morphologic and immunohistochemical features of a series of 75 archival biopsies from patients diagnosed with small B-cell lymphoma, classified according to the typical morphologic and immunohistochemical features that define diagnosis. We identified two cases of small B-cell lymphoma with discordant immunophenotypic and genetic features, and in this paper, we discuss the diagnostic problems posed such cases.

Materials and methods

Tissue samples

Paraffin blocks and the respective stained slides from 75 subsequent patients with small B-cell lymphoma, diagnosed between 2000 and 2005, were retrieved from the archives of the Department of Human Pathology and Oncology, at Siena University Hospital, Italy. Archival hematoxylin–eosin and Giemsa slides were reviewed to confirm diagnosis. Lymphoma cases were classified according to World Health Organization (WHO) criteria [14], by evaluating the histologic and immunohistochemical patterns. All slides were evaluated by two independent experienced pathologists (LL, IK). In cases of discrepancy, the slides were simultaneously reviewed by both observers to achieve a consensus.

Immunohistochemistry

In brief, paraffin-embedded tumor tissue sections (4 μm) were immunostained using the labeled streptavidin biotin (LSAB) method. The sections were deparaffinized in xylene and dehydrated in graded ethanol. Subsequently, the heat-induced epitope retrieval (HIER) method was performed. Slides for CCND1, CD3, CD20, CD23, Bcl2, and Bcl6 staining were immersed in citrate buffer, pH 6.8, and heated in a microwave oven three times for 5 min, while the slides for CD5 and CD10 staining were treated with W-CAP citrate buffer (Bio-Optica, Milan, Italy), pH 6.0, at 95°C for 40 min. Trypsin digestion was used for CD21 antigen. All slides were then treated with 3% hydrogen peroxide in methanol for 30 min to quench the endogenous peroxidase activity. The following monoclonal antibodies were applied for 70 min at room temperature: CCND1 (SP4, 1:100; NEOMARKERS, Fremont, CA), CD3 (1:1,000; NEOMARKERS), CD5 (4C7, 1:50; NEOMARKERS), CD10 (Ab-2, 1:50 NEOMARKERS), CD20 (L26, 1:50; NEOMARKERS), CD21 (1F8, 1:100; DakoCytomation, Glostrup, Denmark), CD23 (Ab-1, 1:100; Bio-Optica), CD79α (HM57, 1:50; DakoCytomation), Bcl2 (124, 1:100; DakoCytomation), and Bcl6 (PG-B6p, 1:50; DakoCytomation). A secondary biotinylated anti-mouse antibody was used for 30 min. The sections were then incubated in streptavidin-peroxidase for 30 min, followed by 3,3′-diaminobenzidine chromogen staining to detect antibody binding. Sections from tonsillar tissue were included as positive controls for CCND1 and CD3, CD5, CD10, CD20, CD21, CD23, CD79α, Bcl-2, Bcl6 antigens, while sections stained by omitting the primary monoclonal antibody served as negative controls.

Fluorescence in situ hybridization

CCND1, BCL2, and c-myc rearrangements were sought by FISH using the CCND1 FISH DNA Probe–Split Signal, the BCL2 FISH DNA Probe–Split Signal, and MYC FISH DNA Probe–Split Signal by means of standard procedures. FISH investigation was performed for CCND1 rearrangement in two cases, while BCL2 and c-myc rearrangements were investigated in one of these two cases. Briefly, paraffin tissue sections (4 μm) were deparaffinized, air dried, immersed in a jar filled with pretreatment solution, and warmed at 98°C for 10 min by means of a Whirlpool JT 356 microwave (Dako). Subsequently, the slides were cooled for 15 min at RT. After two passages in Wash

Buffer, 3 min each, excess buffer was taped off and the slides digested with cold Pepsin for 20 min in a DakoCytomation Hybridizer. Than the slides were washed twice in Wash Buffer for 3 min, dehydrated using increasing graded ethanol series, air-dried, and finally 10 μl of Probe mix were applied to each tissue section. The slides, covered with coverslip and sealed with rubber cement, were than incubated in the DakoCytomation Hybridizer (Dako) according to the manufacturer's recommendation. Next day, slides were treated with stringency buffer at 65°C for 2 min, then placed twice in Wash Buffer for 3 min, dehydrated using increasing graded ethanol series, air-dried, and counterstained applying 15 μl of Fluorescence Mounting Medium. Hybridization signals were visualized using a Leica microscope equipped with a triple-band filter for detecting green fluorescent protein (GFP)/spectrum green, Texas red/spectrum orange, and DAPI/spectrum blue. Images were captured and archived using Leica FW4000 software. One hundred nonoverlapping interphase nuclei were scored for each tumor specimen. In normal nuclei, two yellow fusion signals (2F) can be detected, whereas in nuclei with translocations, a yellow (or red-green juxtaposed) signal is accomplished by one red and one green segregated signal (1F1R1G). All reagents and probes were kindly provided by DakoCytomation Glostrup, Denmark.

Results

Patients

All but two of our 75 cases could be assigned to subtypes of the small B-cell lymphoma on the basis of the site of involvement, lymphomatous mass growth pattern, cytomorphic features, and immunophenotype. Table 1 summarizes the clinicopathological and immunophenotypic characteristics of these cases. However, two cases of small B-cell lymphoma were atypical in terms of morphologic and immunohistochemical features and are described in this study.

Case 1

A male patient of 75 years of age was admitted to Siena Hospital because of abdominal pain. Ultrasound examination showed a mass in the gallbladder wall and a cholecystectomy was performed. Microscopic examination of the gall bladder wall revealed infiltration of the mucosa by a monotonous population of small- to medium-sized neoplastic cells with irregular contoured nuclei and a thin rim of cytoplasm (Fig. 1a). A marginal zone lymphoma-like growth pattern and evident lymphoepithelial lesions involving the superficial epithelium were observed (Fig. 1b).

Immunohistochemical analysis with a large panel of monoclonal antibodies for the diagnosis showed strong positivity for CD20 and CD79α antigens in the whole neoplastic population, confirming their B-cell lineage. The neoplastic lymphoid cells also expressed Cyclin D1 (Fig. 1c). In addition, the neoplastic cells were positive for Bcl2, while scored negative for CD3, CD5 (Fig. 1d), CD10, CD23, and BCL6. Determination of the growth fraction by MIB1 showed a large number of positive nuclei, in up to 40% of neoplastic cells. Residual reactive germinal centers that were focally infiltrated by neoplastic cells were recognized by the presence of CD10, Bcl6, and MIB1 and the absence of Bcl2.

FISH analysis showed a signal pattern indicative of a reciprocal t(11;14)(q13;q32) translocation in more than 40% of the nuclei (Fig. 2).

A Computed tomography (CT) scan examination revealed lymphomatous infiltration in the gastric and duodenal walls and a bone marrow biopsy documented local involvement of lymphoma (stage IV/A). Because the gastrointestinal tract is a common site of extranodal involvement by both MZL and MCL, our case raised the question of whether it was a MZL showing aberrant expression of Cyclin D1 or a MCL which was atypical in that it had lost CD5 expression.

Table 1 Clinicopathological and immunophenotypic characteristics of 73 cases assigned to subtypes of small B-cell lymphomas

Number of cases	Small B-cell lymphoma type	Median age	Gender M/F	Immunophenotype
42	Follicular lymphoma	59.73	27/15	CD20+, CD79a+, CD3−, CD5−, cyclin D1−, bcl-2+, bcl−6+, CD10+, CD23−
11	Mantle cell lymphoma	67.09	8/3	CD20+, CD79a+, CD3−, CD5−, cyclin D1+, bcl−2+, bcl6−, CD10−, CD23−
14	Marginal zone lymphoma	71.92	4/10	CD20+, CD79a+, CD3−, cyclin D1−, CD5−, bcl−2+, bcl−6−, CD10−, CD23−
6	Lymphocytic B-cell lymphoma/chronic lymphocytic leukemia	66	4/2	CD20+, CD79a+, CD3−, cyclin D1−, CD5+, bcl−2+, bcl−6−, CD10−, CD23+

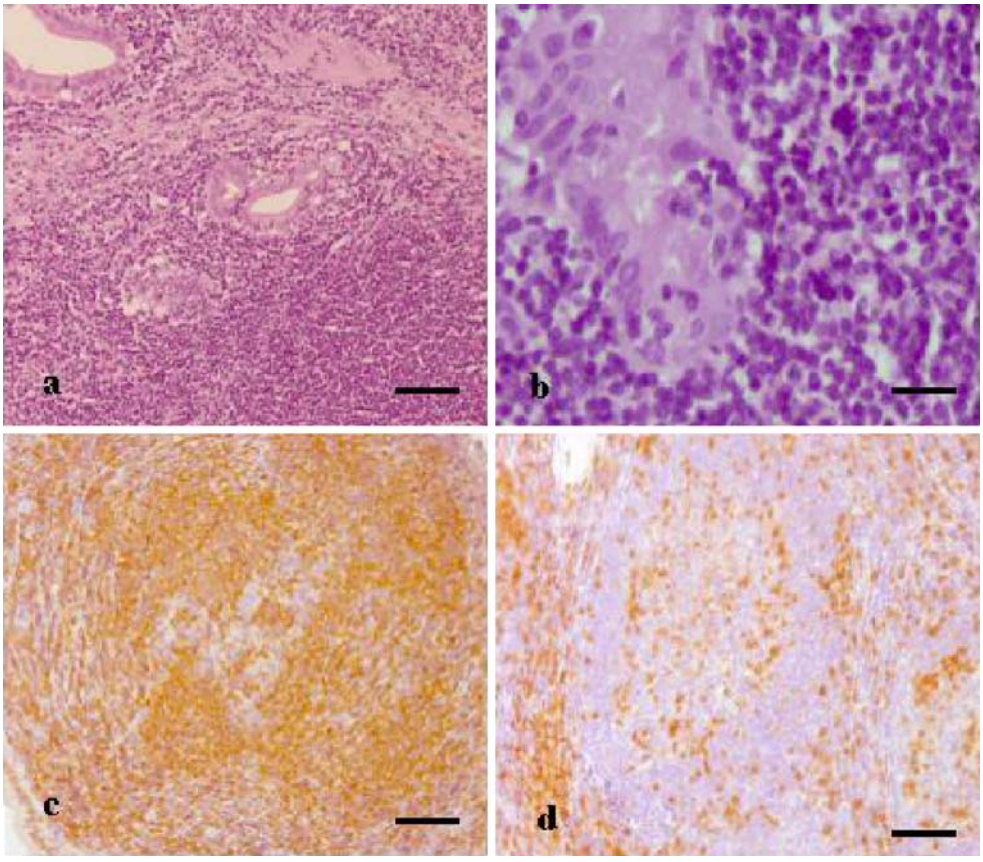

Fig. 1 Case 1. The gallbladder wall revealed infiltration of a monotonous population of small to medium neoplastic cells (HE ×100) (**a**). The high magnification showed evident lymphoepithelial lesion involving the glandular epithelium (HE ×400) (**b**). The neoplastic lymphoid cells were positive for Cyclin D1 (×100) (**c**), whereas they were negative for CD5 (×100) (**d**). *Scale bar* 100 μm

The patient received oral Chlorambucil (10mg daily) for 42 consecutive days and Rituximab (700 mg) in four weekly doses. At restaging, the patient was found to have achieved a partial remission, but residual neoplastic cells, morphologically and immunophenotypically identical to those infiltrating the gallbladder, were documented in different gastric and duodenal biopsies performed at 8 and 11 months after diagnosis. Lymphoepithelial lesions were also observed in the gastric/duodenal mucosa biopsies. The patient underwent surgical excision of the stomach by Billroth 2 technique and is well, with no signs of disease at 24 months from diagnosis.

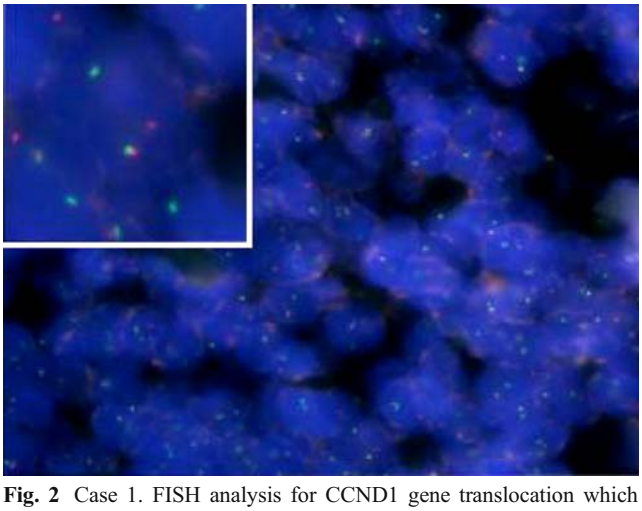

Fig. 2 Case 1. FISH analysis for CCND1 gene translocation which revealed more than 40% of interphase positive nuclei with the classical signal pattern (1F1R1G). *Inset* Higher magnification of a positive nucleus

Case 2

A 74-year-old male patient was admitted to Siena Hospital because of lymphnode enlargements at axillary sites and in the mediastinum. A lymph node was excised from the right axilla.

At histological examination, extensive effacement of lymph node architecture by neoplastic lymphoid cells of small/medium size with irregular or cleaved nuclei and scant cytoplasm was documented. The tumor cells were distributed in an obvious follicular pattern (Fig. 3a), associated with a meshwork of dendritic follicular cells stained for CD21 (Fig. 3b). The immunostain with a large panel of monoclonal antibodies for the diagnosis showed that the neoplastic cells were positive for CD20, CD10 (Fig. 4a), CD79α, Bcl6 (Fig. 4b), Bcl2, and Cyclin D1 (Fig. 4c), whereas the stains for CD3, CD5 (Fig. 4d), and CD23 were negative. A large number of neoplastic cells (>50%) were MIB1 positive. CCND1 gene translocation was observed by FISH in about 50% of the interphase

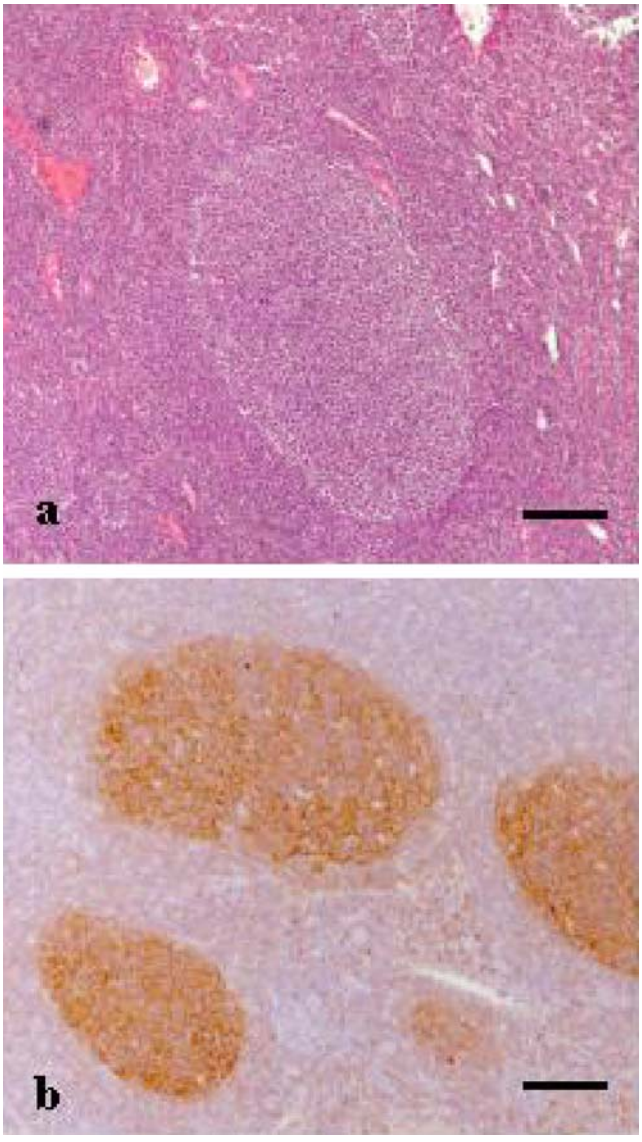

Fig. 3 Case 2. The lymphoid tissue showed a follicular pattern distribution of the B-cells (HE ×50) (**a**). A meshwork of dendritic follicular cells stained for CD21 (HE ×50) (**b**). *Scale bar* 100 μm

nuclei (Fig. 5a), several times accompanied by two or three extra yellow signal, suggesting the possibility of a polisomy of the chromosome 11 (Fig. 5a inset). Translocation of the BCL2 gene was not observed, although tetraploidy of chromosome 18 was highlighted by the presence of four yellow signals (Fig. 5b). No segregated signals indicating translocation of the *c-myc* gene were observed. The majority of nuclei showed four pairs of yellow or closely located red/green signals, suggesting tetrasomy of chromosome 8 (Fig. 5c).

A CT scan demonstrated disease involvement of the axillary and mediastinum lymph nodes and of the spleen, while a bone marrow biopsy scored negative (stage IIIs/A).

The patient received four cycles of Fludarabine (40 mg/day for four consecutive days) and Cyclophosphamide (200 mg/day for four consecutive days). After treatment, lymph nodes and splenomegaly disappeared and the patient remained in good clinical conditions for 1 year, when disease relapsed 1 year from diagnosis. The patient is currently undergoing an additional line of immunochemotherapy treatment.

Discussion

The initial goal of this study was to evaluate the importance of clinical pathological and immunophenotypic analysis in the diagnosis of small B-cell lymphoma cases. Based on the site of involvement, growth pattern of the lymphomatous mass, cytomorphic characteristics, and immunophenotype, all our cases except two were easily assigned to subtypes of small B-cell lymphoma. One of these cases, involving cholecystic and duodenal mucosa infiltration by small/medium-sized neoplastic lymphoid cells with irregular nuclei and scanty cytoplasm, appeared suggestive of MALT lymphoma but was positive for Cyclin D1 protein. Because the gastrointestinal tract is a common site of extranodal involvement by both MZL and MCL, our case raised the question of whether it was a MZL showing aberrant expression of Cyclin D1 or a MCL, which was atypical in that it had lost CD5 expression. An ancillary but inconsistent criterion for the diagnosis of extranodal MZL (MALT-type) is the "monocytoid" aspect of lymphoid cells. An additional helpful criterion for the diagnosis of this clinicopathologic entity is the presence of lymphoepithelial lesions (although similar lesions have occasionally been described in cases of MCL at various mucosal surfaces [10, 19, 31]). These cytomorphologic features were present in our case. However, a typical t(11;14) FISH pattern was visualized on cell nuclei, favoring the diagnosis of a MCL with loss of CD5.

The diagnosis of MCL is based mainly on coexpression of CD5 and Cyclin D1 and MZL is usually negative for both markers. However, immunophenotypic similarities and overlapping immunoprofiling between these two histogenetically different subtypes may be observed [9, 15, 20, 23, 26]. Our case highlights the difficulties in the differentiating between these lymphoproliferative diseases, and further supports the notion that the distinction between MCL and MZL subtypes remains critical. Cases of MCL mimicking MZL have been reported in diverse anatomic sites of involvement, such as palatine tonsils [1], liver [37], and spleen [7, 28].

The second case showed a growth pattern typical of follicular lymphoma, comprising small- to medium-sized cells with irregular or cleaved nuclei lying within a meshwork of follicular dendritic cells. Classical markers were present [CD20, CD79α, CD10, Bcl2, and Bcl6

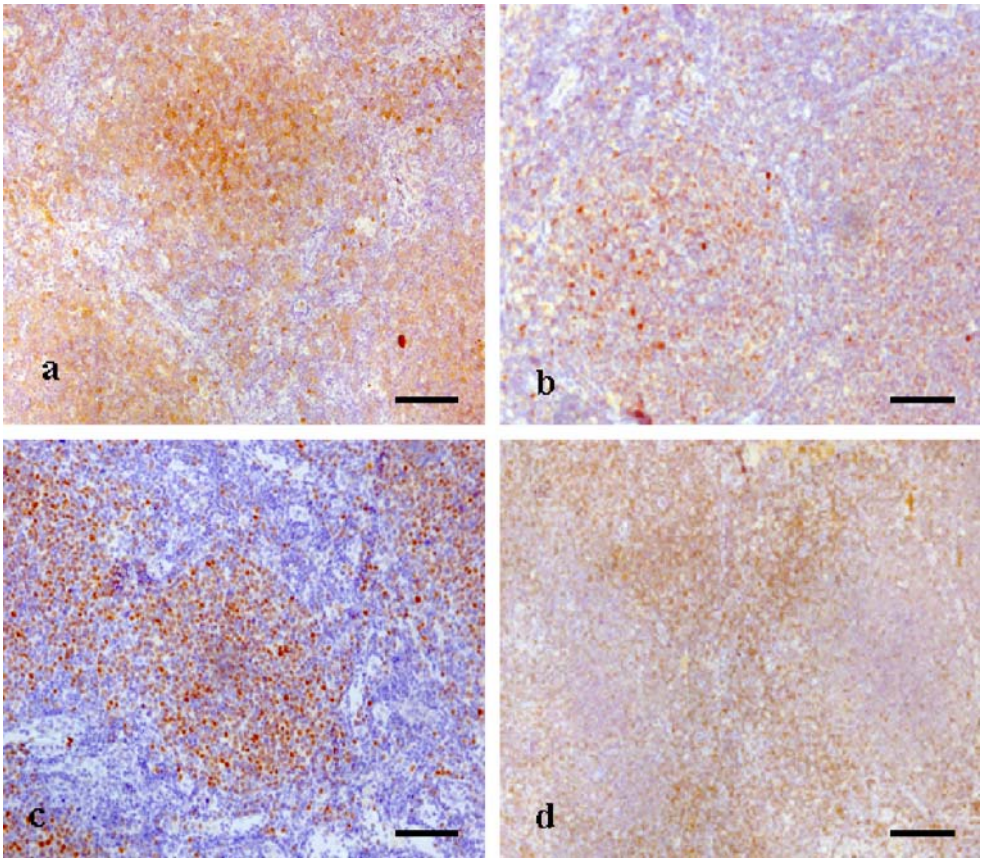

Fig. 4 The neoplastic lymphoid cells were positive for CD10 (**a**) (×50), Bcl6 (×100) (**b**), and Cyclin D1 (×100) (**c**) while they were negative for CD5 (×50) (**d**). *Scale bar* 100 μm

(focally)], but Cyclin D1 was also present. CD3, CD5, and CD23 were all absent. The differential diagnosis was therefore between MCL and FL.

An atypical CCND1 signal pattern consisting of three or two colocalized (F) signals and a variable number of green and red signals was observed in this case and no evidence of c-myc or BCL2 rearrangements were found. Tetrasomy of chromosome 8 and numerical change of chromosome 18 was also observed. This hybridization pattern is similar to a pattern described in several MCLs by Kodet et al. [18]. Numerical chromosomal changes have also been reported in MCLs [16, 24]. In addition, trisomies of 3q, 8q, and tetraploidy were observed in the immunoglobulin variable heavy chain gene (VH)-unmutated MCLs [17].

Given the morphologic and immunophenotypic characteristics, the possibility that this case should represent a composite FL and MCL could have been taken into consideration. However, the detection by FISH results of CCND1 gene translocation in about 50% of the interphase nuclei and not translocation of the BCL2 gene, ruled out this possibility and suggested a diagnosis of MCL with loss of CD5 and aberrant expression of CD10. The clinical significance of immunophenotypic disparity is unknown [6, 39] although a change in surface antigen expression may be documented in cases of MCL with histologic transformation and more aggressive evolution [8, 21]. Mantle cell lymphoma with coexpression of CD5 and CD10 has been reported [6]. CD5 negative MCL are also well documented [20]. However, the strong positivity of CD10 as seen in this case, together with the negativity of CD5 is a rare event and only a few cases have been described [21] including one recently reported on http://www.forumcases.org. This immunophenotype is challenging to interpret in a routine diagnostic setting without the help of molecular analysis.

In conclusion, FISH analysis may be informative in diagnosis of small B-cell lymphomas when histology and immunophenotype are inconclusive. We assume that overlapping morphologic patterns and heterogeneous combined immunophenotypes that are sometimes observed in small B-cell lymphomas could be attributed to genetic abnormalities, such as numerical chromosomal changes. Although the clinical behavior of such cases is not known, it is possible that it may be more aggressive. In our cases, the follow-up is too short to allow any correlation with the other cases included in this study. The question still remains whether such cases should be assigned to a specific lymphoma entity or reported as unclassifiable

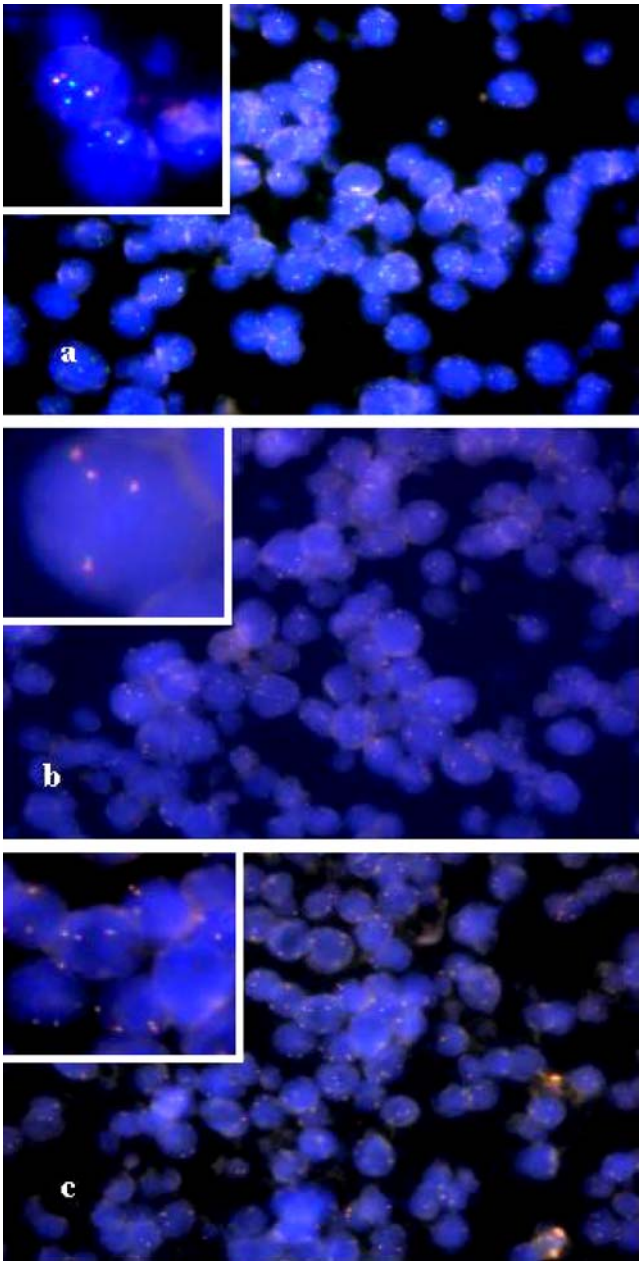

Fig. 5 Case 2. FISH performed for CCND1, BCL2, and c-myc gene translocations: 50% of interphase nuclei were positive for the CCND1 gene translocation (**a**), majority accompanied by extrasignal (*Inset* higher magnification of a nucleus), suggesting the possibilities that polisomy of the chromosome 11 was also present. No cells were positive for the BCL2 gene translocation (**b**); in several nuclei, tetraploidy of chromosome 18 were observed (*Inset* higher magnification of a nucleus). No cells positive for the c-myc gene translocation were highlighted (**c**), although in most if not all nuclei, tetraploidy of the chromosome 8 were found (*Inset* higher magnification of a nucleus)

(with a note detailing the unusual features). Further studies of these rare cases are needed and this will be facilitated if they are recognized in future classification and clinical trials.

Acknowledgements We thank Prof. David Mason, Leukaemia Research Fund Immunodiagnostics Unit, Nuffield Department of Clinical Laboratory Sciences, John Radcliffe Hospital (Oxford, UK), for the helpful discussion and comments.

References

1. Anagnostopoulos I, Foss H-D, Hummel M, Trenn G, Stein H (2001) Extanodal mantle cell lymphoma mimicking marginal zone cell lymphoma. Histopathology 39:561–565
2. Barista I, Romaguera JE, Cabanillas F (2001) Mantle cell lymphoma. Lancet Oncol 2:141–148
3. de Boer CJ, Schuuring E, Dreef E, Peters G, Bartek J, Kluin PM, van Krieken JH. (1995) Cyclin D1 protein analysis in the diagnosis of mantle cell lymphoma. Blood 86:2715–2723
4. de Boer CJ, Kluin-Nelemans JC, Dreef E, Kester MG, Kluin PM, Schuuring E, van Krieken JH (1996) Involvement of the CCND1 gene in hairy cell leukemia. Ann Oncol 7:251–256
5. de Leon E, Alkan S, Huang JC, Hsi ED (1998) Usefulness of an immunohistochemical panel in paraffin-embedded tissues for the differentiation of B-cell lymphomas of small lymphocytes. Mod Pathol 11(11):1046–1051
6. Dong HY, Gorczyca W, Liu Z, Tsang P, Wu CD, Cohen P, Weisberger J (2003) B-cell lymphomas with coexpression of CD5 and CD10. Am J Clin Pathol 119:218–230
7. Elnenaei MO, Jadayel DM, Matutes E, Morilla R, Owusu-Ankomah K, Atkinson S, Titley L, Mandala EM, Catovsky D (2001) Cyclin D1 by flow cytometry as a useful tool in the diagnosis of B-cell malignancies. Leuk Res 25:115–123
8. Felten CL, Stephenson CF, Ortiz RO, Hertzberg L (2004) Burkitt transformation of mantle cell lymphoma. Leuk Lymphoma 45 (10):2143–2147
9. Ferry JA, Yang WI, Zukerberg LR, Wotherspoon AC, Arnold A, Harris NL (1996) CD5+ extranodal marginal zone B-cell (MALT) lymphoma. A low grade neoplasm with a propensity for bone marrow involvement and relapse. Am J Clin Pathol 105(1):31–37
10. Fraga M, Lloret E, Sanchez-Verde L, Orradre JL, Campo E, Bosch F, Piris MA (1995) Mucosal mantle cell (centrocytic) lymphomas. Histopathology 26(5):413–422
11. Haralambieva E, Schuuring E, Rosati S van Noesel C, Jansen P, Appel I, Guikema J, Wabinga H, Bleggi-Torres LF, Lam K, van den Berg E, Mellink C, van Zelderen-Bhola S, Kluin Pl (2004) Interphase fluorescence in situ hybridization for the detection 8q24/MYC breakpoints on routine histologic sections: validation in Burkitt lymphomas from three geographical regions. Genes Chromosomes Cancer 40:10–18
12. Hui P, Howe JG, Crouch J, Nimmakayalu M, Qumsiyeh MB, Tallini G, Flynn SD, Smith BR (2003) Real-time quantitative RT-PCR of cyclin D1 mRNA in mantle cell lymphoma: comparison with FISH and immunohistochemistry. Leuk Lymphoma 44 (6):1385–1394
13. Jadayel D, Matutes E, Dyer MJ, Brito-Babapulle V, Khohkar MT, Oscier D, Catovsky D (1994) Splenic lymphoma with villous lymphocytes: analysis of bcl-1 rearrangements and expression of the cyclin D1 gene. Blood 83(12):3664–3671
14. Jaffe ES, Harris NL, Stein H, Wardiman JW (2001) Mature B-cell Neoplasm World Health Organization Classification of tumours. Pathology and genetics of tumours of haematopoietic and lymphoid tissues. IARC Press, Lyon, France
15. Kaptain S, Zukerberg LR, Ferry JA (1998) Bcl-1/cyclinD1+ CD5- mantle cell lymphoma (Abstract). Mod Pathol 11:133A

16. Katz RL, Caraway NP, Gu J, Jiang F, Pasco-Miller LA, Glassman AB, Luthra R, Hayes KJ, Romaguera JE, Cabanillas FF, Medeiros LJ (2000) Detection of chromosome 11q13 breakpoints by interphase fluorescence in situ hybridization. A useful ancillary method for the diagnosis of mantle cell lymphoma. Am J Clin Pathol 114:248–257
17. Kienle D, Krober A, Katzenberger T, Ott G, Leupolt E, Barth TF, Moller P, Benner A, Habermann A, Muller-Hermelink HK, Bentz M, Lichter P, Dohner H, Stilgenbauer S (2003) VH mutation status and VDJ rearrangement structure in mantle cell lymphoma: correlation with genomic aberrations, clinical characteristics, and outcome. Blood 102(8):3003–3009
18. Kodet R, Mrhalová M, Krsková L, Soukup J, Campr V, Neskudla T, Szepe P, Plank L (2003) Mantle cell lymphoma: improved diagnostics using a combined approach of immunohistochemistry and identification of t(11;14)(q13;q32) by polymerase chain reaction and fluorescence in situ hybridization. Virchows Arch 442:538–547
19. Lavergne A, Brouland JP, Launay E, Nemeth J, Ruskone-Fourmestraux A, Galian A (1994) Multiple lymphomatous polyposis of the gastrointestinal tract. An extensive histopathologic and immunohistochemical study of 12 cases. Cancer 74 (11):3042–3050
20. Liu Z, Dong HY, Gorczyca W, Tsang P, Cohen P, Stephenson CF, Berger CS, Wu CD, Weisberger J (2002) CD5-mantle cell lymphoma. Am J Clin Pathol 118:216–224
21. Morice WG, Hodnefield JM, Kurtin PJ, Hanson CA (2004) An unusual case of leukemic mantle cell lymphoma with a blastoid component showing loss of CD5 and aberrant expression of CD10. Am J Clin Pathol 122:122–127
22. Motokura T, Bloom T, Kim HG, Juppner H, Ruderman JV, Kronenberg HM, Arnold A (1991) A novel cyclin encoded by a bcl1-linked candidate oncogene. Nature (Lond) 350:512–515
23. Onciu M, Berrak SG, Medeiros LJ, Katz RL, Huh YO (2002) Discrepancies in the immunophenotype of lymphoma cells in samples obtained simultaneously from different anatomic sites. Am J Clin Pathol 117:644–650
24. Ott G, Kalla J, Ott MM, Schryen B, Katzenberger T, Muller JG, Muller-Hermelink HK (1997) Blastoid variants of mantle cell lymphoma: frequent bcl-1 rearrangements at the major translocation cluster region and tetraploid chromosome clones. Blood 89 (4):1421–1429
25. Paternoster SF, Brockman SR, McClure RF, Remstein ED, Kurtin PJ, Dewald GW (2002) Technical advance: a new method to extract nuclei from paraffin-embedded tissue to study lymphomas using interphase fluorescence in situ hybridization. Am J Pathol 160:1967–1972
26. Petit B, Chaury M-P, Le Clorennec C, Jaccard A, Gachard N, Moalic-Judge S, Labrousse F, Cogne M, Bordessoule D, Feuillard J (2005) Indolent lymphoplasmacytic and marginal zone B-cell lymphomas: absence of both IRF4 and Ki67 expression identifies a better prognosis subgroup. Haematologica 90:200–206
27. Pruneri G, Fabris S, Baldini L, Carboni N, Zagano S, Colombi MA, Ciceri G, Lombardi L, Rocchi M, Buffa R, Maiolo AT, Neri A (2000) Immunohistochemical analysis of cyclin D1 shows deregulated expression in multiple myeloma with the t(11;14). Am J Pathol 156:1505–1513
28. Piris MA, Mollejo M, Campo E, Menarguez J, Flores T, Isaacson PG (1998) A marginal zone pattern may be found in different varieties of non-Hodgkin's lymphoma: the morphology and immunohistology of splenic involvement by B-cell lymphomas simulating splenic marginal zone lymphoma. Histopathology 33:230–239
29. Remstein E, Kurtin P, James C, Wang XY, Meyer RG, Dewald GW (2002) MALT lymphomas with t(11;18) (q21;q21) and MALT lymphomas with aneuploidy develop along different pathways. Am J Pathol 161(1):63–71
30. Ronchetti D, Finelli P, Richelda R, Baldini L, Rocchi M, Viggiano L, Cuneo A, Bogni S, Fabris S, Lombardi L, Maiolo AT, Neri A (1999) Molecular analysis of 11q13 breakpoints in multiple myeloma. Blood 93:1330–1337
31. Shibata K, Shimamoto Y, Nakano S, Miyahara M, Nakano H, Yamaguchi M (1995) Mantle cell lymphoma with the features of mucosa-associated lymphoid tissue (MALT) lymphoma in an HTLV-I seropositive patient. Ann Hematol 70(1):47–51
32. Specht K, Kremer M, Muller U, Dirnhofer S, Rosemann M, Hofler H, Quintanilla-Martinez L, Fend F (2002) Identification of cyclin D1 mRNA overexpression in B-cell neoplasias by real-time reverse transcription-PCR of microdissected paraffin sections. Clin Cancer Res 8:2902–2911
33. Swerdlow SH, Zukerberg LR, Yang W-I, Harris NL, Williams ME (1996) The morphologic spectrum of non Hodgkin's lymphomas with BCL1/cyclin D1 gene rearrangements. Am J Surg Pathol 20 (5):627–640
34. Tomita S, Kojima M, Imura J, Hori H, Ueda Y, Koitabashi A, Suzuki Y, Nakamura T, Nakamura Y, Mitani K, Terano A, Ohkura Y, Kawamata H, Fujimori T (2003) Extranodal diffuse follicular center lymphoma mimicking mantle cell lymphoma of the intestine. Am J Hematol 74(3):287–289
35. Tsujimoto Y, Jaffe ES, Cossman J, Gorham J, Nowell PC, Croce CM (1985) Clustering of breakpoints on chromosome 11 in human B-cell neoplasms with the t(11;14)chromosome translocation. Nature (Lond) 315:343–345
36. Uchimaru K, Taniguchi T, Yoshikawa M, Asano S, Arnold A, Fujita T, Motokura T (1997) Detection of cyclin D1 (bcl-1, PRAD1) overexpression by a simple competitive reverse transcription-polymerase chain reaction assay in t(11;14)(q13;q32)-bearing B-cell malignancies and/or mantle cell lymphoma. Blood 9:965–974
37. Ueda G, Oka K, Matsumoto T, Yatabe Y, Yamanaka K, Suyama M, Ariyama J, Futagawa S, Mori N (1996) Primary hepatic marginal zone B-cell lymphoma with mantle cell lymphoma phenotype. Virchows Arch 428(4–5): 311–314
38. Vaandrager JW, Schuuring E, Raap A, Philippo K, Kleiverda K, Kluin P (2000) Interphase FISH detection of BCL2 rearrangement in follicular lymphoma using breakpoints flanking probes. Genes Chromosomes Cancer 27:85–94
39. Xu Y, McKenna RW, Kroft SH (2002) Assessment of CD10 in the diagnosis of small B-cell lymphomas. A multiparameter flow cytometry study. Am J Clin Pathol 117:291–300
40. Yatabe Y, Nakamura S, Seto M, Kuroda H, Kagami Y, Suzuki R, Ogura M, Kojima M, Koshikawa T, Ueda R, Suchi T (1996) Clinicopathologic study of PRAD1/cyclin D1 overexpressing lymphoma with special reference to mantle cell lymphoma. A distinct molecular pathologic entity. Am J Surg Pathol 20 (9):1110–1122
41. Zukerberg LR, Yang WI, Arnold A, Harris NL (1995) Cyclin D1 expression in non Hodgkin's lymphomas. Detection by immunohistochemistry. Am J Clin Pathol 103:756–760

Virchows Arch (2006) 449: 328–333
DOI 10.1007/s00428-006-0167-8

ORIGINAL ARTICLE

Katharina Glatz-Krieger · Mona Pache · Coya Tapia · Alain Fuchs · Spasenija Savic · Dieter Glatz · Michael Mihatsch · Peter Meyer

Anatomic site-specific patterns of gene copy number gains in skin, mucosal, and uveal melanomas detected by fluorescence in situ hybridization

Received: 21 December 2005 / Accepted: 25 January 2006 / Published online: 8 March 2006
© Springer-Verlag 2006

Abstract To assess the differences between melanomas of different location and different etiology, 372 malignant melanomas were brought in a tissue microarray format. The collection included 23 acral and 118 non-acral skin melanomas, 9 mucosal melanomas, 100 uveal melanomas, and 122 melanoma metastases. Fluorescence in situ hybridization (FISH) was used to assess copy number changes of the cyclin D1 (CCND1), MDM2, c-myc (MYC), and HER2 genes. FISH analysis revealed distinct differences between melanomas from different locations. CCND1 amplifications were detected in skin melanomas from sites with chronic sun exposure (6 of 32 cases), acral melanomas (4 of 17 cases), and mucosal melanomas (one of ten cases) but not in uveal melanomas. High-level MDM2 amplifications were exclusively present in acral melanomas (2 of 19 cases). MYC copy number gains were detected in 32 of 71 uveal melanomas, five of eight mucosal melanomas, and 6 of 67 melanomas from sites with intermittent sun exposure but not in acral melanomas nor melanomas from sites with chronic sun exposure. Alterations of the MYC gene were associated with advanced tumor stage. There were no high-level HER2 amplifications. Site-specific genetic and epigenetic features may impact the response of melanomas to various anti-cancer drugs and should be considered in future studies on the molecular pathogenesis of malignant melanomas.

K. Glatz-Krieger (✉) · C. Tapia · A. Fuchs · S. Savic · M. Mihatsch · P. Meyer
Institute for Pathology, University of Basel,
Schoenbeinstrasse 40,
CH-4031 Basel, Switzerland
e-mail: Katharina.Glatz@unibas.ch
Tel.: +41-61-2652880
Fax: +41-61-2653194

M. Pache · P. Meyer
University Eye Clinic of Basel,
Basel, Switzerland

D. Glatz
IT Department, University of Basel,
Basel, Switzerland

Keywords Melanoma · Fluorescence in situ hybridization · Tissue array · Amplification

Introduction

There is considerable hope that a new generation of anti-cancer drugs targeting specific genes or molecular pathways may be more efficient in the future. The introduction of trastuzumab (Herceptin), a humanized antibody for the treatment of HER2-positive metastatic breast cancer [9, 29], has pointed out the potential of molecular-targeted therapy. As the results of systemic treatment with classical cytostatic drugs in melanoma patients presenting distant metastases have been discouraging with only a minority of these patients living beyond 1 year [1]. The discovery of frequent mutations of the BRAF gene in malignant melanomas [13] and the subsequent development of BRAF antagonists [7] have raised new hope. If individual molecular features should be targeted in cancer cells, melanoma subgroups with different molecular signatures may be clinically important. It is interesting that there is increasing evidence for distinct molecular characteristics of melanoma subtypes depending on the localization and different levels of sun exposure of the primary tumor [3, 5, 11, 12, 33, 37, 39, 42]. It is tempting to speculate that such differences may be due to a site-specific etiology of melanoma. For example, mutations of the BRAF gene have been shown to be preferentially present in melanomas from sites with intermittent sun exposure [12, 24] and acral melanomas [33] but were nearly inexistent in tumors arising in sites of chronic sun-induced damage, mucosal melanomas [15], and uveal melanomas [10, 14]. Gene amplifications were found to be significantly more frequent in acral and mucosal melanomas than in melanomas from non-acral skin [3, 12]. In addition to the site-specific differences in the degree of genomic instability, there is increasing evidence of distinct patterns of genetic alterations depending on the localization of the primary tumor [12, 41].

To collect more information on possible site-specific molecular differences, we determined the frequency of amplifications of the proto-oncogenes cyclin D1 (CCND1), MDM2, c-myc (MYC), and HER2 in melanomas from different localizations including mucosal and uveal melanomas. For the purpose of this study, we selected a tissue microarray format which allowed us to analyze a total of 372 melanomas on one tissue slide under highly standardized experimental conditions.

Materials and methods

Tumors

Formalin-fixed and paraffin-embedded tissues from 141 primary skin melanomas, 100 uveal melanomas, 9 mucosal melanomas, and 122 metastases (70 lymph node and 52 hematogenous) were brought in a tissue microarray (TMA) format [21]. Primary tumors and corresponding metastases were available from 16 patients and more than one metastasis from 12 patients. Among the 141 primary skin melanomas, there were 37 melanomas located in areas of chronic sun exposure (27 in the head/neck and 10 in the forearm), 78 melanomas located in areas of intermittent sun exposure (45 in the thorax, 8 in the upper arm, and 25 in the legs), 2 anal melanomas (no sun exposure), 23 acral melanomas, and 1 melanoma of unknown location. All melanomas from sites with chronic sun exposure (head/neck and forearm) had marked solar elastosis microscopically. All cases were classified according to the pTNM classification (UJCC, 6th edition, 2003). The stages of skin and primary mucosal tumors were pTis in 6, pT1a in 32, pT1b in 3, pT2a in 27, pT2b in 4, pT3a in 23, pT3b in 14, pT4a in 12, and pT4b in 29. The subtypes of the primary tumors were as follows: superficial spreading (82), nodular (46), lentigo maligna (5), and acral lentiginous (17). The pT stages of the uveal melanomas were pT1a in 3, pT1b in 1, pT2a in 25, pT2b in 27, pT2c in 6, pT3 in 15, and pT4 in 20. pT stage could not be determined in three uveal melanomas. Histologically, a spindle-cell type was present in 50, an epitheloid type in 13, and a mixed type in 37 cases of uveal melanomas. All slides from all tumors were reviewed by one of two pathologists (K.G. for non-uveal melanomas and P.M. for uveal melanomas) to define the histological tumor type and the pathological stage.

A semiautomated arraying instrument was used for TMA construction as described [36]. A representative tissue cylinder of the vertical growth phase was taken for the tissue array from primary tumors in the vertical growth phase (119) and of the radial growth phase from primary tumors in the radial growth phase (22). Of the 25 skin melanomas and 40 uveal melanomas, two tissue cores from the same tumor block were placed in the tissue array.

Tissue samples were collected during 1985–2002 at our institution. The use of the archival material and data in research was approved by the Ethics Committee of the University Hospital Basel.

Fluorescence in situ hybridization

A set of 4-μm TMA sections was used for two-color fluorescence in situ hybridization (FISH). For the proteolytic slide pretreatment, a commercial kit was utilized (Paraffin pretreatment reagent kit, Vysis, Downers Grove, IL, USA). Spectrum Orange-labeled CCND1, MDM2, MYC, and HER2 were used in combination with Spectrum Green-labeled chromosomes 11, 12, 8, and 17 centromeric probes as a reference. All locus-specific probes were obtained from Vysis, IL, USA. Before hybridization, the sections were deparaffinized, air dried, and dehydrated in 70, 85, and 100% ethanol followed by denaturation for 5 min at 74°C in 70% formamide–2× SSC solution. After overnight hybridization at 37°C in a humidified chamber, slides were washed and counterstained with 0.2 μM DAPI in an anti-fade solution. For each tumor, the predominant gene and centromere copy numbers were estimated. A tumor was considered amplified if the ratio of gene probe to centromere probe was ≥2.0.

Statistical analysis

Contingency table analysis and chi-square tests were used to study frequency comparisons of nominal categorized variables.

Results

FISH analysis was successful for CCND1 in 293 (79%), for MDM2 in 301 (81%), for MYC in 271 (73%), and HER2 in 322 (87%) out of the 372 melanoma samples. Non-informative samples were mainly caused by insufficient hybridization, too high background, or absence of tumor cells on arrayed tissues.

CCND1

CCND1 amplifications were found in 8% of 120 primary skin and mucosal melanomas and in 11.2% of 107 metastases from skin melanomas but in none of the 83 uveal melanomas. Among the 21 amplified cases, there were eight tumors with high-level amplifications showing >10 CCND1 signals per tumor cell (Fig. 1). The associations with localization, metastases, and stage are shown in Table 1. It ia interesting that CCND1 amplification was significantly more frequent in acral melanomas and melanomas of the forearm and the head and neck (chronic sun exposure) than in melanomas of the trunk, the legs, and the upper arms (intermittent sun exposure, p=0.001). All melanomas from chronically sun-exposed sites with CCND1 amplifications showed moderate to severe solar elastosis. As lentigo maligna melanomas arise in chronically sun-damaged skin, CCND1 amplifications were more frequent in this subtype than in superficial spreading or nodular melanomas.

MYC

An increase of MYC gene copies was frequently observed in uveal (45.1% of 71) and mucosal (62.5% of 8) melanomas but only rarely in melanomas from sites with intermittent sun exposure (9% of 67) and not from sites with chronic sun exposure or acral sites. In most cases with increased MYC signals, there were only low-level MYC gene copy number gains with the ratio of MYC copies as compared to centromere 8 being 2:1. Clear-cut high-level MYC amplifications with an average ratio of MYC signals per centromere 8 above 5 and the signals occurring in distinct clusters was found in four tumor samples: a nodular melanoma of the upper arm, a nodular melanoma of the elbow, an esophageal melanoma, and a subcutaneous metastasis of a substernal primary. The esophageal melanoma was the only tumor in this study showing high-level amplifications of two genes (CCND1 in addition to MYC).

There was an association between MYC copy number increase and increased tumor stage when all stages were compared (p=0.018). MYC alterations were significantly more frequent in melanomas from the nodular than the superficial spreading type (p=0.002).

MDM2

MDM2 amplifications were found in 3.6% of 139 primary tumors of the skin but not in metastases nor uveal melanomas. Two of five amplified tumors had high-level amplifications (>10 MDM2 copies per cell, Fig. 1). Both were acral melanomas (Table 1).

HER2

One primary tumor from the back skin (Breslow 0.98 mm, pT2) showed a low-level amplification of the HER2 gene (two centromere and five HER2 copies per cell). All the other 322 interpretable primary melanomas and metastases showed no HER2 amplifications.

Results of multiple samples from one patient

For CCND1, MDM2, and HER2, all multiple samples from the same patient showed a consistent result. Among these multiple samples, there were four concordant amplifications of the CCND1 gene [multiple metastases (2×), samples of the same tumor block (1×), and a primary tumor of the esophagus with its lymph node metastasis].

The evaluation of the MYC gene revealed some discrepant results in multiple samples of the same patient. In five uveal melanomas and one skin melanoma, one tissue cylinder had low-level MYC gene copy number gains while the other cylinder of the same tumor block showed a normal MYC copy number as a result of intratumoral heterogeneity. The primary tumor of an esophageal melanoma but not its corresponding lymph node metastasis had a high-level MYC amplification. In another 45 cases with multiple tissue cylinders from one patient, the results of MYC copy numbers of all samples were congruent. Of these 45 cases, 24 had an increased MYC copy number.

Discussion

In this study, the analysis of 372 melanoma tissue samples revealed significant molecular differences between tumors of different sites.

FISH was used to investigate gene amplifications of CCND1, MDM2, MYC, and HER-2. Among these genes, high-level amplifications of CCND1 were most frequent. It is interesting that CCND1 amplification was significantly more frequent in locations with chronic sun exposure (head/neck and forearms) than in locations with intermittent sun exposure (trunk, legs, and upper arms), raising the

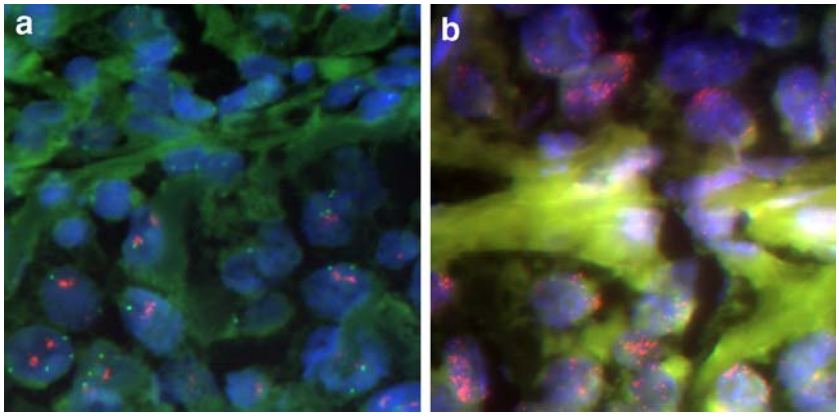

Fig. 1 **a** CCND1 amplification in a lentigo maligna melanoma. Hybridization was done with probes for centromere 11 (*green*) and CCND1 (*red*). Large tumor cells in the *lower half* of the image contain one or two irregularly formed clusters consisting of many closely packed red CCND1 signals and up to four centromere 11 signals. ×640 magnification. **b** MDM2 high-level amplification in acral lentiginous melanoma. Hybridization was done with probes for centromere12 (*green*) and MDM2 (*red*). Large tumor cells with several clusters of MDM2 signals. ×640 magnification

Table 1 Molecular findings, tumor phenotype, stage, and location

		CCND1 (%)	MDM2 (%)	MYC (%)	HER2 (%)
Localization of primary tumor	Uvea	0/83	0/59	32/71 (45.1)	0/78
	Intermittent sun exposure	0/65	3/72 (4.8)	6/67 (9)	1/66 (1.5)
	Chronic sun exposure	6/32 (18.8)[a]	0/32	0/24	0/33
	Acral	4/17 (23.5)[b]	2/19 (10.5)	0/9	0/19
	Mucosa	1/10 (10)	0/8	5/8 (62.5)	0/9
pT (skin primary tumors)	pT1	1/24 (4.2)	3/27 (11.1)	0/25	1/21 (4.8)
	pT2	2/25 (8.0)	0/26	1/25 (4)	0/28
	pT3	3/32 (9.4)	1/34 (2.9)	4/29 (13.8)	0/33
	pT4	5/33 (15.2)	1/32 (3.1)	6/23 (26.1)[c]	0/34
Metastases	Lymph node	8/65 (12.3)	0/60	3/92	0/66
	Distant	5/43 (11.6)[d]	0/46	3/92	0/43
Growth phase	Radial	0/18	1/17 (5.9)	0/17	0/21
	Vertical	11/101 (10.9)	4/107 (3.7)	7/92 (12.0)	1/102 (1.0)
Histologic subtype	Superficial spreading	3/70 (4.3)	3/71 (4.2)	2/67 (6.0)	1/71 (1.4)
	Nodular	3/39 (7.7)	0/37	7/31 (22.6)[e]	0/38
	Lentigo maligna	2/4 (50)	0/5	0/3	0/5
	Acral lentiginous	3/12 (25)	2/13 (15.4)	0/8	0/14

Tumors with CCND1, MDM2, MYC, and HER2 gene probe to centromere probe ratio ≥2.0 detected by FISH. Percentages are indicated in brackets

[a]Site of chronic sun exposure (head/neck and forearm) vs site of intermittent sun exposure (upper arm, leg, and trunk), $p<0.0001$

[b]Acral vs non-acral skin, $p=0.02$

[c]MYC copy number increases when all stages are compared, $p=0.018$

[d]Primary tumors vs metastases, $p<0.0001$

[e]Nodular vs superficial spreading type, $p=0.002$

possibility that CCND1 activation could be particularly important for melanoma development in sites with chronic sun exposure. Our overall frequency and site distribution of CCND1 amplifications in primary skin melanomas is consistent with previous data [12, 34].

The presence of frequent CCND1 amplifications in acral melanomas could be explained by an overall higher level of genetic instability of these tumors involving other molecular pathways than in classical skin melanoma [5, 12].

Our mucosal melanoma with CCND1 amplification had originated from the esophagus where CCND1 amplification occurs at a particularly high frequency in carcinomas as well [35]. A review of our case confirmed the melanoma diagnosis, however. In the same tumor, we additionally detected a high-level MYC amplification illustrating the higher degree of genetic instability in mucosal melanomas [12].

MDM2 was only amplified in five melanomas including two high-level amplifications. Both high-level amplifications were seen in acral melanomas. This finding and the overall low number of MDM2 amplifications are consistent with previous data from Bastian et al. [3]. They found 12q14 copy number gains in 5 of 22 acral melanomas but none in 108 non-acral skin melanomas using CGH and MDM2 amplifications in 1 of 15 acral melanomas by FISH.

Amplifications in acral melanomas but not in non-acral melanomas have been shown to be present in the in situ portion and in the invasive areas at mostly similar levels [2, 3]. It was concluded that the amplifications arise very early during tumor progression in acral melanomas, suggesting that acral melanomas develop a specific amplification-permissive defect early in tumorigenesis unique to the pathogenesis of this tumor type [3, 5]. In most cancers, gene amplifications occur frequently at a late stage and are clearly associated with tumor progression though the mechanisms through which amplifications are generated are largely unknown [23]. The fact that amplifications, in general, occur late in tumorigenesis may explain why amplifications are rather frequent in mucosal melanomas [12] which are usually diagnosed at a late stage.

The unique molecular features in uveal melanomas are not unexpected due to their special location. The chromosomes 1, 3, 6, and 8 are consistently affected by non-random aberrations mainly in the form of chromosomal gains and losses [18, 38]. Additional copies of the long arm of chromosome 8 either by translocation or in the form of an isochromosome i(8q) have been shown to correlate with reduced survival [25]. Parrella et al. [27] had described MYC amplification in 14 of 43 uveal melanomas. These amplifications were of borderline nature typically showing twice as many MYC copies as compared to centromere 8 in FISH analysis. Twice as many gene copies as centromere copies typically reflect a duplication of a large stretch of DNA (e.g., isochromosome formation) rather than a gene-specific amplification event as has been shown in studies of uveal and skin [22, 39] melanomas. By CGH analysis, over-representation of the long arm of chromosome 8 has been reported in 38% of primary melanomas [4]. The poor prognosis associated with extra copies of chromosome 8q may point to the presence of several oncogenes in this region. Ehlers et al. [16] suggest that the DDEF1 gene

located at 8q24 rather than MYC which is also located at 8q24 may function as an oncogene during uveal melanoma progression. The fact that the copy number alterations of the MYC gene are more common in advanced tumors of the nodular subtype has been shown before in studies with limited case numbers [22, 40]. Blocking the expression of MYC with liposomal MYC antisense oligodeoxynucleotides has been reported to inhibit tumor growth and metastases in an in vivo melanoma model [28]. Hopefully, such an approach will finally provide a targeted therapy for selected patients with advanced melanomas.

One skin melanoma showed HER2 amplification according to our definition. This case had two centromere and five HER2 signals which do not constitute a classical amplification. Persons et al. [30] have also reported one HER2 amplification in 40 advanced melanomas. It is not surprising that several studies have proposed HER2 overexpression in up to 80% of melanomas [6, 26] as IHC can yield highly variable results under non-standardized conditions. More recent IHC studies using Food and Drud Administration-approved reagents have described inexistent [17] or a very low rate of detectable HER2 expression (0.9–3%) [19, 31] (own unpublished findings). Altogether, these data strongly argue against a possible therapeutic application of Herceptin in malignant melanoma.

The hypothesis of distinct genetic alterations between melanomas arising in different sites is also supported by the results of recent studies on the frequency of BRAF mutations. BRAF mutations have been observed preferentially in melanomas from skin without chronic sun-induced damage [12] but only rarely or not at all in acral melanomas, melanomas from chronically sun-exposed skin, and mucosal and uveal melanomas [10, 15, 24, 33]. The comparison of aberration frequencies in CGH analysis of melanomas with different sun exposure patterns revealed significant differences between the subgroups defined by location [12, 34]. Altogether, there is increasing evidence for site-specific molecular pathways of melanoma development.

As we know from H&E morphology, malignant melanomas often show considerable intratumoral heterogeneity. On several occasions, this heterogeneity has also been observed at the molecular level [4, 8, 32]. TMAs provide a method for the rapid and simultaneous analysis of up to 1,000 tissue samples in a single experiment under highly standardized conditions. They are not intended for making clinical diagnoses of individual cases but to screen for molecular alterations. The validity of TMA analysis has been shown by comparisons with whole-section analysis in breast, prostate, and brain cancer [20].

In a limited number of cases, we had analyzed more than one sample from the same patient revealing a low number of discordant results. It is interesting that, in one case, a high-level MYC amplification was present in the esophageal primary tumor but not in its lymph node metastasis. A more detailed study of intratumoral heterogeneity will be especially important for the evaluation of potential therapeutic targets that should be present throughout the whole tumor and in its metastases if targeted therapy is to be effective. For that purpose, whole-section slides or several samples of different areas within a given tumor, e.g., of the vertical and radial growth phases, will have to be analyzed.

Due to their genetic characteristics, melanomas may respond differently to various cytotoxic and biologic cancer therapies depending on their body location and the presence or absence of chronic sun-induced damage. The latter can roughly be estimated microscopically by the degree of solar elastosis. In future studies that investigate the molecular pathogenesis of malignant melanomas and in clinical trials with new drug targets, the genetic diversity of melanomas from different sites should be taken into account.

Acknowledgements Katharina Glatz-Krieger and Coya Tapia had been supported by a grant from the "Schweizerische Nationalfonds" and the "SAKK", respectively.

References

1. Balch CM, Soong SJ, Gershenwald JE, Thompson JF, Reintgen DS, Cascinelli N, Urist M, McMasters KM, Ross MI, Kirkwood JM, Atkins MB, Thompson JA, Coit DG, Byrd D, Desmond R, Zhang Y, Liu PY, Lyman GH, Morabito A (2001) Prognostic factors analysis of 17,600 melanoma patients: validation of the American Joint Committee on Cancer melanoma staging system. J Clin Oncol 19:3622–3634
2. Bastian BC (2003) Understanding the progression of melanocytic neoplasia using genomic analysis: from fields to cancer. Oncogene 22:3081–3086
3. Bastian BC, Kashani-Sabet M, Hamm H, Godfrey T, Moore DH 2nd, Brocker EB, LeBoit PE, Pinkel D (2000) Gene amplifications characterize acral melanoma and permit the detection of occult tumor cells in the surrounding skin. Cancer Res 60:1968–1973
4. Bastian BC, LeBoit PE, Hamm H, Brocker EB, Pinkel D (1998) Chromosomal gains and losses in primary cutaneous melanomas detected by comparative genomic hybridization. Cancer Res 58:2170–2175
5. Bastian BC, Olshen AB, LeBoit PE, Pinkel D (2003) Classifying melanocytic tumors based on DNA copy number changes. Am J Pathol 163:1765–1770
6. Bodey B, Bodey Jr B, Groger AM, Luck JV, Siegel SE, Taylor CR, Kaiser HE (1997) Clinical and prognostic significance of the expression of the c-erbB-2 and c-erbB-3 oncoproteins in primary and metastatic malignant melanomas and breast carcinomas. Anticancer Res 17:1319–1330
7. Bollag G, Freeman S, Lyons JF, Post LE (2003) Raf pathway inhibitors in oncology. Curr Opin Investig Drugs 4:1436–1441
8. Casorzo L, Luzzi C, Nardacchione A, Picciotto F, Pisacane A, Risio M (2005) Fluorescence in situ hybridization (FISH) evaluation of chromosomes 6, 7, 9 and 10 throughout human melanocytic tumorigenesis. Melanoma Res 15:155–160
9. Cobleigh MA, Vogel CL, Tripathy D, Robert NJ, Scholl S, Fehrenbacher L, Wolter JM, Paton V, Shak S, Lieberman G, Slamon DJ (1999) Multinational study of the efficacy and safety of humanized anti-HER2 monoclonal antibody in women who have HER2-overexpressing metastatic breast cancer that has progressed after chemotherapy for metastatic disease. J Clin Oncol 17:2639–2648
10. Cohen Y, Goldenberg-Cohen N, Parrella P, Chowers I, Merbs SL, Pe'er J, Sidransky D (2003) Lack of BRAF mutation in primary uveal melanoma. Invest Ophthalmol Vis Sci 44: 2876–2878

11. Cree IA (2000) Cell cycle and melanoma–two different tumours from the same cell type. J Pathol 191:112–114
12. Curtin JA, Fridlyand J, Kageshita T, Patel HN, Busam KJ, Kutzner H, Cho KH, Aiba S, Brocker EB, LeBoit PE, Pinkel D, Bastian BC (2005) Distinct sets of genetic alterations in melanoma. N Engl J Med 353:2135–2147
13. Davies H, Bignell GR, Cox C, Stephens P, Edkins S, Clegg S, Teague J, Woffendin H, Garnett MJ, Bottomley W, Davis N, Dicks E, Ewing R, Floyd Y, Gray K, Hall S, Hawes R, Hughes J, Kosmidou V, Menzies A, Mould C, Parker A, Stevens C, Watt S, Hooper S, Wilson R, Jayatilake H, Gusterson BA, Cooper C, Shipley J, Hargrave D, Pritchard-Jones K, Maitland N, Chenevix-Trench G, Riggins GJ, Bigner DD, Palmieri G, Cossu A, Flanagan A, Nicholson A, Ho JW, Leung SY, Yuen ST, Weber BL, Seigler HF, Darrow TL, Paterson H, Marais R, Marshall CJ, Wooster R, Stratton MR, Futreal PA (2002) Mutations of the BRAF gene in human cancer. Nature 417:949–954
14. Edmunds SC, Cree IA, Di Nicolantonio F, Hungerford JL, Hurren JS, Kelsell DP (2003) Absence of BRAF gene mutations in uveal melanomas in contrast to cutaneous melanomas. Br J Cancer 88:1403–1405
15. Edwards RH, Ward MR, Wu H, Medina CA, Brose MS, Volpe P, Nussen-Lee S, Haupt HM, Martin AM, Herlyn M, Lessin SR, Weber BL (2004) Absence of BRAF mutations in UV-protected mucosal melanomas. J Med Genet 41:270–272
16. Ehlers JP, Worley L, Onken MD, Harbour JW (2005) DDEF1 is located in an amplified region of chromosome 8q and is overexpressed in uveal melanoma. Clin Cancer Res 11: 3609–3613
17. Fink-Puches R, Pilarski P, Schmidbauer U, Kerl H, Soyer HP (2001) No evidence for c-erbB-2 overexpression in cutaneous melanoma. Anticancer Res 21:2793–2795
18. Hausler T, Stang A, Anastassiou G, Jockel KH, Mrzyk S, Horsthemke B, Lohmann DR, Zeschnigk M (2005) Loss of heterozygosity of 1p in uveal melanomas with monosomy 3. Int J Cancer 116:909–913
19. Inman JL, Kute T, White W, Pettenati M, Levine EA (2003) Absence of HER2 overexpression in metastatic malignant melanoma. J Surg Oncol 84:82–88
20. Kallioniemi OP, Wagner U, Kononen J, Sauter G (2001) Tissue microarray technology for high-throughput molecular profiling of cancer. Hum Mol Genet 10:657–662
21. Kononen J, Bubendorf L, Kallioniemi A, Barlund M, Schraml P, Leighton S, Torhorst J, Mihatsch MJ, Sauter G, Kallioniemi OP (1998) Tissue microarrays for high-throughput molecular profiling of tumor specimens. Nat Med 4:844–847
22. Kraehn GM, Utikal J, Udart M, Greulich KM, Bezold G, Kaskel P, Leiter U, Peter RU (2001) Extra c-myc oncogene copies in high risk cutaneous malignant melanoma and melanoma metastases. Br J Cancer 84:72–79
23. Lengauer C, Kinzler KW, Vogelstein B (1998) Genetic instabilities in human cancers. Nature 396:643–649
24. Maldonado JL, Fridlyand J, Patel H, Jain AN, Busam K, Kageshita T, Ono T, Albertson DG, Pinkel D, Bastian BC (2003) Determinants of BRAF mutations in primary melanomas. J Natl Cancer Inst 95:1878–1890
25. Mudhar HS, Parsons MA, Sisley K, Rundle P, Singh A, Rennie IG (2004) A critical appraisal of the prognostic and predictive factors for uveal malignant melanoma. Histopathology 45:1–12
26. Natali PG, Nicotra MR, Digiesi G, Cavaliere R, Bigotti A, Trizio D, Segatto O (1994) Expression of gp185HER-2 in human cutaneous melanoma: implications for experimental immunotherapeutics. Int J Cancer 56:341–346
27. Parrella P, Caballero OL, Sidransky D, Merbs SL (2001) Detection of c-myc amplification in uveal melanoma by fluorescent in situ hybridization. Invest Ophthalmol Vis Sci 42:1679–1684
28. Pastorino F, Brignole C, Marimpietri D, Pagnan G, Morando A, Ribatti D, Semple SC, Gambini C, Allen TM, Ponzoni M (2003) Targeted liposomal c-myc antisense oligodeoxynucleotides induce apoptosis and inhibit tumor growth and metastases in human melanoma models. Clin Cancer Res 9:4595–4605
29. Pegram MD, Lipton A, Hayes DF, Weber BL, Baselga JM, Tripathy D, Baly D, Baughman SA, Twaddell T, Glaspy JA, Slamon DJ (1998) Phase II study of receptor-enhanced chemosensitivity using recombinant humanized anti-p185HER2/neu monoclonal antibody plus cisplatin in patients with HER2/neu-overexpressing metastatic breast cancer refractory to chemotherapy treatment. J Clin Oncol 16:2659–2671
30. Persons DL, Arber DA, Sosman JA, Borelli KA, Slovak ML (2000) Amplification and overexpression of HER-2/neu are uncommon in advanced stage melanoma. Anticancer Res 20:1965–1968
31. Potti A, Hille RC, Koch M (2003) Immunohistochemical determination of HER-2/neu overexpression in malignant melanoma reveals no prognostic value, while c-Kit (CD117) overexpression exhibits potential therapeutic implications. J Carcinog 2:8
32. Ragnarsson-Olding B, Platz A, Olding L, Ringborg U (2004) p53 protein expression and TP53 mutations in malignant melanomas of sun-sheltered mucosal membranes versus chronically sun-exposed skin. Melanoma Res 14:395–401
33. Sasaki Y, Niu C, Makino R, Kudo C, Sun C, Watanabe H, Matsunaga J, Takahashi K, Tagami H, Aiba S, Horii A (2004) BRAF point mutations in primary melanoma show different prevalences by subtype. J Invest Dermatol 123:177–183
34. Sauter ER, Yeo UC, von Stemm A, Zhu W, Litwin S, Tichansky DS, Pistritto G, Nesbit M, Pinkel D, Herlyn M, Bastian BC (2002) Cyclin D1 is a candidate oncogene in cutaneous melanoma. Cancer Res 62:3200–3206
35. Shinozaki H, Ozawa S, Ando N, Tsuruta H, Terada M, Ueda M, Kitajima M (1996) Cyclin D1 amplification as a new predictive classification for squamous cell carcinoma of the esophagus, adding gene information. Clin Cancer Res 2:1155–1161
36. Simon R, Mirlacher M, Sauter G (2004) Tissue microarrays. Methods Mol Med 97:377–389
37. Singh AD, Boghosian-Sell L, Wary KK, Shields CL, De Potter P, Donoso LA, Shields JA, Cannizzaro LA (1994) Cytogenetic findings in primary uveal melanoma. Cancer Genet Cytogenet 72:109–115
38. Sisley K, Cottam DW, Rennie IG, Parsons MA, Potter AM, Potter CW, Rees RC (1992) Non-random abnormalities of chromosomes 3, 6, and 8 associated with posterior uveal melanoma. Genes Chromosomes Cancer 5:197–200
39. Sisley K, Rennie IG, Parsons MA, Jacques R, Hammond DW, Bell SM, Potter AM, Rees RC (1997) Abnormalities of chromosomes 3 and 8 in posterior uveal melanoma correlate with prognosis. Genes Chromosomes Cancer 19:22–28
40. Treszl A, Adany R, Rakosy Z, Kardos L, Begany A, Gilde K, Balazs M (2004) Extra copies of c-myc are more pronounced in nodular melanomas than in superficial spreading melanomas as revealed by fluorescence in situ hybridisation. Cytometry B Clin Cytom 60:37–46
41. van Dijk M, Sprenger S, Rombout P, Marres H, Kaanders J, Jeuken J, Ruiter D (2003) Distinct chromosomal aberrations in sinonasal mucosal melanoma as detected by comparative genomic hybridization. Genes Chromosomes Cancer 36: 151–158
42. White VA, Chambers JD, Courtright PD, Chang WY, Horsman DE (1998) Correlation of cytogenetic abnormalities with the outcome of patients with uveal melanoma. Cancer 83:354–359

Virchows Arch (2006) 449:334–340
DOI 10.1007/s00428-006-0255-9

ORIGINAL ARTICLE

COX-2 expression of ampullary carcinoma: correlation with different histotypes and clinicopathological parameters

Giuseppe Perrone · Daniele Santini · Mariagiovanna Zagami · Bruno Vincenzi · Alfio Verzì · Sergio Morini · Domenico Borzomati · Roberto Coppola · Armando Antinori · Paolo Magistrelli · Giuseppe Tonini · Carla Rabitti

Received: 12 January 2006 / Accepted: 16 June 2006 / Published online: 12 August 2006
© Springer-Verlag 2006

Abstract Epidemiological studies suggest that regular intake of nonsteroidal anti-inflammatory drugs (NSAIDs) are associated with reduced incidence of gastrointestinal cancer. Several lines of evidence indicate that the antineoplastic effect of NSAIDs is attributable to COX-2 inhibition. The aim of our study was to assess COX-2 expression in a series of primary untreated ampullary carcinomas and its possible correlation with clinicopathological parameters. In the present study, 45 surgical specimens of invasive ampullary carcinomas were histologically classified into pancreaticobiliary, intestinal, and unusual types. COX-2 expression by immunohistochemical method was analyzed. High COX-2 expression was detected in 35 (77.8%) ampullary carcinomas. Among these, 20/21 (95.2%) were classified as intestinal, 9/18 (50%) pancreaticobiliary, and 6/6 (100%) unusual type. A significant statistical difference in terms of COX-2 expression was found between pancreaticobiliary vs intestinal type (P=0.002). Furthermore, a negative significant statistical correlation was found between T factor and COX-2 expression (P=0.047). The different COX-2 expression among histopathological types supports the concept of histogenetical difference of ampullary carcinomas. Furthermore, the high rate of COX-2 expression in the intestinal subtype of ampullary carcinoma may represent the rational for a histotype-tailored therapy targeting COX-2.

Keywords Vater · Ampulla · Cancer · Histotype · COX-2

G. Perrone (✉) · M. Zagami · A. Verzì · C. Rabitti
Surgical Pathology, Campus Bio-Medico University,
Via Emilio Longoni,
Rome 83 00155, Italy
e-mail: g.perrone@unicampus.it

D. Santini · B. Vincenzi · G. Tonini
Oncology Unit, Campus Bio-Medico University,
Rome, Italy

S. Morini
Department of Biomedical Research,
Campus Bio-Medico University,
Rome, Italy

D. Borzomati · R. Coppola
General Surgery Department, Campus Bio-Medico University,
Rome, Italy

A. Antinori · P. Magistrelli
General Surgery Department,
Catholic University of the Sacred Heart,
Rome, Italy

Introduction

A growing body of evidence has suggested a correlation between nonsteroidal anti-inflammatory drug (NSAID) use and lower incidence of cancer. The most established data is on the prevention of colorectal [27, 34] and breast cancer [13, 15], but there are also new studies suggesting a similar effect of NSAIDs in many other types of malignant diseases.

The best known target of NSAIDs is the COX enzyme, which catalyses the synthesis of prostaglandins from arachidonic acid. Two isoforms of the COX gene were identified: COX-1, constitutively expressed and related to physiological functions, such as cytoprotection of the stomach and control of platelet aggregation; and COX-2, not detectable in most normal tissues and induced by inflammatory and mitogenic stimuli [30, 33].

A recent number of cell culture and animal model studies has indicated that COX-2-derived prostaglandin E2 (PGE2) promotes carcinogenesis by activating prostaglan-

din E receptor signaling and subsequent promotion of angiogenesis, inhibition of apoptosis, and suppression of immune responses [36].

Angiogenesis is an essential step in the transition of in situ cancers to invasive forms [11, 12] and in the development of distant metastasis [11, 37]. COX-2 stimulates angiogenesis via multiple mechanisms: (1) promotion of the synthesis of vascular endothelial growth factor protein [5, 9]; (2) production of thromboxane A2, PGE2, and prostacyclin, which are direct stimulants of endothelial cells [6, 14, 20]; (3) upregulation of matrix metalloproteinases that are endopeptidases essential for tumor and vascular cell invasion [4, 21]; and (4) inhibition of the production of interleukin-12, a potent antiangiogenic cytokine [32, 35].

Another procancerous effect of the overexpression of COX-2 is the increased resistance to apoptosis [20]. This resistance is caused by the increased production of Bcl-2, an antiapoptotic protein, in response to high levels of PGE2 [5, 29].

Moreover, the increased production of prostaglandins by COX-2 can cause local immune suppression by decreasing the activity of both lymphocytes and natural killer cells and by inhibiting the production of TNF-α that can alter the antitumor immune response [3, 7].

Carcinoma of the ampulla of Vater is one of the smallest cancers that can cause death [17] and only limited studies on COX-2 expression were carried out on surgically removed ampullary carcinomas.

The ampulla of Vater consists of papilla, common channel, distal common bile duct (ampullo-biliary portion), and the distal main pancreatic duct (ampullo-pancreatical portion). The papilla is covered by intestinal mucosa. The inner parts of the ampulla are lined by a simple mucinous epithelium like that of the pancreaticobiliary tree [17–19]. Therefore, ampullary carcinomas may arise from two different types of mucosa, which might reflect the broad histomorphologic spectrum of these tumors [10].

The very special situation of this border between two different types of mucosa should be reflected in the classification of these tumors. Kimura et al. [18], for the first time, have distinguished pancreaticobiliary type and intestinal type of ampullary carcinoma. In 2000, Albores-Saavedra et al. [2] defined the pancreaticobiliary and intestinal types as main types and added the so-called "unusual types."

In the present study, we classified 45 adenocarcinomas of Vater's ampulla by the histomorphologic criteria proposed by Albores-Saavedra et al. Moreover, to the best of our knowledge, for the first time in literature, we examined the expression of COX-2 within different histopathologic types and its possible correlation with pathological parameters.

Materials and methods

Clinical data and tumor specimen acquisition

Material included 45 surgical specimens of invasive ampullary carcinomas. All patients were treated at the Catholic University of the Sacred Heart University and at the University Campus Bio-Medico of Rome from 1988 to 2005 with radical surgical intent. Before surgery all patients were staged by thorax, abdomen, and pelvis computerized tomography scan, by liver palpation and, when indicated, by intraoperative ultrasound of the liver to exclude the presence of distant metastases. All tumors included in the study were limited to the ampulla or were mainly located in the ampulla and secondarily spreading into the neighboring structures.

All specimens were all anatomically examined according to the procedure described by Rosai [26], including evaluation of all anatomic structures (pancreatic duct, ampulla of Vater, common bile duct, and pancreatic head).

Tumors were completely embedded after serial sections of the ampullary region, perpendicularly to the duodenal axis.

Pathological findings were obtained from the pathologists' original reports. In addition to the original pathological reports, microscopic findings (tumor type, differentiation status, and Tumor-Node-Metastasis classification) were reassessed. Tumors were categorized as International Union Against Cancer [31].

Histology

All specimens were fixed in 4% buffered formaldehyde and embedded in paraffin. The samples were sectioned at 5 μm and stained with hematoxylin and eosin. The histological diagnosis was reexamined by two independent pathologists (G. P. and M. Z.) and all tumors were classified histologically according to the criteria published by Albores-Saavedra et al. [2]: The intestinal-type carcinoma is composed of well-formed tubular to elongate glands, complex cribriformed areas and solid nests indistinguishable from colorectal adenocarcinoma (Fig. 1a–c), whereas the pancreaticobiliary-type carcinomas mostly consist of simple or branching glands and small solid nests of cells surrounded by a strikingly desmoplastic stroma (Fig. 1b–d). Tumors with mixed pattern were classified according to their predominant component into the pancreaticobiliary-type or intestinal-type group. Carcinomas of unusual types included undifferentiated, mucinous, signet ring cell, and clear cell carcinomas. Agreement in histological evaluation between the two observers was >90%. In cases of disagreement, a final decision was determined by consensus after reexamination.

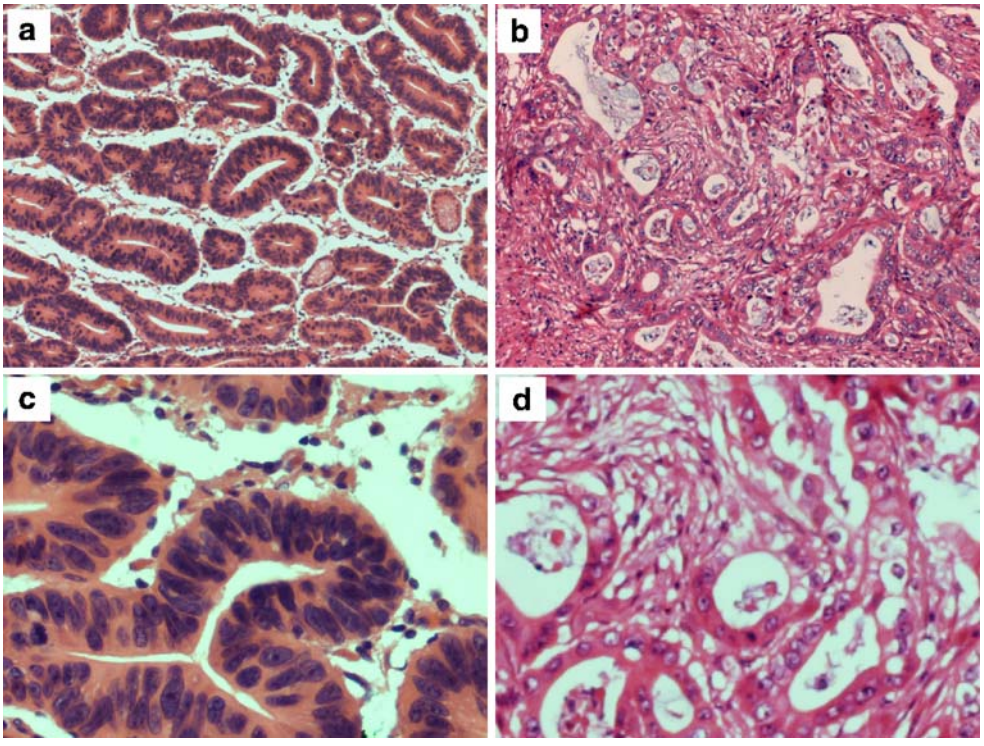

Fig. 1 The intestinal-type carcinoma is composed of well-formed tubular to elongate glands, complex cribriformed areas indistinguishable from colorectal adenocarcinomas (**a**, **c**), whereas the pancreaticobiliary-type carcinomas mostly consist of simple or branching glands surrounded by a strikingly desmoplastic stroma (**b**, **d**). Magnification: **a**, **b** 100×; **c**, **d** 400×

Immunohistochemical staining and quantification

The most representative blocks of each case were selected to be cut into new 3-μm-thick sections for immunohistochemical studies.

Immunohistochemical staining was performed by the streptavidin-biotin method. In brief, sections were deparaffinized. Endogenous peroxidase was blocked by incubation in 3% hydrogen peroxide for 5 min at room temperature. The antibody used was a mouse monoclonal antibody against COX-2 protein (clone CX-294; DakoCy-

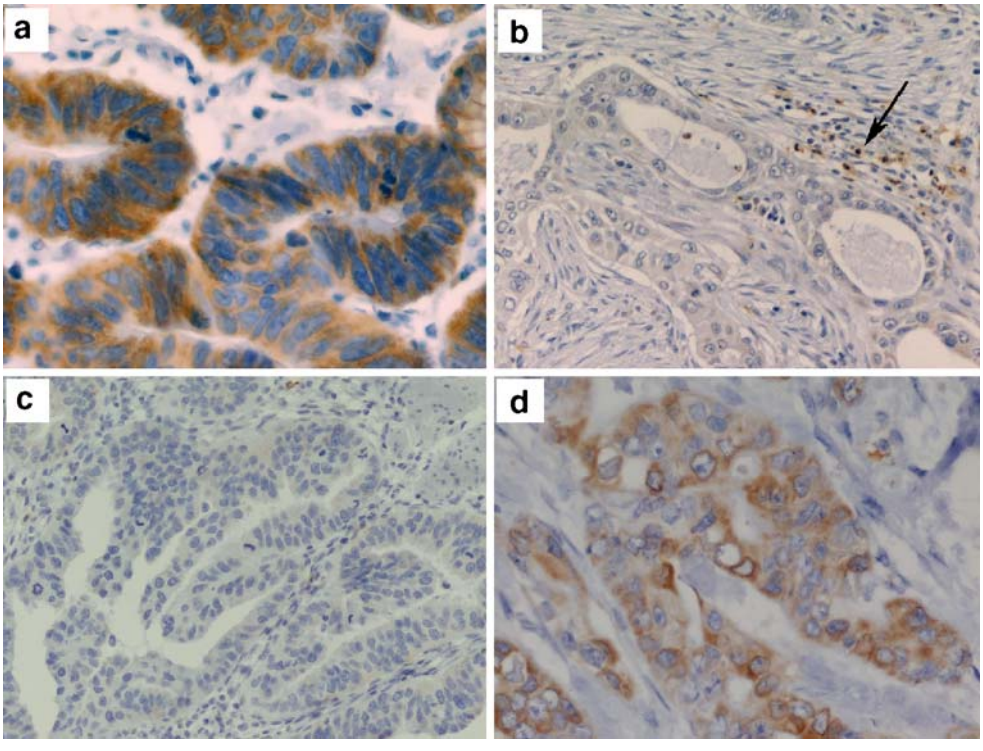

Fig. 2 COX-2 expression staining was cytoplasmatic and granular with staining localized into the tumor cells and not into the surrounding stroma. According to classification in two groups of COX-2 expression, 77.8% of lesions showed high COX-2 expression. In particular, 95.2% of intestinal histotype adenocarcinomas were found to be COX-2-positive **a** and only one case negative **c**, while 50% pancreaticobiliary histotype were found to be COX-2-negative **b** and 50% positive **d**. Macrophages were used as positive internal control (*arrow*). Magnification: 400×

tomation) in a 1:50 dilution at room temperature for 2 h. After washing three times with Tris-buffered saline (TBS), sections were incubated with biotinylated goat anti-mouse/anti-rabbit immunoglobulin G (Dako, Dakopatts, Denmark) for 10 min. They were then washed three times with TBS, treated with streptavidin–peroxidase reagent (Dako, Dakopatts) for 10 min, and again washed with TBS three times. Finally, specimens were incubated in diaminobenzidine for 5 min, followed by hematoxylin counterstaining. Slides were examined by two investigators (G. P. and M. Z.) without knowledge of the corresponding clinicopathological data.

For the evaluation of COX-2 expression, we utilized an immunohistochemical score (IHS) calculated by combining an estimate of the percentage of immunoreactive cells (quantity score) with an estimate of the staining intensity (staining intensity score), as previously described [24]. Percentage of positive tumor cells was categorized as follows: 0, <5%; 1, 5–25%; 2, 26–50%; 3, 51–75%, and 4, >75%. Staining intensity was graded as absent (0), weak (1+), medium (2+), or strong (3+). Theoretically, the overall scores could range from 0 to 12. An IHS score of 9–12 was considered as strong immunoreactivity, 5–8 was considered moderate, 1–4 was considered weak, and 0 was scored as negative. Macrophages were used as positive internal control (Fig. 2) [24]. Furthermore, negative external control slides processed without primary antibody were included for each staining run.

Statistical analysis

Spearman's rank test was applied to establish a correlation between COX-2 expression and tumor local extension (T factor), nodal status (N factors). Fisher's exact test was used to assess relationships of COX-2 expression in different ampullary carcinoma histotypes. Kruskal–Wallis test was used to establish the difference for nonparametric independent variables. *P* values less than 0.05 were regarded as statistically significant in two-tailed tests. SPSS software (version 10.00, SPSS, Chicago, USA) was used for statistical analysis.

Results

Patients' characteristics and histological classification

The main clinicopathological features are summarized in Table 1. The cohort consists of 45 patients with pathological diagnosis of radically resected cancer of the ampulla (25 men and 20 women). The median age at diagnosis was 63 years (range, 38–78). Nine patients (20%) were classified as T1, 19 (42.2%) as T2, 15 (33.3%) as T3, and only 2 (4.4%) as T4. Twenty (44.4%) patients had lymph node metastasis. A positive statistical correlation was found between T and N factor ($P<0.0001$) (Table 4).

Table 1 Clinicopathological parameters

Patients' clinicopathological features	
Total number	45
Median age (range)	63 (range 38–78) years
Gender	
Male vs female	25 vs 20 (55.6 vs 44.4%)
T factor	
1	9 (20%)
2	19 (42.2%)
3	15 (33.3%)
4	2 (4.4%)
N factor	
0	25 (55.6%)
1	20 (44.4%)
Histotype	
Intestinal	21 (46.7%)
Pancreaticobiliary	18 (40%)
Unusual	6 (13.3%)

According to histological criteria published by Albores-Saavedra et al. [2], we found 21 (46.7%) intestinal-type carcinomas, 18 (40%) pancreaticobiliary-type carcinomas, and 6 (13.3%) unusual type carcinomas.

In 29 cases (64.4%), ampullary carcinomas were associated to an epithelial dysplastic transformation of adjacent duodenal mucosa and/or biliopancreatic structures. Adenomatous lesions in 19/45 cases (42.2%) were found (histologically close to intestinal adenomas), while 10/45 cases (22.2%) showed pancreatic intraepithelial neoplasia.

No significant correlation was found between T and N factors and ampullary carcinoma subtypes ($P=0.425$ and 0.863, respectively).

Immunohistochemical staining for COX-2 and its correlation with different histotypes

COX-2 expression staining was cytoplasmatic and granular with staining localized into the tumor cells. Furthermore, macrophages showed a cytoplasmatic staining pattern coherently with our recent paper and were used as internal positive control [24]. The remaining surrounding stroma cells were always negative (Fig. 2).

No significant difference was found between ampullary carcinoma histotypes and COX-2 according to classification in negative, weak, moderate, and strong expression ($P=0.276$). However, when cancers were divided into two groups of COX-2 expression (strong and moderate vs weak and negative), there was a significant statistical difference among histotypes of ampullary carcinoma ($P=0.001$) (Table 2).

Table 2 COX-2 expression in ampullary carcinoma

Histotype	COX-2				P^a	COX-2		P^a
	Negative	Weak	Moderate	Strong		Low (Negative–weak)	High (Moderate–strong)	
Intestinal	0	1	15	5	0.276	1	20	0.001
Pancreaticobiliary	4	5	3	6		9	9	
Unusual	0	0	5	1		0	6	

[a] Kruskal–Wallis test

In particular, when classifying COX-2 expression in high and low, significant statistical difference was found between intestinal vs pancreaticobiliary types (P=0.002). Furthermore, a trend toward significant differences was found between pancreaticobiliary vs unusual types (P=0.052). Finally, no difference was found between intestinal and unusual types (P=1.000) (Table 3).

Correlation between COX-2 expression and clinicopathological parameters

According to classification in two groups of COX-2 expression, 35 lesions (77.8%) showed high COX-2 expression. A negative significant correlation was found between COX-2 and T factor (P=0.047). No significant correlation was found between COX-2 and N factor (P=0.272) (Table 4).

Discussion

Multiple lines of evidence suggest that the enzyme cyclooxygenase, specifically COX-2, may be a promising chemotherapeutic target. COX-2 expression was recently found elevated in several different types of human cancer, suggesting that the presence of COX-2 correlated with cancer development [8, 22, 25, 38, 41].

To date, only limited studies on COX-2 expression were carried out on surgically removed cancers of the ampulla of Vater [1, 16, 23, 28]. In the current study 45 ampullary carcinomas were analyzed for COX-2 expression. Thirty-five lesions (77.8%) showed a high COX-2 expression.

A negative statistical correlation was found between T factor and COX-2 expression (r=−0.298 and P=0.047). This finding may suggest and confirm that as in other tumor diseases [24, 36], COX-2 has a major role in the early phases of neoplastic disease than in advanced ones.

Ampullary carcinomas may arise from two different types of mucosa, which might reflect the broad histomorphologic spectrum of these tumors. On the basis of this concept, following the classification of Albores-Saavedra et al. [2], ampullary carcinomas were distinguished into intestinal, pancreaticobiliary, and unusual types on the basis of histomorphology. To the best of our knowledge, there has been no report focusing on COX-2 expression in different histotypes of ampullary carcinomas.

In the current study, ampullary carcinomas were analyzed for COX-2 expression within different histopathological types. Twenty out of 21 intestinal (95.2%), 9/18 pancreaticobiliary (50%), and 6/6 unusual (100%) types of ampullary carcinomas showed high COX-2 expression. A significant statistical difference in terms of COX-2 expression was established between intestinal and pancreaticobiliary types (P=0.002). Furthermore, a very close to significant difference in terms of COX-2 expression was established between pancreaticobiliary and unusual types carcinomas (P=0.052).

Recent studies have suggested molecular biological differences within histomorphological types of ampullary carcinomas. Zhao et al. [39] demonstrated that K-ras

Table 3 Relationship between COX-2 and ampullary carcinoma histotypes

Groups	COX-2 low, *n* (%)	COX-2 high, *n* (%)	P^a
Intestinal vs pancreaticobiliary type	1 (4.8)–9 (50)	20 (95.2)–9 (50)	0.002
Pancreaticobiliary vs unusual type	9 (50)–0 (0)	9 (50)–6 (100)	0.052
Intestinal vs unusual type	1 (4.8)–0 (0)	20 (95.2)–6 (100)	1.000

[a] Fisher's test

Table 4 Correlation matrix between COX-2 expression and clinicopathological parameters

	COX-2	T
COX-2		
T	r=−0.298 P=0.047	
N	r=−0.167 P=0.272	r=0.529 P<0.0001

Using Spearman test
r Rho correlation coefficient

mutation was found significantly more often in intestinal than in the pancreaticobiliary types and that intestinal type adenocarcinomas show p53 abnormalities more commonly than those of the pancreaticobiliary type. Moreover, Zhou et al. [40] demonstrated that mucin 2 glycoprotein and cytokeratin (CK) 20 were more expressed in intestinal than in pancreaticobiliary type, while CK7 was more expressed in pancreaticobiliary than intestinal type.

Our immunohistochemical finding on ampullary carcinoma demonstrated that an elevated percentage of intestinal type showed a high COX-2 expression. If confirmed by other studies, this result may provide the rational for clinical studies aimed in examining the efficacy of COX-2 inhibitors for the treatment or chemoprevention of this type of ampullary carcinoma. Furthermore, the significant statistical difference found in terms of COX-2 expression between pancreaticobiliary vs intestinal type suggests that these two histotypes of ampullary carcinomas have different molecular biological characteristics and supports the concept of histogenetically different types of ampullary carcinomas. Characterization of these tumors based on histopathology, immunohistochemistry, and molecular anomalies may help to elucidate their etiology, to define different risk profiles, and to program more tailored therapies.

Acknowledgements We thank Alessandra Innocenzi and Giorgio Lescarini for technical support and Maria Crapulli for useful collaboration. The experiments comply with the current laws of the country in which they were performed.

References

1. Agoff SN, Crispin DA, Bronner MP, Dail DH, Hawes SE, Haggitt RC (2001) Neoplasms of the ampulla of vater with concurrent pancreatic intraductal neoplasia: a histological and molecular study. Mod Pathol 14:139–146
2. Albores-Saavedra J, Henson DE, Klimstra DS (2000) Tumors of the gallbladder, extrahepatic bile duct, and ampulla of Vater. In: Rosai J, Sobin L (eds) Atlas of tumor pathology, 3rd series, fascicle 27. Armed Forces Institute of Pathology, Washington DC, pp 259–316
3. Altorki NK, Subbaramaiah K, Dannenberg AJ (2004) COX-2 inhibition in upper aerodigestive tract tumors. Semin Oncol 31:30–35
4. Callejas NA, Casado M, Diaz-Guerra MJ, Bosca L, Martin-Sanz P (2001) Expression of cyclooxygenase-2 promotes the release of matrix metalloproteinases-2 and -9 in fetal rats hepatocytes. Hepatology 33:860–867
5. Cianchi F, Cortesini C, Bechi P, Fantappie O, Messerini L, Vannacci A, Sardi I, Baroni G, Boddi V, Mazzanti R, Masini E (2001) Up-regulation of cyclooxygenase 2 gene expression correlates with tumor angiogenesis in human colorectal cancer. Gastroenterology 121:1339–1347
6. Daniel TO, Liu H, Morrow JD, Crews BC, Marnett LJ (1999) Thromboxane A2 is a mediator of cyclooxygenase-2 dependent endothelial migration and angiogenesis. Cancer Res 59:4574–4577
7. Dannenberg AJ, Altorki NK, Boyle JO, Dang C, Howe LR, Weksler BB, Subbaramaiah K (2001) Cyclooxygenase-2: a pharmacological target for the prevention of cancer. Lancet Oncol 2:544–551
8. Eberhart CE, Coffey RJ, Radhika A, Giardiello FM, Ferrenbach S, DuBois RN (1994) Up-regulation of cyclooxygenase 2 gene expression in human colorectal adenomas and adenocarcinomas. Gastroenterology 107:1183–1188
9. Ferrara N, Gerber HP, LeCouter J (2003) The biology of VEGF and its receptors. Nat Med 9:669–676
10. Fischer HP, Zhou H (2004) Pathogenesis of carcinoma of the papilla of Vater. J Hepatobiliary Pancreat Surg 11:301–309
11. Gately S, Li WW (2004) Multiple roles of COX-2 in tumor angiogenesis: a target for antiangiogenic therapy. Semin Oncol 31:2–11
12. Hanahan D, Weinberg RA (2000) The hallmarks of cancer. Cell 100:57–70
13. Harris RE, Namboodiri KK, Farrar WB (1996) Nonsteroidal antiinflammatory drugs and breast cancer. Epidemiology 7:203–205
14. Inoue H, Takamori M, Shimoyama Y, Ishibashi H, Yamamoto S, Koshihara Y (2002) Regulation by PGE2 of the production of interleukin-6, macrophage colony stimulating factor, and vascular endothelial growth factor in human synovial fibroblasts. Br J Pharmacol 136:287–295
15. Johnson TW, Anderson KE, Lazovich D, Folsom AR (2002) Association of aspirin and nonsteroidal anti-inflammatory drug use with breast cancer. Cancer Epidemiol Biomarkers Prev 11:1586–1591
16. Kim HJ, Sohn TS, Lee KT, Lee JK, Paik SW, Rhee JC (2003) Expression of cyclooxygenase-2 and its correlation with clinicopathologic factors of ampulla of Vater cancer. J Korean Med Sci 18:218–224
17. Kimura W, Ohtsubo K (1988) Incidence, sites of origin, and immunohistochemical and histochemical characteristics of atypical epithelium and minute carcinoma of the papilla of Vater. Cancer 61:1394–1402
18. Kimura W, Futakawa N, Yamagata S, Wada Y, Kuroda A, Muto T, Esaki Y (1994) Different clinicopathologic findings in two histologic types of carcinoma of papilla of Vater. Jpn J Cancer Res 85:161–166
19. Matsubayashi H, Watanabe H, Yamaguchi T, Ajioka Y, Nishikura K, Kijima H, Saito T (1999) Differences in mucus and K-ras mutation in relation to phenotypes of tumors of the papilla of Vater. Cancer 86:596–607
20. Murohara T, Horowitz JR, Silver M, Tsurumi Y, Chen D, Sullivan A, Isner JM (1998) Vascular endothelial growth factor/vascular permeability factor enhances vascular permeability via nitric oxide and prostacyclin. Circulation 97:99–107
21. Nelson AR, Fingleton B, Rothenberg ML, Matrisian LM (2000) Matrix metalloproteinases: biologic activity and clinical implications. J Clin Oncol 18:1135–1149
22. Okami J, Yamamoto H, Fujiwara Y, Tsujie M, Kondo M, Noura S, Oshima S, Nagano H, Dono K, Umeshita K, Ishikawa O, Sakon M, Matsuura N, Nakamori S, Monden M (1999) Overexpression of cyclooxygenase-2 in carcinoma of the pancreas. Clin Cancer Res 5:2018–2024
23. Perrone G, Santini D, Verzi A, Vincenzi B, Borzomati D, Vecchio F, Coppola R, Antinori A, Magistrelli P, Tonini G, Rabitti C (2006) COX-2 expression in ampullary carcinoma: correlation with angiogenesis process and clinicopathological parameters. J Clin Pathol 59(5):492–496
24. Perrone G, Santini D, Vincenzi B, Zagami M, La Cesa A, Bianchi A, Altomare V, Primavera A, Battista C, Vetrani A, Tonini G, Rabitti C (2005) COX-2 expression in DCIS: correlation with

VEGF, HER-2/neu, prognostic molecular markers and clinicopathological features. Histopathology 46:561–568
25. Ristimaki A, Honkanen N, Jankala H, Sipponen P, Harkonen M (1997) Expression of cyclooxygenase-2 in human gastric carcinoma. Cancer Res 57:1276–1280
26. Rosai J (2004) Appendix E. In: Rosai and Ackerman's surgical pathology, 9th edn. Mosby, Edinburgh, pp 2953–2954
27. Rosenberg L, Palmer JR, Zauber AG, Warshauer ME, Stolley PD, Shapiro S (1991) A hypothesis: nonsteroidal anti-inflammatory drugs reduce the incidence of large-bowel cancer. J Natl Cancer Inst 83:355–358
28. Santini D, Vincenzi B, Tonini G, Scarpa S, Vasaturo F, Malacrino C, Vecchio F, Borzomati D, Valeri S, Coppola R, Magistrelli P, Nuzzo G, Picciocchi A (2005) Cyclooxygenase-2 overexpression is associated with a poor outcome in resected ampullary cancer patients. Clin Cancer Res 11:3784–3789
29. Sheng H, Shao J, Morrow JD, Beauchamp RD, DuBois RN (1998) Modulation of apoptosis and Bcl-2 expression by prostaglandin E2 in human colon cancer cells. Cancer Res 58:362–366
30. Smith WL, DeWitt DL, Garavito RM (2000) Cyclooxygenases: structural, cellular, and molecular biology. Annu Rev Biochem 69:145–182
31. Sobin LH, Wittekind C (2002) TNM Classification of malignant tumours, 6th edn. UICC International Union Against Cancer, Wiley-Liss, New York
32. Stolina M, Sharma S, Lin Y, Dohadwala M, Gardner B, Luo J, Zhu L, Kronenberg M, Miller PW, Portanova J, Lee JC, Dubinett SM (2000) Specific inhibition of cyclooxygenase-2 restores antitumor reactivity by altering the balance of IL-10 and IL-12 synthesis. J Immunol 164:361–370
33. Subbaramaiah K, Telang N, Ramonetti JT, Araki R, DeVito B, Weksler BB, Dannenberg AJ (1996) Transcription of cyclooxygenase-2 is enhanced in transformed mammary epithelial cells. Cancer Res 56:4424–4429
34. Thun MJ, Namboodiri MM, Heath CW Jr (1991) Aspirin use and reduced risk of fatal colon cancer. N Engl J Med 325:1593–1596
35. Voest EE, Kenyon BM, O'Reilly MS, Truitt G, D'Amato RJ, Folkman J (1995) Inhibition of angiogenesis in vivo by interleukin-12. J Natl Cancer Inst 87:581–586
36. Wang D, Mann JR, DuBois RN (2005) The role of prostaglandins and other eicosanoids in the gastrointestinal tract. Gastroenterology 128:1445–1461
37. Weidner N (2000) Angiogenesis as a predictor of clinical outcome in cancer patients. Hum Pathol 31:403–405
38. Wolff H, Saukkonen K, Anttila S, Karjalainen A, Vainio H, Ristimaki A (1998) Expression of cyclooxygenase-2 in human lung carcinoma. Cancer Res 58:4997–5001
39. Zhao B, Kimura W, Futakawa N, Muto T, Kubota K, Harihara Y, Takayama T, Makuuchi M (1999) p53 and p21/Waf1 protein expression and K-ras codon 12 mutation in carcinoma of the papilla of Vater. Am J Gastroenterol 94:2128–2134
40. Zhou H, Schaefer N, Wolff M, Fischer HP (2004) Carcinoma of the ampulla of Vater: comparative histologic/immunohistochemical classification and follow-up. Am J Surg Pathol 28:875–882
41. Zimmermann KC, Sarbia M, Weber AA, Borchard F, Gabbert HE, Schror K (1999) Cyclooxygenase-2 expression in human esophageal carcinoma. Cancer Res 59:198–204

Virchows Arch (2006) 449:341–347
DOI 10.1007/s00428-006-0249-7

ORIGINAL ARTICLE

Conjugated linoleic acid reduced metastasized LL2 tumors in mouse peritoneum

Yasuha Sakai · Tomonori Sasahira · Hitoshi Ohmori · Kazuhiro Yoshida · Hiroki Kuniyasu

Received: 5 February 2006 / Accepted: 6 June 2006 / Published online: 8 August 2006
© Springer-Verlag 2006

Abstract The effect of conjugated linoleic acid (CLA) on pre-existent peritoneal metastasis was examined by mouse peritoneal metastasis models. The cell growth of LL2 mouse cancer cells was suppressed by CLA in a dose-dependent manner. CLA-induced growth inhibition was recovered by the exposure to antisense *S*-oligodeoxynucleotide for peroxisome proliferator-activated receptor (PPAR)-γ. C57B6 mice were inoculated with LL2 cells into their peritoneal cavity. Two weeks after inoculation, colonized peritoneal cancer foci (2.2±0.4 mm in diameter) were treated with CLA administrated intraperitoneally (200 or 600 pmol/mouse, twice a week). CLA treatment decreased the number of peritoneal tumors: 8.7±0.6, 5.7±0.6, and 2.3±0.6 in untreated, 200 pmol/mouse CLA, and 600 pmol/mouse CLA groups, respectively ($P<0.0001$). CLA treatment decreased the size of peritoneal tumors: 3.7±1.5, 1.3±0.5, and 1.0±0.4 mm in untreated, 200 pmol/mouse CLA, and 600 pmol/mouse CLA groups, respectively ($P<0.0001$). In CLA-treated tumors, proliferating cells were decreased ($P<0.0001$), whereas apoptotic cells were increased ($P=0.0010$). CLA-treated LL2 tumors showed decrease of PPARγ and EGFR proteins and increase of BAX protein in comparison with untreated tumors. These findings suggest that CLA possesses anti-tumor capability to peritoneal metastasis.

Keywords CLA · Metastasis · Growth inhibition

Abbreviations

CLA	conjugated linoleic acid
PPAR	peroxisome proliferator-activated receptor
EGFR	epithelial growth factor receptor
TGF	transforming growth factor
ODN	transforming growth factor
PCNA	proliferating cell nuclear antigen
TUNEL	terminal deoxynucleotidyl transferase-mediated dUTP nick and labeling

Introduction

Conjugated linoleic acid (CLA) is one of the essential fatty acids and which possesses characteristic bioactive properties [2]. CLA is a mixture of positional and stereo-isomers of octadecadienoate (18:2) [16]. CLA possesses ligand activity to peroxisome proliferator-activated receptor (PPAR)-γ. PPARγ is originally identified to induce adipocyte differentiation [15]. The multiple functions of PPARγ also involved cell growth inhibition and anti-inflammatory effect [1]. PPARγ is a nuclear receptor belonging to the nuclear hormone receptor superfamily

Y. Sakai · T. Sasahira · H. Ohmori · H. Kuniyasu
Department of Molecular Pathology,
Nara Medical University School of Medicine,
Kashihara, Japan

K. Yoshida
Department of Surgical Oncology,
Research Institute for Radiation Biology and Medicine,
Hiroshima University,
Hiroshima, Japan

Present address:
H. Kuniyasu (✉)
840 Shijo-cho,
634-8521 Kashihara, Japan
e-mail: cooninh@zb4.so-net.ne.jp

[1, 3, 7]. PPARγ is dimerized with retinoic X receptor and binds to a specific responsive element within promoter DNA sequence to regulate gene expression [3, 12]. PPARγ initiates the transcription of genes associated with mainly energy homeostasis and proinflammatory cytokines [1, 3, 6, 20].

PPARγ plays a role in transcriptional regulation of cancer-related genes. PPARγ downregulates epithelial growth factor receptor (EGFR) and upregulates Bax, p21Waf-1, and E-cadherin, which are associated with anti-proliferative, pro-apoptotic, and pro-differentiation effects [5, 13, 14, 21]. We previously reported that PPARγ induces EGFR and transforming growth factor (TGF)-α expression by CLA and linoleic treatment in cancer cells [11]. These alterations collectively provide an anti-metastatic effect on cancer cells. The inhibitory effect of PPARγ to cancer metastasis is reported in several cancers, such as non-small cell lung cancer, colon cancer, thyroid cancer, and breast cancer [4, 8, 12, 21].

We previously reported that simultaneously administrated CLA at cancer cell inoculation reduced the number of peritoneal colonization of cancer cells [11]. However, the uncolonized cancer cells are labile to anti-cancer stimuli in comparison to tumor-formed status. In the present study, we revealed the tumor-suppressive effect of CLA on established peritoneal tumors using a mouse peritoneal metastasis model.

Materials and methods

Cell culture

A mouse lung cancer cell line, LL2, was purchased (Dainihon). The cells were routinely maintained in RPMI-1640 (Sigma, St. Louis, MO, USA) containing 10% fetal bovine serum (Sigma) under the condition of 5% CO_2 in air at 37°C. CLA (Calbiochem, Darmstadt, Germany) was dissolved with 70% ethanol (200 nM) for stock solution. For the negative control, the same amount of 70% ethanol was used.

Cell growth

The cells were harvested from 80% confluent monolayer cultures by brief trypsinization with 0.1% trypsin and 0.1% ethylenediamine tetraacetic acid (Sigma). The cells were seeded at density of 10,000 cells per well of 24-well tissue culture plates and treated under the conditions mentioned in the "Results" section. These cell numbers were counted by an autocytometer (Sysmecs, Kobe, Japan) at 48 h after the treatment. Each experiment was repeated three times.

Antisense phosphorothioate (*S*)-oligodeoxynucleotide assay

The 18-mer *S*-oligodeoxynucleotide (ODN) for the antisense sequence from the first to the 18th nucleotide of mouse PPARγ cDNA coding region was synthesized and purified by reverse-phase high-performance liquid chromatography (Sigma Genosys, Ishikari, Japan). The sequence of PPARγ was 5′-ATG GGT GAA ACT CTG GGA-3′ (refer to GenBank NM011146). The sense sequence 18-mer was for negative control. The cells were pretreated with 3 μM antisense or sense *S*-ODN for 6 days, with medium exchanges and additions of antisense or sense *S*-ODN every 2 days. After that, the cells were used for further experiments.

Animal model

C57B6 mice were purchased from Japan SLC (Shizuoka, Japan). The mice were maintained according to the institutional guidelines approved by the Committee for Animal Experimentation of Nara Medical University, in accordance with the current regulations and standards of the Ministry of Health, Labor, and Welfare. The mice were used according to the institutional guidelines when they were 5 weeks old. The cells were briefly trypsinized and washed with Hanks balanced saline solution (HBSS) for three times. The cells suspended by HBSS were injected into the peritoneal cavity by 1×10^7 in each mouse. Eight mice were injected for each group. From 2 weeks after the inoculation, CLA (200 or 600 pmol in 0.2 ml phophate-buffered saline, PBS) was weekly injected into the peritoneal cavity three times. The mice were killed to count the number of metastatic foci in the peritoneal cavity. In another experiment set, mouse survival was observed until 16 weeks after the inoculation.

Immunohistochemistry

Consecutive 4-μm sections were cut from each block, and immunostaining was performed by the immunoperoxidase technique. For proliferating cell nuclear antigen (PCNA) immunostaining, an antigen retrieval method was performed; microwave (500 W) treatment was for 20 min in citrate buffer, pH 6.0. After endogeneous peroxidase block by 3% H_2O_2–methanol for 15 min, those specimens were rinsed with PBS. Anti-PCNA antibody (DAKO, Carpinteria, CA, USA) was used at 0.5 μg/ml for primary antibody and incubated at room temperature for 2 h. The specimens were rinsed with PBS and incubated at room temperature for 1 h with secondary antibody conjugating peroxidase diluted at 0.5 μg/ml (MBL, Nagoya, Japan). All of the specimens were then rinsed with PBS and color was developed by diamino-

benzidine (DAB) solution (DAKO). After being washed with water, the specimens were counterstained with Meyer's hematoxylin (Sigma). Immunostaining of all specimens was performed to ensure the same condition of antibody reaction and DAB exposure. The PCNA-positive cells were counted by microscopic observation on 500 cells and designated by percentage (labeling index, LI).

Terminal deoxynucleotidyl transferase-mediated dUTP nick and labeling method

Apoptotic cells were detected by the terminal deoxynucleotidyl transferase (TdT)-mediated dUTP-biotin nick and labeling (Tunel method). The thin sections were dewaxed, hydrated, and digested by Proteinase K (20 mg/ml, Sigma) 30 min at 37°C. dUTP-biotin (Boehringer-Manheim, Manheim, Germany) was labeled by terminal deoxynucleotidyl transferase reaction (Boehringer-Manheim) in cacodylate buffer in 60 min at 37°C. After blocking nonspecific reactions by a solution containing 5% normal horse serum, the sections were incubated with a 1:50 dilution of a peroxidase-conjugated streptavidine (DAKO) 30 min at room temperature. The all specimens were then rinsed with PBS and color-developed by DAB (DAKO). Then nuclei were counterstaind by hematoxylin (Sigma). Terminal deoxynucleotidyl transferase-mediated dUTP nick and labeling (TUNEL)-positive cells were counted by microscopical observation on 500 cells and designated by percentage (labeling index; LI).

Immunoblot analysis

The whole-cell lysates were prepared as described previously [10]. The 50-μg lysates were subjected to immunoblot analysis in 12.5% sodium dodecyl sulfate–polyacrylamide gels followed by electrotransfer onto nitrocellulose filters. The filters were incubated with primary antibodies and then with peroxidase-conjugated IgG antibodies (MBL). An α-tubulin antibody was used to assess the levels of protein loaded per lane (Oncogene Research Products, Cambridge, MA, USA). The immune complex was visualized by CSA system (DAKO). Anti-PPARγ, anti-EGFR, and anti-Bax (Santa Cruz Biotechnology, Santa Cruz, CA, USA) antibodies were used as primary antibodies.

Statistical analysis

Statistical significance was examined by ANOVA test by using InStat software (Graphpad Software, Los Angeles, CA, USA). Statistical significance was defined as a two-sided *P* value of less than 0.05.

Results

Effect of CLA on growth in LL2 cells

To examine the effect of CLA on the growth of LL2 cells, the LL2 cells were treated with various concentration of CLA for 48 h (Fig. 1). Firstly, we examined the effect of PPARγ antisense and sense *S*-ODNs on PPARγ expression in LL2 cells (Fig. 1a). In antisense *S*-ODN-treated LL2 cells, PPARγ production was suppressed to 13% than in sense *S*-ODN-treated cells. The CLA treatment with exposure to PPARγ sense *S*-ODN showed growth inhibition of LL2 cells in a dose-dependent manner (Fig. 1b). LL2 cells showed 78% growth inhibition by treatment with 10 nM CLA. The exposure to antisense *S*-ODNs for PPARγ significantly reduced CLA-induced growth inhibition in LL2 cells. Antisense-exposed LL2 cells showed 16% growth inhibition by treatment with 10 nM CLA ($P<0.0001$).

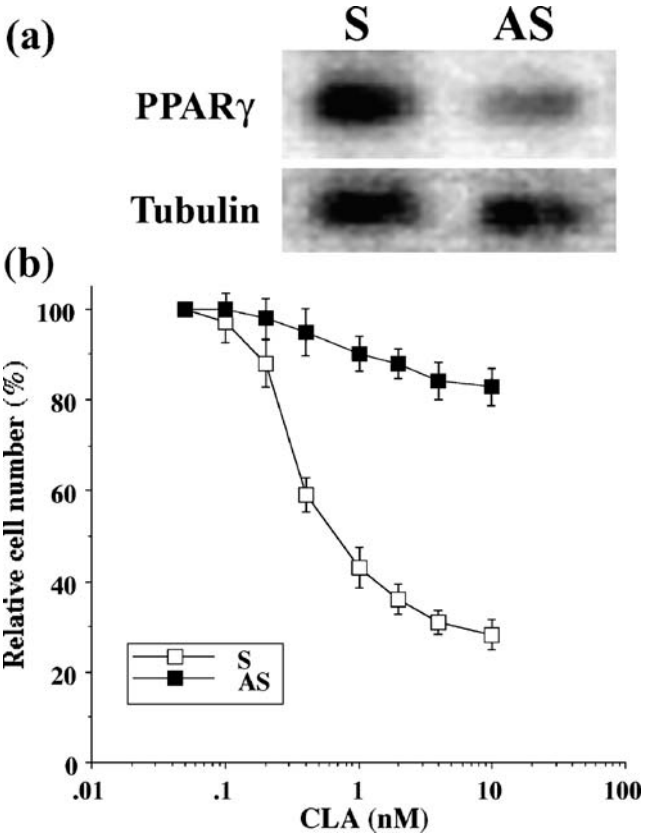

Fig. 1 Effect of CLA on growth of LL2 cells. **a** Effect of sense and antisense *S*-ODN for PPARγ production in LL2 cells. PPARγ protein levels were examined by immunoblotting. Tubulin was served as an internal control. *S*, sense; *AS*, antisense. **b** LL2 cells were treated with various concentration of CLA with sense or antisense *S*-ODN for PPARγ. The relative cell number was standardized by the control cell number of PBS-treated LL2, which is set to 100. *Error bar*, SD

Effect of CLA on reduction of LL2 cells colonized peritoneally

We next examined the effect of CLA on the reduction of metastasized LL2 cells using a syngenic mice models according to the schedule as shown in Fig. 2a. LL2 cells were inoculated by 1×10^7 in the peritoneal cavity of syngenic C57B6 mice. At 2 weeks after inoculation, LL2 cells formed a mean of 8.9 tumors per mouse, which showed 2.2 mm as the mean diameter (Fig. 2b,c). The gross appearance and histology of the tumors before treatment were shown in Fig. 2d,e. Tumors colonized in the serosa of intestine and mesocolon were invaded into the mucosal layer. To treat these established tumors, CLA (200 or 600 pmol/mouse) were intraperitoneally administrated at 2 and 3 weeks after inoculation (Fig. 2a). At 3 weeks after the inoculation, the size and number of the peritoneal tumors was examined (Fig. 2b,c). LL2 cells showed 8.7±0.6 foci per mouse of peritoneal tumors observed in control mice, whereas the numbers of tumors were decreased to 5.7±0.6 and 2.3±0.6 foci per mouse by treatment with CLA (200 and 600 pmol/mouse, respectively, $P<0.0001$). In control mice, tumor size was increase to 3.7±1.5 mm in diameter from that at 2 weeks after inoculation. In contrast, the tumors were significantly smaller in CLA-treated mice than that in control mice and than that in mice at 2 weeks after inoculation ($P<0.0001$). To evaluate the toxicity of CLA, the body weight of mice was assessed (Fig. 2f). Treatment with CLA did not affect body weight of the mice, whereas control mice lost the weight at 3 weeks after inoculation due to tumor growth.

Effect of CLA on proliferation and apoptosis in LL2 tumors

We next examined the effects of CLA on proliferative activity and apoptosis of LL2 cells in tumors by immunohistochemistry (Fig. 3 and Table 1). In untreated tumors, LL2 cells showed high proliferative activity (PCNA LI=72±15%), whereas the CLA-treated cells had significantly suppressed proliferation in a dose-dependent manner ($P<0.0001$). TUNEL-positive apoptotic cells were found in 4±2% LL2 cells in untreated tumors, whereas apoptosis was significantly increased in CLA-treated cells in a dose-dependent manner ($P=0.0010$).

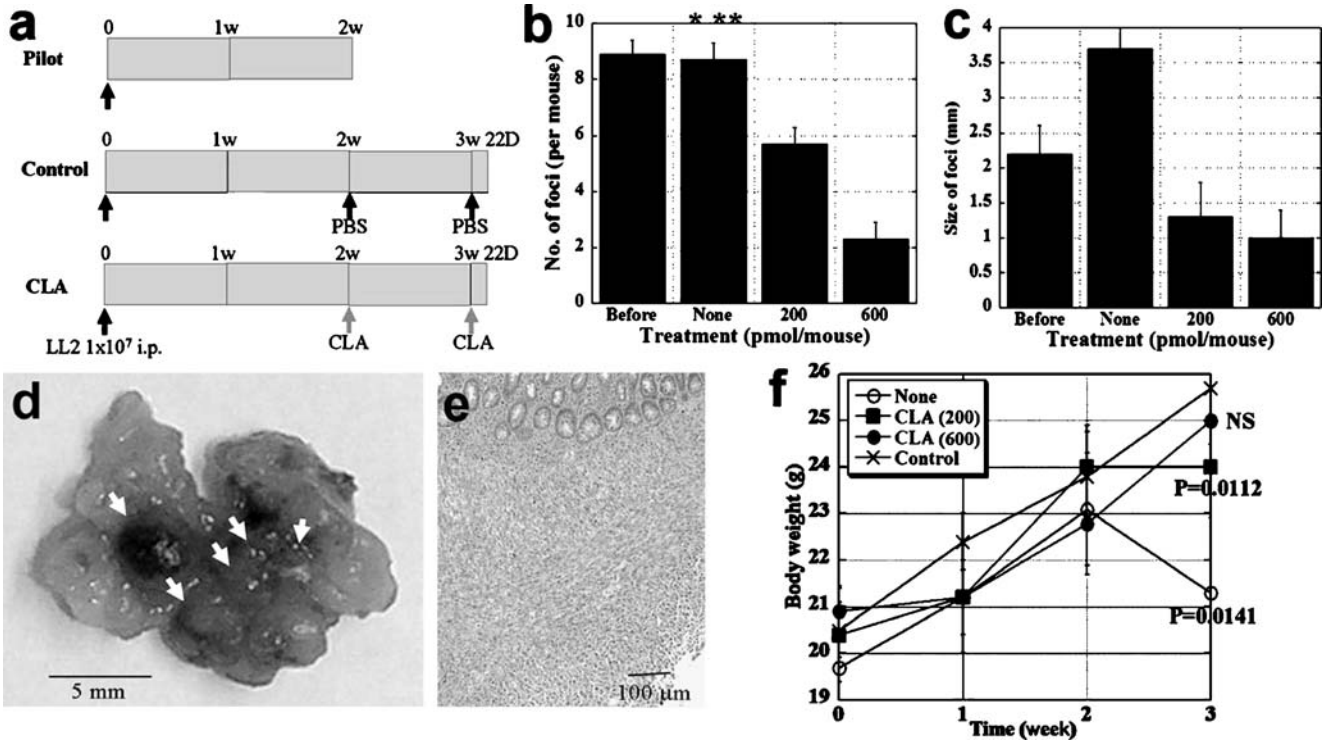

Fig. 2 Effect of CLA on peritoneal metastasis of LL2 cells. **a** Experiment schedule of in vivo CLA treatment. In the pilot group, the mice were killed before CLA treatment to confirm tumor formation. An intraperitoneal administration of CLA (200 or 600 pmol/mouse) or PBS was performed twice. **b**, **c** Number (**b**) and size (**c**) of peritoneal tumors of LL2 cells. **d**, **e** Gross (**d**) and microscopical (**e**) findings of the LL2 peritoneal tumor. LL2 tumor histologically occupied the whole wall of mouse colon. *Arrow*, tumor. **f** Temporal change of body weight of mice. *Error bar*, SD

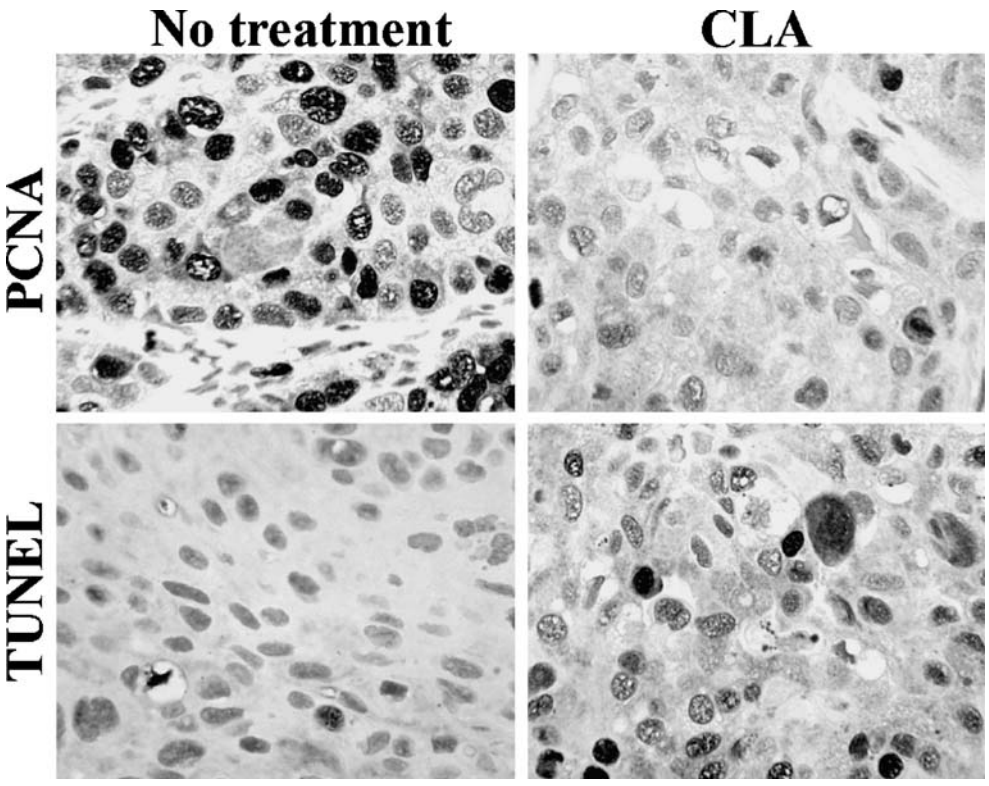

Fig. 3 Effects of CLA treatment on proliferation and apoptosis in LL2 tumors. **a**, **b** The proliferative activity of LL2 tumors with or without CLA treatment (600 pmol/mouse) was examined by PCNA immunohistochemistry. Positive cells were found in 82 and 11% of cells treated with control ethanol and CLA, respectively. **c**, **d** The apoptotic change of LL2 tumors with or without CLA treatment (600 pmol/mouse) was examined by TUNEL method. Positive cells were found in 7 and 32% of cells treated with control ethanol and CLA, respectively. *Bar*, 100 μm

Effect of CLA on protein production of PPARγ, EGFR, and BAX in LL2 tumors

Finally, the protein production of PPARγ, EGFR, and BAX in LL2 tumors treated with or without CLA was assessed (Fig. 4). The protein levels of PPARγ and EGFR were decreased by CLA treatment in a dose-dependent manner. In LL2 tumors treated with 600 pmol/mouse of CLA, the protein levels of PPARγ and EGFR were, respectively, 16 and 12% of those in untreated LL2 tumors. In contrast, BAX protein was increased by CLA treatment in a dose-dependent manner. CLA (600 pmol/mouse) treatment increased BAX protein to 580% in untreated LL2 tumors.

Table 1 Labeling indices of proliferating and apoptotic cells

Treatment	PCNA-positive cells (%)	TUNEL-positive cells (%)
None	72±15	4±2
CLA 200 pmol/mouse	22±8	18±7
CLA 600 pmol/mouse	13±4	33±10
P value[a]	<0.0001	0.0010

[a]Tested by one-way ANOVA

Discussion

In the present study, we revealed that CLA reduced the number and size of the established peritoneal tumors of LL2 cancer cells. We previously reported that the peritoneal colonization of MKN28 and Colo320 cancer cells was inhibited by simultaneous CLA treatment with inoculation [11]. When CLA was administrated intraperitoneally at the same time of cancer cell inoculation, the uncolonized cancer cells were exposed to CLA. This situation resembles an in vitro treatment of cultured cells. CLA in vitro treatment induces growth inhibition, apoptosis, and suppression of invasion in MKN28 and Colo320 cancer cells [11]. To confirm the anti-cancer effect of CLA, we designed the experiment examining CLA effect to established peritoneal cancers in the present study. CLA treatment reduced the number of peritoneal tumors to 64 and 26%, respectively, of untreated mice and the size of tumors to 36 and 27%, respectively, of untreated mice.

CLA is a ligand for PPARγ, which is a member of the hormone receptor family [15, 17]. Our previous report showed that the anti-cancer effects of CLA are derived from PPARγ activation [11]. We confirmed in this study that the anti-cancer effects of CLA disappeared by PPARγ antisense exposure. In the present study, PPARγ antisense treatment recovered CLA-derived growth inhibition in LL2 cells. The activation of PPARγ affects gene expression transcriptionally [3, 7]. We reported that PPARγ activation

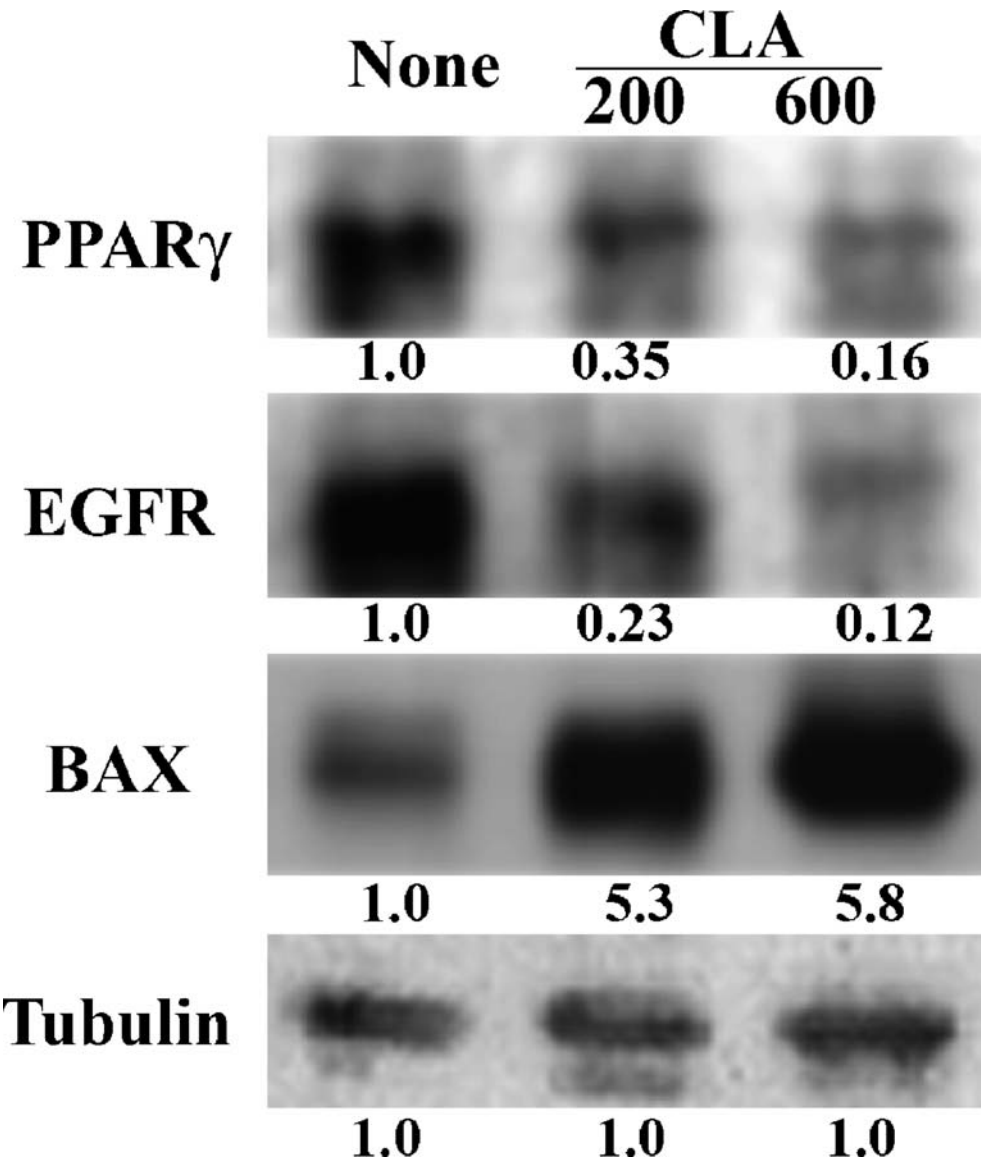

Fig. 4 Effect of CLA treatment on protein levels of PPARγ, EGFR, and BAX in LL2 tumors. The protein expressions of PPARγ, EGFR, and BAX in LL2 tumors were examined by immunoblotting. *Numbers* designate relative signal densities, which are standardized by tubulin expression. The signal density in untreated tumors was set to 1.0. *None*, untreated; *CLA*, CLA-treated; *200*, 200 pmol/mouse; *600*, 600 pmol/mouse

by CLA decreased EGFR and TGF-α and, in contrast, increased Bax [11]. In the present study, the CLA-treated LL2 tumors also showed decreased EGFR and increased Bax proteins. These alterations are associated with growth inhibition and apoptosis in cancer cells. An examination by PCNA and TUNEL in LL2 tumors showed the anti-proliferative and pro-apoptotic effects of CLA. It is interesting to note that the PPARγ protein was decreased by CLA-treated tumors. PPARγ-associated mitogen-activated protein kinase activation increases phosphorylation of PPARγ and downregulates it [9]. This observation suggests that an overdose of CLA might decrease the CLA target, PPARγ, and attenuate CLA anti-tumor effects. A further study on suitable dosage and schedule of CLA treatment is needed to apply CLA to cancer treatment.

A low dose of CLA (200 and 600 pmol/mouse which are, respectively, equivalent to 10 and 30 nM, twice weekly) is indeed effective for anti-cancer treatment. CLA administration showed no obvious side effects, such as impairment of food uptake and weight gain, or disorder of social behaviors. Thus, CLA might be administrated as safe to cancer-burdened individuals. Peritoneal metastasis of gastrointestinal cancer causes poor quality of life in patients [18, 19]. Although the biological effect of CLA in a long treatment needs to be examined in further studies, the use of CLA is a relevant issue for treatment of peritoneal metastasis of cancer.

Acknowledgement The authors thank Mrs. Kaori Isobe for expert assistance with the preparation of this manuscript.

References

1. Bassaganya-Riera J, Hontecillas R, Beitz DC (2002) Colonic anti-inflammatory mechanisms of conjugated linoleic acid. Clin Nutr 21:451–459
2. Belury MA (2002) Dietary conjugated linoleic acid in health: physiological effects and mechanisms of action. Annu Rev Nutr 22:505–531
3. Berger J, Wagner JA (2002) Physiological and therapeutic roles of peroxisome proliferator-activated receptors. Diabetes Technol Ther 4:163–174
4. Bren-Mattison Y, Van Putten V, Chan D, Winn R, Geraci MW, Nemenoff RA (2005) Peroxisome proliferator-activated receptor-γ (PPARγ) inhibits tumorigenesis by reversing the undifferentiated phenotype of metastatic non-small-cell lung cancer cells (NSCLC). Oncogene 24:1412–1422
5. Chen A, Xu J (2004) Activation of PPARγ by curcumin inhibits Moser cell growth and mediates the suppression of the gene expression of cyclinD1 and EGFR. Am J Physiol Gastrointest Liver Physiol 14:14
6. Desreumaux P, Dubuquoy L, Nutten S, Peuchmaur M, Englaro W, Schoonjans K, Derijard B, Desvergne B, Wahli W, Chambon P, Leibowitz MD, Colombel JF, Auwerx J (2001) Attenuation of colon inflammation through activators of the retinoid X receptor (RXR)/peroxisome proliferator-activated receptorγ (PPARγ) heterodimer. A basis for new therapeutic strategies. J Exp Med 193: 827–838
7. Duplus E, Forest C (2002) Is there a single mechanism for fatty acid regulation of gene transcription? Biochem Pharmacol 64: 893–901
8. Galusca B, Dumollard JM, Chambonniere ML, Germain N, Prades JM, Peoc'h M, Estour B (2004) Peroxisome proliferator activated receptor gamma immunohistochemical expression in human papillary thyroid carcinoma tissues. Possible relationship to lymph node metastasis. Anticancer Res 24:1993–1997
9. Hsi LC, Wilson L, Nixon J, Eling TE (2001) 15-Lipoxygenase-1 metabolites down-regulate peroxisome proliferator-activated receptor gamma via the MAPK signaling pathway. J Biol Chem 276:34545–34552
10. Kuniyasu H, Yasui W, Kitahara K, Naka K, Yokozaki H, Akama Y, Hamamoto T, Tahara H, Tahara E (1997) Growth inhibitory effect of interferon-beta is associated with the induction of cyclin-dependent kinase inhibitor p27Kip1 in a human gastric carcinoma cell line. Cell Growth Differ 8:47–52
11. Kuniyasu H, Yoshida K, Sasaki T, Sasahira T, Fujii K, Ohmori H (2006) Conjugated linoleic acid inhibits peritoneal metastasis in human gastrointestinal cancer cells. Int J Cancer 118:571–576
12. Liu H, Zang C, Fenner MH, Possinger K, Elstner E (2003) PPARγ ligands and ATRA inhibit the invasion of human breast cancer cells in vitro. Breast Cancer Res Treat 79:63–74
13. Liu JJ, Huang RW, Lin DJ, Peng J, Wu XY, Lin Q, Pan XL, Song YQ, Zhang MH, Hou M, Chen F (2005) Expression of survivin and bax/bcl-2 in peroxisome proliferator activated receptor-γ ligands induces apoptosis on human myeloid leukemia cells in vitro. Ann Oncol 16:455–459
14. Majumder B, Wahle KW, Moir S, Schofield A, Choe SN, Farquharson A, Grant I, Heys SD (2002) Conjugated linoleic acids (CLAs) regulate the expression of key apoptotic genes in human breast cancer cells. FASEB J 16:1447–1449
15. McCarty MF (2000) Activation of PPARγ may mediate a portion of the anticancer activity of conjugated linoleic acid. Med Hypotheses 55:187–188
16. Miller A, Stanton C, Devery R (2002) Cis 9, trans 11- and trans 10, cis 12-conjugated linoleic acid isomers induce apoptosis in cultured SW480 cells. Anticancer Res 22:3879–3887
17. Moya-Camarena SY, Belury MA (1999) CLA and PPARγ activation. J Nutr 129:2106
18. Sugarbaker PH (2002) New responsibilities in the management of colorectal cancer with peritoneal seeding. Cancer Investig 20:1118–1122
19. Sugarbaker PH, Yu W, Yonemura Y (2003) Gastrectomy, peritonectomy, and perioperative intraperitoneal chemotherapy: the evolution of treatment strategies for advanced gastric cancer. Sem Surg Oncol 21:233–248
20. Tanaka T, Kohno H, Yoshitani S, Takashima S, Okumura A, Murakami A, Hosokawa M (2001) Ligands for peroxisome proliferator-activated receptors α and γ inhibit chemically induced colitis and formation of aberrant crypt foci in rats. Cancer Res 61:2424–2428
21. Yoshizumi T, Ohta T, Ninomiya I, Terada I, Fushida S, Fujimura T, Nishimura G, Shimizu K, Yi S, Miwa K (2004) Thiazolidinedione, a peroxisome proliferator-activated receptor-γ ligand, inhibits growth and metastasis of HT-29 human colon cancer cells through differentiation-promoting effects. Int J Oncol 25:631–639

Virchows Arch (2006) 449:348–357
DOI 10.1007/s00428-006-0258-6

ORIGINAL ARTICLE

Interstitial cells of Cajal could regenerate and restore their normal distribution after disrupted by intestinal transection and anastomosis in the adult guinea pigs

Feng Mei · Bin Yu · Hua Ma · Hong-jun Zhang · De-shan Zhou

Received: 31 March 2006 / Accepted: 16 June 2006 / Published online: 16 August 2006
© Springer-Verlag 2006

Abstract Surgical manipulations of the gastrointestinal (GI) tract usually lead to loss of interstitial cells of Cajal (ICCs). The present study prepared to investigate whether ICCs can regenerate and restore their normal distribution up to 5 months after semitransection and end-to-end anastomosis of small intestines of adult guinea pigs. The segments of anastomosis were studied by immunohistochemistry with anti-KIT, 5-bromo-2′-deoxyuridine (BrdU), stem cell factor (SCF), and neurofilament 200 antibodies and also by transmission electron microscopy (TEM). At early stage, intestinal surgery led to intestinal wall impairment and ICCs loss, and ICCs near the site of anastomosis gradually increased in numbers. About 150 days postoperation, the distribution of ICCs and the microstructure of intestinal wall appeared to be similar with those of the control. By double immunostaining with BrdU and KIT antibodies, a number of proliferated ICCs were seen near the site of transection/anastomosis. Furthermore, KIT ligand, SCF, was mainly observed in the smooth muscle cells (SMCs), which are located close to ICCs. TEM observation revealed a number of immature and mature ICCs in this region. Our results indicated that ICCs could regenerate and restore their normal distribution after intestinal surgery and SMCs might be involved in the regenerated events of ICCs in the adult guinea pig GI tract.

F. Mei · B. Yu · H. Ma · H.-j. Zhang · D.-s. Zhou
Department of Histology and Embryology,
Third Military Medical University,
Chongqing 400038, People's Republic of China

D.-s. Zhou (✉)
Department of Histology and Embryology,
Capital University of Medical Sciences,
Beijing 100054, People's Republic of China
e-mail: dszhou2000@163.com

Keywords Interstitial cells of Cajal · KIT · Intestine · Abdominal surgery · C-kit

Abbreviations

DMP	Deep muscular plexus
GI	Gastrointestinal
ICCs	Interstitial cells of Cajal
IM	Intramuscular
MY	Myenteric plexus
SCF	Stem cell factor
SMCs	Smooth muscle cells

Introduction

Interstitial cells of Cajal (ICCs) are the pacemaker cells that generate and propagate the slow waves in alimentary tract, act as mediators of inputs from the enteric nervous system to gastrointestinal (GI) smooth muscles, and play an important role in the regulation of GI motility [8, 12, 16, 26]. Clinical studies indicate that ICCs are involved in some of GI motility disorders characterized by ICCs reduction and network impairment [4, 15]. Therefore, it was inferred that the deficiency of ICCs might contribute to the disappearance of slow waves and subsequent physical contraction of the smooth muscle in the GI tract [7, 23].

Surgical manipulations of the GI tract usually lead to postoperative GI dysmotilities (e.g., postoperative paralysis of intestine) in the clinic, and it often takes days or even months to recover depending on invasive degree [3]. Recent studies indicate that intestinal surgery results in

functional and morphological alterations of ICCs at the vicinity of the site of transection/anastomosis in the mouse small intestine, such as disappearance of both slow wave and c-kit receptor tyrosine kinase (KIT)-positive cells at 5 h after operation and the expression of KIT partial recovery at 24 h. These alterations of ICCs caused by operation are believed to be involved in short-term disruption of GI motor after surgery [30]. However, long-term alterations of ICCs at the site of transection/anastomosis after GI surgery and whether regeneration or degeneration of ICCs is involved in the recovery of the intestinal microstructure are still unknown. It was suggested that proliferation of ICCs could be detected only in embryonic and neonatal period, but whether ICCs could regenerate and restore their normal distribution after impairment in adult mammals remains essentially unsolved [9, 14, 20]. Therefore, the goal of our present study is to investigate the alterations of ICCs after they are disrupted by semitransection and anastomosis in small intestine of the adult guinea pigs up to 5 months. Immunohistochemical analyses and electron microscopy observation were performed on the specimens through the site of transection/anastomosis, including both oral and aboral ends. Our results indicated that ICCs could regenerate and restore their normal distribution after GI surgery and SMCs, which, expressing stem cell factor (SCF), might be involved in the regenerated events of ICCs.

Materials and methods

Animal treatment

Fifty guinea pigs (male or female, aged 6–8 weeks), purchased from Animal Center of Third Military Medical University (Chongqing, China), were used for intestinal surgeries in our experiments. The guinea pigs were anesthetized with pentobarbital sodium (Nembutal 50 μg/g); then approximately 30 mm of segment of ileum (100–150 mm from the ileocecal sphincter) was exposed; then the semitransection of the full thickness of intestinal the wall (both the longitudinal and circular muscle layer and mucosa) were cut down; and subsequent end-to-end seromuscular anastomosis were performed by using suture thread with 7-0 Ethilon. After absence of obstruction and leakage were confirmed, the abdomen was closed with 5-0 silk suture thread. Three sham-operated guinea pigs, which only underwent the laparotomy, were also prepared. Experimental animals were killed at 5, 10, 30, 50, 70 days and 3 and 5 months after operation by overdose anesthesia with pentobarbital. The experimental animals were performed in accordance with our University of Health Guide for the Care and Use of Laboratory Animals.

Immunohistochemistry

Small intestines that appeared normal in color and size from four animals for each group were used in present studies. Segments of small intestine, 10 mm in length from anastomosis to either end, were removed and opened along the mesenteric border. After enteric contents were washed away with phosphate-buffered saline (PBS), the specimens were quickly frozen with liquid nitrogen in optimal cutting temperature compound and the longitudinal sections through the site of anastomosis (6- to 8-μm-thick) were cut with a cryostat (Leica 1850) and were then fixed with 100% acetone for 15 min (4°C). Immunostaining procedures were done as previously described [10]. ICCs were identified by using a rat monoclonal antibody raised against KIT (ACK2, 5 μg/ml; eBioscience) and immunoreactivity was detected by using a fluorescein isothiocyanate-conjugated secondary antibody (anti-rat IgG, 1:150; Jackson ImmunoResearch Lab) or peroxidase-conjugated secondary antibody (anti-rat IgG, 1:100; DAKO), and horseradish peroxidase reaction was developed in a solution containing 0.05% of 3,3′-diaminobenzidine tetrahydrochloride (DAB; Sigma) in 0.05 M Tris–HCl buffer (pH 7.6) with 0.3% H_2O_2 and the sections were counterstained with hematoxylin after immunohistochemical staining. Detection of SCF or nerve with a mouse monoclonal antibody raised against SCF (5 μg/ml; Santa Cruz, USA) or neurofilament 200 (NF200, 1:100; Boster), respectively, was carried out with the same procedures as described above. The SCF or NF200 positive cells were examined by Cy3-conjugated secondary antibody (anti-mouse IgG, 1:200; Sigma). Control specimens were prepared in a similar manner, but each primary antibody in the incubation solution was omitted. The stained results were examined with a BX51 fluorescence microscope (OLYMPUS, Japan) with an excitation wavelength appropriate for fluorescein isothiocyanate (488 nm) or Cy3 (552 nm).

Detection of regenerated interstitial cells of Cajal

To identify cell proliferation, 5-bromo-2′-deoxyuridine (BrdU, 13 μg/g every 2 days; Sigma) was injected intraperitoneally for three animals of each operated group, i.e., 5-, 10-, 30-, and 50-day groups and nonoperated group until the day before they were killed. For detection of regenerated ICCs, KIT immunocytochemical staining with ACK2 was first carried out as described above and then the stained sections were further fixed in 4% paraformaldehyde in 0.1 M PB at pH 7.2 for 30 min, Baker's solution for 10 min, and 1% glutaraldehyde in the same buffer for 15 min in turn. After rinsing in PBS, the specimens were pretreated with pepsin (0.006%; Sigma) for 30 min at 37°C, followed by partial denaturation of double-stranded DNA

with 4 N HCl for 30 min at 37°C. To reveal BrdU, the sections were incubated with a mouse monoclonal antibody raised against BrdU (3 μg/ml; DAKO) overnight at 4°C and then with Cy3-conjugated secondary antibody (anti-mouse IgG, 1:200; Sigma) for 1 h at 25°C.

Measurement and statistical analysis

Twenty sections were sampled from 100 series of sections of each animal in a systematic random manner. In practice, every fifth section was systematically sampled, the first one being randomly sampled from the first five sections. BrdU/KIT-positive cells within both oral and aboral anastomotic ends were counted. Data were expressed as means±SEM. Differences in the data were evaluated by single factor analysis of variance. $P<0.05$ was taken as a statistically significant difference. The *N* values reported in the text referred to the number of animals in which BrdU injection was performed on. The numbers of KIT/BrdU double positive cells within anastomotic region at different time and different locations, including myenteric plexus (MY), deep muscular plexus (DMP) and intramuscular (IM), were measured and analyzed.

Transmission electron microscopy

According to immunostaining results, the samples from three animals of 70 days postoperative group were performed for the ultrastructural observation. In brief, the pieces of anastomotic region were placed in a fixative made of 2.5% glutaraldehyde and 4% paraformaldehyde in 0.1 M PB at pH 7.2 for 2 h at 4°C. The specimens were washed in the same buffer and subsequently postfixed with 1% osmium tetroxide (OsO_4) in the same buffer for 1 h at 4°C. After osmication, the specimens were rinsed in distilled water and then block-stained with a saturated aqueous uranyl acetate solution for 2 h, dehydrated through a graded series of alcohols, and embedded in Epon 812 resin (TAAB, England). Ultrathin sections were cut using a Reichert ultramicrotome and double-stained with uranyl acetate and lead citrate and observed with Philips Tecnai 10 transmission electron microscope.

Results

On the longitudinal sections through the site of the surgical incision with hematoxylin and eosin staining, the full thickness of the intestinal wall were broken down and each anastomotic end was divided into three areas. The cut ends of intestinal smooth muscle layers were taken as area I, which appeared to be thicker than the normal state for smooth-muscle contraction. Adjacent to this area, where suturation was performed, the muscle layers seemed to be thinner because of sutural tension (area II), while area III, between the oral and aboral ends of serosal surfaces in the anastomosis, showed a triangle-like area (Fig. 1a).

The alterations of distribution of interstitial cells of Cajal in postoperation intestines

In normal and sham-operated animals, many ICCs and their cytoplastic processes forming the networks were usually seen at the MY level, associated with DMP and IM. Five and 10 days postoperation, the longitudinal sections showed that smooth muscle layers and ICCs cellular networks in area I were disrupted by surgery, and IC-MY and IC-DMP were mostly lost in area II, while area III and the site of surgical incision were mainly filled with a large amount of connective tissue where no ICCs-like cells were seen (Fig. 1b). From 10 to 30 days after operation, some ICCs-like cells showed up in areas I, II, and III. Those cells were characterized by oval-shaped nuclei with poor cytoplasm and 1–2 short and thin processes, but they were still irregularly distributed in above areas (Fig. 1c,d). Around 50 days postoperation, the distribution of ICCs-like cells and microstructure of intestinal wall in areas I and II were of partial recovery. On the longitudinal sections, IC-MY and IC-DMP could be distinguishable and their processes were prolonging toward another cut end (Fig. 1e). In 70 days postoperation, the intestinal wall of areas I and II tended to restore normal microstructure, besides the density of IC-MY and IC-DMP was still increased (Fig. 1f), and ICCs-like cells with 2–3 thin processes began to appear in area III (Fig. 1g). In 90 days, the distribution of ICCs in areas I and II tended to restore to normal, but not interconnected yet. About 5 months after operation, along with the recovery of smooth muscle layers, oral and aboral anastomotic ends were interconnected and ICCs-like cells were also redistributed to continue with IC-MY and IC-DMP, respectively (Fig. 1h).

Identification of regenerated interstitial cells of Cajal

Although we observed that ICCs could restore their normal distribution after surgery, it was not clear if regeneration or proliferation of ICCs were involved in this process. Therefore BrdU incorporation was used and double immunostaining with anti-BrdU monoclonal antibody and anti-KIT monoclonal antibody was employed. Only KIT/BrdU double labeling cells with processes were considered as proliferated ICCs. No KIT/BrdU double labeling cells were observed in the intestinal wall of the control and 5 days postoperation of animals, while a large amount of intestinal epithelial cells (Fig. 2a) and some fibroblasts and smooth muscle cells (SMCs) were often incorporated by

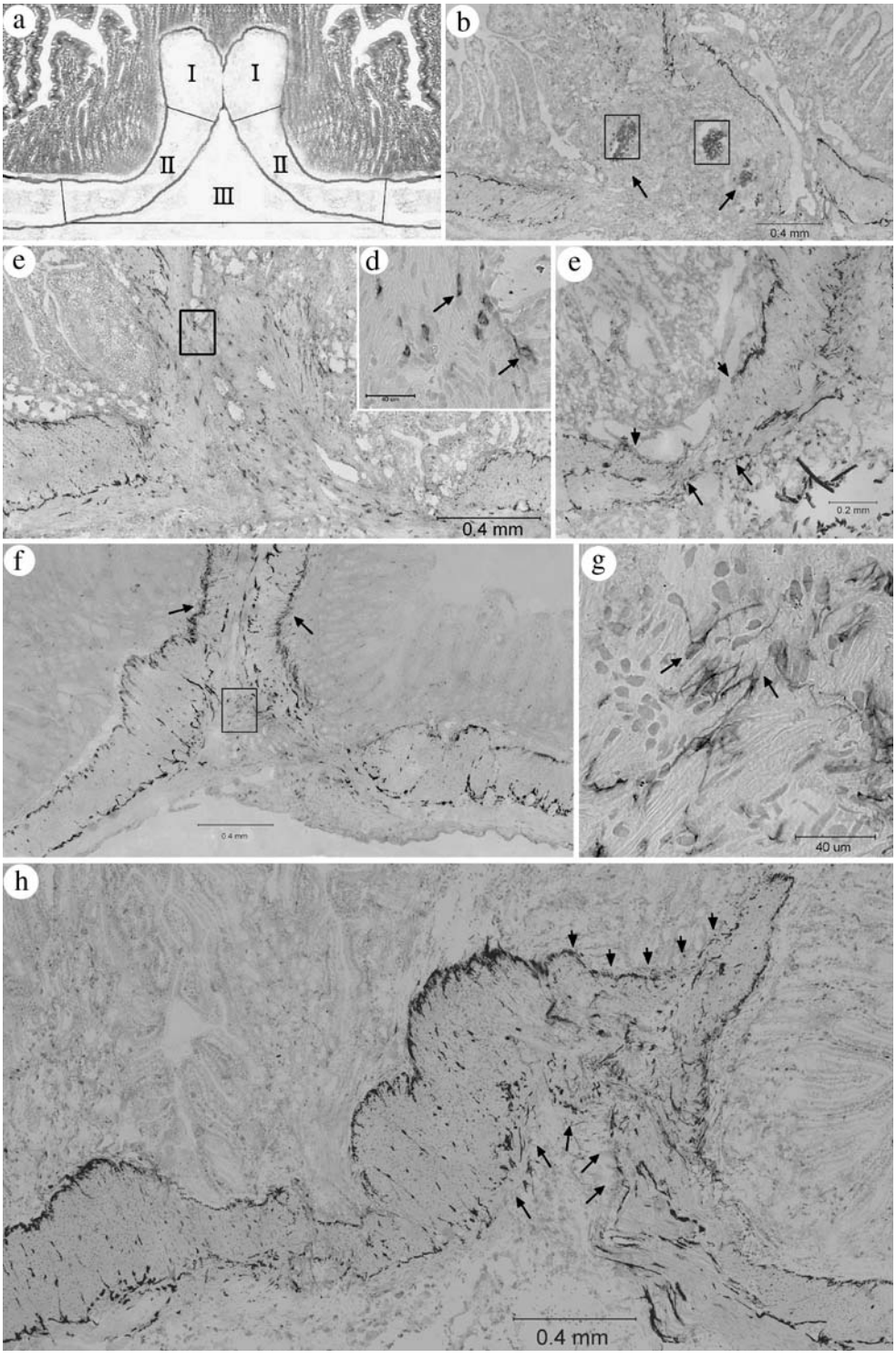

Fig. 1 Longitudinal sections showing alterations of ICCs from 10 to 150 days postoperation with KIT immunohistochemical staining. **a** The rough sketch displaying the three areas of anastomosis: *area I* is the cut ends of intestinal smooth muscle layers; *area II* is the place where suturation was performed; and *area III* is between oral and aboral serosal surface of anastomotic ends that showed a *triangle*-like area. **b** KIT-positive cells in *areas I* and *II* were disrupted and partly lost (*arrows*) 10 days postoperation (*frames* showing suture thread). **c** Some ICCs-like cells irregularly showed up in the three areas at 30 days postoperation. **d** Higher magnification of ICCs-like cells (*arrows*) in *area III* (*frame* in subpanel **c**). **e** ICCs-like cells increased in *areas I*, *II*, and *III* and showed a tendency to form IC-MY (*arrows*) and IC-DMP (*arrowheads*) at 50 days postoperation. **f** IC-DMP and IC-MY in *areas I* and *II* were still increased in density at 70 days (*arrows*) postoperation. **g** Higher magnification showing ICCs-like cells in *area III* with 2–3 slender processes and branches (*arrows*) (*frame* in subpanel **f**). **h** One hundred and fifty days postoperation, oral and aboral anastomotic ends including IC-MY (*arrows*) and IC-DMP (*arrow heads*) that are interconnected. *Scale bar* **b**, **c**, **f**, and **h**=0.4 mm; **d**, **g**=40 μm; and **e**=0.2 mm

BrdU at these animals. Ten-day postoperation, 0~3 (n=3, average 1.48±1.19) KIT/BrdU double staining cells were observed in each oral or aboral anastomotic end, and these cells were mainly seen in the DMP (74%) region or MY (23%) and seldom within smooth muscle layers (3%). It should be noticed that no KIT/BrdU double staining cells were observed in the area that was beyond 2.1 mm from the site of anastomosis. The number of KIT/BrdU double staining cells was gradually increased to 6–10 (n=3, averaged 7.9±2.4) around 30 days after operation. Among them, about 62% were located at the DMP region with enriched cytoplasm and oval-shaped nuclei, and some located around MY (26%) and within smooth muscle layers (12%). Most of them (95%) were distributed within 4.0 mm from anastomotic site to the oral or aboral end (Fig. 2b). Fifty days after operation the number of KIT/

BrdU double staining cells were increased to 14~18 (n=3, average 16.47±1.98). Those cells were nearly located within 6.5 mm from anastomotic site to the oral or aboral end. Among them, 58% were distributed in the places of DMP, 25% in the MY with 2~3 thin and long processes and 17% in the smooth muscle layers (Fig. 2c,d). The statistical analysis showed that the number of regenerated/proliferated ICCs at various times and locations were significantly different (P<0.05), whereas they have no significant difference between the oral and aboral ends of the anastomosis (P>0.05) (Fig. 3a,b).

Stem cell factor, smooth muscle, and nerves in the anastomotic intestinal wall

Previous studies have demonstrated that the KIT-SCF signal pathway is essential to the development and survival of ICCs [13, 24]. To explore the possible roles of the signal pathway during ICCs regeneration, double immunostaining with anti-SCF and anti-KIT antibodies were performed. Strong SCF immunoreactions were mainly observed in SMCs, including the circular and longitudinal SMCs, and weak in neurons of MY, while no SCF immunoreaction was visible in the connective tissue cells (Fig. 4a). By the SCF immunostaining, we found that the longitudinal SMCs began to grow from area II to area III and then toward the opposite side around 30 days postoperation and completely interconnected in about 70 days (Fig. 4b,c). In contrast, the circular smooth muscle layer at the site of the anastomosis did not completely interconnect until 5 months (Fig. 4d). It was noticed that increased ICCs were in higher density and only distributed among SCF-positive SMCs in the region of anastomosis and in area III (Fig. 4e); ICCs were also observed around or within out-growing SMC bundles from area II (Fig. 4f). Meanwhile, immunostaining with anti-NF200 showed that the MY and DMP were also disrupted and they began to regrow out within SMCs 30 days postoperation (data not shown). They were

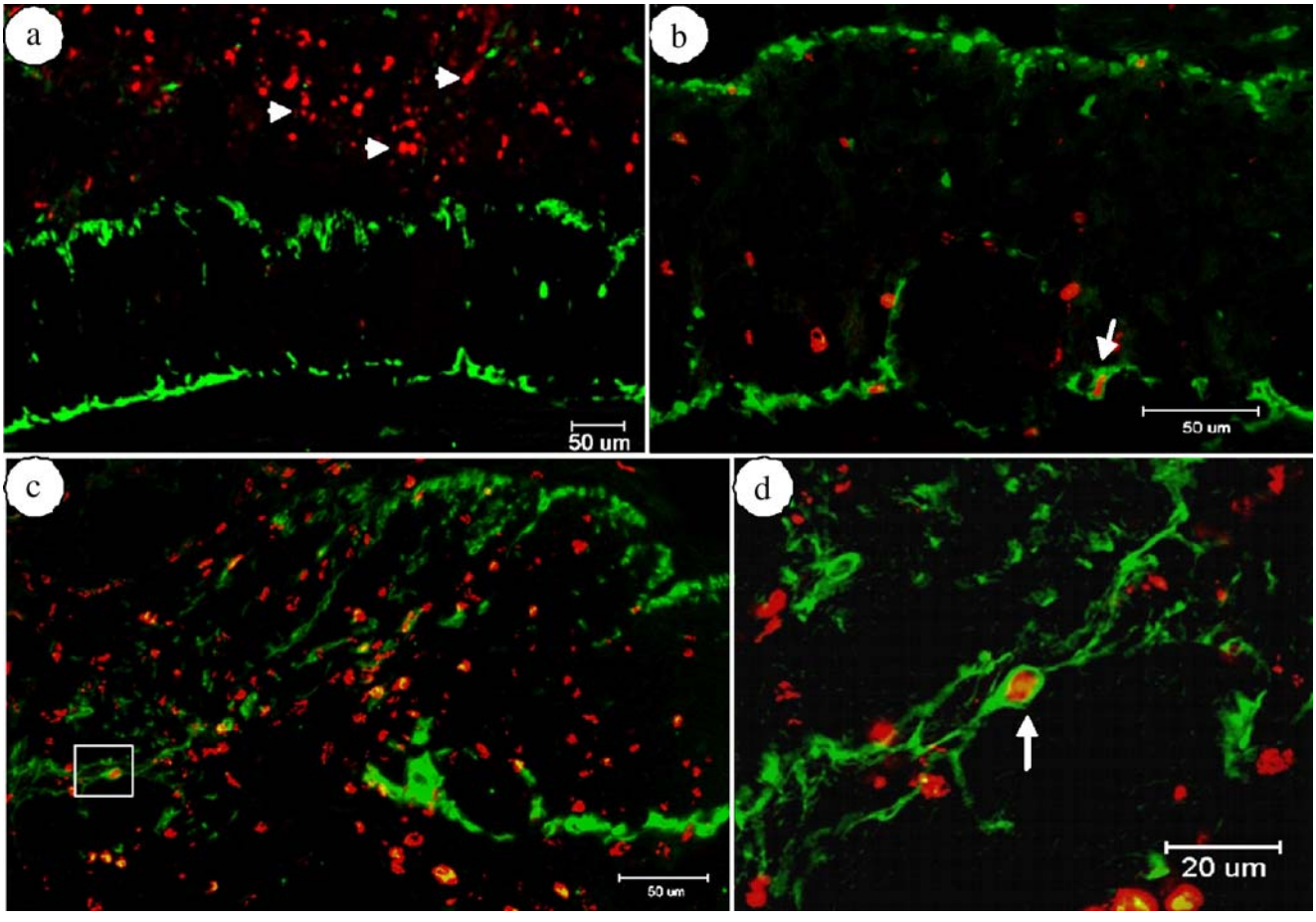

Fig. 2 KIT (*green*)/BrdU (*red*) double staining showing regenerated ICCs. **a** No KIT/BrdU double-staining cells were observed on the longitudinal sections of the control group, while a large number of epithelial cells in the intestine were BrdU-positive (*arrowheads*). **b** KIT/BrdU double-staining cells, as proliferated ICCs, were seen in normal intestinal wall adjacent to anastomosis at 30 days post-operation (*arrow*). **c** Proliferated ICCs were often detected in the site of anastomosis at 50 days postoperation. **d** Higher magnification showing KIT/BrdU double-labeling cells with slender processes (*frame* in subpanel **c**). *Scale bar* **a**–**c**=50 μm; **d**=20 μm

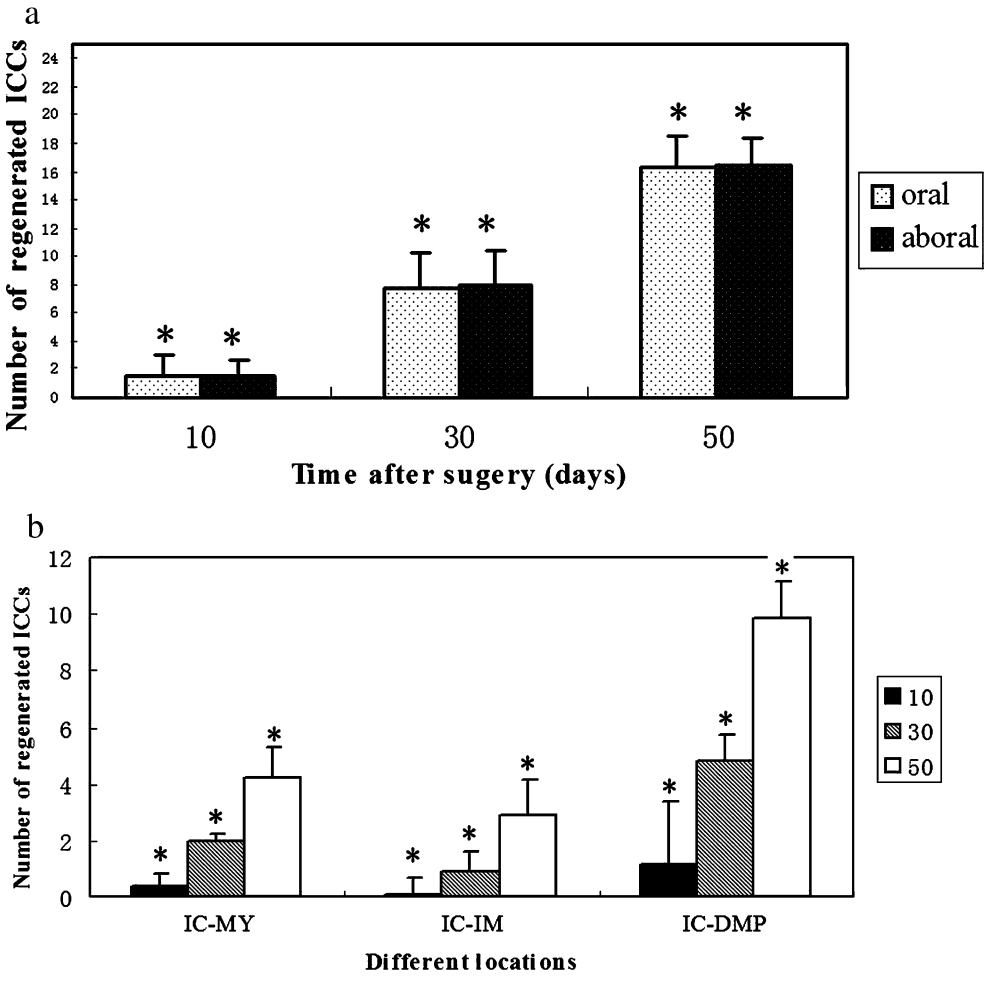

Fig. 3 Account of the number of KIT/BrdU double-staining cells at different time and locations. Each histogram represents the means±SEM. **a** The number of regenerated ICCs was gradually increased from 10-, 30- and 50-day groups of postoperation (*P<0.05). The number of regenerated ICCs was similar between oral and aboral (P>0.05) in each group. **b** The amounts of KIT/BrdU double-staining cells in MY, IM, and DMP regions were significantly different (*P<0.05)

redistributed to continue with MY and DMP at the anastomotic region at 5 months postoperation (Fig. 4g).

Ultrastructural features of the region of anastomosis

As mentioned above, 70 days postoperation animals appeared to be in the middle of the process, so the ultrastructural features of these samples were selectively studied by transmission electron microscopy (TEM). The region of anastomosis was filled with abundant collagen fibers, fibroblasts (Fig. 5a), and some SMCs (Fig. 5b) and a number of mature and immature ICC-like cells were also often seen in this region. The whole ICCs shape including cell bodies and long processes can hardly be viewed in a single profile because ICCs have slender processes. In an ultrathin section, the mature ICCs seemed to be characterized by the presence of many mitochondria, well-developed smooth endoplasmic reticulum, and microtubules (Fig. 5c). However, in the atypical ICCs, immature ones, were characterized by the presence of abundant cytoplasm with numerous free ribosomes, which were essential to the synthesis of structural protein for the cells (Fig. 5d).

Discussion

Clinical and experimental studies have suggested that loss of ICCs are associated with intestinal motor dysfunction and that GI surgeries inevitably lead to loss of ICCs and network impairment [16]. The present study established an animal model and demonstrated that IC-MY and IC-DMP were disrupted, and ICCs were partly lost in anastomotic region 5 days postoperation. These alterations might result from surgical manipulation (e.g., transection or anastomosis), sutural tension, local inflammatory reactions [6], and KIT phenotype loss in parts of ICCs [5]. We found that ICCs-like cells and processes in areas I and II were gradually increased with the increase of time and recovered to normal distribution around 70 days after GI surgery, but were not yet rejoined in area III. It appeared that at 150 days postoperation, the microstructure of the intestinal wall nearly restored to the same as those of the control group, such as ICCs, SMCs, and nerve fibers growing through the site of anastomosis. It was surprising that the distribution of ICCs and the microstructure of the intestinal wall took nearly 5 months to recover. However, we did not

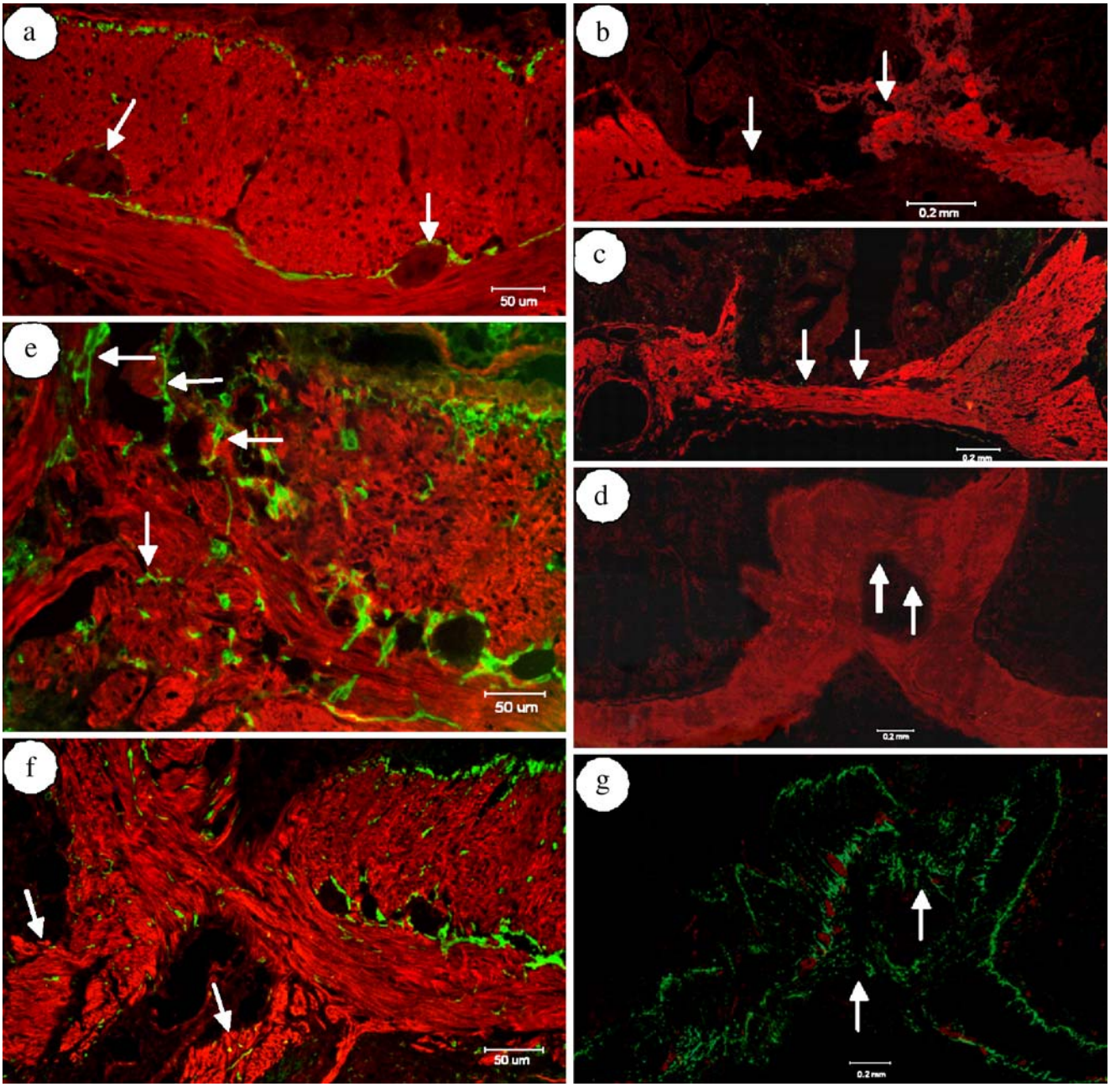

Fig. 4 **a**–**f** KIT(*green*)/SCF(*red*) double staining of the operated intestine. **a** SCF was mainly expressed in SMCs and weakly in neurons (*arrows*). **b**, **c** Longitudinal smooth muscle layer began to grow at 30 days postoperation (*arrows*) (subpanel **b**) and interconnected at 70 days (*arrows*; subpanel **c**). **d** Circular smooth muscle layer interconnected 150 days postoperation (*arrows*). **e** The density of ICC-like cells was higher among the SCF-positive SMCs in the site of anastomosis (*arrows*). **f** In *area III*, ICCs-like cells showed a tendency of outgrowth with SMCs bundles at anastomosis (*arrows*). **g** ACK2 (*green*)/NF200 (*red*) double staining showing that ICCs and nerves reconnected 150 days after surgery and also showing smooth muscle layers (*arrows*). *Scale bar* **a**, **e**, and **f**=50 μm; **b**–**d**, and **g**=0.2 mm

observe any symptoms of GI motility dysfunctions (e.g., vomiting or diarrhea) on our experimental animals, and dysfunction of GI motility after abdominal surgical manipulation usually would not last for such a long time in clinic [1, 21, 22]. The possible interpretations might be the following: (1) ICCs and the enteric nervous system adjacent to anastomosis (>2.4 mm) still kept normal distribution that might compensate the disabled segment of the intestine or operated site; and (2) The anastomotic region is covered by a connective tissue, which might prevent from overdistension, infection, and leakage, and support the transportation of the GI movement. Our results would help clinical surgeons understand prolonged inhibition of bowel motility functions, which often occurred in some patients with GI

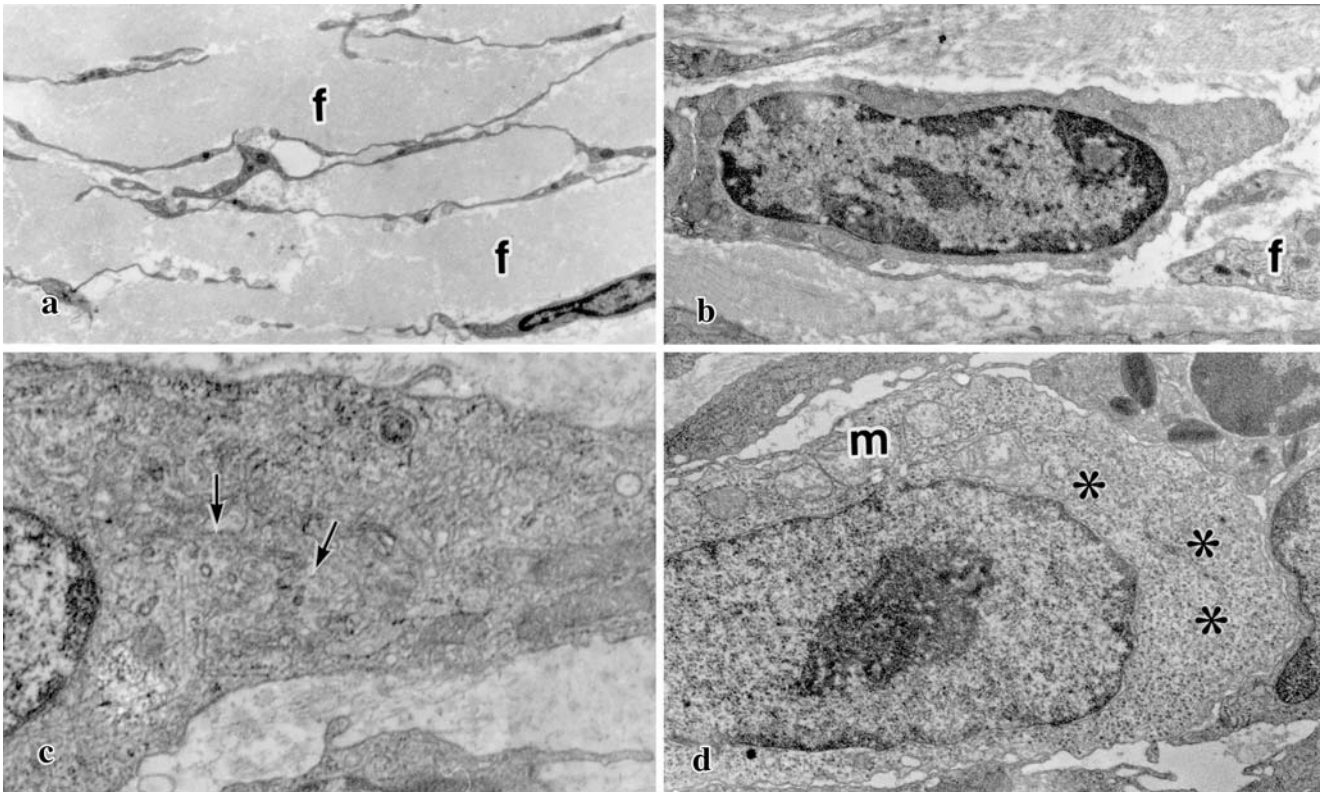

Fig. 5 Electron micrographs showing the region of anastomosis at 70 days postoperation. **a** Low-magnification micrograph of abundant collagen fibers (*f*) and partial processes of the fibroblasts (×4,200). **b** SMC with a number of mitochondria and abundant sarcoplasm was also observed at vicinity of anastomosis (×5,200). **c** A mature ICC-like cell with abundant cytoplasm, smooth endoplasmic reticulum, and a large number of microtubules were seen in the site of anastomosis (×9,000). **d** One of the immature ICC-like cell characterized by the presence of a large amount of free ribosomes (×11,000)

operations. Those might be related to the fact that ICCs were lost in a large amount and took a long time to restore to their normal distribution. Moreover, it was reported that distention and inflammatory factors after GI surgeries might produce a regional pseudoobstruction that might lead to further loss of ICCs and contribute to a longer motility disorders in clinic [1].

Previous studies have demonstrated that ICCs originated from mesenchymal cells [9, 11], and the proliferation of ICCs and extension of the processes are only observed in embryonic and neonatal periods in mammals, and even ICCs, which derive from 6-day neonatal mice, could not increase in number in culture [14, 27], indicating that the proliferation of ICCs depend on the age in vitro. However, after sequential injection of BrdU for 2 weeks, no KIT/BrdU double labeling cells were observed in adult guinea pigs, which hinted that ICCs might have a low renewal rate in the normal condition. Therefore, this animal model was also used to investigate the regenerated events and our results revealed that KIT/BrdU double labeling cells, the proliferated ICCs, were observed 10 days postoperation. The amount of these cells at 50 days postoperation rose about nine times as many as it was at 10 days. They were mainly found in the site of anastomosis and within the intact networks adjacent to this region, while no KIT/BrdU double labeling cells were seen in the control and sham-operated groups. TEM observation also revealed a number of immature ICC-like cells in the regions of anastomosis. All together, our results indicated that ICCs in the adult GI tract still possessed the ability to regenerate in the condition of lost ICCs. However, according to our data, it was not clear that the regenerated ICCs originated from residual ICCs or precursor/stem cells. Basing on morphological features and locations of KIT/BrdU double labeling cells, it was suggested that proliferation of the residual ICCs near the site of anastomosis might be one of the resources, meanwhile mesenchymal stem cells, the precursor of both ICCs and SMCs, could not be excluded [28].

With regard to the factors that might be involved in the proliferation of ICCs, SCF, the ligand of KIT receptor, is considered because KIT–SCF signal pathway plays an important role in the development and survival of ICCs [2, 13]. It has been demonstrated that mutation of c-kit or steel or blockage of KIT–SCF signal pathway with antibody against KIT would lead to the disappearance of ICCs and slow waves and result in distention and paralysis of

intestine [18, 23, 24]. In the present study, the expression of SCF and KIT were measured by double immunostaining, SCF immunoreactions were mainly found in SMCs, and ICCs were nearly in the vicinity of SCF-positive SMCs and among the SMCs bundles, which grew out from area II to area III. These results suggested that SMCs, which are expressing SCF, might be involved in the regenerated events of ICCs after GI surgery. This is coincident with other reports that SMCs alone could provide a suitable microenvironment for the survival of ICCs via expressing SCF [11, 29, 31]. Moreover, besides SMCs, nerves are closely related with ICCs morphologically and physiologically, although it was demonstrated that neither neurons nor glial cells are necessary for the development or survival of ICCs [19, 32] and the expression of SCF in SMCs appears to be sufficient to stimulate growth of ICCs and formation of the cellular network [17, 25]. Furthermore, it appeared that nerve fibers and neurons were not likely to locate to ICCs as tightly as SMCs and expressed SCF weakly in our experiments, but their contributions during the restoration should be carefully studied in the further researches.

In conclusion, our results indicated that ICCs could regenerate and their processes could extend gradually toward the site of anastomosis after being disrupted by intestinal semitransection and anastomosis and finally restore their normal distribution in the adult guinea pigs. SMCs, which are expressing SCF, might be one of the factors that were involved in the regenerated events of ICCs. These results might provide a clue to the understanding and clinical treatment of GI motility disorders.

Acknowledgements We thank Dr. Y. Tang (Department of Histology and Embryology, Chongqing University of Medical Sciences) for critical reading the manuscript. This work was supported in parts by grants no. 30470911 and 30570983 from the National Science Foundation of China (NSFC). Feng Mei and Bin Yu contributed equally to this work.

References

1. Baig MK, Wexner SD (2004) Postoperative ileus: a review. Dis Colon Rectum 47:516–526
2. Beckett EA, Horiguchi K, Khoyi M, Sanders KM, Ward SM (2002) Loss of enteric motor neurotransmission in the gastric fundus of Sl/Sl(d) mice. J Physiol 543:871–887
3. Behm B, Stollman N (2003) Postoperative ileus: etiologies and interventions. Clin Gastroenterol Hepatol 1:71–80
4. Bharucha AE, Philips SF (2001) Slow-transit constipation. Curr Treat Options Gastroenterol 4:309–315
5. Chang IY, Glasgow NJ, Takayama I, Horiguchi K, Sanders KM, Ward SM (2001) Loss of interstitial cells of Cajal and development of electrical dysfunction in murine small bowel obstruction. J Physiol 536:555–568
6. Faussone-Pellegrini MS, Gay J, Vannucchi MG, Corsani L, Fioramonti J (2002) Alterations of neurokinin receptors and interstitial cells of Cajal during and after jejunal inflammation induced by Nippostrongylus brasiliensis in the rat. Neurogastroenterol Motil 14:83–95
7. Isozaki K, Hirota S, Miyagawa J, Taniguchi M, Shinomura Y, Matsuzawa Y (1997) Deficiency of c-kit+ cells in patients with a myopathic form of chronic idiopathic intestinal pseudo-obstruction. Am J Gastroenterol 92:332–334
8. Kito Y, Ward SM, Sanders KM (2005) Pacemaker potentials generated by interstitial cells of Cajal in the murine intestine. Am J Physiol Cell Physiol 288:C710–C720
9. Kluppel M, Huizinga JD, Malysz J, Bernstein A (1998) Developmental origin and Kit-dependent development of the interstitial cells of Cajal in the mammalian small intestine. Dev Dyn 211:60–71
10. Komuro T, Zhou DS (1996) Anti-c-kit protein immunoreactive cells corresponding to the interstitial cells of Cajal in the guinea-pig small intestine. J Auton Nerv Syst 61:169–174
11. Lecoin L, Gabella G, Le Douarin N (1996) Origin of the c-kit-positive interstitial cells in the avian bowel. Development 122:725–733
12. Liu LW, Thuneberg L, Huizinga JD (1998) Development of pacemaker activity and interstitial cells of Cajal in the neonatal mouse small intestine. Dev Dyn 213:271–282
13. Mikkelsen HB, Malysz J, Huizinga JD, Thuneberg L (1998) Action potential generation, kit receptor immunohistochemistry and morphology of steel-Dickie (Sl/Sld) mutant mouse small intestine. Neurogastroenterol Motil 10:11–26
14. Nakahara M, Isozaki K, Vanderwinden JM, Shinomura Y, Kitamura Y, Hirota S, Matsuzawa Y (2002) Dose-dependent and time-limited proliferation of cultured murine interstitial cells of Cajal in response to stem cell factor. Life Sci 70:2367–2376
15. Rolle U, Piotrowska AP, Nemeth L, Puri P (2002) Altered distribution of interstitial cells of Cajal in Hirschsprung disease. Arch Pathol Lab Med 126:928–933
16. Sanders KM, Ordog T, Koh SD, Torihashi S, Ward SM (1999) Development and plasticity of interstitial cells of Cajal. Neurogastroenterol Motil 11:311–338
17. Sanders KM, Ordog T, Ward SM (2002) Physiology and pathophysiology of the interstitial cells of Cajal: from bench to bedside. IV. Genetic and animal models of GI motility disorders caused by loss of interstitial cells of Cajal. Am J Physiol Gastrointest Liver Physiol 282:G747–G756
18. Torihashi S, Ward SM, Nishikawa S, Nishi K, Kobayashi S, Sanders KM (1995) c-kit-dependent development of interstitial cells and electrical activity in the murine gastrointestinal tract. Cell Tissue Res 280:97–111
19. Torihashi S, Yoshida H, Nishikawa S, Kunisada T, Sanders KM (1996) Enteric neurons express steel factor-lacZ transgene in the murine gastrointestinal tract. Brain Res 738:323–328
20. Torihashi S, Ward SM, Sanders KM (1997) Development of c-Kit-positive cells and the onset of electrical rhythmicity in murine small intestine. Gastroenterology 112:144–155
21. Tsukamoto K, Mizutani M, Yamano M, Tagi Y, Takeda M (2000) The effect of SK-896 on post-operative ileus in dogs: gastrointestinal motility pattern and transit. Eur J Pharmacol 401:97–107
22. van der Velden MA, Klein WR (1993) The effects of cisapride on the restoration of gut motility after surgery of the small intestine in horses; a clinical trial. Vet Q 15:175–179
23. Ward SM, Burns AJ, Torihashi S, Sanders KM (1994) Mutation of the proto-oncogene c-kit blocks development of interstitial cells and electrical rhythmicity in murine intestine. J Physiol 480(Pt 1): 91–97
24. Ward SM, Burns AJ, Torihashi S, Harney SC, Sanders KM (1995) Impaired development of interstitial cells and intestinal electrical rhythmicity in steel mutants. Am J Physiol 269: C1577–C1585

25. Ward SM, Ordog T, Bayguinov JR, Horowitz B, Epperson A, Shen L, Westphal H, Sanders KM (1999) Development of interstitial cells of Cajal and pacemaking in mice lacking enteric nerves. Gastroenterology 117:584–594
26. Ward SM, Beckett EA, Wang X, Baker F, Khoyi M, Sanders KM (2000) Interstitial cells of Cajal mediate cholinergic neurotransmission from enteric motor neurons. J Neurosci 20:1393–1403
27. Wester T, Eriksson L, Olsson Y, Olsen L (1999) Interstitial cells of Cajal in the human fetal small bowel as shown by c-kit immunohistochemistry. Gut 44:65–71
28. Wu JJ, Rothman TP, Gershon MD (2000) Development of the interstitial cell of Cajal: origin, kit dependence and neuronal and nonneuronal sources of kit ligand. J Neurosci Res 59:384–401
29. Yamataka A, Kato Y, Tibboel D, Murata Y, Sueyoshi N, Fujimoto T, Nishiye H, Miyano T (1995) A lack of intestinal pacemaker (c-kit) in aganglionic bowel of patients with Hirschsprung's disease. J Pediatr Surg 30:441–444
30. Yanagida H, Yanase H, Sanders KM, Ward SM (2004) Intestinal surgical resection disrupts electrical rhythmicity, neural responses, and interstitial cell networks. Gastroenterology 127:1748–1759
31. Young HM, Ciampoli D, Southwell BR, Newgreen DF (1996) Origin of interstitial cells of Cajal in the mouse intestine. Dev Biol 180:97–107
32. Young HM, Torihashi S, Ciampoli D, Sanders KM (1998) Identification of neurons that express stem cell factor in the mouse small intestine. Gastroenterology 115:898–908

Virchows Arch (2006) 449:358–366
DOI 10.1007/s00428-006-0260-z

ORIGINAL ARTICLE

Differential expression of basement membrane collagen-IV α1 to α6 chains during oral carcinogenesis

Ryo Tamamura · Hitoshi Nagatsuka · Chong Huat Siar · Naoki Katase · Ichiro Naito · Yoshikazu Sado · Noriyuki Nagai

Received: 1 April 2006 / Accepted: 19 June 2006 / Published online: 16 August 2006
© Springer-Verlag 2006

Abstract This study aimed to resolve if basement membrane (BM) collagen α chains undergo remodeling during oral carcinogenesis. Using immunohistochemistry and transmission electron microscopy, we found that BMs in oral epithelial dysplasias (OED: mild, *n*=10; moderate, *n*=10; severe, *n*=10) and carcinoma in situ (CIS) (*n*=10) differed from normal mucosa (*n*=6) and oral epithelial hyperplasia (*n*=5) in showing: (1) excessive lamina densa-like material ultrastructurally, and (2) stronger immunoexpression for α5(IV) than for α1(IV), α2(IV), and α6(IV) chains—findings that implicate these molecules' role as an adhesive template for the attachment and persistence of basal dysplastic cells. Incipient loss of BM integrity in CIS, where α5(IV)/α6(IV) chains were more frequently absent than α1(IV)/α2(IV) chains, suggests that α(IV) network disruption is crucial for progression of dysplastic cells into the extracellular compartment, marking transition into the invasive phase. In carcinomatous BM, the disappearance of α(IV) chains was more severe in poorly differentiated oral squamous cell carcinoma (OSCC) (*n*=10) than in well-differentiated OSCC (*n*=10). In all samples examined, α3(IV) and α4(IV) chains were absent. These findings taken together suggest that BM collagen-IV α chains undergo remodeling where selective increase and loss of these molecules are probably early and late events, respectively, during progression of oral dysplasia to cancer.

Keywords Collagen-IV α chains · Epithelial dysplasia · Carcinoma in situ · Squamous cell carcinoma · Oral carcinogenesis

R. Tamamura · H. Nagatsuka · N. Katase · N. Nagai (✉)
Department of Oral Pathology and Medicine,
Graduate School of Medicine,
Dentistry and Pharmaceutical Sciences, Okayama University,
2-5-1 Shikata-cho,
Okayama 700-8525, Japan
e-mail: nori@md.okayama-u.ac.jp

C. H. Siar
Department of Oral Pathology,
Oral Medicine and Periodontology, Faculty of Dentistry,
University of Malaya,
50603 Kuala Lumpur, Malaysia

I. Naito
Department of Human Morphology,
Graduate School of Medicine,
Dentistry and Pharmaceutical Sciences, Okayama University,
2-5-1 Shikata-cho,
Okayama 700-8525, Japan

Y. Sado
Division of Ultrastructural Biology,
Shigei Medical Research Institute,
Yamada, Okayama 701-0202, Japan

Y. Sado
Division of Immunology, Shigei Medical Research Institute,
Yamada, Okayama 701-0202, Japan

Introduction

Type-IV collagen, the major structural component of basement membranes (BMs), consists of a family of six genetically distinct α chains designated as α1–α6 [24, 32]. Three α chains assemble into triple-helical molecules that further self-associate to form supramolecular networks. Human BM has at least three molecular forms of type-IV collagen, which are tissue-specific in their distribution. The major form is $[\alpha1(IV)]_2\alpha2(IV)$, which is

ubiquitous in all BMs, while α3(IV), α4(IV), and α5(IV) are abundant in lung alveolar and glomerular BMs, and $[\alpha5(IV)]_2\alpha6(IV)$ is mainly localized in the BMs of mammary duct and lobule, epidermis, prostate gland, and smooth muscle cells [3, 6, 8, 24].

The concept that oral carcinogenesis is a two-step process characterized by the initial presence of a precursor lesion that subsequently developed into cancer is well established [2, 26]. According to the World Health Organization, a precursor lesion is defined as "altered epithelium with an increased likelihood for progression to squamous cell carcinoma" [2]. The altered epithelium is characterized by distinct cytological and architectural changes collectively grouped under the term epithelial dysplasia [2]. Oral squamous cell carcinoma (OSCC), which ranks as the sixth most common cancer worldwide, is the most common oral malignancy. It is one of the few cancer types where it is possible to obtain biopsies at all stages of cancer development and progression for purposes of investigating their underlying molecular mechanisms [2].

At present, BMs must be considered not only as a supporting network for various cell types but also as a potential regulator of cell behavior [32]. Among BM components, type-IV collagen provides not only an architectural network, but the different NC1 domains of its constitutive α(IV) chains might also regulate cellular functions and exhibit antiangiogenic or antitumor properties [4, 9]. It is now recognized that collagen-IV has a profound effect on the biological behavior of tumors. Our group has previously investigated and shown that disruption or loss of BM type-IV collagen α chains correlates with tumor invasiveness in ameloblastomas [22], benign and malignant odontogenic tumors [19], and primary oral mucosal melanomas [20]. Similarly, others have also demonstrated the antiinvasive properties of collagen-IV in tumor types including prostate carcinoma [5], colorectal tumors [12], pancreatic adenocarcinomas [13], renal cell carcinoma [16], adenoid cystic carcinoma [17], bronchoalveolar carcinoma [21], breast tumors [23], and basal cell carcinoma [29]. These studies also documented changes in BM collagen-IV α-chain composition in relation to progression from a preneoplastic state to cancer [5, 21, 23]. However, to date, there are no reports investigating the immunolocalization of BM collagen-IV α chains in conjunction with oral carcinogenesis [10, 11, 15, 30, 31]. In this study, chain-specific monoclonal antibodies against six collagen-IV α chains were used to determine the differential distribution of these proteins in archival oral mucosal specimens that showed separately and/or in contiguous manner features of normal oral mucosa, oral epithelial hyperplasia, OED, carcinoma in situ (CIS), and OSCC. In addition, transmission electron microscopy was used to define further these BM changes at the ultrastructural level.

Materials and methods

Tissue samples

The source of the sample used in this study was from the surgical pathology files of the Department of Oral Pathology, Graduate School of Medicine, Dentistry and Pharmaceutical Sciences, Okayama University, Okayama, Japan. Archival formalin-fixed, paraffin-embedded tissue blocks of normal oral mucosa (n=6), oral epithelial hyperplasia (n=5), OED (mild: n=10, moderate: n=10, severe: n=10), oral CIS (n=10), and OSCC (well-differentiated: n=10, poorly differentiated: n=10) were retrieved. Prior ethical approval was obtained, and safety and ethical guidelines were followed in using these human tumor tissues according to the requirements of the institution. The histological diagnoses of OED and OSCC were based on established criteria in current use [2, 26]. New 4-μm-thick sections were prepared for staining with hematoxylin–eosin, periodic acid Schiff solution (Sigma, St. Louis, Missouri, USA) and for immunohistochemical detection of collagen-IV α chains.

Immunohistochemical procedures

The standard avidin–biotin–peroxidase complex (ABC) technique was performed as previously described [19, 20]. Briefly, deparaffinized sections were pretreated for antigen retrieval by autoclave heating (132°C, 3 min) in 10 nM of citrate buffer (pH 3.3, 5 min). These sections were then immersed in 0.3% methanol containing 1% hydrogen peroxide for 30 min, to block endogenous peroxidase, and rinsed in 0.05 M Tris-buffered saline (TBS) (5 min, three times) before immersing in blocking solution (Funakoshi, Japan) for 10 min at room temperature. Thereafter, the sections were covered with the primary antibody and incubated overnight at 4°C. For staining of collagen-IV α1, α2, α3, α4, α5, and α6 chains, the primary antibodies used in this study were rat monoclonal antibodies raised against six different human collagen-IV α chains, and the clones, specificities, and method of production of these antibodies have been detailed elsewhere [14, 27]. The optimal dilutions of these primary antibodies were as follows: α1(IV) and α2(IV) 1:400, α3(IV) 1:100, α4(IV) 1:10, α5(IV) 1:100, and α6(IV) 1:20. The immunoreaction was performed using a Vectastatin peroxidase ABC kit (Vector, Burlingame, California, USA). The antigenic sites were visualized by reacting sections with a mixture of 0.05% 3,3′-diaminobenzidine tetrahydrochloride (Vector) in

0.05 M of Tris–HCl buffer (pH 7.6) containing 0.01% H_2O_2 for 7 min and counterstained with Mayer's hematoxylin. For negative control, sections were treated as above but without the primary antibody. All the control sections were negative. Positive staining control was also included, and, where present in the specimens, internal staining controls were also checked for appropriate reactions with the primary antibody.

Immunostaining of α(IV) chains along the BM of each tissue section was semiquantitatively scored as follows: positive, when α(IV)-chain staining was present; and negative, when α(IV)-chain staining was absent. For OSCC, BM status at the advancing tumor front was considered. Positive staining was further subcategorized into continuous, when no disruptions were found in the staining of α(IV) chain, and discontinuous, when disruptions or short breaks were identified. Statistical analysis was performed using chi-square test, and statistical significance was set at $p<0.05$.

Transmission electron microscopy

Tissue samples containing small regions of BM in selected specimens from light microscopic sections were microdissected out, postfixed in 2.5% glutaraldehyde, and postfixed further in a solution of 1% OsO_4 [18]. These were dehydrated and embedded according to the standard procedure, and thin sections were cut and stained with uranyl acetate–lead citrate and examined with an EF LEO912 transmission electron microscope.

Results

The results are detailed below and illustrated in Figs. 1, 2, 3, 4, 5 and 6.

Immunohistochemical findings

For all specimens examined, no immunoreactivity for α3 (IV) and α4(IV) chains was detected. In OED, CIS, and OSCC, a margin of normal oral mucosa and/or OED present at the periphery of these specimens enabled evaluation of the gradual alteration in α(IV)-chain distribution from normal to abnormal BM.

All six oral mucosas and five oral epithelial hyperplasias demonstrated positive immunostaining for α1(IV), α2(IV), α5(IV), and α6(IV) chains (Figs. 1, 5), and these were expressed as well-defined linear patterns polarized along the BM zones (Fig. 1a–e). Staining was stronger for α1(IV) and α2(IV) chains than for α5(IV) and α6(IV) chains. Limited areas of discontinuous staining identified as short breaks along the BM of oral epithelial hyperplasia were seen in those areas showing marked inflammatory cell infiltration.

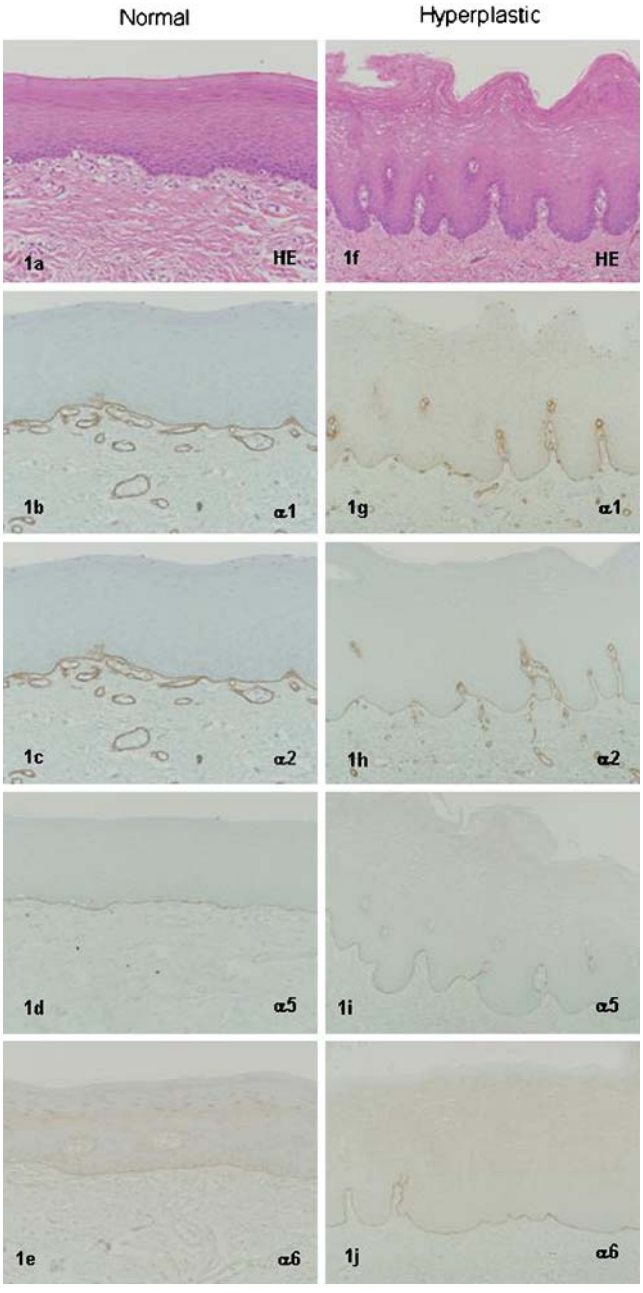

Fig. 1 Immunolocalization of α1(IV), α2(IV), α5(IV), and α6(IV) chains as continuous linear patterns in the basement membranes (*BMs*) of normal oral mucosa (**a**–**e**) and oral epithelial hyperplasia (**f**–**j**). Note that α1(IV) and α2(IV) chains are more strongly expressed than α5 (IV) and α6(IV) chains. Positive α(IV) staining in BM of blood vessels serves as internal control. **a**–**j**, ×100

In BMs of mild, moderate, and severe OED, all four α(IV) chains were predominantly expressed as continuous linear patterns demarcating the dysplastic oral epithelium from the underlying lamina propria (Fig. 2a–r). In moderate and severe OED, staining was strongest for α5(IV) chains

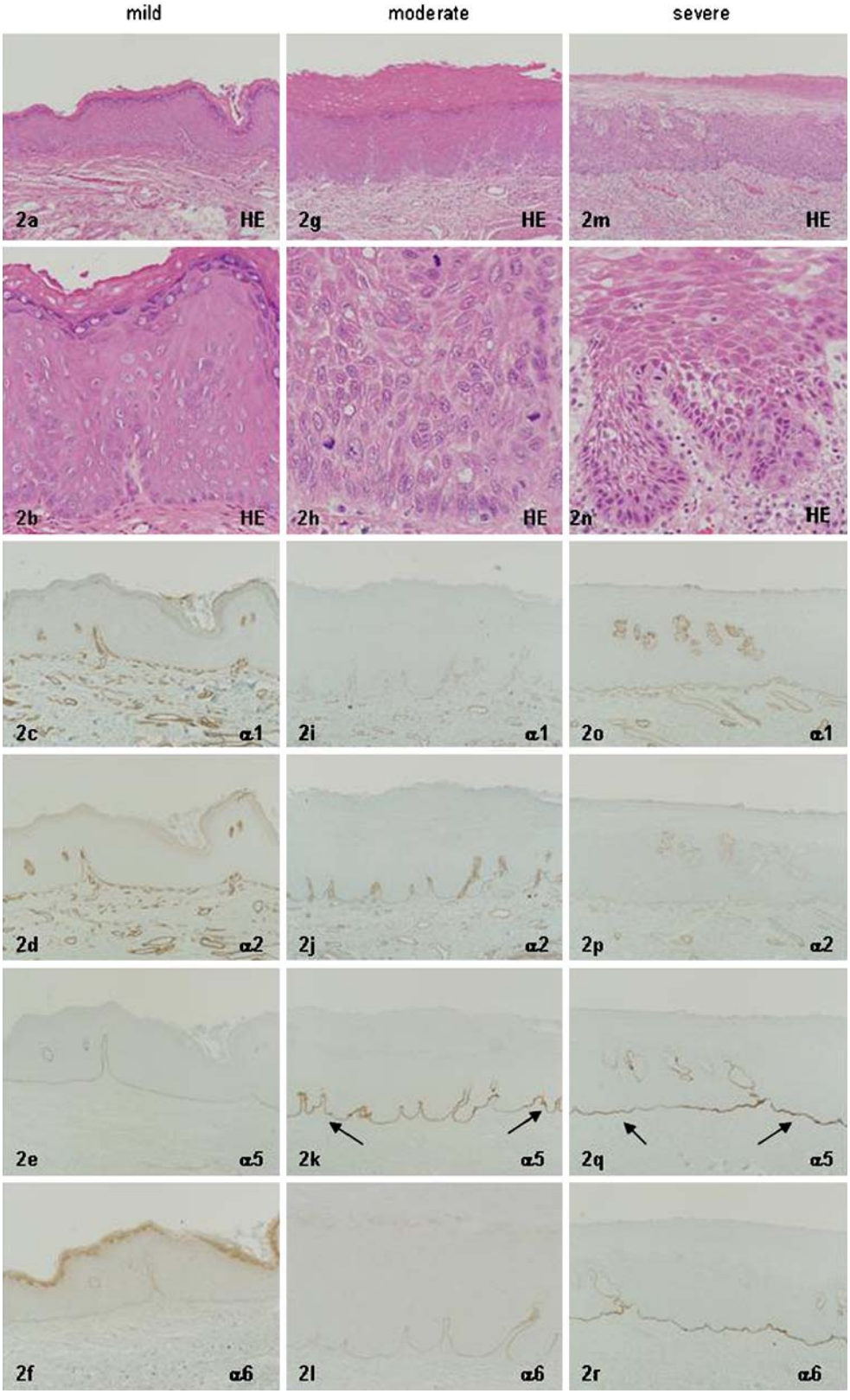

Fig. 2 Immunolocalization of α1(IV), α2(IV), α5(IV), and α6 (IV) chains as continuous linear patterns in the basement membranes (*BMs*) of mild (**a**–**f**), moderate (**g**–**l**), and severe (**m**–**r**) oral epithelial dysplasias (*OED*). Note the strong expression for α5(IV) chains (*arrows*) in BM of moderate (**k**) and severe (**q**) OED. **a**, **c**–**g**, **i**–**m**, **o**–**r**, ×100; **b**, **h**, **n**, ×400

(Fig. 2k,q) than for the other chains. Nonreactivity and disrupted staining at sites of superimposed inflammatory cell infiltration were observed but the frequency of occurrence was low (Fig. 5).

Immunohistochemical staining showed linear expression of all four α(IV) chains in the BM of CIS (Fig. 3a–e, insets), with α5(IV) chains displaying the most intense immunoreactivity (Fig. 3d, inset). Incipient foci of BM

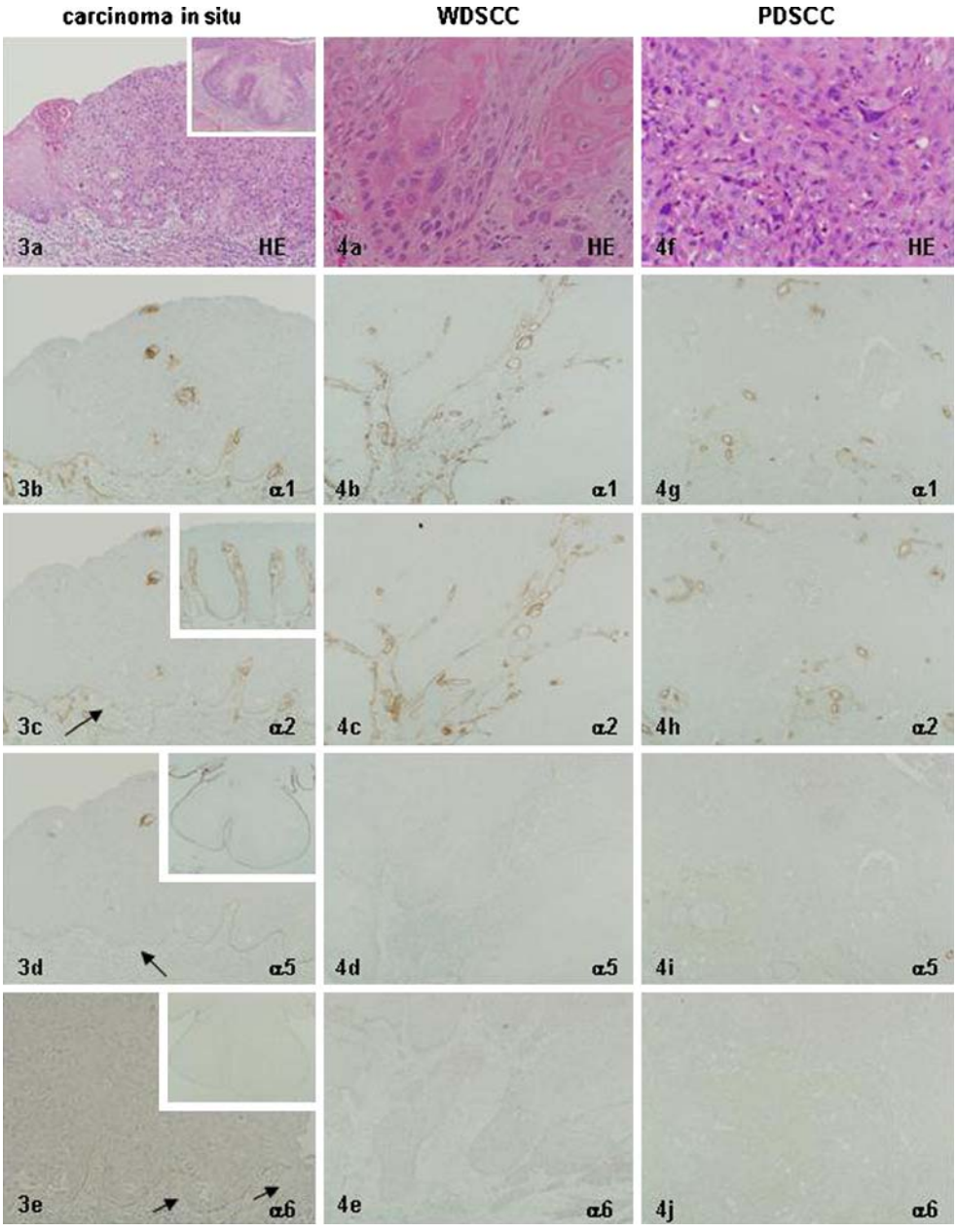

Fig. 3 Immunolocalization of α1(IV), α2(IV), α5(IV), and α6(IV) chains as continuous linear patterns in the basement membrane (*BM*) of carcinoma in situ (*CIS*) (**a**, **b**, **c**–**e** *insets*). Note the strong expression for α5(IV) chains (**d** *inset*). Incipient foci of BM loss characterized by discontinuity in staining (*arrows*) for α2(IV), α5(IV), and α6(IV) chains are observed (**c**–**e**). **a**, **c**, **d** *insets*, ×100; **a**–**d**, ×200

Fig. 4 Immunolocalization of α1(IV), α2(IV), α5(IV), and α6(IV) chains in well-differentiated (**a**–**e**) and poorly differentiated oral squamous cell carcinoma (*OSCC*) (**f**–**j**). Discontinuous staining for α1(IV) and α2(IV) chains and nonreactivity for α5(IV) and α6(IV) chains were observed at the tumor–stromal borders surrounding epithelial islands and nests in well-differentiated OSCC (**b**–**e**), whereas in poorly differentiated OSCC, all four α(IV) chains were not detected. **b**–**e**, **g**–**j**, ×200; **a**, **f**, ×400

disruption characterized by a discontinuous staining pattern for α(IV) chains were also seen but the frequency of occurrence was low (Fig. 3c–e). One case of CIS was immunonegative for all four α(IV) chains (Fig. 5).

In carcinomatous BM, along the advancing tumor front, the disappearance of α5(IV) and α6(IV) chains were more frequent than those of α1(IV) and α2(IV) chains (Fig. 5). Half of the well-differentiated OSCC cases (5/10; 50%) demonstrated loss of expression for α5(IV) and α6(IV) chains ($p<0.05$; Fig. 4d,e), whereas α1(IV) and α2(IV) chains were intermittently expressed at the tumor–stromal interface bordering neoplastic epithelial islands and nests (Fig. 4a–c). In poorly differentiated OSCC, a significant number of cases showed loss of expression for all four α(IV) chains ($p<0.05$; Figs. 4f–j and 5).

Transmission electron microscopic findings

In normal oral mucosa, the BM complex comprised a hemidesmosomal attachment on the epithelial side and a well-defined lamina lucida, lamina densa, and anchoring fibrils within the BM proper (Fig. 6a,b). In OED and CIS, the BM zone demonstrated focal thickenings formed by multiple layers of lamina densa-like material disposed in a wavy or pleated pattern (Fig. 6c,d). Incipient foci of breached BM in CIS were identified as loss of hemi-

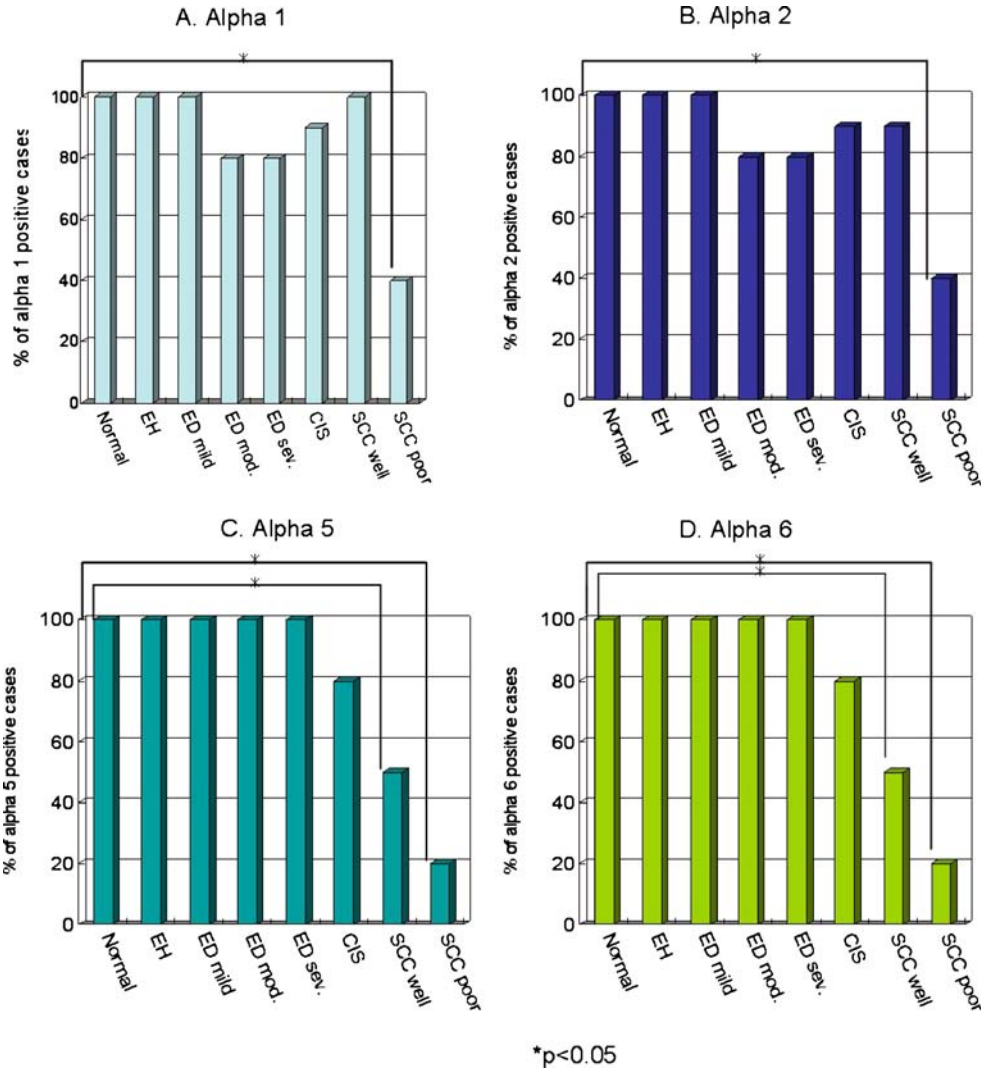

Fig. 5 Results of collagen-IV α-chain immunostaining score calculated based on the percentage of cases showing positive immunoreactivity for each α(IV) chain. Statistical significance for chi-square test is set at $p<0.05$

desmosomal attachments, disruption of the lamina lucida and lamina densa, as well as fragmentation of the anchoring fibrils. In OSCC, only residual fragments of BM comprising lamina lucida and lamina densa were observed.

Discussions

The two-step process of oral carcinogenesis characterized by the initial presence of a precursor lesion that subsequently developed into OSCC provides a unique model for the study of BM protein involvement during these transformation events. Earlier studies using monoclonal or polyclonal antibodies that probably only limit detection of collagen-IV heterotrimeric molecules have variously reported BM collagen-IV macromolecules as being normally expressed, increased, greatly diminished, or even lost in oral premalignant lesions and OSCC [7, 10, 11, 15, 30, 31].

This study is the first to use chain-specific monoclonal antibodies against collagen α1(IV) to α6(IV) chains to detect their localization in the BM of normal oral mucosa, oral epithelial hyperplasia, OED, and OSCC in an attempt to clarify the expression patterns of these molecules during oral carcinogenesis. Our data disclosed that BM associated with oral carcinogenesis differed from normal BM in showing distinctive patterns of α(IV)-chain distribution at specific stages of oral cancer development. We observed that this modification of α(IV)-chain distribution pattern was gradual, that transition from a preinvasive to invasive phase was characterized by a differential gain followed by loss of specific α chains, and that the severity of chain loss increased with higher grades of dysplasia and OSCC. All these findings suggest that alteration in BM collagen-IV α-chain distribution, i.e., remodeling, parallels the progression of neoplastic transformation process in oral epithelium [30]. Immunohistochemical evidence of BM α(IV)-chain remodeling during tumorigenesis has been previously described in cancers involving the prostate [5], pancreas [13], lungs [21], and breast [23], but as in oral carcinogenesis, their

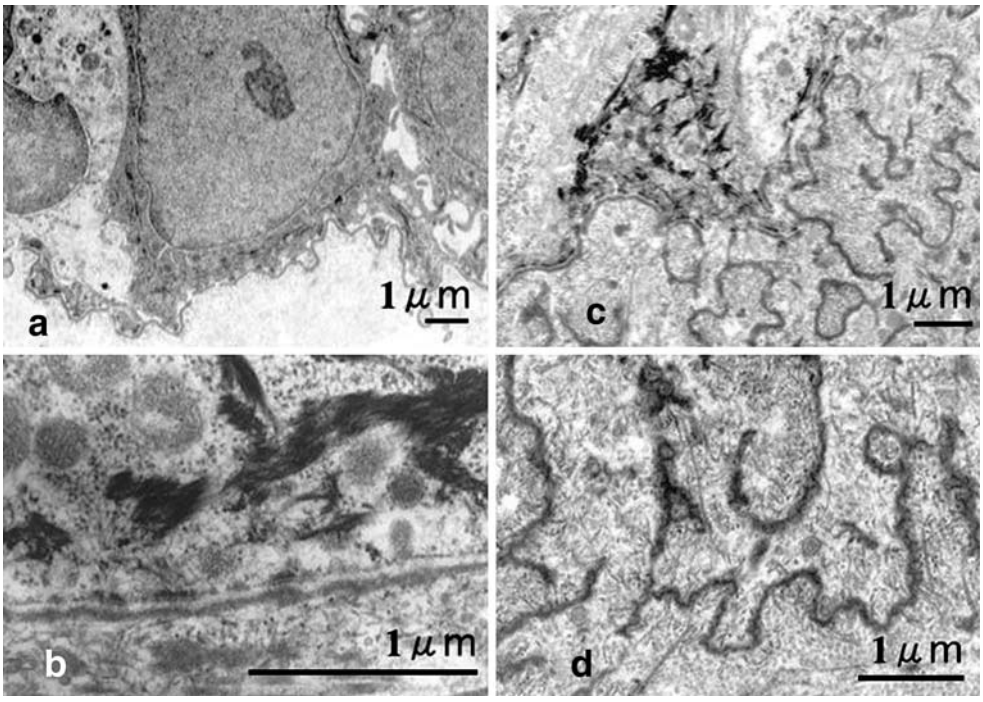

Fig. 6 Transmission electron microscopy of normal oral mucosa showing basement membrane (*BM*) with normal ultrastructural morphology (**a**, **b**). Ultrastructure of oral epithelial dysplasia BM showing excessive deposits of lamina densa-like material in a wavy pattern (**c**, **d**)

precise molecular mechanisms of remodeling remain unclear.

A distinctive feature of oral premalignant BM is the occurrence of focal thickenings consisting of duplications of basal lamina material such as type-IV collagen [7, 10, 11, 15, 30, 31], and these structures were similarly observed in the current study. It has been suggested that the excessive deposition of BM type-IV collagen components probably functions as a selective template for early cancer progression by providing a permissive environment for these altered cells to adhere to the epithelial-connective tissue interface, to persist in a basal position, and to proliferate to dominate the tissue [1]. In the absence of BM proteins for adhesive interactions, these transformed cells will not persist in a premalignant state and will be desquamated.

Another distinctive feature of oral preneoplastic BM is the overexpression of α5(IV) chains especially in moderately/severely dysplastic and in situ oral epithelial lesions. This finding is considered unique because α5(IV) is a novel chain with a restricted distribution [8, 24]. We speculated that aberrant deposition of α5(IV) chains in oral premalignant BM probably has a protective role in providing some resistance and stability to the BM. Abnormal depositions of α5(IV) chains have been identified in the stromal tissues abutting onto tumor islands in odontogenic epithelial neoplasms [19], and in the malignant BMs of prostate carcinomas [5], but there has been no previous description of their occurrence in oral premalignant lesions. In the aorta and some arteries where blood pressure changes significantly, α5(IV)/α6(IV) chains expressed by smooth muscles are believed to have special functions related to mechanical stress and tensile strength during the characteristic contractile activity of these tubular structures [28]. It is plausible that the augmented expression of α5(IV) chains in oral premalignant BM has a similar stabilizing effect on the collagen-IV network.

With the exception of short breaks in BM continuity due to superimposed inflammatory cell infiltration such as observed in oral hyperplastic and dysplastic epithelium, incipient foci of BM disruption characterized by loss of α(IV) chains in CIS lesions herald onset of the invasive phase. A distinctive observation here is that α5(IV)/α6(IV) chains were more frequently absent than α1(IV)/α2(IV) chains. It is known that α1(IV) and α2(IV) chains favor cell migration, whereas the other chains have an antiinvasive phenotype [25]. It is possible that the differential loss of α(IV) chains is crucial to facilitate malignant progression of altered epithelial cells into the extracellular compartment. In bronchoalveolar carcinoma which is recognized as a CIS lesion, the loss of BM α3(IV), α4(IV), and α5(IV)-chain expression and the increase in α1(IV) and α2(IV)-chain expression have been described [21].

At the invasive phase of oral carcinogenesis, we observed that absence and discontinuity in staining for α(IV) chains were more frequent along the BM at the advancing tumor front than in the tumor center. These findings suggest that cancer progression is characterized by BM destruction and stromal invasion followed by quiescence and BM reformation. We further observed that α5(IV)/α6(IV) chains were more frequently absent than α1

(IV)/α2(IV) chains, again presumably to aid stromal invasion [25]. This pattern of differential depletion of α(IV) chains in malignant BM has also been reported in cancers of the prostate [5], pancreas [13], breast [23], and skin [29]. Although the precise mechanism of depletion is unknown, involvement of matrix metalloproteinases has been suggested [21].

In summary, this immunolocalization study demonstrates that specific alterations in the distribution of type-IV collagen α chains in BM occur during oral carcinogenesis, each reflecting the progression of the neoplastic transformation process. However, more studies are needed for further clarification of the biological significance of these changes.

Acknowledgements This study was supported by Grant-in-Aid for JSPS and Scientific Research from the Japanese Ministry of Education, Culture, Sport, Science and Technology (A) No. 15209060 and (C) No. 17591910. The experiments complied with the current laws of the country in which they were performed.

References

1. Andriani F, Garfield J, Fusenig NE, Garlick J (2004) Basement membrane proteins promotes progression of intraepithelial neoplasia in 3-dimensional models of human stratified epithelium. Int J Cancer 108:348–357
2. Barnes L, Eveson JW, Reichert P, Sidransky D (eds) (2005) World Health Organization classification of tumours. Pathology and genetics of head and neck tumours. IARC Press, Lyon
3. Borza DB, Bondar O, Ninomiya Y, Sado Y, Naito I, Todd P, Hudson BG (2001) The NC1 domain of collagen IV encodes a novel network composed of the alpha 1, alpha 2, alpha 5, and alpha 6 chains in smooth muscle basement membranes. J Biol Chem 276:28532–28540
4. Boutad A, Borza DB, Bondar O, Gunwar S, Netzer KO, Singh N, Ninomiya Y, Sado Y, Noelken ME, Hudson BG (2000) Type IV collagen of the glomerular basement membrane. Evidence that the chain specificity of network assembly is encoded by the noncollagenous NC1 domains. J Biol Chem 275:30716–30724
5. Dehan P, Waltregny D, Beschin A, Noel A, Castronovo V, Trygvason K, De Leval J, Foidart JM (1997) Loss of type IV collagen alpha 5 and alpha 6 chains in human invasive prostate carcinomas. Am J Pathol 151:1097–10104
6. Erickson AC, Couchman JR (2000) Still more complexity in mammalian basement membranes. J Histochem Cytochem 48:1291–1306
7. Firth NA, Reade PC (1996) The prognosis of oral mucosal squamous cell carcinoma: a comparison of clinical and histopathological grading and of laminin and type IV collagen staining. Aust Dent J 41:83–86
8. Fleischmajer R, Kuhn K, Sato Y, MacDonald ED 2nd, Perlish JS, Pan TC, Chu ML, Kishiro Y, Oohashi T, Bernier SM, Yamada Y, Ninomiya Y (1997) There is temporal and spatial expression of alpha 1 (IV), alpha 2 (IV), alpha 5 (IV), alpha 6 (IV) collagen chains and beta1 integrins during the development of the basal lamina in an "in vitro" skin model. J Invest Dermatol 109:527–533
9. Floquet N, Pasco S, Ramont L, Derreumaux P, Laronze JY, Nuzillard JM, Maquart FX, Alix AJ, Monboisse JC (2004) The antitumor properties of the α3(IV)-(185–203) peptide from NC1 domain of type IV collagen (tumstatin) are conformation-dependent. J Biol Chem 279:2091–2100
10. Garzino-Demo P, Carrozzo M, Trusolino L, Savoia P, Gandolfo S, Marchisio PC (1998) Altered expression of alpha 6 integrin subunits in oral squamous cell carcinoma and oral potentially malignant lesions. Oral Oncol 34:204–210
11. Giannelli G, Milillo L, Marinosci F, Lo Muzio L, Serpico R, Antonaci S (2001) Altered expression of integrins and basement membrane proteins in malignant and pre-malignant lesions of oral mucosa. J Biol Regul Homeost Agents 4: 375–380
12. Hiki Y, Iyama K, Tsuruta J, Egami H, Kamio T, Suko S, Naito I, Sado Y, Ninomiya Y, Ogawa M (2002) Differential distribution of basement membrane type IV collagen alpha1(IV), alpha2(IV), alpha5(IV) and alpha6(IV) chains in colorectal epithelial tumors. Pathol Int 52:224–233
13. Kadono G, Ishihara T, Yamaguchi T, Kato K, Kondo F, Naito I, Sado Y, Saisho H (2004) Immunohistochemical localization of type IV collagen alpha chains in the basement membrane of the pancreatic duct in human normal pancreas and pancreatic diseases. Pancreas 29:61–66
14. Kagawa M, Kishiro Y, Naito I, Nemoto T, Nakanishi H, Ninomiya Y, Sado Y (1997) Epitope-defined monoclonal antibodies against type-IV collagen for diagnosis of Alport's syndrome. Nephrol Dial Transplant 12:1238–1241
15. Kannan S, Balaram P, Chandran GJ, Pillai MR, Mathew B, Nalinakumari KR, Nair MK (1994) Alterations in expression of basement membrane proteins during tumour progression in oral mucosa. Histopathology 24:531–537
16. Lohi J, Korhonen M, Leio I, Kangas L, Tani T, Kalluci R, Miner JH, Lehto VP, Virtanen I (1997) Expression of type IV collagen α1(IV)–α6(IV) polypeptides in normal and developing human kidney and in renal cell carcinoma and oncocytomas. Int J Cancer 72:43–49
17. Misumi S, Iyama K, Honda Y, Kitano T, Sado Y, Ninomiya Y, Shinohara M (2004) Differential expression of basement membrane type-IV collagen α1, α2, α3, α5 and α6 chains among the histological subtypes of adenoid cystic carcinoma. Virchows Arch 445:54–62
18. Nagai N, Lee YJ, Nagaoka N, Gunduz M, Nakano K, Nojima T, Tsujigiwa H, Gunduz E, Siar CH, Nagatsuka H (2002) Elemental sulphur and alkali elutable melanin detected in oral melanosis and malignant melanoma by energy-filtering transmission electron microscopy. J Oral Pathol Med 31:481–487
19. Nagatsuka H, Siar CH, Nakano K, Tsujigiwa H, Gunduz M, Choufuku H, Lee Y-J, Naito I, Sado Y, Nagai N (2002) Differential expression of collagen IV α1 to α6 chains in benign and malignant odontogenic tumors. Virchows Arch 441:392–399
20. Nagatsuka H, Rivera RS, Gunduz M, Lee Y-J, Tamamura R, Gunduz E, Naito I, Sado Y, Nagai N (2005) Immunolocalization and distribution patterns of type IV collagen alpha chains in oral mucosal melanoma. Virchows Arch 447: 710–716
21. Nakano KY, Iyama KI, Mori T, Yoshioka M, Hiraoka T, Sado Y, Ninomiya Y (2001) Loss of alveolar basement membrane type IV collagen α3, α4, and α5 chains in bronchioloalveolar carcinoma of the lung. J Pathol 194:420–427
22. Nakano K, Siar CH, Nagai N, Naito I, Sado Y, Nagatsuka H, Hoh C, Kurada K, Tsujigiwa H, Gunduz M (2002) Distribution of basement membrane type IV collagen alpha chains in ameloblastoma: an immunofluorescence study. J Oral Pathol Med 31:494–499
23. Nakano S, Iyama K, Ogawa M, Yoshioka H, Sado Y, Oohashi T, Ninomiya Y (1999) Differential tissular expres-

sion and localization of type IV collagen α1(IV), α2(IV), α5 (IV), and α6(IV) chains and their mRNA in normal breast and in benign and malignant breast tumors. Lab Invest 79:281–292
24. Ninomiya Y, Kagawa M, Iyama K, Naito I, Kishiro Y, Seyer JM, Sugimoto M, Oohashi T, Sado Y (1995) Differential expression of two basement membrane collagen genes, COL4A6 and COL4A5, demonstrated by immunofluorescence staining using peptide-specific monoclonal antibodies. J Cell Biol 1:1219–1229
25. Ortega N, Werb Z (2002) New functional roles for non-collagenous domains of basement membrane collagens. J Cell Sci 115(Pt 22):4201–4214
26. Reibel J (2003) Prognosis of oral pre-malignant lesions: significance of clinical, histopathological and molecular biological characteristics. Crit Rev Oral Biol Med 14:47–62
27. Sado Y, Kagawa M, Kishiro Y, Sugihara K, Naito I, Seyer JM, Sugimoto M, Oohashi T, Ninomiya Y (1995) Establishment by the rat lymph node method of epitope-defined monoclonal antibodies recognizing the six different α chains of human type IV collagen. Histochem Cell Biol 104:267–275
28. Seki Y, Naito I, Oohashi T, Sado Y, Ninomiya Y (1998) Differential expression of type IV collagen isoforms, α5(IV) and α6(IV) chains, in basement membranes surrounding smooth muscle cells. Histochem Cell Biol 110:359–366
29. Tanaka K, Iyama K, Kitaoka M, Ninomiya Y, Oohashi T, Sado Y, Ono T (1997) Differential expression of α1(IV), α2(IV), α5(IV), and α6(IV) collagen chains in the basement membrane of basal cell carcinoma. Histochem J 29:563–570
30. Tosios KI, Kapranos N, Papanicolaou SI (1998) Loss of basement membrane components laminin and type IV collagen parallels the progression of oral epithelial neoplasia. Histopathology 33:261–268
31. Wilson DF, De-Jun J, Pierce AM, Wiebkin OW (1999) Oral cancer: role of basement membrane in invasion. Aust Dent J 44:93–97
32. Yurchenco PD, O'Rear JJ (1994) Basal lamina assembly. Curr Opin Cell Biol 6:674–681

Virchows Arch (2006) 449: 367–372
DOI 10.1007/s00428-005-0076-2

CASE REPORT

Jesús Vera · María-Dolores García · Miguel Marigil · Manuel Abascal · Jose-Ignacio Lopez · Luis Ligorred

Biphasic synovial sarcoma of the abdominal wall

Received: 1 July 2005 / Accepted: 19 August 2005 / Published online: 20 July 2006
© Springer-Verlag 2006

Abstract Synovial sarcoma arising in the abdominal wall is a rare tumor. We report a case of a 38-year-old man who complained of abdominal pain. Physical examination revealed a firm mobile mass, 25 cm in diameter, in the left lower abdominal wall. The tumor was first thought to be a sarcoma arising from the omentum or mesentery. During surgery, a large tumor was found attached to the inner surface of the abdominal wall and compressing the gastrointestinal tract. On microscopic examination the tumor corresponded to a biphasic synovial sarcoma immunoreactive for cytokeratins (AE1/AE3, 7 and 19), epithelial membrane antigen and carcinoembryonic antigen in the epithelial tumor cells, for E-cadherin especially in their glandular structure, vimentin, CD99, and CD56 in the spindle cell component and for bcl-2 protein. The tumor recurred at the same site, and clinical course progressed to death 3 months after the initial diagnosis.

Keywords Synovial sarcoma · Abdominal wall · Sarcoma · Carcinosarcoma · Immunohistochemistry

Introduction

Synovial sarcoma is a rare malignancy that occurs chiefly in the soft tissues of the extremities, especially near the large joints, in young adults. However, it may be more rarely found in unexpected sites, such as abdominal and thoracic walls [11, 20, 33], head and neck regions [34], including pharynx, larynx [33], and orbit [37], retroperitoneum [14, 38], mediastinum [40], bone [6], nerves [28], blood vessels [33], as well as visceral organs, such as lungs [44], pleura [16, 26], heart [19], kidneys [3, 23] or prostate [18]. The anterior abdominal wall is a rare location for synovial sarcoma development and, in the English language literature, 44 cases have been published between 1950 and 2005 [1, 11, 17, 20, 25].

The reported data on the frequency of this tumor vary, ranging from 5.6 [42] to 10% [4] among all soft tissue sarcomas.

We describe a case of biphasic synovial sarcoma arising on the anterior abdominal wall and presenting as a peritoneal cavity tumor. Clinical diagnosis of synovial sarcoma of the abdominal wall is virtually impossible, although the presence of stippled amorphous calcification on X-ray should suggest the diagnosis [17].

J. Vera (✉) · M.-D. García · M. Marigil · M. Abascal
Department of Pathology, Hospital General San Jorge,
Avenida Martinez de Velasco, 36,
22071 Huesca, Spain
e-mail: jjvera@salud.aragon.es
Tel.: +34-97-4247000
Fax: +34-97-4247065

J.-I. Lopez
Department of Radiology, Hospital General San Jorge,
Huesca, Spain

L. Ligorred
Department of Surgery, Hospital General San Jorge,
Huesca, Spain

Case report

Clinical history

A 38-year-old man was admitted to the hospital because of a slowly growing abdominal mass in the left lower quadrant of the abdomen. He thought that it had been present for about 1 year. The tumor became painful and increased rapidly in size. General examination was negative except for a huge, movable mass (25 cm in diameter) in the left lower abdominal wall. No other masses were detected anywhere else. Liver and spleen were not palpable, and rectal examination showed negative results. No lymph nodes were palpable. Examination and investigation of the genitourinary system likewise yielded negative results. Routine laboratory investigations were normal. Abdominal X-ray showed amorphous stippled calcification on the left peritoneal cavity. Computed tomography revealed a huge well-demarcated

mass with cystic changes and marginal calcification (Fig. 1a).

Surgical removal of the abdominal tumor was carried out. A large tumor occupying the left, lower quadrant region of the abdominal cavity was found attached to the inner surface of the abdominal wall and compressing the gastrointestinal tract. The tumor was covered by, and loosely adherent to, the greater omentum. Peritoneal ascites, dissemination or metastases were not observed. The peritoneum was intact and left untouched by the tumor. The neoplasm was completely removed with a 1-cm margin of normal tissue together with an omentectomy and sampling of the perigastric lymph nodes. The extirpated tumor proved to be a biphasic synovial sarcoma. A whole-body scan did not reveal any abnormality. Plain X-ray of abdomen, chest and extremities did not reveal any pathology. After surgery, neither local radiation therapy nor chemotherapy was administered. Three months later, the tumor recurred at the same site. This time there were multiple small masses in the peritoneum, firm and slightly mobile and were incompletely resected. Clinical course progressed to death 15 days later. No autopsy was performed.

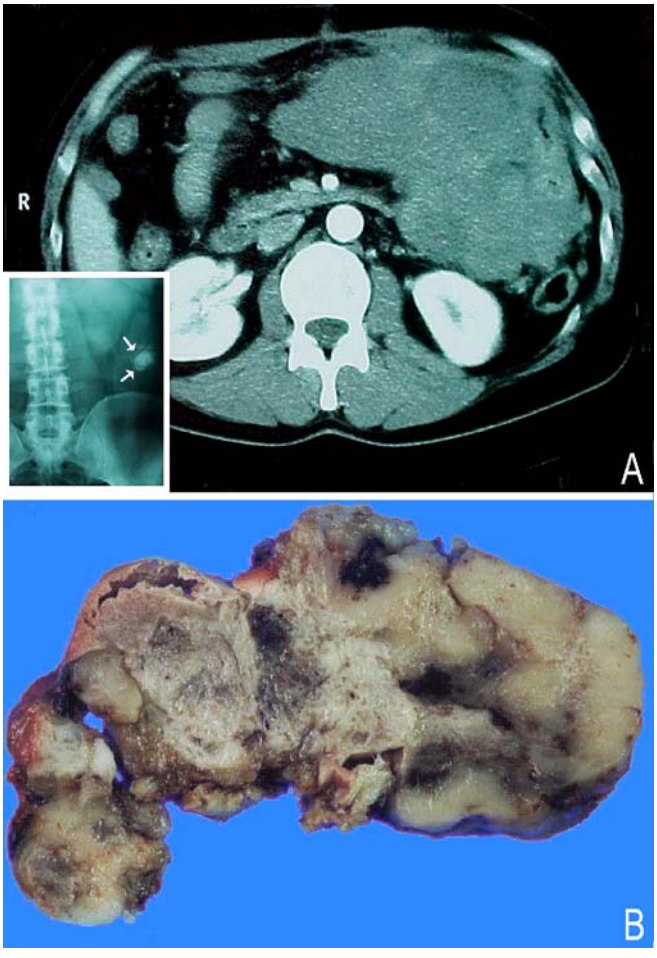

Fig. 1 **a** Computed tomography scan of abdomen showing a large tumor mass occupying the left peritoneal cavity with marginal calcification. *Inset*: amorphous stippled calcification can be seen on abdominal X-ray (*arrows*). **b** The tumor cut surface demonstrated a multicystic mass and areas of solid tissue with hemorrhage and necrosis

Material and methods

The excised specimen was fixed in 10% buffered formalin, embedded in paraffin, cut in 4-μm sections and stained with hematoxylin and eosin, periodic acid–Schiff (PAS) with and without diastase digestion, Alcian blue (pH 2.5) with and without hyaluronidase digestion, and silver impregnation for reticulin. Sections were studied immunohistochemically with automated immunostaining on a Biotek Solutions Tech Mate (TechMate 500; Biotech Solutions, Dako, Glostrup, Denmark) and then incubated in a detection kit (CheMate, code K4001, Dako) according to the manufacturer's instructions. Peroxidase activity was developed with 3-3′-diaminobenzidine (Sigma) to obtain a brown end product. Heat-induced epitope retrieval was performed for all sections via a pressure cooker, as previously described [24]. Representative sections were examined by using positive and negative controls. The following commercially available antibodies were used: epithelial membrane antigen (EMA) (E29, 1:100), α-smooth muscle actin (1A4, 1:50), CD34 (QBEND/10, 1:30; Biogenex, San Ramon, CA, USA), vimentin (V9, 1:200), cytokeratin (AE1/AE3, 1:20), cytokeratin 7 (LP- 5K, 1:10), cytokeratin 19 (b170, 1:100), WT1 (6F-H2, 1:25), calretinin (5A5, 1:100), CD56 (1B6, prediluted), E-cadherin (36B5, prediluted; Novocastra, Newcastle, UK), desmin (D33, 1:100), S-100 protein (S-100, 1:40), carcinoembryonic antigen (CEA) (II-7, 1:100), bcl-2 protein (124, prediluted), CD117 (c-kit, 1:400), anti-human mesothelial cell (HBME-1, prediluted), thrombomodulin (1009, 1:100) and CD99 (12E7, 1.50; Dako, Carpenteria, CA, USA).

Pathological findings

Gross features

Pathological examination revealed a grey-colored tumor mass; it was sharply circumscribed, multilobular, limited by a smooth pseudocapsule and attained a size of 25× 14×7 cm. The cut surface revealed a multicystic mass with areas of solid grey-white to tan with a variegated and friable appearance, and with multiple areas of hemorrhage and necrosis (Fig. 1b).

Microscopic features

Microscopic examination of surgical specimen showed a biphasic growth pattern composed of epithelial and spindled areas (Fig. 2a). However, the proportion of the two components changed in different areas. The epithelial areas showed solid cords, nests and glandular structures (Fig. 2b). The epithelial cells were predominantly cuboidal

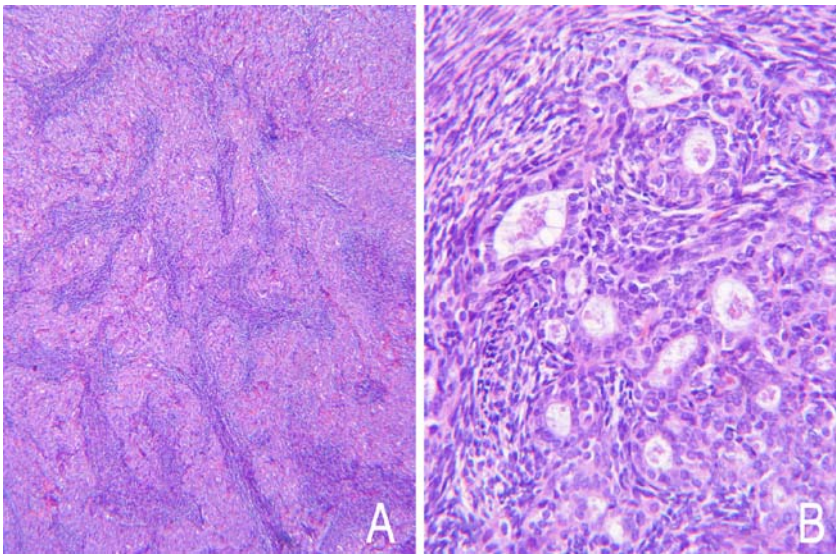

Fig. 2 **a** Biphasic cellular patern with epithelium-like cell component and spindle cell areas (hematoxylin–eosin, 100×). **b** The tumor shows glandular structures in focal areas (hematoxylin–eosin, 400×)

and had a moderate amount of pale-staining cytoplasm with distinctly cellular borders, and round to oval vesicular nuclei. The lumina of the glands contained eosinophilic mucinous material, which was not digestible with diastase or hyalorunidase. The surrounding spindle cell or fibrous component forming solid and compact sheets was composed of densely packed, elongated, fusiform cells (Fig. 3a) with small amounts of indistinct cytoplasm and oval dark-staining nuclei. Silver stain showed abundant reticulin in the spindle areas, in marked contrast to the epithelial portions of the tumor. The frequency of mitoses varied, but their presence was limited to spindle cell areas with five to 15 mitoses per ten high-power fields. Calcification with ossification was present in a small portion of the neoplasm (Fig. 3b). Large amounts of mast cells were found in areas of spindle cells. Necrosis involving less than 30% of the microscopic tumor areas was present. There was no vascular invasion nor direct extension to adjacent structures including omentum, mesentery and abdominal muscles. There were no regional lymph node metastases.

Immunohistochemical features

Immunohistochemically, cytokeratins (AE1/AE3, 7 and 19), EMA and CEA were positive in the cytoplasm of the epithelial tumor cells. Bcl-2 protein was positive in epithelial and spindled components. E-cadherin expression was observed especially in their glandular structure with weak and focal membranous staining. Vimentin and CD56 were expressed by the tumor cells of the spindle cell component. The spindle cells were positive for CD99, with focal membranous staining. The tumor cells were consistently negative for desmin, α-smooth muscle actin, S-100 protein, CD34, calretinina, thrombomodulin, HBME-1, WT-1 and CD117 (Fig. 4).

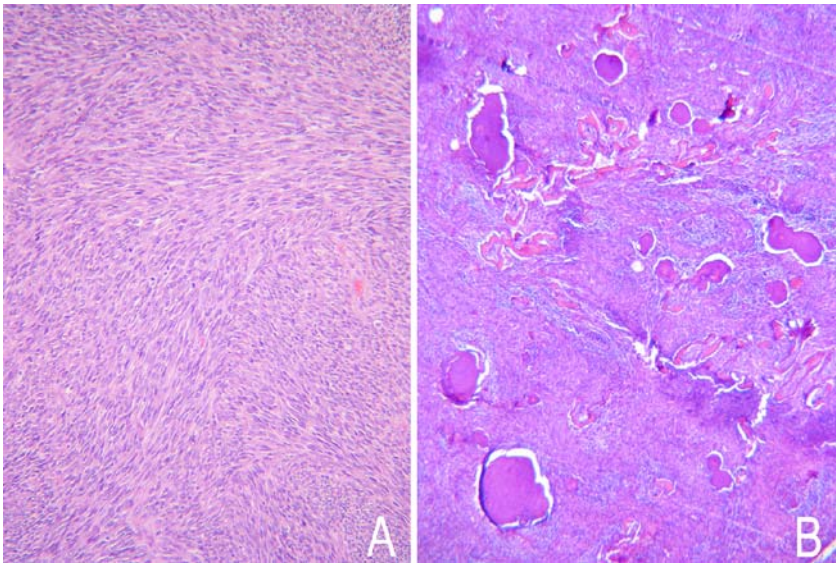

Fig. 3 **a** Spindle-cell areas showing fibrosarcomatous growth pattern composed of densely packed fusiform cells in interweaving fascicles (hematoxylin–eosin, 200×). **b** An area with focal points of calcification is present (hematoxylin–eosin, 200×)

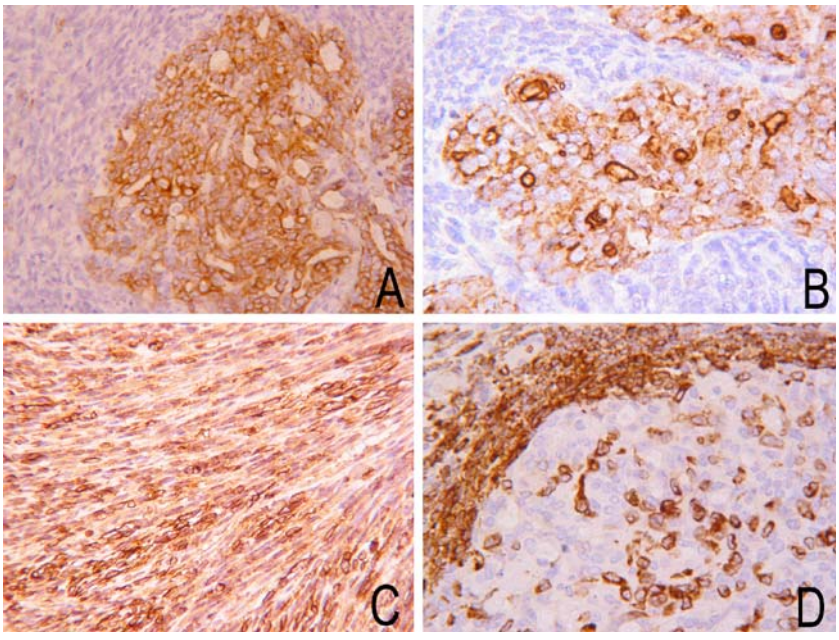

Fig. 4 Epithelial component showing positive immunostaining with antibodies against cytokeratin AE1/AE3 (**a**) and EMA (**b**). Diffuse vimentin staining in the spindle cell component (**c**) and positive bcl-2 staining in both components (**d**)

Discussion

Although the most common location for synovial sarcoma includes the soft tissues of the extremities and the head and neck region, examples of this entity have now been reported in almost all parts of the body [13, 14, 40]. Examples of synovial sarcoma occurring in the anterior abdominal wall are rare, with most accounts consisting of case reports [1, 11, 17, 20–22, 25, 30]. In 1950, Pack and Ariel [30] reported the first two cases of synovial sarcoma arising in the abdominal wall. The survival rate for patients with synovial sarcoma of the abdominal wall is generally similar to that reported for synovial sarcoma [11]. The clinical behavior of synovial sarcoma has been described as being correlated to some morphologic factors such as histologic subtype, mitotic rate [11], percent glandularity [5], tumor necrosis and vascular invasion [32]. Less favorable behavior was also noted when the tumors were large (≥5 cm), and some investigators considered proliferative activity to be an important prognostic factor for this type of tumor [29]. In the present case the tumor displayed morphological features which could indicate poor prognosis such as size of neoplasm, presence of necrosis and a high mitotic rate.

In its classic bimorphic form, with mixed epithelial and spindle cell components, synovial sarcoma is rarely a diagnostic dilemma. However, the differential diagnosis for this tumor in the peritoneum can include other biphasic neoplasms, metastatic carcinoma, spindle cell sarcomas and small round cell tumors. Biphasic synovial sarcoma must be distinguished from mesothelioma and carcinosarcoma. Biphasic peritoneal mesotheliomas are closely related to long-term exposure to asbestos [43], occurring in an older age group and having larger and less uniform nuclei [14]. Also, gross morphologic findings can be quite helpful in such cases; synovial sarcoma will usually present as a lobular mass as opposed to mesothelioma, which has a tendency to grow as a diffuse, plaque-like tumor mass [40]. Although differential diagnosis can be problematic, especially with mixed-type lesions [16, 43], and mast cell infiltration is not a characteristic finding of mesothelioma, hyaluronic acid may be detectable in glandular elements within mesotheliomas, whereas it is absent in the epithelial component of synovial sarcomas. Furthermore, both epithelial and sarcomatoid components of mesotheliomas are positive for vimentin, cytokeratin and EMA by immunohistochemistry [21, 43]. Müllerian adenosarcoma and carcinosarcoma occur mostly in gynaecological organs in older patients; these, and other sarcomatoid carcinomas, are more pleomorphic than synovial sarcoma and have more diffuse cytokeratin positivity [14]. Metastatic carcinoma can be generally ruled out by identifying the atypical spindle cell component surrounding the glands. Also, the nuclei in metastatic adenocarcinoma are more pleomorphic and less uniform than those generally encountered in the glandular elements of synovial sarcoma [40]. Fibrosarcoma, malignant fibrous histiocytoma, malignant haemangiopericytoma, leiomyosarcoma, gastrointestinal stromal tumor, and small round cell sarcomas, including primitive neuroectodermal tumors, display a monophasic growth pattern, and appropriate use of immunohistochemical panels can be required [13]. Also, in the differential diagnosis, extra-renal Wilms' tumors [21] and malignant peripheral nerve sheath tumors with epithelial elements should be considered [11]. The simultaneous use of antibodies to both CD99 and CD56 may be useful in the differential diagnosis because synovial sarcoma will almost always test positive with both antibodies, whereas primitive neuroectodermal tumors will be CD99 positive and CD56 negative, and malignant peripheral nerve sheath tumors will be CD99 negative but CD56 positive [15]. Extra-renal Wilms' tumors occurring in adults are extremely rare; they almost always develop in the retroperi-

toneal and inguinal regions and there have been no reported cases involving the anterior abdominal wall [21].

Although the immunohistochemical profile of synovial sarcoma is extensive [13, 36], it was recently suggested that EMA, cytokeratin AE1/AE3 and E-cadherin, in combination with CD34 negativity, are the most useful and sensitive markers for diagnosing synovial sarcoma [31, 35].

However, the pattern and extent of the immunohistochemical staining, in conjunction with clinical, radiologic, and microscopic features, will usually lead to appropriate classification [11].

Finally, the possibility of a metastases to the abdominal wall from a synovial sarcoma of soft tissue should always be ruled out first before making a diagnosis of primary synovial sarcoma at this site. In the present case, the patient did not have a history or evidence of tumor elsewhere (on clinical or radiographic examination), which supported its primary origin at this site.

The pathogenesis of synovial sarcoma is unresolved. Because of its frequent association with para-articular regions, it was initially postulated that these tumors originated from synovial cells [4]. Moreover, the presence of synovial sarcoma of the abdominal wall, as well those of other extra-articular sites where normal synovial, bursal, or tendon sheath structures do no exist, argues against an origin from arthrogenous mesenchyme [9]. However, many examples have been described in recent years, indicating that these tumors are not related to normal synovium but rather show features of epithelial differentiation [7, 10, 12, 24, 35]. These examples, coupled with their documented occurrence at extra-articular sites, have led to the speculation that these neoplasms could arise from a mutated pluripotential mesenchymal cells present in diverse locations [10, 12].

The characteristic chromosomal translocation t(x;18)(p11.2;q11.2) found in about 90% of synovial sarcomas [5, 8] has been interpreted as being specific to synovial sarcomas and is probably related to the genesis of this tumor [12]. Furthermore, two different types of breakpoint on chromosome X, which correspond to the chimeric genes SYT-SSX1 and SYT-SSX2, have been reported in synovial sarcomas [9, 27, 41]. These two chimeric genes may be related to the histological subtypes monophasic and biphasic. It has been suggested that a high degree of correlation exists, in the sense that nearly all biphasic tumors carry the SYT-SSX1 fusion, whereas most of those with SYT-SSX2 are monophasic [19]. In this way, the problems that may be encountered in the diagnosis of synovial sarcomas located in sites other than the extremities can be largely overcome by the detection of SYT-SSX transcripts by reverse transcriptase-polymerase chain reaction (RT-PCR) in fresh or paraffin-embedded material [2, 10].

Synovial sarcoma can recur locally, usually within 2 years, but sometimes many years later [43]. Metastases occur particularly in the lung, and less commonly in lymph nodes and bone. The preferred treatment is local excision, with wide margins of normal tissue, supplemented by radiation therapy [39], chemotherapy, or both [11].

References

1. Al-Dewachi HS, Sangal BC, Zakaria MA (1981) Synovial sarcoma of the abdominal wall: a case report and study of its fine structure. J Surg Oncol 18:335–344
2. Argani P, Zakowski MF, Klimstra DS, Rosai J, Ladanyi M (1998) Detection of the SYT-SSX chimeric RNA of synovial sarcoma in paraffin-embedded tissue and its application in problematic cases. Mod Pathol 11:65–71
3. Argani P, Faria PA, Epstein JI, Reuter VE, Perlman EJ, Beckwith JB, Ladanyi M (2000) Primary renal synovial sarcoma: molecular and morphologic delineation of an entity previously included among embryonal sarcomas of the kidney. Am J Surg Pathol 24:1087–1096
4. Cadman NL, Soule EH, Kelly PJ (1965) Synovial sarcoma: an analysis of 134 tumors. Cancer 18:613–627
5. Cagle LA, Mirra JM, Storm FK, Roe DJ, Eilber FR (1987) Histologic features relating to prognosis in synovial sarcoma. Cancer 59:1810–1814
6. Cohen IJ, Issakov J, Avigad S, Stark B, Meller I, Zaizov R, Bar-Am I (1997) Synovial sarcoma of bone delineated by spectral karyotyping. Lancet 350:1679–1683
7. Corson JM, Weiss LM, Banks-Schlegel SP, Pinkus GS (1984) Keratin proteins and carcinoembryonic antigen in synovial sarcomas: an immunohistochemical study of 24 cases. Human Pathol 15:615–621
8. Dal Cin P, Rao U, Jani-Sait S, Karakousis C, Sandberg AA (1992) Chromosomes in the diagnosis of soft tissue tumors. I. Synovial sarcoma. Mod Pathol 5:357–362
9. de Leeuw B, Balemans M, Olde Weghuis D, Geurts van Kessel A (1995) Identification of two alternative fusion genes, SYT-SSX1 and SYT-SSX2, in t(x;18) (p11.2; q11.2)-positive synovial sarcoma. Hum Mol Genet 4:1097–1099
10. Dickersin GR (1991) Synovial sarcoma: a review and update, with emphasis on the ultrastructural characterization of the nonglandular component. Ultrastruct Pathol 15:379–402
11. Fetsch JF, Meis JM (1993) Synovial sarcoma of the abdominal wall. Cancer 72:469–477
12. Fisher C (1986) Synovial sarcoma: ultrastructural and immunohistochemical features of epithelial differentiation in monophasic and biphasic tumors. Human Pathol 17:996–1008
13. Fisher C (1998) Synovial sarcoma. Ann Diagn Pathol 2: 401–421
14. Fisher C, Folpe AL, Hashimoto H, Weiss SW (2004) Intra-abdominal synovial sarcoma: a clinicopathological study. Histopathology 45:245–253
15. Folpe AL, Schmidt RA, Chapman D, Gown AM (1998) Poorly differentiated synovial sarcoma: immunohistochemical distinction from primitive neuroectodermal tumors and high-grade malignant peripheral nerve sheath tumors. Am J Surg Pathol 22:673–682
16. Gaertner E, Zeren HE, Fleming MV, Colby TV, Tavis WD (1996) Biphasic synovial sarcoma arising in the pleural cavity: a clinicopathologic study of five cases. Am J Surg Pathol 20:36–45
17. Hale JE, Calder IM (1970) Synovial sarcoma of the abdominal wall. Br J Cancer 24:471–474
18. Iwasaki H, Ishiguro M, Ohjimi Y, Ikegami H, Takenchi T, Kikuchi M, Kaneko Y, Ariyoshi A (1999) Synovial sarcoma of the prostate with t(X;18)(p11.2;q11.2). Am J Surg Pathol 23:220–226
19. Iyenzar V, Lineberger AS, Kerman S (1995) Synovial sarcoma of the heart. Arch Pathol Lab Med 119:1080–1082
20. Karadag O, Altundag K, Elkiran ET, Dikbas O, Gedikoglu G, Kars A (2005) Anterior abdominal wall synovial sarcoma: a rare presentation. Am J Clin Oncol 28:323–324
21. Kashima T, Matsushita H, Kurod M, Takeuchi H, Udagawa H, Ishida T, Hara M, Machinami R (1997) Biphasic synovial sarcoma of the peritoneal cavity with t(x;18) demonstrated by reverse transcriptase polymerase chain reaction. Pathol Int 47:637–641

22. Katenkamp D, Stiller D (1980) Synovial sarcoma of the abdominal wall: Light microscopic, histochemical and electron microscopic investigations. Virchows Arch, A Pathol Anat Histopathol 388:349–360
23. Limon J, Mrozek K, Mandahl N (1991) Cytogenetics of synovial sarcoma: Presentation of ten new cases and review of the literature. Genes Chromosom Cancer 3:338–345
24. Miller RT, Estran C (1995) Heat-induced epitope retrieval with a pressure cooker. Appl Immunohistochem 3:190–193
25. Murphy S, Margarit E (1968) Synovial sarcoma of the abdominal wall. Ann Surg 168:928–930
26. Nicholson AG, Godstraw P, Fisher C (1998) Synovial sarcoma of the pleura and its differentiation from other primary pleural tumors: a clinicopathologic and immunohistochemical review of three cases. Histopathology 33:508–513
27. Noguchi SI, Ueki T, Kawauchi S, Fukuda T, Matsuura H, Sonoda T, Tsuneyoshi M (1997) Establishment and characterization of a new synovial sarcoma cell line, SN-SY-1: special reference to bcl-2 protein and SYT-SSX1 hybrid transcripts. Int J Cancer 72:995–1002
28. O'Connell JX, Browne WL, Gropper PT, Berean KW (1996) Intraneural biphasic synovial sarcoma: an alternative "glandular" tumor of peripheral nerve. Mod Pathol 9:738–742
29. Oda Y, Hashimoto H, Takeshita S, Tsuneyoshi M (1993) The prognostic value of immunohistochemical staining for proliferating cell nuclear antigen in synovial sarcoma. Cancer 72:478–485
30. Pack GT, Ariel IM (1950) Synovial sarcoma (malignant synovioma): a report of 60 cases. Surgery 28:1047–1084
31. Pelmus M, Guillou L, Hostein I, Sierankowski G, Lussan C, Coindre JM (2002) Monophasic fibrous and poorly differentiated synovial sarcoma: immunohistochemical reassessment of 60 t(x;18)(SYT-SSX)-positive cases. Am J Surg Pathol 26:1434–1440
32. Rööser B, Willen H, Hugoson A, Rydholm A (1989) Prognostic factors in synovial sarcoma. Cancer 63:2182–2185
33. Rosai J (2004) Rosai and Akerman's surgical pathology. In: Tumors resembling synovial tissue. Mosby, Edinburgh, pp 2309–2313
34. Roth JA, Enzinger FM, Tannenbaum M (1975) Synovial sarcoma of the neck: a follow-up study of 24 cases. Cancer 35:1243–1253
35. Saito T, Oda Y, Sakamoto A, Tamiya S, Kunikawa N, Hayashi K, Iwamoto Y, Tsuneyoshi M (2000) Prognostic value of the preserved expression of the E-cadherin and catenin families of adhesion molecules and of β-catenin mutations in synovial sarcoma. J Pathol 192:342–350
36. Salisbury JR, Isaacson PG (1985) Synovial sarcoma: an immunohistochemical study. J Pathol 147:49–57
37. Shukla PN, Pathy S, Sen S, Purohit A, Julka PK, Rath GK (2003) Primary orbital calcified synovial sarcoma: a case report. Orbit 22:299–303
38. Smookler BM (1982) Retroperitoneal synovial sarcoma. Am J Clin Pathol 77:686–691
39. Suit HD, Russell WO, Martin RG (1973) Management of patients with sarcoma of soft tissue in an extremity. Cancer 31:1247–1255
40. Suster S, Moran CA (2005) Primary synovial sarcomas of the mediastinum. A clinicopathologic, immunohistochemical, and ultrastructural study of 15 cases. Am J Surg Pathol 29: 569–578
41. Tamborini E, Papini D, Mezzelani A, Riva C, Azzareli A, Sozzi G, Pierotti MA, Pilotti S (2001) C-kit and c-kit ligand (SCF) in synovial sarcoma (SS): an mRNA expression analysis in 23 cases. Br J Cancer 85:405–411
42. Tsuneyoshi M, Yokoyama K, Enjoji M (1983) Synovial sarcoma: a clinicopathologic and ultrastructural study of 42 cases. Acta Pathol Jpn 33:23–29
43. Weis S, Goldblum JR (2001) Enzinger and Weiss's soft tissue tumors. In: Malignant soft tissue tumors of uncertain type. Mosby, St. Louis, pp 1483–1509
44. Zeren H, Moran CA, Suster S, Fishback NF, Koss MN (1995) Primary pulmonary sarcomas with features of monophasic synovial sarcoma: a clinicopathologic, immunohistochemical and ultrastructural study of 25 cases. Human Pathol 26:474–480

Virchows Arch (2006) 449:373–375
DOI 10.1007/s00428-006-0248-8

CASE REPORT

Ectopic epididymal tissue in appendix testis

J. Fernando Val-Bernal · Daniel Val · M. Francisca Garijo

Received: 24 April 2006 / Accepted: 1 June 2006 / Published online: 26 July 2006
© Springer-Verlag 2006

Abstract Aberrant epididymal tissue is uncommon and may be associated with an undescended testis. To the best of our knowledge, aberrant epididymal tissue has not been described in a testicular appendix. We report the case of a 7-year-old boy with left cryptorchidism who underwent a homolateral orchidopexy. At operation, the surgeon removed a pedunculated appendix testis containing an epididymal heterotopia. This Wolffian-derivative tissue was confirmed by the diffuse strong CD10 reactivity of the luminal border of the epithelial cells. Awareness of this aberrant tissue avoids misinterpretation as a transected functional reproductive structure.

Keywords Appendix testis · Hydatid of Morgagni · Wolffian remnants · Müllerian remnants · Epididymis · Embryologic remnants · CD10 · Immunohistochemistry

Introduction

The appendix of the testis, or hydatid of Morgagni, is a small sessile or polypoid structure located at the antero-superior pole of the testis, adjacent to the head of the epididymis. The shape is variable, being either globular, pyriform, flat and leaf-like, forked, or lobed. Grossly, it is most often sessile and varies from 1 to 7 mm in greatest dimension in autopsies [6]. Histologically, it contains a loose connective tissue core, with fibroblasts and smooth muscle cells, a large number of blood vessels, a few dilated lymphatic vessels, and occasional lymphocytes. This structure is covered by a single layer of low columnar or cuboidal Müllerian-type epithelium in continuity, with the mesothelium of the tunica vaginalis at the base. Invaginations of the surface may result in appearance of glandular structures in the core.

The appendix testis is a Müllerian vestige, a remnant of the cranial portion of the Müllerian (paramesonephric) duct [3], and is the homolog of the fimbriated end of the Fallopian tube. This structure is present on about 80 to 92% of testes in adult autopsies [5, 6].

The body and tail of the epididymis is a mesonephric or Wolffian derivative. Epididymal tissue ectopias are uncommon and can be associated with undescended testis [2, 8]. To the best of our knowledge, aberrant epididymal tissue has not been reported in a testicular appendix. We wish to report a case of epididymal heterotopia in an appendix testis.

Clinical history

A 7-year-old boy with left cryptorchidism underwent a homolateral orchidopexy. At operation, the surgeon became aware of a large pedunculated appendix testis, which was removed.

Material and methods

The tissue excised was fixed in 10% neutral buffered formalin and routinely processed to obtain paraffin blocks. Histological sections were stained with hematoxylin and eosin. Additional 5-μm-thick sections were cut, deparaffinized, mounted on precoated slides, and stained with alpha-

J. F. Val-Bernal (✉) · D. Val · M. F. Garijo
Departamento de Anatomía Patológica,
Hospital Universitario Marqués de Valdecilla,
Universidad de Cantabria,
Avda. Valdecilla s/n,
ES-39008 Santander, Spain
e-mail: apavbj@humv.es

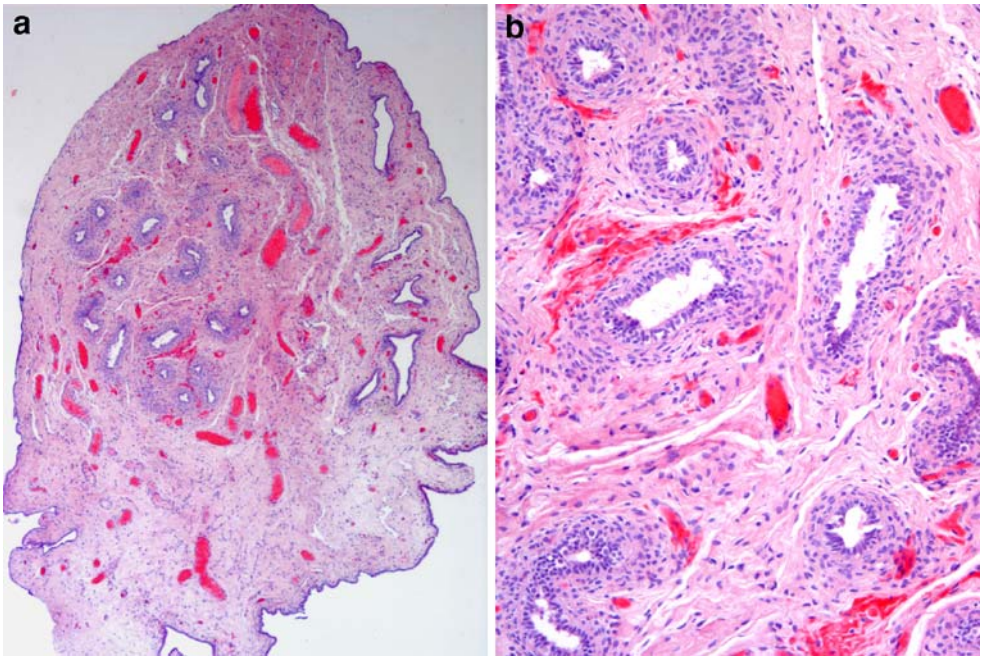

Fig. 1 Longitudinal section of appendix testis with an epididymal ectopia: **a** Aggregates of numerous lumina in a lobular pattern. **b** The surrounding well-defined smooth muscle cell coat is distinct from adjacent stroma

smooth muscle actin antibody (clone 1A4, dilution 1:500, Dako, Glostrup, Denmark) and CD10 antibody (clone 56C6, dilution 1:25, Novocastra Laboratories, Newcastle upon Tyne, UK, pretreated with EDTA). The slides were counterstained with Mayer's hematoxylin (Merck, Darmstadt, Germany) and dehydrated.

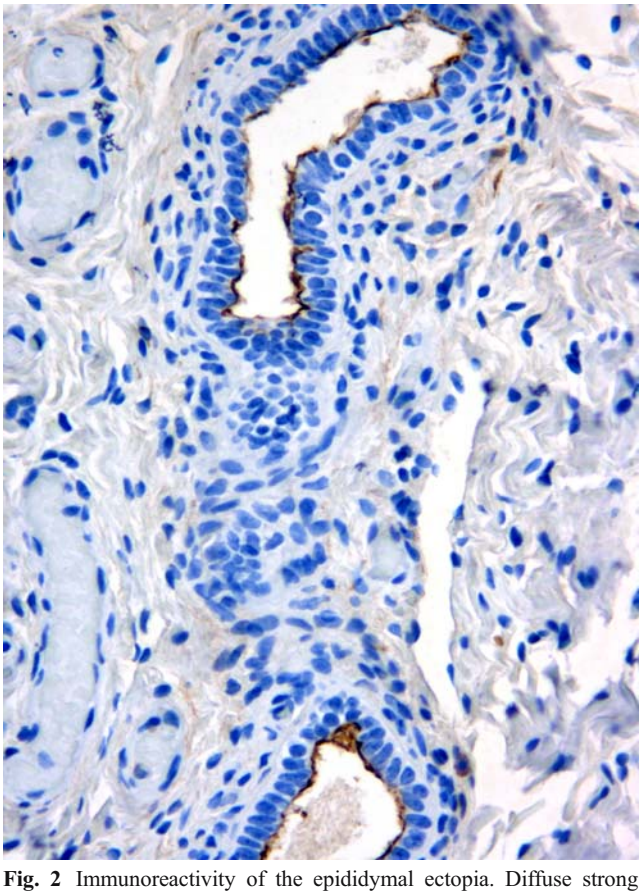

Fig. 2 Immunoreactivity of the epididymal ectopia. Diffuse strong CD10 immunostaining highlights the luminal border of the epithelial cells

Results

The appendix was an oval pedunculated structure measuring 4×3×2 mm. Histologically, it contained a fibrovascular core of loose connective tissue covered by a simple low-columnar epithelium with invaginations into the stroma. Within the core, a cluster of closely arranged tubules lined by columnar epithelium was detected. The outline of the lumina was smooth, with a few tubules showing a tendency toward a stellate configuration (Fig. 1a). These tubules were invested by a small amount of concentrically arranged smooth muscle cells (Fig. 1b). Alpha-smooth muscle actin staining was uniformly strong in the spindle cell coat surrounding the lumina of the ectopic tissue. CD10 positivity, showing a strong membranous staining pattern, was observed in all the tubules (Fig. 2). In contrast, the columnar epithelium covering the surface of the appendix was no reactive.

Discussion

There is a paucity of information describing aberrant epididymal tissue in surgical pathology textbooks, and many pathologists remain unaware of its existence. As far as we know, aberrant epididymal tissue in a testicular

appendix is, for the first time, described in this report. The interpretation of this heterotopia may raise concern in the surgical pathologist that a functional reproductive structure, epididymis, has been surgically interrupted. In a prepubertal male, resolution of this question may be difficult. However, the awareness of the existence of this type of heterotopia will help to solve this problem.

CD10, the common acute lymphoblastic leukaemia antigen, is a 100-kDa integral membrane glycoprotein expressed by lymphoid precursors, germinal center B cells, some myelocytes, renal cell carcinoma, endometrial stromal tumors and Wolffian-derived structures [4]. Reliable expression of CD10 in typical Wolffian-mesonephric derivatives in conjunction with its lack of expression in Müllerian-derived epithelium has been demonstrated by Cerilli et al. [1]. The current study substantiates the identification of an epididymal ectopia through the typical morphology of the aberrant tissue. The heterotopic epididymal tissue was confirmed by its CD10 reactivity, which is concordant with the reactivity of the normal epididymis. Thus, this lesion can securely be differentiated from what remains of the Müllerian duct presenting as single or multiple, tubular or irregular cavities, usually not opening on to the surface on about 40% of testicular appendices [7].

In conclusion, awareness of the presence of aberrant epididymal tissue in testicular appendix avoids misinterpretation as a transected functional reproductive structure.

References

1. Cerilli LA, Sotelo-Avila C, Mills SE (2003) Glandular inclusions in inguinal hernia sacs. Morphologic and immunohistochemical distinction from epididymis and vas deferens. Am J Surg Pathol 27:469–476
2. Gomez-Roman JJ, Mayorga M, Mira C, Buelta L, Fernandez F, Val-Bernal JF (1994) Glandular inclusions in inguinal hernia sacs: a clinicopathologic study of six cases. Pediatr Pathol 14:1043–1049
3. Jacob M, Barteczko K (2005) Contribution to the origin and development of the appendices of the testis and epididymis in humans. Anat Embryol 209:287–302
4. Ordi J, Nogales FF, Palacin A, Márquez M, Pahisa J, Vanrell JA, Cardesa A (2001) Mesonephric adenocarcinoma of the uterine corpus. CD10 expression as evidence of mesonephric differentiation. Am J Surg Pathol 25:1540–1545
5. Rolnick D, Kawanoue S, Szanto P, Bush IM (1968) Anatomic incidence of testicular appendages. J Urol 100:755–756
6. Sahni D, Jit I, Joshi K, Sanjeev (1996) Incidence and structure of the appendices of the testis and epididymis. J Anat 189:342–348
7. Willis RA (ed) (1962) The borderland of embryology and pathology, 2nd edn. Butterworths, London
8. Wollin M, Marshall FF, Fink MP, Malhotra R, Diamond DA (1987) Aberrant epididymal tissue: a significant clinical entity. J Urol 138:1247–1250

Virchows Arch (2006) 449:376–381
DOI 10.1007/s00428-006-0251-0

CASE REPORT

Tumor of the liver (hepatocellular and high grade neuroendocrine carcinoma): a case report and review of the literature

Monica T. Garcia · Pablo A. Bejarano · Maria Yssa · Efren Buitrago · Alan Livingstone

Received: 1 April 2006 / Accepted: 7 June 2006 / Published online: 1 August 2006
© Springer-Verlag 2006

Abstract We describe a rare hepatic collision tumor composed of a hepatocellular carcinoma and a high-grade neuroendocrine carcinoma. The patient, a 50-year-old man, underwent a partial hepatectomy because of a 5.0-cm mass. The tumor had two distinctive patterns. The majority of the tumor was a high-grade neuroendocrine carcinoma with features of a small cell carcinoma that was positive for chromogranin, synaptophysin, and cytokeratin 19 and negative for hepatocellular antigen and alpha-fetoprotein (AFP). The second component was a moderately differentiated hepatocellular carcinoma that was positive for hepatocellular antigen and AFP and negative for neuroendocrine markers. The two tumors were separated by fibrous bands. In areas where they collided, there was no transition or intermingling of cells between the two components, thus, it is different from the combined type of tumors. After removal of the tumor, the patient had intrahepatic and mesenteric recurrences within a follow-up period of 16 months.

Keywords Collision tumor · Combined tumor · Liver neoplasms

M. T. Garcia (✉) · P. A. Bejarano · M. Yssa
Department of Pathology, University of Miami,
Miller School of Medicine–Jackson Memorial Hospital,
1611 NW 12th Avenue, Holtz Building, Room 2042 G,
Miami, FL 33136, USA
e-mail: mgarcia22@med.miami.edu

E. Buitrago · A. Livingstone
Department of Surgery, University of Miami,
Miller School of Medicine,
Miami, FL, USA

Introduction

A collision tumor is an unusual neoplasm that is defined as having two histologically distinct tumors simultaneously involving the same organ with no transition between them. They are different from combined tumors, which are not only contiguous, but also intermingle with each other. In the liver, both types are rare, but the combined type is more frequent. It represents 2.0 to 3.6% of all primary hepatic malignancies [2, 5]. It is postulated that these combined tumors arise from stem cells that evolve into divergent differentiation [3, 13]. The most frequent combined tumor consists of hepatocellular and cholangiocarcinoma (hepatocholangiocarcinoma). Hepatic collision tumors are even rarer with an incidence of 0.1 to 1% [2, 3]. Most of the collision tumors also show a hepatocellular carcinoma accompanied by a cholangiocarcinoma. Single case reports of primary collision tumors include hepatocellular carcinoma with sarcoma [7] and the rare occurrence of hepatocellular carcinoma with neuroendocrine tumor [4], such as the one described in this article.

Clinical history

The patient is a 50-year-old Hispanic man who has a medical history of hepatitis C treated with interferon monotherapy, which was terminated in 1994. Since then, his hepatitis C virus–RNA was not detectable (less than 5 IU/ml). Periodic hepatic ultrasound follow up showed a mass on the left lobe of the liver 3 months before surgery. A CT scan of the abdomen revealed a 5.0-cm mass located in the hepatic segment IV-B (Fig. 1). The serum level of alpha-fetoprotein (AFP) at this time was 1,191 ng/ml. The patient had mild hypoalbuminemia (3.4 g/dl); normal liver

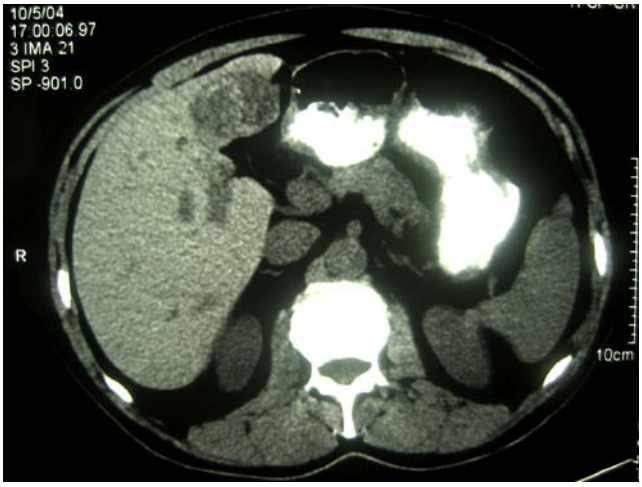

Fig. 1 CT scan of liver showing a 5.0-cm mass in the left lobe with areas of necrosis. Both components cannot be distinguished

enzymes, including 30 U/l aspartate aminotransferase, 45 U/l alanine aminotransferase, and 65 U/l alkaline phosphatase; and total bilirubin of 0.4 mg/dl. CA19-9 and CA125 were normal. CT of chest and extrahepatic abdomen showed no abnormalities. At our institution, a liver core biopsy was performed, which showed an extensively necrotic, epithelial malignant neoplasm (Fig. 2). An intraoperative ultrasound showed that the mass was located in segment IV-B extending to segment V for which an extended left hepatectomy was performed. Intraoperatively, the abdominal cavity, including omentum, peritoneum, intestines, stomach, and pancreas, were free of lesions. The specimen showed both a hepatocellular carcinoma and a neuroendocrine carcinoma. Because of the latter component, an OctreoScan was performed in the 14th day after surgery. There was no evidence of abnormal activity that could have suggested somatostatin receptor positive tumor. A follow-up serum level of AFP was 8.1 ng/ml on the first month after the operation. Four months after surgery, a CT

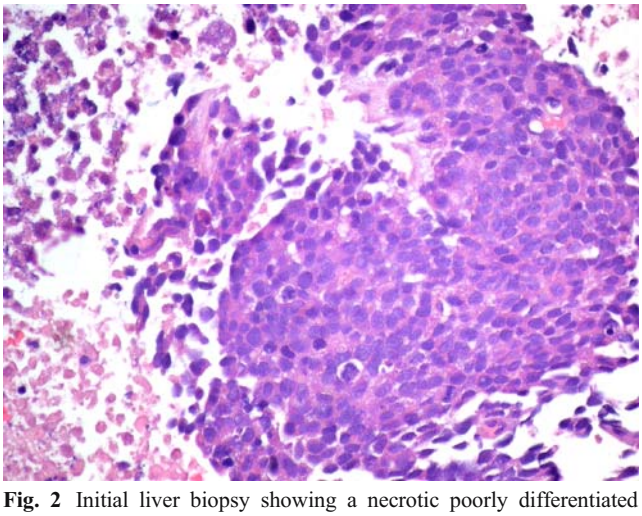

Fig. 2 Initial liver biopsy showing a necrotic poorly differentiated carcinoma (hematoxylin and eosin, ×200)

scan of the abdomen showed 2.5-cm and 1.1-cm nodules in the posterior and anterior segments of the right liver, respectively. Two weeks later, a repeat CT scan of the abdomen with contrast demonstrated a 4.5-cm mass involving segments VII and VIII and a 2.0-cm mass in segment V. The patient was treated with chemoinfusion with 75 mg/m^2 of cisplatin and the right hepatic branch was embolized with Gelfoam. The post chemoembolization arteriogram showed no blood flow to the mass involving segments VII and VIII and less flow to the mass located in segment V. However, there were persistent liver lesions in mid to lower liver lobe. At the time of this procedure, the serum level of AFP was 570 ng/ml and decreased to 213 ng/ml 1 month after. Subsequently, the patient was placed on chemotherapy with doxorubicin. A follow-up CT scan showed an increased size in the liver masses, peripancreatic adenopathy, and multiple nodular densities in the anterior mesenteric area consistent with omental caking. Then, thalidomide and bevacizumab (Avastin®) were added. At last visit on May 2006, the chemotherapy treatment of the patient was still continued and he showed evidence of active disease in the liver and mesenteric areas, which have slightly decreased in size and showed possible necrosis on the last CT. No biopsy was performed to determine the histopathology of the recidivant tumors.

Materials and methods

The liver specimen was fixed with 10% buffered formalin, embedded in paraffin, cut in 4-μm-thick sections, and stained with hematoxylin and eosin using the standard methods. Immunohistochemistry was performed on selected deparaffinized tissue sections using the avidin-biotin-peroxidase method in a Dako AutoStainer (Carpinteria, CA, USA). After antigen retrieval, the following panel of primary antibodies was used: Hep Par1 (hepatocellular antigen, Dako 1:50), AFP (Dako 1:1,500), synaptophysin (Dako 1:10), chromogranin (Dako 1:50), cytokeratin (CK) cocktail (AEI-3: Dako 1:200; HMW: Dako 1:500; and CAM5.2: Becton Dickinson 1:1,500), CK7 (Dako 1:1,500), CK19 (Dako 1:50), CK20 (Dako 1:25), neuron-specific enolase (NSE) (Dako 1:5,000), CD56 (Vision BioSystem 1:50), thyroid transcription factor (TTF)-1 (Dako 1:150), MIB-1 (Dako 1:100), insulin (Dako 1:50), glucagon (Dako 1:2,500), and vasoactive intestinal peptide (VIP) (Chemicon 1:300).

Tissue from paraffin blocks was recovered for electron microscopy, deparaffinized, postfixed in 2% buffered glutaraldehyde, and embedded in Epon epoxy resin. The ultrathin sections were stained with uranyl acetate and lead citrate and examined with a JEOL CX-100 transmission electron microscope.

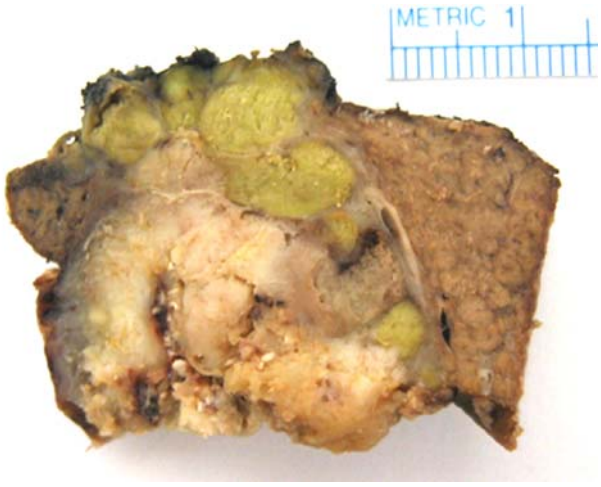

Fig. 3 Cut surface of collision tumor showing the two components. The *green nodular* area represents the hepatocellular component and the *white tan* area corresponds to the neuroendocrine component

Results

Gross findings

The resected specimen consisted of a 220-g 17.5×9.5×7.1-cm portion of a noncirrhotic liver with attached gallbladder. Sections revealed a well circumscribed and demarcated, but nonencapsulated 5.3×4.5×4.0-cm mass that was composed of two sharply defined and distinctive areas (Fig. 3). The first occupied about 70% of the tumor and was tan-white and friable. The second distinct area was green, nodular, and extended into the resection margin. The initial resection margin of the liver showed malignancy on frozen section. Therefore, an additional 3.1-cm resection was performed in which a negative margin was obtained. No satellite lesions were identified. The gallbladder was unremarkable. No lymph nodes were identified.

Histological findings and immunohistochemistry

The initial biopsy showed an extensively necrotic poorly differentiated carcinoma. The neoplastic cells were positive for cytokeratin cocktail and negative for CK7, CK20, TTF1, and Hep Par1. The surgical specimen revealed a hepatic mass that had two distinct morphologies with different immunophenotypic profiles (Figs. 4 and 5). The green and nodular component showed large cells with abnormal nucleoli and abundant eosinophilic cytoplasm. These cells were arranged in cords and plates of various thicknesses separated by sinusoids lined by flat endothelial cells. This component corresponded to a moderately differentiated hepatocellular carcinoma, which was confirmed by immunohistochemical staining, as it was positive for Hep Par1 and AFP. It was negative for synaptophysin, chromogranin, CD56, NSE, CK7, CK19, CK20, and TTF1. The second component corresponding to the tan-white and friable mass contained smaller cells with a lesser amount of cytoplasm and the nuclei had dispersed chromatin. The tumor cells grew in a solid pattern interrupted with pseudoacinar areas and rosette formation. It showed

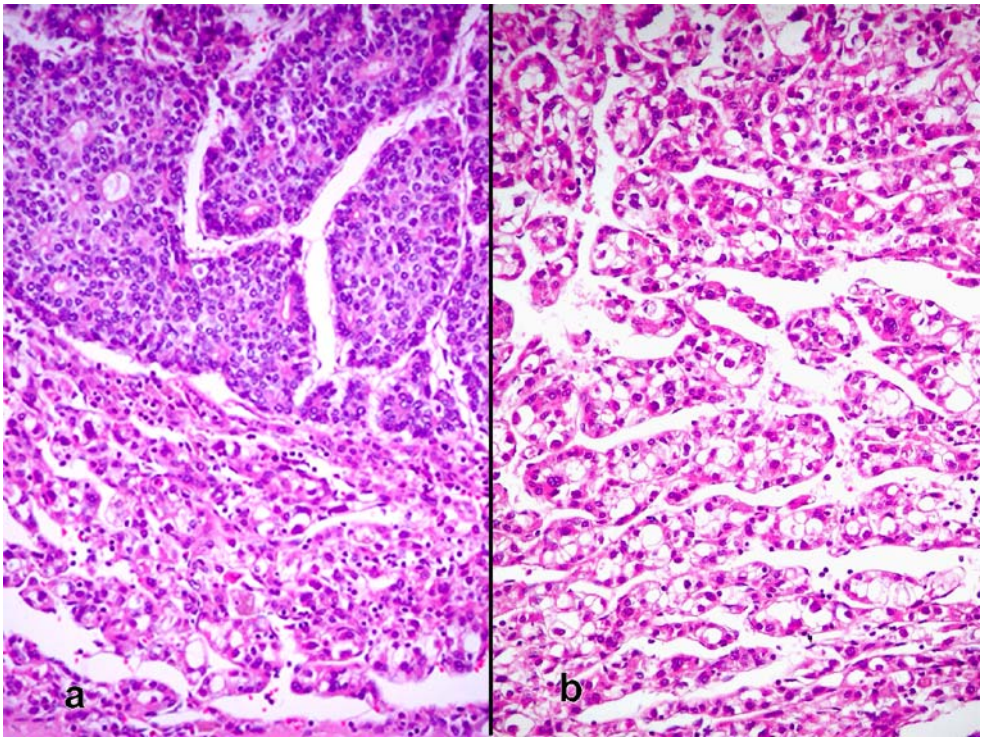

Fig. 4 **a** Sharp demarcation of the both components of moderately differentiated hepatocellular carcinoma and the neuroendocrine carcinoma with the latter showing rosettes (hematoxylin and eosin, ×100). **b** Hepatocellular carcinoma (hematoxylin and eosin, ×200)

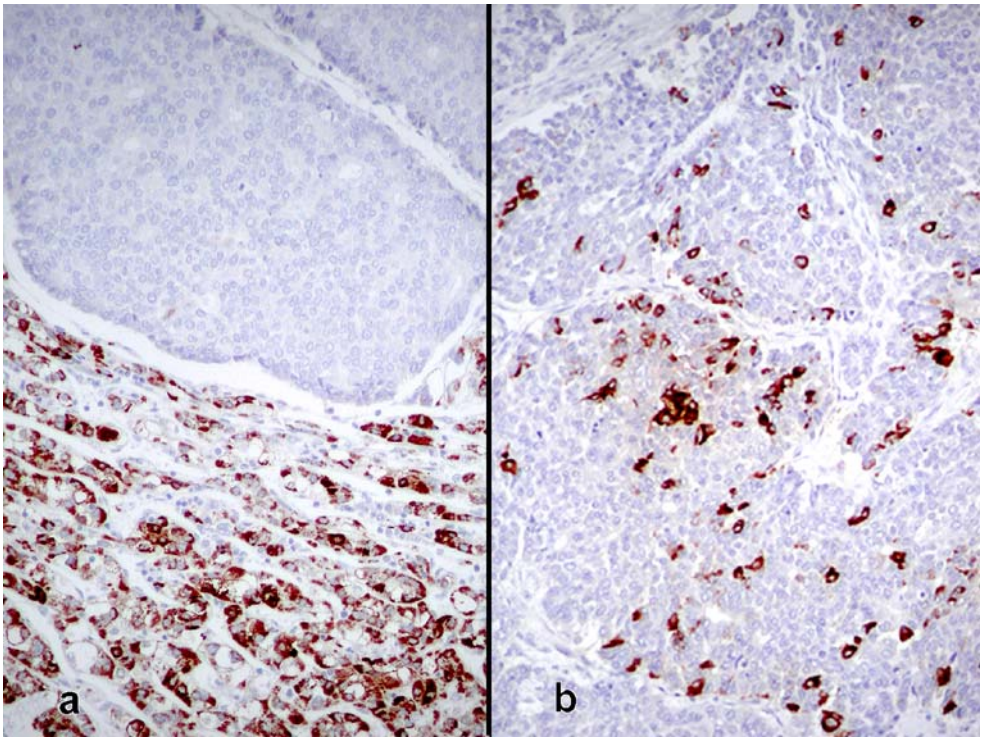

Fig. 5 **a** Borderline area between both tumors showing immunoreactivity for Hep Par1 in the hepatocellular carcinoma, whereas it is negative in the neuroendocrine tumor (immunoperoxidase, ×100). **b** Neuroendocrine carcinoma showing immunoreactivity for chromogranin (immunoperoxidase, ×100)

extensive necrosis and Azzopardi phenomena. This tumor corresponded to a high-grade neuroendocrine carcinoma with features of a small cell carcinoma. It was positive for chromogranin, synaptophysin, NSE, CD56, and VIP; strongly positive for CK19; and negative for Hep Par1, CK7, AFP, CK20, TTF1, insulin, and glucagon. MIB-1 immunostain demonstrated different proliferative activity in both components. The neuroendocrine component showed high proliferative activity (70–80% of the cells were positive) while the hepatocellular component had lower proliferative activity (10–20% of the cells were positive). The tumors were separated from each other by broad fibrous bands. No transition areas were present. Even in the areas of closest proximity the tumors were sharply demarcated and were compressing, rather than infiltrating. The American Joint Committee Classification pathologic staging was determined to be T3NxMx. The nonneoplastic liver showed mild chronic hepatitis and portal fibrosis.

Ultrastructural findings

The cells of hepatocellular carcinoma exhibited giant lysosomes, myelin figures, megamitochondria, and abnormal accumulations of glycogen and different degenerative products. In the neuroendocrine tumor there were cytoplasmic neurosecretory granules that ranged in diameter from 360 to 410 nm and were not present in the hepatocellular carcinoma (Fig. 6).

Discussion

True primary hepatic collision tumors are unusual, but the presence of hepatocellular carcinoma growing synchronously with a neuroendocrine tumor in a patient with no existing extrahepatic tumor is even rarer. We report one such case where the hepatocellular carcinoma grew independently from an adjacent high-grade neuroendocrine carcinoma in a noncirrhotic liver. Although hepatocellular carcinoma is essentially considered a complication of liver

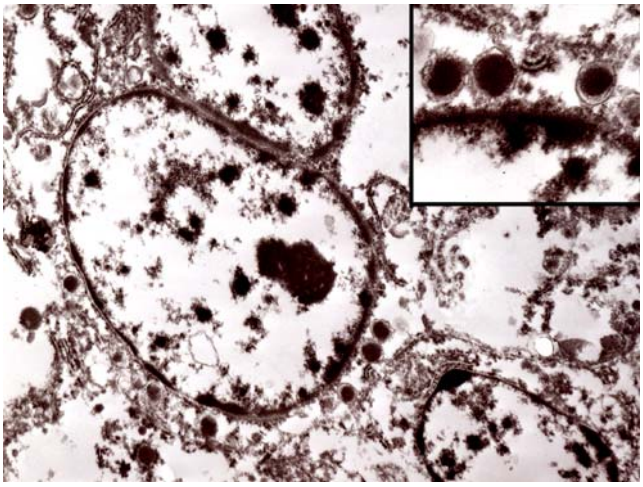

Fig. 6 Ultrastructural findings of the neuroendocrine tumor cells showing dense-core granules that measured up to 410 nm (*inset*; original magnification, ×18,000)

cirrhosis, studies showed that about 20–40% of these tumors develop in noncirrhotic livers [6, 8]. There are a few reports of primary neuroendocrine tumors in the liver combined with hepatocellular carcinoma, but these represented differentiation of the malignant liver cells into a neuroendocrine tumor [1, 15]. The only case that appears to fulfill the criteria for collision tumor is the study reported by Ishida et al. [4]. Their patient was a 72-year-old man with a 3-cm high-grade neuroendocrine carcinoma in segment 8 and a 1.5-cm moderately differentiated hepatocellular carcinoma in segment 5. The liver was cirrhotic and lymph nodes showed metastatic neuroendocrine carcinoma. However, the authors favored the view that the neuroendocrine tumor did not arise de novo and speculated that it was a hepatocellular carcinoma that underwent neuroendocrine differentiation despite the fact that it lacked morphologic, immunohistochemical, and ultrastructural features of hepatocellular carcinoma.

In our case, the two tumors were independent of each other, as evidenced by their gross and microscopic features. Grossly, the tumors were separated by fibrous bands and had distinctly different color qualities. The larger tan-white and friable tumor corresponded with the morphologic features of neuroendocrine carcinoma and comprised about 70% of the mass. The green and more nodular hepatocellular carcinoma was well defined and sharply demarcated from the first tumor by fibrous bands.

Microscopically, both tumors were distinctive morphologically, immunophenotypically, and ultrastructurally. They were separated by fibrous bands and they were in direct contact with each other only focally. Even in the areas of contact, the cellular components were markedly different and did not intermingle. In these areas of juxtaposition the tumors appeared to be pushing rather than infiltrating each other. Also, electron microscopy showed no neuroendocrine features in the hepatocellular carcinoma component. Immunohistochemical stains highlighted the differences between both tumors with one showing an immunophenotype of hepatocellular carcinoma while the other featured neuroendocrine markers. The rosette formation in the neuroendocrine tumor suggests that it could have been initially low or intermediate grade neoplasm that later acquired a more aggressive morphology in the form of a small cell carcinoma. These features distinguish collision tumor from the combined type reported Barsky et al. [1] and Yamaguchi et al. [15] where two tumors showed intermingled cells in the transition zone that could not be morphologically separated. In addition, some of the cells in the previously reported tumors had morphologic features of hepatocellular carcinoma on paraffin sections stained by hematoxylin and eosin sections but displayed neurosecretory granules by electron microscopy. These features support the view that although morphologically different, the tumors may have originated from a liver cell that eventually acquired neuroendocrine features.

Apart from the collision and combined types, neuroendocrine tumors can also occur in an isolated fashion primarily in the liver in the form of carcinoids or high-grade tumors represented by small cell carcinomas [9, 12]. However, the issue regarding the origin of primary neuroendocrine tumors of the liver is not well elucidated yet. Hepatic progenitor cells found in the epithelial lining of intrahepatic bile ducts could potentially serve as the origin of neuroendocrine tumors [10, 11]. This hypothesis is supported by the presence of carcinoids and small cell carcinomas in noncirrhotic livers. In our case, the strong positivity for CK19 in the neuroendocrine component supports the theory that these cells originated from hepatic stem cells. A second hypothesis postulates that a stem cell with pluripotential capability is the precursor for liver cell carcinoma, neuroendocrine malignancies, and other tumors with polyphenotypic expression. This is supported by descriptions of hepatocellular carcinomas with neuroendocrine features [14]. Zhao et al. [16] found neuroendocrine differentiation in 60% of their hepatocellular carcinomas. This high rate is incongruent with the rarity of primary neuroendocrine tumor in the liver.

The prognosis and treatment of hepatic neuroendocrine carcinoma and hepatocellular carcinoma collision tumor are uncertain due to the small number of cases studied. Likewise, it is not known which of the two components carries a negative influence in patients' survival. Clinically, our case had an aggressive clinical behavior during a 16-month follow-up period. The other patients with solitary high-grade neuroendocrine tumors described died within a few months after diagnosis [4]. More cases of collision and combined tumors of this type need to be documented to obtain a better insight on their pathogenesis, behavior, and treatment.

References

1. Barsky SH, Linnoila I, Triche, TJ, Costa J (1984) Hepatocellular carcinoma with carcinoid features. Hum Pathol 15(9):892–894
2. Goodman ZD, Ishak KG, Langloss JM, Sesterhenn IA, Rabin L (1985) Combined hepatocellular-cholangiocarcinoma. A histologic and immunohistochemical study. Cancer 55(1):124–135
3. Haratake J, Hashimoto H (1995) An immunohistochemical analysis of 13 cases with combined hepatocellular and cholangiocellularcarcinoma. Liver 15(1):9–15
4. Ishida M, Seki K, Tatsuzawa A, Katayama K, Hirose K, Azuma T, Imamura Y, Abraham A, Yamaguchi A (2003) Primary hepatic neuroendocrine carcinoma coexisting with hepatocellular carcinoma in hepatitis C liver cirrhosis: report of a case. Surg Today 33 (3):214–218
5. Jarnagin WR, Weber S, Tickoo SK, Koea JB, Obiekwe S, Fong Y, DeMatteo RP, Blumgart LH, Klimstra D (2002) Combined

hepatocellular and cholangiocarcinoma: demographic, clinical, and prognostic factors. Cancer 94(7):2040–2046
6. Monto A, Wright TL (2001) The epidemiology and prevention of hepatocellular carcinoma. Semin Oncol 28(5):441–449
7. Morimoto H, Takada Y, Akita T, Kato Y, Tanigawa N, Muraoka R, Urata Y (1986) A resected case of collision tumor of hepatocellular carcinoma and primary liver rhabdomyosarcoma. J Jpn Surg Soc 87(4):456–463
8. Nzeako UC, Goodman ZD, Ishak KG (1996) Hepatocellular carcinoma in cirrhotic and noncirrhotic livers. A clinico-histopathologic study of 804 North American patients. Am J Clin Pathol 105(1):65–75
9. Pilichowska M, Kimura N, Ouchi A, Lin H, Mizuno Y, Nagura H (1999) Primary hepatic carcinoid and neuroendocrine carcinoma: clinicopathological and immunohistochemical study of five cases. Pathol Int 49(4):318–324
10. Roskams T, Van den Oord JJ, De Vos R, Desmet VJ (1990) Neuroendocrine features of reactive bile ductules in cholestatic liver disease. Am J Clin Pathol 137(5):1019–1025
11. Roskams T, Cassiman D, De Vos R, Libbrecht L (2004) Neuroregulation of the neuroendocrine compartment of the liver. Anat Rec A Discov Mol Cel Evol Biol 280(1):910–923
12. Rückert RI, Rückert JC, Dörffel Y, Rudolph B, Müller JM (1999) Primary hepatic neuroendocrine tumor: successful hepatectomy in two cases and review of the literature. Digestion 60(2):110–116
13. Theise ND, Yao JL, Harada K, Hytiroglou P, Portmann B, Thung SN, Tsui W, Ohta H, Nakanuma Y (2003) Hepatic "stem cell" malignancies in adults: four cases. Histopathology 43(3):263–271
14. Wang J, Dhillon AP, Sankey EA, Wightman AK, Lewin JF, Scheuer PJ (1991) "Neuroendocrine" differentiation in primary neoplasms of the liver. J Pathol 163(1):61–67
15. Yamaguchi R, Nakashima O, Ogata T, Hanada K, Kumabe T, Kojiro M (2004) Hepatocellular carcinoma with an unusual neuroendocrine component. Pathol Int 54(11):861–865
16. Zhao M, Laissue JA, Zimmermann A (1993) "Neuroendocrine" differentiation in hepatocellular carcinomas (HCCs): immunohistochemical reactivity is related to distinct tumor cell types, but not to tumor grade. Histol Histopathol 8(4):617–626

Virchows Arch (2006) 449:382–384
DOI 10.1007/s00428-006-0252-z

CASE REPORT

Primary intracranial leiomyoma: a case report and literature review

Abdullah E. Ali · Mahmood Fazl · Juan M. Bilbao

Received: 19 April 2006 / Accepted: 26 May 2006 / Published online: 8 August 2006
© Springer-Verlag 2006

Abstract We report a case of primary intracranial leiomyoma in 29-year-old woman presented with severe headache. The radiology diagnosis was consistent with meningioma. However, histologically, the tumor had the characteristic appearance of benign smooth muscle. This was confirmed by immunohistochemistry and electron microscopy. Benign metastasizing leiomyoma was excluded by thorough imaging. Although rare, leiomyoma should be considered in the differential diagnosis of well-circumscribed intracranial lesion.

Keywords Intracranial · Benign · Leiomyoma

Abbreviations

AIDS	Acquired immunodeficiency syndrome
CNS	Central nervous system
CT	Computerized tomography
EBV	Epstein Barr virus
MRI	Magnetic resonance imaging

Introduction

The majority of intracranial extraaxial neoplasms are meningiomas. Primary intracranial mesenchymal neoplasms are extremely rare but when they occur, they should be classified similarly to their systemic counterparts. Leiomyomas are benign smooth muscle tumors common to the uterus. Outside the uterus, leiomyomas have been reported in almost every organ in the body [9]. In the central nervous system, they can radiologically mimic meningiomas [7].

A. E. Ali · J. M. Bilbao (✉)
Department of Pathology, Sunnybrook Health Science Centre,
2075 Bayview Avenue, Room E-419,
Toronto, ON M4N 3M5, Canada
e-mail: Juan.Bilbao@sunnybrook.ca

M. Fazl
Department of Neurosurgery, Sunnybrook Health Science Centre,
Toronto, ON M4N 3M5, Canada

Clinical history

A 29-year-old woman, previously healthy, presented complaining of episodic clusters of severe hemicranial headaches for few years. The headache lasted for 10 min and occurred 10–20 times per day. She had no visual symptoms. On examination, there were no focal findings. Magnetic resonance image (MRI) of the brain showed a 1.2-cm extraaxial lesion in the right frontal fossa floor, medial to the sphenoid wing (Fig. 1). Although the lesion was small, surgical resection was done because of the close proximity to the optic nerve. The patient underwent frontal craniotomy. The tumor was attached to the dura. It was carefully resected and sent to the anatomical pathology for processing.

Materials and methods

The specimen was fixed in 10% formalin, embedded in paraffin wax, and cut at 5–8 μm. Immunohistochemical staining was performed using the avidin–biotin peroxidase method. The antibodies used in this study were directed against: smooth muscle actin (1/500, monoclonal, Biogenex), muscle-specific actin (1/25, monoclonal, Enzo), desmin (1/100, monoclonal, Biogenex), caldesmon (1/200, monoclonal, Dako), collagen IV (1/50, monoclonal, Dako),

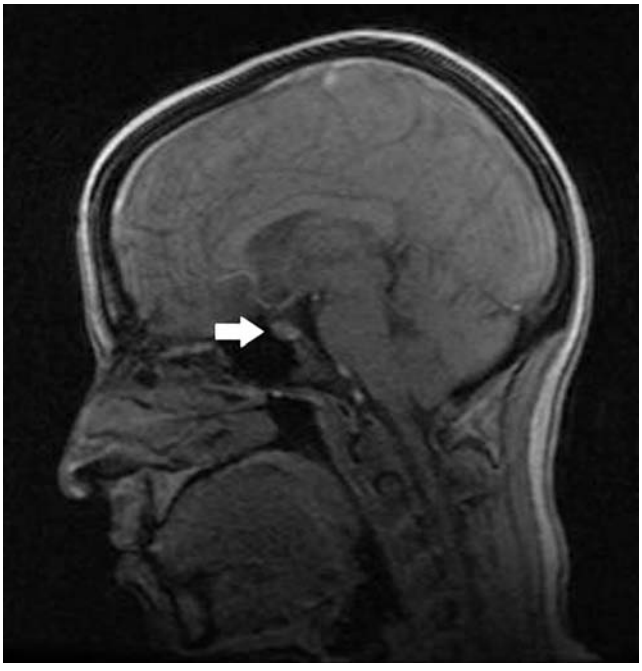

Fig. 1 MRI scan of the brain showing an extraaxial lesion at the base of the frontal fossa floor

pancytokeratin (AE1/AE3, 1/300, monoclonal, Dako), epithelial membrane antigen (1/1,200, monoclonal, Dako), S100 protein (1/1,500, polyclonal, Dako), CD117 (1/400, polyclonal, Dako), estrogen receptor (1/100, monoclonal, Novocastra), progesterone receptors (1/100, monoclonal, Novocastra), CD34 (1/50, monoclonal, Dako), CD30 (1/200, monoclonal, Dako), and Epstein Barr virus (EBV) (1/100, monoclonal, Dako). The tissue for electron microscopy was obtained from the paraffin-embedded material, routinely processed, stained with uranyl acetate, and examined in a ZEISS EM 109 electron microscopy.

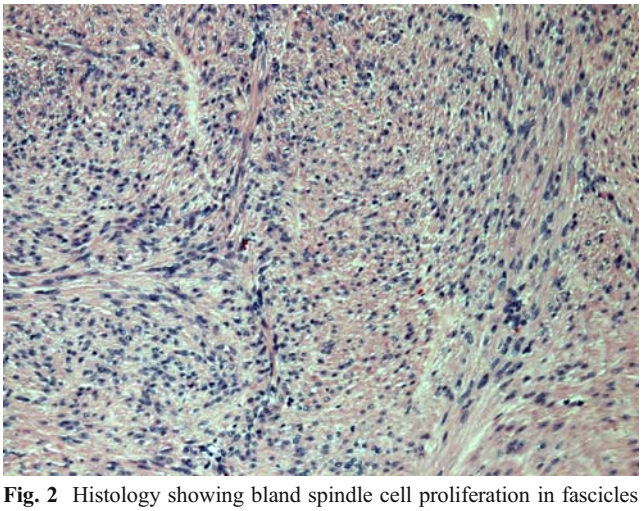

Fig. 2 Histology showing bland spindle cell proliferation in fascicles with abundant eosinophilic cytoplasm. No atypia, increased mitosis, or necrosis is seen (H&E, ×20)

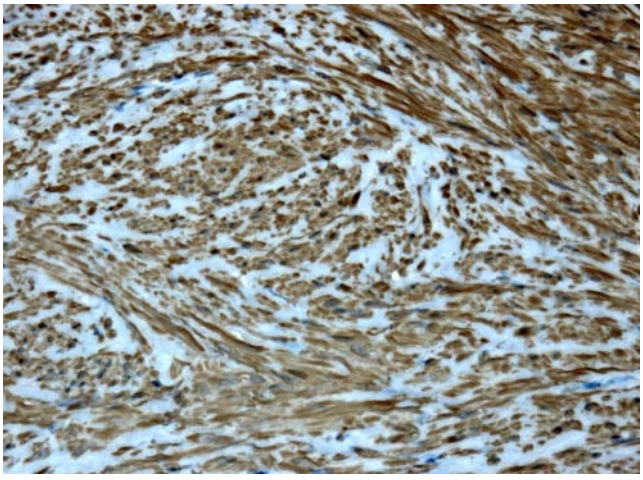

Fig. 3 Immunohistochemistry showing positive caldesmon staining for smooth muscle cells (×20)

Results

The tumor was well circumscribed. Microscopically, the tumor consisted of a bland spindle cell neoplasm composed of intersecting fascicles of cells with abundant eosinophilic cytoplasm, elongated cigar-shaped nuclei without prominent nucleoli (Fig. 2). Mitotic activity was very low, and there was no necrosis. The tumor was immunoreactive to smooth muscle actin, muscle-specific actin, desmin, caldesmon (Fig. 3), and collagen IV, and negative for keratin, epithelial membrane antigen, S100 protein, CD117, estrogen and progesterone receptors, CD34, and CD30. The Ki-67 stained <1% of tumor cells. Immunohistochemical stain for EBV was nonreactive. Electron microscopy showed tumor cells to possess abundant mitochondria and pinocytotic vesicles. The cytoplasm was filled with intermediate filaments (Fig. 4). The findings are charac-

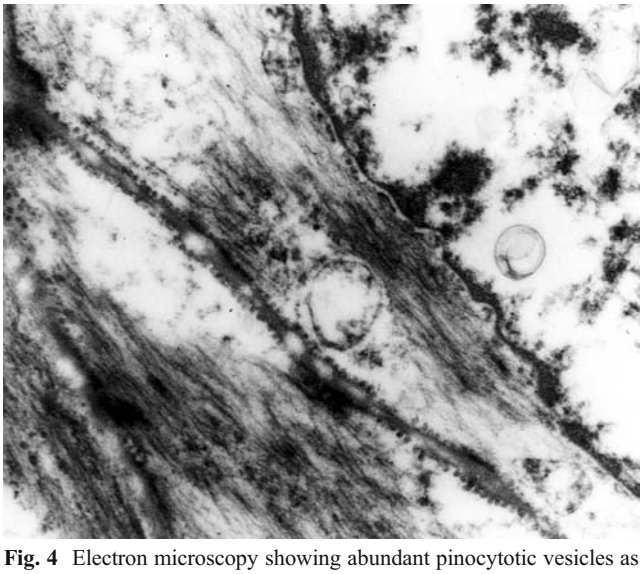

Fig. 4 Electron microscopy showing abundant pinocytotic vesicles as well as cytoplasmic intermediate filaments (×12,000)

Table 1 Reported cases of primary intracranial leiomyoma

	Author	Age	Sex	Site	Size (cm)	Presentation	EBV status	HIV status
1	Kroe et al. [6]	68	F	Intrasellar	2.5–3.0	Visual defect	NA	NA
2	Thierauf and Weiland [10]	Child	F	Suprasellar	4–5	Visual defect	NA	NA
3	Lin et al. [8]	20	F	Left superior temporal and insular gyri	3×2×1	Limb numbness and pain	NA	NA
4	Bette et al. [2]	56	F	Intra- and suprasellar	3.2	Visual defect	NA	NA
5	Bette et al. [2]	34	F	Cavernous sinus	1.2×0.8	Right-sided sixth nerve palsy	Positive	Positive
6	Kim et al. [5]	40	F	Temporoparietal convexity	7×4.5×4	Headache	NA	NA
7	Present case	29	F	Right frontal lobe floor	1.2	Headache	Negative	NA

NA Not available

teristic of smooth muscle differentiation, and a diagnosis of leiomyoma was made. The differential diagnosis of benign metastasizing leiomyoma was entertained but the patient had negative thoracic and abdominal computerized tomography scan as well as gynecological sonography. The final diagnosis was primary central nervous system (CNS) leiomyoma.

Discussion

Primary intracranial mesenchymal tumors are uncommon. Primary CNS smooth muscle tumor is exceedingly rare. Rhabdomyosarcoma accounts for most primary myogenic neoplasms of the CNS reported to date [9]. There is a high incidence of primary CNS smooth muscle neoplasms in immunocompromised individuals. An association with EBV had been demonstrated [1, 9]. The first case of primary intracranial leiomyoma was reported by Kroe et al. in 1968 [6]. The majority of the reported cases were in the sellar region [8]. It has been mistaken as meningioma radiologically [7]. The differential diagnosis of an extra-axial intracranial lesion would include meningioma, schwannoma, hemangiopericytoma, and solitary fibrous tumor. The histology, immunohistochemical profile, and the electron microscopical findings confirmed the smooth muscle origin of this tumor. Another rare differential diagnosis that should not be forgotten, giving the female gender of the patient, is benign metastasizing leiomyoma [3]. This was excluded by thorough imaging.

Several hypotheses were suggested for the origin of this tumor in the CNS. It is presumed that smooth muscle tumors in the CNS may arise from embryonic rests, pluripotential mesenchymal cells, perivascular connective tissue, leptomeninges, or smooth muscle cells of the blood vessels [6, 10]. A separate study suggested the latter origin because of the finding of actin inclusions in the proliferating smooth muscle cells of the adjacent blood vessels similar to those found in the tumor cells [8].

Leiomyomas were recently added to the list of neoplasms showing increasing incidence in acquired immunodeficiency syndrome (AIDS) especially in children [1, 4]. There is an association between EBV infection and the development of leiomyoma in those individuals. One report documents a benign leiomyoma but with EBV positivity in a young female with AIDS. Her tumor behaved aggressively, and she died of extensive intracranial disease [2].

To our knowledge this is the seventh case of primary intracranial leiomyoma [2, 5, 6, 8, 10]. Table 1 summarizes the clinicopathological data of the reported cases of primary intracranial leiomyoma. Although rare, leiomyoma should be considered in the differential diagnosis of a well-circumscribed intracranial extraaxial lesion especially at the sellar or suprasellar regions.

References

1. Bargiela A, Rey JL, Diaz JL (1999) Meningeal leiomyoma in an adult with AIDS: CT and MRI with pathological correlation. Neuroradiology 41(9):696–698
2. Bette K, Kleinschmidt-DeMasters BK, Mierau GW (1998) Unusual dural and skull-based mesenchymal neoplasms: a report of four cases. Hum Pathol 29(3):240–245
3. Goyle KK, Moore DF Jr, Garrett C (2003) Benign metastasizing leiomyomatosis: case report and review. Am J Clin Oncol 26 (5):473–476
4. Karpinski NC, Yaghmai R, Barba D (1999) Case of the month: March 1999—a 26 year old HIV positive male with dura based masses. Brain Pathol 9(3):609–610
5. Kim SH, Youm JY, Song SH, Kim Y, Song KS (1999) Primary intracranial leiomyoma. Case illustration. J Neurosurg 90(1):171
6. Kroe DJ, Hudgins WR, Simmons JC (1968) Primary intrasellar leiomyoma. J Neurosurg 29(2):189–191
7. Lai PH, Yang CF, Huang CH (1998) Primary intracranial leiomyoma. Neuroradiology 40(4):238–241
8. Lin SL, Wang JS, Huang CS (1996) Primary intracerebral leiomyoma: a case with eosinophilic inclusions of actin filaments. Histopathology 28(4):365–399
9. Rosai J (2004) Rosai and Ackerman's surgical pathology, 9th edn. Mosby, St. Louis, MO
10. Thierauf P, Weiland H (1978) Intracranial leiomyoma. Med Welt 29(33):1212–1280

Virchows Arch (2006) 449:385–388
DOI 10.1007/s00428-006-0243-0

LETTER TO THE EDITOR

A malignant mucinous cystic neoplasm arising within a mycrocystic adenoma of the pancreas

Dimas Suarez-Vilela · Francisco Miguel Izquierdo-Garcia · Francisco Iglesias-Dominguez

Received: 16 March 2006 / Accepted: 30 May 2006 / Published online: 1 August 2006
© Springer-Verlag 2006

Sir:

Cystic tumors of the pancreas are a heterogeneous group of neoplasms that includes epithelial tumors (benign, borderline, and malignant) and mesenchymal tumors (benign and malignant). These cystic neoplasms should be differentiated from cystic nontumoral lesions such as pancreatitis-associated pseudocysts, lymphoepithelial cysts, and other cystic lesions [6]. The most important and largest group is that of the epithelial neoplasms, which includes the most common cystic neoplasms: serous cystic neoplasms (SCNs), mucinous cystic neoplasms (MCNs), intraductal papillary-mucinous neoplasms, and solid pseudopapillary neoplasms, but also ductal adenocarcinomas and endocrine tumors with cystic features [6]. In general, SCNs are benign tumors that usually neither relapse nor metastasize and are composed of clear, glycogen-rich cells [2, 6, 7]. Nevertheless, MCNs are a more complex histological group comprising benign and borderline neoplasms and in situ and invasive carcinoma. In some cases of MCN, several patterns of growing or grades of malignancy may be simultaneously found, but irrespective of the histologic appearance of the epithelial component, with or without stromal invasion, pancreatic MCNs should all be considered as mucinous cystadenoma of low-grade malignant potential [6, 9].

D. Suarez-Vilela · F. M. Izquierdo-Garcia · F. Iglesias-Dominguez
Servicio de Anatomia Patológica, Hospital Valle del Nalón,
Polígono de Riaño, S/N,
33920 Riaño (Langreo) Asturias, Spain

F. M. Izquierdo-Garcia (✉)
Servicio de Anatomía Patológica, Hospital de León,
Altos de la Nava s/n,
24008 León, Spain
e-mail: fizquierdo@hleo.sacyl.es

Combined cystic pancreatic neoplasms of serous–mucinous type are very infrequent, with few cases described in the English literature [1, 8]. In this article we report one case of SCN, type serous microcystic adenoma (SMA), combined and intermingled with a MCN, that showed several growth patterns, and foci of invasive adenocarcinoma. We present the case of an 81-year-old woman who came to our hospital because of epigastralgia and dysphagia for the past 3 months. At the serum studies, a light increased level of cancer antigen (CEA) was present (20.2 ngr/mL) and the scanner showed a mass localized in the tail of the pancreas, with radiological features of MA. The ultrasonography and the scanner did not show diffuse or segmental cystic ectasia of the main and secondary pancreatic ducts.

In July 2005, a resection of the body and tail of the pancreas was performed. The patient died 3 months thereafter due to a severe peripancreatic hemorrhage. During this time, she had been operated on again and local relapse and metastases were not found. An autopsy was not performed.

The specimen of pancreatectomy showed a well-delimited mass measuring 9×7×5 cm in size with numerous tiny cysts ranging from 0.1 to 1 cm in diameter. The cysts were filled of serous fluid and surrounded by thin fibrous septa. At the periphery there was a localized, wedge-shaped stromal thickening of cicatricial appearance. The tumor was not related to the main pancreatic duct (Fig. 1). Microscopically, 70% of the tumor corresponded to a typical SMA with cysts of different sizes lined by a single layer of cuboidal or flattened epithelial cells with clear cytoplasms and central, round to oval nuclei with inconspicuous nucleoli. The stroma in between was acellular and collagenous with fibrohyalinzed foci. The peripheral stellate core was composed of hyalinized tissue with a few

Fig. 1 The tumor is well circumscribed and consists of a honeycomb meshwork of small cysts with a few larger interspersed cysts. A peripheral stellate scar is apparent

clusters of minute serous cysts. In many sections, the cysts of the serous tumor were intermingled with other cysts, also of different sizes, lined by tall columnar cells of large eosinophilic cytoplasms, moderate or severe atypia, and pseudostratified nuclei (Fig. 2a). Cells with goblet-like morphology were found admixed with columnar cells. Some of these mucinous cysts showed an intraluminal papillary growth pattern with more atypical nuclei, and in other areas of the mucinous neoplasm, focal stromal infiltration by a mucionus moderately differentiated adenocarcinoma was found (Fig. 3). The stroma of the mucinous tumor showed a fascicular proliferation of elongated cells, abundant collagen, and lymphoplasmacytic infiltrates. In the areas of collision the cystic structures of both tumoral components were enmeshed and the mucinous tumor seemed to infiltrate the serous cysts. With hematoxylin and eosin and ancillary techniques (histochemistry and immunohistochemistry) cysts with a mixed serous–mucinous lining were found, in which the cells were arranged either in a unique layer with a lineal clear-cut limit between

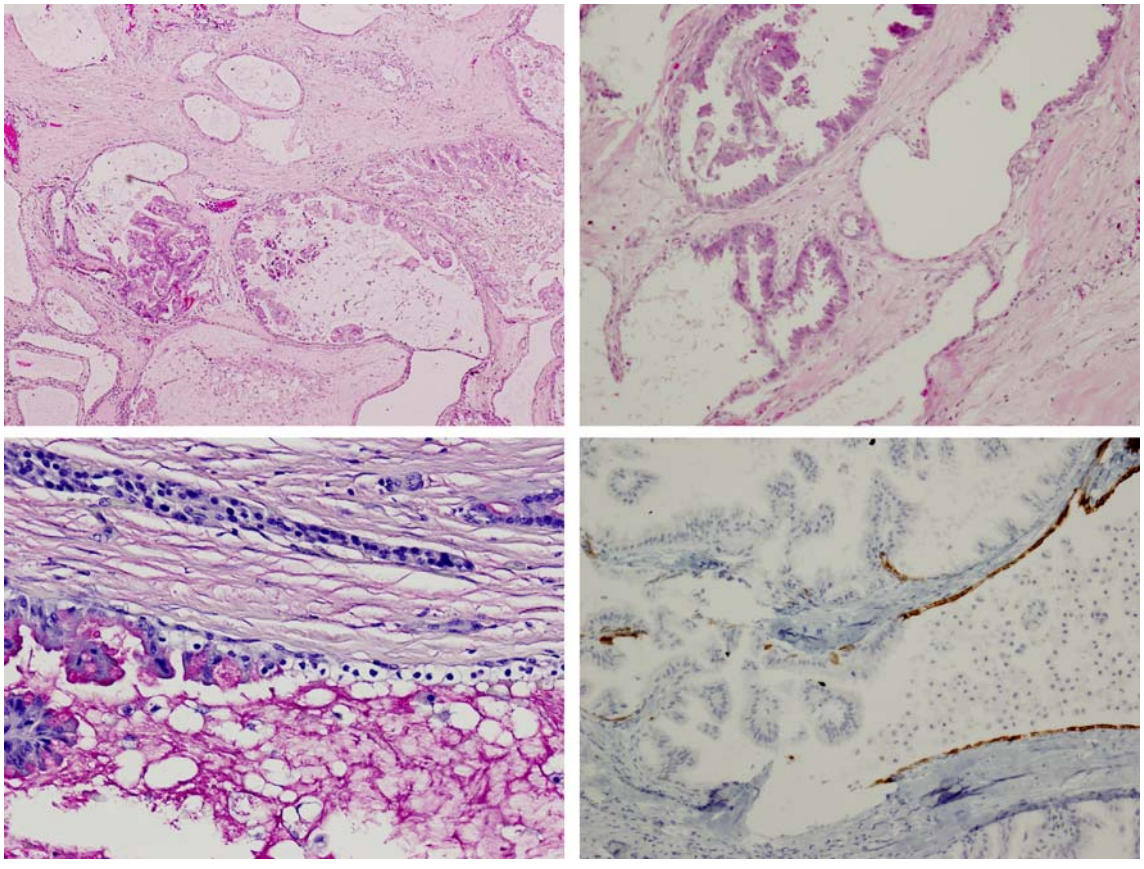

Fig. 2 **a** (upper left) Serous cysts lined by cuboidal cells. The cysts of the central area of the picture show a mixed component of serous cuboidal cells and pseudostratified columnar epithelium with moderate atypia, goblet, and mucinous cells and some papillary structures. **b** (upper right) At higher power, some cysts show mixed serous and mucinous epithelium. **c** (lower left) The columnar cells of the mucinous component present abundant cytoplasmic mucin stained with mucicarmine staining. The serous adjacent cells, in the same cyst, are negative. **d** (lower right) The serous cells of the SMA are positive for α-inhibin. In the cysts with mixed serous and mucinous components, a discontinuous pattern (positive in serous cells and negative in mucinous ones) is observed

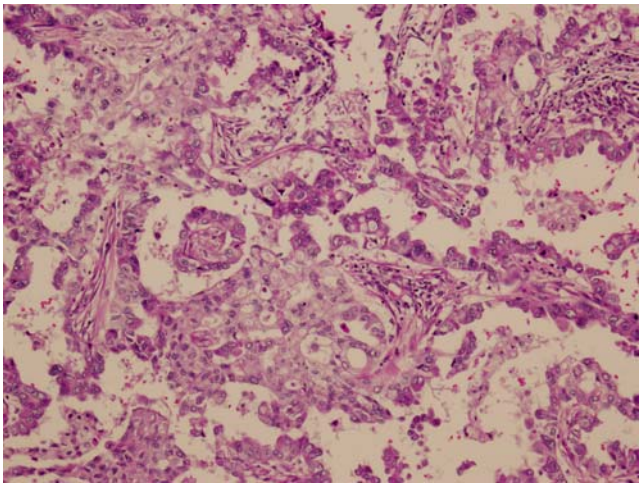

Fig. 3 Infiltrative tumoral pattern with irregular glands and papillae in areas of mucinous component

the two components or in a double layer in which the lower one was composed of serous cells and the luminal one of mucinous cells (Fig. 2b). At the periphery a fibrous capsule surrounded the neoplasm, and none of the tumor components infiltrated it or overpassed it. Neither pancreatic intraepithelial neoplasm nor other significant histologic features were found in the scanty nontumoral pancreatic tissue outside of the capsule of the neoplasm.

The serous cells showed cytoplasmic staining with periodic acid-Schiff technique, being negative after diastase digestion. Alcian blue and mucicarmine stains were also negative. In the mucinous component both columnar and goblet cells were stained with all the techniques just stated, which also remarked the abundant mucinous material inside the lumina of the cysts (Fig. 2C).

On the immunohistochemical study the epithelial cells of the SMA and MCN were positive with Cam5.2, 34βE12, anti-CK7, and anti-EMA antibodies. Focally, both epithelial components were positive for estrogen receptors (70% of the nuclei of the SMA and 15% of the MCN). With the MIB-1 antibody, the proliferation index was 2% for the SMA areas, 15% for the noninfiltrant areas of MCN, and 25% for the infiltrant areas of MCN. Other antibodies marked only one of the types of epithelium. SMA was stained for CK5/6, α-inhibin (Fig. 2d), MUC6, and NSE (focally), whereas MCN showed immunostaining for CD15, CEA, p-53 protein (2% of the nuclei in noninfiltrant and 10% in infiltrant areas of MCN), and HBM-1. All the cells of the MCN stained strongly for MUC1 and to a lesser extent for MUC4, while MUC2 and MUC5 were only expressed in single cells and MUC6 were entirely lacking. Antibodies against vimentin, BerEP4, calretinin, Willms tumor 1 protein, CK20, chromogranin, smooth muscle actin, s-100 protein, CD31, CD34, c-erbB-2, and progesterone receptors were negative on the epithelial cells of both components. The fusiform cells of the stroma of the mucinous neoplasm were positive for vimentin and smooth muscle actin, and focally for calretinin and progesterone receptors. The scanty cells of the stroma of the SMA also showed staining for vimentin and focally for progesterone receptors.

SCNs of the pancreas are a group of uncommon tumors including serous mycrocystic adenoma, serous oligocystic ill-demarcated adenoma, serous solid adenoma, von Hippel–Lindau-associated cystic neoplasm, and serous cystadenocarcinoma. These subtypes have similar histologic features but they are different in their gross appearance, their localization in the pancreas, and their gender distribution [3, 6, 7]. SCNs associated with other neoplasms as collision tumors are very unusual. On this topic, the most frequent combination is SCNs with pancreatic endocrine neoplasms [2]. Occasionally, SCNs are associated with ductal or intraductal papillary-mucionus tumors of the pancreas, but in these cases both tumors are localized in different areas. So, this finding seems to be merely coincidental [4]. SCNs and MCNs found as collision tumors are extremely infrequent. Del Vecchio et al. [8] describe a case of SMA associated with a mucinous cystadenocarcinoma with characteristics very similar to our case. However, macroscopically, in the case of del Vecchio et al. [8], a neoplasm with features of SMA was found, but it presented a more solid area with irregular cysts filled with mucinous material; on the other side, microscopically, the two different components of the tumor were adjacent but not intermingled, and areas intermediate between the two elements were not present. The gross appearance of our case was similar to a classic SMA without evidence of mucinous cysts, and microscopically, in the areas of collision, the serous and mucinous cysts were intermingled and some of them showed a mixed lining with serous and mucinous epithelium on the same cyst. Our immunohistochemical findings agree also with those of del Vecchio et al. [8], but in our findings, α-inhibin and MUC6 were clearly positive on the epithelial cells of the SMA, a finding recently described in this type of tumor [7]. As an unexpected finding, our case showed diffuse staining for MUC1 in the noninvasive component of MCN. This finding is very uncommon inasmuch as MUC1 is positive only in invasive areas of MCNs and very infrequently in noninvasive MCNs that show an eosinophilic cytology, similar to the oncocytic cell type of intraductal papillary-mucinous neoplasms [6]. In reference to the stroma of the SMA and MCN, this finding was similar in both cases, but in our case we found focal expression for progesterone receptors and calretinin on the fusiform cells of the stroma of the MCN, in spite of the fact that it was not ovarian-like, as it is often present in many cases of MCNs [6, 9]. Recently, Abe et al. [1] have described a benign counter-

part, mixed serous and mucinous cystadenoma of the pancreas. Grossly, it showed characteristics of serous oligocystic ill-demarcated adenoma without a mucinous component. The light microscopic findings with hematoxylin and eosin staining and the periodic acid-Schiff reaction were almost consistent with the characteristics of SMA, but the apical portion of the cytoplasms of the neoplastic cells was stained with alcian blue at pH 2.4 and with mucicarmine [1].

SCNs and MCNs of the pancreas are tumors with macroscopic, histologic, histochemical, immunohistochemical, and ultrastructural features clearly differentiated [3, 6, 7, 9]. On the other hand, based on these immunohistochemical and ultrastructural findings, it is thought that SCNs arise from centroacinar cells and MCNs from ductal cells [3, 6, 7, 9]. There are also some molecular differences between both entities. K-ras mutations, as well as other mutations common to pancreatic ductal adenocarcinoma, have been identified in MCNs but not in SCNs, which are often associated with mutations of the von Hippel–Lindau gene [1, 5, 7]. In the case of the findings of del Vecchio et al. [8], the mucinous neoplasm seems to arise inside a preexisting SMA, a finding also present in our case, where, moreover, a sharp limit between both tumoral components does not exist. In the case reported by Abe et al. [1], most of the cells had serous appearances, but some of them showed acid mucopolisacarides at the apical portion of the cytoplasm. These findings raise different hypotheses about hystogenesis and tumorogenesis of the mucinous component in mixed sero-mucinous pancreatic tumors. One possibility is that MCN arises from serous cells of the SCN after mutations in the K-ras gene or other oncogenes; however, an origin of the mucinous component independent of the serous neoplasm should also be considered. In this situation, the molecular oncogenic changes could be developed in the ductal cells of the pancreatic remnant entrapped inside the stroma of some cases of SCNs [3]. Nowadays, it is not possible to predict the prognosis of the cystic sero-mucinous pancreatic tumors because of the few cases reported, but the prognosis is probably related to the histologic features of the mucinous neoplasm [6, 9].

Acknowledgment We very sincerely thank Dr. Klöppel (University of Kiel, Germany) for performing an important part of the immunohistochemical study, mainly the preparation of MUC antibodies, and for confirming our diagnosis.

References

1. Abe H, Kimura W, Mori M, Makuuchi M, Yanagisawam A (2005) Mixed serous cystadenoma with mucinous cystadenoma of the pancreas. Pancreas 31:98–100
2. Alasio M, Vine A, Sanchez A, Dardik H (2005) Pancreatic endocrine tumor coexistent with serous microcystic adenoma: report of a case and review of the literature. Ann Diagn Pathol 9:234–238
3. Alpert LC, Truong LD, Bossart MI, Spjut HJ (1988) Microcystic adenoma (serous cystadenoma) of the pancreas. A study of 14 cases with immunohistochemical and electron-microscopic correlation. Am J Surg Pathol 12:251–263
4. Goh BK, Loh HL, Soo KC (2005) Synchronus pancreatic serous cystic tumor, intraductal papillary mucinous tumor and gastric carcinoma: report of a case. Pancreas 31:195–197
5. Kim SG, Wu TT, Lee JH, Yun YK, Issa JP, Hamilton SR, Rashid A (2003) Comparison of epigenetic and genetic alterations in mucinous cystic neoplasm and serous microcystic adenoma of the pancreas. Mod Pathol 16:1086–1094
6. Kosmahl M, Pauser U, Peters K, Sipos B, Lüttges J, Kremer B, Klöppel G (2004) Cystic neoplasms of the páncreas and tumor-like lesions with cystic features: a review of 418 cases and classification proposal. Virchows Arch 445:168–178
7. Kosmahl M, Wagner J, Peters K, Sipos B, Klöppel G (2004) Serous cystic neoplasms of the pancreas. An immunohistochemical analysis revealing alpha-inhibin, neuron-specific enolase and MUC6 as new markers. Am J Surg Pathol 28:339–346
8. del Vecchio MT, Pergola L, Tripodi SA, Collini A, Forzini L, Cintorino M (2002) Microcystic adenoma associated with a mucinous cystadenocarcinoma: a "collision tumor" of the pancreas. Pancreas 24:106–108
9. Zamboni G, Scarpa A, Bogina G, Iacono C, Bassi C, Talamini G, Sessa F, Capella C, Solcia E, Rickaert F, Mariuzzi GM, Klöppel G (1999) Mucinous cystic tumors of the pancreas. Clinicopathological features, prognosis and relationship to other mucinous cystic tumors. Am J Surg Pathol 23:410–422

Virchows Arch (2006) 449:389–391
DOI 10.1007/s00428-006-0246-x

LETTER TO THE EDITOR

Nephrogenic fibrosing dermopathy with involvement of the dura mater

Adam Saenz · Rajni Mandal · Richard Kradin · E. Tessa Hedley-Whyte

Received: 24 April 2006 / Accepted: 29 May 2006 / Published online: 2 August 2006
© Springer-Verlag 2006

Dear Editor,

Nephrogenic fibrosing dermopathy (NFD) is a recently recognized cutaneous disorder that occurs in patients with end-stage renal disease, but which can also present with systemic involvement [1, 2]. Extracutaneous manifestations of this disease have been reported to involve the subcutaneous tissue, fascia, striated muscle, lungs, and myocardium [3]. Recently, we examined a case of a 71-year-old man with NFD and diffuse calcification of the dura mater of the brain and spinal cord.

The patient's medical history included diet-controlled type 2 diabetes mellitus, hypertension, end-stage renal disease, peripheral vascular disease, atherosclerotic heart disease with anteroseptal myocardial infarction and coronary stenting in August 2005, and a seizure disorder of unknown etiology. He developed rapidly progressing NFD leading to marked flexion contractures of his extremities and debilitating pain. A CT scan of the head revealed prominent dural calcification of the interhemispheric falx and tentorium. The patient's musculoskeletal symptoms did not respond to thalidomide, and he developed an anaphylactic reaction to intravenous immunoglobulin therapy. Due to the progressive nature of his NFD, he chose to discontinue his dialysis and he died at home. A full autopsy was performed.

A. Saenz (✉) · R. Mandal · R. Kradin · E. T. Hedley-Whyte
Massachusetts General Hospital, Department of Pathology,
Harvard Medical School,
55 Fruit Street, Warren 219,
Boston, MA 02114, USA
e-mail: ajsaenz@partners.org

Grossly, the dura mater of the brain (frontal, parietal, and temporal fossa) was yellow, thickened (up to 3 mm), and hard (Fig. 1a,b). The spinal dura mater was also involved but was patchy and spared the cervical cord. The inner surface of the cranial dura mater was covered with a diffuse brown-red rough membrane with neovascularization consistent with an old hemorrhage.

Microscopically, the dura mater was heavily calcified with abundant granulation tissue on the inner surface (Fig. 1). Histology of involved extremity skin revealed marked fibrosis of the papillary and reticular dermis with extension to the fascia and skeletal muscle (Fig. 2). Thick fibrous tracts extended to the pannicular fat, blood vessels, and nerves with fibrosis of the dermis and fascia. There were sparse perivascular mononuclear infiltrates (Fig. 2b). The underlying skeletal muscle had fibrous bands between muscle bundles (Fig. 2d). A Masson trichrome stain of the skin revealed diffuse collagen deposition (Fig. 2c). No comparable changes were found in other organs.

Evidence is mounting to support the idea that nephrogenic fibrosing dermopathy is a systemic fibrosing process that is not limited to the skin. Although extracutaneous evidence of disease was limited to skeletal muscle and dura mater in this case, these findings corroborate the systemic nature of this disorder. Systemic calcification was reported in other cases of NFD [4, 5]. The diffuse calcification of the entire dural cap seen in the present case differs from metaplastic bone in the inner dural and spinal arachnoid membranes. Although the pathogenesis of this disease is uncertain, previous studies have shown increased CD68+, factor XIIIa+ dendritic cells, and TGF-β1 expression in the skin of NFD patients when compared to normal skin, which suggests that activation of the TGF-β1 pathway may contribute to the fibrosing process [3]. In addition, the fibrosis is accompanied by a proliferation of CD34+, which

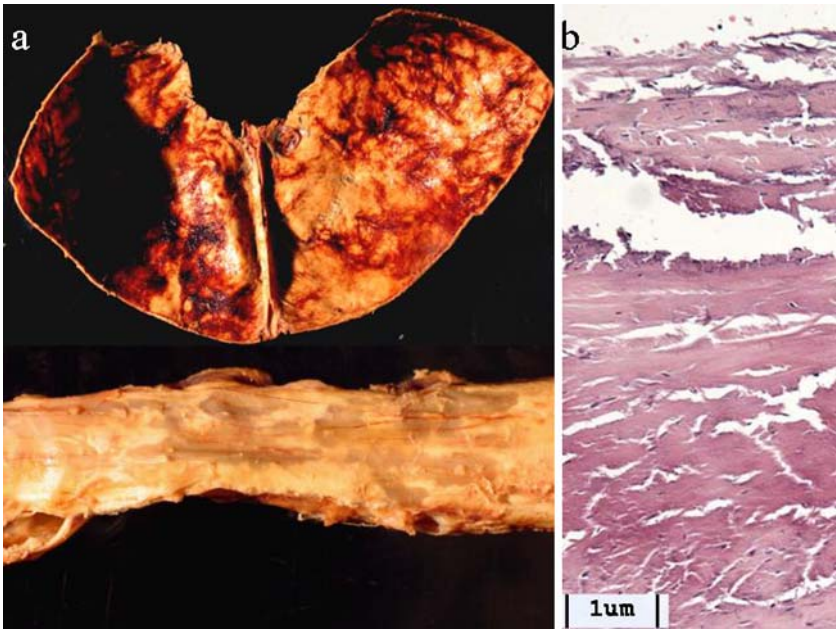

Fig. 1 **a** Dura mater of the brain and spinal cord. The dura is hard and yellow, and the inner surface is covered by a thin subdural membrane. **b** The thickening of the dura mater is due to diffuse calcification (hematoxylin and eosin stain, ×10)

are procollagen+ fibrocytes involved in the inflammatory and proliferative phases of wound repair [6]. However, the etiologic agent for the aberrant fibrosis seen in this disease and the possible therapeutic targets remain unknown.

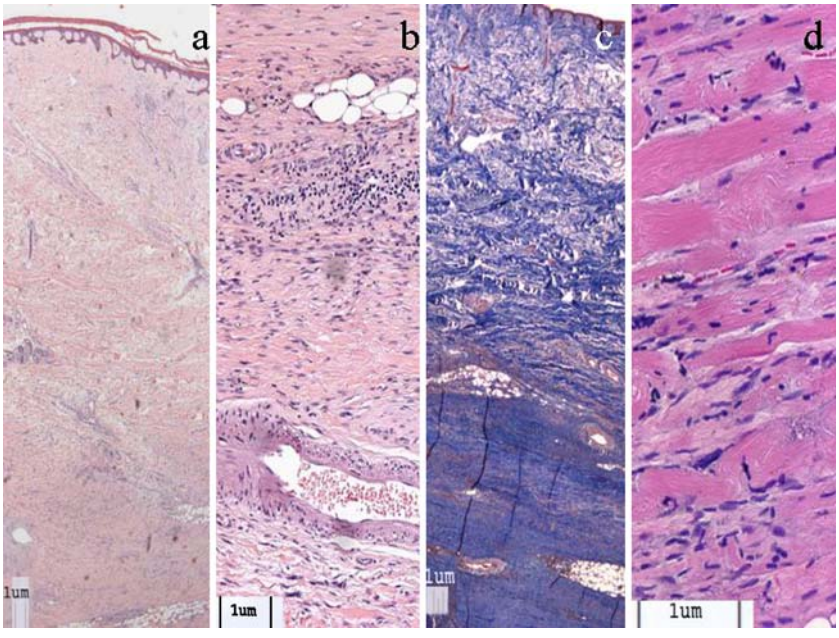

Fig. 2 **a** The skin has marked thickening of the papillary and reticular dermis with extension into the fascia (hematoxylin and eosin stain, ×2, ×10). **b** Fibrous tissue with numerous spindle-shaped fibroblasts extend around adipose tissue **c** Trichrome stain demonstrates diffuse fibrosis of the reticular dermis and the fascia (×10). **d** Skeletal muscle is invaded and replaced by bands of fibrous tissue (×20)

Additional investigation of this disorder with respect to the central nervous system is warranted to further elucidate the pathophysiological derangements of this disease.

References

1. Cowper SE, Su LD, Bhawan J, Robin HS, LeBoit PE (2001) Nephrogenic fibrosing dermopathy. Am J Dermatopathol 23:383–393
2. Daram SR, Cortese CM, Bastani B (2005) Nephrogenic fibrosing dermopathy/nephrogenic systemic fibrosis: report of a new case with literature review. Am J Kidney Dis 46:754–759
3. Jimenez SA, Artlett CM, Sandorfi N, Derk C, Latinis K, Sawaya H, Haddad R, Shanahan JC (2004) Dialysis-associated systemic fibrosis (nephrogenic fibrosing dermopathy). Arthritis Rheum 50:2660–2666
4. Levine JM, Taylor RA, Elman LB, Bird SJ, Lavi E, Stolzenberg ED, McGarvey ML, Asbury AK, Jimenez SA (2004) Involvement of skeletal muscle in dialysis-associated systemic fibrosis (nephrogenic fibrosing dermopathy). Muscle Nerve 30:569–577
5. Ting WW, Stone MS, Madison KC, Kurtz K (2003) Nephrogenic fibrosing dermopathy with systemic involvement. Arch Dermatol 139:903–906
6. Quan TE, Cowper S, Wu SP, Bockenstedt LK, Bucala R (2004) Circulating fbrocytes: collagen-secreting cells of the peripheral blood. Int J Biochem Cell Biol 36:598–606

Virchows Arch (2006) 449:392–393
DOI 10.1007/s00428-006-0266-6

LETTER TO THE EDITOR

Pulmonary hamartoma associated with typical carcinoid/tumorlet

Alberto Cavazza · Massimiliano Paci · Giulio Rossi

Received: 4 May 2006 / Accepted: 29 June 2006 / Published online: 16 August 2006
© Springer-Verlag 2006

Sir,

Pulmonary hamartoma (PH) is a relatively common specimen to be received in the laboratory of Surgical Pathology, and its diagnosis is straightforward in the vast majority of cases. However, some problems may arise when PH is combined with a second neoplasm, a very rare event with a potentially significant impact on prognosis. Both epithelial and mesenchymal tumors have occasionally been described within PH [2, 4]. In this study, we report a hitherto unrecognized association: PH and a bland neuroendocrine proliferation with features of typical carcinoid (TC)/tumorlet.

Our patient was a 65-year-old male, ex-smoker, with an history of left hemicolectomy performed 7 months previously for a moderately differentiated rectal adenocarcinoma (pT3 N1). During the follow-up, a chest X-ray and a computed tomography (CT) scan revealed a well-circumscribed nodule of the lower lobe of the right lung. A videothoracoscopic resection of the nodule was performed. The patient is alive with no evidence of tumor recurrence 6 months after surgery. Grossly, the pulmonary specimen measured 7×3×2 cm and contained a subpleural nodule, 1 cm in diameter, whitish in color, and with pushing margins. Microscopically (Fig. 1), the majority of the tumor had the classical features of PH with lobules of mature cartilage surrounded by fibromyxoid stroma, adipose tissue, and benign epithelial clefts. At the periphery, embedded in the stroma, a second component was present, which extended in the center of the tumor and reached a diameter of 0.6 cm. It consisted of bland epithelioid to spindle cells, with a moderate amount of eosinophilic cytoplasm, "salt and pepper" chromatin and inconspicuous mitotic activity, arranged in anastomosing nodules. No necrosis was evident. The surrounding lung was unremarkable. Immunohistochemically, the cells of the second component were diffusely positive for pan-cytokeratin, chromogranin A, and synaptophysin.

A. Cavazza
Department of Pathology, S. Maria Nuova Hospital,
Reggio Emilia, Italy

M. Paci
Department of Thoracic Surgery, S. Maria Nuova Hospital,
Reggio Emilia, Italy
e-mail: Paci.massimiliano@asmn.re.it

G. Rossi
Section of Anatomic Pathology §, Azienda Policlinico,
Modena, Italy
e-mail: Rossi.giulio@policlinico.mo.it

A. Cavazza (✉)
Unità Operativa di Anatomia Patologica,
Ospedale S. Maria Nuova,
Viale Risorgimento 80,
42100 Reggio Emilia, Italy
e-mail: cavazza.alberto@asmn.re.it

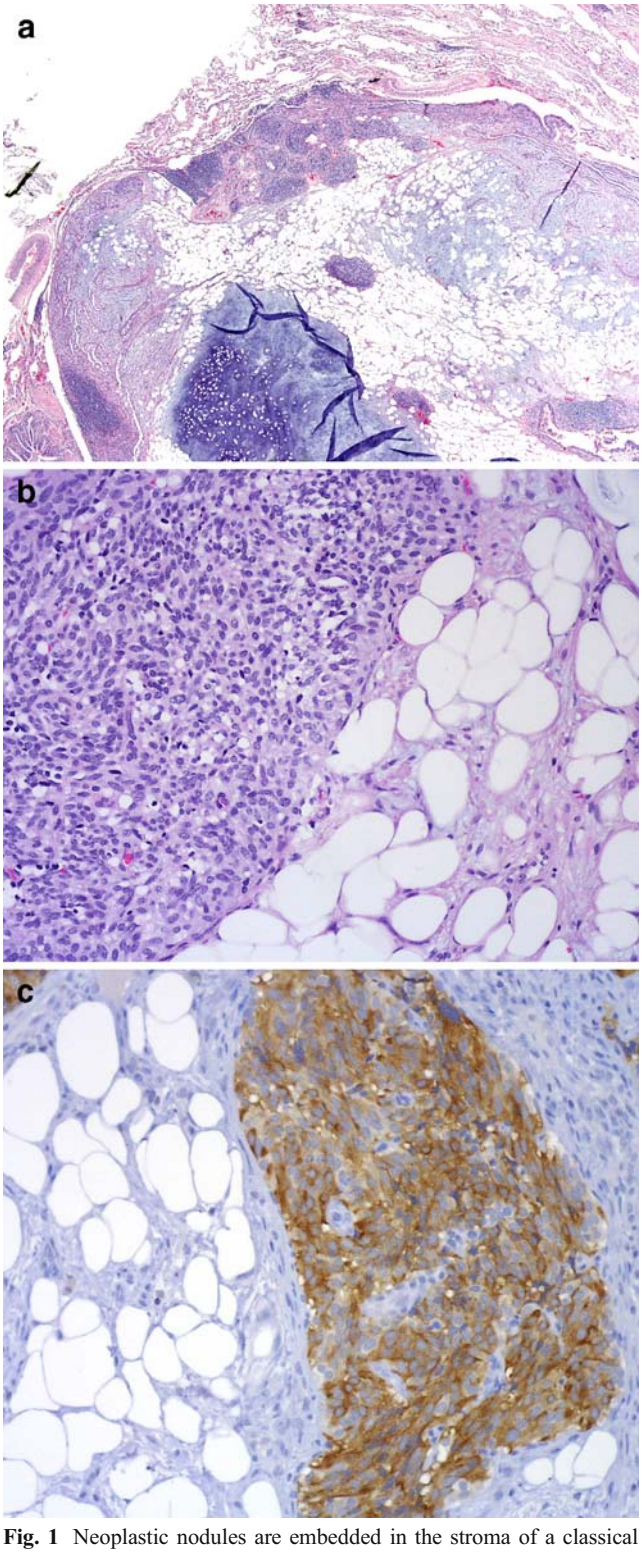

Fig. 1 Neoplastic nodules are embedded in the stroma of a classical pulmonary hamartoma (**a**). The nodules are composed of bland epithelioid to spindle cells (**b**), diffusely immunoreactive with chromogranin A (**c**)

We interpreted this tumor as a TC arising in PH. This interpretation was based on the dimension of the neuroendocrine component (>0.5 cm) [7], but admittedly its multinodular growth made the distinction with a tumorlet quite subjective. This case highlights the need for better criteria to differentiate pulmonary tumorlet from TC. The follow-up of our patient is too brief to be significant; however, the bland morphology of the neuroendocrine component and its small dimension allow to predict a benign clinical behavior.

Although very rare examples of TC combined with acinic cell tumor [3] and adenocarcinoma [1, 5] have been reported in the lung, to the best of our knowledge, this is the first association of TC/tumorlet with PH. General pathologist should be aware that combined PH may rarely occur, to prevent diagnostic mistakes particularly in frozen section [6]. Our observation further expands the spectrum of unusual combinations which can be faced in pulmonary neoplasms.

References

1. Cavazza A, Toffanetti R, Ferrari G, Piana S, Putrino I, Gardini G (2001) Combined neoplasia of the lung: description of a case of adenocarcinoma mixed with typical carcinoid. Pathologica 93: 216–220
2. Pelosi G, Rodriguez J, Viale G, Rosai J (2006) Salivary gland-type tumors with myoepithelial differentiation arising in pulmonary hamartoma. Report of 2 cases of a hitherto unrecognized association. Am J Surg Pathol 30:375–387
3. Rodriguez J, Diment J, Lombardi L, Dominoni F, Tench W, Rosai J (2003) Combined typical carcinoid and acinic cell tumor of the lung: a heretofore unreported occurrence. Hum Pathol 34: 1061–1065
4. Rossi G, Cavazza A, Valli R, Torricelli P, Richeldi L, Rivasi F et al (2003) Atypical lipomatous tumour (lipoma-like liposarcoma) arising in a pulmonary hamartoma and clinically presenting with pneumothorax. Lung Cancer 39:103–106
5. Sen F, Borczuk AC (1998) Combined carcinoid tumor of the lung: a combination of carcinoid and adenocarcinoma. Lung Cancer 21:53–58
6. Sienko A, Allen TC, Zander DS, Cagle PT (2005) Frozen section of lung specimens. Arch Pathol Lab Med 129:1602–1609
7. Travis WD, Brambilla E, Muller-Hermelink HK, Harris CC (2004) Tumours of the lung, pleura, thymus and heart. IARC Press, Lyon, France

Virchows Arch (2006) 449: 394
DOI 10.1007/s00428-006-0295-1
© Springer-Verlag 2006

ANNOUNCEMENTS

21–22 October 2006
Diseases and Tumors of the Salivary Glands
12th Salzburg Weekend Seminar
Auditorium of the Landeskliniken Salzburg, Austria

Course fee:
Euro 150.- Until 30 September 2006 (students: Euro 75.-)
Euro 180 after 1 October 2006
Euro 50.-Histopathological Slide Session (CD-Rom included)

For further information please contact:
Univ.-Doz. Dr. Johann Beck-Mannagetta
Dept. of Oral and Maxillofacial Surgergy/LKS
Müllner Hauptstrasse 48
5020 Salzburg, Austria
Fax: 0043-662-4482884
e-mail: j.beck-mannagetta@salk.at

29 November–1 December 2006
Combined Adult and Congenital Cardiovascular Pathology Course
London, UK

Course Organisers:
M. N. Sheppard, Y. Ho

Course fee:
£ 400.-
£300.- special fee for juniors in training

For further information please contact:
Short Course Office
National Heart and Lung Institute
Dovehouse Street
London SW3 6LY, UK
Fax: 0044 -020-7351-8346
e-mail: shortcourse.NHLI@IC.AC.UK

24–26 January 2007
Theorico-practical Course on Bone and Soft Tissue Tumors
Department of Pathology, Hospital del Mar, Barcelona, Spain

Faculty
Christopher Fletcher, M.D. (Brigham and Women's Hospital, Boston, USA)
Andrew Rosenberg, M.D. (Massachusetts General Hospital, Boston, USA)
Angelo Paolo Dei Tos, M.D. (Hospital of Treviso, Italy)
John Goldblum, M.D. (Cleveland Clinic, Cleveland, USA)
Paola Dal Cin, Ph.D. (Brigham and Women's Hospital, Boston, USA)

For further information please contact:
Francisco Alameda, M.D.
Department of Pathology
Hospital del Mar, Spain
E-mail: 86780@imas.imim.es
or
Esther Oliva, M.D.
Department of Pathology
Massachusetts General Hospital
55 Fruit Street, WRN-2
Boston, MA 02114, USA
E-mail: eoliva@partners.org

Virchows Arch (2006) 449:395–401
DOI 10.1007/s00428-006-0250-1

ORIGINAL ARTICLE

TNM staging of foregut (neuro)endocrine tumors: a consensus proposal including a grading system

G. Rindi · G. Klöppel · H. Alhman · M. Caplin · A. Couvelard · W. W. de Herder · B. Erikssson · A. Falchetti · M. Falconi · P. Komminoth · M. Körner · J. M. Lopes · A-M. McNicol · O. Nilsson · A. Perren · A. Scarpa · J-Y. Scoazec · B. Wiedenmann · and all other Frascati Consensus Conference participants

Received: 11 April 2006 / Accepted: 6 June 2006 / Published online: 12 September 2006
© Springer-Verlag 2006

Abstract The need for standards in the management of patients with endocrine tumors of the digestive system prompted the European Neuroendocrine Tumor Society (ENETS) to organize a first Consensus Conference, which

List of the participants to the "Consensus Conference on the ENETS Guidelines for the Diagnosis and Treatment of Neuroendocrine Gastrointestinal Tumors, Part 1: Foregut Tumors" held in Frascati (Rome, Italy), November 2–5, 2005 (front Authors not listed): R. Arnold, Department of Gastroenterology, Philipps University, Marburg (Germany); W.O. Bechstein, Department of Surgery, Johann-Wolfgang-Goethe-Universität, Frankfurt (Germany); G. Cadiot, Department of Hepatology and Gastroenterology, C.H.U. Bichat-B. Claude Bernard University, Paris (France); E. Christ, Department of Endocrinology, Inselspital, Bern (Switzerland); D. Chung, Department of Gastroenterology, Massachussetts General Hospital, Boston, MA (USA); G. Delle Fave, Department of Digestive and Liver Disease, Ospedale S. Andrea, Rome (Italy); D. Ferone, Department of Endocrinology, Genoa University, Genoa (Italy); P. Goretzki, Department of Surgery, Städtisches Klinikum Neuss, Lukas Hospital, Neuss (Germany); D. Gross, Department of Endocrinology and Metabolism, Hadassah University, Jerusalem (Israel); D. Hochhauser, Department of Oncology, Royal Free University, London (United Kingdom); R. Hyrdel, Department of Internal Medicine, Martin University, Martin (Slovakia); R. Jensen, Department of Cell Biology, National Institute of Health, Bethesda, MD (USA); G. Kaltsas, Department of Endocrinology and Metabolism, Genimatas Hospital, Athens (Greece); F. Keletimur, Department of Endocrinology, Erciyes University, Kayseri (Turkey); R. Kianmanesh, Department of Surgery, UFR Bichat-Beaujon-Louis Mourier Hospital, Colombes (France); W. Knapp, Department of Nuclear Medicine, Medizinische Hochschule Hannover, Hannover (Germany); U.P. Knigge, Department of Surgery, Rigshospitalet Blegdamsuej Hospital, Copenhagen (Denmark); B. Kos-Kuda, Department of Endocrinology, Slaska University, Zabrze (Poland); L. Kvols, Department of Oncology, South Florida University, Tampa, FL (USA); D. Kwekkeboom, Department of Nuclear Medicine, Erasmus MC University, Rotterdam (the Netherlands); V. Lewington, Department of Radiology, Royal Marsden Hospital, Sutton (United Kingdom); R. Manfredi, Department of Radiology, Istituto di Radiologia, Policlinico GB, Verona (Italy); E. Mitry, Department of Hepatology and Gastroenterology, CHV A Pare Hospital, Boulogne (France); B. Niederle, Department of Surgery, Wien University, Vienna (Austria); G. Nikou, Department of Propaedeutic Internal Medicine, Laiko Hospital, Athens (Greece); K. Öberg, Department of Endocrinology, University Hospital, Uppsala (Sweden); J. O'Connor, Department of Oncology, Alexander Fleming Institute, Buenos Aires (Argentina); D. O'Toole, Department of Gastroenterology, Beaujon Hospital, Clichy (France); S. Pauwels, Department of Nuclear Medicine, Catholique de Louvain University, Brussels (Belgium); M. Pavel, Department of Endocrinology, Erlangen University, Erlangen (Germany); U. Plöckinger, Department of Hepatology and Gastroenterology, Charité Universitäts Medizin, Berlin (Germany); J. Ramage, Department of Gastroenterology, North Hampshire Hospital, Hampshire (United Kingdom); J. Ricke, Department of Radiology, Charité Universitäts Medizin, Berlin (Germany); P. Ruszniewski, Department of Gastorenterology, Beaujon Hospital, Clichy (France); R. Salazar, Department of Oncology, Institut Català d'Oncologia, Barcelona (Spain); A. Sauvanet, Department of Surgery, Beaujon Hospital, Clichy (France); M.I. Sevilla Garcia, Department of Oncology, Virgen de la Victoria Hospital, Malaga (Spain); T. Steinmüller, Department of Surgery, Vivantes Humboldt Hospital, Berlin (Germany); A. Sundin, Department of Radiology, Uppsala University, Uppsala (Sweden); B. Taal, Department of Oncology, Netherlands Cancer Centre, Amsterdam (the Netherlands); E. Van Cutsem, Department of Gastroenterology, Gasthuisberg University, Leuven (Belgium); M.P. Vullierme, Department of Gastroenterology, Beaujon Hospital, Clichy (France); S. Wildi, Department of Surgery, Zürich Hospital, Zürich, Switzerland; J.C. Yao, Department of Oncology, University of Texas, Houston, TX (USA).

G. Rindi (✉)
Dipartimento di Patologia e, Medicina di Laboratorio,
Sezione di Anatomia Patologica, Università di Parma,
Via Gramsci, 14,
43100 Parma, Italy
e-mail: guido.rindi@unipr.it

G. Klöppel
Department of Pathology, University of Kiel,
Kiel, Germany

was held in Frascati (Rome) and was based on the recently published ENETS guidelines on the diagnosis and treatment of digestive neuroendocrine tumors (NET). Here, we report the tumor–node–metastasis proposal for foregut NETs of the stomach, duodenum, and pancreas that was designed, discussed, and consensually approved at this conference. In addition, we report the proposal for a working formulation for the grading of digestive NETs based on mitotic count and Ki-67 index. This proposal, which needs to be validated, is meant to help clinicians in the stratification, treatment, and follow-up of patients.

Keywords Neuroendocrine tumors · Gut · Pancreas · Staging · TNM · Grading · Mitotic index · Ki-67 index

Background

It has been known for a long time, and was finally defined within the World Health Organization (WHO) classification of endocrine and digestive tumors, that neuroendocrine tumors (NET) arising at different anatomical sites of the digestive system represent tumor entities that differ in their biology [5, 7, 9, 31]. Several recent publications focused on the application of the "new" WHO classification and proved its effectiveness, supporting the concept that the different endocrine tumor types also differ in their clinical behavior [3, 4, 19, 20, 27, 32].

Malignant gastroenteropancreatic NETs may be fatal, though at a significantly slower pace than their exocrine counterparts. A number of retrospective papers and epidemiological data solidly support such statements [8, 9, 12–14, 21, 24, 25, 32]. This peculiar clinical feature attracted the interest of pathologists very early and was the reason for the special designation of such tumors as "carcinoid" by Oberndorfer [15].

As gastroenteropancreatic NETs are rare [9, 13, 14], it is tempting to lump them together and equate all digestive "carcinoids" with the appendiceal "carcinoid," probably the best known NET with the most benign behavior [28]. However, in recent years it has become clear that gastroenteropancreatic NETs, especially foregut NETs, are heterogeneous in their morphological and biological features. In the last two decades efforts were therefore made by the WHO to define NET features that discriminate true benign behavior (low risk) from low-grade malignant well-differentiated NETs in the different parts of the digestive system. Although the new WHO classification is an important step toward defining the diverse tumor biology of NETs, further efforts are necessary to improve the prognostic assessment of the individual NET.

H. Alhman
Department of Surgery, Gothenburg University,
Gothenburg, Sweden

M. Caplin
Department of Internal Medicine, Royal Free Hospital,
London, UK

A. Couvelard
Department of Pathology, Hôpital Beaujon,
Clichy, France

W. W. de Herder
Department of Internal Medicine,
Erasmus, Rotterdam,
The Netherlands

B. Erikssson
Department of Endocrinology, University Hospital,
Uppsala, Sweden

A. Falchetti
Department of Internal Medicine, University of Florence,
Florence, Italy

M. Falconi
Department of Surgery, University of Verona,
Verona, Italy

P. Komminoth
Department of Pathology, Kantosspital Baden,
Baden, Switzerland

M. Körner
Department of Pathology, University of Bern,
Bern, Switzerland

J. M. Lopes
Department of Pathology, Porto Medical School and IPATIMUP,
University of Porto,
Porto, Portugal

A.-M. McNicol
Department of Pathology, Glasgow Royal Infirmary,
Glasgow, Scotland, UK

O. Nilsson
Department of Pathology, Gothenborg University,
Gothenburg, Sweden

A. Perren
Department of Pathology, Universitätsspital Zürich,
Zürich, Switzerland

A. Scarpa
Department of Pathology, University of Verona,
Verona, Italy

J.-Y. Scoazec
Department of Pathology, University of Lyon,
Lyon, France

B. Wiedenmann
Department of Internal Medicine, Campus Virchow Klinikum,
Berlin, Germany

The demand for standards in the stratification and treatment of patients with gastroenteropancreatic NETs prompted the recently established European Neuroendocrine Tumor Society (ENETS) to define guidelines [22, 33]. Such guidelines underwent scrutiny for consensus in the first of two meetings entitled "Consensus Conference on the ENETS Guidelines for the Diagnosis and Treatment of Neuroendocrine Gastrointestinal Tumors, Part 1: Foregut Tumors" held in Frascati (Rome, Italy) from November 2–5, 2005. During this meeting the clinical need for a tumor–node–metastasis (TNM) classification of gastroenteropancreatic NETs was felt. Here we report the TNM staging classification proposal for foregut NETs that was approved at this consensus conference. In addition, we suggest a simple grading system with some pointers that may help to standardize the prognostic assessment of gastroenteropancreatic NETs.

Materials and methods

Sixty-two experts in the field of digestive endocrine tumors from 20 different countries attended the Consensus Conference. The attendees represented all medical branches involved in managing patients with gastroenteropancreatic NETs. They formed four working groups according to their specific clinical expertise: (1) pathology and genetics (11 participants, all listed as authors and G. Klöppel), (2) surgery (10 participants, including the coauthors H. Alhman and M. Falconi), (3) imaging and radiology (10 participants), (4) medicine and clinical pathology (31 participants, including the coauthors M. Caplin, W.W. de Herder, B. Erikssson, and B. Wiedenmann).

The Conference was divided sequentially into eight sessions devoted to specific topics on an anatomical basis (gastric NET sessions 1–2, duodenal NET, pancreatic NET sessions 1–4, and poorly differentiated endocrine carcinomas). A working booklet with the ENETS guidelines and specific queries had been prepared in advance by the Organizing Committee. The work was organized such that, after a short case presentation in a plenary session, each working group gathered separately to discuss group-specific questions. Once agreement was reached within each group, consensus statements were discussed and approved or rejected by all participants gathered in the plenary session. This procedure was followed for all eight sessions. The TNM staging proposal was made by the

Table 1 Proposal for a TNM classification and disease staging for gastric endocrine tumors

TNM			
T—primary tumor			
TX	Primary tumor cannot be assessed		
T0	No evidence of primary tumor		
Tis	In situ tumor/dysplasia (<0.5 mm)		
T1	Tumor invades lamina propria or submucosa and ≤1 cm		
T2	Tumor invades muscularis propria or subserosa or >1 cm		
T3	Tumor penetrates serosa		
T4	Tumor invades adjacent structures		
	For any T, add (m) for multiple tumors		
N—regional lymph nodes			
NX	Regional lymph nodes cannot be assessed		
N0	No regional lymph node metastasis		
N1	Regional lymph node metastasis		
M—distant metastasis			
MX	Distant metastasis cannot be assessed		
M0	No distant metastases		
M1[a]	Distant metastasis		
Stage			
Disease stages			
Stage 0	Tis	N0	M0
Stage I	T1	N0	M0
Stage IIa	T2	N0	M0
IIb	T3	N0	M0
Stage IIIa	T4	N0	M0
IIIb	Any T	N1	M0
Stage IV	Any T	Any N	M1

[a]M1 specific sites defined according to Sobin and Wittekind [29]

Pathology and Genetics working group and amended and approved by the plenary session of the consensus conference. The grading system was discussed and defined by the Pathology and Genetics working group only.

Results and discussion

The consensus guidelines are reported elsewhere. Here, we report the TNM staging proposal for gastroenteropancreatic NETs of the foregut together with a grading system that may be relevant for the prognostic assessment by the pathologist. The foregut NETs were separated into gastric, duodenal (including ampulla and proximal jejunum), and pancreatic NETs, but were not distinguished according to specific functional activity, main tumor cell type, and specific genetic background.

TNM staging proposal (see Tables 1, 2 and 3)

The currently published TNM format was adopted as working template [29].

Tumor The proposed definition of tumor in situ applies to the stomach only and adheres to the literature [30]. No definition is given for the duodenum and pancreas because none has been agreed upon in spite of recent working proposals [1, 2]. The size limits indicated for T1 are those defined by the WHO for tumors with "benign behavior" according to site-specific clinicopathological correlations [5, 7, 31]. Similarly, for T2 of the stomach and duodenum, the sizes are those indicated for tumors of "uncertain behavior." In the pancreas the size limit given for T2 needs to be validated [5]. Deeply invasive tumors are included under the T3 and T4 definitions, taking into account site-specific features.

Nodes N1 indicates the presence of any single or multiple metastases in regional lymph nodes, according to TNM rules. Although the presence of regional lymph-node metastases is, per se, a negative prognostic factor in gastroenteropancreatic NETs [11], the prognostic significance of the number of metastatic nodes is not known. In light of this, stage 3B of Tables 1, 2 and 3 is proposed to mark the N1 status for future validation.

Distant metastasis M1 indicates the presence of any single or multiple metastases at any distant anatomical site (including nonregional nodes). Because there is evidence that extrahepatic bone metastases are a particularly ominous

Table 2 Proposal for a TNM classification and disease staging for endocrine tumors of the duodenum/ampulla/proximal jejunum

TNM			
T—primary tumor			
TX	Primary tumor cannot be assessed		
T0	No evidence of primary tumor		
T1	Tumor invades lamina propria or submucosa and size ≤1 cm[a]		
T2	Tumor invades muscularis propria or size >1 cm		
T3	Tumor invades pancreas or retroperitoneum		
T4	Tumor invades peritoneum or other organs		
	For any T, add (m) for multiple tumors		
N—regional lymph nodes			
NX	Regional lymph nodes cannot be assessed		
N0	No regional lymph node metastasis		
N1	Regional lymph node metastasis		
M—distant metastases			
MX	Distant metastasis cannot be assessed		
M0	No distant metastases		
M1[b]	Distant metastasis		
Stage			
Disease stages			
Stage I	T1	N0	M0
Stage IIa	T2	N0	M0
IIb	T3	N0	M0
Stage IIIa	T4	N0	M0
IIIb	Any T	N1	M0
Stage IV	Any T	Any N	M1

[a]Tumor limited to ampulla of Vater for ampullary gangliocytic paraganglioma
[b]M1 specific sites defined according to Sobin and Wittekind [29]

Table 3 Proposal for a TNM classification and disease staging for endocrine tumors of the pancreas

TNM			
T—primary tumor			
TX	Primary tumor cannot be assessed		
T0	No evidence of primary tumor		
T1	Tumor limited to the pancreas and size <2 cm		
T2	Tumor limited to the pancreas and size 2–4 cm		
T3	Tumor limited to the pancreas and size >4 cm or invading duodenum or bile duct		
T4	Tumor invading adjacent organs (stomach, spleen, colon, adrenal gland) or the wall of large vessels (celiac axis or superior mesenteric artery)		
	For any T, add (m) for multiple tumors		
N—regional lymph nodes			
NX	Regional lymph node cannot be assessed		
N0	No regional lymph node metastasis		
N1	Regional lymph node metastasis		
M—distant metastases			
MX	Distant metastasis cannot be assessed		
M0	No distant metastases		
M1[a]	Distant metastasis		
Stage			
Disease stages			
Stage I	T1	N0	M0
Stage IIa	T2	N0	M0
IIb	T3	N0	M0
Stage IIIa	T4	N0	M0
IIIb	Any T	N1	M0
Stage IV	Any T	Any N	M1

[a] M1 specific sites defined according to Sobin and Wittekind [29]

sign [6, 20], it is recommended to specify the anatomical site of the metastasis according to the TNM classification rules (PUL, pulmonary; HEP, hepatic; OSS, osseous; etc.) [29].

Staging The proposed staging system lists stage 0 only for the stomach because this is the only anatomical site where Tis is defined. Stage I encompasses the T1 NETs with limited growth. Stage II identifies tumors that are larger in size or more invasive, either T2 or T3, though always in the absence of metastasis. At stage III the increased malignancy refers either to invasion into surrounding structures (stage IIIa) or to the presence of regional node metastasis (stage IIIb). Stage IV always implies the presence of distant metastasis.

Table 4 Grading proposal for foregut (neuro)endocrine tumors

Grade	Mitotic count (10 HPF)[a]	Ki-67 index (%)[b]
G1	<2	≤2
G2	2–20	3–20
G3	>20	>20

[a] 10 HPF: high power field=2 mm^2, at least 40 fields (at 40× magnification) evaluated in areas of highest mitotic density

[b] MIB1 antibody; % of 2,000 tumor cells in areas of highest nuclear labeling

Grading proposal (see Table 4)

Grading It has been widely discussed and generally accepted that no histological grading system effectively predicts the behavior of well-differentiated endocrine tumors. The major obstacle to developing a practically effective grading system is the fact that severe cytological atypia, as, for instance, in pheochromocytomas, has no impact on the clinical behavior and malignancy of such tumors. However, recent studies in well differentiated NETs of the foregut, including the pancreas, and of the midgut have shown the usefulness of a grading system [10, 25, 32]. Thus, well-differentiated endocrine tumors with a more solid appearance and distinct proliferative activity, which also lead to difficulties in the differential diagnosis vs poorly differentiated endocrine carcinomas, seem to have a worse prognosis than NETs without these features [16–18, 22, 23]. It was therefore decided to introduce a grading system that could be of help in distinguishing the well-differentiated NETs into G1 and G2 categories.

As a working suggestion, we propose to apply to foregut NETs a grading system modified from that adopted by the WHO for endocrine tumors of the lung, though exclusively referring to the proliferation status. In brief (see Table 4), three tumor categories are identified: G1, <2 mitosis per

2 mm^2 [10 high power fields (HPF) 40× magnification] and/or Ki-67 index ≤2%; G2, 2–20 mitosis per 2 mm^2 and/or Ki-67 index between 3 and 20%; G3 with 21 or more mitosis per 2 mm^2 and Ki-67 index >20%.

In general, G1 and G2 should refer to well-differentiated NETs displaying diffuse and intense expression of the two general immunohistochemical neuroendocrine markers, chromogranin A and synaptophysin [26]. Punctate necrosis is, per se, indicative of a more aggressive tumor, pointing to a G2 status, which, however, has to be confirmed by the mitotic count. G3 indicates a poorly differentiated neuroendocrine carcinoma. It has high mitotic counts/Ki-67 index, is often associated with fields of necrosis, and shows significantly reduced chromogranin A expression, while maintaining intense staining for synaptophysin. It is relevant to remind here that the diagnosis of G3 carcinoma is based on a specific histologic pattern according to the current WHO criteria [5, 7, 31]. In addition, the clinical behavior of G3 poorly differentiated neuroendocrine carcinomas of the gastroenteropancreatic tract does not necessarily correspond to that of small cell cancers of the lung or of any other sites.

Mitotic count and Ki-67 index We propose that mitoses should be counted on hematoxylin and eosin-stained slides in at least 40 HPFs, where possible. The mitoses should be assessed in areas where they are most frequent after a general slide survey. For Ki-67 assessment, the MIB1 antibody is recommended at the conditions that have been established at the laboratory in question. The Ki-67 index should be assessed in 2,000 tumor cells in areas where the highest nuclear labeling is observed (often but not exclusively at the tumor periphery).

Concluding remarks

Requests for standardization in the management of patients with gastroenteropancreatic NETs recently resulted in the development of several guidelines, including those proposed by ENETS [16, 17, 22, 23]. However, it was never attempted to reach consensus on specific practical issues. The TNM staging system we propose here was developed to meet a clinical need, is based on the current WHO classifications of endocrine and digestive tumors, and is the result of a consensus conference held by specialists involved in the management of digestive endocrine tumor patients. Along the same line, the grading system described here attempts to close the gap between the advances of the most recent WHO classifications and the need for a better prognostic assessment of NETs. It is obvious, of course, that all our proposals have to be validated by future clinicopathological work.

Acknowledgements Support came from grants from Ministry for Instruction University and Research (COFIN 2005) and the University of Parma to G. Rindi. The meeting in Frascati was supported by a generous grant to ENETS from IPSEN Pharmaceutical.

References

1. Anlauf M, Perren A, Meyer CL, Schmid S, Saremaslani P, Kruse ML, Weihe E, Komminoth P, Heitz PU, Klöppel G (2005) Precursor lesions in patients with multiple endocrine neoplasia type 1-associated duodenal gastrinomas. Gastroenterology 128:1187–1198
2. Anlauf M, Wieben D, Perren A, Sipos B, Komminoth P, Raffel A, Kruse ML, Fottner C, Knoefel WT, Monig H, Heitz PU, Klöppel G (2005) Persistent hyperinsulinemic hypoglycemia in 15 adults with diffuse nesidioblastosis: diagnostic criteria, incidence, and characterization of beta-cell changes. Am J Surg Pathol 29:524–533
3. Artale S, Giannetta L, Cerea G, Pedrazzoli P, Schiavetto I, Napolitano M, Veronese S, Bramerio E, Gambacorta M, Vanzulli A, Pisconti S, Pugliese R, Siena S (2005) Treatment of metastatic neuroendocrine carcinomas based on WHO classification. Anticancer Res 25:4463–4469
4. Bajetta E, Catena L, Procopio G, Bichisao E, Ferrari L, Della Torre S, De Dosso S, Iacobelli S, Buzzoni R, Mariani L, Rosai J (2005) Is the new WHO classification of neuroendocrine tumours useful for selecting an appropriate treatment? Ann Oncol 16:1374–1380
5. DeLellis RA, Lloyd RV, Heitz PU, Eng C (eds) (2004) World Health Organization classification of tumours, pathology and genetics of tumours of endocrine organs. IARC, Lyon
6. Gibril F, Doppman JL, Reynolds JC, Chen CC, Sutliff VE, Yu F, Serrano J, Venzon DJ, Jensen RT (1998) Bone metastases in patients with gastrinomas: a prospective study of bone scanning, somatostatin receptor scanning, and magnetic resonance image in their detection, frequency, location, and effect of their detection on management. J Clin Oncol 16:1040–1053
7. Hamilton SR, Aaltonen LA (eds) (2000) World Health Organization classification of tumours, pathology and genetics of tumours of the digestive system. IARC, Lyon
8. Hemminki K, Li X (2001) Familial carcinoid tumors and subsequent cancers: a nation-wide epidemiologic study from Sweden. Int J Cancer 94:444–448
9. Hemminki K, Li X (2001) Incidence trends and risk factors of carcinoid tumors: a nationwide epidemiologic study from Sweden. Cancer 92:2204–2210
10. Hochwald SN, Zee S, Conlon KC, Colleoni R, Louie O, Brennan MF, Klimstra DS (2002) Prognostic factors in pancreatic endocrine neoplasms: an analysis of 136 cases with a proposal for low-grade and intermediate-grade groups. J Clin Oncol 20:2633–2642
11. Jensen RT (1999) Natural history of digestive endocrine tumors. In: Mignon M, Colombel JF (eds) Recent advances in the pathophysiology and management of inflammatory bowel diseases and digestive endocrine tumors. John Libbey Eurotext, Montrouge, pp 192–219
12. Maggard MA, O'Connell JB, Ko CY (2004) Updated population-based review of carcinoid tumors. Ann Surg 240:117–122

13. Modlin IM, Kidd M, Latich I, Zikusoka MN, Shapiro MD (2005) Current status of gastrointestinal carcinoids. Gastroenterology 128:1717–1751
14. Modlin IM, Lye KD, Kidd M (2003) A 5-decade analysis of 13,715 carcinoid tumors. Cancer 97:934–959
15. Öberendorfer S (1907) Karzinoide tumoren des Dünndarms. Frankf Z Pathol 1:426–432
16. Oberg K, Astrup L, Eriksson B, Falkmer SE, Falkmer UG, Gustafsen J, Haglund C, Knigge U, Vatn MH, Valimaki M (2004) Guidelines for the management of gastroenteropancreatic neuroendocrine tumours (including bronchopulmonary and thymic neoplasms). Part I—general overview. Acta Oncol 43:617–625
17. Oberg K, Astrup L, Eriksson B, Falkmer SE, Falkmer UG, Gustafsen J, Haglund C, Knigge U, Vatn MH, Valimaki M (2004) Guidelines for the management of gastroenteropancreatic neuroendocrine tumours (including bronchopulmonary and thymic neoplasms). Part II—specific NE tumour types. Acta Oncol 43: 626–636
18. Oberg K, Kvols L, Caplin M, Delle Fave G, de Herder W, Rindi G, Ruszniewski P, Woltering EA, Wiedenmann B (2004) Consensus report on the use of somatostatin analogs for the management of neuroendocrine tumors of the gastroenteropancreatic system. Ann Oncol 15:966–973
19. Panzuto F, Di Fonzo M, Iannicelli E, Sciuto R, Maini CL, Capurso G, Milione M, Cattaruzza MS, Falconi M, David V, Ziparo V, Pederzoli P, Bordi C, Delle Fave G (2006) Long-term clinical outcome of somatostatin analogues for treatment of progressive, metastatic, well-differentiated entero-pancreatic endocrine carcinoma. Ann Oncol 17:461–466
20. Panzuto F, Nasoni S, Falconi M, Corleto VD, Capurso G, Cassetta S, Di Fonzo M, Tornatore V, Milione M, Angeletti S, Cattaruzza MS, Ziparo V, Bordi C, Pederzoli P, Delle Fave G (2005) Prognostic factors and survival in endocrine tumor patients: comparison between gastrointestinal and pancreatic localization. Endocr Relat Cancer 12:1083–1092
21. Pelosi G, Bresaola E, Bogina G, Pasini F, Rodella S, Castelli P, Iacono C, Serio G, Zamboni G (1996) Endocrine tumors of the pancreas: Ki-67 immunoreactivity on paraffin sections is an independent predictor for malignancy: a comparative study with proliferating-cell nuclear antigen and progesterone receptor protein immunostaining, mitotic index, and other clinicopathologic variables. Hum Pathol 27:1124–1134
22. Plöckinger U, Rindi G, Arnold R, Eriksson B, Krenning EP, de Herder WW, Goede A, Caplin M, Oberg K, Reubi JC, Nilsson O, Delle Fave G, Ruszniewski P, Ahlman H, Wiedenmann B (2004) Guidelines for the diagnosis and treatment of neuroendocrine gastrointestinal tumours. A consensus statement on behalf of the European Neuroendocrine Tumour Society (ENETS). Neuroendocrinology 80:394–424
23. Ramage JK, Davies AH, Ardill J, Bax N, Caplin M, Grossman A, Hawkins R, McNicol AM, Reed N, Sutton R, Thakker R, Aylwin S, Breen D, Britton K, Buchanan K, Corrie P, Gillams A, Lewington V, McCance D, Meeran K, Watkinson A (2005) Guidelines for the management of gastroenteropancreatic neuroendocrine (including carcinoid) tumours. Gut 54(Suppl 4):iv1–iv16
24. Rigaud G, Missiaglia E, Moore PS, Zamboni G, Falconi M, Talamini G, Pesci A, Baron A, Lissandrini D, Rindi G, Grigolato P, Pederzoli P, Scarpa A (2001) High resolution allelotype of nonfunctional pancreatic endocrine tumors: identification of two molecular subgroups with clinical implications. Cancer Res 61:285–292
25. Rindi G, Azzoni C, La Rosa S, Klersy C, Paolotti D, Rappel S, Stolte M, Capella C, Bordi C, Solcia E (1999) ECL cell tumor and poorly differentiated endocrine carcinoma of the stomach: prognostic evaluation by pathological analysis. Gastroenterology 116:532–542
26. Rindi G, Villanacci V, Ubiali A (2000) Biological and molecular aspects of gastroenteropancreatic neuroendocrine tumors. Digestion 45:19–26
27. Ruszniewski P, Ish-Shalom S, Wymenga M, O'Toole D, Arnold R, Tomassetti P, Bax N, Caplin M, Eriksson B, Glaser B, Ducreux M, Lombard-Bohas C, de Herder WW, Delle Fave G, Reed N, Seitz JF, Van Cutsem E, Grossman A, Rougier P, Schmidt W, Wiedenmann B (2004) Rapid and sustained relief from the symptoms of carcinoid syndrome: results from an open 6-month study of the 28-day prolonged-release formulation of lanreotide. Neuroendocrinology 80:244–251
28. Sandor A, Modlin IM (1998) A retrospective analysis of 1570 appendiceal carcinoids. Am J Gastroenterol 93:422–428
29. Sobin LH, Wittekind C (eds) (2002) TNM classification of malignant tumours. Wiley-Liss, New York
30. Solcia E, Bordi C, Creutzfeldt W, Dayal Y, Dayan AD, Fålkmer S, Grimelius L, Havu N (1988) Histopathological classification of nonantral gastric endocrine growths in man. Digestion 41:185–200
31. Solcia E, Klöppel G, Sobin LH (2000) Histological typing of endocrine tumours. Springer, Berlin Heidelberg New York
32. Van Eeden S, Quaedvlieg PF, Taal BG, Offerhaus GJ, Lamers CB, Van Velthuysen ML (2002) Classification of low-grade neuroendocrine tumors of midgut and unknown origin. Hum Pathol 33:1126–1132
33. Wiedenmann B (2004) From ENET to ENETS: a long odyssey in the land of small and rare tumors. Neuroendocrinology 80:1–12

Virchows Arch (2006) 449:402–409
DOI 10.1007/s00428-006-0263-9

ORIGINAL ARTICLE

Secretagogin, a novel neuroendocrine marker, has a distinct expression pattern from chromogranin A

Maode Lai · Bingjian Lü · Xiaoming Xing · Enping Xu · Guoping Ren · Qiong Huang

Received: 9 May 2006 / Accepted: 27 June 2006 / Published online: 6 September 2006
© Springer-Verlag 2006

Abstract Preliminary data suggest that secretagogin (SCGN), a calcium-binding protein identified from our previous proteomics study of colorectal cancers, is a potentially useful neuroendocrine marker. In this study, we further analyzed SCGN expression in normal and tumor tissues from various organ sites compared with three other conventional neuroendocrine markers [chromogranin A (CgA), neuron specific enolase, and synaptophysin]. We found strong SCGN staining in most normal neuroendocrine tissues except in the adrenal cortex. SCGN expression was identified in 140 out of 213 neuroendocrine tumors and 12 conventional carcinomas with neuroendocrine differentiation. In a subset of neuroendocrine tumors, such as gastric neuroendocrine cancers and typical carcinoid tumors of rectum and ovary, SCGN showed strong staining while CgA expression was often negative. It is intriguing to note that SCGN staining was positive in 26 out of 31 small cell lung cancers, more frequently than the other three markers. We conclude that SCGN is a novel neuroendocrine marker that may be useful in routine surgical pathology practice.

Keywords Neuroendocrine tumor · Small cell lung cancer · Gastrointestinal tract · Secretagogin · Chromogranin A

M. Lai (✉) · B. Lü · X. Xing · E. Xu · Q. Huang
Department of Pathology and Pathophysiology,
School of Medicine, Zhejiang University,
Zhejiang, China
e-mail: lmd@zju.edu.cn

G. Ren
Department of Surgical Pathology, the First Affiliated Hospital,
School of Medicine, Zhejiang University,
Zhejiang, China

Introduction

Neuroendocrine system is collectively defined as cells present either in endocrine organs or dispersed throughout the human body (diffuse neuroendocrine system), which can produce neurotransmitter, neuromodulator, or neuropeptide hormones as those identified in neurons [1]. Neuroendocrine tumors, a group of heterogenous tumors in morphology and function arising from neuroendocrine cells, are not uncommon. Their incidence is climbing, primarily due to our increased knowledge and improved detection methods. The presence of scattered neuroendocrine cells in conventional adenocarcinoma is a common finding and their prognostic significance is uncertain [8, 21, 23, 30]. Immunohistochemical staining for neuroendocrine markers is the mainstay for routine diagnosis of neuroendocrine tumors and neuroendocrine differentiation. There is a need for a sensitive and specific neuroendocrine marker.

Generally, there are two catalogs of neuroendocrine markers, specific and generic. The specific markers are antibodies against cell-type-specific regulatory peptides or hormones, such as insulin, glucagon, gastrin, neurotensin, and calcitonin. These markers are highly specific for a subset of neuroendocrine cells and tumors, but they cannot detect most other neuroendocrine cells and tumors, including nonfunctional neuroendocrine tumors. On the other hand, the generic markers are antibodies against certain peptides, which function in the common process of neuroendocrine differentiation, for example, components of secretory granules or nondense core small vesicles. They stain a broad spectrum of neuroendocrine cells and tumors. Neuron-specific enolase (NSE), chromogranin A (CgA), and synaptophysin (Syn) are three conventional generic markers. CgA is considered a golden standard for immu-

nohistochemical and serological identification of normal and neoplastic neuroendocrine cells [24, 27, 28], but it is not highly sensitive for those paucigranulated or agranulated neuroendocrine tumors, including small cell lung cancers (SCLC), pituitary prolactinomas, and rectal and ovarian carcinoid tumors [9, 11, 12, 20]. NSE has the advantage of identifying these tumors because they do not depend on granules. However, their specificity has been challenged [3, 6].

Most generic neuroendocrine markers are first isolated from the neuroendocrine tissues or brain extracts. The gastrointestinal–pancreatic system, which produces more than 30 hormones, is the richest source of neuroendocrine cells beyond the brain. Therefore, it might be a straightforward strategy to discover novel neuroendocrine biomarkers from gastrointestinal tracts. Our recent proteomics study by two-dimensional gel electrophoresis and mass spectrometry (MALDI-TOF) found a novel, downregulated protein secretagogin (SCGN) in colon cancers [29]. This protein did not stain most colonic cancer cells, but invariably expressed in a few small polygonal cells within the lower half of crypts in normal mucosa, a characteristic pattern of intestinal neuroendocrine cells. Wagner et al. [25, 26] first identified SCGN as a pancreatic β-cell-specific calcium-binding protein. SCGN expression in a small number of normal neuroendocrine tissues and tumors was also reported recently [4, 31]. These preliminary findings suggest that SCGN may be a novel neuroendocrine marker. In the current investigation, we analyzed SCGN expression in tumors and normal tissues in various organ sites by immunohistochemistry using the specific antibody for SCGN compared with three other general neuroendocrine markers, CgA, NSE, and Syn. Our study demonstrated that SCGN is a novel reliable and sensitive neuroendocrine biomarker.

Materials and methods

Specimens

Four percent neutral-buffered formaldehyde-fixed, paraffin-embedded blocks of 213 neuroendocrine tumors and 304 nonneuroendocrine tumors were obtained from the archive of the Department of Surgical Pathology, the First Affiliated Hospital, School of Medicine, Zhejiang University, China. Normal tissues adjacent to tumors or those from distant excision margins were available in 113 neuroendocrine tumors and 217 nonneuroendocrine tumors. Two pathologists reviewed the hematoxylin–eosin slides and confirmed the diagnosis. The histological diagnoses are listed in Tables 1 and 2. The Ethics Committee of Biomedicine in Zhejiang University, China authorized this study.

Antibodies

The polyclonal antibody against the recombinant SCGN/glutathione S-transferase fusion proteins (from Ludwig Wagner, University of Vienna, Austria) was diluted to 1:4,000. Three commercial antibodies (Santa Cruz, USA) against CgA (LK 2H10), NSE (E27), and Syn (SP88) were also applied. The dilution for CgA was 1:400, Syn 1:100, and NSE 1:80.

Immunohistochemistry

Immunohistochemical staining was undertaken using the En Vision two-step method (DAKO, Denmark) following the manufacturer's instruction. After deparaffinization and rehydration, the 4-μm tissue sections were subjected to heat-induced antigen retrieval buffer (pH 6.0 citrate buffer) for 20 min in a microwave (Galanze, China), blocked with 3‰ hydrogen peroxide for 15 min at room temperature, incubated with diluted primary antibodies overnight at 4°C, then processed with corresponding ready-to-use peroxidase-conjugated antibodies for 30 min at room temperature, and finally developed with 3,3′-diaminobenzidine as chromogen and counterstained with Mayer's hematoxylin. Staining controls included the omission of primary antiserum as the negative control and normal pancreas tissues (islet) as positive control. All slides were assessed by two pathologists. Only cells with clearcut brownish cytoplasmic or nucleocytoplasmic staining were considered as positive. The tumors were identified as "–" (no immunoreactive cells), "±" (<5% of cells positive), "+" (5–25% of cells positive), "++" (26–50% cells positive), and "+++" (>50% cells positive).

Results

SCGN expression in normal tissues

Generally, SCGN expression is consistent with CgA and Syn expression. Briefly, pituitary gland, pancreas islet, thyroid "C" cells, neuroganglion, nerves, and diffuse neuroendocrine cells along the gastrointestinal and respiratory tracts were SCGN+ (Fig. 1a,b). However, we found weak SCGN staining in the parathyroid gland and adrenal medulla, and negative SCGN staining in the adrenal cortex and thyroid follicular cells. The staining pattern of neuroendocrine cells in gastrointestinal tracts showed minor differences among Syn, CgA, and SCGN. Numerous CgA+ cells appeared in a granular, cone-shaped form. Syn+ cells were round or oval and had abundant foamy cytoplasm. CgA+ and Syn+ cells have few or no protrusions, which rarely extended into the epithelial luminal surface, mimick-

Table 1 Expression of SCGN, CgA, Syn, and NSE in neuroendocrine cancers

Diagnosis	CgA	SCGN	Syn	NSE
WDNET of pancreas	8 (7)/8	8 (8)/8	8 (8)/8	8 (7)/8
Mixed exocrine–endocrine cancer (pancreas)	1/1	1/1	N.A.	N.A.
Pituitary adenoma	9 (4)/10	10 (4)/10	10 (10)/10	10 (6)/10
Adrenal cortical adenoma	2 (0)/11	1 (0)/11	10 (6)/11	6 (2)/11
Pheochromocytoma	11 (11)/12	3 (0)/12	10 (9)/12	10 (7)/12
Paraganglioma	10 (9)/10	12 (3)/20	10 (9)/10	10 (10)/10
Parathyroid adenoma	12 (12)/12	0/12	2 (1)/12	1 (0)/12
Medullary thyroid cancer	6 (6)/6	13 (13)/13	6 (6)/6	6 (6)/6
Thymic carcinoid	5 (5)/5	0/5	5 (5)/5	5 (4)/5
Ovarian carcinoid	0/3	3 (3)/3	2 (2)/3	3 (2)/3
Carcinoid in ovarian teratoma	2 (2)/2	2 (2)/2	2 (2)/2	2 (2)/2
Gastric carcinoid	N.A.	0/1	N.A.	N.A.
Gastric atypical carcinoid	6 (3)/6	6 (5)/6	6 (4)/6	5 (1)/6
Gastric NEC	3 (1)/6	4 (4)/6	4 (2)/6	0/6
Small intestinal carcinoid	2 (2)/2	4 (4)/4	2 (2)/2	2 (2)/2
Small intestinal NEC	N.A.	0/1	N.A.	N.A.
Appendiceal carcinoid	7 (7)/7	6 (6)/7	7 (5)/7	6 (4)/7
Rectal carcinoid	1 (0)/7	7 (7)/7	7 (7)/7	6 (6)/7
Liver carcinoid	N.A.	2 (2)/2	N.A.	N.A.
Liver NEC	N.A.	2 (2)/2	N.A.	N.A.
Lung atypical carcinoid	4 (1)/7	11 (9)/12	4 (4)/7	6 (5)/7
LCNEC	2 (1)/4	3 (2)/6	4 (3)/4	4 (2)/4
SCLC	14 (6)/25	26 (17)/31	13 (11)/25	15 (5)/25
Extra-pulmonary small cell cancer	N.A.	7 (2)/21	N.A.	N.A.
Merkel cell carcinoma	2 (2)/2	9 (5)/10	2 (2)/2	2 (0)/2

The results are given as the number of positive tumors/total number of the tumors. The number of at least ++ are given in the parentheses. *WDNET* Well-differentiated neuroendocrine tumors (i.e., islet cell tumors of pancreas), *NEC* neuroendocrine cancer, *LCNEC* large cell neuroendocrine cancer, *SCLC* small cell lung cancer, and *N.A.* not available

ing so-called "close" endocrine cells. SCGN+ cells invariably showed long protrusion toward the lumen surface (Fig. 1b). Similar staining patterns were also seen in respiratory tracts, but with much fewer SCGN+ cells than in the gastrointestinal tracts. NSE was negative in these diffuse neuroendocrine cells.

SCGN expression was invariably absent in most non-endocrine cells and tissues such as skin, hepatocytes, striated or smooth muscle, collagen, endothelial cells, and lymphocytes. Exceptionally, SCGN expression was found in small bile ducts, Hassall's corpuscles of thymus, renal convoluted tubules, and the intercalated ducts of salivary (parotid) glands.

SCGN expression in neuroendocrine tumors

The immunohistochemical results of SCGN, CgA, NSE, and Syn in neuroendocrine tumors are summarized in Table 1. SCGN expression was identified in 140 out of 213 neuroendocrine tumors. The distribution of SCGN expression in neuroendocrine tumors had common features for CgA, Syn, and NSE. Consistent staining of these four antibodies was found in well-differentiated neuroendocrine tumors (WDNET, i.e., islet cell tumors); medullary thyroid carcinomas; pituitary adenomas; typical carcinoid tumors in small intestine, appendix, and ovarian teratomas; gastric atypical carcinoids; and Merkel cell cancers (Fig. 2a–d).

However, we also noted different expression patterns among these neuroendocrine markers. In typical carcinoid tumors, inconsistent staining remained among SCGN, CgA, NSE, and Syn. CgA did not stain 6/7 rectal and 3/3 ovary carcinoid tumors, whereas SCGN stained all of these carcinoid tumors (Fig. 2e,f). Conversely, all five thymic carcinoid tumors were CgA+, Syn+, and NSE+, but SCGN−. Gastric neuroendocrine cancers were NSE−, but four, three, and four cases expressed SCGN, CgA, and Syn, respectively. It should be noted that SCGN expression was present in three CgA− gastric neuroendocrine cancers. In 11 adrenal cortical adenomas, only 2 were CgA+ and 1 SCGN+, but 10 or 6 were Syn+ and NSE+, respectively. SCGN expression was weak in most pheochromocytomas and paragangliomas, and negative in all 12 parathyroid adenomas. In contrast, CgA staining was strong in all these tumors.

There was another major difference among these neuroendocrine markers in pulmonary endocrine tumors, particularly in SCLC. CgA was expressed in four out of

Table 2 Expression of SCGN in nonneuroendocrine tumors

Histological diagnosis	Cases	SCGN
Benign tumors		
Gastrointestinal stromal tumor	2	–
Conjunctional/intradermal nevus	4	–
Pleomorphic adenoma (parotid)	2	1 (±); N
Schwannoma	4	–
Thymoma	5	–
Mature teratoma	3	–
Ganglioneuroma (adrenal)	2	–
Lung		
Squamous cell carcinoma	12	–
Lung adenocarcinoma	14	–
Bronchioloalveolar carcinoma	5	–
Lung large cell carcinoma	4	1 (+); C
Thyroid		
Follicular adenoma	8	–
Papillary carcinoma	9	–
Follicular carcinoma	5	–
Undifferentiated carcinoma	1	–
Adenocarcinoma		
Stomach	8	2 (±) 1 (+); C
Colorectum	12	2 (±) 1 (+); C
Pancreas	10	2 (+); C
Prostate	21	2 (±) 1 (+); C/N
Breast	9	–
Kidney (clear cell carcinoma)	5	3 (++); C
Ovary	6	–
Endometrium	3	–
Metastatic (unknown)	2	–
Squamous cell carcinoma		
Esophagus	2	–
Skin	3	–
Cervix	3	–
Other carcinoma		
Hepatocellular carcinoma	4	–
Bile duct carcinoma	1	–
Urothelial carcinoma	8	–
Mucoepidermoid carcinoma	3	–
Metastatic nasopharyngeal carcinoma	1	–
Sarcomas		
Hemangiosarcoma	3	–
Rhabdomyosarcoma	4	–
Liposarcoma	5	1 (+); N
Osteosarcoma	3	–
Chondrosarcoma	2	–
Malignant fibrous histiocytoma	4	–
Melanoma	6	–
Stromal sarcoma (uterine)	1	–
Non-Hodgkin's lymphoma	3	–
Spindle cell sarcoma	12	–
Synovial sarcoma	1	1 (±); C
Clear cell sarcoma	2	–
Undifferentiated sarcoma	6	–
Leiomyosarcoma	1	–
Fibrosarcoma	1	–
Epithelioid sarcoma	9	–
Ewing's sarcoma	4	–
Others		
Nephroblastoma	2	1 (±); C
Seminoma	8	–
Embryonic carcinoma	6	–
Medulloblastoma	2	–
Neuroblastoma	2	–
Retinoblastoma	5	–
Olfactory neuroblastoma	7	–
Astrocytoma	11	–
Yolk sac tumor	1	–
Pseudopapillary neoplasm (pancreas)	3	–

The total numbers of tumors are given in the second column. The numbers of positive SCGN staining are given in the third column. The expression categories are given in the parenthesis, which are separated as: "–" (no positive cells), "±" (<5% cells positive), "+" (5–25% of cells positive), "++" (26–50% cells positive), and "+++" (>50% cells positive).
Carcinoid tumor arising in teratoma can be seen in Table 1.
C cytoplasmic staining, *N* nuclear staining, and *N/C* nucleocytoplasmic staining

seven atypical carcinoid tumors and diffusely in one. SCGN and NSE were expressed in 11 out of 12 and 6 out of 7 and diffusely in 9 and 5, respectively. It is intriguing to note that we noticed that SCGN was very sensitive for SCLC, of which 26 out of 31 cases including 4 out of 6 metastatic cancers were SCGN+ and 17 had diffuse and strong expression. Out of 25 primary SCLCs, 14, 13, and 15 were positive, and 6, 5, or 11 were diffusely positive for CgA, NSE, and Syn, respectively (Fig. 2g,h). In SCLC, focal staining of CgA and NSE seemed more common than that of SCGN and Syn. In addition, we also detected SCGN expression in 21 extra-lung small cell cancers from skin, parotid, ureter, bladder, and pharynx, of which only 7 were positive. In large cell neuroendocrine cancer (LCNEC), three out of six were SCGN+, two out of four CgA+, and four out of four NSE+ and Syn+.

SCGN expression in nonneuroendocrine tumors

Most nonneuroendocrine tumors did not express SCGN as shown in Table 2. It is noteworthy that three cases of pseudopapillary neoplasm of pancreas, the mimics of WDNET with unknown histogenesis, were SCGN− and CgA−, although two were Syn+ and NSE+. In this study, there is a group of so-called small round blue cell tumor: olfactory neuroblastoma 7, retinoblastoma 5, medulloblastoma 2, neuroblastoma 2, embryonic rhabdomyosarcoma 2, and Ewing's sarcoma 3. These cancers were SCGN− except for occasional nuclear staining in one neuroblastoma. Syn and NSE were invariably expressed in olfactory neuroblastoma and retinoblastoma, but CgA expression was uncommon. In

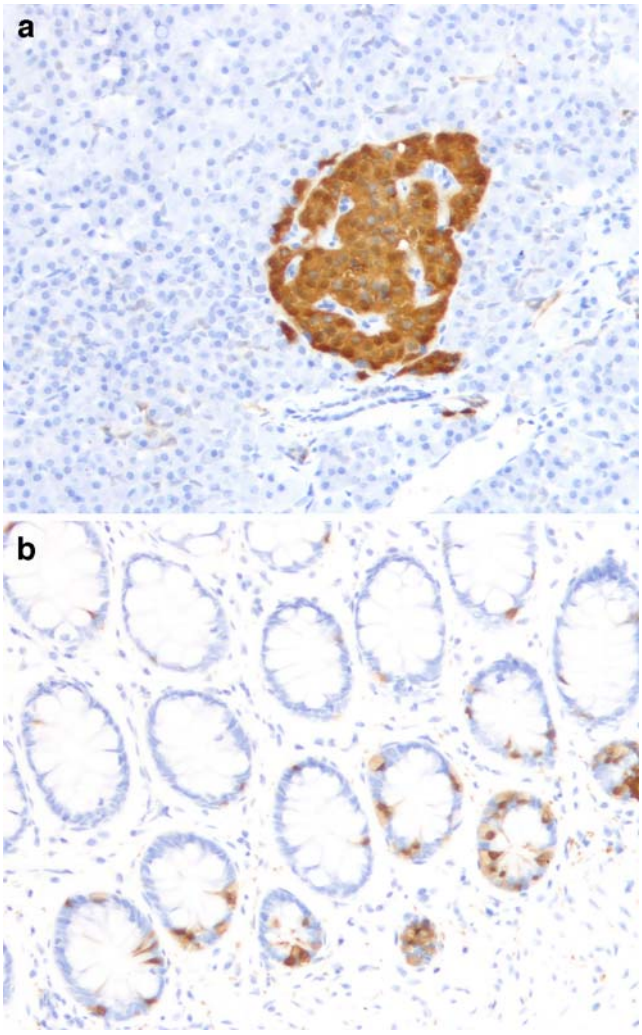

Fig. 1 SCGN expression in normal cells and tissues. **a** SCGN expression was strong in pancreas islet and negative in the exocrine components. **b** SCGN+ cells in gastric mucosa had long protrusions extending toward the luminal surface, mimicking the "open" diffuse neuroendocrine cells

addition, we found less than 10% SCGN+ cells in 12 cases of conventional carcinomas (lung 1, stomach 3, colorectum 3, pancreas 2, and prostate 3). All these cancers invariably showed another antibody expression in keeping with neuroendocrine differentiation. Finally, we also found SCGN expression in a minority of nonneuroendocrine tumors, including renal cell carcinomas (clear cell carcinoma), myxoid liposarcoma, parotid pleomorphic adenoma, and the epithelial component of Wilm's tumor and synovial sarcoma.

Discussion

SCGN, an EF-hand calcium-binding protein, was first identified from a human pancreatic cDNA library by immunoscreening with the murine monoclonal antibody D24 generated using a human insulinoma as immunogen [25, 26]. This gene was mapped to chromosome 6p22.1–22.3. The deduced amino acid sequence, highly homogenous to human calbindin D28K and calretinin, specified a protein of 276 amino acids with calculated molecular mass of 32 kDa and contained six putative tandem repeats of the EF-hand Ca^{2+}-binding domain. SCGN may regulate cell growth and differentiation in neuroendocrine cells. SCGN was abundant in the serial analysis of gene analysis library of the human pancreatic islet, highlighting the potential importance of this protein in hormone secretion [4]. A recent study revealed that this protein seemed to be related to the Ca^{2+} cascade underlying radiotherapy-released pain in cancer metastasis [15]. In this study, we confirmed the sensitivity and specificity of SCGN expression in neuroendocrine tumors. Our results were also supported by a recent study, which was published during our preparation of this manuscript. In that study, only a small number of neuroendocrine tumors, primarily within the hepatogastrointestinal system and lung, were evaluated [2]. Our current study is a thorough survey on SCGN expression in various human tissues and tumors. To our knowledge, it is so far the largest clinical investigation of SCGN expression. More importantly, we had several distinct findings as discussed below.

First, we noted that SCGN showed a distinct complementary expression pattern in a fraction of neuroendocrine tumors, including typical carcinoid tumors of rectum and ovary and gastric neuroendocrine cancers in comparison with CgA, the golden standard marker of neuroendocrine tissues. CgA was frequently absent or only focally expressed in most of these tumors in previous studies [9, 12, 18]. Therefore, SCGN will be of great assistance in diagnosing neuroendocrine tumors in these organ sites. SCGN might also serve as a promising serum biomarker for patients with neuroendocrine tumors because the level of SCGN could be readily measured in serum obtained from patients [2, 5].

The most important clues with potential clinical implications emerged from SCLC. Our data indicated that SCGN is an excellent marker for SCLC. SCLCs are not readily detected by most conventional neuroendocrine markers, including Syn, NSE, and CgA, which reflects the poor differentiation and paucigranules in SCLC [7, 11, 16, 22]. Even with a combined application of several common neuroendocrine antibodies, about 10% of SCLC remained negative. This study also confirmed these findings. It is striking to note that 17 out of 31 SCLCs had diffuse SCGN expression. In diagnostic pathology, small biopsies through endoscopy or core needle biopsy are of ever increasing importance for SCLC because chemotherapy is the first line of therapeutic regimen rather than surgery. Immunohistochemical confirmation of neuroendocrine differentiation becomes crucial under such circumstances, particularly on small biopsy with poor quality of histology. Focal expres-

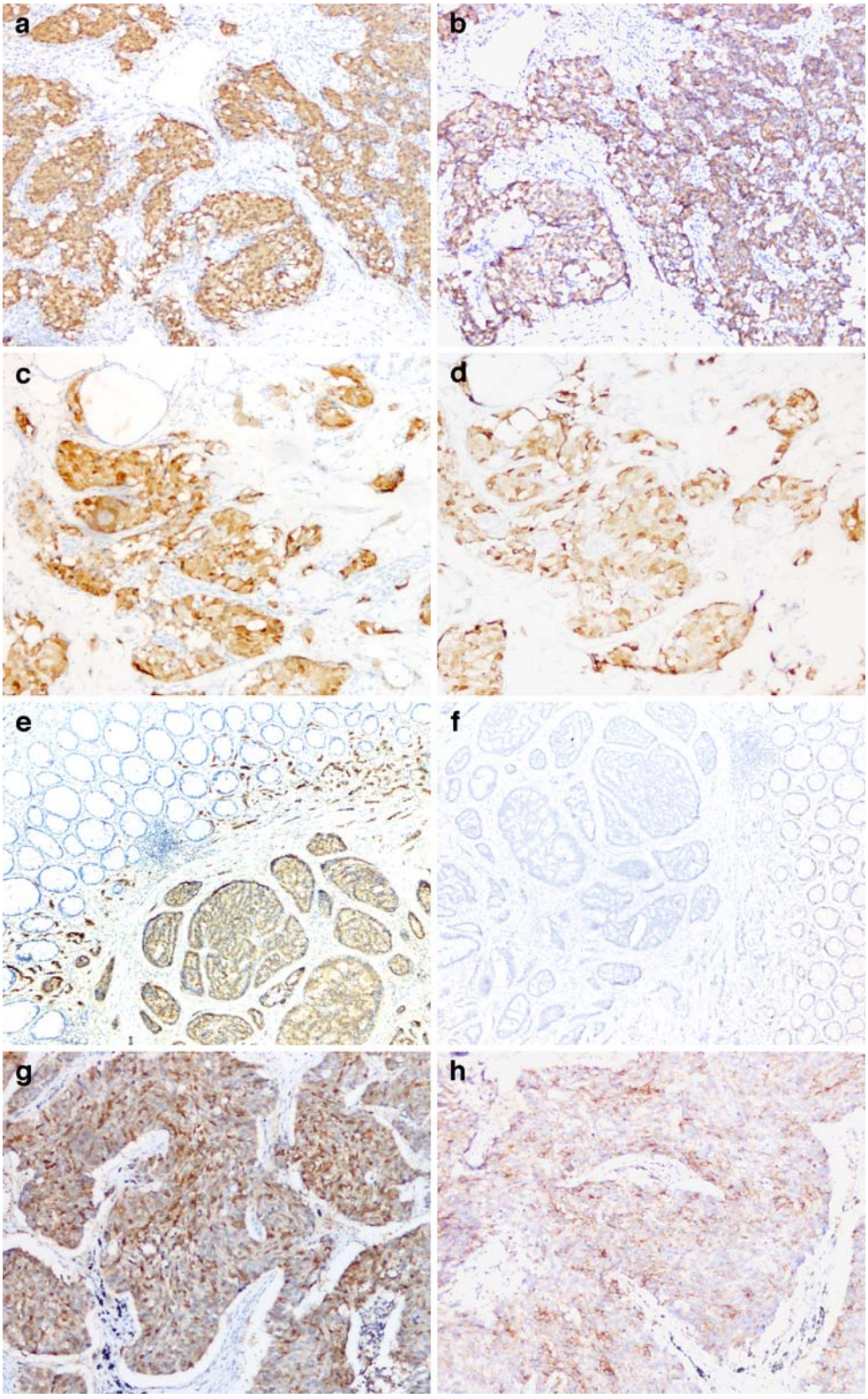

Fig. 2 SCGN expression in neuroendocrine tumors compared with CgA. Pancreatic WDNET (**a**, **b**) and medullary thyroid cancer (**c**, **d**) have strong SCGN and CgA expression (**a**, **c**: SCGN; **b**, **d**: CgA). Rectal typical carcinoid tumor shows intense SCGN staining (**e**) but no CgA staining (**f**). In SCLC, SCGN staining (**g**) is stronger than CgA staining (**h**)

sion means the increased potential of false negative CgA expression in these cases, resulting in diagnostic dilemmas. SCGN may contribute to overcoming such predicaments. It is widely accepted that neural cell adhesion molecules (NCAMs) connoted poor differentiation of neuroendocrine lung tumors and were considered to be the most sensitive marker for SCLC [10, 16]. However, their diagnostic value was limited due to broad immunoreaction beyond neuro-

endocrine tissues, including natural killer cells, squamous cell carcinoma, adenocarcinoma, mesothelioma, etc. Considering focal SCGN expression was only observed in 1 out of 35 conventional lung cancers, we believe that SCGN is more specific than NCAM in SCLC.

Small round blue cell tumors have common morphologic features [17]. The differential diagnosis is important and difficult. Immunoperoxidase staining is essential for differential diagnosis. Unfortunately, several generic neuroendocrine markers display overlapping staining pattern among Merkel cell cancer, small cell cancer, and other cancers. For example, Ewing's sarcoma also expresses NSE, secretogranin II, and neuroblastoma CgA and Syn [13, 14]. In this study, we found that SCGN was only expressed in small cell carcinomas and Merkel cell cancer rather than other small cell tumors, implicating its potential application in the differential diagnosis among these tumors.

Nevertheless, SCGN was not highly sensitive for a subset of neuroendocrine tumors, including parathyroid adenoma, paraganglioma, and adrenal cortical adenoma, which is consistent with the report of Wagner et al. [26]. The differential diagnosis between medullary thyroid cancer and parathyroid tumor is difficult sometimes [19]. Supposedly, SCGN might be helpful under such circumstances when calcitonin staining is not optimal. Simultaneously, we also noted SCGN staining in a minority of nonneuroendocrine tissues and tumors. The underlying mechanism remained unknown, possibly because of post-transcriptional modifications of SCGN in different tissues and tumors.

In summary, in this largest survey of SCGN expression in a broad spectrum of normal human tissues and tumors, we confirmed SCGN expression in normal neuroendocrine tissues and tumors throughout the body. SCGN is a novel neuroendocrine marker that promises complementary significance in diagnostic pathology.

Acknowledgements This manuscript was supported by the Key Foundation from Zhejiang Science and Technology Bureau, China. We thank Professor Ludwig Wagner, University of Vienna, Austria, for providing the polyclonal antibody for SCGN. We are indebted to Dr. Peiguo Chou and Dr. Qing Huang, Department of Pathology, City of Hope National Medical Center, USA, for their kindness in providing several cases of soft tissue tumors, Merkel cell cancers, and extra-lung small cell cancers. We also thank Ms Min Wang for her technical support.

References

1. Barakat MT, Meeran K, Bloom SR (2004) Neuroendocrine tumours. Endocr Relat Cancer 11:1–18
2. Birkenkamp-Demtroder K, Wagner L, Brandt Sorensen F, Bording Astrup L, Gartner W, Scherubl H, Heine B, Christiansen P, Orntoft TF (2005) Secretagogin is a novel marker for neuroendocrine differentiation. Neuroendocrinology 82:121–138
3. Campbell LK, Thomas JR, Lamps LW, Smoller BR, Folpe AL (2003) Protein gene product 9.5 (PGP9.5) is not a specific marker of neural and nerve sheath tumours: an immunohistochemical study of 95 mesenchymal neoplasms. Mod Pathol 16:963–969
4. Cras-Meneur C, Inoue H, Zhou Y, Ohsugi M, Bernal-Mizrachi E, Pape D, Clifton SW, Permutt MA (2004) An expression profile of human pancreatic islet mRNAs by serial analysis of gene expression (SAGE). Diabetologia 47:284–299
5. Gartner W, Lang W, Leutmetzer F, Domanovits H, Waldhausl W, Wagner L (2001) Cerebral expression and serum detectability of secretagogin, a recently cloned EF-hand Ca2+-binding protein. Cereb Cortex 11:1161–1169
6. Gosney JR, Gosney MA, Lye M, Butt SA (1995) Reliability of commercially available immunocytochemical markers for identification of neuroendocrine differentiation in bronchoscopic biopsies of bronchial carcinoma. Thorax 50:116–120
7. Guinee DG Jr, Fishback NF, Koss MN, Abbondanzo SL, Travis WD (1994) The spectrum of immunohistochemical staining of small-cell lung carcinoma in specimens from transbronchial and open-lung biopsies. Am J Clin Pathol 102:406–414
8. Howe MC, Chapman A, Kerr K, Dougal M, Anderson H, Hasleton PS (2005) Neuroendocrine differentiation in non-small cell lung cancer and its relation to prognosis and therapy. Histopathology 46:195–201
9. Kimura N, Pilichowska M, Okamoto H, Kimura I, Aunis D (2000) Immunohistochemical expression of chromogranins A and B, prohormone convertases 2 and 3, and amidating enzyme in carcinoid tumours and pancreatic endocrine tumours. Mod Pathol 13:140–146
10. Lantuejoul S, Moro D, Michalides RJ, Brambilla C, Brambilla E (1998) Neural cell adhesion molecules (NCAM) and expression in neuroendocrine lung tumours. Am J Surg Pathol 22:1267–1276
11. Loy TS, Darkow GV, Quesenberry JT (1995) Immunostaining of pulmonary neuroendocrine carcinomas. An immunohistochemical study with ultrastructural correlations. Am J Surg Pathol 19:173–182
12. Mani S (1994) Carcinoids of the rectum. J Am Coll Surg 179:231–248
13. Molenaar WM, Baker DL, Pleasure D, Lee VM, Trojanowski JQ (1990) The neuroendocrine and neural profiles of neuroblastomas, ganglioneuroblastomas, and ganglioneuromas. Am J Pathol 136:375–382
14. Pagani A, Fischer-Colbrie R, Sanfilippo B, Winkler H, Cerrato M, Bussolati G (1992) Secretogranin II expression in Ewing's sarcomas and primitive neuroectodermal tumours. Diagn Mol Pathol 1:165–172
15. Park HC, Seong J, An JH, Kim J, Kim UJ, Lee BW (2005) Alteration of cancer pain-related signals by radiation: proteomic analysis in an animal model with cancer bone invasion. Int J Radiat Oncol Biol Phys 61:1523–1534
16. Patriarca C, Pruneri G, Alfano RM, Carboni N, Ermellino L, Guddo F, Buffa R, Siccardi AG, Coggi G (1997) Polysialylated N-CAM, chromogranin A and B, and secretogranin II in neuroendocrine tumours of the lung. Virchows Arch 430:455–460
17. Pisick E, Skarin AT, Salgia R (2003) Recent advances in the molecular biology, diagnosis and novel therapies for various small blue cell tumours. Anticancer Res 23:3379–3396
18. Rindi G, Kloppel G (2004) Endocrine tumours of the gut and pancreas tumour biology and classification. Neuroendocrinology 80:12–15
19. Sawady J, Mendelsohn G, Sirota RL, Taxy JB (1989) The intrathyroidal hyperfunctioning parathyroid gland. Mod Pathol 2:652–657
20. Schmid KW, Kroll M, Hittmair A, Maier H, Totsch M, Gasser R, Finkenstett G, Hogue-Angeletti R, Fischer-Colbrie R (1991)

Chromogranin A and B in adenomas of the pituitary. An immunohistochemical study of 42 cases. Am J Surg Pathol 15:1072–1077
21. Scopsi L, Andreola S, Pilotti S, Testori A, Baldini MT, Leoni F, Lombardi L, Hutton JC, Shimizu F, Rosa P (1992) Argyrophilia and granin (chromogranin/secretogranin) expression in female breast carcinomas. Their relationship to survival and other disease parameters. Am J Surg Pathol 16:561–576
22. Senden NH, Timmer ED, de Bruine A, Wagenaar SS, Van de Velde HJ, Roebroek AJ, Van de Ven WJ, Broers JL, Ramaekers FC (1997) A comparison of NSP-reticulons with conventional neuroendocrine markers in immunophenotyping of lung cancers. J Pathol 182:13–21
23. Syversen U, Halvorsen T, Marvik R, Waldum HL (1995) Neuroendocrine differentiation in colorectal carcinomas. Eur J Gastroenterol Hepatol 7:667–674
24. Taupenot L, Harper KL, O'Connor DT (2003) The chromogranin-secretogranin family. N Engl J Med 348:1134–1149
25. Wagner L, Templ E, Reining G, Base W, Weissel M, Nowotny P, Kaserer K, Waldhausl W (1998) Culture of human insulinoma cells: development of a neuroendocrine tumour cell- and human pancreatic islet cell-specific monoclonal antibody. J Endocrinol 156:469–476
26. Wagner L, Oliyarnyk O, Gartner W, Nowotny P, Groeger M, Kaserer K, Waldhausl W, Pasternack MS (2000) Cloning and expression of secretagogin, a novel neuroendocrine and pancreatic islet of Langerhans-specific Ca2+-binding protein. J Biol Chem 275:24740–24751
27. Weiler R, Fischer-Colbrie R, Schmid KW, Feichtinger H, Bussolati G, Grimelius L, Krisch K, Kerl H, O'Connor D, Winkler H (1988) Immunological studies on the occurrence and properties of chromogranin A and B and secretogranin in endocrine tumours. Am J Surg Pathol 12:877–884
28. Wilson BS, Lloyd RV (1984) Detection of chromogranin in neuroendocrine cells with a monoclonal antibody. Am J Pathol 115:458–468
29. Xing X, Lai M, Gartner W, Xu E, Huang Q, Li H, Chen G (2006) Identification of differentially expressed proteins in colorectal cancer by proteomics: down-regulation of secretagogin. Proteomics 6:2916–2923
30. Yu DS, Hsieh DS, Chen HI, Chang SY (2001) The expression of neuropeptides in hyperplastic and malignant prostate tissue and its possible clinical implications. J Urol 166:871–875
31. Zhan X, Evans CO, Oyesiku NM, Desiderio DM (2003) Proteomics and transcriptomics analyses of secretagogin down-regulation in human non-functional pituitary adenomas. Pituitary 6:189–202

Virchows Arch (2006) 449:410–420
DOI 10.1007/s00428-006-0253-y

ORIGINAL ARTICLE

Prognostic value of the International Neuroblastoma Pathology Classification in Neuroblastoma (Schwannian stroma-poor) and comparison with other prognostic factors: a study of 182 cases from the Spanish Neuroblastoma Registry

Octavio Burgues · Samuel Navarro · Rosa Noguera · Antonio Pellín · Amparo Ruiz · Victoria Castel · Antonio Llombart-Bosch

Received: 21 December 2005 / Accepted: 13 June 2006 / Published online: 29 August 2006
© Springer-Verlag 2006

Abstract In addition to clinical and biological factors, further valuable prognostic information in neuroblastoma (Schwannian stroma-poor) (NB) patients is provided by the histopathologic analysis and the application of the International Neuroblastoma Pathology Classification (INPC) system. The objective of this study was to assess the prognostic impact of the INPC classification in a series of NB (Schwannian stroma-poor) and its relation with other prognostic factors. One hundred eighty-two cases of NB were collected from the files of the Spanish Neuroblastoma Registry. Slides were reviewed, and NB cases were grouped into favorable and unfavorable categories according to INPC criteria, taking into account morphological features (mitosis–karyorrhexis index, histological subtype) and patient's age at diagnosis. Other pathological [presence of calcifications, tissular components, and number of mitotic cells per 10 high-power field (HPF)], immunohistochemical (P-glycoprotein and Ki-67 protein expression) and genetic (MYCN amplification and chromosome 1p deletion) features were also studied. Statistical analyses of overall survival with Kaplan–Meier curves and a multivariate study using Cox regression were performed (40.3% of NBs were considered favorable and 59.7% unfavorable). Unfavorable NB showed a mean survival time of 57 months compared with 89 months in favorable cases. Advanced stage, more than ten mitoses per 10 HPF, Ki-67 expression in more than 30% of tumor cells, MYCN oncogene amplification and chromosome 1p deletion were observed more frequently in unfavorable NB. The Cox regression analysis demonstrated that clinical stage (International Neuroblastoma Staging System stage 4) and histological subtype (undifferentiated NB) were the most important factors that influence the overall survival ($p<0.001$). INPC classification results are major prognostic indicators in NB and should be considered in the therapeutic stratification of NB patients.

Keywords Neuroblastoma · Neuroblastic tumors · Pediatric tumors

O. Burgues · S. Navarro (✉) · R. Noguera · A. Pellín · A. Ruiz · A. Llombart-Bosch
Departamento de Patología, Facultad de Medicina de Valencia, Avda. Blasco Ibañez, 17,
E-46010 Valencia, Spain
e-mail: samuel.navarro@uv.es

V. Castel
Pediatric Oncology Unit, Hospital Universitario "La Fe", Valencia, Spain

Introduction

Classically, neuroblastoma (NB) (Schwannian stroma-poor) prognosis is based on two clinical parameters: patient's age at diagnosis and tumor stage [7]. Several established molecular prognostic parameters, such as DNA content (ploidy) [39], MYCN oncogene amplification [45], allelic loss in the short arm of chromosome 1 (1p) [15], and gain of genetic material in chromosome 17 [4, 10], have been progressively introduced as further prognostic indicators. Telomerase activity is being analyzed as a strong new prognostic molecular parameter in NB [42, 43].

Valuable prognostic information is also provided by the histopathologic analyses. Shimada et al. [49] proposed a

classification system for neuroblastic tumors based on the proportion of Schwannian stroma, with a prognostic categorization in favorable or unfavorable subgroups, combining morphological features with the patient's age at diagnosis. Subsequently, Joshi et al. [31, 32] proposed a different age-linked prognostic categorization of NB into two risk groups supported by a new histological grading system, which was later modified [34]. Finally, the system of Shimada et al. [49] was adapted by the International Neuroblastoma Pathology Committee to elaborate on the International Neuroblastoma Pathology Classification (INPC) [47, 48], which standardized a terminology and morphological criteria to classify neuroblastic tumors with prognostic significance.

The immunohistochemical procedures allow the consideration of additional features with actual prognostic value in NB such as P-glycoprotein (the product of the multidrug resistance gene, MDR-1) [13] and the overexpression of the neural growth factor receptor-associated protein Trk-A [5]. The determination of cell proliferation markers such as Ki-67 protein also provides prognostic information on these tumors [44].

In this paper, we review the morphological features of 182 NBs (Schwannian stroma-poor) collected from the files of the Spanish Neuroblastoma Registry, applying the INPC criteria, with the aim of assessing the prognostic impact of this classification and its relation with other clinical, morphological, and biological prognostic factors.

Materials and methods

In this study, 209 NBs (Schwannian stroma-poor) with pathologically valuable material were retrieved from the files of the Spanish Neuroblastoma Registry. The cases were collected between January 1992 and December 1999 from the 26 hospitals enrolled in the Spanish Cooperative Neuroblastoma Study N-II-92 [12]. Each case was diagnosed and staged in accordance with the International Neuroblastoma Staging System (INSS) [6, 7]. Samples of fresh and frozen tumor tissue from the primary tumor or a metastatic site (if it was not available for the primary tumor) were submitted to this reference laboratory. Tumor specimens taken after chemotherapy were excluded from the study. Clinical data from each patient were collected, including sex, date of birth, age at diagnosis, tumor location, INSS stage, clinical follow-up, and final outcome (data available for 182 patients). The cutoff date for the study was June 2000.

Histopathologic analysis Standard procedures were used to prepare hematoxylin-eosin (H&E) sections after paraffin embedding of tumor tissue fixed in 10% buffered formaldehyde. All slides in each tumor were examined by two of the authors with no knowledge of either clinical or genetic abnormalities, and the histological diagnosis based on INPC recommendations [47] was established. The mitosis–karyorrhexis index (MKI) was determined in each tumor according to INPC criteria. Patient's age was taken into account to classify each case into a prognostic subset, favorable or unfavorable, following INPC prognostic categorization [48] (Table 1). Other morphological features considered were the diverse parameter of tissular components found in the slides: percentage of viable tumor cells, percentage of Schwannian stroma, percentage of necrotic tissue (including hemorrhagic and calcified areas) and percentage of other elements (including inflammatory cells, normal tissue, and non-Schwannian stroma), the presence of tumor calcifications, and the number of mitotic cells per 10 HPF.

Immunohistochemical expression of Ki-67 protein (MIB-1; Immunotech; 1:50) was analyzed in all cases following the streptavidin–biotin peroxidase method (LSAB, DAKO) [22]. Antigen retrieval was obtained with microwave heating in a solution of citrate buffer (pH 6). The same technique was performed to assess P-glycoprotein expression using the monoclonal antibody JSB-1 (Centocor; 1:50).

Genetic studies MYCN oncogene amplification was determined in all cases by means of Southern blot analysis of total DNA extracted from frozen tumor samples and fluorescence in situ hybridization (FISH) analysis with a DNA probe [*N*-myc (2p24) red/Alphasatellite 2 Dual-Color, Q-Biogene/mpbio]. To study chromosome 1 status, FISH analysis was performed on tumor touch imprints in 72 NBs

Table 1 Prognostic evaluation of neuroblastoma according to the INPC [48]

INPC type	Age (years)	INPC subtype	MKI	Prognostic group
NB	<1.5	Undifferentiated	Any MKI	Unfavorable
		Poorly differentiated/differentiating	Low/Medium	Favorable
		Any subtype	High	Unfavorable
	1.5–5	Undifferentiated/Poorly differentiated	Any MKI	Unfavorable
		Differentiating	Low	Favorable
		Any subtype	Medium/High	Unfavorable
	>5	Any subtype	Any MKI	Unfavorable

using a chromosome 1 centromeric (1p36 Midi Satellite Probe; green, Q-Biogene/mpbio) and subtelomeric [Chr.1 Classical Satellite (1qh), red, Q-Biogene/mpbio] probe by means of standardized methods [2]. The number of signals was counted in 100 tumor cell nuclei.

Statistical analysis All clinical, morphological, and biological data obtained for each case were filed in a computerized database. A descriptive analysis was performed for each variable included, and associations among these variables were analyzed using the appropriate statistical method (χ^2, Mann–Whitney test, and Kruskal–Wallis test). The Kaplan–Meier method was used to estimate survival rates, and multivariate study using Cox regression procedure was performed. p values ≤ 0.05 were regarded as statistically significant.

Results

Analysis of clinical, biological, and morphological features and their influence on patient's outcome and survival

The clinical, morphological, and biological features of tumors with known follow-up data are listed in Table 2, which also includes the results for their final outcome, p value for bivariate analysis, and statistical test used. Information on the clinical course of 182 patients was available: 135 (74.2%) were alive at the last follow-up, whereas 47 (25.8%) had died of the disease or as a complication of the treatment. Mean observation time was 33.54 months. The 3-year estimated survival rate was 72.9%, with a mean survival rate of 73 months.

The mean age at the moment of diagnosis was 20.5 months. Patients younger than 18 months presented a better outcome and a more prolonged survival (87 months) than older ones. The intermediate age group (1.5–5 years) had the worst survival (44 months), and 51.9% of the patients were dead. Mean age at diagnosis in patients who remained alive was 17 months, nearly half of the patients who died (31.3 months).

Tumors presented in all stages. The number of deaths increased significantly with higher stages. With a mean survival rate of 35 months, 59.3% of INSS stage 4 patients were dead. Behavior of INSS stage 4s NBs was similar to INSS stage 1 tumors (Fig. 1).

MYCN amplification was observed in 29 NBs (16.7%) and was significantly associated with a worse outcome (58.6% were dead) and shorter survival (40 months) than patients without amplification of the gene (17.2% were dead; mean survival, 79 months). By FISH analysis, 27.3% of the NBs studied showed loss of genetic material in the short arm of chromosome 1, a feature that was also related with patient outcome and survival: 44.4% of the patients with this alteration died, with a mean survival rate of 32 months, in contrast to patients without 1p deletion, who for the most part remained alive (87.5%) (mean survival rate, 74 months). All 12 tumors with MYCN amplification in which chromosome 1 was analyzed showed loss of genetic material. INSS stage data were available in 11 of them: 8 (72.7%) were stage 4 tumors, and 3 (27.3%) were stage 3. All but one (91.7%) showed a high MKI. Clinical follow-up information was available in nine of them, and seven (77.8%) were dead.

The immunohistochemical expression of P-glycoprotein was found in 10.3% of 156 NBs analyzed. The percentage of dead patients in the group with P-glycoprotein expression (31.3%) was higher than in the negative group (25.7%), but differences were not statistically significant.

Morphological features According to the INPC diagnostic criteria, 111 (61%) tumors were diagnosed as poorly differentiated NB (PD-NB), 35 (19.2%) as undifferentiated NB (U-NB), and 12 (6.6%) as differentiating NB (D-NB). The remaining 24 (13.2%) cases were tumors with a definitive generic diagnosis of NB, but in which the subtype was impossible to determine because of the paucity of tumor cells or the degree of artifact. These last cases fit into the not otherwise specified (NOS-NB) category. A sample of each subtype is showed on (Fig. 2).

Nearly two-thirds (62.9%) of U-NBs with clinical follow-up had a fatal outcome, with a mean survival rate of 33 months, significantly shorter than in the other subtypes (58–81 months). The best outcome was for D-NB, with only one (8.3%) dead patient. Behavior of tumors regarded as "NOS" was similar to PD-NB, with less than 20% of dead patients (18% in PD-NB, 16.7% in NOS-NB) and a mean survival rate of 80 months (Fig. 3).

Necrosis was significantly related to a higher proportion of dead patients (15.4% in tumors with necrosis vs 8% in tumors without this feature). Inversely, the presence of Schwann cells was associated with a better outcome. A high MKI, more than 6 mitoses per 10 HPF, or Ki-67 expression in more than 30% of tumor cells were features that determined a significant rise in the proportion of dead patients, with a concomitant drop in the mean survival time. We found no differences in outcome between patients whose tumors showed a low or intermediate MKI, most of them (87.9% with low MKI, 85.3% with intermediate MKI) remaining alive at last follow-up.

Multivariate analysis Tumor stage and histological subtype of NB were the factors having a highly significant influence on survival rate. Moreover, INSS stage 4 and undifferentiated subtype of NB were the features with a more negative effect over hazard rate compared with the remaining stages and histological subtypes. Results of the Cox regression procedure are resumed in Table 3.

Table 2 Clinical, morphological, and biological data for each tumor related to outcome

Characteristics	*n*	%	Alive		Dead		*p*[a]	Statistic
			n	%	*n*	%		
Sex								
Boys	104	57.1	76	73.1	28	26.9	0.696	χ^2
Girls	78	42.9	59	75.6	19	24.4		
Age (years)								
<1.5	115	63.2	100	87	15	13	**<0.001**	χ^2
1.5–5	52	28.6	25	48.1	27	51.9		
>5	15	8.2	10	66.7	5	33.3		
Tumor location								
Adrenal	98	55.1	77	78.6	21	21.4	Not performed	Not performed
Paravertebral (abdominal)	28	15.7	23	82.1	5	17.9		
Mediastinal	23	12.9	18	78.3	5	21.7		
Pelvic	7	3.9	7	100	0	0		
Cervical	3	1.7	2	66.7	1	33.3		
Disseminated (no primary site specified)	19	10.7	4	21.1	15	18.9		
Stage (INSS)								
1	47	25.8	46	97.9	1	2.1	**<0.001**	Kruskall–Wallis
2	17	9.3	13	76.4	4	23.6		
3	42	23.1	33	78.6	9	21.4		
4	54	29.7	22	40.7	32	59.3		
4s	22	12.1	21	95.5	1	4.5		
Histologic subtype (INPC diagnosis)								
Undifferentiated NB	35	19.2	13	37.1	22	62.9	**<0.001**	χ^2
Poorly differentiated NB	111	61	91	82	20	18		
Differentiating NB	12	6.6	11	91.7	1	8.3		
NB, NOS	24	13.2	20	83.3	4	16.7		
Tumor calcifications								
Yes	51	28	40	78.4	11	21.6	0.413	χ^2
No	131	72	95	72.5	36	27.5		
Mitotic count (per 10 HPF)								
0	1	0.6	1	100	0	0	**<0.001**	Mann–Whitney
1–5	58	37.4	51	87.9	7	12.1		
6–10	46	29.7	32	69.6	14	30.4		
>10	50	32.3	29	58	21	42		
MKI								
Low	58	36.9	51	87.9	7	12.1	**<0.001**	Mann–Whitney
Intermediate	34	21.7	29	85.3	5	14.7		
High	65	41.4	34	52.3	31	47.7		
Ki-67 protein expression (%)								
≤10	41	23.6	35	85.4	6	14.6	**<0.001**	Mann–Whitney
11–30	70	40.2	58	82.9	12	17.1		
31–50	31	17.8	17	54.8	14	45.2		
>50	32	18.4	18	56.3	14	43.8		
MYCN status								
NO amplificated	145	83.3	120	82.8	25	17.2	**<0.001**	Mann–Whitney
Amplificated	29	16.7	12	41.1	17	58.6		
Del 1p								
Yes	18	27.3	10	55.6	8	44.4	**0.005**	χ^2
No	48	72.7	42	87.5	6	12.5		
p-glicoprotein expression								
Yes	16	10.3	11	68.8	5	31.3	0.634	χ^2
No	140	89.7	104	74.3	36	25.7		
Prognostic categorization (INPC)								
Favorable	64	39.5	60	93.8	4	6.2	**<0.001**	Mann–Whitney
Unfavorable	98	60.5	58	59.2	40	40.8		

[a]Significant associations (p value ≤0.005) in bold

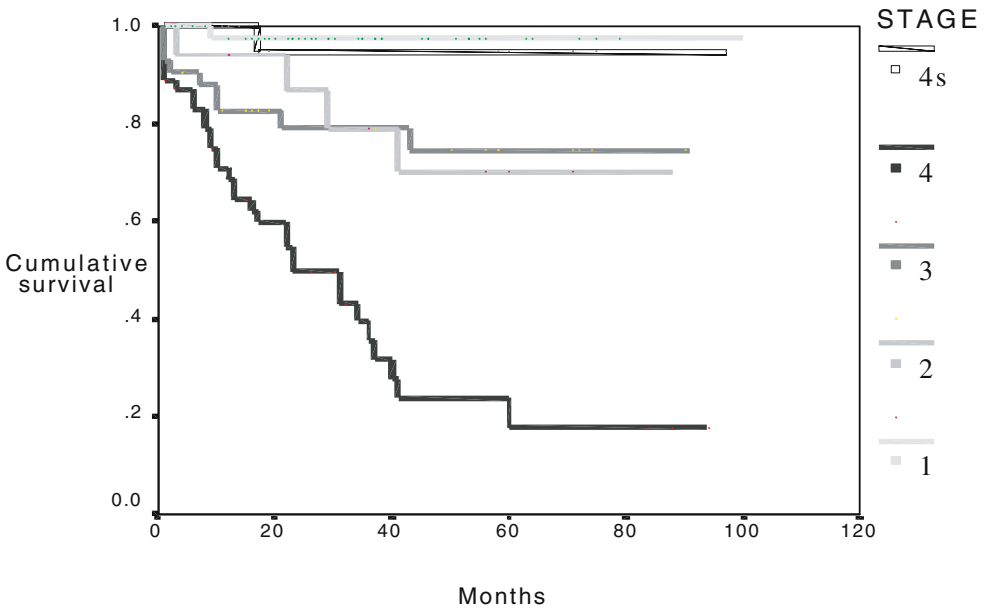

Fig. 1 Differences in patient's survival with regard to INSS stage

Relations between histological subtype of NB and other clinical, morphological, and biological parameters

Poorly differentiated NB and NOS-NB were diagnosed frequently in the first 18 months of life (70%). In contrast, 60% of D-NBs and 63.2% of U-NBs were diagnosed in children older than 1.5 years.

Nearly two thirds of the U-NBs (63.2%) presented as disseminated (INSS stage 4) tumors, whereas PD-NBs and D-NBs were usually localized (INSS stages 1 and 2). Most INSS stage 4s tumors were PD-NBs (66.7%).

The presence of Schwann cells was only significant in D-NB, reaching a mean proportion of 10.3% in this subtype. On the contrary, necrosis was rare in these tumors (2.3%), but reached a mean proportion of 18.2% in slides from U-NB. Tumor calcifications were related to the degree of differentiation of NB, being detected in 60% of D-NBs but in only 18.4% of U-NBs. The proliferative activity

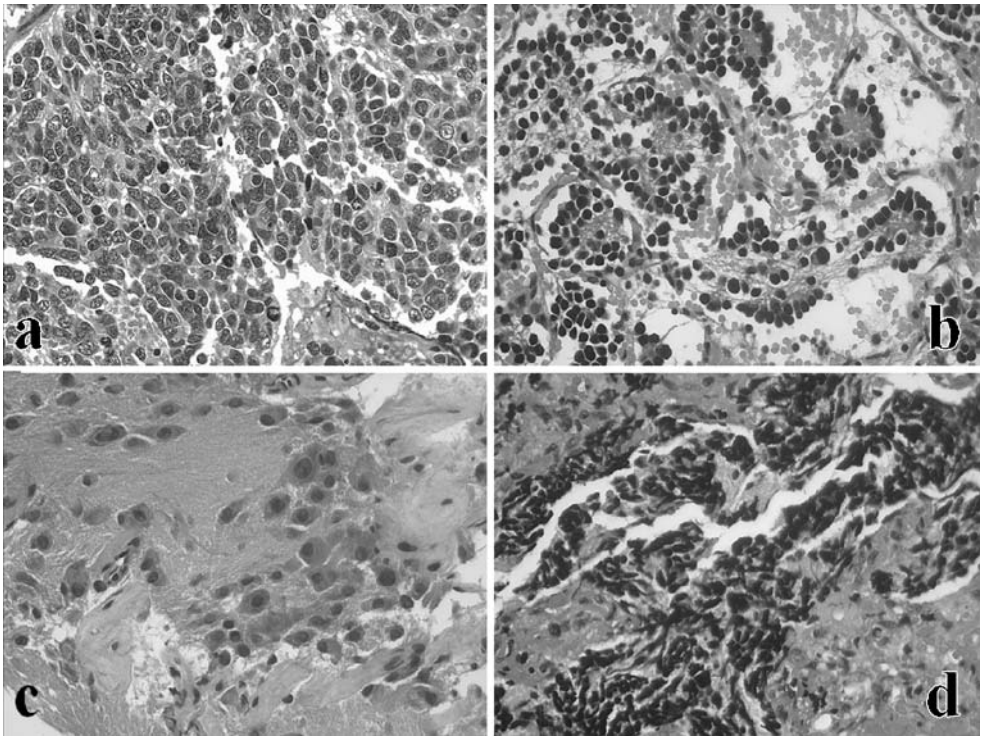

Fig. 2 Histological subtypes of neuroblastoma (Schwannian stroma-poor): **a** undifferentiated NB with high MKI; **b** poorly differentiated NB with Homer–Wright rossettes; **c** differentiating NB; **d** NOS-NB with important artifact. All images are H & E, ×40

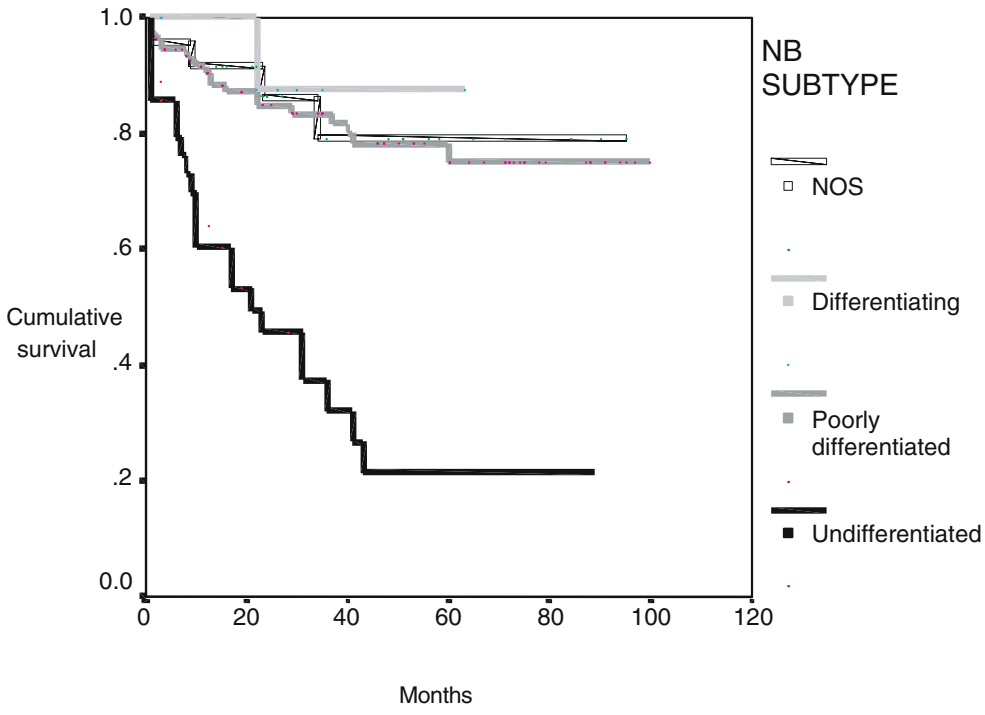

Fig. 3 Variations in survival with regard to the histological subtype of NB

offered marked differences among the NB subtypes, being significantly higher in U-NB compared with the remaining categories. With detail, 72.7% of U-NBs showed a high MKI, more than 10 mitoses were found in 62.5% of them, and Ki-67 nuclear labeling reached a mean percentage of 47.6%. In contrast, D-NBs showed a low MKI (86.7%), less than 5 mitoses (93.3%), and a mean percentage of Ki-67 nuclear labeling of 11.8%.

MYCN oncogene amplification and 1p deletion were found significantly more frequently among U-NB than in remaining subtypes: 45.9% of these tumors showed MYCN amplification, but this feature was found in 16% of NOS-NBs, 9% of PD-NBs, and none in D-NB. 1p deletion was present in seven (70%) of 10 U-NBs, but in only 20–22% in the remaining categories. We could not find any significant differences on P-glycoprotein expression with regard to the histological subtype of NB.

Analysis of the prognostic INPC categorization

Following the INPC criteria, we established the favorable or unfavorable category in 162 patients with available follow-up data. Of the 162 patients, 39.5% of them fitted into the favorable group, whereas the remaining 60.5% were considered as unfavorable. We found an evident association between the prognostic group and outcome: most patients (93.8%) in the favorable group remained alive at last follow-up (Fig. 4), and their mean survival rate (89 months) was significantly higher than those in the unfavorable group (57 months) (Fig. 5). The INPC prognostic system offered a high sensitivity (90.9%), with most of the dead patients located in the unfavorable group (40 of 44 dead patients). However, specificity of this prognostic scheme was low (50.8%) because in this series, half of the patients regarded as unfavorable remained alive at last follow-up.

Table 3 Cox regresion model

Variable ▼	β ▼	*p* ▼	Exp (β) ▼
Stage	Reference category = 1; *p* value <0.001		
2	0.951	0.502	2.588
3	1.090	0.337	2.975
4	2.919	0.005	18.539
4s	0.803	0.571	2.233
Histological subtype of NB	Reference category: undifferentiated NB *p* value <0.001		
PD-NB + D-NB	−1.266	0.003	0.281
NOS	−0.675	0.517	0.508
Cox regresion equation	$H(t)=H_0(t)\ 2.588^{(\text{Stage}=2)}\ 2.975^{(\text{Stage}=3)}\ 18.539^{(\text{Stage}=4)}\ 2.233^{(\text{Stage}=4s)}\ 0.281^{(\text{Subtype}=\text{PD-NB or D-NB})}\ 0.508^{(\text{Subtype}=\text{NOS})}$		

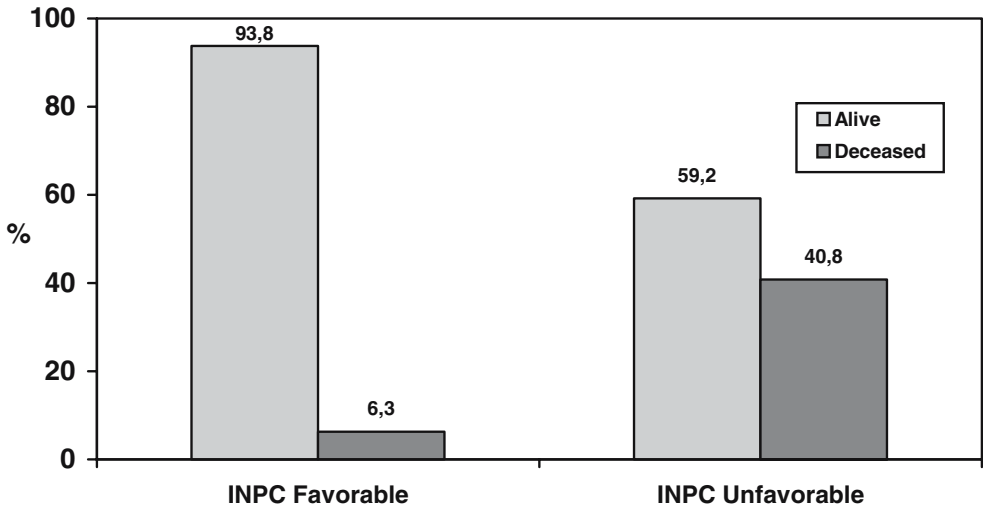

Fig. 4 Differences in the clinical outcome with regard to INPC prognosis

The tumor stage was significantly related to INPC prognosis. Progression in stage implied a higher proportion of unfavorable cases, which reached 89.3% in INSS stage 4 tumors. Results for INSS stage 4s tumors were similar to those of INSS stage 1 tumors, with two thirds of the cases categorized as favorable (65.2% in stage 1; 68.4% in stage 4s).

Regarding the histological composition of the samples, only the proportion of Schwann cells was significantly higher among favorable tumors. The proportion of favorable cases was higher among tumors in which calcifications were found (48.3% vs 36.5% of INPC favorable tumors in the group without calcifications), but differences were not significant.

Tumors with less than five mitoses per 10 HPF were mainly classified as favorable (70.9%), whereas nearly all tumors (98.2%) with more than ten mitoses per 10 HPF belonged to the unfavorable group. The Ki-67 nuclear expression reached a mean value of 40% in unfavorable cases, significantly higher than the mean expression found in favorable tumors (15.8%). In fact, most cases (96.5%) with Ki-67 nuclear expression in more than 30% of tumor cells fell into the unfavorable group.

The presence of MYCN gene amplification or 1p deletion was significantly related to INPC prognosis. Nearly all tumors with MYCN gene amplification were in the unfavorable group (93.1%), the same as for NB showing 1p deletion (84.2% of tumors classified as unfavorable).

Discussion

It has been assumed that NB follows a maturative sequence characterized by a progressive differentiation of tumor cells together with the development of stroma composed mainly of Schwann cells [30, 46]. First attempts to establish a classification of these tumors considered cell differentiation

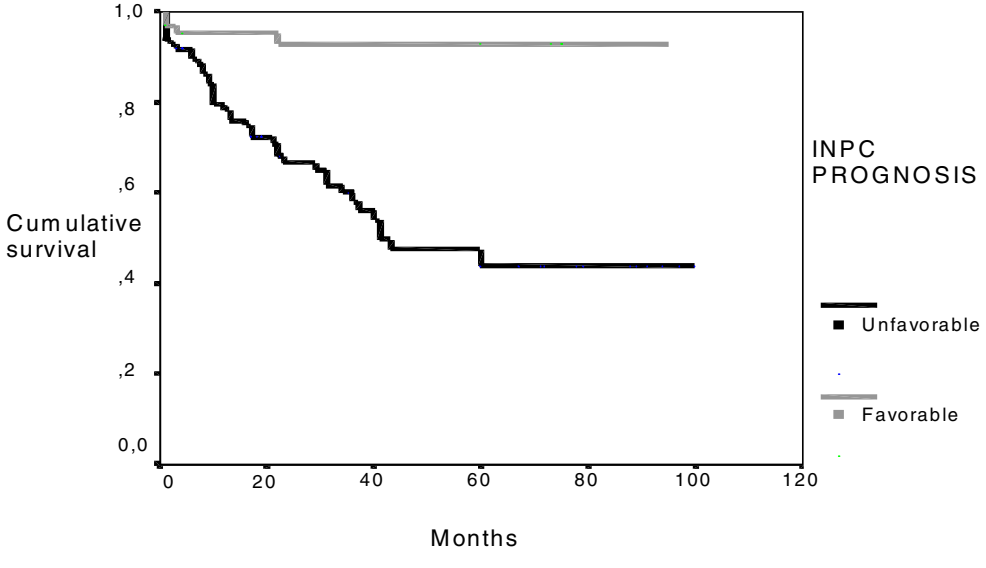

Fig. 5 Differences in survival with regard to INPC prognostic categorization

as the main morphological parameter with prognostic value [3, 28, 40]. Tumor cell differentiation and development of Schwannian stroma were the basis for the classification system and age-linked prognostic categorization proposed by Shimada et al. [49], whose prognostic value was confirmed in subsequent reports [14, 33]. This model was adapted and modified by the International Neuroblastoma Pathology Committee to establish a standard terminology and morphological criteria for the diagnosis of NB, offering a reproducible classification system (the INPC system) that has prognostic value and biological relevance [47, 48].

In this article, we have reviewed 182 NBs (Schwannian stroma-poor) collected from the files of the Spanish Neuroblastoma Registry focusing on pathological features. The INPC diagnostic and prognostic system was applied with the aim of assessing the true prognostic value of this system in our series and its relation with other prognostic factors.

We found patient outcome to be related with histological subtype of NB in such a way that U-NB had a death rate significantly higher than in the other subtypes, and their mean survival time was cut in half. Using a multivariate analysis (Cox regression), the histological subtype of NB was the second most influential factor on survival, closely following tumor stage. INSS stage 4 and undifferentiated histology were the features with a more negative effect on hazard rate.

Tumor necrosis has been related to a worse prognosis in NB [14]. In this series, the proportion of dead patients was significantly higher among tumors with necrosis, which mainly fit into the undifferentiated or "NOS" category. In contrast, the presence of Schwann cells has been related with a better outcome in NB [47, 48]. We found a better outcome for patients whose tumors contained Schwann cells, but this cell type was practically restricted to D-NB. Tumor calcifications have an uncertain biologic significance in NB, but they have been related to a better prognosis in some reports [14, 32], including the INPC report [47]. In our series, they appeared significantly more frequently in D-NB, but differences in outcome with regard to their presence were not significant.

Joshi et al. [32] proposed a grading system for NB based on mitotic rate and the presence of calcifications, these being the morphological factors found to have more impact on prognosis. In our series, mitotic count was significantly related to patient's outcome in such a way that more than six mitoses per 10 HPF implied a remarkable rise in death rate, which was 42% in tumors with more than ten mitoses per 10 HPF. We found mitotic rate to be also related to the histological subtype of NB, being especially high in U-NB. Assessment of mitotic rate in NB can be difficult in practice because of the resemblance of mitotic and karyorrhectic cells. For this reason, the MKI was proposed. These data are obtained from the sum of mitotic and karyorrhectic figures out of 5,000 tumor cells [49]. MKI was one of the features that determined the prognosis in the original Shimada system and, after subsequent reports confirmed its prognostic value [31], it has been maintained as a prognostic factor in the INPC system [48]. In our series, high MKI tumors had a death rate close to 50%, whereas most patients with low or medium MKI tumors remained alive at last follow-up and had a significantly higher mean survival rate. Almost all D-NBs showed a low MKI, whereas this index was high in most U-NBs. Ki-67 protein is an excellent marker for assessing the proliferative activity in tissue [9]. We found significant differences in patient outcome and survival with regard to mean nuclear Ki-67 expression, to the effect that death rate increased markedly when expression was 30% or higher, with a concomitant decrease in mean survival time. In previous reports, low Ki-67 protein expression in NB was related to a better prognosis [24, 44]. U-NB showed a high Ki-67 protein expression (mean value near 50%), significantly higher than in PD-NB and in D-NB (lower than 30%).

Recently, some reports have described prominent nucleoli to be a sign of unfavorable tumor biology and MYCN amplification in U-NB and PD-NB [1, 37]. We are reviewing the slides collected in the Spanish Neuroblastoma Registry to evaluate this parameter (manuscript in preparation).

It is well established that NB of any stage diagnosed in infants have a better prognosis than those diagnosed in children at the same stage [17, 19, 25, 29]. In fact, the main NB prognostic categorization schemes based on morphological parameters were age-linked systems [32, 48, 49].

Tumor stage is also an independent prognostic factor in NB: localized tumors have longer survival rates than disseminated ones [17, 19]. In the multivariate analysis, we found that INSS stage 4 was the parameter with a more negative effect on hazard rate. U-NB appeared as disseminated tumors in the majority of patients, similar to those categorized as NOS, whereas localized tumors predominated among PD-NB and D-NB. INSS stage 4s tumors represented 10% of all NB in our series, a similar proportion to that previously reported [18, 29], and for the most part, they fit into the PD-NB category.

MYCN gene amplification correlates with poor prognosis in NB [8, 16, 20, 45, 52]. We confirmed this fact in our series, in that almost 60% of the patients with MYCN-amplified tumors were deceased, and moreover, we also found a clear relation between this alteration and the histological subtype of NB. MYCN gene amplification appeared in half of the U-NB cases. Previous reports described the presence of a typical phenotype in these amplified NB, being for the most part undifferentiated stroma-poor tumors with a high proliferative activity [21, 38, 50, 52].

Only 72 tumors in our series were studied by means of FISH analysis to assess chromosome 1p status, deletion

being found in 28% of them. As has been previously reported [11, 15, 20, 27, 35], del 1p was related to a worse outcome and a shorter survival rate. We detected this alteration in 70% of the U-NB.

We have classified NB into favorable or unfavorable groups according to the INPC prognostic system. INPC prognosis was significantly related to patient's outcome in such a way that most patients in the favorable group remained alive at last follow-up, whereas the proportion of dead patients was high in the unfavorable group. Mean survival rate for favorable patients was significantly higher than that of unfavorable patients. The INPC prognostic system had a high sensitivity in this series (90.9%): most of the dead patients were in the unfavorable group. However, the specificity of this system was low (50.8%) because half of the patients classified as unfavorable remained alive at last follow-up. The prognostic value of the INPC system has been confirmed in several reports [1, 23, 38, 51]. Recently, the Localised Neuroblastoma European Study Group (LNESG) have shown that the INPC prognostic categorization has a significant impact on outcome prediction in INSS stage 2 localized peripheral NB [41].

In addition to factors that determine INPC prognosis (histological type, MKI, and patient's age at diagnosis), we have found significant associations between the prognostic group and other clinical, morphological, and biological parameters. Progress in the tumor stage is associated with a rise in the proportion of unfavorable cases. Results for INSS stage 4s tumors were similar to those of stage 1 NB and, as is described in the literature, most of them were tumors with favorable features [26, 36]. The rise in mitotic count or in Ki-67 protein labeling index also implied a higher proportion of unfavorable cases. We found MYCN gene amplification and 1p deletion to be significantly more frequent in the unfavorable group. Nearly all tumors with one of these alterations were located in the unfavorable group.

Based upon the present analysis, we can state that, although molecular biology studies have an increasing significance, the histopathologic study is still an important procedure in the study of NB and provides valuable prognostic information. We have confirmed the high sensitivity of the INPC prognostic system, observing that NB in the unfavorable group displays a worse outcome. We have also corroborated the association of clinical, morphological, and biological parameters with their clinical outcome. In this series, NB located in the unfavorable group presented features related to a worse prognosis, INSS stage 4 and undifferentiated histology being the features with a more negative impact on survival.

Acknowledgement Supported by grant no. G03/089 from Instituto Carlos III, Madrid, Spain.

References

1. Ambros IM, Hata H, Joshi VV, Roald B, Dehner LP, Tüchler H, Pötschger U, Shimada H (2002) Morphologic features of neuroblastoma (Schwannian stroma-poor tumors) in clinically favorable and unfavorable groups. Cancer 94:1574–1583
2. Ambros PF, Ambros IM (2001) Pathology and biology guidelines for resectable and unresectable neuroblastic tumors and bone marrow examination guidelines. Med Pediatr Oncol 37:492–504
3. Beckwith JB, Martin RF (1968) Observations on the histopathology of neuroblastomas. J Pediatr Surg 3:106–110
4. Brinkschmidt C, Poremba C, Christiansen H, Simon R, Schafer KL, Terpe HJ, Lampert F, Boecker W, Dockhorn-Dworniczak B (1998) Comparative genomic hybridization and telomerase activity analysis identify two biologically different groups of 4s neuroblastomas. Br J Cancer 77:2223–2229
5. Brodeur GM (1993) TRK-A expression in neuroblastomas: a new prognostic marker with biological and clinical significance (editorial). J Natl Cancer Inst 85:344–345
6. Brodeur GM, Pritchard J, Berthold F, Carlsen NL, Castel V, Castleberry RP, De Bernardi B, Evans AE, Favrot M, Hedborg F, Kaneko M, Kemshead J, Lampert F, Lee R, Look AT, Pearson AD, Philip T, Roald B, Sawada T, Seeger RC, Tsuchida Y, Voute PA (1993) Revisions of the international criteria for neuroblastoma diagnosis, staging, and response to treatment. J Clin Oncol 11:1466–1477
7. Brodeur GM, Seeger RC, Barrett A, Berthold F, Castleberry RP, D'Angio G, De Bernardi B, Evans AE, Favrot M, Freeman AI, Haase G, Hartmann O, Hayes FA, Helson L, Kemshead J, Lampert F, Ninane J, Ohkawa H, Philip T, Pinkerton CR, Pritchard J, Sawada T, Siegel S, Smith EI, Tsuchida Y, Voute PA (1988) International criteria for diagnosis, staging, and response to treatment in patients with neuroblastoma. J Clin Oncol 6:1874–1881
8. Brodeur GM, Seeger RC, Schwab M, Varmus HE, Bishop JM (1984) Amplification of *N*-myc in untreated human neuroblastomas correlates with advanced disease stage. Science 224:1121–1124
9. Brown DC, Gatter KC (1990) Monoclonal antibody Ki-67: its use in histopathology. Histopathology 17:489–503
10. Caron H (1995) Allelic loss of chromosome 1 and additional chromosome 17 material are both unfavourable prognostic markers in neuroblastoma. Med Pediatr Oncol 24:215–221
11. Caron H, Van Sluis P, De Kraker J, Bökkerink J, Egeler M, Laureys G, Slater R, Westerveld A, Voute PA, Versteeg R (1996) Allelic loss of chromosome 1p as a predictor of unfavorable outcome in patients with neuroblastoma. N Engl J Med 334:225–230
12. Castel V, Garcia-Miguel P, Melero C, Navajas A, Navarro S, Molina J, Badal MD, Ruiz-Jimenez JI (1995) The treatment of advanced neuroblastoma. Results of the Spanish Neuroblastoma Study Group (SNSG) studies. Eur J Cancer 31A:642–645
13. Chan HS, Haddad G, Thorner PS, DeBoer G, Lin YP, Ondrusek N, Yeger H, Ling V (1991) P-Glycoprotein expression as a predictor of the outcome of therapy for neuroblastoma. N Engl J Med 325:1608–1614
14. Chatten J, Shimada H, Sather HN, Wong KY, Siegel SE, Hammond GD (1988) Prognostic value of histopathology in advanced neuroblastoma: a report from the Childrens Cancer Study Group. Hum Pathol 19:1187–1198
15. Christiansen H, Lampert F (1988) Tumour karyotype discriminates between good and bad prognostic outcome in neuroblastoma. Br J Cancer 57:121–126
16. Christiansen H, Sahin K, Berthold F, Hero B, Terpe H-J, Lampert F (1995) Comparison of DNA aneuploidy, chromosome 1 abnormalities, MYCN amplification and CD44 expression as prognostic factors in neuroblastoma. Eur J Cancer 31A:541–544

17. Coldman AJ, Fryer CJ, Elwood JM, Sonley MJ (1980) Neuroblastoma: influence of age at diagnosis, stage, tumor site, and sex on prognosis. Cancer 46:1896–1901
18. Evans AE, Chatten J, D'Angio GJ, Gerson JM, Robinson J, Schnaufer L (1980) A review of 17 IV-S neuroblastoma patients at the children's hospital of Philadelphia. Cancer 45:833–839
19. Evans AE, D'Angio GJ, Propert K, Anderson J, Hann HW (1987) Prognostic factors in neuroblastoma. Cancer 59:1853–1859
20. Fong CT, White PS, Peterson K, Sapienza C, Cavenee WK, Kern SE, Vogelstein B, Cantor AB, Look AT, Brodeur GM (1992) Loss of heterozygosity for chromosomes 1 or 14 defines subsets of advanced neuroblastomas. Cancer Res 52:1780–1785
21. George RE, Variend S, Cullinane C, Cotterill SJ, McGuckin AG, Ellershaw C, Lunec J, Pearson AD (2001) Relationship between histopathological features, MYCN amplification, and prognosis: a UKCCSG study. United Kingdom Children Cancer Study Group. Med Pediatr Oncol 36:169–176
22. Giorno R (1984) A comparison of two immunoperoxidase staining methods based on the avidin–biotin interaction. Diagn Immunol 2:161–165
23. Goto S, Umehara S, Gerbing RB, Stram DO, Brodeur GM, Seeger RC, Lukens JN, Matthay KK, Shimada H (2001) Histopathology (International Neuroblastoma Pathology Classification) and MYCN status in patients with peripheral neuroblastic tumors: a report from the Children's Cancer Group. Cancer 92:2699–2708
24. Graham D, Magee H, Kierce B, Ball R, Dervan P, O'Meara A (1995) Evaluation of Ki-67 reactivity in neuroblastoma using paraffin embedded tissue. Pathol Res Pract 191:87–91
25. Grosfeld JL, Schatzlein M, Ballantine TV, Weetman RM, Baehner RL (1978) Metastatic neuroblastoma: factors influencing survival. J Pediatr Surg 13:59–65
26. Hachitanda Y, Hata J (1996) Stage IVS neuroblastoma: a clinical, histological, and biological analysis of 45 cases. Hum Pathol 27:1135–1138
27. Hayashi Y, Kanda N, Inaba T, Hanada R, Nagahara N, Muchi H, Yamamoto K (1989) Cytogenetic findings and prognosis in neuroblastoma with emphasis on marker chromosome 1. Cancer 63:126–132
28. Hughes M, Marsden HB, Palmer MK (1974) Histologic patterns of neuroblastoma related to prognosis and clinical staging. Cancer 34:1706–1711
29. Jereb B, Bretsky SS, Vogel R, Helson L (1984) Age and prognosis in neuroblastoma. Review of 112 patients younger than 2 years. Am J Pediatr Hematol Oncol 6:233–243
30. Joshi VV (2000) Peripheral neuroblastic tumors: pathologic classification based on recommendations of international neuroblastoma pathology committee (modification of Shimada classification). Pediatr Dev Pathol 3:184–199
31. Joshi VV, Cantor AB, Altshuler G, Larkin EW, Neill JS, Shuster JJ, Holbrook CT, Hayes FA, Castleberry RP (1992) Recommendations for modification of terminology of neuroblastic tumors and prognostic significance of Shimada classification. A clinicopathologic study of 213 cases from the Pediatric Oncology Group. Cancer 69:2183–2196
32. Joshi VV, Cantor AB, Altshuler G, Larkin EW, Neill JS, Shuster JJ, Holbrook CT, Hayes FA, Nitschke R, Duncan MH, Shochat SJ, Talbert J, Smith EI, Castleberry RP (1992) Age-linked prognostic categorization based on a new histological grading system of neuroblastomas. A clinicopathologic study of 211 cases from the Pediatric Oncology Group. Cancer 69:2197–2211
33. Joshi VV, Chatten J, Sather HN, Shimada H (1991) Evaluation of the Shimada classification in advanced neuroblastoma with a special reference to the mitosis–karyorrhexis index: a report from the Children's Cancer Study Group. Mod Pathol 4:139–147
34. Joshi VV, Rao PV, Cantor AB, Altshuler G, Shuster JJ, Castleberry RP (1996) Modified histologic grading of neuroblastomas by replacement of mitotic rate with mitosis karyorrhexis index. A clinicopathologic study of 223 cases from the Pediatric Oncology Group. Cancer 77:1582–1588
35. Kaneko Y, Kanda N, Maseki N, Sakurai M, Tsuchida Y, Takeda T, Okabe I, Sakurai M (1987) Different karyotypic patterns in early and advanced stage neuroblastomas. Cancer Res 47:311–318
36. Katzenstein HM, Bowman LC, Brodeur GM, Thorner PS, Joshi VV, Smith EI, Look AT, Rowe ST, Nash MB, Holbrook T, Alvarado C, Rao PV, Castleberry RP, Cohn SL (1998) Prognostic significance of age, MYCN oncogene amplification, tumor cell ploidy, and histology in 110 infants with stage D (S) neuroblastoma: the Pediatric Oncology Group experience—a Pediatric Oncology Group study. J Clin Oncol 16:2007–2017
37. Kobayashi C, Monforte-Munoz HL, Gerbing RB, Stram DO, Matthay KK, Lukens JN, Seeger RC, Shimada H (2005) Enlarged and prominent nucleoli may be indicative of MYCN amplification: a study of neuroblastoma (Schwannian stroma-poor), undifferentiated/poorly differentiated subtype with high mitosis–karyorrhexis index. Cancer 103:174–180
38. Lastowska M, Cullinane C, Variend S, Cotterill S, Bown N, O'Neill S, Mazzocco K, Roberts P, Nicholson J, Ellershaw C, Pearson AD, Jackson MS (2001) Comprehensive genetic and histopathologic study reveals three types of neuroblastoma tumors. J Clin Oncol 19:3080–3090
39. Look AT, Hayes FA, Nitschke R, McWilliams NB, Green AA (1984) Cellular DNA content as a predictor of response to chemotherapy in infants with unresectable neuroblastoma. N Engl J Med 311:231–235
40. Makinen J (1972) Microscopic patterns as a guide to prognosis of neuroblastoma in childhood. Cancer 29:1637–1646
41. Navarro S, Amann G, Beiske K, Cullinane CJ, d'Amore E, Gambini C, Mosseri V, De Bernardi B, Michon J, Peuchmaur M (2006) Prognostic value of International Neuroblastoma Pathology Classification in localized resectable peripheral neuroblastic tumors: a histopathologic study of Localized Neuroblastoma European Study Group 94.01 Trial and Protocol. J Clin Oncol 24:695–699
42. Poremba C, Scheel C, Hero B, Christiansen H, Schaefer KL, Nakayama J, Berthold F, Juergens H, Boecker W, Dockhorn-Dworniczak B (2000) Telomerase activity and telomerase subunits gene expression patterns in neuroblastoma: a molecular and immunohistochemical study establishing prognostic tools for fresh-frozen and paraffin-embedded tissues. J Clin Oncol 18:2582–2592
43. Poremba C, Willenbring H, Hero B, Christiansen H, Schafer KL, Brinkschmidt C, Jurgens H, Bocker W, Dockhorn-Dworniczak B (1999) Telomerase activity distinguishes between neuroblastomas with good and poor prognosis. Ann Oncol 10:715–721
44. Rudolph P, Lappe T, Hero B, Berthold F, Parwaresch R, Harms D, Schmidt D (1997) Prognostic significance of the proliferative activity in neuroblastoma. Am J Pathol 150:133–145
45. Seeger RC, Brodeur GM, Sather H, Dalton A, Siegel SE, Wong KY, Hammond D (1985) Association of multiple copies of the N-myc oncogene with rapid progression of neuroblastomas. N Engl J Med 313:1111–1116
46. Shimada H (1992) Neuroblastoma. Pathology and biology. Acta Pathol Jpn 42:229–241
47. Shimada H, Ambros IM, Dehner LP, Hata J, Joshi VV, Roald B (1999) Terminology and morphologic criteria of neuroblastic tumors. Recommendations by the International Neuroblastoma Pathology Committee. Cancer 86:349–363
48. Shimada H, Ambros IM, Dehner LP, Hata J, Joshi VV, Roald B, Stram DO, Gerbing RB, Lokens JN, Matthay KK, Castleberry RP (1999) The International Neuroblastoma Pathology Classification (the Shimada system). Cancer 86:364–372
49. Shimada H, Chatten J, Newton WA, Sachs N, Hamoudi AB, Chiba T, Marsden HB, Misugi K (1984) Histopathologic prognostic factors in neuroblastic tumors: definition of subtypes

of ganglioneuroblastoma and an age-linked classification of neuroblastomas. J Natl Cancer Inst 73:405–416
50. Shimada H, Stram D, Chatten J, Joshi VV, Hachitanda Y, Brodeur G, Lukens J, Matthay K, Seeger R (1995) Identification of subsets of neuroblastomas by combined histopathologic and N-myc analysis. J Natl Cancer Inst 87:1470–1476
51. Shimada H, Umehara S, Monobe Y, Hachitanda Y, Nakagawara A, Goto S, Gerbing RB, Stram D, Lukens JN, Matthay KK (2001) International neuroblastoma pathology classification for prognostic evaluation of patients with peripheral neuroblastic tumors: a report from the Children's Cancer Group. Cancer 92:2451–2461
52. Tsuda T, Obara M, Hirano H, Gotoh S, Kubomura S, Higashi K, Kuroiwa A, Kakagawara A, Nagahara N, Shimizu K (1987) Analysis of N-myc amplification in relation to disease stage and histologic types in human neuroblastomas. Cancer 60:820–826

Virchows Arch (2006) 449:421–427
DOI 10.1007/s00428-006-0265-7

ORIGINAL ARTICLE

Immunohistochemical detection of bombesin receptor subtypes GRP-R and BRS-3 in human tumors using novel antipeptide antibodies

Solveig Schulz · Christoph Röcken · Stefan Schulz

Received: 10 April 2006 / Accepted: 30 June 2006 / Published online: 12 September 2006
© Springer-Verlag 2006

Abstract Bombesin (BN)-like peptides can stimulate cancer cell growth through binding to their specific G protein-coupled receptors. It is well established that BN receptors are being overexpressed in a subset of human tumors; however, little is known about the cellular and subcellular localization of individual BN receptor subtypes in these tissues. In this study, we developed and characterized novel antipeptide antibodies to the carboxy terminal regions of the gastrin-releasing peptide-preferring bombesin receptor (GRP-R) and the bombesin receptor subtype-3 (BRS-3). Specificity of the antisera was demonstrated by (1) detection of broad bands migrating at M_r 50,000–70,000 in Western blots of membranes from receptor-expressing tissues; (2) cell surface staining of transfected cells; (3) translocation of GRP-R receptor immunostaining after BN exposure; and (4) abolition of tissue immunostaining by preadsorbtion of the antibodies with their immunizing peptides. The distribution of BN receptors was investigated in 74 formalin-fixed, paraffin-embedded human tumors. GRP-R receptors were most frequently detected in breast and prostate carcinomas. BRS-3 receptors were often detected in prostate and pancreatic carcinomas and in pituitary adenomas. Immunoreactive GRP-R and BRS-3 receptors were in many cases predominantly confined to the plasma membrane and uniformly present on nearly all tumor cells. The development of these novel antipeptide antibodies will facilitate the identification of those tumors, which may be targets for diagnostic or radiotherapeutic application of subtype-selective BN analogs.

Keywords Bombesin · Bombesin receptor · GRP-R · BRS-3 · Neoplasm · Antibody · Immunocytochemistry · Western blot

Abbreviations

BN	bombesin
BRS-3	bombesin receptor subtype-3
GRP	gastrin-releasing peptide
GRP-R	gastrin-releasing peptide receptor
NMB	neuromedin B
NMB-R	neuromedin B receptor
HEK	human embryonic kidney
ir	immunoreactivity

Introduction

Bombesin (BN) is a tetradecapeptide, which was first discovered in the skin of the European frog *Bombina bombina* [1]. Subsequently, its mammalian counterparts gastrin-releasing peptide (GRP) and neuromedin B (NMB)

So. Schulz
Department of Obstetrics and Gynecology,
Otto-von-Guericke-University,
39120 Magdeburg, Germany

C. Röcken
Department of Pathology, Otto-von-Guericke-University,
39120 Magdeburg, Germany

St. Schulz (✉)
Department of Pharmacology and Toxicology,
Otto-von-Guericke-University,
Leipziger Strasse 44,
39120 Magdeburg, Germany
e-mail: Stefan.Schulz@Medizin.Uni-Magdeburg.de

C. Röcken
Department of Pathology, Charité Universitätsmedizin Berlin,
Schumannstrasse 20/21,
10117 Berlin, Germany

were discovered [18, 19]. These BN-like peptides were previously detected in a variety of human tissues with preferential expression in nerve fibers [24]. BN-like peptides stimulate a large number of physiological responses such as smooth muscle contraction and secretion from exocrine and endocrine glands [24]. The biological actions of BN-like peptides in humans are mediated by a family of at least three G-protein-coupled receptors namely, the NMB receptor (NMB-R, also called BB1), the GRP receptor (GRP-R, also called BB2), and bombesin receptor subtype-3 (BRS-3, also called BB3) [16, 22]. The affinity of BRS-3 for BN is lower than that of GRP-R and NMB-R. Moreover, GRP and NMB only have a poor potency for BRS-3. Seek for endogenous high-affinity ligand for BRS-3 has not yet been succeeded. Thus, BRS-3 still has to be considered as an orphan G-protein-coupled receptor [31].

BN-like peptides and their receptors were implicated in the development and progression of a variety of human malignancies. BN-like peptides can stimulate growth of lung, breast, and prostate cancer cell lines in vivo and in vitro [2, 38]. Conversely, BN receptor antagonists were shown to inhibit the proliferation of human tumor cells [13, 38]. Whereas the expression of GRP-R receptors in human tumors was well documented, other subtypes such as NMB-R and BRS-3 were poorly investigated in human tissues [5, 7, 11, 17, 28, 39]. Binding sites and mRNA for GRP-R were detected in a large number of human neoplasms such as breast cancer, prostate cancer, ovarian cancer, renal cell cancer, small cell lung cancer, and gastrointestinal stromal tumors [6, 10, 12, 27, 29, 30, 39, 40]. So far, GRP-R protein was only detected in colon cancer by immunocytochemistry [5].

Although it is well established that a subset of human tumors can overexpress BN receptors, the exact cellular and subcellular sites of individual BN receptor subtypes in human neoplastic tissues still need to be fully elucidated. In the present study, we have generated and characterized antibodies directed to the carboxy terminal tail of the BN receptor subtypes GRP-R and BRS-3. We have also developed an immunohistochemical protocol that allows efficient detection of these receptors in formalin-fixed, paraffin-embedded human tissues. The generation of these novel antibodies enabled us to determine the cellular distribution of GRP-R and BRS-3 proteins in a variety of human tumors.

Materials and methods

Patients, tumors, and tissue preparation Seventy-four tumor specimens were retrieved from the archives of the Department of Pathology, Otto-von-Guericke University, Magdeburg, Germany. All tissue specimens had been fixed in formalin and embedded in paraffin. The following tumors were investigated: ductal pancreatic adenocarcinoma (n=5), ductal invasive breast carcinoma (n=10), ovarian carcinoma (n=10), prostate cancer (n=4), thyroid carcinoma (n=6), carcinoid (n=15), pancreatic insulinoma (n=8), growth hormone-producing pituitary adenoma (n=4), pheochromocytoma (n=4), glioblastoma (n=4), and meningioma (n=4). In addition, several fresh tumor specimens were immediately frozen in liquid N_2 and stored at −70°C until Western blot analysis. The following tumors were investigated by Western blotting: breast carcinoma (n=8) and pheochromocytoma (n=4). Adjacent normal tissue was analyzed in four breast carcinomas.

Generation and purification of antipeptide antibodies Polyclonal antisera were generated against the carboxy terminal tail of the BN receptor subtypes GRP-R and BRS-3. The identity of the peptides used for immunizations is given in Table 1. The peptides were synthesized, purified, and coupled to keyhole limpet hemocyanin as previously described [32, 33]. The conjugates were mixed 1:1 with Freund's adjuvant and injected into groups of three rabbits each: rabbit number 9007–9009 for GRP-R antisera production and rabbit number 9013–9015 for BRS-3 antisera production. Animals were injected at 4-week intervals, and serum was obtained 2 weeks after immunizations beginning with the second injection. The specificity of the antisera was initially tested using immunodot blot analysis as previously described [32]. For subsequent analysis, antibodies were affinity purified against their immunizing peptide using the SulfoLink coupling gel according to the instructions of the manufacturer (Pierce, Rockford, IL, USA).

Immunocytochemistry Plasmids encoding the human GRP-R and BRS-3 receptors were obtained from http://www.cdna.org (UMR cDNA Resource Center, Rolla, MO, USA). Human embryonic kidney 293 (HEK-293) cells were stably transfected with the calcium phosphate precipitation method with either GRP-R or BRS-3 and stable transfectants were selected in the presence of 500 μg/ml G418 as previously described [25]. Cells were grown on coverslips overnight and were either not exposed or exposed to 1 μM

Table 1 Amino acid sequences of carboxy terminal regions of human BN receptors

Peptides	Sequences
GRP-R (364–384)	TTCMTSLKS*TNPSVATFSLINGNICHERYV*
BRS-3 (381–399)	TVPGTGSIQMS*EISVTSFTGCSVKQAEDRF*

Amino acid sequences of peptides corresponding to carboxy terminal regions of GRP-R and BRS-3 used to immunize rabbits for antibody production are italicized.

BN (Bachem, Weil am Rhein, Germany). After 30 min, GRP-R-expressing and BRS-3-expressing cells were fixed with Zamboni's solution and incubated with 1 μg/ml anti-GRP-R {9009} and 1 μg/ml anti-BRS-3 {9015} antibodies, respectively, for 2 h at room temperature. Cells were then incubated with cyanine 3.18-conjugated anti-rabbit antibodies (Amersham, Braunschweig, Germany) at a dilution of 1:200 for 1 h at room temperature. Specimens were mounted and examined using a Leica TCS-NT laser scanning confocal microscope as previously described [25, 34].

Western blot analysis Membranes were prepared from fresh tumor specimens. Tissues were lysed in homogenization buffer (5 mM EDTA, 3 mM EGTA, 250 mM sucrose, and 10 mM Tris–HCl at pH 7.6 containing 1 mM phenylmethylsulfonyl fluoride, 1 μM pepstatin A, 10 μg/ml leupeptin, and 2 μg/ml aprotinin), and membranes were pelleted at 20,000×*g* for 30 min at 4°C. Membranes were then dissolved in lysis buffer (150 mM NaCl, 5 mM EDTA, 3 mM EGTA, 20 mM Hepes at pH 7.4 containing 4 mg/ml dodecyl-beta-maltoside and proteinase inhibitors as above) and incubated with 150 μl wheat germ lectin agarose beads (Amersham) for 90 min at 4°C. Beads were washed five times in lysis buffer and adsorbed glycoproteins were eluted with sodium dodecyl sulfate (SDS) sample buffer for 20 min at 60°C. Samples were then subjected to 8% SDS polyacrylamide gel electrophoresis and immunoblotted onto nitrocellulose. Blots were incubated with 1 μg/ml anti-GRP-R {9009} or 1 μg/ml anti-BRS-3 {9015} antibodies followed by peroxidase-conjugated secondary antibodies and enhanced chemiluminescence detection (Amersham). For adsorption controls, the antibody was preincubated with 10 μg/ml of its cognate peptide for 2 h at room temperature.

Immunohistochemistry Seven-micrometer paraffin sections were cut and floated onto positively charged slides and were immunohistochemically stained as previously described [21, 33, 34]. Briefly, sections were dewaxed and microwaved in 10 mM citric acid (pH 6.0) for 20 min at 600 W and subsequently incubated with anti-GRP-R {9009} or anti-BRS-3 {9015} antibodies at a concentration of 2 μg/ml overnight at 4°C. Staining of primary antibody was detected using biotinylated goat anti-rabbit IgG followed by an incubation with avidin-biotinylated peroxidase solution (Vector, Burlingame, CA, USA). Tissue was then rinsed and stained with 3,3′-diaminobenzidine-glucose oxidase for 15 min. Cell nuclei were lightly counterstained with hematoxylin. For immunohistochemical controls, the primary antibody was omitted, replaced by preimmune sera, or adsorbed with several concentrations ranging from 1 to 10 μg/ml of homologous or heterologous peptides for 2 h at room temperature. A tumor known to stain positively was included in each batch of staining as a positive control.

Assessment of staining patterns All slides were evaluated by the same investigator. The presence or absence of staining and the depth of color were noted, as well as the number of cells showing a positive reaction and whether the staining was localized to the plasma membrane. Tumors were only categorized as positive when they exhibited a moderate to strong plasma membrane and/or cytoplasmic staining in the majority of tumor cells, which was easily visible with a low-power (10×) objective.

Results

Characterization of BN receptor antibodies Specificity of the antisera was monitored using immunofluorescent staining of transfected cells. When HEK-293 cells stably transfected with GRP-R were stained with anti-GRP-R antibody {9009}, prominent immunofluorescence localized to the plasma membrane was detected (Fig. 1a). In contrast, no immunofluorescence was detected when BRS-3-expressing cells were stained with anti-GRP-R antibody {9009} (data not shown). When stably transfected HEK-293 cells were stained with anti-BRS-3 antibody {9015}, prominent immunofluorescence localized at the level of the plasma membrane was detected only in BRS-3- but not in GRP-R-expressing cells (Fig. 1c). These results indicate that both GRP-R and BRS-3 antibodies selectively detected their cognate receptor and did not cross-react. After incubation with BN, GRP-R-immunoreactivity (ir) was translocated from the plasma membrane into the cytosol (Fig. 1b). In contrast, such a BN-induced redistribution was not seen in BRS-3-expressing cells (Fig. 1d), indicating that only GRP-R but not BRS-3 was rapidly endocytosed in the presence of BN.

Next, the GRP-R and BRS-3 antisera were tested for possible cross-reactivity with other proteins present in human tissues. When membrane preparations from a human breast carcinoma and adjacent normal tissue were electrophoretically separated and blotted onto nitrocellulose, the anti-GRP-R antibody {9009} detected a broad band migrating at M_r 60,000 to 75,000 and a smaller second band migrating at M_r 40,000 only in breast cancer but not in adjacent normal tissue (Fig. 2a). When membrane preparations from a human pheochromocytoma were electrophoretically separated and blotted onto nitrocellulose, the anti-BRS-3 antibody {9015} detected a broad band migrating at M_r 55,000 to 75,000 (Fig. 2b). All immunoreactive bands were completely abolished by preadsorbtion of the antibodies with 10 μg/ml of their immunizing peptides (Fig. 2a,b).

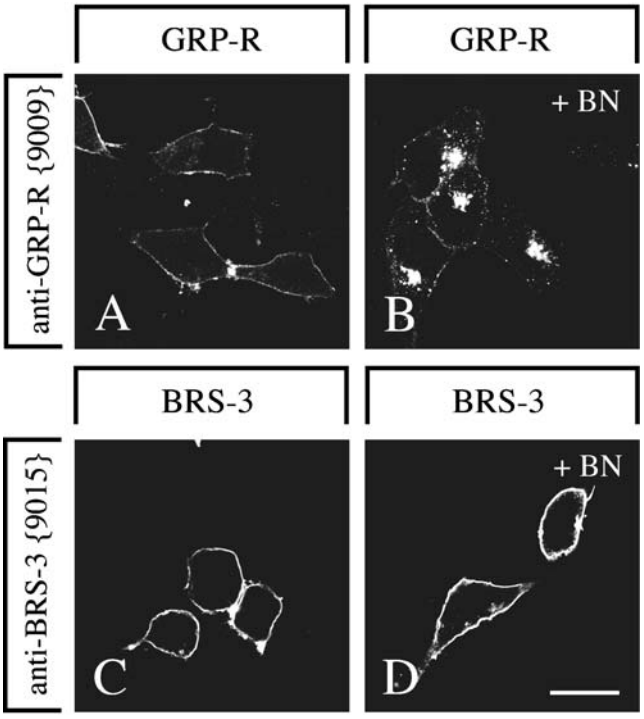

Fig. 1 Characterization of anti-GRP-R and anti-BRS-3 antibodies by immunofluorescent staining of transfected cells. **a**, **b** HEK-293 cells stably transfected to express GRP-R were either not exposed (**a**) or exposed to 1 μM BN for 30 min (**b**), subsequently fixed and immunofluorescently stained with anti-GRP-R {9009} antibody. **c**, **d**, HEK-293 cells stably transfected to express BRS-3 were either not exposed (**c**) or exposed to 1 μM BN for 30 min (**d**), subsequently fixed and immunofluorescently stained with anti-BRS-3 {9015} antibody. Note that in untreated cells, prominent immunofluorescence was localized at the level of the plasma membrane in both GRP-R- and BRS-3-expressing cells. Exposure to BN induced a rapid translocation of GRP-R but not of BRS-3 from the plasma membrane into the cytosol. Representative results from one out of three independent experiments are shown. *BN* Bombesin. *Scale bar*: **a**–**d**=20 μm

BN receptor immunohistochemical staining in neoplastic human tissues The anti-GRP-R and anti-BRS-3 antibodies were then subjected to immunohistochemical staining of human tissues. Initial experiments showed that heat-induced epitope retrieval is required for efficient immunohistochemical staining of paraffin-embedded tissues (data not shown). Two out of three anti-GRP-R antisera yielded essentially identical immunohistochemical staining patterns although with different staining intensities. Similarly, two out of three anti-BRS-3 antisera yielded essentially identical immunohistochemical staining patterns. Immunostaining for each antiserum was completely abolished by preadsorbtion with 10 μg/ml of the immunizing peptide (Fig. 3, insets in c and f). The anti-GRP-R {9009} and the anti-BRS-3 {9015} antibodies produced the most prominent immunostaining and were therefore used throughout the study. The prevalence of BN receptors in human neoplasms is summarized in Table 2. Immunoreactive GRP-R receptors were frequently detected in breast carcinomas (60%) and prostate cancer (50%). GRP-R-ir was also found in 2 out of 5 pancreatic carcinomas (40%) and 2 out of 10 ovarian carcinomas (20%). In contrast, immunoreactive GRP-R receptors were not detected in neuroendocrine tumors, including carcinoid, insulinoma, or pituitary adenoma. GRP-R receptors were also not observed in meningiomas, pheochromocytomas, glioblastomas, or thyroid cancer. Immunoreactive GRP-R were often homogeneously present on the plasma membrane of nearly all tumor cells (Fig. 3a,b). However, a few tumors were observed where GRP-R-ir was predominantly confined to vesicle-like structures within the cytoplasm of the tumor cells (Fig. 3c). Immunoreactive BRS-3 receptors were frequently detected in carcinomas of the prostate (100%) and pancreas (80%), and in growth-hormone-producing pituitary adenomas (75%). In our series, BRS-3-ir was also found in 50% of all breast and ovarian carcinomas as well as in pheochromocytomas and meningiomas. In contrast, immunoreactive BRS-3 receptors were not detected in gut carcinoids, glioblastomas, or thyroid cancer. BRS-3-ir was often seen at the plasma membrane and in vesicle-like structures within the cytoplasm (Fig. 3d–f).

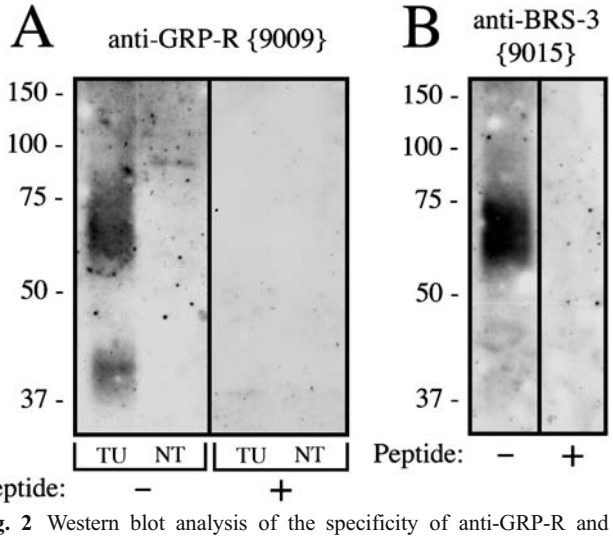

Fig. 2 Western blot analysis of the specificity of anti-GRP-R and anti-BRS-3 antibodies in human tumors. **a** Membrane preparations from a breast carcinoma were separated on 8% SDS polyacrylamide gels, blotted onto nitrocellulose, and incubated with 1 μg/ml anti-GRP-R antibody {9009} in the absence (*minus sign*) or presence (*plus sign*) of 10 μg/ml peptide antigen. **b** Membrane preparations from a pheochromocytoma were separated on 8% SDS-polyacrylamide gels, blotted onto nitrocellulose, and incubated with 1 μg/ml anti-BRS-3 antibody {9015} in the absence (*minus sign*) or presence (*plus sign*) of 10 μg/ml peptide antigen. Blots were developed using enhanced chemiluminescence. Representative results from one out of three independent experiments are shown. *Ordinate*: migration of protein molecular weight markers ($M_r \times 10^{-3}$)

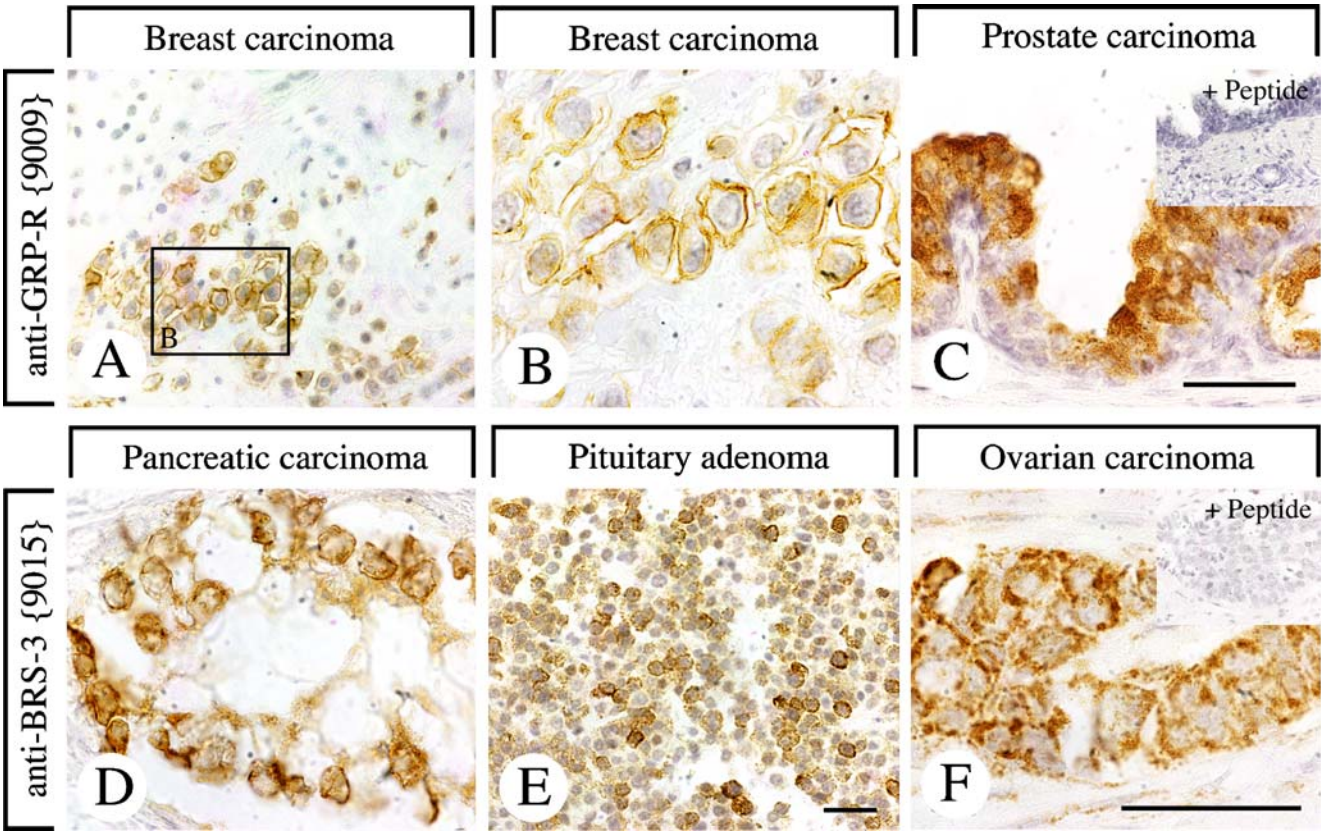

Fig. 3 GRP-R and BRS-3 immunohistochemical staining in human neoplastic tissues. GRP-R immunohistochemical staining in breast cancer (**a**, **b**) and prostate cancer (**c**). BRS-3 immunohistochemical staining in pancreatic carcinoma (**d**), pituitary adenoma (**e**), and ovarian carcinoma (**f**). Sections were incubated with either anti-GRP-R {9009} or anti-BRS-3 {9015} antibodies, sequentially treated with biotinylated anti-rabbit IgG and AB peroxidase solution, and then developed with 3,3′-diaminobenzidine as chromogen (*brown*). Cell nuclei were lightly counterstained with hematoxylin (*blue*). For adsorption controls, primary antibody was incubated with 10 μg/ml of the peptide used for immunizations. Representative results from one out of three independent experiments are shown. *Insets* in subpanels **c** and **f**: peptide adsorption control. *Scale bars*: **a**, **f**=50 μm, **b**, **e**=100 μm, and **c**, **d**=50 μm

Table 2 Prevalence of BN receptors in human tumors

Tumor type (*n*)	Positive cases	
	GRP-R, *n* (%)	BRS-3, *n* (%)
Pancreatic ductal adenocarcinoma (5)	2 (40)	4 (80)
Breast cancer, ductal invasive (10)	6 (60)	5 (50)
Ovarian carcinoma (10)	2 (20)	5 (50)
Prostate cancer (4)	2 (50)	4 (100)
Thyroid cancer (6)	0	0
Carcinoid, midgut (7)	0	0
Carcinoid, hindgut (8)	0	0
Pancreatic insulinoma (8)	0	2 (25)
Pituitary adenoma, growth hormone-producing (4)	0	3 (75)
Pheochromocytoma (4)	0	2 (50)
Glioblastoma multiforme (4)	0	0
Meningioma (4)	0	2 (50)

Discussion

Although it is well established that BN receptors are overexpressed in certain malignancies including breast and prostate cancers, little is known about their cellular and subcellular localization in human tissues. We therefore generated antibodies that exert selective specificity for the human GRP-R and BRS-3 receptors, respectively. We show that the cytoplasmic tail of these receptors can serve as an epitope for the generation of antisera that effectively stain formalin-fixed, paraffin-embedded human tissues. Several lines of evidence indicate that these antibodies specifically detect their targeted BN receptor and do not cross-react. First, in Western blots of membranes from receptor-expressing tumors the antibodies detected broad bands migrating at M_r 50,000 to 75,000, suggesting that GRP-R and BSR-3, like many other G-protein-coupled receptors, exist as glycoproteins in native tissues [21, 25, 33, 34]. Second, the anti-GRP-R and anti-BRS-3 antibodies revealed prominent cell surface staining of GRP-R- and

BRS-3-transfected cells, respectively. The GRP-R but not the BRS-3 immunostaining translocated from the cell surface into the cytosol after BN exposure, indicating rapid agonist-induced endocytosis of the GRP-R receptor. This result was expected because the BSR-3 receptor does not have a high affinity for BN [31]. Third, tissue immunostaining of the anti-GRP-R and BRS-3 antisera was completely abolished by preadsorbtion with homologous but not heterologous peptides. Finally, it should be noted that two out of three GRP-R antisera and two out of three BRS-3 antisera gave similar results.

The availability of GRP-R and BSR-3 antibodies will facilitate further basic morphological investigation of BN receptor expression in human normal and neoplastic tissues. The immunohistochemical BN receptor evaluation offers several major advantages. This method can analyze GRP-R and BRS-3 receptors in routinely processed archival paraffin-embedded material of any diagnostic pathology center. It requires only an immunohistological laboratory to perform the test, which can be carried out without costly and time-consuming receptor autoradiography [12, 17, 28]. The immunohistochemical evaluation of the GRP-R and BRS-3 status of a given tumor specimen can be accomplished in less than 24 h. Although one could expect the immunohistochemical BN receptor determination to be less sensitive than receptor autoradiography with 125I-labeled BN analogs, the sensitivity of the anti-GRP-R {9009} and anti-BRS-3 {9015} antibodies generated and characterized in this study was sufficiently high enough to detect these receptors in human tumors known to express BN receptors in a high percentage, e.g., breast cancer and prostate cancer [12, 17, 28]. In addition, the immunohistochemical BN receptor determination provided a better histological quality and cellular resolution compared to receptor autoradiography. Thus, previously unappreciated cellular localizations of BN receptors in nonneoplastic tissues were uncovered, e.g., expression of GRP-R in human retina and expression of BRS-3 in myenteric neurons and in cells of the anterior pituitary.

The present data confirm the high incidence and high density of GRP-R receptors in prostate and breast carcinomas detected previously by binding autoradiography and reverse transcriptase polymerase chain reaction [12, 17, 28]. The overexpression of BN receptors in certain human tumors may provide the molecular basis for clinical application of BN analogs. BN receptor antagonists are being developed, which were shown to inhibit cancer cell growth in vivo and in vitro [13, 38]. Moreover, a number of BN receptor radioligands were recently successfully used for visualization of GRP-R-expressing breast and prostate cancers [3, 4, 23, 35–37, 41, 42]. An additional clinical application could be the use of BN analogs linked to cytotoxic drugs [8, 9, 14, 15, 20, 26].

In conclusion, we have generated and extensively characterized anti-GRPR and anti-BRS-3 antibodies. The development of these novel antibodies enabled us to visualize GRP-R and BSR-3 in human formalin-fixed, paraffin-embedded tissues. It is now possible to determine the exact cellular and subcellular sites of GRP-R and BRS-3 protein in normal human and neoplastic tissues. The rapid immunocytochemical determination of the BN receptor status may also be helpful in identifying those tumors, which may be targets for diagnostic or radiotherapeutic application of subtype-selective BN analogs.

Acknowledgements We thank Beate Peter and Dana Mayer for skillful technical assistance.

References

1. Anastasi A, Erspamer V, Bucci M (1971) Isolation and structure of bombesin and alytesin, 2 analogous active peptides from the skin of the European amphibians Bombina and Alytes. Experientia 27:166–167
2. Bold RJ, Ishizuka J, Yao CZ, Townsend CM Jr, Thompson JC (1998) Bombesin stimulates in vitro growth of human breast cancer independent of estrogen receptors status. Anticancer Res 18:4051–4056
3. Breeman WA, De Jong M, Bernard BF, Kwekkeboom DJ, Srinivasan A, van der Pluijm ME, Hofland LJ, Visser TJ, Krenning EP (1999) Pre-clinical evaluation of [(111)In-DTPA-Pro(1), Tyr(4)]bombesin, a new radioligand for bombesin-receptor scintigraphy. Int J Cancer 83:657–663
4. Breeman WA, Hofland LJ, de Jong M, Bernard BF, Srinivasan A, Kwekkeboom DJ, Visser TJ, Krenning EP (1999) Evaluation of radiolabelled bombesin analogues for receptor-targeted scintigraphy and radiotherapy. Int J Cancer 81:658–665
5. Carroll RE, Matkowskyj KA, Chakrabarti S, McDonald TJ, Benya RV (1999) Aberrant expression of gastrin-releasing peptide and its receptor by well-differentiated colon cancers in humans. Am J Physiol 276:G655–665
6. Carroll RE, Ostrovskiy D, Lee S, Danilkovich A, Benya RV (2000) Characterization of gastrin-releasing peptide and its receptor aberrantly expressed by human colon cancer cell lines. Mol Pharmacol 58:601–607
7. Chave HS, Gough AC, Palmer K, Preston SR, Primrose JN (2000) Bombesin family receptor and ligand gene expression in human colorectal cancer and normal mucosa. Br J Cancer 82:124–130
8. Engel JB, Keller G, Schally AV, Halmos G, Hammann B, Nagy A (2005) Effective inhibition of experimental human ovarian cancers with a targeted cytotoxic bombesin analogue AN-215. Clin Cancer Res 11:2408–2415
9. Engel JB, Schally AV, Halmos G, Baker B, Nagy A, Keller G (2005) Targeted cytotoxic bombesin analog AN-215 effectively inhibits experimental human breast cancers with a low induction of multi-drug resistance proteins. Endocr Relat Cancer 12:999–1009
10. Fleischmann A, Laderach U, Friess H, Buechler MW, Reubi JC (2000) Bombesin receptors in distinct tissue compartments of human pancreatic diseases. Lab Invest 80:1807–1817
11. Fleischmann A, Waser B, Gebbers JO, Reubi JC (2005) Gastrin-releasing peptide receptors in normal and neoplastic human uterus: involvement of multiple tissue compartments. J Clin Endocrinol Metab 90:4722–4729

12. Gugger M, Reubi JC (1999) Gastrin-releasing peptide receptors in non-neoplastic and neoplastic human breast. Am J Pathol 155:2067–2076
13. Kahan Z, Sun B, Schally AV, Arencibia JM, Cai RZ, Groot K, Halmos G (2000) Inhibition of growth of MDA-MB-468 estrogen-independent human breast carcinoma by bombesin/gastrin-releasing peptide antagonists RC-3095 and RC-3940-II. Cancer 88:1384–1392
14. Keller G, Schally AV, Nagy A, Halmos G, Baker B, Engel JB (2005) Targeted chemotherapy with cytotoxic bombesin analogue AN-215 can overcome chemoresistance in experimental renal cell carcinomas. Cancer 104:2266–2274
15. Kiaris H, Schally AV, Nagy A, Sun B, Armatis P, Szepeshazi K (1999) Targeted cytotoxic analogue of bombesin/gastrin-releasing peptide inhibits the growth of H-69 human small-cell lung carcinoma in nude mice. Br J Cancer 81:966–971
16. Kroog GS, Jensen RT, Battey JF (1995) Mammalian bombesin receptors. Med Res Rev 15:389–417
17. Markwalder R, Reubi JC (1999) Gastrin-releasing peptide receptors in the human prostate: relation to neoplastic transformation. Cancer Res 59:1152–1159
18. McDonald TJ, Jornvall H, Nilsson G, Vagne M, Ghatei M, Bloom SR, Mutt V (1979) Characterization of a gastrin releasing peptide from porcine non-antral gastric tissue. Biochem Biophys Res Commun 90:227–233
19. Minamino N, Kangawa K, Matsuo H (1983) Neuromedin B: a novel bombesin-like peptide identified in porcine spinal cord. Biochem Biophys Res Commun 114:541–548
20. Moody TW, Mantey SA, Pradhan TK, Schumann M, Nakagawa T, Martinez A, Fuselier J, Coy DH, Jensen RT (2004) Development of high affinity camptothecin–bombesin conjugates that have targeted cytotoxicity for bombesin receptor-containing tumor cells. J Biol Chem 279:23580–23589
21. Mundschenk J, Unger N, Schulz S, Hollt V, Steinke R, Lehnert H (2003) Somatostatin receptor subtypes in human pheochromocytoma: subcellular expression pattern and functional relevance for octreotide scintigraphy. J Clin Endocrinol Metab 88:5150–5157
22. Nagalla SR, Barry BJ, Creswick KC, Eden P, Taylor JT, Spindel ER (1995) Cloning of a receptor for amphibian [Phe13]bombesin distinct from the receptor for gastrin-releasing peptide: identification of a fourth bombesin receptor subtype (BB4). Proc Natl Acad Sci USA 92:6205–6209
23. Nock BA, Nikolopoulou A, Galanis A, Cordopatis P, Waser B, Reubi JC, Maina T (2005) Potent bombesin-like peptides for GRP-receptor targeting of tumors with 99mTc: a preclinical study. J Med Chem 48:100–110
24. Ohki-Hamazaki H, Iwabuchi M, Maekawa F (2005) Development and function of bombesin-like peptides and their receptors. Int J Dev Biol 49:293–300
25. Pfeiffer M, Koch T, Schroder H, Klutzny M, Kirscht S, Kreienkamp HJ, Hollt V, Schulz S (2001) Homo- and heterodimerization of somatostatin receptor subtypes. Inactivation of sst (3) receptor function by heterodimerization with sst(2A). J Biol Chem 276:14027–14036
26. Plonowski A, Nagy A, Schally AV, Sun B, Groot K, Halmos G (2000) In vivo inhibition of PC-3 human androgen-independent prostate cancer by a targeted cytotoxic bombesin analogue, AN-215. Int J Cancer 88:652–657
27. Reubi JC, Waser B (2003) Concomitant expression of several peptide receptors in neuroendocrine tumours: molecular basis for in vivo multireceptor tumour targeting. Eur J Nucl Med Mol Imaging 30:781–793
28. Reubi JC, Wenger S, Schmuckli-Maurer J, Schaer JC, Gugger M (2002) Bombesin receptor subtypes in human cancers: detection with the universal radioligand (125)I-[D-TYR(6), beta-ALA(11), PHE(13), NLE(14)] bombesin(6-14). Clin Cancer Res 8:1139–1146
29. Reubi JC, Korner M, Waser B, Mazzucchelli L, Guillou L (2004) High expression of peptide receptors as a novel target in gastrointestinal stromal tumours. Eur J Nucl Med Mol Imaging 31:803–810
30. Reubi JC, Macke HR, Krenning EP (2005) Candidates for peptide receptor radiotherapy today and in the future. J Nucl Med 46 (Suppl 1):67S–75S
31. Ryan RR, Weber HC, Mantey SA, Hou W, Hilburger ME, Pradhan TK, Coy DH, Jensen RT (1998) Pharmacology and intracellular signaling mechanisms of the native human orphan receptor BRS-3 in lung cancer cells. J Pharmacol Exp Ther 287:366–380
32. Schulz S, Pauli SU, Handel M, Dietzmann K, Firsching R, Hollt V (2000) Immunohistochemical determination of five somatostatin receptors in meningioma reveals frequent overexpression of somatostatin receptor subtype sst2A. Clin Cancer Res 6:1865–1874
33. Schulz S, Rocken C, Mawrin C, Weise W, Hollt V (2004) Immunocytochemical identification of VPAC1, VPAC2, and PAC1 receptors in normal and neoplastic human tissues with subtype-specific antibodies. Clin Cancer Res 10:8235–8242
34. Schulz S, Rocken C, Mawrin C (2005) Immunohistochemical localization of CCK1 cholecystokinin receptors in normal and neoplastic human tissues. J Clin Endocrinol Metab 90:6149–6155
35. Scopinaro F, Di Santo GP, Tofani A, Massari R, Trotta C, Ragone M, Archimandritis S, Varvarigou AD (2005) Fast cancer uptake of 99mTc-labelled bombesin (99mTc BN1). In Vivo 19:1071–1076
36. Smith CJ, Volkert WA, Hoffman TJ (2003) Gastrin releasing peptide (GRP) receptor targeted radiopharmaceuticals: a concise update. Nucl Med Biol 30:861–868
37. Smith CJ, Volkert WA, Hoffman TJ (2005) Radiolabeled peptide conjugates for targeting of the bombesin receptor superfamily subtypes. Nucl Med Biol 32:733–740
38. Stangelberger A, Schally AV, Varga JL, Zarandi M, Cai RZ, Baker B, Hammann BD, Armatis P, Kanashiro CA (2005) Inhibition of human androgen-independent PC-3 and DU-145 prostate cancers by antagonists of bombesin and growth hormone releasing hormone is linked to PKC, MAPK and c-Jun intracellular signalling. Eur J Cancer 41:2735–2744
39. Sun B, Halmos G, Schally AV, Wang X, Martinez M (2000) Presence of receptors for bombesin/gastrin-releasing peptide and mRNA for three receptor subtypes in human prostate cancers. Prostate 42:295–303
40. Sun B, Schally AV, Halmos G (2000) The presence of receptors for bombesin/GRP and mRNA for three receptor subtypes in human ovarian epithelial cancers. Regul Pept 90:77–84
41. Van de Wiele C, Dumont F, Vanden Broecke R, Oosterlinck W, Cocquyt V, Serreyn R, Peers S, Thornback J, Slegers G, Dierckx RA (2000) Technetium-99m RP527, a GRP analogue for visualisation of GRP receptor-expressing malignancies: a feasibility study. Eur J Nucl Med 27:1694–1699
42. Zhang H, Chen J, Waldherr C, Hinni K, Waser B, Reubi JC, Maecke HR (2004) Synthesis and evaluation of bombesin derivatives on the basis of pan-bombesin peptides labeled with indium-111, lutetium-177, and yttrium-90 for targeting bombesin receptor-expressing tumors. Cancer Res 64:6707–6715

Virchows Arch (2006) 449:428–434
DOI 10.1007/s00428-006-0254-x

ORIGINAL ARTICLE

Impact of pathology review of stage and margin status of radical prostatectomy specimens (EORTC trial 22911)

Theodorus H. van der Kwast · Laurence Collette · Hein Van Poppel · Paul Van Cangh · Kris Vekemans · Luigi DaPozzo · Jean-François Bosset · Karl H. Kurth · Fritz H. Schröder · Michel Bolla · European Organisation for Research and Treatment of Cancer Radiotherapy and Genito-Urinary Cancer Groups

Received: 27 March 2006 / Accepted: 13 June 2006 / Published online: 29 August 2006
© Springer-Verlag 2006

Abstract Pathological staging and surgical margin status of radical prostatectomy specimens are next to grading the most important prognosticators for recurrence. A central review of pathological stage and surgical margin status was performed on a series of 552 radical prostatectomy specimens of patients, participating in the European Organisation for Research and Treatment of Cancer trial 22911. Inclusion criteria of the trial were pathological stage pT3 and/or positive surgical margin at local pathology. All specimens were totally embedded. Data of the central review were compared with those of local pathologists and related to clinical follow-up. Although a high concordance between review pathology and local pathologists existed for seminal vesicle invasion (94%, κ=0.83), agreement was much less for extraprostatic extension (57.5%, κ=0.33) and for surgical margin status (69.4%, κ=0.45). Review

T. H. van der Kwast
Pathology and Laboratory Medicine,
Mount Sinai Hospital,
Toronto, Canada

L. Collette
European Organisation
for Research and Treatment of Cancer Data Centre,
Brussels, Belgium

H. Van Poppel
Department of Urology,
Universitair Ziekenhuis Gasthuisberg,
Leuven, Belgium

P. Van Cangh
Department of Urology,
Hopital St. Luc,
Brussels, Belgium

K. Vekemans
Department of Urology,
Virga Jesse Ziekenhuis,
Hasselt, Belgium

L. DaPozzo
Department of Urology,
Ospedale San Rafaele,
Milano, Italy

J.-F. Bosset
Department of Radiation Oncology,
Hopital Jean Minjoz,
Besançon, France

K. H. Kurth
Department of Urology,
Academisch Medisch Centrum,
Amsterdam, The Netherlands

F. H. Schröder
Department of Urology,
Erasmus Medical Center,
Rotterdam University,
Rotterdam, The Netherlands

M. Bolla
Department of Radiation Oncology,
Centre Hospitalier Universitaire,
Grenoble, France

T. H. van der Kwast (✉)
Department of Pathology,
University Health Network,
200 Elizabeth Street, 11th Floor,
Toronto, Ontario M5G 2C4, Canada
e-mail: theo.vdkwast@uhn.on.ca

pathology of surgical margin status was a stronger predictor of biochemical progression-free survival in univariate analysis [hazard ratio (HR)=2.16 and p=0.0002] than local pathology (HR=1.08 and p>0.1). The review pathology demonstrated a significant difference between those with and without extraprostatic extension (HR=1.83 and p=0.0017), while local pathology failed to do so (HR=1.05 and p>0.8). The observations suggest that review of pathological stage and surgical margin of radical prostatectomy strongly improves their prognostic impact in multiinstitutional studies or trials.

Keywords Prostatectomy · Stage · Margin status · Interobserver variation · Quality assurance

Introduction

Pathological staging of radical prostatectomy specimens is considered an important tool for the assessment of the prognosis of individual patients and it helps the urologist in decision-making with regard to the installment of adjuvant therapy. Another important role of pathological staging of radical prostatectomy specimens is the definition of a homogeneous patient population to be studied in the context of a clinical study or trial.

To enable an accurate pathological staging, the radical prostatectomy specimens should be processed in a uniform way, allowing the whole specimen to be examined microscopically. Several consensus guidelines on processing and reporting of radical prostatectomy specimens were published recently [9, 14], avoiding confusion and variation among pathologists. Preferentially, the prostatectomy specimens should be totally embedded and the apex and bladder neck should be sectioned in a parasagittal plane for an optimal appreciation of the surgical margins.

The prognostic impact of pathological stage is undisputed; particularly, the invasion of seminal vesicles is considered a highly unfavorable feature. However, as a consequence of widespread prostate-specific antigen (PSA) testing, a stage shift in prostatectomy specimens was noted in recent years [5, 17] and the prognostic significance of pathological stage in current patient populations may have diminished. Although the prognostic impact of surgical margin status is somewhat more controversial, most but not all investigators were able to confirm the prognostic impact of this parameter in multivariate analyses [1, 2, 13, 15].

Another factor that may detract from the prognostic impact of pathological staging and determination of surgical margin is the degree of interobserver variation among pathologists. Most pathologists would agree that a substantial interobserver variation exists for grading of prostate cancer, but this issue has rarely been addressed for pathological staging and surgical margin status [7]. Prostatectomy specimens of the European Organisation for Research and Treatment of Cancer (EORTC) trial 22911 were centrally reviewed as a part of the study protocol designed to study the potential benefit of postoperative external radiotherapy in patients with a pathological stage pT3 prostate cancer and/or positive surgical margins, while negative for locoregional or distant metastasis. The first results of this trial were published recently [3]. Here, we report on the degree of interobserver variation between local pathologists and review pathology (by a single pathologist) for pathological stage, including seminal vesicle invasion and extraprostatic extension, and for surgical margin status. In addition, the prognostic impact of these parameters was analyzed using biochemical recurrence-free survival (PSA failure after prostatectomy) as outcome parameter.

Materials and methods

Patients and surgical specimens

Prostatectomy specimens of 566 participants of the EORTC study 22911 were reviewed, of which 14 belonged to ineligible cases leaving a total of 552 cases (280 in the wait-and-see arm and 272 in the postoperative irradiation arm) eligible. In each participating center the protocol was approved by the local/national ethics review committee. Informed consent was obtained from all patients in accordance with national laws.

The total number of participants of this multiinstitutional trial was 1,005, but only the prostatectomy specimens of 11 major participating hospitals were reviewed.

After formalin fixation, the prostatectomy specimens were totally embedded after inking the outer surface of the specimens essentially using the same protocol for grossing in all participating hospitals [14, 16]. This includes separate embedding of parasagittal sections of the apex and bladder neck margin. Exclusion criteria for pathological review were hormonal therapy before prostatectomy or incomplete embedding of the prostatectomy.

Pathological review

The pathological review was performed by a single pathologist with experience in urogenital pathology (THvdK) and included the examination of all slides of the radical prostatectomy specimen. In addition to Gleason score, pathological stage [Tumor-Node-Metastasis (TNM) 1997], presence of extraprostatic extension, invasion of seminal vesicles, and surgical margin status were recorded. If extraprostatic (or extracapsular) extension was present,

its extent [focal, i.e., extending <1 high power field (hpf), or otherwise extensive, i.e., >1 hpf] and sidedness were recorded. Extraprostatic extension was defined by either infiltration of the carcinoma of the prostatic pseudocapsule into the direct vicinity or beyond the adipose tissue (Fig. 1a) or within the neurovascular bundle beyond the outer contour of the adjacent pseudocapsule (Fig. 1b). Bladder invasion was determined by invasion in the large bundles of smooth muscle, characteristic of the muscularis propria of the urinary bladder. Positive margin status was recorded in case of the presence of tumor cells within the inked margin. For positive surgical margin, apical and nonapical (designated as lateral) involvement was distinguished.

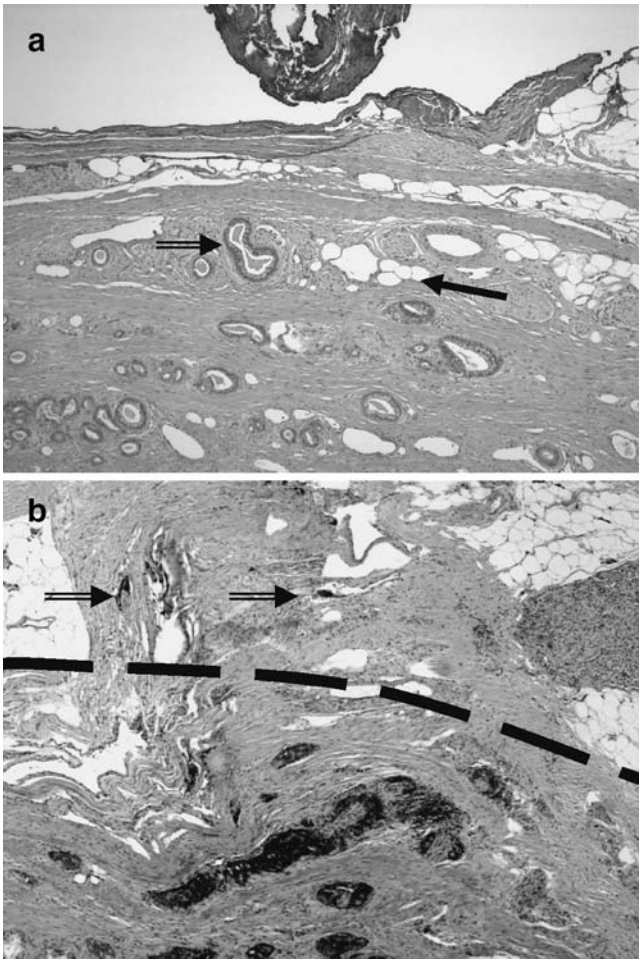

Fig. 1 **a** Micrograph showing adipose tissue (*solid arrow*) at the edge of the pseudocapsule and a single tumor gland (*double-line arrow*) at the level of and beyond the adipose tissue fulfilling the requirement of extraprostatic extension. **b** Micrograph showing infiltration of neurovascular bundle by scattered foci of poorly differentiated carcinoma (*double-line arrow*). The contour of the outer edge of the prostatic pseudocapsule is depicted by the *interrupted line*. Although adipose tissue is not identified in the vicinity of the cancer, this is also considered extraprostatic extension

Follow-up and endpoint

Details of the follow-up of the EORTC trial 22911 were described elsewhere [3]. Clinical follow-up with digital rectal examination and PSA tests were done at 4, 8, and 12 months after treatment, then every 6 months until the end of the fifth year. Chest radiography and bone scans were done every year or in case of clinical or biochemical suspicion of progression. CT scans and liver ultrasound were used for confirmation of progression. Biochemical recurrence was defined as a PSA increase of more than 0.2 ng/ml over the lowest postoperative value measured on three occasions at least 2 weeks apart.

Local recurrence had to be documented by digital rectal examination.

The primary trial endpoint and endpoint of the present analysis is biochemical progression-free survival defined as the time from randomization to first clinical or biochemical recurrence or death due to any cause.

Statistics

Agreement between local pathology and review pathology on the 552 prostatectomy specimens was measured by the total percentage of agreement and by simple kappa statistics [4].

The prognostic value of staging parameters and surgical margin status defined by local and review pathology was analyzed on the 280 cases of the wait-and-see arm of the trial as postoperative irradiation will influence the biochemical and clinical progression-free interval [3]. The prognostic impact of local and review pathology for the different parameters was analyzed by Cox regression model [6] with estimation of hazard ratios (HR) and 95% confidence intervals. Event-free rates were estimated by Kaplan–Meier [12].

Results

The median follow-up time for the 552 patients included in this analysis was 4.7 years. The age range of the patients varied between 47 and 75 years (median 66 years) and preoperative PSA level varied from 0.3 to 159.4 ng/ml (median 12.5 ng/ml) (Table 1). The patients included in this analysis had a slightly better overall prognosis than those excluded from the analysis (p=0.056), probably owing to differences in referral patterns between centers, as can be inferred from the lower rate of positive surgical margins and involvement of seminal vesicles.

Level of agreement between review and local pathology

A total of 552 radical prostatectomies were reviewed for extraprostatic extension, seminal vesicle invasion, and

Table 1 Patient characteristics

Variable	Review pathology performed?		Total (n=1,005)
	No (n=453) Number of patients (%)	Yes (n=552) Number of patients (%)	Number of patients (%)
Age (years)			
Median	64.9	66.0	65.4
Range	47.0–75.1	47.2–75.8	47.0–75.8
Previous short-term neoadjuvant hormonal treatment	46 (10.2)	55 (10.0)	101 (10.0)
Clinical TNM (UICC 1983)			
T0	6 (1.3)	0 (0.0)	6 (0.6)
T1	69 (15.2)	102 (18.5)	171 (17.0)
T2	294 (64.9)	360 (65.2)	654 (65.1)
T3	83 (18.3)	90 (16.3)	173 (17.2)
TX	1 (0.2)	0 (0.0)	1 (0.1)
PSA before surgery (ng/ml, Hybritech equivalent)			
Median	12.3	12.5	12.3
Range	0.3–116.0	0.3–159.4	0.3–159.4
PSA 3 weeks after surgery/before irradiation			
Median	0.2	0.2	0.2
Range	0.0–38.8	0.0–48.7	0.0–48.7
Pathological risk factors (local pathology)			
Positive surgical margins	304 (67.1)	325 (58.9)	629 (62.6)
Capsule perforation	343 (75.7)	431 (78.1)	774 (77.0)
Invasion of the seminal vesicles	132 (29.1)	124 (22.5)	256 (25.5)

UICC Union Internationale Contre Le Cancer (International Union Against Cancer)

surgical margin status. Review data were not available for extraprostatic extension, seminal vesicle invasion, and surgical margin status in 5, 9, and 28 cases, respectively. This was due to incomplete sets of slides or impossibility of interpretation of the histological slides.

Tables 2, 3, 4, and 5 show that the agreement and corresponding kappa value is good for seminal vesicle invasion (Table 2), but mediocre for extraprostatic extension (Table 3) and surgical margin status (Table 4).

The local pathology more frequently judged a case positive for extraprostatic extension (78.1%, 421/552) than the review pathologist (54.5%, 301/552). The review pathologist did not find extraprostatic extension in 35% of the cases judged as extraprostatic extension by local pathology (151/431). In contrast, 19% of the cases scored without extraprostatic extension by local pathology were considered positive for extraprostatic extension by review pathology (23/121).

Surgical margin involvement was recorded in 53.3% by the review pathologist (294/552) and in 58.9% by local pathology (325/552). Negative margins as judged by local pathology were scored positive by review pathology in 26.4% of the cases (60/227) and conversely, 24.9% of the

Table 2 Interobserver variation for seminal vesicle invasion

Review pathology	Local pathology		Total n (%)
	Negative n (%[a]) [%[b]]	Positive n (%) [%[b]]	
Not recorded	8 (89) [2]	1 (11) [1]	9 (2)
Negative	415 (94) [97]	26 (6) [21]	441 (80)
Positive	5 (5) [1]	97 (95) [78]	102 (18)
Total	428 (78)	124 (22)	552 (100)

[a]Percentage of reviewed cases of the category unknown, negative, or positive for seminal vesicle invasion that scored negative or positive at local pathology

[b]Percentage of cases scored negative (second column) or positive by local pathology (third column)

Table 3 Interobserver variation for extraprostatic extension

Review pathology	Local pathology		Total n (%)
	Negative n (%)[a] [%][b]	Positive n (%)[a] [%][b]	
Not recorded	3 (60) [2.5]	2 (40) [0.5]	5 (1)
Negative	95 (39) [79]	151 (61) [35]	246 (45)
Focal	8 (10) [7]	76 (90) [18]	84 (15)
Extensive	15 (7) [12]	202 (93) [47]	217 (39)
Total	121 (22)	431 (78)	552 (100)

[a]Percentage of reviewed cases of the category unknown, negative, focal, or extensive for extraprostatic extension that scored negative or positive at local pathology

[b]Percentage of cases scored negative (second column) or positive by local pathology (third column)

Table 4 Interobserver variation for margin status according to site

Margin status by review pathology	Margin status by local pathology		Total
	Negative (%)[a] [%][b]	Positive (%)[a] [%][b]	
Not recorded	4 (67) [1.8]	2 (33) [0.6]	6 (1)
Negative	149 (65) [66]	81 (35) [25]	230 (42)
Apex positive	11 (17) [5]	54 (83) 17]	65 (12)
Lateral positive	40 (24) [18]	128 (76) [39]	168 (30)
Apex and lateral positive	9 (15) [4]	52 (85) [16]	61 (11)
Not evaluable	14 (64) [6]	8 (36) [2]	22 (4)
Total	227 (41)	325 (59)	552 (100)

[a]Percentage of reviewed cases scored negative or positive at local pathology
[b]Percentage of cases scored negative (second column) or positive by local pathology (third column)

cases that scored positive by local pathology (81/325) were judged negative by the review pathology.

The level of agreement between local and review pathology was similar when the analysis was restricted to the four hospitals contributing more than 75 patients each to the study. Among these four hospitals, however, a large variation in agreement with review pathology existed for extraprostatic extension and surgical margin status. For extraprostatic extension one hospital showed considerably less agreement with review pathology (κ=0.0) than the other three hospitals (κ>0.30). Excluding that hospital, the agreement was κ=0.42 (0.34–0.51). For surgical margin status, there was again significant heterogeneity among the large hospitals (p<0.0001), and agreement was κ=0.64, 0.51, 0.13, 0.18 with review pathology.

In a separate analysis we showed that the year of entry did not influence the level of agreement, neither did it influence seminal vesicle invasion, extraprostatic extension, or margin status (data not shown).

At review pathology a distinction was made between focal and extensive extraprostatic invasion. Analysis of the discrepancies between review and local pathology showed that when the 84 cases with focal extension only were excluded (i.e., only extensive extraprostatic extension at review was considered), the agreement between review and local pathology remained essentially the same (κ=0.31 for extensive extraprostatic extension and κ=0.33 for all cases).

The breakdown of the surgical margin status results according to site is given in Table 4. If review pathology showed a positive surgical margin of the apex (n=126), the local pathology would also judge the margin positive in 83% of the cases, but this proportion dropped to 76% of the cases when only the lateral margin was involved, according to the review pathologist (128/168), and the local pathologist agreed on the negative margin status in only 65% of the cases scored negative by review pathology (149/203).

Influence of review pathology on the prognostic impact of staging parameters

Because postoperative radiotherapy influenced the long-term clinical outcome (biochemical progression-free survival and clinical recurrence), the analysis of the prognostic impact of local and review pathology was restricted to the wait-and-see arm of the trial (n=268 patients with review pathology). Kaplan–Meier analysis for biochemical progression-free survival showed that surgical margin status by review pathology was a stronger predictor compared to local pathology (Fig. 2). HR of positive margins by review pathology for biochemical recurrence was 2.16 (95% CI 1.43–3.26 and p<0.0002), while local pathology surgical margin status was not significantly related to biochemical recurrence (HR=1.08, 95% CI 0.74–1.56, and p>0.1) in univariate analysis.

For extraprostatic extension, including those with focal and extensive extension, review pathology demonstrated a significant difference (in univariate analysis) between the two subsets (HR=1.83, 95% CI 1.25–2.68, and p=0.0017), while local pathology was not able to demonstrate a significant difference (HR=1.05, 95% CI 0.66–1.68, and p>0.1).

Seminal vesicle involvement was a strong predictor of biochemical recurrence when assessed by the review

Table 5 Agreement between review and local pathology

Parameter	Overall agreement (%)	Simple kappa (95% CI)		
		All centers (n=552)	4 Centers with >75 cases (n=461)	7 Centers with <50 cases (n=91)
Seminal vesicle invasion	92.8	0.83[a] (0.77–0.89)	0.83[a] (0.77–0.90)	0.79[a] (0.65–0.93)
Extraprostatic extension	68.2	0.33[a,b] (0.25–0.39)	0.35[a,b] (0.27–0.42)	0.17[a,b] (0.0–0.36)
Surgical margin status	69.4	0.45[a,c] (0.37–0.53)	0.45[a,c] (0.39–0.55)	0.29[a,c] (0.08–0.50)

[a]The cases classified "unknown" or "not evaluable" are excluded.
[b]The categories "focal" and "extensive" are grouped together.
[c]The categories "apex positive," "lateral positive" and "apex and lateral positive" are grouped together.

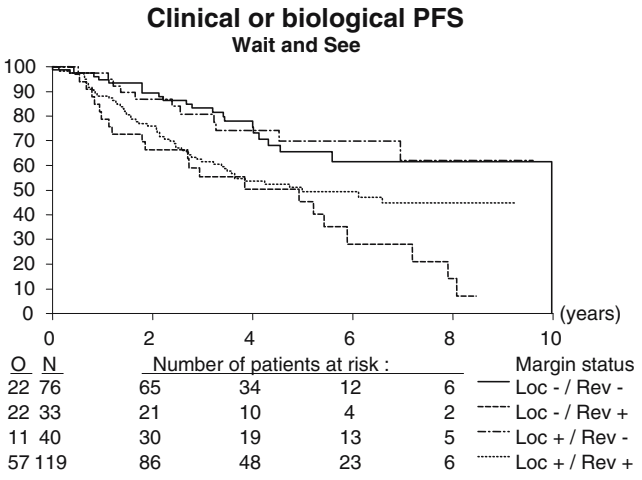

Fig. 2 Kaplan–Meier curves relating the biochemical progression-free survival after prostatectomy based on local and review pathology margin status

pathologist (HR=2.03, 95% CI 1.33–3.10, and P=0.0008) and by the local pathologist (HR=1.99, 95% CI 1.35–2.95, and P=0.0004), owing to the very high agreement between the two assessments.

Discussion

Although it is frequently reported that grading of prostate cancer has a high interobserver variation, irrespective of the grading system used [10, 11] interobserver variation for staging parameters of radical prostatectomy specimens has rarely been investigated. Ekici et al. [7] studied a limited series of prostatectomy specimens from a single institution. They reported a high interobserver variation between the findings in the pathology report and those of the review pathologist, especially for surgical margin status and extraprostatic extension. Similarly, we demonstrate a surprisingly high rate of disagreement on a much larger series of radical prostatectomy specimens retrieved from several large institutions participating in this EORTC study (trial 22911).

All institutions adhered to a similar embedding pathology protocol, including total embedding of the prostatectomy specimen and allowing separate examination of apex and bladder neck, following the guidelines published before [14]. If the centers taken into account are only those attributing more than 75 cases to the trial, the level of (dis) agreement with review pathology remained essentially the same. It is most likely that the discrepancies can be attributed to differences in the interpretation of the findings and/or overlooking of some pathological details related to the investigated parameters. As for surgical margins, during review we strictly adhered to the guideline that tumor cells should really be in contact with ink to consider the margin positive, irrespective of the (minute) distance to the inked surface. This is in line with the finding of Epstein et al. [8] that a close margin (i.e.,<0.1 mm) should not be designated as positive surgical margin because this would not impact the prognosis. Also, lacerations in the capsule were accounted for as they may cause a false-positive diagnosis of positive margins, even though tumor cells may be covered by ink at these sites due to leakage. Similarly, presence of tumor cells in the outer surface of the specimen *not* covered by ink was not considered as evidence for a positive margin.

Current guidelines prescribe that only in the case of covering by ink (applied before the sectioning of the radical prostatectomy specimen) should the margin be considered as positive. It is important to note that application of these rules during our review led to the emergence of surgical margin status as a prognostic parameter, which was maintained after inclusion of the (reviewed) Gleason score in the multivariate analysis. Another potential source for discrepancies concerning the surgical margin status may be the assumption that the mere presence of carcinoma in sections of the apex would automatically signify a positive resection margin. This dates back to the time that in some institutions the apex was cut in a transversal plane precluding a proper evaluation of its resection margins. The observation that in our series the agreement at the apex margin status compared to lateral margin status is only marginally higher (Table 4) is not in line with this explanation.

Overlooking of extraprostatic extension may have played a role in the minority of the cases where review pathology recorded extraprostatic extension where local pathology failed to do so. In that case, comparatively more often, focal extraprostatic extension would be observed by review pathology than in the prostatectomies with consensus between review and local pathology concerning the presence of extraprostatic extension. Because this was not the case, this explanation for the higher frequency of extraprostatic extension during review cannot be maintained. Another potential source for discrepancy may be the judgment of tumor infiltrating the neurovascular bundle. The absence of adipose tissue may lead to underestimation of the presence of extraprostatic extension. Variation in agreement with central review among the four larger hospitals was considerable for both extraprostatic extension (one outlier) and surgical margin status (two outliers). This might suggest that different sets of criteria are being used in different pathology laboratories, while within a pathology laboratory the criteria are relatively uniform.

Similar to the paper by Ekici et al. [7], the level of agreement for seminal vesicle invasion was high. Apparently, most pathologists are aware of the requirement of tumor invasion of the muscular coat of the seminal vesicle in the extraprostatic part of the organ.

A potential limitation of this study may be that only pathological stage T3 cancers and/or those with a positive margin status (at local pathology) were included. Our conclusions are therefore likely to be valid particularly for the subset of patients with more advanced prostate cancer. Nevertheless, our study indicates that the observed strong interobserver variation for surgical margin status and extraprostatic extension bears consequences both directly for optimal patient care and for the outcome of trials on large groups of patients. A further search for the causes underlying the discrepancies is warranted to improve and further specify guidelines on reporting of radical prostatectomy specimens.

Review of radical prostatectomy specimens of participants of a trial is likely to improve the outcome of the study and should be an integrated part of any trial design.

Acknowledgements This publication was supported by grants number 5U10 CA488-21 to 5U10-CA488-34 from the National Cancer Institute (Bethesda, MD, USA) and by a grant from Ligue Nationale contre le Cancer (Comité de l'Isère, Grenoble, France). The content of this paper is solely the responsibility of the authors and does not necessarily represent the official views of the National Cancer Institute or of the Ligue Nationale contre le Cancer.

References

1. Ackerman DA, Barry JM, Wicklund RA, Olson N, Lowe BA (1993) Analysis of risk factors associated with prostate cancer extension to surgical margin and pelvic node metastasis at radical prostatectomy. J Urol 150:1845–1850
2. Blute ML, Bostwick DG, Bergstralh EJ, Slezak JM, Martin SK, Amling CL, Zincke H (1997) Anatomic site-specific positive margins in organ-confined prostate cancer and its impact on outcome after radical prostatectomy. Urology 50:733–739
3. Bolla M, van Poppel H, Collette L, van Cangh P, Vekemans K, Da Pozzo L, de Reijke TM, Verbaeys A, Bosset JF, van Velthoven R, Marechal JM, Scalliet P, Haustermans K, Pierart M, European Organization for Research and Treatment of Cancer (2005) Postoperative radiotherapy after radical prostatectomy: a randomised controlled trial (EORTC trial 22911). Lancet 366:572–578
4. Cohen J (1960) A coefficient of agreement for nominal scales. Educ Psychol Meas 20:37–46
5. Cooperberg MR, Lubeck DP, Mehta SS, Carroll PR, CaPSURE (2003) Time trends in clinical risk stratification for prostate cancer: implications for outcomes (data from CaPSURE). J Urol 170:S21–S25
6. Cox DR (1959) The analysis of exponentially distributed lifetimes with two types of failure. J R Stat Soc B 21:411–421
7. Ekici S, Ayhan A, Erkan I, Bakkaloğlu M, Őzen H (2003) The role of the pathologist in the evaluation of radical prostatectomy specimens. Scand J Urol Nephrol 37:387–391
8. Epstein JI, Sauvageot J (1997) Do close but negative margins in radical prostatectomy specimens increase the risk of postoperative progression? J Urol 157:241–243
9. Epstein JI, Amin M, Boccon-Gibod L, Egevad L, Humphrey PA, Mikuz G, Newling D, Nilsson S, Sakr W, Srigley JR, Wheeler TM, Montironi R (2005) Prognostic factors and reporting of prostate carcinoma in radical prostatectomy and pelvic lymphadenectomy specimens. Scand J Urol Nephrol Suppl 216:34–63
10. Gallee MP, Ten Kate FJ, Mulder PG, Blom JH, van der Heul RO (1990) Histological grading of prostatic carcinoma in prostatectomy specimens. Comparison of prognostic accuracy of five grading systems. Br J Urol 65:368–375
11. Glaessgen A, Hamberg H, Pihl CG, Sundelin B, Nilsson B, Egevad L (2002) Interobserver reproducibility of percent Gleason grade 4/5 in total prostatectomy specimens. J Urol 168:2006–2010
12. Kaplan EL, Meier P (1958) Nonparametric estimation from incomplete observations. J Am Stat Assoc 53:457–481
13. Khan MA, Partin AW (2005) Surgical margin status after radical retropubic prostatectomy. BJU Int 95: 281–284
14. Montironi R, van der Kwast T, Boccon-Gibod L, Bono AV, Boccon-Gibod L (2003) Handling and pathology reporting of radical prostatectomy specimens. Eur Urol 44: 626–636
15. Palisaar RJ, Graefen M, Karakiewicz PI, Hammerer PG, Huland E, Haese A, Fernandez S, Erbersdobler A, Henke RP, Huland H (2002) Assessment of clinical and pathologic characteristics predisposing to disease recurrence following radical prostatectomy in men with pathologically organ-confined prostate cancer. Eur Urol 41:155–1561
16. Stamey TA, McNeal JE, Freiha FS, Redwine E (1988) Morphometric and clinical studies on 68 consecutive radical prostatectomies. J Urol 139:1235–1241
17. Van der Kwast TH, Ciatto S, Martikainen PM, Hoedemaeker R, Laurila M, Pihl CG, Hugosson J, Neetens I, Nelen V, Di Lollo S, Roobol MJ, Maatanen L, Santonja C, Moss S, Schroder FH (2006) Detection rates of high-grade prostate cancer during subsequent screening visits. Results of the European randomized screening study for prostate cancer. Int J Cancer 118:2538–2542

Virchows Arch (2006) 449:435–447
DOI 10.1007/s00428-006-0271-9

ORIGINAL ARTICLE

Tissue microarray profiling of primary and xenotransplanted synovial sarcomas demonstrates the immunophenotypic similarities existing between SYT-SSX fusion gene confirmed, biphasic, and monophasic fibrous variants

Manish Mani Subramaniam · Samuel Navarro · Antonio Pellin · Jose Antonio López-Guerrero · Carmen Carda · Jose Antonio Heredia Alvaro · Pau Lluís Gozalbo Sabater · Antonio Llombart-Bosch

Received: 31 March 2006 / Accepted: 7 July 2006 / Published online: 7 September 2006
© Springer-Verlag 2006

Abstract This paper discusses the diversity of synovial sarcomas (SSs) [biphasic (BSS), monophasic fibrous (MFSS), and poorly differentiated (PDSS)] and tissue microarray (TMA) evaluation of the immunophenotypic and histological progression of SSs in nude mice using three TMAs comprising 11 primary SSs (8 MFSSs, 2 BSSs, and 1 PDSS) and their xenografts. BSS and MFSS progressively transformed to a similar undifferentiated phenotype with loss of glandular component in the xenografts. Epidermal growth factor receptor and SALL2 were expressed in primary tumors and xenografts. Enhanced bcl-2 and bax expression were noted in xenografts. Ki-67 overexpression in xenografts correlated with high mitotic index. Epithelial membrane antigen (EMA) and cytokeratin AE1/AE3 were detected in all original and xenografted SSs. Hierarchical clustering differentiated original MFSS and BSS, but their xenografts clustered together due to similar immunoexpression profile. Our study demonstrates definite phenotypic variability of BSS and MFSS in the xenografts. Differences in immunoexpression for various markers existed between primary tumor and xenografts but not between subtypes. Hierarchical clustering grouped TMA immunostaining data and confirmed immunophenotypic variability; however, it failed to reveal any immunophenotypic differences between SYT-SSX1 and SYT-SSX2 type tumors. Nonetheless, reverse-transcriptase–polymerase chain reaction detected SYT-SSX transcripts in all primary SSs and their xenografts, thereby demonstrating their genetic stability.

M. M. Subramaniam
Department of Pathology, Faculty of Medicine,
University of Valencia,
Valencia, Spain

S. Navarro · A. Pellin · C. Carda · A. Llombart-Bosch (✉)
Department of Pathology, Medical School, University of Valencia,
Avda. Blasco Ibañez, 17,
46010 Valencia, Spain
e-mail: antonio.llombart@uv.es

J. A. López-Guerrero
Molecular Biology Unit,
Fundación Instituto Valenciano de Oncologia,
Valencia, Spain

J. A. Heredia Alvaro · P. L. Gozalbo Sabater
Department of Technology, University of Jaume-I,
Castellon, Spain

Keywords Synovial sarcoma · Nude mice xenografts · Tissue microarrays · Novel markers · Hierarchical cluster analysis

Abbreviations

SS	synovial sarcoma
MFSS	monophasic fibrous synovial sarcoma
BSS	biphasic synovial sarcoma
PDSS	poorly differentiated synovial sarcoma
TMA	tissue microarray
RT-PCR	reverse-transcriptase–polymerase chain reaction
EGFR	epidermal growth factor receptor
SALL2	SAL (*drosophila*)-like 2
IGFBP2	insulin-like growth factor binding protein 2

Introduction

Synovial sarcoma (SS) accounts for 5 to 10% of soft tissue sarcomas and is mainly reported in adolescents and adults aged between 15 and 45 years. More than 85 to 95% arise in the deep soft tissues of the extremities, especially around the knee [40]. Histologically, SS can be classified mainly as biphasic, predominantly epithelial, monophasic fibrous, poorly differentiated, and other unusual subtypes such as cystic, myxoid, calcifying, and bone and/or cartilage-forming forms [12, 40]. Many spindle to round cell sarcomas, especially malignant peripheral nerve sheath tumor (MPNST), fibrosarcoma, leiomyosarcoma, malignant hemangiopericytoma, and Ewing's family tumors (ESFTs), can be confused with monophasic fibrous and poorly differentiated synovial sarcoma (MFSS and PDSS, respectively), whereas biphasic synovial sarcoma (BSS) is easily diagnosed on hematoxylin and eosin (H & E) sections. Immunoreactivity for epithelial membrane antigen (EMA), cytokeratin AE1/AE3, and E-cadherin, in combination with CD34 negativity in a spindle to round cell sarcoma, has been reported as the most sensitive and confirmatory markers in the diagnosis of MFSS and PDSS [14, 33, 39]. Recently, Nielsen et al. [30] has demonstrated the expression of two novel markers: epidermal growth factor receptor (EGFR) and SAL (*Drosophila*)-like 2 (SALL2) in SS by both gene expression profiling and immunohistochemistry, and suggested their expression to be specific for certain keratin-/EMA-negative SSs, differentiating them from other sarcomas, particularly malignant peripheral nerve sheath tumor (MPNST).

The chromosomal translocation t(X;18) (p11.2;q11.2), resulting in the fusion of SYT gene at 18q11 with either SSX1 or SSX2 genes or rarely SSX4, found in more than 90% of the SSs irrespective of the subtypes was suggested to be the primary causal event in tumorigenesis due to the generation of an aberrant SYT-SSX transcript, which codes for a chimeric protein thought to regulate the expression of a particular set of genes [8, 14, 20, 25, 39]. The aberrant SYT-SSX protein acts as a transcriptional cofactor through a repression domain (SSX-RD) on the C terminus of SSX and an activation domain (QPGY) on the SYT portion of the fusion protein [18, 28]. Detection of this translocation or fusion transcripts enables the diagnosis of difficult and unusually located SSs, and is even considered necessary in these doubtful cases [7, 29].

Athymic nude mice readily accept human tumor transplants and constitute a valuable source of material for tumor characterization studies because, to a certain extent, their histology is preserved, and they can also be followed for several generations in successive tumor passages [10, 26, 35]. Nevertheless, there are very few published reports on SS strains transplanted into nude mice, none of which have been followed for successive generations [15, 17, 34].

Nonetheless, even with all these methodologies, the histological characterization of this tumor remains unclear: SS is an intriguing neoplasm displaying many structural patterns with epithelial, epithelioid, spindle, and round cells also associated with myxoid and mucinous deposits. The possibility that this tumor can be a metaplastic carcinoma or a carcinosarcoma has been proposed [11].

Tissue microarray (TMA) is a high-throughput method, which can be effectively used to test the diagnostic utility of various immunomarkers in a large number of specimens, and also aids in comparing the expression of standard markers with new antibodies.

The aim of this study was to analyze 11 primary SSs and their successive xenografts after xenotransplantation into nude mice followed for several tumor passages to characterize the morphological and immunophenotypic changes occurring in the original neoplasm and its successive xenotransplants. In addition, we compare the histology and immunohistochemistry of BSS, MFSS, and PDSS to see if the epithelial phenotype present in the primary tumor persists as such in the nude passages or is lost acquiring MFSS histology or a more undifferentiated configuration (PDSS).

Materials and methods

Tissue samples

A total of 11 primary SSs, including 2 BSSs, 8 MFSSs, and 1 PDSS, were selected for the study. Reverse-transcriptase–polymerase chain reaction (RT-PCR) analysis and direct sequencing detected the SYT-SSX transcripts in 9 of the 11 cases. Frozen material was not available for RT-PCR analysis in the other two cases (cases 4 and 10); however, the fusion transcripts were demonstrated later in the xenografts of one case (case 10), and in the other, the SYT/SSX fusion transcripts could not be demonstrated, and the diagnosis of BSS (case 4) was established by morphological and immunophenotypic approaches.

Xenotransplantation

Several fragments of fresh nonnecrotic tumor of about 3–5 mm in size were transplanted using a trocar into the subcutaneous tissue of the backs of 4- to 6-week-old Balb/c male nude mice (IFA-CREDO, Lyon, France). The successive transfers of the positive tumor passages were performed upon reaching 2- to 5-cc volumes. Growth was positive in all the transplanted cases. The maximum and minimum number of passages obtained were 37 (case 2)

and 2 (case 11), respectively. The specimens were eventually fixed in formalin and paraffin-embedded.

Assembly of TMA

A maximum limit of up to 18 passages was selected for incorporation in the array. These passages were divided into initial (passages 1–5), middle (passages 8, 10, and 12), and terminal (passages 14, 16 and 18) to group the morphological and immunophenotypic variations of the xenotransplants. The primary tumor and the initial, middle, and terminal passages of the 11 cases were assembled in three TMAs consisting of triplicate 1-mm cores using a manual tissue arrayer (Beecher Instr., Inc., Sun. Prairie, WI) with a murine kidney orientation control core in each.

Immunohistochemistry

Five-micrometer sections were obtained from the TMA blocks, and the initial sections were stained with H & E for histological evaluation. Immunohistochemistry was performed for a total of 29 markers comprising standard diagnostic, proliferative, apoptotic, cell cycle regulators, and new markers. The commercial source of the antibodies and the antigen retrieval method adopted for each marker are detailed in Table 1. The staining was performed on a DakoCytomation autostainer and visualized by LSAB (DakoCytomation, Denmark) methodology using 3,3′-diaminobenzidine chromogen as substrate. The DakoCytomation kit was used for manual EGFR immunostaining following the manufacturer's protocol. As controls, known positive tissue sections and negative controls devoid of primary antibody were used. The immunostains were scored by a three-tier system for all the antibodies as follows: negative, 0; mild, 1–25% (1+); moderate, 26–50% (2+); and intense, 51% and above (3+). In situations where there was disconcordance in the triplicate cores, the higher score was taken into consideration. All the sections were evaluated independently by three pathologists (M.M.S., S. N., and A.L.L.B.), and in cases of disagreement in the staining intensity scoring, intensity was determined by consensus.

SYT-SSX fusion gene analysis

RT-PCR was performed on 9 of the 11 primary SSs and their respective three randomly selected passages, including one each from the initial, middle, and the terminal passages. Total RNA extraction from frozen tumor was performed according to the manufacturer's instructions using 1 ml TRIzol reagent (Gibco BRL, Gaithersburg, MD)/50 mg of tissue. Reverse transcription was performed using a Gene Amp RNA-PCR kit (PerkinElmer, Norwalk, CT) under the following conditions: aliquots of 2 μg of total RNA were incubated with 1 μg of 50 μmol/l random hexamers. After incubation at 70°C for 10 min, 4 μl of 25 mmol/l MgCl2, 2 μl of 10 mmol/l dinucleoside triphosphate (dNTPs), 200 U/μl reverse transcriptase, 20 U Rnase inhibitor, and 2 μl tenfold synthesis PCR buffer II were added to obtain 20 μl of reverse-transcription mixture. The conditions of reverse transcription were as described earlier [19]. Two microliters of the resultant cDNA obtained was subjected to PCR amplification with forward and reverse primers as described in the literature [6, 19]. The amplification conditions consisted of denaturation at 95°C for 1 min, annealing at 55°C for 1 min, and extension at 72°C for 1 min for 35 cycles, with a final period of extension at 72°C for 10 min. The products were separated by electrophoresis in 1.5% Tris–borate–EDTA (TBE)-agarose gels and visualized with ethidium bromide. As an internal control for PCR and for quality assessment of the tumor RNAs, a 266-bp portion of CDK4 transcript was amplified with primers as described previously [22]. Negative controls included reactions lacking RNA and RT.

The PCR products were sequenced bidirectionally in an ABI 310 sequencer using the Big Dye terminator v1.1 kit (Applied Bio systems, Inc., Foster City, CA) with the specific primers.

Hierarchical cluster analysis

Hierarchical clustering works in two dimensions. Firstly, the tumors are grouped based on the relatedness of their immunoprofile, and secondly, the antibodies are grouped based on the tumors they stain. Hierarchical clustering uses Cluster and Tree-view programs that can be freely downloaded at http://rana.lbl.gov/EisenSoftware.htm. It is closely based on the average-linkage method of Sokal and Michener [38]. Firstly, Spearman's correlation coefficients are calculated between the antibodies and between the tumors (primary tumor and passages). Secondly, the software constructs a diagonal similarity matrix containing similarity scores between the pairs of antibodies and the tumors based on selected Spearman's correlation metrics. This similarity matrix is then scanned to identify the highest value (representing the most identical pair of antibodies). A node is created joining these two antibodies, and an antibody profile is computed for the node by averaging the observations for the joined elements (missing values are omitted, and the two joined elements are weighted by the number of antibodies they contain). Thus, the antibody cluster is obtained. A similar method is used to obtain the tumor cluster. Finally, the Tree-view program displays the results of the cluster analysis as dendrograms (Fig. 3).

Table 1 Antibodies for immunohistochemistry

Antigen	Clone	Supplier	Dilution	Antigen retrieval
Diagnostic panel				
S100	Polyclonal	DakoCytomation (Denmark)	1/200	None
NSE	MIG-N3		1/200	None
HBA-71	12E7		1/50	None
TRK-A	Polyclonal	Santa Cruz Biotechnology (Santa Cruz, CA, USA)	1/50	None
PGP-9.5	Polyclonal	DakoCytomation	1/50	Pressure cooker[a]
CK	AE1-AE-3		1/50	Pressure cooker
CK-19	B170		1/50	Pressure cooker
EMA	E29		1/200	Pressure cooker
CAM-5.2	5D3	Biogenex (San Ramon, CA, USA)	1/50	Pressure cooker
E-Cadherin	36B5	Novocastra Laboratories, Ltd. (Newcastle, UK)	1/20	Pressure cooker
Cathepsin-D	Polyclonal	DakoCytomation	1/500	Pressure cooker
Vimentin	V9	Novocastra	1/200	Pressure cooker
Collagen-IV	CIV22	DakoCytomation	1/50	Pressure cooker
CD34	QBEND 10		1/50	Pressure cooker
FLI-1	Polyclonal	Santa Cruz	1/25	Pressure cooker
Proliferative markers				
Ki-67	MIB-1	DakoCytomation	1/50	Pressure cooker
Topo Isomerase IIα	3F6	Novocastra	1/20	Pressure cooker
Cellcycle regulators				
Cyclin D1	SP4	Neomarkers (Lab Vision, Fremont, CA, USA)	1/50	HIER using Tris-EDTA buffer (pH 9.0) in water bath for 45 min
p21	F-5	Santa Cruz	1/50	Pressure cooker
p27	SX53G8	DakoCytomation	1/50	Pressure cooker
p16	F12	Santa Cruz	1/100	Pressure cooker
Apoptotic markers				
P53	DO-7	DakoCytomation	1/50	Pressure cooker
Bcl-2	Clone 124		1/50	Pressure cooker
Bcl-X	NC1	Novocastra	1/20	Pressure cooker
Bax	Polyclonal	DakoCytomation	1/50	Pressure cooker
New markers				
EGFR	H11	DakoCytomation	1/50	Incubation in proteinase solution for 15 min
SALL2	Polyclonal	Chemicon (Temecula, CA, USA)	1/200	Pressure cooker
ApoD1	36C6	Novocastra	1/20	Dako Envision
IGFBP2	Polyclonal	Santa Cruz	1/1,000	Pressure cooker

[a] Antigen retrieval carried out in pressure cooker by boiling the slides in 10 mM citrate buffer (pH 6.0) for 3 min at 1.5 atm pressure.
HIER Heat-induced epitope retrieval

Results

Histopathology

The histology was reviewed using conventional full tissue sections to avoid intratumoral heterogeneity and to evaluate tumor necrosis and mitosis. All the primary MFSSs showed fascicles of epithelioid to spindle cells with elongated nuclei and indistinct cytoplasm arranged in either a fibrosarcomatous, hemangiopericytic, and, in some cases, storiform pattern. One primary MFSS (case 8) revealed large myxoid areas, and foci of osseous metaplasia were seen in another (case 11). The necrosis and mitosis were variable in these tumors. Of the two primary BSSs, one (case 5) showed clear-cut biphasic histology characterized by the presence of closely packed glands and intervening stromal spindle cells (Fig. 1). The second (case 4) showed predominantly spindle cells and only isolated foci of tightly packed glands representing the epithelial component.

Four of the eight MFSS nudes retained most of the structure present in the primary tumor throughout all their passages, with spindle cells dominating the histology. The

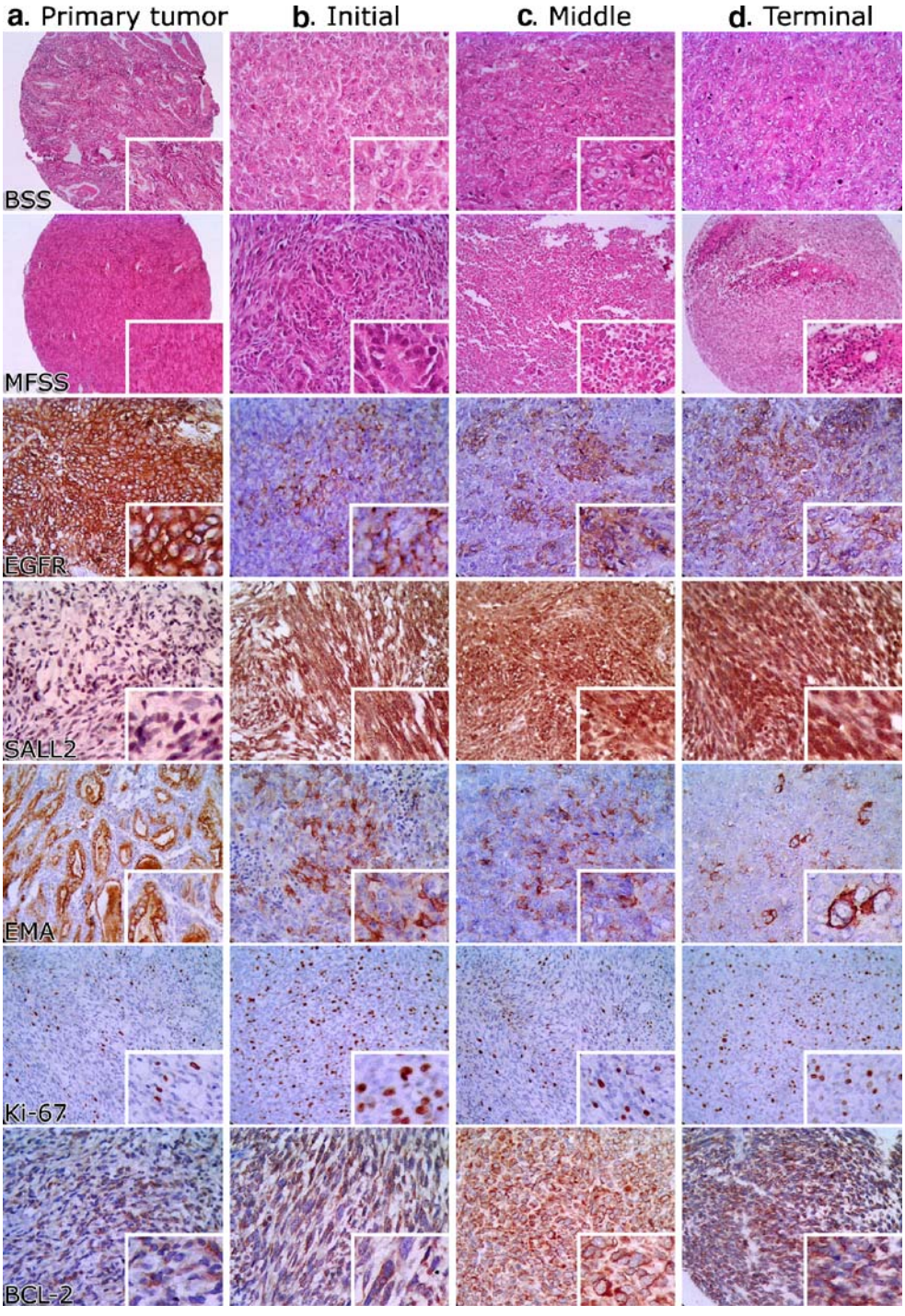

Fig. 1 Histological and immunohistochemical profile of primary SS and the xenografts. *Columns* corresponding to **a**, **b**, **c**, and **d** represent primary tumor, initial, middle, and terminal passages, respectively. The transformation of both primary MFSS and BSS (**a**) to a poorly differentiated pattern comprising sheets of plump epithelioid cells with prominent nucleoli (*inset*) admixed with small round Ewing-like tumor cells forming rosette-like groupings (*insets*) in initial (**b**), middle (**c**) and terminal passages (**d**). Increased necrosis and mitosis also seen in the terminal passages (**d**). EGFR shows intense membranous positivity in primary tumor (**a**) followed by decline in the passages (**b**, **c**, and **d**). SALL2 and Ki-67 shows moderate nuclear positivity in primary tumor (**a**), whereas the passages show intense positivity (**b**, **c**, and **d**). EMA stains the glandular component intensely and the spindle cells focally in the primary tumor; however, the passages show focal positivity in the plump epithelioid cells (*insets*). Bcl-2 shows moderate cytoplasmic positivity in the primary tumor (**a**) and intense positivity in the passages. Original magnifications for **a**–**d**, ×100 and ×400; *insets*, ×600 and ×800, respectively

xenografts of the remaining MFSS, BSS, and PDSS (case 10) showed gradual transition to an epithelioid morphology comprising cells with irregular large round nuclei, prominent nucleoli, and coarse chromatin. Admixed, primitive small round Ewing-like tumor cells, with scarce cytoplasm, forming diffuse compact sheets, pseudorosettes (Fig. 1), and decreasing spindle cell population was observed. The BSS lost its glandular component from the first passage, which was replaced by less-differentiated epithelioid cells intermingled with spindle cells. These changes in cell morphology and histology were detected more extensively in the middle and terminal passages of both the tumor varieties (MFSS and BSS), with the late passages acquiring a more undifferentiated configuration resembling PDSS. Necrosis and mitotic activity increased along the course of the passages in most cases (Fig. 1).

Immunohistochemistry

The immunohistochemistry results of the important markers are summarized in Table 2 and illustrated in detail in Fig. 1. Of the two BSSs, the primary tumor of case 4 lacked the glandular component in all the triplicate cores; therefore, its immunoreactivity was evaluated in the spindle cells.

Novel markers in SS

EGFR showed moderate to intense membranous immunostaining in 5 of the 11 primary tumors (3 MFSSs and 2 BSSs) followed by a decrease to mild or negative staining in their passages (Fig. 1). Three cases were negative for EGFR in both primary tumors and their passages. EGFR was negative in the glandular component of the BSS. No difference in staining was noted between the plump epithelioid, spindle, and the poorly differentiated small round cells.

Mammalian $p150^{Sal2}$ (Sal2, SALL2) belonging to the SALL family of proteins [23] showed an intense nuclear immunostaining. SALL2 was positive in 6 (3 moderate and 3 intense) of the 11 primary SSs. The xenografts of all 11 cases showed an intense positivity (Fig. 1). No immunohistochemical predilection for any particular histological or cellular subtype was noted with SALL2 expression.

ApoDI and insulin-like growth factor binding protein 2 (IGFBP2) displayed sporadic cytoplasmic positivity in occasional xenotransplants of two cases. However, all the primary tumors were negative for both antibodies.

Cell cycle regulators

Cyclin D1 was negative to mildly positive in all 11 primary tumors. In five of these, a relatively increased expression ranging from moderate (3/5) to intense (2/5), especially in the middle and terminal passages, was noted. p16 revealed a very intense nuclear immunoreactivity in the passages compared with the primary tumors. p21 and p27 displayed sporadic mild positivity. The glandular components of the BSS were negative to all the cell cycle proteins except cyclin D1, which was mildly positive.

Apoptotic markers

The apoptotic inhibitor bcl-2 revealed predominantly moderate (5/11) and, in some cases, intense (4/11) perinuclear and cytoplasmic staining in the primary tumors regardless of subtype. The passages of most of the MFSSs showed intense bcl-2 positivity (Fig. 1), whereas on the contrary, mild positivity was noted in the passages of both the BSSs. Bcl-2 stained all the cellular subtypes, including spindle, epithelioid, and primitive round cells, except the glandular components. Bcl-x was negative to mildly positive in the primary tumors and the passages of most of the cases. Bax, the apoptotic promoter, revealed intense cytoplasmic and nuclear positivity in the primary tumors and the xenografts staining all the cellular subtypes, including the epithelial cells of the BSS. p53 showed negative to sporadic positivity.

Proliferative markers

Ki-67 immunostaining was intense in the passages compared with primary tumors in 7 of the 11 cases and correlated with the increasing mitotic activity in the passages (Fig. 1). Topoisomerase IIα levels were comparatively less than Ki-67, comprising mild to moderate immunoreactivity, and failed to correlate with mitotic activity. Only two cases coexpressed both Ki-67 and topoisomerase IIα.

Conventional diagnostic markers

Of the two BSSs, the classic BSS (case 5) showed intense expression of cytokeratin AE1/AE3 and EMA, and moderate staining for CK-19, CAM5.2, and E-cadherin in the glandular elements. The spindle cells were mildly positive for cytokeratin AE1/AE3, EMA, and E-cadherin. The other BSS (case 4), composed of only spindle cells in all the three cores, showed intense expression of EMA and mild positivity for cytokeratin AE1/AE3, E-cadherin, and CAM5.2. The immunoreactivity of epithelial markers declined to focal positive clusters of plump cells in all the passages of the classical BSS (Fig. 1).

In the MFSS category, epithelial markers were expressed in only three of eight cases. Of these three, one showed mild positivity for cytokeratin AE1/AE3 in primary tumor and all its passages. The other two were characterized by negativity of the primary tumors for all the epithelial markers, but coexpression of CK-19 and EMA in one and coexpression of EMA and CAM5.2 in the other were observed, especially in the late passages. Cytokeratin and EMA were positive in all the cell types of MFSSs. E-cadherin was negative in all MFSSs.

The single case of PDSS was mildly positive to cytokeratin AE1/AE3 and EMA. However, its terminal passages displayed moderate positivity for all the epithelial markers. Cathepsin-D was moderate to intense in primary tumors and passages of 6 of 11 SSs. Moderate to intense expression of vimentin in primary tumors and passages was evident. FLI-1 displayed moderate to intense nuclear staining in the middle and terminal passages of four cases. HBA-71, S100, PGP9.5, TRK-A, and NSE were negative to sporadically positive. CD34 was negative in almost all the cases.

Table 2 Immunohistochemical and RT-PCR results of primary and xenografted synovial sarcomas

S.no	Histology	Primary tumor and passages	Novel immunomarke		Apoptotic			Cell cycle regulators		Proliferative		Epithelial Markers				SYT-SSX Transcripts
			EGFR	SALL2	Bcl2	Bcl-x	Bax	CyclinD1	P16	Ki-67	TopoisoIIα	Ck-AE1/AE3	Ck-19	EMA	Cam5.2	
1	MFSS	Primary	N	Mod	N	M	Mod	N	I	N	N	N	N	N	N	SYT-SSX1
		Initial	N	Mod	I	N	I	N	I	M	N	N	N	N	N	SYT-SSX1
		Middle	N	N	I	Mod	I	M	I	I	M	N	N	N	N	SYT-SSX1
		Terminal	N	I	I	Mod	I	M	I	Mod	M	N	N	N	N	SYT-SSX1
2	MFSS	Primary	N	Mod	Mod	N	I	M	Mod	M	M	N	N	N	N	SYT-SSX1
		Initial	N	I	Mod	N	I	M	I	Mod	M	N	N	N	N	SYT-SSX1
		Middle	N	M	I	M	I	N	I	N	N	N	N	N	N	SYT-SSX1
		Terminal	N	M	I	M	I	N	I	M	M	N	N	M	M	SYT-SSX1
3	MFSS	Primary	Mod	N	Mod	N	M	N	M	M	M	N	N	N	N	SYT-SSX1
		First	M	I	I	N	Mod	M	Mod	Mod	Mod	N	N	N	N	FT- NA
		Second	M	I	I	N	I	M	Mod	Mod	M	N	N	N	N	FT-NA
4	B.SS	Primary	I	N	I	M	Mod	N	N	N	N	M	N	I	M	FT-NA
		Initial	M	M	Mod	M	I	Mod	I	M	M	N	N	N	N	FT-NA
		Middle	M	I	M	M	I	I	I	Mod	M	N	N	N	N	FT-NA
		Terminal	N	I	M	M	I	I	I	I	Mod	N	N	N	N	FT-NA
5	B.SS	Primary Sp	I	N	Mod	N	I	N	N	M	N	M	N	M	N	SYT-SSX2
		Primary Ep	N	N	N	N	I	M	N	Mod	N	I	Mod	I	Mod	
		Initial	N	Mod	M	M	I	M	I	M	M	M	N	M	M	SYT-SSX2
		Middle	N	I	N	N	I	M	I	M	M	M	N	M	M	SYT-SSX2
		Terminal	N	I	N	M	I	M	I	M	N	M	N	M	M	SYT-SSX2
6	MFSS	Primary	N	N	Mod	N	I	M	N	Mod	M	N	N	N	N	SYT-SSX1
		Initial	N	M	I	N	I	M	Mod	I	M	N	N	N	N	SYT-SSX1
		Middle	N	I	I	N	I	Mod	Mod	I	M	N	N	N	N	SYT-SSX1
		Terminal	N	I	I	N	I	Mod	I	I	M	N	N	N	N	SYT-SSX1
7	MFSS	Primary	Mod	N	I	N	I	M	Mod	I	Mod	N	N	N	N	SYT-SSX1
		Initial	N	I	I	N	I	N	I	Mod	M	N	N	N	N	SYT-SSX1
		Middle	N	I	I	N	I	N	I	Mod	N	N	N	N	N	SYT-SSX1
		Terminal	N	I	I	M	I	N	I	Mod	N	N	N	N	N	SYT-SSX1
8	MFSS	Primary	N	I	M	M	I	N	N	Mod	M	N	N	N	N	SYT-SSX2
		Initial	M	I	Mod	I	I	N	I	M	N	N	M	M	N	FT-NA
		Middle	Mod	I	I	I	I	Mod	I	Mod	M	N	M	M	N	SYT-SSX2
		Terminal	I	I	I	M	I	Mod	I	I	M	N	M	N	N	FT-NA
9	MFSS	Primary	I	I	Mod	M	I	N	M	M	M	M	N	N	N	SYT-SSX1
		Initial	M	I	I	M	I	N	M	Mod	M	M	N	N	N	SYT-SSX1
		Middle	M	I	I	M	I	M	M	Mod	M	M	N	N	N	SYT-SSX1
		Terminal	N	I	I	M	I	Mod	M	M	N	M	N	N	N	SYT-SSX1
10	PDSS	Primary	Mod	I	I	M	I	N	N	I	Mod	M	N	M	N	FT-NA
		Initial	I	I	M	Mod	I	N	I	M	N	N	N	N	N	SYT-SSX1
		Middle	I	I	I	I	I	N	I	M	M	N	N	N	N	FT-NA
		Terminal	I	I	I	I	I	M	I	I	N	Mod	Mod	M	Mod	SYT-SSX1
11	MFSS	Primary	M	M	I	M	I	M	N	Mod	Mod	N	N	N	N	SYT-SSX2
		first passage	M	I	I	M	I	I	N	I	Mod	N	N	N	N	SYT-SSX2

Note:

MFSS: Monophasic Fibrous Synovial sarcoma, BSS:Biphasic Synovial sarcoma, PDSS: Poorly Differentiated Synovial sarcoma, N: Negative (0), M: Mild (1-25%), Mod: Moderate (26-50%) and I: Intense(50% and above), FT-NA: Frozen tissue not available. Sp:Spindle element , Ep: Epithelial element

RT-PCR assay and sequence analysis

The molecular results are summarized in Table 2 and illustrated in Fig. 2. SYT-SSX1 and SYT-SSX2 transcripts were detected in six and three of the nine primary SSs, respectively. All the six SYT-SSX1 cases were of MFSS subtype, and the three SYT-SSX2 cases consisted of one BSS and two MFSSs. Frozen tissues were not available for the primary PDSS; however, its passages showed the SYT-SSX1 transcript. The SYT-SSX1 and SYT-SSX2 chimeric transcripts of the primary SSs were maintained in all their xenografts.

Hierarchical cluster analysis of TMA immunostaining data

Two distinct analyses were performed to establish the relation between the primary SS and their xenografts. The first one was a global analysis of all the primary tumors and their corresponding xenografts with the entire panel of immunomarkers. The dendrogram in Fig. 3 revealed some interesting cluster formations. One cluster, composed of the two primary BSSs (cases 4 and 5) lying close together at one extreme of the dendrogram, was closely associated with another formed by the passages of a BSS (case 4). The passages of the classical BSS (case 5) were widely dispersed away from the primary tumor, probably due to the decreased staining of epithelial markers in them, compared with intensely expressing primary tumor. Other clusters included one containing three MFSSs (cases 8, 9, and 11) and one PDSS (case 10), and the other was composed of two primary MFSSs (cases 3 and 7), forming a part of a large cluster containing passages of MFSSs (cases 1 and 3). One more interesting cluster depicted the initial passages (1–4) of the BSS (case 5) clustering with the terminal passages (12, 16, and 18) of an MFSS (case 2). We contemplate whether the late expression of epithelial markers in the terminal passages of the MFSS (case 2), indicating epithelial differentiation, can be the reason for their clustering close together with the initial passages of the BSS that were obviously positive. The antibody dendrogram at the top (Fig. 3) shows the grouping of the markers based on their expression pattern and tissue specificity. Apoptotic markers (bcl-2, bax, and p53), proliferative markers (Ki-67 and topoisomerase IIα), and cyclin D1 formed one close cluster. Epithelial markers (keratin AE1/AE3, CK-19, EMA, CAM5.2, and E-cadherin) together with novel markers such as EGFR, SALL2, ApoD1, and IGFBP2 formed a cluster of specific markers of SSs lying separate from a cluster of nonspecific markers such as S100, NSE, and HBA71. EGFR and SALL2 expression neither correlated with each other nor with other markers, suggesting their independent expression. Vimentin formed a separate cluster. A second analysis failed to find any possible difference between the immunophenotype of SYT-SSX1 and SYT-SSX2 type of tumors.

Discussion

Nude mice xenografts offer an excellent system for the study of tumor cell heterogeneity similar to those existing in the human host [15, 35]. Several nude mice studies have

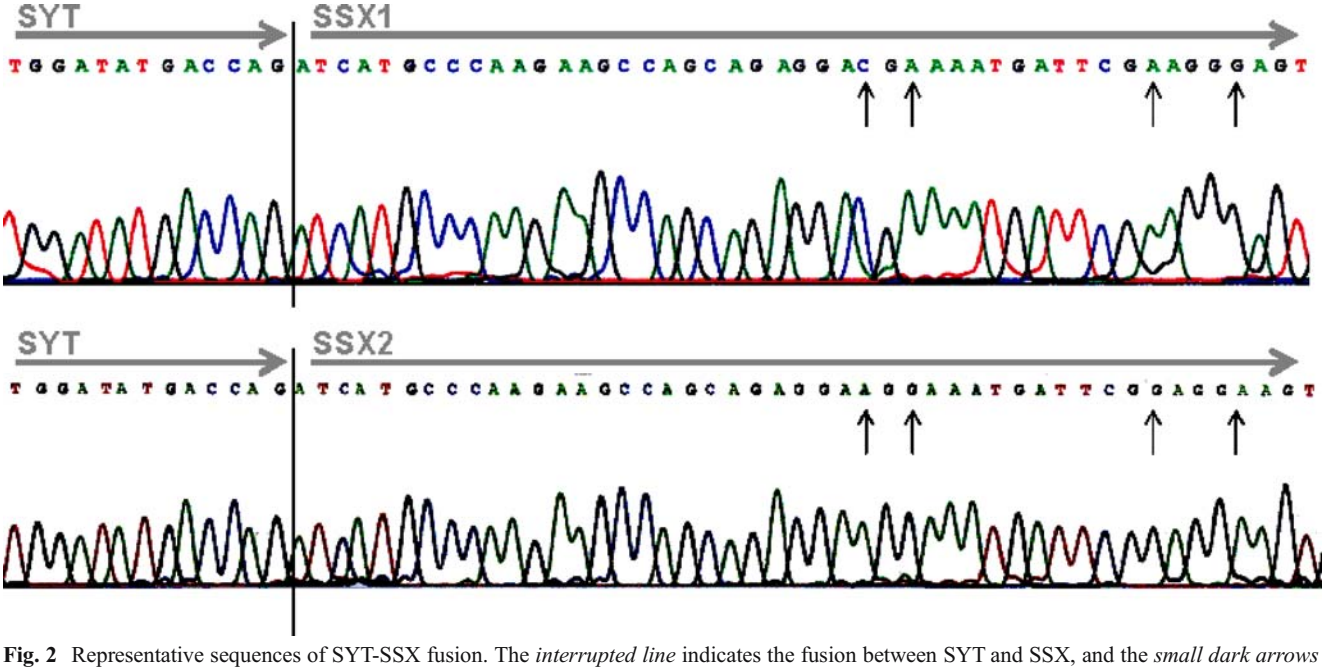

Fig. 2 Representative sequences of SYT-SSX fusion. The *interrupted line* indicates the fusion between SYT and SSX, and the *small dark arrows* indicate the nucleotide differences between the sequences of SYT-SSX1 and SYT-SSX2

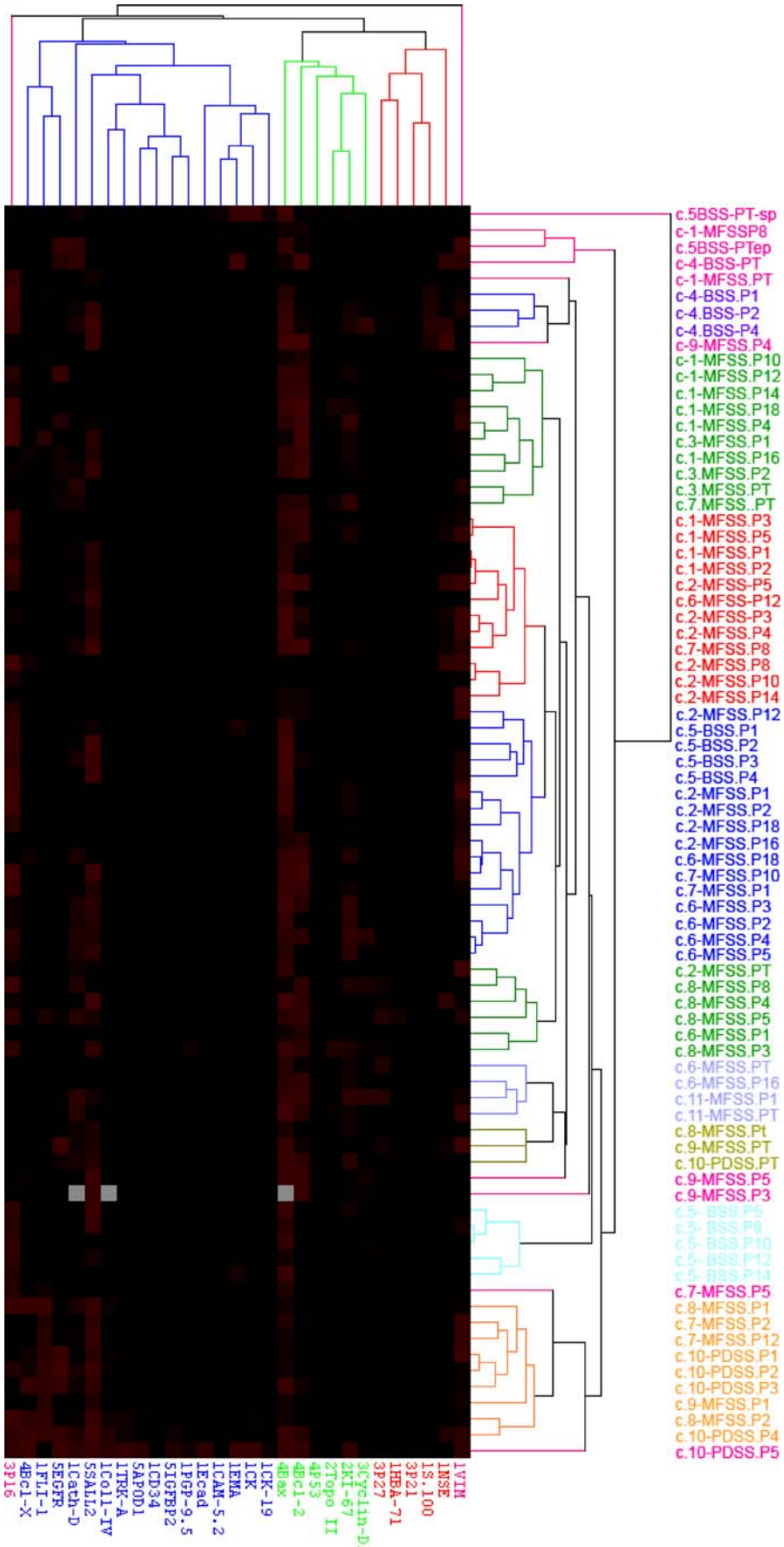

Fig. 3 Hierarchical cluster analysis of immunostaining data of primary SSs and their xenografts. For each antibody indicated at the *bottom* of the figure, cells with intensity 0 are colored *black*, increasing intensity (mild, moderate, and intense) represented in the form of *reds* of increasing intensity, and no available data, is indicated by *white cells*. Dendrogram at the *top* shows antibodies grouped into three clusters, two of which (*blue* and *green*) possess markers specific for SS, whereas the third (*red*) is composed of markers less specific for SS. Vimentin clustered separately. The dendrogram at the *right* shows four significant clusters: the first composed of two primary BSSs (cases 1 and 4) at the *top* (in *pink*), a second cluster (in *purple*) consisting of the passages of the second BSS (case 4) seen closely following the first cluster, the third is made up of three primary MFSSs and one PDSS, and the fourth cluster (in *blue*) is composed of initial passages of BSS (case 5) clustered together with the terminal passages of a MFSS. *PT*, primary tumor; *P*, passage; *sp*, spindle cell component; *ep*, epithelial component

been carried out to analyze the histogenesis, tumor biology, cell differentiation, and heterogeneity of various tumors, including melanomas, neuroblastomas, germ cell neoplasms, epithelial tumors, and bone and soft tissue sarcomas [26]. These studies, being conventional morphological techniques, involved consumption of large quantities of reagents, are labor-intensive, expensive, and achieved an uneven level of standardization.

In the present study, we applied TMA as a high-throughput tool [24] for analyzing the variations in histological (tumor heterogeneity and progression) and immunophenotypic profile of primary SSs xenotransplanted into nude mice. This method enabled us to compare the histological changes and expression patterns of many established and novel markers and their diagnostic sensitivity in multiple primary neoplasms and their xenografts in a single slide. Although studies on tumor progression in various tumors and cell lines using TMA have been published [2], we believe that our study, involving TMA-based immunoprofiling of nude mice xenografts, is the first of its kind.

Morphologically, the most striking feature was the transition of most of the primary tumors to a more undifferentiated neoplasm in the xenografts comprising epithelioid and small round cells, occupying more than five low-power fields [39]. Spindle tumor cells gradually decreased during progression of the primary tumor in the xenografts. These data suggest definite phenotypic variability in the tumors. Our findings contrast with previous studies [20, 32, 34] on SS xenografts and cell lines, where the histology of the original tumor was preserved. However, a change in morphology of an original MFSS to epithelial plaques of large polygonal cells, short spindle cells, and multinucleate giant cells, both in vitro and in vivo, was noted by others [31, 43]. Another series also reported a change in morphology of 30% of their xenotransplants [9]. Increased necrosis and mitotic activity were observed in the xenografts especially in the middle and terminal passages.

We studied the expression profile of a large panel of antibodies using triplicate tissue cores to compensate for tumor heterogeneity because they offer a high concordance rate with standard full sections and low tissue loss rate resulting from various manipulations involved in the immunocytochemical procedures [16]. EGFR declined from moderate to intense membranous staining in the primary tumors to mild or negative staining in the xenografts. The demonstration of EGFR expression at the protein level reiterates the potential for treating SSs with specific EGFR inhibitors. Monoclonal antibodies such as IMC-C25, directed against the external domain of EGFR, or small molecule inhibitors of tyrosine kinase activity such as ZD1839, inhibiting the autophosphorylation of EGFR, have been tested in clinical trials with tumor xenografts [5, 27]. European Organisation for Research and Treatment of Cancer (EORTC) trials are also currently under way for testing the efficacy of small molecule inhibitors of EGFR for anti-EGFR therapy of SS [30].

SALL2 protein is expressed in the fetal renal mesenchyme [37]. In our study, it strongly stained both primary tumors and xenografts. These results show that EGFR and SALL2 are sensitive markers for SS. As non-SSs were not tested for SALL2, we cannot comment on its specificity.

IGF receptor-1 (IGF-1R), crucial in tumor cell growth, has been associated with aggressive phenotype in SS [42]. IGFBP2, an IGF-1 binding protein, is known to regulate IGF-1 signaling in a negative manner by sequestering IGF-1 from its receptor. Its overexpression has been implicated in androgen-independent prostate cancers and high-grade gliomas [4, 13]. Sporadic cytoplasmic positivity for IGFBP2 was noted in spindle and epithelioid cells, a finding also observed by Allander et al. [1]. However, the strong IGFBP2 immunostaining in epithelial elements of all of their BSSs contrasts with the negative epithelial elements of our cases.

ApoD1, a component of the high-density lipoprotein molecule, showed sporadic cytoplasmic positivity in only two cases, similar to the low expression reported in the past [41]. High ApoD expression has been described in dermatofibrosarcoma protuberans, pilocytic astrocytomas, breast, ovarian, and endometrial carcinomas [41].

Genetic alterations of cell cycle regulators are uncommon and considered to be possible secondary events in translocation-associated sarcomas. However, at the protein level, alterations of the G1 checkpoint regulators were associated with poor outcome in SSs [3]. In our cases, cyclin D1 was mildly positive in all the primary tumors, whereas the passages were moderate to intense in some and mild in others. Increased coexpression of cyclin D1 and Ki-67 was seen in only three cases. In others, the absence of coexpression of these two proteins suggests lack of correlation between cyclinD1 and proliferative activity, which can probably be explained due to ectopic expression of cyclinD1, aiding in shortening the G1 interval relative to expression of any single cyclin [3]. p21 and p27 were negative to sporadically positive, and cyclin D1 was mildly positive in the glandular element of BSS, in contrast to Antonescu et al. [3], who found increased expression of cyclin D1 and p21 in the glandular components. However, another study reported p21 to be either negative or only sporadically positive in MFSSs and BSSs [21]. p16 was intensely positive in the passages compared with the primary tumors.

Ki-67 showed relatively increased expression in the xenotransplants and better correlation with mitotic activity than topoisomerase IIα. Increased apoptosis is considered

to be a poor prognostic factor in SS [21]. High levels of bcl-2 expression have been considered as a specific marker for SS, distinguishing it from other spindle cell sarcomas [21]. We noted moderate staining of bcl-2 and intense bax positivity in the primary tumors and intense positivity for both in their passages. Bcl-x was negative to mildly positive. Our data agree with other in vitro and in vivo studies [20, 31]. The intense coexpression of bax and bcl-2 suggests that even apoptotic SS cells express bcl-2 protein due to the promotion of apoptosis by bax in these cells [21].

In the category of established markers, primary BSS showed moderate to intense positivity for all the epithelial markers in the glandular elements and mild staining of the spindle cells. However, focal positivity was retained in all the xenografts. EMA was the most sensitive of the epithelial markers, showing intense membranous positivity in the glandular and spindle elements, a finding in agreement with a past study of a BSS cell line [20]. The epithelial markers were positive in only three of eight MFSSs, of which two revealed expression in the terminal passages, thus confirming the dual differentiation capacity of SS [31, 43].

E-Cadherin, a cell adhesion molecule, was negative in all our MFSSs. Saito et al. [36] also reported low expression of E-cadherin in MFSS and attributed it to the missense mutations in the central region of the E-cadherin gene, thought to play a key role in the adhesion process. They also suggested that reduced E-cadherin expression is the cause for the fibroblastic and spindle-shaped features of MFSS.

RT-PCR revealed six SYT-SSX1-type cases that were MFSSs, whereas the SYT-SSX2 cases included one BSS and two MFSSs. The SYT-SSX transcripts were retained in all the xenografts of all the cases. Association of SYT-SSX1 transcript with BSS has been reported, thereby suggesting its possible permissive role in glandular morphogenesis [19]. In our series, SYT-SSX2 transcript was detected in a BSS with clear glandular formations. However, in the past, rare SYT-SSX2 BSSs with obvious glandular formations have been reported [20, 29].

Hierarchical cluster analysis grouped the primary BSSs and MFSSs separately and differentiated markers specific for SS from nonspecific markers. However, it failed to show any difference in the immunophenotype between SYT-SSX1 and SYT-SSX2 SSs. In addition, differences between the immunoprofile of primary SSs and their xenografts were observed in only two cases, whereas light microscopic evaluation revealed considerable differences between the immunoexpression of primary tumors and the xenografts. We consider that the reasonable explanations for this discrepancy can be a lack of uniformity in the number of passages or a smaller data matrix of our cases. Furthermore, it has been reported that semiquantitative scoring involved in evaluation of immunomarkers leads to data loss involving an element of subjectivity when hierarchical clustering is applied to immunostaining data. In fact, these drawbacks make hierarchical cluster analysis less powerful when applied to immunohistochemical data as opposed to gene microarray data [30].

Our TMA-based morphological and immunohistochemical evaluation of SS xenografts proved to be a high-throughput tool in demonstrating the phenotypic variability of xenografted SSs. Morphological transformation to a poorly differentiated subtype in the xenografts was noted in all cases. Immunohistochemical differences existed in the expression of epithelial, apoptotic, cell cycle, and proliferative markers between the primary tumor and xenografts. Novel markers EGFR and SALL2 were expressed in primary SS and in the xenografts and were found to be independent of expression of other markers. At the molecular level, the primary tumors and their xenografts retained the characteristic SYT-SSX transcripts. Hierarchical cluster analysis served as an efficient tool in grouping the primary SSs and in distinguishing markers specific for SS from those which are nonspecific. In addition, it demonstrates the absence of differences between the primary tumors and their xenografts otherwise observed by histological evaluation. We believe that the present animal model can serve as an important tool in future investigations of cell heterogeneity and differentiation in SS.

Acknowledgements We thank Estela Pons, Alejo Sempere, Francesc Soler, Laura Martinez, and Jose Benavent for their expert technical assistance. Supported by a grant (PI-04/0822) from the FIS (Instituto Carlos-III, Madrid, Spain) and PROTHETS (prognosis and therapeutic targets of Ewing's family of tumors; FP6 contract no. 503036).

Manish Mani Subramaniam received a personal grant from the Spanish Agency for International Cooperation (AECI), Ministry of External Affairs, Spain.

References

1. Allander SV, Illei PB, Chen Y, Antonescu CR, Bittner M, Ladanyi M, Meltzer PS (2002) Expression profiling of synovial sarcoma by cDNA microarrays: association of ERBB2, IGFBP2, and ELF3 with epithelial differentiation. Am J Pathol 161:1587–1595
2. Alonso SR, Ortiz P, Pollan M, Perez-Gomez B, Sanchez L, Acuna MJ, Pajares R, Martinez-Tello FJ, Hortelano CM, Piris MA, Rodriguez-Peralto JL (2004) Progression in cutaneous malignant melanoma is associated with distinct expression profiles: a tissue microarray-based study. Am J Pathol 164:193–203
3. Antonescu CR, Leung DH, Dudas M, Ladanyi M, Brennan M, Woodruff JM, Cordon-Cardo C (2000) Alterations of cell cycle regulators in localized synovial sarcoma: a multifactorial study with prognostic implications. Am J Pathol 156:977–983
4. Bubendorf L, Kolmer M, Kononen J, Koivisto P, Mousses S, Chen Y, Mahlamaki E, Schraml P, Moch H, Willi N, Elkahloun AG,

Pretlow TG, Gasser TC, Mihatsch MJ, Sauter G, Kallioniemi OP (1999) Hormone therapy failure in human prostate cancer: analysis by complementary DNA and tissue microarrays. J Natl Cancer Inst 91:1758–1764
5. Ciardiello F, Caputo R, Bianco R, Damiano V, Pomatico G, De Placido S, Bianco AR, Tortora G (1999) Antitumor effects and potentiation of cytotoxic drug activity in human cancer cells by ZD1839 ("Iressa"), an EGFR-selective tyrosine kinase inhibitor. Clin Cancer Res 6(5):2053–2063
6. Clark J, Rocques PJ, Crew AJ, Gill S, Shipley J, Chan AML, Gusterson BA, Cooper CS (1994) Identification of novel genes, SYT and SSX, involved in the t(X, 18) (p11.2; q11.2) translocation found in human synovial sarcoma. Nat Genet 7: 502–508
7. Coindre JM, Pelmus M, Hostein I, Lussan C, Bui BN, Guillou L (2003) Should molecular testing be required for diagnosing synovial sarcoma? A prospective study of 204 cases. Cancer 98:2700–2707
8. Crew AJ, Clark J, Fisher C, Gill S, Grimer R, Chand A, Shipley J, Gusterson BA, Cooper CS (1995) Fusion of SYT to two genes, SSX1 and SSX2, encoding proteins with homology to the Kruppel-associated box in human synovial sarcoma. EMBO J 2333–2340
9. Donhuijsen K, Budach V, van Beuningen D, Schmidt U (1988) Instability of xenotransplanted soft tissue sarcomas. Morphologic and flow cytometric results. Cancer 61:68–75
10. Engelholm SA, Brunner N, Spang-Thompsen M, Vindlov L (1982) Genetic instability of human solid tumors growth in nude mice. In: Sordat B (ed) Immune deficient animals: 4th international workshop on immunodeficient animals in experimental research, Chexbres. Karger, Basel, pp 339–344
11. Farris KB, Reed RJ (1982) Monophasic, glandular, synovial sarcomas and carcinomas of the soft tissues. Arch Pathol Lab Med 106:129–132
12. Fisher C (1998) Synovial sarcoma. Ann Diagn Pathol 2:401–421
13. Fuller GN, Rhee CH, Hess KR, Caskey LS, Wang R, Bruner JM, Yung WK, Zhang W (1999) Reactivation of insulin-like growth factor binding protein 2 expression in glioblastoma multiforme: a revelation by parallel gene expression profiling. Cancer Res 59:4228–4232
14. Guillou L, Coindre J, Gallagher G, Terrier P, Gebhard S, de Saint Aubain Somerhausen N, Michels J, Jundt G, Vince DR, Collin F, Trassard M, Le Doussal V, Benhattar J (2001) Detection of the synovial sarcoma translocation t(X;18) (SYT-SSX) in paraffin embedded tissues using reverse transcriptase–polymerase chain reaction: a reliable and powerful diagnostic tool for pathologists. A molecular analysis of 221 mesenchymal tumors fixed in different fixatives. Hum Pathol 32:105–112
15. Hajdu SI, Lemos LB, Kozakewich H, Helson L, Beattie EJ Jr (1981) Growth pattern and differentiation of human soft tissue sarcomas in nude mice. Cancer 47:90–98
16. Hoos A, Urist MJ, Stojadinovic A, Mastorides S, Dudas ME, Leung DH, Kuo D, Brennan MF, Lewis JJ, Cordon-Cardo C (2001) Validation of tissue microarrays for immunohistochemical profiling of cancer specimens using the example of human fibroblastic tumors. Am J Pathol 158:1245–1251
17. Ishii S, Yamawaki S, Saki T, Usui M, Ubayama Y, Minami A, Yagi T, Isu K, Kobayashi M (1983) Characteristics of human soft tissue sarcomas in xenografts and in vitro. Clin Orthop Relat Res 173:251–261
18. Kato H, Tjernberg A, Zhang W, Krutchinsky AN, An W, Takeuchi T, Ohtsuki Y, Sugano S, de Bruijn DR, Chait BT, Roeder RG (2002) SYT associates with human SNF/SWI complexes and the C-terminal region of its fusion partner SSX1 targets histones. J Biol Chem 277:5498–5505
19. Kawai A, Woodruff J, Healey JH, Brennan MF, Antonescu CR, Ladanyi M (1998) SYT-SSX gene fusion as a determinant of morphology and prognosis in synovial sarcoma. N Engl J Med 338:153–160
20. Kawai A, Naito N, Yoshida A, Morimoto Y, Ouchida M, Shimizu K, Beppu Y (2004) Establishment and characterization of a biphasic synovial sarcoma cell line, SYO-1. Cancer Lett 204: 105–113
21. Kawauchi S, Fukuda T, Oda Y, Saito T, Oga A, Takeshita M, Yokoyama K, Chuman H, Iwamoto Y, Sasaki K, Tsuneyoshi M (2000) Prognostic significance of apoptosis in synovial sarcoma: correlation with clinicopathologic parameters, cell proliferative activity, and expression of apoptosis-related proteins. Mod Pathol 13:755–765
22. Khatib ZA, Matsushime H, Valentine M, Shapiro DN, Sherr CJ, Look AT (1993) Coamplification of the CDK4 gene with MDM2 and GLI in human sarcomas. Cancer Res 53:5535–5541
23. Kohlhase J, Schuh R, Dowe G, Kuhnlein RP, Jackle H, Schroeder B, Schulz-Schaeffer W, Kretzschmar HA, Kohler A, Muller U, Raab-Vetter M, Burkhardt E, Engel W, Stick R (1996) Isolation, characterization and organ specific expression of 2 novel human zinc finger genes related to *Drosophilia* gene spalt. Genomics 38:291–298
24. Kononen J, Bubendorf L, Kallioniemi A, Barlund M, Schraml P, Leighton S, Torhorst J, Mihatsch MJ, Sauter G, Kallioniemi OP (1998) Tissue microarrays for high-throughput molecular profiling of tumor specimens. Nat Med 4:844–847
25. Lasota J, Jasinski M, Debiec-Rychter M, Szadowska A, Limon J, Miettinen M (1998) Detection of the SYT-SSX fusion transcripts in formaldehyde-fixed paraffin embedded tissue: a reverse transcription polymerase chain reaction amplification assay useful in the diagnosis of synovial sarcoma. Mod Pathol 11:626–633
26. Llombart-Bosch A, Carda C, Boix J, Pellin A, Peydro-Olaya A (1988) Value of nude mice xenografts in the expression of cell heterogeneity of human sarcomas of bone and soft tissue. Pathol Res Pract 183:683–692
27. Mendelsohn J (1997) Epidermal growth factor receptor inhibition by a monoclonal antibody as anticancer therapy. Clin Cancer Res 3:2703–2707
28. Nagai M, Tanaka S, Tsuda M, Endo S, Kato H, Sonobe H, Minami A, Hiraga H, Nishihara H, Sawa H, Nagashima K (2001) Analysis of transforming activity of human synovial sarcoma–associated chimeric protein SYT-SSX1 bound to chromatin remodelling factor Hbrm/ Hsnf2 alpha. Proc Natl Acad Sci USA 98:3843–3848
29. Naito N, Kawai A, Ouchida M, Dan'ura T, Morimoto Y, Ozaki T, Shimizu K, Inoue H (2000) A reverse transcriptase–polymerase chain reaction assay in the diagnosis of soft tissue sarcomas. Cancer 89:1992–1998
30. Nielsen TO, Hsu FD, O'Connell JX, Gilks CB, Sorensen PH, Linn S, West RB, Liu CL, Botstein D, Brown PO, van de Rijn M (2003) Tissue microarray validation of epidermal growth factor receptor and SALL2 in synovial sarcoma with comparison to tumors of similar histology. Am J Pathol 163:1449–1456
31. Noguchi SI, Ueki T, Kawauchi S, Fukuda T, Matsuura H, Sonoda T, Tsuneyoshi M (1997) Establishment and characterization of a new synovial sarcoma cell line, SN-SY-1: special reference to bcl-2 protein and SYT-SSX1 hybrid transcripts. Int J Cancer 72:995–1002
32. Nojima T, Wang YS, Abe S, Matsuno T, Yamawaki S, Nagashima K (1990) Morphological and cytogenetic studies of a human synovial sarcoma xenotransplanted into nude mice. Acta Pathol Jpn 40:486–493

33. Pelmus M, Guillou L, Hostein I, Sierankowski G, Lussan C, Coindre JM (2002) Monophasic fibrous and poorly differentiated synovial sarcoma: immunohistochemical reassessment of 60 t(X;18)(SYT-SSX)-positive cases. Am J Surg Pathol 26:1434–1440
34. Roholl PJ, Rutgers DH, Rademakers LH, De Weger RA, Elbers JR, Van Unnik JA (1988) Characterization of human soft tissue sarcomas in nude mice: evidence for histogenic properties of malignant fibrous histiocytomas. Am J Pathol 131:559–568
35. Rygaard J, Povelsen CO (1969) Heterotransplantation of human malignant tumor to "nude mice." Acta Pathol Microbiol Scand 77:758–760
36. Saito T, Oda Y, Kawaguchi K, Sugimachi K, Yamamoto H, Tateishi N, Tanaka K, Matsuda S, Iwamoto Y, Ladanyi M, Tsuneyoshi M (2004) E-Cadherin mutation and snail overexpression as alternative mechanisms of E-cadherin inactivation in synovial sarcoma. Oncogene 23:8629–8638
37. Sato A, Matsumoto Y, Koide U, Kataoka Y, Yoshida N, Yokota T, Asashima M, Nishinakamura R (2003) Zinc finger protein sall2 is not essential for embryonic and kidney development. Mol Cell Biol 23:62–69
38. Sokal RR, Michener CDA (1958) Statistical method for evaluating systematic relationships. Univ Kans Sci Bull 38:1409–1438
39. Van de Rijn M, Barr FG, Xiong QB, Hedges M, Shipley J, Fisher C (1999) Poorly differentiated synovial sarcoma: an analysis of clinical, pathologic, and molecular genetic features. Am J Surg Pathol 23:106–112
40. Weiss SW, Goldblum JR (2001) Malignant soft tissue tumors of uncertain type. In: Weiss SW, Goldblum JR (eds) Enzinger and Weiss's soft tissue tumors, 4th edn. Mosby, St Louis, pp 1483–1572
41. West RB, Harvell J, Linn SC, Liu CL, Prapong W, Hernandez-Boussard T, Montgomery K, Nielsen TO, Rubin BP, Patel R, Goldblum JR, Brown PO, van de Rijn M (2004) Apo D in soft tissue tumors: a novel marker for dermatofibrosarcoma protuberans. Am J Surg Pathol 28:1063–1069
42. Xie Y, Skytting B, Nilsson G, Brodin B, Larsson O (1999) Expression of insulin-like growth factor-1 receptor in synovial sarcoma: association with an aggressive phenotype. Cancer Res 59:3588–3591
43. Yakushiji T, Yonemura K, Tsuruta J, Nishida K, Kato T, Takagi K (2000) Capacity for epithelial differentiation in synovial sarcoma: analysis of a new human cell line. J Clin Pathol 53:525–531

Virchows Arch (2006) 449:448–454
DOI 10.1007/s00428-006-0261-y

ORIGINAL ARTICLE

Increased numbers of osteoclasts expressing cysteine proteinase cathepsin K in patients with infected osteoradionecrosis and bisphosphonate-associated osteonecrosis—a paradoxical observation?

Torsten Hansen · C. James Kirkpatrick · Christian Walter · Martin Kunkel

Received: 30 March 2006 / Accepted: 25 June 2006 / Published online: 7 September 2006
© Springer-Verlag 2006

Abstract Erosion of the bone is a common problem in patients suffering from infected osteoradionecrosis (IORN) or bisphosphonate-associated osteonecrosis (BON). Besides inflammatory mechanisms and infectious agents, osteoclasts were recently suggested to be specifically involved in the osteolytic mechanisms. We therefore investigated the immunohistochemical labeling of the cysteine proteinase cathepsin K, which plays a central role in osteoclast-mediated bone resorption, in tissue specimens of patients with BON (n=9; four male, five female; mean age=69.2 years) and IORN (n=10; nine male, one female; mean age=60.5 years), and compared the results with control specimens (n=8; six male, two female; mean age=60 years). In all cases, osteoclasts were the predominant cell type expressing cathepsin K. For semiquantitative analysis, we therefore defined osteoclasts as multinuclear giant cells attached to the bone and expressing cathepsin K. Significantly higher numbers of osteoclasts were found for both types of osteonecrosis when compared with the control group (BON+IORN vs controls: P=0.0000036). Within the pathological lesions, IORN cases exhibited significantly less osteoclasts than BON (P=0.00097). Our study verified increased numbers of osteoclasts in patients suffering from BON and IORN. Although it is known that bisphosphonates (and to a lesser extent, irradiation, too) decrease osteoclast function, these findings suggest a critical involvement of osteoclasts in the mechanisms of bone destruction in the respective lesions.

Keywords Head and neck neoplasms · Radiation · Side effects · Infected osteoradionecrosis · Bisphosphonate-associated osteonecrosis · Osteoclast · Cathepsin K · Actinomyces

T. Hansen (✉) · C. J. Kirkpatrick
Institute of Pathology, Johannes Gutenberg-University of Mainz,
Langenbeckstr. 1,
55101 Mainz, Germany
e-mail: hansen@pathologie.klinik.uni-mainz.de

C. Walter · M. Kunkel
Department of Oral and Maxillofacial Surgery,
Johannes Gutenberg-University of Mainz Medical Center,
Mainz, Germany

Introduction

Osteonecrosis of the jaws represents a severe complication in patients treated for malignant tumors. There are two principal groups of patients that are affected with this disorder. The first group suffers from osteoradionecrosis, which has been known for about a century. Nevertheless, it continues to be a risk of radiotherapy in patients suffering from head and neck cancer, with an incidence of 2–35% [2, 30, 32]. Its most severe form, called infected osteoradionecrosis (IORN), frequently presents as a chronic disease that is highly resistant against therapeutic interventions. The clinical symptoms include pain, chronic fistulation, exposed bone, and even extended bone destruction and pathological bone fracture [7, 23, 30]. Among the mechanisms contributing to the development of IORN, damage of the salivary glands and the mucosa by ionizing radiation is discussed as a crucial step resulting in a reduced oral clearance as well as a loss of antimicrobial effects and mucosal integrity [4].

Recently, a second type of osteonecrosis has been observed to involve the jaws during the long term of anticancer treatment. Since the first report by Marx in 2003 [21], numerous case reports and several studies provided strong evidence that patients treated with bisphosphonates can develop necrosis of the jaw bones [1, 5, 6, 14, 19, 22, 28]. Bisphosphonates are synthetic analogs of the naturally

occurring pyrophosphate [6, 26]. They can be grouped into several pharmacologic classes. The most potent class consists of nitrogen-containing bisphosphonates such as alendronate, pamidronate, and zoledronate [26]. They not only accumulate to sites of active bone remodeling, inducing resistance to dissolution by osteoclasts, but are also internalized by osteoclasts, where they inhibit farnesyl diphosphate synthase. This results in suppression of osteoclastic activity and loss of cytoskeletal integrity, leading to apoptosis and cell death [3, 26, 33]. Interestingly, bisphosphonate-associated osteonecrosis (BON) almost always occurs in the jaws [22]. According to Bamias et al. [6], the incidence of BON increases with the time of exposure, from 1.5% among patients treated for 4–12 months to 7.7% for treatment of 37–48 months. Similar to IORN, patients with BON mainly suffer from pain and swelling, and present with exposed bone or fistulae. Most authors favor the view that bisphosphonates induce obliteration of the regional blood vessels and thus lead to avascular bone necrosis [1, 22, 28], but there is also evidence of a proapoptotic effect of bisphosphonates on keratinocytes, which might promote mucosal breakdown [25].

A common problem in both forms of osteonecrosis is extended bone destruction (Fig. 1), which may even end up in pathological fractures and thus needs intensive therapy. The specific mechanisms of bone degradation are still not completely understood. However, several factors are discussed in this context such as genuine bone sequestration, several inflammatory mechanisms, and infectious agents [7, 10, 15, 19, 28, 32]. We recently found remarkable numbers of osteoclasts particularly in tissue specimens of patients with BON. They showed prominent resorption lacunae as a sign of resorptive activity [14]. In order to further explore the role of osteoclasts in bone erosion during osteonecrosis, we analyzed tissue specimens of patients with BON and IORN by immunohistochemistry with antibodies against cathepsin K. This cysteine proteinase is known to play a central role in osteoclast-mediated proteolytic degradation of collagen type I, which is the major organic constituent of the bone matrix [18]. Moreover, numerous studies indicate a predominant expression of cathepsin K in osteoclasts [11, 12, 18, 36], and the enzyme has been suggested to be a good marker for activated osteoclasts [34]. We therefore analyzed cathepsin K expression in BON and IORN semiquantitatively and, in addition, compared the labeling results with control specimens.

Materials and methods

Patient data from the BON group

This population included nine patients (summarized in Table 1 as nos. 1–9: four male, five female; mean age=69.2 years), who were treated with bisphosphonate for bone metastases. Of this cohort, four patients were described previously in a histomorphologic study [14]. The underlying malignancy was breast cancer in four patients, prostate cancer in three patients, and multiple myeloma in two cases. Most of the patients received both pamidronate (Aredia; Novartis, East Hannover, NJ, USA) and zoledronate (Zometa; Novartis). Most commonly, therapy was started by pamidronate and followed by zoledronate. Patients mainly presented with mucosal dehiscence and necrotic bone exposed to the oral cavity together with inflammatory reactions of the surrounding soft tissues. Four patients presented with mandibular bone involvement, four patients had maxillary lesions, whereas one patient presented with the disease occurring in both the maxilla and the mandible. Panoramic X-rays showed regions of osteolysis of the jaws, sometimes with sequester formation.

Fig. 1 Panoramic x-ray of an IORN patient (no. 18) reveals extensive bilateral erosion of the mandibular bone (*arrowheads*)

Table 1 Patients' characteristics and mean values of the osteoclast numbers

Patient no.	Age	Sex	Underlying disease	Complication	Medication (IORN: dose in Gy; BON: medication in months)	Actinomyces	Number of osteoclasts (5 HPF)
1	71	F	MM	BON	Pa: 10, Zo: 48	Yes	8.2
2	56	F	BC	BON	Pa: 30, Zo: 25	Yes	11.6
3	65	M	MM	BON	Pa: 10, Zo: 8	Yes	15.4
4	68	F	BC	BON	Pa: 21, Zo: 28	Yes	15
5	74	M	PC	BON	Zo: 37, Pa: 2	Yes	9.8
6	62	F	BC	BON	Cl: 107, Zo: 57, Bo: 3	Yes	14.8
7	81	F	BC	BON	Zo: 22, Bo: 7	Yes	12.8
8	80	M	PC	BON	Zo: 19	Yes	12
9	67	M	PC	BON	Zo: 14	Yes	21
10	55	F	ACC	IORN	80 Gy	Yes	9.4
11	75	M	SCC	IORN	60 Gy	No	4.6
12	62	M	SCC	IORN	60 Gy	Yes	8.2
13	74	M	SCC	IORN	60 Gy	No	7
14	47	M	SCC	IORN	60 Gy	Yes	11.2
15	49	M	SCC	IORN	60 Gy	Yes	6.8
16	43	M	SCC	IORN	60 Gy	No	9
17	72	M	SCC	IORN	70 Gy	Yes	10.6
18	65	M	SCC	IORN	50 Gy	Yes	6
19	63	M	Adenocarcinoma	IORN	72 Gy	Yes	8.2
20	65	F	SCC	No	No	No	3.8
21	79	M	SCC	No	No	No	1.4
22	51	M	SCC	No	No	No	3.2
23	42	F	SCC	No	No	No	0.8
24	61	M	SCC	No	No	No	3.4
25	56	M	SCC	No	No	No	3
26	66	M	SCC	No	No	No	0.6
27	60	M	SCC	No	No	No	4.8

ACC adenoid cystic carcinoma, *BC* breast cancer, *Bo* bondronate, *BON* bisphosphonate-associated osteonecrosis, *Cl* Clodronate, *F* female, *Gy* Gray, *HPF* high-power field, *IORN* infected osteoradionecrosis, *M* male, *MM* multiple myeloma, *Pa* pamidronate, *PC* prostate cancer, *SCC* squamous cell carcinoma, *Zo* zoledronate

Patient data from the IORN group

The characteristics of the patients are summarized in Table 1 as nos. 10–19. This study population included 10 patients (nine male, one female; mean age=60.5 years). Patients were treated by radiotherapy due to cancer of the head and neck region. Underlying malignancy was squamous cell carcinoma except for two patients, one of them with an adenoid cystic carcinoma (no. 10) and one patient (no. 19) suffering from an adenocarcinoma of the submandibular gland. The mean radiation dose was 63.2 Gy. For diagnostic classification, IORN was defined according to established criteria: bone necrosis following irradiation of osseous tissue (i.e., the jaws) [10, 13, 29]. The clinical symptoms were as follows: signs of infection or sequester formation, local abscess formation, chronic fistula, and necrotic bone exposed to the oral cavity. In all cases, bone involvement was confirmed by radiography and/or computed tomography.

Patient data of the control group

The characteristics of the patients are summarized in Table 1 as nos. 20–27. This population included eight patients (six male, two female; mean age=60 years). All patients of this group underwent major bone resection procedures of primary oral squamous cell carcinomas. None of the patients had previous radiation therapy, chemotherapy, or any other tumor-related treatment. Tissue specimens were taken from tumor-free bone margins.

Tissue preparation, immunohistochemistry, and microscopy

Biopsies were taken from the exposed bone tissues and were routinely fixed in 4% phosphate-buffered saline–formalin and processed according to standard protocols. Decalcification was performed either in trichloric acid (for 24–72 h) or in ethylenediaminetetraacetic acid (EDTA; for 3–8 days). No differences could be observed between these

two procedures concerning the immunohistochemical results. The paraffin-embedded specimens were stained by hematoxylin and eosin (H & E). Subsequent sections were prepared for immunohistochemical technique. Immunohistochemistry was performed using the ABC-method, according to previously described protocols, with primary monoclonal antihuman cathepsin K antibodies (clone 192-12G5; Chemicon, Temecula, CA, USA) in a 1:6,000 dilution. No pretreatment was needed. Tissue sections were examined and photographed with a Zeiss microscope (Axiophot; Oberkochen, Germany; Olympus camera Camedia, Hamburg, Germany).

Tissues were examined by one investigator (T.H.) who was blind to the diagnosis. Osteoclasts were defined according to previous studies as multinuclear cells attached to the bone tissue [25, 33]. For semiquantitative analysis, the number of cathepsin-K-positive multinucleated cells surrounding the bone was evaluated in five high-power fields (HPF=0.307 mm^2).

Statistical analysis

The number of cathepsin-K-positive multinucleated cells was compared for both types of osteonecrosis (BON+IORN) vs controls, BON vs controls, IORN vs controls and BON vs IORN using the nonparametric *U* test according to Wilcoxon, Mann and Whitney [20]. The reported *p* values are two-sided. All calculations were carried out using SPSS for Windows, Version 12 (SPSS Inc., Chicago, IL, USA).

Results

In all tissue specimens examined, osteoclasts could be detected in H & E-stained sections as multinucleated giant cells attached to the bone. They were particularly found in tissue specimens of patients treated with bisphosphonates (BON group) revealing pronounced resorption lacunae (Fig. 2a). Immunohistochemically, cathepsin K was almost exclusively labeled in osteoclasts. Especially in the BON and to a lesser extent in the IORN, large numbers of these cells surrounded areas of both vital and avital bone tissue (Fig. 2b). Moreover, some of the osteoclasts that formed resorption lacunae also showed extracellular expression of cathepsin K (Fig. 2b, inset). In addition, a few positive mononuclear cells were found in the vicinity of the osteoclasts. By contrast, expression of this molecule occurred neither in osteocytes nor in osteoblasts nor in significant numbers of inflammatory infiltrates (which were composed of lymphocytes, plasma cells, and granulocytes). Furthermore, at the site of pseudoepitheliomatous hyper-

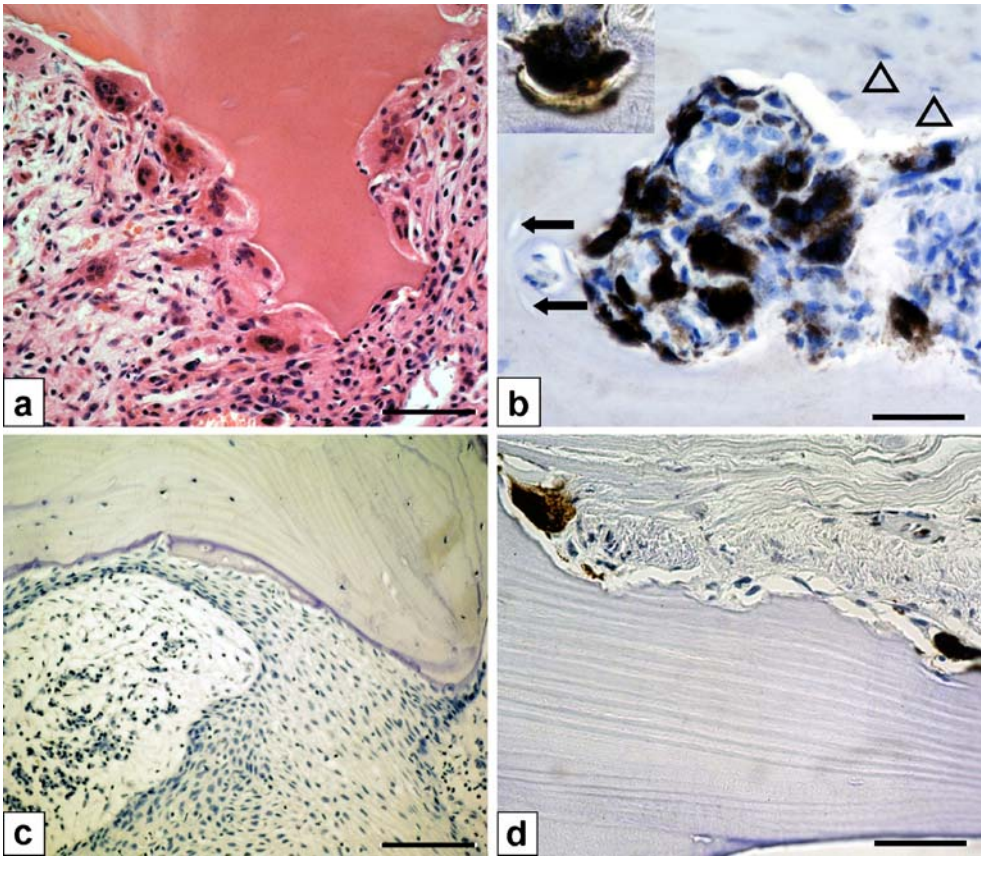

Fig. 2 **a** Standard histology shows bone tissue of a BON case with numerous osteoclasts attached to bone tissue (H & E; bar=75 μm). **b** Immunohistochemistry reveals strong expression of cathepsin K (*brown*) in numerous osteoclasts attached to bone with avital areas (*arrows* show empty osteocyte lacunae) and vital regions in the *upper right part* (*arrowheads*; ABC method; bar=37.5 μm). *Inset* shows strong cathepsin K positivity both in an osteoclast as well as in the extracellular space, i.e., the resorption lacuna. **c** BON case with squamous epithelia attached to bone tissue. The so-called pseudoepitheliomatous hyperplasia displays no expression of cathepsin K (ABC method; bar=75 μm). **d** Control tissue with only a very few osteoclasts revealed by cathepsin K labeling (ABC method; bar=37.5 μm)

plasia, squamous epithelial cells were closely attached to the bone, but they did not reveal positivity for cathepsin K (Fig. 2c). Finally, in the neighborhood of Actinomyces colonies, osteoclasts were not found at all, neither in the IORN nor in the BON group.

Statistical analysis revealed a significantly higher number of osteoclasts for both types of osteonecrosis compared with the controls (P=0.0000036; also Fig. 2d). This holds true when the isolated populations of osteonecroses were compared with the control group (BON vs control: P=0.000082; IORN vs control: P=0.00018). Furthermore, comparison between IORN and BON group showed that the former exhibited significantly less osteoclasts than the latter (P=0.00097). The scatter plot of Fig. 3 displays the osteoclast counts in the three subpopulations. An average of 6.9 osteoclasts/HPF was counted in Actinomyces-negative BON/IORN lesions, whereas 11.3 osteoclasts/HPF could be detected in Actinomyces-positive cases. This difference was only of marginal significance (P=0.057); however, only three lesions without Actinomyces were encountered.

Discussion

Substantial destruction of the jawbone is a major problem in patients suffering from IORN or BON. This disorder often leads to pathological fractures or even gross disfigurement. Recently, we found marked numbers of osteoclasts in tissues received from patients with IORN and especially from patients with BON [14]. In the present study, we investigated the expression of the cysteine proteinase cathepsin K, which plays a central role in osteoclast-mediated bone resorption. We compared the numbers of cathepsin-K-positive osteoclasts in tissue specimens of patients suffering from BON or IORN with respective control tissues.

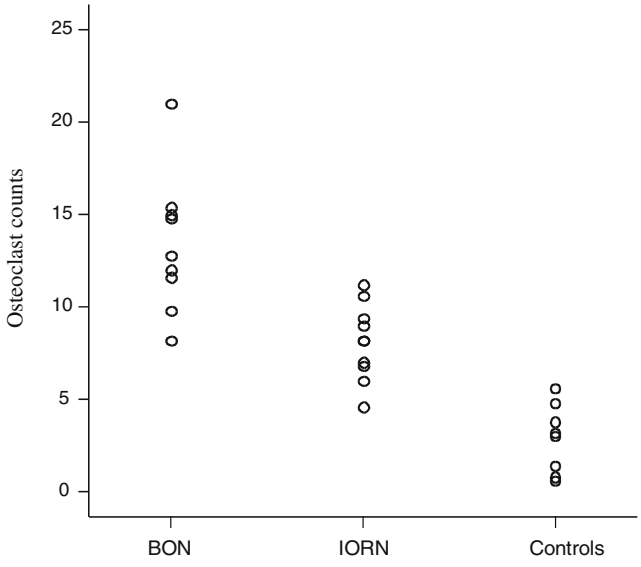

Fig. 3 Scatter plot presents different osteoclast counts in BON, IORN, and controls

Except for few mononuclear cells that most likely represent osteoclast precursors [17, 37], osteoclasts were the almost-exclusive cell type expressing cathepsin K in all tissue specimens examined. This is in line with previous reports on the specificity of cathepsin K for osteoclasts [34]. Therefore, we used cathepsin K positivity in multinucleated giant cells attached to the bone for semiquantitative analysis of the osteoclast content. Semiquantitative analysis revealed significantly larger amounts of osteoclasts in BON and/or IORN than in control probes. Since these cells were attached to both vital and avital bone tissue, this increase is probably not only related to resorption of sequestrated bone as suggested by Kataoka et al. [17], but also leads to degradation of vital and functional bone of the jaws.

Furthermore, immunohistochemistry especially of BON tissue specimens showed extracellular expression of cathepsin K in the resorption lacunae in close contact to the bone matrix. This phenomenon has already been demonstrated by Yamaza et al. using different animal models [36, 37]. In general, it is considered that cathepsin K is a lysosomal proteinase, which is released into the resorption lacunae, where it can degrade collagen type I despite the presence of an acidic pH [36]. Thus, extracellular labeling of this enzyme at the site of resorption lacunae as revealed in the present study can be interpreted as sign of osteoclastic activity. Taken together, these data suggest that osteoclasts are involved in the mechanisms leading to bone erosion of the jaws in patients with IORN and BON.

Interestingly, the numbers of osteoclasts were less frequent in IORN than in BON. This statistically significant difference could be explained by previous studies that showed that radiation primarily inhibits osteoclast formation via a direct effect on radiosensitive, proliferating progenitor cells [29]. Nevertheless, the numbers of osteoclasts were significantly higher in IORN than those in control probes. In addition, it might be surprising that increased osteoclast numbers and especially evidence of osteoclastic activity was recognized in patients who were treated with bisphosphonates in order to inhibit osteoclastic function and recruitment. Altundal and Güvener [3] investigated bone structure in a rat model and found that the number of osteoclasts in animals treated with the amino-bisphosphonate alendronate was significantly lower (P<0.001 on day 28) than that in control animals. By contrast, our data proved substantial increase in osteoclast activity in manifest osteonecrosis, suggesting stimulatory effects that override the influence of both irradiation and bisphosphonates.

In this context, previous models of the interaction between osteoclasts, cytokines, and bacterially induced

bone destruction could be intriguing. Thirty years ago, Garant [8] reported that in a mouse model, osteoclastic activity was associated with dense inflammatory infiltration and large adherent microbial plaques consisting of Actinomyces. Since then, the association between infection with Actinomyces and osteolysis has been demonstrated [15, 35]. This association could be of major interest since several recent studies verified large numbers of Actinomyces-positive biopsies in patients suffering from either IORN or BON [7, 13, 14, 31]. Although only of marginal significance due to the small number of Actinomyces-negative BON/IORN lesions, the higher recruitment of osteoclasts in Actinomyces-positive osteonecrosis as shown in the present study argues for a stimulatory effect of Actinomyces or its associated microbes. Among them, in particular, *Actinobacillus actinomycetemcomitans* is currently discussed as a possible agent [16]. It is commonly detected in patients suffering from periodontitis and recently has also been reported in tissue specimens of IORN patients [31]. In an animal model for periodontitis, it has been demonstrated to lead to significant increase in bone erosion, which is accompanied by an initial increase in proteolytic enzymes such as cathepsin K [9, 24]. However, whether this association also occurs in IORN and/or BON needs to be further investigated.

In summary, the present study provided evidence that osteoclast numbers and activity are significantly increased in IORN and BON as compared with control tissues. Although it is known that bisphosphonates (and to a lesser extent, irradiation, too) decrease osteoclast function, these findings suggest a critical involvement of osteoclasts in the mechanisms of bone destruction in the respective lesions.

Acknowledgments The authors thank Irmtrud Roth and Silke Mitschke, Institute of Pathology, University of Mainz, for their excellent technical assistance.

References

1. Abu-Id MH, Acil Y, Gottschalk J, Kreusch T (2006) Bisphosphonate-associated osteonecrosis of the jaw. Mund Kiefer Gesichtschir 10:72–81
2. Aitasalo K (1986) Bone tissue response to irradiation and treatment model of mandibular irradiation injury. Acta Otolaryngol Suppl 428:1–54
3. Altundal H, Güvener Ö (2004) The effect of alendronate on resorption of the alveolar bone following tooth extraction. Int J Oral Maxillofac Surg 33:286–293
4. Andrews N, Griffiths C (2001) Dental complications of head and neck radiotherapy: part 1. Aust Dent J 46:88–94
5. Bagan JV, Murillo J, Jimenez Y, Poveda R, Milian MA, Sanchis JM, Silvestre FJ, Scully C (2005) Avascular jaw osteonecrosis in association with cancer chemotherapy: series of 10 cases. J Oral Pathol Med 34:120–123
6. Bamias A, Kastritis E, Bamia C, Moulopoulos LA, Melakopulos I, Bozas G, Koutsoukou V, Gika D, Anagnostopoulos A, Papadimitriou C, Terpos E, Dimopoulos MA (2005) Osteonecrosis of the jaw in cancer after treatment with bisphosphonates: incidence and risk factors. J Clin Oncol 34:8580–8587
7. Curi MM, Dib LL, Kowalski LP, Landman G, Mangini C (2000) Opportunistic actinomycosis of the jaws in patients affected by head and neck cancer: incidence and clinical significance. Oral Oncol 36:294–299
8. Garant PR (1976) Light and electron microscopic observations of osteoclastic alveolar bone resorption in rats monoinfected with Actinomyces naeslundii. J Periodontol 47:717–723
9. Garlet GP, Cardoso CR, Silva TA, Ferreira BR, Ávilla-Campos MJ, Cunha FQ, Silva JS (2006) Cytokine pattern determines the progression of experimental periodontal disease induced by Actinobacillus actinomycetemcomitans through the modulation of MMPs, RANKL, and their physiological inhibitors. Oral Microbiol Immunol 21:12–20
10. Glanzmann C, Grätz KW (1995) Radionecrosis of the mandibula: a retrospective analysis of the incidence and risk factors. Radiother Oncol 36:94–100
11. Hansen T, Otto M, Gaumann A, Eckardt A, Petrow PK, Delank KS, Kirkpatrick CJ, Kriegsmann J (2001) Cathepsin K in aseptic hip prosthesis loosening: expression in osteoclasts without polyethylene wear particles. J Rheumatol 28:1615–1619
12. Hansen T, Unger RE, Gaumann A, Hundorf I, Maurer J, Kirkpatrick CJ, Kriegsmann J (2001) Expression of matrix-degrading cysteine proteinase cathepsin K in cholesteatoma. Mod Pathol 14:1226–1231
13. Hansen T, Kunkel M, Kirkpatrick CJ, Weber A (2006) Actinomyces in infected osteoradionecrosis—underestimated? Hum Pathol 37:61–67
14. Hansen T, Kunkel M, Weber A, Kirkpatrick CJ (2006) Osteonecrosis of the jaws in patients treated with bisphosphonates—histomorphologic analysis in comparison with infected osteoradionecrosis. J Oral Pathol Med 35:155–160
15. Happonen RP, Viander M, Pelliniemi L, Aitasalo K (1983) Actinomyces israelii in osteoradionecrosis of the jaws. Oral Surg Oral Med Oral Pathol 55:580–588
16. Henderson B, Nair SP, Ward JM, Wilson M (2003) Molecular pathogenicity of the oral opportunistic pathogen Actinobacillus actinomycetemcomitans. Annu Rev Microbiol 57:29–55
17. Kataoka M, Torisu T, Tsumura H, Hirayama T, Fujikawa Y (2000) Role of multinuclear cells in granulation tissue in osteomyelitis. Acta Orthop Scand 71:414–418
18. Littlewood-Evans A, Kokubo T, Ishibashi O, Inaoka T, Wlodarski B, Gallagher JA, Bilbe G (1997) Localization of cathepsin K in human osteoclasts by in situ hybridization and immunohistochemistry. Bone 20:81–86
19. Lugassy G, Shaham R, Nemets A, Ben-Dor D, Nahlieli O (2004) Severe osteomyelitis of the jaw in long-term survivors of multiple myeloma: a new clinical entity. Am J Med 117:440–441
20. Mann HB, Whitney DR (1947) On a test whether one or two random variables is stochastically larger than the other. Ann Math Stat 18:50
21. Marx RE (2003) Pamidronate (Aredia) and Zoledronate (Zometa) induced avascular necrosis of the jaws: a growing epidemic. J Oral Maxillofac Surg 61:1115–1118
22. Marx RE, Sawatari Y, Fortin M, Broumand V (2005) Bisphosphonate-induced exposed bone (osteonecrosis/osteopetrosis) of the jaws: risk factors, recognition, prevention, and treatment. J Oral Maxillofac Surg 63:1567–1575
23. Millett DT, Chapple IL, Hirschmann PN, Corrigan AM (1990) Septic osteoradionecrosis of the mandible associated with pathological fracture: report of two cases. Clin Radiol 41:408–410

24. Nishida E, Hara Y, Kaneko T, Ikedo Y, Ukai T, Kato I (2001) Bone resorption and local interleukin-1α and interleukin-1β synthesis induced by Actinobacillus actinomycetemcomitans and Porphyromonas gingivalis lipopolysaccharide. J Periodontal Res 36:1–8
25. Reszka AA, Halasy-Nagy J, Rodan GA (2001) Nitrogen-bisphosphonates block retinoblastoma phosphorylation and cell growth by inhibiting the cholesterol biosynthesis pathway in a keratinocyte model for esophageal irritation. Mol Pharmacol 59:193–202
26. Rogers MJ, Gordon S, Benford HL, Coxon FP, Luckman SP, Monkkonen J, Frith JC (2000) Cellular and molecular mechanisms of action of bisphosphonates. Cancer 88:2961–2978
27. Roodman GD (1999) Cell biology of the osteoclast. Exp Hematol 27:1229–1241
28. Ruggiero S, Mehrotra B, Rosenberg T, Engroff S (2004) Osteonecrosis of the jaws associated with the use of bisphosphonates: a review of 63 cases. J Oral Maxillofac Surg 62:527–534
29. Scheven BA, Wassenaar AM, Kawiralang-de Haas EW, Nijweide PJ (1987) Direct and indirect radiation effects on osteoclast formation in vitro. Bone Miner 2:291–300
30. Støre G, Boysen M (2000) Mandibular osteoradionecrosis: clinical behaviour and diagnostic aspects. Clin Otolaryngol 25:378–384
31. Støre G, Eribe ERK, Olsen I (2005) DNA–DNA hybridization demonstrates multiple bacteria in osteoradionecrosis. Int J Oral Maxillofac Surg 34:193–196
32. Thiel HJ (1989) The osteoradionecrosis. Part I: etiology, pathogenesis, clinic, and risk factors. Radiobiol Radiother 30:397–413
33. Thompson K, Dunford JE, Ebetino FH, Rogers MJ (2002) Identification of a bisphosphonate that inhibits isopentenyl diphosphate isomerase and farnesyl diphosphate synthase. Biochem Biophys Res Commun 290:869–873
34. Väänänen K (2005) Mechanism of osteoclast mediated bone resorption—rationale for the design of new therapeutics. Adv Drug Deliv Rev 57:959–971
35. Van Driessche K, van Ranst D, van Offel J, Stevens WJ, De Schepper A, van Marck E, De Clerck LS (2003) Actinomycosis as a rare cause of vertebral osteolysis. Acta Clin Belg 58:296–298
36. Yamaza T, Goto T, Kamiya T, Kobayashi Y, Sakai H, Tanaka T (1998) Study of immunoelectron microscopic localization of cathepsin K in osteoclasts and other bone cells in the mouse femur. Bone 23:499–509
37. Yamaza T, Tsuji Y, Goto T, Kido MA, Nishijima K, Moroi R, Akamine A, Tanaka T (2001) Comparison in localization between cystatin C and cathepsin K in osteoclasts and other cells in mouse tibia epiphysis by immunolight and immunoelectron microscopy. Bone 29:42–53

Virchows Arch (2006) 449:455–461
DOI 10.1007/s00428-006-0256-8

ORIGINAL ARTICLE

Sarcomatoid carcinomas of the lung —are these histogenetically heterogeneous tumors?

Markus Blaukovitsch · Iris Halbwedl · Hannelore Kothmaier · Margit Gogg-Kammerer · Helmut H. Popper

Received: 7 March 2006 / Accepted: 18 June 2006 / Published online: 29 August 2006
© Springer-Verlag 2006

Abstract Sarcomatoid carcinomas (SC) of the lung are a heterogeneous group of nonsmall cell lung carcinomas (NSCLC) containing a sarcoma or sarcoma-like component. SC may represent an epithelial neoplasm undergoing divergent tissue differentiation originating from a single clone. Epithelial–mesenchymal transition (EMT) best describes the origin of the spindle and giant cells. We aimed to define chromosomal aberrations within the subgroups of SC and if EMT does play a role in SC. Twenty-two SC were investigated by chromosomal comparative genomic hybridization (CGH). Immunohistochemical staining was performed with antibodies for E-cadherin, Vimentin, c-Fos, c-Jun, Snail, TGFβ1, Notch1, β-catenin, Glycogen synthase kinase 3β (GSK3β), and Fascin. Gains occurred more frequently than losses (70.5 vs 29.5%). The shortest regions of overlap were gains on chromosomes 8q and 7 followed by 1q, 3q, and 19, supporting the common origin of the different subtypes of SC. The immunohistochemical staining suggests that the sarcomatoid components of SC might have undergone EMT, not triggered by the signaling pathways Notch1, Snail, and TGFβ1, but probably initiated by an upregulation of c-Jun and a consecutive overexpression of Vimentin and Fascin. The Wnt-pathway was not deregulated because combined membrane and cytoplasmic reactivity for β-catenin and GSK3β was observed.

M. Blaukovitsch · I. Halbwedl · H. Kothmaier · M. Gogg-Kammerer · H. H. Popper (✉)
Laboratories for Molecular Cytogenetics,
Environmental and Respiratory Tract Pathology,
Institute of Pathology,
Medical University of Graz,
Auenbruggerplatz 25,
Graz 8036, Austria
e-mail: helmut.popper@meduni-graz.at

Keywords Lung carcinomas · Sarcomatoid carcinomas · Comparative genomic hybridization · CGH · Epithelial mesenchymal transition · Immunohistochemistry · Notch · c-Jun · Vimentin · Fascin

Introduction

Sarcomatoid carcinomas (SC) of the lung are a group of rare malignancies, accounting for approximately 1% of all lung tumors. The average age of diagnosis is 60 years; the men to women ratio is almost 4:1. More than 90% of the patients are smokers or suffered from heavy tobacco abuse in the past [18]. In general, they have a worse prognosis than conventional nonsmall cell lung carcinomas (NSCLC) [15]. This type of malignant neoplasm consists of poorly differentiated NSCLC that contain a component of sarcoma or sarcoma-like differentiation, i.e., spindle and/or giant cells [15].

Five subgroups representing a pathological–morphologic continuum are currently recognized: pleomorphic carcinoma, pure spindle-cell carcinoma, pure giant cell carcinoma, carcinosarcoma, and pulmonary blastoma [18]. Histogenetically, SC may represent malignant epithelial neoplasm undergoing divergent tissue differentiation originating from a single clone [6, 8, 16].

In our present study, we tried to find concordant chromosomal aberrations within these five subgroups of SC to prove their similar histogenesis. It has been proven in the past that the different phenotypically appearing epithelial- and spindle-cell components within some subgroups of SC (urinary bladder and pharynx) might originate from the same clone [17]. Furthermore, epithelial–mesenchymal transition (EMT) could best describe the origin of the sarcoma-like appearing components of the SC [4]. Different

signaling pathways that induce EMT are reported. The best known of these, the Notch, the Wnt, and the c-Jun [5, 9, 11, 21], were investigated in this study by immunohistochemistry (IHC) for key proteins.

The ancient cell-signaling system Notch could imply through Snail transduction the loss of cell polarity, a decrease in intercellular adhesion and an increase of motility, which leads to a mesenchymal phenotype [5]. Alternatively, abnormalities in the Wnt-signaling pathway could generate the mesenchymal appearing cells typical for SC [9]. Finally, we investigated c-Jun, which by synergizing with the activator protein Sp1 and binding to GC-box 1 can enhance Vimentin gene expression. Thus, Vimentin overexpression itself could also lead to EMT [21]. In addition, Fascin might contribute to a migratory phenotype of SC [1, 13].

Materials and methods

Study samples

Twenty-two cases of SC of the lung (including 16 cases of pleomorphic carcinomas, 2 of which have a predominant giant-cell and a minor large-cell component), 1 spindle-cell carcinoma, 2 cases of carcinosarcoma, 1 blastoma, and 2 cases of GC were collected as formalin-fixed, paraffin-embedded tissue blocks from the lung disease archive of the Institute of Pathology, Medical University of Graz, Austria.

DNA isolation

An experienced pathologist classified the tumor samples. Tumors were microdissected with needles, and tumor DNA was isolated from six consecutive, deparaffinized sections. Comparative genomic hybridization (CGH) [12, 20] was essentially done as previously described by Halbwedl et al. [7]. We did not separate the histologically different pleomorphic carcinoma components because in a previous report, no genetic differences between the epithelial- and spindle-cell component were found by CGH [17].

On the average, ten metaphase spreads were evaluated per case. Thresholds for chromosomal gains and losses were set to 1.2 and 0.8, respectively. Telomeres, centromeres, the Y-chromosomes, and gains on well-known CGH critical regions (1p36, 17p, 19p, and 22) were not evaluated. In two cases (one pleomorphic carcinoma and one blastoma), CGH could not be performed due to DNA degradation.

Aberrations of each case were listed in a Microsoft Access© database and displayed in a diagram to show overlapping genetic alterations.

Immunohistochemistry (IHC)

The same 22 paraffin-embedded tissue blocks as used for CGH were investigated. The immunohistochemical staining experiments were performed using primary antibodies and commercially available detection kits as recommended by the manufacturers (Table 1). Using not only tissues recommended by the manufacturer but also normal lung

Table 1 Immunohistochemical staining methods used for each antibody

Antibody for	Clone number, company, clonality	Block[a]	Pretreatment	Detection
E-cadherin	4A2 C7, Zymed, monoclonal	Yes	WB[b], DAKO Epi.[c]	LSAB+AEC[d]
Vimentin	E034, Linaris, monoclonal	Yes	Without pretreatment	CM+DAB[e]
TGF-β1	TB 21, Cymbus Biotech, monoclonal	Yes	MW[f], Na-Citrat pH 6.0	CM+DAB[e]
SNAIL	E-18, Santa Cruz, polyclonal	Yes	MW, Na-Citrat pH 6.0	Multi Link+AEC[g]
Notch1	A6, Neomarkers, monoclonal	Yes	MW, Tris–HCl+5% Urea pH 9.5	HRP+Envis. DAB[h]
c-Jun	H-79, Santa Cruz, polyclonal	Yes	MW, DAKO Tar.[i] pH 9.0	CM+DAB[e]
c-Fos	K-25, Santa Cruz, polyclonal	Yes	MW, Na-Citrat pH 6.0	LSAB+AEC[d]
β-catenin	M3539, Dako, 1:100, polyclonal	Yes	WB[b]	LSAB+AEC[d]
GSK3β	AB8687, Chemicon, 1:100, polyclonal	Yes	MW, Na-Citrat pH 6.0	HRP+Envis. DAB[h]
Fascin	55K2, Chemicon, 1:500	Yes	MW, Na-Citrat pH 6.0	HRP+Envis. DAB[h]

[a] *Blocking* ChemoMate peroxidase-blocking solution
[b] *WB* Waterbath 98°C/ 40 min
[c] *DAKO Epi.* Epitope retrieval solution, Dako
[d] *LSAB+AEC* LSAB peroxidase-blocking solution and AEC substrate chromogen
[e] *CM+DAB* ChemoMate detection kit peroxidase/DAB rabbit/mouse chromogen
[f] *MW* Microwave 160°C/30 min
[g] *MultiLink+AEC* MultiLink 2/3. Antibody and AEC substrate chromogen
[h] *HRP+Envis. DAB* ChemoMate Dako Envision, horseradish peroxidase, rabbit/mouse
[i] *DAKO Tar.* Target retrieval solution pH 9.0, Dako

parenchyma, we tested reactivity and staining intensity. Internal positive and negative controls were identified within the tissue section. After having defined weak and strong stainings (1+ and 3+), the sections were evaluated for the percentage of positively stained tumor cells for each antibody at once (in increments of ten). The site of the reaction was also evaluated as nuclear, cytoplasmic, and membranous.

Statistical analysis of the IHC results was performed using Spearman's rank-sum test for correlation used in Microsoft Excel© add-in program Winstat©.

All patient data were anonymized and thus they were in accordance with the rules of the ethical committee of our University.

Results

In our cases, we found more chromosomal gains than losses (70.5 vs 29.5%). Frequent chromosomal alterations were gains on chromosome 1 (seven cases, 31.8% of all cases), chromosome 8q (six cases, 27.3%), chromosome 3 (six cases, 27.3%), chromosome 7 (five cases, 22.7%), and chromosome 19q (five cases, 22.7%). In addition, we detected gains on chromosomes 11, 12p, 17q, and 20q. Deletions of genetic material were seen only in a few cases (most frequently on chromosomes 4q, 5q, 6q, and 13). Furthermore, two other cases (one pleomorphic carcinoma and one giant-cell carcinoma) did not exhibit any chromosomal aberrations as detected by CGH. In addition, two pleomorphic carcinomas characterized by predominant giant-cell components and minor large-cell carcinomas differed from the other SC by showing gains of 11p and 12p but not the common aberrations on chromosomes 1, 8q, 3, and 7. A detailed karyotype of all chromosomal alterations is shown in Fig. 1.

In all control experiments, the 99% confidence interval was within the thresholds set to 1.2 and 0.8 except of the sex chromosomes. The deviation of the ratio at X-chromosomes was clearly detected in each control experiment hybridized in a sex-mismatch manner.

All immunohistochemical markers were evaluated semi-quantitatively for their staining pattern and intensity. Antibodies for E-cadherin stained the epithelial components of SC more intensively, whereas Vimentin preferentially stained spindle and giant cells. Vimentin not only showed a positive immunoreactivity in the cytoplasm but in a few cases also stained the nuclei (Table 2, Fig. 2a). Immunohistochemical staining of the cell-cycle control proteins c-Jun and c-Fos was mostly confined to the mesenchymal parts of SC. C-Jun (on chromosome 1p32) showed a strongly positive nuclear reaction; however, in most cases also, a cytoplasmic positive immunostaining pattern could be observed (Fig. 2b). C-Fos (mean: 30%, 2+

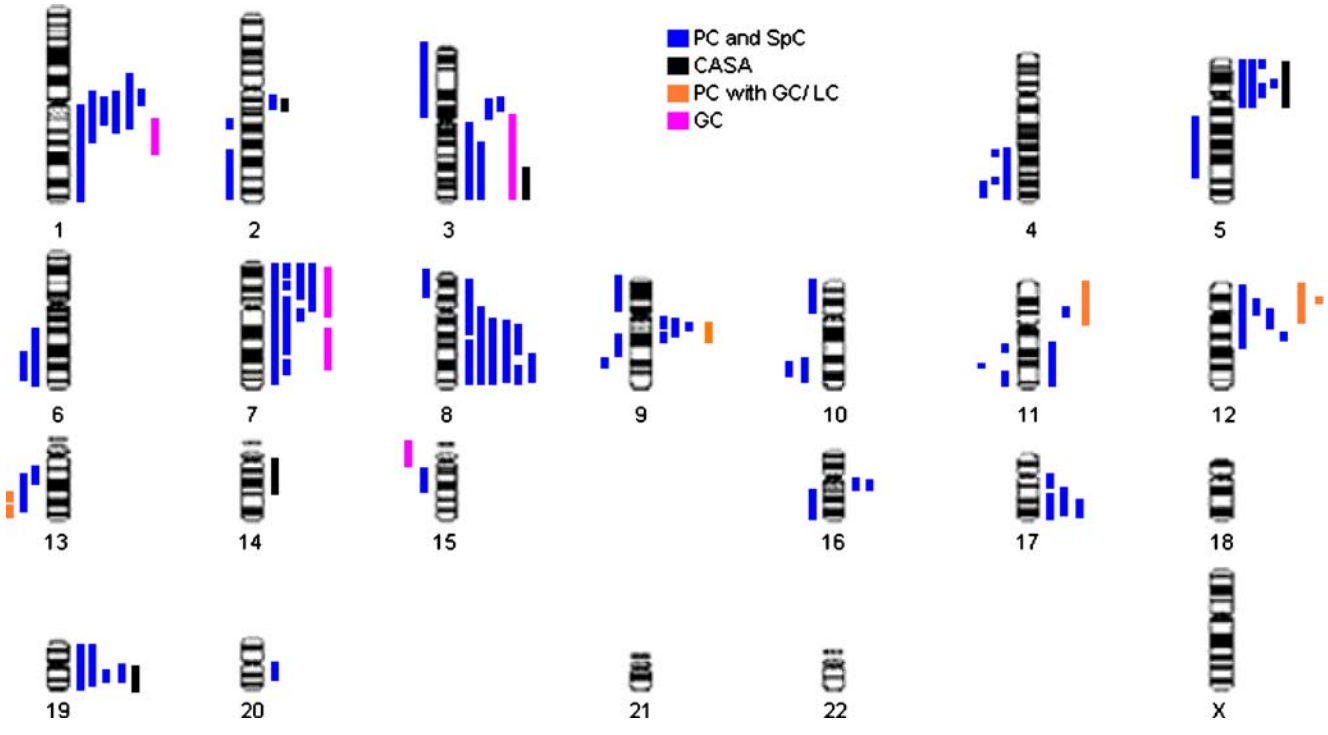

Fig. 1 Overlapping karyograms of sarcomatoid carcinomas. Losses of genetic material are displayed to the *right*, while gains are pictured to the *left* of each chromosome. Pleomorphic carcinoma (*green*), carcinosarcoma (*red*), pleomorphic carcinoma with giant- and large-cell components (*yellow*), pure giant-cell carcinoma (*blue*)

Table 2 Results of the immunohistochemistry

	c-Fos			c-Jun			E-cadherin			Vimentin		TGFβ1		Snail		Notch1		β-catenin			GSK3β			Fascin		
	%	Int.	Loc.	%	Int.	Loc.	%	Int.	Loc.	%	Int.	%	Int.	%	Int.	%	Int.	Loc.	%	Int.	Loc.	%	Int.	Loc.	%	Int.
PC 1	20	2	n	80	2	nc	10	3	nc	10	2	30	3	20	3	80	1	m	50	3	0	0	0	c	30	1
PC 2	40	2	n	60	3	n	5	2	nc	40	3	10	2	30	2	50	1	m	70	3	c	30	3	c	70	1
GC 1	80	3	n	80	3	nc	40	2	nc	5	2	10	2	1	2	70	1	m	90	3	c	50	2	c	90	2
CASA 1	30	2	n	50	2	nmc	0	0	c	10	3	5	2	30	3	80	1	m	60	2	c	30	1	c	40	3
PC 3	5	2	n	30	3	n	0	0	c	30	3	0	0	1	2	20	1	m	70	1	0	0	0	mc	70	2
PC 4	10	2	n	80	2	nc	0	0	nc	90	3	0	0	5	2	70	1	m	60	1	c	40	1	mc	70	3
PC 5	30	2	n	80	3	nmc	10	2	n	0	0	10	1	0	0	20	1	m	70	3	c	10	2	mc	60	1
PC 6	80	3	n	90	3	n	0	0	c	90	3	0	0	20	3	40	2	m	30	1	c	40	3	mc	80	3
PC 7	50	1	n	70	2	nc	0	0	nc	20	3	0	0	10	2	10	1	m	50	2	c	10	2	c	80	2
PC 8	80	2	n	60	3	nc	20	2	c	0	0	20	1	5	2	40	2	m	70	3	c	40	3	c	50	2
PC 9	20	1	n	60	3	n	0	0	c	5	2	0	0	0	0	80	1	m	80	3	c	20	3	0	0	0
PC 10	70	1	nc	95	3	n	0	0	c	80	3	0	0	0	0	10	1	m	70	1	c	70	1	c	60	2
CASA 2	10	1	nc	80	2	nc	70	2	c	5	2	20	1	0	0	20	2	m	70	3	c	30	3	c	60	2
PC/ GC/ LC 11	30	2	n	95	3	n	0	0	nc	50	3	0	0	30	2	30	1	m	40	2	c	90	3	c	70	2
PC 12	20	1	n	80	3	nc	0	0	nc	70	3	0	0	0	0	10	1	m	40	2	c	50	2	mc	70	2
PC/ GC/ LC 13	70	2	nc	70	3	n	0	0	c	60	3	0	0	40	3	20	2	m	10	1	c	40	3	mc	90	3
PC 14	20	1	n	70	2	nc	10	3	nc	20	3	20	1	5	3	70	1	m	70	3	c	50	3	c	60	2
PC 15	30	1	nc	30	2	nc	0	0	nc	30	3	5	1	1	3	60	1	m	30	1	c	70	3	c	50	1
GC 2	40	2	n	20	2	nc	0	0	c	5	3	20	1	70	2	70	1	m	20	2	c	30	2	c	20	2
PC 16	30	2	n	50	3	nc	0	0	nc	40	3	70	3	5	2	70	2	m	60	2	c	30	2	mc	70	3
Blastoma	0	0	0	30	2	c	0	0	c	0	0	0	0	30	3	20	1	nmc	20	2	c	30	1	c	20	1
SpC 17	20	2	nc	30	2	c	0	0	c	30	3	30	2	20	2	60	1	m	30	2	c	40	1	0	0	0

% Percentage of positive cells per case, *int.* intensity of positive reaction ranging 1–3, *loc.* localization of positive staining, *m* membranous, *c* cytosolic, *n* nuclear, *PC* pleomorphic carcinomas, *SpC* pure spindle-cell carcinoma, *CASA* carcinosarcoma, *PC/GC/LC* pleomorphic carcinoma with predominant giant-cell and minor large-cell components, *GC* pure giant-cell carcinoma

intensity) was less intensively stained compared to c-Jun (mean: 70%, 3+ intensity). Weak overall immunoreactivity could be seen for proteins belonging to the Notch1/TGFβ1/Snail signaling pathway. Snail in most SC showed a low percentage of positive cells (mean: 5%); in Notch1, most cells were weakly stained (mean: 45%, 1+). In addition, with both markers only cytoplasmic and no nuclear reaction was seen (see Table 2). Reactivity for TGFβ was overall weak, and only a small percentage of the tumor cells were stained (mean: 5%, 1+).

In addition, diffuse cytoplasmic and membrane-confined staining was seen for Glycogen synthase kinase 3β (GSK3β) (Fig. 2c) and β-catenin (Fig. 2d), both representing the Wnt-signaling pathway. Fascin (fascin 1 and 3 on chromosome 7, fascin 2 on chromosome 17q), an actin-cross-linking protein, showed the strongest reaction of all antibodies used in this study and was remarkably only positive in the mesenchymal parts of SC (Fig. 2e). All results of the immunohistochemical study are given in Table 2.

The statistical analysis (n=22) revealed a strong positive correlation for Fascin and c-Jun, correlation factor r=0.48 (p=0.011), Fascin/Vimentin, r=0.52 (p=0.006), and c-Jun/Vimentin, r=0.37 (p=0.046). In contrast, we did not evaluate any significant positive correlation between Notch/TGFβ1/Snail and Vimentin or Fascin. Because β-catenin did not show a nuclear staining pattern and therefore might not function as a transcription factor, we did not include it in our statistical analysis.

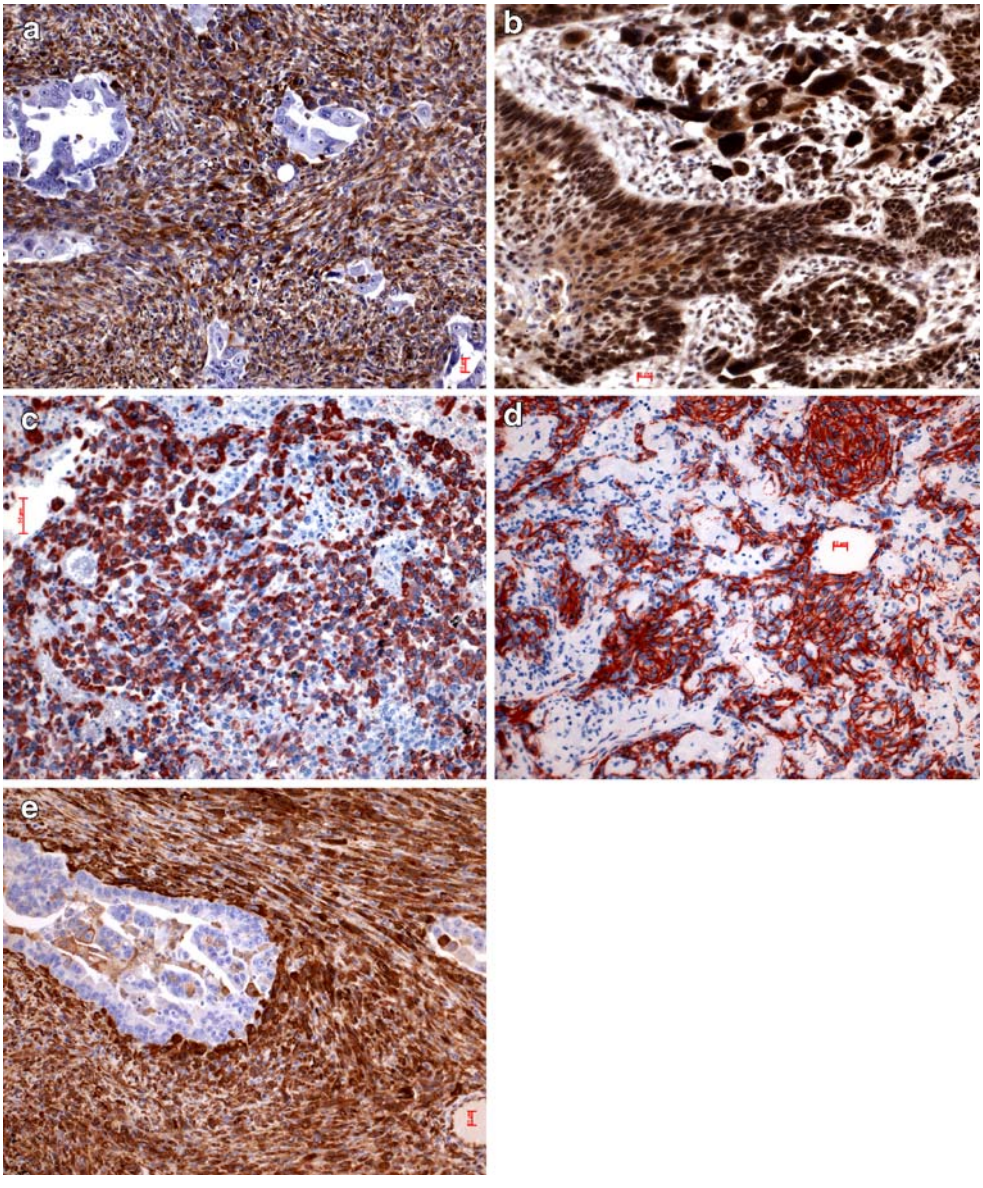

Fig. 2 **a** Immunohistochemistry for Vimentin. In most cases, there is positive reaction in the mesenchymal parts of SC, whereas the differentiated epithelial component is negative. *Bar* 20 μm. **b** Immunohistochemistry for c-Jun. Strong positive nuclear and a focal cytoplasmatic reaction is seen in this SC. There is no difference between the SC components. *Bar* 20 μm. **c** Immunohistochemistry for GSK3β. A positive staining is seen in the cytoplasm. *Bar* 50 μm. **d** Immunohistochemistry for β-catenin. Overall positive reaction at the cell membrane. *Bar* 20 μm. **e** Immunohistochemistry for Fascin. Strong overall reaction in the mesenchymal parts of SC. Most epithelial cells are negative. *Bar* 20 μm

Discussions

CGH results for SC revealed some overlaps of chromosomal aberrations indicating a possible common histogenetic origin of the different subtypes of SC.

Pleomorphic and spindle-cell carcinomas all showed gains on either 8q, 7, 5, 3q, 1 or 19, and 5p. In addition to pleomorphic carcinoma, carcinosarcoma also showed gains on 3q, 5p, and 19. This might be interpreted that carcinosarcoma and pleomorphic and spindle-cell carcinoma are closely related according to their genetic origin, which is also supported by the studies of Rossi et al., Pelosi et al., and Fishback et al. [3, 13–15]. Gains of genetic material on chromosomes 2q and 14q separate carcinosarcoma from the other subtypes of SC. This, however, should be interpreted with caution due to the small numbers of cases investigated.

The chromosomal aberrations of giant-cell carcinomas also showed gains on chromosomes 1q, 3q, and 7, indicating a genetic relation to pleomorphic carcinoma and carcinosarcoma. Nevertheless, chromosomal losses on 13p and 15p were only found in giant-cell carcinoma, probably pointing to the differences in the phenotypic appearance as well as their much more aggressive behavior [3].

The two cases of pleomorphic carcinomas with giant- and large-cell components did clearly show chromosomal alterations, which are not found in the other subgroups of SC. Gains on chromosomes 11p, 12p, 9q, and 17q and losses on 13q were exclusively detected at that type of carcinomas. There was no similarity with pure giant-cell carcinoma; however, the number of cases is probably too small to draw a final conclusion.

Some of the chromosomal aberrations found in SC are not commonly seen in adenocarcinomas (7+ and 12p+) and gains of 1q, 7+, and 8+ not in squamous cell carcinomas [10, 19]. This clearly separates SC from adenocarcinomas and squamous cell carcinomas, although both are the most frequent found components in SC. In one study, the various parts of SC were investigated separately by CGH, and no influence on the chromosomal aberrations was seen [17].

With respect to EMT [2, 4, 5], it seems that the well-known signaling-pathway Notch and its downstream ligands such as TGF-β do not play a crucial role in our cases. Moreover, the combined membranous and cytoplasmic staining for β-catenin and the cytoplasmic staining for GSK3β could implicate a normally regulated Wnt-pathway [9, 11]. The weak staining for E-cadherin might be interpreted as a result of mutation, which would cause β–catenin to dissociate from its membranous partners and shed into the cytoplasm. High expression of GSK3β in the cytoplasm could be an indicator of immediate ubiquitinylation of β-catenin; however, GSK3β needs to be phosphorylated. This was not proven in our experiments.

It is interesting to note that we could show that high nuclear activity of the transcription factor c-Jun might be responsible for the expression of Vimentin in SC, as previously investigated by Wu et al. [21] in cell lines, and probably also Fascin, which is also substantiated by our statistical analysis [13]. Vimentin might therefore be responsible for the EMT and Fascin for an increase in cell motility.

In conclusion, our CGH data point to a close relationship of all subgroups in SC, except the pleomorphic, giant-, and large-cell carcinomas. We provide some evidences that the newly described signaling pathway of c-Jun/ Vimentin acts as probable promoter of EMT in SC. Thus, the members of the c-Jun pathway might be the targets for a new therapeutic treatment concept in these highly aggressive carcinomas.

Acknowledgement This study was supported by the Medical University of Graz.

References

1. Adams JC (2004) Roles of fascin in cell adhesion and motility. Curr Opin Cell Biol 16:590–596
2. Akhurst RJ, Derynck R (2001) TGF-beta signaling in cancer—a double-edged sword. Trends Cell Biol 11:S44–S51
3. Fishback NF, Travis WD, Moran CA, Guinee DG Jr, McCarthy WF, Koss MN (1994) Pleomorphic (spindle/giant cell) carcinoma of the lung. A clinicopathologic correlation of 78 cases. Cancer 73:2936–2945
4. Gotzmann J, Mikula M, Eger A, Schulte-Hermann R, Foisner R, Beug H, Mikulits W (2004) Molecular aspects of epithelial cell plasticity: implications for local tumor invasion and metastasis. Mutat Res 566:9–20
5. Grego-Bessa J, Diez J, Timmerman L, de la Pompa JL (2004) Notch and epithelial-mesenchyme transition in development and tumor progression: another turn of the screw. Cell Cycle 3:718–721
6. Guarino M, Micheli P, Pallotti F, Giordano F (1999) Pathological relevance of epithelial and mesenchymal phenotype plasticity. Pathol Res Pract 6(195):379–389
7. Halbwedl I, Ullmann R, Kremser ML, Man YG, Isadi-Moud N, Lax S, Denk H, Popper HH, Tavassoli FA, Moinfar F (2005) Chromosomal alterations in low-grade endometrial stromal sarcoma and undifferentiated endometrial sarcoma as detected by comparative genomic hybridization. Gynecol Oncol 2:582–587
8. Holst VA, Finkelstein S, Colby TV, Myers JL, Yousem SA (1997) p53 and K-ras mutational genotyping in pulmonary carcinosarcoma, spindle cell carcinoma, and pulmonary blastoma: implications for histogenesis. Am J Surg Pathol 21:801–811
9. Ilyas M (2005) Wnt signalling and the mechanistic basis of tumour development. J Pathol 205:130–144
10. Jiang F, Yin Z, Caraway NP, Li R, Katz RL (2004) Genomic profiles in stage I primary non small cell lung cancer using comparative genomic hybridization analysis of cDNA microarrays. Neoplasia 6:623–635

11. Kallionemi A, Kallionemi OP, Sudar D, Rutovitz D, Gray JW, Waldman F, Pinkel D (1992) Comparative genomic hybridization for molecular cytogenetic analysis of solid tumors. Science 258:818–821
12. Klymkowsky MW (2005) Editorial. β-catenin and its regulatory network. Human Pathol 36:225–227
13. Pelosi G, Fragetta F, Nappi O, Pastorino U, Maisonneuve P, Pasini F, Iannucci A, Solli P, Musavinasab HS, de Manzoni G, Terzi A, Viale G (2003) Pleomorphic carcinomas of the lung show a selective distribution of gene products involved in cell differentiation, cell cycle control, tumor growth, and tumor cell motility: a clinicopathologic and immunohistochemical study of 31 cases. Am J Surg Pathol 27:1203–1215
14. Pelosi G, Scarpa A, Manzotti M, Veronesi G, Spaggiari L, Fragetta F, Nappi O, Benino E, Pasini F, Antonello D, Iannucci A, Maisonneuve P, Viale G (2004) K-ras gene mutational analysis supports a monoclonal origin of biphasic pleomorphic carcinoma of the lung. Mod Path 17:538–546
15. Rossi G, Cavezza A, Sturm N, Migali M, Facciolongo N, Longo L, Maiorana A, Brambilla E (2003) Pulmonary carcinomas with pleomorphic, sarcomatoid, or sarcomatous elements: a clinicopathologic and immunohistochemical study of 75 cases. Am J Surg Pathol 27:311–324
16. Thompson L, Chang B, Barsky SH (1996) Monoclonal origins of malignant mixed tumors (carcinosarcomas). Evidence for a divergent histogenesis. Am J Surg Pathol 20:277–285
17. Torenbeek R, Hermsen MA, Meijer GA, Baak JPA, Meijer CJLM (1999) Analysis by comparative genomic hybridization of epithelial and spindle cell components in sarcomatoid carcinoma and carcinosarcoma: histogenetic aspects. J Pathol 189:338–343
18. Travis W, Brambilla E (2004) Pathology and genetics of tumours of the lung, pleura, thymus and heart. WHO, Lyon
19. Sy SM, Wong N, Lee TW, Tse G, Mok TS, Fan B, Pang E, Johnson PJ, Yim A (2004) Distinct patterns of genetic alterations in adenocarcinoma and squamous cell carcinoma of the lung. Eur J Cancer 40:1082–1094
20. Weiss MM, Hermsen MA, Meijer GA, van Grieken NC, Baak JP, Kuipers EJ, van Diest PJ (1999) Comparative genomic hybridisation. Mol Pathol 52:243–251
21. Wu Y, Zhang X, Zehner ZE (2003) c-Jun and the dominant-negative mutant, TAM67, induce vimentin gene expression by interacting with the activator Sp1. Oncogene 22:8891–8901

Virchows Arch (2006) 449:462–471
DOI 10.1007/s00428-006-0257-7

ORIGINAL ARTICLE

Augmented expression of hepatocytes growth factor activator inhibitor type 1 (HAI-1) in intrahepatic small bile ducts in primary biliary cirrhosis

Motoko Sasaki · Hiroko Ikeda · Hiroaki Kataoka · Yasuni Nakanuma

Received: 28 March 2006 / Accepted: 17 June 2006 / Published online: 29 August 2006
© Springer-Verlag 2006

Abstract The repair system of damaged biliary mucosa was not fully clarified so far in primary biliary cirrhosis (PBC). Given that related factors of the hepatocyte growth factor (HGF) such as HGF activator (HGFA) and HGFA inhibitor type 1 (HAI-1) participate in the repair of injured gastrointestinal mucosa, we investigated the involvement of the HGF/HGFA/HAI-1 system in PBC and control livers. The expression of HGFA, HAI-1, and c-Met was examined in PBC livers (n=24), diseased livers (control, n=30), and normal livers (n=15) by immunohistochemistry and semi-quantitative reverse transcriptase-polymerase chain reaction. We examined the expression of HGFA, HAI-1, and c-Met, and the effect of HGF administration on cell proliferation and wound healing, and HAI expression in cultured mouse biliary epithelial cells (BECs). HAI-1 expression was faint in control livers, whereas it was significantly augmented in damaged small bile ducts, bile ductules, and periportal hepatocytes in PBC (p<0.05). HGFA and c-Met were homogeneously expressed in BECs in PBC and control livers. HAI-1 expression was increased at the front of wound healing and the treatment with HGF-enhanced HAI-1 expression, cell proliferation, and wound healing in cultured BECs. HGF/HGFA/HAI-1 system may participate in biliary mucosal repair as reported in gastrointestinal mucosal repair.

M. Sasaki · H. Ikeda · Y. Nakanuma (✉)
Department of Human Pathology,
Kanazawa University Graduate School of Medicine,
Kanazawa 920-8640, Japan
e-mail: m8sasaki@med.kanazawa-u.ac.jp

H. Kataoka
Department of Pathology II,
Miyazaki Medical College,
Miyazaki, Japan

Keywords Primary biliary cirrhosis · Hepatocytes growth factor (HGF) · HGF activator (HGFA) · HGF activator inhibitor type I (HAI-1) · Biliary epithelial cells

Introduction

Primary biliary cirrhosis (PBC) is an organ-specific autoimmune disease and presents with chronic, progressive cholestasis and liver failure. It usually affects middle-aged women [4] and often leads to liver failure and liver transplantation [9, 18]. PBC is characterized histologically as a cholangitis of small bile ducts (chronic nonsuppurative destructive cholangitis, CNSDC), eventually followed by extensive loss of small bile ducts [9, 14, 18]. PBC is serologically characterized by the presence of antimitochondrial antibodies [9] and B cell- and T cell-mediated immune reaction targeting an inner lipoyl domain of the E2 component of pyruvate dehydrogenase [3, 8, 13, 24]. While there were many studies on immunopathological features and apoptotic processes of biliary epithelial damages, the studies on the homeostasis and repair process of biliary epithelial cells (BEC) are very limited in PBC [17, 20, 21].

Accumulating data suggest that common pathways and factors play a role in mucosal repair of gastrointestinal tract and intrahepatic bile duct [17, 20]. Hepatocyte growth factor (HGF)/scatter factor is thought to play an important role in the regeneration of injured gastrointestinal mucosa by promoting the proliferation and migration of epithelial cells [6, 10]. HGF is secreted by stromal cells as an inactive precursor form, and is specifically activated by HGF activator (HGFA) to the active form [6, 10]. HGFA is also produced as a precursor form and is activated by thrombin

in injured tissues. The activity of HGFA is regulated by two Kunitz type serine proteinase inhibitors: HGFA inhibitor type 1 (HAI-1) and type 2 (HAI-2). HAI-1 is a cell-surface acceptor of activated HGFA and is upregulated in regenerative epithelium relative to normal epithelium in the gastrointestinal tract [6, 10]. The upregulated HAI-1 is suggested to contribute concentrated HGFA activity and efficient pericellular activation of HGF in the injured gastrointestinal mucosa and promote the proliferation and migration of gastrointestinal epithelial cells [6, 10, 11].

Given that HGF and its related factors, such as HGFA and HAI-1, are important in the regeneration of injured gastrointestinal mucosa, we investigated the involvement of these factors in the damaged bile duct lesions in PBC and diseased controls including chronic viral hepatitis (CVH) and extrahepatic biliary obstruction (EBO). In addition, we took advantage of cultured mouse BECs to examine the involvement of HGF/HGFA/HAI-1 system in the repair process of damaged BECs. Although there were several studies regarding the effect of HGF on the cell proliferation [7, 32] and migration of BECs [27], the involvement of the HGFA/HAI-1 system in the repair of biliary mucosa has not yet been studied to our knowledge.

Materials and methods

Classification of intrahepatic biliary tree

The intrahepatic biliary tree is classified into the intrahepatic large and small bile ducts by their size and distributions in the portal tracts [14, 15]. In this study, septal and interlobular bile ducts are called as small bile ducts. Bile ductules were evaluated separately and not included in the small bile ducts.

Liver tissue preparation

A total of 69 liver tissue specimens (all were wedge-biopsied or surgically resected) were collected from the liver disease file of our laboratory and affiliated hospitals. The specimens consisted of 24 PBC livers, 17 CVH livers, 13 livers from EBO, and 15 "histologically normal" livers. All PBC were from the patients fulfilling clinical, serological, and histological characteristics consistent with the diagnosis of PBC and were staged histologically [22, 23]. Sixteen and eight PBC livers were of stages 1/2 and 3/4, respectively. Seven CVH were regarded as F1/2 and ten as F3/4 [2]. Three and 14 out of 17 CVH cases were serologically positive for hepatitis B surface antigen and antihepatitis C viral antibody, respectively. Causes of EBO were obstruction or stenosis of the bile duct at the hepatic hilum or the extrahepatic bile duct due to carcinoma or stone, and the duration of jaundice was less than 1 month. Histologically normal livers were obtained from surgically resected livers for traumatic hepatic rupture or metastatic liver tumor.

Liver tissue samples were fixed in 10% neutral-buffered formalin and embedded in paraffin. More than 20 serial sections, 4-μm-thick, were cut from each block. Several were processed routinely for histopathologic study and the remainder was processed for the following immunohistochemistry.

For the analysis of mRNA expression, frozen liver tissue specimen taken from the patients with PBC (n=14; stages 1/2, n=7; and stages 3/4, n=7), CVH (n=7; F1/2, n=2; and F3/4, n=5), and histologically normal livers (n=12) were used.

Cell culture and treatments of mouse intrahepatic BECs

Mouse intrahepatic BECs were isolated from 8-week-old female BALB/c mice and were purified and cultured as described previously [12, 33]. In several experiments, BECs were treated with 112.5 μM H_2O_2 for 2 h, washed all throughout to remove H_2O_2, and cultured in fresh medium. Recombinant HGF (0–100 ng/ml) (Toyobo, Shiga, Japan) and other recombinant cytokines [interferon (IFN)-γ, 1,000 U/ml; TNF-α, 10 μg/ml; IL-1β, 10 μg/ml; and transforming growth factor (TGF)-β, 8 μg/ml; R&D Systems, Minneapolis, MN, USA] were also used to treat BECs in several experiments.

Immunohistochemistry and semiquantitative evaluation

HGFA and HAI-1 were detected immunohistochemically using mouse monoclonal anti-HGFA (clone A1, dilution 1:200) and anti-HAI-1 (clone 1N7, 1:100) [10], respectively. C-Met was detected using rabbit polyclonal anti-c-Met antibody (1:100; Zymed, South San Francisco, CA, USA). Immunohistochemical staining was performed with pretreatment in microwave oven in citrate buffer (pH 6.0) at 95°C for 20 min as described previously [21]. Negative controls included substituting similar dilution of the control mouse immunoglobulin G (IgG).

The immunohistochemical expression of HGFA, HAI-1, and c-Met in small bile ducts and bile ductules was estimated as positive when more than 5% of cells expressed HGFA, HAI-1, or c-Met. The extent of HAI-1 expression was evaluated as "faint," when HAI-1 was expressed faintly in cytoplasm and/or on lateral cell membrane. The extent was evaluated as "intensive," when the expression of HAI-1 was seen strongly on whole cell membrane of BECs. When a given specimen included

more than three small bile ducts (or bile ductules) evaluated as intensive expression, the specimen was classified as intensive expression of HAI-1. The remaining positive specimens were regarded as faint expression.

Immunofluorescence staining for cultured cells

The BECs growing in Lab-Tek chamber were fixed with 5% buffered formalin and cold methanol for 20 min each. After incubation with 3% bovine serum albumin for blocking, the cells were incubated with either primary antibodies for HGFA (described above) or HAI-1 (rabbit polyclonal antibody [28], 1:100) and c-Met (1:100, rabbit polyclonal, Santa-Cruz Biotechnology, Santa Cruz, CA, USA) for overnight. Then the cells were Alexa-546-labeled or Alexa-488-labeled with goat anti-mouse IgG or anti-rabbit IgG (Molecular Probes, Eugene, OR, USA) for 30 min. The sections were counterstained with 10 μg/ml of 4′- and 6-diamidino-2-phenylindole (DAPI) (Molecular Probes) and were evaluated under conventional fluorescence microscope (Olympus, Tokyo, Japan).

Extraction of RNA and semiquantitative RT-PCR

Total RNA was extracted from the liver tissues or cells with a QIAGEN RNeasy Mini kit (QIAGEN) according to the recommendations of the manufacturer. After cDNA was synthesized, semiquantitative reverse transcriptase polymerase chain reaction (RT)-PCR was carried out as described previously [19]. Primers used for RT-PCR are shown in Table 1. Gel images were evaluated by using NIH image and the expression was normalized as a ratio using human glyceraldehyde-3-phosphate dehydrogenase (G3PDH) or mouse β-actin as a housekeeping gene. Data were expressed as the mean±SD.

Proliferation assays

Viable cell numbers were measured by using WST assay reagent (Roche) according to the recommendations of the manufacturer. BECs (5×10^3 cells/well) were plated in 96-well plates and cultured for 24 h. Then these cells were cultured in the presence or absence of HGF for 48 h. At the end of experiment, the cell proliferation reagent WST-1 (10 μl) was added to each well and incubated for 2 h at 37°C. Optical density (A_{450nm}) was measured using an automatic ELISA plate reader. Each experiment was done in octuplicate.

In vitro wound-healing assay

A wound-healing assay was performed in the presence or absence of HGF (50 ng/ml). BECs (5×10^4 cells/well) were plated in collagen type I-coated 6-well tissue culture plates (IWAKI) and grown to confluence. To inhibit cell proliferation, mitomycin C (Sigma) was added (1.0 μg/ml) 2 h before initiating the wound-healing assay. Confluent monolayers of cells were wounded with a Gilson p10 pipette tip (Amachem, Bedfordshire, UK) and placed in media with and without HGF. Wound widths for each well were evaluated by using NIH image. Ten measurements were performed for each wound before and after 24, 48, and 72 h of the HGF treatment. Each experiment was performed in triplicate. Data are expressed as the percentage reduction in wound width (mean±SD).

Statistical analysis

Statistical analysis for the difference in immunohistochemical study used the Wilcoxon rank sum test. Statistical analysis for the difference in in vitro assays used the Student's *t* test. A *P* value of less that 0.05 was considered significant.

Table 1 Primers for RT-PCR

Gene	GenBank accession no.	Forward primer (5′ to 3′)	Reverse primer (5′ to 3′)	Product size (bp)
Human				
HGFA	nm001528.2	AGGACACAAGTGCCAGATTG	GTTGATCCAGTCCACATAGT	334
HAI-1	BC018702	ATGGAGGCTGCTTGGGCAACA	ACAGGCAGCCTCGTCGGAGG	221 (HAI-1B: 269)
G3PDH	BC023632	GAACGGGAAGCTCACTGGCATGGC	TGAGGTCCACCACCCTGTTGCTG	311
Mouse				
HGFA	nm019447.1	CAAGGACTGTGGCACAGAGA	GATCTCTGTACCATTTCCCAGGAAGCA	298
HAI-1	BC005169.1	ACTGTGCAGAGCTGCCAGAC	AAGACTGGCAAGAGTCCCAG	444
c-Met	Y00671	GAATGTCGTCCTACACGGCC	CAGGGGCATTTCCATGTAGG	727
β-actin	X03765	GCTATGCTCTCCCTCACGCCAT	ACAGCAGCTCAGTAACAGTCCGC	626

Results

Augmented expression of HAI-1 in small bile ducts, bile ductules, and hepatocytes in PBC livers

HGFA The expression of HGFA was homogeneously seen in small bile ducts, bile ductules, and hepatocytes (Fig. 1a, b). There was no difference in the extent of HGFA expression among liver samples of PBC, CVH, EBO, and normal livers.

c-MET c-Met was expressed homogeneously in the cytoplasm of BECs in small bile ducts and bile ductules (Fig. 1c) and no difference was detected between PBC, diseased (control), and normal livers.

HAI-1 The extent of HAI-1 expression in small bile ducts, bile ductules, and hepatocytes is summarized in Table 2. In accordance with the previous report [10], the endothelia of capillaries and lymphatics occasionally showed positive staining.

Small bile ducts and bile ductules

HAI-1 was expressed in BECs of small bile ducts weakly and focally in half of the normal livers and all CVH livers. HAI-1 was not expressed in small bile ducts in the remaining normal livers (Fig. 2a). The extent of HAI-1 expression was significantly high in CVH livers when compared with that of normal livers ($p<0.05$). HAI-1 expression was significantly augmented in small bile ducts in PBC when compared with CVH, EBO, and normal livers ($p<0.05$). Membranous and intensive expression was evident in BECs in injured small bile ducts involved in CNSDC in 22 out of 24 with PBC (Fig. 2b). Intensive expression of HAI-1 was also seen in 4 out of 13 EBO livers. The profile of HAI-1 expression in periportal bile ductules showed similar tendency to that in small bile ducts in PBC and other diseased livers. Intensive membranous expression of HAI-1 was seen in bile ductules in PBC (Fig. 2c) and the extent of HAI-1 expression was significantly high in PBC when compared with CVH, EBO, and normal livers ($p<0.05$).

Hepatocytes

Hepatocellular expression of HAI-1 was rare in control diseased and normal livers, whereas it was significantly frequent in PBC of advanced stage (stages 3 and 4) ($p<0.05$). HAI-1 was expressed in the membrane of periportal hepatocytes (Fig. 2d). Similar membranous expression of HAI-1 was also seen focally in 4 out of 16 PBC of stages 1 and 2 and the extent was significantly high when compared with that in CVH and normal livers ($p<0.05$).

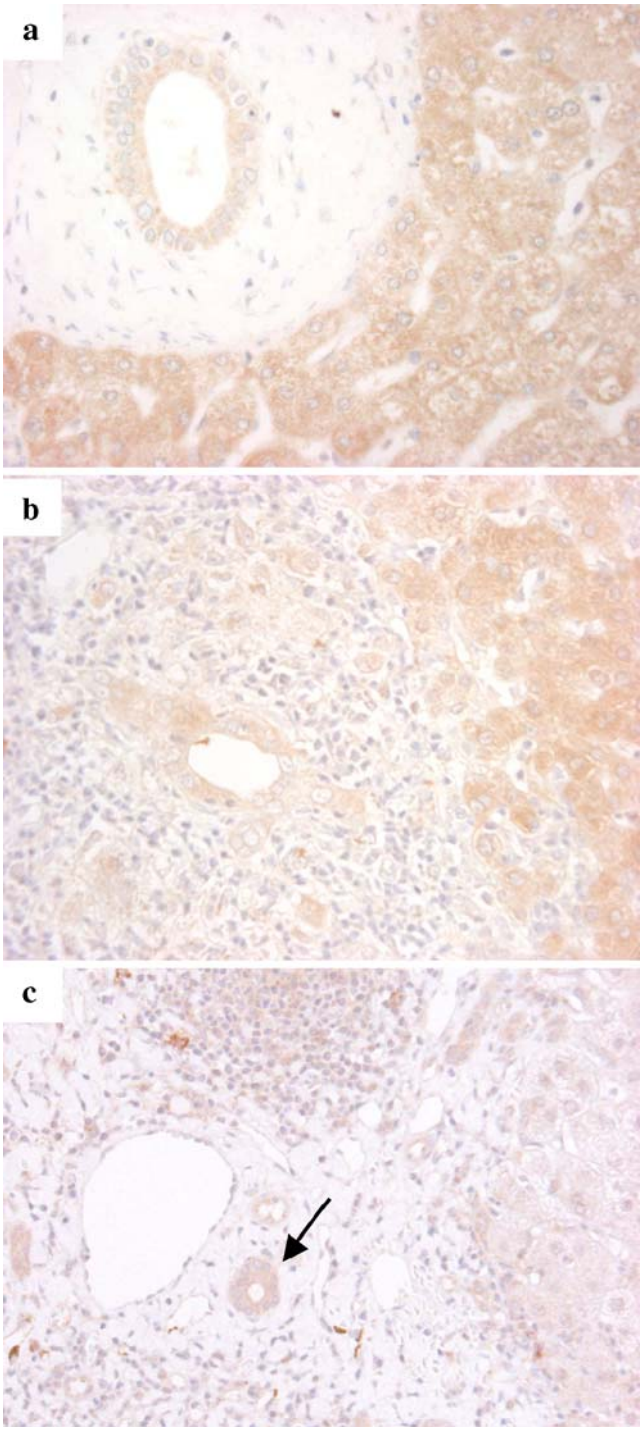

Fig. 1 Expression of HGFA and c-Met in PBC and control livers. **a** HGFA was expressed weakly in cytoplasm of BECs in small bile ducts and hepatocytes homogeneously in normal livers. **b** There was no difference in HGFA expression between PBC and control PBC, stage 2. **a**, **b** Immunostaining for HGFA and hematoxylin, 200×. **c** c-Met expression CVH liver. Immunostaining for c-Met and hematoxylin, 200×

Table 2 The expression of HAI-1 in small bile ducts and bile ductules in PBC and control livers

Diseases	Number of samples	Small bile ducts		Bile ductules		Hepatocytes
		n (%)	[1+, 2+]	*n* (%)	[1+, 2+]	*n* (%)
PBC, stages 1 and 2	16	16 (100)[a,b,c]	[1, 15]	16 (100)[a,b,c]	[1, 15]	4 (25)[a,c]
PBC, stages 3 and 4	8	7 (88)[a]	[1, 7]	8 (100)[a,b,c]	[0, 8]	8 (100)[a,b,c,d]
CVH	17	17 (100)[c]	[16, 1]	17 (100)[c]	[15, 2]	0
EBO livers	13	8 (62)	[4, 4]	8 (62)	[4, 4]	1 (8)
Normal livers	15	8 (54)	[8, 0]	10 (67)	[10, 0]	0

Values in brackets are the number of cases in which faint (1+) and intensive(2+) expression of HAI-1 was detected in more than three small bile ducts.

PBC Primary biliary cirrhosis, *CVH* chronic viral hepatitis, *EBO* extrahepatic biliary obstruction, and *BD* bile ducts

[a] $p<0.05$ vs CVH

[b] $p<0.05$ vs EBO

[c] $p<0.05$ vs normal livers

[d] $p<0.05$ vs PBC, stages 1 and 2

Increased HAI-1 mRNA expression in PBC livers

The representative gel image and the semiquantitative level of HGFA and HAI-1 mRNA expression are shown in subpanels a and b of Fig. 3, respectively.

HGFA HGFA mRNA was expressed constantly in PBC and control livers (Fig. 3a) and there was no difference between PBC and control livers in the level of HGFA mRNA expression (Fig. 3b).

HAI-1 The mRNA expression of HAI-1 was augmented in PBC livers, whereas its expression was low or none in control livers (Fig. 3a). The expression level of HAI-1 was significantly increased in PBC livers when compared with CVH and normal livers ($p<0.05$; Fig. 3b). The HAI-1 mRNA expression was rather high in PBC of stages 3 and 4.

Expression of HGFA and c-Met in cultured BECs

HGFA and c-Met mRNA were detected in cultured BECs by RT-PCR (Fig. 4a). HGFA and c-Met were constantly expressed in the cytoplasm of BECs when detected by immunofluorescent staining (Fig. 4b) and there were few differences by treatment.

HGF enhanced cell proliferation activity and wound healing in cultured BECs

Proliferation assay The administration of HGF (25, 50, 75, and 100 ng/ml) significantly enhanced the proliferation activity of BECs ($p<0.05$; Fig. 5a). The increase of the proliferation activity by HGF administration was dose-dependent (Fig. 5a).

In vitro wound-healing assay The administration of HGF (50 ng/ml) enhanced biliary epithelial wound closure through increased epithelial cell migration (Fig. 5b and Table 3). The percentage of reduction in wound width after 24, 48, and 72 h significantly increased with the administration of HGF (50 ng/ml) when compared to control ($p<0.01$; Table 3).

Administration of HGF, IFN-γ, TNF-α, TGF-β, and oxidative stress increased HAI-1 mRNA expression in BECs

The effect of the treatment with cytokines (HGF, IFN-γ, TNF-α, TGF-β, and IL-1β for 6 h) and oxidative stress caused by H_2O_2 treatment on the expression of HAI-1 was examined in BECs by semiquantitative RT-PCR. The administration of HGF, IFN-γ, TNF-α, and TGF-β significantly increased HAI-1 mRNA expression (HGF, 4.1-fold; IFN-γ, 5.2-fold; TNF-α, 2.9-fold; TGF-β, 6.0-fold) ($p<0.01$; Fig. 6). Oxidative stress caused by H_2O_2 treatment also significantly increased HAI-1 mRNA expression (6.5-fold) when compared to control ($p<0.01$; Fig. 6). IL-1β did not affect the level of HAI-1 mRNA expression (Fig. 6).

Increased expression of HAI-1 at the front of wound healing and enhanced expression by the treatment with HGF and H_2O_2

We examined whether HAI-1 expression was enhanced at the front of wound healing in cultured BECs. In contrast to the weak expression of HAI-1 in control BECs, the expression of HAI-1 was increased at the front of wound healing (Fig. 7). Further increase of HAI-1 expression at the front of wound healing was observed with the administration of HGF (50 ng/ml) (Fig. 7). The

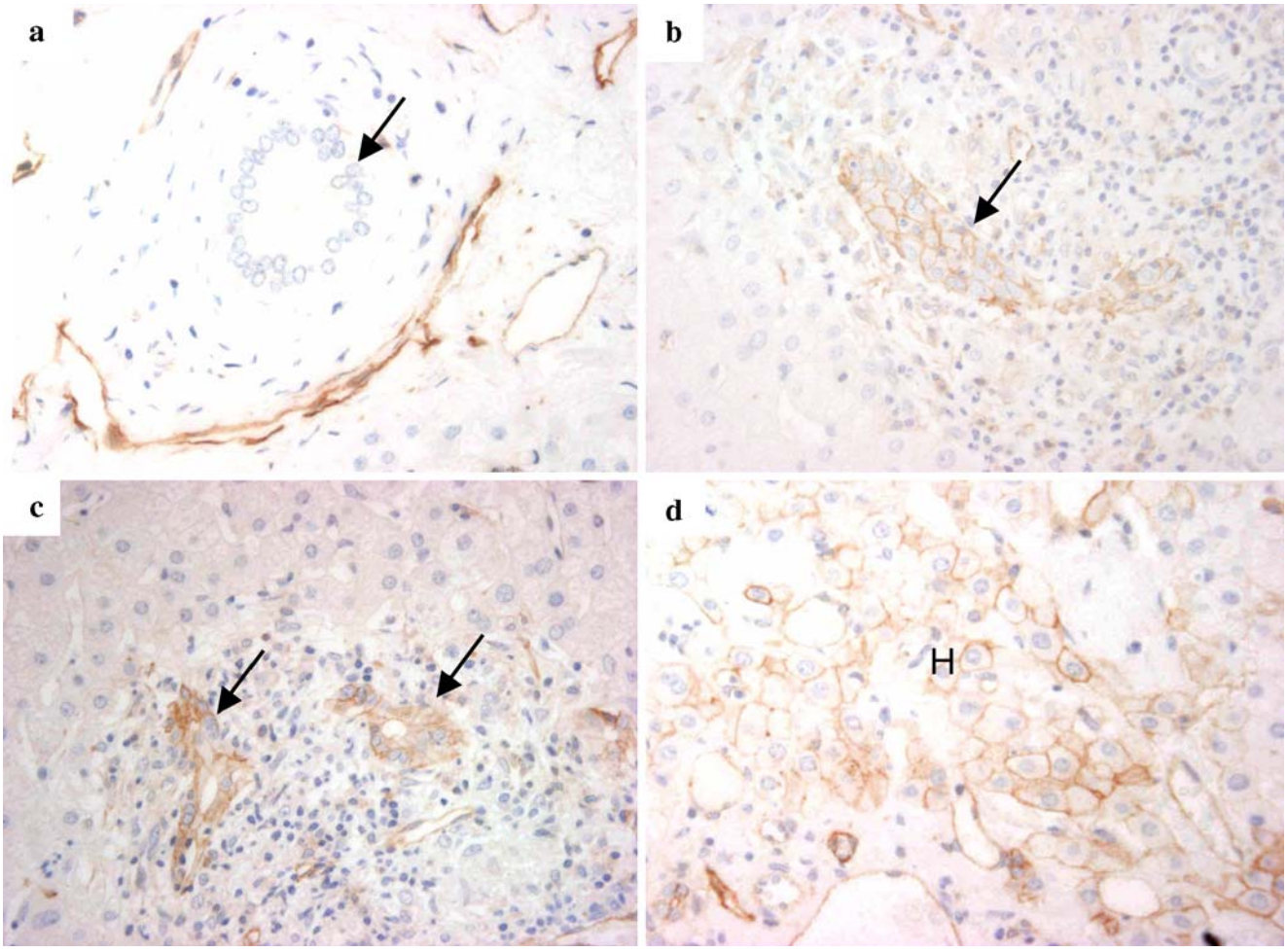

Fig. 2 **a** Expression of HAI-1 in PBC and control livers. HAI-1 was not expressed in BECs of small bile ducts (*arrow*) in normal liver. **b** Normal liver. Intensive and membranous expression of HAI-1 was evident in the damaged small bile ducts involved in chronic nonsuppurative cholangitis (*arrow*), 200×. **c** PBC, stage 2. The expression of HAI-1 in periportal bile ductules tended to be similar to that in small bile ducts, 200×. **d** PBC, stage 3. HAI-1 expression in hepatocytes was significantly frequent in PBC of stages 3 and 4, whereas it was rare in control diseased and normal livers. Immunostaining for HAI-1 and hematoxylin, 200×

treatment with H_2O_2 also increased the expression of HAI-1 (Fig. 7).

Discussion

Healing of a mucosal epithelial lining requires two processes: (1) restitution or spreading and migration of epithelial cells to cover the defect; and (2) regeneration or proliferation of epithelial cells to replace lost cells [29]. HGF and HGF-related factors such as HGFA and HAI-1 are thought to participate in the repair of injured gastrointestinal mucosa by promoting the proliferation and migration of epithelial cells [6]. The present study first revealed that the expression of HAI-1 was augmented in the damaged small bile ducts and bile ductules in PBC livers. The increased expression of HAI-1 mRNA was also detected in PBC livers by semiquantitative RT-PCR in the present study. It is interesting to note that the augmented expression of HAI-1 in damaged bile ducts was similar to that in the injured gastrointestinal mucosa. Weak and focal expression of HAI-1 in intrahepatic BECs in normal livers was consistent with the previous report [10]. HGFA and c-Met were constantly expressed in small bile ducts and bile ductules in PBC and control livers. HGF-enhanced cell proliferation and wound healing in cultured BECs in the present study were as reported previously [1, 7, 27, 32]. HGF has opposing effects on cell growth; HGF stimulates the proliferation of several tumor cell lines [5], whereas it inhibits the proliferation of a number of other tumor cell lines [26]. The present study confirmed the former effect of HGF on BECs.

It is conceivable that the augmented expression of HAI-1 may act as reservoirs of this enzyme on the cell surface and

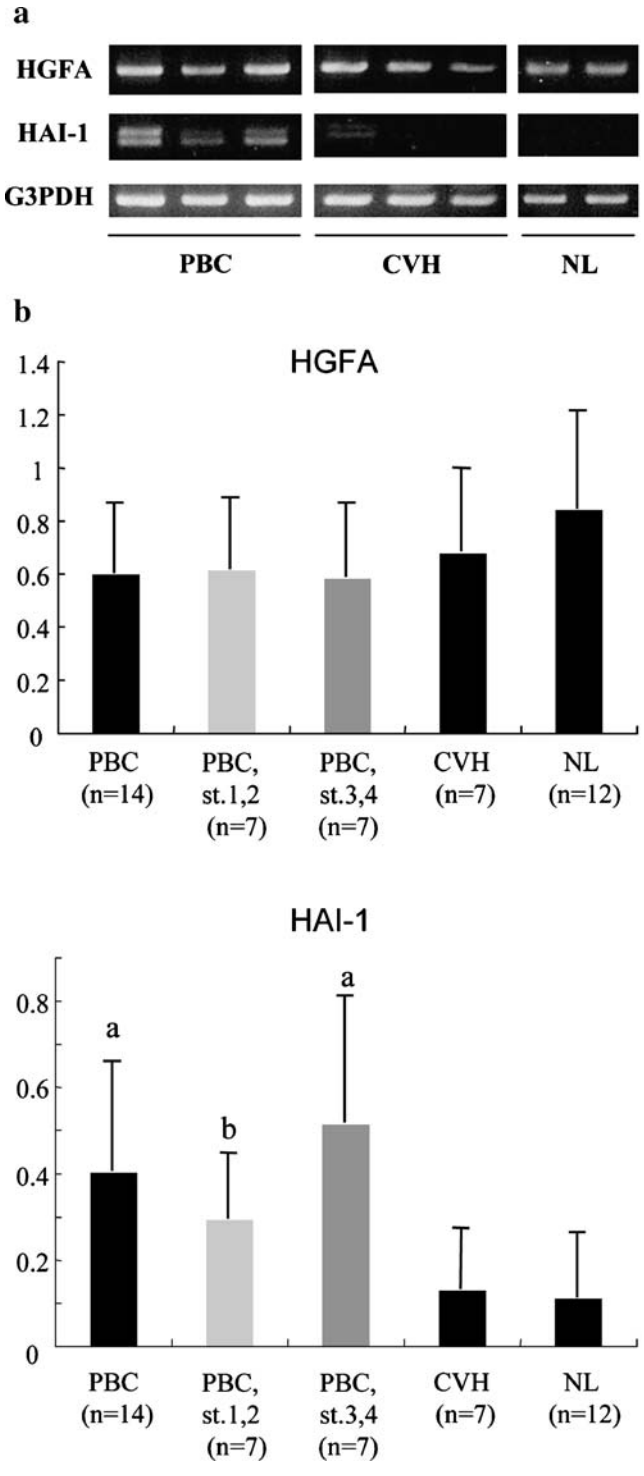

Fig. 3 Semiquantitative RT-PCR for HGFA and HAI-1 mRNA in PBC and control livers. **a** The representative gel image of HGFA and HAI-1 mRNA expression. HGFA mRNA was detected constantly in PBC and control livers. HAI-1 mRNA was detected in all PBC livers and faintly in CVH livers. In normal livers, HAI-1 mRNA was not detected. **b** The semiquantitative level of HGFA and HAI-1 mRNA expression in PBC and control livers. There was no difference between PBC and control livers in the level of HGFA mRNA expression. The level of HAI-1 mRNA was significantly increased in PBC livers when compared with CVH and normal livers. The HAI-1 mRNA expression was rather high in PBC of stages 3 and 4. **a** $p<0.05$ vs CVH and NL; **b** $p<0.05$ vs NL. Gel images were evaluated using NIH image and the expression was normalized as a ratio using human G3PDH as a housekeeping gene. Data were expressed as the mean±SD

contribute to ensure the efficient pericellular activation of HGF at the front of biliary mucosal damage and promote the mucosal repair as suggested in the injured gastrointestinal mucosa [6, 11]. However, the failure of biliary mucosal repair results in progressive bile duct loss in PBC. Therefore, the upregulation of HGF/HGFA/HAI-1 system appears to be insufficient to overcome the biliary mucosal damage in PBC. As a matter of fact, another possibility is that the overexpression of HAI-1 may not function for the increased effect of HGF in damaged biliary mucosa in PBC. We have reported previously that the damaged bile ducts frequently expressed features of cellular senescence in PBC [21]. It is of interest that the augmented expression of HAI-1 showed the colocalization with the expression of senescence markers in the damaged small bile ducts involved in CNSDC. The capacity of bile duct

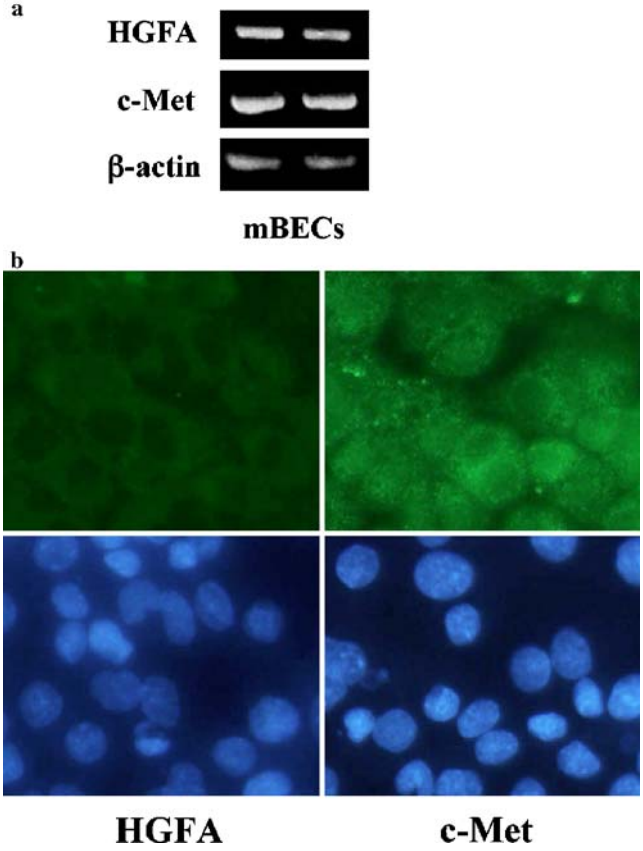

Fig. 4 Expression of HGFA and c-Met in cultured mouse BECs. **a** HGFA and c-Met mRNA were detected in cultured mouse BECs by RT-PCR. **b** HGFA was expressed in the cytoplasm of mouse BECs. Immunofluorescent staining for HGFA and DAPI. **c** c-Met was expressed in the membrane and cytoplasm of mouse BECs. Immunofluorescent staining for c-Met and DAPI

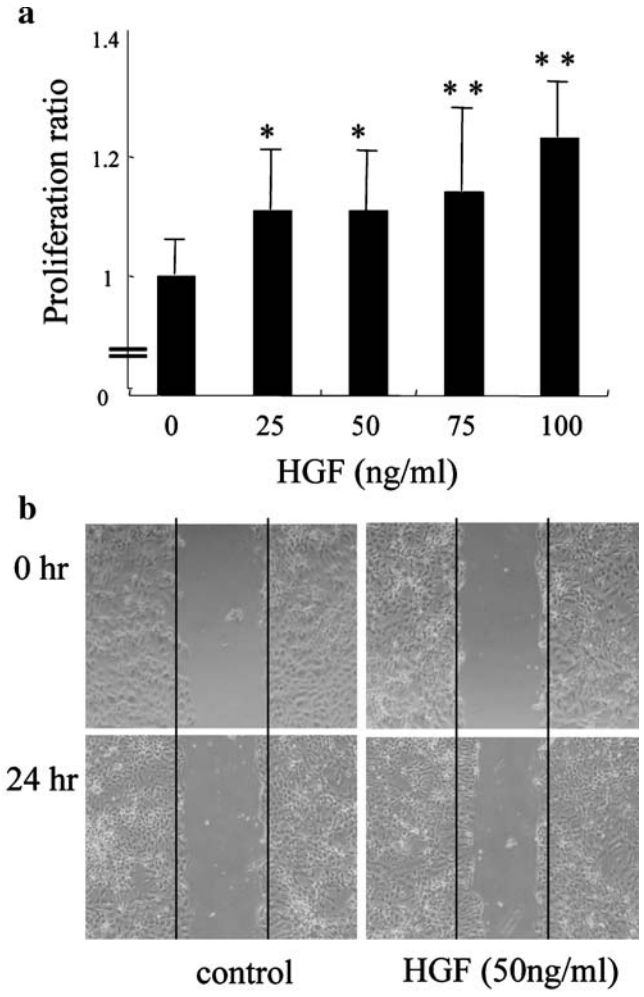

Fig. 5 Effect of HGF on proliferation and wound healing in cultured mouse BECs. **a** Effect of HGF on proliferation of cultured mouse BECs was examined using the proliferative reagent WST-1 and measuring the absorbance at 450 nm. Addition of HGF enhanced the proliferative activities of BECs cultured for 48 h dose-dependently. *p<0.05 and **p<0.01 vs control. The data is shown as ratio of control and presented as the mean±SD. **b** Wound healing in mouse BECs with and without HGF (50 ng/ml). Confluent monolayers of epithelial cells were wounded as described in the "Materials and methods" section. Wound widths and images (20×) were taken before and after 24-h stimulation with and without HGF (50 ng/ml)

proliferation appears to be low in BECs expressing HAI-1 when the cell proliferation was evaluated by the expression of Ki-67 antigen [21]. In fibroblast, the increased expression of plasminogen activator inhibitor-1 is reportedly a senescence marker [31]. Therefore, the increased HAI-1 expression of a marker for cellular senescence in biliary and other epithelial cells may be possible. Further studies are needed to clarify the significance and exact function of HAI-1 in damaged biliary mucosa.

There have been few studies regarding the regulation of HAI-1 expression so far. The present study revealed that HGF and several inflammatory cytokines such as IFN-γ, TGF-β, and TNF-α enhanced the expression of HAI-1 in

Table 3 Percentage of reduction in wound width 24 h after stimulation

Treatment	Time after treatment (h)	Percentage reduction in wound width
Control	24	16.7±6.6
	48	30.5±9.7
	72	59.4±8.4
HGF (50 ng/ml)	24	32.0±5.5[a]
	48	50.3±10.5[a]
	72	73.2±12.1[a]

[a] p<0.01 vs control

BECs. HAI-1 was also upregulated at the front of wound healing in cultured BECs and the administration of HGF

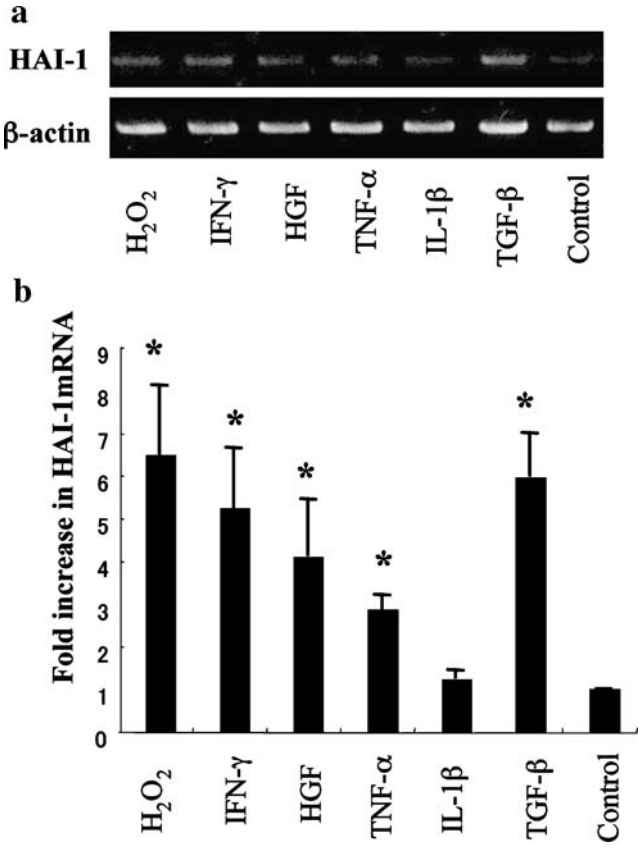

Fig. 6 Effect of cytokines (HGF, IFN-γ, TNF-α, TGF-β, and IL-1β) and oxidative stress caused by H_2O_2 treatment on the expression of HAI-1 in mouse BECs. **a** The representative gel image of HAI-1 mRNA expression by semiquantitative RT-PCR. **b** We examined the effect of cytokines (HGF, 50 ng/ml; IFN-γ, 1,000 U/ml; TNF-α, 10 μg/ml; IL-1β, 10 μg/ml; and TGF-β, 8 μg/ml for 6 h) and oxidative stress (112.5 μM, 2 h) caused by H_2O_2 treatment on the expression of HAI-1 in mouse BECs by semiquantitative RT-PCR. The administration of HGF, IFN-γ, TNF-α, and TGF-β and H_2O_2 treatment significantly increased HAI-1 mRNA expression (HGF, 4.1-fold; IFN-γ, 5.2-fold; TNF-α, 2.9-fold; TGF-β, 6.0-fold; H_2O_2, 6.5-fold). *p<0.01 vs control. IL-1β did not affect the level of HAI-1 mRNA expression. Gel images were evaluated using NIH image and the expression was normalized as a ratio using mouse β-actin as a housekeeping gene. Data were expressed as the mean±SD (n=3)

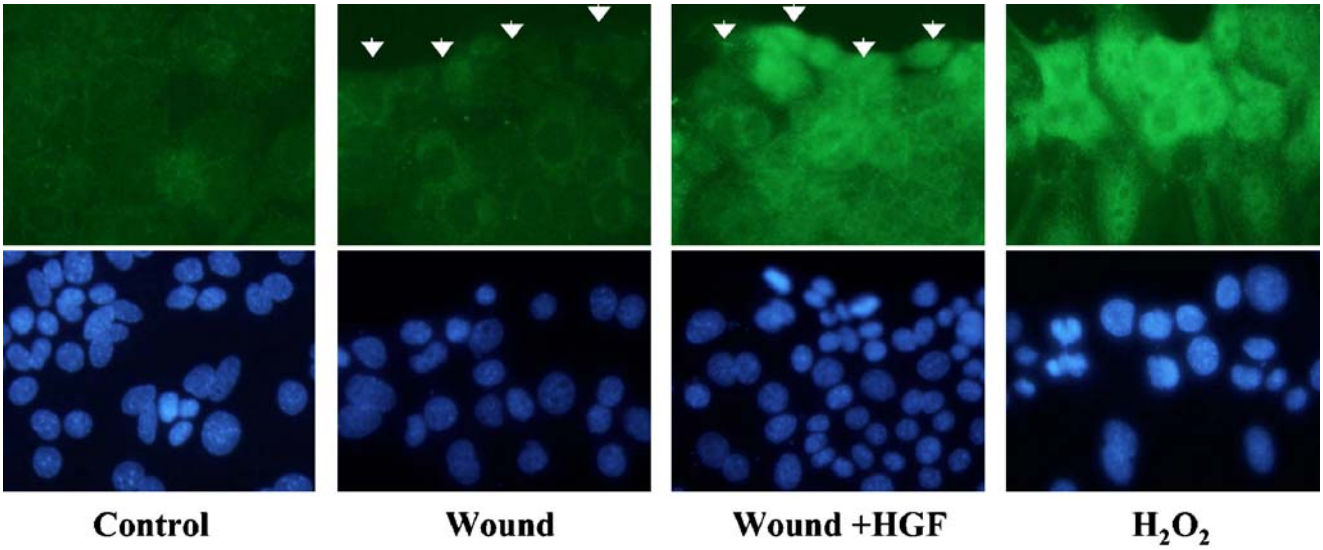

Fig. 7 Increased expression of HAI-1 at the front of wound healing and the enhanced expression by the treatment with HGF and H_2O_2 in mouse BECs. HAI-1 was weakly expressed in control mouse BECs (*left column*). The expression of HAI-1 was increased at the front of wound healing (*second column from left*) when a confluent monolayer of epithelial cells was wounded as described in the "Materials and methods" section. Further increase of HAI-1 expression at the front of wound healing was observed with the administration of HGF (50 ng/ml; *third column*). The treatment with H_2O_2 also increased the expression of HAI-1 (*right column*). *Arrows* indicated the front of wound healing in *second* and *third column*. Immunofluorescent staining for HAI-1 and DAPI

accentuated the expression of HAI-1. Furthermore, oxidative stress by H_2O_2 treatment enhanced HAI-1 expression in the present study. It is well known that a number of cytokines such as HGF, TNF-α, TGF-β, and IFN-γ and oxidative stress were increased in inflammatory lesions around the damaged bile ducts in PBC [16, 25, 30]. Taken together, it is plausible that HGF, inflammatory cytokines, and oxidative stress may enhance the expression of HAI-1 in the damaged bile ducts in PBC.

It is noteworthy that the increased expression of HAI-1 was also detected in the periportal hepatocytes specifically in the advanced stage of PBC. The high level of HAI-1 mRNA in the advanced PBC may reflect the increased hepatocellular expression of HAI-1. Hepatocellular expression of HAI-1 was reported only in fulminant hepatitis so far [10]. Although HGF and other inflammatory cytokines may enhance the expression of HAI-1 in hepatocytes and in BECs, the expression was limited in the advanced stage of PBC. Therefore, chronic cholestasis due to progressive bile duct loss and subsequent oxidative stress may be a main cause for the induction of HAI-1 in hepatocytes. The fact supporting this hypothesis is that an EBO liver expressing HAI-1 in hepatocytes was also cholestatic due to cholangiocarcinoma at hepatic hilum. Furthermore, HAI-1 expression was observed in hepatocytes in other chronic cholestatic liver such as hepatolithiasis in our preliminary study.

In conclusion, HAI-1 expression was augmented in the front of biliary epithelial wound in PBC and cultured BECs. HGF enhanced proliferation and would healing and HAI-1 expression of BECs. These findings suggest that the HGF/HGFA/HAI-1 system may participate in biliary mucosal repair as reported in gastrointestinal mucosa.

References

1. Auth MK, Joplin RE, Okamoto M, Ishida Y, McMaster P, Neuberger JM, Blaheta RA, Voit T, Strain AJ (2001) Morphogenesis of primary human biliary epithelial cells: induction in high-density culture or by coculture with autologous human hepatocytes. Hepatology 33:519–529
2. Desmet V, Gerber M, Hoofnagle J, Manns M, Scheuer P (1994) Classification of chronic hepatitis: diagnosis, grading and staging. Hepatology 19(6):1513–1520
3. Fussey S, Guest J, James O, Bassendine M, Yeaman S (1988) Identification and analysis of the major M2 autoantigens in primary biliary cirrhosis. Proc Natl Acad Sci USA 85:8654–8658
4. Gershwin ME, Mackay IR, Sturgess A, Coppel RL (1987) Identification and specificity of a cDNA encoding the 70 kd mitochondrial antigen recognized in primary biliary cirrhosis. J Immunol 138:3525–3531
5. Halaban R, Rubin JS, Funasaka Y, Cobb M, Boulton T, Faletto D, Rosen E, Chan A, Yoko K, White W et al (1992) Met and hepatocyte growth factor/scatter factor signal transduction in normal melanocytes and melanoma cells. Oncogene 7:2195–2206
6. Itoh H, Kataoka H (2002) Roles of hepatocyte growth factor activator (HGFA) and its inhibitor HAI-1 in the regeneration of injured gastrointestinal mucosa. J Gastroenterol 37(Suppl 14): 15–21
7. Joplin R, Hishida T, Tsubouchi H, Daikuhara Y, Ayres R, Neuberger JM, Strain AJ (1992) Human intrahepatic biliary

epithelial cells proliferate in vitro in response to human hepatocyte growth factor. J Clin Invest 90:1284–1289
8. Kamihira T, Shimoda S, Harada K, Kawano A, Handa M, Baba E, Tsuneyama K, Nakamura M, Ishibashi H, Nakanuma Y, Gershwin ME, Harada M (2003) Distinct costimulation dependent and independent autoreactive T-cell clones in primary biliary cirrhosis. Gastroenterology 125:1379–1387
9. Kaplan M (1996) Primary biliary cirrhosis. New Engl J Med 335:1570–1580
10. Kataoka H, Suganuma T, Shimomura T, Itoh H, Kitamura N, Nabeshima K, Koono M (1999) Distribution of hepatocyte growth factor activator inhibitor type 1 (HAI-1) in human tissues. Cellular surface localization of HAI-1 in simple columnar epithelium and its modulated expression in injured and regenerative tissues. J Histochem Cytochem 47:673–682
11. Kataoka H, Itoh H, Hamasuna R, Meng JY, Koono M (2001) Pericellular activation of hepatocyte growth factor/scatter factor (HGF/SF) in colorectal carcinomas: roles of HGF activator (HGFA) and HGFA inhibitor type 1 (HAI-1). Hum Cell 14:83–93
12. Katayanagi K, Kono N, Nakanuma Y (1998) Isolation, culture and characterization of biliary epithelial cells from different anatomical levels of the intrahepatic and extrahepatic biliary tree from a mouse. Liver 18:90–98
13. Kita H, Matsumura S, He XS, Ansari AA, Lian ZX, Van de Water J, Coppel RL, Kaplan MM, Gershwin ME (2002) Quantitative and functional analysis of PDC-E2-specific autoreactive cytotoxic T lymphocytes in primary biliary cirrhosis. J Clin Invest 109:1231–1240
14. Nakanuma Y, Ohta G (1979) Histometric and serial section observations of the intrahepatic bile ducts in primary biliary cirrhosis. Gastroenterology 76:1326–1332
15. Nakanuma Y, Sasaki M (1989) Expression of blood-group-related antigens in the intrahepatic biliary tree and hepatocytes in normal livers and various hepatobiliary diseases. Hepatology 10:174–178
16. Neuman M, Angulo P, Malkiewicz I, Jorgensen R, Shear N, Dickson ER, Haber J, Katz G, Lindor K (2002). Tumor necrosis factor-alpha and transforming growth factor-beta reflect severity of liver damage in primary biliary cirrhosis. J Gastroenterol Hepatol 17:196–202
17. Nozaki I, Lunz JG 3rd, Specht S, Park JI, Giraud AS, Murase N, Demetris AJ (2004) Regulation and function of trefoil factor family 3 expression in the biliary tree. Am J Pathol 165:1907–1920
18. Portmann B, Nakanuma Y (2001) Diseases of the bile ducts. In: MacSween R, Burt A, Portmann BC, Ishak K, Scheuer P, Anthony P (eds) Pathology of the liver. Churchill Livingstone, London, pp 435–506
19. Sasaki M, Tsuneyama K, Nakanuma Y (2003) Aberrant expression of trefoil factor family 1 in biliary epithelium in hepatolithiasis and cholangiocarcinoma. Lab Invest 83:1403–1413
20. Sasaki M, Tsuneyama K, Saito T, Kataoka H, Mollenhauer J, Poustka A, Nakanuma Y (2004) Site-characteristic expression and induction of trefoil factor family 1, 2 and 3 and malignant brain tumor-1 in normal and diseased intrahepatic bile ducts relates to biliary pathophysiology. Liver Int 24:29–37
21. Sasaki M, Ikeda H, Haga H, Manabe T, Nakanuma Y (2005) Frequent cellular senescence in small bile ducts in primary biliary cirrhosis: a possible role in bile duct loss. J Pathol 205:451–459
22. Scheuer P (1994) Liver biopsy interpretation, 5th edn. Saunders, London
23. Sherlock S, Dooley J (1993) Primary biliary cirrhosis. In: Diseases of the liver and biliary system. Blackwell, London, pp 236
24. Shimoda S, Van de Water J, Ansari A, Nakamura M, Ishibashi H, Coppel RL, Lake J, Keeffe EB, Roche TE, Gershwin ME (1998) Identification and precursor frequency analysis of a common T cell epitope motif in mitochondrial autoantigens in primary biliary cirrhosis. J Clin Invest 102:1831–1840
25. Shiota G, Okano J, Kawasaki H, Kawamoto T, Nakamura T (1995) Serum hepatocyte growth factor levels in liver diseases: clinical implications. Hepatology 21:106–112
26. Shiota G, Rhoads DB, Wang TC, Nakamura T, Schmidt EV (1992) Hepatocyte growth factor inhibits growth of hepatocellular carcinoma cells. Proc Natl Acad Sci USA 89:373–377
27. Strain AJ, Wallace L, Joplin R, Daikuhara Y, Ishii T, Kelly DA, Neuberger JM (1995) Characterization of biliary epithelial cells isolated from needle biopsies of human liver in the presence of hepatocyte growth factor. Am J Pathol 146:537–545
28. Tanaka H, Nagaike K, Takeda N, Itoh H, Kohama K, Fukushima T, Miyata S, Uchiyama S, Uchinokura S, Shimomura T, Miyazawa K, Kitamura N, Yamada G, Kataoka H (2005) Hepatocyte growth factor activator inhibitor type 1 (HAI-1) is required for branching morphogenesis in the chorioallantoic placenta. Mol Cell Biol 25:5687–5698
29. Taupin D, Podolsky DK (2003) Trefoil factors: initiators of mucosal healing. Nat Rev Mol Cell Biol 4:721–732
30. Tsuneyama K, Harada K, Kono N, Sasaki M, Saito T, Gershwin ME, Ikemoto M, Arai H, Nakanuma Y (2002) Damaged interlobular bile ducts in primary biliary cirrhosis show reduced expression of glutathione-S-transferase-pi and aberrant expression of 4-hydroxynonenal. J Hepatol 37:176–183
31. West MD, Shay JW, Wright WE, Linskens MH (1996) Altered expression of plasminogen activator and plasminogen activator inhibitor during cellular senescence. Exp Gerontol 31:175–193
32. Yokomuro S, Tsuji H, Lunz JG 3rd, Sakamoto T, Ezure T, Murase N, Demetris AJ (2000) Growth control of human biliary epithelial cells by interleukin 6, hepatocyte growth factor, transforming growth factor beta1, and activin A: comparison of a cholangiocarcinoma cell line with primary cultures of non-neoplastic biliary epithelial cells. Hepatology 32:26–35
33. Zen Y, Harada K, Sasaki M, Tsuneyama K, Katayanagi K, Yamamoto Y, Nakanuma Y (2002) Lipopolysaccharide induces overexpression of MUC2 and MUC5AC in cultured biliary epithelial cells: possible key phenomenon of hepatolithiasis. Am J Pathol 161:1475–1484

Virchows Arch (2006) 449:472–475
DOI 10.1007/s00428-006-0268-4

CASE REPORT

Primary mantle cell lymphoma of the conjunctiva: a case report

Miltiadis Aspiotis · Spiridon Gorezis · Ioannis Asproudis · Elena Tsanou · Evangelos Papadiotis · Sevasti Kamina · Niki J. Agnantis · Maria Bai

Received: 20 February 2006 / Accepted: 4 July 2006 / Published online: 13 September 2006
© Springer-Verlag 2006

Abstract Primary non-Hodgkin's lymphomas of the conjunctiva are uncommon. They are almost exclusively extranodal marginal zone B-cell lymphomas/mucosa-associated lymphoid tissue lymphomas. In this study, we report an extremely rare case of conjunctival mantle cell lymphoma in a 78-year-old man, presenting as a unilateral epibulbar mass.

Keywords Conjunctiva · Lymphoma · Mantle cell · Cyclin D1

Abbreviations

MALT	mucosa-associated lymphoid tissue
MCL	mantle cell lymphomas
CLL/SCL	chronic lymphocytic leukemia/small cell lymphoma
ENMZL	extranodal marginal zone lymphoma
FCL	follicle center lymphoma
DLBCL	diffuse large B-cell lymphoma

Introduction

Primary ocular adnexal lymphomas represent approximately 10% of orbital neoplasms and 8% of extranodal lymphomas [1, 11]. They are localized in the orbit, the conjunctiva, and the eyelids [15]. Primary conjunctival lymphomas comprise 28% of ocular adnexal lymphomas [15] and 1.5% of conjunctival tumors [12]. Most cases are classified as extranodal marginal zone B-cell lymphomas (ENMZLs) of mucosa-associated lymphoid tissue according to the WHO classification, whereas other types of small B-cell lymphomas or T-cell lymphomas are extremely rare [4, 9, 29].

Mantle cell lymphomas (MCLs) of the ocular adnexa are very rare. They may be primary or secondary and affect patients in the sixth or seventh decade of life [10, 13]. Orbit is the most commonly involved site followed by the lacrimal glands and eyelids [19]. A review of the literature revealed that only three conjunctival MCLs have been reported [3, 4, 25]. In this study, we describe one additional case of primary MCL of the conjunctiva.

Case report

A 78-year-old man patient was admitted to the Ioannina University Clinic of Ophthalmology to undergo a scheduled cataract surgery in his left eye. Routine clinical examination revealed a visual acuity of 5/10 cc—2.00 cyl 90° in his right eye and 7/10 cc—2.00 cyl 90° in his left eye. Slit lamp examination revealed a ruptured posterior lens capsule in his right eye and cataract in his left eye. Furthermore, in the nasal area of the orbital conjunctiva of his right eye, there was an evident enlargement of 1 cm in size, which affected the eyelid movement (Fig. 1). The patient recalled having acknowledged the tumor around 7 months ago but neglected visiting a doctor due to the fact of living in a remote area. The patient underwent an intracapsular cataract surgery in his left eye, and during the

M. Aspiotis · S. Gorezis · I. Asproudis · E. Papadiotis
Department of Ophthalmology, Medical School,
University of Ioannina,
Ioannina, Greece

E. Tsanou · S. Kamina · N. J. Agnantis (✉) · M. Bai
Department of Pathology, Medical School,
University of Ioannina,
Ioannina, Greece
e-mail: gorezis@hotmail.com

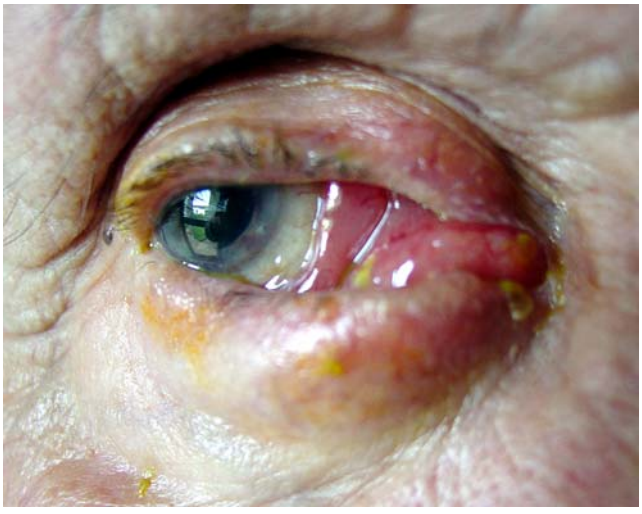

Fig. 1 Mass, 1 cm in size, in the nasal area of the orbital conjunctiva of the right eye

operation, we performed biopsy of the conjunctival tumor in his right eye.

Histological examination of biopsy material (major diameter 1 cm) showed infiltration by monomorphic cell population composed of small- to medium-sized lymphocytes with irregular, indented, or cleaved nuclei, condensed chromatin, and scant cytoplasm (Fig. 2). Basophilic cells with large nucleoli (blast cells) and plasma cells were absent. The growth pattern was diffuse and partially nodular. In the neoplastic tissue, a relatively large number of hyalinized vessels were observed. Surface epithelium was not included in the biopsy material.

Immunohistochemical study revealed that tumor cells were CD45, CD20, CD5, cyclin D1, and BCL-2 positive and CD23, CD10, bcl-6, MUM/IRF4, CD138/Syn-1, and CD3 negative (Fig. 3). Moreover, immunostaining for CD23 and CD35 showed a loose network of follicular dendritic cells in the area with nodular growth pattern. Approximately 40% of the neoplastic cells expressed the cell cycle protein Ki67/MIB-1. The final diagnosis was B-cell non-Hodgkin's lymphoma of MCL type.

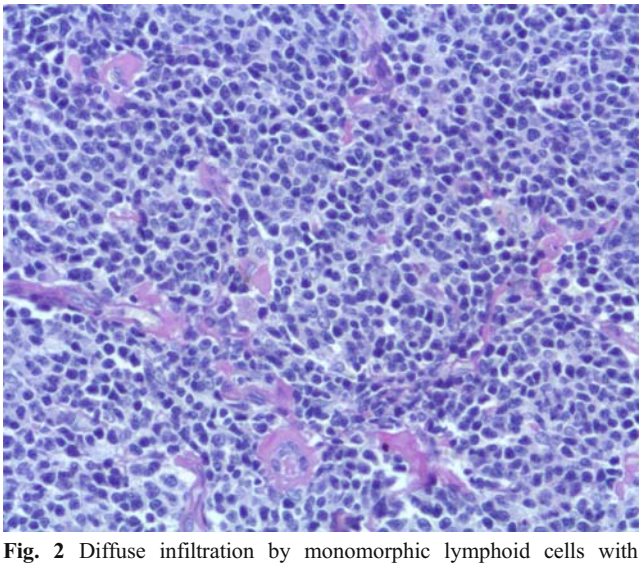

Fig. 2 Diffuse infiltration by monomorphic lymphoid cells with angular or cleaved nuclei and scant cytoplasm (H&E, ×200)

After the pathologist's report, extensive clinical staging was performed. Both physical examination and laboratory assessment revealed no evidence of systemic involvement. The patient denied receiving treatment due to his age and 4 months after diagnosis had not displayed relapse or dissemination of the disease.

Discussions

Primary conjunctival lymphomas are uncommon, and a limited number of cases are reported in the literature (Table 1) [2, 5, 6, 8, 10, 16–18, 20–24, 26, 29]. They are almost all B-cell lymphomas of ENMZL. We present in this study an extremely rare case of primary MCL of the conjunctiva. To our knowledge, three other cases have been reported in the literature [3, 4, 28].

The diagnosis of MCL was based on morphologic and immunophenotypical criteria. Histologically, the reported case showed the main characteristics of MCL monotony of lymphoid infiltrate and absence of blast cells. Moreover, the immunophenotype was consistent with MCL. The neoplastic population expressed CD5 and cyclin D1 antigens and was negative for CD23 and CD10.

The distinction between conjunctival MCLs and other small B-cell lymphomas especially the much more common ENMZL is clinically important. ENMZLs sometimes show a monotonous cell population; however, some blasts are always present, and immunostaining for CD5 is almost always negative. Cyclin D1 is particularly helpful in the differential diagnosis of MCLs, especially in CD5-negative cases, a form that appears to be frequent in the orbit [19]. This protein is expressed in 80–90% of MCLs and is absent in all other B-cell lymphomas with rare exceptions [7]. In one-third of MCL cases, a nodular or partial nodular growth pattern is observed and may be confused with follicular lymphomas (FLs), mainly grade I tumors. In our case, a small area of nodularity was recognized corresponding to preexisting follicles, as it has been confirmed after immunostaining for residual, follicular dendritic cells. The FLs are CD10 and bcl-6 positive, whereas the MCLs are CD5 positive. The differential diagnosis of MCL also includes SCL. This type of lymphoma contains blast cells, and tumor cells coexpress CD5 and CD23 antigens.

It has to be underlined that it is not possible to distinguish histopathologically a primary from a secondary ocular adnexal lymphoma. Thus, it is necessary to include the clinical data to establish the final diagnosis. The stage at

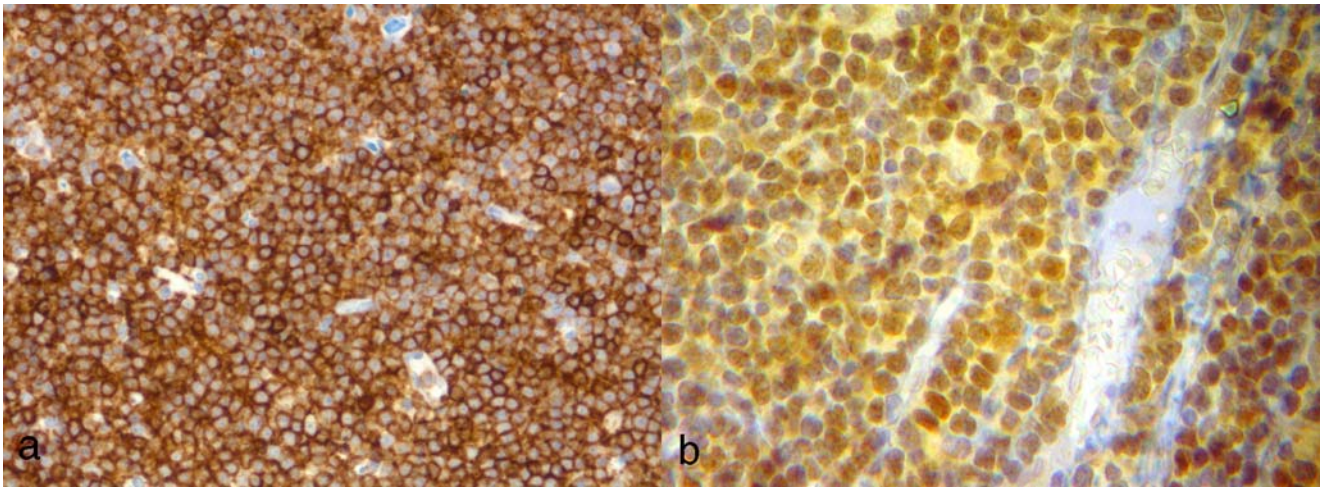

Fig. 3 Immunohistochemical expression of **a** CD5 and **b** cyclin D1 proteins in tumor cells (×200, ×400)

presentation and the histological type have been found to correlate significantly with the final course of primary ocular adnexal lymphoma [3]. Jenkins et al. [14] found that conjunctival lymphomas present the lowest risk of dissemination compared to all other orbital lymphomas. Concerning ocular MCLs, 80% of cases are stage III/IV, and the prognosis is poor with a median overall survival of 57 months [19]. Different chemotherapeutic regimens achieve overall response rates of approximately 70%, with complete remissions in up to 20–40% of cases [25, 27].

Table 1 Results of literature survey on primary conjunctival lymphomas

Author (year)	Number of cases	Histological type
Sharara et al. 2003 [26]	3	ENMZL
	1	LDL
Sasai et al. 2001 [24]	10	ENMZL
	1	Low-grade B-cell lymphoma
	1	DLBCL
	1	Peripheral T-cell lymphoma
Cahill et al. 1999 [4]	3	ENMZL
	1	MCL
Auw-Haedrich et al. 2001 [3]	15	ENMZL
	2	LDL
	1	MCL
White et al. 1995 [28]	2	ENMZL
	1	SCL
	1	MCL
Petrella et al. 1991 [22]	36	ENMZL
Wotherspoon et al. 1993 [29]		
Kurz-Levin et al. 1997 [16]		
Calvo et al. 1997 [5]		
Lee et al. 2001 [17]		
Matteucci et al. 2003 [20]		
Cho et al. 2003 [8]		
Charlotte et al. 2006 [6]		
Akpek et al. 1999 [2]	1	ENMZL
	1	FL
Ellis et al. 1985 [10]	25	Former lymphoma classifications
Knowles et al. 1990 [15]	25	Former lymphoma classifications
Meunier et al. 2004 [21]	49	Low-grade lymphoma
	2	High-grade lymphoma

ENMZL Extranodal marginal zone B-cell lymphoma, *DLBCL* diffuse large B-cell lymphoma, *MCL* mantle cell lymphoma, *SCL* small lymphocytic lymphoma, *FL* follicular lymphoma, *LDL* lymphoplasmacytic lymphoma

References

1. Aisenberg AC (1991) Extranodal lymphoma: presentation, natural history and special treatment considerations. In: Aisenberg AC (ed) Malignant lymphoma. Lea and Fabiger, Philadelphia, pp 235–310
2. Akpek EK, Polcharoen W, Ferry JA, Foster CS (1999) Conjunctival lymphoma masquerading as chronic conjunctivitis. Ophthalmology 106:757–760
3. Auw-Haedrich C, Coupland SE, Kapp A, Schmitt-Graff A, Buchen R, Witschel H (2001) Long term outcome of ocular adnexal lymphoma subtyped according to the REAL classification. Revised European and American Lymphoma. Br J Ophthalmol 85:63–69
4. Cahill M, Barnes C, Moriarty P, Daly P, Kennedy S (1999) Ocular adnexal lymphoma-comparison of MALT lymphoma with other histological types. Br J Ophthalmol 83:742–747
5. Calvo R, Ribera JM, Vaquero M, Garcia O, Moreno I, Feliu E (1997) Low-grade, malt-type, primary B-cell lymphoma of the conjunctiva. Leuk Lymphoma 28:203–207
6. Charlotte F, Doghmi K, Cassoux N, Ye H, Du MQ, Kujas M, Lesot A, Mansour G, Lehoang P, Vignot N, Capron F, Leblond V (2006) Ocular adnexal marginal zone B cell lymphoma: a clinical and pathologic study of 23 cases. Virchows Arch 448:506–516
7. Cheuk W, Wong KO, Wong CS, Chan JK (2004) Consistent immunostaining for cyclin D1 can be achieved on a routine basis using a newly available rabbit monoclonal antibody. Am J Surg Pathol 28:801–807
8. Cho EY, Han JJ, Ree HJ, Ko YH, Kang YK, Ahn HS, Ahn SD, Park CJ, Huh J (2003) Clinicopathologic analysis of ocular adnexal lymphomas: extranodal marginal zone b-cell lymphoma constitutes the vast majority of ocular lymphomas among Koreans and affects younger patients. Am J Hematol 73:87–96
9. Coupland SE, Krause L, Delecluse HJ, Anagnostopoulos I, Foss HD, Hummel M, Bornfeld N, Lee WR, Stein H (1998) Lymphoproliferative lesions of the ocular adnexa. Analysis of 112 cases. Ophthalmology 105:1430–1441
10. Ellis JH, Banks PM, Campbell RJ, Liesegang TJ (1985) Lymphoid tumors of the ocular adnexa. Clinical correlation with the working formulation classification and immunoperoxidase staining of paraffin sections. Ophthalmology 92:1311–1324
11. Freeman C, Berg JW, Cutler SJ (1972) Occurrence and prognosis of extranodal lymphomas. Cancer 29:252–260
12. Grossniklaus HE, Green WR, Luckenbach M, Chan CC (1987) Conjunctival lesions in adults. A clinical and histopathologic review. Cornea 6:78–116 (Review)
13. Isaacson PG, Norton AJ (1994) Lymphomas of the ocular adnexa and eye. In: Nuttall J, Daniels L, Singleton P (eds) Extranodal lymphomas. Churchill Livingstone, Edinburgh, pp 117–129
14. Jenkins C, Rose GE, Bunce C, Wright JE, Cree IA, Plowman N, Lightman S, Moseley I, Norton A (2000) Histological features of ocular adnexal lymphoma (REAL classification) and their association with patient morbidity and survival. Br J Ophthalmol 84:907–913
15. Knowles DM, Jakobiec FA, McNally L, Burke JS (1990) Lymphoid hyperplasia and malignant lymphoma occurring in the ocular adnexa (orbit, conjunctiva, and eyelids): a prospective multiparametric analysis of 108 cases during 1977 to 1987. Hum Pathol 21:959–973
16. Kurz-Levin MM, Flury R, Bernauer W (1997) Diagnosis of MALT lymphoma by conjunctival biopsy: a case report. Graefes Arch Clin Exp Ophthalmol 235:606–609
17. Lee DH, Sohn HW, Park SH, Kang YK (2001) Bilateral conjunctival mucosa-associated lymphoid tissue lymphoma misdiagnosed as allergic conjunctivitis. Cornea 20:427–429
18. Leff SR, Shields JA, Augsburger JJ, Miller RV, Liberatore B (1985) Unilateral eyelid, conjunctival, and choroidal tumours as initial presentation of diffuse large-cell lymphoma. Br J Ophthalmol 69:861–864
19. Looi A, Gascoyne RD, Chhanabhai M, Connors JM, Rootman J, White VA (2005) Mantle cell lymphoma in the ocular adnexal region. Ophthalmology 112:114–119
20. Matteucci C, Galieni P, Leoncini L, Lazzi S, Lauria F, Polito E, Martelli MF, Mecucci C (2003) Typical genomic imbalances in primary MALT lymphoma of the orbit. J Pathol 200:656–660
21. Meunier J, Lumbroso-Le Rouic L, Vincent-Salomon A, Dendale R, Asselain B, Arnaud P, Fourquet A, Desjardins L, Plancher C, Validire P, Chaoui D, Levy C, Decaudin D (2004) Ophthalmologic and intraocular non-Hodgkin's lymphoma: a large single centre study of initial characteristics, natural history, and prognostic factors. Hematol Oncol 22:143–158 (Review)
22. Petrella T, Bron A, Foulet A, Arnould L, Chirpaz L, Michiels R (1991) Report of a primary lymphoma of the conjunctiva. A lymphoma of MALT origin? Pathol Res Pract 187:78–84
23. Reiser M, Josting A, Diehl V, Engert A (2001) Primary lymphoma of the conjunctiva—a rare manifestation of indolent non-Hodgkin's lymphoma. Ann Hematol 80:311–313
24. Sasai K, Yamabe H, Dodo Y, Kashii S, Nagata Y, Hiraoka M (2001) Non-Hodgkin's lymphoma of the ocular adnexa. Acta Oncol 40:485–490
25. Schick U, Lermen O, Unsold R, Hassler W (2004) Treatment of primary orbital lymphomas. Eur J Haematol 72:186–192
26. Sharara N, Holden JT, Wojno TH, Feinberg AS, Grossniklaus HE (2003) Ocular adnexal lymphoid proliferations: clinical, histologic, flow cytometric, and molecular analysis of forty-three cases. Ophthalmology 10:1245–1254
27. Vandenberghe E, De Wolf-Peeters C, Vaughan Hudson G, Vaughan Hudson B, Pittaluga S, Anderson L, Linch DC (1997) The clinical outcome of 65 cases of mantle cell lymphoma initially treated with non-intensive therapy by the British National Lymphoma Investigation Group. Br J Haematol 99:842–847
28. White WL, Ferry JA, Harris NL, Grove AS Jr (1995) Ocular adnexal lymphoma. A clinicopathologic study with identification of lymphomas of mucosa-associated lymphoid tissue type. Ophthalmology 102:1994–2006
29. Wotherspoon AC, Diss TC, Pan LX, Schmid C, Kerr-Muir MG, Lea SH, Isaacson PG (1993) Primary low-grade B-cell lymphoma of the conjunctiva: a mucosa-associated lymphoid tissue type lymphoma. Histopathology 23:417–424

Virchows Arch (2006) 449:476–478
DOI 10.1007/s00428-006-0275-5

CASE REPORT

The aortic coarctation and the Etruscan man: morphohistologic diagnosis of an ancient cardiovascular disease

Rosalba Ciranni · Gino Fornaciari

Received: 20 April 2006 / Accepted: 12 July 2006 / Published online: 29 August 2006
© Springer-Verlag 2006

Abstract Reports of cardiovascular diseases in ancient time are very rare since the material mainly consists of skeletal remains; therefore, these diagnoses can only be carried out indirectly, through the marks left on bones. Here we show a case of coarctation of the aorta diagnosed on bones. Aortic coarctation is a congenital disorder in which a portion of the aorta is narrowed to various extent. A collateral circulation system is enrolled to allow adequate compensation of the blood flow. Collateral vessels may become enlarged, producing a distinctive notching on the pleural surface of the ribs and on adjacent bones. Excavation of a sixth to fifth century B.C. Etruscan tomb revealed three funerary chambers (*celle*) housing 14 skeletal remains of adults. The ribs of one of the male skeleton showed "nail stroke" indentations. Detailed macroscopic examination enabled us to identify them as notching and led to the diagnosis of postductal aortic coarctation. Histological analysis of bone tissue from the notching areas excluded inflammatory and pathological erosive events, supporting the macroscopic diagnosis. The present paper is the first description of aortic coarctation in paleopathology.

Keywords Ribs notching · Hypertension · Collateral circulation

R. Ciranni (✉) · G. Fornaciari
Section of History of Medicine, First Division of Pathology, Department of Oncology, Transplants and Advanced Technologies in Medicine, Pisa University,
56126 Pisa, Italy
e-mail: r.ciranni@do.med.unipi.it

Introduction

An Etruscan chamber tomb, named *Tomba della Selvaccia* (Evil Forest Tomb), was discovered near Siena (Tuscany, Italy). Three rectangular *celle* (archaeological name for funerary Etruscan chambers), organized around a squared vestibule, revealed rich funerary pottery, mainly consisting in *ollae*, *kylikes*, and *olpai* made of the typical Etruscan polished black *bucchero* ware. The presence of an iron ring, a pair of tweezers, and a very interesting bronze *fibula*, together with the pottery, allowed us to date the tomb between the end of the sixth century and the early fifth century B.C.

The 14 human skeletons remains (nine males and five females) were scattered all over the three chambers. Most of the remains were disconnected *ab antiquo*. The anthropological data suggested, for all individuals, to belong to the same family group [7].

Fifteen ribs, found mixed with other human bones showed the typical signs of postductal aortic coarctation. Three ribs, still partially connected to the skeleton, made the attribution to an incomplete male skeleton buried there possible.

It is well-known that coarctation of the aorta is an obstructive congenital heart disorder consisting of an encroachment of variable severity of the aortic lumen. Clinical signs mainly depend on the degree of narrowing of the aorta. The hypertension upstream of the site of restriction forces the blood into the collateral circulation producing a pathological enlargement of intercostal vessels that assume irregular, sinuous shapes. During growth, ribs are constantly subjected to the pulsating loops of engorged arteries, thus generating the notching, which represents a distinctive sign of the disease.

In this paper, we present a detailed macroscopic examination of the pathological ribs and an extensive histological analysis of the bone tissue from the notching area.

Materials and methods

Fifteen ribs (Fig. 1a), belonging to an incomplete skeleton of an adult male about 170 cm tall and aged 40–45 years, were examined macroscopically; the ribs were then anatomically positioned and X-rayed (Gilardoni Apparatus, Italy). X-ray films (Du Pont CRONEX 4 Blue Base film, 30×40 cm) were developed using Agfa developer and fixative. Ten X-rays per rib were performed.

Samples of bone tissue from areas of notching were collected, decalcified, rehydrated according to Sandison [8], and submitted to routine dehydration and paraffin-embedding for histological analysis. Tissue sections were fixed on slides and stained using three different methods: basic staining with hematoxylin–eosin, and differential staining with either periodic acid-Schiff stain or Masson trichrome stain [5, 9]. Slides were examined by light microscopy.

Results

The anthropological data produced by Pardini and Mannucci [7] suggested that the skeleton belonged to a medium-built male. Indices of robustness of the humerus and the femur were average and consistent with each other.

A macroscopic diagnosis of postductal aortic coarctation was readily made since notching was clearly evident on the rib surface. External examination revealed many round-shaped areas of notching, 0.5–1.5 cm in diameter, within the subcostal groove and in proximity to the posterior costal angle (Fig. 1b). Notching was observed through to the lower ribs.

X-ray confirmed the macroscopic diagnosis, showing bilateral, symmetrical notching on the pleural surface of the ribs with no signs of inflammatory sclerosis. Few residual vertebras and the only clavicle found were free of notching.

Histological analysis on hematoxylin–eosin stained samples revealed well-preserved, thinned, and pierced costal bones with evident haversian systems and with no sign of sclerosis or pathological erosion (Fig. 1d). Differential staining showed an increased thickness of the lamellar tissue within the layer of compact bone (Fig. 1c).

Discussion

Coarctation of the aorta is an obstructive congenital disorder representing about 5% of cardiovascular diseases. Frequency in men is three to four times higher than in women. The defect is thought to result from the incomplete development of the aortic arch during organogenesis, but the etiology is unknown. Two classic forms have been described. The infantile preductal form is usually associated with intracardiac anomalies (ventricular septal defect, subaortic stenosis,

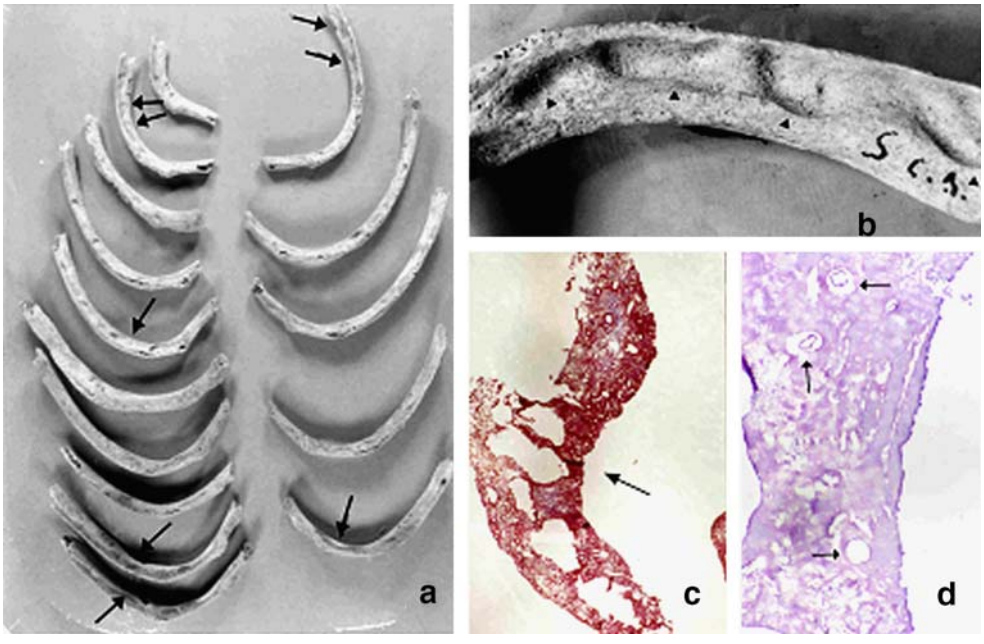

Fig. 1 Inferior view of the 15 ribs belonging to an adult male skeleton buried in the Etruscan tomb *La Selvaccia*. *Arrows* show the distribution of the typical notching due to aortic coarctation (**a**). Inferior aspect of the third left rib showing some notching (*arrows*) inside the subcostal groove (2×; **b**). Differential histology of the transversal section of the third left rib shows the excavation (*arrows*) produced by the pathological development of the artery (6×). The costal bone is pierced but not sclerotic and with no erosive signs (**c**). The costal bone is well-preserved, haversian systems are well-evident (*arrows*), compact bone shows an increased thickness of lamellar tissue at level of the notching (hematoxylin–eosin, 20×; **d**)

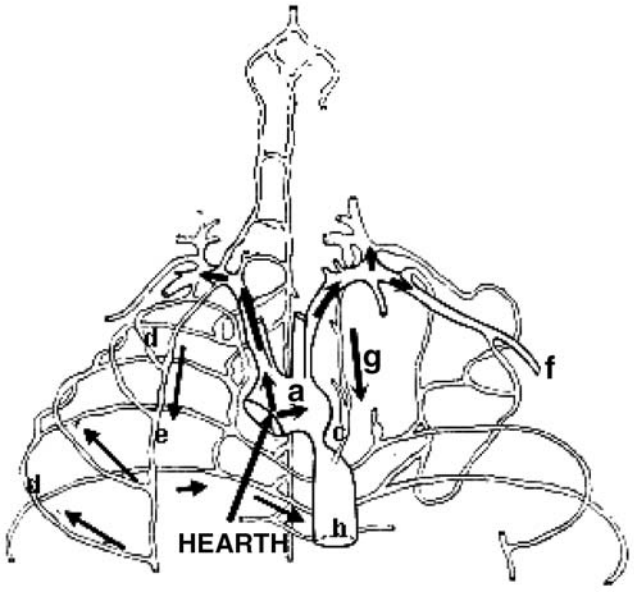

Fig. 2 Diagram showing two of the possible pathways of the collateral circulation between the pre-coarctation arterial branches and the post-coarctation arteries. On the *right*: blood flows into the internal mammary artery (**e**) then spreading into intercostal arteries (**d**), which feed into the aorta descending branch (**b**). On the *left*: blood flows into the succlavia artery (**f**) bypassing coarctation (**c**) trough the esophageal artery (**g**) (*arrows* show the direction of blood flow)

mitral valve defects, etc.) and, from the physiopathologic viewpoint, is classified among the ductus-dependent congenital heart diseases. This form is characterized by high neonatal mortality in the absence of early surgical intervention. The postductal form, mostly asymptomatic during childhood, becomes symptomatic in the adult. Postductal coarctation is characterized by the development of compensatory collateral circulation between pre-coarctation arterial branches and post-coarctation arteries [1, 4].

Figure 2 shows two possible collateral routes. As a consequence of growing blood pressure in the aorta, collateral vessels (i.e., intercostal and internal mammary arteries) may become enlarged producing, in time, notching on the pleural surface of the ribs and onto adjacent bones [1].

Reports of ancient cardiovascular diseases are very rare in paleopathology, and no data are available on aortic coarctation [2]. Atherosclerosis was diagnosed in Egyptian and Peruvian mummies [3]. Recently, Miller et al. [6] have diagnosed a case of myocardial infarction in a mummy. However, paleopathological material mainly consists of skeletal remains; therefore, the diagnosis of cardiovascular diseases can only be carried out indirectly, through the marks left on bones, as in the case of aortic aneurysm [10].

Here we report our findings relative to the skeleton of a medium-built adult man, aged 40–45 years, belonging to a sixth to fifth century B.C. Etruscan population [8]. A macroscopic detailed observation of the ribs revealed distinctive notching that we related to a strong hypertrophy of intercostal arteries as a consequence of aortic coarctation. Histological analysis confirmed the diagnosis and ruled out the possibility of erosive and/or inflammatory disorders.

The man was moderately robust; therefore, he must have coped well with the disease. We hypothesize the development of an extended collateral circulation system to allow adequate compensation of blood flow. In fact, notching was very marked, showing a remarkable increase of the costal artery calibers, and it was observed down through to the lower ribs. Furthermore, anthropological data showed that the main limb bones were well-proportioned, yet indicative of good compensation, while aortic coarctation is often accompanied by unbalanced limb development, with the upper limbs becoming more robust.

We believe that this report is the first well-documented diagnosis of aortic coarctation based on sole skeletal remains. We see it as a step forward to expand the investigation of ancient cardiovascular disease in paleopathological literature.

References

1. Ascenzi A, Mottura G (1971) Trattato di anatomia patologica per il medico pratico. UTET, Torino
2. Aufderheide AC, Rodriguez-Martin C (1998) The Cambridge encyclopedia of human paleopathology. Cambridge University Press, Cambridge, UK
3. Cockburn A, Cockburn E (eds) (1998) Mummies, disease and ancient culture. Cambridge University Press, Cambridge, UK
4. Cotran RS, Kumar V, Robbins SL (2005) Basic pathology. Saunders, Philadelphia, PA
5. Luna LG (ed) (1968) Manual of histologic staining methods of AFIP. McGraw-Hill, New York
6. Miller R, Callas DD, Kahn SE, Ricchiuti V, Apple FS (2000) Evidence of myocardial infarction in mummified human tissue. JAMA 284:831–832
7. Pardini E, Mannucci P (1980) Studio antropologico degli scheletri etruschi (VI°–V° secolo a.C.) ritrovati nella tomba a tre celle scoperta a Selvaccia (Siena). Quaderni di Scienze Antropologiche 5:26–52
8. Sandison AT (1955) The histological examination of mummified material. Stain Technol 30:277–283
9. Schultz M (2001) Paleohistopatology of bone: a new approach to the study of ancient diseases. Am J Phys Anthropol 33:106–147
10. Walker EG (1983) Evidence for prehistoric cardiovascular disease of syphilitic origin on the Northern plains. Am J Phys Anthropol 60(4):499–503

Virchows Arch (2006) 449:479–483
DOI 10.1007/s00428-006-0267-5

CASE REPORT

Hepatosplenic γδ T-cell lymphoma with ring chromosome 7, an isochromosome 7q equivalent clonal chromosomal aberration

Julia Tamaska · Emma Adam · Andras Kozma · Laszlo Gopcsa · Hajnalka Andrikovics · Attila Tordai · Gabriella Halm · Laszlo Bereczki · Eniko Bagdi · Laszlo Krenacs

Received: 8 February 2006 / Revised: 10 June 2006 / Accepted: 30 June 2006 / Published online: 29 August 2006
© Springer-Verlag 2006

Abstract Hepatosplenic T-cell lymphoma is a rare, clinically aggressive lymphoma. Most cases represent a neoplasm of mature non-activated γδ T cells. Isochromosome 7q i(7)(q10) is thought to be the primary cytogenetic abnormality of this disease. In this paper, we describe a hepatosplenic γδ T-cell lymphoma case, with clonal ring chromosome 7 exemplifying an isochromosome 7q equivalent clonal aberration. A 62-year-old female patient presented with thrombocytopenia, isolated hepatosplenomegaly, and extremely high levels of LDH. Bone marrow work-up demonstrated a sinusoidal cytotoxic T-cell infiltrate with blastic features, while molecular studies verified monoclonal rearrangement for both TCR γ and TCR δ genes. Cytogenetics revealed clonal abnormalities including ring chromosome 7, trisomy 8, and der(19), while FISH analysis detected 7q amplification with partial deletion of 7p in ring chromosome 7. To the best of our knowledge, this is the first reported T-cell lymphoma case with ring chromosome 7.

Keywords Hepatosplenic γδ T-cell lymphoma · Cytogenetics · FISH · Ring chromosome 7

J. Tamaska · E. Adam · A. Kozma · L. Gopcsa · H. Andrikovics · A. Tordai · G. Halm
Institute of Hematology and Immunology,
National Medical Center,
Budapest, Hungary

L. Bereczki · E. Bagdi · L. Krenacs (✉)
Laboratory of Tumor Pathology and Molecular Diagnostics,
Institute of Biotechnology,
Bay Zoltan Foundation for Applied Research,
Derkovits fasor 2,
H-6726 Szeged, Hungary
e-mail: krenacsl@bay.u-szeged.hu

Introduction

Hepatosplenic T-cell lymphoma (HSTCL) is a rare, clinically aggressive lymphoma affecting mainly young adult males [2–4, 14]. Most cases represent neoplasm of mature γδ T cells [3, 4, 14, 16]. The patients usually present with thrombocytopenia and isolated hepatosplenomegaly, without lymphadenopathy or significant peripheral blood lymphocytosis [2, 3, 14]. Histologically, HSTCL shows marked sinusoidal involvement in the bone marrow, liver, and spleen [2–4, 14]. Cytogenetically, isochromosome 7q [i(7)(q10)] is reported to be the primary cytogenetic abnormality in HSTCL [1, 3, 5, 7, 13, 16].

In this paper, we describe a case of hepatosplenic γδ T-cell lymphoma with ring chromosome 7, an isochromosome 7q equivalent clonal aberration thus far not reported in T-cell lymphoma.

Clinical history

A 62-year-old native Hungarian female patient presented with thrombocytopenia in July 2003. Based on initial examinations, a presumptive diagnosis of idiopathic thrombocytopenic purpura was made, and corticosteroid therapy was administered with a transient improvement. In August 2003, she was admitted to the Institute of Hematology and Immunology, National Medical Center, Budapest, Hungary due to progressive thrombocytopenic purpura, malaise, fatigue, fever, and arthralgia. Isolated hepatosplenomegaly was found on physical and radiographic examinations. The laboratory parameters at her second admission were as follows: Hgb 10.4 g/l; WBC 4.3×10^9/l; neutrophils 1.72×10^9/l; lymphocytes 1.8×10^9/l; platelets 32×10^9/l; LDH 9,000–16,000 U/l. Comprehensive bone marrow work-up, including flow cytometry, histopathology, cyto-

genetics, and molecular studies, established the diagnosis of hepatosplenic γδ T-cell lymphoma. Combined chemotherapy has been given, which was complicated by gastrointestinal bleeding that occurred on the third day of the first cycle, and the patient died due to left ventricular failure in September 2003.

Materials and methods

Bone marrow samples

Bone marrow smears were stained with May–Grünwald–Giemsa stain. Trephine biopsy specimen was fixed in Schaffer's solution for 16 h, decalcified overnight in 18% EDTA, embedded in paraffin, and routinely stained with hematoxylin and eosin.

Immunophenotyping

Immunohistochemistry was performed on paraffin sections following wet-heat-induced antigen retrieval performed in a pressure cooker and Target Retrieval Solution pH 6.0 (DakoCytomation). Flow cytometry was performed in bone marrow aspirate with FACS Calibur (BD, San Jose, CA, USA). The primary antibodies utilized in the study, including fluorochrome-labeled ones, are displayed in Table 1.

Cytogenetic and FISH analysis

Conventional cytogenetic analysis was performed on the bone marrow aspiration sample. Cells were cultured for 24 h in RPMI 1640 containing 20% fetal calf serum and antibiotics. Colcemid was subsequently added for 2 h, which was followed by standard slide preparation and Giemsa banding. Twenty metaphases were analyzed; the chromosome spreads were interpreted according to the International System for Human Cytogenetic Nomenclature (ISCN 1995). Cell pellets fixed in methanol/acetic acid 3:1 as well as metaphase spreads from conventional cytogenetics were used for FISH analysis. To detect numerical alterations of chromosome 7 as well as alterations of 7q, LSI D7S486/CEP 7 dual color probe (Vysis, Downers Grove, IL, USA) was used, which hybridizes to centromeric 7p11.1–q11.1 as well as the 7q31 regions. CEP 8 probe (Vysis, Downers Grove, IL, USA) was utilized to detect numerical alterations of the chromosome 8. Arm Specific Probe 7p (Oncor, Gaithersburg, MD, USA) was applied for labeling the short arm of chromosome 7. Denaturation, hybridization, and post-hybridization steps were performed according to the manufacturer's instructions. The slides were counterstained with DAPI (Vectashield, Vector Laboratories, Burlingame, CA USA), viewed using a Nikon E600 epifluorescence microscope, and microphotographed with MacProbe 4.3 (Applied Imaging, CA, USA) running on a MacIntosh G4 computer.

Gene rearrangement studies

T-cell receptor (TCR) gene rearrangement studies were performed by PCR amplification of genomic DNA extracted from the bone marrow trephine. The TCRγ gene rearrangement was detected using $V_{\gamma 11}$ and $J_{\gamma 12}$ consensus primers complementary to Vγ1-8 and Jγ1-2 gene segments, respectively [8, 11]. This primer combination is expected to generate bands in the size range of 75–95 base pairs [8]. The TCRδ gene rearrangement was detected according to the BIOMED-2 protocol [11]. PCR products were size-separated by polyacrylamide-gel electrophoresis and visualized by silver staining.

Table 1 Antibodies and results of immunophenotypic analysis in the bone marrow

Antibody Immunohistochemistry	Source	Tumor cells
CD3ε (rabbit polyclonal)	DakoCytomation	+
CD5 (rabbit polyclonal)	Labvision	−
CD8α (C8/144)	DakoCytomation	−
CD56 (56C04)	Labvision	−
TCRβ (βF1)	T-Cell Sciences	−
TIA-1 (26gA10F5)	Immunotech	+
Granzyme B (GrB-7)	DakoCytomation	+/−
Granzyme M (4H10)	Mark J. Smith[a]	+
Tdt (rabbit polyclonal)	DakoCytomation	−
Flow cytometry		
CD3-PE	Becton-Dickinson	+
CD4-FITC	Becton-Dickinson	−
CD5-FITC	Becton-Dickinson	−
CD7-FITC	Becton-Dickinson	+
CD8-PE	Becton-Dickinson	−
CD19-PerCP	Becton-Dickinson	−
CD22-PE	Becton-Dickinson	−
CD45-FITC	Becton-Dickinson	+
CD103-FITC	Becton-Dickinson	−

FITC Fluorescein isothiocyanate, *PE* Phycoerythrin, *PerCP* Peridinin chlorophyll protein, *TCR* T-cell receptor, *Tdt* Terminal deoxyribonucleotidyl transferase

+ Positive, +/− focally positive, − negative

[a] Division of Cancer Immunology, Peter MacCallum Cancer Institute, East Melbourne, Melbourne, Australia

Results

Histopathology and immunophenotyping

The bone marrow trephine biopsy showed marked sinusoidal infiltration with medium- and large-sized monomorphic nucleolated cells with blastic features (Fig. 1) displaying a CD4/CD8 double negative mature T-cell immunophenotype and non-activated cytotoxic lymphocyte antigenic profile (Table 1). The positivity for granzyme M and negativity for TCRβ chain and CD5 suggested γδ T-cell origin. Retrospective analysis of bone marrow smears from the first examination revealed 15% lymphoid cell and a few large cells with a markedly folded nucleus. FACS analysis of the bone marrow showed 68% CD3+ and 57% CD7+ cells in the lymphocytic gate (Table 1).

Cytogenetic and FISH analysis

Conventional cytogenetic studies detected chromosomal abnormalities in 10 of 20 metaphases. The abnormal metaphases showed ring chromosome 7, one extra copy of chromosome 8 and a derivative chromosome 19 (Fig. 2). FISH analysis revealed 7q amplification with partial 7p deletion in the ring chromosome (Fig. 3). Interphase nuclei, analyzed with the same probe set, showed two copies of the centromeric region of chromosome 7 and six copies of band 7q31 (not shown). Trisomy 8 was also detected with interphase FISH.

Gene rearrangement studies

The Vγ1-8/Jγ1-2 PCR displayed a single discrete band within the expected size range, corresponding to monoclonal TCRγ gene rearrangement. The TCRδ PCR revealed monoclonal rearrangements for both Vδ1/Jδ1 and Dδ2/Jδ1 gene segments (Fig. 4) that verified γδ T-cell derivation with Vδ1 gene usage, a common origin of HSTCL cases [10].

Autopsy

The autopsy revealed significant hepatomegaly (2,100 g) and mild splenomegaly (270 g). The splenic parenchyma contained areas of coagulative necrosis, 8 cm in maximum diameter. Liver, spleen, and hypercellular bone marrow displayed a sinusoidal infiltrate composed of CD3+ blastic lymphoid cells consistent with HSTCL (Fig. 1). Segments of the small and large intestines contained partly digested blood, most probably due to thrombocytopenia and capillary bleeding. Presence of severe pulmonary edema confirmed left-sided cardiac failure.

Discussion

HSTCL is an uncommon, but distinct T-cell lymphoma with a characteristic growth pattern and clinical setting. The HSTCL case presented in this paper shares the common

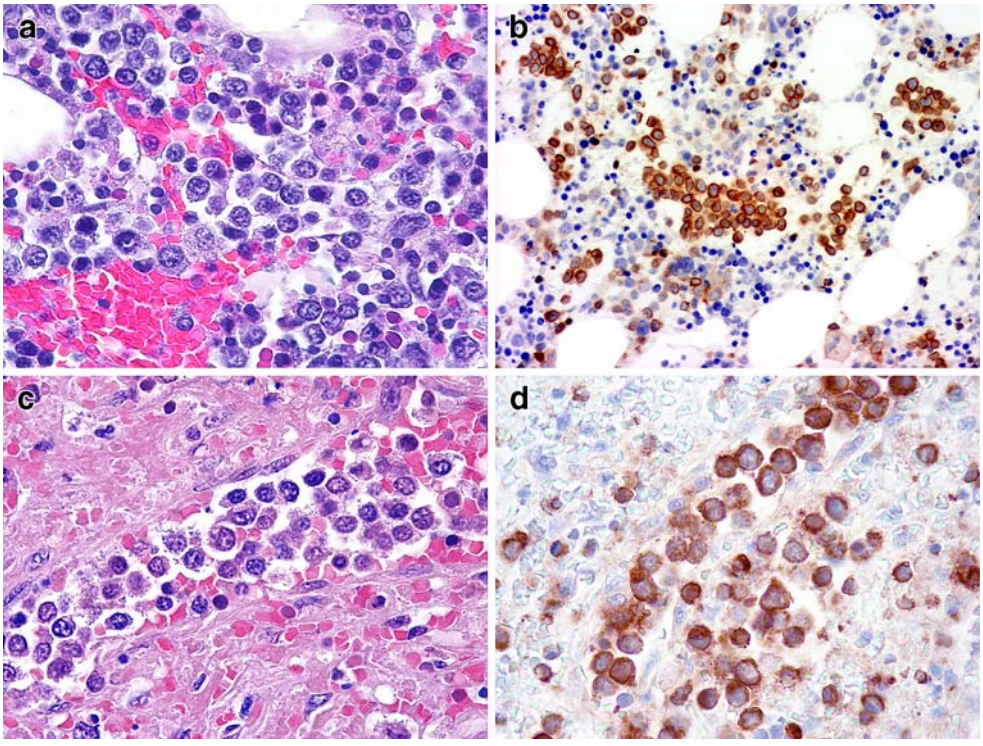

Fig. 1 Histopathology of bone marrow and spleen. **a** Bone marrow trephine biopsy shows a marked sinusoidal accumulation of medium- to large-sized monomorphic blast-like cells. (H and E; original magnification ×600). **b** These atypical intrasinusoidal cells display intense positivity for CD3ε, which is consistent with their T-lymphoid-cell origin. (DakoCytomation Envision+ labeled polymer immunoperoxidase technique; original magnification ×200). **c** Spleen obtained during the autopsy demonstrates sinusoidal infiltration by atypical lymphoid cells establishing splenic involvement. (H and E; original magnification ×600). **d** The intrasinusoidal atypical cells are strongly positive for CD3ε. (DakoCytomation Envision+ labeled polymer immunoperoxidase technique; original magnification ×600)

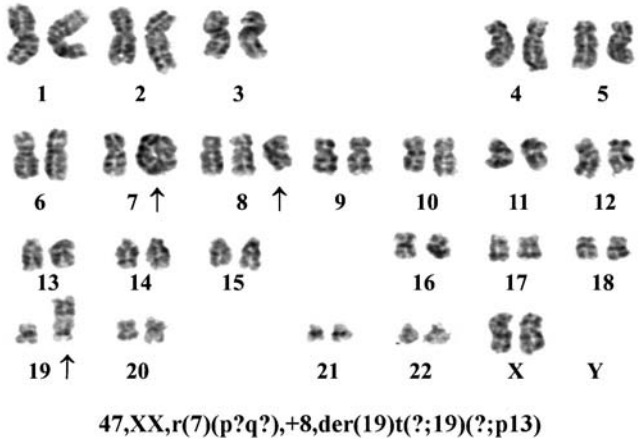

Fig. 2 Conventional karyotype analysis performed on bone marrow aspiration sample shows an abnormal female karyotype with 47 chromosomes, ring chromosome 7, one extra copy of chromosome 8, and a derivative chromosome 19. (Giemsa banding after short-term culture and colcemid inhibition)

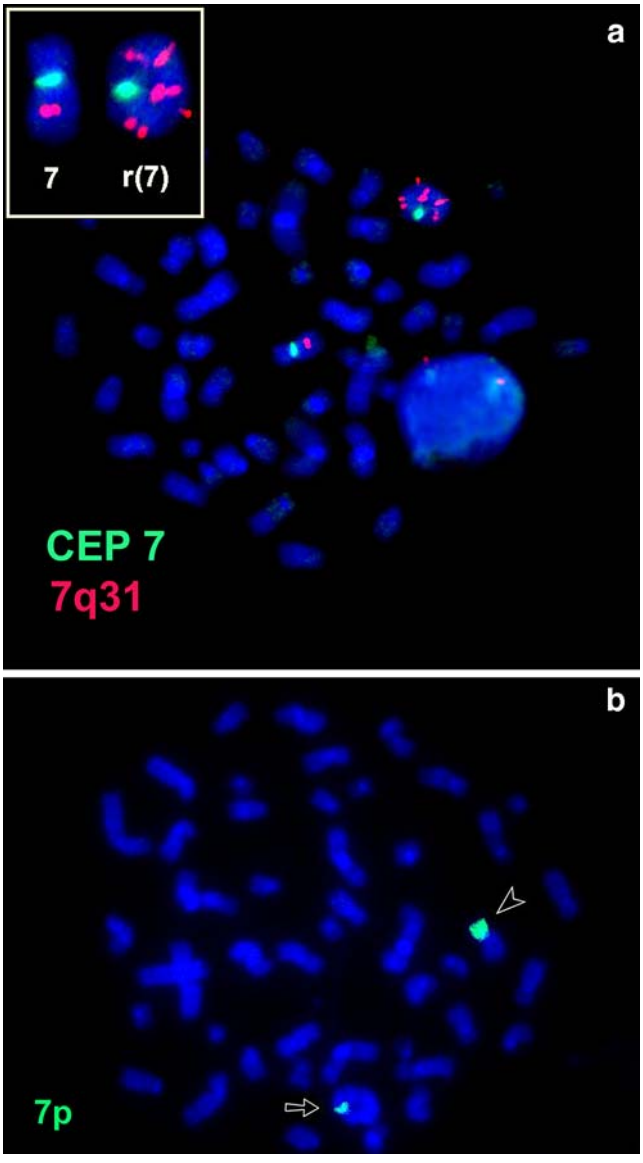

Fig. 3 FISH analysis performed in metaphase spread revealing 7q amplification and a partial 7p deletion in the ring chromosome 7. **a** Dual color probe detecting centromeric 7p11.1–q11.1 region in *green* and 7q31 locus in *red* demonstrates one *green* and one *red* signal in the normal chromosome 7 as well as one *green* and multiple *red* signals in the ring chromosome 7. **b** The 7p specific probe displays strong signal in the normal chromosome 7 (*arrowhead*) and a reduced signal in the ring chromosome 7 (*arrow*), suggesting a partial deletion of the short arm

clinical, morphologic, immunophenotypic, and genotypic features previously reported; however, the karyotypic analysis established the occurrence of clonal ring chromosome 7, instead of common isochromosome 7q. The i(7)(q10), typically occurs in HSTCL, results in the deletion of the short arm of chromosome 7, leading to the loss of tumor suppressor genes located on 7p as well as to the loss of TCR beta gene at 7p15 [5, 16]. Duplication of the long arm, on the other hand, causes excess of oncogenes located on 7q as well as TCR gamma gene at 7q35 [5, 16]. These alterations may play a causal role in the development of HSTCL [5, 16]. In our case, ring chromosome 7 was found, which, similarly to isochromosome 7q, showed 7q amplification, while the 7p was only partially deleted. Our findings indicate that ring chromosome 7 is an isochromosome 7q equivalent alteration, and support the view, which suggests that the overrepresentation of 7q is more important in overgrowing of a malignant clone than the loss of 7p [16]. A ring chromosome is a rare finding in hematologic malignancies and only exceptionally occurs in lymphoproliferative disorders [9, 12, 15]. During our literature search, we have found only two published cases of B-cell lymphomas showing ring chromosome 7 [9, 12], but not a single T-cell lymphoma case was encountered with this clonal chromosomal aberration.

The increasing number of 7q signals has been described in HSTCL cases with cytologic progression [16]. Although it occurred in an immunocompetent person, our case displayed blastic cytomorphological features and had a very poor outcome, which might have been related with the increased number of 7q signals of ring chromosome 7.

Most HSTCL cases represent neoplasms of mature non-activated γδ T cells showing surface TCRγδ expression, homogeneous positivity for cytotoxic granule-associated antigen TIA-1, but weak or negative staining for granzyme B and perforin; the latter two proteins are expressed strongly in activated cytotoxic T cells [1–5, 7, 13, 14, 16]. The expression of the NK-cell and γδ T-cell-restricted serine protease granzyme M is another distinctive feature of a γδ HSTCL [6]. Our case demonstrated both non-activated cytotoxic T-cell phenotype and granzyme M expression; nevertheless, the γδ T-cell derivation was confirmed by the

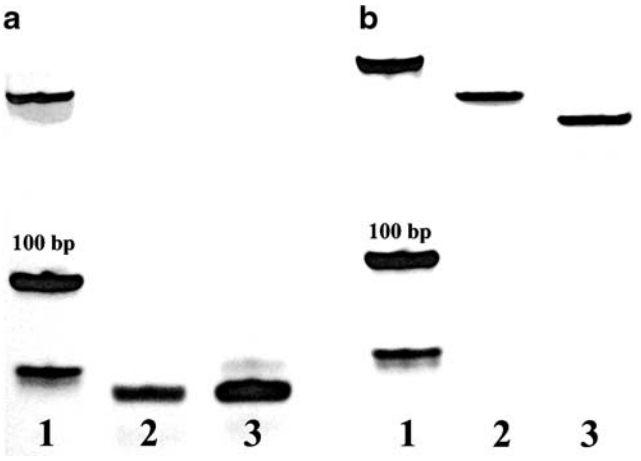

Fig. 4 PCR-based T-cell receptor genotyping confirming γδ T-cell derivation. **a** The Vγ1-8/Jγ1-2 PCR displays a single discrete band within the expected size range (*lane 1*: DNA marker; *lane 2*: positive control; *lane 3*: bone marrow sample), corresponding to monoclonal TCRγ gene rearrangement. **b** PCR for TCRδ gene reveals monoclonal rearrangements for both Vδ1/Jδ1 and Dδ2/Jδ1 gene segments (*lane 1*: DNA marker; *lane 2*: Vδ1/Jδ1; *lane 3*: Dδ2/Jδ1) that verifies γδ T-cell derivation

TCRδ clonality analysis, detecting clonal rearrangement for both Vδ1/Jδ1 and Dδ2/Jδ1 gene segments.

In this paper, we have presented a hepatosplenic γδ T-cell lymphoma that, to the best of our knowledge, is the first published case where the extra copies of 7q were caused by a ring chromosome 7, instead of one or more 7q isochromosomes. This is the first mature T-cell lymphoma case reported with ring chromosome 7.

Acknowledgments The authors thank Dr. Laszlo Kopper (First Department of Pathology, Semmelweis University, Budapest, Hungary) for providing autopsy data. The authors are grateful to Dr. Jon van der Walt FRCPath (Histopathology Department, St Thomas' Hospital, London, UK) for critical reading of the manuscript. This study was supported in part by the Hungarian Scientific Research Fund ('OTKA-T 046663 KON').

References

1. Alonsozana ELC, Stamberg J, Kumar D, Jaffe ES, Medeiros LJ, Frantz C, Schiffer CA, O'Conell BA, Kerman S, Stass SA, Abruzzo LV (1997) Isochromosome 7q: the primary cytogenetic abnormality in hepatosplenic γδ T cell lymphoma. Leukemia 11:1367–1372
2. Belhadj K, Reyes F, Farcet J-P, Tilly H, Bastard C, Angonin R, Deconinck E, Charlotte F, Leblond V, Labouyrie E, Lederlin P, Emile J-F, Delmas-Marsalet B, Arnulf B, Zafrani E-S, Gaulard P (2003) Hepatosplenic γδ T-cell lymphoma is a rare clinicopathological entity with poor outcome: report on a series of 21 patients. Blood 102:4261–4269
3. Cooke CB, Krenacs L, Stetler-Stevenson M, Greiner TC, Raffeld M, Kingma DW, Abruzzo L, Frantz C, Kaviani M, Jaffe ES (1996) Hepatosplenic T-cell lymphoma: a distinct clinicopathologic entity of cytotoxic γδ T-cell origin. Blood 88:4265–4274
4. Farcet JP, Gaulard P, Marolleau JP, Le Couedic J-P, Henni T, Gourdin M-F, Divine M, Haioun C, Yafrani S, Goossens M, Hercend T, Rezes F (1990). Hepatosplenic T-cell lymphoma: sinusal/sinusoidal localization of malignant cells expressing the T-cell receptor γδ. Blood 75:2213–2219
5. Jonveaux P, Daniel MT, Martel V, Maarek O, Berger R (1996) Isochromosome 7q and trisomy 8 are consistent primary non-random chromosomal abnormalities associated with hepatosplenic T γδ lymphoma. Leukemia 10:1453–1455
6. Krenacs L, Smyth MJ, Bagdi E, Krenacs T, Kopper L, Rudiger T, Zettl A, Muller-Hermelink HK, Jaffe EJ, Raffeld M (2003) The serine protease granzyme M is preferentially expressed in NK-cell, γδ T-cell, and intestinal T-cell lymphomas: evidence of origin from lymphocytes involved in innate immunity. Blood 101:3590–3593
7. Lepretre S, Buchonnet G, Stamatoullas A, Lenain P, Duval C, d'Anjou J, Callat M-P, Tilly H, Bastard C (2000) Chromosome abnormalities in peripheral T-cell lymphoma. Cancer Genet Cytogenet 117:71–79
8. McCarthy KP, Sloane JP, Kabarowski JHS, Matutes E, Wiedemann LM (1992) A simplified method of detection of clonal rearrangements of the T-cell receptor-γ chain gene. Diagn Mol Pathol 1:173–179
9. Oscier DG, Gardiner A, Mould S (1996) Structural abnormalities of chromosome 7q in chronic lymphoproliferative disorders. Cancer Genet Cytogenet 92:24–27
10. Przybylski GK, Wu H, Macon WR, Finan J, Leonard DGB, Felgar RE, DiGiuseppe JA, Nowell PC, Swerdlow SH, Kadin ME, Wasik MA, Salhany KE (2000) Hepatosplenic and subcutaneous panniculitis-like γ/δ T cell lymphomas are derived from different Vδ subsets of γ/δ T lymphocytes. J Mol Diagnostics 2:11–19
11. Van Dongen JJM, Langerak AW, Brüggemann M, Evans PAS, Hummel M, Lavender FL, Delabesse E, Davi F, Schuuring E, Garcia-Sanz R, van Krieken JH, Droese J, Gonzalez D, Bastard C, White HE, Spaargaren M, Gonzalez M, Parreira A, Smith JL, Morgan GJ, Kneba M, Macintyre EA (2003) Design and standardization of PCR primers and protocols for detection of clonal immunoglobulin and T-cell receptor gene recombination in suspect lymphoproliferations: report of the BIOMED-2 Concerted Action BMH4-CT98-3936. Leukemia 17:2257–2317
12. Viaggi S, Abbondandolo A, Carbone M, Ottaggio L, Sessarego M, Zupo S, Zunino A (2004) Uncommon cytogenetic findings in a case of splenic marginal zone lymphoma with aggressive clinical course. Cancer Genet Cytogenet 148:133–136
13. Wang C-C, Tien H-F, Lin M-T, Su I-J, Wang C-H, Chuang S-M, Shen M-C, Liu C-H (1995) Consistent presence of isochromosome 7q in hepatosplenic T γδ lymphoma: a new cytogenetic-clinicopathologic entity. Genes Chromosomes Cancer 12:161–164
14. Weidmann E (2000) Hepatosplenic T cell lymphoma. A review on 45 cases since the first report describing the dissease as a distinct lymphoma entity in 1990. Leukemia 14:991–997
15. Werner-Favre C, Beris P, Piguet D, Engel E (1986) Ring chromosomes and hematologic disorders. Cancer Genet Cytogenet 23:265–267
16. Wlodarska I, Martin-Garcia N, Achten R, De Wolf-Peeters C, Pauwels P, Tulliez M, de Mascarel A, Briere J, Patey M, Hagelmeijer A, Gaulard P (2002) Fluorescence in situ hybridization study of chromosome 7 aberrations in hepatosplenic T-cell lymphoma: isochromosome 7q as a common abnormality accumulating in forms with features of cytologic progression. Genes Chromosomes Cancer 33:243–251

Virchows Arch (2006) 449:484–488
DOI 10.1007/s00428-006-0264-8

CASE REPORT

Sebaceous carcinoma of the breast: case report and review of the literature

Masanori Hisaoka · Yuji Takamatsu · Yutaka Hirano · Hironobu Maeda · Tetsuo Hamada

Received: 23 May 2006 / Accepted: 22 June 2006 / Published online: 31 August 2006
© Springer-Verlag 2006

Abstract Sebaceous differentiation has been described in only limited examples of benign and malignant epithelial lesions of the breast. We report a rare case of mammary sebaceous carcinoma to further delineate its morphologic features. Microscopically, the tumor, arising in the right mammary gland of a 63-year-old woman, was composed of well-defined solid sheets or lobules of atypical epithelial cells including many large pale or clear cells with often scalloped nuclei and coarsely vacuolated cytoplasm, in which abundant lipid droplets were identified with oil-red-O staining. Immunohistochemical expressions of cytokeratin, epithelial membrane antigen, and receptors of estrogen and progesterone were detected, whereas GCDFP-15, S-100 protein, vimentin, α-smooth muscle actin, p63, androgen receptor, and the HER2/neu protein were not expressed. Besides, a subset of the tumor cells co-expressed synaptophysin, neurofilament, and PGP9.5, suggesting neuroendocrine differentiation that is a hitherto undescribed phenomenon in the mammary tumors with sebaceous features. This case would expand the morphologic diversity of carcinoma of the breast.

Keywords Breast · Carcinoma · Sebaceous · Neuroendocrine

M. Hisaoka (✉)
Department of Pathology and Oncology, School of Medicine,
University of Occupational and Environmental Health,
1-1 Iseigaoka, Yahatanishi-ku,
Kitakyushu 807-8555, Japan
e-mail: hisaoka@med.uoeh-u.ac.jp

Y. Takamatsu · Y. Hirano
Department of Surgery, Kyushu Rosai Hospital,
1-3-1 Takamatsu, Kuzuhara, Kokuraminami-ku,
Kitakyushu 800-0296, Japan

H. Maeda
Department of Radiology, Kyushu Rosai Hospital,
1-3-1 Takamatsu, Kuzuhara, Kokuraminami-ku,
Kitakyushu 800-0296, Japan

T. Hamada
Department of Surgical Pathology, Kyushu Rosai Hospital,
1-3-1 Takamatsu, Kuzuhara, Kokuraminami-ku,
Kitakyushu 800-0296, Japan

Introduction

Despite some morphologic and developmental links between the mammary gland and skin appendages, sebaceous differentiation is only rarely encountered in benign or malignant epithelial lesions of the mammary gland. Although mammary sebaceous carcinoma was first described as a variant of lipid-secreting carcinoma by van Bogaert and Maldgue in 1977 [15], the recent WHO classification for breast tumors has recognized it as a distinct subtype of invasive breast carcinomas [13]. The number of well-documented cases is still limited [6–8, 12, 16], and we feel that recognition of such a peculiar type of carcinoma is generally poor in this anatomical location. In this report, we describe clinicopathologic features of a case of sebaceous carcinoma of the breast to broaden our knowledge of a morphologic variety of mammary carcinoma.

Case report

A 63-year-old woman was noticed to have a lump in the right breast during a medical checkup. An ultrasonographic

examination revealed a hypoechoic mass with an irregular margin in the upper central aspect of the breast. Mammographically, an opaque mass measuring about 2 cm in size without calcification was identified in the right breast (Fig. 1). Fine needle aspiration cytology strongly suggested invasive ductal carcinoma. Laboratory data on admission were not remarkable, and the serum levels of CEA and CA15-3 were within normal limits. A muscle-preserving radical mastectomy with a regional lymph node dissection was performed.

Materials and methods

The specimen was routinely processed for microscopic, histochemical, and immunohistochemical examinations. Briefly, histological slides of the formalin-fixed, paraffin-embedded tumor tissue were deparaffinized and stained with hematoxylin-eosin, periodic acid-Schiff (PAS), and mucicarmine. The Grimelius argyrophil technique and immunohistochemistry using the following primary antibodies and a labeled polymeric secondary antibody (EnVision system; DAKO Cytomation, Kyoto, Japan) with or without appropriate antigen retrieval were also performed: anti-cytokeratin (AE1/AE3, 1:50, DAKO Cytomation), anti-epithelial membrane antigen (E29, 1:100, DAKO Cytomation), anti-vimentin (V9, 1:30, DAKO Cytomation), anti-α-smooth muscle actin (1A4, 1:150, DAKO Cytomation), anti-S-100 protein (polyclonal, 1:200, DAKO Cytomation), anti-p63 (4A4, 1:30, DAKO Cytomation), anti-synaptophysin (SY38, 1:100, DAKO Cytomation), anti-neurofilament (DA2/FNP7/RMdO20.11, 1:50, Zymed, South San Francisco, CA, USA), anti-chromogranin A (CAK-A3, 1:100, DAKO Cytomation), anti-PGP9.5 (13C4/31A3, 1:400, UltraClone, Isle of Wight, UK), anti-carcinoembryonic antigen (II-7, 1:200, DAKO Cytomation), anti-GCDFP-15 (23A3, 1:50, Novocastra, Newcastle-upon-Tyne, UK), anti-estrogen receptor (1D5, 1:50, DAKO Cytomation), anti-progesterone receptor (1A6, 1:50, Immunotech, Marseille, France), anti-androgen receptor (AR441, 1:50, DAKO Cytomation), anti-HER2/neu (polyclonal, prediluted, DAKO Cytomation), and anti-Ki-67 (MIB-1, 1:50, DAKO Cytomation). Frozen sections were prepared from the formalin-fixed wet tumor tissue and stained with oil-red-O.

Fig. 1 Craniocaudal mammogram of the right breast shows a well-circumscribed opaque mass lesion

Results

Macroscopically, the tumor, measuring 2×1.8×1.5 cm in diameter, was well-demarcated and had the white or grayish cut surface with a firm consistency. The lesion had no connection to the overlying skin or the nipple.

Histologically, the tumor was made up of solid sheets or lobules of a proliferation of polygonal atypical epithelial cells possessing round hyperchromatic or vesicular nuclei, small nucleoli, and eosinophilic fine granular cytoplasm (Fig. 2a). The lobules frequently contained or were partially replaced by large epithelial cells with ample clear, multivacuolated cytoplasm and irregular or often scalloped nuclei (Fig. 2b). An overt ductal structure or squamous or apocrine differentiation was absent. Mitotic figures were readily encountered (more than 10/10 HPF). Although mild stromal invasion of the tumor cells was focally noted, the lesion was almost confined to the mammary gland without intraductal components or necrotic areas. Many tumor cells, particularly multivacuolated cells, had abundant oil-red-O-positive lipid droplets in the cytoplasm (Fig. 2c), whereas they were negatively stained with PAS or mucicarmine staining. Approximately two thirds of the tumor consisted of vacuolated cells with lipid droplets. The Grimelius staining failed to demonstrate darkly granulated, argyrophilic tumor cells. A metastatic deposit was identified in one of the nine axillary lymph nodes examined microscopically.

Immunohistochemically, the tumor cells including large multivacuolated cells were positive for cytokeratin and epithelial membrane antigen (Fig. 2d). Synaptophysin, neurofilament, and PGP9.5 were co-expressed in a subset of the tumor cells mostly lacking vacuolated cytoplasm (Fig. 2e). In addition, the vast majority of tumor cells were positive for the receptors of estrogen and progesterone (Fig. 2f). MIB-1 labeling index was approximately 38%.

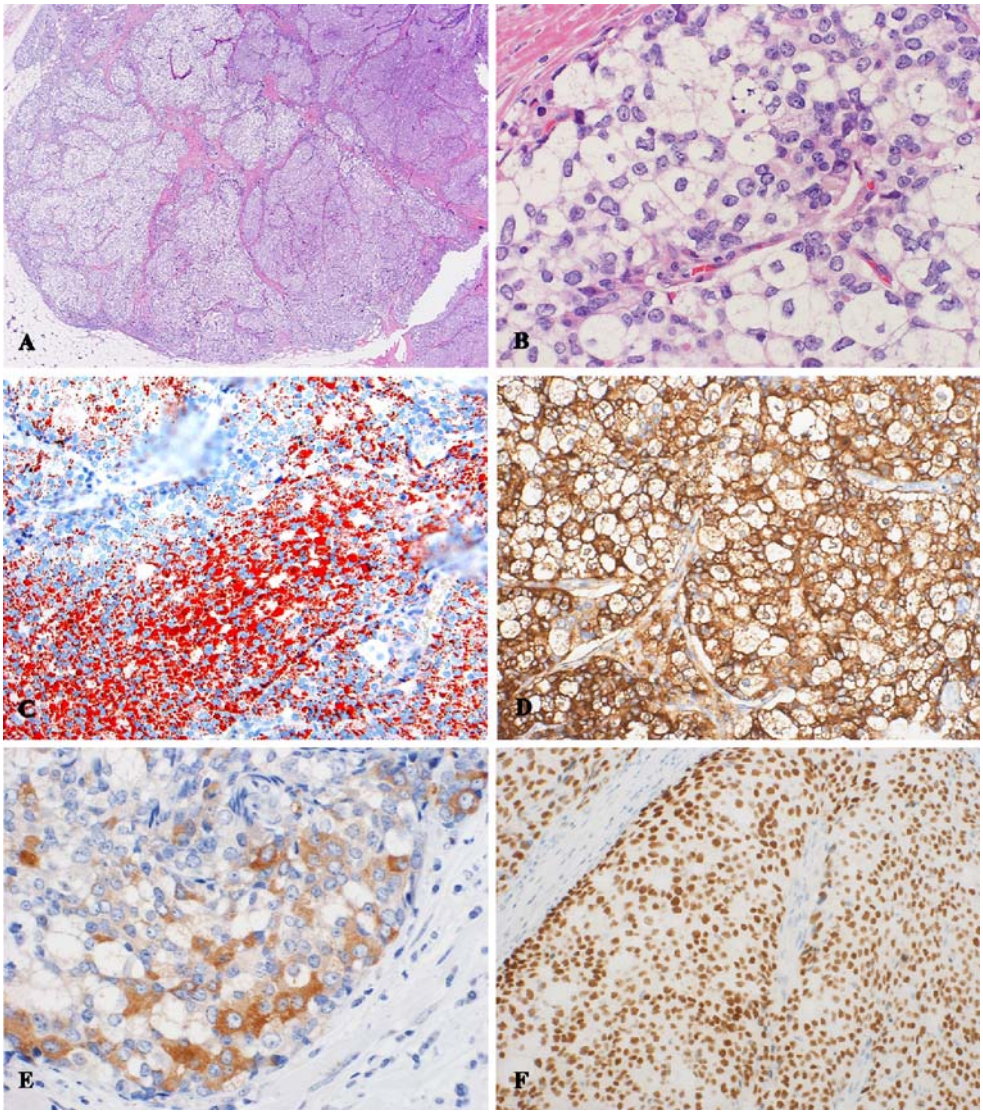

Fig. 2 **a** In a low-power view, the tumor shows a well-delineated, solid sheet-like or lobular configuration (hematoxyline and eosin, ×20). **b** The lobules are made up predominantly of large clear or multivacuolated cells admixed with minor non-vacuolated epithelial cells (hematoxyline and eosin, ×400). **c** Abundant intracytoplasmic neutral lipids are demonstrated in many tumor cells (oil-red-O staining, ×200). **d** Diffuse membranous and bubbly cytoplasmic expression of epithelial membrane antigen is seen (immunohistochemistry, ×200). **e** Some of the tumor cells, mostly of a non-vacuolated phenotype, are positive for synaptophysin (immunohistochemistry, ×400). **f** Nuclear immunoreactivity to estrogen receptor is seen in the vast majority of tumor cells (immunohistochemistry, ×100)

Other immunohistochemical markers examined were essentially negative.

Discussion

Based on the clinicopathologic findings, the current tumor is analogous to those previously reported as mammary carcinoma with sebaceous differentiation or sebaceous carcinoma of the breast [6, 7, 12, 15, 16]. As the initial identification as a variant of lipid-secreting carcinoma [15], sebaceous differentiation has been rarely described in variable morphologic types of mammary carcinoma, such as infiltrating (or invasive) ductal carcinoma, adenoid cystic carcinoma, and a carcinoma with ductal, myoepithelial and squamous elements [6, 7, 12, 14, 16]. In addition, a single case of sebaceous gland metaplasia in intraductal papilloma has been recently described [3]. Another case, also recorded as sebaceous carcinoma of the breast with Muir–Torre syndrome, does not appear to represent a mammary carcinoma, but indeed a cutaneous sebaceous carcinoma because of its dermal localization [8].

The number of previously documented cases with such a peculiar mammary carcinoma with sebaceous differentiation is still very small, and their detailed clinicopathologic information is available in only four examples (Table 1) [6, 7, 12, 16]. According to the reported cases including ours, four of the five patients were women with ages ranging from 45 to 74 years. The lesions were frequently recognized as palpable masses more often in the right breast than in the left, and the size of the tumors ranged from 2.5 to 7.5 cm in diameter. The patients were treated with a

Table 1 Summarized clinicopathologic features of reported sebaceous carcinomas of the breast

Author (year/ref. no.)	Age/ gender	Side	Size	Lymph node metastasis	Histologic feature	Outcome (follow-up period)
Prescott et al. (1992/[7])	74/F	Right	5×4.5×4 cm	–	Invasive ductal carcinoma with squamous and myoepithelial components	NED (6 m)
Mazzella et al. (1995/[6])	55/M	Left	5×4×4 cm	–	Infiltrating ductal carcinoma with intraductal components	NED (10 m)
Tavassoli (1999/[12])	46/F	Right	7.5 cm	–	Carcinoma with squamous morules	No information
Varga et al. (2000/[16])	45/F	Right	2.5 cm	–	Invasive ductal carcinoma with intraductal components	Skin and bone metastases (10 years)
Hisaoka et al. (current case)	71/F	Right	2.5×2×1.5 cm	+ (1 of 9 nodes)	Invasive carcinoma	Recent case

simple or modified radical mastectomy and a regional lymph node dissection. The cases except for ours had no lymph node metastasis at surgery. One case, however, developed distant metastases involving the skin and bones and underwent chemotherapy [16], suggesting that a mammary sebaceous carcinoma is a potentially more aggressive phenotype than presumed previously [12]. Thus, a careful follow-up survey is mandatory in any case with mammary sebaceous carcinoma.

Microscopically, the carcinoma is essentially characterized by a lobular or nested growth pattern of tumor cells variably admixed with those displaying sebaceous differentiation [12, 13]. In contrast to the previously reported carcinomas with sebaceous differentiation [6, 7, 12, 14], our case showed distinct, well-delineated solid and lobular structures without other histologic elements such as squamous and myoepithelial cells or in situ (or intraductal) components. In addition to such a histologic appearance [9], immunohistochemical expressions of cytokeratin and epithelial membrane antigen are conformed to the features of sebaceous carcinoma arising in other anatomical locations such as the skin and the ocular adnexa [1, 11, 16]. However, the status of sex steroid hormone receptors in the mammary lesions appears somewhat different; mammary sebaceous carcinoma tends to express progesterone and/or estrogen receptors, but not that of androgen [6, 12, 16], whereas androgen has been suggested to be a dominant sex hormone influencing a cutaneous counterpart [2, 4]. In the three cases analyzed, a percentage of Ki-67-positive tumor cells was relatively high and ranged from 16 to 38% [12, 16].

The extent of the sebaceous morphology differed among the reported cases [6, 7, 12, 14, 16], and the criteria of mammary sebaceous carcinoma seem ambiguous at this point [12, 13]. Because a non-sebaceous component may display diverse morphologic features, the appellation of sebaceous carcinoma might be suitable for lesions with a prominent sebaceous appearance (e.g., at least half of tumor cells).

It is notable that the current case was immunohistochemically positive for some neuroendocrine markers such as synaptophysin and neurofilament, even if the positivity was confined to cells that were non-vacuolated and non-argyrophilic. The neuroendocrine phenotype is a hitherto undescribed feature in sebaceous carcinoma of the breast or at other sites, although a carcinoid-like trabecular or ribbon-like growth pattern of cells may be seen in subsets of extraocular sebaceous carcinoma and sebaceoma [5]. This phenomenon might represent aberrant or divergent differentiation that may be also encountered in non-sebaceous mammary carcinomas such as mucinous carcinoma and non-mucinous solid carcinoma [10, 13].

Because of the lack of overexpression of the HER2/neu protein in the current case or in the case examined by Varga et al. [16], the protein cannot yet be a molecular therapeutic target for this type of mammary carcinoma.

References

1. Ansai S, Hashimoto H, Aoki T, Hozumi Y, Aso K (1993) A histochemical and immunohistochemical study of extraocular sebaceous carcinomas. Histopathology 22:127–133
2. Bayer-Garner IB, Givens V, Smoller B (1999) Immunohistochemical staining for androgen receptors. A sensitive marker of sebaceous differentiation. Am J Dermatopathol 21:426–431
3. Jiao Y-F, Nakamura S, Oikawa T, Sugai T, Uesugi N (2001) Sebaceous gland metaplasia in intraductal papilloma of the breast. Virchows Arch 438:505–508
4. Kariya Y, Moriya T, Suzuki T, Chiba M, Ishida K, Takeyama J, Endoh M, Watanabe M, Sasano H (2005) Sex steroid hormone

receptors in human skin appendages and its neoplasms. Endocrine J 52:317–325
5. Kazakov DV, Kutzner H, Rutten A, Mukensnabl P, Michal M (2005) Carcinoid-like pattern in sebaceous neoplasms: another distinctive, previously unrecognized pattern in extraocular sebaceous carcinoma and sebaceoma. Am J Dermatopathol 27:195–203
6. Mazzella FM, Sieber SC, Braza F (1995) Ductal carcinoma of the male breast with prominent lipid-rich component. Pathology 27:280–283
7. Prescott RJ, Eyden BP, Reeve NL (1992) Sebaceous differentiation in a breast carcinoma with ductal, myoepithelial and squamous elements. Histopathology 21:181–184
8. Propeck PA, Warner T, Scanlan KA (2000) Sebaceous carcinoma of the breast in a patient with Muir–Torre syndrome. Am J Roentgenol 174:541–542
9. Rao NA, Hidayat LCAA, McLean LCIW, Zimmerman LE (1982) Sebaceous carcinomas of the ocular adnexa: a clinicopathologic study of 104 cases, with five-year follow-up data. Hum Pathol 13:113–122
10. Sapino A, Righi L, Cassoni P, Papotti M, Pietribiasi F, Bussolati G (2000) Expression of the neuroendocrine phenotype in carcinomas of the breast. Semin Diagn Pathol 17:127–137
11. Sinard JH (1999) Immunohistochemical distinction of ocular sebaceous carcinoma from basal cell and squamous cell carcinoma. Arch Ophthalmol 117:776–783
12. Tavassoli FA (1999) Sebaceous carcinoma. In: Medina MP, Greenfield S (eds) Pathology of the breast, 2nd edn. Appleton and Lange, Stamford, pp 555–558
13. Tavassoli FA, Devilee P (2003) World Health Organization classification of tumours: tumours of the breast and female genital organs. IARC, Lyon, pp 46–47
14. Tavassoli FA, Norris HJ (1986) Mammary adenoid cystic carcinoma with sebaceous differentiation. Arch Pathol Lab Med 110:1045–1053
15. van Bogaert LJ, Maldague P (1977) Histologic variants of lipid-secreting carcinoma of the breast. Virchows Arch Pathol Anat 375:345–353
16. Varga Z, Kolb SA, Flury R, Burkhard R, Caduff R (2000) Sebaceous carcinoma of the breast. Pathol Int 50:63–66

Virchows Arch (2006) 449:489–492
DOI 10.1007/s00428-006-0289-z

CASE REPORT

Para-testicular cellular angiofibroma: a rare tumour in a male renal transplant patient

Muna Sabah · Ponnusamy Mohan · Elaine Kay

Received: 15 May 2006 / Accepted: 2 August 2006 / Published online: 7 September 2006
© Springer-Verlag 2006

Abstract Cellular angiofibroma is a rare, benign, mesenchymal neoplasm that should be distinguished from other more aggressive mesenchymal lesions. A 32-year-old male presented with a painless para-testicular mass. Pathological examination showed features characteristic of cellular angiofibroma. He had a history of renal transplantation and was on immunosuppressive drugs. The pathogenesis of cellular angiofibroma is largely undetermined. The role of immunosuppressive therapy in the genesis of this tumour awaits further analysis.

Keywords Cellular angiofibroma · Male · Immunosuppression

Introduction

Cellular angiofibroma was first described in a series of four cases by Nucci et al. [17] in 1997 as a distinctive neoplasm that occurs almost exclusively in the vulval region of middle aged women. Laskin et al. [13] reported a series of 11 cases of similar tumours in the inguinal and scrotal regions in males, and these lesions were designated "angiomyofibroblastoma-like tumours." The World Health Organisation applies the terminology "cellular angiofibroma" to both male and female lesions [5]. Extra-genital locations have been described [6].

The pathogenesis of this tumour is largely undetermined. We describe a case of para-testicular angiofibroma in a 32-year-old male who was on immunosuppressive drugs following renal transplantation.

Clinical history

A 32-year-old man presented with a 1-year history of a painless left scrotal mass, which had gradually increased in size. He had a previous history of end-stage renal failure, secondary to IgA nephropathy, which required cadaveric renal transplantation at the age of 27 and was on immunosuppressive drugs.

Five years following the transplantation, he developed a well-differentiated cutaneous squamous cell carcinoma, which was excised, and a left para-testicular mass.

Ultrasound examination of the testicular region revealed the presence of a solid para-testicular mass (Fig. 1). The mass was postero-lateral to the testis. Left orchidectomy was performed.

Materials and methods

The orchidectomy specimen showed a well-circumscribed mass, measuring 3.5×3×2.5 cm with a firm cut surface. The mass was separated from the testis by a distance of 0.7 cm (Fig. 2). The testis was unremarkable. Sections from the tumour mass were examined, and immunohistochemical

M. Sabah · E. Kay
Department of Histopathology,
Beaumont Hospital and Royal College of Surgeons in Ireland,
Dublin, Ireland

P. Mohan
Department of Urology and Renal Transplant,
Beaumont Hospital and Royal College of Surgeons in Ireland,
Dublin, Ireland

M. Sabah (✉)
Department of Pathology, Education and Research Centre,
The Royal College of Surgeons in Ireland, Beaumont Hospital,
Dublin 9, Ireland
e-mail: munasabah@gmail.com

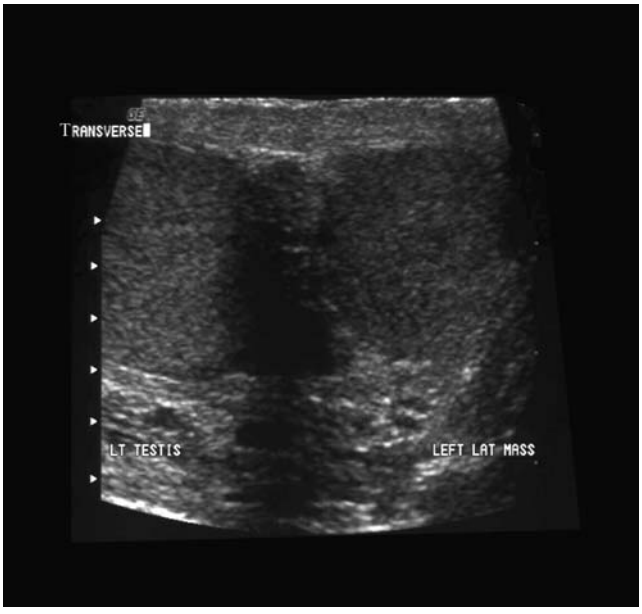

Fig. 1 Ultrasonography of the testis and the para-testicular mass

stains were performed. The antibody clones, dilutions and commercial sources are displayed in Table 1. Heat-induced antigen retrieval was performed, and the incubation period for the antibodies used was 32 min at 37°C.

Results

Haematoxylin- and eosin-stained sections of formalin-fixed, paraffin-embedded tissue revealed a bland spindle cell proliferation arranged in short intersecting fascicles. The stroma was made up of strands of collagen fibres and numerous small- to medium-sized blood vessels, some of which show perivascular hyaline fibrosis (Fig. 3). Foci of myxoid change were present. Mitotic figures were infrequent (1/10 HPFs). There was no evidence of necrosis or haemorrhage. Perivascular and interstitial lymphocytes and mast cells were seen.

The tumour cells showed eosinophilic cytoplasm and tapered nuclei. Focal nuclear pleomorphism was identified and was interpreted as being regenerative in nature. The tumour cells were strongly positive for vimentin and negative for desmin, actin, S100 protein, CD34, CD117, calretinin, epithelial membrane antigen (EMA) and oestrogen and progesterone receptors. At 1-year follow up, the patient was asymptomatic.

Table 1 A list of antibodies used, their clones, dilution and commercial sources

Antibody	Clone	Dilution	Commercial source
Vimentin	V9	1/1,000	DakoCytomation
Desmin	D33	1/75	DakoCytomation
Actin (smooth muscle)	1A4	1/150	DakoCytomation
S100 protein	Polyclonal	1/1,200	DakoCytomation
CD34	QBEnd10	1/30	DakoCytomation
EMA	E29	1/40	DakoCytomation
CD117	Polyclonal	1/30	DakoCytomation
Calretinin	Polyclonal	Neat	Cell Marque
ER	SP1	1/200	NeoMarkers
PR	SP2	1/200	NeoMarkers

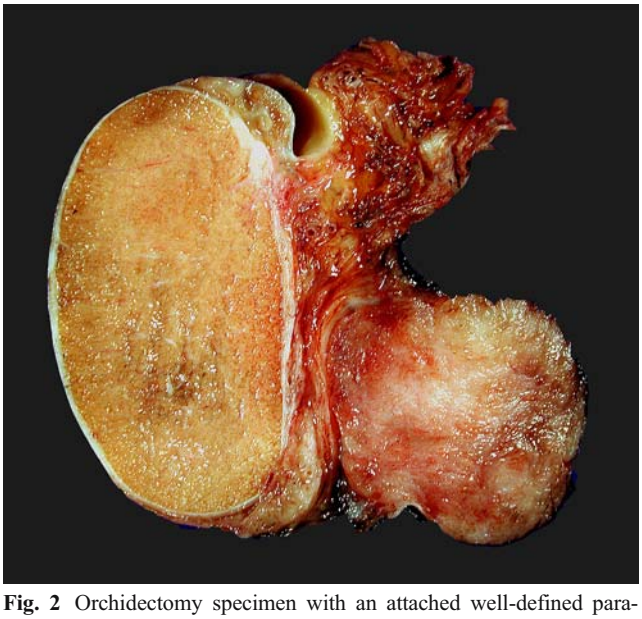

Fig. 2 Orchidectomy specimen with an attached well-defined para-testicular mass

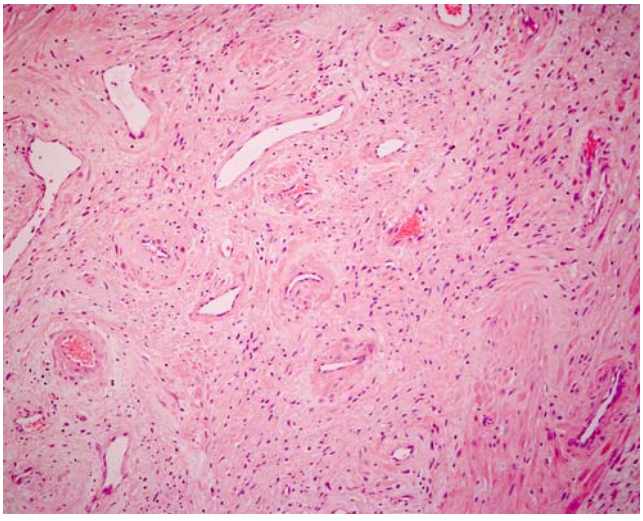

Fig. 3 Haematoxylin and eosin section of cellular angiofibroma showing spindle cell fascicles and numerous hyalinised blood vessels (original magnification ×100)

Discussion

Mesenchymal neoplasms of the genital tract occur predominantly in the uterus and also in the vulva, perineum and pelvic soft tissues. They have also been described in the inguino-scrotal region in males. These tumours often pose a practical diagnostic problem for surgical pathologists, not only because of the rarity of these lesions but also because of their overlapping morphologic features. Cellular angiofibroma is a recently described benign entity. There are few reports in the literature of cellular angiofibroma in the inguino-scrotal region of males. These consist of two series [9, 13] and two case reports [2, 19]. The tumour is well circumscribed and composed of spindle cells with prominent thick-walled stromal blood vessels. Local excision with negative margins is the treatment of choice. The differential diagnosis of this tumour in the inguino-scrotal region is wide and includes aggressive angiomyxoma, angiomyofibroblastoma, smooth muscle tumours, spindle cell lipoma, perineurioma and solitary fibrous tumour. Distinguishing the various entities is clinically important but may be difficult because of the overlapping morphologic features. Immunohistochemistry is of limited value, and histologic examination is the mainstay in the diagnosis of these entities.

Aggressive angiomyxoma is a non-metastasising, locally recurring tumour and therefore should be distinguished from cellular angiofibroma. Rare cases have been described in the genital region in males [8, 16]. The tumour has an infiltrative growth pattern and is composed of spindle cells embedded in a myxoid stroma with prominent blood vessels. The blood vessels are typically surrounded by smooth muscle cells. Mitotic figures are not generally seen. The cells are immunoreactive for vimentin, desmin, actin and CD34.

Angiomyofibroblastoma has been described in the inguino-scrotal region of men [16]. The tumour is well circumscribed and is characterised by alternating hyper- and hypo-cellular areas with numerous thin-walled capillary vessels. The cells have spindle-shaped nuclei with some cases showing epithelioid morphology. The cells typically express desmin and are occasionally actin-positive [16].

Solitary fibrous tumour shows a patternless architecture with alternating hyper- and hypo-cellular areas. The stroma contains keloid-type collagen with haemangiopericytoma-like blood vessels.

Spindle cell lipoma occurs predominantly in the head and neck region but has been described in the groin in males [1]. The lesion has a conspicuous amount of adipose tissue. The stroma contains thick bundles of brightly eosinophilic collagen, and the blood vessels are inconspicuous [9]. The spindle cells are CD34-positive.

Smooth muscle tumours must be distinguished from cellular angiofibroma, given the tendency of cellular angiofibroma to have frequent mitoses and the significance of mitotic activity as being indicative of malignancy if encountered in smooth muscle tumours [16]. The characteristic blood vessels in cellular angiofibroma are helpful features. In addition, the cells in cellular angiofibroma lack the characteristic features of smooth muscle cells, namely, the presence of abundant eosinophilic cytoplasm and cigar-shaped nuclei. Desmin-positive immunostaining has been reported in cellular angiofibroma arising in inguino-scrotal region [13, 16].

Perineurioma is a benign tumour with a whorled growth pattern. The cells are positive for EMA.

The pathogenesis of cellular angiofibroma is largely undetermined. Some studies have identified positive expression of oestrogen and progesterone receptors in lesions from both females [3, 9, 10, 12, 14, 15] and males [9, 13, 19], suggesting that hormonal influences may be implicated in the genesis of these neoplasms [16]. In this case, both oestrogen and progesterone receptors were negative.

The role of immunosuppressive therapy in the tumourigenesis of benign and malignant soft tissue lesions is well documented [4, 7, 11, 18, 20]. This is the first reported case of cellular angiofibroma in an immunosuppressed patient. While this may represent a coincidental finding, the role of long-term immunosuppressive drugs in the genesis of this tumour awaits further analysis.

Acknowledgment The authors thank Professor C. Fletcher for confirming the diagnosis.

References

1. Beham A, Schmid C, Hodl S, Fletcher CD (1989) Spindle cell and pleomorphic lipoma: an immunohistochemical study and histogenetic analysis. J Pathol 158:219–222
2. Canales BK, Weiland D, Hoffman N, Slaton J, Tran M, Manivel JC, Monga M (2006) Angiomyofibroblastoma-like tumors (cellular angiofibroma). Int J Urol 13:177–179
3. Dargent JL, de Saint AN, Galdon MG, Valaeys V, Cornut P, Noel JC (2003) Cellular angiofibroma of the vulva: a clinicopathological study of two cases with documentation of some unusual features and review of the literature. J Cutan Pathol 30:405–411
4. Deyrup AT, Lee VK, Hill CE, Cheuk W, Toh HC, Kesavan S, Chan EW, Weiss SW (2006) Epstein–Barr virus-associated smooth muscle tumors are distinctive mesenchymal tumors reflecting multiple infection events: a clinicopathologic and molecular analysis of 29 tumors from 19 patients. Am J Surg Pathol 30:75–82
5. Fletcher CD, Unni KK, Mertens F (eds) (2002) World Health Organization classification of tumours: pathology and genetics of tumours of soft tissue and bone. IARC Press, Lyon, France, pp 73–74
6. Garijo MF, Val-Bernal JF (1998) Extravulvar subcutaneous cellular angiofibroma. J Cutan Pathol 25:327–332
7. Gomez-Roman JJ, Ocejo-Vinyals G, Sanchez-Velasco P, Nieto EH, Leyva-Cobian F, Val-Bernal JF (2000) Presence of human

herpesvirus-8 DNA sequences and overexpression of human IL-6 and cyclin D1 in inflammatory myofibroblastic tumor (inflammatory pseudotumor). Lab Invest 80:1121–1126
8. Iezzoni JC, Fechner RE, Wong LS, Rosai J (1995) Aggressive angiomyxoma in males. A report of four cases. Am J Clin Pathol 104:391–396
9. Iwasa Y, Fletcher CD (2004) Cellular angiofibroma: clinicopathologic and immunohistochemical analysis of 51 cases. Am J Surg Pathol 28:1426–1435
10. Kerkuta R, Kennedy CM, Benda JA, Galask RP (2005) Vulvar cellular angiofibroma: a case report. Am J Obstet Gynecol 193:1750–1752
11. Lai KN, Lai FM, King WW, Li PK, Siu D, Leung CB, Lui SF (1995) Dermatofibrosarcoma protuberans in a renal transplant patient. Aust NZJ Surg 65:900–902
12. Lane JE, Walker AN, Mullis EN Jr, Etheridge JG (2001) Cellular angiofibroma of the vulva. Gynecol Oncol 81:326–329
13. Laskin WB, Fetsch JF, Mostofi FK (1998) Angiomyofibroblastomalike tumor of the male genital tract: analysis of 11 cases with comparison to female angiomyofibroblastoma and spindle cell lipoma. Am J Surg Pathol 22:6–16
14. McCluggage WG, Ganesan R, Hirschowitz L, Rollason TP (2004) Cellular angiofibroma and related fibromatous lesions of the vulva: report of a series of cases with a morphological spectrum wider than previously described. Histopathology 45:360–368
15. McCluggage WG, Perenyei M, Irwin ST (2002) Recurrent cellular angiofibroma of the vulva. J Clin Pathol 55:477–479
16. Nucci MR, Fletcher CD (2000) Vulvovaginal soft tissue tumours: update and review. Histopathology 36:97–108
17. Nucci MR, Granter SR, Fletcher CD (1997) Cellular angiofibroma: a benign neoplasm distinct from angiomyofibroblastoma and spindle cell lipoma. Am J Surg Pathol 21:636–644
18. Peres E, Mattoo TK, Poulik J, Warrier I (2005) Primitive neuroectodermal tumor (PNET) of the uterus in a renal allograft patient: a case report. Pediatr Blood Cancer 44:283–285
19. Shintaku M, Naitou M, Nakashima Y (2002) Angiomyofibroblastoma-like tumor (lipomatous variant) of the inguinal region of a male patient. Pathol Int 52:619–622
20. Winkelhorst JT, Brokelman WJ, Tiggeler RG, Wobbes T (2001) Incidence and clinical course of de-novo malignancies in renal allograft recipients. Eur J Surg Oncol 27:409–413

Virchows Arch (2006) 449:493–494
DOI 10.1007/s00428-006-0283-5

LETTER TO THE EDITOR

Chondrosarcomatous differentiation of a metastatic leiomyosarcoma of the uterus

Ivan Damjanov · Fang Fan

Received: 28 March 2006 / Accepted: 21 July 2006 / Published online: 16 August 2006
© Springer-Verlag 2006

Sir,

We read with interest the case report of a groin leiomyosarcoma, which, upon recurrence of the primary tumor, showed heterologous osteosarcomatous differentiation [1]. Even though some osteoid formation may be found in malignant fibrous histiocytomas of soft tissues of the giant cell type and so-called malignant mesenchymomas of soft tissues [2], transdifferentiation of soft tissue leiomyosarcomas into osteosarcoma described by Grabellus et al. [1] appears to be extremely uncommon. Hence, their case is unique by all standards.

We would like to report here that unexpected aberrant differentiation or "transdifferentiation" may occur not only in recurrent soft tissue leiomyosarcomas, but also in metastases of malignant smooth muscle cell tumors of the uterus.

The patient was a 42-year-old female who had hysterectomy for uterine leiomyosarcoma in April of 2002. She also had subsequent radiation therapy, which concluded in June 2002. In April 2005, the patient presented with a lump in her right lower quadrant. CT scan showed an enhancing soft tissue mass in the anterior right rectus muscle compatible with metastasis. Fine needle aspiration biopsy proved that the tumor was a leiomyosarcoma, consistent with a metastasis from the primary uterine leiomyosarcoma. The lesion was resected.

Grossly, the tumor was a 2.5-cm well-circumscribed nodular mass with a firm cut surface. Microscopically, the tumor was composed of malignant smooth muscle cells that resembled the original leiomyosarcoma of the uterus (Fig. 1a). In addition to these areas, the metastatic foci contained multiple foci of chondrosarcoma (Fig. 1b). The malignant spindle cells reacted with antibodies to smooth muscle actin (Fig. 1c) and desmin, and the chondrosarcomatous area reacted with the antibody to S-100 (Fig. 1d).

In view of the microscopic findings in the metastatic tumor, we reviewed the slides of the uterine tumor. No signs of chondroblastic differentiation were seen. There were actually no other mesenchymal heterologous elements to indicate that the tumor was a uterine malignant mesenchymoma [3]. Hence, we concluded that the chondrosarcomatous component arose through a novel form of differentiation of the malignant stem cells or transdifferentiation of the original leiomyosarcoma.

In our case, the heterologous differentiation of leiomyosarcoma occurred in the metastasis, whereas in the case reported by Grabellus [1], it occurred in the recurrent tumor. This phenotypic change could have occurred incidentally, but it is also possible that the new conditions

I. Damjanov (✉) · F. Fan
Department of Pathology,
The University of Kansas School of Medicine,
Kansas City, KS 66160, USA
e-mail: idamjano@kumc.edu

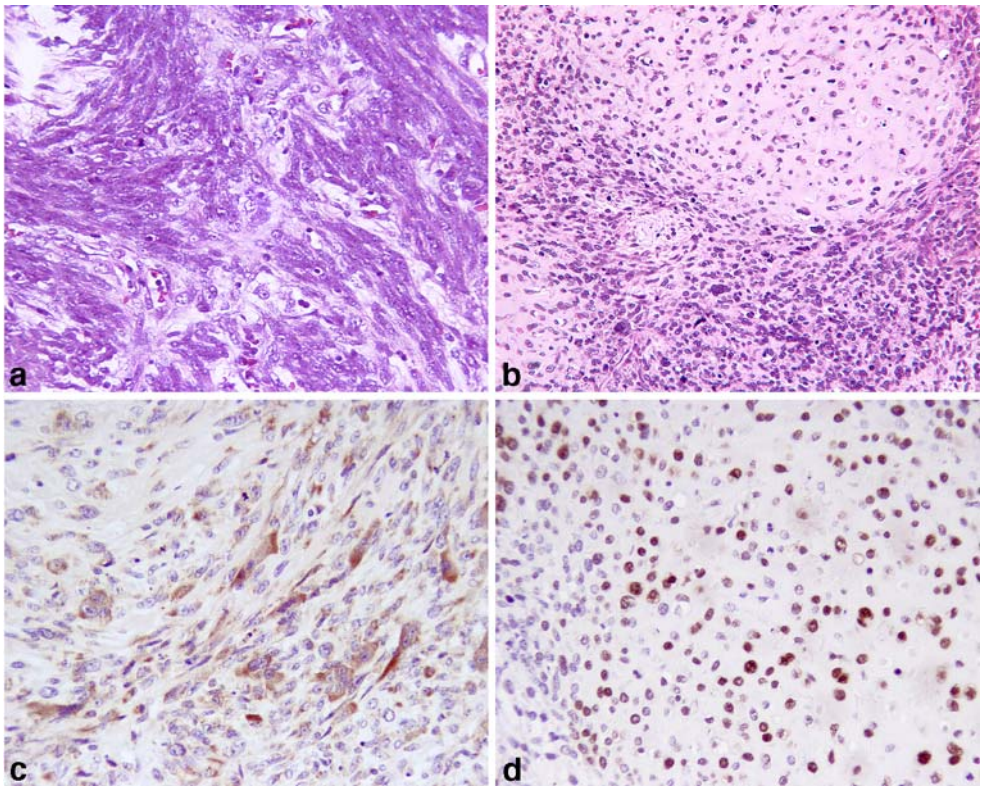

Fig. 1 Metastatic leiomyosarcoma with chondrosarcomatous differentiation. **a** The patient's uterine leiomyosarcoma four years ago. **b** The current metastatic tumor with two components, the leiomyosarcomatous component, and the chondrosarcomatous component. **c** The leiomyosarcomatous component stains with antibodies to smooth muscle actin. **d** The chondrosarcomatous component stains with the antibodies to S-100

of growth at the site of recurrence or metastasis favored aberrant differentiation.

References

1. Grabellus F, Sheu S-Y, Schmidt R, Kuhnen C, Flasshove M, Ruchholtz S, Taeger M, Schmid KW (2006) Recurrent high-grade leiomyosarcoma with heterologous osteosarcomatous differentiation. Virchows Arch 448:85–89
2. Kew CC, Putti TC, Razvi K (2004) Malignant mesenchymoma arising from a uterine leiomyoma in the menopause. Gynecol Oncol 95:712–715
3. Mentzel T, Fletcher CD (1994) Malignant mesenchymomas of soft tissue associated with numerous osteoclast-like giant cells mimicking the so-called giant cell variant of "malignant fibrous histiocytoma." Virchows Arch 424:539–545

Virchows Arch (2006) 449:495–497
DOI 10.1007/s00428-006-0269-3

LETTER TO THE EDITOR

A forgotten Italian pathologist: Angelo Maffucci (1845–1903) and his scientific thought

Rosalba Ciranni

Received: 3 June 2006 / Accepted: 4 July 2006 / Published online: 29 August 2006
© Springer-Verlag 2006

Sir, it often happens that for unknown reasons personages of great talent, culture, and humanity remain disowned by the world although they have contributed with their work to the evolution of knowledge. Angelo Maffucci was one of these people (Fig. 1).

He was born in 1845 in Calitri, (Avellino, Italy), from a well-off farming family. In 1873, he graduated in medicine at the University of Naples and was awarded the Medal of Merit for his active participation in the struggle against cholera at the Hospital for the Incurable. Two years later, in 1875, he started his scientific work as surgeon and pathologist at the Institute of Pathology of the same University [1]. In that period, he described in detail a disease affecting both the cartilage and blood vessels of a woman who had been hospitalized there. She had never suffered from any important diseases, but her body was deformed as a result of skeletal malformations due to the presence of more than 80 tumors that were large: "from a pea [...] to a small orange, to a foetus head" and affected her arms, hands, left humerus, legs, and feet. The patient suffered from frequent and severe haemorrhages caused by the malformed vessels and underwent amputation of one of her arms. Unfortunately, the stump gangrened and soon after the woman died of pyemia [2].

R. Ciranni
Section of History of Medicine, First Division of Pathology,
Department of Oncology,
Transplants and Advanced Technologies in Medicine,
Pisa University,
Pisa, Italy

R. Ciranni (✉)
Department of Oncology, Medical School,
Pisa University,
via Roma 57,
56126 Pisa, Italy

Maffucci performed autopsy and histological examination of the body, and described all the features of this disorder characterized by benign overgrowths of the cartilage (enchondromatosis), and by dark red irregularly shaped patches of skin (multiple cavernous hemangiomas). He reported the case in a manuscript illustrated with a series of handmade sketches and published in an Italian medical journal in 1881 (Figs. 2 and 3) [2]. The disease in question is quite rare (less than 200 cases are reported in literature) and arises during childhood (4–5 years), independent of race and sex.

The etiology is unclear, but genetic involvement of the mesenchymal cells has been hypothesized recently [3]. Maffucci's descriptions are still topical: the venous malformation appeared in the form of soft bluish nodules made up of a spongy matrix organized in large cavernous vascular spaces, full of blood and separated by connectival stroma; the enchondromas seemed to develop from residues of hyaline cartilage, which underwent a process of proliferation and growth [2, 3]. Sixty years later, Alice Carleton called the disease "Maffucci's Syndrome" [4].

Angelo Maffucci was, for a short period, Professor of Pathology at the University of Catania and, in 1884, when the Faculty of Medicine of the University of Pisa inaugurated the new chair of pathology, Maffucci was appointed first director. In Pisa, he founded the Museum and the Institute of Human Pathology where he started his successful career as experimental researcher and teacher. Under his guide, Pisa was probably the first Italian University where students had the possibility to associate theoretical instruction with practical activity [1].

One of his most important experimental scientific contributions was in the field of infectious embryopathology of the anthrax and of tuberculosis [5–7]. In the course of his experiments carried out on fowls, he isolated

Fig. 1 Angelo Maffucci's portrait (particular)

the avian bacillus, asserting, for the first time, that avian tuberculosis has a different aetiology from the bovine and human forms [8, 9]. This revolutionary theory caused a strong scientific conflict with Robert Koch who did not believe in the doctrine of pleomorphism usually applied to bacteria. In spite of the frictions, Maffucci was the only scientist Koch considered worthy of mention, together with Pasteur, as confirmed by the famous speech given in Berlin during the X Internationalen Medicinischen Kongresses in 1890. The same Koch wanted Maffucci to act as vice President in the next conference in London [10].

Ten years later, both for his ideas on experimental pathology and for his modern scientific thought the *Accademia dei Lincei* chose him—instead of Ettore Marchiafava (1847–1935)—to represent Italian pathology abroad.

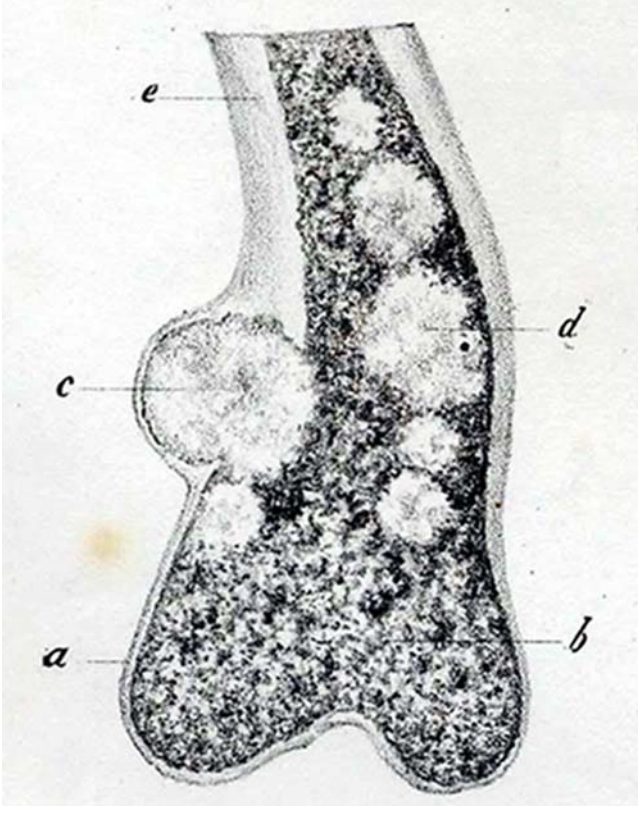

Fig. 2 Maffucci's syndrome: inferior epiphysis of the right femur (3–4 Hartnak). **a** Connecting cartilage; **b** spongy matrix; **c** small enchondroma covered by periosteum; **dd′** cartilaginous nuclei; **e** compact bone. (Maffucci designer, Onufrio incisor, 1881, original legend)

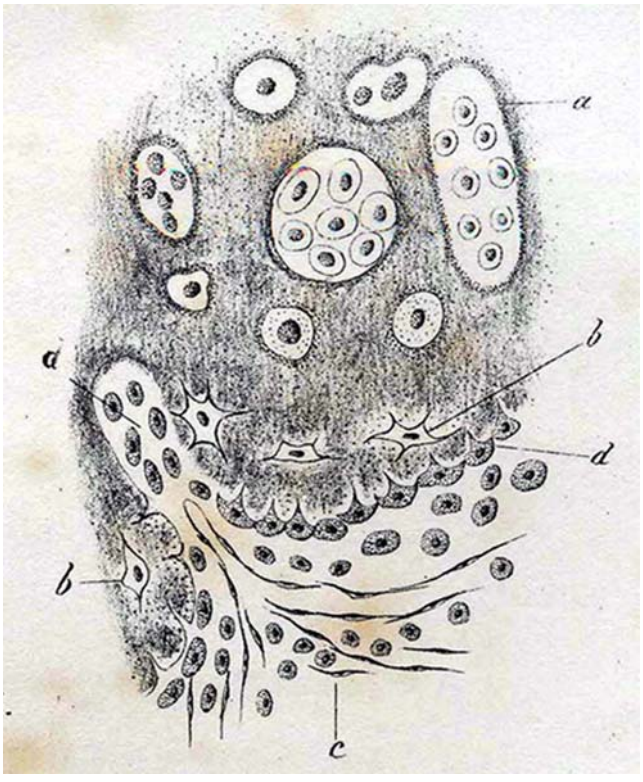

Fig. 3 Maffucci's syndrome: cartilaginous nuclei of the right femour (3–4 Hartnak). **a** Cartilaginous capsula full of cells (*calcified area*); **bb′** bone neoformation whith corpuscles, **c** bone marrow and capillar; **dd′** osteoblastes (Maffucci designer, Onufrio incisor, 1881, original legend)

His studies on infectious embryo-pathology, carried out for about 20 years, represent the most important evidence of his modern conception of experimental pathology. Thanks to his experiments, Maffucci was able to answer five major questions concerning tuberculosis (reaction of the chick embryo to infections and to direct microbic intoxication; the effects of tuberculous chicks on the offspring; the mechanisms of hereditary transmission of the tubercular bacillus and of the relative toxin in mammals (rabbits); the effects of tuberculous mammals on the offspring and the results of tubercular intoxication caused on the female mated to a tuberculous male), providing a solid experimental basis to the knowledge of infectivology in general and of human tuberculosis in particular.

For his important contribution in the field of research and for his brilliant ideas—like that of infecting eggs of fowls artificially to avoid maternal interferences—the National Academy of Sciences awarded him a gold medal in 1903 [11, 12].

In the last years of his life his pioneering research provided the basis for future studies on tubercular vaccines from living bacilli [13].

The most outstanding and original scientific interests of Maffucci can be divided into three important groups: infectious embryo-toxicity, tuberculosis, and micotic aetiology of tumors. His scientific production consists of more than 100 publications (enriched with his massive collection of personal notes, sketchbooks, and watercolors), the reconstruction of which is unfortunately still incomplete. In the pages of a small album that he always carried with him, he methodically outlined the histological profile of the pathologies of the nervous system, in particular, the *cauda equina*, and the hereditary effects of syphilis in the liver, lung, and bones of luetic fetuses. Moreover, he described exhaustively the cellular lesions determined by hepatic cirrhosis and by malignant lymphoma, contributing to demonstrate their occasional infectious aetiology.

His private correspondence with Baumgartner, Camillo Golgi, Bizzozzero, Ziegler, Ettore Marchiafava, and many other colleagues who witnessed that he was held in high esteem and great respect both as a man and scientist by the international scientific community.

He died of malaria in Pisa on 24 November 1903, contributing a large sum to the University for the endowment of a 2-year postgraduate grant for a degree in pathological anatomy [1].

Acknowledgements I would like to thank Dr. Laura Cignoni (C.N. R, Pisa) for revising the English; Patrizia Ciucci, Livia Iannucci and Fabiana Galizia of the Library of the Faculty of Medicine and Surgery (Pisa University).

References

1. Ciranni R, Giuffra V, Maritozzi S, Fornaciari G (2004) Angelo Maria Maffucci (1847–1903) and the beginning of pathological anatomy in Pisa. Med Secoli 16(1):31–41
2. Maffucci AM (1881) Di un caso di encondroma ed angioma multiplo. Contribuzione alla genesi embrionale dei tumori. Mov Med Chir Napoli 13:399–412
3. Cotran RS, Kumar V, Robbins SL (2005) Basic pathology. W.B. Saunders, Pennsylvania
4. Carleton A, Elkington JSC, Greenfield JG, Robb-Smith AHT (1942) Maffucci's Syndrome (dyschondroplasia with haemangeiomata). Q. J. Med 11:203–228
5. Maffucci A (1894) Sulla patologia embrionale infettiva, Il Policlinico (Sez Chir) 1:33–43
6. Maffucci A, Baquis E (1886) Sull'azione del virus carbonchioso sull'embrione di pollo. Rivista internazionale 3:445–460
7. Maffucci A (1888) Sull'infezione tubercolare degli embrioni di pollo. Tip. Nistri, Pisa
8. Maffucci A (1890) Beitrag zur Aetiologie der Tubercolose (Hünertubercolose). Zent Bl Allg Pathol Pathol Anat 10:409–416
9. Maffucci A (1890) Contribuzione all'etiologia della tubercolosi (tubercolosi dei gallinacei). Riforma Med 1:710–721
10. Koch R (1891) Ueber bakteriologische Forschung. In: Verhandlungen des X Internationalen Medicinischen Congresses Berlin, Verlag von August Hirschwald. Berlin 1:35–47
11. Maffucci A (1902) Patologia embrionale infettiva. Intorno alla fisiopatologia dell'embrione. Memoria I. Atti della Reale Accademia dei Lincei, CCXCIX
12. Blaserna P, Cannizzaro S, Grassi B (1905) Relazione sul premio per le scienze fisiche e naturali per l'anno 1903. In: Memorie di Matematica e Fisica della Società Italiana delle Scienze, Reale Accademia dei Lincei Serie 3a. Tomo XIII:18–24
13. Maffucci A, Di Vestea A (1901) Della sieroterapia della tubercolosi. Riv. Igiene e Sanità Pubblica 12:46–57

Virchows Arch (2006) 449: 498
DOI 10.1007/s00428-006-0309-z
© Springer-Verlag 2006

ANNOUNCEMENTS

29 November–1 December 2006
Combined Adult and Congenital Cardiovascular Pathology Course
London, UK

Course Organisers:
M. N. Sheppard, Y. Ho

Course fee:
£ 400.-
£300.- special fee for juniors in training

For further information please contact:
Short Course Office
National Heart and Lung Institute
Dovehouse Street
London SW3 6LY, UK
Fax: 0044 -020-7351-8346
e-mail: shortcourse.NHLI@IC.AC.UK

24–26 January 2007
Theorico-practical Course on Bone and Soft Tissue Tumors
Department of Pathology, Hospital del Mar, Barcelona, Spain

Faculty
Christopher Fletcher, M.D. (Brigham and Women's Hospital, Boston, USA)
Andrew Rosenberg, M.D. (Massachusetts General Hospital, Boston, USA)
Angelo Paolo Dei Tos, M.D. (Hospital of Treviso, Italy)
John Goldblum, M.D. (Cleveland Clinic, Cleveland, USA)
Paola Dal Cin, Ph.D. (Brigham and Women's Hospital, Boston, USA)

For further information please contact:
Francisco Alameda, M.D.
Department of Pathology
Hospital del Mar, Spain
E-mail: 86780@imas.imim.es
or
Esther Oliva, M.D.
Department of Pathology
Massachusetts General Hospital
55 Fruit Street, WRN-2
Boston, MA 02114, USA
E-mail: eoliva@partners.org

Virchows Arch (2006) 449:499–506
DOI 10.1007/s00428-006-0306-2

REVIEW ARTICLE

The grey zone between pure (neuro)endocrine and non-(neuro)endocrine tumours: a comment on concepts and classification of mixed exocrine–endocrine neoplasms

Marco Volante · Guido Rindi · Mauro Papotti

Received: 12 June 2006 / Accepted: 28 August 2006 / Published online: 11 October 2006
© Springer-Verlag 2006

Abstract Terms such as "mixed endocrine–exocrine carcinoma" (MEEC) and "adenocarcinoma with neuroendocrine (NE) differentiation" (ADC-NE) identify tumours belonging to the spectrum of neoplasms with divergent exocrine and (neuro)endocrine differentiation. These tumours display variable quantitative extent of the two components, potentially ranging from 1 to 99%, and variable structural patterns, ranging from single scattered NE cells to a well-defined NE tumour cell population organized in organoid, trabecular or solid growth patterns. In the present report, the grey zone of tumours/carcinomas with mixed NE and non-NE features is explored for various organs. From a practical point of view, MEECs differ from carcinomas with focal NE differentiation by (1) the extension of each component (more than 30%) and (2) the structural pattern of the NE component, either organoid for well-differentiated or solid/diffuse for poorly differentiated cases. In MEECs, the most aggressive cell population drives the clinical behaviour. Conversely, ADC-NE generally do not show a different clinical outcome, compared to the corresponding conventional forms, except for prostatic adenocarcinoma, in which NE cells are a negative prognostic factor. The recognition of MEECs may be of relevance for a targeted therapeutic strategy, foreseeing the use of biotherapies similar to those proposed for pure NE tumours.

M. Volante · M. Papotti (✉)
Department of Clinical and Biological Sciences,
University of Turin and San Luigi Hospital,
Regione Gonzole10,
10043 Orbassano-Torino, Italy
e-mail: mauro.papotti@unito.it

G. Rindi
Department of Pathology, University of Parma,
Parma, Italy

Keywords Neuroendocrine differentiation · Adenocarcinoma · Mixed endocrine–exocrine carcinoma · Diagnosis

Background

Human cancers displaying a combination of neuroendocrine (NE) and conventional (glandular, squamous or urothelial) features are a well-known occurrence in various organs.

The spectrum of (neuro)endocrine and exocrine differentiation in tumours is schematically depicted in Fig. 1. Between the two extremes occupied by pure NE and pure non-NE neoplasms, the spectrum of tumours having mixed divergent differentiation along NE and non-NE lineages displays a variable extension of the two components (potentially ranging from 1 to 99%), and also, variable morphological patterns (ranging from the single NE cell scattered in conventional (adeno)carcinoma cells, to a well-identifiable NE tumour cell population organized in the known organoid, trabecular or solid NE growth patterns). The reverse condition (i.e., focal non-NE differentiation in almost pure NE tumours) is less common, being restricted to small-cell lung carcinomas with focal glandular or squamous components.

Different terms have been employed to label such tumours based on both the extent and the structural patterns of the individual components (Table 1). Among these, the World Health Organization (WHO) classification of endocrine tumours proposed the term "mixed exocrine–endocrine carcinoma" (MEEC) for cases that originated in the pancreas, stomach and appendix [53]. By converse, "adenocarcinoma with NE differentiation" was the most common labeling used in tumours of the breast, prostate and colon [9, 10, 13, 16, 20, 25, 53, 54]. In the lung, both

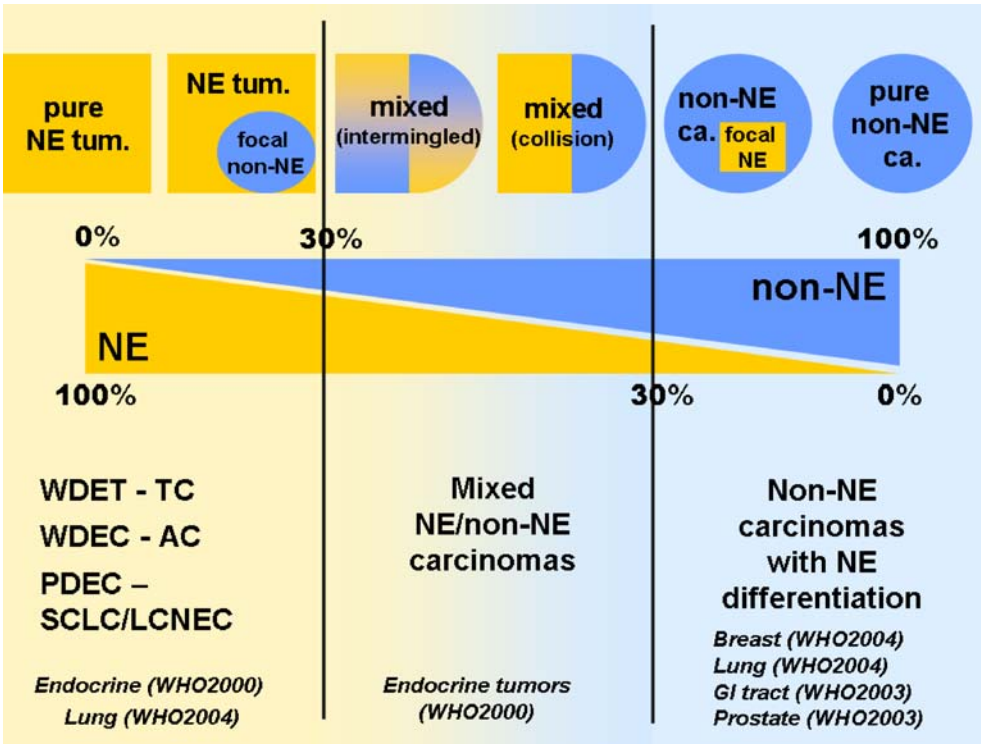

Fig. 1 Schematic representation of NE differentiation in human tumors. *NE* Neuroendocrine, *WDET* well differentiated endocrine tumor, *TC* typical (lung) carcinoid, *WDEC* well-differentiated endocrine carcinoma, *AC* atypical (lung) carcinoid, *PDEC* poorly differentiated endocrine carcinoma, *SCLC* small cell lung carcinoma, *LCNEC* large cell neuroendocrine carcinoma, *GI* gastrointestinal

non-small-cell carcinomas with focal NE differentiation [1, 29] and combined ("mixed") small-cell and non-small-cell carcinomas (most frequently squamous or glandular components) have been reported [56].

Almost 20 years ago, Lewin [34] proposed a nomenclature for mixed exocrine–endocrine tumours in which three separate patterns were recognized: (a) the exocrine and endocrine areas were admixed within the same tumour mass comprising at least one third of the tumour; (b) the phenotypic mixture was at the cellular level, i.e., amphicrine cells composed the whole tumour cell population and (c) the exocrine and endocrine areas were juxtaposed without mixture within the same tumour mass, thus, defining the typical "collision tumour"; this study by Lewin has the merit of introducing the criterion of the extent of the NE cell component, which is, incidentally, the one still currently used (i.e., 30%) and of keeping as a separate entity the so-called collision tumours, which should be kept clearly separate, from both a pathogenetic and a classificative point of view, from the former two entities (as, for example, in the pancreas) [33].

Table 1 Terms in use to define tumors with mixed exocrine–endocrine features

CURRENT TERMINOLOGY
– Mixed exo–endocrine tumor or carcinoma
– Composite glandular–endocrine tumor or carcinoma
– Combined exocrine–NE tumor or carcinoma
– Collision tumor (adenocarcinoma+carcinoid/small cell carcinoma)
– NE differentiated adenocarcinoma
– Adenocarcinoma with (focal) NE differentiation
– (adeno)Carcinoma with divergent differentiation
– Multidirectionally differentiated carcinoma
– Endocrine mucin-producing carcinoma
– Amphicrine tumor
– Adenocarcinoid
– Goblet cell carcinoid
– Mucinous carcinoid

The described morphological, immunophenotypical and terminological heterogeneity in these tumours has, so far, obtained limited clinical attention, mainly due to the low prognostic impact of NE differentiation in conventional (adeno)carcinomas. A possible exception is prostatic adenocarcinoma, in which the NE cell component was shown to be a negative prognostic factor [3, 5, 52].

Aim of the present report is to explore the grey zone of tumours/carcinomas with mixed non-NE and NE features in various organs and to discuss whether a unifying concept for such heterogeneous group of tumours is possible.

Pure (neuro)endocrine tumours

Neuroendocrine tumours classically arise in the gastrointestinal tract, pancreas, lung and thymus. Endocrine glands such as parathyroid, pituitary, thyroid and adrenal may also host neuroendocrine tumours (which are labelled with different terms, including adenoma, carcinoma, medullary

carcinoma, pheochromocytoma, etc). According to the widely used terminology adopted for the lung, the spectrum of NE tumours include typical and atypical (malignant) carcinoids and poorly differentiated (small cell) NE carcinomas [56]. The former two are referred to as well-differentiated endocrine tumour or carcinoma, respectively, according to the WHO classification of endocrine tumours which specifically took into consideration gastroentero–pancreatic NE tumours [14, 25, 53].

The most recent entry of the list of pure NE tumours is the large-cell NE carcinoma (LCNEC), described in 1991 in the lung [55] and now recognized in several other non-NE organs, including parotid, larynx, gallbladder, rectum, kidney, ampulla, urinary bladder, uterus, prostate [12, 17, 18, 21, 24, 36–38, 45]. Also, the other pure forms of NE tumours (carcinoids and small-cell carcinomas) can exceptionally develop in non-NE organs, including the skin, larynx, parotid, breast, gallbladder, uterine cervix, bladder and prostate [9, 10, 16, 20, 26, 49, 54, 59]. Needless to say, these NE tumours are, in all, similar to those developed in other classical locations and differ in morphology and phenotype from carcinomas with NE differentiation.

Ne tumours with focal non-NE component (<30%)

Rare forms of well-differentiated NE tumours (carcinoids) were found to contain a variable amount of exocrine (mucinous) cells, admixed with the neuroendocrine cell population. The tumour cell phenotype differed from that of pure NE or exocrine cells only in the exceptional occurrence of amphicrine elements, so defined by the co-existence of exocrine and neuroendocrine differentiation within the same cell [11, 47]. These tumours were referred to as goblet cell carcinoids or signet ring cell carcinoids or adeno-carcinoids, have been more commonly described in the appendix and are de facto mixed exocrine–endocrine tumours, although the exocrine cell population may not reach the requested threshold of 30% (see below) [53]. Other rare cases have been described, mostly in the pancreas in which a pure NE tumour, functioning or nonfunctioning, had focal areas of acinar [41] or ductal differentiation, never exceeding 5–10% of tumour area [15]. Although it has been suggested that ductular structures may represent an intrinsic neoplastic component of the tumour [15], more recent molecular evidence claimed that the ductular component occasionally found in pancreatic endocrine tumours is the result of entrapment of preexisting nonneoplastic ductules and that the tumours are otherwise not distinctive from conventional pancreatic endocrine tumours [57].

Finally, small-cell carcinomas, mostly of the lung, can grow in combined forms, being this latter sometimes characterized by minimal glandular or squamous component, and are again classified in the group of combined (mixed endocrine–exocrine) carcinomas [56]. Probably, the phenomenon of non-NE-differentiated lineages in predominantly NE tumours is more common than expected and simply has never been thoroughly investigated, in spite of the possible clinical relevance given the higher aggressive potential of transformed exocrine cells. In this respect, several data in breast cancer have indicated that NE-differentiated carcinomas contain a spectrum of mixed amphicrine cell types, including focal apocrine differentiation in tumours with an organoid growth pattern and extensive chromogranin immunoreactivity [50].

Mixed exocrine–endocrine carcinomas (NE or non-NE cells >30%)

The WHO classification of endocrine tumours has incorporated mixed endocrine–exocrine carcinomas (MEEC) in the section on endocrine tumours of the pancreas and briefly commented of these forms in the paragraphs on stomach and appendiceal endocrine tumours [53]. In the pancreas and stomach, these were defined as epithelial malignant tumours characterised by a combination of a predominant exocrine component and a NE cell subpopulation represented by at least one-third of the tumour area [14, 25, 53].

MEEC can be encountered not only in the pancreas [40], but virtually at all sites, being prostate and breast among the most common locations [16, 54] and also in the organs where pure carcinoid tumours are usually found (e.g., gastroenteric tract and lung) [26]. MEECs are distinguished (at least from a morphological viewpoint) from adenocarcinomas with neuroendocrine differentiation by the more limited NE cells component in these latter. In the lung, combined forms are recognized as variants of small-cell carcinoma (code # 8045/3), which contain areas of classical small-cell cancer admixed with foci of squamous or glandular differentiation [56].

In the literature, the definition of MEEC and the distinguishing criteria from carcinomas with NE differentiation are not uniform: some take into account the extension of the NE component only, while others consider type and extent of the observed morphological patterns [9, 10, 20, 34, 49, 59]. This lack of standardization created several controversies in both fields of tumour recognition and treatment of these lesions. In addition, especially in pulmonary and gastroenteropancreatic sites, a relatively wide spectrum (and possibly a continuum) of NE-differentiated tumours does exist including tumours with well-represented (>30% of tumour area) NE cell component and tumours with scattered NE cells only [1, 32, 40, 42, 43, 49].

With regard to the criterion of extension of the NE component within the tumour, the “rule” of at least 30% of

NE-differentiated areas allows to consider as true MEECs those tumours with a well-represented or significant NE cell population, only. On the other hand, however, no reasonable explanation is provided for this limit from both a pathogenetic and histogenetic point of view. In addition, the morphological criterion appears essential for the definition of MEEC and intrinsic to the rule of 30%, as those cases with a well-represented NE component are easily recognized as such (Fig. 1). Indeed, MEECs are the result of intermingling of frankly glandular areas with typical organoid NE areas (in the case of a well-differentiated tumour) or classical small-cell carcinoma areas. This latter pattern is relatively common in lung cancer where it is recognized as a variant (combined small-cell carcinoma, ICD 8045/3) of small-cell carcinoma in the WHO classification of lung tumours [56]. Rarely, this combination has been described in gastrointestinal (Fig. 2a,b), breast and prostatic adenocarcinomas. The criterion of the structural

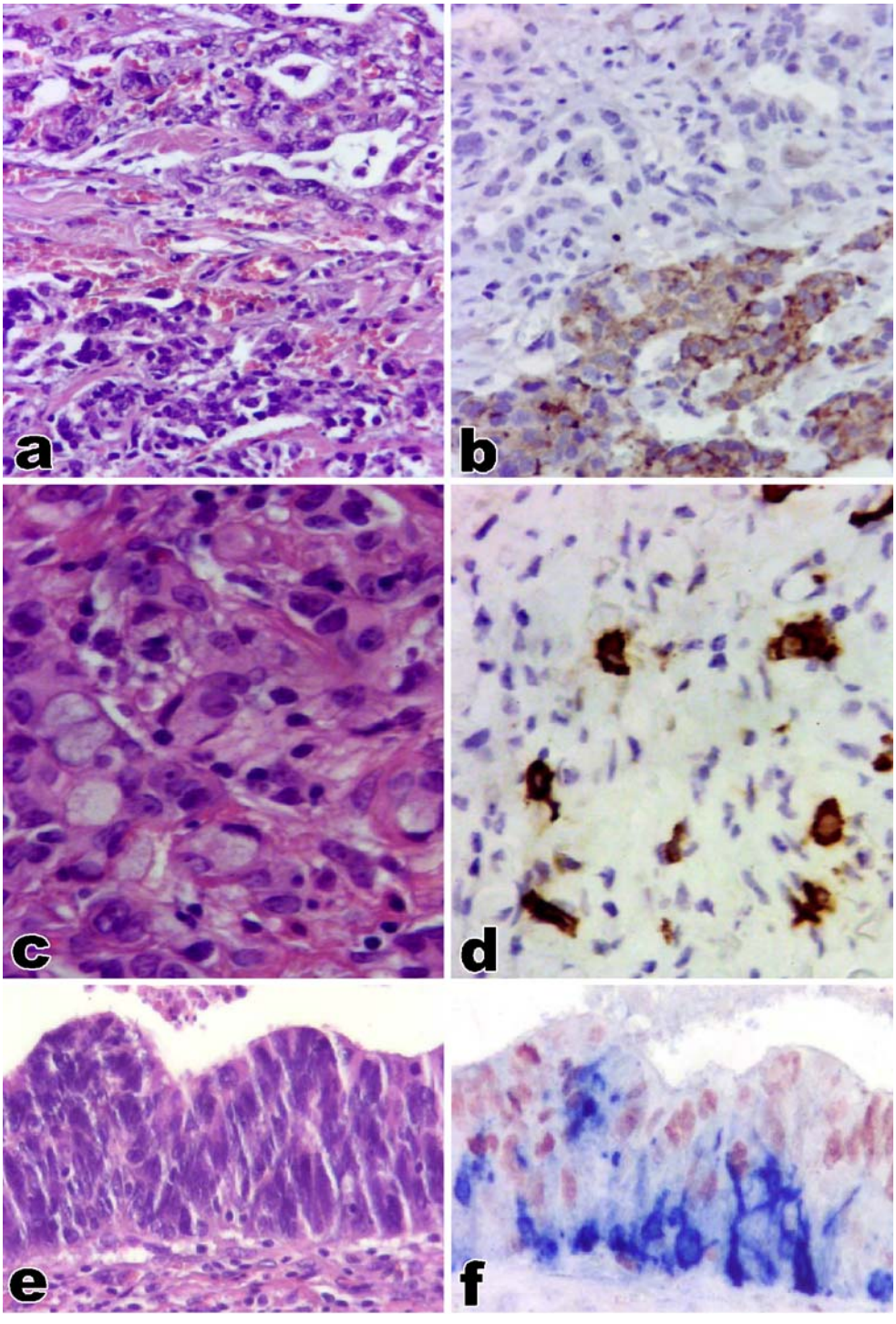

Fig. 2 Different morphological and immunohistochemical patterns in non-NE tumours with NE differentiation. **a**, **b** A case of "mixed" adenocarcinoma (*top*) and poorly differentiated NE (*bottom*) carcinoma of the gallbladder: chromogranin A immunohistochemistry **b** stained positive in the NE component. **c**, **d** Goblet cell carcinoid of the appendix, showing an intimate coexistence of mucin-laden signet ring cells (**c**) with chromogranin A-positive NE cells (**d**). **e**, **f** Colonic adenocarcinoma including basally located NE cells (**f**, *blue color*), showing no evidence of proliferation, as revealed by double immunohistochemical staining with Ki-67 (**f**, *brown color*). (**a**, **c**, **e** H&E; **b**, **d** immunoperoxidase; **f** double immunohistochemical reaction by immunoperoxidase — *brown color* and immuno-alkaline phosphatase—*blue color*; **a**, **b** ×200, **c**, **d** ×600, **e**, **f** ×400)

pattern in the definition of MEEC is relevant to allow separation of conventional adenocarcinoma with a less represented NE cell population randomly spread in the exocrine tumour, in the absence of carcinoid-like or small-cell areas (see below).

A separate comment is deserved for the so-called goblet cell carcinoids (group B of Lewin) [34], which represent an intimate mixture of mucin-laden signet ring cells and highly granulated NE cells in a tumour with classical organoid pattern (Fig. 2c,d). At least in the appendix, goblet cell carcinoids were the first reported examples of mixed exocrine and endocrine tumours and are classified as their pure NE counterparts, according to the current WHO classification of appendiceal carcinoids. Indeed, the relative proportions of the two components are variable, and only in some cases are they large enough to justify a diagnosis of mixed exocrine–endocrine carcinoma. Many other cases have limited mucinous cell population (or more rarely, scant NE cell among signet ring cells and would better fit in the following definition (see below). A case of multiple microscopic signet ring cell carcinoids was reported in the gallbladder, in which many small organoid-patterned carcinoid tumours infiltrated the gallbladder wall and had focal exocrine cell differentiation, in the form of scattered mucin-laden signet ring cells in the neoplastic nests [44]. Only scant amphicrine cells were found by double stainings, and the proportion of signet ring cells did not exceed 20% of the whole tumour. Given the peculiar morphology of goblet cell carcinoids, they should retain their original descriptive terminology.

Non-NE carcinomas with focal NE component (<30%)

Conventional (adeno)carcinomas of various organs, including breast, prostate, lung, colon, stomach and so on, may display specialized differentiation in both exocrine and NE cell lineages. Exocrine differentiation may include mucinous or signet ring cell changes, apocrine differentiation in breast carcinoma, Paneth cell differentiation in gastrointestinal cancer, acinar differentiation in pancreatic cancer, Clara cell features in pulmonary adenocarcinoma or even basaloid features in pulmonary, prostatic or rectal carcinomas [16, 25, 48, 54, 56]. The interest in such rare exocrine differentiation lines was very limited, either due to their rarity and—above all—the lack of significant clinical correlates, with the possible exception of basaloid carcinomas in the lung [8].

On the other hand, foci of NE differentiation have been recognized in non-neuroendocrine carcinomas for many years, employing various methods and markers. Among these, the immunohistochemical detection of chromogranin A is the most popular and reliable test to identify NE cells (Table 2). The interest for NE differentiation in non-NE tumours embraces histogenetic, diagnostic and clinical issues, mostly related to the correct morpho/functional (hormonal) typing of different neoplastic components in both primary and metastatic tumours. Additionally, significant clinical and prognostic correlates were proven in prostatic adenocarcinoma, only, while remaining mostly controversial for cancers at other sites.

Excluding MEEC cases described in the previous paragraph, various patterns of focal NE differentiation (in the range of 1 to 30% of the tumour area) were described. In non-small-cell lung carcinoma, NE differentiation has been reported in up to 36% of cases, depending on the method used to identify NE cells [1, 29], although controversial significant impact on prognosis was reported [29, 46]. Focal NE differentiation is not mentioned in the WHO classification of tumours of the digestive system [25], although there are reports in the literature on the occurrence of NE differentiation in esophageal [26], gastric [42], colorectal [2, 4, 19, 22, 23, 30, 43] and extrahepatic duct carcinomas [28]. The amount of NE cells is variable in

Table 2 Practical algorithm proposed for the identification of NE differentiation in non-NE carcinomas

Search for neuroendocrine differentiation		
When?	Upon request by the clinician (e.g., prostatic adenocarcinoma with high chromogranin blood levels and/or in hormonal escape)	
	Recognized organoid, solid, trabecular or small cell areas present in an otherwise conventional (adeno)carcinoma	
	Clinical history of previously resected NE tumor	
Where?	Organs classically hosting NE tumors (e.g., digestive tract, lung)	
	Non-NE organs in which NE differentiation has been described	
	Commonly: prostate, breast, colon, stomach, lung (NSCLC)	
	Occasionally: uterus, skin, kidney, gallbladder, parotid, larynx, etc.	
How?	Immunostainings first choice	Chromogranin A
	Second choice	Synaptophysin, CD56, others
	Additional	Ki67 (cell proliferation) somatostatin receptors (targeted therapy)
What has to be reported [based on extent + architecture of NE component]		
1 Mixed exocrine–endocrine carcinoma (MEEC)		
2 (adeno)Carcinoma with (focal) NE differentiation		

these tumours and is related to the method used to identify such NE differentiation [43].

Immunoreactivity for chromogranin A is generally the easiest and commonest procedure, which allows to detect NE differentiation in up to 25% of cases. In the breast, more or less extensive NE differentiation foci were described in conventional lobular or ductal carcinomas [49, 54, 59] and are kept separate from the exceptional "carcinoid tumours" of the breast and the NE carcinoma subtype, both of which display NE features in more than 50% of tumour cells [54]. In the prostate and bladder, NE differentiation has been described in a fraction of prostatic and bladder adenocarcinomas [6, 27]. In the former tumour, the prognostic implications of increased chromogranin blood levels (produced by the NE cell population) have been reported, being a remarkable unfavourable prognostic indicator in both surgically treated and hormonally treated patients [3, 5].

The extent of NE-differentiated cells in prostatic adenocarcinoma is highly heterogeneous. Generally, it is limited to scant chromogranin A reactive cells located in a basal position of neoplastic acini. The amount of NE cells increases with increasing Gleason's grade being maximal in solid or trabecular areas, also in association with a small tumour cell size. Histological material obtained after hormonal treatment of a prostatic carcinoma, sometimes shows extensive areas of NE differentiation (occasionally exceeding the threshold of 30%, although a diagnosis of MEEC has never been considered in this context), especially in the case of hormone refractory tumours [5, 16, 27]. It is interesting to note that increased NE cells were reported in rectal adenocarcinomas after chemotherapy or radiotherapy likely reflecting the relative resistance of low proliferating NE cells to conventional antiblastic therapy [51].

It has to be mentioned that none of the studies reported so far in the literature on NE differentiation in prostate or other types of cancer took into consideration the extent of the sampling as a potential source of discrepancy. In fact, in most instances, the focal NE-differentiated component is not equally distributed within a tumour but may be considerably heterogeneous in different areas, therefore, making equivocal the rule of the 30% cutoff. From a practical point of view, adequate sampling (i.e., one paraffin block for each centimeter of tumour size) is, therefore, necessary to rule out the presence or quantify the extent of a NE component and a panel of pan-NE markers may have a higher sensitivity than a single antibody. Moreover, a totally different approach consists in counting NE single scattered cells positive by immunohistochemistry (i.e., at low power field) as compared to estimating the extent of a morphologically NE-patterned area within a lesion. All these aspects have not been considered, to date, in any classification scheme, but would deserve major consideration.

The nature of NE cells in non-NE carcinomas is controversial. In some cases, they were considered terminally differentiated cells, with no proliferative potential, and therefore, although associated to the neoplastic growth, probably not of neoplastic nature [42] (Fig. 2e,f). In other cases, a consistent NE cell population is observed, representing true neoplastic cells of divergent differentiation outgrowing the adenocarcinoma cell component, often after hormonal therapy in the case of prostatic adenocarcinoma [5, 27]. In the pancreas, it has been well documented that the morphological features and the proliferative activity may segregate non-neoplastic from neoplastic NE cells in the context of a non-NE carcinoma, thus, defining different types of ductal adenocarcinomas with scattered endocrine cells [40].

Summary and conclusion

We have summarized the spectrum of currently known NE-differentiated tumours, including pure forms (well-differentiated tumour/carcinoma-carcinoid/malignant carcinoid, poorly differentiated small- and large-cell NE carcinoma) and mixed tumours. In this latter group, the label proposed by the WHO [53] of "mixed exocrine–endocrine carcinomas" is of practical efficacy taking into consideration at least two major diagnostic parameters: (1) extension of each component (at least 30%), and (2) structural features of the NE components as well-differentiated organoid or solid/diffuse growth patterns.

All other carcinomas containing a variable amount of NE cells below one-third of the entire tumour cell population, and more frequently, when scattered in an otherwise glandular growth pattern, are referred to as (adeno) carcinomas with focal NE differentiation. In MEECs, the most aggressive cell population drives the clinical behaviour, in general, of the well-differentiated NE component of MEECs following the natural history of the exocrine carcinoma while MEEC cases with small-cell carcinoma component follow the disease progression of this latter. Conversely, adenocarcinoma with focal NE differentiation generally does not show any difference in the clinical outcome, as shown in studies in the breast, lung and gastrointestinal tract [10, 29, 35, 46, 49, 58]. A notable exception is prostatic adenocarcinoma, in which the presence of chromogranin A-positive NE cells is an unfavourable prognostic factor [3, 5, 52]. The recognition of such tumours may be of relevance for better addressing the therapeutic strategy, and possibly, for evaluating also in mixed endocrine–exocrine tumours the same biotherapies proposed for pure NE tumours [39].

New insights may come from the analysis of the mechanisms leading to the development of both MEEC

and divergent NE differentiation in conventional carcinomas. Several studies defined the role of specific transcription factors (i.e., the family of basic helix–loop–helix–bHLH–factors, including the human achaete–scute homologue 1-hASH1) playing a pivotal role in the development and differentiation of neuronal and endocrine cells of foregut and midgut derivation [7, 31] and that have been found, by means of alternative techniques, to be expressed in NE carcinomas from various sites. Indeed, such transcriptional molecules appear as a promising tool for the identification of functional NE differentiation in MEECs.

Acknowledgement This work is supported by grants from the Italian Ministry of University (ex 60% to MP, GR and MV).

References

1. Abbona G, Papotti M, Viberti L, Macri L, Stella A, Bussolati G (1998) Chromogranin A gene expression in non-small cell lung carcinomas. J Pathol 186:151–156
2. Atasoy P, Ensari A, Demirci S, Kursun N (2003) Neuroendocrine differentiation in colorectal carcinomas: assessing its prognostic significance. Tumori 89:49–53
3. Berruti A, Mosca A, Tucci M, Terrone C, Torta M, Tarabuzzi R, Russo L, Cracco C, Bollito E, Scarpa RM, Angeli A, Dogliotti L (2005) Independent prognostic role of circulating chromogranin A in prostate cancer patients with hormone-refractory disease. Endocr Relate Cancer 12:107–115
4. Blumenfeld W, Chandhoke DK, Sagerman P, Turi GK (1996) Neuroendocrine differentiation in gastric adenocarcinomas. An immunohistochemical study. Arch Pathol Lab Med 120:478–481
5. Bollito E, Berruti A, Bellina M, Mosca A, Leonardo E, Tarabuzzi R, Cappia S, Ari MM, Tampellini M, Fontana D, Gubetta L, Angeli A, Dogliotti L (2001) Relationship between neuroendocrine features and prognostic parameters in human prostate adenocarcinoma. Ann Oncol 12S:159–164
6. Bollito ER, Pacchioni D, Lopez-Beltran A, Volante M, Terrone C, Casetta G, Mari M, DePompa R, Cappia S, Papotti M (2005) Immunohistochemical study of neuroendocrine differentiation in primary glandular lesions and tumours of the urinary bladder. Anal Quant Cytol Histol 27:218–224
7. Borges M, Linnoila RI, vandeVelde HJK, Chen H, Nelkin BD, Mabry M, Baylin SB, Ball DW (1997) An achaete–scute homologue essential for neuroendocrine differentiation in the lung. Nature 386:852–855
8. Brambilla E, Moro D, Veale D, Brichon PY, Stoebner P, Paramelle B, Brambilla C (1992) Basal cell (basaloid) carcinoma of the lung: a new morphologic and phenotypic entity with separate prognostic significance. Hum Pathol 23:993–1003
9. Brambilla E, Lantuejoul S, Sturm N (2000) Divergent differentiation in neuroendocrine lung tumors. Semin Diagn Pathol 17:138–148
10. Capella C, La Rosa S, Uccella S, Billo P, Cornaggia M (2000) Mixed endocrine–exocrine tumors of the gastrointestinal tract. Semin Diagn Pathol 17:91–103
11. Chejfec G, Capella C, Solcia E, Jao W, Gould VE (1985) Amphicrine cells, dysplasias, and neoplasias. Cancer 56:2683–2690
12. Crafa P, Milione M, Azzoni C, Pilato FP, Pizzi S, Bordi C (2003) Pleomorph poorly differentiated endocrine carcinoma of the rectum. Virchows Arch 442:605–610
13. DeLellis RA, Tischler AS, Wolfe HJ (1984) Multidirectional differentiation in neuroendocrine neoplasms. J Histochem Cytochem 32:899–904
14. DeLellis RA, LLoyd R, Heitz PU (eds) (2004) World Health Organization classification of tumors, pathology and genetics—tumors of endocrine organs. IARC, Lyon
15. Deshpande V, Selig MK, Nielsen GP, Fernandez-del Castillo C, Lauwers GY (2003) Ductulo-insular pancreatic endocrine neoplasms: clinicopathologic analysis of a unique subtype of pancreatic endocrine neoplasms. Am J Surg Pathol 27:461–468
16. Eble JN, Sauter G, Epstein JI, Sesterhenn IA (2004) World Health Organization classification of tumours, pathology and genetics—tumours of the urinary system and male genital organs. IARC, Lyon
17. Evans AJ, Al-Maghrabi J, Tsihlias J, Lajoie G, Sweet JM, Chapman WB (2002) Primary large cell neuroendocrine carcinoma of the urinary bladder. Arch Pathol Lab Med 126:1229–1232
18. Evans AJ, Humphrey PA, Belani J, van der Kwast TH, Srigley JR (2006) Large cell neuroendocrine carcinoma of prostate: a clinicopathologic summary of 7 cases of a rare manifestation of advanced prostate cancer. Am J Surg Pathol 30:684–693
19. Foley EF, Gaffey MJ, Frierson HF Jr (1998) The frequency and clinical significance of neuroendocrine cells within stage III adenocarcinomas of the colon. Arch Pathol Lab Med 122:912–914
20. Foschini MP, Eusebi V (2000) Divergent differentiation in endocrine and nonendocrine tumors of the skin. Semin Diagn Pathol 17:162–168
21. Gilks CB, Young RH, Gersell DJ, Clement PB (1997) Large cell neuroendocrine [corrected] carcinoma of the uterine cervix: a clinicopathologic study of 12 cases. Am J Surg Pathol 21:905–914
22. Grabowski P, Schindler I, Anagnostopoulos I, Foss HD, Riecken EO, Mansmann U, Stein H, Berger G, Buhr HJ, Scherubl H (2001) Neuroendocrine differentiation is a relevant prognostic factor in stage III–IV colorectal cancer. Eur J Gastroenterol Hepatol 13(4):405–411
23. Grabowski P, Schonfelder J, Ahnert-Hilger G, Foss HD, Heine B, Schindler I, Stein H, Berger G, Zeitz M, Scherubl H (2002) Expression of neuroendocrine markers: a signature of human undifferentiated carcinoma of the colon and rectum. Virchows Arch 441:256–263
24. Greene L, Brundage W, Cooper K (2005) Large cell neuroendocrine carcinoma of the larynx: a case report and a review of the classification of this neoplasm. J Clin Pathol 58:658–661
25. Hamilton SR, Aaltonen L (2000) World Health Organization Classification of tumors. Pathology and genetics—tumors of the digestive system. IARC, Lyon
26. Hamilton K, Chiappori A, Olson S, Sawyers J, Johnson D, Washington K (2000) Prevalence and prognostic significance of neuroendocrine cells in esophageal adenocarcinoma. Mod Pathol 13:475–481
27. Helpap B, Kloppel G (2002) Neuroendocrine carcinomas of the prostate and urinary bladder: a diagnostic and therapeutic challenge. Virchows Arch 440:241–248
28. Hong SM, Kim MJ, Pi DY, Jo D, Yu E, Ro JY (2005) Neuroendocrine differentiation in extrahepatic bile duct carcinomas and its prognostic significance. Hum Pathol 36:732–740
29. Howe MC, Chapman A, Kerr K, Dougal M, Anderson H, Hasleton PS (2005) Neuroendocrine differentiation in non-small cell lung cancer and its relation to prognosis and therapy. Histopathology 46:195–201
30. Indinnimeo M, Cicchini C, Memeo L, Stazi A, Provenza C, Ricci F, Mingazzini PL (2002) Correlation between chromogranin-A expression and pathological variables in human colon carcinoma. Anticancer Res 22:395–398

31. Ito T, Udaka N, Okudela K, Yazawa T, Kitamura H (2003) Mechanisms of neuroendocrine differentiation in pulmonary neuroendocrine cells and small cell carcinoma. Endocr Pathol 14:129–133
32. Jain D, Eslami-Varzaneh F, Takano A, Ayer U, Umashankar R, Muller R, Klimstra D (2005) Composite glandular and endocrine tumors of the stomach with pancreatic acinar differerentiation. Am J Surg Pathol 29:1524–1529
33. Kloppel G (2000) Mixed exocrine–endocrine tumors of the pancreas. Semin Diagn Pathol 17:104–108
34. Lewin K (1987) Carcinoid tumors and the mixed (composite) glandular–endocrine cell carcinomas. Am J Surg Pathol 11:71–76
35. Makretsov N, Gilks CB, Codman AJ, Hayes M, Huntsman D (2003) Tissue microarray analysis of neuroendocrine differentiation and its prognostic significance in breast cancer. Hum Pathol 34:1001–1008
36. Moukassa D, Leroy X, Bouchind'homme B, Saint F, Lemaitre L, Gosselin B (2000) Primary large cell neuroendocrine carcinoma of the kidney: morphologic and immunohistochemical features of two cases. Ann Pathol 20:357–360
37. Nagao T, Sugano I, Ishida Y, Tajima Y, Munakata S, Asoh A, Yamazaki K, Muto H, Konno A, Kondo Y, Nagao K (2000) Primary large-cell neuroendocrine carcinoma of the parotid gland: immunohistochemical and molecular analysis of two cases. Mod Pathol 13:554–561
38. Nassar H, Albores-Saavedra J, Klimstra DS (2005) High-grade neuroendocrine carcinoma of the ampulla of vater: a clinicopathologic and immunohistochemical analysis of 14 cases. Am J Surg Pathol 29:588–594
39. Oberg K, Kvols L, Caplin M, DelleFave G, DeHerder W, Rindi G, Ruszniewski P, Woltering EA, Wiedenmann B (2004) Consensus report on the use of somatostatin analogs for the management of neuroendocrine tumors of the gastroenteropancreatic system. Ann Oncol 15:966–973
40. Ohike N, Jurgensen A, Pipeleers-Marichal M, Kloppel G (2003) Mixed ductal-endocrine carcinomas of the pancreas and ductal adenocarcinomas with scattered endocrine cells: characterization of the endocrine cells. Virchows Arch 442:258–265
41. Ohike N, Kosmahl M, Kloppel G (2004) Mixed acinar–endocrine carcinoma of the pancreas. A clinicopathological study and comparison with acinar-cell carcinoma. Virchows Arch 445:231–235
42. Ooi A, Hayashi H, Katsuda S, Nakanishi I (1992) Gastric carcinoma cells with endocrine differentiation show no evidence of proliferation. Hum Pathol 23:736–741
43. Pagani A, Papotti M, Abbona GC, Bussolati G (1995) Chromogranin gene expression in colorectal adenocarcinomas. Mod Pathol 8:626–632
44. Papotti M, Galliano D, Monga G (1990) Signet ring cell carcinoid of the gallbladder. Histopathology 17:255–259
45. Papotti M, Cassoni P, Sapino A, Passarino G, Krueger JE, Albores-Saavedra J (2000) Large cell neuroendocrine carcinoma of the gallbladder: report of two cases. Am J Surg Pathol 24:1424–1428
46. Pelosi G, Pasini F, Sonzogni A, Maffini F, Maisonneuve P, Iannucci A, Terzi A, De Manzoni G, Bresaola E, Viale G (2003) Prognostic implications of neuroendocrine differentiation and hormone production in patients with Stage I non-small cell lung carcinoma. Cancer 97:2487–2497
47. Reis-Filho JS, Schmitt FC (2001) Amphicrine gastric carcinoma. Arch Pathol Lab Med 125:1513–1514
48. Rosen PP, Oberman HA (1992) Atlas of tumor pathology. Tumors of the mammary gland. AFIP, Washington, pp 157–243
49. Sapino A, Righi L, Cassoni P, Papotti M, Pietribiasi F, Bussolati G (2000) Expression of the neuroendocrine phenotype in carcinomas of the breast. Semin Diagn Pathol 17:127–137
50. Sapino A, Righi L, Cassoni P, Papotti M, Bussolati G (2001) Neuroendocrine differentiation in breast carcinoma. Mod Pathol 14:768–776
51. Shia J, Tickoo SK, Guillem JG, Qin J, Nissan A, Hoos A, Stojadinovic A, Ruo L, Wong WD, Paty PB, Weiser MR, Minsky BD, Klimstra DS (2002) Increased endocrine cells in treated rectal adenocarcinomas: a possible reflection of endocrine differentiation in tumor cells induced by chemotherapy and radiotherapy. Am J Surg Pathol 26:863–872
52. Slovin SF (2006) Neuroendocrine differentiation in prostate cancer: a sheep in wolf's clothing? Nat Clin Pract Urol 3:138–144
53. Solcia E, Kloppel G, Sobin LH (2000) World Health Organization International histological classification of tumors. Histological typing of endocrine tumors. Springer, Berlin Heidelberg New York, pp 56–68
54. Tavassoli FA, Devilee P (2003) World Health Organization classification of tumours, pathology and genetics—tumours of the breast. IARC, Lyon, pp 32–34
55. Travis WD, Linnoila RI, Tsokos MG, Hitchcock CL, Cutler GB Jr, Nieman L, Chrousos G, Pass H, Doppman J (1991) Neuroendocrine tumors of the lung with proposed criteria for large-cell neuroendocrine carcinoma. An ultrastructural, immunohistochemical, and flow cytometric study of 35 cases. Am J Surg Pathol 15:529–553
56. Travis WD, Brambilla E, Muller-Hermelink HK, Harris CC (2004) World Health Organization Classification of tumors, pathology and genetics—tumors of the lung, pleura, thymus and heart. IARC, Lyon, pp 19–20; 31–34
57. van Eeden S, de Leng WW, Offerhaus GJ, Morsink FH, Weterman MA, de Krijger RR, Kloppel G, Klimstra DS (2004) Ductuloinsular tumors of the pancreas: endocrine tumors with entrapped nonneoplastic ductules. Am J Surg Pathol 28:813–820
58. vanKrimpen C, Elferink A, Broodman CA, Hp WC, Pronk A, Menke M (2004) The prognostic influence of neuroendocrine differentiation in breast cancer: results of a long-term follow-up study. Breast 13:329–333
59. Volante M, Sapino A, Papotti M, Pacchioni D, Bussolati G (2004) Neuroendocrine differentiation patterns in various organs (including lung, breast, skin, and urogenital tract). In: Lloyd RV (ed) Endocrine pathology. Differential diagnosis and molecular advances. Humana, Totowa, USA, pp 345–358

Virchows Arch (2006) 449:507–512
DOI 10.1007/s00428-006-0305-3

ORIGINAL ARTICLE

Invasive carcinomas of the male breast: a morphologic study of the distribution of histologic subtypes and metastatic patterns in 778 cases

Ana M. Burga · Oluwole Fadare · Ruth A. Lininger · Fattaneh A. Tavassoli

Received: 30 May 2006 / Accepted: 24 August 2006 / Published online: 13 October 2006
© Springer-Verlag 2006

Abstract The current investigation was conducted to evaluate the proportional distribution of the various histologic subtypes (including newly recognized variants) of male breast carcinomas, to determine whether any histologic subtypes occur with a frequency that is markedly discordant with the expected frequencies from published data on parallel female breast tumors. We also aimed to document the distribution of malignancies metastatic to the breast. Seven hundred fifty-nine archived cases of primary invasive carcinoma involving the male breast were retrieved and subcategorized into histologic subtypes according to contemporary criteria. Six hundred forty-three (84.7%) tumors were pure infiltrating ductal carcinoma (IDC) not otherwise specified. The most common of the remainder included papillary carcinoma with invasion in the form of IDC (n=34), mixed IDC and mucinous carcinoma (n=26), and pure mucinous carcinoma (n=21). In 19 cases, metastases from other sites involved the breast, most commonly (58%) cutaneous melanoma. Invasive carcinoma of the male breast appears to display a morphologic spectrum and distribution of histologic subtypes that is comparable to those of the female breast, with some expected variation. Compared with published experience on their female counterparts, there is a two-fold increase in the frequency of invasive papillary carcinoma in the male breast. Finally, the most common tumor metastatic to the male breast in this series was cutaneous melanoma.

Keywords Male · Breast · Carcinoma · Papillary · Cancer

The opinions and assertions contained herein are the private views of the authors and are not to be considered official or as necessarily reflecting the opinion of the United States Government or any of its subsidiaries.

A. M. Burga · R. A. Lininger · F. A. Tavassoli
Department of Gynecologic and Breast Pathology,
Armed Forces Institute of Pathology,
Washington, DC, USA

O. Fadare · F. A. Tavassoli
Department of Pathology, Yale University School of Medicine,
New Haven, CT, USA

A. M. Burga
Department of Pathology, Englewood Hospital,
Englewood, NJ, USA

O. Fadare
Department of Pathology, Wilford Hall Medical Center,
Lackland Air Force Base,
San Antonio, TX, USA

O. Fadare
Department of Pathology,
University of Texas Health Science Center at San Antonio,
San Antonio, TX, USA

R. A. Lininger
Department of Pathology, University of North Carolina,
Chapel Hill, NC, USA

O. Fadare (✉)
Department of Pathology, Wilford Hall Medical Center,
2200 Bergquist Dr., Ste 1,
Lackland AFB, TX 78236, USA
e-mail: oluwolefadare@yahoo.com

Introduction

Breast cancer in males is relatively uncommon, with approximately 1,450 newly diagnosed cases annually in the United States, and an associated mortality rate that accounts for less than 0.2% of all cancer-related deaths in men [1, 4, 9, 15, 17, 20, 28]. However, recent epidemiologic studies suggest that the incidence of male breast

cancer has been steadily increasing [7, 14]. Utilizing data from the National Cancer Institute's Surveillance, Epidemiology and End Results database for the 26-year period between 1973 and 1998, Giordano et al. [7] found that the incidence of male breast cancer increased from 0.86 to 1.08 per 100,000 population. This increasing incidence, in addition to the better elucidation of the role of BRCA2 mutations in male breast cancer, has renewed interest in specifically identifying the underlying pathogenesis of male breast cancer and clarifying the specific differences, if any, between male and female breast cancer.

On a broad demographical level, male and female breast cancers are fundamentally similar with the main differences lying in older age of occurrence and lower incidence of the former. However, significant differences have been noted between male and female breast cancers with respect to the expression of a variety of biologic factors, including hormone receptors such as estrogen receptor, progesterone receptor, c-erbB-2, estrogen-inducible proteins such as pS2, Cathepsin D, hsp27, proteins related to basement membrane and extracellular matrix degradation such as the urokinase system of plasminogen activation and their inhibitors, and protooncogenes such as bcl-2 [2, 6, 7, 18, 21, 22, 24, 27]. At the morphologic level, male ductal intraepithelial neoplasia (ductal carcinoma in situ), in contrast to similar lesions in females, displays a distinct histologic profile in which the majority of tumors are of the papillary type, with cribriform, micropapillary, and solid types being much less common [13]. In particular, the comedo-type of DIN (comedo DCIS) is notably rare in the male breast [13]. For invasive carcinomas, the female and male tumors are morphologically indistinguishable [26] and many published studies on male breast cancer frequently represent the major histologic subtypes of nonlobular breast carcinoma, such as ductal, medullary, mucinous, and papillary [3, 7, 8, 12, 19, 22, 25]. However, these studies generally do not have the distribution and relative frequencies of the various histologic subtypes as their main focus, and as such, pathologically important distinctions such as signet ring vs colloid carcinoma (both subsumed under mucin producing carcinoma), or metaplastic carcinoma vs infiltrating duct carcinoma not otherwise specified are not emphasized. Over- or underepresentation of a particular histologic subtype in male breast cancers may provide valuable insight into the etiopathogenetic differences between male and female breast cancers and may provide an important nidus for further studies.

In this study, we investigated the frequencies and distribution of the various histologic subtypes in a large data set of invasive carcinomas seen at a large tertiary center over a 40-year period. Our goals are to document these frequencies and distribution and to see whether any histologic subtypes are notably distinct in frequency of occurrence in the male breast, as compared with historical published data on similar lesions in the female breast. The frequencies and sites of origin of metastatic tumors to the male breast during the study period were also investigated.

Materials and methods

After approval from our institutional research review committee, cases of invasive carcinoma involving the male breast diagnosed between 1957 and 1997 were retrieved from the archived institutional files of the Armed Forces Institute of Pathology (AFIP, Washington DC, USA). The available records and slides on each patient were reviewed. All cases with ambiguous gender (even if one among the multiple entries for gender was coded as female rather than male) were excluded (n=38). Diagnostic designations were assigned according to contemporary WHO criteria [23]. All special types of carcinoma inclusive of mucinous, tubular, secretory, adenoid cystic, lobular, metaplastic, etc. (n=116) were reviewed extensively; many of these cases had been evaluated repeatedly as part of various previously published studies from the department and slides of good quality were available on these cases for review. Among the 643 cases of infiltrating duct carcinoma not otherwise specified, only cases with good quality and adequate representative slides (n=365) were graded, using the modified Scarf–Bloom Richardson scoring system. On 78 cases, the slides were so old that we could only confirm the presence of a ductal type carcinoma. The other 200 cases did not have all of the patients' slides pertaining to the lesion available and the final interpretation was based on the descriptions of morphology in the AFIP files. Because cases sent to AFIP are mostly for confirmation of diagnosis, information about therapy beyond what was in the surgical pathology report or the accompanying cover letter are generally not available. Some patients had repeated material sent to AFIP as the lesion recurred, which is how follow-up information was collected in a small subset of cases.

Information about age, operative procedure, nodal excision, and distant metastases were retrieved from the patients' AFIP files. Diagnostic designations were assigned largely based on morphologic and not immunohistochemical features since in many cases there were no blocks or unstained slides available for additional studies. Thirty of these cases were the subject of a previous report [13], which focused on in situ carcinomas and were reported in 1998. Another 113 cases, 8 of which were ductal in situ and another 9 papillary carcinomas, were subject of another report in 1969 [19] Cases of nonhematopoietic or lymphoreticular malignancies metastatic to the male breast during this period were also catalogued.

Results

Seven hundred and seventy-eight cases of breast carcinoma were reported as involving the male breast during the study period. Seven hundred fifty-nine of these cases were considered primary to the breast and 19 as metastatic to it. The patients ranged in age from 9 to 94 years (mean 61 years). The age distribution available for 520 cases was as follow: 8 were ≤30 years, 22 were ≤40 years, 205 were 41 to 60 years, 251 were 61 to 80 years, and 34 were over 80 years of age. Among the 490 for whom the racial information was available, 401 were Caucasian, not of Hispanic origin, 82 were Black, not of Hispanic origin, 6 were Asians or Pacific Islander, 1 was Hispanic, and the race was unknown for 269. The carcinomas ranged from ≤1 mm (microinvasive) to 12 cm. Many of the cases with multifocal early invasion of 1 to 7 mm were associated with large solitary or multifocal papillary intraductal carcinomas. The various histologic subtypes and their proportional distribution are outlined in Table 1, whereas representative images are illustrated in Fig. 1. Pure *infiltrating duct carcinoma not otherwise specified* was the most common histologic subtype, representing 84.7% of all cases. Six hundred forty-three cases were in the latter group, including 34 cases associated with Paget's disease, 17 cases with prominent apocrine features in <50% of tumor volume (i.e., insufficient to qualify as apocrine carcinomas), 4 cases with prominent medullary features (tumor circumscription, cellular syncytia, sparse lymphocytic infiltrate), 2 cases of infiltrating duct carcinoma with signet ring cells (<5% of tumor volume), 3 cases of infiltrating duct carcinoma with focal clear cells (<5% of tumor volume), and 3 cases of carcinoma with osteoclast-like giant cells. Papillary intraductal carcinoma with invasion in the form of infiltrating duct carcinoma represented 4.5% (34/759 each) of all cases. Other well-represented histologic subtypes or combinations included mixed mucinous and infiltrating duct carcinoma (n=26, 3.4%), pure mucinous carcinoma (21, 2.8%), and adenoid cystic carcinoma (n=8,1.05%). Other variants each constituted less than 1% of all cases (Table 1). Notably, there were three cases of lobular carcinoma. As noted previously, these diagnoses were not based on immunohistochemical confirmation by immunostain for E-cadherin, but all three showed archetypal morphologic features of lobular carcinoma with loosely cohesive single cell files and rare intracytoplasmic lumens. Two of these cases had evidence of lobular development in the surrounding breast but the slides available for review did not show lobular intraepithelial neoplasia (LIN). There were also three cases of mixed lobular and ductal carcinomas, in which these areas were spatially separate. The youngest patient, a 9-year-old boy was the only one with pure secretory carcinoma. Five of 759 cases were microinvasive (invasive focus less than 1 mm in maximum size in a predominantly intraepithelial lesion); three of these five cases were multifocal, whereas the other two were unifocal. Of the 365 cases of infiltrating duct carcinoma not otherwise specified that were graded, 104 were grade 1, 137 were grade 2, and 124 were grade 3. Among the 93 with lymph nodes available for assessment, 61 (66%) cases had axillary metastases. Forty of the women with axillary node metastases also had distant metastases. The most common distant metastatic sites were lung, adrenal glands, and bone. In addition, there were 19 examples of metastases to the breast that were documented. Of these, 58% (11/19) were cutaneous melanomas, and 21% (4/19), 10% (2/19), and 10% (2/19) represented carcinomas from the prostate, lung, and larynx, respectively.

Table 1 Distribution of the various histologic subtypes in 778 invasive carcinomas involving the male breast

Histologic subtype	Number of cases	Percentage
Infiltrating duct carcinoma not otherwise specified, including[a]	643	84.7
Carcinoma associated with Paget's disease	34	
Carcinoma with prominent apocrine features	17	
Carcinoma with medullary features	4	
Carcinoma with osteoclast-like giant cells	3	
Carcinoma with focal signet rings	2	
Carcinoma with focal clear cells	2	
Pleomorphic carcinoma	2	
Carcinoma with no notable distinctive features	579	
Papillary intraductal carcinoma with invasion in the form of infiltrating duct carcinoma	34	4.48
Mixed infiltrating duct and mucinous carcinoma	26	3.4
Pure mucinous carcinoma	21	2.8
Adenoid cystic carcinoma	8	1.05
Tubular carcinoma	6	0.8
Small cell carcinoma	6	0.8
Invasive lobular carcinoma	3	0.39
Solid neuroendocrine carcinoma	3	0.39
Mixed lobular and ductal carcinoma	3	0.39
Adenocarcinoma with spindle cell metaplasia	2	0.26
Pure signet ring carcinoma (no in situ component)	1	0.13
Invasive cribriform carcinoma	1	0.13
Secretory carcinoma	1	0.13
Squamous cell carcinoma	1	0.13
Total	759	100
Metastatic lesions	19	
Final total	778	

[a]Subsets included for information only (not WHO categories)

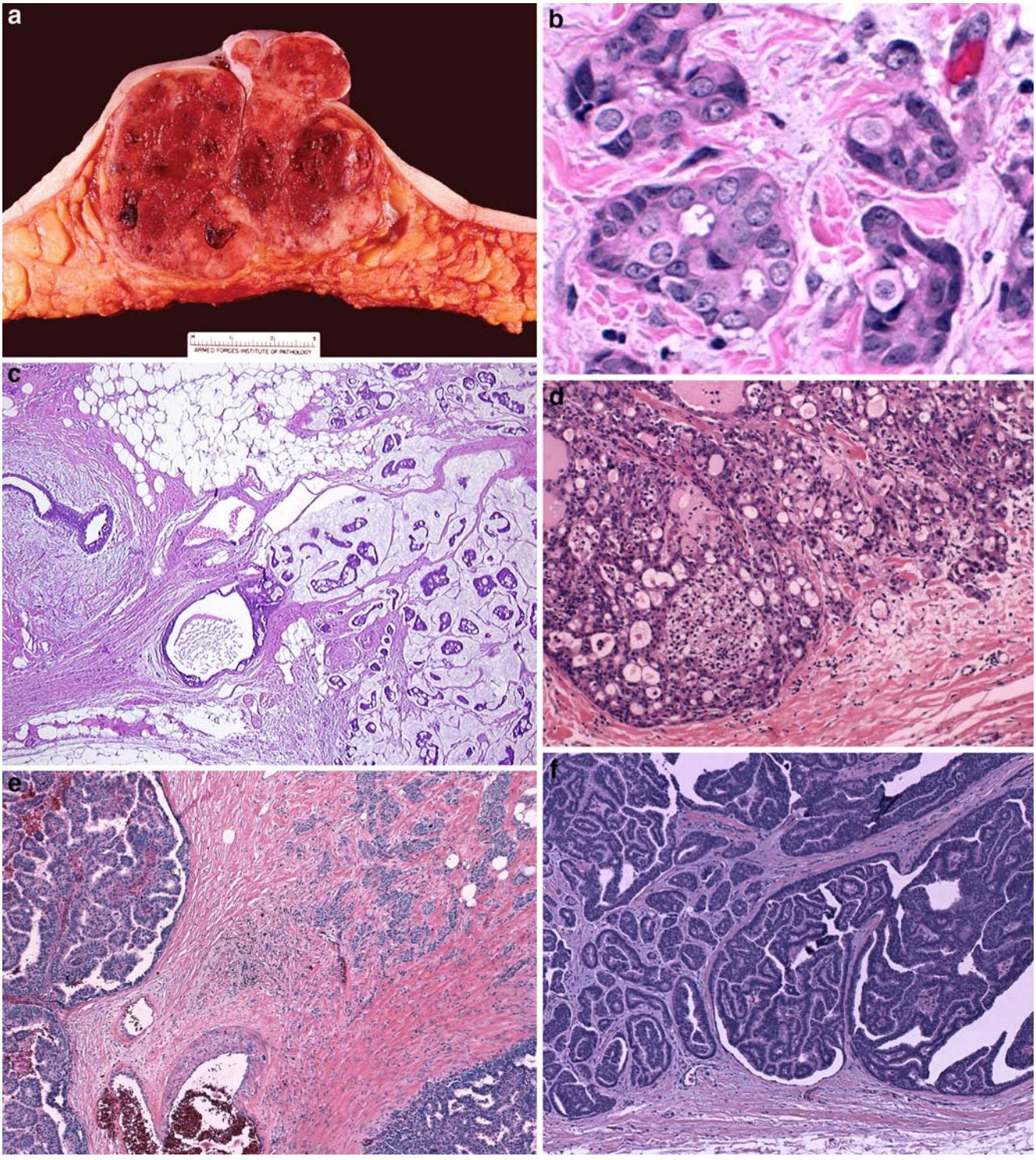

Fig. 1 Representative pathologic images of the various histologic subtypes. **a** and **b** Gross and microscopic images of infiltrating duct carcinoma, the most frequently encountered histologic subtype (**b** original magnification ×160). **c** A colloid (*mucinous*) carcinoma (*right field*) occurring in a gynecomastoid breast (*left field*) (original magnification ×100). **d** The single case of a secretory carcinoma was in a 9-year-old boy, the youngest patient in this series (original magnification ×140). **e** and **f** Examples of papillary intraductal carcinoma with invasion in the form of infiltrating duct carcinoma [original magnifications: ×100 (**e**), ×120 (**f**)]

Discussion

The frequency, distribution, and morphologic spectrum of the various histologic subtypes of male breast cancer as compared with its female counterpart may provide a valuable insight into the etiology and/or pathogenesis of both. This was perhaps best illustrated in the study of ductal carcinoma in situ by Hittmair et al. [13]. The authors showed that in the male breast, papillary DCIS occurred with a much higher frequency (46% of pure lesions) than expected, while solid, micropapillary, and cribriform patterns occurred with a much lower frequency (22% of pure DCIS combined). Notably, only 5 of 114 cases were of comedo-type DCIS and only 7 of 114 cases were considered high grade. The authors concluded that predominance of papillary patterns among intraepithelial male breast lesions is a reflection of the relative abundance of ducts and the poorly developed terminal-ductal lobular units in male breast. Given the rarity of true comedo DIN in male breast, the authors speculated that the fully developed lobular environment and the female type hormonal milieu may be a requirement for development of comedo DIN [13].

In this study, we investigated in detail the frequencies and distribution of the various histologic subtypes in a large data set of invasive carcinomas seen at a large tertiary center over a 40-year period. Our findings suggest that invasive carcinoma of the male breast displays a morphologic spectrum and distribution of histologic subtypes that is comparable to invasive carcinoma of the female breast and that no specific histologic subtypes are notably over- or underrepresented with the exception of papillary and lobular variants.

Papillary intraductal carcinomas basically assumed an infiltrating duct carcinoma pattern once they invaded the stroma (Fig. 1e,f). A papillary component was present in 34 (4.5%) of 759 cases, representing the second most common histologic subtype. These papillary carcinomas appeared to have invaded either through massive expansion and total disruption of ductal confines with typical invasive patterns at their periphery or only focally disrupted the duct wall and invaded the surrounding stroma as an infiltrating duct carcinoma. The latter represents approximately 2% [5] of female breast invasive carcinomas and appears overrepresented in males. In a large population-based study, Giordano et al. [7] reported that 2.6% of invasive malignancies in males were papillary carcinomas, as compared with 0.6% in females ($p<0.0001$). However, the differences between males and females with respect to the frequencies of the other histologic subtypes were also statistically significant. The significance of the papillary histologic subtype or papillary architecture in male ductal carcinoma requires further investigation but is most probably related to the architecture of the male mammary duct system with dominance of larger ducts.

The possibility of metastases to the breast should be considered when evaluating breast masses particularly if there is a history of cancer elsewhere. Nineteen cases of carcinoma metastatic to the male breast were seen over this study period, representing 2.4% (19/778) of all nonhematopoietic or lymphoreticular malignancies. This is again a twofold increase comparable to the 1.2% reported in female breast malignancies over a 10-year period [11]. Of the 19 metastatic tumors, 58% (11/19) were cutaneous melanomas, and 21% (4/19), 10% (2/19), and 10% (2/19) represented carcinomas from the prostate, lung, and larynx, respectively. It is interesting to note that prostatic carcinoma, which has been the subject of most reports of carcinomas metastatic to the male breast [10], was not the most common metastatic tumor in this series. The number of metastatic tumors in this series is relatively small, which is a limitation in interpreting the distribution of originating sites. Nonetheless, in the investigation of metastatic tumors to the male breast of an unknown primary site, our findings provide additional data on some of the most likely sites.

This study also confirms the occurrence of lobular carcinoma in the male breast. Three cases of invasive lobular carcinoma, diagnosed purely on a morphologic basis, were present among 759 cases (0.4%). Three additional cases of mixed lobular and ductal carcinoma were also diagnosed over this period (0.4%). Joshi et al. [16] found one (4%) lobular carcinoma out of 27 cases, while Goss et al. [8] found 4 (1.9%) cases out of a total of 229. In the series of Giordano et al. [7], lobular carcinomas constituted 1.5% for their male breast cancers. It is noteworthy that all of these cases were interpreted as lobular based on morphology without E-cadherin immunostain confirmation.

In summary, invasive carcinoma of the male breast appears to display a morphologic spectrum and distribution of histologic subtypes, which is comparable to invasive carcinoma of the female breast with some variation. As expected, lobular carcinoma is exceedingly rare but was encountered in this series. There appears to be a twofold increase in the frequency of invasive papillary carcinoma and metastatic cancers to the male breast as compared to published data in the female breast. Finally, the most common tumor metastatic to the male breast in this series was cutaneous melanoma.

Acknowledgement Ana M. Burga and Oluwole Fadare are equal contributors and coequal first authors.

References

1. American Cancer Society (2004) Cancer facts and figures 2004. American Cancer Society, Atlanta
2. Dawson PJ, Paine TM, Wolman SR (1992) Immunocytochemical characterization of male breast cancer. Mod Pathol 5:621–625

3. de Perrot M, Deleaval J, Robert J, Spiliopoulos A (2000) Thirty-year experience of surgery for breast carcinoma in men. Eur J Surg 166:929–931
4. Donegan WL, Redlich PN (1996) Breast cancer in men. Surg Clin North Am 76:343–363
5. Fisher ER, Palekar AS, Redmond C, Barton B, Fisher B (1980) Pathologic findings from the National Surgical Adjuvant Breast Project (protocol no. 4) VI. Invasive papillary cancer. Am J Clin Pathol 73:313–322
6. Fox SB, Day CA, Rogers S (1991) Lack of c-erbB-2 oncoprotein expression in male breast carcinoma. J Clin Pathol 44:960–961
7. Giordano SH, Cohen DS, Buzdar AU, Perkins G, Hortobagyi GN (2004) Breast carcinoma in men: a population-based study. Cancer 101:51–57
8. Goss PE, Reid C, Pintilie M, Lim R, Miller N (1999) Male breast carcinoma: a review of 229 patients who presented to the Princess Margaret Hospital during 40 years: 1955–1996. Cancer 85:629–639
9. Gradishar W (2000) Male breast cancer. In: Harris J, Lippman M, Morrow M, Osborne C (eds) Diseases of the breast, 2nd ed. Williams & Wilkins, Philadelphia, pp 661–667
10. Green LK, Klima M (1991) The use of immunohistochemistry in metastatic prostatic adenocarcinoma to the breast. Hum Pathol 22: 242–246
11. Hajdu S, Urban JA (1972) Cancers metastatic to the breast. Cancer 20:1691–1696
12. Heller KS, Rosen PP, Schottenfeld D, Ashikari R, Kinne DW (1978) Male breast cancer: a clinicopathologic study of 97 cases. Ann Surg 188:60–65
13. Hittmair AP, Lininger RA, Tavassoli FA (1998) Ductal carcinoma in situ (DCIS) in the male breast: a morphologic study of 84 cases of pure DCIS and 30 cases of DCIS associated with invasive carcinoma—a preliminary report. Cancer 15(83):2139–2149
14. Hodgson NC, Button JH, Franceschi D, Moffat FL, Livingstone AS (2004) Male breast cancer: is the incidence increasing? Ann Surg Oncol 11:751–775
15. Jepson AS, Fentiman IS (1998) Male breast cancer. Int J Clin Pract 52:571–576
16. Joshi MG, Lee AKC, Loda M, Camus MG, Peterson C, Heatley GJ, Hughes KS (1996) Male breast carcinoma: an evaluation of prognostic factors contributing to a poor outcome. Cancer 77: 490–498
17. Landis SH, Murray T, Bolden S, Wingo PA (1999) Cancer statistics, 1999. CA Cancer J Clin 49:8–31
18. Meijer-van Gelder ME, Look MP, Bolt-de Vries J, Peters HA, Klijn JG, Foekens JA (2001) Clinical relevance of biologic factors in male breast cancer. Breast Cancer Res Treat 68:249–260
19. Norris HJ, Taylor HB (1969) Carcinoma of the male breast. Cancer 23:1428–1435
20. Ravandi-Kashani F, Hayes TG (1998) Male breast cancer: a review of the literature. Eur J Cancer 34:1341–1347
21. Rogers S, Day CA, Fox SB (1993) Expression of cathepsin D and estrogen receptor in male breast carcinoma. Hum Pathol 24:148–151
22. Rudan I, Rudan N, Basic N, Basic V, Rudan D (1997) Differences between male and female breast cancer. II. Clinicopathologic features. Acta Med Croatica 51:129–133
23. Tavassoli FA, Devilee P (eds) (2003) World health organization classification of tumours. Pathology and genetics of tumours of the breast and female genital organs. IARC Press, Lyon
24. Temmim L, Luqmani YA, Jarallah M, Juma I, Mathew M (2001) Evaluation of prognostic factors in male breast cancer. Breast 10: 166–175
25. Visfeldt J, Scheike O (1973) Male breast cancer. I. Histologic typing and grading of 187 Danish cases. Cancer 32:985–990
26. Wainwright JM (1927) Carcinoma of the male breast. Ann Surg 14:836–857
27. Weber-Chappuis K, Bieri-Burger S, Hurlimann J (1996) Comparison of prognostic markers detected by immunohistochemistry in male and female breast carcinomas. Eur J Cancer 32A:1686–1692
28. Weiss JR, Moysich KB, Swede H (2005) Epidemiology of male breast cancer. Cancer Epidemiol Biomark Prev 14:20–26

Virchows Arch (2006) 449:513–519
DOI 10.1007/s00428-006-0294-2

ORIGINAL ARTICLE

Expression of Epstein–Barr virus (EBV)-encoded latent membrane proteins and STAT3 activation in nasopharyngeal carcinoma

Maike Buettner · Nicole Heussinger · Gerald Niedobitek

Received: 3 July 2006 / Accepted: 7 August 2006 / Published online: 11 October 2006
© Springer-Verlag 2006

Abstract The Epstein–Barr virus (EBV) is associated with virtually all cases of undifferentiated nasopharyngeal carcinoma (NPC), and it was proposed that the EBV-encoded transforming protein, latent membrane protein (LMP) 1, may play a role in the neoplastic process. It was proposed recently that LMP1 expression in epithelial cells may be regulated through a loop involving activated signal transducer and activator of transcription 3 (STAT3), LMP1, LMP1-mediated induction of interleukin (IL)-6 expression and STAT3 activation through the IL-6 receptor. This autoregulatory loop may be suppressed by another viral protein, LMP2A, an effect which in turn can be overcome by exogenous IL-6. Here we show that, as expected, expression of LMP1 and LMP2A tend to be exclusive in NPC tumours. Rare cases showing a co-expression of both proteins can be explained by STAT3 activation via the receptors for IL-6 or epidermal growth factor. STAT3 activation was a consistent feature of NPC tumour cells. However, in most cases, this was not accompanied by detectable expression of LMP1, suggesting either that LMP2A expression may suffice to suppress LMP1 expression or that additional factors may be operational. This study emphasises the need to correlate in vitro results with observational studies of ex vivo tumour tissues.

Keywords Epstein–Barr virus · Nasopharyngeal carcinoma · Hodgkin lymphoma · Latent membrane protein · STAT3

M. Buettner (✉) · N. Heussinger · G. Niedobitek
Pathologisches Institut, Friedrich-Alexander-Universität,
Krankenhausstr. 8-10,
91054 Erlangen, Germany
e-mail: maike.buettner@patho.imed.uni-erlangen.de

Introduction

A role of signal transducers and activators of transcription (STATs), especially of STAT3 and STAT5, in oncogenesis has been well-established in recent years [4, 5]. It was shown in vitro that constitutive activation of STAT3 can induce transformation in immortalised fibroblasts [5]. Moreover, STAT3 was implicated in the development of epithelial and lymphatic malignancies such as breast cancer [3], multiple myeloma [22], squamous cell carcinoma of head and neck (SCCHN) [26] and in the Epstein–Barr virus (EBV) associated tumours, nasopharyngeal carcinoma (NPC) and Hodgkin lymphoma (HL) [9, 16, 25]. It might therefore be speculated that EBV could promote oncogenesis by interacting with the STAT pathway.

EBV-associated tumours display different patterns of viral protein expression [21]. A set of nine viral, so-called latent proteins [EBV-encoded nuclear antigens (EBNA) 1 to 6, latent membrane proteins (LMP) 1, 2A, 2B] is expressed in EBV-immortalised lymphoblastoid cell lines and in lymphoproliferations occurring in immunosuppressed individuals [21]. This form of EBV infection is termed latency III. In this context, expression of LMP1, the major transforming viral protein, is regulated through EBNA2, whose expression is initiated before that of LMP1 [1]. In EBV-associated Hodgkin lymphomas and nasopharyngeal carcinomas, viral latent gene expression is restricted to EBNA1, LMP1, LMP2A and LMP2B (latency II) [21]. LMP1 expression is directed by two distinct promoters that contain elements responsive to members of the STAT family [9]. It was proposed recently that in the absence of EBNA2, phosphorylated STAT3 may activate one of these LMP1 promoters (L1-TR) [9]. Physiologically, phosphorylation and activation of STAT3 is the result of cytokine-mediated signalling, e.g. through the IL-6 receptor [17] or

of direct phosphorylation through receptor tyrosine kinases such as the epidermal growth factor receptor (EGFR) [26].

Previous studies have demonstrated a constitutive activation of STAT3 in Hodgkin and Reed–Sternberg (HRS) cells of Hodgkin lymphoma [18]. In keeping with this, LMP1 is consistently expressed in EBV-positive HL cases in the absence of EBNA2 [21]. NPC are also generally held to display a latency II pattern of viral proteins [21]. In vitro, a model has been suggested for epithelial and NPC cell lines, with a positive autoregulatory loop between LMP1 expression and STAT3 activation via IL6 [10]. However, at the protein level, LMP1 is detectable only in approximately 20 to 60% of cases [11, 19]. Recently, it was demonstrated that in epithelial cells, LMP2A may be able to down-regulate expression of LMP1 [27]. Since LMP2A is frequently expressed in NPC [15], this may explain the low levels of LMP1 expression. However, the inhibitory effect of LMP2A on LMP1 expression may be overcome by exogenous IL-6 [27], and in HRS cells, LMP1 and LMP2A are frequently co-expressed [20], suggesting that this effect may be cell lineage and context dependent. Based on these observations, we hypothesised that in NPC, expression of LMP1 and LMP2A should be mutually exclusive and that activated STAT3 should be detectable in LMP1-positive, but not in LMP1-negative, cases. To test these hypotheses, we have examined by immunohistochemistry the expression of LMP1 and LMP2A and the nuclear localisation of activated STAT3 in a series of NPC tumour biopsies.

Materials and methods

Tissues and cell lines

Paraffin wax blocks of 22 HL biopsies and of 20 NPC biopsies were retrieved from the files of the Institute for Pathology, Erlangen, and from the Institute of Pathology, Würzburg. All materials were submitted for diagnostic purposes and were used in accordance with national ethical principles.

The EBV-negative keratinocyte cell line RHEK-1 and an LMP-1 transfected subclone RHEK-1/LMP-1 were kindly provided by L.S. Young, Birmingham, UK. The EBV-negative HL cell lines L428, KMH-2 and HDLM-2 were obtained from Deutsche Sammlung von Mikroorganismen und Zellkulturen, Braunschweig, Germany. All cell lines were maintained in RPMI 1640 medium plus 5–10% fetal bovine serum and penicillin and streptomycin as antibiotics.

Snap-frozen samples of the NPC xenografts C15, C17 and C19 [7] were kindly provided by L.S. Young, and three snap-frozen NPC biopsies were a kind gift by John Nicholls, Hong Kong.

Immunohistochemistry and antibodies

Dewaxed paraffin sections were rehydrated and then treated with 3% H_2O_2 for 10 min at room temperature to block endogenous peroxidase when appropriate. For antigen retrieval, sections were treated in a steam cooker (Biocarta Europe, Hamburg, Germany) at 120°C for up to 150 s in 0.1 M citrate buffer, pH 6.0.

After incubation with primary antibodies (Table 1), biotin-labelled polyclonal rabbit anti-mouse (1:100, DakoCytomation, Hamburg), polyclonal rabbit anti-rat (1:100, DakoCytomation), or polyclonal goat anti-rabbit (1:100, DakoCytomation) were added for 30 min at room temperature.

Sections were then incubated with streptavidin-biotinylated horseradish peroxidase complex or alternatively with streptavidin-biotinylated alkaline phosphatase complex (both DakoCytomation). For STAT3-P and LMP2A, this procedure was followed by tyramide signal amplification as described previously [13, 15]. Immobilised biotin was visualised with streptavidin-biotinylated alkaline phosphatase complex (ABC-AP, DakoCytomation). Fast Red (Sigma-Aldrich, Steinheim, Germany) or aminoethyl carbazole (AEC, Zymed Laboratories, Berlin, Germany) were used as chromogens.

In situ hybridization

Expression of the small EBV-encoded nuclear RNAs was detected in tumour cells using in situ hybridization as described previously [24].

RNase protection assay

Expression of IL-6 RNA transcripts was detected in cell lines using the RNase protection assay as described

Table 1 Antibodies used in immunohistochemistry

Antibody Specificity	Source	Species	Clone or serum
STAT3	Santa Cruz, Heidelberg, Germany	Mouse	F-2
Phospho- STAT3 (Tyr 705)	Cell Signaling Beverly, USA	Rabbit	polyclonal
EGRF	Novocastra, Medac Hamburg, Germany	Mouse	EGFR.25
LMP-1	DakoCytomation, Hamburg, Germany	Mouse	CS.1-4
LMP2A	E. Kremmer, Munich, Germany	Rat	15F9, 4E11

previously [29]. A Riboquant multi-probe template set (hCK-2, BD Pharmingen, Heidelberg, Germany) was used according to the manufacturer's instructions. The set included DNA templates specific for IL-12p35, IL-12p40, IL-10, IL-1α, IL-1β, IL-1R, IL-6, IFNγ, L32, GAPDH .

Results

STAT3, Phospho-STAT3 and EGFR in HL and NPC

Using the STAT3-specific reagent, which detects inactive cytoplasmic and phosphorylated active nuclear STAT3, nuclear labelling of HRS cells was observed in all HL cases (21/21, Table 2, Fig. 1a). In addition, a cytoplasmic STAT3-specific staining was seen in HRS cells of most HL cases (19/21, Fig. 1a). Phosphorylated STAT3 (Phospho-STAT3) presented with a nuclear localisation in HRS cells in 100% (20/20) of HL cases (Fig. 1b). Moreover, nuclear labelling of many small lymphocytes was observed, which was not detected using the STAT3-specific reagent (Fig. 1b).

In NPC, 95% (19/20) of cases showed a nuclear and 100% (20/20) a cytoplasmic staining for STAT3 in tumour cells (Table 3). In the majority of cases, less than 50% of tumour cells, and often only single scattered tumour cells, expressed STAT3 in the nuclei. A nuclear expression in more than half of the tumour cells was observed in one case only. Nuclear Phospho-STAT3 was detected in the epithelial tumour cells of 95% (18/19) of NPC samples. Again the number of positive tumour cells was variable. In general, staining obtained with both reagents was weaker in NPC than in HL cases, whilst non-neoplastic lymphocytes present in the lymphoid stroma showed strong nuclear Phospho-STAT3 reactivity similar to that observed in HL. Using the Phospho-STAT3 reagent, an additional cytoplasmic and membranous staining was found in 100% (19/19) of NPC biopsy samples, in keeping with the known cross-reactivity of this antibody with the EGFR (manufacturer's information). As expected, all NPC (19/19) expressed EGFR in the tumour cells, whereas no staining was seen in the HL cases.

EBV latent gene expression and STAT3 activation

Seven of 21 HL cases were EBV-positive and expressed LMP1. A co-expression of LMP2A and LMP1 was seen in three of seven cases. Twenty-two percent of the NPC samples (4/18) were LMP1-positive and 50% (9/18) were LMP2A-positive. The expression of the LMP1 and LMP2A

Table 2 STAT3, Phospho-STAT3, EGFR expression and EBV infection in HL

	Type	STAT3 n/c	Phospho-STAT3 n/c	EGFR m	EBER n	LMP-1 m	LMP-2 m
HL01	NS	+++/+++	+++/−	−	−	−	−
HL02	NS	+++/+++	+++/−	nd	−	−	−
HL03	NS	+++/+++	+++/−	−	−	−	−
HL04	NS	+/+	+/−	nd	−	−	−
HL05	NS	+++/+++	+++/−	−	−	−	−
HL06	NS	+++/+	+++/−	−	+	+	−
HL07	NS	+/−	+/−	nd	−	−	−
HL08	NS	+++/+++	++/−	nd	−	−	−
HL09	NS	++/+++	++/−	nd	+	+	+
HL10	MC	++/+++	+++/−	nd	+	+	−
HL11	MC	+++/+++	+++/−	−	+	+	+
HL12	MC	+++/+++	+++/−	−	−	−	−
HL13	MC	+++/+++	+++/−	−	−	−	−
HL14	MC	+/+	+/−	−	−	−	−
HL15	MC	++/++	+/−	−	+	+	−
HL16	MC	+++/+++	+++/−	−	+	+	+
HL17	MC	++/+++	++/−	nd	+	+	−
HL18	MC	+++/+++	nd	nd	−	−	−
HL19	NLP	+++/+++	+++/−	−	−	−	−
HL20	NLP	++/+++	nd	nd	−	−	−
HL21	NLP	+++/−	+++/−	−	−	−	−
HL22	NLP	nd	+/−	−	−	−	−

nd not determined; *n* nucleus; *c* cytoplasm; *m* membrane
A single plus sign denotes <20%, two plus signs denote 20–50%, while three plus signs denote >50%.

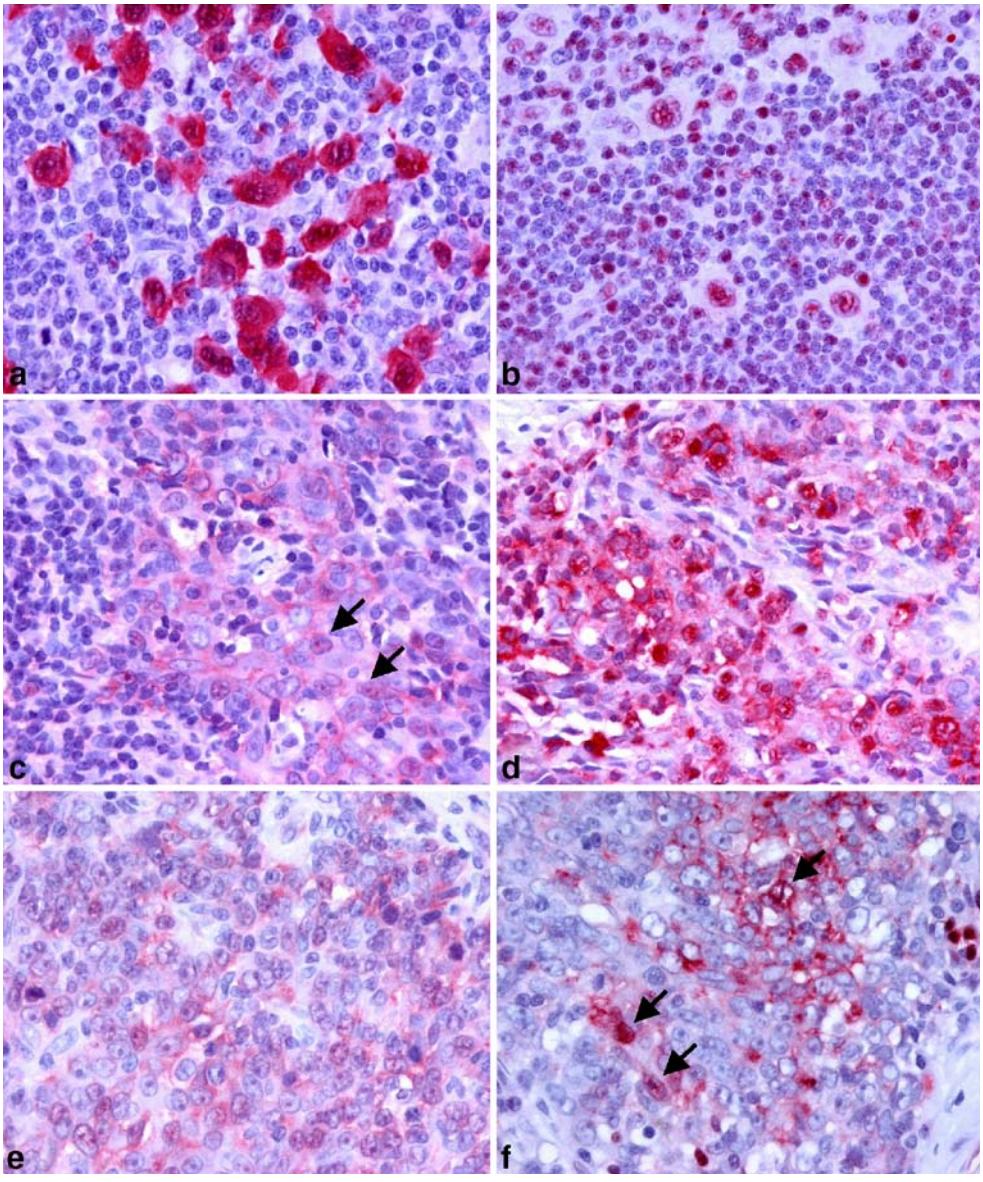

Fig. 1 STAT3 is expressed in the cytoplasm and nuclei of Hodgkin and Reed–Sternberg cells (**a**), while Phospho-STAT3 is detected in the nuclei of Hodgkin and Reed–Sternberg cells and in scattered lymphocytes in the inflammatory infiltrate (**b**). In nasopharyngeal carcinoma, STAT3 is weakly expressed in the cytoplasm and in the nuclei of a few scattered tumour cells (**c** and **e**). With the Phospho-STAT3-specific reagent, a nuclear and a membranous and cytoplasmic labelling was obtained in nasopharyngeal carcinoma (**d** and **f**)

was mutually exclusive in this series of NPC cases. No correlation was seen between the expression of STAT3 or the activation state of STAT3 and the infection of EBV or the expression of LMP1 or LMP2A. Specifically, expression levels of STAT3 were not higher in LMP1-positive than in LMP1-negative cases.

IL-6 expression in cell lines and tumour biopsies

IL-6 was expressed in all three HL cell lines as detected by RPA. In control epithelial RHEK-1 cells, IL-6 was expressed at a low basal level and expression was induced by LMP1 (data not shown). In the NPC xenografts C15, C17 and C19 (data not shown), no substantial IL-6 RNA levels were detected, whereas in tumour biopsies of three NPC patients, IL-6 was consistently present, though at low levels (Fig. 2).

Discussion

The aim of the present investigation was to evaluate the in vivo relevance of a model that suggested for epithelial cells an autoregulatory loop, in which STAT3 induces the expression of LMP-1 via the L1-TR promoter. LMP-1 induces IL-6 expression through the NFκB pathway, and IL-6 in turn activates STAT3 after interaction with IL-6 receptor [10, 27]. LMP2A interferes with this circuit by suppressing the NFκB pathway and, thereby, IL-6 expression, leading to a down-regulation of LMP1 expression [27]. This negative effect, however, can be overcome by exogenous IL-6 [27].

In our study, the presence of activated STAT3 was a common phenomenon in both NPC and HL, supporting studies that implied a role of STAT3 in the pathogenesis of NPC and HL [9, 16, 25]. It has been proposed that LMP1

Table 3 STAT3, Phospho-STAT3, EGFR expression and EBV infection in NPC

	Type	STAT3 n/c	Phospho-STAT3 n/c	EGFR m	EBER n	LMP-1 m	LMP-2 m
NPC01	III	++/+++	++/+++	+	+	−	+
NPC02	III	+/++	+/++	+	+	+	−
NPC03	III	+/++	+/++	+	+	−	+
NPC04	III	+/+++	+/+++	+	+	−	+
NPC05	III	+/+++	+/+++	nd	+	−	+
NPC06	III	−/++	−/++	+	+	−	−
NPC07	III	++/+++	++/+++	+	+	−	+
NPC08	III	++/+++	+/+	+	+	−	+
NPC09	III	++/+++	++/+++	+	+	−	+
NPC10	III	+/++	+/++	+	+	+	−
NPC11	III	++/+++	++/++	+	+	−	−
NPC12	III	++/+++	++/+++	+	+	−	+
NPC13	III	++/+++	++/+++	+	+	+	−
NPC14	I	++/+++	+/++	nd	−	−	−
NPC15	III	++/+++	+/++	+	+	−	−
NPC16	III	+++/+++	+++/+++	+	+	−	−
NPC17	III	+/++	nd	+	+	−	−
NPC18	III	+/+++	+/++	+	+	+	−
NPC19	I	+/+++	+/+++	+	−	−	−
NPC20	III	+/+	+/++	+	+	−	+

A plus sign denote <20%, two plus signs denote 20–50%, while three plus signs denote >50%.

expression in the context of latency II, i.e. in the absence of EBNA2, is mediated through STAT3 responsive elements in the L1-TR promoter [9, 10]. In keeping with this, expression of LMP1 was observed in all EBV-positive HL cases. In contrast, most NPC cases were negative for LMP1 as detected by immunohistochemistry although active nuclear STAT3 was regularly detected in a proportion of tumour cells. Stewart et al. [27] recently reported that LMP2A expression may down-regulate LMP1 in epithelial cells. In keeping with this, expression of LMP1 and LMP2A were mutually exclusive in our NPC cases. However, both proteins are frequently co-expressed in HL, and we have observed co-expression of LMP1 and LMP2 in two of four additional NPC cases not included in the current study due to a lack of available tissue sections for analysis of STAT3 expression (unpublished observation). The occasional co-expression of LMP1 and LMP2A may be explained by the effect of exogenous IL-6 [27]. The frequent presence of IL-6 expressing non-malignant cells has been demonstrated for both HL and NPC [2, 14], and is confirmed for IL-6 in this study using RPA analysis of NPC biopsy samples. It is not known, however, if the IL-6 receptor is expressed in NPC tumour cells. Activation of STAT3 in NPC tumour cells can also be explained by the activity of EGFR, which is consistently expressed in NPC, in keeping with previous studies [12, 24, 28]. This implicates a function of EGFR in STAT3 activation in NPC as has been proposed for SCCHN [8, 23]. We confirm that IL-6 expression is induced by LMP1 in an LMP1-transfected keratinocyte cell line consistent with previous reports [10, 27]. However, whilst in HL expression of IL-6 in the HRS cells correlates with the expression of LMP1, no such relationship has been established for NPC [2], and we show that IL-6 is not expressed in three transplantable NPC cell lines. Moreover, we show now that there is no correlation between expression of LMP1 (or LMP2A) with the detection of activated STAT3 in NPC tissues. Thus, whilst the expression of LMP1 in the presence of LMP2A in NPC and in HL can be explained by exogenous effects, mediated through receptors for IL-6 or EGF, the absence of detectable LMP1 expression in NPC biopsies in the presence of nuclear STAT3 is more difficult to explain. It is possible, that in the cellular environment of NPC tumour cells, STAT3 induces only low levels of LMP1 expression, below the threshold of detection of our immunohistochemical assay. Indeed, it is well-known that using highly sensitive nested PCR methods, low levels of LMP1 RNA transcripts can be detected in all NPC cases [6]. The biological relevance of these rare transcripts, however, remains uncertain. The fact that in most NPC cases STAT3 activation was not accompanied by detectable expression of LMP1 suggests that either LMP2A expression may suffice to suppress LMP1 expression in most cases or that additional factors may operate in NPC, which suppress

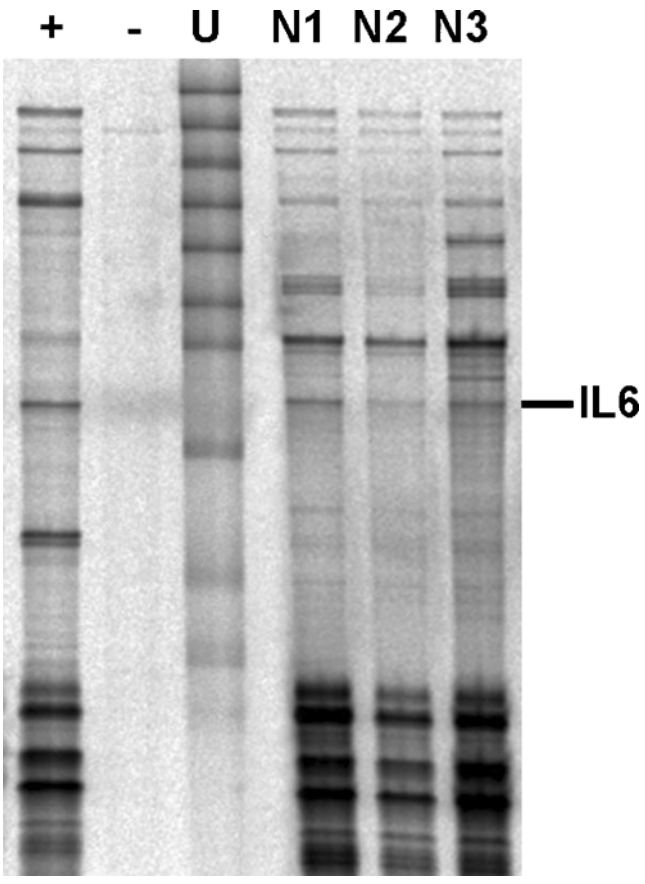

Fig. 2 RPA analysis of IL-6 expression in snap-frozen nasopharyngeal carcinoma biopsies. Each unprotected probe (*U*) migrates slower than the corresponding protected band due to flanking sequences in the probe that are not protected by mRNA. A variable, but consistent, expression of IL-6 RNA is detected in three NPC biopsies (*N1–N3*)

LMP1 expression in most cases. Thus, this study emphasises the need to correlate in vitro results with observational studies of ex vivo tumour tissues.

Acknowledgements We thank G. Ott, Würzburg, for kindly providing paraffin-embedded NPC specimens; L.S. Young, Birmingham, UK for providing snap-frozen samples of the NPC xenografts C15, C17 and C19; and John Nicholls, Hong Kong for three snap-frozen NPC biopsies. This work was supported by a grant from the Wilhelm Sander Foundation.

References

1. Abbot SD, Rowe M, Cadwallader K, Ricksten A, Gordon J, Wang F, Rymo L, Rickinson AB (1990) Epstein–Barr virus nuclear antigen 2 induces expression of the virus-encoded latent membrane protein. J Virol 64:2126–2134
2. Beck A, Pazolt D, Grabenbauer GG, Nicholls JM, Herbst H, Young LS, Niedobitek G (2001) Expression of cytokine and chemokine genes in Epstein–Barr virus-associated nasopharyngeal carcinoma: comparison with Hodgkin's disease. J Pathol 194: 145–151
3. Berclaz G, Altermatt HJ, Rohrbach V, Siragusa A, Dreher E, Smith PD (2001) EGFR dependent expression of STAT3 (but not STAT1) in breast cancer. Int J Oncol 19:1155–1160
4. Bowman T, Garcia R, Turkson J, Jove R (2000) STATs in oncogenesis. Oncogene 19:2474–2488
5. Bromberg JF, Wrzeszczynska MH, Devgan G, Zhao Y, Pestell RG, Albanese C, Darnell JE Jr (1999) Stat3 as an oncogene. Cell 98:295–303
6. Brooks L, Yao QY, Rickinson AB, Young LS (1992) Epstein–Barr virus latent gene transcription in nasopharyngeal carcinoma cells: coexpression of EBNA1, LMP1, and LMP2 transcripts. J Virol 66:2689–2697
7. Busson P, Ganem G, Flores P, Mugneret F, Clausse B, Caillou B, Braham K, Wakasugi H, Lipinski M, Tursz T (1988) Establishment and characterization of three transplantable EBV-containing nasopharyngeal carcinomas. Int J Cancer 42:599–606
8. Chan KS, Carbajal S, Kiguchi K, Clifford J, Sano S, DiGiovanni J (2004) Epidermal growth factor receptor-mediated activation of Stat3 during multistage skin carcinogenesis. Cancer Res 64:2382–2389
9. Chen H, Lee JM, Zong Y, Borowitz M, Ng MH, Ambinder RF, Hayward SD (2001) Linkage between STAT regulation and Epstein–Barr virus gene expression in tumors. J Virol 75:2929–2937
10. Chen H, Hutt-Fletcher L, Cao L, Hayward SD (2003) A positive autoregulatory loop of LMP1 expression and STAT activation in epithelial cells latently infected with Epstein–Barr virus. J Virol 77:4139–4148
11. Fahraeus R, Fu HL, Ernberg I, Finke J, Rowe M, Klein G, Falk K, Nilsson E, Yadav M, Busson P et al (1988) Expression of Epstein–Barr virus-encoded proteins in nasopharyngeal carcinoma. Int J Cancer 42:329–338
12. Fujii M, Yamashita T, Ishiguro R, Tashiro M, Kameyama K (2002) Significance of epidermal growth factor receptor and tumor associated tissue eosinophilia in the prognosis of patients with nasopharyngeal carcinoma. Auris Nasus Larynx 29:175–181
13. Greiner A, Tobollik S, Buettner M, Jungnickel B, Herrmann K, Kremmer E, Niedobitek G (2005) Differential expression of activation-induced cytidine deaminase (AID) in nodular lymphocyte-predominant and classical Hodgkin lymphoma. J Pathol 205:541–547
14. Herbst H, Samol J, Foss HD, Raff T, Niedobitek G (1997) Modulation of interleukin-6 expression in Hodgkin and Reed–Sternberg cells by Epstein–Barr virus. J Pathol 182:299–306
15. Heussinger N, Buttner M, Ott G, Brachtel E, Pilch BZ, Kremmer E, Niedobitek G (2004) Expression of the Epstein–Barr virus (EBV)-encoded latent membrane protein 2A (LMP2A) in EBV-associated nasopharyngeal carcinoma. J Pathol 203:696–699
16. Hsiao JR, Jin YT, Tsai ST, Shiau AL, Wu CL, Su WC (2003) Constitutive activation of STAT3 and STAT5 is present in the majority of nasopharyngeal carcinoma and correlates with better prognosis. Br J Cancer 89:344–349
17. Kisseleva T, Bhattacharya S, Braunstein J, Schindler CW (2002) Signaling through the JAK/STAT pathway, recent advances and future challenges. Gene 285:1–24
18. Kube D, Holtick U, Vockerodt M, Ahmadi T, Haier B, Behrmann I, Heinrich PC, Diehl V, Tesch H (2001) STAT3 is constitutively activated in Hodgkin cell lines. Blood 98:762–770
19. Niedobitek G, Young LS, Sam CK, Brooks L, Prasad U, Rickinson AB (1992) Expression of Epstein–Barr virus genes and of lymphocyte activation molecules in undifferentiated nasopharyngeal carcinomas. Am J Pathol 140:879–887
20. Niedobitek G, Kremmer E, Herbst H, Whitehead L, Dawson CW, Niedobitek E, von Ostau C, Rooney N, Grasser FA, Young LS (1997) Immunohistochemical detection of the Epstein–Barr virus-

encoded latent membrane protein 2A in Hodgkin's disease and infectious mononucleosis. Blood 90:1664–1672
21. Niedobitek G, Meru N, Delecluse HJ (2001) Epstein–Barr virus infection and human malignancies. Int J Exp Pathol 82:149–170
22. Quintanilla-Martinez L, Kremer M, Specht K, Calzada-Wack J, Nathrath M, Schaich R, Hofler H, Fend F (2003) Analysis of signal transducer and activator of transcription 3 (Stat 3) pathway in multiple myeloma: Stat 3 activation and cyclin D1 dysregulation are mutually exclusive events. Am J Pathol 162:1449–1461
23. Rubin Grandis J, Zeng Q, Drenning SD (2000) Epidermal growth factor receptor-mediated stat3 signaling blocks apoptosis in head and neck cancer. Laryngoscope 110:868–874
24. Sheen TS, Huang YT, Chang YL, Ko JY, Wu CS, Yu YC, Tsai CH, Hsu MM (1999) Epstein–Barr virus-encoded latent membrane protein 1 co-expresses with epidermal growth factor receptor in nasopharyngeal carcinoma. Jpn J Cancer Res 90:1285–1292
25. Skinnider BF, Elia AJ, Gascoyne RD, Patterson B, Trumper L, Kapp U, Mak TW (2002) Signal transducer and activator of transcription 6 is frequently activated in Hodgkin and Reed–Sternberg cells of Hodgkin lymphoma. Blood 99:618–626
26. Song JI, Grandis JR (2000) STAT signaling in head and neck cancer. Oncogene 19:2489–2495
27. Stewart S, Dawson CW, Takada K, Curnow J, Moody CA, Sixbey JW, Young LS (2004) Epstein–Barr virus-encoded LMP2A regulates viral and cellular gene expression by modulation of the NF-kappaB transcription factor pathway. Proc Natl Acad Sci USA 101:15730–15735
28. Sung FL, Poon TC, Hui EP, Ma BB, Liong E, To KF, Huang DP, Chan AT (2005) Anti-tumor effect and enhancement of cytotoxic drug activity by cetuximab in nasopharyngeal carcinoma cells. In Vivo 19:237–245
29. Teichmann M, Meyer B, Beck A, Niedobitek G (2005) Expression of the interferon-inducible chemokine IP-10 (CXCL10), a chemokine with proposed anti-neoplastic functions, in Hodgkin lymphoma and nasopharyngeal carcinoma. J Pathol 206:68–75

Virchows Arch (2006) 449:520–528
DOI 10.1007/s00428-006-0274-6

ORIGINAL ARTICLE

Expression of E-cadherin transcriptional regulators in ovarian carcinoma

Sivan Elloul · Ilvars Silins · Claes G. Tropé · Avi Benshushan · Ben Davidson · Reuven Reich

Received: 8 March 2006 / Accepted: 12 July 2006 / Published online: 6 October 2006
© Springer-Verlag 2006

Abstract Unlike most epithelial cancers, E-cadherin expression is upregulated in ovarian carcinoma effusions compared with corresponding primary tumors. In the present study, we analyzed the anatomic site-specific expression of transcription factors that negatively regulate E-cadherin in ovarian carcinoma. Using reverse-transcription polymerase chain reaction, mRNA in situ hybridization, and Western blotting, we analyzed the expression and localization of the Snail, Slug, and SIP1 transcription factors and E-cadherin in 78 effusions, 41 primary carcinomas, and 15 solid metastases. Slug mRNA and protein expression was highest in metastases (p=0.042 and p<0.001, respectively). Snail mRNA was comparable at all anatomic sites, but higher protein expression was found in primary tumors and solid metastases compared with effusions (p<0.001). SIP1 mRNA expression was higher in effusions (p<0.001) compared to other sites. Confocal microscopy analysis of fresh and cultured cells from effusion specimens revealed cytoplasmic localization of the Snail protein in primary tumor cells, with a nuclear shift following culturing of these cells. In conclusion, E-cadherin and its negative regulators show site-dependent expression in ovarian carcinoma. In solid tumors, E-cadherin is negatively regulated by Snail and Slug. In effusions, SIP1 may be the main regulator of E-cadherin, but with a lesser level of suppression compared with primary tumors and solid metastases.

Keywords Ovarian carcinoma · E-cadherin · Transcriptional repressors

Reuven Reich is affiliated with the David R. Bloom Center for Pharmacy at the Hebrew University.

S. Elloul · R. Reich
Department of Pharmacology and Experimental Therapeutics,
School of Pharmacy, Faculty of Medicine,
The Hebrew University of Jerusalem,
Jerusalem 91120, Israel

I. Silins · C. G. Tropé
Department of Gynecologic Oncology,
National Hospital–Norwegian Radium Hospital,
University of Oslo,
Montebello,
0310 Oslo, Norway

B. Davidson (✉)
Department of Pathology,
National Hospital–Norwegian Radium Hospital,
University of Oslo,
Montebello,
0310 Oslo, Norway
e-mail: ben.davidson@radiumhospitalet.no

A. Benshushan
Department of Obstetrics and Gynecology,
Hadassah Medical Center, Hebrew University,
Jerusalem 91120, Israel

Introduction

Epithelial mesenchymal transition (EMT) is a normal process during embryonic morphogenesis in multicellular organisms, in which embryonic mesenchymal cells are formed and become motile following the loss of epithelial cell polarity [12, 30]. During embryogenesis, EMT is tightly regulated in a spatial and temporal fashion to ensure proper homing and reversion of cells to a nonmotile phenotype following migration to a destined location. In recent years, EMT has been recognized as a potential mechanism for cancer progression [29]. In contrast to the embryonic process, cancer cells undergoing EMT have lost specific target recognition and are usually equipped with

autocrine loops of growth signals, mechanisms to evade apoptosis, and the potential to elicit angiogenesis for independent nutrient supply [12].

A central event mediating EMT is the shift from E-cadherin to N-cadherin expression [29]. E-cadherin, the prototype member of the classical cadherin family, is localized to the surface of epithelial cells in regions of cell–cell contact known as adherens junctions and maintains cell polarity and normal epithelial structure [4, 23]. In most epithelial cancers, E-cadherin-mediated cell–cell adhesion is lost concomitantly with progression towards a malignant phenotype [4, 15]. E-cadherin loss occurs in several ways: (1) mutational inactivation of the human E-cadherin gene (CDH1), as in gastric carcinoma of the diffuse type and infiltrating lobular breast carcinoma [13, 21]; (2) hypermethylation of the DNA encoding E-cadherin, which leads to downregulation of E-cadherin mRNA [31]; (3) repression by transcription factors, mediated through a region in the E-cadherin promoter that contains two E-boxes [31].

Two members of the Snail family of transcription factors, Snail and Slug, have been shown to downregulate E-cadherin transcription [29]. Snail has been shown to downregulate E-cadherin in hepatocellular [17], gastric [27], and oral [32] carcinomas and in melanoma [24]. Snail upregulates the expression of matrix metalloproteinases (MMP) [19, 33] and mesenchymal molecules such as fibronectin and vimentin and downregulates the epithelial markers cytokeratin 18, desmoplakin, and Muc1, as well as claudin and occludin, which play an important role in epithelial tissue polarity [20, 16]. Slug was shown to downregulate E-cadherin in breast cancer [14]. Other transcription factors that are able to repress E-cadherin in cell line models are SIP1 and E47 [29].

Carcinoma of the ovary is the leading cause of death from gynecological cancer in western countries, mainly due to its detection at an advanced stage when the chance for cure is poor [11]. Ovarian carcinoma primarily metastasizes to the serosal cavities and is commonly associated with the accumulation of malignant peritoneal and pleural effusions [8, 9]. However, ovarian carcinoma does not follow the classical model of EMT, as evidenced by the upregulation of E-cadherin expression in ovarian carcinoma effusions compared with corresponding primary tumors [7], suggesting that E-cadherin is not a tumor suppressor molecule in this cancer. To elucidate the mechanisms for E-cadherin downregulation in the subset of effusions in which cancer cells show reduced expression of this molecule, we recently analyzed the expression of Snail, Slug, and SIP1 in ovarian and breast carcinoma effusions. We found mRNA expression of all three factors at this anatomic site and reported on the prognostic role of SIP1 and Snail in ovarian and breast carcinoma, respectively [10]. However, in view of the site-related differences in E-cadherin expression in ovarian carcinoma, we hypothesized that its negative regulators may be differentially expressed in primary tumors, solid metastases, and effusions. The present study addresses this question and expands our data to protein expression of Snail and Slug in clinical material and in vitro.

Materials and methods

Tumors All specimens and relevant clinical data were obtained from the Department of Gynecologic Oncology at the Norwegian Radium Hospital. Informed consent was obtained according to National Norwegian and Institutional Guidelines. Data related to specimen handling and diagnosis are detailed in our previous paper [10].

The analyzed material consisted of 78 fresh nonfixed malignant peritoneal (=54) and pleural (=24) effusions, 41 primary carcinomas and 15 solid metastases (Total=134). Five of the primary tumors and one metastasis were from patients with effusion specimens. In addition, matched primary tumor and omental metastasis were available from two patients, with an additional lymph node metastasis from one of these two patients. Clinicopathologic data were available for most patients and are detailed in Table 1. Solid metastases consisted of 11 omental lesions, two vaginal, one peritoneal, and one lymph node metastases. Effusions were centrifuged and frozen as cell pellets immediately upon arrival to our department. Solid tumor specimens were similarly immediately snap-frozen in liquid nitrogen. Frozen sections were obtained from all solid tumors to verify the presence of sufficient (>50%) tumor and the absence of necrosis. E-cadherin protein expression data were previously published for specimens obtained during 1998–1999 [7].

Reverse-Transcription Polymerase Chain Reaction (RT-PCR) Total RNA from all 134 samples was extracted using a commercial kit (Tri-Reagent, Sigma, St. Louis, MO). Using the M-MLV Reverse Transcriptase, 0.5 μg of total RNA was reverse transcribed (Promega, Madison, WI), with incubation of 2 h at 37°C, followed by 5 min at 95°C, and diluted to 1:5 with RNase-free water. RT-PCR was performed on cDNA samples using a DNA thermal cycler (Eppendorf Mastercycler gradient, Eppendorf, Hamburg, Germany) with Reddymix PCR master mix (ABgene, Surrey, UK), RNase-free water and primers as follows: *E-cadherin*: sense 5′-TCCATTTCTTGGTCTACGCC-3′, antisense 5′-CACCTTCAGCCAACCTGTTT-3′ (product size=361 bp) [28]; *Snail*: sense 5′-TGCGCGAATCGGCGACCC-3′, antisense 5′-CTAGAGAACCGCTTCCCGCAG-3′ (product size=600 bp) [24]; *Slug*: sense 5′-GCCTCCAAAAAGCCAAACTACTA-3′, antisense 5′-

Table 1 Clinicopathologic data of the study cohort

Parameter		Material (number of patients)		
		Effusions (70)	Primary (41)	Metastasis (14)
Age (years)	Mean (range)	60 (35–79)	60 (34–84)	62 (48–78)
FIGO stage	I	0	2	0
	II	1	3	0
	III	35	22	11
	IV	34	6	3
	NA[a]	0	8	0
Grade	I	6	5	1
	II	22	11	1
	III	32[b]	18[c]	12
	NA	10	7	0
Residual disease	<2 cm	34	25	6
	≥2 cm	28	7	6
	NA	8	9	2
Histology	Serous	57	33	9
	Mucinous	1	0	0
	Clear cell	4	3	1
	Endometrioid	0	2	1
	Mixed epithelial	4	3	0
	Undifferentiated	3	0	3
	NA	1	0	0

[a] NA=not available, including specimens from inoperable patients and patients operated in other hospitals for whom full clinicopathological data were not available.
[b] Including four patients with clear cell carcinomas.
[c] Including three patients with clear cell carcinomas.

GTGTGCTACACAGCAGCCAGATT-3′ (product size=888 bp); *SIP1*: sense 5′-GCGGCATATGGTGACACA CAA-3′, antisense 5′-TGCCACTAAAC CCGTGTGTA-3′ (product size=466 bp) [27]; *28S*: sense 5′-GTTCACCCA CTAATAGGG AACGTGA-3′, antisense 5′-GGATTCTG ACTTAGAGGCG TTCAGT-3′ (product size=212 bp) [18]. Products were separated on 1.5% agarose gels, isolated using the Invisorb Spin DNA extraction kit (Invitek GmbH, Berlin, Germany), and sequenced. The HT-1080 fibrosarcoma cell line was used as control in all Snail, Slug, and SIP1 reactions. An endometrial carcinoma biopsy was used as control for the E-cadherin RT-PCR reaction. Gels were photographed by the KODAK EDAS 290 system. Densitometer analysis of films was performed using a computerized image analysis (NIH IMAGE 1.63) program. Snail, Slug, SIP1, and E-cadherin mRNA levels were established by calculating the target molecule/28S ratio (all cases scored for band size compared to a control sample derived from the HT-1080 cell line, E-cadherin scored for band size compared to a control sample derived from the endometrium specimen). Measurements were made at the linear phase of the reaction.

In situ mRNA hybridization (ISH) Snail mRNA expression was analyzed in 65 effusions and 91 corresponding solid tumors (40 primary carcinomas, 51 solid metastases). Solid metastases consisted of 29 omental, 8 peritoneal, and 4 intestinal lesions, as well as 10 biopsies from other anatomic sites. These specimens were from a series that has been previously analyzed for mRNA and protein expression of metastasis- and cancer-associated molecules (reviewed in Refs. [8, 9]). Twenty-two of the 65 effusions were also analyzed using RT-PCR. The remaining effusions and all solid tumors were part of our cohort collected between 1998 and 2000 and were different from the cases analyzed using RT-PCR. Specific Brigati tail-labeled antisense oligonucleotide DNA probe for the Snail mRNA transcript [17] was obtained from Sigma. The specificity of the probe was verified using a sense probe (Sigma). A poly d(T)20 oligonucleotide probe (Research Genetics, Huntsville, AL) was used to verify the integrity and lack of degradation of mRNA in each sample. cDNA probes were hyperbiotinylated. The stock dilution was diluted with probe diluent (Research Genetics) immediately before use. Tissue sections (4-μm-thick) of formalin-fixed, paraffin-embedded specimens were mounted on ProbeOn Plus slides (Fisher Scientific, Pittsburgh, PA). Sectioning was performed in RNase-free water. ISH was carried out using the microprobe manual staining system (Fisher Scientific) [25]. Hybridization of the probes was carried out as previously described [6]. Positive enzymatic reaction in this assay stained dark blue. An infiltrating duct carcinoma of the breast shown to express Snail mRNA in pilot studies was used as positive control in each hybridization reaction. Control for endogenous alkaline phosphatase included treatment of the sample in the absence of the probe and the use of the chromogen alone.

Staining in carcinoma and stromal cells was scored as negative, focal, or diffuse, corresponding to staining in 0%, 1–20%, and 21–100% of cells, respectively. At least 500 cells were scored, when present. No specimen contained less than 100 tumor cells.

Western blot analysis Seventy-four effusions, 30 primary carcinomas, and 10 solid metastases were analyzed for Snail and Slug protein expression. All these specimens were part of the material that was analyzed for Snail and Slug mRNA expression. Aliquots of each specimen extract, containing 30 μg of protein, were resolved by 12% SDS-PAGE. The separated extracts were electrophoretically transferred onto Immobilon PVDF membrane (Millipore, Bedford, MA) in a transfer buffer. The membrane was incubated with an anti-Snail antibody (Sigma) or an anti-Slug antibody (Santa Cruz Biotechnology, Santa Cruz, CA). The anti-Snail antibody was raised in a rabbit that has been injected with a peptide containing the N-Terminal region of Snail protein conjugated

to KLH (MPRSFLVRKPSDPNRLPNYC). The membrane was also incubated with preimmune serum and with the antibody and the peptide used for injection to ensure band specificity. Both Snail and Slug proteins are of 29-kDa size.

Immunofluorescence Human fibrosarcoma cells (HT-1080) and ovarian tumor cells isolated from a peritoneal effusion were grown on glass cover slips. Cells from effusion specimens were also collected on slide to preserve the tumor structure. Following TRAIL treatment, the cells were washed with phosphate-buffered sulfate (PBS) and fixed in 4% paraformaldehyde for 15 min. Subsequently, cells were washed in PBS and, after blocking with staining buffer (2% bovine serum albumin and 0.1% Triton X-100 in PBS) for 30 min at room temperature, were incubated with the Snail or Slug antibody. Following washes in PBS, cells were incubated with an antirabbit Alexa Fluor 488 antibody (Molecular Probes, Eugene, OR) for an additional 60 min and were mounted in FluoroGuard antifade reagent (Bio-Rad Laboratories, Hercules, CA). Cells were viewed and photographed using confocal microscopy with ×63 magnification at an excitation wavelength of 488 nm.

Statistical analysis Data were analyzed using the SPSS-PC package (version 12.0, Chicago, IL). Comparative analyses of tumor cell expression results in effusions, primary tumors, and solid metastases using RT-PCR and IB (continuous variables) were performed using the Kruskal–Wallis *H* test (for analysis of all three sites) or Mann–Whitney test (for analysis of two sites). Comparative analyses of Snail ISH data (noncontinuous variable) were performed using the Wilcoxon signed ranks test. All statistical analyses were two sided.

Results

E-cadherin is differentially expressed at different anatomic sites in ovarian carcinoma Our first objective was to analyze E-cadherin mRNA expression levels in the specimens using PCR. E-cadherin mRNA was found in 29/41 (71%) primary ovarian tumors. In metastases, 12/15 (80%) samples were positive. E-cadherin mRNA was found in 75/78 (96%) effusion specimens (Fig. 1a). E-cadherin mRNA expression level was significantly higher in ovarian effusions in comparison with solid tumors (mean rank: 81 in effusions vs 48 in primary tumors and 52 in metastases, $p<0.001$, Kruskal–Wallis *H* test; Fig. 1b). These results are in agreement with our data analyzing E-cadherin protein expression in a previous cohort (Fig. 2a–c) [7].

Snail, Slug, and SIP1 expression in ovarian carcinoma Snail mRNA was found in 38/41 (93%) primary tumors and 14/15 (93%) metastases. In ovarian effusions, we found Snail mRNA in 68/78 (87%) specimens (Fig. 3). Statistical analysis did not show any significant difference between the three groups (Kruskal–Wallis *H* test, $p>0.05$).

Snail expression was additionally analyzed using ISH to demonstrate that this transcription factor localizes to carcinoma cells. ISH analysis showed Snail mRNA expression in carcinoma cells in 43/65 (66%) effusions (30 focal, 13 diffuse), 15/40 (37%) primary tumors (12 focal, 3 diffuse), and 17/51 (33%) solid metastases (14 focal, 3 diffuse) (Fig. 2d–f). This difference was not significant (Wilcoxon signed ranks test, $p>0.05$). Peritumoral stromal cells expressed Snail mRNA in only four primary tumors and five metastases. The less frequent Snail expression using ISH may be attributed to the lower sensitivity of the method, whereas the different relationship

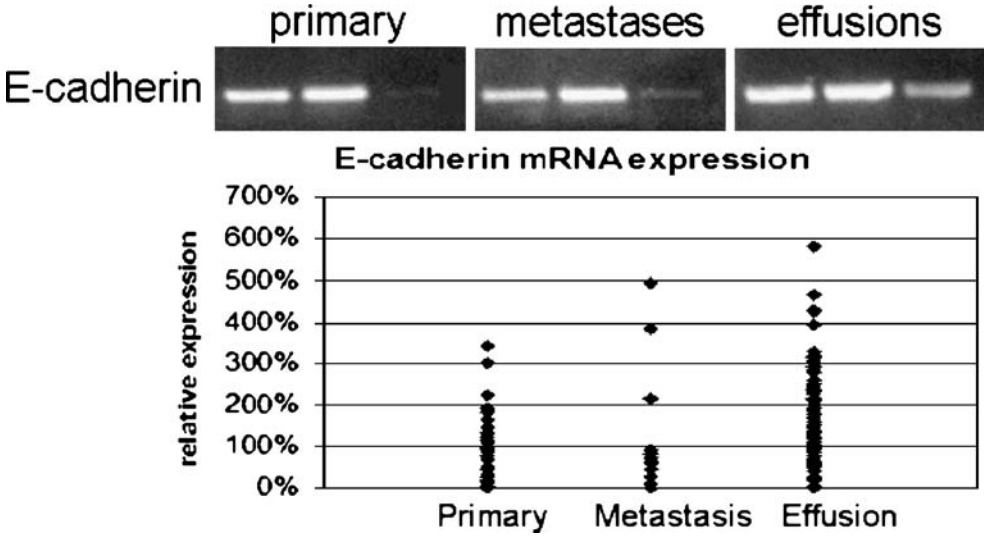

Fig. 1 RT-PCR analysis of E-cadherin mRNA expression in nine representative specimens chosen as examples for the entire cohort (three primary tumors, three solid metastases, three effusions; **a**). Expression differences between tumor cells at different sites, with higher E-cadherin expression in effusions ($p<0.001$; **b**)

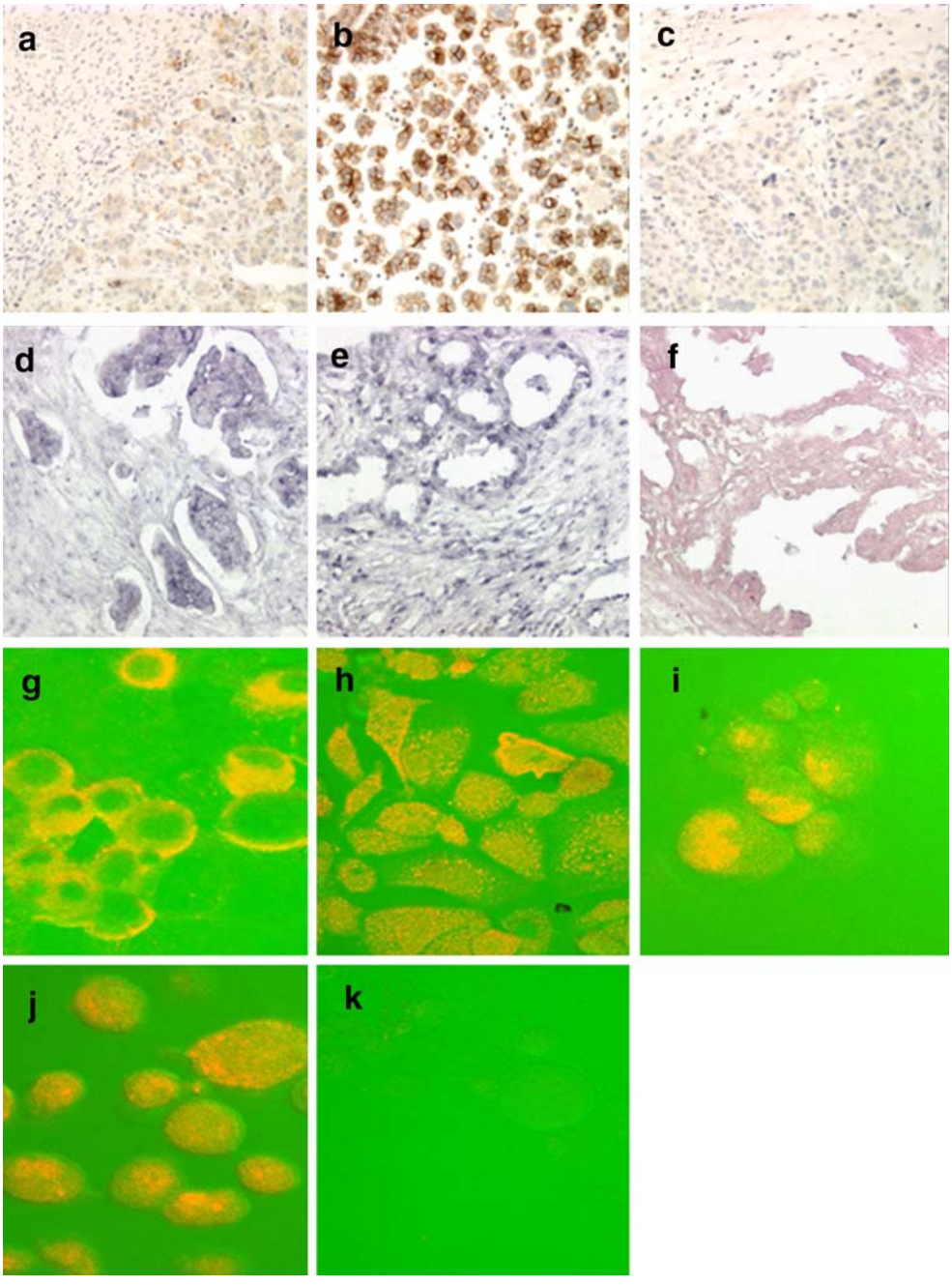

Fig. 2 E-cadherin, Snail, and Slug expression using immunohistochemistry, ISH, and confocal microscopy. **a–c** Immunocytochemistry for E-cadherin in primary carcinoma (**a**), effusion (**b**), and omental metastasis (**c**) from the same patient. Expression is highest in the effusion specimen. **d–f** ISH analysis of Snail mRNA expression. Primary tumor (**d**) and omental metastasis (**e**) show Snail mRNA expression. **f** A Snail-negative ovarian carcinoma. Cells are counterstained with nuclear fast red. **g–k** Confocal microscopy. Uncultured cells show only cytoplasmic Snail expression (**g**). In contrast, cells grown on culture dish show nuclear expression of this transcription factor (**h**). Slug protein is located to the nucleus in both uncultured (**i**) and cultured (**j**) cells. Negative control is shown in **k**. [ISH: NBT-BCIP staining, counterstained with nuclear fast red]

between effusions, primary tumors, and metastases may reflect the different cohorts analyzed. However, both the RT-PCR and ISH tests show no significant differences in Snail mRNA expression levels in carcinoma cells at these three anatomic sites.

In contrast to Snail mRNA, Snail protein expression was markedly different between effusions, primary tumors, and solid metastases. Using a polyclonal anti-Snail antibody, we detected Snail protein in 72/74 (97%) effusions, 30/30 (100%) primary carcinomas, and 10/10 (100%) solid metastases. However, expression levels were markedly different, as reflected by mean expression of 17% of control levels in effusions compared with 118% in primary tumors and 127% in solid metastases. This difference was significant (mean rank: 38 in effusions vs 92 in primary tumors and 97 in metastases, $p<0.001$, Kruskal–Wallis H test; Fig. 4) and was also seen in comparative analysis of the five matched primary tumors and effusions ($p=0.036$, Mann–Whitney U test). This discrepancy between mRNA and protein expression results as related to anatomic site may indicate an additional regulation level of Snail at the translational or posttranslational level.

Slug mRNA expression was found in 39/41 (95%) primary ovarian carcinomas. In metastases, Slug mRNA

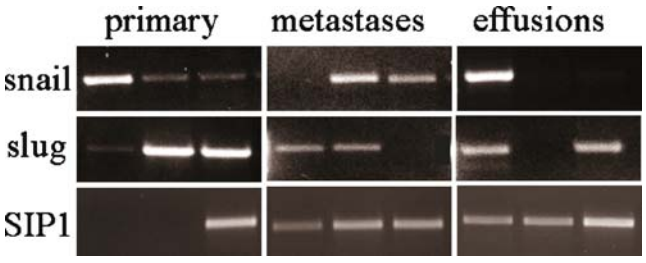

Fig. 3 RT-PCR analysis of Snail, Slug, and Sip1 mRNA expression in nine specimens (three primary tumors, three solid metastases, three effusions). Cases are representative specimens chosen as examples for the entire cohort. The metastasis in the *third lane* in the Slug analysis has weak expression that may be difficult to discern in the figure but was detected in the densitometric analysis

expression was found in all 15 specimens (100%). In effusions, Slug mRNA expression was found in 56/78 (72%) of the specimens (Fig. 3). Slug mRNA level was significantly higher in metastases compared with effusions (mean rank: 59 in metastases vs 44 in effusions, p=0.042, Mann–Whitney test).

Slug protein expression, analyzed by Western blot, showed comparable, though more pronounced, differences. We detected Slug protein in 13/74 (18%) effusions, 21/30 (70%) primary carcinomas, and 10/10 (100%) solid metastases. Mean expression was 2% of control levels in effusions compared with 25% in primary tumors and 62% in solid metastases. This difference was significant (mean rank values were 18 for effusions, 36 for primary tumors, and 51 for metastases, Kruskal–Wallis H test, p<0.001; Fig. 4). In contrast to Snail protein expression, we found significant difference between primary tumors and metastases in Slug protein expression using Mann–Whitney U test (mean rank: 29 for metastases vs 17 for primary tumors, p=0.002). The results for Slug protein were concurrent with the mRNA results, in contrast to the Snail expression, as indicated above.

In primary tumors, Slug protein was found to be inversely correlated with E-cadherin mRNA (p=0.002). This inverse correlation may indicate a negative regulation at this tumor site.

SIP1 mRNA expression was analyzed using RT-PCR in our cohort samples. SIP1 mRNA in primary ovarian tumors was found in 39/41 (95%) of the specimens. In metastases, SIP1 mRNA expression was found in all of the 15 samples (100%). In effusions, 77/78 (99%) of the specimens expressed SIP1 mRNA (Fig. 3). SIP1 mRNA expression levels were significantly higher in the effusions in comparison with primary tumors and solid metastases (mean rank: 81 for effusions, 43 for primary tumors, 63 for metastases, p<0.001, Kruskal–Wallis H test). This difference was reproduced in comparative analysis of the five matched primary tumors and effusions (p=0.008, Mann–Whitney U test).

Results for the RT-PCR and Western blotting experiments are summarized in Table 2.

Protein localization of Snail and Slug in the tumor cells Using confocal immunofluorescence microscopy, we analyzed Snail and Slug protein localization within the cells. The lack of correlation between Snail mRNA and protein expression in effusions may suggest that the Snail protein becomes dysfunctional in these specimens. To evaluate this hypothesis, we analyzed the Snail protein localization in fresh effusions samples using a cytospin centrifuge that concentrated the cells to one spot on the slide without damaging the tumor structure. As control, we put the cells on a cover slip in a culture dish and grew them for 24 h. Surprisingly, we found that Snail protein localization is growth condition dependent. In the "natural state" of the tumor cells, we found only a cytoplasmic staining and no nuclear localization. In contrast, when the same cells were grown in a culture dish, we observed nuclear expression of Snail in addition to cytoplasmic staining. This redistribution was associated with mild reduction (approximately 20% when corrected for 28S levels) of E-cadherin mRNA in the cultured cells (Fig. 5).

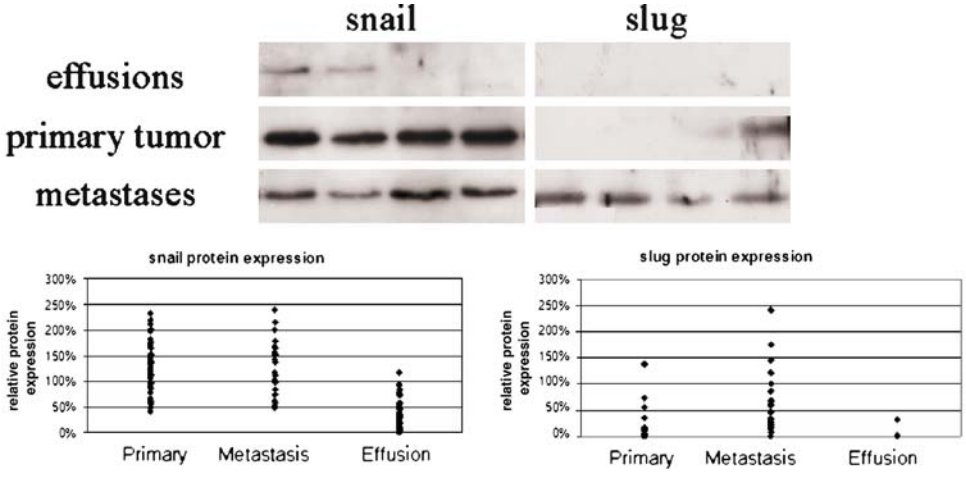

Fig. 4 Western blot analysis of Snail and Slug expression in 12 specimens (four primary tumors, four solid metastases, and four effusions). Cases are representative specimens chosen as examples for the entire cohort. Graphs show site-related distribution, with significantly higher Snail expression in effusions (p<0.001), and higher Slug protein expression in metastases

Table 2 Summary of the study results

Molecule	Mean rank (Kruskal–Wallis *H* test)			*P* value
	Effusions	Primary	Metastasis	
E-cadherin mRNA	81	48	52	<0.001
Snail mRNA	65	68	77	0.543
Snail protein	38	92	97	<0.001
Slug mRNA	63	69	85	0.106[a]
Slug protein	18	36	51	<0.001
SIP1 mRNA	81	43	63	<0.001

[a] Slug mRNA level was significantly higher in metastases compared with effusions in a two-parameter analysis (mean rank: 59 in metastases vs 44 in effusions, p=0.042, Mann–Whitney U test).

On the other hand, Slug protein was concentrated in the nucleus both in cultured and uncultured cells, indicating that the expression of this protein is not growth condition dependent (Fig. 2g–k).

Discussion

Loss of epithelial cell adhesion is a central event in carcinoma progression. E-cadherin, the major adhesion molecule in epithelial tissue, is lost in many types of cancer, resulting in invasion and metastasis [4, 29, 30]. Studies of gastric, breast, and ovarian carcinomas have shown that downregulation of E-cadherin expression in primary tumors may be followed in certain cases by elevated expression in solid metastases [3, 7, 22]. During cancer progression, we witness several cycles of epithelial–mesenchymal transition and mesenchymal–epithelial transition as part of cancer cell dissemination. In the present study, we found that E-cadherin expression is site related and that it changes in the course of ovarian tumor progression as a result of altered regulation mechanism. In ovarian carcinoma effusions, E-cadherin expression was much higher than its expression in solid tumors. These results are in agreement with our previously published results [7] and are reflected in the different architecture of carcinoma cells at these anatomic sites. In effusions, cells are in cluster-like structure and tend to form cohesive groups in the vast majority of cases, with more accentuated expression of E-cadherin at the cell–cell borders compared to the periphery of the clusters, whereas in primary tumors, E-cadherin is lost in most cells. It is possible that in the peritoneal or pleural microenvironment, such re-expression of E-cadherin provides survival advantage to the cancer cells. Surprisingly, in terms of patient survival, the re-expression of E-cadherin in effusions is a cellular event that is associated with better prognosis [10].

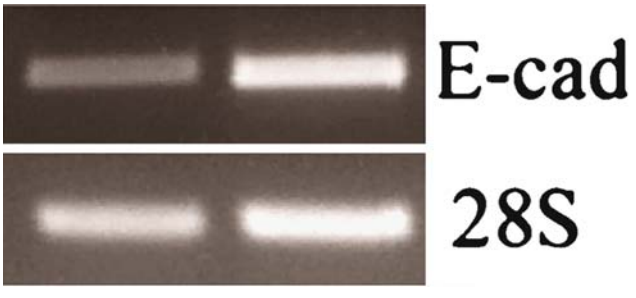

Fig. 5 RT-PCR for E-cadherin mRNA in cultured (*left*) and uncultured (*right*) effusion cells. E-cadherin mRNA level is mildly lower in the cultured cells after correction for 28S level

Since E-cadherin gene mutation in ovarian carcinoma is very rare [27], the alteration in E-cadherin expression along the disease progression may be attributed to two epigenetic mechanisms, including hypermethylation of the promoter and downregulation of the transcription, by inhibitory transcription factors. In many tumors and cell lines, E-cadherin has been shown to be regulated by the Snail, Slug, and SIP1 transcription factors [1, 2, 5, 14, 17, 24, 26, 32]. Our results indicate differential expression of these transcription factors at different anatomic sites in ovarian carcinoma. Snail protein was shown to be more highly expressed in primary tumors and solid metastases compared with effusions in the analysis of the entire material and in the limited comparison of five matched primary carcinomas and effusions. At these sites, it may function as an inhibitory transcription factor. The fact that the Snail protein results did not correlate with the mRNA results may indicate an additional posttranslational regulation mechanism. Recently, it has been shown that Snail protein is highly unstable, with a short half-life of approximately 25 min [34]. Snail protein can be phosphorylated by GSK-3β at two different sites. Phosphorylation of one motif leads to nuclear export of Snail, which makes the transcription factor a nonfunctional one. Phosphorylation of the second motif leads to β-Trcp-mediated ubiquitination. β-Trcp is a destruction box that overlaps with the phosphorylated motif and has to be phosphorylated to bind its substrates [34]. Our confocal microscopy study of Snail protein localization indicates that this protein is not present in the nucleus and may thus be phosphorylated and then exported from the nucleus, becoming dysfunctional regarding E-cadherin regulation. Surprisingly, we found differential protein localization under different culture conditions. In the effusions, Snail protein was found only in the cytoplasm and not in the nucleus, a fact that may indicate a phosphorylation process and functional inactivation that take place at this anatomic site. In contrast, cultured cells showed both cytoplasmic and nuclear staining that may allow Snail functional activation. This redistribution was associated with mild reduction of E-cadherin mRNA in the cultured cells, a finding that requires further research. Snail

is strongly expressed in solid tumors, a fact that suggests that at these sites, Snail acts as a typical inhibitory transcription factor. On the other hand, in ovarian effusions, Snail protein is weakly expressed, a finding that may indicate an inactivation process of Snail at this anatomic site, possibly mediated by GSK-3β as suggested [34].

Slug protein and mRNA expression correlated. At both expression levels, Slug was highly expressed in solid tumors in comparison with its expression in effusions, where it was almost totally silenced. In view of the upregulated expression of E-cadherin protein and mRNA in ovarian carcinoma effusions, with concomitant down-regulation in Slug protein and mRNA at this anatomic site, we hypothesize that loss of Slug may be considered as one of the mechanisms regulating the re-expression of E-cadherin in effusions following metastasis from the primary tumor. We additionally found that Slug expression is independent of growth conditions and is most likely transcriptionally regulated.

SIP1 mRNA expression was found to be significantly higher in effusions compared to solid tumors. This was also seen in the analysis of five matched effusions and primary tumors, despite the small number of cases. These results indicate a functional inactivation of SIP1 in ovarian carcinoma. Since there is no reliable commercially available SIP1 antibody, we can only assume that SIP1 is undergoing some modification that affects its cellular localization, similar to the mechanism by which Snail becomes nonfunctional.

In summary, we analyzed protein and mRNA expression of E-cadherin and its negative regulators Snail, Slug, and SIP1 in ovarian carcinoma at three anatomic sites—primary tumors, effusions, and solid metastases. Our results indicate that both E-cadherin and its regulators are differentially expressed at these sites. In solid tumors, E-cadherin is negatively regulated by Snail and Slug. The negative regulation by Snail and Slug is lost in effusions. Snail is posttranslationally regulated, probably by phosphorylation, which leads to nuclear export, a process that makes the protein nonfunctional, and degradation. Slug, on the other hand, is probably negatively regulated at the transcriptional level.

References

1. Batlle E, Sancho E, Franci C, Dominguez D, Monfar M, Baulida J, Garcia de Herreros A (2000) The transcription factor snail is a repressor of E-cadherin gene expression in epithelial tumour cells. Nat Cell Biol 2:84–89
2. Bolos V, Peinado H, Perez-Moreno MA, Fraga MF, Esteller M, Cano A (2003) The transcription factor Slug represses E-cadherin expression and induces epithelial to mesenchymal transitions: a comparison with Snail and E47 repressors. J Cell Sci 116:499–511
3. Bukholm IK, Nesland JM, Borresen-Dale AL (2000) Re-expression of E-cadherin, alpha-catenin and beta-catenin, but not of gamma-catenin, in metastatic tissue from breast cancer patients. J Pathol 190:15–19
4. Cavallaro U, Christofori G (2004) Cell adhesion and signalling by cadherins and Ig-CAMs in cancer. Nat Rev Cancer 4:118–132
5. Comijn J, Berx G, Vermassen P, Verschueren K, van Grunsven L, Bruyneel E, Mareel M, Huylebroeck D, van Roy F (2001) The two-handed E box binding zinc finger protein SIP1 downregulates E-cadherin and induces invasion. Mol Cell 7:1267–1278
6. Davidson B, Goldberg I, Gotlieb WH, Kopolovic J, Ben-Baruch G, Nesland JM, Berner A, Bryne M, Reich R (1999) High levels of MMP-2, MMP-9, MT1-MMP and TIMP-2 mRNA correlate with poor survival in ovarian carcinoma. Clin Exp Metastasis 17:799–808
7. Davidson B, Berner A, Nesland JM, Risberg B, Berner HS, Tropé CG, Kristensen GB, Bryne M, Flørenes V-A (2000) E-cadherin and alpha-, beta-, and gamma-catenin protein expression is up-regulated in ovarian carcinoma cells in serous effusions. J Pathol 192:460–469
8. Davidson B, Risberg B, Reich R, Berner A (2003) Effusion cytology in ovarian cancer: new molecular methods as aids to diagnosis and prognosis. Clin Lab Med 23:729–754
9. Davidson B (2004) Malignant effusions: from diagnosis to biology. Diagn Cytopathol 31:246–254
10. Elloul S, Elstrand MB, Nesland JM, Tropé CG, Kvalheim G, Goldberg I, Reich R, Davidson B (2005) Snail, Slug, and Smad-interacting protein 1 as novel parameters of disease aggressiveness in metastatic ovarian and breast carcinoma. Cancer 103:1631–1643
11. Goff BA, Mandel L, Muntz HG, Melancon CH (2000) Ovarian carcinoma diagnosis. Cancer 89:2068–2075
12. Gotzmann J, Mikula M, Eger A, Schulte-Hermann R, Foisner R, Beug H, Mikulits W (2004) Molecular aspects of epithelial cell plasticity: implications for local tumor invasion and metastasis. Mutat Res 566:9–20
13. Hajra KM, Fearon ER (2002) Cadherin and catenin alterations in human cancer. Genes Chromosomes Cancer 34:255–268
14. Hajra KM, Chen DY, Fearon ER (2002) The SLUG zinc-finger protein represses E-cadherin in breast cancer. Cancer Res 62:1613–1618
15. Hanahan D, Weinberg RA (2000) The hallmarks of cancer. Cell 100:57–70
16. Ikenouchi J, Matsuda M, Furuse M, Tsukita S (2003) Regulation of tight junctions during the epithelium-mesenchyme transition: direct repression of the gene expression of claudins/occludin by Snail. J Cell Sci 116:1959–1967
17. Jiao W, Miyazaki K, Kitajima Y (2002) Inverse correlation between E-cadherin and Snail expression in hepatocellular carcinoma cell lines in vitro and in vivo. Br J Cancer 86:98–101
18. Lambert CA, Colige AC, Munaut C, Lapiere CM, Nusgens BV (2001) Distinct pathways in the over-expression of matrix metalloproteinases in human fibroblasts by relaxation of mechanical tension. Matrix Biol 20:397–408
19. Miyoshi A, Kitajima Y, Sumi K, Sato K, Hagiwara A, Koga Y, Miyazaki K (2004) Snail and SIP1 increase cancer invasion by upregulating MMP family in hepatocellular carcinoma cells. Br J Cancer 90:1265–1273
20. Nieto MA (2002) The snail superfamily of zinc-finger transcription factors. Nat Rev Mol Cell Biol 3:155–166
21. Nollet F, Berx G, van Roy F (1999) The role of the E-cadherin/catenin adhesion complex in the development and progression of cancer. Molec Cell Biol Res Commun 2:77–85
22. Oka H, Shiozaki H, Kobayashi K, Tahara H, Tamura S, Miyata M, Doki Y, Iihara K, Matsuyoshi N, Hirano S et al (1992) Immunohistochemical evaluation of E-cadherin adhesion mole-

cule expression in human gastric cancer. Virchows Arch A Pathol Anat Histopathol 421:149–156
23. Pecina-Slaus N (2003) Tumor suppressor gene E-cadherin and its role in normal and malignant cells. Cancer Cell Int 3:17
24. Poser I, Dominguez D, de Herreros AG, Varnai A, Buettner R, Bosserhoff AK (2001) Loss of E-cadherin expression in melanoma cells involves up-regulation of the transcriptional repressor Snail. J Biol Chem 276:24661–24666
25. Reed JA, Manahan LJ, Park CS, Brigati DJ (1992) Complete one-hour immunocytochemistry based on capillary action. Biotechniques 13:434–443
26. Risinger JI, Berchuck A, Kohler MF, Boyd J (1994) Mutations of the E-cadherin gene in human gynecologic cancers. Nat Genet 7:98–102
27. Rosivatz E, Becker I, Specht K, Fricke E, Luber B, Busch R, Hofler H, Becker KF (2002) Differential expression of the epithelial–mesenchymal transition regulators snail, SIP1, and twist in gastric cancer. Am J Pathol 161:1881–1891
28. Tai CT, Lin WC, Chang WC, Chiu TH, Chen GTC (2003) Classical cadherin and catenin expression in normal myometrial tissues and uterine leiomyomas. Mol Reprod Dev 64:172–178
29. Thiery JP (2002) Epithelial–mesenchymal transitions in tumour progression. Nat Rev Cancer 2:442–454
30. Thiery JP (2003) Epithelial–mesenchymal transitions in development and pathologies. Curr Opin Cell Biol 15:740–746
31. Van Aken E, De Wever O, Correia da Rocha AS, Mareel M (2001) Defective E-cadherin/catenin complexes in human cancer. Virchows Arch 439:725–751
32. Yokoyama K, Kamata N, Hayashi E, Hoteiya T, Ueda N, Fujimoto R, Nagayama M (2001) Reverse correlation of E-cadherin and snail expression in oral squamous cell carcinoma cells in vitro. Oral Oncol 37:65–71
33. Yokoyama K, Kamata N, Fujimoto R, Tsutsumi S, Tomonari M, Taki M, Hosokawa H, Nagayama M (2003) Increased invasion and matrix metalloproteinase-2 expression by snail-induced mesenchymal transition in squamous cell carcinomas. Int J Oncol 22:891–898
34. Zhou BP, Deng J, Xia W, Xu J, Li YM, Gunduz M, Hung MC (2004) Dual regulation of Snail by GSK-3beta-mediated phosphorylation in control of epithelial–mesenchymal transition. Nat Cell Biol 6:931–940

Virchows Arch (2006) 449:529–538
DOI 10.1007/s00428-006-0285-3

ORIGINAL ARTICLE

Histopathologic indicators of recurrence in meningiomas: correlation with clinical and genetic parameters

Yoo-Jin Kim · Ralf Ketter · Wolfram Henn · Klaus D. Zang · Wolf-Ingo Steudel · Wolfgang Feiden

Received: 11 July 2006 / Accepted: 26 July 2006 / Published online: 3 October 2006
© Springer-Verlag 2006

Abstract Meningiomas in general are circumscribed slow-growing tumors. However, despite gross total resection, tumor relapse and patients' outcome are still an issue. Risk stratification based on histomorphology alone remains problematic. This study explored the independent prognostic value of potential risk factors among 206 patients who underwent meningioma resection and followed-up until death or a median of 44 months. The statistical analysis considered clinical data, histomorphologic parameters, cytogenetic findings, Ki-67 immunoreactivity, and activity of tissue non-specific alkaline phosphatase (ALPL). Recurrence-free survival estimates were computed and prognostic factors were identified using Cox proportional hazards model. Independent predictors of recurrence included (1) anaplasia; (2) mitotic index ≥20/10 high-power fields; (3) subtotal tumor resection; (4) loss of short arm of chromosome 1 (1p−); and (5) Ki-67 labeling index (LI) >12%. Among totally resected WHO grade I meningiomas, neither histopathologic nor clinical parameters were predictive, whereas 1p− was the only independent prognostic factor. ALPL did not reach significance in the multivariate modeling, however, the fast and low-cost histochemical detection of ALPL expression could be proved as a highly sensitive screening method for 1p−. In particular, biologically aggressive meningiomas of histologically benign or "borderline" phenotype could be therefore identified by ALPL detection followed by 1p in situ hybridization.

Keywords Meningioma recurrence · Prognosis · Ki-67 · Alkaline phosphatase · Cytogenetics

Y.-J. Kim (✉) · W. Feiden
School of Medicine, Institute of Neuropathology,
Saarland University,
Bldg. 90.3,
66421 Homburg-Saar, Germany
e-mail: yoo.jin.kim@uniklinikum-saarland.de

R. Ketter · W.-I. Steudel
Department of Neurosurgery, School of Medicine,
Saarland University,
Homburg/Saar, Germany

W. Henn · K. D. Zang
School of Medicine, Institute of Human Genetics,
Saarland University,
Homburg/Saar, Germany

Introduction

Meningiomas are tumors that arise from the leptomeningeal covering of the brain and the spinal cord, accounting for 15% to 20% of all central nervous system tumors [26]. According to the current World Health Organization (WHO) histological grading system, three grades of meningiomas with increasing risk of recurrence are distinguished [14]. Benign or common-type tumors with a low rate of recurrence (7% to 20%) are assigned to Grade I. Grade II meningiomas include atypical meningiomas as well as the rare chordoid and clear cell (intracranial) variants and exhibit a higher risk of recurrence (29% to 40%). Grade III meningiomas are anaplastic meningiomas with high mitotic activity (≥20/10 high-power fields) and/or obviously malignant cytology as well as the rare variants, papillary and rhabdoid meningiomas. Recurrence rate of anaplastic meningiomas is suggested to be 50% to 78%. While the application of histomorphologic criteria can be considered as a means of risk stratification, the prognostic impact of the proposed criteria—particularly the mitotic thresholds distinguishing

between the three different grades—are not irrevocable in individual cases [25]. Regarding the recurrence rate of up to 20% in histologically benign meningiomas [8] on the one hand, and the variable recurrence rate among atypical meningiomas on the other, accurate risk estimation in individual cases based on histomorphologic criteria alone remains problematic. Apart from histomorphologic parameters, incompleteness of tumor resection is known to be the major risk factor of recurrence. However, 7–20% of gross totally resected meningiomas tend to recur—even phenotypically benign tumors. Therefore, an adequate prognosis of biological behavior and individual assessment of recurrence risk requires additional prognostic factors or markers.

It is well-known, that high expression of immunohistochemically detectable markers of proliferative activity, e.g. Ki-67 antigen, indicates a more aggressive behavior and thus, a higher risk of recurrence. However, the determination of the independent predictive value of Ki-67 as well as the appropriate quantitation method still needs to be cleared.

Cytogenetically, meningiomas are characterized by monosomy 22 as a typical primary aberration [33] and progression-associated secondary aberrations, of which monosomy of the short arm of chromosome 1 (1p−) is the most important. Monosomy 1 or loss of the distal part of the short arm of chromosome 1 was found to be correlated with higher histologic grade and with a higher recurrence rate in meningiomas [6, 10, 12, 18, 32]. The tissue non-specific isoform of alkaline phosphatase (ALPL), located on 1p36.1–p34, is strongly active in normal arachnoid cells and in cells of common-type meningiomas, but in contrast, enzyme activity lacks in meningiomas with deletion of 1p. Since karyotyping by means of classic cytogenetics is laborious and not a routine part of tumor diagnostics, the histochemical detection of the loss of ALPL was introduced by Niedermayer et al. [20] as a fast and low-cost technique for the detection of 1p−. The gene, encoding ALPL, is suggested as a putative and not yet identified tumor suppressor gene on chromosome 1p. Beyond its role as enzyme marker for 1p−, loss of ALPL activity could be applied as a predictor of recurrence, as it has been recently demonstrated—at least in univariate manner—by Bouvier et al. [4]. However, neither the independent predictive value of 1p− and loss of ALPL expression nor the correlation of ALPL to 1p− has yet been clarified in a multivariate setting and among a large cohort.

The presented study aims to identify independent prognostic factors and to reveal complex interrelationships among clinical data, histomorphologic parameters, proliferative marker, histochemical expression of ALPL, and cytogenetic parameters in a multivariate approach.

Materials and methods

Patients and clinical data

The retrospective cohort study is based on the data of 265 patients with initial diagnosis of meningioma operated on 1997–2002 at the Department of Neurosurgery, Saarland University. This subset consists of all meningioma patients within the given period where vital tumor tissue was available for histochemical detection of alkaline phosphatase. Mean age (±SD; range) was 59 (±13 years; 4–88 years). The cohort consisted of 186 females and 79 males (sex distribution 7:3). 13 patients (median age at diagnosis 61 years; SD ±9.6; range 51–78) died because of disease within a mean period of 11 months after surgery. Patients were followed-up for a mean period of 44 months (range 6–96 months). After 6 months, 59 patients were lost to follow-up and were not considered in the statistical analyses. Clinical data recorded included dates of birth and death, gender, tumor location, date of surgery for primary and recurrent tumor resections, date of recurrence/regrowth as defined radiologically (CT or MRI), extent of resection, and grossly apparent invasion of adjacent structures. The extent of resection was documented along the guidelines suggested by Simpson [28]. Complete surgical extirpation of the tumor (gross total resection: GTR) was defined as Simpson grade I or II, corresponding to macroscopically determined complete tumor resection with bipolar coagulation of the dural insertion.

Histomorphology

All available slides from primary meningiomas as well as additional hematoxylin and eosin or specially stained slides in all cases were reviewed by two independent pathologists (Y.K. and W.F.) who were unaware of the patients outcomes. When there were discrepancies for parameters between the two investigators, the case was examined simultaneously by both observers and the results were recorded after an agreement was reached. According to the predominant feature or growth pattern, each tumor was assigned to a histologic prototypical guise (meningotheliomatous, fibrous, transitional, microcystic, secretory, lymphoplasmocyte-rich, xanthomatous or otherwise metaplasia, atypical, clear cell, chordoid, papillary, rhabdoid, and anaplastic) and graded according to the current WHO criteria [14]. Further histologic parameters, including hypercellularity, nuclear polymorphism, macronucleoli, small cell formation with high nuclear to cytoplasmic ratio, patternless architecture, inflammatory infiltrate, macrophages/foamy cells, calcification, necrosis, brain invasion, invasion of structures other than the brain, and mitotic index were evaluated in each case. Brain invasion was defined as irregular projections of tumor or tumor cells into

adjacent central nervous system parenchyma without an intervening layer of leptomeninges. Except for mitoses, all parameters were recorded as either absent or present. The mitotic index (MI) was defined as the highest count in 10 consecutive high-power fields (HPF; 1 HPF=0.16 mm^2). According to the mitotic thresholds as suggested by Perry et al. [22] and adopted by the WHO, a MI <4 was defined as "0", MI greater or equal to 4 and less than 20 as "1", and MI ≥20 as "2".

Ki-67 immunohistochemical analysis

For each case, formalin-fixed and paraffin-embedded specimens were sectioned at 3 μm, deparaffinized, and treated with microwave antigen retrieval (2×10 min at 700 W and 350 W, respectively). Slides were incubated for 1 h in a humid chamber at 37°C with a monoclonal antibody directed against Ki-67 (clone KiS5, 1:50; DakoCytomation, Glostrup, Denmark). Biotinylated secondary antibodies were detected using the streptavidin/horseradish peroxidase method and diaminobenzidine as chromogen. Percentage of immuno-positive tumor cells were determined in digital images of 5 HPF of the highest labeling in each case using an automated image analysis device as described by Kim et al. [11]. The computer-based method is described and provided for free at the morphometry section of http://www.uniklinikum-saarland.de/neuropathologie [11].

Histochemical reaction of ALPL

For each case, histochemical detection of alkaline phosphatase was performed in cryostat sections and/or smear preparations

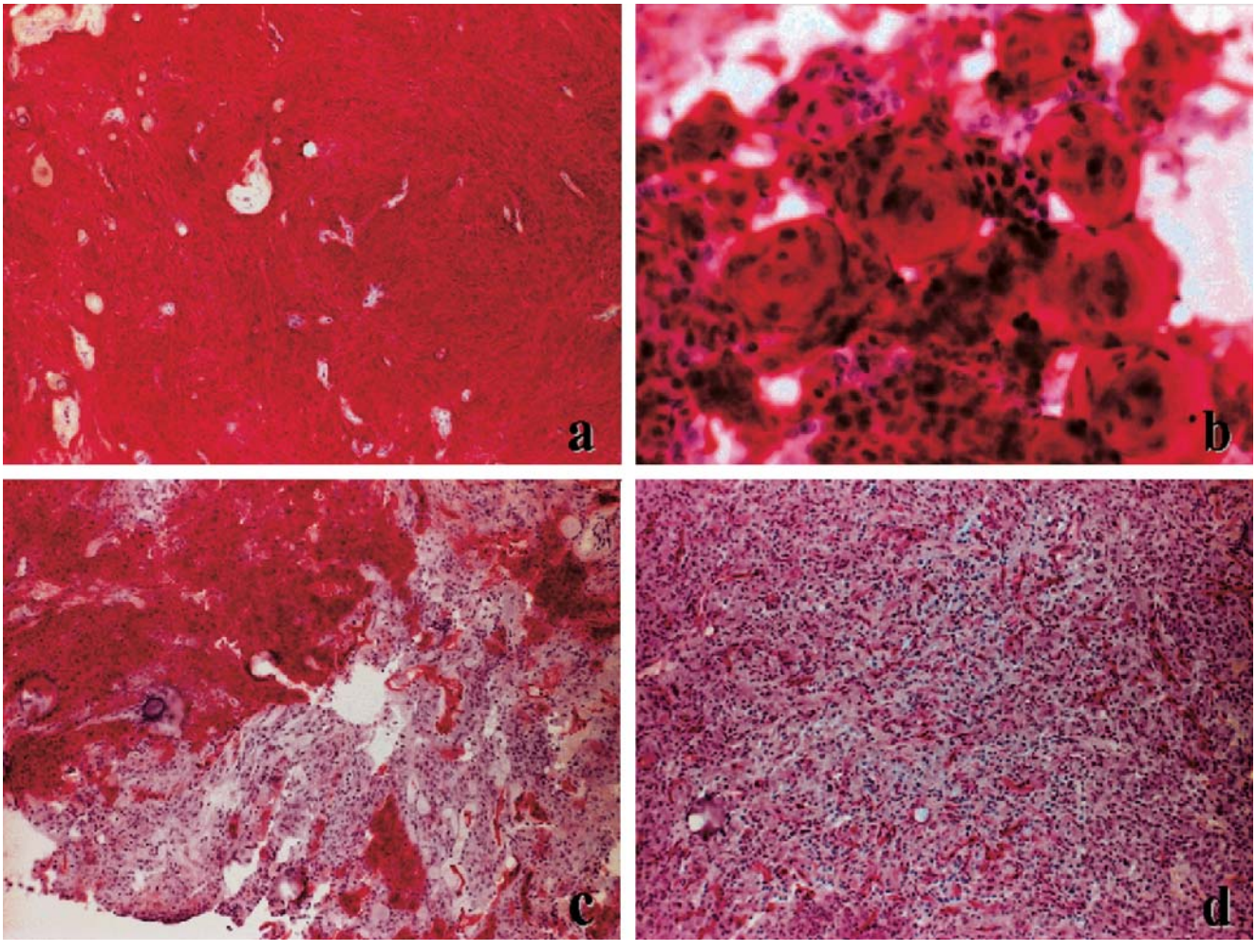

Fig. 1 Histochemical expression patterns of ALPL (tissue non-specific alkaline phosphatase) in meningiomas. (**a**) Positive enzyme activity in meningothelial tumor cells. Cryostat section of a common-type meningothelial meningioma, objective ×10. (**b**) Same tumor specimen, close up view of ALPL detection obtained in smear preparation, objective ×40. Strong enzyme activity, in particular, in whorl formations. (**c**) Atypical meningioma with partial loss of ALPL activity, displaying an alternate pattern of ALPL expression, objective ×10. Well-differentiated whorl formations exhibiting positive enzyme activity alternate with less differentiated tumor areas with loss of ALPL activity. (**d**) Meningioma with complete lack of ALPL activity. Only the endothelium of blood vessels serving as intrinsic positive control exhibit enzyme activity (objective ×10)

Table 1 Association of clinicopathological parameters, Ki-67 LI, ALPL expression, and cytogenetic findings with meningioma recurrence in 206 patients; univariate analysis, chi-square test

	Relative recurrence risk (%)		*p*
Clinical parameters			
Age >65 years	19		0.0011
Sex (female vs male)	11 vs 19		n.s.
Convexity vs other locations	12 vs 9 (WHO °I:8 vs 3)		0.02 (0.0152)
GTR vs STR	12 vs 47		<0.001
Local infiltration	28		<0.001
	STR and GTR	GTR only	
Histopathologic parameters			
Hypercellularity	26	22	0.004 (<0.001)
Small cell formation	25	23	0.003 (<.001)
Macronucleoli	32	25	<0.001
Necrosis	33	29	<0.001
Brain invasion vs non-invasion	28 vs 10		0.03
WHO grade			
II vs I	18 vs 9	18 vs 5	0.09 (0.004)
III vs I and II	75 vs 11	75 vs 8	<0.001
Mitotic index			
≥4/10 HPF	38	39	<0.001
≥20/10 HPF	83	83	<0.001
Ki-67 LI			
>8%	29	27	0.006 (<0.001)
>12%	42	42	0.0052 (<0.001)
ALPL			
At least partial loss	21	18	0.004 (<0.001)
Complete loss	27	25	0.003 (<0.001)
Karyotype			
1p− vs others	45	45	<0.001

Ki-67 LI=Ki-67 labeling index; ALPL=tissue non-specific alkaline phosphatase; *p*=*p* value of chi-square test; n.s.=not significant; GTR=gross total resection; STR=subtotal resection; 1p−=partial or complete deletion of the short arm of chromosome 1; *p* values calculated for the GTR subset only are put in parenthesis

as described previously by Niedermayer et al. [20]. Briefly, histochemical detection of ALPL was done at room temperature with hexazotized triamino-tritolyl-methane-chloride (Neufuchsin; Merck, Darmstadt, Germany) and naphthol-AS-MX phosphate (Sigma-Aldrich, Buchs, Switzerland) at a pH of 8.8. Staining reaction was stopped after 30 min. Positive reactions in the endothelium of the blood vessels served as intrinsic positive control. According to the staining pattern, meningiomas were assigned to (1) ALPL positive with uniform reaction in all tumor cells (Fig. 1a,b); (2) partial loss of ALPL expression with loss of enzyme activity in more than 50% of tumor cells in clearly identifiable tumor areas (Fig. 1c), as suggested by Bouvier et al. [4]; and (3) complete lack of ALPL expression in tumor cells (Fig. 1d).

Karyotyping

Tissue specimens from tumors were obtained freshly during surgery and processed according to previously described methods [13]. Briefly, the cell cultures were grown in Dulbecco's modified Eagle's minimal essential medium supplemented with 10% fetal calf serum and antibiotics. Chromosome preparation from primary cultures, GTG-banding, and karyotyping followed standard procedures. In 197 meningiomas of our study group, cytogenetic findings were obtained. These cases, which represent a part of the cytogenetic meningioma database, founded and characterized by Zang [31], and continuously investigated by Ketter et al. [10], were subdivided into five cytogenetic subgroups: (1) meningiomas with normal chromosome set; (2) with monosomy 22 as the sole cytogenetic aberration; (3) markedly hypodiploid meningiomas with loss of further autosomes in addition to monosomy 22, but with intact chromosome 1; (4) tumors with deletions of the short arm of a chromosome 1 (1p−); and (5) the rare cyogenetic subtype of meningiomas with hyperdiploid chromosome set, with or without detectable loss of chromosome 22 or 1p.

Statistical analysis

Survival times and recurrence-free survival times were computed and distributions were estimated using the Kaplan–Meier method. Univariate correlation of each

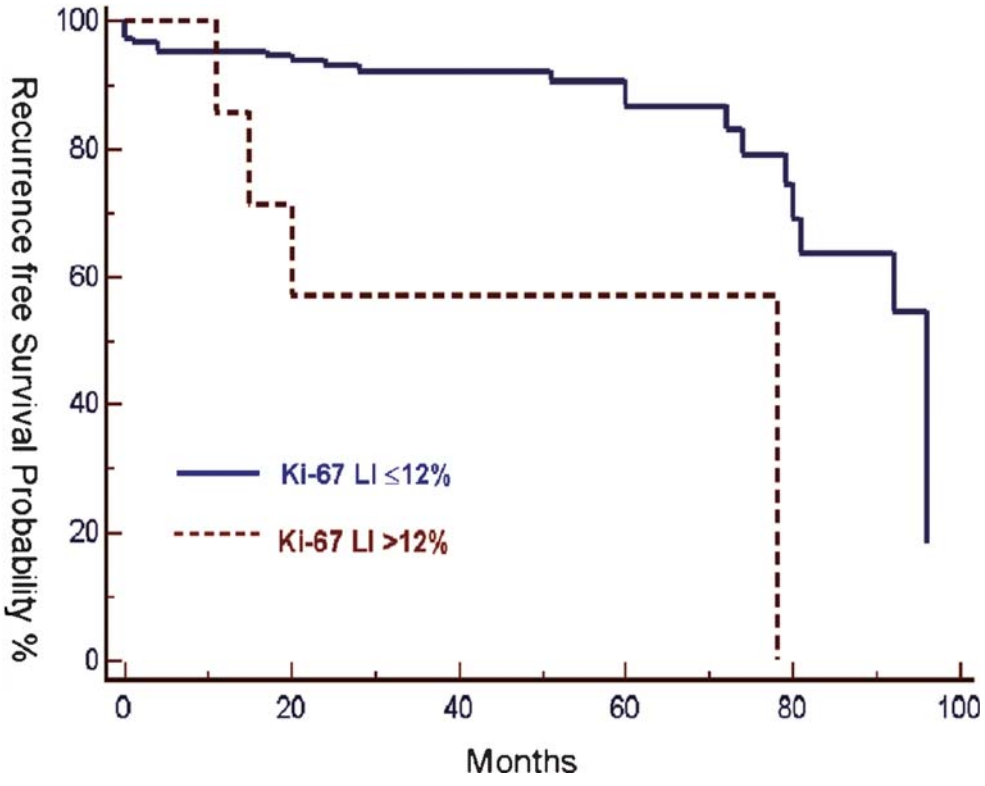

Fig. 2 Recurrence-free survival based on Ki-67 labeling index (LI) in the subset of gross totally resected meningiomas, $n=181$

parameter regarding recurrence was analyzed by using the chi-square test (Table 1). For this purpose, all qualitative variables were dichotomized and recorded as either absent or present. Receiver operator characteristic (ROC) was performed for Ki-67 LI, to define cut off values and for dichotomization. Threshold value for patient's age was defined at 65 years (≤65 years="0"; >65 years="1"). Cox proportional hazard modeling techniques were used to identify independent predictors of recurrence. Age adjusted risk estimations were calculated for (1) the entire cohort and (2) only WHO grade I and II meningiomas, excluding anaplastic meningiomas.

Results

Based on strict histological criteria according to the current WHO grading system [14], 227 tumors were classified as WHO grade I, 30 tumors as WHO grade II, and 8 tumors as WHO grade III meningiomas.

There were no significant differences in the follow-up periods for different WHO grades or brain-invasive meningiomas: We revealed a mean follow-up period of 44 months in the cohort of WHO grade I meningiomas, 46 months in grade II meningiomas, and 44 months in grade III meningiomas. The mean follow-up period for the subset of brain-invasive meningiomas was 55 months and in detail, 57 months for WHO grade I brain-invasive meningiomas and 51 months for WHO grade II or III brain-invasive meningiomas.

A gross total resection (GTR) was reached in 240 cases, in 25 tumors only a subtotal resection (STR) was achieved. Without exception, the latter were assigned to WHO grade I tumors. The majority of these tumors, which underwent STR was located at the base of the skull (18/25).

The overall recurrence rate was 11% ($n=31$). The relative risk of recurrence (RR) was significantly higher for meningiomas with STR (9/25, RR=36%) than for those having undergone GTR (22/240, RR=9%). Relapses were evident after a mean period of 45 months; 48 months after GTR and 36 months after STR, respectively. Tumor location at convexity was significantly associated with loss of ALPL activity and with 1p− or hyperdiploidy. In the subset of WHO grade I meningiomas, convexity meningiomas exhibited a significantly higher risk of recurrence than meningiomas in other locations ($p=0.0152$).

The recurrence rates in the WHO grade I meningiomas was 5% regarding only the GTR subset (11/204), 9% (20/229) regarding also the STR subset. Recurrences were recorded in 18% (5/28) of WHO grade II meningiomas and 75% (6/8) of anaplastic meningiomas. Brain invasions were observed in 14 tumors (9 WHO grade I, 2 grade II, and 3 grade III meningiomas) within 42 cases where central nervous system parenchyma was assessable. Recurrence rate among the few brain-invasive meningiomas was 28% (4/14). All of these recurrent brain-invasive tumors were either atypical or anaplastic.

ROC revealed a Ki-67 LI >8% as a cut off point with a convenient sensitivity/specificity ratio (0.63 to 0.65),

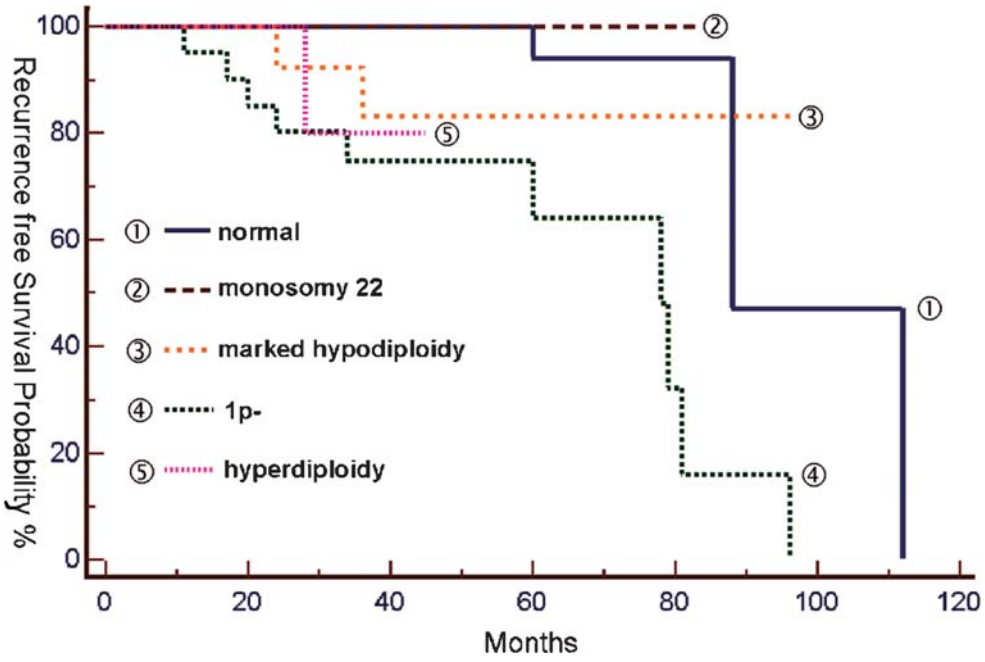

Fig. 3 Recurrence-free survival based on cytogenetic findings in the subset of gross totally resected meningiomas, $n=179$; part of the cytogenetic meningioma data base, Institute of Human Genetics, Saarland University, described in detail by Zang [31] and Ketter et al. [10]

however, sufficient specificity was reached at a threshold value up to LI 12% (specificity >98%). The relative area under the ROC-curve was 0.708. The Mann–Whitney *U* test for testing the discriminatory power of Ki-67 LI was significant ($p<0.05$).

The results of the univariate analyses of clinicopathological parameters and cytogenetic findings are summarized in Table 1.

Independent prognostic factors for recurrence-free survival within the entire cohort (GTR and STR) as revealed by Cox regression included (1) anaplasia ($p<0.001$), (2) almost always in combination with MI ≥20/10 HPF ($p=0.0062$), (3) 1p− ($p=0.0077$), (4) Ki-67 LI >12% ($p=0.0181$), and (5) STR ($p=0.0037$) as further independent predictors. These variables (excluding STR) provided prognostic information also within the subset of tumors that underwent GTR and adjusted for age, tumor site, and histomorphologic parameters. Ki-67 LI >8% was found to be univariately associated with recurrence, but did not reach significance in the multivariate modeling. However, significance in the multivariate setting was reached when the cut off point was scaled up to 12%. Recurrence-free survival

Table 2 Karyotype and pathologic findings

	Cytogenetic subsets ($n=197$)[a]				
	Normal ($n=95$)	Monosomy 22 ($n=45$)	Hypodiploid ($n=19$)	1p− ($n=31$)	Hyperdiploid ($n=7$)
Tumorsite					
Convexity	32 (33%)	22 (48%)	11 (57%)	25 (80%)[b]	5 (71%)
WHO grade					
I	87 (92%)	43 (96%)	15 (79%)	14 (45%)	5 (71%)
II	8 (8%)	2 (4%)	4 (21%)	11 (35%)	1 (14%)
III	0 (0%)	0 (0%)	0 (0%)	6 (19%)	1 (14%)
Histologic subtype					
Meningothelial	40 (41%)	8 (18%)	3 (16%)	3 (10%)	0 (0%)
Fibroblastic	10 (10%)	26 (57%)[b]	7 (37%)	8 (26%)	2 (29%)
Transitional	6 (6%)	8 (18%)	4 (21%)	1 (3%)	0 (0%)
Median Ki-67 LI [%] range	3.5 (0–24)	4.8 (0.7–15.3)	5.8 (0–13.3)	6.9 (0–35)	4 (0–9.4)
Recurrence[c] (recurrence rate)	3/71 (4%)	0/29 (0%)	2/18 (11%)	10/22 (45%)	1/5 (20%)

Ki-67 LI=Ki-67 labeling index

[a] Part of the cytogenetic meningioma data base, Institute of Human Genetics, Saarland University, founded and characterized by Zang [31] and described in detail by Ketter et al. [10]

[b] Significant chi-square test statistics

[c] Only cases followed-up at least 6 months after surgery, $n=154$

Table 3 ALPL expression pattern and pathologic and genetic factors

	ALPL expression (n=265)			
	Positive (n=97)	Partial loss (n=98)	Complete loss n=70)	p
Tumorsite				
Convexity	21 (21%)	62 (63%)	50 (71%)	<0.001[a]
WHO grade				
I	94 (97%)	43 (96%)	15 (79%)	<0.001
II	2 (2%)	2 (4%)	4 (21%)	
III	1 (1%)	0 (0%)	0 (0%)	
Median Ki-67 LI [%] (range)	3 (0.2–18.1)	5 (0.5–25)	5 (0.4–24)	
Cases with Ki-67 LI >8%	8 (8%)	15 (15%)	17 (24%)	<0.025
Cytogenetics (n=197)				<0.001
Normal karyotype	54 (71%)	25 (35%)	16 (33%)	
Monosomy 22	16 (21%)	15 (15%)	7 (14%)	
Marked hypodiploid	3 (4%)	8 (11%)	8 (16%)	
1p−	3 (4%)	13 (18%)	15 (31%)	
Hyperdiploidy	0 (0%)	4 (6%)	3 (6%)	

ALPL=tissue non-specific alkaline phosphatase; Ki-67 LI=Ki-67 labeling index; 1p−=partial or complete deletion of short arm of chromosome 1; p=p value of chi-square test

[a] Partial or complete loss compared to positive ALPL cases, respectively

based on Ki-67 LI is displayed in Fig. 2. Cox regression modeling regarding only the subset of totally resected WHO grade I meningiomas revealed 1p− as the only independent predictor of recurrence (p=0.0077). Recurrence-free survival based on cytogenetic findings is displayed in Fig. 3. Among specific histologic WHO grade I variants, there was no evidence of statistically significant associations with recurrence.

Cytogenetically, "fibroblastic" meningiomas had a significantly higher rate of monosomy 22 as compared to the other subsets (p<0.05) (Table 2). Meningiomas with 1p– showed a higher proliferative potential in terms of Ki-67 LI as well as significantly higher rate of histologic dedifferentiation.

Partial or complete loss of ALPL was strongly associated with a higher WHO grade (II or III) and higher Ki-67 LI (p<0.025). A partial or complete loss of ALPL expression indicated 1p− with a sensitivity of 90% and a positive predictive value of 90%, however, specificity was low (44%). Loss of enzyme activity was significantly associated with tumor recurrence in the univariate analysis (Table 1), whereas no significant contribution was assessable in the multivariate modeling. Associations of ALPL expression pattern to tumor site, histopathologic parameters, and cytogenetic findings are displayed in Table 3.

Discussion

The appropriate risk stratification in individual meningioma patients based on pathological features without overgrading or undergrading is difficult at best [5]. Among histologic parameters, high cellularity, invasion of the brain, large number of mitoses, prominent nucleoli and cell necrosis appear to correlate with aggressive behavior [9]. The three-step grading system of meningiomas, distinguishing well-differentiated, atypical, or anaplastic meningiomas along the guidelines suggested by Perry et al. [22] and adopted by the WHO [14] admits a risk estimation based on histomorphologic criteria. However, the precise grading of meningiomas is not always possible and treatment planning will consider clinical variables [5] and likewise, the post-operative treatment regime will consider further prognostic factors, which may predict the individual clinical course. Among these potential risk factors, incomplete removal is well-known as a prognostic unfavorable finding, as it could be confirmed in the multivariate statistics presented here. Subtotal tumor resection was reported as a prognostic indicator, independent from the histologic grade already used by Simpson [28] and subsequently, by others [8, 15, 22].

However, on the other hand, independent from the extent of resection, meningiomas with histologic anaplasia and/or high mitotic activity (≥20/10 HPF) exhibit a very high risk of recurrence. The recurrence rate of 75% in our series of anaplastic meningiomas is comparable with the recurrence rates of 78% reported by Jääskeläinen et al. [8] or 72% by Maier et al. [15].

Brain invasion suggests a greater likelihood of recurrence and as reported by Perry et al. [22], brain-invasive histologically common-type meningiomas behave similarly to atypical meningiomas in general. We also found a significantly higher rate of recurrence in brain-invasive

meningiomas (relative risk: 28%), but in contrast, all of the recurrent meningiomas with brain invasion were of atypical or anaplastic type — whereas none of the brain-invasive WHO grade I meningiomas recurred. Due to the confounding in histologic grade, brain invasion did not reach significance in the multivariate modeling. It has to be mentioned, that the number of recorded brain invasion among the investigated cohort was small, thus, limiting the significance of these findings. However, in our series, atypical and anaplastic meningiomas are significantly overrepresented in the subset of brain-invasive meningiomas, suggesting, that brain invasion rate may increase with the histologic grade of dedifferentiation.

Patient's age at diagnosis is another reported prognostic factor. Statistic analyses of over 9,000 patients with meningioma based on the National Cancer Data Base revealed patient's age at diagnosis ≥65 years [16] as a multivariately significant negative prognostic factor. Concordantly, in our study, age at diagnosis showed a highly significant association with shorter recurrence-free survival in univariate analysis, although age did not reach significance in the multivariate modeling.

Among the histologic features, mitotic activity is known to exhibit the most powerful prognostic impact. Perry et al. [22] have found a notable increase in the rate of recurrence among totally resected meningiomas with four or more mitoses per 10 high-power fields. This mitotic threshold is adopted as a grading criterion for atypical meningiomas in the current WHO classification. Despite a univariate association with recurrence, the multivariate analysis presented here did not reveal any independent predictive capability at a mitotic threshold ≥4/10 HPF. However, there was no doubt in the prognostic impact of apparently increased mitotic activity with the excess of MI ≥20. The overlap in the ranges of mitotic indices among different studies are well-known and may be due to different counting techniques, variation in field sizes, institutional bias, and inter-observer variability [5, 22]. Thus, these data reflect the need for careful interpretation of MI in meningioma grading, in particular, if mitotic thresholds are suggested as single grading criterion only.

A quantitative approach in the assessment of cell proliferation is the determination of the Ki-67 LI. The prognostic impact of Ki-67 LI is indisputable, since many studies have demonstrated the correlation between proliferation index and tumor grade and/or tumor recurrence in meningiomas [1, 7, 12, 21] and finally, since the prognostic role of Ki-67 is advocated in the current WHO classification [14]. We have found a Ki-67 LI >12% as independent predictor of recurrence adjusted for age, tumor site, and histologic parameters, including mitotic index. The proposed threshold value is comparable with the threshold values of Ki-67 LI >10%, proposed by Ho et al. [7] and recently by Torp et al. [30] for distinguishing recurrent vs non-recurrent meningiomas. In atypical and anaplastic meningiomas, Ki-67 LI allows to identify meningiomas at high risk of recurrence independently from histomorphology or mitotic activity. However, since levels of Ki-67 LI exceeding 10% are implausible in meningiomas of conventional type, this criterion is not suited to distinguish recurrent vs non-recurrent WHO grade I meningiomas. This is supported by the findings of Roser et al. [24] who investigated the prognostic significance of Ki-67 LI in 600 meningiomas. They came to the same conclusion, that Ki-67 is not a statistically significant predictor of survival time in totally resected WHO grade I meningiomas. The determination of Ki-67 LI is a subjective task and the counting techniques vary, which leads to a remarkable overlap in the values recorded for typical, atypical, and anaplastic lesions, as well as for recurring vs non-recurring tumors among reported data [1, 7, 12, 19, 21, 30]. Therefore, it remains problematic to suggest universal Ki-67 LI values for determining recurrence risk [14]. The standardization of the Ki-67 LI assessment and computed image analysis approach may lead to more robust and comparable data.

In contrast to the mentioned prognostic parameters, we found deletion of 1p as the only independent predictor of recurrence also among WHO grade I meningiomas. This is supported by Al-Mefty et al. [2] who demonstrated a complex karyotype, including loss of 1p present ab initio in histologically lower-grade tumors, which later on recurred and upgraded to a higher-grade tumor — contradicting the popular model of stepwise clonal evolution. These and the presented data confirm our previously reported findings [10], which emphasize the prognostic evidence of loss of 1p independently from histologic grade. Our data also suggest, that the histochemical detection of ALPL expression is an appropriate, fast, and low-cost as well as specific and sensitive screening method for identification of those cases with 1p−. We therefore could confirm our previously reported thesis [20] and the recent findings of Bouvier et al. [4], that ALPL, which is encoded in 1p36.1–p34, could be applied as enzyme marker for 1p−. Niedermayer et al. suggested one or more putative tumor suppressor genes located on the distal, ALPL encoding region of chromosome 1 [20]. The strong correlation between ALPL activity loss and monosomy 1p led also to the presumption that the ALPL gene itself might act as a tumor suppressor gene, with one allele being deleted and the remaining ALPL allele inactivated by deletion, mutation, or genomic imprinting [18]. Updated genomic sequencing studies support the hypothesis of a two-step inactivation of the ALPL gene during progression of meningiomas by deletion plus promoter methylation [23]. Recent studies have

demonstrated consistent regions of deletion on 1p36.21 [17] and on 1p33–p34 [29] as well as on 1p34–p32 [3], suggesting that putative suppressor genes are actually located on 1p36–p32. Apart from the significant correlation to 1p−, our data also suggest that loss of ALPL is associated with a higher histologic grade, higher proliferation potential, and higher rate of recurrence. However, in contrast to the univariate modeling as mentioned by previous reports [4, 20], loss of ALPL activity did not contribute significantly to the prediction of recurrence in the multivariate modeling. On the one hand, this may be founded in the remarkable loss of histochemical reaction due to the susceptibility of this histochemical reaction to the state of preservation of tumor tissue, which leads to an inferior predictive potential compared to confounding predictors. On the other hand, equivocal representativeness of cells growing in cell culture, low percentage of cells with 1p− and also small deletions on chromosome 1p cause low sensitivity of classic cytogenetic methods. This results in a misleading discrepancy between ALPL reaction and cytogenetic findings and in individual cases the loss of ALPL activity do not correspond to a deletion of 1p, because the presumptive deletion was not detected by means of classic metaphase cytogenetic methods. Interphase techniques such as fluorescence in situ hybridization (FISH) are more sensitive and accurate in the detection of the deletion of 1p and may result in a higher concordance between ALPL expression and genetic findings. For the comparability of data, we applied the cut off point of at least 50% enzyme negative tumor cells for heterogenous pattern of ALPL expression (ALPL+/−) as suggested by Bouvier et al. [4]. Regarding the arbitrary assessment of this cut off point on the one hand and the low sensitivity of the metaphase cytogentic method on the other, the moderate concordance between ALPL+/− and detectable loss of 1p has to be reconceived. Despite its minor role as independent risk factor itself, we suggest that ALPL expression keeps a key role as a sensitive screening method for 1p−, in particular if the enzyme activity is lacking in a histologically common-type meningioma.

Apart from 1p−, allelic losses of other chromosomal arms, e.g. 10q or 14q, are further cytogenetic aberrations suggested to be progression-associated [27]. In the presented study, these aberrations were subsumed in the group "markedly hypodiploid meningiomas with intact 1p". A more detailed and differentiated analysis of specific chromosomal aberrations is given by Zang [31]. A multiparametric analysis in more than 600 cytogenetically characterized cases is the subject of current studies and will provide a more instructive insight into the genetics and biology of meningiomas (Ketter et al., preliminary data presented at the Meeting of the Neurooncology Section of the German Society of Neurosurgery, October 2005).

Conclusions

Anaplasia, incomplete tumor resection, Ki-67 LI >12%, and 1p− are independent predictors of recurrence in meningiomas. Independent from mitotic activity, a Ki-67 LI >12% indicates a high risk of recurrence among atypical or anaplastic meningiomas. Deletion of the short arm of chromosome 1 also indicates histologically common-type meningiomas with higher risk of recurrence. The fast and low-cost histochemical detection of ALPL expression is suggested as a highly specific screening method for potential 1p−. In particular, recurrence prone meningiomas of histologically benign or "borderline" phenotype could be therefore identified sensitively by ALPL detection followed by 1p in situ hybridization.

Acknowledgement The authors gratefully thank Mr. Craig Washington for the editorial help.

References

1. Abramovich CM, Prayson RA (1999) Histopathologic features and MIB-1 labeling indices in recurrent and nonrecurrent meningiomas. Arch Pathol Lab Med 123:793–800
2. Al-Mefty O, Kadri PA, Pravdenkova S, Sawyer JR, Stangeby C, Husain M (2004) Malignant progression in meningioma: documentation of a series and analysis of cytogenetic findings. J Neurosurg 101:210–218
3. Bello MJ, de Campos JM, Vaquero J, Kusak ME, Sarasa JL, Rey JA (2000) High-resolution analysis of chromosome 1p alterations in meningioma. Cancer Genet Cytogenet 120:30–36
4. Bouvier C, Liprandi A, Colin C, Giorgi R, Quilichini B, Metellus P, Figarella-Branger D (2005) Lack of alkaline phosphatase activity predicts meningioma recurrence. Am J Clin Pathol 124:252–258
5. Burger PC, Scheithauer BW, Vogel FS (eds) (2002) Surgical pathology of the nervous system and its coverings. Churchill Livingstone, New York
6. Cai DX, Banerjee R, Scheithauer BW, Lohse CM, Kleinschmidt-Demasters BK, Perry A (2001) Chromosome 1p and 14q FISH analysis in clinicopathologic subsets of meningioma: diagnostic and prognostic implications. J Neuropathol Exp Neurol 60: 628–636
7. Ho DM, Hsu CY, Ting LT, Chiang H (2002) Histopathology and MIB-1 labeling index predicted recurrence of meningiomas. A proposal of diagnostic criteria for patients with atypical meningiomas. Cancer 94:1538–1547
8. Jääskeläinen J, Haltia M, Servo A (1986) Atypical and anaplastic meningiomas: radiology, surgery, radiotherapy, and outcome. Surg Neurol 25:233–242
9. Kepes JJ (1986) Presidential address: the histopathology of meningiomas. A reflection of origins and expected behavior? J Neuropathol Exp Neurol 45:95–107
10. Ketter R, Henn W, Niedermayer I, Steilen-Gimbel H, Konig J, Zang KD, Steudel WI (2001) Predictive value of progression-associated chromosomal aberrations for the prognosis of meningiomas: a retrospective study of 198 cases. J Neurosurg 95:601–607
11. Kim YJ, Romeike BFM, Uszkoreit J, Feiden W (2006) Automated nuclear segmentation in the determination of the Ki-67 labeling-index in meningiomas. Clin Neuropathol 25:67–73

12. Kolles H, Niedermayer I, Schmitt C, Henn W, Feld R, Steudel WI, Zang KD, Feiden W (1995) Triple approach for diagnosis and grading of meningiomas: histology, morphometry of Ki-67/Feulgen stainings, and cytogenetics. Acta Neurochir (Wien) 137:174–181
13. Limon J, Dal Cin P, Sandberg AA (1986) Application of long-term collagenase disaggregation for the cytogenetic analysis of human solid tumors. Cancer Genet Cytogenet 23: 305–313
14. Kleihues P, Cavenee WK (eds) (2000) Pathology and Genetics, Tumours of the nervous system. IARC Press, Lyon
15. Maier H, Ofner D, Hittmair A, Kitz K, Budka H (1992) Classical, atypical, and anaplastic meningioma: three histopathological subtypes of clinical relevance. J Neurosurg 7:616–623
16. McCarthy BJ, Davis FG, Freels S, Surawicz TS, Damek DM, Grutsch J, Menck HR, Laws ER Jr (1998) Factors associated with survival in patients with meningioma. J Neurosurg 88: 831–839
17. Murakami M, Hashimoto N, Takahashi Y, Hosokawa Y, Inazawa J, Mineura K (2003) A consistent region of deletion on 1p36 in meningiomas: identification and relation to malignant progression. Cancer Genet Cytogenet 140:99–106
18. Müller P, Henn W, Niedermayer I, Ketter R, Feiden W, Steudel WI, Zang KD, Steilen-Gimbel H (1999) Deletion of chromosome 1p and loss of expression of alkaline phosphatase indicate progression of meningiomas. Clin Cancer Res 5: 3569–3577
19. Nakasu S, Li DH, Okabe H, Nakajima M, Matsuda M (2001) Significance of MIB-1 staining indices in meningiomas. Comparison of two counting methods. Am J Surg Pathol 5:472–478
20. Niedermayer I, Feiden W, Henn W, Steilen-Gimbel H, Steudel WI, Zang KD (1997) Loss of alkaline phosphatase activity in meningiomas: a rapid histochemical technique indicating progression-associated deletion of a putative tumor suppressor gene on the distal part of the short arm of chromosome 1. J Neuropathol Exp Neurol 56:879–886
21. Perry A, Stafford SL, Scheithauer BW, Suman VJ, Lohse CM (1998) The prognostic significance of MIB-1, p53, and DNA flow cytometry in completely resected primary meningiomas. Cancer 82:2262–2269
22. Perry A, Stafford SL, Scheithauer BW, Suman VJ, Lohse CM (1997) Meningioma grading. An analysis of histological parameters. Am J Surg Pathol 21:1455–1465
23. Prowald A, Ketter R, Zang K, Steudel WI (2003) Two-step inactivation of the tissue non-specific alkaline phosphatase (ALPL) gene during progression of meningiomas by deletion plus promoter methylation. Genes Chromosomes Cancer 9:81
24. Roser F, Samii M, Ostertag H, Bellinzona M (2004) The Ki-67 proliferation antigen in meningiomas. Experience in 600 cases. Acta Neurochir 146:37–44
25. Rosenblum MK, Bilbao JM, Ang LC (2004) Meningiomas. In: Rosai J (ed) Rosai and Ackerman's surgical pathology. Mosby, New York, pp 2564–2572
26. Russell DS, Rubinstein LJ (eds) (1990) Pathology of tumors of the nervous system. Lippincott Williams and Wilkins, Baltimore
27. Simon M, von Deimling A, Larson JJ, Wellenreuther R, Kaskel P, Waha A, Warnick RE, Tew JM Jr, Menon AG (1995) Allelic losses of chromosomes 14, 10, and 1 in atypical and malignant meningiomas: a genetic model of meningioma progression. Cancer Res 55:4696–4701
28. Simpson D (1957) The recurrence of intracranial meningiomas after surgical treatment. J Neurol Neurosurg Psychiatry 20:22–39
29. Sulman EP, White PS, Brodeur GM (2004) Genomic annotation of the meningioma tumor suppressor locus on chromosome 1p34. Oncogene 23:1014–1020
30. Torp SH, Lindboe CF, Gronberg BH, Lydersen S, Sundstrom S (2005) Prognostic significance of Ki-67/MIB-1 proliferation index in meningiomas. Clin Neuropathol 24:170–174
31. Zang KD (2001) Meningioma: a cytogenetic model of a complex benign human tumor, including data on 394 karyotyped cases. Cytogenet Cell Genet 93:207–220
32. Zang KD (1982) Cytological and cytogenetical studies on human meningioma. Cancer Genet Cytogenet 6:249–274
33. Zang KD, Singer H (1967) Chromosomal constitution of meningiomas. Nature 216:84–85

Virchows Arch (2006) 449:539–545
DOI 10.1007/s00428-006-0286-2

ORIGINAL ARTICLE

Liver glycogen bodies: ground-glass hepatocytes in transplanted patients

Pablo A. Bejarano · Monica T. Garcia · Maria M. Rodriguez · Phillip Ruiz · Andreas G. Tzakis

Received: 28 March 2006 / Accepted: 31 July 2006 / Published online: 22 September 2006
© Springer-Verlag 2006

Abstract Ground-glass hepatocytes have been described in Lafora's disease, fibrinogen deposition, hepatitis B, type IV glycogenosis, and alcohol aversion (cyanamide) therapy. We encountered ground-glass hepatocytes with intracytoplasmic inclusions in four liver biopsies from three transplanted patients who had none of the above-mentioned underlying diseases. One patient was a 4-year-old boy who had a kidney transplant for severe ureterovesical reflux. Patient 2 was a 52-year-old man who had two liver transplants because of hepatitis C. The third patient was a 7-month-old girl who underwent a multivisceral transplant because of necrotizing enterocolitis and liver failure induced by total parenteral nutrition. The patients developed liver abnormalities from 45 days to 4 years after their transplants. The livers showed conspicuous ground-glass hepatocytes in 90% of the children's samples and 30% of the adult liver cells. The cytoplasmic bodies stained strongly for Gomori methenamine-silver; they were positive for periodic acid-Schiff without diastase, but negative after diastase digestion. They were negative for colloidal iron and hepatitis B core and surface antigens. Electron microscopy revealed non-membrane bound aggregates of glycogen. Idiopathic ground-glass hepatocytes occur in transplanted patients and represent accumulation of altered glycogen. However, their clinical significance and cause are not entirely elucidated.

Keywords Inclusions · Glycogen · Ground-glass hepatocytes

P. A. Bejarano (✉) · M. T. Garcia · M. M. Rodriguez · P. Ruiz
Department of Pathology, University of Miami School of Medicine, Jackson Memorial Hospital,
1611 NW 12th Ave Holtz Bldg, Room 2042,
Miami, FL 33136, USA
e-mail: pbejaran@med.miami.edu

A. G. Tzakis
Department of Surgery, University of Miami School of Medicine, Miami, FL, USA

Introduction

The term ground-glass hepatocyte refers to the presence of large, homogeneous, and weakly eosinophilic cytoplasmic bodies in the liver cells. They were first described in certain types of hepatitis [9, 7] and have been noted in a variety of conditions, including Lafora's disease (myoclonus epilepsy), hepatitis B, type IV glycogenosis, alcohol aversion therapy, fibrinogenosis, hepatocellular carcinoma, and drug-related changes. Although their morphologic appearance may be similar, their composition and clinical correlation are diverse. This report describes intracytoplasmic inclusion bodies with ground-glass appearance in the livers of three patients who had received kidney and liver transplants and who had none of the conditions currently known to be associated with ground-glass hepatocytes. Only one similar case in a transplant patient has been described in the peer-reviewed literature [23] and four in an abstract form [25].

Case reports

Case 1

A 4-year-old African-American boy underwent cadaveric kidney transplant due to prune belly syndrome with

vesicoureteral reflux grade IV. One year after transplant and while receiving tacrolimus (4 mg/day, last whole blood level 12.7 ng/ml), methylprednisolone, lansoprazole, baby aspirin, erythropoietin, iron, and multivitamins, the patient presented with total bilirubin of 2.1 mg/dl (normal range 0.2–1.3), direct bilirubin of 1.1 mg/dl (normal range 0.0–0.4), aspartate aminotransferase (AST) of 39 U/l (normal range 15–46), alanine aminotransferase (ALT) of 31 U/l (normal range 21–72), gamma glutamyl transpeptidase (GGTP) at 50 U/l (normal range 15–73), and alkaline phosphatase of 39 U/l (normal range 117–357). Other laboratory tests included blood glucose level of 97 mg/dl (normal range 75–110), creatinine of 0.7 mg/dl (normal range 0.4–0.7), and negative serology tests for hepatitis B. A liver biopsy was performed and revealed chronic hepatitis with mild inflammatory activity and bridging fibrosis. The most prominent feature of the biopsy was the presence of diffusely distributed large ground-glass hepatocytes with pale cytoplasmic inclusions in about 90% of the liver cells. Due to the possibility of drug-related hepatotoxicity, tacrolimus was discontinued and the patient was started on rapamycin. After 6 weeks, laboratory tests revealed a normal bilirubin level (0.3 mg/dl). No further liver biopsies have been obtained. The patient is doing fine 30 months after the transplant, but his fasting glucose level was slightly elevated (118 ng/dl).

Case 2

A 52-year-old white man with a history of hepatitis C underwent two liver transplants. The second transplant was performed due to recurrent chronic hepatitis and allograft rejection and required therapy with interferon and ribavirin. He was negative for hepatitis B. His post-transplant course was complicated by ascending cholangitis due to *Cryptosporidium* infection and pulmonary aspergillosis, from both of which he eventually recovered. Four years later, the laboratory tests showed hepatitis C RNA viral load 1,730,000 IU/ml, alkaline phosphatase=1195 U/l, GGTP=412 U/l, AST=68 U/l, ALT=46 U/l, and creatinine=6.7 mg/dl. At this time, the patient was receiving ribavirin, testosterone, magnesium, ursodiol, candesartan, calcium, and tacrolimus (4 mg/day; last whole blood level, 5 ng/ml). Two liver biopsies were performed within a month and showed changes suggestive of early chronic rejection, minimal to mild grade of chronic hepatitis, and progressively increasing number of ground-glass hepatocytes located mostly in zone 1. At 60 months follow-up after the transplant, the patient developed anemia attributed to chronic idiopathic myelofibrosis. A liver biopsy at this time showed features of chronic rejection, chronic hepatitis, and rare hepatocytes with cytoplasmic inclusions similar to those seen previously, but much less conspicuous. His fasting glucose level was 172 mg/dl.

Case 3

A 7-month-old girl, who developed necrotizing enterocolitis and liver failure induced by total parenteral nutrition, underwent a multivisceral transplant that included the intestine, stomach, pancreas, spleen, and liver. She had no central nervous system abnormalities. Follow-up biopsies of the intestine and stomach did not reveal rejection. Forty-five days after the transplant, she developed a lung fungal infection. The AST was 40 U/l, ALT 29 U/l, alkaline phosphatase 429 U/l, and albumin 2.7 gm/dl. (normal range 3.9–5.0). A percutaneous liver biopsy was performed to rule out fungal infection. It showed no fungi or definitive features of rejection. However, the biopsy was remarkable due to widespread and panacinar presence of cytoplasmic inclusions in the hepatocytes. At the time of the liver biopsy, she was receiving tacrolimus 1.0 mg/day. Other medications included xanopex, valganciclovir, prevacid, and prednisolone. She was hepatitis B-negative. The total follow-up was 17 months with no clinical liver abnormalities. However, her fasting glucose level was 142 mg/dl. A liver biopsy has not been performed since finding the cytoplasmic inclusions.

A list of medications administered to the patients by the time of the biopsy findings is presented in Table 1.

Materials and methods

The core biopsy tissues were fixed in 10% buffered formalin and embedded in paraffin. Hematoxylin and eosin (H&E)-stained slides of four liver core biopsies from the three patients were examined by light microscopy. The following histochemical stains were performed: trichrome, periodic acid-Schiff (PAS) with and without diastase, Gomori methenamine-silver (GMS), and colloidal iron. Deparaffinized sections were incubated with hepatitis B surface (Dako, 1:10,000, mouse) and core antigens (Dako, 1:100, rabbit) and immunostained by an indirect biotin–avidin method in the Dako Autostainer Plus (Dako, CA).

Electron microscopy

Tissue was obtained from the paraffin blocks and ultrastructural analysis was performed in two patients. It was deparaffinized and postfixed in buffered 1% osmium tetroxide. The block was stained with 8% uranyl acetate and embedded in Epon. The thick sections were stained with toluidine blue in order to select the areas for evaluation. Thin sections were stained with lead citrate and examined with a JEOL CX-100 transmission electron microscope.

Table 1 Doses and indications of drugs taken by the patients

Patient 1	Patient 2	Patient 3
Tacrolimus (immunosupressive), 4 mg/day	Tacrolimus, 4 mg/day	Tacrolimus, 1 mg/day
Prednisolone (immunosupressive), 4 mg/day	Peg interferon (hepatitis C), 180 μg/week	Daclizumab (immunosuppressive), 18 mg/week
Prevacid (esophageal reflux), 15 mg/day	Ribavirin (hepatitis C), 200 mg/day	Valganciclovir (CMV), 70 mg/day
Aspirin (anticoagulant), 80 mg/day	Testosterone (body mass builder), 5 g/day	Prevacid, 5 mg/day
Erythropoietin (anemia), 3,600 units/week	Magnesium (deficiency), 400 mg/day	Prednisolone, 6 mg/day
Iron (anemia), 40 mg/day	Ursodiol (to improve bile flow) 1,200 mg/day	
Multivitamins	Candesartan (hypertension), 16 mg/day	
	Labetalol (hypertension), 600 mg/day	
	Calcium (bone loss), 2,600 mg/day	

CMV Cytomegalovirus

Results

Histologic findings

The most striking feature observed in the four liver core biopsies of these three patients was the presence of enlarged ground-glass hepatocytes with prominent pale eosinophilic round to oval intracytoplasmic bodies that occupied most of the cell and displaced the nuclei toward the periphery (Fig. 1a). There were kidney-shaped cytoplasmic bodies that encroached the nucleus of the hepatocytes. Some of the inclusions had a subtle vacuolization and others were surrounded by a crescent-shaped halo that separated them from the cell membrane (Fig. 1b). The glassy hepatocytes in the biopsies from the children were diffusely distributed in a panacinar fashion involving all three zones of the liver and occupying about 90% of the sample. The two biopsies from the adult patient showed clusters of hepatocytes with inclusion bodies, located mostly in the periportal areas and involving approximately 30% of the tissues. In all patients, the intracytoplasmic inclusions were strongly positive with PAS, but negative after diastase digestion (Fig. 1c,d). They had a light gray-blue color with trichrome and sharp black color with GMS stain (Fig. 1e,f). Colloidal iron stain was negative. They were negative for hepatitis B core and surface antigens by immunohistochemistry. The donor biopsy tissues at the time of transplantation were normal.

Ultrastructural findings

On electron microscopic examination, the ground-glass hepatocytes exhibited an eccentrically located nucleus and distorted organelles displaced toward the periphery of the cell by intracytoplasmic low electron-dense inclusions. The cytoplasmic inclusions consisted of non-membrane bound aggregates of beta glycogen granules admixed with few irregularly dilated smooth endoplasmic reticulum and some lipid droplets (Fig. 1g,h). Not all the inclusions were of the same size. They ranged from 9 to 19 μm, and the larger inclusions were associated with distortion of the hepatocyte nucleus. The surrounding mitochondria were swollen and the smooth endoplasmic reticulum was slightly dilated.

Discussion

None of the three patients had the clinical manifestations or histologic features of the known conditions to cause ground-glass hepatocytes. The morphologic differential diagnoses for ground-glass hepatocytes on H&E-stained sections includes fibrinogen deposition, Lafora's disease, type IV glycogenosis, use of cyanamide and disulfiram ("antabuse") for the treatment of alcoholism, chronic hepatitis B, and drug-related changes. Although H&E-stained slides show marked similarity regardless of the cause, the inclusion bodies in these entities are distinguished on clinical grounds, as well as by histochemical, immunohistochemical, and ultrastructural analysis. The first descriptions of these cytoplasmic inclusion bodies are attributed to Klinge and Bannasch [9] who observed them in patients receiving drugs including cholorpromazine and barbiturates. The "ground-glass" term, however, was coined when they were observed in patients with hepatitis B [7]. Fibrinogen may randomly accumulate in the liver and gives a ground-glass appearance to hepatocytes [3, 4] in patients with hypofibrinogenemia. However, fibrinogen can cause ground-glass hepatocytes and storage disease in the absence of hypofibrinogenemia [12, 13] as it has been observed in hepatocellular carcinoma as well [14]. Lafora's disease is manifested by seizures, dementia, and myoclonus. The liver shows large slightly eosinophilic bodies in the periportal hepatocytes. These ground-glass bodies stain positive for colloidal iron. It is postulated that in Lafora's disease, there is a carbohydrate metabolism abnormality. This assumption is supported by the fact that the inclusion bodies represent stored polyglucosans [26]. Type IV glycogen-storage disease is a rare entity caused by a deficiency of the

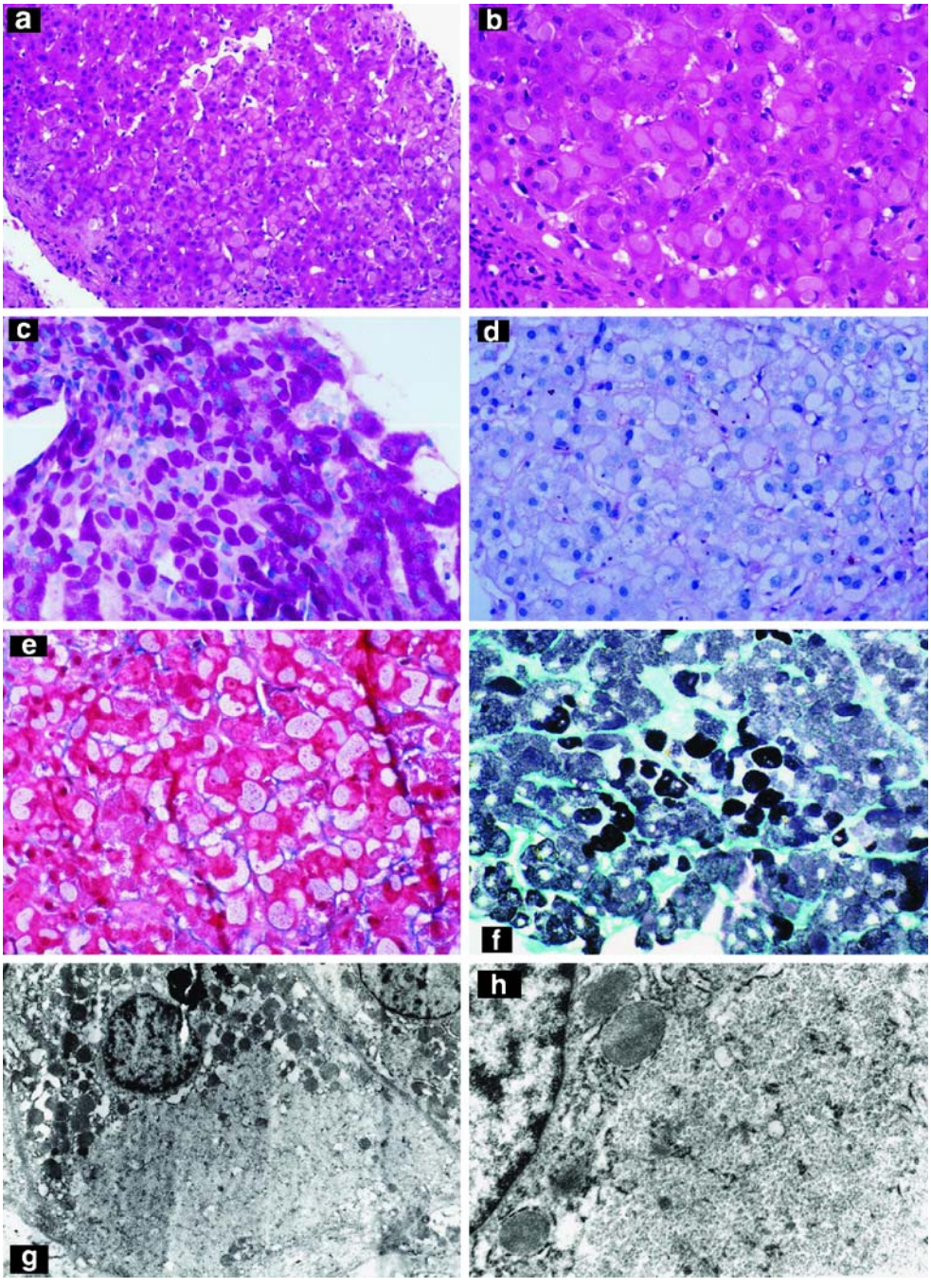

Fig. 1 **a** Needle biopsy tissue from patient 1. Panacinar distribution of ground-glass hepatocytes (H&E, 100×). **b** The cytoplasmic inclusions vary in size and some of them are kidney-shaped (H&E, 400×). **c**, **d** The inclusions are strongly PAS-positive and negative after digestion with diastase (PAS/PAS with diastase, 400×). **e** On trichrome stain, the inclusions display a light gray-blue color. (Trichrome, 400×). **f** The GMS stain enhances the inclusions with a sharp black color (GMS, 400×). **g**, **h** A hepatocyte demonstrating a large inclusion that displaces the cytoplasmic organelles and is composed of numerous beta-glycogen granules, some irregularly dilated smooth endoplasmic reticulum, and lipid droplets. (12,000×, 25,000×)

branching enzyme and characterized by the generalized accumulation of an abnormally organized and poorly soluble glycogen. Patients present in infancy with liver failure, hepatosplenomegaly, failure to thrive, and gastrointestinal symptoms. Death occurs before the third year of life due to cirrhosis. The liver shows deposits of abnormal glycogen, mostly in the periportal hepatocytes, appearing as large bodies that stain similarly to Lafora's bodies. Because of its frequency and historical baggage, chronic hepatitis B is unavoidable as the first differential diagnosis that a pathologist considers when encountering ground-glass hepatocytes. The cytoplasmic inclusions related to cyanamide [20] or disulfiram [22] uses for the treatment of alcoholism have been described as periportal round or ovoid pale ground-glass bodies. By using antibodies against a polyglucosan, Hashimoto et al. [8] found by immunoelectron microscopy that the immunoreactivity was present in glycogen granules of the ground-glass bodies and concluded that in this disorder there was an accumulation of abnormal glycogen that could be formed due to faulty glucose metabolism. Although the documentation has not been firm for the use of other drugs, scant reports claim association with the presence of ground-glass hepato-

cytes [9]. They include rifampicin, chlorpromazine, benzodiazepine and barbiturates [1, 18, 21].

At this point our cases would be considered idiopathic. A summary of the characteristics and differential histologic diagnosis appears in the Table 2. In our three patients, the histochemical qualities and clinical information ruled out the possibilities of type IV glycogen-storage disease, fibrinogen deposition, hepatitis B, or the drugs implicated so far to explain the presence of extensive ground-glass hepatocytes. The cytoplasmic inclusions in our patients demonstrated identical histochemical characteristics with those of the Lafora's disease and ultrastructural features similar to those associated with the use of cyanamide. However, none of our patients had clinical findings of myoclonus epilepsy, dementia, or alcohol aversion therapy. Interestingly, in both conditions, Lafora's disease and cyanamide therapy, the ground-glass inclusions appear to be a consequence of an alteration in the intrahepatic glycogen-related to glucose metabolism [20, 26], which may account for their morphohistochemical similarities, and thus, resembling the features seen in our three cases. The proximity of the glycogen rosettes to the smooth endoplasmic reticulum would support a functional effect. The progressive hepatic accumulation of glycogen could probably be secondary to systemic metabolic signals with increased glycogen synthesis or inhibition of glycogenolysis.

Two cases reported by Ng et al. [15] had no association to the clinical entities reviewed. One of their patients had venoocclusive disease and the other presenile dementia. Their inclusion bodies resembled Lafora's bodies and, thus, share similarities to the ones in our cases. A similar case described by Wills [23] is that of a 54-year-old man who underwent a kidney transplant and 11 months later developed liver disease with the presence of ground-glass hepatocytes. Because of the presence of glycogen rosettes, he termed them "glycogen bodies," supporting the view that the alteration on his case and in the cases reported by Ng and us are related to an interference with the structure and/or metabolism of glycogen. At this point, the cases by Ng, Wills, and our own would fall in the category of idiopathic ground-glass hepatocytes. Wisell et al. [25], in an abstract form, mentioned four bone marrow and solid organ transplanted patients that showed ground-glass changes in their liver biopsies. They also observed similar changes in four more patients who had HIV infection, kidney dialysis, and inflammatory bowel disease. The hepatocytes in their cases showed changes essentially identical to the ground glass seen in chronic HBV, with well-circumscribed, gray-glass inclusions surrounded by a rim of normal cytoplasm. All of their cases were negative for HBsAg immunostaining and/or HBV serological testing. They termed the finding pseudo ground-glass change. Their inclusions were PAS positive and diastase-sensitive and had ultrastructual features of abnormally organized glycogen, thus similar to our observations. What appears to be a common denominator among the cases by Wills [23], Wisell [25], and ours is that most patients are immunosupressed.

The alternative we are left with is to consider the possibility of drug toxicity. Our patients received long-term therapy with tacrolimus. Tacrolimus is a potent immunosuppressive medication that is known to cause alterations in glucose metabolism, neurotoxicity, nephrotoxicity, gastrointestinal toxicity, and hepatotoxicity [19]. Tacrolimus-associated hepatotoxicity is characterized by an increase in ALT or conjugated bilirubin to more than twice the upper limit of normal and a 50% decrease of the excess over the upper normal limit within 1 week to 1 month after withdrawal [6]. Evaluation of the laboratory data obtained at the time of the biopsies and the clinical follow-up revealed that the patient in case 1 met the criteria suggestive for drug-related hepatotoxicity, while the second showed

Table 2 Differential diagnosis of ground-glass hepatocytes

Technique	Hepatitis B	Fibrinogen	Glycogenosis IV	Cyanamide	Lafora's disease	Drug-induced	Idiopathic
PAS	−	−	+	+	+	−	+
D-PAS	−	−	±	−	±−	−	−
Orcein	+	−	−	−	−	−	−
Hepatitis B	+	−	−	−	−	−	−
Fibrinogen	−	+	−	−	−	−	−
GMS	−	−	+	+	+	−	+
EM	Abundant SER with filaments of hepatitis B antigens [24]	Amorphous granular or fibrillar material [3]	Core of 60–65 Å abnormal glycogen surrounded by normal-appearing glycogen [2]	Hyperplastic dilated SER, lipid droplets, lamellar structures and β-glycogen granules [22]	60 Å short fibrils and disrupted ER [16]	Hypertrophic SER [21]	β-glycogen granules, lipid droplets, a few dilated SER

+ Positive, − negative, ± weakly positive, *SER* smooth endoplasmic reticulum, *EM* electron microscopy

nonspecific elevations of the GGTP and alkaline phosphatase that have been stable even after continuing tacrolimus. A higher number of hepatocytes was involved by glycogen bodies in the child than the adult. This may be related to the fact that the serum level of tacrolimus was much higher in the child than the adult. In the third patient, the parenchyma liver function tests were not elevated. Therefore, as to the clinical significance of these cytoplasmic inclusions, it is unclear at this point if they represent either an adaptive response to the drug or an early manifestation of hepatic injury. It is interesting that tacrolimus has been implicated in the development of hepatoxicity and post-transplantation diabetes mellitus particularly in older patients. Between 24 to 33% of patients on tacrolimus develop diabetes [5, 11, 17]. The pathogenesis of post-transplant diabetes in these patients is not completely understood. It has been postulated that there is pancreatic beta-cell toxicity [10]. It is tempting to speculate that the altered glycogen accumulation in hepatocytes may be related to the eventual hyperglycemia in these patients. In fact, two of our patients developed high levels of glucose and one had borderline high values. It is possible that the presence of glycogen bodies in the livers of patients taking tacrolimus is the initial change in the metabolism of glycogen and glucose at molecular level before high glycemia levels become evident, thus serving as a predictor for hyperglycemia. Although, the majority of patients at our center receive tacrolimus, cases showing liver cytoplasmic inclusions are rare. In the cases described by Wisell et al. [25], no single common medicine was identified, though most of their patients were on at least one steroid. The latter drug has been also associated with diabetes after transplantation [10]. The intervals between the transplants and the finding of glycogen bodies in the biopsies were markedly different among our three patients. However, the number of cases is small to draw any conclusion based on these differences.

In summary, transplant patients may show in their liver biopsies large intracytoplasmic inclusions bodies characterized by glassy appearance that resemble those observed on Lafora's disease and enter in the histologic differential diagnosis of ground-glass hepatocytes. They stain positive for PAS, negative for PAS with diastase, and positive for GMS. They are accumulations of altered glycogen. Additional studies are needed to determine their clinical significance and relationship to hepatic biochemical abnormalities.

References

1. Alonso-Marti C, Moreno A, Barat A, Solera JC, Oliva H (1990) Co-existence of hepatocyte ground-glass inclusions from several causes. Histopathology 6:304–307
2. Bannayan GA, Dean WJ, Howell RR (1976) Type IV glycogen-storage Disease. Am J Clin Pathol 66:702–709
3. Brennan SO, Wyatt J, Medicina D, Callea F, George PM (2000) Fibrinogen brescia hepatic endoplasmic reticulum storage and hypofibrogenaemia because of a gamma 284 Gly-Arg mutation. Am J Pathol 157:189–196
4. Callea F, De Vos R, Togni R, Tardanico R, Vanstapel MJ, Desmet VJ (1986) Fibrinogen inclusion in liver cells: a new type of ground-glass hepatocyte. Immune light and electron microscopic characterization. Histopathology 10:65–73
5. Emre S, Genyk Y, Schluger LK, Fishbein TM, Guy SR, Sheiner PA, Schwartz ME (2000) Treatment of tacrolimus-related adverse effects by conversion of cyclosporine in liver transplant recipients. Transpl Int 13:73–78
6. Fisher A, Mor E, Hytiroglou P, Emre S, Boccagni P, Chodoff L, Sheiner P, Schwartz M, Thung SN, Miller C (1995) FK506 Hepatotoxicity in liver allograft recipients. Transplantation 59:1631–1632
7. Hadziyannis S, Gerber MA, Vissoulis C, Popper H (1973) Cytoplasmic hepatitis B antigen in "ground-glass" hepatocytes of carriers. Arch Pathol 96:327–330
8. Hashimoto K, Hoshii Y, Takahashi M, Mitsuno S, Hanai N, Watanabe Y, Ishihara T (2001) Use of a monoclonal antibody against Lafora bodies for the immunocytochemical study of ground-glass inclusions in hepatocytes due to cyanamide. Histopathology 39:60–65
9. Klinge O, Bannasch P (1968) Zur Vermehrung des glatten endoplasmatischen Retikulum in Hepatocyten Menschlicher Leberpunktate. Verh Dtsch Ges Pathol 52:568–573
10. Marchetti P (2005) New-onset diabetes after liver transplantation: from pathogenesis to management. Liver Transpl 11:612–620
11. Martínez-Dolz L, Almenar L, Martínez-Ortiz L, Arnau MA, Chamorro C, Moro J, Osa A, Rueda J, García C, Palencia M (2005) Predictive factors for development of diabetes mellitus post-heart transplant. Transplant Proc 37:4064–4066
12. Marucci G, Morandi L, Macchia S, Betts CM, Tardio ML, Dal Monte PR, Pession A, Foschini MP (2003) Fibrinogen storage disease without hypofibrinogenaemia associated with acute infection. Histopathology 42:22–25
13. Medicina D, Fabbretti G, Brennan SO, George PM, Kudryk B, Callea F (2001) Genetic and immunological characterization of fibrinogen inclusion bodies in patients with hepatic fibrinogen storage and liver disease. Ann N Y Acad Sci 936:522–525
14. Moon WS, Yu HC, Chung MJ, Kang MJ, Lee DG (2000) Pale bodies in hepatocellular carcinoma. J Korean Med Sci 5:516–520
15. Ng IOL, Sturgess RP, Williams R, Portmann B (1990) Ground-glass hepatocytes with Lafora body like inclusions-histochemical, immunohistochemical and electronmicroscopic characterization. Histopathology 17:109–115
16. Nishimura RN, Ishak KG, Reddick R, Porter R, James S, Barranger JA (1980) Lafora disease: diagnosis by liver biopsy. Ann Neurol 8:409–415
17. Rodrigo E, de Cos MA, Fernández-Fresnedo G, Sánchez B, Ruiz JC, Piñera C, Palomar R, Cotorruelo JG, Gómez-Alamillo C, de Castro S, de Francisco AL, Arias M(2005) Higher initial tacrolimus blood levels and concentration–dose ratios in kidney transplant recipients who develop diabetes mellitus. Transplant Proc 37:3819–3820
18. Scheuer PJ, Summerfield JA, Lal S, Sherlock S (1974) Rifampicin hepatitis. A clinical and histological study. Lancet 16:421–425
19. Spencer CM, Goa KL, Gillis JC (1977) Tacrolimus. An update of its pharmacology and clinical efficacy in the management of organ transplantation. Drugs 54:925–975
20. Thomsen P, Reinicke V (1981) Ground glass inclusions in liver cells in an alcoholic treated with cyanamide (Dipsan). Liver 1: 67–73

21. Thomsen P, Poulsen H, Petersen P (1976) Different types of ground glass hepatocytes in human liver biopsies: morphology, occurrence and diagnostic significance. Scand J Gastroenterol 11:113–119
22. Vazquez JJ, Pardo-Mindan J (1979) Liver cell injury (bodies similar to Lafora's) in alcoholics treated with disulfiram (Antabuse). Histopathology 3:377–384
23. Wills EJ (1992) Ground glasslike hepatocytes produced by glycogen-membrane complexes ("glycogen bodies"). Ultrastruct Pathol 16:491–503
24. Winckler K, Junge U, Creutzfeldt W (1976) Ground-Glass hepatocytes in unselected liver biopsies. Ultrastructure and relationship to hepatitis B surface antigen. Scand J Gastroenterol 11:167–170
25. Wisell J, Haas M, Boitnott J, Anders R, Hart J, Lewis J, Abraham SC, Torbenson M (2006) Pseudo-ground glass changes in liver biopsies (Abstract). Mod Pathol 19:282
26. Yokota T, Ishihara T, Yoshida H, Takahashi M, Uchino F, Hamanaka S (1988) Monoclonal antibody against polyglucosan isolated from the myocardium of a patient with Lafora disease. J Neuropathol Exp Neurol 47:572–577

Virchows Arch (2006) 449:546–553
DOI 10.1007/s00428-006-0273-7

ORIGINAL ARTICLE

Expression of endothelin 1 and its angiogenic role in meningiomas

Laura Boldrini · Sabina Pistolesi · Silvia Gisfredi · Silvia Ursino · Greta Alì · Nicola Pieracci · Fulvio Basolo · Giuliano Parenti · Gabriella Fontanini

Received: 11 May 2006 / Accepted: 11 July 2006 / Published online: 30 September 2006
© Springer-Verlag 2006

Abstract Meningiomas are one of the most frequent central nervous system tumours. Although slow-growing at times, they continue to be a cause of morbidity and mortality. The endothelin (ET) family consists of three isoforms: ET-1 is the most abundant one. ET-1 may be involved in meningioma tumourigenesis in concert with other growth factors, in particular with angiogenic agents. We analysed ET-1 expression by immunohistochemistry and its activating system by reverse-transcription–polymerase chain reaction in 56 cases of meningioma. We found an association between high-grade meningiomas and high ET-1 expression levels (p=0.002). Moreover, we evaluated the potential angiogenic role of ET-1, finding an elevated microvessel count in tumours with high ET expression levels (p=0.004). ET-1 may contribute to meningioma growth by inducing formation of new blood vessels. The finding that ET-1 expression positively correlates with vascular endothelial growth factor (VEGF) expression in meningiomas (p=0.03) also supports the hypothesized modulating effect of ET-1 on angiogenesis. Thus, the influence of the ET system on the progression of meningiomas may occur through stimulation of VEGF. The association of ET-1 and meningioma represents a potential area for therapeutic intervention with selective ET inhibitors. Additional clinical studies will be needed before inhibitors can be incorporated in clinical practice.

Keywords Endothelin 1 · Angiogenesis · Meningiomas

Abbreviations

CNS	central nervous system
ECE-1	endothelin-converting enzyme 1
ET	endothelin
ET-1	endothelin 1
GAPDH	glyceraldehyde-3-phosphate dehydrogenase
VEGF	vascular endothelial growth factor
Flt-1	fms-like tyrosine kinase 1
WHO	World Health Organization
MVC	microvessel count
RT-PCR	reverse-transcription–polymerase chain reaction
GPCR	G-protein-coupled receptor

Introduction

Meningiomas are one of the most frequent central nervous system (CNS) tumours, accounting for 13–27% of all primary intracranial tumours [28]. Although slow-growing at times, they continue to be a major cause of morbidity and mortality. The primary therapy for meningioma is surgical intervention, with the likelihood of recurrence inversely related to the extent of resection [9].

Great interest exists in evaluating new molecular markers that may also serve as potential therapeutic targets to improve tumour control, with special regard to unresectable cases due to hazardous locations and to relapsed cases that have exhausted surgical and radiation

L. Boldrini (✉) · S. Pistolesi · S. Gisfredi · S. Ursino · G. Alì · F. Basolo · G. Fontanini
Department of Surgery, University of Pisa,
via Roma 57,
56100 Pisa, Italy
e-mail: l.boldrini@med.unipi.it

N. Pieracci · G. Parenti
Department of Neuroscience, University of Pisa,
56100 Pisa, Italy

treatment options. A new and exciting area of research involves the abnormal expression of different growth factors and/or their receptors in tumoural development and progression.

The endothelin (ET) family consists of three isoforms (ET-1, ET-2 and ET-3), all of which contain 21 amino-acid residues. ET-1 is the most abundant isoform and has been best characterized [11].

The *endothelin 1* gene encodes a precursor peptide, preproendothelin 1, which is cleaved firstly by a neutral endopeptidase to form proendothelin 1, or big ET-1, and in a second step by ET-converting enzyme 1 (ECE-1) to ET-1 [29]. This proteolytic cleavage of Trp–Val bond by ECE-1 is critical to the functions of ET-1 because the precursors have negligible biological activity [1]. Endothelin 1 exerts its physiological action via two receptors, ETA and ETB, which are G-protein-coupled transmembrane receptors.

Increased expression of ET-1 has been shown in various human malignancies such as ovarian, colorectal, and prostate cancer [3, 20, 25, 30], suggesting a potential role of ET-1 expression in tumour development [36]. Pagotto and colleagues [27] provided evidence that ET-1 represents an important growth factor for meningiomas acting via ETA. Endothelin 1 may be involved in meningioma tumourigenesis in concert with other growth factors, in particular with other angiogenic agents [10], but up to now, none of the several aspects regarding the potential role of ET have been clarified. In a recent study by Knowles and coworkers [19], the role of the vasoactive peptide ET-1 in tumour angiogenesis is reviewed. They demonstrated that ET-1 has a direct angiogenic effect on endothelial and perivascular cells, and also an indirect action through the increased release of the potent pro-angiogenic vascular endothelial growth factor (VEGF).

In our study, the hypothesized modulating effect of ET-1 on angiogenesis is supported by the finding that ET-1 expression positively correlates with neovascularization and VEGF expression in meningiomas, as was also previously shown in ovarian [30], breast [37] and colorectal tumours [31] and gliomas [32]. Thus, in a similar way, the influence of the ET system on the progression of meningiomas may occur through stimulation of VEGF.

Materials and methods

Specimens

Fifty-six patients who had undergone macroscopically complete surgical resection (Simpson 1 and 2) of intracranial meningiomas at the U.O. of Neurosurgery, University of Pisa, were analysed. The most common histologic type was typical meningioma (46 cases, 82.14%), followed by atypical/anaplastic subtype (10 cases, 17.86%). Histopathological diagnoses were made following the World Health Organization (WHO) guidelines [18, 21] and evaluated in formalin-fixed, paraffin-embedded samples after staining with haematoxylin–eosin.

Random samples were processed (one block per centimetre of tumour) and independently evaluated by two pathologists. No significant differences were found between their histological reports. Tumours were classified as typical (grade I, 46 cases), atypical (grade II, 8 cases) and anaplastic (grade III, 2 cases). This classification was performed according to the number of mitosis, presence and grade of anaplasia, and number and evidence of nucleoli. Among typical meningiomas, the tumours were classified as 22 transitional, 9 meningothelial, 5 syncytial, 4 fibrous, 4 psammomatous, 1 angiomatous and 1 microcystic.

Cases were enrolled after surgical removal of the lesion and pathological confirmation, but before radiation therapy. Tumour samples obtained at surgery were in part paraffin-embedded for histological processing and in part immediately frozen in liquid nitrogen and stored at −80°C for reverse-transcription–polymerase chain reaction (RT-PCR) analyses.

Immunohistochemical evaluation

All the immunostainings were performed on formalin-fixed and paraffin-embedded samples of all the cases using specific antibodies. Immunoreaction was displayed using the avidin–biotin–peroxidase complex (ABC) method. Peroxidase activity was visualized with diaminobenzidine. Counterstaining was performed with haematoxylin. Negative checks were carried out by omitting the primary antibodies. In all cases, the immunohistochemistry evaluation was independently determined by two pathologists. Each observer evaluated the slides without any knowledge of the counts made by the other; there were no significant differences in the results found by the two pathologists.

For the ET expression, the sections were incubated for 1 h at 25°C with rabbit anti-ET polyclonal antibody (Chemicon International Inc., Temecula, CA, USA; dilution 1:100). Anti-ET is raised against a synthetic octapeptide containing the carboxyterminal heptapeptide common to ET-1, ET-2 and ET-3. After the primary antibodies, a biotinylated secondary one was applied and followed by detection using the ABC method (Vector Laboratories, Burlingame, CA, USA); the ABC method was used by developing immunoreaction with diaminobenzidine. Light counterstaining was performed with haematoxylin. Incubation of parallel slides omitting the first antibody was performed as negative control. For each sample, ET expression was evaluated as the percentage of positive

cells in a total of at least 1,000 tumour cells. Microvascular count (MVC) was determined using anti-FVIII polyclonal antibody (Ventana Medical System, ready to use for the Ventana automated slide stainer) to better visualize the endothelial cells and, consequently, the microvessels. A single microvessel was defined as any brown immunostained endothelial cell separated from adjacent microvessels, tumour cells and other connective tissue elements. Each sample was examined first at low power (×10) to identify the three areas with the highest number of microvessels; these were then carefully counted in the areas at ×25 magnification, and the average count was recorded. The expression of VEGF (monoclonal antibody, dilution 1:100; Ventana) was assessed according to the percentage of immunoreactive cells out of a total of at least 1,000 neoplastic cells.

RNA extraction

Total RNA was extracted from frozen tissue samples using an RNeasy mini kit (Qiagen, M-Medical s.r.l., Florence, Italy); the RNeasy procedure represents a novel technology which combines the selective binding properties of a silica-gel-based membrane with the speed of the microspin principle. Biological samples are first lysed and homogenized in the presence of a highly denaturing guanidinium isothiocyanate-containing buffer, which immediately inactivates RNases to ensure isolation of intact RNA. Ethanol is added to provide appropriate binding conditions, and the sample is then applied to an RNeasy mini spin column where the total RNA binds to the membrane, and contaminants are efficiently washed away. High-quality RNA is then eluted in 30 μl of water. Purified RNA was digested with RNase-free DNase to guarantee that RNA was completely free of DNA contamination.

RT-PCR analysis

A constant amount of total RNA (1 μg) was reverse-transcribed at 42°C for 60 min in a total 20 μl reaction volume using an ImProm-II RT system (Promega, Promega Italia S.r.l, Milan, Italy) and then amplified using the Gene Amp PCR System 2400 (PerkinElmer, Applied Biosystem, CA, USA). PCR was performed at least in triplicate in a standard 50-μl reaction mixture consisting of 10 mM Tris–HCl, 50 mM KCl, 1.5 mM $MgCl_2$ (pH 8.3), 0.2 mM dinucleoside triphosphates (dNTPs), 50 pmol of each sense and antisense primer, and 2.5 U of Amplitaq DNA Polymerase (EUROBIOTAQ, Eurobio, Les Ulis, France). As a negative control the cDNA template was omitted in the reaction.

PCR primers for ET-1 cDNA were 5′-TTGAGATCT GAGGAAC CCG-3′ for forward primer and 5′-TACG GAACAACGTGCTCG-3′ for reverse primer (Clontech Laboratories, Inc., Palo Alto, CA, USA); amplification was performed for 30 s at 95°C, 30 s at 58°C, 30 s at 72°C for 30 cycles and in an additional extension step for 10 min.

PCR primers for ECE-1 cDNA were 5′-AGTATGA CAAGGACG GGAACC-3′ for forward primer and 5′-CTTACCAGACTTCGCACTTGT-3′ for reverse primer; amplification was performed for 30 s at 94°C, 30 s at 55°C, 30 s at 72°C for 29 cycles and in an additional extension step for 10 min.

PCR primers for ET receptors cDNA were as follows: ETA forward primer, 5′-TGGCCTTTTGATCACAAT GACTTT-3′ and reverse primer, 5′-TTTGATGTGGCA TTGAGCATACAGGTT-3′; ETB forward primer, 5′-ACTGGCCATTTGGAGCTGAGATGT-3′ and reverse primer, 5′-CTGCATGCCACTTTTCTTTCTCAA-3′. Thirty cycles of amplification were performed under the following conditions: melting at 95°C for 1 min; annealing at 57 and 58°C, respectively, for 1 min; extension at 72°C for 30 s, and in an additional step for 7 min.

Amplified PCR products were run on a 1.5% agarose gel containing 0.5 μg/ml ethidium bromide. The following bands were visualized: 354 bp for ET-1; 459 bp for ECE-1; and 302 and 428 bp for ETA and ETB, respectively.

Amplification for VEGF was performed for 1 min at 94°C, 1 min at 55°C and 1 min at 72°C for 40 cycles. Lastly, an additional extension step was performed for 2 min. PCR primers for VEGF cDNA were as follows: forward primer, 5′-TCACCGCCTTGGCTT GTCACAT-3′; and reverse primer, 5′-TGGATCCATGAACTTTCTGCTGTC-3′. Three bands were detected: 452, 584 and 656 bp, corresponding to the VEGF isoforms 121, 165 and 189, respectively [12].

PCR primers for Flt-1 cDNA were 5′-GCGCTCGA GAGCATC ACTCAG-3′ for forward primer and 5′-GCGCGGCCGCAGTAAAATCCA-3′ for reverse primer; amplification was performed for 30 s at 95°C, 30 s at 62°C, 30 s at 72°C for 35 cycles, and in an additional extension step for 7 min. The amplified PCR product of 287 bp was run on a 1.5% agarose gel containing 0.5 μg/ml ethidium bromide.

The presence of a 412-bp PCR band, amplified with specific primers for glyceraldehyde-3-phosphate dehydrogenase (GAPDH) with the same cDNAs, was used as an internal control. PCR primers for GAPDH cDNA were as follows: forward primer, 5′-CGATGCTGGCGCTGAG TAC-3′; and reverse primer, 5′-CGTTCAGCTCAGGGATG ACC-3′. As a negative control the cDNA template was omitted in the reaction.

VEGF-competitive PCR

To obtain the quantification of VEGF mRNA levels, we used a technique based on a competitive PCR approach

using a non-homologous internal standard called VEGF competitor. We constructed a 600-bp VEGF competitor as previously described [5]: a titration assay was made to evaluate the opportune competitor dilutions to be used. Competitive PCR reactions were then performed, adding dilutions of VEGF competitor to aliquots of cDNA derived from 8 μg of total RNA. The relative densitometric measure of the electrophoretic bands was then plotted, and the point of equal intensity between the bands of the competitor PCR MIMIC and target gene was taken as concentration of the cDNA samples.

Statistical analysis

All statistical analyses were carried out using Statistica software (Stat-soft). A χ^2 test was used to analyse the associations between the different variables. The a priori level of significance was set at a p value of less than 0.05.

Results

Clinicopathological parameters

All histological subtypes were present in the series analysed, and the histologic grade according to the WHO classification showed a preponderant incidence of grade I tumours (82.14%). The cases consisted of 18 males and 38 females (mean age, 65.03 years; median age, 67 years; range from 34 to 76 years). Seven cases presented recurrence during the period of observation (Table 1).

Among the clinicopathological parameters, no statistical association was found between the level of ET expression and gender, tumour histotype and age (Table 1). In contrast, the majority of high-grade (G_{II}–G_{III}) meningiomas showed high ET levels (χ^2 test; p=0.002) (Table 1). In our series, seven cases had recurrences, and four of them showed a concomitantly high level of ET and a high grade (II–III); however, the number of meningiomas with relapses was too small for finding a statistical association with ET-1 levels (χ^2 test; p=0.25) (Table 1).

ET system mRNAs in meningiomas

Among the tumour samples, 35.71% of cases resulted positive for ET-1 messenger, 60.71% for ECE-1, 80.36% for ETA and 32.14% for ETB. Examples of electrophoretic runs are shown in Fig. 1. The positivity for ET-1 correlated with the expression of the converting enzyme ECE-1 (χ^2 test; p=0.005) and with the expression of the ET receptor ETA (χ^2 test; p=0.03). No association was found between ET-1 and ETB receptor expression.

Table 1 ET-1 protein expression level according to clinical–pathological characteristics

Clinicopathological parameters	ET-1 protein expression level		
	Low	High	p
Gender			
Females	26	12	0.18
Males	9	9	
Histotype			
Transitional	15	7	0.07
Meningothelial	6	3	
Syncytial	4	1	
Fibrous	3	1	
Psammomatous	4	0	
Angiomatous	1	0	
Microcystic	0	1	
Anaplastic	0	2	
Atypical	2	6	
Age			
Low (≤67)	21	9	0.06
High (>67)	12	14	
Grade			
G_I	33	13	0.002*
G_{II}–G_{III}	2	8	
Relapses			
Yes	3	4	0.25
No	32	17	

ET-1 Endothelin 1
*Significant p value <0.05

Final quantified ET-1 messenger levels were expressed as a ratio to GAPDH expression; assuming the median value of 1.25 of ET expression relative to GAPDH, we distinguished tumours with low from tumours with high ET-1 mRNA expression.

Immunohistochemistry for ET-1

An immunohistochemical analysis of ET expression was performed to confirm the positivity obtained with molecular techniques and to provide accurate ET protein localization. The ET-1 immunostaining was mostly localized in the cytoplasm. The pattern of staining in a significant case with high ET-1 protein expression level is shown in Fig. 2. A weak immunoreactivity with the anti-ET-1 antibody was seen in all cancer samples with low ET-1 mRNA expression (χ^2 test; p=0.03), confirming the RT-PCR results. For each tumour sample analysed, the percentage of positive cells for ET-1 staining was evaluated, and the median value (7.5% of positive cells for ET-1) was assumed as the cut-off to distinguish tumours with low (35 cases, 62.5%) from tumours with high ET-1 protein expression.

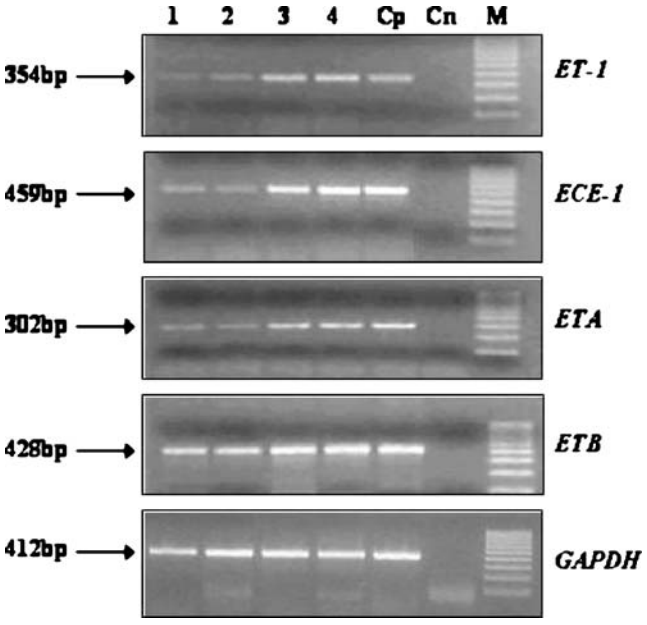

Fig. 1 Endothelin system mRNAs expression detected by RT-PCR. The presence of a 412-bp PCR band amplified with specific primers for GAPDH with the same cDNA was used as an internal control (ET-1/GAPDH ratio, 0.5 and 0.7, respectively, for low-grade meningiomas; 1.2 and 1.4, respectively, for high-grade meningiomas). *Cn*, negative control; *Cp*, positive control; *lanes 1–2*, low-grade meningiomas (I); *lanes 3–4*, high-grade meningiomas (II_III); *M*, molecular weight marker (100-bp ladder, Pharmacia)

Microvessel count and ET-1 expression

For one sample there was no availability of material for microvessel count (MVC) analysis. Figure 3 shows a representative example of analysis of vessel density. The median value of ten microvessels (mean MVC, 15.49) was assumed as the cut-off to distinguish tumours with high vascularization (21/55, 38.14%) from tumours with low MVCs (34/55, 61.82%). A significant association between microvascular density and ET expression was found; tumours with high ET-1 protein expression showed an elevated number of microvessels (χ^2 test; p=0.004) (Table 2).

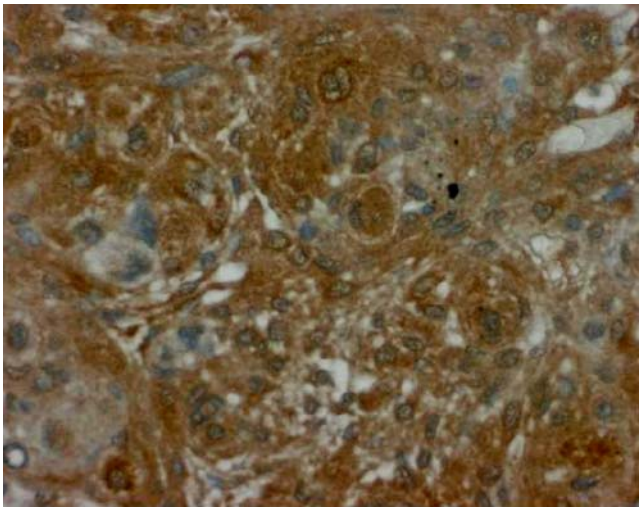

Fig. 2 Endothelin 1 (*ET-1*) expression by immunohistochemistry (×20). ET-1 immunostaining in one representative sample of high-grade meningioma with high expression level. Figure shows an intense and diffuse cytoplasmic stain in almost all the neoplastic cells

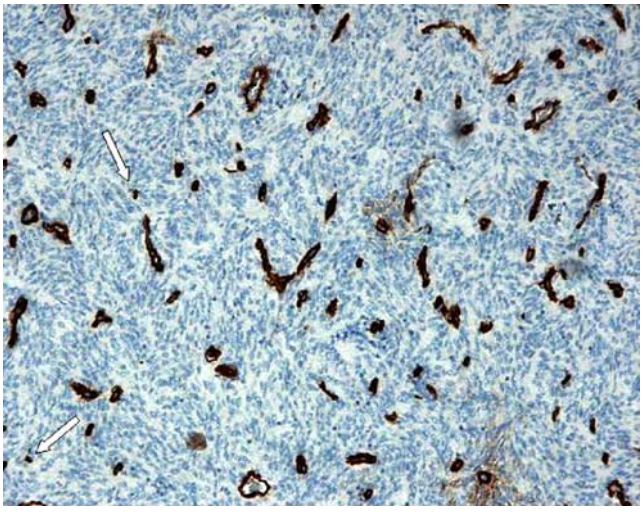

Fig. 3 Microvessel density (×10). Microvessel count detected by immunohistochemical staining in one representative sample of meningioma. *Arrows* indicate two examples of microvessels

Relation between VEGF and ET-1 mRNA expression

Fifty-two cases of meningioma were immunohistochemically analysed for VEGF expression (Fig. 4). Assuming the median value of positive cells for VEGF (median value, 20%; mean, 31.44%), we identified 29 tumours with low VEGF expression (29/52, 55.77%) and 23 tumours with a high percentage of positive cells for VEGF. A significant association was found between high ET expression and elevated VEGF levels (χ^2 test; p=0.03) (Table 3).

The expression of Flt-1, VEGF receptor, was evaluated by RT-PCR (Fig. 5); all the samples were positive, with a high expression in 66% of the cases.

Table 2 Relation between ET-1 protein expression level and microvessel count

Clinicopathological parameters	ET-1 protein expression level		
	Low	High	*p*
MVC			
Low (≤10)	26	8	0.004*
High (>10)	8	13	

MVC Microvessel count
*Significant *p* value <0.05

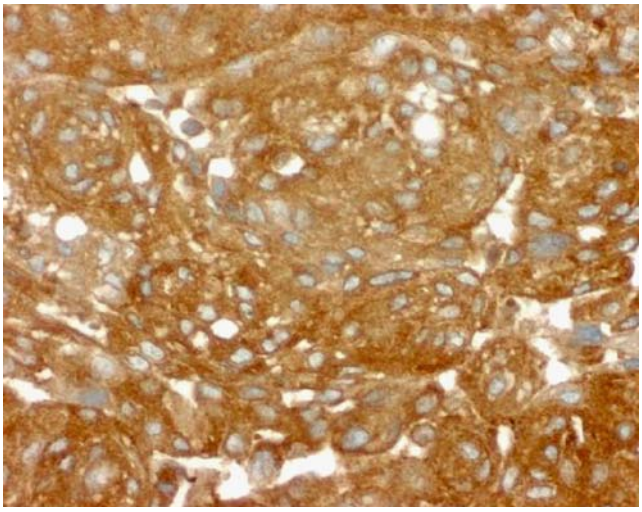

Fig. 4 Vascular endothelial growth factor (*VEGF*) expression by immunohistochemistry (×20). VEGF immunostaining in one representative sample of high-grade meningioma with high expression level. Figure shows an intense and diffuse cytoplasmic stain in almost all the neoplastic cells

In a limited number of 36 cases, due to a lack of availability of material for all the cases, we also evaluated *VEGF* expression by a competitive PCR approach; the exact number of VEGF cDNA molecules was calculated, and, according to the median value (500 VEGF cDNA molecules), we distinguished tumours with high (15/36) from tumours with low VEGF mRNA expression. The results of VEGF mRNA expression, obtained by competitive RT-PCR, agreed with data concerning the VEGF protein expression (χ^2 test; p=0.04) and the Flt-1 receptor expression (χ^2 test; p=0.0019), confirming the relation between VEGF and ET-1 messenger levels (data not shown).

Discussion

Several studies have demonstrated an abnormal expression of different growth factors and/or their receptors in meningiomas [2, 17, 22, 34, 35]. Endothelins are an example of such mediators; ET-1 is the best characterized to date and exerts its effects by binding to two distinct cell-surface ET receptors, ETA and ETB. Both receptors belong to the G-protein-coupled receptor (GPCR) family; ETA is the predominant receptor in cancer biology, with less evidence for ETB [26].

Table 3 Relation between ET-1 protein expression level and vascular endothelial growth factor expression level

Clinicopathological parameters	ET-1 protein expression level		
	Low	High	*p*
VEGF			
Low (≤20%)	22	7	0.03*
High (>20%)	11	12	

VEGF Vascular endothelial growth factor
*Significant *p* value <0.05

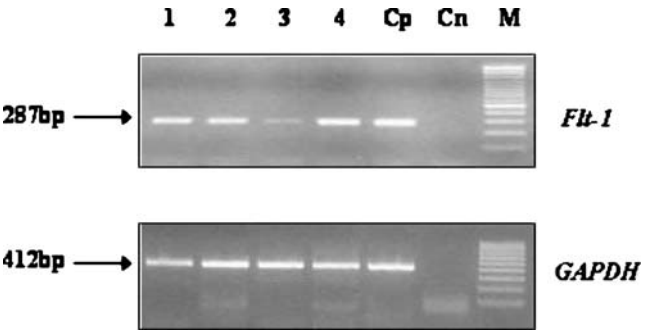

Fig. 5 Flt-1 receptor expression detected by RT-PCR. The presence of a 412-bp PCR band amplified with specific primers for GAPDH with the same cDNA was used as an internal control. *Cn*, negative control; *Cp*, positive control; *lanes 1–4*, representative positive samples of meningiomas; *M*, molecular weight marker (100-bp ladder, Pharmacia)

Pagotto et al. analysed the cases of 35 patients and provided evidence that ET-1, acting via ETA receptor, plays a role in the mechanism of meningioma tumourigenesis, hypothesizing its participation in the angiogenic process [27]. In our study concerning 56 cases of meningioma, we confirmed the expression of ET-1 and the converting enzyme ECE-1 involved in the generation of the active form of ET-1 in this kind of brain tumour. Expression of both ETA and ETB receptors was also confirmed in our series; in general, the presence of mRNA for a given receptor may be taken as evidence of synthesis of that receptor, although no conclusion may be drawn as to functional status of the receptor. The receptor may be fully functional and inserted into the cell membrane, but it can also be differentially modulated by post-translational modifications [13, 15]. Moreover, we evaluated the potential angiogenic role of *ET-1*, demonstrating the association between intense vascularization and high ET expression levels. Endothelin 1 expression/upregulation may contribute to meningioma growth by inducing the formation of new blood vessels.

ET-1 may modulate various stages of neovascularization, including endothelial cell proliferation, migration, invasion, protease production and tube formation. The precise sequence of intracellular signaling events involved in ET-1-induced migration of brain microvessel endothelial cells is not known. Studies using various cell types have demonstrated that ET-1 can activate such enzymes as protein kinase C (PKC), cyclic adenosine monophosphate (cAMP)-dependent protein kinase (PKA), phosphatidylino-

sitol 3-kinase (PI3-K), Ras, and non-receptor protein tyrosine kinases, probably of the Src family, leading to the activation of each of the three main mitogen-activated protein kinase (MAPK) modules (ERK, p38, JNK) [23]. This finding is consistent with the complex character of migration and angiogenesis in general, which has been demonstrated to involve multiple parts of the cell machinery. Because the regulation of VEGF production is a critical event in tumour angiogenesis, including meningioma tumourigenesis as we previously demonstrated [6], we can postulate that in pathological conditions such as cancer, ET-1 and VEGF with its receptor Flt-1 may have a complementary and coordinated role during neovascularization. Our data demonstrated that increased expression of ET-1 was significantly associated with increased VEGF expression in meningiomas, and these results were consistent with recent findings in ovarian [30] and lung cancer [7].

The overall recurrence rate of meningiomas has been reported to be approximately 20%, with higher rates (30–40%) reported in patients who undergo less than complete resection (partial resection or biopsy) [16, 24]. In addition, recurrence rates are higher for the more aggressive histologic variants, with 5-year recurrence rates of 38% for atypical meningiomas and 78% for anaplastic meningiomas [16]. The high recurrence rate in partially resected meningiomas has led to the use of additional therapy designed to improve tumour control. Radiotherapy is frequently administered after partial resection and has been shown to decrease or delay recurrence. Moreover, the symptomatic meningiomas in surgically hazardous locations (i.e. cavernous sinus) can be positively impacted by additional therapies, as can also residual and recurrent diseases after surgery and radiotherapy [8]. With regard to all these cases, there is a need to develop new biologic, genetic and chemotherapeutic strategies; the control of recurrent tumours [4] continues to be a clinical challenge [14, 33], and, in this context, ET seems to be an interesting target.

Early prophylactic intervention with an ET inhibitor may decrease tumourigenic progression in patients with anaplastic neoplasms. The consistent overexpression of ET-1 we found in high-grade meningiomas suggests that ET may play an important functional role from the earliest hyperproliferative stages to the later stages of invasive disease.

The rationale for the combination of inhibitors of ET with ionizing radiation is that of a potentially attractive use for recurrent or anaplastic meningioma. The association of ET-1 and meningioma represents a potential area for therapeutic intervention with selective ET inhibitors either as an adjunct therapy or in combination with radiation therapy. Additional clinical studies will be needed before inhibitors of ET can be incorporated into clinical practice.

References

1. Ahmed SI, Thompson J, Coulson JM, Woll PJ (2000) Studies on the expression of endothelin, its receptor subtypes, and converting enzymes in lung cancer and in human bronchial epithelium. Am J Respir Cell Mol Biol 22:422–431
2. Antoniades HN, Galanopoulos T, Neville-Golden J, Maxwell M (1992) Expression of insulin-like growth factors I and II and their receptor mRNAs in primary human astrocytomas and meningiomas; in vivo studies using in situ hybridization and immunocytochemistry. Int J Cancer 50:215–222
3. Asham E, Shankar A, Loizidou M, Fredericks S, Miller K, Boulos PB, Burnstock G, Taylor I (2001) Increased endothelin-1 in colorectal cancer and reduction of tumour growth by ET (A) receptor antagonism. Br J Cancer 85:1759–1763
4. Barbaro NM, Gutin PH, Wilson CB, Sheline GE, Boldrey EB, Wara WM (1987) Radiation therapy in the treatment of partially resected meningiomas. Neurosurgery 20:525–528
5. Boldrini L, Calcinai A, Silvestri V, Basolo F, Lucchi M, Mussi A, Angeletti CA, Bevilacqua G, Fontanini G (1999) Quantitation by competitive PCR assay of vascular endothelial growth factor in non-small cell lung carcinomas. Int J Oncol 14:161–168
6. Boldrini L, Gisfredi S, Ursino S, Faviana P, Lucchi M, Melfi F, Mussi A, Basolo F, Fontanini G (2004) Angiogenesis in intracranial meningiomas: immunohistochemical and molecular study. Neuropathol Appl Neurobiol 30:118–125
7. Boldrini L, Gisfredi S, Ursino S, Faviana P, Lucchi M, Melfi F, Mussi A, Basolo F, Fontanini G (2005) Expression of endothelin-1 is related to poor prognosis in non-small cell lung carcinoma. Eur J Cancer 41:2828–2835
8. Chamberlain MC, Blumenthal DT (2004) Intracranial meningiomas: diagnosis and treatment. Expert Rev Neurother 4:641–648
9. DeMonte F (2001) Current management of meningiomas. Oncology 9:83–96
10. Economos K, MacDonald PC, Casey ML (1992) Endothelin-1 gene expression and biosynthesis in human endometrial HEC-1A cancer cells. Cancer Res 52:554–557
11. Fagan KA, Mc Murtry IF, Rodman DM (2001) Role of endothelin-1 in lung disease. Respir Res 2:90–101
12. Fontanini G, Boldrini L, Chine S, Pisaturo F, Basolo F, Calcinai A, Lucchi M, Mussi A, Angeletti CA, Bevilacqua G (1999) Expression of vascular endothelial growth factor mRNA in non-small-cell lung carcinomas. Br J Cancer 79:363–369
13. Freedman NJ, Ament AS, Oppermann M, Stoffel RH, Exum ST, Lefkowitz RJ (1997) Phosphorylation and desensitization of human endothelin A and B receptors. Evidence for G protein-coupled receptor kinase specificity. J Biol Chem 272:17734–17743
14. Goldsmith BJ, Wara WM, Wilson CB, Larson DA (1994) Postoperative irradiation for subtotally resected meningiomas. A retrospective analysis of 140 patients treated from 1967 to 1990. J Neurosurg 80:195–201
15. Horstmeyer A, Cramer H, Sauer T, Muller-Esterl W, Schroeder C (1996) Palmitoylation of endothelin receptor A. Differential modulation of signal transduction activity by post-translational modification. J Biol Chem 271:20811–20819
16. Jaaskelainen J, Haltia M, Servo A (1986) Atypical and anaplastic meningiomas: radiology, surgery, radiotherapy, and outcome. Surg Neurol 25:233–242
17. Johnson MD, Federspiel CF, Gold LI, Moses HL (1992) Transforming growth factor a and transforming growth factor receptor/3 expression in human meningioma cells. Am J Pathol 141:633–642
18. Kleihues P, Louis DN, Scheithauer BW, Rorke LB, Reifenberger G, Burger PC, Cavanee WK (2002) The WHO classification of

tumors of the nervous system. J Neuropathol Exp Neurol 61:215–225
19. Knowles J, Loizidou M, Taylor I (2005) Endothelin-1 and angiogenesis in cancer. Curr Vasc Pharmacol 3:309–314
20. Levin ER (1995) Endothelins. N Engl J Med 333:356–363
21. Louis DN, Scheithauer BW, Budka H, von Deimling A, Kepes JJ (2000) Meningiomas. In: Kleihues P, Cavanee WK (eds) Pathology and genetics of tumors of the nervous system. IARC, Lyon, pp 176–184
22. Maxwell M, Naber SP, Wolfe HJ, Galanopoulos T, Hedley-Whyte TE, Black PM, Antoniades HN (1990) Coexpression of platelet-derived growth factor (PDGF) and PDGF-receptor genes by primary human astrocytomas may contribute to their development and maintenance. J Clin Invest 85:131–140
23. Milan J, Charalambous C, Elhag R, Chen TC, Li W, Guan S, Hofman FM, Zidovetzki R (2006) Multiple signaling pathways are involved in endothelin-1-induced brain endothelial cell migration. Am J Physiol Cell Physiol 291:C155–C164
24. Mirimanoff RO, Dosoretz DE, Linggood RM, Ojemann RG, Martuza RL (1985) Meningioma: analysis of recurrence and progression following neurosurgical resection. J Neurosurg 62:18–24
25. Nelson JB, Chan-Tack K, Hedican SP, Magnuson SR, Opgenorth TJ, Bova GS, Simons JW (1996) Endothelin-1 production and decreased endothelin B receptor expression in advanced prostate cancer. Cancer Res 56:663–668
26. Nelson J, Bagnato A, Battistini B, Nisen P (2003) The endothelin axis: emerging role in cancer. Nat Rev Cancer 3:110–116
27. Pagotto U, Arzberger T, Hopfner U, Sauer J, Renner U, Newton CJ, Lange M, Uhl E, Weindl A, Stalla GK (1995) Expression and localization of endothelin-1 and endothelin receptors in human meningiomas. J Clin Invest 96:2017–2025
28. Rachlin JR, Rosenblum ML (1991) Etiology and biology of meningiomas. Raven, New York
29. Rubanyi GM, Polokoff MA (1994) Endothelins: molecular biology, biochemistry, pharmacology, physiology, and pathophysiology. Pharmacol Rev 46:325–415
30. Salani D, Di Castro V, Nicotra MR, Rosano L, Tecce R, Venuti A, Natali PG, Bagnato A (2000) Role of endothelin-1 in neovascularization of ovarian carcinoma. Am J Pathol 157:1537–1547
31. Shankar A, Loizidou M, Aliev G, Fredericks S, Holt D, Boulos PB, Burnstock G, Taylor I (1998) Raised endothelin 1 levels in patients with colorectal liver metastases. Br J Surg 85:502–506
32. Stiles JD, Ostrow PT, Balos LL, Greenberg SJ, Plunkett R, Grand W, Heffner RR (1997) Correlation of endothelin-1 and transforming growth factor beta 1 with malignancy and vascularity in human gliomas. J Neuropathol Exp Neurol 56:435–439
33. Taylor BW Jr, Marcus RB Jr, Friedman WA, Ballinger WE Jr, Million RR (1988) The meningioma controversy: postoperative radiation therapy. Int J Radiat Oncol Biol Phys 15:299–304
34. Todo T, Adams EF, Rafferty B, Fahlbusch R, Dingermann T, Werner H (1994) Secretion of interleukin-6 by human meningioma cells: possible autocrine inhibitory regulatory of neoplastic cell growth. J Neurosurg 81:394–401
35. Weisman AS, Raguet SS, Kelly PA (1987) Characterization of the epidermal growth factor receptor in human meningioma. Cancer Res 47:2172–2176
36. Wulfing P, Diallo R, Kersting C, Wulfing C, Poremba C, Rody A, Greb RR, Bocker W, Kiesel L (2003) Expression of endothelin-1, endothelin-A, and endothelin-B receptor in human breast cancer and correlation with long-term follow-up. Clin Cancer Res 9:4125–4131
37. Wulfing P, Kersting C, Tio J, Fisher RJ, Wulfing C, Poremba C, Diallo R, Bocker W, Kiesel L (2004) Endothelin-1, endothelin-A-, and endothelin-B-receptor expression is correlated with vascular endothelial growth factor and angiogenesis in breast cancer. Clin Cancer Res 10:2393–2400

Virchows Arch (2006) 449:554–560
DOI 10.1007/s00428-006-0284-4

ORIGINAL ARTICLE

Spindle cell rhabdomyosarcoma in adults: clinicopathological and immunohistochemical analysis of seven new cases

Thomas Mentzel · Cornelius Kuhnen

Received: 25 May 2006 / Accepted: 25 July 2006 / Published online: 30 September 2006
© Springer-Verlag 2006

Abstract Rhabdomyosarcoma (RMS) is currently classified into embryonal RMS, including its botryoid and spindle cell variants, alveolar RMS, including a solid variant, and pleomorphic RMS. In children and adolescents embryonal RMS occurs in a younger age group than alveolar RMS, and pleomorphic RMS is almost always seen in older adults. Most recently rare spindle cell and sclerosing, pseudovascular RMS have been reported in adults as well. We analysed the clinicopathological and immunohistochemical features of seven new cases of spindle cell RMS arising in adult patients. Five patients were male and two were female and the age of the patients ranged from 38 to 76 years. Four neoplasms arose on the lower extremities and one case each on the forearm, the lateral aspect of the neck and the penis. Five neoplasms were completely excised, in one incompletely excised neoplasm additional chemotherapy was given, and in one patient a biopsy was done only so far. All neoplasms arose in subcutaneous and deep soft tissues with dermal involvement in one case, and the size of the neoplasms ranged from 4 to 19 cm in largest diameter. Histologically, a plump or diffuse infiltration was seen, and all neoplasms were mainly composed of cellular bands and fascicles of atypical spindle-shaped tumour cells containing enlarged and atypical nuclei associated with a variable number of rhabdomyoblasts. In addition, focal areas reminiscent of sclerosing, pseudovascular RMS were noted in three cases, and in two cases each small solid areas with pleomorphic tumour cells as well as scattered round tumour cells were present. Proliferative activity ranged from 1 to 60 mitoses in 10 high-power fields and tumour necrosis was evident in four cases. Immunohistochemically, all neoplasms tested stained variably positive for desmin, myf-4, WT1 and CD 99, whereas fast myosin was positive in only two out of seven cases. In addition, five out of seven cases tested stained focally positive for alpha-smooth muscle actin. The remaining antibodies (h-caldesmon, S-100 protein, CD 34, pancytokeratin and epithelial membrane antigen) were all negative. Follow-up information was available in five patients (range from 10 to 48 months) and revealed lung metastases in two patients who died of disease within a short period. In summary, spindle cell rhabdomyosarcoma represents a rare neoplasm in adulthood characterized clinically by a rather poor prognosis, and shows a broad morphological spectrum including most likely the sclerosing, pseudovascular variant. Immunohistochemically, tumour cells in RMS stain positively for CD 99 and WT1 as well, which is of importance in the differential diagnosis to other mesenchymal neoplasms, whereas fast myosin does not represent a reliable marker for RMS in adults.

Keywords Rhabdomyosarcoma · Myogenic sarcomas · Soft tissue neoplasms · Immunohistochemistry

T. Mentzel (✉)
Dermatopathologische Gemeinschaftspraxis,
Siemenstrasse 6/1,
88048 Friedrichshafen, Germany
e-mail: tmentzel@w-4.de

C. Kuhnen
Department of Pathology, Ruhr-University of Bochum,
Bochum, Germany

Introduction

Rhabdomyosarcoma (RMS) in adults represents a very rare malignant mesenchymal neoplasm. Whereas embryonal RMS (including the anaplastic, botryoid and

spindle cell subtypes) and alveolar RMS predominate in children and adolescents, pleomorphic RMS occurs almost exclusively in adult patients. On the other hand embryonal RMS is seen in adults as well, and occurs most frequently in visceral and genitourinary locations. Alveolar RMS in adults is distributed evenly between the head and neck region and the extremities [7, 10]. It has been shown convincingly that the histological subtype of RMS does not reliably predict patient survival in adults [7, 10, 15], in striking contrast to children and adolescents in which three prognostically significant subtypes are distinguished [16]. As in other types of sarcomas in adults, patient age, tumour size, extent of disease, and margin status after resection represent the most important predictors of outcome in adult patients with RMS [10]. Pleomorphic RMS in adults occurs predominantly in middle-aged male patients in the lower extremities and follows an aggressive clinical course with an overall poor prognosis; metastases have been reported in between 50 and 60% of patients and up to 70% of affected patients died of disease [6]. Histologically, pleomorphic RMS is composed of large atypical, pleomorphic and often multinucleated tumour cells with abundant eosinophilic cytoplasm and pleomorphic nuclei admixed with a variable number of pleomorphic rhabdomyoblasts staining variably positive for myogenic immunohistochemical markers [9]. Most recently the spindle cell and sclerosing, pseudovascular variants of RMS in adults have been described [8, 14, 15]. In this study we present seven new cases of spindle cell RMS arising in adults and discuss the morphological spectrum of this variant and its immunohistochemical markers.

Materials and methods

The cases were retrieved from routine and consultation files of the authors; Case 4 has been submitted for publication in detail elsewhere [11]. The specimens were obtained by surgical excision, fixed in 10% buffered formalin, and processed routinely for paraffin embedding. Four micrometer-thick sections were stained with haematoxylin and eosin. In addition, sections were stained immunohistochemically by the labelled Streptavidin Biotin (LSAB) technique using commercially available antibodies; appropriate positive and negative controls were used in each case. The used antibodies, their sources, and dilutions are summarized in Table 1. Clinical and follow-up information were obtained from the referring clinicians and pathologists (see Acknowledgements).

Results

Clinical findings

The clinical data of the seven patients are summarised in Table 2. The neoplasms were seen in five male and two female patients aged between 38 and 76 years. Four neoplasms arose on the lower extremities and one case each on the left forearm, the lateral neck and the penis, respectively. Five neoplasms have been completely excised, in Case 7 an incomplete excision was performed and additional chemotherapy was given, and in Case 6 a biopsy was done so far only. In five cases additional follow-up information were available (ranging from 10 to 48 months) and revealed lung metastases in Cases 1 and 4; both patients died of disease within less than 2 years.

Table 1 Antibodies used for immunohistochemical analysis

Antigen	Clone	Dilution	Source
ASMA	1A4	1:300	DAKO
Desmin	D33	1:200	DAKO
Caldesmon	h-CD	1:200	DAKO
Myf-4	LO26	1:40	Novocastra
Fast myosin	MY-32	1:400	SIGMA
WT1	6F-H2	1:400	Novocastra
CD 99	12E7	1:200	DAKO
S-100 protein	polyclonal	1:2000	DAKO
Pancytokeratin	MNF116	1:100	DAKO
EMA	Mc5	1:400	Biogenex
CD 34	HPCA-1	1:100	Becton & Dickinson

ASMA — alpha-smooth muscle actin
EMA — epithelial membrane antigen

Table 2 Clinical details of seven cases of spindle cell RMS arising in adults

Case	Age/ sex	Site	Size (cm)	Follow-up
1	38/M	Forearm	13×7×6	Lung MTS/DOD at 2 years
2	57/M	Hip region	18×12×19	NSR at 46 months
3	63/F	Lower leg	15×9×4	NA
4	62/M	Lower leg	11×9×10	Lung MTS/DOD at 12 months
5	76/F	Thigh	4×2.5×4	NSR at 15 months
6	41/M	Penis	Biopsy	NA
7	51/M	Neck	8×6×4	NSR at 48 months

M — male; F — female; MTS — metastases; DOD — died of disease; NSR — no sign of recurrence; NA — not available

Pathological findings

Grossly, the size of the neoplasms ranged from 4 to 19 cm. The neoplasms arose in subcutaneous and deep soft tissues (Fig. 1) with dermal involvement in Case 2. Histologically, all neoplasms were composed mainly of atypical spindle-shaped tumour cells with pale eosinophilic cytoplasm and enlarged fusiform nuclei that were arranged at least focally in cellular bands and fascicles mimicking occasionally the herringbone growth pattern seen in rare fibrosarcoma of adults (Fig. 2). A diffuse infiltration of pre-existing tissue was noted in Case 5 (Fig. 3), whereas a rather plump invasion into surrounding structures was present in the remaining cases. The atypical spindled tumour cells in all cases were admixed with a variable number of enlarged plump spindle- or polygonal-shaped rhabdomyoblasts containing abundant eosinophilic cytoplasm and hyperchromatic, eccentrically placed enlarged nuclei (Figs. 2 and 5). Mitoses, including atypical forms ranged from 2 (Case 7) to 60 (Case 2) per 10 high-power fields, and tumour necrosis was present in four cases. The neoplasms contained a variable number of blood vessels, and in Case 7 a prominent haemangiopericytoma-like

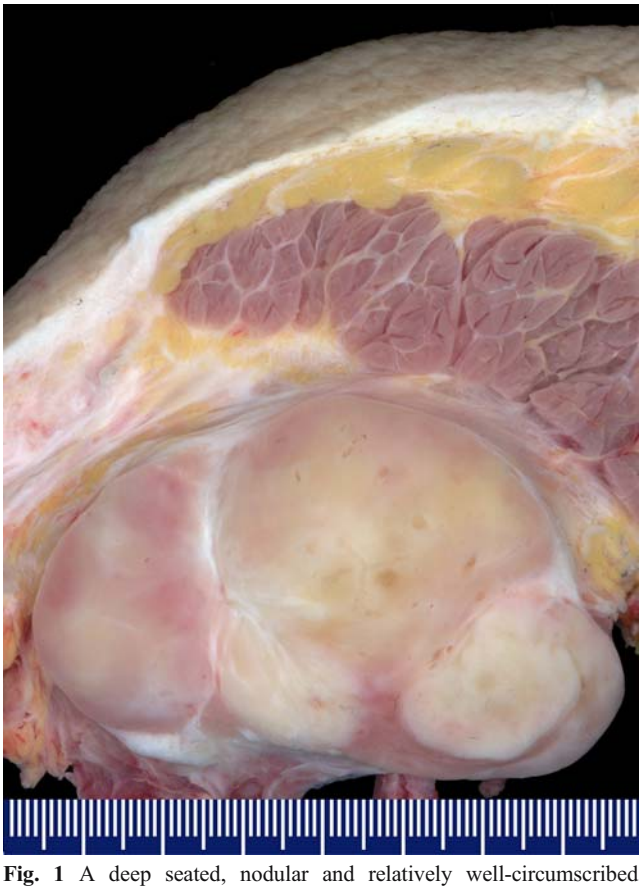

Fig. 1 A deep seated, nodular and relatively well-circumscribed neoplasm is seen in Case 7

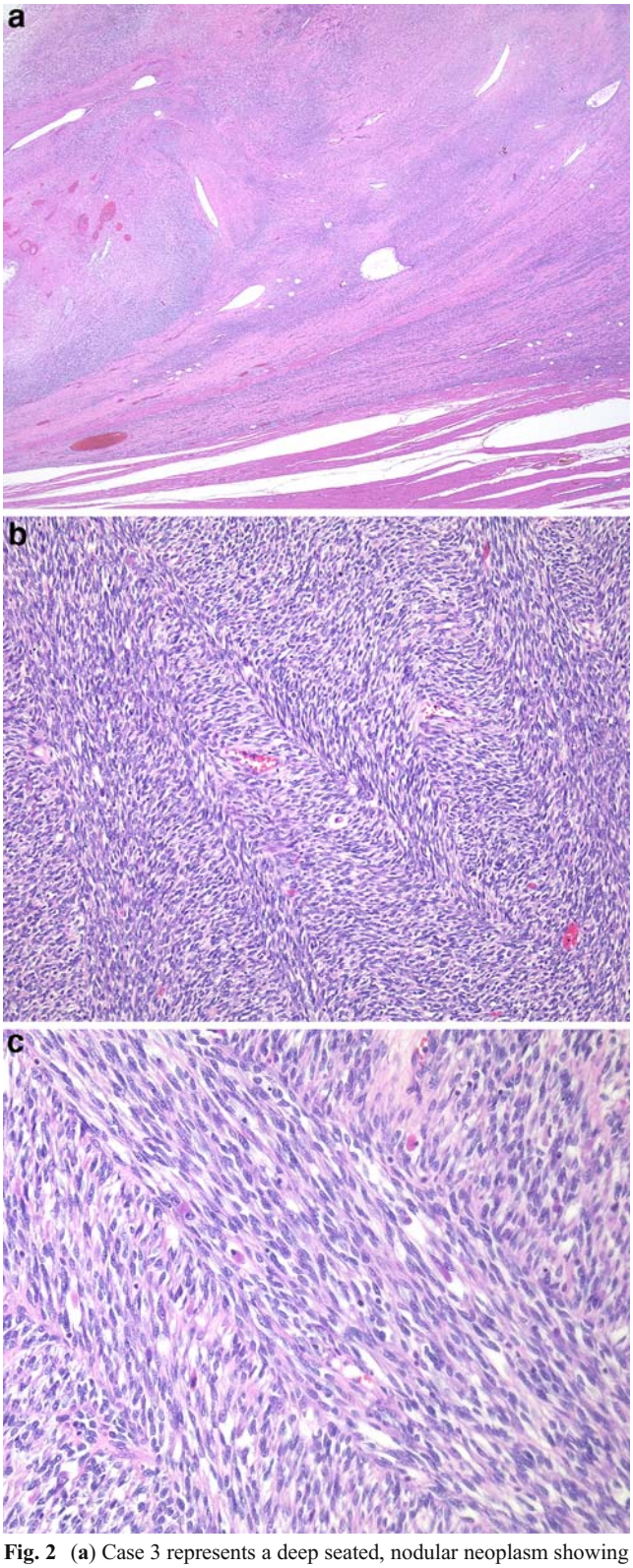

Fig. 2 (**a**) Case 3 represents a deep seated, nodular neoplasm showing a variable cellularity. (**b**) Histologically, all neoplasms were composed of atypical spindled cells often arranged in a herringbone growth pattern. (**c**) Scattered rhabdomyoblasts containing abundant eosinophilic cytoplasm and eccentrically placed nuclei were seen in all cases

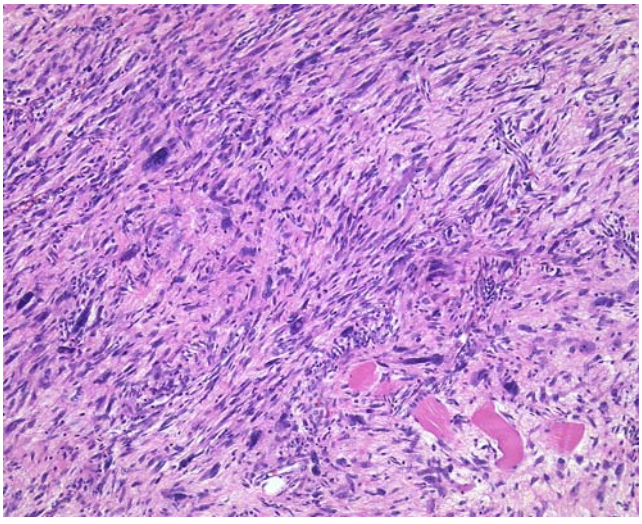

Fig. 3 A diffuse infiltration of pre-existing structures was noted in Case 5. Note the presence of scattered enlarged, atypical tumour cells

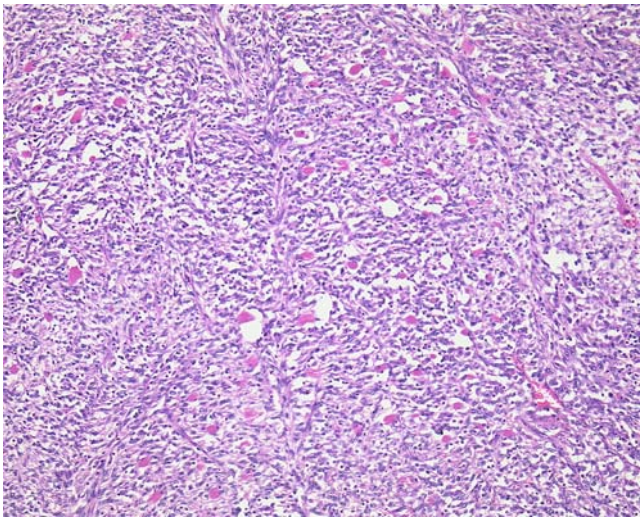

Fig. 5 Scattered round tumour cells were noted in Case 4. Note the presence of numerous rhabdomyoblasts

vasculature has been observed. Obvious lymphovascular invasion was not identified in any of the cases.

It is interesting to note that in Cases 1, 3, and 4 tumour areas with lower cellularity and abundant collagenous stroma showing prominent hyaline sclerosis and pseudovascular spaces have been observed (Fig. 4). In addition, in Cases 2 and 5 small solid tumour areas with enlarged pleomorphic tumour cells were present, and in Cases 4 and 6 scattered round tumour cells were seen (Fig. 5).

Immunohistochemically, tumour cells in all cases stained variably positive for desmin and myf-4 (Fig. 6), and in addition a strong cytoplasmic staining for WT1 and CD 99 was noted (Fig. 7). In all cases only few tumour cells, obvious rhabdomyoblasts and spindled tumour cells, showed a nuclear expression of myf-4. In contrast a focal

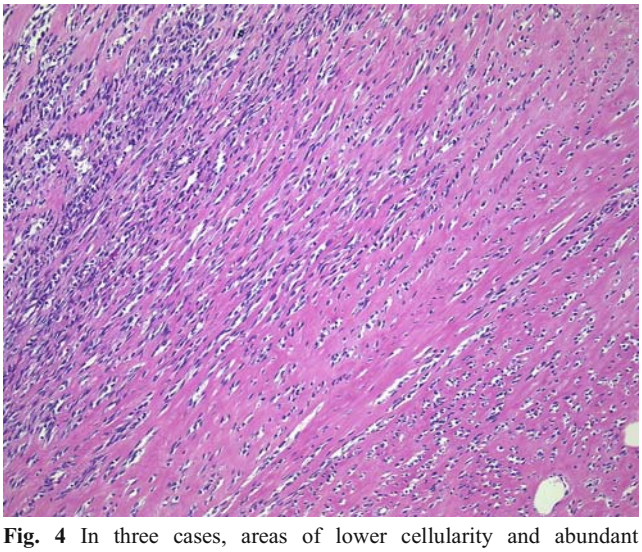

Fig. 4 In three cases, areas of lower cellularity and abundant collagenous stroma mimicking morphological features of sclerosing rhabdomyosarcoma were noted

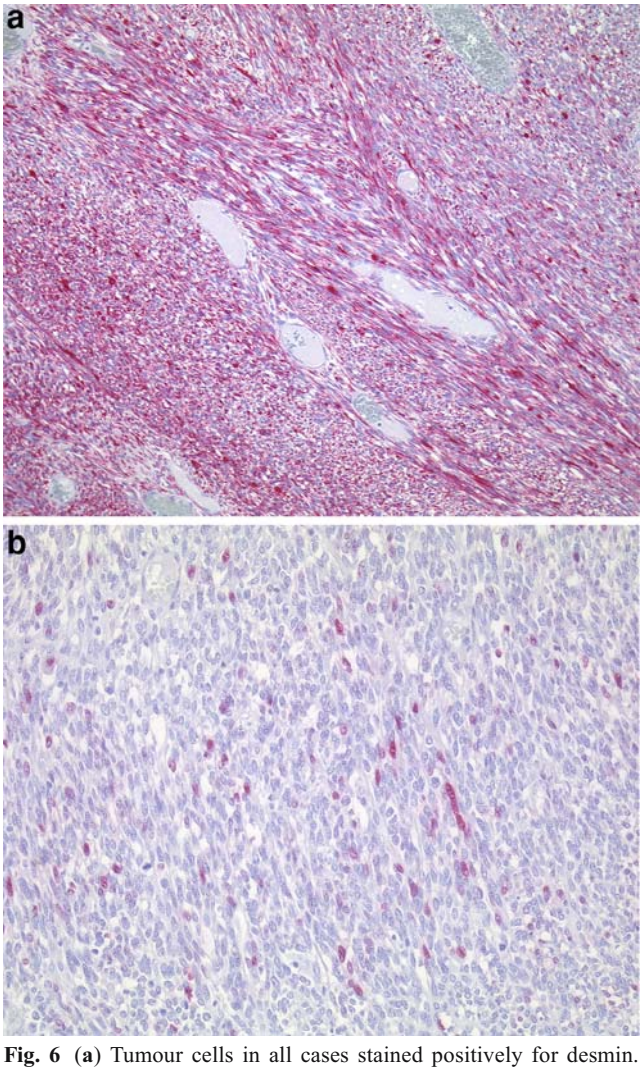

Fig. 6 (**a**) Tumour cells in all cases stained positively for desmin. (**b**) Scattered tumour cells showed a nuclear expression of myf-4 in all cases

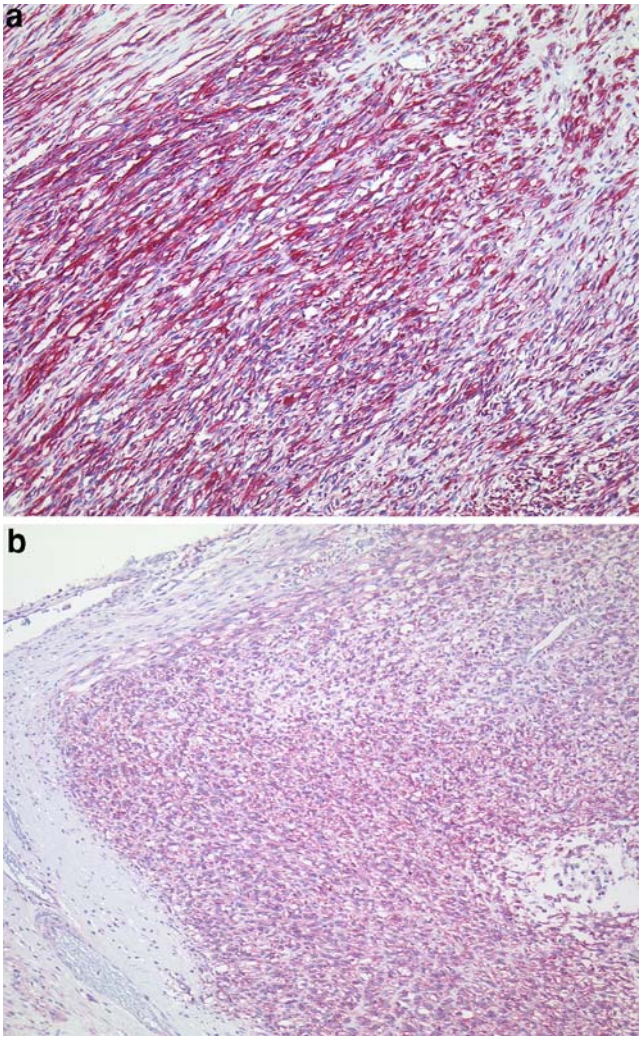

Fig. 7 (**a**) Neoplastic cells in all cases stained strongly positive for WT1. (**b**) A cytoplasmic expression of CD 99 was noted in all cases

staining for alpha-smooth muscle actin was present in five cases and for fast myosin in two cases only (Table 3). The remaining antibodies (h-caldesmon, S-100 protein, pancytokeratin, epithelial membrane antigen and CD 34) were negative in all cases tested.

Discussion

The current classification of RMS has been shown to distinguish subtypes with significant morphological, molecular, clinical, and prognostic differences, which emphasizes the need for exact diagnosis in order to achieve proper treatment of the affected patients. This is especially of importance in cases of RMS arising in children and adolescents, where three prognostically relevant subgroups are defined and treated by different protocols. Embryonal RMS arising in children and adolescents is characterized clinically by a relatively good prognosis, especially the botryoid and spindle cell subtypes which have an excellent prognosis in this age group [2, 12, 16]. In contrast, cases of alveolar RMS, including its solid variant, show a worse clinical outcome, and the rare anaplastic RMS, that represents in most cases embryonal RMS with sheets of bizarre cells with giant nuclei set in a collagenous stroma, and numerous, also atypical mitoses, has a poor survival.

Table 3 Results of (positive) immunohistochemical stainings

Case	Desmin	ASMA	Myf-4	Fast myosin	WT1	CD 99
1	Focal +	–	Focal +	Focal +	+	+
2	+	Focal +	Focal +	–	+	+
3	Focal +	sc +	Focal +	–	+	+
4	Focal +	Focal +	Focal +	–	+	+
5	Focal +	Focal +	Focal +	–	Focal +	+
6	+	–	Focal +	Focal +	+	+
7	+	Focal +	Focal +	–	+	+

ASMA — alpha-smooth muscle actin; sc — single cells

Rare cases of RMS arising in adult patients are characterized clinically by poor outcome irrespective of the morphological subtype [7, 10]. This is also true for the most recently delineated spindle cell variant of RMS in adults in which up to 40% of patients had uncontrolled local disease, 25% developed metastases, and 17% died of disease [15]. This finding is confirmed in the present study in which two out of five patients with clinical follow-up information developed multiple metastases and died of disease within a short time period. Spindle cell RMS in adults that arises in contrast to spindle cell RMS in children and adolescents most frequently on the extremities and in the head and neck region, is composed predominantly of atypical spindle-shaped tumour cells arranged in cellular fascicles and bands reminiscent to what is seen in rare fibrosarcoma in adults, leiomyosarcoma or malignant peripheral nerve sheath tumour. The spindled tumour cells contain an ill-defined pale eosinophilic cytoplasm and enlarged fusiform nuclei, and are admixed with a variable number of enlarged plump spindle- or polygonal-shaped rhabdomyoblasts containing abundant eosinophilic cytoplasm and hyperchromatic, eccentrically placed enlarged nuclei. These rhabdomyoblasts represent a significant diagnostic clue on H&E stainings.

Occasionally, and this was seen also in two cases of the presented series, scattered tumour cells showing a rather rounded and/or epithelioid morphology may be present in spindle cell RMS [15]. In addition, few pleomorphic tumour cells were seen in Cases 2 and 5 raising the differential diagnosis to pleomorphic RMS. However, given that the majority of tumour tissue in these two cases was composed of cellular spindle cell fascicles and rhabdomyoblasts containing a single nucleus (lacking bizarre pleomorphic rhabdomyoblasts seen in pleomorphic RMS), the

diagnosis of spindle cell RMS containing scattered pleomorphic cells was preferred. It is interesting to note that areas of lower cellularity and abundant collagenous stroma showing prominent hyaline sclerosis and pseudovascular spaces reminiscent of the features of sclerosing pseudovascular RMS, a further rare subtype of RMS arising in children and adults [3, 8, 14], also mentioned briefly in previous reports as well [15], were present in three of the reported cases. Given that cases of otherwise typical spindle cell RMS may contain areas with prominent hyaline sclerosis, and that otherwise cases of sclerosing, pseudovascular RMS may show focally an increased cellularity with long spindle cells fascicles (Fig. 2 in [14]), sclerosing RMS belongs most likely into the spectrum of spindle cell RMS. Cytogenetically, gain of chromosome 11 and loss of chromosome 22 has been reported in one case of sclerosing RMS, and a link with the embryonal subtype of RMS was suggested [4]. However, in a second report loss of material from the region 10q22 and of the chromosome Y as well as a trisomy of chromosome 18 has been found suggesting that sclerosing (spindle cell) RMS is different from embryonal RMS cytogenetically [11]. Given different clinical, morphological, and cytogenetic findings, spindle cell RMS in adults does not represent a variant of embryonal RMS. Further cases have to be studied in order to prove whether spindle cell RMS is characterized by reproducible cytogenetic changes.

Immunohistochemistry plays an important role in the diagnosis and differential diagnosis of spindle cell RMS. As in previous reports, also the present study emphasizes that desmin and myf-4 represent the most reliable markers. In contrast to cases of alveolar RMS, characterized by a strong and uniform expression of this marker [5], a nuclear expression of myf-4 was found in scattered cells in all cases only, confirming previous results [8, 15]. As said before, spindled tumour cells stained positively for this marker in addition to obvious rhabdomyoblasts [15]. In contrast, it seems that fast myosin does not represent a very sensitive marker for spindle cell RMS. It is interesting to note that all cases stained strongly positive for WT1 and CD 99 emphasizing that WT1 represents a further sensitive, but not specific marker for RMS [1], and that the cytoplasmic expression of CD 99 has to be considered in the differential diagnosis of CD 99 positive neoplasms.

A number of mesenchymal neoplasms has to be distinguished from spindle cell RMS. Rare fibrosarcoma in adults and sclerosing epithelioid fibrosarcoma do not contain rhabdomyoblasts and neoplastic cells are negative for desmin and myf-4. Malignant Triton tumour (malignant peripheral nerve sheath tumour with rhabdomyoblastic differentiation) arises often from a large peripheral nerve and in patients with known neurofibromatosis, but morphological distinction may be problematic especially in cases of malignant peripheral nerve sheath tumour with prominent heterologous rhabdomyoblastic differentiation. However, the presence of perivascular tumour cell accentuation, cytomorphology and focal myxoid changes in areas of malignant peripheral nerve sheath tumour are helpful morphological clues in the distinction of both entities. Tumour cells in leiomyosarcoma are negative for myf-4 but stain positively for h-caldesmon in many cases, and obvious rhabdomyoblasts are not evident. Given the diffuse infiltration of pre-existing structures by atypical myogenic cells in Case 5, also (low-grade) myofibroblastic sarcoma [13] may enter the differential diagnosis of spindle cell RMS. However, tumour cells in (low-grade) myofibroblastic sarcoma do not express myf-4, and rhabdomyoblasts are not seen. Immunohistochemical markers are also of help in distinguishing spindle cell carcinoma and spindle cell as well as desmoplastic malignant melanoma, especially in the head and neck region of elderly patients.

In summary, the reported cases of spindle cell RMS arising in adult patients emphasize that spindle cell RMS in this age group represents a high-grade sarcoma that arises frequently on the extremities and the head and neck region, in striking contrast to spindle cell RMS in children and adolescents characterized by an excellent prognosis and arising predominantly in the paratesticular location. In addition, the histological features of the described cases widen the morphological spectrum of this entity, and it seems most likely that sclerosing RMS belongs in the spectrum of spindle cell RMS. Immunohistochemically, desmin, myf-4, WT1 and CD 99 are sensitive markers for spindle cell RMS and play an important role in the differential diagnosis to other spindle cell sarcomas.

Acknowledgements The authors thank the following clinicians and pathologists for providing the cases and clinical information when available: Dr. H. Graupner, Wesel (Case 1), Dr. W. Foss, Paderborn (Case 2), Professor Dr. H. Frenzel, Karlsruhe (Case 3), Dr. D. Drücke, Bochum (Case 4), Dr. Professor Dr.H.U. Steinau (Cases 5 and 7), and Dr. P. Schabbauer, Neubrandenburg (Case 6) all Germany.

References

1. Carpentieri DF, Nichols K, Chou PM (2002) The expression of WT1 in the differentiation of rhabdomyosarcoma from other pediatric small round blue cell tumors. Mod Pathol 15:1080–1086
2. Cavazzana AO, Schmidt D, Ninfo V, Harms D, Tollot M, Carli M, Treuner J, Betto R, Salviati G (1992) Spindle cell rhabdomyosarcoma: a prognostically favorable variant of rhabdomyosarcoma. Am J Surg Pathol 16:229–235
3. Chiles MC, Parham DM, Qualman SJ, Teot LA, Bridge JA, Ullrich F, Barr FG, Meyer WH; Soft Tissue Sarcoma Committee of the Children's Oncology Group (2004) Sclerosing rhabdomyosarcomas in children and adolescents: a clinicopathologic review of 13 cases from the Intergroup Rhabdomyosarcoma Study Group and Children's Oncology Group. Pediatr Dev Pathol 7:583–594

4. Croes R, Debiec-Rychter M, Cokelaere K, De Vos R, Hagemeijer A, Sciot R (2005) Adult sclerosing rhabdomyosarcoma: cytogenetic link with embryonal rhabdomyosarcoma. Virchows Arch 446:64–67
5. Dias P, Chen B, Dilday B, Palmer H, Hosoi H, Singh S, Wu C, Li X, Thompson J, Parham D, Qualman S, Houghton P (2000) Strong immunostaining for myogenin in rhabdomyosarcomas is significantly associated with tumors of the alveolar subclass. Am J Pathol 156:399–408
6. Esnaola NF, Rubin BP, Baldini EH, Vasudevan N, Demetri GD, Fletcher CDM, Singer S (2001) Response to chemotherapy and predictors of survival in adult rhabdomyosarcoma. Ann Surg 234:215–223
7. Ferrari A, Dileo P, Casanova M, Bertuelli R, Meazza C, Gandola L, Navarria P, Collini P, Gronchi A, Olmi P, Fossati-Bellani F, Casali PG (2003) Rhabdomyosarcoma in adults. A retrospective analysis of 171 patients treated at a single institution. Cancer 98:571–580
8. Folpe AL, McKenney JK, Bridge JA, Weiss SW (2002) Sclerosing rhabdomyosarcoma in adults. Report of four cases of a hyalinizing, matrix-rich variant of rhabdomyosarcoma that may be confused with osteosarcoma, chondrosarcoma, or angiosarcoma. Am J Surg Pathol 26:1175–1183
9. Furlong MA, Mentzel T, Fanburg-Smith JC (2001) Pleomorphic rhabdomyosarcoma in adults: a clinicopathologic study of 38 cases with emphasis on morphologic variants and recent skeletal specific markers. Mod Pathol 14:595–603
10. Hawkins WG, Hoos A, Antonescu CR, Urist MJ, Leung DH, Gold JS, Woodruff JM, Lewis JJ, Brennan MF (2001) Clinicopathologic analysis of patients with adult rhabdomyosarcoma. Cancer 91:794–803
11. Kuhnen C, Herter P, Leuschner I, Mentzel T, Drücke D, Jaworska M, Johnen G (2006) Sclerosing pseudovascular rhabdomyosarcoma — immunohistochemical, ultrastructural, and genetic analysis indicating a distinct subtype of rhabdomyosarcoma. Virchows Arch (in press)
12. Leuschner I, Newton WA, Schmidt D, Sachs N, Asmar L, Hamoudi A, Harms D, Maurer HM (1993) Spindle cell variants of embryonal rhabdomyosaroma in paratesticular region. A report of the Intergroup Rhabdomyosarcoma Study. Am J Surg Pathol 17:221–230
13. Mentzel T, Dry S, Katenkamp D, Fletcher CDM (1998) Low-grade myofibroblastic sarcoma: analysis of 18 cases in the spectrum of myofibroblastic tumors. Am J Surg Pathol 22:1228–1238
14. Mentzel T, Katenkamp D (2000) Sclerosing, pseudovascular rhabdomyosarcoma in adults. Clinicopathological and immunohistochemical analysis of three cases. Virchows Arch 436:305–311
15. Nascimento AF, Fletcher CDM (2005) Spindle cell rhabdomyosarcoma in adults. Am J Surg Pathol 29:1106–1113
16. Newton WA, Gehan EA, Webber BL, Marsden HB, van Unnik AJ, Hamoudi AB, Tsokos MG, Shimada H, Harms D, Schmidt D (1995) Classification of rhabdomyosarcomas and related sarcomas. Pathologic aspects and proposal for a new classification — an Intergroup Rhabdomyosarcoma Study. Cancer 76:1073–1085

Virchows Arch (2006) 449:561–564
DOI 10.1007/s00428-006-0287-1

CASE REPORT

Anaplastic large-cell non-Hodgkin's lymphoma of the breast in periprosthetic localisation 32 years after treatment for primary breast cancer—a case report

Florian Rudolf Fritzsche · Stefan Pahl · Iver Petersen · Mick Burkhardt · Anja Dankof · Manfred Dietel · Glen Kristiansen

Received: 21 July 2006 / Accepted: 1 August 2006 / Published online: 16 September 2006
© Springer-Verlag 2006

Abstract Primary, as well as secondary, lymphomas of the breast are rare diseases and might, in some cases, be misdiagnosed as breast cancer on routine hematoxylin/eosin stainings. We report a case of an anaplastic large cell lymphoma in a 72-year-old woman with a history of breast cancer treated with breast-ablative surgery and a subsequent silicon implant 32 years ago. Clinically, she presented with an ulceration of the skin, which had developed within a few months. On conventional histology, the tumor cells were mimicking poorly differentiated invasive ductal carcinoma with a prominent leukocytic infiltrate. The immunoprofile of the tumor showed negativity for cytokeratins and led to the diagnosis of a CD30-positive anaplastic large cell lymphoma.

Keywords Lymphoma · Breast cancer · ALCL · C-ALCL · Immunohistochemistry

Introduction

Non-Hodgkin's lymphomas (NHL) of the breast are, as any non-carcinomas, very rare events, which comprise less than 1% of all breast malignancies [26]. To our knowledge, there is no epidemiologic data about breast lymphomas so far. Most publications on this topic are case reports or small series of single institutions. Lin et al. [14] analysed a series of 21 primary and 19 secondary NHLs in the breast, finding a median age of 67 and 61 years and a predominance of intermediate or poor differentiation and of the diffuse large-cell type. Primary and secondary lymphomas of the breast are indistinguishable on morphologic grounds [1] and seem to occur equally frequent [21]. B cell NHLs seem to be more common than T cell NHLs [20, 24]. Some of the lymphomas of the breast reported were initially diagnosed as carcinomas [14, 20], which, because of the vastly different treatment options, underlines the importance for the surgical pathologist to be aware of this uncommon disease when confronted with a poorly differentiated neoplasm in the breast. Clinically, most lymphomas of the breast present as a solid mass with or without mammographic findings [23], although diffuse firm infiltrating anechoic mastitis-like processes have also been described [8]. Cases of NHL arising from an intramammary lymph node in elderly patients have been published [22].

F. R. Fritzsche · S. Pahl · I. Petersen · M. Burkhardt · A. Dankof · M. Dietel · G. Kristiansen (✉)
Institute of Pathology, Charité Universitätsmedizin Berlin,
Schumannstr. 20/21,
10117 Berlin, Germany
e-mail: glen.kristiansen@charite.de

Case report

Clinical data

We report a case of a 72-year-old woman with a history of breast cancer 32 years ago. The slides of the primary histology were not available due to transgression of the storage obligation time (30 years). After primary ablative surgery, 32 years ago, she received several reconstruction operations resulting in a prosthetic breast reconstruction with a polyurethane-coated silicon implant 16 years ago. Anamnestically, no systemic therapy was administered. The implant was removed half a year ago. The material sent in for histology at this time was unsuspicious. Apart from two strokes 3 years ago, a transitional ischemic attack 2 years ago and a penicillin allergy, the patient's history was non-contributory. The patient presented to the physician a 25-

mm skin ulceration of her left breast that arose above the prosthesis in the course of a few months. The lesion was excised with free margins of at least 7 mm to all directions and a depth of 25 mm and was sent to the pathologist with the clinical suspicion of recurrent carcinoma.

Histologic findings

Histologically, the lesion presented as a subepithelial infiltrate of partially disperse single-cells and partially trabecular and solid clusters of highly pleomorphic cells (Fig. 1). The epithelioid tumor cells were large with blast-like appearance, severe cellular and nuclear atypias with large nuclei and nucleoli and up to 26 mitoses per 10 high power fields. The tumor infiltrates were found discontinuously growing from the skin ulceration into the deep and cranial resection margins. The tumor cells were accompanied by a dense infiltrate of lymphocytes, neutrophil and eosinophil granulocytes, macrophages and very few giant cells. Initially, we suspected a highly dedifferentiated carcinoma and immunostained for hormone receptors and c-erbB2 and also for pancytokeratin for confirmation of epithelial origin of the neoplasm (Fig. 2). As all these markers turned out to be negative, we immunostained for vimentin CD3, CD4, CD5, CD8, CD15, CD20, CD23, CD30, CD34, CD43, CD45, CD56, CD68, CD79a, EBV, EMA, TdT, bcl-2, HMB45, S-100, EMA, Mib-1, PAX-5 and ALK. The tumor cells showed a strong cytoplasmic expression of CD30 and a weak and partial expression of CD4, CD5 and CD56. The proliferative fraction, determined by Mib-1, was above 80%. All other markers were negative in the tumor cells. This constellation allows for two possible diagnoses that are important to differentiate: systemic secondary cutaneous anaplastic large-cell CD30-positive and ALK-negative NHL (ALCL) or primary cutaneous CD30-positive anaplastic large cell lymphoma (C-ALCL).

Discussion

The distinction between these two entities (ALCL vs C-ALCL) is not trivial but of great therapeutic importance. Unfortunately, both entities are morphologically quite similar, and, in some cases, careful clinical staging is the most important factor for this decision. Multinucleated giant cells and Reed–Sternberg-like cells occur more often in C-ALCL. C-ALCLs are typically positive for CD30, CD4, cytotoxic granule-associated proteins (e.g. perforin, granzyme B) and HECA-452 [10]. They are negative for EMA and ALK. Usually, the prognosis of C-ALCL is quite good (about 90% 5-year survival), and, apart from local therapies (surgical excision, radiotherapy), there is no need

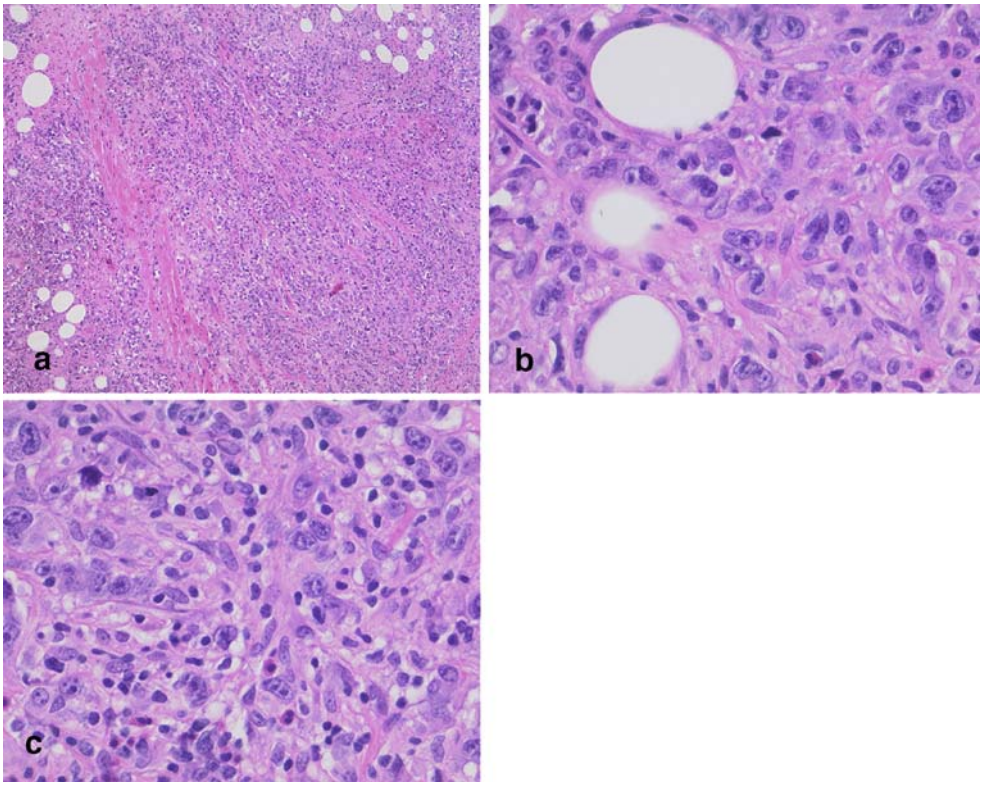

Fig. 1 **a** Hematoxylin/eosin (*H/E*) staining of the tumor with cohesive-like tumor cell clusters and leukocytic infiltrate (magnification 50×). **b**, **c** H/E staining with tumor cell clusters (magnification 1000×)

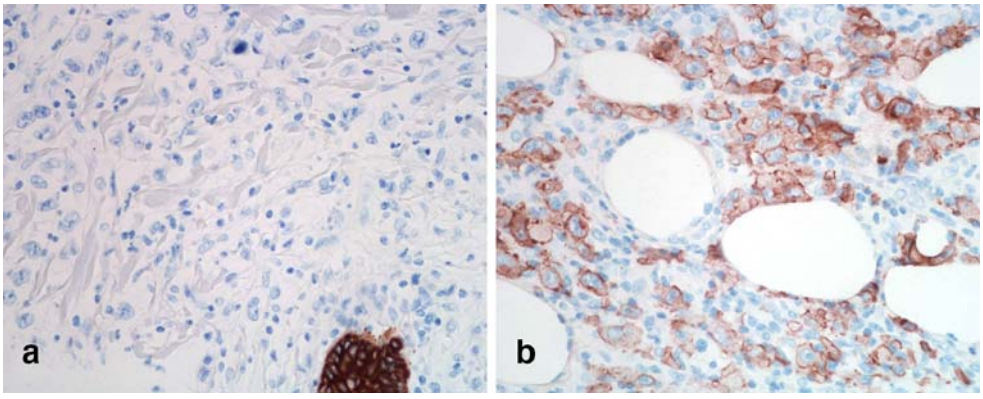

Fig. 2 **a**, **b** Immunohistologic staining for pancytokeratin (**a**) with negative tumor cells and for CD30 with strong cytoplasmic expression in the tumor cells (magnification 400×)

for a systemic treatment, unless extracutaneous lesions occur. Unlike the cutaneous form, systemic ALCLs are often positive for ALK and EMA [10]. Systemic ALCL often stain for CD2, CD4, cytotoxic granule-associated proteins and CD43.

While ALK-positive systemic ALCL are more often in younger male patients, ALK-negative ones are associated with advanced age and show no sexual predominance. The skin is the most frequent extranodal site involved by systemic ALCL, but ALK-negative ALCLs are somewhat less frequently found outside of lymph nodes. In three fourths of the cases, the patient presents with B symptoms, which was not the case in our patient. While all kinds of ALK-positive ALCL contain cells with eccentric kidney-shaped nuclei, often with pronounced perinuclear eosinophilia, ALK-negative ALCL are less well characterized [10]. The cells in the latter type are larger, more pleomorphic and exhibit prominent nucleoli. Since ALK-negative ALCL differ from ALK-positive ones by an older age of onset, a lack of gender predominance and a worse prognosis, it is not clear whether they may even represent different entities [10].

Only about 2% of the extranodal NHLs are located in the breast, most of them are of the B cell type. Some cases of mucosa-associated lymphatic tissue (MALT) lymphomas have been published [9, 13, 27]. Two T cell NHL described by Tan and Sng [20] were large-cell anaplastic lymphomas. In our case, the lymphoma was located in the left breast, but most lymphoma cases were reported in the right breast [1, 21]. The criteria that have to be fulfilled for the diagnosis of primary lymphoma of the breast are an adequate pathological specimen, close proximity of mammary tissue and lymphomatous infiltrate, no prior diagnosis of extramammary lymphoma and no concurrent widespread lymphoma except concomitantly involved ipsilateral lymph nodes [25]. Our case met only two of these criteria, as no residual glandular breast tissue was present and as the patient refused any further diagnostic or therapeutic options and has, according to this standard, to be considered as secondary lymphoma of the breast. Realizing the different prognostic and therapeutic implications of primary C-ALCL and secondary cutaneous systemic ALCL, this distinction cannot be made without the clinical staging data.

Generally, the peak incidence for lymphomas of the breast seems to be around the sixth decade, although some cases occurred in the third decade [23]. Associations with autoimmune diseases have been described [5]. As lymphomas of the breast are rare diseases, prognostic data on this entity are rare and rely on small study groups. Generally, the prognosis and outcome depend on the histology of the lymphoma regardless whether primary or secondary [2, 5, 16, 17, 24]. However, this is not the case for ALCL, and for statistical reasons and for further research, this matter should be addressed anyway. The 5-year overall survival in the small cohort of Vignot et al. [24] was only 29% with a median survival time of 21.5 months while Vigliotti et al. [23] reported a 10-year survival rate of 71%. We can confirm the difficulty in the differential diagnosis between undifferentiated carcinoma and lymphoma of the breast on hematoxylin/eosin morphologic basis. To clarify this differential diagnosis, immunohistochemistry is mandatory. In a poorly differentiated neoplasm of the breast, the absence of estrogen receptor, progesterone receptor and c-erbB2 in addition to a missing in situ component should alert the pathologist to ascertain the histogenesis of the neoplasm by immunohistochemistry. Should cytokeratins be negative, additional immunohistochemical analyses for leukocyte markers, malignant melanoma (S100 protein, HMB-45) and sarcoma (desmin, smooth muscle actin, CD34) should follow.

Until now, including our case, 11 cases of lymphoma of the breast in association with breast prosthesis have been published. Cook et al. [4] described one follicular lymphoma, Duvic et al. [6], Gaudet et al. [7], Sahoo et al. [18] and Keech and Creech [11] reported together seven cases of T cell lymphomas and Said et al. [19] and Kraemer et al. [12] found together two cases of B cell lymphomas in patients with breast implants. It is interesting to note that in the

reported prosthesis-associated cases, unlike the other breast lymphoma cases, the T cell lymphomas predominate. It remains speculative whether potential triggers like stimulation of the immune system by silicon leakage, implant-associated staphylococcus infections or toluene diamine leakage from polyurethane foam covers are of importance in these rare cases.

Still, epidemiologically, the breast cancer risk for women with implants seems not to be elevated, although a potential risk for sarcomas and hematologic cancers was found [3].

In contrast to breast carcinomas, there are very limited data on therapeutic options for lymphomas of the breast. Two recently published studies of Liu et al. [15] and Vigliotti et al. [23] recommended a sequence of full-dose (anthracycline-containing) chemotherapies and radiotherapy. If the lymphoma in the reported case was a manifestation of a systemic ALCL, a systemic therapy would be mandatory. Should it be a primary cutaneous anaplastic large-cell tumor, the local surgical or radiotherapeutical treatment would be sufficient. Unfortunately, in our case, the patient refused any further diagnostic or therapeutic approaches.

References

1. Arber DA, Simpson JF, Weiss LM, Rappaport H (1994) Non-Hodgkin's lymphoma involving the breast. Am J Surg Pathol 18:288–295
2. Ariad S, Lewis D, Cohen R, Bezwoda WR (1995) Breast lymphoma. A clinical and pathological review and 10-year treatment results. S Afr Med J 85:85–89
3. Brinton LA, Brown SL (1997) Breast implants and cancer. J Natl Cancer Inst 89:1341–1349
4. Cook PD, Osborne BM, Connor RL, Strauss JF (1995) Follicular lymphoma adjacent to foreign body granulomatous inflammation and fibrosis surrounding silicone breast prosthesis. Am J Surg Pathol 19:712–717
5. Domchek SM, Hecht JL, Fleming MD, Pinkus GS, Canellos GP (2002) Lymphomas of the breast: primary and secondary involvement. Cancer 94:6–13
6. Duvic M, Moore D, Menter A, Vonderheid EC (1995) Cutaneous T-cell lymphoma in association with silicone breast implants. J Am Acad Dermatol 32:939–942
7. Gaudet G, Friedberg JW, Weng A, Pinkus GS, Freedman AS (2002) Breast lymphoma associated with breast implants: two case-reports and a review of the literature. Leuk Lymphoma 43:115–119
8. Grubstein A, Givon-Madhala O, Morgenstern S, Cohen M (2005) Extranodal primary B-cell non-Hodgkin lymphoma of the breast mimicking acute mastitis. J Clin Ultrasound 33:140–142
9. Hakoda Y, Gotoh A, Kuriyama Y, Kusama M, Koyanagi Y, Serizawa H, Mukai K, Ohyashiki K (2001) Breast MALT lymphoma: potential relationship between hormonal environment and female sex hormone receptor expression in lymphoma cells. Leuk Lymphoma 42:1157–1159
10. Jaffe ES, Harris NL, Stein H, Vardiman JW (2006) World Health Organization classification of tumours. Pathology & genetics: tumours of the haematopathologic and lymphoid tissue. IARC Press, Lyon
11. Keech JA Jr, Creech BJ (1997) Anaplastic T-cell lymphoma in proximity to a saline-filled breast implant. Plast Reconstr Surg 100:554–555
12. Kraemer DM, Tony HP, Gattenlohner S, Muller JG (2003) Lymphoplasmacytic lymphoma in a patient with leaking silicone implant. Haematologica 88:ELT30
13. Kraemer DM, Weissinger F, Reimer P, Kunzmann V, Rudiger T, Wilhelm M (2003) Female patient with a history of Hashimoto's thyroiditis, diagnosed with MALT lymphoma of both breasts. Onkologie 26:277–280
14. Lin Y, Govindan R, Hess JL (1997) Malignant hematopoietic breast tumors. Am J Clin Pathol 107:177–186
15. Liu MT, Hsieh CY, Wang AY, Pi CP, Chang TH, Huang CC, Huang CY (2005) Primary breast lymphoma: a pooled analysis of prognostic factors and survival in 93 cases. Ann Saudi Med 25:288–293
16. Loughrey MB, Windrum P, Catherwood MA, Alexander HD, Markey GM, McManus DT, Morris TC (2004) WHO reclassification of breast lymphomas. J Clin Pathol 57:1213–1214
17. Ryan GF, Roos DR, Seymour JF (2006) Primary non-Hodgkin's lymphoma of the breast: retrospective analysis of prognosis and patterns of failure in two Australian centers. Clin Lymphoma Myeloma 6:337–341
18. Sahoo S, Rosen PP, Feddersen RM, Viswanatha DS, Clark DA, Chadburn A (2003) Anaplastic large cell lymphoma arising in a silicone breast implant capsule: a case report and review of the literature. Arch Pathol Lab Med 127:e115–e118
19. Said JW, Tasaka T, Takeuchi S, Asou H, de Vos S, Cesarman E, Knowles DM, Koeffler HP (1996) Primary effusion lymphoma in women: report of two cases of Kaposi's sarcoma herpes virus-associated effusion-based lymphoma in human immunodeficiency virus-negative women. Blood 88:3124–3128
20. Tan PH, Sng IT (1996) Breast lymphoma—a pathologic study of 14 cases. Ann Acad Med Singap 25:783–790
21. Topalovski M, Crisan D, Mattson JC (1999) Lymphoma of the breast. A clinicopathologic study of primary and secondary cases. Arch Pathol Lab Med 123:1208–1218
22. Venizelos ID, Tatsiou ZA, Vakalopoulou S, Mandala E, Garipidou V (2005) Primary non-Hodgkin's lymphoma arising in an intramammary lymph node. Leuk Lymphoma 46:451–455
23. Vigliotti ML, Dell'olio M, La Sala A, Di Renzo N (2005) Primary breast lymphoma: outcome of 7 patients and a review of the literature. Leuk Lymphoma 46:1321–1327
24. Vignot S, Ledoussal V, Nodiot P, Bourguignat A, Janvier M, Mounier N, Cherel P, Floiras JL, Turpin F (2005) Non-Hodgkin's lymphoma of the breast: a report of 19 cases and a review of the literature. Clin Lymphoma 6:37–42
25. Wiseman C, Liao KT (1972) Primary lymphoma of the breast. Cancer 29:1705–1712
26. Young JL Jr, Ward KC, Wingo PA, Howe HL (2004) The incidence of malignant non-carcinomas of the female breast. Cancer Causes Control 15:313–319
27. Zobolas B, Sakorafas GH, Kourakli I, Tsiotou AG (2002) Bilateral, primary, low-grade, diffuse B-cell lymphoma of mucosa-associated lymphoid tissue (MALT) of the breast. Breast J 8:382

Virchows Arch (2006) 449:565–571
DOI 10.1007/s00428-006-0281-7

CASE REPORT

Eccrine ductal and acrosyringeal differentiation of the breast epithelium—a lesion associated with some metaplastic breast carcinomas

Tibor Tot

Received: 24 April 2006 / Accepted: 20 July 2006 / Published online: 3 October 2006
© Springer-Verlag 2006

Abstract Two cases of metaplastic breast carcinoma associated with eccrine ductal metaplasia in the surrounding breast tissue are reported. The metaplastic epithelium deviated from the normal in its immunophenotype not expressing glandular cytokeratins (Cam 5.2) and estrogen receptors, being maspin-positive, and resembling morphologically different segments of dermal eccrine duct and acrosyringium. In addition, in one of the cases, basalioma-like intraductal cell proliferation was observed, also showing focal acrosyringeal differentiation. The invasive carcinomas, one of them representing "syringomatous squamous tumor of the breast" while the other diagnosed as high-grade metaplastic carcinoma, also showed focal eccrine and acrosyringeal differentiation and intensive diffuse maspin expression. These previously unrecognized metaplastic changes of the breast epithelium may represent precursor lesions of certain types of metaplastic breast carcinomas.

Keywords Breast · Eccrine metaplasia · Metaplastic carcinoma · Basalioma-like change · Maspin

Introduction

Eccrine differentiation characterizes some rare lesions of the breast, such as syringomatous adenoma of the nipple [14] and syringomatous squamous tumor [17], the latter representing a rare variant of low-grade adenosquamous carcinoma, which in turn is a part of the wide spectrum of metaplastic carcinomas [18]. Sweat gland-type tumors of the breast, identical to their counterparts in the skin, have occasionally been reported [9, 21]. The origin of these lesions is still unclear as these tumors, although sharing morphologic features with skin eccrine tumors, do not develop from the sweat glands. Eccrine metaplasia of the ductal or lobular epithelium, on the other hand, is not a generally recognized element of the otherwise very wide morphologic spectrum of the normal breast tissue.

In this paper, we report two cases of metaplastic breast carcinoma associated with noninvasive epithelial structures showing striking morphological and immunohistochemical similarity to the epithelium of the dermal eccrine ducts and, in part, resembling the area of the opening of these ducts within the epidermis, the acrosyringium. Up to our best knowledge, this kind of eccrine ductal metaplasia and acrosyringeal differentiation has not been previously described.

Materials and methods

The first case was submitted to the author in consultation from an outside institution, while the second one was from the files of the Department of Pathology, Central Hospital in Falun, Sweden. The cases were worked up using the large-section histology technique described elsewhere in details [19]. Immunophenotyping of the lesions was carried out in the DAKO autostainer using the standard procedure and original reagents of the manufacturer. The following primary antibodies were used: anti-human epithelial membrane antigen (EMA) clone E29, anti-human estrogen receptor clone 1D5, anti-human progesterone receptor clone PgR 636, c-erbB-2 oncoprotein A0485, and anti-human smooth muscle actin (SMA) clone 1A4, and p63 clone 4A4, all from Dako Glostrup Denmark, anti-cytokeratin

T. Tot (✉)
Department of Pathology, Central Hospital,
791 82 Falun, Sweden
e-mail: tibor.tot@ltdalarna.se

Cam 5.2 from Becton Dickinson, human cytokeratin 14 clone LL002 and anti-human maspin clone EAW24 from Novocastra, and anti-cytokeratin 5/6 clone D5/16 B4 from Boehringer Mannheim Biochemica.

Results

Case 1

A 62-year-old woman was operated with sector resection for an invasive ductal carcinoma NOS in the upper lateral quadrant of her right breast 12 years before detection of a palpable tumor mass and mammographically suspicious microcalcifications in the lower lateral quadrant of the same breast. Actually, two separate foci of invasive cancer were detected, both radiologically and on macroscopic examination, one of them measuring 1 cm and representing a well-differentiated invasive ductal carcinoma NOS. The other tumor was initially diagnosed as metaplastic breast carcinoma measuring 25 mm. All the tumors were c-erbB-2- and estrogen and progesterone receptor (ER and PR)-negative. The patient was operated with sector resection and reoperated with mastectomy; no lymph node metastasis was found.

The 25-mm tumor exhibited islands of epithelial structures lying in a fibromatosis-like stroma. The epithelial component showed partly squamous differentiation with keratinization, and even lumina delineated with cuticle-like substance. No reaction with Cam 5.2 but a strong and diffuse staining with maspin, cytokeratin 5/6 (CK 5/6), and cytokeratin 14 (CK 14) was observed on immunohistochemical examination in these structures. A diffuse nuclear staining with p63 was also evidenced, but many of the luminal cell nuclei remained unstained. The inner surface of the gland-like lumina stained intensively with EMA (Fig. 1a–f). On second opinion, the diagnosis of low-grade

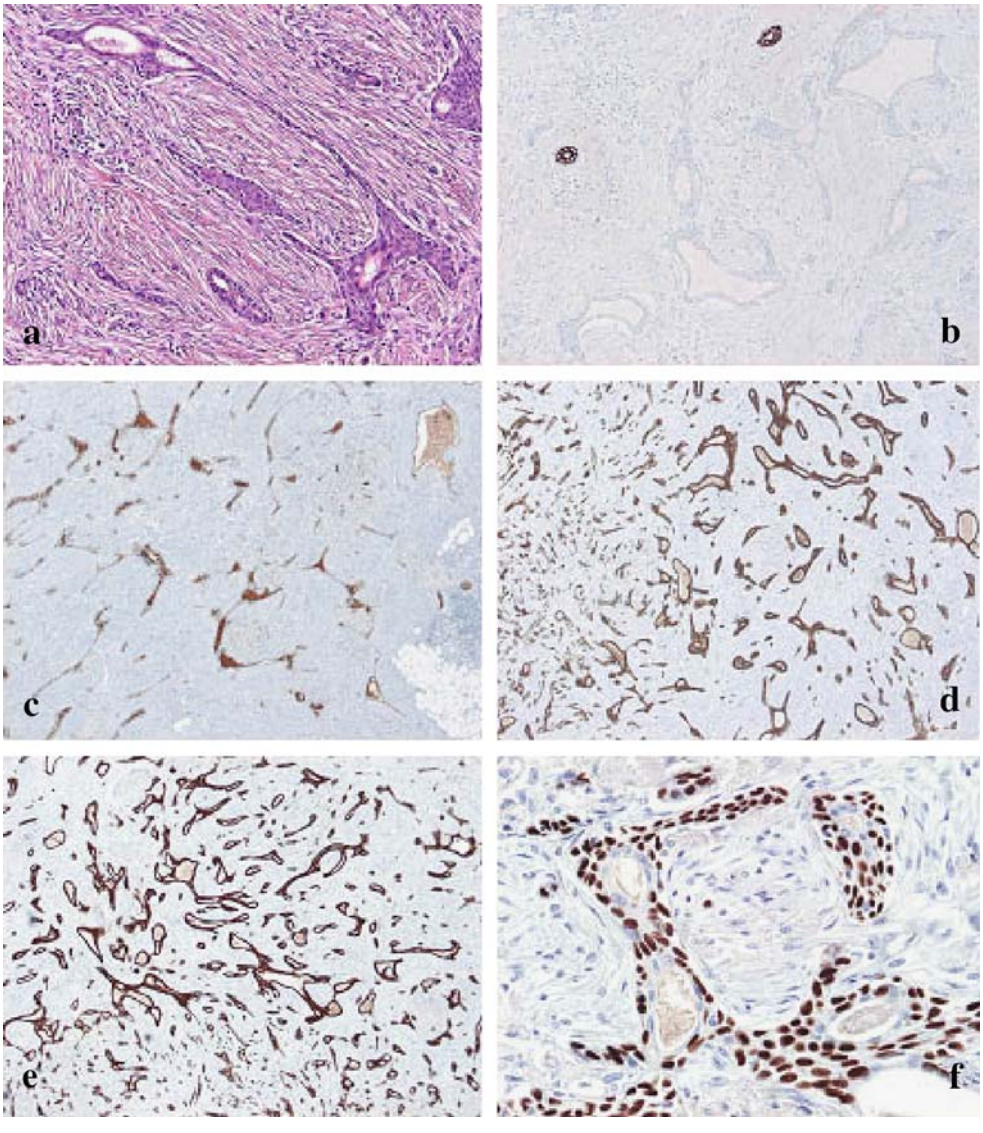

Fig. 1 Syringomatous squamous tumor of the breast. Fibromatosis-like stroma and epithelial structures with squamous differentiation and eccrine duct-like lumina, H&E (**a**). Cam 5.2 immunostaining without reaction in the tumor structures; note the positively stained normal ducts (**b**). Intensive and widespread luminal positivity with EMA (**c**). Intensive cytoplasmic CK 5/6 positivity in the tumor cells (**d**). Intensive nuclear and cytoplasmic maspin positivity in the tumor cells (**e**). Intensive nuclear p63 positivity in the tumor cells; some luminal cells remained unstained (**f**)

adenosquamous carcinoma of the breast with features of syringomatous squamous tumor was suggested.

Surrounding this tumor, particular changes called for attention. Plenty of altered lobules containing acinus-like structures with Cam 5.2-, ER-, and PR-negative but maspin-positive (both nuclear and cytoplasmic positivity) two-layered or sometimes multilayered epithelium were seen; those of them having a lumen showed intensive luminal positivity for EMA. These structures showed an intense nuclear positivity with p63, but some luminal cells remained unstained. As this epithelium was morphologically, and by its immunophenotype, identical to the epithelium of different segments of the eccrine ducts of the skin, we used the term "eccrine duct lobules" to delineate these lobules from their normal counterparts. The stroma of these lobules was more cellular and more compact than the normal intralobular stroma, and SMA-positive myofibroblasts were regularly present in it. Some eccrine duct lobules showed only partial metaplasia also containing some Cam 5.2-positive, ER-positive acini with maintained myoepithelial cell layer. The acini and the terminal ducts showing eccrine ductal epithelium could contain an attenuated myoepithelial cell layer, but typically it was absent even in two-layered structures (Fig. 2a–g). Eccrine duct lobules were not observed in association with the two ductal carcinoma NOS within the same breast.

Case 2

A 64 year-old woman presented with a palpable lump in the upper medial quadrant of her right breast. On mammography, a 13-mm circular tumor mass was found without associated microcalcifications. The diagnosis of invasive carcinoma was proved preoperatively with core biopsy. Sector resection and intraoperative sentinel node examination were performed.

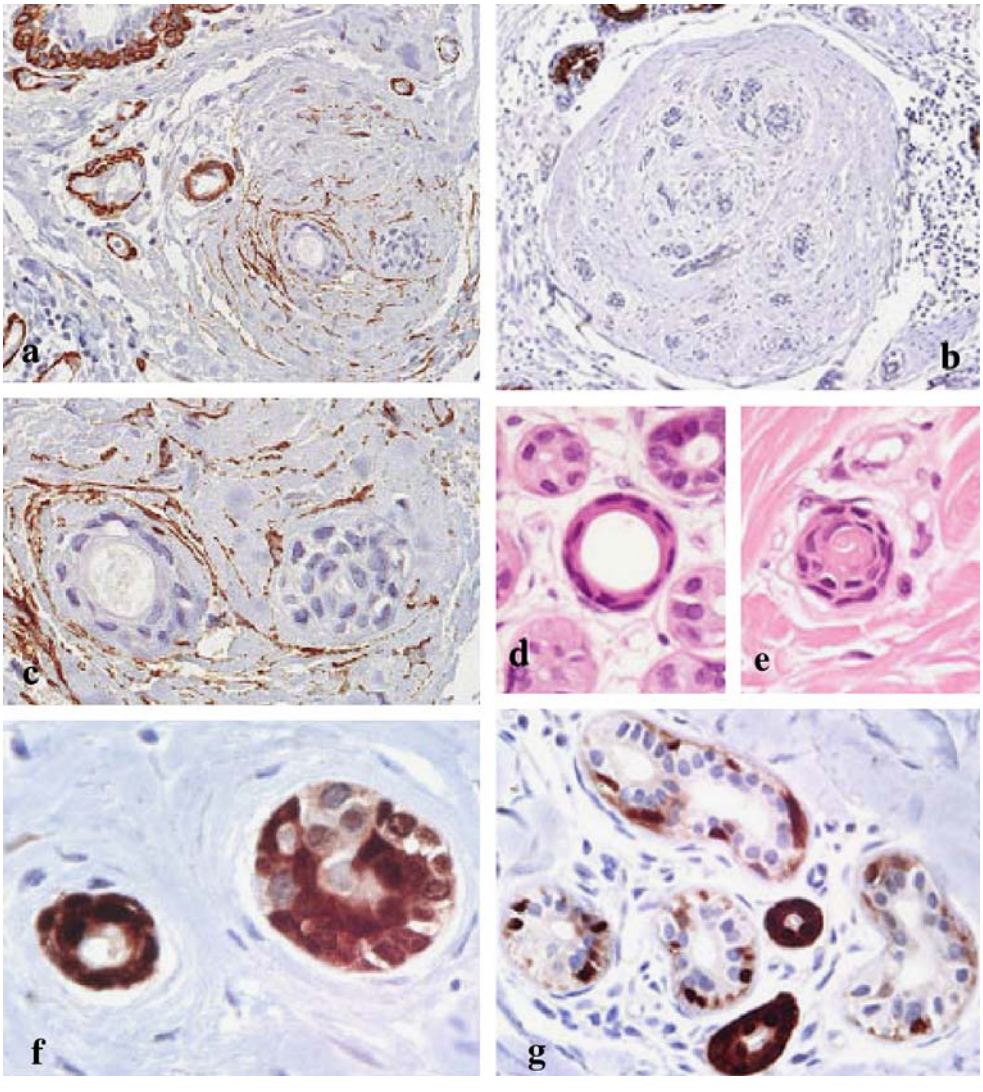

Fig. 2 Eccrine duct lobules. A lobule with dense stroma with SMA-positive cells (**a**). The epithelial structures of the eccrine duct lobule showed no reaction with Cam 5.2; note the positively stained normal acini in the surroundings (**b**). A detail from (**a**) with two acini lined by bilayered (*left*) and multilayered (*right*) epithelium. The myoepithelial cell layer is absent (**c**). For comparison, segments of normal dermal eccrine duct are demonstrated (**d**, **e**). Intensive nuclear and cytoplasmic maspin positivity [deeper level corresponding to (**c**)] (**f**). Eccrine gland of the skin: the duct is intensively stained with maspin showing both nuclear and cytoplasmic positivity in both cell layers; in the secretory glands, maspin expression is restricted to the basal cell layer (**g**)

An 11×5×3 cm large specimen was received and worked up with large section technique (Fig. 3). In addition to a 13×12-mm invasive carcinoma, a 70×30-mm large area of extensive intraductal/intralobular epithelial proliferation was found. The invasive component showed a focal squamous differentiation and a matrix-rich stroma. The cells of the invasive component were only focally reactive to Cam 5.2 but more intensively and diffusely to CK 5/6 and CK 14. They also demonstrated intense nuclear and cytoplaspic maspin positivity and focally nuclear p63 positivity. Eccrine duct-like lumina showing apical positivity to EMA were also evidenced. The invasive tumor showed high-grade cellular and nuclear atypia and large number of mitoses, among them atypical. The tumor was ER-, PR-, c-erbB-2-negative, aneuploid with high S-phase on flow cytometric measurement, and was diagnosed as high-grade metaplastic carcinoma of the breast.

The extensive in situ epithelial proliferation in the described area was polymorphous. Partly, lobules resembling the eccrine duct lobules were seen, with terminal ducts and acini with two-layered or multilayered Cam 5.2-negative, ER- and PR-negative, but maspin-positive epithelium with EMA-positive lumina sometimes delineated by cuticle (Fig. 4). More prominently, ducts and lobules containing solid growth of basaloid cells were seen with obvious palisading on the periphery, resembling the typical histological appearance of skin basaliomas (Fig. 5a–d). Within these structures, the foci of cells with eosinophilic cytoplasm and EMA-positive lumina appeared. This phenomenon was regarded for a probably neoplastic basaloid cell proliferation with eccrine ductal and acrosyringeal differentiation. These structures were ER-, PR-, and c-erbB-2-negative and maspin-positive (Fig. 6) and stained variably with CK 5/6 and CK 14 and only focally with p63. The myoepithelial cell layer around these structures was regularly preserved.

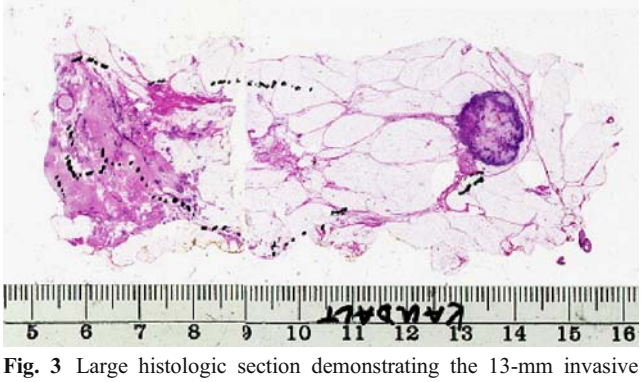

Fig. 3 Large histologic section demonstrating the 13-mm invasive carcinoma and the marked area of extensive intraductal changes. Reconstruction of the original tissue slice, which was bisected and embedded in two large paraffin blocks

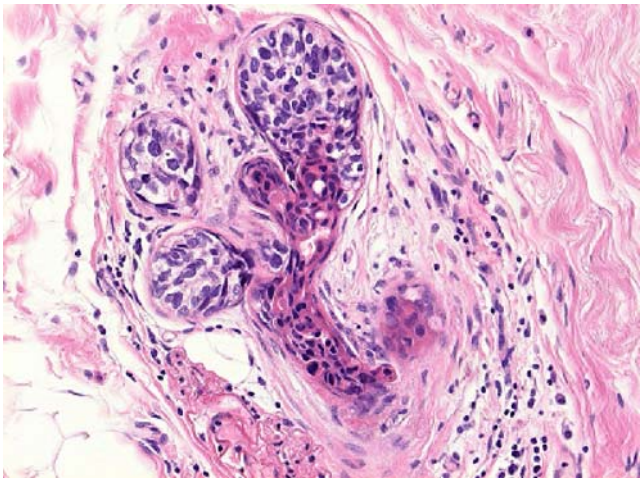

Fig. 4 A lobule with eccrine ductal metaplasia of the epithelium of the terminal duct

Discussion

Eccrine ductal metaplasia, eccrine duct lobules, and basalioma-like in situ lesions with acrosyringeal differentiation observed in association with metaplastic carcinomas of the breast seem to be unique features of the presented cases, which were previously unrecognized in the literature. While apocrine differentiation is very frequent in normal breast tissue and nonneoplastic and neoplastic breast lesions, eccrine differentiation is not evidenced. The apocrine epithelium, which is morphologically clearly deviating from the normal ductal and acinar epithelium of the breast, is easy to recognize. To distinguish eccrine glands from breast ducts and acini is, however, very difficult as all these structures are similar in their morphology and immunophenotype. The bilayered dermal duct of the eccrine as well as apocrine glands of the skin is, however, Cam 5.2-negative, SMA-negative, and maspin-positive [in contrast to the acinar (secretory) component of the eccrine glands with Cam 5.2-positive luminal cells and nuclear and cytoplasmic maspin and cytoplasmic SMA positivity restricted to the basal layer] [11] (Table 1). A thin layer of eosinophilic cuticle may delineate the lumina of these ducts. These features when exhibited by the epithelium in breast ducts and lobules are clearly deviating from the normal and allow the recognition and identification of eccrine ductal metaplasia. Although apocrine dermal ducts are identical to eccrine dermal ducts in their phenotype, we avoided terms like “apocrine ductal metaplasia” and “apocrine/eccrine ductal metaplasia” to underline the differences between the usual apocrine metaplasia and the lesions described above. When the eccrine epithelium in the breast is multilayered with a central lumen, it resembles the most superficial (epidermal) part of the eccrine duct, the acrosyringium, thus the term acrosyringeal differentiation of the breast epithelium is proposed.

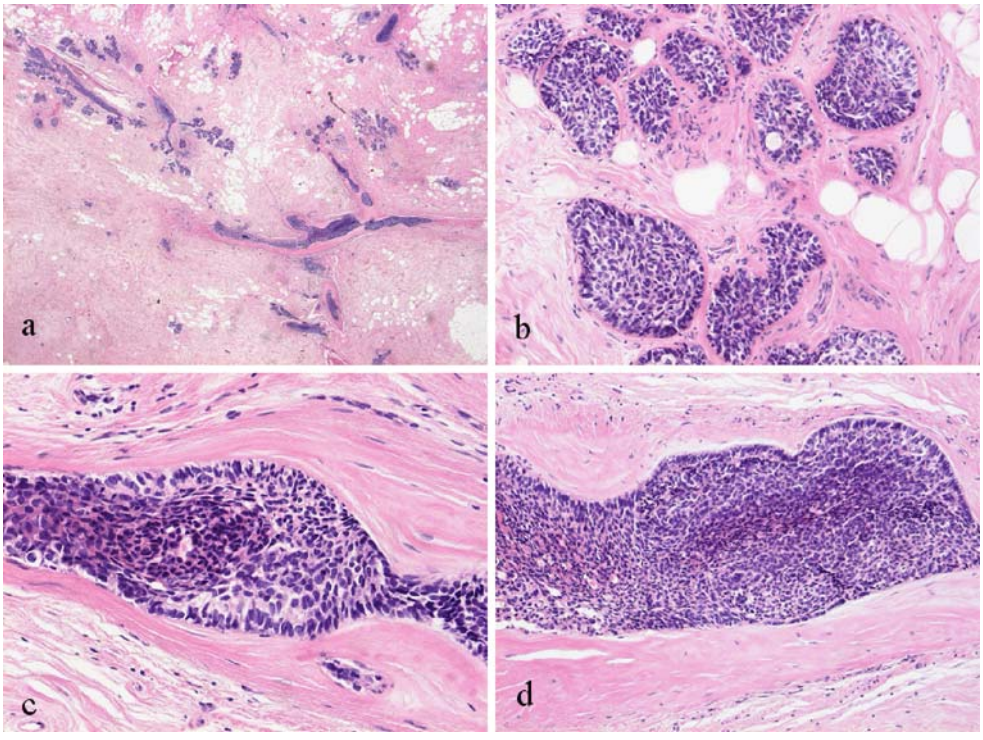

Fig. 5 Basalioma-like changes. Scanning magnification showing the maintained normal ductal–lobular architecture (**a**). Acini (**b**) and ducts (**c**, **d**) filled with basaloid cells. Note the palisading on the periphery of these structures and the eccrine differentiation in (**c**)

Vina and Wells [22] suggested that clear cell metaplasia of the breast represents eccrine differentiation of the breast epithelium and recommended the term "eccrine metaplasia" for this well-recognized aberration in normal breast lobules. Irrespective of the correctness of these observations, the metaplastic changes described in the present report are different. While clear cell change may represent a differentiation toward eccrine glands, the metaplastic changes in our two cases showed similarities not to glandular part of the eccrine sweat gland of the skin but to the epithelium of the dermal eccrine duct.

Although maspin was originally isolated from the mammary epithelium and mammary carcinomas, the normal breast epithelium shows only a faint and focal cytoplasmic maspin expression in routine immunohistochemistry; the myoepithelium in the breast, however,

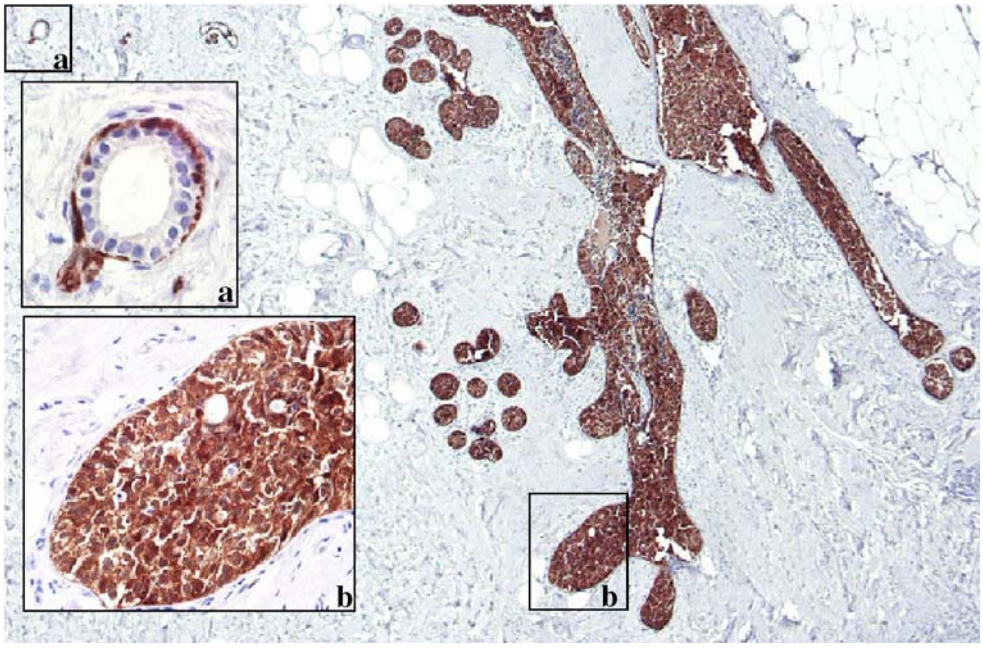

Fig. 6 Basalioma-like changes showing intensive maspin positivity. Magnified detail containing a normal ductile: staining restricted to myoepithelial cell layer (**a**). Another magnified detail showing diffuse nuclear and cytoplasmic reaction (**b**)

Table 1 The typical phenotype of eccrine duct lobules compared to normal breast epithelium and normal eccrine sweat gland

	Normal breast ducts and lobules	Dermal eccrine glands	Dermal eccrine duct	Eccrine duct lobules in the breast
Cam 5.2	+	+	−	−
ER	+	−	−	−
CK 5/6	−/+	+	+	+/−
SMA	+[a]	+[a]	−	−
Maspin	+[a]	+[a]	+	+

[a] Staining of myoepithelial/basal cells only

consistently expresses maspin both in nuclei and in cytoplasm. Thus, the maspin expression pattern of the normal mammary ducts and acini and the acinar (secretory) part of the normal eccrine glands of the skin is identical [11]. On the other hand, the eccrine ducts of the skin regularly demonstrate intense nuclear and cytoplasmic maspin positivity in both their cell layers deviating clearly from the acinary part of the skin glands. The same maspin expression pattern was observed in the metaplastic changes described in this study: the eccrine duct lobules as well as the basalioma-like epithelial proliferations showed intensive and diffuse maspin positivity. Thus, maspin seems to represent a specific marker of eccrine duct and acrosyringeal differentiation in the breast. Furthermore, as demonstrated by Reis-Filho et al. [13], maspin is regularly expressed by metaplastic carcinomas of the breast, suggesting that eccrine metaplasia may represent a precursor lesion of some metaplastic breast carcinomas.

Basaliomas of the skin may show eccrine differentiation and also may develop from the dermal eccrine ducts [5, 16]. Skin adnexal differentiation in basaliomas may reflect a common origin of the basaloid and the adnexal epithelium from an embryonic stem cell. The basaloid differentiation associated with eccrine ductal differentiation in our second demonstrated case may also be a manifestation of such biphasic differentiation. Like some skin basaliomas, the basaloid cell proliferation in our second case expressed maspin but lacked the diffuse expression of p63 typical of skin basaliomas [11, 12].

Since 1940, Oliver [8] suggested that breast tumors resembling dermal syringomas may develop as a result of squamous metaplasia of the preexisting breast epithelium. Squamous metaplasia is relatively common in breast lesions [10] and may sometimes exhibit signs of skin adnexal differentiation [6, 15], a phenomenon not reported in connection with metaplastic breast carcinomas. Describing four cases of syringomatous squamous tumor of the breast, Suster et al. [17] postulated that the pathogenesis of these tumors remains unclear in the lack of established precursor lesions. In our cases, eccrine duct lobules were present in the immediate vicinity of the metaplastic carcinomas and could represent such precursor lesion. The further argument for this possibility is that in our first case, the occurrence of eccrine duct lobules was limited to the area surrounding the syringomatous squamous tumor and was not observed in association with the two invasive ductal carcinomas of the same breast. In our second case, the area of eccrine ductal and acrosyringeal differentiation with and without basalioma-like proliferations was very large, probably involving a whole sick lobe [20], but these changes were also found in the vicinity of the metaplastic carcinoma. Thus, one of the possibilities is that the metaplastic carcinomas in our cases have developed from the described precursor lesions; the other option is the simultaneous development of the metaplastic and neoplastic lesions from progenitor cells of the same type.

Metaplastic carcinomas of the breast belong to the category of "basal-like" tumors lacking ER, PR, and c-erbB-2 expression [4] but expressing CK 5 [2] and/or CK 14 [7], p63 [1, 13], maspin [13], and other "basal" markers. With squamous and skin adnexal metaplasia, as in our cases, the metaplastic tumors may also lose the expression of glandular-type cytokeratins. Basal-like carcinomas are recognized increasingly more often after the studies postulating that they (in contrast to other invasive carcinomas of the breast) originate from CK 5-positive stem cells [2]. Distinguishing metaplastic and basal-like breast carcinomas is mainly dependent of the metaplastic features of the first category and can be problematic if only immunohistochemical criteria are used. Bryan et al. [3] have recently characterized a subgroup of ductal carcinoma in situ of the breast with basal-like phenotype probably representing the precursor of invasive basal-like breast carcinomas. These high-grade intraductal lesions seem to be different from the intraductal lesions described in the present report suggesting that the basal-like tumors and the metaplastic lesions may be different in their origin.

In summary, two cases with particular epithelial lesions associated with metaplastic breast carcinomas are reported. These lesions are eccrine ductal metaplasia of the breast epithelium, acrosyringeal metaplasia, development of eccrine duct lobules, and basalioma-like intraductal cell proliferation. These lesions are morphologically, and in their immunophenotype, almost identical to different parts of dermal duct of the sweat gland or some skin basaliomas. These previously unrecognized metaplastic changes of the breast epithelium may represent precursor lesions of certain types of metaplastic breast carcinomas.

Acknowledgments The author is grateful to his excellent colleagues Sante Olling, M.D., Ph.D., Pia Waldenbäck, M.D., and Anders Åkerlund, M.D., Central Hospital Gävle-Sandviken, Sweden, for all their help in connection with the consultation case.

References

1. Azoulay S, Lae M, Freneaux P, Merle S, Al Ghuzlan A, Chnecker C, Rosty C, Klijanienko J, Sigal-Zafrani B, Salmon R, Fourquet A, Sartre-Garau X, Vincent-Salomon A (2005) KIT is highly expressed in adenoid cystic carcinoma of the breast, a basal-like carcinoma associated with favourable outcome. Mod Pathol 18 (12):1623–1631
2. Boecker W, Buerger H (2003) Evidence of progenitor cells of glandular and myoepithelial cell lineages in the human adult female breast epithelium: a new progenitor (adult stem) cell concept. Cell Prolif 1(Suppl 36):73–84
3. Bryan BB, Schnitt SJ, Collins LC (2006) Ductal carcinoma in situ with basal-like phenotype: a possible precursor to invasive basal-like breast cancer. Mod Pathol 19:617–621
4. Foulkes WD, Stefansson IM, Chappius PO, Begin LR, Goffin JR, Wong N, Trudel M, Akslen LA (2003) Germline BRCA1 mutations and basal epithelial phenotype in breast cancer. J Natl Cancer Inst 95:1482–1485
5. Heenan PJ, Bogle MS (1993) Eccrine differentiation in basal cell carcinoma. J Invest Dermatol 100:295S–299S
6. Hurt MA, Diaz-Arias AA, Rosenholz MJ, Havey AD, Stephenson HE (1989) Posttraumatic lobular squamous metaplasia of the breast: an unusual pseudocarcinomatous metaplasia resembling squamous (necrotizing) sialometaplasia of salivary glands. Mod Pathol 1:385–390
7. Jones C, Nonni AV, Fulford L, Merrett S, Chaggar R, Eusebi V, Lakhani SR (2001) CGH analysis of ductal carcinoma of the breast with basaloid/myoepithelial cell differentiation. Br J Cancer 85:422–427
8. Oliver RL (1940) Metaplasia in the breast. Arch Surg 41:714–722
9. Panico L, D'Antonio A, Chiacchio R, Delrio P, Petrella G, Pettinato G (1996) An unusual, recurring breast tumor with features of eccrine spiradenoma: a case report. Am J Clin Pathol 106:665–669
10. Reddick RS, Jennette C, Askin FB (1985) Squamous metaplasia of the breast. An ultrastructural and immunologic evaluation. Am J Clin Pathol 84:530–533
11. Reis-Filho JS, Torio B, Albergaria A, Schmitt FC (2002) Maspin expression in normal skin and usual cutaneous carcinomas. Virchows Arch 441:551–558
12. Reis-Filho JS, Torio B, Albergaria A, Schmitt FC (2002) p63 expression in normal skin and unusual cutaneous carcinomas. J Cutan Pathol 29(9):517–523
13. Reis-Filho JS, Milanezi F, Paredes J, Silva P, Pereira EM, Maeda SA, de Carvalho LV, Schmitt FC (2003) Novel and classic myoepithelial/stem cell markers in metaplastic carcinomas of the breast. Appl Immunohistochem Mol Morphol 11(1):1–8
14. Rosen PP (1983) Syringomatous adenoma of the nipple. Am J Surg Pathol 7:739–745
15. Salm R (1957) Epidermoid metaplasia in mammary fibroadenoma with formation of keratin cysts. J Pathol 74:221–223
16. Sanchez NP, Winkelmann RK (1982) Basal cell tumor with eccrine differentiation (eccrine epithelioma). J Am Acad Dermatol 6:514–518
17. Suster S, Moran CA, Mark AH (1991) Syringomatous squamous tumors of the breast. Cancer 67:2350–2355
18. Tavassoli FA, Devilee P (eds) (2003) Tumours of the breast and female genital organs. World Health Organization Classification of Tumours. IARC, Lyon, pp 39–40
19. Tot T, Tabár L, Dean PB (2002) Practical breast pathology. Thieme, Stuttgart, New York, pp 116–123
20. Tot T (2005) DCIS, cytokeratins and the theory of the sick lobe. Virchows Arch 447:1–8
21. Urso C (1996) Syringomatous breast carcinoma and correlated lesions. Pathologica 88:196–199
22. Vina M, Wells CA (1989) Clear cell metaplasia of the breast: a lesion showing eccrine differentiation. Histopathology 15:85–92

Virchows Arch (2006) 449:572–578
DOI 10.1007/s00428-006-0282-6

CASE REPORT

Sclerosing pseudovascular rhabdomyosarcoma—immunohistochemical, ultrastructural, and genetic findings indicating a distinct subtype of rhabdomyosarcoma

Cornelius Kuhnen · Peter Herter · Ivo Leuschner · Thomas Mentzel · Daniel Druecke · Malgorzata Jaworska · Georg Johnen

Received: 28 April 2006 / Accepted: 20 July 2006 / Published online: 3 October 2006
© Springer-Verlag 2006

Abstract Sclerosing (pseudovascular) rhabdomyosarcoma in adults has been described as a rare variant of rhabdomyosarcoma characterized by extensive hyaline fibrosis and pseudovascular growth patterns. We describe another case of this rhabdomyosarcoma subtype including ultrastructural and genetic findings—the lesion presented in a 62-year-old male patient in the left lower leg. The tumor was located within the deep soft tissue with maximum diameter of 11.8 cm and skin ulceration. Ultrastructural analysis revealed irregularly distributed disorganized filaments without clear evidence of Z-bands and a richly collagenized matrix. Using comparative genomic hybridization, a sharply delineated loss of chromosomal region 10q22, loss of chromosome Y, and a gain of chromosome 18 (trisomy) were detected. Reciprocal translocations t(1;13) and t(2;13)(q35;q14) which are characteristic of alveolar rhabdomyosarcoma could be excluded. These findings, while showing a relation to other rhabdomyosarcoma subtypes, represent a relatively circumscribed genetic defect pattern in sclerosing (pseudovascular) rhabdomyosarcoma that is somewhat different from patterns described in most other rhabdomyosarcoma subtypes. Six months after tumor resection, the patient presented with metastatic disease. Further studies should concentrate on the identification of genes especially on chromosomal region 10q22 to elucidate more aspects in the pathogenesis of this rhabdomyosarcoma subtype.

Keywords CGH · Genetics · Immunohistochemistry · Rhabdomyosarcoma · Sclerosing pseudovascular · Ultrastructure

Abbreviations

CGH	comparative genomic hybridization
RT-PCR	reverse transcriptase-polymerase chain reaction
RMS	rhabdomyosarcoma
SRMS	sclerosing pseudovascular rhabdomyosarcoma
TEM	transmission electron microscopy

C. Kuhnen (✉) · M. Jaworska · G. Johnen
Institute of Pathology, Limb tumor registry,
University Hospital Bergmannsheil,
Bürkle-de-la-Camp-Platz 1,
44789 Bochum, Germany
e-mail: Cornelius.Kuhnen@ruhr-uni-bochum.de

P. Herter
Max-Planck-Institute for Molecular Physiology,
Otto-Hahn-Straße 11,
44227 Dortmund, Germany

I. Leuschner
Institute of Pathology, University Hospital Schleswig-Holstein,
Campus Kiel, Michaelisstraße 11,
24105 Kiel, Germany

T. Mentzel
Dermatopathologische Gemeinschaftspraxis,
Siemensstr. 6/1,
88048 Friedrichshafen, Germany

D. Druecke
Department of Plastic and Hand Surgery-Burn Centre,
Limb Tumor Registry, University Hospital Bergmannsheil,
Bürkle-de-la-Camp-Platz 1,
44789 Bochum, Germany

G. Johnen
BGFA (Research Institute for Occupational Medicine),
University Hospital Bergmannsheil,
Bürkle-de-la-Camp-Platz 1,
44789 Bochum, Germany

Introduction

Sclerosing (pseudovascular) rhabdomyosarcoma (SRMS) in adults has been described for the first time by Mentzel and Katenkamp in 2000 as an unusual and previously unrecognized variant of RMS [15]. This first series included three cases of this type of RMS. In 2002, Folpe et al. [5] reported four additional cases which they called sclerosing RMS; these authors categorized the former described cases by Mentzel and Katenkamp and their own cases as one identical entity that might be a true distinct subtype within the spectrum of RMS. Three additional cases of this variant were included in a series of adult spindle cell rhabdomyosarcoma [17], one case was described as a lesion at the base of tongue [10] and so far, 14 cases in children and adolescents have been described [2, 19]. Recently, a single case was reported by Croes et al. [3], applying cytogenetics with SRMS for the first time. Based on their analysis, Croes et al. concluded, however, that SRMS does not represent a distinct subtype of RMS, but suggested a close relationship of SRMS with embryonal RMS. We present immunohistochemical, ultrastructural, molecular, and cytogenetic findings in another case of SRMS and discuss the findings with respect to categorization of this neoplasm in the spectrum of RMS.

Clinical history

A 62-year-old male patient presented with a swelling of the lower left leg. The skin was ulcerated within an area of 8× 7 cm. A biopsy was taken and consequently the lesion was entirely resected, partly marginally. Six months after tumor resection, the patient presented with lung metastases and pleural spread of disease and was living with disease 10 months after biopsy diagnosis.

Materials and methods

The specimen was fixed in a 4% buffered formalin solution and paraffin-embedded. 3–5 μm thick sections were stained with hematoxylin and eosin. Freshly obtained tumor tissue of the surgical specimen was snap-frozen in liquid nitrogen for further genetic analysis and fixed in glutaraldehyde for ultrastructural analysis. Informed patient's consent was obtained concerning all analyses and especially concerning genetic analyses regarding possible inherited chromosomal imbalances. Immunohistochemistry was performed on selected paraffin sections using a standard alkaline phosphatase anti alkaline phosphatase method described elsewhere [14]. Antibodies against the following antigens were used: Desmin (Dako-Cytomation, clone D33, 1:100), muscle-specific actin (Dako-Cytomation, clone HHF35, 1:400), MyoD1 (Dako-Cytomation, clone MyoD1, 5.8A, 1:50), myf-4 (myogenin: Novocastra, clone LO26, 1:30), smooth-muscle actin (Biogenex, 1:50), myoglobin (Dako-Cytomation, polyclonal, 1:10), vimentin (Dako-Cytomation, clone V9), 1:8,000), CD99 (Dako-Cytomation, clone 12E7, 1:25), cytokeratins (Dako-Cytomation, clones MNF116, 1:100, and AE1/AE3, 1:10), EMA (Dako-Cytomation, clone E29, 1:50), CD 31 (Dako-Cytomation, clone JC70A, 1:1,000), CD 34 (Immunotech, clone QBEND10, 1:2,000), factor VIII-associated antigen (Dako-Cytomation, clone, 1:9,000), S-100 protein (Biogenex, clone 15E2E2, 1:100), NSE (Dako-Cytomation, clone BB5/NC/VI-H14, no dilution), and Ki 67 (Dako-Cytomation, clone MIB-1, 1:800). Immunostaining scores were used according to Folpe et al. [5] (negative: <5% of cells positive; 1+: 5–25% cells positive; 2+: 26–50% cells positive; 3+: >50% cells positive). For transmission electron microscopy (TEM), small pieces of tumor tissue were fixed with 2.5% glutaraldehyde and postfixed with 1% osmium tetroxide, degraded in an ascending series of ethanol, processed through propylene oxide, and embedded in epoxy resin. Semithin sections were stained with toluidine blue, and appropriate areas were selected for the study of ultrastructure. To improve contrast, ultrathin sections were stained with uranyl acetate followed by lead citrate and then investigated with a ZEISS 902 electron microscope. The ultrastructural characterization of myofilaments and structures defining a skeletal muscle differentiation referred to the criteria proposed by Erlandson [4]. For reverse transcriptase-polymerase chain reaction (RT-PCR), RNA extraction from paraffin-embedded tissue was performed as published previously [11, 18] with several modifications. After deparaffinization with Xylol, the tissue was lysed in 0.5 ml of 2% proteinase K solution at 56°C. RNA was extracted from the lysate with 2 ml Trizol® (phenol/guanidine isothiocyanate reagent, Invitrogen) according to the manufacturer's protocol. 1 μg total RNA was reverse-transcribed. Primer pairs for amplification of the PAX3/FKRH and PAX7/FKHR fusion transcripts [produced by the t(2;13)(q35;q14), and t(1;13)(p36;q14)] were selected according to the NCBI GenBank sequences, generating fragments less than 300 bp in consideration of the limited cDNA fragment size. PCR was performed using 5-μl cDNA template. For control of RNA quality and reverse transcription, the *gapdh* RNA of the tumor tissue was amplified. Validation of PCR products was done by automated sequencing (ABIprism 310, Perkin Elmer). Comparative genomic hybridization (CGH) was performed as described elsewhere [12]. The software package Quips (Applied Imaging, Newcastle, UK) has been used for evaluation of CGH data. Freshly frozen tumor tissue (20 sections, 10 μm each) was microdissected to assure 80–90% tumor purity. In addition, a patient's blood sample (20 ml) was analyzed concerning possible inherited chromosomal imbalances.

DNA was isolated with a QIAamp tissue kit (Qiagen, Hilden, Germany). Tumor and reference DNA were labeled by nick translation. Labeling and CGH were performed as described previously [12, 13]. Twelve metaphases were recorded and evaluated, their ratio profiles averaged and 95% confidence intervals calculated using the Quips software package. Thresholds for gains and losses were set to 1.18 and 0.82, respectively. A sample from healthy muscle tissue served as negative control, a tumor cell line with known defects (MPE 600; Vysis/Abbott, Wiesbaden, Germany) as positive control.

Results

Gross findings

The tumor was totally resected en bloc with a rim of noninvolved soft tissue at the margins, partly marginal resection. The lesion was ovally shaped, relatively well circumscribed, and presented as a soft to firm mass located within the deep muscles of the lower leg. The neoplasm showed an extend already to the subcutis and dermis causing skin ulceration. Maximum tumor sizes were 11.8×9.5×10.5 cm. The cut surface was characterized by a soft to firm consistency, whitish, with focal areas of hemorrhage (Fig. 1a).

Microscopic immunohistochemical findings

The neoplasm consisted mainly of relatively evenly distributed round and spindle-shaped tumor cells embedded within a hyalinized, sclerotic matrix. The tumor cells formed nests and anastomosing chords. Some more solid areas were characterized by an increased cellular density and larger areas of the neoplasm contained tumor cells arranged in short fascicles with elongated cells in a fibrotic,

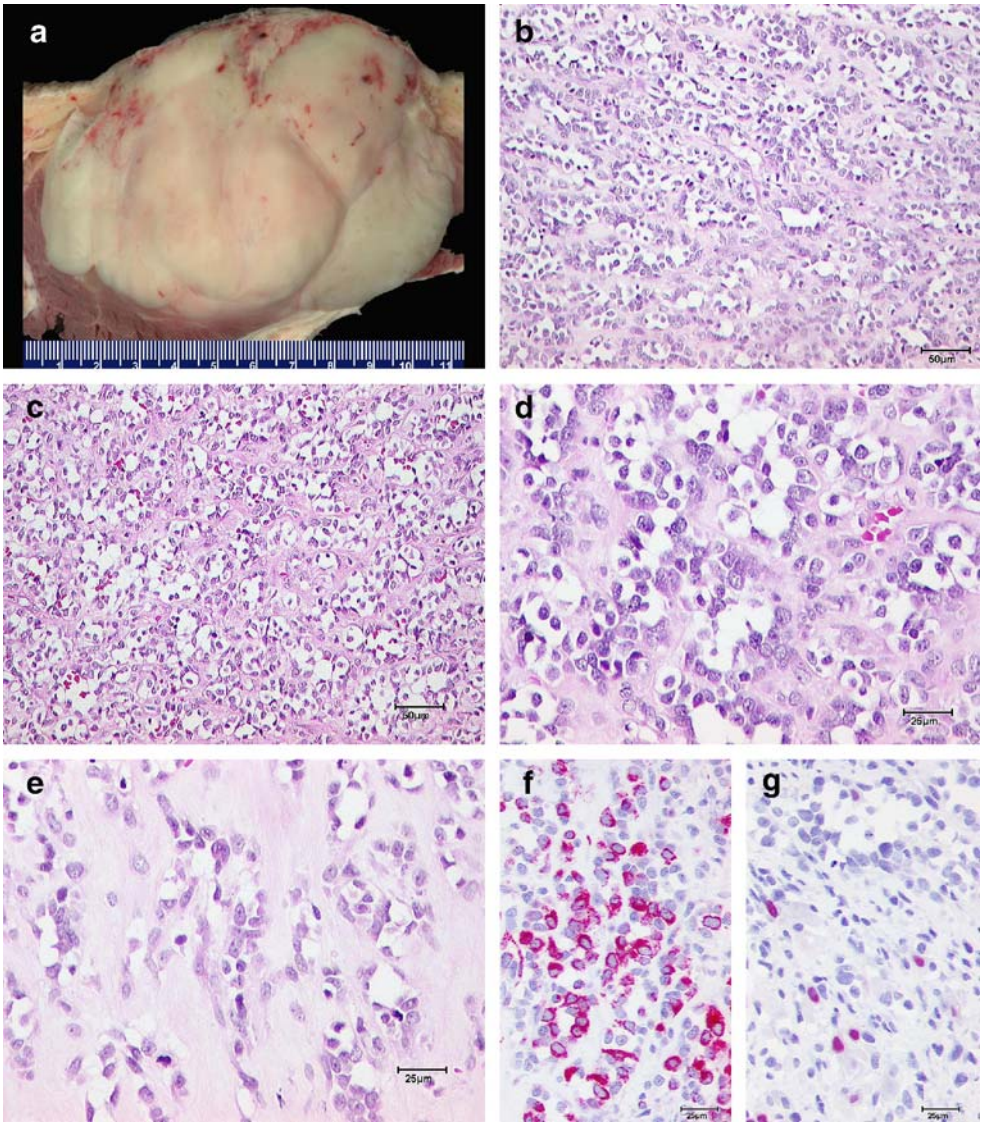

Fig. 1 Macroscopic and microscopic findings in sclerosing (pseudovascular) rhabdomyosarcoma. **a** White cut surface of deeply seated tumor with hemorrhagic areas and protrusion of the overlying, partly ulcerated skin, tumor size in this photograph around 11 cm. **b** Tumor cells arranged in pseudovascular aggregates. **c** Tumor cells showing a clear cytoplasm/cytoplasmic vacuolization. **d** Relatively small tumor cells, partly with eosinophilic cytoplasm and fibrotic matrix, slight microalveolar growth pattern. **e** Rhabomyoblastic tumor cells with faintly eosinophilic cytoplasm lying in densely sclerotic stroma, pseudovascular spaces. **f** Strong cytoplasmic immunoreactivity for desmin. **g** Nuclear immunoreactivity for myogenin (myf-4)

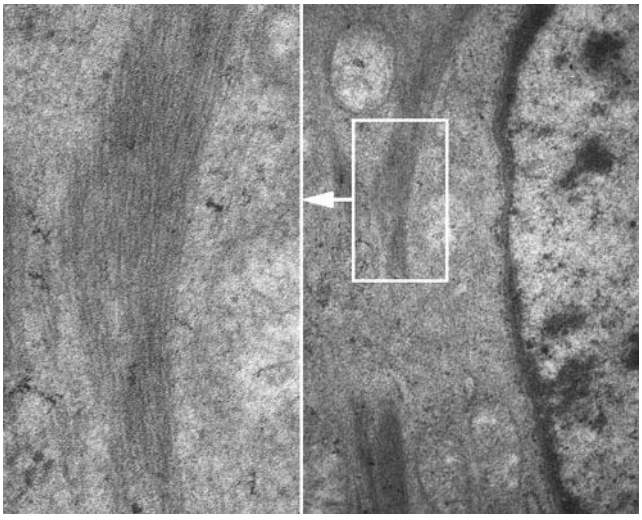

Fig. 2 Ultrastructure of a tumor cell showing loosely arranged and in general disorganized fibrils intracytoplasmatically without well-formed Z-bands or abortive Z-bands (primary magnification of figure to the *right*: 20,000×; inset of figure to the *right* with higher magnification to the *left*)

hyalinized stroma. No vascular invasion was obvious. A striking pseudovascular growth pattern was created by anastomosing spaces that were lined by tumor cells with tufts and pseudopapillae. This growth pattern was reminiscent of angiosarcoma. Overall, the tumor stroma was composed of hyalinized collagen without matrix calcification. Some tumor cells contained small amounts of eosinophilic cytoplasm but without rhabdomyoblastic strap cells, multinucleated cells, or tumor cell lacunae. No glycogen was noted (PAS-staining negative). The nuclei usually showed only faint to moderate pleomorphism with weak hyperchromatism and small, inconspicuous nucleoli. The mean mitotic rate was 7 per 10 high power field (=HPF, ×40, evaluation of a total of 140 HPF); in general, the more cellular, less sclerotic regions exhibited an increased mitotic activity (up to a maximum of 18 mitoses per 10 HPF in cellular areas). Small areas of coagulation necrosis (≤50% of tumor extension) were evident. The tumor showed the same morphological aspect in the biopsy and resection specimen (Fig. 1b–e). Only focally, a slight microalveolar growth pattern (Fig. 1d) developed, but no large alveoli, characteristic of alveolar RMS, could be detected.

Immunohistochemically, the tumor cells were diffusely cytoplasmatically reactive for desmin (++, 40% positive tumor cells) (Fig. 1f), muscle-specific actin (HHF 35) (++, 45% positive tumor cells, predominant dot-like staining pattern), and vimentin (+++, 90–100% positive tumor cells), a strong membraneous reactivity was noted for CD99 (+++, 90–100% positive tumor cells). Approximately 80% of tumor cells showed a strong positive nuclear

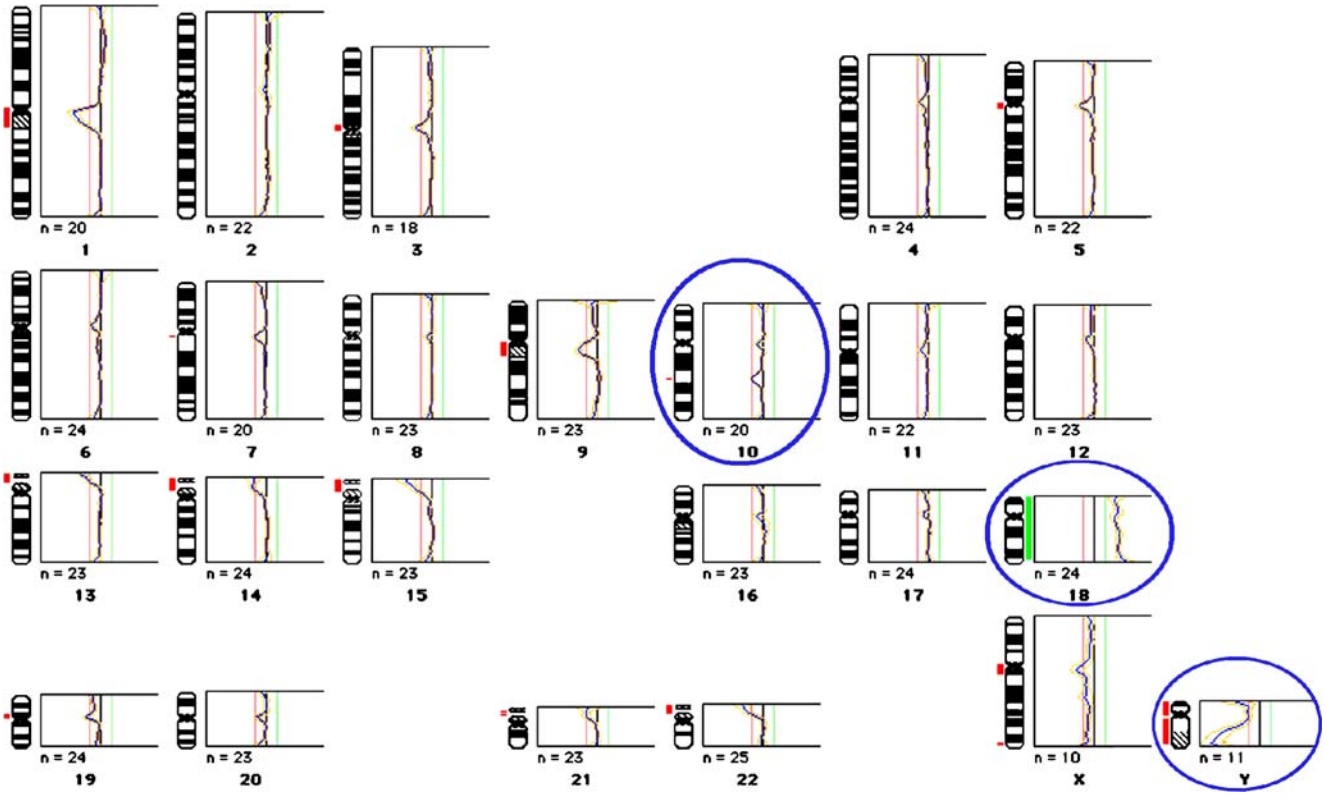

Fig. 3 CGH sum karyogram revealing three chromosomal imbalances: a narrow defect area that showed a loss at 10q22, a gain of the whole of chromosome 18 (trisomy), a loss of the Y chromosome (each of these chromosomes surrounded by a *blue circle*)

staining for MyoD1, only some tumor nuclei for myf-4 (myogenin) (Fig. 1g). No reactivity could be detected with antibodies against smooth-muscle actin, myoglobin, cytokeratins, EMA, CD 31, CD 34, factor VIII-associated antigen, S-100, and NSE. The Ki-67-proliferation index (antibody MIB-1) was approximately 20% (in hot spots).

Ultrastructural findings

Ultrastructurally, the tumor cells contained loosely arranged and in general disorganized fibrils intracytoplasmatically (Fig. 2). True distinction between thin and thick myofibrils was not possible. Well-formed Z-bands, abortive Z-bands or ribosome/myofibril complexes could not be detected. The abundant developed tumor matrix was characterized ultrastructurally by densely arranged collagen bundles.

RT-PCR

Molecular pathological investigations could not identify chimeric RNA transcripts due to a t(1;13) p36;q14) or t(2;13)(q35;q14) using RT-PCR.

Comparative genomic hybridization

The CGH profile revealed a total of three chromosomal imbalances: a gain of the whole of chromosome 18 (trisomy), a loss of the Y chromosome and a narrow defect area that showed a loss at 10q22 (Fig. 3). No inherited chromosomal imbalances and no cytogenetic defects were detected when analyzing the patient's normal blood sample.

Final diagnosis Sclerosing, pseudovascular RMS.

Discussion

SRMS represents a rare subtype within the spectrum of RMS with only 26 cases being described so far in the English written literature [2, 3, 5, 10, 15, 17, 19]. Its true nature as a distinctive entity of RMS has been discussed intensely and controversially. The results presented in this study delineate ultrastructural and genetic findings that give insights into additional aspects of this rare variant of RMS.

Pleomorphic RMS usually follows a quite aggressive clinical course with overall poor prognosis [6, 7, 9], seemingly worse than other pleomorphic sarcomas [16]. From seven originally described patients who suffered from sclerosing (pseudovascular) rhabdomyosarcoma, two patients developed metastatic disease [5, 15]. The most common recent case was diagnosed with multiple metastases 12 months after surgery [3]. In the patient described in this study, lung and pleural metastases occurred 6 months after tumor resection, indicating an aggressive clinical course. Based on short periods of follow-up in the original papers and the own observation, only limited information is available at the moment concerning the final clinical outcome of this rare variant of RMS.

Ultrastructure

Electron microscopy revealed irregularly arranged filaments within the tumor cells. These filaments showed diameters of about 10–20 nm and appeared as bundles of disorganized fibrils. The filaments might represent disorganized myofibrils, although a clear distinction, e.g., between thin and thick myofilaments could not be obtained. Taken together, a true myogenous nature of the filaments observed in our case cannot be definitively proved, but might be possible.

Molecular genetics and cytogenetics

Molecular pathological investigations could not identify chimeric RNA transcripts due to a t(1;13)(p36;q14) or t(2;13)(q35;q14) using RT-PCR. Thus, the characteristic translocations of alveolar rhabdomyosarcoma are not a feature of SRMS in our case. In addition, the observed staining patterns of immunohistochemistry with strong expression of MyoD1 in nearly each tumor nuclei and only focal positivity for myogenin—a finding identical to the results of Folpe et al. [5] in their series—further does not favor a relationship of SRMS with alveolar RMS.

The frequency and pattern of chromosomal imbalances of the index case is somewhat different from that of alveolar RMS and embryonal RMS. Both subtypes show numerous gains and losses, including high-level amplifications, with an average of 6.9 defects per case using comparative genomic hybridization [1, 20]. The recent report by Croes et al. [3] was the first to describe a classical cytogenetic analysis of a SRMS case. The six defects were mostly gains of whole chromosomes (11, 16, 18, and 21) that, in view of the authors, were indications for a close relationship to embryonal RMS. In contrast, our case has only three defects that—as a pattern—are not frequently found in CGH results of most alveolar and embryonal RMS. However, a recently published investigation of seven pleomorphic RMS reports, besides many other chromosomal imbalances (12.4 defects/case on average), a gain of chromosome 18 in one case (14%), and partial gains of 18 in three more cases (43%), as well as losses on chromosome 10 with a smallest region of overlap around 10q23 in five of seven cases (71%) [8].

The resolution of the CGH method is usually limited to 10–20 megabasepairs. While high-level amplifications of smaller regions can be found more easily, small losses are

usually difficult to detect. In our case, a combination of fresh tissue of good quality, careful microdissection, and relatively low tumor heterogeneity resulted in excellent material for CGH with low background noise. The resulting averaged ratio profiles with narrow 95% confidence intervals allowed a clear detection of the small defect on chromosome 10 (10q22) in this case of a SRMS, which otherwise would have been lost in the background noise. It seems possible that more RMS might carry small deletions in that region that evade detection by classical CGH. Thus, the narrow region around 10q22 might hint at an interesting locus for genes involved in sarcomagenesis or tumor progression in RMS, especially in the sclerosing pseudovascular variant. There are several putative tumor suppressor genes at 10q22–23, some of them involved in colon cancer. The chromosomal region 10q22.3 harbors the gene of BMPR1A (bone morphogenetic protein receptor, type 1A), the *PJI* gene (polyposis, juvenile intestinal) as well as the *CD* gene (Cowden disease). The adjacent 10q23.31 region carries the *PTEN* gene (phosphatase and tensin homolog), which codes for a cell cycle regulator. Further analysis of the 10q region, preferably with higher resolution methods like matrix-CGH (array CGH) or fluorescence in situ hybridization (FISH), should yield an answer to the question which genes are affected in SRMS and whether small deletions are present in other subtypes of RMS as well. The gain of the whole of chromosome 18 (trisomy) as well as the loss of the Y chromosome cannot be finally evaluated at the moment. In general, trisomies and loss of Y are common nonspecific findings in several malignancies. It remains to be discussed whether these chromosomal changes represent decisive events for the pathogenesis of SRMS.

Taken together, immunohistochemical, ultrastructural, and genetic analyses do not support a clear categorization of our case as either embryonal, alveolar, or pleomorphic subytype of RMS. Although the CGH findings are partly similar to changes in pleomorphic RMS, but less comparable to alveolar and embryonal RMS, the summarized results argue against a pleomorphic variant. Not taking differences in the applied methods into account, the cytogenetic differences between the results obtained by Croes et al. and our own findings probably reflect the variability in this tumor entity. Therefore, more cases of this rare neoplasm have to be analyzed by CGH or comparable methods to allow an unambiguous classification of SRMS on the genetic level.

Acknowledgements The authors gratefully acknowledge the excellent technical assistance of Cornelia Troske (Institute for Pathology, University Hospital Bergmannsheil, Bochum, Germany), Alice Kasprzynski (Max-Planck-Institute for Molecular Physiology, Dortmund, Germany), and Matthias Krams, M.D. (Institute of Pathology, University Hospital Schleswig-Holstein, Campus Kiel, Germany).

References

1. Bridge JA, Liu J, Qualman SJ, Suijkerbuijk R, Wenger G, Zhang J, Wan X, Baker KS, Sorensen P, Barr FG (2002) Genomic gains and losses are similar in genetic and histologic subsets of rhabdomyosarcoma, whereas amplification predominates in embryonal with anaplasia and alveolar subtypes. Genes Chromosomes Cancer 33:310–321
2. Chiles MC, Parham DM, Qualman SJ, Teot LA, Bridge JA, Ullrich F, Barr FG, Meyer WH, Soft Tissue Sarcoma Committee of the Children's Oncology Group (2004) Sclerosing rhabdomyosarcomas in children and adolesents: a clinicopathologic review of 13 cases from the Intergroup Rhabdomyosarcoma Study Group and Children's Oncology Group. Pediatr Dev Pathol 7:583–594
3. Croes R, Debiec-Rychter M, Cokelaere K, De Vos R, Hagemeijer A, Sciot R (2005) Adult sclerosing rhabdomyosarcoma: cytogenetic link with embryonal rhabdomyosarcoma. Virchows Arch 446:64–67
4. Erlandson RA (1994) Rhabdomyoma and rhabdomyosarcoma. In: Diagnostic transmission electron microscopy of tumors. Raven Press, New York, pp 700–710
5. Folpe AL, McKenney JM, Bridge JA, Weiss SW (2002) Sclerosing rhabdomyosarcoma in adults—report of four cases of a hyalinizing, matrix-rich variant of rhabdomyosarcoma that may be confused with osteosarcoma, chondrosarcoma or angiosarcoma. Am J Surg Pathol 26:1175–1183
6. Furlong MA, Mentzel T, Fanburg-Smith JC (2001) Pleomorphic rhabdomyosarcoma in adults: a clinicopathologic study of 38 cases with emphasis on morphologic variants and recent skeletal muscle-specific markers. Mod Pathol 14:595–603
7. Gaffney EF, Dervan PA, Fletcher CDM (1993) Pleomorphic rhabdomyosarcoma in adulthood. Analysis of 11 cases with definition of diagnostic criteria. Am J Surg Pathol 17:601–609
8. Gordon A, McManus A, Anderson J, Fisher C, Abe S, Nojima T, Pritchard-Jones K, Shipley J (2003) Chromosomal imbalances in pleomorphic rhabdomyosarcomas and identification of the alveolar rhabdomyosarcoma-associated PAX3-FOXO1A fusion gene in one case. Cancer Genet Cytogenet 140:73–77
9. Hollowood K, Fletcher CDM (1994) Rhabdomyosarcoma in adults. Semin Diagn Pathol 11:47–57
10. Knipe TA, Chandra RK, Bugg MF (2005) Sclerosing rhabdomyosarcoma: a rare variant with predeliction for the hand and neck. Laryngoscope 115:48–50
11. Krams M, Claviez A, Heidorn K, Krupp G, Parwaresch R, Harms D, Rudolph P (2001) Regulation of telomerase activity by alternate splicing of human telomerase reverse transcriptase mRNA in a subset of neuroblastomas. Am J Pathol 159:1925–1932
12. Krismann M, Adams H, Jaworska M, Müller KM, Johnen G (2000) Patterns of chromosomal imbalances in benign solitary fibrous tumours of the pleura. Virchows Arch 437:248–255
13. Krismann M, Müller KM, Jaworska M, Johnen G (2002) Molecular cytogenetic differences between histological subtypes of malignant mesotheliomas: DNA cytometry and comparative genomic hybridization of 90 cases. J Pathol 197:363–371
14. Kuhnen C, Herter P, Muller O, Muehlberger T, Krause L, Homann H, Steinau HU, Muller KM (2000) β-Catenin in soft tissue sarcomas: expression is related to proliferative activity in high-grade sarcomas. Mod Pathol 13:1005–1013
15. Mentzel T, Katenkamp D (2000) Sclerosing, pseudovascular rhabdomyosarcoma in adults—clinicopathological and immunohistochemical analysis of three cases. Virchows Arch 436:305–311
16. Miettinen M (1988) Rhabdomyosarcoma in patients older than 40 years of age. Cancer 62:2060–65
17. Nascimento AF, Fletcher CDM (2005) Spindle cell rhabdomyosarcoma in adults. Am J Surg Pathol 29:1106–1113

18. Poremba C, Schell C, Hero B, Christiansen H, Schaefer KL, Nakayama J, Berthold F, Juergens H, Boecker W, Dockhorn-Dworniczak B (2000) Telomerase activity and telomerase subunits gene expression patterns in neuroblastoma: a molecular and immunohistochemical study establishing prognostic tools for fresh-frozen and paraffin-embedded tissues. J Clin Oncol 18: 2582–2592
19. Vadgama B, Sebire NJ, Malone M, Ramsay AD (2004) Sclerosing rhabdomyosarcoma in childhood: case report and review of the literature. Pediatr Dev Pathol 7:391–396
20. Weber-Hall S, Anderson J, McManus A, Abe S, Nojima T, Pinkerton R, Pritchard-Jones K, Shipley J (1996) Gains, losses, and amplification of genomic material in rhabdomyosarcoma analyzed by comparative genomic hybridization. Cancer Res 56:3220–3224

Virchows Arch (2006) 449:579–584
DOI 10.1007/s00428-006-0279-1

CASE REPORT

Adamantinoma-like Ewing's sarcoma with EWS-FLI1 fusion gene: a case report

Hiromasa Fujii · Kanya Honoki · Yasunori Enomoto · Takahiko Kasai · Akira Kido · Itsuto Amano · Makiko Kumamoto · Toru Morishita · Yoshio Mii · Akitaka Nonomura · Yoshinori Takakura

Received: 16 June 2006 / Accepted: 18 July 2006 / Published online: 3 October 2006
© Springer-Verlag 2006

Abstract Recent studies have advocated the genotypic and phenotypic delineation of a novel Ewing's sarcoma histologic variant showing epithelial features defined as "adamantinoma-like Ewing's sarcoma". We described an 18-year-old girl with a primary small round-cell sarcoma of the right tibia showing polyphenotypic differentiation with epithelioid features. The neoplastic cells had mainly round or oval nuclei with fine chromatin with a portion of epithelial arrangements. The immunohistochemical analysis showed the epithelial markers of cytokeratin 5/6/18, AE1/AE3, and cytokeratin high molecular weight were stained especially in the foci with epithelioid features, as well as MIC2, S100, and NSE. The diagnosis of the lesion was confirmed as Ewing's sarcoma by the presence of the EWS-FLI1 fusion transcript, and could be defined as the so-called "adamantinoma-like Ewing's sarcoma". After wide excision and high-dose chemotherapy with peripheral blood stem cell transfusion, the patient has been well and continuously event-free for 3 years since the initial diagnosis.

Keywords Adamantinoma · Ewing's sarcoma · Epithelioid · Immunohistochemistry · EWS-FLI1 fusion gene

Abbreviations

VCR	vincristine
CBDCA	carboplatin
CYC	cyclophosphamide
HDCT	high-dose chemotherapy
IFM	ifosphamide
I-PAM	melphalan
NSE	neuron-specific enolase
PBSCT	peripheral blood stem cell transfusion
RT-PCR	reverse transcriptase-polymerase chain reaction
α-SMA	α-smooth muscle actin
THP	piarubicin
VP-16	etoposide

H. Fujii · K. Honoki (✉) · A. Kido · Y. Takakura
Department of Orthopedic Surgery, Nara Medical University,
840 Shijo-cho,
Kashihara, Nara 634-8521, Japan
e-mail: kahonoki@nmu-gw.cc.naramed-u.ac.jp

Y. Enomoto · T. Kasai · A. Nonomura
Department of Diagnostic Pathology, Nara Medical University,
840 Shijo-cho,
Kashihara, Nara 634-8521, Japan

I. Amano · M. Kumamoto
Hematology and Oncology Unit, Department of Medicine,
Nara Medical University,
840 Shijo-cho,
Kashihara, Nara 634-8521, Japan

T. Morishita · Y. Mii
Department of Orthopedic Surgery,
National Hospital Organization Nara Medical Center,
840 Shijo-cho,
Kashihara, Nara 634-8521, Japan

Introduction

Ewing's sarcoma is a highly malignant skeletal or extraskeletal tumor mainly affecting children. This type of tumor was originally defined in 1921 by James Ewing as a primitive malignant tumor characterized by uniform, densely packed small cells, without distinct cytoplasmic borders or prominent nucleoli [7, 25], and it is now considered to be of neuroectodermal origin. The differential diagnosis includes rhabdomyosarcoma, neuroblastoma, and lymphoma, which are referred to as small, round, blue cell tumors [25]. Over 90% of Ewing's sarcomas are genetically characterized by chromosomal translocation of t(11;22)

(q24;q21) [1, 24], resulting in fusion of the *EWS/FLI-1* gene [28], and the transcripts of the fusion gene have been established as a specific diagnostic tool for Ewing's sarcoma.

Adamantinoma is a rare tumor defined as a low-grade malignancy composed of epithelial cells in a fibrous or osteofibrous stroma [5, 21]. The tumor occurs almost exclusively in the long bones, most commonly in the anterior cortex and middle third of the tibial diaphysis [5]. The cellular origin of adamantinoma remains controversial. Adamantinoma has a wide histologic spectrum and sometimes shows epithelial-to-mesenchymal transition ("sarcomatoid dedifferentiation") [14].

van Haelst et al. reported the case of a 13-year-old girl with a tumor located in the metatarsus, with a differential diagnosis between adamantinoma and atypical Ewing's sarcoma [27]. Several reports have been published regarding "adamantinoma-like Ewing's sarcoma" or vice versa, i.e., "Ewing-like adamantinoma" [17–19]; however, very limited number of cases have been confirmed with molecular diagnosis of Ewing's sarcoma specific fusion transcripts.

Bridge et al. described three cases of Ewing's sarcomas with adamantinoma-like features, having EWS-FLI-1 fusion transcripts in the nuclei of cytokeratin immunoreactive cells, suggesting genotypic and phenotypic delineation of a novel Ewing's sarcoma histologic variant, adamantinoma-like Ewing's sarcoma [2]. In contrast, Hauben et al. reported that 12 cases of adamantinoma lacked both EWS-FLI-1 and EWS-ERG fusion transcripts [12]. The most recent and larger study reported by Folpe et al. described that 3 of 56 cases (5%) showed "adamantinoma-like" features expressing high molecular weight cytokeratins with genetic confirmation [9].

The current report describes a case of Ewing's sarcoma having adamantinoma-like features, both clinically and histologically with confirmatory fusion gene transcript.

Clinical history

An 18-year-old Japanese woman complained of pain in the right calf when she was running in December 2002. She did not have any previous history of trauma. The pain persisted and did not decline over the following several months. In April 2003, she consulted an orthopedist in the local community hospital, and this revealed a tumor in her right tibia. Radiography showed a well-demarcated, multi-lobular, radiolucent lesion in the tibial diaphysis, extending from the proximal region to half of the distal region with a thin cortex lacking any distinct periosteal reaction (Fig. 1a). Magnetic resonance imaging showed that the major axis of the lesion measured 17 cm in length (Fig. 1b). Laboratory data were unremarkable and an extensive work-up, including chest computed tomography and technetium sintigraphy, revealed no other lesions.

Open biopsy was subsequently performed. The tumor consisted of small round cells with portions of dense eosinophilic matrices (Fig. 2a,b) showing positive immunoreactivity to S-100 protein and NSE, which led to a diagnosis of Ewing's sarcoma. The patient was referred to our university hospital in June 2003.

After preoperative chemotherapy consisting of two courses of vincristine (VCR, 1.3 mg/m^2), cyclophosphamide (CYC, 2 g/m^2), and pirarubicin (THP, 50 mg/m^2), two courses of ifosphamide (IFM, 14 g/m^2) and etoposide (VP-16, 20 mg/m^2), and 45 Gy radiotherapy, wide excision of two-thirds of the upper portion of the tibial diaphysis was performed, and the defect was replaced by a prosthesis in October 2003. This was followed by postoperative high-dose chemotherapy (HDCT) consisting of carboplatin (CBDCA, 1.6 g/m^2), VP-16 (1 g/m^2), and melphalan (I-PAM, 180 mg/m^2) with peripheral blood stem cell transfusion (PBSCT). She has shown continuous disease-free status with no evidence of local recurrence or distant metastatic lesions in 3 years since the initial

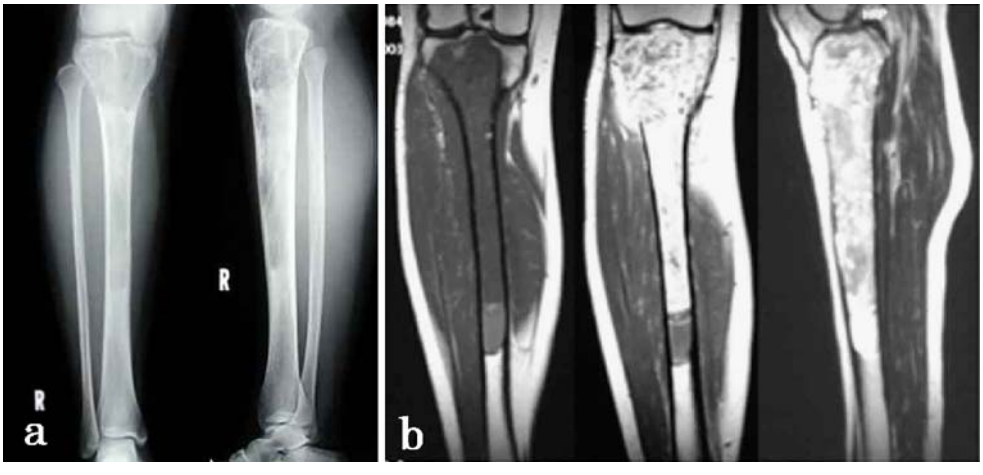

Fig. 1 **a** Radiograph showing well-demarcated, multi-lobular, radiolucent lesion in the tibial diaphysis, extending from the proximal region to the distal half; **b** magnetic resonance imaging showing that the major axis of the lesion measured 17 cm long

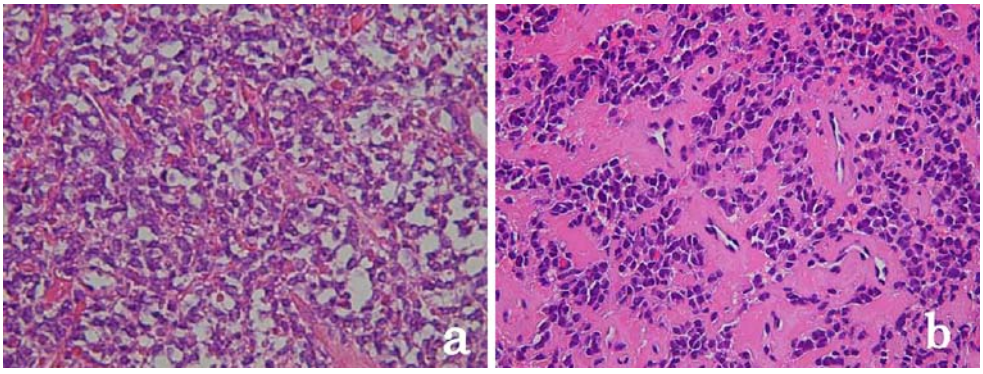

Fig. 2 **a** The histological appearance of biopsy specimen showing tumor composed of small round blue cell, ×200; **b** the portion with dense eosinophilic matrix, ×200

diagnosis, and functional status was 80% of Enneking's grading system [6].

Materials and methods

The patient was diagnosed with Ewing's sarcoma at initial biopsy. After referral to our hospital, she was treated preoperatively with IFM, VP-16, THP, VCR, and CYC combined with radiotherapy, followed by tumor-wide-area excision and artificial joint replacement. The whole tumor specimen was fixed in buffered formalin, embedded in paraffin, and sent for pathological investigation; a part of the specimen was snap-frozen for genetic analysis.

Sections were routinely stained with hematoxylin and eosin, and periodic acid-Schiff (PAS) staining with or without diastase digestion, and stained with Azan. Immunohistochemistry for protein CD99 (1:50~100; Dako N1593, CA, USA), CD45 (LCA) (1:1600; Dako), CD31 (1:30; Dako), CD34 (1:25~50; Dako N1632), cytokeratin AE1/AE3 (Predilute; Zymed Laboratories, CA, USA), cytokeratin 5/6/18 (1:100; Novocastra Laboratories, UK), high molecular CK (1:80; Dako), cytokeratin 7 (1:50; Novocastra), cytokeratin 20 (1:50; Novocastra), HHF35 (1:50~100; Dako N1567), factor VIII (1:150; Novocastra), S-100 (1:3000; Dako), neuron-specific enolase (NSE) (1:200; Novocastra), synaptophysin (1:80; Dako), chromgranin A (1:100; Dako), CEA (1:25~50; Dako N1586), α-smooth muscle actin (α-SMA) (1:100; Dako), vimentin (1:100; Dako), and EMA (1:80; Dako) was performed on formalin-fixed, paraffin-embedded tissues.

Genetic analysis by reverse transcriptase-polymerase chain reaction (RT-PCR) to detect the fusion genes was performed using RNA from snap-frozen tumor specimens taken at the time of operation. The sequences of primer sets used for RT-PCR were 5′-CTA CAA TGA GCT GCG TGT GGC-3′ and 5′-CAG GTC CAG ACG CAG GAT GGC-3′ for β-actin, 5′-TCC TAC AGC CAA GCT CCA AGT C-3′ and 5′-ACT CCC CGT TGG TCC CCT CC-3′ for EWS-FLI1. The product of RT-PCR was purified and sequenced using an ABI Prism Sequencer.

Results

The tumor was removed along with almost two-thirds of the proximal portion of the tibia and part of the muscles including the anterior tibia and the toe extensors. Gross appearance of the resected specimen from the surgery showed an intramedullary tumor extended from epiphysis to diaphysis without any distinct periosteal reaction.

Histologically, the tumor cells lay scattered in the tibial diaphysis, diffusely proliferating within an area of necrosis. There was also abundant blood vessel formation and intratumoral hemorrhage. The neoplastic cells had mainly round or oval nuclei with fine chromatin, single small nucleoli (Fig. 3a), and an eosinophilic matrix without distinctive cell borders. In addition, there was cystic space formation and several nest formations with epithelioid clusters showing basaloid patterns (Fig. 3b) and squamoid patterns with keratinization (Fig. 3c), and tubular patterns (Fig. 3d). Tumor cells infiltrated the periosteum and surrounding muscles; however, no further extension was observed at the edge of the resected specimen. The response to preoperative chemotherapy was very poor, evaluated as grade 2 using the Huvos grading system, also classified as moderate effect (solid areas of remnant viable tumor) proposed by van der Woude HJ et al. [10, 26]. A moderate number of tumor cells showed PAS-positive cytoplasmic granularity, but neither collagen fibers nor osteoid were detected with Azan stain.

The immunohistochemical findings are summarized in Table 1. The immunoreactivity was evaluated as negative if staining found in less than 5% of neoplastic cells, partially positive in 5–50%, and positive in more than 50%. The tumor cells were positive for NSE, S-100, CD99, cytokeratin 5/6/18, AE1/AE3, and high-molecular weight cytokeratin 20, vimentin, CEA, and negative for cytokeratin 7, synatophysin, chromograninA, CD45 (LCA), CD 31, CD 34, factor VIII, LCA, α-SMA, HHF35. The epithelial makers such as cytokeratin 5/6/18, cytokeratin high-molecular weight, AE1/AE3 and EMA showed particularly prominent staining in the cells with epithelioid features.

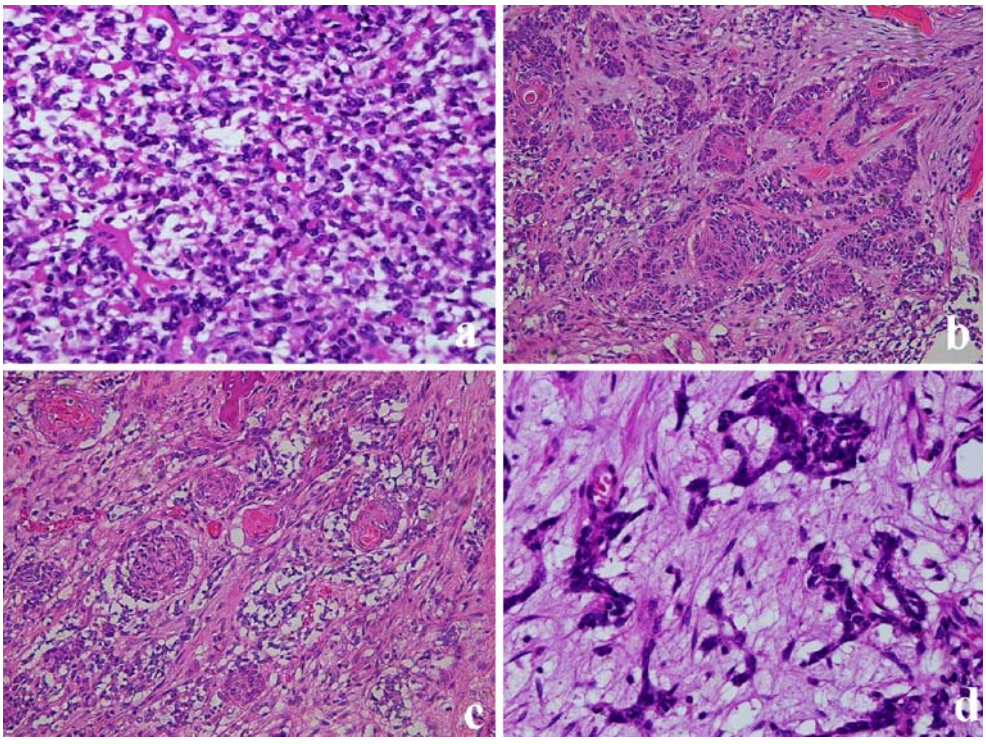

Fig. 3 **a** Neoplastic cells showing mainly round or oval nuclei with fine chromatin, single small nucleoli, ×200; 112×82 mm (150×150 DPI); **b** neoplastic cells showing several nest formations with epithelioid clusters showing keratinoid, ×100; 112×84 mm (150×150 DPI); **c** neoplastic cells showing squamoid features, ×100; 112×85 mm (150×150 DPI); **d** neoplastic cells showing tubular patterns, ×200; 111×84 mm (150×150 DPI)

RNA was extracted from the snap-frozen specimen and RT-PCR was performed to detect fusion transcripts. The results showed the EWS-FLI1 fusion transcript in tumor tissue (Fig. 4) and confirmed it as a type 1 variant of this type of fusion gene by sequencing. No EWS-ERG fusion transcript was found (data not shown).

Because of the insufficient response to preoperative chemotherapy, we used HDCT, which consisted of CBDCA, VP-16 and I-PAM with PBSCT, in addition to the conventional protocol with VCR, THP, CYC, and irinotecan (CPT-11, 100 mg/m^2) in combination with 20 Gy radiotherapy. The patient has remained alive for 3 years after initial diagnosis with continuous event-free status. The function of the knee was excellent in accordance with Enneking's grading system [6].

Discussion

The present report describes a polyphenotypic round-cell sarcoma, with the primary site being the right tibia. The presence of the EWS-FLI1 fusion transcript in the present tumor was strongly supportive of Ewing's sarcoma; however, the clinical, histologic, and immunohistochemical features were atypical.

Ewing's sarcoma is a highly malignant small round-cell tumor of neuroectodermal origin. Diagnosis of this type of tumor is based on its histochemical and immunohistochemical characteristics. The cells of Ewing's sarcoma usually contain glycogen (PAS-positive, digested by diastase) and are immunoreactive for NSE, vimentin, and S-100 protein. A recent study demonstrates that it also shows high immunoreactivity for CD99, which is indicative of high

Table 1 The results of immunohistochemical study

Antigen	Small round-cell region	Squamoid/ basaloid cell region	Tubular cell region
CD99 (MIC2)	++	+	++
Cytokeratin HMW	−	++	+
AE1/AE3	+	++	+
Cytokeratin 5/6/18	−	++	+
Cytokeratin 7	−	−	−
Cytokeratin 20	−	+	−
EMA	−	+	+
S-100	++	+	++
NSE	++	+	++
Synatophysin	−	−	−
ChromograninA	−	−	−
Vimentin	+	−	+
CD45 (LCA)	−	−	−
CD31	−	−	−
CD34	−	−	−
Factor VIII	−	−	−
a-SMA	−	−	−
HHF35	−	−	−
CEA	+	+	+
PAS	+	+	+

− negative, + partially positive, ++ positive

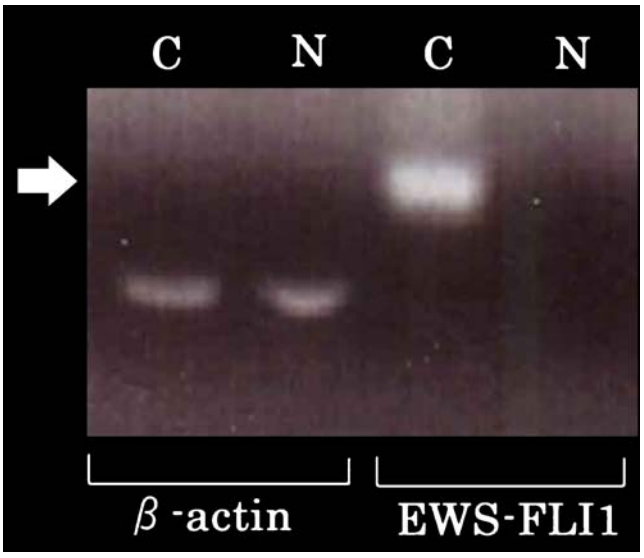

Fig. 4 Results of RT-PCR demonstrating an EWS-FLI1 fusion transcript (*arrow*) in the tumor sample. *C* Case; *N* negative control. The β-actin was used as an internal control

expression of the *MIC2* gene product [8]. Over 90% of Ewing's sarcoma and primitive neuroectodermal tumors are genetically characterized by t(11;22), resulting in fusion of the *EWS-FLI1* gene. Adamantinoma of the long bones is a rare tumor and defined as a relatively low-grade malignant tumor with epithelial features. Hazelbag et al. reported about 32 patients who had had an adamantinoma of the long bones, and about 5 histological patterns of differentiation that are characteristic of adamantinoma were observed, including the basaloid, spindle-cell, tubular, squamous, and osteofibrous dysplasia-like subtypes [15]. This epithelial nature is further demonstrated by immunoreactivity for cytokeratins [13]. Ewing's sarcoma and adamantinoma are not generally considered to be related lesions and showed totally different biological behavior and prognostic nature. However, several cases have been described since 1975, demonstrating tumors with microscopic, immunohistochemical or ultrastructural features of both Ewing's sarcoma and adamantinoma [17–19, 27]. The most recent report by Folpe et al. defined the untypical Ewing's sarcoma as "adamantinoma-like", typical primitive neuroectodermal tumor, spindle-cell sarcoma-like, sclerosing, and large-cell type, and "adamantinoma-like" type consisted of 5% of this type of tumor [9].

In the present case, the tumor was diffusely extended with a well-demarcated, multi-lobular radiolucent lesion in the tibial diaphysis, extending from the proximal region to the distal half, lacking the distinct periosteal reaction usually observed in Ewing's sarcoma. The pathological findings indicated that it mainly consisted of small round cells, but some showed epithelioid features by both histological and immunohistochemical analysis. The cytological features of small round cells, the presence of glycogen and immunoreactivity for NSE, S-100, and CD99 were consistent with Ewing's sarcoma, and the expression of EWS-FLI1 fusion gene by RT-PCR confirmed this diagnosis. The distinctive feature of this tumor was the presence of nests of cells with epithelioid features demonstrated by positive staining for epithelial markers such as cytokeratin 5/6/18, AE1/AE3, and high-molecular-weight cytokeratin.

Several reports have demonstrated expression of cytokeratins CK8 and 18, and AE1/AE3 was found in about 20% of Ewing's sarcoma by immunohistochemistry [11, 20]. Bridge et al. reported a variant Ewing's sarcoma with epithelioid features and proposed the term "adamantinoma-like Ewing's sarcoma" [2]. Folpe et al. described that three cases of "adamantinoma-like" Ewing's sarcoma showed a distinctly nested, epithelioid growth pattern with surrounding desmoplasia, and characteristically expressed high-molecular-weight cytokeratins and pan-cytokeratins [9]. The current case showed distinctive characteristic features of this pattern. The small round-cell regions were positive only for AE1/AE3. Squamoid/basaloid cell regions were positive for cytokeratin HMW, AE1/AE3, cytokeratin 5/6/18, and cytokeratin 20, but not cytokeratin 7. Tubular cell regions were positive for cytokeratin HMW, AE1/AE3, cytokeratin 5/6/18 (Table 1).

There will be a possible argument on the differential diagnosis between Ewing's sarcoma and adamantinoma, i.e., "adamantinoma-like Ewing sarcoma" vs "Ewing-like adamantinoma". The present case showed sufficient evidence for Ewing's sarcoma with immunoreactivity for NSE, S-100 and CD99. Moreover, the presence of EWS-FLI1 fusion gene transcript was strongly supportive for the diagnosis of Ewing's sarcoma. The histogenesis of this lesion is not clear; however, Ewing's sarcoma is considered to be derived from primitive, pluripotential stem cells [22] that may differentiate into cells with mesenchymal, epithelial, and neuronal features. This may result in expression of phenotypes showing both epithelial and neuroectodermal differentiation in Ewing's sarcoma.

Appropriate treatment of this lesion has not yet been established, but it should be performed along with standard pre- and postoperative chemotherapy and wide surgical excision for Ewing's sarcoma. Recently, the risk-adapted treatment strategy has been proposed including HDCT with PBSCT [23]. However, the role of HDCT with or without PBSCT in the treatment of sarcomas has not yet been established, and the previous studies demonstrated that HDCT with PBSCT in the treatment of Ewing's sarcoma have limited benefits [3, 4, 16]. Although the risk of this variant of Ewing's sarcoma has not been fully defined, as the surgical specimen showed a poor response to preoperative chemotherapy in this case, we treated with postoperative HDCT and PBSCT, and the outcome has been excellent with continuous event-free status for 2.5 years after initial diag-

nosis. Further study will be needed to clarify the differences of prognosis and chemosensitivity between conventional Ewing's sarcoma and Ewing's sarcoma with epithelioid features, i.e. "adamantinoma-like Ewing's sarcoma".

We presented a case of Ewing's sarcoma showing epithelioid features resembling adamantinoma-like keratinoid, squamoid, tubular patterns with immunoreactivity for cytokeratin 5/6/18, AE1/AE3 and high-molecular-weight cytokeratin as well as NSE, S-100, and CD-99. The tumor contained the EWS-FLI1 fusion transcript, which strongly supported the diagnosis for Ewing's sarcoma. This case could be defined as a so-called "adamantinoma-like Ewing's sarcoma," and the HDCT with PBSCT combined with wide surgical resection would be beneficial for the treatment of this type of tumors.

Acknowledgement The authors thank Prof. Takayuki Nojima, Department of Pathology, Kanazawa Medical University, for his critical comments on this paper.

References

1. Aurias A, Rimbaut C, Buffe D, Dubousset J, Mazabraud A (1983) Translocation of chromosome 22 in Ewing's sarcoma. C R Seances Acad Sci III 296:1105–1107
2. Bridge JA, Fidler ME, Neff JR, Degenhardt J, Wang M, Walker C, Dorfman HD, Baker KS, Seemayer TA (1999) Adamantinoma-like Ewing's sarcoma: genomic confirmation, phenotypic drift. Am J Surg Pathol 23:159–165
3. Burdach S, Jurgens H, Peters C, Nurnberger W, Mauz-Korholz C, Korholz D, Paulussen M, Pape H, Dilloo D, Koscielniak E (1993) Myeloablative radiochemotherapy and hematopoietic stem-cell rescue in poor-prognosis Ewing's sarcoma. J Clin Oncol 11:1482–1488
4. Burdach S, Meyer-Bahlburg A, Laws HJ, Haase R, van Kaik B, Metzner B, Wawer A, Finke R, Gobel U, Haerting J, Pape H, Gadner H, Dunst J, Juergens H (2003) High-dose therapy for patients with primary multifocal and early relapsed Ewing's tumors: results of two consecutive regimens assessing the role of total-body irradiation. J Clin Oncol 21:3072–3078
5. Campanacci M, Giunti A, Bertoni F, Laus M, Gitelis S (1981) Adamantinoma of the long bones. The experience at the Institute Orthopedico Rizzoli. Am J Surg Pathol 5:533–542
6. Enneking WF, Dunham W, Gebhardt MC, Malawar M, Pritchard DJ (1993) A system for the functional evaluation of reconstructive procedures after surgical treatment of tumors of the musculoskeletal system. Clin Orthop 286:241–246
7. Ewing J (1972) Classics in oncology. Diffuse endothelioma of bone. James Ewing. Proceedings of the New York Pathological Society, 1921. CA Cancer J Clin 22:95–98
8. Fellinger EJ, Garin-Chesa P, Triche TJ, Houvos AG, Rettir WJ (1991) Immunohistochemical analysis of Ewing's sarcoma cell surface antigen p30/32^{MIC2}. Am J Pathol 139:317–325
9. Folpe AL, Goldblum JR, Rubin BP, Shehata BM, Liu W, Dei Tos AP, Weiss SW (2005) Morphologic and immunophenotypic diversity in Ewing family tumors. A study of 66 genetically confirmed cases. Am J Surg Pathol 29:1025–1033
10. Glasser DB, Lane JM, Huvos AG, Marcove RC, Rosen G (1992) Survival, prognosis, and therapeutic response in osteogenic sarcoma. The Memorial Hospital experience. Cancer 69:698–708
11. Gu M, Antonescue CR, Guiter G, Huvos AG, Ladanyi M, Zakowski MF (2000) Cytokeratin immunoreactivity in Ewing's sarcoma. Prevalence in 50 cases confirmed by molecular diagnostic studies. Am J Surg Pathol 24:410–416
12. Hauben E, van den Broek LCJM, van Marck E, Hogendoom PCW (2001) Adamantinoma-like Ewing's sarcoma and Ewing's-like adamantinoma. The t(11;22), t(21;22) status. J Pathol 195:218–221
13. Hazelbag HM, Fleuren GJ, van den Broek LJ, Taminiau AH, Hogendoorn PC (1993) Adamantinoma of the long bones: keratin subclass immunoreactivity pattern with reference to its histogenesis. Am J Surg Pathol 17:1225–1233
14. Hazelbag HM, Laforga JB, Roels HJ, Hogendoorn PC (2003) Dedifferentiated adamantinoma with revertant mesenchymal phenotype. Am J Surg Pathol 27:1530–1537
15. Hazelbag HM, Taminiau AHM, Fleuren GJ, Hogendoorn PCW (1994) Adamantinoma of the long bones. A clinicopathological study of thirty-two patients with emphasis on histological subtype, precursor lesion, and biological behavior. J Bone Joint Surg Am 76:1482–1499
16. Horowitz ME, Kinsells TJ, Wexler LH, Belasco J, Triche T, Tsokos M, Steinberg SM, McClure L, Longo DL, Steis RG (1993) Total-body irradiation and autologous bone marrow transplant in the treatment of high-risk Ewing's sarcoma and rhabdomyosarcoma. J Clin Oncol 11:1911–1918
17. Ishida T, Kikuchi F, Oka T, Machinami R, Kojima T, Iijima T, Higaki S, Imamura T (1992) Case report 727: juxtacortical adamantinoma of humerus (simulating Ewing tumor). Skelet Radiol 21:205–209
18. Lipper S, Kahn LB (1983) Case report 235: Ewing-like adamantinoma of the left radial head and neck. Skeletal Radiol 10:61–66
19. Meister P, Konrad E, Hubner G (1979) Malignant tumor of humerus with features of "adamantinoma" and Ewing's sarcoma. Pathol Res Pract 166:112–122
20. Moll R, Lee I, Gould VE, Berndt R, Roessner A, Franke WW (1987) Immunocytochemical analysis of Ewing's tumors. Patterns of expression of intermediate filaments and desmosomal proteins indicate cell type heterogeneity and pluripotential differentiation. Am J Pathol 127:288–304
21. Moon NF, Mori H (1986) Adamantinoma of the appendicular skeleton—updated. Clin Orthop Relat Res 204:215–237
22. Riggi N, Cironi L, Provero P, Suva ML, Kaloulis K, Garcia-Echeverria C, Hoffmann F, Trumpp A, Stamenkovic I (2005) Development of Ewing's Sarcoma from primary bone marrow-derived mesenchymal progenitor cells. Cancer Res 65:11459–11468
23. Rodriguez-Galindo C, Spunt SL, Pappao AS (2003) Treatment of Ewing Sarcoma family of tumors: current status and outlook for the future. Med Pediatr Oncol 40:276–287
24. Turc-Carel C, Philip I, Berger MP, Philip T, Lenoir GM (1984) Chromosome study of Ewing's sarcoma (ES) cell lines. Consistency of a reciprocal translocation t(11;12)(q24;q12). Cancer Genet Cytogenet 12:1–19
25. Ushigome S, Machinami R, Sorensen PH (2002) Ewing sarcoma/primitive neuroectodermal tumor (PNET). In: Fletcher CDM, Unni KK, Mertens F (ed) WHO classification of tumors. Pathology and genetics of tumors of soft tissue and bone. IARC, pp 153–154
26. van der Woude HJ, Bloem JL, Taminiau AH, Nooy MA, Hogendoorn PC (1994) Classification of histopathologic changes following chemotherapy in Ewing's sarcoma of bone. Skelet Radiol 23:501–507
27. van Haelst UJGM, de Haas van Dorsser AH (1975) A perplexing malignant bone tumor. Highly malignant so-called adamantinoma or non-typical Ewing's sarcoma. Virchows Arch A Pathol Anat Histol 365:63–74
28. Zucman J, Delattre O, Desmanze C, Plougastel B, Joubert I, Melot T, Peter M, De Jong P, Rouleau G, Aurias A (1992) Cloning a characterization of the Ewing's sarcoma and peripheral neuroepithelioma t(11;22) translocation breakpoints. Genes Chromosomes Cancer 5:271–277

Virchows Arch (2006) 449:585–590
DOI 10.1007/s00428-006-0291-5

CASE REPORT

Intrahepatic sarcomatoid cholangiocarcinoma of round cell variant: a case report and immunohistochemical studies

Katsuaki Sato · Hiroshi Murai · Yoshimichi Ueda · Shogo Katsuda

Received: 3 March 2006 / Accepted: 4 August 2006 / Published online: 11 October 2006
© Springer-Verlag 2006

Abstract Sarcomatoid transformation was observed in 4.5% of autopsied cases of intrahepatic cholangiocarcinoma. Here, we report a case of intrahepatic sarcomatoid cholangiocarcinoma with round cell feature, extremely rare variant. An 87-year-old man was incidentally found to have a tumor in the left lobe of the liver by abdominal computed tomography scans. The patient was clinically diagnosed to have intrahepatic cholangiocarcinoma and received palliative care without specific treatment. He died of hepatic insufficiency 3 months after the diagnosis. The autopsied liver specimens showed a reddish gray tumor of 4.0×2.8 cm in size. Histologically, the tumor was centrally hemorrhagic and necrotic and was composed of tubular adenocarcinoma and a round cell component, which has an eccentrically located nucleus and eosinophilic cytoplasm without mucin production. Immunohistochemically, the adenocarcinoma cells expressed cytokeratin 19 and β-catenin in their cytoplasm, with E-cadherin and CD44s at the plasma membrane. In the round cells, cytokeratin 19 and vimentin was detected in their cytoplasm and CD44s at the plasma membrane. E-cadherin immunoreactivity was weakly present in their cytoplasm and β-catenin was negative. Loss or reduction of the E-cadherin and β-catenin expressions and overexpression of CD44s in the round cells are suggested to be contributed to the high propensity for lymphatic permeation and poor prognosis.

Keywords Intrahepatic sarcomatoid cholangiocarcinoma · Round cell variant · E-cadherin · β-catenin · CD44s

K. Sato (✉) · Y. Ueda · S. Katsuda
Department of Pathophysiological and Experimental Pathology,
Kanazawa Medical University,
1-1Daigaku, Uchinada Kahoku,
Ishikawa 920-0293, Japan
e-mail: sato-k@kanazawa-med.ac.jp

H. Murai
Department of Geriatric Medicine, Kanazawa Medical University,
Ishikawa, Japan

Introduction

Sarcomatoid transformation has been observed in carcinomas in various organs. In the liver, sarcomatoid transformation was present in 3.9% (14 of 355) to 9.4% (55 of 579) of hepatocellular carcinoma (HCC) autopsy cases [10, 11] and 4.5% (7 of 155) of cholangiocarcinoma cases [17]. The sarcomatoid components usually show spindle-shaped cells, pleomorphic cells or multinucleated giant cells in previously reported cases of intrahepatic sarcomatoid cholangiocarcinoma (ISC) [5, 6, 8, 9, 14, 16, 17, 20, 21] and combined hepatocellular and cholangiocellular carcinoma with sarcomatoid changes [5, 15, 18]. However, intrahepatic cholangiocarcinoma (ICC) with round cell feature is extremely rare [16].

Cell adhesion molecules are considered to be involved in tumor invasion and metastasis. Cadherins are Ca^{2+}-dependent cell–cell adhesion molecules that interact with catenins, which are submembranous cytoplasmic proteins termed α-, β-, and γ-catenin [19]. Reduced expressions of E-cadherin, which are constantly expressed in epithelial cells, and catenins have been reported in many cancers. In cholangiocarcinoma, down-regulated expressions of E-cadherin and β-catenin have been reported to be significantly correlated with high grade tumors but not with vascular invasion and metastasis [2].

CD44 standard (CD44s) is a cell adhesion molecule, specifically a transmembrane glycoprotein that functions as

a hyaluronate receptor, which may modulate cell–cell or cell–matrix interactions [23]. Aberrant expressions of CD44 have been observed in a variety of carcinomas [23]. In the bile duct, normal epithelial cells never express CD44s, even weakly or focally, in a nonspecific manner [2, 23, 24]. There have been a few reports of aberrant CD44s expressions in bile duct carcinoma cells, although no relationships of the CD44s immunoreactivity with the tumor grade, vascular invasion, and metastasis were noted [2, 24].

To date, no studies have investigated the above-described molecules in cholangiocarcinoma with sarcomatoid transformation. Here, we described a case of ISC of round cell variant and examined the differences between the immunohistochemical profiles of the tubular adenocarcinoma and the round cells, with particular focus on E-cadherin, β-catenin, and CD44s.

Clinical history

An 87-year-old man was incidentally found to have elevated ductal enzyme levels. His family history was unremarkable. He had never suffered from liver disease. Laboratory data revealed a moderately elevated serum level of carcinoembryonic antigen (16.2 ng/ml) and a highly elevated level of CA19-9 (2,894 U/ml). The serum level of alpha-fetoprotein was within the normal range. Hepatitis B surface antigen and anti-hepatitis C virus antibody in the serum were negative. Abdominal computed tomography (CT) scans showed a tumor in the left lobe of the liver. The patient was clinically diagnosed to have ICC. He received palliative care without surgery or chemotherapy and died of hepatic insufficiency and bronchopneumonia 3 months after the diagnosis. An autopsy was performed 1 h after death.

Materials and methods

The autopsy liver specimens were fixed in 10% neutral-buffered formalin and embedded in paraffin. Tissue sections, 4 μm in thickness, were used for hematoxylin and eosin (HE) staining, special staining, and immunohistochemical examination. Primary antibodies used in this study are listed in Table 1. Detection was achieved with automated immunostainer (Ventana Medical System, Tucson, AZ, USA).

Ultrastructural analysis was performed for autopsied liver specimens which is fixed in 10% neutral-buffered formalin, postfixed in 2% osmium tetroxide, dehydrated, and embedded in epoxy resin. Ultrathin sections were examined under electron microscope (JEM1200EXII, Japan Electron Optics Laboratory, Tokyo, Japan).

DNA extracted from submicrodissected paraffin-embedded tissue was analyzed by polymerase chain reaction-single strand conformational polymorphism (PCR-SSCP) to screen for mutations in exons 5–8 of the *p53* gene. The primers used for PCR amplification were as follows: exon 5 (5′-TGTTCACTTGTGCCCTGACT-3′ and 5′-CAGCCCT GTCGTCTCTCCAG-3′), exon 6 (5′-CCCAGGCCTCT

Table 1 Antibodies used for immunohistochemical studies and findings of both the adenocarcinoma and sarcomatoid components

Antibodies	Clone	Source	Dilution	Findings	
				Adenocarcinoma component	Sarcomatoid component
CK7	OV-TL 12/30	Dako, Glostrup, Denmark	1:50	+	P+
CK19	RCK108	Dako	1:50	+	+
CK7+8	CAM5.2	Becton-Dickinson, San Jose, CA, USA	Prediluted	+	+
Vimentin	V9	Dako	1:100	−	+
CA19-9	1116NS19-9	Cisbio international, Cèze Cedex, France	1:10	+	−
Hepatocyte	OCH1E5	Dako	1:25	−	−
Desmin	D33	Dako	1:100	−	−
Myoglobin	Polyclonal	Dako	1:9,000	−	−
Myogenin	F5D	Dako	1:100	−	−
MyoD1	5.8A	Dako	1:100	−	−
Mitochondria	AE-1	Leinco Technologies, St Louis, MO, USA	1:10	+	+
p53 protein	Bp53-12	IBL, Gunma, Japan	1:5000	+	−
E-cadherin	NCH-38	Dako	1:50	M+	W, C+
β-catenin	17C2	Novocastra, Newcastle upon Tyne, UK	1:100	W, C+	−
CD44s	DF1485	Novocastra	1:80	M+	M+
Ki-67	MIB-1	Dako	1:50	35.8%	49.7%

CK Cytokeratin, + positive, − negative, *W* weakly, *P* partially, *M* membranous, *C* cytoplasmic

GATTCCTCA-3′ and 5′-CAACCACCCTTAACCCCTCC-3′), exon 7 (5′-ACTGGCCTCATCTTGGGCCT-3′and 5′-TGTGCAGGGTGGCAAGTGGC-3′), and exon 8 (5′-TAAATGGGACAGGTAGGACC-3′and 5′-TCCACCGCTTCTTGTCCTGC-3′), respectively.

Results

At autopsy, the gross appearance of the tumor, which measured 4.0×2.8 cm, was reddish gray to tan in color with massive hemorrhagic necrosis (Fig. 1). Microscopically, the tumor was mostly necrotic and viable tumor cells were only identified in the periphery. The tumor was composed of two different components: moderately differentiated tubular adenocarcinoma and round cell elements (Fig. 2a). In the former portion, conglutinated atypical glands had proliferated with a fibrous stroma (Fig. 2b). In the latter portion, noncohesive round cells showed sarcomatoid appearances with eccentrically located nuclei and abundant eosinophilic cytoplasm (Fig. 2c). Multinucleated giant cells were scattered throughout the area (Fig. 2d). Round cells showed numerous lymphatic invasions into the liver and direct invasion into the gallbladder wall. No HCC component was detected. Lymph node metastasis, which was detected at the hepatic hilum and around the common bile duct, had resulted in obstructive jaundice. Metastatic nodules of round cells were identified in the bilateral adrenal glands. There was no evidence of cirrhosis, hepatolithiasis, or sclerosing cholangitis in the background liver. Mucin production of round cells was not detected in periodic acid Schiff (PAS), mucicarmine, and alcian blue stainings.

The immunohistochemical profiles of the two types of tumor cells are summarized in Table 1. The round cells were positive for cytokeratin (CK) 19 (Fig. 3a) and vimentin, but CK 7 expression was reduced. E-cadherin expression was lost at the membrane and weakly found in the cytoplasm (Fig. 3b), while no immunoreactivity for β-catenin was detected (Fig. 3c). The round cells in the lymphatic vessels and stromal invasive sites demonstrated marked CD44s expression at the membrane (Fig. 3d). The tubular adenocarcinoma cells expressed CK19 (Fig. 3e) and β-catenin (Fig. 3g) in their cytoplasm, with E-cadherin (Fig. 3f) and CD44s (Fig. 3h) at the plasma membrane. Round cells and multinucleated giant cells presented immnoreactivity for mitochondria densely in the paranuclear cytoplasm. Nuclear expression of p53 protein was found in the adenocarcinoma cells. No specific expression of rhabdomyogenic markers was found for desmin, myoglobin, myogenin, or MyoD1. Electron micrographs revealed accumulation of large mitochondria in the cytoplasm of the round cells and multinucleated giant cells (Fig. 4). No band shifting was detected in exons 5–8 of the *p53* gene by PCR-SSCP analysis in both adenocarcinoma and round cell components.

Fig. 1 Macroscopic appearance of the cut surface of the autopsied liver demonstrating a tumor of 4.0×2.8 cm in size, with hemorrhage and necrosis (*arrowhead*)

Discussion

ISC is an uncommon variant of ICC and sarcomatoid component exhibited spindle-shaped cells in almost previously reported cases [5, 8, 15, 16, 20, 21]. Furthermore, ISC of round cell feature is very rare. Nakajima et al. [16] report a case of ICC comprised papillary carcinoma and round cells. Sasaki et al. [20] described a case of ISC composed of adenosquamous carcinoma, spindle-shaped cells, multinucleated giant cells, and round cells resembling rhabdomyosarcoma cells. Because the round cells of the present case apparently seemed to be rhabdomyosarcoma cells, displayed no mucin in their cytoplasm, and expressed both cytokeratins and vimentin, we considered this tumor as a sarcomatoid carcinoma. However, the round cells were not rhabdomyosarcoma or rhabdoid cells, as myogenic markers were not expressed by immunohistochemistry, and a whorl of intermediate filaments was not confirmed by ultrastructural study. Electron micrographs confirmed that the accumulation of mitochondria was attributable to the eosinophilic paranuclear cytoplasm. ICC with rhabdoid phenotype was reported by Honda et al. [7] and Lim et al. [12] but made no mention of ultrastructural findings.

Sarcomatous transformation occasionally appears in HCC cases treated with anticancer therapy, particularly, transcatheter arterial embolization (TAE) [11]. The present tumor was distinguished from HCC due to its negative immunoreactivity for an anti-hepatocyte antibody (OCH1E5). There have been no previous reports concerning the relationship between ISC and anticancer therapy. The previously reported cases of a round cell variant ICC and the present case had received neither TAE nor chemotherapy. It is, therefore, reasonable to consider that sarcomatoid transformation is a biologically natural

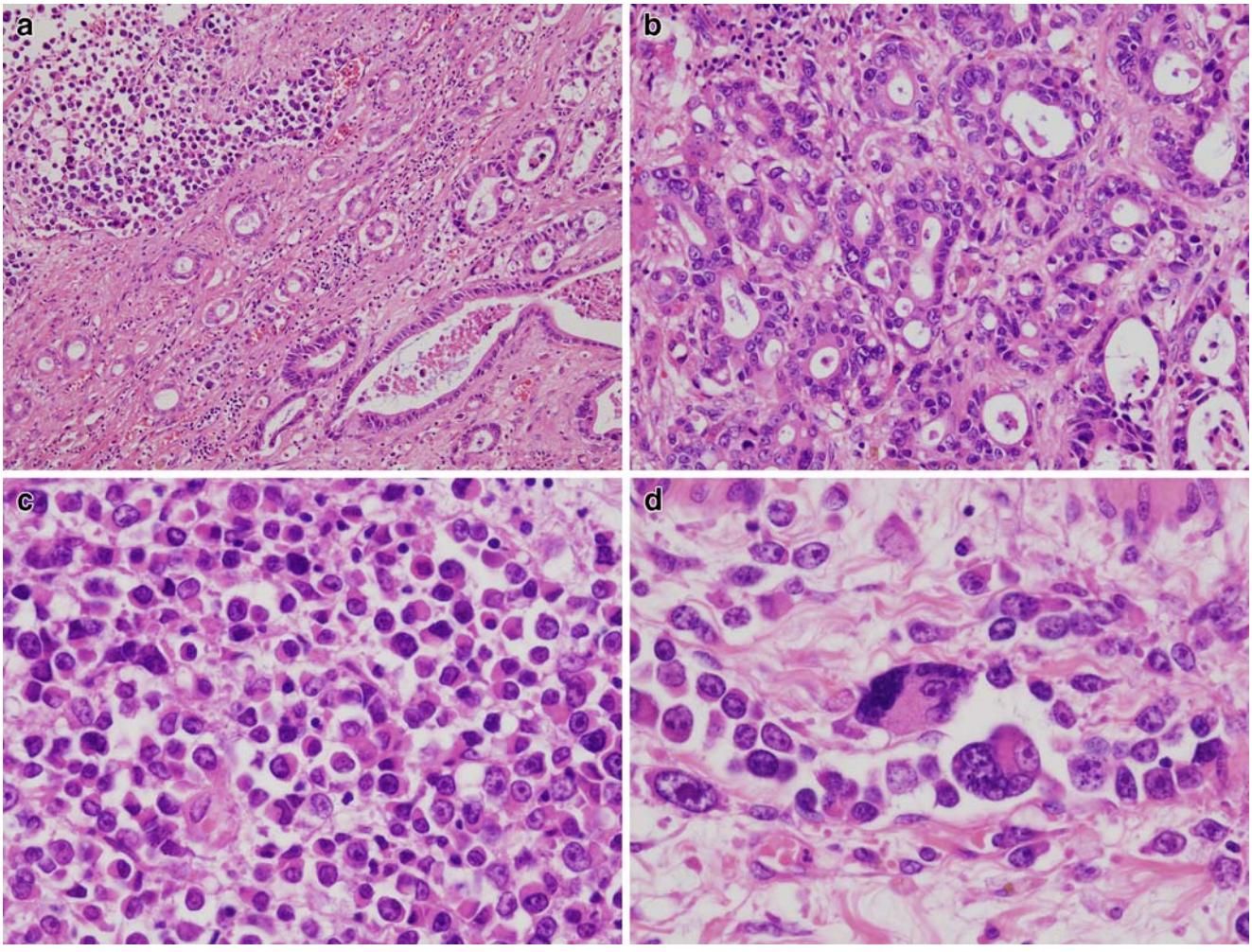

Fig. 2 Histological appearances of the tumor (Hematoxylin and eosin staining). **a** Tubular adenocarcinoma (*lower right*) and sarcomatoid components with round feature (*upper left*) are observed in the periphery, ×100. **b** Tubular adenocarcinoma composed of small atypical glands, ×200. **c** Sarcomatoid round cells are noncohesive and have eccentric large vesicular nuclei, prominent nucleoli, and abundant paranuclear eosinophilic cytoplasm, ×400. **d** Multinucleated giant cells are shown, ×400

course of tumor progression rather than a secondary event due to artificial treatment.

In ISC, sarcomatoid component usually coexists with cholangiocarcinoma component. The previously reported cases of ISC showed cytokeratin expressions in both the adenocarcinoma and sarcomatoid components [5–7, 9, 15, 20, 21]. In the present case, immunohistochemical positivity for CK19, which is restricted to the biliary epithelium within the liver, was detected in both the adenocarcinoma component and round cells. Therefore, the round cell component can reasonably be considered to have transformed from the cholangiocarcinoma cells. Differences in the immunoreactivities for CK7, vimentin, and CA19-9 between adenocarcinoma and round cells suggest that alterations in genetic expressions and phenotypic changes occur during sarcomatoid transformation. By immunohistochemistry, the expression of p53 protein was different between adenocarcinoma and round cells, but no mutation was detected in exons 5–8 of the *p53* gene in both components.

Normal bile duct epithelial cells show immunoreactivities for E-cadherin and β-catenin on the plasma membrane [2]. Reductions of these molecules were detected in cholangiocarcinoma and correlated with high-grade character [2]. The expressions of E-cadherin and β-catenin contribute to the maintenance of the normal morphology and polarity of bile ducts [2]. In the present case, immunohistochemical staining for E-cadherin revealed diffuse membranous expression in the adenocarcinoma component and weak cytoplasmic expression in the round cell component. The β-catenin immunoreactivity was weakly positive in the adenocarcinoma component and negative in the round cells. Loss of the membranous expression and cytoplasmic localization of E-cadherin have been reported to be associated with functional and structural disorders [22]. Loss of the membranous expres-

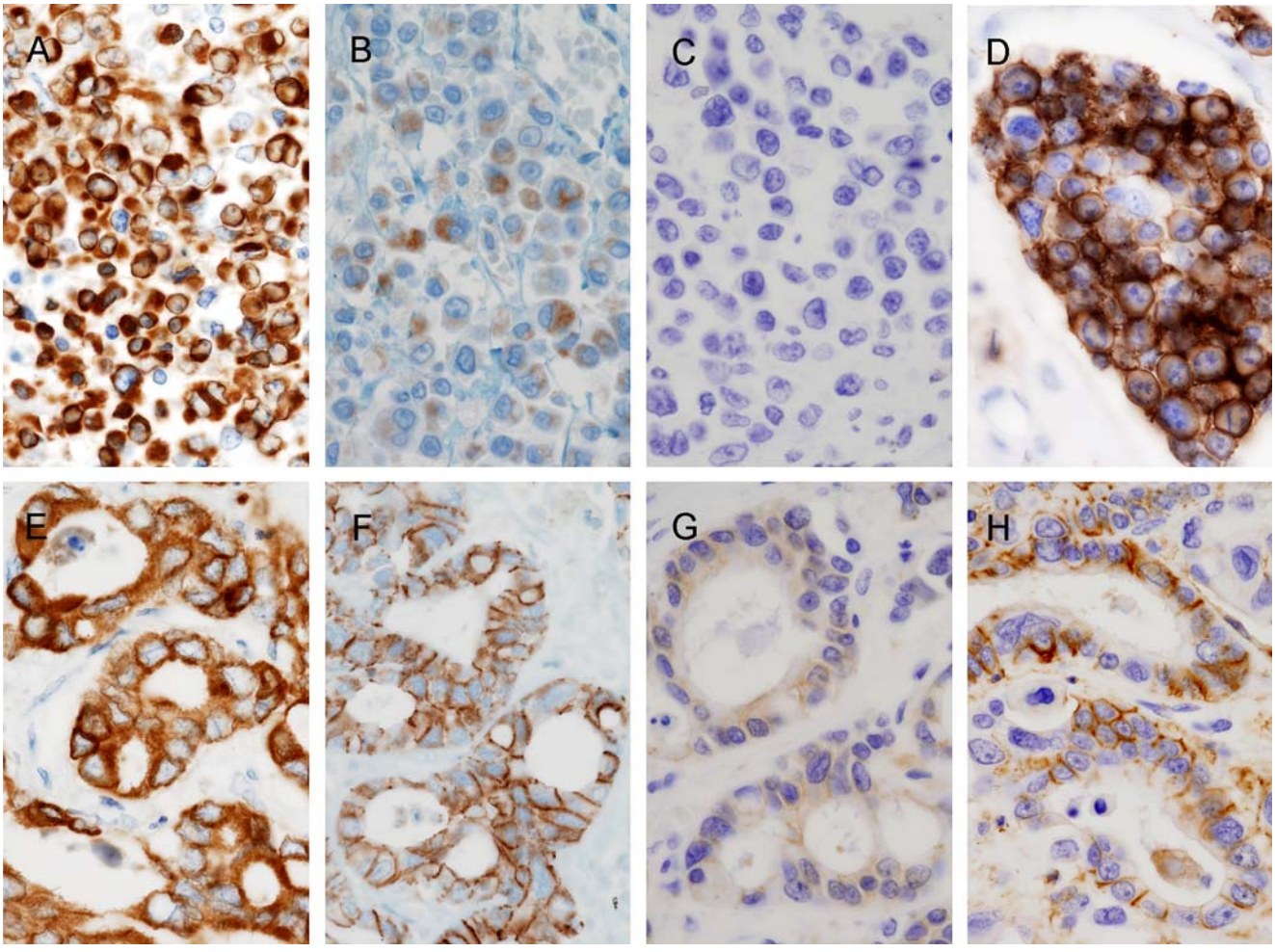

Fig. 3 Immunohistochemical findings of the tumor cells, ×400. The round cells express CK19 in the cytoplasm (**a**) and E-cadherin weakly in the cytoplasm (**b**), but no β-catenin expression is detected (**c**). The round cells in the lymph vessels express CD44s at the plasma membrane (**d**). The tubular adenocarcinoma cells express CK19 in the cytoplasm (**e**), E-cadherin at the membrane around the cell (**f**), β-catenin weakly in the cytoplasm (**g**) and CD44s at the lateral plasma membrane (**h**)

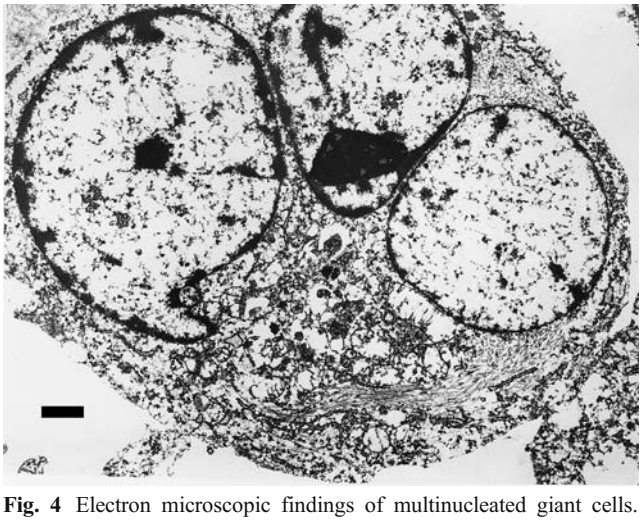

Fig. 4 Electron microscopic findings of multinucleated giant cells. Large mitochondria are accumulated in cytoplasm. *Scale bar*=1 μm

sions of E-cadherin and β-catenin may play an important role in disruption of the histologic architecture and aggressive behavior for invasion and metastasis of the round cell component.

CD44s is aberrantly expressed at the membrane of cholangiocarcinoma cells [2]. However, its roles in tumor invasion and lymph–vascular penetration have not been fully elucidated. In HCC, upregulation of CD44 was related to vascular invasion [13]. In contrast, reduced or loss of CD44 expression is associated with lymph-vascular permeation in invasive micropapillary carcinoma of the breast, endometrial carcinoma, and colon carcinoma [1, 3, 4]. In the present case, the round cells showed a distinct membranous expression of CD44s. The CD44s immunoreactivity was more intense in the round cells than in the adenocarcinoma cells. The results suggest that aberrant overexpression of CD44s may be involved in marked

lymph–vascular invasion by sarcomatoid cholangiocarcinoma cells as has been reported for HCC.

In conclusion, ISC with a round cell phenotype is an aggressive variant of ICC. Loss or reduction of the membranous expressions of E-cadherin and β-catenin and upregulation of CD44s in the round cell component may be associated with the high propensity for lymph–vascular permeation.

Acknowledgements The authors thank Ms. Yumi Tsubata (Department of Pathology, Kanazawa Medical University Hospital) for immunohistochemistry and Ms. Yoshiiku Okanemasa (Department of Pathology, Kanazawa Medical University Hospital) for electron micrographs.

References

1. Asao T, Nakamura J, Shitara Y, Tsutsumi S, Mochiki E, Shimura T, Takenoshita S, Kuwano H (2000) Loss of standard type of CD44 expression in invaded area as a good indicator of lymph-node metastasis in colorectal carcinoma. Dis Colon Rectum 43:1250–1254
2. Ashida K, Terada T, Kitamura Y, Kaibara N (1998) Expression of E-cadherin, alpha-catenin, beta-catenin, and CD44 (standard and variant isoforms) in human cholangiocarcinoma: an immunohistochemical study. Hepatology 27:974–982
3. Fujita N, Yaegashi N, Ide Y, Sato S, Nakamura M, Ishiwata I, Yajima A (1994) Expression of CD44 in normal human versus tumor endometrial tissues: possible implication of reduced expression of CD44 in lymph-vascular space involvement of cancer cells. Cancer Res 54:3922–3928
4. Gong Y, Sun X, Huo L, Wiley EL, Rao MS (2005) Expression of cell adhesion molecules, CD44s and E-cadherin, and microvessel density in invasive micropapillary carcinoma of the breast. Histopathology 46:24–30
5. Haratake J, Horie A (1991) An immunohistochemical study of sarcomatoid liver carcinomas. Cancer 68:93–97
6. Haratake J, Yamada H, Horie A, Inokuma T (1992) Giant cell tumor-like cholangiocarcinoma associated with systemic cholelithiasis. Cancer 69:2444–2448
7. Honda M, Enjoji M, Sakai H, Yamamoto I, Tsuneyoshi M, Nawata H (1996) Case report: intrahepatic cholangiocarcinoma with rhabdoid transformation. J Gastroenterol Hepatol 11:771–774
8. Imazu H, Ochiai M, Funabiki T (1995) Intrahepatic sarcomatous cholangiocarcinoma. J Gastroenterol 30:677–682
9. Kaibori M, Kawaguchi Y, Yokoigawa N, Yanagida H, Takai S, Kwon AH, Uemura Y, Kamiyama Y (2003) Intrahepatic sarcomatoid cholangiocarcinoma. J Gastroenterol 38:1097–1101
10. Kakizoe S, Kojiro M, Nakashima T (1987) Hepatocellular carcinoma with sarcomatous change. Clinicopathologic and immunohistochemical studies of 14 autopsy cases. Cancer 59: 310–316
11. Kojiro M, Sugihara S, Kakizoe S, Nakashima O, Kiyomatsu K (1989) Hepatocellular carcinoma with sarcomatous change: a special reference to the relationship with anticancer therapy. Cancer Chemother Pharmacol 23 Suppl:S4–S8
12. Lim BJ, Kim KS, Lim JS, Kim MJ, Park C, Park YN (2004) Rhabdoid cholangiocarcinoma: a variant of cholangiocarcinoma with aggressive behavior. Yonsei Med J 45:543–546
13. Mathew J, Hines JE, Obafunwa JO, Burr AW, Toole K, Burt AD (1996) CD44 is expressed in hepatocellular carcinomas showing vascular invasion. J Pathol 179:74–79
14. Matsuo S, Shinozaki T, Yamaguchi S, Takami Y, Obata S, Tsuda N, Kanematsu T (1999) Intrahepatic cholangiocarcinoma with extensive sarcomatous change: report of a case. Surg Today 29:560–563
15. Nakajima T, Kubosawa H, Kondo Y, Konno A, Iwama S (1988) Combined hepatocellular-cholangiocarcinoma with variable sarcomatous transformation. Am J Clin Pathol 90:309–312
16. Nakajima T, Kondo Y, Miyazaki M, Okui K (1988) A histopathologic study of 102 cases of intrahepatic cholangiocarcinoma: histologic classification and modes of spreading. Hum Pathol 19:1228–1234
17. Nakajima T, Tajima Y, Sugano I, Nagao K, Kondo Y, Wada K (1993) Intrahepatic cholangiocarcinoma with sarcomatous change. Clinicopathologic and immunohistochemical evaluation of seven cases. Cancer 72:1872–1877
18. Papotti M, Sambataro D, Marchesa P, Negro F (1997) A combined hepatocellular/cholangiocellular carcinoma with sarcomatoid features. Liver 17:47–52
19. Pignatelli M, Vessey CJ (1994) Adhesion molecules: novel molecular tools in tumor pathology. Hum Pathol 25:849–856
20. Sasaki M, Nakanuma Y, Nagai Y, Nonomura A (1991) Intrahepatic cholangiocarcinoma with sarcomatous transformation: an autopsy case. J Clin Gastroenterol 13:220–225
21. Shimada M, Takenaka K, Rikimaru T, Hamatsu T, Yamashita Y, Kajiyama K, Taguchi K, Shirabe K, Sugimachi K (2000) Characteristics of sarcomatous cholangiocarcinoma of the liver. Hepatogastroenterology 47:956–961
22. Shiozaki H, Tahara H, Oka H, Miyata M, Kobayashi K, Tamura S, Iihara K, Doki Y, Hirano S, Takeichi M, Mori T (1991) Expression of immunoreactive E-cadherin adhesion molecules in human cancers. Am J Pathol 139:17–23
23. Sneath RJ, Mangham DC (1998) The normal structure and function of CD44 and its role in neoplasia. Mol Pathol 51:191–200
24. Washington K, Telen MJ, Gottfried MR (1997) Expression of cell adhesion molecule CD44 in primary tumors of the liver: an immunohistochemical study. Liver 17:17–23

Virchows Arch (2006) 449:591–596
DOI 10.1007/s00428-006-0276-4

CASE REPORT

Primary hepatic lymphoma with spindle cell components: a case report

Hiroko Hayashi · Hiroshi Ohtani · Takashi Ueda · Junzo Yamaguchi · Kunihide Izawa · Takahiro Hayashida · Yoshikazu Higami · Isao Shimokawa

Received: 1 March 2006 / Accepted: 13 July 2006 / Published online: 19 September 2006
© Springer-Verlag 2006

Abstract Diffuse large B-cell lymphoma (DLBCL) with spindle cell components is extremely rare and often misdiagnosed as carcinoma or sarcoma. Here, we present a case of primary DLBCL with spindle cell components arising in the liver, for which a preoperative diagnosis by needle biopsies was unsuccessful. The patient was a 70-year-old man with a continuous cough. Thoracic computed tomography incidentally detected a mass of 5 cm in diameter in his liver. The initial and second needle biopsies from the liver mass were pathologically diagnosed as suspicious for sarcomatoid hepatocellular carcinoma. He underwent an extended left hepatectomy. Histological examination revealed a diffuse or epithelioid arrangement of round and polygonal cells, mixed with the fascicles of spindle-shaped cells. Immunohistochemically, all the morphological types of tumor cells showed positive reactions for a lymphocytic marker (CD45RB) and B-cell markers (CD20 and CD79a). Double-immunostaining revealed that the spindle-shaped tumor cells expressed CD20, but never expressed alpha-smooth muscle actin. Malignant lymphoma with a spindle cell morphology is quite uncommon, and this variant can be a diagnostic pitfall, especially in tiny biopsy specimens. We emphasize that pathologists should be reminded of lymphoma as a differential diagnosis of spindle cell tumors.

H. Hayashi (✉) · H. Ohtani · T. Hayashida · Y. Higami · I. Shimokawa
Department of Pathology and Gerontology,
Nagasaki University Graduate School of Biomedical Science,
1-12-4 Sakamoto,
Nagasaki City, Nagasaki 852-8523, Japan
e-mail: dm04013y@stcc.nagasaki-u.ac.jp

T. Ueda · J. Yamaguchi · K. Izawa
Department of Surgery,
National Hospital Organization Saga National Hospital,
Saga, Japan

Keywords Diffuse large B-cell lymphoma · Liver · Spindle cell morphology · Sarcomatoid hepatocellular carcinoma

Introduction

Primary hepatic lymphoma (PHL) is confined to the liver with no lymph node, spleen, or bone marrow involvement. PHL is rare, representing approximately 0.4% of extranodal non-Hodgkin lymphoma and approximately 0.01% of non-Hodgkin lymphoma [8]. Diffuse large B-cell lymphoma (DLBCL) with spindle cell features is extremely rare, and to the best of our knowledge, there have been no previous reports of such cases arising in the liver. This rarity and morphological inconsistency can often result in pathological misdiagnosis. Here, we describe a case of PHL with a spindle cell morphology, including the possible origin of the spindle cells, and briefly review the literature.

Clinical history

A 70-year-old man with a history of hypertension and type 2 diabetes mellitus presented with a cough. Thoracic computed tomography (CT) incidentally found a mass in his liver. On admission, liver function tests were slightly elevated: aspartate aminotransferase (AST), 54 IU/L (normal range, 2–40 IU/L); alanine aminotransferase (ALT), 62 IU/L (2–43 IU/L); lactate dehydrogenase (LDH), 315 IU/L (120–230 IU/L); alkaline phosphatase (ALP), 299 IU/L (100–340 IU/L); and gamma glutamyl transpeptidase (γ-GTP), 110 IU/L (5–65 IU/L). Serological tests for hepatitis B virus (HBV) and hepatitis C virus (HCV) were negative. No tumor markers, including alpha-fetoprotein (AFP) and carcinoembryonic antigen (CEA), were

elevated. Abdominal CT showed a low-density area measuring 5 cm in diameter in the left hepatic lobe (segment 4), which was weakly and gradually stained by contrast CT. A selective angiogram of the superior mesenteric artery and celiac artery did not demonstrate any obvious tumor vascularity. Although the first and second needle biopsy specimens showed both necrosis and sarcomatoid patterns, which were suspicious for sarcomatoid hepatocellular carcinoma (Fig. 1a and b), immunostaining with antihepatocyte and anticytokeratin antibodies did not confirm this diagnosis. The tumor was considered to be malignant due to its significant cytological atypia and compact cellularity, and an extended left hepatectomy was performed. The tumor was diagnosed as DLBCL with spindle cell components. No palpable lymph node swelling or involvement of the hematolymphoid system was found on abdominal and thoracic CT scans. Furthermore, the lymph nodes within the hepatoduodenal ligament were not swollen. Peripheral blood cell counts were in their normal ranges and bone marrow aspiration showed no evidence of abnormal lymphocytes. Therefore, the preoperative staging of our patient was clinical stage IEA using the modified (Cotswolds revision) Ann Arbor staging system [16]. After the operation, chemotherapy including rituximab and cyclophospamide, doxorubicin, vincristine, and prednisone (CHOP) was given. He was diagnosed with primary lung cancer at 8 months after the operation but showed no signs of recurrence of the lymphoma during the 24-month follow-up.

Materials and methods

Specimens were fixed in 10% buffered formalin, sectioned and routinely stained with hematoxylin and eosin. Immunohistochemistry was carried out using antibodies against CD45RB (Dako, Kyoto, Japan), CD20 (Dako), CD79a (Dako), CD45RO (Dako), CD30 (Dako), ALK (Dako), CD4 (Novocastra, Newcastle, UK), CD5 (Dako), CD8 (Novocastra), CD10 (Zymed), hepatocytes (Dako), cytokeratin (Novocastra), cyclin-D1 (Dako), bcl-2 (Dako), p53 protein (Dako), MIB-1 (Dako), and alpha-smooth muscle actin (SMA; Nichirei, Tokyo, Japan) using the avidin–biotin peroxidase method. For the antibodies against CD79a, CD30, ALK, CD4, CD5, CD8, CD10, hepatocytes, cytokeratin, cyclin-D1, bcl-2, and MIB-1, the sections were pretreated using an autoclave procedure for antigen retrieval.

To identify the nature of the spindle-shaped cells, we immunostained serial sections with a series of anti-CD20 antibody alone, anti-SMA antibody + anti-CD20 antibody (double-immunostaining), and anti-SMA antibody alone in that order. Double-immunostaining for SMA and CD20 was initially performed using a primary anti-SMA antibody and alkaline phosphatase-labeled polymer with a secondary antimouse antibody [Histofine Simple Stain AP (M); Nichirei] and was developed with 5-bromo-4-chloro-3-indolyl phosphate/nitroblue tetrazolium (BCIP/NBT), which produced a dark blue stain. Subsequently, the sections were incubated with a primary anti-CD20 antibody and peroxidase-labeled polymer with a secondary antimouse antibody [Histofine Simple Stain MAX-PO (M); Nichirei] and were developed with 3,3′-diaminobenzidine, which produced a brown stain.

Results

The resected liver tumor was 10×6 cm, yellow to gray in color, solid, and well-circumscribed (Fig. 2). Microscopic examination revealed a diffuse or epithelioid pattern of round and polygonal cells mixed with the fascicles of spindle cells (Fig. 3a and b). All the tumor cells had irregularly shaped vesicular and hyperchromatic nuclei with a few membrane-bound nucleoli. The spindle-shaped cells represented approximately 20% of all tumor cells, and most of them showed nuclear atypia (Fig. 3b). Scattered tingible body macrophages and Reed Sternberg-like giant cells were present (Fig. 3a). At the periphery of the tumor, the tumor cells infiltrated along the sinusoids with little stromal reaction or necrosis (Fig. 3c). In contrast, the central portion of the tumor showed geographic necrosis and stromal fibrosis in some regions, and spindle cells were

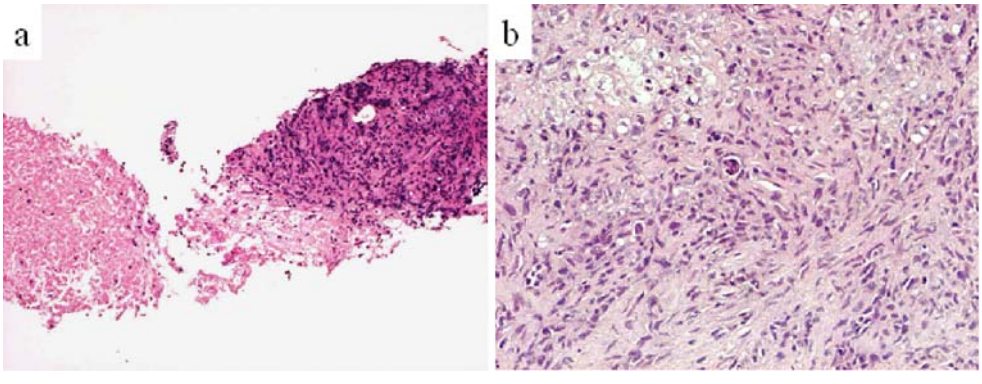

Fig. 1 Microscopic appearances of the liver biopsies. **a** Initial biopsy specimen showing conspicuous artifacts and necrosis. **b** Second biopsy specimen showing epithelioid (*upper*) and sarcomatoid (*lower*) patterns in a background of fibrosis (H & E staining)

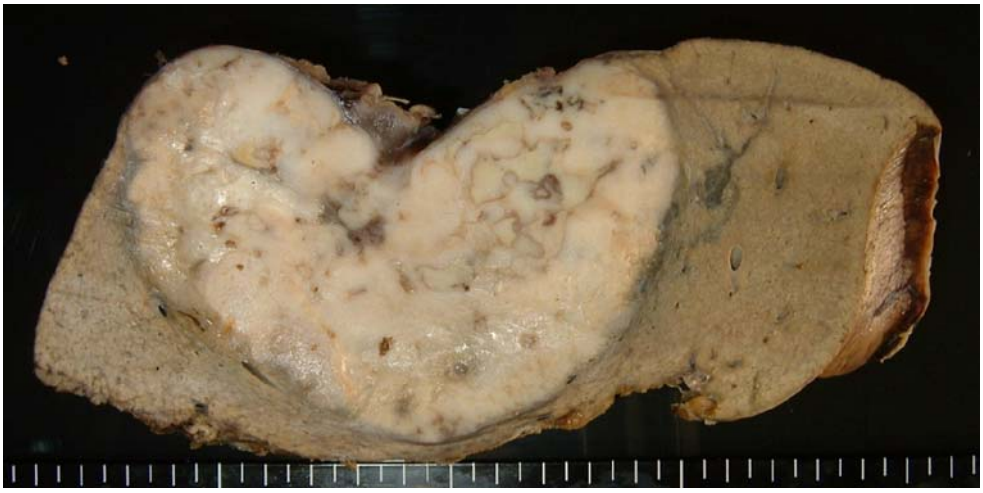

Fig. 2 Cut surface of the liver tumor showing geographic necrosis

more prominent in the background of collagens (Fig. 3b). Noninfiltrated liver showed no remarkable changes.

Immunohistochemically, all the morphological types of tumor cells showed positive staining for CD45RB, CD20 (Figs. 3d and 4b), and CD79a and were negative for CD45RO, CD30, ALK, CD4, CD5, CD8, CD10, hepatocyte, cytokeratin, cyclin-D1, bcl-2, and p53 protein. The MIB-1 labeling index was approximately 40%. The series of stained serial sections revealed that the spindle-shaped tumor cells were positive for CD20, but negative for SMA (Fig. 4b and c). SMA immunostaining was present in the vascular wall and long spindle cells with elongated cytoplasmic processes (Fig. 4c). The double-immunostaining revealed that none of the CD20-positive cells expressed SMA (Fig. 4d).

Discussion

The spectrum of DLBCL is extremely broad and includes many variants [19]. Among these morphological variants, DLBCL with spindle cell features is extremely rare [4, 19], and there have been no reports of this variant of DLBCL arising in the liver to date. Table 1 shows a summary of the available data for 13 cases, including the present case [3, 9–11, 19, 23]. The age range is from 24 to 89 years, and the ratio of males to females is 6:7. The most common location

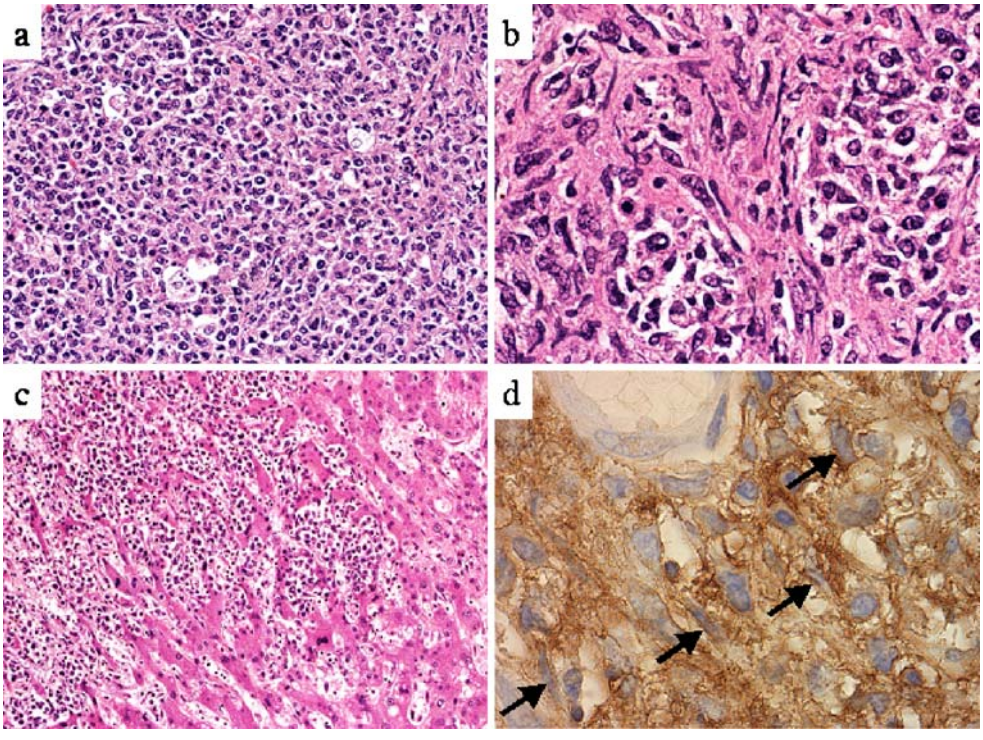

Fig. 3 Various histologies of the surgical specimen. **a** Tingible body macrophages in compact tumor cells. **b** High magnification image of spindle-shaped tumor cells with significant nuclear atypia. **c** Tumor cells infiltrating along the sinusoids (H & E staining). **d** Spindle-shaped tumor cells (*arrows*) showing CD20-positive immunostaining

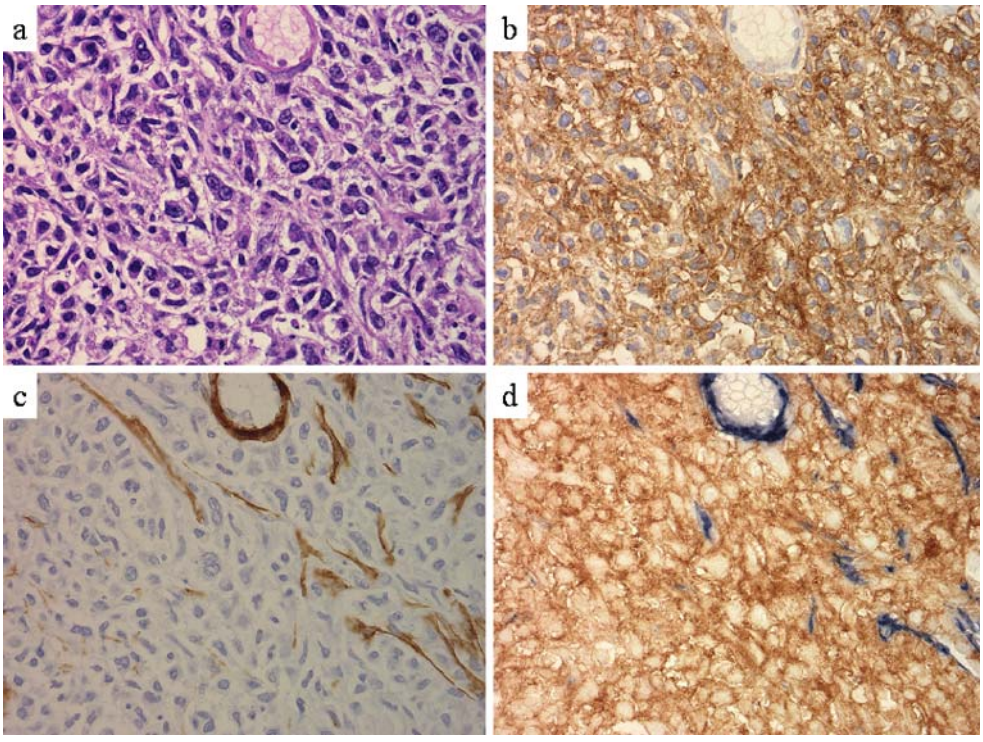

Fig. 4 Series of stained serial sections photographed at the same site. **a** Polymorphic lymphoma cells with many spindle cells (H & E staining). **b** All the lymphoma cells show CD20-positive immunostaining. **c** Only long spindle cells with elongated cytoplasmic processes and the vascular wall show SMA-positive immunostaining. **d** Lymphoma cells are positive for CD20 (*brown*), but negative for SMA (*dark blue*), as evaluated by double-immunostaining for SMA and CD20

is skin, with 10 of the 13 cases (77%) present in skin or soft tissue. More than half (6 of 10 cases) of the initial pathological diagnoses are sarcoma or sarcomatoid carcinoma. In almost all the cases, the pathological diagnosis is made by immunohistochemistry. In the current case, preoperative diagnosis by needle biopsies was unsuccessful because we could not include malignant lymphoma as a differential diagnosis for spindle cell tumors, and the paucity of tumor material did not provide any suggestive information of malignant lymphoma. However, the surgical specimen revealed scattered tingible body macrophages and sinusoid infiltration of tumor cells, which are characteristics of malignant lymphoma [5]. Immunohistochemical staining of both the biopsy and surgical specimens confirmed the pathological diagnosis.

It has been reported that lymphoma cells may assume a spindle configuration when they infiltrate bone and soft tissues [4, 13, 19]. Lymphoma cells are also occasionally spindle-shaped in the absence of a stromal influence. It is currently believed that the spindle formation probably results from aberrations in the cytoskeleton, and Nozawa et al. [19] reported that SMA expression may be associated with the spindle morphology of lymphoma cells. On the other hand, lymphoma with spindle cell features has been reported to be associated with an exuberant mesenchymal reaction [13, 14], which predominantly occurs in the peripheral portion of the tumor, and the spindle cells lack nuclear atypia [4]. In the current case, spindle-shaped tumor cells with nuclear atypia were present throughout the tumor and consistently showed CD20 and CD79a expression, but never SMA expression. The observation of SMA-positive spindle cells with irregularly elongated processes suggests that most of these cells were not true tumor cells and could instead represent proliferating myofibroblasts, possibly derived from hepatic stellate cells, pericytes, or stromal cells [6]. Therefore, spindle cells in PHL can consist of at least two types of cells, that is, lymphoma cells with the spindle-shape change and non-neoplastic cells probably representing myofibroblasts. Although the exact mechanism of the spindle-shape changes in lymphoma cells remains unknown, the appearance of the immunostaining in the current case is of considerable interest and could bring about better understanding of the mechanism.

Due to its microscopic morphology, especially in the skin, this variant is easy to misdiagnose as spindle cell sarcoma, poorly differentiated carcinoma, dendritic cell sarcoma, or inflammatory pseudotumor [23]. Follicular dendritic cell sarcoma has also been reported to mimic diffuse large cell lymphoma [7]. In these cases, immunohistochemical examination is quite useful for a differential diagnosis.

PHL itself is rare, representing 0.4% of extranodal non-Hodgkin lymphoma and 0.016% of all non-Hodgkin lymphoma [8]. PHL is confined to the liver with no lymph node, spleen, or bone marrow involvement. Since the clinical, biological, and radiological features of PHL are usually nonspecific, as seen in our case, the diagnosis is made by liver biopsy with histological and immunohisto-

Table 1 Reports of DLBCL with spindle cell features (including the present case)

Case no.	Age/ sex	Organs involved	Size (mm)	Initial pathological diagnosis	Final pathological diagnosis	Reference
1	64/M	Inguen, retroperitoneum, diaphragm, and chest wall	60	Soft-tissue sarcoma	Malignant lymphoma[a]	Fung [9]
2	59/F	Skin of back	35×35	ND	ND	Cerroni et al. [3]
3	89/F	Skin of scalp	40×50	ND	ND	Cerroni et al. [3]
4	30/F	Skin of forehead	ND	Spindle cell squamous carcinoma, atypical fibroxanthoma, or melanoma	B-cell lymphoma	Cerroni et al. [3]
5	69/M	Skin behind ear	ND	ND	ND	Cerroni et al. [3]
6	54/M	Skin of sternum	ND	Dermatofibrosarcoma	B-cell lymphoma of the large cell type	Cerroni et al. [3]
7	73/F	Skin of scalp	40	Poorly differentiated histiocytic lymphoma	Spindle-cell B-cell lymphoma	Goodlad [10]
8	78/F	Upper arm	20×15	Sarcoma versus spindle cell carcinoma	DLBCL[b]	Wang et al. [23]
9	48/M	Skin of submaxilla	10×8	Suspicious for lymphoma	DLBCL[b]	Wang et al. [23]
10	51/M	Orbit, nasal mucosa, and paranasal sinuses	25×15	Inflammatory pseudotumor	DLBCL[b]	Wang et al. [23]
11	24/F	Chest wall and mediastinum	20×9	Spindle cell sarcoma or malignant fibrous histiocytoma	DLBCL[b]	Wang et al. [23]
12	32/F	Uterine cervix	110	DLBCL[c]	DLBCL[c]	Kahlifa et al. [11]
13	70/M	Liver	100×60	Sarcomatoid HCC	DLBCL[c]	Present case

ND not described, *DLBCL* diffuse large B-cell lymphoma. *HCC* hepatocellular carcinoma
[a] Malignant lymphoma, diffuse large noncleaved cell type, with extensive sclerosis and B-cell phenotype
[b] DLBCL with prominent spindle cell features
[c] DLBCL with a spindle cell component

chemical examinations [2]. The majority of PHL cases is DLBCL [2, 15, 20]. Other histologies have been described in less than 5% of cases [15, 18, 20] and include diffuse lymphoma of the mucosa-associated lymphoid tissue (MALT) type [2, 17], mixed small and large cell, lymphoblastic, diffuse immunoblastic, diffuse histiocytic, mantle cell, and small noncleaved or Burkitt lymphoma. The initial misdiagnoses in PHL have been embryonic sarcoma, granulomatous cholangitis, inflammatory pseudotumor, and granulomatous hepatitis [17, 21].

Although the etiology of PHL is unknown, Bronowicki et al. [2] described 31 PHL cases, among which their largest series of PHL patients showed a high prevalence of HCV infection, specifically 6 (21%) of 28 cases. However, our case was HCV-negative.

The prognosis of PHL is variable. The median survival is 15.3 months and the survival range is 3–123.6 months [1]. Treatment options for PHL include surgery, chemotherapy, radiation, or varying combinations of these modalities [18, 21]. In patients with low-volume localized disease, surgical resection alone has been performed with a good outcome [22]. However, PHL is also a chemosensitive disease, and CHOP-based regimens generally appear to be chosen [20]. Due to the small number of reported cases, the viability of the optimal treatment for patients with PHL is still debated. Although we believe that chemotherapy is essential after a pathological diagnosis to avoid oversurgery [2], surgery followed by adjuvant chemotherapy is one of the treatment options for patients with localized disease, as carried out in our present case [2, 12, 18].

In summary, we report here the first case of primary hepatic DLBCL with spindle cell components. Most of these spindle cells were lymphoma cells with the spindle-shape change, although a small number of non-neoplastic myofibroblastic cells were scattered. The pathological diagnosis by needle biopsy alone was very difficult due to not only poor materials but also its rarity and morphological inconsistency. This morphological variant can be a serious pitfall for histological diagnosis, and immunohistochemical studies are very useful for a differential diagnosis. However, the crucially important aspects for pathologists are for them to be aware that lymphoma can show a spindle cell morphology and to include malignant lymphoma as a differential diagnosis when the clinical information indicates a nonspecific liver tumor.

References

1. Avlonitis VS, Lions D (1999) Primary hepatic lymphoma: a review. Eur J Surg 165:725–729
2. Bronowicki JP, Bineau C, Fergier P, Hermine O, Brousse N, Oberti F, Rousselet MC, Dharancy S, Gaulard P, Flejou JF, Cazals-Hatem D, Labouyrie E (2003) Primary lymphoma of the liver: clinical-pathological features and relationship with HCV infection in French patients. Hepatology 37:781–787
3. Cerroni L, El-Shabrawi-Caelen L, Fink-Puches RF, LeBoit PE, Kerl H (2000) Cutaneous spindle-cell B-cell lymphoma. Am J Dermatopathol 22:299–304
4. Chan JKC, Buchanan R, Fletcher CDM (1990) Sarcomatoid variant of anaplastic large-cell Ki-1 lymphoma. Am J Surg Pathol 14:983–988
5. Emile JF, Azoulay D, Gornet JM, Lopes G, Delvart V, Samuel D, Reynes M, Bismuth H, Goldwasser F (2001) Primary non-Hodgkin's lymphomas of the liver with nodular and diffuse infiltration patterns have different prognoses. Ann Oncol 12:1005–1010
6. Enzan H, Himeno H, Iwamura S, Saibara T, Onishi S, Yamamoto Y, Hara H (1994) Immunohistochemical identification of Ito cells and their myofibroblastic transformation in adult human liver. Virchows Arch 424:249–256
7. Fonseca R, Tefferi A, Strickler JG (1997) Follicular dendritic cell sarcoma mimicking diffuse large cell lymphoma: a case report. Am J Hematol 55:148–155
8. Freeman C, Breg JW, Cutler SJ (1972) Occurrence and prognosis of extranodal lymphomas. Cancer 29:252–260
9. Fung CHK, Antar S, Lo TYJ (1993) Actin-positive spindle cell lymphoma. Arch Pathol Lab Med 117:1053–1055
10. Goodlad JR (2001) Spindle-cell B-cell lymphoma presenting in the skin. Br J Dermatol 145:313–317
11. Kahlifa M, Buckstein R, Perez-Ordonez B (2003) Sarcomatoid variant of B-cell lymphoma of the uterine cervix. Int J Gynecol Pathol 22:289–293
12. Kitabayashi K, Hasegawa T, Ueno K, Saito H, Kosaka T, Takashima S, Kurose N, Nojima T (2004) Primary hepatic non-Hodgkin's lymphoma in a patient with chronic hepatitis C: report of a case. Surg Today 34:366–369
13. Kluin PM, Slootweg PJ, Schuurman HJ, Go DMDS, Rademakers LHPM, Putte SCJ, Unnik JAM (1984) Primary B-cell malignant lymphoma of the maxilla with a sarcomatous pattern and multilobated nuclei. Cancer 54:1598–1605
14. Lanham GR, Weiss SW, Enzinger FM (1989) Malignant lymphoma: a study of 75 cases presenting in soft tissue. Am J Surg Pathol 13:1–10
15. Lei KI (1998) Primary non-Hodgkin's lymphoma of the liver. Leuk Lymphoma 29:293–299
16. Listar TA, Crowther D, Sutcliffe SB, Glatstein E, Canellos GP, Young RC, Rosenberg SA, Coltman CA, Tubiana M (1989) Report of a committee convened to discuss the evaluation and staging of patients with Hodgkin's disease: Cotswolds meeting. J Clin Oncol 7:1630–1636
17. Maes M, Depardieu C, Dargent JL, Hermans M, Verhaeghe JL, Delabie J, Pittaluga S, Troufleau P, Verhest A, Wolf-Peeters CD (1997) Primary low-grade B-cell lymphoma of MALT-type occurring in the liver: a study of two cases. J Hepatol 27: 922–927
18. Noronha V, Shafi NQ, Obando A, Kummar S (2005) Primary non-Hodgkin's lymphoma of the liver. Crit Rev Oncol Hepatol 53:199–207
19. Nozawa Y, Wang J, Weiss LM, Kikuchi S, Hakozaki H, Abe M (2001) Diffuse large B-cell lymphoma with spindle cell features. Histopathology 38:177–179
20. Page RD, Romaguera JE, Osborne B, Medeiros LJ, Rodriguez J, North L, Sanz-Rodriguez C, Cabanillas F (2001) Primary hepatic lymphoma. Cancer 92:2023–2029
21. Santos ES, Raez LE, Salvatierra J, Morgensztern D, Shanmugan N, Neff GW (2003) Primary hepatic non-Hodgkin's lymphomas: case report and review of the literature. Am J Gastroenterol 98:2789–2793
22. Scoazec JY, Degott C, Brousse N, Barce J, Molas G, Potet F, Benhamou JP (1991) Non-Hodgkin's lymphoma presenting as a primary tumor of the liver: presentation, diagnosis and outcome in eight patients. Hepatology 13:870–875
23. Wang J, Sun NCJ, Nozawa Y, Arber DA, Chu P, Chang KL, Weiss LM (2001) Histological and immunohistochemical characterization of extranodal diffuse large-cell lymphomas with prominent spindle cell features. Histopathology 39:476–481

Virchows Arch (2006) 449:597–599
DOI 10.1007/s00428-006-0290-6

LETTER TO THE EDITOR

Prostatic ductal adenocarcinoma mimicking villous adenoma of the urethra

Katsuaki Sato · Hironori Tachibana · Toyonori Tsuzuki · Yoshimichi Ueda · Shogo Katsuda

Received: 25 July 2006 / Accepted: 4 August 2006 / Published online: 19 September 2006
© Springer-Verlag 2006

Dear Editor,

Prostatic ductal adenocarcinoma (PDA) is a rare variant of a prostatic adenocarcinoma, accounting for less than 1% [5]. Usually, PDAs grow in irregular complicated papillary or cribriform pattern, of which nuclear atypia is marked [5]. We report a case of PDA with bland cytological and structural atypia mimicking villous adenoma, suggesting a diagnostic pitfall.

A 73-year-old man presented with a complaint of hematuria. A digital rectal examination revealed normal-sized prostate with no nodules, and the serum level of prostate-specific antigen (PSA) was within normal range. Urine cytology showed a few clusters composed of atypical cells with mildly increased N/C ratio and irregular nuclei, suspicious of malignancy. Ultrasonography characterized a tumor in the neck of the urinary bladder, 1.8 cm in maximal diameter (Fig. 1a, arrow), while urethrocystoscopy demonstrated a papillary tumor protruding into the prostatic urethra. Transurethral resection of the tumor was performed.

Histologically, the resected specimen showed tumor fragments mainly comprised of simple papillary-growing components associated with a fibrovascular stalk, similar to villous adenoma (Fig. 1b). Serrated and cribriform figures were partially seen. The tumor cells appeared as tall columnar cells with pseudostratified nuclei and abundant cytoplasm (Fig. 1c). Cytological atypia was characteristically minimal. Cytoplasmic mucin was not detected by periodic acid-Schiff or Alcian blue staining. Immunohistochemically, the tumor cells diffusely expressed PSA (Fig. 1d) and androgen receptor and focally expressed prostatic acid phosphatase. Furthermore, α-methylacyl-CoA racemase (P504S) and prostate-specific membrane antigen were weakly positive, but cytokeratin (CK) 7 and CK20 were negative. Ki-67 (MIB-1) positivity was approximately 20%. Transrectal needle biopsy of the prostate was performed, and one of the six specimens demonstrated conventional acinar adenocarcinoma with a Gleason score of 3+3=6. The patient received hormonal therapy, and there was no evidence of local recurrence or distant metastasis 1 year after the tumor resection.

PDA was first described as endometrial carcinoma of the prostatic utricle by Melicow and Pachter in 1967 [4]. The carcinoma has now been confirmed to originate from the prostatic duct, not derived from the Müllerian duct. The tumor growth can be subdivided into two patterns: centrally located papillary tumor protruding into the prostatic urethra such as this case, and peripherally located tumor diffusely involved in the transitional or peripheral zone of the prostate [5]. Histologically, tall columnar epithelium with pseudostratified nuclei and eosinophilic or amphophilic cytoplasm proliferate in a papillary and tubulopapillary fashion, resembling an endometrial carcinoma, and are nominated as type A. Type B shows cribriform patterned or solid growth with frequent comedonecrosis and marked nuclear atypia. Type A almost matches with *adenocarcinoma of the primary prostatic ducts*, and type B with *adenocar-*

K. Sato (✉) · Y. Ueda · S. Katsuda
Department of Pathophysiological and Experimental Pathology,
Kanazawa Medical University,
1-1 Daigaku, Uchinada, Kahoku,
Ishikawa 920-0293, Japan
e-mail: sato-k@kanazawa-med.ac.jp

H. Tachibana
Department of Urology, Kanazawa Medical University,
Ishikawa, Japan

T. Tsuzuki
Department of Pathology and Laboratory Medicine,
Nagoya Second Red Cross Hospital,
Nagoya, Japan

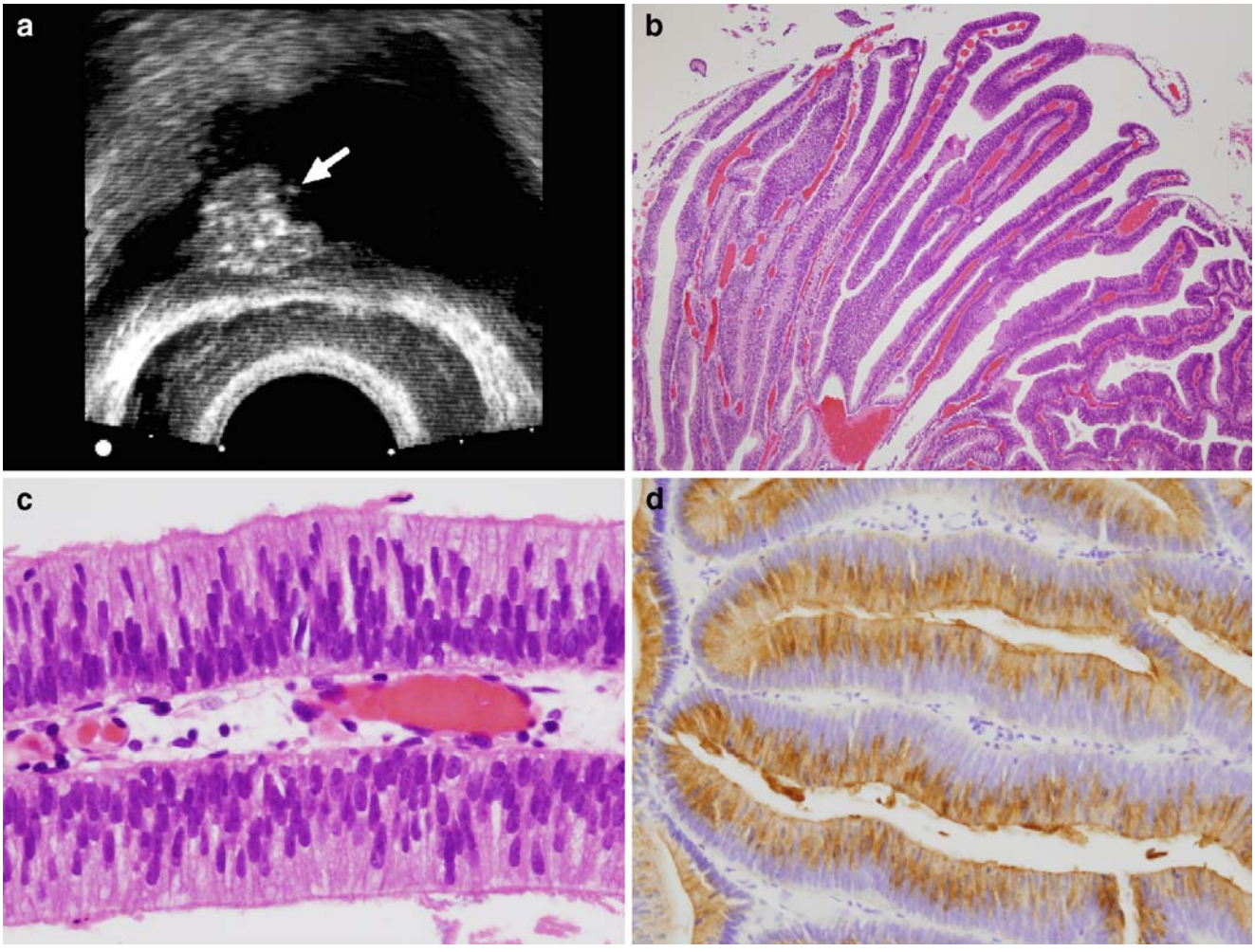

Fig. 1 **a** Ultrasonographic appearance showing a polypoid lesion in the bladder neck. **b** Lower magnification of the tumor presenting mainly villous pattern. H&E staining. **c** Higher magnification demonstrating bland cytological atypia and no cytoplasmic mucin. H&E staining. **d** Immunohistochemistry for prostate-specific antigen showing positive reaction in the cytoplasm

cinoma of the secondary prostatic ducts, as reported by Dube et al. [2] Cytological atypia of PDA is characteristically higher than that of conventional acinar carcinoma: irregular chromatin distribution, distinct nucleoli, and frequent mitotic figures. However, in some cases of type A, the cytological atypia is minimal as this case, and small biopsy specimens can hardly be diagnosed as a carcinoma [5].

The present case showed a papillary tumor projecting into the prostatic urethra with bland cytologic features. This centrally located tumor was histologically type A and probably developed from the primary prostatic duct. The differential diagnosis in this case included villous adenoma of the urethra, which is a rare benign tumor in the urothelium. Morphological similarity is a papillary structure being comprised of columnar epithelium with nuclear pseudostratification and mild cytological atypia. The difference on HE section is in cytoplasmic mucin; villous adenoma cells secrete mucin but PDA cells contain no mucin in the cytoplasm. Immunohistochemically, PDAs are positive for PSA, but villous adenomas are negative. Villous adenoma is commonly reactive to CK7, CK20, and carcinoembryonic antigen but PDA is not. Immunohistochemical findings in this case were consistent with a PDA.

Both centrally and peripherally located PDAs can present simultaneously, and a centrally located PDA is sometimes admixed with conventional acinar adenocarcinoma as in the present case [5]. An examination of the entire prostate is critical in PDA cases to prepare a therapeutic strategy. Also in villous adenoma, histological examination of the entire specimens is needed because adenocarcinoma commonly coexists. The usual treatment for a PDA is the same as that for an acinar adenocarcinoma, although antiandrogen therapy is less effective for a PDA than for acinar adenocarcinomas [5].

Dube et al. [2] reported that the 5-year survival rate was 42.8% for a PDA of primary duct origin (type A) and 24.2%

for a PDA of secondary duct origin (type B), and the prognosis for type A is analogous to that for acinar adenocarcinoma. The rate for type B is significantly worse than that for type A; however, it is not clear if cytological atypia correlates with prognosis [5]. PDAs of secondary duct origin might have a greater malignant potential than PDAs of primary duct origin. Recently, many studies have described that PDAs have a more aggressive nature than previously thought. Christensen et al. [1] stated that PDAs, most cases in the report were of secondary duct origin, were in an advanced stage at presentation, examining from radical prostatectomized specimens, and had shorter time for recurrence than acinar adenocarcinomas in a similar clinical stage. Previous cases described as *endometrioid carcinoma of the prostate* approximately correspond to a type A PDA of primary duct origin. A case of a pure form of type A without acinar adenocarcinoma components can have a favorable course after deep transurethral resection [3]. The patient in this study received hormonal therapy and presented no local recurrence or distant metastasis at 1 year after tumor resection. Further studies will be needed to better clarify the biological nature of PDAs and the differences in prognosis between types A and B.

In conclusion, it is essential that PDA should be included in differential diagnosis of papillary tumors with minimal cytological atypia in the prostatic urethra, and confirmation by mucin staining or immunohistochemistry is needed in small samples.

References

1. Christensen WN, Steinberg G, Walsh PC, Epstein JI (1991) Prostatic duct adenocarcinoma. Findings at radical prostatectomy. Cancer 67:2118–2124
2. Dube VE, Farrow GM, Greene LF (1973) Prostatic adenocarcinoma of ductal origin. Cancer 32:402–409
3. Elgamal AA, Van de Voorde W, Van Poppel H, Vandeursen H, Baert L, Lauweryns J (1994) Exophytic papillary prostatic duct adenocarcinoma with endometrioid features, occurring in prostatic urethra after TURP. Urology 43:737–742
4. Melicow MM, Pachter MR (1967) Endometrial carcinoma of prostatic utricle (uterus masculinus). Cancer 20:1715–1722
5. Yang XJ, Cheng L, Helpap B, Samaratunga H (2004) Ductal adenocarcinoma. In: Eble JN, Sauter G, Epstein JI, Sesterhenn (eds) World Health Organization classification of tumours. Pathology and genetics of tumours of the urinary system and male genital organs. IARC, Lyon, pp 199–201

Virchows Arch (2006) 449:600–602
DOI 10.1007/s00428-006-0292-4

LETTER TO THE EDITOR

Prostatic tissue ectopia within the seminal vesicle: a potential source of confusion with seminal vesicle involvement by prostatic adenocarcinoma

Sean K. Lau · Peiguo G. Chu

Received: 5 June 2006 / Accepted: 15 August 2006 / Published online: 3 October 2006
© Springer-Verlag 2006

Dear Editor:

Ectopic prostatic tissue is an unusual but not uncommon finding in the genitourinary tract. Aberrant prostatic tissue occurs most commonly in the urethra [4] and urinary bladder [3], but has also been observed in the testis [9], epididymis [6], penis [11], cervix, and vagina [7]. The presence of benign ectopic prostatic glandular elements within the seminal vesicle is extremely rare, with only a single report in the literature describing this unusual finding [10]. Herein, we present an additional case of ectopic prostate tissue involving the seminal vesicle. Recognition and awareness of this phenomenon is important so as not to confuse this particular lesion with secondary involvement of the seminal vesicle by prostatic carcinoma.

An asymptomatic 65-year-old male presented with a screening serum prostate-specific antigen level of 2.47 ng/ml. A transrectal ultrasound-guided biopsy of the prostate was subsequently performed, which revealed a prostatic adenocarcinoma, Gleason score 3+3=6. Following discussion of therapeutic options, the patient underwent a robotic-assisted laparoscopic prostatectomy. The patient's postoperative course was unremarkable, and he is presently alive and well with no evidence of recurrent tumor or metastasis 10 months following surgery.

The resected prostate measured 4.5×3.5×3.0 cm and weighed 57 g. Histologic sections of the prostate showed an acinar prostatic adenocarcinoma, Gleason score 3+3=6, involving both sides of the gland. There was no evidence of perineural invasion, extraprostatic extension, or involvement of the surgical margins by the tumor.

S. K. Lau (✉) · P. G. Chu
Department of Pathology, City of Hope National Medical Center,
1500 East Duarte Road,
Duarte, CA 91010, USA
e-mail: SLau@coh.org

The right seminal vesicle measured 3.1×2.0×1.0 cm and the left seminal vesicle measured 2.8×1.2×1.1 cm. Microscopic evaluation demonstrated no involvement of the seminal vesicles by prostatic adenocarcinoma. However, a 6.0-mm well-demarcated proliferation of closely packed glands was observed within the smooth muscle wall of the left seminal vesicle (Fig. 1a). Histologically, the glands were distinct from the adjacent seminal vesicle (Fig. 1b) and resembled the ducts and acini of the normal central zone of the prostate [8], exhibiting architectural complexity with irregular contours, papillary infoldings, and epithelial arches, imparting a cribriform appearance (Fig. 1c). The glands were lined by a double-layered epithelium comprised of an inner luminal cell layer and an outer basal cell layer. The inner luminal layer was composed of columnar cells with pseudostratified nuclei and granular cytoplasm (Fig. 1d). Nuclei were uniform and without prominent nucleoli. A continuous basal cell layer was present around the glands, composed of flattened cuboidal cells with scant amounts of cytoplasm. Corpora amylacea were present in several of the gland lumina. The glands exhibited strong and diffuse positive immunoreactivity for prostate-specific antigen (PSA; Fig. 2a) and prostatic acid phosphatase (PAP), establishing the prostatic nature of the lesion. High molecular weight keratin/34βE12 and p63 confirmed the presence of basal cells (Fig. 2b), and no expression of P504S/AMACR was observed (Fig. 2c), excluding a diagnosis of prostatic malignancy involving the seminal vesicle.

Artifactual displacement of benign prostatic glands into the seminal vesicle secondary to tangential tissue sectioning was considered. However, the glandular focus was observed in a section of the seminal vesicle sampled away from its connection with the prostate; therefore, the lesion was felt to represent ectopic prostatic tissue.

Aberrant non-neoplastic prostatic tissue within the seminal vesicle is an extremely uncommon finding. Salem et al. [10]

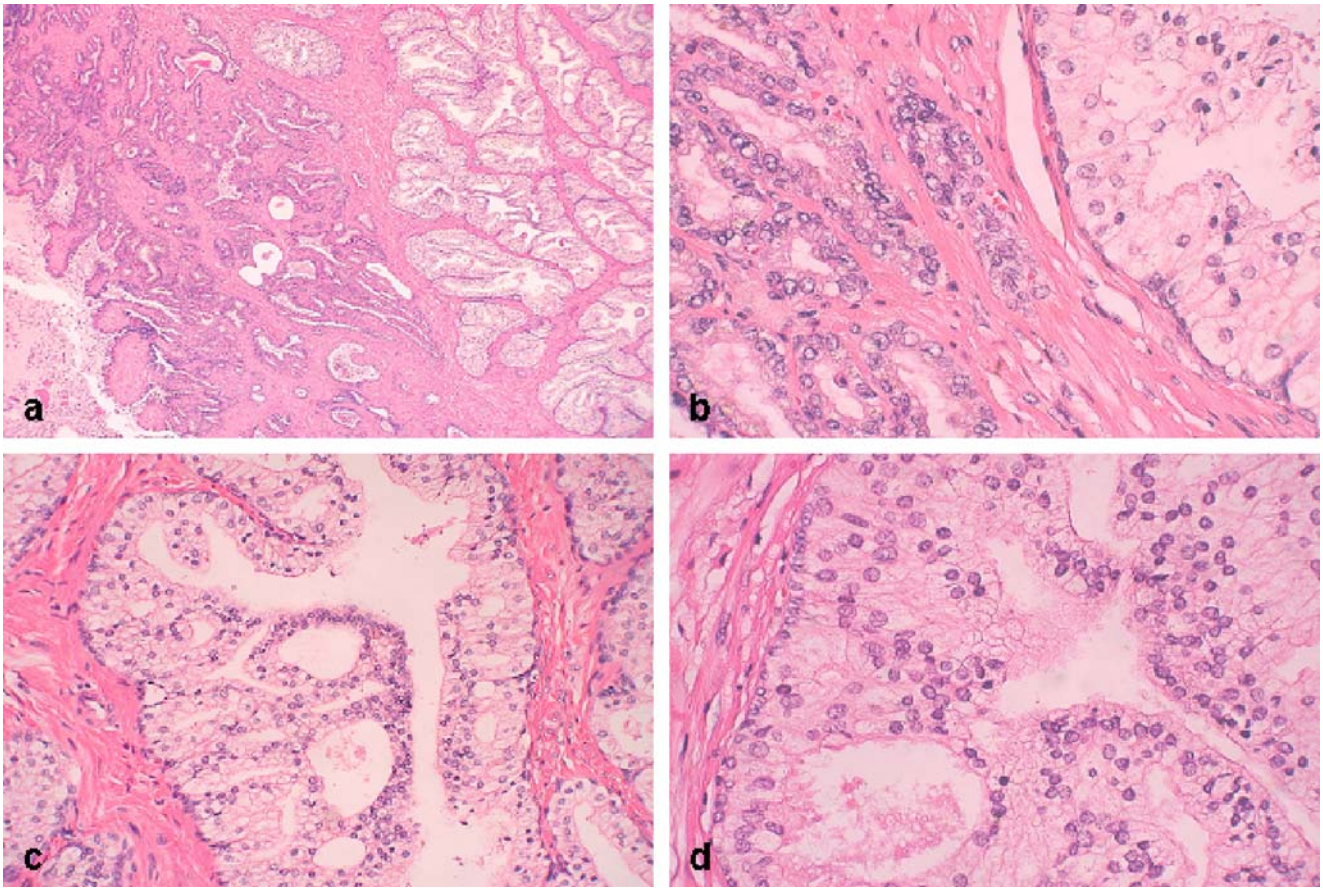

Fig. 1 **a** Ectopic prostatic tissue (*right*) involving the seminal vesicle (*left*; original magnification ×40). **b** The prostatic glands (*right*) are morphologically distinct from the adjacent seminal vesicle (*left*; original magnification ×400). **c** The prostatic glands exhibit a complex cribriform architecture (original magnification ×200). **d** The lining epithelium is comprised of cytologically bland pseudostratified columnar cells. A basal cell layer is also evident (original magnification ×400)

described a case of ectopic prostatic tissue in the seminal vesicle of 67-year-old male who had undergone a radical cystoprostatectomy for bladder malignancy. Examination of the specimen showed a high-grade urothelial carcinoma of the urinary bladder and a concurrent, organ-confined adenocarcinoma of the prostate, Gleason score 2+2=4. A 5.0-mm nodule comprised of prostatic glandular tissue was observed in the left seminal vesicle away from its attachment to the prostate. This ectopic focus showed no architectural or cytologic features of malignancy, and the presence of an intact basal cell layer was confirmed by positive immunoreactivity for keratin 34βE12. Benign prostatic glands have also been observed in a case of a seminal vesicle cyst [2].

The finding of benign prostate glands in the seminal vesicle may be explained by the overlapping embryonic origins of the two organs. The prostate develops during the 12th week of gestation from epithelial evaginations that appear along the urethra. The seminal vesicles are derived from outpouchings of the Wolffian duct and are of mesodermal origin. Although the prostate is generally regarded to be of endodermal origin, there is evidence to suggest that the central zone, which is situated posteriorly towards the base of the prostate, may be derived from the mesodermal Wolffian duct similar to the seminal vesicles. The central zone exhibits distinctive morphologic features that differ from the other anatomic zones of the prostate including a complex glandular architecture, pseudostratified columnar epithelium, and more granular cytoplasm [8]. In addition, immunohistochemical studies have shown that the pattern of expression of various proteins by the central zone is more similar to that of the seminal vesicle than to other regions of the prostate [5]. The observation that the prostatic central zone is absent in some patients with absence of Wolffian duct structures also supports the concept that the central zone of the prostate, like the seminal vesicles, is mesodermally derived [1].

Both the present case and the case previously reported by Salem et al. [10] noted the presence of central zone type histology in the ectopic prostatic tissue present in the seminal vesicle. This suggests that the presence of prostatic tissue in this particular location could be attributed to the shared embryologic origins of the central zone of the prostate and seminal vesicles, and perhaps results from anomalous development of the Wolffian duct.

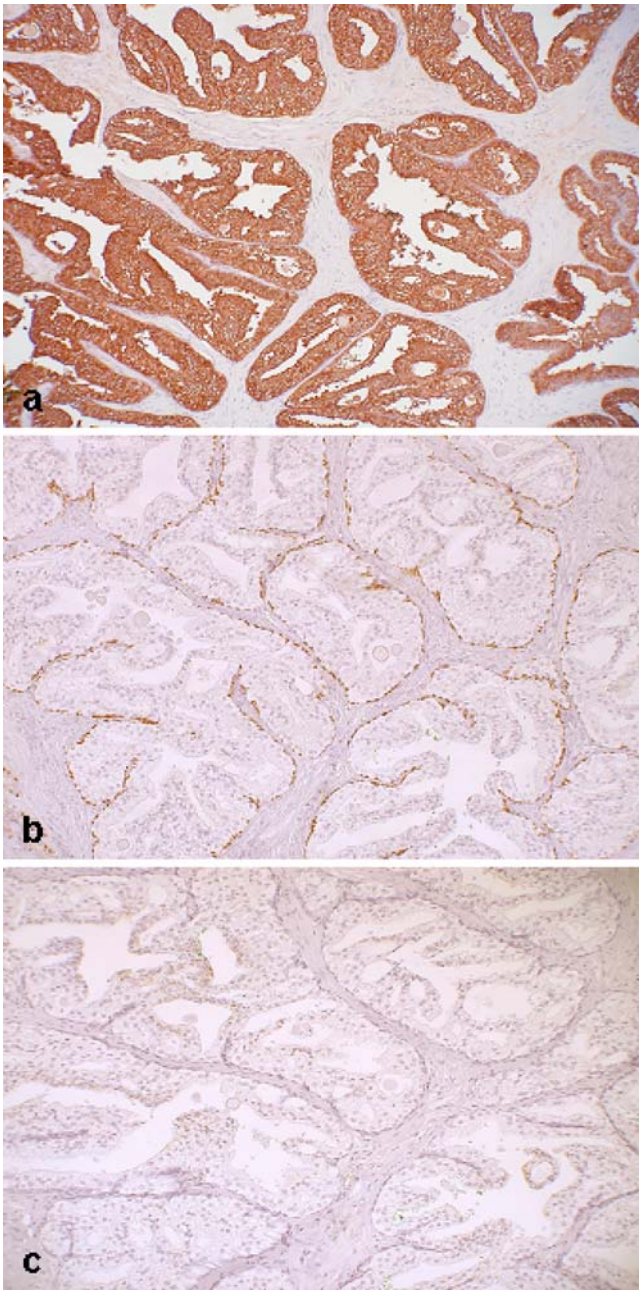

Fig. 2 **a** The focus of ectopic glands shows strong immunoreactivity for PSA (original magnification ×100). **b** Immunohistochemistry for p63 highlights an intact basal cell layer (original magnification ×100). **c** The ectopic prostate tissue is negative for P504S/AMACR (original magnification ×100)

Recognition of prostatic tissue ectopia involving the seminal vesicle is straightforward once the diagnosis is considered. The ectopic glandular proliferation is morphologically distinct from the branching configuration of the background seminal vesicle glands and lacks the significant nuclear atypia commonly seen in seminal vesicle epithelium. Prostatic differentiation can be demonstrated with the use of immunohistochemistry for PSA and PAP. The presence of ectopic prostatic tissue within the seminal vesicle should not be mistaken for seminal vesicle involvement by prostatic carcinoma, as misdiagnosis in this setting has important clinical implications in regards to staging, prognosis, and treatment. Prostatic tissue ectopia is a benign lesion and lacks typical microscopic features of prostatic adenocarcinoma such as an infiltrative architecture, absence of basal cells, and nuclear atypia in the form of nuclear enlargement and prominent nucleoli. The benign nature of the prostatic glands can be confirmed using immunohistochemistry; immunoreactivity for basal cell markers such as 34βE12 or p63 will demonstrate the presence of an intact basal cell layer, and no expression of AMACR should be observed.

Although clearly a rare occurrence, it is important to appreciate that benign prostatic ectopia can arise within the seminal vesicle. Awareness of this entity is important so as not to confuse such ectopic foci with seminal vesicle involvement by prostatic carcinoma. Once considered, the diagnosis can usually be established on morphologic grounds and can be easily confirmed utilizing immunohistochemistry.

References

1. Argani P, Walsh PC, Epstein JI (1998) Analysis of the prostatic central zone in patients with unilateral absence of Wolffian duct structures: further evidence of the mesodermal origin of the prostatic central zone. J Urol 160:2126–2129
2. Aslan DL, Pambuccian SE, Gulbahce HE, Tran ML, Manivel JC (2006) Prostatic glands and urothelial epithelium in a seminal vesicle cyst: report of a case and review of pathologic features and prostatic ectopy. Arch Pathol Lab Med 130:194–197
3. Bellezza G, Sidoni A, Cavaliere A (2005) Ectopic prostatic tissue in the bladder. Int J Urol 12:1066–1068
4. Butterick JD, Schnitzer B, Abell MR (1971) Ectopic prostatic tissue in urethra: a clinocopathological entity and a significant cause of hematuria. J Urol 105:97–104
5. Laczko I, Hudson DL, Freeman A, Feneley MR, Masters JR (2005) Comparison of the zones of the human prostate with the seminal vesicle: morphology, immunohistochemistry, and cell kinetics. Prostate 62:260–266
6. Lee LY, Tzeng J, Grosman M, Unger PD (2004) Prostate gland-like epithelium in the epididymis: a case report and review of the literature. Arch Pathol Lab Med 128:e60–e62
7. McCluggage WG, Ganesan R, Hirschowitz L, Miller K, Rollason TP (2006) Ectopic prostatic tissue in the uterine cervix and vagina: report of a series with a detailed immunohistochemical analysis. Am J Surg Pathol 30:209–215
8. McNeal JE (1997) Prostate. In: Sternberg S (ed) Histology for pathologists. Lippincott-Raven, Philadelphia, pp 997–1017
9. Milburn JM, Bluth EI, Mitchell WT Jr (1994) Ectopic prostate in the testicle: an unusual cause of a solid testicular mass on ultrasonography. J Ultrasound Med 13:578–580
10. Salem CE, Gibbs PM, Highshaw RA, Reuter VE, Cote RJ (1996) Benign ectopic prostatic tissue involving the seminal vesicle in a patient with prostate cancer: recognition and implications for staging. Urology 48:490–493
11. Willis RA (1962) Developmentally heterotopic tissues. In: The borderland of embryology and pathology, 2nd edn. Butterworth, Washington, pp 315–350

Virchows Arch (2006) 449:603–605
DOI 10.1007/s00428-006-0298-y

LETTER TO THE EDITOR

Unexpected and potentially misleading TTF-1 expression: a word of caution

Abbas Agaimy · Peter H. Wünsch

Received: 9 August 2006 / Accepted: 21 August 2006 / Published online: 28 September 2006
© Springer-Verlag 2006

Dear Editor,

Thyroid transcription factor-1 (TTF-1) is a cell-specific transcription protein expressed in normal epithelial cells of the lung (type II pneumocytes and Clara cells) and the thyroid (both follicular and calcitonin-producing C-cells) [1, 2]. This immunoreactivity is fairly retained in the neoplastic descendants of these cell types, a finding of high diagnostic utility in the routine surgical pathology practice. The high sensitivity and specificity of TTF-1 in pulmonary adenocarcinoma have been validated in different studies [1–3, 8]. Among non-pulmonary, non-thyroid neoplasms tested, only rare cases of colorectal adenocarcinoma and two cases of ovarian carcinoma showed a variable TTF-1 expression, depending on the antibody used [2]. The consistent lacking of TTF-1 in reactive and neoplastic mesothelial lesions has qualified this marker as an additional negative marker in the panel used to distinguish pulmonary adenocarcinoma from diffuse malignant mesothelioma of the pleura [9]. In the routine practice, an unequivocal TTF-1 immunoreactivity in a metastatic adenocarcinoma of unknown origin is used as an evidence for a pulmonary origin. Likewise, finding TTF-1 positive epithelial cells in body cavity effusions strongly suggests a metastatic pulmonary carcinoma [3, 7, 8]. In this report, we demonstrate the potential diagnostic confusion and pitfalls that may be caused by unexpected TTF-1 reactivity in pleural effusion cells and in metastatic adenocarcinoma of unknown primary.

The first patient was a 77-year-old man who was admitted to hospital because of cough and unexplained pleural effusion. Pleural cytology performed on three different occasions revealed activated mesothelial cells in a fibrinous inflammatory background with scattered aggregates of mildly to moderately atypical epithelial cells forming gland-like and papillary structures (Fig. 1a). These latter cells were immunoreactive for CK7 (1:500, Dako), HEA125 (1:100, Linaris) and TTF-1 (8G7G3/1, 1:100, Dako; Fig. 1b), but were negative for calretinin (polyclonal, 1:75, Zytomed), HBME-1 (1:50, Linaris) and CK5/6 (1:20, Zytomed). The findings were initially interpreted as suspicious for metastatic adenocarcinoma of probable pulmonary origin. However, imaging procedures failed to reveal a primary tumour neither in the lung nor in other organs. A thoracoscopy was performed, and multiple pleural biopsies were taken from representative areas. Histological examination (after serial sectioning) showed extensive pleural empyema with necrotizing pneumonia involving the adherent peripheral lung tissue. No neoplastic elements could be detected. Based on the clinicopathological findings and the immunohistochemical profile, these cells were reinterpreted as reactive alveolar epithelial cells released into the pleural cavity as a consequence of the extensive pleuropulmonary damage. The patient was alive with no evidence of a neoplastic disease 18 months later.

The second patient was a 70-year-old woman who was investigated for non-specific lower abdominal symptoms. Ultrasound examination revealed a large retroperitoneal mass (clinically thought to represent a malignant lymphoma or a sarcoma). An ultrasound-guided core biopsy revealed a high-grade adenocarcinoma with focally prominent papillary pattern (Fig. 2a). An initial diagnosis of metastatic

A. Agaimy (✉) · P. H. Wünsch
Institut für Pathologie, Klinikum Nürnberg,
Prof.-Ernst-Nathan-Strasse 1,
90419 Nürnberg, Germany
e-mail: abbas.agaimy@klinikum-nuernberg.de

P. H. Wünsch
e-mail: wuensch@klinikum-nuernberg.de

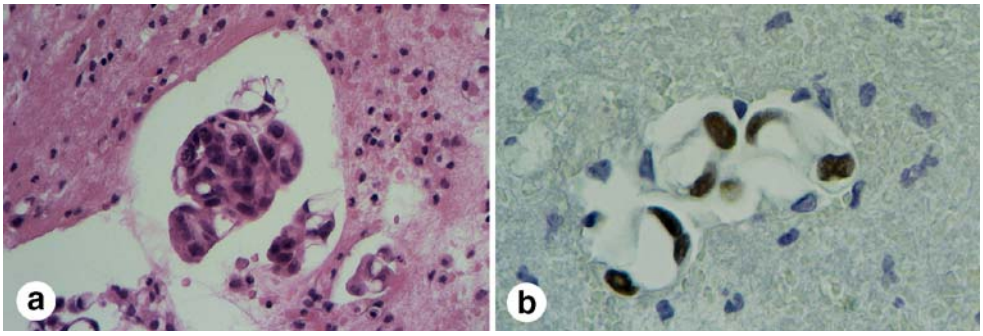

Fig. 1 **a** Reactive alveolar epithelial cells forming gland-like structures in a fibrinous background. **b** Strong nuclear staining for TTF-1

papillary serous adenocarcinoma of probable ovarian origin was rendered. Surprisingly, immunohistochemistry revealed, in addition to reactivity for CK7, a strong nuclear staining in almost all tumour cells for TTF-1 (Fig. 2b). Thyroglobulin (polyclonal, 1:1,800, Dako) was not expressed in the tumour cells. As these findings were difficult to interpret, a close pulmonary investigation to exclude an occult primary was recommended. Further clinical work-up revealed a large left ovarian mass that was completely surgically resected, together with an adherent colon segment, the uterus and the right unremarkable ovary. Histological examination showed a primary ovarian malignant mullerian mixed tumour (MMMT) consisting of an admixture of high-grade papillary serous adenocarcinoma and non-specific sarcoma (Fig. 2c). Immunohistochemically, the carcinomatous component had a similar profile as the metastasis with a strong nuclear staining for TTF-1 (Fig. 2d). The sarcomatous component was high grade expressing only vimentin.

TTF-1 has emerged as a useful marker in the histogenetic classification of primary and metastatic neoplasms derived from the thyroid and the lungs. In the daily practice, the finding of TTF-1 immunoreactive glandular epithelial cells in an unexplained body cavity effusion strongly suggests a metastatic pulmonary carcinoma [3, 7, 8]. The first case in this report illustrates the potential diagnostic confusion that may arise if regenerative alveolar epithelium is exfoliated into the pleural cavity as a result of peripheral pleuropulmonary damage. Such epithelial cells may show a remarkable degree of reactive/regenerative atypia caused by the underlying pathology, as in the current case. Without an active pathologist–clinician intercommunication, it would be impossible to distinguish such a reactive finding from a metastatic neoplastic process. We are not aware of any report in the literature documenting a similar finding. Not considering this rare phenomenon may result in a disastrous over-treatment of the patient. The differential diagnosis includes mainly reactive mesothelial hyperplasia, which may show glandular and papillary formations. However, reactive mesothelial cells have a distinct immunoprofile (CK7+/HEA125−/calretinin+/TTF-1−) different from that of pulmonary epithelium (CK7+/HEA125+/calretinin−/

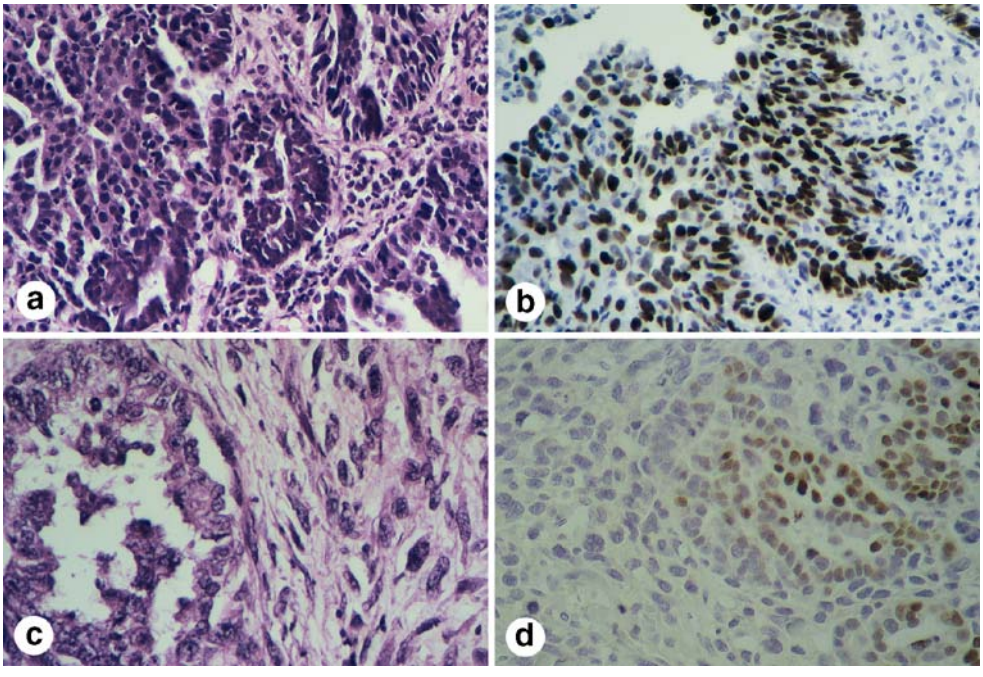

Fig. 2 **a** High-grade papillary carcinoma as the sole component of MMMT metastatic to the retroperitoneum. **b** TTF-1 is expressed in almost all cells. **c** Primary ovarian MMMT with high-grade carcinomatous (*left*) and sarcomatous component (*right*). **d** TTF-1 reactivity in the epithelial component (lacking staining in the sarcomatous area and a weaker staining at the interphase between the two components)

TTF-1+). To our knowledge, TTF-1 reactivity has not been demonstrated in reactive mesothelial cells. A pulmonary adenocarcinoma was excluded by thorough clinical–radiological examination and thoracoscopic pleural sampling. The pleural empyema was obviously secondary to the necrotizing pneumonia.

The second case illustrates the potential diagnostic pitfall when applying immunohistochemical marker for histogenetic or topographic typing of metastatic carcinoma of unknown primary. Metastatic pulmonary adenocarcinoma may rarely present as a unilateral or bilateral ovarian mass strikingly mimicking primary ovarian cancer, both grossly and histologically [5, 6]. In challenging cases, this differential diagnostic issue may be solved only by immunohistochemical methods. In this regard, the consistent detection of TTF-1 in pulmonary adenocarcinoma and its almost lacking expression in ovarian adenocarcinoma proved to be of a great diagnostic value [1, 6]. However, a recent report has documented a strong expression of TTF-1 in two primary ovarian carcinomas (one each serous and endometrioid carcinoma) among 166 cases (1.2%) [4]. The spectrum of TTF-1 expressing ovarian lesions other than conventional ovarian cancer is relatively limited, encompassing mainly benign and malignant struma ovarii, strumal carcinoid and ovarian metastasis from lung and thyroid carcinoma. TTF-1 expression has not been previously reported in MMMT. It may be a reflection of the capability of MMMT for multidirectional differentiation towards a pulmonary or a thyroid phenotype similar to the wide spectrum of sarcomatous differentiation in MMMT. An occult pulmonary neoplasm was excluded by appropriate clinical and radiological procedures.

In summary, we documented a potentially misleading TTF-1 immunoreactivity in reactive alveolar epithelium in pleural effusion cytology and in the carcinomatous component of an occult primary ovarian MMMT metastatic to the retroperitoneum. Both cases underscore the high significance of pathologist–clinician intercommunication for a proper interpretation of unexpected/unusual histological and immunohistochemical findings for an optimal patient management.

References

1. Chang YL, Lee YC, Liao WY, Wu CT (2004) The utility and limitation of thyroid transcription factor-1 protein in primary and metastatic pulmonary neoplasms. Lung Cancer 44:149–157
2. Comperat E, Zhang F, Perrotin C, Molina T, Magdeleinat P, Marmey B, Regnard J-F, Audouin J, Camilleri-Broet S (2005) Variable sensitivity and specificity of TTF-1 antibodies in lung metastatic adenocarcinoma of colorectal origin. Mod Path 18: 1371–1376
3. Gomez-Fernandez C, Jorda M, Delgado PI, Ganjei-Azar P (2002) Thyroid transcription factor 1. A marker for lung adenocarcinoma in body cavity fluids. Cancer 96:289–293
4. Graham AD, Williams ARW, Salter DM (2006) TTF-1 expression in primary ovarian epithelial neoplasia. Histopathology 48:764–765
5. Householder J, Han A, Edelson MI, Eager JM, Rosenblum NG (2002) Immunohistochemical confirmation of pulmonary papillary adenocarcinoma metastatic to ovaries. Arch Pathol Lab Med 126:1101–1103
6. Irving JA, Young RH (2005) Lung carcinoma metastatic to the ovary. A clinicopathologic study of 32 cases emphasizing their morphologic spectrum and problems in the differential diagnosis. Am J Surg Pathol 29:997–1006
7. Jang KY, Kang MJ, Lee DG, Chung MJ (2001) Utility of thyroid transcription factor-1 and cytokeratin 7 and 20 immunostaining in the identification of origin in malignant effusions. Anal Quant Cytol Histol 23:400–404
8. Ng WK, Chow JCY, Ng PKH (2001) Thyroid transcription factor-1 is highly sensitive and specific in differentiating metastatic pulmonary from extrapulmonary adenocarcinoma in effusion fluid cytology specimens. Cancer 96:43–48
9. Ordonez NG (2005) Immunohistochemical diagnosis of epithelioid mesothelioma. An update. Arch Pathol Lab Med 129:1407–1414

Virchows Arch (2006) 449:606–607
DOI 10.1007/s00428-006-0293-3

LETTER TO THE EDITOR

Passion for pathology: beauty is in the eye of the beholder

Anna Batistatou · Konstantinos Charalabopoulos

Received: 1 August 2006 / Accepted: 15 August 2006 / Published online: 3 October 2006
© Springer-Verlag 2006

Dear Editor,

We read with great interest the editorial by G. Bussolati on the mental processes that lead to pathological diagnoses [2], which is the first published approach to this process. We would like to stress/add a few points that we think are of great importance. Besides the perception of form, color is important for detecting objects and patterns that would otherwise not be noticed. We all know from experience that black and white microscopic figures loose much of their information content. A haematoxylin–eosin-stained glass slide makes us look twice if it is over-stained with haematoxylin, since we have unconsciously associated "bluish" with hypercellular/suspicious lesions. Color opponency, simultaneous color contrast and color constancy are the key features of color vision. Color is coded in the retina and in the lateral geniculate nucleus by color-opponent cells and processed in the cortex by concentric double-opponent cells in the blob zones (area V1 of the cortex) [3].

According to neurobiologists, memory has stages (short-term, long-term) and is often localized in different places in the nervous system. Based on the way information is stored and recalled, memory can be classified as implicit or explicit. The former can be reported verbally and involves the medial temporal lobe system, while the latter does not require conscious awareness and involves various perceptual pathways. Based on the editorial, it is certain that both types of pathology memory exist. Furthermore, "cognition", defined as the sum of the processes by which the sensory (visual) input is transformed, reduced, elaborated, stored, recovered and used, is very important in pathology. As Ulrich Meisser has stated: the world of experience is produced by the man who experiences it [3]. Or according to the well-known statement: beauty is in the eye of the beholder. Indeed, microscopic images can constitute art since they have form and beauty [1]. Moreover, pathologists worldwide, when looking at a slide under the microscope, are alert not only to the clues that will lead to the correct diagnosis but also to the incidental appearance of known forms and images of the three-dimensional world (Fig. 1). Thus, hearts, faces, animals, flowers and trees are always welcomed findings, particularly after a hard day's work on the microscope, and help the observing pathologist keep his passion for pathology alive.

A. Batistatou (✉)
Department of Pathology,
University of Ioannina Medical School,
Ioannina, Greece
e-mail: abatista@cc.uoi.gr

K. Charalabopoulos
Clinical Unit, Department of Physiology,
University of Ioannina Medical School,
Ioannina, Greece

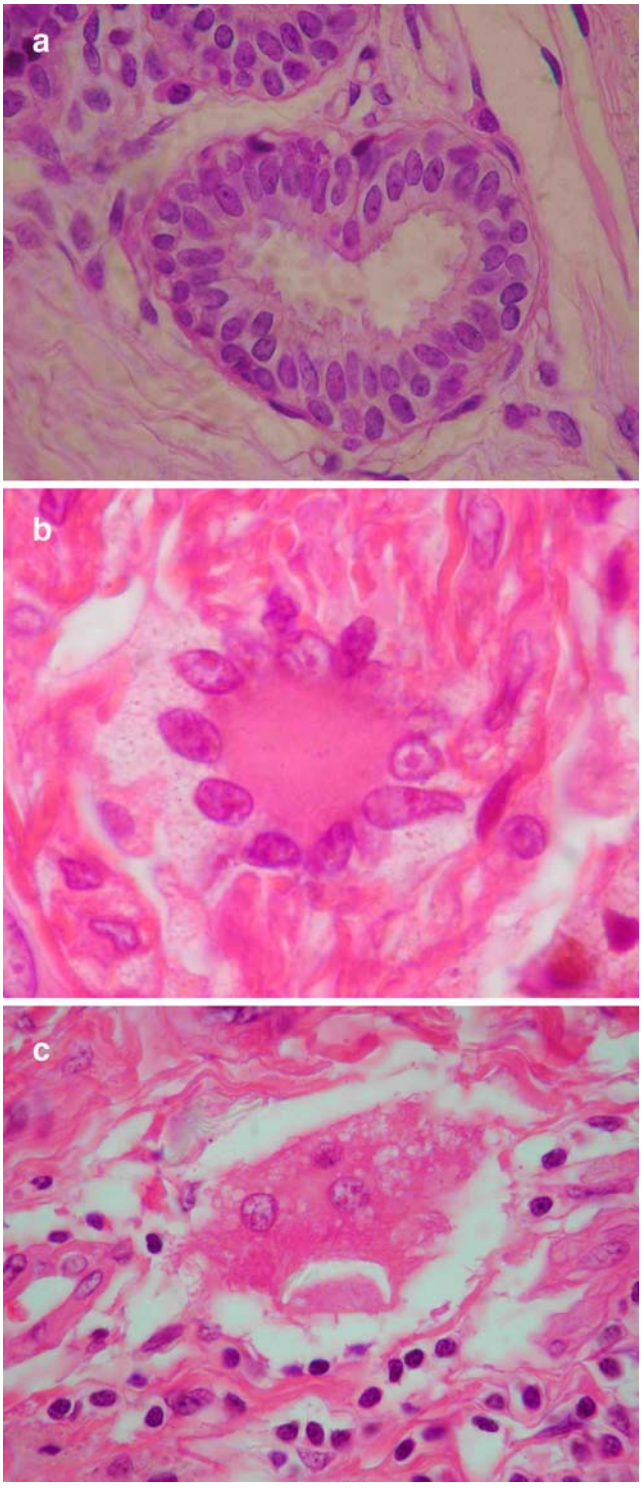

Fig. 1 Passion for pathology. **a** Heart-shaped breast duct, **b** flower-shaped giant cell, **c** face-shaped giant cell with foreign body (haematoxylin–eosin, original magnification ×400)

References

1. Batistatou A, Charalabopoulos KA (2005) The art of science: transitional cell carcinoma of the bladder and Golconda. Med Hypotheses 65:970–971
2. Bussolati G (2006) Dissecting the pathologist's brain: mental processes that lead to pathological diagnoses. Virchows Arch 448:739–743
3. Kandel ER, Schwartz JH, Jessell TM (1995) Essentials of neural science and behavior. International edition. Prentice Hall, London

Virchows Arch (2006) 449: 608
DOI 10.1007/s00428-006-0332-0
© Springer-Verlag 2006

ANNOUNCEMENTS

24–26 January 2007
Theorico-practical Course on Bone and Soft Tissue Tumors
Department of Pathology, Hospital del Mar, Barcelona, Spain

Faculty
Christopher Fletcher, M.D. (Brigham and Women's Hospital, Boston, USA)
Andrew Rosenberg, M.D. (Massachusetts General Hospital, Boston, USA)
Angelo Paolo Dei Tos, M.D. (Hospital of Treviso, Italy)
John Goldblum, M.D. (Cleveland Clinic, Cleveland, USA)
Paola Dal Cin, Ph.D. (Brigham and Women's Hospital, Boston, USA)

For further information please contact:
Francisco Alameda, M.D.
Department of Pathology
Hospital del Mar, Spain
E-mail: 86780@imas.imim.es
or
Esther Oliva, M.D.
Department of Pathology
Massachusetts General Hospital
55 Fruit Street, WRN-2
Boston, MA 02114, USA
E-mail: eoliva@partners.org

Virchows Arch (2006) 449:609–616
DOI 10.1007/s00428-006-0245-y

ORIGINAL ARTICLE

Discrepancies in the diagnosis of intraductal proliferative lesions of the breast and its management implications: results of a multinational survey

Mohiedean Ghofrani · Beatriz Tapia · Fattaneh A. Tavassoli

Received: 10 March 2006 / Accepted: 31 May 2006 / Published online: 13 October 2006
© Springer-Verlag 2006

Abstract To measure discrepancies in diagnoses and recommendations impacting management of proliferative lesions of the breast, a questionnaire of five problem scenarios was distributed among over 300 practicing pathologists. Of the 230 respondents, 56.5% considered a partial cribriform proliferation within a duct adjacent to unequivocal ductal carcinoma in situ (DCIS) as atypical ductal hyperplasia (ADH), 37.7% of whom recommended reexcision if it were at a resection margin. Of the 43.5% who diagnosed the partially involved duct as DCIS, 28.0% would not recommend reexcision if the lesion were at a margin. When only five ducts had a partial cribriform proliferation, 35.7% considered it as DCIS, while if ≥20 ducts were so involved, this figure rose to 60.4%. When one duct with a complete cribriform pattern measured 0.5, 1.5, or 4 mm, a diagnosis of DCIS was made by 22.6, 31.3, and 94.8%, respectively. When multiple ducts with flat epithelial atypia were at a margin, 20.9% recommended reexcision. Much of these discrepancies arise from the artificial separation of ADH and low-grade DCIS and emphasize the need for combining these two under the umbrella designation of ductal intraepithelial neoplasia grade 1 (DIN 1) to diminish the impact of different terminologies applied to biologically similar lesions.

M. Ghofrani · B. Tapia · F. A. Tavassoli (✉)
Department of Pathology, Yale University School of Medicine,
Lauder Hall (LH) 222, 310 Cedar St.,
New Haven, CT 06510, USA
e-mail: Fattaneh.Tavassoli@Yale.edu

Present address:
B. Tapia
Department of Pathology and Immunology,
Washington University School of Medicine,
St. Louis, MO, USA

Keywords Breast · Ductal carcinoma in situ · Hyperplasia · Interobserver variability · Ductal intraepithelial neoplasia

Introduction

The concept of atypical hyperplasia was introduced decades ago within the continuum of intraductal breast proliferations, a continuum which encompasses benign proliferations of usual ductal hyperplasia to high-grade ductal carcinoma in situ (DCIS) [3–5, 7, 15, 32]. The term atypical ductal hyperplasia (ADH) was used initially for a vaguely defined group lesions that had "some but not all of the requisite features of ductal carcinoma in situ" [21]. Subsequently, the qualitative similarity to low-grade DCIS (LG-DCIS) was stressed, and quantitative measures were introduced to separate ADH from DCIS [21, 31].

Totally arbitrary boundaries were drawn to separate ADH from LG-DCIS, a separation that resulted in drastically different management approaches in the 1980s—i.e., mastectomy for those diagnosed as DCIS and follow-up for those with a diagnosis of ADH. Now, even with widespread use of conservative surgery, patient management differs significantly depending on whether a lesion is diagnosed as ADH or DCIS. The two most notable approaches for this separation have been based on: (a) the definition by Page et al. [21] who defined the minimum requirement for LG-DCIS as complete involvement of at least two spaces by a proliferation that cytologically and architecturally resembles DCIS and (b) the definition of Tavassoli and Norris [31] who required complete involvement of one or more ducts by a cribriform or micropapillary proliferation of uniform cells with low-grade nuclei exceeding 2 mm in aggregate diameter for a diagnosis of LG-DCIS. According to either of these two definitions, any intraductal prolifer-

ative lesion that demonstrated the qualitative cytologic and architectural features of LG-DCIS but failed to pass the defined quantitative threshold was to be designated as ADH.

Since then, no objective molecular, ultrastructural, immunohistochemical, or morphometric feature has been identified to reliably distinguish ADH from LG-DCIS [1, 11, 15, 16, 18, 25]. Therefore, the distinction of the two continues to be based solely on application of the arbitrary criteria mentioned above. Frequently cited studies in the literature, which have attempted to calculate the relative risk of various proliferative lesions, may have claimed to adhere to the criteria of Page et al. have actually deviated from the two-space rule and have accepted single-space involvement as DCIS, thereby blurring the distinction between levels of hyperplasia and atypia and diminishing the practical utility of such a distinction [8].

We conducted a survey 15 and 20 years postintroduction of these two sets of criteria to determine how much uniformity or discrepancy exists in the interpretation of these lesions and how it would impact current patient management.

Materials and methods

To investigate pathologists' approach to selected problems in the diagnosis and management of intraductal proliferative lesions of the breast, a questionnaire was prepared with diagrammatic representations of five potentially problematic scenarios in breast pathology dealing with intraductal proliferative lesions (Figs. 1, 2, 3, 4, 5). It was decided to use diagrammatic representations rather than glass slides to facilitate distribution of the survey among a greater number of pathologists and to ensure that the participants focused on the same diagnostic issue, given the presence of certain lesions in the background. The questionnaire also inquired whether the respondents considered breast pathology their area of expertise, the average number of breast biopsies and lumpectomies or mastectomies they signed out each week, the practice setting in which they worked in (academic, community, or private), and how long they had been in practice.

The questionnaire was distributed among over 300 pathologists who were either known for their expertise and specialization in breast pathology in various countries or who were interested in the field as evidenced by their participation in educational courses dedicated to breast pathology. If a participant left a response in the questionnaire blank, that response was considered null and excluded from calculations. Also, for all questions regarding diagnosis and management of lesions illustrated in the questionnaire, the respondents were given the option of choosing one of the two answers (i.e., ADH vs DCIS, Yes vs No). The responses of the small minority who chose both were similarly excluded from analyses. Also, if a participant responded to the questions regarding average number of biopsies or lumpectomies/mastectomies a week by providing a numeric range, the average value of the range was considered for calculations. The collected responses were anonymized and tabulated in a custom Microsoft Access database (Microsoft Corporation, Redmond, WA, USA), and custom queries were written for data analysis. Statistical significance of the results was evaluated using chi-square and *t* tests.

Results

A total of 230 completed questionnaires were received and included in the study. Of the 230 respondents, 93 (40.4%) considered breast pathology their area of expertise, while 130 (56.5%) did not consider themselves experts but had special interest or responsibility for signing out breast pathology. The respondents signed out an average and standard deviation of 10.1±9.5 biopsies and 7.5±7.8 lumpectomies or mastectomies a week. These figures were 14.4±11.4 biopsies and 10.3±9.0 lumpectomies or mastectomies a week for the responding pathologists who considered breast pathology their area of expertise and 6.9±6.0 biopsies and 5.3±6.0 lumpectomies or mastectomies a week for those who did not. *T* test showed the differences between the means in these two groups to be statistically significant ($p<0.0001$ for both biopsies and lumpectomies/mastectomies).

Academic pathologists constituted 85 (37.0%) of the respondents, while 113 (49.1%) of the respondents worked in community hospitals and 20 (8.7%) in private laboratories. Nine pathologists (3.9%) worked in more than one practice setting. Sixty-five pathologists (28.3%) had been practicing pathology for less than 5 years, 37 (16.1%) for 6 to 10 years, and 125 (54.3%) had over 10 years of practice experience.

As shown in Fig. 1, the first question addressed whether respondents considered a partially involved duct adjacent to unequivocal cribriform DCIS as ADH or DCIS and, depending on their response, whether they would recommend reexcision if this partially involved duct was less than 0.1 mm from the excision margin. Of the 230 respondents, 130 (56.5%) considered this partial cribriform proliferation as ADH and, among these respondents, 49 (37.7%) recommended reexcision of the ADH if it were close to the excision margin. On the other hand, of the 100 (43.5%) who diagnosed this partially involved duct as DCIS, 28 (28.0%) would not recommend reexcision if the lesion were close to the excision margin. Although chi-square analysis showed that pathologists who made a diagnosis of DCIS were significantly more likely

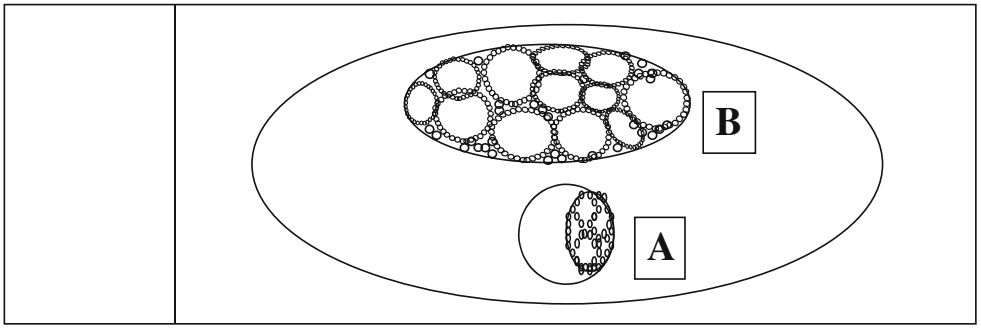

Fig. 1 The first scenario assessed how pathologists would diagnose a partially involved duct adjacent to unequivocal cribriform DCIS, and whether they would recommend reexcision if it were less than 0.1 mm from a resection margin

"A" is a single duct with unequivocal cribriform grade 1 DCIS
"B" is a duct with partial involvement by a cribriform pattern located <0.1 mm from the margin.
1. What is your diagnosis for duct "B"?
____ DCIS
____ ADH
2. Would you recommend re-excision?
____ Yes
____ No

to recommend reexcision compared to those who made a diagnosis of ADH ($p<0.001$), the final impact on patient management was that, regardless of the diagnosis, 116 (50.4%) would recommend to have a reexcision while 108 (47.0%) would not.

Question 2 documented how respondents categorized a partial cribriform proliferation involving a few (five) or numerous (20 or more) ducts (Fig. 2). When only five ducts had a partial cribriform proliferation, 82 (35.7%) of the respondents considered it as DCIS. With ≥20 ducts so involved, 139 (60.4%) of the respondents designated the changes as DCIS. Chi-square testing showed this difference to be statistically significant ($p<0.001$).

In Question 3, as shown in Fig. 3, the minimum size requirement for diagnosis of LG-DCIS in a single duct was addressed. When a single duct with a complete cribriform pattern measured 0.5, 1.5, or 4 mm, a diagnosis of DCIS was made by 52 (22.6%), 72 (31.3%), and 218 (94.8%) of the respondents, respectively. Chi-square testing confirmed that pathologists were significantly more likely to diagnose DCIS if the single duct measured >2 mm ($p<0.001$).

Question 4 addressed the approach to management of flat epithelial atypia when it was present in multiple ducts located within less than 0.1 mm from the excision margin (Fig. 4). In this scenario, when multiple ducts with flat epithelial atypia were close to an excision margin, 48 respondents (20.9%) recommended reexcision.

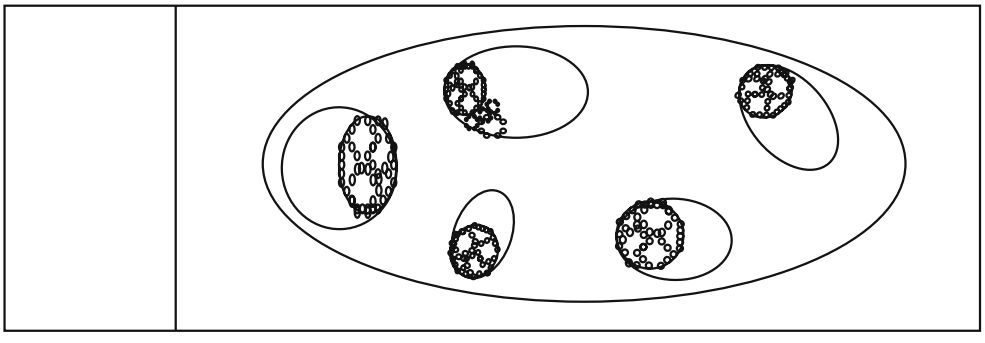

Fig. 2 In question 2, participants were asked whether the number of partially involved ducts affects their decision to make a diagnosis of ADH

There are multiple ducts (5) with partial cribriform proliferation; there is no necrosis.
1. What is your diagnosis?
____ DCIS
____ ADH
2. What would your diagnosis be if > 20 ducts showed the same finding?
____ DCIS
____ ADH

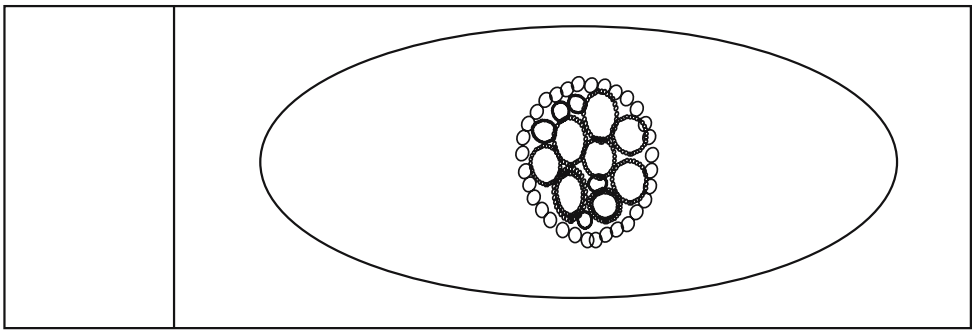

Fig. 3 Responses to question 3 demonstrated what pathologists thought was the lowest size threshold required to make a diagnosis of DCIS

There is a single 1.5 mm duct with classic cribriform nuclear grade 1 pattern; there is no necrosis.

1. What is your diagnosis?
   ____ DCIS
   ____ ADH
2. What would your diagnosis be if the duct were 0.5mm?
   ____ DCIS
   ____ ADH
3. What would your diagnosis be if the duct were 4mm?
   ____ DCIS
   ____ ADH

Finally, question 5 evaluated how respondents measured invasive carcinoma when two foci of stromal microinvasion (measuring less than 1 mm each) emanated from two opposite poles of a 1-cm duct with high-grade comedo-type DCIS (Fig. 5). Of the 230 respondents, 185 (80.4%) measured these as two separate foci of microinvasion (less than 1 mm each), while 37 (16.1%) considered the total size of invasive carcinoma as the aggregate diameter of the high-grade DCIS plus the two microinvasive foci, namely, 1.19 cm.

Chi-square testing was performed to compare the responses of expert breast pathologists and nonexperts to all five questions. No statistically significant difference was found between the two groups in the proportion of responses to any of the questions.

Discussions

These results indicate that 15 and 20 years postintroduction of criteria for separation of ADH from DCIS [21, 31], interobserver variability in the diagnosis of intraductal proliferative lesions of the breast has not diminished. Given the significance of margin involvement or proximity in current management of DCIS, this survey demonstrates an

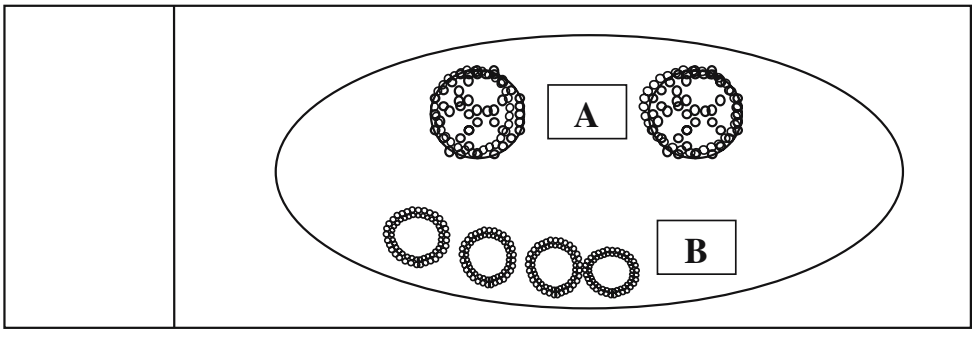

Fig. 4 Question 4 evaluated how participants would manage flat epithelial atypia close to a resection margin

The cribriform grade 1 DCIS (A) is more than 5mm from the inked margin.
Multiple ducts with flat epithelial atypia are within < 0.1 mm of the inked margin (B).
Would you recommend re-excision?

____ Yes
____ No

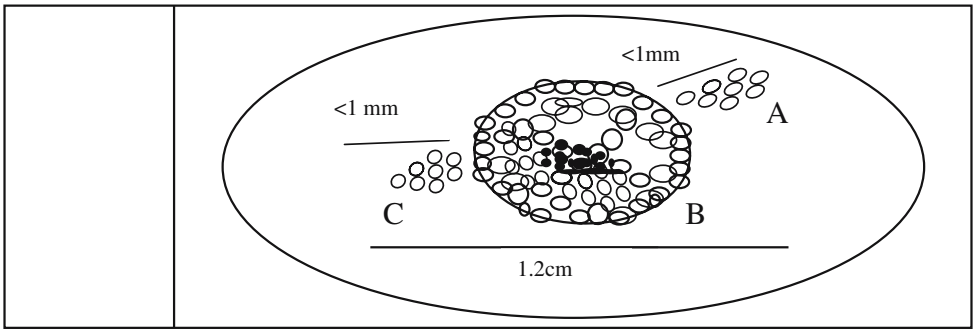

Fig. 5 Question 5 surveyed how pathologists measured invasive carcinoma in the presence of multifocal microinvasion

There is a single duct (B) with high grade DCIS and comedo-necrosis and two unequivocal foci of stomal invasion, each <1mm, at opposite poles of the duct (A and C)

1. The size of the invasive carcinoma is:
   _____ Two separate foci of microinvasion, <1mm each (A and C)
   _____ The sum of A+B+C (approximately 1.2cm)

even wider variability that exists in the management of such lesions and ultimately patient care.

In a survey done by Rosai in 1991, 17 ductal and lobular proliferative breast lesions were distributed among five experts in breast pathology [24]. The participants were asked to categorize such lesions, which had already been circled on glass slides, as either hyperplasia, atypical hyperplasia, carcinoma in situ, or "other" (to be specified) based on the diagnostic criteria they used in their daily practice. In that study, there was no a single case in which all five pathologists agreed on the diagnosis, and there were only three cases (18%) in which four of the five pathologists agreed. Also, some pathologists tended to make more malignant diagnoses than others. In his report, Rosai considered this interobserver variability to be unacceptably high and suggested the adoption of a terminology such as mammary intraepithelial neoplasia with a grading system similar to that which was being used for the uterine cervix.

A possible explanation for such a high degree of interobserver variability set forth in that report was that the pathologists were not using a standard set of criteria. Therefore, a year later, Schnitt et al. [27] tried a different approach to assess interobserver variability in the diagnosis of intraductal proliferative lesions of the breast. In their 1992 survey, they asked six experts in breast pathology to evaluate 24 proliferative ductal lesions. In this survey, the participating pathologists agreed to use the criteria of Page et al., and 15 teaching slides representing classic examples of usual ductal hyperplasia, atypical ductal hyperplasia, and noncomedo DCIS were circulated among the six pathologists to foster concordance before initiation of the study. The specific area of interest on each study slide was indicated by masking all the surrounding tissue so that all the participants focused on the same lesion and to prevent any bias that may result from assessment of changes in the surrounding breast tissue. The participants in this survey were asked to adhere to the provided criteria rather than the ones they used in their daily practice. Despite all these efforts, there was complete agreement among all six pathologists in only 14 (58%) of the 24 cases and among five or more pathologists in 17 cases (71%). The most common diagnostic problem was the distinction of atypical hyperplasia from DCIS in six cases. Although this study showed a significant improvement in interobserver agreement compared to Rosai's survey, the persistence of significant differences among expert breast pathologists even under optimal and highly artificial conditions conveyed a more widespread problem in the pathology community with potential impact on patient management.

Responses to the current survey also demonstrate that although criteria to distinguish ADH from DCIS have been introduced over two decades ago, there is still no agreement on how to categorize these two types of mammary intraductal proliferation. While the sole partially involved duct described in question 1 would not qualify as DCIS according to the criteria set forth by either Page et al. or Tavassoli and Norris, 43.5% of practicing pathologists, nevertheless, diagnosed it as DCIS. This might seem logical because the partially involved duct probably reflects an extension of the same process present in the nearby unequivocal cribriform DCIS. However, the fact remains that there is no consensus on what to designate a partially involved duct adjacent to unequivocal LG-DCIS and how to manage such a lesion when it is near or on the surgical excision margin [10]. Even among the respondents who considered the partially involved duct in question 1 as ADH, more than a third recommended reexcision if it were close to the margin of resection, and of those who considered this partially involved duct as DCIS, close to 30% would not recommend reexcision even if the in situ carcinoma were within 0.1 mm of the resection margin.

This interobserver variability in diagnosis and management was so high that, in the end, patients would have an almost 50:50 chance of having a reexcision or not, regardless of the diagnosis of the partially involved duct as ADH or DCIS. This was due to a combination of the high proportion diagnosing it as DCIS and the high proportion of those who recommended reexcision even though they interpreted it as ADH. Obviously, the impact of this issue goes beyond simply margin involvement; it is also crucial in the assessment of lesion size, resulting in widely varied assessment of size/extent of LG-DCIS.

Question 2 addressed the concept of extensive ADH. Cognizant of the fact that available criteria require complete involvement of duct cross sections for a diagnosis of low-grade (cribriform or micropapillary) variants of DCIS, it was surprising to find that even when only five ducts were involved by a partial cribriform proliferation, over 35% of the respondents considered it as DCIS. Furthermore, when greater than 20 ducts were partially involved by such a cribriform proliferation, the proportion of respondents who treated it as DCIS rose significantly to over 60%. Chi-square testing showed that as the number of partially involved ducts increased, the number of patients diagnosed with cancer significantly increased. Nevertheless, even with drastic differences in the number of involved ducts (5 vs ≥20), there was no unanimity in the diagnosis of carcinoma in situ vs atypical hyperplasia.

This scenario has become increasingly more frequent since the introduction of screening mammography. It was not addressed in the criteria introduced by either Page et al. or Tavassoli and Norris because both those retrospective studies were based on predominantly premammographic era biopsies. With the increasing number of such "extensive ADH" cases (≥20 partially involved ducts) seen in her consultation practice, Tavassoli suggested that even when these are designated as extensive ADH due to strict adherence to previously defined criteria, they should be managed as DCIS and reexcised if close to or at the margin of resection [29].

Question 3 demonstrated that the majority of respondents used the 2-mm size criterion rather than the two spaces in diagnosing DCIS. When the single duct described in the question measured greater than 2 mm (4 mm), close to 95% of the respondents considered it DCIS. However, if this single duct measured less than 2 mm, i.e., 0.5 or 1.5 mm, 22.6 and 31.3% of the respondents considered it DCIS, respectively. Although this difference in the probability of diagnosing DCIS when the lesion measured less than or greater than 2 mm was statistically significant, it is interesting to note that over 30% of the respondents considered a single duct measuring 1.5 mm as DCIS and over 20% designated a single duct measuring only 0.5 mm as carcinoma in situ despite the fact that these two scenarios meet neither the criteria of Page et al., which require two completely involved spaces not otherwise specified as to size [21], nor the criteria of Tavassoli and Norris, which require one or more spaces greater than 2 mm in maximal cross-sectional diameter [31]. Even with a substantial 4 mm duct, 5.2% did not designate the lesion as DCIS presumably because of the two-space requirement of Page et al. These responses demonstrate that in the current day to day practice of pathology, some women with a 0.5-mm lesion would be diagnosed as having DCIS, with a reexcision if it were close to or at the resection margin, and most probably radiation therapy, whereas some women with 4 mm lesions interpreted as ADH would get no reexcision, would be simply followed up, or at most would enter some form of prevention trial with hormone therapy [2, 9].

Question 4 in our survey documented the confusion that exists regarding the management of flat epithelial atypia, with over 20% of respondents recommending reexcision if the lesion were close to an excision margin. As a result, over a fifth of the patients would have reexcision, while the remaining 80% would not.

The last question showed the various approaches pathologists take in measuring invasive carcinoma when multifocal early invasion emanating from a single duct is present. Although over 80% of respondents would consider foci of invasion less than 1 mm emanating from opposite poles of a duct with DCIS as microinvasion, slightly over 16% of respondents would measure DCIS with its associated microinvasion from opposite poles as one continuous invasive carcinoma, which would entail a drastically different treatment approach.

The results of this survey raise numerous questions about studies performed in different countries and even different institutions within the same country regarding risk factors, treatment, prognosis, and outcome of intraductal proliferative lesions of the breast, which include LG-DCIS and/or ADH—a significant proportion of mammographically detected noninvasive lesions. Even when the criteria used are explicitly stated, application of criteria varies remarkably among pathologists and from one study to the next. Certainly, the issues raised in this study are not uncommon but have not been specifically addressed in any of the major single-, multiinstitutional, or multinational studies on DCIS cases that include LG-DCIS. Most if not all such studies lack a central review of the diagnosis and even many rely on multiple pathologists at sometimes multiple institutions. This study also illustrates that 15 to 20 years of education of pathologists at local, national, and international courses has not helped much in increasing the level of agreement and uniformity in the diagnosis and interpretation of these common lesions using the criteria available for separating ADH from LG-DCIS. Chi-square

testing failed to reveal any statistically significant difference in the response behavior of expert breast pathologists and pathologists who did not consider themselves experts.

Since the institution of widespread screening mammography, the number of early, LG-DCIS lesions that are diagnosed has dramatically increased [13, 14, 19]. How partially involved ducts, often spread around completely involved ducts, are interpreted could change the size/extent of the lesion by several centimeters. This potentially undermines the internal consistency and comparability of epidemiological studies and clinical trials regarding such lesions.

In his 1991 survey, Rosai lamented the fact that there were no known morphometric, ultrastructural, immunohistochemical, or molecular features to distinguish ADH from LG-DCIS [24]. Unfortunately, this issue continues to be the case [1, 11, 15, 16, 18, 25]. Pathologists must assign lesions within the ADH–DCIS continuum to one end of the spectrum or the other based on the morphologic features present on an H&E-stained slide and an arbitrary set of quantitative criteria that cannot be applied to every lesion encountered. Not only the subjective nature of interpreting the morphologic findings but also the existence of different and in some cases conflicting diagnostic criteria create considerable interobserver variability in distinguishing ADH from LG-DCIS.

This diagnostic variability in turn leads to confusion regarding the optimal management approach to such intraductal proliferative lesions because a diagnosis of LG-DCIS is automatically associated with a significantly worse prognosis and usually requires a more drastic surgical approach compared to ADH. Furthermore, the negative impact of the diagnosis of "carcinoma", albeit an in situ one, on patients' psychological well-being (depression and anxiety) has been well documented [12, 23] and should be a consideration in the choice of optimal terminology.

Molecular, immunohistochemical, and morphologic similarities indicate that the only difference between ADH and LG-DCIS is a quantitative one [1, 11, 15, 16, 18, 25]. The claim that separation of ADH from LG-DCIS is justified based on the development of carcinomas post-ADH in either breast while those that develop after LG-DCIS occur in the same breast is questionable [20, 22, 26]. Over a period of 23 years, three papers have appeared on this topic based on a group of 28 women with a median follow-up of 31 years, noting that the invasive carcinomas that occur after LG-DCIS treated by biopsy alone develop in the same breast and in the same quadrant from which the original biopsy with DCIS was taken. Seven of the 11 women who developed subsequent invasive carcinoma were diagnosed within 10 years of the DCIS biopsy, 1 was diagnosed within 12 years, and the remaining 3 developed infiltrating carcinomas over 23–42 years. The authors conclude that these results "indicate a striking dividing point biologically and histopathologically between LG-DCIS lesions and the cytologically similar but lesser lesions of ADH" [26]. When 7 of the 28 women developed invasive carcinoma within 10 years, one wonders why the remaining patients were not contacted to receive appropriate therapy for their disease rather than continuing the study for another 20 years.

Judging from the microscopic description and the sampling documented for these 28 cases, a substantial number of these lesions were probably not low grade because they had some atypia and/or necrosis, albeit not diffusely, suggesting that those who died within 10 years most likely had substantial amount of residual disease and/or higher grade DCIS lesions [6]. The gross and pathologic features of these 28 cases are described in detail in the initial paper published in 1982, which did not refer to them as low grade [20]. Therefore, it is more likely that this study reflects the natural history of a wide variety of intraductal carcinomas, only some of which were LG-DCIS. A more simple explanation for any differences that might exist between ADH and LG-DCIS in the frequency of subsequent progression would be that a minuscule lesion, once totally removed, results in near equalization of the risk for subsequent development of carcinoma in the two breasts of that individual patient. A more extensive process, however, is less likely to be completely eliminated by conservative surgical excision alone, leading to the development of recurrences at the same site due to residual disease [6].

A recent epidemiological study has shown a nearly equal incidence rate (5.4 vs 4.5/1,000 person-years) for development of subsequent invasive carcinoma in either breast after a diagnosis of DCIS among close to 37,700 patients diagnosed between January 1988 and December 2002, many of whom were treated by surgery and radiation therapy [17]. This confirms the fact that once a DCIS is adequately treated, it results in equalization of risk for either breast. Furthermore, it indicates that complete excision is an adequate therapy for small lesions. Therefore, complete excision with adequate margins should be explored further as the only therapy for small DIN 1 (DCIS grade 1) lesions that do not exceed 3–4 mm in maximum extent, particularly when there is no evidence of even any flat epithelial atypia around the DCIS.

It seems only logical to adopt a terminology in which two morphologically identical lesions are not given diagnostic designations as different as "hyperplasia" and "carcinoma". The use of the DIN terminology may help solve this problem [28, 30]. Although the DIN terminology does not claim to reduce interobserver variability, it

diminishes the effect of drastically different designations for similar lesions by including the spectrum of atypical ductal hyperplasia and LG-DCIS under the umbrella designation of grade 1 DIN.

References

1. Allred DC, O'Connell P, Fuqua SA, Osborne CK (1994) Immunohistochemical studies of early breast cancer evolution. Breast Cancer Res Treat 32:13–18
2. Arpino G, Laucirica R, Elledge RM (2005) Premalignant and in situ breast disease: biology and clinical implications. Ann Intern Med 143(6):446–457
3. Ashikari R, Huvos AG, Snyder RE, Lucas JC, Hutter RV, McDivitt RW, Schottenfeld D (1974) A clinicopathologic study of atypical lesions of the breast. Cancer 33:310–317
4. Ashikari R, Huvos AG, Snyder RE, Sharma R, Kirch R, Schottenfeld D (1980) A clinicopathologic study of atypical lesions of the breast further follow up. Pathol Res Pract 166:481–490
5. Azzopardi JG (1979) Problems in breast pathology. Saunders, Philadelphia
6. Bellamy CO, McDonald C, Salter DM, Chetty U, Anderson TJ (1993) Noninvasive ductal carcinoma of the breast: the relevance of histologic categorization. Hum Pathol 24:16–23
7. Black MM, Barclay TH, Cutler SJ, Hankey BF, Asire AJ (1972) Association of atypical characteristics of benign breast lesions with subsequent risk of breast cancer. Cancer 29:338–343
8. Bodian CA, Perzin KH, Lattes R, Hoffmann P, Abernathy TG (1993) Prognostic significance of benign proliferative breast disease. Cancer 71:3896–3907
9. Burstein HJ, Polyak K, Wong JS, Lester SC, Kaelin CM (2004) Ductal carcinoma in situ of the breast. N Engl J Med 350:1430–1441
10. Ceilley E, Jagsi R, Goldberg S, Kachnic L, Powell S, Taghian A (2004) The management of ductal carcinoma in situ in North America and Europe: results of a survey. Cancer 101:1958–1967
11. Chuaqui RF, Zhuang Z, Emmert-Buck MR, Liotta LA, Merino MJ (1997) Analysis of loss of heterozygosity on chromosome 11q13 in atypical ductal hyperplasia and in situ carcinoma of the breast. Am J Pathol 150:297–303
12. De Morgan S, Redman S, White KJ, Cakir B, Boyages J (2002) "Well, have I got cancer or haven't I?" The psycho-social issues for women diagnosed with ductal carcinoma in situ. Health Expect 5:310–318
13. Ernster VL, Barclay J (1997) Increases in ductal carcinoma in situ (DCIS) of the breast in relation to mammography: a dilemma. J Natl Cancer Inst Monogr 22:151–156
14. Ernster VL, Ballard-Barbash R, Barlow WE, Zheng Y, Weaver DL, Cutter G, Yankaskas BC, Rosenberg R, Carney PA, Kerlikowske K, Taplin SH, Urban N, Geller BM (2002) Detection of ductal carcinoma in situ in women undergoing screening mammography. J Natl Cancer Inst 94:1546–1554
15. Goldenberg VE, Goldenberg NS, Sommers SC (1969) Comparative ultrastructure of atypical ductal hyperplasia, intraductal carcinoma, and infiltrating ductal carcinoma of the breast. Cancer 24:1152–1169
16. Lakhani SR, Collins N, Stratton MR, Sloane JP (1995) Atypical ductal hyperplasia of the breast: clonal proliferation with loss of heterozygosity on chromosomes 16q and 17p. J Clin Pathol 48:611–615
17. Li CI, Malone KE, Saltzman BS, Daling JR (2006) Risk of invasive breast carcinoma among women diagnosed with ductal carcinoma in situ and lobular carcinoma in situ, 1988–2001. Cancer 106:2104–2112
18. O'Connell P, Pekkel V, Fuqua SA, Osborne CK, Clark GM, Allred DC (1998) Analysis of loss of heterozygosity in 399 premalignant breast lesions at 15 genetic loci. J Natl Cancer Inst 90:697–703
19. Osteen RT, Cady B, Chmiel JS, Clive RE, Doggett RL, Friedman MA, Hussey DH, Kraybill WG, Urist MM, Winchester DP (1994) 1991 national survey of carcinoma of the breast by the Commission on Cancer. J Am Coll Surg 178:213–219
20. Page DL, Dupont WD, Rogers LW, Landenberger M (1982) Intraductal carcinoma of the breast: follow-up after biopsy only. Cancer 49:751–758
21. Page DL, Dupont WD, Rogers LW, Rados MS (1985) Atypical hyperplastic lesions of the female breast: a long-term follow-up study. Cancer 55:2698–2708
22. Page DL, Dupont WD, Rogers LW, Jensen RA, Schuyler PA (1995) Continued local recurrence of carcinoma 15–25 years after a diagnosis of low grade ductal carcinoma in situ of the breast treated only by biopsy. Cancer 76:1197–1200
23. Rakovitch E, Franssen E, Kim J, Ackerman I, Pignol JP, Paszat L, Pritchard KI, Ho C, Redelmeier DA (2003) A comparison of risk perception and psychological morbidity in women with ductal carcinoma in situ and early invasive breast cancer. Breast Cancer Res Treat 77:285–293
24. Rosai J (1991) Borderline epithelial lesions of the breast. Am J Surg Pathol 15:209–221
25. Ruiz A, Almenar S, Callaghan RC, Llombart-Bosch A (1999) Benign, preinvasive and invasive ductal breast lesions. A comparative study with quantitative techniques: morphometry, image- and flow cytometry. Pathol Res Pract 195:741–746
26. Sanders ME, Schuyler PA, Dupont WD, Page DL (2005) The natural history of low-grade ductal carcinoma in situ of the breast in women treated by biopsy only revealed over 30 years of long-term follow-up. Cancer 103:2481–2484
27. Schnitt SJ, Connolly JL, Tavassoli FA, Fechner RE, Kempson RL, Gelman R, Page DL (1992) Interobserver reproducibility in the diagnosis of ductal proliferative breast lesions using standardized criteria. Am J Surg Pathol 16:1133–1143
28. Tavassoli FA (1998) Ductal carcinoma in situ: introduction of the concept of ductal intraepithelial neoplasia. Mod Pathol 11:140–154
29. Tavassoli FA (1999) Pathology of the breast, 2nd edn. Appleton & Lange, Stamford, CT
30. Tavassoli FA (2005) Breast pathology: rationale for adopting the ductal intraepithelial neoplasia (DIN) classification. Nat Clin Pract Oncol 2:116–117
31. Tavassoli FA, Norris HJ (1990) A comparison of the results of long-term follow-up for atypical intraductal hyperplasia and intraductal hyperplasia of the breast. Cancer 65:518–529
32. Wellings SR, Jensen HM, Marcum RG (1975) An atlas of subgross pathology of the human breast with special reference to possible precancerous lesions. J Natl Cancer Inst 55:231–273

Virchows Arch (2006) 449:617–621
DOI 10.1007/s00428-006-0296-0

ORIGINAL ARTICLE

Proliferating activity in columnar cell lesions of the breast

Jean-Christophe Noel · Isabelle Fayt · Sergio Fernandez-Aguilar · Frederic Buxant · Rachel Boutemy

Received: 20 June 2006 / Accepted: 20 August 2006 / Published online: 6 October 2006
© Springer-Verlag 2006

Abstract With the introduction of mammographic screening, columnar cell lesions (CCLs) are observed more and more frequently because they are often associated with microcalcifications. Until now, the proliferative activity of these lesions has not been previously evaluated. Ki67 index was performed by immunohistochemistry in CCLs without atypia [columnar cell change (CCC) n=20 and columnar cell hyperplasia without atypia (CCH without atypia) n=20], flat epithelial atypia (FEA DIN1A n=20), low-grade intraductal carcinoma (DIN1C n=20), high-grade intraductal carcinoma (DIN 2–3 n=20). Adjacent terminal duct-lobular unit (TDLU) of normal breast tissue served as control. Ki-67 index is extremely low and close in CCLs without atypia (CCC mean 0.1% and CCH mean 0.76%) and paradoxically is lower than in normal TDLU (mean 2.4%) (p<0.001). In the FEA, in comparison with normal TDLU and CCLs without atypia, the Ki67 is higher (mean 8.2%) (p<0.001) but extremely close to those of DIN1C (mean 8.9%) (p=0.6 NS). Lastly, the Ki67 index is higher in DIN 2–3 (mean 25.4%) than in CCLs without atypia and FEA (p<0.001). CCLs are disparate lesions having in common cells with columnar configuration but different proliferative characteristics. These data represent findings of biological interest which could help us to better understand these controversial lesions.

Keywords Columnar cell lesions · Breast · Flat epithelial atypia · Intraductal carcinoma · DIN · Proliferation · Ki67

J.-C. Noel · I. Fayt · S. Fernandez-Aguilar · F. Buxant · R. Boutemy
Unit of Senology, Erasme University Hospital,
Free University of Brussels,
Brussels, Belgium

J.-C. Noel (✉)
Department of Pathology, Clinic
of Senology, Erasme University Hospital,
808 route de Lennik,
1070 Brussels, Belgium
e-mail: jenoel@ulb.ac.be

Introduction

With the instauration of screening mammography on Belgium, columnar cell lesions of the breast are discovered more and more frequently on mammograms because they are often associated with abnormal calcifications (ACR3-4) [1, 5, 21]. Histologically, columnar alterations appear as transformation of the terminal duct unit from a low cuboïdal epithelium to tall columnar epithelium [1, 10, 14–16, 19, 20, 23]. According, to Schnitt et al. and the WHO Working Group on the Pathology and Genetics of Tumours of the Breast, columnar cell lesions (CCLs) have been divided into two categories: columnar cell change and columnar cell hyperplasia (manifested by >2 cell layers) without atypia (nonatypical CCLs) and flat epithelial atypia (FEA) (DIN 1A) which design CCLs with low-grade/monomorphic-type cytologic atypia that lacked the architectural features of atypical ductal hyperplasia or low-grade ductal carcinoma in situ (DCIS) [14, 19–21, 24]. Several studies have suggested that FEA are morphologic precursors to DCIS, and invasive carcinoma particularly, low-grade invasive ductal carcinoma and tubular carcinoma [4, 6, 7, 15, 17, 22]. These data have been corroborated by the discovery of common molecular abnormalities in these lesions [2, 12, 13, 22]. The control of cell cycle appears as a fundamental event in carcinogenesis, but until now, the

proliferating activity in CCLs has been poorly investigated. Therefore, the aim of this present study is to assess the proliferating activity in CCLs without atypia [columnar cell change (CCC) and columnar cell hyperplasia (CCH)] and flat epithelial atypia (FEA) and to compare it with those of terminal duct-lobular unit (TDLU) normal breast tissue, low (DIN1C), and high (DIN 2–3) grade intraductal carcinoma. We used for that immunohistochemistry with Ki67 antigen. Ki67 is a human nuclear protein, which is expressed in all active parts of the cell cycle G1, S, G2, and mitosis but absent in resting and quiescent cells (G0) [3]. During interphase, the antigen can be exclusively detected within the nucleus, whereas in mitosis most of the protein is relocated to the surface of the chromosomes. The antigen is rapidly degraded as the cell enters the nonproliferative state, and there appears to be no expression of Ki67 during DNA repair processes [3].

Materials and methods

Sixty cases of CCLs have been investigated. The lesions were distributed as follow:

a) Forty cases of CCLs without atypia (CCC n=20 and CCH without hyperplasia n=20)
b) Flat epithelial atypia (FEA) (n=20).

To increase the reproducibility in the diagnosis of the CCLs and FEA, the strict criteria recently described by Schnitt et al. and O'Malley et al. were applied and are summarized in Table 1 [14]. Adjacent normal TDLU (n=20), DIN1C (n=20), and DIN 2–3 (n=20) served as controls.

For immunohistochemistry, the antigen retrieval method was performed. In brief, 4-μm paraffin sections were placed on silanized slides, dewaxed in xylene, and rehydrated in decreasing concentrations of ethanol. While immersed in citrate buffer (pH 6.0), slides were placed in a calibrated warm water bath (95–99°C) for 60 min to perform epitope retrieval. Tissues were then incubated for 2 h, at room temperature with the primary antibodies Ki67 (clone MIB1, dilution: 1/50, Dako, Glostrup, Denmark). The UltraVision Labeled Polymer (Lab Vision, Fremont, USA) was used for the subsequent steps according to the manufacturer's instructions. Chromogenic development was accomplished using diaminobenzidine–hydrogen peroxide. Slides were then slightly counterstained with hematoxylin, dehydrated, and applied with coverslips. To control for nonspecific binding of the primary antibody preparation were substituted as the first layer of the serial sections. Positive control consisted on normal human tonsil. The pathological acini previously marked on the slides were examined for Ki67 reactivity under ×20 objective by two independent observers who were blinded to outcome. As the proliferation in normal breast and pathological lesions may not occur necessarily uniformly, a minimum of 1,000 nuclei per case were counted and there was agreement between observers in more than 90 of cases. Disagreements in evaluation were resolved by review and discussion at a multiheaded microscope.

Statistical analysis

Comparison of the data was performed using the Student's t test (two-tailed). Statistical significance was defined as $p<0.01$.

Results

The proliferative activity as measured by the Ki67 appears extremely close in CCC (mean 0.1%) and CCH without atypia (mean 0.76%) (p=0.06 NS) and paradoxically is lower than in normal TDLU (mean 2.4%) ($p<0.001$). In the FEA, in comparison with normal TDLU, CCC, and CCH without atypia, the KI-67 is higher (mean 8.2%) ($p<0.001$) but extremely close of those of DIN1C lesion (mean 8.9%) (p=0.6 NS). Finally and not surprisingly, the Ki67 is higher

Table 1 Diagnostic criteria used to qualify columnar cell lesions (CCLs) without atypia (columnar cell change and columnar cell hyperplasia) and flat epithelial atypia (FEA) (DIN 1A)

Columnar cell change (CCC)	Columnar cell hyperplasia (CCH)	Flat epithelial atypia (FEA)
Distended acini lined by one to two cell layers with uniform ovoid or elongated nuclei perpendicular to basement membrane without nucleoli or only inconspicuous nucleoli	Distended acini lined by more two-cell layers with stratification but without Roman bridges, micropapillary tufts or secondary lumens. The cells showed the same characteristic seen in columnar cell change	Distended acini lined by cells showing cytologic atypia seen in low-grade DCIS. The lining cells are generally round, more rarely ovoid with or without nucleoli but lack polarity and are not perpendicular to basal membrane. Flat growth pattern without Roman brigdes, micropapillary tufts or secondary lumens as seen in ADH or DCIS
Apical snouts present but not prominent	Apical snouts present and prominent	Apical snouts present and prominent
Luminal secretion possible but not prominent	Luminal prominent secretion often present	Luminal prominent secretion often present
Calcifications possible	Calcifications frequently present	Calcifications frequently present

Table 2 Ki67 immunohistochemical reactivity, expressed as mean (±SD) percentage of positive cells

Normal TDLU *N*=20	CCC *N*=20	CCH *N*=20	FEA *N*=20	DIN 1C *N*=20	DIN 2–3 *N*=2O
2.4±0.9	0.1±0.06	0.76±0.2	8.2±1.9	8.9±3.5	25.4±6.8

TDLU Terminal duct-lobular unit, *CCC* columnar cell change, *CCH* columnar cell hyperplasia, *FEA* flat epithelial atypia, *DIN 1C* ductal intraepithelial neoplasia grade 1 c/ductal carcinoma in situ low grade, *DIN 2–3* ductal intraepithelial neoplasia grade 2–3/ductal carcinoma in situ intermediate and high grade.

in DIN 2–3 (mean 25.4%) than in CCC, CCH without atypia, and FEA ($p<0.001$). All results are summarized in the Table 2 and illustrated in Fig. 1.

Discussion

This last decade, the diagnostic of CCLs increase drastically because the vast majority of these lesions are associated with abnormal calcifications of the calcium phosphate type (ACR3 or 4) discovered on screening mammograms [1, 5, 10, 14]. CCLs are composed of a spectrum of epithelial pathologies going from nonatypical columnar cell change with or without hyperplasia to flat epithelial atypia (FEA) which is characterized by intraductal flat alteration with the replacement of the native epithelial cells by a single or 3–5 layers of moderately atypical cells [14, 19–21, 24]. Combining these entities into a single-family lead to a possible belief that they have a biological relationship. To clarify the issue, as loss of

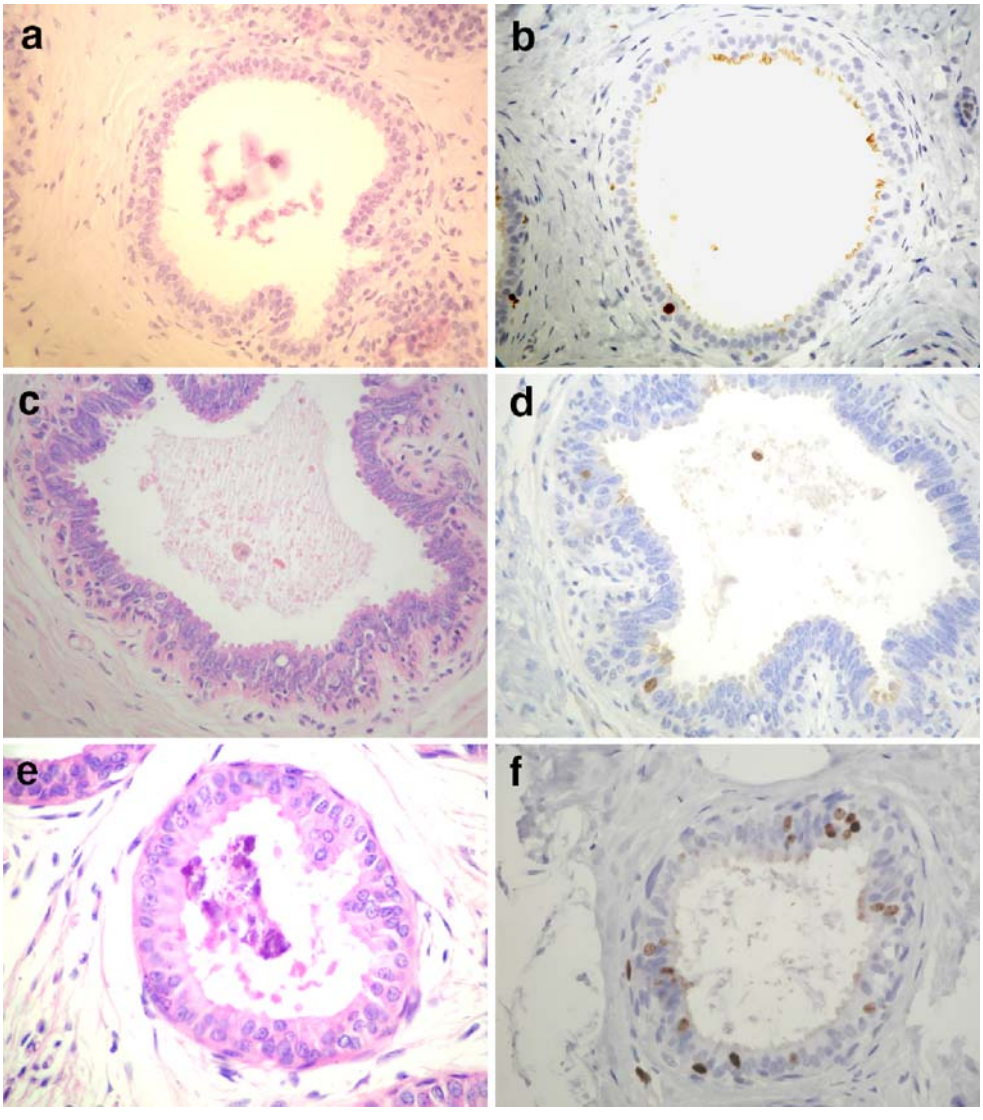

Fig. 1 **a** and **b** Columnar cell lesions without hyperplasia and atypia [columnar cell change (CCC)] (**a** H&E; **b** Ki67 immunohistochemistry). **c** and **d** Columnar cell lesions with hyperplasia but without atypia [columnar cell hyperplasia (CCH)] (**c** H&E; **d** Ki67 immunohistochemistry). **e** and **f** Columnar cell lesions with atypia [flat epithelial atypia (FEA)] (**e** H&E; **f** Ki67 immunohistochemistry)

control of cell division and/or inappropriate stimulation of cell growth appear as a fundamental event in carcinogenesis and tumor development, we have evaluated the proliferative activity of CCLs. Ki67 which is an epitope of a nuclear and nucleolar protein that is specifically expressed throughout the whole cell cycle of proliferating cells with exception of the G0 phase [3]. In the present study, we have clearly demonstrated, at least if the histological criteria of Schnitt et al. and O'Malley et al. are applied, that columnar cell lesions are disparate lesions having in common cells with columnar configuration but different proliferative characteristics. Indeed, in CCC and CCH without atypia, Ki67 index appears extremely low (<1%) and is statistically significant ($p<0.001$) lower than in FEA (mean 8.2%) and paradoxically than in adjacent TDLU (mean 2.4%). It remains difficult to explain the lower rate of proliferation in CCLs without atypia in comparison with TDLU of normal breast tissue. However, it is possible that CCC without atypia represent only a simple transformation of TDLU from low cuboidal to tall columnar epithelium without modification of the proliferative properties. Recent molecular studies showing an absence of mutational change in simple columnar changes seem to confirm these data [2]. It is also possible that CCLs without atypia in comparison to normal TDLU are less sensitive from a proliferative point of view to the effects of menstrual cycle, age, oral contraceptive, or hormone replacement therapy. Lastly, if KI-67 labeling occurs throughout the cell cycle, the Ki67 positivity, however, may not always accurately reflect proliferative activity particularly in cells with a long G1 phase [3]. Our results suggest that CCLs with and without atypia are different proliferative entities. Therefore, these findings could help us to clarify CCLs difficult to categorize using conventional morphological criteria. Indeed, if a recent study performed by experts in breast pathology on selected digital images conclude that the diagnosis of FEA and its distinction from CCLs without atypia is highly reproductible with the use of available criteria; others are less enthusiastic [14, 23]. For them, many of cytological and morphological changes distinguishing these lesions appear so subtle that inexperienced (or not) pathologist can easily confuse it [23]. However, the recognition of FEA is of clinical importance because these lesion are classically associated with atypical ductal hyperplasia (ADH), DIN 1C, tubular carcinoma, and lobular neoplasia [4, 6, 7, 9, 15, 17, 18]. It is interesting to note that we have also demonstrated that FEA and low-grade intraductal carcinoma (DIN 1C) have a close proliferative activity (FEA mean 8.2%; DIN1C mean 8.9%; $p=0.6$). These data are in accordance with the original description of Azzopardi who considered FEA as "clinging carcinoma monomorphic type" [1, 15, 24]. Firstly, because FEA and DIN 1C are frequently associated and share similar immunohistochemical profiles with overexpression of estrogen receptors, progesterone receptors, and keratins 5 and 19 [9, 11, 22, 25]. Secondly, because we and others have showed that FEA are frequently merging with DIN 1C [4, 15, 21, 22].

In conclusion, CCLs represent a range of proliferative lesions going from low-proliferative one (CCC and CCH without atypia) to high-proliferative (FEA). These data represent findings of biological interest which could help us to better understand these lesions and maybe their clinical significance and management which remains controversial [8, 10, 16, 18, 21].

References

1. Azzopardi JG (1978) Problems in breast pathology. WB Saunders, Philadelphia, pp 193–202
2. Dabbs DJ, Carter G, Fudge M, Peng Y, Swalsky P, Finkelstein S (2006) Molecular alterations in columnar cell lesions of the breast. Mod Pathol 19:344–349
3. Endl E, Gerdes J (2000) The Ki-67 protein: fascinating forms and unknown function. Exp Cell Res 257:231–237
4. Fernandez-Aguilar S, Simon P, Buxant F, Simonart T, Noel JC (2005) Tubular carcinoma of the breast and associated intraepithelial lesions: a comparative study with invasive low-grade ductal carcinomas. Virchows Arch 447:683–687
5. Fraser JL, Raza S, Chorny K, Connolly J, Schnitt S (1998) Columnar alteration with prominent apical snouts and secretions: a spectrum of changes frequently present in breast biopsies performed for microcalcifications. Am J Surg Pathol 22: 1521–1527
6. Guerra-Wallace MM, Christensen WN, White RL (2004) A retrospective study of columnar alteration with prominent apical snouts and secretions and association with cancer. Am J Surg 188:395–398
7. Goldstein NS, O'Malley BA (1997) Cancerization of small ectatic ducts of the breast by ductal carcinoma in situ cells with apocrine snouts. A lesions associated with tubular carcinoma. Am J Clin Pathol 107:561–566
8. Jacobs T, Connolly J, Schnitt S (2002) Non malignant lesions in breast core needle biopsies: to excise or not to excise. Am J Surg Pathol 26:1095–1110
9. Koerner FC, Oyama T, Maluf H (2001) Morphological observations regarding the origins of atypical cystic lobules (low-grade clinging carcinoma of flat type). Virchows Arch 439:523–530
10. Nasser SM (2004) Columnar cell lesions: current classification and controversies. Semin Diagn Pathol 1:18–24
11. McLaren B, Gobbi H, Schuyler P, Olson S, Parl F, Dupont W, Page D (2005) Immunohistochemical expression of estrogen receptor in enlarged lobular units with columnar alteration in benign breast biopsies: a nested case-control study. Am J Surg Pathol 29:105–108
12. O'Connel P, Pekkel V, Fuqua S, Osborne CK, Allred DC (1994) Molecular genetic studies of early breast cancer evolution. Breast Cancer Res Treat 32:5–12
13. O'Connell, Pekkel V, Fuqua SA, Osborne CK, Clark GM, Allred DC (1998) Analysis of loss of hererozygosity in 399 premalignant breast lesions at 15 genetic loci. J Natl Cancer Inst 90:697–703

14. O'Malley FP, Moshin SK, Badve S, Bose S, Collins LC, Ennis M, Kleer CG, Pinder SE, Schnitt SJ (2006) Interobserver reproducibility in the diagnosis of flat epithelial atypia of the breast. Mod Pathol 19:172–179
15. Oyama T, Iijma K, Takei H, Horiguchi J, Lino Y, Nakajima T, Koerner F (2000) Atypical cystic lobules: an early stage in the formation of low-grade ductal carcinoma in situ. Breast Cancer 7:326–331
16. Page DL, Jensen RA (1996) Hypersecretory hyperplasia with atypia in breast biopsies. What is the proper level of clinical concern? Pathol Case Rev 1:36–40
17. Rosen PP (1999) Columnar cell hyperplasia is associated with lobular carcinoma in situ and tubular carcinoma. Am J Surg Pathol 23:1561
18. Shaaban A, Sloane J, West C, Moore F, Jarvis C, Williams E, Foster C (2002) Histopathologic types of benign breast lesions and the risk of breast cancer: case-control study. Am J Surg Pathol 26:421–430
19. Schnitt SJ, Vincent-Salomon A (2003) Columnar cell lesions of the breast. Adv Anat Pathol 10:113–124
20. Schnitt SJ (2003) Columnar cell lesions of the breast. Pathol Case Rev 8:201–210
21. Schnitt SJ (2003) The diagnosis and management of preinvasive breast disease: flat epithelial atypia-classification, pathologic features and clinical significance. Breast Cancer Res 5:263–268
22. Simpson P, Gale T, Reis-Filho J, Jones C, Parry S, Sloane J, Hanby A, Pinder S, Lee A, Humphreys S, Ellis I, Lakhani S (2005) Columnar cell lesions of the breast: the missing link in breast cancer progression? A morphological and molecular analysis. Am J Surg Pathol 29:734–746
23. Tan PH, Selvarajan S, Yap W, Hanby A (2005) Pathological diagnosis of columnar cell lesions of the breast: are there issues of reproducibility? J Clin Pathol 58:705–709
24. Tavassoli FA, Hoefler H, Rossi J (2003) Intraductal proliferative lesions. In: Tavassoli FA, Devilee P (eds) World Health Organization classification of tumours. Pathology and genetics of tumours. Pathology and genetics of tumours of the breast and female genital organs. IARC Press, Lyon, France, pp 63–73
25. Tremblay G, Deschenes J, Alpert L, Quenneville L (2005) Overexpression of estrogen receptors in columnar cell change and in unfolding breast lobules. Breast J 11: 326–332

Virchows Arch (2006) 449:622–627
DOI 10.1007/s00428-006-0310-6

ORIGINAL ARTICLE

The significance of modified Gleason grading of prostatic carcinoma in biopsy and radical prostatectomy specimens

Burkhard Helpap · Lars Egevad

Received: 15 May 2006 / Accepted: 5 September 2006 / Published online: 8 November 2006
© Springer-Verlag 2006

Abstract At an International Society of Urological Pathology consensus conference in 2005, the Gleason grading system for prostatic carcinoma underwent its first major revision. Gleason pattern 4 now includes most cribriform patterns and also fused and poorly formed glands. Our aims were to compare the grade distributions and assess the agreement between biopsy and radical prostatectomy specimens for the modified and conventional Gleason grading. More than 3,000 radical prostatectomy (RP), needle biopsies (NB) and transurethral resection specimens were assigned modified Gleason score (GS). In NB, modified GS 3+3=6 and 3+4=7a were almost equally common, while in RP, 3+4=7a was most common followed by 4+3=7b. After application of the modified GS on NB, a substantial shift in GS distribution occurred: The proportion of GS 6 and 7 were 48 and 26%, respectively, with conventional Gleason grading as compared to 22 and 68%, respectively, with modified grading. In 368 men, the agreement between NB and RP with a modified GS 6, 7a, 7b and 8–10 in NB was 28, 88, 68 and 64–100%, respectively. The overall agreement improved from 58 to 72% ($p<0.001$) compared to conventional GS. The higher agreement with modified Gleason grading may facilitate therapeutic decisions.

B. Helpap (✉)
Department of Pathology, Center of Uropathology,
General Hospital Hegau-Bodensee-Klinikum Singen,
Academic Hospital of the University of Freiburg,
P.O. Box 720, 78207 Singen, Germany
e-mail: pathologie@hbh-kliniken.de

L. Egevad
Department of Pathology and Cytology, Karolinska Hospital,
Stockholm, Sweden

L. Egevad
International Agency for Research on Cancer (IARC),
Lyons, France

Keywords Adenocarcinoma of the prostate · Modified Gleason grading · Core needle biopsy · Radical prostatectomy

Introduction

In 1966, Gleason first presented his grading system for prostatic carcinoma (Fig. 1a). The Gleason grading is now universally acknowledged and also endorsed by the WHO [13, 19–22]. During the preparation of the last edition of the WHO classification of prostatic carcinomas, other grading systems were also discussed, such as the modified histocytological WHO grading of Mostofi from 2002 and the Helpap subgrading system [13, 19, 23, 25, 33], but only the Gleason grading was finally included in the new WHO classification. When the Gleason grading was introduced, the clinical and diagnostic steps to find prostate cancer and the therapeutic consequences of this diagnosis differed from today's practice. The basis of the Gleason grading system was the morphological experience from simple prostatectomy or transurethral resection specimens. Core needle biopsies were very rare at that time, and radical prostatectomy as performed today was virtually unknown.

The Gleason grading was slightly modified twice in 1966/1967 and 1974/1977 and then unchanged until 2005 [9, 10, 19, 20, 22, 29–31]. After the publication of the new WHO classification of tumours of the urinary system and male genital organs in 2004 [13], there was a continued discussion about Gleason grading of needle biopsies. This issue was debated at the International Consultation on Prediction of Patient Outcome in Prostate Cancer sponsored by the WHO in Stockholm 2004, and some modifications of the Gleason grading were suggested [1]. A recommendation was given to separately report the Gleason score for

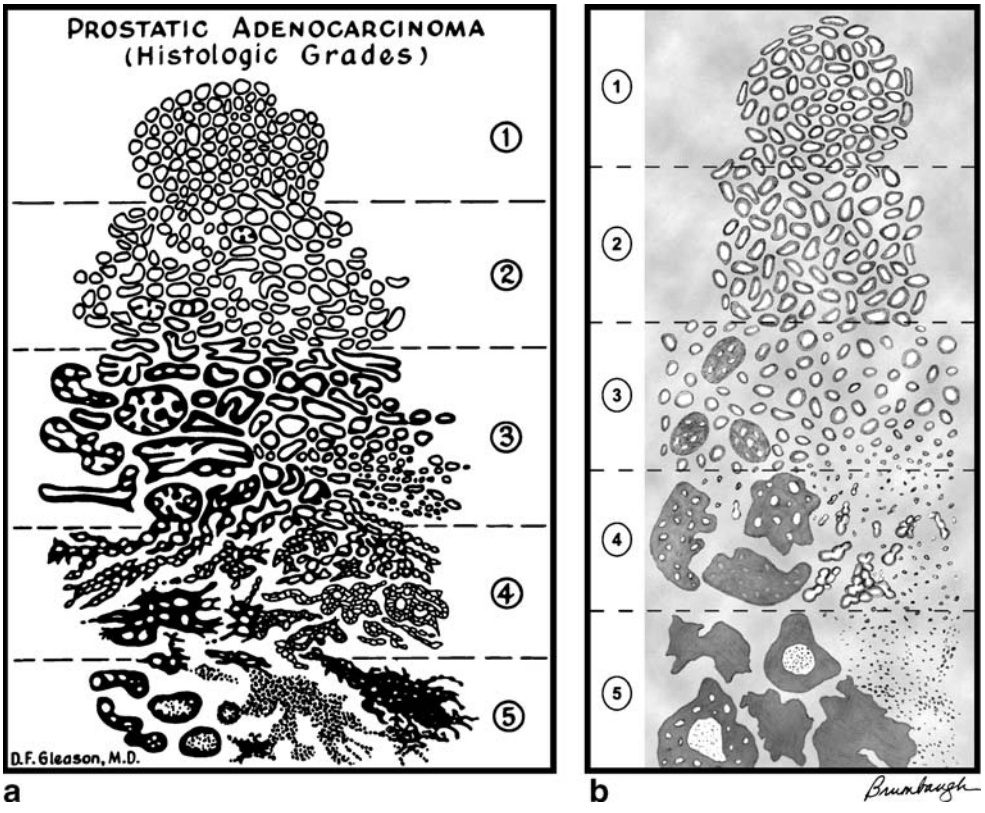

Fig. 1 Schematic representations of conventional (**a**) and modified (**b**) Gleason grading system. The most important changes between them are within patterns 3 and 4. In the modified system, most cribriform patterns and also poorly defined glands are included in pattern 4. Reproduced from [14] with permission of Lippincott Williams and Wilkins, Baltimore, MD, USA

each recognizable core. It was also suggested that tertiary patterns of higher grade in needle biopsies should influence the Gleason score [32].

To clarify how the Gleason grading system is applied in practice, a survey was recently circulated among 91 experts in genitourinary pathology in countries around the world [8]. Of 67 responding participants, only 13 and 36%, respectively, ever diagnosed a Gleason score of 2 to 4 on needle biopsies, and 88% of those who did so assigned a Gleason score 4 to <1% of cancers. Cribriform Gleason pattern 3 was acknowledged by 88%, but a majority of them would classify less than 20% of cribriform patterns as Gleason pattern 3. Two thirds included incomplete or poorly defined glands in Gleason pattern 4 (Fig. 2). Although only 26% defined Gleason score on needle biopsies as primary + tertiary Gleason pattern, a majority would mention a tertiary pattern separately. The conclusion was that there was a need to standardize the application of Gleason grading both in terms of interpretation of patterns and reporting of the grade. Therefore, the International Society of Urological Pathology (ISUP) decided to organize a consensus conference, which took place in San Antonio, TX, in 2005 [14]. Essentially the same experts who participated in the survey study were invited to the consensus meeting. The Gleason grading system for prostatic carcinoma now underwent its first major revision including both pattern interpretation and compiling and reporting of grade information. The definition of Gleason patterns 3 and 4 was modified, and the use of Gleason patterns 1 and 2 on needle biopsy and radical prostatectomy specimens was restricted. It was decided that focal areas of high-grade cancer in needle biopsies should be included in the Gleason score.

To be clinically useful, a grading system must be reproducible, and there must be a reasonable agreement between biopsies and surgical specimens [18]. The overall

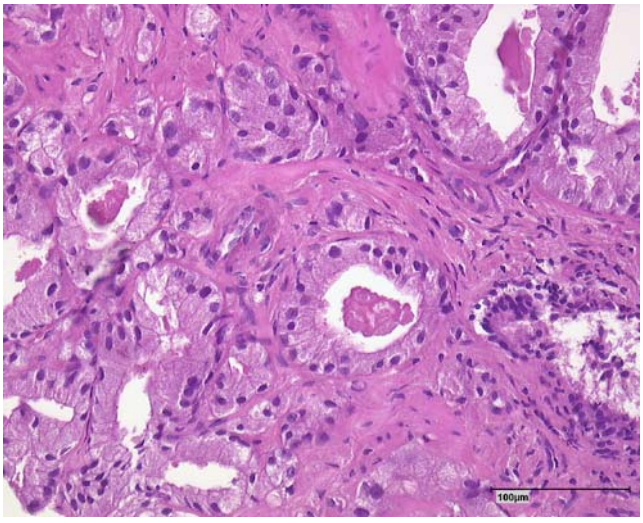

Fig. 2 Adenocarcinoma of the prostate with both complete, circumscribed glands and poorly formed glands corresponding to a modified Gleason score 3+4=7. H&E

agreement of the Gleason score between biopsy and radical prostatectomy specimens has generally only been between 35 and 45% [2–6, 16, 27, 28, 31, 34–37]. This relatively poor agreement is caused by undergrading of low-grade carcinomas in needle biopsies, while the agreement is more exact when high-grade carcinomas are diagnosed [16, 28, 31, 37]. Biopsies have been found to under-grade in 24–60% (pooled data 45%) and over-grade in 5–32% (pooled data 10.4%) [11]. Although other grading systems have better results with regard to biopsy and radical prostatectomy agreement as, e.g. the old and new WHO grading or the nucleolar subgrading of Helpap, the Gleason grading became the preferred grading system [13, 15, 23, 25, 33]. It would be clinically very important if the modified Gleason grading could contribute to a better agreement because the Gleason score is one of the most significant prognostic factors of prostatic carcinoma.

Therefore, we have estimated the modified Gleason scores of all prostatic carcinomas in needle biopsy, radical prostatectomy and transurethral tissue resections specimens of 1 year at the Department of Pathology, General Hospital Singen. A separate series of biopsies have been regraded for a comparison of the distribution of the grading systems. Furthermore, the correlation and agreement of Gleason scores were assessed between needle biopsy and radical prostatectomy specimens, both with the conventional and the modified Gleason grading system.

The study demonstrates the changed distributions of the Gleason scores with modified grading, which may be significant for the post-operative prediction of Gleason scores and its influence on therapeutic strategies.

Materials and methods

In 2004, 3,215 adenocarcinomas of the prostate were diagnosed by histological analysis at the Department of Pathology, General Hospital Singen, including 2,502 core needle biopsies, 533 radical prostatectomy specimens and 180 transurethral resection specimens. The prostate tissue was formalin-fixed, usually in 4% formaldehyde. Biopsy specimens were fixed 12 h, while transurethral resection and radical prostatectomy specimens were fixed 24–36 h. Radical prostatectomy specimens were worked up according to a modified Stanford method [36]. Every second section was embedded in paraffin. The transurethral resection material was embedded completely in paraffin when suspicious for malignancy. After paraffin embedment, specimens were cut at 3 μm and stained with hematoxylin and eosin. With low microscopic magnification (4–10× lens magnification), prostatic carcinomas were graded according to the modified Gleason grading system, and the scores were assessed (Fig. 1b) [14]. Every core needle biopsy was graded, and a final Gleason score (global Gleason score) was assessed for all core needle biopsies of every patient. In 20 cases of Gleason score 4+3=7, a tertiary pattern 5 (less than 5%) was included in the final Gleason score.

Modified and conventional Gleason grading (Fig. 1a and b) were compared by regrading 368 radical prostatectomy specimens and the available preoperative biopsies, and we estimated the agreement of conventional and modified Gleason scores between both tissue specimens. The radical prostatectomy specimens were received from 1/1996 to 12/2000. Gleason scores 7 were divided into 3+4=7a and 4+3=7b and scores 9 to 4+5=9a and 5+4=9b. A distinction between Gleason scores 7a and 7b and between 9a and 9b was not routinely made in the original pathology reports.

For statistical analysis, chi-square was used. A p value of <0.05 was considered significant.

Results

The distribution of modified Gleason scores in 3,215 prostate specimens is presented in Fig. 3. The most frequent Gleason score of biopsies and radical prostatectomy specimens was 7 (52.8 and 81.8%, respectively), while Gleason score 5 was the most common grade in transurethral resection specimens (28.9%). Gleason scores 7–10 were more common in radical prostatectomy specimens than in needle biopsies (94.4 and 66.7%, respectively, $p<0.001$) and more common in needle biopsies than in transurethral resection specimens (66.7 and 43.9%, respectively, $p<0.001$). Gleason score 3+4=7a was more common than 4+3=7b in all specimen types. In needle biopsies, radical prostatectomy specimens and transurethral resection specimens, Gleason score 7a were 69.3, 67.2 and 79.4%, respectively, for all Gleason score 7 cases.

The major changes in Gleason score distribution after regrading 368 needle biopsy cases were that Gleason scores 2–4 decreased from 2.7 to 0% ($p<0.001$), Gleason score 5 decreased from 12.2 to 0.3% ($p=0.18$), Gleason score 6 decreased from 48.4 to 22.0%, but Gleason score 7 increased from 25.5 to 67.9% ($p<0.001$; Tables 1 and 2). Similarly, after regrading 368 radical prostatectomy specimens, Gleason scores 2–5 decreased from 6.3 to 0% ($p=0.008$), Gleason score 6 decreased from 32.3 to 6.3% ($p<0.001$) and Gleason score 7 increased from 35.9 to 82.9% ($p<0.001$; Tables 1 and 2). The overall exact agreement between Gleason score of core needle biopsies and radical prostatectomy specimens with conventional and modified Gleason grading were 58 and 72%, respectively ($p<0.001$; Tables 1 and 2). With modified Gleason grading, the agreement was 28.4% for a biopsy Gleason score 6, 88.5% for Gleason score 3+4=7a, 68.0% for Gleason score 4+3=7b and 73.3–100% for Gleason scores 8–10.

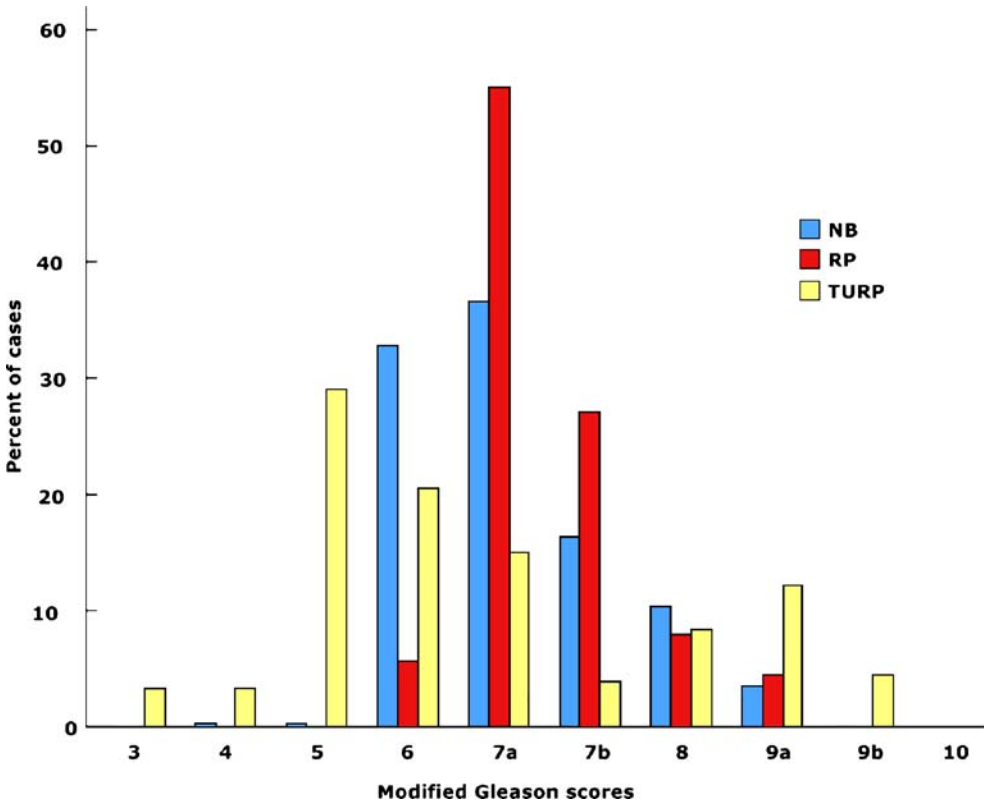

Fig. 3 Distribution of modified Gleason scores (*GS*) in needle biopsies (*NB*), radical prostatectomy (*RP*) specimens and transurethral resection (*TURP*) specimens. The grading was performed by two uropathologists

Discussion

In recent years, there has been a discrepancy between the original version of the Gleason grading and how it is applied in practice [8]. The ISUP consensus meeting in 2005 was organized with the purpose to standardize both the perception of histological patterns and how the grade information is compiled and reported [14].

In contrast to incidental carcinoma in transurethral resection material from the transition zone of the prostate, carcinomas with Gleason patterns 1 to 2 or Gleason scores 2 to 4 are generally not seen in the peripheral zone. Therefore, these Gleason scores are very unlikely to be diagnosed in core needle biopsies, which mainly sample the peripheral zone [8, 12–14, 17]. A recommendation was issued by the ISUP that with extremely rare exceptions, a Gleason score of 1+1=2 should not be diagnosed in any type of specimen, and that Gleason score 4 should rarely, if ever, be diagnosed on needle biopsies. Furthermore, the consensus was that cribriform

Table 1 Correlation of Gleason scores of prostatic carcinomas after conventional Gleason grading in needle biopsies (NB) and radical prostatectomy specimens (RP)

GP	GS	NB		RP		Agreement
		Number	Percent	Number	Percent	Percent
2+1	3	1		1		
2+2	4	9	2.7	3	1.0	33.3
2+3	5	45	12.2	23	6.3	51.1
3+3	6	178	48.4	119	32.3	66.9
3+4	7a	94	25.5	132	35.9	71.2
4+3	7b	–		–		–
4+4	8	35	9.6	85	23.1	41.2
4+5	9	6	1.6	5	1.4	83.3
5+5	10	–		–		
			368	100.0	368	100.0

The grading was performed by two uropathologists.
GP Gleason patterns, *GS* Gleason score

Table 2 Correlation of modified Gleason scores of prostatic carcinomas in needle biopsies (NBX) and radical prostatectomy (RP) specimens

GP	GS	NB		RP		Agreement
		Number	Percent	Number	Percent	Percent
2+3	5	1	0.3	0	0	0
3+3	6	81	22.0	23	6.3	28.4
3+4	7a	184	50.0	208	56.5	88.5
4+3	7b	66	17.9	97	26.4	68.0
3+4/ 4+3	7	250	67.9	305	82.9	81.9
4+4	8	25	6.8	25	6.8	100.0
4+5	9	11	3.0	15	4.0	73.3
5+5	10	–		–		
		368	100.0	368	100.0	

The grading was performed by two uropathologists.
GP Gleason patterns, *GS* Gleason score

patterns are not allowed within Gleason pattern 2 in contrast to Gleason's original diagram. When regrading needle biopsies in the present study, no specimens were assigned a Gleason score of 2 to 4, which is in line with these recommendations.

Similar to the results of our own consultation service for prostatic carcinomas, reference centers for prostatic carcinomas in the USA and Scandinavia have reported frequent undergrading of prostatic carcinomas in biopsy specimens [8, 14, 24]. We have observed that Gleason score 3+3=6 carcinoma is often undergraded on needle biopsies by external pathologists. Very often, small nests of Gleason 3 pattern (score 6) are misclassified as pattern 1 or 2 (scores 2, 3 or 4) carcinomas. The results of this study support the notion that Gleason patterns 1 and 2 should not be used in diagnostic biopsies. Such patterns may be diagnosed in incidental adenocarcinomas (T1a–b) detected on transurethral resection specimens from the transition zone of the prostate [12, 14, 17].

However, the most important modifications of pattern interpretation proposed by the ISUP meeting pertained to patterns 3 and 4. In the original description by Gleason, cribriform patterns were assigned either a Gleason pattern 3 or 4 depending on the shape of the cribriform glands. There is now an increased understanding that invasive cribriform carcinoma is a relatively aggressive disease. Therefore, it was now recommended that most cribriform carcinomas should be assigned a Gleason pattern 4 rather than 3, and that cribriform glands must be small and round to qualify for pattern 3. The ISUP consensus meeting emphasized that Gleason pattern 4 should also include ill-defined glands with poorly formed glandular lumina, a relatively common pattern that was not incorporated in the original definition of pattern 4 (Fig. 2). It is unclear how this pattern used to be graded, but the incomplete structure of some of the glands may have been overlooked to be included into Gleason pattern 3. With the ISUP modifications, some cases that used to be interpreted as Gleason score 6 are now considered Gleason score 7.

Even before the ISUP revision of the Gleason grading, the most frequent Gleason scores in needle biopsies and radical prostatectomy specimens were Gleason scores 6 and 7, respectively [37]. Therefore, the modification of the Gleason grading system may both change the distribution of Gleason scores and the agreement of Gleason scores between specimens. The most common grade in needle biopsies with conventional Gleason grading in this study was Gleason score 6, while with modified grading, a Gleason score 7 was the most frequent. In the literature, Gleason score 6 is often reported to be the most common Gleason score of needle biopsy specimens. This may be explained by pattern interpretation (cribriform and some poorly formed glands have been interpreted as pattern 3), but could also be attributed to the current stage shift with more and more cancers detected at an early stage.

In the current study, the overall exact agreement between Gleason score of needle biopsies and radical prostatectomy specimens improved from 58 to 72% with modified Gleason grading. Compared to previous reports [2–6, 16, 27, 28, 31, 34–38], this is an excellent concordance. Preoperative identification of a high-grade tumour component is clinically important. Gleason pattern 4 may be either undergraded in needle biopsies or not sampled. Therefore, a significant disagreement exists between biopsies and radical prostatectomy specimens for Gleason scores 6, 7a and 7b [7, 21, 26]. Notably, the agreement of modified Gleason score 3+4=7a between needle biopsies and radical prostatectomies at 88.5% was very high compared to Gleason score 3+3=6 (28.4%) and 4+3=7b (68.0%). In comparison to this high level of agreement, the concordance of conventional Gleason grading was only moderate, corresponding to the upper end of the range (28–68%) reported in the literature [2–6, 9, 10, 16, 18, 27, 28, 31, 34–38].

Hence, the modified Gleason grading minimizes undergrading of prostatic carcinomas in biopsies and improves the agreement between biopsies and radical prostatectomy specimens. By providing a more accurate prognostic information before treatment, the modified Gleason grading contributes to a safer treatment decision.

References

1. Amin M, Boccon-Gibod L, Egevad L, Epstein JI, Humphrey PA, Mikuz G, Newling D, Nilsson S, Sakr W, Srigley JR, Wheeler TM, Montironi R (2005) Prognostic and predictive factors and reporting of prostate carcinoma in prostate needle biopsy specimens. Scand J Urol Nephrol 39:20–33
2. Bonkhoff H (2005) Gleason grading: diagnostic criteria and clinical implications. Pathologe 26:422–432
3. Bostwick DG (1994) Gleason grading of prostatic needle biopsies. Correlation with grade in 316 matched prostatectomies. Am J Surg Pathol 18:796–803
4. Bostwick DG (1994) Grading prostate cancer. Am J Clin Pathol 102:38–59
5. Carlson GD, Calvanese CB, Kahane H, Epstein JI (1998) Accuracy of biopsy Gleason scores from a large uropathology laboratory: use of a diagnostic protocol to minimize observer variability. Urology 51:525–529
6. Cookson MS, Fleshner NE, Soloway SM, Fair WR (1997) Correlation between Gleason score of needle biopsy and radical prostatectomy specimen: accuracy and clinical implications. J Urol 157:559–562
7. Dunn RL, Shah R, Zhou M (2002) Global Gleason score, highest Gleason score, or weighted Gleason score: what Gleason score should be reported in prostate needle biopsies. Mod Pathol 15:161A–669A
8. Egevad L, Allsbrook WC, Epstein JI (2005) Current practice of Gleason grading among genitourinary pathologists. Hum Pathol 36:5–9
9. Egevad L, Granfors T, Karlberg L, Bergh A, Stattin P (2002) Percent gleason grade 4/5 as prognostic factor in prostate

cancer diagnosed at transurethral resection. J Urol 168:509–513
10. Egevad L, Granfors T, Karlberg L, Bergh A, Stattin P (2002) Prognostic value of the Gleason score in prostate cancer. BJU Int 89:538–542
11. Egevad L, Norlen BJ, Norberg M (2001) The value of multiple core biopsies for predicting the Gleason score of prostate cancer. BJU Int 88:716–721
12. Epstein JI (2000) Gleason score 2–4 adenocarcinoma of the prostate on needle biopsy: a diagnosis that should not be made. Am J Surg Pathol 24:477–478
13. Epstein H, Algaba F, Allbrook WC et al (2004) Acinar adenocarcinoma. In: Eble JN, Sauter G, Epstein JI, Sesterhenn IA (eds) World Health Organization classification of tumors. Pathology and genetics: tumours of the urinary system and male genital organs. IARC, Lyon, France, pp 179–184
14. Epstein JI, Allsbrook WC, Amin MB, Egevad L, and the ISUP Grading Committee (2005) The 2005 International Society of Urological Pathology (ISUP) consensus conference on Gleason grading of prostatic carcinoma. Am J Surg Pathol 29(9):1228–1242
15. Gallee MP, Ten Kate FJ, Mulder PG, Blom JH, van der Heul RO (1990) Histological grading of prostatic carcinoma in prostatectomy specimens. Comparison of prognostic accuracy of five grading systems. Br J Urol 65:368–375
16. Garnett JE, Oyasu R, Grayhack JT (1984) The accuracy of diagnostic biopsy specimens in predicting tumor grades by Gleason's classification of radical prostatectomy specimens. J Urol 131:690–693
17. Gaudin PB, Epstein JI (1995) Adenosis of the prostate. Histologic features in needle biopsy specimens. Am J Surg Pathol 19:737–747
18. Glaessgen A, Hamberg H, Pihl CG, Sundelin B, Nilsson B, Egevad L (2002) Interobserver reproducibility of percent Gleason grade 4/5 in total prostatectomy specimens. J Urol 168:2006–2010
19. Gleason DF (1966) Classification of prostatic carcinomas. Cancer Chemother (Rep Part) 50:125–128
20. Gleason DF (1977) Histologic grading and clinical staging of prostatic carcinoma. In: Tannenbaum M (ed) Urologic Pathology: the prostate. Lea and Felbiger, Philadelphia, pp 171–198
21. Gleason DF (1992) Histological grading of prostate cancer: a perspective. Hum Pathol 23:273–279
22. Gleason DF, Mellinger GT (1974) Prediction of prognosis for prostatic adenocarcinoma by combined histological grading and clinical staging. J Urol 111:58–64
23. Helpap B (1993) Review of the morphology of prostatic carcinoma with special emphasis on subgrading and prognosis. J Urol Pathol 1:3–20
24. Helpap B (2005) Small suggestive lesions of the prostate. Histological and immunohistochemical analyses—report of the uropathology consultation service. Pathologe 26:398–404
25. Helpap B, Böcking A, Dhom G, Kastendiek R, Leistenschneider W, Müller HA (1985) Klassifikation, histologisches und zytologisches Grading sowie Regressionsgrading des Prostatakarzinoms. Eine Empfehlung des pathologisch-urologischen Arbeitskreises "Prostatakarzinoms". Pathologe 6:3–7
26. Herman CM, Kattan MW, Scardino PT, Wheeler TW (1999) Predominant Gleason pattern is a significant predictor of disease progression in Gleason score 7 prostate cancer. Mod Pathol 12:97A
27. Kramer SA, Spahr J, Brendler CB, Glenn JF, Paulson DF (1980) Experience with Gleason's histopathologic grading in prostatic cancer. J Urol 124:223–225
28. Lang PH, Narayan P (1983) Understaging and undergrading of prostate cancer. Argument for postoperative radiation of adjuvant therapy. Urology 21:113–118
29. Mellinger GT (1977) Prognosis of prostatic carcinoma. Recent Results Cancer Res 61–72
30. Mellinger GT, Gleason DF, Bailar J 3rd (1967) The histology and prognosis of prostatic cancer. J Urol 97:331–337
31. Mills SE, Fowler JE (1986) Gleason histologic grading of prostatic carcinoma. Correlations between biopsy and prostatectomy specimens. Cancer 57:346–349
32. Mosse CA, Magi-Galluzzi C, Tsuzuki T, Epstein JI (2004) The prognostic significance of tertiary Gleason pattern 5 in radical prostatectomy specimens. Am J Surg Pathol 28:394–398
33. Mostofi FK, Sesterhenn IA, Davis CJ (2002) Histological typing of prostate tumours. In: World Health Organization international histological classification of tumours. Springer, Berlin Heidelberg New York
34. Partin AW, Kattan MW, Subong EN, Walsh PC, Wojno KJ, Oesterling JE, Scardino PT, Pearson JD (1997) Combination of prostate-specific antigen, clinical stage, and Gleason score to predict pathological stage of localized prostate cancer: a multi-institutional update. JAMA 277:1445–1451
35. Spires SE, Cibull ML, Wood DP Jr, Miller S, Spires SM, Banks ER (1994) Gleason histologic grading in prostatic carcinoma. Correlation of 18-gauge core biopsy with prostatectomy. Arch Pathol Lab Med 118:705–708
36. Stamey TA, McNeal JE, Freiha FS, Redwine E (1988) Morphometric and clinical studies on 68 consecutive radical prostatectomies. J Urol 139:1235–1241
37. Steinberg DM, Sauvageot J, Piantadosi S, Epstein JI (1997) Correlation of prostate needle biopsy and radical prostatectomy Gleason grade in academic and community settings. Am J Surg Pathol 21:566–576
38. Young RH, Srigley JR, Amin MB, Ulbright TM, Cubilla AL (2000) Tumors of the prostate gland, seminal vesicles, male urethra, and penis. In: Rosai J, Sobin LH (eds) Atlas of tumor pathology. AFIP, Washington, pp 111–216

Virchows Arch (2006) 449:628–636
DOI 10.1007/s00428-006-0315-1

ORIGINAL ARTICLE

ADAM8 expression in prostate cancer is associated with parameters of unfavorable prognosis

Florian R. Fritzsche · Monika Jung · Chuanliang Xu · Anja Rabien · Hanka Schicktanz · Carsten Stephan · Manfred Dietel · Klaus Jung · Glen Kristiansen

Received: 8 July 2006 / Accepted: 11 September 2006 / Published online: 8 November 2006
© Springer-Verlag 2006

Abstract Gene products of the A disintegrin and metalloprotease (ADAM) family are critically involved in carcinogenesis and tumor progression of various solid tumors. Little is known about ADAM8 in prostate cancer. In our quest for novel diagnostic tissue markers of prostate cancer, we aimed to evaluate the expression of ADAM8 in prostate cancer and to correlate it with clinicopathological parameters. One hundred twenty-eight clinicopathologically characterized prostate cancer patients, with available follow-up data, were immunostained for ADAM8. Additionally, ADAM8 mRNA expression was quantified by real-time reverse transcription polymerase chain reaction (n=59). ADAM8 protein expression was significantly associated with higher pT status, positive nodal status, and higher Gleason scores. Still, a significant prognostic value for the prostate-specific antigen relapse-free survival of ADAM8 could not be demonstrated. The differentiality of ADAM8 expression on protein and on mRNA level was low and partially inconclusive. Therefore, despite of its significant association with conventional parameters of an unfavorable prognosis, ADAM8 adds only limited information to the conventional histopathological assessment of prostate cancer.

Keywords Prostate cancer · ADAM8 · qRT-PCR · Immunohistochemistry

F. R. Fritzsche · H. Schicktanz · M. Dietel · G. Kristiansen (✉)
Department of Pathology, Charité-Universitätsmedizin Berlin,
Schumannstrasse 20-21,
10117 Berlin, Germany
e-mail: glen.kristiansen@charite.de

M. Jung · C. Xu · A. Rabien · C. Stephan · K. Jung
Institute of Urology, Charité-Universitätsmedizin Berlin,
Berlin, Germany

Introduction

Prostate cancer is estimated to have 234,460 new cases for the year 2006, which makes it by far the most common cancer in men. Causing an estimated 27,350 deaths, it is the third most common cause of death from cancer in the USA [10]. These numbers underscore that the importance of prostate cancer cannot be underestimated from the medico-scientific and the socioeconomic points of view. In search for new treatment options and a more precise assessment of this malignancy, several potential therapy targets and candidate biomarkers, e.g., CD24, Bcl-1, Bcl-2, p53, c-erbB2, CD44, Ep-CAM, and EGF, have been reported [6, 14, 24]. In this study, we focused on a member of the "A disintegrin and metalloprotease" (ADAM) family, a group of genes that consists of several proteins fulfilling different functions, e.g., in spermatogenesis, cell adhesion, myogenesis, and neurogenesis and leukocyte infiltration [18, 27], and that have recently been associated with progression in renal cell cancer, lung cancer, and brain tumors [9, 21, 25].

ADAM8 (synonym CD156) is a transmembrane protein [28] of 824 amino acids coded by a gene located on chromosome 10q26.3 [29]. Unlike other transmembrane proteins, ADAMs generally consist of a protease domain in addition to the adhesion domain. This structure of ADAMs was found to be related to soluble snake venom proteins, which lead to hemorrhage and destruction of the basement membrane [2, 26]. ADAM8 is strongly expressed in inflammatory cells in experimental asthma [12]. Furthermore, the ADAM8-dependent activation of CD23, leading to the production of IgE and inflammatory cytokines, supported the idea of a potential role of ADAM8 in allergic and inflammatory processes [5]. ADAM8 has also been shown to be expressed in various cell types of the CNS [22]

and was thought to influence intercellular interactions by adhesion molecule cleavage [19]. Autocatalytic remnants of ADAM8 in the cell membrane seem to be of importance for cell adhesion and cell fusion [23]. In contrast to other proteolytic proteins, which can be inhibited by tissue inhibitors of metalloproteinases (TIMP1–4), the proteolytic activity of ADAM8 appears to function independently of TIMPs [1, 23]. Upregulation of other ADAMs has already been demonstrated in various cancer types [3, 4, 7, 15] including prostate cancer [11, 16, 17]. Ishikawa et al. [9] found ADAM8 expressed in 47–79% of different cancer types on a tissue microarray of 363 cases. ADAM8 expression was associated with higher tumor stage in adenocarcinomas of the lung and has been proposed as a serum marker for lung cancer [9]. Functionally, the expression of ADAM8 was demonstrated to increase the migratory activity of mammalian cells [9]. Roemer et al. [21] suggested ADAM8 as a tumor marker for renal cell carcinomas. They found mRNA over-expression of ADAM8 significantly associated with shorter patient survival and a predictor of distant metastasis.

In this study, we aimed to evaluate ADAM8 expression on a protein and transcript level to clarify a diagnostic or prognostic value of ADAM8 in prostate cancer.

Materials and methods

Patients

One-hundred and twenty-eight patients who underwent a radical prostatectomy for prostate cancer, which was diagnosed at the Institute of Pathology of Charité-Universitätsmedizin Berlin between 1992 to 2001, were enclosed in this study. From 1992 to 1999, the prostatectomies were performed by open surgery (n=80, 62.5%), while from 2000 onward they were done almost exclusively laparoscopically (n=48, 37.5%). Patient age ranged between 47 and 73 years with a median of 62. The prostate was completely embedded, and histological diagnosis was established according to the guidelines of the World Health Organization. Preoperative prostate-specific antigen (PSA) levels ranged from 0.03 to 150.0 with a median of 9.2 ng/ml. Twenty-seven patients had received anti-androgenic hormone therapy before surgery. All cases had a postoperative PSA level below 1 ng/ml. Cases were selected according to tissue availability and were not stratified for any known preoperative or pathological prognostic factors. As patients with systemic disease (pM1 or pN1; assessed by intraoperative frozen-section histology) at the time of diagnosis did not undergo prostatectomy, they could not be included in this study. Clinical follow-up data including survival time was available for all patients included. The median follow-up time of all cases was 41 months, ranging between 4 and 180 months. The median follow-up time of patients without a PSA relapse was 48 months (range 10 to 180). Forty-seven patients (36.7%) experienced a PSA relapse (PSA>1 ng/ml) after a median time of 28 months (range 4 to 88). Eight patients (6.25%) with postoperatively confirmed nodal metastases (pN1) were enclosed. For six patients, no nodal status was available (pNx). There was no adjuvant treatment administered to any of the patients until relapse occurred. The clinicopathological data of the cases are described in Table 1.

Immunohistochemistry

Formalin-fixed, paraffin-embedded tissue was freshly cut (3 μm). The sections were mounted on Superfrost slides (Menzel Gläser, Braunschweig, Germany), dewaxed with xylene and gradually hydrated. Antigen retrieval was achieved by pressure cooking in 0.01 M citrate buffer for

Table 1 Association between the protein expression of ADAM8 in prostate cancer and clinicopathological parameters

	Total	Low ADAM8	High ADAM8	p Value
All cases	128	78 (60.9%)	50 (39.1%)	
Age				0.206
≤63	70	39 (55.7%)	31 (44.3%)	
>63	58	39 (67.2%)	19 (32.8%)	
Pre-OP PSA[a]				0.094
≤9.1 ng/ml	64	45 (70.3%)	19 (29.7%)	
>9.1 ng/ml	58	32 (55.2%)	26 (44.8%)	
pT Status				0.206
pT2	66	44 (66.7%)	22 (33.3%)	
pT3+	62	34 (54.8%)	28 (45.2%)	
pN Status[b]				0.053
pN0	95	61 (64.2%)	34 (35.8%)	
pN1	8	2 (25.0%)	6 (75.0%)	
Histological grade (WHO)[c]				0.468
G1/2	70	45 (64.3%)	25 (35.7%)	
G3	58	33 (56.9%)	25 (43.1%)	
Gleason sum[c]				0.259
3–6	46	31 (67.4%)	15 (32.6%)	
7–10	80	45 (56.3%)	35 (43.8%)	
PSA relapse				0.351
No	81	52 (64.2%)	29 (35.8%)	
Yes	47	26 (55.3%)	21 (44.7%)	
Residual tumor[d]				0.856
R0	68	41 (60.3%)	27 (39.7%)	
R1	59	37 (62.7%)	22 (37.3%)	

[a] Preoperative PSA was not available for six cases.
[b] Twenty-five cases were pNx.
[c] For two cases, no Gleason score was given in the report.
[d] One case was Rx.

5 min. The primary ADAM8 antibody (polyclonal rabbit antibody, Cedarlane Laboratories, Hornby, Canada) was diluted 1:200 using a background reducing dilution buffer (DAKO, Hamburg, Germany). The primary antibody was incubated at room temperature for 1 h. Detection took place by the conventional labeled streptavidin–biotin method (LSAB-kit, DAKO) with alkaline phosphatase as the reporting enzyme according to the manufacturer's instructions. Fast-Red (Sigma-Aldrich, Munich, Germany) served as chromogen. Afterwards, the slides were briefly counterstained with hematoxylin and aqueously mounted.

Evaluation of the immunohistochemical stainings

The immunostainings were independently evaluated by two genitourinary pathologists who were blinded for patient outcome. For better reproducibility, we aimed to keep our scoring system of the immunostaining simple by semiquantitatively scoring the staining intensity of ADAM8 as negative (0), weak (1), moderate (2), or strong (3). Immunoreactivity in less than 5% of the tumor cells was scored as negative.

Microdissection

Fifty-nine matched malignant and nonmalignant prostate cancer samples from the years 1999 to 2003 were manually microdissected (tumor and normal tissue) from frozen sections. Cases were selected according to availability of frozen tissue and were not stratified for any known preoperative or pathological prognostic factors. Cases used for microdissection and mRNA preparation were different from the cohort used for immunohistochemistry. The clinicopathological parameters of this cohort were as follows: pT2: 34 (58%), pT3/4: 25 (42%); R0: 33 (56%), R1: 25 (42%), and Rx: 1 (2%); pN0: 18 (30%), pN1: 1 (2%), and pNx: 40 (68%). Gleason sum (GS) of microdissected areas were: GS4 2 (3%), GS5 2 (3%), GS6 30 (51%), GS7 16 (27%), GS8 8 (14%), and GS10 1 (2%). Six patients received anti-androgenic therapy before prostatectomy. The median preoperative PSA serum level was 7.40 ng/ml. Follow-up data was available for 53 patients with a median follow-up time of 34 months (range 11 to 69 months). Thirteen patients experienced a PSA relapse after a median of 15.8 months (range 1.3 to 48 months).

Microdissection was conducted as described [13]. Briefly, frozen tissue samples were sectioned (8 μm) and mounted on Superfrost slides (Menzel Gläser) and quickly stained with hematoxylin. Histopathological selection and evaluation of malignant and nonmalignant areas for microdissection was carried out by a single pathologist. From 20 consecutive slides, tissue areas were manually scraped and collected for RNA isolation.

RNA isolation

The total RNA isolation was performed by RNeasy Micro Kit (Qiagen, Hilden, Germany) according to the manufacturer's instructions. The samples were applied on a RNeasy MinElute spin column for selective binding of RNA at a silica gel membrane. After different washing steps and a DNA digestion step, high quality RNA was eluted with 30 μl RNase-free water. RNA content of samples was measured with the NanoDrop ND-1000 Spectrophotometer (NanoDrop Technologies, Wilmington, USA).

First strand cDNA synthesis

cDNA synthesis was performed with the Transcriptor First Strand cDNA Synthesis Kit (Roche Applied Science, Penzberg, Germany) using a maximum of 1 μg RNA in the reaction. Before cDNA synthesis, RNA samples were incubated at 65°C for 10 min for denaturation of RNA secondary structures. Kit-included random hexamer primers were applied for first strand cDNA synthesis after the following procedure: 10 min at 25°C for primer annealing, 30 min at 55°C for reverse transcription step, 5 min at 85°C for inactivation of Transcriptor Reverse Transcriptase, then cooling on ice. The cDNA volume amounted to 20 μl. Tubes were stored at −20°C up to subsequent real-time PCR.

Quantitative real-time PCR

Real-time reverse transcription polymerase chain reaction (RT-PCR) was performed on the LightCycler Instrument (Roche). As described recently, we also measured the housekeeping gene hypoxanthine–phosphoribosyl–transferase (*HPRT1*) in the same cDNA samples [21]. The *HPRT* gene is stably expressed in prostate and was used as endogenous reference gene for normalization of ADAM8 mRNA expression [20]. HPRT was quantified with the LightCycler h-HPRT Housekeeping Gene Set (Roche). Both PCR products were detected by fluorescence resonance energy transfer technique using each two specific hybridization probes labeled with different fluorophores. The amplifications were performed with a "hot start" Taq DNA Polymerase included in the FastStart DNA Master ^{PLUS} HybProbes. The PCR reaction volume was 20 μl in the LightCycler capillaries including always 2 μl cDNA. Final concentrations were 1 μM for each of the ADAM8 primers and 0.2 μM for each of the probes each. The following were also added: 1 μl dimethyl sulfoxide and 4 μl 5× conc. FastStart DNA Master ^{PLUS} Hybridization Probes. ADAM8 PCR run conditions were: initial activation step of Taq DNA polymerase at 95°C for 15 min, amplification cycles of denaturation at 95°C for 10 s, annealing at 59°C

for 25 s, and elongation at 72°C for 25 s. The temperature transition rate was 20°C/s in each step. PCR runs were finished after 42 cycles. The HPRT-PCR conditions and the reaction mixture were in accordance with the kit instructions (Roche).

Each PCR run included a no-template control, a standard cDNA pool with known ADAM8, and HPRT mRNA content for quantification as well as a cDNA sample for intra- and inter-run precision control. For both gene-specific PCRs, calibration curves were generated, and the PCR efficiencies were calculated.

The PCR efficiency was 1.91 for ADAM8 and 2.00 for HPRT. The intra-run and between-run variations of quantities did not exceed 13.2% for ADAM8 and 11.7% for HPRT, respectively. For relative quantification, the nondimensional ratio of ADAM8 to HPRT was calculated.

Statistical analysis

Statistical analysis was performed using SPSS, version 13.0. Fisher's exact and chi-square tests were applied to assess the statistical significance of the associations between expression of ADAM8 and various clinicopathological parameters. Wilcoxon test was used to assess intergroup differences. Correlations were calculated according to Spearman. Univariate survival analysis was carried out according to Kaplan–Meier, while differences in survival curves were assessed with the log-rank test. Cox regression model was used for multivariate survival analyses. P values <0.05 were considered significant.

Results

ADAM8 immunostaining in prostate cancer and adjacent normal prostate tissue

Sixty one percent (78 of 128) of the prostate cancer cases showed no (0, 13.3%) or a weak (1+, 47.7%) cytoplasmic staining for ADAM8, while 39% (50 of 128) of cases revealed a moderate (2+, 32.0%) to strong (3+, 7.0%) ADAM8 expression (Fig. 1). The ADAM8 expression in the normal prostate tissue was none to weak in 84.4% (108 of 128) of conclusive cases and moderate to strong in 15.6% (20 of 128). The mean staining intensity of cancerous and normal tissue was 1.33 and 1.05, respectively, while the median staining intensity of both tissue types was 1. Still, this difference in mean staining intensities of tumor and normal tissue was highly significant ($p<0.001$). Prostatic intraepithelial neoplasia (PIN) was present in 75 (58.6%) of the 128 cases. None or weak ADAM8 expression appeared in 48.0%, moderate or strong in 52.0% of the PIN with a mean staining intensity of 1.57 and a median of 2 (Fig. 1). In 32 cases, ADAM8 expression was higher in PIN than in the normal tissue (equal in 43 cases) and higher in 8 cases than in invasive prostate cancer

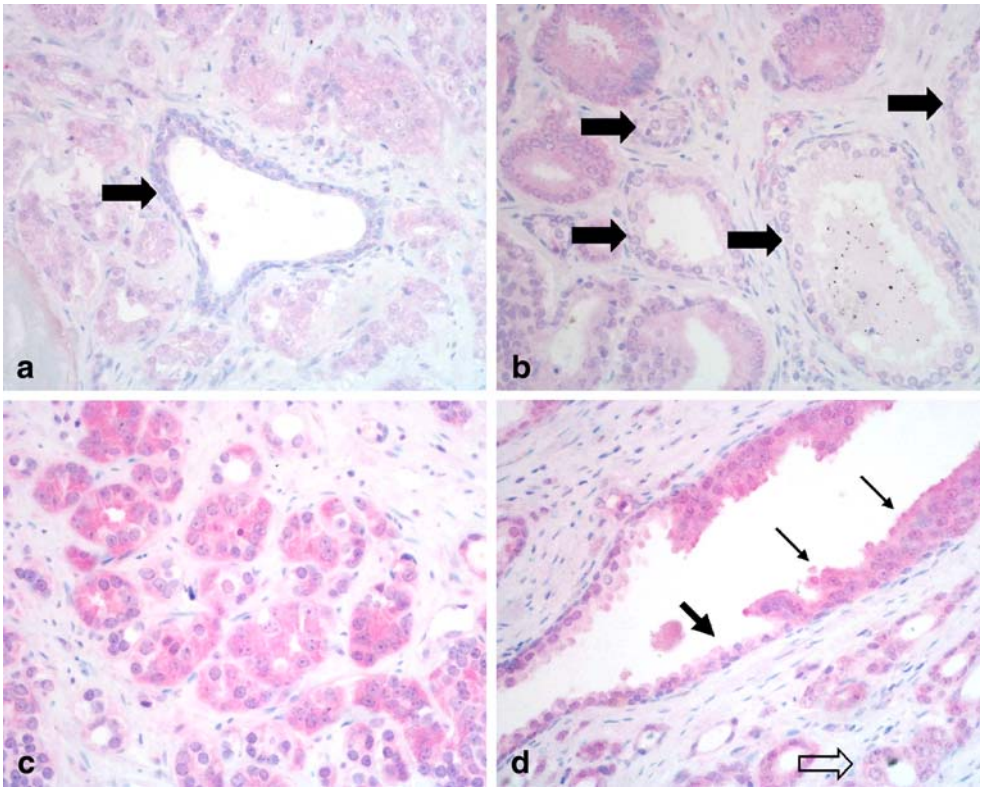

Fig. 1 Immunohistological expression of ADAM8. **a**, **b** Glandular prostate cancer tissue displaying moderate to strong ADAM8 protein expression adjacent to normal prostate glands with distinctly weaker expression of ADAM8. **c** Prostate cancer tissue showing strong ADAM8 protein expression. **d** Prostatic intraepithelial neoplasia (*small arrows*) with strong ADAM8 expression sharply marked off from the normal prostatic epithelium (*bold arrow*) and surrounding microglandular prostate cancer (*unfilled arrow*)

Table 2 Correlation of ADAM8 protein expression in prostate cancer with clinicopathological parameters

ADAM8	pT Status	pN Status	Gleason sum	Grading	Pre-OP PSA	Age	*R* status
CC	0.177	0.261	0.218	0.086	0.096	−0.028	−0.047
p	0.046	0.008	0.014	0.334	0.295	0.756	0.601
N	128	103	126	128	122	128	127

CC Correlation coefficient, *p* two-sided significance, *N* number of cases, *R status* residual tumor

(lower in one case and equal in 66 cases). These differences in the ADAM8 expression between PIN and normal tissue ($p<0.001$) and PIN and invasive carcinoma ($p=0.021$) were statistically significant.

For further statistical analyses, we dichotomized groups by the median (1) into ADAM8-positive (>1) vs ADAM8-negative (≤1) tumors.

ADAM8 expression, clinicopathological correlations, and survival times

In bivariate correlations, the ADAM8 expression of the tumor was significantly correlated with an advanced pT status, positive nodal status, and higher Gleason scores (Table 2).

In univariate survival analysis, cumulative survival curves were calculated according to the Kaplan–Meier method. We analyzed the impact of ADAM8 expression, preoperative PSA, patient age, type of surgery, pT status, tumor grade, Gleason score, and residual tumor status on PSA relapse-free survival time. All conventional prognostic markers of prostate cancer reached statistical significance (Table 3). ADAM8-positive tumors revealed a slight trend for shortened relapse-free survival times (Fig. 2), which failed to reach significance ($p=0.218$). Subsequently, the effects of ADAM8 expression were analyzed in various subgroups defined by the parameters mentioned above. Although the trend for shortened, relapse-free survival times of ADAM8-positive tumors could repeatedly be demonstrated, significance was reached in none of these groups (data not shown).

Quantitative RT-PCR

To reduce the inter-run variability, the paired samples of nonmalignant and malignant tissue areas were measured in one PCR run. Interestingly, the normalized ADAM8

Table 3 Univariate survival analysis (Kaplan–Meier): PSA relapse times according to clinicopathological factors and ADAM8 expression

Characteristic	No. of cases	No. of events	3-year PSA relapse rate (±SE) in %	p Value
ADAM8 expression				0.218
Low	78	26	27.7±5.2	
High	50	21	30.8±6.9	
Pre-OP PSA				0.005
≤9.1 ng/ml	64	16	21.4±5.3	
>9.1 ng/ml	58	28	36.6±6.6	
Age				0.660
≤63 years	70	31	30.0±5.6	
>63 years	58	20	27.5±6.1	
Type of surgery				0.240
Open surgery	80	36	31.6±5.2	
Laparoscopy	48	11	23.4±6.6	
pT status				0.004
pT1/2	66	16	19.5±5.1	
pT3/4	62	31	38.3±6.3	
Histological grade (WHO)				<0.001
G1/2	70	13	13.4±4.2	
G3	58	34	48.1±7.0	
Gleason sum				0.003
1–6	46	10	15.7±5.4	
7–10	80	36	37.6±5.7	
Residual tumor				0.043
R0	68	19	25.1±5.5	
R1	59	27	33.4±6.3	

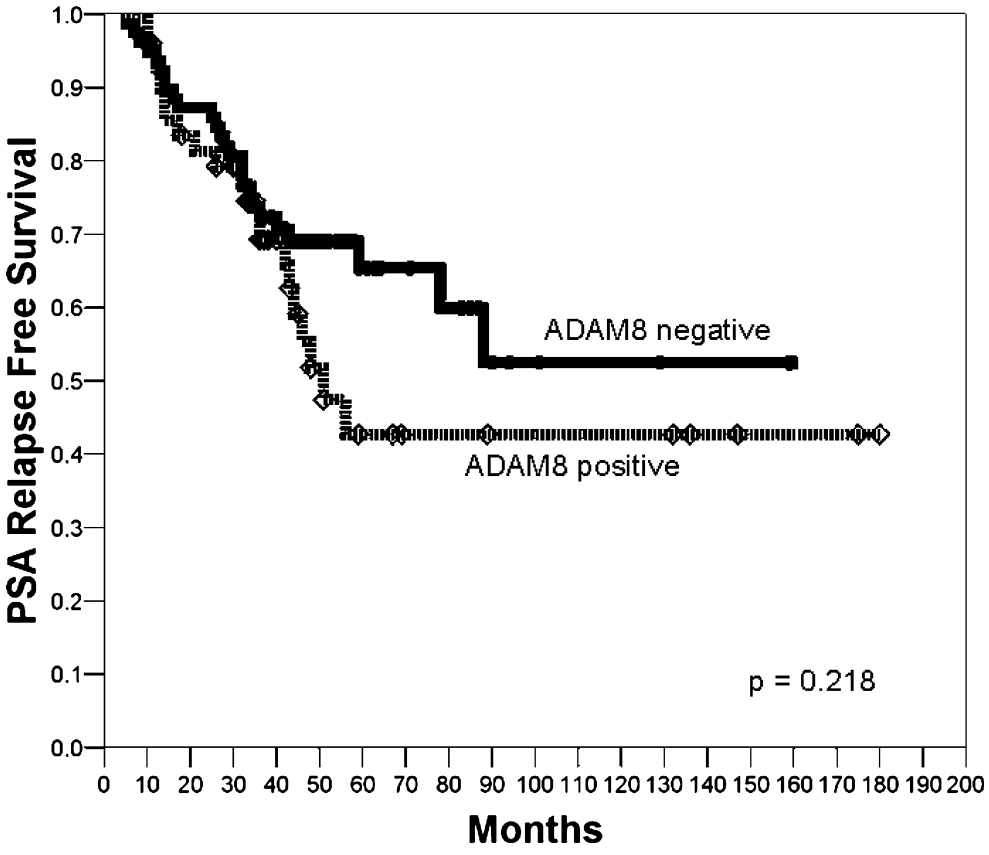

Fig. 2 PSA relapse-free survival curve for ADAM8. A slight trend towards shorter PSA relapse-free survival times for patients with ADAM8-positive tumors can be recognized, but remains insignificant

expression was significantly lower in malignant samples than in matched nonmalignant samples (medians, 0.622 vs 0.864; Wilcoxon test, $p<0.001$; Fig. 3a). In 18 (30.5%) prostate cancer cases, ADAM8 was expressed at higher levels compared to the expression in matched benign tissue (Fig. 3b). Using the change fold>2 definition to differentiate up- and downregulation, in the majority of cases ($n=36$, 61%) there was no difference between malignant and nonmalignant samples. In 21 cases (35.6%), ADAM8 mRNA expression was lower, and in two cases (3.4%) ADAM8 mRNA expression was higher in the cancerous tissue than in matching normal tissue. However, no significant associations of ADAM8 mRNA expression with pT status, Gleason sum of the microdissected area/

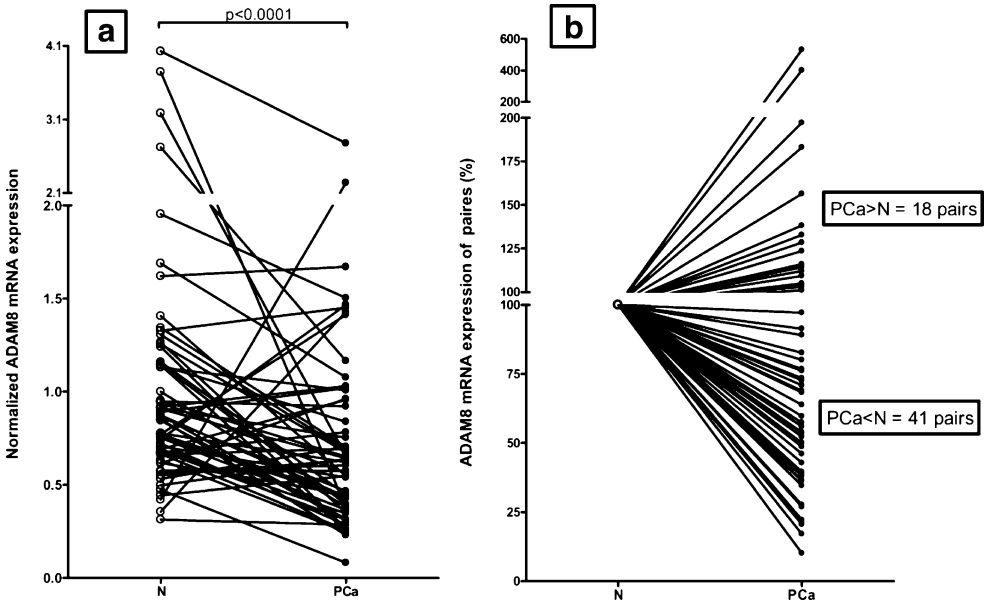

Fig. 3 ADAM8 mRNA expression. **a** Normalized ADAM8 mRNA expression values in nonmalignant (*unfilled dots*, *left*) and malignant tissue of matched paired samples after prostatectomy (*filled dots*, *right*). Differences between the paired samples were highly significant (Wilcoxon signed rank test). **b** Prostate cancer cases grouped according to whether ADAM8 mRNA expression in the carcinoma is higher (*top part*) or lower (*bottom part*) in comparison to the paired normal prostate tissue

prostatectomy specimen, preoperative PSA value, surgical margin status, or PSA relapse were found (Table 4). There were no changes to Table 4 leading to any significance when the change fold>2 approach was used for the calculation.

Discussion

This is the first study to evaluate ADAM8 expression in the prostate. ADAM8 was known to take part in inflammatory processes and was already found in various human carcinomas [8, 9, 12, 21]. In the present study, we found a significantly stronger mean ADAM8 protein expression in cancerous tissue in comparison to normal tissue, which might be taken as a hint towards its importance in this malignancy. On the other hand, as the median ADAM8 protein expression in normal and cancerous tissue is equal and differences in mean expression are minimal, this upregulation seems to be of little use diagnostically, even if statistically significant. Interestingly, in contrast to the immunohistological findings, ADAM8 mRNA expression was significantly downregulated in the tumor in comparison to normal prostate tissue. Again, this finding was put into perspective when a change fold>2 definition was used to assess differential gene expression, since then the majority of cases showed no differences between tumor and normal tissue. Still, ADAM8 mRNA was rather downregulated in the tumor. This discrepancy of the direction of differential ADAM8 expression between mRNA and protein level remains puzzling, but might be negligible given the minimal differentiality on both levels. Still, it might hint at different post-translational regulatory mechanisms in cancerous and normal prostate, but it could also be due to the differences in the cohorts used for immunohistochemistry and RT-PCR.

In three former studies on ADAM8 in lung, renal cell cancer, and brain tumors, over-expression of ADAM8 has been associated with worse prognostic parameters or even with shorter survival times in renal cancer [9, 21, 25]. In the present study on prostate cancer, we could not demonstrate a significant association of ADAM8 expression with PSA relapse-free survival times, although a trend was suggested. In the study of Roemer et al. on renal carcinomas, ADAM8 expression was the best predictor of distant metastases. We found a highly significant correlation of the ADAM8 expression with a positive nodal status. But with only eight nodal positive cases, this number was too small to make nodal status a significant marker of PSA relapse-free survival in our cohort (log rank $p=0.623$, data not shown). Certainly, this could question the validity of the strong correlation of ADAM8 expression with a positive nodal status, but it also might explain why this strong correlation did not lead to a significant prediction of the PSA relapse-

Table 4 Association between ADAM8 mRNA expression in prostate cancer and clinico-pathological parameters

	Total	Low ADAM8	High ADAM8	*p* Value
All cases	59	41 (69.5%)	18 (30.5%)	
Age				0.389
≤63	37	24 (64.9%)	13 (35.1%)	
>63	22	17 (77.3%)	5 (22.7%)	
Pre-OP PSA[a]				1.000
≤9.1 ng/ml	30	21 (70.0%)	9 (30.0%)	
>9.1 ng/ml	26	19 (73.1%)	7 (26.9%)	
pT Status				1.000
pT2	34	24 (70.6%)	10 (29.4%)	
pT3+	25	17 (68.0%)	8 (32.0%)	
Histological grade (WHO) PS				0.395
G1/2	24	15 (62.5%)	9 (37.5%)	
G3	35	26 (74.3%)	9 (25.7%)	
Gleason sum MA				1.000
3–6	34	24 (70.6%)	10 (29.4%)	
7–10	25	17 (68.8%)	8 (32.0%)	
Gleason sum PS				0.533
3–6	16	10 (62.5 %)	6 (37.5%)	
7–10	43	31 (72.1%)	12 (27.9%)	
PSA relapse[b]				1.000
No	40	28 (70.0%)	12 (30.0%)	
Yes	13	9 (69.2%)	4 (30.8%)	
Residual tumor[c]				0.151
R0	33	26 (78.8%)	7 (21.2%)	
R1	25	15 (60.0%)	10 (40.0%)	

PS Prostatectomy specimen, *MA* microdissected area
[a] Preoperative PSA was not available for three cases.
[b] Follow-up data was available for 53 patients.
[c] One case was Rx.

free survival time of ADAM8. Moreover, the significant association of ADAM8 positivity with higher pT status and Gleason scores further supports the general notion of ADAM8 as a marker of unfavorable outcome, which might be of significance in the group of nodal positive tumors, which is clearly underrepresented in our study. This is in line with functional findings for ADAM8 showing its ability to cleave adhesion molecules, thereby allowing easier stromal invasion of cancer cells [19]. Furthermore, the demonstrated increase of migratory activity of lung cancer cells by ADAM8 could lead to more aggressive, faster growing, and bigger tumors resulting in higher pT stages [9]. Scholmann et al. [22] have shown the induction of ADAM8 by tumor necrosis factor-alpha, which also might play a role in prostate cancer. The finding of a significantly higher protein expression of ADAM8 in PIN in comparison to both invasive tumor and normal tissue might also be taken as a hint at a possible transient overexpression of ADAM8 in the carcinogenesis of prostate cancer, which clearly warrants further study.

In conclusion, we are the first to describe ADAM8 expression in prostate cancer. Interestingly, we found ADAM8 protein expression significantly associated with parameters of unfavorable prognosis. About 40% of the tumors were moderately to strongly positive for ADAM8, which might be a potential target for novel therapeutics, but the differentiality of ADAM8 expression was low. Therefore, the diagnostic value of ADAM8 seems limited. The post-translational processing of ADAM8 and possible blocking or downregulating mechanisms and the role of ADAM8 in carcinogenesis and metastasis of prostate cancer should be the focus of further studies.

Acknowledgements We are grateful to Britta Beyer for excellent technical assistance. The continuous support of Ilka Olson and Dr. Marius Fritzsche is greatly acknowledged.

References

1. Amour A, Knight CG, English WR, Webster A, Slocombe PM, Knauper V, Docherty AJ, Becherer JD, Blobel CP, Murphy G (2002) The enzymatic activity of ADAM8 and ADAM9 is not regulated by TIMPs. FEBS Lett 524:154–158
2. Bjarnason JB, Fox JW (1995) Snake venom metalloendopeptidases: reprolysins. Methods Enzymol 248:345–368
3. Blanchot-Jossic F, Jarry A, Masson D, Bach-Ngohou K, Paineau J, Denis MG, Laboisse CL, Mosnier JF (2005) Up-regulated expression of ADAM17 in human colon carcinoma: co-expression with EGFR in neoplastic and endothelial cells. J Pathol 207:156–163
4. Carl-McGrath S, Lendeckel U, Ebert M, Roessner A, Rocken C (2005) The disintegrin-metalloproteinases ADAM9, ADAM12, and ADAM15 are upregulated in gastric cancer. Int J Oncol 26:17–24
5. Fourie AM, Coles F, Moreno V, Karlsson L (2003) Catalytic activity of ADAM8, ADAM15, and MDC-L (ADAM28) on synthetic peptide substrates and in ectodomain cleavage of CD23. J Biol Chem 278:30469–30477
6. Hammond ME, Fitzgibbons PL, Compton CC, Grignon DJ, Page DL, Fielding LP, Bostwick D, Pajak TF (2000) College of American Pathologists Conference XXXV: solid tumor prognostic factors—which, how and so what? Summary document and recommendations for implementation. Cancer Committee and Conference Participants. Arch Pathol Lab Med 124:958–965
7. Held-Feindt J, Paredes EB, Blomer U, Seidenbecher C, Stark AM, Mehdorn HM, Mentlein R (2006) Matrix-degrading proteases ADAMTS4 and ADAMTS5 (disintegrins and metalloproteinases with thrombospondin motifs 4 and 5) are expressed in human glioblastomas. Int J Cancer 118:55–61
8. Higuchi Y, Yasui A, Matsuura K, Yamamoto S (2002) CD156 transgenic mice. Different responses between inflammatory types. Pathobiology 70:47–54
9. Ishikawa N, Daigo Y, Yasui W, Inai K, Nishimura H, Tsuchiya E, Kohno N, Nakamura Y (2004) ADAM8 as a novel serological and histochemical marker for lung cancer. Clin Cancer Res 10:8363–8370
10. Jemal A, Siegel R, Ward E, Murray T, Xu J, Smigal C, Thun MJ (2006) Cancer statistics, 2006. CA Cancer J Clin 56:106–130
11. Karan D, Lin FC, Bryan M, Ringel J, Moniaux N, Lin MF, Batra SK (2003) Expression of ADAMs (a disintegrin and metalloproteases) and TIMP-3 (tissue inhibitor of metalloproteinase-3) in human prostatic adenocarcinomas. Int J Oncol 23:1365–1371
12. King NE, Zimmermann N, Pope SM, Fulkerson PC, Nikolaidis NM, Mishra A, Witte DP, Rothenberg ME (2004) Expression and regulation of a disintegrin and metalloproteinase (ADAM) 8 in experimental asthma. Am J Respir Cell Mol Biol 31:257–265
14. Kristiansen G, Sammar M, Altevogt P (2004) Tumour biological aspects of CD24, a mucin-like adhesion molecule. J Mol Histol 35:255–262
13. Kristiansen G, Pilarsky C, Wissmann C, Kaiser S, Bruemmendorf T, Roepcke S, Dahl E, Hinzmann B, Specht T, Pervan J, Stephan C, Loening S, Dietel M, Rosenthal A (2005) Expression profiling of microdissected matched prostate cancer samples reveals CD166/MEMD and CD24 as new prognostic markers for patient survival. J Pathol 205:359–376
15. Lendeckel U, Kohl J, Arndt M, Carl-McGrath S, Donat H, Rocken C (2005) Increased expression of ADAM family members in human breast cancer and breast cancer cell lines. J Cancer Res Clin Oncol 131:41–48
16. McCulloch DR, Akl P, Samaratunga H, Herington AC, Odorico DM (2004) Expression of the disintegrin metalloprotease, ADAM-10, in prostate cancer and its regulation by dihydrotestosterone, insulin-like growth factor I, and epidermal growth factor in the prostate cancer cell model LNCaP. Clin Cancer Res 10:314–323
17. McCulloch DR, Harvey M, Herington AC (2000) The expression of the ADAMs proteases in prostate cancer cell lines and their regulation by dihydrotestosterone. Mol Cell Endocrinol 167:11–21
18. Nath D, Slocombe PM, Webster A, Stephens PE, Docherty AJ, Murphy G (2000) Meltrin gamma(ADAM-9) mediates cellular adhesion through alpha(6)beta(1)integrin, leading to a marked induction of fibroblast cell motility. Mol Cell Endocrinol 113(Pt 12):2319–2328
19. Naus S, Richter M, Wildeboer D, Moss M, Schachner M, Bartsch JW (2004) Ectodomain shedding of the neural recognition molecule CHL1 by the metalloprotease-disintegrin ADAM8 promotes neurite outgrowth and suppresses neuronal cell death. J Biol Chem 279:16083–16090
20. Ohl F, Jung M, Xu C, Stephan C, Rabien A, Burkhardt M, Nitsche A, Kristiansen G, Loening SA, Radonic A, Jung K (2005) Gene expression studies in prostate cancer tissue: which reference gene should be selected for normalization? J Mol Med 83:1014–1024

21. Roemer A, Schwettmann L, Jung M, Stephan C, Roigas J, Kristiansen G, Loening SA, Lichtinghagen R, Jung K (2004) The membrane proteases adams and hepsin are differentially expressed in renal cell carcinoma. Are they potential tumor markers? J Urol 172:2162–2166
22. Schlomann U, Rathke-Hartlieb S, Yamamoto S, Jockusch H, Bartsch JW (2000) Tumor necrosis factor alpha induces a metalloprotease-disintegrin, ADAM8 (CD 156): implications for neuron–glia interactions during neurodegeneration. J Neurosci 20:7964–7971
23. Schlomann U, Wildeboer D, Webster A, Antropova O, Zeuschner D, Knight CG, Docherty AJ, Lambert M, Skelton L, Jockusch H, Bartsch JW (2002) The metalloprotease disintegrin ADAM8. Processing by autocatalysis is required for proteolytic activity and cell adhesion. J Biol Chem 277: 48210–48219
24. Sivridis E, Touloupidis S, Giatromanolaki A (2002) Immunopathological prognostic and predictive factors in prostate cancer. Int Urol Nephrol 34:63–71
25. Wildeboer D, Naus S, Amy Sang QX, Bartsch JW, Pagenstecher A (2006) Metalloproteinase disintegrins ADAM8 and ADAM19 are highly regulated in human primary brain tumors and their expression levels and activities are associated with invasiveness. J Neuropathol Exp Neurol 65:516–527
26. Wolfsberg TG, Primakoff P, Myles DG, White JM (1995) ADAM, a novel family of membrane proteins containing A disintegrin and metalloprotease domain: multipotential functions in cell–cell and cell–matrix interactions. J Cell Biol 131:275–278
27. Yamamoto S, Higuchi Y, Yoshiyama K, Shimizu E, Kataoka M, Hijiya N, Matsuura K (1999) ADAM family proteins in the immune system. Immunol Today 20:278–284
28. Yoshida S, Setoguchi M, Higuchi Y, Akizuki S, Yamamoto S (1990) Molecular cloning of cDNA encoding MS2 antigen, a novel cell surface antigen strongly expressed in murine monocytic lineage. Int Immunol 2:585–591
29. Yoshiyama K, Higuchi Y, Kataoka M, Matsuura K, Yamamoto S (1997) CD156 (human ADAM8): expression, primary amino acid sequence, and gene location. Genomics 41:56–62

Virchows Arch (2006) 449:637–646
DOI 10.1007/s00428-006-0299-x

ORIGINAL ARTICLE

The expression of metaloproteinases-2 and -9 is different according to the patterns of growth and invasion in squamous cell carcinoma of the penis

Fernando A. Soares · Isabela Werneck da Cunha · Gustavo Cardoso Guimarães · Sueli Nonogaki · Rodrigo Sousa Madeira Campos · Ademar Lopes

Received: 3 March 2006 / Accepted: 22 August 2006 / Published online: 27 October 2006
© Springer-Verlag 2006

Abstract Squamous cell carcinoma (SCC) of the penis is characterized by different patterns of growth and local invasion. The matrix metalloproteinases (MMPs) is a family of proteolytic enzymes that are involved in the degradation of extracellular matrix to allow the migration of tumor cells. The present study examined whether the expression of MMP-2 and -9 is correlated with the patterns of tumor growth and invasion in penile SCC. The expression of MMP-2 and -9 was examined immunohistochemically in samples of 115 patients. The cases were divided in three groups according to the patterns of growth and invasion: group 1, exophytic growth and pushing pattern of invasion; group 2, endophytic growth and invasion in large sheets of cells; and group 3, endophytic growth and invasion in small group or isolated cells. Tumors with MMP-2 and -9 overexpression are deeply invasive and present an invasion pattern of small groups of cells. Also, expression of MMP-2 changed from membrane to cytoplasm in invasive tumors, maybe representing activation of MMP-2. These findings allow us to conclude that the less differentiated tumors, which are more invasive and with a pattern of invasion in small group of cells, are associated with the overexpression of MMPs.

F. A. Soares (✉) · I. W. da Cunha · S. Nonogaki
Department of Anatomic Pathology,
Medical and Research Center Hospital do Câncer A C Camargo,
#211 Antonio Prudente Street, 1st floor,
São Paulo, São Paulo 01509-010, Brazil
e-mail: fasoares@hcancer.org.br

G. C. Guimarães · R. S. M. Campos · A. Lopes
Department of Pelvic Surgery,
Medical and Research Center Hospital do Câncer A C Camargo,
#211 Antonio Prudente Street, 1st floor,
São Paulo, São Paulo 01509-010, Brazil

Keywords Penile cancer · Squamous cell carcinoma of the penis · Metalloproteinases · Extracellular matrix degradation · Tumor invasion

Introduction

Squamous cell carcinoma (SCC) of the penis is a major problem in developing countries, and comprehends 2% of the tumors in Brazilian males [27]. One of the most characteristic clinical features of penile SCC is its capacity to invade locally and metastasize to regional lymph nodes. The stage of the tumor is the most important prognostic factor, as the regional lymph node metastasis and depth of invasion are very important to patient survival [6, 7, 27]. The World Health Organization recently recognized several histological types of penile carcinoma [7] such as SCC, warty carcinoma [5], verrucous carcinoma, papillary carcinoma, sarcomatoid (spindle cell) carcinoma [37], and adenosquamous. The most common histological type is the usual SCC. Following patterns common in other types of SCC, the progression in the penis probably presents the same natural history of other mucosa, such as the cervix and aerodigestive tract, with hyperplastic, low-grade, and high-grade lesions [36]. So, hyperplastic and/or dysplastic epitheliums are frequently seen in adjacent tumor areas [7]. There are three main growth patterns in penile SCC: superficially spreading with horizontal growth and superficial invasion; and vertical growth, which is deeply invasive and multicentric pattern [7]. The invasion pattern is an important prognostic determinant [6]. Although these morphological aspects are well known, there is no paper exploiting why some tumors are predominantly exophytic and why others are deeply invasive.

The process of invasion of an epithelial tumor is quite complex and requires degradation of extracellular matrix

and of the epithelial/vascular basal membrane [31]. Both expression and activation of proteolytic enzymes are a pivotal step in the tumor progression [10]. The matrix metalloproteinases (MMPs) constitutes a family of highly homologous extracellular zinc- and calcium-dependent endopeptides with enzymatic activity against almost all protein components of the extracellular matrix [10, 31]. Nowadays, MMPs are grouped according to their structures [10]. There are eight distinct structural classes of MMPs: five are secreted and three are membrane-type MMPs [10].

The enzymes known as gelatinases (or type IV collagenases) are now classified as secreted MMP of the gelatin-binding structural class [10]. They are characterized based in a fibronectin-like domain and a gelatin-binding domain, and the main two elements are MMP-2 (gelatinase A, 72-kDa gelatinase, and neutrophil gelatinase) and MMP-9 (gelatinase B, and 92-kDa gelatinase) [10]. Gelatinases are able to cleave both the denatured forms of collagen and type IV collagen found in the basement membrane. Gelatinases were associated with tumor progression, invasion, and clinical behavior in several neoplasms. The expressions of MMP-2 and -9 are gradually higher according to the degree of cervical intraepithelial neoplasia and cervical invasive carcinomas [3, 8, 14]. MMP-9 is upregulated in preinvasive lesions of the bronchial epithelium, increasing the expression as the severity of the lesion progresses, and therefore suggesting an important role in basement membrane remodeling [15]. MMPs were implicated in the invasion and metastasis in several tumors, and the relationship between the expression of MMP and the prognosis was described in SCC of several primary sites, such as the cervix [8, 16], head, neck [9, 18–20, 24–26, 29, 38, 39], esophagus [21], and lung [35]. Also, MMP-9 was implicated in invasion depth and vascular invasion in SCCs of the esophagus [30] and it is also correlated with worse prognosis in lung adenocarcinoma [32].

To the best of our knowledge, no paper has explored the expression of MMP-2 and -9 in penile SCC and its relationship with the invasion and morphological growth pattern. In the current study, we analyzed the expression of MMP-2 and -9 in a series of 115 patients with SCC of the penis, and we correlated how the expression of these enzymes is related with the morphological growth pattern of the tumors.

Materials and methods

Tissue specimens

Paraffin-embedded tissue specimens from 115 previously treated patients with usual penile SCC were available for this study. Verrucous and warty carcinomas were not included in the study. The patient population ranges in age from 24 to 79 years, with a median age of 52 years. All tumor sections available from each case were evaluated. Hematoxylin and eosin slides from each tumor underwent pathological review, and blocks, which best represent growth pattern for that tumor, were selected. The cases were further divided according to the differentiation pattern of growth and invasion in three groups: (1) group 1, tumors with an exophytic pattern of growth and pushing pattern of invasion; (2) group 2, endophytic pattern of growth and invasion with large sheets of cells; and (3) group 3, endophytic pattern of growth and invasion in small group of cells.

Immunohistochemistry

Immunohistochemical (IHC) staining for MMP-2 and -9 was performed on formalin-fixed, paraffin-embedded tissue sections. The 4-μm sections were dewaxed, and after hydrogen peroxide treatment (0.3% in absolute methanol for 30 min), these were immersed in a citrate buffer solution (0.01 M sodium citrate at pH 6.0) and boiled in a microwave oven at 700 W (three times, 5 min each). This was followed by rinsing the distilled water and phosphate-buffered saline (PBS). Immunostaining was performed using monoclonal antibodies against MMP-2 (Oncogene, USA; clone 75-7F7) and against MMP-9 (Oncogene; clone 56-2A4). The sections were incubated with primary antibody (1:40 working dilution for MMP-2, 1:80 for MMP-9). All antibodies were incubated overnight at 4°C in a humidified chamber. After being washed with PBS, secondary antibody was added, followed by preformed streptavidin-biotin reagents (kit StrepABComplex/HRP Duet mouse/rabbit, DAKO, USA). Localization of the antigen was visualized using the chromogen 0.05% 3,3′-diaminobenzidine in Tris–HCl buffer. Tissue sections were then counterstained in diluted Harris hematoxylin, dehydrated, cleared with xylene, and mounted with Permount.

IHC scoring

The IHC scoring was performed by two evaluators (FAS and IWC). The scorers were blinded to the outcome and clinical aspects of each tumor specimen. After scanning it in low power field to choose the most stained area, at least ten fields were evaluated under high power. The presence of a clearly visible dark brown precipitation was considered an immunoreaction. Evaluation of MMP-2 and -9 stains included the proportion of reactive cells within the tumors and the staining intensity. The proportion score described the estimated fraction of positively stained tumor cells using the following grading system: 0, <1% of positive cells; 1, 1–10% of tumors cells

stained; 2, 11–50% of tumors cells stained; 3, 51–90% of tumor cells stained; and 4, >90% of tumor cells stained. The intensity score represented the estimated staining intensity (0: no visible reaction, 1: weak, 2: moderate, and 3: strong reaction intensity). For statistical analysis, we considered the sum between intensity and number of cells. The cases were considered negatives when the sum was 0 or 1; weakly positive when the sum was between 1 and 4; and positive when the sum was higher than 4. The reactions were further analyzed according to the localization of the immunodeposits, and they were divided into two patterns of reaction: membrane staining and membrane plus cytoplasmatic staining. The pattern of MMP-2 and -9 expression was also evaluated on the adjacent nonneoplastic epithelium and in intraepithelial carcinoma areas.

Statistical analysis

Statistical analysis were done using GraphPad Prism version 4.00b for Windows, GraphPad Software, San Diego, CA, USA (http://www.graphpad.com). The data of the three groups in association with the expression of MMP-2 and -9 were analyzed by the chi-square or Fisher's exact test. Values were considered significantly different when the p value was lower than 0.05.

Results

Histological features

Among the 115 cases of surgically resected tumors analyzed, there were 28 cases with exophytic growth and pushing pattern of invasion (group 1), 50 cases with endophytic pattern of growth and invasion with large sheets of cells (group 2). There were also 37 cases with an endophytic pattern of growth and invasion in small groups of cells (group 3).

As we have pointed out in the "Materials and methods," all cases were usual SCC, and any special histological type was included. With regard to the histological grade of differentiation, all tumors in group 1 were classified as well-differentiated SCC. In the group 2, there are 18 cases of well-differentiated SCC, and 32 tumors classified as moderately differentiated. Finally, in group 3 there were 14 cases of moderately differentiated SCC, 23 poorly differentiated SCC, and no cases of well-differentiated SCC.

With regard to the invasion level, all tumors in the group 1 have superficial invasion of the *corpus spongiosum*. In the group 2, 16 out of 50 infiltrate the corpus cavernosum and the other 34 infiltrate the corpus spongiosum only. Finally, group 3 was characterized by deep invasion (*corpus cavernosum*) in 35 out 37 cases.

Immunohistochemistry

The overall results of the MMP-2 and -9 expression of the three groups are given in Table 1. Table 2 shows the distribution of the MMP-2 immunostaining according to the cell localization of the deposits.

Metaloproteinase-9 immunohistochemistry

Adjacent nonneoplastic epithelium showed a very constant feature with positively stained cells restricted to the basal layer and no stains were visualized in intermediate and superficial cells (Fig. 1a). Cases with atypical hyperplasia and intraepithelial neoplasia showed an increase of positive cells. Figure 1b,c shows a marked transition between an area of nonneoplastic epithelium and intraepithelial neoplasia The dysplastic area showed an overexpression of MMP-9 in most of the dysplastic cells. This transition area is

Table 1 Expression of MMP-9 and MMP-2 in SCC of the penis according the growth and invasion pattern

Groups	MMP-9[a]			MMP-2[b]		
	N (%)	WP (%)	P (%)	N (%)	WP (%)	P (%)
Group 1[c] (n=28)	24 (86)	4 (14)	0 (0)	3 (11)	23 (82)	2 (7)
Group 2[d] (n=50)	19 (38)	16 (32)	15 (30)	3 (6)	6 (12)	41 (82)
Group 3[e] (n=37)	4 (11)	9 (24)	24 (65)	1 (3)	3 (8)	33 (89)

N Negative, *WP* weakly positive, and *P* positive

[a] Statistical differences in MMP-9 expression (p<0.0001) and when the groups are taken in comparison (group 1 vs group 2, p=0.0001; group 1 vs group 2, p<0.0001; and group 2 vs group 3, p=0.002).

[b] Statistical differences in MMP-2 expression in the three groups was significant (p<0.0001) and when we compared group 1 against group 2 (p=0.002) and against group 3 (p<0.0001). However, there are no differences between groups 2 and 3 (p=0.6239).

[c] Penile SCC with exophytic pattern of growth and pushing borders at invasion front

[d] SCC with an endophytic pattern of growth and invasion with large sheets of cells

[e] SCC with an endophytic pattern of growth and invasion in small group of cells

Table 2 Expression of MMP-2 in SCC of the penis according to the localization of the reaction

Groups	MMP-2[a]		
	Negative (%)	Membrane (%)	Membrane+ cytoplasm (%)
Group 1[b] (n=28)	3 (11)	23 (82)	2 (7)
Group 2[c] (n=50)	3 (6)	24 (48)	23 (46)
Group 3[d] (n=37)	1 (3)	6 (16)	30 (81)

[a] The statistics tests showed differences between groups 1 and 2 (p=0.0051), groups 1 and 3 (p<0.0001), and groups 2 and 3 (p<0.004).
[b] Penile SCC with exophytic pattern of growth and pushing borders at invasion front
[c] SCC with an endophytic pattern of growth and invasion with large sheets of cells
[d] SCC with an endophytic pattern of growth and invasion in small group of cells

shown in detail in Fig. 1c. The expression of MMP-9 is upregulated on intraepithelial neoplasia foci (Fig. 1d,e). It is interesting to note that basal cells lost its MMP-9 expression and cells on the intermediate and superficial layer were strongly positive, including cells in mitosis. In the case where neoplastic cells fill all stratified epithelium (in situ carcinoma), we can observe atypical large MMP-9 positive cells replacing basal cells beside areas where some reserve basal cells still are MMP-9-negative (Fig. 1f).

Figure 2 shows examples of MMP-9 expression in all groups. All weakly positive and positive specimens showed a cytoplasmatic pattern of reaction. In the specimens from 28 tumors characterized as group 1, only 4 cases (14%) showed a weak positive cytoplasmatic reaction of MMP-9 and 24 cases (86%) showed no immunodeposits (Fig. 2a). A positive pattern was characterized by immunostaining of the inner cell layer with basal cells showing no expression in a similar pattern of some in situ carcinomas. MMP-9 expression was evident in 31/50 cases (62%) in group 2, with 15 specimens (30%) presenting a strong positive immunostaining and 19 cases (38%) showing negative reaction. In Fig. 2c we can observe the expression of MMP-9 in all tumor nests, but there is a stronger reaction on the basal layer The keratinized cells are weaker when compared with undifferentiated cells located on the basal layer. Finally, MMP-9 expression was detected in 33/37 in group 3 specimens (89%), with 24 cases (65%) showing a strong cytoplasmatic reaction (Fig. 2d–f). Figure 2d shows tumor infiltration through corpus spongiosum of the penis, and Fig. 2e,f shows a small infiltrating group of cells strongly stained with MMP-9. The observed differences in MMP-9 expression in the three groups were strongly significant (p<0.0001), and these were maintained when the groups were taken in comparison (group 1 vs group 2, p=0.0001; group 1 vs group 2, p<0.0001, and group 2 vs group 3, p= 0.002). The total number of cases in each group can be seen in Table 1.

Metaloproteinase-2 immunohistochemistry

Figure 3 shows the pattern of expression of MMP-2 in the nonneoplastic epithelium and in the intraepithelial neoplasia. Expression of MMP-2 was restricted to the cytoplasm of basal cells in a nonneoplastic mucosa and to intermediate cells, which showed a weakly positive expression (Fig. 3a). In the hyperplastic epithelium the number of positive cells increased with the degree of hyperplasia as shown in Fig. 3b. It is interesting to note that the expression pattern changes from cytoplasmatic to membrane stain in more superficial cells. When the mucosa begins to present atypical cells and architectural modifications, there is a layer of undifferentiated cells just above the basal layer (proliferative compartment) in which there is no expression of MMP-2 (Fig. 2b). This aspect can be observed in detail in Fig. 3c. In areas of carcinoma in situ (Fig. 3d), proliferating cells, which constitute the basal layer, do not express MMP-2. However, when the cells are differentiated by superficial layers, they acquire the ability to express MMP-2 in a membrane pattern. This pattern is very similar to what was shown with MMP-9 immunostains.

Figure 4 shows the pattern of MMP-2 expression in the different groups, and the number of cases expressing MMP-2 in each group is demonstrated in Table 1. Immunoreactivity for MMP-2 was detected in tumor cells in the great majority of the tumors. In the specimens from 28 tumors characterized as group 1, MMP-2 expression was observed in 25/28 cases (91%). However, all but two showed a weak positive immunoreaction (Fig. 4a,b). MMP-2 expression was evident in 46/50 cases (62%) in the group 2 but, different from the group 1 tumors, the majority of the specimens showed strong positive reaction (41/50) and only six cases showed the same pattern of weakly positive deposits (Fig. 4c,d). The immunoreaction observed in the group 3 tumors was quite similar to what was observed in group 2 tumors having 36/37 positive tumors and 33 of them with a strong positive reaction (Fig. 4e,f). The observed differences in MMP-2 expression in the three groups were significant (p<0.0001) and when we compared group 1 against group 2 (p=0.002) and against group 3 (p<0.0001); nevertheless there are no differences between groups 2 and 3 (p=0.6239).

The cell localization of MMP-2 immunoreaction was significantly different between the groups (Table 2, p<0.0001). In the group 1 specimens, almost all positive cases showed a very well-defined membrane pattern with only two cases where the deposits could be identified in the cytoplasm. These two cases are the same ones that

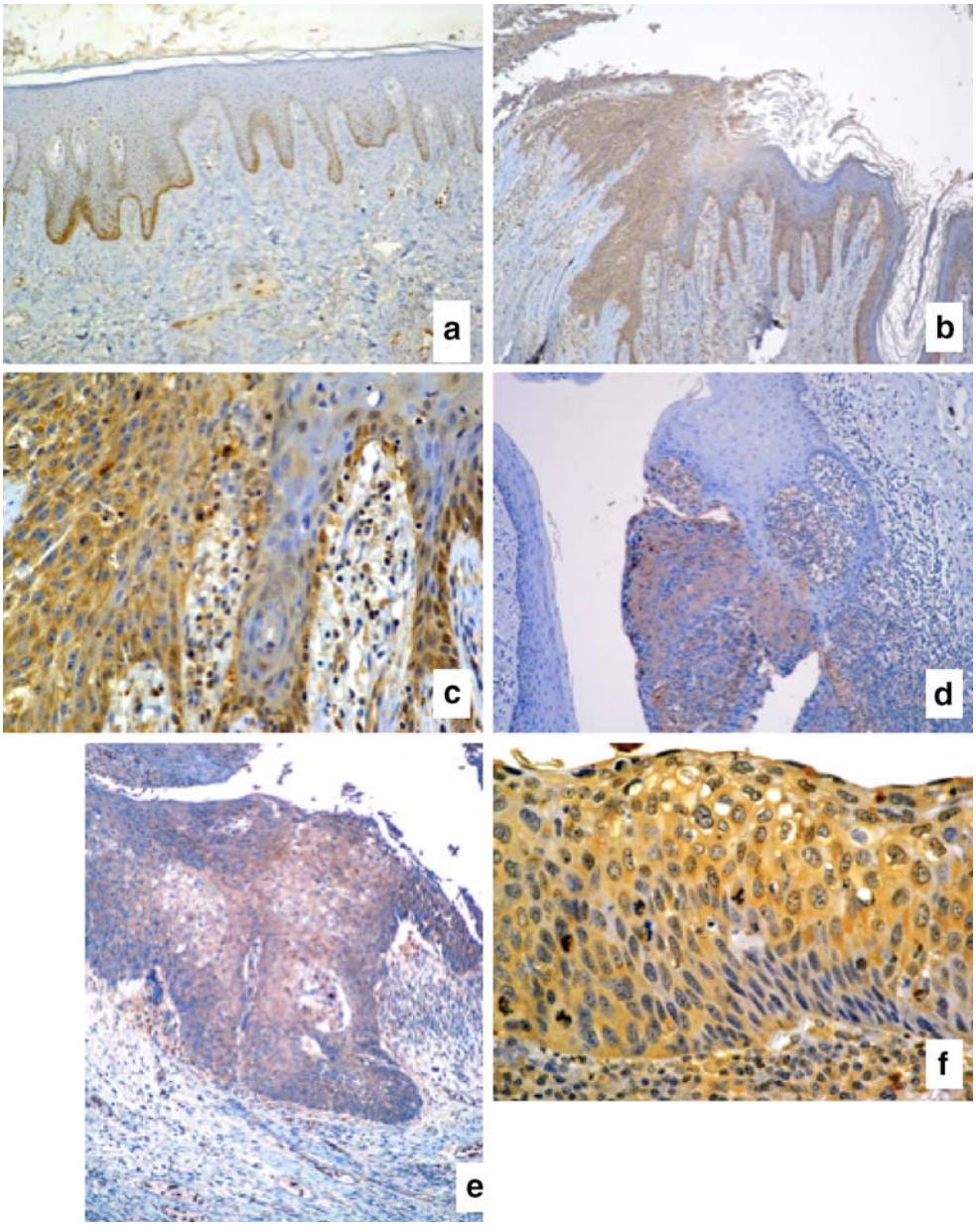

Fig. 1 Expression of MMP-9 in nonneoplastic epithelium, hyperplastic epithelium, and intraepithelial neoplasm. In nonneoplastic mucosa, positive cells are restricted to the basal layer (**a**). **b** and **c** Transition between nonneoplastic epithelium and dysplastic epithelium with a marked increase of MMP-9 expression. Expression of MMP-9 is upregulated in intraepithelial neoplasia foci (**d**, **e**), but basal cells lost MPP-9 expression. **f** Intraepithelial neoplasia where most of the cells are MMP-9-positive. At the *lower right corner*, note how reserve basal cells do not express MMP-9, similar to dysplastic epithelium

showed a strong positive reaction. As we pointed out before, although there were no differences in the number of specimens with the expression of MMP-2 between tumors of groups 2 and 3, the pattern of reaction was completely different. From the 47 positive cases of the group 2, 24 cases exclusively showed a membrane expression, and the other 23 also showed a cytoplasmatic stain (Fig. 4d). In group 3, from 36 positive cases, only 6 specimens showed a membrane pattern and in the 30 remaining cases we could detect membrane plus cytoplasm stain (Fig. 4e). The reaction was even stronger in deeper invasive tumor cells nests (Fig. 4f). The statistics tests showed differences between groups 1 and 2 ($p=0.0051$), groups 1 and 3 ($p<0.0001$), and groups 2 and 3 ($p<0.004$).

Discussion

SCC of the penis is a major problem in developing countries, with emphasis in Central and South America [7]. In Brazil, it is a common tumor especially in the Northeast area of the country, and it is highly associated with cervical cancer incidence [1].

The great majority of penile cancers are usually SCC but they have a heterogenous pattern of growth. They should be separated from “verruciform” tumors. The latter includes several histological types such as giant condyloma acuminatum, warty (condylomatous carcinomas) and verrucous carcinomas, and papillary SCCs. The pattern of growth in usually SCC of the penis, and consequently the depth of invasion are an important prognostic determinant [11, 27].

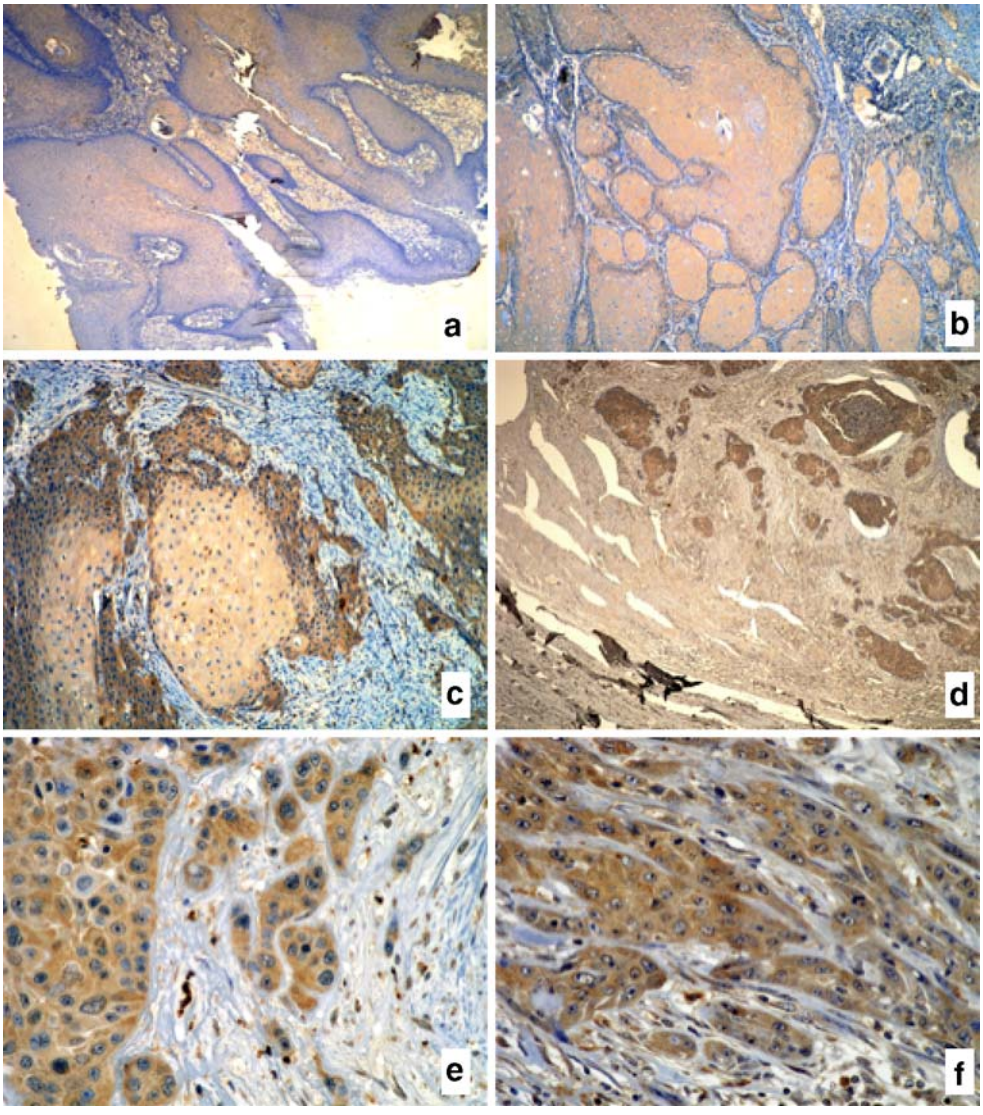

Fig. 2 Weak positive reaction was observed in exophytic tumors, and only in superficial cells in a similar pattern observed in dysplastic epithelium (**a**). Tumors with pushing borders at the invasion front show expression of MMP-9, but basal layer expression is stronger than in the superficial cells (**b**, **c**). Groups 2 and 3 overexpressed MMP-9 in the invasive front, especially in a small group of tumor cells, as demonstrated in subpanels **d**, **e**, and **f**

Other important factors to predict the final outcome are histological differentiation and vascular invasion [12, 13, 27]. In this paper, we classify cases of penile SCC by the invasion pattern. Similar grading systems, using a combination of tumor grade and depth of invasion, were proposed before and so far they showed a good correlation with lymph node metastasis and mortality index [4, 28, 33].

Although these growth and invasion patterns are well recognized, there is no paper in the literature addressing why some tumors have a more infiltrative pattern of invasion with usually a consequently worse prognosis, and why others have pushing and not infiltrative borders and behave more indolently. Recently, our group demonstrated that MPP-9 expression is an independent risk factor for disease recurrence [17], and invasion pattern of small group of cells are important to determine the risk of lymph node metastases [20]. In the present study, we were able to demonstrate that the expression of MMP-2 and -9 are different according to the growth and invasion patterns. The importance of MMPs and its inhibitors in tumor biology are well known and several clinical trials trying to inhibit their action are currently on progress. However, the first results are quite disappointing [31]. MMPs are proteolytic enzymes that regulate several cell functions, which are important to the genesis of neoplasms, to the progression and biological behavior as cell growth, differentiation, apoptosis, migration, and invasion, and to the regulation of tumor angiogenesis and immune surveillance [10]. In tumors with exophytic pattern of growth and pushing borders, we have observed a less frequent expression of MMP-2 and -9 in contrast with flat and highly invasive tumors. Also, the histological grade and deepness of invasion correlated very consistently with the growth/invasion pattern. Almost all exophytic tumors were well-differentiated SCC, with pushing borders, do not invade corpus cavernosum and do not overexpress MMPs. For the other side, poorly differentiated tumors with invasion pattern of small group of cells frequently invade deeply

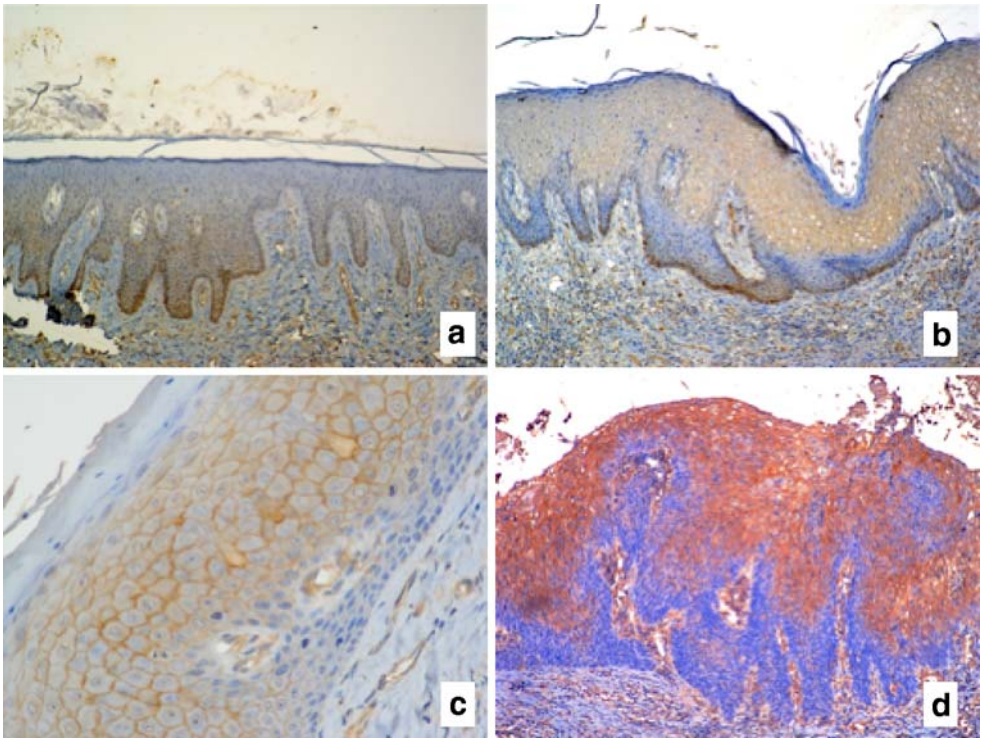

Fig. 3 Expression of MMP-2 was restricted to cytoplasm of the basal cells in nonneoplastic mucosa (**a**). There is an increase of the number of cells expressing MMP-2 in the hyperplastic epithelium (**b**). In contrast with basal cells, superficial cells show a membrane pattern of MMP-2 expression (**c**). In areas of carcinoma in situ (**d**), proliferating cells do not express MMP-2, and there is an overexpression of superficial cells in a membrane pattern

(corpus cavernosum) and overexpress basal membrane MMPs. Therefore, the ability to degrade basal membrane determined by expression/activation of MMP-2 and -9 is a characteristic of less-differentiated tumors, and this fact might be one of the causes that determine whether a penile SCC is locally aggressive.

Another interesting point was to observe the pattern of expression of MMP-2 and -9 during tumor progression. MMP-9 expression is restricted to a basal layer of the epithelium in normal and hyperplasia without atypia and when the severity of the lesion evolves, more superficial cells overexpress MMP-9. One very interesting observation was that undifferentiated basal cells in high-grade lesions are negative. However, atypical cells, including those in mitosis, strongly expressed MMP-9 (Fig. 1f). This observation creates a hypothesis that basal membrane degradation occurs only when all epithelial layers are replaced by neoplastic cells, with high capacity of gelatinases expression. Low-grade and superficially invasive tumors mimic this pattern of expression of MMP-9 (Fig. 2a). Immunoexpression of MMP-9 in basal cells of cervical [3, 14], skin [23], and bronchial hyperplastic epithelium [15], with the intensity and frequency in intraepithelial carcinoma increasing, was demonstrated previously by other authors. However, they had not been correlated with the pattern of invasion. Davidson et al. [8] demonstrated MMP-9 expression in only half of the cases of cervical intraepithelial neoplasia, but the authors did not report low-grade lesions. Another evidence that MMP levels are correlated with tumor progression was provided by Jordan et al. [22]. These authors examined changes in MMP-1, -2, and -9 mRNA expression in 34 oral dysplasias, in which 19 of them had progressed to invasive cancer. The levels of MMP-9 and -1 mRNA in oral mucosa dysplasia that progressed to oral cancer were higher than in cases of oral mucosa dysplasia that did not progressed to SCCs. Besides that, both groups had lower levels when compared to invasive SCCs [22].

One of the most striking findings in our study was the membrane expression of MMP-2 in dysplastic and well-differentiated lesions. MMP-2 is a secreted form of MMP, and it is not a membrane-MMP. Membrane MMPs are covalently linked to the cell membrane and the members of this family includes MMP-14, -15, -16, -17, -24, and -25. The secreted MMPs can also be localized in the cell surface by bindings to integrins [2] or to CD44 [40, 41]. There is also the possibility of interactions with cell-surface-associated molecules and with extracellular MMPs inducer, among others [34]. Therefore, membrane expression of MMP-2 in dysplastic and well-differentiated tumors may indicate the integrity of the MMP–integrin complex. As the tumor progresses and becomes more aggressive and invasive, the secreted MMP-2 is seen on the cytoplasm plus membrane staining. Another possible explanation is that all MMP are secreted in an inactivated form and after cleavage they become enzymatically active. MMPs are active during the early stages of tumorigenesis, contributing to the formation of a microenvironment that promotes extracellular matrix and basal membrane degradation. The antibodies used in the present study recognize both form of

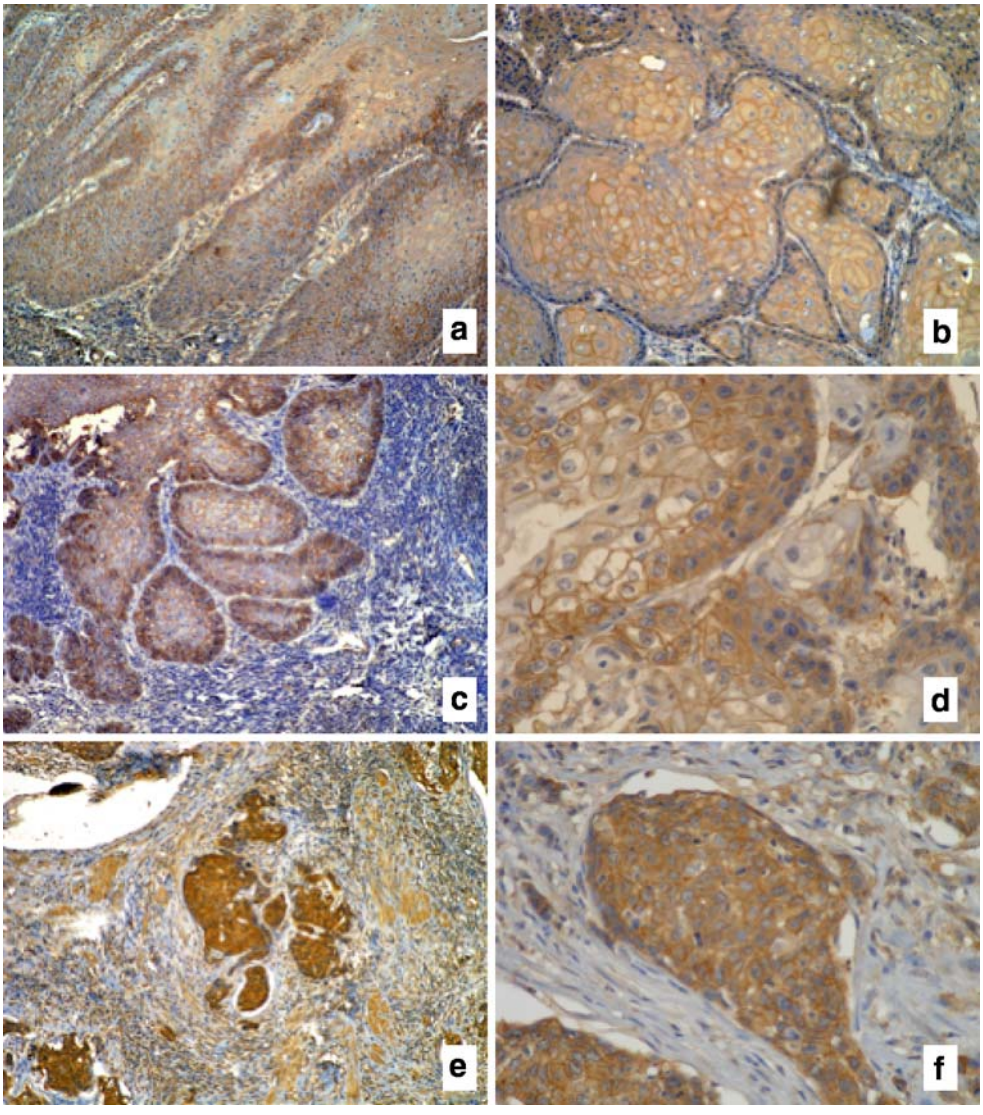

Fig. 4 Expression of MMP-2 in SCCP. **a**, **b** Expression of MMP-2 in exophytic tumors in a membrane pattern on superficial cells and negative on basal cells. **c**, **d** Expression of MMP-2 in tumors with pushing borders at the invasive front, mainly on the superficial layer and weak expression in basal cells. **e**, **f** MMP-2 expression in tumors of groups 2 and 3. All tumor cells overexpress MMP-2 localized in the cell's membrane and cytoplasm

MMP-2 and -9, noncleaved and cleaved. It is possible that the dramatic change from membrane staining in intraepithelial lesions and less invasive tumors to cytoplasmatic pattern in frankly invasive lesions represents the enzyme activation phenomenon. But further studies using functional assays are necessary to clarify this point.

Our results demonstrated a correlation between growth and invasion patterns and the overexpression of MMP-2 and -9. Isolated cells and small groups of invasive cells overexpressed both gelatinases when compared with tumors characterized by exophytic growth and pushing borders at invasion front. Several papers have correlated the pattern of invasion in SCC and overexpression of MMPs. Kurahara et al. [24] studied 96 biopsies from patients with SCC of the oral mucosa. The cases were classified into four groups according to the pattern of invasion. The authors found out that there is a strong relationship between the pattern of invasion and expression of the MMP-2 and -9, with overexpression of the enzymes in the most aggressive tumors, which is similar with the results obtained in the present study. A similar result was obtained by O'Charoenrat et al. [29] who analyzed SCC from several primary sites of the head and neck. In this paper, the authors only found a relation with the invasive pattern for MMP-9 mRNA levels, and did not do so for MMP-1, -2, -7, and -11 [29]. Also, in esophagus carcinomas the expression of MMP-9 was more frequent in tumors, which were deeply invasive [30]. There is a lot of controversy about the expression of MMP-2 and -9 and histological grade. We demonstrated that in penile SCC the expressions of MMP-2 and -9 are usually less-differentiated and locally aggressive.

It is very disappointing how there are only few papers that address the molecular aspects of the penile SCC in contrast to SCC from other primary sites. Papers analyzing even the most common molecules involved with carcinogenesis and tumor progression are scarce in the literature. We know almost nothing about penile SCC genetics and molecular markers, especially when we compare the

knowledge about SCCs from other sites, such as cervical and head/neck tumors. Further studies are necessary for a better understanding of the molecular particularities and to establish the prognostic factors in this rare, but very important neoplasm.

Acknowledgements The authors would like to acknowledge Mr. Renato Soares for the English grammar review, and Mr. Carlos Ferreira Nascimento and Mr. Severino Ferreira for their technical assistance.

References

1. Bosch FX, Cardis E (1990) Cancer incidence correlations: genital, urinary and some tobacco-related cancer. Int J Cancer 49:178–184
2. Brooks PG, Stromblad S, Sanders LC, von Schalscha TL, Aimes RT, Stetler-Stevenson WG, Quigley JP, Cheresh DA (1996) Localization of matrix metalloproteinase MMP-2 to the surface of invasive cells by interaction with integrin alpha v beta 3. Cell 85:683–693
3. Brummer O, Bohmer G, Hollwitz B, Flemming P, Petry KU, Kuhnle H (2002) MMP-1 and MMP-2 in the cervix uteri in different steps of malignant transformation—an immunohistochemical study. Gynecol Oncol 84:222–227
4. Cubilla AL, Caballero C, Piris A, Reuter VE, Alcabes P (2000) Prognostic index (PI): a novel method to predict mortality in squamous cell carcinoma of the penis. Lab Invest 80:97A
5. Cubilla AL, Velazques EF, Reuter VE, Esther O, Mihm MCJ, Young RH (2000) Warty (condylomatous) squamous cell carcinoma of the penis: a report of 11 cases and proposed classification of "verruciform" penile tumors. Am J Surg Pathol 24:505–512
6. Cubilla AL, Piris A, Pfanni R, Rodriguez I, Agüero F, Young RH (2001) Anatomic levels: important landmarks in penectomy specimens: a detailed anatomic and histologic study based on examination of 44 cases. Am J Surg Pathol 25:1091–1094
7. Cubilla AL, Ayala G, Dillner J, Reuter VE, Schellhammer PF, Von Krogh G, Horenblas S (2004) Malignant epithelial tumors of the penis. In: Eble JN, Sauter G, Epstein JI, Sesterhenn IA (eds) World Health Organization classification of tumors. Pathology and genetics. Tumors of the urinary system and male genital organs. IARC Press, Lyon, France, pp 281–290
8. Davidson B, Goldberg I, Kopolovic J, Lerner-Geva L, Gotlieb WH, Weis B, Ben-Baruch G, Reich R (1999) Expression of matrix metalloproteinase-9 in squamous cell carcinoma of the uterine cervix—clinicopathologic study using immunohistochemistry and mRNA in situ hybridization. Gynecol Oncol 72:380–386
9. de Vicente JC, Fresno MF, Villalain L, Vega JA, Hernandez VG (2005) Expression and clinical significance of matrix metalloproteinase-2 and matrix metalloproteinase-9 in oral squamous cell carcinoma. Oral Oncol 41:283–293
10. Egeblad M, Werb Z (2002) New functions for the matrix metalloproteinases in cancer progression. Nat Rev Cancer 2:161–174
11. Emerson RE, Ulbright TM, Eble JN, WA G, Eckert GJ, Cheng L (2001) Predicting cancer progression in patients with penile squamous cell carcinoma: the importance of depth of invasion and vascular invasion. Mod Pathol 14:963–968
12. Ficarra V, Martignoni G, Maffei N, Cerruto MA, Novara G, Cavalleri S, Artibani W (2002) Predictive pathological factors of lymph nodes involvement in the squamous cell carcinoma of the penis. Int Urol Nephrol 34:245–250
13. Ficarra V, Zattoni F, Cunico SC, Galleti TP, Luciani L, Fandella A, Guazzieri S, Maruzzi D, Sava T, Siracusano S, Pilloni S, Tasca A, Martignoni G, Gardiman M, Tardanico R, Zambolin T, Cisternino A, Artibani W, Gruppo Uro-Oncologico del Nord Est (Northeast Uro-Oncological Group) Penile Cancer Project (2005) Lymphatic and vascular embolizations are independent predictive variables of inguinal lymph node involvement in patients with squamous cell carcinoma of the penis: Gruppo Uro-Oncologico del Nord Est (Northeast Uro-Oncological Group) Penile Cancer data base. Cancer 103:2507–2516
14. Gaiotto MA, Focchi J, Ribalta JL, Stavale JN, Baracat EC, Lima GR, Guerreiro da Silva ID (2004) Comparative study of MMP-2 (matrix metalloproteinase 2) immune expression in normal uterine cervix, intraepithelial neoplasias, and squamous cells cervical carcinoma. Am J Obstet Gynecol 190:1278–1282
15. Galateau-Salle FB, Luna RE, Horiba K, Sheppard MN, Hayashi T, Fleming MV, Colby TV, Bennett W, Harris CC, Stetler-Stevenson WG, Liotta L, Ferrans VJ, Travis WD (2000) Matrix metalloproteinases and tissue inhibitors of metalloproteinases in bronchial squamous preinvasive lesions. Hum Pathol 31:296–305
16. Garzetti GG, Ciavattini A, Lucarini G, Goteri G, Romanini C, Biagini G (1996) The 72-kDa metalloproteinase immunostaining in cervical carcinoma: Relationship with lymph node involvement. Gynecol Oncol 60:271–276
17. Guimarães GC, Lopes A, Campos RSM, Zequi SC, Leal MLO, Carvalho AL, Cunha IW, Soares FA (2006) Front pattern of invasion in squamous cell carcinoma of the penis: new prognostic factor for predicting risk of lymph node metastases. J Urol 68:148–153
18. Guttman D, Stern Y, Shpitzer T, Ulanovski D, Druzd T, Feinmesser R (2004) Expression of MMP-9, TIMP-1, CD-34 and factor-8 as prognostic markers for squamous cell carcinoma of the tongue. Oral Oncol 40:798–803
19. Hong SD, Hong SP, Lee JI, Lim CY (2000) Expression of matrix metalloproteinase-2 and -9 in oral squamous cell carcinomas with regard to the metastatic potential. Oral Oncol 36:207–213
20. Imanishi Y, Fujii M, Tokumaru Y, Tomita T, Kanke M, Kanzaki J, Kameyama K, Otani Y, Sato H (2000) Clinical significance of expression of membrane type 1 matrix metalloproteinase and matrix metalloproteinase-2 in human head and neck squamous cell carcinoma. Hum Pathol 31:895–904
21. Ishibashi Y, Matsumoto T, Niwa M, Suzuki Y, Omura N, Hanyu N, Nakada K, Yanaga K, Yamada K, Ohkawa K, Kawakami M, Urashima M (2004) CD147 and matrix metalloproteinase-2 protein expression as significant prognostic factors in esophageal squamous cell carcinoma. Cancer 101:1994–2000
22. Jordan RC, Macabeo-Ong M, Shiboski CH, Dekker N, Ginzinger DG, Wong DT, Schmidt BL (2004) Overexpression of matrix metalloproteinase-1 and -9 mRNA is associated with progression of oral dysplasia to cancer. Clin Cancer Res 10:6460–6465
23. Kobayashi T, Onoda N, Takagi T, Horl H, Hattori S, Nagai Y, Tajima S, Nishikawa T (1996) Immunolocalizations of human gelatinase (type IV collagenase, MMP-9) and TIMP (tissue inhibitor of metalloproteases) in normal epidermis and some epidermal tumors. Arch Dermatol Res 288:239–244
24. Kurahara S-I, Shinohara M, Ikebe T, Nakamura S, Beppu M, Hiraki A, Takeuchi H, Shirasuna K (1999) Expression of MMPs, MT-MMP, and TIMPs in squamous cell carcinoma of the oral cavity: correlations with tumor invasion and metastasis. Head Neck 21:627–638
25. Kusukawa J, Sasaguri Y, Shima I, Kameyama T, Morimatsu M (1993) Expression of matrix metalloproteinase-2 related to lymph node metastasis of oral squamous cell carcinoma. A clinicopathologic study. Am J Clin Pathol 99:18–23
26. Liu WW, Zeng ZY, Wu QL, Hou JH, Chen YY (2005) Overexpression of MMP-2 in laryngeal squamous cell carcinoma:

a potential indicator for poor prognosis. Otolaryngol Head Neck Surg 132:395–400
27. Lopes A, Hidalgo GS, Kowalski LP, Torloni H, Rossi BM, Fonseca FP (1996) Prognostic factors in carcinoma of the penis: multivariate analysis of 145 patients treated with amputation and lymphadenectomy. J Urol 156:1637–1642
28. McDougal WS (1995) Carcinoma of the penis: improved survival by early regional lymphadenectomy based on the histological grade and depth of invasion of the primary lesion. J Urol 154:1364–1366
29. O'Charoenrat P, Rhys-Evans PH, Eccles SA (2001) Expression of matrix metalloproteinases and their inhibitors correlates with invasion and metastasis in squamous cell carcinoma of the head and neck. Arch Otolaryngol Head Neck Surg 127:813–820
30. Ohashi K, Nemoto T, Nakamura K, Nemori R (2000) Increased expression of matrix metalloproteinase 7 and 9 and membrane type 1-matrix metalloproteinase in esophageal squamous cell carcinomas. Cancer 88:2201–2209
31. Overall CM, López-Otin C (2002) Strategies for MMP inhibition in cancer: innovations for the post-trial era. Nat Rev Cancer 2:657–672
32. Pinto CA, Carvalho PE, Antonangelo L, Garippo A, da Dilva AG, Soares F, Younes R, Beyruti R, Takagaki T, Saldiva P, Vollmer RT, Capelozzi VL (2003) Morphometric evaluation of tumor matrix metalloproteinase 9 predicts survival after surgical resection of adenocarcinoma of the lung. Clin Cancer Res 9:3098–3104
33. Solsona E, Ibarra I, Rubio J, Casanova JL, Ricos JV, Calabulg C (2001) Prospective validation of the association of local tumor stage and grade as a predictive factor for occult lymph node micrometastasis in patients with penile carcinoma and clinically negative lymph nodes. J Urol 165:1506–1509
34. Stemlicht MD, Werb Z (2001) How matrix metalloproteinases regulates cell behaviour. Annu Rev Cell Dev Biol 17:463–516
35. Tokuraku M, Sato H, Murakami S, Okada Y, Watanabe Y, Seiki M (1995) Activation of the precursor of gelatinase A/72 kDa type IV collagenase/MMP-2 in lung carcinomas correlates with the expression of membrane-type matrix metalloproteinase (MT-MMP) and with lymph node metastasis. Int J Cancer 64:355–359
36. Velazques EF, Cubilla AL (2003) Lichen sclerosus in 68 patients with squamous cell carcinoma of the penis: frequent atypias and correlation with special carcinoma variants suggests a precancerous route. Am J Surg Pathol 27:1448–1453
37. Velazques EF, Melamed J, Barreto JE, Agüero F, Cubilla AL (2005) Sarcomatoid carcinoma of the penis: a clinicopathologic study of 15 cases. Am J Surg Pathol 29:1152–1158
38. Yorioka CW, Coletta RD, Alves F, Nishimoto IN, Kowalski LP, Graner E (2002) Matrix metalloproteinase-2 and -9 activities correlate with the disease-free survival of oral squamous cell carcinoma patients. Int J Oncol 20:189–194
39. Yoshizaki T, Maruyama Y, Sato H, Furukawa M (2001) Expression of tissue inhibitor of matrix metalloproteinase-2 correlates with activation of matrix metalloproteinase-2 and predicts poor prognosis in tongue squamous cell carcinoma. Int J Cancer 95:44–50
40. Yu Q, Stamenkovic I (1999) Localization of matrix metalloproteinase 9 to the cell surface provides a mechanism to CD44-mediated tumor invasion. Genes Dev 13:35–48
41. Yu W-H, Woessne JFJ, McNeish JD, Stamenkovic I (2002) CD44 anchors the assembly of matrilysin/MMP-7 with heparan-binding epidermal growth factor precursor and ErbB4 and regulates female reproductive organ remodeling. Genes Dev 16:307–323

19, 22, 23, 26, 30]. It is likely that T3N0 patients with few (six to nine) lymph nodes recovered should be considered at a high risk for missing positive nodes, and adjuvant therapy can be advised [6, 18, 26]. Over time, several authors have proposed a different number of lymph nodes, ranging from 6 to 17 [5, 9, 12, 13, 21, 24], but the tumor–node–metastasis (TNM) system recommends that at least 12 lymph nodes is a sufficient number for an accurate identification of regional metastatic disease [25].

The aim of the present paper was to establish if the 12 lymph nodes recommended by TNM is a sufficient number for a correct staging system of rectal cancer. Previous studies about the minimum number of lymph nodes to be recovered in colorectal cancer have been performed using retrospective analysis and statistical correlation between the number of lymph nodes detected for each specimen and the number of metastases discovered [1, 5, 9, 10, 20, 27]. Conversely, we first planned a prospective study that compared the mean number of lymph nodes recovered in the same surgical specimen at two different moments: the routine sampling and the resampling performed by a second pathologist with expertise in gastrointestinal pathology. The study was performed on 50 cases of patients with pT2N0 and pT3N0 rectal cancer, with a minimum number of 12 lymph nodes recovered at first sampling, histologically proven to be negative for metastases. A correlation was made between the total mean number of lymph nodes recovered, the number of metastases disclosed, and the original pTN stage. The present study first showed that 18.7% of pT3 patients with rectal cancer had been understaged if less than 26 lymph nodes had been recovered.

Materials and methods

Between January 2001 and December 2005, two surgical pathologists of different institutions (Istituto Nazionale per lo Studio e la Cura dei Tumori of Milan and San Luigi–Santi Currò Hospital of Catania), with expertise in gastrointestinal pathology (S.A. and P.G.), performed a resampling of the perirectal adipose tissue from 50 cases of pT2 and pT3 rectal adenocarcinomas (mid and lower one third of the rectum) to ascertain if some lymph nodes had been previously missed at first sampling. The cases to be resampled were selected on the basis of the following strict criteria:

(1) All patients underwent rectal resection with total mesorectal excision.
(2) The sampling of surgical specimens was performed according to the guidelines for rectal cancer, including the examination of the distal resection margin and the circumferential resection margin of the mesorectum, the latter by sampling a 1-mm-thick slice of adipose tissue from the whole surface of this margin [2].
(3) Only tumors with a minimum number of 12 lymph nodes recovered routinely by manual dissection and later proven to be histologically negative for metastasis were included in the study.

In practice, surgical specimens are sent unfixed to a pathologist, opened longitudinally, straightened without stretching, and pinned to a corkboard. All surgical samples were fixed in 10% buffered formalin for 24 h. Lymph nodes were isolated by manual dissection without fat-clearing technique, as it has been shown to be a reliable and

Table 1 Comparison between the number of lymph nodes recovered, metastasis detection, and pN-staging before and after the second sampling in patients with pT2 rectal cancer

Case number	1° Sampling Met./LNs	pTN	2° Sampling Met./LNs	Met./total LNs	Final stage
1	0/16	pT2 N0	0/8	0/24	pT2 N0
2	0/33	pT2 N0	0/6	0/39	pT2 N0
3	0/12	pT2 N0	0/5	0/17	pT2 N0
4	0/13	pT2 N0	0/14	0/27	pT2 N0
5	0/15	pT2 N0	0/8	0/23	pT2 N0
6	0/20	pT2 N0	0/10	0/30	pT2 N0
7	0/12	pT2 N0	0/4	0/16	pT2 N0
8	0/25	pT2 N0	0/3	0/28	pT2 N0
9	0/19	pT2 N0	0/14	0/33	pT2 N0
10	0/17	pT2 N0	0/10	0/27	pT2 N0
11	0/17	pT2 N0	0/8	0/25	pT2 N0
12	0/13	pT2 N0	0/5	0/18	pT2 N0
13	0/35	pT2 N0	0/1	0/36	pT2 N0
14	0/17	pT2 N0	0/1	0/18	pT2 N0
15	0/32	pT2 N0	0/3	0/35	pT2 N0
16	0/23	pT2 N0	0/4	0/27	pT2 N0
17	0/14	pT2 N0	0/7	0/21	pT2 N0
18	0/12	pT2 N0	0/10	0/22	pT2 N0

Met. Number of metastatic lymph nodes, *LNs* number of lymph nodes recovered

reproducible technique [1, 3, 20]. After the routinary sampling by one of the pathologists of the two different anatomical pathology sections, the residual perirectal adipose tissue of each case in which at least 12 lymph nodes had been recovered was maintained in formalin. Histological examination of lymph nodes was routinely conducted without performing serial sections. Only the cases histologically proven to be negative for lymph node metastases were selected, and the corresponding residual perirectal adipose tissue was retrieved from formalin and resampled by the two different pathologists (one for each institution) with expertise in gastrointestinal pathology. Definitive histological diagnosis was delayed for 24–36 h and rendered after performing the second sampling. The pathologic stage of the entire series (first + second sampling) was defined according to the TNM system [25]. Distal and circumferential margins were tumor-free in all cases selected. All patients are still in follow-up.

Results

The routinely pathologic sampling of the 50 surgical specimens selected revealed that 18 tumors were pT2N0, and the remaining 32 tumors were pT3N0 (Tables 1 and 2). The median number of lymph nodes from the first routine sampling was 19.1 (range 12–35) and 17.8 (range 12–33) in the pT2N0 and pT3N0 group, respectively (Table 3).

In all cases, the pathologist performing the second manual sampling identified new lymph nodes that had been previously missed, with a number varying from 1 to 24 lymph nodes (Tables 1 and 2). The maximum number of lymph nodes missed in a single surgical specimen at the first sampling was 14 in the T2 group and 24 in the T3 group (Tables 1 and 2). The total (first + second sampling) mean number of lymph nodes recovered was 25.8 (range 16–39) for the T2 group and 26.8 (range 13–39) for the T3 group (Table 3).

Table 2 Comparison between the number of lymph nodes recovered, metastasis detection, and pN-staging before and after the second sampling in patients with pT3 rectal cancer

Case number	1° Sampling Met./LNs	pTN	2° Sampling Met./LNs	Met./total LNs	Final stage	∅ Metastatic lymph nodes (mm)	∅ Metastases
1	0/13	pT3 N0	1/21	1/34	pT3 N1	4.6	3 mm
2	0/14	pT3 N0	1/11	1/25	pT3 N1	4.9	3.2 mm
3	0/18	pT3 N0	1/5	1/23	pT3 N1	3.4	2.5 mm
4	0/19	pT3 N0	1/10	1/29	pT3 N1	4.8	2.7 mm
5	0/25	pT3 N0	1/11	1/36	pT3 N1	2.4	2.4 mm
6	0/12	pT3 N0	1/8	1/20	pT3 N1	2.4	1.8 mm
7	0/13	pT3 N0	0/12	0/25	pT3 N0	–	
8	0/12	pT3 N0	0/14	0/26	pT3 N0	–	
9	0/12	pT3 N0	0/1	0/13	pT3 N0	–	
10	0/19	pT3 N0	0/3	0/22	pT3 N0	–	
11	0/22	pT3 N0	0/15	0/37	pT3 N0	–	
12	0/12	pT3 N0	0/5	0/17	pT3 N0	–	
13	0/12	pT3 N0	0/4	0/16	pT3 N0	–	
14	0/12	pT3 N0	0/9	0/21	pT3 N0	–	
15	0/12	pT3 N0	0/9	0/21	pT3 N0	–	
16	0/24	pT3 N0	0/6	0/30	pT3 N0	–	
17	0/21	pT3 N0	0/12	0/33	pT3 N0	–	
18	0/16	pT3 N0	0/22	0/38	pT3 N0	–	
19	0/33	pT3 N0	0/1	0/34	pT3 N0	–	
20	0/22	pT3 N0	0/11	0/33	pT3 N0	–	
21	0/18	pT3 N0	0/21	0/39	pT3 N0	–	
22	0/22	pT3 N0	0/10	0/32	pT3 N0	–	
23	0/20	pT3 N0	0/5	0/25	pT3 N0	–	
24	0/28	pT3 N0	0/11	0/39	pT3 N0	–	
25	0/13	pT3 N0	0/5	0/18	pT3 N0	–	
26	0/30	pT3 N0	0/2	0/32	pT3 N0	–	
27	0/14	pT3 N0	0/24	0/38	pT3 N0	–	
28	0/24	pT3 N0	0/8	0/32	pT3 N0	–	
29	0/12	pT3 N0	0/1	0/13	pT3 N0	–	
30	0/12	pT3 N0	0/2	0/14	pT3 N0	–	
31	0/18	pT3N0	0/5	0/23	pT3N0		
32	0/17	pT3N0	0/4	0/21	pT3N0		

Met. Number of metastatic lymph nodes, *LNs* number of lymph nodes recovered, ∅ maximum diameter

Table 3 Correlation between mean number of lymph nodes of the first and second sampling with pN-stage

PT stage	Mean number of LNs (1° sampling)	pN-Stage	Mean number of LNs (1°+2° sampling)	Final pN-stage
T2 (18 pts)	19.1 (range 12–35)	N0	25.8 (range 16–39)	N0 (18 pts)
T3 (32 pts)	17.8 (range 12–33)	N0	26.8 (range 13–39)	N0 (26 pts) N1 (6 pts)

pts Number of patients, *LNs* number of lymph nodes recovered

No metastasis was found in the lymph nodes recovered in the second sampling of patients with pT2 stage (Tables 1 and 3), whereas lymph node metastasis was detected in 6 out of 32 (18.7%) patients with pT3 stage (Tables 2 and 3). Accordingly, the overall final pN stage remained unchanged in 88% of patients and, more specifically, in 100% of pT2 and 81.3% of pT3 patients (Tables 1, 2 and 3). In the pT3N1 patients, the second sampling increased the mean number of lymph nodes recovered from 16.6 (range 12–25) to 27.8 (range 20–36; Table 4). Notably, only one metastatic lymph node was detected for each single case of this subgroup (Table 2). The maximum diameter of the single metastatic lymph node, measured on the histological slide by micrometer ocular, was 4.9 mm (2.4 to 4.9 mm; Table 2).

Residual lymphatic tissue was identified in five out of six metastatic cases. Metastasis size, measured on the histological slide by micrometer ocular, ranged from 1.8 to 3.2 mm (Table 2). Only in one case was a small (2.4 mm) round-shaped neoplastic nodule in the perirectal tissue interpreted as lymph node metastasis according to the TNM system [25].

It was noteworthy that most of the cases (five out of six) with missed metastatic lymph nodes were detected in specimens in which a maximum number of 19 lymph nodes had been previously recovered at the first sampling (Table 2).

Discussion

It is widely known that a meticulous search of lymph nodes in the perirectal adipose tissue is crucial for a correct staging system. In all cases of the present series of rectal adenocarcinomas, we first showed that, even if at least 12 lymph nodes are identified during the first routine sampling, a variable number of lymph nodes, ranging from 1 to 24, are missed. Although this finding seems to be alarming, we point out that a correct overall pN stage, including pT2 and pT3 patients, was achieved in a high percentage of cases (88%) at the first routine manual dissection. All pT2 patients maintained their pN0 stage despite the mean number of lymph nodes recovered increased from 19.1 (first sampling) to 25.8 (second sampling). This could be explained by a lower metastatic biological potential for pT2 colorectal cancers, indicating that these tumors can be correctly staged with 12 lymph nodes recovered.

In regard to pT3 patients, we showed that there is an 18.7% chance of identifying metastatic lymph nodes if the mean number of lymph nodes recovered in the same surgical specimens increased from 17.8 at the first sampling to 26.8 after the second sampling. The mean number 26.8 of lymph nodes in our study is near to that obtained by Leibl et al. [20] who found that 80 and 90% of specimens with lymph node metastases had 26 (or fewer) and 30 (or fewer) lymph nodes recovered, respectively. Notably, the above-mentioned study of Leibl et al. and our present findings support the validity of Goldstein's [10] hypothesis who, performing statistical analyses in a large series of colorectal cancers, suggested that the predictive probability of identifying the single lymph node metastasis in a theoretical surgical specimen of colorectal cancer with a single lymph node metastasis increases up to 80% if about 30 lymph nodes are recovered.

In the present study, metastases occurred in small-sized (<5 mm) lymph nodes, and interestingly, all patients had only a single metastatic lymph node. These findings raise the controversial issue about the minimum number of lymph nodes to be recovered for each specimen. In agreement with other authors, we believe that an ideal minimum number of lymph nodes to be recovered does not exist [8, 10], likely being only a statistical concept that cannot be applied for each single patient. In fact, the number of lymph nodes can greatly vary according to individual biological variation (tumor stage and associated inflammatory response), quality of surgical excision, and the pathologist performing the sampling of peri(colon)-rectal adipose tissue at different pathologic institutions [17, 20, 22, 27–29]. The latter seems to be crucial, as the present study showed that a resampling of perirectal adipose tissue by a second pathologist with expertise in gastrointestinal pathology has retrieved meta-

Table 4 Correlation between pN-stage and mean number of lymph nodes in understaged pT3 patients

No. of patients	Mean number of LNS (1° sampling)	pN-stage	Mean number of LNS (1°+2° sampling)	Final stage
6	16.6 (range 12–25)	N0	27.8 (range 20–36)	N1

No. Number, *LNs* number of lymph nodes recovered

static lymph nodes that had been missed at the first sampling in 18.7% of pT3 patients. However, we admit that the manual isolation of lymph nodes from the perirectal adipose tissue is objectively difficult, despite the pathologist's diligence, as many lymph nodes are small in size (<5 mm) and can be easily missed or crushed during sampling. This is further supported by one case of our series in which the single metastatic lymph node of 2.4 mm in maximum diameter was missed at first sampling, despite 25 lymph nodes had been recovered. Accordingly, we suggest that pathologists should handle with care the perirectal adipose tissue during manual lymph node dissection even if they had been able to detect a number of lymph nodes larger than recommended (12 lymph nodes) by the TNM system. Practically, as we have shown that most missed metastatic lymph nodes were detected in specimens in which a maximum number of 19 lymph nodes had been originally recovered, we strongly suggest a resampling of pT3NO specimens if less than 20 lymph nodes have been recovered.

References

1. Andreola S, Leo E, Belli F, Bufalino R, Tomasic G, Lavarino C, Baldini T, Meroni E (1996) Manual dissection of adenocarcinoma of the rectum specimens for detection of lymph node metastases smaller than 5 mm. Cancer 77:607–612
2. Andreola S, Leo E, Belli F, Bonfanti G, Sirizzotti G, Greco P, Valvo F, Tomasic G, Gallino GF (2001)Adenocarcinoma of the lower third of the rectum surgically treated with a <10-mm distal clearance: preliminary results in 35 N0 patients. Ann Surg Oncol 8:611–615
3. Andreola S, Zucchini N, Greco P (2001) Il chirurgo e il patologo: un rapporto in evoluzione. Ital J Proctol 20:73–75
4. Baxter NN, Virnig DJ, Rothenberger DA, Morris AM, Jessurun J, Virning BA (2005) Lymph node evaluation in colorectal cancer patients: a population-based study. J Natl Cancer Inst 97:219–225
5. Caplin S, Cerottini JP, Bosman FT et al (1998) For patients with Duke's B (TNM stage II) colorectal carcinoma, examination of six or fewer lymph nodes is related to poor prognosis. Cancer 83:666–672
6. Cianchi F, Palomba A, Boddi V, Messerini L, Pucciani F, Perigli G, Bechi P, Cortesini C (2002) Lymph node recovery from colorectal tumor specimens: recommendation for a minimum number of lymph nodes to be examined. World J Surg 26:384–389
7. Cohen AM, Minsky BD, Schilsky RL (1997) Cancers of the gastrointestinal tract: cancer of the colon. In: DeVita VT Jr, Hellman S, Rosenberg SA (eds) Cancer principles and practice of oncology. Lippincott-Raven, Philadelphia, pp 1144–1196
8. Cserni G, Vinh-Hung V, Burzykowski T (2002) Is there a minimum number of lymph nodes that should be histologically assessed for a reliable nodal staging of T3N0M0 colorectal carcinoma? J Surg Oncol 81:63–69
9. Goldstein NS, Sanford W, Coffey M, Layfield LJ (1996) Lymph node recovery from colorectal resection specimens removed for adenocarcinoma. Trends over time and a recommendation for a minimum number of lymph nodes to be recovered. Am J Clin Pathol 106:209–216
10. Goldstein NS (2002) Lymph node recoveries from 2427 pT3 colorectal resection specimens spanning 45 years. Recommendations for a minimum number of recovered lymph nodes based on predictive probabilities. Am J Surg Pathol 26:179–189
11. Gumus M, Yumuk PF, Atalay G, Aliustaoglu M, Maculuoglu B, Dane F, Caglar H, Sengoz M, Turhal S (2005) What is the optimal number of lymph nodes to be dissected in colorectal cancer surgery? Tumori 91:168–172
12. Hermanek P (1991) Onkologische Chirurgie/Pathologsch-anatomische Sicth. Langenbecks Arch Chir Suppl:277–281
13. Hernanz F, Revuelta S, Redondo C, Madrazo C, Castillo J, Gomez-Fleitas M (1994) Colorectal adenocarcinoma: quality of the assessment of lymph node metastases. Dis Colon Rectum 37:373–377
14. Herrera L, Villarreal JR (1992) Incidence of metastases from rectal adenocarcinoma in small lymph nodes detected by a clearing technique. Dis Colon Rectum 35:783–788
15. Herrera-Ornelas L, Justiniano J, Castillo N, Petrelli NJ, Stulc JP, Mittelman A (1987) Metastases in small lymph nodes from colon cancer. Arch Surg 122:1253–1256
16. Hida J, Mori N, Kubo R, Matsuda T, Morikawa E, Kitaoka M, Sindoh K, Yasutomi M (1994) Metastases from carcinoma of the colon and rectum detected in small lymph nodes by the clearing method. J Am Coll Surg 178:223–228
17. Horzic M, Kopljar M (2005) Minimal number of lymph nodes that need to be examined for adequate staging of colorectal cancer—factors influencing lymph node harvest. Hepato-gastroenterology 52:86–89
18. Joseph NE, Sigurdson ER, Yhanlon AL, Wang H, Mayer RJ, MacDonald JS, Catalano PJ, Haller DG (2003) Accuracy of determining nodal negativity in colorectal cancer on the basis of the number of nodes retrieved on resection. Ann Surg Oncol 10:213–218
19. Law CH, Wright FC, Rapanos T, Alzahrani M, Hanna SS, Khalifa M, Smith AJ (2003) Impact of lymph node retrieval and pathological ultra-staging on the prognosis of stage II colon cancer. J Surg Oncol 84:120–126
20. Leibl S, Tsybrovskyy O, Denk H (2003) How many lymph nodes are necessary to stage early and advanced adenocarcinoma of the sigmoid colon and upper rectum? Virchow Arch 443:133–138
21. Maurel J, Launoy G, Grosclaude P et al (1998) Lymph node harvest reporting in patients with carcinoma of the large bowel. A French population based study. Cancer 82:1482–1486
22. Miller EA, Woosley J, Martin CF, Sandler RS (2004) Hospital-to-hospital variation in lymph node detection after colorectal resection. Cancer 101:1065–1071
23. Sarli L, Bader G, Iusco D, Salvemini C, Mauro DD, Mazzeo A, Regina G, Roncoroni L (2005) Number of lymph nodes examined and prognosis of TNM stage II colorectal cancer. Eur J Cancer 41:272–279
24. Scott KWM, Grace RH (1989) Detection of lymph node metastases in colorectal carcinoma before and after fat clearance. Brit J Surg 76:1165–1167
25. Sobin LH, Wittekind C (eds) (2002) TNM classification of malignant tumors. In: International Union Against Cancer (UICC), 6th edn. Wiley-Liss, New York
26. Swanson RS, Compton CC, Stewart AK, Bland KI (2003) The prognosis of T3N0 colon cancer is dependent on the number of lymph nodes examined. Ann Surg Oncol 10:65–71
27. Thorn CC, Woodcock NP, Scott N, Verbeke C, Scott SB, Ambrose NS (2004) What factors affect lymph node yield in surgery for rectal cancer? Colorectal Dis 6:356–361
28. Wong JH, Johnson DS, Hemmings D, Hsu A, Imai T, Tominaga GT (2005) Assessing the quality of colorectal cancer staging: documenting the process in improving the staging of node-negative colorectal cancer. Arch Surg 140:881–886
29. Wright FC, Law CH, Last L, Khalifa M, Arnaout A, Naseer Z, Klar N, Gallinger S, Smith AJ (2003) Lymph node retrieval and assessment in stage II colorectal cancer: a population-based study. Ann Surg Oncol 10:903–909
30. Yoshimatsu K, Ishibashi K, Umehara A, Yokomizo H, Yoshida K, Fujimoto T, Watanabe K, Ogawa K (2005) How many lymph nodes should be examined in Dukes' B colorectal cancer? Determination on the basis of cumulative survival rate. Hepato-gastroenterology 52:1703–1706

Virchows Arch (2006) 449:652–659
DOI 10.1007/s00428-006-0300-8

ORIGINAL ARTICLE

Histological risk markers for non-cardia early gastric cancer

Pattern of mucin expression and gastric cancer

Akiko Shiotani · Ken Haruma · Noriya Uedo · Hiroyasu Iishi · Ryu Ishihara · Masaharu Tatsuta · Mitutaka Kumamoto · Yukinori Nakae · Shingo Ishiguro · David Y. Graham

Received: 22 May 2006 / Accepted: 23 August 2006 / Published online: 13 October 2006
© Springer-Verlag 2006

Abstract There are limited data regarding the prognostic value of the pattern of mucin expression in IM. To examine the role of the type of IM and pattern of mucin expression in IM as histological risk markers of gastric cancer, 80 patients with a history of endoscopic mucosal resection (EMR) for early gastric cancer and 80 sex and age-matched controls were studied. Serum levels of pepsinogen (PG) were measured by RIA, and MUC2, MUC5AC and MUC6 were evaluated immunohistochemically. There is a significant association between types of IM and atrophic scores or PG levels. The most incomplete IM (type II and III) preserving gastric mucin is the gastric and intestinal mixed (GI) type, whereas the complete type is the intestinal (I) type especially in the corpus lesser curve. Gastric cancer was most significantly associated with incomplete IM in the corpus lesser curve (OR=6.4; 95% CI, 2.0–21, p=0.002). Asynchronous multiple lesions were associated with incomplete IM in the corpus greater curve (OR=4.8; 95% CI, 1.4–16, p=0.01). Classification of IM obtained using fixed-point biopsy samples may enhance the ability of surveillance programs to detect patients at increased risk of gastric cancer.

Keywords Early gastric cancer · Type III intestinal metaplasia · MUC2 · MUC5AC · MUC6

A. Shiotani · K. Haruma
Department of Internal Medicine, Kawasaki Medical School, Okayama, Japan

N. Uedo · H. Iishi · R. Ishihara · M. Tatsuta
Department of Gastrointestinal Oncology, Osaka Medical Center for Cancer and Cardiovascular Diseases, Osaka, Japan

M. Kumamoto · Y. Nakae
Department of Medicine, Aishinkai Nakae Hospital, Wakayama, Japan

S. Ishiguro
Department of Pathology, Osaka Medical Center for Cancer and Cardiovascular Diseases, Osaka, Japan

D. Y. Graham
Department of Medicine, VA Medical Center and Baylor College of Medicine, Houston, TX, USA

A. Shiotani (✉)
577 Matsushima, Kurashiki, Okayama Prefecture 701-0192, Japan
e-mail: shiotani@med.kawasaki-m.ac.jp

Introduction

The pathogenesis of gastric cancer is a multifactorial process in which both environmental and host-related factors play significant roles. The risk of developing gastric cancer is closely related to *Helicobacter pylori*-associated progressive gastric inflammation [2, 5, 26, 32]. The degree of damage is initially most severe in the antrum, but over time the damage progresses into the gastric corpus and can be visualized as an advancing atrophic border, which involves the lesser curve more rapidly than the greater curve [2, 8, 16, 22]. Intestinal type gastric cancers are thought to evolve through a multi-step process starting with superficial gastritis and progressing through atrophy, followed by the development of dysplasia, and finally carcinoma [1]. The role of intestinal metaplasia (IM) in the transition from superficial gastritis to cancer is unclear. There are data suggesting that cancer and IM arise from different cell lineages such that IM may not be a precursor lesion but rather is likely a marker for increased risk [6, 17, 29].

Gastric IM was classified as complete (small intestine) or incomplete (colonic) using immunohistochemical staining techniques and into three types based on the staining pattern of its mucins: I (complete), and II and III (incomplete). Type I is the most common type; Paneth cells are present and goblet cells secrete sialomucins. Types II and III are characterized by the presence of columnar cells and goblet cells secreting sialomucins and/or sulfomucins, and columnar cells secret sialomucins in type II and sulfomucins in type III [12]. Although several studies have suggested that patients with type III IM may be at a higher risk for development of gastric cancer [3, 34], the predictive value of type I and type II IM remains unclear.

Mucins are heavily glycosylated proteins that constitute the major component of the mucous protective layer above mucous surfaces. Core proteins for 12 human mucins (MUC1, 2, 3, 4, 5AC, 5B, 6, 7, 8, 9,11,12) were identified [15, 23, 30, 39]. The normal gastric mucosa shows cell type specific expression of MUC1, 5AC, and 6, and does not express MUC2. Alterations of the expression pattern of mucins were described in carcinoma and IM. Loss of expression of MUC5AC and increased mucin heterogeneity were reported in gastric cancer, whereas under-expression of MUC1, MUC5AC and MUC6 and de novo expression of MUC2 were described in IM. IM was also classified based upon the cell classification status using both gastric and intestinal phenotypic markers [19, 36–38]. In that system, IM is divided into two major types; a gastric and intestinal mixed (GI) type, and a solely intestinal (I) type. MUC5AC and MUC6, galactose oxidase-Schiff, etc. are markers of gastric phenotype, and MUC2, CD10, Villin, sucrase, etc. are intestinal phenotypic markers [19, 35–38].

In retrospective studies, type III IM was found in 75% to 90% of cases of intestinal type gastric cancer that underwent surgical resections [13, 24]. The presence of type III IM was also associated with an increased risk of developing early gastric cancer [3, 14, 28] but not with diffuse type gastric carcinoma [20].

IM is a manifestation of atrophic mucosa occurring in patients with chronic *H. pylori* gastritis. Type I IM is commonly found in random biopsies of patients with *H. pylori* infection and the prevalence increases with age. Because detection of IM in routinely obtained endoscopic biopsy materials is common, its presence alone is not considered a reliable marker for identifying patients in whom surveillance is indicated [11]. In addition, biopsies taken repeatedly from predetermined points showed that neither the presence nor the type of IM was constant [7].

There are a number of studies suggesting that the presence of type III IM may be a risk factor for the intestinal type gastric cancer. However, the majority of these studies involved surgical specimens of human stomach with gastric cancer [8, 18, 24, 25] such that while it is possible to conclude that type III IM is frequently present in patients with gastric cancer, little can be said regarding its predictive value. The same problem is present regarding the role of altered mucin expression pattern in IM as most of the studies have come from patients who already had gastric cancers. There are no data regarding the potential value of mucin expression pattern as a risk factor for gastric cancer using fixed-point biopsy samples. We previously used endoscospic biopsies from predetermined sites and found that the presence of IM at the corpus lesser curve was the prevalent finding in patients with early gastric cancer [32].

The aim of the present study was to examine the usefulness of typing of IM and the pattern of mucin expression in IM. We compared the histopathological findings in patients with a history of EMR for early gastric cancer with a suitable control group to identify markers useful to identify patients at increased risk of having or developing gastric cancer.

Materials and methods

This was a case-control study in patients who previously had endoscopic mucosal resection (EMR) for early gastric cancer. The study was performed at the Osaka Medical Center for Cancer and Cardiovascular Diseases and the Aishinkai Nakae Hospital in Japan. Patients were enrolled for the study between November 2003 and November 2005.

Patients

Patients with prior medical EMR for early stage, non-cardiac intestinal type gastric cancer without lymph node metastasis were age and sex-matched with control patients who underwent endoscopy for follow-up of peptic ulcer or for health screening. Patients were excluded if they had received eradication therapy for *H. pylori* infection, used anti-secretory drugs or non-steroidal anti-inflammatory drugs (NSAIDs), or had predisposing factors of hemorrhagic disease or chronic diseases such as insulin-dependent diabetes mellitus, cirrhosis or renal failure. Drinking and smoking were defined as regular intake when respective consumption was more than 35 g of ethanol and 5 cigarettes per day, respectively.

The study was approved by the Osaka Medical Center for Cancer and Cardiovascular Diseases Ethical Committee, and informed consent was obtained from each patient. The biopsy samples from a subpopulation of these patients (40 controls and 40 gastric cancer patients) were also used in studies regarding loss of Sonic Hedgehog as an indicator of *H. pylori*-induced atrophic gastritis progressing to gastric

cancer and for histological and serum risk markers for non-cardia early gastric cancer [31, 32].

Endoscopic finding of gastric cancer

EMR was done in patients with intestinal type cancers in which the depth of invasion was clinically limited to the mucosa. Patients were followed up at least once per year after EMR. Experienced endoscopists performed all endoscopies.

IM and atrophy grading

Two specimens each were obtained from the greater curvature of the antrum 3 cm proximal to the pylorus and the mid-point of the greater and lesser curvature of the gastric body. A 4-point visual analogue scale was used to grade the mucosal biopsies ranging from zero (absent/normal) to three (maximal intensity) for IM and atrophy [4]. The grading was determined twice for each slide by a single pathologist who was blinded to the previous histological scores and other experimental results. The average histological scores were for the analyses.

Immunohistochemistry

Three adjacent sections 4 μm thick were cut onto each of three polylysine-coated glass slides. The sections were deparaffinized, washed in phosphate–buffer–saline (PBS) and autoclaved for 10 min in sodium citrate buffer for antigenic retrieval. For immunostaining, sections were incubated with diluted primary mouse monoclonal antibodies against MUC2, MUC5AC, MUC6 (Novocastra Laboratories, Newcastle, UK) at a dilution of 1:200, 1:500, 1:500, respectively, at room temperature for 1 h. After washing in PBS, the sections were incubated for 1 h with an anti-mouse immunoglobulin conjugated to horseradish peroxidase dextran labeled polymer using an EnVision TM peroxidase mouse system (DAKO, Carpinteria, CA, USA). The sections were washed in PBS, stained in 0.05% diaminobenzidine hydrochrolide (DAB) solution for 5 min, and counterstained with haematoxylin. After dehydration with xylene, the sections were mounted under a glass coverslip.

Subtyping IM

Biopsies were stained with Alcian blue (AB)/high-iron diamine (HID) to categorise IM as complete type (Type I) or incomplete type (Type II and III). Slides were immersed in HID solution for 20 h at room temperature, then rinsed with deionised water, and stained with 1% AB (pH 2.5) for 2 min. IM subtyping was done according to the system used by Fillipe et al. [12] as follows: Type I, non-secretory absorptive cells and sialomucin secreting goblet cells; Type II, few absorptive cells, columnar cells secreting sialomucin, and goblet cells secreting mainly sialomucin but occasionally sulphomucin; Type III, columnar cells secreting predominantly sulphomucin and goblet cells secreting sialomucin or sulphomucin.

Assay for serum levels of pepsinogen (PG) I and PG II

Blood samples were collected just before endoscopic examination. Serum levels of PG I and PG II were measured by radioimmunoassay (RIA).

Diagnosis of *H. pylori* infection

H. pylori infection was diagnosed by specific IgG *H. pylori* antibodies analyzed by an enzyme-linked immunosorbent assay (ELISA) kit (E plate, Eiken Kagaku Inc, Tokyo).

Statistical analyses

Values were expressed as the mean±SD or median and 25–75% range whichever was appropriate. Mantel–Haenszel chi square analyses, Kruskal–Wallis and the non-parametric Mann–Whitney *U* test were performed to measure differences. Analysis of proportions among the three different groups was performed using chi square analyses. Comparisons were made between those with cancer and the entire control group and control subjects with IM. After comparison by Kruskal–Wallis, Dunn's methods were used to isolate the groups that differ from the others.

Mantel–Haenszel statistics were used to assess the relationship between gastric cancer and histopathological findings showing the odds ratio (OR) and 95% confidence interval (CI). Risk factors for gastric cancer were analyzed by multivariate logistic regression analyses. A two sided p value of less than 0.05 was considered statistically significant. All statistical computations were performed using SPSS (version 11.0 for Windows, SPSS Inc, Chicago, IL).

Results

The study groups consisted of 80 patients with a prior EMR for non-cardiac early gastric cancer and 80 age and sex-matched controls. Demographic and clinical characteristics of the study groups are shown in Table 1. Multiple malignant lesions were found in 30 patients (asynchronous 15, synchronous 15); the remaining 50 had single lesions. Malignant lesions in 42 patients were located in the lower stomach (antrum or angulus), and 29 patients had lesions in the upper stomach (corpus). In the remaining nine patients, malignant lesions were located in the two different locations. Malignant lesions in 20 patients were depressed

Table 1 Patient demographic and clinical characteristics

	Control (n=80)	Cancer (n=80)	p values
Age mean (SD)	68 (9)	68 (8)	0.85*
Sex male/female	60/20	60/20	
Current smokers	31.3%	33.8%	0.80**
Regular alcohol intake	48.9%	41.3%	0.53**
H. pylori positive	82.5%	87.5%	0.51**

p values; *unpaired t test, **by Mantel–Haenszel chi square analyses

type and those in 50 patients were protruded type. Finally, ten patients had both types of malignant lesions.

The IM scores for each region of the stomach were significantly higher in the cancer group than in the control group (Fig. 1). There is a significant association between atrophic scores and types of IM in the corpus lesser curve (p<0.001). The frequency of type III IM increased along with the scores of atrophy (Fig. 2). The ratio between the concentration of PG I and PG II (PG I/II) was significantly lower in the type II and type III groups compared to the group without IM (p<0.01). The PG I/II ratio was inversely related to the presence of type III IM and was significantly lower (p<0.05) in the type III group than in the type I group (Fig. 3).

In the gastric mucosa without IM, MUC5AC expression was detected in the foveolar epithelium and mucous neck cells of both the antrum and corpus. MUC6 expression was detected in the pyloric glands of the antrum and the mucous cells of the neck zone of the corpus. MUC2 was only detected in the mucosa with IM. MUC2 expression displayed a vacuolar staining in most goblet cells. In the gastric mucosa with type I IM, MUC5AC in the goblet cells was detected in 46% in the antrum and 13% in the corpus (Fig. 4). In the gastric mucosa with type II and type III IM,

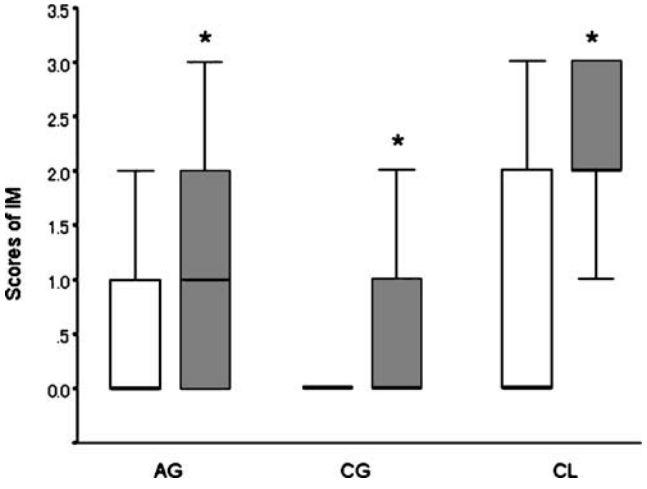

Fig. 1 Comparison of IM scores between patients with gastric cancer (▪) and control subjects (▫). The *ends of the boxes* define the 25th and 75th percentiles with the bold line at the median and *error bars* define the 10th and 90th percentiles. *p<0.001; p values by Mann–Whitney U test. AG, antrum greater curve; CG, corpus greater curve; CL, corpus lesser curve

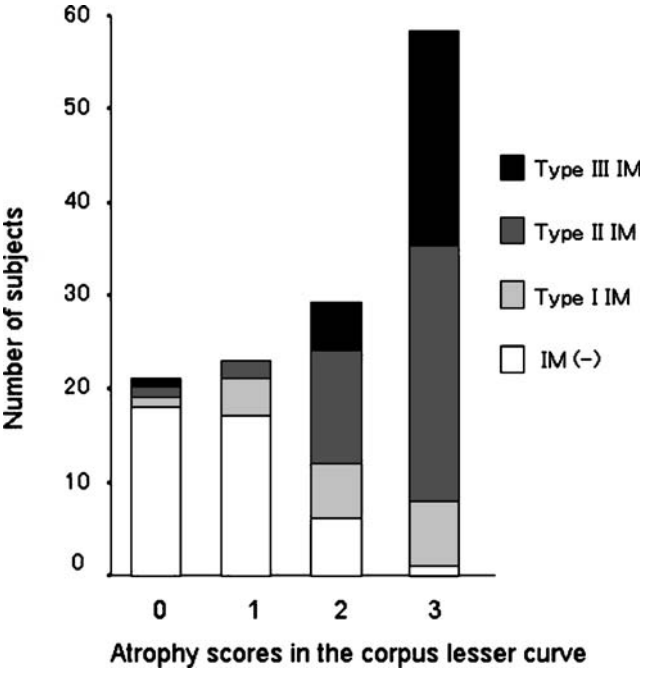

Fig. 2 Correlation between types of IM and atrophic scores in the corpus lesser curve. The frequency of type III IM increased along with the scores of atrophy (p<0.001, by Kruskal–Wallis)

MUC5AC was detected in 83% and 94% of patients, respectively, in the antrum and 57% and 90%, respectively, in the corpus (Figs. 4 and 5). In contrast, expression of MUC6 in IM in the antrum was present in 46% of patients with type II IM and 50% of patients with type III (Table 2).

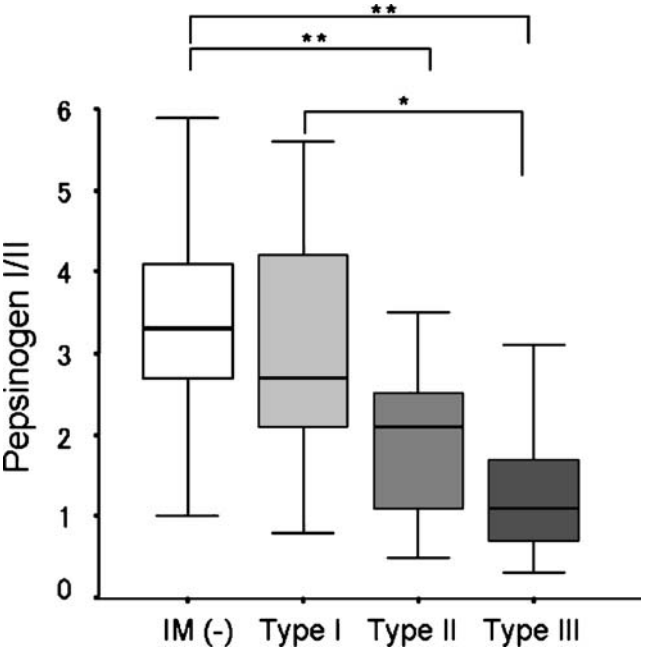

Fig. 3 Comparison of the ratio between the concentration of PG I and PG II (PG I/II). The PG I/II was significantly lower in the type II and type III groups compared to the control group (p<0.01). The PG I/II ratio was inversely related to the presence of type III IM and was significantly lower in the type III group than in the type I group (p<0.05). *p<0.05, **p<0.01 by Dunn's methods

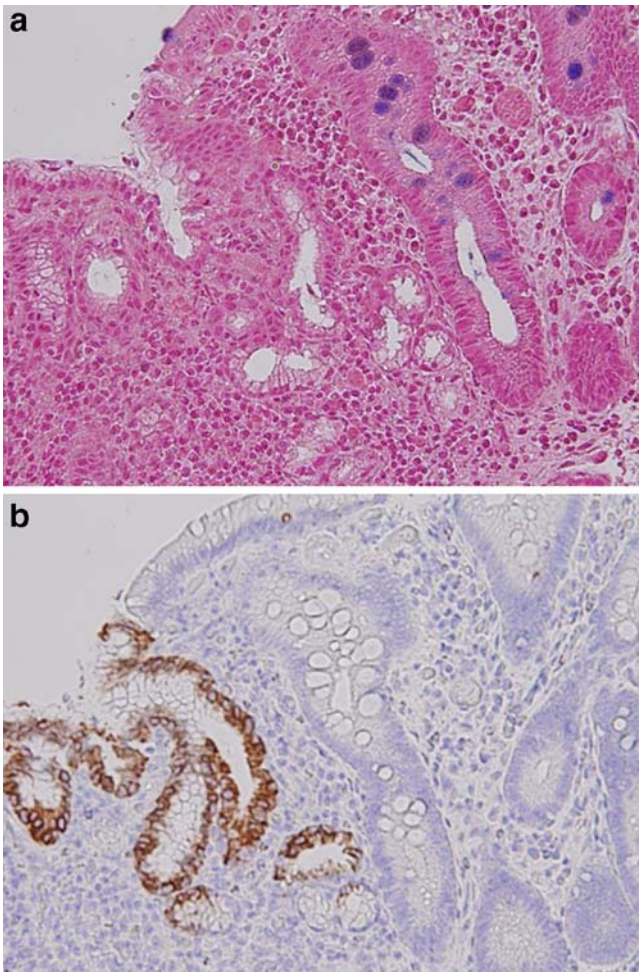

Fig. 4 Immunohistochemical staining of serial sections of type I (*) and II (**) IM in the antrum greater curve (original magnification ×40). **a**. High-iron diamine–alcian blue (HID–AB) staining shows goblet cells stained in *blue* (sialomucin) of type I IM (*) and cells stained in *brown* (sulphomucin) of type II IM (**). **b**. MUC5 was detected in the mucosa without IM and type I IM (*)

Gastric cancer was associated with a higher frequency of incomplete IM (types II and III) and IM expressing MUC5AC (Table 3). The sensitivity and specificity of detecting incomplete IM in either point were 86% and 65% (OR=11, 95% CI 5.1–25, $p<0.001$). Those of type III IM were 55% and 95% (OR=22; 95% CI 7.5–67, $p<0.001$), and IM with MUC5AC expression were 81% and 69%, respectively (OR=8.9, 95% CI 4.3–19, $p<0.001$).

Among the patients with IM, the presence of type III IM in the antrum and corpus lesser curve, and incomplete and GI mixed type MUC5AC expressing IM in each part were

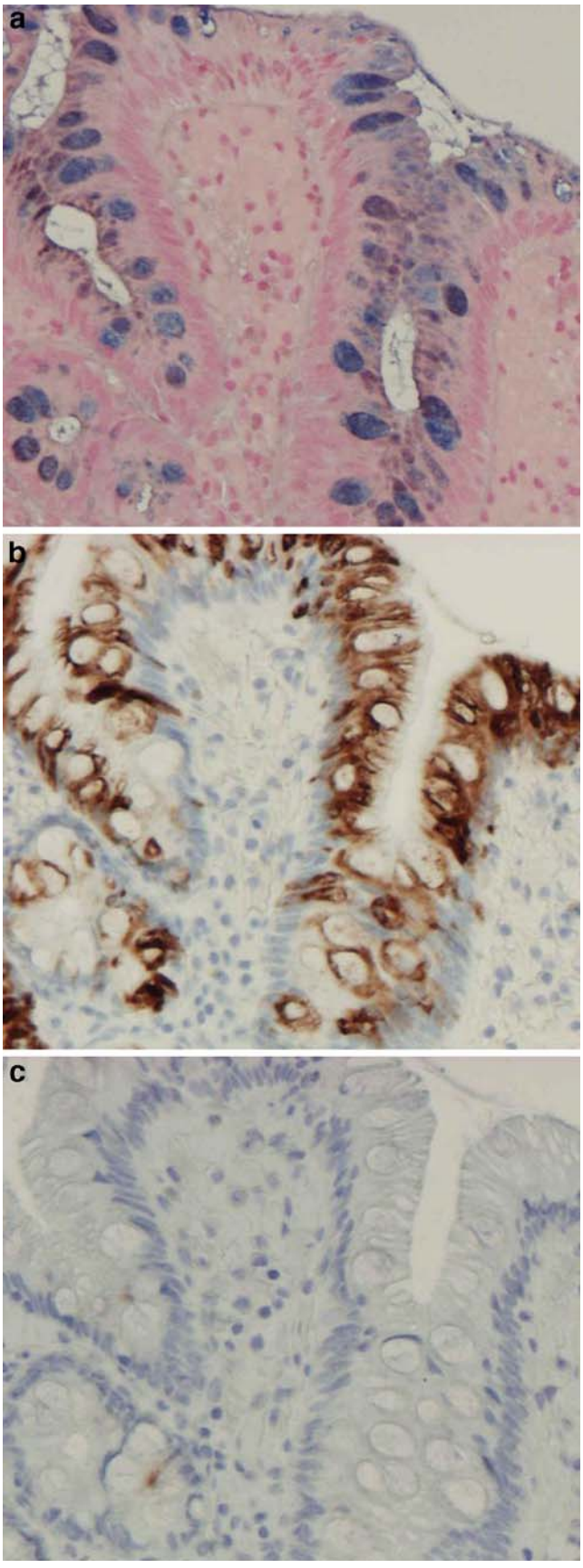

Fig. 5 MUC2 and MUC5AC immunohistochemical staining of serial sections of type III IM in the corpus lesser curve (original magnification ×40). **a**. High-iron diamine–alcian blue (HID–AB) staining shows goblet cells and columnar cells stained in *brown* (sulphomucin). **b**. MUC5AC was detected in the goblet cells and in the columnar cells. **c**. IM does not express MUC6

Table 2 Correlation of HID–AB staining and expression of MUC5AC and MUC6

	MUC5AC, MUC2 of GI type IM (%)	*p* values	MUC6, MUC2 of GI type IM (%)	*p* values
Antrum*		<0.001		<0.001
Type I IM *n*=13	46		39	
Type II IM *n*=40	83		46	
Type III IM *n*=31	94		50	
Corpus *		<0.001		<0.001
Type I IM *n*=40	13		5.0	
Type II IM *n*=65	57		19	
Type III IM *n*=39	90		52	

*Antrum, antrum greater curve; Corpus, Corpus lesser and greater curve. IM, intestinal metaplasia; GI type, gastric and intestinal mixed type. *p* values by chi square analyses

significant risk factors for gastric cancer (Table 4). However, in a multivariate analysis among those factors, gastric cancer was significantly associated with a higher frequency of incomplete IM (types II or III) in the corpus lesser curve (OR=6.4; 95% CI, 2.0–21, p=0.002).

Asynchronous multiple lesions were associated with incomplete IM in the corpus greater curve (OR=4.8; 95% CI, 1.4–16, p=0.01). However, there was no significant association between types of IM and locations of malignant lesions.

Discussion

In this study, we confirmed that MUC5AC expression was observed most often in type III IM. Previous studies examined biopsy samples or surgical specimens taken from the gastric mucosa adjacent to carcinomas, and MUC1 and MUC5AC together with MUC2 were expressed in every case with IM types II and III [27, 33]. A recent study from Japan examined the pyloric regions of stomachs resected for gastric cancer and showed that MUC5AC was expressed in 38% of type I glands, 78% of type II, and 91% of type III IM [35]. These results are similar to those reported here. The most incomplete IM (type II and III) preserving gastric mucin is the GI mixed type, whereas the complete type is the type I IM especially in the corpus lesser curve.

Gastric cancer risk increases with age and is highest in those with severe atrophic gastritis. We found that incomplete IM in the corpus lesser curve is common in patients with gastric cancer. The presence of incomplete IM at this location is indicative of the presence of corpus atrophy, which is a known risk factor for an increased risk of the intestinal type gastric cancer [31, 32]. The fact that multivariate analysis showed a better association of the type of IM with the presence of gastric cancer than the score of atrophy suggests that, in an examination using a limited number of biopsy specimens, the type of IM may better reflect the severity and extent of atrophy. This notion is consistent with our results showing an inverse correlation between the type of IM, the PG I/II and the severity of corpus atrophy.

Using a systematic endoscopic protocol with fixed-point biopsy samples, we previously showed that the scores for IM in the corpus greater curve and the scores for atrophy in the corpus lesser curve were significantly higher in patients with multiple malignant lesions compared to those with a single lesion [32]. This study extended those findings showing that the presence of incomplete IM in the corpus greater curve was an additional histological risk marker for recurrent new malignant lesions. Kabashima et al. reported that the incidence of IM expressing gastric phenotype in non-neoplastic mucosa within 5 mm from the margins of carcinoma cells was higher in the patients with multiple early gastric cancer lesions than in the patients with a single lesion [21].

This study suggests that the type and location of IM provides important additional information regarding the

Table 3 Comparison of histological findings between the cancer group and the control

	Control	Cancer	*p* values
Type I/Type II/Type III IM			
AG	10/16/3	4/26/28	<0.001
CG	5/4/0	12/18/4	<0.001
CL	15/14/3	8/33/33	<0.001
MUC5AC, MUC2 GI type IM			
AG	11/18	7/51	<0.001
CG	8/1	27/9	<0.001
CL	18/15	20/56	<0.001

AG, antrum greater curve; CG, corpus greater curve; CL, corpus lesser curve. IM, intestinal metaplasia; GI type, gastric and intestinal mixed type. *p* values by chi square analyses

Table 4 Comparison of the prevalence of type of intestinal metaplasia among the subjects with intestinal metaplasia

	OR (95% CI)	*p* values
Type III IM		
AG	14 (4.0–49)	<0.001
CG	–	–
CL	18 (5.2–62)	<0.001
Type II & III IM		
AG	7.1 (3.5–14)	<0.001
CG	7.1 (2.3–22)	0.001
CL	18 (8.2–41)	<0.001
MUC5AC, MUC2 GI type IM		
AG	6.6 (3.3–13)	<0.001
CG	10 (1.3–82)	0.03
CL	10 (4.8–21)	<0.001

AG, antrum greater curve; CG, corpus greater curve; CL, corpus lesser curve. IM, intestinal metaplasia; GI type, gastric and intestinal mixed type; OR, odds ratio; CI, 95% confidence interval

extent and severity of gastric atrophy and thus the risk of developing gastric cancer. Changes in the type of IM could also reflect the amount of genetic damage that has taken place and/or changes in the intragastric environment (e.g., development of low acid secretion). For example, hypoacidity might allow stem cell differentiation in a particular direction to IM and independently to cancer [10, 31]. Recent studies investigating relationship between genetic alterations and cellular phenotypes in cancer and IM have provided evidence that the phenotypic expression in cancer and precancerous lesions of the stomach is strongly dependent on genetic changes [9], and that cancer and IM may arise from different cell lineages [6, 17, 29, 36]. Tatematsu and colleagues used the classification of IM using gastric and intestinal cell phenotypic markers, and hypothesized that IM phenotype shift from GI mixed type to I type [35–37]. Intestinalization progresses from GI mixed type to I type in non-cancerous and cancerous tissue independently. However, our results do not support the concept of IM phenotype shift from mixed type to intestinal type as incomplete IM appeared to follow complete IM and was correlated with the PG I/II ratio and with the severity of corpus atrophy. The pathogenesis of IM and actual relationship to gastric cancer remains unclear and additional studies are warranted to explore the relationship.

Our study using targeted biopsies showed that the most incomplete IM preserving gastric mucin is the GI type, whereas the complete type is the type I IM especially in the corpus lesser curve, and that IM type was associated with the presence of early gastric cancer. These data suggest that patients with incomplete IM in the corpus lesser curve are likely to have severe atrophic pangastritis and such patients are at increased risk of developing gastric cancer. Moreover, the presence of incomplete IM in the corpus greater curve was an additional histological risk marker for recurrent new malignant lesions. In conclusion, the classification of IM by histochemical detection using biopsy samples obtained from fixed-points may enhance the ability of surveillance programs to detect patients at increased risk of either having or developing gastric cancer.

Acknowledgements The authors thank all the laboratory technicians in the Department of Pathology, Osaka Medical Center for Cancer and Cardiovascular Diseases for the expert technical assistance.

References

1. Correa P (1984) Chronic gastritis as a cancer precursor. Scand J Gastroenterol Suppl 104:131–136
2. Correa P (1995) *Helicobacter pylori* and gastric carcinogenesis. Am J Surg Pathol 19(Suppl 1):S37–S43
3. Dinis-Ribeiro M, Lopes C, da Costa-Pereira A, Guilherme M, Barbosa J, Lomba-Viana H, Silva R, Moreira-Dias L (2004) A follow up model for patients with atrophic chronic gastritis and intestinal metaplasia. J Clin Pathol 57:177–182
4. Dixon MF, Genta RM, Yardley JH, Correa P (1996) Classification and grading of gastritis. The updated Sydney System. International Workshop on the Histopathology of Gastritis, Houston 1994. Am J Surg Pathol 20:1161–1181
5. Dixon MF (2001) Prospects for intervention in gastric carcinogenesis: reversibility of gastric atrophy and intestinal metaplasia. Gut 49:2–4
6. Egashira Y, Shimoda T, Ikegami M (1999) Mucin histochemical analysis of minute gastric differentiated adenocarcinoma. Pathol Int 49:55–61
7. El-Zimaity HM, Ramchatesingh J, Saeed MA, Graham DY (2001) Gastric intestinal metaplasia: subtypes and natural history. J Clin Pathol 54:679–683
8. El-Zimaity HM, Ota H, Graham DY, Akamatsu T, Katsuyama T (2002) Patterns of gastric atrophy in intestinal type gastric carcinoma. Cancer 94:1428–1436
9. Endoh Y, Sakata K, Tamura G, Ohmura K, Ajioka Y, Watanabe H, Motoyama T (2000) Cellular phenotypes of differentiated-type adenocarcinomas and precancerous lesions of the stomach are dependent on the genetic pathways. J Pathol 191:257–263
10. Faller G, Dimmler A, Rau T, Spaderna S, Hlubek F, Jung A, Kirchner T, Brabletz T (2004) Evidence for acid-induced loss of Cdx2 expression in duodenal gastric metaplasia. J Pathol 203:904–908
11. Fennerty MB (2003) Gastric intestinal metaplasia on routine endoscopic biopsy. Gastroenterology 125:586–590
12. Filipe MI, Potet F, Bogomoletz WV, Dawson PA, Fabiani B, Chauveinc P, Fenzy A, Gazzard B, Goldfain D, Zeegen R (1985) Incomplete sulphomucin-secreting intestinal metaplasia for gastric cancer. Preliminary data from a prospective study from three centres. Gut 26:1319–1326
13. Filipe MI, Barbatis C, Sandey A, Ma J (1988) Expression of intestinal mucin antigens in the gastric epithelium and its relationship with malignancy. Hum Pathol 19:19–26
14. Filipe MI, Munoz N, Matko I, Kato I, Pompe-Kirn V, Jutersek A, Teuchmann S, Benz M, Prijon T (1994) Intestinal metaplasia types and the risk of gastric cancer: a cohort study in Slovenia. Int J Cancer 57:324–329
15. Gendler SJ, Spicer AP (1995) Epithelial mucin genes. Annu Rev Physiol 57:607–634
16. Graham DY, Shiotani A (2005) The time to eradicate gastric cancer is now. Gut 54:735–738
17. Hattori T (1986) Development of adenocarcinomas in the stomach. Cancer 57:1528–1534
18. Iida F, Kusama J (1982) Gastric carcinoma and intestinal metaplasia. Significance of types of intestinal metaplasia upon development of gastric carcinoma. Cancer 50:2854–2858
19. Inada K, Tanaka H, Nakanishi H, Tsukamoto T, Ikehara Y, Tatematsu K, Nakamura S, Porter EM, Tatematsu M (2001) Identification of Paneth cells in pyloric glands associated with gastric and intestinal mixed-type intestinal metaplasia of the human stomach. Virchows Arch 439:14–20
20. Jass JR, Filipe MI (1981) The mucin profiles of normal gastric mucosa, intestinal metaplasia and its variants and gastric carcinoma. Histochem J 13:931–939
21. Kabashima A, Yao T, Sugimachi K, Tsuneyoshi M (2000) Gastric or intestinal phenotypic expression in the carcinomas and background mucosa of multiple early gastric carcinomas. Histopathology 37:513–522
22. Kimura K, Satoh K, Ido K, Taniguchi Y, Takimoto T, Takemoto T (1996) Gastritis in the Japanese stomach. Scand J Gastroenterol Suppl 214:17–20, discussion 21–13
23. Lapensee L, Paquette Y, Bleau G (1997) Allelic polymorphism and chromosomal localization of the human oviductin gene (MUC9). Fertil Steril 68:702–708

24. Matsukura N, Suzuki K, Kawachi T, Aoyagi M, Sugimura T, Kitaoka H, Numajiri H, Shirota A, Itabashi M, Hirota T (1980) Distribution of marker enzymes and mucin in intestinal metaplasia in human stomach and relation to complete and incomplete types of intestinal metaplasia to minute gastric carcinomas. J Natl Cancer Inst 65:231–240
25. Matsuzaki H, Shimada S, Uno K, Tsuruta J, Ogawa M (1998) Novel subtyping of intestinal metaplasia in the human stomach: brain-type glycogen phosphorylase expression in the proliferative zone and its relationship with carcinogenesis. Am J Clin Pathol 109:181–189
26. Meining A, Morgner A, Miehlke S, Bayerdorffer E, Stolte M (2001) Atrophy–metaplasia–dysplasia–carcinoma sequence in the stomach: a reality or merely an hypothesis? Best Pract Res Clin Gastroenterol 15:983–998
27. Reis CA, David L, Correa P, Carneiro F, de Bolos C, Garcia E, Mandel U, Clausen H, Sobrinho-Simoes M (1999) Intestinal metaplasia of human stomach displays distinct patterns of mucin (MUC1, MUC2, MUC5AC, and MUC6) expression. Cancer Res 59:1003–1007
28. Rokkas T, Filipe MI, Sladen GE (1991) Detection of an increased incidence of early gastric cancer in patients with intestinal metaplasia type III who are closely followed up. Gut 32:1110–1113
29. Saito A, Shimoda T, Nakanishi Y, Ochiai A, Toda G (2001) Histologic heterogeneity and mucin phenotypic expression in early gastric cancer. Pathol Int 51:165–171
30. Shankar V, Pichan P, Eddy RL Jr, Tonk V, Nowak N, Sait SN, Shows TB, Schultz RE, Gotway G, Elkins RC, Gilmore MS, Sachdev GP (1997) Chromosomal localization of a human mucin gene (MUC8) and cloning of the cDNA corresponding to the carboxy terminus. Am J Respir Cell Mol Biol 16:232–241
31. Shiotani A, Iishi H, Uedo N, Ishiguro S, Tatsuta M, Nakae Y, Kumamoto M, Merchant JL (2005) Evidence that loss of sonic hedgehog is an indicator of *Helicobater pylori*-induced atrophic gastritis progressing to gastric cancer. Am J Gastroenterol 100:581–587
32. Shiotani A, Iishi H, Uedo N, Kumamoto M, Nakae Y, Ishiguro S, Tatsuta M, Graham DY (2005) Histologic and serum risk markers for noncardia early gastric cancer. Int J Cancer 115:463–469
33. Silva E, Teixeira A, David L, Carneiro F, Reis CA, Sobrinho-Simoes J, Serpa J, Veerman E, Bolscher J, Sobrinho-Simoes M (2002) Mucins as key molecules for the classification of intestinal metaplasia of the stomach. Virchows Arch 440:311–317
34. Tahara E (1995) Genetic alterations in human gastrointestinal cancers. The application to molecular diagnosis. Cancer 75:1410–1417
35. Tanaka H, Tsukamoto T, Mizoshita T, Inada K, Ogasawara N, Cao X, Kato S, Joh T, Tatematsu M (2005) Expression of small intestinal and colonic phenotypes in complete intestinal metaplasia of the human stomach. Virchows Arch 447:806–815
36. Tatematsu M, Tsukamoto T, Inada K (2003) Stem cells and gastric cancer: role of gastric and intestinal mixed intestinal metaplasia. Cancer Sci 94:135–141
37. Tsukamoto T, Inada K, Tanaka H, Mizoshita T, Mihara M, Ushijima T, Yamamura Y, Nakamura S, Tatematsu M (2004) Down-regulation of a gastric transcription factor, Sox2, and ectopic expression of intestinal homeobox genes, Cdx1 and Cdx2: inverse correlation during progression from gastric/intestinal-mixed to complete intestinal metaplasia. J Cancer Res Clin Oncol 130:135–145
38. Tsukamoto T, Mizoshita T, Mihara M, Tanaka H, Takenaka Y, YamamuraY, Nakamura S, Ushijima T, Tatematsu, M (2005) Sox2 expression in human stomach adenocarcinomas with gastric and gastric-and-intestinal-mixed phenotypes. Histopathology 46:649–658
39. Williams SJ, McGuckin MA, Gotley DC, Eyre HJ, Sutherland GR, Antalis TM (1999) Two novel mucin genes down-regulated in colorectal cancer identified by differential display. Cancer Res 59:4083–4089

not be completely reliable. It is necessary to search for new biomarker(s) capable of providing a better prediction of the metastatic potential of malignant SGN.

Constitutive expression of the *NM23*gene was shown to suppress metastasis in vitro as well as in human tumor cohorts [9, 14, 25, 29]. Moreover, decreased levels of NM23 protein was shown to be associated with aggressive biologic behaviors such as a reduced disease-free period, a poor overall survival rate, and lymph node metastasis. NM23 was also correlated with poorly differentiated grades of melanoma and malignancies of the breast, stomach, ovary, cervix, and liver [8, 14–16]. However, this inverse correlation is not consistently seen in malignancies of all tissue origins. In neuroblastoma and pancreatic carcinoma, an opposite trend was reported, while in other malignancies, such as colorectal, thyroid, and lung carcinomas, it does not correlate with neoplastic aggressiveness [3, 12, 14].

An inverse correlation between NM23 expression and the metastatic potential of adenoid cystic carcinoma and mucoepidermoid carcinoma of the salivary glands was previously reported [17, 28, 31]. In addition, positive NM23 immunostaining is more frequently seen in benign SGN, when compared to malignant SGN [13]. However, a recent study showed no correlation between NM23 immunostaining and the biological behavior of salivary gland adenocarcinomas [5]. These different results have led to some controversy regarding the role of NM23 in SGN and while these differences may be due to either the antibody used, the immunohistochemical methods or the tissue specificity, there remains a question regarding the linkage of NM23 to SGN metastatic potential. In this study, we analyzed SGN specimens to better understand the role of NM23 in the metastatic potential of SGN.

To evaluate whether NM23 could be a biomarker for predicting the metastatic potential of SGN, immunolocalization of NM23 was characterized in SGN exhibiting different biological behaviors: (a) to quantify and compare the NM23 immunostaining indices of various SGN whose biologic behavior ranges from benign to distant metastasis, and (b) to evaluate whether the NM23 immunostaining index could be used to discriminate primary malignancies with no evidence of metastasis from primary malignancies with evidence of metastasis.

Materials and methods

The present study was approved by the Committees for Ethics on Research of the institutions where it was performed.

Fifty-six samples of salivary gland tumors were collected from the archives of the Oral Pathology Service of the Federal University of Uberlândia and the Center of Research and Training for Cancer A. C. Camargo (all institutions from Brazil). There were 16 pleomorphic adenomas (PA), 21 adenoid cystic carcinomas (ACC) and 19 mucoepidermoid carcinomas (MEC). All of the cases were reviewed and categorized according to the WHO classification of salivary gland tumors [2].

Medical records of the patients were reviewed and clinic-pathological data were collected. Evidence of metastasis was confirmed with one or more of the following studies: radiographs, computerized tomography scan or magnetic resonance image; and/or histological evidence of local/distant metastases. The mean follow-up period was 6.9±5.7 years with a range from 2 to 31 years. For analytic purposes, four groups were delineated according to the observed biological behavior of the lesions. These four groups are benign (n=16), primary malignancies with no evidence of metastasis (n=6 ACC and 9 MEC), primary malignancies with evidence of metastasis (n=10 ACC and 5 MEC), and metastatic implants (n=5 ACC and 5 MEC). There were five pairs of ACC and four pairs of MEC sampled from the primary sites and their metastatic implants. Most of the malignant lesions were located in major salivary glands and had clinically advanced staging as shown in Tables 1, 2 and 3.

Avidin–biotin–peroxidase immunohistochemical technique was employed to localize the distribution of NM23 in the tissue specimens. Briefly, 3 μm formalin-fixed paraffin tissue sections were mounted on 3-aminopropyltriethoxysilane (Sigma-Aldrich, USA) coated slides and the antigens of interest were retrieved with EDTA (1 mM, pH 8.0) in a microwave environment. Endogenous biotin and peroxidase activity was blocked with biotin blocking system (Dako Cytomation, USA) and H_2O_2 solution, respectively. The primary monoclonal antibodies used to detect the NM23 antigen were NCLnm23-37.6 and NCLnm23-2-NM301 (Novocastra Labs., Newcastle, UK) at 1:600 and 1:400 dilutions, respectively. After overnight incubation in a humidified chamber at room temperature, the antibody binding sites were visualized with the chromogen diaminobenzidine (Sigma-Aldrich, USA) and the nuclei were counterstained with Meyers' hematoxylin. Negative control was performed as above, without primary antibody. As a positive control, tissue fragments of an infiltrating ductal carcinoma of the breast known to be strongly NM23-positive were used. Fragments of non-neoplastic salivary glands were also used to evaluate the distribution of NM23 in normal salivary gland tissue.

The presence and distribution of chromogen precipitation in the tissue, as well as the pattern of its distribution were recorded. For purpose of quantitation, an immunostaining index was scored in each sample where the index is the percentage of cytoplasmic NM23-positive cells in an area of 1,000 neoplastic cells [19]. Correlation between the immunostaining indices using the two primary antibodies in this study was determined by the Spearman test. The mean

Table 1 Clinical features, histopathology and NM23 immunostaining index of the primary malignancies with no evidence of metastasis investigated in the present study

Case	Diagnosis	Primary site	TNM staging	Histological pattern	Index of NM23 immunostaining (%)
1	ACC	Parotid gland	IV	Cribriform	31.2
2	ACC	Parotid gland	II	Cribriform/tubular	15.5
3	ACC	Submandibular gland	IV	Cribriform	0.0
4	ACC	Submandibular gland	IV	Cribriform/tubular	0.0
5	ACC	Maxilla	III	Cribriform	0.0
6	ACC	Palate	III	Cribriform/tubular	35.5
7	MEC	Parotid gland	N/A	Low grade	62.4
8	MEC	Parotid gland	IV	High grade	60.2
9	MEC	Parotid gland	II	Low grade	86.9
10	MEC	Parotid gland	IV	Low grade	8.3
11	MEC	Submandibular gland	IV	Low grade	0
12	MEC	Palate	IV	Moderate grade	3.4
13	MEC	Maxilla	IV	Low grade	65.8
14	MEC	Posterior mandibular ridge	N/A	High grade	88.9
15	MEC	Posterior mandibular ridge	IV	Low grade	14.7

ACC=adenoid cystic carcinoma, MEC=mucoepidermoid carcinoma, N/A=not available

Table 2 Clinical features, histopathology and NM23 immunostaining index of the primary malignancies with evidence of metastasis investigated in the present study

Case	Diagnosis	Primary site	TNM staging	Histological pattern	Site of metastasis and/or corresponding case in Table 3	Index of NM23 immunostaining (%)
16	ACC	Submandibular gland	IV	Cribriform	Lung, refer to case #31	0.0
17	ACC	Parotid gland	IV	Tubular	Lymph node, refer to case #32	54.2
18	ACC	Submandibular gland	IV	Cribriform	Lung, refer to case #33	16.3
19	ACC	Submandibular gland	IV	Cribriform	Lung, refer to case #34	1.3
20	ACC	Submandibular gland	IV	Cribriform	Lung, refer to case #35	6.1
21	ACC	Submandibular gland	IV	Solid	Lymph node	2.3
22	ACC	Submandibular gland	II	Cribriform	Lymph node	0.0
23	ACC	Submandibular gland	IV	Solid	Lymph node	43.9
24	ACC	Submandibular gland	IV	Solid	Lymph node, lung	95.5
25	ACC	Submandibular gland	IV	Cribriform	Lung	8.0
26	MEC	Parotid gland	IV	High grade	Lymph node, refer to case #36	72.9
27	MEC	Parotid gland	IV	High grade	Lymph node, refer to case #37	51.8
28	MEC	Floor of the mouth	IV	High grade	Lymph node, refer to case #38	83.6
29	MEC	Parotid gland	IV	High grade	Lymph node, refer to case #39	5.1
30	MEC	Parotid gland	IV	High grade	Lymph node	93.4

ACC=adenoid cystic carcinoma, MEC=mucoepidermoid carcinoma

Table 3 Clinical features, histopathology and NM23 immunostaining index of the metastatic implants investigated in the present study

Case	Diagnosis	Location	Histological pattern	Primary site and/or corresponding case in Table 2	Index of NM23 immunostaining (%)
31	ACC	Lung	Solid	SMG, refer to case #16	13.8
32	ACC	Lymph node	Solid	SMG, refer to case #17	0.0
33	ACC	Lung	Cribriform	SMG, refer to case #18	27.2
34	ACC	Lung	Cribriform	SMG, refer to case #19	15.7
35	ACC	Lung	Solid	SMG, refer to case #20	0.0
36	MEC	Lymph node	High grade	PG, refer to case #26	0.0
37	MEC	Lymph node	High grade	PG, refer to case #27	55.6
38	MEC	Lymph node	High grade	FOM, refer to case #28	16.6
39	MEC	Lymph node	High grade	PG, refer to case #29	60.0
40	MEC	Lymph nodes	High grade	PG	10.2

ACC=adenoid cystic carcinoma, MEC=mucoepidermoid carcinoma, SMG=submandibular gland, PG=parotid gland, FOM=floor of mouth

NM23 immunostaining indices were compared between the four delineated groups by Mann–Whitney U or Kruskal–Wallis non-parametric statistical tests. Only probabilities of alpha-error less than 0.05 were considered significant.

Results

Immunostaining intensity with the antibody NCLnm23-37.6 was stronger than that with NCLnm23-2-NM301 regardless of the histologic typing of the SGN. There was a strong correlation between the indices of immunostaining reaction obtained with these two antibodies ($p<0.001$). The data presented in this report were the results of NCLnm23-37.6.

The NM23 protein was primarily seen in the cytoplasm of the salivary gland cells. In PA, both luminal and non-luminal (myoepithelial) cells were positive for NM23, but a stronger immunostaining was observed in the luminal cells (Fig. 1). In MEC, a strong NM23 immunostaining was seen in the intermediate and luminal cells of the cystic and solid areas. The mucous, clear and caliciform cells were negative (Fig. 2). In ACC, NM23 was observed in both luminal and non-luminal cells, albeit a strong reaction was restricted to the luminal cells in a fashion similar to that seen in PA (Fig. 3). The staining was also more intense in the cells of solid areas (not shown).

Due to the rarity of SGN malignancies, only ACC and MEC were available for evaluation at the time of this study. For convenience, "malignant SGN" and "ACC and MEC" will be used interchangeably in this report despite the fact that there are malignant SGN other than ACC and MEC.

The clinical, histopathologic and immunostaining data of the investigated cases are presented in Tables 1, 2 and 3. In summary, cytoplasmic NM23 was present in 12 out of 16 (75.0%) of the PA (mean index=29.4±30.3%) and in 24 out of 30 (80.0%) of the primary malignant SGN (mean

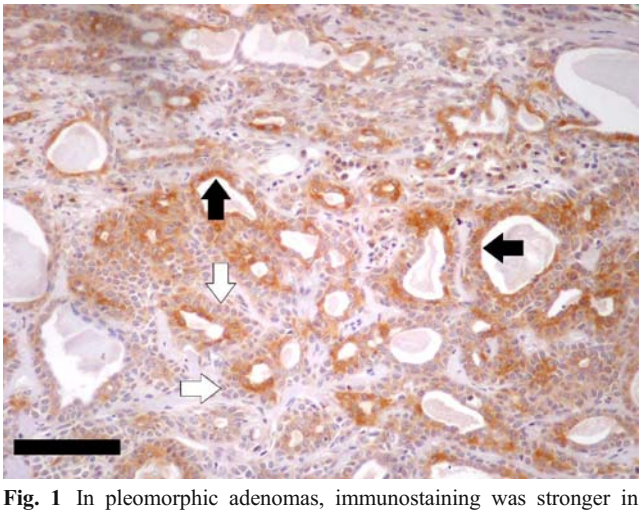

Fig. 1 In pleomorphic adenomas, immunostaining was stronger in luminal cells (black arrows) than in myoepithelial, non-luminal (white arrows) cells. Streptavidin–biotin–peroxidase, scale bar=100 μm

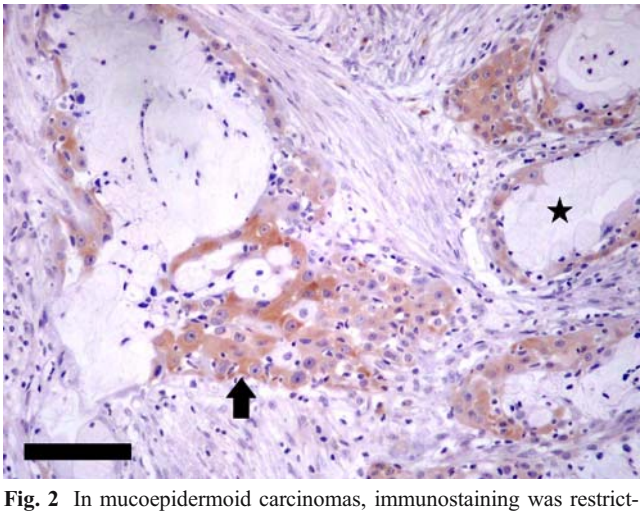

Fig. 2 In mucoepidermoid carcinomas, immunostaining was restricted to epidermoid and intermediate cells (arrows) while mucous and clear cells were negative (star). Streptavidin–biotin–peroxidase, scale bar=50 μm

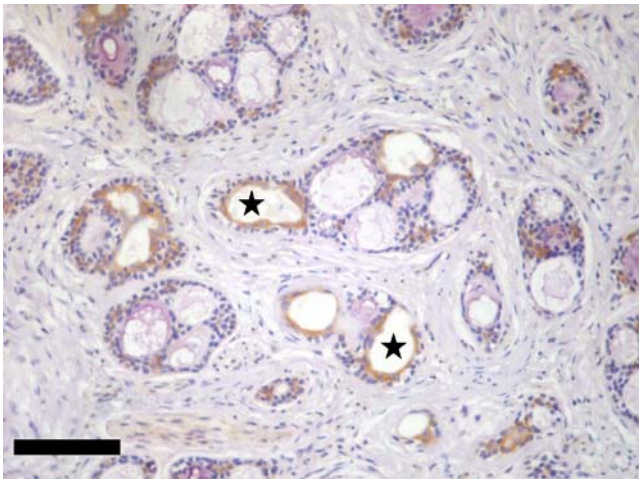

Fig. 3 In this cribriform adenoid cystic carcinoma, NM23 immunostaining was more evident in the cells underlying the luminal spaces (stars). Streptavidin–biotin–peroxidase, scale bar=100 μm

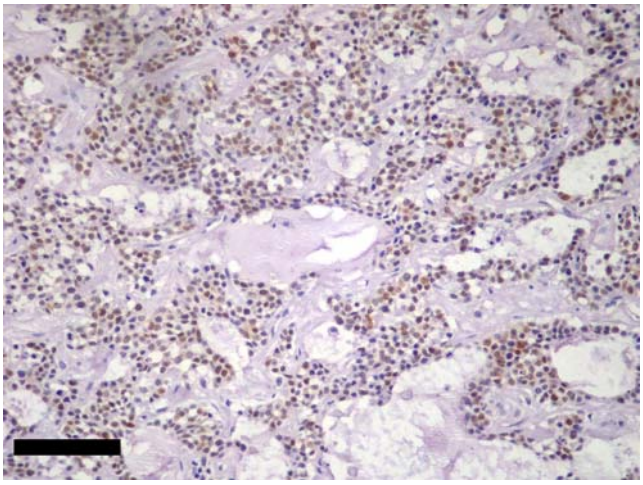

Fig. 4 Nuclear NM23 immunolocalization was observed in this adenoid cystic carcinoma. Streptavidin–biotin–peroxidase, scale bar=100 μm

index=33.6±34.4%). Among these 24 out of 30 malignancies, NM23 was found in 11 out of 15 (73.3%) of the primary malignancies with no evidence of metastasis (mean index=31.5±32.9%), and in 13 out of 15 (86.7%) of the primary malignancies with evidence of metastasis (mean index=35.6±36.9%). In addition, NM23 was found in six out of ten (60.0%) metastatic implants (mean index=18.9±22.5%). Statistically, there was no significant difference of the NM23 immunostaining index between benign and primary malignant tumors (p=0.79), nor among primary malignancies with no evidence of metastasis, primary malignancies with evidence of metastasis, and their metastatic implants (p=0.51). However, there is a trend showing a decreased NM23 expression in metastatic implants compared to their primary lesions. This trend can be seen in ACC (mean index=11.3% vs 22.8%) and MEC (mean index=26.4% vs 61.4%).

It is interesting to note that NM23 protein was seen in the nuclei of the neoplastic cells in 10 out of 15 primary malignancies with evidence of metastasis (four out of five MEC and six out of ten ACC) and their metastatic implants (six out of ten cases) (Fig. 4). This pattern was not observed in PA and primary SGN malignancies without evidence of metastasis.

Discussion

The NM23 protein (or nucleoside-diphosphate kinase) was associated with metastasis suppression experimentally [29]. Clinic-pathologically, there were reports that decreased or negative immunostaining of this protein may be associated with the development of metastasis of human malignancies from various tissue origins [8, 14, 25, 30]. However, this inverse relationship in salivary gland neoplasms has been controversial. It was found conclusively in some studies [11, 17, 28, 31] but inconclusively in one study [5]. In the present study by using an alternative, behavior-driven method to revisit this issue, we did not find any correlation between the metastatic potential of SGN and NM23 protein. Nevertheless, we did observe two interesting trends: decreased cytoplasmic NM23-positive cell populations in metastatic implants compared to their primary counterparts and nuclear NM23-positive cells solely seen in lesions with a history of metastasis and their metastatic implants.

In the present study, NM23 protein was immunohistochemically detected in 75.0% of PA, 68.7% of ACC, and 92.8% of MEC. These findings are similar to those reported previously [17, 28]. Of those 56 SGNs studied, the NM23 protein was found to be located in the cytoplasm of 75% of benign tumors, 73.3% of primary malignancies with no evidence of metastasis, 86.6% of primary malignancies with evidence of metastasis, and 60% of metastatic implants. Statistical analysis did not demonstrate a consistent correlation between NM23 expression and the metastatic potential of SGN. Our findings were consistent with a previous report [5]. However, it was reported that negative NM23 immunostaining in malignant SGN is associated with a higher frequency of metastasis [17, 28]. A recent study showed that benign SGN were significantly associated with more frequent NM23 immunostaining reactions compared to the malignancies of SGN [13]. These contradictions illustrate that the interpretation of NM23 as a biological behavior marker in SGN remains elusive.

One possible explanation for the discrepancies is the diversity of the NM23 family combined with the selection of particular detecting antibodies. The NM23 family consists of 8 members, namely, NM23-H1 to NM23-H8.

NM23-H1 and NM23-H2 are abundant and most studied [1, 6, 20, 26]. Historically, several antibodies raised against NM23 were analyzed with respect to a wide range of neoplasms [5, 12, 16, 22, 23, 27]. Many studies were completed before the characterization of all members of the NM23 family and consequently it is not clear which family member was identified. Thus, it is difficult to interpret and compare the results. To make sure that the distribution of NM23 in this study was representative, we employed two clones of antibody available commercially: NCLnm23-37.6 and NCLnm23-2-NM301. The 37.6 monoclonal antibody binds to the H1 isoform of NM23, but may cross-react with the H2 isoform, while the NM301 clone is specific for binding to the H1 isoform only (information obtained from Novocastra Labs., Newcastle, UK). In the present work, less intense immunostaining was obtained with the NM301 clone, but similar histo-morphological distribution of NM23-positive cells was observed using both antibodies, resulting in a strong statistical correlation between the immunostaining indices of these two antibodies. Similar result was also found in colorectal carcinomas [18]. Thus, we believed that the distribution of NM23 protein in the SGN of this study is representative and the data of this study are reliable.

Many qualitative and semiquantitative methods for the evaluation of NM23 immunostaining were applied to the study of salivary gland neoplasms. In common, all of these protocols established empiric and heterogeneous cut-off values to determine positivity or negativity [5, 12, 17, 27, 28, 31]. Yet, in our study there was no empiric cut-off value. Only those with immunostaining indices of zero were considered negative. Our results are not consistent with the conclusions of four different groups [13, 17, 28, 31]. This discrepancy may be due to different data analysis methods. Therefore, our data were re-analyzed with two different alternatives: by tumor growth pattern and by overexpressed cell population. Clusters of lesions with distinct histomorphology growth pattern (e.g. cribriform vs solid patterns) believed to be associated with certain biological behavior were compared with the NM23 expression levels of the clusters. This method was unable to demonstrate any conclusive differences among the studied lesions. Furthermore, it is debatable for almost all immunohistochemical evaluations if the analysis should be best based on the number of cells with over-expression regardless of the overall staining index, or based on the overall staining index regardless of the local areas of over-expression [15, 16, 21, 24]. With this in mind, each case was re-evaluated and re-defined using the positive reaction at three different cut-off values where more than 30%, 25%, or 10% of cells demonstrate over-expression. None of these evaluations reached different conclusions (data not shown).

Although our data did not support an inverse relationship between NM23 and the metastatic potential of SGN, there were trends showing (a) cytoplasmic NM23-positive cell populations in metastatic implants were decreased compared to their primary counterparts and (b) nuclear NM23 was exclusively seen in the primary SGN with evidence of metastasis and their metastatic implants. This nuclear NM23 staining pattern was consistent with those findings in normal and neoplastic thyroid [3], as well as cutaneous fibrohistiocytic tumors [21]. A recent report claimed that NM23-H1 and NM23-H2 are transiently internalized into the nuclei late in the G1 phase of the cell cycle, and are excluded from the nuclei during the S phase [6]. This cell cycle-dependent NM23 localization would explain the interesting trends seen in this study. It is possible that in our model, the NM23 protein in SGN malignant cells was internalized from the cytosol into the nucleus of those cells capable of metastasis. The amount of internalized NM23 is likely increased above the baseline to a level detectable by immunohistochemistry. As a result, there were decreased cytoplasmic NM23-positive cell populations and nuclear NM23 was seen solely in the metastasizing/metastatic cells. The cause-and-effect of this above baseline internalization of NM23 in metastasizing/metastatic cells is beyond the scope this study. It could be the over-internalized nuclear NM23 that triggers the metastasis cascade or metastasizing/metastatic cells to allow more NM23 molecules to be accumulated intra-nuclearly. One way or the other, it is clear that there is an above normal amount of nulcear NM23 seen only in malignant cells of primary SGN with evidence of metastasis and in cells of metastatic implants. Thus, this nuclear NM23 could be a good marker for identifying SGN neoplastic cells capable of metastasis. This interpretation is based on a small sample size. In the future, further study on a larger scale will shed more light on the potential application of nuclear NM23 protein.

In conclusion, our results demonstrate that the level of cytoplasmic NM23 protein was not associated with the metastatic potential of SGN. However, the exclusive presentation of NM23 protein in the nuclei of metastasizing/metastatic cells suggested that the nuclear NM23 protein could be a biomarker for SGN capable of metastasis.

Acknowledgments This study was financially supported by the National Council for Research and Development (CNPq) and by the Research Supporting Foundation of Minas Gerais (FAPEMIG), Brazil.

The authors acknowledge Dr. Charles F. Shuler for the grammatical review.

References

1. Amrein L, Barraud PA, Daniel JY, Perel Y, Landry M (2005) Expression patterns of nm23 genes during mouse organogenesis. Cell Tissue Res 5:1–14

2. Barnes L, Eveson JW, Reichart P, Sindransky D (2005) World Health Organization Classification of Tumours. Pathology and genetics of head and neck tumours. IARC Press, Lyon
3. Bertheau P, De La Rosa A, Steeg PS, Merino MJ (1994) NM23 protein in neoplastic and nonneoplastic thyroid tissues. Am J Pathol 145:26–32
4. Bevilacqua G, Sobel ME, Liotta LA, Steeg PS (1989) Association of low nm23 RNA levels in human primary infiltrating ductal breast carcinomas with lymph node involvement and other histopathological indicators of high metastatic potential. Cancer 49:5185–5190
5. Birek C, Chung W, Mcneill K (1998) Heterogeneous expression of NM23-H1 putative oncossupressor-protein in salivary gland neoplasms. Oral Surg Oral Med Oral Pathol Oral Radiol Endo 86:215
6. Bosnar MH, Gunzburg J, Bago R, Brecevic K, Weber I, Pavelic J (2004) Subcellular localization of A and B Nm23/NDPK subunits. Exp Cell Res 298:275–284
7. Bradley PJ (2001) Distant metastases from salivary glands cancer. ORL J Otorhinolaryngol Relat Spec 63:233–242
8. Charpin C, Bouvier C, Garcia S, Martini F, Andrac L, Lavaut MN, Allasia C (1997) Automated and quantitative immunocytochemical assays of nm23/NDPK protein in breast carcinomas. Int J Cancer 74:416–420
9. de la Rosa A, Williams RL, Steeg PS (1995) Nm23/nucleoside diphosphate kinase: toward a structural and biochemical understanding of its biological functions. Bioessays 17:53–62
10. Ellis GL, Auclair P (1996) Tumors of the salivary glands. Atlas of tumor pathology, series 3, fascicle 17. Armed Forces Institute of Pathology, Washington, pp155–175
11. Fan Z, Beresford PJ, Oh DY, Zhang D, Lieberman J (2003) Tumor suppressor NM23-H1 is a granzyme A-activated DNase during CTL-mediated apoptosis, and the nucleosome assembly protein SET is its inhibitor. Cell 112:659–672
12. Gazzeri S, Brambilla E, Negoescu A, Thoraval D, Veron M, Moro D, Brambilla C (1996) Overexpression of nucleoside diphosphate/kinase A/nm23-h1 protein in human lung tumors: association with tumor progression in squamous carcinoma. Lab Invest 74:158–167
13. Gong L, Chen ZL, Hu J, Huo HY (2004) Expression of p16 and nm23 genes in salivary gland tumours. Huaxi Kouqiang Yixue Zazhi 22:155–157 (article in Chinese)
14. Hartsough MT, Steeg PS (2000) Nm23/nucleoside diphosphate kinase in human cancers. J Bioenerg Biomembranes 32:301–308
15. Heimann R, Fergunson DJ, Hellman S (1998) The relationship between nm23, angiogenesis, and the metastatic proclivity of node-negative breast cancer. Cancer Res 58:2766–2771
16. Heimann R, Lan F, Mcbride R, Hellman S (2000) Separating favorable from unfavorable prognostic markers in breast cancer: the role of E-cadherin. Cancer Res 60:298–304
17. Jin H, Li J, Chen X (1997) Significance of nm23 expression in malignant carcinoma of salivary gland. Zhonghua Kouquiang Yixue Zazhi 32:341–343 (article in Chinese)
18. Kapitanovic S, Cacev T, Berkovic M, Popovic-Hadzija M, Radosevic S, Seiwerth S, Spaventi S, Pavelic K, Spaventi R (2004) nm23-H1 expression and loss of heterozygosity in colon adenocarcinoma. J Clin Pathol 57:1312–1318
19. Kiyoshima T, Shima K, Kobayashi I, Matsuo K, Okamura K, Komatsu S, Rasul AME, Sakai H (2001) Expression of p53 tumor suppressor gene in adenoid cystic and mucoepidermoid carcinomas of the salivary glands. Oral Oncol 37:315–322
20. Lakso M, Steeg PS, Westphal H (1992) Embryonic expression of nm23 during mouse organogenesis. Cell Growth Differ 3:873–879
21. Lee CS, Clarke RA, Tran KT, Kearsley JH, Chou ST (1999) nm23 protein expression and p53 immunoreactivity in cutaneous fibrohistiocytic tumors. Pathology 31:123–126
22. Lu Y, Zhou Z, He Z, Yang C (1995) Anti-metastasis gene nm23 expression in buccal cancer studied by immunohistochemistry stain. Huaxi Yike Daxue Xuebao 26:367–370 (article in Chinese)
23. Ohta Y, Nozaki Z, Nozawa H, Kamesui T, Tsunezuka, Oda M, Watanabe G (2001) The predictive value of vascular endothelial growth factor and nm23 for the diagnosis of occult metastasis in non-small cell lung cancer. Jpn J Cancer Res 92:361–366
24. Otsuki K, Alcalde RE, Matsumura T, Kimura N (1997) Immunohistochemical analysis of nucleoside diphosphate kinases in oral squamous cell carcinomas. Oncology 54:63–68
25. Ouatas T, Salerno M, Palmieri D, Steeg PS (2003) Basic and translational advances in cancer metastasis: nm23. J Bioenerg Biomembranes 35:73–79
26. Postel EH (1999) Cleavage of DNA by human NM23-H2/nucleoside diphosphate kinase involves formation of a covalent protein-DNA complex. J Biol Chem 274:22821–22829
27. Sawan A, Lascu I, Veron M, Anderson JJ, Wright C, Horne CHW, Angus B (1994) NDP-K/nm23 expression in human breast cancer in relation to relapse, survival, and other prognostic factors: an immunohistochemical study. J Pathol 172:27–34
28. Shi H, He R, Qiu W (1997) nm23 expression and its correlation with lung metastasis in human salivary adenoid cystic carcinoma. Zhonghua Kouquiang Yixue Zazhi 32:4–6 (article in Chinese)
29. Steeg PS, Bevilacqua LK, Thorgeirsson UP, Talmadge JE, Liotta LA, Sobel ME (1988) Evidence for a novel gene associated with low tumor metastatic potential. J Natl Cancer Inst 80:200–204
30. Takes RP, Baatenburg de Jong RJ, Schuuring E, Hermans J, Vis AA, Litninov SV, van Krieken JH (1997) Markers for assessment of nodal metastasis in laryngeal carcinoma. Arch Otolaryngol Head Neck Surg 123:412–419
31. Xu S, Wu M, Yang Y, Wang J, Chen Z (2001) Detection of proteins and mRNA of p16, p53, and nm23 in mucoepidermoid carcinoma of salivary glands and their prognostic significance. Zhonghua Binglixue Zazhi 30:273–275 (article in Chinese)

cycle, which prevents progression from G1 to S phase by inhibiting the catalytic activity of CDK4 or CDK6/cyclin D complex and subsequently Rb protein phosphorylation [9, 15]. Loss of normal p16 activity in melanoma is mainly due to inactivating mutations or to deletions of the CDNK2A locus.

The purpose of this study is to investigate the expression of p16 in relation with the histopathologic features and the clinical course in patients with malignant melanoma of the sinonasal tract. To this aim, we examined the expression of p16 by immunohistochemistry in a series of 37 sinonasal melanomas. Furthermore, we performed interphase fluorescence in situ hybridization (FISH) for the 9p21 locus in a subset of cases.

Methods

Immunohistochemistry

Paraffin sections (5-μm thickness) were dewaxed and hydrated, and after the inactivation of endogenous peroxidase with 3% hydrogen peroxidase for 20 min, they were submitted to an antigen retrieval procedure with microwave oven heating at 97°C for 40 min in 10× citrate buffer, followed by several washes in Tris/HCl buffer (Wash Buffer 10×). The primary antibody (clone E6H4, DakoCytomation) was applied at 1:25 dilution and the reaction was visualized using the En Vision/HRP Plus mouse kit (DAKO) with aminoethylcarbazol (AEC, LabVision Corporation) as chromogen. Nuclei were lightly counterstained with haematoxylin.

Evaluation of the immunostaining was performed by two pathologists (AF and DM). Positivity was estimated by assessing the percentage of positive cells in 10 high power (40× objective) fields. Cases showing nuclear or both nuclear and cytoplasmic staining in >20% of tumour cells were considered positive for p16.

Fluorescence in situ hybridization for 9p21 region

Fluorescence in situ hybridization (FISH) analysis was carried out on 4-μm sections placed on positively charged slides and air-dried overnight at 56°C. Rehydration of the sections was followed by pretreatment in 0.2 mol/l HCl for 20 min at room temperature and pretreatment in 1 mol/l sodium thiocyanate at 80°C for 30 min. Then the sections were enzymatically digested with protease (2,500–3,000 U/mg in NaCl, pH 2.0) for 12 min at 37°C and subsequently fixed in 10% buffered formalin at room temperature for 10 min. Dual-target, dual-colour FISH assay was performed using the LSI 9p21 spectrum orange/CEP9 spectrum green (Vysis, Downers Grove, IL) centromeric probe for chromosome 9 and locus-specific probe for band 9p21 directly labelled with orange and green fluorochromes. Ten microlitres of probe was applied to the selected area on each slide and covered with a glass coverslip sealed with rubber cement. Simultaneous probe/specimen denaturation at 84°C for 10 min with subsequent overnight incubation at 37°C was performed in the HYBrite hybridization chamber (Vysis Inc.). Slides were then immersed in posthybridization solution 0.4× standard saline citrate (SSC)/0.3% NP40 for 2 min at 73°C and in 2× SSC/0.1% NP40 for 1 min at room temperature. After dehydration in a ethanol series, 10 μl of 4,6-diamino-2-phenyindole-2-hydrocloride (DAPI) (Vysis Inc.) was applied to all the sections for chromatin counterstaining. The fluorescent signals were analysed under a fluorescence microscope Leica DM RD (Leica Mikrosystems Vertrieb GmbH, Germany): the 9p21 sequence was visualized with a Rand B Phycoeritrin filter, the chromosome 9 centromere sequence was visualized with a fluorescein isothiocyanate (FITC) filter and the nuclei were identified with a DAPI filter. Signals were scored in at least 100 non-overlapping nuclei with intact morphology. Non-neoplastic cells were used as a control for the probe pair. Heterozygous deletions were defined as >50% nuclei containing either one signal of locus-specific 9p21 probe and ≥2 signals of reference CEP 9 probe.

Statistical analysis

Statistical tests were performed using the SPSS software (release 14.0, SPSS Inc., Chicago, IL). The relationship between p16 expression and clinico-pathologic variables was assessed by the two-tailed Fisher's exact test or by the Pearson's chi-squared method. Overall survival curves and disease-free survival curves were obtained using the Kaplan–Meier method and compared using the log-rank test. All p values resulted from the use of two-sided statistical tests. $p<0.05$ was considered significant.

Results

Patients

A total of 37 cases of primary mucosal melanoma of the nasal cavities and paranasal sinuses were retrieved from our files. The patients were 24 women and 13 men, ranging in age between 48 and 96 years at presentation (median, 77 years). Twenty-three tumours were located in the nasal cavities, 10 involved both the nasal cavities and paranasal sinuses or orbit, whereas in 4 patients, the anatomic site was a paranasal sinus. Follow-up data were available for 32 patients (mean follow-up, 29.3 months). Six patients (18.8%) developed lymph node metastases,

whereas distant metastases occurred in 7 (21.9%). Fifteen patients (46.9%) died of the disease after a mean follow-up period of 37.7 months.

Haematoxylin- and eosin-stained slides from all cases were reviewed, and the following parameters were recorded for each tumour: type of surface epithelium (squamous or cylindrical); ulceration (present or absent); pagetoidism (present or absent), junctional activity (present or absent) and melanin pigment (present or absent); architecture of growth (alveolar, diffuse or mixed); cell type (epithelioid, spindle, mixed). Since in most cases, the material available for review was fragmented, an accurate measurement of tumour thickness was impossible.

Histopathologic features

The type of surface epithelium could be assessed in 26 lesions. In most cases, there were areas of squamous metaplasia (80.7%), whereas respiratory type epithelium was observed only in five instances (19.3%). In addition, almost all cases (32 of 37, 86.4%) presented areas of ulceration of the surface. Junctional activity of the neoplasm was noted in 13 lesions, and pagetoid spread within the epithelium was observed in nine tumours, although these features could not be assessed in all cases. Presence of ulceration and fragmentation of the material precluded an accurate measurement of tumour thickness. However, an attempt to measure tumour thickness from the surface to the point of greatest infiltration in the mucosa could be done in 29 lesions, which measured between 0.2 and 2.5 cm, with a mean of 0.9 cm. Melanin pigment was present in tumour cells of 18 lesions (48.6%), whereas an infiltrate of melanophages was observed in 7 lesions (19%). The majority of tumours (29, 78.3%) showed a diffuse architecture of growth, whereas in the remaining cases, tumour cells were arranged in an alveolar pattern. The appearance of tumour cells was variable, with most cases being characterised by an epithelioid morphology (67.5%) and the remaining showing a spindle cell (8.1%) or mixed/pleomorphic (24.4%) morphology.

Immunohistochemical analysis

Nuclear and cytoplasmic positivity for p16 was observed in 15 melanomas (40.5%) (Fig. 1a), 10 of which showed >20% of positive tumour cells. Immunostaining was also present in surface and glandular epithelia. Overall, 27 melanomas (72.9%) showed loss of p16 expression, with 22 cases being negative and 5 cases showing only few scattered positive cells (Fig. 1b). All cases with spindle or mixed cytology showed loss of p16, whereas this was present in 60% of tumours with epithelioid appearance (p=0.01). Loss of p16 expression was more frequently seen in melanomas with alveolar architecture (87.5%) than in tumours with diffuse architecture (68.9%), but this difference was not significant (p=0.4). There was no correlation between p16 status and any other pathologic feature in our series of sinonasal melanomas (Table 1).

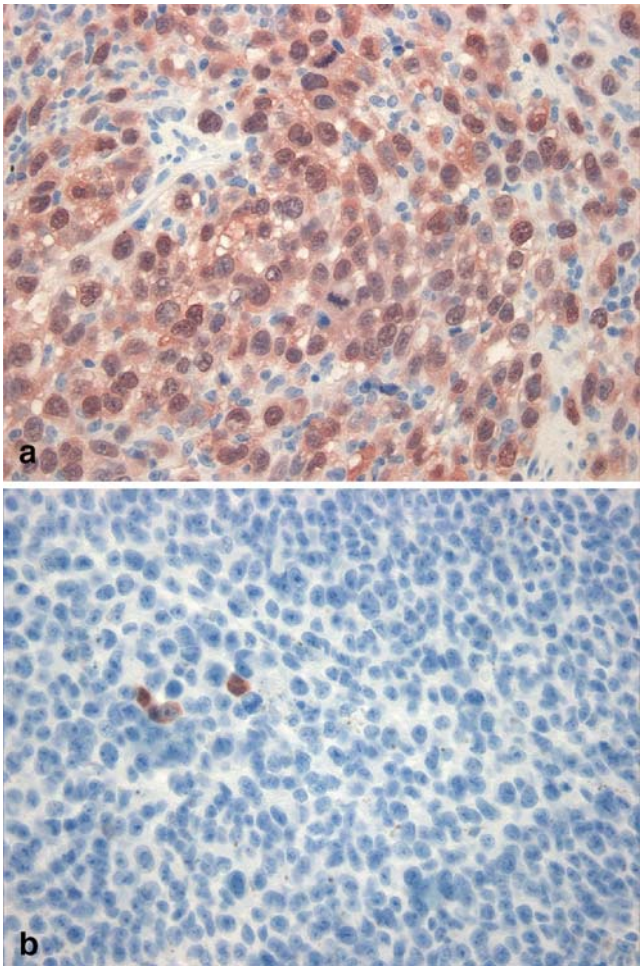

Fig. 1 Sinonasal melanoma showing diffuse nuclear and cytoplasmic staining for p16 (**a**). The case depicted in **b** shows loss of p16 expression, with only few scattered cells showing nuclear and cytoplasmic positivity

Of 32 patients with available follow-up, 15 (46.9%) died of the disease (follow-up ranging between 2 and 201 months; mean, 30.3 months). There was no correlation between p16 expression and presence of lymph node or distant metastases (p=0.57 and 0.24, respectively). The 5-year overall survival rate was 44.4% in the present series. p16 status did not influence overall survival (p=0.29) and disease-free survival (p=0.19).

FISH analysis

Interphase FISH analysis was successfully performed in 17 cases. Of these, 11 showed deletion of the 9p21 region

Table 1 Correlation between p16 immunohistochemical expression, the results of FISH analysis of 9p2.1 region and clinico-pathological parameters in sinonasal melanoma

	p16 immunohistochemistry		Statistical analysis, *P*
	0–20% (*n*=27, 72.9%)	21–100% (*n*=10, 27.1%)	
FISH 9p2.1			
Normal (35.3%)	1 (16.6%)	5 (83.4%)	–
Deletion (64.7%)	10 (90.9%)	1 (9.1%)	
Architecture			
Alveolar (21.7%)	7 (87.5%)	1 (12.5%)	0.4
Diffuse (78.3%)	20 (68.9%)	9 (31.1%)	
Cytology			
Epithelioid (67.5%)	15 (60%)	10 (40%)	0.01
Spindle/mixed (32.5%)	12 (100%)	0 (0%)	
Lymph node metastasis			
No (81.2%)	19 (73.1%)	7 (26.9%)	0.57
Yes (18.8%)	5 (83.3%)	1 (16.7%)	
Distant metastasis			
No (78.1%)	20 (80%)	5 (20%)	0.24
Yes (21.9%)	5 (62.5%)	3 (37.5%)	

(Fig. 2), which in one case consisted of an homozygous deletion. Overall, there was a good agreement with the results of the immunohistochemical analysis: 10 of the 11 cases with 9p21 deletion showed loss of protein expression, whereas 5 of the 6 cases with no alteration of the 9p21 region showed unaltered levels of protein expression (Table 1).

Discussion

The clinico-pathologic features of our series are substantially similar to those previously reported in the literature.

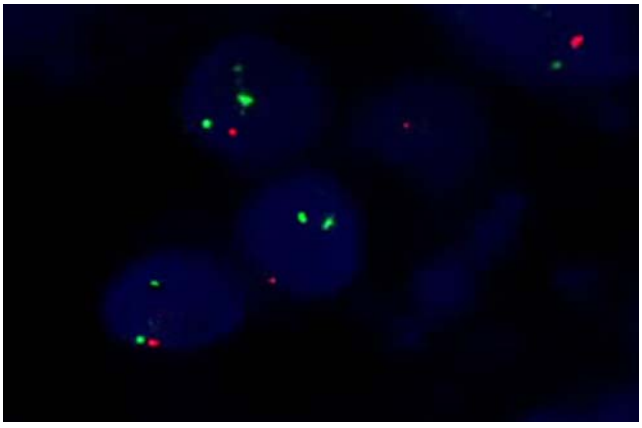

Fig. 2 FISH analysis showing deletion of the 9p21 locus in a case of sinonasal melanoma (same case of Fig. 1b). Two *green signals* corresponding to the centromeric probe for chromosome 9 can be seen, whereas only one *orange signal* corresponding to the 9p21 locus is present

Sinonasal melanoma is a rare tumour characterised by advanced age at diagnosis, which is usually performed when the tumour has reached considerable dimensions due to the late development of symptoms. This explains the poor prognosis with a reported 5-year survival rate of about 40%, which is consistent with that observed in the present series [20]. Overall, these features clearly separate sinonasal melanoma from cutaneous melanoma, which is far more common, occurs in younger patients and is associated with a relatively low mortality, in relation with the high rate of early diagnoses [4]. Such differences may be due to different molecular events leading to the development of these tumours.

Indeed, there is increasing evidence that distinct genetic pathways determine the development of malignant melanoma, and these pathways appear to be related to the exposure to ultraviolet light. In this view, mucosal melanomas share some similarities with melanomas arising in areas relatively protected from the sun like acral melanomas since both groups are characterised by a significantly higher degree of chromosomal aberrations than melanomas arising in other cutaneous regions [5].

So far, only few studies have attempted to characterise the genetic alterations present in sinonasal melanoma. Van Dijk and coworkers [21] evaluated chromosomal aberrations in a series of 14 sinonasal melanomas using comparative genomic hybridization (CGH). They observed a high frequency of gains at 1q, 6p and 8q, whereas losses of chromosome 9 were present in 50% of cases [21]. In a more recent molecular study of cutaneous and mucosal melanoma, deletion of the CDNK2A locus was the most commonly observed genomic loss [5]. In addition, mucosal and acral melanomas more frequently showed losses of the

CDNK2A locus in comparison with melanomas arising in skin with or without sun-induced damage [5].

In our series of 37 primary malignant melanomas of the nasal cavities and paranasal sinuses, loss of p16 expression was found in 72.9% of the tumours. This is a higher rate than that observed in studies previously conducted on cutaneous melanomas where loss of p16 expression determined by immunohistochemical analysis occurred in about 50% of the invasive lesions [11, 13, 14, 17, 18]. Previous immunohistochemical studies of p16 expression in sinonasal melanoma resulted in similar rate of protein loss [12]. In addition, loss of heterozygosity (LOH) analysis conducted in a case of nasal melanoma and in the adjacent nasal melanosis using a flanking marker for the p16 gene showed LOH in the area of melanosis and complete loss of both alleles within the tumour [8]. Thus, loss of p16 for deletion of the CDNK2A locus may play a major role in the deregulation of cell-cycle control pathways occurring in sinonasal melanoma, and it is likely to be an early event in the development of this tumour.

To investigate the mechanisms involved in the loss of p16 expression in sinonasal melanoma, we evaluated the status of the 9p21 locus in a subset of cases by FISH analysis. We found that all but one cases showing loss of p16 expression at the protein level had deletion of the 9p21 locus, including one tumour with homozygous deletion. Other possible mechanisms for reduced p16 expression include promoter hypermethylation and gene mutation, which may involve the other allele. However, even if hemizygosity for p16 were present, a reduction in functional protein to 50% of normal levels could be sufficient to reduce p16 levels to below the threshold for immunohistochemical detection [17].

In cutaneous melanoma, loss of p16 expression has been correlated with poor prognosis in patients with vertical growth phase lesions [18] and in tumours with Breslow thickness equal or more than 1.0 mm [11]. In addition, cytoplasmic immunostaining for p16 has been recognised as a predictor of negative sentinel lymph node status [11]. In our series of sinonasal melanoma, no association was detected between p16 expression and clinical features, including age, sex, lymph node or distant metastases, as well as with patients' survival. This may be so since in sinonasal melanomas, the diagnosis is delayed in most cases for the absence of symptoms until the tumour has reached large dimensions so that the local control of the disease is often difficult to reach.

In summary, our study is the first attempt to assess the frequency of p16 alteration in a relatively large series of sinonasal melanomas. Loss of p16 expression appears to be a frequent event in this group of mucosal melanoma, occurring at higher frequency than cutaneous melanoma, and it appears to be mainly related to deletion of 9p21 region. At variance from cutaneous melanoma, loss of p16 expression is not correlated with the prognosis of patients affected by sinonasal melanoma.

References

1. Batsakis JG, Regezi JA, Solomon AR, Rice DH (1982) The pathology of head and neck tumors: mucosal melanomas. Head Neck Surg 4:404–418
2. Batsakis JG, Cove H (1994) Melanosis, melanocytic hyperplasia, and primary malignant melanoma of the nasal cavity. Cancer 44:1424–1433
3. Berthelsen A, Andersen AP, Jensen S, Hansen HA (1984) Melanomas of the mucosa in the oral cavity and the upper respiratory passages. Cancer 54:907–912
4. Chang AE, Karnell LH, Menck HR (1998) The National Cancer Data Base report on cutaneous and noncutaneous melanoma: a summary of 84,836 cases from the past decade. The American College of Surgeons Commission on Cancer and the American Cancer Society. Cancer 83:1664–1678
5. Curtin JA, Fridlyand J, Kageshita T, Patel HN, Busam KJ, Kutzner H, Cho KH, Aiba S, Brocker EB, LeBoit PE, Pinkel D, Bastian BC (2005) Distinct sets of genetic alterations in melanoma. N Engl J Med 353:2135–2147
6. Franquemont DW, Mills SE (1991) Sinonasal malignant melanoma. A clinicopathologic and immunohistochemical study of 14 cases. Am J Clin Pathol 96:689–697
7. Freedman HM, DeSanto LW, Devine KD, Weiland LH (1973) Malignant melanoma of the nasal cavity and paranasal sinuses. Arch Otolaryngol 97:322–325
8. Hofbauer GF, Boni R, Simmen D, Mihic D, Nestle FO, Burg G, Dummer R (2002) Histological, immunological and molecular features of a nasal mucosa primary melanoma associated with nasal melanosis. Melanoma Res 12:77–82
9. Kamb A, Gruis NA, Weaver-Feldhaus J, Liu Q, Harshman K, Tavtigian SV, Stockert E, Day RS III, Johnson BE, Skolnick MH (1994) A cell cycle regulator potentially involved in genesis of many tumor types. Science 264:436–440
10. Lund V (1982) Malignant melanoma of the nasal cavity and paranasal sinuses. J Laryngol Otol 96:347–355
11. Mihic-Probst D, Mnich CD, Oberholzer PA, Seifert B, Sasse B, Moch H, Dummer R (2006). p16 expression in primary malignant melanoma is associated with prognosis and lymph node status. Int J Cancer 118:2262–2268
12. Padilla Parrado M, Saez Castillo AI, Galan Morales JT, Orradre Romeo JL, Delgado Quero AL, Sanchez Carrion S (2001) Melanoma maligno de fosas nasales. Estudio retrospectivo. Analisis de la expresion de p53 y p16INK4. An Otorrinolaringol Ibero Am 28:303–316
13. Piccinin S, Doglioni C, Maestro R, Vukosavljevic T, Gasparotto D, D'Orazi C, Boiocchi M (1997) p16/CDKN2 and CDK4 gene mutations in sporadic melanoma development and progression. Int J Cancer 74:26–30
14. Reed JA, Loganzo F Jr, Shea CR, Walker GJ, Flores JF, Glendening JM, Bogdany JK, Shiel MJ, Haluska FG, Fountain JW et al (1995) Loss of expression of the p16/cyclin-dependent kinase inhibitor 2 tumor suppressor gene in melanocytic lesions correlates with invasive stage of tumor progression. Cancer Res 55:2713–2718
15. Serrano M, Hannon GJ, Beach D (1993) A new regulatory motif in cell-cycle control causing specific inhibition of cyclin D/CDK4. Nature 366:704–707
16. Sharpless NE, Chin L (2003) The INK4a/ARF locus and melanoma. Oncogene 22:3092–3098

17. Sparrow LE, Eldon MJ, English DR, Heenan PJ (1998) p16 and p21WAF1 protein expression in melanocytic tumors by immunohistochemistry. Am J Dermatopathol 20:255–261
18. Straume O, Sviland L, Akslen LA (2000). Loss of nuclear p16 protein expression correlates with increased tumor cell proliferation (Ki-67) and poor prognosis in patients with vertical growth phase melanoma. Clin Cancer Res 6:1845–1853
19. Trapp TK, Fu YS, Calcaterra TC (1987) Melanoma of the nasal and paranasal sinus mucosa. Head Neck Surg 113:1086–1089
20. Thompson LD, Wieneke JA, Miettinen M (2003) Sinonasal tract and nasopharyngeal melanomas: a clinicopathologic study of 115 cases with a proposed staging system. Am J Surg Pathol 27:594–611
21. van Dijk M, Sprenger S, Rombout P, Marres H, Kaanders J, Jeuken J, Ruiter D (2003) Distinct chromosomal aberrations in sinonasal mucosal melanoma as detected by comparative genomic hybridization. Genes Chromosomes Cancer 36:151–158
22. Wenig BM, Dulguerov P, Kapadia SB, Prasad ML, Fanburg Smith JC, Thompson LDR (2005) Neuroectodermal tumours. In: Barnes L, Eveson JW, Reichart P, Sidranski D (eds) World Health Organization classification of tumours. Pathology and genetics of head and neck tumours. IARC Press, Lyon, pp 65–75

been found to play an important role in tumor progression in association with angiogenesis, anaerobic metabolism, buffering of the intracellular compartment, and the induction of growth factors.

It has also been reported that the overexpression of HIF-1α is associated with a worse prognosis in patients with human malignant diseases including oligodendrogliomas and breast, head and neck, cervix, endometrial, and oropharyngeal cancers [1–3, 16, 29, 39, 43], whereas the HIF-1α expression has been reported to be associated with a favorable prognosis in recent studies, such as lung cancer and renal cell carcinoma [13, 31, 46]. The effect of HIF-1α expression on the prognosis of soft-tissue sarcomas has not yet been studied. Therefore, the aim of this study was to investigate whether HIF-1α protein expression has a prognostic impact in soft-tissue sarcomas.

Materials and methods

Study population and tissue preparation

The tissue samples that were used for this study were obtained from patients who underwent an open biopsy or a surgical resection at the Department of Orthopedic Surgery, Mie University Graduate School of Medicine after obtaining informed consent according to the institutional review board guidelines. Immediately after surgical removal, the tissue samples were fixed in 10% buffered formalin solution and embedded in paraffin 24 h later (for the histological analysis). Paraffin-embedded tumor tissue samples, measuring 4 μm in thickness, were placed on silanized slides (Dako Japan, Kyoto, Japan) and stained with hematoxylin and eosin. The histological sections of all patients were diagnosed by well-trained pathologists.

In all cases, immunohistochemical staining was used to diagnose spindle-cell sarcomas according to World Health Organization classification [14]. Immunostain was performed with the following antibodies: α-smooth muscle actin (SMA) (clone 1A4, 1/100 dilution; DAKO Japan), desmin (clone D33, 1/100 dilution; DAKO Japan), S-100 protein (polyclonal, 1/1,000 dilution; DAKO Japan), neuron-specific enolase (NSE) (clone BBS/NC/VI-H14, 1/200 dilution; DAKO Japan), pan-cytokeratin (CK) (clone 5D3 and LP34, 1/100 dilution; Novocastra Laboratories, UK), and epithelial membrane antigen (EMA) (clone E29, 1/100 dilution; DAKO Japan).

Leiomyosarcomas were diagnosed when tissue samples contained immunoreactivity for α-SMA and desmin. Synovial sarcomas were diagnosed when tissue samples contained immunoreactivity for pan-CK and EMA (Fig. 1a,b). Moreover, RNA extraction and reverse transcriptase polymerase chain reaction analysis were performed to detect SYT–SSX fusion gene transcripts. SYT–SSX fusion gene transcripts were detected in all tumors diagnosed as synovial sarcomas. In malignant peripheral nerve sheath tumors (MPNSTs), the immunoreactivity for S-100 protein and NSE was used for the diagnosis. Malignant fibrous histiocytomas (MFHs) were diagnosed primarily based on the morphological appearance in consideration of the results of no reactivity for immunostain, as being of storiform-pleomorphic type in 24 patients and of myxoid type (including myxofibrosarcoma) in five patients. There was no patient demonstrating either giant-cell type or inflammatory type.

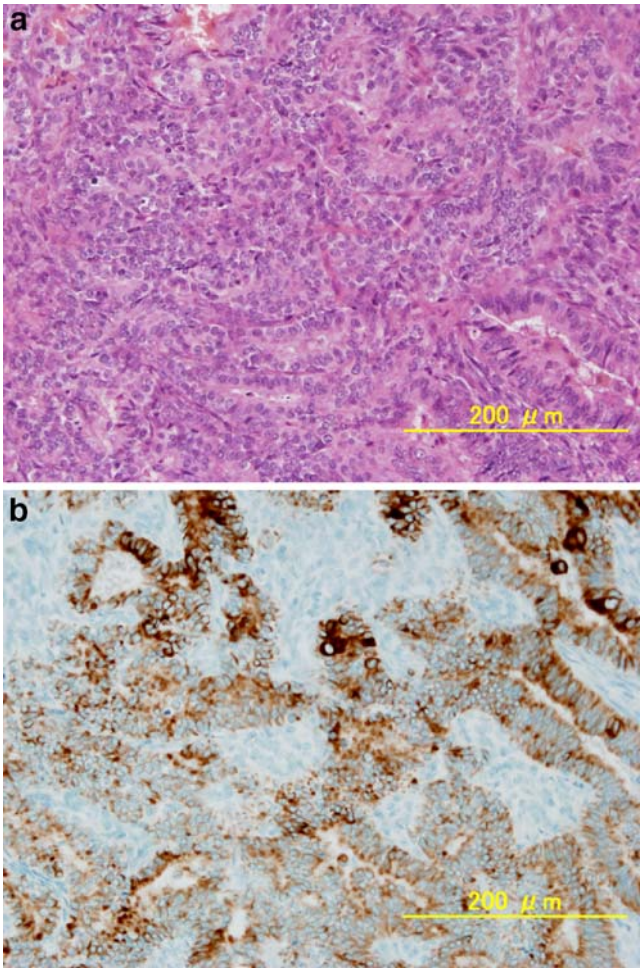

Fig. 1 **a** [Hematoxylin and eosin (H&E) stain, ×100] Specimens from a 15-year-old girl with biphasic synovial sarcoma, which has epithelial and spindle-cell components. **b** (Immunostain, ×100) Strong positivity for pan-cytokeratin in the tumor cytoplasm

Clinical and pathologic analysis

The details of clinicopathologic features are listed in Table 1. The series comprised 49 patients (23 men and 26 women). The median age of all patients was 63 years (range, 12–85). The median follow-up for all patients was 39 months (range, 5–181). The 49 tumor samples consisted

Table 1 Details of patient characteristics

Characteristics	No. of all patients (N=49)	No. of patients except for M1 (N=42)
Gender		
Male	23	19
Female	26	23
Age (years)		
≦59	19	17
≧60	30	25
Location		
Upper extremities	8	7
Lower extremities	25	22
Trunk	16	13
Size (cm)		
<5	10	9
≧5	39	33
Depth		
Superficial	7	7
Deep	42	35
Histology		
MFH	29	26
Synovial sarcoma	12	10
Leiomyosarcoma	4	3
MPNST	4	3
Primary or recurrence		
Primary	40	34
Recurrence	9	8

M1: patients with distant metastasis when distinct diagnosis was obtained

MFH malignant fibrous histiocytoma, *MPNST* malignant peripheral nerve sheath tumor

of 40 primary lesions and nine local recurrences. Seven patients had distant metastases at initial treatment. The histological diagnosis included 29 MFHs, 12 synovial sarcomas, four leiomyosarcomas, and four MPNSTs.

All patients underwent a complete tumor resection with a wide margin during the initial surgery at our hospital. Most patients underwent a limb-sparing resection, except for one patient who had an amputation.

Immunohistochemical analysis

Paraffin-embedded tumor tissue specimens measuring 4 μm in thickness were placed on silanized slides (Dako Japan, Kyoto, Japan) and then deparaffinized in xylol. Antigen retrieval was performed with 0.01 M citrate buffer at 97°C for 45 min. After cooling for 60 min and washing in PBS, automated immunohistochemistry was achieved with Ventana EX system using a DAB universal kit (Ventana Medical Systems, Tucson, AZ, USA), in which the visualization of bound antibodies was performed using the streptavidin-biotinylated complex method. The mouse monoclonal anti-HIF-1α antibody (clone Mab H1α67, NB 100-105; Novus Biologicals, Littleton, CO, USA) was diluted 1:1,000 in antibody diluent buffer (Dako, Japan). For proliferation studies, we performed the mouse Ab MIB-1 (Dako Japan), which recognizes the nuclear-cell proliferation-related Ki-67 antigen at 1:50 dilution. The slides were washed and then were incubated with secondary anti-mouse IgG antibody. 3-3′ diaminobenzidine tetrahydrocholoride (DAB) was used for coloration. Hematoxylin was used as the final nuclear counterstain.

In this study, the expression of HIF-1α was assessed semi-quantitatively by two parameters, the percentage of stained nucleus in tumor cells and the staining intensity, as suggested by the previous report [2, 39]. The percentage of positive cells was rated as follows: 0 point, cases with ≦10% positive cells were rated as negative, regardless of staining intensity; 2 points, 11–50% positive cells; 3 points, 51–80% positive; and 4 points, >80% positive cells. The staining intensity was rated as follows; 1 point, weak intensity; 2 points, moderate intensity; and 3 points, strong intensity. The points for the percentage of positive cells and staining intensity were added, and the specimens were categorized into four groups according to their overall score; negative expression, ≦10% cells stained positive, regardless of intensity, 0–2 points; weak expression, 3 points; moderate expression, 4–5 points; and strong expression, 6–7 points.

The expression of Ki-67 was assessed based on the percentage of cells showing nuclear staining.

Statistics and analysis

The chi-square test was used to analyze the associations between clinical-pathological variables. The chi-square test was used instead of Fisher's exact test, as there were no subgroup sizes less than 5. The metastasis-free survival (MFS) was defined as the time from the initial treatment to the date of clinically documented distant metastasis. The overall survival (OS) was defined as the time from the initial treatment to the date of death attributed to soft-tissue sarcoma.

For a prognostic analysis, the Kaplan–Meier survival analysis and log-rank tests were performed excluding the seven patients with distant metastases. For a multivariate analysis, a Cox proportional hazards regression model was used to identify the statistically significant differences in the survival and estimate hazard ratios and 95% confidence intervals. Prognostic variables identified by univariate analysis with $P<0.2$ were entered into a Cox multivariate analysis model. A p value <0.05 was considered to be significant. The analysis was performed using the StatView statistical software package (version 5.0; SAS Institute, Cary, NC, USA).

Results

Expression of HIF-1α and associations between HIF-1α expression and clinico-pathologic variables

An immunohistochemical analysis showed the nuclear accumulation of HIF-1α protein in 35 (71.4%) soft-tissue tumor samples. The expression of HIF-1α is summarized in Table 2 according to the histological diagnoses. The expression of HIF-1α was negative in 14 (28.6%) cases, weak in nine (18.4%) (Fig. 2a–c), moderate in 17 (35.4%), and strong in nine (18.4%) (Fig. 2d–f). In all samples that showed the nuclear accumulation of HIF-1α protein, HIF-1α expression was diffusely observed throughout the section. The chi-square test was used to analyze the associations between the HIF-1α expression and the clinico-pathologic variables. The level of HIF-1α expression was not associated with the histological diagnoses, patient's age, tumor size, tumor depth, distant metastasis, and expression of Ki-67 (data not shown).

Prognostic analysis

We next compared the MFS and OS of patients showing a high (strong and moderate) expression of HIF-1α with those of patients showing a low (weak and absent) expression of HIF-1α. For a prognostic analysis, the Kaplan–Meier survival analysis and log-rank tests were performed in 42 patients with spindle-cell sarcoma excluding the seven patients with distant metastases. A univariate analysis demonstrated the HIF-1α expression to be not associated with MFS (P=0.0858; Fig. 3a), but it was associated with a poor OS (P=0.029; Fig. 3b). In a univariate analysis, there were no significant differences between OS and other prognostic factors including the patient's age, gender, tumor size, tumor depth, and the expression of Ki-67 (Table 3).

Table 2 Expression of HIF-1α protein in the 49 patients with spindle-cell sarcoma

Histological diagnosis	Result of immunostaining			
	Negative	Weak	Moderate	Strong
MFH (N=29)	10	5	7	7
Synovial sarcoma (N=12)	4	2	4	2
Leiomyosarcoma (N=4)	0	1	3	0
MPNST (N=4)	0	1	3	0
Total (N=49)	14 (28.6%)	9 (18.4%)	17 (34.7%)	9 (18.4%)

HIF Hypoxia-inducible factor, *MFH* malignant fibrous histiocytoma, *MPNST* malignant peripheral nerve sheath tumor

A multivariate analysis demonstrated the expression of HIF-1α to be the only independent prognostic factor for OS (P=0.018; Table 4).

Discussion

Spindle-cell sarcomas that arise in soft tissue often show an aggressive clinical course. A subset of patients with this disease remains at high risk for tumor-related mortality. Biomarkers, which can predict the high-risk patients are very important because such biomarkers may be a useful indicator for determining whether adjuvant therapeutic modalities such as irradiation and chemotherapy should be performed. In soft-tissue sarcomas, the tumor size, tumor location, and histologic grade have been shown to be important prognostic factors [20]. However, these prognostic factors do not always reliably predict the patient's outcome because there is histologic herterogeneity, which reflects the biologic behavior of soft-tissue sarcomas.

Intratumoral hypoxia has been reported to induce a rapid increase of HIF-1 protein in tumor cells [21, 41], thus leading to the stimulation of numerous target genes. Recently, many experimental studies have helped to clarify that HIF-1α plays an important role in angiogenesis of malignant neoplasms [30]. Moreover, numerous researchers have been interested in the mechanism that regulates angiogenesis related to HIF-1α protein, because HIF-1α has a potential of therapeutic target of anti-cancer drugs [21, 42]. However, little is known about the clinical implications of HIF-1α expression in the prognosis of patients with soft-tissue sarcomas. In the present study, we examined the expression of HIF-1α protein in spindle-cell sarcoma and found that the overexpression of HIF-1α protein has an impact as a biomarker of tumor aggressiveness.

In previous reports, most cancers showed an intense HIF-1α expression in the area adjacent to necrosis and invading tumor margins because hypoxia is the main regulator of HIF-1α [4, 45, 50]. However, we observed HIF-1α protein diffused throughout the section. These results suggest that HIF-1α protein in sarcoma cells may be regulated by several non-oxygen-dependent mechanisms [42, 45]. Cytokines and other signaling molecules such as insulin-like growth factor (IGF), epidermal growth factor (EGF), and interleukin-1 induce HIF-1α synthesis through either the phosphatidylinositol 3-kinase (PI3K) or mitogen-activated protein kinase (MAPK) pathways [27, 37].

Furthermore, HIF-1α stability increases in response to genetic alterations. For instance, the loss of function mutations in tumor suppressor genes, such as PTEN and VHL, may influence the stability of HIF-1α [27, 42, 51]. In addition, the expression of oncogenes, such as V-SRC, has also been

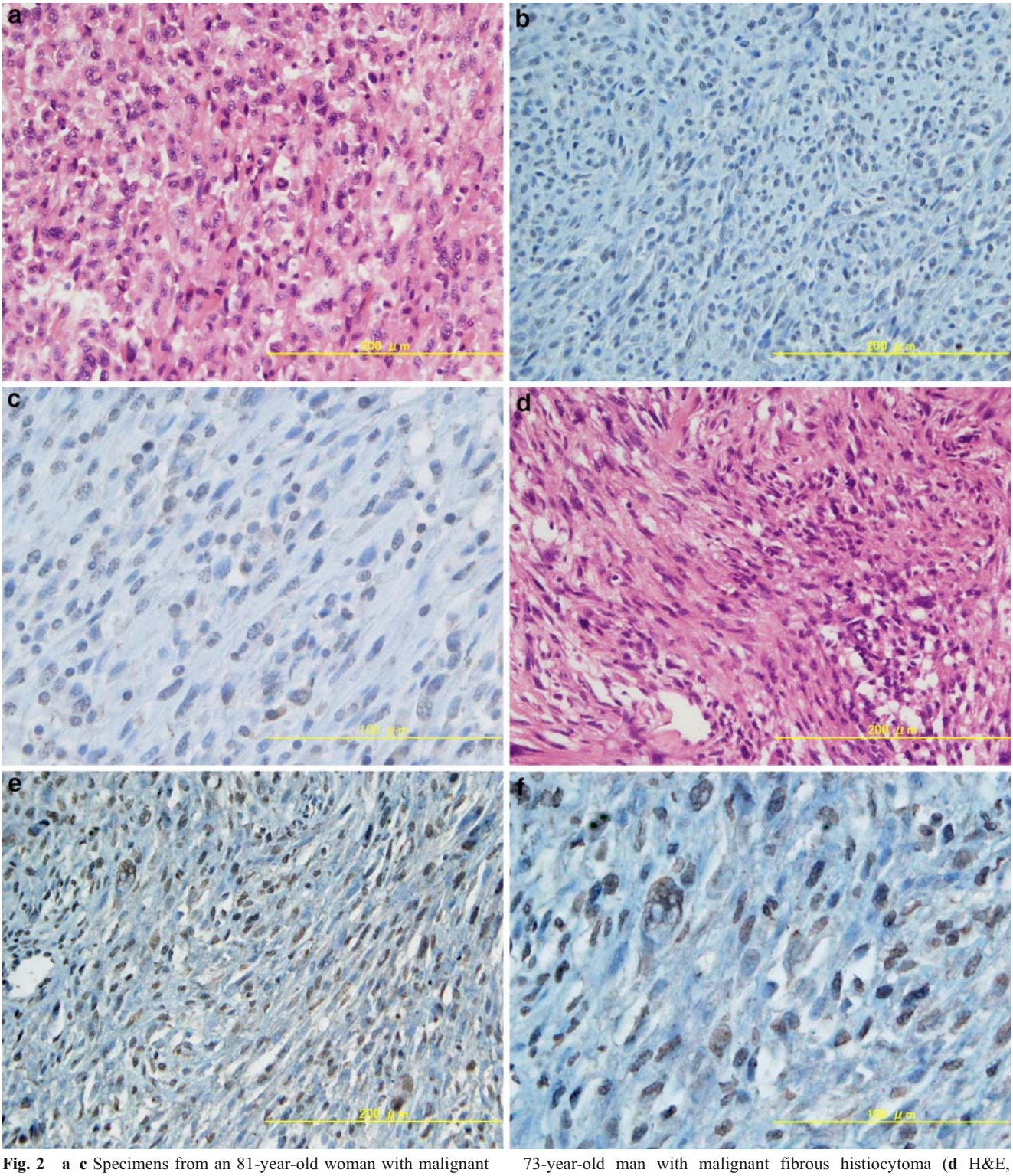

Fig. 2 **a**–**c** Specimens from an 81-year-old woman with malignant fibrous histiocytoma (**a** H&E, ×200) showing a weak expression of HIF-1α (**b**, **c** Immunostain; **b** ×200, **c** ×400). **d**–**f** Specimens from a 73-year-old man with malignant fibrous histiocytoma (**d** H&E, ×200) showing a strong expression of HIF-1α (**e**, **f** immunostain; **e** ×200, **f** ×400)

implicated in the HIF-1α expression at normoxia [26]. Consequently, the diffuse expression of HIF-1α in sarcomas may be caused not by tumor hypoxia, but by an oncogene, a tumor suppressor gene, and other signaling molecules.

The patients with a strong or moderate expression of HIF-1α had a significantly shorter overall survival rate compared to those having a weak or negative expression based on a univariate analysis and a multivariate analysis.

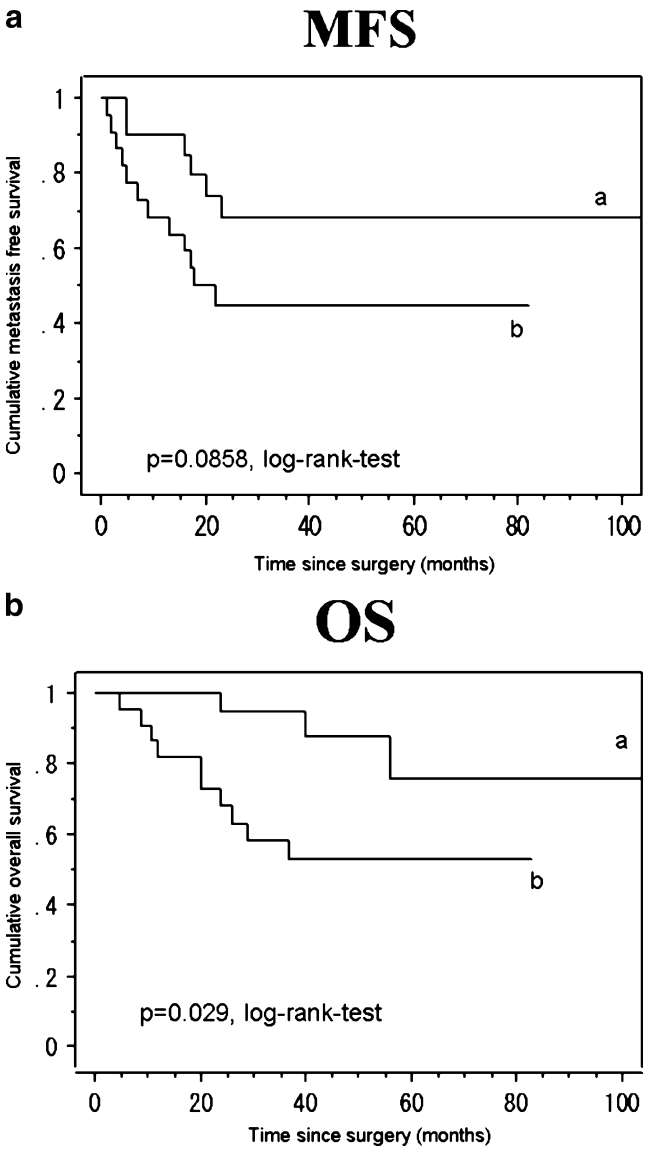

Fig. 3 **a** Cumulative metastasis-free survival (MFS) of **a** patients with a negative or weak expression of HIF-1α, compared with **b** patients with a moderate or strong expression in spindle-cell sarcomas. **b** The cumulative overall survival (OS) of **a** patients with a negative or weak expression of HIF-1α, compared with **b** patients with a moderate or strong expression in spindle-cell sarcomas. Kaplan–Meier curves confirmed that the overall survival rates for patients with moderate or strong expression of HIF-1α were significantly reduced

Known HIF-1-inducible proteins, which might be important in sarcoma cell biology, include CA IX, Glut-1, EPO, inducible nitric oxide synthase (iNOS), and VEGF. Although we have not yet examined the expression of these HIF-1α-inducible proteins, some previous reports have demonstrated the relationship between the expression of HIF-1α-inducible protein and disease prognosis in soft-tissue sarcoma. CA IX is a transmembrane glycoprotein that is involved in the maintenance of intracellular pH in hypoxic

Table 3 Univariate survival analysis in 42 patients with spindle-cell sarcoma

Prognostic factor	No. of the patients	5-year survival rate (%)	*p* value[1]
Patient's age (years)			
<59	19	73.5	0.055
≧60	23	54.4	
Gender			
Male	17	63.7	0.93
Female	25	65.5	
Size (cm)			
<5	9	88.9	0.19
≧5	33	59.3	
Depth			
Superficial	7	85.7	0.37
Deep	35	61.7	
Ki-67			
<30%	32	70.9	0.175
≧30%	10	42.2	
HIF-1α			
Low	20	75.4	0.029
High	22	52.9	

Low means negative/weak; high means moderate/strong
HIF Hypoxia-inducible factor
[1] Log-rank test

environment, and it was reported to be a good predictor for a poor prognosis in patients with deep, large, high-grade soft-tissue sarcoma [32]. The VEGF expression and microvessel density (MVD) are not identified as prognostic markers in soft-tissue sarcomas, but there have been some studies that demonstrated the VEGF expression and MVD to be associated with histological grading [7, 18, 38]. The expression of HIF-1α correlated with the VEGF expression and microvessel density [4, 6, 30]. The distribution of

Table 4 Multivariate analysis of the overall survival of 42 patients with spindle-cell sarcoma

Characteristic	Relative risk	95% confidence interval	*P* value
Patient's age (years)			
(<59 vs ≧60)	–	–	0.080
Tumor size (cm)			
(<5 vs ≧5)	–	–	0.188
Ki-67 (%)			
(<30 vs ≧30)	–	–	0.456
HIF-1α			
(Low vs High)	5.14	1.33–19.88	0.018

Low means negative/weak; high means moderate/strong
HIF hypoxia-inducible factor

microvessels within soft-tissue sarcomas, which are usually induced by VEGF, is also homogeneous and diffuses inside the tumor mass [44, 48]. Therefore, it seems that angiogenesis via HIF-1α may thus play an important role in tumorgenesis.

Among the previously reported biomarkers, the significance of p53 and bcl-2 as prognostic markers still remains controversial [9, 10, 33, 34]. p27 protein is a major regulator of the G1-S transition of the cell cycle and it has been shown to be an independent prognostic factor in patients with synovial sarcoma [28] and leiomyosarcoma [11]. Ki-67 antigen is a proliferation marker that is synthesized throughout most of the cell cycle, and an overexpression of this nuclear protein is associated with tumor progression [17]. Ki-67 has been found to be associated with the prognosis in soft-tissue sarcoma in several independent studies [22, 24]. In the present report, although there was a tendency for a poor prognosis in patients with a high expression of Ki-67, we could not find any significant association between the expression level of Ki-67 and the clinical outcome. This may be due to the fact that we examined only spindle cell sarcomas and excluded liposarcomas.

In the present study, no significant differences were observed between the expression level of HIF-1α and the histological diagnoses, although patients with a strong or moderate expression of HIF-1α had a significantly shorter overall survival rate compared to those with a weak or negative expression based on both a univariate analysis and a multivariate analysis. These results mean that the expression of HIF-1α does not depend on cell differentiation of the signal but on tumor biological aggressiveness. Therefore, HIF-1α might be a useful biomarker in spindle-cell sarcoma, regardless of its subtype. We need to investigate a larger number of samples and plan cohort studies to improve the accuracy of the present study because soft-tissue sarcomas often consist of histologic heterogeneous subtypes.

In conclusion, immunohistochemically, the expression of HIF-1α protein was negative in 14 (28.6%) cases, weak in nine (18.4%), moderate in 17 (35.4%), and strong in nine (18.4%). The HIF-1α protein was accumulated in the nucleus, and it was observed diffusely throughout the specimens of soft-tissue sarcomas. The patients with a strong or moderate expression of HIF-1α had a significantly shorter overall survival rate in comparison to those with a weak or negative expression based on a univariate analysis and a multivariate analysis. These results suggest that overexpression of HIF-1α protein is an independent prognostic marker for soft-tissue sarcomas. There is a possibility that the overtreatment of patients with less aggressive tumors within spindle-cell sarcoma might thus be avoided by examining the expression of HIF-1α. Larger numbers of patients with soft-tissue sarcoma should therefore be studied in future prospective studies.

Acknowledgement We thank the secretarial staff of the Department of Orthopedic Surgery, Mie University School of Medicine, for their generous cooperation.

References

1. Aebersold DM, Burri P, Beer KT, Laissue J, Djonov V, Greiner RH, Semenza GL (2001) Expression of hypoxia-inducible factor-1α: a novel predictive and prognostic parameter in the radiotherapy of oropharyngeal cancer. Cancer Res 61:2911–2916
2. Birner P, Schindl M, Obermair A, Plank C, Breitenecker G, Oberhuber G (2000) Overexpression of hypoxia-inducible factor 1α is a marker for unfavorable prognosis in early-stage invasive cervical cancer. Cancer Res 60:4693–4696
3. Birner P, Gatterbauer B, Oberhuber G, Schindl M, Rossler K, Prodinger A, Budka H, Hainfellner JA (2001) Expression of hypoxia-inducible factor-1α in oligodendrogliomas: its impact on prognosis and on neoangiogenesis. Cancer 92:165–171
4. Bos R, Zhong H, Hanrahan CF, Mommers EC, Semenza GL, Pinedo HM, Abeloff MD, Simons JW, van der Wall E (2001) Levels of hypoxia-inducible factor-1α during breast carcinogenesis. J Natl Cancer Inst 93:309–314
5. Brizel DM, Scully SP, Harrelson JM, Layfield LJ, Bean JM, Prosnitz LR, Dewhirst MW (1996) Tumor oxygenation predicts for the likelihood of distant metastasis in human soft tissue sarcoma. Cancer Res 56:941–943
6. Carmeliet P, Dor Y, Herbert JM, Fukumura D, Brusselmans K, Dewerchin M, Neeman M, Bono F, Abramovitch R, Maxwell P, Koch C, Ratcliffe P, Moons L, Jain RK, colleen D, Keshert E (1998) Role of HIF-1α in hypoxia-mediated apoptosis, cell proliferation, and tumor angiogenesis. Nature 394:485–490
7. Chao C, Al-Saleem T, Brooks JJ, Rogatko A, Kraybill WG, Eisenberg B (2001) Vascular endothelial growth factor and soft tissue sarcomas: tumor expression correlates with grade. Ann Surg Oncol 8:260–267
8. Chen C, Pore N, Behrooz A, Ismail-Beigi F, Maity A (2001) Regulation of glut1 mRNA by hypoxia-inducible factor-1. Interaction between H-ras and hypoxia. J Biol Chem 276:9519–9525
9. Cordon-Cardo C, Latres E, Drobnjak M, Oliva MR, Pollack D, Woodruff JM, Marechal V, Chen J, Brennan MF, Levine AJ (1994) Molecular abnormalities of mdm2 and p53 genes in adult soft tissue sarcomas. Cancer Res 54:794–799
10. Dan'ura T, Kawai A, Morimoto Y, Naito N, Toshida A, Inoue H (2002) Apoptosis and expression of its regulatory proteins in soft tissue sarcomas. Cancer Lett 178:167–174
11. Dobashi Y, Noguchi T, Nasuno S, Katayama K, Kameya T (2001) CDK-inhibitor-associated kinase activity: a possible determinant of malignant potential in smooth muscle tumors of the external soft tissue. Int J Cancer 94:353–362
12. Feldser D, Again F, Iyer NV, Pak B, Ferreira G, Semenza GL (1999) Reciprocal positive regulation of hypoxia-inducible factor 1α and insulin-like growth factor 2. Cancer Res 59:3915–3918
13. Fillies T, Werkmeister R, van Diest PJ, Brandt B, Joos U, Buerger H (2005) HIF1-alpha overexpression indicates a good prognosis in early stage squamous cell carcinomas of the oral floor. BMC Cancer 5:84
14. Fletcher CDM, Unni KK, Mertens FE (2002). Pathology and genetics of tumours of soft tissue and bone. In: Fletcher CDM, Unni KK, Mertens FE (eds) World Health Organization classification of tumours. IARC, Lyon

15. Forsythe JA, Jiang BH, Iyer NV, Agani F, Leung SW, Koos RD, Semenza GL (1996) Activation of vascular endothelial growth factor gene transcription by hypoxia-inducible factor 1. Mol Cell Biol 16:4604–4613
16. Fyles A, Milosevic M, Headley M, Pintilie M, Levin W, Manchul L, Hill RP (2002) Tumor hypoxia has independent predictor impact only in patients with node-negative cervix cancer. J Clin Oncol 20:680–687
17. Gerdes J, Lemke H, Baisch H, Wacker HH, Schwab U, Stein H (1984) Cell-cycle analysis of a cell proliferation-associated human nuclear antigen defined by the monoclonal antibody Ki-67. J Immunol 133:1710–1715
18. Graeven U, Andre N, Achilles E, Zornig C, Schmiegel W (1999) Serum levels of vascular endothelial growth factor and basic fibroblast growth factor in patients with soft-tissue sarcoma. J Cancer Res Clin Oncol 125:577–581
19. Greene FL, Page DL, Fleming ID et al (eds) (2002) AJCC cancer staging manual, 6th edn. Springer, Berlin Heidelberg New York
20. Guillou L, Coindre JM, Bonichon F, Nguyen BB, Terrier P, Collin F, Vilain MO, Mandard AM, Le Doussal V, Leroux A, Jacquemier J, Duplay H, Sastre-Garau X and Costa J (1997) Comparative study of the National Cancer Institute and French Federation of Cancer Centers Sarcoma Group grading systems in a population of 410 adult patients with soft tissue sarcoma. J Clin Oncol 15:350–362
21. Harris AL (2002) Hypoxia: a key regulatory factor in tumor growth. Nat Rev Cancer 2:38–47
22. Heslin MJ, Cordon-Cardo C, Lewis JJ, Woodruff JM, Brennan MF (1998) Ki-67 detected by MIB-1 predicts distant metastasis and tumor mortality in primary, high grade extremity soft tissue sarcoma. Cancer 83:490–497
23. Hockel M, Schlenger K, Aral B, Mitze M, Schaffer U, Vaupel P (1996) Association between tumor hypoxia and malignant progression in advanced cancer of the uterine cervix. Cancer Res 56:4509–4515
24. Hoos A, Stojadinovic A, Mastorides S, Urist MJ, Polsky D, Di Como CJ, Brennan MF, Cordon-Cardo C (2001) High Ki-67 proliferative index predicts disease specific survival in patients with high-risk soft tissue sarcomas. Cancer 92:869–874
25. Jemal A, Tiwari RC, Murray T, Ghafoor A, Samuels A, Ward E, Feuer EJ, Thun MJ (2004) Cancer statistics, 2004. CA Cancer J Clin 54:8–29
26. Jiang BH, Agani F, Passaniti A, Semenza GL (1997) V-SRC induces expression hypoxia-inducibe factor 1 (HIF-1) and transcription of encoding vascular endothelial growth factor and enolase 1: involvement of HIF-1 in tumor progression. Cancer Res 57:5328–5335
27. Jiang BH, Jiang G, Zheng JZ, Lu Z, Hunter T, Vogt PK (2001) Phosphatidylinositol 3-kinase signaling controls levels of hypoxia-inducible factor 1. Cell Growth Differ 12:363–369
28. Kawauchi S, Goto Y, Liu XP, Furuya T, Oga A, Oda Y, Tsuneyoshi M, Ihara K, Sasaki K (2001) Low expression of p27 (Kip1), a cyclin-independent kinase inhibitor, is a marker of poor prognosis in synovial sarcoma. Cancer 91:1005–1012
29. Koukourakis MI, Giatromanolaki A, Sivridis E, Simopoulos C, Turley H, Talks K, Gatter KC, Harris AL (2002) Hypoxia-inducible factor (HIF1A and HIF2A), angiogenesis, and chemoradiotherapy outcome of squamous cell head-and-neck cancer. Int J Radiat Oncol Biol Phys 53:1192–1202
30. Kuwai T, Kitadai Y, Tanaka S, Onogawa S, Matsutani N, Kaio E, Ito M, Chayama K (2003) Expression of hypoxia-inducible factor-1α is associated with tumor vascularization in human colorectal carcinoma. Int J Cancer 105:176–181
31. Lidgren A, Hedberg Y, Grankvist K, Rasmuson T, Vasko J, Ljungberg B (2005) The expression of hypoxia-inducible factor 1α is a favorable independent prognostic factor in renal cell carcinoma. Clin Cancer Res 11:1129–1135
32. Maseide K, Kandel RA, Bell RS, Catton CN, O'Sullivan B, Wunder JS, Pintilie M, Hedley D, Hill RP (2004) Carbonic anhydrase IX as a marker for poor prognosis in soft tissue sarcoma. Clin Cancer Res 10:4464–4471
33. Molina P, Pellin A, Navarro S, Boix J, Carda C, Llombart-Bosch A (1997) Analysis of p53 and mdm2 proteins in malignant fibrous histiocytoma in absence of gene alteration: prognostic significance. Virchows Arch 435:596–605
34. Nakanishi H, Ohsawa M, Naka N, Uchida A, Ochi T, Aozasa K (1997) Immunohistochemical detection of bcl-2 and p53 proteins and apoptosis in soft tissue sarcoma: their correlations with prognosis. Oncology 54:238–244
35. Nordsmark M, Hoyer M, Keller J, Nielsen OS, Jensen OM, Overgaard J (1996) The relationship between tumor oxygenation and cell proliferation in human soft tissue sarcomas. Int J Radiat Oncol Biol Phys 35:701–708
36. Nordsmark M, Overgaard M, Overgaard J (1996) Pretreatment oxygenation predicts radiation response in advanced squamous cell carcinoma of the head and neck. Radiother Oncol 41:31–39
37. Richard DE, Berra E, Gothie E, Roux D, Pouyssegur J (1999) p42/p44 mitogen-activated protein kinases phosphorylate hypoxia-inducible factor 1α (HIF-1α) and enhance the transcriptional activity of HIF-1. J Biol Chem 274:32631–32637
38. Saenz NC, Heslin MJ, Adsay V, Lewis JJ, Leung DH, LaQuaglia MP, Brennan MF (1998) Neovascularity and clinical outcome in high-grade extremity soft tissue sarcomas. Ann Surg Oncol 5:48–53
39. Schindl M, Schoppmann SF, Samonigg H, Hausmaninger H, Kwasny W, Grant M, Jakesz R, Kubista E, Birner P, Oberhuber G (2002) Overexpression of hypoxia-inducible factor 1α is associated with an unfavorable prognosis in lymph node-positive breast cancer. Clin Cancer Res 8:1831–1837
40. Semenza GL, Wang GL (1992) A nuclear factor induced by hypoxia via de novo protein synthesis binds to the human erythropoietin gene enhancer at a site required for transcriptional activation. Mol Cell Biol 12:5447–5454
41. Semenza GL (2000) Hypoxia, clonal selection, and the role of HIF-1 in tumor progression. Crit Rev Biochem Mol Biol 35:71–103
42. Semenza GL (2003) Targeting HIF-1 for cancer therapy. Nat Rev Cancer 3:721–732
43. Sivridis E, Giatromanolaki A, Gatter KC, Harris AL, Koukourakis MI, Tumor and Angiogenesis Research Group (2002) Association of hypoxia-inducible factors 1α and 2α with activated angiogenic pathways and prognosis in patients with endometrial carcinoma. Cancer 95:1055–1063
44. Tomlinson J, Barsky SH, Nelson S, Singer S, Pezeshki B, Lee MC, Eilber F, Nguyen M (1999) Different patterns of angiogenesis in sarcomas and carcinomas. Clin Cancer Res 5:3516–3522
45. Vleugel MM, Greiler AE, Shvarts A, van der Groep P, van Berkel M, Aarbodem Y, van Tinteren H, Harris AL, van Diest PJ, van der Wall E (2005) Differential prognostic impact of hypoxia induced and diffuse HIF-1α expression in invasion breast cancer. J Clin Pathol 58:172–177
46. Volm M, Koomagi R (2000) Hypoxia-inducible factor (HIF-1) and its relationship to apoptosis and proliferation in lung cancer. Anticancer Res 20:1527–1533
47. Wang GL, Jiang BH, Rue EA, Semenza GL (1995) Hypoxia-inducible factor 1 is a basic-helix-loop-helix-PAS heterodimer regulated by cellular O2 tension. Proc Natl Acad Sci USA 92:5510–5514

48. West CC, Brown NJ, Mangham DC, Grimer RJ, Reed MWR (2005) Microvessel density dose not predict outcome high grade soft tissue sarcoma. Eur J Surg Oncol 31:1198–1205
49. Wykoff CC, Beasley NJ, Watson PH, Turner KJ, Pastorek J, Sibtain A, Wilson GD, Turley H, Talks KL, Maxwell PH, PughCW, Ratcliffe PJ, Harris AL (2000) Hypoxia-inducible expression of tumor-associated carbonic anhydrases. Cancer Res 60:7075–7083
50. Zhong H, De Marzo AM, Laughner E, Lim M, Hilton D, Zagzag D, Buechler P, Isaacs WB, Semenza GL, Simons JW (1999) Overexpression of hypoxia-inducible factor 1α in common human cancers and their metastases. Cancer Res 59:5830–5835
51. Zundel W, Schindler C, Haas-Kogan D, Koong A, Kaper F, Chen E, Gottschalk AR, Ryan HE, Johnson RS, Jefferson AB, Stokoe D, Giaccia AJ (2000) Loss of PTEN facilitates HIF-1-mediated gene expression. Genes Dev 14:391–396

with alveolar macrophages belongs to the first line of defense against inhaled toxic substances. It is not clear which factors protect against exposure of bronchial epithelium to exogenous toxic agents such as the ones present in cigarette smoke.

Over the past decade, oncological studies aiming to elucidate mechanisms of cytostatic drug resistance have identified some molecules pivotal to protect cells against xenobiotics. Tumor cells that are resistant to a certain cytostatic drug are often also resistant to other structurally and functionally unrelated natural product drugs. This feature is termed multidrug resistance (MDR). Many MDR-related proteins can act as cellular efflux pumps, resulting in decreased intracellular concentrations of drugs at the site of action. Several MDR mechanisms have been identified, mediated by members of the "ATP-binding cassette" (ABC) transporter superfamily, e.g., multidrug resistance-associated protein 1 (MRP1) and P-glycoprotein (P-gp, encoded by the MDR1 gene) [2, 9]. MRP1 can transport glutathione (GSH) conjugates such as the inflammatory mediator leukotriene C4, as well as substrates in the presence of GSH, thereby decreasing intracellular concentrations of toxic compounds [7]. P-gp effluxes toxic compounds out of the cells and is present in for example apical membranes in the liver, intestine, and kidney. Another protein associated with MDR is lung resistance-related protein (LRP), the human major vault protein. Vaults are cytosolic structures that may compartmentalize drugs to protect intracellular target [4, 18, 19].

Limited data are available on MDR proteins in normal lung tissue [22]. Immunohistochemical studies have shown the presence of MRP1, P-gp, and LRP in normal bronchial epithelium [1, 17, 24]. MRP1 mRNA was first detected in small cell lung cancer and is highly expressed in normal human lung [2, 8, 21]. In this study, MRP1 expression may be pivotal in the protection against oxidative stress generated by, e.g., cigarette smoke by exporting GSH conjugates or substances in the presence of GSH out of the cells. Reduced GSH is one of the major antioxidants in the lung. It is present in high levels in each cell and in epithelial lining fluid [12]. Besides its role in MDR, lower MRP1 transcript levels were found to be associated with more severe disease in cystic fibrosis patients who have defective function of the ABC transporter cystic fibrosis transmembrane conductance regulator [3].

In the present study, we investigated whether altered expression of MRP1 or other MDR-related proteins is associated with COPD. As a first step to elucidate this, the expression and localization of MRP1, P-gp, and LRP in bronchial epithelium was studied in COPD patients and healthy controls using immunohistochemistry. We primarily analyzed the normal epithelium component (basal, ciliated, and goblet cells). In addition, the expression in areas with squamous metaplasia was evaluated. Furthermore, we assessed whether expression of these proteins was associated with disease status and smoking history.

Materials and methods

Patients and healthy controls

The characteristics of the participating COPD patients and healthy controls of two study groups are listed in Table 1. In both studies, patients with atopy, asthma, and other pulmonary diseases were excluded. Classification of patients was defined according to the global initiative for chronic obstructive lung disease (GOLD) criteria [10]. The local medical ethics committee for human studies approved the protocols. Informed written consent was obtained from the participating subjects.

Study group 1: COPD and healthy ex-smokers

Bronchial biopsies (frozen tissue) were collected from 26 individuals, who were classified in two groups based on clinical data and smoking history as described previously [15] (Table 1). In brief, this study consisted of 15 COPD patients (11 moderate and 4 severe COPD) and 11 healthy subjects (no history of pulmonary disease and normal lung function) with similar pack years. All had quitted smoking for at least 1 year (on average 14 years). Inhaled corticosteroids were discontinued at least 1 month before the study, and patients treated with oral corticosteroids or antibiotics or having had a respiratory tract infection in the month before the study were excluded.

Study group 2: mild to very severe COPD patients

Lung tissue (frozen tissue) was obtained from surgical procedures in 21 individuals as described previously [23]. In brief, patients were classified in two groups primarily based on clinical data (lung function) which were confirmed by routine histological examination of lung tissue (Table 1). The first group (n=12) consisted of patients with severe and very severe COPD, resected for unilateral or bilateral lung transplantation with severe airway obstruction (forced expiratory volume in one second (FEV_1) 10–45% predicted, FEV_1/VC 14–56%). The second group (n=9) comprised lung tissue obtained from patients with mild to moderate COPD (FEV_1 52–101% predicted, FEV_1/VC 36–75%), undergoing therapeutic partial resection, (bi)lobectomy, or pneumonectomy for pulmonary carcinoma. Lung tissue distant from the tumor (when possible from noninvolved lobes) was selected for our studies. Both groups comprised current and ex-smokers.

Table 1 Characteristics of study groups

	Study 1		Study 2	
	COPD (moderate and severe)	Healthy	COPD (very severe and severe)	COPD (mild and moderate)
Number of individuals	15	11	12	9
Gender (M/F)	11/4	8/3	5/7	7/2
Age (years±SD)	64±7	58±8	48±7	66±7
Smoking (pack years±SD)	34±17	25±15	23±12	40±10
FEV_1 (% predicted±SD)	58±14	104±11	20±10	75±18
FEV_1/VC (%±SD)	49±9	75±4	25±11	58±13

Mild, moderate, severe, and very severe COPD defined by the Global Initiative for Chronic Obstructive Lung Disease [10]
FEV_1 Forced expiratory volume in one second, *VC* vital capacity, *SD* standard deviation

Immunohistochemistry

The anti-P-gp monoclonal antibody C219 was purchased from Alexis (San Diego, CA, USA) and used in the recommended dilution. All other monoclonal antibodies used were produced by our group, and immunohistochemical methods were described earlier (R.J.S. and G.L.S.) [16, 20]. We used antibody MRPr1 for MRP1, C219 for P-gp, and LRP56 for LRP. For positive controls, normal human lung (MRP1, LRP) or liver (P-gp) was stained, and for negative controls, irrelevant antibodies were used. All biopsies and lung tissues of each study were stained in one procedure for the particular antigen.

Evaluation of immunohistochemistry on bronchial biopsies and lung tissue

All proteins were scored for intensity of staining in bronchial epithelial cells (i.e., basal, ciliated, and goblet cells) with a semiquantitative score: 0 = no staining; 1 = weak; 2 = moderate; 3 = strong. When squamous metaplasia was present in a biopsy, evaluation of metaplasia staining was performed separately from normal bronchial epithelium in the same biopsy. Groups were compared both by including and excluding the scored values for the metaplastic epithelium. Special attention was paid to cellular localization of expression. Two observers (W.T. and M.D.) performed all evaluations of bronchial biopsies and lung tissues individually in a blinded fashion. Most sections stained variable for MRP1, P-gp, or LRP in epithelium, and parts with the most intense staining were evaluated for scoring.

Some biopsies and lung tissues had to be excluded for further analysis because of limited quality of the tissue section, resulting in different numbers of individuals per staining.

Statistical evaluation

Differences in intensity of expression in the immunohistochemical staining between groups were analyzed using nonparametric Mann Whitney *U* tests (two-tailed). Correlations between variables were evaluated with Spearman's rank correlation test (two-tailed). Values of $p<0.05$ were considered statistically significant. Statistical analyses were performed with SPSS 10 (SPSS, Chicago).

Results

Study group 1: COPD and healthy ex-smokers

MRP1 expression was lower in normal bronchial epithelium of COPD patients (n=11) compared to healthy controls (n=8) (p=0.029; Fig. 1). P-gp expression was very low to absent in both COPD patients and healthy controls, and LRP expression was variable. P-gp as well as LRP expression in COPD patients was not different from healthy controls (Fig. 1b,c).

MRP1 was mainly present in basal cell layers of normal bronchial epithelium of both COPD patients and healthy controls. Representative pictures of MRP1 staining in normal bronchial epithelium of a COPD patient and a healthy control are shown in Fig. 2a,b. P-gp was located at the apical side of bronchial epithelium. LRP was usually present in the cytoplasm of all epithelial layers. In general, areas with squamous metaplasia stained moderately or strongly for MRP1 with the most intense staining in suprabasal cells (Fig. 2c), while P-gp staining was absent in these areas. When intense MRP1 staining in metaplastic epithelium was included in the analysis (metaplasia in COPD: 4 out of 11; metaplasia in controls: three out of eight), MRP1 expression was still significantly lower in the COPD group (p=0.038).

MRP1, P-gp, and LRP expression was not related to lung function parameters or number of pack years in the combined COPD and healthy control group.

Study group 2: mild to very severe COPD patients

MRP1 expression was lower in the group with (very) severe COPD (n=10) compared to mild and moderate

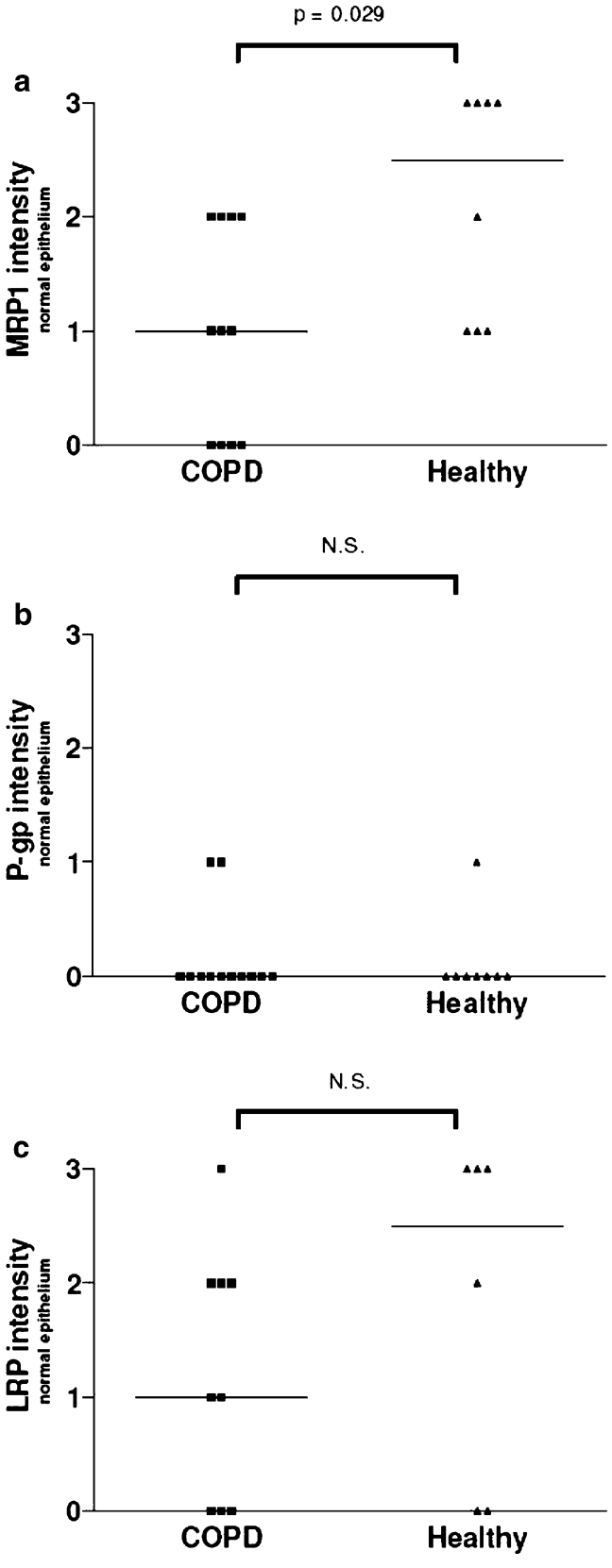

◀ **Fig. 1** **a** MRP1 intensities in normal bronchial epithelium of patients with COPD and healthy controls. There was a lower expression (p=0.029) in patients with COPD (n=11) compared to healthy controls (n=8). **b** Similar comparison for P-gp, and **c** for LRP. P-gp expression is low or absent, and both P-gp and LRP do not show any difference between COPD and healthy controls

COPD (n=9) (p=0.047) (Fig. 3). P-gp and LRP expression was not different between groups.

MRP1 in the lower airways was mainly detected at the basolateral membranes of bronchial epithelial cells, as it was in bronchial biopsies (Fig. 2d). The strongest expression of P-gp was in the cilia (Fig. 2e). LRP staining was expressed in all epithelial layers with a very intense staining in the cytoplasm of cells at the luminal side (Fig. 2f). Metaplastic epithelium was not detected in these lower airways.

MRP1, P-gp, and LRP expression was not related to lung function parameters or number of pack years in the combined mild to very severe COPD group.

Discussions

The present study describes for the first time a diminished MRP1 expression in bronchial epithelium of carefully characterized COPD patients with moderate to severe disease (FEV_1 ranging from 36 to 79% predicted) compared to healthy controls, all ex-smokers with similar pack years of cigarette smoking, and duration of smoking cessation (study group 1). A similar observation was found in airway sections of patients with severe or very severe COPD (FEV_1 20±10% predicted) compared to patients with mild to moderate COPD (FEV_1 75±18% predicted) (study group 2).

We detected a predominantly high MRP1 expression in squamous metaplastic epithelium, especially in suprabasal cells. Exposure of bronchial epithelium to cigarette smoke causes squamous metaplasia and therefore, the higher expression of MRP1 as observed in metaplastic epithelium may be a result of smoking and may have important clinical consequences in oxidative defense. It might represent an ultimate attempt to resist the toxic effect after repeated cigarette smoke exposures. In our study, the number of pack years did not correlate with MRP1, P-gp, and LRP expression in bronchial epithelium, suggesting that the cumulative amount of cigarettes smoked does not influence the diminished MRP1 expression in COPD.

MDR-related proteins such as MRP1 and P-gp are highly expressed in normal human airways but the function of these proteins in the lung is unknown [1, 5, 17, 22]. In a previous study, we observed high MRP1, P-gp, and LRP expression and lower breast-cancer resistance protein expression in bronchial and bronchiolar epithelium of normal human and murine lung [17]. MRP2, MRP3, and MDR3 P-gp were either undetectable or were present in

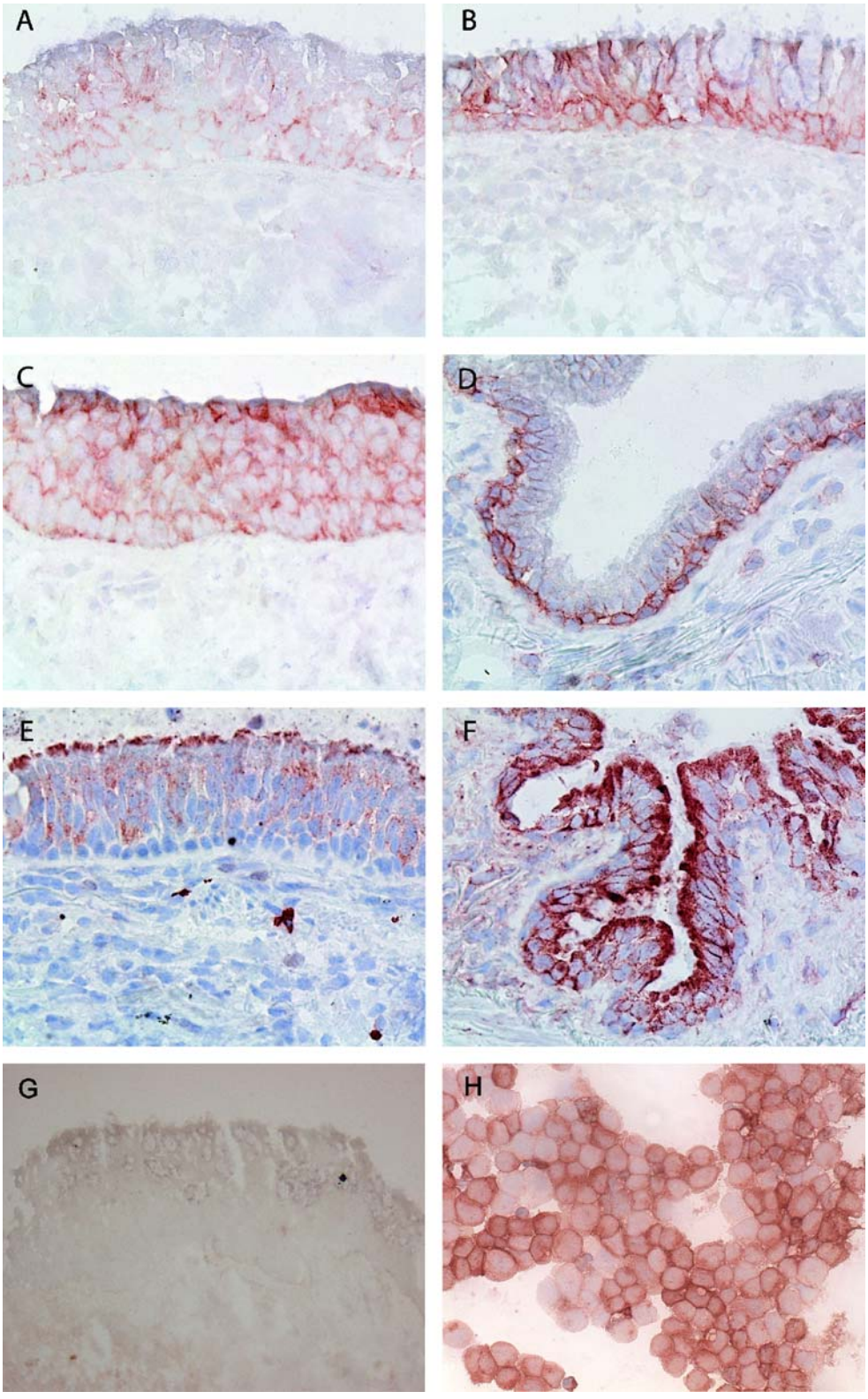

Fig. 2 Immunohistochemical staining of MRP1, P-gp, and LRP in bronchial biopsies or lung tissue of COPD patients and healthy controls. Staining in bronchial biopsies of **a** MRP1 (weak expression) in normal epithelium of COPD patient, **b** MRP1 (high expression) in normal epithelium of healthy control, and **c** MRP1 (high expression) in metaplastic epithelium of COPD patient. Representative staining of **d** MRP1, **e** P-gp, and **f** LRP tissue in lung tissue of COPD patients. **g** Negative control, employing nonrelevant species (rat) and isotype-matched monoclonal antibody LMR42. **h** Positive control for MRP1 staining of GLC4/ADR small cell carcinoma cell line

very low levels in these lung tissues. The normal physiological role of MDR proteins is detoxification of toxic substances in the body. The high expression of MRP1, P-gp, and LRP in the lung may therefore indicate that these proteins play distinct roles in the protection against inhaled toxic substances.

The MRP1 protein, together with GSH, can play an important role in the antioxidant defense of epithelial cells

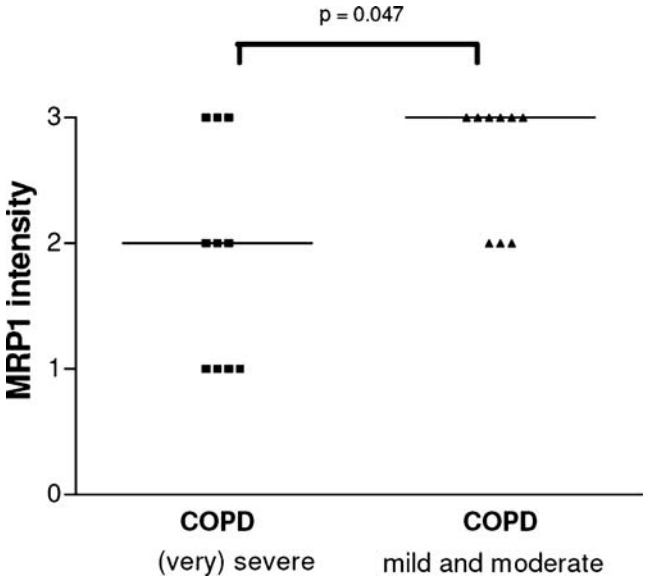

Fig. 3 MRP1 intensities in lung tissue of patients with COPD. There was a lower expression (p=0.047) in patients with severe and very severe COPD (n=10) compared to patients with mild and moderate COPD (n=9)

and in handling the redox status of a cell. A recent study identified MRP1-dependent transport of a tobacco-specific carcinogen (NNAL-*O*-glucuronide) in the presence of GSH [6]. This suggests that MRP1 plays an important role in the protection against lung cancer-inducing agents such as the ones present in cigarette smoke.

At present, it is unclear whether the lower expression level of MRP1 in COPD is implied in a cause or effect relationship. The reduced expression of MRP1 might be associated with increased vulnerability for COPD ("cause"), as this lower MRP1 may result in impaired antioxidant defense and in impaired clearance of xenobiotics such as cigarette smoke. Alternatively, MRP1 may be downregulated concurrent with development of COPD ("effect"). Functional studies of MRP1 in epithelial cells of COPD patients should shed further light on the role of MRP1 in COPD pathogenesis.

Conclusions

MRP1 expression in bronchial biopsies of COPD patients was lower compared to healthy controls. In addition, MRP1 expression was lower in patients with (very) severe COPD compared to mild and moderate COPD. Our findings indicate that diminished MRP1 expression in normal bronchial epithelium is associated with COPD. The exact role in COPD pathogenesis is to be revealed by further functional studies.

Acknowledgements This work was supported by a grant from the Netherlands Asthma Foundation (NAF 97.35). The authors thank Dr. W.J. Sluiter for the critical evaluation of statistical analyses and Mrs. Adriana Pijnenborg for the excellent technical support. The authors declare that their experiments comply with the current laws of the country in which they were performed (i.e., the Netherlands).

References

1. Brechot JM, Hurbain I, Fajac A, Daty N, Bernaudin JF (1998) Different pattern of MRP localization in ciliated and basal cells from human bronchial epithelium. J Histochem Cytochem 46:513–517
2. Cole SP, Bhardwaj G, Gerlach JH, Mackie JE, Grant CE, Almquist KC, Stewart AJ, Kurz EU, Duncan AM, Deeley RG (1992) Overexpression of a transporter gene in a multidrug-resistant human lung cancer cell line. Science 258:1650–1654
3. Hurbain I, Sermet-Gaudelus I, Vallee B, Feuillet MN, Lenoir G, Bernaudin JF, Edelman A, Fajac A (2003) Evaluation of MRP1-5 gene expression in cystic fibrosis patients homozygous for the delta F508 mutation. Pediatr Res 54:627–634
4. Kitazono M, Sumizawa T, Takebayashi Y, Chen ZS, Furukawa T, Nagayama S, Tani A, Takao S, Aikou T, Akiyama S (1999) Multidrug resistance and the lung resistance-related protein in human colon carcinoma SW-620 cells. J Natl Cancer Inst 91:1647–1653
5. Lechapt-Zalcman E, Hurbain I, Lacave R, Commo F, Urban T, Antoine M, Milleron B, Bernaudin JF (1997) MDR1-Pgp 170 expression in human bronchus. Eur Respir J 10:1837–1843
6. Leslie EM, Ito K, Upadhyaya P, Hecht SS, Deeley RG, Cole SP (2001) Transport of the beta-O-glucuronide conjugate of the tobacco-specific carcinogen 4-(methylnitrosamino)-1-(3-pyridyl)-1-butanol (NNAL) by the multidrug resistance protein 1 (MRP1). Requirement for glutathione or a non-sulfur-containing analog. J Biol Chem 276:27846–27854
7. Muller M, Meijer C, Zaman GJ, Borst P, Scheper RJ, Mulder NH, de Vries EG, Jansen PL (1994) Overexpression of the gene encoding the multidrug resistance-associated protein results in increased ATP-dependent glutathione S-conjugate transport. Proc Natl Acad Sci U S A 91:13033-13037
8. Nooter K, Westerman AM, Flens MJ, Zaman GJ, Scheper RJ, van Wingerden KE, Burger H, Oostrum R, Boersma T, Sonneveld P (1995) Expression of the multidrug resistance-associated protein (MRP) gene in human cancers. Clin Cancer Res 1:1301–1310
9. Pastan I, Gottesman MM, Ueda K, Lovelace E, Rutherford AV, Willingham MC (1988) A retrovirus carrying an MDR1 cDNA confers multidrug resistance and polarized expression of P-glycoprotein in MDCK cells. Proc Natl Acad Sci U S A 85:4486–4490
10. Pauwels RA, Buist AS, Calverley PM, Jenkins CR, Hurd SS (2001) Global strategy for the diagnosis, management, and prevention of chronic obstructive pulmonary disease. NHLBI/WHO Global Initiative for Chronic Obstructive Lung Disease (GOLD) Workshop summary. Am J Respir Crit Care Med 163:1256–1276
11. Pryor WA, Stone K (1993) Oxidants in cigarette smoke. Radicals, hydrogen peroxide, peroxynitrate, and peroxynitrite. Ann NY Acad Sci 686:12–27
12. Rahman I, MacNee W (1999) Lung glutathione and oxidative stress: implications in cigarette smoke-induced airway disease. Am J Physiol 277:L1067–L1088
13. Rahman I, Morrison D, Donaldson K, MacNee W (1996) Systemic oxidative stress in asthma, COPD, and smokers. Am J Respir Crit Care Med 154:1055–1060
14. Repine JE, Bast A, Lankhorst I (1997) Oxidative stress in chronic obstructive pulmonary disease. Oxidative stress study group. Am J Respir Crit Care Med 156:341–357

15. Rutgers SR, Timens W, Kaufmann HF, van der Mark TW, Koeter GH, Postma DS (2000) Comparison of induced sputum with bronchial wash, bronchoalveolar lavage and bronchial biopsies in COPD. Eur Respir J 15:109–115
16. Scheffer GL, Kool M, Heijn M, de Haas M, Pijnenborg AC, Wijnholds J, van Helvoort A, de Jong MC, Hooijberg JH, Mol CA, van der Linden M, de Vree JM, van der Valk P, Elferink RP, Borst P, Scheper RJ (2000) Specific detection of multidrug resistance proteins MRP1, MRP2, MRP3, MRP5, and MDR3 P-glycoprotein with a panel of monoclonal antibodies. Cancer Res 60:5269–5277
17. Scheffer GL, Pijnenborg AC, Smit EF, Muller M, Postma DS, Timens W, van der Valk P, de Vries EG, Scheper RJ (2002) Multidrug resistance related molecules in human and murine lung. J Clin Pathol 55:332–339
18. Scheffer GL, Schroeijers AB, Izquierdo MA, Wiemer EA, Scheper RJ (2000) Lung resistance-related protein/major vault protein and vaults in multidrug-resistant cancer. Curr Opin Oncol 12:550–556
19. Scheffer GL, Wijngaard PL, Flens MJ, Izquierdo MA, Slovak ML, Pinedo HM, Meijer CJ, Clevers HC, Scheper RJ (1995) The drug resistance-related protein LRP is the human major vault protein. Nat Med 1:578–582
20. Schroeijers AB, Scheffer GL, Reurs AW, Pijnenborg AC, Abbondanza C, Wiemer EA, Scheper RJ (2001) Detection of the Mr 110,000 lung resistance-related protein LRP/MVP with monoclonal antibodies. J Histochem Cytochem 49:1379–1385
21. Thomas GA, Barrand MA, Stewart S, Rabbitts PH, Williams ED, Twentyman PR (1994) Expression of the multidrug resistance-associated protein (MRP) gene in human lung tumours and normal tissue as determined by in situ hybridisation. Eur J Cancer 30A:1705–1709
22. van der Deen M, de Vries EG, Timens W, Scheper RJ, Timmer-Bosscha H, Postma DS (2005) ATP-binding cassette (ABC) transporters in normal and pathological lung. Respir Res 6:59
23. van Straaten JF, Coers W, Noordhoek JA, Huitema S, Flipsen JT, Kauffman HF, Timens W, Postma DS (1999) Proteoglycan changes in the extracellular matrix of lung tissue from patients with pulmonary emphysema. Mod Pathol 12:697–705
24. Wright SR, Boag AH, Valdimarsson G, Hipfner DR, Campling BG, Cole SP, Deeley RG (1998) Immunohistochemical detection of multidrug resistance protein in human lung cancer and normal lung. Clin Cancer Res 4:2279–2289

immune syndrome, called the immune restoration inflammatory syndrome (IRIS), due to the rapid increase in CD4+ T lymphocytes [5, 10, 31]. This clinical deterioration is a result of an exuberant inflammatory response toward previously diagnosed or incubating opportunistic pathogens, as well as a response toward other as yet undefined antigens [5, 10, 31].

The development of a granulomatous reaction after peripheral blood CD4+ T-cell recovery suggests a causative relationship between the initiation of HAART and the occurrence of a "sarcoid-like" process mimicking sarcoidosis lesions observed in an HIV-negative population. These paradoxical reactions have been reported in cases of lymph nodes or pulmonary parenchyma infected with *Mycobacterium avium* complex or *Mycobacterium tuberculosis* [23, 25, 28, 29]. However, in most of the cases of "sarcoid-like" lesions, there is no acid-fast bacilli identified morphologically or by culture [20, 22, 34].

Polymerase chain reaction (PCR) using oligonucleotide primers specific for *M. tuberculosis* gene fragments has been largely used in previous studies to identify tuberculosis (TB) infection from stored, formalin-fixed, paraffin-embedded tissue [12, 15, 16, 26, 32]. Data obtained from PCR on whole tissue sections must be evaluated critically due to the elevated occurrence of false-positive and false-negative results [2, 14, 24]. In this regard, we have previously demonstrated that PCR analysis of formalin-fixed, deparaffinized sections after laser capture microdissection (LCM) of granulomas was efficient for the detection of *M. tuberculosis* and that this association between PCR and LCM may reduce false-positive and false-negative results [30].

The aim of this study was to search for the presence of *M. tuberculosis* in the sarcoid-like granulomas observed in IRIS associated with HAART-treated AIDS patients by performing PCR on formalin-fixed, deparaffinized sections after LCM of granulomas. Results were compared to those obtained on samples with a confirmed microbiological diagnosis of TB and on samples with typical features of sarcoidosis obtained from HIV-negative patients.

Materials and methods

Patients and samples

All patients signed an informed consent form for this study, and the protocol was approved by the Ethics Committee of the University of Nice (PHRC 2001).

The clinical samples included three groups:

Group 1 The files of the Department of Pathology of Pasteur Hospital (Nice, France) were searched from 1999 through 2005 for cases of sarcoid-like lesions in HIV patients treated with HAART: 14 HAART-treated HIV patients with cervical and/or mediastinal lymph nodes, pulmonary parenchyma, or cutaneous disorders were included. The main clinical and epidemiological data and TB exposure are summarized in Table 1. All patients were French Caucasians living in Nice. The clinical signs at the time of IRIS diagnosis included fever (eight cases), pulmonary symptoms (five cases), a cervical lymphadenopathy (six cases), and a cutaneous lesion (two cases).

Group 2 Fifteen formalin-fixed, paraffin-embedded tissue (FFPE) samples were selected from the files of Department of Pathology of Nice. In all of them, the histological examination revealed caseating granulomas consistent with lesions of TB. The 15 samples were Ziehl-Neelsen positive. In all cases, the corresponding clinical material was culture positive for *M. tuberculosis*.

Group 3 Twelve FFPE tissue samples (displaying non-caseating granulomas) were selected from the files of the Department of Pathology of Nice. Histological and clinical evidence in all of these cases was suggestive of sarcoidosis. Ziehl-Neelsen staining performed on the above samples failed to reveal any acid-fast bacilli. Corresponding clinical material taken from these patients and examined using a microbiological method was in all cases culture negative for *M. tuberculosis*.

Immunohistochemical study

Immunohistochemistry was performed on deparaffinized sections of the different samples taken in group 1 and in group 2. An immunohistochemical study was carried out using an avidin–biotin–peroxidase complex (Vector Laboratories, Burlingame, CA, USA) and mouse anti-CD45 (Dako, Trappes, France; dilution: 1:200), anti-CD3 (Dako, Trappes, France; dilution: 1:200), anti-CD4 (Dako, Trappes, France; dilution: 1:200), anti-CD8 (Neomarkers, CA, USA; dilution: 1:100), and anti-CD68 (Dako, Trappes, France; dilution: 1:100).

Laser capture microdissection of specimens, deparaffinization, and DNA extraction

LCM of specimens, deparaffinization, and DNA extraction were performed as previously described [30]. Briefly, before microdissection, the 5-μm-thick tissue sections were cut from the paraffin block and mounted on uncoated and uncharged slides. The first slide was stained with hematoxylin–eosin (HE) to determine the position of the granulomas and other tissue landmarks in the section (Fig. 1), then the

Table 1 Summary of clinical and epidemiological data

Patient	Gender	Age (years)	HIV risk factor	Antecedents	Previous TB exposure	CD4 (mm^3)	Biopsies	HAART regimen[a]	Duration of HAART (months)
1	M	22	Hom.	PCP	No	248	Mediastinal lymph node	EFU/TFV/ 3TC/ABC	3
2	F	28	Het.	Tuberculosis	Yes	232	Skin	EFV/3TC/ ABC	6
3	M	34	IVDA	PCE PMLE	No	256	Skin	AZT/3TC/ NVP	8
4	M	51	IVDA	Cerebral toxoplasmosis	No	211	Mediastinal lymph node	AZT/3TC/ NVP	6
5	F	38	IVDA	Esophageal candidiasis	Yes	343	Cervical lymph node	EFV/3TC/ ABC	5
6	M	25	Hom.	Anal herpes	No	223	Cervical lymph node	TFV/3TC/ NVP	11
7	F	33	Het.	Esophageal candidiasis	No	241	Cervical lymph node	EFV/TFV/ 3TC/ABC	10
8	M	45	IVDA	Tuberculosis	Yes	208	Mediastinal lymph node	EFV/TFV/ ABC	7
9	M	29	Hom.	PCP	Yes	327	Mediastinal lymph node	AZT/3TC/ NVP	8
10	M	35	Hom.	PMLE	No	333	Mediastinal lymph node	AZT/3TC/ NVP	5
11	F	27	IVDA	Virus B hepatitis	No	287	Cervical lymph node	TFV/3TC/ NVP	9
12	M	42	IVDA	HIV neuropathy	No	222	Mediastinal lymph node	EFV/TFV/ ABC	10
13	M	55	Hom.	PCP	Yes	277	Cervical lymph node	TFV/3TC/ NVP	6
14	M	38	Hom.	Esophageal candidiasis	No	299	Mediastinal lymph node	AZT/3TC/ NVP	8

[a] Drugs used in HAART regimens included nucleoside analogue: [lamivudine (3TC), zidovudine (AZT), Abacavir (ABC)], nucleotide analogues: tenofovir (TFU), and nonnucleoside reverse transcriptase inhibitors: efavirenz (EFV), nevirapine (NVP)

IVDA Intravenous drug abuse, *Hom.* homosexuality, *Het.* heterosexuality, *PCP Pneumocystis carinii* pneumonia, *PMLE* progressive multifocal leukoencephalitis, *TB* tuberculosis

next steps were carried out as previously described [30]. Microdissected tissues were deparaffinized by adding 1 ml of xylene in each Eppendorf tube, and the samples were gently mixed for 20 min at 65°C. The samples were then processed as previously described [30]. For the digestion of the tissue, distilled water containing proteinase K (100 μg/μl; Sigma, Paris), Tris–HCl (20 mM; pH 8), EDTA (20 mM; Sigma), and SDS (2%) was added for 72 h at 55°C. DNA was purified using a Microcon 50 device (AMICON, OH, USA). The absorbance at 260 and 280 nm was determined in a spectrophotometer (Ultraspec 2000, USA) to assess the DNA concentration and purity. In parallel, the quantification of DNA after microdissection and extraction of cells was performed using the PicoGreen fluorescence method as previously described [1]. Briefly, microtiter plates were read in LS50B spectrofluorimeter with plate reading attachment (Perkin-Elmer/Applied Biosystems, Paris, France). PicoGreen-stained samples were excited at 485 nm. Triplicate aliquots were evaluated for each point between 0.060 and 600 ng, and the average was graphed. For PCR amplification, the amount of DNA purified from the microdissected samples was ranged between 0.5 and 0.7 ng.

Polymerase chain reaction and controls

The different steps were performed as previously described [30]. Briefly, 1 μl of extracted DNA was combined in a final volume of 50 μl containing 50 mM KCl, 10 mM Tris–HCl at pH 8.3, dH_20, 1.5 mM $MgCl_2$, dNTPs (200 μM; Invitrogen, Paris, France), and primer 1 and primer 2. PCR was based upon the amplification of a 123-bp fragment of the IS*6110* insertion element as described by Eisenach et al. [11]. The sequences of the primers used for amplification were IS*6110* 5′ (5′-3′ CCTGCGAGCGTAGGCGTCGG) (primer 1) and IS*6110* 3′ (5′-3′ CTCGTCCAGCGCCGC TTCGG) (primer 2) (Invitrogen). Taq polymerase (1.25 U) (Invitrogen) was added, and the conditions for PCR analy-

sis were as follows: 35 cycles at 94°C for 5 min, 67°C for 1 min, and 72°C for 40 sec (Perkin-Elmer Thermal Cycler; CA, USA). After the last cycle, 8 μl of amplified DNA with 2 μl of bromophenol blue Ficoll was loaded in each lane of a 1.5% agarose, ethidium bromide-stained gel. Four different sets of controls were performed. To control contamination during the DNA isolation procedure and to determine specificity, DNA was isolated from human paraffin-embedded non-TB granulomas in parallel with other samples. Ten formalin-fixed, paraffin-embedded non-TB specimens were used. Five specimens were from lymph nodes of HIV-negative patients with pyoepithelioid granulomas caused by *Bartonella* sp. infection, and five specimens were from lymph nodes of HIV patients, which presented atypical mycobacteriosis (with positive culture for *M. avium-intracellulare*). For each tissue sample, the amplification of the β-actin gene served as a control for successful DNA isolation. The primers used for amplification were β-actin 5′, 3′-AGCGGGAAATCGTGCGTG and β-actin 3′, 5′-CAGGGTACATGGTGGTGC (Invitrogen, Paris, France). In each PCR experiment, a control without DNA (paraffin block without tissue) was included. Finally to evaluate the sensitivity of the system in paraffin-embedded tissues, acid-fast positive bacilli were counted in a 5-μm-thick tissue section that was culture positive for *M. tuberculosis*. The DNA was extracted as described above from seven adjacent 5 μm sections of the block, prepared for PCR, and serial dilutions of the sample were tested.

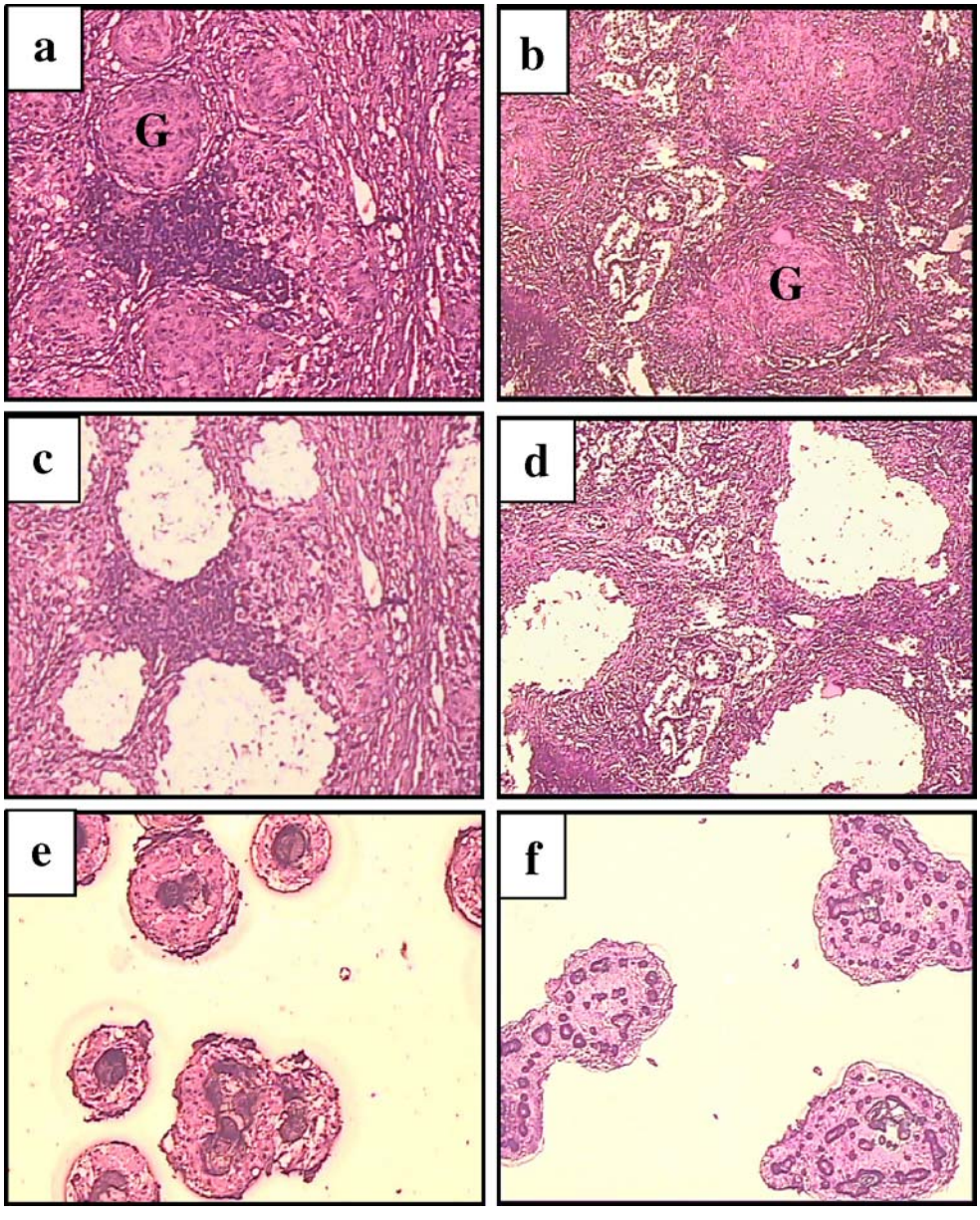

Fig. 1 Isolation of lymph-node sarcoid-like (**a**, **c**, **e**) and caseating (**b**, **d**, **f**) granulomas by laser capture microdissection. (**a**, **b**) Deparaffinized section before microdissection (G: granuloma). **c**, **d** The same section after microdissection. (**e**, **f**) Captured granulomas on a thermoplastic cap

Results

Sarcoid-like granulomas observed in HAART-treated patients demonstrated infiltration by CD4+ and CD8+ T lymphocytes

Immunostaining of paraffin-embedded tissue sections revealed that the sarcoid-like granulomas (group 1) were predominantly infiltrated by CD3 (Fig. 2a) lymphocytes of the CD4 subset (Fig. 2c). Moreover, immunohistochemistry showed low CD8 expression of the T cells infiltrating the granulomas (Fig. 2e). Anti-CD68 immunostaining confirmed the presence of numerous macrophages among the infiltrated cells (Fig. 2g). Caseating granulomas (group 2) were infiltrated by CD3 (Fig. 2b) lymphocytes of both the CD4 (Fig. 2d) and CD8 (Fig. 2f) subsets. Histiocytes and multinucleated giant cells were strongly stained with anti-CD68 antibody (Fig. 2h).

PCR from microdissected sarcoid-like granulomas in HAART-treated patients, sarcoidosis granulomas, and TB granulomas

PCR performed on microdissected sarcoid-like granulomas obtained from one 5 μm section of each specimen was negative in 14 cases (Fig. 3). PCR from microdissected TB granulomas obtained from one 5 μm section of each specimen was strongly positive in 15 cases, whereas PCR from microdissected sarcoidosis was negative in all cases (Fig. 3). All controls performed on atypical mycobacteriosis and pyoepithelioid granulomas were negative for PCR performed on microdissected granulomas (Fig. 3). Negative results were also obtained from the paraffin block without tissue (Fig. 3).

Discussion

Granulomatous inflammation of different organs, particularly of the lungs and the lymph nodes, and less frequently of the skin, kidneys, liver, and duodenum, has been described in patients responding to HAART [23, 25, 28]. These granulomas can be associated with the presence of different pathogens, most commonly *M. tuberculosis* [9, 10, 23, 25, 28]. Sarcoid-like disease, also considered as IRIS, is observed less frequently in patients responding to HAART [20, 22, 34].

In the present work, all cases of sarcoid-like lesions observed in HAART-treated patients showed CD4+ T cells in granulomas, an observation which is associated with a very low number of CD8+ T cells. Granulomas were composed of a majority of epithelioid macrophages in association with a few giant cells, without a necrotic area. Previous studies have demonstrated similar sarcoid-like lesions in HIV-positive patients treated with HAART [20, 22, 34]. In comparison, caseating granulomas showed numerous CD3+ T cells of both CD4+ and CD8+ subsets.

There is a need to differentiate histologically the different types of IRIS, particularly the infectious IRIS and the sarcoid IRIS, because the treatment strategy is different. In this regard, the goal of the present work was to determinate if sarcoid-like lesions associated with HAART could be linked to the presence of *M. tuberculosis*, even though Ziehl-Neelsen staining and/or culture was negative. We used a PCR-based method to examine sarcoid-like lesions microdissected by laser capture because we showed in a previous study that this technology can be used to improve the detection of *M. tuberculosis* in tissue. In the present study, we failed to detect the presence of *M. tuberculosis* DNA in sarcoid-like lesions observed in HAART-treated patients. In parallel, by using the same technology, we failed to detect the presence of *M. tuberculosis* DNA in sarcoidosis occurring in HIV-negative patients. The pathogenesis of granulomas associated with IRIS in AIDS is actually not well understood. The involvement of CD4+ T cells could explain the occurrence of this disorder after the addition of interleukin-2 therapy to HAART [18]. The occurrence of sarcoid-like granuloma most probably involves naive and IL-2 receptor-positive CD4+ T cells rather than memory T cells which have been thought to be implicated in MAC exacerbation [18, 28, 33]. Exceptionally, HIV-associated sarcoidosis has been reported in patients not receiving HAART [6]. However, in this latter condition, tissue examination showed a majority of CD8+ T cells infiltrating in granulomas. The role of *M. tuberculosis* in the pathogenesis of sarcoidosis is still debated [9]. Some previous studies have demonstrated, by PCR performed on whole deparaffinized sections, the presence of *M. tuberculosis* DNA in sarcoidosis lesions [8, 27]. Conversely, another study did not detect *M. tuberculosis* DNA or ribosomal RNA of *M. tuberculosis* using the same methodology [13]. In our work, we failed to detect the presence of *M. tuberculosis* DNA in our series of HIV-negative sarcoidosis lesions by using an LCM approach.

In conclusion, as the use of HAART increases around the world, physicians and pathologists managing patients with HIV infection will encounter increasing numbers of patients with IRIS. Management of these conditions is often problematic, in particular distinguishing them from opportunistic infections or drug toxicity. In the present work, we could not detect *M. tuberculosis* DNA in sarcoid-like lesions observed in HAART-treated patients. Therefore, these lesions do not represent an active TB infection. It is thus important to understand the pathogenesis of IRIS in order for treatment strategies to be developed. In this regard, further studies should be undertaken to look for (a)

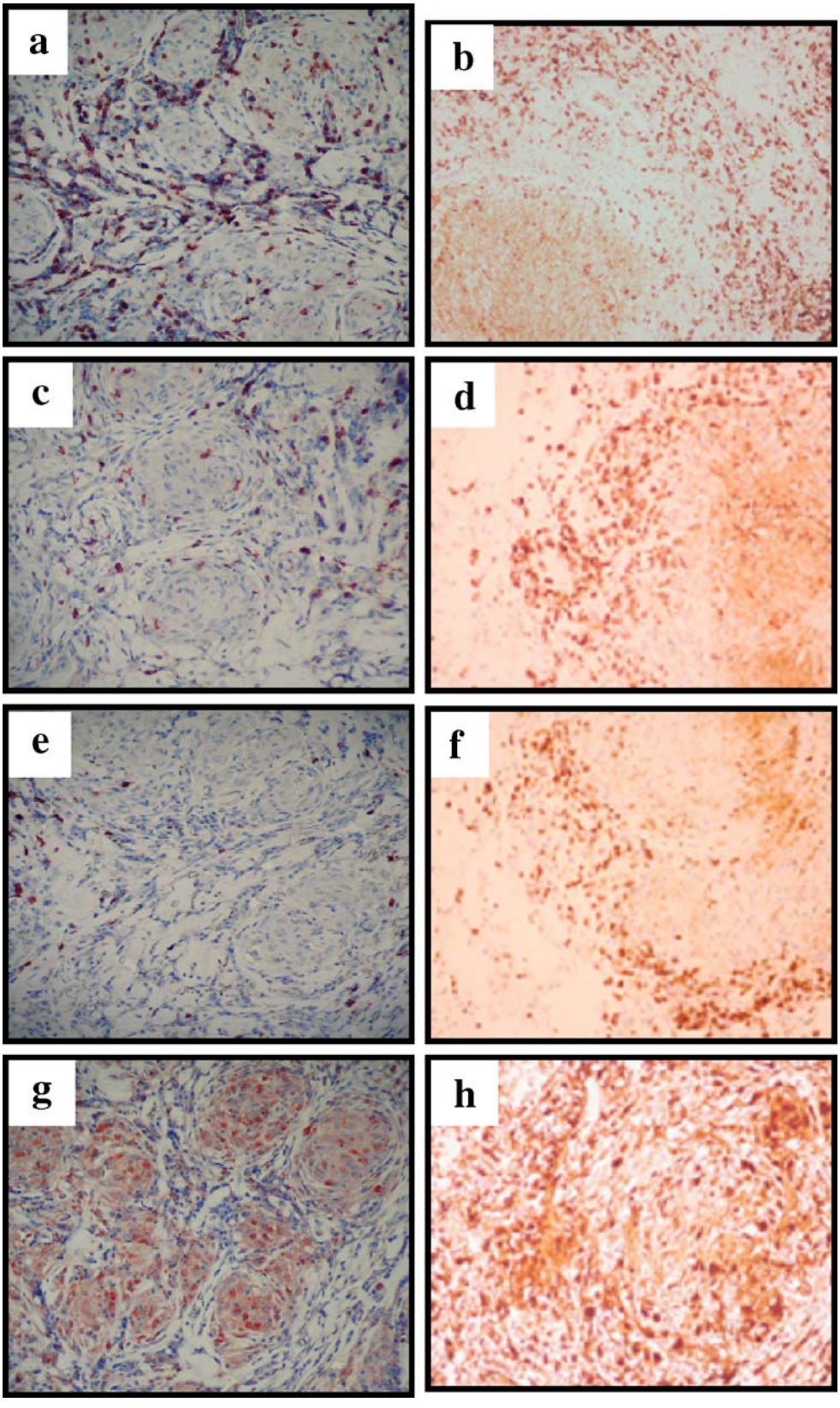

Fig. 2 Sarcoid-like granulomas: anti-CD3 (**a**), anti-CD4 (**c**), anti-CD8 (**e**), and anti-CD68 (**g**) immunostaining. Caseating granulomas: anti-CD3 (**b**), anti-CD4 (**d**), anti-CD8 (**f**), and anti-CD68 (**h**) immunostaining. Immunoperoxidase, original magnification ×320

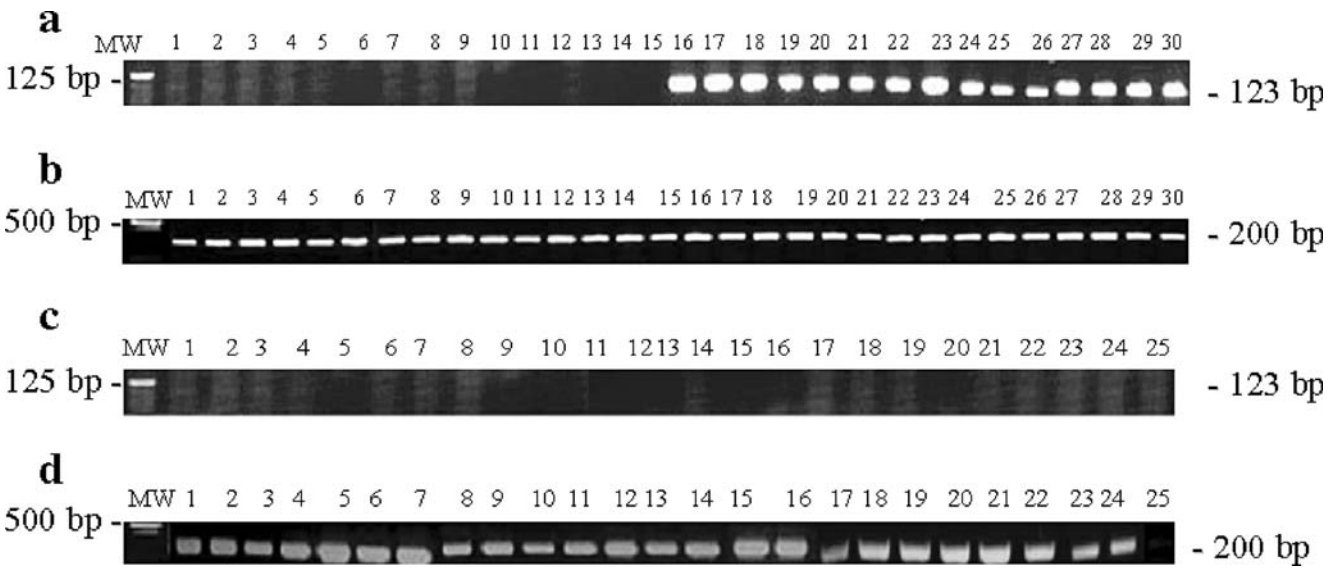

Fig. 3 Analysis of PCR products from DNA of microdissected granulomas from formalin-fixed, paraffin-embedded tissues amplified with primers specific for *M. tuberculosis* DNA. The products were separated by electrophoresis on a 1.5% agarose gel. *MW* Molecular weight marker (fragment length: 125 and 500 bp). **a** *Lanes 1–14* PCR from sarcoid-like granulomas in AIDS patients with IRIS. *Lanes 15–30* PCR from tuberculous granulomas with acid-fast bacilli performed on formalin-fixed, paraffin-embedded tissue section. **b** PCR amplification of the β-actin gene from the microdissected areas. **c** *Lanes 1–12* PCR from sarcoidosis granulomas. *Lanes 13–18* PCR from specimens of pyoepithelioid granulomas. *Lanes 19–24* Granulomas with atypical mycobacteria (culture from fresh specimens were positive for *M. avium-intracellulare*). *Lane 25* PCR from paraffin block without tissues. **d** PCR amplification of the β-actin gene from the microdissected areas

yet unidentified antigen(s) that induce(s) sarcoid-like granulomas in IRIS diagnosed in HAART-treated HIV patients.

Acknowledgments This work was supported by the PHRC Regional 2001 (Centre Hospitalo-Universitaire de Nice) (SL, ES, VH, JM, PD, PH). The authors wish to thank Dr. Michel Mouroux (CHPG, Monaco) for his support and Dr. Ellen Van Obbergen for reading this manuscript.

References

1. Ahn SJ, Costa J, Emanuel JR (1996) PicoGreen quantification of DNA: effective evaluation of samples pre- or post-PCR. Nucleic Acids Res 24:2623–2625
2. Cabras AD, Kremer M, Schulz S, Werner M, Hummel M, Komminoth P, Hofler G, Hofler H (2000) Quality assessment in diagnosis molecular pathology: experience from a German–Austrian–Swiss multicenter trial. Virchows Arch 437:46–51
3. Carr A, Cooper DA (2000) Adverse effects of antiretroviral therapy. Lancet 356:1423–1430
4. Carr A (2002) Improvement of the study, analysis, and reporting of adverse events associated with antiretroviral therapy. Lancet 360:81–85
5. Cheng VCC, Yuen K-Y, Chan WM, Wong SS, Ma ES, Chan RM (2000) Immunorestitution disease involving the innate and adaptive response. Clin Infect Dis 30:882–892
6. Coots LE, Lazarus AA (1989) Sarcoidosis diagnosed in a patient with known HIV infection. Chest 96:201–202
7. Deayton J, Mocroft A, Wilson P, Emery VC, Johnson MA, Griffiths PD (1999) Loss of cytomegalovirus (CMV) viraemia following highly active antiretroviral therapy in the absence of specific anti CMV therapy. AIDS 13:1203–1206
8. Drake WP, Pei Z, Pride DT, Collins RD, Cover TL, Blaser MJ (2002) Molecular analysis of sarcoidosis tissues for mycobacterium species DNA. Emerg Infect Dis 8:1334–1341
9. Du Bois RM, Goh N, McGrath D, Cullinan P (2003) Is there a role for microorganisms in the pathogenesis of sarcoidosis? J Intern Med 253:4–17
10. Emery S, Lane HC (1997) Immune reconstitution in HIV infection. Curr Opin Immunol 9:568–572
11. Eisenach KD, Cave MD, Bates JH, Crawford JT (1990) Polymerase chain reaction amplification of a repetitive DNA sequence specific for *Mycobacterium tuberculosis*. J Infect Dis 161:977–981
12. Frevel T, Schafer KL, Totsch M, Bocker W, Dockhorn-Dwoniczak (1999) PCR based detection of mycobacteria in paraffin wax embedded material routinely processed for morphological examination. Mol Pathol 52:283–288
13. Ghossein RA, Ross DG, Salomon RN, Rabson AR (1994) A search for mycobacterial DNA in sarcoidosis using the polymerase chain reaction. Am J Clin Pathol 101:733–737
14. Greer CE, Peterson SL, Kiviat NB, Manos MM (1991) PCR amplification from paraffin-embedded tissues. Effects of fixative and fixation time. Am J Clin Pathol 95:117–124
15. Hardman WJ, Benian GM, Howard T, McGowan JE Jr, Metchock B, Murtagh JJ (1996) Rapid detection of mycobacteria in inflammatory necrotizing granulomas from formalin-fixed, paraffin-embedded tissue by PCR in clinically high risk patients with acid-fast stain and culture negative tissue biopsies. Am J Clin Pathol 106:384–389
16. Ikonomopoulos JA, Gorgolis VG, Kastrinakis NG, Zacharatos PV, Kokotas SN, Evangelou K, Kostsinas AG, Manolis EN, Kittas CN (2000) Sensitive differential detection of genetically related mycobacterial pathogens in archival material. Am J Clin Pathol 114:940–950

17. Kalkut G (2005) Antiretroviral therapy: an update for the non-AIDS specialist. Curr Opin Oncol 17:479–484
18. Kuekrek H, Schlingmann T, Valdez H, Boehm BO, Pollard RB, Mitsuyasu R, Goebel F-D, Lederman MM, Lehmann PV, Tary-Lehmann M (2005) Differential effect of interleukin-2 treatment on primary and secondary immunizations in HIV infected individuals. AIDS 19:1967–1974
19. Lassalle S, Cervera P, Hofman V, Mari M, Dellamonica P, Hofman P (2005) Le syndrome lipodystrophique associé aux traitements antirétroviraux: aspects anatomo-cliniques. Ann Pathol 25:309–317
20. Mirmirani P, Maurer TA, Herndier B, McGrath M, Weinstein MD, Berger TG (1999) Sarcoidosis in a patient with AIDS: a manifestation of immune restoration syndrome. J Am Acad Dermatol 41:285–286
21. Mocroft A, Ledergerber B, Katlama C, Kirk O, Reiss P, d'Arminio Monforte A, Knysz B, Dietrich M, Philips AN, Lundgren JD, EuroSIDA Study Group (2003) Decline in the AIDS and death rates in the EuroSIDA study: an observational study. Lancet 362:22–29
22. Naccache JM, Antoine M, Wislez M, Fleury-Feith J, Okenhendler E, Mayaud C, Cadranel J (1999) Sarcoid-like pulmonary disorder in human immunodeficiency virus-infected patients receiving antiretroviral therapy. Am J Respir Crit Care Med 159:2009–2013
23. Navas E, Martin-Davilla P, Moreno L, Pintado V, Casado JL, Fortun J, Perez-Elias MJ, Gomez-Mamapaso E, Moreno S (2002) Paradoxical reactions of tuberculosis in patients with the acquired immunodeficiency syndrome who are treated with highly active antiretroviral therapy. Arch Intern Med 162:97–99
24. Pan LX, Diss TC, Isaacson PG (1995) The polymerase chain reaction in histopathology. Histopathology 26:201–207
25. Philipps P, Kwiatkowski MB, Copland M, Craib K, Montaner J (1999) Mycobacterial lymphadenitis associated with the initiation of combination antiretroviral therapy. J Acquir Immune Defic Syndr Hum Retrovirol 20:122–128
26. Popper HH, Winter E, Hofler G (1994) DNA of *Mycobacterium tuberculosis* in formalin-fixed, paraffin-embedded tissue in tuberculosis and sarcoidosis detected by polymerase chain reaction. Am J Clin Pathol 101:738–741
27. Popper HH, Klemen H, Hoefler GB, Winter E (1997) Presence of mycobacterial DNA in sarcoidosis. Hum Pathol 28:796–800
28. Race EM, Adelson-Mitty J, Kriegel GR, Barlam TF, Reimann KA, Letvin NL, Japour AJ (1998) Focal mycobacterial lymphadenitis following initiation of protease-inhibitor therapy in patients with advanced HIV-1 disease. Lancet 351:252–255
29. Salama C, Policar M, Venkataraman M (2003) Isolated pulmonary *Mycobacterium aviumcomplex* infection in patients with human immunodeficiency virus infection: case reports and literature review. Clin Infect Dis 37:35–40
30. Selva E, Hofman V, Berto F, Musso S, Castillo L, Santini J, Dellamonica P, Hofman P (2004) The value of polymerase chain reaction detection of *Mycobacterium tuberculosis* in granulomas isolated by laser capture microdissection. Pathology 36:77–81
31. Shelburne SA III, Hamill RJ, Rodriguez-Barradas MC, Greenberg SB, Atmar RL, Musher DW, Gathe JC Jr, Visnegarwala F, Trautner BW (2002) Immune reconstitution inflammatory syndrome: emergence of a unique syndrome during highly active antiretroviral therapy. Medicine (Baltimore) 81:213–827
32. Totsch M, Bocker W, Brommelkamp E, Fille M, Kreczy A, Ofner D, Scmid KW, Dockhorn-Dworniczak B (1996) Diagnostic value of different PCR assays for the detection of mycobacterial DNA in granulomatous lymphadenopathy. J Pathol 178:221–226
33. Vento S, Cainelli F, Temesgen Z (2006) Interleukin-2 therapy and CD4+ T cells in HIV-1 infection. Lancet 367:93–94
34. Wittram C, Fogg J, Farber H (2001) Immune restoration syndrome manifested by pulmonary sarcoidosis. AJR Am J Roentgenol 177:1427

Materials and methods

The Institute of Pathology of the Milan University is the Reference Center of the Lombardy Region (nine million inhabitants) for the project "Legislative measures for anatomo-pathological and forensic-pathological intervention targeting the prevention, knowledge and identification of the SIDS cases" [28]. This project imposes, on the basis of a specific decree, that all suspected cases of SIDS must be sent to our Institute for anatomopathological examination, together with the relative clinical-anamnestic data, a careful reconstruction of the death scene, and of the events surrounding the discovery of the dead infant. On this basis, we collected 128 sudden infant death victims with clinical diagnosis of SIDS or suspect of SIDS. The performance of a complete autopsy with in-depth histology on serial sections, particularly of the brainstem and of the cardiac conduction system, in accordance with our necropsy protocol [34, 36], allowed us to diagnose 20 non-SIDS cases, in which decease was due to serious documented pathologies, 6 cases of borderline-SIDS, with insufficient features to explain the death [43], and 102 cases of SIDS (Table 1). Additional 40 infants dying suddenly and unexpectedly were excluded from this study, due to the lack of the brainstem and/or of the cardiac conduction system after incorrect or incomplete autopsy sampling performed from the cooperating regional centers.

The SIDS group consisted of Caucasian infants, 64 (62.74%) males and 38 (37.26%) females, ranging in age at the time of death from 1 to 12 months. Pregnancy had run a normal course in all cases. None of the mothers had any significant pathology.

Table 1 Death diagnoses in 132 infant sudden death victims

Sudden death classification	Anatomopathological findings	Number of cases
Non-SIDS (20 cases)	Hypertrophic cardiomyopathy	8
	Hyperacute myocardial infarction	3
	Pericarditis	1
	Cardiac fibroma	1
	Dilated cardiomyopathy	1
	Bronchopneumonia	2
	Biliary atresia	2
	Congenital toxoplasmosis	1
	Peritonitis	1
Borderline-SIDS (6 cases)	Viral encephalitis of brainstem nuclei	3
	Hemangioendothelioma of the area postrema	1
	Necrosis of the tractus solitarii nucleus	1
	T-lymphocytic leptomeningitis of the ventral medullary surface	1
SIDS (102 cases)	Brainstem alterations	78
	No brainstem alterations	24

The control group consisted of the 20 non-SIDS age-matched infant cases deceased of various causes documented at autopsy (Table 1).

Ethical approval

Ethical consent is not required for our study as the Institute of Pathology is the referral National center for the study of sudden unexpected and unexplained infant and perinatal death, according to the Italian Law no. 31 of 2-02-2006 "Regulations for Diagnostic Post Mortem Investigation in Victims of Sudden Infant Death Syndrome (SIDS) and Unexpected Fetal Death".

Risk factors evaluation

For each victim, anamnestic and epidemiological data were collected in a specific questionnaire included in our protocol. The variables commonly referred as risk factors for SIDS were classified, according to Guntheroth's criteria [10], as "non-preventable" and "preventable". The non-preventable variables were: sex, age, and time of death. Preventable risk factors included: parental cigarette smoking, prone position in the crib, and formula feeding. In the parental smoking group, particular attention was given to the maternal habit. Eighty-one mothers (79.4%) were active smokers, routinely smoking 3–15 cigarettes/day during and after pregnancy, and 21 were nonsmokers (20.6%).

The time of death was classified in terms of both season (spring, summer, autumn, and winter) and hour, defining the night as the period between 10 p.m. and 7.30 a.m. and the day between 7.31 a.m. and 9.59 p.m.

Other variables reported in the literature, that include maternal substance abuse, socioeconomic status, birth weight, soft bedding, cosleeping, and overheating, were not considerable in this study. In fact, none of the mothers used drugs, high doses of caffeine, sedatives or alcohol. Poor prenatal and postnatal care, related to low socioeconomic status, was indicated only in three cases; the birth weight was generally within normal limits (≥2,500 g); all the subjects slept in a crib, usually in the parent's room, with no-soft pillows and mattresses; thermal stress, was never reported.

Statistical analysis

The significance of differences between group parameters was evaluated by χ^2 test (SigmaStat version 3.0; SPSS). The selected level of significance was $p<0.01$, two-tailed.

Necropsy protocol

Autopsies were performed within 24 h after the death had occurred. Multiple samples from all organs were fixed in

10% phosphate-buffered formalin, processed and embedded in paraffin; 5-μm sections for each specimen were stained with hematoxylin–eosin.

In addition to the routine necropsy procedures, our autopsy protocol included the study of serial sections of the autonomic, central and peripheral nervous system, and of the cardiac conduction system.

Briefly, the brainstem, from the pontomesencephalic portion to the lower pole of the inferior olivary nucleus, was cut into four blocks. Transverse serial sections were made through the blocks at 30-μm intervals. For each level, twelve 5-μm sections were obtained with a total number of sections ranging from 900 to 1,400 for each case. The sections were stained with hematoxylin/eosin and Klüver–Barrera for histological analysis and treated with specific antibodies for immunohistochemical evaluation of neurotransmitters (catecholamines and somatostatin) involved in cardiorespiratory activity, for gliosis (GFAP method) and apoptosis. The pertinent nuclei were outlined, namely, the arcuate nucleus, the hypoglossus nucleus, the dorsal vagus motor nucleus, the tractus solitarii nucleus, the ambiguous nucleus, and the ventrolateral reticular formation in the medulla oblongata; the locus coeruleus, the parabrachial/Kölliker–Fuse complex in the pons and mesencephalon [23, 34, 36, 43]. Diagnoses of hypodevelopment, including nuclear hypoplasia and neuronal delayed maturation, of the arcuate nucleus [25, 32, 34] and of the hypoglossus nucleus [44] were established according to previously described criteria.

For the cerebellum examination, sections of both cerebellar hemispheres, including the vermis and hilus of the dentate nucleus, were obtained. Cerebellar blocks were serially sectioned. For each case, two 5-μm sections were stained with hematoxylin/eosin and Klüver–Barrera. Additional sections were subjected to immunohistochemistry, particularly for apoptosis detection. Diagnosis of altered cerebellar cortex was established according to our previously described criteria [26].

The cardiac conduction system was removed in two blocks: the first included the sinoatrial node and the crista terminalis, the second contained the atrioventricular node, His bundle down to the bifurcation, and bundle branches. These two blocks were serially cut at intervals of 40-μm (levels) and stained alternately with hematoxylin-eosin and Azan [35, 36, 42].

Morphometric analysis

The morphometric analysis with three-dimensional reconstruction was performed with an Image-Pro Plus Image Analyzer (Media Cybernetics, Silver Spring, Maryland, USA). The research was carried out particularly on the arcuate nucleus (ArcN) in both sides of the medulla oblongata in the same specimen. The following parameters were evaluated: arcuate neuronal density [number of neurons per unit area (mm^2)] and arcuate nucleus volume. All the neurons were counted in transverse sections, coplanar, with clearly defined edges and with a distinct nucleolus, and examined with the optical microscope at ×20 magnification. The volume of the ArcN was measured by three-dimensional reconstruction. A computer program developed by Voxblast (VayTek, Fairfield, Iowa) was used to digitize and display serial sections reconstructions, and to obtain volumetric measurements of the selected cell populations. Every tenth section, the outer boundaries of the arcuate nucleus was traced. The tracings were digitized by computer and then registered to reestablish their original positions relative to one another. The fourth ventricle and central canal served as landmarks for registration. The brainstem was reconstructed from the cervicomedullary to the pontomedullary junction [32].

Immunohistochemical methods

Tyrosine hydroxylase (TH) immunohistochemistry For TH immunostaining, the sections were rinsed three times in 0.1 M Trizma buffered saline (TBS) followed by a 48-h incubation at 4°C with a 1/500 dilution of primary rabbit antiserum to TH (Novocastra Laboratories, Newcastle, UK). The dilutions were prepared with a solution of 1% normal goat serum (NGS) and 0.25% Triton X-100 in 0.1 M Tris–saline. This was followed by a 2.5-h incubation with biotinylated goat anti-rabbit immunoglobulin G (IgG) (Vector Laboratories, Burlingame, CA, USA) diluted 1/200 with 1% NGS in Tris–saline. The tissue was then incubated for 2 h with the avidin–biotin complex diluted 1/100 with 1% NGS in Tris–saline (Vector). Between each incubation, the sections were rinsed three times with 1% NGS in Tris–saline. The sections were then treated for 6 min with a 0.05% solution of 3,3'diamino–benzidine and 0.01% hydrogen peroxide, rinsed in phosphate buffer, mounted on gel-coated slides, cleared in xylene and coverslipped with Depex mounting medium.

Somatostatin (SS) immunohistochemistry To neutralize endogenous peroxidase, sections were pretreated with a solution of 0.3% hydrogenase peroxide for 20 minutes. After rinsing in buffer, sections were exposed for 48 h to the specific primary antiserum (Novocastra Laboratories, Newcastle, UK) diluted 1:150 at 25°C. After 10 min in buffer, the site of antigen–antibody reaction was revealed with anti-rabbit immunoglobulin followed by peroxidase–antiperoxidase complex. The unlabeled antiserum was placed on the sections for 2 h, diluted 1:200 at room temperature. The sections were then exposed to peroxidase–antiperoxidase complex for 2 h at a dilution of 1:200.

The sites of peroxidase activity were visualized with 0.3% hydrogen peroxide in buffer containing 0.04% diaminobenzidine tetrahydrochloride and 0.5 g nickel ammonium sulfate.

Apoptosis immunohistochemistry The sections were deparaffinized and incubated with 20 μg/ml proteinase K (Sigma). After blocking the endogenous peroxidase with 3% hydrogen peroxide, deoxynucleotidyl transferase (TdT 0.3 U/ml) was used to incorporate digoxigenin-conjugated deoxyuridine (dUTP 0.01 mM/ml) into the ends of DNA fragments. The signal of TdT-mediated dUTP Nick End Labeling (TUNEL) was then detected by an antidigoxigenin antibody conjugated with peroxidase (Apoptag Peroxidase in situ Apoptosis Detection kit, Oncor, Gaithersburg, MD, USA). Counterstaining was performed by immersing the slides in methyl green for 10 min.

GFAP immunohistochemistry To reveal the reactive astrocytes the sections were stained by the indirect immunoperoxidase method with antibody to the glial fibrillar acidic protein (GFAP) (bovine GFAP, Novocastra, Newcastle, Tyne, UK). The GFAP dilution was 1:200; the time of incubation 1 h. Sections were then counterstained with Mayer's hematoxylin. Astrocytes were counted if they displayed a GFAP-positive cytoplasm and counterstained nucleus.

For all the immunohistochemical methods, negative controls were prepared by replacing the respective primary antibodies with PBS in the incubation. In these procedures, staining always failed to occur.

Immunohistochemistry evaluation

To evaluate the immunoreactivity for TH protein and apoptosis, we applied a rating system for each method, based on the examination of all the immunostained sections along the caudorostral extension of the brainstems. Only neurons with intense brown staining were considered to be positive.

We quantified the scoring for each brainstem nucleus as follows:

– No positive neuron, or presence of weakly immunostained neurons
\+ A number of positive neurons ≤30% (moderate positivity)
++ A number of positive neurons >30% (strong positivity)

The scores, referred to bilateral sides of every nucleus, were assigned by two independent and blinded observers and comparison among the data was performed to evaluate the interobserver reproducibility. In cases of discordance among the investigators, the case was reviewed and discussed until a unanimous result was obtained.

As regards to gliosis, the density and the ratio of reactive astrocytes in braistem and cerebellum sections were evaluated. A case was considered as positive when a percentage higher than 25% of immunopositive cells was detected.

Results

The in-depth anatomopathological examination, following our guidelines, led to exclusion from our study of 20 non-SIDS and six borderline cases, thus reducing the number of effective SIDS victims to 102 (Table 1).

Histopathologic, morphometric, and immunohistochemical examination of the central autonomic nervous system revealed, in 78 cases of the SIDS group (76.47%), various anomalies of the brainstem nuclei related to cardiorespiratory control. The main brainstem findings were:

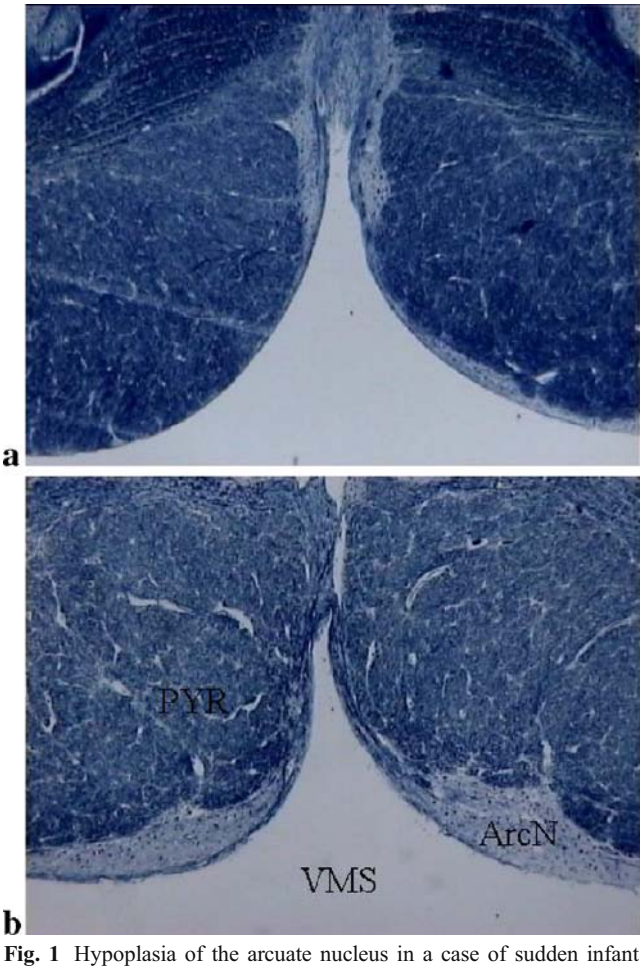

Fig. 1 Hypoplasia of the arcuate nucleus in a case of sudden infant death syndrome (**a**), compared with a normal arcuate nucleus (**b**). *ArcN* arcuate nucleus, *PYR* pyramid, *VMS* ventral medullary surface. Klüver–Barrera, ×25

1) Hypodevelopment of the arcuate nucleus (Fig. 1). In particular, hypoplasia of the arcuate nucleus was observed in 58 cases (56.86%). In 21 SIDS victims the hypoplasia was bilateral, extending throughout the whole arcuate nucleus; in 26 cases, there was partial hypoplasia, generally confined to the inferior two thirds and in 11, there was monolateral hypoplasia, prevalently involving the right portion. In addition, delayed neuronal maturation of the arcuate nucleus, despite a normal structure, was found in 18 SIDS cases. No hypodevelopment abnormalities of the arcuate nucleus were found in control cases. The diagnosis of arcuate nucleus hypoplasia was substantiated by the morphometric analysis. On the basis of the histologic structure of the nucleus, we divided the analyzed cases into three subsets: group A, SIDS cases with arcuate nucleus hypodevelopment; group B, SIDS cases with normal structure of the arcuate nucleus, and group C, control cases with normal arcuate nucleus. The volume of the hypoplastic arcuate nucleus (SIDS-group A) was on average 2.98 $mm^3 \pm 0.47$, significantly lower than mean volume of the group B (SIDS with normal structure of the arcuate nucleus): 8.85 $mm^3 \pm 0.35$, and of the control group C: 9.26 $mm^3 \pm 1.82$ ($p=0.0021$). The considerable developmental reduction of the arcuate nucleus was associated with a marked cell depletion, as indicated by the mean neuronal density of the group A (317 ± 25 neurons/mm^2), with respect to the mean density of the group B (1490 ± 281 neurons/mm^2), and of the group C (1536 ± 151 neurons/mm^2).
2) Intense positivity for somatostatin in the hypoglossus nucleus (Fig. 2), revealing a delayed maturation of its neurons, was detected in 55 cases (53.93%)of SIDS. Somatostatin-positive neurons were also detected in the hypoglossus nucleus of two control cases (10%), with statistically significant difference between the two groups ($p<0.01$; χ^2 test).
3) Negativity for tyrosine hydroxylase, an enzyme involved in catecholamine synthesis, in the pontine locus coeruleus, was detected in 65 cases (63.72%). In cases of death of known causes, locus coeruleus showed a tyrosine hydroxylase-positive score.
4) Strong diffuse gliosis (Fig. 3), an aspecific marker of pathologic processes, in the brainstem was observed in 41 cases (40.19%) of SIDS. Gliosis was detected also in control cases with a percentage of reactive astrocytes was lower than 25%.
5) Hypoplasia of the hypoglossus nucleus was observed in 15 cases (14.70%). No hypoplasia of the hypoglossus nucleus was found in control cases.

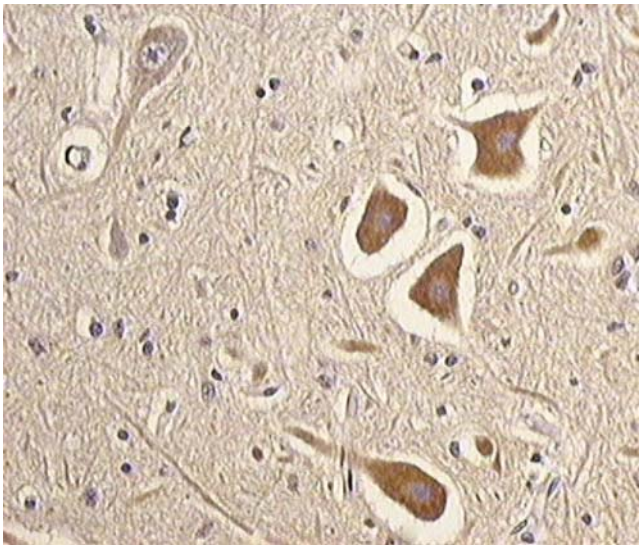

Fig. 2 Somatostatin-positive neurons of the hypoglossus nucleus in a case of sudden infant death syndrome. Somatostatin immunostain, ×200

Alterations of the cerebellar cortex (immaturity of the external granular layer, apoptosis of the Purkinje cells, and apoptosis of the inner granular layer) were detected in 54 cases (52.94%), while were absent in control cases.

As concerning the mediastinal autonomic nervous system, neural immaturity and increase in small intensely fluorescent (SIF) cells in the sympathetic upper cervical ganglion was observed in 8.82% of the SIDS victims, while these were not detected in the control cases. Hyperplastic aorticopulmonary paraganglia, secondary to hypoxia, was detected in 23.53% of the SIDS cases and was absent in control cases. Frequently, in the same case, two or more of these anomalies were detected.

Regarding the cardiac conduction system, we observed accessory pathways, mainly Mahaim fibers (Fig. 4), in 22.54% of victims and, rarely, James (4.90%) and Kent fibers (1.96%). Mahaim fibers were detected in 5% of control cases, without a statistically difference; James and Kent fibers were absent in controls. Dispersion or septation

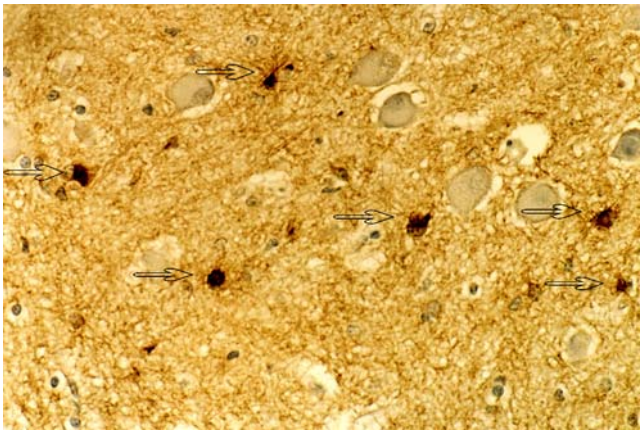

Fig. 3 Reactive astrocytes (*arrows*) in the inferior olivary nucleus in a case of sudden infant death syndrome. GFAP immunostain, ×40

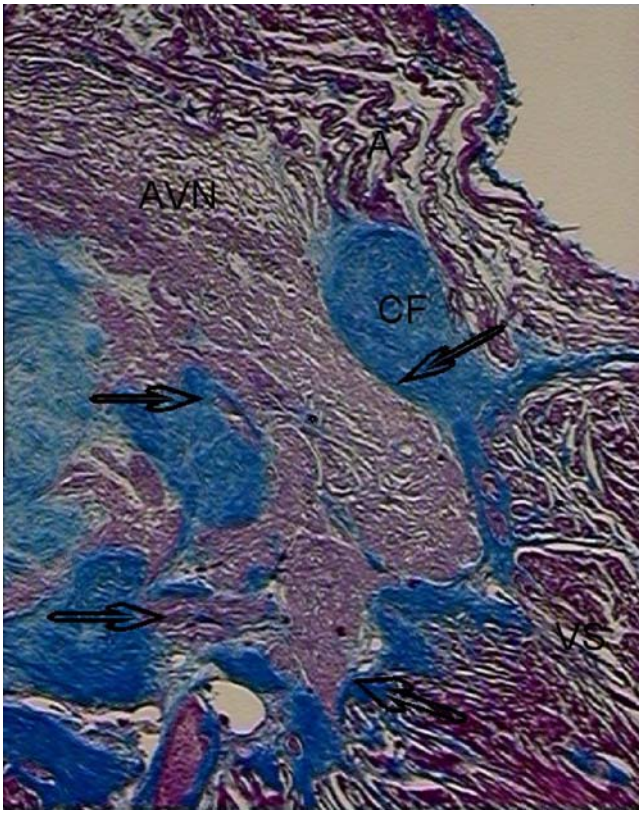

Fig. 4 Nodoventricular accessory pathway of Mahaim type (*arrows*) bridging the atrioventricular node (*AVN*) directly to the interventricular septum (*VS*), in a case of sudden infant death syndrome. *CF* central fibrous body; *A* right atrium. Trichrome Heidenhain (Azan), ×25

of the atrioventricular node and/or His bundle were detected in 41.17% of the SIDS and in 15% of control cases. These findings were frequently associated to autonomic nervous system alterations in SIDS cases.

Most of the SIDS cases occurred under 6 months of age, particularly between 2 and 4 months (45.1% of the cases); males were more affected than females (62.74 vs 37.26%), and the distribution of deaths in the year featured a winter peak (44.12%). No night or day hour of death was more frequent in our SIDS group (Table 2).

The incidence of the preventable behaviors is represented in Table 3. Infants sleeping face down have about the same rate of SIDS as those sleeping on their back (50.98 and 49.02%, respectively). A high percentage of SIDS victims (79.41%) had been exposed to cigarette smoke, particularly from the mother, during pregnancy and after birth. Formula feeding is also a frequent feature in SIDS victims (64.71% of cases).

The different risk factors were correlated with the brainstem findings (Table 4). A statistically significant relation was found only between maternal smoke and brainstem alterations. In fact, the distribution of the most significant variables into the two groups of SIDS (with and without brainstem abnormalities, respectively), showed that maternal cigarette smoking was the risk factor almost always present in SIDS cases with morphological and/or functional anomalies of brainstem structures ($p<0.01$, χ^2 test). None of the other relevant features (prone position, formula feeding, male sex, 2–4 months of age, and winter months of death) was statistically different between the 2 SIDS groups (ns, χ^2 test) (Table 4) (Fig. 5).

Table 2 Distribution of the non-preventable variables in SIDS cases ($n=102$)

Variables	Number of cases	Percentage
Age (months)		
<2	18	17.65
2–4	46	45.10
4–6	23	22.55
≥6	15	14.70
Sex		
Male	64	62.74
Female	38	37.26
Death season		
Spring	20	19.60
Summer	10	9.80
Autumn	27	26.48
Winter	45	44.12
Death time (24 h clock)		
Night (from 10 p.m. to 7.30 a.m.)	50	49.10
Day (from 7.31 a.m. to 9.59 p.m.)	52	50.90

Discussion

SIDS is a long-debated problem, centered upon the respiratory (apnea), cardiac (arrhythmogenic), and visceral-deranged motion (glottid–aesophagus–gastric spasm) theories [47, 48, 52], concerning still scarcely understood causative mechanisms.

Table 3 Distribution of the preventable variables in SIDS

Variables	Number of cases	Percentage
Sleep position		
Prone	52	50.98
Supine	50	49.02
Maternal smoking		
Negative	21	20.59
Positive	81	79.41
Feeding		
Maternal (only)	36	35.29
Formula (or mixed: formula + maternal)	66	64.71

Table 4 Distribution of risk factors among SIDS without and with brainstem alterations in a total of 102 SIDS victims

Risk factor	SIDS group I (n=24) number of cases (%)	SIDS group II (n=78) number of cases (%)
Preventable		
Maternal smoking (81 cases)	7 (8.64)	74[a] (91.36)
Prone position (52 cases)	12 (23.08)	40 (76.92)
Formula or mixed feeding (66 cases)	14 (21.21)	52 (78.79)
Non-preventable		
Male sex (64 cases)	17 (26.56)	47 (73.43)
2–4 months age (46 cases)	15 (32.61)	31 (67.39)
Winter months (45 cases)	11 (24.44)	34 (75.56)

SIDS Sudden infant death syndrome, *SIDS group I* SIDS cases without brain alterations (n=24 cases), *SIDS group II* SIDS cases with brainstem alterations (n=78 cases)

It can be underlined that neurogenic factors are interplaying in all such theses, also in the cardiac arrhythmogenic one, in which the conduction system (the accessory pathways namely) are subject to strict autonomic control [47, 48]. Thereby SIDS seems to represent a paradigmatic model for sudden death from conduction-cum-neural derangements, attempted by cardiorespiratory abnormality.

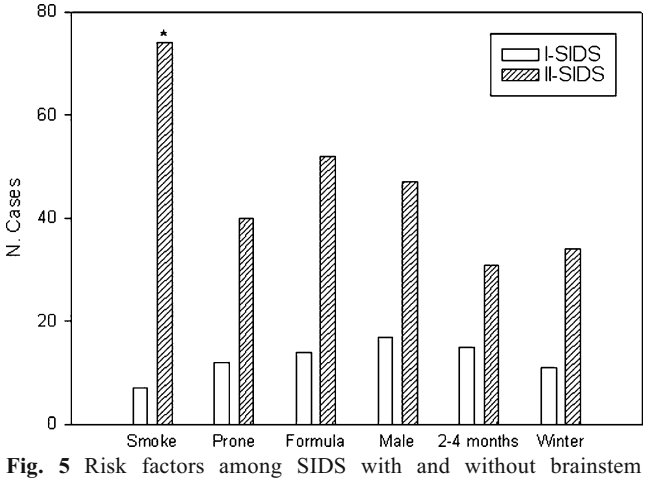

Fig. 5 Risk factors among SIDS with and without brainstem abnormalities. Distribution of the risk factors among the two groups of SIDS (with and without brainstem abnormalities) in a total of 102 SIDS victims. Maternal cigarette smoking was a risk factor significantly associated with SIDS cases characterized by morphological and/or functional anomalies of the brainstem (*p<0.01, χ^2 test). None of the other variables analyzed (prone position, formula or mixed feeding, male sex, 2–4 months of age, and winter months of death) was statistically different between the two groups (ns, χ^2 test). *I-SIDS* SIDS cases without brainstem alterations; *II-SIDS* SIDS cases with brainstem alterations

In the majority of past and present studies reported in the literature, sudden infant deaths continue to be attributed to SIDS, despite no or inadequate performance of autopsy, without the necessary examination of the nervous system. Even if different authors have underlined that SIDS is a diagnosis by exclusion with no pathognomonic findings at autopsy [53, 54], the proposed necropsy protocols, even in a recent report [20], mainly concern general features, i.e., evaluation of the nutritional status, the presence of petechial hemorrhages, thymic stress, foci of chronic inflammatory cells, above all in the respiratory system.

No current advice for autopsy examination in suspected cases of SIDS contemplates our guidelines, presented and approved at the 7th International Conference on SIDS [33]. In fact, we proposed that the diagnosis of SIDS can be effective only after a complete autopsy including an in-depth histological examination of the cardiorespiratory innervation and specialized myocardium, performed by an experienced pathologist, as described on our web site [35] and published in international journals [34, 36]. Our study also includes the search for possible physiological defects of the brainstem, evaluating by immunohistochemistry the presence of important neurotransmitters involved in the cardiorespiratory activity (namely, catecholamines and somatostatin).

In this study, the anatomopathological examination allowed us to recognize, among a group of 128 postnatal sudden deaths, collected on the basis of a specific Lombardy regional decree [28], 20 cases of non-SIDS in whom the death was due to significant organic diseases, and six cases of borderline-SIDS, with insufficiently severe findings to explain the cause of death. Thus, our examination allowed us to reduce by 20% the SIDS clinical diagnoses within this group of sudden infant deaths.

In the remaining group of 102 cases of undoubted SIDS, we identified frequent developmental abnormalities of the brainstem, particularly the hypoplasia of the arcuate nucleus, an important chemoreceptorial cardiorespiratory center of the ventral medullary surface, as well as abnormalities of the cardiac conduction system.

It is important to retain that the cardiorespiratory control is exerted primarily by the vagus, by an arc abutting of the brainstem nuclei [50], with an ill-recognized interplay of the glossopharyngeal nerve. Therefore, the neuropathological involvement of the vagal–glossopharyngeal neuronal circuitry is adapt to explain some lethal vagal reflexogenic mechanisms for SIDS quoted in the literature as “dive; feigned death” and/or “Ondine’s curse” reflex [37, 48].

In this large sample of SIDS victims, we aimed to reexamine these alterations, partially described in our previous works [21, 22, 24, 25, 34, 43], evaluating for the first time the role and the significance of the main risk factors up to now reported in epidemiological works [1, 2,

8, 9, 12, 27, 31, 45]. We omitted in our evaluation several variables, such as maternal substance abuse, socioeconomic status, birth weight, soft bedding, cosleeping, and overheating because they did not represent risk features for the SIDS cases collected in this study.

We subdivided the effective risk factors, following Guntheroth's suggestion [10], into "preventable" and "nonpreventable".

Among the nonpreventable risk factors, it was evident that males were more vulnerable than females (62.7% vs 37.3%), particularly between the ages of 2 and 4 months (45.1%) and in the winter period (44.1%) (Table 2). The winter peak of SIDS deaths is probably associated with increased respiratory illness. In fact, such infants often have documented upper respiratory infections in the days preceding death. Infections may thus represent a stress factor that contributes to the demise of a vulnerable infant [3, 4].

In the group of the modifiable behaviors, maternal cigarette smoking was the most important preventable risk factor for SIDS, reported in 79.41% of the cases. The incidence of smoking mothers mounts to 91.36% in the victim group with morpho-functional brainstem alterations (Table 4).

Several authors have attempted to explain why infants of smoking mothers are at higher risk of SIDS [6, 7, 13, 54]. The most common belief is that environmental smoke may influence the arousal mechanism, a key feature in the apnea theory for SIDS [6, 55].

On the basis of results of the Children's Hospital and Harvard Medical School of Boston [18, 40, 41], of our previous research [21, 22, 24, 25] and of the present study, we support the hypothesis of a close relation between maternal cigarette smoking during pregnancy and many abnormal processes in human brain development. In particular, in case of prenatal smoke exposure, carbon monoxide, a gaseous combustion product of nicotine, may readily cross by passive diffusion the placenta, where it binds to hemoglobin. Consequently, the carboxyhemoglobin inhibits the release of oxygen into fetal tissues causing hypoxia especially in the most susceptible organs, including the brain. Indeed, smoking in utero may strongly interfere with brain biology, giving rise not only to the structural developmental abnormalities of the arcuate nucleus, but also to decreased noradrenergic activity of the locus coeruleus and to increased somatostatin positivity in the hypoglossus nucleus. All these abnormalities can have an adverse effect on cardiorespiratory control and subsequently lead to sudden death.

Breastfeeding did not emerge from our analysis as related to a risk reduction of SIDS. In fact, even if many SIDS victims were formula-fed (64.71%), the difference is not statistically significant (Fig. 5).

Additionally, in our study, the prone sleeping position was not found to be a significant feature related to the brainstem alterations. The frequency of the prone position in the crib was 50.9%, whereas infants sleeping on their backs accounted for 49.02% of the SIDS victims (Table 3). Probably, despite the fact that the parents had received information about sleeping position at the birth of their infant, in accordance with the Lombardy Region guidelines for SIDS prevention, these babies were likely placed prone for sleep. Thus, improved educational efforts for parents should continue to focus on encouraging the supine position. In fact, in very many epidemiological reports of the last 15 years [2, 11, 14, 15, 17, 39, 46, 52], the prone position has been identified as the major risk factor for SIDS. Several authors suggest that prone sleeping provokes an array of problems, including rebreathing of carbon dioxide, reflex lowering of vasomotor tone, blunting of arousal responses and alterations of sleep patterns, all of which can potentially cause death.

However, our study must be differentiated from the many evaluations reported in the literature, none of which was related to an in-depth postmortem examination. Even the basic epidemiological work by Carpenter et al. [5], based on data for more than 60 variables in 754 SIDS cases collected in 20 European centers, that ascribes 48% of deaths to sleeping in the lateral or prone position, did not contemplate this aspect, which is indispensable in our view. Although these authors maintain that only cases submitted to necropsy are included in the study, the referred international autopsy protocol did not include histological examination of the autonomic nervous system.

Despite marked reductions in rates over the past decade, ascribed to avoidance of the prone sleeping position, SIDS is still responsible for more infant deaths than any other cause of death during the first year of life [19, 31]. According to our statistical analysis related to brainstem findings (Table 4, Fig. 5), we do not believe that SIDS is dependent on this single variable and stress that other features should be attributed importance in the effort to protect infants from sudden death.

Conclusions

In our statistical analysis, maternal smoking during pregnancy was found to be the most important preventable risk factor for SIDS, related to morphological and/or functional alterations of brainstem centers (Fig. 5). So, other than putting infants in a supine sleeping position, maternal smoking dissuasion must be the next most important issues to be considered for a strong second preventive campaign.

In addition, air pollution, particularly in the Lombardy Region, where the victims of this study come from, and

which features high rates of both gases (carbon monoxide, nitrogen dioxide, ozone, and sulfur dioxide) and particulate matter (above all PM_{10}, with a median diameter inferior to 10 μm) [49], could have an important influence in determining SIDS. We postulate that gas pollutants in particular, likewise cigarette smoke, can cross the placenta during pregnancy in the maternal blood, and lead to structural and/or functional impairments of the central nervous system.

Finally, as recently suggested by Hunt [16], it must be underlined that SIDS is probably a physiopathological response to a variety of mechanisms determined by gene-environment interactions, i.e., the same risk factors could have very different effects in infants with a different genetic constitution. Preventable risk factors can thus interact in complex ways with specific gene mutations and/or polymorphisms that yield phenotypes susceptible to sudden and unexpected death in infancy.

Now that sequencing of the human genome has been completed, studies need to be carried out to elucidate the molecular basis of the SIDS. Therefore, the delineation also of genetic risk factors for SIDS is the future necessary step to identify vulnerable phenotypes and specific strategies for preventing in these subjects fatal responses to high risk environmental perturbations.

Acknowledgments The authors thank Dr. Graziella Alfonsi and Dr. Lorella Terni for their precious technical assistance. This study was supported by the Region of Lombardy (project no. 49210–24.3.00 "Program of research and intervention for the reduction of the risk of sudden infant death syndrome—SIDS—and unexpected fetal death"), by "Lino Rossi" Research Center for the study and prevention of unexpected perinatal death and sudden infant death syndrome (SIDS) fundings (Rectorial Decree n. 225678 of 23/04/04), and by the Ministry of Foreign Affairs (joined project of particular relevance no. 269/P/0085087 "Anatomopathologic and genetic study of the unexplained perinatal death and SIDS"), Milan, Italy. The funding source had no involvement in study design, in the collection, analysis, and interpretation of data, in the writing of the report, and in the decision to submit the paper for publication.

References

1. Alm B, Wennergren G, Norvenius G, Skjaerven R, Irgens LM (1999) Caffeine and alcohol as risk factors for sudden infant death syndrome. Arch Dis Child 81:107–111
2. American Academy of Pediatrics, Task Force on Infant Sleep Position and Sudden Infant Death Syndrome (2000) Changing concepts of sudden infant death syndrome: implications for infant sleeping environment and sleep position. Pediatrics 105: 650–656
3. Blackwell CC, Weir DM, Busuttil A (2001) A microbiological perspective. In: Byard RW, Krous HF (eds) Sudden infant death syndrome: problems, progress and possibilities. Arnold, London, pp 182–208
4. Carmichael EM, Goldwater PN, Byard RW (1996) Routine microbiological testing in sudden and unexpected infant death. J Paediatr Child Health 32:412–415
5. Carpenter RG, Irgens LM, Blair PS, England PD, Fleming P, Huber J, Jorch G, Schreuder P (2004) Sudden unexplained infant death in 20 regions in Europe: case control study. Lancet 363:185–191
6. Chang AB, Wilson SJ, Masters IB, Yuill M, Williams J, Hubbard M (2003) Altered arousal response in infants exposed to cigarette smoke. Arch Dis Child 88:30–33
7. Chong DSY, Yip PSF, Karlberg J (2004) Maternal smoking: an increasing unique risk factor for sudden infant death syndrome in Sweden. Acta Paediatr 93:471–478
8. Douglas AS, Alexander E, Allan TM, Helms PJ (1996) Seasonality of birth in sudden infant death syndrome. Scott Med J 41:39–43
9. Guntheroth W, Spiers PS (1996) Are bedding and rebreathing suffocation a cause of SIDS? Pediatr Pulmonol 22:335–341
10. Guntheroth W (1999) Causation of SIDS: a critical review. Proceedings of the International Symposium on SIDS. October 4–5, Milan, Italy, pp 53–60
11. Harrison LM, Morris JA, Telford DR, Brown SM, Jones K (1999) Sleeping position in infants over 6 months of age: implications for theories of sudden infant death syndrome. FEMS Immunol Med Mictobiol 25:29–35
12. Hoffman HJ, Hillman L (1992) Epidemiology of the sudden infant death syndrome: maternal, neonatal and postneonatal risk factors. Clin Perinatol 19:717–737
13. Horne RS, Franco P, Adamson TM, Groswasser J, Kahn A (2004) Influences of maternal cigarette smoking on infant arousability. Early Hum Dev 79:49–58
14. Hunt CE, Shannon DC (1992) Sudden infant death syndrome and sleeping position. Pediatrics 90:115–118
15. Hunt CE, Lesko SM, Vezina RM et al (2003) Infant sleep position and associated health outcomes. Arch Pediatr Adolesc Med 157:469–474
16. Hunt CE (2005) Gene-environment interactions: implications for sudden unexpected deaths in infancy. Arch Dis Child 90:48–53
17. Kattwinkel J, Brooks J, Myerberg D (1992) American academy of pediatrics, task force on infant positioning and SIDS. Pediatrics 89:1120–1126
18. Kinney HC, O'Donnel TJ, Kriger P, White WF (1993) Early developmental changes in H3-nicotine binding in the human brainstem. Neuroscience 55:1127–1138
19. Kochanek KD, Murphy SL, Anderson RN, Scott C (2004) Deaths: final data for 2002. Natl Vital Stat Rep 53:1–115
20. Krous HF, Beckwith JB, Byard RW, Rognum TO, Bajanowski T, Corey T, Cutz E, Hanzlick R, Keens TG, Mitchell EA (2004) Sudden infant death syndrome and unclassified sudden infant deaths: a definitional and diagnostic approach. Pediatrics 114:234–238
21. Lavezzi AM, Ottaviani G, Mauri M, Matturri L (2004) Hypoplasia of the arcuate nucleus and maternal smoking during pregnancy, in perinatal and infant sudden unexpected death. Neuropathology 24:284–289
22. Lavezzi AM, Ottaviani G, Matturri L (2004) Role of somatostatin and apoptosis in breathing control in sudden perinatal and infant unexplained death. Clin Neuropathol 23:304–310
23. Lavezzi AM, Ottaviani G, Rossi L, Matturri L (2004) Cytoarchitectural organization of the parabrachial/Kölliker-Fuse complex in man. Brain Dev 26:316–320
24. Lavezzi AM, Ottaviani G, Mingrone R, Matturri L (2005) Analysis of the human locus coeruleus in perinatal and infant sudden unexplained deaths. Possible role of the cigarette smoking in the development of this nucleus. Brain Res Dev Brain Res 154:71–80
25. Lavezzi AM, Ottaviani G, Matturri L (2005) Adverse effects of prenatal tabacco smoke exposure on biological parameters of the developing brainstem. Neurobiol Dis 20:601–607

26. Lavezzi AM, Ottaviani G, Mauri M, Matturri L (2006) Alterations of biological features of the cerebellum in sudden perinatal and infant death. Curr Mol Med 6:429–435
27. L'Hoir MP, Engelberts AC, VanWell GT, Bajanowski T, Helweg-Larsen K, Huber J (1998) Sudden unexpected death in infancy: epidemiologically determined risk factors related to pathological classification. Acta Paediatr 87:1279–1287
28. Lombardy Regional Decree no. 11693 of 06-20-02 "Legislative measures on adoption of anatomo-pathological and forensic-pathological intervention targeted on the prevention, knowledge, and identification of the sudden infant death cases". http://users.unimi.it/~pathol/pdf/decreto.pdf. Accessed: June 1st, 2005
29. Markestad T, Skadberg B, Hordvik E, Morild I, Igrens L (1995) Sleeping position and sudden infant death syndrome (SIDS): effect of an intervention programme to avoid prone sleeping. Acta Paediatr 84:375–378
30. Mathews TJ, Menacker F, MacDorman MF (2003) Infant mortality statistics from the 2001 period linked birth/infant death data set. Natl Vital Stat Rep 52:1–28
31. Matthews T, McDonnell M, McGarvey C, Loftus G, O'Regan M (2004) A multivariate time based analysis of SIDS risk factors. Arch Dis Child 89:267–271
32. Matturri L, Biondo B, Suarez-Mier MP, Rossi L (2002) Brain stem lesions in the sudden infant death syndrome: variability in the hypoplasia of the arcuate nucleus. Acta Neuropathol (Berl) 104:12–20
33. Matturri L, Lavezzi AM, Rossi L (2002) Proposal to modify the definition of SIDS, with regard to the post mortem exam. In: Proceedings of the 7th SIDS International Conference. Florence, Italy; August 31–September 4, 2002, p 103
34. Matturri L, Ottaviani G, Alfonsi G, Crippa M, Rossi L, Lavezzi AM (2004) Study of the brainstem, particularly the arcuate nucleus, in sudden infant death syndrome (SIDS) and sudden intrauterine unexplained death (SIUD). Am J Forensic Med Pathol 25:44–48
35. Matturri L, Ottaviani G, Alfonsi G, Rossi L, Lavezzi AM. Guidelines in pathological and forensic-medical diagnostics of sudden unexpected infant (SIDS) and fetal death. Lombardy Region Project for reduction of the risk for SIDS and/or Sudden Fetal Death. Available at: http://users.unimi.it/~pathol/sids/linee_guida_e.html. Accessed: June 1st, 2005
36. Matturri L, Ottaviani G, Lavezzi AM (2005) Techniques and criteria in pathologic and forensic-medical diagnostics of sudden unexpected infant and perinatal death. Am J Clin Pathol 124:259–268
37. Matturri L, Ottaviani G, Lavezzi AM (2005) Sudden infant death triggered by dive reflex. J Clin Pathol 58:77–80
38. Mitchell EA, Thach BT, Thompson JMD, Williams S (1998) Changing infant's sleep position increases inner-city infants. JAMA 280:336–340
39. Moon RY, Omron R (2002) Determinant of infant sleep position in an urban population. Clin Pediatr 41:569–573
40. Nachmanoff DB, Panigrahy A, Filiano JJ, Mandell F, Sleeper LA, Valdes-Dapena M, Krous HF, White WF, Kinney HC (1998) Brainstem H3-nicotine receptor binding in the sudden infant death syndrome. J Neuropathol Exp Neurol 57:1018–1025
41. Nattie E, Kinney H (2002) Nicotine, serotonine, and sudden infant death syndrome. Am J Respir Crit Care Med 166:1544–1549
42. Ottaviani G, Matturri L, Rossi L, James TN (2003) Crib death: further support for the concept of fatal cardiac electrical instability as the final common pathway. Int J Cardiol 92:17–26
43. Ottaviani G, Matturri L, Bruni B, Lavezzi AM (2005) Sudden infant death syndrome "gray zone" disclosed only by a study of the brain stem on serial sections. J Perinat Med 33:165–169
44. Ottaviani G, Matturri L, Mingrone R, Lavezzi AM (2006) Hypoplasia and neuronal immaturity of the hypoglossal nucleus in sudden infant death. J Clin Pathol 59:497–500
45. Person TLA, Lavezzi WA, Wolf BC (2002) Cosleeping and sudden unexpected death in infancy. Arch Pathol Lab Med 126:343–345
46. Rambaud C, Guilleminault C (2004) "Back to Sleep" and unexplained death in infants. Sleep 27:1359–1366
47. Rossi L, Matturri L (1995) Anatomo-histological features of the heart's conduction system and innervation in SIDS. In: Rognum TO (ed) Sudden infant death syndrome: new trends in the nineties. Scandinavian University Press, Oslo, pp 207–212
48. Rossi L, Matturri L (1995) Cardiac conduction system in health disease cardiac conduction and nervous system in health disease and sudden death: an anatomoclinical overview. Osp Maggiore 89:239–257
49. Schweda D (2000) Air pollution and health in urban areas. Rev Environ Health 15:13–41
50. Spyer KM (1981) Neuronal organization and control of the baroreceptor reflex. Rev Physiol Biochem Pharmacol 88:23–31
51. Taylor JA, Davis RL (1996) Risk factors for the infant prone sleep position. Arch Pediatr Adolesc Med 150:834–837
52. Valdès-Dapena M (1985) Are some crib-deaths sudden cardiac deaths? J Am Coll Cardiol 5:11B
53. Valdès-Dapena M, Mc Freeley PA, Hoffman HJ, Damus KH, Franciosi RR, Allison DJ, Jones M, Hunter JC (1993) Histopathology atlas for the sudden infant death syndrome. Armed Forces Institute of Pathology, Washington DC
54. Willinger M, James LS, Catz C (1991) Defining the Sudden infant death syndrome (SIDS): deliberations of an expert panel convened by the National Institute of Child Health Development. Pediatr Pathol 11:677–684
55. Wisborg K, Kesmodel U, Henriksen TB, Olsen SF, Secher NJ (2001) Exposure to tobacco smoke in utero and risk of stillbirth and death in the first year of life. Am J Epidemiol 154:322–327

logical changes occur within these areas of wrinkling, specifically disintegration of the internal elastic membrane and proliferation of smooth muscle cells. The morphologic appearance of these areas (periodic furrowing perpendicular to the longitudinal axis) might be better described by the term 'rhythmic wrinkling' (RW). This type of wrinkling is distinctly different from the longitudinal intimal wrinkling ('tree-barking') of the ascending thoracic aorta observed in tertiary syphilis.

Until now, the topographic distribution of RW has only been described in general terms in the literature [13]. The topographical distributions of atherosclerotic lesions, fatty streaks (FS), and raised lesions (RL) have been previously described in the thoracic and abdominal aorta by investigators of the Pathobiological Determinants of Atherosclerosis in Youth (PDAY) study [9, 11, 12]. In the course of these studies, RW was thought to be an artifact and, therefore, not included in the grading or descriptions of lesions. Spurred by the possibility that RW may indeed be associated with atherosclerosis, the main purpose of this study was to determine their prevalence and extent in 15- to 34-year-old subjects from the PDAY study, to map their precise topographical distributions in the aorta, and to investigate their possible relationship to both fatty streaks (FS) and the more advanced atherosclerotic lesions, specifically raised lesions (RL).

Materials and methods

Study design

Cases used for this study were obtained from the Pathobiological Determinants of Atherosclerosis in Youth (PDAY) study. The PDAY study consisted of 15 cooperating centers that adopted a Standard Operating Protocol and Manual of Procedures to collect specimens and data and submit them to central laboratories for analysis. A statistical coordinating center received all data pertaining to each case from the collection centers and laboratories. Detailed descriptions of methods have been previously published [9, 11, 12].

Subjects

A total of 2,650 out of 2,876 cases from the PDAY study were used for this study, as 226 cases with either a missing thoracic or abdominal aorta were excluded. The 2,650 PDAY cases were comprised of 15- to 34-year-old persons, blacks, whites, men, and women, who died of accidents, homicides, or suicides. All PDAY case deaths were trauma-related, and cases with a history of cardiovascular disease were excluded.

Specimen handling and definition of arterial lesions

The dissection and preservation of the arteries have been previously described in detail [9, 20]. In summary, PDAY investigators bisected the aorta longitudinally and fixed the left half in 10% neutral buffered formalin, which was subsequently stained with a fat stain, specifically Sudan IV, for identification and visual grading of atherosclerotic lesions. A FS was an area of the intimal surface stained by Sudan IV. A RL was a firm, elevated intimal lesion, sometimes partially or completely covered by sudanophilic deposits. As a group, RL included fibrous plaques (FP), calcified lesions, and complicated lesions, defined as FP with areas of hemorrhage, ulcer, or thrombus. Raised lesions within this young age group were rarely complicated. RW is characterized by grossly visible periodic ('rhythmic'), often interlaced, rows of linear wrinkled intima that extend perpendicular to the longitudinal axis of the aorta. Areas of RW are recorded as present whether they were in areas devoid of fatty streaks, within areas of fatty streaks, or at the edges of RL. Cases in which RL and RW coexist were not difficult to record because the RW was located on the edges (or surrounding) the RL. The surrounding edges were outlined as an area of RW (excluding the RL). Fatty streaks, on the other hand, were graded as FS regardless of whether they were present within an area of RW or an area devoid of RW.

Grading atherosclerotic lesions by computerized image analysis

In the PDAY study, the morphometry laboratory at The Ohio State University scanned 35-mm color transparencies of each Sudan-IV-stained aorta at a resolution of 512×256 pixels by 8-bit gray scale to capture areas of FS. Using a Gould Vicom IP9527 image processing system, anatomic landmarks (branch points of arteries, ostia) in the aorta were identified, and an algorithm converted each digitized image into a standardized rendition (template) of the artery. Those arteries identified by pathologists as positive for RL were photographed and a black and white print was prepared. The intimal areas occupied by RL were identified and marked by pathologists on the photograph. The morphometry laboratory then scanned the marked print and converted the image into the same type of standard template as that used for fatty streaks.

In this analysis, standardized renditions for the arteries of each case were generated on transparent plastic sheets from the same templates used in the PDAY study. The transparencies were marked for areas of rhythmic wrinkling, and then sent to The Ohio State University where the image analysis system that produced maps of the topographic distribution of FS and RL was used to estimate the percent of

intimal surface involved with rhythmic wrinkling and generated topographical maps for this study. An algorithm computed the fraction of pixels in the image of each artery involved with each particular lesion, and the ratio of 'lesion' pixels to that of the entire area was taken to represent the percent of intimal surface involved. The prevalence at each pixel location was determined by the presence or absence of lesion indicated at that pixel location for the study case. Areas of equal prevalence were then displayed in topographical maps as areas of common color or banded color.

Unlike previous PDAY projects where the percent surface area involvement of atherosclerotic lesions was based on the average estimate of three independent pathologists gradings, the determinations of percent surface area involvement for FS, RL, and RW used in this study were all done by computerized image analysis.

Statistical analyses

The effects of race, sex, and 5-year-age groups on the prevalence of each type of lesion was analyzed using logistic regression, with the effects of sex, race, and age as covariates [7]. Two-factor interactions among significant covariates were investigated. The effects of sex, race, and 5-year age groups on percent surface area involved with lesions were analyzed using analysis of variance [3]. The linear models included the same factors as the logistic models. To better satisfy the assumptions underlying the statistical analysis, we applied a logarithmic transformation to the percent of surface area involved with lesions, with a small constant (0.1) added to avoid the logarithm of zero.

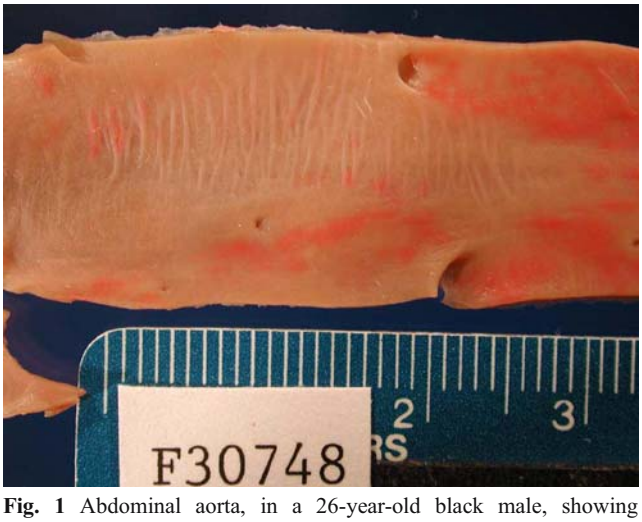

Fig. 1 Abdominal aorta, in a 26-year-old black male, showing rhythmic wrinkling as grossly visible alternating rows extending perpendicular to the longitudinal axis

Results

Figure 1 is an example of an area of RW within the aorta of a 26-year-old black man. It clearly shows the characteristic periodic, often interlaced, rows of linearly wrinkled intima that extend perpendicular to the longitudinal axis of the aorta. The appearance and texture of the RW varies from barely visible and non-palpable to easily visible as an area of wrinkling, and palpable. In each case, there are alternating bands with some that are straight and perpendicular to the longitudinal axis of the aorta, and others that are slightly curved and intersecting the neighboring bands. The latter appearance of curved, intersecting wrinkles occurs more so at the periphery of the area of involvement, and seems to suggest a spiraling or helical nature. In an intact thoracic artery, areas of RW appear to turn from the dorsal to the ventral aspect in the region of the aortic arch. In unstained arteries, the areas of RW are white and distinctly visible. After Sudan IV staining, these same areas of RW are less visible within areas of FS, but are still identifiable.

Prevalence

The overall prevalence of FS, RW, and RL in this study was found to be 100, 34, and 32%, respectively. In the thoracic aorta, the prevalence of FS, RW, and RL was 100, 19, and 6%, respectively, while the prevalence of RW was greater in whites than blacks (21.3 vs 16.1%, p=0.0006) and greater in men than in women (19.5 vs 15.8%, p=0.0363). The prevalence for RL in the thoracic aorta was similar in blacks and whites (5.9 vs 5.3%, p=0.5398) and in women and men (5.7 vs 5.5%, p=0.8972).

In the abdominal aorta, the prevalence of FS, RW, and RL was 100, 27, and 26%, respectively. The prevalence of RW in the abdominal aorta was greater in whites than blacks (32 vs 24%, p<0.0001) and greater in men than in women (29 vs 23%, p=0.0096). The prevalence of RL in the abdominal aorta was also greater in whites than blacks (28 vs 24%, p=0.0253), but there was no apparent difference in prevalence of RL between men and women (26 vs 25%, p=0.7745) in the abdominal aorta.

Table 1 shows the prevalence of FS, RW, and RL in both segments of the aorta stratified by race, sex, and 5-year-age group. In the thoracic aorta, there are no differences between men and women in the prevalence of FS (100%), or RW (p=0.8334), but there is a suggestion of a difference in RL (p=0.0603). There also appear to be differences in prevalence between blacks and whites for RW (p=0.0828) and RL (0.0844); however, they do not reach the level of significance. RL increase with increasing age (p<0.0001), but no age effect was seen for RW (p=0.6765). Despite the fact that no significant level of RW difference was found

Table 1 Prevalence (%) of fatty streaks (FS), rhythmic wrinkling (RW), and raised lesions (RL) in the thoracic and abdominal aorta by race, sex and 5-year age groups

		Thoracic aorta			Abdominal aorta		
Age group	*N*	FS	RW	RL	FS	RW	RL
White men							
15–19	195	100	20.00	1.03	100	32.31	3.59
20–24	234	100	23.93	0.43	100	35.90	11.97
25–29	271	100	22.51	5.17	100	30.26	32.47
30–34	233	100	21.46	16.74	100	37.34	60.09
Black men							
15–19	233	100	20.17	1.29	100	20.17	1.29
20–24	309	100	18.12	0.97	100	27.51	13.59
25–29	314	100	18.79	7.01	100	26.75	32.80
30–34	209	100	10.05	13.88	100	19.62	52.15
White women							
15–19	70	100	21.43	0.00	100	21.43	5.71
20–24	89	100	20.22	0.00	100	30.34	14.61
25–29	94	100	15.96	1.06	100	24.47	28.72
30–34	88	100	19.32	12.50	100	23.86	54.55
Black women							
15–19	65	100	13.85	0.00	100	12.31	1.54
20–24	71	100	15.49	2.82	100	29.58	11.27
25–29	94	100	11.70	7.45	100	19.15	27.66
30–34	81	100	8.64	18.52	100	24.69	48.15
p value							
Sex			0.8334	0.0603		0.3948	0.4995
Race			0.0828	0.0844		0.1407	0.6985
Age			0.6765	0.0001		0.8136	<0.0001

for either age or race, it is interesting to note that in the thoracic aorta, there seem to be large decreases in the prevalence in the older age groups of black men and women, compared to the younger groups.

In the abdominal aorta, the prevalence of RL significantly increases with increasing age ($p<0.0001$). There are no significant differences in prevalence of RL between men and women ($p=0.4995$) or between blacks and whites ($p=0.6985$). There are also no differences in prevalence of RW between men and women ($p=0.3948$), or blacks and whites ($p=0.1407$). Rhythmic wrinkling appears to increase across the first two age groups in black men and white women, then decreases with increasing age in black men and white women; however, there are no significant differences by age groups ($p=0.8136$).

Topographic distributions

Figure 2 shows the topographical distribution of the prevalence of FS, RW, and RL in the thoracic aorta (top half) and the abdominal aorta (bottom half). In the thoracic aorta, there are clearly defined lesion-prone and lesion-resistant areas. For each age group, the highest prevalence (darkening colors) of FS occurs at the dorsal surface between the paired intercostal ostia, while the ventral surface is devoid of FS with the exception of the most distal aspect. The highest prevalence of RW also occurs along intercostal ostia from the distal end to midway of the thoracic aorta where areas of RW turn to extend more ventrally. The thoracic aorta is essentially devoid of RL until the 30- to 34-year-old-age group. In this age group, the distribution of RL follows the same pattern as that of FS and RW in the distal half. However, in the proximal half, the distribution of RL follows more closely that of RW, with a similar turn from the dorsal to the ventral aspect.

As in the thoracic aorta, the abdominal aorta demonstrates clearly defined lesion-prone and lesion-resistant areas. Although areas of FS formation in the abdominal aorta are more diffuse and not as clearly defined as in the thoracic aorta, the prevalence is greater in the dorsal than in the ventral aspect of the abdominal aorta. Areas of RW and RL are more sharply defined than are areas of FS. Regions of high prevalence of RW and RL occur in the dorsal aspect with clearly defined areas from just proximal to the

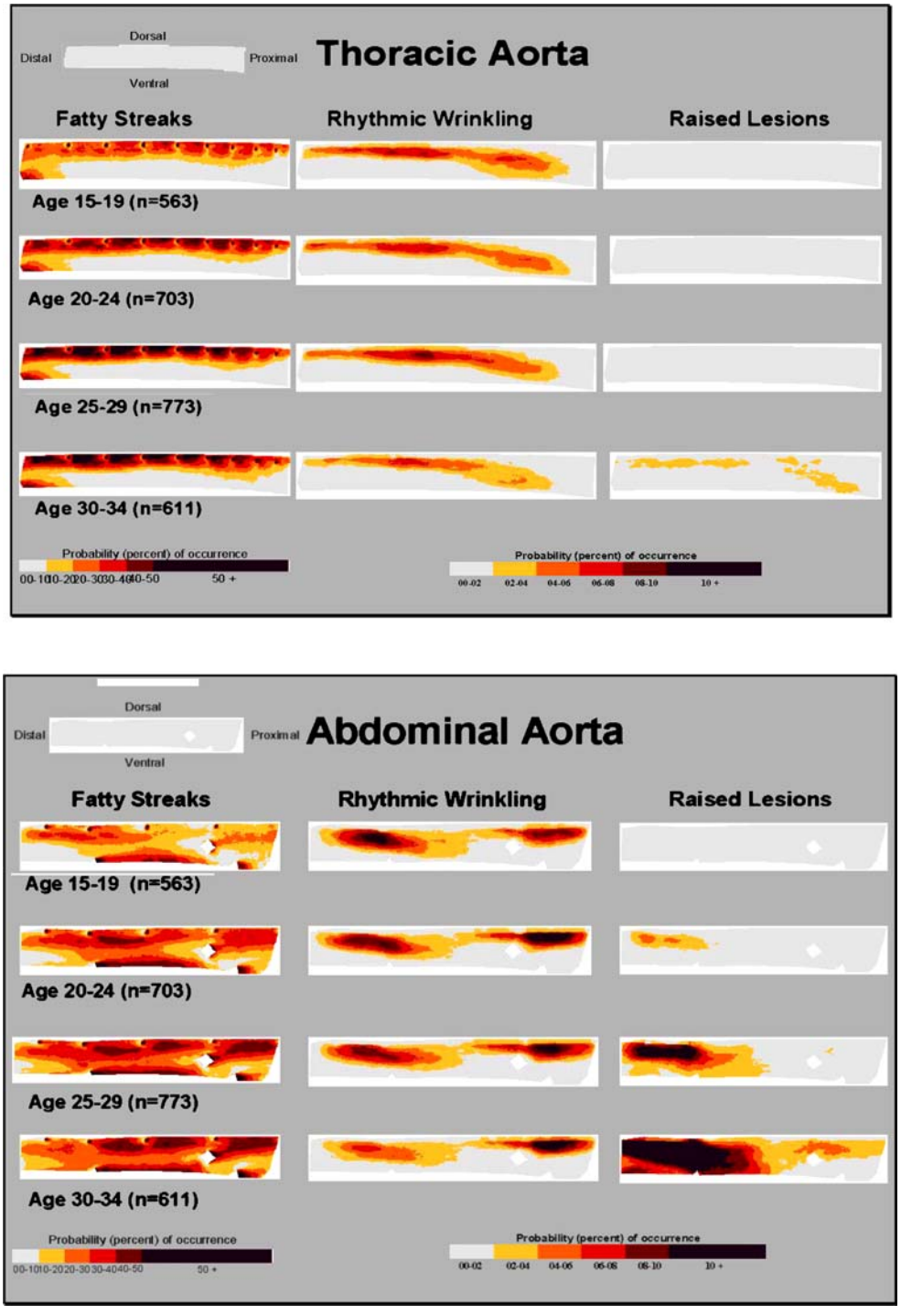

Fig. 2 Topographical distribution maps of fatty streaks, rhythmic wrinkling, and raised lesions in the thoracic and abdominal aorta by 5-year age groups

bifurcation of the iliacs to midway between the inferior mesenteric and superior mesenteric ostia and just proximal to the renal artery ostium.

Mean extent of lesions

Table 2 and Fig. 3 show the percent of intimal surface area involved with FS, RW, and RL by race, sex, and 5-year age group for both segments of the aorta. Large standard deviations demonstrate the great individual variability among cases of the same age, race, and sex.

In the thoracic aorta, the mean percent intimal surface area involved with FS is greater in blacks than whites ($p<0.0001$) and greater in men than women ($p=0.0026$). The mean percent intimal surface area involved with RW is greater in whites than in blacks ($p=0.0004$), and seems to

Table 2 Percent of intimal surface involved with fatty streaks (FS), raised lesions (RL), and rhythmic wrinkling (RW) by sex, race, and 5-year age groups

				Thoracic aorta			Abdominal aorta		
Sex	Race	Age group	*N*	FS Mean (SD)	RL Mean (SD)	RW Mean (SD)	FS Mean (SD)	RL Mean (SD)	RW Mean (SD)
Males	White	15–19	195	12.72 (11.81)	0.07 (0.98)	1.62 (3.99)	15.32 (13.91)	0.40 (3.34)	3.78 (7.50)
		20–24	234	17.38(14.28)	0.10 (1.54)	2.11 (5.08)	21.77 (17.06)	0.73 (2.98)	3.28 (6.24)
		25–29	271	19.21(14.01)	0.15 (090)	2.66 (6.66)	26.42 (19.69)	2.53 (5.56)	3.00 (6.26)
		30–34	233	18.34 (14.61)	0.60 (0.07)	1.55 (3.59)	25.63 (18.99)	6.74 (10.34)	3.18 (6.30)
	Black	15–19	233	18.45 (13.15)	0.08 (1.02)	2.13 (5.53)	17.70 (13.97)	0.06 (0.82)	1.96 (4.78)
		20–24	309	22.121 (16.18)	0.06 (0.92)	1.55 (4.40)	25.10 (19.51)	0.47 (1.51)	2.21 (4.65)
		25–29	314	21.14 (15.24)	0.30 (1.75)	1.87 (4.84)	25.13 (20.67)	2.91 (7.14)	2.54 (5.78)
		30–34	209	23.87 (17.49)	0.80 (3.28)	0.78 (2.99)	27.96 (20.79)	6.65 (11.90)	1.47 (3.75)
Females	White	15–19	70	11.42 (10.98)	0.00 (0.00)	2.10 (5.06)	20.70 (15.74)	0.08 (0.36)	1.68 (4.12)
		20–24	89	13.09 (11.09)	0.00 (0.00)	2.54 (6.22)	27.93 (18.11)	0.61 (2.04)	3.07 (6.40)
		25–29	94	16.35 (12.79)	0.01 (0.09)	1.25 (3.57)	36.36 (20.70)	2.34 (5.51)	2.74 (6.18)
		30–34	88	17.21 (14.69)	0.69 (3.05)	2.52 (6.58)	32.53 (18.92)	8.37 (12.67)	1.67 (4.31)
	Black	15–19	65	13.90 (12.25)	0.00 (0.00)	1.08 (3.04)	20.46 (19.54)	0.02 (0.16)	1.59 (6.80)
		20–24	71	18.84 (16.05)	0.02 (0.10)	1.36 (4.58)	32.74 (22.42)	0.71 (2.54)	2.74 (7.83)
		25–29	94	23.12(14.09)	0.29 (1.55)	1.09 (3.77)	37.45 (20.69)	2.33 (5.24)	1.77 (5.66)
		30–34	81	23.32 (14.68)	2.36 (8.13)	0.89 (3.61)	37.40 (20.73)	8.51 (15.11)	1.75 (3.92)
p values									
Sex				0.0026	0.763	0.0764	<0.0001	0.5881	0.0058
Race				<0.0001	0.3293	0.0004	0.4202	0.218	<0.0001
Age				<0.0001	<0.0001	0.0616	<0.0001	<0.0001	0.9649

Lesion values are arithmetic means

be greater, but not significantly so, in men than in women (p=0.0764). In addition, there appears to be an age-related trend of decreasing extent of RW in black men and black women (p=0.0616). A significant age-by-race interaction (p=0.0139, not shown) was found for RW, and this is probably due to the decrease in extent of RW with increasing age for black men and black women, but not for white men and white women. There are no significant differences for mean extent of RL between females and males (p=0.7630) or between blacks and whites (p=0.3293).

In the abdominal aorta, the surface area involved with FS has a greater mean percent in males than females (p<0.0001), but there are no significant differences between blacks and whites (p=0.4202). The mean percent of surface area involved with RW is greater in whites than in blacks (p<0.0001) and men than in women (p=0.0058). Whites have a mean percent of surface area involved with RL greater than blacks (p=0.0218), but there does not appear to be any differences by gender (p=0.5881).

In both the thoracic and the abdominal aorta, the mean percent of surface area involved with FS and RL increases with increasing age across all race-by-sex groups. The extent of RW increases in the younger age groups followed by a decrease in the oldest age group, suggesting an inverse relationship of RW with both FS and RL.

Discussion

Results from this study show that RW is highly prevalent in the aorta, with greater prevalence in the abdominal than the thoracic segment. Overall prevalence of RW in this study is 34%, which is lower than the 68% previously reported by Vikhert et al. [15] and 74% reported by Tanimura et al. [13]. The Vikhert studies also observed a higher proportion of cases with fibrous plaques, but this would be expected as the cases in that study spanned a much larger age range. There were also a number of environmental, ethnic, and life-style differences between the two prior studies and the current study populations, which may account for these differences. Nevertheless, the high prevalence of RW in this study as well as those reported in prior studies strongly underscores the need to determine the etiology and pathology of RW and its role, if any, in the development of advanced lesions of atherosclerosis. A very limited histological evaluation indicates an absence of fat but a proliferation of smooth muscle within the intima of the aorta in the areas of RW. More extensive histological studies are needed to further classify RW and determine what role, if any, this lesion, along with the grossly defined transition lesion [8] and the histologically defined type III transition lesion [10], plays in the overall developmental scheme of atherosclerosis.

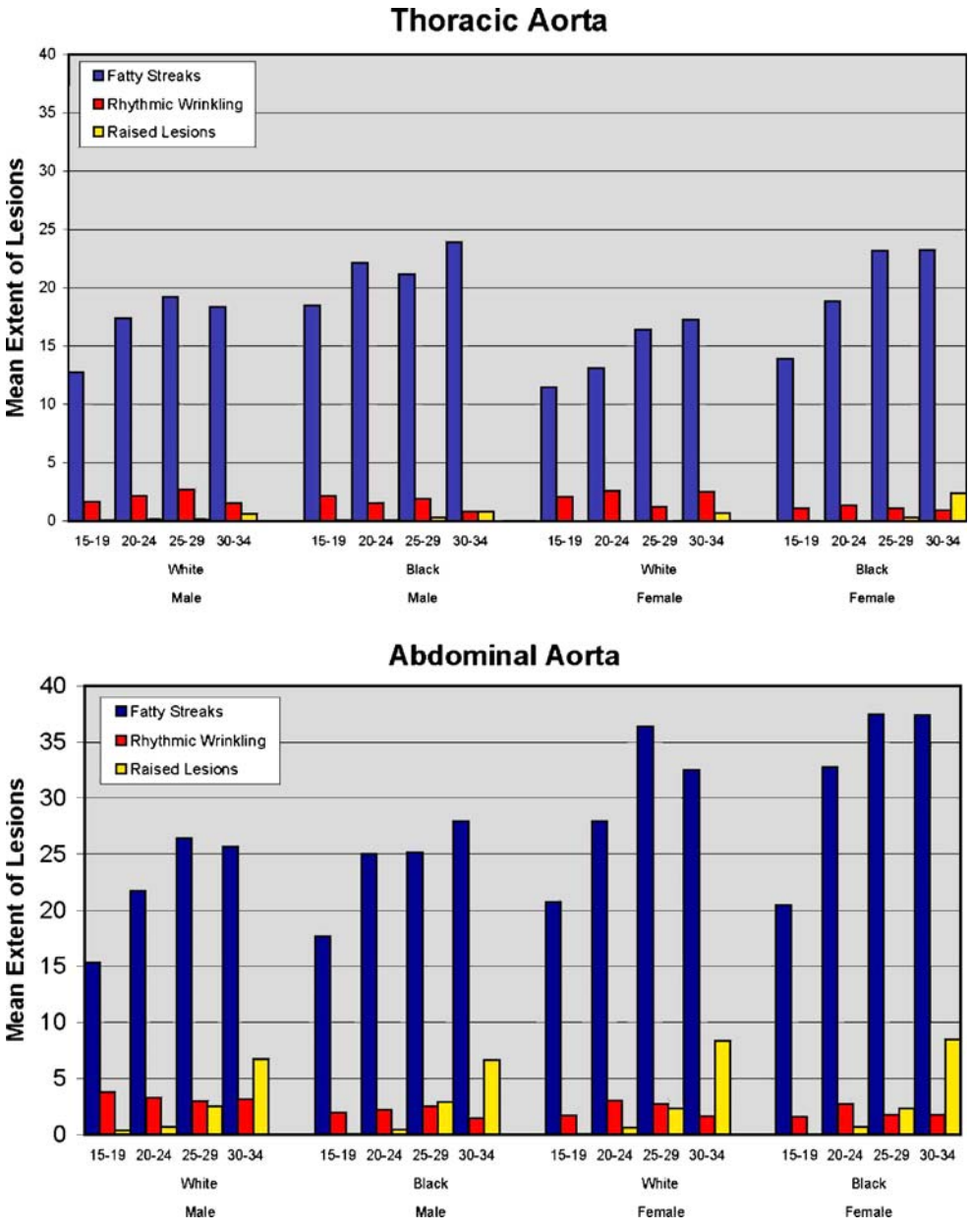

Fig. 3 Mean extent of fatty streaks (*FS*), rhythmic wrinkling (*RW*), and raised lesions (*RL*) in the thoracic and abdominal aorta by sex, race, and 5-year age groups

One of the main objectives of this study was to investigate the relationship of RW to both FS and RL. Fatty streaks were found in 100% of aortas examined in this study, which is consistent with Holman et al. [5] who also found 100% prevalence of FS in aortas beginning at age 3. There was little evidence to suggest a relationship between FS and RW. However, we did find suggestions of an inverse relationship between RW and RL. As observed in Table 2 and in the topographical probability maps for RW and RL, as the mean extent and probability of RW decreases with increasing age, the mean extent and probability of RL increases. For example, in Fig. 2 we see that in the thoracic aorta, as the probability of RW decreases in the 25- to 29- to the 30- to 34-year-old age groups, RL begins to appear in the same pattern as RW. The distribution of RW in the thoracic aorta follows the intercostal ostia from the distal end to midway of the thoracic aorta where areas of RW turn to extend more ventrally. The thoracic aorta is devoid of RL until the 30- to 34-year-old age group, where the distribution follows the same pattern as that of RW in the distal half, along intercostal ostia, with the same turning effect from dorsal to ventral in the proximal aspect.

The topographical distribution of FS is similar to that of RW and RL in the dorsal aspect of the distal thoracic aorta between the intercostal ostia; however, it does not follow the same distribution as RW and RL in the proximal aspect. Although analysis of variance does not indicate that there is

a significant age effect on RW in the abdominal aorta, the topographical distribution maps do strongly suggest a decrease in RW with increasing age, particularly in the distal aspect of the abdominal aorta just proximal to the bifurcation of the iliac arteries. At the same time that the extent of RW decreases, RL appears and continues to increase with age within the same distribution as the RW, suggesting RL replaces RW. In the abdominal aorta proximal to the renal artery ostia, there is an increase in the extent of RW until the 20- to 24-year-old age group followed by a slight decrease in the older age groups.

The distribution of FS in the abdominal aorta is more extensive and diffuse compared to the thoracic aorta, and does not follow the distribution of RL as clearly as does RW. These findings in both the thoracic and abdominal aorta demonstrate that RW and RL occur in the same areas of the vessels with RW appearing at a younger age than RL. It also suggests that RW, occurring at a younger age than RL, may subsequently contribute to the formation of RL within the aorta. The observation of an apparent age-dependence of RW in the age-stratified topographical probability plots shows the strength of this methodology. It allows one to see a virtual time-lapse image of specific areas of lesion progression, as opposed to the analysis of variance (ANOVA) methodology that ascribes equal treatment to all lesion areas.

Based on the current study, we suggest those areas in which RW and RL coexist may represent RW as a precursor in the formation of fibrous plaques. These findings are based not only on the topographical maps present in this study, which suggest areas of coexistence, but also on the gross observation of different stages of lesion progression involving RW including (1) barely visible, non-palpable areas of RW, (2) more prominent and easily visible, often palpable, areas of RW, (3) confluent and merging areas of wrinkling, and (4) RW and RL coexisting within the same area.

To date, the etiology of RW has not been established. It is possible that the development of RW and its progression to advanced lesions is influenced by hemodynamics. It may be that the dynamics of blood flow (regions of low shear stress and turbulence created at arterial bifurcations or ostia and arterial branches) result in damage to the endothelium, thereby activating endothelial cells in the aortic intima and initiating the proliferation and migration of smooth muscle cells from the media into the intima, leading to the development of advanced atherosclerotic plaques. In 1989, Vikhert and Zhdanov [18] described the histological alterations and formally stated that the occurrence of RW is most likely associated with hemodynamic effects specifically, sites of RW cause severe local hemodynamic disturbances, and, therefore, may contribute to the progression of areas of RW to advanced atherosclerosis. Earlier, Crawford et al. [1] analyzed high-resolution casts of the femoral and coronary arteries made at physiologic pressure, and found small longitudinal ridges in portions of arteries with no visible lesions of atherosclerosis. He further reported that these ridged areas were replaced by plaques and demonstrated that, based on hemodynamics, the orientation of the ridges correlated with the expected direction of secondary surface flow streamlines.

In summary, this study provides evidence that (1) the prevalence of RW is fairly high in the aorta, and these lesions occur in a specific distribution in both the thoracic and abdominal aorta; (2) RW seems to precede the development of RL with RL occurring in the same topographical areas as RW, and (3) RW may be associated with the subsequent development of advanced atherosclerosis, particularly raised lesions. The precise topographical distributions of FS, RW, and RL developed in this study may provide a basis for future studies to compare the anatomic and physiological characteristics of these areas of the aorta. This study represents the necessary first step for future studies aimed at revealing the nature of biochemical, cellular, and structural factors that cause RW and its pathogenesis.

References

1. Crawford DW, Barndt R, Back LH (1976) Surface characteristics of normal and atherosclerotic human arteries including observations suggesting interaction between flow and intimal morphology. Lab Invest 34(5):463–470
2. Doerr W, Daugs J (1963) Uber eine funktionelle Struktur der Aortenwand. In: W. Doerr (ed) Perfusionstheorie der Arteriosklerose. Stuttgart. Thieme pp 44–68
3. Draper NR, Smith H (1966) Applied regression analysis. New York, NY, Wiley and Sons, pp 407
4. Ernst P (1916) Uber eine funktionelle Struktur der Aortenwand Beitr Pathol Anat Allg Pathol 63:141
5. Holman RL, McGill HC Jr, Strong JP, Geer JC (1958) The natural history of atherosclerosis: the early aortic lesions as seen in New Orleans in the middle of the 20th century. Am J Pathol 34:209–235
6. Jipp P (1963) Uber die rhythmischen Strukturen der Aortenintima. Arch Kreislaufforsch 41:252–268
7. Kleinbaum DG, Kupper LL, Morgenstern H (1982) Epidemiologic research: principles and quantitative methods. Von Nostrand Reinhold, New York, NY
8. McGill HC, McMahan CA, Zieske AW, Sloop GD, Walcott JV, Troxclair DA, Malcom GT, Tracy RE, Oalmann MC, Strong JP for the Pathobiological Determinants of Atherosclerosis in Youth (PDAY) Research Group (2000) Associations of coronary heart disease risk factors with the intermediate lesion of atherosclerosis in youth. Arterioscler Thromb Vasc Biol 20:1998–2004
9. Pathobiological Determinants of Atherosclerosis in Youth (PDAY) Research Group (1993) Natural history of aortic and coronary atherosclerotic lesions in youth. Arterioscler Thromb Vasc Biol 13(9):1291–1298
10. Stary HC, Chandler AB, Dinsmore RE, Fuster V, Glagov S, Insull W, Rosenfeld ME, Schwartz CJ, Wagner WD, Wissler RW (1995) A definition of advanced types of atherosclerotic lesions and a

histological classification of atherosclerosis: a report from the Committee on Vascular Lesions of the Council on Arteriosclerosis. Am Heart Assoc Monogr Circ 92(5):1–20
11. Strong JP, For the Pathobiological Determinants of Atherosclerosis in Youth (PDAY) Research Group (1995) Natural history and risk factors for early human atherogenesis. Clin Chem 41(1):134–138
12. Strong JP, Malcom GT, McMahan CA, Tracy RE, Newman WP III, Herderick EE, Cornhill JF (1999) Prevalence and extent of atherosclerosis in adolescents and young adults: implications for prevention from the Pathobiological Determinants of Atherosclerosis in Youth Study. JAMA 281(8):727–735
13. Tanimura A, Cho T, Saito Y, Nakashima T (1986) Role of "Wave Line" (Doerr; Wellenlinie) of aorta in atherosclerosis. Angiology 37(4):272–280
14. Thoma R (1921) Uber die intima der arterien. Virchows Arch 230:1–45
15. Vikhert AM, Sternby NH, Livshits AM, Duskova J (1994) Rhythmic structures and atherosclerosis in the aorta. Atherosclerosis 106(2):129–137
16. Vikhert AM, Zhdanov VS (1970) Rhythmic structures of aortic intima. Arch Pathol 32(7):68–72
17. Vikhert AM, Zhdanov VS, Osis YG (1988) Role of rhythmical structures of the aortic intima in the development of atherosclerosis. Ter Arh 60(12):7–12
18. Vikhert AM, Zhdanov VS (1989) Role of rhythmic structures of aortic intima in the development of atherosclerosis. Zentralbl Allg Pathol 135(6):607–617
19. Wagner H (1954) Rhythmic structures and thrombotic deposits of aortic intima; morphogenesis of diffuse thickening of intima and of arteriosclerotic cushion. Schweiz Z Pathol Bakteriol 17(3):258–588
20. Wissler RW (1991) USA multicenter study of the pathobiology of atherosclerosis in youth. Ann N Y Acad Sci 623:26–39

the same dysplastic lineage or had developed independently (de novo). The concept of field cancerization was evaluated in this case of long-standing colitis.

Clinical history

An 83-year-old woman, known to have UC for at least 16 years, was admitted to the hospital because of severe colitis-related complications. Endoscopy showed active inflammation in the distal part of the colon with ulceration and several polypoid lesions with a large mass at 40 cm from the anorectal junction being most suspicious for DALM/carcinoma. Histological biopsies revealed inflammatory bowel disease, compatible with UC, and multifocal low- and high-grade dysplasia in the rectosigmoid part of the colon. Subsequently, a proctocolectomy with ileostomy was performed. Three polypoid DALM-like lesions were seen in, respectively, the proximal sigmoid, mid-sigmoid (largest lesion), and proximal rectum, all harboring adenocarcinoma. Three locoregional lymph nodes revealed metastatic adenocarcinoma.

Materials and methods

The cancers were graded and staged according to the 2002 UICC TNM (tumor–node–metastasis) classification [10]. Only paraffin-embedded materials were available for genomic array analysis. Slides containing triplicates of ~3,500 BAC–PAC clones spaced at density along the full genome were used [6, 11]. Tumor and reference DNAs were labeled with (1) Cy3- and Cy5-2′-deoxycytidine 5′-triphosphates (Amersham Bioscience, Roosendaal, The Netherlands) according to a random priming protocol from the Bio-Prime labeling system (Invitrogen, Carlsbad, CA,

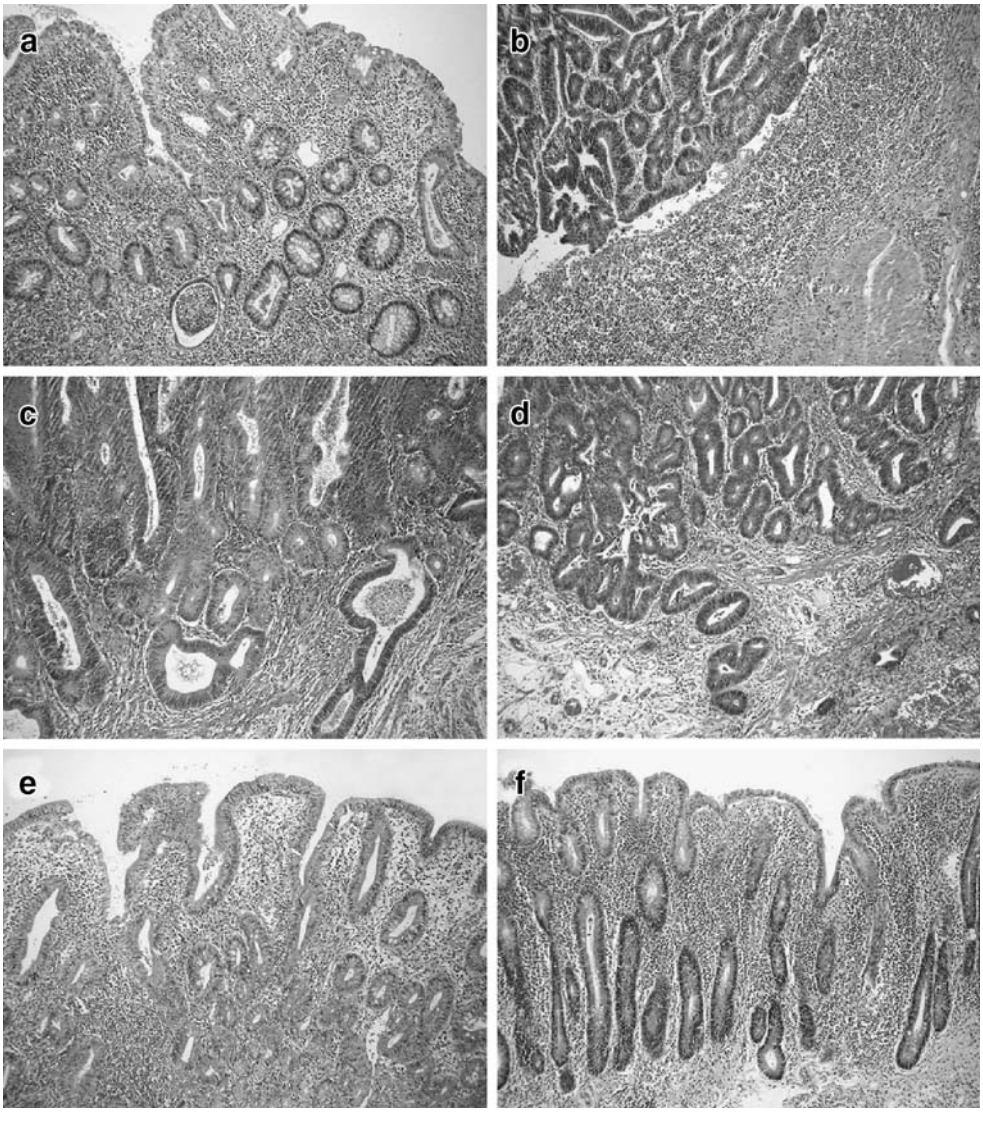

Fig. 1 Images of hematoxylin- and eosin-stained tissue sections (10× objective). **a** Rectal mucosa showing chronic active inflammation and cryptitis. **b** The T2 cancer in the mid-sigmoid illustrating adenocarcinoma infiltrating the muscularis propria (*right lower corner*). **c** The T1 cancer in the proximal sigmoid. **d** The T1 carcinoma in the proximal rectum infiltrating the submucosa. **e** Dysplastic mucosa directly adjacent to the rectal carcinoma. **f** Atypical mucosa in the distal rectum compatible with low-grade dysplasia

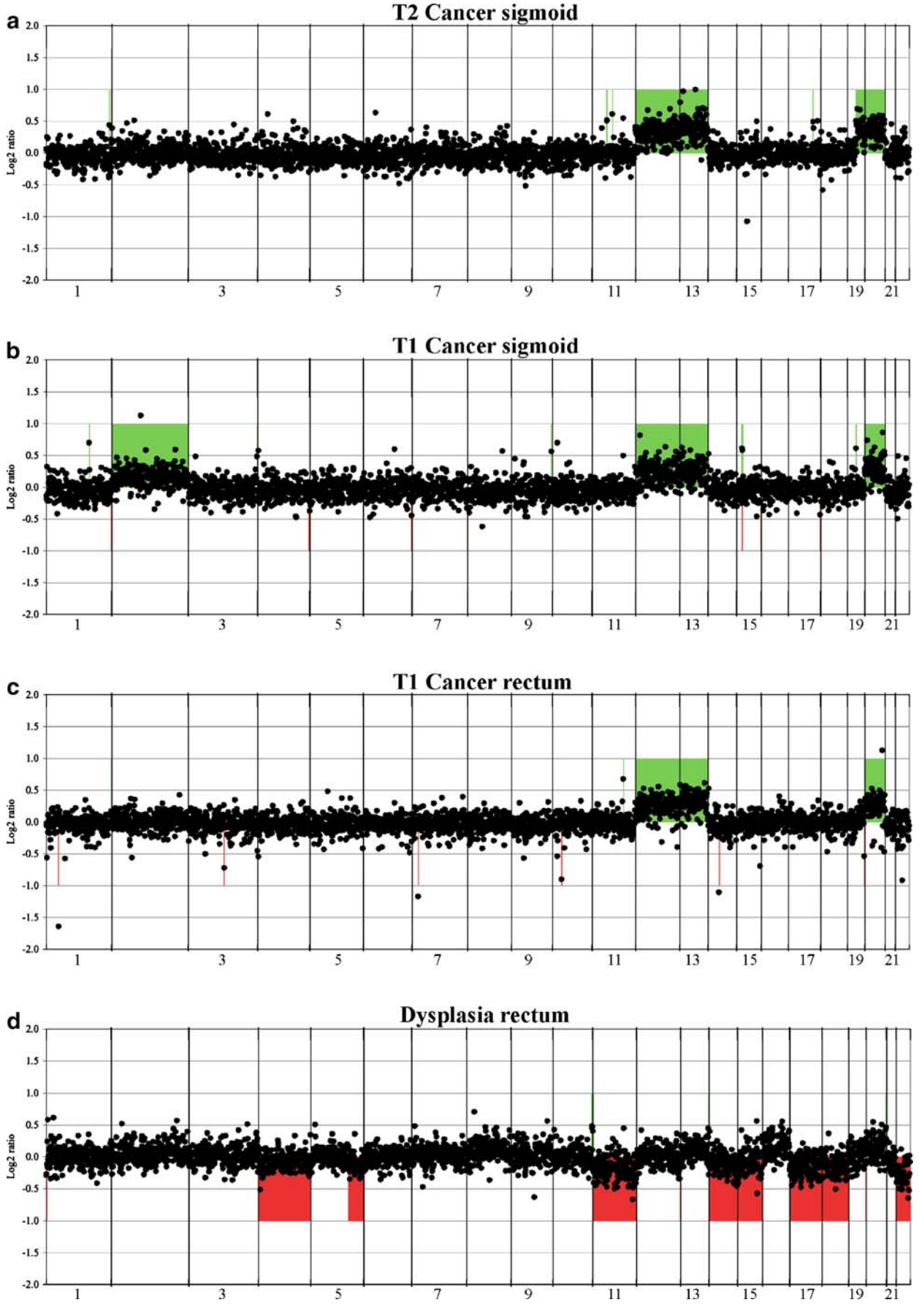
a
T2 Cancer sigmoid
b
T1 Cancer sigmoid
c
T1 Cancer rectum
d
Dysplasia rectum
Log2 ratio
2.0
1.5
1.0
0.5
0.0
-0.5
-1.0
-1.5
-2.0
1
3
5
7
9
11
13
15
17
19
21

◀ **Fig. 2** Log_2 ratios along the genome (chromosome 1–22) illustrating genomic imbalances defined by array-based CGH (gains *green*, losses *red*) of the three carcinomas and distal rectal mucosa. **a–c** CGH patterns of the T2 mid-sigmoid, the T1 proximal sigmoid, and the T1 proximal rectal cancers, respectively, all carrying gains of chromosomes 12, 13q, and 20. In addition, the T2 cancer shows gain of 19q, whereas the T1 carcinoma in the proximal sigmoid displays gain of whole chromosome 2. **d** Low-grade dysplasia in the distal rectum showing a completely different CGH pattern of alterations, i.e., losses of chromosomes 4, 5q, 11, 14q, 15q, 17, 18, and 22q

USA) and (2) Cy3 and Cy5 conjugates from the Universal Linkage System (ULS, Kreatech Biotechnology, Amsterdam, The Netherlands). Thus, all reactions were performed in duplicate. In general, ULS-labeled samples showed higher resolution in CGH of paraffin-embedded DNAs as compared to random priming. Consequently, the ULS-labeled DNAs were used for evaluation [5].

Microsatellite instability (MSI) analysis and immunohistochemistry (IHC) of cancer-associated genes were performed as described before [12]. For MSI markers, *BAT25* and *BAT26* were used. Briefly, after PCR, the products were separated by electrophoresis on a polyacrylamide gel, and the films were evaluated by visual inspection. IHC was carried out with primary antibodies against *MLH1* (Pharmingen, Alphen aan den Rijn, The Netherlands), *MSH2* (Pharmingen), *MSH6* (Pharmingen), *PMS2* (Pharmingen), *MYC* (Santa Cruz Biotechnology, Santa Cruz, CA, USA), *cyclin D1* (Lab Vision Neomarkers, Fremont, CA, USA), *β-catenin* (Transduction Laboratories, San Jose, CA, USA), and *E-cadherin* (Euro-Diagnostica, Arnhem, The Netherlands). As a positive control, a cytokeratin antibody was used; as a negative control, the primary antibody was omitted. Immunoreactivity was visualized with the Envision kit (Dako, Heverlee, Belgium), and the protein expression patterns were evaluated.

Results

Histopathological examination of the proctocolectomy specimen revealed inactive colitis in the proximal and middle part of the colon, but active inflammation and ulceration in the distal part. Three malignant tumors compatible with DALM were discriminated: a large lesion in the mid-sigmoid containing a T2 adenocarcinoma, a T1 cancer in the proximal sigmoid, and another T1 tumor in the proximal rectum. These cancers were situated at 40, 44, and 24 cm of the anorectal junction, respectively. All tumors were surrounded by multifocal flat (non-adenomatous) dysplasia. The histologies are illustrated in Fig. 1. The three invasive carcinomas showed an overlapping CGH pattern of genomic alterations with concomitant gains of chromosomes 12pq, 13q, and 20pq (Fig. 2). In addition, in all three carcinomas, MSI analysis with polymorphic markers *BAT25* and *BAT26* did not reveal instability, and several cancer-related proteins showed identical immunostaining profiles (Fig. 3). IHC of the mismatch repair genes *MLH1*, *PMS2*, *MSH2*, and *MSH6* detected conserved protein expression for all four genes. Tumor suppressor *E-cadherin* revealed comparable patterns of membranous staining, and *β-catenin* was strongly positive in all of the three cancers. The oncogenes *MYC* and *cyclin D1* both showed immunohistochemical protein overexpression. However, dysplastic mucosa distal to the three cancers displayed a completely different pattern of genomic changes (Fig. 2, Table 1). Dysplastic mucosa adjacent to the rectal cancer was not informative (not shown).

Discussion

The high degree of similarity between the CGH profiles of the three malignancies supports a monoclonal origin of the tumor cells. Based on our data (unpublished) and literature data [1, 13], UC-related neoplasms show frequent losses of 4p, 5q, 8p, 17p, and 18q with gains of 5p, 8q, 13q, and 20q. However, whole chromosome 12 gain is not a frequent finding. It is seen in less than 10% of cases, which would result in a P value below 0.001 for three synchronous tumors. Thus, recurrent combination of gains of chromosomes 12pq, 13q, and 20pq in all three malignancies strongly suggests that these cancers originate from the same preneoplastic lineage. This is also supported by the MSI and IHC analyzes as well as the presence of another clonal lineage in the distal rectum, which only showed chromosomal losses. All of these data are in favor of monoclonality and make field cancerization unlikely.

It cannot be fully excluded that these multiple cancers arose in three different colonic adenomas. The pattern of genomic imbalances in sporadic colorectal carcinomas is characterized by gains of chromosomes 7, 8q, 13q, and 20q and losses of 17p and 18q [3]. Again, whole chromosome 12 gain is not a frequent alteration. However, the clinical, endoscopic, and histological findings are better compatible with DALM-related malignancy in UC. Further, the overlapping pattern of chromosomal aberrations does not support three simultaneously occurring adenoma-carcinoma events.

The cancer risk in UC is well documented, but information is sparse concerning synchronous colitis-related adenocarcinomas. Only one well-documented report is present in the literature [7]. The authors describe a UC patient with extensive dysplasia involving nearly the entire colon and four DALM-related adenocarcinomas. The molecular profiles of the neoplastic lesions, defined by *P53* and *RAS* mutations, differed, supporting a polyclonal nature and field cancerization. However, these four cancers were distributed through the entire large bowel, whereas our three carcinomas all arose within a 20-cm colonic

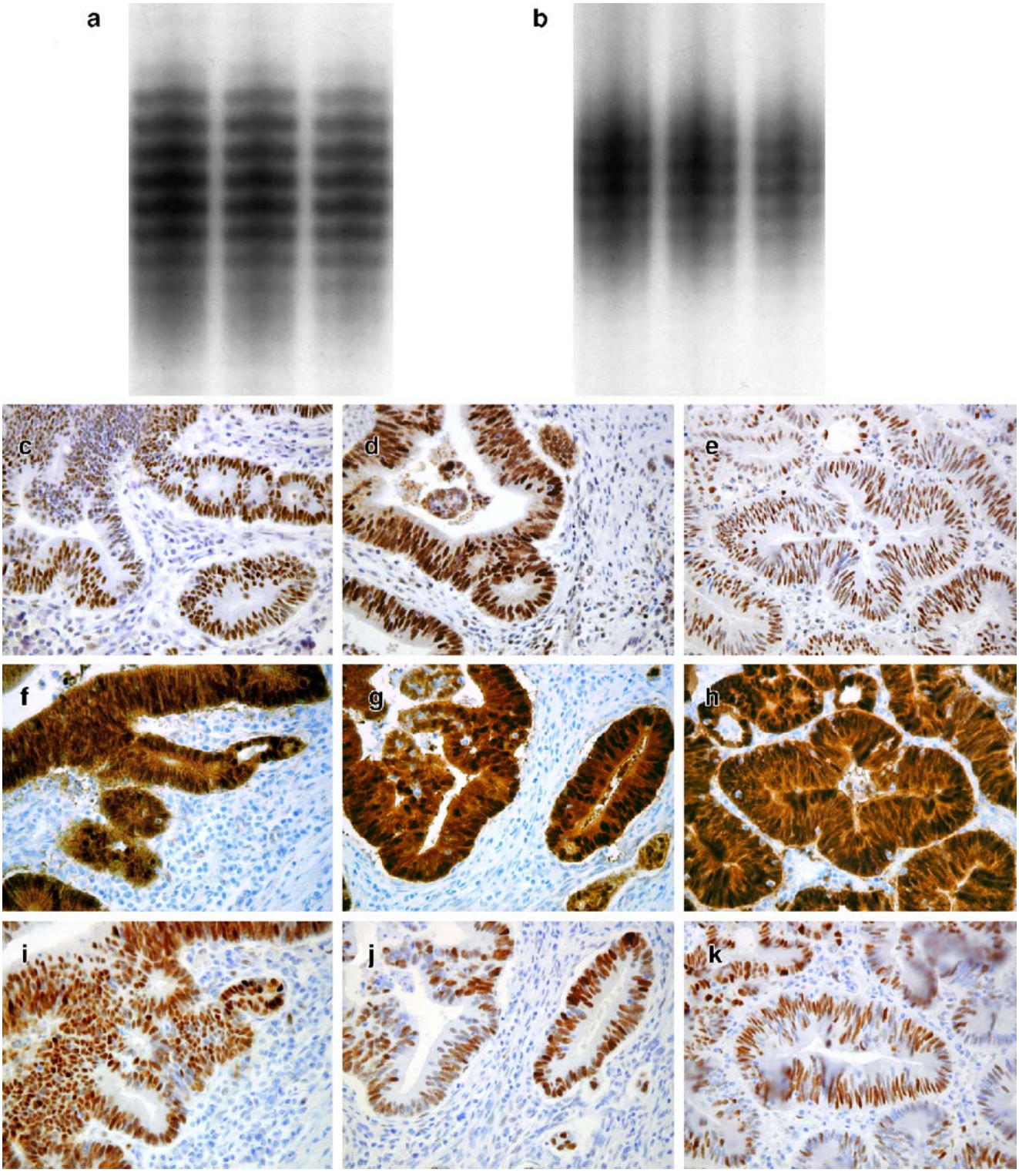

Fig. 3 MSI analysis and IHC (40× objective) of the three colitis-related adenocarcinomas. **a**, **b** MSI evaluation of polymorphic markers *BAT25* (**a**) and *BAT26* (**b**) displaying an identical microsatellite (*stable*) pattern for both markers (as compared to normal muscle control). **c–e** IHC reveals conserved protein expression of mismatch repair gene *MSH2* in the T2 mid-sigmoid, the T1 proximal sigmoid, and the T1 proximal rectal cancers, respectively. **f–h** Same, *β-catenin*, showing strong nucleocytoplasmic staining of the tumor cells indicating activation of the *Wnt*-pathway. **i–k** Same, *cyclin D1*, illustrating protein over-expression of this oncogene

Table 1 Clinical and experimental data

Sample	Site	Appearance	Histology	Grade[a]	T-stage[b]	CGH alterations[c]
1	Mid-sigmoid	Polypoid (DALM)	Adenocarcinoma	1	2	**+12pq**, **+13q**, +19q, **+20pq**
2	Proximal sigmoid	Polypoid (DALM)	Adenocarcinoma	1	1	**+2pq**, +12pq, **+13q**, **+20pq**
3	Proximal rectum	Polypoid (DALM)	Adenocarcinoma	1	1	**+12pq**, **+13q**, **+20pq**
4	Proximal rectum	Flat	Dysplasia	Low		No alterations[d]
5	Distal rectum	Flat	Dysplasia	Low		−4pq, −5q, −11pq, −14q, −15q, −17pq, −18pq, −22q

[a] Tumor grade: 1 = well differentiated
[b] Tumor node metastasis classification according to the UICC (2002): 1 = invasion of submucosa; 2 = extension into muscularis propria
[c] Overlapping alterations in bold
[d] Lack of alterations possibly caused by strong admixture of non-lesional cells

segment. Thus, in our case, a single preneoplastic (dysplastic) clone was, firstly, capable of colonizing a distinct bowel segment by an extensive lateral spread and secondly, able to give rise to three invasive cancers. This unique multifocal neoplasm allowed us to increase our knowledge of field cancerization in colitis-associated malignancies.

References

1. Aust DE, Willenbucher RF, Terdiman JP, Ferell LD, Chang CG, Moore DH, Molinaro-Clark A, Baretton GB, Loehrs U, Waldman FM (2000) Chromosomal alterations in ulcerative colitis-related and sporadic colorectal cancers by comparative genomic hybridization. Human Pathol 31:109–114
2. Blackstone MO, Riddell RH, Rogers BH, Levin B (1981) Dysplasia-associated lesion or mass (DALM) detected by colonoscopy in long-standing ulcerative colitis: an indication for colectomy. Gastroenterology 80:366–374
3. Douglas EJ, Fiegler H, Rowan A, Halford S, Bicknell DC, Bodmer W, Tomlinson IP, Carter NP (2004) Array comparative genomic hybridization analysis of colorectal cancer cell lines and primary carcinomas. Cancer Res 64:4817–4825
4. Ekbom A, Helmick C, Zack M, Adami HO (1990) Ulcerative colitis and colorectal cancer. A population-based study. N Engl J Med 323:1228–1233
5. Jong K, Marchiori E, Meijer G, Vaart AV, Ylstra B (2004) Breakpoint identification and smoothing of array comparative genomic hybridization data. Bioinformatics 12:3636–3637
6. Knijnenburg J, Szuhai K, Giltay J, Molenaar L, Sloos W, Poot M, Tanke HJ, Rosenberg C (2005) Insights from genomic microarrays into structural chromosome rearrangements. Am J Med Genet 132:36–40
7. Lyda MH, Noffsinger A, Belli J, Fischer J, Fenoglio-Preiser CM (1998) Multifocal neoplasia involving the colon and appendix in ulcerative colitis: pathological and molecular features. Gastroenterology 115:1566–1573
8. Odze RD, Brown CA, Hartmann CJ, Noffsinger AE, Fogt F (2000) Genetic alterations in chronic ulcerative colitis-associated adenoma-like DALMs are similar to non-colitic sporadic adenomas. Am J Surg Pathol 24:1209–1216
9. Riddell RH, Goldman H, Ransohoff DF, Appelman HD, Fenoglio CM, Haggitt RC, Ahren C, Correa P, Hamilton SR, Morson BC (1983) Dysplasia in inflammatory bowel disease: standardized classification with provisional clinical applications. Human Pathol 14:931–968
10. Sobin LH, Wittekind C (2002) International Union Against Cancer (6th edn). Wiley, New York
11. Van Dekken H, Wink JC, Vissers KJ, van Marion R, Koppert LB, Tilanus HW, Siersema PD, Tanke HJ, Szuhai K, Hop WCJ (2006) Genomic analysis of early adenocarcinoma of the esophagus or gastro-esophageal junction: tumor progression is associated with alteration of 1q and 8p sequences. Genes Chromosomes Cancer 45:516–525
12. Westenend PJ, Schutte R, Hoogmans MM, Wagner A, Dinjens WN (2005) Breast cancer in an *MSH2* gene mutation carrier. Human Pathol 36:1322–1326
13. Willenbucher RF, Aust DE, Chang CG, Zelman SJ, Ferrell LD, Moore DH, Waldman FM (1999) Genomic instability is an early event during the progression pathway of ulcerative-colitis-related neoplasia. Am J Pathol 154:1825–1830

ded in paraffin and stained with hematoxylin and eosin. To highlight the cytoplasmic granularity of the oncocytes, we also performed a phosphotungstic acid hematoxylin (PTAH) stain. Immunohistochemical stains were performed in selected blocks. Staining using a standard avidin–biotin complex technique was performed for epithelial membrane antigen (EMA, MC5, Ventana, prediluted), keratin 19 (CK19, Vector, 1:50), keratin 7 (CK7, Dako, 1:100), low-molecular-weight keratin (LMWK, Becton Dickinson, Cam 5.2, 1:50), high-molecular-weight keratin (HMWK, Ventana 34BE12, prediluted), keratin 5/6 (CK5/6, Dako, 1:50), keratin 14 (CK14, Vector, 1:100), keratin 20 (CK20, Dako, 1:100), S-100 (Ventana, polyclonal, prediluted), p63 (Vector, 1:50), muscle-specific actin (MSA, Dako, 1:100), smooth-muscle actin (SMA, Ventana, prediluted), and calponin (Dako, 1:100). All immunohistochemical stains were performed in an automated Ventana BenchMark® instrument (Tucson, AZ) with routine positive and negative controls.

Results

The tumor measured 3×2.5×2 cm and was described as well demarcated with nodular, white, and solid appearance. The tumor was surrounded by a thin capsule of fibrous tissue and was composed of variable-sized sheets of oncocytes admixed with mature adipose tissue (Fig. 1a). Approximately, 30–40% of the tumor was composed of adipose tissue, with the remaining being composed of oncocytes. The oncocytes showed abundant, intensely eosinophilic granular cytoplasm and contained a small, round, centrally placed nucleus with conspicuous nucleolus. A second cell population composed of small densely eosinophilic cells with pyknotic nuclei, commonly referred to as "dark" cells, was also identified (Fig. 1b). The oncocytes were arranged predominantly in acinar or microglandular patterns with variable-sized sheets. There were scattered mature sebaceous glands admixed with the oncocytes (Fig. 1c). PTAH stain demonstrated strong and diffused cytoplasmic granularity consistent with abundant mitochondria within the tumor cells (Fig. 1d). Often, the sebaceous glands were surrounded by small lymphoid aggregates. No necrosis, cellular atypia, mitotic activity, or invasion was identified. The adjacent parotid gland was unremarkable and showed no sebaceous or oncocytic changes.

Immunohistochemically, the oncocytes were strongly and diffusely positive for LMWK and CK7 (Fig. 2a). CK19, CK5/6, and HMWK showed a peculiar pattern of expression mostly by cells located at the periphery of acini (Fig. 2b–d). A variable number of oncocytes, many of them also located at the periphery of neoplastic acini, showed a nuclear expression of p63 (Fig. 2e). EMA highlighted the luminal surface of the oncocytes, whereas their cytoplasm was negative. Only terminally differentiated sebaceous cells were strongly positive for EMA and CK14 (Fig. 2f). Ductal basal and parabasal cells in the sebaceous glands were positive for CK19, CK5/6, and HMWK (Fig. 2b,c). The basal and parabasal cells in the ducts of sebaceous glands also expressed p63. CK20 was negative. No myoepithelial cells were present in the tumor as MSA, SMA, and calponin, were negative. Only the adipocytes in the mature adipose tissue were positive for S-100.

Discussion

Oncocytic lipoadenoma is a recently described benign salivary gland neoplasm composed of an oncocytic epithelial component intimately admixed with mature adipose tissue [2, 8]. The clinical and pathologic features of the cases reported in the English literature are summarized in

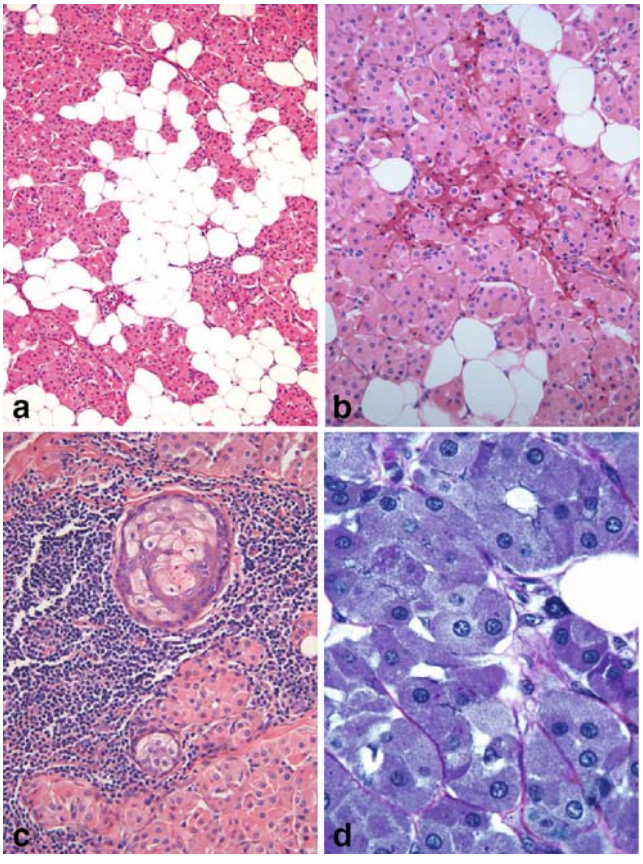

Fig. 1 **a** Sheets of oncocytes admixed with mature adipose tissue are characteristic of oncocytic lipoadenoma. **b** Oncocytic lipoadenoma demonstrating a mixture of "light" and "dark" cells. **c** Oncocytes with sebaceous glands surrounded by small lymphocytes. **d** PTAH demonstrating diffused cytoplasmic granularity consistent with large numbers of mitochondria within the tumor cells

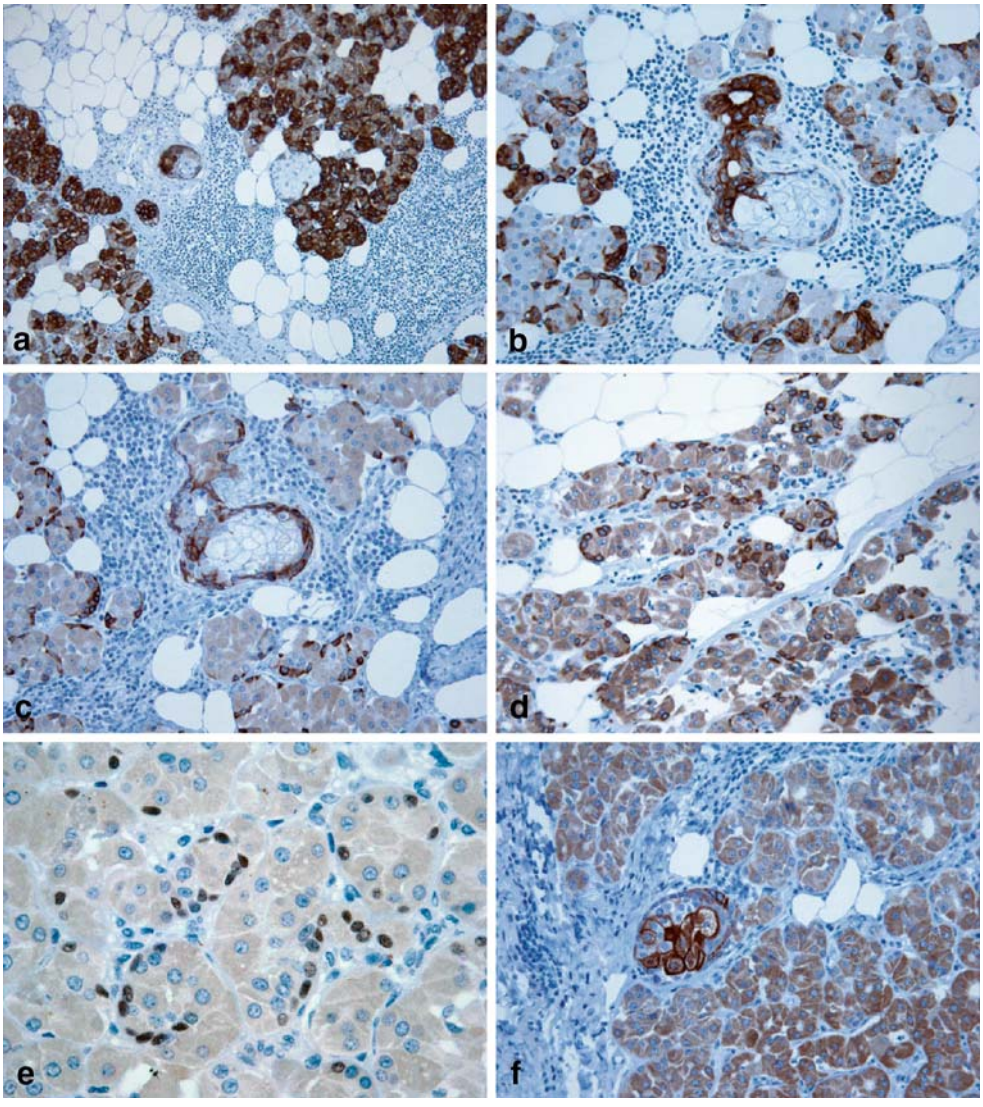

Fig. 2 **a** Oncocytic lipoadenoma showing diffused strong expression of CK7. The sebaceous cells are negative. **b** CK19 is expressed by ductal cells in sebaceous glands and peripheral cells at the periphery of neoplastic acini. Most oncocytes are negative as are sebaceous cells. **c** CK5/6 is positive in cells mainly located at the periphery of neoplastic acini and sebaceous glands. Oncocytes and sebaceous cells are negative. **d** HMWK-staining cells at the periphery of the acini. **e** Nuclear expression of p63 is seen in some cells of this oncocytic lipoadenoma. **f** CK14 is positive only in sebaceous glands. The oncocytes are negative but note their non-specific cytoplasmic granular staining

Table 1. All three cases have affected major salivary glands of adult women. Oncocytic lipoadenomas are encapsulated neoplasms composed of oncocytes similar to those of conventional salivary gland oncocytomas with "light" and "dark" cells [2, 5]. In addition, oncocytic lipoadenoma shows a mature adipose tissue within the tumor capsule, a feature not present in conventional oncocytomas [3]. The presence of this capsule also separates oncocytic lipoadenoma from oncocytosis, a condition defined as "the formation of micronodules as a result of oncocytic metaplasia and hyperplasia of small and large ducts" [3, 5]. Our case expands the morphologic spectrum of oncocytic lipoadenoma because, in addition to the oncocytic and adipose tissue elements, the tumor demonstrated sebaceous metaplasia, a hitherto unreported association. Sebaceous differentiation in benign salivary gland tumors, other than sebaceous adenoma and sebaceous lymphadenoma, has been variously reported as being relatively uncommon [5] to "reasonably" frequent [4] and has been noted in pleomorphic adenoma, oncocytoma, sialoblastoma, and Warthin tumor [3, 5]. Oncocytic lipoadenoma should be added to the list of benign salivary gland neoplasms with the potential of developing sebaceous metaplasia.

Table 1 Salivary gland oncocytic lipoadenoma (clinical features)

	Sex	Age	Site	Size (cm)	Follow-up
Hirokawa et al. [7]	Female	66	Submandibular gland	11	AND, 30 months
Kato and Horie [8]	Female	57	Parotid gland	4.5	NA
Current case	Female	47	Parotid gland	3.0	AND, 6 months

AND alive no disease, *NA* not available.

The pathologic diagnosis of benign oncocytic neoplasms in salivary gland is relatively straightforward, a fact that may explain the paucity of studies investigating their keratin profile [9, 11]. We found that the oncocytes in this oncocytic lipoadenoma were diffusely and strongly positive for LMWK and CK7. These results are in agreement with previous reports that indicate that between 100 and 90% of conventional salivary gland oncocytomas are positive for LMWK and CK7, respectively [9, 11]. We noted that the oncocytes demonstrated a typical luminal pattern when stained with EMA, a pattern recently described by Ozolek et al. [9], and are consistent with the ultrastructural presence of glandular lumens and luminal cell differentiation [4]. We also found that most of the oncocytes were negative for high-molecular-weight keratins—investigated by HMWK and CK5/6—and CK19; however, we noted a subpopulation of cells expressing these keratins. In addition, many of these cells also demonstrated nuclear staining for p63. This expression pattern for keratin suggests the presence of a dual epithelial population within this tumor, a finding in agreement with previous observations in conventional oncocytomas [1, 6]. Askew et al. [1] regarded this dual cell population as being composed of "epithelial" and "myoepithelial" oncocytes; however, subsequent ultrastructural [4, 6] and immunophenotypical [9, 11] observations have failed to demonstrate a myoepithelial component in salivary gland oncocytomas. Gustafsson et al. [6] suggested that this dual cell population—one packed with mitochondria and virtually without filaments and the second showing fewer mitochondria but with large amounts of keratin filaments—likely represented different degrees of "pure" epithelial differentiation rather than ductal and myoepithelial differentiation. The nature of this second cell population in our tumor remains unclear. The expression of CK5/6, HMWK, and p63 by these tumor cells in this oncocytic lipoadenoma are suggestive of partial basal-cell differentiation [10], although lack of CK14 staining and expression of CK19 are not features seen in normal basal cells. The presence and nature of a dual epithelial population with ductal and possibly aberrant basal-cell differentiation in oncocytic lesion of salivary glands warrant further investigation. The lack of staining for actins and calponin in our case supports the absence of a myoepithelial participation in oncocytic lipoadenoma.

References

1. Askew JB Jr, Bentinck DC, Jenson AB, Fechner RE (1971) Epithelial and myoepithelial oncocytes. Ultrastructural study of a salivary gland oncocytoma. Arch Otolaryngol 93:46–54
2. Barnes L, Eveson JW, Reichart P, Sidransky D (2005) Tumors of the salivary glands. World Health Organization classification of tumors. Pathology and genetics head and neck. IARC Press, Lyon, pp 209–281
3. Brandwein MS, Huvos AG (1991) Oncocytic tumors of major salivary glands: a study of 68 cases with follow-up of 44 patients. Am J Surg Pathol 15:514–528
4. Dardick I, Kini S, Bradley G, Lee L, Leong I (2006) Salivary gland tumor cytopathology, oral and surgical pathology. Pathology Images Inc., Ottawa
5. Ellis GL, Auclair PL (1996) Benign epithelial neoplasms. In: Rosai J, Sobin LH (eds) Tumors of the salivary glands. Atlas of tumor pathology, third series. Armed Forces Institute of Pathology, Washington, District of Columbia, pp 39–153
6. Gustafsson H, Kjorell U, Carlsoo B (1985) Cytoskeletal proteins in oncocytic tumors of the parotid gland. Arch Otolaryngol 111:99–105
7. Hirokawa M, Shimizu M, Manabe T, Ito J, Ogawa S (1998) Oncocytic lipoadenoma of the submandibular gland. Human Pathol 29:410–412
8. Kato M, Horie Y (2000) Oncocytic lipoadenoma of the parotid gland. Histopathology 36:285–286
9. Ozolek JA, Bastacky SI, Myers EN, Hunt JL (2005) Immunophenotypic comparison of salivary gland oncocytoma and metastatic renal cell carcinoma. Laryngoscope 115:1097–1100
10. Reis-Filho JS, Simpson PT, Martins A, Preto A, Gartner F, Schmitt FC (2003) Distribution of p63, cytokeratins 5/6 and cytokeratin 14 in 51 normal and 400 neoplastic human tissue samples using TARP-4 multi-tumor tissue microarray. Virchows Arch 443:122–132
11. Thompson LD, Wenig BM, Ellis GL (1996) Oncocytomas of the submandibular gland. A series of 22 cases and a review of the literature. Cancer 78:2281–2287

Results and discussion

The lung revealed a 1.3-cm well-circumscribed soft yellow nodule with bulging cut surface (Fig. 1). Microscopic examination showed that the tumor was comprised almost entirely of lipid-laden CD68+ macrophages. The tumor cells were diffusely immunopositive for Factor XIIIa, ALK-1, and vimentin. Follicular structures (Fig. 2) were identified throughout the tumor. Cells comprising the follicular structures stained intensely for ALK-1, CD1a, fascin, and S100. The tumor showed diffuse cytoplasmic staining for fat as judged by Oil-Red-O, but the follicular structures were largely devoid of fat (Fig. 3). Special stains for bacteria, fungus, and mycobacteria were negative. HHV-8 antigen was expressed by the majority of tumor cells as judged by immunostaining (Fig. 4). Infrequent and scattered cells were positive for CD21 and smooth muscle actin. An EBV RNA probe was negative. The patient's prior Hodgkin lymphoma was negative for both HHV-8 and EBV expression.

According to the current World Health Organization (WHO) classification [14], "inflammatory myofibroblastic tumor" (IMT) includes tumors previously classified as inflammatory pseudotumor, fibroxanthoma, fibrous histiocytoma, pseudosarcomatous myofibroblastic tumor, invasive fibrous tumor of the tracheobronchial tree, xanthogranuloma, plasma cell granuloma, or plasma cell granuloma–histiocytoma complex [12]. As suggested by these terms, the recognized histologies included under the rubric of "IMT" are varied.

IMT is currently thought to represent either a low-grade mesenchymal malignancy or reactive inflammation [14]. In the present case, the tumor cells were comprised virtually entirely of CD68+, Factor XIIIa+, and ALK-1+ macrophages. It was distinguished by the presence of unusual epithelioid follicular structures scattered throughout the lesion. CD1a, fascin, and S100 staining was limited to cells in the follicular structures. ALK-1 expression was enhanced in the follicular structures with weak staining of the adjacent tumor cells. Factor XIIIa staining was diminished in the follicles. CD34 stained blood vessels in the tumor, but the tumor cells were negative.

Fig. 1 Lung contains a well-circumscribed yellow tumor with bulging cut surface

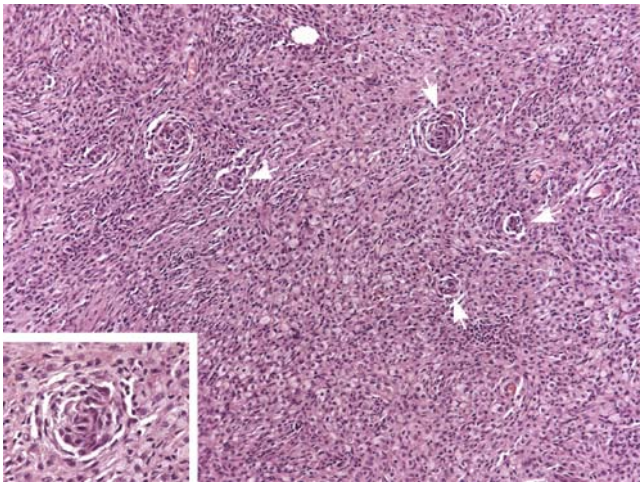

Fig. 2 The tumor shows xanthomatous macrophages and discrete follicular structures (*arrowheads*). The follicular structures include spindled and foamy mesenchymal cells (H&E. Original magnifications ×100, *inset* ×400)

Factor XIIIa was expressed diffusely by the xanthomatous macrophages. Factor XIIIa is a plasma transglutaminase that plays a critical role in the cross-linking of the fibrin clot. It is synthesized by human pulmonary macrophages and dermal dendrocytes. Factor XIIIa labels cells of a variety of benign reactive lesions, including xanthogranuloma, xanthoma disseminatum, and dermatofibroma. The presence of Factor XIIIa+ cells in the present tumor supports its classification as a xanthogranuloma [3], whereas the absence of myofibroblastic differentiation argues against a myofibroblastic lineage.

Cells within the follicular structures were distinguished by their specific staining for CD1a, fascin, ALK-1, and S100. These lesions crudely resembled the follicular structures that are seen in Castleman's disease [10]. Rosai and others have suggested that IMTs are proliferative disorders of the accessory immune system. The latter includes T- and B-cell-related dendritic cells, as well as the so-called fibroblastic reticulum cells, myoid cells, and dictyocytes [8]. Pileri et al. have reported that dendritic cell neoplasms and Langerhans cell tumors express CD68, CD1a, and S100, comparable to the cells seen in the follicular structures of the present case [9]. Fascin expres-

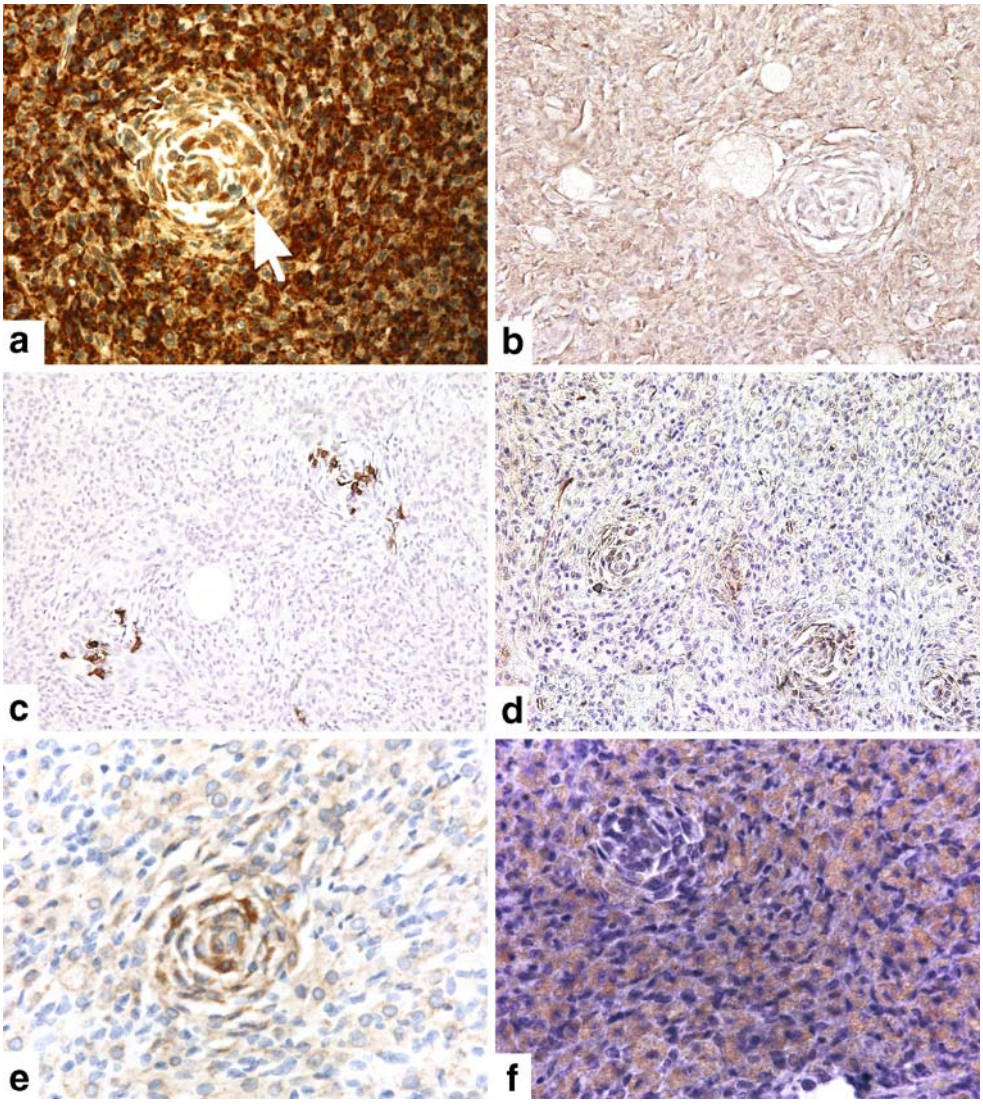

Fig. 3 **a** Tumor cells stain diffusely positive for CD68 in both follicular structures (*arrow*) and extrafollicular cells (peroxidase. Original magnification ×400). **b** Factor XIIIa stain is most pronounced in extrafollicular cells (peroxidase. Original magnification ×200). **c** CD1a stain is exquisitely limited to follicular structures (peroxidase. Original magnification ×200). **d** Fascin staining is concentrated in follicular structures (peroxidase. Original magnification ×200). **e** ALK-1 stains the tumor cells diffusely with enhanced expression within follicular structures (peroxidase. Original magnification ×400). **f** Fat is diffusely present in extrafollicular macrophages and is diminished within the follicular structures (Oil-Red-O. Original magnification ×400)

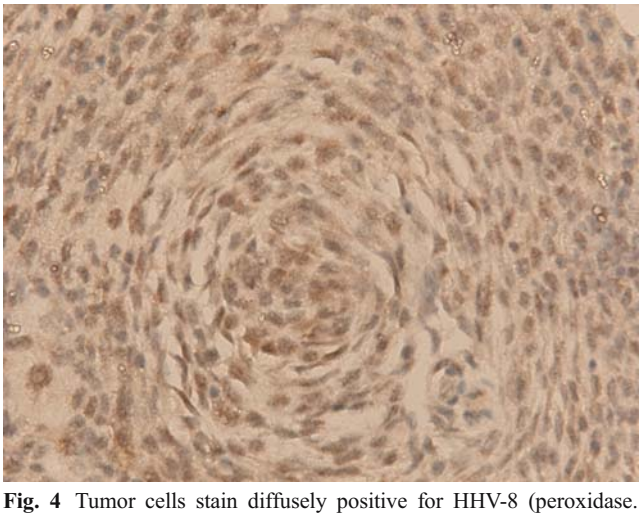

Fig. 4 Tumor cells stain diffusely positive for HHV-8 (peroxidase. Original magnification ×400)

sion has been reported in the T-cell-related interdigitating dendritic cell lineage, including closely related Langerhans cells [8]. ALK-1 has been demonstrated in approximately 40% of IMT, but its cell of origin in these tumors is uncertain [14]. The localization of accessory dendritic cells in the follicular structures of the present case suggests their ability to organize into compartmentalized microstructures within the tumor.

Table 1 Infections that yield the morphological changes of inflammatory myofibroblastic tumor

Organism	IMT-related morphologies	Reference(s)
Actinomyces	Yes	[12]
Campylobacter jejuni	Yes	[12]
Histoplasma	Yes	[12]
Q fever	Yes	[7]
Mycobacteria	AIDS, kidney transplant	[1, 2, 13]
Human herpes virus-8	Yes	[5, 6]

The expression of HHV-8 genes has been previously reported in pulmonary IMT [4–6]. Gomez-Roman et al. identified HHV-8 molecular transcripts in five cases of pulmonary IMT. The proteins encoded by these transcripts included human homologous oncoproteins (viral cyclin-D), inflammatory cytokines (viral IL-6), and inhibitors of apoptotic pathways (viral FLIP and viral Bcl-2), mostly expressed in a latent viral replicative stage [6].

Tumors with histologies comparable to IMT have been observed in a variety of other infections including *Campylobacter jejuni*, *Actinomyces*, *Coxiella burnetti*, and *Histoplasma* [7, 12]. Atypical mycobacterial infection has been associated with spindle-cell pseudotumors of lymph nodes [1, 2, 13], skin [1], and bone marrow [13] in patients with acquired immunodeficiency syndrome (AIDS) (see Table 1). A spindle-cell pseudotumor associated with *Mycobacterium tuberculosis* has also been reported in a transplant patient [11]. In most of these cases, the patients have been immunosuppressed.

The present case appears to represent a proliferation of Factor XIIIa+ xanthomatous macrophages with compartmentalized accumulation of Langerhans cells and no myofibroblastic differentiation. It further suggests possible links between Hodgkin disease, treatment-related immunosuppression, opportunistic infection by HHV-8, and benign proliferation of the accessory immune cells. The specific role of HHV-8 infection in eliciting this response is uncertain. Although the current WHO system of classification simplifies the diagnosis of pulmonary inflammatory pseudotumors, by virtue of including a wide variety of morphologic patterns under the category of IMT, there is concern that it may potentially obfuscate associations between morphology and specific pathogenesis. Further consideration of this issue is warranted.

Acknowledgments Funding was provided by the Massachusetts General Hospital Pathology Service James Homer Wright Pathology Laboratories. The experiments performed comply with the current laws of the United States of America.

References

1. Brandwein M, Choi HS, Strauchen J, Stoler M, Jagirdar J (1990) Spindle cell reaction to nontuberculous mycobacteriosis in AIDS mimicking a spindle cell neoplasm. Evidence for dual histiocytic and fibroblast-like characteristics of spindle cells. Virchows Arch A Pathol Anat Histopathol 416:281–286
2. Chen KT (1992) Mycobacterial spindle cell pseudotumor of lymph nodes. Am J Surg Pathol 16:276–281
3. Dabbs DJ (2002) "Immunohistochemistry of skin tumors". Diagnostic immunohistochemistry. Churchill Livingstone, New York, p 318
4. Ding Y, Saylors RL, Brown H, Parham DM (2002) Pulmonary inflammatory pseudotumor with HHV-8. Am J Surg Pathol 26:1089–1091
5. Gomez-Roman JJ, Ocejo-Vinyals G, Sanchez-Velasco P, Nieto EH, Leyva-Cobian F, Val-Bernal JF (2000) Presence of human herpesvirus-8 DNA sequences and overexpression of human IL-6 and cyclin D1 in inflammatory myofibroblastic tumor (inflammatory pseudotumor). Lab Invest 80:1121–1126
6. Gomez-Roman JJ, Sanchez-Velasco P, Ocejo-Vinyals G, Hernandez-Nieto E, Leyva-Cobian F, Val-Bernal JF (2001) Human herpesvirus-8 genes are expressed in pulmonary inflammatory myofibroblastic tumor (inflammatory pseudotumor). Am J Surg Pathol 25:624–629
7. Lipton JH, Fong TC, Gill MJ, Burgess K, Elliott PD (1987) Q fever inflammatory pseudotumor of the lung. Chest 92:756–757
8. Nonaka D, Birbe R, Rosai J (2005) So-called inflammatory myofibroblastic tumour: a proliferative lesion of fibroblastic reticulum cells? Histopathology 46:604–613
9. Pileri SA, Grogan TM, Harris NL, Banks P, Campo E, Chan JKC, Favera RD, Delsol G, Wolf-Peeters CD, Falin B, Gascoyne RD, Gaulard P, Gatter KC, Isaacson PG, Jaffe ES, Kluin P, Knowles DM, Mason DY, Mori S, Müller-Hermelink H-K, Piris MA, Ralfkiaer E, Stein H, Su I-J, Warnke RA, Weiss LM (2002) Tumours of histiocytes and accessory dendritic cells: an immunohistochemical approach to classification from the International Lymphoma Study Group based on 61 cases. Histopathology 41:1–29
10. Schnitzer B (2000) The Reactive Lymphadenopathies. In: Knowles DM (ed) Neoplastic hematopathology. Williams and Wilkins, Philadelphia, PA, pp 537–568
11. Sekosan M, Cleto M, Senseng C, Farolan M, Sekosan J (1994) Spindle cell pseudotumors in the lungs due to Mycobacterium tuberculosis in a transplant patient. Am J Surg Pathol 18:1065–1068
12. Travis WD, Colby TV, Koss MN, Rosado-de-Christenson ML, Müller NL, Talmadge E, King J (2002) Miscellaneous diseases of uncertain etiology: inflammatory myofibroblastic tumor (inflammatory pseudotumor). In: King DW (ed) Atlas of nontumor pathology: non-neoplastic disorders of the lower respiratory tract. Armed Forces Institute of Pathology, Bethesda, Maryland, pp 857–867
13. Umlas J, Federman M, Crawford C, O'Hara CJ, Fitzgibbon JS, Modeste A (1991) Spindle cell pseudotumor due to Mycobacterium avium-intracellulare in patients with acquired immunodeficiency syndrome (AIDS). Positive staining of mycobacteria for cytoskeleton filaments. Am J Surg Pathol 15:1181–1187
14. Yousem SA, Tazelaar HD, Manabe T, Dehner LP (2004) Inflammatory myofibroblastic tumor. In: Travis WD, Brambilla E, Müller-Hermelink HK, Harris CC (eds) Pathology and genetics of tumours of the lung, pleura, thymus and heart. IARC Press, Lyon, pp 105–106

tests, complete blood count, and coagulation tests were normal. Testing for hepatitis B surface antigen and hepatitis C antibodies were negative. Echinococcal serology was negative. Serum tumor markers (alpha-fetoprotein, CA 19-9, and carcinoembryonic antigen) were within the normal range. Abdominal ultrasonography detected in the liver a well-delineated, unilocular, avascular, hypoechoic lesion of 60 mm in diameter located in the medial segment of the left lobe (segment IV). On unenhanced computed tomography (CT), the lesion was hyperdense relative to surrounding liver parenchyma (Fig. 1). At contrast material-enhanced CT, the lesion was not enhanced with well-defined margin and an internal calcification. Magnetic resonance imaging at 1.5 T was performed for more detailed examination. The lesion appeared homogeneously hyperintense relative to surrounding liver parenchyma on T1 and T2-weighted images. It was also not enhanced after Gd-DTPA administration. The diagnosis of a cystic lesion with protein content was done and laparoscopic surgical removal of the lesion was indicated.

The lesion was subcapsularly located in the segment IV of the liver and attached to the gallbladder. There was no communication between the lesion and the gallbladder as demonstrated by a cholangiography performed during surgery. The lesion was removed with the gallbladder by enucleation.

Materials and methods

The specimen was routinely formalin-fixed, paraffin-embedded, and cut. Microscopic slides were stained by hematoxylin–phloxine–saffron, periodic acid Schiff, and Alcian blue. Immunohistochemical stainings were performed using the labeled streptavidin–biotin method in a Bond-Max (Vision Biosystems) autostainer with the following antibodies : cytokeratin 5/6 (Dakocytomation), cytokeratin 7 (Dakocytomation), cytokeratin 19 (Dakocytomation), cytokeratin 20 (Dakocytomation), TTF-1 (LabVision), oestrogen receptor (Dakocytomation), and progesterone receptor (Biogenex).

Fig. 1 Unenhanced CT scan showing an hyperdense lesion with well-defined margin in the segment IV of the liver

Results

Macroscopically, the lesion consisted of a thin walled cyst measuring 60×40 mm. The internal and external surfaces were smooth (Fig. 2). The content was mucinous with a high level of CA19-9 (361 U/ml; normal<33 U/ml). At histological examination, the cyst was lined mainly by a regular squamous epithelium without keratin formation (Fig. 3a). The squamous epithelium cells expressed cytokeratin 5/6 (Fig. 3a) and cytokeratin 19. Cytokeratin 7 was expressed in the superficial squamous cells. Cytokeratin 20, TTF-1, estrogen receptor, and progesterone receptor immunostainings were negative. After extensive sampling, a ciliated pseudostratified columnar epithelium with some goblet cells was focally identified (Fig. 3b). Goblet cells were alcian blue, PAS, and PAS-diastase positive (Fig. 3b). The ciliated epithelium expressed cytokeratin 7 and cytokeratin 19. Cytokeratin 20, TTF-1, estrogen receptor, and progesterone receptor immunostainings were negative. There were no foci of ulceration or inflammation. The other layers of the wall were a loose subepithelial connective tissue, smooth-muscle bundles, and a fibrous capsule where we found occasional small bile duct. The lesion was totally examined and there was no epithelial dysplasia or carcinoma.

Discussion

CHFC is a rare usually benign lesion of the liver that arise from the embryonic foregut like esophageal cyst and

Fig. 2 Macroscopy of the lesion with the gallbladder showing a thin whitish walled cyst, without ulceration

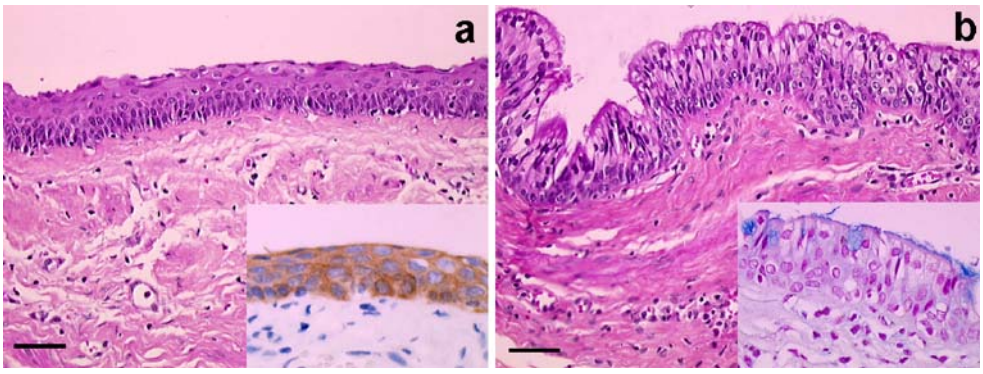

Fig. 3 Histology of the lesion (hematoxylin–phloxin–saffron, scale bar 50 μm). **a** Most areas corresponded to a squamous epithelium without dysplasia, expressing cytokeratin 5/6 (*inset*). **b** Some rare areas showed a ciliated pseudostratified columnar epithelium with alcian blue positive goblet cells (*inset*)

bronchogenic cyst. The latter is usually found in the mediastinum, but some intraabdominal or retroperitoneal cases have been described. In bronchogenic cysts, there is cartilage or respiratory glands and the epithelium is ciliated with possible focal or extensive squamous metaplasia. Esophageal cysts stay close to the esophageal wall, have a double layer of smooth muscle, and the lining epithelium may be squamous, ciliated, or a mixture. A ciliated cyst with no distinctive feature of bronchogenic or esophageal cyst is referred to as a foregut cyst [13]. It is usually a solitary unilocular asymptomatic lesion incidentally found on radiologic imaging. Rarely it causes portal hypertension by hepatic vein compression or jaundice by hepatic duct compression. The mean age of diagnosis is 50 years and there is a slight male predilection [11]. CHFC is usually located in the left liver lobe with a strong predilection for the segment IV, but it is also described in the right liver lobe, the gallbladder, the pancreas, or in retroperitoneal location [1, 5, 8]. One case communicated with the gallbladder through a duct [6]. The histological hallmark of CHFC is the presence of a pseudostratified ciliated epithelium. A ciliated epithelium is also present in mullerian cysts. Retroperitoneal mullerian cysts have been described, but there is no case of intrahepatic mullerian cyst described so far to our knowledge [7]. Moreover in mullerian cysts, the epithelium is unistratified, without goblet cells and there is usually estrogen and/or progesterone receptor expression by the epithelial cells [7].

It is interesting to note that although squamous epithelium is frequently observed in bronchogenic and esophageal cysts, it is very rare is hepatic foregut cysts. Indeed, it has never been described in the largest series including one with an extensive literature review [1, 11]. To our knowledge, the only three cases of CHFC with squamous metaplasia described so far were always associated with a squamous carcinoma [2, 3, 12]. This could suggest that squamous metaplasia in CHFC is rare, and that when it appears, it rapidly degenerates into carcinoma. The presence of foci of dysplasia in association with the squamous carcinoma in these cases suggest a progression from nondysplastic epithelium to dysplasia and then to carcinoma. Squamous metaplasia has also been described in biliary cysts also associated with squamous carcinoma [9]. Finally, some cases of squamous liver cysts without any other qualification have been reported [10]. The origin of these cysts remains unclear and they could correspond to ciliated foregut or biliary cysts with extensive squamous metaplasia.

Because CHFC is the only known ciliated lesion in the liver, aspiration cytology can give the diagnosis when it shows ciliated epithelial cells admixed with hepatocytes and mucous cells [4]. However, in case of extensive squamous metaplasia as in our case, it can miss the diagnosis. Because some cases of squamous carcinoma have been described in CHFC, surgical removal of the lesion may be more appropriate than close follow-up or sclerosing therapy.

To conclude, squamous epithelium may be seen in liver cysts. An extensive sampling of the lesion is then recommended to identify possible foci of squamous carcinoma and to classify more precisely the histological type of the lesion that could correspond to a biliary cyst or a CHFC.

References

1. Chatelain D, Chailley-Heu B, Terris B, Molas G, Le Cae A, Vilgrain V, Belghiti J, Degott C, Flejou JF (2000) The ciliated hepatic foregut cyst, an unusual bronchiolar foregut malformation: a histological, histochemical, and immunohistochemical study of 7 cases. Hum Pathol 31:241–246
2. de Lajarte-Thirouard AS, Rioux-Leclercq N, Boudjema K, Gandon Y, Ramee MP, Turlin B (2002) Squamous cell carcinoma arising in a hepatic forgut cyst. Pathol Res Pract 198:697–700
3. Furlanetto A, Dei Tos AP (2002) Squamous cell carcinoma arising in a ciliated hepatic foregut cyst. Virchows Arch 441:296–298
4. Hornstein A, Batts KP, Linz LJ, Chang CD, Galvanek EG, Bardawil RG (1996) Fine needle aspiration diagnosis of ciliated hepatic foregut cysts: a report of three cases. Acta Cytol 40:576–580
5. Kajiya Y, Nakajo M, Ichinari N, Yamazumi K, Otuji T, Tanaka T (1997) Retroperitoneal foregut cyst. Abdom Imaging 22:111–113

6. Koletsa T, Tzioufa V, Michalopoulos A, Apostolidis S, Papadopoulos B, Hytiroglou P (2005) Ciliated hepatic foregut cyst communicating with the gallbladder. Virchows Arch 446:200–201
7. Konishi E, Nakashima Y, Iwasaki T (2003) Immunohistochemical analysis of retroperitoneal mullerian cyst. Hum Pathol 34:194–198
8. Munshi IA, Parra-Davila E, Casillas VJ, Sleeman D, Levi JU (1998) Ciliated foregut cyst of the pancreas. HPB Surg 11:117–119
9. Pliskin A, Cualing H, Stenger RJ (1992) Primary squamous cell carcinoma originating in congenital cysts of the liver. Report of a case and review of the literature. Arch Pathol Lab Med 116:105–107
10. Schullinger JN, Wigger HJ, Price JB, Benson M, Harris RC (1983) Epidermoid cysts of the liver. J Pediatr Surg 18:240–242
11. Vick DJ, Goodman ZD, Deavers MT, Cain J, Ishak KG (1999) Ciliated hepatic foregut cyst: a study of six cases and review of the literature. Am J Surg Pathol 23:671–677
12. Vick DJ, Goodman ZD, Ishak KG (1999) Squamous cell carcinoma arising in a ciliated hepatic foregut cyst. Arch Pathol Lab Med 123:1115–1117
13. Wheeler DA, Edmondson HA (1984) Ciliated hepatic foregut cyst. Am J Surg Pathol 8:467–470

Virchows Arch (2006) 449:734
DOI 10.1007/s00428-006-0341-z

ANNOUNCEMENTS

© Springer-Verlag 2006

24–26 January 2007

Theorico-practical Course on Bone and Soft Tissue Tumors

Department of Pathology, Hospital del Mar, Barcelona, Spain

Faculty

Christopher Fletcher, M.D. (Brigham and Women's Hospital, Boston, USA)

Andrew Rosenberg, M.D. (Massachusetts General Hospital, Boston, USA)

Angelo Paolo Dei Tos, M.D. (Hospital of Treviso, Italy)

John Goldblum, M.D. (Cleveland Clinic, Cleveland, USA)

Paola Dal Cin, Ph.D. (Brigham and Women's Hospital, Boston, USA)

For further information please contact:

Francisco Alameda, M.D.
Department of Parthology
Hospital del Mar, Spain
E-mail: 86780@imas.imim.es
or
Esther Oliva, M.D.
Department of Pathology
Massachusetts General Hospital
55 Fruit Street, WRN-2
Boston, MA 02114, USA
E-mail: eoliva@partners.org